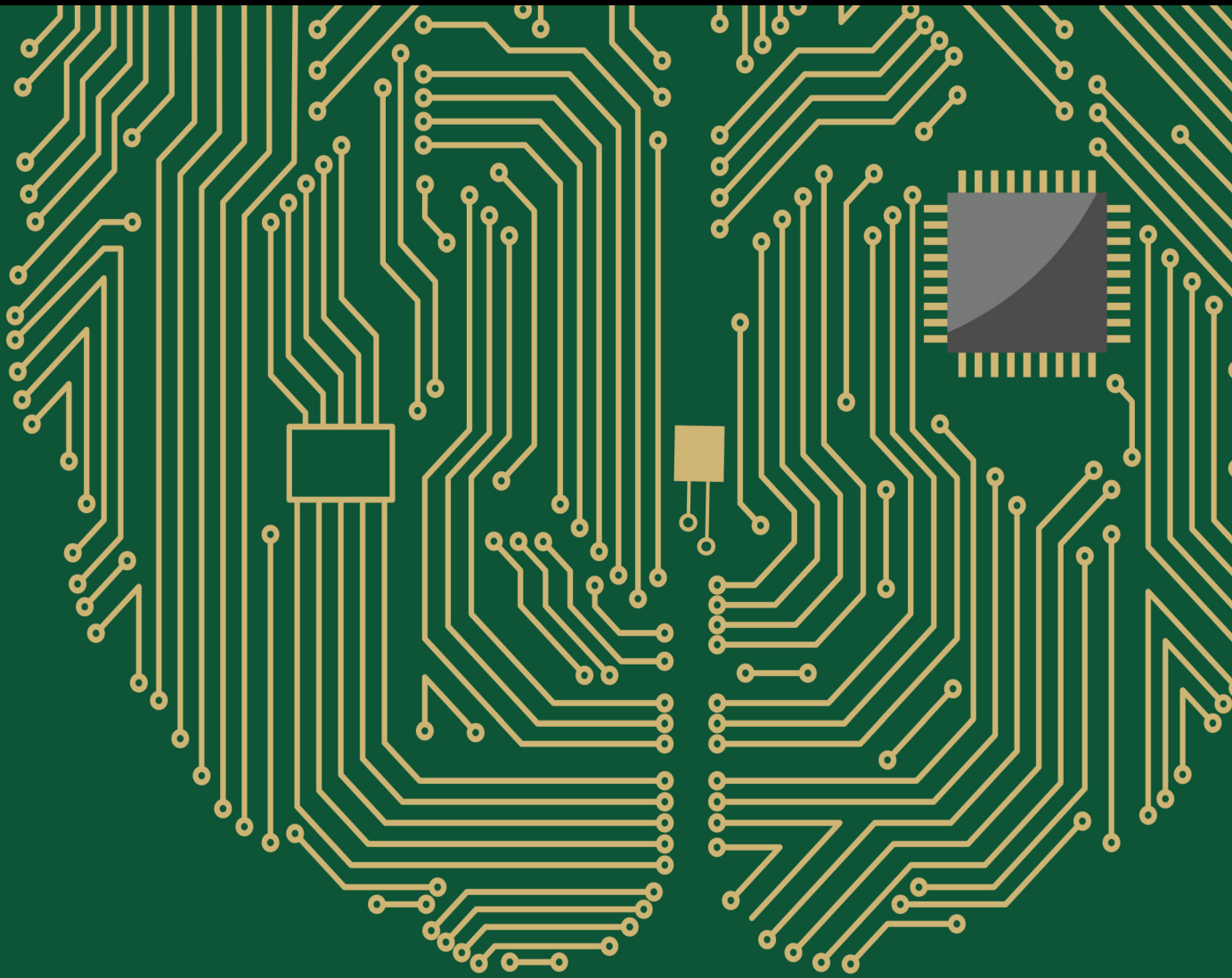# Human Behavior Modelling in Engineering Management under Industry 4.0

Lead Guest Editor: Huihua Chen
Guest Editors: Xiao-Wei Luo, Hanliang Fu, Zhangpeng Tian, and Ruoyu Jin

Human Behavior Modelling in Engineering Management under Industry 4.0

Human Behavior Modelling in Engineering Management under Industry 4.0

Lead Guest Editor: Huihua Chen
Guest Editors: Xiao-Wei Luo, Hanliang Fu, Zhangpeng Tian, and Ruoyu Jin

Contents

Contents

Contents

Contents

Contents

Retraction

Retracted: Sports Economic Operation Index Prediction Model Based on Deep Learning and Ensemble Learning

Computational Intelligence and Neuroscience

This article has been retracted by Hindawi following an investigation undertaken by the publisher [1]. This investigation has uncovered evidence of one or more of the following indicators of systematic manipulation of the publication process:

(1) Discrepancies in scope

(2) Discrepancies in the description of the research reported

(3) Discrepancies between the availability of data and the research described

(4) Inappropriate citations

(5) Incoherent, meaningless and/or irrelevant content included in the article

(6) Peer-review manipulation

The presence of these indicators undermines our confidence in the integrity of the article's content and we cannot, therefore, vouch for its reliability. Please note that this notice is intended solely to alert readers that the content of this article is unreliable. We have not investigated whether authors were aware of or involved in the systematic manipulation of the publication process.

Wiley and Hindawi regrets that the usual quality checks did not identify these issues before publication and have since put additional measures in place to safeguard research integrity.

We wish to credit our own Research Integrity and Research Publishing teams and anonymous and named external researchers and research integrity experts for contributing to this investigation.

The corresponding author, as the representative of all authors, has been given the opportunity to register their agreement or disagreement to this retraction. We have kept a record of any response received.

References

[1] C. Yang and J. Chen, "Sports Economic Operation Index Prediction Model Based on Deep Learning and Ensemble Learning," *Computational Intelligence and Neuroscience*, vol. 2022, Article ID 9085349, 12 pages, 2022.

Retraction

Retracted: Value Proposition for Enabling Construction Project Innovation by Applying Building Information Modeling

Computational Intelligence and Neuroscience

This article has been retracted by Hindawi following an investigation undertaken by the publisher [1]. This investigation has uncovered evidence of one or more of the following indicators of systematic manipulation of the publication process:

(1) Discrepancies in scope

(2) Discrepancies in the description of the research reported

(3) Discrepancies between the availability of data and the research described

(4) Inappropriate citations

(5) Incoherent, meaningless and/or irrelevant content included in the article

(6) Peer-review manipulation

The presence of these indicators undermines our confidence in the integrity of the article's content and we cannot, therefore, vouch for its reliability. Please note that this notice is intended solely to alert readers that the content of this article is unreliable. We have not investigated whether authors were aware of or involved in the systematic manipulation of the publication process.

Wiley and Hindawi regrets that the usual quality checks did not identify these issues before publication and have since put additional measures in place to safeguard research integrity.

We wish to credit our own Research Integrity and Research Publishing teams and anonymous and named external researchers and research integrity experts for contributing to this investigation.

The corresponding author, as the representative of all authors, has been given the opportunity to register their agreement or disagreement to this retraction. We have kept a record of any response received.

References

[1] H. Liu, Q. Ju, N. Zhao, H. Li, and M. J. Skibniewski, "Value Proposition for Enabling Construction Project Innovation by Applying Building Information Modeling," *Computational Intelligence and Neuroscience*, vol. 2022, Article ID 2586307, 13 pages, 2022.

Research Article

The Influence of Mutual Assistance of Construction Workers with Different Personality Traits on Team Safety

Keqing Li [ID],[1] **Ting-Kwei Wang** [ID],[2] **Anyuan Yu** [ID],[1] **and Jieh-Haur Chen** [ID][3]

[1]*School of Management Science and Real Estate, Chongqing University, Chongqing 400045, China*
[2]*Department of Civil Engineering, National Kaohsiung University of Science and Technology, Kaohsiung 80778, Taiwan*
[3]*Department of Civil Engineering, National Central University, Taoyuan 32001, Taiwan*

Correspondence should be addressed to Ting-Kwei Wang; tingkwei@nkust.edu.tw

Construction workers' unsafe behaviors are closely related to construction safety performance. Most existing studies on construction workers' personality traits and safety behaviors have ignored the flexibility of worker mix at construction sites, the dynamics of workers' behaviors, and the complexity of environmental risks at construction sites. Based on the cognitive process of construction workers' safety behaviors and from the perspective of personality traits, this research establishes an agent-based model of steelworkers' mutual assistance behavior. The AnyLogic platform is adopted to show emerging phenomena in complex problems. Through simulation experiments, the optimized configuration of construction team members under different risk environments can be obtained. This research is conducive to project managers to understand the influence of construction workers' mutual assistance on team safety, assess workers' potential for safe work before recruitment, and carry out active safety management from the source instead of looking for the cause of the accident afterward, making safety management theory more realistic and dynamic.

1. Introduction

According to statistics, the construction industry employs approximately 6%–10% of the labor force but accounts for 20%–40% of occupational fatal accidents [1]. The frequent occurrence of accidents makes the safety problem of building construction very serious. Researchers [2–4] analyzed the relevant data on accidents and found that the unsafe behavior of the construction personnel was the fuse for the accident. Even in the same situation, construction workers will have different behaviors. This is because, besides being affected by environmental factors, workers' behavior is also affected by personal characteristics. Many studies [5, 6] have identified personality as one factor that significantly affects workers' safety performance. Personality can also be used to explain and predict human behavior and job performance [7]. Florez and Cortissoz [8, 9] show that workgroups with similar personalities can speed up project progress. Also, personality has been proven to be related to

risk perception [10], risk propensity [10], risk preference [11], unsafe behavior [11], and social behavior [12]. Although researchers have explored the relationship between workers' unsafe behaviors and personality traits, existing studies hardly consider the dynamic effects of personality traits on worker behavior and interactions between workers and the external environment.

Complex construction tasks exist on the construction site. Some traditional research methods, such as the field observation method [13] and qualitative analysis method [14], can only analyze the static state of the project but cannot capture the processes of on-site dynamic changes. Therefore, it is necessary to investigate methods that can capture the nature of dynamic site changes as well as the impacts of different personality traits.

Computer simulation technology provides a good way to solve complex systemic problems [15]. By reproducing relevant scenarios in the real world and setting parameter ranges in simulation experiments to observe changes at the

macro level, the shortcomings of traditional analysis methods such as limited data, excessive interference factors, and difficulty in controlling variables [16] can be effectively avoided. Agent-based modeling (ABM) is a classic research method to explore changes in macroscopic results caused by microinteractions [17]. Aiming at the workers in the construction team and considering the mutual assistance of on-site workers and workers and the interactions with the external environment, an agent model is established in this study based on the cognitive process of behavior.

2. Literature Review

2.1. Big Five Personality Traits and Behaviors.
In the construction industry, many researchers studied the factors that influence individual unsafe behaviors from the perspective of psychology. Neal and Griffin [18] proposed that personality traits affect safety behaviors and can affect safety results. Lingard and Rowlinson [19] found that there are almost no workplaces where personality does not affect work-related behaviors. Since accidents are caused by a series of events and the agents of these events are a person. Therefore, it is vital to understand the relationship between the personality characteristics of people and the high incidence of human error accidents on construction sites [20]. The Big Five personality traits, proposed by McCrae and Costa [21], are the version accepted by most psychologists, including five dimensions of extraversion, agreeableness, conscientiousness, neuroticism, and openness. In interviews, self-descriptions and observations, as well as a wide range of participants of different ages and different cultures, showed consistency [22].

Many researchers have studied the correlation between Big Five personality traits and the unsafe behavior of construction workers. Geller [23] took construction workers as the research object and explored the correlation between the five characteristics of the Big Five personality traits and unsafe behaviors through a questionnaire survey. Similarly, Clarke [24] also found that workers' accident tendency is closely related to their personality traits. Although an individual's personality traits do not directly determine whether unsafe behaviors occur, they can have an important impact on the main actions in the process of unsafe cognition. As far as risk perception is concerned, different individuals have different perceptions of risks. Different individuals have different cognitions and understandings of the origin of different risks, the composition of risks, and the severity of risks [25].

Chauvin et al. [26] found that the environment faced by construction workers is complex and changeable when performing work tasks. When making risk decisions, they are often affected by personality factors. Myers et al. [27] found that the perception of risk is closely related to individual differences based on research. The risk assessment also involves the individual's risk tolerance. Risk tolerance is related to the number of risks, the qualitative characteristics of the hazards, the perceived benefits of risks, and personal acceptability. Faced with the same risk situation, everyone's risk tolerance is different. Risk tolerance is affected by factors such as personal characteristics, expected consequences, and safety culture [28]. Thanki [29] found a correlation between personality traits and risk tolerance. Bye and Lamvik [30] also proposed that personality traits are related to risk tolerance.

2.2. The Cognitive Process of Safe Behavior.
Many researchers found that the unsafe behaviors of construction workers mainly caused accidents. For the unsafe behavior of construction workers, the mechanism of unsafe behavior is the sorting out of the influencing factors of unsafe behavior and the construction of interrelationship to clarify the position and role of each influencing factor in the chain of unsafe behavior, which is a further deepening based on the analysis of influencing factors. With the in-depth study of psychology and social cognitive processes, Fang et al. [31] began to explain the mechanism of unsafe behavior from the perspective of safety cognition. Goh et al. [32] borrowed from the theory of planned behavior [33] to analyze and believes that unsafe behavior is the result of rational decision-making by construction workers. Chi et al. [34] pointed out that workers' unsafe behaviors are misjudgments or wrong decisions made in the cognitive process. From a physiological point of view, construction workers' cognitive status can also be assessed by valence, arousal, and dominance index in the valence-arousal-dominance (VAD) model [35], which can be measured by electroencephalography (EEG) [36]. By analyzing the three broadly influential cognitive models: Rasmussen's step-ladder model [37], Wickens et al.'s model of human information processing [38], and the IDAC model [39], Fang et al. [31] summarized the cognitive process of construction workers' unsafe behaviors into five stages: discovering information, understanding information, thinking and responding, choosing a response, and implementing the response. Among them, the failure of the choice response is the most important cause of unsafe behavior. Ye et al. [40] sorted out the influencing factors in the cognitive process and discussed the impact of the failure of the cognitive process on construction workers' unsafe behavior from the individual and the environment. The research summarizes the cognitive process into four stages: obtaining information, understanding information, choosing response, and taking action. Although there are differences in the details involved, these models all emphasize risk perception, risk assessment, and decision-making.

2.3. Workers' Mutual Assistance and Construction Safety.
With the continuous improvement and progress of various mechanisms in human society, the emotions and instincts of cooperation and mutual assistance between individuals have become increasingly mature [41]. The behavior of mutual assistance is very important to the work and life of the individual. Herman [42] believes that mutual assistance behavior is when others have certain needs, the behavior for satisfying the real needs of others. Anderson and Williams [43] believe that helping others deal with the problems encountered in work and life, that is, the behavior of colleagues in favor of others is a mutual assistance behavior.

In the construction and production activities, the team is not only closely related to the equipment, machinery, tools, and materials required in the construction and production activities but also the most basic organization that implements the various rules and regulations, construction technology, and on-site management activities in the construction enterprise. In the construction team, most of the construction workers come from the same place. They are not only the relationship of colleagues at work but also the relationship of friends in life. No matter in life or work, construction workers will care about their workers, help and cooperate, and strengthen emotional exchanges in daily activities. Mutual help behavior not only helps team members better establish interpersonal relationships and better adapt to the surrounding environment but also has important significance in completing construction tasks safely and improving the overall performance of the team.

In the field of construction safety, many researchers have researched the mutual assistance behavior of construction workers. Liang et al. [44] believe that workers often surpass team leaders and managers and have a more social influence on workers. Some researchers [45–47] regard worker mutual assistance as a dimension to evaluate the safety atmosphere of construction and verify the relationship between the safety mutual assistance of workers and workers and the safety atmosphere of the organization. Burt et al. [46] have further realized that workers who care about the safety of their colleagues play an important role in improving safety performance. The active care of workers may overcome (or supplement) the need for management to continuously monitor safety-related behaviors. Workers help ensure the safety of their colleagues by taking on this responsibility. Suppose the dominant attitude of each worker is to care about each other, and each worker actively identifies hazards and reminds workers. In that case, the safety performance of the team will be improved. Osama Jannadi et al.'s [48] research also shows that mutual safety assistance between colleagues positively impacts safety performance.

Safety mutual help between workers is mostly in the form of communication, such as reminding workers to abide by safety rules, sharing hazard information with workers, and discussing past accidents and safety improvement measures [45, 49]. These exchanges and mutual help will not only bring about the flow of information and knowledge and other organizational resources but also positively impact the members of the organization. Knowledge and experience sharing among colleagues can better promote performance [50]. Through safe and mutual help exchanges with workers, construction workers not only make it easier for construction workers to master the operating methods of the tools and machinery used but also avoid unsafe behaviors to the greatest extent.

3. Research Gap

Existing studies have explored the correlation between personality traits and the work behavior of construction workers through questionnaires, focusing on the psychological factors of the agents of construction activities. However, each worker's behavior is not the direct result of a factor but rather a combination of personal characteristics, mutual assistance with others, and interaction with the external environment. In a site environment with complex construction tasks, the variability of behavior caused by different personality traits, the interactivity caused by mutual assistance and cooperation with workers, and the dynamism caused by real-time adjustment of their behavior according to site changes make the interactive behavior of individual construction personnel at the individual level lead to changes at the project level.

Thus, traditional research methods, such as the field observation method and qualitative analysis, are only possible to analyze the project situation in a static state but not to capture the dynamic changing processes. In addition, although these studies can find universal rules and provide certain guiding significance, they ignore the composition of workers' personality traits, the interactions between workers and the external environment, and the influence of construction workers' mutual assistance on team safety. Furthermore, those studies do not consider the degree of environmental risk on the construction site.

4. Research Methodology

4.1. Overview. Due to the complexity of the construction tasks, characteristics of the individuals, and the changing environment, it is more difficult to use traditional methods to study the behavior changes of construction workers and their dynamic effects [51]. Using computer simulation technology to study the behavioral activities of interaction in building construction can actively change the parameters for control, avoid the interference of unrelated external factors on the experimental results, and achieve real experimental and control effects. It can also create a new research space for construction safety-related behaviors of construction workers from the perspective of technical methods [16].

In this study, firstly, based on the findings of existing literature, the relationship between the five personality traits in the Big Five personality theory and the key parameters (risk perception, risk tolerance) in the cognitive process of unsafe behavior of construction workers was synthesized. Then, based on the workers' key parameter attributes and their external environment, whether they perform unsafe behaviors or not is determined. Finally, while the cognitive process of workers' unsafe behaviors occurs, the possibility of cooperation and mutual assistance between workers and their surrounding colleagues is considered to explore the impact of individual behaviors on the overall team safety.

This study adopts an ABM approach to solve the problem of inconvenient control of variables such as external environmental factors and an individual's actual situation when personality trait factors are involved. A variety of combinations of workers with different personality traits are realized by dynamically adjusting the relevant parameters in order to explore the different combinations of workers' mutual assistance on the overall unsafe team behavior. This study simulates the impacts of safety and mutual assistance of workers with different personality traits on team safety and provides an optimized combination plan for team workers.
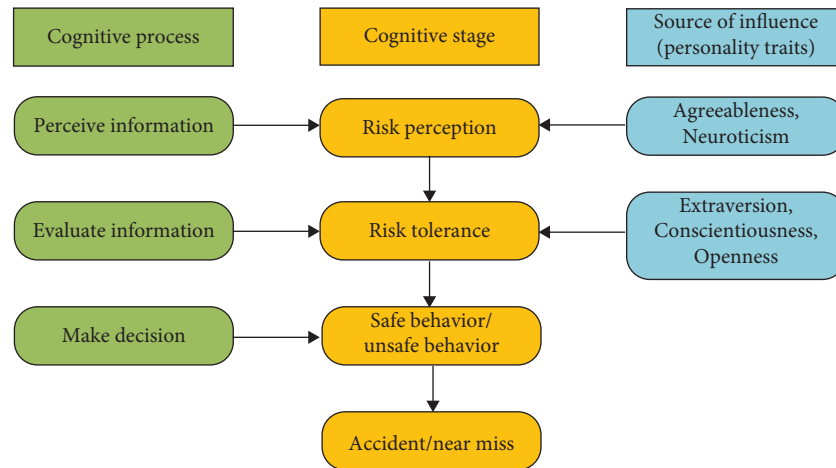
FIGURE 1: Framework of decision-making in the cognitive process of unsafe behavior of construction workers.

4.2. Model Framework. In recent years, research on theoretical models of cognition has matured and improved, providing a strong foundation for the scientific study and explanation of individual cognitive processes in many fields. The cognitive process of construction workers' unsafe behavior can be divided into three stages: perceiving information, evaluating information, and making decisions [52]. In the stage of perceiving information, workers perceive the risks from external information. This means the subjective judgment and assessment of the current danger when the individual is in an environment where danger may occur [53]. The risk level perceived by an individual is not only related to the true risk level [54], but risk perception is also affected by personal beliefs, attitudes, judgments, and feelings [55]. In studies on the Big Five personality traits and individual perceived risk, perceived risk is influenced by agreeableness [54] and neuroticism [26]. According to Sjöberg [54] and Chauvin et al. [26], the more neurotic and agreeableness of an individual, the more risks they feel. Individuals with high agreeableness scores may prefer safer solutions or alternatives to reduce their discomfort [56]. During the evaluation information phase, construction workers consider the level of acceptance of risk to assess the level of injury and benefit from the behavior. The risk evaluation process can be determined by comparing the perceived risk with the risk tolerance the individual can bear. Hunter [57] defines risk tolerance as "The amount of risk that an individual is willing to accept when pursuing a certain goal." According to this definition, it can be found that risk tolerance includes two aspects: subjectivity (the degree that an individual can tolerate) and goal (total risk). Wang et al. [58] verified that the psychological characteristics of construction workers significantly impact risk tolerance through questionnaires and structural equation models. Individuals' acceptance of risk is related to their extroversion [30], openness [29], and due conscientiousness [28]. In the decision-making phase, workers make judgments based on a combination of information from the first two phases as well as physiological and skill factors. The first two cognitive stages, perceived and evaluated information, are important for the safety of construction workers. Therefore, risk perception and risk tolerance in the two stages will be selected as key parameters in the model, and the influence of personality traits on these two parameters will be investigated. The framework of decision-making in the cognitive process of unsafe behavior of construction workers is shown in Figure 1.

4.3. Agent-Based Model Development. Establish an agent-based model according to the cognitive process of safe behavior, which is composed of (1) a description of the environment and the agent (2) defining the mutual assistance rules between the agent and the interaction rules between the agent and the external environment (3) model validation [59]. Each of these model components is explained in detail below.

4.3.1. Defining Environment and Agent. In the agent-based model, the virtual construction site environment is set according to the grid form proposed by Lu et al. [60]. The area is set to $40 * 40$ (each grid represents $1\,m^2$ of space); the task volume is included in the site (range 0–20); and the risk level (range 0–1) has two parameters. Different grids have different tasks and risk levels as shown in Figure 2. Among them, parameters 1–9 are the initial parameters of the environment (1–2) and the agents (3–9) that need to be set when the model is constructed and are mainly set according to existing studies [44, 61]. Parameters 10–21 are process parameters calculated when the model is running, and the calculation method is executed according to the define interaction rules.

Because steelworkers have the highest occupational disease and injury rate [62], the workers in the model are set as steelworkers. Considering that the death rate of tower crane-related accidents is relatively serious and the location is relatively fixed, more importantly, the tower crane is easy to be noticed by colleagues' safety warnings and avoid accidents [63]. So the hazard source is set as a tower crane and placed in the center of the site.
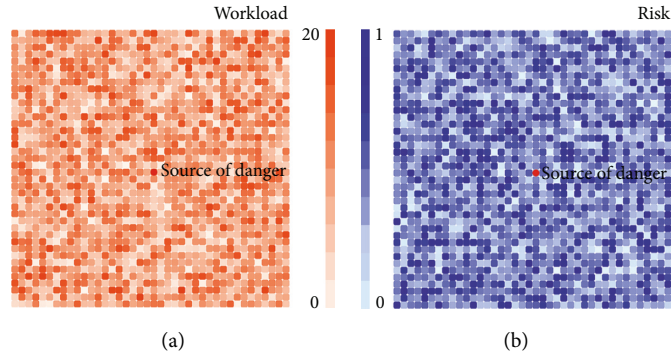
FIGURE 2: Virtual construction site: (a) workload and (b) risk level view (generated by AnyLogic software).

TABLE 1: Model parameter setting.

No.	Parameter name	Parameter meaning	Initialization value
1	riskLevel	Construction site environmental risks	Triangular (0, 0.5, 1)
2	workload	Construction site tasks	Triangular (0, 10, 20)
3	workerNum	Number of workers	20
4	id	Worker's ID	—
5	extroversion (E)	Worker's extroversion	N (0.5, 0.13)
6	agreeableness (A)	Worker's agreeableness	N (0.5, 0.13)
7	conscientiousness (C)	Worker's conscientiousness	N (0.5, 0.13)
8	neuroticism (N)	Worker's neuroticism	N (0.5, 0.13)
9	openness (O)	Worker's openness	N (0.5, 0.13)
10	riskPerception (RP)	Risk perception of worker	—
11	riskTolerance (RT)	Risk tolerance of worker	—
12	unsafeBehavior (UB)	Unsafe behavior of worker	—
13	safeHelpBehavior (SHB)	Mutual assistance of workers	—
14	numberOfUnsafeBehaviors	Number of worker's unsafe behaviors	—
15	numberOfSafeBehaviors	Number of worker's safe behaviors	—
16	unsafeBehaviorRate	Unsafe behavior rate	—
17	numberOfAccidents	Number of accidents	—
18	numberOfNear-missingAccidents	Number of near-missing	—
19	ratioOfAccidentsToNearMisses	Ratio of accidents to near-missing	—
20	unsafeBehaviorReductionRate	Unsafe behavior reduction rate	—
21	accidentRate	Accident rate	—

Steelworkers are the main agents of the model, and each worker has the following state variables: ID number, Big Five personality traits (extraversion, conscientiousness, agreeableness, neuroticism, and openness), risk perception, risk tolerance, and unsafe behavior. Based on the size of the construction team, the number of workers on site is set to 20. Before each simulation model runs, the grid unit's risk value and task amount are assigned different values to simulate different construction situations. The five personality traits of construction workers are assigned different values, representing their heterogeneous attributes. Among them, different personality traits will affect the behavior and decision-making in performing tasks. Based on the statistical research of Schmitt et al. [61], the distribution of personality traits in each dimension follows the normal distribution, and the model sets its range from 0 to 1. To exclude extreme traits, the worker's traits range from 0.1 to 0.9, which is set to obey the normal distribution of N (0.5, 0.13) through analysis. The on-site environmental risks and on-site tasks are set to a medium level that obeys

the triangular distribution [44]. Table 1 shows the parameter settings for the construction of the benchmark model (the model that has set the relevant initial parameters of the agent).

4.3.2. Defining Interaction Rules. This research assumes that construction workers have two states: task-Searching and task-Executing. In task-Searching, the grid unit where the worker is currently located has no tasks, and at this time, the agent needs to move to the grid with tasks, and its state also changes from task-Searching to task-Executing. Since injuries or accidents usually occur in the task execution process rather than the task search process, this research mainly focuses on the cognitive process of safety behavior during the task execution process.

(1) The Decision-Making Rules of the Cognitive Process. According to the conclusion of the cognitive model, workers mainly experience three stages: perception information,
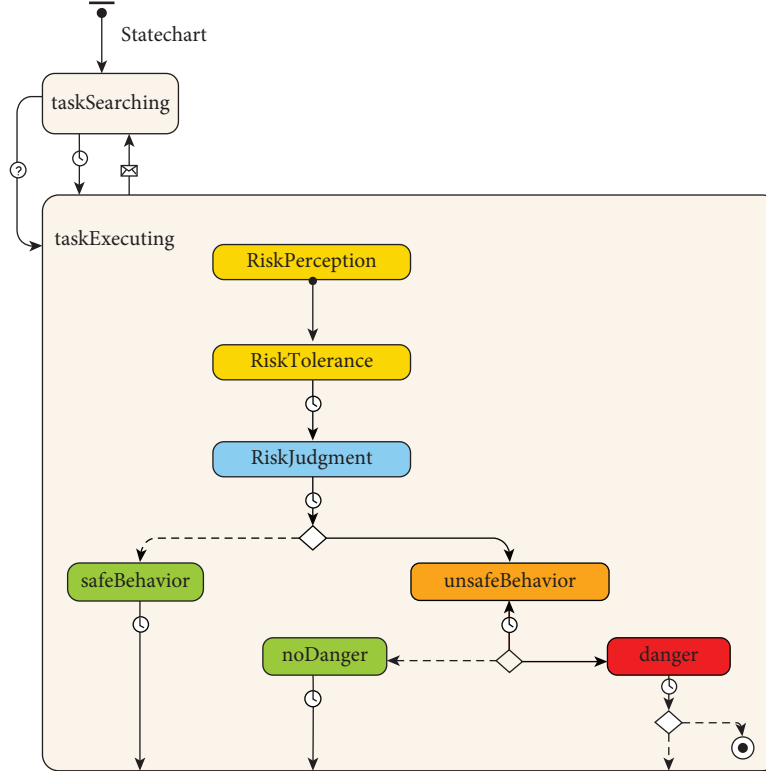
FIGURE 3: Modeling logic of workers' construction safety behavior based on the cognitive model.

evaluation information, and decision-making response, in the process of cognition of unsafe behaviors, corresponding to the three states of risk perception, risk tolerance, and safe behavior or unsafe behavior. The modeling logic is shown in Figure 3.

In the stage of perceiving information, workers will make subjective judgments and assessments of hazards. Risk perception can be affected by actual risk levels [54] and individual factors [55].

Chauvin et al. [26] found that construction workers face complex and changeable environments when performing work tasks, and they are often affected by personality factors when making risky decisions. Even facing the same environmental risk, the risk perceived by one worker may be different from that of another colleague. Therefore, the risk perception in the model is determined by the actual risk value of the current environment and the personality traits of the worker. Individuals with a high level of agreeableness tend to view risk as a higher risk factor [26]. In contrast, people with high neuroticism scores are prone to anxiety and tend to be conservative in the face of risks [64]. According to Sjöberg [54] and Chauvin et al. [26], the more neurotic and agreeableness of an individual, the more risks they feel. An individual with high agreeableness scores may prefer safer solutions or alternatives to reduce their discomfort [56]. Therefore, risk perception can be determined by agreeableness and neuroticism from the perspective of personality traits. To ensure the balance of contribution, the proportion is set to 0.5. Based on the above analysis, the model can express risk perception by the following formula:

$$\mathrm{RP}_i^t = \mathrm{ER}_i^t * \left(0.5 * \frac{a_i}{A} + 0.5 * \frac{n_i}{N} \right), \tag{1}$$

where RP_i^t: worker i's risk perception at time t, ER_i^t: the actual risk value of worker i's environment at time t, a_i: the agreeableness score of workers i, A: the maximum value in the value range of agreeableness, n_i: the neuroticism score of workers i, and N: the maximum value in the value range of neuroticism.

When workers perceive risk, they will conduct an informal assessment based on their situation, that is, assess the degree of risk that can be tolerated. Williams and Noyes [65] believe that risk tolerance is a personal assessment of risk and the corresponding comfort or discomfort to the risk. It depends on the level of confidence that controls the uncertainty of the situation. Studies have found a correlation between risk tolerance and personality traits [28–30]. Oehler and Wedlich [66] found that people with high extraversion have a higher risk tolerance, and openness positively correlates with risk-taking behavior [67]. The results of the study by Pak and Mahmood [68] show a significant negative correlation between conscientiousness and risk tolerance. Therefore, the risk tolerance set in the model is determined by the extraversion, openness, and conscientiousness of the personality traits. To ensure the balance of the distribution of traits and avoid the influence caused by a relatively high proportion of a certain trait, the proportional coefficients of the three traits are set to be 1/3 in the model. In addition to being related to their personality traits, they will also be affected by the organizational climate so that workers will adjust their behavior to conform to group norms. Moreover,

the behavioral role models of coworkers can have a significant impact on individual workers and can provide individual workers with relevant information on acceptable behaviors on site [69]. Therefore, each worker will know the risk tolerance of other colleagues as a result of being affected by the safety climate of the construction team. And, due to the existence of the memory utility, the worker's risk tolerance is also determined by the average value of the risk tolerance of other workers on site in the previous time unit determined. The proposed model in this research assumes that the worker's personality traits and the influence of external colleagues have the same contribution to risk tolerance, both at 50%. Based on the above analysis, this model sets the following formula:

$$\mathrm{RT}_i^t = 50\% * \left(\frac{1}{3} * \frac{e_i}{E} + \frac{1}{3} * \frac{o_i}{O} - \frac{1}{3} * \frac{c_i}{C} \right) + 50\% * \frac{1}{m} \sum_{j=1}^{m} RT_j^{t-1}.$$

(2)

Here, RT_i^t: the risk tolerance of worker i at time t, e_i: extraversion score of worker i, E: the maximum value in the value range of extraversion, o_i: worker i's openness score, O: the maximum value in the value range of openness, c_i: worker i's conscientiousness score, C: the maximum value in the value range of conscientiousness, m: the number of other workers on site, and RT_j^{t-1}: the risk tolerance of worker j at $t-1$.

In the decision-making stage, workers make risky behavior decisions based on perceived risks and their risk tolerance. The theory of risk steady-state points out that risk perception and risk tolerance are the two main aspects that determine risk behavior [70]. Workers will compensate for the behavior if the perceived risk exceeds the internal threshold (i.e., the current risk tolerance). In the proposed model, if the perceived risk exceeds the worker's current risk tolerance, then the worker will perform safe behavior to prevent accidents. Conversely, if the perceived risk does not exceed the worker's current risk tolerance, then the worker will take unsafe behavior. Based on the above analysis, this research proposes the following formula:

$$\mathrm{UB}_i^t = \begin{cases} 1, \mathrm{RP}_i^t < \mathrm{RT}_i^t, \\ 0, \mathrm{RP}_i^t > \mathrm{RT}_i^t. \end{cases}$$

(3)

Here, UB_i^t: worker i's unsafe behavior state at time t, 1: take unsafe behavior, and 0: take safe actions.

Since there is no danger when taking unsafe behaviors, it may be safe and sound, which is only a near-missing event [71]. Therefore, the model assumes that when workers take unsafe behaviors, if the environment happens to be in an unsafe state, then an accident will occur; otherwise, no danger will occur, and only a near-missing accident will occur. Based on the above analysis, this model sets the following formula:

$$D_i^t = \begin{cases} 1, & \mathrm{UB}_i^t = 1, \mathrm{ER}_i^t > \mathrm{random.uniform}\,(0, 1), \\ 0, & others. \end{cases}$$

(4)

Here, D_i^t: the dangerous state of worker i at time t, ER_i^t: the actual risk value of worker i's environment at time t, and

random.uniform (0, 1): generate a uniformly distributed floating-point number between [0, 1].

After experiencing a dangerous state, the worker's risk tolerance will change. If unsafe behaviors are taken, but no danger occurs, workers' tolerance for risks will increase and become riskier [72]. If accidents occur after unsafe behaviors, workers' risk tolerance will be weakened. That is, risk tolerance will decrease. Among them, the degree of reduction of risk tolerance is greater than the degree of increase. The purpose of the research is not to accurately measure the change value of the risk tolerance of workers after mutual assistance but to reflect the changes of different combinations of workers under different environmental risks. Therefore, after multiple simulations to observe the value range of risk tolerance, setting the reduction coefficient and the increase coefficient to 0.1 and 0.5, respectively, indicates that the change range is different. Because workers with different personality traits have different sensitivity to danger, their risk tolerance changes after the dangerous state are not the same. Therefore, after the dangerous state, the worker's risk tolerance change value is set in the model as follows:

$$\mathrm{RT}_i^{t+1} = \begin{cases} \mathrm{RT}_i^t, \mathrm{UB}_i^t = 0, \\[2mm] \mathrm{RT}_i^t - 0.1 * \left(\frac{1}{3} * \frac{e_i}{E} + \frac{1}{3} * \frac{o_i}{O} - \frac{1}{3} * \frac{c_i}{C} \right), \mathrm{UB}_i^t = 1, D_i^t = 1, \\[2mm] \mathrm{RT}_i^t + 0.05 * \left(\frac{1}{3} * \frac{e_i}{E} + \frac{1}{3} * \frac{o_i}{O} - \frac{1}{3} * \frac{c_i}{C} \right), \mathrm{UB}_i^t = 1, D_i^t = 0. \end{cases}$$

(5)

Here, RT_i^{t+1}: the risk tolerance of worker i at $t+1$.

(2) Decision-Making Rules for Mutual Assistance Behavior. When construction workers are task-Executing, they will randomly engage in safe mutual assistance behaviors with surrounding workers. In the five dimensions of the Big Five personality traits, agreeableness reflects the orientation of interpersonal relationships such as trust, understanding, sympathy, and altruism [73]. Agreeableness people are good at cooperating, like to help others, and have strong empathy. Therefore, this model sets an agreeableness value as a switch for triggering safety mutual assistance behavior. According to Table 1, the agreeableness follows a normal distribution with a mean of 0.5. Therefore, it is assumed in the model that when the agreeableness of workers is higher than the average, there is an altruistic tendency and mutual assistance with other workers. Based on this, this model sets formula (6). To more accurately simulate the limitations of human perception and behavior in the actual construction environment, the range of safe mutual assistance behavior is set to workers within a radius of three meters from the workers [74].

$$\mathrm{SHB} = \begin{cases} 1, & a_i > 0.5, \\ 0, & others. \end{cases}$$

(6)
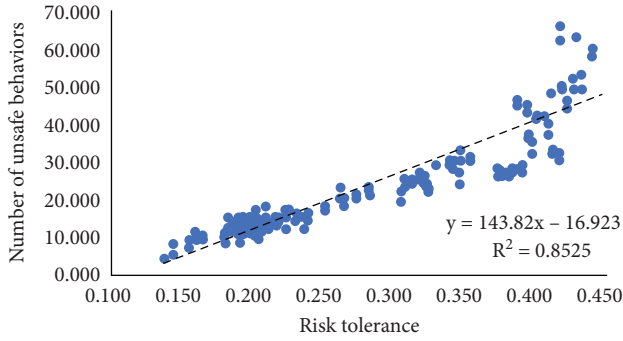
FIGURE 4: The relationship between the average risk tolerance of construction workers and the number of unsafe behaviors.

FIGURE 5: The relationship between the average risk perception level of construction workers and the number of unsafe behaviors.

Here, SHB: safe mutual assistance behavior and a_i: the agreeableness score of worker i.

Learning behavior is closely related to the process of mutual assistance. Mutual assistance from others can help individuals clarify concepts, improve problem-solving skills, and increase retention. Mutual assistance is one of the prerequisites for external learning [75]. Interaction can bring about information exchange, knowledge acquisition [76], and obvious behavior changes [77]. Mutual assistance behavior is one of the important manifestations of the interactive process. After workers undergo safe mutual assistance during construction, both participants will have new cognition and understanding of construction safety, so the feedback to the individuals of both participants is a positive behavior change rather than a negative impact. So set in the model; the two participants have a certain improvement in risk perception after mutual assistance behavior and are also more risk-conscious. Run the model multiple times to observe the value range of risk perception and set the increased value to 0.01. Based on the above analysis, this model proposes the following formula:

$$RP_i^{t+1} = RP_i^t + 0.01. \tag{7}$$

4.3.3. Model Verification. The purpose of model verification is to ensure that the simulation model can reasonably express the logic of the real world to solve the problem to be studied [78]. Zeigler et al. [79] divided the verification method into replicative validity (i.e., "the model matches data obtained from the real world"), predictive validity (i.e., "the model matches data before being acquired from the real world"), and construct validity (i.e., "the model truly reflects how the real world operates"). At the same time, Sargent [80] proposed that an appropriate verification method should be selected according to the purpose of the model. This paper aims to explore the role of construction workers with different personality traits on safety-related behaviors based on the cognitive mechanism of safety behaviors, rather than to make accurate predictions of safety behaviors. Therefore, the verification of this model will focus on replicative validity and construct validity.

First, a qualitative consistency test of replicative validity was carried out for the model. It can be seen from Figure 4
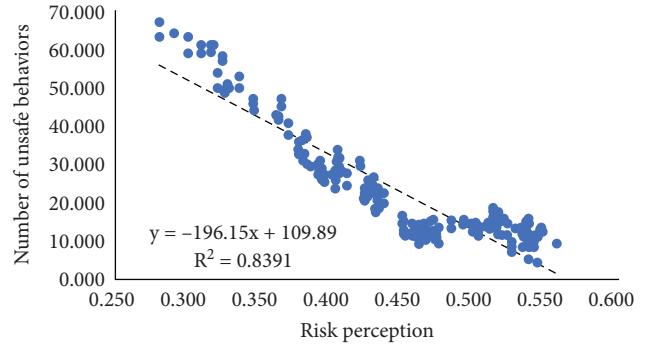
that the overall risk tolerance level of construction workers in the benchmark model is directly proportional to the number of unsafe behaviors (the total number of unsafe behaviors taken by workers in the team from the beginning of the task to the current model time; $R^2 = 0.852$, $p < 0.001$). That is, the higher the level of construction workers who can tolerate risks, the more unsafe behaviors may occur during the execution of the task. This result is supported by existing literature in many fields. Ji et al. [81] interviewed pilots and used questionnaires to analyze the relationship between pilots' behavioral decision-making and risk tolerance. The results showed that the higher the risk tolerance, the fewer safe behaviors. Davidson [82] found that the higher the coal miners' tolerance to risk, the greater the risk of their decision-making plans by studying the process of coal miners' final behavior selection. In construction, Ma [83] established a construct equation model, conducted empirical analysis, and found that the risk tolerance of construction workers was significantly negatively correlated with safety behavior.

The simulation results are consistent with existing studies on the relationship between risk perception and unsafe behavior. As shown in Figure 5, the unsafe behavior of construction workers will be inhibited by their risk perception level ($R^2 = 0.839$, $p < 0.001$). Under the same level of risk environment, the more risks construction workers can perceive and the more comprehensive, the higher the probability of taking safe actions. Existing studies also support this result. The research of Xia et al. [84] found that the more risks construction workers perceive, the more they can recognize the potential dangers in the current state and thus can choose safe behaviors to prevent themselves from accidents. Huang et al. [85] found that risk perception and unsafe behavior have a significant negative correlation through a survey of front-line workers in Chinese construction projects. Xia et al. [86] found that improving the risk perception of construction workers can play a positive role in safe behavior.

To ensure the quantitative consistency of replicative validity, this study implemented the benchmark model 50 times, calculated the mean value of important indicators, and compared the results with the empirical data of previous studies. Among them, the unsafe behavior rate (formula (8)) is 0.35 (standard deviation = 0.006), which is consistent with

the research results of Sa et al. [87] and Fang and Wu [88]. Both studies have found that one-third of workers are unsafe at the construction site. Also, according to Heinrich's [89] triangle rule, every major accident will cause 29 serious accidents and 300 near-missing accidents. That is, the ratio of accidents to near-missing accidents (formula (9)) is roughly 1:10. Execute the benchmark model 50 times and calculate that the ratio of accidents to near-missing events is 1:8.6, which is near the value of the triangle rule. Finally, the average accident rate is calculated and compared with the relevant accident statistics. The benchmark model is executed 50 times, and the accident rate (formula (10)) is calculated to be 3.3, which is the same as the 2016 Occupational Injury and Disease Incident Rate (3.0) published by the U.S. Bureau of Labor Statistics [90] very close. Therefore,

TABLE 2: Big Five personality parameter settings in the experiment (extraversion as an example).

	Group A	Group B
E	0.3	0.3
	0.3	0.7
	0.7	0.7
A	$N(0.5, 0.16)$	$N(0.5, 0.16)$
C	$N(0.5, 0.16)$	$N(0.5, 0.16)$
N	$N(0.5, 0.16)$	$N(0.5, 0.16)$
O	$N(0.5, 0.16)$	$N(0.5, 0.16)$

the quantitative consistency between the simulation results and the empirical data is proved.

$$\text{unsafe behavior rate} = \frac{\text{number of unsafe behaviors}}{\text{number of un safe behaviors} + \text{number of safe behaviors}}, \tag{8}$$

$$\text{ratio of accidents to near misses} = \frac{\text{number of accidents}}{\text{number of nearmissing accidents}}, \tag{9}$$

$$\text{accident rate} = \frac{\text{number of accidents}}{\text{number of unsafe behaviors} + \text{number of safe behaviors}}. \tag{10}$$

In terms of construct validity, this study uses three methods to enhance the construct validity of the model. First, the agent's behavioral rules and interaction rules are based on theories that have been established and verified in the social science literature (such as cognitive science theory, risk homeostasis theory, and Big Five personality traits). Secondly, the influencing factors of parameters (such as risk perception and risk tolerance) are derived from the research results of the existing literature. Finally, the initialization of model parameters refers to the common principles in existing empirical research and related construction simulation literature [52, 60].

5. Experiments and Results

5.1. Experimental Design. Based on the parameters set by the benchmark model, this study changed the risk level of the construction environment. The model kept running until the changes in each variable have stabilized (elapse of 80 model time units).

In the experiment, the construction workers in the construction team were divided into two groups (A and B), and each group has ten workers. The five dimensions of the personality traits of the construction workers have two levels, high and low. For example, extraversion is divided into high-level extraversion (i.e., extroversion, denoted by 0.7) and low-level extroversion (i.e., introversion, denoted by 0.3). The variable traits of the two groups of workers will take a combination of high and low levels. The personality traits of other dimensions all obey the normal distribution. In the benchmark model, all traits are set to follow a normal

distribution. Take the extraversion as an example. The experiment sets the parameters as shown in Table 2 to explore the relevant effects of different combinations of extraversion. Different levels of environmental risk are set by changing the mode value of the triangular distribution, as shown in Figure 6.

5.2. Simulation Results. Figures 7–11, respectively, show the combination of construction workers with different personality traits in high-, medium-, and low-risk environments. After the cognitive process of unsafe behavior and the process of mutual assistance, they reflect the change in the rate of unsafe behavior reduction on the overall level of the construction team (i.e., the ratio of the difference between the number of unsafe behaviors before and after the safe mutual assistance behavior and the number of unsafe behaviors before mutual assistance). It should be pointed out that the average unsafe behavior rate of construction workers within the construction team in the baseline model was reduced by 53% in the medium-risk environment.

It can be seen from Figure 7 that with the increase of environmental risks, the average unsafe behavior reduction rate of the three types of extraverted combination forms of team workers is getting lower. This is because the high-risk environment is relatively more dangerous and prone to accidents. The resulting warning effect will prompt workers to pay more attention to construction safety. As far as the combination is concerned, regardless of the high or low environmental risk, the team with the same number of high- and low-extroverted workers has the largest reduction rate of unsafe behavior, and the overall safety performance of the
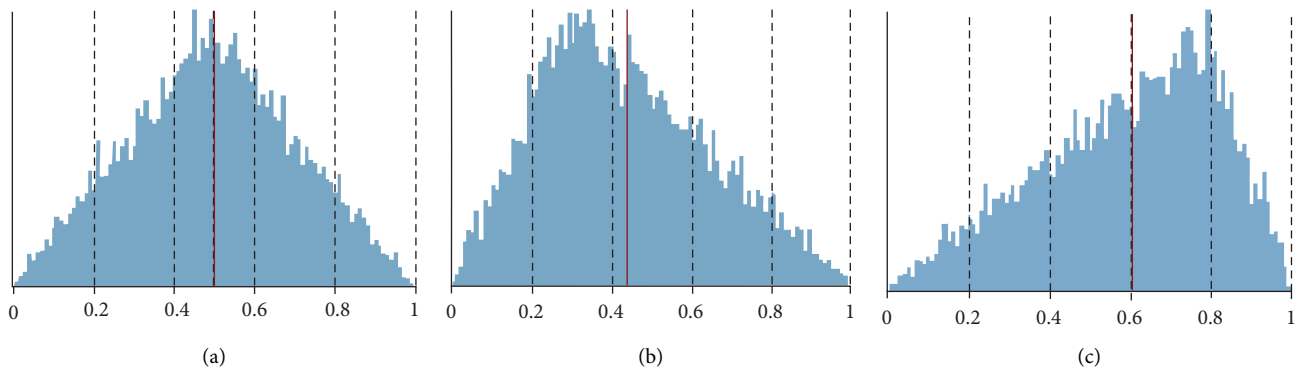
FIGURE 6: Different environmental risk levels (indicated by triangular distribution function): (a) medium risk triangular (0, 1, 0.5), (b) low risk triangular (0, 1, 0.3), and (c) high risk triangular (0, 1, 0.8).
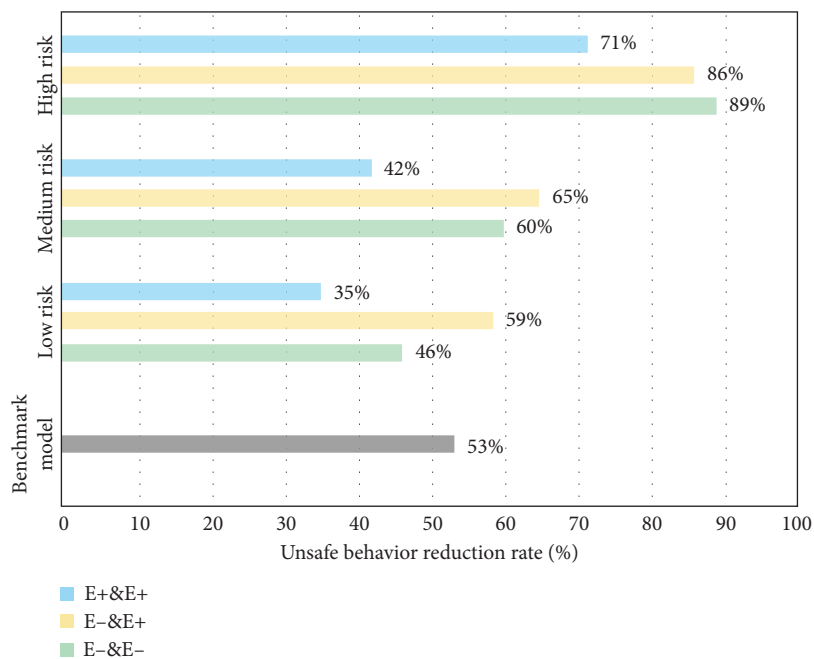
FIGURE 7: The reduction rate of unsafe behaviors of construction workers with different levels of extroversion (E) under different risk environments.

team has the best improvement effect. The team with more highly extroverted workers has the lowest reduction rate of unsafe behavior, which is caused by the characteristics of highly extroverted individuals who like to take risks and pursue excitement.

In Figure 8, as far as the combination is concerned, regardless of the high or low environmental risk, teams with the same number of agreeableness workers have the greatest reduction in unsafe behaviors. At this time, the overall safety behavior of the team has the best improvement, especially in the medium- and high-risk environments by about 90%. This may be because workers with different levels of agreeableness are more efficient in learning safety in mutual assistance behaviors, thereby reducing the occurrence of unsafe behaviors.

Figure 9 shows that with the increase in environmental risk levels, the average incidence of unsafe behaviors of the

three types of conscientious combination of team workers is getting lower. This is because the environmental risk becomes higher, the greater the impact of conscientiousness; workers will carefully assess the safety situation before performing tasks and act more cautiously so that there are fewer unsafe behaviors. Especially in a high-risk environment, in teams with more highly conscientious workers or teams with the same number of high- and low-conscientious workers, the unsafe behavior of construction workers after mutual assistance is reduced by about 90%.

It can be found in Figure 10 that in terms of the combination form, regardless of the level of environmental risk, team workers with the same number of high- and low-neurotic workers have the greatest reduction in unsafe behavior, and the improvement of team safety behavior is the best, especially in the high-risk environment; it is reduced to 85%. Teams with more highly neurotic or less
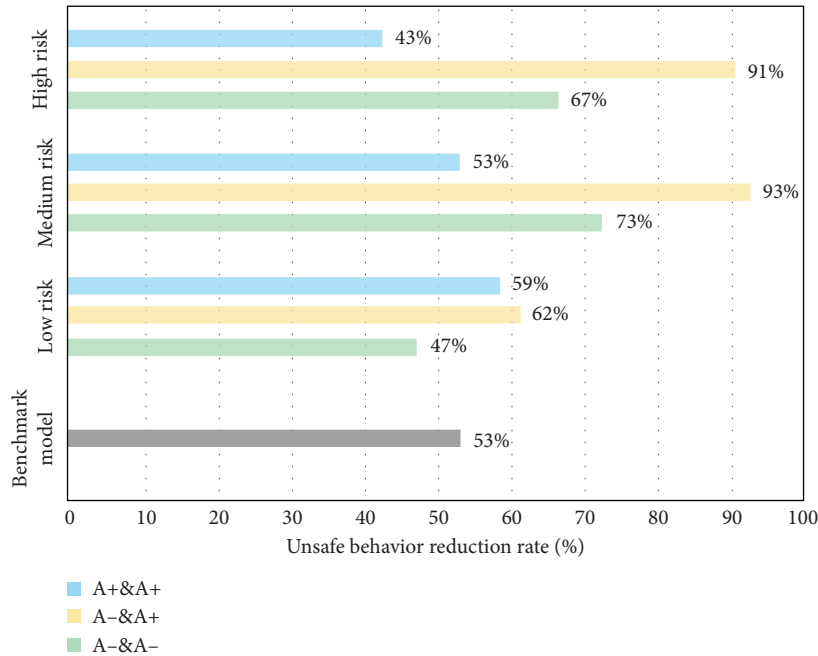
FIGURE 8: The reduction rate of unsafe behaviors of construction workers with different levels of agreeableness (A) under different risk environments.
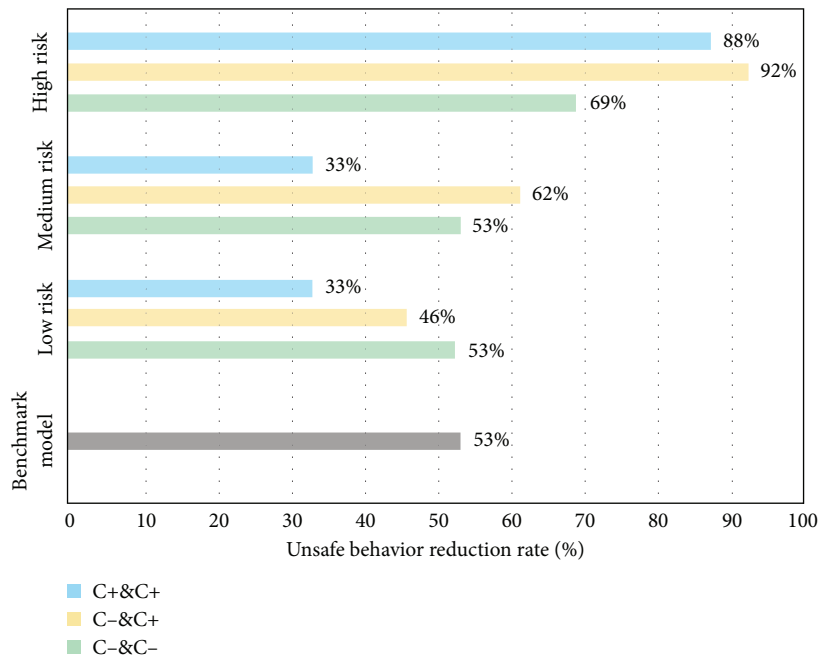
FIGURE 9: The reduction rate of unsafe behaviors of construction workers with different conscientiousness (C) levels under different risk environments.

neurotic workers are more effective in reducing unsafe behaviors in medium to high risks but are less effective in low-risk environments. This may be due to workers' safety mentality being more relaxed and emotionally stable and will not always worry about accidents in low-risk environments.

Figure 11 shows that in a low-risk environment, the reduction rates of unsafe behaviors of workers in a combination of the three types of openness levels after mutual assistance

are very small, all of which are around 50%. In a medium-risk environment, when the overall openness of the team is at the mid-to-high level, mutual assistance has the best effect on safety. While in a high-risk environment, the overall openness and consistency of the team are more important. The overall reduction rate of unsafe behaviors in teams with high or low overall openness after mutual assistance is nearly 80%, which can effectively improve team performance.
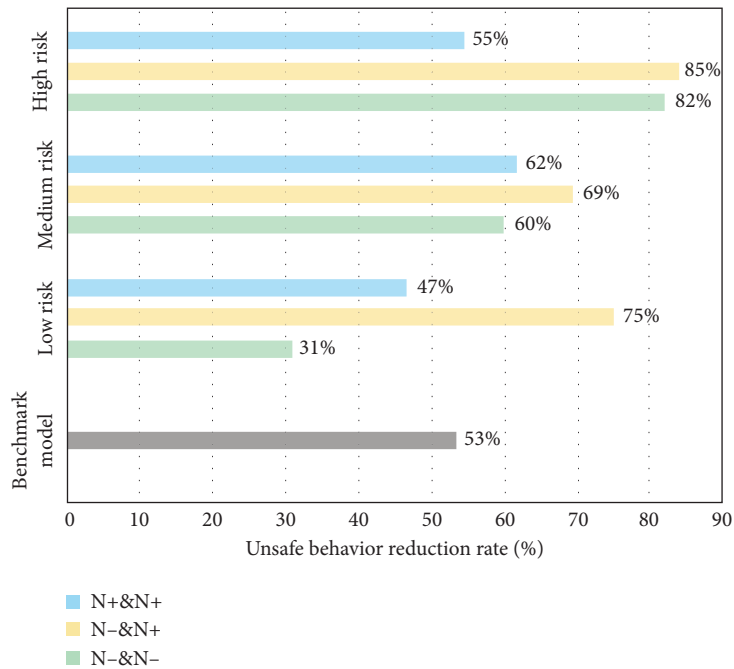
FIGURE 10: The reduction rate of unsafe behaviors of construction workers with different neuroticism (N) levels under different risk environments.
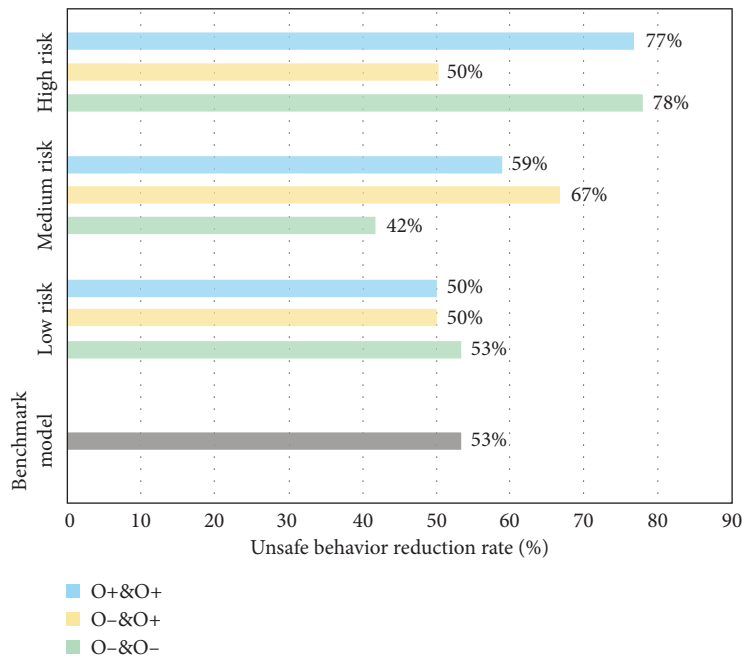
FIGURE 11: The reduction rate of unsafe behaviors of construction workers with different openness (O) levels under different risk environments.

Based on the results of the above experiments, according to the idea that the higher the rate of unsafe behavior reduction after the mutual assistance of the construction workers of the team is, the better the improvement of safety performance. It can analyze the best combination of different personality traits to improve the overall safety level of the team under various levels of environmental risks as shown in Table 3.

In a low-risk environment, when the number of high and low levels of extravert, agreeable, and neurotic workers in the team is similar, and there are more low-conscientious and low-neurotic workers, the effect of improving team safety is best. In a medium-risk environment, the team has the best potential for safety performance when the team has much the same as the workers with high and low levels of each trait. In a high-risk environment, when the number of high and

TABLE 3: The best combination of workers' personality traits under various levels of environmental risks to improve safety performance.

Environmental risk level	Low		Medium		High	
Group	Group A	Group B	Group A	Group B	Group A	Group B
Extroversion	High	Low	High	Low	Low	Low
Agreeableness	High	Low	High	Low	High	Low
Conscientiousness	Low	Low	High	Low	High	Low
Neuroticism	High	Low	High	Low	High	Low
Openness	Low	Low	High	Low	Low	Low

low levels of agreeable, conscientious, and neurotic workers in the team is almost identical and there are more low-extraversion and low-openness workers, the team's safety behavior improvement effect is best after worker safety mutual assistance. It can be found that when the number of workers with high and low levels of extraversion, agreeableness, and neuroticism is nearly equal, regardless of the level of environmental risk, mutual assistance improves the overall safety of the construction team.

6. Discussion and Conclusion

This paper mainly explores the change difference in the overall unsafe behavior of the workers after the safety mutual assistance of workers with different personality traits. First, based on the occurrence mechanism of unsafe behaviors of construction workers, the critical processes in the cognitive process of unsafe behaviors are extracted: risk perception, risk tolerance, and decision-making. Existing studies indicate that the Big Five personality traits affect the risk perception and risk tolerance in the process of individual unsafe behaviors and indirectly determine whether unsafe behaviors of construction workers occur.

Agent-based modeling (ABM) is used in this paper as a bottom-up and micro-to-macro classical modeling approach. At the same time, the research analyzes the relationship between construction workers and workers and the relationship between construction workers and the external construction environment to establish individual behavior rules and interaction rules that are consistent with the actual construction context. The individual worker's personality trait, an inherent attribute that cannot be easily changed later in life, determines each worker's unique outwardly expressive behavior and decision-making style. By setting up worker agents possessing different traits in the agent-based model and arranging various combinations of workers in the team, it is possible to maximize the simulation of the behavioral differences of workers with different personality traits in the real environment and measure the impact of such differences on overall team safety performance. This paper explores the optimal combination of workers with varying traits of personality in various risk environments from the perspective of psychology, providing a new way to improve the safety performance of teams in different situations and ultimately deepen the understanding of the complex system in construction.

By introducing the Big Five personality traits theory into the research of the construction industry, combined with the agent-based modeling method in the complex system theory, this paper is conducive to understanding the cognitive process of construction workers' unsafe behavior and the differences in the results of unsafe behavior from the perspective of psychology. According to the conclusions of the simulation analysis, this research proposes corresponding management measures to improve construction safety from the perspective of enterprise human resources and personnel arrangements based on personality traits and actively manages from the source to improve the level of construction safety performance.

Data Availability

The data used to support the findings of this study are included within the article.

Conflicts of Interest

The authors declare that they have no conflicts of interest.

Acknowledgments

References

[1] A. A. Raheem and J. W. Hinze, "Disparity between construction safety standards: a global analysis," *Safety Science*, vol. 70, pp. 276–287, 2014.

[2] R. A. Haslam, S. A. Hide, A. G. Gibb et al., "Contributing factors in construction accidents," *Applied Ergonomics*, vol. 36, no. 4, pp. 401–415, 2005.

[3] H. W. Heinrich, *Industrial Accident Prevention: A Scientific Approach*, McGraw-Hill, New York, 1959.

[4] A. Suraji, A. R. Duff, and S. J. Peckitt, "Development of causal model of construction accident causation," *Journal of Construction Engineering and Management*, vol. 127, no. 4, pp. 337–344, 2001.

[5] Y. A. Báez, M. A. Rodríguez, J. Limón, and D. A. Tlapa, "Model of Human Reliability for Manual Workers in Assembly Lines," in *Proceedings of the 2014 IEEE International Conference on Industrial Engineering and Engineering Management*, pp. 1448–1452, Selangor, Malaysia, May 2014.

[6] H.-C. Seo, Y.-S. Lee, J.-J. Kim, and N.-Y. Jee, "Analyzing safety behaviors of temporary construction workers using structural equation modeling," *Safety Science*, vol. 77, pp. 160–168, 2015.

[7] R. P. Tett and D. D. Burnett, "A personality trait-based interactionist model of job performance," *Journal of Applied Psychology*, vol. 88, no. 3, pp. 500–517, 2003.

[8] L. Florez and J. C. Cortissoz, "Probability Density Function for Predicting Productivity in Masonry Construction Based on the Compatibility of a Crew," in *Proceedings of the 25th Annual Conference of the International Group for Lean Construction*, pp. 655–662, Heraklion, Greece, March 2017.

[9] L. Florez and J. C. Cortissoz, "Using workers compatibility to predict labor productivity through cluster analysis," *Procedia Engineering*, vol. 196, pp. 359–365, 2017.

[10] C. M. Wang, B. B. Xu, S. J. Zhang, and Y. Q. Chen, "Influence of personality and risk propensity on risk perception of Chinese construction project managers," *International Journal of Project Management*, vol. 34, no. 7, pp. 1294–1304, 2016.

[11] J. Zhang, P. Xiang, R. Zhang, D. Chen, and Y. Ren, "Mediating effect of risk propensity between personality traits and unsafe behavioral intention of construction workers," *Journal of Construction Engineering and Management*, vol. 146, no. 4, Article ID 04020023, 2020.

[12] J. J. Jaccard, "Predicting social behavior from personality traits," *Journal of Research in Personality*, vol. 7, no. 4, pp. 358–367, 1974.

[13] L. M. Baker, "Observation: a complex research method," *Library Trends*, vol. 55, no. 1, pp. 171–189, 2006.

[14] J. Ritchie, L. Spencer, and W. O'Connor, *Carrying Out Qualitative Analysis*, 2003.

[15] Y. Y. Ke, "Research on the Chinese industrialized construction migrant workers from the perspective of complex adaptive system: combining the application of SWARM computer simulation technology," *Wireless Personal Communications*, vol. 102, no. 4, pp. 2469–2481, 2018.

[16] Z. Jiang, D. Fang, and M. Zhang, "Understanding the causation of construction workers' unsafe behaviors based on system dynamics modeling," *Journal of Management in Engineering*, vol. 31, no. 6, Article ID 04014099, 2015.

[17] C. M. Macal and M. J. North, *Tutorial on Agent-Based Modeling and Simulation, 2005 Winter Simulation Conference*, pp. 2–15, WSC 05, Orlando, FL, 2005.

[18] A. Neal and M. A. Griffin, *Safety Climate and Safety at Work*, 2004.

[19] H. Lingard and S. M. Rowlinson, *Occupational Health and Safety in Construction Project Management*, Taylor & Francis, Harzing, 2005.

[20] F. Sherratt, "Exploring 'Zero Target' safety programmes in the UK construction industry," *Construction Management & Economics*, vol. 32, no. 7-8, pp. 737–748, 2014.

[21] R. R. McCrae and P. T. Costa, "Personality trait structure as a human universal," *American Psychologist*, vol. 52, no. 5, pp. 509–516, 1997.

[22] D. C. Funder, *Accuracy in Personality Judgment: Research and Theory Concerning an Obvious Question*, Accuracy in Personality Judgment: Research and Theory Concerning an Obvious Question, Washington, DC, 2001.

[23] S. Geller, "The fitting solution to respiratory hazards," *Psychology of safety*, vol. 6, pp. 12–14, 2004.

[24] S. Clarke, "The relationship between safety climate and safety performance: a meta-analytic review," *Journal of Occupational Health Psychology*, vol. 11, no. 4, pp. 315–327, 2006.

[25] M. Loosemore, J. Raftery, and C. Reilly, *Risk Management in Projects*, Taylor & Francis, Harzing, 2006.

[26] B. Chauvin, D. Hermand, and E. Mullet, "Risk perception and personality facets," *Risk Analysis*, vol. 27, no. 1, pp. 171–185, 2007.

[27] J. R. Myers, D. H. Henderson-King, and E. I. Henderson-King, "Facing technological risks: the importance of individual differences," *Journal of Research in Personality*, vol. 31, no. 1, pp. 1–20, 1997.

[28] T. Rundmo, "Employee images of risk," *Journal of Risk Research*, vol. 4, no. 4, pp. 393–404, 2001.

[29] H. T. Hod, "Risk tolerance dependent on what? Demographics or personality type: findings from an empirical research," *Risk*, vol. 6, 2015.

[30] R. Bye and G. Lamvik, "Organizational culture and risk perception," *Zagadnienia Eksploatacji Maszyn*, vol. 42, pp. 131–146, 2007.

[31] D. Fang, C. Zhao, and M. Zhang, "A cognitive model of construction workers' unsafe behaviors," *Journal of Construction Engineering and Management*, vol. 142, no. 9, Article ID 04016039, 2016.

[32] Y. M. Goh and N. F. Binte Sa'adon, "Cognitive factors influencing safety behavior at height: a multimethod exploratory study," *Journal of Construction Engineering and Management*, vol. 141, no. 6, Article ID 04015003, 2015.

[33] I. Ajzen, "The theory of planned behavior," *Organizational Behavior and Human Decision Processes*, vol. 50, no. 2, pp. 179–211, 1991.

[34] S. Chi, S. Han, and D. Y. Kim, "Relationship between unsafe working conditions and workers' behavior and impact of working conditions on injury severity in US construction industry," *Journal of Construction Engineering and Management*, vol. 139, no. 7, pp. 826–838, 2013.

[35] B. Q. Cheng, C. J. Fan, H. L. Fu, J. L. Huang, H. H. Chen, and X. W. Luo, "Measuring and computing cognitive statuses of construction workers based on electroencephalogram: a critical review," *Ieee Transactions on Computational Social Systems*, pp. 1–16, 2022.

[36] S. Gannouni, A. Aledaily, K. Belwafi, and H. Aboalsamh, "Adaptive emotion detection using the valence-arousal-dominance model and EEG brain rhythmic activity changes in relevant brain lobes," *IEEE Access*, vol. 8, pp. 67444–67455, 2020.

[37] J. Rasmussen, *Information Processing and Human-Machine Interaction*, An approach to cognitive engineering, 1986.

[38] C. D. Wickens, J. G. Hollands, S. Banbury, and R. Parasuraman, *Engineering Psychology and Human Performance*, Psychology Press, Hove, East Sussex, 2015.

[39] Y. Chang and A. Mosleh, "Cognitive modeling and dynamic probabilistic simulation of operating crew response to complex system accidents: Part 5: dynamic probabilistic simulation of the IDAC model," *Reliability Engineering & System Safety*, vol. 92, no. 8, pp. 1076–1101, 2007.

[40] G. Ye, H. Yue, J. Yang et al., "Understanding the socio-cognitive process of construction workers' unsafe behaviors: an agent-based modeling approach," *International Journal of Environmental Research and Public Health*, vol. 17, no. 5, p. 1588, 2020.

[41] P. Kropotkin, *Mutual Aid: A Factor of Evolution*, Courier Corporation, North Chelmsford, 2012.

[42] B. Herman, "Mutual aid and respect for persons," *Ethics*, vol. 94, no. 4, pp. 577–602, 1984.

[43] S. E. Anderson and L. J. Williams, "Interpersonal, job, and individual factors related to helping processes at work," *Journal of Applied Psychology*, vol. 81, no. 3, pp. 282–296, 1996.

[44] H. Liang, K.-Y. Lin, S. Zhang, and Y. Su, "The impact of coworkers' safety violations on an individual worker: a social contagion effect within the construction crew," *International*

Journal of Environmental Research and Public Health, vol. 15, no. 4, p. 773, 2018.

[45] M. Brondino, S. A. Silva, and M. Pasini, "Multilevel approach to organizational and group safety climate and safety performance: Co-workers as the missing link," *Safety Science*, vol. 50, no. 9, pp. 1847–1856, 2012.

[46] C. D. Burt, B. Sepie, and G. McFadden, "The development of a considerate and responsible safety attitude in work teams," *Safety Science*, vol. 46, no. 1, pp. 79–91, 2008.

[47] H. C. Lingard, T. Cooke, and N. Blismas, "Group-level safety climate in the Australian construction industry: within-group homogeneity and between-group differences in road construction and maintenance," *Construction Management & Economics*, vol. 27, no. 4, pp. 419–432, 2009.

[48] M. Osama Jannadi, "Impact of human relations on the safety of construction workers," *International Journal of Project Management*, vol. 13, no. 6, pp. 383–386, 1995.

[49] C. D. B. Burt, K. L. Gladstone, and K. R. Grieve, "Development of the considerate and responsible employee (CARE) scale," *Work & Stress*, vol. 12, no. 4, pp. 362–369, 1998.

[50] J. H. Dyer and N. W. Hatch, "Relation-specific capabilities and barriers to knowledge transfers: creating advantage through network relationships," *Strategic Management Journal*, vol. 27, no. 8, pp. 701–719, 2006.

[51] J. M. Epstein and R. Axtell, *Growing Artificial Societies: Social Science from the Bottom up*, Brookings Institution Press, Washington, D.C., USA, 1996.

[52] B. Choi and S. Lee, "An empirically based agent-based model of the sociocognitive process of construction workers' safety behavior," *Journal of Construction Engineering and Management*, vol. 144, no. 2, Article ID 04017102, 2018.

[53] M. R. Hallowell and J. A. Gambatese, "Population and initial validation of a formal model for construction safety risk management," *Journal of Construction Engineering and Management*, vol. 136, no. 9, pp. 981–990, 2010.

[54] L. Sjöberg, "Factors in risk perception," *Risk Analysis*, vol. 20, no. 1, pp. 1–12, 2000.

[55] A. S. Akintoye and M. J. MacLeod, "Risk analysis and management in construction," *International Journal of Project Management*, vol. 15, no. 1, pp. 31–38, 1997.

[56] M. Lauriola and I. P. Levin, "Personality traits and risky decision-making in a controlled experimental task: an exploratory study," *Personality and Individual Differences*, vol. 31, no. 2, pp. 215–226, 2001.

[57] D. R. Hunter, *Risk Perception and Risk Tolerance in Aircraft Pilots*, Federal Aviation Administration Washington DC Office of Aviation Medicine, 2002.

[58] J. Wang, P. X. Zou, and P. P. Li, "Critical factors and paths influencing construction workers' safety risk tolerances," *Accident Analysis & Prevention*, vol. 93, pp. 267–279, 2016.

[59] C. M. Macal and M. J. North, "Tutorial on agent-based modelling and simulation," *Journal of Simulation*, vol. 4, no. 3, pp. 151–162, 2010.

[60] M. Lu, C. M. Cheung, H. Li, and S.-C. Hsu, "Understanding the relationship between safety investment and safety performance of construction projects through agent-based modeling," *Accident Analysis & Prevention*, vol. 94, pp. 8–17, 2016.

[61] D. P. Schmitt, J. Allik, R. R. McCrae, and V. Benet-Martínez, "The geographic distribution of Big Five personality traits: patterns and profiles of human self-description across 56 nations," *Journal of Cross-Cultural Psychology*, vol. 38, no. 2, pp. 173–212, 2007.

[62] I. W. Fung, T. Y. Lo, and K. C. Tung, "Towards a better reliability of risk assessment: development of a qualitative & quantitative risk evaluation model (QREM) for different trades of construction works in Hong Kong," *Accident Analysis & Prevention*, vol. 48, pp. 167–184, 2012.

[63] S. G. Pratt, S. M. Kisner, and P. H. Moore, "Machinery-related fatalities in the construction industry," *American Journal of Industrial Medicine*, vol. 32, no. 1, pp. 42–50, 1997.

[64] W. K. Hofstee, B. de Raad, and L. R. Goldberg, "Integration of the big five and circumplex approaches to trait structure," *Journal of Personality and Social Psychology*, vol. 63, no. 1, pp. 146–163, 1992.

[65] D. J. Williams and J. M. Noyes, "How does our perception of risk influence decision-making? Implications for the design of risk information," *Theoretical Issues in Ergonomics Science*, vol. 8, no. 1, pp. 1–35, 2007.

[66] A. Oehler and F. Wedlich, "The relationship of extraversion and neuroticism with risk attitude, risk perception, and return expectations," *Journal of Neuroscience, Psychology, and Economics*, vol. 11, no. 2, pp. 63–92, 2018.

[67] N. Nicholson, E. Soane, M. Fenton-O'Creevy, and P. Willman, "Personality and domain-specific risk taking," *Journal of Risk Research*, vol. 8, no. 2, pp. 157–176, 2005.

[68] O. Pak and M. Mahmood, "Impact of personality on risk tolerance and investment decisions," *International Journal of Commerce and Management*, vol. 25, no. 4, pp. 370–384, 2015.

[69] R. Gao, A. P. Chan, W. P. Utama, and H. Zahoor, "Multilevel safety climate and safety performance in the construction industry: development and validation of a top-down mechanism," *International Journal of Environmental Research and Public Health*, vol. 13, no. 11, p. 1100, 2016.

[70] G. J. S. Wilde, "The theory of risk homeostasis: implications for safety and health," *Risk Analysis*, vol. 2, no. 4, pp. 209–225, 1982.

[71] B. H. W. Guo, T. W. Yiu, V. A. González, and Y. M. Goh, "Using a pressure-state-practice model to develop safety leading indicators for construction projects," *Journal of Construction Engineering and Management*, vol. 143, no. 2, Article ID 04016092, 2017.

[72] M. Shin, H.-S. Lee, M. Park, M. Moon, and S. Han, "A system dynamics approach for modeling construction workers' safety attitudes and behaviors," *Accident Analysis & Prevention*, vol. 68, pp. 95–105, 2014.

[73] P. T. Costa and R. R. McCrae, *Revised NEO Personality Inventory (NEO-PI-R) and Neo Five-Factor Inventory (NEO-FFI)*, Psychological Assessment Resources, Florida, 1992.

[74] H. Strasburger, I. Rentschler, and M. Jüttner, "Peripheral vision and pattern recognition: a review," *Journal of Vision*, vol. 11, no. 5, p. 13, 2011.

[75] D. Lei, J. W. Slocum, and R. A. Pitts, "Designing organizations for competitive advantage: the power of unlearning and learning," *Organizational Dynamics*, vol. 27, no. 3, pp. 24–38, 1999.

[76] F. Therin, *"Learning-based strategy, toward a new model of strategic behaviour"*, Grenoble Ecole de Management (Post-Print) hal-00451450, HAL, 2003.

[77] R. J. Marzano, *A Theory-Based Meta-Analysis of Research on Instruction*, 1998.

[78] P. Ormerod and B. Rosewell, *Validation and Verification of Agent-Based Models in the Social Sciences, International Workshop on Epistemological Aspects of Computer Simulation in the Social Sciences*, pp. 130–140, Springer, Berlin, Heidelberg, 2006.

[79] B. Zeigler, T. Kim, and H. Praehofer, *Theory of Modeling and Simulation: Integrating Discrete Event and Continuous Complex Dynamic Systems*, Academic Press, Boston, 2000.

[80] R. G. Sargent, "Verification and validation of simulation models," in *Proceedings of the 2010 winter Simulation Conference*, pp. 166–183, IEEE, 2010.

[81] M. Ji, X. You, J. Lan, and S. Yang, "The impact of risk tolerance, risk perception and hazardous attitude on safety operation among airline pilots in China," *Safety Science*, vol. 49, no. 10, pp. 1412–1420, 2011.

[82] J. Davidson, *Cognitive Behavior Therapy, Basics and beyond*, LWW, Philadelphia, 2013.

[83] Z. Ma, *Research on the Impact of Construction Workers' Risk Tolerance on Unsafe Behaviors, Master*, Dongbei University of Finance and Economics, China, 2017.

[84] N. Xia, Q. Xie, X. Hu, X. Wang, and H. Meng, "A dual perspective on risk perception and its effect on safety behavior: a moderated mediation model of safety motivation, and supervisor's and coworkers' safety climate," *Accident Analysis & Prevention*, vol. 134, Article ID 105350, 2020.

[85] Y. P. Huang, X. Q. Wang, R. X. Ding, and N. N. Xia, *Risk Perception, Risk Propensity, and Unsafe Behavior: An Empirical Study of Workers in Chinese Construction Industry*, in *Proceedings of the IEEE International Conference on Industrial Engineering and Engineering Management (IEEM)*, pp. 1121–1125, Bali, Indonesia, December 2016.

[86] N. Xia, X. Wang, M. A. Griffin, C. Wu, and B. Liu, "Do we see how they perceive risk? An integrated analysis of risk perception and its effect on workplace safety behavior," *Accident Analysis & Prevention*, vol. 106, pp. 234–242, 2017.

[87] J. Sa, D.-C. Seo, and S. D. Choi, "Comparison of risk factors for falls from height between commercial and residential roofers," *Journal of Safety Research*, vol. 40, no. 1, pp. 1–6, 2009.

[88] D. Fang and H. Wu, "Development of a safety culture interaction (SCI) model for construction projects," *Safety Science*, vol. 57, pp. 138–149, 2013.

[89] H. W. Heinrich, *Industrial Accident Prevention. A Scientific Approach*, McGraw-Hill book Company, 1941.

[90] USBLS U.S.B.o.L.S., *Table 1-Incidence Rates-Detailed Industry Level-2019*, U.S. Bureau of Labor Statistics, 2019.

Review Article

Exploring the Application of BIM Technology in the Whole Process of Construction Cost Management with Computational Intelligence

Dan Tang and Kongling Liu [ORCID]

School of Architecture and Engineering, Hunan Institute of Engineering, Xiangtan, Hunan 411100, China

Correspondence should be addressed to Kongling Liu; konglingliu@hnie.edu.cn

The construction industry is a labor-intensive industry in China. In recent years, as people's living standards have risen, so have their requirements for the functionality, appearance, and comfort of buildings. The amount of information attached to construction projects is also increasing, especially for some modern large-scale construction projects. Due to the long construction period and a large amount of information in the construction process, the difficulty of project engineering management has also increased significantly. At the same time, with the gradual development and improvement of China's market economy system, the prices of labor and materials in the construction industry continue to rise, and the huge consumption of energy and resources no longer meets the strategic requirements of sustainable development. Therefore, construction project cost management is facing a huge impact, the actual effect of construction project cost management work is not good, and the phenomenon of uncontrolled construction project investment commonly occurs. The use of BIM software to build a building information model can integrate information from all stages of the project and facilitate the participation and cooperation of all project entities. Cost management is carried out before the actual construction of the project, thus realizing the whole process of cost management and effectively avoiding the occurrence of actual costs exceeding the budget after the project is completed. The study analyses the suitability of applying BIM technology to the whole process of construction project cost management with computational intelligence and explains the value and advantages of BIM in the whole process of construction project cost management. On this basis, this research provides a specific analysis of the application of BIM technology in the process of cost management at various stages of the whole process of construction projects and thus puts forward suggestions that can solve the obstacles that may be encountered in the whole process of cost management of construction projects in China.

1. Introduction

As one of the oldest industries in the world, the construction industry has always played a very important role in the history of human development. The construction industry has an irreplaceable position in China's national economic growth and social and economic development and has become an important pillar industry of the national economy [1]. In recent years, influenced by the national macrocontrol policies, the development of China's construction industry has gradually slowed down, but the construction industry output value in China's national economy still occupies a large proportion, and the proportion is increasing year by year trend. For a long time, the construction industry has been a labor-intensive industry in China, and the phenomenon of low efficiency and high construction costs is more common [2]. As living standards improve, people are demanding more and more information about the function, appearance, and comfort of buildings, and the amount of information attached to construction projects is increasing [3]. In the course of the actual construction of a project, changes are often made due to design failures or communication problems between the parties involved, especially for modern large-scale construction projects with large

investment scales. Due to the large number of construction units involved and the long construction cycle, the difficulty of project management is greatly increased, and the problem of cost management is particularly acute [4]. However, because of the lack of overall planning for the whole life cycle of China's construction industry management, the attention of project participants is still only on a certain stage of the life cycle and a certain partial business. For instance, the traditional cost management model is unable to achieve information sharing throughout the construction life cycle [5]. Therefore, in order to ensure the effectiveness of engineering projects and reduce the waste of resources, it is necessary to improve the engineering management model, especially cost management which plays an important role in engineering management [6]. The effective use of information technology in the processing of various relevant information to achieve the whole process of project cost management can fundamentally reduce engineering changes and delays, thus reducing costs and maximizing the benefits of the project.

The three main objectives of construction project management are cost [7], quality [8], and duration [9]. With the continuous development of modern construction material technology, quality and duration are no longer universal issues in the construction industry. In the competitive environment of economic globalization, construction cost has become the focus of attention in the construction industry [10]. The most direct effect of the serious waste and low productivity caused by the lagging application of information technology in the construction industry is reflected in the cost [11]. Thus, how to use modern science and technology to reasonably control the cost of construction has become an urgent task for the construction industry. For a long time, experts and scholars at home and abroad have been committed to research the whole process of cost management of construction projects. They hope that, through the continuous management and control of the whole process of construction project cost, the organic link between each stage can be established, so as to realize the whole process and all-round project cost management [12–14]. However, at present, there is still a clear division of labor between design and construction in China's construction industry, and the vast majority of construction project management models adopt the DBB (Design, Bid, and Build) model. This model can hinder the transmission of information between the various stages of engineering construction and poor communication between the parties involved, making it difficult to implement whole process cost management for construction projects [15]. In this context, people began to explore a large number of new technologies and management models, such as three-dimensional mapping [16], lean construction management model [17], integrated project delivery management model [18], BIM model [19], system dynamic model [20], and electroencephalogram model [21], the purpose of which is to build bridges between the various stages of the project and the various parties involved, so as to reduce information communication obstacles, so that the whole process of construction project cost management can be implemented.

Currently, 3D graphics technology has been implemented in the budgeting software, allowing users to quickly implement 3D graphics modeling in the budgeting software, and the system will automatically calculate and summarize the quantity information and establish a link with the cost estimation database to generate cost estimates. The system will automatically calculate the summary quantity information and establish a link with the cost estimate database to generate cost estimates [22]. This model supports the construction of geometric operations and spatial topology relationships, which not only improves the accuracy of cost estimates but also improves intelligence and automation [23]. However, there are several problems with this technology. For instance, there is not yet a good interface between cost forecasting and design, which prevents the direct use of design information and affects the efficiency of cost forecasting and control. Furthermore, there is no intuitive link between building components and cost information, and when design changes or changes in cost parameters occur, they need to be adjusted item by item in each system, which is less efficient.

With the rapid development of information technology today, information resources have become one of the three strategic resources in the new century. Along with the continuous development of Internet technology and the data industry, the capacity and performance of computer hardware have also been upgraded, which has made it possible for the development of information technology in all industries [24]. In China, the level of informatization in the electronics and manufacturing industries is already at a high level, and the models generated by information technology have significantly improved the productivity of these industries, but the informatization of the construction industry is still in its infancy. Informatization in the construction industry refers to the use of information technology, such as computer technology, communication technology, control technology, and information security technology, to transform and upgrade the technical means and production organization of the construction industry, thereby improving the management level and core competitiveness of construction enterprises. In developed countries such as Europe and the USA, where information technology in the construction industry started earlier, the application of information technology in construction enterprises has become more common, mainly in the extensive use of BIM [25]. BIM is a new concept that has emerged in the construction industry in recent years. Its introduction and development have placed higher demands on decision-makers and participants in engineering and construction projects in terms of collaborative work and application management for information sharing. In terms of modeling, BIM is based on three-dimensional digital technology, with the database formed by the three-dimensional model as the core [26]. The whole modeling process not only contains the professional design concepts of designers from various disciplines but also contains information on the whole process from design to construction and even completion and final demolition. From the application point of view, the model is based on the

parametric design and is an object-oriented, parametric, and intelligent digital representation of the building, supporting various operations in construction projects and containing engineering information that is all interrelated [27]. Based on the parametric, visual, collaborative, and information-sharing advantages of BIM models, BIM can facilitate the early involvement of all parties involved in construction projects. In addition, the application of BIM can help constructors make the most effective decisions and use BIM to participate in construction project management during the construction process, thereby reducing project duration, controlling project risks, and promoting the smooth implementation of the whole process cost management.

The understanding of what BIM means varies due to the different levels of understanding of BIM. The most straightforward understanding of BIM is that it is a production tool that is used as a platform on which all information related to a construction project is placed to create a building model that simulates the real situation of the building [28]. BIM is also a new management concept, as the building model created through BIM can accommodate information from all stages of the building construction process and can be updated at any time to facilitate the participation and cooperation of all parties involved in the project, thus achieving whole life cycle management from design to construction, operation, and even demolition. With the support of BIM technology, all parties involved in the project can visualize the results of the design through BIM software. With the help of BIM, communication between the various project participants is made easier. Through construction simulations, they can identify any design irregularities in advance, thus reducing the need for rework due to changes and optimizing the design [29]. Cost management before the actual construction of the project can prevent the actual cost of the project from exceeding the budget after completion. As a result, the emergence and application of BIM technology provide a reference for the realization of whole process cost management [30]. However, there are still a few cases of BIM being used in construction projects in China, but research on BIM has already started. Some universities have set up BIM research groups to research BIM theory, BIM software, and BIM applications [31]. The research and development of BIM and the use of BIM technology to build an information platform to facilitate the efficient implementation of the whole process of construction project cost management will be a key focus of future research and development in the field of construction project costing in China.

In this context, this paper investigates the whole process of cost management of project construction based on BIM technology, focusing on the whole process of cost control of engineering construction projects from conceptual design to construction and completion and handover. In addition, this research focuses on the application of BIM technology in the whole process cost management of construction projects as an example and proposes a proven solution for BIM technology in the whole process cost management of construction projects.

2. Construction Cost Management

The construction cost refers to the construction price of an item of engineering construction. In a broad sense, construction cost covers construction cost, installation cost, municipal cost, power cost, water cost, and communication cost. The meaning of construction cost can be understood in two different ways from the perspective of the owner and the contractor, respectively. From the owner's point of view, the construction cost is the total one-off cost of the planned reproduction of fixed assets, the formation of corresponding intangible assets, and the laying down of working capital, i.e., the investment in the fixed assets of the construction project. On the other hand, from the contractor's point of view, the construction cost is the price of the construction and installation work and the total price of the construction work expected or formed in the land market, the technical labor market, and the equipment market, and other trading activities.

2.1. Current Status of Construction Cost Management in China. At the present stage, China's construction cost management mode is a whole process construction cost management mode in which fixed-price pricing and bill-of-contract pricing coexist. The whole process of cost management refers to reasonable determination and effective control of project costs throughout the entire process from the decision-making stage to the completion and acceptance of the project. To facilitate the establishment of economic relations between the parties in the process of construction and to meet the requirements of construction management, budget estimates are required for each stage of construction. Each construction stage and its corresponding budget estimates are shown in Figure 1.

In recent years, with the improvement of the bidding system and the continuous development of the quota standard, the cost management level of China's construction industry has been significantly improved, and cost consultancy has become a relatively mature profession. However, the level of cost management of construction projects in China still has a large gap with that of developed countries, and the current situation of cost management of construction projects in China is not optimistic. From the perspective of project cost management, each stage of cost management can reflect common features. The relationship between the various stages of a construction project also inevitably requires that the cost management of each stage is also coherent with each other. The entire construction project cost management should form an organic whole, so that all parties involved in the construction project can be the first to know the occurrence and changes in construction investment and cost. Therefore, the whole process of cost management of construction projects is the most advantageous management mode at present. At the same time, the current situation of cost management in China's construction projects and many problems that have been revealed have made whole process cost management an inevitable trend.
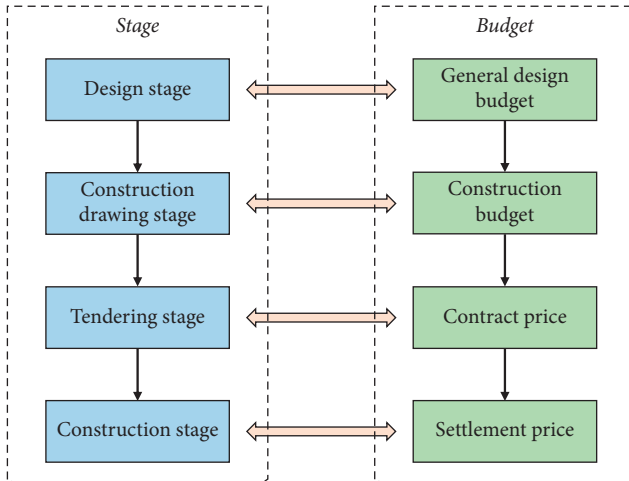
FIGURE 1: Construction stage and its corresponding budget estimates.

FIGURE 2: Framework of BLM.

2.2. Building Lifecycle Management.

Building lifecycle management (BLM) is a digital approach to creating, managing, and sharing information about the capital assets of a project throughout its construction. The core idea is to integrate the design, construction, and management processes through information integration and collaborative working. BLM covers all aspects of the full project lifecycle, including component design, document management, cost forecasting, construction management, project management, and visualization in the decision phase, implementation phase, and operational phase. The construction information is characterized by the large volume, diversity, and frequent changes, and the difficulty of managing project information is exacerbated by the large number of parties involved. The starting point of BLM is to solve the challenges of project information management, including information creation, management, and sharing. The process of creating information involves the selection of solutions and the integration of relevant information to ensure the accuracy of the information, including project solutions, spatial geometric properties, bills of materials, product structures, and cost information. An important way to achieve the creation of information is through the use of BIM technology.

The realization of the concept needs to rely on the support of relevant technical software. As shown in Figure 2, BIM technology completes the collection and creation of basic building information data, and each participant extracts and uses project information through their respective data interfaces to realize the value-added final realization of the project concept.

The core purpose of BLM technology is to solve the problem of information creation, information management, and information sharing in the whole life cycle of a construction project, and the process of its realization can be expressed in Figure 3.

2.3. Building Information Modeling.

Building information modeling (BIM) is the process of creating and managing building information. It is a technique for modeling the
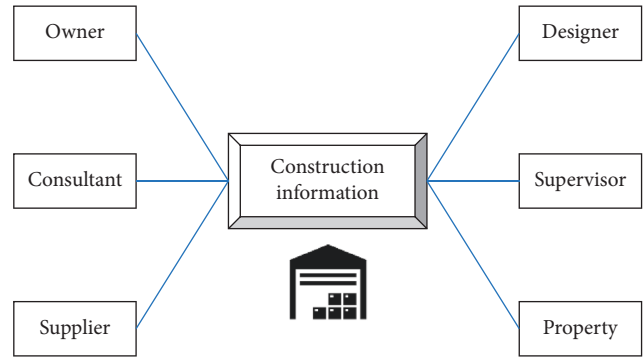
entire construction project through one or more building information databases and is a parametric model containing a variety of information. Through technology-based design software, designers can input parametric information directly into the database in a graphical environment, without the need to expend more effort on abstract two-dimensional drawings, to obtain objects with a range of characteristics to represent the basic properties of a building. In recent years, with the widespread application of modern computer technology in the construction industry, BIM technology has slowly been realized. The application and promotion of BIM technology is not only a technical upgrade to the construction industry but also a revolution to the traditional concept of construction engineering.

With the support of BIM technology, designers can carry out a comparative analysis of multiple solutions, thus minimizing the impact of design changes or professional conflicts on construction projects and providing security for project decisions. Designers can directly create parametric 3D building models through BIM-related software, putting more effort into the design rather than wasting a lot of time on 2D output drawings. Figure 4 reflects the difference between the design process based on BIM and the traditional design process.

The key to BIM applications is how to solve the problem of information expression, information transfer, and information exchange. For a long time, it has been difficult to exchange information between different software due to the large differences in data formats between them. To solve this problem, the most effective way is to develop a data file standard that all software can support so that all software can exchange information with each other through this data file standard. For this reason, a number of standards have been implemented internationally to regulate the representation and exchange of different data, and three of the more popular ones are industry foundation class (IFC), information delivery manual (IDM), and international framework for dictionaries (IFD). As shown in Figure 5, IFC, IDM, and IFD form the basis for information exchange on the BIM platform, ensuring the smooth transfer and sharing of information on construction projects and thus maximizing the value of the BIM technology platform. IDM is the process of defining the types of information that need to be exchanged between different phases and objects and the methods of
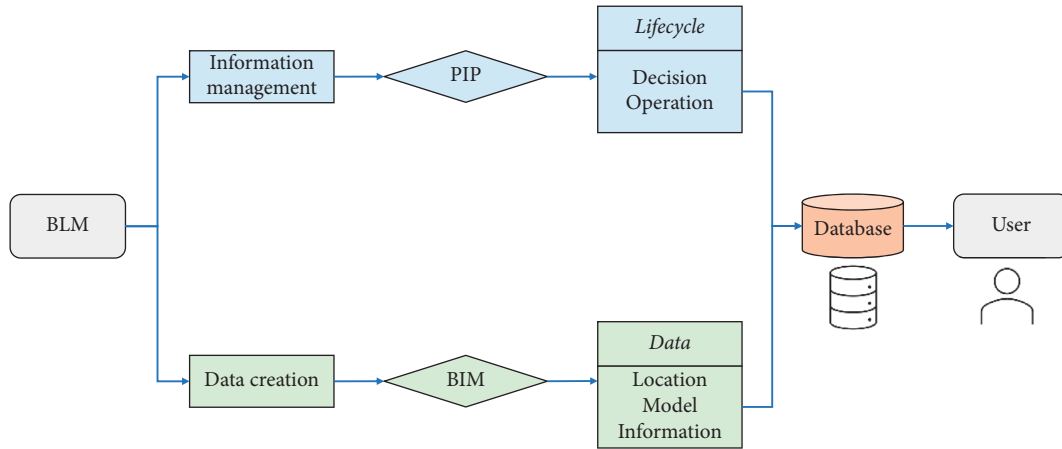
FIGURE 3: Realization process of BLM.
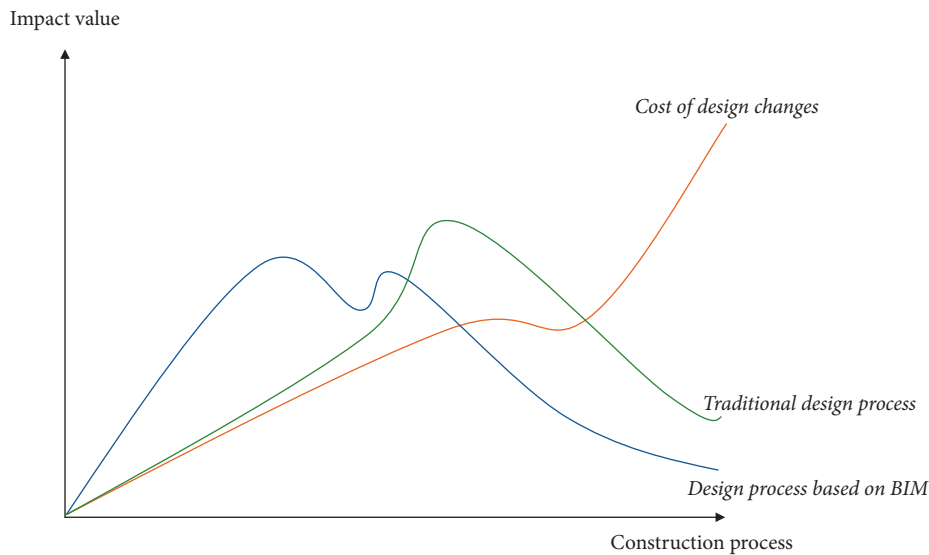
FIGURE 4: Difference between design process based on BIM and traditional design process.

exchange and ensuring that these information exchange processes are properly understood and used. The relationship between FC and IDM can be understood as the IFC is like a pharmacy with all the medicines, while the IDM is a prescription for a particular disease or a particular patient. That is, the IFC supports all business requirements between all projects and all phases, while the IDM supports one business requirement for one project and one phase, and it is the IDM that decides which IFC information is needed for this business.

3. BIM-Based Construction Cost Management

The first step in cost budgeting is quantity surveying. The biggest advantage of building information model quantity surveying over traditional drawing surveying is that it minimizes the need for manual surveying.

3.1. Investment Decision Stage. The investment decision stage is the most crucial step in the construction of a project, where different investment options are economically and technically justified, and the best option is selected after comparison. A mistake in decision-making can often bring irreparable losses to the enterprise and even plunge it into an economic crisis, so the investment decision stage of the project needs to be given high priority. The content of the investment decision stage is the basis for determining the cost of the project, and a correct investment decision requires an accurate grasp of the costs of each option. Therefore, on the premise of technical feasibility, it is essential to make investment estimates for each option. The use of Excel archives has been a further development, but for many reasons, the amount of data that can be accumulated is small. Historical data are less structured, less calculable, and more cumbersome to accumulate. The BIM model has construction data, technical data, quantity data, cost data, schedule data, and application data that can be restored when comparing and selecting investment options and can be displayed in a three-dimensional mode. As shown in Figure 6, the model of a project with a similar history can be changed and innovated according to the program characteristics of the new project, so that the cost and total amount
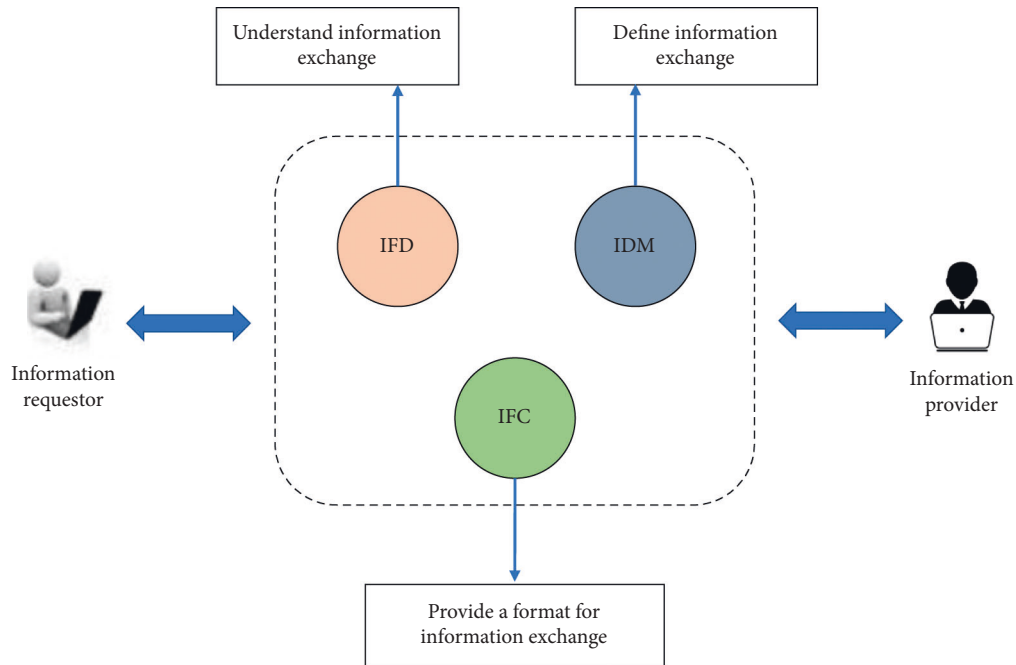
FIGURE 5: Information exchange among IFC, IDM, and IFD.
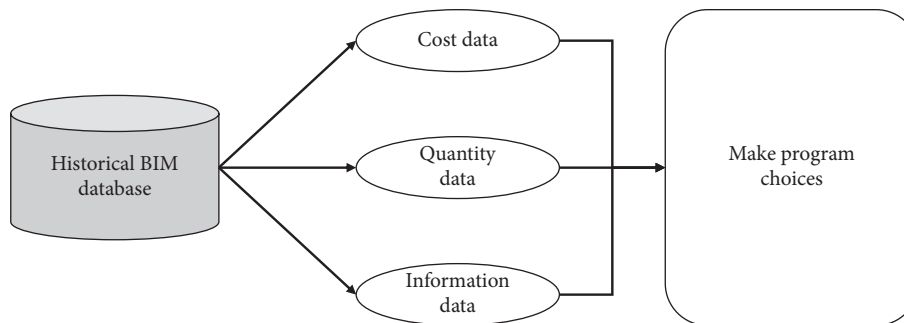
FIGURE 6: Program choice based on BIM.

of work can be calculated for several costs programs. Based on this procedure, the selection of the overall solution is made easier, making it much more efficient and helping to design future solutions.

3.2. Design Stage. The preparation of estimates at the design stage depends on the depth of the design, the degree of completeness of the information, and the requirements for the accuracy of the estimates. When design information is insufficient, budgets for similar projects can be selected as a basis for preparation after analysis and adjustment of co-efficients. If the information on similar projects is not available, the budget estimates will be prepared using in-dicators. When the design has reached a certain depth and a detailed list of equipment, a sketch of the pipeline alignment, building and structure type, and technical requirements for construction can be provided, and the estimate is prepared on the basis of quotas and cost indicators.

It is now generally accepted that cost management at the design stage should focus on limit design, i.e., the initial

scheme design should be based on investment estimates. Nowadays, it is not easy to achieve a reasonable limit design based on traditional manual algorithms and engineering budgeting methods. Firstly, the varying technical levels of the designers and the lack of cost control thinking mean that the tasks of the different disciplines are separate, and co-ordination and control have to be carried out regularly. Furthermore, the lack of adequate cost information in the design drawings due to the current design approach means that cost consultancy work and design work cannot be synchronized, and design proposals cannot be revised in a timely manner due to the constraints of cost indicators. As shown in Figure 7, with the introduction of BIM technology, the designer can extract some of the relevant design indi-cators from the model database for a more rapid limit de-sign, thus achieving the goal of an economical and reasonable design. Along with this objective, construction information and the corresponding quantity information can be obtained by the cost engineer and compared with the information in the database, so that the estimated price can be derived more quickly. The reasonableness of the design
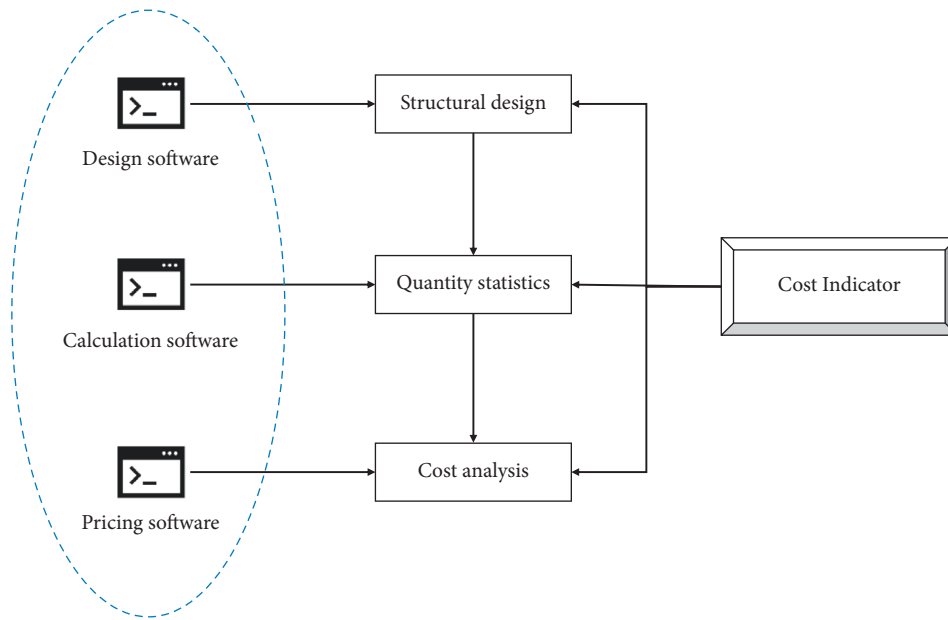
FIGURE 7: Construction limit design process.
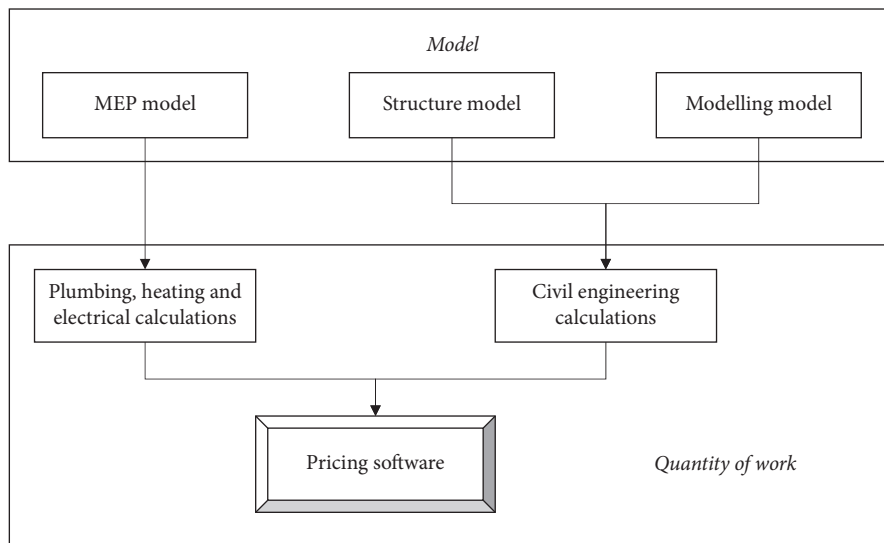
FIGURE 8: Interface relationship between design and calculation software.

indicators is then verified, and the value engineering approach is combined with the control of construction and use costs based on the whole project cycle, thus optimizing the design solution. The BIM model's real-time modeling and accounting of costs can be used as a basis for designers and cost engineers to carry out real-time and simultaneous calculations and analyses of the cost of the units designed, so that the information obtained can be used to optimize every detail of the design scheme, thus enabling limit design to be achieved.

The establishment of a great BIM model is highly valued by engineering cost practitioners, different professions have different BIM models, and the quality of the BIM model has a direct impact on the outcome of the project. Figure 8 illustrates the interface relationship between design and calculation software. Many domestic costing-related software companies are doing their best to develop relevant model data interfaces to implement the model design. Their efforts have been tested in several engineering cases, and some results have gradually been achieved. With the promulgation of national standards for the interface from design to measurement, this technology is gradually being accepted by engineers.

4. Conclusion

In the current construction industry, there are many participants and a huge amount of information. Traditional construction cost management methods and information communication mechanisms have been unable to meet the

requirements of modern construction project cost management work and must be committed to exploring new ways of working and information transmission channels to realize the whole process of construction project cost management. Only in this way can China's current construction project cost management be optimized, the overall cost control level of the industry be improved, and the waste of energy and resources be reduced, so that we can ultimately stand out in the fierce international competitive environment. In order to realize the whole process of cost management of construction projects, this study applies BIM technology to it. BIM is suitable for the whole process of cost management in construction projects. It can be used to effectively improve the efficiency of cost management at all stages and control the total cost of construction projects. BIM establishes an information-sharing platform to share information and improve the efficiency of cost management at each stage. In addition, BIM technology can achieve coordination and cooperation in cost management between all stages and all parties involved, thus realizing BIM-based cost management for the whole construction process, which is the key to solving the current problems of cost management for the whole construction process in China.

However, this paper is only a theoretical study and discussion of how to achieve BIM-based construction cost management, and there are still the following problems to be solved. Firstly, further research should be carried out on the creation of a computer-literate API interface to BIM software data and a database of BIM correspondence with lists and quotations. In addition, it is necessary to explore how to establish working methods and communication mechanisms between the various stages of the project and between the various parties involved in specific business operations based on BIM.

Data Availability

The labeled datasets used to support the findings of this study are available from the corresponding author upon request.

Conflicts of Interest

The authors declare that they have no conflicts of interest.

Acknowledgments

References

[1] W. Zhu, Z. Zhang, X. Li, W. Feng, and J. Li, "Assessing the effects of technological progress on energy efficiency in the construction industry: a case of China," *Journal of Cleaner Production*, vol. 238, Article ID 117908, 2019.

[2] Y. Wang, G. Ye, Y. Zhang, P. Mu, and H. Wang, "Is the Chinese construction industry moving towards a knowledge- and technology-intensive industry?" *Journal of Cleaner Production*, vol. 259, Article ID 120964, 2020.

[3] S. Durdyev, S. Ismail, and N. Kandymov, "Structural equation model of the factors affecting construction labor productivity," *Journal of Construction Engineering and Management*, vol. 144, no. 4, Article ID 04018007, 2018.

[4] S. Demirkesen and B. Ozorhon, "Impact of integration management on construction project management performance," *International Journal of Project Management*, vol. 35, no. 8, pp. 1639–1654, 2017.

[5] N. O. M. T. Altawati, N. Kim-Soon, A. R. Ahmad, and A. A. Elmabrok, "A review of traditional cost system versus activity based costing approaches," *Advanced Science Letters*, vol. 24, no. 6, pp. 4688–4694, 2018.

[6] C. Colapinto, R. Jayaraman, and S. Marsiglio, "Multi-criteria decision analysis with goal programming in engineering, management and social sciences: a state-of-the art review," *Annals of Operations Research*, vol. 251, no. 1-2, pp. 7–40, 2017.

[7] S. Ahmed, "A review on using opportunities of augmented reality and virtual reality in construction project management," *Organization, Technology & Management in Construction: An International Journal*, vol. 11, no. 1, pp. 1839–1852, 2019.

[8] R. Lotfi, Z. Yadegari, S. H. Hosseini, A. H. Khameneh, E. B. Tirkolaee, and G. W. Weber, "A robust time-cost-quality-energy-environment trade-off with resource-constrained in project management: a case study for a bridge construction project," *Journal of Industrial and Management Optimization*, vol. 18, no. 1, p. 375, 2022.

[9] H. Erol, I. Dikmen, and T. Birgonul, "Measuring the impact of lean construction practices on project duration and variability: a simulation-based study on residential buildings," *Journal of Civil Engineering and Management*, vol. 23, no. 2, pp. 241–251, 2016.

[10] A. Isaksson and H. Linderoth, "Environmental considerations in the Swedish building and construction industry: the role of costs, institutional setting, and information," *Journal of Housing and the Built Environment*, vol. 33, no. 4, pp. 615–632, 2018.

[11] Y. Zhang, Z. Guo, J. Lv, and Y. Liu, "A framework for smart production-logistics systems based on CPS and industrial IoT," *IEEE Transactions on Industrial Informatics*, vol. 14, no. 9, pp. 4019–4032, 2018.

[12] G. Wu, C. Liu, X. Zhao, and J. Zuo, "Investigating the relationship between communication-conflict interaction and project success among construction project teams," *International Journal of Project Management*, vol. 35, no. 8, pp. 1466–1482, 2017.

[13] S. C. Paul, Y. W. D. Tay, B. Panda, and M. J. Tan, "Fresh and hardened properties of 3D printable cementitious materials for building and construction," *Archives of Civil and Mechanical Engineering*, vol. 18, no. 1, pp. 311–319, 2018.

[14] C. Z. Li, F. Xue, X. Li, J. Hong, and G. Q. Shen, "An Internet of Things-enabled BIM platform for on-site assembly services in prefabricated construction," *Automation in Construction*, vol. 89, pp. 146–161, 2018.

[15] J. Park and Y. H. Kwak, "Design-Bid-Build (DBB) vs. Design-Build (DB) in the U.S. public transportation projects: the choice and consequences," *International Journal of Project Management*, vol. 35, no. 3, pp. 280–295, 2017.

[16] R. G. Sayre, D. J. Wright, S. P. Wright et al., "A three-dimensional mapping of the ocean based on environmental data," *Oceanography*, vol. 30, no. 1, pp. 90–103, 2017.

[17] L. Koskela, A. Ferrantelli, J. Niiranen, E. Pikas, and B. Dave, "Epistemological explanation of lean construction," *Journal of Construction Engineering and Management*, vol. 145, no. 2, Article ID 04018131, 2019.

[18] S. M. E. SepasgozarSepasgozar, R. Karimi, S. Shirowzhan, M. Mojtahedi, S. Ebrahimzadeh, and D. McCarthy, "Delay causes and emerging digital tools: a novel model of delay analysis, including integrated project delivery and PMBOK," *Buildings*, vol. 9, no. 9, p. 191, 2019.

[19] B. Cheng, K. Lu, J. Li, H. Chen, X. Luo, and M. Shafique, "Comprehensive assessment of embodied environmental impacts of buildings using normalized environmental impact factors," *Journal of Cleaner Production*, vol. 334, Article ID 130083, 2022.

[20] R. Yuan, F. Guo, Y. Qian et al., "A system dynamic model for simulating the potential of prefabrication on construction waste reduction," *Environmental Science and Pollution Research*, vol. 29, no. 9, pp. 12589–12600, 2022.

[21] B. Cheng, C. Fan, H. Fu, J. Huang, H. Chen, and X. Luo, "Measuring and computing cognitive statuses of construction workers based on electroencephalogram: a critical review," *IEEE Transactions on Computational Social Systems*, pp. 1–16, 2022.

[22] F. Ning, Y. Shi, M. Cai, W. Xu, and X. Zhang, "Manufacturing cost estimation based on a deep-learning method," *Journal of Manufacturing Systems*, vol. 54, pp. 186–195, 2020.

[23] Z. Xu, L. Zhang, H. Li, Y. H. Lin, and S. Yin, "Combining IFC and 3D tiles to create 3D visualization for building information modeling," *Automation in Construction*, vol. 109, Article ID 102995, 2020.

[24] T. C. Li and Y. E. Chan, "Dynamic information technology capability: concept definition and framework development," *The Journal of Strategic Information Systems*, vol. 28, no. 4, Article ID 101575, 2019.

[25] R. Santos, A. A. Costa, J. D. Silvestre, T. Vandenbergh, and L. Pyl, "BIM-based life cycle assessment and life cycle costing of an office building in Western Europe," *Building and Environment*, vol. 169, Article ID 106568, 2020.

[26] F. Tang, T. Ma, J. Zhang, Y. Guan, and L. Chen, "Integrating three-dimensional road design and pavement structure analysis based on BIM," *Automation in Construction*, vol. 113, Article ID 103152, 2020.

[27] S. Wu, N. Zhang, X. Luo, and W. Z. Lu, "Intelligent optimal design of floor tiles: a goal-oriented approach based on BIM and parametric design platform," *Journal of Cleaner Production*, vol. 299, Article ID 126754, 2021.

[28] H. Chen, L. Hou, G. K. Zhang, and S. Moon, "Development of BIM, IoT and AR/VR technologies for fire safety and upskilling," *Automation in Construction*, vol. 125, Article ID 103631, 2021.

[29] X. Li, J. Xu, and Q. Zhang, "Research on construction schedule management based on BIM technology," *Procedia Engineering*, vol. 174, pp. 657–667, 2017.

[30] Y. Deng, Z. Rao, and L. Cai, "Comprehensive Evaluation of BIM Calculation Quantity in Domestic Construction Engineering Based on Fuzzy Comprehensive Evaluation," *Computational Intelligence and Neuroscience*, vol. 2021, Article ID 3292376, 21 pages, 2021.

[31] H. Liu, Q. Ju, N. Zhao, H. Li, and M. J. Skibniewski, "Value Proposition for Enabling Construction Project Innovation by Applying Building Information Modeling," *Computational Intelligence and Neuroscience*, vol. 2022, Article ID 2586307, 13 pages, 2022.

Research Article

Health State Assessment of Industrial Equipment Driven by the Fusion of Digital Twin Model and Intelligent Algorithm

Shuai Wang [ID],[1] Yabin Wang [ID],[1] Xiaoyu Liu,[2] Jinguo Wang,[1] and Zhuo Wang[1]

[1]*Army Engineering University of PLA, Shijiazhuang Campus, Department of Equipment Command and Management, Shijiazhuang 050003, China*
[2]*State Grid Hebei Electric Power Co., Ltd., Marketing Service Center, Shijiazhuang 050035, China*

Correspondence should be addressed to Yabin Wang; wangyabin123@163.com

Equipment health state assessment is of great significance to improve the efficiency of industrial equipment maintenance support and realize accurate support. Using the method driven by the fusion of digital twin model and intelligent algorithm can make the equipment health state assessment more suitable for the "accuracy" requirement of equipment support. Taking the neural network algorithm as an example, this paper studies the method of unit level health state assessment of equipment driven by the fusion of digital twin model and intelligent algorithm. The principle and opportunity of equipment health state assessment based on digital twin model are analyzed, the equipment health state grade is redefined from the data-driven perspective, the selection principles of assessment parameters are established, and the unit level health state assessment model of equipment based on digital twin model and neural network algorithm is established. The proposed method is implemented by programming with Python, and the effectiveness of the method is verified by a case study. It provides support for further research of equipment-level health state assessment and the decision-making of equipment maintenance and provides reference for the study of the combination of digital twin model and other intelligent algorithms for health state assessment.

1. Introduction

The introduction should be succinct, with no subheadings. Limited figures may be included only if they are truly introductory and contain no new results.

Industrial equipment is the foundation of production-oriented enterprises, and its health state directly affects the production efficiency of enterprises. In order to improve its core competitiveness, enterprises must try to improve the healthy operation time of equipment and reduce the investment in equipment maintenance support as much as possible, so as to save costs and increase profits. Therefore, production-oriented enterprises urgently need to realize accurate equipment maintenance support.

Facing the characteristics of industrial equipment, such as complex structure and function, various degradation conditions, and various failure modes, studying its performance degradation rules and health state assessment method, and timely assessing the health state of equipment can guide enterprises to make optimal support decisions, which is of great significance for enterprises to carry out accurate support [1–3].

Based on the methods of fuzzy comprehensive assessment [4], combined weighting model [5], neural network model [6], and Bayesian network model [7], research works have studied the equipment health state assessment from the qualitative perspective or probability of failure perspective. However, most of the existing research results on the assessment of equipment health state give the level of failure probability, which cannot solve the problem of when the equipment fails and when to carry out maintenance to achieve the best efficiency. The assessment is vague and cannot meet the requirements of accurate equipment support.

The fusion application of digital twin technology and intelligent algorithm provides a way to solve this problem.

After continuous exploration, the digital twin modeling technology of industrial equipment has matured. Using the established digital twin model for data analysis and algorithm implementation has become a new research focus of the practical application of digital twin technology. The combination of digital twin technology and intelligent algorithm can give full play to the advantages of digital twin model in mastering a large amount of equipment historical data, real-time data, and empirical knowledge and give full play to the advantages of intelligent algorithm in finding rules through machine learning, so as to obtain high-precision results. Taking the combination of digital twin technology and neural network algorithm as an example, this paper studies the equipment health state assessment method driven by the fusion of digital twin model and intelligent algorithm.

2. Analysis of Equipment Health State Assessment Based on Digital Twin Model

2.1. Basic Concepts. Equipment health state assessment is the assessment of the ability of equipment and its components to perform its design functions [8, 9]. Health assessment of equipment can effectively ensure the healthy and safe operation of equipment and provide technical support for equipment maintenance and repair decision-making [10].

Equipment health state assessment based on digital twin model is to assess the health state of equipment by using a large amount of data mastered by digital twin model and intelligent algorithm on the basis of digital twin model.

Equipment is composed of replaceable units that perform different functions. Equipment health state assessment can be divided into equipment level assessment and unit level assessment. The equipment level assessment is to assess the overall health state of the equipment. The unit level assessment is used to assess the health state of the replaceable unit of the equipment. The overall health state of equipment is affected by the health state of each unit. This paper mainly studies the method of unit level health state assessment of equipment in use stage based on digital twin model and neural network algorithm, so as to provide basis for equipment use units to research the equipment level health state assessment and make equipment support decisions.

2.2. Principle of Assessment. With the increase of equipment operation time, the health state of each component of equipment deteriorates according to different rules, and the health degree decreases continuously. The degradation curve of equipment health state is shown in Figure 1 [10].

It can be seen from the figure that the equipment generally does not fail instantaneously but has state degradation after operation for a period of time, and the degradation process is gradually accelerated under the action of various stresses until it is degraded enough to affect the realization of equipment functions, resulting in failure [11]. The degradation curve of equipment health state is an irregular decreasing curve, which cannot be described by analytical method. However, as long as the relevant

parameters representing equipment health state are found, the degradation rules of equipment health state can be found.

The purpose of health state assessment is to identify and monitor in a timely manner the relevant parameters that represent the health state of the equipment, to find the best maintenance time between the state degradation point and the functional failure point, to repair the equipment before it is close to failure, and to reduce excessive maintenance and save equipment support cost before ensuring normal operation of the equipment. At the same time, the maintenance equipment is prepared in advance to reduce the waiting time of the equipment [12].

2.3. Opportunity of Assessment. Equipment health state assessment based on digital twin model can realize real-time state assessment and master the health state of equipment at any time. In practical work, the combination of centralized assessment and assessment can be adopted at any time. In general, the assessment of the affiliated equipment shall be performed once a day and arranged in the idle time of the equipment at night, so as to avoid affecting the operation of the equipment and the accuracy of the assessment. Under special circumstances, when major changes or emergencies occur to the equipment, it can be assessed at any time. Through the assessment, the health state of the equipment can be mastered in time, and the corresponding countermeasures can be prompted, such as failure early warning, spare parts allocation demand, and equipment maintenance demand.

3. Digital Twin Technology and Neural Network Algorithm

Combining digital twin technology with neural network algorithm and giving full play to their respective advantages, we can obtain a high-precision assessment model.

3.1. Equipment Support Model Based on Digital Twin. Digital twin is a technology that creates virtual models of physical entities in a digital way. It simulates the behavior of physical entities in the real environment with the help of data and adds or expands new capabilities for physical entities through virtual and real interactive feedback, data fusion analysis, decision iterative optimization, and other means [13]. Based on a large number of advanced technologies such as sensor technology and big data technology, digital twin technology realizes the functions of automatic measurement, automatic recording, active uploading, active analysis, active early warning, auxiliary decision-making, and so forth with high data consistency and reliability; it is favored by research in various fields of production and life, such as engineering manufacturing, aerospace, smart city, smart grid, and system operation and maintenance.

The research of digital twin technology originates from the life cycle management of equipment. It has great matching and many advantages in the application of equipment maintenance support, which can greatly improve
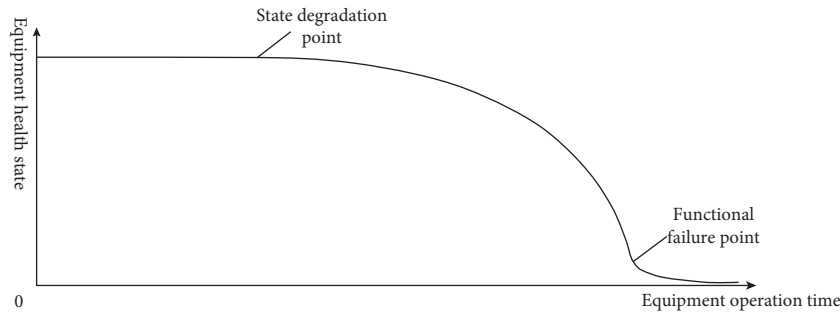
FIGURE 1: Degradation curve of equipment health state.

the initiative and accuracy of equipment maintenance support. NASA combines the physical system with its equivalent virtual system, studies the failure prediction and elimination method of complex systems based on digital twins, and applies it to the health management of plane, aircraft, launch vehicles, and other flight systems [14]. By combining the ultrahigh fidelity aircraft virtual model with the structural deviation and temperature calculation model affecting flight, the structural science center of the US Air Force Research Laboratory has carried out the life prediction of aircraft structure based on digital twins and summarized the technical advantages of digital twins [15]. Reference [16] introduced the digital twin five-dimensional model into prognostics and health management (PHM) and proposed a method of PHM based on digital twin.

At present, the digital twin modeling technology of industrial equipment has matured; [17] has studied and given the equipment support model based on digital twin, as shown in Figure 2.

The equipment support model based on digital twin is divided into four parts: physical layer, twin layer, application layer, and connection layer. In the process of operation, the physical layer transmits the real-time data to the twin layer. The twin layer provides data support to the application layer through data collection and processing and uses the processing results to guide the operation of entities in the physical layer. The application layer uses the data given by the twin layer to provide application services to equipment managers, assist equipment maintenance support decision-making, and act on the physical layer. The connection layer plays the role of internal and external communication of the model, transfers data between various layers within the model, and establishes communication with other relevant digital twin models.

Through the operation of digital twin model, the physical system and the cyber model can be synchronized, making it possible to analyze data online [18, 19]. Using the equipment support model based on digital twin, we can realize the real mapping of virtual equipment model to physical equipment entities, accurately reflect the actual situation of physical equipment, provide support for accurate equipment health state assessment, failure prediction, and spare parts demand prediction, better realize the timely maintenance support of equipment, and reduce the overall support cost [20].

3.2. Basic Principle of Neural Network. Artificial neural network system refers to a technical system that uses engineering technology to simulate the structure and function of the human brain neural network. It is a large-scale parallel nonlinear complex network system and is called neural network for short [21]. The neural network has good self-learning ability, nonlinear mapping, and fault tolerance [22] and has been widely used in classification, pattern recognition, prediction, signal processing, expert system, and other fields [23]. As long as there are enough hidden layers and hidden nodes, the neural network can approach any nonlinear mapping relationship, and its learning algorithm belongs to the global approximation method, so it has good generalization ability [24].

The typical neural network structure consists of three layers of neurons, namely, input layer, hidden layer, and output layer, as shown in Figure 3. Each layer is composed of several neurons, which are fully connected, and bias nodes (represented by (b) are added in the input layer and hidden layer. Through the continuous correction of the connection weights of each layer, the error convergence is realized, and finally a reliable neural network model is obtained to realize the required functions.

Due to the large difference in the probability of different results, the training dataset of neural network is usually imbalanced, which requires the use of algorithms such as granular computing and random forest to identify the optimal granularity and refine the imbalanced dataset [25, 26].

Programming with Python or other languages can realize the processing of training dataset, as well as the establishment and training of neural network model, and the neural network model that meets the training requirements can be used to realize the functions of data fitting, classification, clustering, and so on.

4. Equipment Health State Grade under Data Drive

The health state of equipment is described by health state grade. At present, the research on health state grade is mostly described by qualitative description or failure probability, which cannot adapt to the data-driven health state assessment method. To adapt to the data-driven health state assessment and provide support for the assessment, it is
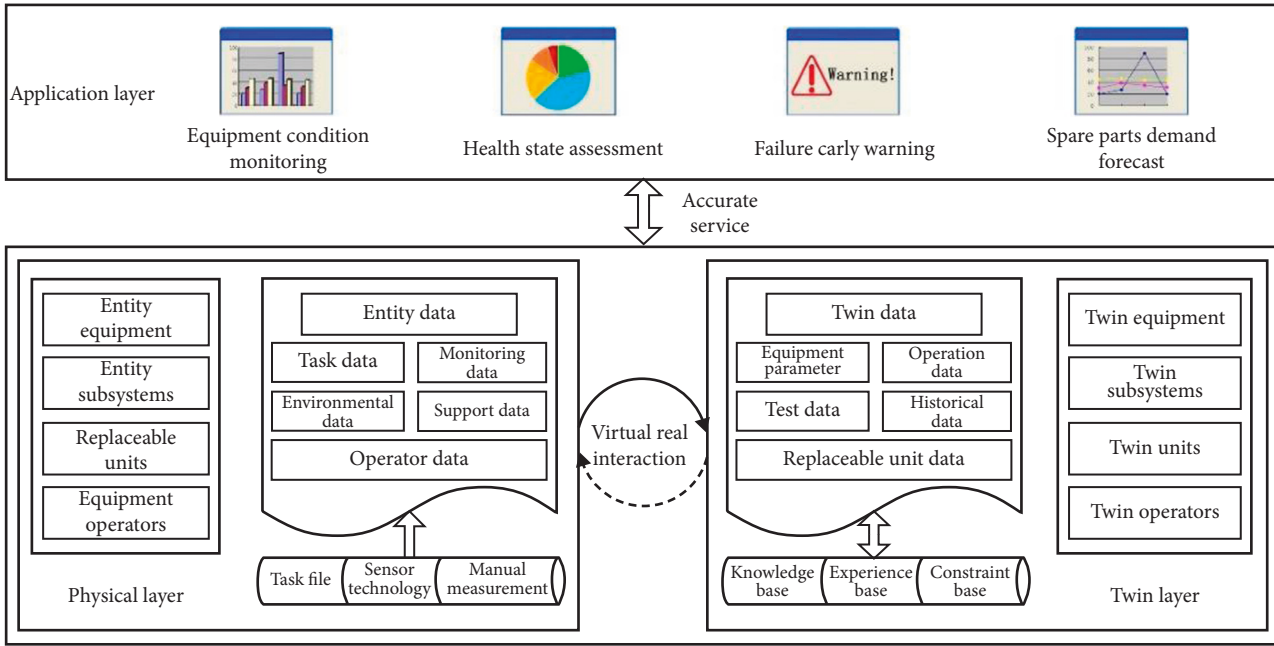
Figure 2: Equipment support model based on digital twin.
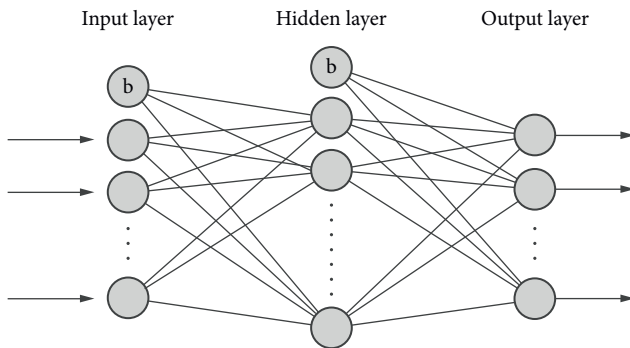
Figure 3: Typical neural network structure.

necessary to redefine the health state grade from the data-driven perspective.

According to the degradation curve of equipment health state and the support cycle of equipment maintenance equipment, the health state of equipment replaceable units is divided into five grades: health, subhealth, attention, danger, and failure, which are defined from the perspective of digital drive, as shown in Figure 4 and Table 1.

Health. The equipment is healthy and has good performance, and all indicators are in good condition, which is suitable for long-term operation. For such equipment, only daily maintenance is required.

Subhealth. The equipment performance degrades to a certain extent, but it does not affect the normal operation of the equipment. The failure is almost impossible to occur in the next 30 days. For such equipment, while doing well in daily maintenance, it is necessary to strengthen condition monitoring.

Attention. The equipment performance degradation is serious and can be detected obviously. Failure may occur in the next 30 days. For such equipment, it is necessary to strengthen condition monitoring, prepare for repair, and query the inventory of spare parts. If the inventory is insufficient, spare parts shall be allocated in time.

Danger. The equipment performance degradation is very serious, which has affected the operation quality of equipment. Failure may occur in the next 7 days. For such equipment, it needs to be repaired immediately during the scheduled downtime.

Failure. The equipment failure has occurred and the function of the equipment has been affected. Such equipment can only be shut down for repair.

5. Assessment Method of Equipment Health State

In the process of equipment health state assessment driven by the fusion of digital twin model and intelligent algorithm, the physical layer of digital twin model is responsible for connecting with the physical equipment through various sensors to obtain the most real original data and provide the data to the twin layer. The twin layer is responsible for preliminary statistical analysis of the obtained data, obtaining the analyzed twin data and transmitting it to the application layer for use. The application layer is responsible for using the obtained twin data to complete the task of health state assessment through intelligent algorithm. The information transmission between each layer is uniformly scheduled and transmitted through the connection layer. The data flow diagram of equipment health state assessment
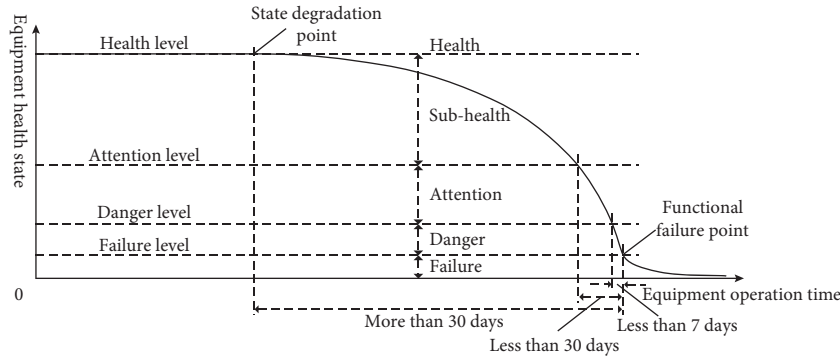
FIGURE 4: Equipment health state grade.

TABLE 1: Detailed table of equipment health state grade.

Health state grade	Grade identification	State performance	Definition under digital drive	Maintenance measures
Health	1	Good performance, all indicators are in good condition, suitable for long-term operation.	All indicators are in good condition.	Carry out the daily maintenance.
Subhealth	2	The performance degrades to a certain extent, but it does not affect the normal operation of the equipment.	The failure is almost impossible to occur in the next 30 days.	Carry out the daily maintenance and strengthen condition monitoring.
Attention	3	The performance degradation is serious and can be clearly detected.	Failure may occur in the next 30 days.	Strengthen condition monitoring, prepare for repair, and allocate spare parts in time.
Danger	4	The performance degradation is very serious, which has affected the operation quality of equipment.	Failure may occur in the next 7 days.	Repair at the right time.
Failure	5	A failure has occurred and the function of the equipment has been affected.	Failure has occurred.	Shutdown for repair.

driven by the fusion of digital twin model and intelligent algorithm is shown in Figure 5.

A large number of papers have been studied on the establishment of digital twin model, as well as the application of sensor and preliminary statistical analysis of data, which will not be repeated in this paper. This paper mainly studies the process of health state assessment in the application layer of digital twin model, combined with intelligent algorithm.

The basic idea of equipment health state assessment driven by the fusion of digital twin model and intelligent algorithm is as follows:

(1) Select assessment parameters.

(2) Obtain parameter data from the digital twin model.

(3) Assess health state through an intelligent algorithm.

(4) Give assessment conclusions and suggestions.

Taking the neural network algorithm as an example, the specific process of equipment health state assessment driven by the fusion of digital twin model and intelligent algorithm is shown in Figure 6.

5.1. Select Assessment Parameters. The health state of equipment can be characterized by a series of state parameters. As long as the parameters are selected comprehensively and reasonably, the health state of equipment can be characterized [27]. The state parameters commonly used in equipment mainly include temperature, vibration, pressure, speed, and acceleration, such as water temperature, oil temperature, oil pressure, amplitude, and frequency. At the same time, the analysis data of relevant parameters after preliminary analysis are also the characterization of the health state of the equipment, such as water temperature at startup, oil pressure at startup, maximum water temperature, minimum oil pressure, temperature rise speed, temperature 10 minutes after startup, steady-state temperature, and abnormal vibration characteristics.

When selecting assessment parameters, attention should be paid to the following aspects:

(1) The assessment parameters are not limited to the determinants of equipment health state and can also be related factors of health state, that is, the factors that will change due to the change of health state. As long as it can reflect some or several changes in the health state of equipment, it can be used as the selection object. When selecting assessment parameters, the most closely related state parameters should be selected as much as possible from the perspective of failure inducing mechanism.
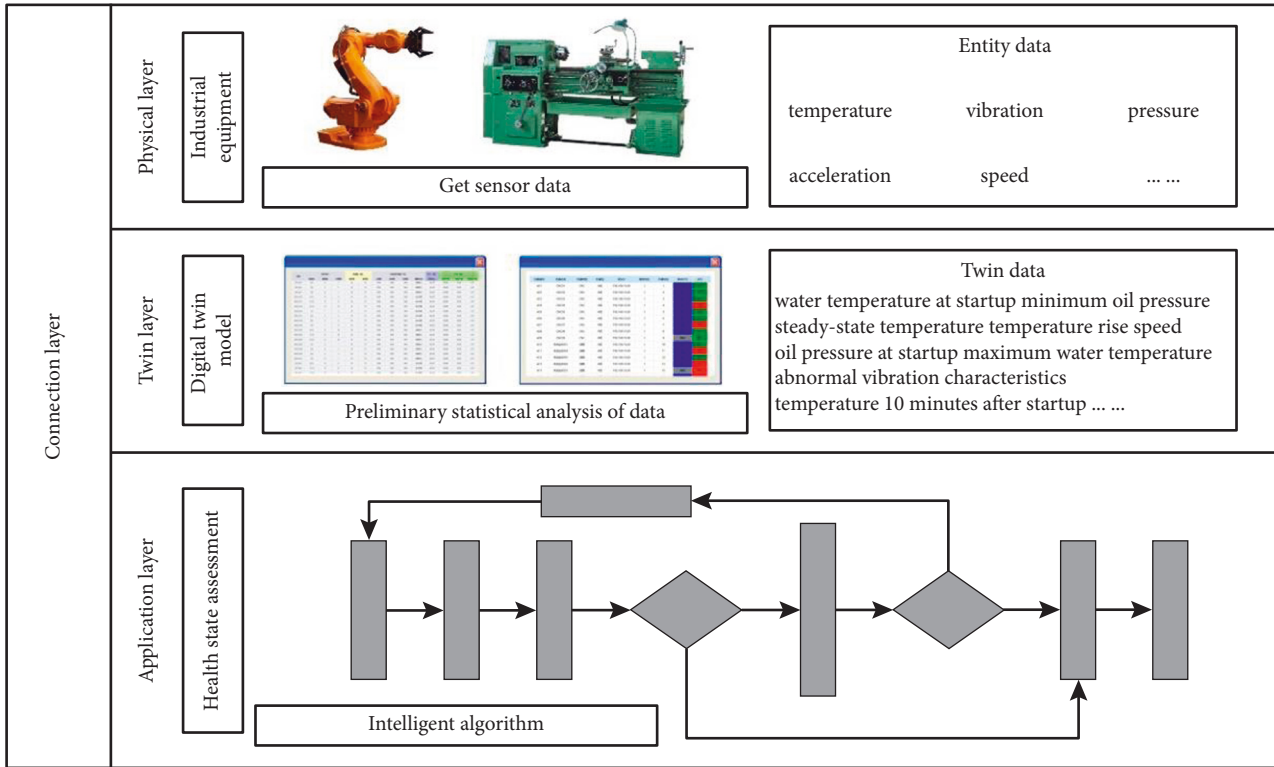
FIGURE 5: Schematic diagram of the data flow.

(2) When selecting assessment parameters, we should take into account the principles of correlation and measurability, should comprehensively analyze and optimize measurable state parameters from the perspective of existing measurement technology, and should not put forward too high requirements for the measurability of parameters. If too many sensors are added, not only will the cost be greatly increased, but also the normal operation of the equipment may be affected. The analysis of equipment state data can be strengthened, and the analysis of relevant data can be used to solve the problem that some data cannot be measured.

(3) The selected parameters should not be too many or too few. On the premise of reflecting the changes of equipment health state from the perspective of intelligent assessment, the assessment parameters should be selected as few as possible.

If it is found that the training result is not good enough in the process of training the neural network model, it shows that the correlation between the selected parameters and the equipment health state is not strong; that is, the parameter selection is not reasonable. At this time, it is necessary to reselect the state parameters with strong correlation with the equipment health state as the assessment parameters of the equipment health state.

5.2. Query Parameter Data from Digital Twin Model. Using sensor technology, digital twin model can obtain a large amount of state data efficiently, establish the real mapping between the virtual model and the physical entity,

and truly reflect the real-time state of equipment. At the same time, the digital twin model has sufficient historical and empirical data, which can be used as the support of data analysis.

Querying parameter data from digital twin model is to query and collect relevant data of assessment parameters in digital twin model, including current data, historical data, and empirical data, as the basis for further analysis. If no relevant data is queried from the digital twin model, the digital twin model needs to be adjusted.

5.3. Adjust Digital Twin Model. When establishing the digital twin model, the common parameters of equipment are mainly considered. If some selected parameters are not collected in the digital twin model and it is necessary to collect these parameters for health state assessment, it is necessary to adjust the digital twin model, add corresponding sensors, collect these parameters, and collect relevant historical and empirical data.

5.4. Preprocess Data. To meet the needs of neural network algorithm, the input data need to be preprocessed in two aspects: state data normalization and grade data formatting.

(1) State data normalization. The state data of the input data of the neural network model should be normalized according to a certain method to avoid the influence of different data value range on the results. There are many normalization algorithms, and appropriate methods can be selected according to the characteristics of data. Here, a simple method of
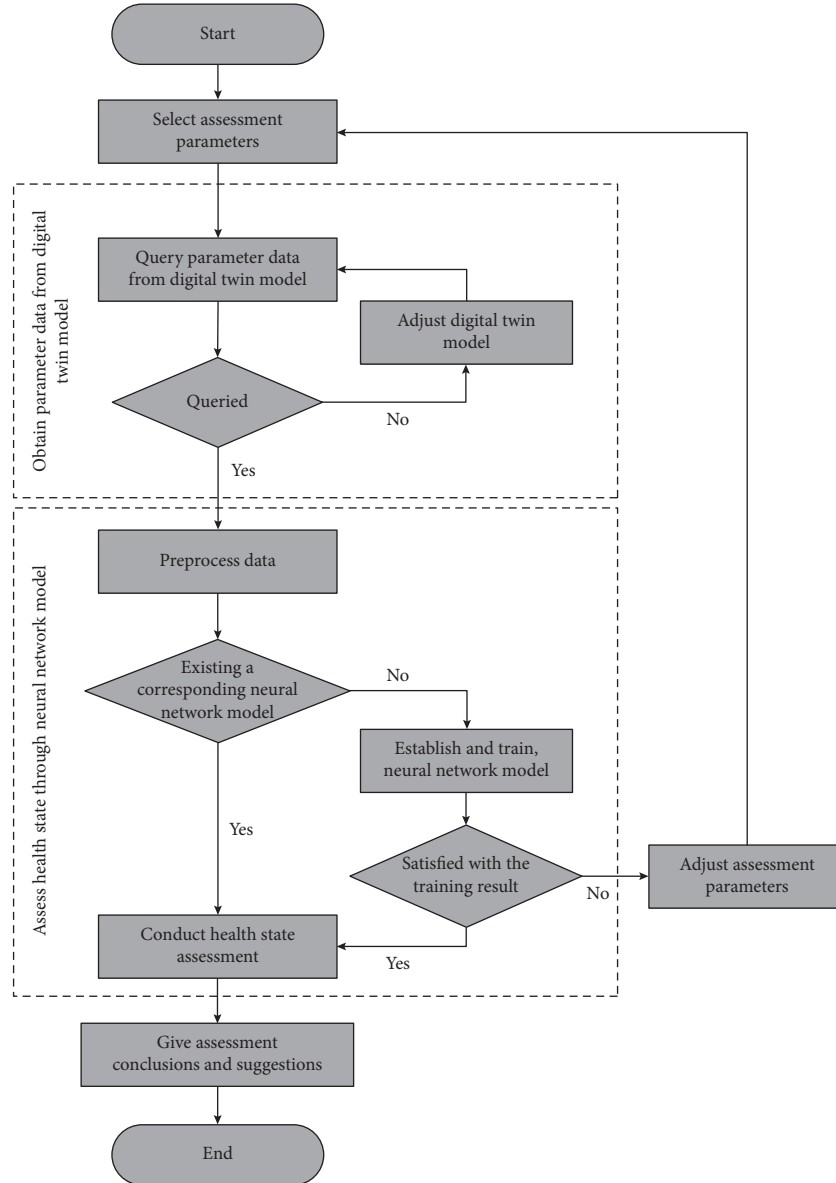
FIGURE 6: Assessment process.

maximum linear conversion is introduced as an example. The conversion equation is

$$x' = \frac{(x - x_{\min})}{(x_{\max} - x_{\min})},\qquad(1)$$

where x' is the value after normalization, x is the value before normalization, $x_{\min}$ is the minimum value of the sample, and $x_{\max}$ is the maximum value of the sample.

(2) Grade data formatting. The grade data of the input data of the neural network model shall be marked by a one-dimensional array in the format of 0-1. For example, if the health state of the equipment is divided into five grades, the grade data of the five grades shall be represented by a one-dimensional array [1,0,0,0,0], [0,1,0,0,0], [0,0,1,0,0], [0,0,0,1,0], and [0,0,0,0,1], as shown in Table 2.

TABLE 2: Grade data format.

Health state grade	Grade identification	Grade data format
Health	1	[1,0,0,0,0]
Subhealth	2	[0,1,0,0,0]
Attention	3	[0,0,1,0,0]
Danger	4	[0,0,0,1,0]
Failure	5	[0,0,0,0,1]

5.5. Establish and Train the Neural Network Model. In the stage of state assessment through the neural network model, if the assessed unit has established and trained the corresponding neural network model in the early stage, it can directly use this model for health state assessment. Otherwise, it should use the data obtained from digital twin model to establish and train the neural network model and assess the training result of the model. The established neural network model should also be retrained once a year.

5.5.1. Design the Model. The number of nodes in the input layer is represented by n, which is equal to the number of selected assessment parameters. The more assessment parameters, the more nodes.

The number of nodes in the output layer is represented by m, which is the number of required classifications. For example, if the equipment health state is divided into 5 grades, the number of nodes in the output layer is $m = 5$.

The hidden layer is designed as one hidden layer, and the number of nodes is represented by n_1. It is calculated according to (2), and the number of nodes with the best training result is set after many tests within the value range.

$$n_1 = \sqrt{n + m} + a, \tag{2}$$

where n_1 is the number of hidden layer nodes, m is the number of output layer nodes, n is the number of input layer nodes, and a is a constant between 1 and 10.

After adding bias nodes in the input layer and hidden layer, respectively, the neural network design is shown in Figure 7.

5.5.2. Train the Model. Distinguish the input data, so that 75% of the data is used for model training and 25% of the data is used for model testing. Write the neural network algorithm program in Python; we can train the neural network model. By continuously correcting the connection weights of each node in each layer, the error convergence can be realized and a reliable neural network model can be obtained.

5.5.3. Assess the Training Result. After the training of neural network model is completed, the training result of the model can be assessed and the accuracy of the model can be given through the model error and the classification effect of the model on the training data and test data. If the training effect meets the needs of assessment, the model can be used for health state assessment. If the training effect is not good enough, it indicates that the selected assessment parameters are not strongly correlated with the equipment health state. The assessment parameters should be adjusted according to the selection principle of assessment parameters, and the neural network model should be reestablished.

5.5.4. Retrain the Model. The established neural network model should be retrained regularly, and the newly collected actual operation data should be substituted into the model as input data, so as to increase the amount of data and improve the accuracy of the model. Since one year is generally a cycle of equipment operation and support and relatively complete operation and support data can be obtained at the end of the year, the retraining is generally conducted once a year and arranged at the end of each year.

5.6. Conduct Health State Assessment. After obtaining the data from the digital twin model and establishing and training the neural network model, we can use the state data
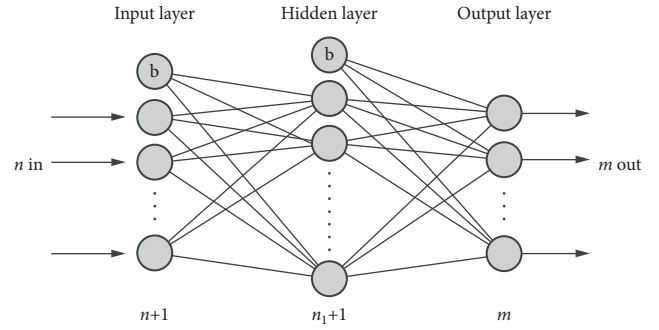
FIGURE 7: Neural network design.

and neural network model to assess the health state of equipment. After preprocessing the parameter data reflecting the current state of the equipment according to the same method as the input data and inputting them into the trained neural network model, the current health state grade of the equipment can be obtained, which directly reflects the health state of the equipment.

5.7. Give Assessment Conclusions and Suggestions. According to the health state assessment result, combined with the knowledge base and expert system of digital twin model, we can give the health state assessment conclusion, describe the current health state of the equipment, and present equipment maintenance suggestions, so as to help equipment managers better carry out equipment support and give full play to the maximum efficiency of the equipment.

6. Case Study

We take the engine fuel system of a certain equipment as an example to assess its health state. The engine fuel system is a replaceable unit of the equipment.

6.1. Select Assessment Parameters. According to the characteristics of engine fuel system, the pressure of high-pressure oil pipe is selected as the measurement basis, and six parameters are selected as the assessment parameters of the health state of the engine fuel system, as shown in Table 3.

6.2. Obtain and Preprocess Data. 3000 groups of historical data can be obtained from the built engine digital twin model as the input data of the neural network model, and the data are preprocessed. Part of the preprocessed data is shown in Table 4.

6.3. Establish and Train the Neural Network Model. We can write a program in Python to establish and train the neural network model.

The number of input layer nodes $n = 6$ and the number of output layer nodes $m = 5$ of the neural network model can be determined by 6 state parameters and 5 health state grades. According to (2), the number of hidden layer nodes n_1 can

TABLE 3: Health state assessment parameters.

Parameter number	Parameter content
Parameter 1	Pressure at the beginning of fuel injection
Parameter 2	Maximum fuel pressure
Parameter 3	Submaximum fuel pressure
Parameter 4	Width of the rising phase of pressure waveform
Parameter 5	Height difference between the highest point and the lowest point of pressure waveform
Parameter 6	Area of pressure waveform in an injection cycle

TABLE 4: Part of the preprocessed data.

Parameter 1	Parameter 2	Parameter 3	Parameter 4	Parameter 5	Parameter 6	Grade identification				
0.28	0.80	0.17	0.51	0.91	0.32	0	1	0	0	0
0.30	0.04	0.25	0.25	0.34	0.05	1	0	0	0	0
0.79	0.33	0.14	0.18	0.69	0.20	1	0	0	0	0
0.53	0.21	0.27	0.85	0.88	0.57	0	0	1	0	0
0.28	0.84	0.24	0.21	0.11	0.90	1	0	0	0	0
0.22	0.61	0.17	0.38	0.52	0.97	0	1	0	0	0
0.80	0.57	0.59	0.60	0.42	0.45	0	0	1	0	0
0.78	0.69	0.17	0.79	0.83	0.32	0	0	1	0	0
0.03	0.54	0.87	0.07	0.04	0.79	0	1	0	0	0
0.76	0.42	0.50	0.49	0.78	0.61	0	1	0	0	0
0.10	0.67	0.06	0.03	0.54	0.48	1	0	0	0	0
0.57	0.62	0.92	0.53	0.48	0.82	0	0	0	1	0
0.96	0.82	0.44	0.16	0.45	0.25	1	0	0	0	0
0.96	0.96	0.10	0.27	0.37	0.42	1	0	0	0	0
0.45	0.15	0.18	0.42	0.66	0.72	1	0	0	0	0
0.90	0.74	0.06	0.11	0.00	0.74	0	1	0	0	0
0.04	0.62	0.58	0.65	0.04	0.51	0	0	1	0	0
0.80	0.16	0.58	0.43	0.88	0.34	0	1	0	0	0
0.83	0.57	0.19	0.51	0.67	0.67	0	0	0	1	0
0.14	0.65	0.65	0.02	0.16	0.10	1	0	0	0	0
0.83	0.83	0.65	0.44	0.21	0.48	0	1	0	0	0
0.08	0.44	0.56	0.56	0.32	0.92	0	1	0	0	0
0.38	0.88	0.16	0.74	0.21	0.05	1	0	0	0	0
0.31	0.75	0.98	0.33	0.18	0.88	0	1	0	0	0
0.50	0.36	0.72	0.12	0.77	0.10	1	0	0	0	0
. . .	. . .	. . .	. . .	. . .	. . .	. . .	. . .	. . .	. . .	. . .

be selected from 4 to 13. Through many experiments, when the number of hidden layer nodes $n_1 = 13$, the model training effect is the best. Thus, the neural network model can be established.

The neural network model is trained by using the preprocessed input data. After many times of training, the satisfactory training result is obtained, as shown in Figure 8. It can be seen that the error of the neural network model decreases gradually through training. In the final neural network model, the correct rate of training data is 92.93%, the correct rate of test data is 91.87%, and the correct rate of all input data is 92.67%. The correct rate of the test data is close to that of the training data, and the error results only appear in the adjacent state of the actual results, indicating that the model does not overfit, and its correct rate is high, which can meet the requirements of the assessment model.

6.4. Conduct Health State Assessment. After extracting the current state information of the engine fuel system from the digital twin model and preprocessing, the state data can be obtained, as shown in Table 5.

After running the neural network model and entering the state data into the model, the assessment result can be obtained, as shown in Figure 9.

It can be seen that the assessment result of the current state is [0.0000, 0.1573, 0.5573, 0.1907, 0.000], suggesting that the engine fuel system is in the "Attention" state at this time. The assessment result is consistent with the actual situation.

6.5. Give Assessment Conclusions and Suggestions. Through the assessment, the engine fuel system is in the state of "Attention" at this time. Combined with the grading principle and referring to the knowledge base and experience base in the digital twin model, the assessment conclusion is that the performance degradation of the engine fuel system is serious and failure may occur in the next 30 days. The assessment suggestions are as follows: strengthen condition monitoring, prepare for repair, and allocate spare parts in time.

The above case shows that using the fusion driven method of digital twin model and neural network algorithm
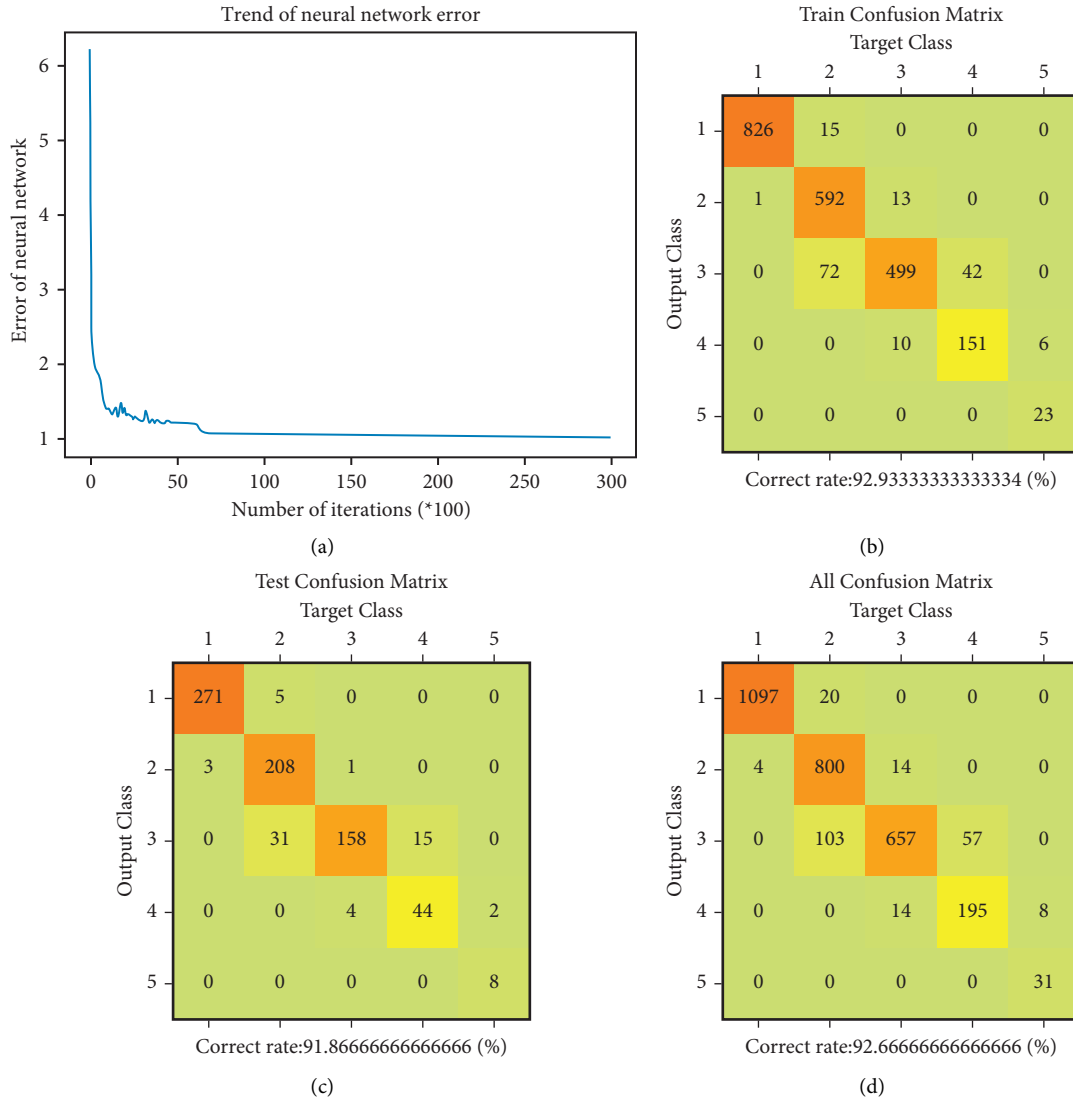
FIGURE 8: Training result of neural network. (a) Trend of neural network error. (b) Train confusion matrix. (c) Test confusion matrix. (d) All confusion matrix.

TABLE 5: State data after preprocessing.

Parameter 1	Parameter 2	Parameter 3	Parameter 4	Parameter 5	Parameter 6
0.86	0.81	0.71	0.58	0.49	0.07
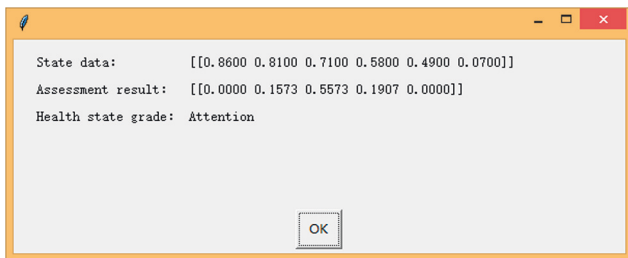
FIGURE 9: Conduct health state assessment.

can effectively realize the assessment of equipment health state and obtain intuitive and accurate assessment results.

7. Discussion

The above method defines a data-driven health state grade and uses the fusion drive of digital twin model and neural network algorithm to assess the health state of equipment and achieves the expected results.

This problem can also be solved by SOTA methods such as fuzzy comprehensive assessment, combined weighting model, and Bayesian network model, but because these methods are mostly assessed from the qualitative perspective or probability perspective, the assessment results are relatively fuzzy, which cannot meet the requirements of equipment support accuracy.

Compared with these methods, this method has the following characteristics:

(1) Faster. Using this method, real-time health state assessment can be realized. Because the digital twin model is established in advance and the way to obtain data is established, the data acquisition is faster. Because the training of neural network model is completed in advance and the training results can be used for many times, the assessment process is also faster.

(2) More accurate. In this method, the intelligent algorithm is used to make full use of the advantages of big data and find the failure rules suitable for each equipment. It avoids the process of determining the weight through expert scoring in some traditional methods and eliminates the interference of human factors, and the result is more accurate and objective. It meets the needs for accurate support.

(3) Better adapt to new requirements. The data-driven state grade is redefined to define the state with data, which meets the needs of big data-driven mode. The complex calculation process of some traditional methods is avoided, and the model can be used many times after training, which reduces the amount of calculation of state assessment and meets the needs of big data processing.

(4) More practical. The traditional health state assessment can only be used to count the state of batch equipment and master the overall state of equipment. This method can be used to assess the equipment group, single equipment, and a part of equipment. The assessment results can be used to reliably judge the health state of equipment, guide the support decision-making, and improve the active of equipment support.

(5) More automated. From data collection to processing to assessment, the whole process of assessment is automated, which saves labor, improves work efficiency, and greatly reduces the error rate.

(6) Portable. For new equipment that lacks a large amount of data support, the parameter data in the assessment model of similar equipment can be transplanted as empirical data to become the initial data of new equipment to bring the initial support data of new equipment closer to reality and provide support for the support decision of new equipment.

8. Conclusions

Equipment health state assessment is of great significance to realize equipment accurate support. Taking the neural network algorithm as an example, this paper studies the method of unit level health state assessment of equipment driven by the fusion of digital twin model and intelligent algorithm. The equipment health state grade is redefined from the data-driven perspective, and the unit level health state assessment model of equipment based on digital twin

model and neural network algorithm is established. The effectiveness of the method is verified by case study. Support is provided for further research of equipment-level health state assessment and the decision-making of equipment maintenance.

This paper mainly studies the method of health state assessment based on the combination of neural network algorithm and digital twin model. In fact, there are many intelligent algorithms that can be combined with digital twin model for equipment health state assessment. Different equipment or different replaceable units may need to use different algorithms according to their characteristics, but the method of combination with digital twin model is the same. The combination of digital twin model and other algorithms for health state assessment can be further studied in the future.

Data Availability

The raw data used to support the findings of the study can be obtained from the corresponding author upon request.

Conflicts of Interest

The authors declare that they have no conflicts of interest regarding this work.

Acknowledgments

References

[1] Y. Wang, J. Zhao, Z. Cheng, and Z. Yang, "Integrated decision on spare parts ordering and equipment maintenance under condition based maintenance strategy," *Eksploatacja i Niezawodnosc – Maintenance and Reliability*, vol. 17, no. 4, pp. 591–599, 2015.

[2] J. A. Kay and S. Malik, "Impact of improper installation, maintenance and servicing of electrical equipment in forest products industries," *IEEE Transactions on Industry Applications*, vol. 56, no. 4, pp. 3359–3367, 2020.

[3] C. L. Melchor-Hernández, F. Rivas-Dávalos, S. Maximov, V. Coria, and J. Guardado, "A model for optimizing maintenance policy for power equipment," *International Journal of Electrical Power & Energy Systems*, vol. 68, pp. 304–312, 2015.

[4] L. Zhou, Y. Feng, and J. Gu, "Missile quality assessment based on fuzzy theory," *Ordnance Industry Automation*, vol. 39, no. 8, pp. 60–66, 2020.

[5] J. An, T. Xu, X. Zeng, Z. Li, and G. Zhu, "Equipment quality condition assessment under fusion information based on combination weighting," *Control and Decision*, vol. 33, no. 9, pp. 1693–1698, 2018.

[6] J. Pei, J. An, and W. Wang, "Navy missile quality status hierarchy and evaluation," *Computer & Digital Engineering*, vol. 44, no. 12, pp. 2309–2313, 2016.

[7] D. Hao, J. Zhao, S. Zhang, and Y. Fang, "Research on military equipment quality evaluation method based on bayes theory," *Equipment Environmental Engineering*, vol. 13, no. 4, pp. 168–175, 2016.

[8] Y. Yao, Y. Wu, Y. Feng, and J. Zhao, "Health condition assessment of equipment," *Modern Defence Technology*, vol. 40, no. 5, pp. 156–161, 2012.

[9] B. L. Ferrell, "Air vehicle prognostics & health management," in *Proceedings of the 2000 IEEE Aerospace Conference*, vol. 6, pp. 145-146, Big Sky, MT, USA, March 2000.

[10] G. Liao, *Data-driven Methods of Equipment Health Assessment and Maintenance Decision-Making*, Huazhong University of Science and Technology, Wuhan, China, 2016.

[11] X. Wu and S. Li, "Health assessment and fault diagnosis model of GIS intelligent substation based on digital twin," *Hebei Electric Power*, vol. 40, no. 3, pp. 15–18, 2021.

[12] S. B. Rathnayaka, K. Y. See, and K. R. Li, "Inductively coupled on-line impedance measurement for condition monitoring of electrical equipment," *IET Science, Measurement & Technology*, vol. 12, no. 3, pp. 382–387, 2018.

[13] F. Tao, W. Liu, J. Liu et al., "Digital twin and its potential application exploration," *Computer Integrated Manufacturing Systems*, vol. 1, pp. 1–18, 2018.

[14] M. Grieves and J. Vickers, *Digital Twin: Mitigating Unpredictable, Undesirable Emergent Behavior in Complex Systems. Transdisciplinary Perspectives on Complex Systems*, Springer International Publishing, Berlin, Germany, pp. 85–113, 2017.

[15] E. J. Tuegel, A. R. Ingraffea, T. G. Eason, and S. M. Spottswood, "Reengineering aircraft structural life prediction using a digital twin," *International Journal of Aerospace Engineering*, vol. 2011, Article ID 154798, 14 pages, 2011.

[16] F. Tao, M. Zhang, Y. Liu, and A. Nee, "Digital twin driven prognostics and health management for complex equipment," *CIRP Annals*, vol. 67, no. 1, pp. 169–172, 2018.

[17] Y. Wang, S. Wang, and J. Wang, "Digital twin model of equipment maintenance management in modern enterprises," in *Proceedings of the 2021 7th International Conference on Materials, Mechanical Engineering and Automation Technology (MMEAT2021)*, pp. 1–6, Article ID 012088, Dali, China, May 2021.

[18] J. Leng, M. Zhou, Y. Xiao et al., "Digital twins-based remote semi-physical commissioning of flow-type smart manufacturing systems," *Journal of Cleaner Production*, vol. 306, Article ID 127278, 17 pages, 2021.

[19] J. Leng, D. Yan, Q. Liu et al., "Digital twin-driven joint optimisation of packing and storage assignment in large-scale automated high-rise warehouse product-service system," *International Journal of Computer Integrated Manufacturing*, vol. 34, no. 7-8, pp. 783–800, 2021.

[20] S. Wang, Y. Wang, and J. Wang, "Spare parts demand forecasting method of modern enterprises based on digital twin model," *International Journal of Modeling, Simulation, and Scientific Computing*, vol. 13, Article ID 2250045, 18 pages, 2022.

[21] Q. Shi, L. Wang, X. Shi, and M. Zhao, *Decision and Modeling of Systems*, National Defense Industry Press, Beijing, 2016.

[22] L. Han, *Theory, Design and Application of Artificial Neural Network*, Chemical Industry Press, Beijing, 2007.

[23] F. Yue, Q. Yan, T. Xu, and M. Zhao, "Application of BP neural network in quality evaluation of equipment in use stage," *Journal of Sichuan Ordnance*, vol. 31, no. 11, pp. 56–59, 2010.

[24] P. Alapuranen and J. Schroeder, "Complex artificial neural network with applications to wireless communications," *Digital Signal Processing*, vol. 119, Article ID 103194, 6 pages, 2021.

[25] J. Leng, Q. Chen, N. Mao, and P. Jiang, "Combining granular computing technique with deep learning for service planning under social manufacturing contexts," *Knowledge-Based Systems*, vol. 143, pp. 295–306, 2018.

[26] J. Leng, G. Ruan, Y. Song et al., "A loosely-coupled deep reinforcement learning approach for order acceptance decision of mass-individualized printed circuit board manufacturing in Industry 4.0," *Journal of Cleaner Production*, vol. 280, Article ID 124405, 2021.

[27] W. G. Chen, J. X. Wang, F. Wan, and P. Wang, "Review of optical fibre sensors for electrical equipment characteristic state parameters detection," *High Voltage*, vol. 4, no. 4, pp. 271–281, 2019.

Research Article

NTM-Based Skill-Aware Knowledge Tracing for Conjunctive Skills

Qiang Huang [iD],[1] **Wei Su** [iD],[1] **Yuantao Sun** [iD],[2] **Tianyuan Huang**,[1] and **Juntai Shi**[1]

[1]*School of Information Science and Engineering, Lanzhou University, Lanzhou 730000, China*
[2]*Ant Group, Hangzhou, China*

Correspondence should be addressed to Wei Su; suwei@lzu.edu.cn

Knowledge tracing (KT) is the task of modelling students' knowledge state based on their historical interactions on intelligent tutoring systems. Existing KT models ignore the relevance among the multiple knowledge concepts of a question and characteristics of online tutoring systems. This paper proposes a neural Turing machine-based skill-aware knowledge tracing (NSKT) for conjunctive skills, which can capture the relevance among the knowledge concepts of a question to model students' knowledge state more accurately and to discover more latent relevance among knowledge concepts effectively. We analyze the characteristics of the three real-world KT datasets in depth. Experiments on real-world datasets show that NSKT outperforms the state-of-the-art deep KT models on the AUC of prediction. This paper explores details of the prediction process of NSKT in modelling students' knowledge state, as well as the relevance of knowledge concepts and conditional influences between exercises.

1. Introduction

With the development of intelligent tutoring systems (ITSs) and the emergence of massive open online courses (MOOCs) [1, 2], knowledge tracing plays an important role in improving the efficiency of personalized learning platforms. Knowledge tracing is the task of modelling students' knowledge state based on their historical interactions to predict students' mastery of knowledge concepts (KCs), where a KC can be an exercise, a skill, or a concept [3, 4].

In order to better model students' knowledge state, various knowledge-tracing models have been proposed. In previous studies, Bayesian knowledge tracing (BKT) is a powerful knowledge-tracing model. BKT models students' knowledge concept state by using a hidden Markov model (HMM) for each KC [5].

As deep learning develops, a lot of deep learning models have been applied in KT. Chris Piech applies the recurrent neural network (RNN) to model the student learning process for the first time and proposes deep knowledge tracing (DKT) [6–9]. The dynamic key-value memory network (DKVMN) uses a static memory called key and a dynamic memory called value to discover latent relations between exercises and knowledge concepts [10, 11]. Self-attentive

knowledge tracing (SAKT) proposes a self-attention-based KT model to model the students' knowledge state, with exercises as attention queries and students' past interactions as attention keys/values [3, 12–15].

However, the aforementioned works only focus on students' exercise interactions and ignore the relations between questions and skills. It cannot model students' knowledge state accurately by merely focusing on students' interactions. Knowledge tracing models begin to pay attention to the structure of the knowledge concepts [16–18].

Deep hierarchical knowledge tracing models students' knowledge state by capturing the hierarchical structure of questions and knowledge concepts [16]. Neil Heffernan's latest work considers the question information to which the knowledge concept belongs [17]. Graph-based knowledge tracing considers the influence among neighboring knowledge concepts [19–22]. The bipartite graph is an effective structural model to capture latent relations between questions and skills [18]. This method is effective, but the amount of calculation is huge because it needs to extract questions and skills, respectively. Thus, it is difficult to be regarded as a streamlined and effective knowledge-tracing model.

None of the above KT models make full use of the multiknowledge concept information of the questions.

Existing knowledge tracing models cannot capture latent relations between questions and concepts concisely and effectively. We know that questions are generally composed of multiple knowledge concepts, which are actually closely related. In order to better model the students' learning process, our model is constructed by using neural Turing machines (NTMs), which are an instance of memory-augmented neural networks (MANNs) that have a large external memory capacity [23–25]. Therefore, on the basis of above deep knowledge tracing models, we propose an NTM-based skill-aware knowledge-tracing model. The highlight of our work is to utilize the knowledge concept composition information of questions to model the students' knowledge state more accurately and to discover more latent relevance among knowledge concepts effectively. The contributions of this paper are concluded as follows:

(i) We process the real-world KT datasets in detail and discover new characteristics of online tutoring systems and knowledge tracing datasets.

(ii) We design a question-skill dictionary algorithm to obtain the conjunctive skills of questions. The input encoding contains both students' answering interaction information and the related knowledge concept information.

(iii) We apply neural Turing machines into knowledge tracing innovatively to enhance the memory capacity of our model and to predict students' mastery of knowledge concepts accurately and discover knowledge concept substructure effectively.

(iv) We propose a novel NTM-based skill-aware knowledge-tracing model for conjunctive skills and apply a novel loss optimization function to deep knowledge tracing to enhance the model's ability of skill awareness. Our model considers the conjunctive knowledge concept information contained in a question in the process of modelling the students' knowledge state; thus, our model outperforms existing KT models.

The rest of this paper is organized as follows: Section 2 presents a brief overview of related work in the field of knowledge tracing. In Section 3, we formulate the process for NSKT to perform the knowledge-tracing task. Then, Section 4 introduces the characteristics and classifications of online tutoring systems. The details of the NSKT model are provided in Section 5. The experimental results and the comparison of models' performance in the real-world datasets are given in Section 6. In Section 7, we discuss in detail the process of NSKT in modelling the students' knowledge state. Section 8 presents the conclusions and future studies of this work.

2. Related Work

In this section, we present a brief overview of the models and methods of related work in the field of knowledge tracing, which can be classified into two main categories, as shown in Table 1.

TABLE 1: Related work.

Models	Methods	Categories
IRT	Logistic model	Statistical model
BKT	Bayesian model	
DKT	Long short-term memory network	Deep learning models
DHKT	Long short-term memory network	
DKVMN	Memory-augmented neural network	
SAKT	Self-attention	

2.1. Item Response Theory. Item response theory is the most commonly used cognitive model to predict students' mastery of knowledge concepts before knowledge tracing was proposed in 1995 [26, 27]. On the basis of IRT, the students' knowledge state cognitive model based on factor analysis was later proposed: LFA [28] and PFA [29]. These logistic regression models predict students' mastery of knowledge concepts by analyzing the relationship among factors that have an impact on students' answering accuracy [30, 31].

2.2. Knowledge Tracing. Bayesian knowledge tracing (BKT) models the students' knowledge state by using the hidden Markov model (HMM) for a single knowledge concept, which is represented as a set of binary latent variables [5].

With the rise of deep learning, deep knowledge tracing (DKT) was proposed in [6], which regards students' historical interactions as time sequences and models the students' knowledge state by the recurrent neural network (RNN). The experimental results show that DKT has the powerful ability of modelling the students' knowledge state. After DKT, a lot of deep KT models have been proposed to improve the AUC of the prediction of students' mastery of knowledge concepts. However, most of these deep knowledge-tracing models only focus on students' interactions on knowledge concepts and ignore the structural relationship between questions and knowledge concepts.

2.3. Question-KC Relation in Knowledge Tracing. Cen et al. proposed the two IRT models (additive factor model (AFM) and conjunctive factor model (CFM)) to model the conjunctive skills in the student datasets [32]. Both the AFM and CFM consider the conjunctive skills information contained in an item to predict the probability of students answering the item correctly.

Deep hierarchical knowledge tracing begins (DHKT) to focus on the hierarchical relationship between knowledge concepts and questions to predict the performance of students [16]. DHKT trains a question embedding by the average embeddings of the skills belonging to the question. The model using the bipartite graphs can capture relationships between knowledge concepts and questions effectively and systematically to pretrain question embeddings for each question [18]. Neil Heffernan's latest work begins to focus on the architecture of knowledge concepts and questions too [17].

TABLE 2: Notations.

Notations	Description
p	Problem/question
q	KC (skill/concept)
a	Answer correctness to the knowledge concept (KC) q
c	Answer correctness to related knowledge concept (RKC)
M	Number of unique KCs in the KT dataset
P	Probability
S	The RKCs
H	Interaction sequence of a student: $\{h_1, \ldots, h_{|H|}\}$
D	Dataset
E	Encoding
KC	Knowledge concept
RKC	Related knowledge concept
Dic	Dictionary

3. Problem Formulation

Generally, KT can be formulated as a supervised sequence learning problem: the student's interaction tuple at the timestamp t, $h_t = (q_t, a_t)$ that represents the combination of which skill (exercise) was answered and if the skill was answered correctly, so $a_t \in \{0, 1\}$, $q_t \in \{q_i\}_{i=1}^M$, where M is the number of unique exercises in datasets. Given the student's past exercise interactions, $H_t = \{h_0, \ldots, h_t\}$, the goal of KT is to predict the probability that the student will answer question q_{t+1} correctly at the next timestamp $t + 1$, $P(a_{t+1} = 1/q_{t+1}, H_t)$ [3, 6, 10].

It can be seen that existing KT models only focus on students' exercise interactions, so they are difficult to predict students' mastery of skills effectively. The notations used in this paper are shown in Table 2.

Definition 1. Related knowledge concepts (RKCs): the related knowledge concepts (RKCs) refer the other knowledge concepts S that compose the question p with a knowledge concept q, where S and q are mutual conjunctive knowledge concepts (skills).

The Algorithm 1 processes the skills and the questions of the dataset to obtain a dictionary Dic with the question number as the key and conjunctive skills of the question as the value, while conjunctive skills are the skills that make up the same question. The time complexity of Algorithm 1 is $\mathcal{O}(n^2)$. In this paper, we use KC shown in Table 2 to represent skill. Let S be the RKCs related to KC q of the answering question p, where $S = \{x/x \in \text{Dic}_p, x \neq q\}$ is illustrated in Figure 1(a).

The skill-aware knowledge tracing model can be formulated as follows: the student's interaction at the timestamp t, $h_t' = (p_t, q_t, a_t, S_t, c_t)$, where a_t is the correctness to the question p_t on skill q_t, S_t are the of RKCs of KC q_t, c_t is the correctness to RKCs S_t. Given the student's past interactions, $H_t' = (h_0', \ldots, h_t')$, we can predict the probability that the student will answer next KC q_{t+1} correctly at the timestamp $t + 1$, $P(q_{t+1}) = P(a_{t+1} = 1/q_{t+1}, H_t')$ or predict students' mastery of holistic knowledge concepts, $\{P(q_i)\}_{i=1}^M$.

4. Online Tutoring Systems

The online tutoring systems can be classified into two categories:

4.1. Question-Level Online Tutoring Systems. In question-level online tutoring systems, students answer the question directly. If the question is answered correctly or incorrectly, all KCs (skills) of the question are answered correctly or incorrectly too. So if a student has answered q_t correctly or incorrectly, then they must answer the RKCs S_t correctly or incorrectly too, which is illustrated in Figure 1(b). Because q_t and S_t are from the same question, so in question-level online tutoring systems, for a student's interaction at the timestamp t: $(p_t, q_t, a_t, S_t, c_t)$,

$$c_t = a_t. \tag{1}$$

4.2. Skill-Level Online Tutoring Systems. The question-answering situation in skill-level online tutoring systems is much more complicated than that of the question-level online tutoring system. Students can individually answer one of the skills in the question and can answer this skill once or multiple times. So if a student answers KC_1 correctly, it does not mean that the student must answer KC_2 correctly, which is shown in Figure 1(c).

Superficially, there is no obvious answering correctness relationship between skill q_t and the related skill set S_t. However, there are a large number of students answering examples shown in Table 3 in skill-level online tutoring systems, indicating that if a student answers q_t incorrectly many times, even if he finally answers q_t correctly, which demonstrates that his mastery of skill q_t is very poor, and similarly, he has poor mastery of S_t. It is very likely that he will answer q_t's-related skills S_t incorrectly. So the student's mastery of q_t, $P(q_t)$ and the student's mastery of S_t, $P(S_t)$ are close:

$$P(q_t) \approx P(S_t). \tag{2}$$

This finding is strongly supported by the actual responses of students in skill-level online tutoring systems. So in skill-level online tutoring systems, according to formula (2), we can assume.

$$c_t \approx a_t, \tag{3}$$

as shown in Table 4.

5. Method

In this section, we will give a detailed introduction of our NSKT framework, of which, the overview architecture is given in Figure 2.

5.1. Model. The model consists of an encoding layer and a neural network layer. In order to better model the students' knowledge state, the model is constructed with

Input: question list L^p; skill list L^q; dictionary Dic; dataset $D = \{(q_i, p_i)\}_{i=0}^{|D|-1}$ composed of skills and questions.
Output: Dic
(1) Dic **initialization**
(2) L^p **initialization**
(3) $\mu \leftarrow 0$
(4) **for each** $i \leftarrow 0, 1, \ldots, |D| - 1$ **do**
(5)   **if** $D(p)_i$ **not in** L^p **then**
(6) $L_\mu^p \leftarrow D(p)_i$
(7) $\mu \leftarrow \mu + 1$
(8)   **end**
(9) **end**
(10) **for each** $i \leftarrow 0, 1, \ldots, \mu - 1$ **do**
(11) $\eta \leftarrow 0$
(12) L^q **initialization**
(13)   **for each** $j \leftarrow 0, 1, \ldots, |D| - 1$ **do**
(14)   **if** $D(p)_j == L_i^p$ **and** $D(q)_j$ **not in** L^q **then**
(15) $L_\eta^q \leftarrow D(q)_j$
(16) $\eta \leftarrow \eta + 1$
(17)   **end**
(18)   **end**
(19) $\text{Dic}_{L_i^p} \leftarrow L^q$
(20) **end**
(21) **return** Dic

ALGORITHM 1: Question-skill dictionary algorithm.

(a)   (b)   (c)
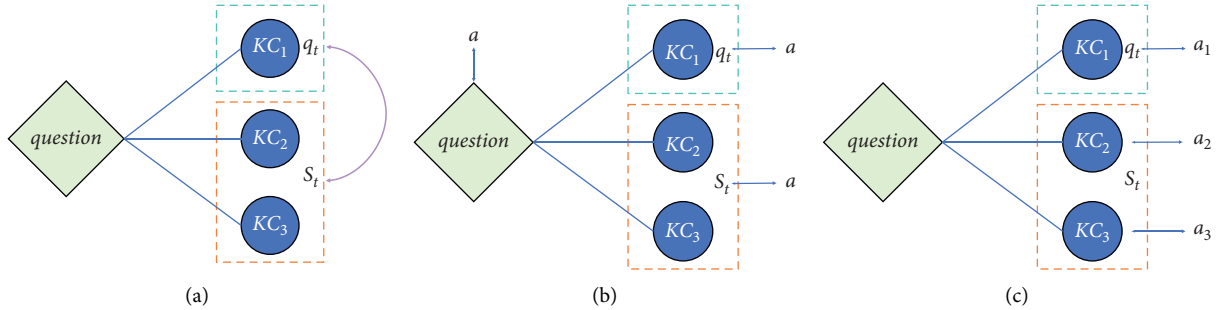
FIGURE 1: Illustrations. (a) Illustration of RKC S related to KC q, where S and q are mutual conjunctive skills. (b) Illustration of the question-level online tutoring system, where a denotes answer correctness to a question. (c) Illustration of the skill-level online tutoring system, a_1 denotes answer correctness to KC1, a_2 denotes answer correctness to KC_2, and so on a_3.

TABLE 3: Example of a student answering question 33 in skill-level online tutoring systems. Question 33 is composed of skill $s11$ and $s21$. The student answers $s11$ incorrectly three times $t_1 - t_3$ in succession. Even if he answers $s11$ correctly at the timestamp t_4, his mastery of $s11$ is very poor and his mastery of $s11$'s-related skill $s21$ is not good too, so it is very likely to answer $s21$ incorrectly, in fact, he answers $s21$ incorrectly at the timestamp t_5.

Timestamp	Skill	Correctness
t_1	$s11$	0
t_2	$s11$	0
t_3	$s11$	0
t_4	$s11$	1
t_5	$s21$	0

the neural Turing machine, which is an instance of memory-augmented neural networks (MANNs) that offer the ability to quickly encode and retrieve new information [23].

TABLE 4: The relationship between a_t and c_t in skill-level online tutoring systems.

timestamp	q_t	a_t	S_t	c_t
t_1	$s11$	0	$s21$	0
t_2	$s11$	0	$s21$	0
t_3	$s11$	0	$s21$	0
t_4	$s11$	1	$s21$	1
t_5	$s21$	0	$s11$	0

5.2. Input Features

5.2.1. Answer Information Encoding. Let E^q be the encoding of the student's interaction tuple (q, a), thus $E^q = [e_i^q] \in \{0, 1\}^{2M}$:

$$e_i^q = \begin{cases} 1, & \text{if } i = q + a \times M, \\ 0, & \text{otherwise} \end{cases} \tag{4}$$
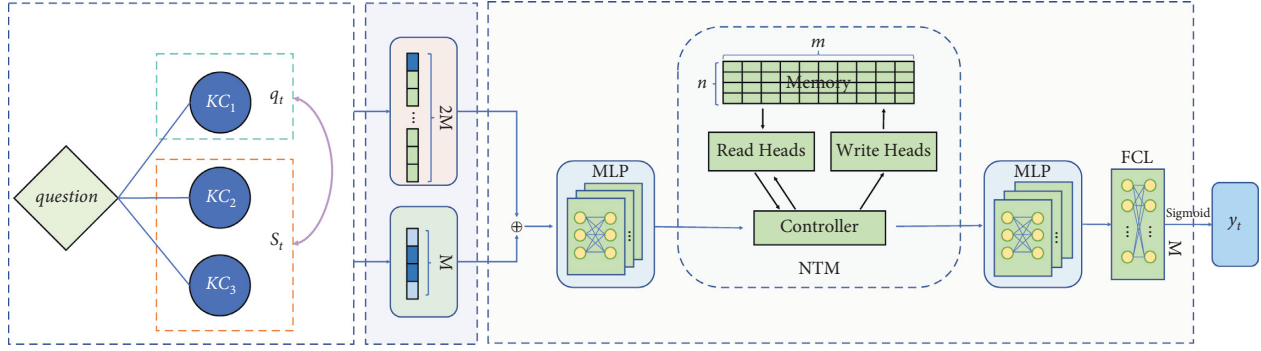
FIGURE 2: The NSKT framework overview.

5.2.2. RKC Information Encoding.

The information of the set S of RKCs related to KC q is encoded E^s with a length of M: $E^s = [e_i^s] \in \{0, 1\}^M$:

$$e_i^s = \begin{cases} 0 & i \notin S, \\ 1 & i \in S. \end{cases} \tag{5}$$

5.3. Neural Turing Machines.

Neural Turing machines are an instance of memory-augmented neural networks (MANNs) that extend the capabilities of neural networks by coupling them to external memory resources. Experiments show that neural Turing machines have stronger memory capabilities than the LSTM [23], which is very suitable for modeling the students' knowledge state [33–35]. Figure 3 shows a high-level diagram of the neural Turing machine architecture.

As can be seen from Figure 3, the NTM is composed of 4 modules: controller, read heads, write heads, and memory. The controller can be a feed-forward neural network or a recurrent neural network [23, 34] and has read and write heads that access the external memory matrix.

5.4. Reading.

Let $\mathbf{M}_t$ be the external memory content which is a $n \times m$ memory matrix at the timestamp t, where n is the number of memory locations and m is the vector dimension at each memory location. The n elements $w_t(i)$ of $\mathbf{w}_t$, which is a vector of weightings over the n locations emitted by a read head at the timestamp t, obey the following constraints:

$$\sum_i w_t(i) = 1, 0 \le w_t(i) \le 1, \forall i. \tag{6}$$

Let $\mathbf{r}_t$ be the read vector of a length m returned by the head at the timestamp t:

$$\mathbf{r}_t \leftarrow \sum_i w_t(i) \mathbf{M}_t(i). \tag{7}$$

5.5. Writing.

The memory matrix $\mathbf{M}_t$ at the timestamp t is modified by the erase vector $\mathbf{e}_t$ and the add vector $\mathbf{a}_t$:

$$\begin{aligned} \widetilde{\mathbf{M}}_t(i) &\leftarrow \mathbf{M}_{t-1}(i)\left[1 - w_t(i)\mathbf{e}_t\right] \\ \mathbf{M}_t(i) &\leftarrow \widetilde{\mathbf{M}}_t(i) + w_t(i)\mathbf{a}_t. \end{aligned} \tag{8}$$
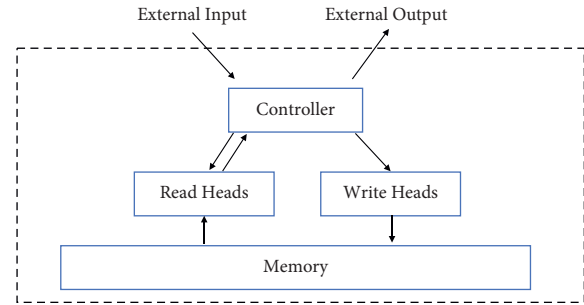
FIGURE 3: Neural Turing machine architecture.

5.6. Addressing Mechanisms

5.6.1. Focusing on Content.

Each head produces a length m key vector $\mathbf{k}_t$ that is used to compute the normalised weighting w_t^c as follows:

$$w_t^c(i) \leftarrow \frac{\exp\left(\beta_t K\left[\mathbf{k}_t, \mathbf{M}_t(i)\right]\right)}{\sum_j \exp\left(\beta_t K\left[\mathbf{k}_t, \mathbf{M}_t(j)\right]\right)}, \tag{9}$$

where β_t is a positive key strength generated by the controller and the similarity measure K is cosine similarity:

$$K[\mathbf{u}, \mathbf{v}] = \frac{\mathbf{u} \cdot \mathbf{v}}{\|\mathbf{u}\| \times \|\mathbf{v}\|}. \tag{10}$$

5.6.2. Focusing on Location.

The location-based addressing mechanism is designed to facilitate both simple iterations across the locations of the memory and random-access jumps. It does so by implementing a rotational shift of a weighting as follows [23].

Firstly, the interpolation gate g_t is used to blend between the weighting $\mathbf{w}_{t-1}$ and the weighting $\mathbf{w}_t^c$:

$$\mathbf{w}_t^g \leftarrow g_t \mathbf{w}_t^c + (1 - g_t)\mathbf{w}_{t-1}. \tag{11}$$

Furthermore, the model uses a one-dimensional convolution shift kernel to convolve the current weighting w_t^g:

$$\widetilde{w}_t(i) \leftarrow \sum_{j=0}^{n-1} w_t^g(j) s_t(i - j), \tag{12}$$

where $\mathbf{s}_t$ is the shift weighting generated by the controller.

To correct the blur that occurs due to the convolution operation, each head emits one further scalar $\gamma_t \geq 1$ whose effect is to sharpen the final weighting as follows:

$$w_t(i) \leftarrow \frac{\widetilde{w}_t(i)^{\gamma_t}}{\sum_j \widetilde{w}_t(j)^{\gamma_t}}. \tag{13}$$

5.7. Controller. The NTM controller in our model is the long short-term memory network [36], which can be formulated by the formulas as follows:

$$
\begin{aligned}
\mathbf{f}_t &= \sigma\big(\mathbf{w}_f[\mathbf{h}_{t-1}, \mathbf{x}_t] + \mathbf{b}_f\big), \\
\mathbf{i}_t &= \sigma\big(\mathbf{w}_i[\mathbf{h}_{t-1}, \mathbf{x}_t] + \mathbf{b}_i\big), \\
\mathbf{o}_t &= \sigma\big(\mathbf{w}_o[\mathbf{h}_{t-1}, \mathbf{x}_t] + \mathbf{b}_o\big), \\
\mathbf{c}_t &= \mathbf{f}_t \odot \mathbf{c}_{t-1} + \mathbf{i}_t \odot \tanh\big(\mathbf{w}_c[\mathbf{h}_{t-1}, \mathbf{x}_t] + \mathbf{b}_c\big), \\
\mathbf{h}_t &= \mathbf{o}_t \odot \tanh(\mathbf{c}_t).
\end{aligned}
\tag{14}
$$

$\mathbf{i}, \mathbf{f}, \mathbf{o}, \mathbf{c}, \mathbf{h}$ are the activation matrices of the input gate, the forget gate, the output gate, the memory cell, and the hidden state matrix, respectively. $\mathbf{w}$ and $\mathbf{b}$ are the weight matrix and the bias vector of the corresponding gate, respectively. $\odot$ denotes the Hadamard product. σ and tanh denote the sigmoid and hyperbolic tangent function, respectively:

$$\sigma(x) = \frac{1}{1 + \exp(-x)}, \tag{15}$$

let logits $\in \mathbb{R}^M$ be the output of the last neural network of the NSKT model, the student's mastery of knowledge concepts predicted by the model at the timestamp t is

$$\mathbf{y}_t = \sigma(\text{logits}), \tag{16}$$

where $\mathbf{y}_t \in \mathbb{R}^M$.

5.8. Optimization. The loss function of the model consists of two parts, namely, the answering interaction loss $\mathscr{L}_1$ and the related knowledge concept information loss $\mathscr{L}_2$. Let ℓ be the binary cross entropy loss:

$$\ell(p, a) = -(a \log p + (1 - a)\log(1 - p)). \tag{17}$$

We optimize the average cross entropy loss of the student's interactions as follows:

$$\mathscr{L}_1 = \frac{\sum_t \ell\big(\mathbf{y}_t^{\mathbf{T}} \delta(q_{t+1}), a_{t+1}\big)}{|H| - 1}, \tag{18}$$

where $\delta(q_{t+1})$ is the one-hot encoding of KC q_{t+1} at the timestamp $t + 1$, $|H|$ is the total number of the student's interactions, and $\mathbf{T}$ denotes transpose operation.

The average cross-entropy loss of the related knowledge concept information is

$$\mathscr{L}_2 = \frac{\sum_t \sum_{i=1}^{|S_{t+1}|} \ell\big(\mathbf{y}_t^{\mathbf{T}} \delta(q_i), c_i\big)}{\sum_t |S_{t+1}|}, \tag{19}$$

where $q_i \in S_{t+1}$, c_i is the correctness to skill q_i.

The loss for a single student is represented by $\mathscr{L}$, which is as follows:

$$
\begin{aligned}
\mathscr{L} &= \lambda \mathscr{L}_1 + (1 - \lambda)\mathscr{L}_2 \\
&= \lambda \frac{\sum_t \ell\big(y_t^T \delta(q_{t+1}), a_{t+1}\big)}{|H| - 1} + (1 - \lambda)\frac{\sum_t \sum_{i=1}^{|S_{t+1}|} \ell\big(y_t^T \delta(q_i), c_i\big)}{\sum_t |S_{t+1}|} \\
&= \sum_t \left(\lambda \frac{\ell\big(y_t^T \delta(q_{t+1}), a_{t+1}\big)}{|H| - 1} + (1 - \lambda)\frac{\sum_{i=1}^{|S_{t+1}|} \ell\big(y_t^T \delta(q_i), c_i\big)}{\sum_t |S_{t+1}|} \right),
\end{aligned}
\tag{20}
$$

where the hyperparameter λ is the coefficient that determines the proportion of the answering information loss and the related information loss. We use an optimizer to optimize our model. Let Θ be the minimum of $\mathscr{L}$, thus, the training objective of NSKT is as follows:

$$\Theta \leftarrow \text{optimizer}(\mathscr{L}). \tag{21}$$

5.9. Skill Awareness. The student's past interactions in online tutoring systems: $H_t' = \{h_0', \dots, h_t'\}$, where $h' = (q_t, a_t, S_t, c_t)$ denotes that the student interaction tuple at the timestamp t. The set of knowledge concepts Set_q that students have answered actually so far is represented as follows:

$$\text{Set}_t^q = \{q_i\}_{i=1}^t. \tag{22}$$

The set of knowledge concepts (skills) Set^S answered by NSKT so far is represented as follows:

$$\text{Set}_t^S = S_1 \cup \dots \cup S_t. \tag{23}$$

As shown in Figure 4, when the student answers the next skill q_{t+1} at the next timestamp $t + 1$, even if the student has not answered questions related to skill q_{t+1} before, $q_{t+1} \notin \text{Set}_t^q$, but if NSKT has awareness of skill q_{t+1} so far, $q_{t+1} \in \text{Set}_t^S$, NSKT can predict the student's mastery of skill q_{t+1} accurately.

6. Experiments

In this section, we give a detailed explanation of datasets and experiments conducted to evaluate the performance of the NSKT model and other KT models in three real-world open-source knowledge tracing datasets.

6.1. Datasets. To evaluate KT models' performance, we use three datasets collected from online learning platforms. These three datasets are widely used real-world datasets in KT.

(i) ASSISTments2009 (https://sites.google.com/site/assistmentsdata/home/2009-2010-assistment-data) (ASSIST09) is provided by the ASSISTment online tutoring platform and is the most widely used dataset in knowledge tracing.

(ii) ASSISTments2017 (https://sites.google.com/view/assistmentsdatamining/dataset/) (ASSIST17) is
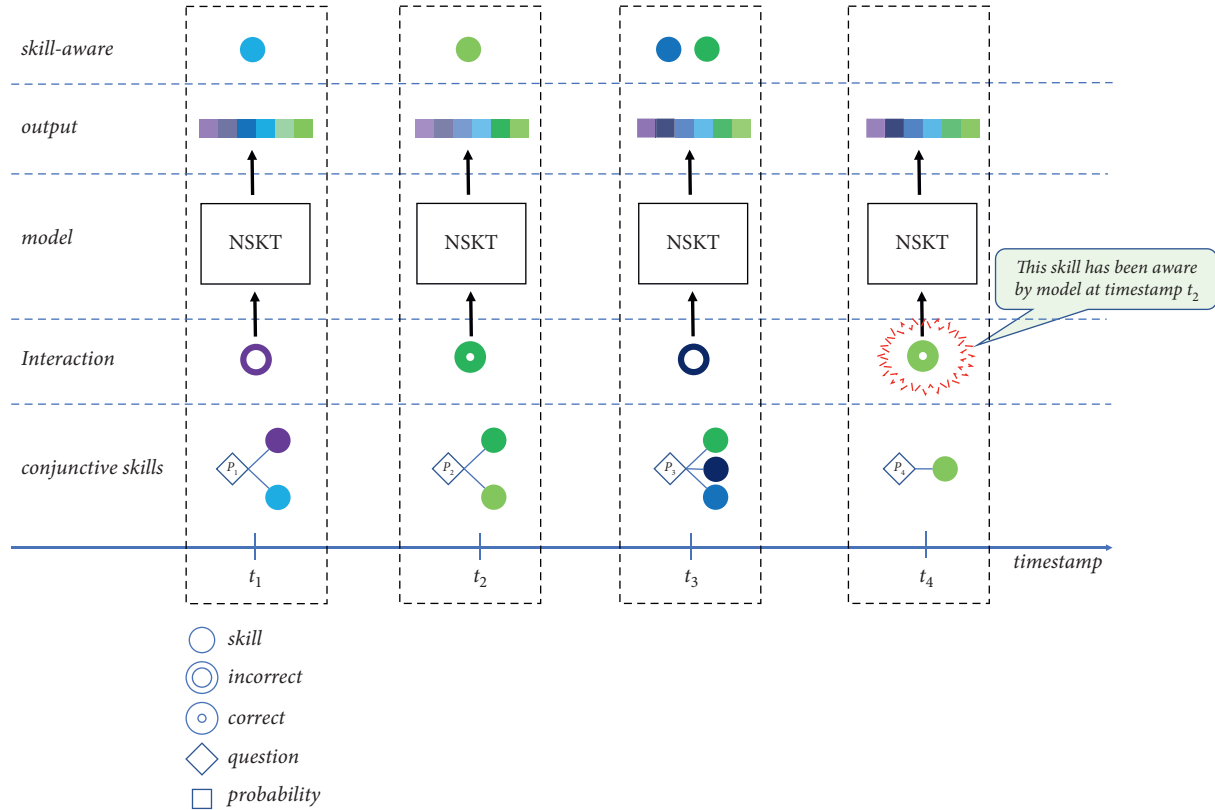
FIGURE 4: The process of skill awareness in NSKT. Different skills are indicated by different colors.

TABLE 5: The statistics of the three datasets.

	Students	Skills	Questions	Interactions (K)	MIN[a]	MAX[b]	AVG[c]
ASSIST09	4,162	124	26,688	526[d]	0	3	0.316
ASSIST17	1,709	102	3,162	942	0	2	0.472
EdNet	784,309	189	13,169	962	0	6	1.388

The symbol [a] indicates the minimum value of $|S|$, where 0 means that the question is a single KC (skill) question. The symbol [b] indicates the maximum value of $|S|$. The symbol [c] indicates the average value of $|S|$. The symbol [d]K stands for a thousand.

provided by the 2017 ASSISTments data mining competition and is the latest ASSISTments dataset with the most student responses.

(iii) EdNet (https://github.com/riiid/ednet) is the dataset of all student-system interactions collected over 2 years by Santa, a multiplatform AI tutoring service with more than 780 K users in Korea available through Android, iOS, and Web [37]. We conducted our experiments on EdNet-KT1 which consists of students' question-solving logs and is the record of Santa collected since April 2017 by following the question-response sequence format.

The complete statistical information for the three datasets is shown in Table 5.

The details about the columns in datasets are shown as follows:

ASSISTments:

(i) user_id: the ID of the student

(ii) problem_id: the ID of the problem

(iii) skill_id: the ID of the skill associated with the problem

(iv) 1: Correct on the first attempt
0: Incorrect on the first attempt,

EdNet:

(i) user_id: the ID of the student.

(ii) question_id: the ID of the question.

(iii) tags: the expert-annotated tags for each question.

(iv) correct_answer: the correct answer of each question recorded as a character between a and d inclusively.

(v) user_answer: the answer that the student submitted was recorded as a character between a and d inclusively.

6.2. Dataset Characteristics

(i) ASSIST09 and EdNet: For multiple skill questions, the records of students' interactions will be repeated with different skill taggings and each record

represents the student response to a skill of the question [38].

(ii) ASSIST17: similar to the ASSIST09 dataset, each record in ASSIST17 represents the student response to a skill of the question. However, we noticed the special features of this dataset. A large number of users in the ASSIST17 dataset only answered one skill of multiple skill questions and answered this skill one or more times. The number of multiple skill questions in this situation accounted for 44.88% of the total number of questions answered by students. That is, the student answers one or more skills of multiple skill questions, and the number of responses to a skill may be given once or multiple times.

6.3. Compared Models and Implementation Details.
To show the performance of our model and demonstrate the improvement of our model to existing KT models, we compare NSKT against the state-of-the-art KT models. We give the reference GitHub repositories of some KT models.

(i) BKT [5]: Bayesian knowledge tracing uses the hidden Markov model (HMM) to model the students' latent knowledge state as a set of binary variables. We use pyBKT (https://github.com/CAHLR/pyBKT) to implement BKT and set the model parameters: seed = 42, num_fits = 1.

(ii) DKT-LSTM [6]: the DKT-LSTM is the standard deep knowledge-tracing mode. We implemented DKT (https://github.com/chrispiech/DeepKnowledgeTracing) with the LSTM with tanh activation.

(iii) DKT-NTM: DKT is implemented by using the neural Turing machine (https://github.com/MarkPKCollier/NeuralTuringMachine).

(iv) DKVMN [10]: the DKVMN (https://github.com/jennyzhang0215/DKVMN) is a variation of MANNs, which uses a static memory called key and a dynamic memory called value to model the students' knowledge state.

(v) SAKT [3]: SAKT (https://github.com/shalini1194/SAKT) is the KT model based on the self-attention architecture with exercises as attention queries and students' past interactions as attention keys/values.

(vi) DSKT: the skill-aware deep knowledge-tracing model is implemented with the LSTM and tanh activation. We dynamically set the value of the coefficient λ to explore the best performance of DSKT.

(vii) NSKT: NSKT is an NTM-based skill-aware knowledge tracing. We test the performance of NSKT with different values of the coefficient λs to optimize the model's performance.

For all models, we use the Adam optimizer with learning_rate = 0.001, beta1 = 0.9, beta2 = 0.999, and

epsilon = $1e - 8$ to optimize. The minibatch size and the maximum length of the sequence for all datasets are set to 32 and 100, respectively. We perform standard five-fold cross-validation to evaluate all the KT models in this paper. We conduct experiments on the server with an 8-core 2.50 GHz Intel(R) Xeon(R) Platinum 8163 CPU and 64 GB memory.

6.4. Experimental Results

6.4.1. Models' Performance.
We use the area under the receiver operating characteristic curve (AUC) as an evaluation metric to compare prediction performance among the KT models mentioned in Section 6.3. A higher AUC indicates better performance. The test AUC results in the three real-world datasets for all KT models are shown in Table 6. From the experiment results, we can find the following observations:

(i) NSKT performs better than the other competing KT models in all datasets and achieves the average test AUC of 85.38%, 82.35%, and 80.81% in ASSIST09, ASSIST17, and EdNet, respectively.

(ii) DSKT performs better than the DKT-LSTM, achieves the average test AUC of 84.88%, 81.27%, and 79.71% in datasets ASSIST09, ASSIST17, and EdNet, respectively, gaining an average performance improvement of 0.82% (DKT-LSTM achieves the AUC of 84.45%, 80.04%, and 78.91%). NSKT performs better than the DKT-NTM, gaining an average performance improvement of 1.33% (DKT-NTM achieves the AUC of 84.53%, 80.51%, and 79.49%).

(iii) The DKT-NTM model has a better performance than the standard DKT-LSTM in knowledge tracing. The DKT-NTM achieves the average test AUC of 84.53%, 80.51%, and 79.49% in the three datasets, respectively, while the standard DKT-LSTM achieves the average test AUC of 84.45%, 80.04%, and 78.91% in the three datasets, respectively.

(iv) The performance of NSKT is better in dataset ASSIST17, which has more complex data features than those of ASSIST09 and EdNet. NSKT gains an average performance improvement of 2.31% in ASSIST17 compared to the standard DKT-LSTM while improving AUC by 0.93% and 0.90% in ASSIST09 and EdNet, respectively. It proves that NSKT is better in mining hidden information from complex educational data features to improve the accuracy of prediction.

Figure 5 shows the training process of KT models in the three KT datasets. It shows that the DKVMN and SAKT can learn faster than other KT models. The training speed of the DKT-LSTM, DKT-NTM, DSKT, and NSKT is close, but the test AUC of NSKT is the best.

We set the probability to KC q_t predicted by KT models: $P(q_t)$, and assume that students will answer KC q_t correctly if $P(q_t) > = 0.5$ and if $P(q_t) < 0.5$, the student will answer q_t incorrectly:

TABLE 6: Test AUC results for all datasets (%).

	BKT	DKT-LSTM	DKT-NTM	DKVMN	SAKT	DSKT	NSKT
ASSIST09	72.06	84.45	84.53	84.37	84.70	84.88	**85.38**
ASSIST17	65.25	80.04	80.51	80.55	81.25	81.27	**82.35**
EdNet	66.28	78.91	79.49	79.72	79.83	79.71	**80.81**

Bold values indicate the best performance.
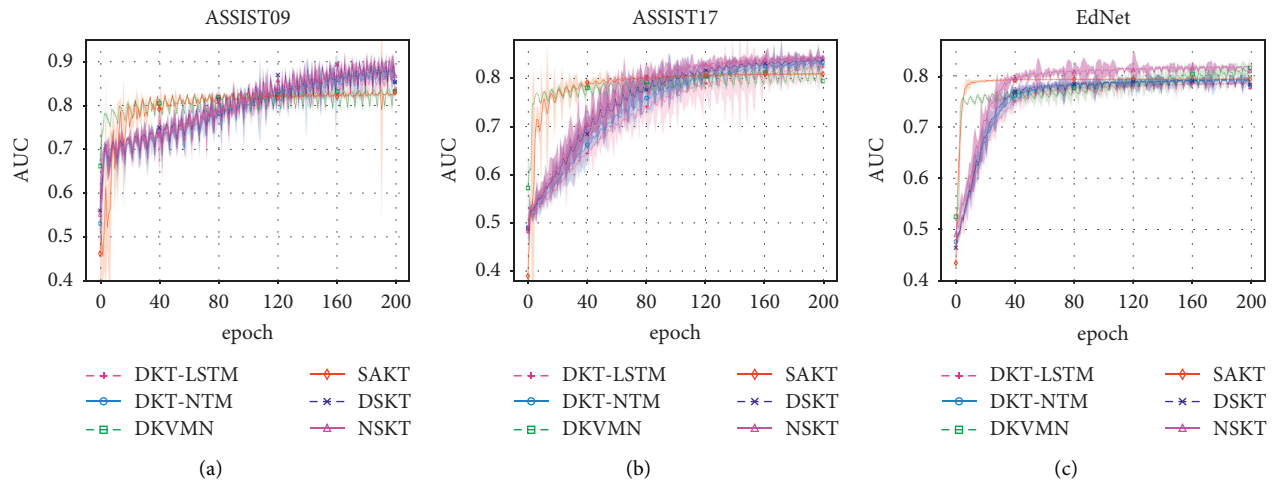
FIGURE 5: The dynamics for training models in the KT datasets with the best hyperparameter selection for each model and each dataset individually. Each line plots the mean over multiple runs, while the corresponding root mean square error (RMSE) is shown as the shaded area around the mean. (a) ASSIST09. (b) ASSIST17. (c) EdNet.

$$a'_t = \begin{cases} 0 & P(q_t) < 0.5, \\ 1 & P(q_t) > = 0.5. \end{cases} \tag{24}$$

If $a'_t = a_t$, it means that models can predict correctly. Thus, the accuracy of prediction for KT models in the datasets is shown in Figure 6.

Figure 7 shows the performance of DSKT and NSKT under different λ values and the value of λ when models achieve the best performance. From Figure 7, we can draw the following conclusions: the test AUC of DSKT and NSKT is not ideal with a small λ value. However, as the value of λ increases, the test results of DSKT and NSKT get better and better; thus, we recommend $\lambda \geq 0.9$.

6.5. Friedman-Aligned Rank Test.
We perform the Friedman-aligned rank test [39] on the AUC test results of the KT models shown in Table 6 by the following formula:

$$X^2 = \frac{12}{nk(k+1)} \sum R_i^2 - 3n(k+1), \tag{25}$$

where R_i is the sum of the ranks of the i-th sample, k is the number of groups of samples, and n is the number of samples in each group. The probability distribution of X^2 can be approximated by that of the chi-squared distribution with $k - 1$ degrees of freedom χ^2_{k-1}. Now, we test the null hypothesis, which is as follows:

H$_0$: there is no significant difference in the performance of the KT models.

The P value P of the Friedman-aligned rank test on test AUC results is

$$P(\chi^2_{k-1} \geq X^2) = 0.013 < 0.05. \tag{26}$$

Then, we reject the null hypothesis H$_0$, which indicates a significant difference in the performance of the KT models.

6.6. Execution Time.
We compared the execution time of KT models per 200 batches in each dataset shown in Figure 8. As shown in Figure 8, the BKT model requires the least execution time to train the same size of data. This is because the BKT is not a deep learning knowledge tracing model, and it needs to train fewer parameters. For deep learning knowledge tracing models, the execution times of the DKT-LSTM, DKVMN, and SAKT are close and the execution times of the DKT-NTM and DSKT are close. The execution time of the DKT-NTM is more than that of the DKT-LSTM. The reason can be that the NTM takes more time to access its own external memory matrix. NSKT considers the conjunctive skills of the questions during the training process and needs to access the NTM's external memory matrix to enhance the memory ability of the model. Hence, NSKT has the most execution time, but this is also the reason why NSKT performs better in modelling the students' knowledge state.

The experimental results show that the NTM-based skill-aware knowledge-tracing model has a strong ability to capture the relevance among knowledge concepts and can enhance the model's ability of skill awareness for conjunctive skills and improve the accuracy of prediction in modelling
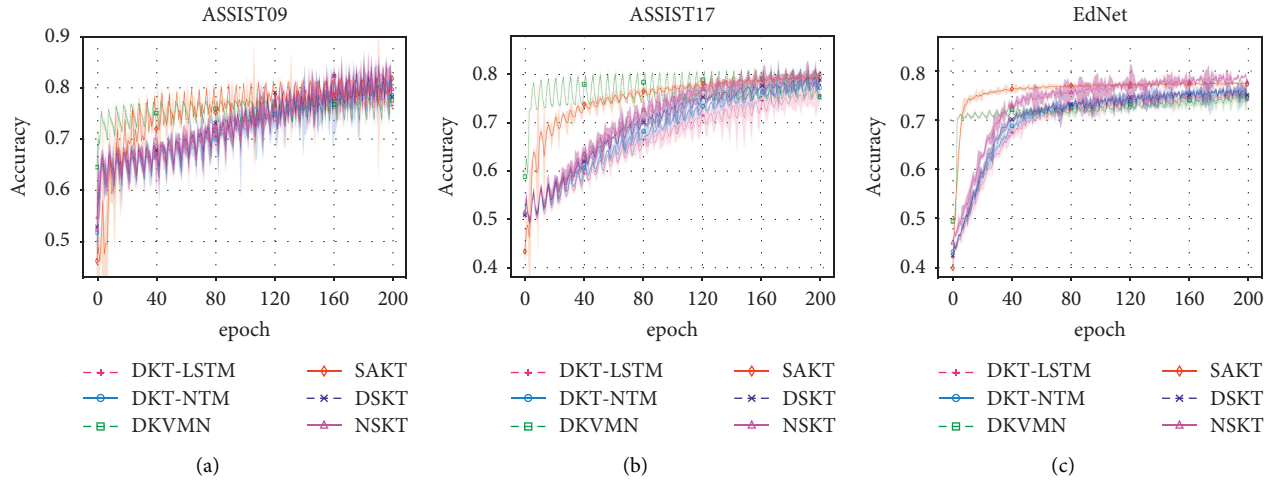
Figure 6: The accuracy of prediction for training models in the KT datasets with the best hyperparameter selection for each model and each dataset individually. Each line plots the mean over multiple runs, while the corresponding root mean square error (RMSE) is shown as the shaded area around the mean. (a) ASSIST09. (b) ASSIST17. (c) EdNet.
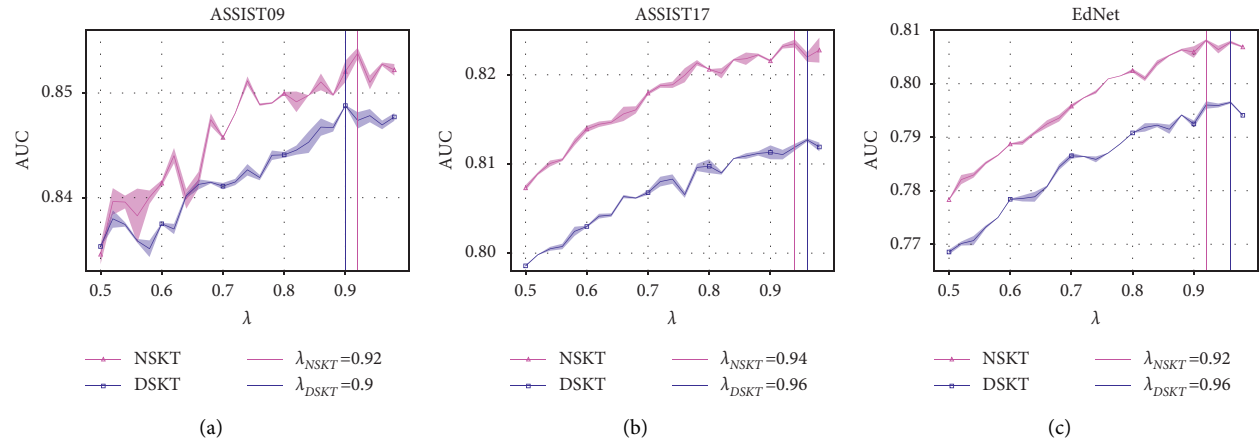
Figure 7: The average test AUC of NSKT and DSKT with different λ values in datasets. Each line plots the mean over multiple runs, while the corresponding root mean square error (RMSE) is shown as the shaded area around the mean. (a) ASSIST09. (b) ASSIST17. (c) EdNet.
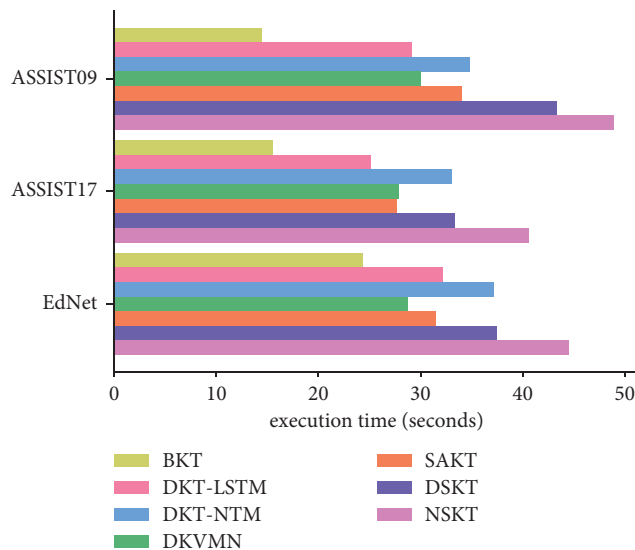
Figure 8: The comparison of the KT models' execution time per 200 batches in each dataset.

the students' knowledge state. Experiments demonstrate that NSKT is effective.

7. Discussion

In this section, we discuss the details of the prediction process of the KT model in modelling the students' knowledge state, as well as the relevance of knowledge concepts and conditional influence between exercises.

7.1. Prediction Process. In our opinion, an excellent KT model not only can predict the probability that students will answer questions correctly at the next timestamp accurately but also can perform well in modelling the students' holistic knowledge concept state.

Analyzing the prediction process of KT models can show the performance of NSKT. We randomly select a student sample U_1 from the ASSIST09 dataset, and the detailed process of DKT and NSKT modelling U_1's knowledge state is shown in Figure 9.

It can be seen from Figure 9(a) that although DKT performs fairly well in prediction, DKT only focuses on the knowledge concepts to be predicted at the next timestamp and does not care about the U_1's mastery of other knowledge concepts. Therefore, after U_1 answers $s32$ correctly $(s32, 1)$ at the timestamp t_3, the model's predicted probability of $s32$ decreases rapidly, indicating that U_1's mastery of $s32$ is getting worse and worse, which should not be consistent with the U_1's real knowledge state shown in Table 7. Because of lacking related knowledge concept (RKC) information, DKT's prediction accuracy and prediction breadth are not ideal.

As shown in Figure 9(b), we use two heatmap subfigures to show the process of modelling the U_1's knowledge state on NSKT. The x-axis of the lower subfigure is the sequence of U_1's interactions (q_t, a_t) and the y-axis is the skill index. The x-axis of the upper subfigure is the RKC S_t and the y-axis is the index of the RKCs S_i.

Because U_1 answers skill 32 (abbreviated as $s32$) correctly $(s33, 1)$ in the first three timestamps $t_1 - t_3$, the predicted probability of $s32$ gets higher and higher and the color of $s32$ in the y-axis of the lower subfigure gets brighter and brighter. As shown in the x-axis of the upper subfigure, $s33$ is the related knowledge concept of $s32$ in the first three timestamps $t_1 - t_3$; thus, the predicted probability of $s33$ gets higher and higher and the color of the $s33$ in the y-axis of the upper subfigure gets brighter and brighter too.

In the next three timestamps $t_4 - t_6$, U_1 answers s33 correctly $(s33, 1)$ in succession, the predicted probability of $s33$ gets higher and higher and the color of $s33$ in the y-axis of the lower subfigure gets brighter and brighter. $s32$ is the related knowledge concept of $s33$, so the predicted probability of $s32$ continues to increase, and the color of $s32$ in the y-axis of the upper subfigure gets brighter and brighter too and remains at a relatively high value.

In the next three timestamps $t_7 - t_9$, U_1 continues to answer $s33$ correctly $(s33, 1)$; however, this $s33$ is a single skill without related knowledge concepts, so only the

predicted probability of $s33$ gets higher and higher and the color of $s33$ in the y-axis of the lower subfigure gets brighter and brighter.

At the last timestamp t_{10}, U_1 answer $s37$ correctly $(s37, 1)$, so the predicted probability of $s37$ gets higher and higher and the color of $s32$ in the y-axis of the lower subfigure gets brighter and brighter. Because $s55$ is the related knowledge concept of $s37$, so the predicted probability of $s55$ gets higher and higher and the color of $s55$ in the y-axis of the upper subfigure gets brighter and brighter too.

In contrast, we randomly select a student sample U_2 with a low answering accuracy shown in Table 8.

The process of DKT and NSKT modelling the U_2's knowledge state is shown in Figure 10. It can be seen from Figure 10(a) that DKT models the U_2's knowledge state almost accurately, but the prediction breadth is not enough.

As shown in Figure 10(b), NSKT, like DKT, models the U_2's knowledge state accurately and performs better in prediction breadth. At the timestamp t_4, U_2 answers $s95$ incorrectly many times, the predicted probability of $s95$ gets lower and lower and the color of $s95$ in the y-axis of the lower subfigure gets darker and darker. As shown in the x-axis of the upper subfigure, $s2$ is the related knowledge concept of $s95$; thus, the predicted probability of $s2$ gets lower and lower and the color of $s33$ in the y-axis of the upper subfigure gets darker and darker too.

It can be concluded from Figures 9 and 10 that NSKT performs better in prediction accuracy and prediction breadth and can better model the students' knowledge state. NSKT not only focuses on students' mastery of the knowledge concept to be predicted at the next timestamp but also focuses on the students' mastery of the related knowledge concepts. This is where NSKT is superior to other existing KT models, and NSKT performs better in modelling the students' knowledge state than DKT [4].

7.2. Pearson Correlation Coefficient. In this paper, we use the Pearson correlation coefficient as the metric to measure the correlation among skills. By estimating the covariance and standard deviation of the sample, we can get the sample Pearson coefficient r:

$$r_{(X,Y)} = \frac{\sum_{i=1}^{n} (X_i - \overline{X})(Y_i - \overline{Y})}{\sqrt{\sum_{i=1}^{n} (X_i - \overline{X})^2} \sqrt{\sum_{i=1}^{n} (Y_i - \overline{Y})^2}}. \quad (27)$$

Figures 11 and 12 show the comparison of skill Pearson correlations of U_1's interactions and U_2's interactions on DKT and NSKT, respectively. Figures 11(a) and 12(a) show the skill Pearson correlation on DKT, and Figures 11(b) and 12(b) show the skill Pearson correlation on NSKT. It can be seen from the figures that DKT can only mine the correlation among the skills that have been answered in the past, indicating that DKT cannot effectively discover the relevance among knowledge concepts. As shown in Figures 11(b) and 12(b), NSKT can discover the correlation among four skills, while DKT can only discover among three. For example, it can be seen from Figure 11(b) that the Pearson correlation between $s32$ and $s55$ on NSKT of U_1's interactions is

(a)

(b)
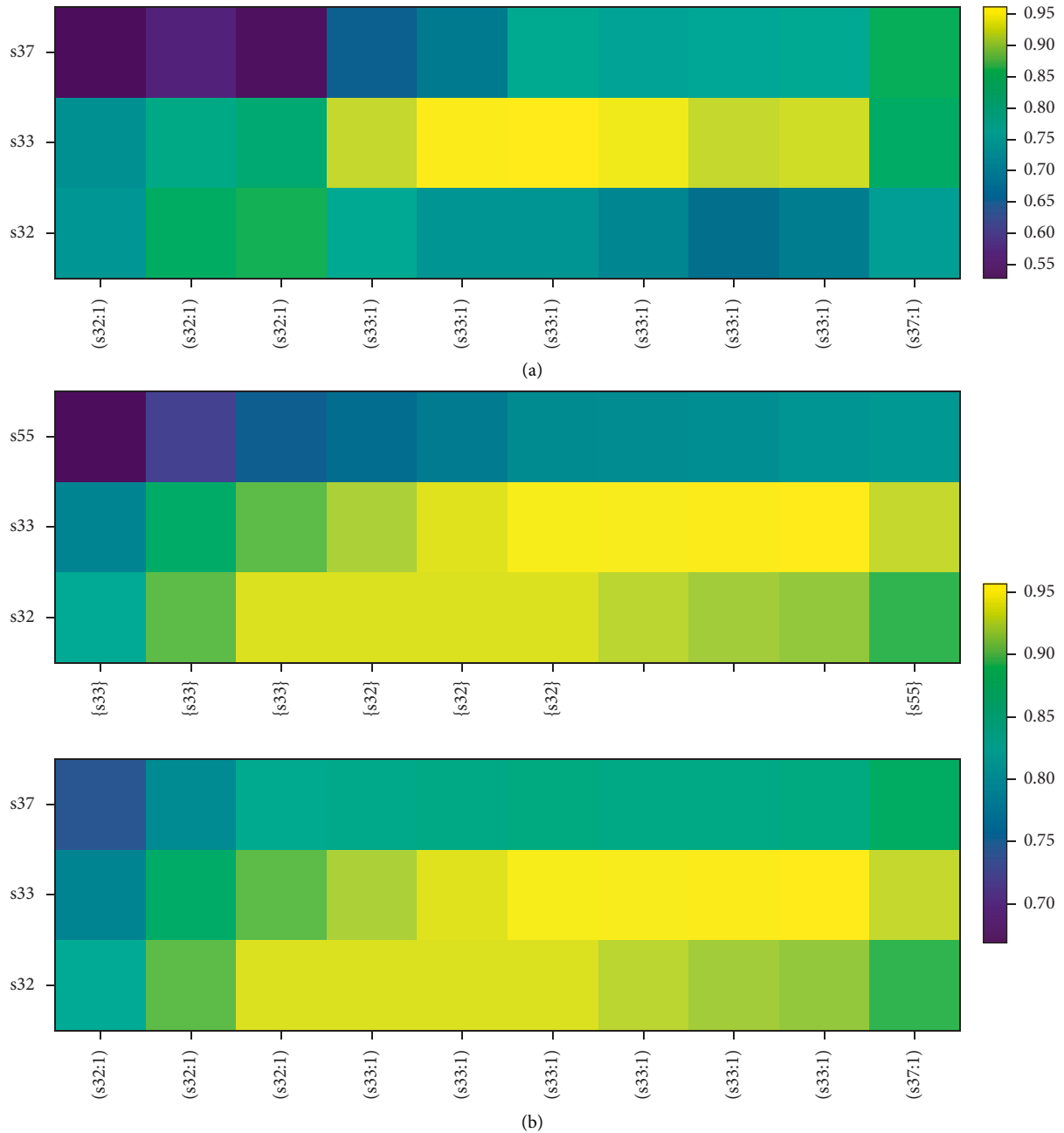
Figure 9: Comparison of the prediction process of U_1 on DKT and NSKT. The color of the heatmap indicates the predicted probability that U_1's mastery of skills after interaction (q_t, a_t) at the timestamp t. The yellower the color, the higher the probability. (a) Heatmap for the prediction process of DKT. The x-axis is the sequence of U_1's interactions $(q_t; a_t)$ and the y-axis is the skill index. (b) Heatmap for the prediction process of NSKT. The x-axis of the lower subfigure is the sequence of U_1's interactions $(q_t; a_t)$ and the y-axis is the skill index. The x-axis of the upper subfigure is the RKC S_t and the y-axis is the skill index of the RKCs S_t.

Table 7: Skill maps of ASSIST09 and U_1's interaction accuracy.

Skill index	Skill name	Accuracy (%)
32	Ordering positive decimals	100
33	Ordering fractions	100
37	Addition whole numbers	100
55	Absolute value	100

Table 8: Skill maps of ASSIST17 and U_2's interaction accuracy.

Skill index	Skill name	Accuracy (%)
2	Point plotting	30
4	Reading graph	100
34	Equation solving	50
95	Divisibility	30
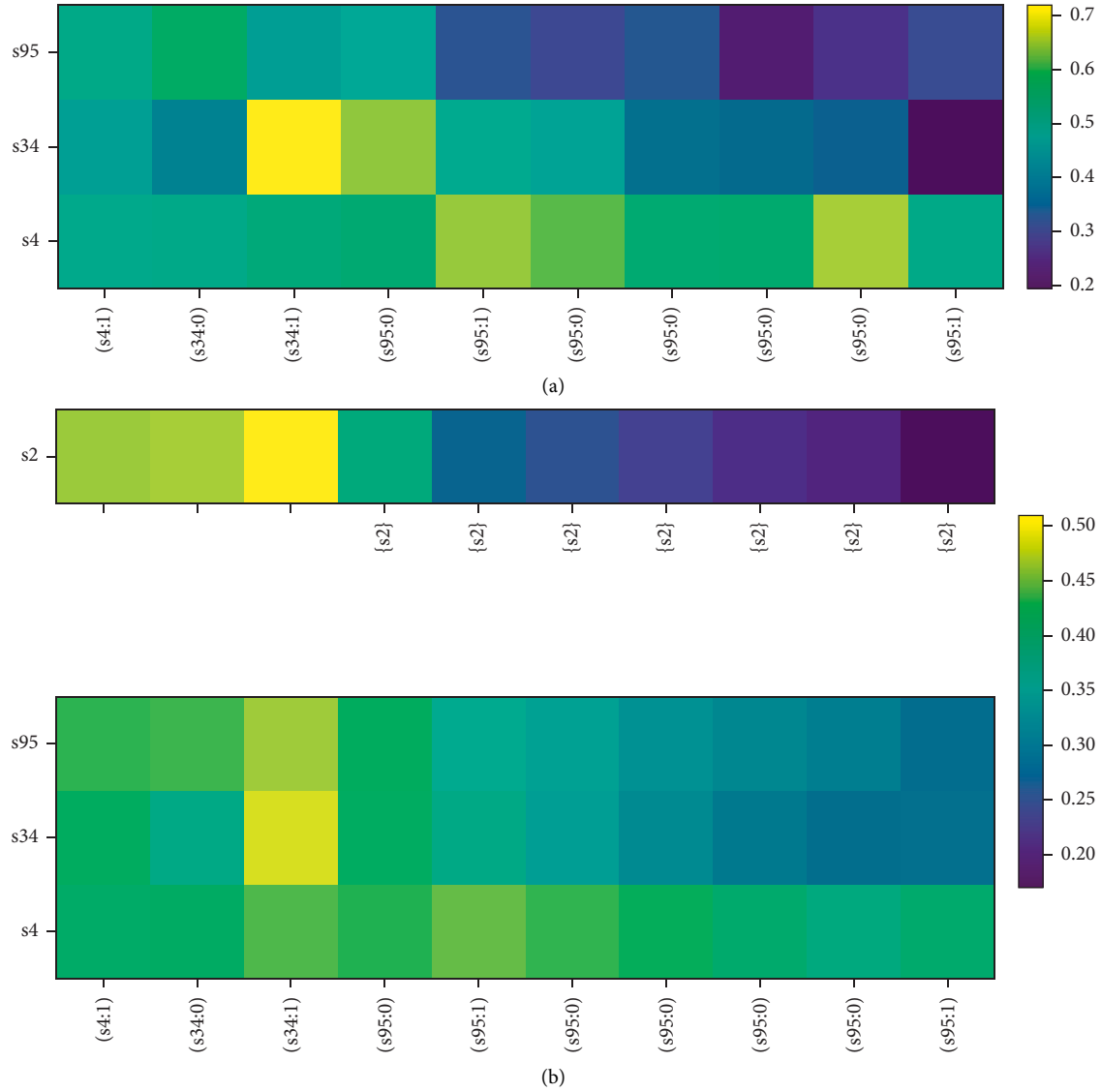
FIGURE 10: Comparison of the prediction process of U_2 on DKT and NSKT. The color of the heatmap indicates the predicted probability that U_2's mastery of skills after interaction (q_t, a_t) at the timestamp t. The yellower the color, the higher the probability. (a) Heatmap for the prediction process of DKT. The x-axis is the sequence of U_2's interactions $(q_t; a_t)$ and the y-axis is the skill index. (b) Heatmap for the prediction process of NSKT. The x-axis of the lower subfigure is the sequence of U_2's interactions $(q_t; a_t)$ and the y-axis is the skill index. The x-axis of the upper subfigure is the RKC S_t and the y-axis is the skill index of the RKCs S_t.

$r_{(s32,s55)} = 0.31$, which means there is a weak positive correlation between $s32$ and $s55$.

The Pearson correlation between $s33$ and $s55$ on NSKT of U_1's interactions is $r_{(s33,s55)} = 0.92$, which means there is a strong positive correlation between $s33$ and $s55$. Through the above examples, we can conclude that NSKT performs better in the ability of discovering latent relevance among knowledge concepts than existing KT models.

7.3. Knowledge Concepts' Discovery. NSKT can learn latent knowledge concept substructure among skills without expert annotations and can cluster related skills into a cluster, which denotes a knowledge concept (KC) class [6].

Figure 13 shows the visualization of using k-means to cluster the skill representation vectors, which have been performed by the t-SNE method [40, 41]. All skills are clustered into eight clusters, and each cluster can represent a knowledge concept class. Skills in the same cluster are labeled with the same color, and those skills have strong relevance and similarity. For example, $s32$ and $s33$ do have a strong relevance and similarity because they are very close in Figure 13, which further proves that NSKT has a stronger ability of discovering skill latent relevance information than existing KT models.

We have explored latent conditional influence between exercises by

$$J_{i \longrightarrow j} = \frac{y(j/i)}{\sum_k y(j/k)},$$ (28)

where $y(j/i)$ is the correctness probability assigned by NSKT to exercise j when exercise i is answered correctly in the first
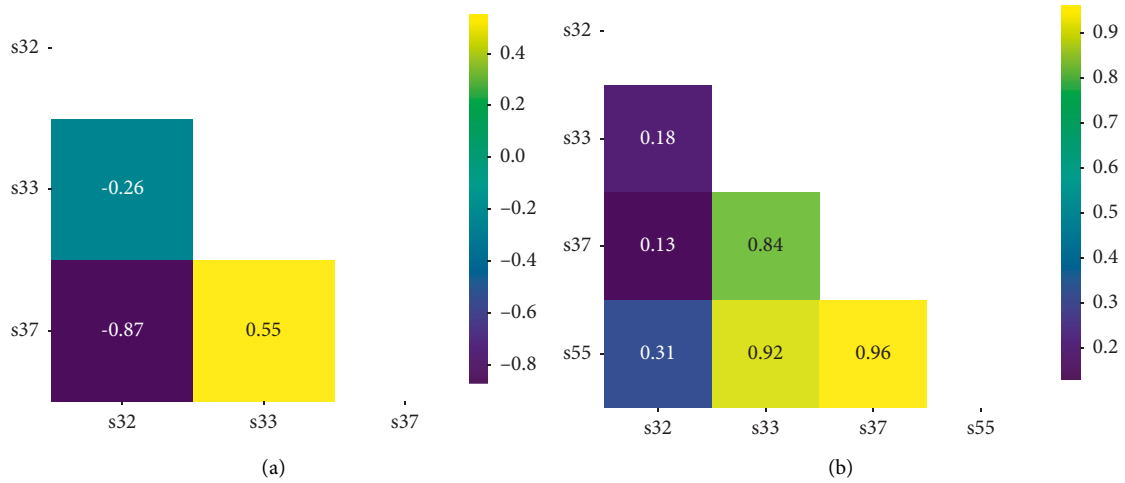
FIGURE 11: Comparison of U_1's interaction skill Pearson correlations on DKT and NSKT ((a) DKT and (b) NSKT). Both the x-axis and the y-axis are the skills in U_1's interactions.
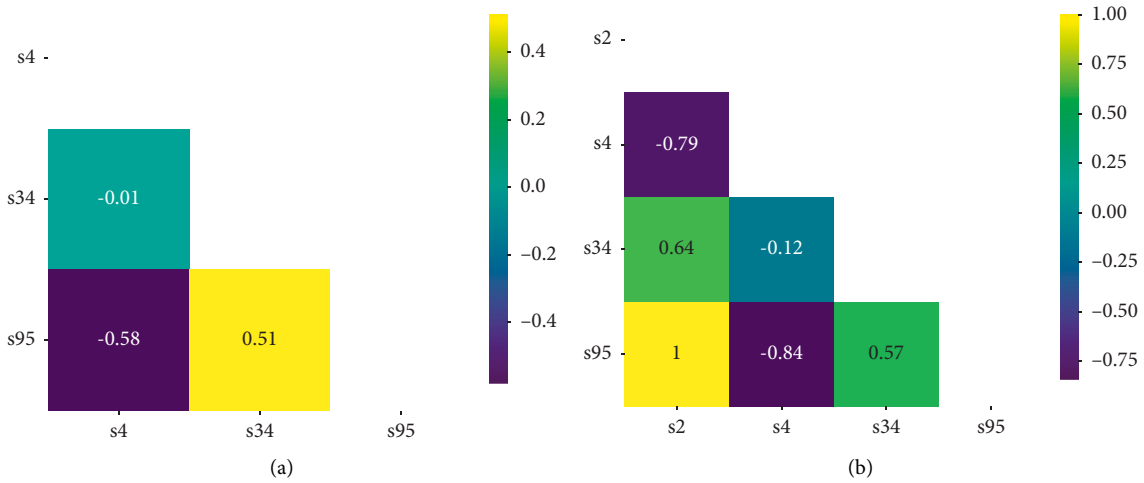
FIGURE 12: Comparison of U_2's interaction skill Pearson correlations on DKT and NSKT ((a) DKT and (b) NSKT). Both the x-axis and the y-axis are the skills in U_2's interactions.

FIGURE 13: Knowledge concept visualization in ASSIST09 and conditional influences between exercises.

time step [6]. We have shown a latent conditional influence relationship among the exercises corresponding to Figure 9(b) interactions. We have marked them with arrow symbols in Figure 13. The line width indicates connection strength, and nodes may be connected in both directions. We only show edges with an influence threshold greater than 0.08. Attached ASSIST09 skill maps are shown in Figure 13 (we only show 110 skills with the skill name).

8. Conclusion

In this work, we proposed a novel NTM-based skill-aware knowledge-tracing model for conjunctive skills, which can capture the relevance among the multiple knowledge concepts of questions to predict students' mastery of knowledge concepts (KCs) more accurately and to discover more latent relevance among knowledge concepts effectively. In order to better model the students' knowledge state, we adopt the neural Turing machines, which use the external memory matrix to augment memory ability. Furthermore, NSKT relates knowledge concepts (KCs) to related knowledge concepts (RKCs) as a whole to enhance the model's ability of skill awareness and improve prediction accuracy and prediction breadth. Experiments in the real-world KT datasets demonstrate that the NTM-based knowledge concept skill-aware knowledge-tracing model (NSKT) outperforms existing state-of-the-art KT models in modelling the students' knowledge state and discovering latent relevance among knowledge concepts.

For future studies, we will focus on mining hidden associations among knowledge concepts and building students' personalized answering paths in intelligent tutoring systems. Furthermore, we will construct the holistic structure of knowledge concepts to enhance students' understanding of how the overall knowledge affects each other.

Data Availability

The datasets used to support the findings of this study are included within the article and are available from the corresponding author on reasonable request too.

Conflicts of Interest

The authors declare that they have no conflicts of interest.

Acknowledgments

References

[1] J. Self, "Theoretical foundations for intelligent tutoring systems," *Journal of Artificial Intelligence in Education*, vol. 1, no. 4, pp. 3–14, 1990.

[2] M. Feng, N. Heffernan, and K. Koedinger, "Addressing the assessment challenge with an online system that tutors as it assesses," *User Modeling and User-Adapted Interaction*, vol. 19, no. 3, pp. 243–266, 2009.

[3] S. Pandey and G. Karypis, "A self-attentive model for knowledge tracing," in *Proceedings of the 12th International Conference on Educational Data Mining*, pp. 384–389, Montréal, Canada, July 2019.

[4] C. K. Yeung and D. Y. Yeung, "Addressing two problems in deep knowledge tracing via prediction-consistent regularization," in *Proceedings of the 5th Annual ACM Conference on Learning at Scale*, pp. 1–10, London, UK, June 2018.

[5] A. T. Corbett and J. R. Anderson, "Knowledge tracing: modeling the acquisition of procedural knowledge," *User modelling and user-adapted interaction*, vol. 4, no. 4, pp. 253–278, 1995.

[6] C. Piech, J. Spencer, J. Huang et al., "Deep knowledge tracing," in *Proceedings of the 28th Advances in Neural Information Processing Systems*, pp. 505–513, Montreal, Canada, December 2015.

[7] S. Shen, Q. Liu, E. Chen et al., "Convolutional knowledge tracing: modeling individualization in student learning process," in *Proceedings of the 43rd International ACM SIGIR Conference on Research and Development in Information Retrieval*, pp. 1857–1860, New York, NY, USA, July 2020.

[8] W. Wang, T. Liu, L. Chang, T. Gu, and X. Zhao, "Convolutional recurrent neural networks for knowledge tracing," in *Proceedings of the 2020 International Conference on Cyber-Enabled Distributed Computing and Knowledge Discovery (CyberC)*, pp. 287–290, Chongqing, China, July 2020.

[9] V. Mandalapu, J. Gong, and L. Chen, "Do we need to go deep? Knowledge tracing with big data," 2021, https://arxiv.org/abs/2101.08349.

[10] J. Zhang, X. Shi, I. King, and D. Y. Yeung, "Dynamic key-value memory networks for knowledge tracing," in *Proceedings of the 26th international conference on World Wide Web*, pp. 765–774, Perth, Australia, April 2017.

[11] S. Liu, R. Zou, J. Sun et al., "A hierarchical memory network for knowledge tracing," *Expert Systems with Applications*, vol. 177, Article ID 114935, 2021.

[12] T. Oya and S. Morishima, "LSTM-SAKT: LSTM-encoded SAKT-like transformer for knowledge tracing," 2021, https://arxiv.org/abs/2102.00845.

[13] S. Pu, M. Yudelson, L. Ou, and Y. Huang, "Deep knowledge tracing with transformers," in *Proceedings of the 21st International Conference on Artificial Intelligence in Education*, pp. 252–256, Ifrane, Morocco, July 2020.

[14] S. Pandey and J. Srivastava, "RKT: relation-aware self-attention for knowledge tracing," in *Proceedings of the 29th ACM International Conference on Information & Knowledge Management*, pp. 1205–1214, Ireland, Europe, October 2020.

[15] Y. Choi, Y. Lee, J. Cho et al., "Towards an appropriate query, key, and value computation for knowledge tracing," in *Proceedings of the Seventh ACM Conference on Learning @ Scale*, pp. 341–344, Chicago, IL, USA, August 2020.

[16] T. Wang, F. Ma, and J. Gao, "Deep hierarchical knowledge tracing," in *Proceedings of the 12th International Conference on Educational Data Mining*, pp. 671–674, Montréal, Canada, July 2019.

[17] A. Ghosh, N. Heffernan, and A. S. Lan, "Context-aware attentive knowledge tracing," in *Proceedings of the 26th ACM SIGKDD International Conference on Knowledge Discovery & Data Mining*, pp. 2330–2339, New York, NY, USA, August 2020.

[18] Y. Liu, Y. Yang, X. Chen, J. Shen, H. Zhang, and Y. Yu, "Improving knowledge tracing via pre-training question

embeddings," in *Proceedings of the 29th International Joint Conference on Artificial Intelligence*, pp. 1577–1583, Yokohama, Japan, January 2020.

[19] H. Nakagawa, Y. Iwasawa, and Y. Matsuo, "Graph-based knowledge tracing: modelling student proficiency using graph neural network," in *Proceedings of the IEEE/WIC/ACM International Conference on Web Intelligence*, pp. 156–163, Thessaloniki, Greece, October 2019.

[20] Q. Liu, Z. Huang, Y. Yin et al., "Ekt: exercise-aware knowledge tracing for student performance prediction," *IEEE Transactions on Knowledge and Data Engineering*, vol. 33, no. 1, pp. 100–115, 2021.

[21] S. Tong, Q. Liu, W. Huang et al., "Structure-based knowledge tracing: an influence propagation view," in *Proceedings of the 20th International Conference on Data Mining*, pp. 541–550, Sorrento, Italy, November 2020.

[22] Y. Yang, J. Shen, Y. Qu et al., "GIKT: a graph-based interaction model for knowledge tracing," in *Proceedings of the European Conference on Machine Learning and Principles and Practice of Knowledge Discovery in Databases*, pp. 299–315, Bilbao, Spain, September 2020.

[23] A. Graves, G. Wayne, and I. Danihelka, "Neural turing machines," 2014, https://arxiv.org/abs/1410.5401.

[24] M. Collier and J. Beel, "Implementing neural turing machines," in *Proceedings of the 27th International Conference on Artificial Neural Networks*, pp. 94–104, Rhodes, Greece, October 2018.

[25] A. Graves, G. Wayne, M. Reynolds et al., "Hybrid computing using a neural network with dynamic external memory," *Nature*, vol. 538, no. 7626, pp. 471–476, 2016.

[26] F. Lord, *Applications of Item Response Theory to Practical Testing Problems*, Erlbaum Associates, Mahwah, NJ, USA, 1980.

[27] F. Lord, "A Theory of Test Scores," *Psychometric monographs*, vol. 17, 1952.

[28] H. Cen, K. Koedinger, and B. Junker, "Learning factors analysis - a general method for cognitive model evaluation and improvement," in *Proceedings of the International Conference on Intelligent Tutoring Systems*, pp. 164–175, Jhongli, Taiwan, June 2006.

[29] P. I. Pavlik, H. Cen, and K. R. Koedinger, "Performance factors analysis–a new alternative to knowledge tracing," in *Proceedings of the 14th International Conference on Artificial Intelligence in Education*, pp. 531–538, Brighton, England, July 2009.

[30] K. H. Wilson, Y. Karklin, B. Han, and C. Ekanadham, "Back to the basics: Bayesian extensions of irt outperform neural networks for proficiency estimation," in *Proceedings of the 9th International Conference on Educational Data Mining*, pp. 539–544, Raleigh, North Carolina, June 2016.

[31] Y. Su, Z. Cheng, P. Luo et al., "Time-and-Concept enhanced deep multidimensional item response theory for interpretable knowledge tracing," *Knowledge-Based Systems*, vol. 218, Article ID 106819, 2021.

[32] H. Cen, K. Koedinger, and B. Junker, "Comparing two IRT models for conjunctive skills," in *Proceedings of the Intelligent Tutoring Systems*, pp. 796–798, Montreal, Canada, June 2008.

[33] S. Malekmohamadi Faradonbe, F. Safi-Esfahani, and M. Karimian-kelishadrokhi, "A review on neural turing machine (NTM)," *SN Computer Science*, vol. 1, no. 6, p. 333, 2020.

[34] A. Santoro, S. Bartunov, M. Botvinick, D. Wierstra, and T. Lillicrap, "One-shot learning with memory-augmented neural networks," 2017, https://arxiv.org/abs/1605.06065.

[35] J. Zhao, S. Bhatt, C. Thille, N. Gattani, and D. Zimmaro, "Cold start knowledge tracing with attentive neural turing machine," in *Proceedings of the Seventh ACM Conference on Learning @ Scale*, pp. 333–336, Chicago, IL, USA, June 2020.

[36] S. Hochreiter and J. Schmidhuber, "Long short-term memory," *Neural Computation*, vol. 9, no. 8, pp. 1735–1780, 1997.

[37] Y. Choi, Y. Lee, D. Shin et al., "EdNet: a large-scale hierarchical dataset in education," in *Proceedings of the 21st International Conference on Artificial Intelligence in Education*, pp. 69–73, Ifrane, Morocco, July 2020.

[38] X. Xiong, S. Zhao, E. G. Van Inwegen, and J. E. Beck, "Going deeper with deep knowledge tracing," in *Proceedings of the 9th International Conference on Educational Data Mining*, pp. 545–550, Raleigh, NC, USA, June 2 2016.

[39] M. Friedman, "The use of ranks to avoid the assumption of normality implicit in the analysis of variance," *Journal of the American Statistical Association*, vol. 32, no. 200, pp. 675–701, 1937.

[40] L. Van Der Maaten and G. Hinton, "Visualizing data using t-SNE," *Journal of Machine Learning Research*, vol. 9, no. 11, pp. 2579–2605, 2008.

[41] J. MacQueen, "Some methods for classification and analysis of multivariate observations," in *Proceedings of the 5th Berkeley symposium on mathematical statistics and probability*, vol. 1, no. 14, pp. 281–297, Oakland, California, January 1967.

Research Article

Effect of Industrial Robots on Employment in China: An Industry Level Analysis

Yantong Zhao [1,2] **Rusmawati Said,** [1] **Normaz Wana Ismail,** [1] **and Hanny Zurina Hamzah** [1]

[1] School of Business and Economics, University Putra Malaysia, 43400 Serdang, Selangor, Malaysia
[2] College of Confucian Business, Jining University, Qufu 273155, Shandong, China

Correspondence should be addressed to Yantong Zhao; gs60065@student.upm.edu.my and Rusmawati Said; rusmawati@upm.edu.my

China has been the world's largest market for industrial robots since 2013. Industrial robots improve accuracy, safety, and efficiency in industrial production but have a substantial impact on the labor market. This investigation uses the task-based model to explore the relationship between industrial robots and employment across industries. This study uses industrial robot data from the International Federation of Robotics and employment data from the China Statistical Yearbook from 2010 to 2019 to examine robot applications' influencing mechanisms on labor demand in different industries in China. The results show a significant positive correlation between robots' exposure and labor demand for IT, health and social services, science research and technical services, and management of water conservancy and environmental industries. Based on the results, the use of robots promotes high-skilled talent employment and some third-sector employment, like education, food and beverages, utilities, household appliances, and transport. However, multiple regression analysis reveals that the use of robots has reduced employment in traditional industries such as agriculture and mining.

1. Introduction

The issue of the potential impact of robots on the labor market has received considerable attention. The popularity of artificial intelligence and new robot designs has significantly influenced both the economy and society. At the beginning of the 20th century, the famous economist, John Maynard Keynes, predicted that humankind would have a new employment challenge, that is, "technological unemployment" [1]. Rapid progress in the fields of artificial intelligence and robotics has begun to solve major problems in terms of productivity and the acceleration of the replacement of labor by robots. This introduces tremendous challenges having to do with the human workforce [2]. According to application, robots can be classified as repetitive-tasks robots, medical robots, guarding robots, domestic-purpose robots, astronomical robots, entertainment robots, mining robots, defense and military robots, agriculture robots, and remote-areas robots [3]. A recent study by the McKinsey Global Institute

(MGI) pointed out that robots will replace 400 to 800 million people in the world by 2030. In the rapid development of automation, up to 31% of working hours in China will be automated [4]. To what extent will robots replace human workers in the future? Is the rapid development of artificial intelligence and robotics responsible for introducing positive opportunities or challenges? This set of questions has become a global issue that cannot be ignored.

Since 2015, artificial intelligence has seen explosive growth in China, attracting significant attention from all social sectors. In September 2017, the government released a document entitled, "New Generation Artificial Intelligence Development Plan." This plan urges China to seize the global command of artificial intelligence by the year 2030 and incubate 10 trillion Yuan in industrial output. As an essential component of artificial intelligence, robot applications have become a critical fulcrum for transforming China from manufacturing to higher-quality economic development. More robots are utilized from the IFR (IFR, 2019) data than

ever before. The operational stock of robots measures the number of robots currently deployed. The working stock of robots in the world rose from 1.02 million in 2009 to 2.73 million units in 2019 with a steady upward trend. China, Japan, the United States, South Korea, and Germany constitute the five major industrial robot markets. They account for about 70% of the global import and export in trade in robots and their installation. The data from the past ten years show that robot operations in China are in a state of continuous growth. At the same time, the United States, Germany, Japan, and South Korea have experienced zero or even negative growth in the rate of robot ownership in the past ten years. China has been the world's largest market for industrial robots since 2013. The number of robot installation was about 550 units in 1990. After ten years of slow augmentation, robot installations increased from 5525 units in 2009 to 156,000 units in 2017. In 2017 and 2018, China's total industrial robot installations accounted for 38% of the global total. In 2019, a total of 140,000 units were installed which is 9% less than that in 2018 but still higher than the total robots installed in Europe and the United States. With the acceleration of artificial intelligence development, robots have had a greater impact on labor force employment. Against this backdrop, it is necessary to systematically study the technical progress of robots and their effect on the labor market from the perspective of economic method and theory.

Both the government and private enterprise in China have expended a tremendous amount of money to promote and support technological innovation in terms of artificial intelligence and robots' development. The rise of human-machine collaborations has affected all areas of the modern world, from work to everyday life and beyond. However, it is difficult to answer the question of whether robots are responsible for creating or eliminating employment opportunities. More than 100,000 new industrial robots were installed in the United States industry (IFR, 2019), mainly in the automotive industry where the employment increased by 230,000 jobs from 2010 to 2015 [5]. Although, certain occupations may disappear in local communities, the total number of jobs may increase globally. In addition to changing the jobs quantity, the nature and characteristics of employment and labour are likely to change fundamentally. As one of the largest developing countries with a transitional economy, the rapid popularization of robotic technology will undoubtedly have a profound dual effect on human resource management in the market. Previous studies about the impact of robots on the labor market, however, are inconsistent. Most studies of these studies have only been conducted in developed countries [6–9]. Although a few studies have investigated the development of robotics and artificial intelligence and the corresponding economic impact on China [10–12], most studies have focused on the theoretical dimension or country, provincial, and firm levels [13–15]. A wide gap also exists between China's robotic development and its impact. Systematic empirical studies are lacking on the relationship between industrial robots and China's employment in different industries and skills. This investigation aims to explore the relationship between industrial robots and employment across industries. This study

uses the International Federation of Robotics (IFR)'s industrial robot data and employment data from the China Statistical Yearbook to construct a penetration index for industrial robots in China. Thus, we examine the influence of robot deployment on labor demand in China. We also analyze the potential impact of robots on economic outcomes, which may provide the Chinese government with guidance for economic growth and employment in the future.

The paper organization is as follows: the next section reviews the existing theoretical and empirical literature on industrial robots' impact on economic and labor markets. Section 3 describes research methods, with a particular focus on the theoretical framework, data description, and the empirical model. The last section represents a summary of the research.

2. Literature Review

With the rapid development of artificial intelligence technology, a new era of technological revolution and industrial transformation is gradually taking shape. It is an era in which robots are changing manufacturing processes and life patterns [16]. The rapid development of the international robot market has become an important phenomenon that cannot be ignored in terms of its consequences for economic life. This section reviews the existing theoretical and empirical literature on the impact of industrial robots on the economy and labor market.

Some scholars believe that technological innovation leads to social progress and reduces the importance of human resources in the production sector, which increases the unemployment rate [2, 17, 18]. In examining this proposition, Susskind developed a task-based model. He argues that using intelligent machines can reduce relative wages and the income share of the labor force, while leading to a high unemployment rate [17]. Frey and Osborne developed a model based on the Gaussian process to classify more than 700 detailed occupations in the United States according to their susceptibility to automation based on data from the United States Department of Labor's Occupational Classification Database. The results of this line of investigation show that about half of jobs in the United States will be challenged by automation in the next decades [2]. Acemoglu and Restrepo [18] examine the competition between human labor and robots in terms of different production tasks. They conclude that the use of robots will reduce employment and lower the laborers' salaries. Their analysis is based on the usage of industrial machines, employment, and wage changes to return in the United States (IFR). According to the results of each additional robot in every thousand workers, the employed population ratio decreases by 0.18%~0.34%, and the wage decreases by 0.25%~0.5%. This negative effect Indicates that the application of robots has a significant negative impact on the employment and wage in the commuting field [18].

Many scholars also support the view that innovation positively affects employment [19–21]. Bloom et al. estimate that, due to the extensive integration of artificial intelligence

technology into daily life, between 2010 and 2030, the world will develop 734 million new jobs [19]. Acemoglu and Restrepo [20] argue that, from the standpoint of the development history of science and technology, in the long run, technological progress will lead to the development of new employment opportunities. In this respect, the compensation effect produced by new jobs can offset the substitution effect caused by automation [20]. Similarly, Gregory et al. [21] examined data from 27 European countries from 1999 to 2010. They found that conventional forms of technological change led capital to replace labor in the production process, reducing employment by about 9.6 million jobs. In comparison, the spillover effect on product demand brought about by technological progress led to an increase of nearly 21 million jobs. On the whole, technological progress has had a net positive impact on employment in the European labor force [21].

A series of empirical studies have shown that unskilled labor and capital are substitutes, while skilled labor and capital are complementary [22–25]. For example, when machine prices fall, firms reduce the use of unskilled labor. In contrast, when the prices of machinery fall, manufacturers increase the use of equipment, and the demand for skilled labor increases because equipment operation requires skilled labor. According to the study, a 10% decrease in equipment prices leads to a 5% decrease in the use of unskilled labor and a 5% increase in the use of skilled labor [26]. This finding is widely known as the capital–skill complementary hypothesis, which has several important policy implications. For example, the hypothesis suggests that technological advances, such as the rapid drop in the cost of computing in recent decades, may significantly influence income inequality. This effect exists because technological progress causes an increase in demand for skilled labor and a decrease in demand for unskilled labor.

The impact of technological progress on the employment of laborers with different skills shows that highly skilled laborers can quickly master and adapt to new technologies; and, in this sense, skilled labor has a complementary relationship with new technologies. However, unskilled labor is limited by its level of human capital since unskilled laborer are unable to master new technologies quickly. For this reason, its risks are replaced by new technologies. As with the progress of traditional technology, artificial intelligence will increase the demand for and employment opportunities for skilled labor. This will create a substitution effect for unskilled labor [27–29]. In this respect, Acemoglu and Restrepo [20] point out that artificial intelligence and robot learning have enabled robots to make breakthroughs in analysis, problem-solving, and the performance of complex and unconventional tasks. It is also possible that robots can do the work of highly skilled workers instantly. By constructing a theoretical model, they found that the skilled labor force replaced by a high-skilled labor force might compete with low-skilled workers and be competent for other jobs. The employment creation effect of artificial intelligence on the labor force is thus concentrated in high- and low-skill positions, and the substitution effect is centered on medium-skill positions. This labor force has

comparative advantages in terms of communication, service, innovation, and research and development (R&D) [20]. Artificial intelligence is complementary to the labor force in these sectors and can, in fact, create jobs.

The substitution and creation effects on labor caused by intelligent robots produce changes in labor supply and demand, and they can ultimately lead to changes in wage equilibrium. Previous studies have also explored the impact of robots on labor compensation from various perspectives. Some researchers conclude that intelligent robots can quickly replace workers in certain jobs and thereby reduce wages. The two-phase overlapping generations model proposed by Benzell et al. illustrates the idea that the operation of intelligent robots will cause labor's share of national income to decrease in the long run [30]. Similarly, DeCanio [31] uses the Houthakker model [32] to briefly evaluate the influence of intelligent robots on labor compensation in the United States [31]. Cabrales et al. demonstrated that the threat of robot replacement does not affect the efforts of workers [33]. According to DeCanio's results, if the job substitution elasticity of humans and robots exceeds 1.9, then the expansion of robots will induce salary reductions.

Several studies have examined the impact of robot adoption on the labor market in China [12–15]. Fan et al. examined the impact of rising labor costs on the adoption of industrial robots by Chinese companies. A 10% increase in the minimum wage between 2008 and 2012 increased the probability of a company adopting a robot by 0.11% points. Higher minimum wages have a significant impact on the adoption of robots for firms that are more productive, located in coastal areas, private, and skilled labor-intensive [13]. Tang et al. found that the adoption of robots and highly skilled workers are complementary. After adopting robots, companies hire more highly skilled and educated workers. Therefore, the adoption of robots has resulted in an employment skill bias among Chinese enterprises [12]. Du and Lin systematically investigated the impact of adopting industrial robots on total factor productivity in different regions according to the panel data of Chinese provinces from 2006 to 2019. The results showed a U-shaped relationship between the adoption of industrial robots and total factor productivity [14]. Fu et al. studied the labor markets of 74 economies using international panel datasets from 2004 to 2016. The study found that the adoption of industrial robots is associated with a significant increase in labor productivity and total employment in developed economies, whereas the impact is not significant in developing countries, where increased robot adoption is associated with a significant decline in the labor share of GDP. In both developed and developing countries, increased robot adoption is associated with a substantial increase in income inequality [15].

3. Research Methods

3.1. Theoretical Framework. For investigating the effect of industrial robots on employment, our research uses the task-based model with automation technology [7]. Firstly, we introduce the basic model, and then, in the second part, we replace the automated capital with robots to analyze the

impact of robots on the labor market. In this way, we obtain the labor quantity under equilibrium conditions.

(I). Basic model: task-based model with automation technology

Assume that the economy produces only one good Y, accomplished by a series of tasks $y(i)$, and the production function is as follows:

$$Y = \left(\int_{N-1}^{N} y(i)^{\sigma - 1/\sigma} di \right)^{\sigma/\sigma - 1}, \tag{1}$$

where σ is elasticity of substitution. An increase in N implies that a new complex task appears. An increase in $N - 1$ also means that the old task disappears.

Labor can produce any task. Capital is unable to produce complex new tasks. Assume that $I \in [N-1, N]$, when tasks $i < I$, it is feasible to produce with capital. If $i > I$, tasks I must be produced by labor. When $i < I$, the production function of task i is as follows:

$$y(i) = k(i) + \gamma(i) \cdot l(i), \tag{2}$$

where $\gamma(i)$ is labor productivity, $l(i)$ is labor, and $k(i)$ is capital.

When $i \geq I$, the production function of task i is as follows:

$$y(i) = \gamma(i) \cdot l(i). \tag{3}$$

The cost of each task is as follows:

$$p(i) = \begin{cases} \min\left\{ r, \dfrac{W}{\gamma(i)} \right\}, & i \leq I, \\[3mm] \dfrac{W}{\gamma(i)}, & i > I. \end{cases} \tag{4}$$

Where r is capital rent and W is wage. From equations (2)–(4), we can get the following equation:

$$y(i) = Y \cdot p(i)^{-\sigma},$$

$$y(i) = \begin{cases} Y \cdot \left[\min r, \dfrac{W}{\gamma(i)} \right]^{-\sigma}, & i \leq I, \\[4mm] Y \left[\dfrac{W}{\gamma(i)} \right]^{-\sigma}, & i > I. \end{cases} \tag{5}$$

We use robots only when the cost of using the robot is less than that of labor. There exists a unique $\tilde{I}$ such that $r = W/\gamma(\tilde{I})$. For task $\tilde{I}$, the production cost is equal for labor and capital. Let $I^* = \min\{I, \tilde{I}\}$. All tasks are produced with capital if $i \leq I^*$, while all tasks are produced with labor if $i > I^*$.

So, the demand for capital and labor is as follows:

$$k(i) = \begin{cases} Y r^{-\sigma}, & i \leq I^*, \\ 0, & i > I^*, \end{cases} \quad \text{and}$$

$$l(i) = \begin{cases} 0, & i \leq I^*, \\[3mm] Y \left(\dfrac{W}{\gamma(i)} \right)^{-\sigma}, & i > I^*. \end{cases} \tag{6}$$

When the capital and labor market clear, the following equations hold:

$$(I^* - N + 1) Y \cdot r^{-\sigma} = K,$$

$$Y \cdot \int_{I^*}^{N} \left(\frac{W}{\gamma(i)} \right)^{-\sigma} di = L^s, \tag{7}$$

$$(I^* - N + 1) \cdot p^{1-\sigma} + \int_{I^*}^{N} \left(\frac{W}{\gamma(i)} \right)^{1-\sigma} di = 1.$$

(II). Task-based model for robots and employment

Suppose that there are C regions in the economy, and each region has I industries. The output of each region is Y_C, and the output of each industry in the region is Y_{ci}, $c \in C$. Consumption of the region is X_C, and the consumption of the region for each industry is X_{ci}. Suppose that there is no trade, then we get the following equation:

$$\begin{aligned} Y_C &= X_C, \\ Y_{ci} &= X_{ci}, \\ Y_C &= \left(\sum_{i \in I} v_i^{1/\sigma} \cdot Y_{ci}^{\sigma - 1/\sigma} \right)^{\sigma/\sigma - 1}, \end{aligned} \tag{8}$$

where v_i is the share of industry i, σ is substitution elasticity, and $\sum_{i \in I} v_i = 1$, the price is p_{ci}^X for industry i's output. Output is produced by combining capital K with continuous tasks $s \in [0, 1]$. A task can be produced by robots or labor. $x_{ci}(s)$ shows the quantity of task s.

$$X_{Ci} = A_{Ci} \left[\min_{s \in [0,1]} \{ x_{Ci}(s) \} \right]^{\alpha} \cdot K_{Ci}^{1-\alpha}. \tag{9}$$

According to the basic model in I, there is a boundary θ_i when tasks $s \leq \theta_i$. Tasks can be performed using labor or robots while they must be performed using labor if tasks $s > \theta_i$.

$$X_{Ci} = \begin{cases} \gamma_M \cdot M_{Ci}(s) + \gamma_L L_{Ci}(s), & s \leq \theta_i, \\ \gamma_i \cdot L_{Ci}(s), & s > \theta_i, \end{cases} \tag{10}$$

where γ_M and γ_L are productivity of robot and labor, respectively. $M_{Ci}(s)$ and $L_{Ci}(s)$ are numbers of robots and labors in task s, respectively.

Robots are produced using investment I_C with $M_C = D \cdot (1 + \eta) I_C^{1/1+\eta}$. So $Y_C = C_C + I_C$. C_C is the consumption of household. Let L_C is the labor supply and W_C is

wage. The rental price of robot is R_C^M and nonrobot capital is fixed at K_C with price R_C^k.

We use robot only when its cost is less than that of using labor (i.e., $R_C^M/V_M < W_C/\gamma_L$). Let $\pi_C = 1 - R_C^M/\gamma_M/W_C/\gamma_L$. We use robot when $\pi_C > 0$. Now, we look at the impact of robots on employment. We get the following equations:

$$M_C = D \cdot (1 + \eta) \cdot I_C^{1/1+\eta},$$
$$I_C = D^{-1-\eta} \cdot (1 + \eta)^{-1-\eta} \cdot M_C^{1+\eta}, \qquad (11)$$
$$C_C = Y_C - I_C = Y_C - D^{-1-\eta} \cdot (1 + \eta)^{-1-\eta} \cdot M_C^{1+\eta}.$$

In region c, the following equations define the first-order condition for the representative household:

$$W_C = B C_C^{\psi} \cdot L_C^{\varepsilon}$$
$$= B \cdot \left[Y_C - D^{-1-\eta} \cdot (1 + \eta)^{-1-\eta} \cdot M_C^{1+\eta} \right] \cdot L_C^{\varepsilon}. \qquad (12)$$

For robots, we obtain the following equation:

$$R_C^M = \frac{dI_C}{dM_C},$$
$$R_C^M = D^{-1-\eta} \cdot (1 + \eta)^{-1-\eta} \cdot (1 + \eta) \cdot M_C^{\eta+1-1}, \qquad (13)$$
$$R_C^M = D^{-1-\eta} \cdot (1 + \eta)^{-\eta} \cdot M_C^{\eta}.$$

Price of industry i is marginal cost, so we get the following equation:

$$p_{Ci}^X = \frac{1}{A_{Ci}} \cdot \left[\theta_i \frac{R_C^M}{\gamma_M} + (1 - \theta_i) \frac{W_C}{\gamma_L} \right]^{\alpha} \cdot \left(R_C^k \right)^{1-\alpha}. \qquad (14)$$

The share of labor in tasks is as follows:

$$S_{Ci}^L = \frac{W_C L_{Ci}}{\partial p_{Ci}^X X_{Ci}}$$
$$= \frac{(1 - \theta_i)(W_C/\gamma_L)}{\theta_i \left(R_C^M/\gamma_M \right) + (1 - \theta_i)(W_s/\gamma_L)}, \qquad (15)$$

αS_{Ci}^L is the share of labor in the value added of industry i. $1 - \alpha$ of total cost are paid to capital.

$$\sum_{i \in I} v_i \left(p_{Ci}^X \right)^{1-\sigma} = 1. \qquad (16)$$

From (15), we get the wage in the region c: $W_C \cdot L_{Ci} = \alpha S_{Ci}^L \cdot p_{Ci}^X \cdot X_{Ci}$

$$W_C L_C = \sum_{i \in I} \alpha S_{Ci}^L v_i p_{Ci}^{X/1-\sigma} \cdot Y_C. \qquad (17)$$

Similarly, the demand for robot and capital can be represented as follows:

$$R_C^M \cdot M_C = \sum_{i \in I} \alpha \left(1 - S_{Ci}^L \right) v_i \cdot p_{Ci}^{X\,1-\sigma} \cdot Y_C, \qquad (18)$$
$$R_C K_C = (1 - \alpha) \cdot Y_C.$$

Because the added-value of industry i is $v_i \cdot p_{Ci}^{X,1-\sigma} \cdot Y_C$ and labor share is $S_{Ci}^L \alpha$, using (14) and (15) we get the following equation:

$$\sum_{i \in I} vi \left(p_{ci}^x \right)^{1-\sigma} = 1. \qquad (19)$$

Then,

$$L_{Ci} = (1 - \theta_i) \left(\frac{\alpha(1 - \alpha)(1 - \alpha/\alpha) v_i}{\gamma_L A_{Ci}^{1/\alpha}} \right) p_{Ci}^{X1-\sigma-(1/\alpha)} Y_C^{1/\alpha} K_C^{\alpha-1/\alpha}. \qquad (20)$$

Taking the log form as follows:

$$\ln L_{Ci} = \ln (1 - \theta_i) + \ln \frac{\alpha(1 - \alpha)^{1-\alpha/\alpha} v_i}{\gamma_L A_i^{1/\alpha}} - \left(\sigma + \frac{1}{\alpha} - 1 \right) \ln p_{Ci}^X$$
$$+ \frac{1}{\alpha} \ln Y_C + \frac{\alpha - 1}{\alpha} \ln K_C. \qquad (21)$$

Differentiating both sides, we obtain the following equation:

$$d \ln L_{Ci} = -\frac{1}{1 - \theta_i} d\theta_i + \frac{1}{\alpha} d \ln Y_C - \left(\sigma + \frac{1}{\alpha} - 1 \right) d \ln p_{Ci}^X. \qquad (22)$$

There are three different forces of robots that affect labor demand, as shown in (22). The first part is the displacement effect. When θ_i increases, it means that more robots are involved in replacing labor and this effect always reduces the labor force. The second part is a positive productivity effect. Automation reduces costs and increases productivity and labor demand among industries. Finally, workers can be transferred from the automated tasks to the nonautomated tasks, and thus they can specialize in the performance of new tasks.

3.2. Data Description

3.2.1. Exposure to Robots. Robotics data for industries comes from the IFR (IFR, 2019). The IFR compiled annual robot use data for 50 countries from 1993 to 2019. The use of the IFR data for studying changes in employment and robot adoption has been widely reported in the literature. Using the robot data, Acemoglu and Restrepo [7], Graetz and Michaels [6], Dauth et al. [9], Carbonero et al. [34], and Chiacchio et al. [8] have explored the impact of robot adoption on employment in the United States, Germany, and different EU countries [7–9, 34]. We use data from the period between 2010 and 2019 since robots in China have been growing rapidly since the early 2000s. Table 1 lists 13 industries for which we collected robot data. Similar to Du and Lin [14], we compare these industries with those in the Chinese national standard (GB/T 4754–2017). In this industry classification standard, there are 13 industries, as shown in column 3 of Table 1. The first column of Table 1 represents the industries with robot data. The second column is the industry label, such as information technology (IT) and scientific research and technical (R&T) services. More robots are utilizing the IFR (IFR, 2019) data than ever. The number of robots

TABLE 1: List of all industries based on the China National Standard (GB/T 4754-2017).

Included in robotics data	Label	Code description
√	Agriculture	Agriculture, forestry, animal husbandry and fishery
√	Mining	Mining
√	Manufacturing	Manufacturing
√	Utilities	Production and supply of electricity, heat, gas and water
√	Construction	Construction
√	Transport	Transport, storage and post
√	IT	Information transmission, software and information technology
√	Food and beverages	Hotels and catering services
√	Science R&T	Scientific research and technical services
√	Chemical	Management of water conservancy, environment
√	Household appliances	Services to households, repair and other services
√	Education	Education
√	Pharmaceuticals	Health and social service

Notes. Table 1 lists 13 industries for which we collected robot data from IFR. We compared these with the industries in the Chinese national standard (GB/T 4754-2017) as shown in column 3 of Table 1. The first column of Table 1 represents the industries with robot data. The second column is the industry label, such as information technology (IT) and scientific research and technical (R&T) services.

currently utilized was measured by the operational stock of robots.

China's use of industrial robots began in the early 1970s but developed slowly thanks to abundant labor resources and backward technology. The popularity of robots began to increase in the mid-1980s during the period of reform and opening up. Robots were listed as the key national scientific research program in the seventh five-year plan. When the National High Technology Research and Development Program ("863" Program) of China was launched, the theme of intelligent robots was created, and robotics was listed as a crucial field in the "Made in China 2025" document.

From the robot operation data for the most recent ten years, it is evident that the robot operations in China have been in a state of continuous growth. At the same time, the United States, Germany, Japan, and South Korea have experienced zero growth or even negative change in the rate of robot ownership in the past ten years. Since 2013, China has been the world's largest industrial robot market. Figure 1 shows robot installations in China between 1999 and 2019 measured as the number of units. The number of robot installations was about 550 units in 1990. After ten years of slow growth, robot installations increased from 5525 units in 2009 to 156,000 in 2017. In 2017 and 2018, China's industrial robot installations accounted for 38% of the world's total. In 2019, a total of 140,000 units were installed, which is 9% less than that in 2018 but still greater than the total number of robots installed in Europe and the United States.

3.2.2. Labor Market Data. The China Statistical Yearbook compiled by the National Bureau of Statistics of China covers the employment numbers for each industry from 2010 to 2019. Figure 2 displays the industrial data to identify the trend of the change in the number of people employed from 2010 to 2019.

We divide industries into four categories based on sectors and employment trends. The first group (A) is the industries where employment has tended to rise, including IT, pharmaceuticals, science R&T, and chemicals. The second group (B) includes agriculture and mining. Their employment has followed a downward trend for the last ten years. The third group (C) is the rest of the tertiary sector, including education, food and beverages, utilities, household appliances, and transportation. In these industries, employment has remained unchanged over the decade of the study period. The fourth group (D) is the industries in the secondary sector, including construction and manufacturing, with a growing trend of employment until 2013 but decline since 2014. The first is the industries where employment is rising, including IT, pharmaceuticals, science R&T, and chemicals. Based on Table 2, these four industries require a relatively high level of education and about 70% of employees have a college degree or above. For example, the proportion of college, university, and graduate and higher level attainment of urban employed persons in the IT industry in 2019 was 27.5, 39.4, and 4.7, respectively.

3.2.3. Control Variables. Different theories exist in the literature regarding the effect of technological progress on employment, among them classical theory, Marxist theory, neoclassical theory, new growth theory, Schumpeter's innovation theory, and business cycle theory. Up to now, several studies have revealed a correlation between technological progress and employment [19–21, 35–38]. Brouwer et al. [35] conducted two innovative studies in the Netherlands to estimate the effects of technological progress on employment. They found a positive effect caused by product-related R&D activities but an adverse effect in relation to overall R&D investments [35]. Greenan and Guellec [39] used market research in France from 1991 to analyze employment growth from 1986 to 1990. They found positive effects for both process and product innovation, with more muted effects for process innovations [39]. Bloom et al. estimated that, thanks to progress in artificial intelligence, more than 700 million new jobs will be created between 2010 and 2030 globally [19]. Acemoglu and Restrepo believe that, from the perspective of the history of science and technology, while rendering certain jobs obsolete,
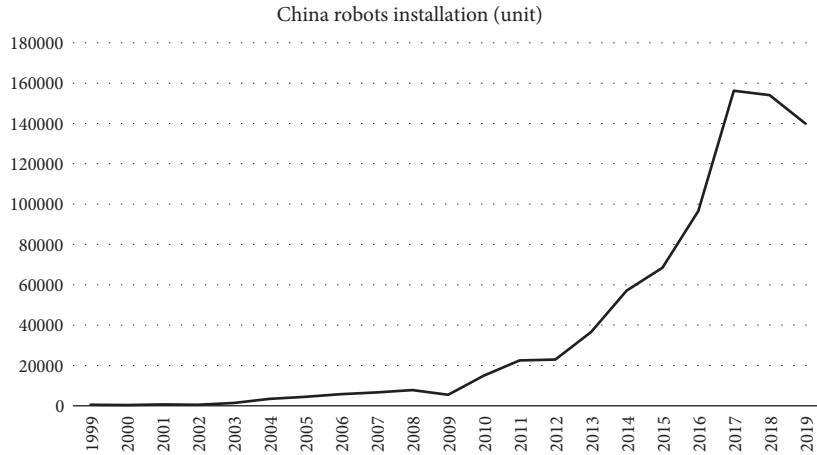
FIGURE 1: China's robots installations from 1999 to 2019. (Source: IFR, 2019).
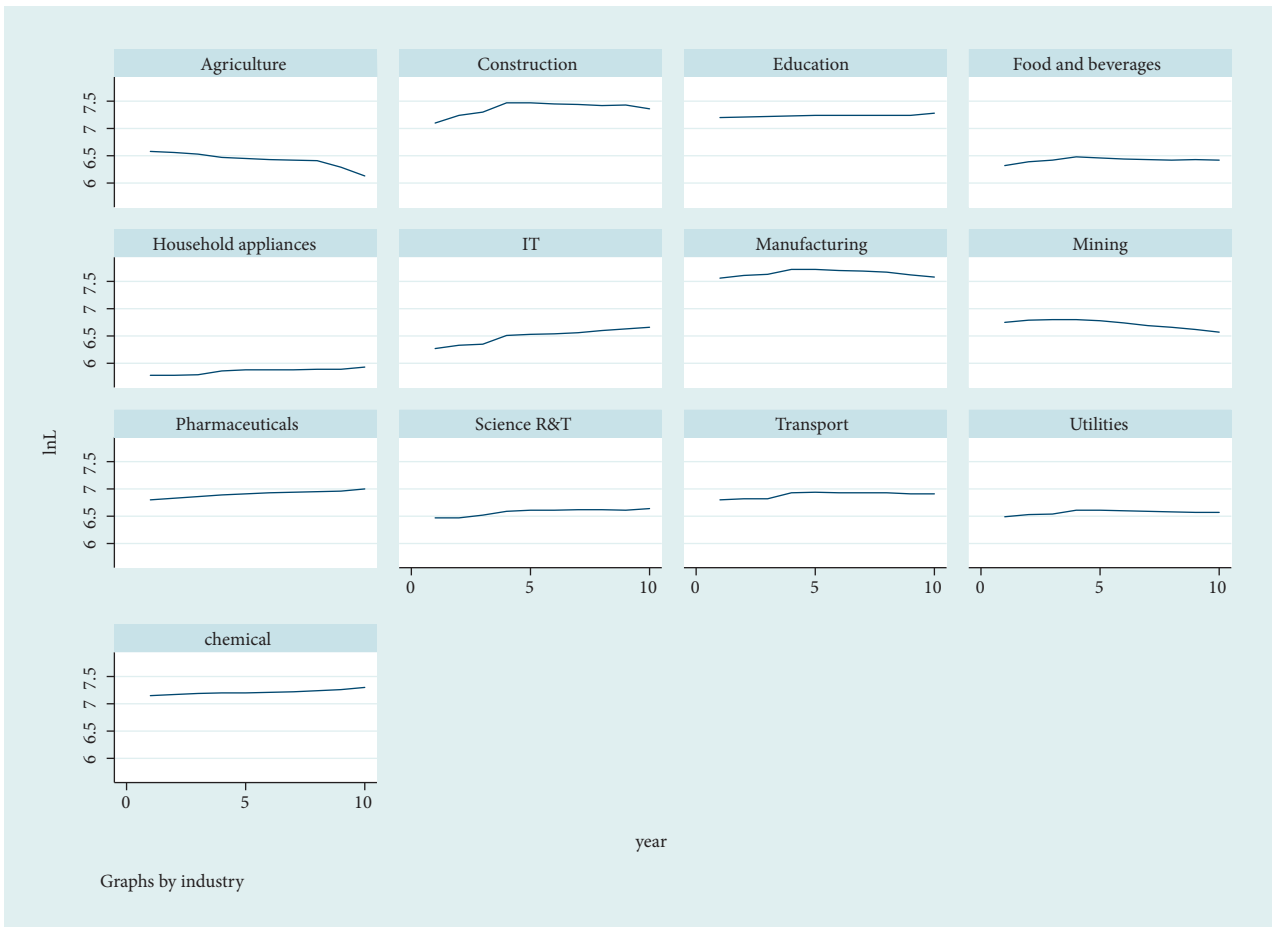
FIGURE 2: Employed persons by industry from 2000 to 2019. Notes: The results were graphed using Stata 15. This figure displays the industrial data to identify the trend of the change in the number of people employed from 2010 to 2019.

technological innovation will create many more new jobs in the long-run. The compensation effect produced by the new positions can offset the substitution effect [20]. Gregory et al. studied data from 27 European countries during the period from 1999 to 2010. They found that conventional substitution resulting from technological change led capital to replace labor in production, thereby eliminating about 9.6 million jobs. In comparison, the spillover effect from product demand brought about by technological progress led to an increase of nearly 21 million jobs. On the whole, technological progress has had a positive impact on employment levels for the European labor force [21].

Table 2: Educational attainment of urban employed persons by industry in 2019.

Industries	Total	Junior secondary school and below	Senior secondary school	Medium vocational education	High vocational education	College	University	Graduate and higher level
Agriculture	100	89.4	6.6	1.5	0.2	1.5	0.7	0.0
Mining	100	36.4	21.7	12.0	2.6	16.2	10.5	0.7
Manufacturing	100	47.4	18.4	9.4	1.7	13.3	9.0	0.8
Utilities	100	20.4	18.3	10.8	2.5	24.4	21.6	2.1
Construction	100	61.9	14.7	4.6	0.9	10.0	7.4	0.4
Transport	100	46.3	21.2	8.4	1.9	13.5	8.3	0.3
IT	100	8.8	10.7	6.7	2.0	27.5	39.4	4.7
Science R&T	100	9.9	10.2	5.2	2.1	23.0	38.9	10.7
Chemical	100	44.6	14.5	6.5	1.7	16.2	15.1	1.3
Households	100	53.6	19.7	7.8	1.8	10.8	6.0	0.2
Education	100	8.8	6.6	5.8	1.9	23.7	45.0	8.3
Pharmaceuticals	100	10.9	8.0	10.6	2.3	30.2	33.4	4.5

Source. China Population Statistics Yearbook (2019).

Table 3: Descriptive statistics.

Group	Variables	Min	Max	Mean	Std. dev	Observations		
Group A	lnL	2.28	3.30	2.80	0.30	$N = 40$	$n = 4$	$T = 10$
	lnRobot	−1.54	2.60	0.70	0.87	$N = 40$	$n = 4$	$T = 10$
	lnFDI	3.81	6.32	5.07	0.71	$N = 40$	$n = 4$	$T = 10$
	lnRD	4.91	7.18	5.77	0.72	$N = 40$	$n = 4$	$T = 10$
Group B	lnL	2.13	2.80	2.57	0.18	$N = 20$	$n = 2$	$T = 10$
	lnRobot	−1.79	0.48	-0.94	0.69	$N = 20$	$n = 2$	$T = 10$
	lnFDI	3.98	5.34	4.96	0.36	$N = 20$	$n = 2$	$T = 10$
	lnRD	3.90	6.32	5.18	0.99	$N = 20$	$n = 2$	$T = 10$
Group C	lnL	1.78	3.28	2.59	0.47	$N = 50$	$n = 5$	$T = 10$
	lnRobot	−1.51	2.19	0.58	1.09	$N = 50$	$n = 5$	$T = 10$
	lnFDI	2.60	5.75	4.85	0.78	$N = 50$	$n = 5$	$T = 10$
	lnRD	2.92	4.88	4.11	0.60	$N = 50$	$n = 5$	$T = 10$
Group D	lnL	3.10	3.72	3.51	0.17	$N = 20$	$n = 2$	$T = 10$
	lnRobot	−1.89	2.25	0.31	1.44	$N = 20$	$n = 2$	$T = 10$
	lnFDI	4.96	6.72	5.89	0.76	$N = 20$	$n = 2$	$T = 10$
	lnRD	4.17	7.21	5.37	1.17	$N = 20$	$n = 2$	$T = 10$

Expenditure on R&D, contractual value deals in domestic technical markets (CVD), foreign direct investment (FDI), imports of capital goods, technology purchases, patent citations, and the index of industrial robots are some of the most commonly used indicators of technological change. Interestingly, all of these indicators catch different dimensions of technology. This study uses expenditure on R&D activities and FDI to model technological progress. The amounts of FDI and R&D for each industry were obtained from 2010 to 2019 from the China Statistical Yearbook.

Since the new millennium, China's R&D expenditure has increased at an average annual rate of about 20%. R&D expenditure has expanded from 89.6 to 2443 billion Yuan in 2000 and 2020, respectively, accounting for 0.89% to 2.40% of GDP. Especially eight years ago, China became the world's second-largest consumer, which is a major phenomenon in terms of its global economic status and deserves attention. From 2000 to 2016, China's contribution to the worldwide R&D economic expansion was 27.4%, close to the 29.5% growth of the United States.

3.3. The Empirical Model.
According to our discussion in the theoretical framework, there are three forces about the power of robots affecting employment, including displacement, productivity, and composition effects [7]. To explore the total impact of robots on employment in different industries, we can posit the following formula:

$$\ln L_{it} = \alpha_0 + \alpha_1 \ln \text{RobotExposure}_{it} + x_{it}^L + \varepsilon_{it}, \quad (23)$$

where L_{it} is the level of employment; robot exposure refers to the penetration of industrial robots in industry i in year t, which is equal to the stock of industrial robots in Chinese industry i in t years divided by the employment level of i industry in China in year t; and x_{it}^L represents other factors affecting labor demand. In our empirical model, we use R&D

TABLE 4: Effects of robots on employment of the four group.

	Group A			Group B			Group C			Group D		
	(1) OLS	(2) FE	(3) RE	(1) OLS	(2) FE	(3) RE	(1) OLS	(2) FE	(3) RE	(1) OLS	(2) FE	(3) RE
lnRobot	0.258**	0.108***	0.258***	−0.177	−0.194***	−0.177	0.039	0.047***	0.045***	0.121	0.137**	0.121**
	(3.76)	(13.28)	(7.66)	(−4.54)	(−8.55)	(−6.46)	(1.53)	(6.49)	(2.62)	(0.69)	(2.63)	(2.35)
lnFDI	−0.402**	−0.032	−0.402***	−0.047	0.021	−0.047	0.311***	−0.018	−0.072*	−0.006	0.190	−0.006
	(−4.78)	(−1.38)	(−9.75)	(−0.95)	(0.49)	(−1.04)	(−7.39)	(−0.99)	(−1.79)	(−0.03)	(1.12)	(−0.08)
lnRD	0.057	0.029	0.057	−0.065	0.172**	−0.065***	0.641***	0.018	0.084**	−0.014	−0.004	−0.014
	(1.72)	(0.92)	(1.54)	(−2.17)	(2.21)	(−3.07)	(5.19)	(1.14)	(2.24)	(−0.15)	(−0.10)	(−0.35)
_Cons	4.331***	2.717***	4.331***	2.979**	1.401**	2.979***	1.460**	2.592***	2.572***	3.579	2.368**	3.579***
	(8.02)	(12.12)	(17.28)	(50.32))	(2.64)	(14.54)	(2.90)	(27.49)	(11.36)	(2.29)	(2.22)	(7.28)
N	40	40	40	20	20	20	49	49	49	20	20	20
R^2	0.73	0.901		0.890	0.792		0.793	0.427		0.782	0.276	
F	.	119.941			25.39		51.884	14.268		.	3.752	

Notes. This table reports the impact of industrial robots on employment of the four groups. The dependent variable is employment at the industrial level. All other variables are defined in Section 3.2. OLS is the pooled regression and FE, RE are the fixed and random effect model, respectively. t statistics are reported in parentheses. ***, **, and * indicate significance at the 1%, 5%, and 10% levels, respectively.

and FDI as control variables. To standardize the data, we took log form for all the variables.

The correlation between robot exposure and employment was tested using panel data, which provides richer models and estimation methods than cross-sectional data. An extreme strategy for estimating panel data is pooled regression as cross-section data, requiring each individual in the sample to have exactly the same regression equation. The disadvantage of pooled regression is that it ignores the heterogeneity of individuals, which may relate to explanatory variables and lead to inconsistent estimates.

In practice, a compromise estimation strategy is often adopted; it is assumed that individual regression equations have the same slopes but different intercepts to capture heterogeneity. This model is called the individual-specific effects model and is formulated as below.

$$y_{it} = x'_{it}\beta + z'_i\delta + u_i + \varepsilon_{it} \ (i = 1, \ldots, n; t = 1, \ldots, T),$$
$$L^D = F(W, Q^D, T), \tag{24}$$

where z_i is a time-invariant individual characteristic. x_{it} can vary with individuals and over time. The disturbance term consists of $u_i + \varepsilon_{it}$, called composite error term. Among them, the unobserved random variable u_i is the intercept term representing individual heterogeneity, namely individual effects. ε_{it} is a disturbance term that varies with individual and time, known as idiosyncratic error.

If u_i relates to an explanatory variable, it signals the fixed effects (FE) model. If u_i is not correlated with all explanatory variables (x_{it}, z_i), it implies the random effects (RE) model. Hence, this research use the Hausman check if this model follows FE or RE model.

4. Results

4.1. The Empirical Results. Table 3 shows the descriptive statistics of the relevant variables used in this paper. These statistics are the mean, maximum, minimum, standard deviation, and number of observations. For example, the minimum, maximum, mean, and standard deviation of the log form of employment in group A are 2.28, 3.30, 2.80, and

0.30, respectively. T is years, n represents four industries in the first group, and the number of observations is 40. Table 4 shows the statistical results for the above groups. There is a significant positive correlation between robots' exposure and labor demand for Group A. These results show that the use of robots promotes high-skilled employment. A 10% increase in robot density leads to a 1.1% rise in high-tech jobs. The Hausman test statistics reject the null hypothesis of the RE model and accept the FE model at a 5% statistically significant level. Also, the resulted F statistics reject the pool regression and accept the FE model.

Group B shows a significant negative correlation between robots' exposure and labor demand. According to the Hausman test and F test, the FE model is superior to the RE and pooled regression model. Another finding was that R&D promotes employment in traditional industries according to the FE model, which explains the fact that various technological transformations or upgrades have a corresponding effect on workers. China is predominantly agricultural and very populous. According to the National Bureau of Statistics, employment in primary industries, mainly agriculture, accounted for 50% of the total workforce in 2001, 37% in 2010, and only 24% in 2020.

The proportion of the population employed in primary industry has declined year by year. Of the country's more than 600 million farmers, very few are engaged in the agricultural sector. More people have chosen to enter secondary and tertiary industries to go elsewhere for work or to start a small business. With the rapid development and industrialization of China, the R&D of agricultural robots has been gradually expanding. Agricultural robots can be engaged in planting, spraying pesticides, harvesting, and other field operations, and they can play an essential role in animal husbandry. This not only saves human resource costs but also improves quality control ability and enhances resilience. For the mining industry, there are many problems with underground production operations in coal mines: high accident rates, harsh operating conditions, serious environmental pollution, and high disaster risk. Faced with high-risk underground operations, robots have become an essential means of achieve the safe and efficient production

TABLE 5: Result of regression analysis of different estimation methods of the four groups.

	Group A		Group B		Group C	
	(4) FE_Robust	(5) LSDV	(4) FE_Robust	(5) LSDV	(4) FE_Robust	(5) LSDV
lnRobot	0.108***	0.108***	0.194**	−0.194**	0.047***	0.047***
	(13.93)	(13.34)	(−20.59)	(−19.94)	(9.34)	(8.92)
lnFDI	−0.032	−0.032	0.021	0.021	−0.018	−0.018
	(−1.07)	(−1.03)	(0.29)	(0.28)	(−1.56)	(−1.49)
lnRD	0.029	0.029	0.172	0.172	0.018	0.018
	(0.76)	(0.73)	(4.18)	(4.04)	(1.06)	(1.01)
_Cons	2.717***	3.082***	1.401	1.166	2.592***	3.237***
	(12.01)	(13.82)	(2.51)	(1.84)	(31.15)	(40.29)
N	40	40	20	20	49	49
R^2	0.909	0.993	0.805	0.929	0.478	0.996
F	2.1e + 04	.	.	.	269.906	.

Notes. This table reports the results of the robustness test in Section 4.2. FE_Robust is FE using clustering robust standard and LSDV is least-squares dummy variables regression. The dependent variable is employment at the industrial level. All other variables are defined in Section 3.2. t statistics are reported in parentheses. ***, **, and * indicate significance at the 1%, 5%, and 10% levels, respectively.

goals in coal mines. To achieve safety of coal miners, it is a general trend for robots to replace miners in underground operations. Coal mine production will therefore develop toward the use of unmanned, autonomous, intelligent, and highly efficient robots in the future. Artificial intelligence technology can play an irreplaceable role in that and diversified artificial intelligence technology can be applied to coal mine robots. Although the current application of artificial intelligence in the field of industrial coal mining is still in a period of exploration, with the increasing application of artificial intelligence technology in the field of coal mining, it is imperative to build unmanned mines.

For Group C, after the Hausman test and F test, the FE model is superior to the RE model and pooled regression. Table 4 indicates that the use of robots has a positive effect on the third employment sector. Robots have been used in the service industry for decades. Helpmate, a service robot created in the 1980s by Joseph F·Engelberger, the so-called "father of robotics," delivers meals, medicine, and supplies to hospital patients [16]. Helpmate, of course, is a square box, impersonal and rudimentary. Service robots are growing fast in Japan in another direction: entertainment robots. In recent years, robots have been increasingly used in the service industry. As Engelberger predicted, robots are more likely to be used in the service industries, including maintenance, repair, transportation, cleaning, security, rescue, and domestic tasks and nursing [16]. In recent years, modern information technologies have developed rapidly including cloud computing, the "Internet of Things," artificial intelligence, and "big data." A series of proactive policies continued to develop, including the transformation of the real economy, cross-border e-commerce, and support for rural e-commerce. Also, new forms of online retail and orders have risen, creating a large number of new jobs in wholesale and retail trade, hotels, and restaurant industries.

In Group D, the results of the Hausman and LR tests in MLE support the RE model against the FE and pooled regression models. Nonetheless, the LM test results suggest a pooled regression against the RE model. In this group, there is no significant correlation between robot density and employment in the secondary sector. Secondary industries

involve many industries, such as steel manufacturing, automobile production, and wired and wireless communication. Some companies have tried to liberate front-line workers by using industrial robots in recent years. Foxconn, the largest mobile phone manufacturer, uses industrial robots to perform the tasks previously performed by workers on production lines. Now, some domestic manufacturing enterprises have begun to replace front-line operators with industrial robots, improving their efficiency.

4.2. Robustness Check. Table 5 shows the results of different estimated regression methods on the employment of robots. The regression results of FE using clustering robust standards in Table 5 show that robots have a positive relationship with the employment of the first and third groups, and a negative relationship with the employment of the second group. Both of them are significantly valid at 0.05, which indicates that the use of industrial robots increases employment in tertiary sectors and high-tech industries, but is ineffective in employment in agriculture and mining industries. Table 5 shows that the results obtained by different regression estimation methods (i.e., FE_Robust and LSDV) are the same, which verifies the validity and robustness of the basic FE regression and the empirical results.

In addition to using different regression methods, we add a lagged core explanatory variable for endogeneity problems. In this paper, the lag variable L.lnRobot of explanatory variable lnRobot is used as a substitute variable to conduct regression tests. Table 6 shows the results. The coefficients of lag variable L.lnRobot on the employment of the three groups are 0.096, -0.202, and 0.033, respectively, and significant at the 1% level, indicating that the regression results are still robust after considering endogeneity.

Following [40], the equation of demand for labor is as follows:

$$L^D = F(W, Q^D, T), \tag{25}$$

where L^D is labor demand or the desired level of employment, W is the wage rate, Q^D is the output or product

TABLE 6: Adding lagged core explanatory variables to deal with endogeneity.

	Group A (6) lnL	Group B (6) lnL	Group C (6) lnL
L.lnRobot	0.096*** (12.10)	−0.202*** (−7.83)	0.033*** (4.45)
lnFDI	−0.028 (−1.24)	0.015 (0.35)	−0.015 (−0.85)
lnRD	0.060* (1.91)	0.180* (1.95)	0.035** (2.29)
_Cons	2.552*** (12.56)	1.340** (2.16)	2.535*** (25.97)
N	36	18	44
R^2	0.887	0.774	0.293
F	93.396	20.750	8.265

Notes. This table reports the results of the robustness test in Section 4.2. The lag variable L.lnRobot of explanatory variable lnRobot is used as a substitute variable to conduct regression test. The dependent variable is employment at the industrial level. All other variables are defined in Section 3.2. t statistics are reported in parentheses. ***, **, and * indicate significance at the 1%, 5%, and 10% levels, respectively.

TABLE 7: Result of FE model by adding control variables for intervention.

	Group A (7) lnL	Group B (7) lnL	Group C (7) lnL
lnRobot	0.0876*** (8.00)	−0.160* (−2.05)	0.035* (1.78)
lnFDI	−0.0306 (−1.37)	0.040 (0.69)	−0.026 (−1.26)
lnRD	−0.00840 (−0.26)	0.199* (2.00)	0.016 (1.06)
lnWage	−0.132 (−0.56)	−0.142 (−0.36)	0.531** (2.68)
lnVA	0.204 (1.29)	−0.121 (−0.40)	−0.409** (−2.08)
_Cons	2.766*** (5.14)	2.399 (1.21)	1.858*** (3.92)
N	40	20	49
R^2	0.916	0.765	0.493
F	86.743	13.561	11.119

Notes. This table reports the results of the robustness test in Section 4.2. The dependent variable is employment at the industrial level. We add wage and value-added (VA) in our model as control variables. All other variables are defined in Section 3.2. t statistics are reported in parentheses. ***, **, and * indicate significance at the 1%, 5%, and 10% levels, respectively.

demand, and T is the technology. We add wage and value-added (VA) in our model, and the robot, R&D, and FDI represent technology. Table 7 displays that industrial robot still has a significant impact on employment under the model of increasing control variables, indicating that the regression results are still robust after the intervention of increasing control variables.

4.3. Discussion of the Results.

According to the capital–skill complementarity hypothesis discussed in the literature review, technological progress leads to an increase in demand for skilled labor and a decrease in demand for unskilled labor. An initial objective of this study was to identify the relationship between industrial robot adoption and China's employment in different industries and skills. Our results suggested that an association existed between robot adoption and employment across industries. There is a significant positive correlation between robots' exposure and labor demand for high-skilled employment and third sector employment. A 10% increase in robot density leads to a 1.1% rise in high-tech jobs. However, multiple regression analysis reveals that robots have reduced employment in traditional industries such as agriculture and mining. This study supports evidence from previous observations [11, 12, 41, 42] that industrial robots are a skilled-biased technology change.

Using data about Germany, Dauth et al. found that industrial robots reduce manufacturing employment, but the reduced employment is offset by increased employment in the tertiary industry [9]. The industry-based estimates in this study are inconsistent with those of Acemoglu and Restrepo [7], which are based on data about the United States. Their findings showed that the negative effects of robot adoption on employment are mainly felt in highly mechanized industries, such as automobile manufacturing, chemical, pharmaceutical, and food manufacturing. Robotic applications will promote labor employment in industries such as finance, the public sector, and nonrobotized

manufacturing [7]. These results are inconsistent for two reasons. First, compared with developed countries such as the United States, China's robot adoption is still in its early stages. The first adopters of robotic production technology can use this competitive advantage to expand their market share, thereby increasing the demand for labor. This role is particularly prominent in the capital- or technology-intensive industries, such as information transmission, software and information technology, communication equipment, and computer and other electronic equipment manufacturing. Second, with the rise in labor costs in China, labor-intensive industries such as construction, manufacturing, and mining face more prominent cost pressures, indicating that such industries have more substantial economic incentives to replace labor with robots.

5. Conclusion

Our study aims to assess how robots contribute to the employment of different industries and skills. The results of this investigation show a significant positive correlation between robots' exposure and labor demand for the third sector of employment. The results show that the use of robots promotes high-skilled talent employment. However, multiple regression analysis reveals that the use of robots has reduced employment in traditional industries such as agriculture and mining. This study represents the first comprehensive assessment of how industrial robots contribute to the employment of different industries and skills of China. A limitation of this study is that the robot data is only from 2010, because the use of robots in China has started late but has increased rapidly since the 2000s. The use of robots affects not only employment but also other aspects of the labor market and the economy as a whole. There is still uncertainty

about whether robot technical progress impacts wage inequality. Further work needs to be done to establish whether the application of robots is conducive to improving the labor share of national income. Much uncertainty still exists about the relationship between the industry robots, total factor productivity, and added-value of China. Further research needs to examine more closely the links between industrial robots and productivity.

The robot industry will be the main engine of economic growth in the next few years. The progress of robotics is inevitable. There will be unprecedented significant development and improvement in the field of robotics. We must accept this trend and seize this opportunity to leap into economic development. Obviously, under the state's leadership, robot technology as a whole is helping to promote positive economic growth, and it has become an opportunity for people to find jobs again. The findings of this study have a number of important implications for future practice. Studying the impact of robots on economic outcomes may provide guidelines for governments about China's economic growth and employment in the future.

This study showed that the employment promotion effect of robot adoption mainly lay in the middle- and high-skilled labor groups, indicating that intelligent manufacturing provided by robots needs a large medium- and high-skilled labor force to match it. The average skill level in China's current labor force was low, and the low-skill labor force accounted for a large proportion of the total labor force. Therefore, China should further strengthen the guidance and expenditure on vocational skill education and training, provide abundant labor resources for intelligent manufacturing, and reduce frictional unemployment caused by technological change.

We also found the employment substitution effect of robot adoption in traditional industries, such as agriculture and mining. The government should provide more guidance and support for unemployment insurance, job-transfer training, and especially new skills learning. The government should also alleviate the employment impact of new technology adoption on traditional industries and ensure a fuller and higher employment quality.

We provide three recommendations for the education system. First, higher vocational education should be developed. The state can establish and improve the majors of artificial intelligence and robotics, train high-skilled professors, and establish practice bases to cultivate intelligent, automated, and information-based technical workers. Second, re-employment training should be strengthened. In addition to the existing higher vocational colleges, the government should support the establishment of more re-employment training centers. Subsidies should be increased for the return of low-skilled young people to advance their studies and for the unemployed to undergo re-employment training; this would reduce re-education costs for both groups and enable them to acquire competent skills in intelligent, automated, and information-based production positions. Finally, relevant preferential policies should be introduced to guide the flow and transfer of labor among various industries of the national economy in an orderly manner so that citizens do not need to bear more costs for acquiring new labor skills and positions.

Data Availability

All variables used in this study are listed with the sources in the following: Industrial Robot: robotics data for industries comes from the International Federation of Robotics (2019). Source: https://ifr.org/worldrobotics/. Employment: the number of employed persons in urban units by sector. Source: China Statistical Yearbook compiled by the National Bureau of Statistics of China. https://data.stats.gov.cn/english/. Education: educational attainment of urban employed persons by sector and sex. Source: China population and employment Statistics yearbook complied by Department of Population and Employment National Bureau of Statistics of China. https://www.yearbookchina.com/. FDI: Foreign Direct Investment by sector, investment actually utilized. Source: China Statistical Yearbook compiled by the National Bureau of Statistics of China. https://data.stats.gov.cn/english/. R&D: intramural expenditure on R&D of R&D institutions by industrial sector in which the R&D institutions served. Source: China Statistical Yearbook on Science and Technology. https://www.yearbookchina.com/. Wage: average Wage of Employed Persons in Urban Units by _Sector. Source: China Statistical Yearbook compiled by the National Bureau of Statistics of China. https://data.stats.gov.cn/english/. Value-added: Value-added by Sector. Source: China Statistical Yearbook compiled by the National Bureau of Statistics of China. http://www.stats.gov.cn/tjsj/ndsj/2019/indexeh.htm.

Conflicts of Interest

The authors declare that there are no conflicts of interest.

References

[1] J. M. Keynes, *Treatise on Money*, papamoa press, Tauranga New Zealand, 1930.

[2] C. B. Frey and M. A. Osborne, "The future of employment: how susceptible are jobs to computerisation?" *Technological Forecasting and Social Change*, vol. 114, pp. 254–280, 2017.

[3] G. Singh and V. K. Banga, "Robots and its types for industrial applications," *Materials Today Proceedings*, vol. 60, no. 3, pp. 1779–1786, 2022.

[4] J. Manyika, M. Chui, M. Miremadi et al., "A future that works: AI, automation, employment, and productivity," *McKinsey Global Institute Research Technical Report D*, vol. 60, pp. 1–135, 2017.

[5] R. Gosine and P. Warrian, "Digitalizing Extractive Industries: State-Of-The-Art to the Art-Of-The-Possible: Opportunities and Challenges for Canada," *Munk School of Global Affairs*, University of Toronto, Toronto, Canada, 2017.

[6] G. Graetz and G. Michaels, "Robots at work," *The Review of Economics and Statistics*, vol. 100, no. 5, pp. 753–768, 2018.

[7] D. Acemoglu and P. Restrepo, "Robots and jobs: evidence from US labor markets," *Journal of Political Economy*, vol. 128, no. 6, pp. 2188–2244, 2020.

[8] F. Chiacchio, G. Petropoulos, and D. Pichler, "The Impact of Industrial Robots on EU Employment and Wages: A Local

Labor Market Approach (No. 2018/02)," *Bruegel working paper*, vol. 15, 2018.

[9] W. Dauth, S. Findeisen, J. Sudekum, and N. Woessner, "German Robots-The Impact of Industrial Robots on Workers," vol. 7, 2017.

[10] G. Zhou, G. Chu, L. Li, and L. Meng, "The effect of artificial intelligence on China's labor market," *China Economic Journal*, vol. 13, no. 1, pp. 24–41, 2020.

[11] H. Ma, Q. Gao, X. Li, and Y. Zhang, "AI development and employment skill structure: a case study of China," *Economic Analysis and Policy*, vol. 73, pp. 242–254, 2022, https://doi.org/10.1016/j.enpol.2014.04.029.

[12] C. Tang, K. Huang, and Q. Liu, "Robots and skill-biased development in employment structure: evidence from China," *Economics Letters*, vol. 205, Article ID 109960, 2021.

[13] H. Fan, Y. Hu, and L. Tang, "Labor costs and the adoption of robots in China," *Journal of Economic Behavior & Organization*, vol. 186, pp. 608–631, 2021.

[14] L. Du and W. Lin, "Does the application of industrial robots overcome the Solow paradox? Evidence from China," *Technology in Society*, vol. 68, Article ID 101932, 2022.

[15] X. M. Fu, Q. Bao, H. Xie, and X. Fu, "Diffusion of industrial robotics and inclusive growth: labor market evidence from cross country data," *Journal of Business Research*, vol. 122, pp. 670–684, 2021.

[16] J. F. Engelberger, "Health-care robotics goes commercial: the 'HelpMate' experience," *Robotica*, vol. 11, no. 6, pp. 517–523, 1993.

[17] D. Susskind, "A model of technological unemployment," *Economics Series Working Papers*, vol. 819, 2017.

[18] D. Acemoglu and P. Restrepo, "Secular stagnation? The effect of aging on economic growth in the age of automation," *The American Economic Review*, vol. 107, no. 5, pp. 174–179, 2017.

[19] D. E. Bloom, M. McKenna, and K. Prettner, "Demography, Unemployment, Automation, and Digitalization: Implications for the Creation of (Decent) Jobs, 2010–2030 (No. w24835)," *National Bureau of Economic Research*, https://doi.org/10.1093/oxrep/grq038, 2018.

[20] D. Acemoglu and P. Restrepo, "Low-skill and high-skill automation," *Journal of Human Capital*, vol. 12, no. 2, pp. 204–232, 2018.

[21] T. Gregory, A. Salomons, and U. Zierahn, "Racing with or against the Machine? Evidence from Europe," *Evidence from Europe (July 15, 2016). ZEW-Centre for European Economic Research Discussion Paper, (16-053)*, vol. 20, no. 2, pp. 869–906, 2016.

[22] Z. Griliches, "Capital-skill complementarity," *The Review of Economics and Statistics*, vol. 51, no. 4, pp. 465–468, 1969.

[23] A. P. Bartel and F. R. Lichtenberg, "The comparative advantage of educated workers in implementing new technology," *The Review of Economics and Statistics*, vol. 69, no. 1, pp. 1–11, 1987.

[24] C. Goldin and L. F. Katz, "The origins of technology-skill complementarity," *Quarterly Journal of Economics*, vol. 113, no. 3, pp. 693–732, 1998.

[25] H. David and D. Dorn, "The growth of low-skill service jobs and the polarization of the US labor market," *The American Economic Review*, vol. 103, no. 5, pp. 1553–1597, 2013.

[26] K. B. Clark and R. B. Freeman, "How Elastic Is the Demand for Labor? (No. W0309)," *National Bureau of Economic Research*, vol. LXII, no. 2, pp. 509–520, 1979.

[27] S. Machin and J. Van Reenen, "Technology and changes in skill structure: evidence from seven OECD countries," *Quarterly Journal of Economics*, vol. 113, no. 4, pp. 1215–1244, 1998.

[28] G. M. Cortes, "Where have the middle-wage workers gone? A study of polarization using panel data," *Journal of Labor Economics*, vol. 34, no. 1, pp. 63–105, 2016.

[29] G. Lordan and D. Neumark, "People versus machines: the impact of minimum wages on automatable jobs," *Labour Economics*, vol. 52, pp. 40–53, 2018.

[30] S. G. Benzell, L. J. Kotlikoff, G. LaGarda, and J. D. Sachs, "Robots Are Us: Some Economics of Human Replacement (No. W20941)," *National Bureau of Economic Research*, vol. 53, 2015.

[31] S. J. DeCanio, "Robots and humans - complements or substitutes?" *Journal of Macroeconomics*, vol. 49, pp. 280–291, 2016.

[32] H. S. Houthakker and W. Hildenbrand, "Market Demand: Theory and Empirical Evidence," vol. 62, 1995.

[33] A. Cabrales, P. Hernandez, and A. Sanchez, "Robots, labor markets, and universal basic income," *Humanities and Social Sciences Communications*, vol. 7, no. 1, pp. 1–8, 2020.

[34] F. Carbonero, E. Ernst, and E. Weber, "Robots Worldwide: The Impact of Automation on Employment and Trade," Report number: 36, International Labour Organization, Geneva, Switzerland, 2020.

[35] E. Brouwer, A. Kleinknecht, and J. O. Reijnen, "Employment growth and innovation at the firm level," *Journal of Evolutionary Economics*, vol. 3, no. 2, pp. 153–159, 1993.

[36] N. M. Yunus, R. Said, and W. N. W. Azman-Saini, "Spillover effects of FDI and trade on demand for skilled labour in MALAYSIAN manufacturing industries," *Asian Academy of Management Journal*, vol. 20, no. 2, pp. 1–27, 2015.

[37] R. U. S. M. A. W. A. T. I. Said, A. S. M. A. D. D. Y. Haris, and R. McNabb, "Changes in relative demand for labor in Malaysia (1984-1997) using a decomposition approach," *International Journal of Economics and Management*, vol. 2, no. 1, pp. 157–178, 2008.

[38] A. Haris and R. Said, "Social security wealth and early retirement in public pension scheme," *International Journal of Economics and Management*, vol. 6, no. 2, pp. 346–359, 2012.

[39] N. Greenan and D. Guellec, "Technological innovation and employment reallocation," *Labour*, vol. 14, no. 4, pp. 547–590, 2000.

[40] R. G. Ehrenberg, R. S. Smith, and K. F. Hallock, *Modern Labor Economics: Theory and Public Policy*, Routledge, Oxfordshire, UK, 2021.

[41] B. Ni and A. Obashi, "Robotics technology and firm-level employment adjustment in Japan," *Japan and the World Economy*, vol. 57, Article ID 101054, 2021.

[42] A. Haris and R. Said, "Social security wealth and early retirement in public pension scheme," *International Journal of Economics and Management*, vol. 6, no. 2, pp. 346–359, 2012.

Research Article

Comprehensive Evaluation of the Tendency of Vertical Collusion in Construction Bidding Based on Deep Neural Network

Wenxi Zhu [iD],[1,2] **Kaizhi Cheng** [iD],[1] **Yabin Guo** [iD],[3] **and Yun Chen** [iD][1]

[1]*School of Traffic and Transportation Engineering, Changsha University of Science and Technology, Changsha 410114, China*
[2]*Key Laboratory of Highway Engineering (Changsha University of Science & Technology), Ministry of Education, Changsha, China*
[3]*Yunji Smart Engineering Co., Ltd., Shenzhen 518000, China*

Correspondence should be addressed to Kaizhi Cheng; 20101040114@stu.csust.edu.cn

To effectively diagnose and monitor the vertical collusion in construction project bidding, this paper developed a comprehensive evaluation model with deep neural network and transfer learning. By this model, the collusion characteristics of bidders, tenderers, and bid evaluation experts were mined from limited data set hidden and collusion tendency was evaluated. Firstly, 18 evaluation indicators were established from literature review, court file summarization, typical case analysis, and expert consultation. Then, a comprehensive evaluation model was developed with the deep neural network and transfer learning. Finally, the model was trained and tested with the collected data set. The test results showed that the developed model achieved 87.3% identification accuracy in collusion tendency evaluation of different subjects.

1. Introduction

There are many problems in the process of project construction, especially the collusion phenomenon in the bidding stage [1, 2]. In addition, the collusion in bidding has become more and more prominent due to factors such as information asymmetry, inadequate supervision, imperfect system, and unscientific management [3], and the concealment and non-detectability of the bidding collusion in construction projects are gradually increasing [4].

For the problem of vertical collusion in bidding for construction projects, a lot of research has been conducted by scholars, mainly including: in terms of the motivation of collusion behavior, Aoyagi [5] deduced the equilibrium conditions of collusion between bidders and tenderers and analyzed the distribution of benefits after collusion; Zarkada-Fraser and Skitmore [6] studied the factors influencing bidder collusion based on their psychology, attitude, and behavior when colluding; Pesendorfer [7] stated that the two main ways of tenderer-bidder collusion were compensation and subcontracting; Lugovskyy et al. [8] stated that cooperation experience, reputation, and initiative were the main

factors that lead to collusion between regulators and bidders; Dotoli et al. [9] showed that inadequate government oversight of bidding collusion and low penalty costs led to invalid oversight and occurred collusion; Friedman [10] found that the high rate of return (financial interest) was the underlying motive for collusion by analyzing the causes of collusion. Scholars also found that the psychology of the participants had some influence on collusive bidding [11]; cost asymmetry and unreasonable offers were the "triggers" for collusion [12, 13]. In terms of collusion prevention, Zhang [14] analyzed the possibility of collusion based on the project properties, market environment, collusion costs, and collusion benefits, and also constructed a three-party game model, which showed that reducing regulatory costs, improving regulatory tools, increasing penalties, and benefits for participants can strongly curb collusion; Cavill and Cavill [15] pointed out that strengthening the accountability of the stakeholders involved in bidding, improving their respective responsibilities, and efficiently fulfilling their obligations have important effects on preventing the collusion; Rahman et al. [16] emphasized the importance of maintaining information symmetry, guaranteeing information security,

TABLE 1: Cases of bid conspiracy crimes in China judgements online (partial).

No.	Release date	Case	Case no.	Court name
1	July.7 2020	Tenderers used the convenience of their jobs to illegally accept property from bidders for their benefit.	(2020) No.2 Yue crime	Guangdong high People's court
2	Oct.2 2020	Bidders borrowed the qualifications of other enterprises to obtain qualifications.	(2020) No.53 11E crime	Huanggang intermediate people's court, Hubei province
3	Aug.31 2020	Bidders borrowed qualifications, agreed on bid prices, and participated in bidding.	(2020) No.67 05 Zhe crime	Zhejiang Huzhou intermediate people's court
4	June.28 2019	Tenderers and bidders negotiated on bid prices, programs, and other contents before bidding	(2019) No.2181 supreme court civil	Supreme people's court of the people's republic of China
5	Nov.6 2019	Bidders bribed tenderers in return for bid information before bid publicity.	(2019) No.1507 01 Yue crime	Guangzhou intermediate people's court, Guangdong province
6	Dec.31 2019	Being a member and leader of the bid evaluation committee, the bidder participated in whole process of the evaluation.	(2019) No.5242 supreme court civil	Supreme People's court of the people's republic of China
7	Sep.21 2018	Bid evaluation experts made use of their job convenience to make profit for bidders for illegal properties against bid evaluation regulation.	(2018) No.7 0921 chuan crime	Pengxi county people's court
8	Dec.6 2018	Bidders undertook projects in the form of bidding after obtaining information about bidding in advance from the tenderers.	(2018) No.1055 0103 Hei crime	Harbin Nangang district people's court

and preserving data privacy in the process of against collusion, and proposed the signing of privacy bid agreement as a governance measure; Boone and Mulherin [17] and Ishiguro [18] indicated that the fundamental way to eliminate the occurrence of collusion in bidding was to establish a bidding supervisory body and gave full play to the regulatory role of the acting government, and handled timely for supervision efficiency; Howlader et al. [19] detected vertical collusion in bidding by constructing an SNA network model of individuals, organizations, communities and other participants and achieved good results; Van Den Heuvel [20] deterred bidding stakeholders' willingness to collude by feature analysis of vertical collusion in bidding and trace to the master and follower of bidding combined with genetic algorithm. Scholars also considered the psychology of participants [21] and the probability density function of auction price [22], etc. on collusion prevention.

To sum up, most of the studies on collusion in bidding of construction projects are focused on the analysis of collusion subjects and influencing factors, while the studies on evaluating and determining collusion tendency are relatively rare. In view of the constant change of vertical collusion in bidding for construction projects, more difficulty in collusion detection, unavailability of the evaluating data, deficiency in sample, and complex correlation among indicators, a comprehensive evaluation model of the tendency of vertical collusion in bidding for construction projects was developed based on deep neural network (DNN). Firstly, through literature research, file summarization, case analysis, and expert consultation, 18 evaluation indicators were determined for the tendency of bidders, tenderers, and bid evaluation experts to collude; secondly, a comprehensive evaluation model based on deep neural network was developed, and 130 cases were collected as the training set and test set of DNN model input data; at last, the stable DNN model could effectively evaluate the tendency of vertical collusion in bidding, which can help to prevent vertical collusion targetedly.

2. Methodology

2.1. Data Collection

(1) Literature review: In China National Knowledge Infrastructure (CNKI) and Web of Science (WOS), the keywords "collusion", "bidding collusion", and "bidding corruption" were searched. In order to avoid potential influence from age-old literature, 847 papers in the past 5 years (from 2015 to 2020) were chosen as data samples, including 291 from the general journal, 187 from master or doctor thesis, and 369 from the core and above journals.

(2) Summarization of court files: In the study of bid collusion, court files give sufficient resources of real cases, so it is necessary to make full use of this data source. For its case abundance and authenticity, bid conspiracy registered in China Judgements Online from 2015 to 2020 were researched and summarized in this paper. Table 1 shows some cases of crimes.

(3) Typical case analysis: The typical cases of bidding were searched and summarized from the Chinese government procurement network, Chongqing public resources trading network, and other websites. Table 2 shows some typical examples of collusion on the website.

2.2. Expert Consultation.
By qualitatively analyzing and summarizing the collected collusive data, five experts in the field of bidding in China were consulted on the vertical collusion among the tenderers, bidders, and bid evaluation experts. Table 3 shows the profile of the expert panel. Three specific questions were included. Generalized indicators were extracted by recording and analyzing the original expert responses.

TABLE 2: Bidding collusion cases (partial).

No.	Publishing platform	Collusive practice	Company name
1	https://www.ccgp.gov.cn/	Provide false materials to win bid	XX Co., Ltd.
2	https://ggzyjyjgj.cq.gov.cn/	Bid evaluation experts were inclined to the intended bidders.	XX Co., Ltd.
3	https://www.ccgp.gov.cn/	Bidders provided false materials to meet the tender requirements.	XX Greening Co., Ltd.
4	https://jycg.hubei.gov.cn/	Tenderers used their positions or power to unintentionally or intentionally authorize bid evaluation experts to give high scores to specific bidders.	XX environmental construction Co., Ltd.
5	Other sites	Tenderers broke the rules to facilitate intended bidders	XX consulting Co.

TABLE 3: Profile of the expert panel.

Employer	Position	Years of experience	Largest project ever managed/consulted
Contractor	Project manager	19	RMB ¥ 1.1 billion
Consultant	Deputy manager	16	RMB ¥ 3.5 billion
Academia	Professor	20	RMB ¥ 64 million

Question 1: What do you think are the general manifestations or behaviors of tenderers when they are involved in collusion?

Question 2: Based on the bidders' behavior provided by us, what do you think will the bidders do when they are involved in collusion?

Question 3: In your opinion, what are the main bias practices of bid evaluation experts in bidding activities?

2.3. Deep Neural Network.

The main shallow machine learning models are Support Vector Machines (SVM) [23], boosting models [24], and maximum entropy models [25], etc. The emergence of BP algorithms has effectively promoted the development of deep neural network represented by Multi-Layer Perceptron (MLP) [26]. Compared with shallow machine learning models, deep neural network models are characterized by deep network layers, large number of network model parameters, and strong learning ability, which has triggered a wave of scholars' research in this field. For example, Zhu and Shan [27] established a high-dimensional neural network model to comprehensively evaluate the probability of public engineering project investment risk. Langkvist et al. [28] pointed out that the deep neural network has three advantages: breaking through data limitations, considering complex interactions, and avoiding overfitting problems. Takeuchi and Lee and Ding et al. [29, 30] both used deep neural network to explore the trend of stock price fluctuations, and verified the model through empirical research. Dixon et al. [31] have proven through a large number of cases that deep neural network has the advantages of fusion and analysis of multiple information, thus forming a more effective information set for follow-up research. Pei et al. [32] applied the white box testing framework to the deep neural network system to further improve the performance of the deep learning system. Ma et al. [33] transplanted the mature combined testing technology from traditional software testing to the deep neural network system, during the test, the technology of using combined test coverage to guide the generation of test cases was proposed and achieved good results. Sun et al. [34] proposed a set of relatively complete and systematic test standards based on the characteristics and applicability of deep neural network, which provided strong support for follow-up research, etc. DNN is a neural network model with several hidden layers added, also known as MLP. Among several common structures of deep learning, DNN is superior in strong feature extraction ability, simple model structure, low training difficulty, and fast convergence speed, etc. Considering the problems that the data of the indicators for comprehensive evaluation of vertical collusion in bidding of construction projects are not easy to obtain, insufficient sample size and complex interrelationship, as well as the characteristics and requirements of comprehensive evaluation of tendency of vertical collusion, this study used DNN model to conduct the comprehensive evaluation.

2.3.1. Structure of DNN.

Deep neural network generally consists of an input layer, a number of hidden layers, and an output layer (as shown in Figure 1), and the layers are fully connected to each other, i.e., any neuron in layer i must be connected to any neuron in layer $i + 1$. In terms of the small local model, the data in DNN, same as perceptron's, is transferred among different neurons by linear function $z = \sum w_i x_i + b$ and function $\sigma(z)$, where xi represents the input from the ith neuron, w_i is the connection weight of the ith neuron, and b represents the offset, and the learning process of the neural network is essential to continuously adjust the connection weights and neuron offsets between the neurons to get closer to the output of the training samples.

2.3.2. Application of DNN.

The training and testing process of deep neural network includes training, determining parameters, testing, and checking network accuracy (as in Figure 2).
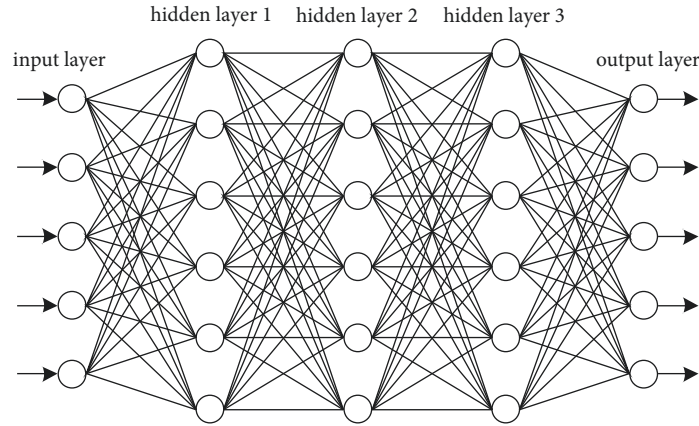
FIGURE 1: DNN basic structure.
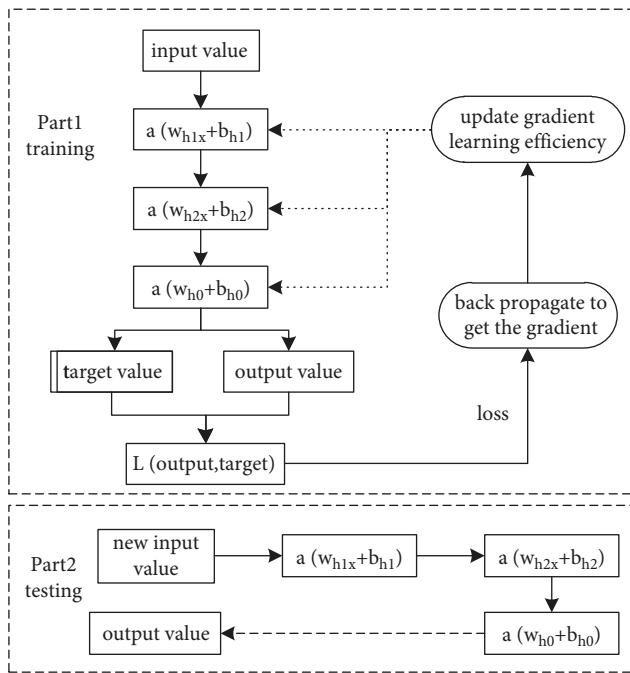
FIGURE 2: DNN basic implementation process.

FIGURE 3: Research flow.

2.4. Research Flow. Specific to small data set, this paper developed the model by employing DNN method and transfer learning algorithm, in which the obtained tendency evaluation value of tenderers, bidders, and bid evaluation experts were as input. Transfer learning can apply the knowledge learned in a domain or a task to another domain or task. Given a source domain Ds and a learning task Ts in the source domain, a target domain Dt and the corresponding learning task Tt, the goal of transfer learning is to use the knowledge in Ds and Ts to complete the task Tt in Dt. This method can be used when there is insufficient data. Combining the transfer learning with deep neural network can reduce the sample size requirement of DNN model, so as to adapt to the small dataset of vertical collusion in bidding in order to obtain a high comprehensive evaluation accuracy. The flow of the developed evaluation model is shown in Figure 3.
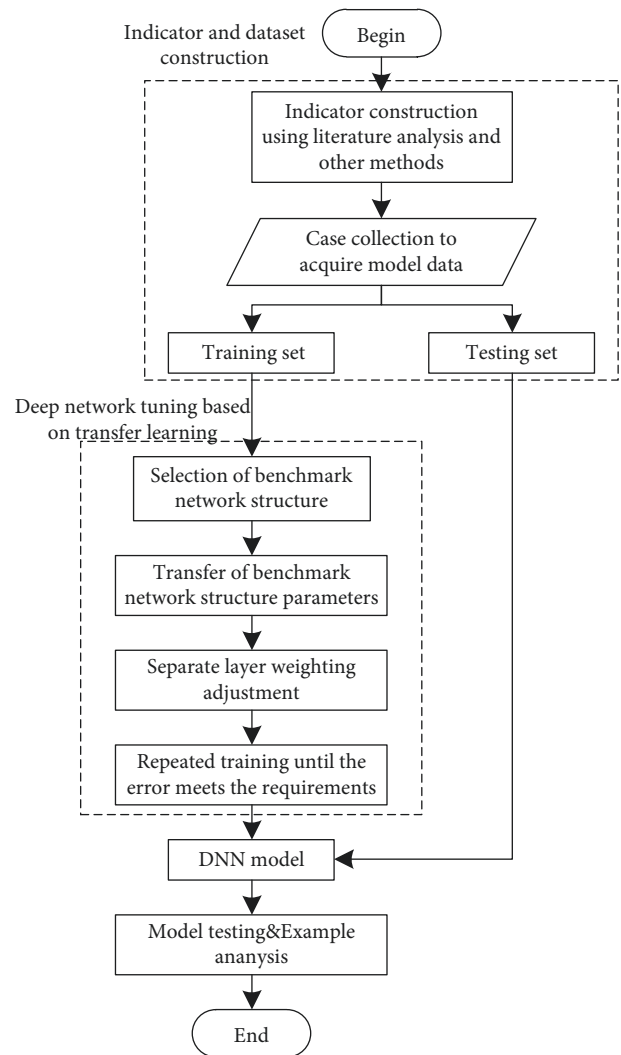
3. Results

Based on the keywords in literature, collusion in typical cases, and the causes in the court files, the frequency of collusion of bidders and tenderers is plotted as shown in Figure 4.
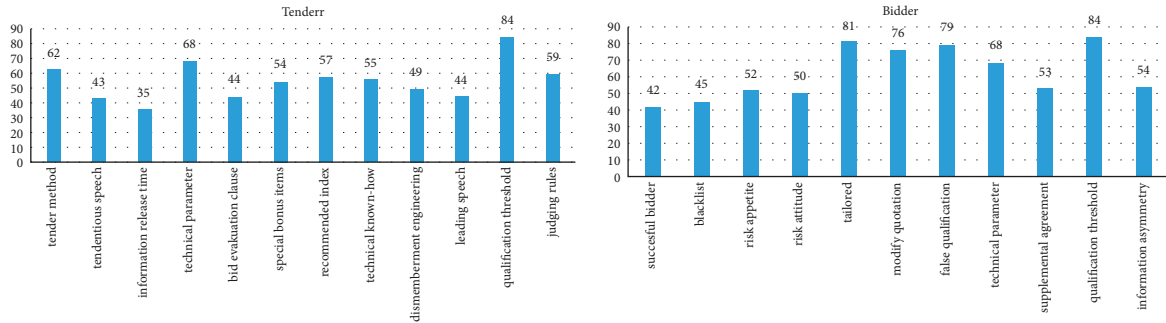
Figure 4: Indicator frequency of tenderers and bidders' collusion.

Based on the collected keywords of collusive practices of bidders and tenderers, the three questions were interviewed to experts and their original judgment was recorded. Grounded on the collated expert consultation results, indicators and explanations were reached for evaluating actors in construction projects bids, shown in Table 4. The range of model input values for all indicators was [1, 10].

4. Development of the DNN Model

4.1. Data input. In this study, a total of 130 cases were collected (due to the large number of participants, only the data of the top 5 bidders were obtained for each case), and divided into two parts: training samples and testing samples. In terms of the ratio of training and test sample settings, Zhang and Zhao [35] set 90% as the training set and 10% as the test set when building a neural network model of user Q&A-related variables and monthly sales of clothing; Wen et al. [36] randomly divided the data into 80% of the training set and 20% of the test set when building a neural network with effective wave height inversion set; Ding et al. [37] used the improved lion swarm algorithm to optimize the neural network model for the housing price prediction problem by using the first 70% of the data samples as training samples and the last 30% as test samples, etc. In view of the concealment of vertical collusion in bidding, the correlation among monitoring indicators and the difficulty in obtaining indicator data, this study took about 60% training samples and about 40% test samples, i.e., 75 training samples (former 60 collusive cases and latter 15 non-collusive cases) and 55 test samples (former 40 collusive cases and rest 15 normal cases) (see Table 5).

4.2. Transfer Learning. A parameter-based transfer learning approach was used in this study, on the premise that some parameters or prior distributions were shared between the source and target tasks model. The algorithm achieved knowledge transfer by finding these shared parameters or prior distributions and processing them. The unique advantages of transfer learning have caused widespread application by scholars: Liao et al. and Liu et al. [38, 39] used the transfer learning algorithm to complete the text detection task and the edge detection task on the basis of the visual geometric group network structure; Wu et al. [40] used the transfer learning algorithm to control the ship name

identification, and considerable test results were obtained. Considering the concealment of vertical collusion in bidding and the complex relationship between indicators, the study improved the model with the help of parameter transfer algorithm, aiming to improve the accuracy of vertical collusion evaluation.

In the tendency evaluation analysis, Hu [41] studied electricity consumption characteristics and constructed a tracking monitoring model for electricity theft users with the help of improved BP neural network to conduct deep monitoring of electricity users. The main reasons for using this model as a transfer learning source were: (1) the similarity of electricity consumption characteristics and vertical collusion evaluation indicators as source domains; (2) the outputs of the two models are basically the same, one is the theft suspicion coefficient, and the other is the tendency of vertical collusion; (3) the indicator data is readily available from inner system of an electric power company, where the electricity consumption data is abundant and easily accessible; hereafter, the specific process of the comprehensive evaluation model based on transfer learning algorithm in this study, see Figure 5.

Among them, the fine-tuning method of the model was as follows: the relevant parameters of the source model were transferred to the target model; the weights of some layers were fixed to adjust the weights of other layers, and the process was repeated until the error between the output value of the model and the actual value meets the requirements; at this time, the optimal weights between layers were obtained. Suppose there were P samples to train, where X_{pi} = the ith input value of p, n, q, m = the respective number of nodes in each layer, V_{ki} = the weight from node i in the input layer to node k in the hidden layer, w_{jk} = the weight from node k in the hidden layer to node j in the output layer, and the activation function was the sigmoid function. The forward input process of this model network is as follows.

The output from input layer to the hidden layer is

$$Z_{pk} = g(\text{net}_{pk}),$$
$$= g\left(\sum_{i=0}^{n} v_{ki} - x_{ki} + \theta_k\right), \quad k = 0, 1, 2, \ldots, q. \tag{1}$$

The output from the hidden layer to the output layer is

TABLE 4: Comprehensive evaluation indicator system.

Subjects	Indicators	Indicator description
Tenderer	Valid bid ratio X_{11}	The ratio of valid bids to total bids. The range of value is 0–100%. The tenderer, on purpose of boosting cooperative bidder's success rate, may reduce the valid bid rate in some way to let the activity less competitive.
	Selection of tendering method X_{12}	Dismemberment (unreasonable) or normal bidding activities (reasonable). One is to split project to evade due tender procedure, and the other is to set specific conditions to change the public tender to invited tender, awarding "benefits" to collusive bidders.
	Tenderers convey tendentious information X_{13}	Yes or no. The tenderers pass project-related information to collusive bidders or persuade other bid evaluation experts privately to make the related enterprise win the bid.
	Release timeliness of bidding information X_{14}	Some tenderers may change the tender release time for collusive bidders' consideration, resulting in information not accessible simultaneously to advance winning rate.
	Setting reasonability of technical parameter X_{15}	Some unreasonable arrangements, for instance, changing range value to specific value, may be done towards to bidders by tenderers.
	Tendency of tender requirements X_{16}	Tenderers may require previous business contacts such as construction performance or similar project experience as tender premise to preclude other participants.
	Extra credit bias X_{17}	Tenderers may set unreasonable qualification conditions such as the size of registered capital, geography, years of operation, and employees in bid preparation as a way to increase the evaluation score of collusive bidders.
	Rationality of evaluation setting X_{18}	Normally evaluation in bid documents should be made in regard to actual project situation, past experience, and relevant regulations, practically the tenderers may set inclined standard and unscientific weight to favor collusive bidders.
Bidder	Bid winning rate X_{21}	The residual difference indicator is examined. When the residual difference between the actual and predicted winning bids falls outside a certain interval, it indicates that the bidder has a tendency to collude with the tenderers partly.
	Special requirements compliance X_{22}	The conformity of unreasonable conditions such as the scale of registered capital, geographical area, years of operation, and employees in tender.
	Reassessment rate X_{23}	The value range is 0–100%. When the supervisory authority finds that the bidder's conditions are consistent with the evaluation factors listed in the agreements or that the bidder has unreasonable practices, it will ask the experts to re-evaluate.
	Authenticity of bidding materials X_{24}	Yes or no. During the review of the bidders' materials, the tenderers may know the materials have problems but keep silent, and then tacit collusion of both sides occurs.
	Similarity of technical bid parameters X_{25}	The value range is 0–100%. The technical content similarity between tender party and bidder party, expressed as the overlapping content accounting for the total technical content.
	Fitness to business documents X_{26}	The value range is 0–100%. The degree of business conformity (such as project performance, and enterprise qualification) specified in tender documents, expressed as similar content accounting for total content of the business bid.
	Type of bidder risk appetite X_{27}	Aggressive, positive, balanced, robust, and conservative. Risk appetite has a significant positive effect on the tendency of collusion, and aggressive risk appetite further stimulates the occurrence of collusive practices.
	Degree of mastery of key project information X_{28}	The tenderers may deliberately conceal key information about the project and only let collusive bidders know the information to ensure their dominance in the bid evaluation process.
Bid evaluation expert	Deviation of expert score X_{31}	The deviation range is examined. There are horizontal deviation and vertical deviation. The experts may be suspicious of collusion when two deviations exceed the range ($\pm 10\% \sim \pm 20\%$).
	Reward strength of bid evaluation X_{32}	The strength of rewards for bid evaluation experts largely reflects whether experts adopt collusive practice, and the greater the strength of rewards based on previous good evaluations, the less likelihood experts' collusion will occur.
	Rigor of bid evaluation process X_{33}	In the bid evaluation process, the experts select the team leader randomly; the experts are guided by the tenderer's comments and actions and do not question the bid evaluation methods or the experts make targeted remarks.
	Expert type X_{34}	Randomly selective experts are tested on personality and psychological scales, and then define according to results as 4 types: Capricious, ambitious without knowledge, independent, and opinion leader, with sequence of decrease in collusion.

TABLE 5: Data set classification.

Sample type	Quantity (abnormal & normal)
Training sample	75 (60 + 15)
Test sample	55 (40 + 15)
Total	130

$$Y_{pk} = g(\text{net}_{pj}),$$
$$= g\left(\sum_{k=0}^{q} w_{jk} z_{pk} + \theta_j\right), \quad k = 0, 1, 2, \ldots, m. \tag{2}$$

The total model error is

$$E = \sum_{p=1}^{P} E_p,$$
$$= \frac{1}{2} \sum_{p=1}^{P} \sum_{j=1}^{m} (t_{pj} - y_{pj})^2. \tag{3}$$

where E_p = the sample error, t_{pj} = the expected output, and y_{pj} = the model output.

The inverse process uses the gradient descent method to adjust the weight values, and the calculation process is as follows.

The weights between layers are updated as follows:

$$\Delta w_{jk} = -\eta \frac{\partial E}{\partial w_{jk}},$$
$$= \eta \sum_{p=1}^{P} \left(-\frac{\partial E_p}{\partial w_{jk}}\right), \tag{4}$$
$$= \eta \sum_{p=1}^{P} \left(-\frac{\partial E_p}{\partial \text{net}_{pj}} \cdot \frac{\partial \text{net}_{pj}}{\partial w_{jk}}\right).$$

where η = the learning rate.

The output layer error is

$$\delta_{pj} = -\frac{\partial E_p}{\partial \text{net}_{pj}},$$
$$= -\frac{\partial E_p}{\partial y_{pj}} \cdot \frac{\partial E_{pj}}{\partial \text{net}_{pj}}. \tag{5}$$

The hidden layer node weights are updated as:

$$\Delta v_{ki} = -\eta \frac{\partial E}{\partial v_{ki}},$$
$$= \eta \sum_{p=1}^{P} \left(-\frac{\partial E}{\partial v_{ki}}\right), \tag{6}$$
$$= \eta \sum_{p=1}^{P} \left(-\frac{\partial E_p}{\partial \text{net}_{pk}} \cdot \frac{\partial \text{net}_{pk}}{\partial w_{ki}}\right).$$

The hidden layer error is

$$\delta = -\frac{\partial E_p}{\partial \text{net}_{pk}},$$
$$= -\frac{\partial E_p}{\partial z_{pk}} \cdot \frac{\partial z_{pk}}{\partial z_{pk}}. \tag{7}$$

4.3. Training and Testing of Network

4.3.1. Transfer of the Benchmark Network Structure. In this study, the configuration 10-6-1(number of inputs-number of hidden layer neurons-number of output) of DNN model for tracking and monitoring electricity theft users was used as the benchmark network structure based on the transfer learning algorithm to develop a DNN model for comprehensive evaluation [41], and the benchmark network parameters are shown in Table 6.

4.3.2. Optimization and Training. For the characteristics of the evaluation of bidding vertical collusion tendency, the transferred benchmark network was debugged in this study, specifically: considering the small sample size of the evaluation indicators of the participants in the vertical collusion and the data correlation is more complicated, increased network dimensions, and adjusted the number of neurons. The compact network structure is conducive to get the optimal conclusion through less training data. Due to the difference in collusion evaluation indicators among bidders, tenderers, and bid evaluation experts, two different network structures were designed to match the comprehensive evaluation; the configuration of tenderer & bidder network. The training parameters of DNN-based comprehensive evaluation model for bidders, tenderers, and bid evaluation experts are finally determined in Table 7.

Specifically, the mean squared error MSE was generally chosen as loss function for the training of DNN models, as shown in the following equation.

$$\text{MSE} = \frac{1}{mp} \sum_{r=1}^{p} \sum_{j=1}^{m} (\hat{y}_{rj} - y_{rj})^2, \tag{8}$$

where m = the number of output nodes, $\hat{y}_{rj}$ = the expected output value of the network, p = the number of training samples, and y_{rj} = the actual output of the network. Sigmoid, the activation function of hidden layer and output layer, also functioned as threshold function of neural network, mapped its variables to interval from 0 to 1 with input interval whole real number and output internal [0, 1], satisfying the designed need for comprehensive vertical collusive evaluation. The expression of the sigmoid function is shown in the following equation.

$$f(x) = \frac{1}{1 + e^{-x}}. \tag{9}$$
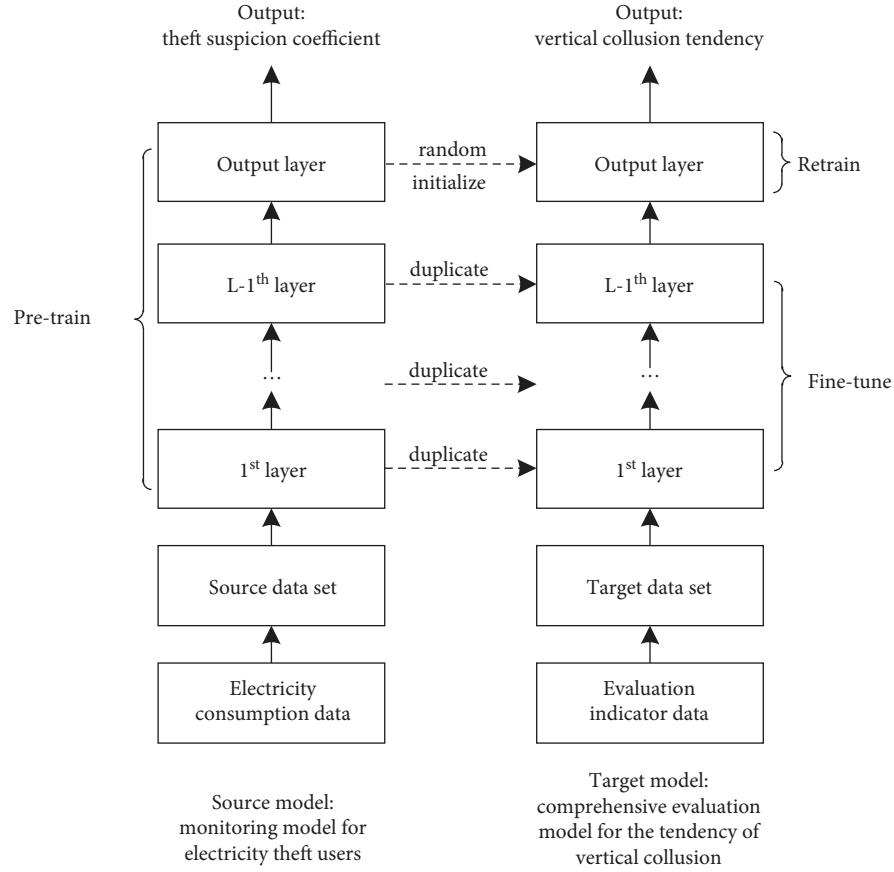
FIGURE 5: Parameter transfer process.

TABLE 6: Training parameters of the Benchmark network.

Parameter	Value
Configuration	[10, 6, 1]
Number of layer (n)	3
Activation function of hidden layer	Sigmoid
Learning rate	0.02
Loss function	Mean squared error (MSE)
Iteration	2000
Output layer activation function	Sigmoid

TABLE 7: Training parameters of the developed DNN model.

Parameter	Value	
Configuration	Tenderer&Bidder	[8, 4, 2, 1]
	Expert	[4, 2, 1]
Number of layer (n)	Tenderer&Bidder	4
	Expert	3
Activation function of hidden layer	Sigmoid	
Learning rate	0.5	
Loss function	MSE	
Iteration	2000	
Output layer activation function	Sigmoid	

According to the training results, the configuration of the developed model is obtained as shown in Figure 6.

In this study, the Python 3.9 code was implemented for model training, and the output target value of collusion case was set as any value in [0.3, 1] and the output target value of normal case was set as any value in [0, 0.3] during training [42].

In the tenderer and bidder network structure, the input layer was the value of the vertical collusion indicator of tenderer and bidder, value range [1, 10], input randomly based on actual situation; the hidden layer, the optimal number determined by constant adjustment, was 2 layers with 4 and 2 neurons, respectively; the output layer was any value in tenderer and bidder collusion tendency interval (0, 1). In addition, in movement of twice dimension reduction in achievement of higher accuracy for tendency evaluation, the weight distribution matrices were matrix 8×4 and 4×2, respectively. In the 3rd dimension degradation, the weight distribution matrix from $L3$ to $L4$ was matrix 2×1 with [0.169, −0.317] in tender network and matrix 2×1 with [0.404, 0.827] in bidder network.

Since there were only 4 indicators for evaluating the collusion behavior of bid evaluation experts, this paper adjusted the dimensions of the comprehensive evaluation DNN network towards experts referring to the DNN network for tenderers and bidders. In the bid evaluation expert network structure, the input layer was the value of the bid evaluation expert vertical collusion indicators, value range [1, 10], input randomly based on actual situation; the hidden layer, the optimal number determined by constant adjustment, was 1 layer with 2 neurons; the output layer was any value in bid expert collusion tendency interval (0, 1). In
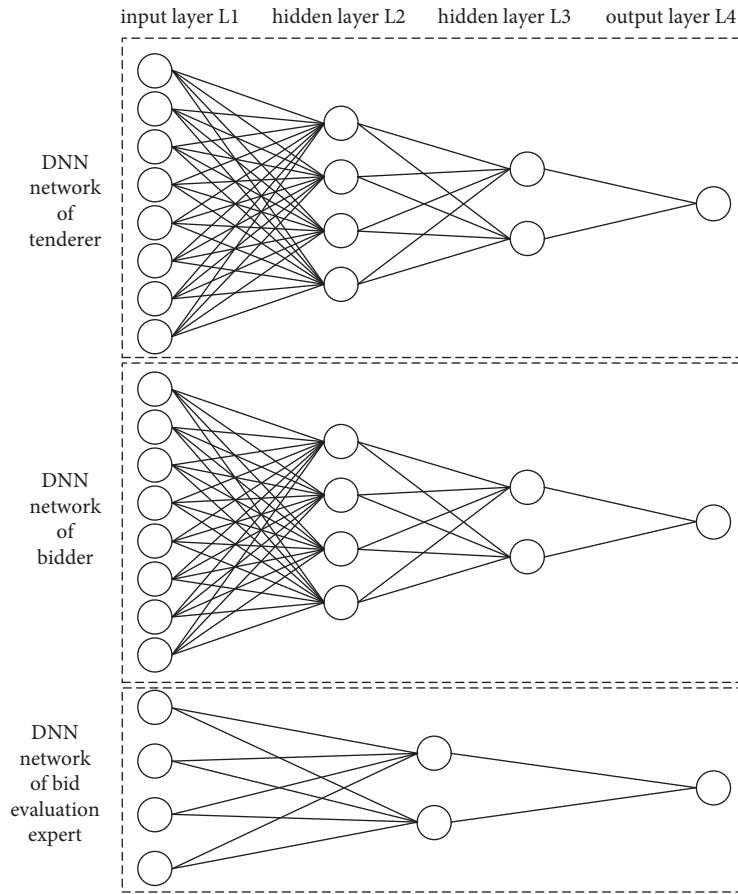
FIGURE 6: Configuration of the developed model.

reach of high accuracy for comprehensive tendency evaluation model in bid evaluation expert's party, the weight distribution matrix in first dimension reduction was matrix 4×2, the second dimension, namely, from $L2$ to $L3$, was matrix 2×1 with [0.044, 0.075].

4.3.3. Gradient Descent of the Error.

Since the loss function used in the model was the minimized loss function, the model output error could be solved by gradient descent algorithm. In this study, the number of iterations was set to 2000 when training the developed model, and it was found that the mean square error of training samples was close to 0 (see Figure 7). Thus, the final determined network parameters and weight distribution matrix could reflect that the developed model was regarded as reliable. In this study, in order to alleviate or avoid the problem of overtraining, an early termination algorithm was carried to mitigate overfitting, i.e., the training was terminated as soon as the overfitting trend of the model was detected.

4.3.4. Testing.

The test was conducted using the aforementioned 55 test samples, and the results are shown in Table 8. The experimental results showed that the developed model predicted 48 correct and 7 incorrect, with a comprehensive accuracy of 87.3%, which was high, further
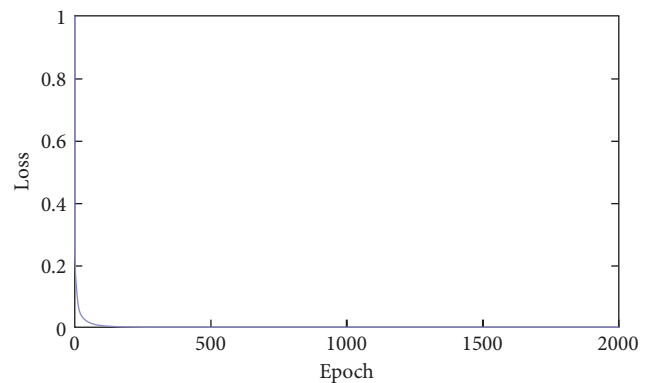
FIGURE 7: Training effect.

TABLE 8: Accuracy of model test results.

Case collusion type	Total	Incorrect number	Correct rate (%)
Tenderer & bidder & expert	11	2	81.82
Tenderer & bidder	21	2	90.48
Bidder & expert	8	0	100
Normal	15	3	80

TABLE 9: Collusion evaluation level.

Participate	Evaluation levels and collusion tendency intervals			
Tenderer	Stronger [0.84, 1]	Strong [0.39, 0.84)	Weak [0.23, 0.39)	Weaker [0, 0.23)
Bidder	Stronger [0.76, 1]	Strong [0.30, 0.76)	Weak [0.23, 0.30)	Weaker [0, 0.23)
Expert	Stronger [0.85, 1]	Strong [0.50, 0.85)	Weak [0.25, 0.50)	Weaker [0, 0.25)

TABLE 10: Inputs for the model (3 regulatory experts).

Indicator	X_{11}	X_{12}	X_{13}	X_{14}	X_{15}	X_{16}	X_{17}	X_{18}
Tenderer	5, 5, 5	3, 4, 3	7, 7, 8	4, 5, 5	8, 7, 8	8, 7, 7	6, 5, 6	8, 8, 7
Indicator	X_{21}	X_{22}	X_{23}	X_{24}	X_{25}	X_{26}	X_{27}	X_{28}
Bidder $A1$	3, 3, 4	8, 7, 7	1, 1, 1	1, 2, 2	9, 9, 9	8, 8, 8	6, 6, 6	6, 5, 5
Bidder $A2$	3, 3, 3	8, 7, 8	1, 1, 1	2, 1, 1	8, 8, 8	7, 7, 7	5, 5, 5	6, 5, 6
Bidder $A3$	3, 3, 3	6, 5, 4	1, 1, 1	1, 2, 1	5, 5, 5	4, 4, 4	4, 4, 4	6, 6, 5
Bidder A4	2, 2, 2	6, 5, 5	1, 1, 1	1, 1, 1	4, 4, 4	4, 4, 4	4, 4, 4	4, 3, 3
Indicator	X_{31}		X_{32}		X_{33}		X_{34}	
Expert	7, 8, 7		4, 3, 5		8, 7, 8		6, 6, 7	

indicating that the model could be regarded as reliable and accurate.

5. Model Application and Discussion

5.1. Background. In bid evaluation of a provincial highway mainline site construction project, the expert panel finally locked 4 candidates, in the order of $A1$, $A2$, $A3$, and $A4$. The project department determined the first and the second winning candidates according to the number of labor teams to be recruited and the recommended order of winning candidates.

Combined with the obtained evaluating indicators of the tenderers, bidders, and bid evaluation experts, the following improper practices were found in the bidding activity after repeated review and continuous retroactive tracking of the indicators by the government supervisory department: (1) in the process of preparing bidding documents, the tenderers added "special technology", and "enterprise qualification", and the scoring criteria and scoring indicators in bid evaluation part were unreasonable; (2) in the bidding process of $A1$, the tenderer leaked relevant bidding information to the enterprise before bidding announcement, what was more, the tenderer used his position to inform the enterprise of important information about the required materials; (3) during the bidding process of $A2$, the tenderer set "limited number system" pre-qualification conditions for him; selected the bid evaluation experts at his will, and finally designated his next bid evaluation experts by the enterprise; (4) $A3$ and $A4$ participated in the bidding in accordance with normal procedures, and no abnormalities were found in the indicators; (5) during bid evaluation, the bid evaluation team deliberately gave $A2$ high score at tenderer's instruction, and made obvious tendentious remarks.

5.2. Comprehensive Evaluation of the Tendency of Vertical Collusion. Wu [42] established a model for measuring the strength of the tendency of bidders and tenderers to collude based on evidence-based reasoning approach, and concluded

that the strength level could be divided into weaker (0–0.3), weak (0.3–0.5), strong (0.5–0.8), and stronger (0.8–1), and the strong level reflect the existence of collusion between the two parties. Through comparative analysis, in this case, the collusion evaluation level is as shown in Table 9, which provides some theoretical reference significance for the comprehensive evaluating level of the tendency of collusion of the model output value.

The input values of the model are shown in Table 10, each caught by three regulatory experts' investigating and tracking indicators of the tenderer, 4 bidders, and bid evaluation experts.

The above three sets of values were applied to the developed model and run in Python 3.9, respectively, and the results are shown in Table 11.

Based on the output results, we could get that there was a high probability of collusion in the bidding activity, and the colluding subjects were the tenderers, $A1$ bidder, $A2$ bidder, and bid evaluation experts.

5.3. Discussion. Based on the tendency indicators of vertical collusion in bidding and the comprehensive tendency model of vertical collusion, four types of prevention suggestions for vertical collusion in bidding can be put forward, namely, routine prevention, early warning prevention, moderate prevention, and severe prevention.

(1) Routine prevention faces the situation that the actors are labeled weaker with the developed model. Preventive measures are mainly routine check, irregular check, special check, and emphasized check to materials and practices of the body of tenderer, bidder, and bid evaluation expert in the implementation process.

(2) Early warning prevention suits for monitoring the weak assessed by the developed model, and the preventive measures are mainly to monitor the whole process of bidding activities dynamically, compare bidding data at multiple levels, and review

TABLE 11: Output values of the model (3 regulatory experts).

Output	Tenderer	Bidder $A1$	Bidder $A2$	Bidder $A3$	Bidder $A4$	Bid evaluation expert
Expert 1	0.8559	0.8083	0.7053	0.2019	0.2456	0.7997
Expert 2	0.8553	0.8089	0.7055	0.2023	0.2458	0.8001
Expert 3	0.8562	0.8091	0.7049	0.2020	0.2451	0.7998

bidding problems in all aspects with the help of intelligent technologies such as 5 G communication network, Internet of Things, and cloud computing. At the same time, the blockchain multi-point storage technology for data confidentiality management, identification system to strengthen expert management and other intelligent technologies can combine to guarantee the whole process, multi-level and all-around strict review of bids, judges, evaluation, and management of bidding activities in construction projects.

(3) Moderate prevention applies to those scored strong doers evaluated by the developed model, and the preventive measures mainly include the implementation of commitment system, joint and several penalty system and heavy fine system. In addition, giving full play to the advantages of trading platform facilities and resources and real-time interaction of network information, it is suggested that the relevant supervisory department and government legal department should reasonably reorganize the business process to effectively prevent collusion in construction bidding.

(4) Severe prevention adapts to the stronger participants marked by the developed model, and the preventive measures mainly include introducing social credit code system and weaving a detailed and sound credit record system for those bidding-related parties. With this system, any relevant activities are always observed, recorded, and exposed on the designated platform haunting psychology of daring not collusion. Moreover, expending supervision role of public service and third party, constantly innovating supervisory ideas, improving supervisory methods, and maintaining supervisory concepts, all are organically bonded to a systematic supervision mechanism to monitor the whole stage of bidding.

6. Conclusions

This study developed a deep neural network model for comprehensive evaluation of the tendency of vertical collusion with the help of transfer learning, subdivided to 4-layer model (8-4-2-1) for tenders, 4-layer model (8-4-2-1) for bidders, and 3-layer model (4-2-1) for bid evaluation experts. The collected 130 cases were trained and tested to the established DNN model, and the result of 87.3% accuracy said the model was reliable. Depending on comprehensive evaluation results of the model, four types of collusion prevention suggestions are proposed: routine, early warning, moderate, and severe. The specific measures for routine

prevention include routine check, irregular check, special check, and emphasized check; early warning prevention include strengthening the audit strength of participating parties, improving the transparency of bidding activities, and popularizing intelligent technology; the moderate prevention are mainly implementing the commitment system, strengthening the public reporting channels, and improving electronic bidding; the severe prevention falls on temporary inclusion in blacklist, encouraging joint departmental supervision, and establishing a new regulatory mechanism bridging the whole bidding process. The comprehensive evaluation model of tendency of vertical collusion behavior developed in this study has some reference value for the standardization of bidding market in China and other countries.

Since the comprehensive evaluation executed in this study needs to fully consider various factors, the study needs to be further explored and improved, mainly in the following two aspects: on one hand, the differences in corporate culture and local customs have not been taken into account when obtaining the comprehensive evaluation indicators, which need to be considered in future research; on the other hand, there is some subjectivity in data collection by using expert consultation as input value, thus subsequent collection means of evaluation data waits for deep exploration to be close to actual situation.

Data Availability

The data used to support the findings of this study are available from the corresponding author upon request.

Conflicts of Interest

The authors declare that they have no conflicts of interest.

Acknowledgments

References

[1] Y. Wang, "Analysis of project management problems and countermeasures of China's government investment projects," *Rural Economy and Technology*, vol. 27, pp. 100-101, 2016.

[2] R. Messick, *Curbing Fraud, Corruption, and Collusion in the Roads sector*, The World Bank Group, Washington DC, 2011.

[3] Y. K. Kim and J. Kim, "Optimal collusion-proof auctions," *Journal of Economic Theory*, vol. 144, no. 2, pp. 565–603, 2009.

[4] Y. Chen, M. L. Chen, and J. Li, "Collusion behavior analysis of tenderers and bidders of government-invested project based on group cases method," *Transportation Enterprise Management*, vol. 34, pp. 92–95, 2019.

[5] M. Aoyagi, "Bid rotation and collusion in repeated auctions," *Journal of Economic Theory*, vol. 112, no. 1, pp. 79–105, 2003.

[6] A. Zarkada-Fraser and M. Skitmore, "Decisions with moral content: collusion," *Construction Management & Economics*, vol. 18, no. 1, pp. 101–111, 2000.

[7] M. Pesendorfer, "A study of collusion in first-price auctions," *The Review of Economic Studies*, vol. 67, no. 3, pp. 381–411, 2000.

[8] V. Lugovskyy, D. Tucker, and S. Tucker, "An experimental investigation of overdissipation in the all pay auction," *European Economic Review*, vol. 54, no. 8, pp. 974–997, 2010.

[9] M. Dotoli, N. Epicoco, M. Falagario, F. Costantino, and N. Costantino, "A Nash equilibrium simulation model for the competitiveness evaluation of the auction based day ahead electricity market," *Computers in Industry*, vol. 65, no. 4, pp. 774–785, 2014.

[10] L. Friedman, "A competitive-bidding strategy," *Operations Research*, vol. 4, no. 1, pp. 104–112, 1956.

[11] D. S. Ni and X. Guan, "Governance of bid-rigging in the bidding," in *Proceedings of the 19th International Conference on Industrial Engineering and Engineering Management*, pp. 1213–1221, Springer, Berlin, Heidelberg, 2013.

[12] J. Miklós-Thal, "Optimal collusion under cost asymmetry," *Economic Theory*, vol. 46, no. 1, pp. 99–125, 2011.

[13] P. Ballesteros-Pérez, M. Skitmore, R. Das, and M. L. del Campo-Hitschfeld, "Quick abnormal-bid-detection method for construction contract auctions," *Journal of Construction Engineering and Management*, vol. 141, no. 7, pp. 1–11, 2015.

[14] C. Zhang, "Game analysis of collusion and supervision between agents and contractors of government investment projects," *Journal of Jiaxing University*, vol. 23, pp. 74–79, 2011.

[15] M. Cavill and S. Cavill, "Accountability to prevent corruption in construction projects," *Journal of Construction Engineering and Management*, vol. 134, no. 9, pp. 729–738, 2008.

[16] M. S. Rahman, A. Basu, S. Bhuiyan, and M. Z. A. Bhuiyan, "Privacy-friendly secure bidding for smart grid demand-response," *Information Sciences*, vol. 379, pp. 229–240, 2017.

[17] A. L. Boone and J. H. Mulherin, "Do private equity consortiums facilitate collusion in takeover bidding?" *Journal of Corporate Finance*, vol. 17, no. 5, pp. 1475–1495, 2011.

[18] S. Ishiguro, "Collusion and discrimination in organizations," *Journal of Economic Theory*, vol. 116, no. 2, pp. 357–369, 2004.

[19] J. Howlader, A. Pal, and T. D. Pal, "Secure receipt-free sealed-bid electronic auction," *Communications in Computer and Information Science*, vol. 40, pp. 228–239, 2009.

[20] G. Van Den Heuvel, "The parliamentary enquiry on fraud in the Dutch construction industry collusion as concept between corruption and state-corporate crime," *Crime, Law and Social Change*, vol. 44, no. 2, pp. 133–151, 2006.

[21] K. Daniel and T. Amos, "Choices, values, and frames," *American Psychologist*, vol. 39, pp. 44–65, 1984.

[22] L. Weinschelbaum and F. Weinschelbaum, "The effect of corruption on bidding behavior in first-price auctions," *European Economic Review*, vol. 53, no. 6, pp. 645–657, 2009.

[23] A. Urtubia, R. León, and M. Vargas, "Identification of chemical markers to detect abnormal wine fermentation using support vector machines," *Computers & Chemical Engineering*, vol. 145, Article ID 8, 2021.

[24] R. Rousseau and P. Rousseau, "An enhanced model of particle radiation properties in high ash gas-particle dispersion flow through industrial gas-to-steam heat exchangers," *Fuel*, vol. 285, Article ID 119153, 2021.

[25] J. Jin, C. Mi, W. Xu, Q. Wang, and H. Wei, "Grey relational maximum entropy weight model considering expert judgment information," *Chinese Management Science*, vol. 20, pp. 135–143, 2012.

[26] C. Qiu, X. Wu, Z. Luo et al., "Simultaneous inverse design continuous and discrete parameters of nanophotonic structures via back-propagation inverse neural network," *Optics Communications*, vol. 483, Article ID 126641, 2021.

[27] W. Zhu and M. Shan, "Neural network method for risk evaluation of public engineering projects," *Journal of Harbin Engineering University*, vol. 27, pp. 142–146, 2006.

[28] M. Längkvist, L. Loutfi, and A. Loutfi, "A review of unsupervised feature learning and deep learning for time-series modeling," *Pattern Recognition Letters*, vol. 42, pp. 11–24, 2014.

[29] L. Takeuchi and Y. Y. A. Lee, *Applying Deep Learning to Enhance Momentum Trading Strategies in Stocks*, Stanford University, Technical Report. Stanford, CA, USA, 2013.

[30] X. Ding, Y. Hang, T. Liu, and J. Duan, "Deep learning for event-driven stock prediction," in *Proceedings of the 24th International Conference on Artificial Intelligence*, pp. 2327–2333, AAAI, California, USA, 2015.

[31] M. Dixon, D. Klabjan, and J. H. Bang, "Implementing deep neural networks for financial market prediction on the Intel Xeon Phi," in *Proceedings of the WHPCF 2015: 8th Workshop on High Performance Computational Finance - Held in Conjunction with SC 2015: The International Conference for High Performance Computing, Networking, Storage and Analysis*, 2015.

[32] K. Pei, Y. Cao, J. Jana, and S. Jana, "DeepXplore," *GetMobile: Mobile Computing & Communications*, vol. 22, no. 3, pp. 36–38, 2019.

[33] L. Ma, F. Zhang, and M. Xue, *Combinatorial Testing for Deep Learning Systems*, arXiv:1806.07723, 2018.

[34] Y. Sun, X. Huang, and D. Kroening, *Testing Deep Neural Networks*, arXiv:1803.04792, 2018.

[35] Y. Zhang and P. Zhao, "Influence of user questions and answers based on BP neural network on monthly sales of clothing products," *Silk*, vol. 58, pp. 70–75, 2021.

[36] B. Wen, W. Tang, and Y. Tian, "Retrieval of effective wave height field of high frequency radar based on BP neural network," *Journal of Huazhong University of Science and Technology (Nature Science Edition)*, vol. 49, pp. 114–119, 2021.

[37] Y. Ding, M. Wang, J. Li, P. Li, Z. Guo, and Y Chen, "Characterization of a 3-hydroxyanthranilic acid 6-hydroxylase involved in paulomycin biosynthesis," *Biochemical and Biophysical Research Communications*, vol. 543, pp. 8–14, 2021.

[38] M. Liao, B. Shi, and X. Bai, *Text Boxes: A Fast Text Detector with a Single Deep Neural Network*, vol. 46, pp. 4161–4167, AAAI, California, USA, 2017.

[39] Y. Liu, M. M. Cheng, X. Bian et al., "Richer convolutional features for edge detection," *IEEE Transactions on Pattern Analysis and Machine Intelligence*, vol. 41, no. 8, pp. 1939–1946, 2019.

[40] S. Wu, B. Liu, and S. Xu, "A two-stage ship plate location algorithm combining deep feature transfer and fusion," *Journal of Computer Aided Design and Graphics*, vol. 32, pp. 628–634, 2020.

[41] M. Hu, *Research on User Behavior Characteristic Analysis and Electric Stealing Identification Method Based on Electric Power Marketing Data*, Shandong University, Shandong, China, 2020.

[42] C. Wu, *Research on the Intensity Calculation of the Collusion Tendency between the Tenderer and the Bidder in the Government Investment Projects*, Changsha University of Science and Technology, Hunan, China, 2018.

Research Article

Dematel-ISM-Based Study of the Impact of Safety Factors on Urban Rail Tunnel Construction Projects

Liang Ou [iD]**, Yun Chen** [iD]**, Jing Zhang** [iD]**, and Chongsen Ma** [iD]

School of Traffic & Transportation Engineering, Changsha University of Science and Technology, Hunan 410000, China

Correspondence should be addressed to Liang Ou; ouliang@stu.csust.edu.cn

The factors affecting urban rail tunnel construction projects are very complex and are influenced by many factors such as the social environment, the construction process, and the way construction is managed. These influencing factors interact with each other, leading to the complexity of the development risks of this type of project. However, at present, the research on engineering construction risk is mainly focused on the field of housing construction, and there are few researches on the risk of urban tunnel construction. At the same time, with the continuous development of urbanization, the coverage of urban underground rail transport is increasing, so it is of great theoretical and practical significance to study the construction process of urban underground tunnels. This paper uses the literature collection method and the LDA model to initially identify the impact factors, and on this basis, the final set of evaluation impact factors is determined by means of expert interviews. Based on the set of influencing factors, the Dematel-ISM model was used to obtain a comprehensive analysis of the factors affecting urban rail tunnel construction projects by comparing topological maps and obtaining a Dematel-ISM model diagram with a cause-effect reachable hierarchy. Finally, the results obtained are applied to the actual development to verify the validity of the model. The results of the study show that construction operation, sequence arrangement, and procedure selection are the key influencing factors for safety risks in urban rail tunnel construction projects.

1. Introduction

Transport infrastructure refers to transport engineering facilities that provide public services for social production and residents' lives and is a public service system used to ensure the normal conduct of social and economic activities in a country or region, mainly including railway, highway, aviation, water transport, road and bridge, tunnel, port, and other construction contents. With the continuous development of China's economy, the construction of China's transport infrastructure has made significant developments since 1978. Transport facilities have achieved the transformation from constraining economic development to basically adapting to the level of economic development. By the end of 2020, China's total road mileage reached 5,198,100 kilometers, and railway operating mileage reached 146,300 kilometers, with highways and high-speed railways reaching 161,000 kilometers and 39,800 kilometers, respectively. Both

have achieved leapfrog development, and China has also made greater development in shipping. Urban railways, as an important part of the transport infrastructure, have been developed rapidly in recent years. However, urban rail transit inevitably encounters many problems in the construction process, especially in the construction process, as the location of the construction is mostly the city center, and the requirements for construction technology are more stringent. Therefore, this paper will study the risk of tunnel construction in the process of urban rail transit construction, which is of great practical significance.

At present, there are few studies on unsafe behavior and unsafe factors in the construction of urban rail tunnels, and the research content is usually biased towards the purely technical level. Fewer studies have been conducted on the relationship between the risk factors from a management perspective. Therefore, this paper adopts a Dematel-ISM linkage approach to gradually construct an explanatory

structural model to understand the key factors and structures affecting the safety of the construction process of urban rail tunnels and to provide suggestions for the control of unsafe behavior in urban rail tunnel construction. Based on the clarification of the key factors and structures affecting the safety of urban rail tunnel construction, ideas and strategies are proposed for the impact of risk-cause pairs.

The Dematel method was developed in the 1970s by Prof. Gabus and Fontela of the Geneva Research Centre and is commonly used to address the relationships between factors in the analysis of complex systems [1]. The method uses mathematical theory to analyze the relationship between the criteria and the strength of their effects by observing the degree of interaction between them and to model the structure of the indicators. In recent years, due to its wide applicability and introduction has received much attention and has been applied in a large number of applications and with the continuous optimization by many scholars, the method has made great progress in the fields of systems engineering, management science, project management, and safety management. In the Dematel method, there are three main expert information expressions as follows: point estimation judgment information, fuzzy number estimation judgment information, and grey number estimation information. Dytczak and Ginda pointed out through experimental analysis that there is a big controversy on how to use the Dematel algorithm and further made suggestions on how to carry out optimization [2]. Bai and Sarkis put forward grey-based Dematel and fused successful key factors for a business project in practical [3]. Lee et al. resolved the infeasibility of Dematel [4]. However, the comprehensive influence matrix (TIM) in Dematel can provide more information than the reachable matrix, so the combination of Dematel and ISM methods can achieve the complementary advantages and integration of the two methods; at the same time, there are also many studies combining Dematel method with ANP, AHP, and VIKOR methods [5–10]. These methods replace the evaluation matrix of the above methods with the constructed TIM matrix, but some scholars point out that the mismatch between the use of Dematel and ANP scales can have some impact on the rationality of the combination of methods [11].

The explanatory structure model (ISM) was proposed by Warfield in 1973, and the method is mainly used to analyze the constituent elements and interdependencies of complex systems. The ISM method forms a top-down arranged hierarchical diagram by decomposing the constituent elements of a complex system and transporting them through the system topology.

This paper further explores the risk influencing factors for sustainable transport infrastructure development in China and analyzes the project using the Dematel method and the ISM method, making the role of the relationship between the fuzzy, entangled risk influencing factors in the development process clear and providing a topological model for the continuous development of transport infrastructure development.

The innovation of this paper is mainly reflected in the following two points:

(i) This study analyzes the impact of safety factors on urban rail tunnel construction projects based on Dematel-ISM and identifies key impact indicators, which are important for controlling the process of urban rail tunnel construction and ensuring construction safety.

(ii) In this study, the LDA model was used to extract risk factors from the safety factors of previous urban rail tunnel construction projects, which is more scientific and reasonable than traditional methods.

2. Influencing Factors and Index System Construction

In order to construct an evaluation index system for transport infrastructure development, the first step of the thesis selects the LDA topic model to carry out topic semantic identification of the 500 highly cited papers collected and selects high-frequency words for risk factor extraction at the best topic count, and the second step is to use the Delphi method to screen the main influencing factors from the preliminary collated risk influencing factors for sustainable development of transport infrastructure.

2.1. A Determination of Impact Factor Evaluation Indicators for Sustainable Development of Transport Infrastructure Based on LDA Theme Model

2.1.1. Extraction of Risk Theme Words Based on LDA Model. The thesis selected the LDA topic model for data mining of selected research texts; data mining is also known as knowledge discovery in databases. By processing a large amount of random data, information containing patterns or values in the text is extracted. Text mining processes textual information and can be used to analyze and refine the themes implied behind the text through technology. Text mining has been used extensively in processing large amounts of irregular text. The thesis chooses latent Dirichlet allocation (LDA) topic model to process selected text data. The LDA model is a commonly used topic model that automatically extracts potential topics from large-scale texts. LDA does not require manual processing of relevant preliminaries during recognition and is an unsupervised machine learning algorithm that can be more efficient in the large-scale text processed. The LDA topic model is artificial in that individual documents are made up of implied topics, and the words in the documents make up the implied topics. The logical structure of the LDA model is shown in Figure 1.

The thesis uses the Gensim and Numpy libraries to construct an LDA topic model after setting up a specialized thesaurus and deactivating words. The LDA topic model is based on a Bayesian model. By counting the input text, the number of words in each of the M documents is recorded. The distribution of topics and the distribution of words in each topic are found for each document. The LDA topic model is currently used in information management and user comment analysis.

As the thesis focuses on Chinese issues, it was searched on CNKI using the keywords "tunnel," "construction," and
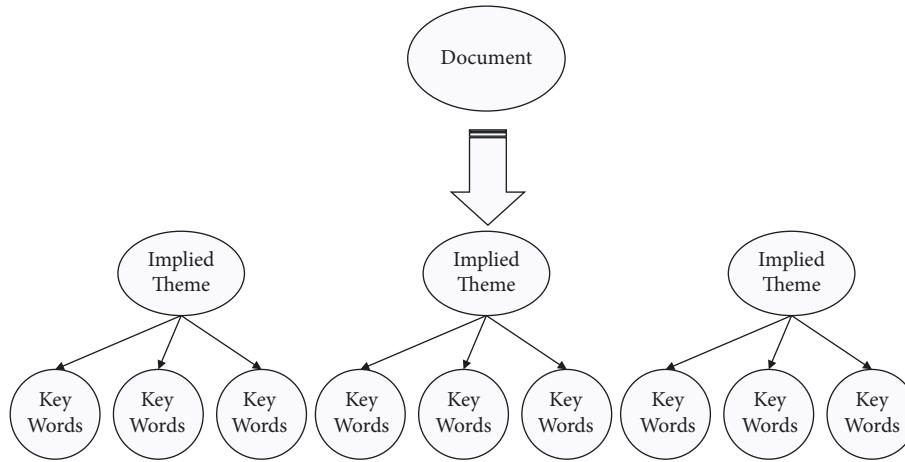
FIGURE 1: LDA model of the banking theme topology.

"risk," and 81 core papers and 16 incident reports with high relevance from 2000 to 2021 were selected as the initial source data. The 81 core papers and 16 incident reports with high relevance from 2000 to 2021 were selected as the initial source data for analysis. After downloading, 55 texts were retained after the initial manual screening. The model perplexity of the analyzed texts is shown in Figure 2.

Through Figure 2, it can be found that the article has the least confusion when the topic is selected as 8. The paper selects topic = 7, 8, 9; analyzes the obtained data; and finds that the best results are obtained when the topic is selected as 8. The results of the analysis of high-frequency topic words in the LDA model part are shown in Table 1.

2.2. Preliminary Risk Influencing Factors Determination.

Since the thesis addresses the risk of sustainable development of transportation infrastructure, the probability of generation of relevant factors has a small impact on the study. After referring to the subject terms, each subject term is statistically organized and the collated preliminary impact indicators for key risks are shown in Table 2.

The paper identifies the initial risk factors after the subject terms are advanced through the LDA subject matter model. The final evaluation metrics will be determined through the Delphi method. The Delphi method is a commonly used expert scoring method, which was proposed by RAND in 1946. The method collects expert opinions and eventually achieves a unified opinion among the investigators.

Steps of the paper to determine the final evaluation indicators are as follows:

(i) Clarify the survey objectives, survey purposes, and survey methods and create questionnaires as needed. The method and precautions for filling out the survey questionnaire are explained. The thesis selects the Likert seven-level scale to make the questionnaire. The relative importance among the indicators is judged by means of an expert interview survey. Duplicate indicators and those with less influence were screened out.

FIGURE 2: Topic perplexity of LDA model.

(ii) Expert panel members were identified. Ten experts related to theory and practice were selected for this study. Through interviews with experts and questionnaire filling, evaluation indicators are determined based on Table 2. The surveyed experts included government staff, university teachers, relevant researchers, and related practitioners. For the information on survey personnel (see Table 3).

(iii) A questionnaire (see Table 4) was sent to the selected experts by face-to-face communication or letter. And each expert's opinion on the indicators was sought.

(iv) The returned questionnaire results were statistically analyzed, and after collecting the questionnaire data, the questionnaire data were processed using SPSS AU software, and after determining that the data reliability validity met the requirements, the indicators were censored according to the factor loadings. And the final results were returned to each expert.

After the experts discussed the 29 influencing factors, 24 influencing factors with greater practical significance were finally summarized (see Table 5).

TABLE 1: Analysis results of some high-frequency subject words in LDA model.

Topic 0		Topic 1		Topic 2		Topic 3	
Word	Prob	Word	Prob	Word	Prob	Word	Prob
Tunnel	0.026	Tunnel	0.018	Engineering	0.011	TBM	0.022
Project	0.020	Shield	0.013	Production	0.007	Construction	0.019
Construction	0.015	Construction	0.013	Municipalities	0.007	Tunneling	0.011
Assessment	0.010	Subway	0.009	Management	0.007	Tunneling	0.009
Grade	0.008	Technology	0.005	Accidents	0.006	Pipeline	0.009
. . .		. . .		. . .		. . .	
Topic 4		Topic 5		Topic 6		Topic 7	
Word	Prob	Word	Prob	Word	Prob	Word	Prob
Construction	0.022	Production	0.019	Tunnel	0.011	Construction	0.023
Accidents	0.008	Accidents	0.011	House	0.010	Tunnel	0.018
Rebar	0.005	Emergency response	0.009	Waterlogging	0.008	Structure	0.014
Work	0.005	Shield	0.008	Shield	0.007	Deformation	0.013
Management	0.005	Rail transit	0.007	Underground	0.007	Control	0.011
. . .		. . .		. . .		. . .	

TABLE 2: Statistics of factors influencing sustainability in transportation.

No.	Factor name
1	Stratigraphic conditions
2	Complex hydrological situation
3	Complex underground pipelines
4	Site disturbance
5	Complex surrounding building conditions
6	Poor climatic conditions
7	Accuracy of survey data
8	Design reasonableness
9	Reasonableness of scheme selection
10	Project scale
11	Process selection
12	Tunnel type
13	Construction technology risks
14	Informatization
15	Monitoring and measurement
16	Worker's working condition
17	Work sequence arrangement
18	Equipment use
19	Uncoordinated construction relationship
20	Poor safety awareness
21	Improper installation and commissioning of equipment
22	Improper application of new technology
23	Comprehensive quality of construction unit
24	Construction organization design
25	Safety technical measures
26	Safety hazard rectification
27	Safety education
28	Safety inspection
29	Emergency preparedness

TABLE 3: Basic information of the research experts.

Work area	Number	Title	Average years of service
Government worker	2	—	3
Professoriat	3	Pro.Dr.	15
Researcher	3	PhD	6
Relevant employees	2	Manager	5

TABLE 4: Transportation infrastructure impact relevance score.

Factor name	1	2	3	4	5
Poor stratigraphic conditions					
Complex hydrological situation					
Complex underground pipelines					
Site disturbance					
. . .					
Safety inspection situation					
Emergency plan					

Note: Please fill in the questionnaire according to the actual situation. Scores 1 to 9 indicate that the risk impact is minimal to large.

3. Dematel-ISM Modeling of Safety Influencing Factors in Urban Rail Tunnel Construction Projects

The core idea of this paper is to combine the Dematel method with ISM to reflect the impact of each safety influence factor on the project in the process of urban rail tunnel construction more clearly and reasonably. Compared with text and symbols, the Dematel-ISM method expresses the results more intuitively and clearly and reduces the inverse influence of experts' personal subjective factors on the results on the basis of clear and accurate reflection of the cause-effect relationships seen in each element. In this method, the influencing factors are considered as nodes, and the nodes with causal relationships are linked using directed line segments. In the obtained directed topology diagram, if an element is active, it is called an activity element, and the system containing an Activity element is called extension variable system. In a directed topology diagram, elements are said to form a loop if they are reachable to each other. A reasonable ISM-directed topology diagram requires the presence of a nonloop system. The intercept is set reasonably through the expert interview guided to determine the correlation and hierarchy among the influencing factors and to determine the influence relationship between the factors. The basic process of constructing a model based on the model is as follows (see Figure 3).

TABLE 5: Index system of construction safety in an urban rail tunnel.

Indicator categories	Indicator names	Indicator symbols
Geological conditions	Stratigraphic conditions	R_{11}
	Complex hydrological situation	R_{12}
Construction environment	Complex underground pipelines	R_{21}
	Site disturbance	R_{22}
	Complex surrounding building conditions	R_{23}
	Poor climatic conditions	R_{24}
Planning and design	Accuracy of survey data	R_{31}
	Design reasonableness	R_{32}
	Reasonableness of scheme selection	R_{33}
Construction technology	Project scale	R_{41}
	Process selection	R_{42}
	Tunnel type	R_{43}
	Construction technology risk	R_{44}
	Informatization	R_{45}
	Monitoring and measurement	R_{46}
	Worker operation	R_{47}
	Work sequence arrangement	R_{48}
	Equipment use	R_{49}
Management factors	Uncoordinated construction relationship	R_{51}
	Poor safety awareness	R_{52}
	Comprehensive quality of construction unit	R_{53}
Safety factors	Safety technical measures	R_{61}
	Safety education	R_{62}
	Safety inspection situation	R_{63}
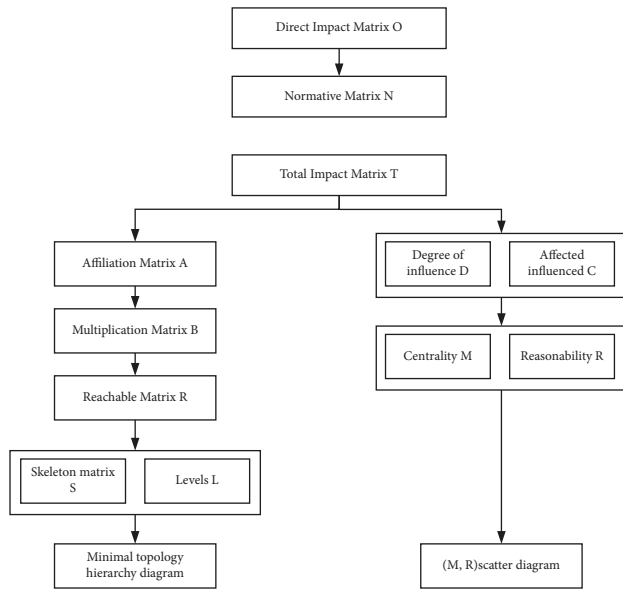
FIGURE 3: Dematel-ISM modeling of safety influencing factors.

3.1. Total Impact Matrix Establishment and Specification.

Twenty-four influencing indicators of construction safety of urban rail tunnel are quantified by the Dematel method for factor analysis, and on the basis of the quantitative analysis, a direct influence matrix O was formed. The direct impact matrix O should be normalized. The formula is as follows:

$$N = \frac{O}{\max \sum_{j=1}^{n}} = O_{ij} = \left(X_{ij} \right)_{n*n}. \tag{1}$$

The normative direct relation matrix N is aggregated by accumulating all direct and indirect relationships, and the sum of all direct and indirect relationships of each factor should be identified to obtain the total impact matrix T as follows:

$$T = N(I - N)^{-1}, \tag{2}$$

where I is the unit matrix.

The direct impact O matrix of construction safety indicators of the urban rail tunnel is shown in Table 6, and the total impact T matrix is shown in Table 7.

3.2. The Dematel Factors Analysis.

The cause degree and centrality of each factor of construction safety in the urban rail tunnel should be calculated to obtain the level and weight of each factor. The main steps are as follows:

(i) Set D represents the comprehensive influence of each factor on all other factors. Set C represents the comprehensive affected degree of all other factors on each factor.

(ii) Set $D + C(M)$ represents the correlation degree of this factor in the system, which is called centrality. Set D-C (R) denotes the cause degree of this factor in the system, which is called reasonability. The sets D, C, M, and R of construction safety indicators of the urban rail tunnel are shown in Table 8, and the (M, R) scatter diagram is shown in Figure 4.

$D + C$ means the significance of the factor centrality in the system; the greater the value, the more important the

TABLE 6: Direct impact O matrix of safety indicators of urban rail tunnel.

	R_{11}	R_{12}	R_{21}	R_{22}	R_{23}	R_{24}	R_{31}	R_{32}	R_{33}	R_{41}	R_{42}	R_{43}	R_{44}	R_{45}	R_{46}	R_{47}	R_{48}	R_{49}	R_{51}	R_{52}	R_{53}	R_{61}	R_{62}	R_{63}
R_{11}	0	2	4	4	3	0	3	3	4	3	4	3	4	0	3	3	3	1	0	2	1	4	4	4
R_{12}	3	0	1	2	2	0	3	3	4	2	4	1	2	0	3	3	3	1	0	3	1	4	4	4
R_{21}	0	0	0	0	1	0	3	2	4	1	2	1	1	0	2	0	3	2	0	0	0	3	3	3
R_{22}	0	0	0	0	4	0	0	0	1	0	0	0	1	0	4	1	1	1	0	2	1	4	1	1
R_{23}	0	0	5	0	0	0	4	5	5	3	4	3	4	1	3	1	3	3	1	2	0	2	2	3
R_{24}	1	3	0	0	1	0	1	0	0	1	3	0	2	0	0	1	3	1	1	2	0	1	1	1
R_{31}	0	0	0	0	0	0	0	5	5	4	4	4	4	0	4	3	3	1	1	2	0	3	3	3
R_{32}	0	0	0	3	2	0	0	0	4	3	3	3	3	1	3	1	2	1	0	1	0	1	1	1
R_{33}	0	0	0	3	3	0	0	3	0	2	5	2	3	1	2	2	2	1	0	1	0	1	1	1
R_{41}	0	0	0	2	0	0	1	2	1	0	2	4	4	0	3	3	4	1	2	2	1	2	2	2
R_{42}	0	0	0	4	0	0	0	5	5	3	0	3	3	2	2	3	5	2	1	2	1	4	3	3
R_{43}	0	0	0	1	0	0	0	3	3	3	4	0	3	0	2	2	5	2	1	2	1	3	3	3
R_{44}	0	0	0	0	0	0	0	0	1	1	0	1	0	0	0	1	1	0	0	2	0	4	3	2
R_{45}	0	0	0	1	0	0	0	0	3	1	2	0	0	0	3	2	2	1	1	0	4	0	0	0
R_{46}	0	0	0	0	0	0	0	0	0	1	0	0	0	4	0	1	0	0	0	4	2	3	3	3
R_{47}	0	0	0	5	0	0	0	0	0	0	0	0	0	3	5	4	0	5	4	3	2	4	3	3
R_{48}	0	0	0	3	0	0	0	0	1	0	2	0	3	4	1	3	0	3	4	1	1	2	2	2
R_{49}	0	0	0	1	0	0	0	0	0	0	0	0	0	1	0	1	2	4	0	1	1	1	1	1
R_{51}	0	0	0	0	0	0	0	0	0	0	0	0	0	1	5	1	4	4	1	0	0	2	0	0
R_{52}	0	0	0	0	0	0	0	0	0	0	0	0	0	0	0	0	0	0	0	0	1	3	3	3
R_{53}	0	0	0	2	0	0	0	0	0	0	0	0	0	3	4	2	5	4	4	1	0	0	3	3
R_{61}	0	0	0	1	0	0	0	0	0	0	0	0	0	2	0	0	1	0	0	0	3	1	0	2	2
R_{62}	0	0	0	3	0	0	0	0	0	0	0	0	0	3	0	1	3	1	4	0	1	1	1	0	1
R_{63}	0	0	0	3	0	0	0	0	0	0	0	0	0	3	0	1	0	0	1	0	1	1	1	1	0

factor; $D - C$ means the influence of a certain factor on other factors. The factor whose value is greater than 0 means more influence on other factors and is denoted as the reason factor. The factor whose value is less than 0 means more influence by others and is denoted as result factor. Each factor should be normalized to obtain weight according to its $D + C(M)$ value.

From the factors analysis of construction safety in the urban rail tunnel, R_{11} (stratigraphic conditions), R_{12} (complex hydrological situation), R_{23} (complex surrounding building conditions), and R_{31} (accuracy of survey data) have the highest reasonability, which means the greatest impact on other factors. R_{48} (construction operation), R_{47} (sequence arrangement), and R_{42} (procedure selection) have the highest centrality, which means the fundamental impact on the construction safety of the urban rail tunnel.

3.3. ISM Factor Analysis and Reachable Matrix Establishment.

Since the Dematel factors analysis on themselves belongs to each factor interaction correspondence, the unit matrix I is used to indicate the influence value of factors on themselves. The comprehensive influence relationship of factors in the whole system can be replaced by multiplication matrix B.

$$B = T + I. \tag{3}$$

In matrix B, if $b_{ij} = 0$, it shows that factor b_i has no effect on b_j; otherwise, b_i has an effect on b_j. The matrix B obtained in Dematel factors includes not only the existence of factor relationships but also the degree of scope of factors interaction. Therefore, the matrix B calculated by Dematel can be simplified to reachable matrix R, which shows the reachable

hierarchical structure of the urban rail tunnel safety index system.

The reachable matrix R is used to reflect a directed topological hierarchy graph that can link each influencing safety factor of an urban rail tunnel through a certain path. The threshold value $\lambda = 0.016$ is determined according to the actual situation and the influence strength, which the purpose of threshold setting is to discard the less influential relationship and simplify the factor relationship, so as to clearly express the main system structure level. The matrix R is simplified according to the following formula. The matrix R of the urban rail tunnel safety index system is shown in Table 9.

$$R = (r_{ij}) = \begin{cases} 0, r_{ij} < \lambda, \\ 1, r_{ij} \geq \lambda. \end{cases} \tag{4}$$

3.4. Topological Hierarchy Diagram Establishment.

There is a reachable set R, a prior set Q, and a common set A from the matrix R, where $T = R \cap Q$ to further get the relationship levels of interaction among factors. All the factors of each row correspond to a path value of 1 are called reachable sets $R(i)$. All the factors of each corresponding column value of 1 are called the prior set $Q(i)$. The common set of the reachable set $R(i) \cap Q(i)$ and the prior set is called $T(i)$. The topological hierarchy extraction process of the urban rail tunnel safety index system can be seen in Table 10.

By comparing directed topological diagrams, the influencing factors of construction safety in the urban rail tunnel are analyzed comprehensively to determine the correlation and hierarchy among the influencing factors and determine

TABLE 7: Total impact T matrix of construction safety indicators of urban rail tunnel.

	R_{11}	R_{12}	R_{21}	R_{22}	R_{23}	R_{24}	R_{31}	R_{32}	R_{33}	R_{41}	R_{42}	R_{43}	R_{44}	R_{45}	R_{46}	R_{47}	R_{48}	R_{49}	R_{51}	R_{52}	R_{53}	R_{61}	R_{62}	R_{63}
R_{11}	0.002	0.032	0.070	0.115	0.066	0.000	0.059	0.082	0.107	0.078	0.102	0.077	0.129	0.033	0.100	0.097	0.108	0.060	0.021	0.080	0.045	0.131	0.124	0.123
R_{12}	0.048	0.002	0.023	0.080	0.047	0.000	0.056	0.076	0.099	0.058	0.096	0.041	0.090	0.030	0.092	0.091	0.098	0.054	0.019	0.089	0.042	0.120	0.115	0.114
R_{21}	0.000	0.000	0.002	0.027	0.024	0.000	0.051	0.049	0.083	0.032	0.052	0.031	0.050	0.016	0.055	0.026	0.075	0.053	0.011	0.023	0.013	0.076	0.074	0.074
R_{22}	0.000	0.000	0.005	0.013	0.067	0.000	0.005	0.009	0.026	0.008	0.009	0.006	0.035	0.014	0.077	0.030	0.031	0.029	0.006	0.050	0.026	0.083	0.036	0.036
R_{23}	0.000	0.000	0.082	0.044	0.013	0.000	0.071	0.110	0.119	0.077	0.100	0.076	0.119	0.045	0.091	0.059	0.102	0.083	0.035	0.070	0.024	0.086	0.082	0.096
R_{24}	0.018	0.049	0.004	0.022	0.021	0.000	0.021	0.014	0.018	0.027	0.062	0.011	0.057	0.015	0.019	0.038	0.073	0.033	0.026	0.051	0.013	0.043	0.041	0.041
R_{31}	0.000	0.000	0.001	0.044	0.011	0.000	0.002	0.101	0.107	0.086	0.091	0.085	0.113	0.030	0.100	0.086	0.094	0.048	0.034	0.069	0.025	0.095	0.092	0.090
R_{32}	0.000	0.000	0.003	0.075	0.042	0.000	0.004	0.019	0.084	0.064	0.069	0.063	0.081	0.035	0.075	0.043	0.065	0.038	0.013	0.042	0.017	0.052	0.047	0.046
R_{33}	0.000	0.000	0.005	0.077	0.057	0.000	0.005	0.067	0.026	0.049	0.098	0.049	0.083	0.037	0.061	0.059	0.067	0.040	0.014	0.043	0.018	0.054	0.048	0.048
R_{41}	0.000	0.000	0.001	0.061	0.007	0.000	0.017	0.044	0.034	0.014	0.048	0.074	0.098	0.026	0.074	0.077	0.098	0.042	0.047	0.059	0.036	0.070	0.066	0.064
R_{42}	0.000	0.000	0.001	0.105	0.015	0.000	0.002	0.094	0.103	0.065	0.026	0.064	0.095	0.061	0.070	0.086	0.122	0.065	0.035	0.066	0.042	0.109	0.088	0.086
R_{43}	0.000	0.000	0.001	0.052	0.009	0.000	0.002	0.062	0.067	0.062	0.081	0.015	0.087	0.026	0.060	0.065	0.115	0.059	0.032	0.060	0.036	0.086	0.082	0.081
R_{44}	0.000	0.000	0.000	0.012	0.002	0.000	0.000	0.003	0.019	0.019	0.005	0.019	0.014	0.006	0.008	0.026	0.025	0.010	0.004	0.042	0.007	0.075	0.060	0.043
R_{45}	0.000	0.000	0.000	0.035	0.005	0.000	0.001	0.008	0.056	0.023	0.041	0.006	0.020	0.021	0.065	0.053	0.055	0.033	0.026	0.014	0.077	0.022	0.019	0.019
R_{46}	0.000	0.000	0.000	0.014	0.001	0.000	0.000	0.001	0.005	0.018	0.004	0.002	0.014	0.072	0.012	0.029	0.012	0.012	0.005	0.073	0.044	0.062	0.062	0.061
R_{47}	0.000	0.000	0.001	0.105	0.007	0.000	0.001	0.002	0.012	0.006	0.009	0.003	0.076	0.107	0.090	0.034	0.109	0.089	0.062	0.056	0.088	0.082	0.077	0.076
R_{48}	0.000	0.000	0.000	0.070	0.006	0.000	0.001	0.005	0.027	0.007	0.039	0.005	0.070	0.085	0.038	0.072	0.029	0.067	0.074	0.034	0.037	0.058	0.053	0.052
R_{49}	0.000	0.000	0.000	0.028	0.002	0.000	0.000	0.001	0.003	0.002	0.003	0.001	0.028	0.014	0.025	0.044	0.074	0.012	0.024	0.025	0.025	0.030	0.028	0.028
R_{51}	0.000	0.000	0.000	0.017	0.002	0.000	0.000	0.001	0.008	0.003	0.007	0.001	0.030	0.099	0.032	0.081	0.082	0.032	0.012	0.010	0.048	0.016	0.015	0.014
R_{52}	0.000	0.000	0.000	0.008	0.001	0.000	0.000	0.000	0.001	0.000	0.000	0.000	0.009	0.002	0.004	0.006	0.004	0.006	0.001	0.005	0.020	0.053	0.053	0.053
R_{53}	0.000	0.000	0.000	0.058	0.004	0.000	0.000	0.002	0.009	0.004	0.007	0.002	0.072	0.086	0.054	0.103	0.089	0.086	0.030	0.020	0.023	0.074	0.071	0.070
R_{61}	0.000	0.000	0.000	0.023	0.002	0.000	0.000	0.000	0.002	0.001	0.001	0.001	0.040	0.004	0.006	0.022	0.006	0.007	0.002	0.054	0.021	0.011	0.041	0.040
R_{62}	0.000	0.000	0.000	0.060	0.004	0.000	0.000	0.001	0.004	0.002	0.002	0.002	0.060	0.011	0.028	0.059	0.031	0.075	0.007	0.028	0.026	0.034	0.015	0.030
R_{63}	0.000	0.000	0.000	0.053	0.004	0.000	0.000	0.001	0.003	0.002	0.001	0.001	0.054	0.004	0.022	0.007	0.006	0.021	0.002	0.024	0.020	0.028	0.025	0.008

TABLE 8: Dematel factors analysis of construction safety in urban rail tunnel.

	D	C	M	R	Weight
R_{11}	1.839	0.069	1.908	1.771	0.046
R_{12}	1.581	0.083	1.664	1.498	0.040
R_{21}	0.897	0.201	1.098	0.696	0.026
R_{22}	0.601	1.198	1.799	−0.596	0.044
R_{23}	1.581	0.418	1.999	1.163	0.048
R_{24}	0.720	0.000	0.720	0.720	0.018
R_{31}	1.406	0.297	1.703	1.109	0.041
R_{32}	0.976	0.751	1.727	0.224	0.042
R_{33}	1.003	1.021	2.024	−0.018	0.049
R_{41}	1.056	0.706	1.761	0.350	0.042
R_{42}	1.400	0.953	2.353	0.447	0.057
R_{43}	1.139	0.636	1.775	0.503	0.043
R_{44}	0.399	1.526	1.925	−1.128	0.047
R_{45}	0.600	0.882	1.482	−0.282	0.036
R_{46}	0.506	1.258	1.764	−0.753	0.043
R_{47}	1.090	1.294	2.384	−0.204	0.057
R_{48}	0.829	1.570	2.400	−0.741	0.058
R_{49}	0.398	1.055	1.453	−0.657	0.035
R_{51}	0.512	0.542	1.053	−0.030	0.026
R_{52}	0.226	1.086	1.312	−0.860	0.032
R_{53}	0.868	0.774	1.643	0.094	0.040
R_{61}	0.283	1.548	1.831	−1.265	0.044
R_{62}	0.482	1.413	1.894	−0.931	0.046
R_{63}	0.287	1.395	1.682	−1.109	0.041
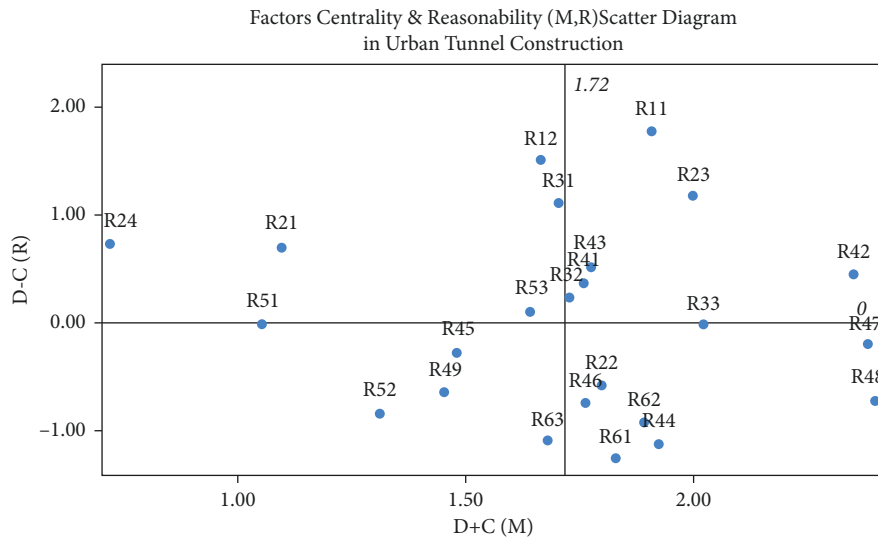
FIGURE 4: Factors centrality and reasonability (M, R) scatter diagram.

the influencing relationship among factors. The basic process of constructing the model according to this is shown in Table 11.

From the topological hierarchy extraction process, the levels can be shown in Table 11.

According to the relationship between the confrontation hierarchy extracted process and levels, the directed topological hierarchy diagram can be drawn as shown in Figure 5.

As shown in Figure 5, the root cause factors set of R_{24} (climatic conditions), R_{11} (stratigraphic conditions), R_{12} (complex hydrological situation), R_{23} (complex surrounding building conditions), and R_{31} (accuracy of survey data), which are at the bottom of the system and are not affected by other factors, can directly or indirectly affect other factors within the system. The features of factors up to down are from superficial to essential, which means dominant levels are from level 4 to level 7. As shown in figures, factors of R_{23} (complex surrounding building conditions), R_{31} (accuracy of survey data), R_{32} (design reasonableness), R_{48} (construction operation), R_{47} (sequence arrangement), and R_{42} (procedure selection) are the dominant function factors of great importance, which means their fundamental impact on

TABLE 9: Reachable matrix R of urban rail tunnel safety index system.

	R_{11}	R_{12}	R_{21}	R_{22}	R_{23}	R_{24}	R_{31}	R_{32}	R_{33}	R_{41}	R_{42}	R_{43}	R_{44}	R_{45}	R_{46}	R_{47}	R_{48}	R_{49}	R_{51}	R_{52}	R_{53}	R_{61}	R_{62}	R_{63}
R_{11}	1	1	0	0	1	0	1	1	1	1	1	1	1	1	1	1	1	1	1	1	1	1	1	1
R_{12}	1	1	1	1	1	0	1	1	1	1	1	1	1	0	1	1	1	1	0	1	1	1	1	1
R_{21}	0	0	1	1	1	0	1	1	1	0	0	0	1	0	1	1	1	1	0	1	0	1	1	1
R_{22}	0	0	0	1	1	0	0	0	1	1	1	1	1	1	1	1	1	1	0	1	1	1	1	1
R_{23}	0	0	1	1	1	0	1	1	1	1	1	1	1	0	1	1	1	1	1	1	1	1	1	1
R_{24}	1	1	0	1	1	1	1	1	0	1	1	1	1	1	0	1	1	1	1	1	1	1	1	1
R_{31}	0	0	0	1	0	0	1	1	1	1	1	1	1	1	0	1	1	1	1	1	1	1	1	1
R_{32}	0	0	0	1	1	0	0	1	1	1	1	1	1	1	1	1	1	1	0	1	0	1	1	1
R_{33}	0	0	0	1	1	0	0	0	1	1	1	1	1	1	1	1	1	1	0	1	0	1	1	1
R_{41}	0	0	0	1	0	0	0	0	0	1	1	1	1	1	1	1	1	1	1	1	1	1	1	1
R_{42}	0	0	0	1	0	0	0	0	0	0	1	0	1	1	1	1	1	1	0	1	1	1	1	1
R_{43}	0	0	0	1	0	0	0	0	0	0	0	1	1	1	1	1	1	1	1	1	1	1	1	1
R_{44}	0	0	0	0	0	0	0	0	0	0	0	0	1	0	1	1	0	0	0	0	0	1	1	0
R_{45}	0	0	0	1	0	0	0	0	0	0	0	0	0	1	1	1	1	1	0	1	0	1	1	1
R_{46}	0	0	0	0	0	0	0	0	0	0	0	0	0	0	1	1	1	1	0	0	0	1	1	1
R_{47}	0	0	0	1	0	0	0	0	0	0	0	0	0	0	0	1	1	1	1	1	1	1	1	1
R_{48}	0	0	0	1	0	0	0	0	0	0	0	0	0	0	0	0	1	1	0	0	0	1	1	1
R_{49}	0	0	0	1	0	0	0	0	0	0	0	0	0	0	0	0	0	1	0	0	0	1	1	1
R_{51}	0	0	0	0	0	0	0	0	0	0	0	0	0	0	0	1	1	0	1	1	1	1	1	1
R_{52}	0	0	0	0	0	0	0	0	0	0	0	0	0	0	0	0	0	0	0	1	1	0	0	0
R_{53}	0	0	0	1	0	0	0	0	0	0	0	0	0	0	0	0	0	0	0	1	1	1	1	1
R_{61}	0	0	0	1	0	0	0	0	0	0	0	0	1	0	1	1	1	1	0	1	1	1	1	1
R_{62}	0	0	0	1	0	0	0	0	0	0	0	0	1	0	1	1	1	1	0	1	1	1	1	1
R_{63}	0	0	0	1	0	0	0	0	0	0	0	0	1	0	1	0	0	1	0	1	1	1	1	1

TABLE 10: Topological hierarchy extraction process of urban rail tunnel safety index.

i	$R(i)$	$Q(i)$	$A = R \cap Q$
R11	1, 2, 5, 7, 8, 9, 10, 11, 12, 13, 14, 15, 16, 17, 18, 19, 20, 21, 22, 23, 24	1, 2, 6	1, 2
R12	1, 2, 3, 4, 5, 7, 8, 9, 10, 11, 12, 13, 14, 15, 16, 17, 18, 19, 20, 21, 22, 23, 24	1, 2, 6	1, 2
R21	3, 4, 5, 7, 8, 9, 10, 11, 12, 13, 15, 16, 17, 18, 20, 21, 22, 23, 24	3, 4, 6	3, 4
R22	4, 5, 9, 13, 15, 16, 17, 18, 20, 21, 22, 23, 24	2, 3, 4, 5, 7, 8, 10, 11, 12, 14, 16, 17, 18, 21, 22, 23, 24	4, 5, 16, 17, 18, 21, 22, 23, 24
R23	3, 4, 5, 7, 8, 9, 10, 11, 12, 13, 14, 15, 16, 17, 18, 19, 20, 21, 22, 23, 24	1, 2, 3, 4, 5, 6, 8, 9	3, 4, 5, 8, 9,
R24	1, 2, 3, 4, 5, 6, 7, 8, 9, 10, 1116, 17, 18, 19, 20, 22, 23, 24	6	6
R31	4, 7, 8, 9, 10, 11, 16, 17, 18, 19, 20, 22, 23, 24	1, 2, 3, 5, 6, 7	7
R32	4, 5, 6, 8, 9, 10, 11, 12, 13, 14, 15, 16, 17, 18, 20, 22, 23, 24	1, 2, 3, 5, 7, 8, 9, 10, 11, 12,	5, 8, 9, 10, 11, 12,
R33	4, 5, 8, 9, 10, 11, 12, 13, 14, 15, 16, 17, 18, 19, 20, 21, 22, 23, 24	1, 2, 3, 4, 5, 7, 8, 9, 10, 11, 12, 14, 17	4, 5, 8, 9, 10, 11, 12, 14, 17,
R41	4, 8, 9, 10, 11, 12, 13, 14, 15, 16, 17, 18, 19, 20, 21, 22, 23, 24	1, 2, 3, 5, 7, 8, 9, 10, 11, 12, 14,	8, 9, 10, 11, 12, 14,
R42	4, 8, 9, 10, 11, 12, 13, 14, 15, 16, 17, 18, 19, 20, 21, 22, 23, 24	1, 2, 3, 5, 7, 8, 9, 10, 11, 12, 14, 17	8, 9, 10, 11, 12, 14, 17
R43	4, 8, 9, 10, 11, 12, 13, 14, 15, 16, 17, 18, 19, 20, 21, 22, 23, 24	1, 2, 3, 5, 7, 8, 9, 10, 11, 12,	8, 9, 10, 11, 12
R44	13, 16, 17, 20, 22, 23, 24	1, 2, 3, 4, 5, 7, 8, 9, 10, 11, 12, 13, 14, 16, 17, 18, 19, 21, 22, 23, 24	13, 16, 17, 22, 23, 24
R45	4, 9, 10, 11, 13, 14, 15, 16, 17, 18, 19, 22,	1, 2, 5, 7, 8, 9, 10, 11, 12, 14, 15, 16, 17, 19, 21, 23, 24	9, 10, 11, 14, 15, 16, 17, 19,
R46	14, 15, 16, 20, 21, 22, 23, 24	1, 2, 3, 4, 5, 7, 8, 9, 10, 11, 12, 14, 15, 16, 17, 18, 19, 21, 23	14, 15, 16, 21, 23, 24
R47	4, 13, 14, 15, 16, 17, 18, 19, 20, 21, 22, 23, 24	1, 2, 3, 4, 5, 7, 8, 9, 10, 11, 12, 13, 14, 15, 16, 17, 18, 19, 21, 23	4, 13, 14, 15, 16, 17, 18, 19, 21, 23
R48	4, 9, 11, 13, 14, 15, 16, 17, 18, 19, 20, 21, 22, 23, 24	1, 2, 3, 4, 5, 7, 8, 9, 10, 11, 12, 13, 14, 16, 17, 18, 19, 21, 23	4, 9, 11, 13, 14, 16, 17, 18, 19, 21, 23
R49	4, 13, 15, 16, 17, 18, 19, 20, 21, 22, 23, 24	1, 2, 3, 4, 5, 7, 8, 9, 10, 11, 12, 14, 16, 17, 18, 19, 21, 23, 24	4, 16, 17, 18, 19, 21, 23, 24
R51	13, 14, 15, 16, 17, 18, 19	1, 5, 6, 7, 10, 11, 12, 14, 16, 17, 18, 19, 21	14, 16, 17, 18, 19
R52	20, 21, 22, 23, 24	1, 2, 3, 4, 5, 7, 8, 9, 10, 11, 12, 16, 17, 18, 20, 21, 22, 23, 24	20, 21, 22, 23, 24
R53	4, 13, 14, 15, 16, 17, 18, 19, 20, 21, 22, 23, 24	1, 2, 4, 5, 7, 10, 11, 12, 15, 16, 17, 18, 19, 20, 21, 22, 23, 24	4, 15, 16, 17, 18, 19, 20, 21, 22, 23, 24
R61	4, 13, 16, 20, 21, 22, 23, 24	1, 2, 3, 4, 5, 6, 7, 10, 11, 12, 15, 16, 17, 18, 20, 21, 22, 23, 24	4, 13, 16, 20, 21, 22, 23, 24
R62	4, 13, 15, 16, 17, 18, 20, 21, 22, 23, 24	1, 2, 3, 4, 5, 6, 7, 10, 11, 12, 13, 15, 16, 17, 18, 20, 21, 22, 23, 24	4, 13, 15, 16, 17, 18, 20, 21, 22, 23, 24
R63	4, 13, 15, 18, 20, 21, 22, 23, 24	1, 2, 3, 4, 5, 6, 7, 10, 11, 12, 13, 15, 16, 17, 18, 20, 21, 22, 23, 24	4, 13, 15, 18, 20, 21, 22, 23, 24

TABLE 11: Hierarchy extraction levels.

Levels	Factors
Level 1	$R63, R62, R61, R44$
Level 2	$R22, R46, R49, R52$
Level 3	$R51, R45, R33, R53$
Level 4	$R45, R47, R48$
Level 5	$R32, R42, R43, R23$
Level 6	$R12, R11, R31, R21$
Level 7	$R24$
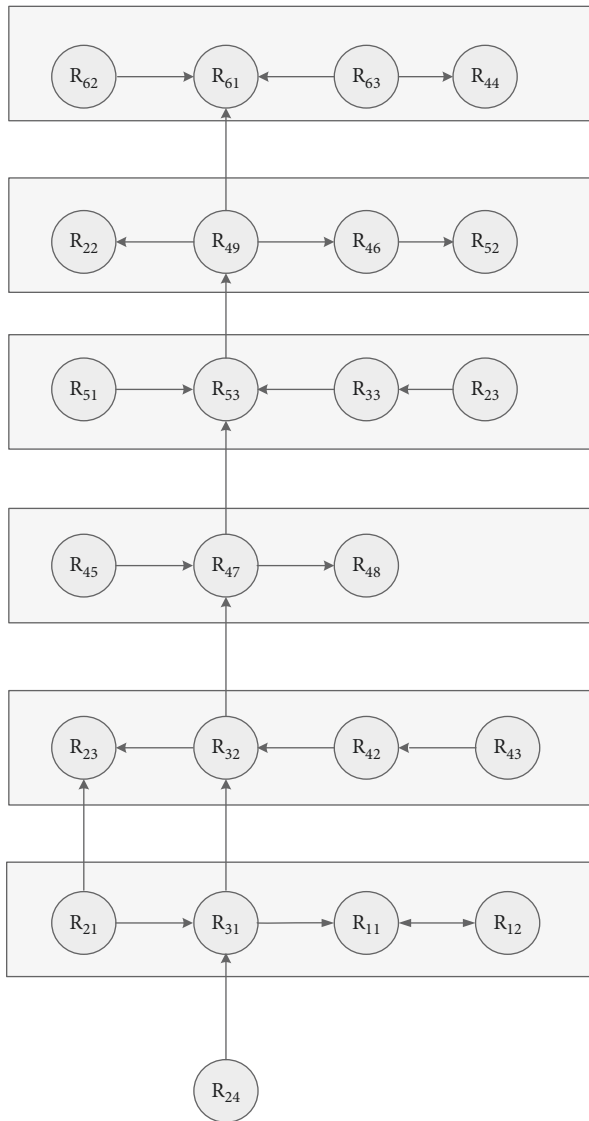
FIGURE 5: Topological hierarchy diagram of urban rail tunnel safety index.

construction safety of urban rail. It can be found that geological conditions, planning and design, and construction technology are more important indicator categories in the safety of urban railway tunnel construction, which should be paid more attention. It also can be noted that by combining the weight analysis of factors in Table 9, R_{48} (construction operation), R_{47} (sequence arrangement), and R_{42} (procedure selection) have the greatest centrality and

importance for the construction safety of urban rail, which means that the choice of technology and the effectiveness of its implementation during construction have a dominant influence on construction safety in urban railways.

4. Conclusions

This paper studies the risk of tunnel construction in the process of urban rail transit construction. It adopts a Dematel-ISM linkage approach to gradually construct an explanatory structural model to understand the key factors and structures affecting the safety of the construction process of urban rail tunnels. This paper uses the literature collection method and the LDA model to initially identify the impact factors, and on this basis, the final set of evaluation impact factors is determined by means of expert interviews. Based on the research 6 clarification of the 24 key factors affecting the safety of urban rail tunnel construction can be obtained, then the Dematel-ISM model was used to obtain a comprehensive analysis of the factors affecting urban rail tunnel construction projects by comparing topological maps and obtaining a Dematel-ISM model diagram with a cause-effect reachable hierarchy. Finally, the results obtained are applied to the actual development to verify the validity of the model.

From the research, it can be found that the root cause factors set of R_{24} (climatic conditions), R_{11} (stratigraphic conditions), R_{12} (complex hydrological situation), R_{23} (complex surrounding building conditions), and R_{31} (accuracy of survey data), which are at the bottom of the system and are not affected by other factors, can directly or indirectly affect other factors and result within the system, which should be paid more attention. It can be found especially during the prior period that the most direct safety impact factors come from geological conditions, climatic conditions, and complex surrounding conditions. Therefore, on the basis of fully collecting and possessing accurate information, professional experts should be invited to improve the accuracy and rationality of conditions research in this phrase. During the prior period, the possible changes in the conditions of the project shall be fully considered, and the disposal plan shall be made for relevant changes to reduce the possible impact of unpredictable changes in conditions.

It also notes reachable hierarchy diagram that R_{31} (accuracy of survey data), R_{32} (design reasonableness), R_{48} (construction operation), R_{47} (sequence arrangement), and R_{42} (procedure selection) are the dominant function factors of great importance, which means their fundamental impact on construction safety of urban rail. It can be found that planning and design and construction technology are more important indicator categories in the safety of urban railway tunnel construction, which should be paid more attention. Design and construction periods are also important for the safety of the urban railway tunnel. Combing the weight analysis of factors, R_{48} (construction team arrangement), R_{47} (sequence arrangement), and R_{42} (procedure selection) have the greatest centrality for construction safety of urban rail, and the calculations imply that the choice of technology and the effectiveness of its implementation have a dominant

influence on construction safety in urban railways during construction, which means we should pay full attention to the construction standards, reasonable construction arrangement, and team arrangement. This paper puts forward the important influencing factors that may have a great impact on the safety of urban railway tunnel construction, which can provide some reference for the construction of relevant projects and improve the investment efficiency. At present, further research is needed on the relationship of factors contained in the study and the impact degree on the project caused by the relationship between them. Therefore, it is necessary to conduct in-depth research on the practical cases of urban railway tunnel construction.

In this study, the risk factors were extracted using the LDA model, and based on this, the relationship between the influencing factors was investigated using the Dematel-ISM method. However, the process of determining the relationships between the factors relies heavily on expert scoring, which is highly subjective, and does not take into account the impact of information technology and industrial clustering on tunnel construction risks.

Data Availability

The raw data supporting the conclusions of this article will be made available by the authors, without undue reservation.

Conflicts of Interest

The authors declare that they have no conflicts of interest regarding this work.

Acknowledgments

References

[1] J. Michnik, "Weighted Influence Non-linear Gauge System(WINGS)-an analysis method for the systems of inter related components," *European Journal of Operational Research*, vol. 228, no. 3, 2013.

[2] M. Dytczak and G. Ginda, "Is explicit processing of fuzzy direct influence evaluations in DEMATEL indispensable?" *Expert Systems with Applications*, vol. 40, no. 12, pp. 5027–5032, 2013.

[3] C. Bai and J. Sarkis, "A grey-based DEMATEL model for evaluating business process management critical success factors," *International Journal of Production Economics*, vol. 146, no. 1, pp. 281–292, 2013.

[4] H. S. Lee, G. H. Tzeng, W. Yeih, J. W. Yu, and C. Y. Shing, "Revised DEMATEL:resolving the infeasibility of DEMATEL," *Applied Mathematical Modelling*, vol. 37, no. 10/11, pp. 6746–6757, 2013.

[5] M. Shakerian, A. Choobineh, J. Mehdi, M. Alimohammadlou, M. Nami, and J. Hasanzadeh, "Interactions among cognitive factors affecting unsafe behavior: integrative fuzzy DEMATEL ISM approach," *Mathematical Problems in Engineering*, vol. 2020, Article ID 8952624, 18 pages, 2020.

[6] X. Wan, Y. Zhang, R. Wang et al., "Causation of metro operation accidents in China: calculation of network node importance based on DEMATEL and ISM," *Complexity*, vol. 2021, Article ID 2397203, 16 pages, 2021.

[7] J. Chen, "Improved DEMATEL-ISM integration approach for complex systems," *PLoS One*, vol. 16, no. 7, 2021.

[8] Y. Zhang and Y. Song, "Identification of food safety risk factors based on intelligence flow and dematel-ism (decision making trial and evaluation laboratory-interpretive structural modeling)," *Dyna*, vol. 95, no. 1, pp. 418–424, 2020.

[9] P. Chen, B. Cai, M. Wu, and Y. Zhao, "Obstacle analysis of application of blockchain technology in power data trading based on improved DEMATEL-ISM method under fuzzy environment," *Energy Reports*, vol. 8, pp. 4589–4607, 2022.

[10] J. He and J. Zhu, "Key drivers of the emergency capabilities of integrated elderly services supply chains," *Information Resources Management Journal*, vol. 35, no. 1, pp. 1–20, 2022.

[11] Q. Zhang and Y. Xi, "Vulnerability and impact mechanism of urban waste resource utilization network," *Economics and Management*, no. 10, pp. 168–183, 2016.

Research Article

Analyzed and Simulated Prediction of Emission Characteristics of Construction Dust Particles under Multiple Pollution Sources

Wei Liu [1] Xiaohui Huang [1] Huapeng Chen,[1,2] and Luyao Han[1]

[1]School of Civil Engineering and Architecture, East China Jiaotong University, Nanchang 330013, China
[2]Civil Engineering Department of Engineering Science University of Greenwich, London, UK

Correspondence should be addressed to Wei Liu; liuweijx13@163.com and Xiaohui Huang; huangxiaohui_gz@163.com

Dust pollution in construction sites is an invisible hazard that is often ignored as a nuisance. Regulatory and engineering control methods are predominantly used for its mitigation. To control dust, dust-generating activities and their magnitudes need to be established. While researchers have comprehensively studied dust emissions of construction work, prediction of dust concentrations based on work phases and climatic conditions is still lacking. To overcome the above knowledge gap, this article selected two construction stages of a project to monitor dust generation using the HXF-35 dust sampler. Based on the collected data, dust emission characteristics of these two stages are studied, and dust emission characteristics under multiple pollution sources are analyzed. Based on the results, a BP neural network model is built to perform simulations of dust emission concentrations in different work areas and predict construction dust concentrations under different conditions. Except few, the majority of the work areas monitored have exceeded the allowable upper limit of TSP concentration stipulated by relevant standards. In addition, dust emission differences of work areas are pronounced. The results verified that the BP neural network dust concentration prediction model is feasible to be used to predict dust concentration changes in different work faces under different climate conditions and to provide a scientific base for pollution control. This study provides several practical solutions where the prediction of dust concentrations at designated work areas will allow construction companies early warning to implement mitigation measures before it becomes a serious health hazard. In addition, it provides an opportunity to re-evaluate those hazardous work in the light of these revelations. The outcome of this study is both original and useful for both construction companies and regulatory agencies. It can better predict the concentration of construction dust in different operating areas and different weather conditions and provide a guide for the prevention and control of construction dust.

1. Introduction

With the rapid economic development, China's construction industry has been ushered into a period of large-scale construction and infrastructure development. The increasing scale of construction activities, including building construction, building demolition, equipment installation, and so on, has aggravated particle pollution. The majority of construction activities are in-situ and organized in the open air. In addition, material transportation, loading and unloading, and stockpiles of earthwork cause large-scale unavoidable emissions. The large particles of these emissions tend to settle down near the construction site after being raised. However, small particles tend to flow with the wind

and enter the atmosphere to form suspended solids that are commonly known as construction dust [1]. According to past research, construction dust has been considered to be an important source of particle pollution [2–4].

The formation of construction dust has been widely studied by scholars for years, which included dust monitoring technologies [5], dust emission factors [6, 7], dust diffusion rules [8–10], dust pollution characteristics [11, 12], health hazard evaluation [13–15], and dust prevention and control measures [16]. So far, instrument sampling has been the most commonly used method to monitor construction dust particle concentration. Gao [17] measured the TSP (total suspended particulate) concentration using the HXF-35 dust sampler and the TSP as a monitoring index of

construction dust. In response to the complexity and uniqueness of construction sites, Ma [18] adopted unmanned aerial vehicles and image recognition technologies to design an automatic monitoring system of construction dust pollution sources and analyzed construction dust from three aspects: tests for construction dust pollution sources, identification of construction dust polluted areas, and characteristic comparison of construction dust pollution sources.

In order to quantify dust data acquired from monitoring, researchers have employed construction dust emission factors and emissions via three commonly used research methods [19]: exposure profiling method, four-dimensional Flux model, and Flux-FDM method. Tian [20] built a mathematical model, a four-dimensional flux model, which is similar to the exposure profiling method proposed by the U.S. Environmental Protection Agency, and a set of construction dust emission monitoring plan matched with this model. The model also combined the actually measured data of more than 40 construction sites for a quantitative assessment of emissions and emission factors of construction dust. After analyzing relevant data of a Tianjin building construction site, Zhao [21] set up the Flux-FDM model, which is used for the estimation of PM10 emissions of construction, and combined the dust emission factors and construction dust influencing factors obtained through the nonlinear fitting. They found wind velocity and the superficial dust water content are key factors that affect dust emissions. However, construction dust emission is not only subjected to the influence of climate factors, but also to the monitoring height, construction intensity, and other factors.

In the studies of emission characteristics of construction dust particles, Tian [22] studied the vertical and horizontal diffusion laws of construction dust at the boundary of the construction site by monitoring the change of the dust fall concentration near the construction site. They found construction dust fall concentration is inversely proportional to the square of height on the same plane of the construction site boundary. The same correlation was also observed between the dust concentration and the square of the distance from the monitoring point to the center on the same height. Li [23] chose typical residential construction projects in Beijing and set up dust concentration collection points in major work areas during three different periods, namely earthworks, frame, and partitions and interior decoration. They conducted on-site monitoring with TSP as the monitoring index. By comparing the dust pollution status of different construction activities, Li [24] analyzed dust emission characteristics and major distribution principles, and the results suggested that dust emissions of different construction activities significantly differed from each other in terms of their concentration, which, to be specific, showed that the dust concentration during the construction of frame is lower than that of the earthworks. The emission intensity of the former is more stable, and the overall dust concentration of the partitioning and interior decoration stage was high but stable. Hou [25] selected the construction sites in Mentougou District and Daxing District of Beijing as the monitoring objects and used the light scattering method and

the gravimetric method to measure the dust at different points of the construction site. The results suggested that the dust concentration distribution characteristics are different in different areas of the earthwork construction site. The dust concentration of the foundation pit is much higher than that of the main entrance and downwind area, and the construction site with poor dust prevention level is more likely to produce high-concentration dust pollution.

To sum up, researchers have comprehensively studied dust emissions characteristics of construction work, but most researches have focused on the analysis of the overall dust emission levels and characteristics of the entire construction site. Nevertheless, research into dust emissions characteristics of different work phases of construction is still lacking. The construction process is not homogenous and hence different work phases generate different dust concentrations, dust types, and hazards. A building's construction process goes through three distinctly unique stages: foundation, frame, and internal partitions/finishes. Different from the first two stages, the third mainly happens indoor. Therefore, dust generated during the third stage would not influence the external environment, and the dust characteristics are significantly different from those of the other two stages. Meanwhile, researchers have also done a lot of work in the prediction of construction dust particles. In the establishment of construction dust prediction models, researchers mostly use traditional multiple linear regression models [26, 27], but they have great limitations and cannot capture the relationship between the concentration of dust emission particles and dust monitoring factors, resulting in predictions are not accurate. While a back propagation (BP) neural network can overcome this limitation very well, it can build a very complex nonlinear model, which can well reflect the nonlinear relationship between particle concentration and dust monitoring factors [28].

Hence, in order to accurately portray the dust emission concentration of outdoor construction, this article mainly focuses on the first two stages, namely foundation and construction of the frame of a building. Based on the field data monitoring, dust emission characteristics of these two stages are studied, and dust emission characteristics under multiple pollution sources are analyzed. Meanwhile, a BP neural network model is built using the monitored data. This model is employed to perform simulation analysis of dust emission concentrations in different work areas and predict construction dust concentrations under different conditions.

2. Division of Work Areas and Layout of Monitoring Points

The foundation and construction of frames are the main stages of a building construction, whose activities are quite different. Foundation work mainly includes preparation of site, excavation, slope support, filling disposal, rebar processing, concreting, etc. Among them, excavation, slope support, and filling would form part of the foundation excavation. Therefore, the foundation excavation area is chosen as a monitoring point. Activities in the rebar processing area and concreting area differ from each other

TABLE 1: Profile of dust monitoring points.

Construction stage	Monitoring points	Construction dust types	Major activities
Foundation	Foundation excavation area	Silicious dust	Soil excavation, slope support, earthwork compaction
	Rebar processing area	Silicious dust	Rebar transportation, processing, and storage
	Concrete mixing area	Cement dust	Concrete mixing and transportation
	Road area	Silicious dust	Earthworks and construction material transportation
Structural frame	Floor area	Silicious dust	Rebar binding, erection of formwork, scaffolding work, and demolition
	Concrete mixing area	Cement dust	Concrete mixing and transportation
	Rebar processing area	Silicious dust	Rebar transportation, processing, and storage
	Timber formwork area	Timber dust	Timber formwork and other timber processing
	Road area	Silicious dust	Transportation of premixed concrete and other construction materials

significantly; therefore, they should be two separate monitoring points. The construction of the frame mainly covers formwork, bar bending, rebar processing, concrete mixing, concrete pouring, and timberwork. Additionally, activities such as formwork demolition and setup, floor rebar binding, concrete pouring, and scaffolding are all done on the construction floor or nearby. Since these work areas are close to each other and have a similar construction environment, the floor work area is set up as a monitoring point. Meanwhile, the rebar processing area, concrete mixing area, and timberwork area are set up as other monitoring points. Moreover, vehicles transporting construction materials during these two stages can easily raise road dust. Therefore, the road area where the vehicles travel in and out of the site was set up as a monitoring point. The profile of all monitoring points in this research is presented in Table 1.

As shown in Table 1, there are 9 monitoring points set up for the two construction stages. The type of dust in different work areas varies different, which primarily includes silicious dust, cement dust, and timber dust. As the most commonly seen dust type, silicious dust generally comes from the soil, which is diffused into the air through natural wind and by vehicles. Cement dust is generally caused by the dust settlement during the loading and unloading of cement bags, transportation process, and dust diffusion during the feeding process, which is common in the concrete mixing area. Timber dust refers to the dust generated during the erection of timber formwork [29].

3. Construction Dust Monitoring

3.1. Monitoring Index, Equipment, and Methods. At present, there are four main monitoring indicators to measure construction dust, namely dust fall, TSP, PM10, and PM2.5. The total suspended particle (TSP) is defined as the suspended particle whose aerodynamic diameter is smaller than $100\,\mu$m, and from a particle size perspective, TSP includes particulate matter 10 (PM10) [30]. The increasing mass concentration of TSP in the air can increase the morbidity of chronic obstructive pulmonary diseases, cardiovascular diseases, cerebrovascular diseases, and acute respiratory tract infections [31, 32]. Compared with direct monitoring of PM10 concentrations, monitoring TSP concentrations is less expensive and simpler to operate and can increase the

density of monitoring sites and enable larger data collections [33]. Therefore, considering the scientificity and operability of monitoring indicators, combined with the consideration of construction site conditions and dust monitoring costs, the TSP concentration in the air is chosen as the construction dust monitoring indicator. In this research, the TSP concentration is monitored using the dust sampler HXF-35. Measurement results of this instrument can accurately reflect the position and occurrence time of dust pollution and realize multipoint simultaneous monitoring to acquire mass data.

This research refers to the Chinese national standard, "Determination of Dust in the Air of Workplace–Part 1: Total Dust Concentration" and uses the filter membrane increment method for measurement. Before sampling, the filter membrane is weighed. During the process of sampling, the dust sampler HXF-35 is installed on an A-frame holder. Under the obligation of not influencing the construction operations, the sampling point can be kept as close to the operator as practically possible, and the sampling flow rate is set to be 20 L/min. After the end of sampling, all samples are taken back to the lab for weighing and data recording. The TSP concentration can be given by the following equation:

$$c = \frac{m_2 - m_1}{V * t} * 1000, \tag{1}$$

where c denotes the total dust concentration (mg/m^3), m_2 denotes the membrane quality after sampling (mg), m_1 denotes the membrane quality before sampling (mg), V denotes the sampling flow (mg), and t denotes the sampling time (min).

Because of sharp differences in dust concentration at different monitoring points, the monitoring points should be selected according to the practical situations. If there is no serious dust within the vicinity, the sampling time should be above 60 min. If the monitoring point is severely affected by pollution, the sampling time should be controlled within 30 min. The dust concentration of every monitoring point should be monitored for at least four different periods of a day to ensure the completeness and accuracy of dust data. In addition to dust monitoring of different work areas, meteorological data should be recorded, including, temperature, wind velocity, and humidity.

(a)

(b)

(c)

(d)

Figure 1: Location of the project.

3.2. Overview of the Project Monitored. This research chose a residential construction project in the Donghu District of Nanchang, as shown in Figure 1. Nanchang is located at $115°27'$ $-116°35'$ E and $28°10'$ $-$ $29°11'$ S, which is characterized by a moist monsoon climate of the mid-subtropical region with a pleasant temperature and ample sunlight. The average annual temperature of Nanchang is between $17°C$ and $18°C$, and its average annual precipitation is around 1,600 mm. The meteorological conditions in Nanchang are characterized by a high frequency of calm wind, a high frequency of atmospheric stability, and a high frequency of near-earth inversion layers. The frequencies of calm winds in the four seasons are 25.9%, 24.8%, 21.4%, and 26.6%, respectively. During the calm wind period, the wind speed is small, about grades 1-2, and the temperature inversion phenomenon lasts for a long time, which inhibits the diffusion and dilution of atmospheric pollutants in Nanchang. According to relevant researches, calm wind and temperature inversion are the most important meteorological conditions that cause serious air pollution [34].

TABLE 2: Concentrations of dust at different monitoring points of work areas.

Construction periods	Dust monitoring points	Dust types	Average concentration (mg/m³)	Scope of excess multiple	Measurement point yield (%)	Variance
Foundation	Foundation excavation area	Silicious dust a	0.988	0.000–0.320	72.000	0.042
	Rebar processing area	Silicious dust a	1.103	0.000–0.590	70.000	0.082
	Concrete mixing area	Cement dust b	7.392	0.000–3.440	37.000	10.017
	Road area	Silicious dust a	4.287	0.000–5.650	13.000	3.391
Structural frame	Floor area	Siliciousdust a	1.148	0.000–0.600	60.000	0.066
	Concrete mixing area	Cement dust b	2.093	—	100.000	0.791
	Rebar processing area	Silicious dust a	1.374	0.000–0.740	38.000	0.127
	Timber formwork area	Timber dust c	8.697	0.000–3.740	12.000	4.855
	Road area	Silicious dust a	2.124	0.000–2.200	30.000	0.860

Note. The concentration of silicious dust, cement dust, and timber dust is a, PC-PWA = 1 mg/m³, b, PC-PWA = 4 mg/m³, and c, PC-PWA = 3 mg/m³ [35], respectively.

4. Dust Concentration Emission Characteristics

4.1. Dust Concentration Monitoring Result.
According to the "Occupational Exposure Limit for Hazardous Agents in the Work-place," it can be seen that the standard limit of dust concentrations is related to dust types. In order to compare the dust emission concentration of different work areas, this article chose the standard limit for different types of dust concentration to calculate the average concentration, excess multiple, measurement point yield, and other indices, as shown in Table 2.

As shown in Table 2, the average construction dust concentration of the foundation during excavation is 0.988, which is the lowest of value and falls within the allowable limit of the silicious dust. There are two reasons for this. Firstly, the soil water content in the construction area is high, which retards the formation of dust. Secondly, earthwork is mainly carried out by large machinery, whose tracks can help consolidate the soil beneath, preventing the generation of dust. The dust emissions of the road area and the concrete mixing area are severe. The average dust concentration, dust concentration peak, and sample variance of the concrete mixing area are 7.392, 17.760, and 10.017, respectively, which are considerably higher than those of other work areas. The average dust concentration of the road area is 4.287, which is around four times the average dust concentration of the foundation area and rebar processing area. This suggests that concrete processing and vehicular traffic are the main sources of dust during the foundation work.

During the construction of the frame, the average dust concentration of timber formwork area is 8.697, which is around eight times the average of the floor area and exceeds the average of the concrete mixing area and the road area by four-folds. The measurement point yield of the work area is just 12%, meaning that the dust emissions are severe in the timber formwork area and also constitute the main dust source of this stage. This is mainly caused by a tight workspace, which slows down dust diffusion. Emissions from the road area are the second largest for this stage, whose average dust concentration, measurement point yield, and sample variance are all below those of the timber formwork area. The average dust concentration of the concrete mixing area is below that of the floor work area and the rebar processing area. The dust concentration of the concrete mixing area is within the allowable standard, its exceeding multiple is 0, and its measurement point yield is 100%. All these data suggest that dust emissions of the concrete mixing area are slightly lower than those of the floor area and the rebar processing area. Compared with the floor work area, the rebar processing area has a higher average concentration, exceeding multiple, and measurement point yield, implying that dust emissions of the latter are more severe than those of the former; because the dust pollution in the vertical direction of the spread is limited, the dust concentration of the floor area decreases constantly with the increase of floors.

4.2. Comparison of Construction Dust in the Same Work Area but at Different Stages.
Table 3 summarizes the average construction dust concentration, average exceeding multiple, and variation of the indices during earthwork and structural frame stages. Overall, with the exception of the rebar processing area, a decrease in the average construction dust concentration and average exceeding multiple could be observed, when construction activities move from the foundation to the structural frame.

Based on average concentration, emissions in the rebar processing area are on an upward trend, because of the heavy demand placed on rebar for the structural frame. Though road area is the major dust source during foundation, it decreases by more than 50% when construction moves to the

TABLE 3: Comparison of construction dust in the same work area at different stages of construction.

Monitoring point	Average concentration (mg/m^3)			Average exceeding multiple		
	Foundation	Structural frame	Variation	Foundation	Structuralframe	Variation
Rebar processing area	0.988	1.374	39.070	0.590	0.740	25.420
Concrete mixing area	7.392	2.089	−71.730	3.440	0.000	−100.000
Road area	4.287	2.124	−50.450	5.650	2.200	−61.060

structural frame. There are two main reasons for the decline. Firstly, there is more bare soil during the earthwork as most pavements have not been hardened. However, by the time construction moves over to the structural frame, most of these road surfaces are hardened, reducing dust raised by vehicles. Secondly, during the structural frame, there are fewer vehicles transporting soil from and to the site. The dust concentration of concrete mixing during earthworks is three times higher than that of structural frame. This is mainly because concrete is transported using a pump for pouring into the formwork, whereas for foundation, a pump is not used. The cement, before entering the compression pump, has full contact and reaction with water and aggregates, thus evading the generation of cement dust.

From the average exceeding multiple perspective, vehicle movements cause severe dust during both foundation and structural frame stages. As to dust emissions of the rebar processing area and the road area, their average exceeding multiple varies significantly and drops by a large margin. In particular, the average exceeding multiple of the concrete mixing area during the structural frame has dropped to zero.

4.3. Comparison of Work Areas with Major Construction Dust Emissions. Table 4 summarizes work areas with severe construction dust emissions in the two stages. During foundation work, road area, concrete mixing area, and rebar processing area are the main dust-generating areas. However, during the construction of structural frame, timber formwork area, road area, and rebar processing areas have emerged as major dust-generating areas.

A comparison of average dust concentration and average exceeding multiple of the three work areas is shown in Figure 2. The highest average excess multiple is found for the road area, which is five times as high as that of the other two. Hence, these three work areas should be the key areas for construction dust prevention and control during construction.

5. Establishment of Dust Concentration Prediction Model Based on the BP Neural Network

Considering the complexity of building construction process, multiple work phases, high emission randomness, and difficulty of quantifying dust pollution, it is very important to model dust concentrations at different work phases. Therefore, this research conducts a simulation prediction of dust particle concentration at different work areas in an attempt to build a construction dust particle concentration prediction model using the BP neural network.

TABLE 4: Comparison of work areas with severe dust emissions.

Serial number	Foundation	Structural frame
1	Road area	Timber formwork area
2	Concrete mixing area	Road area
3	Rebar processing area	Rebar processing area
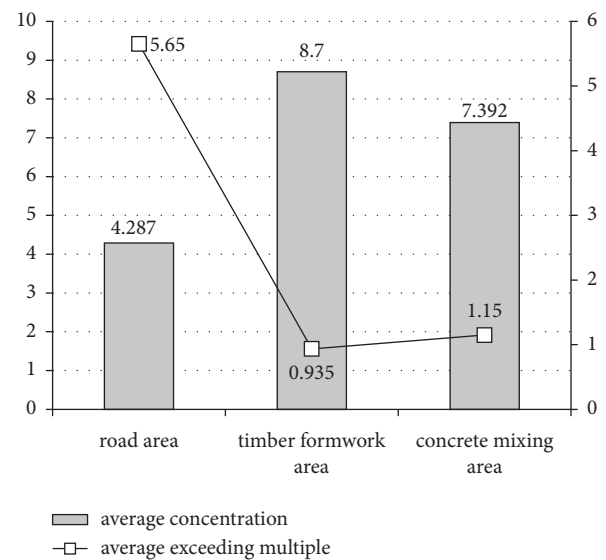
FIGURE 2: Comparison of dust concentration and excess multiple in work areas with severe emissions.
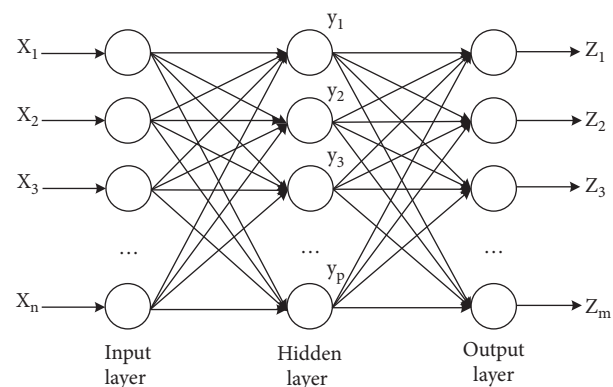
FIGURE 3: BP neural network structure.

5.1. Overview of the BP Neural Network. As one of the most widely used models, the BP neural network has found applications in many fields [36–38]. The BP neural network is defined as a feedforward neural network or backpropagation
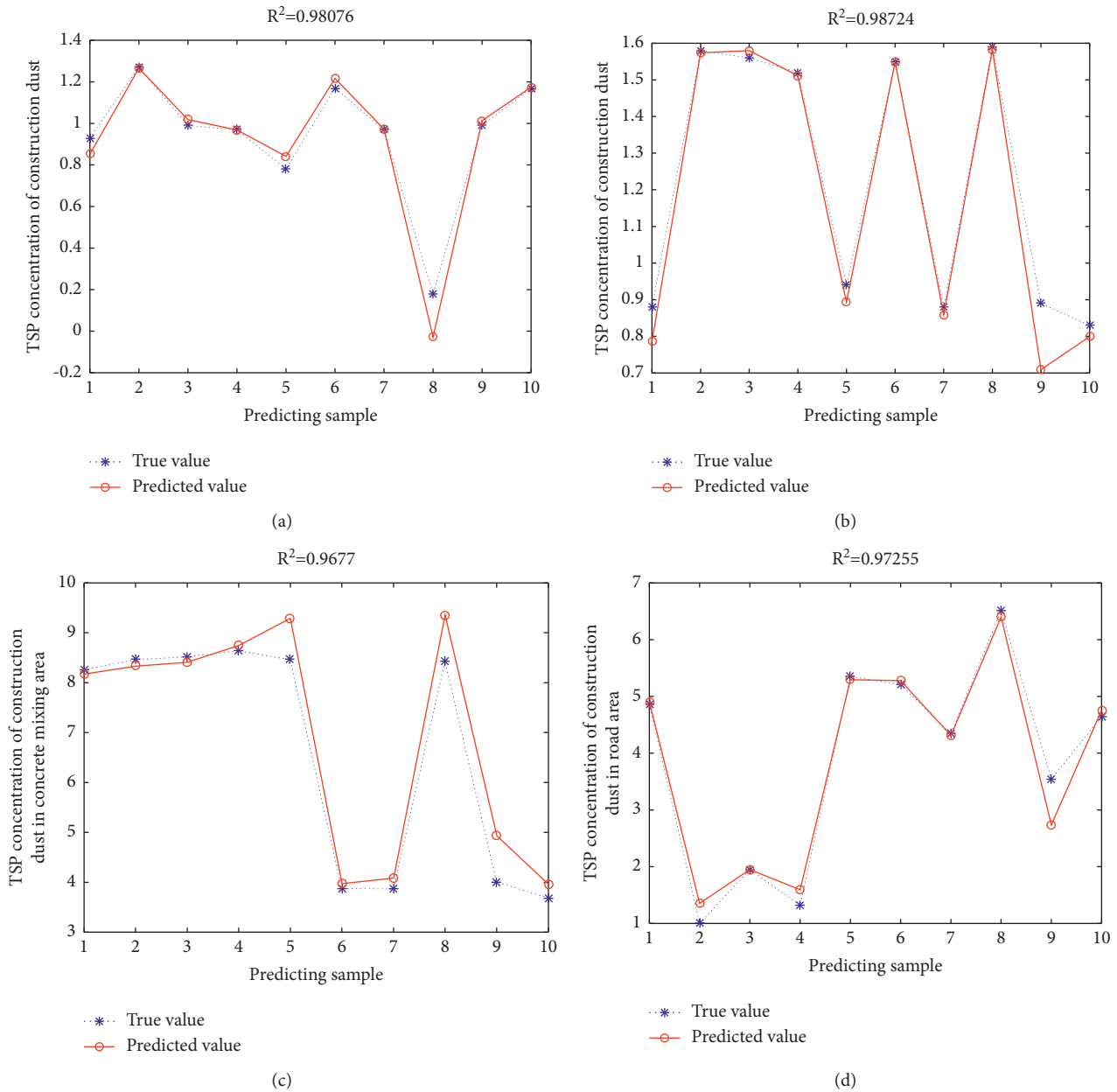
FIGURE 4: Comparison between the predicted values and the measured values of dust particle concentration during the foundation stage: (a) foundation excavation area, (b) rebar processing area, (c) concrete mixing area, and (d) Road area.

neural network, which is characterized by the forward propagation of signals and backward propagation of errors. Generally speaking, the BP neural network consists of the input layer, hidden layer, and output layer [39], and its structure is presented in Figure 3. The optimization capacity of the BP neural network has a close bearing on its structure—a structure characterized by variability, nonlinearity, error tolerance, self-adaption, and autonomous learning.

5.2. Dust Concentration Prediction Model. The neural network model adopted in this research to build the construction dust concentration prediction model features a three-layer network structure, in which there are three neurons in the input layer, namely the temperature, moisture, and wind velocity [40]. The initial hidden layer has 20 neurons, and the output layer has one neuron that is dust concentration. In other words, it is a model with a 3-20-1 three-layer network structure. Meanwhile, MATLAB2016a is adopted as the numerical computing platform. Before prediction, the BP neural network should first receive network model training to get equipped with the ability of memorization and prediction. To the end, the "Rand" function is used to acquire 60 samples from every monitoring point, and the first 50 samples are adopted as the training set, while the other 10 as the test set. The iteration items are set as 100, and the learning rate is taken as 0.01.

TABLE 5: Dust particle concentration of different work areas.

Construction periods	Work areas	$R2$
Foundation	Foundation excavation area	0.9807
	Rebar processing area	0.9872
	Concrete mixing area	0.9677
	Road area	0.9726
Structural frame	Floor area	0.9749
	Concrete mixing area	0.9097
	Rebar processing area	0.9556
	Timber formwork area	0.9608
	Road area	0.9988

TABLE 6: Regression analysis results of the predicted output and the target data of different work areas.

Construction stage	Work areas	Training	Validation	Test	All
Foundation	Foundation excavation area	0.9937	0.9459	0.9833	0.9859
	Rebar processing area	0.9968	0.9135	0.9583	0.9746
	Concrete mixing area	0.9821	0.869	0.9098	0.9586
	Both sides of road	0.9986	0.9913	0.9966	0.9973
Structural frame	Floor area	0.9917	0.9777	0.9908	0.9837
	Concrete mixing area	0.9986	0.9894	0.9988	0.9962
	Rebar processing area	0.9962	0.9956	0.9721	0.9921
	Timber formwork area	0.9968	0.7586	0.9442	0.9885
	Both sides of road	0.9996	0.9949	0.9953	0.9978

5.3. Dust Concentration Simulation of Different Work Areas. The model with a 3-20-1 network structure thus built is used to conduct simulated prediction of various work areas. Figure 4 shows the actually measured values and predicted values of the dust emission concentration of different work areas of the foundation stage. Table 5 shows the correlation coefficient of simulation prediction of different work areas during the foundation and structural frame stages. Hence, R2 below denotes the decision coefficient of regression analysis, which is 0.9807, 0.98724, 0.9677, and 0.97255 in the foundation area, rebar processing area, concrete rebar area, and road area of the foundation stage, respectively. The prediction results and the actually measured value show a high degree of fitting, indicating favorable simulation prediction effects as shown in Figure 4. From Table 5, it can be seen that R2 of the floor work area, concrete mixing area, rebar processing area, timber formwork area, and road area are 0.9749, 0.9097, 0.9556, 0.9608, and 0.9988, respectively. Combining the results of Table 4 with the results of Figure 4, the neural network training results of different work areas in the structural frame stage are favorable.

Table 6 shows the regression results of the predicted output and the target data of different work areas during the two stages. Figure 5 shows the regression analysis results of the predicted output and the target data of the road area during the structural frame stage, where training, validation, test, and all represent the regression coefficient R of the training samples, verification samples, test samples, and integrated samples, respectively. The regression coefficients are above 90% as shown in Table 6 and are generally close to 1. By combining the results demonstrated in Figure 5, it is concluded that the model generates favorable simulation prediction results. It also shows the feasibility of developing a construction dust emission

concentration prediction model based on the BP neural network.

6. Discussion

Research results suggest that, during the construction period, dust emissions of different work areas differ from each other significantly, which aligns with the previous research findings [41]. However, numerical simulations of construction dust at present are mostly based on the gas-solid two-phase flow theory to simulate the diffusion based on rules of the wind velocity, height of the generation source, and dust concentration [42, 43]. It is not based on the characteristics of on-site construction activities and their influences on dust emissions. This is a major gap in the extant literature, and hence some of the highly polluting areas are neglected in auditing and monitoring schemes. In order to fill the above gap in the knowledge, this research chose the wind velocity, temperature, and moisture as input factors to build a construction dust simulation prediction model for different work areas of a construction site, focusing primarily on two work stages that happen in the open air. Hence, the model considers not only the influence of the meteorological conditions, but also the influence of construction activities on dust emissions. The regression coefficients show that the predicted values and the measured values demonstrate good agreement. Therefore, the established model should be capable of well-predicting construction dust concentration changes in different work areas and under different weather conditions and providing a scientific base for its control, diffusion, and pollution.

In order to verify the validity of the construction dust prediction model, ten test samples are randomly chosen
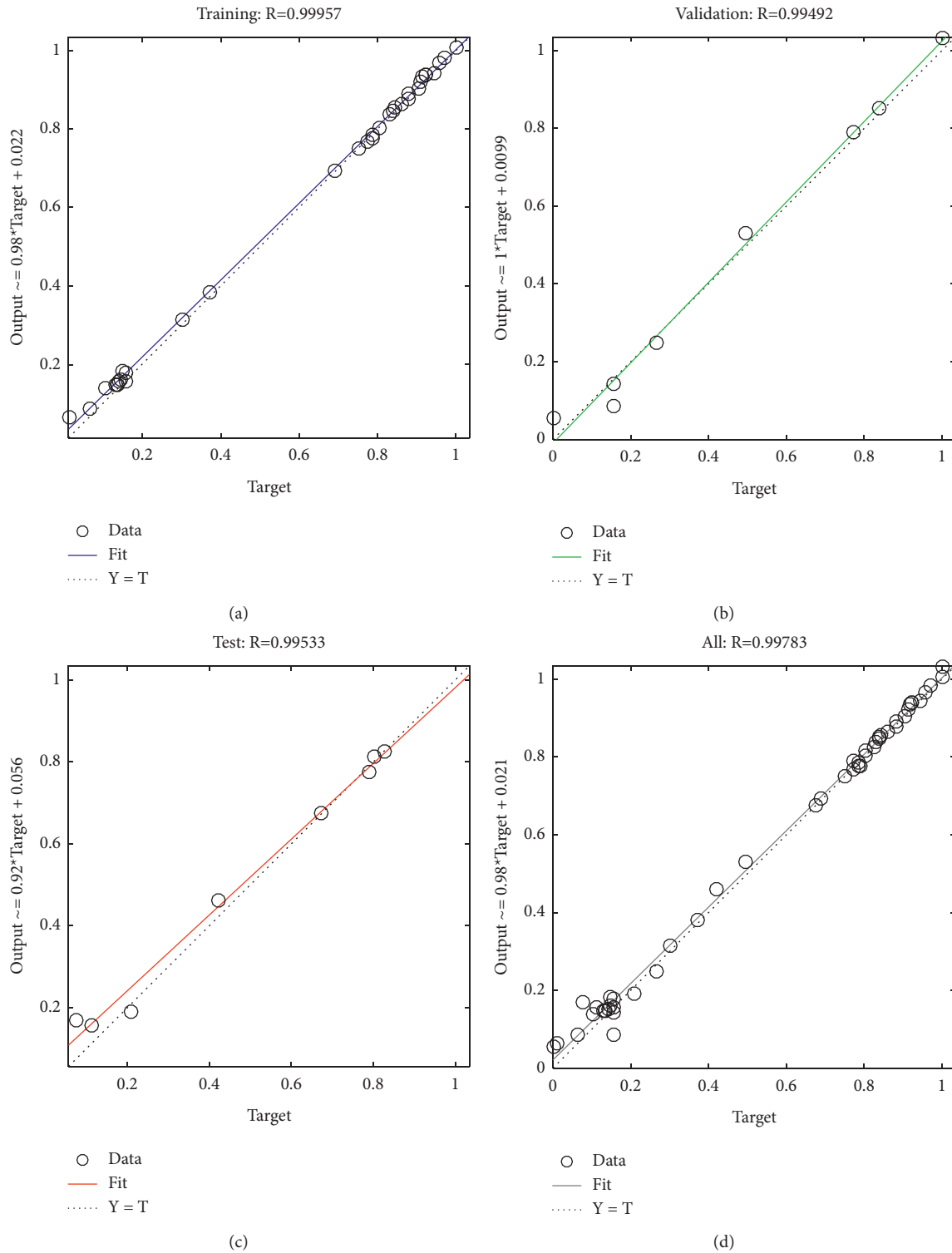
Figure 5: Regression analysis results of the road area during the structural frame stage: (a) training: $R = 0.99957$, (b) validation: $R = 0.99492$, (c) test: $R = 0.99533$, and (d) all: $R = 0.99783$.

from the road area during the construction of the structural frame for prediction as shown in Table 7. The relative error between the predicted values and the actual values of the ten samples are all around 0.01, meaning that the construction dust prediction model proposed by this article can obtain favorable results. In addition, the neural network construction dust prediction model is easy to use and well demonstrate the prediction results in the form of curves. The prediction of dust concentrations in different work areas of a construction site has several positive implications. It allows the construction company to monitor dust levels at different stages of work and plan strategic interventions before it is

TABLE 7: Predicted results of the road area during the structural frame.

Index	1	2	3	4	5	6	7	8	9	10
Measured value	2.65	2.58	2.98	0.87	2.98	3.18	0.95	3.20	3.15	2.65
Predicted value	2.64	2.62	3.04	0.93	3.01	3.19	0.99	3.15	3.15	2.64
Relative error (%)	0.32	1.91	1.88	4.27	1.11	0.53	3.99	1.44	0.06	0.32

too late. It could prevent dust-related long-term illnesses among workers who are routinely involved in such tasks.

For example, an investigation by the Australian Broadcasting Cooperation (ABC, 2019) revealed that the workers who are involved in installing stone kitchen bench-tops have reported silicosis due to exposure to silica dust (http://www.aap.com.au/,2019). The report states "doctors are worried Australia is facing the worst occupational lung disease crisis since the peak of the asbestos disaster" as number of stonemasons in New South Wales, Victoria, Australian Capital Territory, and Queensland have been reported to the hospital with accelerated silicosis of alarming levels. However, the builders involved in residential construction in Australia have never been on the spotlight for any violation of WHS laws related to dust pollution. The reason is, construction dust is considered as "nuisance dust" because most auditing and monitoring (if all happens) is based on the overall measurement results rather than on designated areas. Based on these overall measurements, the site does not exceed the regulatory thresholds set by the Environmental Project Agency (EPA) of Australia. However, if measurements were taken at different work areas, some areas could be well above those limits. Therefore, the prediction of dust concentrations at designated work areas should be a high priority for construction companies. Furthermore, regulatory agencies should avoid blanket rulings on construction sites as different activities have varying dust generation potential, some of which could be very harmful to workers and the neighboring community.

7. Conclusion

Due to the complexity, continuity, and time-varying characteristics of construction dust emissions, traditional regression prediction models cannot accurately predict the concentration of the dust emissions. Therefore, in order to simulate construction dust under multiple pollution sources, this article monitored dust emissions during two important stages of a residential construction project, namely foundation and structural frame. The study identified training and learning samples for the neural network, compiled the learning and training algorithm, and built the neural network model reflecting dust emission concentrations in different work areas. Based on the results of simulation prediction, the output data of the BP neural network model demonstrate a favorable and ideal correlation, and compared with the traditional regression model, the dust concentration prediction model established by the BP neural network is feasible to be used to predict dust concentration changes in different work areas and under different climate conditions, which can provide a scientific base for pollution control.

The majority of work areas have exceeded the allowable upper limit of TSP concentration stipulated by relevant standards. This means that most work areas are suffering from the serious concentration of dust pollution under multiple pollution sources. The dust emission differences of work areas are pronounced. To be specific, the areas with serious dust emission concentrations during foundation include the road area, concrete mixing area, and rebar processing area. The areas with serious dust emission concentrations during the construction of structural frame include the timber formwork area, road area, and rebar processing area. While the road area in foundation construction, concrete mixing area, and wood formwork area in structure construction are the key areas of dust emission in construction period.

The prediction of dust concentrations in designated work areas will provide construction companies with an early warning to implement mitigation measures before it becomes a serious health hazard. In addition, it provides an opportunity to re-evaluate those hazardous work in the light of these revelations. Although this study showed that the BP neural network could develop such early warning, the study only used two stages of a long and laborious construction process as a demonstration. Further research is needed in other stages and activities to evaluate the true potential of BP neural network simulations and to demonstrate their suitability. Further research into other stages of construction could reveal activities that are prone to severe dust emissions which at present are not considered as hazardous by builders or regulatory bodies.

Data Availability

The data used to support the findings of this study are available from the corresponding author upon request.

Conflicts of Interest

The authors declare that there are no conflicts of interest regarding the publication of this article.

Acknowledgments

References

[1] M. C. Todd and C. Cavazos-Guerra, "Dust aerosol emission over the sahara during summertime from cloud-aerosol lidar with orthogonal polarization (CALIOP) observations," *Atmospheric Environment*, vol. 128, pp. 147–157, 2016.

[2] Y. Huang, C. J. Hu, H. R. Cheng, and Z. Wang, "Emission inventory and spatial distribution characteristics of particulate matters from dust source in Wuhan, China," *Journal of Wuhan University (Natural Science Edition)*, vol. 64, no. 4, pp. 354–362, 2018.

[3] B. Lu, J. Dong, and Z. Xiang, "Discussion on Hangzhou dust pollution control measures," *Environmental Science and Management*, vol. 38, no. 07, pp. 83–86, 2013.

[4] S. Vardoulakis and Kassomenos, "Sources and factors affecting PM10 levels in two European cities: implications for local air quality management," *Atmospheric Environment*, vol. 42, no. 17, pp. 3949–3963, 2008.

[5] F. Fang and Y. L. Ding, "Comparative research and analysis of manual monitoring and online monitoring of dust on building construction sites," *China Population, Resources and Environment*, vol. 27, no. S1, pp. 45–47, 2017.

[6] H. Xiao, X. C. Yang, Q. C. Wu et al., "Estimate emissions of construction fugitive dust in Xi'an," *Acta Scientiae Circumstantiae*, vol. 39, no. 1, pp. 222–228, 2019.

[7] G. E. Muleski and C. Cowherd, *Particulate Emission Measurements from Controlled Construction Activities*, Midwest Research Institute, Kansas City, 2001.

[8] N. Stevulova, A. Estokova, M. Holub, and Singovszka, "Characterization of demolition construction waste containing asbestos, and the release of fibrous dust particles," *Applied Sciences*, vol. 10, no. 11, p. 4048, 2020.

[9] Y. F. Xue, Z. Zhou, Y. H. Huang, T. Nie, L. Nie, and J. P. Qin, "Fugitive dust emission characteristics from building construction sites of Beijing," *Environmental Sciences*, vol. 38, no. 06, pp. 2331–2337, 2017.

[10] Y. H. Huang, G. Tian, J. P. Qin, G. Li, and B. L. Yan, "Characteristics of fugitive dust pollution in different construction phases," *Environmental Sciences*, vol. 28, no. 12, pp. 2335–2888, 2017.

[11] L. K. Zhang, L. J. Li, L. Jiang et al., "Spatial and temporal distribution characteristics and fugitive dust emission of building sites in Beijing," *Environmental Sciences*, vol. 40, no. 01, pp. 135–142, 2019.

[12] S. Liang, Q. Y. Fu, Q. Z. Liu et al., "The pollution characterizations of fugitive dust of a typical construction site during the structure construction period in autumn in Shanghai," *Environmental Pollution and Control*, vol. 40, no. 12, pp. 135–142, 2018.

[13] D. E. Van, A. Pronk, S. Spaan et al., "Quartz and respirable dust in the Dutch construction industry: a baseline exposure assessment as part of a multidimensional intervention approach," *Annals of Occupational Hygiene*, vol. 58, no. 6, pp. 724–738, 2014.

[14] X. D. Li, S. Su, and T. J. Huang, "Health damage assessment model for construction dust," *Journal of Tsinghua University*, vol. 55, no. 1, pp. 50–55, 2015.

[15] J. Li, P. Mao, J. W. Wei, L. Y. Jin, and J.-F. Yuan, *Journal of Civil Engineering and Management*, vol. 35, no. 06, pp. 208–214, 2018.

[16] N. E. Tjoe, S. Hilhorst, T. Spee et al., "Dust control measures in the construction industry," *Annals of Occupational Hygiene*, vol. 47, no. 3, pp. 211–218, 2003.

[17] Y. J. Gao, J. W. Huo, and X. C. Jia, "Research into dust monitoring and measures of construction sites based on big data," *Building Structure*, vol. 49, no. S1, pp. 1003–1007, 2019.

[18] G. X. Ma, Y. Han, J. F. Lu, J. Yao, and S. You, "Design and implementation of automatic monitoring system for constructional fugitive dust pollution sources based on UAV," *Environmental Monitoring in China*, vol. 34, no. 01, pp. 151–156, 2018.

[19] Q. Jia, A. A. Nadhir, and K. Sven, "Measurement of dust emission from a road construction using exposure-profiling method," *Natural Science*, vol. 5, no. 12, pp. 1255–1263, 2013.

[20] G. Tian, Y. H. Huang, and G. Li, "Establishment and application of four-dimensional fluxes emission factor model for construction fugitive dust," *Environmental Sciences*, vol. 30, no. 04, pp. 1003–1007, 2009.

[21] P. S. Zhao, Y. C. Feng, Y. F. Zhang et al., "Research and application of quantitative model of construction dust emission factors," *China Environmental Science*, vol. 29, no. 06, pp. 567–573, 2009.

[22] G. Tian, G. Li, B. L. Yan, Y. H. Huang, and J. P. Qin, "Spatial dispersion laws of fugitive dust from construction sites," *Environmental Sciences*, no. 01, pp. 259–262, 2008.

[23] X. D. Li, S. Su, T. J. Huang, Y. Lin et al., "Monitoring and comparative analysis of construction dust at earthwork and main structure construction stages," *China Safety Science Journal*, vol. 24, no. 05, pp. 126–131, 2014.

[24] X. D. Li, S. Su, and T. J. Huang, "Field monitoring and analysis of fugitive dust in construction at rough decoration stage," *China Safety Science Journal*, vol. 24, no. 08, pp. 103–106, 2014.

[25] Y. F. Hou, M. Xing, and Y. Pan, "Analysis of dust emission characteristics and key influencing factors of construction sites in Beijing earthwork stage," *Environmental Pollution and Prevention*, vol. 43, no. 02, pp. 171–177+181, 2021.

[26] H. H. Xie, X. F. Ma, and Y. P. Zhao Y, "Prediction of dust dispersion in highway construction based on regression prediction," *Highways*, vol. 66, no. 05, pp. 89–92, 2021.

[27] Q. R. Fu, "Research on haze prediction method based on multiple linear regression," *Computer Science*, vol. 43, no. S1, pp. 526–528, 2016.

[28] L. Z. Shi, Q. H. Deng, and C. Lu, "Prediction of PM(10) mass concentration of atmospheric particulate matter based on BP artificial neural network," *Journal of Central South University*, vol. 43, no. 05, pp. 1969–1974, 2012.

[29] M. Y. Cheng, C. L. Wu, and Y. P. Lin, "Analysis of dust pollution characteristics of construction engineering sites in Shenzhen," *Technology and Market*, vol. 24, no. 04, pp. 163-164+166, 2017.

[30] D. Tartakovsky, D. M. Broday, and E. Stern, "Evaluation of AERMOD and CALPUFF for predicting ambient concentrations of total suspended particulate matter (TSP) emissions from a quarry in complex terrain," *Environmental Pollution (Amsterdam, Netherlands)*, vol. 179, pp. 138–145, 2013.

[31] N. H. Hsieh and C. M. Liao, "Assessing exposure risk for dust storm events-associated lung function decrement in asthmatics and implications for control," *Atmospheric Environment*, vol. 68, pp. 256–264, 2013.

[32] Z. H. Zhang and F. Wu, "Health impairment due to building construction dust pollution," *Journal of Tsinghua University*, vol. 48, no. 06, pp. 922–925, 2008.

[33] T. J. Huang, X. D. Li, S. Su, and S. K. Liu, "Monitoring and analysis of dust pollution during earthwork construction stage of construction engineering," *Journal of Safety and Environment*, vol. 14, no. 03, pp. 317–320, 2014.

[34] C. X. Yan, X. Zhou, and H. M. Zhang, "Study on the temporal and spatial variation characteristics and influencing factors of ambient air pollution in Nanchang City," *Resources and Environment in the Yangtze River Basin*, vol. 28, no. 06, pp. 1446–1459, 2019.

[35] GBZ 2 1 2007, *Occupational Exposure Limits for Hazardous Agents in the Workplace*, Ministry of Health of the People's Republic of China, China, 2007.

[36] N. Kumari, S. Garg, A. Singhal et al., "Optimizing pretreatment of *Leucaena leucocephala* using artificial neural networks (ANNs)," *Bioresource Technology Reports*, vol. 7, Article ID 100289, 2019.

[37] J. Zhao, Y. F. Tao, and A. H. Wang, "Application of BP neural network algorithm to professional machinery quick design," *Machinery Design & Manufacturer*, vol. 57, no. 07, pp. 34–38, 2019.

[38] B. L. Sun, H. Sun, C. N. Zhang, J. Shi, and Y. Zhong, "Forecast of air pollutant concentrations by BP neural network," *Acta Scientiae Circumstantiae*, vol. 37, no. 05, pp. 1864–1871, 2017.

[39] D. L. Zhang, D. N. Huang, and C. Zhang, "Application of BP neural network based on genetic algorithm in the inversion of density interface," *Journal of Jilin University (Earth Science Edition)*, vol. 47, no. 02, pp. 580–588, 2017.

[40] S. B. Fan, G. Li, and G. Tian, "Fugitive dust emission characteristics from construction site by field measure," *Environmental Science & Technology*, vol. 34, no. S2, pp. 209–211+266, 2011.

[41] P. Zhao, Z. F. Li, and R. Y. Deng, "Numerical simulation of dust diffusion characteristics during earthwork construction," *Journal of Safety and Environment*, vol. 21, no. 04, pp. 1743–1749, 2021.

[42] J. T. Deng, Y. D. Huang, and Q. Zhang, "A CFD study on effects of fence height on migration and diffusion of construction dust," *Environmental Engineering*, vol. 32, no. 04, pp. 83–86, 2014.

[43] L. R. Wu and D. Wang, "Stimulation of dust migration and concentration change law during powered support advance in fully mechanized top-coal caving face based on Fluent," *Mining Safety & Environmental Protection*, vol. 42, no. 05, pp. 29–33, 2015.

Hindawi

Research Article

Design of Optimization Algorithm for Configuration of Amateur Sports Training Equipment in Smart City Community

Yuehong Wan [ID] [1] **and Hong Tang**[2]

[1]*Physical Education College of Jiangxi Normal University, Nanchang 330022, China*
[2]*School of Information Engineering, East China Jiaotong University, Nanchang 330013, China*

Correspondence should be addressed to Yuehong Wan; 002409@jxnu.edu.cn

Community amateur sports training equipment is necessary to ensure the development of national fitness activities. It is found that the design concept of community public sports space in China is not perfect, the structural layout is not reasonable, the stock space is not optimized, and the resource allocation is not balanced. In particular, there is a lack of indoor fitness facilities and sports venues in the community, and the people's "fitness where to go" is still a difficult problem. In the smart city construction, the resource integration and optimization of community amateur sports training facilities have also been further developed. Considering various influencing factors, this paper establishes a location model of community amateur sports training facilities with the least total cost and convenience. Aiming at the practical optimization problem with high complexity, an improved adaptive weight multiobjective particle swarm optimization (PSO) model is proposed. These parameters in the algorithm were adjusted dynamically, which balanced the overall search ability and partial improvement ability of the PSO algorithm and completed the optimal scheduling of community amateur sports training equipment configuration while ensuring the optimal global solution. Experimental results show that the algorithm's efficiency and searching ability have been further promoted. It also has an excellent performance in solving the complex location problem of community amateur sports training facilities.

1. Introduction

In January 2019, the CPC Central Committee clearly proposed to take people's yearning for a better life as the starting point and focus of spatial planning [1]. Improve the quality of the living environment [2]. Improve the quality of people's life [3]. Community amateur sports facilities are an important carrier for public fitness activities [4]. It is a necessary condition to ensure the development of national fitness activities. For improving national physical quality. Achieve high quality of life. The cause of national fitness continued to develop. The supply and service level of community amateur sports facilities continued to improve. The "six sides" project of national fitness has been preliminarily constructed as the main content. A relatively sound public service system for national fitness covering urban and rural areas [5]. According to the report on the development

of Chinese mass sports (2014) issued by the State Administration of sports in 2014. The number of sports parks in China is 1662, according to the statistical survey data of national sports venues in 2019. In 2019, there will be 823500 national fitness paths in China. 76800 fitness trails, according to the statistical bulletin of national economic and social development in 2020 [6]. By the end of 2020, there were 3.713 million sports venues in China.

However, the effective supply of community amateur sports facilities in China is insufficient. The utilization rate of existing facilities is low. Popular and convenient amateur sports facilities are still seriously insufficient [7]. These have formed a serious contradiction between supply and demand with the growing fitness demand of the public [8]. "Land grabbing," "noise disturbing residents," "elderly occupying the stadium," and other events occur frequently [9]. People's "fitness where to go" has become the focus of social

attention. Hindering the development process of the national fitness project [10]. Under the tight situation of land resources, reasonable optimization of the existing community amateur sports facilities is occurred [11]. "Make the best use of everything" so that community amateur sports facilities can meet and guide people's sports and fitness needs.

Focus on the convenience and benefit of the people. China has implemented policies and measures such as the "six sided project" of mass sports. Increase the effective supply of community amateur sports facilities [12]. Community amateur sports facilities around the masses are also stepping up the layout and construction. However, the layout method of "sticking to the seams" is usually adopted according to the actual situation in the specific implementation process. There is still a lack of echo with the surrounding environment and necessary humanistic care [13]. "Basketball and fitness dance conflict case" and "fitness dance disturbing residents" were once pushed to the commanding height of public opinion. The lack of sports fitness venues and facilities and the disturbing fitness activities have fully exposed the defects and deficiencies in community amateur sports facilities [14]. The official website of the Sichuan Provincial People's government once listed "unscientific setting of square dance venues, nonstandard management and noise disturbing residents" as one of the "ten things that the masses are most dissatisfied with." To some extent, this also reflects the unsatisfactory layout planning of community amateur sports facilities in China. The accessibility of community amateur sports facilities was not fully considered in the planning and site selection [15]. It is not enough to meet the time and space needs of different people and the needs of fitness activities with multilevel and diversified configuration [16]. Especially in the context of rapid aging, community amateur sports facilities show some problems, such as insufficient scale, unreasonable function allocation, and poor accessibility. It has seriously affected the demand for outdoor activities of the elderly [17]. It is of great significance to pay attention to improving the accessibility and convenience of community amateur sports facilities in geographical space and the safety, fitness, and entertainment of content space [18].

Health is the premise of a happy life. Health is the foundation of a country to create a better future. Health is the strength of national prosperity. National fitness is the foundation of building a sports power [19]. Achieve national health through national fitness, and then achieve the goal of a well-off society in an all-around way. It is also the internal requirement of accelerating the construction of a sports power [20].

The supply of community amateur sports facilities is insufficient and unbalanced. Insufficient supply is mainly reflected in the single supply type of venues around the masses [21]. In particular, there is a lack of indoor fitness facilities and sports health service platforms in the community. People's "fitness where to go" is still a difficult problem.

With the rapid development of China's economy and people's increasing concern for health, community amateur

sports facilities, as an infrastructure for national service, are developing rapidly across the country [22]. It has had a major impact on people's lives and health. Community amateur sports facilities are the core configuration of public sports space. To a large extent, it determines the development of national fitness. Community amateur sports facilities' spatial distribution and location must be reasonable and scientific [23]. Its location optimization has always been an important planning problem in most cities. It is also an issue of concern and concern to scholars. Because of its nonlinearity, high complexity, and many constraints, the traditional mathematical model can not obtain the global optimal solution [24]. The particle swarm optimization algorithm has a strong global optimization ability [25]. The group parallel search method is used to calculate and solve, with high efficiency and fast convergence speed [26]. In this paper, the improved adaptive weight multiobjective PSO is used to solving model, which is applied to the location problem of community amateur sports facilities with constraints, and good results are obtained.

2. Methodology

2.1. User Satisfaction Model. In order to improve users' satisfaction and fitness experience during the construction of community amateur sports facilities, users' satisfaction is judged by the distance of community amateur sports facilities. According to the questionnaire survey, the satisfaction is shown in Table 1.

Therefore, if you want to improve user satisfaction, you need to ask for the time period of going to the fitness place $[S_g, F_g]$. The longer the journey time, it will directly reduce user satisfaction. There is a negative correlation between user satisfaction and journey time; that is, the longer the journey time, the worse the user satisfaction will be. The satisfaction function is shown in the following formula:

$$S_g = 1 - \frac{S_g^d - S_g^r}{F_g - S_g}, \tag{1}$$

where S_g^d is the ideal travel time and S_g^r is the actual travel time. At the same time, the AHP is used to determine the key degree of amateur sports facilities in each community to users. The weight of facility g is recorded as M_g, and the total user satisfaction of all facilities is recorded as shown in the following formula:

$$S = \sum_{g \in G} S_g \cdot M_g. \tag{2}$$

In order to let users experience the practicability and economy of the community amateur sports facilities optimization model, the total satisfaction acceptable to users is recorded as A, combined with the lowest cost model.

$$\sum_{g \in G} S \cdot M_g > A. \tag{3}$$

2.2. User Demand Fluctuation Model. Compared with users, the main purpose of optimal configuration is to realize the

Table 1: Satisfaction survey.

Distance (m)	Time spent (min)	Satisfaction
[0, 500]	[0, 8]	Very satisfied
[500, 1000]	[8, 15]	Satisfied
[1000, 1500]	[15, 23]	Basically satisfied
[1500, 2000]	[23, 30]	Dissatisfied

use demand of fitness equipment. In this topic, the use frequency of equipment is selected as the fluctuation degree of user demand. Therefore, if the fluctuation degree of user demand is smaller, the use frequency of fitness equipment is more stable. Divide the day into 48 time periods, each of which is 30 minutes. The optimization objective function is shown in the following formula:

$$d = \max_{1 \leqslant n \leqslant N} \sum_{g=1}^{G} e_g^h - \min_{1 \leqslant n \leqslant N} \sum_{g=1}^{G} e_g^h, \tag{4}$$

where e_g^h is the usage frequency of facility g in period h. G is the total number of facilities. $g = 1$ indicates the first facility. The smaller the final result, the smaller the fluctuation of user demand.

2.3. Multiobjective Processing. The multiobjective optimization is processed by the method of square sum weighting, and the optimal value f_x of each objective function is obtained, respectively. Since it is impossible to achieve the optimal situation of each objective at the same time and try to ensure that it approaches the ideal situation, the weighted evaluation function is constructed as follows:

$$F(I) = \sum_{x=3}^{t} M_x \left[\frac{f_x(I) - f_x}{f_x} \right]^2. \tag{5}$$

The optimal solution of multiobjective optimization is obtained through (5). M is the weight coefficient, which can reflect the importance of each objective in the optimization process. Based on this, the unified function of the multi-objective optimization problem in this paper can be constructed.

$$F(I) = M_C \left(\frac{C_{\min}}{C_{\min}\Delta} - 1 \right) + M_S \left(\frac{S_{\max}}{S_{\max}\Delta} - 1 \right) + M_d \left(\frac{d_{\min}}{d_{\min}\Delta} - 1 \right), \tag{6}$$

where $C_{\min}\Delta$, $S_{\max}\Delta$, and $d_{\min}\Delta$ represent the optimal value of facility cost, user satisfaction, and fluctuation degree of user demand, respectively.

2.4. Standard PSO Algorithm. PSO is a classical intelligent algorithm based on mutual cooperation to find the most appropriate solution [27]. Compared with other algorithms, it does not have too many complex parameters and is easier to implement. In this text, a multiobjective PSO algorithm (IAW-MOPSO) with an improved weight strategy is proposed to consider the fitness of the whole particle. It can not only solve multiple objective optimization problems but also optimize faster. At the same time, in the search principle of

the optimal solution, it combines the idea of nonsupported sorting and the method of Pareto optimal appropriate allocation and uses the cooperative relationship between particles to constantly update the optimal solution of particles, so as to solve the problem. Finally, the particle set with the best fitness is selected.

The core of the PSO algorithm is to determine the overall best value and local best value of the particle by changing the next movement through its own experience and the better in the population [28]. The update process is shown in the following formula:

$$\begin{cases} q_{x+1} = mq_{x+1} + c_1 \cdot \text{rand} \cdot \left(U_{\text{best}_x} - I_x \right) + c_2 \cdot \text{rand} \cdot \left(a_{\text{best}_x} - I_x \right), \\ I_{x+1} = I_x + q_{x+1}, \end{cases} \tag{7}$$

where q_x is the velocity of particles. I_x is the position of particles. U_{best_x} is the best position found so far for each particle. a_{best_x} is the best position in all groups. Rand() is a random function between 0 and 1. q_{x+1} is the $x + 1$ particle velocity. I_{x+1} is the position of the $x + 1$ particle. c_1 and c_2 are learning factors. m is the dynamic weight value of particle swarm. Update inertia weights with nonlinear variations as follows:

$$m_v = \frac{m_{\max} - [v(m_{\max} - m_{\min})]}{n_{\max}}, \tag{8}$$

where v is the current iteration number. m_v is the weight value updated in the v iteration. $m_{\max}$ and $m_{\min}$ are the maximum and minimum values of m set artificially. $n_{\max}$ is the maximum iteration number.

2.5. Improvement of PSO Algorithm. Compared with other intelligent algorithms, the PSO algorithm is simpler to set parameters in the process of solving problems, and simpler to understand compared with other bionic algorithms. The difference is that the PSO algorithm does not need coding, so it does not have the solving accuracy limitation brought by coding in other bionic algorithms. However, it still has the problem that the universal intelligent algorithm is better for single objective optimization and easy to fall into some of the most optimal when carrying out multiobjective optimization. To solve this problem, this paper promotes the standard PSO. It not only dynamically adjusts the inertia weight and learning factor but also introduces dynamic time-varying control factors to restrict the position update amplitude of particles, because the nonlinear time-varying adjustment of parameters can obtain better algorithm performance than linear adjustment. These parameters are adjusted by nonlinear dynamic adaptive time-varying adjustment strategy. The inertial weight m is the most important parameter in the multiobjective PSO. With the increase of m, the overall search ability of the algorithm will be promoted, and with the decrease of m, the part search ability of the algorithm will be promoted.

The improved PSO algorithm optimizes the configuration of community amateur sports training equipment, and the management unit can adjust the community amateur

sports training facilities on this basis. The improvement process of this algorithm is as follows:

(1) Calculate the current fitness value of all particles

(2) Update and iterate the new generation of particles and count the particles whose fitness value is more than and less than the average value in the population

(3) Using nonlinear dynamic inertial weights to update m, the global and local searching ability of PSO is improved

$$
m = \begin{cases} m_{\min} - \dfrac{(f_{\mathrm{mean}} - f_{\min})\Delta m}{(f_q - f_{\min})}, & f_{\mathrm{mean}} \leq f_q, \\[3mm] m_{\max}, & f_{\mathrm{mean}} > f_q, \end{cases} \tag{9}
$$

where $m_{\max}$ and $m_{\min}$ show the maximum and minimum values of m, respectively, $\Delta m = (m_{\max} - m_{\min})$. F_{mean} show the current particle fitness value. F_q show the current particles average fitness value. $f_{\min}$ show the current particles minimum fitness value. m changes with the fitness value of particles.

When the f_{mean} of the particles tends to be uniform, or vice versa. The particle whose f_{mean} is better than f_q and its corresponding m is smaller, which protects the particle. For the particle below f_q, its corresponding m is larger, so that the particle will move towards a better search area.

2.6. Dynamic Parameter Update Strategy.

In particle swarm optimization, inertia weight ω function of is to keep the particle in the motion state of the previous moment, and its value has an important influence on the convergence of the algorithm. The basic PSO algorithm sets the inertia weight as a fixed value, and its search result is very poor. The main function of the learning factor is to adjust the proportion of individual optimal position and overall optimal position in speed update to balance the overall search ability and part search ability of the algorithm. In order to make the algorithm more flexible and reliable, this paper adopts the parameter dynamic adjustment strategy. The following formula conveys all the details:

$$
\omega = \omega_{\max} - \frac{(\omega_{\max} - \omega_{\min})n}{N_{\max}},
$$

$$
c_1 = c_{\max} - \frac{(c_{\max} - c_{\min})n}{N_{\max}}, \tag{10}
$$

$$
c_2 = c_{\min} + \frac{(c_{\max} - c_{\min})n}{N_{\max}},
$$

where $\omega_{\max}$ show the maximum value of inertia weight, respectively. $\omega_{\min}$ show the minimum value of inertia weight, respectively. $N_{\max}$ show the maximum number of iterations. $C_{\max}$ show the maximum value of learning factor, respectively. $C_{\max}$ show the minimum value of learning

factor, respectively. At the initial stage of the algorithm iteration, the inertia weight value is large, the initial speed of particles changes rapidly, the algorithm has a fairly strong overall search ability, the learning factor c_1 value is large, and the c_2 value is small, so the algorithm has a fairly strong individual cognitive ability. With the iteration of the algorithm, the inertia weight decreases, the change of particle velocity slows down, the value of learning factor c_1 decreases and the value of c_2 increases. The algorithm has a strong global cognitive ability.

The variation curve of each parameter is shown in Figures 1–3.

2.7. Model Solving Process.

Aiming at the optimal allocation strategy of amateur sports training equipment in the smart city community, this paper studies the improved adaptive weight multi-objective PSO algorithm.

When solving the multiobjective problem, the optimal individual can be selected through the Pareto hierarchical sorting principle, and finally, the Pareto optimal solution set can be obtained. The specific multiobjective scheduling operation process is as follows:

Step 1: coding strategy. The coding strategy adopts binary coding, and each particle represents a feasible solution of the multiobjective problem. All particles are designed as "gh" dimension 0–1 matrix $I = (i_{xy})_{gh}$, where i_{xy} represents the x flexible load, and the y period is selected as the working period, $\sum_{y=1}^{g} i_{xy} = 1, \quad x = 1, 2, \ldots, h$ which means that each equipment selects a period for operation. The particle velocity is expressed by $q = (q_{xy})_{gh}$.

Step 2: system and algorithm initialization. Determine the load model to be dispatched, and inputting the operation time, power, model, and other basic parameters of each load. Setting the particle swarm size as U_{size}, the maximum number of iterations, $n_{\max}$ and other algorithm parameters, initialize the particle swarm and the external file set at the same time, and each particle is randomly distributed in the feasible solution space and given an initial velocity within a given range.

Step 3: determining extremal value. The fitness value of each particle was calculated. The historical optimal position was recorded as the individual extreme value. The global optimal solution was found in the external archive set. The best solution was selected as the global extreme value by comparison with the individual optimal solution.

Step 4: update the velocity and displacement of particles according to equation (7).

Step 5: update the weight according to equation (9).

Step 6: update location. According to the fitness updating historical best U_{best} and overall best a_{best}, the current particle fitness value is compared with the previously determined optimal solution. If the current optimal solution is better, the extreme value is replaced.
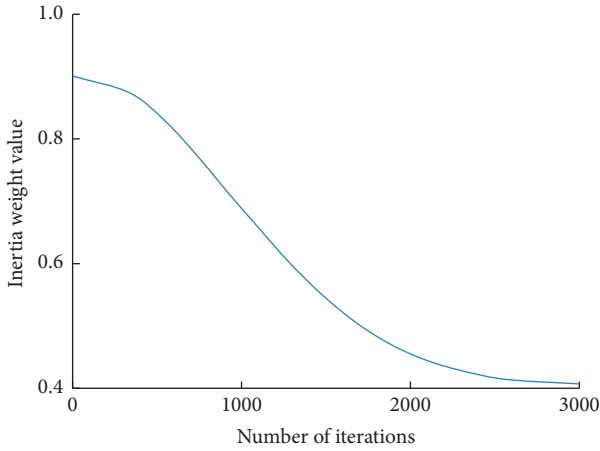
FIGURE 1: Inertia weight value change curve.
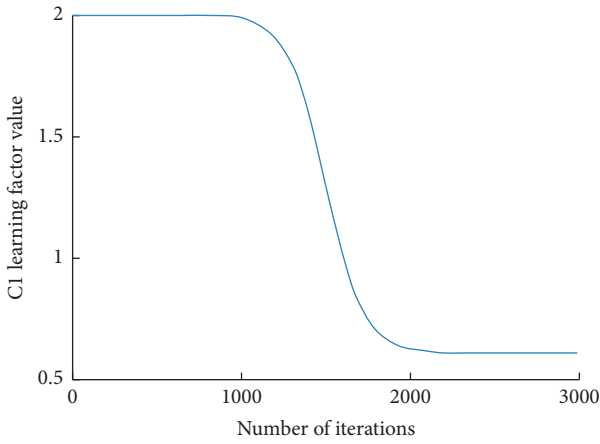
FIGURE 2: C_1 learning factor value change curve.

FIGURE 3: C_2 learning factor value change curve.

TABLE 2: Community location coordinates and fitness demand.

Community serial number	Coordinate	Demand (person-time)
1	(200, 1500)	125
2	(600, 800)	132
3	(1500, 300)	128
4	(2000, 1500)	112
5	(600, 2000)	116
6	(1000, 2500)	119
7	(3000, 1500)	111
8	(1500, 200)	135

Step 7: update the external file set. Retaining the currently found optimal solution set, then merge the solution set found in the latest iteration with the current optimal, and selecting the nondominated optimal again.

Step 8: judge whether the termination conditions are met. If the conditions are met, the algorithm terminates the iteration and outputs the optimal solution set, the optimized community amateur sports training equipment and facilities. Conversely, return to step 4 to continue optimization as shown in Figure 4.

3. Result Analysis and Discussion

To prove the algorithm's effectiveness in solving complex and multiconstraint problems in reality, it is applied to solve the location of community amateur sports training facilities. The location coordinates of 8 communities are collected. The coordinates of each community and the total amount of fitness needs are shown in Table 2.

It is planned to build amateur sports training facilities within the range of $200 \leq x$ and $y \leq 3000$ to minimize the initial construction cost and the total cost of users. To meet the timeliness requirements of users' fitness, it is agreed that the maximum distance between sports training facilities and the community shall not be greater than 2000 m. The use loss cost is set as 2 yuan/person time. The construction cost is different in different subregions: within the coordinate range of $200 \leq x$, $y \leq 1500$, the construction cost is 30000 yuan. Within $1500 < x$, $y \leq 3000$ coordinates, the construction cost is 35000 yuan; within the coordinate range of $200 \leq x \leq 1500$, $1500 < y \leq 3000$, the construction cost is 40000 yuan. Within the coordinate range of $1500 < x \leq 3000$, $200 \leq y \leq 1500$, the construction cost is 25000 yuan. According to the given constraints, the optimal location coordinates of community amateur sports training facilities are determined by using the proposed improved PSO optimization model to minimize the total operation cost. The distribution of construction costs is shown in Table 3. The total operating cost analysis is shown in Table 4.

The proposed algorithm is compared with the standard PSO algorithm ($c1$ and $c2$ are constant, and inertia weight decreases linearly). The dynamic adaptive PSO algorithm runs the corresponding program. The change of fitness function value is shown in Figure 5. A comparison of the operation time of different algorithms is shown in Figure 6. The location results of community amateur sports training facilities are shown in Figure 7.

The improved PSO algorithm based on the dual mechanism proposed in the paper is used to solve the

TABLE 3: Distribution of construction costs.

Sports facilities serial number	Position coordinates	Construction cost (yuan)
1	$x \in [200, 3000), y \in (0, 1500]$	30000
2	$x \in (1500, 3000), y \in (0, 3000]$	35000
3	$x \in [200, 1500], y \in (1500, 3000]$	40000
4	$x \in (1500, 3000], y \in [200, 1500]$	25000

TABLE 4: Total operating cost analysis table.

Coordinate	Construction cost (yuan)	Demand (person-time)	Wreck a cost (yuan)	Total operating cost (yuan)
(200, 1500)	30000	125	250	30250
(600, 800)	30000	132	264	30264
(1500, 300)	35000	128	256	35256
(2000, 1500)	35000	112	224	35224
(600, 2000)	40000	116	232	35232
(1000, 2500)	40000	119	238	35238
(3000, 1500)	25000	111	222	35222
(1500, 200)	25000	135	270	35270
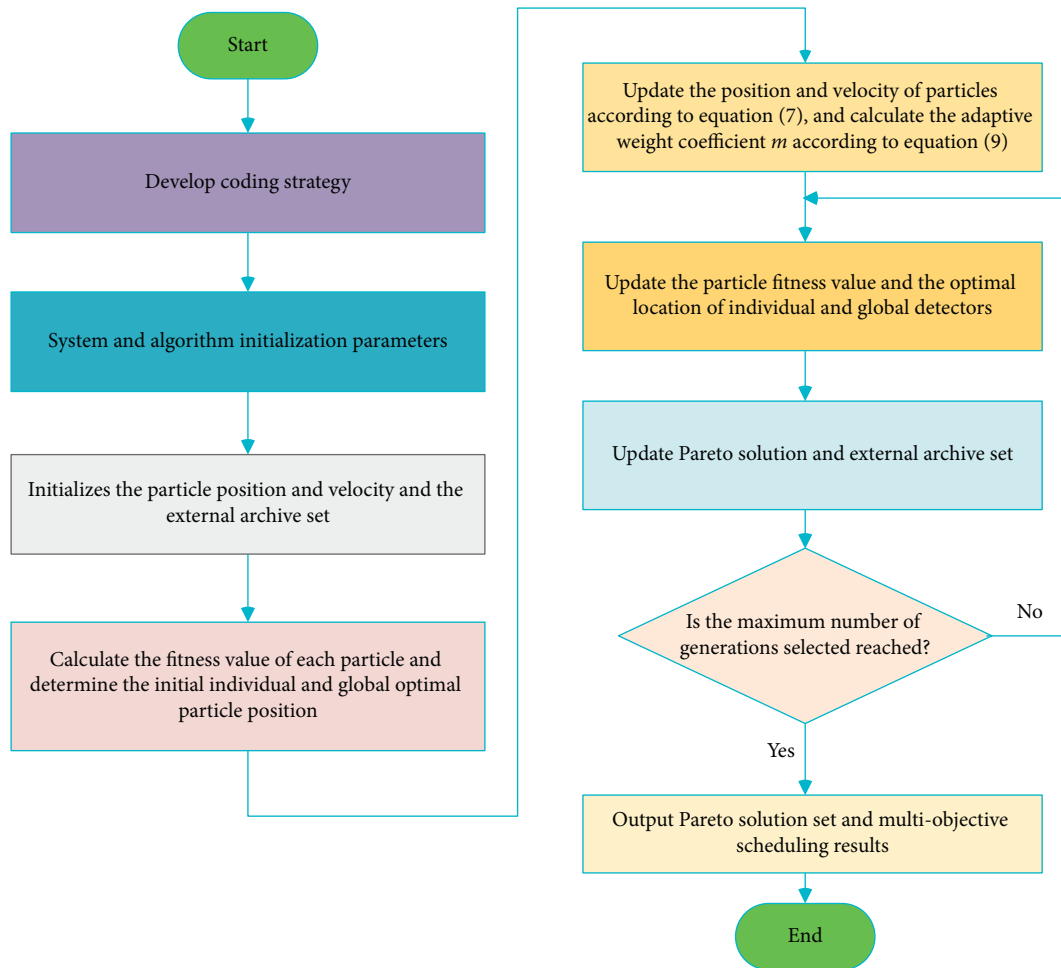
FIGURE 4: Improved MOPSO algorithm flow chart.

location problem of community amateur sports training facilities, which has good convergence. The number of iterations to obtain the optimal solution is about 40 times, the best distribution center coordinates (513.77, 599.99), and the minimum total cost of construction and later distribution is 1228 million yuan. The standard PSO algorithm and the dynamic adaptive PSO algorithm can not converge to the global optimum, although the solution results are close to
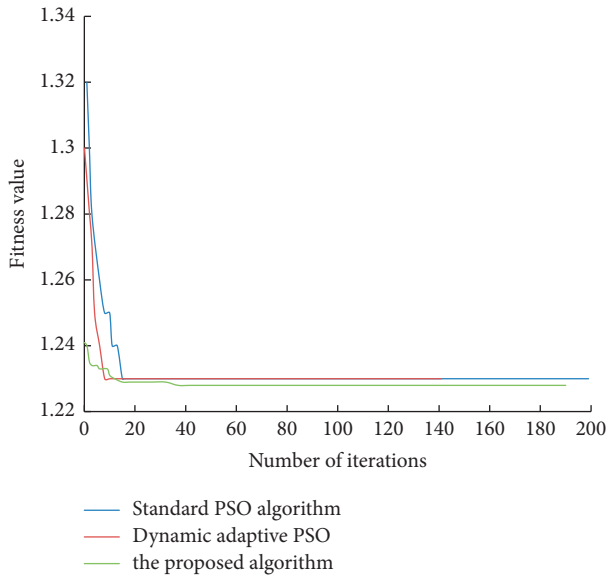
Figure 5: Comparison diagram of changes in fitness function values.
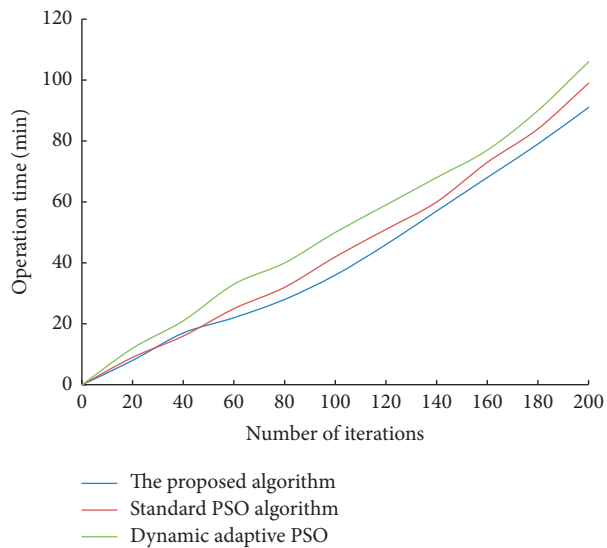
Figure 6: Comparison of operation time of different algorithms.
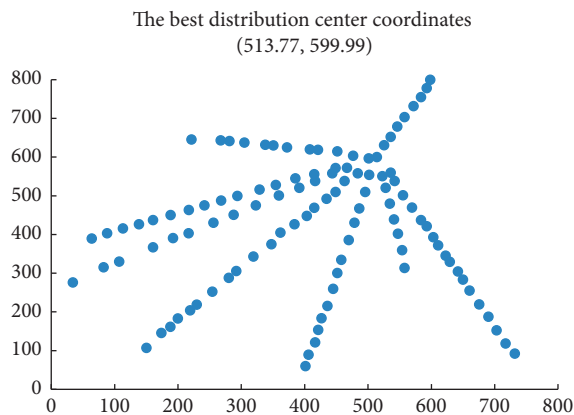
Figure 7: Site selection results of community amateur sports training facilities.

the solution results of the former. This paper constructs the mathematical model of community amateur sports training facility location and solves the optimal community amateur sports training facility location scheme through the improved PSO algorithm. The obtained scheme can significantly reduce the total cost to the minimum. Therefore, the PSO algorithm based on a dual mechanism has achieved the desired results in solving the location problem of community amateur sports training facilities, which has a very positive significance.

4. Conclusion

The traditional PSO is dynamically self-adjusted and optimized from inertial weight and acceleration factors, and dynamically changing control factors are added to improve the efficiency. Results show that the performance of PSO is improved significantly by the dynamic adaptive adjustment of multiple parameters, and the overall optimization ability of the improved is enhanced. The improved PSO can be used to solve nonlinear and complex problems such as path planning and automatic control. Through the application of the sports training facility location model, which proved the accuracy of the location selection model and adaptive weighting based on improved multiobjective PSO to solve complex optimization problems the effectiveness of the adaptive weighting based on improved multiobjective PSO to improve the easy to fall into part optimum, the disadvantage of poor robustness, the model is applied to sports training facility location problem solving, it has good dynamic observation and convergence. In the next step, we will continue to optimize the algorithm and apply the model to solve other problems, such as commercial location and constantly optimize and improve it.

Data Availability

The labeled dataset used to support the findings of this study are available from the corresponding author upon request.

Conflicts of Interest

The authors declare that there are no conflicts of interest.

Acknowledgments

References

[1] A. P. Nasution, E. A. Wibowo, R. Ramdani, and T. Rofiqah, "Urgensity of environmental management system implementation on oil palm plantation management policies in north sumatera," *Journal of Social Transformation and Regional Development*, vol. 3, no. 1, pp. 1–6, 2021.

[2] S. Schindler and J. M. Kanai, "Getting the territory right: infrastructure-led development and the re-emergence of spatial planning strategies," *Regional Studies*, vol. 55, no. 1, pp. 40–51, 2021.

[3] S. Koistinen, L. Olai, K. Ståhlnacke, A. Falt, and A. Ehrenberg, "Oral health-related quality of life and associated factors among older people in short-term care," *International Journal of Dental Hygiene*, vol. 18, no. 2, pp. 163–172, 2020.

[4] K. Wodniak, "Social leverage of sporting mega-events and co-production. The case study of Orlik facilities in Poland after EURO 2012," *International Journal of Sport Policy and Politics*, vol. 13, no. 1, pp. 85–104, 2021.

[5] Y. Paik, S. Kang, and R. Seamans, "Entrepreneurship, innovation, and political competition: how the public sector helps the sharing economy create value," *Strategic Management Journal*, vol. 40, no. 4, pp. 503–532, 2019.

[6] H. Mishchuk, S. Bilan, H. Yurchyk, L. Akimova, and M. Navickas, "Impact of the shadow economy on social safety: the experience of Ukraine," *Economics & Sociology*, vol. 13, no. 2, pp. 289–303, 2020.

[7] J. Wang and B. Lv, "Big data analysis and research on consumption demand of sports fitness leisure activities," *Cluster Computing*, vol. 22, no. S2, pp. 3573–3582, 2019.

[8] J. L. Rice, D. A. Cohen, J. Long, and J. R. Jurjevich, "Contradictions of the climate-friendly city: new perspectives on eco-gentrification and housing justice," *International Journal of Urban and Regional Research*, vol. 44, no. 1, pp. 145–165, 2020.

[9] S. Fried, A. Avigdor, B. Bielorai et al., "Early and late hematologic toxicity following CD19 CAR-T cells," *Bone Marrow Transplantation*, vol. 54, no. 10, pp. 1643–1650, 2019.

[10] B. R. Belcher, J. Zink, A. Azad, C. E. Campbell, S. P. Chakravartti, and M. M. Herting, "The roles of physical activity, exercise, and fitness in promoting resilience during adolescence: effects on mental well-being and brain development," *Biological Psychiatry: Cognitive Neuroscience and Neuroimaging*, vol. 6, no. 2, pp. 225–237, 2021.

[11] J. R. Pate and D. Bragale, "Challenges of an established amateur sport: e," *Journal of Amateur Sport*, vol. 5, no. 1, pp. 50–75, 2019.

[12] T. Bradbury, R. Mitchell, and K. Thorn, "Moving forward: business model solutions for amateur sport clubs," *Managing Sport and Leisure*, vol. 26, no. 3, pp. 189–205, 2021.

[13] G. E. Thibault, "Humanism in medicine: what does it mean and why is it more important than ever?" *Academic Medicine*, vol. 94, no. 8, pp. 1074–1077, 2019.

[14] A. Latham and J. Layton, "Kinaesthetic cities: s," *Progress in Human Geography*, vol. 44, no. 5, pp. 852–876, 2020.

[15] T. Şahin, S. Ocak, and M. Top, "Analytic hierarchy process for hospital site selection," *Health Policy and Technology*, vol. 8, no. 1, pp. 42–50, 2019.

[16] A. M. Briggs, E. Houlding, R. S. Hinman et al., "Health professionals and students encounter multi-level barriers to implementing high-value osteoarthritis care: a multi-national study," *Osteoarthritis and Cartilage*, vol. 27, no. 5, pp. 788–804, 2019.

[17] H. C. Xu, W. S. Jang, and Y. H. Pan, "Study on the improvement of elderly activity demand in outdoor public space in urban communities-A case study of wuhan in China," *Journal of the Korea Convergence Society*, vol. 11, no. 1, pp. 141–150, 2020.

[18] S. Gao, C. Li, Y. Rong, Q. Yan, W. Liu, and Z. Ma, "The places–people exercise: understanding spatial patterns and the formation mechanism for urban commercial fitness space in changchun city, China," *Sustainability*, vol. 14, no. 3, 1358 pages, 2022.

[19] J. Liu, "The development and promotion of three-man basketball in ordinary colleges and universities based on the background of national fitness," *Academic Journal of Humanities & Social Sciences*, vol. 2, no. 2, pp. 93–97, 2019.

[20] D. J. Harper, C. Carling, and J. Kiely, "High-intensity acceleration and deceleration demands in elite team sports competitive match play: a systematic review and meta-analysis of observational studies," *Sports Medicine*, vol. 49, no. 12, pp. 1923–1947, 2019.

[21] D. M. Studdert and M. A. Hall, "Disease control, civil liberties, and mass testing — calibrating restrictions during the COVID-19 pandemic," *New England Journal of Medicine*, vol. 383, no. 2, pp. 102–104, 2020.

[22] V. S. Litvinenko, "Digital economy as a factor in the technological development of the mineral sector," *Natural Resources Research*, vol. 29, no. 3, pp. 1521–1541, 2020.

[23] C. Gomez-Gonzalez, C. Nesseler, and H. M. Dietl, "Mapping discrimination in europe through a field experiment in amateur sport," *Humanities and Social Sciences Communications*, vol. 8, no. 1, pp. 1–8, 2021.

[24] J. P. Wallner, "Structural constraints for dynamic operators in abstract argumentation," *Argument & Computation*, vol. 11, no. 1-2, pp. 151–190, 2020.

[25] N. Dhanachandra and Y. J. Chanu, "An image segmentation approach based on fuzzy c-means and dynamic particle swarm optimization algorithm," *Multimedia Tools and Applications*, vol. 79, no. 25-26, pp. 18839–18858, 2020.

[26] F. Agostinelli, S. McAleer, A. Shmakov, and P. Baldi, "Solving the Rubik's cube with deep reinforcement learning and search," *Nature Machine Intelligence*, vol. 1, no. 8, pp. 356–363, 2019.

[27] J. Tang, G. Liu, and Q. Pan, "A review on representative swarm intelligence algorithms for solving optimization problems: applications and trends," *IEEE/CAA Journal of Automatica Sinica*, vol. 8, no. 10, pp. 1627–1643, 2021.

[28] H. Chen, D. L. Fan, L. Fang et al., "Particle swarm optimization algorithm with mutation operator for particle filter noise reduction in mechanical fault diagnosis," *International Journal of Pattern Recognition and Artificial Intelligence*, vol. 34, no. 10, Article ID 2058012, 2020.

Research Article

A Data-Driven Customer Profiling Method for Offline Retailers

Huahong Zuo,[1] **Sike Yang,**[2] **Hailong Wu** ⓘ**,**[3] **Wei Guo,**[3] **Lina Wang,**[4] **Xiao Chen,**[5] **and Yingqiang Su**[5]

[1]*Wuhan Chuyan Information Technology Co., Ltd., Wuhan 430050, China*
[2]*Center of Information, Hubei Tobacco Monopoly Bureau, Wuhan 430000, China*
[3]*College of Computer Science and Technology, Zhejiang University of Technology, Hangzhou 310023, China*
[4]*The Southeast Digital Economy Development Research Institute, Quzhou 32400, Zhejiang, China*
[5]*Jingzhou Tobacco Monopoly Bureau of Hubei Province, Jingzhou 434000, China*

Correspondence should be addressed to Hailong Wu; whl512@zjut.edu.cn

In order to accelerate the transformation of offline retailers and improve sales by using big data technology, this paper proposes a data-driven customer profile modeling method based on the collected historical purchase records of offline consumers. This method is mainly divided into three aspects: (1) an incremental RFM model is designed to classify the value of historical consumers and support the dynamic update of the model, which is more efficient than the traditional RFM model; (2) the commodity preference of different types of customers is analyzed by the TGI model, so as to guide the retail terminal to optimize the marketing strategy; (3) a commodity purchase behavior prediction model based on LSTM is proposed, which can predict the commodity that each customer may purchase in the future, so as to optimize the retail strategy. According to extensive experiments based on a true tobacco dataset, the incremental RFM model can save 80% more time than the traditional method, and our proposed prediction model can achieve 59.32% accuracy, which is better than other baselines.

1. Introduction

In recent years, with the transformation and upgrading of offline retail stores, smart point-of-sale terminals have become popular, enabling offline retail stores to collect consumers' historical purchase records. By analyzing these consumer data, offline retailers can optimize their resource allocation and increase consumer stickiness, which is helpful to attract consumers and improve their sales.

However, how to form an accurate and knowledge of consumers' consumption motivation, consumption ability, consumption preference, consumption habits, and consumption trends through the analysis of consumers' purchase behavior records is the main challenge at present. Therefore, this paper proposes a data-driven customer profile modeling method, which mainly includes coarse-grained value classification and preference analysis of customers, as well as fine-grained purchase behavior prediction.

Based on the consumers' purchase behavior collected by the POS terminals, we firstly use the RFM model [1] to evaluate the customers' value according to their consumption recency, consumption frequency, and consumption monetary. This paper also proposes an incremental optimization on the RFM model.

With the continuous generation of new consumer purchase behavior data, an efficient update strategy is designed to avoid the repeated reading of historical data and unnecessary redundant calculation, so as to speed up the update efficiency of the RFM model. At the same time, this paper introduces TGI (target group index) model [2], analyzes consumers' consumption habits according to their consumption records, and describes consumers' preferences according to their groups, which is conducive to recommending their preferred products according to people.

In addition, in order to help retail terminals achieve fine-grained precision marketing, this paper designs a

purchase prediction model based on LSTM (long short term memory) [3], which is used to predict the commodity that the consumer is most likely to buy in the future based on his/her historical purchase behavior. To eliminate the preference biases between customers, the model takes the historical commodities purchased by a consumer in the last five times and the commodity most frequently in history as the model input and finally predicts the commodity that the consumer is most likely to buy in the future. Because the historical purchase behavior has a chronological relationship, this paper uses the LSTM model to model it. In addition, the model also uses the embedding layer [4] of the neural network to embed commodities and maps the original independent commodities into low-dimensional vectors, which can improve the prediction accuracy of the model.

The main contributions of this paper are as follows:

(1) An incremental RFM model updating method is proposed, which can quickly update the old RFM model with the continuous accumulation of data.

(2) We propose to use the TGI model to analyze the preference of customer groups rather than individuals, which is useful to alleviate individual bias.

(3) A commodity purchase prediction model based on LSTM is proposed; it outperforms other baselines by 1.31% accuracy.

The organization of this paper is as follows: Section 2 mainly introduces the incremental RFM model; Section 3 mainly introduces the TGI model; Section 4 mainly introduces the commodity purchase prediction model based on LSTM; Section 5 carries out extensive experiments to verify the effectiveness of the proposed methods; related work is introduced in Section 6; finally, Section 7 summarizes the work of this paper.

2. Customer Classification Based on Incremental RFM Model

In this section, we will first introduce the relevant knowledge of the traditional RFM model, then propose our incremental RFM model update method, and finally help understand with a simple example.

2.1. Introduction of Traditional RFM Model. RFM model is usually used to evaluate customer churn tendency, loyalty, and customer value. This model depicts the customer dynamically through three indexes, recency, frequency, and monetary consumption. Recency means the time interval since the last transaction; frequency means the number of transactions in the last n months; monetary means the total cost in the last months.

The RFM model calculates the overall average value of the three indicators, records them as r_{avg}, f_{avg}, and m_{avg}, r_{avg}, and then marks the corresponding indicators as 0 or 1 according to the relationship between each customer's own RFM indicators and the average value, that is,

$$sr_i = \begin{cases} 1, & r_i < r_{avg}, \\ 0, & r_i \geq r_{avg}, \end{cases}$$
$$sf_i = \begin{cases} 1, & f_i > f_{avg}, \\ 0, & f_i \leq f_{avg}, \end{cases} \qquad (1)$$
$$sm_i = \begin{cases} 1, & m_i > m_{avg}, \\ 0, & m_i \leq m_{avg}. \end{cases}$$

Based on the above formula, each customer can be marked with three 0/1 marks and finally can be classified into 8 types of consumers as shown in Table 1.

2.2. Incremental RFM. The three indicators of the RFM model are real-time; that is, the recency, frequency, and monetary of consumption will change with the passage of time and the generation of orders. At the same time, consumers' consumption habits and consumption demand are not invariable. It may change at any time due to consumers' new attempts, age growth, and other factors. The grab and prediction of consumers' consumption habits should be based on the "current situation." Therefore, in order to obtain the latest RFM model, it is necessary to consider the newly generated consumption data based on historical consumption data. However, if we use the traditional calculation method to recalculate the RFM model for historical data and newly generated data, it will be very time-consuming, especially when the scale of historical data is very large. Therefore, in this section, we propose an incremental RFM calculation method to efficiently update the RFM model by counting relevant indicators of newly generated consumption data based on the historical RFM model.

For historical data, the RFM index of each consumer i is recorded as R_i^{old}, F_i^{old}, M_i^{old}. For the newly added data, the RFM index of consumer j is recorded as R_j^{new}, F_j^{new}, M_j^{new}. In order to update the old RFM model, we need to consider the new data. At this time, the following three situations will occur:

Case 1: the consumer u has purchase records in both historical data and new data:

$$R_u = R_u^{new},$$
$$F_u = F_u^{old} + F_u^{new}, \qquad (2)$$
$$M_u = M_u^{old} + M_u^{new}.$$

Case 2: the consumer u only has purchase record in the historical data, and there is no purchase record in the new data:

$$R_u = R_u^{old} + I,$$
$$F_u = F_u^{old}, \qquad (3)$$
$$M_u = M_u^{old},$$

where I indicates the time interval of new data. If we update the RFM model every month, then $I = 30$.

Table 1: Consumer classification of RFM model.

Consumer classification	Type	Recency	Frequency	Monetary
Important value consumers	1	1	1	1
Important development consumers	2	1	0	1
Important maintain consumers	3	0	1	1
Important retain consumers	4	0	0	1
General value consumers	5	1	1	0
General development consumers	6	1	0	0
General maintain consumers	7	0	1	0
General retain consumers	8	0	0	0

Case 3: the consumer u only has a purchase record in the new data, but there is no purchase record in the historical data:

$$
\begin{aligned}
R_u &= R_u^{\text{new}}, \\
F_u &= F_u^{\text{new}}, \\
M_u &= M_u^{\text{new}}.
\end{aligned}
\tag{4}
$$

After the RFM indicators of each consumer are updated, the average value of each indicator needs to be calculated before consumers can be classified. Suppose that the consumer set in the historical data is recorded as U^{old}, including N^{old} consumers, and the average RFM values of the historical data are $R_{\text{avg}}^{\text{old}}$, $F_{\text{avg}}^{\text{old}}$, $M_{\text{avg}}^{\text{old}}$. Suppose that the consumers in the new data are recorded as a combination of consumers U^{new}, including N^{new} consumers who have purchase behavior in the historical data, and N_2^{new} consumers who have no purchase behavior in the historical data, and then they meet $N_1^{\text{new}} + N_2^{\text{new}} = N^{\text{new}}$. The average value of each index of the updated RFM model can be calculated by the following formula:

$$
\begin{aligned}
F_{\text{avg}} &= \frac{\left(F_{\text{avg}}^{\text{old}} \times N^{\text{old}} + \sum_{j \in U^{\text{new}}} F_j^{\text{new}}\right)}{\left(N^{\text{old}} + N_2^{\text{new}}\right)}, \\
M_{\text{avg}} &= \frac{\left(M_{\text{avg}}^{\text{old}} \times N^{\text{old}} + \sum_{j \in U^{\text{new}}} M_j^{\text{new}}\right)}{\left(N^{\text{old}} + N_2^{\text{new}}\right)}, \\
R_{\text{avg}} &= \frac{\left(\sum_{i \in U'} \left(R_i^{\text{old}} + 30\right) + \sum_{j=1}^{N^{\text{new}}} R_j^{\text{new}}\right)}{\left(N^{\text{old}} + N_2^{\text{new}}\right)},
\end{aligned}
\tag{5}
$$

where $U' = U^{\text{old}} - (U^{\text{old}} \cap U^{\text{new}})$ represents the consumer set with purchase records only in the historical data.

3. Examples

Assume that we have obtained RFM results for four consumers based on the historical data, as shown in Table 2:

Table 2: Consumer RFM table based on historical data statistics.

Consumer	Recency	Frequency	Monetary
$u1$	33	3	28
$u2$	34	1	27
$u3$	36	3	26
$u4$	37	1	59

The average value of each indicator can be calculated:

$$
\begin{aligned}
r_{\text{avg}} &= \frac{1}{4}\left(33 + 34 + 36 + 37\right) = 35, \\
f_{\text{avg}} &= \frac{1}{4}\left(3 + 1 + 3 + 1\right) = 2, \\
m_{\text{avg}} &= \frac{1}{4}\left(28 + 27 + 26 + 59\right) = 35.
\end{aligned}
\tag{6}
$$

Then, according to the relationship between the RFM data of each consumer and the average value, calculate the scoring of each consumer in the three indicators, and $u1$ is used as an example:

$$
\begin{aligned}
r_1 &= 33 < r_{\text{avg}} = 35 \Rightarrow sr_1 = 0, \\
f_1 &= 3 > f_{\text{avg}} = 2 \Rightarrow sf_1 = 1, \\
m_1 &= 28 > f_{\text{avg}} = 35 \Rightarrow sm_1 = 0.
\end{aligned}
\tag{7}
$$

Similarly, the scoring matrix of all consumers can be obtained, as shown in Table 3:

According to Table 1, the consumer classification results of the four consumers are shown in Table 4:

It is assumed that another month has passed on the basis of Table 2, and the data volume of one month has been increased, and the RFM statistics of this month are shown in Table 5:

A new consumer $U5$ is added, which has not appeared in Table 2 before. In addition, $U2$ and $U4$ are not recorded in Table 5 because they have not bought goods within this month.

According to Tables 2 and 5, it can be calculated that $N^{\text{old}} = 4$, $N_2^{\text{new}} = 1$, $F_{\text{avg}}^{\text{old}} = 2$, $M_{\text{avg}}^{\text{old}} = 35$, $U' = \{u2, u4\}$, so according to the formula in Section 2.2,

$$
\begin{aligned}
F_{\text{avg}}^{\text{new}} &= \frac{2 * 4 + 2 + 1 + 2}{4 + 1} = 2.6, \\
M_{\text{avg}}^{\text{new}} &= \frac{35 * 4 + 18 + 15 + 18}{4 + 1} = 38.2, \\
R_{\text{avg}}^{\text{new}} &= \frac{(34 + 30 + 37 + 30 + 10 + 2 + 5)}{4 + 1} = 29.6.
\end{aligned}
\tag{8}
$$

It can be seen that the incremental method does not need to traverse the historical data to obtain the historical RFM value, which saves much time.

3.1. Product Preference Analysis Based on TGI Index. Target group index (TGI), also known as the target group index, can reflect the strength or weakness of the target

Table 3: Consumer RFM scoring table based on historical data statistics.

Consumer	Recency	Frequency	Monetary
u1	0	1	0
u2	0	0	0
u3	1	0	0
u4	1	1	1

Table 4: RFM results based on historical data statistics.

Consumer	Classification
u1	General maintain
u2	General retain
u3	General develop
u4	Important value

Table 5: RFM results in the latest month.

Consumer	Recency	Frequency	Monetary
u1	10	2	18
u3	2	1	15
u5	5	2	18

group within a specific research scope. In short, it is the preference of the target group for an object or feature

$$\text{TGI} = \frac{\text{Proportion of certain characteristics in the target group}}{\text{Proportion of groups with the same characteristics in the population}} * 100\%. \tag{9}$$

TGI index represents the difference of different groups on the same problem. TGI index equal to 100 indicates the average level, and an index higher than 100% indicates that such consumers pay more attention to a certain problem than the overall level. For example, assume that there are 35% of people smoke in China, and 50% of Chinese men smoke. Therefore, we can calculate that $\text{TGI} = 50/35 * 100\% = 142\%$, indicating that Chinese men prefer smoking than women.

Based on the classification results of the RFM model in Section 2, we will use the TGI model to analyze the preference of different categories of customers for various goods. The general flow of analysis is shown in the Figure 1.

Firstly, we will use the RFM model to classify customers (red arrow part), then select the four goods with the highest sales volume from the historical data for analysis, and calculate the TGI index of eight types of consumers (blue arrow part). Through the TGI index, we can analyze the preferences of different types of customers, so as to provide suggestions for the replenishment of retail terminals in the future.

4. The Commodity Purchase Prediction Model Based on LSTM

Consumers' purchase behavior can be regarded as sequential data, and traditional machine learning can be used. However, the ability of traditional machine learning methods to

compared with all members. The TGI index can be calculated by the following formula:

capture time-series correlation characteristics is weak, while the recursive neural network (RNN) [5] in deep learning can handle time-series correlation data well. Therefore, in this section, we will use the framework of the recursive neural network to predict commodity purchase behavior.

4.1. Introduction of the LSTM Model. The traditional RNN model structure is shown in Figure 2. The data of each time step is composed of the input data of the current time and the data of the previous time step. Each edge of the input and output has weights, which are W, U and V respectively. RNN network mainly includes two important processes, forward propagation of data and backward propagation of gradients. The parameters of the model are adjusted through forward and backward propagation to optimize the network. However, the traditional RNN model will have the problem of vanishing gradient or exploding gradient [6] with the increase of time step, so someone later optimized the RNN model and proposed the long and short memory neural network (LSTM) [3].

On the basis of RNN, LSTM adds input gate, output gate, and forget gate to make the model selectively remember important data and forget unimportant data and further optimize the prediction method of RNN. The input gate determines the update of information, and the output gate
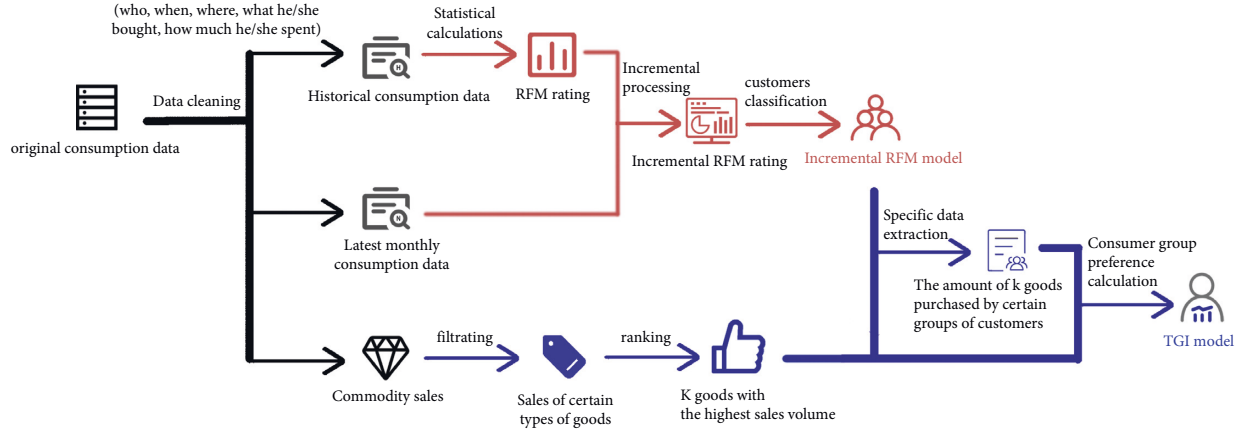
Figure 1: TGI analysis process.
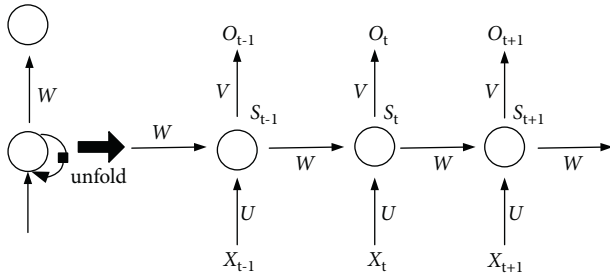
Figure 2: RNN model.

Figure 3: LSTM model.

determines the information output of the cell state. Through the gate structure, important information is saved, and unnecessary information is forgotten to improve the memory of long-term sequences. The calculation of each gate of LSTM is shown in equations (10)–(15). The structure of LSTM is shown in Figure 3.

$$f_t = \sigma\left(W.\left[h_{t-1}, x_t\right] + b_i\right), \quad (10)$$

$$\widetilde{C}_t = \tanh\left(W_C.\left[h_{t-1}, x_t\right] + b_i\right), \quad (11)$$

$$i_t = \sigma\left(W_i.\left[h_{t-1}, x_t\right] + b_c\right), \quad (12)$$

$$C_t = f_t * C_{t-1} + i_t * \widetilde{C}_t, \quad (13)$$

$$o_t = \sigma\left(W_o\left[h_{t-1}, x_t\right] + b_o\right), \quad (14)$$

$$h_t = o_t * \tanh\left(C_t\right). \quad (15)$$

4.2. The Prediction Model Based on LSTM. In this section, we design a commodity purchase prediction model based on LSTM, as shown in Figure 4. Firstly, it takes the commodities purchased by the consumer for the first five times as the time-series feature, which is recorded as $X1$, $X2$, $X3$, $X4$, and $X5$. It also takes the most frequently purchased commodity in history as the additional feature, which is recorded as $TzX6$. The model inputs them into the embedding layer [7] and maps each commodity into a low-dimensional vector
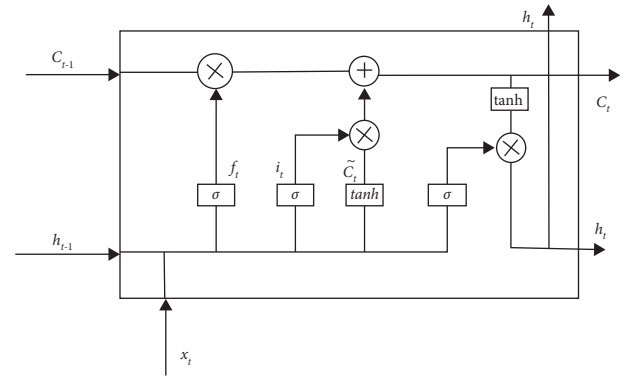
representation. The vector representation of each commodity implies the correlation between commodities and their respective characteristics, which can help the prediction model better analyze the historical behavior of consumers.

After embedding, $X1$ to $X5$ are fed into LSTM neural network and output the final hidden layer result P. The hidden layer result P integrates the characteristics of the consumer's previous five purchase behaviors and then maps to a deeper feature space through a layer of full connection, which is recorded as P_C.

As an additional feature, the most frequently purchased commodity in the consumer's history has no sequential relationship with the commodities that are purchased in the last five times, so it is not processed by LSTM neural network. We input the embedding representation of $TzX6$ into a fully connected layer and map it to P_A, whose dimensions are the same dimension as P_C, written as TZ_C. Then, we concatenate P_C and TZ_C and fed them into two fully connected layers to produce the final prediction result $Y\_predict$.

Because there are many commodities that can be predicted, the prediction task actually is a multiclassification problem. Therefore, the final model output $Y\_predict$ is a multidimensional vector, and the corresponding number of each dimension in the vector represents the probability that the consumer purchases the corresponding commodity. We
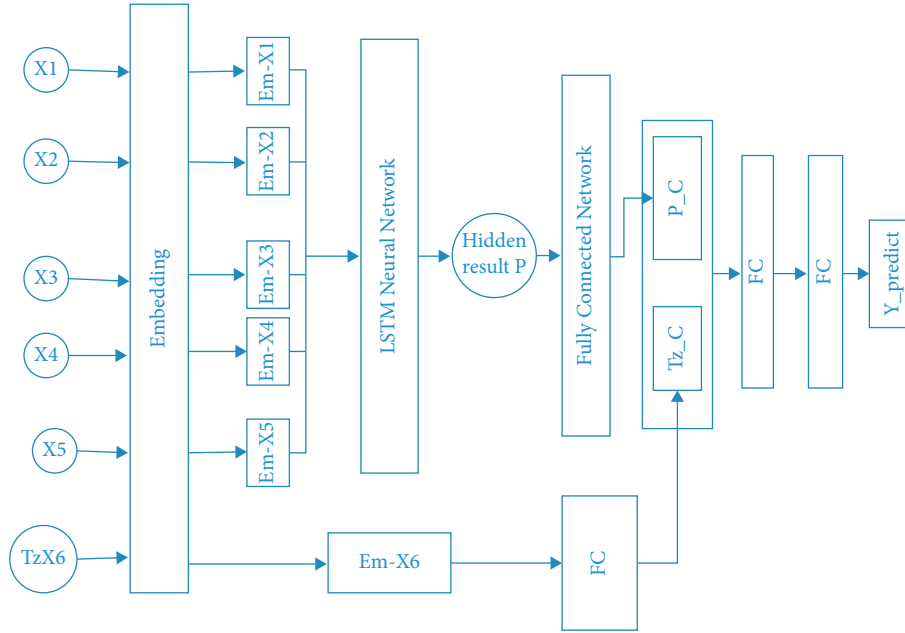
FIGURE 4: The architecture of the prediction model.

can take the commodity represented by the one dimension with the greatest probability as the final prediction result.

Therefore, we adopt the cross-entropy loss [8] as the loss function of the model. Then, we adopt the Adam [9] gradient optimization algorithm to optimize model parameters according to the error between prediction and ground truth.

5. Experiments

In this section, we will use the real consumer consumption records collected by cigarette sales terminals in a prefecture level city of Hubei Province from June 9, 2019, to March 9, 2021, for experimental verification. Our experimental data is from the real purchase records generated by customers in commodity enterprises. On this basis, we preprocessed and annotated the data. Each record of data contains the customer's last five purchases, the most frequently purchased commodity and labels. Through data cleaning and preprocessing, the final data includes 371089 consumers and 51095 purchase records, including 1655 cigarette brands.

Firstly, we conduct efficiency experiments on the incremental RFM model to study the time cost in updating the RFM model in different ways and verify the effects of the incremental calculation method proposed in this paper. Secondly, we display the TGI results of the top-4 cigarette brands based on classified consumers by the RFM model. Finally, we test the accuracy of the prediction model based on LSTM and compare its accuracy with different classification models, so as to verify the prediction effect of the proposed model. At the same time, we also conducted some ablation experiments to analyze the performance differences of the model under different conditions.

In the purchase prediction experiment, we conducted a 10-fold cross validation and then calculated the average and standard deviation of the experimental results as the final performance of models.

5.1. RFM Efficiency Experiments.
In order to compare the update efficiency of the incremental RFM model before and after optimization, based on the data of one and a half years (2019/6/9–2020/2/9), we compared the calculation time after adding new data of different D days, in which D takes 7, 14, 21, 28, 35, and 42. In order to avoid accidental errors, we run the program several times to calculate the average running time (see Figure 5).

As can be seen from Figure 5, with the increase of new data, the incremental RFM model can save about 5 seconds than the tradition RFM model, which means that our proposed method can greatly improve the efficiency of update the model (the updating model).

5.2. TGI Results.
According to statistics, the four kinds of cigarettes with the highest sales volume in history are yellow crane tower (soft blue), Liqun (new version), Yellow Crane Tower (hard wonder), and Red Golden Dragon (soft boutique). Figure 6 shows the TGI index of eight categories of customers.

Taking Yellow Crane Tower (soft blue) as an example, the TGI index of important value consumers is 929.925%, which is much higher than the measurement standard of 100%, which shows that important value consumers have a high preference for Yellow Crane Tower (soft blue) compared with other consumers; the TGI index of important retained consumers is only 48.125%, far lower than 100%. In proportion, few important retained consumers buy Yellow Crane Tower (soft blue).

If the four products with the highest sales volume are compared horizontally, it is not difficult to find that these
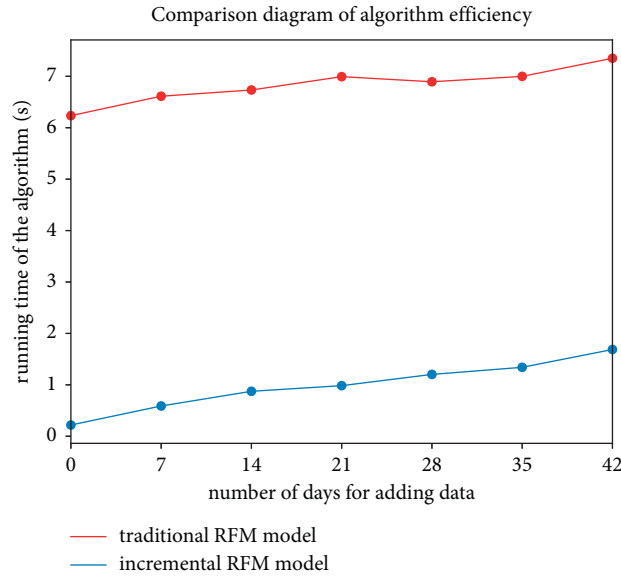
FIGURE 5: Comparison of RFM model efficiency.
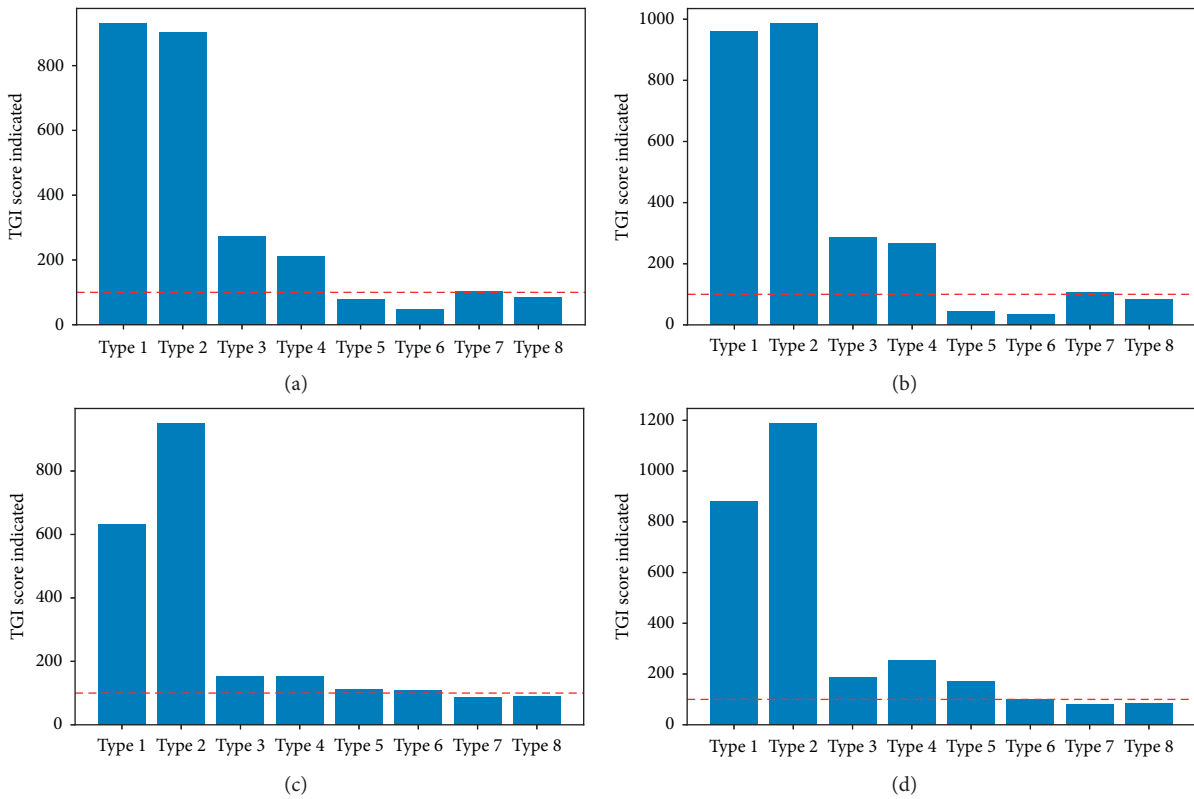
FIGURE 6: TGI index of TOP-4 well-sell cigarettes by different categories of customers. (a) Yellow crane tower (soft blue). (b) Liqun (new version). (c) Yellow crane tower (hard wonder). (d) Red golden dragon (soft boutique).

four products are more popular with the four types of consumers: general maintenance consumers, important maintenance consumers, general value consumers, and important value consumers, especially the important maintenance consumers and important value consumers, while the Yellow Crane Tower (hard wonder) and Red Golden Dragon (soft Boutique) are also popular with important development consumers. In contrast, important value consumers prefer Liqun (new version), important maintenance consumers and important development consumers prefer Hongjinlong (soft boutique), and important retention consumers prefer yellow crane tower (hard spectacle).

5.3. Accuracy Evaluation of the Prediction Model Based on LSTM. In this section, we will compare the accuracy of the cigarette purchase prediction model based on LSTM proposed in this paper with other machine learning algorithms, including support vector machine (SVM) [10], random forest (RF) [11], decision tree (DT) [12], and XGBoost [13]. The parameters of each model are determined according to the prediction results after careful grid search.

Figure 7 shows the accuracy comparison results of the five methods, where the blue bar represents the average accuracy and the green bar represents the standard deviation of accuracy. It can be seen from the figure that the method proposed in this paper achieves the highest accuracy, reaching 59.32%. It is 1.31% better than the second-place method (XGBoost). And the standard deviation of the method proposed in this paper is lower, which shows that our method has better robustness and can better deal with data anomalies.

Secondly, in the comparison methods, we can see that the prediction algorithm based on the tree is better than SVM, probably because the prediction model based on tree can potentially describe the temporal relationship of purchase behavior according to the splitting order of tree nodes.

5.4. Ablation Study. In this section, we will compare the impact on the LSTM cigarette purchase prediction model by 3 key factors, which are the embedding layer in the model, and the characteristics of the most frequently purchased cigarettes in the data, and the characteristics of the previous *K* purchases.

5.5. Influence on Prediction Effect of the Embedding Layer. In this section, we study the impact of the embedding layer by comparing the prediction accuracy of models with and without an embedding layer (see Figure 8).

In Figure 8, the blue bar graph represents the mean value of accuracy and the green bar represents the standard deviation of accuracy. When there is an embedded layer in the model, the average accuracy rate reaches 59.32%, which is 16.77% higher than that without this layer. It can be found that the average accuracy rate is greatly improved. In addition, the standard deviation of accuracy is also reduced by 1.86% compared with that without the embedding layer, indicating that the prediction effect of the model is more stable when this layer is added. Therefore, the embedding layer is useful to improve the prediction accuracy of the model.

5.6. Effects of the Most Frequently Purchased Commodity. In this section, we study the impact of the most frequently purchased good by comparing the prediction accuracy of models with and without this feature, and the results are shown in Figure 9.

In Figure 9, the blue bar represents the average value of accuracy and the green bar represents the standard deviation of accuracy. It can be seen from the figure that the accuracy with *TzX6* in the feature reaches 59.32%, which is 7.62%
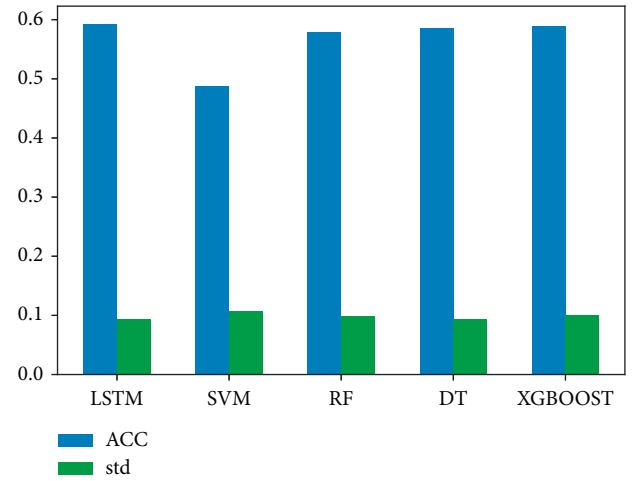
FIGURE 7: Comparison of model evaluation results.
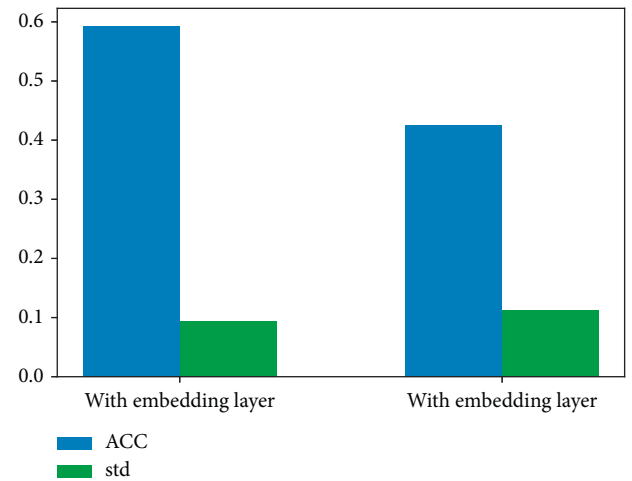
FIGURE 8: Comparison of effect with and without embedding layer.
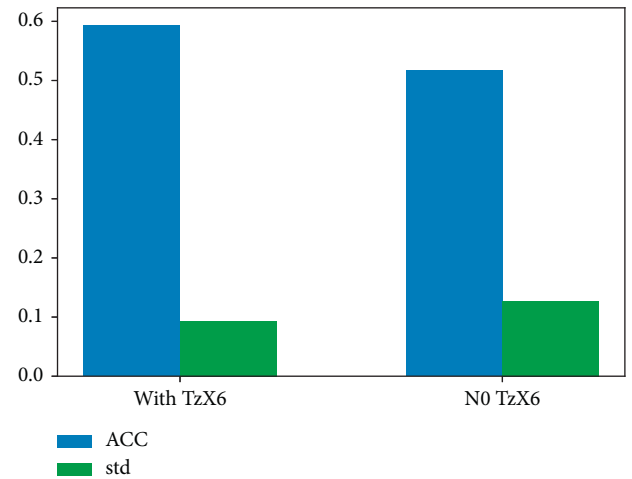
FIGURE 9: Comparison of effect with and without *TzX6* feature.

higher than that without *TzX6*. In addition, the standard deviation is reduced by 3.4%, which makes the prediction effect of the model more accurate and more stable.

5.7. Effects of Previous K Purchase Records. In this section, we compare the impact on the prediction effect of consumers' recent K different purchase behaviors.

Figure 10(a) compares the average accuracy of five different K consumption records. It can be seen from the figure that the prediction accuracy first decreases and then increases with the increase of the K value. When K is 5, the accuracy of the model is more than 0.92% higher than the average accuracy when K is 2, 3, and 4. It is interesting that when we only consider the latest purchase record, the model achieves the best performance. It indicates that the consumer's purchase behavior is most related to his/her latest purchase behavior and his/her long-term behavior.

In Figure 10(b), it compares the standard deviation of accurate values of five different K values. It can be seen that, among the last four K values, the standard deviation of five consumption records is the smallest, reaching 9.32%, indicating that the prediction effect is the best and most stable when $K = 5$. Similarly, when $K = 1$, although the standard deviation is relatively small, the randomness of the customer's latest record is relatively large, which cannot explain the customer's long-term consumption preference and consumption habits. Therefore, considering the prediction effect and significance of each K value, five is a better choice than one.

6. Related Work

The main work of this paper is to carry out customer profiling work, so we first investigate the work related to the customer profiling. Besides, we improve the traditional RFM model and classify customers by the incremental RFM model. And we solve the commodity purchase predictions problem. Therefore, we further investigate the related work into the RFM model and commodity purchase predictions.

Customer profiling: In the trend of a big data environment, customer profiling is used more and more in online shopping and offline retail. In 2016, Li et al. [14] used the K-means algorithm to divide different cigarette attributes and customer attributes and proposed the retailer with the format of the grocery store, the market type of city, the regional type of school district, and the business scale of medium scale. Customers recommend flue-cured cigarettes. In the product recommendation problem in 2019, Zhou et al. [15] proposed a multimodel stacking ensemble (MMSE) algorithm for the personalized product recommendation problem, which is mainly divided into data analysis and model construction. In the data analysis section, Zhou et al. proposed a feature model containing six feature clusters. They designed a sampling algorithm to balance the ratio of positive and negative samples through k-means clustering and undersampling. In the construction of customer profile in the new retail environment proposed by Wang [16], the author takes the customer of offline stores and online stores on the "Tesco on Campus" platform as the research object, based on the essential attribute characteristics of customers, consumer behavior characteristics. There are three dimensions of time and space features, and the data is analyzed by clustering, and the RFM model is constructed using the time and space feature dimensions. Different from the above work, the incremental RFM model is first proposed, and then it used to classify customers. And we solve the commodity purchase predictions problem. This approach helps us construct customer profiling from multiple perspectives.

RFM model: Different researchers have improved the traditional RFM model to varying degrees. For example, Ye [9] designed the online consumer value RFM from three dimensions. Wei [17] proposed adding customer demographic characteristics to the RFP model by combining qualitative and quantitative analysis, breaking the traditional collaborative filtering algorithm based on the RFM model. Anitha and Patil [18] combined the RFM model and K-means clustering method to classify customers. Khajvand et al. [19] extended the RFM model and introduced a new counting parameter to classify customers. You et al. [20] used the RFM and decision-making models for precision marketing. Different from the above work, starting from the update efficiency of the RFM model, this paper proposes an incremental RFM calculation method. Based on historical RFM model, it counts relevant indicators of newly generated consumption data and quickly updates the RFM model.

Commodity purchase predictions: Commodity purchase predictions mostly use machine learning and deep learning methods in purchase behavior prediction. With the gradual deepening of research, some multistage hybrid models have been derived from the single initial model. Ge et al. [21] established an overall customer behavior feature model by constructing customer behavior feature engineering and designed a customer purchase behavior prediction method based on deep forest, which achieved an efficient behavior prediction training effect. XGBoost algorithm is based on Bagging strategy in commodity purchase prediction proposed by Dongqing and Chengji [22]. After that, researchers gradually realized that commodity purchase prediction is essentially a time-series prediction problem. Therefore, some e-commerce commodity prediction problems use related single models or multistage hybrid models based on deep learning and neural network models. For example, Xuyang and Fengjing [23] proposed a prediction model based on the combination of LSTM and random forest. In commodity purchase predictions, Yin et al. [24] designed a customer profiling based on TF-IDF customer cigarette preference prediction algorithm model based on a tobacco company, combining customer portraits and customer preference prediction. The character data author uses TF-IDF to analyze and predict the customer's emotional tendency towards commodity. The text-based data predicts the customer's preference value for cigarettes by calculating
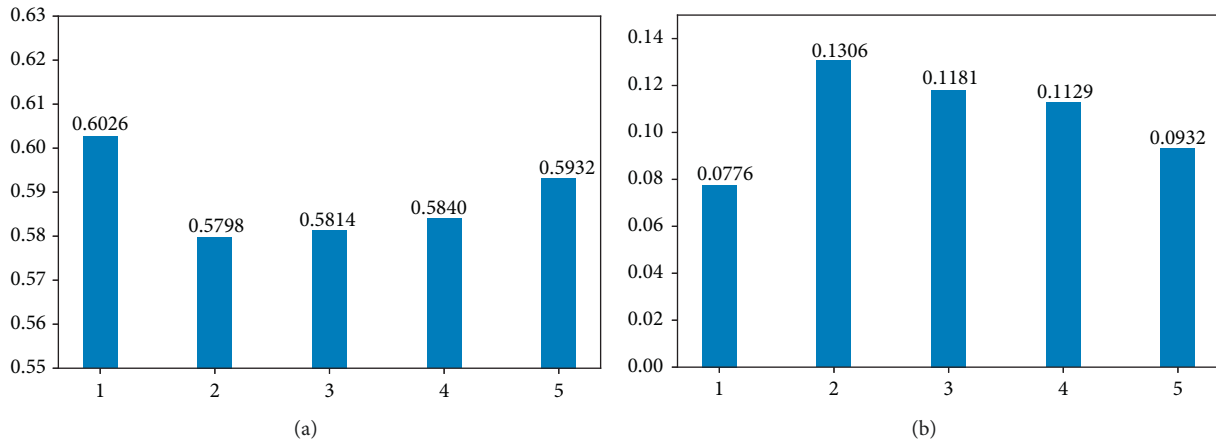
FIGURE 10: Comparison of different K consumption records. (a) Average accuracy. (b) Average standard deviation.

the similarity of the data. Due to the lack of mature customer preference and commodity purchase predictions models in cigarette companies, the TF-IDF prediction model only considers the purchase frequency of customers and does not consider the time-series nature of commodity purchase predictions. Different from the above work, based on the LSTM model, this paper uses six fine-grained features to make predictions, and the fine-grained data include the last five purchases of consumers and the most frequently purchased goods. Commodity purchase predictions consider the customer's commodity purchase frequency and the timing of the customer's purchase behavior and can make dynamic and accurate predictions based on changes in customer behavior in recent times.

7. Conclusions

This paper proposes a consumer profiling method from three aspects by using the historical purchase records of consumers collected by retail terminals. Firstly, an incremental RFM model is designed to classify customers' value and judge whether customers are valuable and loyal. The incremental RFM model can achieve model update in a shorter time than the traditional method. Then, the TGI model is used to analyze the preference of classified customers. Although we only analyze the top four well-sell cigarette brands in experiments, it can be easily extended to other goods of interest. Finally, we propose a commodity purchase prediction model based on LSTM to predict which commodity will be bought by each customer in the future. We take the customer's last five purchase records and the most frequently purchased commodity in history as the input features and adopt semantic embedding and LSTM model to predict the final results. Through experiments on real cigarette purchase data, it is verified that the model can achieve the best prediction accuracy, reaching 59.32%.

In future work, we will continue to optimize the commodity prediction model, hoping to mine the patterns of consumer interest changes and improve the prediction accuracy of the model.

Data Availability

The dataset used were collected from the tobacco monopoly bureau and are not publicly accessible.

Conflicts of Interest

The authors declare that they have no conflicts of interest.

Acknowledgments

References

[1] R. G. Martínez, R. A. Carrasco, C. Sanchez-Figueroa, and D. Gavilan, "An rfm model customizable to product catalogues and marketing criteria using fuzzy linguistic models: case study of a retail business," *Mathematics*, vol. 9, no. 16, p. 1836, 2021.

[2] A. M. AlBedah, M. K. Khalil, A. A. Khalil, and A. T. Elolemy, "Use of the target group index survey to evaluate the cigarette smoking profile in Saudi Arabia," *Saudi Medical Journal*, vol. 32, no. 10, pp. 1055–1059, 2011.

[3] J. Park, Y. Kim, I. Eom, and K. Lee, "Economic load dispatch for piecewise quadratic cost function using hopfield neural network," *IEEE Transactions on Power Systems*, vol. 8, no. 3, pp. 1030–1038, 1993.

[4] J. Dong, J. Wang, and S. Chen, "Knowledge graph construction based on knowledge enhanced word embedding model in manufacturing domain," *Journal of Intelligent and Fuzzy Systems*, vol. 41, no. 2, pp. 3603–3613, 2021.

[5] T. Mikolov, K. Chen, G. Corrado, and J. Dean, "Efficient Estimation of Word Representations in Vector Space," 2013, https://arxiv.org/abs/1301.3781.

[6] H. H. Tan and K. H. Lim, "Vanishing Gradient Mitigation with Deep Learning Neural Network Optimization," in *Proceedings of the 2019 7th International Conference on Smart Computing & Communications (ICSCC)*, IEE, Sarawak, Malaysia, June 2019.

[7] M. Martinez and R. Stiefelhagen, "Taming the Cross Entropy Loss," in *proceedings of the German Conference on Pattern Recognition*, Springer, Berlin, Germany, February 2018.

[8] A. KingaD, "A method for stochastic optimization. Anon," in *Proceedings of the InternationalConferenceon Learning Representations*, SanDego, CA, USA, May 2015.

[9] H. Z. Ye, "The research of online number customer value based on the new 3d customer segment mode," *Statistics & Information Forum*, vol. 31, pp. 96–101, 2016.

[10] S. Mengshu, H. Yuansheng, X. Xiaofeng, and L. Dunnan, "China's coal consumption forecasting using adaptive differential evolution algorithm and support vector machine," *Resources Policy*, vol. 74, Article ID 102287, 2021.

[11] E. A. Atumo, T. Fang, and X. Jiang, "Spatial statistics and random forest approaches for traffic crash hot spot identification and prediction," *International Journal of Injury Control and Safety Promotion*, vol. 29, no. 2, pp. 207–216, 2021.

[12] M.-J. Jun, "A comparison of a gradient boosting decision tree, random forests, and artificial neural networks to model urban land use changes: the case of the seoul metropolitan area," *International Journal of Geographical Information Science*, vol. 35, no. 11, pp. 2149–2167, 2021.

[13] J. Luo, Z. Zhang, Y. Fu, and F. Rao, "Time series prediction of covid-19 transmission in America using lstm and xgboost algorithms," *Results in Physics*, vol. 27, Article ID 104462, 2021.

[14] B. Li, Y. Wang, and Y. Liu, "K-means-based customer profile and intelligent recommendation application in the big data environment," *Modern Computer Professional Edition*, vol. 33, no. 24, 2016, (in Chinese).

[15] A. Zhou, K. Ren, X. Li, and W Zhang, "MMSE: A Multi-Model Stacking Ensemble Learning Algorithm for purchase prediction," in *Proceedings of the 2019 IEEE 8th Joint International Information Technology and Artificial Intelligence Conference (ITAIC)*, pp. 96–102, IEEE, Chongqing, China, May 2019.

[16] Xi Wang, "Construction of the customer profile based on the new retail environment," *Enterprise Technology and Development*, vol. 37, no. 01, pp. 228–230, 2021.

[17] Z. Wei, *Research on Personalized Recommendation Methods of Physical Retail Enterprises Based on Rfm Model*, Lanzhou University of Finance and Economics, China, 2018.

[18] P. Anitha and M. M. Patil, "Rfm Model for Customer purchase Behavior Using K-Means Algorithm," *Journal of King Saud University-Computer and Information Sciences*, vol. 34, no. 5, 2019.

[19] M. Khajvand, K. Zolfaghar, S. Ashoori, and S. Alizadeh, "Estimating customer lifetime value based on rfm analysis of customer purchase behavior: case study," *Procedia Computer Science*, vol. 3, pp. 57–63, 2011.

[20] Z. You, Y.-W. Si, D. Zhang, X. Zeng, S. C. Leung, and T. Li, "A decision-making framework for precision marketing," *Expert Systems with Applications*, vol. 42, no. 7, pp. 3357–3367, 2015.

[21] S. Ge, J. Ye, and M. He, "Deep forest-based user purchase behavior prediction model," *Computer Science*, vol. 46, no. 09, pp. 190–194, 2019, (in Chinese).

[22] X. Dongqing and Z. Chengji, "Application of xgboost algorithm based on bagging strategy in commodity purchase prediction," *Modern Information Technology*, vol. 1, pp. 80–82, 2017.

[23] L. Xuyang and S. Fengjian, "Lstm and random forest buying behavior prediction model," *Journal of Qingdao University (Natural Science Edition)*, vol. 33, pp. 17–20, 2018.

[24] J. Yin, X. Liang, Z. Liu, and Z. Lu, "User preference prediction model research and customer profile label application," *Electronic Technology and Software Engineering*, vol. 9, no. 24, 201–202, 2020, (in Chinese).

Research Article

Research on the Training and Management of Industrializing Workers in Prefabricated Building with Machine Vision and Human Behaviour Modelling Based on Industry 4.0 Era

Junwu Wang [iD],[1,2] **Yinghui Song** [iD],[1] **Chunbao Yuan** [iD],[3] **Feng Guo** [iD],[1,2] **Yanru Huangfu,**[4] **and Yipeng Liu** [iD][1,2]

[1]*School of Civil Engineering and Architecture, Wuhan University of Technology, Wuhan 430070, China*
[2]*Hainan Research Institute, Hainan Research Institute, Sanya 572019, China*
[3]*China Construction Seventh Engineering Division Corp Ltd, Shenzhen 518129, China*
[4]*School of Art and Design, Zhengzhou University of Light Industry, Zhengzhou 450002, China*

Correspondence should be addressed to Chunbao Yuan; 262895@whut.edu.cn

As countries around the world pay more and more attention to the sustainable development of the construction industry, the prefabricated building model has become the best construction type to achieve energy conservation and emission reduction. However, the prefabricated building entails higher technical requirements, and the workers involved in the construction must be trained to reduce the risks. For China, where the demographic dividend is gradually disappearing, how to quickly promote the industrializing workers process has become an urgent issue. This research focuses on the training and management of industrializing workers in prefabricated building. First, the facial images of the participants were collected from the actual test data, and the changes of participants' facial expressions were analyzed through multitask convolutional neural network-Lighten Facial Expression Recognition (MTCNN-LFER). The results of the analysis were plugged into the facial expression recognition and evaluation model for industrializing workers training in this research to calculate the weights, and then all the weights were clustered through the improved SWEM-SAM method. The results show the following: (1) the values of objective data were used to judge the participating workers' mastery of each knowledge and to evaluate whether they are qualified. (2) The evaluation results were used to analyze the risk events that may be caused by participating workers.

1. Introduction

With the development of global economy and engineering technology, the urbanization and industrialization of each country are also advancing [1], and the advancement of electronic intelligence technology has enabled the world industrial level to move into a New Era of Industry 4.0. In today's world of advocating resource conservation and sustainable development, the traditional construction model consumes a large amount of resources [2, 3] and produces a huge amount of construction waste that causes great damage to the environment. Therefore, the Chinese government has proposed the 14th Five-Year Plan and the long-range goals

for 2035 [4], in which prefabricated building model was promoted widely to drive sustainable development of the world environment. Since the prefabricated building model is not yet mature in China, there is a high technical requirement for workers. Besides, as China's population distribution changes, China is gradually entering an ageing society and the demographic dividend is rapidly declining. The Chinese government has proposed to accelerate the process of industrialized workers to ensure sufficient numbers of professionals and high-quality technologies in the construction industry.

According to data released by the Ministry of Housing and Urban-Rural Development of the PRC, this study

investigated safety accidents in the construction industry between 2009 and 2020 [5]. 96.17% of accidents with casualties were caused by workers' unsafe behaviours. 284 safety accidents in prefabricated buildings were reported in 2020 alone, with an average casualty rate of 1.63 people per accident [6]. Besides, 72.64% of the economic and legal problems leading to project delays stemmed from the failure of relevant practitioners to fulfil their obligations in accordance with contracts and laws and regulations. Therefore, a strict control of the training and management system for industrialized workers in prefabricated building is of greater significance in origin-tracing of accidents in such projects and can promote the stable and standardized development of the construction industry as a whole [7].

At present, the construction of prefabricated buildings worldwide is through the combination of prefabricated components and cast-in-place technology, the design concept of which is similar to the structural strength of cast-in-place buildings. The main design method is to connect the prefabricated elements to the cast-in-place structure by solid longitudinal reinforcement connections and then technical processes are implemented to the joints of the whole building structure in order to achieve safety and durability that match the architectural design level [8]. As finished products, prefabricated components have high requirements on humidity, storage space, and maintenance methods in terms of production, transportation, and storage. Considering construction, the longitudinal reinforcement connection technology of prefabricated buildings is quite complex with a large number of joints and splicing gaps, and the waterproofing and insulation of walls are technically challenging [9]. Therefore, prefabricated buildings require workers with higher technical skills.

The traditional worker training system is only a two-phase process from training to employment, and the workers are rural migrant workers with a mobile work nature. As these workers are poorly educated generally, they usually rely on "experience" and tend to ignore the correct mechanical operation steps or the standardized and safe construction sequence, which has posed great engineering hidden dangers to the whole project. In recent years, with the advancement of industrialized workers, the relevant training system has incorporated the concept of assessment. But the practice of determining whether the training standards are met only based on the workers' test scores leads to neglect of workers' mastery of knowledge in different situations. It results in redundant training or muddling through the test, which will cause economic losses to the company and even failure to detect safety hazards in time.

In summary, based on the development background of China's construction industry, how to establish a training system with sound risk control for industrialized workers to ensure the quality of the advancement of the industrializing workers and to reduce the incidence of various risks in the construction industry is an urgent problem to be solved at present. This research uses human behaviour modelling as the grassroots theory, adopts a combination of artificial intelligence and machine vision to recognize and analyze the facial expressions of workers undergoing industrializing

worker training tests, and decomposes the test results of workers in different emotional contexts, so as to establish a facial expression recognition and evaluation model for industrializing worker training. Then the calculation results were clustered through the improved SWEM-SAM method to evaluate the effects of the worker training and to uncover the hidden risks and hazards in this worker group.

The rest of the research is organized as follows. In Section 2, literature research on basic theory involved in this paper is conducted to find theoretical support. Section 3 introduces the methods adopted in this research and improvement points. In Section 4, a facial expression recognition and evaluation model for industrializing worker training is established and four different scenarios are analyzed. In Section 5, the actual test data are plugged into the model for analysis. Section 6 discusses the analysis results, the correctness of the model, and the trends of the interpretation results and concludes the research to provide theoretical directions for further research.

2. Literature Review

2.1. Human Behaviour Modelling. Human behaviour modelling is an interdisciplinary mathematical modelling method that evaluates what is happening and predicts what will happen through the external behaviour of humans. It has been successfully applied in a number of disciplines. Human behaviour is modelled based on rationality to find optimal solutions [10, 11], but, in practice, much human behaviour is found to deviate from rationality.

Steyn investigated contingency reserves in engineering projects and modelled workers' behaviour at construction sites, so as to use the model to predict contingency reserves and prevent economic overruns of the project and possible shortening of construction period [12]. Meel et al. investigated personnel management in chemical plants and analyzed the management relationship between plant risk calculations and human behaviour patterns to study the correlation between unsafe human behaviour and training the workers received [13, 14]. Zhang et al. analyzed risk factors of man-made accidents in underground engineering by modelling human behaviour from three aspects of safety cognition, behaviour, and physiological states of humans and proposed how to control man-made risk causes [15]. Ronchi modelled dynamic evacuation behaviour of the crowd in fire scenarios by starting with big data analysis. He put forward a theory of management and prevention of disasters caused by crowd gathering by the fitting analysis of large bulk of data of movement patterns of each individual in the crowd and their state performance [16]. Asilian-Mahabadi et al. surveyed a large number of relevant practitioners by studying the prerequisites for unsafe behaviour of front-line workers and managers in civil engineering and discussed the ability of human behaviour models to accurately expose the risk causes of unsafe worker behaviour [17]. van der Kleij and Leukfeldt analyzed the status quo of unsafe behaviour in cyberspace and proposed a new network resilience framework that integrates resilience engineering and human behaviour models. A pilot study of more than 60

small- and medium-sized enterprises in the Netherlands was conducted, the results of which could provide solid recommendations for organizations to better address cyberthreats [18]. Bai and Qian conducted a study on the validity and reliability of the human behaviour cognition factor and found that higher ratings of the people involved in such models had a greater contribution to quality assurance and safety behaviour in construction projects [19].

There are many similar studies that can reflect the existence of a management relationship between human behaviour modelling and accident risk, which means trends of human behaviour can be used to predict the likelihood of risk occurrence. This study aims to identify hidden risks in engineering by analyzing the distribution of workers' test scores.

2.2. Emotional Expressions in Facial Expressions.

Human facial expressions vary significantly under different emotions and the changes in facial expressions caused by each emotion are basically the same regardless of the country to which the person belongs. Therefore, studies related to emotion communication through facial expressions are mostly associated with human behaviour. Words can sometimes deceive, but a momentary change in facial expressions is difficult to hide.

Suhr et al. started with the rising crime rate of automated bank teller machines. As the machine's sensing system could not accurately determine sabotage, the offenders' facial expressions captured by the camera were identified, especially during the sabotage period, to build a model of facial expressions of emotion, and finally a correlation between facial expressions and insecure behaviour was identified [20]. Pantano collected data on the facial expressions of a large group of consumers when they were engaged in consumer behaviour to build a machine learning model and employed facial expression recognition system to evaluate consumer behaviour and activities, allowing salespeople to guide consumers according to their emotional activities [21]. Israel and Schonbrodt measured the physiological phenomena generated by changes in facial expressions (including facial electromyography, heart rate changes, and brain electrical changes) to create a benchmark test emotion evaluation system based on machine learning algorithms and found that human emotional changes could affect human behaviour [22]. Liu et al. proposed a multilabel and distributed learning approach to analyze students' facial expressions in the classroom and assessed teaching quality by observing respondents' facial expressions. Corresponding improvement suggestions on teaching models were proposed to educational administrators [23]. Monaro et al. used machine learning methods to identify facial microexpressions with the study subject of criminals in interrogation and introduced the concept of speaker cognitive load to determine whether criminals lied to conceal the truth during questioning with the help of machine vision. Given the same control group experiment, judgment by facial expressions was correct 78% of the time, compared to the 57% of human judges [24]. In the healthcare industry,

Altameem and Altameem developed a multimodal visualization analysis method by detecting facial expressions on patients to provide emergency treatment for patients through facial expression changes caused by adverse emotions [25]. De la Torre-Luque et al. found that emotion recognition is a key process of social cognition which reflects a person's maximal social adaptability. By comparing the facial expressions of a great number of normal people with those of psychopaths, a theoretical model for emotional decoding of human behaviour and facial expressions was developed [26]. Riquelme et al. collected a large amount of facial expression data of drivers and extracted feature codes to develop a driver fatigue monitoring system, which detects the driver's mouth aspect ratio, blinking frequency, and head tilt angle to determine whether the driver is in fatigue and alerts control staff in time, so as to avoid traffic accidents [27]. In a study on classroom teaching, Schneider et al. found that facial expressions are expressions of mental activity and that different facial expressions have a greater impact on learning efficiency. The analysis of the emotional state of facial expressions provides effective suggestions for educational administrators to improve students' learning efficiency [28].

Through the above scholars' research, it is found that changes in facial expressions can convey the inner activities of human beings, which is a great aid to judging the mental state of the test subjects.

2.3. Industrializing Worker Training.

"Industrializing workers" refers to, in China where the demographic dividend is gradually disappearing, the process by which construction worker teams, mainly migrant workers, are reeducated, assessed, and qualified to engage in industrial production with long-term work effectiveness. With 200 million mobile migrant workers in China, migrant workers need to receive instruction and education in industrial production ideas, science and technology, the use of wearable devices, and efficient and safe workforce regulations to become industrializing workers.

He's study found that vocational education occupies a greater proportion of worker industrialization, suggesting a connection model that combines higher vocational education and industrializing worker training in conjunction with the talent cultivation models in construction vocational colleges [29]. Wang and Ji conducted a research on the demand for construction workers in different development stages of construction industrialization, analyzed the differences between construction workers in developed countries and in China in various aspects, and pointed out the significance of safety education for industrializing workers and implementation of labor security system on promoting industrializing workers [30]. In a study on the risk cognition of Spanish workers, Rodriguez-Garzon et al. found that the industrial transformation efficiency of workers was related to working population mobility. By aggregation and clustering analysis, it was found that the worker groups who received multiple trainings had stronger risk perception ability [31]. In the industrial transformation

of workers in the construction of a laboratory at the Graz University of Technology, Karre et al. found that the key to transformation lied in supervision system and technical training should be strengthened [32]. Ke analyzed the complexity of the evolution from migrant workers to industrializing workers in the construction industry in China on the basis of CAS theory and made recommendations based on an agent-based modelling [33]. Hatami and Kakavand deemed that behaviour modification plays an indispensable part in worker industrialization and proposed the PRECEDE-PROCEED approach to evaluate the educational intervention effectiveness of occupational safety training on industrializing workers. As a result, the programme greatly reduced unsafe behaviour [34]. Radhakrishnan et al. combined the industrializing worker training system with artificial intelligence by using IVR technology to simulate accidents in a virtual environment and transmit the perception data of the trainers [35]. Cao et al. adopted a CHAID decision tree and chi-square analysis from the aspect of construction safety to explore the primary and secondary influencing factors and unrelated factors in education and training for industrializing workers. A five-factor method for training effectiveness was proposed [36].

Most of the previous studies have applied methods of traditional education industry to industrializing worker training, exploring the potential correlation between worker training effects and the reduction of accident probability. Combined with previous findings, this research focuses on the management relationship between training effect and risk factors occurrence in engineering.

In the previous studies, the calculation of risk and effect assessment was often based on the experts' criteria and ignored the influence of subjective wills. For example, it is difficult to know whether an expert is sensitive to a certain influencing factor and therefore the objective rules of development are ignored in the scoring. Moreover, the common mathematical model evaluation methods do not take into account the randomness and ambiguity of the evaluated objects, so the evaluation results sometimes differ greatly from the real situation. With the reduction of China's demographic dividend, the policy of industrializing workers has become an excellent strategy for China to address the coming huge labor shortage. There is still a large research gap on how to ensure the quality of training and education for industrializing workers. To fill this gap and make a combination to the prospect of highly intelligent industrial development in the context of Industry 4.0, this paper combines AI machine vision with an evaluation system as a theoretical basis. The industrial worker training evaluation system is improved by considering the combined effect of workers' personal influence and experts' subjective will, so that the industrial worker training evaluation results can make timely and effective rectification of hidden engineering problems in the existing project management process of prefabricated buildings construction projects.

3. Methods

3.1. Face and LFER Facial Expression Recognition Based on Multitask Convolutional Neural Network. A large number of algorithms for image segmentation and artificial intelligence

recognition already exist, and each algorithm is designed for different areas. For the background of this research, the MTCNN face recognition algorithm is selected for individual objects, and, because of the need for real-time evaluation of facial expressions, the Lighten Facial Expression Recognition (LFER) is chosen and improved as human facial expression recognition algorithm, and the FER2013 dataset is used for expression classification and recognition training.

3.1.1. MTCNN Human Face Recognition Method. The high accuracy of the MTCNN face recognition algorithm comes from the organic combination of face detection and facial landmark detection. In the face classification and bounding-box regression stage, the main framework of MTCNN is similar to that of the Cascade algorithm and can be decomposed into a three-layer network structure. Before detection, the images are transformed to different sizes and image pyramids are constructed to accommodate face images of different pixels.

The MTCNN implementation process mainly adopts the method of candidate box plus classifier to realize fast and efficient face detection. The three cascade networks are P-Net for fast candidate box, R-Net for candidate box filtering selection, and O-Net for generating face landmarks and face boundaries [37].

The training data for the MTCNN algorithm was sourced from the Wider and CelebA databases. Wider gives the face detection data and marks the coordinate information of the bounding box, and CelebA provides the five landmark coordinate points [38].

(1) P-Net. The Proposal Network (P-Net) consists of a fully convolutional network. Rough feature extraction and boundary calibration of image pyramid are realized through fully convolutional networks (FCN), and the Nonmaximum Suppression (NMS) and bounding-box regression are used for border filtering and adjustment. The initial filtering transmits possible face region images determined by classifier to the next layer of the network.

In the screening process, each input sample should be represented by a cross-entropy loss function, which requires the use of positive and negative samples. The probability calculation formula for the face is shown in the following equation:

$$L_i^{\text{det}} = -\left(y_i^{\text{det}}\log(p_i) + \left(1 - y_i^{\text{det}}\right)\left(1 - \log(p_i)\right)\right). \tag{1}$$

(2) R-Net. The Refined Network consists of a convolutional neural network with an additional fully linked layer, which is more complex than the P-Net. The images transmitted from P-Net are further filtered and adjusted to achieve high-precision filtering and optimization of face image regions.

In the process of border regression, for each candidate box, the loss between the predicted offset and the true coordinate offset needs to be calculated. The formula for calculating the regression loss by Euclidean distance is shown in the following equation:

$$L_i^{\text{box}} = \left\| \widehat{y}_i^{\text{box}} - y_i^{\text{box}} \right\|_2^2. \tag{2}$$

(3) O-Net. The Output Network has one more layer of convolutional neural network than R-Net and regresses the facial feature points of the filtered face image. The image features are saved in bulk to optimize the model performance. Finally, the coordinates of the top left and bottom right corners are output for plotting bounding boxes and five face image feature points are output.

Feature coordinate point location is similar to that of candidate box regression, in which the Euclidean distance between the candidate feature coordinate offsets and the true coordinate offsets needs to be calculated to obtain the overall loss function. The formula for calculating the regression loss from the Euclidean distance in the landmark sample and the overall loss function are shown in the following equation:

$$L_i^{\text{landmark}} = \widehat{y}_i^{\text{landmark}} - y_{i2}^{\text{landmark2}},$$

$$\min \sum_{j=1}^{N} \sum_{j \in \{\text{det,box,landmark}\}} \alpha_j \beta_i^j L_i^j. \tag{3}$$

An image structure overlay and deconstructed diagram of the three-layer network structure are shown in Figure 1.

3.1.2. Lighten Facial Emotional Recognition Method. Human facial expression recognition relies on the classification of human face images collected by face recognition algorithms, equivalent to adding a classifier to the face recognition algorithm. LFER uses an annual deep convolutional network to fuse face expression feature extraction and classification into an end-to-end network. VGG-16/19 and ResNet-18/101/164 are employed in expression recognition and classification. Dropout is added before the full linked layer to increase the robustness of the algorithm model and prevent overfitting. An increase in robustness will improve the stability of the model and increase its recognition ability. Overfitting will lead to a lack of dispersion, thus increasing the probability of misjudgment. The seven categories of expressions were feeling disgusted, angry, sad, worried, neutral, happy, and surprised. The full linked layer in VGG and ResNet is removed, and the concept of loss function and cross-entropy is introduced. The calculation process of cross-entropy is shown in the following equation [39]:

$$J(\theta) = -\frac{1}{m} \sum_{i=1}^{m} \left[y^i \log\left(h_\theta\left(x^i\right)\right) + \left(1 - y^i\right) \log\left(1 - h_\theta\left(x^i\right)\right) \right]. \tag{4}$$

The LFER algorithm uses Network Slimming and binarization methods for model compression to speed up recognition and employs Batch Normalization (BN) to reduce computation amount. The images of low BN indicator will be removed. The BN calculation formula is shown as follows:

$$\widehat{z} = \frac{(z_{\text{in}} - \mu\beta)}{\sqrt{\sigma_\beta^2 + \varepsilon}; z_{\text{out}} = \gamma\widehat{z} + \beta}. \tag{5}$$

3.2. Structural Entropy Weight Method. In information theory, entropy represents the measure of uncertainty of a dataset. The absolute value of entropy becomes larger as the uncertainty of the information expressed in the dataset increases, and the value of entropy contains more information. Correspondingly, the smaller the value of entropy is, the poorer the information it contains and the more homogeneous the meaning of the representative indicator is.

Since SEWM has the function of both quantitative and qualitative analysis, it can be called an objective empowerment method in which the variation of values depends on the dispersion of the calculated dataset. The basic process of SEWM calculation is as follows: firstly, making a combination with Delphi method and fuzzy analysis method. The fuzzy analysis method is used to fuzzify the experts' scores and quantify the ranking according to the subjective will of the experts. After the quantification is completed, the normalization process is performed. Then, cognitive blindness degree analysis and entropy calculation are performed for the quantitative order of experts' judgments, and the possible bias due to the subjective opinions of experts is corrected. Finally, the weighting value is calculated [40]. The detailed calculation and formula are shown below.

3.2.1. Arranging the Quantization Order of the Datasets. According to the Delphi method, k experts in the relevant fields are selected to fill out the questionnaire. The basis of data acquisition in this paper is built on machine vision, so the sample data of answers from k relevant workers can be used as the data source. The questionnaire taken by the original Delphi method is replaced by a random fixed number of classified questions from the question bank.

The importance of the sample data is obtained by the positive and negative selection method considering facial expressions in this paper, where 1 is an important indicator and n unimportant. For the i samples and j indicators in the dataset, where $1 \leq i \leq k$ and $1 \leq j \leq n$, the representation performed by the a_{ij} array is shown as follows:

$$a_{ij} = \begin{bmatrix} a_{11} & \cdots & a_{1n} \\ \vdots & \ddots & \vdots \\ a_{k1} & \cdots & a_{kn} \end{bmatrix}. \tag{6}$$

3.2.2. Making Normalization of Indicators: Homogenization of Heterogeneous Indicators. Each indicator may have inconsistent measurement units in statistical decision-making, so it is necessary to standardize the sorted datasets and convert the relative values of indicators into absolute values to solve inconsistent measurement methods for different indicators. Since the normalization of the data group value is an absolute value, the greater the difference in the Hamming distance of each normalized data, the greater the dispersion.
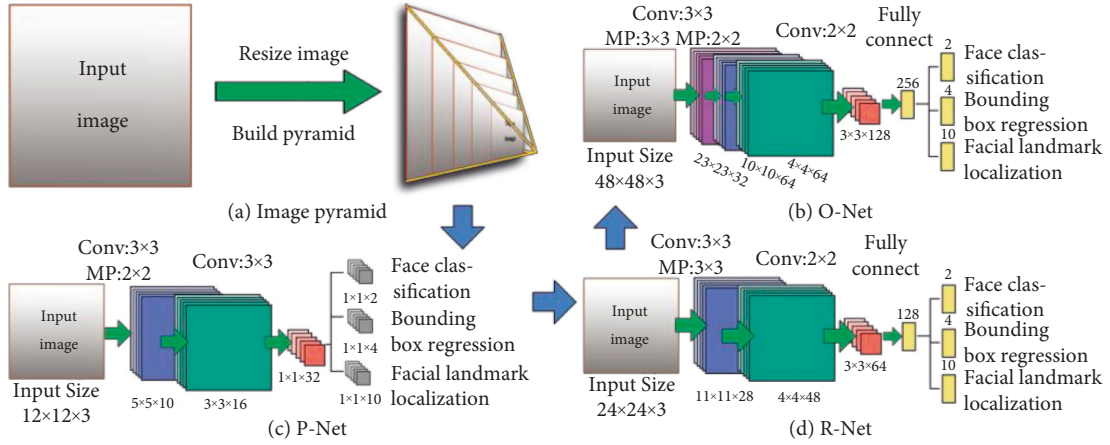
FIGURE 1: The image structure overlay and deconstruction of the P-Net, R-Net, and O-Net network structures. (a) Image pyramid. (b) O-Net. (c) P-Net. (d) R-Net.

The normalization processing method is related to the calculation method, as shown in (7) and (8):

Positive indicators:

$$a'_{ij} = \frac{a_{ij} - \min\{a_{1j}, a_{2j}, \ldots, a_{nj}\}}{\max\{a_{1j}, a_{2j}, \ldots, a_{nj}\} - \min\{a_{1j}, a_{2j}, \ldots, a_{nj}\}}. \quad (7)$$

Negative indicators:

$$a'_{ij} = \frac{\max\{a_{1j}, a_{2j}, \ldots, a_{nj}\} - a_{ij}}{\max\{a_{1j}, a_{2j}, \ldots, a_{nj}\} - \min\{a_{1j}, a_{2j}, \ldots, a_{nj}\}}. \quad (8)$$

To simplify the formula, the normalized data a'_{ij} is still denoted by a_{ij}.

3.2.3. Weight Calculation for Qualitative Analysis and Quantitative Analysis.

Relying on the concept of entropy weight method, the quantitative analysis data is revised, where I is the order in the data group and m is the conversion parameter whose values are usually equal to $j + 2$ ($m = j + 2$) [40]. The quantitative analysis correction is shown as follows:

$$\mu(I) = -\frac{\ln(m - I)}{\ln(m - 1)}. \quad (9)$$

Substituting a_{ij} into the above formula, the quantitative analysis correction array b_{ij} is obtained. The expert cognitive blindness degree analysis parameter Q_j is introduced. The calculation formula of Q_j is shown as follows:

$$Q_j = \left| \frac{\left\{ \left[\max\{b_{1j}, b_{2j}, \ldots, b_{nj}\} - b_j \right] + \left[\min\{b_{1j}, b_{2j}, \ldots, b_{nj}\} - b_j \right] \right\}}{2} \right|. \quad (10)$$

The perception of the relevant respondents for the indicator is defined as x_j and the standardized weights are calculated. The calculation process is shown in the two following equations:

$$x_j = b_j(1 - Q_j). \quad (11)$$

$$\omega_j = \frac{x_j}{\sum_{j=1}^{n} x_j}. \quad (12)$$

3.3. Similarity Aggregation Method.

For the possibility of fuzzy numbers and uniform or normal distribution, the linguistic terms and sentiment labels of the relevant descriptions are expressible as affiliation functions of different values. In previous risk assessments, triangular and trapezoidal fuzzy numbers were mostly used. For qualitative and comparative analysis, converting collected data into fuzzy numbers is more adaptable than converting them into probability distributions [41]. In this study, it is necessary to use the improved SAM to convert the data into fuzzy numbers for aggregation and then to evaluate the effect through weight calculation.

This study proposes an improved SAM that introduces the concept of emotional expression when inputting data and changes the previous expert evaluation system to the facial expression recognition dataset of the surveyed person. The method quantifies the change in respondents' emotions during the test through human behaviour modelling, and the resulting fuzzy numbers are corrected based on multiple factors. In previous studies, some scholars selected experts' position, duration of practice, age, and education as rank divisions [42].

The improved SAM calculation processes are as follows:

(1) Suppose that there are E_i experts, where $1 \le i \le k$. Calculate the consistency $S(\widetilde{R_u}, \widetilde{R_v})$ of quantitative data for each expert (respondent), where R_u and R_v are the fuzzy numbers of S. The formula of quantitative data consistency is shown as follows:

$$S(\widetilde{R_u}, \widetilde{R_v}) = 1 - \frac{1}{5 \sum_{i=1}^{5} |a_i - b_i|}, \quad (13)$$

a_i and b_i represent the evaluation parameter values of different qualitative analysis. The larger the S value, the more unified the opinions of experts (respondents).

(2) Subsequently, the Delphi method was used for secondary quantitative analysis, combined with credibility to improve the reliability of aggregated analysis results. Finally, the consistency $WA(E_u)$ of weighted agreement (absolute value) is calculated, and the relative consistency $RA(E_u)$ and the consistency coefficient $RC(E_u)$ of the expert dataset are calculated according to the expert's $WA(E_u)$. In previous studies, some scholars introduced the concept of relaxation factor δ, $\delta \epsilon [0, 1]$. When the value of δ approaches 1, it means that the experts' judgment weight is the main basis; when the value of A tends to 0, it means that $RC(E_u)$ is an indicator of the relative value of experts' judgments. Finally, the summary results of experts' opinions are calculated to obtain the overall fuzzy number $\widetilde{R}$. The calculation formula of $\widetilde{R}$ is

$$\widetilde{R} = \sum_{u=1}^{M} \left[RC(E_u) \times \widetilde{R_u} \right]. \quad (14)$$

4. Data Survey and Model Establishment

4.1. Data Investigation and Collection. The data for this study, done with the assistance of Python 3.8 programming language, were obtained from the results of the responses to the questions drawn from the question bank, which were all multiple-choice questions about knowledge related to safety in assembled buildings, divided into five sections: Knowledge about Engineering Project Management (KPM), Cautions at Construction Site (CCS), Prefabricated Component Hoisting and Installation (PHI) Knowledge, Emergency Accident Handling Methods (EAM), and Laws and Regulations Related to Construction (LRC). As respondents took the training test, cameras were used to capture their facial expressions, recorded at 30 frames per second, with a 10-second response time for each question and a final 2-second answer checking phase. The footage is then split at 15-frame intervals. Twenty face images are collected for each question, and each respondent can provide 2000 face images for analysis. The pseudocode of collecting facial expression data for the industrializing worker training test is shown in Algorithm 1.

Subsequently, every 20 images were formed into a data group for expression analysis using the MTCNN-LFER model. Firstly, the acquired images are decomposed into image pyramids and then imported into the three-layer volume and network P/R/O-Net for expression analysis and recognition. The recognition process is shown in Figure 2. Then the probability of emotions is determined based on the relative coordinates of the expression features, and the output of the determination is shown in Figure 3.

4.2. Evaluation Model of Facial Expression Recognition for Industrializing Worker Training. Quantitative analysis of the collected data is required before the construction of the expression recognition evaluation model. The difference between the data collection phase of this study and the establishment of previous evaluation models is that previous evaluation models mostly use the mechanism of expert scoring, while that in this study is derived from the respondents' status while taking the answer test. This study uses the Likert's seven-level scale method to assign different categories of facial expression recognition (including disgusted, angry, sad, worried, neutral, happy, and surprised) from 1 to 7 points. The formula for preliminary scoring is shown in Equation (15). t is the moment, p_{emo} is the bias probability for each expression, and S_{l7} is the assigned score on the 7-point Likert scale. S_r is the parameter for correct or incorrect answers, and when the answer is correct, S_r is 1.2; otherwise, S_r is 0.8. The division of expression scores based on Likert's seven-level scale is shown in Figure 4 [43].

$$W_{emo} = \sum_{t=1}^{20} \sum_{p_{emo}=1}^{7} \left(\frac{p_{emo} \times S_{l7}}{n} \right) S_r. \quad (15)$$

However, the assignment of expressions is not the final "expert score," because the data comes from training tests, and the answers will be right or wrong. However, in the process of testing, workers may be unskilled in the operation of electronic equipment or emotionally resulting in deviations in the visual area. Furthermore, there is a possibility that when a worker encounters an uncertain option, he guesses the correct option by luck. Monaro et al. [24] defined the concept of error and hesitation degree in the research of facial expression detection deception. Through the survey, it was found that, due to differences in education, gender, age, and other influencing factors, different people will have abnormal facial expressions when they make judgment. According to the average conditions of Chinese workers, the range of the error degree τ is 0.6514 ± 0.1343, and that of hesitation degree v is 0.4875 ± 0.098 [24].

In view of the above situation, this article expresses the worker's facial expression changes and corresponding moments of each question with images and selects 4 curved surfaces and curves under abnormal mood fluctuations as special images for analysis. The four abnormal images are shown in Figure 5. According to the fluctuation trend of the four curves, it can be analyzed as the four following situations.

Situation 1. When the respondents first saw the topic, the expression was worried, indicating that the worker did not understand the randomly selected topic and felt worried. But, in the subsequent reading stage, workers who are skilled in training knowledge tend to be natural in their expressions. After finishing reading the questions, if the workers have a good memory of the correct answers, their facial expressions will turn into a happy state and will turn into a natural look during the answer verification stage.

(1) Import the video recorded by workers during the test into the program.
(2) if cap.grab ():
(3)   numframe + = 1
(4)   if numframe %15 = = 1: # Screenshot of dismantling the video.
(5)   flag, frame = cap.retrieve ()
(6)   end if
(7) Save the video split images to the specified path, and the naming rule is str(numframe/15).
(8) Import the image disassembled by video.
(9) $i = 0$; $m = 0$; $t = 0$
(10)   if≤100:
(11) $i + = 1$
(12)   if $t \leq 20$:
(13) $t + = 1$; $m + = 1$
(14)   Import the image numbered T for expression recognition, and input the recognition data into m rows.
(15)   end if
(16)   Arrange the positive and negative expression choice array by Eq. (3).
(17)   The array is normalized by Eq. (4) and (5).
(18)   The standardized weights are calculated by Eq. (6)–(9).
(19) end if

ALGORITHM 1: Pseudocode of facial expression data collection for industrializing worker training test.
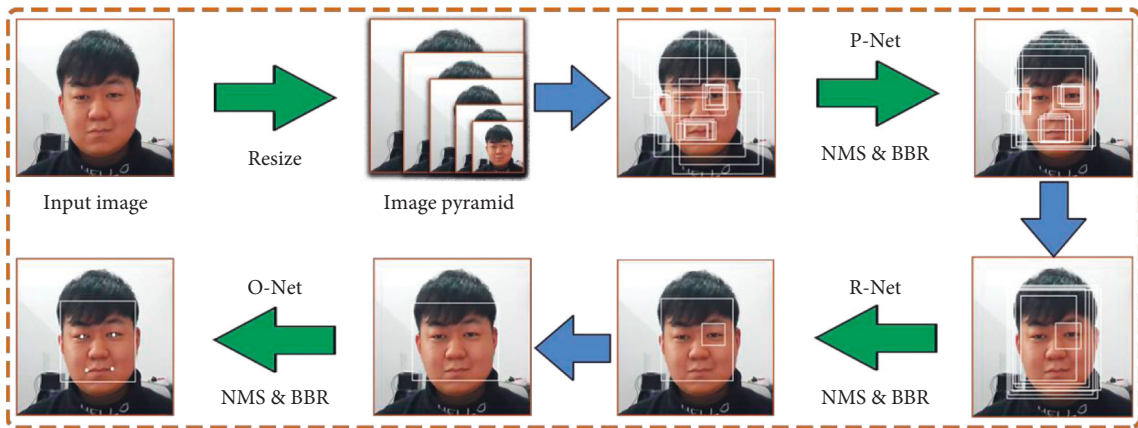
FIGURE 2: Face image recognition and feature calibration process.
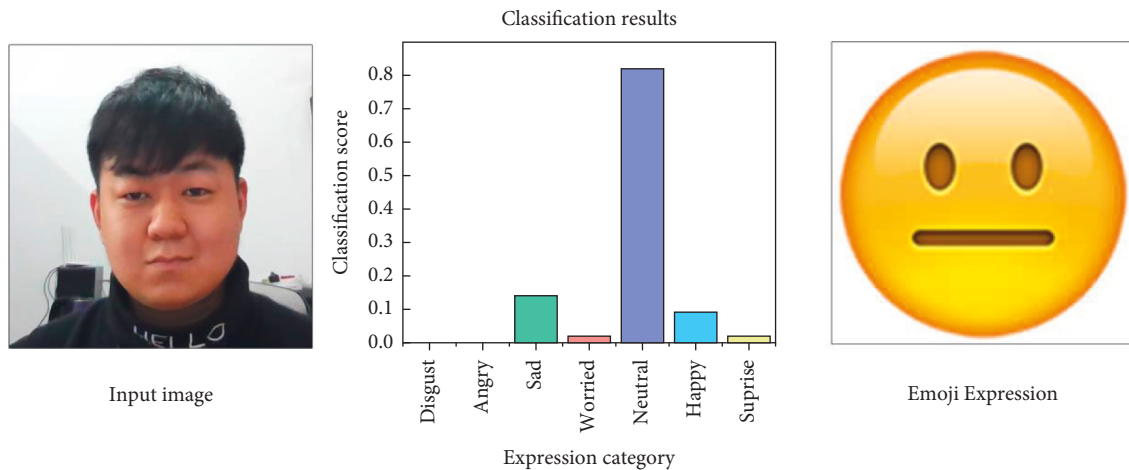
FIGURE 3: The result of facial expression judgment.

FIGURE 4: Expression score division based on Likert's seven-level scale.
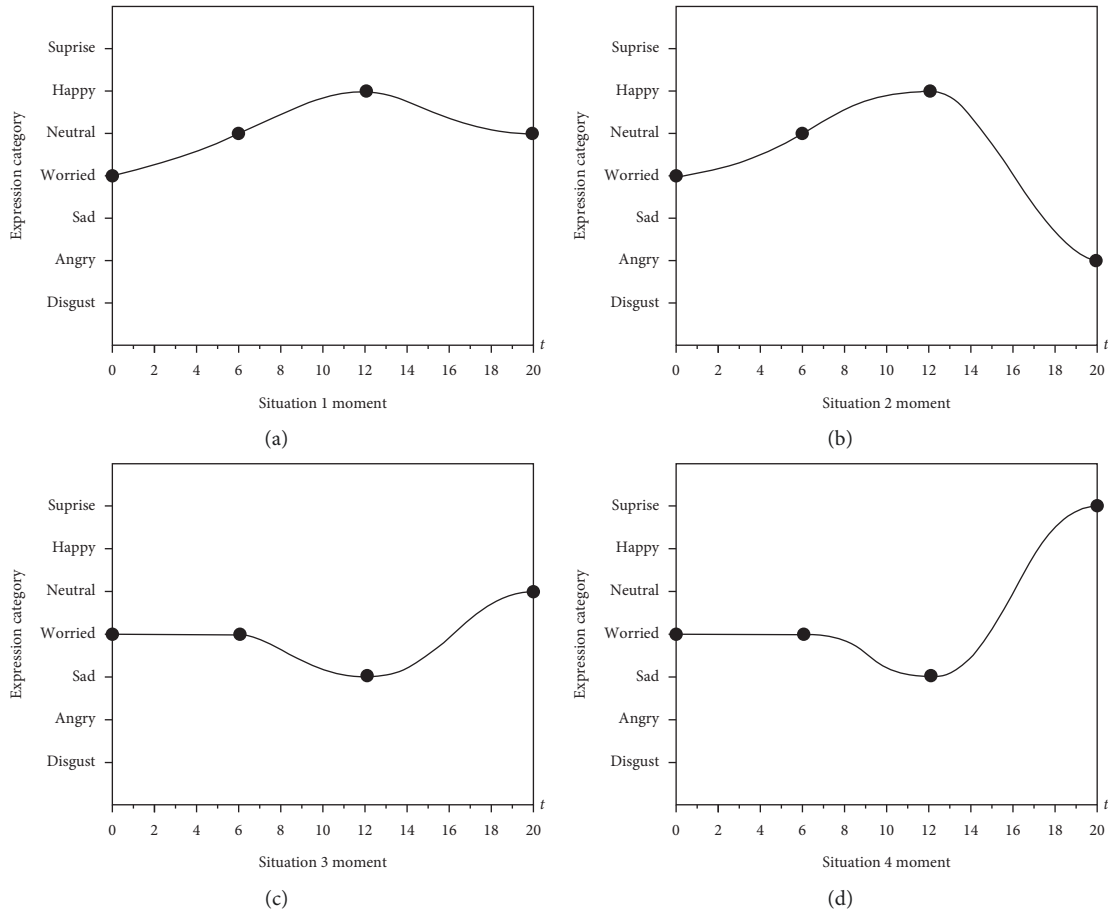
FIGURE 5: Diagram of four abnormal mood fluctuations. (a) Situation 1. (b) Situation 2. (c) Situation 3. (d) Situation 4.

Situation 2. Before the answer verification, it is the same as situation 1. When checking the answers, if the worker is fully sure of the knowledge points involved in the question, but when making choices, it may be due to operational errors or incorrect memory, which may cause the worker to have a short period of frustration during the test. In order to eliminate the worker's wrong operation and memory error, the error degree τ ($\tau = 0.7$) is introduced for the first time to correct the evaluation score of the worker's answers.

Situation 3. When workers are not very familiar with randomly selected questions, they will maintain a worried look at the initial reading stage; then when thinking about the questions further, they will show sadness and regret expressions due to the vague memory. In the answer verification stage, as the

wrong answer is expected, the worker's expression will return to a sad look, worrying about the next question.

Situation 4. Before the answer verification stage, it is similar to situation 3. When checking the answers, they will feel surprised because of the unexpected correct answers. However, the workers' choices under this emotion are only done through luck and guessing, so this study introduces hesitation degree v ($v = 0.45$) to modify the evaluation score of the workers' answers [44].

Based on the four situations of emotional changes in industrializing workers training test under normal conditions, this paper establishes an emotional analysis and evaluation process for industrializing workers training test. The process is shown in Figure 6.
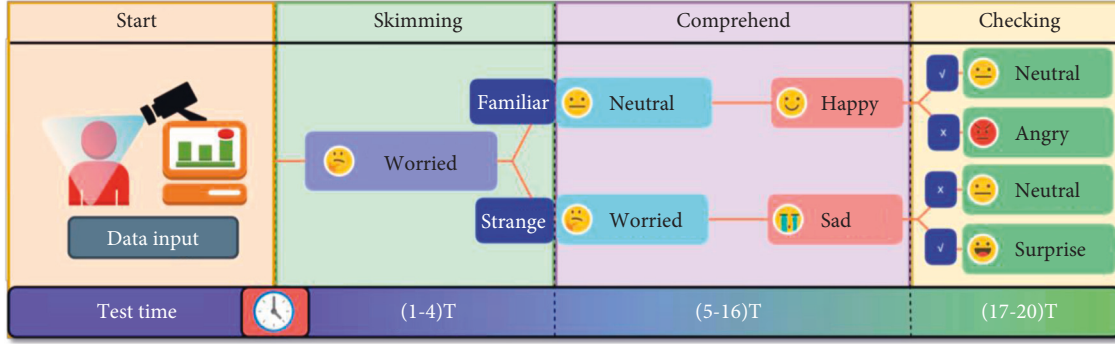
FIGURE 6: Evaluation process of sentiment analysis of industrializing worker training test.

According to process analysis, (15) is improved with the introduction of the concepts of error and hesitancy degree. The improved expression score division weight calculation method is shown as follows:

$$W_{emo} = \left(\sum_{t=1}^{4} \sum_{p_{emo}=1}^{7} \left(\frac{p_{emo} \times S_{l7}}{n} \right) + \sum_{t=5}^{16} \sum_{p_{emo}=1}^{7} \left(\frac{p_{emo} \times S_{l7}}{n} \tau \right) + \sum_{t=17}^{20} \sum_{p_{emo}=1}^{7} \left(\frac{p_{emo} \times S_{l7}}{n} v \right) \right) S_r. \tag{16}$$

All data collected in this study were entered into the evaluation process, and the results were calculated with SEWM-SAM to derive the final weight ranking. The highest weight value is the most significant point of the model source data.

5. Result

This survey study relies on a prefabricated building project at Langfang Airport Free Trade Port, which is implementing a career path promotion for industrializing workers. After training and reeducation of the workers, a worker who had recently violated engineering regulations was selected and surveyed and analyzed by using the model developed in this paper. The testing system in this study draws 100 questions at a time from a pool of safety knowledge questions, with 20 questions in each of the five professional directions. Two thousand images and 14,000 cells of analysis data were collected for a single worker.

5.1. Facial Expression Recognition Score Based on MTCNN-LFER. Taking the multiple-choice questions in the construction site precautions test as an example, the collected images of respondents' expressions at that time were analyzed and imported into the facial expression recognition evaluation model for industrializing worker training in this study for score evaluation. According to the grading level of the education industry, 75% of the highest value is taken as the pass line. The process of image analysis and data extraction imported into the model is shown in Figure 7. The facial expression analysis data are shown in Table 1.

The data scores of 20 moments for each question were brought into the model of this paper and calculated by equation (16) to get W_{emo} value for each question. The values are shown in Table 2.

Find the average of W_{emon}, which is $\overline{W_{emon}}$ of the current question, indicating the average value of the standard scoring of this question in the evaluation system, which can be used as SWEM expert scoring data.

5.2. Numerical Solution of SEWM Weight. The test questions were graded into 5 first-level indicators and 20 second-level indicators by analyzing the collected image expression emotion data. The 5 first-level indicators are KPM, CCS, PHI, EAM, and LRC, and the 20 second-level indicators correspond to the questions under each first-level indicator. The expression scores of different moments represent the scoring values of experts. The weights of second-level indicators related to Section A are shown in Table 3.

After calculating the weights of the second-level indicators of the five sections, the values are used as the reference data for conducting the comparative solution. First, the extreme values of the second-level indicators' weights are transformed into fuzzy arrays, whose classifications are shown in Table 4. The weight of a single second-level indicator is multiplied by the corresponding grade score to find the average value, and the approximate integer solutions are the data of the first-level indicators. Then the data are substituted into equations (6)–(12) to get the weights of the first-level indicators. The weights of the first-level indicators are shown in Table 5.

From the first level and second level of indicator weight values, it can be analyzed that the expression data plays a decisive role in the evaluation of each question, and the change of the values can be divided into 3 segments, where the middle segment has the greatest influence, and when the good emotion overlaps with the correct option, the final comprehensive weight value will be larger.
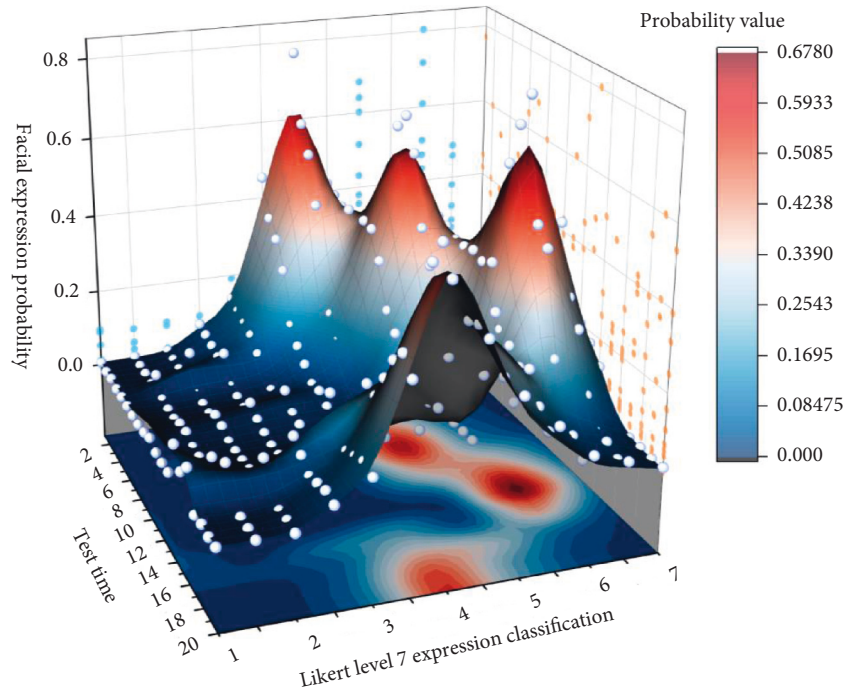
(a)
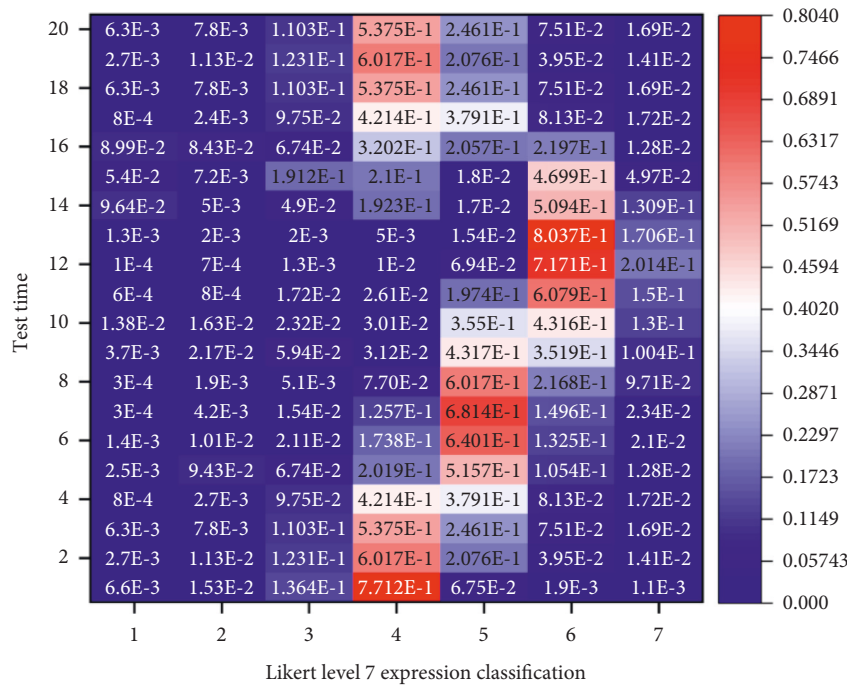
(b)

FIGURE 7: Facial expression analysis and data extraction process. (a) Surface map. (b) Determining the numerical thermal distribution map.

5.3. Analysis of the Significance of SAM

5.3.1. Establishing Linguistic Fuzzy Sets.
In this study, five levels of fuzzy classification languages are used for expert inspiration. The fuzzy linguistic number set is determined by trapezoidal fuzzy numbers. The hazard impact assessment levels are shown in Table 6. In this study, 20 questions in each section are used to assess the understanding of surveyed workers on the 5 sections, and the total fuzzy number is derived from the formula to measure the implementation effect of industrializing worker training, where the relative weights of the sections are equal to the weights of the first-level indicators of each section.

The fuzzy language set of the expert evaluation classification is substituted into (13) as the parameters a_i and b_i,

TABLE 1: Facial expression analysis data.

Time	Disgusted	Angry	Sad	Worried	Neutral	Happy	Surprised
1	0.0066	0.0153	0.1364	0.7712	0.0675	0.0019	0.0011
2	0.0027	0.0113	0.1231	0.6017	0.2076	0.0395	0.0141
3	0.0063	0.0078	0.1103	0.5375	0.2461	0.0751	0.0169
4	0.0008	0.0027	0.0975	0.4214	0.3791	0.0813	0.0172
5	0.0025	0.0943	0.0674	0.2019	0.5157	0.1054	0.0128
6	0.0014	0.0101	0.0211	0.1738	0.6401	0.1325	0.0210
7	0.0003	0.0042	0.0154	0.1257	0.6814	0.1496	0.0234
8	0.0003	0.0019	0.0051	0.0771	0.6017	0.2168	0.0971
9	0.0037	0.0217	0.0594	0.0312	0.4317	0.3519	0.1004
10	0.0138	0.0163	0.0232	0.0301	0.3550	0.4316	0.1300
11	0.0006	0.0008	0.0172	0.0261	0.1974	0.6079	0.1500
12	0.0000	0.0007	0.0013	0.0101	0.0694	0.7171	0.2014
13	0.0012	0.0020	0.0020	0.0051	0.0154	0.8037	0.1706
14	0.0964	0.0050	0.0490	0.1923	0.0170	0.5094	0.1309
15	0.0539	0.0072	0.1912	0.2101	0.0180	0.4699	0.0497
16	0.0899	0.0843	0.0674	0.3202	0.2057	0.2197	0.0128
17	0.0008	0.0027	0.0975	0.4214	0.3791	0.0813	0.0172
18	0.0063	0.0078	0.1103	0.5375	0.2461	0.0751	0.0169
19	0.0027	0.0113	0.1231	0.6017	0.2076	0.0395	0.0141
20	0.0063	0.0078	0.1103	0.5375	0.2461	0.0751	0.0169

TABLE 2: W_{emon} value considering the error degree, hesitation degree, and correctness rate.

Time (t)	W_{emon}	Time (t)	W_{emon}	Time (t)	W_{emon}	Time (t)	W_{emon}
1	0.5554	6	0.4922	11	0.5842	16	0.4177
2	0.5964	7	0.5026	12	0.61049	17	0.2885
3	0.6146	8	0.5316	13	0.6125	18	0.2765
4	0.6411	9	0.5322	14	0.5080	19	0.2684
5	0.4501	10	0.5511	15	0.4739	20	0.2765

Note. $\tau = 0.7$; $v = 0.45$; $S_r = 1.2$.

TABLE 3: The weights of second-level indicators related to Section A.

No.	Disgusted	Angry	Sad	Worried	Neutral	Happy	Surprised
1	0.0066	0.0153	0.1364	0.7712	0.0675	0.0019	0.0011
2	0.0027	0.0113	0.1231	0.6017	0.2076	0.0395	0.0141
3	0.0063	0.0078	0.1103	0.5375	0.2461	0.0751	0.0169
4	0.0008	0.0027	0.0975	0.4214	0.3791	0.0813	0.0172
5	0.0025	0.0943	0.0674	0.2019	0.5157	0.1054	0.0128
6	0.0014	0.0101	0.0211	0.1738	0.6401	0.1325	0.0210
7	0.0003	0.0042	0.0154	0.1257	0.6814	0.1496	0.0234
8	0.0003	0.0019	0.0051	0.0771	0.6017	0.2168	0.0971
9	0.0037	0.0217	0.0594	0.0312	0.4317	0.3519	0.1004
10	0.0138	0.0163	0.0232	0.0301	0.3550	0.4316	0.1300
11	0.0006	0.0008	0.0172	0.0261	0.1974	0.6079	0.1500
12	0.0000	0.0007	0.0013	0.0101	0.0694	0.7171	0.2014
13	0.0012	0.0020	0.0020	0.0051	0.0154	0.8037	0.1706
14	0.0964	0.0050	0.0490	0.1923	0.0170	0.5094	0.1309
15	0.0539	0.0072	0.1912	0.2101	0.0180	0.4699	0.0497
16	0.0899	0.0843	0.0674	0.3202	0.2057	0.2197	0.0128
17	0.0008	0.0027	0.0975	0.4214	0.3791	0.0813	0.0172
18	0.0063	0.0078	0.1103	0.5375	0.2461	0.0751	0.0169
19	0.0027	0.0113	0.1231	0.6017	0.2076	0.0395	0.0141
20	0.0063	0.0078	0.1103	0.5375	0.2461	0.0751	0.0169
b_{11}	2.1117	2.1116	2.1056	2.0812	2.0819	2.0848	2.1067
Q_{11}	1.0576	1.0575	1.0542	1.0463	1.0446	1.0507	1.0556
x_{11}	0.1217	0.1214	0.1140	0.0963	0.0929	0.1057	0.1171
w_{11}	0.1582	0.1579	0.1483	0.1252	0.1208	0.1374	0.1522

TABLE 4: The classification of the fuzzy array of the secondary indicator mapping.

Numerical interval	Level classification score
(0.1200,0.1300]	5
(0.1300,0.1400]	4
(0.1400,0.1500]	3
(0.1500,0.1600]	2
(0.1600,0.1700]	1

TABLE 5: The weight values of the first-level indicators.

Name	KPM	CCS	PHI	EAM	LRC	Name	KPM	CCS	PHI	EAM	LRC
Data1	3	4	1	2	2	Data11	5	3	3	4	2
Data2	4	3	2	1	3	Data12	4	5	5	3	1
Data3	4	2	1	3	1	Data13	3	4	3	3	3
Data4	4	2	1	3	3	Data14	4	2	2	5	4
Data5	4	4	2	3	2	Data15	1	5	5	5	2
Data6	3	2	1	4	4	Data16	5	5	4	4	3
Data7	4	5	1	3	5	Data17	5	4	2	3	4
Data8	3	3	2	1	2	Data18	3	3	4	4	2
Data9	2	4	1	3	1	Data19	4	4	3	5	1
Data10	1	4	1	4	3	Data20	2	1	2	3	2
b_t	1.5266	1.5063	1.7968	1.5375	1.7030	w_{1t}	0.3803	0.2078	0.0584	0.3681	0.0145
Q_t	0.7200	0.8449	0.9635	0.7309	1.0096	Rank	1	3	4	2	5
x_t	0.4274	0.2336	0.0656	0.4137	0.0163						

TABLE 6: Scale table of fuzzy language set.

Fuzzy numbers	Linguistic terms	Corresponding sections
Slight influence	(0, 0, 0.1, 0.2, 0.2)	—
Mild influence	(0.2, 0.3, 0.4, 0.4, 0.5)	1, 5
Moderate influence	(0.4, 0.4, 0.5, 0.6, 0.6)	2
Severe influence	(0.5, 0.6, 0.6, 0.7, 0.8)	4
Significant influence	(0.8, 0.8, 0.9, 1, 1)	3

Note: "—" means none.

TABLE 7: Fuzzy aggregation indicators calculation data of experts' opinions.

Variable name	Value	Variable name	Value
WA(E_1)	0.7465	RA(E_4)	0.2022
WA(E_2)	0.8414	RA(E_5)	0.2213
WA(E_3)	0.5966	CC(E_1)	0.2838
WA(E_4)	0.7660	CC(E_2)	0.2123
WA(E_5)	0.8387	CC(E_3)	0.1072
RA(E_1)	0.1970	CC(E_4)	0.2804
RA(E_2)	0.2220	CC(E_5)	0.1163
RA(E_3)	0.1574		

and the evaluation data of each section are aggregated through SAM. Because the relaxation factor requires a large number of actual events to be tested, as a new method proposed for the training of industrializing workers, this study refers to relevant literature and takes the general value of the relaxation factor $\beta = 0.5$ as the test.

5.3.2. Acquiring Aggregation Fuzzy Numbers. A calculation of the consistency of the fuzzy language scale array to which each section belongs is made. The calculation process is as follows: $S(\widetilde{R}_1, \widetilde{R}_2) = 1 - [(0.4 - 0.2) + (0.4 - 0.3) + (0.5 - 0.4) + (0.6 - 0.4) + (0.6 - 0.5)]/5 = 0.86$. The results are substituted into the calculation of the weighted agreement degree WA(E_n) and the relative agreement degree RA(E_n). Then the relaxation factor is used to calculate the expert agreement coefficient, for example, CC$(E_1) = 0.5 \times 0.3706 + (1 - 0.5) \times$ RA(E_1). Substituting the expert weighted agreement degree, relative agreement degree, and agreement coefficient into (14), the overall fuzzy number R can be calculated. The calculation data of experts' opinions fuzzy aggregation indicators are shown in Table 7.

Through aggregation calculation, the aggregation total fuzzy number $\widetilde{R} = (0.3909, 0.5309, 0.5990, 0.4590, 0.6590)$ of expert opinion aggregation is obtained. The aggregated total fuzzy number and the second-level indicators are made into a cluster analysis, as shown in Figure 8. According to the images of the data group, it can be seen from the feedback from the training test of industrializing workers that the worker has the worst knowledge of relevant construction laws and regulations, which is in line with the fact that he has made mistakes in the project funds recently.

According to the statistics of the correct rate of the questions in the 5 sections, the correct rates of the questions in Section 2, 3, and 5 are all more than 75%, indicating that the worker has passed the test in these areas. However, with the score gap in Section 5 being too huge, it is necessary to verify whether it is personal reasons or a faulty training system that caused this result.
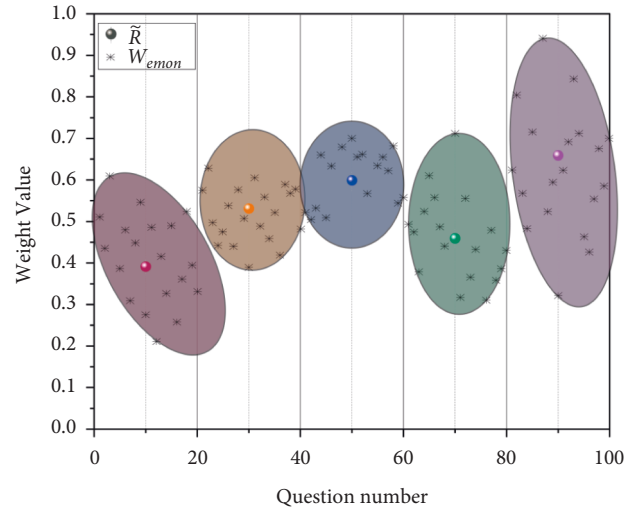
FIGURE 8: Cluster analysis of industrializing worker training management system.

5.4. Model Validation. This study relies on a prefabricated building project at Langfang Airport Free Trade Port and conducts surveys and statistics after the construction of the project. A total of 17 engineering hidden dangers and accidents were found in the acceptance stage. The 17 hidden dangers and accidents were classified according to the 5 first-level indicators in this study. The classified statistical graph of the number of hidden dangers and accidents in the Langfang Airport Free Trade Port prefabricated building projects is shown in Figure 9.

In this study, 10 workers who participated in the construction of prefabricated buildings in Langfang Airport Free Trade Port were randomly selected for training effect assessment, and the results were calculated. The aggregated total fuzzy number values are shown in Table 8.

The aggregated total fuzzy number of training assessment of 10 workers was compared with the number of engineering hidden dangers and accidents in the acceptance stage of Langfang Airport Free Trade Port. The association chart between industrializing workers' training assessment results and potential dangers and accidents in Langfang Free Trade Port project is shown in Figure 10.

From the comparison in the figure, it can be found that the aggregated total fuzzy number value of the worker's training assessment results is positively correlated with the probability of occurrence of such hidden dangers and accidents in the engineering projects that the worker is engaged in. As can be seen from Figure 10, the group of workers in the project at Langfang City Airport Free Trade Port was not well trained in CCS, PHI, and LRC, so the project has many hidden dangers and accidents in the
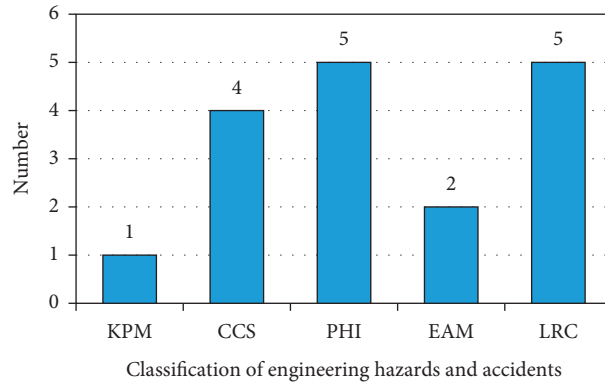
Figure 9: Statistical graph of the number of hidden dangers and accidents in the Langfang Airport Free Trade Port prefabricated building projects.

Table 8: Aggregate total fuzzy number values for the training assessment of the 10 workers.

	KPM	CCS	PHI	EAM	LRC
$\tilde{R}_1$	0.3909	0.5309	0.5990	0.4590	0.6590
$\tilde{R}_2$	0.3167	0.5792	0.6451	0.3367	0.6237
$\tilde{R}_3$	0.3094	0.4920	0.6142	0.3105	0.6064
$\tilde{R}_4$	0.4380	0.5134	0.6279	0.3751	0.5834
$\tilde{R}_5$	0.4957	0.3978	0.5764	0.3417	0.5739
$\tilde{R}_6$	0.3227	0.5142	0.5342	0.3697	0.4896
$\tilde{R}_7$	0.3275	0.4935	0.6302	0.4217	0.5860
$\tilde{R}_8$	0.3410	0.4792	0.6017	0.4100	0.6176
$\tilde{R}_9$	0.3639	0.5406	0.5798	0.3817	0.6010
$\tilde{R}_{10}$	0.3867	0.5273	0.6014	0.4630	0.6427
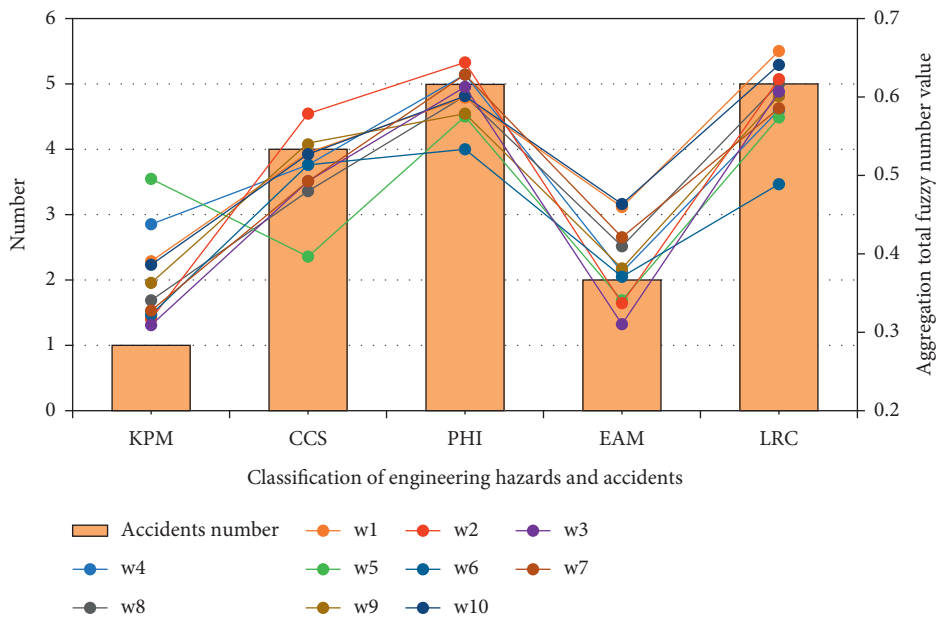
Figure 10: Association chart between industrializing workers' training assessment results and potential dangers and accidents in Langfang Free Trade Port project.

acceptance stage, with 4, 5, and 5 cases, respectively, which proves the correctness of the model proposed in this study.

6. Discussion and Conclusion

6.1. Discussion. In the process of building the model, MTCNN-LFER was used to analyze the respondents' facial expressions in real time in order to conform to objective facts, and four situations were analyzed according to the characteristics of expression changes under different mental activities. In previous evaluation system, respondents' feedback was only scored based on their performance results. For example, in Scenario 2, the respondents' misselection would be directly judged as a wrong situation according to the conventional evaluation system. However, their initial judgments are valid. Inaccurate evaluation results will lead to wrong final rating, thus affecting workers' training enthusiasm. For construction units, wrong evaluation leads to redundant training course arrangement, which affects the efficiency of workers' industrialization process and also wastes a lot of financial and material resources [33].

However, there is another situation, such as Situation 4, where the worker guesses the correct option. For this case, the traditional evaluation method does not consider whether the worker has a solid knowledge of the question but only recognizes that the worker's choices are correct and thus determines that the worker has a high level of mastery of such knowledge. According to the description of human behaviour, humans always make constant rather than consistent and repetitive guesses about the unknown. The worker will choose another answer when the correctly guessed question is retested in a short time. For workers, with the help of good luck to save time and effort, they do not need to master engineering-related knowledge. However, for construction units, workers who muddle through with this trick may cause greater property damage or even affect engineering safety and cause malignant casualty accidents. Therefore, it is necessary to introduce relevant parameters to modify the model to ensure that the model is suitable for the development rule of objective facts, so that the applicability of the evaluation system is stronger, which will have guiding significance for similar industries.

According to the final weight calculation and cluster analysis results, it was found that, in some knowledge sections, although a small number of them scored high and the final composite score was higher compared with other sections, there was a large dispersion, which proved that workers did not have a firm grasp of such knowledge and still many knowledge points needed to be checked and remedied. Therefore, even though the overall score is the highest, there is still a need for training and education. In engineering construction, muddling through is never an option, as workers with poor knowledge may have a great impact on the entire project. In Li et al.'s study, it was noted that unsafe behaviour in engineering is related not only to the workers' own behaviour but also to cognitive biases in different contexts. Poor worker handling can also contribute to engineering accidents; however, the correctness of the handling is related to the way the worker chooses to deal with the problem [45].

The weight solution of this study for each question can also give feedback on the proficiency of the question in the section to which it belongs; in particular, the test after training can reflect whether workers have evasive behaviour for a certain knowledge point. Chen has suggested in previous research that workers will often adopt unsafe behaviours to ensure that progress is efficient [46]. This type of problem can be explained by the pattern presented by the group industrial worker training test to explain the current engineering safety climate problem that exists in the group of industrial workers.

For example, a worker has insufficient knowledge about construction phase reports when answering questions, and most of the workers in the construction team have this situation; then it can be inferred that the construction is in poor quality. The root of this can be found to be a hidden line of conflict of interest between the worker, the construction unit, and the regulator [47]. The quality of training of the group can thus be screened to identify more hidden dangers that affect the economy and safety of engineering under the policy of industrializing worker training process.

According to the model validation, it can be seen from the calculation and analysis of the evaluation results of the training management of industrializing workers in this study that hidden dangers and accidents in engineering projects are closely related to the skills mastered by workers. In all construction stages of engineering projects, the management of industrializing worker training can be improved to eliminate possible hazards and stop accidents in time to ensure safe, economical, and stable construction and production of the engineering project.

6.2. Conclusion. This paper is based on the background that the Chinese government proposes to accelerate the process of industrializing workers in response to the rapid reduction of the domestic demographic dividend and the rapid weakening of the labor advantage in the era of Industry 4.0. The artificial intelligence machine vision and fuzzy mathematical evaluation system are combined to test the workers who receive industrializing training and record the information related to the change of facial expressions and the correct rate of assessment when the workers receive the test assessment. In addition, the evaluation model of facial expression recognition for industrializing worker training is used to conduct qualitative and quantitative analysis and finally arrive at the aggregated information results. The main conclusions of this study are as follows:

(1) The expert scoring mechanism in the evaluation model is improved by using machine vision to analyze the changes in workers' facial expressions during the test to determine their mental activities, effectively preventing the waste of money and time for subsequent training due to wrong operations. It also prevents workers from guessing the answers and ignoring the forgotten knowledge points, which reduces the possibility of more safety accidents and property damage to the project.

(2) The questions of each section are converted into primary and secondary indicators to conduct an aggregation consistency analysis, and the weight of each indicator and the significance of the aggregation analysis are used to indicate the degree of mastery of the tested workers on the knowledge of each section. According to the discrete degree of each question, we can check whether it is a common problem of the construction workers and can timely find out the safety, economic, or management hazards.

In this paper, although the necessity of objective facts is considered to the greatest extent when analyzing and mathematically modelling the changes in facial expressions of workers doing the test, there still exist the following deficiencies:

(1) There is no evaluation or research analysis of workers' psychological states. Actually, the differences in personalities and psychological states may affect the accuracy of emotions conveyed through facial expressions during the test.

(2) In analyzing the dispersion of each knowledge point, only the problems of the workers were considered, but, in fact, it is possible that some irregularities caused by "traditional experience" of the industry lead to workers not recognizing the standardized operation, or some people with management authority forbid workers to follow the standardized practice of construction or project handling.

These deficiencies can be refined in future research and solved by multiobjective optimization methods.

Data Availability

The case analysis data used to support the findings of this study are available from the corresponding author upon request.

Conflicts of Interest

The authors declare that there are no conflicts of interest.

Acknowledgments

References

[1] J. Zuo, S. Pullen, R. Rameezdeen et al., "Green building evaluation from a life-cycle perspective in Australia: a critical review," *Renewable and Sustainable Energy Reviews*, vol. 70, pp. 358–368, 2017.

[2] Q. Shi, J. D. Chen, and L. Y. Shen, "Driving factors of the changes in the carbon emissions in the Chinese construction industry," *Journal of Cleaner Production*, vol. 166, pp. 615–627, 2017.

[3] B. Q. Cheng, K. Lu, J. C. Li, H. H. Chen, X. W. Luo, and M. Shafique, "Comprehensive assessment of embodied environmental impacts of buildings using normalized environmental impact factors," *Journal of Cleaner Production*, vol. 334, Article ID 130083, 2022.

[4] L. Y. Chen, X. Gao, C. X. Hua, S. T. Gong, and A. B. Yue, "Evolutionary process of promoting green building technologies adoption in China: a perspective of government," *Journal of Cleaner Production*, vol. 279, Article ID 123607, 2021.

[5] N. Hong, *Ministry of Housing and Urban-Rural Development of the People's Republic of China*, China Academy of Urban Planning and Design, Beijing, 2021.

[6] R. D. Hislop, "national construction safety accident data "released", it is imperative to promote VR site safety training," 2020, http://www.ycc333.com/Article/2020qgjzaq.html.

[7] Z. H. Wang, L. Li, Y. X. Zhang, and W. T. Wang, "Bond-slip model considering freeze-thaw damage effect of concrete and its application," *Engineering Structures*, vol. 201, Article ID 109831, 2019.

[8] Z. Q. Lv and D. Zhang, "Analysis of the life cycle stage of prefabricated buildings," *IOP Conf. Ser.: Earth Environ. Sci*, vol. 330, 2019.

[9] S. S. Yu, Y. F. Liu, D. J. Wang, A. S. Bahaj, Y. Wu, and J. P. Liu, "Review of Thermal and Environmental Performance of Prefabricated Buildings: Implications to Emission Reductions in China," *Renewable & Sustainable Energy Reviews*, vol. 137, 2021.

[10] G. Zhou, J. Xue, H. Wang, and Q. Zhang, "Analysis on Human Safety Behavior Mode during the Production Process," *Taishan Academic Forum - Project on Mine Disaster Prevention and Control*, pp. 203–210, 2014.

[11] Y. P. Guo, W. M. Cheng, L. R. Wu et al., "Diagnosis and assessment of human unsafe behavior," *Progress in Safety Science and Technology*, vol. 6, pp. 613–616, 2006.

[12] H. Steyn, "Managing contingency reserves in project schedules and budgets," in *Proceedings Of The iemc'01: change management and the new industrial revolution*, pp. 400–405, IEEE, Albany, NY, USA, 7 October 2001.

[13] A. Meel, W. D. Seider, and U. Oktem, "Analysis of management actions, human behavior, and process reliability in chemical plants. I. Impact of management actions," *Process Safety Progress*, vol. 27, no. 1, pp. 7–14, 2008.

[14] A. Meel, W. D. Seider, and U. Oktem, "Analysis of management actions, human behavior, and process reliability in chemical plants. II. Near-miss management system selection," *Process Safety Progress*, vol. 27, no. 2, pp. 139–144, 2008.

[15] J. S. Zhang, G. Fu, S. Du, and H. Y. Zhang, "Human-based risk management methods in underground engineering," in *Proceedings Of The 2009 international symposium on risk control and management of design*, pp. 79–82, IEEE, Shanghai, China, 26 December 2009.

[16] E. Ronchi, "A fire safety engineering perspective on crowd evacuation dynamics: comment on "Human behaviours in evacuation crowd dynamics: from modelling to "big data" toward crisis management" by Nicola Bellomo," *Physics of Life Reviews*, vol. 18, pp. 48-49, 2016.

[17] H. Asilian-Mahabadi, Y. Khosravi, N. Hassanzadeh-Rangi, E. Hajizadeh, and A. H. Behzadan, "A qualitative investigation of factors influencing unsafe work behaviors on construction

projects," *Work-a Journal of Prevention Assessment & Rehabilitation*, vol. 61, no. 2, pp. 281–293, 2018.

[18] R. van der Kleij and R. Leukfeldt, "Cyber resilient behavior: integrating human behavioral models and resilience engineering capabilities into cyber security," *Advances in Intelligent Systems and Computing*, vol. 960, pp. 16–27, 2020.

[19] X. P. Bai and C. Qian, "Factor validity and reliability performance analysis of human behavior in green architecture construction engineering," *Ain Shams Engineering Journal*, vol. 12, no. 4, pp. 4291–4296, 2021.

[20] J. K. Suhr, S. Eum, H. G. Jung, G. Li, G. Kim, and J. Kim, "Recognizability assessment of facial images for automated teller machine applications," *Pattern Recognition*, vol. 45, no. 5, pp. 1899–914, 2012.

[21] E. Pantano, "Non-verbal evaluation of retail service encounters through consumers' facial expressions," *Computers in Human Behavior*, vol. 111, 2020.

[22] L. S. F. Israel and F. D. Schonbrodt, "Predicting affective appraisals from facial expressions and physiology using machine learning," *Behavior Research Methods*, vol. 53, no. 2, pp. 574–592, 2021.

[23] T. T. Liu, J. X. Wang, B. Yang, and X. Wang, "Facial expression recognition method with multi-label distribution learning for non-verbal behavior understanding in the classroom," *Infrared Physics & Technology*, vol. 112, 2021.

[24] M. Monaro, S. Maldera, C. Scarpazza, G. Sartori, and N. Navarin, "Detecting deception through facial expressions in a dataset of videotaped interviews: a comparison between human judges and machine learning models," *Computers in Human Behavior*, vol. 127, 2022.

[25] T. Altameem and A. Altameem, "Facial expression recognition using human machine interaction and multi-modal visualization analysis for healthcare applications," *Image and Vision Computing*, vol. 103, 2020.

[26] A. De la Torre-Luque, A. Viera-Campos, A. C. Bilderbeck et al., "Relationships between social withdrawal and facial emotion recognition in neuropsychiatric disorders," *Progress in Neuro-Psychopharmacology & Biological Psychiatry*, vol. 113, 2022.

[27] F. Riquelme, R. Olivares, F. Mu駒z, X. Molinero, and M Serna, "Hypo-driver: a multiview driver fatigue and distraction level detection system," *Cmc-Computers Materials & Continua*, vol. 71, no. 1, pp. 1999–2007, 2022.

[28] S. Schneider, F. Krieglstein, M. Beege, and G. D. Rey, "The impact of video lecturers' nonverbal communication on learning - an experiment on gestures and facial expressions of pedagogical agents," *Computers & Education*, vol. 176, Article ID 104350, 2022.

[29] L. He, "Research on the connectivity between higher vocational education and industrial worker training in the development of construction industry," *International Conference on Social Sciences and Society ICSSS 2015)*, vol. 2 71, pp. 68–72, 2015.

[30] N. Wang and Y. B. Ji, "The analysis on construction workers for sustainable development of construction industrialization," *Proceedings of the 1st International Conference on Sustainable Construction & Risk Management*, vol. I, pp. 864–869, 2010.

[31] I. Rodriguez-Garzon, V. Lucas-Ruiz, M. Martinez-Fiestas, and A. Delgado-Padial, "Association between perceived risk and training in the construction industry," *Journal of Construction Engineering and Management*, vol. 141, Article ID 04014095, 2015.

[32] H. Karre, M. Hammer, M. Kleindienst, and C. Ramsauer, "Transition towards an industry 4.0 state of the leanlab at Graz university of technology," *7th Conference on Learning Factories Clf*, vol. 9, pp. 206–213, 2017.

[33] Y. Y. Ke, "Research on the Chinese industrialized construction migrant workers from the perspective of complex adaptive system: combining the application of SWARM computer simulation technology," *Wireless Personal Communications*, vol. 102, no. 4, pp. 2469–2481, 2018.

[34] F. Hatami and R. Kakavand, "The effect of educational intervention on promoting safe behaviors in textile workers," *International Journal of Occupational Safety and Ergonomics*, vol. 3, 2021.

[35] U. Radhakrishnan, K. Koumaditis, and F. Chinello, "A systematic review of immersive virtual reality for industrial skills training," *Behaviour & Information Technology*, vol. 40, no. 12, pp. 1310–1339, 2021.

[36] Z. H. Cao, T. Chen, and Y. Q. Cao, "Effect of occupational health and safety training for Chinese construction workers based on the chaid decision tree," *Frontiers in Public Health*, vol. 9, 2021.

[37] Z. P. Zhao, N. N. Zhou, L. Zhang, H. L. Yan, Y. Xu, and Z. X. Zhang, "Driver fatigue detection based on convolutional neural networks using em-cnn," *Computational Intelligence and Neuroscience 2020*, vol. 2020, Article ID 7251280, 11 pages, 2020.

[38] K. P. Zhang, Z. P. Zhang, Z. F. Li, and Y. Qiao, "Joint face detection and alignment using multitask cascaded convolutional networks," *IEEE Signal Processing Letters*, vol. 23, no. 10, pp. 1499–1503, 2016.

[39] "Facial-Expression-Recognition.Pytorch," 2021, https://github.com/WuJie1010/Facial-Expression-Recognition.Pytorch.

[40] H. Wu, S. Liu, D. H. Liu, and J. W. Wang, "Hse risk assessment of major sewage transport tunnel projects at the construction stage based on the structuralentropy weight method and the cloud model," *Advances in Civil Engineering 2020*, vol. 2020, Article ID 8882903, 12 pages, 2020.

[41] X. X. Guo, J. Ji, F. Khan, L. Ding, and Y. Q. Yang, "Fuzzy bayesian network based on an improved similarity aggregation method for risk assessment of storage tank accident," *Process Safety and Environmental Protection*, vol. 149, pp. 817–830, 2021.

[42] M. Yazdi and S. Kabir, "A fuzzy bayesian network approach for risk analysis in process industries," *Process Safety and Environmental Protection*, vol. 111, pp. 507–519, 2017.

[43] "Facial Expressions Reference Project," 2021, https://chronicdoodler.deviantart.com.

[44] A. Ullah, J. Wang, M. S. Anwar et al., "Fusion of machine learning and privacy preserving for secure facial expression recognition," *Security and Communication Networks*, vol. 2021, Article ID 6673992, 12 pages, 2021.

[45] H. J. Li, H. H. Chen, Z. Y. Zhao, X. D. Hu, B. Q. Cheng, and J. L. Huang, "Tunnel construction workers' cognitive biases and unsafe behaviors: the mediating effects of risk perceptions," *Advances in Civil Engineering*, vol. 2020, Article ID 8873113, 10 pages, 2020.

[46] H. H. Chen, H. J. Li, and Y. M. Goh, "A review of construction safety climate: definitions, factors, relationship with safety behavior and research agenda," *Safety Science*, vol. 142, Article ID 105391, 2021.

[47] Y. H. Song, J. W. Wang, D. H. Liu, Y. R. Huangfu, F. Guo, and Y. P. Liu, "The influence of government's economic management strategies on the prefabricated buildings promoting policies: analysis of quadripartite evolutionary game," *Buildings*, vol. 11, pp. 444–10, 2021.

Research Article

Portfolio Optimization Model for Gold and Bitcoin Based on Weighted Unidirectional Dual-Layer LSTM Model and SMA-Slope Strategy

Qianyi Xue [1,2] **Yuewei Ling** [1,3] **and Bingwei Tian** [1,4]

[1]*Institute for Disaster Management and Reconstruction, Sichuan University, Chengdu 610207, China*
[2]*College of Computer Science, Sichuan University, Chengdu 610207, China*
[3]*Pittsburgh Institute, Sichuan University, Chengdu 610207, China*
[4]*West China Hospital of Sichuan University, Chengdu 610041, China*

Correspondence should be addressed to Bingwei Tian; bwtian@scu.edu.cn

Portfolio optimization is one of the most complex problems in the financial field, and technical analysis is a popular tool to find an optimal solution that maximizes the yields. This paper establishes a portfolio optimization model consisting of a weighted unidirectional dual-layer LSTM model and an SMA-slope strategy. The weighted unidirectional dual-layer LSTM model is developed to predict the daily prices of gold/Bitcoin, which addresses the traditional problem of prediction lag. Based on the predicted prices and comparison of two representative investment strategies, simple moving average (SMA) and Bollinger bands (BB), this paper adopts a new investment strategy, SMA-slope strategy, which introduces the concept of k-slope to measure the daily ups and downs of gold/Bitcoin. As two typical financial products, gold and Bitcoin are opposite in terms of their characteristics, which may represent many existing financial products in investors' portfolios. With a principle of $1000, this paper conducts a five-year simulation of gold and Bitcoin trading from 11 September 2016 to 10 September 2021. To compensate for the SMA and BB that may miss buying and selling points, 4 different parameters' values in the k-slope are obtained through particle swarm optimization simulation. Also, the simulation results imply that the proposed portfolio optimization model contributes to helping investors make investment decisions with high profitability.

1. Introduction

Industry 4.0 was first introduced in 2013, defining "the transition from a time when people worked with computers to when computers work without humans." The world is witnessing the development of information technology and the widespread use of computers. The emergence of Industry 4.0 has impacted global financial markets and continues to drive technological iterations in the financial field [1]. Portfolio optimization has always been a popular topic in modern financial research, and investors with different capital levels have to face the problem of portfolio selection [2]. The optimal portfolio selection yields the highest expected return within an acceptable risk range [3], but high returns usually come with high risks [4]. Technical analysis uses historical long-term and

short-term stock trends to help investors make informed and profitable trading decisions [5]. Zhu and Zhou pointed out that technical analysis can add value to stocks when their returns are predictable. It contributes to identifying trading opportunities when there are uncertainties about stock returns [6]. Portfolio optimization in the real world is a very difficult and complex mathematical problem [7]. Based on the technical analysis, the portfolio optimization of gold and Bitcoin is divided into two subproblems, daily price prediction and decision algorithms of investment strategies.

1.1. Price Prediction. Intelligence in manufacturing is considered an essential hallmark of Industry 4.0, driven by the boom and maturity of new information and communication

technologies applied to industrial processes and products [8]. The growth of available information in industrial plants has contributed to the widespread use of machine learning in addressing specific industrial needs [9]. In the era of Industry 4.0, prediction is a hot topic, especially the ability to predict events related to industrial assets and production processes [10]. With the vigorous development of artificial intelligence (AI), many optimization techniques based on machine learning and deep learning have favored many investors, which are applied to predict the prices of financial products, especially stock price prediction. There are many optimal methods for stock price prediction, but no perfect solution has been developed yet. Stock prices are affected by multiple factors in the stock market, and the mechanisms of these factors are incredibly complex. Changes in investor sentiment are also a major cause for changes in stock prices, which are usually analyzed by sentiment analysis. With evaluation of the causal relationship between VIX and BTC, Chi concluded that Bitcoin is not a safe asset in a climate of fear, which contributes to obtaining the most risk returns [11]. Moreover, some external factors like the black swan event are difficult to predict but significantly impact stock prices. For example, the COVID-19 pandemic is a black swan event for financial markets [12].

Time-series forecasting is traditionally performed in econometrics using the autoregressive integrated moving average (ARIMA) model [13]. But some problems of the ARIMA model are gradually emerging as it is applied in different fields: (1) As a linear model, it is difficult for the ARIMA model to establish nonlinear relationships between variables. (2) Given that stock prices are usually noisy, volatile, and nonparametric, it should be a complex nonlinear problem. However, the error of the ARIMA model cannot have a constant standard deviation. Kane found that although the problem in the ARIMA model can be solved to a certain extent using the ARIMA-GARCH model, there are some problems of the optimization of parameters in the generalized autoregressive conditional heteroskedasticity (GARCH) model [14]. Sai optimized the kernel function of the support vector machine (SVM) and used the optimized model to predict and analyze the investment stock index, which performed significantly better than the ARIMA model [15]. With the development of neural networks and the superiority of long short-term memory (LSTM) in natural language processing tasks, LSTM has been applied to the same time-series stock price prediction problem. Ma compared the performances of three models in stock price prediction, the ARIMA model, the artificial neural network (ANN) model, and the LSTM model. Mahas found that the LSTM model performs better because of its improvement on the vanishing gradient problem [16]. Yurtsever noticed that LSTM performed the best by comparing three multivariate time-series models (LSTM, Bi-LSTM, and GRU), using six indicators of crude oil price, consumer price index, stock market index, effective exchange rate, interest rate, and gold price as model inputs [17]. Saifi proved that the LSTM-based prediction model is slightly better than other prediction models (GRU, DNN, and RNN) in Bitcoin price prediction (regression) [18]. Selvin et al. tested the performance of CNN, LSTM, and RNN on the same sliding window and concluded that CNN can capture short-term trend changes and achieve better results than LSTM and RNN because CNN does not rely on any previous information to make predictions. It only uses the current data window to make predictions [19]. Fleischer et al. used LSTM to evaluate predictions for cryptocurrencies such as Bitcoin and pointed out that the results seemed promising as the predicted values deviate very little from the true values. Still, upon closer inspection, it turned out that the prediction lags by a day since stock prices follow the random walk theory, which means that the nature of their movement follows a random walk; that is, changes in prices are not necessarily the result of previous changes [20].

1.2. Investment Strategy. Decision-making, a kind of human behavior aimed at achieving a specific goal, occurs in every activity of human society [21]. An investment strategy is a set of rules to guide investors in trading decisions. The right investment strategy is critical to an investor's success, which requires every investor to analyze as much of the available data as possible [22]. The simple moving average (SMA) and Bollinger bands (BB) are common investment strategies. SMA uses two moving averages, a long period and a short period moving average, which is straightforward to help investors make decisions [23]. Liu and Malik proposed a neural network-based framework to improve profit generation, where SMA effectively measures the volatility of stocks [24]. SMA has good stability, which is not influenced by temporary price fluctuations. BB consist of three lines, the upper, the middle, and the lower. BB can be used to recognize volatility and trends of the price, which allow investors to realize the breakouts. BB were applied to identify stocks with the highest profitability [25]. However, SMAs do not react promptly enough to rapid price changes at market reversal points, and BB overly reply to current market movements. The flaws of SMA and BB may cause investors to miss suitable and favorable buying and selling opportunities. In addition to providing the right time to buy and sell, the buy and sell ratio is also the focus of the investment strategy. Particle swarm optimization (PSO) was adopted to optimize the trading setups of Bitcoin [26]. Zhu et al. applied PSO to a metaheuristic approach to solving the intractability of portfolios [27]. Also, Butler and Kazakov pointed out that PSO can offer better trading results [28].

1.3. Contribution. This paper adopts the technical analysis to establish a portfolio optimization model based on the unidirectional dual-layer LSTM model and the SMA-slope strategy. The unidirectional dual-layer LSTM model is developed to predict gold and Bitcoin's daily average price data, which realizes one of the most important goals of Industry 4.0, intelligent prediction. It is a common approach to designing portfolios with an investment horizon greater than one year based on daily data [29]. Also, we propose a weighting method to address the traditional problem of prediction lags. The unidirectional dual-layer LSTM model is trained and tested on the two datasets, daily gold prices

(London Bullion Market Association, 9 November 2021) and daily Bitcoin prices (NASDAQ, 9 November 2021). Gold and Bitcoin are two diametrically opposed financial products due to their widely varying volatility trends and opposed characteristics, such as linearity and stability. Also, this paper introduces the SMA-slope strategy. The SMA-slope strategy uses PSO to determine the optimal buying and selling ratio. It also increases the buying and selling points using the concept of k-slope based on the SMA strategy, which solves the insensitivity of the SMA strategy to short-term price fluctuations. The introduction of the k-slope reflects a kind of human behavior, as investors do not tend to change their existing views until they are convinced of new plausible trends [30]. Simulation is a key technology in the era of Industry 4.0 [31]. With an initial principal of $1,000 and different trading commissions as a prerequisite, we compare the SMA-slope strategy to the SMA and BB strategies by simulating 5 years of actual trading from 2016 to 2021.

At present, most researches focus on the price prediction and investment strategies of stocks. Based on the technical analysis of stocks, this paper considers the portfolio optimization for gold and Bitcoin. Gold and Bitcoin are typical products of the financial market, which have opposite characteristics. The study of the portfolio optimization of these two financial products contributes to optimizing the portfolio of various products with different characteristics in the financial market. Also, more attention has been paid to regression evaluation indicators like RMSE and MAPE while predicting prices. Few studies have focused on the performance of times-series models on stocks and gold/Bitcoin in terms of prediction lags. The prediction lag is a traditional problem of time-series problem, and researches have shown that LSTM can solve it to some extent [32]. This paper focuses on the prediction lag and employs a lag metric (up and down accuracy) to assess the performance. A small sliding window is used to forecast, and predicted prices for the next few days obtained by the model are weighted. The specific weights are obtained from various tests, which improve the accuracy of the rise and fall. Moreover, few papers provide a comparative analysis of the SMA strategy and Bollinger band strategy, and the buying and selling points due to these two strategy measures are not addressed. In this paper, the SMA-slope strategy is proposed based on the concept of k-slope, which conduces improving the sensitivity to reasonable buying and selling points.

2. Methodology

2.1. Feature Selection. Based on the literature review [33, 34] and data availability, we select 18 features: simple moving average (SMA), relative change (RC), exponential moving average (EMA), moving average convergence/divergence (MACD), relative strength index (RSI), Bollinger bands, and so on. These features will be used as input vectors to the LSTM model for training. The LSTM model is used to predict the daily average prices of gold/Bitcoin.

The simple moving average (SMA) over the last k days is calculated by (1) as follows:

$$\text{SMA}_k = \frac{p_{n-k+1} + p_{n-k+2} + \cdots + p_n}{k} = \frac{1}{k} \sum_{i=n-k+1}^{n} p_i, \quad (1)$$

where p_i is the value of the gold/Bitcoin on the i-th day.

The relative change (RC) of the simple moving average is calculated by (2) as follows:

$$\text{RC} = \ln\left(\frac{\text{SMA}_1}{\text{SMA}_5}\right), \quad (2)$$

where SMA_1 is the simple moving average over the last 1 day and SMA_5 is the simple moving average over the last 5 days.

The exponential moving average (EMA) over the last n days is calculated by (3) as follows:

$$\text{EMA}_i = \begin{cases} p_1, & i = 1, \\ \left(\frac{n-1}{n+1}\right)\text{EMA}_{i-1} + \left(\frac{2}{n+1}\right)p_i, & i > 1, \end{cases} \quad (3)$$

where p_i is the value of the gold/Bitcoin on the i-th day.

The differential value (DIF) is calculated by (4) as follows:

$$\text{DIF}_i = \text{EMA}_i(12) - \text{EMA}_i(26), \quad (4)$$

where $\text{EMA}_i(12)$ is the exponential moving average over the last 12 days on the i-th day and $\text{EMA}_i(26)$ is the exponential moving average over the last 26 days on the i-th day.

The differential exponential average (DEA) is calculated by (5) as follows:

$$\text{DEA}_i = \begin{cases} 0, & i = 1, \\ (0.8)\text{DEA}_{i-1} + (0.2)\text{DIF}_i, & i > 1, \end{cases} \quad (5)$$

where DIF_i is the differential value of the gold/Bitcoin on the i-th day.

The moving average convergence/divergence (MACD) is calculated by (6) as follows:

$$\text{MACD}_i = 2\left(\text{DIF}_i - \text{DEA}_i\right), \quad (6)$$

where DIF_i is the differential value of the gold/Bitcoin on the i-th day and DEA_i is the differential exponential average of the gold/Bitcoin on the i-th day.

The growth periods over the last 14 days are characterized by the value of the gold/Bitcoin being higher than the value of the previous day; that is, $p_i > p_{i-1}$. The gross growth (GG) over the last 14 days is calculated by (7) as follows:

$$\text{GG} = \sum_{i=n-13}^{14} \left(p_i - p_{i-1}\right), \quad (7)$$

where p_i is the value of the gold/Bitcoin on the i-th day.

The decline periods over the last 14 days are characterized by the value of the gold/Bitcoin being not higher than the value of the previous day; that is, $p_i \leq p_{i-1}$. The gross decline (GD) over the last 14 days is calculated by (8) as follows:

$$GD = \sum_{i=n-13}^{14} (p_{i-1} - p_i). \tag{8}$$

The relative strength (RS) is calculated by (9) as follows:

$$RS = \frac{GG}{GD}, \tag{9}$$

where GS is the gross growth and GD is the gross decline.

The relative strength index (RSI) is calculated by (10) as follows:

$$RSI = 100 - \frac{100}{1 + RS}, \tag{10}$$

where RS is the relative strength.

The Bollinger bands refer to the upper Bollinger band, middle Bollinger band, and lower Bollinger band, which can reflect the value volatility of gold/Bitcoin over time. The middle Bollinger band (MBB) over the last 20 days is calculated by (11) as follows:

$$MBB = \frac{1}{20} \sum_{i=n-19}^{n} p_i, \tag{11}$$

where p_i is the value of the gold/Bitcoin on the i-th day.

The upper Bollinger band (UBB) over the last 20 days is calculated by (12) as follows:

$$UBB = MBB + 2\sigma, \tag{12}$$

where MBB is the middle Bollinger band and σ is the standard deviation of the value of the gold/Bitcoin over the last 20 days.

The lower Bollinger band (LBB) over the last 20 days is calculated by (13) as follows:

$$LBB = MBB - 2\sigma, \tag{13}$$

where MBB is the middle Bollinger band and σ is the standard deviation of the value of the gold/Bitcoin over the last 20 days.

2.2. Price Prediction with LSTM Model.

Recurrent neural network (RNN) can reflect the sequence-related characteristics of financial time-series data, but it has the problem of gradient disappearance or gradient explosion. Also, its mining of historical information for financial time-series data is very limited. LSTM is a special RNN that can well handle the long-term dependencies of time-series data [35]. Therefore, the LSTM model is an improved RNN model, to some extent. Figure 1 shows the network structure of the LSTM. The basic unit of the LSTM model is a memory block, which includes a memory cell and three gate structures that control the state of the memory cell, forget gate, input gate, and output gate. To be specific, the forget gate decides to forget the useless historical information from the memory cell state, the input gate decides the influence of the current input data on the memory cell state, and the output gate decides the output information.

Firstly, the information that needs to be eliminated from the cell is determined by the forget gate (f_t) of the (14) as follows:

$$f_t = \sigma(b_f + W_f x_t + U_f h_{t-1}), \tag{14}$$

where σ is the sigmoid activation function, which represents the amount of information retained, x_t is the current input vector, and h_t is the currently hidden layer vector. b_t, x_t, and x_t are the bias, the input weight, and the loop weight of the forget gate, respectively.

Next, the information state is updated in the cell. The external input gate (i_t) is controlled by a sigmoid activation function of the (15) as follows:

$$g_t = \sigma(b_g + W_g x_t + U_g h_{t-1}). \tag{15}$$

Meanwhile, the cell state (C_t) is updated on the basis of C_{t-1} by (16) as follows:

$$C_t = f_t * C_{t-1} + g_t * \tanh(b_c + W_c x_t + U_c h_{t-1}), \tag{16}$$

where C_t represents the state of the memory cell at time t.

Finally, the information output is controlled by the output gate (O_t) of the (18) as follows:

$$h_t = (O_t)\tanh(C_t), \tag{17}$$

$$O_t = \sigma(b_o + W_o x_t + U_o h_{t-1}). \tag{18}$$

We firstly build two models, unidirectional dual-layer LSTM model and bidirectional LSTM model, which aim to predict the average daily prices of Bitcoin after 1 day based on the prices in the previous 8 days. We compare the forecast results for different size time windows for the prices of gold/Bitcoin, respectively.

Furthermore, in order to address the problem of prediction lag, we adopt further optimizations to alleviate it and improve the accuracy of ups and downs. We expand the range of predictions, the average price 3 days after is based on the previous n-day prediction, and the up- and downtrend of prices (trend) is expressed in terms of yields over the next three days.

The up- and downtrend of prices (trend) is calculated by (19) as follows:

$$\text{trend} = \gamma_1 * \frac{\text{price}(n+1)}{\text{price}(n)} + \gamma_2 * \frac{\text{price}(n+2)}{\text{price}(n+1)}$$
$$+ \gamma_3 * \frac{\text{price}(n+3)}{\text{price}(n+2)}, \tag{19}$$

where $\gamma_i \cdot (i = 1, 2, 3)$ is the weight of the fluctuation rate for the next three days, price(n) is the price of yesterday for the n-th day, and price(i) $(i = n+1, n+2, n+3)$ is the predicted price for the next three days.

The final predicted result (Result) is calculated by (20) as follows:

$$\text{Result} = \text{trend} \times \text{price}(n). \tag{20}$$

We select 5 indicators as evaluation criteria for model performance: mean square error (MSE), root-mean-square deviation (RMSD), coefficient of determination (R^2), mean
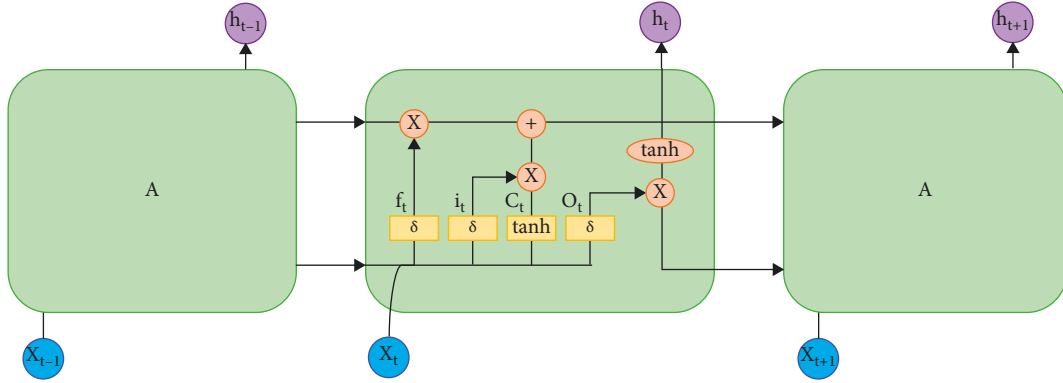
FIGURE 1: LSTM network structure.

absolute percentage error (MAPE), and accuracy of ups and downs predictions (Accuracy).

The mean square error (MSE) is calculated by (21) as follows:

$$MSE = \frac{1}{n} \sum_{i=1}^{n} (y_i - \widehat{y}_i)^2, \quad (21)$$

where y_i is the true value and $\widehat{y}_i$ is the predicted value of y_i.

The root-mean-square error (RMSE) is calculated by (22) as follows:

$$RMSE = \sqrt{MSE} = \sqrt{\frac{\sum_{i=1}^{n} (\widehat{y}_i - y_i)^2}{n}}, \quad (22)$$

where MSE is the mean square error.

The coefficient of determination (R^2) is calculated by (23) as follows:

$$R^2 = 1 - \frac{SS_{res}}{SS_{tot}} = 1 - \frac{\sum_{i=1}^{n} (y_i - \overline{y})^2}{\sum_{i=1}^{n} (y_i - \widehat{y}_i)^2}, \quad (23)$$

where SS_{res} is the sum of squares of residuals, SS_{tot} is the total sum of squares, y_i is the true value, $\overline{y}$ is the mean of true values, and $\widehat{y}_i$ is the predicted value of y_i.

The mean absolute percentage error (MAPE) is calculated by (24) as follows:

$$Mape = \frac{100\%}{n} \sum_{i=1}^{n} \left| \frac{y_i - \widehat{y}_i}{y_i} \right|, \quad (24)$$

where y_i is the true value and $\widehat{y}_i$ is the predicted value of y_i.

2.3. Trading Strategies

2.3.1. Strategy Establishment. With an initial principle of $1000, we set the specified buy position ratio, sell position ratio, and buy position ratio for the first time/after clearance before starting the trading process. Figure 2 is the structure diagram of the strategy backtesting framework. Firstly, the daily price of gold/Bitcoin is predicted through the weighted unidirectional dual-layer LSTM model. Next, we determine whether today is a trading day and the appropriate time to buy or sell according to different strategies. In this way, we can derive nine different buy and sell combinations for gold and Bitcoin. Figure 3 shows the detailed trading strategy. For

the date of simultaneous buy or sell, we adopt the PSO to obtain the optimal buying and selling ratio of gold and Bitcoin, where the objective function is to maximize the profit. Finally, we summarize the state of the asset, including the total assets, the assets of gold, the assets of Bitcoin, and the empty asset. The experiment led by Schmidt and Traub showed that loss aversion is a common human behavior in most situations [36]. When the loss reaches 3% or 5% of the initial principle, all positions will be cleared so that the loss will be stopped in time.

2.3.2. Strategy Process

(1) Simple Moving Average Strategy. We choose two specific indicators, the long-term simple moving average (SMA) of 15 days average daily prices and the short-term SMA of 5 days. When the short-term SMA exceeds the long-term SMA, the asset has an upward trend, implying that it is suitable for buying. When the short-term SMA moves down and intersects with the long-term SMA, the asset has a downward trend, making it suitable for selling.

(2) Bollinger Bands Strategy. Bollinger bands (BB) indicate areas of support and resistance. A set of parameters can be adopted according to the length of time under various situations. We select 20 days and use 2 as the multiplicative parameter before standard deviation because the proposed combination is the most commonly employed standard and interests many investors [37]. When the average daily price of gold/Bitcoin exceeds the upper Bollinger lines, the price of the asset continues to rise, which implies that a sell operation should be considered conservatively. When the average daily price of gold/Bitcoin is lower than the lower Bollinger lines, the price of the asset continues to fall, which indicates that a buying operation should be considered conservatively.

(3) SMA-Slope Strategy. We establish a new strategy called the SMA-slope strategy by introducing a new concept of k-slope based on SMA. The parameter k of the k-slope refers to the number of days where the slope is consecutively positive/negative. The k-slope is used to increase the buy and sell points, which promote the investment to generate more excellent interest rates.
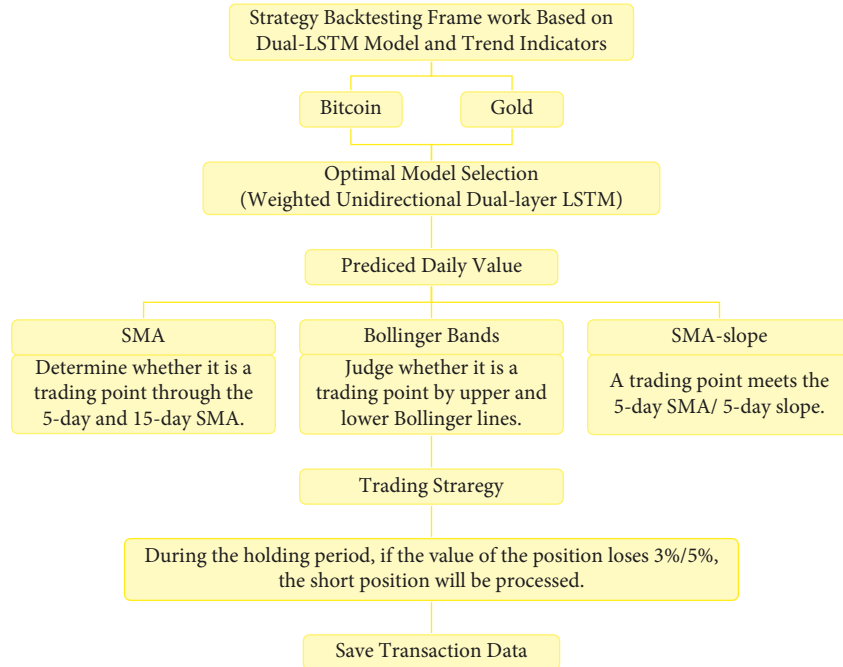
FIGURE 2: Structure diagram of the strategy backtesting framework.
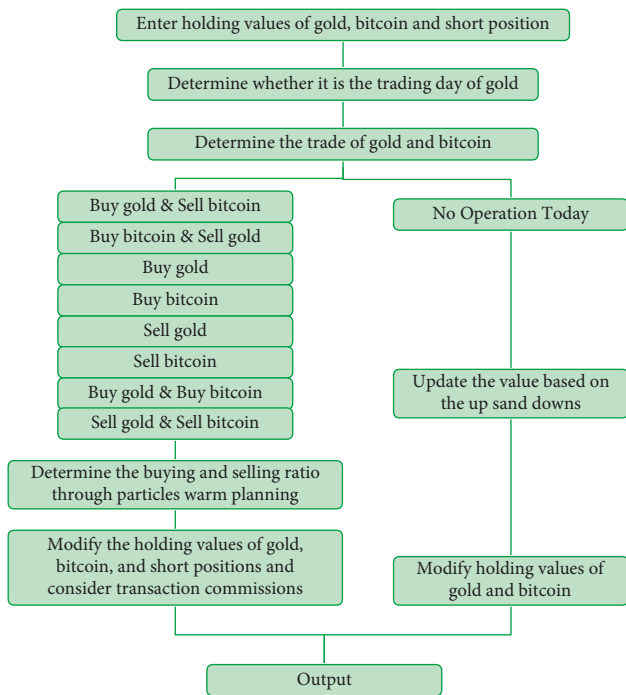
FIGURE 3: Flowchart of trading strategy.

We calculate the ratio of positive/negative slopes for gold/Bitcoin for k consecutive days (Table 1). It can be easily noticed that, by introducing the concept of k-slope, many k make the number of days that meet the trading conditions exceed the number of days to trade formed by SMA and BB strategies only. When $k > 10$, the number of days that meet the trading conditions is less. Therefore, we set traversals and search to range from k to [1, 12]. Considering that the SMA strategy has

outperformed the Bollinger band strategy, we incorporate the k-slope into the SMA strategy to form the SMA-slope strategy, which can create more trading days than the SMA strategy. Also, it makes gold and Bitcoin more likely to be traded simultaneously, so we expect better results by using PSO.

The k-slope of gold/Bitcoin represents how aggressively the price rises or falls, which can be used for trend identification to establish a trading bias. A positive slope dictates a bullish bias, while a negative slope dictates a bearish bias. However, the k-slope follows a trend or price point, which cannot predict a trend. In order to treat the problems of possible lags, we apply the predicted price of today and the actual data of yesterday to calculate today's slope.

The k-slope (s_i) is calculated by (25) as follows:

$$s_i = \frac{\widehat{y}_i - y_{i-1}}{1 \text{ day}}, \tag{25}$$

where y_{i-1} is the true value on the $(i-1)$-th day and $\widehat{y}_i$ is the predicted value of y_i.

When $k > 2$, if the slopes for consecutive k days are both positive and negative and the absolute value of the slope for the most recent day is less than the absolute value of the slope today, we will consider it as a possible buying/selling point. Directional movement is also important for analyzing the slope. When the k-slope continues to be positive and has a slowing trend, we decide that this is an appropriate selling point; when the k-slope continues to be negative and has a slowing trend, we decide that this is an appropriate buying point. To sum up, when $k > 1$, we consider $s_i > 0$ as a selling point and $s_i < 0$ as a buying point.

We set the number of consecutive days that Bitcoin has a positive slope as BITCOIN_k_positive, and the value that meets the requirements represents a suitable time to sell Bitcoin on that day. We set the number of consecutive days

TABLE 1: The ratio positive/negative slopes for gold/Bitcoin for k consecutive days.

k	Gold (1826 days)									Bitcoin (1826 days)								
	2	3	4	5	6	7	8	9	10	2	3	4	5	6	7	8	9	10
Positive (%)	38	32	28	26	24	22	21	20	19	42	36	32	30	27	25	24	23	23
Negative (%)	34	27	24	21	19	18	16	15	14	31	25	21	19	16	15	13	12	11

that Bitcoin has a negative slope as BITCOIN_k_negative, and the value that meets the requirements represents a suitable time to buy Bitcoin on that day. GOLD_k_positive and GOLD_k_negative are defined similarly. We perform a traversal search with the range from 1 to 12 for these four parameters to find the optimal value for k in the k-slope.

3. Results

3.1. Performance of LSTM Model Based on Feature Selection. Figures 4 and 5 represent correlation coefficients of all features with daily average price of gold/Bitcoin. The darker the colour, the smaller the influence of the feature on the value of gold/Bitcoin. Also, the lighter the colour, the greater the influence of the feature on the value of gold/Bitcoin. The value of gold has a large correlation coefficient with all features of SMA and Bollinger bands, implying a strong positive correlation. In particular, the correlation coefficients of 5-day SMA and 5-day EMA reach 1.0, which is a perfect positive correlation. Therefore, these characteristics can have a greater impact on the value of gold. The correlation coefficients of RC, RSI, and MACD were 0.05, 0.12, and 0.02, respectively, showing a positive weak correlation.

The value of Bitcoin has a strong correlation coefficient with all the characteristics of the simple moving average, exponential moving average, and Bollinger bands, even reaching 1.0 on the 5-day and 10-day SMA and EMA. Therefore, these characteristics can have a noticeable impact on the value of Bitcoin. The correlation coefficients of RC, RSI, and MACD are 0.02, 0.00, and 0.00, respectively, and there is almost no correlation. However, since only 18 indicators are selected in this paper, all indicators with weak correlations are reserved.

Table 2 represents the result of the performance comparison of LSTM models. It can be seen that the unidirectional dual-layer LSTM model is better than the bidirectional LSTM model in every index. As a result, we initially choose the unidirectional dual-layer LSTM as the basic model.

Δt and m in Table 2 refer to the average daily price data of consecutive trading Δt days as a time window to input the model training, which aims to predict the profit situation after m days. Therefore, it can use the predicted price data of m days to predict the short-term price trend.

Secondly, we compare different sizes of the time window (Δt), where 1, 5, and 8 are chosen.

Table 3 represents the performance of unidirectional dual-layer LSTM model with time windows of 1, 5, and 8. It is obvious that the 5 indicators are not particularly different. Given that we pay more attention to the accuracy of ups and downs predictions (Accuracy), we choose the unidirectional

dual-layer LSTM model with time windows of 5 to predict the average daily price of Bitcoin.

In the same way, a unidirectional dual-layer LSTM model with time windows of 8 is chosen to predict the average daily price of Bitcoin.

As shown in Figure 6, prediction lag is sometimes encountered, where the predicted average daily price of Bitcoin lags behind the change in the actual situation. It may lead to a decrease in the accuracy of ups and downs (Accuracy).

As shown in Tables 4 and 5, it can be inferred that, compared with $m = 1$, the accuracies of ups and downs (Accuracy) have more than 25% growth. Therefore, we can conclude that the model has been significantly improved. In addition, whether it is Bitcoin or gold, the result with a weight ratio of 0.4 : 0.5 : 0.1 performs better than the result with a weight ratio of 0.4 : 0.32 : 0.28. Hence, we choose a weight ratio of 0.4 : 0.5 : 0.1 to build the model.

According to the model we selected and improved, we predict the average daily prices of gold and Bitcoin, as shown in Figures 7 and 8. It can be clearly seen that the prediction lag with $m = 3$ has been alleviated. To sum up, with a time window of 5, the unidirectional dual-layer LSTM model predicting the next 3 days is the best for Bitcoin average daily price prediction. Also, with a time window of 8, the unidirectional dual-layer LSTM model predicting the next 3 days is the best one for gold average daily price prediction.

3.2. Financial Strategy Results. A 5-year trading simulation is conducted based on a $1000 principal. For the sake of concise and convenient representation, the symbols we will use frequently in the next two sections are explained in Table 6. The initial conditions of the simulation are as follows: the sell position ratio is 20%, the buy position ratio is 50%, the buy position ratio for the first time/after clearance is 70%, and the transaction commissions of Bitcoin and gold are 2% and 1%, respectively.

3.2.1. Performance of the SMA-Slope Strategy

(1) Optimal Value of k in k-Slope for Gold. As the number of consecutive days with negative slopes for gold (GOLD_k_negative) increases, the number of buying points for gold decreases, but the upper limit of the gold asset increases. As the number of consecutive days with positive slopes for gold (GOLD_k_positive) increases, the number of selling points for gold decreases, but the upper limit of the gold asset increases. From Table 7, it can be concluded that long-term holding is more suitable for gold, while frequent reading operations are not appropriate. By analyzing gold assets under different settings of four parameters, we find that when
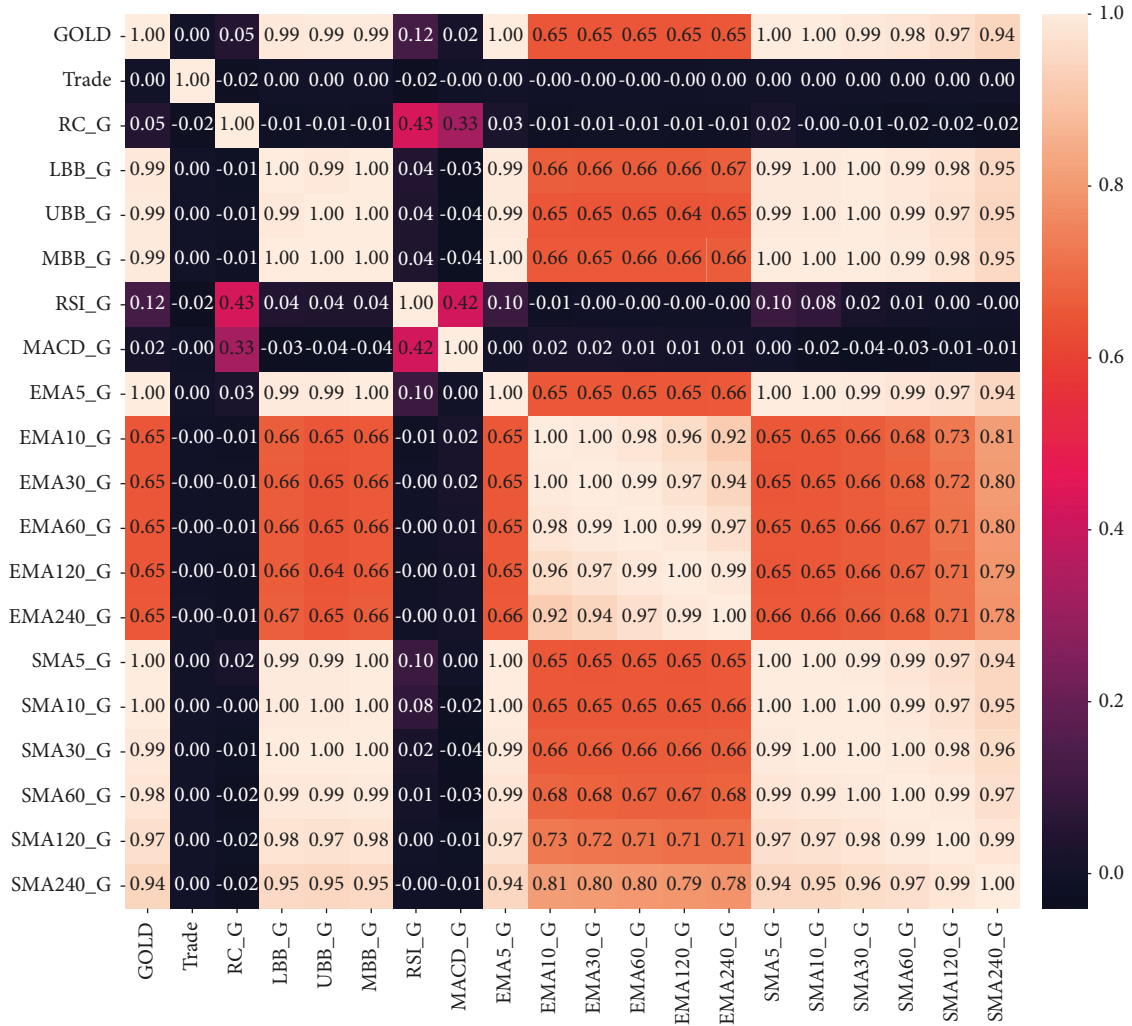
FIGURE 4: Correlation coefficients of all features with gold values.

GOLD_k_negative and GOLD_k_positive take 9 at the same time, the gold assets can reach the highest. Moreover, selling points have a more significant impact on gold assets because GOLD_k_positive can distinguish different gold assets while GOLD_k_negative cannot. When the buying and selling points are the same, the results of the SMA-slope strategy are better than those of the SMA strategy due to the influence of Bitcoin on gold. It increases the number of days to buy and sell both gold and Bitcoin at the same time, which contributes to better results of asset allocation.

(2) Optimal Value of k in k-Slope for Bitcoin. As the number of consecutive days with negative slopes for Bitcoin (BITCOIN_k_negative) decreases, the number of buying points for Bitcoin increases, and the upper limit of Bitcoin assets increases. As the number of consecutive days with positive slopes for Bitcoin (BITCOIN_k_positive) decreases, the number of selling points for Bitcoin increases, and the upper limit of Bitcoin assets increases. From Table 8, we can draw the conclusion that Bitcoin is more suitable for short-term holding. The buying point has a greater impact on Bitcoin because buying points can partition the Bitcoin asset,

while selling points cannot. When the selling points are the same, the SMA-slope strategy far outperforms the SMA results because the SMA-slope strategy increases the buying point for Bitcoin. With more days to buy and sell both gold and Bitcoin simultaneously, more proper asset allocation can be obtained.

(3) Optimal Values of k in k-Slope for the Portfolio. We perform a global search for four k-slope parameters, and the optimal solution set is shown in (26) as follows:

$$\begin{cases} \text{BITCOIN}\_k\_\text{negative} = 1, \\ \text{BITCOIN}\_k\_\text{positive} \geq 8, \\ \text{GOLD}\_k\_\text{negative} \geq 7, \\ \text{GOLD}\_k\_\text{positive} = 5, \end{cases} \quad (26)$$

Bitcoin has 1567 buying points and 52 selling points, while gold has 31 buying points and 99 selling points. This optimal solution set confirms previous conclusions; that is, selling points play a decisive role in gold assets, and buying point is crucial for Bitcoin.
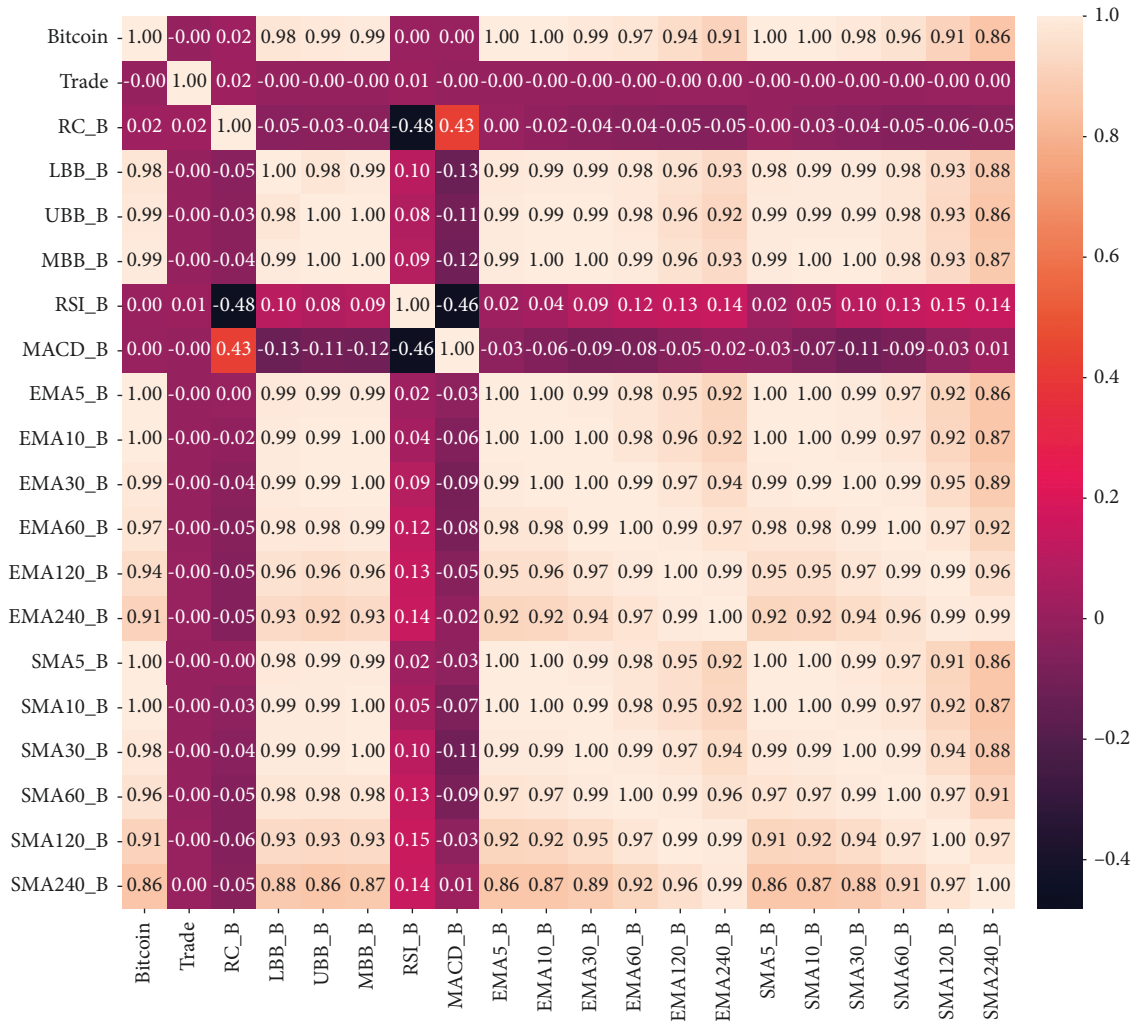
Figure 5: Correlation coefficients of all features with Bitcoin values.

Table 2: Performance comparison of LSTM models.

Model	Δt	m	MSE	RMSE	R^2	MAPE	Accuracy (%)
Unidirectional dual-layer LSTM	8	1	751150.9776	866.6897	0.9962	2.8881	46.9163
Bidirectional LSTM	8	1	752803.4835	867.6425	0.9962	2.8641	45.5044

Table 3: Performance comparison with different sizes of the time window of the LSTM model.

Model	Δt	m	MSE	RMSE	R^2	MAPE	Accuracy (%)
	1	1	731372.9356	855.2034	0.9963	2.9109	46.6410
Unidirectional dual-layer LSTM	5	1	739981.2836	860.2216	0.9962	2.8791	47.7974
	8	1	751150.9776	866.6897	0.9962	2.8881	46.9163

However, at this time, 99% or more of the total assets are composed of Bitcoin assets, and the holding ratio also exceeds 99% of the total positions. This is a very aggressive, risky behavior that does not conform to normal human behaviors. However, this set can be ignored by setting the empty, gold, and Bitcoin ratio not to be extreme. Table 9 shows the optimal asset results by global search.

Figure 9 presents the results of different BITCOIN_k_negative and GOLD_k_positive investment simulations. It

can be noticed that the best results are obtained when the value of BITCOIN_k_positive is 1. Similarly, Figure 10 presents the changes in gold assets at different BITCOIN_k_negative, and we can see that the more the proportion of Bitcoin, the smaller the proportion of gold and the more the total assets. Under different BITCOIN_k_negative, better results are obtained when the value of GOLD_k_positive is 7, but as the number of buying points for Bitcoin decreases, GOLD_k_positive moves to a smaller value to obtain the

Figure 6: Predicted values of Bitcoin by unidirectional dual-layer LSTM model.

Table 4: Performance comparison with different weights for gold of the LSTM model.

Model	γ_1	γ_2	γ_3	MSE	RMSE	R^2	Mape	Accuracy (%)
Unidirectional dual-layer LSTM $(\Delta t = 8, m = 3)$	0.4	0.32	0.28	354788.3113	595.6410	0.9982	2.1194	73.7885%
	0.4	0.5	0.1	253736.0019	503.7221	0.9987	1.5871	82.0485%

Table 5: Performance comparison with different weights for Bitcoin of the LSTM model.

Model	γ_1	γ_2	γ_3	MSE	RMSE	R^2	Mape	Accuracy (%)
Unidirectional dual-layer LSTM $(\Delta t = 5, m = 3)$	0.4	0.32	0.28	354788.3113	595.6410	0.9982	2.1194	73.7885
	0.4	0.5	0.1	253736.0019	503.7221	0.9987	1.5871	82.0485

Figure 7: Predicted values of gold by weighted unidirectional dual-layer LSTM model.
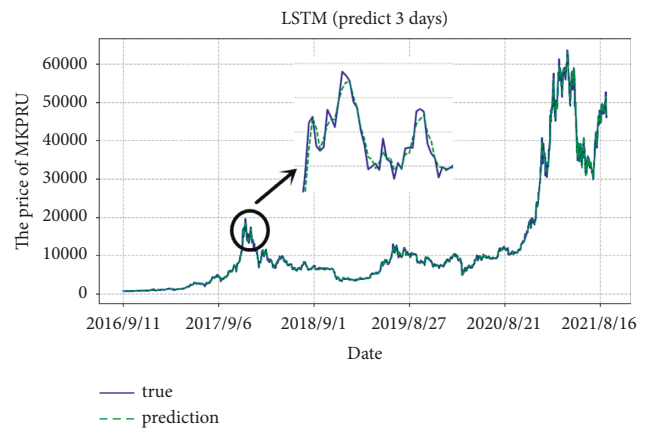
Figure 8: Predicted values of Bitcoin by weighted unidirectional dual-layer LSTM model.

optimal solution. The portfolio has the tendency to decrease the proportion of gold and increase the proportion of Bitcoin in order to get a higher profit.

3.2.2. Comparison of SMA, BB, and SMA-Slope Strategies. From Table 10, as for the performance of the annual percentage rate (APR) of the portfolio consisting of gold and Bitcoin, the SMA-slope strategy is better than the SMA strategy, and the SMA strategy is better than the BB strategy. The empty, gold, and Bitcoin have unbalanced asset allocations with high risk when SMA-slope and BB

strategies perform best. It also confirms the possibility that investors may substitute Bitcoin for gold in a portfolio for higher risk-adjusted returns [38]. In the SMA-slope strategy, without pursuing the minimum value, we can get a set of slope values, which contributes to more balanced asset allocation, and the APR is higher than that of the SMA strategy. As shown in Table 11, the SMA-slope strategy dramatically increases the number of buying points of Bitcoin and changes the selling points of gold. It can be speculated that the SMA-slope strategy adjusts the number of trading times for gold and Bitcoin on the same day to get better results.

TABLE 6: Notations used in this section.

Symbol	Definition
Gold	Accumulated holding value of gold.
Bitcoin	Accumulated holding of Bitcoin.
Short	Cumulative remaining value of assets.
Total	Cumulative total value of assets.
Buy position ratio	The ratio of value of assets that are bought to the cumulative remaining value of assets.
Sell position ratio	The ratio of value of assets that are sold to the cumulative remaining value of assets.
Buy position ratio for the first time/after clearance	Buy position ratio for first purchase at the beginning and the first purchase after short position.

TABLE 7: Number of buying and selling points for gold and corresponding asset values at different slopes.

GOLD_k_negative	Gold buying points	Gold assets range ($)	GOLD_k_positive	Gold selling points	Gold assets range ($)
10,11,12	31	[2.58, 5473.44]	10,11,12	37	[863.20, 5304.65]
9	**31**	**[2.61, 5497.88]**	**9**	**40**	**[894.96, 5497.88]**
7,8	31	[2.58, 5473.44]	8	40	[894.96, 5371.01]
6	33	[1.92, 3979.27]	7	45	[905.68, 5473.44]
5	36	[1.78, 3664.29]	6	67	[553.25, 3264.70]
4	45	[1.32, 1487.55]	5	99	[349.40, 1990.88]
3	63	[1.34, 1042.88]	4	156	[173.06, 1056.99]
2	98	[1.20, 960.06]	3	298	[33.91, 138.46]
			2	576	[1.20, 4.04]
SMA	31	[2.61, 5473.44]	SMA	37	[877.41, 5181.83]

TABLE 8: Number of buying points and selling points for Bitcoin and corresponding asset values at different slopes.

BITCOIN_k_negative	Bitcoin buying points	Bitcoin assets range ($)	BITCOIN_k_positive	Bitcoin selling points	Bitcoin assets range ($)
11,12	46	[1117.15, 6960.06]	**8,9,10,11,12**	**52**	**[1127.11, 34864.58]**
10	47	[1102.19, 7181.45]	7	54	[1111.62, 33071.92]
9	48	[1118.53, 6994.15]	6	57	[1093.92, 31634.04]
8	51	[970.53, 6676.25]	5	62	[1081.70, 30123.10]
7	54	[1026.62, 6351.62]	4	73	[1064.18, 27314.72]
6	70	[1565.28, 8649.57]	3	103	[1068.01, 23883.65]
5	108	[2062.81, 11227.64]	2	155	[1026.62, 20596.88]
4	175	[2434.13, 12411.84]	1	239	[970.53, 18015.70]
3	336	[4101.21, 21453.82]			
2	735	[6283.13, 32608.38]			
1	**1567**	**[7816.49, 34864.58]**			
SMA	46	[1226.95, 7127.42]	SMA	52	[1226.95, 7127.42]

TABLE 9: Optimal asset results by global search.

BITCOIN_k_negative	BITCOIN_k_positive	GOLD_**k_negative**	GOLD_**k_positive**	Empty ($)	Gold assets ($)	Bitcoin assets ($)	Total assets ($)
1	8	7	5	134.641	176.012	36950.113	37260.767
1	8	8	5	134.659	176.035	36954.796	37265.490
1	8	9	5	134.659	176.035	36954.796	37265.490
1	9	7	5	134.659	176.035	36954.796	37265.490
1	9	8	5	134.659	176.035	36954.796	37265.490
1	9	9	5	134.659	176.035	36954.796	37265.490
1	Null	7	5	134.659	176.035	36954.796	37265.490
1	8	Null	5	134.659	176.035	36954.796	37265.490
1	Null	Null	5	134.659	176.035	36954.796	37265.490
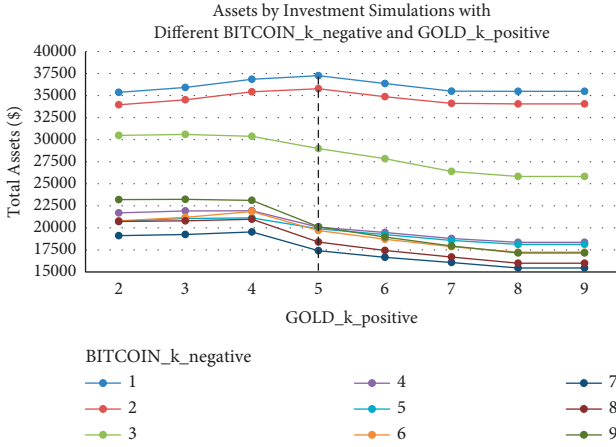
Figure 9: Assets by investment simulations with different BITCOIN_k_negative and GOLD_k_positive.
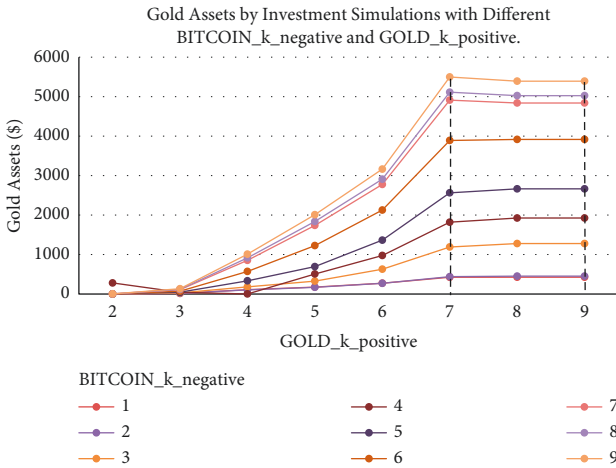
Figure 10: Gold assets by investment simulations with different BITCOIN_k_negative and GOLD_k_positive.

3.3. Analysis of Operational Factors Affecting Investment Results.

The proper asset allocation is key to achieving the goal of high return and risk tolerance. Rebalancing will be employed when the asset allocation is out of line, which will provide the best relative return on risk [39]. Therefore, we set the BITCOIN_k_negative as 5 and GOLD_k_positive as 5 to further analyze the SMA-slope strategy. Results with these settings avoid extreme imbalances in the ratio of gold and bitcoin.

3.3.1. Buy Position Ratio Analysis. Figures 11–13 are the analysis of buy position ratio under 3 strategies. For the SMA strategy, when we fix the gold/bitcoin sell position ratio of 20% each time and adjust the proportion of the short position each time we buy, it is evident that the APR is adjusted from 72.0% to 84.4%. The growth rate of the APR is proportional to the buy position ratio. The Bollinger band strategy shows that its annual interest rate has nothing to do with the buying position ratio, implying that the strategy is

highly conservative. Its proportion of gold and Bitcoin is highly unbalanced. For the SMA-slope strategy, it can be found that the annual interest rate shows a parabolic trend, and the total assets will fall back as the position increases to warn investors. When the buy position ratio is adjusted to 70%, the maximum APR is 83.0%. However, as the buy position ratio becomes closer to 100%, the APR shows a downward trend.

Moreover, the SMA-slope strategy obtains a better solution when the buy position ratio is within the interval [40%, 80%]. When the buy position ratio is adjusted to 40%, the difference between the APRs of the SMA and SMA-slope strategies is at most 8%. Considering risk factors, it is generally not recommended for investors to use all amounts of cash to buy assets at one time, especially for Bitcoin, which is highly volatile. Therefore, with careful consideration, the SMA-slope strategy performs better in response to adjusting the buy position ratio.

3.3.2. Sell Position Ratio Analysis. We try to explore the performance of the SMA strategy in extreme cases, that is, sell only a tiny percentage of gold/Bitcoin at one time. When we set the buy position ratio to 60% (Figure 14), it can be seen that the growth of the annual interest rate has a linear relationship with the sell position ratio. The higher the sell position ratio, the lower the annual interest rate. The position ratio between the holding value of Bitcoin and gold and the short position value is about 3 : 6:1, a stable ratio. We want to explore whether this ratio relationship is still satisfied in extreme cases (Figure 15). We figure out that when the sell position ratio is 1%, the final short position value is only 32.6, the value of Bitcoin holdings reaches 48436.5, and the total assets reach \$51711.0, where the Bitcoin share becomes 93.7%. It is dangerous behavior. Although the data shows that a lower sell position ratio can finally greatly promote the growth of total assets, it is still a dangerous behavior requiring alertness.

3.3.3. Buy Position Ratio for the First Time/after Clearance Analysis. We have conducted a detailed analysis of the purchases when the current gold/Bitcoin position value is 0 under different strategies; that is, we adjust the buy position ratio for the first time/after short positions to explore its impact on the annual interest rate. We set the sell position ratio as 20% and the buy position ratio as 50%, aiming to find the changes in annual interest rate under different buy position ratios for the first time/after short positions. It can be found that, under the SMA strategy (Figure 16), the annual interest rate and the buy position ratio for the first time/after short positions have a linearly increasing relationship. Moreover, the value of empty, Bitcoin, and gold has increased, and the proportion is relatively balanced. Under the Bollinger band strategy (Figure 17), the annual interest rate has no effect on buy position ratios for the first time/after short positions, and the total assets remain at \$4815.8. It confirms the conservative nature of the Bollinger band strategy again, avoiding short positions to the greatest extent.

TABLE 10: Comparison of the results of different strategies.

Strategy							Empty ($)	Gold assets ($)	Bitcoin assets ($)	Assets ($)	Annual percentage rate (APR) (%)
BITCOIN_k_negative	BITCOIN_k_positive	GOLD_k_negative	GOLD_k_positive								
	1		8	7		5					
SMA-slope	**1**					**5**	**134.64**	**176.01**	**36950.11**	**37260.77**	**106.18**
SMA-slope	1		Null	Null		9	159.22	426.08	34906.09	35491.40	104.19
SMA-slope	5		Null	Null		5	4251.05	696.73	14953.83	19901.61	81.88
SMA-slope	5		NULL	Null		9	3653.54	2664.75	11812.30	18130.59	78.52
SMA-slope	9		Null	Null		7	4411.51	5497.70	8037.65	17946.8	78.15
SMA							3976.98	5181.83	6960.06	16118.87	74.37
BB							≈0	≈0	4950.74	4950.74	37.70

TABLE 11: Selling and buying points for different strategies.

Strategy	Bitcoin buying points	Bitcoin selling points	Gold buying points	Gold selling points
BB	449	76	50	1105
SMA	46	52	31	37
SMA-slope (best)	1567	52	31	99
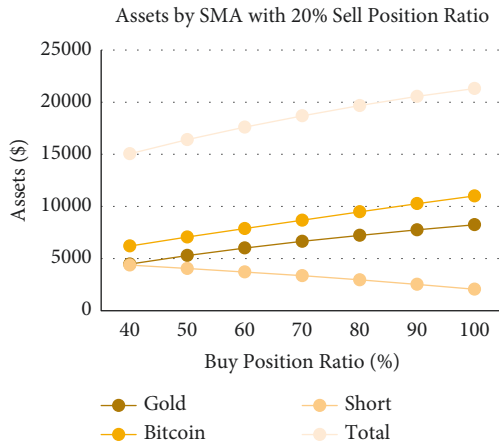
FIGURE 11: Assets by SMA strategy with 20% sell position ratio and different buy position ratio.

FIGURE 12: Assets by Bollinger bands strategy with 20% sell position ratio and different buy position ratio.

FIGURE 13: Assets by SMA-slope strategy with 20% sell position ratio and different buy position ratio.

FIGURE 14: Assets by SMA strategy with 60% buy position ratio and different sell position ratio.

FIGURE 15: Assets by SMA strategy with 100% buy position ratio and different sell position ratio.

3.3.4. Different Transaction Commissions of Gold/Bitcoin.
As shown in Figures 18–21, the assets show a linear relationship with different transaction commissions of gold/Bitcoin for SMA and SMA-slope models. Also, with the increase of the transaction commission of gold/Bitcoin, the total asset decreases linearly.

Tables 12 and 13 show the effects on the two models when the transaction commission of gold/Bitcoin changes. The average sensitivity (average rate of change) of the SMA strategy to changes in Bitcoin transaction commission is 36%, and the average sensitivity of the SMA-slope strategy is 47. Additionally, SMA and SMA-slope strategies are
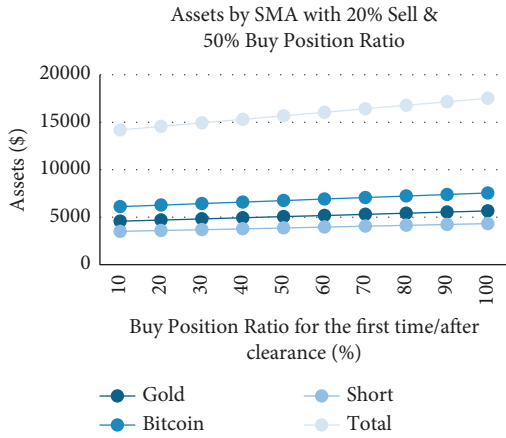
Figure 16: Assets by SMA strategy with 20% sell and 50% buy position ratio and different buy position ratio for the first time/after clearance.
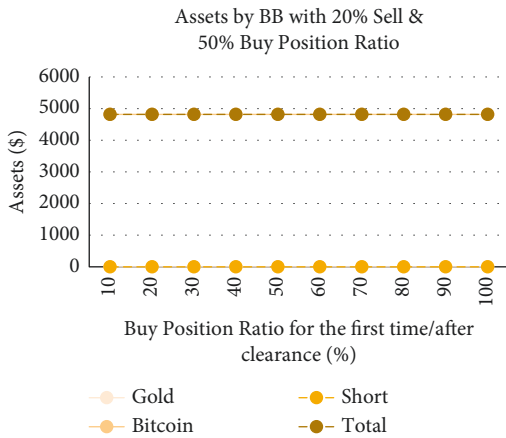
Figure 17: Assets by Bollinger band strategy with 20% sell and 50% buy position ratio and different buy position ratio for the first time/after clearance.
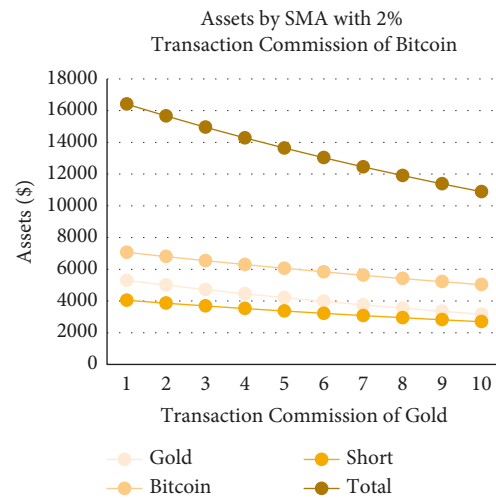
Figure 18: Assets by SMA strategy with 2% transaction commission of Bitcoin and different transaction commissions of gold.
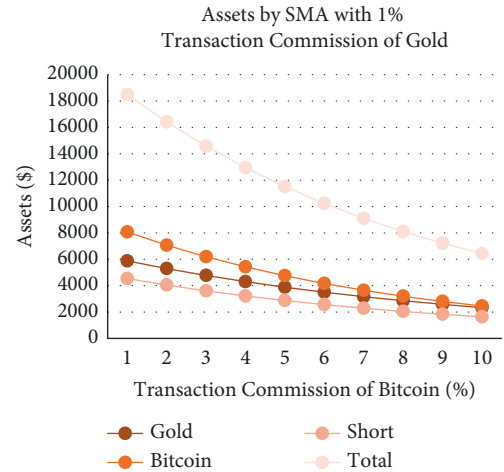
Figure 19: Assets by SMA strategy with 1% transaction commissions of gold and different transaction commission of Bitcoin.
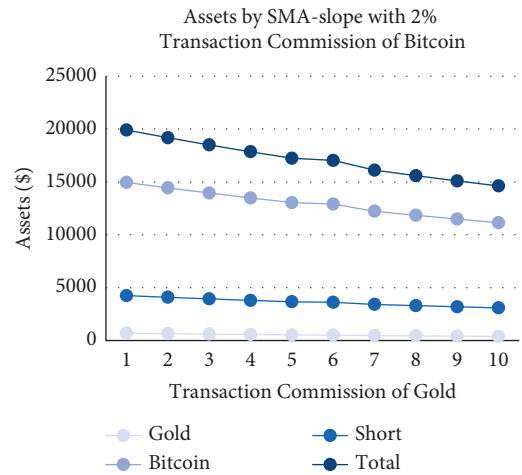
Figure 20: Assets by SMA-slope strategy with 2% transaction commission of Bitcoin and different transaction commissions of gold.
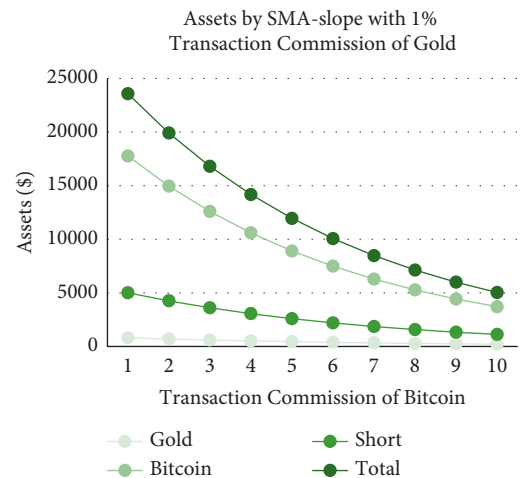
Figure 21: Assets by SMA-slope strategy with 1% transaction commission of gold and different transaction commissions of Bitcoin.

Table 12: Effects on SMA and SMA-slope strategies by changes in transaction commission of Bitcoin.

Transaction commission of gold (%)	Transaction commission of Bitcoin (%)	SMA		SMA-slope	
		Total assets ($)	Rate of change (%)	Total assets ($)	Rate of change (%)
1	1	18490.8	−13	23570.5	−18
1	2	16410.6	0	19901.6	0
1	3	14570.8	11	16794.1	16
1	4	12943	21	14163.5	29
1	5	11502.6	30	11937.9	40
1	6	10227.5	38	10056.2	49
1	7	9098.4	45	8466	57
1	8	8098.3	51	7123.1	64
1	9	7212.1	56	5989.6	70
1	10	6426.6	61	5033.5	75

Table 13: Effects on SMA and SMA-slope strategies by changes in transaction commission of gold.

Transaction commission of gold (%)	Transaction commission of Bitcoin (%)	SMA		SMA-slope	
		Total assets ($)	Rate of change (%)	Total assets ($)	Rate of change (%)
1	2	16410.6	−5	19901.6	−4
2	2	15663	0	19179.9	0
3	2	14953.4	5	18497.2	4
4	2	14279.6	9	17850.9	7
5	2	13639.9	13	17238.6	10
6	2	13032.3	17	17027.6	11
7	2	12455.2	20	16107.4	16
8	2	11906.9	24	15584.6	19
9	2	11385.9	27	15088	21
10	2	10890.9	30	14616	24

sensitive to gold transaction commission changes with an average sensitivity of 17%.

To sum up, due to the relatively gentle change of gold, the two models are less sensitive to changes in the transaction commission. However, because of the significant volatility and extensive fluctuation range of Bitcoin, the two models are more sensitive to it. Moreover, the sensitivity of the SMA-slope strategy is higher than that of the SMA strategy, and the highest rate of change is 75%.

4. Discussion

We have built a portfolio optimization model for gold and Bitcoin with high profitability to help investors make trading decisions. By sliding window and a weighted method for three days, we achieve a high accuracy of ups and downs for the unidirectional dual-layer LSTM model. Also, with the introduction of the k-slope and slight adjustments for the asset allocation, higher returns are realized by the SMA-slope strategy compared to common SMA and BB strategies. However, there are still some improvements that can be completed in the future work. Firstly, risk factors should be taken into more consideration. The current optimal set is a hazardous solution with highly unbalanced asset allocation. A fixed rule and some rebalancing methods can be conducted to avoid risks caused by inappropriate portions of different assets. Secondly, the relationship between gold and

Bitcoin can be explored while we currently train and test the LSTM model for prediction separately. The internal influence mechanism between gold and Bitcoin may play an essential role in predicting daily prices [40]. Thirdly, the window size can be dynamic as time goes by. Fix window size is used in the current model, limiting temporal modeling in deep learning neural networks because the data defined by the window size is only modeled and unsuitable for dealing with long-term dependencies in time-series data [41]. Also, the sliding window may be more suitable for Bitcoin than gold. Finally, in the context of Industry 4.0, AI technology can be applied more in the prediction model and the simulation for practical trading processes. Many alternatives for the LSTM model may contribute to higher accuracy for daily price prediction. AI can be described as a set of techniques for modeling and simulation environmental systems, such as artistic neural networks and reinforcement learning [42]. More use of AI technology may make trading simulations more realistic.

5. Conclusion

This paper establishes a portfolio optimization model for gold and Bitcoin, including a weighted unidirectional dual-layer LSTM model to predict the daily prices and the SMA-slope strategy for trading decision-making. We also carry out trading simulations for gold and Bitcoin with an initial

principal of \$1000 for further exploration. The weighted unidirectional dual-layer LSTM model is trained by daily prices of gold/Bitcoin and their related financial indicators. In order to make the simulation more in line with the actual, we adopt a sliding window for daily price prediction. For evaluation matrices, in addition to some common indicators like R^2 and RMSE, we pay more attention to the accuracy of ups and downs, which has a more direct relationship with trading decision-making. Changes in the financial market do not always obey the regular common rules or follow the same cycle. The predicted prices are obtained for the following 3 days, and a weighted method is used on them for higher accuracy of ups and downs, which reduces prediction lags to catch trends of prices better. In this paper, we compared three strategies, SMA strategy, BB strategy, and SMA-slope strategy. By analyzing results from various simulations, the SMA-slope strategy is considered the best choice for obtaining relatively high returns and avoiding extremely unbalanced asset allocation, where four parameters in the k-slope can be adjusted to achieve different outcomes. We focus on the operation derails involved in the investment processes and conclude that buy position ratios, sell position ratios, buy position ratios for the first time/after clearance, and transaction commissions of gold/Bitcoin all significantly impact the assets, which also have a more substantial effect on the performance of strategies.

Data Availability

The data included in this paper are available without any restriction.

Conflicts of Interest

The authors declare that there are no conflicts of interest regarding the publication of this paper.

Acknowledgments

References

[1] B. Machkour and A. Abriane, "Industry 4.0 and its implications for the financial sector," *Procedia Computer Science*, vol. 177, pp. 496–502, 2020.

[2] M. Dia, "A portfolio selection methodology based on data envelopment analysis," *INFOR: Information Systems and Operational Research*, vol. 47, no. 1, pp. 71–79, 2009.

[3] R. Vetschera and A. T. de Almeida, "A PROMETHEE-based approach to portfolio selection problems," *Computers & Operations Research*, vol. 39, no. 5, pp. 1010–1020, 2012.

[4] J.-M. Martel, N. T. Khoury, and M. Bergeron, "An application of a multicriteria approach to portfolio comparisons," *Journal of the Operational Research Society*, vol. 39, no. 7, pp. 617–628, 1988.

[5] R. D. Edwards, J. Magee, and W. H. C. Bassetti, *Technical Analysis of Stock Trends*, CRC Press, New York, NY, USA, 2018.

[6] Y. Zhu and G. Zhou, "Technical analysis: an asset allocation perspective on the use of moving averages☆," *Journal of Financial Economics*, vol. 92, no. 3, pp. 519–544, 2009.

[7] H. Markowitz, "Portfolio selection," *The Journal of Finance*, vol. 7, no. 1, pp. 77–91, 1952.

[8] A. Diez-Olivan, J. Del Ser, D. Galar, and B. Sierra, "Data fusion and machine learning for industrial prognosis: trends and perspectives towards Industry 4.0," *Information Fusion*, vol. 50, pp. 92–111, 2019.

[9] R. S. Michalski, J. G. Carbonell, and T. M. Mitchell, *Machine Learning: An Artificial Intelligence Approach*, Tioga Pub. Co, Palo Alto, CA, USA, 1983.

[10] A. Diez Oliván, "Machine Learning for Data-Driven Prognostics: Methods and Applications," Doctoral dissertation, UniversitatPolitècnica de València, Valencia, Spain, 2017.

[11] C.-W. Su, Y. Xi, R. Tao, and M. Umar, "Can Bitcoin be a safe haven in fear sentiment?" *Technological and Economic Development of Economy*, vol. 28, no. 2, pp. 268–289, 2022.

[12] L. Morales and B. Andreosso-O'Callaghan, "Covid19: global stock markets 'black swan,'" *Critical Letters in Economics & Finance*, vol. 1, no. 1, pp. 1–14, 2020.

[13] B. Y. Qu and P. N. Suganthan, "Constrained multi-objective optimization algorithm with an ensemble of constraint handling methods," *Engineering Optimization*, vol. 43, no. 4, pp. 403–416, 2011.

[14] G.-F. Deng, W.-T. Lin, and C.-C. Lo, "Markowitz-based portfolio selection with cardinality constraints using improved particle swarm optimization," *Expert Systems with Applications*, vol. 39, no. 4, pp. 4558–4566, 2012.

[15] T.-J. Chang, N. Meade, J. E. Beasley, and Y. M. Sharaiha, "Heuristics for cardinality constrained portfolio optimisation," *Computers & Operations Research*, vol. 27, no. 13, pp. 1271–1302, 2000.

[16] H. Kellerer, R. Mansini, and M. G. Speranza, "Selecting portfolios with fixed costs and minimum transaction lots, Annals of Operations Research," *Annals of Operations Research*, vol. 99, no. 1/4, pp. 287–304, 2000.

[17] M. Yurtsever, "Gold price forecasting using LSTM, Bi-LSTM and GRU," *European Journal of Science and Technology*, vol. 31, pp. 341–347, 2021.

[18] S. Velankar, S. Valecha, and S. Maji, "Bitcoin price prediction using machine learning," in *Proceedings of the 2018 20th International Conference on Advanced Communication Technology (ICACT)*, pp. 144–147, Chuncheon, South Korea, February 2018.

[19] S. Selvin, R. Vinayakumar, E. A. Gopalakrishnan, V. K. Menon, and K. P. Soman, "Stock price prediction using LSTM, RNN and CNN-sliding window model," in *Proceedings of the 2017 International Conference on Advances in Computing, Communications and Informatics (ICACCI)*, pp. 1643–1647, Udupi, India, September. 2017.

[20] J. Fleischer, G. von Laszewski, C. Theran, and Y. J. Parra Bautista, "Time series analysis of blockchain-based cryptocurrency price changes," 2022, https://arxiv.org/abs/2202.13874.

[21] T. Silva, P. R. Pinheiro, and M. Poggi, "A more human-like portfolio optimization approach," *European Journal of Operational Research*, vol. 256, no. 1, pp. 252–260, 2017.

[22] B. Yerznkyan, T. M. Gataullin, and S. T. Gataullin, "Solow models with linear labor function for industry and

enterprise," *Montenegrin Journal of Economics*, vol. 17, no. 1, pp. 111–120, 2021.

[23] J. Stanković, I. Marković, and M. Stojanović, "Investment strategy optimization using technical analysis and predictive modeling in emerging markets," *Procedia Economics and Finance*, vol. 19, pp. 51–62, 2015.

[24] C. Liu and H. Malik, "A new investment strategy based on data mining and Neural Networks," in *Proceedings of the 2014 International Joint Conference on Neural Networks (IJCNN)*, pp. 3094–3099, Beijing, China, July 2014.

[25] G. Parambalath, E. Mahesh, P. Balasubramanian, and P. N. Kumar, "Big data analytics: a trading strategy of nse stocks using bollinger bands analysis," *Advances in Intelligent Systems and Computing*, vol. 839, 2018.

[26] M. Z. Jaworski, "Particle Swarm Optimization of Custom Bitcoin Trading Algorithm," BS Thesis, University of Twente, Enschede, Netherlands, 2022.

[27] H. Zhu, Y. Wang, K. Wang, and Y. Chen, "Particle Swarm Optimization (PSO) for the constrained portfolio optimization problem," *Expert Systems with Applications*, vol. 38, no. 8, Article ID 10161, 2011.

[28] M. Butler and D. Kazakov, "Particle swarm optimization of bollinger bands," *Lecture Notes in Computer Science*, vol. 6234, pp. 504–511, 2010.

[29] C. León, "Portfolio optimization and long-term dependence," *SSRN Electronic Journal*, 2010.

[30] J. P. Singh and P. Dey, "Risk measurement, nonlinearities and chaos," *Singapore Management Review*, vol. 24, no. 2, pp. 47–59, 2002.

[31] M. M. Gunal, *Simulation for Industry 4.0: Past, Present, and Future*, Springer, Cham, Switzerland, 2019.

[32] S. Hochreiter and J. Schmidhuber, *LSTM Can Solve Hard Long Time Lag Problems*, papers.nips, 1996.

[33] Z. Hu, Y. Zhao, and M. Khushi, "A survey of forex and stock price prediction using deep learning," *Applied System Innovation*, vol. 4, no. 1, p. 9, 2021.

[34] E. Beyaz, F. Tekiner, X.-j. Zeng, and J. Keane, "Comparing technical and fundamental indicators in stock price forecasting," in *Proceedings of the 2018 IEEE 20th International Conference on High Performance Computing and Communications; IEEE 16th International Conference on Smart City; IEEE 4th International Conference on Data Science and Systems (HPCC/SmartCity/DSS)*, pp. 1607–1613, Exeter, UK, June. 2018.

[35] H. Ouyang, K. Huang, and H. Yan, "Prediction of financial time series based on LSTM neural network," *Chinese Journal of Management Science*, vol. 28, no. 4, pp. 27–35, 2020.

[36] U. Schmidt and S. Traub, "An experimental test of loss aversion," *Journal of Risk and Uncertainty*, vol. 25, no. 3, pp. 233–249, 2002.

[37] L. Kai Jie Shawn, T. T. Hisarli, and N. Shi He, "The profitability of a combined signal approach: bollinger bands and the ADX," *SSRN Electronic Journal*, 2013.

[38] I. Henriques and P. Sadorsky, "Can bitcoin replace gold in an investment portfolio?" *Journal of Risk and Financial Management*, vol. 11, no. 3, p. 48, 2018.

[39] M. A. Harjoto and F. J. Jones, "Rebalancing strategy for stocks and bonds asset allocation," *The Journal of Wealth Management*, vol. 9, no. 1, pp. 37–44, 2006.

[40] J. Fajou and A. McCarren, "Forecasting gold prices using temporal convolutional networks," *SSRN*, vol. 3105, 2021.

[41] D. Tomar, P. Tomar, A. Bhardwaj, and G. R. Sinha, "Deep learning neural network prediction system enhanced with best window size in sliding window algorithm for predicting domestic power consumption in a residential building," *Computational Intelligence and Neuroscience*, vol. 2022, Article ID 7216959, 14 pages, 2022.

[42] W. de Paula Ferreira, F. Armellini, and L. A. De Santa-Eulalia, "Simulation in industry 4.0: a state-of-the-art review," *Computers & Industrial Engineering*, vol. 149, Article ID 106868, 2020.

Hindawi

Research Article

The Compound Effect of Spatial and Temporal Resolutions on the Accuracy of Urban Flood Simulation

Xiting Li,[1,2] Leizhi Wang [iD],[2] Haolan Zhou,[3] Yintang Wang,[2] Kaijie Niu,[2] and Lingjie Li[2]

[1]*Tianjin University, Tianjin 300350, China*
[2]*Nanjing Hydraulic Research Institute, Nanjing, Jiangsu 210029, China*
[3]*South China Agricultural University, Guangzhou, Guangdong 510642, China*

Correspondence should be addressed to Leizhi Wang; wanglz@nhri.cn

Flood disaster is one of the critical threats to cities. With the intellectualization tendency of Industry 4.0, refined urban flood models can effectively reproduce flood inundation scenarios and support the decision-making on the response to the flood. However, the spatiotemporal variability of rainfall and the spatial heterogeneity of the surface greatly increase the uncertainties in urban flood simulations. Therefore, it is crucial to account for spatiotemporal variability of rainfall events and grids of the model as accurately as possible to avoid misleading simulation results. This study aims to investigate the effect of temporal resolutions of rainfall and spatial resolutions of the model on urban flood modeling in small urban catchments and to explore a proper combination of spatiotemporal schemes. The IFMS Urban (integrated flood modeling system, urban) is used to construct a one-dimension and two-dimension coupled urban flood model in the typical inundated area in Dongguan, China. Based on five temporal resolutions of rainfall input and four spatial resolutions, the compound effect of spatiotemporal resolutions on the accuracy of urban flood simulations is systematically analyzed, and the variation characteristics are investigated. The results show that the finer the temporal resolution is, the higher the simulation accuracy of the maximum inundated water depth. Considering the spatial resolution, as the spatial grid becomes smaller, the relative error of the maximum inundated water depth decreases, but it also shows some nonlinear characteristics. Therefore, the smaller grid does not always mean a better simulation. The spatial resolution has a greater impact on the flood simulation accuracy than the temporal resolution. The simulation performance reaches the best when the grid interval is 100 m and the rainfall input interval is 5 min, 10 min, or 15 min. Affected by other factors such as terrain slope, the simulation accuracies under different spatiotemporal resolutions present complex nonlinear characteristics. The mechanisms of the compound effect of the spatiotemporal resolutions on the model simulation and the effect of underlying surface and topography on model simulation will be the focus of in-depth exploration for the future urban flood model.

1. Introduction

With booming urbanization, the flood-inducing factors and hazard bearing bodies have experienced great changes in recent years. Many large and medium-sized cities around the world have suffered from frequent floods, which seriously threaten the safety of life and property of urban residents [1–3]. As an important basis for urban flood emergency control and risk management, the urban flood model is very important in real-time simulation, early warning, and risk assessment of floods. In recent years, under the background of Industry 4.0, the algorithms, calculation data, and computing power have greatly improved [4]. The spatio-temporal resolutions of urban flood models are becoming higher, and the decision-making is more intelligent. However, the fine-resolution simulation brings computational pressure and increases the uncertainties in the urban flood simulation. Due to the diverse underlying urban surface, the fast runoff process, and the short response time, its hydrological characteristics in urban regions show high spatiotemporal heterogeneity [5, 6]. Therefore, the urban flood model generally has strong resolution dependence, and the

simulation accuracy is constrained by the spatiotemporal resolutions [7–9]. To improve the simulation accuracy, we need to conduct in-depth and systematic research on the impact of spatiotemporal resolutions on the simulation accuracy of urban flood models.

Rainfall is one of the key driving factors of urban hydrological processes and is of high spatiotemporal variability [10, 11]. Variations of the rainfall spatiotemporal resolutions can affect the rainfall-runoff response time and water yield in the hydrological model [11]. Therefore, it is important to simulate the hydrological response with an appropriate spatiotemporal resolution of rainfall [12, 13]. A large number of studies have proved that for small urban catchments, urban flood simulation should use the rainfall data on at least 1–15 min time resolution and 100–1000 m spatial resolution [14–16]. Bruni et al. [17] analyzed the relationship between the urban catchment area and the required spatiotemporal resolutions of rainfall data and showed that for small urban catchments with less than 700 hectares, the urban hydrological simulation requires the rainfall data with at least a 5 min time resolution and a 1.7 km spatial resolution. In addition, the sensitivity of different hydrological models to the spatiotemporal resolutions of rainfall differs significantly, with the physical model being more sensitive than the conceptual model [18–20]. Aronica et al. [21] found that the Storm Water Management Model (SWMM) is more sensitive to rainfall temporal resolution than hydrological parameters. Meselhe et al. [22] compared the HMS (hydrologic modeling system) conceptual model with the physics-based hydrological model MIKE SHE. They found that the latter is more sensitive to rainfall temporal resolution. Gires et al. [23] found that the 1D/2D (one-dimension/two-dimension) coupled model, Multi-Hydro, is more sensitive to rainfall variability than the simpler 1D model. Many other studies also found that in small urban catchments, the time-scale variation of rainfall data has a greater impact on urban hydrodynamic models [24, 25]. To sum up, for a densely built and highly impermeable urban catchment, the output of the urban flood model is very sensitive to the rainfall spatiotemporal resolutions, and the bias of output increases obviously as the resolutions decrease.

Most urban flood models are distributed hydrological models based on grid data. The hydrological process is also sensitive to the spatial distribution of the underlying surface of the watershed [9]. The computational efficiency of the model and the accuracy of the simulations are often affected by the spatial resolution of the grid and the accuracy of input data [26, 27]. In the early 1960s, the importance of the spatial resolution of input data is recognized by scholars [28, 29]. Since then, many scholars have studied the spatial resolution of hydrological models. They found that the conclusions are different in different study areas. The model of high spatial resolution can lead to the systematic underestimation of peak flow [30, 31]. Ichiba et al. [27] found that increasing spatial resolution can reduce peak flow and total flow. The effect of spatial resolution of the grid on model performance is nonlinear, and higher mesh accuracy does not necessarily lead to better simulation. Zhang and Montgomery [32]

found that a spatial resolution of 10 m can greatly improve the simulations than 30 m and 90 m, while that of 2 m or 4 m only improves the model slightly. The above studies show that the difference in spatial resolutions will change the loss of underlying surface information and the complexity of the surface runoff between adjacent grids, which has a nonlinear impact on the simulations. Therefore, in the modeling process of the urban flood, the appropriate spatial resolution should be selected according to the comprehensive analysis of the calculation characteristics of the model, the characteristics of the underlying surface of the study area, and the accuracy of the input data.

To sum up, there have been extensive studies on evaluating the accuracy of urban flood simulation unilaterally from the temporal resolution of rainfall data or spatial resolution of the grids. These studies show that the effects of temporal resolution and spatial resolution on the simulation accuracy are obvious and nonlinear. So, the compound effects of grid spatial resolution and rainfall temporal resolution on the simulation accuracy should be more complicated. However, there are few studies on this aspect. To this end, we take the typical flooded area in Dongguan, China, as the study area (Section 2.1) and collect topographic and sewer network data (Section 2.2). The distributed urban flood model IFMS Urban (Section 3.1) is used to construct the coupling model of the 1D urban drainage network model and 2D surface hydrodynamic model in the study area, and the model is validated by using the high temporal resolution rainfall data and observed historical inundation events (Sections 2.2 and 3.3). Then, we explore the effects of rainfall temporal resolution and model spatial resolution on the maximum inundation water depth and the submerged water depth hydrograph based on five temporal resolutions of rainfall input and four spatial resolutions(Sections 4.1 and 4.2). Furthermore, we analyze the compound effects of different spatiotemporal resolutions on the accuracy of urban flood simulations (Section 4.3). Conclusions can be found in Section 5.

2. Study Domain and Data

2.1. Study Domain. The study site, Guancheng District of Dongguan City, is located on the south-central east coast of the Pearl River estuary, Guangdong Province, China (within E119°31′-114°15′, N22°39′-23°09′). It covers approximately 13.31 km^2 (Figure 1(a)). The study area represents a typical urban area with a density of human structures such as houses, commercial buildings, and roads. When the city is hit by heavy rainfall, the topographic characteristics of the study area make the flood converge to the middle from the sides south and north and finally discharge into the Dongyin Canal in the east.

2.2. Data Collection

2.2.1. Topographic Data. The basic geographic data provided by the Urban Planning Bureau of Dongguan City (UPBDC) included a remote-sensing image and a digital elevation model (DEM). The resolution of the remote-sensing and
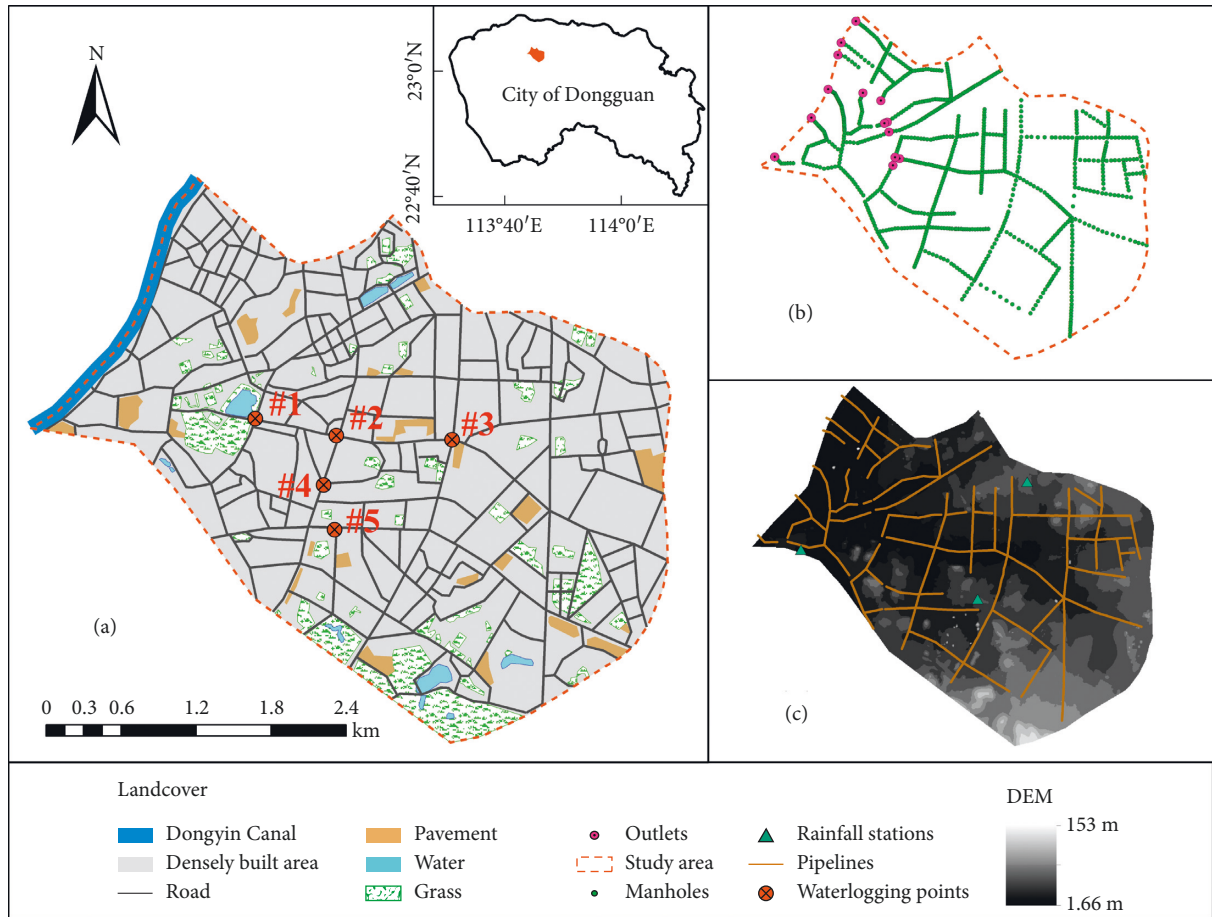
FIGURE 1: (a) Location and landcover conditions of the study area in which five numbers from #1 to #5 labeled with distribution of waterlogging points: #1 People's Park; #2 Dongzong Road; #3 Yinshan Street; #4 Dongcheng West Road; #5 Yonghuating. (b) shows the sewer network with manholes and outlets. (c) Top view of the DEM overlaid with the pipeline and rainfall station layer of the study area.

DEM are 5 m and 0.5 m, respectively. The former was used to distinguish the land use types of the underlying surface, and the latter was used to calculate the elevation and slope of the 2D grid.

2.2.2. Sewer Network Data. The sewer network data (Figures 1(b) and 1(c)) that were obtained from UPBDC is mainly based on the combined system. Most of the pipelines do not meet the design return period of one year, and most of the pipelines are less than 1000 mm in diameter, which is easy to cause waterlogging in the lower terrain.

2.2.3. Rainfall Data. In this research, two rainstorm events that occurred on August 30, 2018, and May 7, 2015, were used for model calibration and impact study of temporal and spatial scale, respectively. The maximum 24-hour cumulative rainfall of the two rainstorm events exceeded 50 mm, resulting in waterlogging in the study area. Three rainfall stations, which collect rainfall data at an interval of every 5 min, are located in and around the study area (Figure 1(c)). The rainfall of 10 min, 15 min, 30 min, and 1 h temporal scale was accumulated from the rainstorm of May 7, 2015.

Meteorological Bureau of Dongguan City provided the corresponding rainfall records.

2.2.4. Observed Historical Inundation Events. Generally, it is difficult to calibrate and validate the urban inundation model due to a lack of detailed observation of inundation events [2]. Therefore, in many cases, either a partial calibration/validation of the model or an indirect validation/verification based on testimonial reports is sought [33, 34]. In this research, the process of inundation depth in the inundation area in Yonghuating, Dongcheng Road West, and Dongzong Road on August 30, 2018, was observed for the calibration and verification of the urban flood model. The data on maximum inundation depth and distribution of inundation area on May 7, 2015, were collected and released by the Water Authority of Dongguan City.

3. Methodology

3.1. IFMS Urban. IFMS Urban couples the SWMM with a 2D surface hydrodynamic model that is conducted based on an adaptive grid and finite volume method, which can automatically identify the region with a large parameter

gradient and the boundary between dry and wet, adjust the grid size, accurately simulate the dynamic change of water flow propagation, and can be applied to the actual flood simulation [35]. The IFMS Urban efficiently calculates the urban flood process in the complex urban area with frequent waterlogging and achieves good calculation accuracy, which provides technical support for this paper.

3.1.1. 1D Urban Drainage Network Model.

The urban drainage system consists of water inlets, drainage pipes, drainage pumping stations, and river channels at the outlets of the pipe network. The 1D model can use three methods of dynamic wave method, kinematic wave method, and steady flow method to calculate the drainage pipeline confluence. The governing equation is specifically the following formulas:

$$\frac{\partial Q}{\partial x} + \frac{\partial A}{\partial t} = 0, \tag{1}$$

where Q is the discharge, A is the discharge section area, t represents the time, and x represents the distance.

$$gA\frac{\partial H}{\partial x} + \frac{\partial \left(Q^2/A\right)}{\partial x} + \frac{\partial Q}{\partial t} + gAS_f = 0, \tag{2}$$

where H represents the water depth, g represents the gravitational acceleration, and S_f is the slope gradient of friction resistance.

3.1.2. 2D Surface Hydrodynamic Model.

In order to establish a special well-balanced scheme technique for dealing with source term due to bottom topography constructed, this paper develops a well-balanced Godunov-type scheme of the second-order accuracy for 2D shallow water equation with mesh. As above, the MUSCL method is used to reconstruct the variable values on both sides of the unit interface $U_{i+1/2}^{L/R}$ and the Roe format is selected to solve interface flux in the evolutionary step. Regarding the discretization of the source term, the bed slope term is discretized by characteristic classification, and the resistance source term is discretized implicitly.

The 2D shallow water equation of depth-averaged can be abbreviated as follows:

$$\frac{\partial h}{\partial t} + \frac{\partial hu}{\partial x} + \frac{\partial hv}{\partial y} = 0,$$

$$\frac{\partial hu}{\partial t} + \frac{\partial}{\partial x}\left[hu^2 + \frac{1}{2}gh^2\right] + \frac{\partial huv}{\partial y} = S_x, \tag{3}$$

$$\frac{\partial hu}{\partial t} + \frac{\partial hvu}{\partial x} + \frac{\partial}{\partial y}\left[hv^2 + \frac{1}{2}gh^2\right] = S_y,$$

where h represents the water depth, u is the flow velocity of x-direction, v is the flow velocity of y-direction; S_x and S_y are the source terms.

3.1.3. Algorithm of Coupled Model.

The 1D urban drainage network model and 2D surface hydrodynamic model are coupled by calculating the exchange water volume, which is substituted into their respective model for calculation and update to the next step. The exchange water volume can be calculated through the following equation:

$$Q = M\left(H_{\text{node}} - H_{\text{surface}}\right)W_{\text{crest}}\sqrt{2g\left|H_{\text{node}} - H_{\text{surface}}\right|}$$
$$\cdot \frac{\left|H_{\text{node}} - H_{\text{surface}}\right|}{\left|\max\left(H_{\text{node}}, H_{\text{surface}}\right) - H_g\right|}, \tag{4}$$

where H_{Surface} is the head of land surface, H_{node} is the head of drainage pipeline, M is the discharge coefficient, W_{crest} is the width or perimeter of manhole, and H_g is the surface elevation.

3.2. Evaluation of Modeling Results.

The calibration process has been evaluated using error indicators including Nash-Sutcliffe efficiency coefficient (NSE), maximum inundation depth relative error (RE_P), and maximum inundation depth appearance time absolute error (AE_T) for the simulated and observed values. The error indicators are formulated as in the following equations:

$$\text{NSE} = 1 - \frac{\sum_{i=1}^{N}\left(q_i^{\text{obs}} - q_i^{\text{sim}}\right)^2}{\sum_{i=1}^{N}\left(q_i^{\text{obs}} - \overline{q}^{\text{obs}}\right)^2}, \tag{5}$$

where q_i^{obs} is the observed value of an event i, q_i^{sim} is the simulated value of an event i, N is the number of observed values, and $\overline{q}^{\text{obs}}$ is the average of observed values.

$$\text{RE}_P = \frac{\left|q_P^{\text{obs}} - q_i^{\text{sim}}\right|}{q_P^{\text{obs}}} \times 100\%, \tag{6}$$

where q_P^{obs} is the observed value of maximum inundation depth, q_P^{sim} is the simulated value of flood peak maximum inundation depth.

$$\text{AE}_T = T_P^{\text{obs}} - T_P^{\text{sim}}, \tag{7}$$

where T_P^{obs} is the observed value of maximum inundation depth appearance time, and T_P^{sim} is the simulated value of maximum inundation depth appearance time.

In order to compare the results from different rainfall temporal resolution and 2D grid scale and also to compare the effect of the composition of the rainfall temporal resolution and 2D grid scale, different measures were used. In addition to the common error indicators such as RE_P and AE_T, we also used the coefficient of determination (R^2) to compare the correlation of two inundation depth series. The closer R^2 to 1, the higher the correlation between the two inundation depth series. R^2 is specifically as follows:

$$R^2 = \frac{\sum\left(Y_A - \overline{Y_A}\right)^2 - \sum\left(Y_A - Y_B\right)^2}{\sum\left(Y_A - \overline{Y_A}\right)^2}, \tag{8}$$

where Y_A is the value of the inundation depth series A, $\overline{Y_A}$ is the mean value of the inundation depth series A, and Y_B is the value of the inundation depth series B.

3.3. Model Validation

3.3.1. Model Setup. The model is set up based on the drainage network. The study area is generalized into 999 pipes, 1011 manholes, and 12 outlets. The parameters for the model include the section size of the drainage network, the two-dimensional (2D) grid elevation, the subcatchment slope, and the 2D grid pervious surface ratio. The section parameters of the drainage network are obtained from the actual survey data. The 2D grid elevation and the subcatchment slope are determined based on the DEM data. The 2D grid pervious surface ratio is extracted from the remote sensing images over the study area. The empirical parameters of the model include the impervious area Manning's roughness, the depression storage for the pervious area, and the infiltration related parameters. The empirical parameters are calibrated according to the SWMM user manual and the hydrogeological characteristics of the study area, as shown in Table 1. The rainwater in the study area flows through the pipeline by gravity and is finally discharged into the Dongyin Canal. According to historical data, the water level of the Dongying Canal is low and does not affect the outflow of the pipeline. Therefore, the model boundary outflow condition is set to free outflow. The modeling time step is set to 20 s, and the total simulation time is 24 h. The setting can ensure that the pipeline network system has no inflow. The accumulated water in the pipeline has been emptied when the simulation ends under each input rainfall condition.

3.3.2. Model Validation. In this section, we validate the IFMS Urban model by using the rain and flood event on August 30, 2018, as an example. The rainfall poured heavily in the study area from 11:00 to 16:00, within which rainfall amount accounted for over 80% of the total in the day. Thus, a 5 h storm event spanning from 11:00 to 16:00 was used as model rainfall data.

A summary of the simulations performed is given in Figure 2 and Table 2. The model can well predict the flood occurring and receding at the typical waterlogging points of Yonghuating, Dongcheng West Road, and Dongzong Road. These results confirm that the simulation of flood processes is reasonably well, with NSE for all waterlogging points exceeding 0.75. The RE_P and AE_T ranged approximately from 11.11% to 17.50% and from 5 min to 12 min, respectively. All of them are within the allowable error range required by the Standard for Hydrological Information and Hydrological Forecasting of China. Furthermore, the results of Dongcheng West Road are better than other waterlogging points, with NSE, RE_P and AE_T being 0.86, 11.11%, and 5 min, respectively. In conclusion, the above results show that the parameters of the model are set reasonably, and the model has good applicability in the study area. The model is reliable and is suitable for the subsequent analysis.

Table 1: Values of empirical parameters.

Number	Parameter	Value
1	Manning's roughness for impervious area	0.013
2	Manning's roughness for pervious area	0.230
3	Depression storage on impervious area (mm)	2.500
4	Depression storage on pervious area (mm)	5.000
5	Roughness of pipe	0.014
6	Maximum infiltration rate (mm·h^{-1})	104.000
7	Minimum infiltration rate (mm·h^{-1})	12.000
8	Attenuation coefficient	8.500
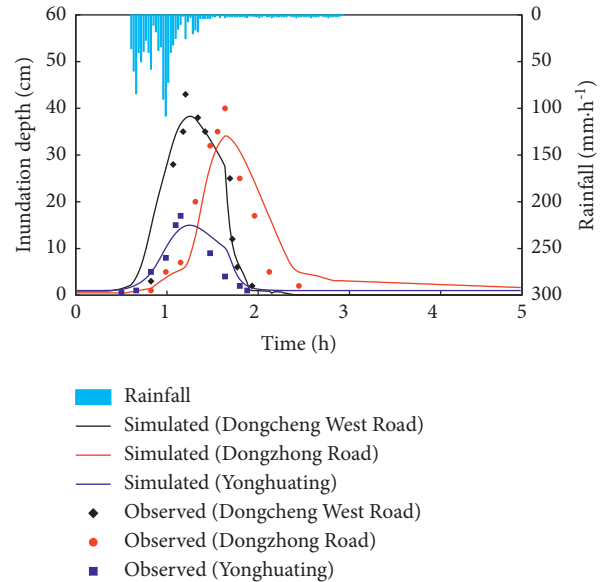
Figure 2: Simulation results of flood processes at typical waterlogging points.

Table 2: Simulation error statistics.

	Dongcheng west road	Yonghuating	Dongzong road
NSE	0.86	0.78	0.80
RE_P	11.11%	17.64%	17.50%
AE_T/min	5	8	12

4. Results and Discussion

4.1. Effect of Rainfall Temporal Resolution. Table 3 and Figure 3 show the maximum inundation water depth and RE_P at five typical waterlogging points under five temporal resolutions. With the increase of rainfall temporal resolution, the maximum inundation water depth gradually decreases and RE_P increases. However, the effect of the rainfall temporal resolution on the maximum inundation water depth is small on the whole. Increasing the time step of rainfall input from 5 min to 30 min, the variation range of the maximum inundation water depth at the five waterlogging points is within 5 cm, while the variation range of RE_P is less than 8%. RE_P at waterlogging points based on the 1 h temporal resolution is larger than the other four temporal resolutions, with that in Dongcheng West Road being the largest (13.73%). The errors of the maximum inundation

TABLE 3: Maximum inundation water depth at five typical waterlogging points under five temporal resolutions.

Waterlogging points	Maximum inundation water depth (cm)					
	Observation	5 min	10 min	15 min	30 min	1 h
Dongcheng west road	60	58.81	58.17	57.97	56.75	53.19
Dongzong road	25	23.65	23.61	23.34	23.21	22.19
Yonghuating	30	28.20	28.19	28.15	28.05	25.88
People's park	17	16.69	16.62	16.51	16.21	15.36
Yinshan street	22	21.17	21.11	20.90	20.84	20.12
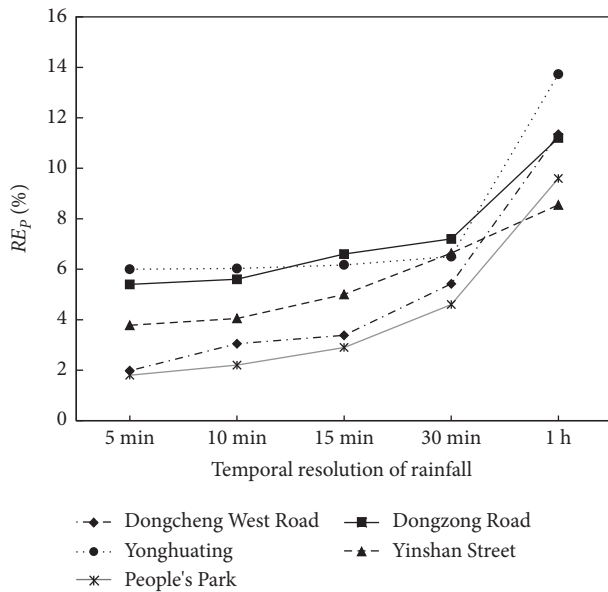
FIGURE 3: Relative errors of maximum inundation water depth (RE_P) at five typical waterlogging points under five rainfall temporal resolutions.

water depth at the waterlogging points increase with the temporal interval of rainfall input, but the overall increase is not large.

The occurrence time of the maximum inundation water depth (referred to as the peak time of inundation water depth) at waterlogging points has a high correlation with the temporal resolution of rainfall input. As shown in Table 4, with the increase of the temporal resolution of rainfall input, the time between the peak time of inundation water depth at waterlogging points and the rainfall peak time (referred to as the lag time) also increases. The lag time of the 10 min and 15 min rainfall input intervals at the five waterlogging points is short (only 0–3 min). The lag time of the 30 min and 1 h rainfall input intervals changes a lot. Compared with the 5 min time interval, the lag time is, respectively, extended by 7–13 min and 23–36 min.

With the increase of rainfall input interval, the correlation between the submerged water depth and the rainfall at waterlogging points decreases. The deformation degree of the submerged water depth hydrograph at waterlogging points becomes larger. Taking the waterlogging point, Yonghuating, as an example (as shown in Figure 4), the rainfall peaks twice at about 1 h and 2 h. Correspondingly, there are two obvious waterlogging processes in 1-2 h and

TABLE 4: Lag time of maximum inundation depth to rainfall peak under five temporal resolutions.

Waterlogging points	Lag time (min)				
	5 min	10 min	15 min	30 min	1 h
Dongcheng west road	63	63	66	76	90
Dongzong road	80	83	83	93	116
Yonghuating	30	33	36	43	63
People's park	60	63	63	70	83
Yinshan street	63	63	66	70	86
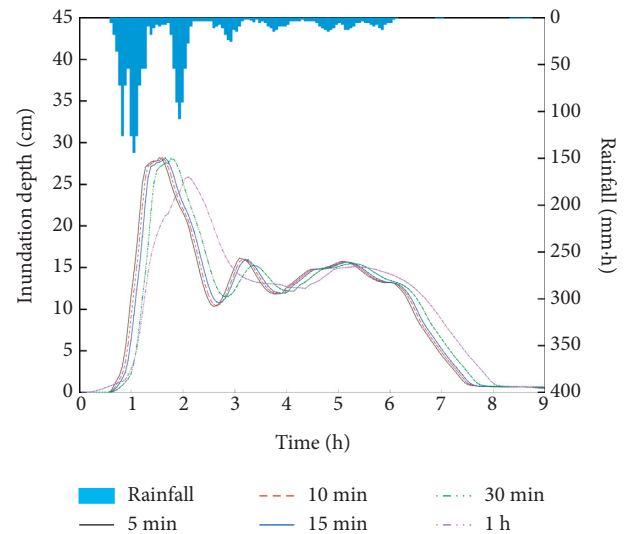
FIGURE 4: The hydrographs of inundation under five rainfall temporal resolutions at Yonghuating.

3-4 h under the 5 min, 10 min, 15 min, and 30 min rainfall temporal resolutions at Yonghuating, and the results have a good correlation with the rainfall observation. The submerged water depth hydrograph under the 1 h rainfall temporal resolution has only one obvious waterlogging process. Compared with the waterlogging processes under other temporal resolutions, the maximum inundation depth is lower and the corresponding occurrence time is later. Using the coefficient of determination (R^2), this study further analyzes how well the shape of submerged water depth hydrographs under 10 min, 15 min, 30 min, and 1 h rainfall input resolutions at five typical waterlogging points match that of the hydrograph under the 5 min resolution (Figure 5). With the increase of temporal interval, the coefficient of determination decreases, and the difference between submerged water depth hydrographs increases. The
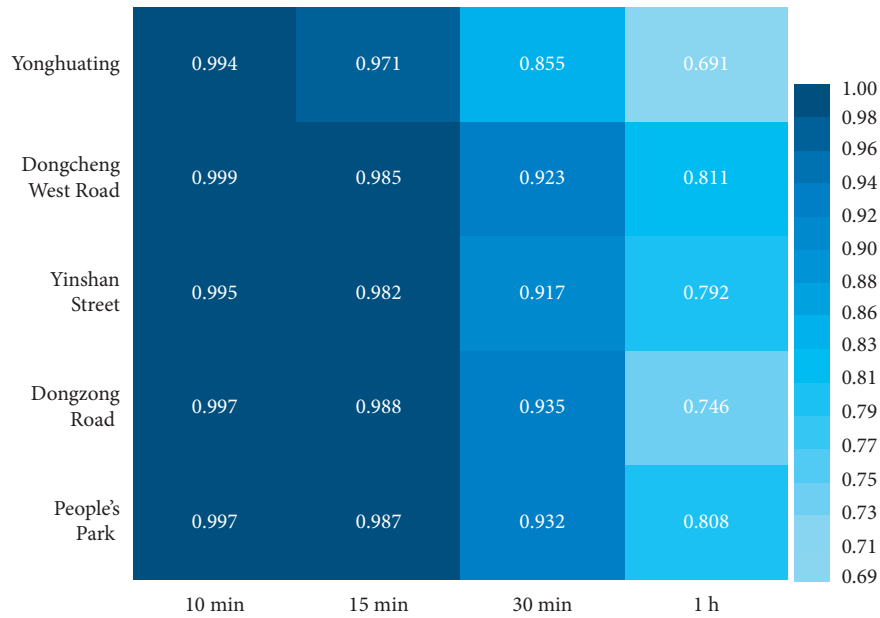
Figure 5: The coefficients of determination of inundation hydrograph between four rainfall temporal resolutions and the 5 min resolution.

shape for the 10 min and 15 min resolutions is in good agreement with the submerged water depth process under 5 min resolution, and R^2 are all higher than or equal to 0.97. However, there are certain differences of hydrographs between 1 h and 5 min resolutions, and the R^2 is only 0.69–0.81.

4.2. Effect of the 2D Spatial Resolution of Model Grids. The study area is used as the meshing area to generate four kinds of mixed 2D meshes of triangles and quadrilaterals with spatial scales of 50 m × 50 m, 100 m × 100 m, 150 m × 150 m and 200 m × 200 m. According to the remote sensing images, we analyze the land use type of the underlying surface and set the impervious area and roughness of the simulations under four spatial resolutions. The grid elevations for the four spatial resolutions are all obtained by inverse distance weighted interpolation based on a DEM with a resolution of 5 m.

As shown in Table 5 and Figure 6, the effect of grid spatial resolution on the model simulation is nonlinear. It means that the smaller spatial resolution does not correspond to the higher accuracy of model outputs. With the increase of grid spatial interval, the maximum inundation depth decreases and the absolute error (AE) of the maximum inundation depth increases on the whole. When the grid spatial resolution is increased from 50 m to 150 m, the maximum inundation depth decreases, and its variation range is small. All AE is within 4 cm and RE_P is less than or equal to 6%, while those of the 200 m grid are larger than the other resolution simulations. The maximum inundation depths with a spatial resolution of 50 m at the five typical waterlogging points are all overestimated. Except for Yinshan Street, RE_P of the 50 m grid is higher than that of the 100 m grid at other four waterlogging points.

There are significant correlations between the slope and the grid spatial resolution of the catchments of waterlogging points and the hydrological characteristics. As the spatial resolution becomes larger, the calculation accuracy of the waterlogging point with large slope of catchment area decreases obviously. The DEM and flow direction of main roads in the study area and around each waterlogging point are shown in Figure 7. On one hand, the three areas of Yinshan Street, Dongzong Road, and People's Park are located in the low-lying central of the study area, where the rain and floods in the eastern, northern, and southern parts of the study area are concentrated. But due to the flat terrain from the Yinshan Street to the People's Park, the converged rain and floodwater cannot be discharged in time, resulting in waterlogging in the three areas. When the grid resolution is increased from 50 m to 200 m, the simulation results at Yinshan Street, Dongzong Road, and People's Park are less affected by the grid size. All AE is less than 3 cm and RE_P is less than 13%. On the other hand, small-scale rain and floods are gathering in the mountainous southeast of the study area, mainly located in Yonghuating and Dongcheng West Road. The slope in the catchment areas is larger than that in other waterlogging areas. When the grid resolution is increased from 50 m to 150 m, AE and RE_P in Yonghuating and Dongcheng West Road have a small variation range, while AE and RE_P at the 200 m grid have increased obviously, reaching 7.07–27.26 cm and 23.6–45.43%, respectively. In the urban flood model, the spatial grid is the basic unit of the runoff calculation of the model. The slope and other properties of the underlying surface have a direct impact on the runoff calculation. In this study, most of the study area is continuous urban hard ground or green space. With the increase of the spatial grid interval, the generalization of the terrain and underlying surface information is greater, and variation details of the urban terrain and

TABLE 5: Maximum inundation depth and AE (cm) at typical waterlogging points under four spatial resolutions.

Waterlogging points	Observed value of maximum inundation depth	50 m × 50 m		100 m × 100 m		150 m × 150 m		200 m × 200 m	
		Maximum inundation depth	AE	Maximum inundation depth	AE	Maximum inundation depth	AE	Maximum inundation depth	AE
Dongcheng west road	60	61.39	−1.39	60.98	−0.98	58.81	1.19	34.13	27.26
Dongzong road	30	30.55	−0.55	29.55	0.45	28.20	2.35	23.48	7.07
Yonghuating	25	27.25	−2.50	24.00	1.00	23.65	1.35	22.82	2.18
People's park	22	22.45	−0.45	21.39	0.61	21.16	0.84	19.15	2.85
Yinshan street	17	18.20	−1.20	17.50	−0.50	16.69	0.31	15.25	1.75
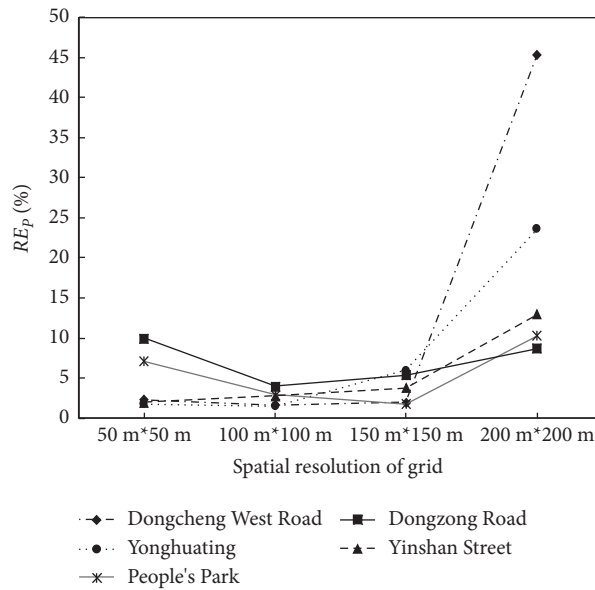
FIGURE 6: Variations of RE_P at typical waterlogging points under four grid spatial resolutions.

underlying surface are covered up. Therefore, the simulations at Yonghuating and Dongcheng West Road where there is larger slope are more affected by the spatial resolution.

4.3. The Compound Effect of Rainfall Temporal Resolution and Grid Spatial Resolution.

In this study, four rainfall temporal resolutions of 5 min, 10 min, 15 min, and 30 min are selected to be matched with three grid spatial resolutions of 50 m × 50 m, 100 m × 100 m and 150 m × 150 m. Thus, 12 experiments with different spatial and temporal resolutions are conducted. The IFMS Urban model is used to simulate the 12 experiments, and the compound effects of spatiotemporal resolutions on flood simulations have been compared and analyzed.

As shown in Figure 8, the effect of spatial resolution at typical waterlogging points is greater than that of rainfall temporal resolution. For the grids with different resolutions, with the increase of rainfall temporal resolution from 5 min to 30 min, the maximum inundation depth at typical waterlogging points has a small variation range, and RE_P is less than 3%. The effects of the 5 min, 10 min, and 15 min temporal resolutions are very close. For different rainfall temporal resolutions, with the increase of grid spatial interval, RE_P at typical waterlogging points greatly changes with nonlinear characteristics. For the waterlogging points of Dongcheng West Road and Yonghuating with a large slope, large grids have a larger influence on the simulation results, while for the flat Dongzong Road and People's Park, small grids have a larger influence on the simulation results.

In urban flood simulation, the finer spatiotemporal resolution does not mean more accurate simulation results. For the 50 m grids, the maximum inundation depth is overestimated under different rainfall temporal resolutions. The finer the temporal resolution is, the greater the overestimation is. At the five typical waterlogging points, RE_P with the spatiotemporal resolutions of 5 min and 50 m is relatively large, ranging from 1.8% to 10%. In contrast, the water depth range that decreases with the increase of rainfall temporal resolution is small. It is not enough to compensate for the overestimated water depth range under the high-precision grid and RE_P is still larger than that of the 100 m grid. For the grid of 100 m, the overall simulations are better than those of 50 m and 150 m. The 5 min × 100 m, 10 min × 100 m, and 15 min × 100 m resolutions can achieve
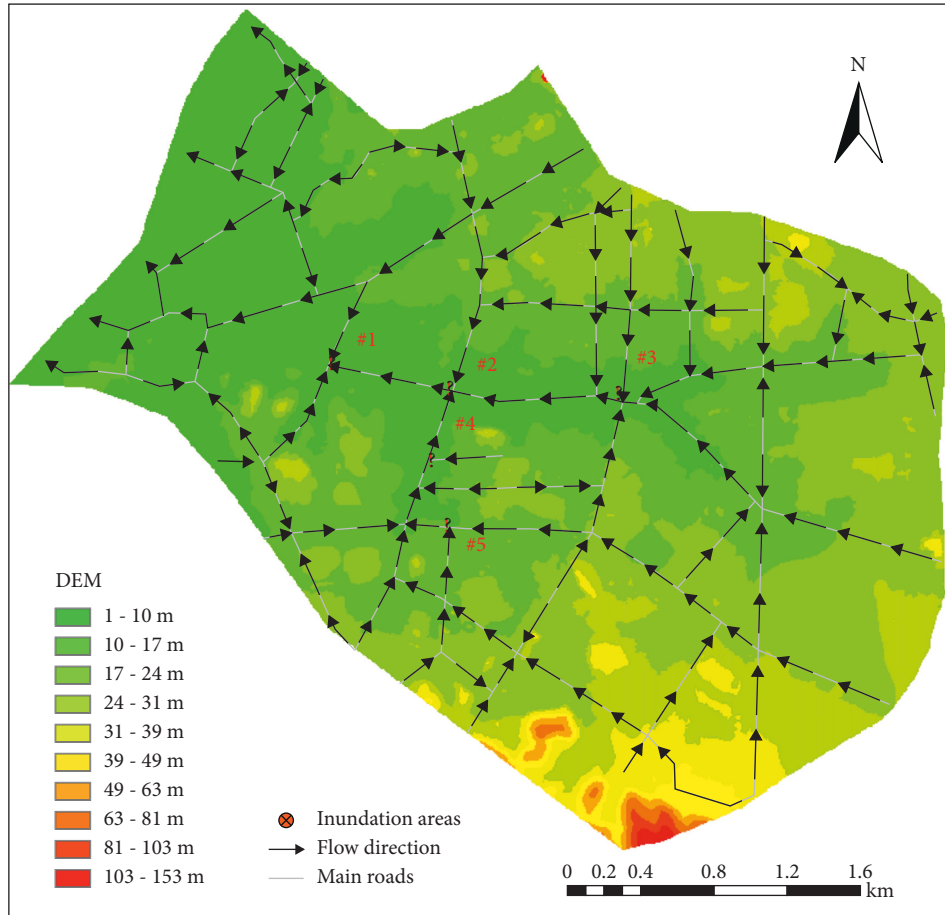
FIGURE 7: Topography and flow direction of main roads in the study area (The five waterlogging points numbered #1 to #5 are People's Park, Dongzong Road, Yinshan Street, Dongcheng West Road, and Yonghuating).

(a)

(b)

FIGURE 8: Continued.

(c)

(d)

(e)
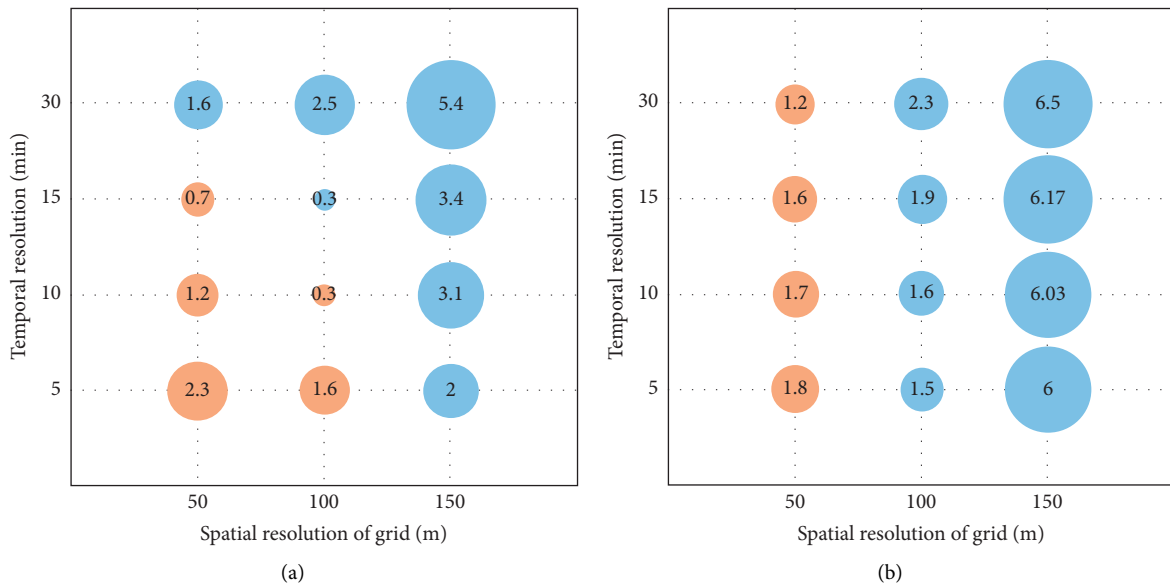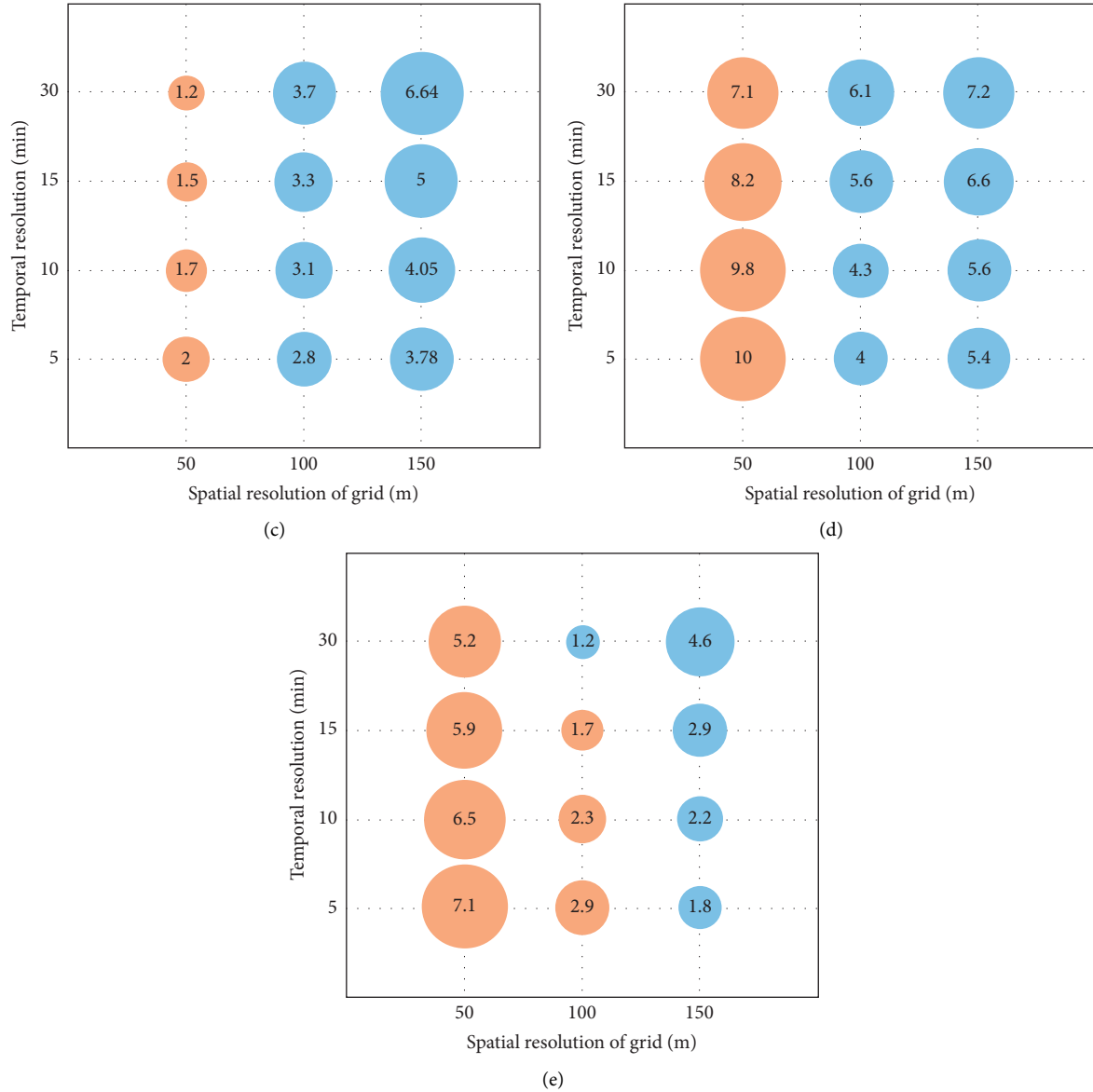
Figure 8: Bubble charts of the relative error of maximum inundation depth (RE_P) for 12 experiments with different rainfall temporal resolutions and grid spatial resolutions. The size of the bubble represents the range of RE_P. The yellow and blue colors represent that the simulated maximum inundation depth is higher and lower than the observation, respectively.

the best simulations at different typical waterlogging points, and their RE_P ranges from 0.3% to 6.1%. For the grid of 150 m, the maximum inundation depth of typical water-logging points is underestimated. With the increase of rainfall temporal resolution, the maximum inundation depth decreases and the RE_P increases. By judging the compound effect of rainfall temporal resolution and grid spatial resolution on the simulations, we find the simulation results are better with the 5 min, 10 min, or 15 min rainfall temporal resolution and the 100 m grid spatial resolution.

5. Conclusions

This study utilized the IFMS Urban model that couples SWMM and 2D hydrodynamic model to analyze the

response of the flood process of urban to different spatio-temporal resolutions. The typical waterlogged area, Guan-cheng District of Dongguan City, China, was selected as the study area. The variation characteristics of maximum in-undation water depth and inundation process were inves-tigated based on five rainfall temporal resolutions and four grid spatial resolutions. The main conclusions are as follows:

With the increase of rainfall temporal resolution, the accuracy of the simulated maximum inundation depth decreases, the time interval between the occurrence of the maximum inundation depth and the peak time of rainfall is prolonged, and the shape of the submerged water depth hydrograph changes greatly, which means the inundation process correlation with the rainfall process is decreased. Compared with the temporal resolution of 5 min, 10 min,

15 min, or 30 min, the 1 h temporal resolution has a greater influence on urban flood simulation.

For the effect of grid spatial resolution, the effect of grid resolution on urban flood simulation is nonlinear. With the increase of grid interval, the maximum inundation depth decreases and RE_P presents an overall increasing trend. For the fine 2D grids, the maximum inundation depth is overestimated, and the simulations at the waterlogging points with larger slopes are more affected by the spatial resolution.

In this study, the grid spatial resolution has a greater effect on the simulations at typical waterlogging points than the rainfall temporal resolution. It is not the case that the finer spatial and temporal resolutions are, the higher the accuracy of the simulation will be. The simulations perform better with the 5 min, 10 min, or 15 min rainfall temporal resolution and 100 m grid spatial resolution. For the area with the large slope in the catchment areas, using a 2D grid with a smaller grid spatial interval can obviously improve the computational accuracy of the model.

In this study, we have not considered the influence of terrain slope and vertical structure on the urban flood model. In the future, we will focus on the mechanisms of the compound effect of the spatiotemporal resolutions, and on how the model accuracy is affected by the type and slope of underlying surface.

Data Availability

The rainfall records are provided by the Meteorological Bureau of Dongguan City. The data of maximum inundation depth and distribution of inundation area on May 7, 2015, were collected and released by the Water Authority of Dongguan City. The basic geographic data provided by the Urban Planning Bureau of Dongguan City included a remote-sensing image and a digital elevation model. The sewer network data was provided by the Urban Planning Bureau of Dongguan City.

Conflicts of Interest

The authors declare that they have no conflicts of interest to report regarding the present study.

Acknowledgments

References

[1] Z. Zheng, J. Gao, Z. Ma et al., "Urban flooding in China: main causes and policy recommendations," *Hydrological Processes*, vol. 30, no. 7, pp. 1149–1152, 2016.

[2] X. Wu, Z. Wang, S. Guo, W. Liao, Z. Zeng, and X. Chen, "Scenario-based projections of future urban inundation within a coupled hydrodynamic model framework: a case study in Dongguan city, China," *Journal of Hydrology*, vol. 547, pp. 428–442, 2017.

[3] X. Li and Y. Wang, "Construction of urban flood disaster emergency management system using scenario construction technology," *Computational Intelligence and Neuroscience*, vol. 2022, Article ID 8048327, 10 pages, 2022.

[4] Z. Li, Y. He, X. Lu, H. Zhao, Z. Zhou, and Y. Cao, "Construction of smart city Street landscape big data-driven intelligent system based on Industry 4.0," *Computational Intelligence and Neuroscience*, vol. 2021, Article ID 1716396, 11 pages, 2021.

[5] I. Emmanuel, H. Andrieu, E. Leblois, and B. Flahaut, "Temporal and spatial variability of rainfall at the urban hydrological scale," *Journal of Hydrology*, vol. 430-431, pp. 162–172, 2012.

[6] A. Gires, I. Tchiguirinskaia, D. Schertzer, A. Schellart, A. Berne, and S. Lovejoy, "Influence of small scale rainfall variability on standard comparison tools between radar and rain gauge data," *Atmospheric Research*, vol. 138, pp. 125–138, 2014.

[7] J. Cantone and A. Schmidt, "Improved understanding and prediction of the hydrologic response of highly urbanized catchments through development of the Illinois urban hydrologic model," *Water Resources Research*, vol. 47, no. 8, p. 8538, 2011.

[8] Z. Zhou, J. A. Smith, L. Yang et al., "The complexities of urban flood response: flood frequency analyses for the Charlotte metropolitan region," *Water Resources Research*, vol. 53, no. 8, pp. 7401–7425, 2017.

[9] X. Cao, H. Lyu, G. Ni, F. Tian, Y. Ma, and C. S. B. Grimmond, "Spatial scale effect of surface routing and its parameter upscaling for urban flood simulation using a grid-based model," *Water Resources Research*, vol. 56, no. 2, 2020.

[10] M. C. Ten Veldhuis, Z. Zhou, L. Yang, S. Liu, and J. Smith, "The role of storm scale, position and movement in controlling urban flood response," *Hydrology and Earth System Sciences*, vol. 22, no. 1, pp. 417–436, 2018.

[11] W. Schilling, "Rainfall data for urban hydrology: what do we need?" *Atmospheric Research*, vol. 27, no. 1–3, pp. 5–21, 1991.

[12] F. Fabry, A. Bellon, M. R. Duncan, and G. L. Austin, "High resolution rainfall measurements by radar for very small basins: the sampling problem re-examined," *Journal of Hydrology*, vol. 161, no. 1–4, pp. 415–428, 1994.

[13] H. Lyu, G. Ni, X. Cao, Y. Ma, and F. Tian, "Effect of temporal resolution of rainfall on simulation of urban flood processes," *Water*, vol. 10, no. 7, p. 880, 2018.

[14] G. Bruni, R. Reinoso, N. C. Van de Giesen, F. H. L. R. Clemens, and J. A. E. Ten Veldhuis, "On the sensitivity of urban hydrodynamic modelling to rainfall spatial and temporal resolution," *Hydrology and Earth System Sciences*, vol. 19, no. 2, pp. 691–709, 2015.

[15] V. P. Singh, "Effect of spatial and temporal variability in rainfall and watershed characteristics on stream flow hydrograph," *Hydrological Processes*, vol. 11, no. 12, pp. 1649–1669, 1997.

[16] R. Berndtsson and J. Niemczynowicz, "Spatial and temporal scales in rainfall analysis — some aspects and future perspectives," *Journal of Hydrology*, vol. 100, no. 1–3, pp. 293–313, 1988.

[17] F. Lobligeois, V. Andréassian, C. Perrin, P. Tabary, and C. Loumagne, "When does higher spatial resolution rainfall information improve streamflow simulation? an evaluation

using 3620 flood events," *Hydrology and Earth System Sciences Discussions*, vol. 10, no. 10, Article ID 12485, 2013.

[18] W.-Y. Yang, Z. Li, T. Sun, and G.-H. Ni, "Better knowledge with more gauges? Investigation of the spatiotemporal characteristics of precipitation variations over the Greater Beijing Region," *International Journal of Climatology*, vol. 36, no. 10, pp. 3607–3619, 2016.

[19] C. Obled, J. Wendling, and K. Beven, "The sensitivity of hydrological models to spatial rainfall patterns: an evaluation using observed data," *Journal of Hydrology*, vol. 159, no. 1–4, pp. 305–333, 1994.

[20] E. Cristiano, M. C. Ten Veldhuis, and N. Van de Giesen, "Spatial and temporal variability of rainfall and their effects on hydrological response in urban areas - a review," *Hydrology and Earth System Sciences*, vol. 21, no. 7, pp. 3859–3878, 2017.

[21] G. Aronica, G. Freni, and E. Oliveri, "Uncertainty analysis of the influence of rainfall time resolution in the modelling of urban drainage systems," *Hydrological Processes*, vol. 19, no. 5, pp. 1055–1071, 2005.

[22] E. A. Meselhe, E. H. Habib, O. C. Oche, and S. Gautam, "Sensitivity of conceptual and physically based hydrologic models to temporal and spatial rainfall sampling," *Journal of Hydrologic Engineering*, vol. 14, no. 7, pp. 711–720, 2009.

[23] A. Gires, A. Giangola-Murzyn, J.-B. Abbes, I. Tchiguirinskaia, D. Schertzer, and S. Lovejoy, "Impacts of small scale rainfall variability in urban areas: a case study with 1D and 1D/2D hydrological models in a multifractal framework," *Urban Water Journal*, vol. 12, no. 8, pp. 607–617, 2014.

[24] S. Ochoa-Rodriguez, L. P. Wang, A. Gires et al., "Impact of spatial and temporal resolution of rainfall inputs on urban hydrodynamic modelling outputs: a multi-catchment investigation," *Journal of Hydrology*, vol. 531, no. 2, pp. 389–407, 2015.

[25] L. Yang, J. A. Smith, M. L. Baeck, and Y. Zhang, "Flash flooding in small urban watersheds: storm event hydrologic response," *Water Resources Research*, vol. 52, no. 6, pp. 4571–4589, 2016.

[26] J. Dehotin and I. Braud, "Which spatial discretization for distributed hydrological models? Proposition of a methodology and illustration for medium to large-scale catchments," *Hydrology and Earth System Sciences*, vol. 12, no. 3, pp. 769–796, 2008.

[27] A. Ichiba, A. Gires, I. Tchiguirinskaia, D. Schertzer, P. Bompard, and M.-C. Ten Veldhuis, "Scale effect challenges in urban hydrology highlighted with a distributed hydrological model," *Hydrology and Earth System Sciences*, vol. 22, no. 1, pp. 331–350, 2018.

[28] J. Amorocho, "Discussion of "predicting storm runoff on small experimental watersheds"," *Journal of the Hydraulics Division*, vol. 87, no. 2, pp. 185–191, 1961.

[29] N. E. Minshall, "Predicting storm runoff on small experimental watersheds," *Journal of the Hydraulics Division*, vol. 86, no. 8, pp. 17–38, 1960.

[30] M. Eddy, *Storm Water Management Model Volume 1—Final Report*, Environmental Protection Agency, Washington, DC, USA, 1971.

[31] A. Goldstein, R. Foti, and F. Montalto, "Effect of spatial resolution in modeling stormwater runoff for an urban block," *Journal of Hydrologic Engineering*, vol. 21, no. 11, Article ID 06016009, 2016.

[32] W. Zhang and D. R. Montgomery, "Digital elevation model grid size, landscape representation, and hydrologic simulations," *Water Resources Research*, vol. 30, no. 4, pp. 1019–1028, 1994.

[33] N. M. Hunter, P. D. Bates, S. Neelz et al., "Benchmarking 2D hydraulic models for urban flooding," *Proceedings of the Institution of Civil Engineers-Water Management*, vol. 161, no. 1, pp. 13–30, 2008.

[34] B. Russo, D. Sunyer, M. Velasco, and S. Djordjević, "Analysis of extreme flooding events through a calibrated 1D/2D coupled model: the case of Barcelona (Spain)," *Journal of Hydroinformatics*, vol. 17, no. 3, pp. 473–491, 2015.

[35] W. Yu, J. Ma, Y. Yin, H. Yu, B. Wu, and J. Mu, "2D Hydrodynamic model based on adaptive grid," *China Flood & Drought Management*, vol. 32, no. 3, pp. 66–72, 2022.

Hindawi

Research Article

An Optimization Method for Enterprise Resource Integration Based on Improved Particle Swarm Optimization

Aifang Guo [ID], Lina Zhu, and Lingjie Chang

Department of Economy and Trade, Changzhi Vocational and Technical College, Changzhi 046000, China

Correspondence should be addressed to Aifang Guo; fenling123@163.com

An enterprise's development and growth are inextricably linked to rational and efficient resource integration and optimization. This study focuses on the reorganization and integration of industrial elements inside the firm from the standpoint of resource integration. The ideal resource integration strategy is investigated by integrating the industrial parts of a certain enterprise in order to increase the efficiency of project completion and lower enterprise expenses. The enterprise's internal material and human resources are limited, but it is frequently necessary to execute numerous activities at the same time, and each activity must meet multiple goals. This research investigates how to properly integrate and schedule resources while attaining different goals. This research proposes using an enhanced particle swarm optimization technique (IPSO) to combine firms' internal resources. In order to address the issue of uneven particle dispersion caused by random population initialization, IPSO incorporates chaos theory into particle population initialization. The logistic mapping sequence generates a huge number of particles, and the particles with the highest quality are chosen for initialization. This can increase particle quality, allowing particles to be spread equally during setup. In the late stage, the classic particle swarm optimization algorithm (PSO) has a slow convergence rate, causing the algorithm to readily slip into a local optimal solution. This research proposes a dynamic inertia weight update approach based on fitness value. In the later stages of the algorithm, this strategy can improve the convergence speed and quality of the global optimal solution, allowing the particles to do a global search and eventually identify the population's ideal solution. Furthermore, IPSO creates a fitness function depending on task completion time. IPSO is used to test the performance of an enterprise's resource integration case. Experiments show that the method utilized can swiftly locate the ideal solution, complete the integration, and optimization of enterprise resources in the shortest job completion time, and for the least amount of money.

1. Introduction

Rapid advancements in science and technology have resulted in rapid economic growth. Economic development also poses difficulties for the management and operation of various businesses. To stand firm in today's rapidly changing society, businesses must not only have a long-term development plan on the outside but also a reasonable and efficient resource integration mechanism on the inside. The ability of an enterprise to screen, acquire, and combine various heterogeneous resources in the process of operation, including both the macrolevel that the enterprise obtains resources from the external environment where it is located, and the internal the microlevel of resource allocation. Some academics divide enterprise resource integration capabilities

into macrolevel categories based on this. The macrolevel enterprise resource integration capabilities include enterprises' ability to reconstruct operating rules and predict corporate strategies and risks in advance, whereas the microlevel enterprise resource integration capabilities include enterprises' ability to allocate, stimulate, and combine various existing resources. Existing research has examined the factors that may influence the development of enterprise resource integration capabilities in various contexts. According to the resource-based viewpoint, an enterprise is a collection of resources that can be obtained in a variety of ways. Resources are an important factor in an enterprise's long-term development. If a company wants to gain a competitive advantage and establish a market presence, it must invest in valuable resources and management skills.

Unrepeatable strategic management resources that can assist companies in successfully managing their businesses and obtaining additional compensation. At the moment, many scholars support the theory of resource-based view, and most studies are aimed at the impact of a specific type of enterprise's own resources on enterprise performance. Many of the results of the experimental analyses are consistent with resource-based theory. The uniqueness and nonreplicability of resources can play a role in the operation of businesses, forming competitive advantages and determining enterprise performance. Each enterprise's management resources are unique, and they have varying degrees of importance at each stage of the enterprise's operation. It can be defined as the various human, financial, and material resources that business managers manage in their daily operations. The good operation of the enterprise's resources can achieve the management goals of the enterprise.

Enterprise managers with varying management capabilities deal with their management resources in various ways. Reasonable resource allocation and utilization can result in satisfactory operational results. According to reference [1] the materials owned by the enterprise cannot directly create performance and obtain benefits for the enterprise. Professional resource integration talents, on the other hand, can integrate the enterprise's static resources and generate benefits for the enterprise. Differences in management resources will result in differences in resource allocation efficiency, resulting in differences in corporate performance. According to reference [2], each company has distinct management resources and management employees with different talents. As a result, each business will develop its own management style. This type of management disparity resulting from resource differences will have an impact on the company's performance. Firms with a wealth of management resources outperform their competitors. External mergers and acquisitions by businesses, according to reference [3], might boost a company's ability to manage resources swiftly. The outside offers fresh resources and management strategies to the company, which will boost the company's ability to adapt to changes in the external environment while also promoting its growth. Rich management resources, according to reference [4], can assist businesses optimize and alter their organizational structure to react to changing external market conditions. At the same time, businesses can create long-term plans and alter their management practices as needed. Reference [5] demonstrates that firms can strengthen their market position by fully utilizing management resources. To summarize, resources play an essential role in the development of enterprises, and management resources play a positive function in enhancing firm performance, according to resource-based theory. The better the managerial resources, the better the company's performance.

Enterprise resource management optimization's ultimate goal is to maximize the company's benefits. To optimize earnings, different companies have different criteria. It mostly entails optimizing earnings and reducing the time it takes to execute tasks. To do this, the enterprise's material and human resources must be integrated and dispatched in a

reasonable manner. Enterprise resource integration and scheduling are NP-complete problems [6, 7]. Particle swarm algorithms [8–10], ant colony algorithms [11–13], simulated annealing algorithms [14–16], and genetic algorithms [17–19] are currently available that can solve NP-complete problems. The PSO algorithm has the advantages of fast convergence speed, easy operation, and the algorithm is convenient for global optimization, but it also has disadvantages such as easy to fall into local optimum and low search accuracy. Aiming at these problems, this paper proposes an IPSO algorithm, and applies it to the instance of enterprise resource integration and scheduling. In order to verify the performance of the method used in this paper, the experimental results obtained through simulation experiments show that the IPSO algorithm has a good effect on solving the problem of enterprise resource integration.

2. Information Construction of Enterprise Resource Management

2.1. Enterprise Resource Management Platform. Business resources are not only the most significant aspect of an enterprise's internal environment, but they are also the prerequisites for enterprise resource integration. Enterprise management is now completely reliant on computers, and the advancement of information technology has expedited the reform of internal management and resource management in businesses. As a result, a series of information systems focused on the integration and deployment of enterprise resources have emerged. The system can help with resource integration and give a platform for all employees to quickly acquire tasks and resources. Figure 1 depicts the enterprise resource integration optimization platform's design structure.

Figure 1 depicts a three-tier architecture for an enterprise resource integration platform. The acquisition layer gathers the data that the system requires. The resource integration layer supports various resource release and interface negotiation models, as well as evaluating and classifying the released data before storing it in various databases. To achieve intelligent business resource integration, the resource application layer executes application processing on diverse enterprise information resources.

2.2. Optimization of Enterprise Resource Integration. Optimizing enterprise resource integration mainly starts from four aspects: resource creation, resource use, integration, and effect evaluation. The relationship and interaction of these four aspects are shown in Figure 2.

(1) Theory is an important basis for guiding actual production. Constructivist theory mainly emphasizes the initiative and situational nature of resource integration. Resource integration is not a stimulus to passively receive information, but to actively process external information according to the corporate background. When the resource content is related to the needs of the enterprise, the enterprise should propose appropriate resource integration and
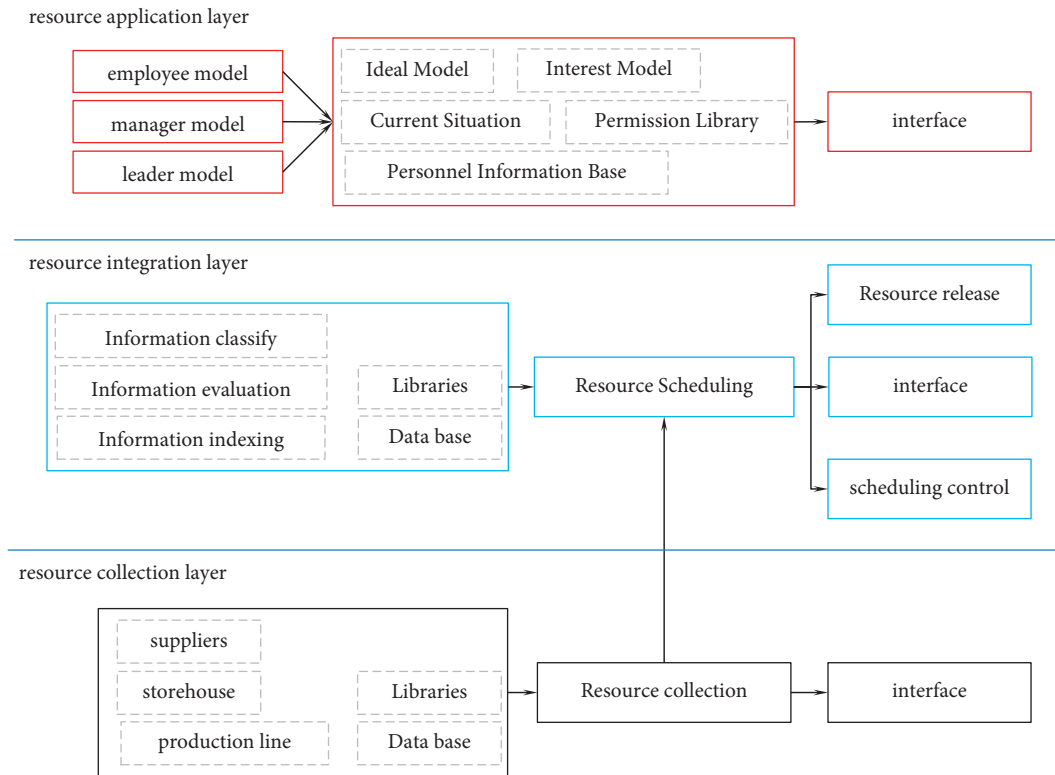
FIGURE 1: Architecture of enterprise resource integration platform.
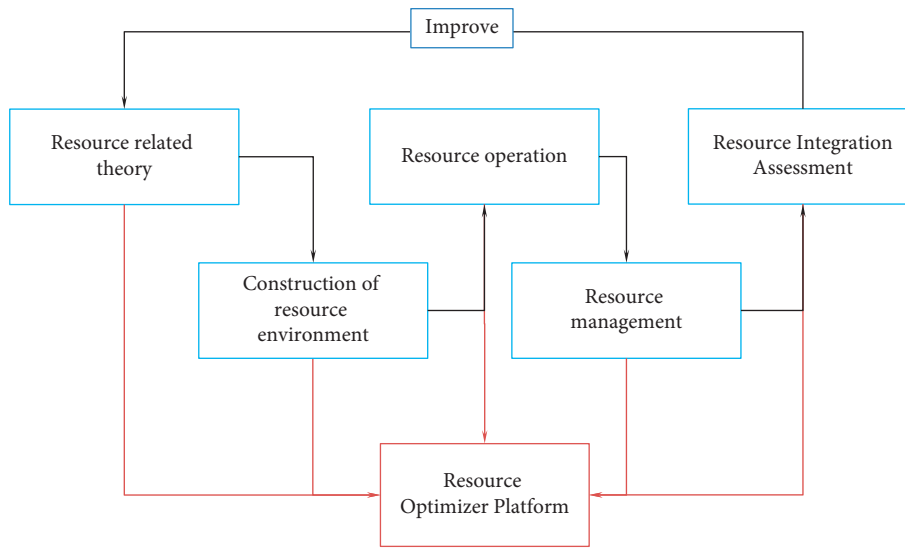
FIGURE 2: Optimization of enterprise resource integration.

allocation strategies to deal with various tasks. The resource integration dependence theory mainly emphasizes that the survival of the entire enterprise organization needs to absorb resources from the surrounding environment, and the interaction between the organization and the control resources in other environments is carried out.

(2) Resource creation. Resource creation should take enterprise managers as the main body and employees'

needs as the fundamental starting point, so as to encourage employees, managers, and leaders to work together. Build a resource environment dominated by service resources to ensure the reliability of resources, thereby providing guarantees for sustainable development of resources.

(3) Independent integration management includes user information maintenance, resource information maintenance, and integration strategy. User

information maintenance requires periodic updates and confidentiality of information. Enterprises need to set confidential information goals, formulate information integration plans, determine integration progress, and select integration resources to achieve self-maintenance. Resource information maintenance is to store and update resource information. Integrate and optimize resources based on integration strategies.

(4) Evaluation is the guarantee for resource integration. With the goal of resource integration and optimization, the design evaluation process is shown in Figure 3. Figure 3 shows that evaluation is an important indicator to measure the rational integration of resources and is the driving force behind the integration of resources and information within an enterprise. To evaluate based on the integration of platform resources, it is not only necessary to analyze each link but also to evaluate the effect of self-integration of employee information in a timely manner.

3. Enterprise Resource Integration and Optimization of IPSO Algorithm

3.1. Introduction to PSO. Suppose a population X is searched in a D-dimensional space, and each population consists of H particles. Each particle in the population can be represented as a solution to the problem. $X_i(t)$ to represent the position of the i-th particle in the t-th iteration of the population. $V_i(t)$ is the velocity of the particle at the t-th iteration in the population. S_i represents the self-optimal solution of the i-th particle, and S_{best} represents the optimal solution of the entire particle population. The mathematical expression formula of each variable is as follows:

$$
\begin{aligned}
X(t) &= \{X_1(t), X_2(t), \ldots, X_H(t)\}, \\
X_i(t) &= (x_{i1}(t), x_{i2}(t) \ldots, x_{iD}(t)), \\
V_i(t) &= (v_{i1}(t), v_{i2}(t) \ldots v_{iD}(t)), \\
S_i &= (S_{i1}, S_{i2}, \ldots, S_{iD}), \\
S_{best} &= (S_1, S_2, \ldots, S_D).
\end{aligned}
\tag{1}
$$

PSO updates the state of the particle through the particle's velocity and position; equation (2) is the velocity update expression, and equation (3) is the position update expression:

$$
v_i(t+1) = wv(t) + e_1 g_1 (S_i(t) - x_i(t)) + e_2 g_2 (S_{best} - x_i(t)),
\tag{2}
$$

$$
x_i(t+1) = x_i(t) + v_i(t+1),
\tag{3}
$$

where w is the inertia weight coefficient, which is used to determine how much velocity is retained after the last iteration; $e1$, $e2$ are the learning factors of the algorithm. Usually, both parameters are set to 2. $g1$, $g2$ are random numbers whose values are between [0, 1]; t is the number of
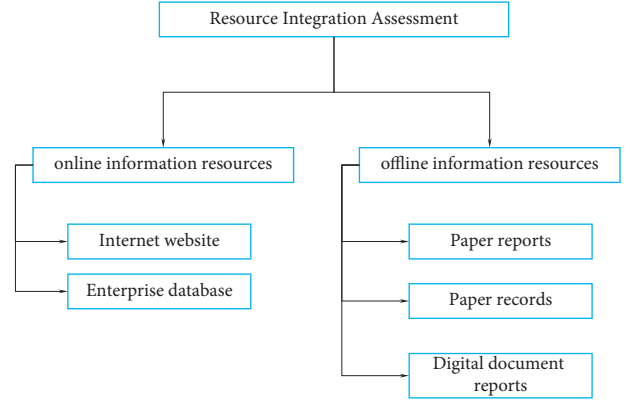
Figure 3: Enterprise resource integration assessment process.

iterations variable; and T is the maximum number of iterations. $[X_{min}, X_{max}]$ is the value range of position, and $[V_{min}, V_{max}]$ is the value range of velocity. The fitness value function f is used to judge the quality of particles. The size of the fitness function value indicates the pros and cons of the problem solution. After the particles are iterated, equation (4) is the update formula of the individual optimal value. When the maximum number of iterations is reached, the algorithm stops iterating:

$$
S_i = \begin{cases} X_i(t), & f(X_i(t)) > f(S_i), \\ S_i, & f(X_i(t)) \le f(S_i). \end{cases}
\tag{4}
$$

The flow of the PSO algorithm is shown in Figure 4. The specific implementation steps of PSO are as follows:

Step 1: Initialize the particle swarm. Given $t = 0$, bring the value of t into the particle velocity formula and position formula, and determine the initial position of the particle as $X_i(0)$ and the initial velocity as $V_i(0)$. Set all parameter values related to the algorithm, such as H, D, T, w, $e1$, $e2$, $g1$, $g2$.

Step 2: Calculate the fitness value of each particle.

Step 3: Set the fitness value of the current position of the particle as the optimal solution S_i of the particle itself. Set the optimal solution in the initial population as S_{best}.

Step 4: Update the particles.

① Update the position of the particle according to equation (3), and update the velocity of the particle according to equation (2).
② Judging the velocity and position of the current particle within a given range.
③ Calculate the fitness value of each particle, and then update S_i according to equation (4). Compare the fitness value of the individual optimal position and the group optimal position to update S_{best}.

Step 5: Judge whether the end condition is met, if the end condition is met, then step 6 is executed. Otherwise, the number of iterations is increased by 1, and step 4 is executed.

Step 6: Output S_{best}, and the algorithm ends.

Figure 4: PSO flow chart.

$$w = w_{\max} - \frac{w_{\max} - w_{\min}}{T} \times t, \tag{5}$$

where $w_{\max}$ represents the maximum inertia weight value, and $w_{\min}$ represents the minimum inertia weight value. In the early stage of the algorithm search, because the number of iterations is relatively small, the value of w will be large, which is convenient for particles to search globally. In the later stage of the algorithm search, as the value of t increases, the value of w will become smaller, which makes it easier for the particle to find the local optimal solution.

Inspired by the above strategies, this paper proposes a new method to update inertia weights. This method also dynamically updates the inertia weight based on the size of the fitness value. f_{avg} represents the average fitness value of the population. f_i represents the fitness value of the particle currently being iterated, $i = 1, 2, 3, \ldots H, H$ is the population size. The inertia weight value ranges from 0.4 to 0.9. The inertia weight expression used in this paper is as follows:

$$v_i(t + 1) = wv_i(t) + e_1 g_1 \left(S_{\text{best}} - x_i(t)\right),$$

$$s.Tw = \begin{cases} w_{\min} + \dfrac{f_{\text{avg}} - f_i}{f_{\text{avg}}}, & f_i \leq f_{\text{avg}}, \\[4mm] w_{\max} - \dfrac{f_i - f_{\text{avg}}}{f_{\text{avg}}}, & f_i \geq f_{\text{avg}}. \end{cases} \tag{6}$$

Chaos theory has different chaotic mapping methods, this paper adopts Logistic mapping. The principle of logistic mapping is the regression equation. Logistic maps are well ergodic and the particles are evenly distributed over their range. Its regression equation is as follows:

$$y_{k+1, j} = 4y_{k, j}\left(1 - y_{k, j}\right) y_{k, j} \in (0, 1), \tag{7}$$

where k is the number of iterations, and y_{kj} is the population sequence. This article will use chaos theory to initialize the population. PSO uses the chaotic sequence to produce a large number of particles during initialization and selects the particles with better quality as the initial particles of the population. This ensures that the particles are uniformly distributed in the solution space and the quality of the particles can be guaranteed.

(1) The steps to initialize using the chaotic sequence are as follows:

Step 1. Randomly generate a number $y_{0,0}$ in [0, 1].
Step 2. Bring $y_{0,0}$ into equation (8) for iteration to generate the sequence y_{kj}.
Step 3. Repeat step 2 until $k = 2^*H$;
Step 4. Map the generated sequence to the solution space of the population according to equation (8) so that 2^*H particles can be obtained.

$$x_{k, j} = a + y_{k, j}(b - a), \tag{8}$$

where $a = X_{\min}$, $b = X_{\max}$.
Step 5. Select the optimal H particles from the generated 2^*H particles as the initial population.

3.2. IPSO Algorithm. Due to the slow convergence speed of the traditional PSO late stage, this will result in the inability to perform global search in the particle late stage. Aiming at this problem, this paper improves the update method of inertia weight value, which can improve the convergence ability and search ability of the algorithm. In addition, since the population initialization of PSO is random, this will inevitably lead to a part of the particles far away from the optimal solution and affect the quality of the particles. Therefore, in this paper, chaos theory is added to the population initialization process to improve the particle quality and optimization ability.

Choosing an appropriate inertia weight w is the key to improving the convergence and optimization capabilities of PSO. The size of the inertia weight value determines the optimization ability of the algorithm. When the inertia weight value is small, the local optimization ability of the algorithm is better. When the inertia weight value is large, the global optimization ability of the algorithm is better. However, in the traditional PSO, the inertia weight value is set to a fixed value; so many studies have proposed various improvement strategies for the inertia weight to make the optimization ability of the algorithm the best. Among the many improvement strategies, the improvement ideas of the following strategies are very good. The strategy can update the inertia weight value according to the number of iterations. The ability of particle local optimization and global optimization is balanced by dynamically adjusting the w value. The mathematical expression for this strategy is as follows:

(2) The implementation steps of particle swarm optimization based on chaos theory are as follows:

Step 1. Population initialization based on chaos theory. Set the initial iteration number t to 0, and other parameters in the algorithm.

Step 2. Calculate the fitness value of the selected H particles with good quality.

Step 3. Set the fitness value of the current position of the particle as the optimal solution S_i of the particle itself. Set the optimal solution in the initial population as Sbest.

Step 4.Update the particle's position and velocity:

① Update the velocity and position of the particle according to the relevant update formula.

② Determine whether the current particle velocity and position are beyond the feasible range.

③ Update S_i and Sbest according to equation (4).

Step 5. Determine whether the end condition is reached. If the end condition is reached, execute step 6. If not, increase the number of iterations by 1, and execute step 4.

Step 6. Output S_{best}, and the algorithm ends.

4. Construction and Solution of Resource Integration Model Based on IPSO

4.1. Model Building. A single project has a clear project goal in the project planning stage and is divided into several tasks through work breakdown, and these tasks are all serving the project goal. Generally speaking, the scope of project objectives includes three dimensions: cost, time, and quality. In the multiproject management environment, the implementation of all projects of the enterprise serves the enterprise strategy. Project resource scheduling meets the project's time requirements for different resources as much as possible and strives to keep the completion time of all projects as short as possible. At the same time, such scheduling will inevitably involve organizational resources, so how to improve the utilization efficiency of organizational resources becomes a problem. In addition, the project leader will also pay attention to cost and quality issues. On the one hand, he hopes to reduce the project budget and improve the project income, and on the other hand, the quality should be as high as possible.

Under the premise of limited total resource supply, the multiproject resource scheduling problem can be regarded as the superposition of resource scheduling problems in multiple tiny time intervals. Therefore, it is possible to take a certain period of time during the execution of the project for analysis. Suppose the multiproject resource scheduling problem involves m mutually independent projects and n resource supply types. Within the time interval ΔT, there are e processes in progress in project i. Where the quantity of the kth resource required by the jth process is denoted as $z_{i,j,k}$, the quantity of the obtained resource is denoted as $n_{i,j,k}$, and the total supply of this type of resource is Z_k. Once the construction period delay in project i causes losses, the total cost of

delaying the project per unit time is recorded as s_i. Δt_i represents the engineering delay time of project i within the time interval ΔT. With the goal of minimizing project losses due to insufficient resource supply, the objective function is established, as follows:

$$Z = \min \sum_{i=1}^{q} \Delta t_i s_i, \tag{9}$$

where s_i is a known quantity, which can be known from the contract; Δt_i is an unknown quantity, which is determined by the quantity $z_{i,j,k}$ of resources obtained by the process j performed by the project i in the time period ΔT. Under the condition that the total supply of various resources is limited, $n_{i,j,k}$ should meet the restrictive conditions:

$$\sum_{i=1}^{q} \sum_{j=1}^{q} n_{ijk} \le Z_k, k = 1, 2, \ldots, w. \tag{10}$$

In the time period ΔT, the number of resources required by the critical path process in project i is z_{izk}, and the number of resources obtained is lick. Let t_{iz} denote the planned working time of the critical path, $t_{iz} = \Delta T$, and t'_{iz} denote its actual working time. From the principle that the total consumption of each resource in the same process remains unchanged, that is, $z_{izk}t_{iz} = n_{izk}t'_{iz}$, $t'_{iz} = z_{izk}t_{iz}/n_{izk}$, $k = 1, 2, \ldots, w$. Therefore, the delay time of the critical path of project i can be expressed and known as

$$\Delta t_i = \Delta t_{iz} = \frac{z_{izk} - n_{izk}}{n_{izk}}. \tag{11}$$

In the same way, for any process on the noncritical path in project i, mark the number of required resources as r_{isk}, and the number of obtained resources as n_{isk}, within the time period ΔT, the planned working time of this path is t_{if}, and the time difference is t_{is}. The delay time is expressed as follows:

$$\Delta t_{is} = \max \left\{ \frac{t_{is}(z_{\text{isk}} - n_{isk})}{n_{\text{isk}}} \right\}. \tag{12}$$

In order to ensure that the critical path of project i does not change, the difference between the delay time of the noncritical path and the time difference owned by the process should not exceed the delay time of the key process, namely,

$$\Delta t_{is} - T_{is} \le \Delta t_i. \tag{13}$$

In the actual project implementation, the construction of any process may require multiple resources at the same time, and a certain proportional relationship must be satisfied between different resources to coordinate and promote the process forward. In resource scheduling, under any circumstances, for the ongoing process j in project i, the supply quantity of resources and the demand quantity should satisfy the following proportional relationship:

$$n_{ijk} = \eta_{ij}z_{jk}, \quad k = 1, 2, \ldots, w, 0 < \eta_{ij} \le 1, \tag{14}$$

where η_{ij} represents the resource allocation coefficient related to each process j under construction within the time interval ΔT.

To sum up, substituting equations (7) and (11) into equations (9), (10) and (13) respectively, we get

$$Z = \min\left[\Delta T \sum_{i=1}^{q} s_i \left(\frac{1}{\eta_{iz}} - 1\right)\right], \tag{15}$$

$$\sum_{i=1}^{q} \sum_{j=1}^{q} \eta_{ij} z_{ijk} \le Z_k, \quad k = 1, 2, \ldots, w, \tag{16}$$

$$t_{is}\eta_{iz} \le \Delta T \eta_{is}. \tag{17}$$

Equations (15)–(17) constitute a mathematical model of enterprise resource scheduling in a multiproject environment with limited resources.

4.2. Model Solution.

The IPSO algorithm is proposed to be used for enterprise resource integration and scheduling. In order to verify the effectiveness of the proposed algorithm for enterprise resource integration scheduling, this paper introduces the method into a practical case. A company has a total of four projects to be completed within a certain period of time, and there are three types of resources needed and available. Each project has a different number of processes. Every project has strict delivery time requirements. The loss cost M_i ($i = $ P1,P2,P3,P4) of each item per delay unit time is 1000 for M_{P1}, $M_{P2} = 800$, $M_{P3} = 1500$, $M_{P4} = 1800$. Table 1 is a breakdown of the resource requirements of the enterprise to complete each project, where ΔT is set to 5.

Substitute the data shown in Table 1 into the resource integration model shown in equation (15), and the obtained formula is as follows:

$$\min z = 5 * 1000\left(\frac{1}{x_3} - 1\right) + 5 * 800\left(\frac{1}{x_5} - 1\right) + 5 * 1500\left(\frac{1}{x_6} - 1\right) + 5 * 1800\left(\frac{1}{x_{10}} - 1\right),$$

$$s.t. 18x_1 + 15x_2 + 10x_3 + 29x_4 + 17x_5 + 13x_6 + 21x_7 + 16x_8 + 23x_9 + 18x_{10} \le 150$$

$$25x_1 + 27x_2 + 16x_3 + 18x_4 + 23x_5 + 26x_6 + 10x_7 + 18x_8 + 15x_9 + 11x_{10} \le 190$$

$$9x_1 + 16x_2 + 35x_3 + 18x_4 + 12x_5 + 11x_6 + 14x_7 + 23x_8 + 14x_9 + 8x_{10} \le 150$$

$$4x_3 \le 5x_1$$

$$2x_3 \le 5x_2$$

$$3.5x_5 \le 5x_4 \tag{18}$$

$$4x_6 \le 5x_7$$

$$4.5x_{10} \le 5x_8$$

$$3x_{10} \le 5x_9$$

$$0 < x_i < 1,$$

where x_1, x_2, x_3 represents the resource allocation coefficient of process P11, P12, P13; x_4, x_5 represents the allocation coefficient of process P21, P22, x_6, x_7 represents the resource allocation coefficient of process P31, P32; x_8, x_9, x_{10} represents the resource allocation coefficient of process P41, P42, P43.

For the above mathematical programming model, the standard particle swarm optimization algorithm and the new PSO optimization algorithm proposed in this paper are used to solve the problem, respectively. The parameter settings of the algorithm are evolution times $T = 600$, population size $D = 300$, and parameter $e_1 = 1.532$, $e_2 = 1.541$, the error $\varepsilon = 0.0001$.

In addition, Figure 5 shows the simulation results of the two algorithms. It can be seen from the figure that the average value of the project loss cost obtained by the standard particle swarm optimization method is larger than the result obtained by the new particle swarm optimization algorithm. According to the discrete degree of the objective function, the simulation results of the new particle swarm optimization algorithm are more concentrated, while the simulation results of the standard PSO [20] are more scattered.

After the above comparison and analysis of the simulation results of the two algorithms, it is concluded that compared with the standard particle swarm optimization algorithm, the improved particle swarm optimization algorithm in this paper has higher stability and better convergence.

TABLE 1: Details of enterprise resource requirements.

Project	Process	Required time	Time difference	Resource R1	Resource R2	Resource R2
P1	P11	4	0	18	25	9
	P12	2	2	15	27	16
	P13	5	2.5	10	16	35
P2	P21	3.5	3	29	18	18
	P22	5	2	17	23	12
P3	P31	5	1.5	13	26	11
	P32	4	2	21	10	14
P4	P41	4.5	3	16	18	23
	P42	3	1	23	15	14
	P43	5	3	18	22	8
Resource requirements				**180**	**200**	**160**
Max supplies				150	190	150
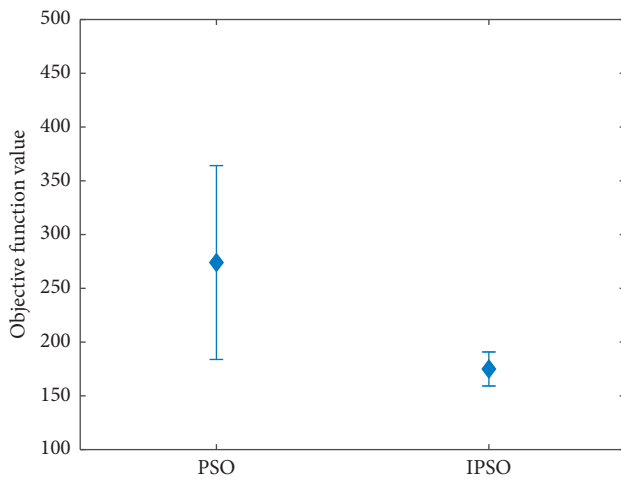
FIGURE 5: Comparison of project loss costs obtained by different algorithms.

According to the resource allocation coefficients obtained by the PSO and IPSO algorithms, the allocation of each resource among different projects is calculated, and the resource allocation of the two algorithms is obtained as shown in Tables 2 and 3.

Observing the data in Table 2, it can be seen that the allocation of resource R1 based on PSO is 136.17, the allocation of resource R2 is 152.63, and the allocation of resource R3 is 121.07. There is a large gap between the calculated allocation and supply of each resource. This shows that the allocation of resources is not reasonable. The delay times for the three operations of project P1 are 1.489, 3.119, and 2.765, respectively. The planned time differences corresponding to these three processes are 0, 2, and 2.5, respectively. The delay time calculated based on PSO is larger than the planned time difference. This shows that resource integration based on PSO is not very effective. The delay times for the two processes of project P2 are 2.120 and 2.221 respectively. The planned time differences corresponding to these two processes are 3 and 2, respectively. It can be seen that the process P21 can be completed within the set time difference, but the process P22 cannot be completed within the set time difference. The delay times for the two processes of project P3 are 1.765 and 0.815

respectively. The planned time differences corresponding to these two processes are 1.5 and 2, respectively. It can be seen that the process P32 can be completed within the set time difference, but the process P31 cannot be completed within the set time difference. The delay times for the three operations of project P4 are 2.642, 0 and 2.812, respectively. The planned time differences corresponding to these three processes are 3, 1, and 3, respectively. From the comparison data, it can be seen that these three processes can be completed within the set time difference. To sum up, in the resource integration scheme based on the PSO algorithm, except for P4, which can be completed according to the set time difference, other projects cannot be completed within the set time difference.

Observing the data in Table 3, it can be seen that the allocation of resource R1 based on IPSO is 159.74, the allocation of resource R2 is 175.89, and the allocation of resource R3 is 137.41. The calculated allocation of each resource is very close to the available Supply amount. This shows that the allocation of resources is more reasonable. In the results calculated based on IPSO, the delay times for the three processes of project P1 are 1.622, 2.120 and 3.235, respectively. The planned time differences corresponding to these three processes are 0, 2, and 2.5, respectively. The delay time calculated based on IPSO is larger than the planned time difference. The delay times for the two processes of project P2 are 1.522 and 1.767, respectively. The planned time differences corresponding to these two processes are 3 and 2, respectively. It can be seen that both steps P21 and P22 can be completed within the set time difference. The delay time for the 2 processes of project P3 is 0.521,0 respectively. The planned time differences corresponding to these two processes are 1.5 and 2, respectively. It can be seen that both steps P31 and P32 can be completed within the set time difference. The delay times for the three processes of project P4 are 2.764, 1.656, and 2.701, respectively. The planned time differences corresponding to these three processes are 3, 1, and 3, respectively. From the comparison data, it can be seen that this process P41 and P43 can be completed within the set time difference, and P42 cannot be completed within the set time difference. To sum up, in the resource integration scheme based on the PSO algorithm, except for P2 and P3, which can be completed according to the set time difference,

TABLE 2: Details of the actual allocation of enterprise resources based on PSO.

Project	Process	Required time	Time difference	Resource R1	Resource R2	Resource R2	Partition coefficient	Delay value
	P11	4	0	13.33	18.51	6.66	0.7403	1.489
P1	P12	2	2	12.38	22.28	13.20	0.8251	3.119
	P13	5	2.5	6.56	10.49	22.95	0.6557	2.765
P2	P21	3.5	3	13.20	8.20	8.20	0.4553	2.120
	P22	5	2	9.29	12.57	6.56	0.5465	2.221
P3	P31	5	1.5	13.00	26.00	11.00	1	1.765
	P32	4	2	19.50	9.29	13.00	0.9287	0.815
	P41	4.5	3	14.08	15.84	20.24	0.8798	2.642
P4	P42	3	1	23.00	15.00	14.00	1	0
	P43	5	3	11.84	14.47	5.26	0.6576	2.812
Original resource requirement				180	200	160		
Actual allocation of each resource				136.17	152.63	121.07		
Max supplies				160	190	150		

TABLE 3: Details of the actual allocation of enterprise resources based on IPSO.

Project	Process	Required time	Time difference	Resource R1	Resource R2	Resource R2	Partition coefficient	Delay value
	P11	4	0	17.21	23.90	8.60	0.9561	1.622
P1	P12	2	2	15.00	27.00	16.00	1	2.120
	P13	5	2.5	7.76	12.41	27.14	0.7755	3.235
P2	P21	3.5	3	24.54	15.23	15.23	0.8462	1.522
	P22	5	2	12.48	16.88	8.81	0.7341	1.767
P3	P31	5	1.5	11.33	22.66	9.59	0.8715	0.521
	P32	4	2	21.00	10.00	14.00	1	0
	P41	4.5	3	12.06	13.57	17.34	0.7539	2.764
P4	P42	3	1	22.20	14.48	13.51	0.9652	1.656
	P43	5	3	16.16	19.75	7.18	0.8978	2.701
Original resource requirement				180	200	160		
Actual allocation of each resource				159.74	175.89	137.41		
Max supplies				160	190	150		
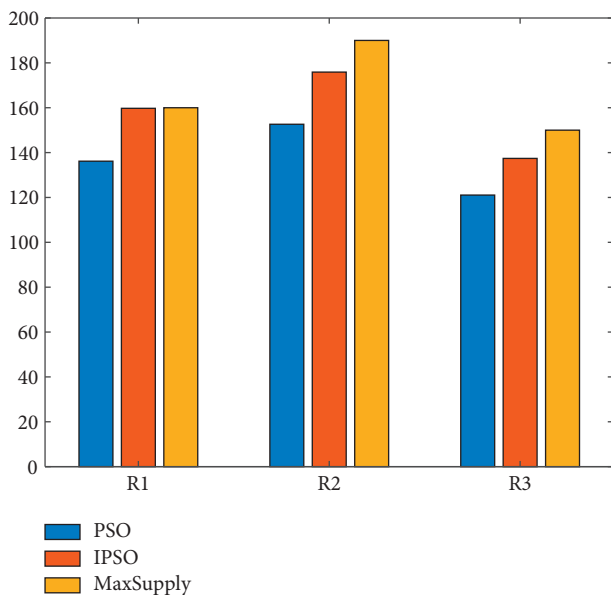
FIGURE 6: Comparison of resource allocation of different algorithms.

other projects cannot be completed within the set time difference.

In order to compare the resource integration and allocation schemes obtained by the two methods more intuitively, screen out the optimal resource allocation scheme, and give a resource allocation comparison chart, as shown in Figure 6. In the figure, MaxSupply represents the amount of resources that the enterprise can supply. From the data in the figure, it can be seen that the allocation of the three resources based on IPSO is the closest to the maximum supply. However, there is still a big gap between the distribution scheme based on PSO and the maximum supply.

5. Conclusion

In the process of continuous operation and development of enterprises, there will definitely be some problems in the use and deployment of internal resources. In order to optimize the integration and allocation of enterprise resources, this paper proposes to use an optimization algorithm to allocate resources. Its purpose is to efficiently complete the delivery of each project within the contracted construction period. Based on the traditional PSO algorithm, this paper proposes

an IPSO algorithm. Firstly, to solve the problem of uneven particle distribution caused by random initialization of the population, the algorithm adds chaos theory to the initialization of particle population. It uses the Logistic mapping sequence to generate a large number of particles, and selects the particles with better quality for initialization, which improves the quality of the particles and enables the particles to be evenly distributed during initialization. Secondly, the late convergence speed of particle swarm optimization algorithm is slow, which makes it easy to fall into the local optimal solution. Aiming at this problem, a dynamic inertia weight update method based on fitness value is designed. This can improve the convergence speed in the later stage of the algorithm, improve the quality of the global optimal solution, and enable the particles to perform a global search and finally find the optimal solution of the population. Finally, a fitness function based on task completion time is designed, and the IPSO algorithm is applied to the integration and optimization of internal resources of the enterprise. Compared with the standard particle swarm optimization algorithm, the IPSO algorithm has higher stability and better convergence. In the experimental part, a set of optimal solutions are selected to solve the resource allocation of each project process in the experimental example. The results show that the IPSO algorithm can produce better results for this kind of resource allocation problem. It can not only allocate the limited enterprise resources reasonably, but also minimize the total project loss caused by the delay of the construction period. The optimization results show that the IPSO algorithm proposed in this paper can effectively integrate and schedule the internal resources of the enterprise and improve the operation efficiency of the enterprise.

Data Availability

The labeled data set used to support the findings of this study is available from the corresponding author upon request.

Conflicts of Interest

The author declares that there are no conflicts of interest.

Acknowledgments

References

[1] B. Wernerfelt, "A resource-based view of the firm," *Strategic Management Journal*, vol. 5, no. 2, pp. 171–180, 1984.

[2] D. J. Teece, G. Pisano, and A. Shuen, "Dynamic capabilities and strategic management," *Strategic Management Journal*, vol. 18, no. 7, pp. 509–533, 1997.

[3] D. G. Sirmon, "Managing firm resources in dynamic environments to create value: looking inside the black box," *Academy of Management Review*, vol. 32, no. 1, pp. 173–192, 2007.

[4] D. Hillman and C. Blom, "Optimizing process efficiency in a multi-stream keying environment," *TODAY-The Journal of Work Process Improvement*, vol. 9, no. 6, p. S10, 2009.

[5] S. C. Lonial and R. E. Carter, "The impact of organizational orientations on medium and small firm performance: a resource-based perspective," *Journal of Small Business Management*, vol. 53, no. 1, pp. 94–113, 2015.

[6] H. Hoorfar and A. Bagheri, "NP-completeness of chromatic orthogonal art gallery problem," *The Journal of Supercomputing*, vol. 77, no. 3, pp. 3077–3109, 2021.

[7] A. Kulmburg and M. Althoff, "On the co-NP-completeness of the zonotope containment problem," *European Journal of Control*, vol. 62, pp. 84–91, 2021.

[8] D. Zhang, R. Chi, J. Li, X. Chi, and T. Zhu, "Cuckoo optimization algorithm visual positioning system based on particle swarm algorithm," *Advances in Intelligent Automation and Soft Computing*, vol. 80, pp. 16–21, 2022.

[9] M. E. C. Bento, "A hybrid particle swarm optimization algorithm for the wide-area damping control design," *IEEE Transactions on Industrial Informatics*, vol. 18, no. 1, pp. 592–599, 2022.

[10] M. Quarto, G. D'Urso, and C. Giardini, "Micro-EDM optimization through particle swarm algorithm and artificial neural network," *Precision Engineering*, vol. 73, pp. 63–70, 2022.

[11] Y.-q. Chen, J.-l. Guo, H. Yang, Z.-q. Wang, and H.-l. Liu, "Research on navigation of bidirectional A∗ algorithm based on ant colony algorithm," *The Journal of Supercomputing*, vol. 77, no. 2, pp. 1958–1975, 2021.

[12] L. Yun and H. Lu, "Diagnosis strategy design method based on ant colony algorithm," *Journal of Physics: Conference Series*, vol. 1894, no. 1, Article ID 012081, 2021.

[13] M. Sharifian, N. Abdolvand, and S. Rajaee Harandi, "Context-based expert finding in online communities using ant colony algorithm," *Journal of Information Systems and Telecommunication (JIST)*, vol. 8, no. 30, pp. 130–139, 2020.

[14] S. Nayeri, R. Tavakkoli-Moghaddam, Z. Sazvar, and J. Heydari, "A heuristic-based simulated annealing algorithm for the scheduling of relief teams in natural disasters," *Soft Computing*, vol. 26, no. 4, pp. 1825–1843, 2022.

[15] V. F. Yu, H. Susanto, P. Jodiawan, T.-W. Ho, S.-W. Lin, and Y.-T. Huang, "A simulated annealing algorithm for the vehicle routing problem with parcel lockers," *IEEE Access*, vol. 10, pp. 20764–20782, 2022.

[16] S. Ren, M. Gao, M. Wang, and Y. Li, "Polarized laser backscattering of atmospheric cloud distribution based on simulated annealing algorithm," *Mathematical Problems in Engineering*, vol. 2021, no. 1, 9 pages, Article ID 6635828, 2021.

[17] A. Zemliak, "A modified genetic algorithm for system optimization," *COMPEL: The International Journal for Computation & Mathematics in Electrical & Electronic Engineering*, vol. 41, no. 1, pp. 499–516, 2022.

[18] F. Hajati, A. Rezaee, and S. Gheisari, "Genetic algorithms for scheduling examinations," *Advanced Information Networking and Applications*, vol. 227, pp. 524–532, 2021.

[19] M. Bortolini, C. Cafarella, E. Ferrari, F. G. Galizia, and M. Gamberi, "Reconfigurable manufacturing system design using a genetic algorithm," *Sustainable Design and Manufacturing*, vol. 262, pp. 130–139, 2022.

[20] Q. Wang, X.-L. Fu, G.-F. Dong, and T. Li, "Research on cloud computing task scheduling algorithm based on particle swarm optimization," *Journal of Computational Methods in Science and Engineering*, vol. 19, no. 2, pp. 327–335, 2019.

Research Article

Research on an Intelligent Identification and Classification Method of Complex Holes in Triangle Meshes for 3D Printing

Shanhui Zhang [D],[1] **Wei Wei** [D],[2] **and Wei Wu** [D][2]

[1]*School of Control Science and Engineering, Shandong University, Jinan, Shandong 250061, China*
[2]*Shandong Shanda Hoteam Software Co., Ltd, Jinan, Shandong 250101, China*

Correspondence should be addressed to Shanhui Zhang; zsh@sdu.edu.cn

In triangular mesh models, the repair of complex hole poses a difficult problem, which always causes serious repair defects. Therefore, it is needed to develop an intelligent identification and classification method of complex holes to reduce repair difficulties. First, the topological structure of the complex hole is studied and all the holes are divided into single holes and continuous holes depending on whether there are intersection points. Second, to tackle the nesting and connecting of complex continuous holes, a decomposition method of multiply connected domains based on intersection points is proposed to partition or reconstruct complex continuous holes into single holes. Based on the different geometric structures, single holes are classified into five common hole types and a corresponding identification method of single holes is presented. Finally, an experiment is carried out to verify the repair quality and efficiency of the proposed method. Compared with Geomagic software, the proposed method can automatically identify and partition complex holes with fewer defects and similar efficiency. It can reduce the difficulties of repairing complex holes and enable the repair of complex holes based on existing methods. It is shown that the method can be applied to complex hole repair of 3D printing models without the participation of technicians.

1. Introduction

As a rapidly developing manufacturing technology, 3D printing technology (also known as additive manufacturing technology or rapid prototyping technology) is gradually entering various fields and playing an important role [1, 2]. Compared with traditional manufacturing technology, 3D printing technology can better meet the modern green concept and presents a favourable trend in the green manufacturing industry. In 3D printing technology, triangle meshes are characterized by simplicity, straightforwardness, and expressiveness [3]. Thus, it becomes a widely used form of a geometric model and gradually proves to be an important basis of 3D printing technology. However, in the construction and acquisition of mesh models, holes are often generated, affecting the appearance and quality of 3D printed models. Therefore, the identification and repair of the holes in the triangle mesh model become the key to improving the quality of 3D printing.

At present, the identification and repair of triangle mesh holes are mostly carried out manually, with low efficiency and high requirements of operators' skills. Automatic hole identification and repair algorithms often regard all holes as single holes. Most research focuses on the repair method of single holes and disregards the processing and partitioning of complex holes, single hole geometry, and the topological relationship between relevant holes. This results in unsatisfactory model repair and new defects, such as self-intersecting surfaces, highly refracted edges, and degenerate triangles.

Therefore, to improve the quality of hole repair and to lower the reliance on specialized technicians, it is necessary to study the intelligent identification and partitioning method of complex holes in triangle meshes. The technical route of the paper is shown in Figure 1. First, the mesh model is checked and preprocessed. Second, the complex holes are identified and segmented and continuous holes are partitioned into single holes. Third, all the single holes are
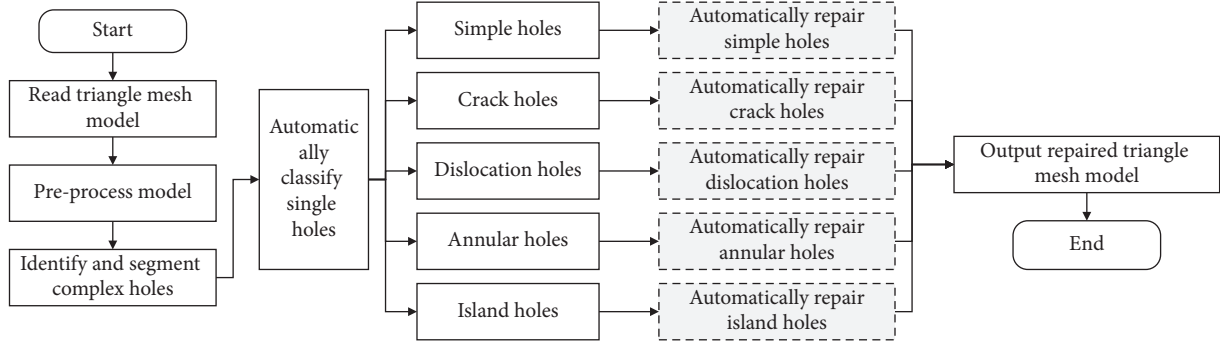
Figure 1: Technical route.

automatically classified into specific single holes, such as the simple hole, crack hole, and annular hole. Finally, the appropriate hole repair methods are chosen and the ideal triangle mesh model is output. The results show that the proposed method can accurately identify, partition, and repair complex holes with intersection points. The main contributions are summarized as follows:

(1) A decomposition method of multiply connected domains based on intersection points is proposed to partition or reconstruct complex continuous holes into single holes. It can greatly improve the structure and size of the complex holes and can mostly avoid the intersection of various hole lines.

(2) An identification method of single holes is researched to divide single holes into five common hole types, which can reduce the difficulties of repairing complex holes and enable the repair of complex holes based on existing repair methods of single holes.

(3) The proposed repair process is completely automated, replacing the manual judgment and repair operation, reducing the dependence on professionals. At the same time, it can achieve high efficiency, similar to Geomagic.

2. Related Work

Hole identification and extraction is a critical preliminary process for hole repair. Given the considerable amount of data generated from the conversion from solid model to point cloud or grid, the data processing is time-consuming with low efficiency if holes are identified and extracted through repeated traversal. Therefore, the efficiency and accuracy of identification and extraction will directly affect the efficiency and quality of subsequent repair. The existing hole identification and extraction methods can be divided into two categories according to the data type: hole identification based on point cloud data and that based on grid [4, 5].

There are many methods for hole identification based on point cloud data [6–9]. Milroy et al. [10] identified the boundary of holes by calculating the extreme value of curvature. This method can generate good results in areas with small curvature changes and relatively smooth surfaces,

but less so when the model curvature changed dramatically. Orriols and Binefa [11] adopted the least squares method to identify and query holes, which was also not suitable for drastic curvature changes. Bendels et al. [12] used the minimum spanning tree to detect feature points of the point cloud boundary, but the complete extraction of the boundary still needed to be further improved. Liu [13] calculated the barycentre of sampling points and that of sampling points in the neighborhood to efficiently extract the hole boundary according to the distance ratio of various points. Alrashdan et al. [14] used the neural network method to automatically extract the boundary points, but the boundary points with small change of normal vector were easily to be missed, so that the extracted boundary might not be complete, and it was also time-consuming.

The grid-based hole identification method is also a focal point of research. In computer graphics, grid is a very basic representation method, and it can be obtained by point cloud data reconstruction or 3D model transformation. Triangular mesh is the most widely used form because of its simplicity, straightforwardness, and expressiveness. Zhan and Zhang [15] proposed the area expansion method to identify hole boundary and to form the Delaunay triangulation of point cloud data. Chen et al. [16] projected the object model onto a two-dimensional plane and used the interior angles of the projected polygon in the plane and related theories to automatically identify the holes. Li et al. [17] proposed a hole identification method based on the winged-edge data structure, in which all the holes of the model can be obtained through one traversal, greatly improving the efficiency of hole identification. However, in practical 3D printing application, the point cloud data obtained by traversal may be unevenly distributed, which may easily lead to a situation where multiple holes share a boundary vertex [18]. Therefore, the above algorithms cannot accurately identify such complex holes, and it will cause repair defects, such as self-intersecting surfaces and structure change.

Based on the above hole identification methods, many scholars have conducted in-depth studies on the hole-filling of triangle mesh models, among which the typical repair methods were as follows: the feature plane is calculated based on the point distribution of holes and the points of holes were projected onto the feature plane for partitioning. Then, implicit function [19], radial basis function [20, 21],

and the wave-front method [22] were used to map the points on the feature plane to the 3D model. The surface of the filled hole obtained by this method was often well shaped, but it was only applicable under extremely limited conditions. The method worked ideally for simple holes, but as for complex holes, mapping failure or errors may occur, leading to inferior hole filling. Therefore, a large number of scholars have proposed the classification and filling methods for complex holes.

Jun [23] proposed an algorithm of subdividing complex holes into simple holes before repairing them, providing a solution for the subdivision and repairing of holes with self-intersecting boundaries in the projection process. However, it was not conducive to dealing with other types of complex holes, especially with the challenge of self-intersecting boundaries in the nonprojection process. Inspired by this method, Li et al. [17] presented and created an algorithm based on edge expansion, which split the holes into flatter ones considering the spatial shape of holes. The method cannot deal with self-intersecting boundaries, and the complex holes were in fact just a simple hole with complex curvature changes. Lai et al. [24] mulled the processing of island holes and proposed a hole filling algorithm based on B-spline surfaces, fitting the vertices near holes to B-spline surfaces. This method focused on the topological accuracy and smoothness of the connection between new meshes and existing ones. Feng et al. [25] proposed a fast filling method for triangle meshes based on the hole size. The holes were classified into small holes, medium holes, and large holes according to their size, and different filling algorithms were used for different types of holes. However, the classification method only factored in the size of holes while ignoring the complex topological form of holes, thus leading to subpar filling results for complex holes. Wen et al. [26] proposed a method for automatic identification and repair of real defect holes, but it was only applicable in simply connected domains and ignored the topological form of the complex missing area. Therefore, the above studies lack the identification and segmentation of complex multiconnected domain holes, especially of the holes with self-intersecting boundaries.

To sum up, the repair methods for a specific type of holes, especially for simple holes, are relatively sophisticated, having delivered good repair results in previous research. However, the identification and partitioning of complex holes and the corresponding repair methods vary with each case. Adopting a uniform repair method will lead to self-intersecting surfaces in hole repair and unsatisfactory repair outcomes. At the same time, the human-computer interaction is often adopted in hole repair with ultralow identification and repair efficiency. In this case, the repair outcomes depend on the precision of the repair algorithm and the operator's skills. In order to solve this problem, based on the topological form of holes, ways must be found to intelligently identify and partition complex holes with multiconnected domains and self-intersecting boundaries. Thus, a method of automatically detecting, identifying, and partitioning of holes in triangle mesh models should be proposed, aiming at the nested and crossed characteristics of complex continuous holes. It can make up for the deficiency of various simple hole repair methods in complex holes.

3. Identification and Partitioning of Complex Holes

3.1. Features of Single Holes and Continuous Holes. Through compiling and analyzing the data of hole repair failure cases in the triangle mesh model, it is found that the failure often occurs when multiple holes are adjacent or nested to each other. It leads to mapping failure and thus unsatisfactory repair outcomes. In order to solve this problem, it is necessary to analyze the characteristics of such holes and differentiate them from single holes. Through analyzing many cases, it is found that the main difference is whether there are intersection points connecting multiple hole lines. On this basis, all the holes are classified into two types.

(1) Single holes: the points on the hole line can be connected in turn to form a closed loop with a unique solution. This is shown in Figure 2(a).

(2) Continuous holes: a continuous hole consists of multiple single holes, and there are one or more intersection points between the single holes. It offers multiple ways of representing each individual closed loop. As shown in Figure 2(b), four points A, B, C, and D of the continuous hole are the intersection points of multiple hole lines. When the counter-clockwise direction is defined positive, the continuous hole boundary can be identified as A-P1-A-B-P5-B-C-P6-P4-C-P3-D-P2-D-A.

3.2. Identification of Single Holes and Continuous Holes. Because of the large difference between repairing single holes and continuous holes in triangle meshes in terms of difficulties and methods, it is an essential step to classify and identify all holes and determine whether they are single holes or continuous holes before hole repair. Before identification, it is necessary to preprocess the input triangle mesh model and quickly establish the topological structure of the model's facets, edges, and vertices. According to the relationship between facets and edges of the triangle mesh model, all simply connected domains of the triangle mesh model are obtained, and each simply connected domain is regarded as a part. Free edges are found for each part, and all free edges are connected from end to end according to the connection between edges and points to obtain hole lines, so the basic information of all holes is obtained, including hole lines, hole directions, and the relationship between holes and parts. Among them, a free edge refers to an edge connected with only one facet. A hole line refers to the closed line formed by connecting the ends of free edges in each set, maintaining the topological relationship of the original triangle mesh model.

On this basis, an identification process of single holes and continuous holes is put forward, as shown in Figure 3. First, all the free edges of the hole lines are found by obtaining the basic information of the hole. The sets of free
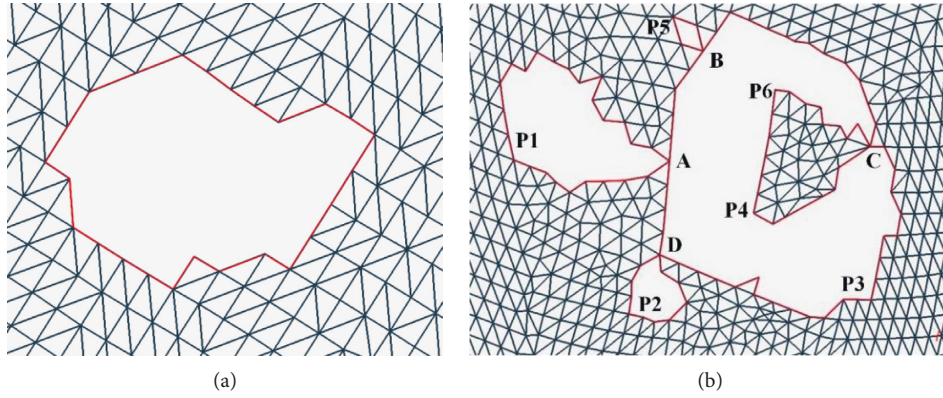
FIGURE 2: Examples of (a) single hole and (b) continuous hole.
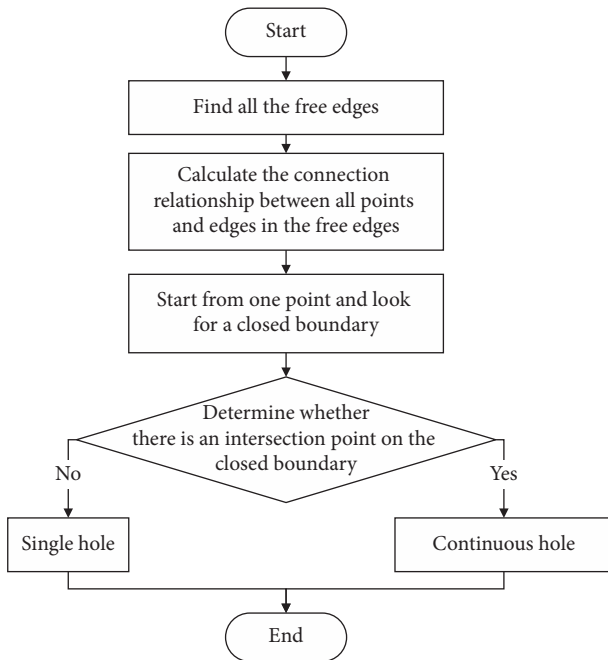
FIGURE 3: Identification process of single holes and continuous holes.

edges are discovered. Second, according to the topological structure relationship between each edge and each vertex, the connection between all points and edges in the free edges is calculated. Third, starting from any point, the closed boundaries are found according to the relation of connection. Then, it is judged whether there is an intersection point on the closed hole lines. If not, a single hole is output; if so, it is a continuous hole, and the corresponding boundary information is output to facilitate the subsequent partitioning of continuous holes.

3.3. Segmentation Method of Continuous Holes. In order to facilitate the repair of triangle mesh models, the complex continuous holes must be divided into single holes to improve the accuracy and repair quality of each single hole repair algorithm. The nesting and connection of the hole

lines in continuous holes are likely to cause errors in the partitioning of multiple holes. To solve this problem, a decomposition method of multiply connected domains based on intersection points is proposed to segment and reconstruct the hole lines of continuous holes. The specific steps are shown in Figure 4.

Step 1: detect the boundary of continuous holes.

Based on the information obtained during identification, the boundary of the continuous hole is detected, and the corresponding hole line is formed in the counterclockwise direction. For example, the continuous hole boundary in Figure 2(b) is A-P1-A-B-P5-B-C-P6-P4-C-P3-D-P2-D-A, and four intersection points A, B, C, and D are identified.

Step 2: divide the boundary line.

According to the intersection points of continuous holes, the inner area of continuous holes is divided into several separate holes. For example, the boundary of continuous holes in Figure 2(b) can be divided into five separate holes, namely, A-P1-A, B–P5–B, C–P6–P4–C, D-P2-D, and A-B-C-P3-D-A.

Step 3: distinguish the inner holes from outer ones.

The points on the hole line are projected onto the plane, and the positional relations of each hole are calculated according to the relative inner and outer relations between the points and the polygon. If the points of a hole L1 are all outside of another hole L2, it is assumed that L1 is outside of L2. If a hole line is not inside any of the holes, it is an outer hole, and if a hole line is inside one of the holes, it is an inner hole.

Step 4: judge whether it is an outer hole.

If the outer hole does not contain the inner hole, jump to Step 7; otherwise, continue with Step 5. It can be concluded that the outer holes in the continuous holes in Figure 2(b) are A-P1-A, B–P5–B, D-P2-D, and A-B-C-P3-D-A and the inner hole is C–P6–P4–C, which is included by the outer holes A-B-C-P3-D-A.

Step 5: identify and determine the new boundary point.

For an outer hole that contains an inner hole, the intersection point in its hole line must be found, and
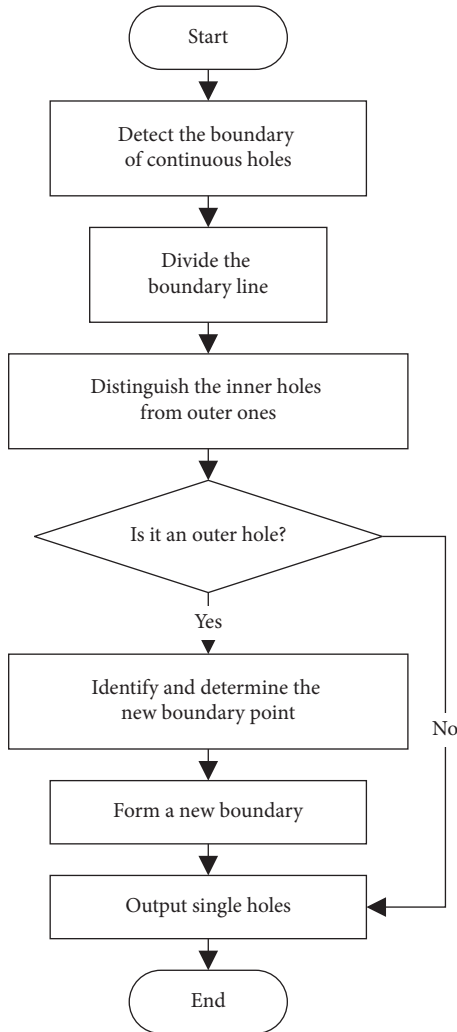
FIGURE 4: Segmentation process of continuous holes.

FIGURE 5: Determination of the subsequent boundary point of an outer hole line.
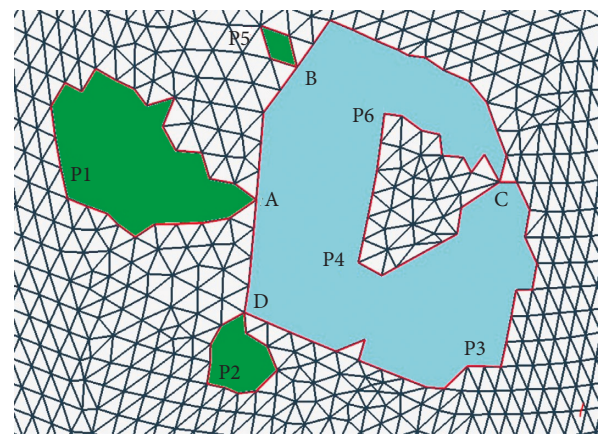
FIGURE 6: Single hole identification and output.
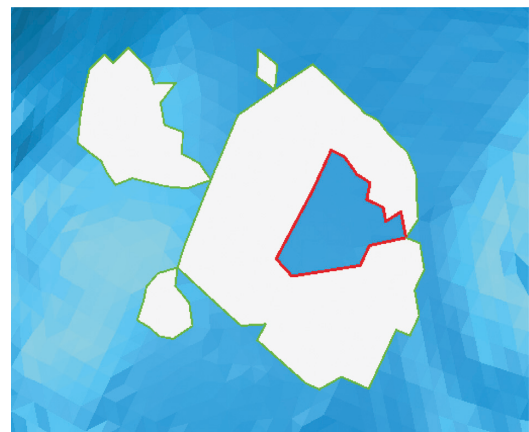
FIGURE 7: Hole identification result of Geomagic.

there are three important edges connected to the intersection point, namely, the first edge connecting to the previous index point of the current outer hole line and the second and third edge connecting to two neighbouring index points in the inner hole line. Calculate the included angle between the first edge and the second and third edge. Select the neighbouring index point with the smallest included angle as the new boundary point. For example, Figure 5 shows that C1, C2, and C3 are the three important edges, and the included angle ∠1C2 is less than angle ∠1C3. Thus, the next boundary point is calculated to be in the direction of ray C2, that is, in the direction of P6, rather than P4.

Step 6: form a new boundary.

Starting from the new boundary point, all the points on the inner hole are inserted into the boundary of the outer hole in accordance with the connection order on the boundary, and the outer and inner edges of the hole are combined. In other words, in the example, the inner hole C–P6–P4–C is inserted into the outer hole A-B-C-P3-D-A and the new boundary line is A-B-C-P6-P4-C-P3-D-A.

Step 7: output single holes.

All the holes that meet the conditions are output as a single hole, with the boundary lines given. According to this method, the example outputs four single holes with the boundary lines A-P1-A, B–P5–B, D-P2-D, and A-B-C-P6-P4-C-P3-D-A. The filled area as shown in Figure 6 is four single holes surrounded by four boundary lines.

(a)   (b)
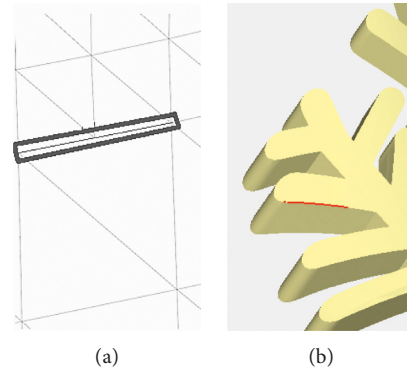
Figure 8: Crack hole. (a) Triangle mesh example. (b) Model example.

(a)   (b)
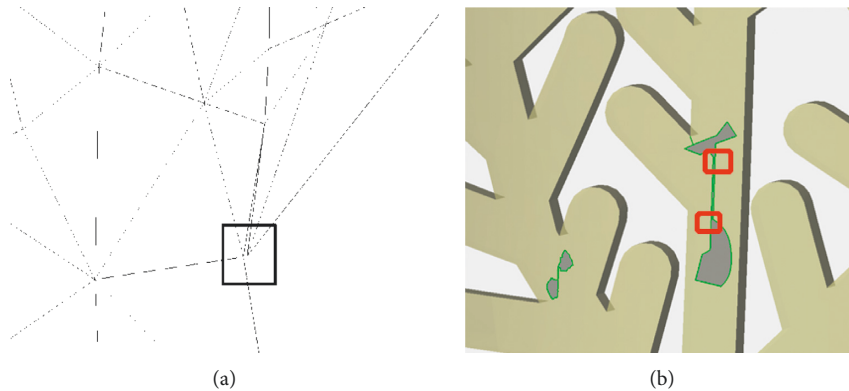
Figure 9: Dislocation hole. (a) Triangle mesh example. (b) Model example.

Step 8: end.

When the hole in this case is processed by traditional hole identification methods and software such as Geomagic, C–P6–P4–C can be easily identified and be output as a single hole. If filled based on this, the model obtained will not be desirable and a large number of self-intersecting surfaces will be created. As shown in Figure 7, both the green and red hole lines are identified as single holes, but the inner red hole line will intersect with the outer hole line during repair, obviously inconsistent with the actual hole.

4. Types of Single Holes and the Intelligent Identification Method

4.1. Types of Single Holes. After the complex continuous holes are divided into single holes, the geometry of each single hole still varies, posing challenges to the hole repair process. Therefore, by analyzing causes of self-intersecting surfaces based on the geometry of the hole and the current sophisticated hole repair methods, the single hole is further classified into five types: crack hole, dislocation hole, annular hole, simple hole, and island hole. Their respective characteristics are as follows:

(1) Crack hole: if the included angle and the cumulative included angle of any two sides forming the hole boundary are less than the set angle threshold, such a single hole is defined as a crack hole. Its shape resembles a straight line. The general rule of thumb is that the angle threshold is set between 5° and 10°, which is used to determine whether the hole resembles a straight line. The cumulative angle refers to the sum of angles between all boundary edges starting from the first edge. Crack holes, which occur in modelling or format conversion, are linear bad edges that are not sewn together at the surface joints. There are no triangles missing, but the adjacent triangles are not connected, as shown in Figure 8. Therefore, the crack holes are more suitable for repairing by stitching the boundary points and then optimizing the subdivision.

(2) Dislocation hole: if the distance between the points on the hole edge and on the nearest edge is very short (less than the set distance threshold), such holes are called dislocation holes, as shown in Figure 9(a). The distance threshold is also an empirical value and is generally set to about 0.1–0.5 mm. If it is less than this value, the hole is fixed by kneading the triangles together, generally without affecting the shape of the model; if it is above the set threshold, the hole is considered as a simple hole and can be repaired by adding triangle surfaces, which will not cause too many narrow and long triangles. As shown in Figure 9(b), both the red parts are dislocation holes.
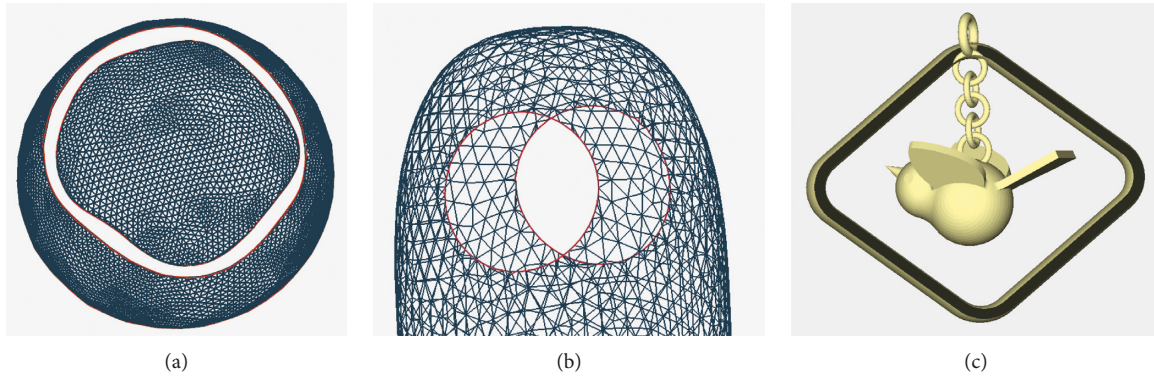
FIGURE 10: Annular hole. (a) Triangle mesh example—coplanar annular hole. (b) Triangle mesh example—parallel annular hole. (c) Model example.
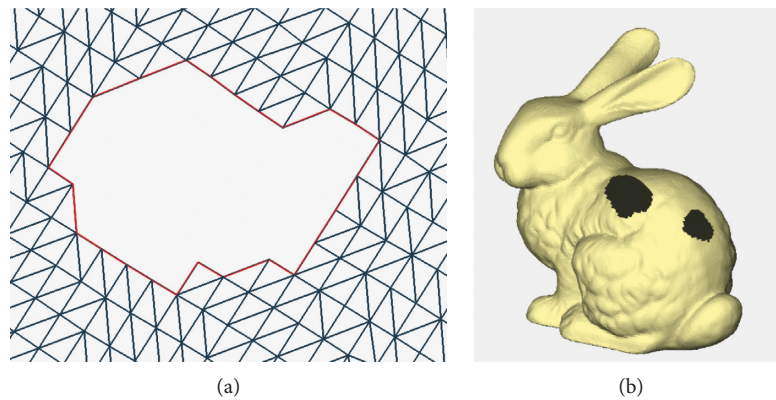
FIGURE 11: Simple hole. (a) Triangle mesh example. (b) Model example.

After judgment, the holes can be partitioned into simple holes and crack holes by merging the surfaces of dislocation holes.

(3) Annular hole: it refers to a hole composed of two boundary lines, nearly coplanar or parallel, with similar shapes and without intersection points, as indicated in Figure 10. There is an approximate coplanar or parallel relationship between the positions of the two annular closed curves, which is generally seen in the cross section or the profile of the model. The repair method of firstly stitching two hole boundaries and then optimizing the triangulation and fitting the surface is suitable.

(4) Simple hole: it refers to a single hole with no triangle surface data inside and only one closed boundary, as shown in Figure 11. It is the simplest type of single holes, and it is the type of hole that most repair methods are applicable to.

(5) Island hole: it refers to the existence of an independent grid area composed of triangle surfaces inside a hole, as shown in Figure 12. This individual grid area is called an island, and the number of islands can be one or more. According to the size of the islands, different repair methods can be selected,

such as the multidirectional advancing method [27] and variational implicit surfaces [4].

4.2. Intelligent Identification Method of Single Holes. After the identification and the segmentation of complex holes into single holes, the shapes of single holes are still different. To prevent various repair defects, different repair methods should be adopted according to hole types. Therefore, an intelligent identification method of single holes is researched to avoid human errors, which can judge the types of five holes in turn and realize the automatic and accurate identification of single holes. The specific judgment process is shown in Figure 13. It is described as follows.

Step 1: preprocess the model.

Traverse all the parts of the triangular model and output the basic information of every single hole, for instance, vertexes, free edges, and boundaries. This step provides a data basis for other steps.

Step 2: judge whether there is a crack hole.

Calculate the included angle and the cumulative included angle of any two edges that constitute the single hole. If the value is less than the set threshold value, output the hole as a crack hole; if not, proceed to Step 3.
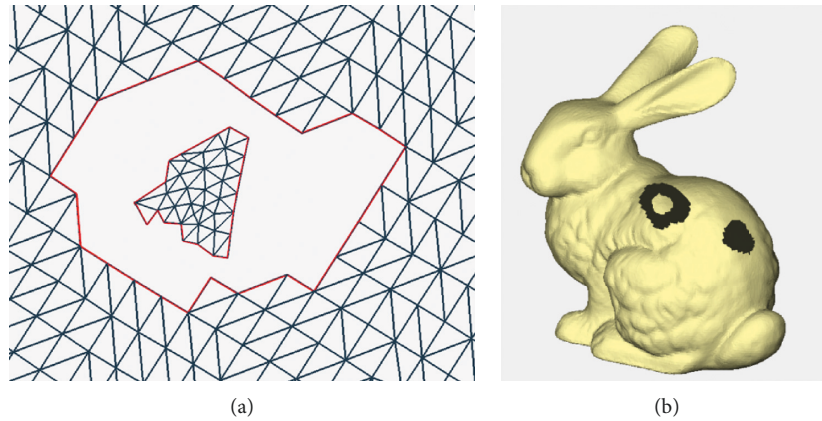
FIGURE 12: Island hole. (a) Triangle mesh example. (b) Model example.
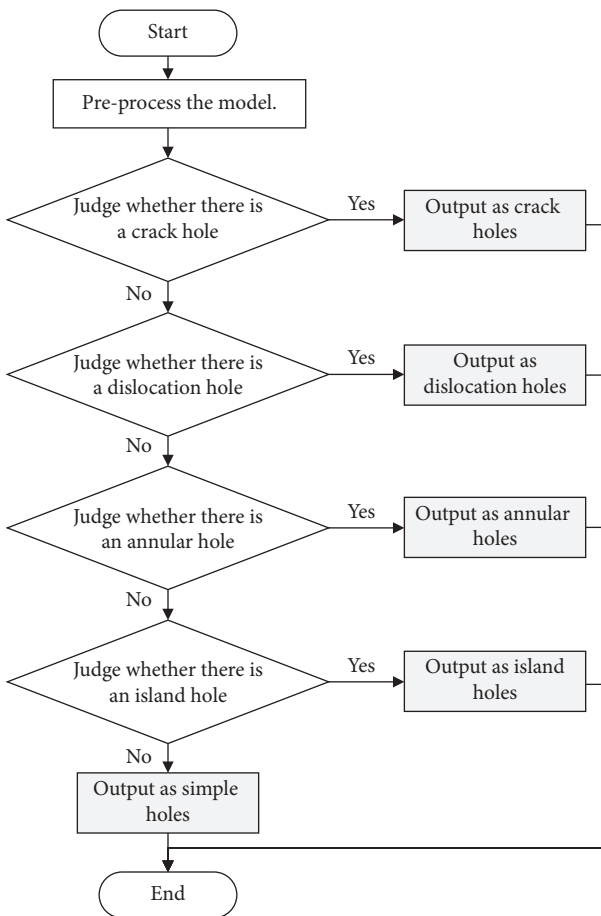
FIGURE 13: Identification process of single holes.

Step 3: judge whether there is a dislocation hole.

Calculate the distance between points on the single hole and on their nearest edges. If it is less than the set distance, the current point is the dislocation point and output the hole as a dislocation hole; if not, continue with Step 4.

Step 4: judge whether there is an annular hole.

Determine whether there are two boundaries that are the closest and most similar to each other and whether

the gravity center of one boundary is within another boundary on the fitting plane. If so, output the hole as an annular hole; if not, proceed to Step 5.

Step 5: judge whether there is an island hole.

Determine whether there are one or more boundaries that are inside another boundary. If so, output it as an island hole; if not, output it as a simple hole.

Step 6: end.

5. Experimental Results and Discussion

As few studies have been conducted on the classification and identification method of the complex holes with intersection points in triangle mesh models, it is difficult to find a targeted algorithm for comparison. For this reason, the well-known commercial software Geomagic is selected to determine the identification and repair effect of the proposed method. All the developed algorithms are implemented in C++ by using Visual Studio 2013 and tested on a PC equipped with an Intel® Core i7-4790 processor and 8 GB of RAM on Windows 10. In the process of comparison, various proven methods in repairing different single holes can be chosen. Crack holes and dislocation holes are repaired through the suture or kneading of the corresponding points. Annular holes, simple holes, and island holes are repaired with the variational implicit surface algorithm [28–30].

Taking the backpack model in Figure 14 as an example, the model has a complex hole, including multiple single holes and complex continuous holes. All single holes and continuous holes can be identified by the proposed hole identification method. The red lines represent continuous holes, and the green lines represent single holes. Two sets of continuous holes are identified, that is, the area surrounded by dash-dotted lines. By means of the continuous hole segmentation method, the upper continuous hole can be merged into a complete single hole and the lower continuous hole can be divided into five simple holes. Therefore, it has been verified that this method can be applied to identify and to partition complex holes. It can provide effective preprocessing that facilitates subsequent hole repair.
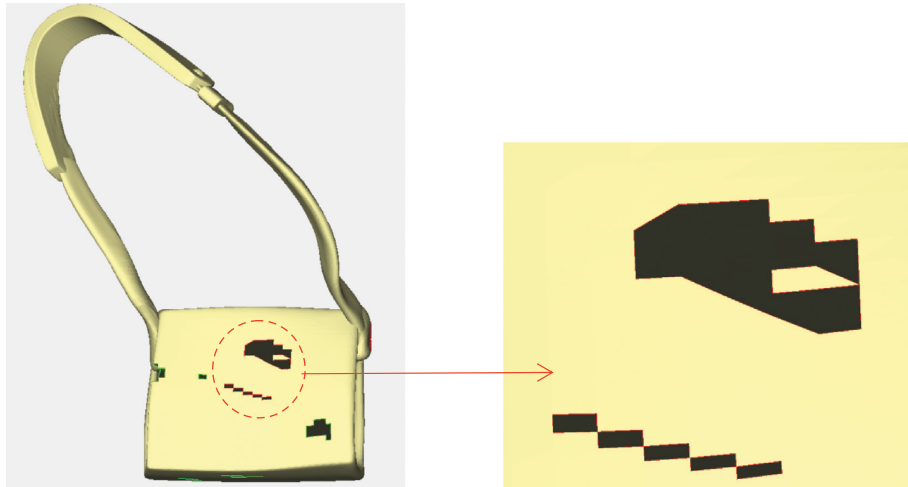
FIGURE 14: Backpack example model.

(a)

(b)
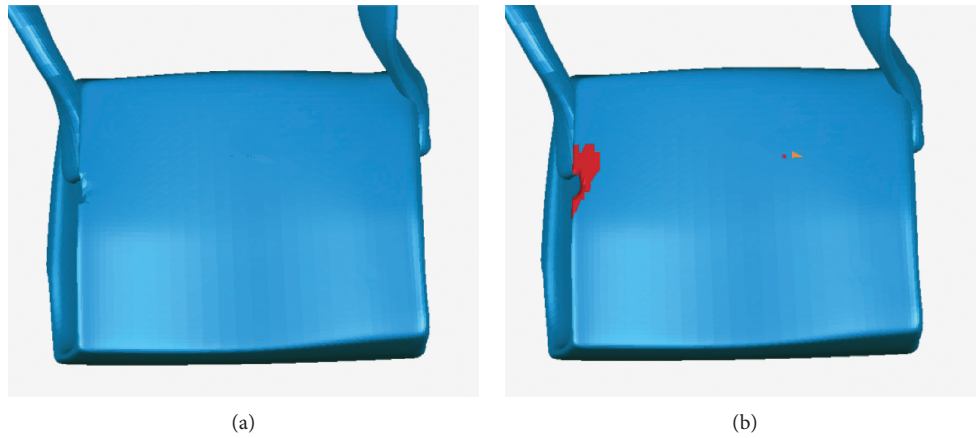
FIGURE 15: Comparison of repair results—continuous holes of a backpack model. (a) Repaired with the proposed method. (b) Repaired with Geomagic.

(a)

(b)
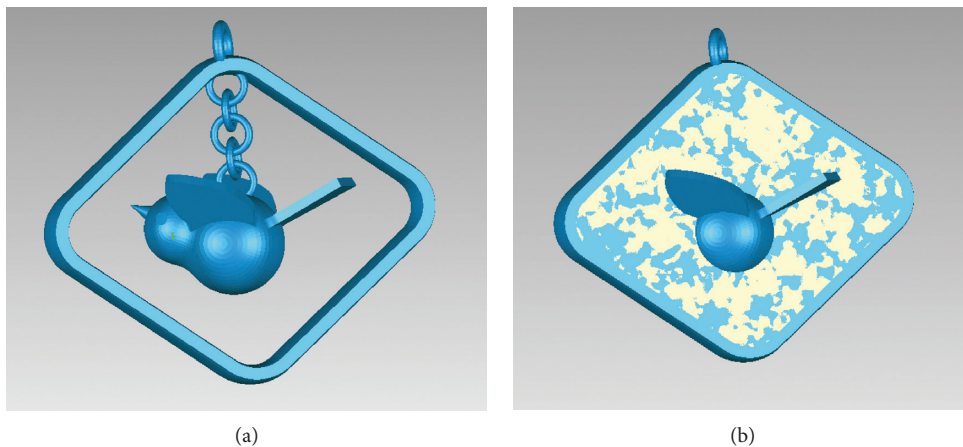
FIGURE 16: Comparison of repair results—annular holes of a bird pendant model. (a) Repaired with the proposed method. (b) Repaired with Geomagic.
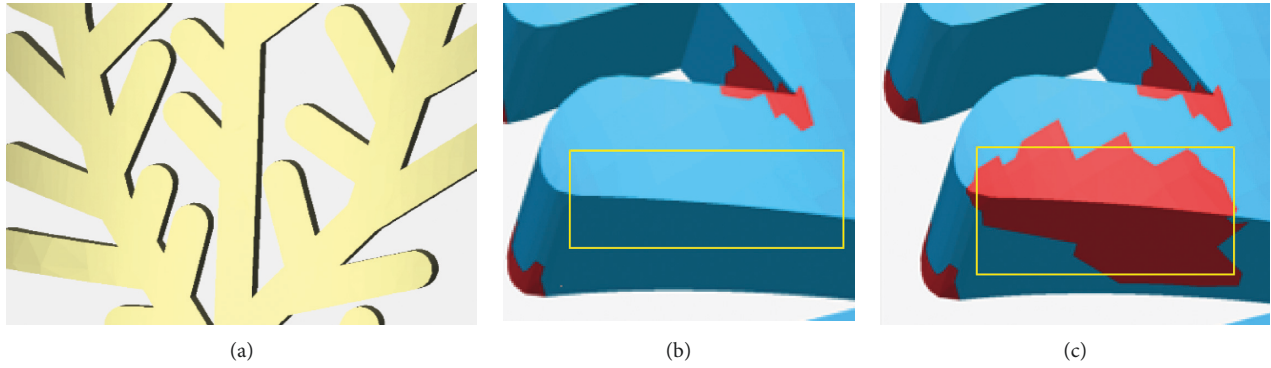
FIGURE 17: Comparison of repair results—crack holes and dislocation holes of a leaf model. (a) Repaired with the proposed method. (b) Enlarged view repaired with the proposed method. (c) Enlarged view repaired with Geomagic.
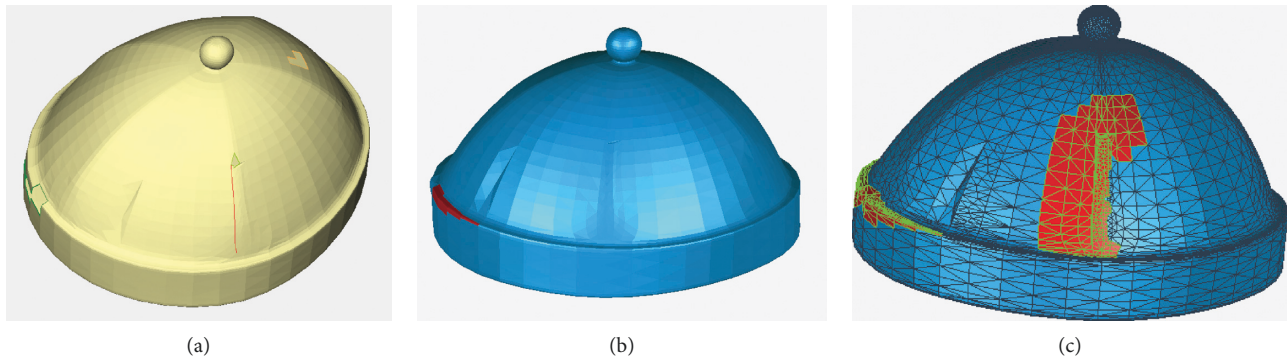
FIGURE 18: Comparison of identification and repair results—complex holes of a hat model. (a) Original model with holes. (b) Repaired with the proposed method. (c) Repaired with Geomagic.

The repair result of the algorithm proposed in this paper is compared with Geomagic. In terms of the identification and repair of continuous holes, the proposed method can accurately complete the complex hole segmentation and repair, but the commercial software generates multiple spikes and a large number of highly refracted edges, as shown in Figure 15. In terms of the identification and repair of annular holes, the model is corrected after being repaired with the proposed method and many self-intersecting surfaces are produced with Geomagic, which destroy the original structure of the model, as shown in Figure 16.

In terms of the identification and repair of crack holes and dislocation holes, as shown in Figure 17, the repaired crack holes and dislocation holes are located in the yellow box. The model structure is normal after being repaired by the proposed method, and the repaired region does not produce self-intersecting and highly refractive edges. After the repair of Geomagic, a number of self-intersecting surfaces, highly refractive edges, and surrounding degenerate triangles, indicated by the red area, are generated. After the degenerate triangles are deleted, it has been found that there are obvious degenerate surfaces in the repaired model, which is not conducive to the subsequent editing and 3D printing of the model.

For the identification and repair of complex holes, the hat model and the ornament model are also chosen for

validation, as shown in Figures 18 and 19. In the hat model, eight crack holes and three simple holes were identified and partitioned. In the ornament model, one annular hole, two simple holes, and one island hole were identified. After using the identification and repair methods in this paper, the models are all better treated. By contrast, there is an obvious error in the repair of annular holes with Geomagic for the ornament model. The error is circled by a red line, as shown in Figure 19.

To accurately check the repair quality, the above two repaired models were scanned by a grid doctor. In terms of the six types of repair defects, including nonmanifold edges, self-intersections, highly-creased edges, spikes, small components, and small holes, Geomagic is found to generate more defects such as spikes, highly creased edges, and self-intersections, while the model repaired by the proposed method has fewer defects and a higher repair quality. The repair time of the proposed method is equivalent to Geomagic; thus, the repair efficiency is acceptable. Specific comparison information is shown in Table 1.

Through the above examples, it can be found that the complex continuous holes containing intersection points can be segmented and all kinds of holes can be accurately identified with the proposed method, as shown in Table 2. Subsequently, the existing mature methods can be used to repair corresponding holes and the repaired models have

(a) (b) (c)
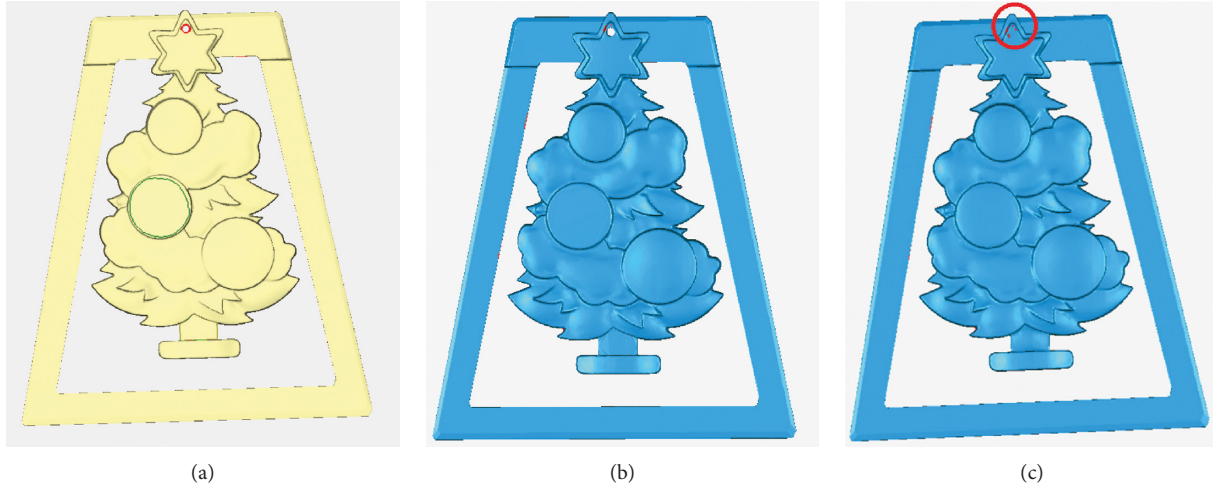
FIGURE 19: Comparison of identification and repair results—complex holes of an ornament model. (a) Original model with holes. (b) Repaired with the proposed method. (c) Repaired with Geomagic.

TABLE 1: Comparison of repair results after inspection.

Models	Methods	Nonmanifold edges	Self-intersections	Highly creased edges	Spikes	Small components	Small holes	Repair time (s)
Hat	Geomagic	0	100	64	24	0	0	0.093
	The proposed method	0	0	0	12	0	0	0.090
Ornament	Geomagic	0	188	113	0	0	0	0.082
	The proposed method	0	0	26	0	0	0	0.086

TABLE 2: Comparison of hole identification and repair results.

Models	Methods	Continuous holes	Simple holes	Crack holes	Dislocation holes	Annular holes	Island holes
Backpack	Geomagic	×	√	—	—	—	—
	The proposed method	√	√	—	—	—	—
Bird pendant	Geomagic	—	—	—	—	×	—
	The proposed method	—	—	—	—	√	—
Leaf	Geomagic	—	—	×	×	—	—
	The proposed method	—	—	√	√	—	—
Hat	Geomagic	—	√	×	—	—	—
	The proposed method	—	√	√	—	—	—
Ornament	Geomagic	—	√	—	—	×	√
	The proposed method	—	√	—	—	√	√

"×" represents that the model has such holes and the method is not workable; "√" represents that the model has such holes and the method is workable; "—" represents that the model does not have such holes.

fewer repair defects and a higher repair quality. However, some of these holes cannot be well segmented and identified with Geomagic without the participation of professionals. The proposed repair process is completely automated, replacing the manual judgment and repair operation, reducing the dependence on professionals.

6. Conclusion

In this work, an intelligent identification and classification method of complex holes is proposed. It can identify,

partition, and reconstruct complex holes into single holes based on the intersection points connecting multiple hole lines and classify all the single holes into five types, such as crack holes, dislocation holes, annular holes, simple holes, and island holes. Thus, proper hole repair algorithms can be selected according to the type of the single holes. Compared with Geomagic software, the proposed method can mostly avoid the intersection of various hole lines and reduce the defects of traditional hole repair methods, but it can achieve similar efficiency. The proposed method provides a new idea for the automatic hole repair of triangle meshes without the

participation of professionals and can be widely used in 3D printing model repair.

In future work, first, the identification method of boundary holes that do not have closed hole lines should be researched. Second, it is recommended to select and study more accurate repair algorithms for some single holes with large curvature variations to further improve the repair results.

Data Availability

The data used to support the findings of this study are included within the article.

Conflicts of Interest

The authors declare that there are no conflicts of interest regarding the publication of this paper.

Acknowledgments

References

[1] I. Karakurt and L. Lin, "3D printing technologies: techniques, materials, and post-processing," *Current Opinion in Chemical Engineering*, vol. 28, pp. 134–143, 2020.

[2] D. A. W. Rahito, D. Wahab, and A. Azman, "Additive manufacturing for repair and restoration in remanufacturing: an overview from object design and systems perspectives," *Processes*, vol. 7, no. 11, 802 pages, 2019.

[3] Q. Wang, P. F. Yang, Y. Y. Jiang, G. Zhang, and L. Huang, "A topology structure repair algorithm for triangular mesh model," in *Proceedings of the 13th International Conference on Embedded Software and Systems (ICESS)*, Chengdu, China, October 2016.

[4] J. Wang, *Research on approaches to filling complex holes in triangular mesh models*, Ph.D. Thesis, Dalian University of Technology, Dalian, 2020.

[5] Z. Yang, "Quadrilateral mesh boundary classification and editing," in *Proceedings of the 2017 ACM SIGCSE Technical Symposium on Computer Science Education*, pp. 789-790, New York, NY, USA, March 2017.

[6] V. S. Nguyen, A. Bac, and M. Daniel, "Boundary extraction and simplification of a surface defined by a sparse 3D volume," in *Proceedings of the Third Symposium on Information and Communication Technology*, New York, NY, USA, August 2012.

[7] Z. P. Liao, K. Liu, and Y. Xiang, "Boundary points extraction method of planar point cloud based on multi-threshold," *Journal of Computer Applications*, vol. 36, pp. 1933–1937, 2016.

[8] D. Z. Sun, H. D. Liu, Y. Shi, and C. Cai, "Boundary feature abstraction of unorganized points based on kernel density estimation," *Transactions of the Chinese Society for Agricultural Machinery*, vol. 44, pp. 275–279+268, 2013.

[9] L. J. Tong and J. C. Zheng, "Secondary extraction algorithm for scattered point cloud surface boundary," *Computer Engineering*, vol. 43, pp. 252–256, 2017.

[10] M. Milroy, C. Bradley, and G. Vickers, "Segmentation of a wrap-around model using an active contour," *Computer-Aided Design*, vol. 29, no. 4, pp. 299–320, 1997.

[11] X. Orriols and X. Binefa, "Finding breaking curves in 3D surfaces, Pattern Recognition and Image Analysis," in *Proceedings of the Iberian Conference on Pattern Recognition and Image Analysis*, pp. 681–688, Berlin, Heidelberg, June 2003.

[12] G. H. Bendels, R. Schnabel, and R. Klein, "Fragment-based surface in painting," in *Eurographics Symposium on Geometry Processing*, M. Desbrun and H. Pottmann, Eds., Eurographics Association, Montreal, Canada, 2005.

[13] L. Q. Liu, *Processing Algorithms on Scattered point Cloud*, Ph.D. Thesis, Northwest University, Xian, 2010.

[14] A. Alrashdan, S. Motavalli, and B. Fallahi, "Automatic segmentation of digitized data for reverse engineering applications," *IIE Transactions*, vol. 32, no. 1, pp. 59–69, 2000.

[15] X. Zhan and J. S. Zhang, "Research on algorithm of integrating boundary extraction and triangle mesh generation of point cloud," *Computer Simulation*, vol. 30, pp. 272–275, 2013.

[16] J. Chen, C. H. Gao, and B. W. He, "Automatic recognition of boundary features of non-closed triangulation model," *Machinery Design & Manufacture*, vol. 11, pp. 147–149, 2011.

[17] G. Li, X.-Z. Ye, and S.-Y. Zhang, "An algorithm for filling complex holes in reverse engineering," *Engineering with Computers*, vol. 24, no. 2, pp. 119–125, 2008.

[18] Z. L. Wei, Y. X. Zhong, C. L. Yuan, and R. Li, "Research on smooth filling algorithm of large holes in triangular mesh model," *China Mechanical Engineering*, vol. 8, pp. 949–954, 2008.

[19] Q. Wang, *Research and Application of Triangular Mesh Models Transition and Hole Repairing Algorithm*, Ph.D. Thesis, Nanjing University of Aeronautics and Astronautics, Nanjing, 2007.

[20] S. Liu and C. C. Wang, "Quasi-interpolation for surface reconstruction from scattered data with radial basis function," *Computer Aided Geometric Design*, vol. 29, no. 7, pp. 435–447, 2012.

[21] J. Wang and M. M. Oliveira, "Filling holes on locally smooth surfaces reconstructed from point clouds," *Image and Vision Computing*, vol. 25, no. 1, pp. 103–113, 2007.

[22] X. Wang, X. Liu, L. Lu, and B. J. B. X. Li, "Automatic hole-filling of CAD models with feature-preserving," *Computers & Graphics*, vol. 36, no. 2, pp. 101–110, 2012.

[23] Y. Jun, "A piecewise hole filling algorithm in reverse engineering," *Computer-Aided Design*, vol. 37, no. 2, pp. 263–270, 2005.

[24] J. Y. Lai and S. H. Hsu, "On the development of a hole filling algorithm for triangular meshes," *Journal of the Chinese Institute of Engineers*, vol. 30, no. 5, pp. 877–889, 2007.

[25] C. Feng, J. Liang, M. Ren, and G. W. S. Qiao, "A fast hole-filling method for triangular mesh in additive repair," *Applied Sciences*, vol. 10, no. 3, 969 pages, 2020.

[26] P. Z. Wen, Y. Q. Lei, and M. L. Sun, "Defective hole identification and hole-filling for 3D reconstruction mesh models," *Application Research of Computers*, vol. 37, pp. 1234–1238, 2020.

[27] S. Li, C. C. Ma, and F. Lu, "Island hole repairing based on multi-directional advancing method," *China Mechanical Engineering*, vol. 30, no. 20, pp. 2473–2479, 2019.

[28] G. Turk and J. F. O'Brien, "Modelling with implicit surfaces that interpolate," *ACM Transactions on Graphics*, vol. 21, no. 4, pp. 855–873, 2002.

[29] X. Jin, H. Sun, and Q. Peng, "Subdivision interpolating implicit surfaces," *Computers & Graphics*, vol. 27, no. 5, pp. 763–772, 2003.

[30] T. Karkanis and A. J. Stewart, "Curvature-dependent triangulation of implicit surfaces," *IEEE Computer Graphics and Applications*, vol. 21, no. 2, pp. 60–69, 2001.

Research Article

A Cooperative Lightweight Translation Algorithm Combined with Sparse-ReLU

Xintao Xu [ID],[1,2] **Yi Liu** [ID],[2] **Gang Chen** [ID],[2] **Junbin Ye** [ID],[2] **Zhigang Li** [ID],[2] **and Huaxiang Lu** [ID][2,3,4,5]

[1]*School of Microelectronics, University of Science and Technology of China, Hefei, China*
[2]*Institute of Semiconductors, Chinese Academy of Sciences, Beijing, China*
[3]*Materials and Optoelectronics Research Center, University of Chinese Academy of Sciences, Beijing, China*
[4]*College of Microelectronics, University of Chinese Academy of Sciences, Beijing, China*
[5]*Semiconductor Neural Network Intelligent Perception and Computing Technology Beijing Key Laboratory, Beijing, China*

Correspondence should be addressed to Gang Chen; chengang08@semi.ac.cn

In the field of natural language processing (NLP), machine translation algorithm based on Transformer is challenging to deploy on hardware due to a large number of parameters and low parametric sparsity of the network weights. Meanwhile, the accuracy of lightweight machine translation networks also needs to be improved. To solve this problem, we first design a new activation function, Sparse-ReLU, to improve the parametric sparsity of weights and feature maps, which facilitates hardware deployment. Secondly, we design a novel cooperative processing scheme with CNN and Transformer and use Sparse-ReLU to improve the accuracy of the translation algorithm. Experimental results show that our method, which combines Transformer and CNN with the Sparse-ReLU, achieves a 2.32% BLEU improvement in prediction accuracy and reduces the number of parameters of the model by 23%, and the sparsity of the inference model increases by more than 50%.

1. Introduction

Machine translation, an essential branch of computational linguistics, is a process of translating source language into the target language by computer. Translation has extremely high requirements for translators, and at the same time, there is a lack of professional translators, so machine translation has made significant progress in international exchanges [1]. In recent years, deep learning technology has developed rapidly. Researchers have introduced neural network into language model, which can better process the representation of common and rare words. For example, a recurrent neural network (RNN) can adapt to any sentence length and process the context recurrently to get the final result. Transformer applies the attention mechanism to machine translation and has better translation quality than traditional methods.

Compared with traditional statistical machine translation, which requires elaborate features, the flexibility of existing machine translation based on neural networks is greatly improved. Methods based on RNN and its derived models such as GRU and LSTM need to learn the long-distance dependencies of each input word vector. The principle is to use the embedding layer to map sentences to the embedding space and then use the hidden layer to compute the knowledge obtained in the previous step. As multiple hidden layers compute sequentially, calculations within a single hidden layer are executed sequentially and cannot be carried out in parallel. Different from the scheme of the RNN model that continuously accumulates input information, the Transformer network uses the Encoder-Decoder structure.

Because of its stacking self-attention layer and point-by-point full connection layer, the recursive structure in RNN is eliminated, and the network based on Transformer has the advantage of high parallelism. Transformer offers significant improvements to machine translation, but at the cost of a

large number of parameters. The number of BERT large parameters is 334M, the number of BERT base parameters is 109M, and the number of IB-BERT large parameters is 293M. Due to its large number of parameters and low sparsity of parameters, it is generally applied to the server side, and there is no suitable edge side Transformer algorithm. The existing RNN model must wait for all previous input processing to be completed before processing the next input, which is a bottleneck when processing long sequences. The number of operations required by the RNN model to correlate information from two arbitrary input or output positions increases as the position distance increases. This makes extracting complicated dependencies between far-away positions more difficult. Therefore, RNN is difficult to parallel, which is not conducive to hardware acceleration, and the translation effect is not ideal. On the other hand, the hardware-implementation-friendly CNN can not effectively process location information and is not effective in machine translation tasks when applied alone.

It is an effective method for hardware deployment of the neural network to reduce parameter storage and transmission amount and reduce the dependence on hardware data transmission bandwidth by using the compressed sparse matrix method. And it has little influence on algorithm accuracy. The premise of this scheme is that the sparsity of algorithm parameters is high enough. The weight parameters of the Transformer have not been optimized for sparsity, which is difficult to be applied to hardware accelerated by a compressed sparse matrix [2, 3]. The traditional ReLU activation function adopted by Transformer models such as [4] does not improve the sparsity of the neural network algorithm to the maximum extent. An appropriate activation function is an important measure to improve network performance and reduce the number of network parameters.

The hardware deployment machine translation algorithm must meet the requirements of lightweight and maintain high-precision translation results. At the same time, in order to further reduce the difficulty of deployment on edge devices, the algorithm optimization must improve the sparsity of weight parameters, so as to use the sparse matrix compression method for hardware deployment. To solve the above problems, this research proposes a new activation function that can improve the algorithm accuracy and parameter sparsity at the same time and designs a cooperative machine translation algorithm combining CNN to extract local features and Transformer to process sequence information. Our method combined with Sparse-ReLU improved the BLEU score of the algorithm to 35.24, increased the sparsity by more than 150%, and controlled the total number of parameters within 38M. Our main contributions are as follows:

(1) A new activation function, Sparse-ReLU, is proposed and applied to the machine translation model. The BLEU score of the IWSLT14 German-English translation task is enhanced from 34.29 to 35.16 by using the model whose parameter scale is 36.42 M. The number of parameters has been reduced, and more than 50% of sparsity has grown. Meanwhile, Sparse-ReLU can improve the translation effect.

(2) A Transformer structure with low number of parameters is proposed, which only uses three attention heads and a 7-layer encoder and decoder. The number of parameters of this structure is only 36.42 M, which solves the problem that Transformer is too large to be deployed on the hardware.

(3) A CNN structure for machine translation tasks is proposed and combined with a Transformer to optimize the network. The number of parameters of the overall algorithm is 37.99 M. The BLEU score is increased from 35.16 to 35.24.

1.1. Related Works.

The machine translation algorithm based on the neural network generally adopts the Encoder-Decoder model to deal with the machine translation task [5]. The encoder takes the source sentence as input and calculates a real expression value. The decoder inputs the real expression value and generates the target translation. CNN, RNN, and Transformer are the classical algorithms for constructing the Encoder-Decoder structure.

Machine translation jobs can be processed serially using an approach based on RNN and its derivatives LSTM [6, 7] and GRU [8]. It has the advantage of high extraction ability in processing series information. For example, the RNN-based algorithm [9, 10] generates dynamic context representation through its Encoder-Decoder architecture based on attention mechanism. Research [11] creates target phrases with fixed source statement representation. To make the RNN and its derivative networks deeper and better, [12] employs a residual strategy and skip connections to further the RNN development.

The Transformer based algorithm [4] and its variants [5, 13–16] achieve the most advanced results on multiple language pairs only based on the attention mechanism. Research [13] improves the effect by increasing the scale of model parameters. Still, increasing the number of parameters means that more extensive data sets are needed, and the training is more complicated. It is not suitable for hardware, especially edge devices. CNN-based algorithms [17, 18] are concerned because of their high parallelism. Among them, [17] proposes a CNN-based machine translation algorithm with higher parallelism and a shorter long-term dependency than RNN.

Machine translation projects employ a variety of Transformer structures to optimize the size of the model and precision, as well as the bandwidth required for hardware deployment. Research [2] proposes a pruning algorithm to increase model sparsity and deploy the model on GPU, and research [19] proposes a sparse matrix calculation method. Both of them reduced the bandwidth requirements of matrix calculation on hardware. One is to improve the activation functions such as the ReLU and SoftMax. Research [20] introduces a novel activation function WReLU for lightweight neural network design. Research [16] introduces a random calculation method to replace the traditional SoftMax calculation, which reduces the calculation complexity and improves the speed. Research [14] is a collaborative processing scheme that combines the advantages of
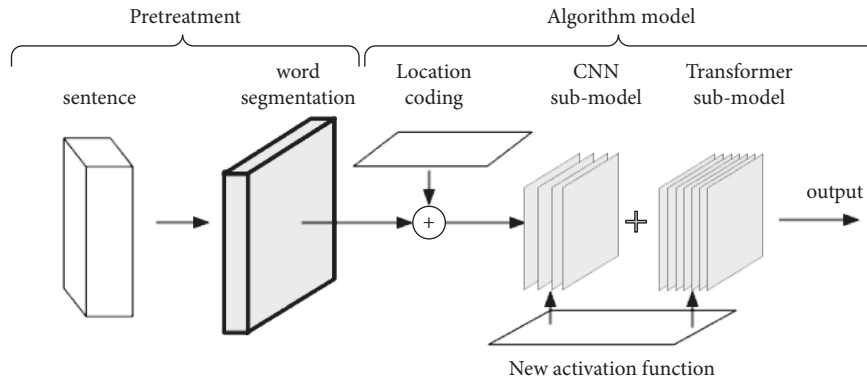
FIGURE 1: Overall structure of the algorithm.

multiple networks, and it combines BiLSTM and recurrent attention for machine translation tasks.

These works have effectively promoted the development of machine translation. However, most of the existing Transformer schemes dealing with machine translation tasks only use the attention mechanism and lack the research results combined with the CNN model. Most optimized networks are still too large, and there are defects in input sequence order when using the RNN model to process sequence information. The effect of processing sequence information using the CNN model is not ideal, making them challenging to deploy in edge devices. Based on these, the new activation function Sparse-ReLU, CNN submodel structure, Transformer submodel structure, and cooperation scheme proposed in this research achieve a better effect under a particular parameter scale condition.

1.2. Method. Unlike prior machine translation Transformer algorithms, this study proposes a Transformer model with few parameters, a CNN submodel, and a novel activation function Sparse-ReLU. CNN and Transformer submodels use Sparse-ReLU to optimize the effect. The three of them cooperate in dealing with machine translation tasks. CNN can process local information of word vectors and extract multiple features containing position-coding, and the attention mechanism can process local features extracted by CNN rather than input sentences. Figure 1 shows the process of our algorithm.

Figure 1 depicts the translation process. The input and output of the algorithm model are symbol sequences, and the word segmentation operation of the input symbol sequence uses the BPE word segmentation method. The position-coding operation embeds the position information into the symbol sequence obtained by word segmentation. The CNN submodel extracts the features of sentences containing location coding information. The Transformer submodel further extracts the output information of the CNN submodel. Both submodels use Sparse-ReLU.

2. Model Structure

2.1. Activation Function That Can Improve Sparsity and Accuracy. Most neural network algorithms currently

require activation functions to introduce nonlinear operations. However, activation functions such as sigmoid have the disadvantages of complex hardware implementation and high resource consumption in algorithm deployment. When implementing the algorithm in hardware, sparse matrix acceleration is a viable option, and sparse matrix acceleration necessitates high weights sparsity. The ordinary activation function can not maximize sparsity matrix compression technology. Based on this, this research proposes a new activation function Sparse-ReLU for hardware optimization. The activation function has the advantages of low hardware implementation cost and low computing time like the traditional ReLU function. It solves the disadvantages of limited representation ability and insufficient flexibility of the conventional ReLU function.

For machine translation and other applications in natural language processing, real-time computing requirements are high. Because of its low power consumption and small area, the edge devices cannot effectively deploy translation algorithms with huge parameters. In particular, the Transformer algorithm, although the translation effect is good, can only be deployed on the server-side. It is of great significance to realize the activation function with high flexibility and simple hardware implementation.

The activation function designed in this research can improve the sparsity and accuracy of neural networks. The expression is shown in formulas (1)–(4), in which the range of parameter a is $(0, 1)$, the content of b is $(0,1)$, which satisfies $a < b$ and $c < d$, and both a and b need to meet the relationships of $0.125x$, to complete the multiplication calculation only through the hardware shift operation. As shown in formula (1)–(3), the three subfunctions of Sparse-ReLU are y_0, y_1, and y_2.

$$y_0 = 0, \tag{1}$$

$$y_1 = a \times (x - c), \tag{2}$$

$$y_2 = b \times (x - d). \tag{3}$$

The function of the subfunction $y_0 = 0$ shown in Formula (1) is to set the activation value of the neural network to 0 and improve the sparsity of its activation value. The
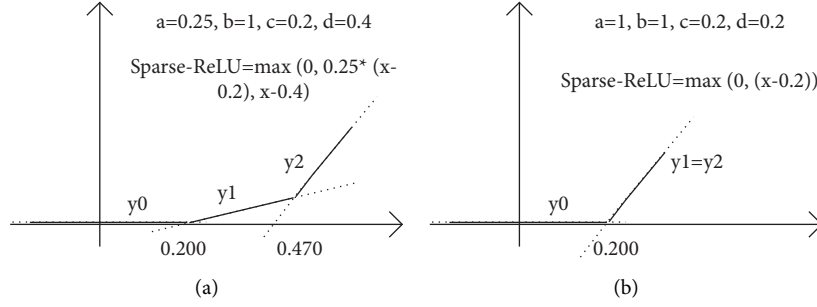
Figure 2: Sparse-ReLU function.

traditional ReLU function sets the input of all negative numbers to 0 and the positive part to itself. The y_0 function in this research puts the output to 0 no matter what the input is. However, doing so will cause all information to be lost, so formulas (2) and (3) are required to retain the information. Taking the maximum value of the three subfunctions can obtain the formula of Sparse-ReLU.

$$\text{Sparse} - \text{ReLU} = f(x) = \max_{x \in (-\infty, +\infty)} (y_0, y_1, y_2). \quad (4)$$

When determining parameters a, b, c, and d, the functions with large c and d are preferred under the same translation effect, improving the sparsity of the weights and activations of neural network. When setting the parameters of Sparse-ReLU to $a = 0.25$, $b = 1$, $c = 0.2$, and $d = 0.4$ in Figure 2(a), the translation effect of the activation function is the best. According to the formula, the traditional ReLU function is a subset of the activation function designed in this research. Figure 2(b) is the image of setting parameters $a = 1$, $b = 1$, $c = 0.2$, $d = 0.2$ to make $Y1 = Y2$ in Sparse-ReLU. In this case, Sparse-ReLU degenerates into an offset traditional ReLU function. Furthermore, ReLU is a subset of Sparse-ReLU, and the characterization power of Sparse-ReLU is higher.

In this research, Sparse-ReLU replaces the traditional function to provide nonlinear characteristics for the network. It is applied between two fully connected layers or between the CNN layer and the fully connected layer in the network. Parameters a, b, c, and d in Sparse-ReLU are found through training, to make the effect of the network model better than that of the traditional ReLU activation function. According to the iterative experiment, the German-English translation task of IWSLT14 dataset performs best when the parameters are $a = 0.25$, $b = 1$, $c = 0.1$, and $d = 0.4$. After determining parameters in Sparse-ReLU, combined with the pruning operation, the sparsity of the network model is improved. Unlike other sparsity improvement methods, this activation function can enhance the sparsity of weight parameters and the sparsity of activation, which is convenient for further hardware acceleration using a sparse matrix.

Because it can efficiently use shift and addition operations to realize the activation function in hardware and complete the prediction task of the model based on Sparse-ReLU, Sparse-ReLU can obtain multiple zero values, in which the experimental statistics are more than 50% higher than the value close to zero in the ordinary ReLU activation

value. So, it can effectively improve the network sparsity. It has the characteristics of low resource consumption in hardware implementation and can enhance the sparsity of neural network parameters and the accuracy of the model prediction. Figure 3 shows the application of Sparse-ReLU in the model, as discussed in Section 1.2.

2.2. Transformer and CNN Submodels Combined with Sparse-ReLU.
Figure 1 shows the overall design, which is made up of a CNN and a Transformer submodel. We will introduce the Transformer structure used in this research in detail.

The Transformer structure has a high ability to extract sequence information. Figure 4 shows the Transformer structure in this research, composed of the residual layer, multihead attention layer, Sparse-ReLU layer, and layer normalization. As shown in Table 1, the parameters of each Transformer structure are listed. It has the characteristics of low parameter quantity. The Encoder combines Sparse-ReLU, which can improve prediction accuracy.

The CNN submodel needs to process the input sentences and extract the features without changing the size of the feature map. Convolution can improve the extraction ability of local features of the network. Figure 5 shows the CNN submodel. After the sentence is entered into the model, it needs to go through embedding and position-coding operation and then carry out layer normalization operation. Finally, utilizing two-dimensional CNN to process the sentence coding results containing position information. Figure 5 shows the CNN structure, where Len is the sentence length.

The input channel of CNN is 1, the output channel is the length of the word vector, that is, 512 channels, the size of convolution kernel is (5,512), the stride step is 1, and the size of padding is two zeros for rows and no padding for columns. The dimension of the feature map before CNN processing is (Len, 512), Len is the sentence length, and the dimension of the feature map after CNN is (512, Len). After dimension transformation and Sparse-ReLU, the fully connected layer maps the result to another dimension and makes the residual connection with the original input. Table 2 lists the detailed measurements of each structure of CNN.

2.3. Collaborative Processing Scheme between CNN and Transformer Submodels.
Considering the strong ability of

(a)   (b)
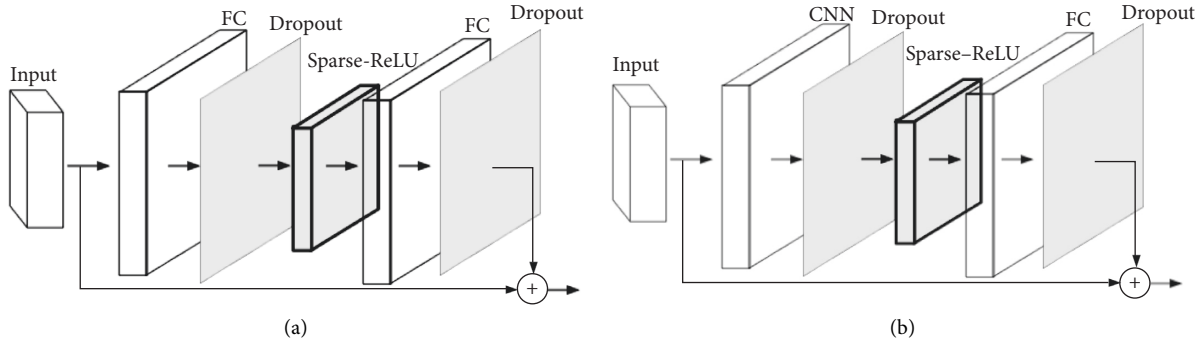
FIGURE 3: The deployment method of Sparse-ReLU function.
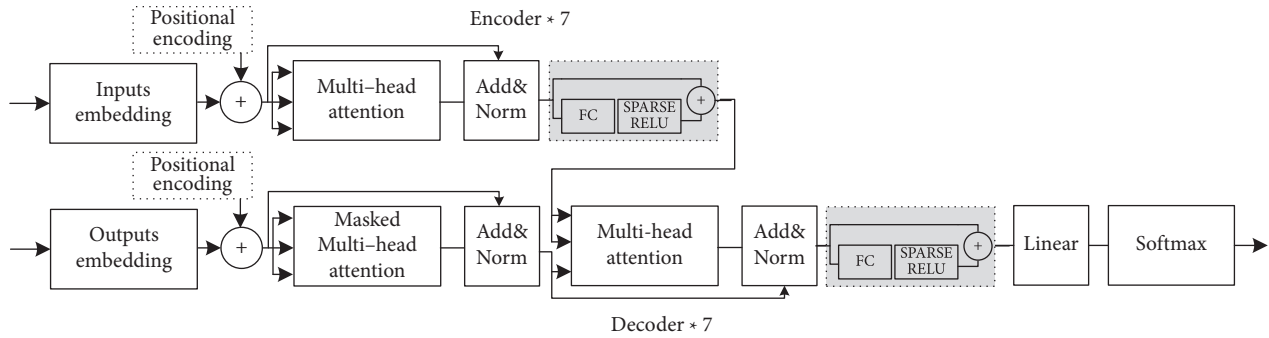
FIGURE 4: Structure of Transformer submodel.

TABLE 1: Transformer submodel size.

Description	Substructure	Layer name	Size
Encoder	MultiHeadAttention	cast_queries	(512, 384)
		cast_keys_values	(512,768)
		cast_output	(384,512)
		softmax	softmax
		layer_norm	eps = 1e-05
		LayerNorm	eps = 1e-05
	PositionWiseFCNetwork	fc_1	(512,1024)
		fc_2	(1024,512)
		Sparse-ReLU	Sparse-ReLU : $a = 0.25, b = 1, c = 0.2, d = 0.4$
Decoder	Embedding	Embedding	(10000, 512)
	MultiHeadAttention	tgt_emb	(10000, 512)
	MultiHeadAttention	pos_emb	(10000, 512)
	PositionWiseFCNetwork	Sparse-ReLU	Sparse-ReLU : $a = 0.25, b = 1, c = 0.1, d = 0.4$
Output	LayerNorm	LayerNorm	eps = 1e-05
	Fc	Fc	(512,10000)

CNN to extract local features, the combination of Transformer and CNN submodels can effectively improve the power of the algorithm to extract local features. There are a variety of cooperative processing strategies for multinetworks, including the concatenation operation method [21], result addition method [22], result point multiplication method [23], and matrix transformation after the concatenation operation. The model in research [21] adopted the method of submodules in series, effectively combined CNN and attention, and proposed an end-to-end ResNet structure model, which was used to extract local features, and summarized the local feature sequence through the attention

mechanism. This research discusses the impact of CNN and Transformer on machine translation tasks. Figure 6 shows the details of various collaborative processing schemes discussed in this research. The CNN submodel of Figure 6 is the structure in Figure 5. Encoder and decoder are also the forms discussed in Figure 4.

To make the size of the matrix output of the CNN submodel be the same as that of the attention submodel, we set the number of output channels of the convolution kernel to be 512, which is the same as the length of the word vector in the matrix output of attention submodel. Figure 6(a) shows the scheme that the attention submodel learns the
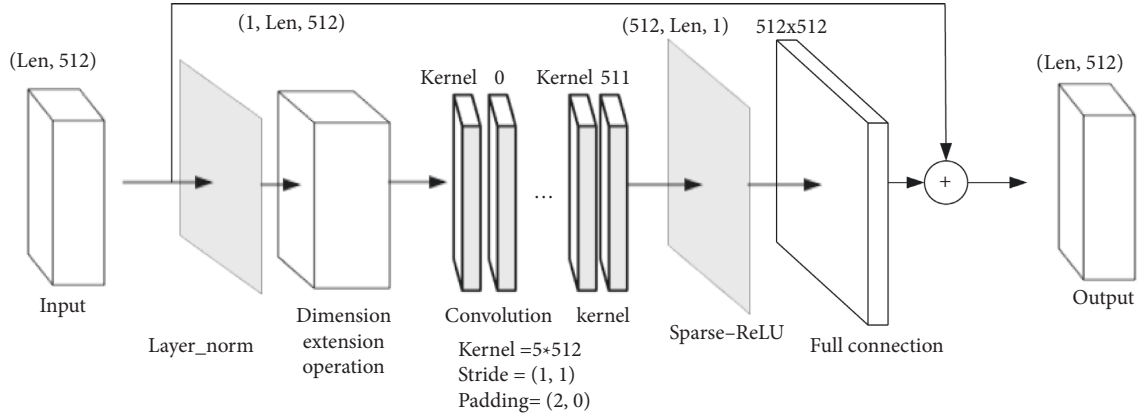
Figure 5: Structure of CNN submodel.

Table 2: CNN submodel size.

Description	Substructure	Layer name	Size
Pretreatment	Embedding and location coding	Embedding	(10000, 512)
CNN	Convolution submodel	LayerNorm	eps = 1e-05
		Conv2d	in_ch = 1, out_ch = 512, kernel = (5, 512), stride = (1, 1), pad = (2, 0)
		Linear	(512, 512)
	Activation function	Sparse-ReLU	Sparse-ReLU : $a = 0.25, b = 1, c = 0.1, d = 0.4$
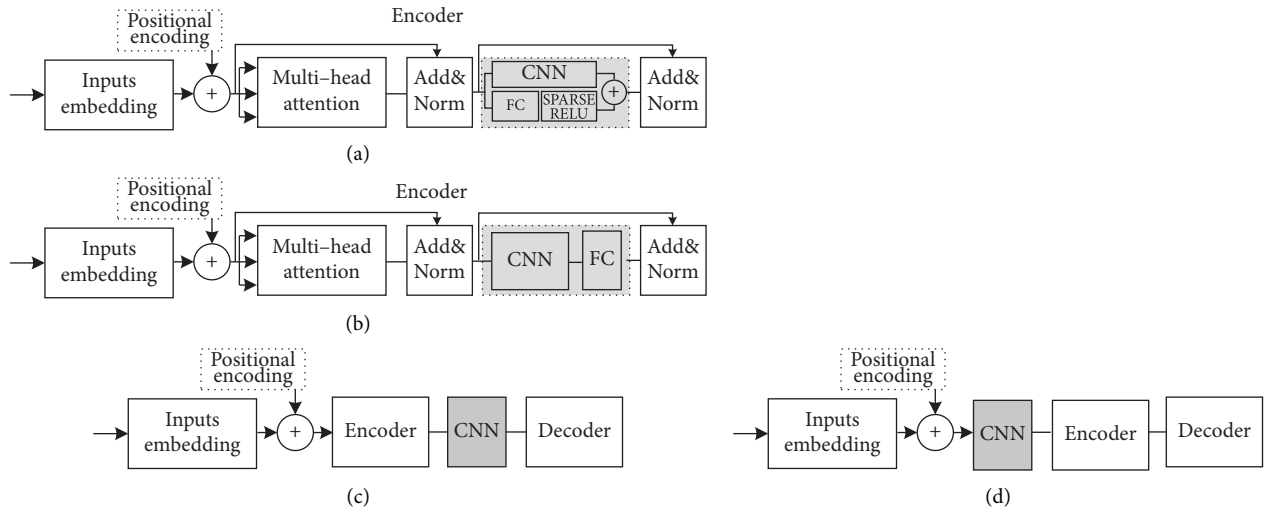
Figure 6: Collaborative scheme of transformer and CNN submodel.

feature of input data, and the feed-forward module consisting of a CNN and a fully connected layer processes the result of attention computation, which is illustrated with the gray box. As shown in Figure 7, the output characteristic matrix of the feed-forward module is the result of the addition of a CNN and a fully connected layer. Figure 6(b) shows how to add a CNN submodel after the multihead attention layer of the encoder in the Transformer. Figure 6(c) uses the attention submodel to summarize the feature sequence from the original sentence, then uses a CNN submodel with a ResNet structure to extract local features from the features summarized by the attention submodel, and finally uses the decoder submodel to decode the target text.

Figure 6(d) shows that the CNN submodel first processes the input sentence and learns the local features of the sentence. The Transformer submodel extracts the sequence features processed by the CNN submodel. After the encoder operation in the Transformer, it is handed over to the decoder submodel for decoding operation again.

2.4. Algorithm Model. Figure 8 shows the details of the model in this research. According to the introduction of the previous three sections, the model in this research mainly includes the convolutional neural network feature extraction layer, encoder layer, and decoder layer. Table 3 shows the structural parameters of the algorithm.
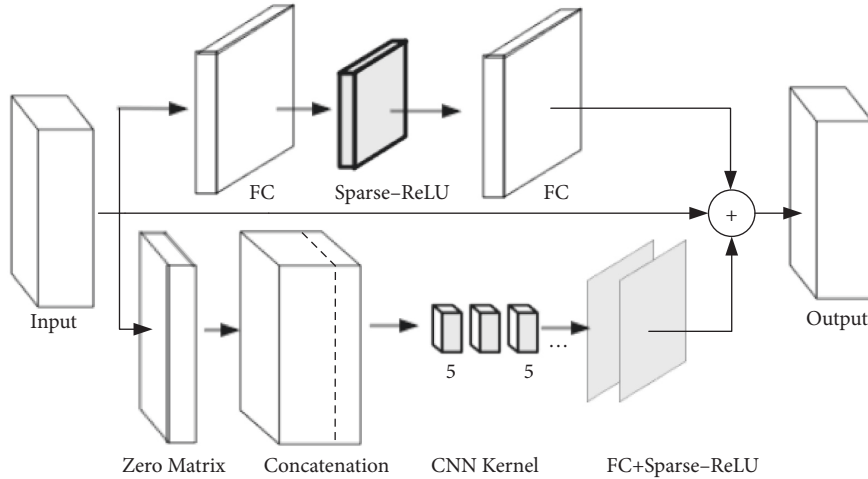
FIGURE 7: Structural details of CNN in Figure 6(a).
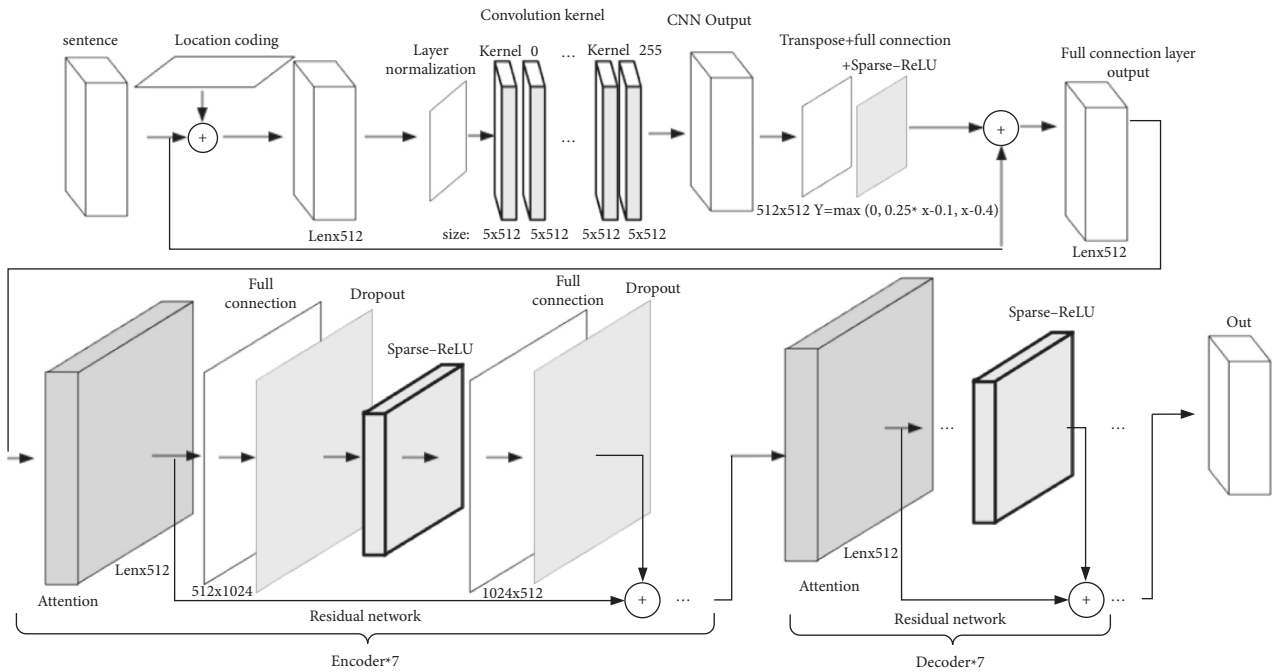
FIGURE 8: Final translation model combined with Sparse-ReLU.

TABLE 3: Parameters of the model.

Parameter name	Small model
d_model	512
n_heads	3
d_queries	128
d_values	128
d_inner	1024
n_layers	7
max_len	300
cnn_kernel	(5,512)
beam_size	5

TABLE 4: Experimental environment.

CPU	Intel(R) Xeon(R) silver 4116 CPU @ 2.10 GHz
Experiment framework	PyTorch 1.4.0
GPU	8 TITAN XP graphics cards
CUDA	CUDA 10.2
OS	Ubuntu 16.04.12

3. Experiment and Result Analysis

3.1. Machine Translation Dataset and Word Segmentation Algorithm. This research selects the German-English translation task for the experiment, and the dataset is IWSLT14. The training set contains 160250 sentences, and the testing set uses 6750 independent sentences [24].

The input and output of the translation algorithm are symbol sequences. These symbols are the basic units of sentences. Because extensive vocabulary cannot be naturally decomposed into words, using words as the basic units

TABLE 5: Translation results of the model.

Standard results	Results of this research
And of course, we all share the same adaptive imperatives	And of course, we all share the same adaptive applications
We're all born. We all bring our children into the world	We're all born. We bring children to the world
And the great indicator of that, of course, is language loss	And the key indicator for this is the extinction of languages

TABLE 6: The comparison results between this model and others (German-English translation task using IWSLT14 dataset).

		BLEU	Size M	Model
Research [17]		23.1	—	Encoder model based on 6-layer CNN.
Research [28]		28.83	—	Tag-less backtranslation
Research [29]		29.9	—	Linear transformer
Research [16]		34.4	—	Random feature attention
Research [30]		34.8	285	Pay less attention with lightweight CNN
		35.20	296	Pay less attention with dynamic CNN
Traditional transformer model [4]		34.44	49.27	Traditional transformer model
This paper scheme	Small model + Sparse-ReLU	34.29	36.42	Small transformer
		35.16		Sparse-ReLU + Small transformer
	Small model + Sparse-ReLU + CNN	35.24	37.99	Sparse-ReLU + small transformer + CNN

to form sentences will make it challenging to train the algorithm. An alternative is to use word segmentation algorithms such as [19, 25] to learn subwords from the dataset. This research uses the method of research [19] for word segmentation, which introduced the BPE algorithm variant for word segmentation, which can encode the available vocabulary with the vocabulary of variable length subword units. In this experiment, the size of the word table is 10000.

3.2. Evaluation Metric. Many automatic evaluation metrics have been proposed in the machine translation task to evaluate the quality of translation results. This research adopts the most popular BLEU [26] evaluation. It summarizes the overlapping words and phrases between machine translation and reference results. The translation results judged by the BLEU evaluation metric are highly consistent with those considered by human beings and have become a de facto translation evaluation standard after being proposed. This research does not use single testing set for BLEU score evaluation but combines multiple testing sets for score evaluation.

3.3. Experimental Environment and Model Training. This experiment uses 8 Titan XP graphics cards. PyTorch version is 1.4.0, and the CUDA version is 10.2. Table 4 lists the detailed configuration used in the experiment.

The algorithm uses a dropout operation to prevent training overfitting to ensure the training quality [27]. We use the dropout operation before the layer normalization of the CNN submodel, multihead attention submodel, encoder and decoder submodel output, and final output layer. Table 3 lists the network parameter configuration. The step of warmup is 8000. In the prediction process, a beam search algorithm is used instead of a greedy algorithm to obtain better prediction results, where the beam size is 5.

3.4. Result Analysis

3.4.1. BLEU Score Comparison. This model is being used to test German-English translation tasks. Table 5 lists the translation results of this algorithm and expected results.

Table 6 lists the comparison between the translation results of various types of machine translation algorithms and the algorithms in this research. The parameter size of the algorithm proposed in this research is 37.99 M, and the BLUE score reaches 35.24, which is 52.554% higher than other schemes such as research [17], 17.860% higher than research [29], and 2.442% higher than research [16]. The score of the algorithm model in this work is enhanced by 2.323% compared to the classic Transformer model [4], and the parameter size is decreased by 11.28 M, which is reduced by 23%. Compared with Dynamic CNN [30], the score of the proposed algorithm is 1.264% higher, and the parameter size is decreased by 247.01 M, which is reduced by 87%. Compared with the Transformer using the ReLU, the score of the Transformer using Sparse-ReLU is improved by 0.87 scores from 34.29 scores to 35.16 scores, an increase of 2.54%. The score of the optimization result using Sparse-ReLU and CNN is 35.24, an increase of 2.77%.

According to the four cooperation schemes between CNN and Transformer designed in Section 2.3, Table 7 lists the translation results obtained by the seven structures. The CNN structure of structure 2 is the one-dimensional CNN proposed in Figure 7, and the other CNN structures are the two-dimensional CNN submodel structure proposed in Figure 5. The input channel is 1, and the Transformer submodule is the structure proposed in Section 2.2. The input and output channels are word vector lengths, and the word vector dimension is the input channel of the convolution kernel. Using structure 7, when the convolution kernel size is 5×512, the BLEU score achieves the best result of 35.24 points.

TABLE 7: Comparison of translation results of different structures between CNN and Transformer (512 convolution output channels).

Structural details	Convolution type	Convolution kernel size	BLEU
Structure 1: Figure 6(a)	2d convolution	Same as structure 7	34.32
Structure 2: Figure 6(a)	1d convolution	in_ch = 512, kernel = (5, 1), stride = (1, 0), pad = 0	34.15
Structure 3: Figure 6(b)	2d convolution	in_ch = 1, kernel = (3, 512), stride = (1, 0), pad = (1, 0)	31.46
Structure 4: Figure 6(b)	2d convolution	Same as structure 7	33.61
Structure 5: Figure 6(c)	2d convolution	Same as structure 7	30.86
Structure 6: Figure 6(d)	2d convolution	in_ch = 1, kernel = (7, 512), stride = (1, 0), pad = (3, 0)	34.37
Structure 7: Figure 6(d) (This research adopts)	2d convolution	in_ch = 1, kernel = (5, 512), stride = (1, 0), pad = (2, 0)	35.24
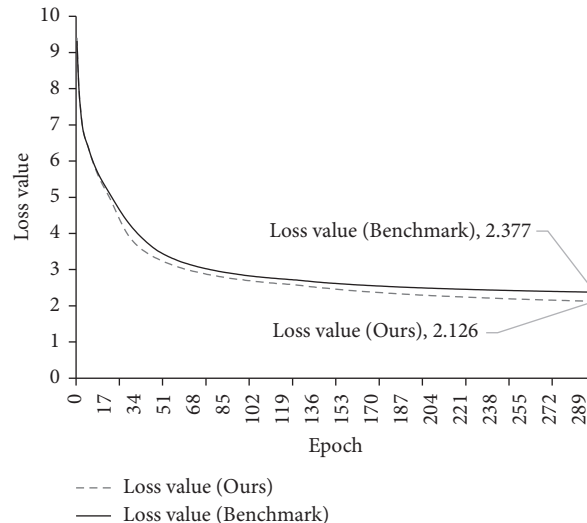
FIGURE 9: Falling curve of loss value of each structure.

TABLE 8: Influence of Sparse-ReLU on model sparsity.

Sparse-ReLU parameters	Formula	Relative loss value	Relative sparsity
$a = 1$, $b = 1$, $c = 0$, $d = 0$	$Y = \max(0, x)$	100% (Baseline)	100% (Baseline)
$a = 1$, $b = 1$, $c = 0.2$, $d = 0.2$	$Y = \max(0, x\text{-}0.2)$	100.92%	127.09%
$a = 1$, $b = 1$, $c = 0.4$, $d = 0.4$	$Y = \max(0, x\text{-}0.4)$	114.68%	150.96%
$a = 0.25$, $b = 1$, $c = 0.2$, $d = 0.4$	$Y = \max(0, 1/4(x\text{-}0.2), x\text{-}0.4)$	57.80%	150.95%

Figure 9 shows the comparison results of the decline curves of loss during different structure training. The solid line in the figure is the loss decline curve of the benchmark model, and the dotted line is the loss decline curve of the Transformer model with CNN and Sparse-ReLU. Compared with the benchmark model, the loss reduction speed of the model with CNN and Sparse-ReLU is much higher than that of the benchmark model. Under the same 300 epochs, the loss value is reduced by 10.6%.

3.4.2. Sparsity Comparison. Table 8 lists the effects of Sparse-ReLU and ReLU on the sparsity of the algorithm. Compared with the conventional ReLU function, the Sparse-ReLU proposed in this research increases the sparsity of the relevant layer by 150.95% and reduces the loss value by 42.2%. Both indexes have an excellent optimization effect.

When the parameters of the new activation function are set to $a = 0.25$, $b = 1$, $c = 0.2$ and $d = 0.4$, the algorithm is pruned to improve the sparsity of the parameters. Table 9

lists the effects of traditional and new activation functions on the sparsity of the model when the model adopts different pruning algorithms. Table 9 shows that, compared with L1 norm pruning, the random unstructured pruning algorithm and Sparse-ReLU jointly improve the sparsity of the weight to 78.26% and the sparsity of the activation value of the tested layer to more than 120%.

The bar graph of key information in the above two tables is shown in Figure 10. Figure 10(a) shows that the Sparse-ReLU used in this paper significantly decreases the loss value and improves the sparsity when training the model compared with ReLU. According to Figure 10(b), when the model with Sparse-ReLU uses different pruning algorithms, it can further improve the sparsity with little accuracy loss.

4. Conclusion

This paper proposed a cooperative machine translation algorithm based on CNN and Transformer submodels combined with Sparse-ReLU, where the CNN is used to extract

TABLE 9: Experimental results of the combination of Sparse-ReLU and pruning algorithm.

Pruning algorithm	Set parameters	Relative activations sparsity	Relative loss value	Weights sparsity
No pruning + Sparse-ReLU	\	100% (Baseline)	100% (Baseline)	0.00% (Baseline)
L1Unstructured + Sparse-ReLU	0.3	121.22%	173.60%	22.58%
	0.5	122.97%	195.12%	68.47%
RandomUnstructured + Sparse-ReLU	0.3	120.18%	120.42%	65.99%
	0.2	120.55%	110.79%	48.70%
	0.4	120.70%	288.05%	78.26%
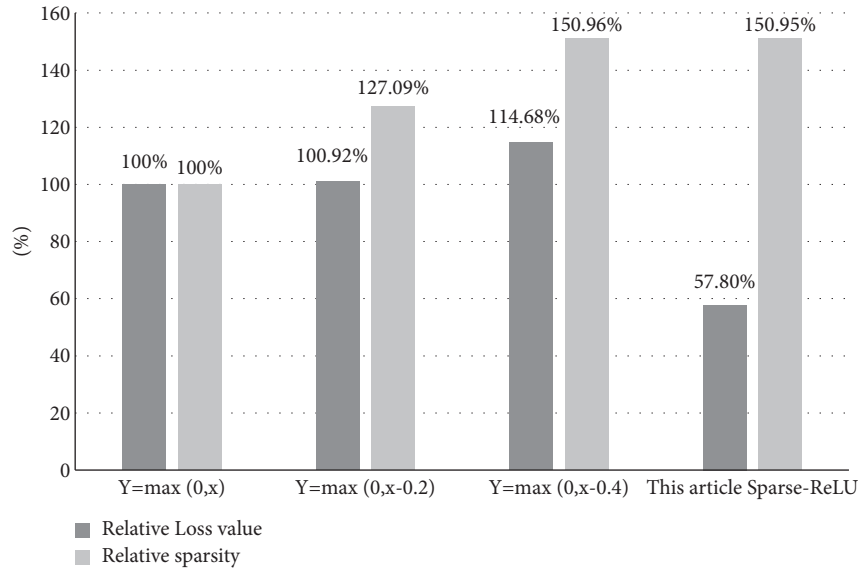
(a)
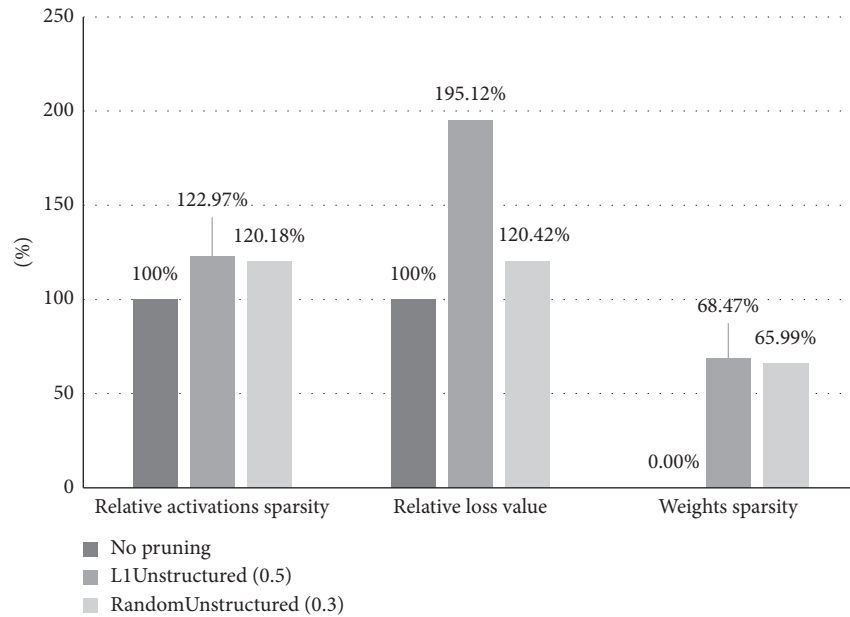
(b)

FIGURE 10: The influence of Sparse-ReLU on sparsity and accuracy.

local features of sentences containing location information, the Transformer is used to further extract sequence features, and the Sparse-ReLU can optimize the algorithm. Compared with the traditional counterpart, the count of parameters decreased by 23% with accuracy increased by 2.77%, and the sparsity increased by 50%. Consequently, Transformer and CNN parameters are only 36.42 M and 1.57 M, respectively. Test results show that the proposed scheme can effectively improve the accuracy of model translation and the sparsity of activation and weight value.

In future works, the author of this research will continue to study the collaborative scheme between CNN and Transformer and the parameter training method of Sparse-ReLU, hoping to achieve better results.

Data Availability

The experimental data used to support the findings of this study are included within the article. The dataset data used to support the findings of this study are available from the corresponding author upon request.

Conflicts of Interest

The authors declare that there are no conflicts of interest regarding the publication of this paper.

Authors' Contributions

Xintao Xu and Yi Liu contributed equally to this article.

Acknowledgments

References

[1] S. Maruf, F. Saleh, and G. Haffari, "A survey on document-level neural machine translation," *ACM Computing Surveys*, vol. 54, no. 2, pp. 1–36, 2022.

[2] M. Zhu, T. Zhang, Z. Gu, and Y. Xie, "Sparse tensor core: algorithm and hardware co-design for vector-wise sparse neural networks on modern gpus," in *Proceedings of the 52nd Annual IEEE/ACM International Symposium on Micro-architecture*, pp. 359–371, Columbus, OH, USA, October 2019.

[3] X. Xie, Z. Liang, P. Gu, and A. Basak, "Spacea: sparse matrix vector multiplication on processing-in-memory accelerator," in *Proceedings of the 2021 IEEE International Symposium on High-Performance Computer Architecture (HPCA)*, pp. 570–583, IEEE, Seoul, Korea, March 2021.

[4] A. Vaswani, N. Shazeer, N. Parmar et al., "Attention is all you need," in *Proceedings of the Advances in Neural Information Processing Systems*, pp. 5998–6008, Long Beach, CA, USA, December 2017.

[5] A. Fan, S. Bhosale, H. Schwenk, and Z. Ma, "Beyond English-centric multilingual machine translation," *Journal of Machine Learning Research*, vol. 22, no. 107, pp. 1–48, 2021.

[6] B. Talafha, A. Abuammar, and M. Al-Ayyoub, "Atar: attention-based LSTM for arabizi transliteration," *International Journal of Electrical and Computer Engineering*, vol. 11, no. 3, pp. 2327–2334, 2021.

[7] B. Pathak, S. Mittal, K. Shinde, and P. Pawar, "Comparison between LSTM and RNN Algorithm for Speech-To-Speech Translator," in *Proceedings of the International Conference on Communication Circuits, and Systems*, pp. 15–21, Daegu, Korea, May 2021.

[8] P. Shalu and M. Meera, "Neural machine translation for English to Hindi using GRU," 2021, https://easychair.org/publications/preprint/w7f4.

[9] D. Bahdanau, K. Cho, and Y. Bengio, "Neural machine translation by jointly learning to align and Translate," *Computer Science*, vol. 7, 2014.

[10] J. L. Elman, "Finding structure in time," *Cognitive Science*, vol. 14, no. 2, pp. 179–211, 1990.

[11] I. Sutskever, O. Vinyals, and Q. V. Le, "Sequence to sequence learning with neural networks," in *Proceedings of the Advances in Neural Information Processing Systems*, pp. 3104–3112, Montreal, Canada, December 2014.

[12] J. Zhou, Y. Cao, X. Wang, P. Li, and W. Xu, "Deep recurrent models with fast-forward connections for neural machine translation," *Transactions of the Association for Computational Linguistics*, vol. 4, pp. 371–383, 2016.

[13] B. Zhang, P. Williams, and I. Titov, "Improving massively multilingual neural machine translation and zero-shot translation," 2020, https://arxiv.org/abs/2004.11867.

[14] Z. Yang, Z. Hu, Y. Deng, and C. Dyer, "Neural machine translation with recurrent attention modeling," 2016, https://arxiv.org/abs/1607.05108.

[15] M. Dehghani, S. Gouws, O. Vinyals, and K. Łukasz, "Universal transformers," 2018, https://arxiv.org/abs/1807.03819.

[16] H. Peng, N. Pappas, and D. Yogatama, "Random feature attention," 2021, https://arxiv.org/abs/2103.02143.

[17] J. Gehring, M. Auli, D. Grangier, and N. Dauphin, "A convolutional encoder model for neural machine translation," 2016, https://arxiv.org/abs/1611.02344.

[18] J. Gehring, M. Auli, D. Grangier, and N. D. Yann, "Convolutional sequence to sequence learning," in *Peds of the International Conference on Machine Learning PMLR*, pp. 1243–1252, Sydney, Australia, August 2017.

[19] R. Sennrich, B. Haddow, and A. Birch, "Neural machine translation of rare words with subword units," 2015, https://arxiv.org/abs/1508.07909.

[20] Y. Liu, X. Guo, and K. Tan, "Novel activation function with pixelwise modeling capacity for lightweight neural network design," *Concurrency and Computation: Practice and Experience*, Article ID e6350, 2021.

[21] M. Hammad, P. Pławiak, K. Wang, and U. R. Acharya, "ResNet-Attention model for human authentication using ECG signals," *Expert Systems*, vol. 38, no. 6, Article ID e12547, 2021.

[22] Z. Zhang, Q. Wu, Y. Wang, and F. Chen, "Exploring region relationships implicitly: image captioning with visual relationship attention," *Image and Vision Computing*, vol. 109, no. 10, Article ID 104146, 2021.

[23] S. F. Bhat, I. Alhashim, and P. Wonka, "Adabins: depth estimation using adaptive bins," in *Proceedings of the IEEE/CVF Conference on Computer Vision and Pattern Recognition*, pp. 4009–4018, Nashville, TN, USA, June 2021.

[24] M. Cettolo, J. Niehues, and S. Stüker, "Report on the 11th iwslt evaluation campaign," in *Proceedings of the 2014 International Workshop on Spoken Language Translation*, vol. 57, Hanoi, Vietnam, December 2014.

[25] T. Kudo and J. Richardson, "SentencePiece: a simple and language independent subword tokenizer and detokenizer for neural text processing," in *Proceedings of the 2018 Conference on Empirical Methods in Natural Language Processing: System Demonstrations*, Brussels, Belgium, December 2018.

[26] K. Papineni, S. Roukos, T. Ward, and W. Zhu, "BLEU: a method for automatic evaluation of machine translation," in *Proceedings of the Annual Meeting Of The Association For Computational Linguistics*, Philadelphia, PA, USA, July 2002.

[27] N. Srivastava, G. Hinton, A. Krizhevsky, and S. Ruslan, "Dropout: a simple way to prevent neural networks from overfitting," *Journal of Machine Learning Research*, vol. 15, no. 1, pp. 1929–1958, 2014.

[28] I. Abdulmumin, B. S. Galadanci, and G. Aliyu, "Tag-less back-translation," pp. 1–31, 2021, https://arxiv.org/abs/1912.10514.

[29] A. Katharopoulos, A. Vyas, N. Pappas, and F. Fleuret, "Transformers are rnns: fast autoregressive transformers with linear attention," in *Proceedings of the International Conference on Machine Learning PMLR*, pp. 5156–5165, New York, NY, USA, July 2020.

[30] F. Wu, A. Fan, A. Baevski, and A. Michael, "Pay less attention with lightweight and dynamic convolutions," 2019, https://arxiv.org/abs/1901.10430.

Hindawi

Research Article

High-Performance Concrete Strength Prediction Based on Machine Learning

Yanning Liu [iD]

Shanxi Polytechnic College, Taiyuan 030006, China

Correspondence should be addressed to Yanning Liu; liuyanning960220@163.com

High-performance concrete is a new high-tech concrete, produced using conventional materials and processes, with all the mechanical properties required for concrete structures, with high durability, high workability, and high volume stability of the concrete. The compressive strength of high-performance concrete has exceeded 200 MPa. 28-d average strength between 100 to 120 MPa of high-performance concrete has been widely used in engineering. Compressive strength is one of the important parameters of concrete, and carrying out concrete compressive strength prediction is of high reference value for concrete design. Eight variables related to concrete strength are used as the input of the machine learning algorithm, and the compressive strength of HPC is used as the object of study. 60 samples are constructed as the dataset by concrete preparation, and the prediction of compressive strength of HPC is carried out by combining the XGBoost algorithm. In addition, SVR algorithm and RF algorithm are also performed on the same dataset. The results show that the XGBoost model has the highest prediction accuracy among the three machine learning models, and the XGBoost algorithm scores 0.9993 for $\mathbf{R}^2$ and 1.372 for RMSE on the test set. The XGBoost algorithm has high prediction accuracy in predicting the compressive strength of HPC, and the choice of model is important for improving the prediction accuracy.

1. Introduction

High-performance concrete (HPC) is a new type of high technology concrete, which is produced using conventional materials and processes [1]. The production process requires the incorporation of external admixtures that improve the properties of concrete, adding high durability, workability, and volumetric stability on top of improving the mechanical properties of concrete. The excellent performance of HPC makes it widely used in various fields of the construction industry. A lot of practical experience in engineering proves that controlling the quality of concrete is extremely important for the safety and durability of building structures. As a core element of concrete quality control and an important basis for structural design and construction, the 28-d compressive strength of concrete specimens after curing is a key parameter in the design of concrete structures and an important indicator of the engineering performance of HPC. It is a key parameter in the design of concrete structures and

an important indicator of the engineering performance of HPC. In engineering practice, whether the strength of HPC meets the design requirements is the primary issue, the ordinary orthogonal experimental method to determine the compressive strength of HPC is relatively time-consuming, and the procedure is cumbersome and costly. In order to meet the requirements of timely presumption and early control of concrete quality in construction, it is important to develop and improve the early concrete strength prediction technology adapted to the actual project and continuously improve the prediction accuracy to improve the construction quality and speed up the construction schedule. Therefore, it is of high economic value and practical guidance to predict the strength of HPC quickly and accurately [2].

As one of the most widely used and largest construction materials for modern engineering structures in the world today, concrete materials have played an important role in the process of economic development and social progress. With the development of capital construction and the

advancement of construction technology, the scale of engineering construction is becoming more ambitious, the structural forms are more replicated, and the requirements of the construction industry for concrete performance have increased. HPC is developed on the basis of high-strength concrete, and the definition of HPC varies from country to country. In general, HPC should have high permeability, high volumetric stability, appropriately high compressive strength, and good workability. It can be seen that the prediction of the strength of HPC not only is of theoretical value, but also has a high practical engineering value.

In recent years, with the rapid development of artificial intelligence technology, various industries are combining new artificial intelligence technologies for self-empowerment, and engineering-based research based on machine learning and deep learning has continued. Many machine learning theories have been applied to concrete-related research, mainly including artificial neural networks [3], support vector [4], and integration algorithms [5]. Erdal et al. [6] predicted the strength of HPC based on wavelet transform neural network model, and the prediction accuracy was good. Yuan et al. [7] proposed two hybrid neural networks, genetic optimization BP neural network, and ANFIS, to predict the strength of concrete, and compared the results with the ordinary BP neural network model, and the results showed that the prediction accuracy of the hybrid neural network model was greatly improved. Daneshvar and Behnood [8] used random forest algorithm to build a dynamic-elastic mode prediction model for asphalt concrete, and the prediction accuracy could reach 94.62%. Ren et al. [9] proposed a convolutional neural network for semantic segmentation of cracks based on computer vision technology, which provides a new method for health monitoring of tunnels. Cui et al. [10] introduced the attention mechanism into the semantic segmentation task of concrete cracks and proposed a convolutional neural network with AttUnet to achieve accurate semantic segmentation of cracks. Chun et al. [11] carried out the study of internal damage of reinforced concrete structures based on random forest algorithm and achieved accurate prediction results. Chou et al. [12] proposed an improved least squares support vector regression algorithm to improve the accuracy of high-performance concrete compressive strength prediction by parameter optimization. Behnood et al. [13] used M5P algorithm to study high-performance concrete compressive strength prediction by constructing model trees from high-latitude data. Zhou et al. [14] used 10 supervised learning algorithms for rock-burst prediction based on 246 sets of rock-burst cases and compared the prediction results of different algorithms.

Concrete-related research based on machine learning has been carried out and achieved some results. Farouk and Jinsong [15] explored machine learning in concrete strength prediction by using four machine learning algorithms, SVM, ANN, MLR, and SWR, to predict the strength of UHPC-NSC interface bond. Kim et al. [16] used CatBoost algorithm to predict FRP-concrete interface bond strength as an improved ensemble machine learning method with better performance metrics when compared with histogram gradient boosting algorithm and extreme gradient boosting

algorithm and random forest. Tran et al. [17] used six machine learning models such as GB algorithm, XGB algorithm, support vector regression, and hybrid models with particle swarm optimization, i.e., GB_PSO, XGB_PSO, and SVR_PSO, to predict the strength of recycled compressive strength of concrete. Researchers often compare multiple methods to select the optimal model for concrete strength prediction, but there is a lack of case studies on strength prediction of HPC. In this paper, three machine learning algorithms, RF, SVR, and XGBoost, are used to predict the compressive strength of HPC based on the quality characteristics of HPC. Also, cement dosage, age, water, coarse aggregate, fine aggregate, high-efficiency water reducing agent, fly ash, and mineral powder are used as multiple features and input to construct the machine learning model dataset. Training testing, along with comparing the accuracy of different models in applying to the prediction of compressive strength of HPC, and selecting the optimal model applicable to the prediction of compressive strength of concrete, can also be helpful in constructing the machine learning model dataset.

2. Concrete Preparation and Datasets

The concrete specimens were prepared using Southern P-O 42.5 grade cement, Guodian Shuang liao Class I fly ash, Huibei Mining crushed stone with continuous grading from 5 to 31.5 mm, Rong Shun quartz sand with fineness modulus of 2.29, and poly-carboxylic acid high-efficiency water reducing agent from Wuhan Harbor Research Institute Co. The powdered poly-carboxylic acid high-efficiency water reducing agent (water reduction rate of 23%) and alkyl-phenol ethylene oxide compound air-entraining agent were added during mixing, in which the high-efficiency water reducing agent accounted for 0.2%~0.8% of the cement mass and the air-entraining agent accounted for 0.8%~1.2% of the cement mass. The amount of HPC and air-entraining agent and the ratio of sand, cement, and water were adjusted experimentally according to the desired workability, including flowability, cohesiveness and water retention, and slump measured using a slump cone.

The HPC molding and mixing procedure include starting the mixer, putting in cement, fly ash, quartz sand, and other powders, dry mixing three minutes, adding water and water reducing agent, and mixing for three to five minutes. After the mixing is completed, the mix is poured into the steel mold, and after shaking and smoothing, the mold is covered with plastic film to prevent rapid moisture dissipation and left to stand at room temperature for 48 hours before demolding. The slump was measured to be 220 mm, with good fluidity, cohesion, and water retention. The test method was in accordance with GB/T 50081-2016 "test method for mechanical properties of ordinary concrete," and a total of 60 sets of data samples were produced.

A scientific and reasonable dataset is the key to achieve accurate prediction of concrete strength, which is mainly related to cement. Concrete strength is mainly related to variables such as cement dosage, age, water, coarse aggregate, fine aggregate, high-efficiency water reducing

agent, fly ash, and mineral powder. Therefore, the values of the above indicators need to be measured during the preparation of the specimens as the input to the machine learning model, and the output is the compressive strength value of the concrete.

3. Predictive Methods of HPCS

3.1. RF Algorithm. Bagging is the process of training multiple base classifiers on a dataset and then voting on the results obtained from the base classifiers as the final classification result. Random forest (RF) algorithm is an extended variant of bagging. Due to its excellent performance in data classification, it is often used in recent years for strength prediction of various types of concrete [18]. Based on the integration of the decision tree as the base classifier, RF further introduces random attribute selection in the training process of the decision tree. It selects the splitting feature by measuring the impurity of the feature division result and calculating the information gain. From the root node, according to the feature division condition and the principle of minimum purity of nodes, splitting downward until the rule is satisfied, the final prediction result is the weighted average of the results of each decision tree.

Information entropy is often used as a measure of the purity of a dataset. Let the proportion of the k-th class of data to all datasets X be p_k ($k = 1, 2, \ldots, n$); then, the information entropy of the dataset X is defined as equation (1) [19]. The smaller the value of $H(X)$, the less chaotic and purer the dataset X.

$$H(X) = -\sum_{k=1}^{n} p_k \log_2 p_k. \tag{1}$$

Assuming that the discrete feature α is used to classify the dataset X, I classification results are generated, where the I-th classification result contains all the data, denoted as X_I. The information entropy of X_I is calculated according to equation (1), and considering that different classification results contain different amounts of data, each classification result is given a weight of $|X_I|/|X|$, indicating that the more data the classification result has, the greater the role of the classification result, so the information gain obtained by using feature α to divide the dataset X is calculated in equation (2). Generally speaking, the larger the value of $\text{Gain}(D, \alpha)$ is, the more the complexity of the dataset is reduced after the feature a is used for splitting, and the more obvious the classification result is.

$$\text{Gain}(D, \alpha) = H(X) - \sum_{i=1}^{I} \frac{|X_I|}{|X|} H(X_I). \tag{2}$$

RF randomly selects m subsamples from the original dataset with put-back, and then randomly selects k features when training a single decision tree, and chooses the optimal features from these k features to split the nodes, which makes the random forest model not easily overlearn the features of the training set and reduces the variance of the model.

3.2. SVR Algorithm. The support vector regression algorithm is an application of SVM (support vector machine) to the regression problem, where the SVR creates a "spacing band" on both sides of the linear function with ε, also called the SVR creating a "spacing band" on both sides of the linear function with a spacing of ε, also known as tolerance bias, and does not calculate losses for all samples falling into the spacing band; i.e., only the support vector affects its functional model, and the optimized model is derived by minimizing the total losses and maximizing the spacing [20]. The basis consists of two main principles. One is that the model allows ε error between the predicted value $f(x)$ and the true value y. The second is that the loss function of the model is parameter updated only when the absolute value of the difference between $f(x)$ and y is greater than varepsilon. The SVR model constructs a band of model parameter nonupdating regions with $f(x)$ as the center and $\pm\varepsilon$ as the broadband.

Given the training data $D = \{(x_1, y_1), (x_2, y_2), \ldots, (x_m, y_m)\}$, the regression model $f(x) = w^T x + b$ is obtained by machine learning so that $f(x)$ is as close to y as possible. For the sample (x, y), traditional regression models usually calculate the loss directly based on the difference between the model output $f(x)$ and the true output y. The loss is 0 when and only when $f(x)$ is exactly equal to y. It follows that the SVR problem can be described by

$$L(w, y_i, f(x_i)) = \min_{w,b} \frac{1}{2}\|w\|^2 + C \sum_{i=1}^{m} l(f(x_i) - y_i), \tag{3}$$

where w is the normal vector, C is the regularization constant, L is the model optimization objective function, $f(x_i)$ is the predicted value of the model, and y_i is the true label value of the data.

The SVR algorithm uses a kernel function that allows mapping to a higher dimensional space and thus solves the classification of nonlinearities. The classification idea is simple, which is to maximize the interval between the sample and the decision surface. In addition, the SVR algorithm has better classification results. However, it is more difficult for processing large samples for large-scale data training, while the concrete strength prediction problem studied in this paper does not belong to large-scale data training and can achieve better prediction results using SVR algorithm.

3.3. XGBoost Algorithm. The idea of boosting algorithm is to integrate many weak classifiers together to form a strong classifier. XGBoost is also known as extreme gradient boosting. It is widely used in classification and regression fields because of its fast, efficient, and accurate operations and strong generalization ability [21]. Parameters such as the amount of cement used in concrete can affect its strength and durability, and XGBoost is often used to study the complex interrelationships between multiple influencing factors and their performance indicators [22]. XGBoost supports user-defined objective functions and evaluation functions, and for samples with missing values of features, it

can automatically learn its splitting direction. The core concept is to learn new features by adding trees, fitting the residuals of the final prediction, and then obtaining the sample scores, which can be summed up for each tree to obtain the final prediction score of the sample. For n labeled samples with m features, it uses G additive functions to predict scores, and the specific process is shown in

$$y_{\text{pre}} = \sum_{g=1}^{G} f_g(x_i), \quad f_g \in F;$$

$$F = \left\{ f(x) = w_{q(x)}\left(q: R^m \longrightarrow T, w \in R^T\right) \right\}, \tag{4}$$

where F represents the space of regression trees, $f(x)$ is one of the regression trees, and $w_{q(x)}$ represents the independent structure score of each T-leaf tree. The objective function of XGBoost is defined as

$$L = \sum_{i=1}^{n} l(y_i^*, y_i) + \sum_{g=1}^{G} \Omega(f_g);$$

$$\Omega(f_g) = \gamma T + \frac{1}{2} \mu w^2, \tag{5}$$

where l denotes the loss function of the model, Ω is the regularization term, T denotes the number of leaf nodes, w is the fraction of leaf nodes, while γ and μ represent the control coefficients to prevent overfitting. To speed up the optimization, a Taylor second-order expansion can be used, as shown in

$$L(t) = \sum_{i=1}^{n} \left[l\left(y_i, y_i^{*\,(t-1)}\right) + k_i f_t(x_i) + \frac{1}{2} h_i f_t^2(x_i) \right] + \gamma T$$

$$+ \frac{1}{2} \mu \sum_{i=1}^{T} w_i^2. \tag{6}$$

By adding the loss function of the samples, the samples an be recombined. And finally using the vertex formula to find the optimal w and the objective function formula L as shown in equation.

$$w_i' = -\frac{K_i}{H_i + \mu};$$

$$L = -\frac{1}{2} \sum_{i=1}^{T} \frac{K_i^2}{H_i + \mu} + \gamma T, \tag{7}$$

where $K_i = \sum_{i \in I_j} k_i$ and $H_i = \sum_{i \in I_j} h_i$. XGBoost combines the traditional greedy algorithm with an approximation algorithm to find the best splitting point by enumerating several possible candidates based on the percentile method and then calculating the best splitting point according to equation (7). XGBoost uses various methods to avoid overfitting, such as introducing regularization, row sampling, and feature sampling, and also adds handling of sparse data. In addition, XGBoost has other advantages, such as the ability to perform parallel processing, which results in a significant speedup; a high degree of flexibility, with customizable optimization

goals and evaluation criteria; and built-in cross-validation, which allows cross-validation to be used in each boosting iteration. Combining the above advantages of XGBoost in classification algorithms, this paper selects XGBoost as one of the main alternative models for HPCS. The modeling steps of XGBoost are shown in Figure 1.

Firstly, we define the algorithm function and call the XGBoost function to build the network model; then, we set the initial parameters and input the training set to train the model, adjusting the weights every time until the training error is minimized or the required maximum training times are reached; after training, we store the current network file and input the validation set to compare the evaluation metrics to determine whether it is optimal or not, and so on until all parameters are optimal; then, we enter the testing phase and evaluate the model to obtain the corresponding metrics to complete the classification experiment of HPCS.

4. Experimental Results and Analysis

For the purpose of selecting the most suitable prediction model for HPCS, this paper uses the comparative experimental method. Specific concrete samples are prepared in the laboratory, and the data are preprocessed after understanding the characteristics of each data, so as to select the model with the best prediction performance based on machine learning theory. The overall technical route is shown in Figure 2.

In order to compare and analyze the performance of three machine learning methods, RF, SVR, and XGBoost, on the concrete compressive strength dataset, this paper selects R^2 and RMSE from the commonly used machine learning evaluation metrics. Where the root mean square error (RMSE) mainly measures the accuracy of the model, the smaller its value, the higher the prediction accuracy of the model. The correlation coefficient (R^2) characterizes the closeness between the predicted value of the model and the true value of the data, and the closer the R^2 is to 1, the higher the prediction accuracy of the model. The mathematical formula is shown in

$$R^2 = \frac{\sum_i \left(y_{\text{obs}} - y_{\text{pre}}\right)^2}{\sum_i \left(y_{\text{obs}} - \overline{y_{\text{obs}}}\right)^2};$$

$$\text{RMSE} = \sqrt{\frac{\sum_i \left(y_{\text{obs}} - y_{\text{pre}}\right)^2}{n}}. \tag{8}$$

4.1. Comparative Analysis of Model Results. Before comparing the prediction results of each model, the *GridSearch* method is used to optimize the parameters of various models for making the prediction results of each model more accurate. The results of the parameter optimization are shown in Table 1. Eight influencing factors such as cement use, age, water, coarse aggregate, fine aggregate, high-efficiency water reducer, fly ash, and mineral powder are selected as input variables, and 28-d compressive strength was taken as the prediction target to construct the initial index system of the
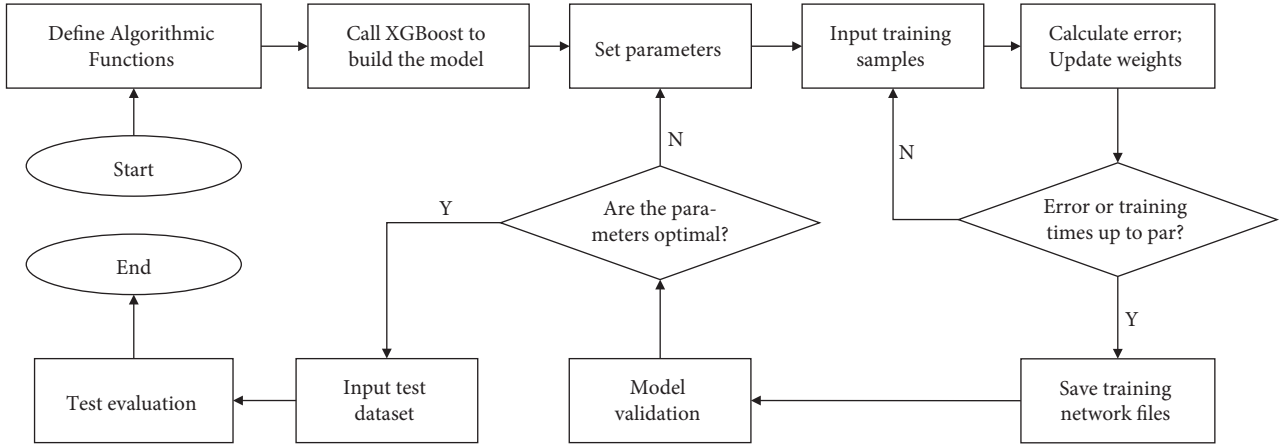
Figure 1: XGBoost modeling steps.
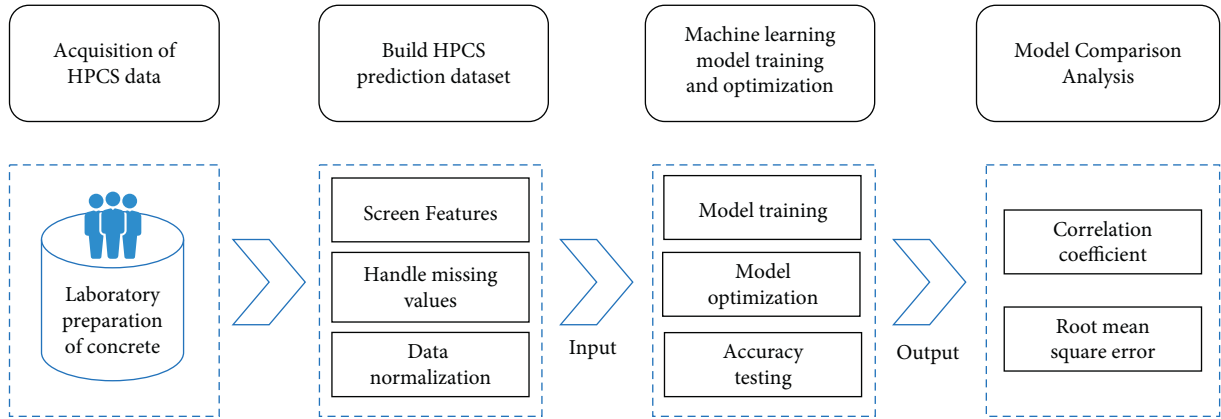
Figure 2: Technical route of HPCS prediction.

high-performance concrete compressive strength prediction model. The original dataset was randomly divided into 10 parts according to the ratio of 8 : 2, of which 80% was used as the training set and the rest as the test set. In this paper, there are 60 sets of data samples, 48 sets are divided into training set, and the remaining 12 sets are test sets. We perform statistical analysis on the prediction results of each model, and the comparison results in test sets are listed in Figure 3.

Analysis of Figure 3 shows that, overall, for the error measure RMSE, the XGBoost model has the lowest error prediction 1.372, followed by RF 2.347 and finally SVR 2.656. In terms of the correlation coefficient R^2, all three models get the desired value; that is, the concrete strength data in this paper are convincing. The correlation coefficient of the XGBoost model reaches 0.9993, reaching the maximum value of the three. The results of these two evaluation indexes fully illustrate the superiority of XGBoost algorithm in HPCS prediction, which can be used as a favorable reference for future prediction work.

4.2. Prediction Result Analysis of XGBoost.
XGBoost implements a general tree boosting algorithm. In view of the good performance of XGBoost algorithm in HPCS prediction, this

Table 1: Parameter configuration.

Algorithm	Parameter optimization
RF	n_estimators = 500, max_depth = 18, min_samples_split = 4
SVR	Kernel = "rbf," C = 1010, gamma = 0.56
XGBoost	n_estimators = 500, max_depth = 6, learning_rate = 0.01

paper analyzes the operation results of XGBoost in detail to better illustrate the adaptability of this method.

The statistical results of the comparison between the HPCS prediction results of the XGBoost model and the actual compressive strength are shown in Figures 4 and 5.

When training is performed, the XGBoost algorithm achieves good results, and the actual values are almost indistinguishable from the predicted values. Therefore, in order to visualize the prediction effect of the training set, Figure 4 shows the actual values as the horizontal coordinates and the predicted values as the vertical coordinates, and the distribution of each data point basically coincides with the line $y = x$. The composition of concrete strength data in the training set ranges from 20 MPa to 70 MPa, the RMSE is 0.341, and R^2 is 0.9989 after XGBoost training. This indicates that XGBoost has a very excellent prediction performance in the training phase.

FIGURE 3: Comparison of test set evaluation results.

FIGURE 5: XGBoost testing set result.

FIGURE 4: XGBoost training set result.

prediction model will greatly dominate the preparation of concrete. As a simple example, with the prediction model, it is possible to filter the dosage range of important indicators such as cement dosage according to the actual demand. This greatly reduces the number of pre-experiments conducted and the time to conduct them, which also saves experimental materials and speeds up the efficiency of experiments. Nowadays, there are still some problems in concrete prediction, such as lack of sample data, lack of representativeness, inability to reflect the sensitivity of input parameters, and narrow scope of application of the model. Concrete prediction, as a typical multivariate, nonlinear system, requires the incorporation of reasonable data processing methods such as machine learning to be performed. This paper uses comparisons to select a better quality method that can better serve HPC in practical engineering for problems such as proportioning optimization.

5. Conclusion

With the large-scale development of transportation infrastructure, how to use the available data to make accurate prediction of concrete strength, so as to feed back to optimize the concrete mix design, has become a hot topic of research in the academic and engineering circles nowadays. The strengths of the HPCs we prepared ranged from 20 MPa to 70 MPa. To better investigate the nonlinear relationship between HPCS and the eight influencing factors, machine learning approaches are used to solve this problem. In order to find the most suitable algorithm to strength prediction, three commonly used and effective methods, RF, SVR, and XGBoost, are selected using comparative analysis. Through data preprocessing and parameter optimization, all three methods achieve a nice prediction state, and the results of the study can provide some reference for machine learning in the field of concrete strength prediction research. The R^2 values of the three methods are all above 0.9, and the model fitting effect is good. By comparing the performance capability of RF, SVR, and XGBoost algorithms on the same dataset, it is found that XGBoost has the highest prediction

Figure 5 reveals that although XGBoost achieves good outcomes on the training set, there is no overfitting, and the performance on the training set is also outstanding. In general, for different strengths of high-performance concrete, the predictions of the XGBoost model are very close to the true values of the test set, and the dashed and solid lines are generally in the same direction. The RMSE on the training set is 1.372, while the R^2 is 0.993. The trend of the two lines in the figure shows that the strength prediction performance of concrete with strengths in the interval of 40–50 MPa is better than that of 50–70 MPa. Judging from the performance on the training set and validation set, the XGBoost prediction model has strong adaptability and superiority in HPCS prediction and can better guide the prediction of compressive strength of HPC.

The construction industry is pursuing higher and higher quality of construction, and the strength of concrete is often a key influencing factor of that. How to prepare high-performance concrete is an important topic in civil engineering materials science, and a high-performance concrete strength

accuracy and the lowest RMSE value of 1.372, which can be applied to HPCS prediction.

The prediction method in this paper has high precision; therefore, it will serve the experimental design of the laboratory. In addition, machine learning algorithms can also identify the most sensitive intensity influencers, which can also be used for future research.

Data Availability

The labeled datasets used to support the findings of this study are available from the corresponding author upon request.

Conflicts of Interest

The authors declare no conflicts of interest.

Acknowledgments

References

[1] A. Kumar, H. C. Arora, N. R. Kapoor et al., "Compressive strength prediction of lightweight concrete: machine learning models," *Sustainability*, vol. 14, no. 4, p. 2404, 2022.

[2] S. Chithra, S. S. Kumar, K. Chinnaraju, and F. Alfin Ashmita, "A comparative study on the compressive strength prediction models for High Performance Concrete containing nano silica and copper slag using regression analysis and Artificial Neural Networks," *Construction and Building Materials*, vol. 114, pp. 528–535, 2016.

[3] S. Kekez, "Application of artificial neural networks for prediction of mechanical properties of CNT/CNF reinforced concrete," *Materials*, vol. 14, no. 19, p. 5637, 2021.

[4] W. Jiang, Y. Xie, W. Li, J. Wu, and G. Long, "Prediction of the splitting tensile strength of the bonding interface by combining the support vector machine with the particle swarm optimization algorithm," *Engineering Structures*, vol. 230, no. 7, Article ID 111696, 2021.

[5] H. W. Song, A. Ahmad, F. Farooq et al., "Predicting the compressive strength of concrete with fly ash admixture using machine learning algorithms," *Construction and Building Materials*, vol. 308, Article ID 125021, 2021.

[6] H. I. Erdal, O. Karakurt, and E. Namli, "High performance concrete compressive strength forecasting using ensemble models based on discrete wavelet transform," *Engineering Applications of Artificial Intelligence*, vol. 26, no. 4, pp. 1246–1254, 2013.

[7] Z. Yuan, L. N. Wang, and X. Ji, "Prediction of concrete compressive strength: research on hybrid models genetic based algorithms and ANFIS," *Advances in Engineering Software*, vol. 67, pp. 156–163, 2014.

[8] D. Daneshvar and A. Behnood, "Estimation of the dynamic modulus of asphalt concretes using random forests algorithm," *International Journal of Pavement Engineering*, vol. 3, pp. 1–11, 2020.

[9] Y. Ren, J. Huang, Z. Hong et al., "Image-based concrete crack detection in tunnels using deep fully convolutional networks," *Construction and Building Materials*, vol. 234, Article ID 117367, 2020.

[10] X. Cui, Q. Wang, J. Dai, X. Yanjin, and Y. Duan, "Intelligent crack detection based on attention mechanism in convolution neural network," *Advances in Structural Engineering*, vol. 24, no. 9, pp. 1859–1868, 2021.

[11] P. J. Chun, I. Ujike, K. Mishima, M. Kusumoto, and S. Okazaki, "Random forest-based evaluation technique for internal damage in reinforced concrete featuring multiple nondestructive testing results," *Construction and Building Materials*, vol. 253, Article ID 119238, 2020.

[12] J. S. Chou, A. D. Pham, and P. Anh-Dyc, "Smart artificial firefly colony algorithm-based support vector regression for enhanced forecasting in civil engineering," *Computer-Aided Civil and Infrastructure Engineering*, vol. 30, no. 9, pp. 715–732, 2015.

[13] A. Behnood, V. Behnood, M. M. Gharehveran, and K. E. Alyamac, "Prediction of the compressive strength of normal and high-performance concretes using M5P model tree algorithm," *Construction and Building Materials*, vol. 142, pp. 199–207, 2017.

[14] J. Zhou, X. B. Li, and H. S. Mitri, "Classification of rockburst in underground projects: comparison of ten supervised learning methods," *Journal of Computing in Civil Engineering*, vol. 30, no. 5, Article ID 04016003, 2016.

[15] A. I. B. Farouk and Z. Jinsong, "Prediction of interface bond strength between ultra high-performance concrete (UHPC) and normal strength concrete (NSC) using a machine learning approach," *Arabian Journal for Science and Engineering*, vol. 47, pp. 5337–5363, 2022.

[16] B. Kim, D. E. Lee, G. Hu, Y. Natarajan, S. Preethaa, and A. P. Rathinakumar, "Ensemble machine learning-based approach for predicting of FRP-concrete interfacial bonding," *Mathematics*, vol. 10, no. 2, p. 231, 2022.

[17] V. Tran, V. Q. Dang, and L. S. Ho, "Evaluating compressive strength of concrete made with recycled concrete aggregates using machine learning approach," *Construction and Building Materials*, vol. 323, Article ID 126578, 2022.

[18] J. Zhang, G. Ma, Y. Huang, J. sun, F. Aslani, and B. Nener, "Modelling uniaxial compressive strength of lightweight self-compacting concrete using random forest regression," *Construction and Building Materials*, vol. 210, pp. 713–719, 2019.

[19] K. Madian, I. Ilyas, H. Hammady, M. Ouzzani, and E. Ahmed, "Learning to identify relevant studies for systematic reviews using random forest and external information," *Machine Learning*, vol. 102, 2016.

[20] X. Peng, "TSVR: an efficient twin support vector machine for regression," *Neural Networks*, vol. 23, no. 3, pp. 365–372, 2010.

[21] H. Baker, M. R. Hallowell, and J. P. Tixier, "AI predicts independent construction safety outcomes from universal attributes," *Automation in Construction*, vol. 118, 2019.

[22] W. Dong, Y. Huang, B. Lehane, and M. Guowei, "XGBoost algorithm-based prediction of concrete electrical resistivity for structural health monitoring-ScienceDirect," *Automation in Construction*, vol. 114, p. 114, 2020.

Hindawi

Research Article

Testing the Effects of the Digital Linguistic Landscape on Engineering Education for Smart Construction

Lin Xu,[1] **Jingxiao Zhang** [ID],[2] **Yin Yuan,**[1] **Junwei Zheng,**[3] **Simon P. Philbin,**[4] **Brian H. W. Guo,**[5] **and Ruoyu Jin** [ID][6]

[1]*School of Foreign Languages, Northwest University, Xi'an 710127, China*
[2]*School of Economics and Management, Chang'an University, Xi'an 710064, China*
[3]*Faculty of Civil Engineering and Mechanics, Kunming University of Science and Technology, Kunming 650500, China*
[4]*School of Engineering, London South Bank University, London SE10AA, UK*
[5]*Department of Civil & Natural Resources Engineering, University of Canterbury, Christchurch, New Zealand*
[6]*School of Built Environment and Architecture, South Bank University, London, UK*

Correspondence should be addressed to Jingxiao Zhang; zhangjingxiao964@126.com

This study investigates the mechanism of digital linguistic landscapes in enabling engineering education for smart construction according to the educational dimensions of A (ability), S (skill), and K (knowledge). A questionnaire survey was conducted based on the core concepts of the informative dimension and symbolic dimension in digital language landscape as well as the ability dimension, knowledge dimension, and skill dimension in engineering education. Structural equation modeling (SEM) was used as the test method. The results of the research demonstrate that the informative dimension and symbolic dimension are two main aspects of DLL in education of engineering students for smart construction. Additionally, DLL has a significant positive impact on the ability, knowledge, and skill education of engineering students for smart construction. The research has theoretical and practical significance, as it not only enriches research on the relationship between DLL and engineering education for smart construction but also expands the theoretical understanding of engineering education from the perspective of linguistics. Furthermore, the study explores the path of the practical application of digital language landscape to engineering education for smart construction.

1. Introduction

The construction industry faces a number of pressing challenges, including improving the level of productivity and responding to the high level of fragmentation and complexity as well as leveraging the emerging opportunities by digital transformation [1, 2]. Indeed, the construction industry has already started to adopt digital technologies to improve the operational performance of industrial activities, including virtual reality, Internet of Things, and machine learning [3]. Moreover, the requirement for smart buildings is rapidly becoming an inherent constituent of policies associated with the design and development of buildings for the future [4]. Therefore, smart construction has been

proposed as a new concept for the construction industry to adopt in order that the sector can fully capitalize on the opportunities afforded by digital transformation. Smart construction systems have huge potential to improve the efficiency of construction industry [5]. Specifically, they empower the engineering production system and promote the interconnection of engineering construction processes, including online and offline integration, resource, and element collaboration [6, 7]. In this context, the 21st century engineers and architects must be able to deal with the rapid pace of technological change and successfully navigate the highly interconnected world of industry [8]. Facing such profound changes in the construction industry triggered by digital technologies in the new era, there is an increasing

demand for engineering students who are suitable for engaging in smart construction. Such students need to meet the requirements for the future development of the construction industry and to adapt to the transformation and upgrading of the industry [1, 3]. This also requires changes at the educational level [9].

The current basis for the education of engineering students suitable for smart construction fails to adequately integrate with digital technologies. There is a need to make changes to the engineering education system from different perspectives, including the digital linguistic landscape as well as aspects of the new industrial technology, information, and humanistic literacy. Therefore, it is necessary to change the traditional mode of educating smart construction engineering students to adopt a new approach that is suited to the digital context of the construction industry. Consequently, this study focuses on addressing the following question: Does the digital linguistic landscape play a role in the development of smart construction-related abilities, skills, and knowledge as part of engineering education? What is the mechanism of action?

Educating engineering students who possess smart construction capabilities faces various challenges, which can be summarized in four main areas. Firstly, the educational mode for enhancing the innovation awareness and ability of students is comparatively singular in nature. On this matter and in the case of China, Chen and Ding [10] identified that there is still a large gap between the innovation level of the country's construction industry and that of the developed countries, and this gap is especially prominent in the field of smart construction. Besides, university-level engineering students in general do not have a good understanding of the importance of innovation awareness and possess the capacity for innovation [11]. In addition, their awareness of the need to learn innovation skills and knowledge is currently limited [12]. In developing countries, educational programs have often been using out-of-date teaching methodologies, whereby students listen to lectures delivered by academic faculty without any practical applications or hands-on experience. This provokes a decrease in students' attention span and motivation and makes them become bored with the learning process [13, 14].

Secondly, the path for cultivating internationalized engineering students in the construction industry in China is somewhat narrow. In the context of the globalization trend and the "Belt and Road" initiative, there is a growing need for internationalized engineering students [15]. Engineering universities often prefer to establish long-term and stable cooperation with world-class universities, research institutions, and enterprises [16]. This kind of cooperation could provide good opportunities for engineering students in academic exchanges, engineering practice, and visits [17, 18]. However, resources are limited, and the number of students is large, while the opportunity to go abroad for exchange is not enough, which makes engineering students at this stage disconnected from the international advanced engineering concepts and academic ideas and often results in a lack of international vision and global awareness in engineering practice [19].

Thirdly, the knowledge horizon of engineering students in many cases is too narrow. China's engineering knowledge system needs improvement, and while the knowledge obtained by students is comprehensive, there are still difficulties in responding to industrial development trends and other arising technological challenges [20]. The current professional settings of engineering education are bounded by the traditional engineering disciplines, which often pay too much attention to the systemic nature of the disciplines themselves and ignore the interconnection between the knowledge across disciplines [21].

Fourthly, the digital linguistic landscapes are insufficient in number. The quantity of digital linguistic landscapes in the education environment of engineering students is far from enough. This not only serves to weaken the influence of the language environment itself on the cultivation of engineering students' consciousness, thinking, and cultural heritage [7] but also installs certain obstacles to the cognitive ability of such students [22]. This affects their learning ability and also decreases the significance of the digital information platform on the education of students suitable for smart construction through difficulties adapting to the rapid changes in the era of digitalization and information technology.

In view of this, digitalization is a way of information processing and representation and a technical method to store, transmit, process, handle, and apply information carriers (i.e., text, pictures, images, and signals) in digitally encoded form (usually binary). Digitalization is developing fast and has become a powerful tool for digital planning, construction, and operations, for instance, in the case of digital twins [23]. Digitalization and digital transformation have become a major research trend. Kohtamaki et al. [24] researched the relationship between digitalization and servitization, Ferreira et al. [25] studied the benefits of digitalization, and Verhoef et al. [26] researched the strategies of digital transformation. Digital linguistic landscape refers to the linguistic landscape in digital space. Linguistic landscapes have multiple roles in the development of students, as they can be powerful tools for education, language learning, critical thinking, language activism, and so on [27, 28]. Therefore, as an information platform for displaying the linguistic landscape through digital technology, digital linguistic landscape is a tool to broaden the influence of linguistic landscapes. The information provided by the digital linguistic landscape is rich, diversified, and internationalized, and its presentation media are diverse. Language and symbolic information on digital websites, digital signage, digital media, and other media all belong to digital linguistic landscapes. Therefore, the application of the digital linguistic landscape concept to the education of engineering students suitable for smart construction provides rich, diversified, and multilingual knowledge information and thereby strengthens the humanities of smart construction engineering students while also promoting the digital capabilities of engineering students.

The study aims to explore and test the mechanism of digital linguistic landscape on the education of engineering students suitable for smart construction through the use of

the "ASK" (i.e., ability, skill, and knowledge) educational model based on the digital linguistic landscape platform. There is no relevant research on digital linguistic landscape for engineering talents cultivation at home and abroad, and this study has certain groundbreaking significance. This study has the following theoretical implications for the engineering education for smart construction: (1) defining the digital linguistic landscape; (2) expanding the theoretical scope of smart construction engineering education from the perspective of linguistics and providing the theoretical basis for the linguistic landscape atmosphere of the education; (3) exploring a new path to educate engineering students for smart construction and further enriching the research on the education path of smart construction-related engineering students.

2. Literature Review

2.1. Engineering Education for Smart Construction Students. According to the World Federation of Engineering Organization (WFOE), engineering capacity building, as a driver for sustainable socioeconomic development, has become a globally recognized priority [29]. Therefore, it is necessary to study the capacities of smart construction engineering students.

A search of the keywords "smart construction engineering students' qualities" and "abilities" in domestic and foreign mainstream databases showed that there was no relevant literature. In order to summarize the core qualities of engineering students suitable for smart construction more accurately, the core competence standards for graduates of the Washington Accord, Sydney Accord, and FEANI, as well as the domestic standards for the connotation of engineering students' qualities, were analyzed and extracted. This was carried out from the perspective of professional certification of engineering education at home and abroad, focusing on the keywords "smart construction," "engineering students," "qualities," "competence," and "abilities." After carefully screening the relevant literature, 10 of the core qualities were finally selected to analyze and summarize the core qualities of engineering students, as shown in Table 1.

From Table 1, it can be observed that, in the context of "New Engineering," the quality of engineering students mainly focuses on lifelong learning ability, engineering innovation ability, engineering thinking ability, interdisciplinary and integration ability, communication, and cooperation ability, as well as engineering knowledge and professional skills. On this basis and combined with the new requirements for professional students relevant to smart construction [1, 40–44], the core qualities of engineering students' in smart construction were summarized as follows:

(a) Engineering innovation ability: innovation is critical to economic and social prosperity [45]. Educating engineering students for smart construction who are innovative is the key to building a dynamic and successful economy [12]. The focus of cultivating the innovation ability of engineering students suitable for smart construction is to enhance their

TABLE 1: Core qualities of engineering students.

	A	B	C	D	E	F	G
FEANI [30]	✓		✓			✓	✓
Sydney Accord [31]	✓		✓	✓	✓	✓	
Washington Accord [32]	✓		✓		✓	✓	✓
IEC [33]	✓		✓	✓	✓	✓	✓
Cutler et al. [34]		✓	✓		✓	✓	✓
Klein-Gardner et al. [35]			✓		✓	✓	
Siller et al. [36]		✓	✓		✓	✓	✓
Stieff et al. [37]		✓	✓				
Hu and Li [38]	✓	✓				✓	✓
CEEAA [39]	✓		✓	✓	✓	✓	✓
Proposed index in this research		✓	✓		✓	✓	✓

Notes. A, lifelong learning ability; B, innovation ability; C, international ability; D, engineering thinking ability; E, interdisciplinary ability; F, Knowledge; G, Skill.

engineering innovation abilities and knowledge and develop a greater understanding of the opportunities associated with adopting new technologies [39, 46, 47].

(b) International ability: internationalization is the process of integrating an international or intercultural dimension into the teaching, research, and service functions of a higher education institution [48, 49]. At present, there is no common definition of internationalized students in the academic field. Thus, this study summarized the international ability of students as intercultural communication ability, cooperation ability, international thinking, and vision, as well as global awareness of international competencies [35, 50, 51].

(c) Engineering thinking ability: engineering thinking is a form of "invisible" consciousness activity, which is a kind of nonlogical and comprehensive way of thinking adopted by engineering students based on the elements of engineering philosophy and engineering knowledge for the purpose of planning engineering entities [52–54]. The engineering thinking abilities of engineering students suitable for smart construction include interrogative and systematic thinking, critical thinking, and the ability to solve complex engineering problems [32, 39].

(d) Lifelong learning ability: lifelong learning ability is the prerequisite to ensuring the continuous development and improvement of smart construction engineering students. Engineering students must have the awareness and ability of lifelong learning in order to adapt to the development of industrial technology and meet the requirements of modern production systems [55]. Lifelong learning refers to having an awareness of independent and lifelong learning and the ability to continuously learn and adapt to development. The specific connotations are (1) the ability to recognize the necessity of independent and lifelong learning in the context of social development and (2) the ability to learn

independently, including the ability to understand technical problems and summarize and ask questions [39].

(e) Interdisciplinary ability: with the emergence of new industrial clusters, an education to develop an interdisciplinary ability for engineering students to meet the needs of economic development and smart construction is an emerging trend in the construction industry [56, 57]. It is the ability to integrate resources across disciplines while breaking through the limitations of individual knowledge boundaries [38, 58]. This includes the ability to think across disciplines and also integrate knowledge across disciplines [59, 60].

(f) Knowledge of engineering: engineering students suitable for smart construction need to master the basic theoretical knowledge necessary for the main engineering disciplinary area in a systematic manner [61]. The engineering knowledge necessary for smart construction students includes mathematics, natural science, engineering fundamentals, and expertise, which are useful for solving complex engineering problems [39, 62]. Smart construction education also needs to include the basic theory and knowledge of related disciplines, such as materials science, mechanical engineering, and digital skills and knowledge, so as to achieve the integration of information technology and engineering knowledge [1, 63].

(g) Engineering skill: professional skills of engineering students suitable for smart construction include both hard and soft skills. Hard skills refer to generic skills in specified engineering majors, such as design and development, application of modern tools, project management and financial analysis, research and study, and engineering analysis [31, 32, 64], while soft skills include exploring and management skills as well as communication skills [65–67].

2.2. Linguistic Landscape.

Landry and Bourhis [68] were the first to introduce and use the concept of "linguistic landscape" and defined it as "the language of public road signs, advertising billboards, street names, place names, commercial shop signs, and public signs on government buildings combines to form the linguistic landscape of a given territory, region, or urban agglomeration." The linguistic landscape has two main types of functions, namely, informative and symbolic. The informative function of language signs indicates the borders of the territory inhabited by a linguistic group and also the availability of a specific language to communicate in that territory. On the contrary, the symbolic function refers to the perception that members of a language group have of the value and status of their languages as compared to other languages [68].

Since the concept of linguistic landscapes was proposed, many researchers have conducted studies on the subject, which reached a climax in 2006. In 2015, John Benjamins, a well-known Dutch publishing group, launched "Landscapes: An International Journal," marking the maturation of the study of linguistic landscapes [69, 70].

The traditional topics on linguistic landscape include the spread of English, the phenomenon of multilingualism, the gap between language policy and concrete implementation, and the vitality of minority languages that continue to attract academia's attention [71], while new research areas have also emerged, including the linguistic landscape in virtual space and multimodal data-semiotic landscapes, such as [72–74].

Digital linguistic landscape is a new topic, and there is little relevant research on the matter, and this includes the virtual linguistic landscape. Virtual linguistic landscape or cyber linguistic landscape can be viewed as innovative subareas of the digital linguistic landscape. The development of virtual linguistic landscape research is still slow and mostly concentrates on exploring the presentation mode and linguistic forms of virtual linguistic landscape.

2.3. Digital Linguistic Landscape.

With the development of society and technology, eye tracking, virtual reality (VR), and other technologies have enabled people to extend their understanding of social space from "real space" to "virtual space" [75, 76]. The linguistic landscape with a multimodal combination of sound, picture, image, and color has become an emerging form of expression [77, 78]. In addition, with the growth of multilingual capabilities in digital communication, multilingual options in virtual spaces have become more popular, and linguistic landscapes can be defined not only in physical spaces but also in virtual spaces, such as electronic spaces, popular culture, and the Internet [79].

Digital linguistic landscape refers to the linguistic landscape in digital space. In a microsense, it is a controlled linguistic landscape space formed by combining traditional public road signs, billboards, and store signs with text, images, images, and 2D codes using various digital technologies. In a macrosense, it is the process, method, and technology of collecting, monitoring, analyzing, simulating, creating, and reproducing linguistic landscape information with the help of computer technology, multimedia technology, Internet technology, AI, VR, simulation and sensing technology, and other digital technologies. From a technical perspective, digital linguistic landscape is different from the traditional signage to express the linguistic landscape.

Digital linguistic landscape is an information platform for displaying linguistic landscapes through digital technology. Further, it is a tool for sharing language information. The information provided by digital linguistic landscapes is rich, diversified, and internationalized, and its media are diverse, such as digital websites, digital signage, digital media, and other media [80, 81]. Among them, digital signage refers to the multimedia professional audio-visual system that releases business, financial, and entertainment information through large-screen terminal displays in large shopping malls, supermarkets, hotel lobbies, restaurants, theaters, and other public places [82, 83].

Digital linguistic landscapes not only present linguistic information from around the world and are an important

gateway to knowledge, information, and skills but also are tools for people to understand the cultures of various countries and enrich their understanding of the world [73, 84]. Digital linguistic landscape is an extension of the physical linguistic landscape, which also has informative and symbolic functions. The informative function of the digital linguistic landscape includes information delivering function, information indicating function, and information mediation function. The information delivering function is manifested in the form of linguistic information at an intuitive level [85]; the information indicating function is manifested in the form of multimodal linguistic landscapes that serve as an aid to comprehension or emphasis [86]; and the information mediation function is manifested in the form of short, guiding messages that point to a broader pool of relevant information resources [74]. The symbolic function of digital linguistic landscape refers to its ability to reflect market trends and current social conditions [87, 88], as the information of digital linguistic landscape is shared, convenient, and expandable to facilitate the wide dissemination of social phenomena [89], and its information most directly reflects often the most cutting-edge social hotspots and trends. Besides, the information dissemination medium relies on the latest digital technology. Based on these features, digital linguistic landscape is a carrier that reflects current situations and market trends.

3. A Priori Model and Hypotheses

3.1. Theoretical Supporting Model: ASK. The supporting model "ASK" (also known as KSA) was applied to investigate the mechanism of the digital language landscape on the education of engineering students in smart construction. ASK, a benchmark of the American Council on Education, primarily aimed to assess the capabilities of a prospective job applicant [90]. In federal personnel guidance, KSAs are defined as the factors that identify higher qualified candidates from a group of individuals with varying levels of skills and knowledge [91, 92]. At present, the ASK model is mainly applied to the education of enterprise personnel and management, and it has also been explored in higher education and training of medical human resources. For example, at the level of personnel training, Stahl and Luczak [93] investigated personnel planning in concurrent engineering with KSA. From the perspective of higher education, Hu et al. [94] investigated the impact of the KSA competency enhancement framework on nonengineering students' competencies.

In the ability dimension of the model, this study examined innovation ability and international ability. The ASK model constructed in this study is shown in Figure 1.

3.2. Hypotheses. Based on the ASK education model for smart construction engineering, the hypotheses of the mechanism of digital linguistic landscape for smart construction education are proposed.

3.2.1. Digital Linguistic Landscape and the Smart Construction Ability of Engineering Students. With the advancement of China's new era of industrialization, an important mission of higher education institutions focused on engineering education is to cultivate innovative engineering students and provide support for the development of industrialization so as to meet the demand for continuous innovation. Innovation ability refers to the ability of people to discover new problems, propose new ideas, and new ways to solve problems through innovative thinking activities and produce new products, new technologies, or new methods through innovative and practical activities on the basis of rich knowledge and broad horizon [95]. Innovation ability is mainly a comprehensive ability formed by the interaction of such elements as knowledge horizon, innovation awareness, innovation thinking, and innovation skills [46]. Digital linguistic landscapes carry information that is diverse in presentation and rich in content, which helps to enrich knowledge and broaden horizons. It also has the potential to influence the acquisition and development of abilities at the consciousness level through the expansion of information and the diversification of information channels. Thus, the following research hypothesis was proposed regarding the digital linguistic landscape's role in the development of innovation ability for engineering students suitable for smart construction:

> H1: digital linguistic landscapes have a significant positive impact on the innovation ability of engineering students suitable for smart construction.

This study classifies intercultural communication ability, global awareness, and global vision as international abilities. Global vision requires students to be able to think and deal with problems from the perspective of global industrial development and seek opportunities for international development in a complex and changing international environment [96, 97]. Global awareness is a habit of mind that focuses on understanding and grasping the trends of the times [98]. Intercultural communication skills of smart engineering students cannot be developed without knowledge input and the practices of global engineering programs and immersive research experience abroad [99]. From the informative dimension of the digital linguistic landscape, it covers a wide range of information on humanities and history at home and abroad, as well as a wide range of languages, providing a global range of resources and a wide range of channels for inputting knowledge. From the symbolic dimension, the digital linguistic landscape provides a convenient medium to obtain information, a channel to understand the international market situation, and a facilitator to develop international thinking habits. Thus, the following research hypothesis was proposed regarding the digital linguistic landscape's role in the development of international ability of engineering students suitable for smart construction:

> H2: digital linguistic landscapes have a significant positive impact on the international ability of engineering students suitable for smart construction.
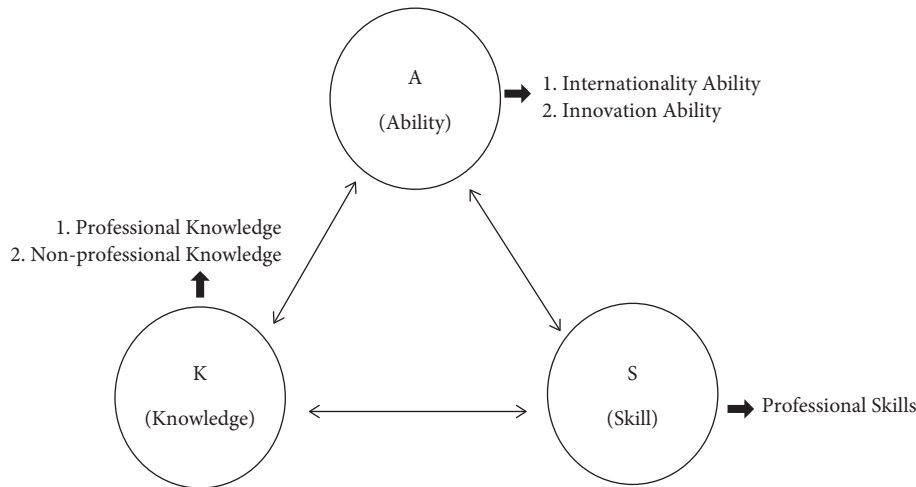
FIGURE 1: ASK education model for smart construction engineering.

3.2.2. Digital Language Landscape and Knowledge Acquisition by Engineering Students Suitable for Smart Construction. The education of engineering students in developed countries focuses on improving the professional knowledge and comprehensive quality of engineers and involves a wide range of courses covering multidisciplinary knowledge [100, 101]. The education mode of engineering students in the United States emphasizes liberal education in humanities, mathematics, and science. This involves a basic education in many disciplines with the goal of educating general engineering students, focusing on the integration of arts and science, enabling an adequate coverage of science and engineering, and supporting interdisciplinary [102, 103], whereas the education mode of engineering students in German universities mainly emphasizes the combination of basic education in humanities and social sciences and professional knowledge education and focuses on practical engineering education, with the goal of educating senior engineering students with a broad knowledge base [104–106].

A research report of the Chinese Academy of Engineering identified that engineering and technology students need to have more professional science and technology awareness and more solid engineering expertise as well as humanities and social knowledge [38]. Indeed, it can be seen that engineering students suitable for smart construction need not only to have the theoretical knowledge of their professions but also to learn the basic knowledge of multidisciplinary, humanities, and social sciences. Since the informative dimension of the digital linguistic landscape provides rich knowledge and information and basic knowledge of humanities and social sciences, as well as interdisciplinary knowledge, it is therefore able to play a key role in expanding the knowledge horizon of engineering students. In terms of the symbolic dimension, the digital linguistic landscape has the characteristics of information sharing, convenience, and expansion, which has the potential to impact the knowledge learning ability of students. Thus, the following research hypothesis was proposed regarding the digital linguistic landscape's role in the

education of knowledge acquisition of engineering students suitable for smart construction:

> H3: digital linguistic landscapes have a significant positive impact on the knowledge acquisition of engineering students suitable for smart construction.

3.2.3. Relationship between Digital Linguistic Landscape and Skills Training of Engineering Students. The overall scale and development level of China's construction industry continues to grow, but the construction industry still suffers from low skill quality of construction industry workers, imperfect skill education system, shortage of highly skilled personnel, and other problems, which seriously restricts the transformation of the construction industry. The provision of professional and systematic theoretical knowledge is an effective support to cultivate the skills of construction students [107, 108]. Indeed, China's Ministry of Education [39] proposed that, on the basis of the necessary basic theoretical knowledge and expertise, students should master the basic ability and basic skills to engage in the practical work in their professional fields. Therefore, in order to improve the skills mastery of smart construction engineering students, it is necessary to strengthen their professional theoretical knowledge base. As a platform for information provision and a medium for knowledge sharing, the digital language landscape plays a supporting role in the acquisition of skills and theories. Hence, the following research hypothesis was proposed regarding the digital linguistic landscape's role in the skill training of engineering students suitable for smart construction:

> H4: digital linguistic landscapes have a significant positive impact on the skills training of engineering students suitable for smart construction.

3.2.4. The Dimensions of Digital Language Landscape. Digital linguistic landscapes have informative and symbolic functions. The knowledge dimension in the ASK model derives from the informative function of the digital linguistic

landscape, which provides the source and support for the K in the ASK model. The symbolic function of the digital linguistic landscape can provide directions for the development of abilities and skills by reflecting current conditions and market trends. In view of this, the following research hypothesis was proposed on the role dimensions of digital linguistic landscape:

> H5: informative dimension and symbolic dimension are two main aspects of the DLL in the education of engineering students suitable for smart construction.

Based on the above hypotheses, the DLL-ASK model of the mechanism of digital language landscape on smart construction student educating was constructed, as shown in Figure 2.

4. Methods

4.1. Survey Design, Sample, and Procedure. A questionnaire was designed to survey the relations between DLL and engineering education. The questionnaire consists of two main parts, with four questions focusing on the background of participants and thirty-six statements to measure international ability, innovation ability, knowledge, skills, and informative and symbolic dimension of DLL (see Appendix). For the items in the second part, a 5-point Likert scale was used, with 1 indicating "strongly disagree" and 5 indicating "strongly agree."

The survey was designed and administered to collect data from September 28, 2021, to October 15, 2021, and was conducted in the form of online distribution on Sojump, a questionnaire platform. The survey was randomly sent to engineering college students, engineering professional teachers, and practitioners. In order to ensure the authenticity and objectivity of the survey data, the questionnaire was answered anonymously, and the purpose and the confidentiality of the study were informed in advance to reduce the privacy concerns of the survey respondents. A total of 193 responses were received.

As can be seen from Table 2, among the participants in the questionnaire survey, 1.05% of them are doctoral students and above, 10.47% are master's students, and 98.43% are bachelor's students and above, which reflects that the overall education level of the respondents in this survey is high. The statistics on the level of intercultural communication ability show that those who said they are not fluent in English account for the most (64.77%), while those who are fluent account for only 30.57%, and 4.66% said they could not communicate at all. This highlights that the overall intercultural communication level of college engineering students is low.

4.2. Data Analysis

4.2.1. Treatment of Data. In order to ensure the quality of data collected before commencing data analysis, all the completed questionnaires ($N = 193$) were checked against systematic response patterns and more than 5% missing items, as suggested by [109–111]. All questionnaires were completely answered. In view of the small proportion of engineering teachers and practitioners, their relevant data and questions (2nd question, years of working) were excluded, so 2 out of 193 completed questionnaires were dropped from the data set. To code responses for data analysis, the researchers identified each item as being favorable or unfavorable toward its factor to be measured, as suggested by Seo [109]. Items that score lower than 3 represent unfavorable; otherwise, they represent favorable.

4.2.2. Statistical Analysis. Data were analyzed with structural equation modeling (SEM) procedures, and MPLUS software was used to construct the SEM analysis of the DLL-ASK mechanism. This study used different types of indexes of overall fit for evaluating SEM models, including x^2/degrees of freedom ratio (x^2/df), Comparative Fit Index (CFI), Tucker-Lewis Index (TLI), and the root mean square error approximation (RMSEA).

(1) Absolute Fit Indexes. Absolute fit indexes typically evaluate "badness of fit." x^2/df and root mean square error of approximation (RMSEA) are two commonly used absolute fit indexes.

The model is regarded as acceptable, if the value of x^2/degrees of freedom ratio is less than two. MacCallum et al. [112] suggested that a value of 0.01, 0.05, and 0.08 of RMSEA indicates excellent, good, and mediocre fit, respectively.

(2) Incremental Fit Indexes. Incremental fit indexes typically evaluate "goodness of fit," as larger values indicate a better fit between hypothesized model and data. Commonly used incremental fit indexes include Bentler and Bonett's Normed Fit Index (NFI), Comparative Fit Index (CFI), Tucker-Lewis Index (TLI), and the Incremental Index of Fit (IFI), among which CFI and DFI were used in this study. A CFI value > 0.95 (ranging from 0.00 to 1.00) was considered representative of a well-fitting model. TLI value close to 0.95 represents indicative of a good fit [113].

5. Results

5.1. Descriptive Statistics. Correlations among all the dimensions are reported in Table 3, showing that all variables were significantly correlated ($p < 0.05$), and none of the correlation values exceeds the threshold value of 0.9, which suggests that the multicollinearity problem does not exist between the items [114].

5.2. Exploratory Factor Analysis. KMO and Bartlett's sphericity tests were conducted using SPSS software, and the results are shown in Table 4. The KMO value of the questionnaire sample was 0.864, and Bartlett's test value was less than 0.001, indicating that the sample is suitable for exploratory factor analysis (EFA) and the data information could be extracted effectively.

This study used SPSS24.0 software for the EFA to identify the dimensionality of the survey. After reducing the dimensionality of 36 factors, a total of 6 common factors were
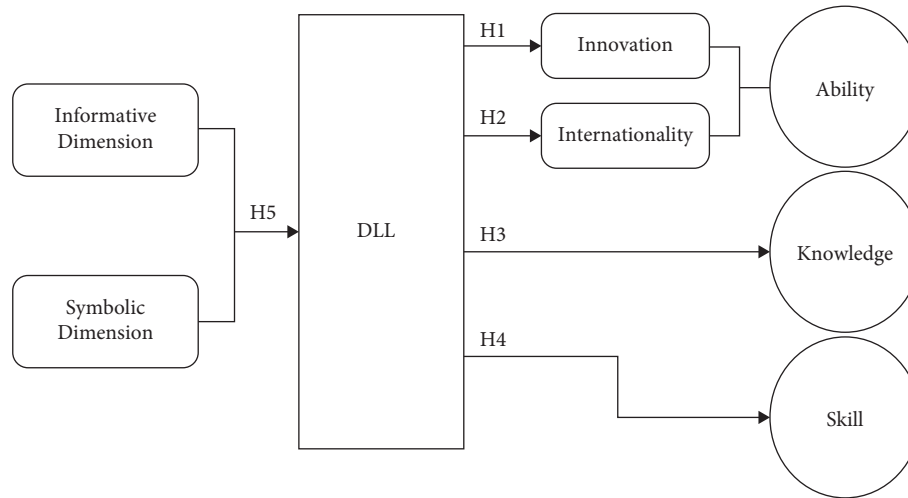
Figure 2: DLL-ASK model.

Table 2: Sample information table.

Items	Options	%
Degree	Associate/bachelor	86.91
	Master	10.47
	Doctor and above	1.05
English level	Else	1.57
	Very fluent	1.55
	Fluent	29.02
	Not fluent	64.77
	Cannot speak at all	4.66

Table 3: Correlations among variables.

Dimensions	A-I	A-CX	K	S	DLL-Info	DLL-Sym
A-I	1					
A-CX	0.264**	1				
K	0.560**	0.151*	1			
S	0.225**	0.203**	0.255**	1		
DLL-Info	0.318**	0.233**	0.263**	0.359**	1	
DLL-Sym	0.222**	0.187*	0.305**	0.412**	0.525**	1

**Correlation is significant at the 0.01 level. *Correlation is significant at the 0.05 level.

Table 4: KMO and Bartlett's test.

KMO and Bartlett's test		
KMO		0.864
Bartlett test of sphericity	Approx. Chi-square	9892.396
	df	1081
	Sig.	0.000

extracted, as shown in Table 5, and the cumulative variance explained by the extracted 6 factors was 70.614%, which proved that the extracted 6 factors could explain the original data of the questionnaire well.

Rotated component matrix result is shown in Table 6, and it can be seen that the classification of each question item corresponds exactly to the dimensional settings, indicating that the settings of each question item under the six dimensions are reasonable.

5.3. Testing the Measurement Model. The reliability of variables can be tested by Cronbach's alpha coefficient if $\alpha > 0.6$, indicating that the dimension is valid, and the larger it is, the better its reliability is. The results of the reliability test using SPSS software are shown in Table 7. It can be seen that the α values of variables are all greater than 0.7, and the CITC values of all measurement items are greater than 0.3, which shows that the data of each variable meet the requirements of reliability.

Then, the validity of factors was tested by confirmatory factor analysis (CFA). The CFA results are shown in Table 8. The results showed that the KMO values of these research variables are higher than 0.7, and Bartlett's test value is less than 0.001, representing statistically significant. Meanwhile, the factor loadings of items are all larger than 0.5, and the cumulative variance explained is above 50%. It represents each measurement item that belongs to the corresponding variable, and the dimension has good discriminant validity and convergent validity and meets the requirements needed for the study, so it can be tested by SEM.

5.4. Structural Model. The results of SEM analysis of the DLL-ASK mechanism are shown in Figure 3, and the specific coefficient results are shown in Table 9. The results of the SEM fit index are within the acceptable range, as x^2/df is 1.789 < 3, CFI is 0.950 > 0.90, TLI is 0.946 > 0.90, and RMSEA is 0.064 < 0.80. It can be seen that the DLL-ASK model constructed in this paper fits well.

According to the results of the SEM in Figure 3 and Table 9, it was found that the digital linguistic landscape contains an informative dimension and a symbolic dimension with factor loadings of 0.768 and 0.760, respectively. At the same time, the digital linguistic landscape variable consisting of these two dimensions has

TABLE 5: Common factors.

Component	Initial eigenvalues			Extraction sums of squared loadings			Rotation sums of squared loadings		
	Total	% of variance	Cumulative %	Total	% of variance	Cumulative %	Total	% of variance	Cumulative %
1	10.903	30.287	30.287	10.903	30.287	30.287	5.910	16.416	16.416
2	4.603	12.787	43.074	4.603	12.787	43.074	5.776	16.044	32.460
3	3.800	10.556	53.629	3.800	10.556	53.629	4.878	13.549	46.009
4	2.688	7.467	61.097	2.688	7.467	61.097	3.241	9.004	55.013
5	2.010	5.583	66.680	2.010	5.583	66.680	3.071	8.530	63.543
6	1.416	3.934	70.614	1.416	3.934	70.614	2.545	7.071	70.614
7	1.169	3.247	73.861						
8	0.975	2.709	76.570						
9	0.917	2.548	79.118						
10	0.869	2.413	81.531						
11	0.814	2.260	83.791						
12	0.718	1.995	85.786						
13	0.641	1.780	87.566						
14	0.603	1.674	89.240						
15	0.572	1.590	90.830						
16	0.555	1.542	92.372						
17	0.495	1.374	93.746						
18	0.435	1.209	94.955						
19	0.401	1.113	96.068						
20	0.351	0.975	97.043						
21	0.340	0.944	97.987						
22	0.230	0.638	98.625						
23	0.102	0.283	98.907						
24	0.076	0.210	99.118						
25	0.048	0.133	99.251						
26	0.044	0.123	99.374						
27	0.038	0.105	99.479						
28	0.033	0.092	99.571						
29	0.032	0.089	99.660						
30	0.025	0.070	99.731						
31	0.025	0.069	99.799						
32	0.023	0.063	99.863						
33	0.018	0.050	99.912						
34	0.015	0.042	99.954						
35	0.011	0.031	99.985						
36	0.005	0.015	100.000						

Extraction method: principal component analysis.

a positive effect on international ability, with a path coefficient of 0.361 ($p < 0.001$), and also a positive effect on innovation ability, with a path coefficient of 0.229 ($p < 0.05$), assuming that path H1 and H2 are established. Among them, the digital linguistic landscape has more influence on the formation of international ability. In addition, there is a significant positive effect of digital linguistic landscape on knowledge, with a path coefficient of 0.397 ($p < 0.001$), and the same to skill, with a path coefficient of 0648 ($p < 0.001$), proving that the hypotheses paths H3 and H4 are tenable. Considering the effect of digital linguistic landscape on ability, this result shows that digital linguistic landscape has the most significant effect on skills training of engineering students suitable for smart construction.

The hypothesis H5 that the digital linguistic landscape contains both informative and symbolic dimensions holds true, and the digital linguistic landscape combines together the two dimensions to educate engineering students suitable for smart construction. Features 6 (providing rich linguistic information), 7 (providing domestic and foreign human history), and 8 (providing interdisciplinary knowledge) of the informative dimension play the most significant role, and features 4 (reflecting foreign market trends) and 5 (reflecting domestic market trends) of the symbolic dimension play the most obvious role.

6. Discussion

This study aims to test the mechanism of the digital linguistic landscape in engineering education for smart construction. The results underscore the importance of digital linguistic landscape in educating engineering students in smart construction. DLL plays a significant role in educating the international ability and innovation

Table 6: Rotated component matrix.

Items	Components					
	1	2	3	4	5	6
A-I1	0.946					
A-I2	0.928					
A-I3	0.922					
A-I4	0.926					
A-I5	0.934					
A-I6	0.933					
A-CX1			0.956			
A-CX2			0.966			
A-CX3			0.962			
A-CX4			0.971			
A-CX5			0.965			
K1		0.917				
K2		0.924				
K3		0.933				
K4		0.907				
K5		0.923				
K6		0.925				
DLL-Info1				0.542		
DLL-Info2				0.376		
DLL-Info3				0.362		
DLL-Info4				0.543		
DLL-Info5				0.657		
DLL-Info6				0.725		
DLL-Info7				0.656		
DLL-Info8				0.602		
DLL-Sym1						0.486
DLL-Sym2						0.388
DLL-Sym3						0.341
DLL-Sym4						0.761
DLL-Sym5						0.850
S1					0.566	
S2					0.730	
S3					0.602	
S4					0.682	
S5					0.690	
S6					0.606	

Extraction method: principal component analysis.

ability of engineering students suitable for smart construction.

The findings have significant implications for the specification of the education objectives in regard to the ASK dimensions. The results identify the acting path of DLL on ability, knowledge, and skill education. To be specific, the path to enhance the international ability of engineering students for smart construction is mainly to improve the international competitiveness, cross-cultural communication ability, and broad international horizon. In addition, the path to enhance the innovation ability of the students is mainly to improve the innovation awareness, innovation thinking, and innovation skills, whereas the path to educate the underpinning knowledge of the students is mainly to enrich students' knowledge reserve, broaden their knowledge horizon, and enhance knowledge learning motivation. Furthermore, the improvement of the personal skill level of engineering students is of primary importance in skills training.

Table 7: CITC and Cronbach's a coefficient of variables.

Dimensions	Variables	Items	CITC	α
Ability: international ability	A: A-I	A-I1	0.995	0.976
		A-I2	0.983	
		A-I3	0.980	
		A-I4	0.985	
		A-I5	0.987	
		A-I6	0.985	
Innovation ability	A-CX	A-CX1	0.947	0.928
		A-CX2	0.975	
		A-CX3	0.967	
		A-CX4	0.976	
		A-CX5	0.973	
Knowledge	K	K1	0.930	0.972
		K2	0.971	
		K3	0.975	
		K4	0.972	
		K5	0.979	
		K6	0.972	
Skill	S	S1	0.405	0.781
		S2	0.618	
		S3	0.465	
		S4	0.551	
		S5	0.582	
		S6	0.557	
Informative dimension of DLL	DLL-Info	DLL-Info1	0.461	0.763
		DLL-Info2	0.323	
		DLL-Info3	0.396	
		DLL-Info4	0.431	
		DLL-Info5	0.489	
		DLL-Info6	0.525	
		DLL-Info7	0.532	
		DLL-Info8	0.513	
Symbolic dimension of DLL	DLL-Sym	DLL-Sym1	0.450	0.708
		DLL-Sym2	0.382	
		DLL-Sym3	0.345	
		DLL-Sym4	0.539	
		DLL-Sym5	0.614	

The innovation ability is an indispensable ability for engineering students suitable for smart construction [12, 95]. Digital linguistic landscape influences innovative thinking through feature 1 of the informative dimension (extensive information access) and features 2 and 3 of the symbolic dimension (reflecting market trends), innovative awareness through feature 5 of the informative dimension (diverse forms of information presentation), and innovative

TABLE 8: Confirmatory factor analysis results of variables.

Dimensions	Variables	Items	Factor loadings	KMO	P	Explained variance ratio (%)
Ability: international ability	A: A-I	A-I1	0.987	0.927	<0.001	98.110
		A-I2	0.991			
		A-I3	0.990			
		A-I4	0.990			
		A-I5	0.988			
		A-I6	0.996			
Innovation ability	A-CX	A-CX1	0.967	0.927	<0.001	96.154
		A-CX2	0.985			
		A-CX3	0.984			
		A-CX4	0.981			
		A-CX5	0.967			
Knowledge	K	K1	0.951	0.946	<0.001	95.320
		K2	0.982			
		K3	0.981			
		K4	0.979			
		K5	0.978			
		K6	0.951			
Skill	S	S1	0.960	0.818	<0.001	74.118
		S2	0.615			
		S3	0.887			
		S4	0.888			
		S5	0.655			
		S6	0.692			
Informative dimension of DLL	DLL-Info	DLL-Info1	0.783	0.768	<0.001	81.749
		DLL-Info2	0.920			
		DLL-Info3	0.939			
		DLL-Info4	0.892			
		DLL-Info5	0.783			
		DLL-Info6	0.838			
		DLL-Info7	0.820			
		DLL-Info8	0.670			
Symbolic dimension of DLL	DLL-Sym	DLL-Sym1	0.599	0.713	<0.001	79.622
		DLL-Sym2	0.958			
		DLL-Sym3	0.912			
		DLL-Sym4	0.900			
		DLL-Sym5	0.855			

skills through feature 1 (helping to understand digital technology) of the symbolic dimension. Digital linguistic landscape influences innovative skills through integrating the informative dimension and the symbolic dimension to cultivate the innovation ability of engineering students suitable for smart construction.

Digital linguistic landscape enhances cross-cultural communication ability through feature 6 (providing rich linguistic information) in the informative dimension and broadens international vision through feature 8 (rich interdisciplinary knowledge). Also, DLL improves international competitiveness through features 4 and 5 (reflecting domestic and international current conditions) in the symbolic dimension and integrates the informative dimension and symbolic dimension work together to cultivate the international ability of engineering students suitable for smart construction. Cultivation of the international ability of engineering students suitable for smart construction enables the students to become the leaders of the construction industry of the future [15].

Digital linguistic landscape educates the knowledge dimension of smart construction engineering students by enriching the professional and nonprofessional knowledge reserve of students through feature 4 (providing diversified foreign language information) and feature 6 (providing rich languages) of the informative dimension of digital linguistic landscape and broadens the knowledge horizon through feature 8 (rich interdisciplinary knowledge) of the informative dimension and features 2–5 of the symbolic dimension (reflecting market trends and current conditions). To broaden the knowledge horizons and enhance knowledge learning motivation through informative dimension feature 2 (easy access to information) and feature 5 (multimodal information presentation form) allow integration of two dimensions to cultivate the knowledge dimension of smart construction engineering students.

The specific path of the digital linguistic landscape for the skill education of engineering students suitable for smart construction is to train the skill of smart construction students through features 2 (easy access to

Note: $x^2/df = 1.789$, CFI = 0.950, TLI = 0.946, RMSEA = 0.064.
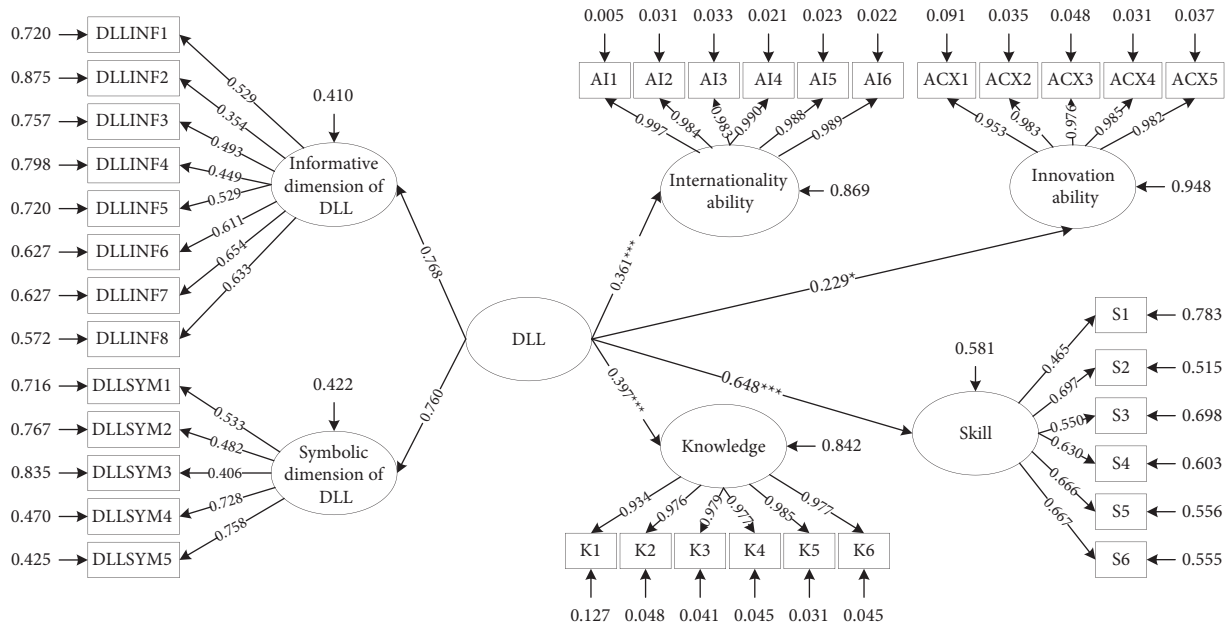
FIGURE 3: SEM results. *Notes*. x^2/df = 1.789, CFI = 0.950, TLI = 0.946, and RMSEA = 0.064. $^*p < 0.05$; $^{***}p < 0.001$.

TABLE 9: SEM coefficiency results.

Paths	Coefficiency	Standard error	p value	95% confidence intervals	Hypotheses
DLL⟶international ability	0.361	0.099	***	[0.168; 0.524]	Support
DLL⟶innovation ability	0.229	0.109	*	[0.015; 0.443]	Support
DLL⟶knowledge	0.397	0.093	***	[0.214; 0.550]	Support
DLL⟶skill	0.648	0.115	***	[0.423; 0.836]	Support

Notes. $^*p < 0.05$; $^{***}p < 0.001$.

TABLE 10: Questionnaire statements.

Items	Specific statements
1	Understanding domestic and international current conditions can help people enhance one's international competitiveness
2	Understanding market trends helps people enhance international competitiveness
3	Access to information on foreign language knowledge can help enhance one's intercultural communication skills
4	Access to rich linguistic information can help enhance one's intercultural communication skills
5	Access to information on humanities and social sciences helps to develop one's international perspective
6	Access to multidisciplinary knowledge helps to broaden one's global vision
7	Understanding domestic and international current situation helps to enhance one's innovation awareness
8	Understanding market trends helps enhance one's innovative thinking
9	Understanding the latest digital technology helps enhance one's innovative skills
10	Diversified access to information helps enhance one's innovative thinking
11	Diversified forms of information presentation can help enhance one's innovative thinking
12	Access to more language information helps to strengthen one's professional knowledge base
13	Access to foreign language knowledge helps enhance one's nonspecialized knowledge base
14	Understanding multidisciplinary knowledge helps broaden one's knowledge horizon
15	Understanding domestic and international market trends helps broaden one's knowledge horizons
16	Easy access to language information helps to increase motivation to learn
17	Access to a wide range of language information helps to increase motivation to learn
18	Knowledge of the latest digital technologies helps to strengthen one's skills
19	Understanding more knowledgeable information helps to strengthen one's skills
20	Understanding domestic and international current conditions helps strengthen one's skills
21	Knowledge of domestic and international market trends helps strengthen one's skills
22	Knowledge of foreign language information helps strengthen one's skills
23	Easy access to information helps strengthen personal skills

TABLE 10: Continued.

Items	Specific statements
24	DLL can increase people's access tunnels to information
25	DLL makes it easier for people to access information
26	DLL allows people to share information resources
27	DLL multimodality increases people's interest in it
28	DLL provides various languages
29	DLL provides a wealth of linguistic information
30	DLL helps people understand the history of people at home and abroad
31	DLL can provide access to multidisciplinary knowledge
32	DLL provides access to the latest digital technologies
33	DLL provides access to domestic current situations
34	DLL provides access to foreign current situations
35	DLL helps people study foreign market trends
36	DLL helps people study domestic market trends

information), feature 4 (providing multiple foreign language information), and feature 6 (providing rich language information) of the informative dimension of digital linguistic landscape.

Educating the ability of engineering students in smart construction is the driver and support for the development of the smart construction industry [115]. Knowledge has been identified as a key driving force for innovation [95]. Thus, the development of the knowledge dimension also indirectly acts on the improvement of the innovation ability. By improving the skill level, smart construction students can improve their skill level and thereby be more able to adapt to society and meet its changing needs more quickly [99]. Therefore, it is necessary to strengthen the application of DLL in engineering education.

7. Conclusion

This research investigates the influence factors on the education of engineering students suitable for smart construction. The study divided the qualities of engineering students suitable for smart construction into the three dimensions of ability, knowledge, and skill based on the ASK model, and a DLL-ASK hypothesis model was subsequently constructed. Based on this approach, the DLL-ASK model was surveyed and tested using a questionnaire and SEM.

The results of the study identify the following: (1) The informative dimension and symbolic dimension are two main aspects of the DLL in engineering education for smart construction. (2) DLL has a significant positive impact on the ability, knowledge, and skills of engineering students suitable for smart construction. (3) DLL educates the ability, knowledge, and skills of engineering students for smart construction by transmitting rich language information and multilingual information as well as reflecting market trends at home and abroad. The research results are consistent with the DLL-ASK hypothesis model, and therefore, the DLL-ASK model is supported.

Based on the above results, the following suggestions are made on how to educate engineering students for smart construction from the informative dimension and symbolic dimension of the digital linguistic landscape:

(1) Increase the amount of digital linguistic landscapes in engineering education. It is highly important to enhance the use and edification of digital linguistic landscape in the real engineering student training environment or digital space learning environment. Through strengthening the edification and influence of digital linguistic landscape in smart construction training, it is more likely to gradually improve the ability and skills of students and broaden their knowledge horizon as well. Specific measures include increasing the amount of digital signage on campus, using digital media to support the education process, and establishing a digital linguistic landscape network platform for information sharing.

(2) Pay more attention to the content of digital language landscape information. Digital language information is most directly accessed and absorbed by students, so this feature can be harnessed to present the education contents to smart construction engineering students through the carrier of the digital language landscape. For example, for the cross-cultural communication ability of engineering students, the skills to enhance abilities or access to resources can be presented through multimodal presentation such as voice, image, and QR code.

(3) Make full use of digital language landscape technology guidance role. As the embodiment of digital technology, digital language landscape has a significant impact on the technical development of engineering students for smart construction. By learning the application of digital technology, smart construction students can better and faster integrate the trend of social development and meet the changing needs of the construction industry.

Therefore, it is necessary to periodically update the digital language landscape medium and use the latest technology-supported digital signage so as to connect digital technology with smart construction technology.

The limitation of this study is that although the participants appear to be representative of engineering students in China's higher education, there is nevertheless a lack of involvement of teachers and practitioners. Moreover, the participants were limited to Chinese engineering students, and there was a lack of involvement of international students. Therefore, future research should adopt a larger sample size with a wider range of participants to further examine the external validity of the study.

Appendix

Questionnaire

Linguistic landscape includes physical landscapes formed by language, such as language appearing on public signs such as public street signs, billboards, street names, place names, and store signboards. It also includes language information on virtual media such as digital signage, electronic billboards, and network video advertisements. Digital linguistic landscape is a platform for displaying linguistic landscape information through digital technology, a medium for carrying linguistic information in virtual space, such as QR codes, digital advertisements, and multimedia videos.

The survey is anonymous, and the data of this questionnaire is for academic research use only. Your honest, personal opinions are greatly appreciated and help us a lot. Thanks for your time!

(I) Demographic traits

(1). Your identity: ☐Engineering Practitioner ☐Engineering Teacher ☐Engineering Learner
(2). How long have you been working in this industry: _____
(3). Your major: _____
(4). Your education: ☐university or college ☐postgraduate ☐doctor ☐else

(II) Your evaluations of the following roles' degree

Five choices are listed below each question, from 1 indicating "strongly disagree" to 5 indicating "strongly agree" (Table 10).

Data Availability

The data used to support the findings of the study could be obtained from the corresponding author upon request.

Conflicts of Interest

The authors declare that they have no conflicts of interests or personal relationships that could have appeared to influence the work reported in this paper.

Authors' Contributions

Jingxiao Zhang contributed to the conception of the study, Lin Xu and Yin Yuan performed the experiment, Yin Yuan and Junwei Zheng contributed significantly to analysis and manuscript preparation, Yin Yuan and Jingxiao Zhang performed the data analyses and wrote the manuscript, P. Philbin and Brian H.W. Guo helped perform the analysis with constructive discussions, and Ruoyu Jin contributed to the revision and polishing of the paper.

Acknowledgments

References

[1] L. Ding, "System thinking on cultivation mode for innovative intelligent construction talents," *Research in Higher Education of Engineering*, vol. 05, pp. 1–4+29, 2019.

[2] C. Santelices, R. Herrera, and F. Muñoz, "Problemas en la gestión de calidad e inspección técnica de obra: un estudio aplicado al contexto chileno," *Revista ingeniería de construcción*, vol. 34, no. 3, pp. 242–251, 2019.

[3] M. Bilal, L. O. Oyedele, J. Qadir, and K. Munir, "Big Data in the construction industry: a review of present status, opportunities, and future trends," *Advanced Engineering Informatics*, vol. 30, no. 3, pp. 500–521, 2016.

[4] A. Ghaffarianhoseini, U. Berardi, H. AlWaer, S. E. Chang, and A. Ghaffarianhoseini, "What is an intelligent building? Analysis of recent interpretations from an international perspective," *Architectural Science Review*, vol. 59, no. 5, pp. 338–357, 2016.

[5] D. Liu, W. Lu, and Y. Niu, "Extended technology-acceptance model to make smart construction systems successful," *Journal of Construction Engineering and Management*, vol. 144, no. 6, 2018.

[6] Z. Yang, Y. Wang, and C. Sun, "Emerging information technology acceptance model for the develoment of smart construction system," *Journal of Civil Engineering and Management*, vol. 24, no. 6, pp. 457–468, 2018.

[7] J. Zhang, Z. Zhang, S. P. Philbin, H. Huijser, Q. Wang, and R. Jin, "Toward next-generation engineering education: a case study of an engineering capstone project based on BIM technology in MEP systems," *Computer Applications in Engineering Education*, vol. 30, no. 1, pp. 146–162, 2022.

[8] B. Becerik-Gerber and K. Kensek, "Building information modeling in architecture, engineering, and construction: emerging research directions and trends," *Journal of Professional Issues in Engineering Education and Practice*, vol. 136, no. 3, pp. 139–147, 2010.

[9] L. E. Bernold, "Paradigm shift in construction education is vital for the future of our profession," *Journal of Construction Engineering and Management*, vol. 131, no. 5, pp. 533–539, 2005.

[10] K. Chen and L. Ding, "Development of key domain- relevant technologies for smart construction in China," *Chinese Journal of Engineering Science*, vol. 23, no. 4, pp. 64–70, 2021.

[11] G. T. Anderson and IEEE, "An approach to teaching innovation processes in engineering," in *Proceedings of the 3rd Interdisciplinary Engineering Design Education Conference (IEDEC)*, pp. 1–5, Santa Clara, CA, USA, March 2013.

[12] J. Zhang, R. Li, H. Li, M. Skitmore, and P. Ballesteros-Perez, "Improving the innovation ability of engineering students: a Science and Technology Innovation Community organisation network analysis," *Studies in Higher Education*, vol. 46, no. 4, pp. 851–865, 2021.

[13] P. Ponce, A. Molina, E. O. L. Caudana, G. B. Reyes, and N. M. Parra, "Improving education in developing countries using robotic platforms," *International Journal on Interactive Design and Manufacturing*, vol. 13, no. 4, pp. 1401–1422, 2019.

[14] R. Navon, "The last lecture: the need for civil engineering education to stimulate thinking instead of only teaching," *Journal of Construction Engineering and Management*, vol. 146, no. 5, 2020.

[15] A. G. Ball, H. Zaugg, R. Davies, and I. Tateishi, "Identification and validation of a set of global competencies for engineering students," *International Journal of Engineering Education*, vol. 28, no. 1, pp. 156–168, 2012.

[16] A. D. Wisneski, L. Huang, B. Hong, and X. Wang, "Tsinghua-johns hopkins joint center for biomedical engineering research: scientific and cultural exchange in undergraduate engineering," in *Proceedings of the 33rd Annual International Conference of the IEEE Engineering-In-Medicine-And-Biology-Society (EMBS)*, pp. 3620–3623, Boston, MA, USA, August 2011.

[17] H. Nishiguchi, Y. Yagyu, and F. Ishinuki, "Scientific exchanging meetings with overseas students for improvement of technical communication in English," in *Proceedings of the 8th IEEE/SICE International Symposium on System Integration (SII)*, pp. 151–156, Meijo Univ, Nagoya, Japan, December 2015.

[18] J. H. Zheng, T. Fuhrmann, B. Q. Xu et al., "Curriculum design and German student exchange for sino-German bachelor program majored in optoelectronics engineering," in *Proceedings of the 14th Conference on Education and Training in Optics and Photonics (ETOP)*, PEOPLES R CHINA, Hangzhou, May 2017.

[19] W. Lu, Y. Peng, Q. Shen, and H. Li, "Generic model for measuring benefits of BIM as a learning tool in construction tasks," *Journal of Construction Engineering and Management*, vol. 139, no. 2, pp. 195–203, 2013.

[20] G. Lu and T. Li, "Reflections of the paths of constructing and developing emerging engineering education," *Research in Higher Education of Engineering*, vol. 03, pp. 20–26, 2017.

[21] L. B. Wu, H. Yuan, S. Q. Gao et al., *Nitric Oxide: Biology and Chemistry*, vol. 57, pp. 21–29, 2016.

[22] A. Damci, "Impact of personal demographics on civil engineers' motivators: case study of Turkey," *Journal of Management in Engineering*, vol. 32, no. 2, 2016.

[23] B. Weber-Lewerenz, "Corporate digital responsibility (CDR) in construction engineering—ethical guidelines for the application of digital transformation and artificial intelligence (AI) in user practice," *SN Applied Sciences*, vol. 3, no. 10, p. 801, 2021.

[24] M. Kohtamaki, V. Parida, P. C. Patel, and H. Gebauer, "The relationship between digitalization and servitization: the role of servitization in capturing the financial potential of digitalization," *Technological Forecasting and Social Change*, vol. 151, p. 119804, 2020.

[25] J. J. M. Ferreira, C. I. Fernandes, and F. A. F. Ferreira, "To be or not to be digital, that is the question: firm innovation and performance," *Journal of Business Research*, vol. 101, pp. 583–590, 2019.

[26] P. C. Verhoef, T. Broekhuizen, Y. Bart et al., "Digital transformation: a multidisciplinary reflection and research agenda," *Journal of Business Research*, vol. 122, pp. 889–901, 2021.

[27] G. Shang, "Linguistic landscape and language teaching: from resource to tool," *Chinese Journal of Language Policy and Planning*, vol. 2, no. 2, p. 9, 2017.

[28] E. Shohamy and S. Waksman, "Linguistic landscape as an ecological arena: modalities, meanings, negotiations, education," in *Linguistic Landscape:Expanding the Scenery*, E. S.&D. Gorter, Ed., pp. 313–331, 2008.

[29] Wfeo, "World federation of engineering organization," *Committee on Engineering Capacity Building*, 2017, http://www.wfeo.org.

[30] FEANl, "FEANl:Competence of professional engi-neers/ EUR ING(April2005)," 2005, https://www.feani.org/webfeani/.

[31] "The Sydney Accord," 2013, https://www.ieagreements.org/assets/Uploads/Documents/Policy/Graduate-Attributes-and-Professional-Competencies.

[32] "The Washington Accord," https://www.academia.edu/12050366/Washington_Accord.

[33] Iec, "International engineering Alliance.International engineering Alliance.International engineering alliance—APEC agreement," 2017, http://www.ieagreements.orglagreements/apec.

[34] S. Cutler, M. Borrego, and ieee, "developing global competence in graduate engineering and science students through an IGERT international internship program," in *Proceedings of the 40th Annual Frontiers in Education Conference*, Arlington, VA, USA, October 2010.

[35] S. S. Klein-Gardner, A. Walker, and Asee, "Defining global competence for engineering students," in *Proceedings of the ASEE Annual Conference and Exposition*, Vancouver, CA, USA, June 2011.

[36] T. J. Siller, A. Rosales, J. Haines, and A. Benally, "Development of undergraduate students' professional skills," *Journal of Professional Issues in Engineering Education and Practice*, vol. 135, no. 3, pp. 102–108, 2009.

[37] M. Stieff, S. Scopelitis, M. E. Lira, and D. Desutter, "Improving representational competence with concrete models," *Science Education*, vol. 100, no. 2, pp. 344–363, 2016.

[38] W. Hu and Z. Li, "Research on international representative engineering talents key competences model," *Research in Higher Education of Engineering*, vol. 04, pp. 81–87, 2021.

[39] Ceeaa, "China engineering education accreditation association," *General Criteria for Accreditation of Engineering*

Education, 2018, https://www.ccf.org.cn/c/2018-11-05/654410.shtml.

[40] D. Coelho, L. L. Tundisi, K. S. Cerqueira, and J. R. D. S. Rodrigues, "Microalgae: cultivation aspects and bioactive compounds," *Brazilian Archives of Biology and Technology*, vol. 62, 2019.

[41] K. Mehta and I. Gorski, "Engineering careers in social innovation and global sustainable development [commentary]," *IEEE Technology and Society Magazine*, vol. 36, no. 4, pp. 55–61, 2017.

[42] F. Gerber and K. J. Mammen, "Eastern Cape employers' views on the strengths and weaknesses of civil engineering diplomates entering the workplace," *Journal of the South African Institution of Civil Engineers*, vol. 61, no. 1, pp. 38–51, 2019.

[43] J. Zhang, W. Wu, and H. Li, "Enhancing building information modeling competency among civil engineering and management students with team-based learning," *Journal of Professional Issues in Engineering Education and Practice*, vol. 144, no. 2, 2018.

[44] A. Alroomi, H. D. Jeong, and G. D. Oberlender, "Evaluation of methods to retain cost estimating competencies using structural equation modeling," *Journal of Management in Engineering*, vol. 32, no. 1, 2016.

[45] A. R. Carberry, E. M. Gerber, and C. K. Martin, "Measuring the innovation self-efficacy of engineers," *International Journal of Engineering Education*, vol. 34, no. 2, pp. 590–598, 2018.

[46] J. Lin, "On outstanding engineers' innovation ability training," *Research in Higher Education of Engineering*, vol. 05, pp. 1–17, 2012.

[47] D. M. Ferguson and M. W. Ohland, "What is engineering innovativeness?" *International Journal of Engineering Education*, vol. 28, no. 2, pp. 253–262, 2012.

[48] B. J. Knight, "Internationalisation: elements and checkpoints," in *Ottawa: Canadian Bureau for International Education*, Canada, 1994.

[49] J. Knight, "Internationalization remodeled: definition, approaches, and rationales," *Journal of Studies in International Education*, vol. 8, no. 1, pp. 5–31, 2004.

[50] S. Bains and IEEE, "Teaching technical communication to engineering students at scale," in *Proceedings of the IEEE International Professional Communication Conference (ProComm)*, pp. 83–89, Aachen, Germany, July 2019.

[51] A. Fleury and M. T. L. Fleury, *Brazilian Multinationals: Competences for Internationalization*, Cambridge University Press, 2011.

[52] M. Frank and D. Elata, "Developing the capacity for engineering systems thinking (CEST) of freshman engineering students," *Systems Engineering*, vol. 8, no. 2, pp. 187–195, 2005.

[53] A. Azerni and Ieee, "Benefits of teaching systems thinking as part of an fngineering curriculum," in *Proceedings of the 49th IEEE Frontiers in Education Conference (FIE)*, Univ. Cincinnati, Cincinnati, OH, USA, October 2019.

[54] S. Bell, A. Chilvers, L. Jones, and N. Badstuber, "Evaluating engineering thinking in undergraduate engineering and liberal arts students," *European Journal of Engineering Education*, vol. 44, no. 3, pp. 429–444, 2019.

[55] J. D. Stolk and R. Martello, "Can disciplinary integration promote students' lifelong learning attitudes and skills in project-based engineering courses?" *International Journal of Engineering Education*, vol. 31, no. 1, pp. 434–449, 2015.

[56] E. A.-R. Blakeney, S. Kang, K. Henrikson, and J. T. C. Liu, "Implementation and evaluation of team science training for interdisciplinary teams in an engineering design program," *Journal of Clinical and Translational Science*, vol. 5, no. 1, 2021.

[57] L. R. Lattuca, D. B. Knight, H. K. Ro, and B. J. Novoselich, "Supporting the development of engineers' interdisciplinary competence," *Journal of Engineering Education*, vol. 106, no. 1, pp. 71–97, 2017.

[58] R. Munasinghe and Ieee, "Multidisciplinary research projects for engineering students - Part II," in *Proceedings of the 40th Southeastern Symposium on System Theory*, pp. 405–409, New Orleans, LA, USA, March 2008.

[59] G. S. Stump, J. C. Hilpert, J. Husman, Wt Chung, and W. Kim, "Collaborative learning in engineering students: gender and achievement," *Journal of Engineering Education*, vol. 100, no. 3, pp. 475–497, 2011.

[60] T. Healy, G. P. Smestad, and J. Gonzalez, "A project-based interdisciplinary program in sustainable energy," in *Proceedings of the 3rd Interdisciplinary Engineering Design Education Conference (IEDEC)*, pp. 148–152, Santa Clara, CA, USA, March 2013.

[61] J. Zhang, H. Xie, and H. Li, "Competency-based knowledge integration of BIM capstone in construction engineering and management education," *International Journal of Engineering Education*, vol. 33, no. 6b, pp. 2020–2032, 2017.

[62] R. G. Roberts, "A case study to motivate engineering students to do mathematical proofs," *International Journal of Electrical Engineering Education*, vol. 40, no. 4, pp. 231–242, 2003.

[63] C. B. Tatum, "Learning construction engineering: why, what, and how?" *Journal of Construction Engineering and Management*, vol. 144, no. 3, 2018.

[64] R. A. Rahman, S. Alsafouri, P. Tang, and S. K. Iyer, "Comparing building information modeling skills of project managers and BIM managers based on social media analysis," in *International Conference on Sustainable Design, Engineering and Construction (ICSDEC)*, vol. 145, pp. 812–819, Arizona State Univ, Coll Avenue Commons, May 2016.

[65] P. Caratozzolo, A. Alvarez-Delgado, and S. Hosseini, "Strengthening critical thinking in engineering students," *International Journal on Interactive Design and Manufacturing*, vol. 13, no. 3, pp. 995–1012, 2019.

[66] V. Caggiano, T. Redomero-Echeverria, J. L. Poza-Lujan, and A. Bellezza, "Soft skills in engineers, a relevant field of research: exploring and assessing skills in Italian engineering students," *Ingeniería e Investigación*, vol. 40, no. 2, pp. 81–91, 2020.

[67] T. Hegazy, M. Abdel-Monem, D. A. Saad, and R. Rashedi, "Hands-on exercise for enhancing students' construction management skills," *Journal of Construction Engineering and Management*, vol. 139, no. 9, pp. 1135–1143, 2013.

[68] R. Landry and R. Y. Bourhis, "Linguistic landscape and ethnolinguistic vitality: an empirical study," *Journal of Language and Social Psychology*, vol. 16, no. 1, pp. 23–49, 1997.

[69] D. Gorter, "Linguistic landscapes and trends in the study of schoolscapes," *Linguistics and Education*, vol. 44, pp. 80–85, 2018.

[70] D. Gorter and J. Cenoz, "Theoretical development of linguistic landscape studies," *Linguistic Landscape. An international journal*, vol. 6, no. 1, pp. 16–22, 2020.

[71] D. Gorter, "Linguistic landscapes in a multilingual world," *Annual Review of Applied Linguistics*, vol. 33, pp. 190–212, 2013.

[72] M. Berezkina, "'Language is a costly and complicating factor': a diachronic study of language policy in the virtual public sector," *Language Policy*, vol. 17, no. 1, pp. 55–75, 2018.

[73] B. Busse, "Practices of discursive urban place-making in Brooklyn, New York: (hidden) digital and embodied discourse," *Text & Talk*, vol. 41, no. 5-6, pp. 617–641, 2021.

[74] T. Hiippala, A. Hausmann, H. Tenkanen, and T. Toivonen, "Exploring the linguistic landscape of geotagged social media content in urban environments," *Digital Scholarship in the Humanities*, vol. 34, no. 2, pp. 290–309, 2019.

[75] B. Jordan, "Blurring boundaries: the real and the virtual in hybrid spaces," *Human Organization*, vol. 68, no. 2, pp. 181–193, 2009.

[76] D. Dunlevy, P. Martin, and M. Neele, Eds., *Linguistic Landscape*, vol. 5, no. 3, 2019.

[77] J. Morales, R. Montes, N. Zermeno, J. Duran, and F. Herrera, "The use of fuzzy linguistic information and fuzzy delphi method to validate by consensus a questionnaire in a blended-learning environment," *Communications in Computer and Information Science*, vol. 855, pp. 137–149, June 2018.

[78] G. Simungala and H. Jimaima, "Towards an appreciation of individual positionality and the global-local interface: facebook Actorhood in Zambia," *Journal of Multicultural Discourses*, vol. 16, no. 3, pp. 227–244, 2021.

[79] K. Bolton, "World Englishes and linguistic landscapes," *World Englishes*, vol. 31, no. 1, pp. 30–33, 2012.

[80] U. Keles, B. Yazan, and A. Giles, "Turkish-English bilingual content in the virtual linguistic landscape of a university in Turkey: exclusive de facto language policies," *International Multidisciplinary Research Journal*, vol. 14, no. 1, pp. 1–19, 2020.

[81] J. Shibliyev, "Genel hdgkdd," *Bilig*, vol. 90, pp. 67–91, 2019.

[82] H. Limerick, R. Hayden, D. Beattie, O. Georgiou, and J. Muller, "User engagement for mid-air haptic interactions with digital signage," in *Proceedings of the 8th ACM International Symposium on Pervasive Displays (Pervasive Displays)*, Palermo, Italy, June 2019.

[83] D. Sheppard, N. Felker, and J. Schmalzel, "Development of voice commands in digital signage for improved indoor navigation using google assistant SDK," in *Proceedings of the 14th IEEE Sensors Applications Symposium (SAS)*, Sophia Antipolis, France, March 2019.

[84] E. Adami, "Book review: communicating beyond language: everyday encounters with diversity and the linguistic landscape of chinatown: a sociolinguistic ethnography," *Visual Communication*, vol. 17, no. 2, pp. 263–268, 2018.

[85] J. M. Magno, "Linguistic landscape in cebu city higher education offering communication programs," *Asia Pacific Journal of Multidisciplinary Research*, vol. 5, no. 1, p. 2, 2017.

[86] I. W. Mulyawan, "Reading visual design of outdoor signs in Kuta (A case study of multimodal linguistic landscapes)," *Cogent Arts & Humanities*, vol. 7, no. 1, p. 1748987, 2020.

[87] T. Kopylova and L. Kilina, "The media image of the country in political discourse: speech methods of creation," *Mundo Eslavo-Journal of Slavic Studies*, vol. 19, pp. 77–88, 2020.

[88] V. Kerry, *Language in Society*, vol. 47, no. 3, pp. 473-474, 2018.

[89] J. R. E. Leimgruber, "Global multilingualism, local bilingualism, official monolingualism: the linguistic landscape of Montreal's St. Catherine Street," *International Journal of Bilingual Education and Bilingualism*, vol. 23, no. 6, pp. 708–723, 2020.

[90] H. S. Al-Khalifa, *Applying Knowledge, Skills and Abilities in Undergraduate Research Seminar Course*, IEEE, 2013.

[91] T. M. Ho-Kim, "Knowledge, skills and abilities of international business MajorsWhat we teach them versus what companies need them to know," *Journal of Teaching in International Business*, vol. 19, 2007.

[92] U. Control, *The Importance of KSA's (Knowledge, Skills and Abilities) in the Federal Application Process*, u.s.center for disease control & prevention, 2013.

[93] J. Stahl and H. Luczak, "Personnel planning in concurrent engineering: a case study," *Human Factors and Ergonomics in Manufacturing*, vol. 10, no. 1, pp. 23–44, 2000.

[94] C.-C. Hu, H.-C. Yeh, and N.-S. Chen, "Enhancing STEM competence by making electronic musical pencil for non-engineering students," *Computers & Education*, vol. 150, 2020.

[95] S. M. Asio, J. A. Cross, and S. Ekwaro-Osire, "Factors affecting innovation in engineering design teams: an empirical investigation of student team perceptions," *International Journal of Engineering Education*, vol. 34, no. 4, pp. 1159–1173, 2018.

[96] S. Kulturel-Konak, A. Konak, G. E. Kremer, and I. Esparragoza, "Assessment of engineering students' global awareness knowledge, strategic processing and interest," *International Journal of Engineering Education*, vol. 35, no. 2, pp. 519–534, 2019.

[97] D. Render, I. Jimenez-Useche, and C. A. Calahan, "Cultivating global mindsets without leaving campus: building interculturally competent engineer," in *Proceedings of the IEEE Frontiers in Education Conference (FIE)*, Indianapolis, IN, USA, October 2017.

[98] S. Chipperfield, S. Kulturel-Konak, and A. Konak, "Assessing students' global awareness," in *Proceedings of the 5th IEEE Integrated STEM Education Conference (ISEC)*, pp. 151-152, Princeton, New Jersey, March 2015.

[99] L. Hahn, L. Sorenson, and Ieee, "Developing engineering students' language and cultural skills for academic and professional success," in *Proceedings of the IEEE Frontiers in Education Conference (FIE)*, Madrid, Spain, October 2014.

[100] D. Lopez-Fernandez, P. P. Alarcon, and E. Tovar, "Motivation in Engineering Education A framework supported by evaluation instruments and enhancement resources," in *Proceedings of the IEEE Global Engineering Education Conference (EDUCON)*, pp. 421–430, Tallinn Univ. Technol, Tallinn, Estonia, March 2015.

[101] A. J. Lopez-Martin, "Attracting prospective engineering students in the emerging European space for higher education," *IEEE Transactions on Education*, vol. 53, no. 1, pp. 46–52, 2010.

[102] S. K. Najid, S. A. Osman, M. Z. Omar et al., "Perception of faculty engineering and built environment's students towards the benefit of industrial training," *Procedia - Social and Behavioral Sciences*, vol. 60, pp. 157–162, 2012.

[103] H. K. Sardana and P. P. Arya, "Training evaluation of engineering students: a case study," *International Journal of Engineering Education*, vol. 19, no. 4, pp. 639–645, 2003.

[104] E. S. Fritzsche, J. Schlingensiepen, and R. Kordts-Freudinger, "Study motivation and academic emotions in engineering students A case study in German higher education," in *Proceedings of the IEEE Global Engineering Education Conference (EDUCON) - Emerging Trends and Challenges of Engineering Education*, pp. 563–570, Santa Cruz de Tenerife, Spain, April 2018.

[105] L. Plumanns, D. Janssen, and R. Vossen, "Ready for future international challenges: promoting intercultural competencies," in *Proceedings of the 19th European Conference on Knowledge Management (ECKM)*, pp. 708–715, Univ Padua, Padua, Italy, Septemper 2018.

[106] N. Strenger, M. Petermann, and S. Frerich, "Going abroad A discipline-specific approach to promote the mobility of German engineering students," in *Proceedings of the 8th IEEE Global Engineering Education Conference (EDUCON)*, pp. 226–229, Athens, Greece, April 2017.

[107] K. G. Nelson, D. F. Shell, J. Husman, E. J. Fishman, and L. K. Soh, "Motivational and self-regulated learning profiles of students taking a foundational engineering course," *Journal of Engineering Education*, vol. 104, no. 1, pp. 74–100, 2015.

[108] Y. Reyes-Gonzalez, N. Martinez-Sanchez, A. Diaz-Sardinas et al., "Conceptual clustering: a new approach to student modeling," in *Intelligent Tutoring Systems*, vol. 87, pp. 70–76, Revista Facultad De Ingenieria-Universidad De Antioquia, 2018.

[109] D. C. Seo, "An explicative model of unsafe work behavior," *Safety Science*, vol. 43, no. 3, pp. 187–211, 2005.

[110] B. H. W. Guo, T. W. Yiu, and V. A. González, "Predicting safety behavior in the construction industry: development and test of an integrative model," *Safety Science*, vol. 84, pp. 1–11, 2016.

[111] B. H. W. Guo, T. W. Yiu, and V. A. González, "Does company size matter? Validation of an integrative model of safety behavior across small and large construction companies," *Journal of Safety Research*, vol. 64, pp. 73–81, 2018.

[112] R. C. MacCallum, M. W. S. Browne, and H. M. Sugawara, "Power analysis and determination of sample size for covariance structure modeling," *Psychological Methods*, vol. 1, no. 2, pp. 130–149, 1996.

[113] L. Hu and P. M. Bentler, "Cutoff criteria for fit indexes in covariance structure analysis: conventional criteria versus new alternatives," *Structural Equation Modeling: A Multidisciplinary Journal*, vol. 6, pp. 1–55, 1999.

[114] J. F. Hair, *Multivariate Data Analysis*, Pearson Prentice Hall, 2006.

[115] J. Zhang, H. Xie, and H. Li, "Exploring the cognitive structure and quality elements: building information modeling education in civil engineering and management," *International Journal of Engineering Education*, vol. 32, no. 4, pp. 1679–1690, 2016.

Research Article

Application of Mathematical Methods Based on Improved Fuzzy Computing in Building and Urban Design in the Environment of Industry 4.0

Chuan Duan (ID)

School of Architecture and Civil Engineering, Xihua University, Chengdu 610039, China

Correspondence should be addressed to Chuan Duan; duan_chuan@mail.xhu.edu.cn

In order to improve the performance of the urban building in urban design, this paper uses the mathematical method based on an improved fuzzy calculation to construct an intelligent building and urban design system. Moreover, this paper quantitatively studies the pedestrian wind environment of high-rise buildings and determines the optimal building aerodynamic shape and optimal building layout in the full wind direction. In addition, based on the results of the whole watershed analysis of CFD numerical simulation, this paper reveals the mechanism of building shape and layout in the pedestrian wind environment of high-rise buildings. Finally, this paper constructs an intelligent model to improve the effect of urban architectural design. Through the model research results, we can see that the urban design intelligent system proposed in this paper meets the needs of urban design in the environment of Industry 4.0.

1. Introduction

In the context of Industry 4.0, there are very few cases where the development of AI application science is supported by mainstream architects and urban designers. Early claims of artificial intelligence have raised concerns that the core jobs and competencies of architects and urban designers will be displaced. At the same time, when expectations fail to materialize, there is a loss of interest and funding for AI in building and urban design. However, interest in AI has picked up again since the second decade of the twenty-first century. Advances in technology, changing attitudes towards computer science in general, the emergence of big data and data analytics, the widespread use of civics, the rediscovery of civic design, the emergence of civic design science, and large-scale open online design approaches are working together to advance a more positive outlook for AI in building and urban design and may lead to compelling outcomes.

At present, the phenomenon of blindly copying foreign architectural creations is common in domestic building and urban design, which is obviously in mourning with the idea of a "harmonious society". In response to this phenomenon, we believe that we should not only actively absorb the good parts of the foreign building in architectural creation. What is more important is to absorb the excellent ideas in the development of foreign cities, such as the idea of focusing on the coordinated development of individual buildings and the city as a whole, to consider the issue of architectural creation in the context of macro urban society. Therefore, in order to realize a "harmonious society", it is necessary to emphasize the concept of coordination between people, buildings, and the environment in architectural creation.

The huge demand in the construction market and the relatively affluent social and economic conditions have led to the phenomenon of the one-sided pursuit of form and blind pursuit of novelty in the field of urban and architectural design. This "impetuous" design idea is reflected in the urban environment. First of all, various construction projects compete with each other to become the city's logo and image projects. It is conceivable that every building strives to highlight its individual image and play a leading role in the

city. The result is a cluttered urban landscape and weakens the overall appearance of the city. In addition, driven by the concept of the supremacy of form, urban architectural design is seriously plagiarized, applying some avant-garde and trendy fashion designs in the world, ignoring the specific base environment and cultural connotation; this leads to the disappearance of the environmental identity and cultural identity of urban areas. Many traditional urban areas and historical areas have been completely "renovated" after renovation, cutting off the social life network of the original residents, and the architectural form has become a false stage setting. The root cause of these problems lies in the neglect of the relationship between the part and the whole in creative activities and the lack of respect for the urban environment and regional culture. This self-centered view of creation will inevitably bring chaos to the overall urban environment, which is not conducive to the construction of a "harmonious society". Therefore, we should adhere to the people-oriented scientific development concept, deal with the relationship between architecture and the city from an overall perspective, and realize the harmonious development of people, buildings, and the environment.

From urban planning and design to architectural design, it is a "three-stage" relationship from the whole to the group and then to the individual [1]. If the individual building is taken out and analyzed again, the overall volume of the building, the volume transition relationship, and the detail processing will form a "three-stage" relationship [2]. In this way, when the building is enlarged into a system, the details of the near-human scale are at its most microscopic level. However, the building volume observed from the city's perspective becomes its macro scale, and it is observed from the perspective of the street, that is, urban design [3].

This paper combines the mathematical method of improving fuzzy calculation to construct the intelligent building and urban design system and improves the effect of urban architectural design through the intelligent model.

2. Related Work

The methods and capabilities of urban architectural planning and design continue to develop with the advancement of science and technology. In the early urban architectural planning, due to the use of traditional manual drawings for design, there were many problems due to the limitation of technology such as low labor efficiency, long design and design cycles of drawings, and error-prone architectural planning and design information. It is difficult to exchange and store design files and design results [4] and so on. The improvement of the economic level and the acceleration of the urbanization process affect the needs of urban architectural planning and design, and the traditional manual drawing method cannot handle a large number of design documents quickly and accurately. Information technology and CAD software have begun to be popularized on a large scale, various industries have also begun to enter the digital age, and the "electronic design" system of the urban architectural planning and design industry has emerged as the times require [5]. The electronic construction report design

system adopts CAD electronic drawings in a unified and standardized format, which can quickly extract and calculate and analyze the information to be designed for the building, complete the automatic quantitative accounting of design indicators, realize electronic filing, and dynamically store architectural project design plans. The precise data processing capability of CAD provides efficient and accurate design technology for architectural planning, and the specification standards and accounting indicators formulated by electronic design make the design results reasonable and serious [6]. With the increasingly complex development of urban architecture, urban planning and design need more comprehensive and objective analysis, and the CAD technology based on a two-dimensional plane is difficult to realize the image description of urban three-dimensional geospatial information [7].

At the beginning of the twenty-first century, the rapid development of 3D GIS technology made the concept of the digital city begin to be valued by people. The 3D visualization analysis of the architectural space environment in the digital city has become the development direction of architectural planning and design [8]. 3D GIS technology can be used for urban architectural planning and design. Comprehensive, intuitive, and scientific decision analyses are provided. In recent years, the fusion technology of BIM and GIS has attracted much attention in many industries, and its application in urban architectural planning and design has also entered the stage of research and exploration. BIM technology is widely used in some developed countries abroad [9]. Professional architectural engineering software based on BIM technology includes Revit and Infraworks series software products of Autodesk Company of the United States, ArchiCAD software of Graphisoft Company of Hungary, and MicroStation TriForma software of Bentley Company [10]. These large software developers provide comprehensive solutions for the needs of different stages of construction projects and the management goals of different professions. However, at present, most of these softwares are aimed at single building projects, which have poor support for terrain data and limited data capacity, which cannot meet the needs of urban planning and design in a three-dimensional environment. On the other hand, geographic information system (GIS) software is also moving closer to BIM. The processing of spatial data is a feature of GIS [11], and the storage, expression, and analysis of large-scale terrain spatial data are the strength of GIS, which just makes up for the shortcomings of traditional BIM software in infrastructure construction projects in a large-scale environment [12]. BIM and GIS are different in the geometric and semantic expressions of model objects. The key to their integrated application lies in the fusion of model data. With the in-depth research on the integration of BIM and GIS technology, although relevant personnel of various majors has completed the exchange of information and data through simple model conversion, similar methods only save part of the semantic information, resulting in obvious limitations in the application of BIM [13]. At present, the research on BIM and GIS integration mainly focuses on two aspects, one is the integration of basic data models, and the other is the
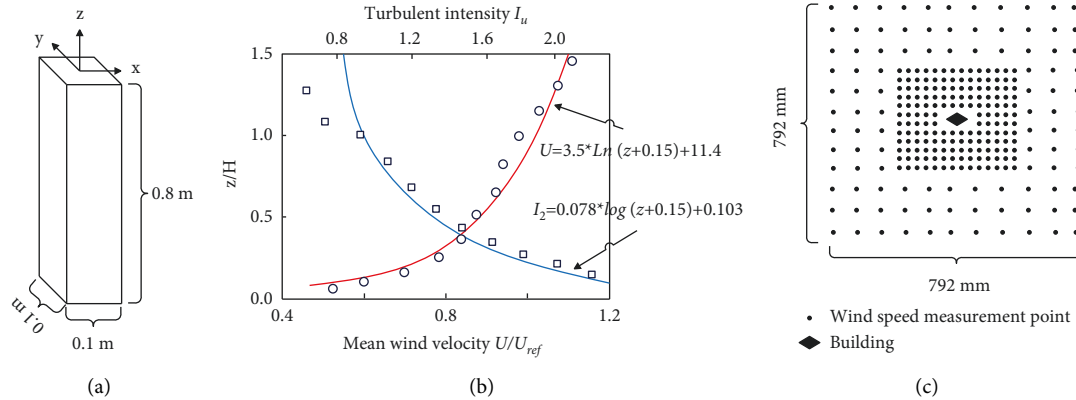
FIGURE 1: Basic model parameters. (a) Model size. (b) Average wind speed profile and turbulence intensity. (c) Distribution map of measuring points.

integration of existing data formats. The former analyzes the different expression types of BIM and GIS model objects and establishes a unified expression model for the two [14].

At this stage, most research directions are mainly focused on the latter, integrating model data in different formats, such as IFC Explorer developed by the Karlsruhe University of Technology in Germany, BIM Server developed by the Eindhoven University of Technology in the Netherlands, and Navisworks software developed by Autodesk [15]. Among them, IFCExplorer CityGML is committed to the seamless integration of the BIM standard model format IFC and the GIS standard model format CityGML, but it is difficult to achieve indiscriminate conversion between the two standard models, and it is still at the lower level of detail of the research model conversion [16]. BIMServer software supports the understanding and management of various BIM model structures, and at the same time, it can realize the simple conversion of BIM to GIS models. However, its functions are limited to data management and transformation and cannot achieve application analysis [17]. In addition, the conversion between its BIM and GIS models still has problems such as poor quality of the converted model and lack of semantics. Although Navisworks can realize the integrated analysis and application of BIM data sets, it is mainly based on a simple file system, so it is difficult to process large-scale data and the efficiency is low. And its support for GIS data can only be achieved through the conversion of third-party software, which will inevitably lose a lot of real information during the conversion process [18].

3. Architecture and Urban Design Based on Improved Fuzzy Computing

The structural model used in this paper is a single building with a square cross section. The scale ratio used in the numerical simulation is consistent with the experiment, which is $1 : 500$, and the size after the scale is $D_x \times D_y \times D_z = 0.1 \times 0.1 \times 0.8 m$ (Figure 1(a)), and Figure 1(b) shows the distribution of measuring points around the building. All the measuring points are located at the pedestrian

height, and a total of 280 measuring points are arranged. The distribution range of measuring points is $X \times Y = 0.792 \times 0.792$ m (the center point of the building is the origin of coordinates), which is about 8 times the cross-sectional area of the calculated model. The height H of the building is taken as the reference height, and $U_{\text{ref}} = 11.3$m/s, $I_u = 11.6\%$ at the reference height. Existing research conclusions show that, for the fitting of regions with lower heights, the logarithmic wind profile is better than the exponential wind profile. Since this paper studies the pedestrian wind environment at the pedestrian height (the height is 2 meters), in order to ensure the accuracy of the numerical simulation, the logarithmic wind profile is used for calculation. The distribution map of the measuring points is shown in Figure 1(c).

3.1. Calculation Domain and Boundary Condition Setting. In the CFD numerical simulation, the dimensions of all models are consistent with the wind tunnel test, and the size of the three-dimensional computational domain is set to $D_x \times D_y \times D_z = 15H \times 10H \times 6H$ (Figure 2). After calculation, the corresponding blocking rate is less than 3%, which meets the corresponding requirements.

The inlet of the computational domain is set to velocity inlet, the outlet is set to pressure outlet, and the boundary conditions on both sides and the top boundary are symmetric boundary conditions (symmetry).

The model is structured and meshed with ICEM CFD software. In meshing, because the Reynolds number of the fluid in the near-wall region is low during the flow process, in order to ensure the full development of turbulence, the mesh in the near-wall region must be refined. On the other hand, since different turbulence models have different requirements for mesh quality, it is necessary to divide meshes of different sizes according to the selected turbulence model.

In the CFD calculation, the size of the first layer grid of the model is often determined by calculating the size of the $y+$ value. The relevant calculation steps are as follows.

(1) It calculates the Reynolds number *Re*
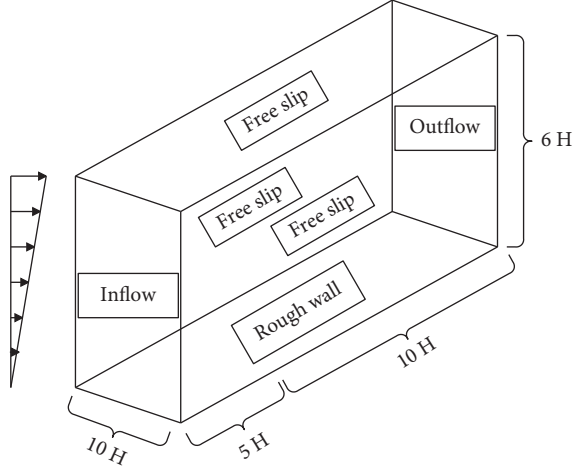
FIGURE 2: Computational domain and boundary condition settings (square).

$$R_e = \frac{\rho U L}{\mu}. \tag{1}$$

(2) It calculates the wall friction coefficient C_f

$$C_f = \left(2 \log_{10} R_e - 0.65\right)^{-2.3} \left(R_e \leq 10^9\right). \tag{2}$$

(3) It calculates the wall shear stress τ_w

$$\tau_w = C_f \times \frac{1}{2} \rho U^2. \tag{3}$$

(4) It calculates the grid height of the first layer

$$u^* = \sqrt{\frac{\tau_w}{\rho}}, \qquad (4)$$
$$\Delta y = \frac{y^+ \mu}{\rho u^*}.$$

When meshing, it is often necessary to divide different meshes according to different calculation models. In order to facilitate the calculation, this paper uniformly selects $Y^+ = 15$ for mesh division, the corresponding first-layer mesh size is set to $\Delta y = 0.0005m$ after calculation, and the corresponding mesh schematic diagram and calculation conditions are set as shown in Figure 3.

In order to verify the influence of the mesh size on the calculation results, the working condition RANS-1 is used as the reference condition to verify the influence of different mesh sizes on the calculation results. Two sets of grids with different sizes were established on the basis of the working condition SCRS-1. The minimum grid size of the refined grid is 0.0005 m, the minimum grid size of the sparse grid is 0.002 m, and other related settings remain unchanged. The corresponding mesh numbers are as follows. The total number of refined meshes is about 9×10^7, and the number of sparse meshes is about 4×10^7. The comparison chart of different size grids is shown in Figure 4.

In the numerical simulation study in the pedestrian wind environment, the accuracy of the simulation calculation cannot be guaranteed due to the low height of pedestrians, which are easily affected by the ground roughness. Therefore, one of the key issues of CFD numerical simulation is to meet the requirement of wind speed self-sustainability in the empty flow domain, that is, to ensure that the flow characteristics of the flow field remain consistent in the horizontal direction when the fluid passes the ground surface.

In the CFD calculation, we first calculate an airflow field before starting the model calculation, from which we obtain the average wind profile at the entrance, exit, and three locations of the model. The wind profile without corresponding adjustment is shown in Figure 5, and it can be found that the unadjusted wind profile does not achieve good retention at lower altitudes. At this altitude, the wind speed profile is significantly affected, resulting in a change in wind speed. In order to keep the wind speed uniform at lower heights, the self-sustainability of the wind speed is achieved by modifying the wall function and roughness parameters in this paper.

It can be found that in the wind field after debugging, the wind speeds of the inlet and outlet surfaces are consistent, thus ensuring the accuracy of the numerical simulation in this paper.

When evaluating the pedestrian wind environment around a building, the wind speed ratio R_i is often used for analysis, and its related definition is as follows:

$$R_i = \frac{V_i}{V_0}, \tag{5}$$

where V_i is the wind speed at the pedestrian height at the measuring point around the building (this paper is 2 meters above the ground), and V_0 is the wind speed at the entrance pedestrian height when there is no building [19].

In order to find the turbulence model with the best match between the predicted results and the experimental results, the turbulence model is judged by three evaluation indicators. The corresponding parameters are as follows:

(1) The indicator q is

$$q = \frac{1}{M} \sum_{i=1}^{M} n_i,$$
$$n_i = \begin{cases} 1 & \left|\dfrac{R_{i\,\exp} - R_{iCFD}}{R_{i\,\exp}}\right| \leq 0.2 \text{ or } \left|R_{i\,\exp} - R_{iCFD}\right| \leq 0.2 \\ 0 \end{cases} \tag{6}$$

(2) The average error δ is

$$\delta = \frac{1}{M} \sum_{i=1}^{M} \left|R_{\text{iexp}} - R_{\text{iCFD}}\right|. \tag{7}$$

(3) The mean square error σ is

$$\sigma = \sqrt{\frac{1}{M} \sum_{i=1}^{M} \left(R_{\exp} - R_{iCFD}\right)^2}. \tag{8}$$
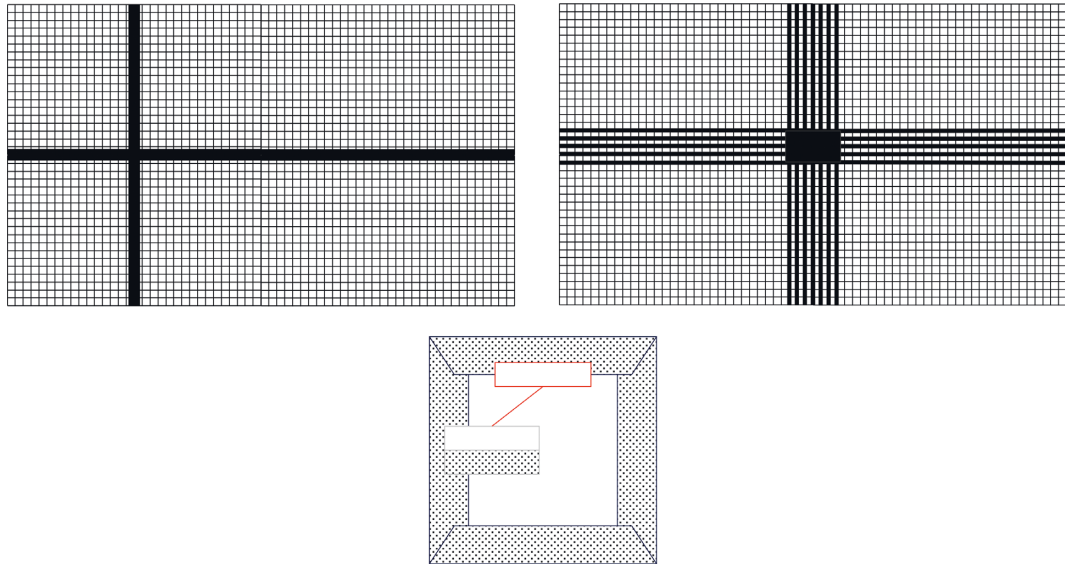
FIGURE 3: Schematic diagram of grid distribution (square).

| (a) | (b) | (c) |
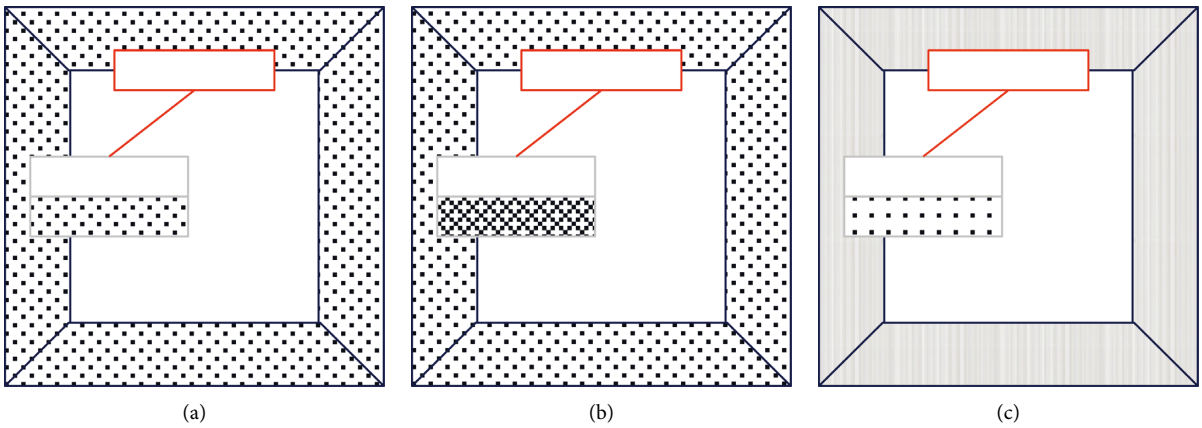
FIGURE 4: Grid independence analysis (square). (a) Basic network. (b) Encrypted Network. (c) Sparse network.

| (a) | (b) |
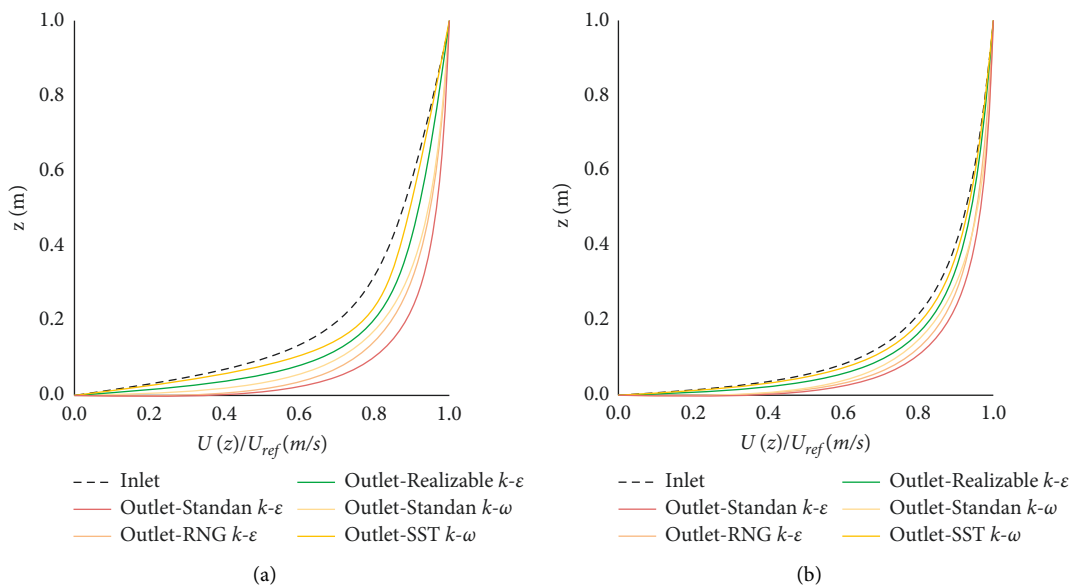
FIGURE 5: Comparison of inlet and outlet wind speed profiles under different conditions. (a) Unadjusted wind profile comparison. (b) Adjusted wind profile comparison.
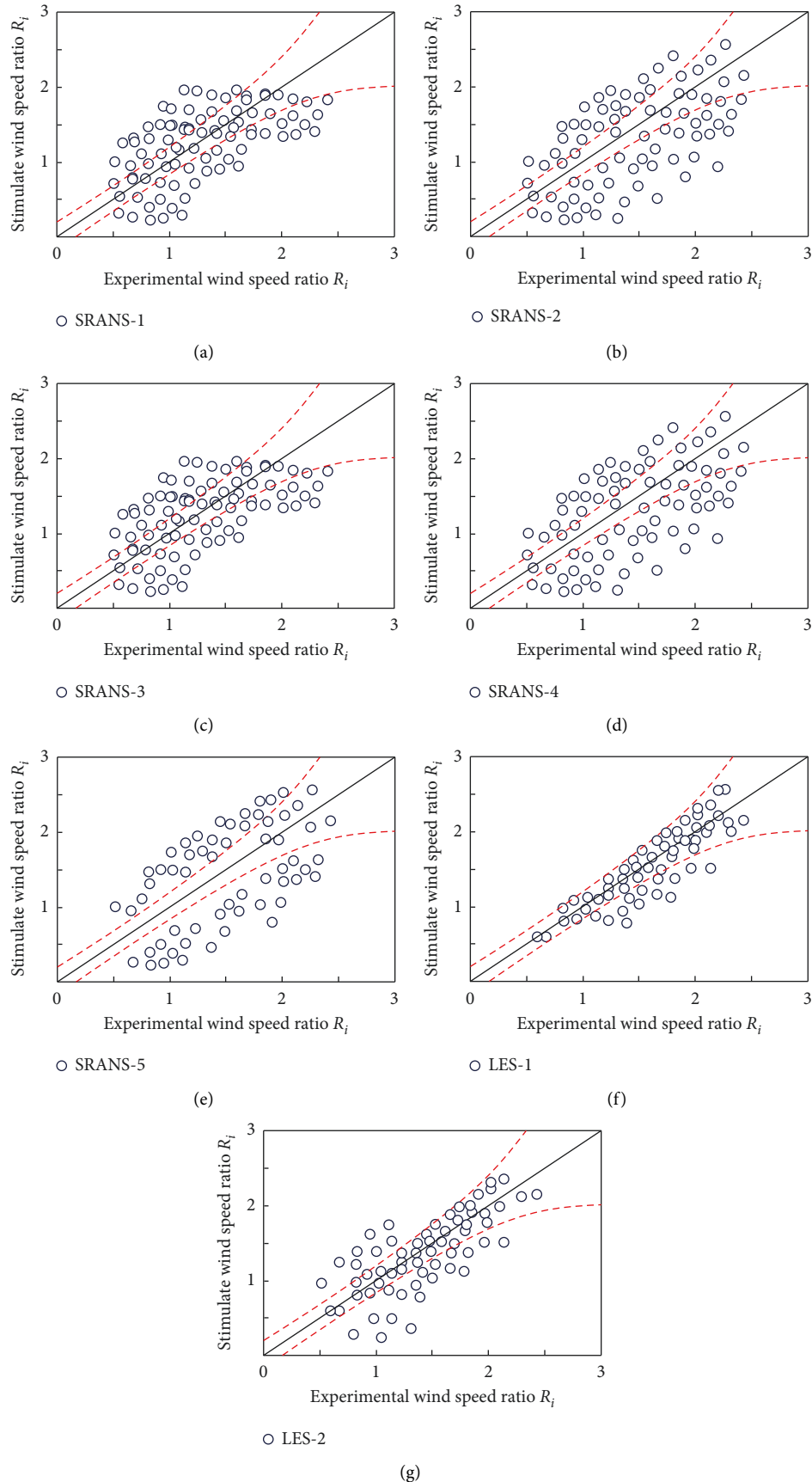
Figure 6: Distribution results of evaluation index q value under different working conditions. (a) Standard K-ε model. (b) RNG K-ε model. (c) Realizable K-ε model. (d) Standard K-ε model. (e) SST K-ε model. (f) ARFE method. (g) CDRFG method.
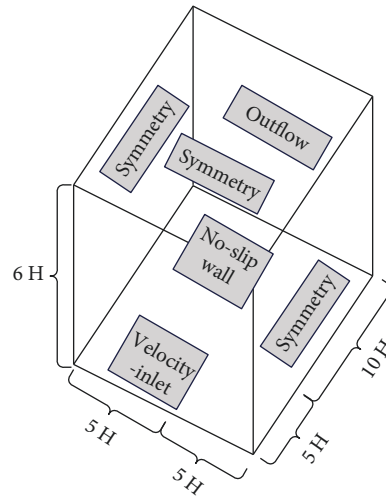
FIGURE 7: Computational domain and boundary condition settings (building group).

(a)

(b)

(c)

(d)
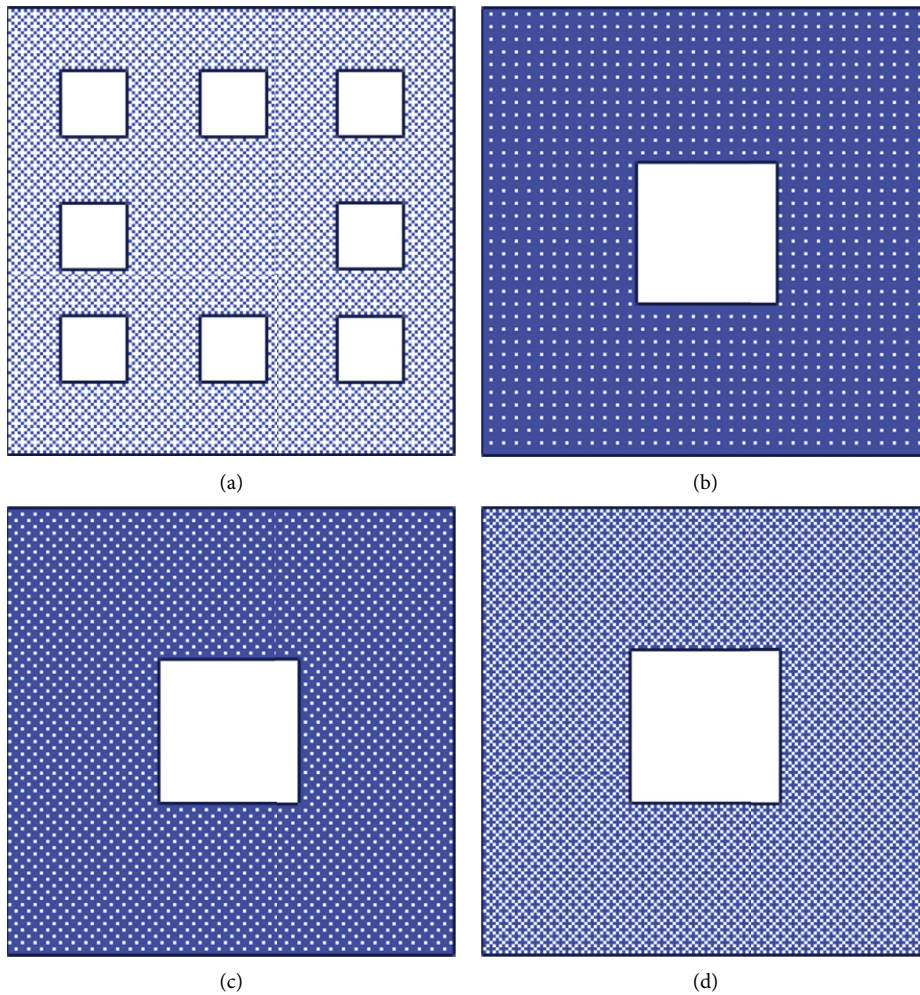
FIGURE 8: Grid independence analysis (building group). (a) Global network. (b) Sparse network. (c) Base network. (d) Encryption network.

In the above three formulas, M is the number of measuring points, and R_{iexp}, $R_{iCF\ D}$ is the wind tunnel test result and CFD simulation result at the i-th measuring point, respectively.

After sorting out the wind tunnel test data, a total of 244 valid data measurement points are collected in the wind tunnel test. Through statistical analysis of these 244 different measuring points, it is found that there are 77 low wind
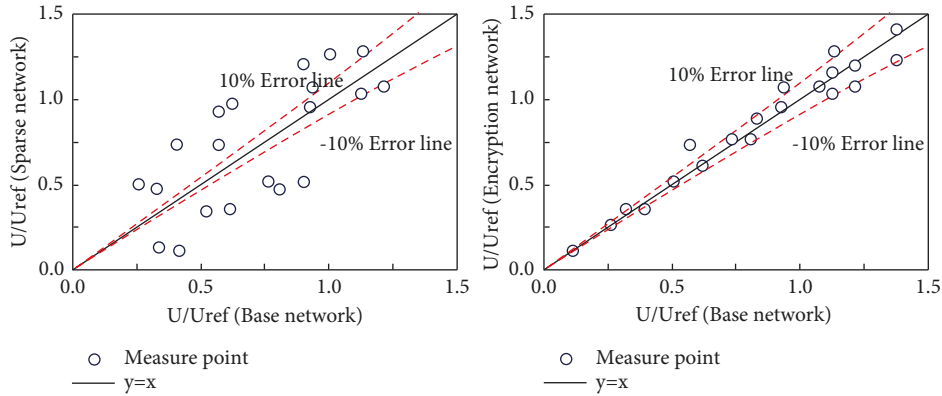
FIGURE 9: Comparison of wind speeds at different measuring points (buildings).
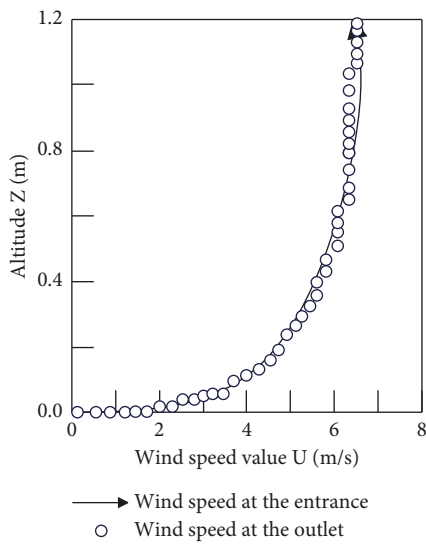
FIGURE 10: Comparison of inlet and outlet wind speed profiles under different working conditions (building group).
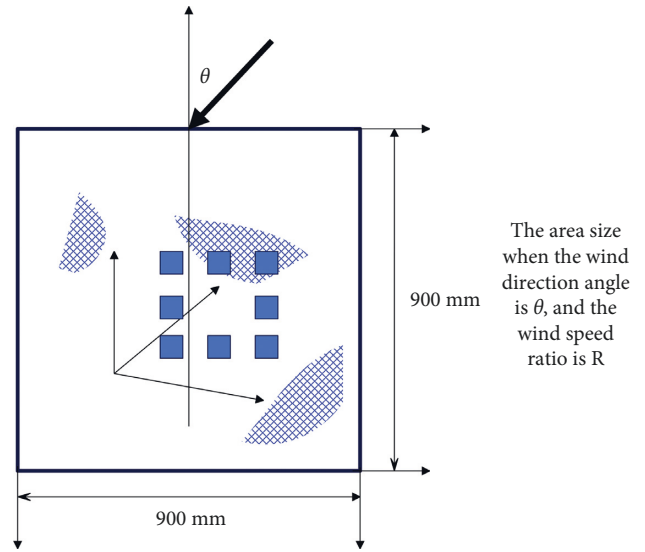
FIGURE 11: Schematic diagram of the calculation of $\theta_{R,\theta}$.

speed measuring points (wind speed ratio R_i is less than 1.0) and 167 high wind speed measuring points (wind speed ratio R_i is greater than 1.0). Therefore, the distribution map of the corresponding simulation results is first given (Figure 6).

From the distribution results of the index q, there is a certain error between different working conditions of the SRAMS model, but the error is mainly concentrated in the low wind speed area, that is, the area where the wind speed ratio R_i is less than 1.0. On the other hand, it performs well in the high wind speed area, that is, the area where the wind speed ratio R_i is greater than 1.0. This is mainly due to the fact that the SRNS model cannot accurately simulate the flow separation phenomenon in the wake area of the building, which makes it poorly simulated in the low wind speed area. The LES condition performs well in both low wind speed and high wind speed regions.

In the CFD numerical simulation, the dimensions of all models are kept consistent with the wind tunnel test. The size of the computational domain is 15H (length) × 10H (width) × 6H (height) (as shown in Figure 7), and the blockage rate of the CFD numerical simulation is less than 3%, which

meets the requirements of computational wind engineering and does not need to be revised. The structured grid is used for division, and the grid is refined at the building wall. The grid height of the first floor is 0.0002 meters. According to the preliminary simulation results, the y value of the building surface is about 30, the grid growth rate is set to 1.1, and the total number of grids for all working conditions is 7×10^7 ∼ 9×10^7.

This paper takes the square enclosed layout as an example to verify the grid independence. First, a set of basic grids is established. The height of the first layer grid is 0.0002 meters, the grid growth rate is set to 1.1, and the total number of grids is about 7 million. Secondly, another two sets of grids of different sizes are distributed and established. The grid size of the first layer of the sparse grid is 0.0004 meters, the grid growth rate is 1.1, and the total number of grids is about 4 million. The mesh size of the first layer of the refined mesh is 0.0001 meters, the mesh growth rate is 1.1, and the total number of meshes is about 11 million. The corresponding grid size comparison chart is shown in Figure 8. Furthermore, different grids are used to simulate the pedestrian wind environment, and the
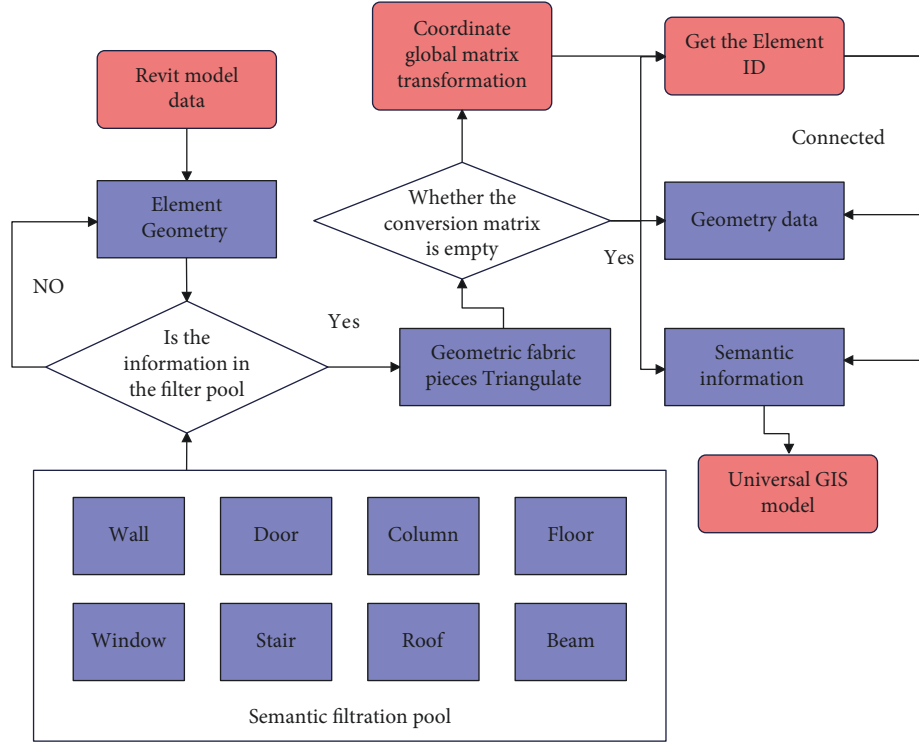
FIGURE 12: Application process of the mathematical method based on improved fuzzy calculation in building and urban design.

calculation results of 26 different measuring points are obtained. The corresponding results are compared in Figure 9.

It can be clearly found that there is a significant difference in the calculation results between the sparse grid and the basic grid, while the difference between the refined grid and the basic grid is very small. This is enough to show that using the basic grid for simulation can not only ensure the calculation accuracy but also ensure that the computing resources are consumed as little as possible, so all the calculation case grids in this chapter are divided according to the basic grid method.

It can be seen from the foregoing that the self-sustainability of the wind speed must be ensured first before CFD numerical simulation is carried out. In this paper, the self-sustainability of wind speed is achieved by modifying the wall function and roughness parameters. The relevant simulation results are shown in Figure 10. The results show that the velocity profiles of the inlet and outlet are relatively consistent and have good self-sustainability in the verification results of the empty wind field.

When evaluating the pedestrian wind environment around a building, the wind speed ratio R_i is often used for analysis, and its related definition is as follows:

$$R_i = \frac{V_i}{V_0}, \tag{9}$$

where V_i is the wind speed at the pedestrian height at the measuring point around the building (this paper is 2 meters above the ground), and V_0 is the wind speed at the entrance pedestrian height when there is no building.

In order to quantitatively analyze the impact of building shape and layout on the pedestrian wind environment of high-rise buildings, this paper uses the maximum wind speed ratio R_{max} and the normalized accelerated area ratio A^{**} to evaluate the wind environment of the building group. The relevant definitions are as follows:

$$R_{max,\theta} = \max(R_{i,\theta}),$$

$$A_{R,\theta}^* = \frac{A_{R,\theta}}{A_T},$$

$$R_{max} = \max(R_{max,\theta}),$$

$$R_{min} = \min(R_{max,\theta}), \tag{10}$$

$$A_{max^*} = \max(A_{R,\theta}^*),$$

$$A_{min^*} = \min(A_{R,\theta}^*),$$

$$A_{R,arg}^* = \frac{1}{N} \sum A_{R,\theta}^*,$$

where $R_{i,\theta}$ is the wind speed ratio in the evaluation area when the wind direction angle is θ, and A_T is the area of the evaluation area. According to the distribution of measuring points, the size of this area is $900 \times 900 \text{mm}^2$. $\theta_{R\theta}$ is the size of the area where the wind direction angle is θ and the wind speed ratio in the area is greater than R (Figure 11).

TABLE 1: Evaluation of architectural and urban design effects.

Number	City design	Number	City design	Number	City design
1	77.73	26	74.89	51	72.16
2	74.16	27	80.02	52	77.88
3	70.21	28	75.51	53	76.07
4	74.21	29	75.06	54	81.58
5	80.27	30	73.25	55	83.74
6	76.40	31	73.41	56	74.14
7	78.11	32	69.83	57	82.05
8	81.21	33	73.41	58	77.35
9	79.30	34	83.55	59	81.83
10	71.06	35	83.59	60	78.62
11	76.57	36	74.58	61	74.05
12	83.50	37	72.94	62	83.96
13	72.94	38	70.72	63	81.90
14	70.08	39	69.63	64	81.18
15	69.94	40	78.15	65	77.22
16	75.85	41	71.83	66	80.56
17	75.67	42	77.15	67	78.62
18	82.61	43	82.67	68	73.14
19	82.39	44	80.56	69	79.49
20	78.42	45	79.20	70	79.93
21	72.81	46	74.98	71	70.61
22	80.63	47	71.22	72	80.45
23	70.59	48	73.28	73	71.19
24	83.27	49	77.99	74	71.76
25	77.91	50	82.50	75	76.45

TABLE 2: User experience evaluation of urban design.

Number	User experience	Number	User experience	Number	User experience
1	84.17	26	86.03	51	79.97
2	80.32	27	77.55	52	84.71
3	85.38	28	74.59	53	83.20
4	77.41	29	76.95	54	79.83
5	79.55	30	76.04	55	86.98
6	78.61	31	76.00	56	78.19
7	74.66	32	77.55	57	82.80
8	79.65	33	79.73	58	74.43
9	74.12	34	79.06	59	86.00
10	79.25	35	85.93	60	84.08
11	73.26	36	75.26	61	76.00
12	85.37	37	83.04	62	77.24
13	74.69	38	83.38	63	73.88
14	77.81	39	73.57	64	84.99
15	74.33	40	82.82	65	74.01
16	83.27	41	77.29	66	83.80
17	85.23	42	81.82	67	83.52
18	84.34	43	86.01	68	76.88
19	73.82	44	74.03	69	85.64
20	80.35	45	76.39	70	83.58
21	82.51	46	73.88	71	86.91
22	76.22	47	83.24	72	82.34
23	82.53	48	78.80	73	73.42
24	73.25	49	82.78	74	81.34
25	84.09	50	74.67	75	86.60

It can be known from the previous definition that the size of the R value in $A_{R,\theta}$ should be a value greater than 1.0. Regarding the specific value of R, in the absence of meteorological statistics, in order to meet the comfort of the wind environment, the wind speed ratio of the dominant wind direction should not be greater than. Therefore, when conducting research in this paper, $R_i = 1.2$ is selected for research; that is, the magnitude of $A_{R,\theta}$ is calculated for wind environment assessment.

4. Application of Mathematical Methods Based on Improved Fuzzy Computing in Building and Urban Design in the Environment of Industry 4.0

The intelligent model covers the structure and related facilities of the building in all aspects of design, construction, and operation management. It is necessary to simplify the BIM model for different applications, filter the geometric and semantic data irrelevant to the visual analysis, and extract the key elements required for the approval of building spacing. The specific process of extracting key elements is shown in Figure 12.

On the basis of the above research, the effect of the model proposed in this paper is verified. The model in this paper mainly assists the architectural structure design and human experience in urban architectural design. Therefore, this paper combines the simulation test to evaluate the effect of architectural and urban design and evaluates the architectural experience. The results shown in Tables 1 and 2 are obtained.

From the above research, we can see that the urban design intelligent system proposed in this paper meets the needs of urban design in the environment of Industry 4.0.

5. Conclusion

The urban building has a significant impact on the city block in which it is located. In its sheer size and population alone, it is of obvious importance to the concentration of urban blocks, to pedestrians on the street, and to the streetscape itself. Moreover, these can be attributed to the environmental relationship of tall buildings, which must be the subject of effective urban design in a certain location. At this level, the development of urban building can be controlled by planners through local planning. Due to their relative volume and height, high-rise buildings have a great impact on the existing surrounding environment and the scale of the city. Whether standalone or blended into an urban environment, the larger the building's mass, the greater the impact. This paper combines the mathematical method of improving fuzzy calculation to construct the intelligent building and urban design system and improves the effect of urban architectural design through the intelligent model. The simulation results show that the urban design intelligent system proposed in this paper meets the needs of urban design in the environment of Industry 4.0.

Data Availability

The labeled dataset used to support the findings of this study is available from the corresponding author upon request.

Conflicts of Interest

The authors declare that they have no competing interests.

Acknowledgments

References

[1] H. R. Abed, W. A. Hatem, and N. A. Jasim, "Adopting BIM technology in fall prevention plans," *Civil Engineering Journal*, vol. 5, no. 10, pp. 2270–2281, 2019.

[2] S. Ahmed, "Barriers to implementation of building information modeling (BIM) to the construction industry: a review," *Journal of civil engineering and construction*, vol. 7, no. 2, pp. 107–113, 2018.

[3] C.-J. Chen, S.-Y. Chen, S.-H. Li, and H.-T. Chiu, "Green BIM-based building energy performance analysis," *Computer-Aided Design and Applications*, vol. 14, no. 5, pp. 650–660, 2017.

[4] A. Dainty, R. Leiringer, S. Fernie, and C. Harty, "BIM and the small construction firm: a critical perspective," *Building Research & Information*, vol. 45, no. 6, pp. 696–709, 2017.

[5] R.-R. Dong, "The application of BIM technology in building construction quality management and talent training," *Eurasia Journal of Mathematics, Science and Technology Education*, vol. 13, no. 7, pp. 4311–4317, 2017.

[6] M. O. Fadeyi, "The role of building information modeling (BIM) in delivering the sustainable building value," *International Journal of Sustainable Built Environment*, vol. 6, no. 2, pp. 711–722, 2017.

[7] L. Joblot, T. Paviot, D. Deneux, and S. Lamouri, "Literature review of Building Information Modeling (BIM) intended for the purpose of renovation projects," *IFAC-PapersOnLine*, vol. 50, no. 1, Article ID 10518, 2017.

[8] I. Kim, J. Choi, E. A. L. Teo, and H. Sun, "Development of K-BIM e-Submission prototypical system for the openBIM-based building permit framework," *Journal of Civil Engineering and Management*, vol. 26, no. 8, pp. 744–756, 2020.

[9] Y.-C. Kim, W.-H. Hong, J.-W. Park, and G.-W. Cha, "An estimation framework for building information modeling (BIM)-based demolition waste by type," *Waste Management & Research: The Journal for a Sustainable Circular Economy*, vol. 35, no. 12, pp. 1285–1295, 2017.

[10] M. N. Kocakaya, E. Namlı, and Ü. Işıkdağ, "Building information management (BIM), a new approach to project management," *Journal of sustainable construction materials and technologies*, vol. 4, no. 1, pp. 323–332, 2019.

[11] A. Koutamanis, J. Heuer, and K. D. Könings, "A visual information tool for user participation during the lifecycle of school building design: BIM," *European Journal of Education*, vol. 52, no. 3, pp. 295–305, 2017.

[12] T. Mandičák, P. Mesároš, and M. Tkáč, "Impact of management decisions based on managerial competencies and skills developed trough BIM technology on performance of construction enterprises," *Pollack Periodica*, vol. 13, no. 3, pp. 131–140, 2018.

[13] A. Okakpu, A. GhaffarianHoseini, J. Tookey, J. Haar, A. Ghaffarianhoseini, and A. Rehman, "A proposed framework to investigate effective BIM adoption for refurbishment of building projects," *Architectural Science Review*, vol. 61, no. 6, pp. 467–479, 2018.

[14] I. Othman, Y. Y. Al-Ashmori, Y. Rahmawati, Y. Mugahed Amran, and M. A. M. Al-Bared, "The level of building information modelling (BIM) implementation in Malaysia," *Ain Shams Engineering Journal*, vol. 12, no. 1, pp. 455–463, 2021.

[15] X. Qin, Y. Shi, K. Lyu, and Y. Mo, "Using a TAM-TOE model to explore factors of Building Information Modelling (BIM) adoption in the construction industry," *Journal of Civil Engineering and Management*, vol. 26, no. 3, pp. 259–277, 2020.

[16] L. Ustinovičius, A. Puzinas, J. Starynina, M. Vaišnoras, O. Černiavskaja, and R. Kontrimovičius, "Challenges of BIM technology application in project planning," *Engineering Management in Production and Services*, vol. 10, no. 2, pp. 15–28, 2018.

[17] P. Wu, R. Jin, Y. Xu, F. Lin, Y. Dong, and Z. Pan, "The analysis of barriers to bim implementation for industrialized building construction: a China study," *Journal of Civil Engineering and Management*, vol. 27, no. 1, pp. 1–13, 2021.

[18] S.-M. Luo, J. Xu, and B.-K. Li, "Practice and exploration on teaching reform of engineering project management course in universities based on BIM simulation technology," *Eurasia Journal of Mathematics, Science and Technology Education*, vol. 14, no. 5, pp. 1827–1835, 2018.

[19] J. Yang and X. Fu, *The Centre of City: Wind Environment and Spatial Morphology*, Springer, Berlin, Germany, 2020.

Research Article

Empirical Research on the Critical Success Factors of Construction Program

Chunmei Zhou, Zheng He [ID], Ping Hu, and Hongyan Yan [ID]

Department of Construction Management, Hunan University of Finance and Economics, Changsha 410205, Hunan, China

Correspondence should be addressed to Hongyan Yan; yanhongyan@hufe.edu.cn

Academic Editor: Andrea Loddo

Scientific identification of the factors that underpin the success of construction program can effectively promote the success of construction program. Based on literature statistics, this paper developed the measurement items of key success factors of construction program in Chinese context. Based on exploratory factor analysis, seven key success factors of construction program were extracted. Then, the excellence model of construction program was constructed by referring to the ideas, concepts, and theoretical mechanisms of EFQM model. The research conclusions of this paper provide a systematic and holistic guidance for the successful implementation of the program by the construction program organization and promote the success of the program.

1. Introduction

With the economic development having been switched from high-speed development to high-quality development, China is now facing a critical period of development mode transformation, economic structure optimization, and growth momentum conversion. Against this background, the construction industry needs to achieve high-quality development through transformation and upgrading. With the continuous expansion of the scale of the construction industry and the implementation of national strategies such as "Belt and Road Initiative" and "New Urbanization," the number and scale of construction programs are increasing day by day, and the construction program aims to pursue higher values and benefits and achieve the expected goals through unified coordination and management of multiple projects so as to promote the high-quality development of the construction industry. Compared with an individual project, the construction program is not only larger in scale, but also characterized with higher complexity, longer duration, higher cost, and greater risk, and it also has more significant social and economic impact [1]. Therefore, it is of particular importance to think about how to promote the success of the construction program so as to facilitate the

upgrading and transformation of the construction industry and further enhance the competitiveness of the industry. The key success factors of the construction program are the factors that are managed and influenced by the organization in an effort to promote the success of the program. Clarifying the key success factors of the construction program can help managers to figure out the management priorities and difficulties and allocate resources rationally to achieve the purpose of promoting the success of the program [2].

At present, the academic circles in foreign countries have conducted a large number of theoretical and empirical studies on the key success factors of the program, and the scholars have set forth different views on this matter [3,4]. With the development of the theory of construction program management, the research on the key success factors of construction program has gradually developed. Scholars such as Haadir et al. [5] (2011) believe that good communication, support from senior executives, monitoring and feedback, correct project goals, teamwork, power decentralization, and adequate financial support are the key factors to ensure the success of the construction program. Scholars such as Patanakul et al. [6] (2016) put forward six key factors to promote the success of construction programs, namely, the pursuit of nonfinancial target benefits, product

service life, multiple stakeholders, complexity, political environment, and compliance with mandatory project management procedures; scholars such as Gamil et al. [7] (2017) believe that the establishment of an appropriate certification system for contractors and consulting agencies, reasonable cost and time planning, effective communication and co-ordination platforms, and advanced technologies are the key factors for the success of the construction program; Shao et al. [8] (2018) believe that, apart from adequate financial support, delivery capability, organizational capability, innovation capability, organizational adaptability, project flexibility, and organizational stability are also key success factors for the program.

The research results mentioned above have enriched the theoretical system of the key success factors of the construction program and formed a general key success factor model of the construction program. However, the researchers have not reached a unified conclusion as to the key factors that influence the construction program. At the same time, cultural and industrial discrepancy may affect the applicability of the key success factor frameworks of construction program proposed by different scholars (Shao et al., 2012 [9]), and Pellegrinelli et al. [10] (2007) also emphasized the importance of environment for program management. Therefore, it is necessary to study the key success factors of construction program in our country based on the Chinese context. Based on literature statistics and exploratory factor analysis, this paper refines the key success factors of the construction program and builds an excellence model of the construction program by referring to the ideas, concepts, and theoretical mechanism of the EFQM model. The research in this article provides a new framework system of critical success factors for construction program managers and helps them to quickly clarify the dimensions of project management, improve management levels, define development directions, and promote the success of construction programs.

2. Definition of Success Criteria for Construction Programs

There is a causal relationship between the success criteria of the construction program and the key success factors, and different key success factors will be identified for different success criteria. Therefore, defining the meaning and the success criteria of the construction program is the basis for scientifically identifying the key success factors of the program. Based on the previous research, this paper develops the standard measurement items for the success of construction programs in the Chinese context based on literature statistics and China's construction program management practices. On the basis of the data collected by the questionnaire survey, the SPSS22.0 statistical analysis software is adopted as an auxiliary tool to carry out exploratory factor analysis for the success criteria of the construction program, and the success criteria of the construction program are extracted: the success of the construction program management, the success of the

construction program organization strategy, and the harmony of the stakeholders of the construction program.

3. Theoretical Construction of Key Success Factors of Construction Program

At present, the research on the key success factors of construction program is still in its infancy worldwide, and there are few related documents. Seven papers on the key success factors of construction program published in international authoritative journals were selected. By comparing and analyzing the key success factors between construction projects and construction programs, the results indicate that more emphasis is put on the key influence of "executive support," "clear goals," and other factors on the success of the construction program, while more emphasis is put on the key influence of factors such as "team member ability" and "team communication" and other factors on the success of the construction project.

Literature analysis lays the foundation for identifying the key success factors of construction program. Due to the differences in the construction environment of the programs in various countries, this paper draws on the statistical conclusions of literature, the 66 key success factors of construction program proposed by scholars such as Sarmad Kiania [11], and the in-depth interviews carried out with university scholars, program managers, program executives, and other experts to explore the key factors affecting the success of the construction program in China. Also, this paper supplements and discovers the hidden factors of the construction program and summarizes the measurement items for the key success factors of the construction program in the Chinese context, as shown in Table 1.

4. Empirical Analysis of Key Success Factors of Construction Program Based on Exploratory Factor Analysis

This paper adopts questionnaire survey to carry out empirical research on the key success factors of construction program, and a total of 32 valid questionnaires were collected. The subjects of the survey are company executives, program managers, program management support personnel/auxiliary personnel, etc. Most of the subjects are highly educated and have relatively rich work experience, so the questionnaire results are representative, reliable, and authentic.

4.1. Adaptability Test of Factors. In order to analyze the quality of the questionnaires, this paper needs to test the reliability and validity of the scale data. The output results suggest that the correlation coefficient matrix is "nonpositive definite matrix." Neither KMO nor Bartlett's test shows the results. The main reasons mainly come from two aspects: (1) The sample size is too small while there are too many indicators. (2) The correlation between certain variables is too strong. There are 40 measurement items for the key success factors of the construction program, but only 32

TABLE 1: Measurement items of key success factors of construction program.

Key success factors measurement items of construction program
SF1. Clear vision, strategic goals, and mission.
SF2. Well-defined and realistic organizational goals.
SF3. Well aware of opportunities and threats for industry development.
SF4. Have a positive organizational culture and organizational structure system.
SF5. Have a clear and documented accountability system.
SF6. Have a good communication and management system.
SF7. Strategic support from executives.
SF8. The senior executives fully trust and authorize the program/subproject management team.
SF9. The strategic alignment between the objectives of the program and the technology.
SF10. Correct feasibility study.
SF11. Reasonable program financing method.
SF12. Reasonable program delivery system.
SF13. Allocate correct and sufficient resources to each subproject such as funds, materials, and equipment.
SF14. Stable employment of the employee system.
SF15. Regular evaluation of the objectives of the program and subprojects.
SF16. Adequate communication among program stakeholders.
SF17. Clear program objectives, deliverables, and benefits.
SF18. The consistency of the program objectives and organizational strategy.
SF19. Outstanding program/project manager.
SF20. Familiar with the exact information needs of executives.
SF21. Correct program cost estimation.
SF22. Appropriate program budget allocation.
SF23. Effective program cost management.
SF24. Reasonable program/subproject schedule.
SF25. Effective program/subproject schedule management.
SF26. Effective program quality management.
SF27. Effective program change management.
SF28. Effective communication management to control disputes and conflicts.
SF29. Effective risk management.
SF30. Effective stakeholder management.
SF31. Reasonable distribution of benefits among stakeholders.
SF32. Reasonably adjust and guide the program/subproject performance based on the strategic objectives.
SF33. The program manager pays attention to the mutual influence between the program/subproject targets.
SF34. Use mature tools, techniques, and management processes in program management.
SF35. Use integrated and coordinated management to achieve strategic goals.
SF36. There are enough program management business cases/plan charters for reference.
SF37. Provide continuous financial support according to the program budget.
SF38. Powerful and integrated program management office.
SF39. The government's policy affirmation and support for the program.
SF40. Government departments provide efficient services for the program implementation.

questionnaires were effectively collected. The main reason is that the management idea of the construction program has not been effectively promoted in China's program practice. Therefore, there is a need to process the data in order to analyze the key success factors of construction program. The main measure taken is to reduce the number of measurement items. Through the analysis of the correlation of indicators, eleven items were deleted from the key success factor measurement items of the construction program, so as to meet the requirements of the quality inspection of the factor analysis, as shown in Table 2.

4.2. Structural Factor Variant.
SPSS 22.0 tool was used to perform exploratory factor analysis on the scale data, and the common factor is extracted based on the standard where the feature value is greater than 1 and the cumulative contribution rate is greater than 80%, and the factor analysis results are shown in Table 3.

TABLE 2: KMO and Bartlett's validity test.

Kaiser–Meyer–Olkin	Questionnaire adequacy measurement	0.645
Bartlett's sphericity test	χ^2	1035.466
	Df (degree of freedom)	406
	Sig. (significance level)	0.000

From the results in Table 3, it can be seen that the cumulative variance contribution rate explained by the first 6 common factors is 80.583%, indicating that these 6 factors have integrated 80.583% of the information of original 29 success factors from the key success factors of the construction program, which can basically reflect the essential information of the sample.

4.3. Factor Variable Explanation.
In order to further explain the 6 common factors that have been extracted, the maximum variance orthogonal rotation method is used to

TABLE 3: Initial and rotated factor variation contribution rate of indicators.

Factors	Initial eigenvalue			Rotated sum of squares loaded			Rotated sum of squares loaded	
	Total (%)	Variance (%)	Cumulative (%)	Total (%)	Variance (%)	Cumulative (%)	Total (%)	Variance (%)
1	15.985	55.121	55.121	15.985	55.121	55.121	4.875	16.810
2	1.896	6.536	61.657	1.896	6.536	61.657	4.390	15.139
3	1.587	5.474	67.131	1.587	5.474	67.131	4.255	14.673
4	1.431	4.934	72.064	1.431	4.934	72.064	4.101	14.143
5	1.382	4.765	76.829	1.382	4.765	76.829	3.173	10.943
6	1.089	3.754	80.583	1.089	3.754	80.583	2.574	8.876
...								
29	0.001	0.003	100.000					

perform factor rotation on the extracted factors. The rotated factor loading matrix is shown in Table 4. The value in the factor loading matrix reflects the importance of the corresponding key success factor index of the construction program to each factor.

Factor 1 explains the measurement items of SF11, SF36, SF6, SF4, and SF5 and reflects that the completeness of the construction program organization and management system directly affects the success or failure of the construction program, so it is named the organization/management standard system completeness factor.

Factor 2 explains the measurement items of SF27, SF13, SF26, SF29, SF25, and SF37, reflects the connotation of the whole process management of the construction program, and shows that the effective management of the whole process of the construction program is the key factor to promote the success of the program, so it is named excellent program management factor.

Factor 3 explains the measurement items of SF34, SF20, SF19, SF33, SF38, and SF14 and reflects that high competency of the construction program management team can effectively promote the success of the program. Therefore, it is named the excellent program management team factor.

Factor 4 explains the measurement items of SF18, SF40, SF12, SF3, SF39, and SF1. It is divided into two factors since it cannot effectively explain the key success factors of specific construction programs. SF18, SF12, and SF1 explain the organization strategy and goal of construction programs, indicating that organizational strategy has a guiding role in the implementation of the program. Organizational strategy is the basis for the success of the program, so it is named the organizational strategy/clear target factor; SF40 and SF39 explain the role of government support in promoting the success of the construction program, and it is named the government support factor.

Factor 5 explains the measurement items of SF16, SF31, and SF30 and reflects the interest demands and cooperation of the stakeholders of the construction program, so it is named the stakeholder cooperation factor.

Factor 6 explains the measurement items of SF7 and SF8, indicating that the support of senior executives is inseparable from the success of the program, and it is named the senior executive support factor.

TABLE 4: Rotated factor loading matrix of key success factors of construction program.

Factor 1	
Component	Factor loading
SF11	0.876
SF36	0.800
SF6	0.622
SF4	0.594
SF5	0.576
Factor 2	
SF27	0.825
SF13	0.662
SF26	0.653
SF29	0.620
SF25	0.612
SF37	0.609
SF23	0.540
Factor 3	
SF34	0.824
SF20	0.777
SF19	0.669
SF33	0.615
SF38	0.589
SF14	0.443
Factor 4	
Component	Factor loading
SF18	0.791
SF40	0.726
SF12	0.615
SF3	0.586
SF39	0.555
SF1	0.465
Factor 5	
SF16	0.854
SF31	0.640
SF30	0.623
Factor 6	
SF7	0.781
SF8	0.577

4.4. Results and Discussion

4.4.1. Organizational Strategy/Clear Target Factor. Organizational strategy and goals are the blueprint and outlook for the strategic goals and mission scope of the construction program. The implementation of any project/

program is inseparable from a clear organizational strategy and target.

The achievability of the project objectives is the prerequisite for the smooth implementation of a construction project. Researches have shown that the formulation of an implementable plan can substantively improve the possibility of achieving overall success and project progress, thereby improving project performance [12]. Therefore, it is the initial and prior task to formulate reasonable and implementable strategic goals when building the construction program, and clarifying the project/Program targets will help the stakeholders of the construction program to figure out their responsibilities and facilitate the smooth implementation of the project/program. Researchers, such as Shenhar et al. [13] (2001), believe that the organization's strategy and project targets should be well-aligned to ensure their complementarity and directional consistency so as to promote the success of the construction program.

4.4.2. Senior Executives Support Factor. Senior executive support refers to the phenomenon that the senior executives provide various resources as well as written and verbal support to the program team during the whole process of building the construction program. Existing studies believe that senior executive support is one of the necessary conditions for project success (Crosby [14], 2012). Senior executives are the core personnel of project/program and the executive to accomplish organizational strategy and target; through the tactic/strategic support of the senior executives to the project/program, the project/program management process can be improved, which can have a positive impact on the project and program objectives and thereby improve the performance of the program (Duan Zhicheng [15], 2013).

Senior executive support promotes the success of the construction program mainly through the following aspects: The senior executives promise to complete the program; pay attention to the progress of the construction program; actively participate in the program and provide necessary support; ensure that the project/program has an appropriate priority.

4.4.3. Completeness Factor of Organization/Management and Other Normative Systems. Standardization of the organization and management system is the basic element for the success of construction projects/programs. By constructing a positive organization culture and establishing a reasonable organization structure for the construction program, the ability of the organization and individuals can be effectively boosted and the effectiveness of the policy and strategic goals can be improved, so that the management efficiency of construction project/program can be raised to promote the success of the program [15].

The organization of the construction program is determined by the strategic goal of the program, and the organization is an important foundation and support for the realization of the strategic target. Construction program management is a highly integrated management, and the program organization should also achieve the unity of powers, responsibilities, and benefits to ensure that the organization can effectively perform its functions. The larger the construction program and the more complex the task, the more it is necessary to build an effective organization and adopt the correct work process to comprehensively consider the program's targets and resources, so that the program management can be well-organized and the program's strategic targets can be achieved. The positive culture of the construction program has an important impact on the employees participating in the construction program and the program itself (Zuo, Zillante [16], 2005). At the same time, the project/program organizational culture can promote the governance of the project/program, boost employees' work enthusiasm, reduce contradictions and conflicts, and help to harmonize the atmosphere among organizations (Yang et al. [17], 2018).

4.4.4. Excellent Program Management Team Factor. The construction program management team includes the team members with the construction program managers as the core, the management technology used by the managers/team, the application of capabilities, and the needs of the managers/team. Scholars such as Belassi et al. (1996) [18] believe that the management skill of the project manager department is the most important key factor for project success; scholars such as Kog et al. (1999) [19] found that the key factors affecting project success include the project manager's emphasis on the project and the experience of the project manager, etc. Therefore, it is helpful to select an experienced and capable construction program/project manager to improve the organization and individual capabilities and formulate effective strategies and integrate internal and external resources, so as to improve the efficiency of the construction program/project management and effectively promote the success of the program/project [15].

As the core team of the whole process management, the construction program management team plays an important role in dealing with some complex situations and systems and ensuring the implementation of the construction program and the successful delivery of the program. The construction program management office is a project management organization specially set up for project management, which influences the success of the program by providing practical methods for construction program management. The ability of the members of the construction program management team is matched with the application of technology; that is, the stronger the ability of the program team members, the higher the technical requirements, which is conducive to the success of the project. The manager of the construction program can also resolve the errors and conflicts of a certain subproject or unit by allocating resources to ensure the realization of the goal of the construction program.

4.4.5. Excellent Program Management Factor. According to project management theory, project management ability is the key to ensuring project value addition. Construction

program management is the key stage for the completion of the construction program products, which must rely on scientific and effective management methods to grasp the critical points of implementation so as to promote the success of the program. Research results show that 62.4% of experienced project/program managers believe that when the project/program management is successful, the project/program will generally succeed [20]. In this sense, effective program management is the foundation of the success of program [21].

The implementation of the construction program involves the scope, time, cost, quality, human resources, communication, resources, information and risk, and other management fields of the program. In light of the traditional "iron triangle-time management, cost management, quality management", etc., it is necessary to take effective control measures under target constraints. At the same time, control measures shall also be strengthened in management areas such as resource management, information management, and risk management.

4.4.6. Stakeholder Cooperation Factor. The needs, expectations, requirements, and behaviors of the stakeholders of the construction program can impose influence on or are affected by the program to varying degrees. Their duty-performing ability and level of performance are directly related to the success or failure of the program. The satisfaction of the different interest needs of the stakeholders of the construction project/program and the harmonious relationship between the stakeholders, which benefit all participants, are important factors for the success of the project group; and the inability to achieve effective cooperation among the stakeholders of the project/program will cause organizational chaos [22] and may lead to project/program failure.

Strengthening the communication, coordination, and cooperation among the stakeholders of the construction program\project is essential to the stakeholder relationship management of the construction program. It can promote timely communication, reduce adverse effects, avoid conflicts between departments, and resolve incidents that hinder progress and can help to create a coordinated and harmonious environment and improve the management level and operational efficiency of the entire program, thereby promoting the success of the program.

4.4.7. Government Support Factor. In the decision-making and construction of major construction projects/program, the role of the government is irreplaceable, and the relationship between the government and the construction program is inseparable.

Program construction is a large-scale project which entails a lot of attention from the government, and governmental approval is required for various processes involved during the construction process of the program. At the same time, the government also plays a role in the supervision and management of the program construction. Studies have found that the government, which supervises

and regulates the implementation process of the construction program through supervisory and regulatory institutions, can achieve the purpose of preventing corruption and promoting the program performance. Efficient public institutions have a great impact on the success of the project [23], and the higher the efficiency of the government, the faster the construction of the project/program, and the more likely the project/program will be successful. By providing effective guarantees and policy support, the government can promote the success of the program [24]. The support of national policies greatly encourages the government executives to support the construction of the program. The government executives effectively promote the performance of the program by facilitating the project's preliminary consultation and approval process. Government credit is equally important to the success of the project, and the trustworthiness of all stakeholders in the project/program is vital to the continuation of cooperation, and any party's breach of contract may lead to the termination of the project/program.

5. Excellence Model of Construction Program

The EFQM model is the first excellence model selected by the European Foundation for Quality Management through evaluation. The EFQM model measures project performance and shows the ideal strategy and targets of the project to elevate its performance to the highest level (Wongrassamee et al. [25], 2003). Although the analytical methods used by the EFQM model are vastly different from those used in the field of engineering project management, it is found that that there have been research results achieved by applying the EFQM model in construction field [26] according to papers published in this field. The EFQM model embodies the key influence between the facilitation factors (process) and organizational performance (results). Therefore, this paper attempts to introduce the EFQM model into the mechanism of interaction between the key success factors and the success criteria of the construction program to build an excellence model for the construction program.

This paper refers to the thought of Westerveld [27] (2003) to apply the EFQM model in the project success field. Its hypothesis is to divide project management into two fields, namely, the result field and the facilitation field. The result field represents the project success criterion and the facilitation field represents the key success factors. In this light, this paper interprets the key success factors of the construction program as the facilitation field and the success criteria of the construction program as the result field.

In the facilitation field of the excellence model of the construction program, leadership is a behavior in which managers in an organization use their power to exert influence on their subordinates in order to achieve the goals of the organization. Senior executive support refers to the support of senior executives to their subordinates, and leadership can be interpreted as senior executive support; the personnel, policies and strategies, partners, and resources covered by the facilitation field can be, respectively, interpreted as excellent program management team, clear
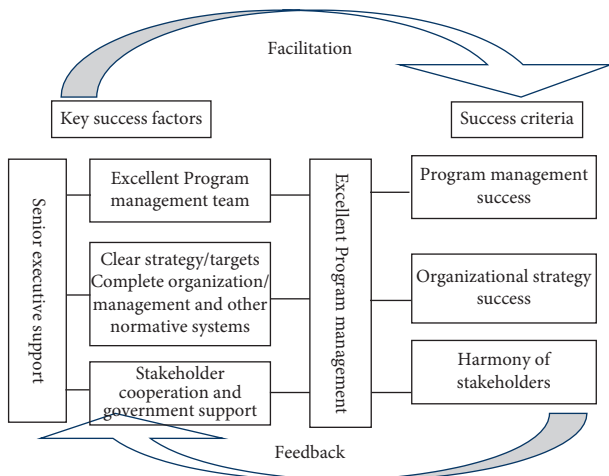
FIGURE 1: Excellence model of construction program.

strategies/targets, complete organization/management, and stakeholder cooperation and government support; the process reflects the whole process of constructing the program, and therefore the process can be deemed as excellent program management. In the result field of the construction program excellence model, the dimensions of personnel results and customer satisfaction correspond to the harmony (satisfaction) of stakeholders; social influence reflects the long-term performance of the organization, that is, the success of the organization's strategy; corporate performance is interpreted by the success of project management.

Based on the above analysis, this paper constructs an excellence model of the construction program, which reveals the relationship between the success of the program and the key success factors as well as the enabling paths, as shown in Figure 1.

The excellence model of the construction program based on the EFQM model organically combines the "success criteria of construction program" in the success result field and "key success factors of construction program" in the facilitation field. The two constitute a facilitation-feedback relationship; that is, the key success factors of the construction program facilitate the success of the program while the success of the program reacts upon the whole process management of the program. The scientific definition of the success criteria of the construction program plays a guiding role in defining the key success factors of the construction program managers in the whole process management of the program and helps the managers to judge and effectively control the key success factors.

6. Conclusion

Key success factors of the program play a decisive role in determining the success of the construction program. Therefore, in-depth and systematic research on the key success factors of the program will help the construction program organization to focus on the investment in key factors and increase the likelihood of program success.

Based on literature statistics, this paper explores the key factors affecting the success of construction programs in China, supplements and excavates the hidden factors of the construction program, and develops the measurement items for the key success factors of the construction program in the Chinese context. Using the data collected by the questionnaire survey, SPSS22.0 statistical analysis software is used as an auxiliary tool for exploratory factor analysis of the key success factors of the construction program, and the key success factors of the construction program are refined: Key success factors in seven dimensions, including clear organizational strategy/targets, senior executive support, government support, organization/management and other standard systems, excellent program management team, stakeholder cooperation, and excellent program management. The ideas, concepts, and theoretical mechanisms of the EFQM model construction program are drawn on to organically integrate the "success criteria of construction program" in the result field and "key success factors of the construction program" in the facilitation field to construct an excellence model of the construction program.

The key success factors of the construction program and the excellence model of the construction program established in this paper provide a directional guide for the systematic and holistic success of the implementation of the program by the construction program organization. Real-time monitoring and process control are carried out during the implementation of the program to make the implementation of the program more flexible, reduce the risk of the program, and promote the success of the program.

Data Availability

All data are included in the manuscript.

Conflicts of Interest

The authors declare that they have no conflicts of interest.

Acknowledgments

References

[1] H. Yan, H. Elzarka, C. Gao, Z. Feilian, and W. Tang, "Critical success criteria for programs in China: construction companies' perspectives," *Journal of Management in Engineering*, vol. 35, no. 1, Article ID 04018048, 2019.

[2] A. P. C. Chan, D. Scott, and A. P. L. Chan, "Factors affecting the success of a construction project," *Journal of Construction Engineering and Management*, vol. 130, no. 1, pp. 153–155, 2004.

[3] M. K. Buniya, I. Othman, R. Yosia Sunindijo et al., "Critical success factors of safety program implementation in construction program in Iraq," *International Journal of Environmental Research and Public Health*, vol. 18, no. 16, 2021.

[4] Z. He and H. Chen, "An ISM-based methodology for inter-relationships of critical success factors for construction program in ecologically fragile regions: take korla, China as an example," *Applied Sciences*, vol. 11, no. 10, 2021.

[5] S. A. Haadir and K. Panuwatwanich, "Critical success factors for safety program implementation among construction companies in Saudi Arabia," *Procedia Engineering*, vol. 14, pp. 148–155, 2011.

[6] P. Patanakul, Y. H. Kwak, O. Zwikael, and M. Liu, "What impacts the performance of large-scale government projects?" *International Journal of Project Management*, vol. 34, no. 3, pp. 452–466, 2016.

[7] Y. Gamil, I. A. Rahman, S. Nagapan, and A. E Nashwan, "Qualitative approach on investigating failure factors of Yemeni mega construction program[C].MATEC web of conferences," *EDP Sciences*, vol. 103, Article ID 03002, 2017.

[8] J. Shao, "The moderating effect of program context on the relationship between program managers' leadership competences and program success," *International Journal of Project Management*, vol. 36, no. 1, pp. 108–120, 2018.

[9] J. Shao, R. Müller, and J. R. Turner, "Measuring program success," *Project Management Journal*, vol. 43, no. 1, pp. 37–49, 2012.

[10] S. Pellegrinelli, D. Partington, C. Hemingway, Z. Mohdzain, and M. Shah, "The importance of context in programme management: an empirical review of programme practices," *International Journal of Project Management*, vol. 25, no. 1, pp. 41–55, 2007.

[11] S. Kiani, V. Yousefi, S. Haji Yakhchali, and A. Mellatdust, "Identifying program critical success factors in construction industry," *Management Science Letters*, vol. 4, no. 6, pp. 1325–1334, 2014.

[12] E. J. Jaselskis and D. B. Ashley, "Optimal allocation of project management resources for achieving success," *Journal of Construction Engineering and Management*, vol. 117, no. 2, pp. 321–340, 1991.

[13] A. J. Shenhar, D. Dvir, O. Levy, and A. C. Maltz, "Project success: a multidimensional strategic concept," *Long Range Planning*, vol. 34, no. 6, pp. 699–725, 2001.

[14] P. Crosby, "Key success drivers," *International Journal of Information Technology Project Management*, vol. 3, no. 2, pp. 1–20, 2012.

[15] Z. Duan and C. Tong, "Research on identification of engineering project management factors and interrelationship model[J]," *Journal of AnHui University (Philosophy and Social Sciences Edition)*, vol. 37, no. 3, pp. 150–156, 2013.

[16] J. Zuo and G. Zillante, "Project culture within construction program: a literature review," in *Proceedings of the 13th Annual Conference of the International Group for Lean Construction*, pp. 353–361, Sydney, New South Wales, January 2005.

[17] D. Yang, Q. He, Q. Cui, and S. C Hsu, "Organizational citizenship behavior in construction megaProgram," *Journal of Management in Engineering*, vol. 34, no. 4, Article ID 04018017, 2018.

[18] W. Belassi and O. I. Tukel, "A new framework for determining critical success/failure factors in projects," *International Journal of Project Management*, vol. 14, no. 3, pp. 141–151, 1996.

[19] Y. C. Kog, D. K. H. Chua, P. K. Loh, and E. J. Jaselskis, "Key determinants for construction schedule performance," *International Journal of Project Management*, vol. 17, no. 6, pp. 351–359, 1999.

[20] A. Collins and D. Baccarini, "Project success - a survey," *Journal of Construction Research*, vol. 05, no. 2, pp. 211–231, 2004.

[21] H. Li and K. Liu, "Research on the development of management model for construction project group," *Journal of Xihua University·Natural Science*, vol. 30, no. 2, pp. 88–91, 2011.

[22] J. R. Turner, "Five necessary conditions for project success," *International Journal of Project Management*, vol. 5, no. 22, pp. 349-350, 2004.

[23] L. I. U. Wan-lin, Q. U. Chun-li, X. Yuan, and W. Jiang, "Critical success factors for PPP projects from A three-dimension perspective," *Journal of Engineering Management*, vol. 32, no. 1, pp. 115–119, 2018.

[24] Y. Zhang and H. A. O. Shengyue, "Influence of critical success factors of PPP project on performance:based on the analysis of five critical success factors," *Journal of Civil Engineering and Management*, vol. 36, no. 5, pp. 157–164, 2019.

[25] S. Wongrassamee, J. E. L. Simmons, and P. D. Gardiner, "Performance measurement tools: the balanced scorecard and the EFQM excellence model," *Measuring Business Excellence*, vol. 7, no. 1, 2003.

[26] M. Vukomanovic, M. Radujkovic, and M. M. Nahod, "EFQM excellence model as the TQM model of the construction industry of southeastern Europe," *Journal of Civil Engineering and Management*, vol. 20, no. 1, 2014.

[27] E. Westerveld, "The Project Excellence Model®: linking success criteria and critical success factors," *International Journal of Project Management*, vol. 21, no. 6, 2003.

Research Article

Garment Design Models Combining Bayesian Classifier and Decision Tree Algorithm

Xiaoyu Yan [ID] [1,2] **and Shuo Ma** [ID]

[1]*College of Fine Arts and Design, Hebei Institute of Communications, ShiJiazhuang 050000, China*
[2]*Faculty of Art & Design, Universiti Teknologi, Mara 40450, Shah Alam, Malaysia*

Correspondence should be addressed to Shuo Ma; mmashuo2019@163.com

With the rapid economic development and rising consumption levels in recent years, people are becoming more and more demanding in terms of style and fashion of clothes. As a result, customer demand for personalised clothing is increasing and the need to respond quickly to consumer demands is also becoming a competitive issue for clothing companies. The automation and intelligence of the garment design and production process is an important part of the implementation of intelligent manufacturing in the garment industry and a necessary way to transform and upgrade the garment industry. Successful clothing styles always have a distinct style identity. The style of the garment can not only conveys the designer's vision but also express the emotional needs of the consumer. In contrast, traditional garment design involves only designers and a single style. With so many styles available, the user has only been able to combine them repeatedly and has not been able to create an innovative design. In addition, apparel design and product development is still a highly empirical task. To be specific, most apparel companies can only respond to a rapidly changing market by increasing the number of designers. However, this blind expansion of staff inevitably leads to increased production costs. As a result, how to effectively develop garment products without relying on the empirical knowledge of garment designers is one of the important issues in achieving intelligent manufacturing in garment enterprises. With the rapid development of computer and network technologies, artificial intelligence, machine learning, and expert systems are widely used in various industries. Nevertheless, the application of these advanced technologies in the field of garment design is still not deep enough. This is mainly due to the uncertainty and imprecision of garment design knowledge. Also, with the rapid development of the fashion industry and the arrival of the trend of personalisation, people's demand for clothing has gradually shifted from mass appeal in terms of comfort and aesthetics to personalisation in terms of self-polishing and temperament. The personalisation of clothing encompasses a wide range of preferences in terms of style and fit. The bottom-up design process and the relatively independent setup of functional modules in traditional clothing technology have prevented the different design levels from being interlinked. This does not reflect the composition of the garment elements in the process of forming features and makes it difficult to grasp the overall design state of the garment. Therefore, in order to address these above issues, this paper proposes a garment design model based on the Bayesian classifier and decision tree algorithm to investigate how computer technologies can be applied to model garment design knowledge. This model can enable inexperienced designers to develop garment products quickly and efficiently to meet the customisation needs of customers, thus enhancing the market competitiveness of garment enterprises.

1. Introduction

As an indispensable product for people, clothing has the combined attributes of physiological protection, mobility support, and self-expression [1]. As a result, the design of clothing is based on a combination of protection, fit, personal preference, and social aesthetics. With the rapid economic growth of recent years and the rapid development of clothing-related industries, the supply of clothing products has been greatly enriched [2]. People's demands for clothing have long gone beyond physiological and safety needs to focus on social needs, personality preferences, and

self-realisation. The choice of clothing, in terms of style, stylistic details, and size, has gradually changed from a simple, comfortable, mass-market design to a personalised design that is based on fit, self-fashioning, and self-fulfillment [3]. With the widespread popularity of e-commerce, consumers' demand for personalised products has become increasingly strong [4]. In this context, traditional garment customisation models are no longer able to meet the needs of consumers due to their long production cycles and monotonous styles [5]. As a result, there is a need to provide a personalised apparel design model to achieve zero distance interaction with the customer, thus reducing production costs for the company and increasing customer satisfaction. The personalisation process must be supported by detailed theoretical methods and technical guidance [6]. The modern model of garment design consists mainly of style design, structure design, and process design. The main task of style design is to draw up renderings and style drawings, the main task of structural design is to development patterns, and the main task of process design is to produce process guidance documents [7, 8]. As shown in Figure 1, style design, structure design, and process design are interlinked and they can form the main part of modern garment design. The needs of consumers in the market have changed with the rise in material and cultural standards of living, from the traditional economical to the enjoyable. As a result, traditional mass production methods are no longer able to meet consumers' needs for fashion and individuality [9]. Today, in the pursuit of individuality and fashion, people have new requirements for bespoke garment designs that inspire confidence and satisfaction. Consumers want to participate in the customisation process, expressing their needs through interactive customisation and being able to customise the style of their clothing according to their own wishes [10]. In this way, consumers are better able to personalise their own designs independently and thus create personalised garments for themselves that match their own aesthetics, which has been the most popular industry chain strategy in recent years.

China is currently the world's largest producer, consumer, and exporter of textiles and clothing. As a result, the garment industry plays a vital role in China's national economy [11]. The realisation of intelligent manufacturing in apparel enterprises is of great significance to the upgrading of China's overall manufacturing level. Also, the realisation of intelligent garment design is an important part of the implementation of intelligent manufacturing in apparel enterprises [12]. However, the garment industry is typically a low-tech and labour-intensive industry. With the rapid development of the economy, the consumption habits of customers are constantly changing and the demand for personalisation is increasing [13]. In this context, garment companies need to constantly improve the efficiency of their product development in order to cope with the fierce competition in the market [14, 15]. Over the past hundred years, the production model of apparel companies has evolved from artisanal production to mass production and then to mass customisation in order to keep pace with market changes and customer needs. Mass customisation
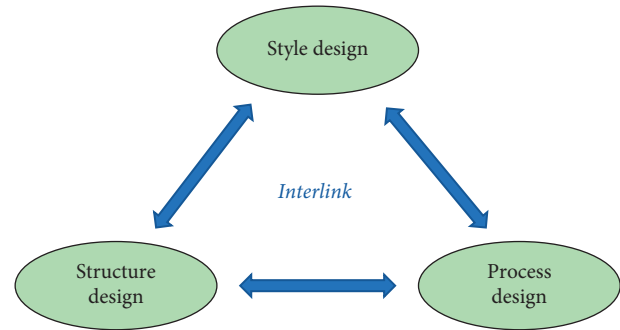
Figure 1: Relationship among style design, structure design, and process design.

requires garment manufacturers to produce customised garment products quickly and in large quantities to suit different customer sizes and individual requirements [16]. However, the individual needs of customers increase the difficulty of developing apparel products and prolong the product development cycle. The fast-changing market requires apparel companies to react quickly and shorten the product development cycle as much as possible [17]. In other words, there is always a serious conflict between the individual needs of customers and the demands of the market on product development cycles. In the future, the market will change even more dramatically and consumers' personalisation needs will tend to increase [3]. The question of how to improve the efficiency of apparel product development and shorten the product development cycle while satisfying consumer needs has been a difficult one for apparel companies. There are currently two ways to solve this problem. Firstly, more apparel product developers could be hired to work on the design and production of garments [18]. In addition, the current design methods and processes could be revamped. Hiring more experienced apparel product developers is currently the main solution to this problem, but this approach would significantly increase the cost of product development and would not be conducive to a competitive position in the marketplace [19]. It is clear that optimising and innovating design methods and processes is an effective way of overcoming these challenges in product development for apparel companies.

Clothing is an essential part of the culture of human society and an important expression of human spiritual civilisation [20]. Although the domestic garment industry has been developing for 30 to 40 years, it still seems to be a relatively traditional industry. The traditional domestic garment industry is labour-intensive and has always suffered from low production levels, serious homogenisation of products, and low brand awareness. In recent years, with the emergence and rapid development of big data [21], cloud computing [22], intelligent manufacturing [23], and e-commerce [24], it has become possible to shift from high-end tailoring to large-scale personalised tailoring. This possibility will accelerate the transformation of the garment industry towards the Internet. This breakthrough in the traditional thinking of the manufacturing industry has led to a shift from a closed manufacturing system to an open,

direct-to-consumer production model, allowing consumers to participate directly in the design and production of garments. This type of consumer participation in personalisation has led to the development of a more dynamic apparel industry and an optimised industrial structure. Large-scale personalised tailoring is set to become an important trend in the future development of clothing [25]. The traditional garment design process is shown in Figure 2. This process can be generally divided into three parts: design object determination, garment concept design, and garment production. The first step is to analyse the customer's needs and to define the design plan and concept. While collecting the source material around the design concept and plan, the customer's body size information is collected. A series of variations on the source material is then drawn up, based on the designer's inspiration and experience, to produce a graphic style drawing, which includes the basic elements of the design. Furthermore, the shape of the silhouette, structure, and details of the garment are constructed by dividing, combining, building up, and arranging the three elements. The garment structure is then transformed from a flat to a three-dimensional form by using flat or three-dimensional cutting methods. The three-dimensional shape is then evaluated and fed back into the design for correction and adjustment. Finally, the output is used to assess the feasibility of the finished garment and to adjust the garment structure.

The apparel product development department is one of the core departments of an apparel company [26]. The quality of an apparel product depends to a large extent on the skill level of the product developer. Traditionally, garment design and pattern development is a highly empirical task. After all, a junior apparel product developer needs several years of practical experience to become proficient in apparel design or pattern development. Experienced designers and pattern makers are therefore a scarce resource for an apparel company, and their departure can have a serious impact on the company [27]. During the product development phase, designers, pattern makers, and craftsmen need to communicate and collaborate with each other repeatedly in order to develop a satisfactory garment. This process is tedious and time-consuming and requires the product developer to have a wealth of experience and knowledge. Therefore, there is a pressing need for apparel companies to move away from the traditional overreliance on experienced designers and pattern makers and to be able to develop satisfactory garment products quickly. This will reduce the reliance on designers and pattern makers and increase the efficiency of product development and reduce development costs. The fit of garments is always one of the main concerns of apparel developers and consumers [28]. Fit assessment is a constant part of the apparel product development process, with designers repeatedly trying on samples to check whether a garment is feasible and whether it fits properly. Currently, the fit of a garment can only be analysed by trying on a real garment in person or on a human platform. This process is cumbersome and can significantly increase the cost of developing a garment. While the advent of virtual fitting technology can assist apparel developers in checking the viability of a garment, it cannot effectively determine the fit of a garment. As a result, it is quite important for product development to be able to assess the fit of garments without the need for a real fitting.

With the rapid development of computer information technology in recent years, artificial intelligence [29], machine learning [30], expert systems [31], and system dynamics [32] have been widely used in various industries. However, in the apparel industry, particularly in the area of apparel design and fit assessment, the use of computers is not yet sufficiently advanced. The main reason for this is the uncertainty and inaccuracy of knowledge about garment design and fit assessment. After all, this type of knowledge is more difficult to extract and represent by computer. Recent research has shown that the tacit knowledge involved in apparel design can also be extracted, expressed, and applied through mathematical modelling and computer simulation. It is in this context that this study proposes a model for apparel design based on the Bayesian classifier as well as decision tree algorithm. The model allows for the mathematical modelling of the expert knowledge required for garment design, thus enabling less experienced designers to develop garment products and assess their fit quickly and efficiently.

2. Relevant Algorithm

Mathematical modelling of garment design is the basis for the automation and intelligence of apparel design. Currently, linear regression models are widely used for knowledge modelling in the field of garment design and pattern development, mainly because they are simple to understand and practical. However, there are many aspects of garment design that do not lend themselves to the use of linear regression for knowledge modelling. As a result, this section mainly introduces Bayesian classifiers, decision trees, and neural network algorithms to provide the necessary theoretical support for the construction of garment design models.

2.1. Feature Selection. The main function of feature selection is to eliminate the features with interference factors and find the information feature subset with the least dimension but stronger discrimination ability. With the rapid growth of data scale, the sample size increases and the dimension of feature becomes higher and higher. Furthermore, with the rapid growth of irrelevant features or noise data, the effectiveness of the algorithm gradually decreases. As a result, feature selection is quite necessary, which can select the most effective feature from the original data, so as to reduce the dimension of dataset and improve the performance of learning algorithm. Figure 3 shows the basic framework for feature selection.

2.2. Bayesian Classifier. Most datasets contain a large number of features, and when training a dataset for classification, it can be seen that the degree to which the features contained in the dataset affect the classification results varies.
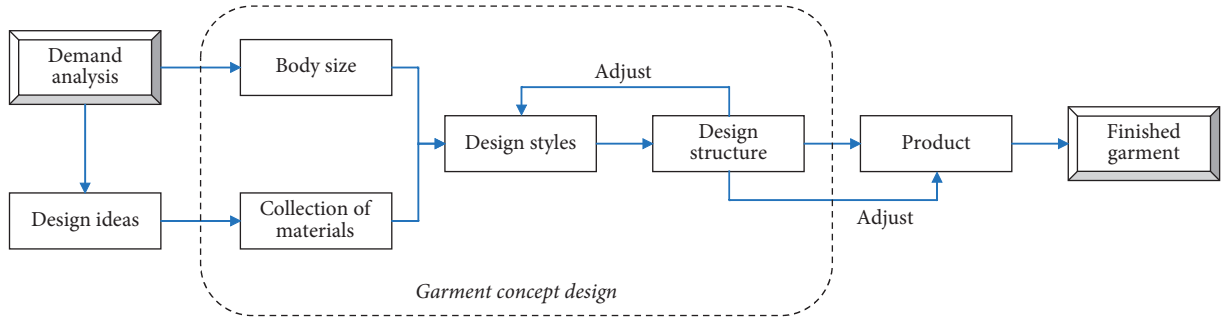
FIGURE 2: Traditional garment design process.
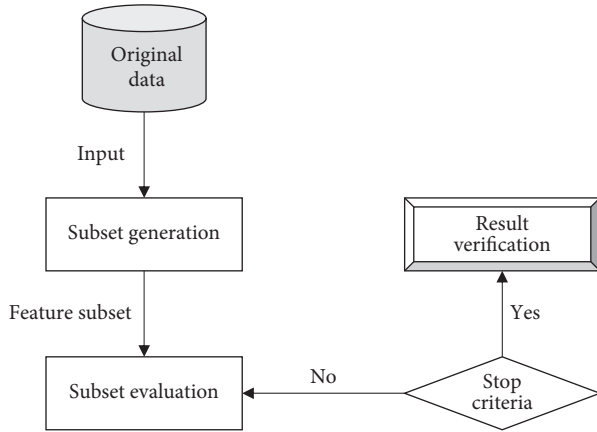
FIGURE 3: Basic framework for feature selection.

Generally, the more features there are, the better the classification results are. However, much of the data in the database are unprocessed and contain too many confounding factors that can affect the classification results to some extent, and feature selection can solve this problem. As a result, before using the Bayesian classifier algorithm, feature selection is required in order to obtain a better performance of the trained classifier.

Bayesian classifiers are machine learning algorithms built on the basis of Bayes' theorem. As an early type of Bayesian classifier, the plain Bayesian classifier has high classification or prediction efficiency and good adaptation to new samples. The plain Bayesian classifier treats the properties of classes as isolated and independent of each other, i.e., the class conditions are independent of each other. This hypothesis allows for the handling of otherwise complex class-attribute relationships, and although some data information is lost, the amount of arithmetic involved in the classification process is significantly reduced.

Let $S = \{s_1, s_2, s_3, \ldots, s_n\}$ denote the training dataset, which contains n samples. Also, let $s_i = \{d_{i1}, d_{i2}, d_{i3}, \ldots, d_{im}, k_i\}$ represent the non-category and category attribute values of the ith sample in the training dataset. Therefore, the detailed implementation process can be seen as follows:

(1) Construct the structure of Bayesian classifier.

According to the different values of the class attributes of the training samples, the root node of the non-class attributes is used to construct the structure of the Bayesian model.

(2) Construct parameter table.

According to the training dataset $S = \{s_1, s_2, s_3, \ldots, s_n\}$ and the structure of Bayesian classifier, the relevant parameters can be learned and the parameter table can be constructed.

(3) Calculate posteriori probability.

For a sample $(d_1, d_2, \ldots, d_m)$, the calculation process of its posteriori probability is shown as follows:

$$
\begin{aligned}
P(k^i|d) &= \frac{P(k^i|d) \times P(k^i)}{P(d)} \\
&= \theta \times P(k^i) \times \prod_{j=1}^{m} P(d_1|k^i),
\end{aligned}
\tag{1}
$$

where θ refers to the regular factor of one constant and k^i refers to the value of the category variable.

(4) Distribution of samples.

After obtaining the posteriori probability, the samples can be distributed to the specified attribute.

To sum up, the detailed implementation process of applying the Bayesian classifier can be seen in Figure 4.

2.3. Decision Tree. As shown in Figure 5, decision tree is a knowledge representation method similar to tree organization. All non-leaf nodes of a decision tree represent the non-category attributes of sample data, while all leaf nodes represent the category attributes of sample data. Any unbranched branch in a decision tree, from root to branch to leaf, represents a knowledge rule. The method of knowledge expression and application of decision tree is to make recursive judgment from the root node according to each attribute value of the sample to be evaluated until the leaf node is given to belong to a certain category.

Decision tree algorithm uses information entropy and gain degree in information theory as classification basis to study the classification of things or events. The adequacy of information transfer depends on the degree of uncertainty of the system. The smaller the uncertainty of the system is, the more sufficient the information transfer will be, and vice versa. Therefore, in order to transmit information adequately,
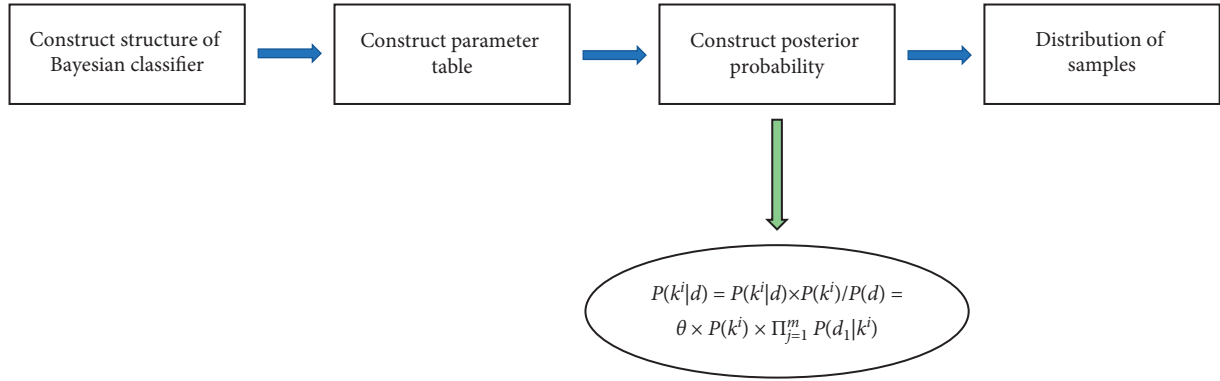
FIGURE 4: Implementation process of applying Bayesian classifier.
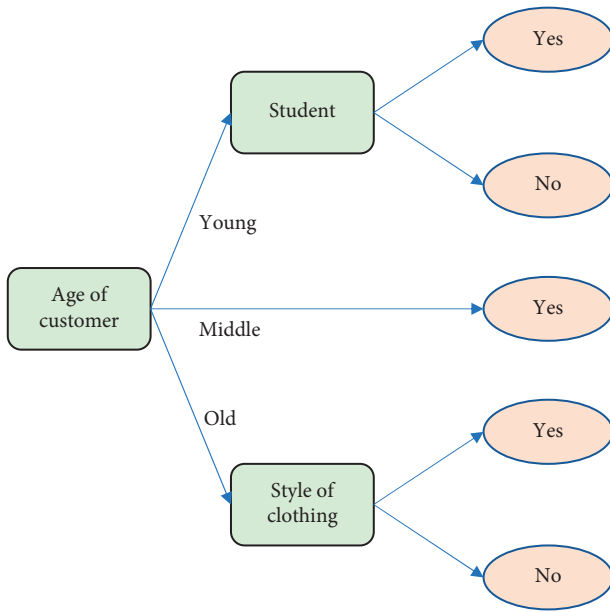
FIGURE 5: Example of decision tree.

system uncertainty must be ensured as little as possible. The decision tree algorithm applies the information gain value as the criterion to judge the uncertainty of the system, selects the maximum attribute of the information gain value as the test attribute, and divides the training sample set according to the different values of the test attribute. The calculation method of information gain value is given below.

Let D represent the set of d training samples, and let a denote the number of attribute values. Then, calculation of information entropy is shown below:

$$I(d_1, d_2, \ldots, d_a) = -\sum_{i=1}^{a} P_i \times \ln(P_i), \qquad (2)$$

where P_i refers to the probability of the ith sample.

Next, the calculation of information entropy generated by dividing samples by attribute X is shown below:

$$Y(X) = \sum_{i=1}^{m} \frac{d_{1i} + d_{2i} + \ldots + d_{mi}}{D} \times I(d_1, d_2, \ldots, d_a). \qquad (3)$$

Finally, the calculation of the information gain value generated by dividing the sample set s by attribute X is shown below:

$$G(X) = I(d_1, d_2, \ldots, d_a) - Y(X). \qquad (4)$$

When machine learning algorithm is used to construct classification model, it is necessary to reserve some samples in the total sample set for testing and verifying the prediction accuracy of the built model.

2.4. Neural Network. The human brain is an advanced intelligent signal processing system, which consists of a large number of interconnected neurons, each of which has a series of processing and transmission of electrochemical signals it receives. The electrochemical signal transmission process is as follows. First, the synapse receives a large number of electrochemical signals, which are transmitted through the dendrites to the cell body. The inhibitory and stimulating parts of the electrochemical signal are then superimposed on each other. When the cumulative effect reaches and exceeds a certain threshold, the cell body is excited and outputs an electrochemical signal. Finally, the electrochemical signal is transmitted from the axon to the adjacent neurons, and so on. The neural network structure of the human brain is made up of two parts: nature and learning. In the continuous learning process of external things, some links between neuron cells will slowly disappear, and when these existing links disappear, a large number of new links will be generated. The neural network of the brain continuously learns new knowledge from real things, gradually changes the structure of the network, and can produce new cognition of things.

Artificial neural network is an intelligent information processing system based on the working principle of brain neural network. In the construction process of artificial neural network, it is necessary to simulate the main functions of biological neuron cells first and construct the human neuron model with similar functions. As shown in Figure 6, the output function of the artificial neuron model has various forms.
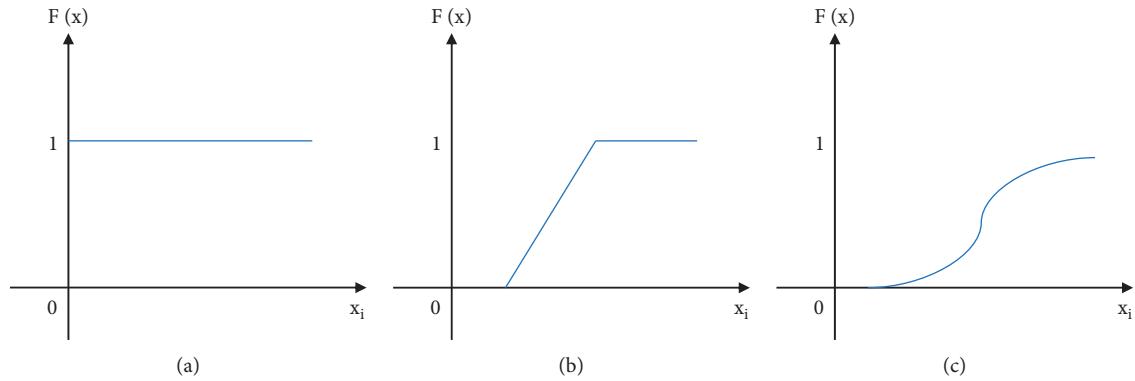
Figure 6: Output function of the artificial neuron model.
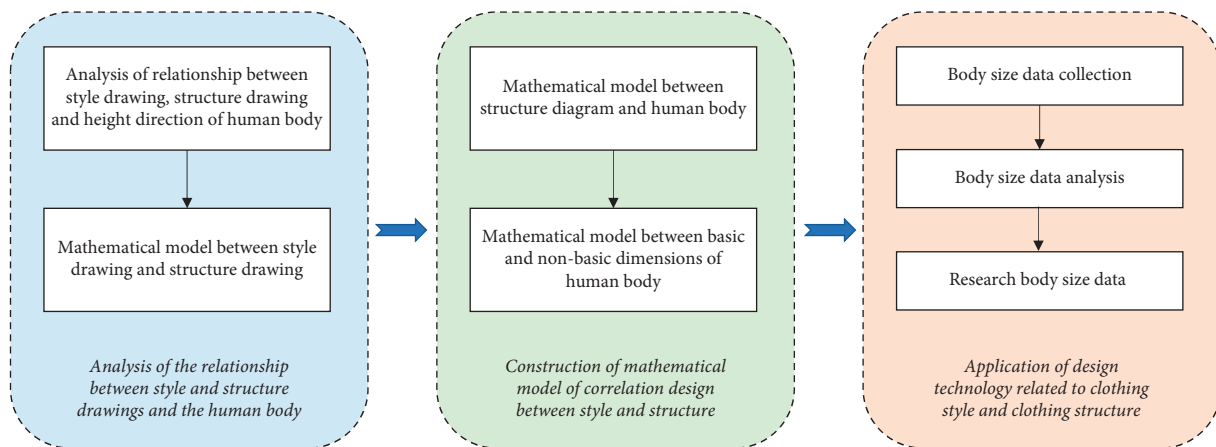
Figure 7: Stye and structure correlation design.

3. Garment Design Model

3.1. Style and Structure Correlation Design. The style diagram is used to express the designer's design concept in concrete terms. The structure of a garment is a flat pattern presentation of the garment pieces based on the style diagram. There is a close relationship between the design of the garment style and the construction of the garment, but currently in the garment industry, the two are separate departments, with the designer designing the style and the pattern maker designing the construction. In the product development phase, designers need to communicate with pattern makers in order to avoid poor understanding of styles. The separation of the design and structure of the garment is one of the main reasons for the long product development cycle. If the design and structure of the garment were integrated, the development cycle would be much shorter. To be specific, the stye and structure correlation design can be seen in Figure 7.

3.2. Construction of Mathematical Model. How to obtain satisfactory clothing style is also a problem worth considering. However, due to the complexity of clothing style, the coding scheme based on spline key point parameters has

great instability. Therefore, the model can not only generate new styles but also get user satisfaction.

Body size is the basis of clothing structure design, and clothing style design is based on the comparison of clothing and human body, without measuring the real body size. If the body size is also given to the pattern drawing, then there is a link between the design and structural design of clothing. The basis of the association design technology between garment style and garment structure proposed in this chapter is to assign human body size to the pattern drawing, so that the garment style design and structural design are integrated based on the common human body size. Compared with the traditional fashion design method, this method is a novel design method. Therefore, the design idea of multi-factor combination-driven is based on the analysis of the essence of things to the characteristics and forms of elements, and its methods and related technologies have a wide range of applications. However, in the aspect of clothing design, especially those requiring individuation, most current studies regard the correlation between elements as the influence of one or several parameters and determine these parameters through experience or data fitting. This single reasoning method is difficult to reveal the interaction of different elements and has great limitations.

According to the function and use of clothing, people's perception of clothing can be divided into functional image and emotional image. Functional image mainly expresses the perception of specific functional strength of clothing. Emotional image can meet the needs of functional image on the premise of a certain clothing design, if only the modelling is consistent with the user's personal preferences. Compared with other elements of clothing, specific elements and styles have a greater impact on specific user image and present a stable state of psychological association. Therefore, the research on users' clothing image preference can fully explore the clothing elements and the rules of modelling construction and design the clothing to meet the personalised expectation.

4. Conclusion

This study states the intelligent clothing design system, starting from the research point of clothing style, and human-machine interaction as a main way of clothing innovation design. According to the analysis of users' needs, the style is described, and the style of clothing is studied and analysed to achieve the expression of users' needs. Combined with the characteristics of men's suit design based on biological genes, Bayesian classifier and decision tree algorithm are used to design the suit. Neural network technology was used to extract and express the gene of clothing style samples to obtain the main component gene characteristics of clothing style. Then, this research analyses its characteristics and raises up a kind of new gene definition, sorts out the influence clothing design element, as well as carries on the parametric design.

The research in this paper provides a certain theoretical basis for clothing design and fit evaluation. However, in view of the limitations of knowledge level and research conditions, the following aspects should be explored in the later stage to further improve the research content. First of all, subsequent studies can collect different body size data for different customer groups. In addition, the data are used to construct the correlation design model of clothing style and clothing structure, so that the final design of clothing products will be more targeted. Furthermore, a series of dynamic clothing pressures can be measured, and the dynamic clothing pressures with time series characteristics can be taken as the input of the model. In this case, the prediction accuracy and reliability of garment fit evaluation model based on machine learning are expected to be further improved.

Data Availability

The labeled dataset used to support the findings of this study is available from the corresponding author upon request.

Conflicts of Interest

The authors declare that there are no conflicts of interest.

Acknowledgments

References

[1] K. Lee, H. Choi, J. H. Choi, and T. Kim, "Development of a data-driven predictive model of clothing thermal insulation estimation by using advanced computational approaches," *Sustainability*, vol. 11, no. 20, p. 5702, 2019.

[2] A. Majumdar, S. K. Sinha, M. Shaw, and K. Mathiyazhagan, "Analysing the vulnerability of green clothing supply chains in South and Southeast Asia using fuzzy analytic hierarchy process," *International Journal of Production Research*, vol. 59, no. 3, pp. 752–771, 2021.

[3] Y. Zhao, "Manufacturing personalization models based on industrial big data," *Journal of Discrete Mathematical Sciences and Cryptography*, vol. 21, no. 6, pp. 1287–1292, 2018.

[4] G. Deepak and D. Kasaraneni, "OntoCommerce: an ontology focused semantic framework for personalised product recommendation for user targeted e-commerce," *International Journal of Computer Aided Engineering and Technology*, vol. 11, no. 4/5, pp. 449–466, 2019.

[5] L. Macchion, R. Fornasiero, and A. Vinelli, "Supply chain configurations: a model to evaluate performance in customised productions," *International Journal of Production Research*, vol. 55, no. 5, pp. 1386–1399, 2017.

[6] I. Maldini, P. J. Stappers, J. C. Gimeno-Martinez, and H. A. M. Daanen, "Assessing the impact of design strategies on clothing lifetimes, usage and volumes: the case of product personalisation," *Journal of Cleaner Production*, vol. 210, pp. 1414–1424, 2019.

[7] M. Shi, Y. Wei, L. Chen, D. Zhu, T. Mao, and Z. Wang, "Learning a shared deformation space for efficient design-preserving garment transfer," *Graphical Models*, vol. 115, Article ID 101106, 2021.

[8] X. Tao, X. Chen, X. Zeng, and L. Koehl, "A customized garment collaborative design process by using virtual reality and sensory evaluation on garment fit," *Computers & Industrial Engineering*, vol. 115, pp. 683–695, 2018.

[9] K. Ma, L. Wang, and Y. Chen, "A resource sharing mechanism for sustainable production in the garment industry," *Sustainability*, vol. 10, no. 2, p. 52, 2017.

[10] W.-K. Jung, H. Kim, Y.-C. Park, J.-W. Lee, and E. S. Suh, "Real-time data-driven discrete-event simulation for garment production lines," *Production Planning & Control*, vol. 33, no. 5, pp. 480–491, 2020.

[11] L. Zhang, T. Wu, S. Liu, S. Jiang, H. Wu, and J. Yang, "Consumers' clothing disposal behaviors in Nanjing, China," *Journal of Cleaner Production*, vol. 276, Article ID 123184, 2020.

[12] E. Eşme and B. Karlık, "Design of intelligent garment with sensor fusion for rescue teams," *Journal of the Faculty of Engineering and Architecture of Gazi University*, vol. 34, no. 3, pp. 1187–1200, 2019.

[13] A. S. Joshi, S. Gupta, G. Kanahasabai, and E. P. Ijjina, "IIntelligent garment detection using deep learning," *Handbook of Intelligent Computing and Optimization for Sustainable Development*, pp. 49–67, 2022.

[14] O. Bongomin, J. I. Mwasiagi, E. O. Nganyi, and I. Nibikora, "Improvement of garment assembly line efficiency using line balancing technique," *Engineering Reports*, vol. 2, no. 4, Article ID e12157, 2020.

[15] K. Kashiwagi and E. Iwasaki, "Effect of agglomeration on technical efficiency of small and medium-sized garment firms in Egypt," *African Development Review*, vol. 32, no. 1, pp. 14–26, 2020.

[16] J. Bae, P. Lund-Thomsen, and A. Lindgreen, "Global value chains and supplier perceptions of corporate social responsibility: a case study of garment manufacturers in Myanmar," *Global Networks*, vol. 21, no. 4, pp. 653–680, 2021.

[17] S. Weber, "Reuse recycle repair remanufacture," *Alternatives Journal*, vol. 43, no. 3-4, pp. 80–86, 2018.

[18] M. Feori-Payne and E. McKinney, "Apparel product developers: an exploration through the lens of work analysis," *Journal of Global Fashion Marketing*, vol. 12, pp. 1–17, 2021.

[19] M. Salahuddin and L. Romeo, "Wearable technology: are product developers meeting consumer's needs?" *International Journal of Fashion Design, Technology and Education*, vol. 13, no. 1, pp. 58–67, 2020.

[20] L. Zhao, L. Guo, R. Zhang, X. Xie, and X. Ye, "mmGaitSet: multimodal based gait recognition for countering carrying and clothing changes," *Applied Intelligence*, vol. 52, no. 2, pp. 2023–2036, 2022.

[21] M. Dong, X. Zeng, L. Koehl, and J. Zhang, "An interactive knowledge-based recommender system for fashion product design in the big data environment," *Information Sciences*, vol. 540, pp. 469–488, 2020.

[22] S. C. Sethuraman, P. Kompally, S. P. Mohanty, and U. Choppali, "MyWear: a novel smart garment for automatic continuous vital monitoring," *IEEE Transactions on Consumer Electronics*, vol. 67, no. 3, pp. 214–222, 2021.

[23] B. Lüthje, "Platform capitalism 'made in China'? Intelligent manufacturing, taobao villages and the restructuring of work," *Science Technology & Society*, vol. 24, no. 2, pp. 199–217, 2019.

[24] M. R. Hoque, R. Boateng, and R. Boateng, "Adoption of B2B e-commerce in developing countries: evidence from ready made garment (RMG) industry in Bangladesh," *Pacific Asia Journal of the Association for Information Systems*, vol. 9, no. 1, pp. 55–74, 2017.

[25] E. Fernández, C. Ayas, M. Langelaar, and P. Duysinx, "Topology optimisation for large-scale additive manufacturing: generating designs tailored to the deposition nozzle size," *Virtual and Physical Prototyping*, vol. 16, no. 2, pp. 196–220, 2021.

[26] S. Guo, T.-M. Choi, and B. Shen, "Green product development under competition: a study of the fashion apparel industry," *European Journal of Operational Research*, vol. 280, no. 2, pp. 523–538, 2020.

[27] C. Homburg, D. Jozić, and C. Kuehnl, "Customer experience management: toward implementing an evolving marketing concept," *Journal of the Academy of Marketing Science*, vol. 45, no. 3, pp. 377–401, 2017.

[28] K. Liu, X. Zeng, P. Bruniaux, J. Wang, E. Kamalha, and X. Tao, "Fit evaluation of virtual garment try-on by learning from digital pressure data," *Knowledge-Based Systems*, vol. 133, pp. 174–182, 2017.

[29] B. Cheng, C. Fan, H. Fu, J. Huang, H. Chen, and X. Luo, "Measuring and computing cognitive statuses of construction workers based on electroencephalogram: a critical review," *IEEE Transactions on Computational Social Systems*, vol. 9, pp. 1–16, 2022.

[30] Y. Qian, S. Chen, J. Li et al., "A decision-making model using machine learning for improving dispatching efficiency in Chengdu Shuangliu airport," *Complexity*, vol. 2020, Article ID 6626937, 16 pages, 2020.

[31] B. Cheng, K. Lu, J. Li, H. Chen, X. Luo, and M. Shafique, "Comprehensive assessment of embodied environmental impacts of buildings using normalized environmental impact factors," *Journal of Cleaner Production*, vol. 334, Article ID 130083, 2022.

[32] K. Liu, J. Wang, E. Kamalha, V. Li, and X. Zeng, "Construction of a prediction model for body dimensions used in garment pattern making based on anthropometric data learning," *Journal of the Textile Institute*, vol. 108, no. 12, pp. 2107–2114, 2017.

Research Article

Identification Method of Citrus Aurantium Diseases and Pests Based on Deep Convolutional Neural Network

Yuke Lin,[1] Jin Xu,[2] and Ying Zhang [ID] [3]

[1]*Department of Communication Engineering Chongqing College of Electronic Engineering, Chongqing 401331, China*
[2]*Dabashan Branch of Chongqing Academy of Chinese Materia Medica, Chongqing 400065, China*
[3]*Disinfection and Vector Control Institute of Chongqing Center for Disease Control and Prevention, Chongqing 400042, China*

Correspondence should be addressed to Ying Zhang; 200719027@cqcet.edu.cn

The traditional identification methods of Citrus aurantium diseases and pests are prone to convergence during the running process, resulting in low accuracy of identification. To this end, this study reviews the newest methods for the identification of Citrus aurantium diseases and pests based on a deep convolutional neural network (DCNN). The initial images of Citrus aurantium leaves are collected by hardware equipment and then preprocessed using the techniques of cropping, enhancement, and morphological transformation. By using the neural network to divide the disease spots of Citrus aurantium images, accurate recognition results are obtained through feature matching. The comparative experimental results show that, compared with the traditional recognition method, the recognition rate of the proposed method has increased by about 11.9%, indicating its better performance. The proposed method can overcome the interference of the external environment to a certain extent and can provide reference data for the prevention and control of Citrus aurantium diseases and pests.

1. Introduction

Citrus aurantium (bitter orange) is an herbal medicine collected in the Chinese Pharmacopoeia, and its medicinal source is the dried fruit of the Rutaceae plant lime and its cultivars. The green peel is harvested in July, cut in half from the middle, and dried in the sun or at a low temperature. Citrus aurantium is bitter, acrid, sour, and warm and has the functions of regulating qi and unblocking the stomach, promoting qi, and stopping bloating. It is mainly used to treat diseases such as qi stagnation in the chest, distending pain, undissolved food accumulation, phlegm-rheum collecting internally, gastroptosis, anus prolapse, uterine prolapse, etc. Citrus aurantium is produced in many places in China, mainly in Hunan and Jiangxi provinces. Specifically, Citrus aurantium from Xingan County, Jiangxi Province, is also known as Shangzhou Citrus aurantium and Sanhu Citrus aurantium, with the characteristics of thick pulp, eversion like raspberry, and many orange petals. Its medicinal ingredients are better than other varieties, and it is listed as a protected product of China's National Geographical Indication [1]. With the development of the Citrus aurantium industry, the variety of the diseases and pests of Citrus aurantium has increased and the degree of damage has worsened. It is urgently needed to find ways to quickly and accurately diagnose Citrus aurantium diseases and take corresponding control measures.

In terms of diseases and pests detection, the commonly used method is to manually identify with the naked eye by agricultural experts. This method can compare plant insect and pest samples based on external characteristics, such as shape, color, etc., to obtain identification results. However, because manual identification has certain limitations and subjectivity, and humans cannot continuously work for a long time, the accuracy of manual identification is low, and it is labor-intensive. This has led to the contradiction between the growing demand for identification of crop diseases and pests and the shortage of identification staff in China [2]. For this reason, researchers have put forward a method for the identification of Citrus aurantium pests by combining

computer technology and image processing technology. So far, the research fields related to crop disease image recognition have made some progress and achieved many research results. The existing research results include the proposal of pest identification method based on deep learning [3], machine vision [4], and spatial pyramid pooling [5].

At present, most of the image features are extracted by artificial design or through spectral discrimination. However, the traditional identification methods of Citrus aurantium diseases and pests are prone to convergence during the running process, resulting in low accuracy of identification. Different environmental conditions have a great impact on the recognition results, and the robustness and accuracy are poor. To this end, this study introduces a DCNN algorithm. The DCNN algorithm is a combination of the deep learning algorithm and the convolutional neural network (CNN) algorithm, which solves the problem that the traditional CNN is prone to convergence and falls into local minimum points during the propagation process. In the DCNN algorithm, deep learning technology is used to automatically classify extract features of the images. The application of DCNN method to the identification of Citrus aurantium diseases and pests can improve the identification efficiency and provide effective technical support for the control of Citrus aurantium diseases and pests.

2. Experimental Materials and Methods

2.1. Acquiring the Images of Citrus Aurantium Diseases and Pests. Firstly, the test object of Citrus aurantium was selected. Then, under natural lighting conditions, CCD cameras were to collect the images of Citrus aurantium diseases and pests under three automatic exposure modes with image resolution of 2048×1536, 1600×1200, and 1024×768, respectively. The images were saved in the unity environment in the same format. The specific steps of acquiring the images of Citrus aurantium diseases and pests are shown in Figure 1.

The images of Citrus aurantium diseases and pests were collected in three time periods, morning, middle, and evening. The collection points are randomly and uniformly distributed in the specified area. The camera was made parallel as much as possible to the plane where the leaves of the Citrus aurantium were located to prevent obvious deformation [6].

2.2. Image Preprocessing. There is a certain degree of irrelevant image information in both healthy and diseased Citrus aurantium images. Image preprocessing is to enhance relevant information and eliminate irrelevant information to the greatest extent, thereby improving the reliability of image recognition.

The different sizes of the images are not conducive to the convolution operation in the subsequent network training, and the main information is located in the middle area of the image. Therefore, images should be cropped in batches before classification and identification, and a final image size

of 256×256 in the middle area should be selected. While simplifying the dataset, the number of datasets should remain unchanged, and the information of major diseases should be retained.

Furthermore, the image is directly compressed or expanded into a deep convolutional network model, which requires a fixed input image size. The input format required by the ResNet network model is 224×224, and the input format required by the Inception-v3 network model is 299×299 [7].

Image enhancement techniques include grayscale, binarization, filtering, and smoothing, etc. The commonly used RGB image is subjected to weighting processing on the three components of R, G, and B and then used as grayscale value. The process can be expressed as

$$\text{Gray} = 0.299R + 0.587G + 0.114B, \tag{1}$$

where R, G, and B represent the three components of the color image of Citrus aurantium, respectively, and the calculation result is the gray value of the pixel. On this basis, all the pixels of the original image are calculated, and the grayscale processing result of the color image is obtained. Using the grayscale histogram of the image, the image is divided into objects and backgrounds using a threshold. The expression is as follows:

$$g(x, y) = \begin{cases} 1, & f(x, y) > T, \\ 0, & f(x, y) \leq T, \end{cases} \tag{2}$$

where $f(x, y)$ is the pixel value of point $g(x, y)$ and T is the global threshold of the segmented image. Then, the median filter algorithm is used to filter the images. The median filtering algorithm uses some neighborhood pixels around the pixel to be processed to form a region space, arranges the gray values of all pixels in the region space from small to large or from large to small into a series, and then uses the middle value in the series as the gray value of the center point, as shown by

$$g'(i, j) = \text{Med}\{g(x, y), (x, y) \in S\}. \tag{3}$$

A new image can be obtained by performing the same processing on each pixel in the image in sequence [8]. In equation (3), if there is an odd number of pixels in the field space S, then the gray value of the pixel in the middle after sorting is taken as the gray value of the center point; if there is an even number of pixels in the field space S, the gray value of the middle two pixels is used as the gray value of the center point.

2.2.1. Multiple Morphological Transformation. Mathematical morphology usually has four basic operations, namely, erosion, dilation, closing, and opening [9]. In this study, two transformation methods, i.e., erosion and dilation, are mainly used in processing the images of Citrus aurantium. The corrosion operation is to eliminate boundary points and shrink the boundary inward. Target area of the image of Citrus aurantium is set as the set A which is subjected to
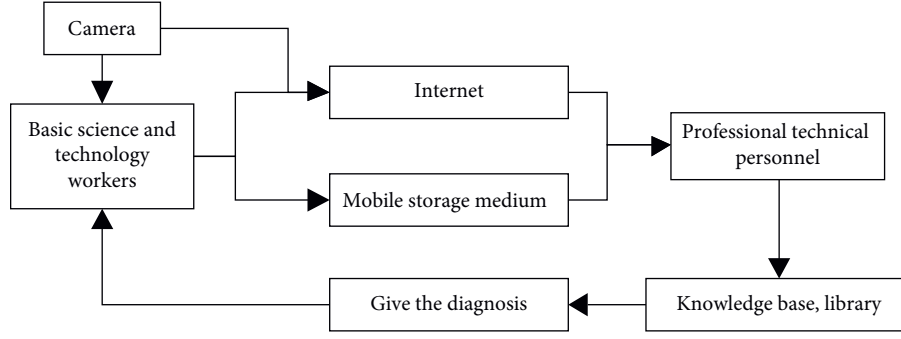
FIGURE 1: Flow chart of the image acquisition of Citrus aurantium diseases and pests.

convolution operation with the kernel B. The processing results are as follows:

$$A \ominus B = \{x \mid (B)_x \subseteq A\}. \quad (4)$$

Equation (4) shows that, after translating B by x pixels, its solution still exists in the set A; then it is said to be eroded by A. Corrosion is mainly manifested as image shrinkage. Furthermore, the role of dilation is to blend the surrounding environment into the target area, so that the boundary expands outward. The result of processing the set A expanded by the set B can be expressed as

$$A \oplus B = \{x \mid [(B)_x \subseteq A] \neq \varnothing\}. \quad (5)$$

When performing polymorphic transformation on an image, the operation of first eroding and then dilating is called the opening operation, which can eliminate the small noise inside the image and smooth the boundary of the object. The operation of first dilating and then eroding is called the closing operation, which can fill the small holes inside the image and smooth the boundaries of objects [9]. After many times of opening and closing operations on the image of Citrus aurantium, morphological transformation is performed on it.

2.2.2. Image Normalization.
The role of the normalization operation in probability theory is to present the statistical distribution of the sample, and the interval is normalized to [0, 1]; then the interval presents the coordinate distribution [10]. To this end, the Z-score method is used to normalize the disease image dataset into the [0, 1] interval to meet the data input requirements of the deep convolutional network model. Its mathematical expression is

$$y' = \frac{y - \mu}{\sigma^2}, \quad (6)$$

where y represents the disease image dataset, the initial μ represents the mean value of the Citrus aurantium disease and pest data, and the parameter σ represents the variance of the Citrus aurantium diseases and pests data.

2.3. Constructing a DCNN.
A DCNN is divided into input layer, feature extraction layer, and output layer from the perspective of data flow [11]. From the structural point of view, the DCNN consists of one or more convolutional layers, pooling layers, and fully connected layers. The two-dimensional image is used as the direct input of the network, and the middle part of the network is alternately connected by convolutional layers and pooling layers. The output layer is usually composed of a fully connected layer and a classifier, and the constructed DCNN structure is shown in Figure 2.

As can be seen from Figure 2, the DCNN consists of three convolutional layers, two pooling layers, and two fully connected layers. The size of the handwritten digit image input is 32×32. In the feature extraction layer, the convolutional layer receives the feature map of the previous layer and affines the convolution of the previous layer with the current layer [12]. The result of the operation is calculated, and the feature map of the layer is obtained through the activation function.

$$\begin{cases} y_j^m = f\left(u_j^m\right), \\ u_j^m = \sum_{i \in M_j} x_j^m * k_{ij}^m + b_j^m, \end{cases} \quad (7)$$

where y_j^m and u_j^m represent the feature map and net activation of the j th convolution kernel of the m th convolution layer, b_j^m represents the bias parameter, k_{ij}^m represents the weight of the j th convolution kernel of the m th layer, and $f(\cdot)$ and $*$ represent the nonlinear activation functions and convolution operator, respectively. The downsampling layer of the DCNN performs aggregation statistics on the upper-layer feature maps through local correlation. By reducing the feature dimension, the signal-to-noise ratio can be improved, and local features can be fused to generate new features [13]. The downsampling extraction of the input feature map can be expressed as

$$\begin{cases} y_j^m = f\left(u_j^m\right), \\ u_j^m = \beta_j^m \, \mathrm{down}\left(x_j^{m-1}\right) + b_j^m, \end{cases} \quad (8)$$

where down$(\cdot)$ represents the downsampling function and β_j^m represents the weight of the j th convolution kernel of the m th downsampling layer. By rasterizing the input pixel values, the two-dimensional feature map is converted into a one-dimensional feature column, and then the output feature map of the fully connected layer is obtained by weighted summation and nonlinear activation function operation:
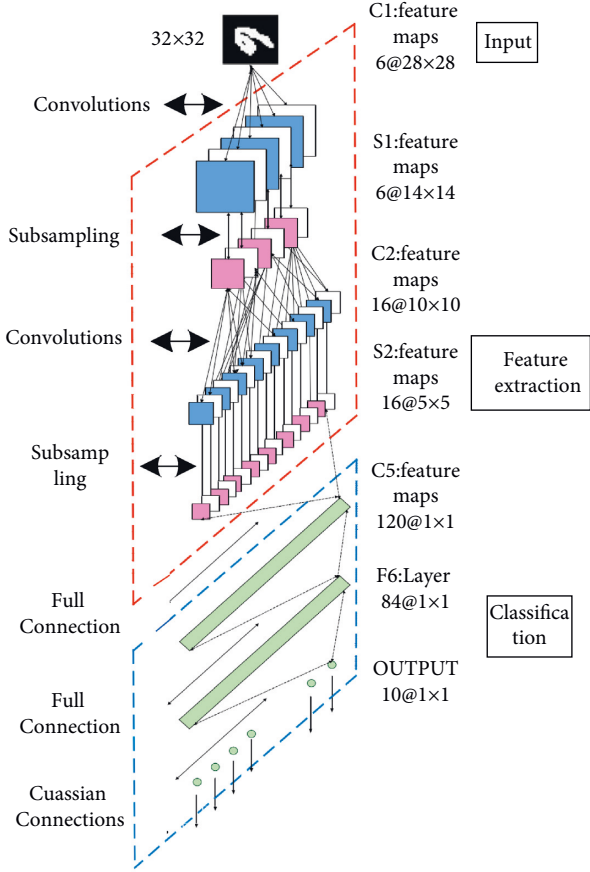
FIGURE 2: Structure diagram of DCNN.

$$u^m = \omega^m x_j^{m-1} + b_j^m, \tag{9}$$

where ω^m represents the weight parameter of the fully connected layer. To improve the recognition accuracy or meet the needs of specific tasks, multiple auxiliary layers such as dropout, local response normalization, local contrast normalization, and linear activation units are also inserted into the hidden layer in this study [14]. The activation function in the DCNN selects the sigmoid function which has the characteristics of monotonically increasing and inverse functions and can map variables to [0, 1]. The sigmoid function expression is given by

$$\text{Sigmoid}(\alpha) = \frac{1}{(1 + e^{-\alpha})}. \tag{10}$$

The image corresponding to the sigmoid function is shown in Figure 3.

2.4. Segmentation of the Image Area of Citrus Aurantium Disease Spots.
For the Citrus aurantium image, in the context of DCNN, HSI is selected as the color space. Among them, the I component has nothing to do with the color information of the image, while the H and S components are closely related to people's perception of color. Based on this feature, when H belongs to [70, 200] and S belongs to [0.17, 1], the green area of crop leaves can be roughly represented. Using
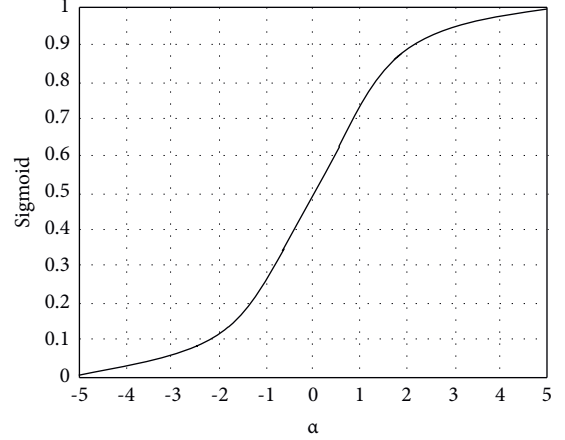
FIGURE 3: Sigmoid function curve.

the HSI color gamut, the above areas are erased to achieve the purpose of filtering the chlorophyll [15]. Then the gray values of all pixels are traversed to maximize the inter-class variance, and the obtained T is the required threshold. The color interval of each pixel is determined by the solved threshold value to realize the segmentation of pixel values. The final disease spot segmentation result can be obtained by merging multiple segmentation regions.

2.5. Extracting the Characteristics of the Diseases and Pests of Citrus Aurantium.
Using the feature extraction part in the DCNN, the extraction of the diseases and pests features of Citrus aurantium in the image is realized from the aspects of color and texture.

2.5.1. Color Features.
In order to find out the core features of color suitable for Citrus aurantium diseases and pests, according to the color difference of these diseases and pests, multiple characteristic parameters are selected as the color features [16]. We define r_j, g_j, and b_j as the red, green, and blue components of the i th pixel, respectively, and the hue, saturation, and luminance component values of the i th pixel of the converted HSI color space are represented as H_i, S_i, and I_i. Then, the extraction of each color feature can be expressed as

$$\begin{cases} \overline{r} = \dfrac{1}{N} \sum_{i=1}^{N} r_i, \quad \overline{b} = \dfrac{1}{N} \sum_{i=1}^{N} b_i, \quad \overline{g} = \dfrac{1}{N} \sum_{i=1}^{N} g_i, \\[4mm] \overline{H} = \dfrac{1}{N} \sum_{i=1}^{N} H_i, \quad \overline{S} = \dfrac{1}{N} \sum_{i=1}^{N} S_i, \quad \overline{I} = \dfrac{1}{N} \sum_{i=1}^{N} I_i, \end{cases} \tag{11}$$

where $\overline{r}$, $\overline{b}$, $\overline{g}$, $\overline{H}$, $\overline{S}$, and $\overline{I}$ represent the mean values of the red, green, and blue components and the hue, saturation, and luminance components, respectively.

2.5.2. Texture Features.
In the field of pattern recognition, texture analysis is a very important work, which involves the details of the image, such as pattern gray distribution,

gradient direction, roughness, and so on. Because the disease spots produced by different diseases of Citrus aurantium are always different in texture, the texture feature is selected as the supplement of the color feature, and the two cooperate with each other to avoid the defects of single feature classification. Select the gray level cooccurrence matrix to extract texture features. This method mainly obtains its cooccurrence matrix by calculating the grayscale image and then obtains a series of scalars by calculating the grayscale image to represent the texture information of the image. At any point on the grayscale image, another point is kept a certain distance from the point, and the point pair has a grayscale value [17]. Assuming that the grayscale sequence of the image is, then the grayscale values of the two pixels have a total of combinations. On the entire grayscale image, count the number of occurrences of each to obtain a statistical matrix of, which is called the grayscale co-occurrence matrix, and then normalize this matrix to obtain the joint probability matrix of the grayscale distribution of the image. Based on this model, energy, entropy, and moment of inertia are calculated as texture feature quantities, respectively.

By integrating the extraction results of color features and texture features in the collected images of Citrus aurantium diseases and pests, the extraction results of comprehensive features of Citrus aurantium diseases and pests can be obtained.

2.6. Identifying Citrus Aurantium Diseases and Pests.
In the DCNN constructed in this study, the extracted image features are resubstituted. Through network training and iteration, the classification results can be obtained, that is, the function of identifying Citrus aurantium diseases and pests.

The training process of DCNN can be divided into two stages: forward propagation and back propagation. Forward propagation is to obtain the calculation result to be inferred, and back propagation is to update the parameters according to the gradient calculated by the loss. The algorithm calculates the output and loss of each layer through forward propagation of the network and calculates the gradient of the network through back propagation [18]. The parameters are then gradient updated according to the stochastic gradient descent algorithm. After continuous learning to make the final loss meet the accuracy requirements, the parameter values of each layer of the network can be retained without reinitialization the next time the network is used [19].

For the identification of Citrus aurantium diseases and pests, it is necessary to set a comparison standard to clarify the color and texture differences between normal Citrus aurantium and abnormal ones, and to set a specific identification and comparison standard map according to the severity of the disease and pest [20]. Then, the similarity between the standard Citrus aurantium image features in the database and the pest features extracted from the DCNN is calculated to realize the matching of pest features. The calculation formula is given by

$$\text{Sim}\left(F_x, F_y\right) = \left(\sum_{i=1}^{n} \left|F_{x_i} - F_{y_i}\right|^p\right)^{1/p}, \tag{12}$$

where F_x and F_y represent the extracted image features and standard Citrus aurantium diseases and pests features in the database, respectively, and the variable p takes a constant value. By setting the similarity threshold value and combining the results in equation (12), we can obtain the class and severity degree of Citrus aurantium diseases and pests, that is, to obtain the identification results of Citrus aurantium diseases and pests.

3. Results and Analysis

In order to test the performance of the proposed identification method based on DCNN, the following test experiments are designed.

In the experiment, the traditional method based on machine vision (the method in reference [4]) and the method based on spatial pyramid pooling (the method in reference [5]) were used for comparison, including traditional recognition methods and algorithm optimization methods. The recognition rates of different methods were calculated and compared in the same experimental environment.

3.1. Selecting the Citrus Aurantium Sample Dataset.
Three different experimental datasets were employed in the experiment, namely, MalayaKew dataset, P1antVillage dataset, and AES-CD2020 dataset. These MalayaKew leaf datasets were from the Royal Botanic Gardens in Kew, UK, and contain two subsets, MK-D1 and MK-D2, with a total of 44 classes. MK-D1 is a leaf image dataset that performs multi-angle rotation expansion on the collected images to form a training set with 2282 samples and a test set with 528 samples. MK-D2 is an image set formed by local cropping and multi-angle rotation expansion of all leaves in MK-D1. The training set of MK-D2 has 788 images per class, and the testing set has 200 images per class. The P1antVillage dataset is a set of images that contain the health and disease of a variety of plants. There are 38 classes of healthy and diseased images related to crop diseases, more than 50,000 images, and the number of each class of images is uneven.

This study selected 10,478 leaf images of Citrus aurantium collected by P1antVillage, including images of healthy leaves and 5 classes of diseased leaves. The above two experimental sample datasets mainly provide comparison for the experiment. The AES-CD2020 dataset is a dataset composed of images shot on-site. The images in the AES-CD2020 dataset have different sizes, shooting angles, backgrounds, and lighting, etc. The environmental conditions are shown in Figure 4.

All the images in the experimental training set are equally divided into 5 groups, with 200 images in each group. The specific composition of each group of images is
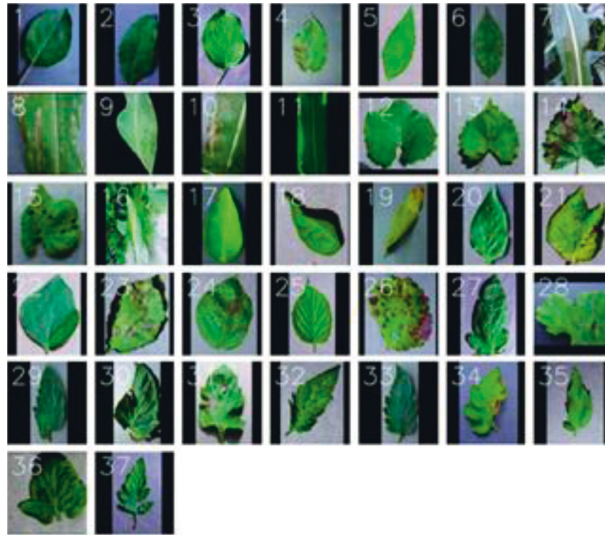
FIGURE 4: Schematic diagram of training set samples in the experiment.

TABLE 1: Experimental group setting.

Serial number	1	2	3	4	5
Number of healthy citrus aurantium samples (piece)	66	93	74	85	83
Number of samples of fructus aurantii with leaf blight (piece)	24	17	36	19	27
Leaf spot disease fructus aurantii sample number (piece)	31	25	40	22	25
Powdery mildew fructus aurantii sample quantity (piece)	45	28	11	25	23
Number of samples of thrips citrus (piece)	34	37	39	49	42

TABLE 2: Results of recognition rate.

Serial number		Number of correctly identified samples (piece)	Recognition rate (%)
1		175	87.5
2		173	86.5
3	Method of reference [4]	171	85.5
4		174	87
5		177	88.5
Average		174.0	87.0
1		182	91
2		184	92
3	Method of reference [5]	185	92.5
4		183	91.5
5		181	90.5
Average		183.0	91.5
1		196	98
2		199	99.5
3	Method of this paper	198	99
4		199	99.5
5		197	98.5
Average		197.8	98.9

shown in Table 1. The data in Table 1 is set as the identification standard data of the experiment.

3.2. *Experimental Environment.* The experiments were designed using the Caffe framework. Caffe is an open source tool for deep learning with CNNs. Caffe supports the languages of are C++ and CUDA and provides MATLAB, Python interfaces, and command lines, where the set_mode interface can be used to switch between CPU and GPU. The selected Citrus aurantium sample dataset was preprocessed to generate a database format. First, Caffe was used to read the data, and then training was performed. Net completed the initialization of the network layer, and

Solver was used to control the model training process. During the training process and at the end of the training, several trained models were saved. Through the configuration of the experimental environment, it is ensured that the constructed DCNN could run normally in the experimental environment.

3.3. Testing Process and Results Analysis of the Identification Methods. The recognition rate is used as the indicator for evaluating the algorithm performance. It can be directly obtained by calculating the ratio of the number of correctly identified samples to the total number of all identified samples. The prepared experimental sample data was imported into the experimental environment, and the resolution of the data sample was adjusted to 600×600. At the same time, the three methods for comparison were imported into the experimental environment in the form of program codes. The identification results were obtained by retrieving data samples.

By comparing the output recognition results with the dataset in Table 1, the results of recognition rate can be obtained, as shown in Table 2.

According to the data in Table 2, the average recognition rates of the methods in [4] and [5] are 87.0% and 91.5%, respectively. By comparison, the DCNN-based identification method proposed in this research shows an average recognition rate of 98.9%, indicating its best performance.

4. Conclusions

In order to achieve effective control and prevention of Citrus aurantium diseases and pests, this study designs a DCNN-based method for identifying Citrus aurantium diseases and pests. The method uses the relevant hardware equipment to collect the initial Citrus aurantium leaf images and complete the image preprocessing. The recognition results are obtained through feature matching.

(1) In order to verify the effectiveness of the proposed method, relevant experiments have been conducted. The experimental results show that the recognition rate of the proposed method is about 11.9% higher than that of the traditional recognition methods, verifying its high recognition rate.

(2) The reason for the high reliability of the proposed method is that it realizes the preprocessing of the initial Citrus aurantium image data through cropping, enhancement, and morphological transformation, etc. This fundamentally avoids the influence of environmental factors on the recognition results.

(3) By using the neural network to divide the disease spots of Citrus aurantium images, accurate recognition results are obtained through feature matching. The proposed method can overcome the interference of the external environment to a certain extent and can provide reference data for the prevention and control of Citrus aurantium diseases and pests.

Data Availability

The labeled dataset used to support the findings of this study is available from the corresponding author upon request.

Conflicts of Interest

The authors declare no conflicts of interest.

Acknowledgments

References

[1] Y. B. Liu, B. Lei, Y. Cao, J. Y. Tang, and L. Hu, "Maize diseases identification based on deep convolutional neural network," *Chinese Agricultural Science Bulletin*, vol. 34, no. 36, pp. 165–170, 2018.

[2] H. X. Li, C. F. Long, M. Zeng, and J. Shen, "A detecting method for the rape pests based on deep convolutional neural network," *Journal of Hunan Agricultural University (Natural Sciences)*, vol. 45, no. 5, pp. 114–118, 2019.

[3] S. Yang, Q. Feng, J. H. Zhang, W. Sun, and G. P. Wang, "Identification method for potato disease based on deep learning and composite dictionary," *Transactions of the Chinese Society for Agricultural Machinery*, vol. 51, no. 7, pp. 22–29, 2020.

[4] Z. J. Shang, H. Zhang, C. Zeng, M. Le, and Q. Zhao, "Automatic orientation method and experiment of Fructus aurantii based on machine vision," *Journal of Chinese Agricultural Mechanization*, vol. 40, no. 7, pp. 119–124, 2019.

[5] B. Zhang, M. H. Zhang, and Y. Z. Chen, "Crop pest identification based on spatial pyramid pooling and deep convolution neural network," *Transactions of the Chinese Society of Agricultural Engineering*, vol. 35, no. 19, pp. 209–215, 2019.

[6] H. M. Cai, Y. T. Sui, Z. Zhang, and X. Y. Zeng, "Crop disease recognition based on depthwise separable convolutional neural network," *Journal of Anhui Agricultural Sciences*, vol. 47, no. 11, pp. 244–246+252, 2019.

[7] Y. L. Yang, C. J. Ouyang, L. Li, T. Liao, and P. J. Tang, "Image recognition of rice diseases based on deep convolutional neural network," *Journal of Jinggangshan University (Natural Sciences Edition)*, vol. 40, no. 2, pp. 38–45, 2019.

[8] J. D. Yang, T. Yang, T. Miao et al., "Recognition of powdery mildew disease of strawberry leaves based on con-volutional neural network," *Jiangsu Journal of Agricultural Sciences*, vol. 34, no. 3, pp. 527–532, 2018.

[9] Y. Zhang, C. N. Wang, and N. N. Qin, "Optimize methods for identifying plant pests and diseases," *Seed Science & Technology*, vol. 38, no. 7, pp. 77-78, 2020.

[10] M. S. Long, C. J. Ouyang, H. Liu, and Q. Fu, "Image recognition of Camellia oleifera diseases based on convolutional neural network & transfer learning," *Transactions of the Chinese Society of Agricultural Engineering*, vol. 34, no. 18, pp. 194–201, 2018.

[11] B. Y. Shi, J. Q. Li, L. Zhang, and J. Li, "Recognition model of crop pests and diseases images based on CNN," *Computer Systems & Applications*, vol. 29, no. 6, pp. 89–96, 2020.

[12] B. N. Su, "Image processing based rice pest and disease identification technology," *Information Technology & Informatization*, vol. 43, no. 5, pp. 96–98, 2018.

[13] Y. J. Gao, Y. M. Wang, Y. Q. Chen, and Y. H. Zhang, "Research on visualization and recognition method of crop disease and insect pests based on GIS," *Journal of Catastrophology*, vol. 35, no. 2, pp. 28–31, 2020.

[14] M. Jiang, Y. M. Shen, J. Y. Zhang, Y. Rao, and W. Dong, "Research on rice diseases and pests diagnosis based on deep learning," *Journal of Luoyang Institute of Science and Technology (Natural Science Edition)*, vol. 29, no. 4, pp. 78–83, 2019.

[15] G. Hu, X. Yang, Y. Zhang, and M. Wan, "Identification of tea leaf diseases by using an improved deep convolutional neural network," *Sustainable Computing: Informatics and Systems*, vol. 24, no. 11, pp. 1028–1035, 2019.

[16] G. Geetharamani and J. A. Pandian, "Identification of plant leaf diseases using a nine-layer deep convolutional neural network," *Computers & Electrical Engineering*, vol. 76, pp. 323–338, 2019.

[17] Z. Liu, X. Zheng, Z. Xiao et al., "Research on integrated algorithm based on convolutional neural network for rice disease identification," *Journal of Physics: Conference Series*, vol. 1646, no. 1, pp. 66–70, 2020.

[18] Z. Shu, Y. Yang, N. Xing, Y. Wang, Q. Wang, and H. Kuang, "Structural characterization and immunomodulatory activity of a pectic polysaccharide (CALB-4) from Fructus aurantii," *International Journal of Biological Macromolecules*, vol. 116, pp. 847–856, 2018.

[19] Q. Zhang and F. Feng, "The effects of different varieties of aurantii fructus Immaturus on the potential toxicity of zhi-zi-hou-Po decoction based on spectrum-toxicity correlation analysis," *Molecules*, vol. 24, no. 23, p. 4254, 2019.

[20] X. Q. Luo, S. S. Li, H. F. Chen, and W. Yang, "Study on HPLC fingerprint of genuine regional drug of aurantii fructus in Jiangxi," *Chinese Journal of New Drugs*, vol. 27, no. 24, pp. 2949–2953, 2018.

Research Article

Multimedia Automation Access Control of Big Data Open Resources Based on Blockchain

Nan Zhao ⓘ,[1] **Hui Su** ⓘ,[2] **QingSheng Han** ⓘ,[1] and **Yan Zhao** ⓘ[1]

[1]*Beijing Institute of Economics and Management, Beijing 100102, China*
[2]*Unit 78111 of PLA, Chengdu 610011, China*

Correspondence should be addressed to Nan Zhao; 2016214241@smail.jsut.edu.cn

In order to better mine the value of data, the author proposes a research on the automatic access control of big data open resources multimedia based on blockchain and introduces big data access control BBAC-BD (blockchain-based access control mechanism for big data environment). The author designed a strategy management contract based on the Bloom filter, as a probabilistic data structure with extremely high space utilization efficiency and proposed the strategic management contract (PAP CONTRACT) and the strategic decision contract (PDP CONTRACT). In this way, the nontampering, auditability, and verifiability of the access control information are guaranteed; then, the access control method based on smart contracts is adopted to realize the user-driven, whole-process transparent, and dynamic and automatic access control of big data resources. The simulation results show that the greater the ratio of n/k, the better the optimization effect, and the greater the ratio, the lower the corresponding misjudgment rate, but it will also take up more space costs. At the same time, the true value of the false positive rate is generally less than the theoretical value of the false positive rate. When the performance of Hash (strategy to retrieve) is better, the result of Hash distribution is more uniform. Under the condition of $m = 3$, the misjudgment rate acceptable for the expected use can be achieved, and the increase in the number of Hashes will not bring a significant increase in revenue. Freed from the traditional model of providing access control services based on third parties, solve the problem of transparency of authority judgments; at the same time, through smart contracts, based on the strategy published by the resource owner on the blockchain, realize automatic access control to big data resources; and make the judicial process more flexible and the judgment result more credible. The BBAC-BD mechanism realizes a safe, reliable, and transparent new access control architecture, and it can effectively promote the safe circulation and sharing of big data.

1. Introduction

Human society is accompanied by social networks, e-commerce, and mobile communications, and the rise of the Internet of Things, which has entered the era of big data with data volume, big data analysis, and prediction based on distributed computing. This can make decisions more precise of what people are seeing is just the tip of the iceberg of the true value of big data [1]. Smartphones and wearable devices make every change of our behavior, position, and even physiological information become data that can be recorded and analyzed, but these big data are stored and controlled by various government agencies, business alliances, scientific research institutions, and even individuals,

and the phenomenon of "data islands" is formed [2]. Interconnect and sharing of these scattered big data, in order to obtain products and services of great value, is an urgent need coexisting in business, scientific research, public services, and other fields [3]. In order to realize big data sharing, it is first necessary to connect separate and decentralized data sources [4]. However, due to the lack of detailed and transparent institutional standards, open policies, and pricing mechanisms between enterprises, scientific research institutions, and government departments, it is difficult to achieve fairness and equality between sharing parties [5]. Data diversification, storage structure, and interaction standards are not uniform, and the lack of a transparent communication environment is also hindering data

interaction; the technical architecture of big data access control is shown in Figure 1 [6]. These problems together r cause data connection difficulties. Therefore, a transparent and open data connection method is urgently needed to record data information, access conditions, standards, and other related information to achieve interconnection. Fundamentally speaking, the issue of "data islands" is mainly related to interest and security issues. The data are kept by a large data platform or other intermediary organization. Once the data are uploaded, the owner loses the right to control the data. Regardless of whether it is a government agency or an Internet company, it is very sensitive to data, and once it is leaked, it will have a great social impact.

2. Literature Review

In response to this research question, the author of [7]aimed at third-party collection and control of personal data security vulnerabilities, leading to the problem of user privacy leakage; a distributed personal data management system based on blockchain is proposed to ensure users own and control their private data. For all blockchain transactions, Ansart et al. are transparently embodied in the public network that leads to the leakage of transaction privacy, and they proposed the use of the Hawk protocol based on smart contracts; the agreement encrypts the communication between the parties to the contract to ensure the absolute security of information [8]. Liu et al. addressed the issue of data security and privacy in the Internet of Things, proposed a lightweight blockchain application suitable for IoT devices, and in the smart home scene, they practiced and verified its security, confidentiality, integrity, and availability [9]. Yin et al. adopted an encrypted smart contract, protected public privacy files through public and private keys, and provided auditing and tracking [10]. In terms of data storage and authenticity verification, Xu, J. et al. made an in-depth discussion on the future impact of the audit industry based on big data analysis and blockchain technology, and studied how to incorporate blockchain into future audit procedures based on the existing theoretical framework [11]. Yu et al. proposed using blockchain to build a secure global named storage system, including the three-tier architecture of the blockchain-based naming system. The naming system is divided into three layers: data layer, routing layer, and blockchain layer [12]. Zhang et al. proposed a method for ensuring the authenticity of microbial sampling robot data based on the bitcoin blockchain, which makes the robot not be interfered by human factors in the process of collecting data, especially the malicious tampering behavior of third-party regulatory agencies [13]. Fan et al. aimed at the three types of credibility problems existing in the current Internet of Things data sharing management and proposed blockchain-based solutions, including a decentralized Internet of Things data sharing architecture and smart contract collection [14]. Ling et al. built an access control architecture for the Internet of Things to provide a more flexible management plan [15]. Bera et al. proposed a resource access control method based on blockchain technology and combined XACML with bitcoin to realize the reliable authority control

mechanism based on rules [16]. On the basis of the current research, the author proposes a research on the automatic access control of big data open resources multimedia based on blockchain, using the big data access control BBAC-BD mechanism based on blockchain; it also elaborated and analyzed the basic framework and process of access control in detail. At the same time, for access control strategies based on blockchain transactions and entity attribute information management methods, with the increase of policy rules, the success rate of strategic judgments has decreased, and the BBAC-BD mechanism has realized a safe, reliable, and transparent new access control architecture, and it can effectively promote the safe circulation and sharing of big data.

3. Methods

3.1. Big Data Access Control Architecture. Big data access control involves the collection, aggregation, management, and control of big data resources. The big data access control architecture is mainly composed of 6 parts: data layer, resource aggregation layer, infrastructure layer, transaction layer, consensus layer, and access control contract layer. Each layer structure cooperates with each other and performs its own duties to form a complete big data access control architecture [17].

(1) Data layer: real big data resources, including structured data, unstructured data, and semistructured data distributedly stored in different locations and logically managed by the resource aggregation layer [18];

(2) Resource convergence layer: resource management of big data resources based on blockchain technology to realize the convergence of big data resources from different sources. Although real big data resources are in fact distributed and stored by different data owners, but through blockchain technology, it logically forms a unified management of big data resources. The author's research focuses on the access control mechanism, and the resource aggregation layer will not elaborate [19].

(3) Infrastructure layer: the blockchain platform provides infrastructure for big data access control. It is the foundation of the whole architecture, and the nodes and minors of the entire network are required to maintain the normal operation of the system. It is the carrier of big data access control platform transactions and smart contracts. The transaction layer, contract layer, and resource aggregation layer are all upper-layer applications based on blockchain.

(4) Transaction layer: it includes 4 types of access control transactions: data transaction, strategy transactions, attribute transactions, and contract transactions. Data transactions are used to manage big data resources, which serve at the resource convergence layer. Policy transactions are used to manage access control policies, including the release, update, and sale of strategies to provide data support for PAP
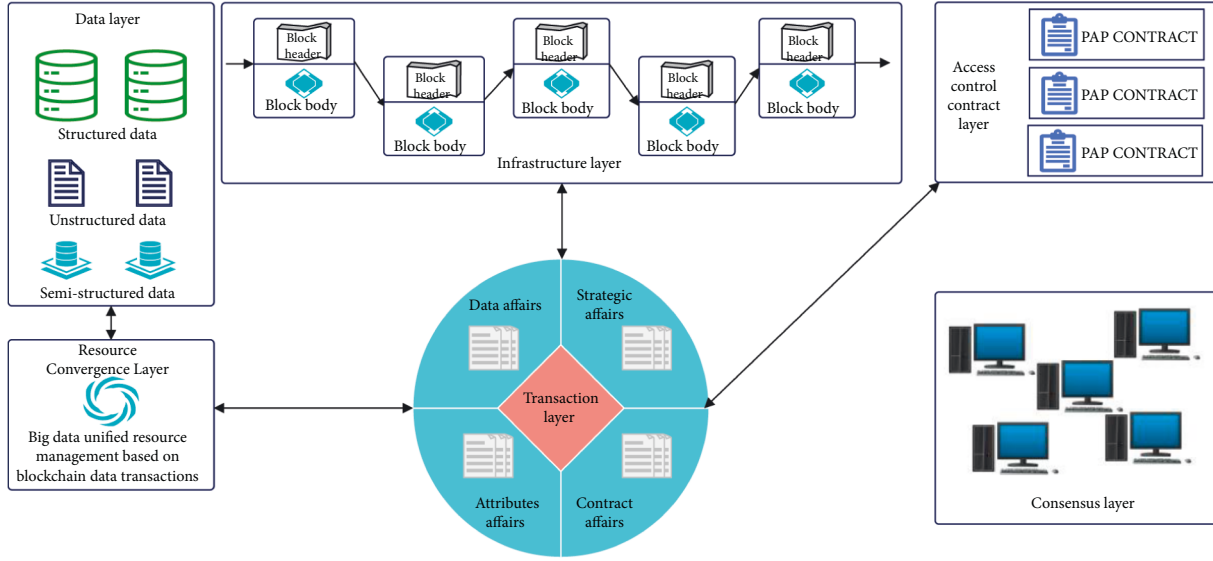
FIGURE 1: Data access control technology architecture.

CONTRACT at the contract layer. Attribute transactions are used to manage the attributes of entities, including the release, update, and sale of properties to provide data support for the contract layer AA CONTRACT, and contract transactions are used to provide an operating environment for smart contracts, which serve at the contract layer [20];

(5) Consensus layer: it mainly includes consensus mechanism, through various consensus algorithms, in order to ensure the consistency and authenticity of access control data among distributed nodes, so as to reach a stable consensus among nodes [21];

(6) Access control contract layer: it includes three types of contracts: PAP CONTRACT, PDP CONTRACT, and AA CONTRACT; PAP CONTRACT is used for access control strategy management, PDP CONTRACT is used for access control request judgment, and AA CONTRACT is used for entity attribute management.

In order to obtain the initial judgment matrix $EQ = (eqij)_{m \times m}$, there are m matrices $E = (e1, e2, \ldots, em)$, and the matrix is concentrated in the importance of ei and ej for binary comparison, which is shown in the following formula:

$$eqij = \begin{cases} 0, & ei < ej, \\ 0.5, & ei = ej, \\ 1, & ei > ej. \end{cases} \quad (1)$$

Convert the initial judgment matrix into a fuzzy consistent matrix, which is shown in the following formula:

$$\begin{cases} qij = \dfrac{qi - qj}{2m} + 0.5, \\ qi = \displaystyle\sum_{k}^{m} = 1eq_{ik}. \end{cases} \quad (2)$$

Calculate the weight vector $W = (w_1, w_2, \ldots, w_m)^T$ of each evidence of a certain m characteristic, which is shown in the following formula:

$$w_i = \frac{\sum_{k}^{m} = 1qik - 0.5}{m(m-1)/2}. \quad (3)$$

Next, the evaluation value matrix of the user behavior characteristic is calculated, and the value on the diagonal of the matrix obtained from the evidence matrix $E = (eij)_{m \times n}$ and the weight matrix $W = (w_{ij})m \times n$ according to $E \times W^T$ is the characteristic evaluation value matrix $F = (f1, f2, \ldots fn)$. The behavioral credit of the final user is shown in the following formula:

$$current\_T(u) = 1 - F \times W_f^T = 1 - \sum_{i=1}^{n} fiwi. \quad (4)$$

$current\_T(u)$ represents the user's current credit rating, and $W_f = (W_{f1}, W_{f2}, \ldots, W_{fn})$ represents the weight of the user's behavioral characteristics. When the user logs in for the first time to perform access control, the system will generate the first historical credit according to the user's software and hardware operations: $History\_T_1(u) = Current\_T_1(u)$. As the number of visits increases gradually, the user's historical credit needs to be gradually changed according to the passage of time as shown in the following formula:

$$History\_T(u) = \begin{cases} 0, & n = 0, \\ \displaystyle\sum_{i=1}^{n} (Final\_Ti(u) \times ti), & n > 0, \\ \displaystyle\sum_{i=1}^{n} ti. \end{cases} \quad (5)$$

$Final\_T_i(u)$ corresponds to the user's final credit at the end of each visit and t_i records the access time. This parameter calculates the total time from the user's login to the end of the user's exit from the system. When $n = 0$, it means that the user has logged into the system for the first time and has no

corresponding historical credit value. When a user visits for the first time, there is no historical credit, and the recommended credit will have a certain reference value. The user's recommended credit is calculated based on the credit between the user and other service organizations. Assuming that there are n credible access organizations $s = (s_1, s_2, \ldots, s_n)$, T and N representing the historical credit value and the number of successful visits of users of service organizations s_i and u_i, respectively, then the expression of the recommended credit is shown in the following formula:

$$
\text{Recommend\_}T(u) = \begin{cases} 0, & n = 0, \\[2ex] \dfrac{\sum_{j=1}^{n}\left(Nj \times T_{ui}^{si}\right)}{\sum_{j=1}^{n} Nj}, & n > 0. \end{cases} \tag{6}
$$

There is a competitive relationship between the chain generated by the honest node and the chain generated by the attacker. When the honest node is ahead, the chain of the honest node is extended by one block; otherwise, the chain of the attacker is extended by one block. The attacker successfully fills the gap behind z blocks, which is similar to the gambler bankruptcy problem, and then the attacker fills the gap and catches up with the honest chain. The probability is shown in the following formula:

$$
q_z = \begin{cases} 1, & p \leq q, \\[2ex] \left(\dfrac{q}{p}\right)^z, & p > q, \end{cases} \tag{7}
$$

where p represents the probability of an honest node gaining ownership of the next node, q represents the probability of an attacker gaining ownership of the next node, and qz represents the attacker filling the gap z blocks behind. When $p > q$, the probability of the attacker successfully attacking the next block decreases with the increase of z. Assuming that honest blocks take the average expected time to generate a block, the potential progress of the attacker is calculated according to the Poisson distribution, and the expected value is shown in the following formula:

$$
\lambda = z \frac{q}{p}. \tag{8}
$$

In order to calculate the probability that the attacker will generate nodes and catch up with the honest nodes in the chain when the attacker is behind, the probability is pz. We compare the Poisson distribution of blocks obtained by the attacker with the potential attack speed and the probability that the attacker can catch up with the honest nodes. The probabilities are multiplied to obtain the following formula:

$$
p_z = \sum_{k=0}^{\infty} \frac{\lambda^k e - \lambda}{k} \cdot \begin{cases} \left(\dfrac{q}{p}\right)^{(z-k)}, & k \leq z, \\[2ex] 1, & k > z. \end{cases} \tag{9}
$$

After simplification, the formula is

$$
\begin{aligned} p_z &= 1 - \sum_{k=0}^{z} \frac{\lambda k_e - \lambda}{k} \cdot \left(1 - \left(\frac{q}{p}\right)^{(z-k)}\right) \\[2ex] &= 1 - \sum_{k=0}^{z} \frac{(zq/p)^k e - zq/p}{k} \cdot \left(1 - \left(\frac{q}{p}\right)^{(z-k)}\right). \end{aligned} \tag{10}
$$

3.2. BBAC-BD Workflow. In the BBAC-BD (blockchain-based access control mechanism for big data environment) proposed by the author, the access control workflow is an extension of the standard ABAC model workflow. The access control workflow can be divided into two phases: the preparation phase and the execution phase. The preparation phase is mainly for the management of access control strategies and attributes, including the release, update, and withdrawal of policies and attributes and the response to the results of the policy and attribute query, and the execution phase is mainly for the judgment, response, and execution of the access request [22].

(1) Preparation stage: from the property release direction to the blockchain, release property, and property relationship information, AA (attribute authority) CONTRACT collects and integrates attribute information in blockchain transactions in advance, for PEP (policy enforcement point) CLIENT and PAP (point administration point) CONTRACT, from the policy release direction, the access control policy is released in the blockchain. PAP CONTRACT combines attribute information to describe, collect, and integrate access control strategies in blockchain transactions, for PDP (policy decision point) CONTRACT to make an access request decision.

(2) Execution stage: when PEPCLIENT receives a request from a user to perform a certain operation on a certain resource, PEPCLIENT analyzes the subject, object, and operational semantics of the original access request, generates an attribute-based access request AAR based on the attribute information obtained from AACONTRACT, sends AAR to PDP CONTRACT, PDP CONTRACT queries PAP CONTRACT for the access control policy set related to the requested big data resource, makes an access control decision, and sends the judgment result response back to PEP CLIENT. According to the response result by PEP CLIENT, authorize access to big data resources, since the access control policy is stored in the blockchain, policy information is verifiable, traceable, and nontamperable to anyone. The access control of big data resources gets rid of the traditional centralized access control management, possible single points of failure, and transparency of access control decisions. It realizes the distributed management of the access control strategy and effectively improves the robustness and credibility of the system. In addition, the decision process of the

access control strategy is realized through the form of smart contract, with no need for the involvement of a third-party central agency, and avoids the possible ultravires behavior of the third-party center, based on the blockchain system to realize the automatic judgment of access control under consensus. It is a truly decentralized access control mechanism, which meets the access control management requirements of big data resources [23].

3.3. Transaction Storage in the Blockchain.

In the blockchain, data are stored in the blockchain in the form of transactions, we use the form of transactions in the blockchain to manage access control policies, the transaction data in the block are stored in the data structure of the Merkle tree based on the HashHash algorithm, and the transaction data of inconsistent size are mapped into a fixed-size character string through a HashHash algorithm, stored on the leaf nodes of the Merkle tree. The nonleaf nodes of the Merkle tree store the HashHash values of its child nodes. The blockchain includes physical accounts, data blocks, transaction set data, and configuration data. The data view relationship between them is shown in Figure 2.

(1) Physical account: it is the initiator of various transaction requests and the owner of related data in the blockchain. It is the actual owner of the data resources in the access control mechanism and has a pair of public and private keys generated by the PKI system. In the system, the account is uniquely identified by the public key, and the transaction data published by the resource owner need to be signed by the entity account with a private key for other users to verify the authenticity of transactions in the block [24];

(2) Data block: it is the underlying data in the blockchain network, and multiple blocks together form a chain structure, persist the transaction processing results within a certain period of time in an immutable form.

(3) Transaction set data: it is based on the access control mechanism of the blockchain and stores data for performing actual business activities, including access control transactions and smart contract transactions. Access control transactions are used for the management of access control policies; it mainly covers the release, update, and cancellation of policy information in policy management. Smart contract transactions are used in the decision process of access control, in response to access requests and generating access control responses. Issuing transactions on the blockchain requires tokens that consume a certain amount of data, as the user's expenses for using blockchain services.

(4) Configuration data: it is the configuration information required for the normal operation of the blockchain system, including configuration information such as protocol version number and communication node information.
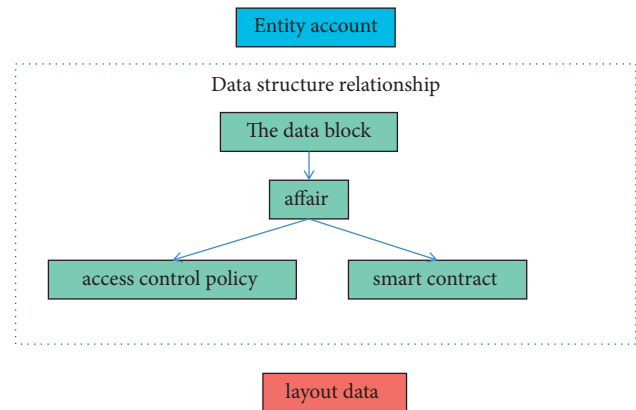
Figure 2: The relationship between data view entities in the block.

3.4. Smart Contract for BBAC-BD.

(1) Strategic management contract (PAP CONTRACT).

The flow of the PAP CONTRACT is shown in Algorithm 1.

PAP CONTRACT algorithm flow description.

Analyze the AAR to obtain the requested resource attribute information rttrTuple; traverse the strategic transaction data blocks in each block of the blockchain; obtain the attribute Bloom filter (BF) corresponding to the strategy transaction data block. According to the Hash function corresponding to the BF, calculate the Hash value corresponding to rttrTuple. If the Hash value obtained by calculating rAttrTuple and the corresponding bit in BF are all 1, then add the strategy in the data block in RELEVANT_POLICY_SET; otherwise, there is no rttrTuple related strategy in the data block. When the traversal of strategy transactions in all blocks is completed, return resource-related policy set RELEVANT_POLICY_SET to PDP for permission judgment.

(2) The strategy decision process is carried out by the strategy decision contract (PDP CONTRACT), and the contract flow is shown in Algorithm 2.

PDP CONTRACT algorithm flow description.

Put all pending decisions into UNKNOWN_SET, as a predecision strategy set; traverse the predecision strategy; and get 4 strategy decision result sets:

PERMINT_RESULT_SET DENY_RESULT_SET UNSATISFY_RESULT_SET UNKNOWN_RESULT_SET. According to the judgment result set, the final judgment result of the AAR request is obtained: if there is a conflicting judgment result, the final judgment result is obtained after the conflict is processed, and conflict handling can be based on the principle of affirmative priority or negative priority for conflict resolution.

4. Results and Analysis

4.1. Strategy Retrieval Efficiency Test.

This experiment is aimed at the management method based on the Bloom filter strategy and performed testing on the optimization effect of strategy retrieval efficiency. In the experiment, matching query tests were performed on test sets of different query

---

(i) Input: attribute access request AAR and blockchain blocks
(ii) Output: resource-related policy set RELEVANT_POLICY_SET

Algorithm 1: Strategy management contract (PAP CONTRACT).

(i) Input: attribute access request AAR, access control policy set POLICY_SET;
(ii) Output: strategy decision result PERMIT, DENY, UNKNOWN, and UNSATISFY.

Algorithm 2: PDP CONTRACT.

Table 1: Strategy retrieval test results 1.

Serial number	n/k	m test value	M optimal value	Query size	True false positive rate	Theoretical misjudgment rate	Total delay	Single time delay
1	20	3	14	4000	0.1975	0.2721	432	0.118
2	20	3	14	8000	0.1869	0.2721	798	0.079
3	20	6	14	4000	0.0321	0.0331	762	0.198
4	20	6	14	8000	0.0298	0.0331	1484	0.187
5	20	14	14	4000	0.0074	0.0076	985	0.257
6	20	14	14	8000	0.0095	0.0076	2062	0.255
7	20	20	14	4000	0.0029	0.0141	1247	0.332

Table 2: Strategy retrieval test results 2.

Serial number	n/k	m test value	M optimal value	Query size	True false positive rate	Theoretical misjudgment rate	Total delay	Single time delay
8	20	20	14	8000	0.0098	0.0141	2 462	0.328
9	10	3	7	4000	0.9356	1.7451	484	0.124
10	10	7	7	4000	0.792	0.891	I 134	0.285
11	5	3	3	4000	9.12	9.21	837	0.229
12	2	1	1	4000	39.51	39.29	762	0.192
13	2	2	1	4000	39.76	40.12	812	0.203

scales, set different parameters for the Bloom filter to test the error rate and retrieval delay, which were used to evaluate the impact of different parameters of the Bloom filter on retrieval performance. The calculation method of single time delay is total time delay/total number of matches. The optimization effect is mainly through the strategic management contract. The retrieval delay of the strategy is measured. The smaller the delay, the higher the execution efficiency, and the better the search optimization effect. From the test results of Tables 1 and 2, we can see that the larger the ratio of n/k, the better the optimization effect, and the larger the ratio, the lower the corresponding misjudgment rate, but at the same time, it will take up more space and cost. At the same time, the true value of the false positive rate is generally less than the theoretical value of the false positive rate [25].

The results of Figures 3 and 4 show that, when the performance of Hash is better, that is, the result of Hash distribution is more uniform, under the condition of $m = 3$. The misjudgment rate acceptable for the expected use can be achieved, the increase in the number of Hashes will not bring a significant increase in revenue. Therefore, when conditions
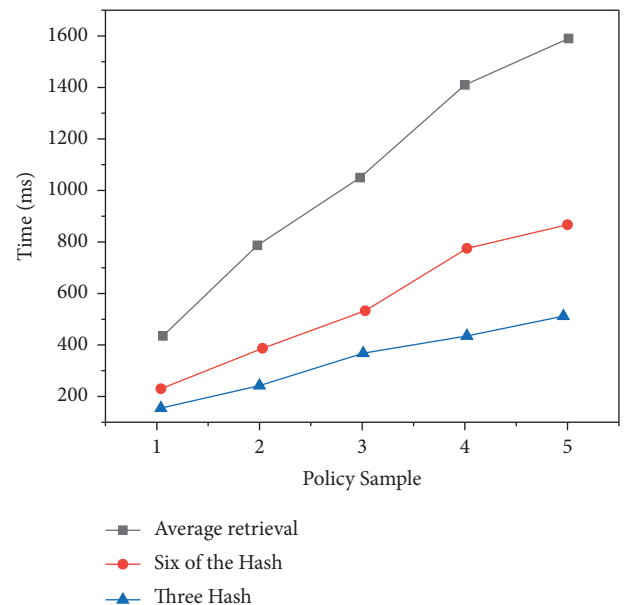
Figure 3: Comparison of strategy retrieval performance.
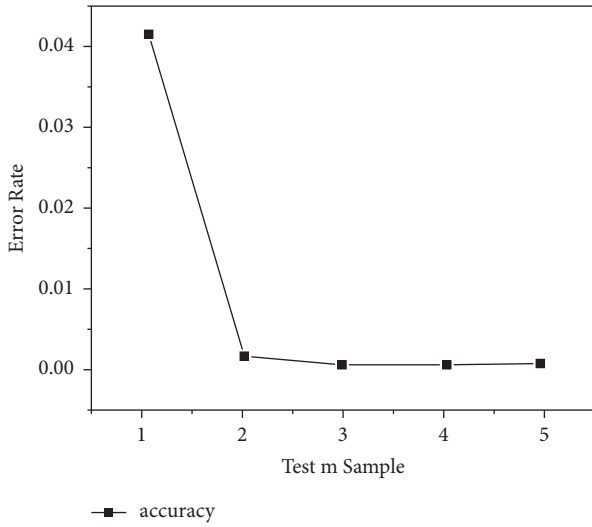
FIGURE 4: M value affects the accuracy of retrieval results.

FIGURE 5: Comparison of strategy decision performance.

permit, try to expand the value of n/k and can effectively improve query performance. This is mainly due to the Bloom filter's attribute keyword filtering process of policy detection, the retrieval time is less affected by the scale of the strategy set, so compared to the traversal retrieval process, strategy retrieval and matching based on the Bloom filter can achieve high performance and strategy retrieval based on the Bloom filter can effectively save cache space, reduce the number of requests to the cache, and improve the efficiency of strategy query and the isolation of strategy management services.

4.2. Strategy Decision Function Test. In order to verify the effectiveness of the BBAC-BD access control mechanism, the author under different scales of strategies, judgment function of access control strategy based on smart contract, performed a functional test; the test content includes the efficiency of the strategy decision and the success rate of the

FIGURE 6: Comparison of the success rate of strategy decision results.

decision result. The PolicySamples of 1 to 5 groups correspond to 1000, 2000, 3000, 4000, and 5000 single strategy test set samples, respectively. The test set sample constructs 800 different access requests for 80 user identities; each logo has an average of 5 attribute values, and each request is sent randomly 5 times. The strategy decision delay is obtained by calculating the average response delay of all requests as shown in Figures 5 and 6.

As can be seen from Figure 5, the strategy decision delay is directly related to the strategy scale, with the increase of strategy rules, the delay of access control decision has increased significantly. At the same time, it can be seen from Figure 6 that, as the strategy rules increase, the strategy decision success rate decreases.

5. Conclusion

The author proposes a research study on the automatic access control of big data open resources multimedia based on blockchain. The author uses the big data access control BBAC-BD mechanism based on blockchain. It also elaborated and analyzed the basic framework and process of access control in detail. At the same time, access control strategies based on blockchain transactions and entity attribute information management methods explain that, with the increase of strategy rules, the success rate of strategy decisions decreases. The BBAC-BD mechanism implements a safe, reliable, and transparent new access control architecture, which can effectively promote the safe circulation and sharing of big data. Through smart contracts, based on the strategy released by the resource owner to the blockchain, the automatic access control of big data resources is realized, the judgment process is more flexible, and the judgment results are more credible. The BBAC-BD mechanism is safe, reliable, and transparent. The new access control architecture can effectively promote the safe circulation and sharing of big data. This is because there are

some conflicting strategies in the strategy set. For conflicting strategies, the strategic judgment contract cannot get a consistent judgment result, it should be noted that the author has not yet introduced the strategy conflict handling part into the strategy judgment contract, the conflict resolution has not been effectively resolved, and this part of the content will continue to be improved in the follow-up research work.

Data Availability

The data used to support the findings of this study are available from the corresponding author upon request.

Conflicts of Interest

The authors declare that they have no conflicts of interest.

Acknowledgments

References

[1] Z. Li, H. Guo, A. V. Barenji, W. M. Wang, and Y. Guan, "A sustainable production capability evaluation mechanism based on blockchain, lstm, analytic hierarchy process for supply chain network," *International Journal of Production Research*, vol. 58, no. 24, pp. 7399–7419, 2020.

[2] B. Huabai and B. Jiaqi, "Research on the improvement of village governance efficiency based on blockchain technology," *Journal of Agricultural Science*, vol. 12, no. 9, 2020.

[3] S. Gao, G. Piao, J. Zhu, X. Ma, and J. Ma, "Trustaccess: a trustworthy secure ciphertext-policy and attribute hiding access control scheme based on blockchain," *IEEE Transactions on Vehicular Technology*, vol. 69, no. 6, pp. 5784–5798, 2020.

[4] E. B. Sifah, Q. Xia, K. O. B. O. Agyekum et al., "Chain-based big data access control infrastructure," *The Journal of Supercomputing*, vol. 74, no. 10, pp. 4945–4964, 2018.

[5] X. Zheng, M. Li, Y. Chen, J. Guo, and W. Hu, "Blockchain-based secure computation offloading in vehicular networks," *IEEE Transactions on Intelligent Transportation Systems*, no. 99, pp. 1–15, 2020.

[6] R. Xu, Y. Chen, E. Blasch, and G. Chen, "Exploration of blockchain-enabled decentralized capability-based access control strategy for space situation awareness," *Optical Engineering*, vol. 58, no. 4, p. 1, 2019.

[7] None, "Call and calendar," *Computer*, vol. 48, no. 7, pp. 81–83, 2015.

[8] M. Ansart, S. Epelbaum, G. Gagliardi et al., "Reduction of recruitment costs in preclinical ad trials. validation of automatic pre-screening algorithm for brain amyloidosis," *Statistical Methods in Medical Research*, vol. 29, no. 1, pp. 151–164, 2019.

[9] L. Liu, C. Wang, H. Zhang, Y. Tang, and Z. Zhang, "Automatic monitoring method for surface deformation of coastal area based on time series analysis," *Journal of Coastal Research*, vol. 93, no. sp1, 2019.

[10] Z. Yin, C. Du, J. Liu, X. Sun, and Y. Zhong, "Research on auto-disturbance-rejection control of induction motors based on ant colony optimization algorithm," *IEEE Transactions on Industrial Electronics*, no. 4, p. 1, 2017.

[11] J. Xu, K. Xue, H. Tian, J. Hong, and D. S. L. Wei, "An identity management and authentication scheme based on redactable blockchain for mobile networks," *IEEE Transactions on Vehicular Technology*, vol. 69, no. 6, pp. 6688–6698, 2020.

[12] G. Yu, X. Zha, X. Wang et al., "Enabling attribute revocation for fine-grained access control in blockchain-iot systems," *IEEE Transactions on Engineering Management*, vol. 67, no. 4, pp. 1213–1230, 2020.

[13] N. Zhang and K. Zheng, "Research and design of the architecture of the marine logistics information platform based on big data," *Journal of Coastal Research*, vol. 106, no. sp1, p. 628, 2020.

[14] K. Fan, Y. Ren, Y. Wang, H. Li, and Y. Yang, "Blockchain-based efficient privacy preserving and data sharing scheme of content-centric network in 5g," *IET Communications*, vol. 12, no. 5, pp. 527–532, 2018.

[15] X. Ling, Y. Le, J. Wang, and Z. Ding, "Hash access: trustworthy grant-free iot access enabled by blockchain radio access networks," *IEEE Network*, vol. 34, no. 1, pp. 54–61, 2020.

[16] B. Bera, S. Saha, A. K. Das, N. Kumar, and P. Lorenz, "Blockchain-envisioned secure data delivery and collection scheme for 5g-based iot-enabled internet of drones environment," *IEEE Transactions on Vehicular Technology*, vol. 69, no. 8, pp. 9097–9111, 2020.

[17] S. Biswas, K. Sharif, F. Li, and S. Mohanty, "Blockchain for e-health-care systems: easier said than done," *Computer*, vol. 53, no. 7, pp. 57–67, 2020.

[18] X. Wei and C. Qin, "Risk early-warning model of ocean international trade based on svm," *Journal of Coastal Research*, vol. 93, no. sp1, p. 785, 2019.

[19] A. Fioravanti, G. Fico, D. Salvi, R. I. García-Betances, and M. T. Arredondo, "Automatic messaging for improving patients engagement in diabetes management: an exploratory study," *Medical, & Biological Engineering & Computing*, vol. 53, no. 12, pp. 1285–1294, 2015.

[20] M. Hooshyar, D. Wang, S. Kim, S. C. Medeiros, and S. C. Hagen, "Valley and channel networks extraction based on local topographic curvature and k-means clustering of contours," *Water Resources Research*, vol. 52, no. 10, pp. 8081–8102, 2016.

[21] H. Lu, C. Jin, X. Helu, C. Zhu, and Z. Tian, "Autod: intelligent blockchain application unpacking based on jni layer deception call," *IEEE Network*, vol. 35, no. 99, pp. 1–7, 2020.

[22] G. Pin, G. Fenu, V. Casagrande, D. Zorzenon, and T. Parisini, "Robust stabilization of a class of nonlinear systems controlled over communication networks," *IEEE Transactions on Automatic Control*, no. 99, p. 1, 2020.

[23] L. Zhang, "Application research of automatic generation technology for 3d animation based on ue4 engine in marine animation," *Journal of Coastal Research*, vol. 93, no. sp1, p. 652, 2019.

[24] A. Macaranas, A. N. Antle, and B. E. Riecke, "What is intuitive interaction? balancing users' performance and satisfaction with natural user interfaces," *Interacting with Computers*, vol. 27, no. 3, pp. 357–370, 2015.

[25] Y. Dong, S. Xiao, H. Ma, and L. Chen, "Research on quantum authentication methods for the secure access control among three elements of cloud computing," *International Journal of Theoretical Physics*, vol. 55, no. 12, pp. 5106–5117, 2016.

Research Article

Grounded Theory and Social Psychology Approach to Investigating the Formation of Construction Workers' Unsafe Behaviour

Yu Han,[1] **Xuezheng Li,**[1] **Zhida Feng,**[2] **Ruoyu Jin** [ID],[3] **Joseph Kangwa,**[4] **and Obas John Ebohon**[3]

[1]*Faculty of Civil Engineering and Mechanics, Jiangsu University, 301 Xuefu Road, Zhenjiang 212013, Jiangsu, China*
[2]*Faculty of Management, Jiangsu University, 301 Xuefu Road, Zhenjiang 212013, Jiangsu, China*
[3]*School of Built Environment and Architecture, London South Bank University, 103 Borough Rd, London SE10AA, UK*
[4]*School of Architecture and Built Environment, University of Wolverhampton, Wolverhampton, UK*

Correspondence should be addressed to Ruoyu Jin; jinr@lsbu.ac.uk

There have been limited studies analyzing the causes of construction workers' unsafe behaviour from the social psychology perspective. Based on a Grounded Theory approach, this study first identified and defined seven coded categories related to workers' dangerous behaviour on construction sites. The original qualitative data were obtained from individual site interviews conducted with 35 construction professionals. These main categories were found connected to workers' status of safety awareness and sense of danger, which affected the type of unsafe behaviours, i.e., proactive, passive, or reactive behaviour. By further integrating social cognitive psychology theories into workers' behavioural decision-making process, the formation mechanism framework and diagram were developed to describe construction workers' unsafe behaviours based on the dynamic process of balancing the individual desires and perceived safety risks. This study advances the body of knowledge in construction safety behavioural management by performing in-depth theoretical analysis regarding workers' internal desires, activated by external scenarios and intervened by a personal safety cognition system, which could result in different motivations and various behavioural outcomes. It is argued that safety cognition serves as a mediated moderation system affecting behavioural performance. Practical suggestions on developing a proper safety management system incorporating safety education in guiding construction workers' site behaviours are presented.

1. Introduction

Construction is generally recognized as a risky industry with high injuries and accidents [1–2]. Besides accidents/incidents and other quantitative measurements (e.g., injury rate), reactive indicators for safety performance and proactive measures have also been developed in construction, such as behaviour-based safety and safety climate/culture [3, 4]. Existing studies (e.g., [5–7]) focusing on these proactive measurements have commonly adopted the questionnaire survey approach. Potential drawbacks of conducting the questionnaire survey method include some questions being incorrectly completed, questions being misunderstood, requiring follow-up in-depth research, and being unsuitable for investigating long and complex issues [8]. In addition, the multiscale data collected through a questionnaire survey may not be sufficient to depict construction workers' subtle mental status and psychological state when conducting unsafe behaviours. Construction site workers before, during, and right after making a behavioural decision could present a dynamic and mixed internal mechanism influenced by external scenarios (e.g., the project's tight schedule). Likewise, an advanced workflow originates from workers' inner desires, which may be

activated by an external scenario and mediated by personal safety cognition, resulting in safety behavioural decisions.

As the alternative approach, qualitative studies (e.g., semistructured interviews) are also adopted in construction safety research, followed by qualitative analysis to define categories related to a specific safety issue, for example, causes of fall accidents from roofs [9]. More alternative analysis approaches from other fields, such as Grounded Theory from social studies, have been applied in the construction field. So far, there have been limited studies [10, 11] that have applied Grounded Theory to construction safety. The rationale of using Grounded Theory in this study to explore the causes of workers' unsafe behaviour is not concurrent with the methodology from prior studies of construction safety. These issues, as mentioned earlier, are mainly due to the desire to link dangerous behaviour to construction sites to a social psychological definition. Furthermore, the desire to articulate the mechanism of workers' behavioural decision formulation process from the perspective of human psychology and what drives the tenants for such desires and motivations is yet another objective. Research questions in social psychology, such as by what processes attitudes towards an object affect behaviour towards the object [12], can be applied in construction safety behaviour to provide a theoretical guide in safety management.

Aiming to address the above issues, this study was designed to answer the following research questions: (1) what are the internal and external causes of construction workers' unsafe behaviour and (2) how would human psychological desires and motivations lead to different behavioural outcomes? This study addresses the research scenarios in construction workers' unsafe behaviours depicting the unique psychological mechanism of behavioural decisions. An alternative method called Grounded Theory is adopted for qualitative analysis. Therefore, this study is seen to contribute to the in-depth theory of the formation of workers' unsafe behaviour by linking workers' behaviour to their safety cognition, internal desire, and the ultimate behavioural outcome. The study provides both theoretical and practical guides for effective construction safety management. Theoretically, it postulates a framework of how internal human desires, insinuated by the mediation and moderation effects of safety cognition, could lead to different behavioural decisions and outcomes; practically, this study sequences the extent to which construction workers' safety behaviours towards a safer and less risky manner can manifest.

2. Literature Review

2.1. Safety Behaviour.
Safety behaviour is a critical theme in managing safety [13]. It crosses different fields such as driving [14], fire service [15], and agriculture [16]. Innovative research theories and methods are required to promote behavioural safety studies [13]. Up to 95% of workplace accidents have been caused by unsafe acts [17]. Occupational safety behaviour significantly affects workplace performance [18]. The management of safety behaviour was identified by

Goh and Ayskar Ali [19] as one key challenge in improving construction safety management. [20] described the intervention process to correct unsafe behaviours by measuring and comparing the frequency, duration, and rate of behaviours before and after the intervention, aiming to change dangerous behaviours. The behaviour-based safety (BBS) could enhance safety performance by monitoring preestablished safety behaviours in construction [21]. However, when adopting behaviour-based management in construction, Lingard and Rowlinson [22] found the behaviour-based limitation and suggested that safe behaviour could only be achieved when a basic safety infrastructure is in place. Further, Eckenfelder [23] criticized BBS for being time-consuming and costly, as safety investment would interact with the construction workforce to affect safety performance [24]. Nevertheless, Cooper [25] showed positive outcomes of applying BBS in improving safety performance. Similarly, the empirical study conducted by Choudhry [26] showed that BBS could be used in any country's culture based on effective communication on-site and committed management. Critical success factors for BBS have been identified, including employee engagement, satisfaction with safety training, and trust relationships among workers [20]. These factors affecting safety behaviour, such as work engagement and management commitment [27], could be important indicators in the safety climate framework.

2.2. Safety Climate.
In the dynamic construction safety management system, Guo et al. [28] suggested considering the interrelationships among factors within the system. One factor within the management system is defined as a safety climate within the workforce. Attitudes towards safety are considered one of the main indicators of safety climate [5]. Safety climate can be measured by workers' safety perceptions [29], and it reflects workers' perception of the role of safety in their jobs [30]. In the safety climate study conducted by Li et al. [7] in China's construction industry, workers' self-perception of safety (e.g., safety awareness), their involvement in safety (e.g., self-protection), peer interaction (e.g., communication and cooperation), safety environment, management involvement, and safety personnel support (e.g., foremen behaviour) were defined as major dimensions. Similar safety climate indicators such as risk perception, workers' perception of safety management, and management attitudes can be found in multiple other studies (e.g., [31, 32]). The effect of safety climate on safety performance has been identified in several previous studies [33, 34]. Safety climate can be multilevel and can be divided into subgroup safety climates according to workers' job position [35, 36] and other subgroup factors such as demographic features [37].

2.3. Safety Cognition.
A safety climate forms a culture that involves knowledge transfer at the organizational level [38] and engages social cognitions [39]. Implicit memory significantly affects unconscious cognition in making judgements [40, 41]. Cognition directly influences behaviour [42]. Individual safety cognition is critical to enhancing safety
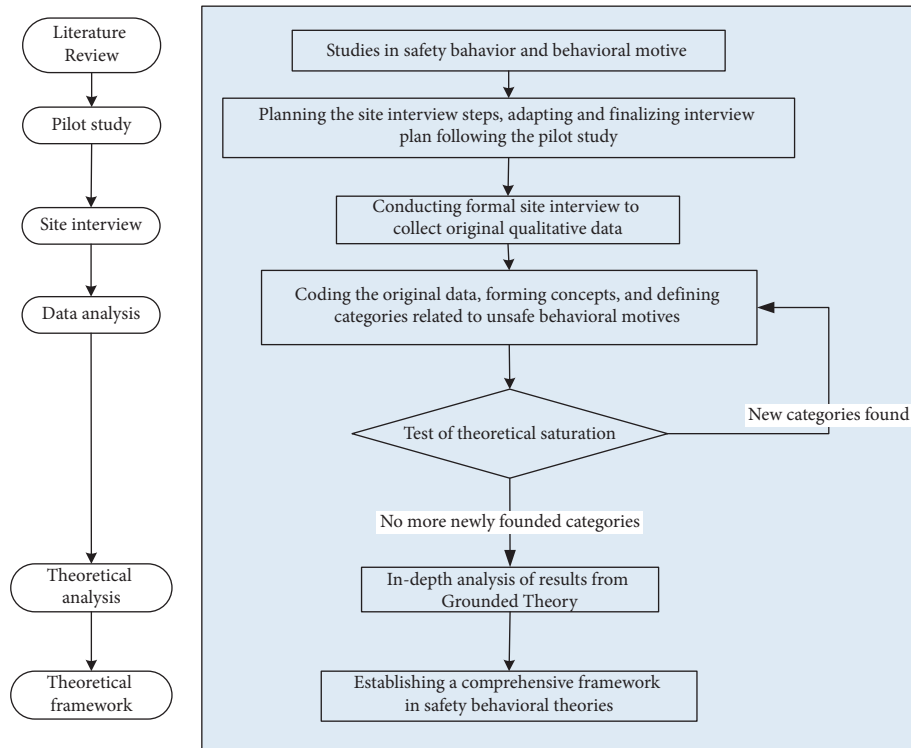
FIGURE 1: Description of the research workflow.

performance in the construction industry [43]. Social awareness can be divided into the implicit and explicit levels [39]. The implicit social cognition reflects individuals' internal assumptions that could influence behaviour and group perceptions [44]. In the construction industry, workers' implicit safety cognition is formed based on their prior work scenarios, which further build their safety knowledge [45, 46]. The implicit safety cognition further affects workers' intuition or basic assumptions, which, together with prior scenarios and safety knowledge, affect workers' safety perceptions [39]. Safety perception constitutes the explicit social cognition [46], which, to some degree, is equated to a safety climate based on the measurement criteria [47].

3. Methodology

Investigation of research questions such as "how construction workers form their unsafe behaviours" requires in-depth research as this type of question involves complex issues. Qualitative methods (e.g., site interviews with workers) could overcome the barriers encountered in the questionnaire survey-based approach by investigating the formation of workers' unsafe behaviours. A more qualitative approach can explore insights into human beings' opinions, attitudes, experiences, and behaviours [48]. Face-to-face site interview with individual construction workers to collect qualitative data on reasons for risk-taking behaviours has been adopted in some existing studies, including Guo et al. [28] and Man et al. [11], who assumed the Grounded Theory approach. Grounded Theory aims to generate or discover a theory from data systematically obtained from social research [49]. It has

been successfully adopted to understand a concept or phenomenon in different fields, such as higher education [50], housing policies [51], and healthcare [52]. The methodology adopted in this study is illustrated in Figure 1.

The data analysis method shown in Figure 1 involves the three-step Grounded Theory approach, namely, open, axial, and selective coding, as Strauss and Corbin [53, 54] advised. After capturing the causes of workers' unsafe behaviours, theoretical saturation is tested by utilising the remaining data to ensure that no more new concepts or categories would be found. The Grounded Theory is based on an explanatory approach to investigate a specific occurrence in an inductive way which favours the exact explanation of the phenomenon studied [55]. Researchers also followed other methodological guides in adopting Grounded Theory in this study, specifically: (1) early stages of data collection may involve purposeful sampling [56] as evidenced in the example of MacDonald [57]; (2) as data collection and analysis progress, e.g., concepts and categories summarized and refined from data [58], ideas, and tentative hypotheses could emerge [59]; and (3) pursing theories through data and theoretical sampling [60]. Following the interviews with workers, the qualitative data were recorded and analyzed using the intelligent voice core technological tool developed by iFlytek [61], which assisted speech recognition by analyzing the oral characteristics of human beings.

3.1. Design of Interview Questions. Following the review of safety behaviour-related literature, the open-ended questions for site interviews with construction workers were designed.

TABLE 1: Descriptions of five general questions asked during the formal site interview.

No.	Question	Purpose
1	Could you describe the most unforgettable safety accident that you have heard of or experienced?	This is a starting and guiding question to motivate the interviewee to feel comfortable and become more engaged in the interview process by recalling their past site stories or experience. It also aims to spark the interviewee's thinking about safety.
2	What do you think about the cause of construction safety accidents? For example, are they more due to human mistakes or other reasons?	This commentary question aims to let the interviewee analyze the cause of accidents from the standpoint of a bystander who was not directly involved in the accident. It seeks to capture the core view of the interviewee as a nonbiased witness. It also guides the interviewee to pay attention to human factors related to unsafe behaviours gradually.
3	From your experience, were there some site behaviours of yourself that you feel could be dangerous?	This question serves as a transitional point aiming to shift the focus to the unsafe behaviour of the interviewee. In addition, it aims to let the interviewee realize their prior hazardous behaviour. The question was asked in a self-reflective approach, motivating the interviewee to recall and evaluate their dangerous behaviours (if any).
4	Why did you still decide to behave unsafely if you had realized the danger related to your unsafe behaviour?	This is a core question, continuing from the previous question to obtain the exact reasons that cause site workers to behave unsafely. In addition, it aims to capture site workers' psychological or mental status right before, during, and after conducting unsafe behaviours.
5	What unsafe behaviours do you see other people conduct? And what do you think are the main reasons why they behave unsafely?	This is a wrap-up question by shifting the focus from the interviewee themselves back to others. The interviewee answers the question again as a bystander to evaluate why peers behave unsafely. It is designed to acquire more in-depth thoughts related to unsafe behaviours. Also, because the initial question has been sensitive by asking the self-related dangerous behaviour, this question can relieve the nerve of the interviewee and allow the interviewee further to provide more information.

They underwent the pilot study to ensure that these questions were valid, transparent, and easily understood. Before conducting the pilot study, the research ethics approval was gained from Jiangsu University. A consent form would be provided to each interview invitee before conducting the interview. It was ensured that no personal or company information would be stored in a database. Invitees to participate in the interview would be provided with a clear guide of the purpose of the study, and they could decide whether or not to accept the interview request. They were also allowed to withdraw or terminate the process during the interview.

Considering the generally low level of education that workers had received in China's construction industry and other facts that they tended to hide or withhold sensitive information related to their unsafe behaviours to the interviewer, these questions were designed as simple as possible to be not technical. In April 2018, before conducting the formal site interview, a pilot study involving five site workers was asked these predesigned questions to evaluate the appropriateness and effectiveness of the discussion. These five participants worked as project managers, safety staff, site technicians, crew supervisors, and steelworkers. Their age ranged from 33 to 52, with site experience varying from 9 to 31 years. The interview with each participant lasted from 18 to 57 minutes. Following the pilot study, researchers in this study found that generally, interviewees would be happy to share their experiences regarding safety issues with others when they were just bystanders not involved. However, they would be more nervous or concerned when asked of themselves as the party directly involved in safety issues, despite that they were told that the interview was confidential and anonymous. Therefore, in the finalized questions listed in Table 1, the interview with each participant was designed to start with a relaxing atmosphere in a storytelling style by sharing his or her own site experience.

The five basic questions in Table 1 were designed to be open-ended as they can be easily extended to discover more details contributing to site workers' unsafe behaviour or behavioural decision. They considered the potential psychological status of interviewees progressively. Researchers asked guidance and descriptive and summative questions by starting with the general question with the interviewee as a bystander or witness, then shifting the interviewee's role to be the party directly involved in unsafe behaviour, and finally back to the role as a bystander. Basic information related to dangerous behaviour can be obtained from answers to these questions. More insightful or detailed information could also be acquired by directing these open-ended questions.

3.2. Background Information of Interviewees. Echoing Cutcliffe [56] and MacDonald [57], who indicated the adoption of purposeful sampling in collecting data, this study recruited interviewees based on the critical features known to the researchers. These key features included knowledge or

TABLE 2: Background information of the 35 interviewees.

No.	Age	Site experience (years)	Education level	Profession	Interview duration (min: sec)
1	55	30	Primary school	Concrete worker	27 : 42
2	32	13	Community college	Safety staff	24 : 55
3	50	30	High school	Project manager	43 : 00
4	40	8	Middle school	Crew foreman	30 : 59
5	30	5	Primary school	Electrical worker	28 : 27
6	25	8	High school	Ironworker	41 : 59
7	29	10	Middle school	General contractor's site employee worker	23 : 22
8	26	1	Master	Safety staff	32 : 21
9	23	1	Community college	General contractor's site employee	30 : 58
10	29	12	Community college	Crew foreman	42 : 46
11	27	2	Bachelor	Quality inspector	39 : 33
12	53	13	High school	Concrete worker	23 : 11
13	36	20	Middle school	Electrical worker	32 : 29
14	52	10	No education	Painter	25 : 14
15	48	20	High school	Office administrator	32 : 02
16	37	10	Primary school	Form worker	19 : 56
17	35	10	Bachelor	Quality inspector	37 : 48
18	35	10	Primary school	Ironworker	28 : 05
19	53	32	Middle school	Concrete worker	31 : 56
20	50	30	Middle school	Steelworker	27 : 07
21	60	10	Middle school	Site signal coordinator	27 : 17
22	50	20	Middle school	Steelworker	37 : 47
23	42	24	Middle school	Steelworker	18 : 09
24	50	30	Bachelor	Project manager	47 : 07
25	30	12	Middle school	Concrete worker	25 : 34
26	27	2	Bachelor	Technical support staff	26 : 58
27	25	1	Bachelor	Technical support staff	32 : 47
28	53	30	Primary school	Form worker	26 : 38
29	43	20	Middle school	Form worker	33 : 17
30	54	30	Primary school	Form worker	30 : 29
31	60	40	Primary school	Form worker	27 : 46
32	43	25	Middle school	Concrete worker	27 : 48
33	52	33	Primary school	Steelworker	30 : 05
34	30	7	High school	Form worker	35 : 24
35	45	23	Middle school	Steelworker	40 : 28

experience on the studied phenomenon of interest, availability and willingness to participate, and the ability to communicate experiences and opinions expressively and reflectively, which were defined by Palinkas et al. [62] for purposeful sampling. A total of 35 participants were recruited in the formal site interview conducted from May 2018 to March 2019 in the southeast coastal region of China. The reasons for recruiting participants from the eastern coastal region of China can be more in the prior studies of researchers (i.e., [37, 46]). Basically, as the economically active region of China, the east coastal region attracted labours from the rest of the country to work in the construction industry. These construction workers were also referred to as migrant workers that were considered representative of the workforce sample. The qualitative data for Grounded Theory-based analysis were based on the interview of 30 participants. The remaining five participants' answers to interview questions were used for the later theoretical saturation test described in Figure 1. The background information of the 35 interviewees is provided in Table 2. The professions of interviewees included project manager, quality inspector, general contractor's site

workers, safety staff, crew supervisors, and workers from different trades. The average site experience was 16 years in the interviewee sample, and 60% of them had an education level below or at middle school. The average time lasted in each interview was around 29 minutes.

3.3. Interview Process. A semistructured interview was conducted individually for each participant. The interview process was designed to be interactive, allowing the mutual discussion and questions between the interviewer and the interviewee. Interviewees were encouraged to express their opinions freely. Considering that site workers usually have heavy daily duties in a relatively confined and stressful work environment, the interviews were generally conducted in the evenings after participants completed their daily tasks and were in a relaxing mental state. During each interview, the researcher started with an icebreaker to allow the interviewee to feel comfortable. The interviewer (i.e., the researcher) encouraged the interviewee to move forward with the safety behaviour-related theme by adopting the questions listed in Table 1, simultaneously enabling the

TABLE 3: List of concepts causing unsafe behaviours according to open coding.

Typical example(s) from interviewee's verbal messages	Concept	Frequency
"Sometimes, I prefer not to wear the safety belt when working at a height because that saves my effort."	Saving efforts	34
"The main reason for some unsafe actions is to make more money in less time."	Gaining more income	13
"I don't want to pay much attention to following these cumbersome steps. On the contrary, I want to ignore it and finish my work as soon as possible."	Increasing productivity	10
"The reality is that workers must follow their managers' demands to complete the given tasks in a fast way."	Being pressured	10
"Some guys feel that they are very skilled to perform tasks."	Being overconfident	10
"When the schedule is tight, the boss asks us to work overtime and maintain the efficiency."	Meeting schedule requirements	9
"The main reason for unsafe behaviour is to save time."	Saving time	7
"They think it is their freedom to not wear a hard hat"; "If the manager wants them to wear the hard hat, they may still not fasten the tie of the hat."	Being unwilling to be regulated	6
"The weather in the summer is hot, and not wearing the protective equipment makes me feel more comfortable."	Feeling more comfortable	6
"The manager asks us to do things fast and complete the tasks quickly; otherwise, we could lose our job."	Following the manager's demand	5
"Older and more experienced folks can do things fast without risks"; "Older guys think they know things well enough and do not need to follow the safety education."	Following personal experience	5
"Safety accidents occurred very rarely on sites where I work during my past five years' career. I don't think I would be that unlucky." "They think they are lucky enough to be accident-free by not wearing the safety boots."	Holding a "fortunate" mindfulness	5
"Some guys are rebellious and do not want to follow what their managers say."	Being against the safety demand	4
"Sometimes we want to relax a bit after considerable experience site work, without realizing site safety risks."	Relaxing	4
"A crew foreman just learned that he was about to be fired. He hammered a nail into an electrical cable to show his anger before he left. Later a fire accident happened when the cable was powered."	Venting the negative emotion	3
"Some younger workers behave unsafely to show their own 'tough-guy' image."	Showing off self-capability	3
"Two different woodwork teams needed tower cranes to transport materials, and conflicts happened. Both teams did not want to calm down. One of them broke the electrical cable of the tower crane on purpose."	Escaping responsibilities	3
"Two apprentices were working together with their mentor. One of the apprentices was trying to impress the mentor during the installation of scaffolding when the mentor was not around for a moment. He climbed into the scaffold trying to operate, but later he fell off from scaffolding and was injured."	Demonstrating own skills	3
"This type of part-time guys deliberately waste time, not doing jobs safely."	Dawdling	3
"I just want to operate the machine myself to see how it works."	Satisfying curiosity	2
"The wastes from saw-cuts fell on flammable things, but workers are hungry and want to have their lunch. So they ignore that."	Being anxious to finish work	2
"Some guys walk along the steel pipes without fall protection just to feel excited."	Seeking excitement	2
"Arguments may happen between different trade teams because of interests of conflict."	Defending for the benefit of their team	2
"If everyone else is working unsafely to complete work on time, I will follow them."	Following peer behaviours	2

Note. Table 1 does not cover coding concepts only mentioned once by the 30 interviewees. They include maintaining self-esteem, meeting self-vanity, helping others in an emergency, and horseplaying.

interviewee to be comfortable. Following each response from the interviewee, the interviewer would then continue by asking, "what you just said is insightful. Do you have any other things to share with me?" With each interviewee's full consent and approval, the interview was voice-recorded.

4. Results from Grounded Theory Analysis

The categorization process involves the cyclical workflow of analyzing, inducing, and summarizing the sentences and keywords from original voice messages conveyed by the

interviewees. Coding is a crucial job in the analysis and summary. It involves labelling interviewees' answers and selecting, distinguishing, and categorizing the qualitative data. Therefore, the three main steps, including open, axial, and selective coding, were conducted progressively and concurrently.

4.1. Open Coding Results. Open coding intends to define concepts and categories. The main objective of open coding is to disaggregate original data and reform the concepts until

there is no more suitable code to replace the resulting and improved concepts. Glaser [63] suggested using the gerund format as being more ideal for exploring the concepts of Grounded Theory, for example, "saving effort" instead of "to save effort," as shown in Table 3. In this study, the original data were analyzed on a single-word basis, with the actual words in the text labelled to define the initial factors. During the induction and summarization processes, interviewees' sentences were compared and matched, and prototypical keywords were marked. Initial concepts were extracted based on these labelled concepts and semantic meanings within sentences. Finally, all concepts with similar or consistent attributes were classified into initially coded categories. For example, in the original verbal message, "I feel it cumbersome to wear a safety belt, making me not flexible to do my job," the keywords "cumbersome" and "not flexible" were extracted to form the initial concept of "avoiding cumbersome operation." In another verbal message, "Guys would like to find the most convenient way to work, and it is common to find an easier way to save time," the keywords "convenient" and "to save time" were captured. These similar keywords from other messages were found during open coding, and they were formed into the initial category defined as "saving efforts."

The 255 messages conveyed by the 30 selected interviewees were initially obtained by adopting the iFLYTEK [61] tool. The research team performed a second round of screening by removing codes not related to construction safety. 158 messages were finalized and converted into coded concepts. Table 3 displays some of the concepts associated with typical examples from interviewees' original verbal statements.

These concepts in Table 3 are further coded into initial categories as shown in Table 4.

The open-coding results reveal that site workers who conduct unsafe behaviours may be due to their psychological needs (e.g., seeking excitement) or motivations (e.g., increasing income). It is also indicated that workers' unsafe behaviours are affected by external conditions or site scenarios. For instance, they may desire to follow their peers' behaviours, follow the demand from their team leader to work fast, or even simply help others in an emergency.

4.2. Axial Coding Results.

Following the open coding, axial coding aims to establish a more generalized category through cluster analysis to discover internal connections between these initial categories identified in Table 4. It can be found from Tables 3 and 4 that some of the concepts are strongly correlated, for example, saving time and pursuing work efficiency. According to the behavioural intention and motivations reflected in the open coding, these initially coded categories are redefined into seven main categories listed in Table 5.

These seven main categories listed in Table 5 could be further divided into three different scenarios: (1) reducing physical work, saving time, and increasing income are motivations that workers hold to enhance their input-to-output efficiency. Workers desire to meet these personal needs. Under

this scenario, they behave unsafely in a proactive way to achieve personal needs; (2) relieving stress and wishing to be part of the team are scenarios that drive workers to adjust themselves in a specialized circumstance, although it may not be their original intention to make these adjustments. They adopt unsafe behaviours to cater to the external scenario (e.g., managers' demand to work fast) in a passive manner; (3) different from the prior two scenarios, workers desire to help others, especially under emergent situations, despite their lack of safety knowledge or competency. Their unsafe behaviour manifests reactively.

4.3. Selective Coding Results.

The principles of selective coding were defined by Strauss and Corbin [53, 54] as the process of selecting the main category, relating it to other types, and analyzing the relationships between categories. Selective coding was conducted through text analyses to identify the internal connections for each main category defined from axial coding, workers' individual safety perception, and the corresponding and resulting unsafe behaviour type. Each coded main category is listed in Table 5, with individuals' safety perception status, and the potential behavioural outcomes are described in Table 6.

It is seen that individual desire or needs, activated by one of these main categories, linked to the unique perception status, could potentially lead to unsafe behaviour. Based on the qualitative data obtained and processed from the initial steps, the safety perception status of individuals can be defined in distinct types according to their safety awareness and fear of danger. The perception status described in Table 6 indicates that safety education is imperative for individuals to be equipped with sufficient safety awareness and the correct perceptions of the ensuing danger. Their unsafe behavioural outcome can also be divided into proactive, passive, and reactive types. These various perception statuses and types of the behavioural effect can further be described as (1) the intention of saving time, reducing labour inputs, or increasing personal income, all of which have the potential to reward the respective workers themselves; moreover, behind the income-driven motivations is the devastating effect of proactive unsafe behaviours; (2) relieving stress and the desire to be part of the team could induce workers to behave unprofessionally due to the external stress or peer pressure; and (3) in a less common case, helping or rescuing others on-site under emergency also causes unsafe behaviours. This scenario can be defined as workers' reactive behaviour stimulated by unexpected stresses.

4.4. Test of Theoretical Saturation.

Following the preliminary three-step coded analysis of qualitative data from the 30 interviewees, data from the remaining five interviewees were adopted for the theoretical saturation test. Following the same three-step analysis in Grounded Theory, no new concepts or categories were different from the previously defined categories. Therefore, it was indicated that the current coded categories and their connections, as described in Table 6, had encapsulated the significant causes and features of unsafe behaviours on construction sites

TABLE 4: Initial categories summarized through open coding.

Initially coded category	Defined feature	Mentioned by number of interviewees
Saving effort	Some workers consider the standard practice cumbersome and desire that the task be completed in a relatively more straightforward manner, such as throwing tools to deliver them between peers, crossing the safety fence, installing the scaffolding without fall protection, and randomly placing tools/materials on-site for the sake of convenience.	13
Gaining more income	Some workers perform their jobs with sicknesses or fatigue to gain more income or bonus.	11
Being overconfident	Some workers underestimate the risk of their behaviours and overestimate their capability to control risks.	8
Fearing losing jobs	Some workers opt to do unsafe work if their managers require them to finish on time or catch up with the construction schedule.	7
Meeting the scheduling needs	Some workers work overtime under fatigue to catch up with the scheduling requirements.	7
Saving time	Some workers skip steps in the standard construction workflow by violating safety regulations to save time. Some crew miss the safety education just to gain more time performing site duties.	7
Pursuing work efficiency	Some workers desire to complete duties in less time and behave in more risky ways, such as dropping the concrete formwork and scaffolding fasteners and manually carrying heavy items on-site.	5
Coping with safety inspection	Some site workers conceal or temporarily hide site items that do not comply with safety regulations to cope with periodic safety inspections from authorities or third parties.	5
Relying on personal experience	Some workers highly rely on their past site experience to judge the risk of their behaviour, and some unsafe behaviours may occur due to their long-term risk-taking habits or experience.	5
Holding the "being lucky" mindset	Some workers underestimate the safety issues, being even more "optimistic" towards safety if their past violation of safety rules did not cause accidents. However, they also believe that they would not be unfortunate to be involved in accidents.	5
Seeking comfort	Workers feel that wearing a hard hat, fastening safety belts, or using other safety protective equipment would make them even more uncomfortable in the hot weather.	4
Following the manager's demands	Workers feel unable to resist the commands of their crew leader. They feel obliged to perform risky duties and require high professional skills beyond their capability. As a result, they violate safety regulations to prevent project delays.	4
Resisting being regulated	When facing the blame or punishment for a safety violation, some workers turn out to be rebellious and feel unfairly treated and desire to continue their unsafe behaviours.	4
Reducing fatigue or pressure	Labour-intense duties and uncomfortable site conditions (noisy and hot) make workers feel exhausted and drive them irritable. As a result, some may smoke, snore, or even drink alcohol on-site.	3
Expressing emotions	Some workers are annoyed and angered for several reasons, including being rudely treated or blamed by site management personnel, family issues, and fairly punishment; as a result, they behave on purpose against the demands of their managers as a way to express their anger, such as by not attending mandatory safety education.	3
Escaping responsibilities	Some site workers lack a sense of responsibility, feel reluctant to be part of the site inspection, hide unsafe conditions or not report safety accidents, or blame others for the aroused safety issues.	3
Revenging	Conflicts may happen between workers and management personnel or among different trades. Some site workers seek opportunities to revenge by damaging others' work outputs.	3
Demonstrating capability	Some workers desire to impress their managers and demonstrate their capabilities by behaving differently from their peers.	3
Showing a "tough guy" image	Some workers desire to show their "tough guy" image to their peers and line managers. They do not follow management guidelines and pretend that they are experienced and know what they would perform, resulting in risky behaviours and safety violations.	2

TABLE 4: Continued.

Initially coded category	Defined feature	Mentioned by number of interviewees
Idling	Some part-time workers do not care about safety or perform their high-quality jobs. Instead, they mainly focus on gaining their daily income by spending their time on-site.	2
Hurrying to complete work	Once upon completing their daily duties, some workers are anxious to return home by finishing the last piece of work in a hurry and further cause accidents, e.g., falling from height.	2
Satisfying curiosity	Some workers feel curious and operate equipment (e.g., tower crane) without proper training.	1
Seeking excitement	Some workers behave unsafely by jumping on-site, throwing tools to deliver them, horseplaying, or playing in dark and confined spaces (e.g., basement, culverts).	1
Following peers	Although they do not agree with some unsafe actions conducted by co-workers, some workers still decide to follow their peers' unsafe behaviours to be social in their workgroup.	1
Maintaining self-esteem	When some workers feel insulted on-site, they may react in an extreme or unsafe way to defend their self-esteem.	1
Enhancing self-vanity	Some workers perform risky tasks beyond their control to gain praise from others.	1
Disturbing other trade teams' work	Some workers use the tools or equipment from other trade groups without permission just to benefit their group.	1
Reacting in emergency	Some workers, although without sufficient safety training, react in an emergency by trying to help others in danger.	1
Avoiding being monitored	Some workers deliberately hide from their managers to act unsafely.	1
Being distracted	Some workers are thinking of other nonwork-related things when working on-site.	1

TABLE 5: Coded main categories linked to initially coded categories.

Main category	Initially coded categories	The intention or motivation of unsafe behaviours
Reducing physical work	Saving effort; coping with safety inspection; seeking comfort; idling	Minimizing discomfort at work; reducing labour input
Reducing time input	Saving time; pursuing work efficiency; hurrying to complete work	Reducing the time spent on performing duties
Meeting internal desires	Being overconfident; relying on personal experience; holding the "being lucky" mindset; resisting being regulated; expressing emotions; escaping responsibilities; revenging; showing a "tough guy" image; demonstrating capability; satisfying curiosity; seeking excitement; enhancing self-vanity; maintaining self-esteem; avoiding being monitored; being distracted	Meeting a specific psychological need or desire; seeking a specific type of internal satisfaction (e.g., curiosity)
Relieving stress at work	Fearing of losing jobs; meeting the scheduling needs; following the manager's demands; reducing fatigue or pressure	Relieving stress driven by a specific type of external scenario
Increasing income	Gaining more income	Gaining more income from work
Being part of the team	Following peers; disturbing other trade teams' work	Demonstrating self-conformance to the own social or workgroup
Helping others	Reacting in emergency	Saving others from danger despite self-incompetency

comprehensively. Further discussion and in-depth theoretical analysis could then be conducted.

5. Discussion

5.1. Analytic Framework in the Formation of Safety Behavioural Decision. Following the Grounded Theory analysis, the process from construction workers' internal desires or motivations to behavioural outcomes is analyzed by introducing the social psychology theories as demonstrated in Figure 2.

5.1.1. Definition of the Analytic Framework Involving Mediated Moderation Effects in Safety Behavioural Outcomes. The framework shown in Figure 2 is considered a combination of mediation and moderation, according to Baron and Kenny [64]. The difference between a moderator (e.g., implicit safety cognition) and a mediator (e.g., explicit awareness) lies in that a moderator serves as an independent variable. Still, a mediator works as an intervening factor between an independent variable and the outcome [64]. As seen in Figure 2, workers' implicit safety cognition is at the

TABLE 6: Internal connections for each coded category, individual status of safety perception, and the corresponding behavioural outcome.

Connection among each coded category, individual safety perception status, and potential behavioural outcome	Definition
Reducing physical work → With safety awareness but without fear of danger → Proactive unsafe behavior	Before conducting unsafe behaviour, workers have a certain understanding of the risk involved in their unsafe actions. However, they either underestimate the danger, hold the "fortunate" mindset believing that accidents are not likely to occur to themselves, or desire to seek convenience or comfort.
Reducing time input → With safety awareness but without fear of danger → Proactive unsafe behavior	Before conducting unsafe behaviour, workers have a certain understanding of the risk involved in their unsafe actions. However, they underestimate the danger or hold the belief that they should not be that unlucky to become victims of accidents. They also care more about completing site work in less time.
Meeting internal desires → With safety awareness but without fear of danger → Proactive unsafe behavior	Before conducting unsafe behaviour, workers thoroughly understand the risk involved in their unsafe actions. But they also desire to satisfy specific internal needs by ignoring or underestimating the danger and violating safety rules.
Relieving stress at work → Without safety awareness but with fear of danger → Passive unsafe behavior	Before conducting unsafe behaviour, workers have a certain degree of fear of the potential danger. However, they still run dangerous behaviours due to stress caused by external scenarios and improper safety awareness due to a lack of professional knowledge.
Increasing income → With safety awareness but without fear of danger → Proactive unsafe behavior	Before conducting unsafe behaviour, workers have a specific understanding of the risk involved in their unsafe actions. However, they underestimate the danger or hold the belief that they should not be that unlucky to become victims of accidents. They also care more about earning more rather than safety.
Being part of the team → Without safety awareness but with fear of danger → Passive unsafe behavior	Before conducting unsafe behaviour, workers have a certain degree of fear of the potential danger. But they lack sufficient knowledge of the risk related to their hazardous behaviour. Peers' unsafe behaviour would encourage them more to behave unsafely in order to show themselves as part of the team.
Helping others → Without safety awareness and without fear of danger → Reactive unsafe behavior	Workers may not have sufficient safety knowledge of risks, and nor do they fear the danger involved. They desire to help other people on-site, under unexpected conditions or emergencies.

same level as the external scenario as an independent variable that may affect the outcome, which is the worker's behavioural decision of whether to behave unsafely. The external methods can activate these coded main categories shown in Table 5, such as the desire to save effort or gain more income. According to Scheier [65] and Snyder [66], self-monitoring or self-consciousness, once becoming the moderator variable, can improve the traits and attitudes. In this study, workers' self-monitoring or self-consciousness of safety can be reflected in the implicit safety cognition as moderating variables to the external scenarios. In this dynamic framework involving multiple variables affecting the behavioural outcome, self-monitoring within the implicit safety cognition, as a moderator variable, divides workers into subgroups according to their traits, for example, by demographic factors [67], job trades [68], or experience level [37]. These subgroup factors could cause workers' safety perceptions [46].

5.1.2. Extending the Social Psychology Theory into Safety Behavioural Science.
Applying the social phycology theory described in Baron and Kenny [64] and following the dynamic framework displayed in Figure 2, it is seen that the implicit safety cognition moderates the effects of the external scenarios in their behavioural decision, and the explicit safety cognition works as the mediator who could significantly intervene the decision. The behavioural decision could be different depending on the interacted effects of these variables. This interacted effect can be through different routes by extending the theory of Baron and Kenny [64]. The implicit cognition and the external scenario may significantly affect the behavioural decision (as seen in the dashed lines in Figure 3 from implicit safety cognition and external scenario to the outcome). The interaction of explicit cognition and external scenario indicates moderation. Explicit cognition can mediate the relation from the external scenario to the outcome, meaning that the external distraction from these aforementioned coded categories (e.g.,
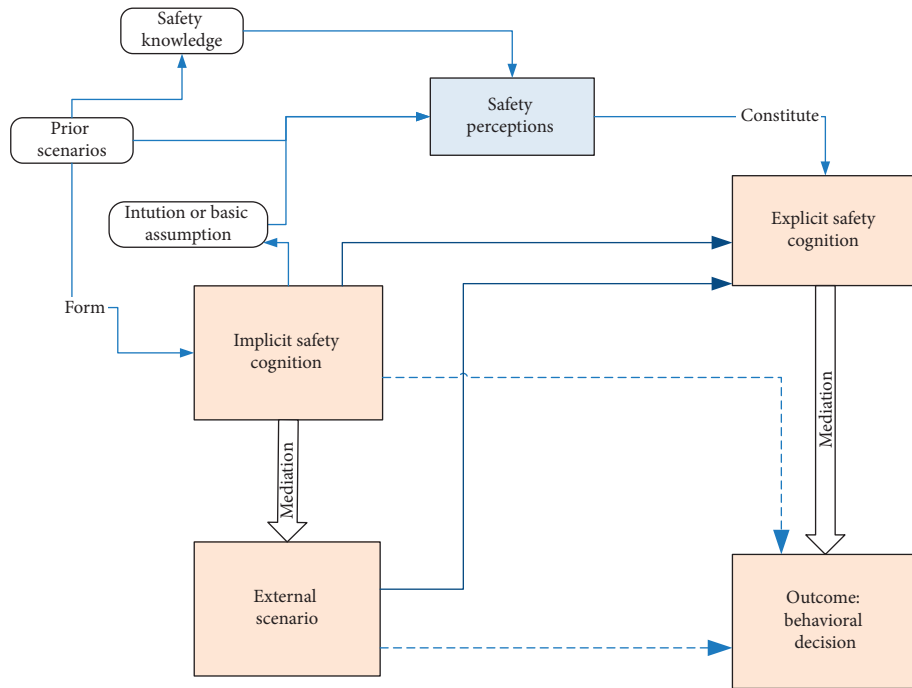
FIGURE 2: Analytic framework of mediated moderation informing construction workers' safety behavioural decision (source adapted by integrating the theories of Baron and Kenny [64] and Han et al. [46]).
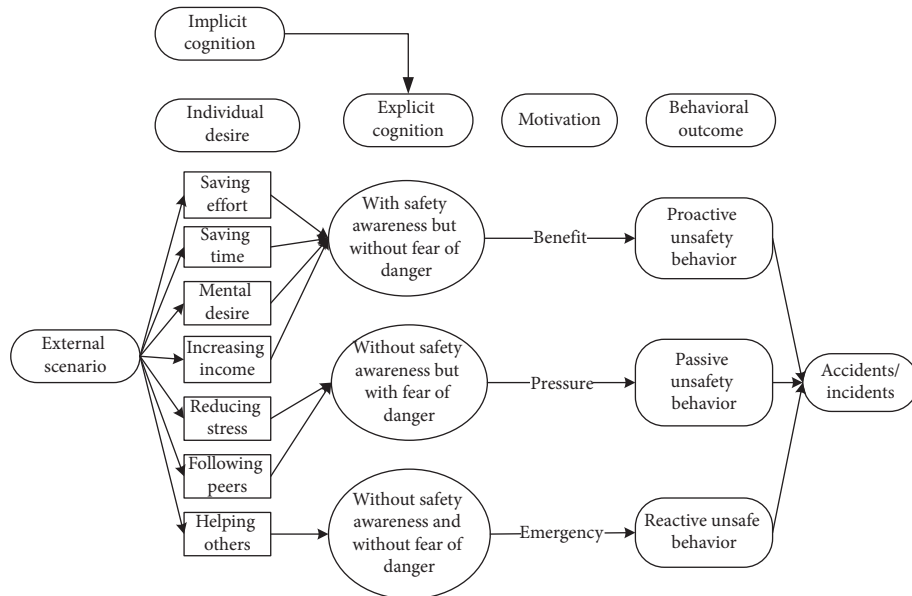
FIGURE 3: Diagram describing the formation of workers' unsafe behaviours driven by various individual desires under different explicit cognition patterns.

desire to increase personal income) does not necessarily cause unsafe behaviours if the worker has the correct safety perception to resist the temptations activated by the external scenarios. If that mediation is complete, these temptations that are driven by the external site scenarios to work unsafely would not result in unsafe behaviours. Indeed, to strengthen the explicit safety cognition (i.e., safety climate), implicit safety cognition should strongly affect clear awareness.

By extending the social psychology theory described by Baron and Kenny [64], it is indicated that the interaction effect from explicit cognition and the initial external scenario would strongly affect the behavioural decision. However, through the mediation effect from clear cognition, and depending on the level of mediation, workers could redirect their own safety behaviours from being risky to behaving safely. This level of deviation

would highly depend on the effectiveness of safety programs [69] and safety training [46] which could improve a positive safety climate.

5.2. Formation Mechanism of Construction Workers' Unsafe Behaviours.
The analytic framework shown in Figure 2 can be further extended into the formation process based on the coded categories generated from Grounded Theory. Continued from Table 6, it is seen that unsafe behavioural outcomes are formed through one of the dynamic routes shown in Figure 3. Therefore, for any unsafe behaviour to occur, an external scenario that activates one individual desire, intervened by personal safety cognition, would drive the formation of the dominating motivation (i.e., benefit, stress, or emergency). It is stated in the Self-Determination Theory [70] that distinct types of motivations drive human behaviour. The motivation-driven behaviours could be performed to simply satisfy the innate psychological needs [71]. This need or desire is a necessary condition but not a sufficient condition for unsafe behaviour.

5.2.1. Individual Desire Is Linked to Construction Workers' Unsafe Behaviour.
The seven individual desires listed in Figure 3 reflect the need for workers and can be considered reasonable and regular human needs. Compared to other industries, the construction industry has more adverse and diverse site working conditions (e.g., hot to cool outdoor environments) and is deemed riskier in terms of health and safety. The subcontracted work in China's construction industry is more commonly based on a fixed amount, meaning that workers would gain the same payment by completing the given tasks. Hence, many workers prefer to save labour input and time to complete a fixed amount of work. Many workers migrate to urban areas of more economically developed regions in China in search of better-paying jobs. They may feel socially isolated and desire to be part of a social group. Therefore, they tend to follow peers' behaviours. The social outcome, defined by Man et al. [11], could be considered necessary for workers to enhance their image or status in the social system. External factors could also increase the probability of unsafe behaviour.

In many cases, construction projects in the urban areas of China are under a tight schedule to meet deadlines. As a result, it is common to see site workers committing to work overtime, including weekends. Therefore, any demands from the management that work should be completed earlier would result in more stress.

It should be a concern if workers' unsafe behaviours originate from their reasonable and rational human needs. It could be said that the unsafe behaviour is a by-product of the site work, meaning that the personal desire or conditions do not necessarily result in dangerous behaviours. It is not possible to eliminate these internal needs. What is more practical and feasible in safety management is to provide proper education by targeting workers' common personal needs, primarily to prevent them from conducting unsafe behaviours.

5.2.2. The Effect of Safety Cognition on Unsafe Behaviours.
Unsafe behaviours could allow an individual worker to achieve their own desired outcomes with positive or negative consequences (e.g., injuries). Therefore, before making a behavioural decision, each individual has to weigh the risk and benefits associated with a decision [72]. Indeed, construction workers would perceive it as worthwhile in trying a risky approach if there is a significant return from pursuing such unsafe behaviour. An immediate example is when having to save the lives of people in case of emergency or just simply to demonstrate their own "tough guy" syndrome [10] to peers and managers. Over time, and with sufficient safety awareness and perception of danger, workers may not decide to behave unsafely despite the benefits brought by the risky behaviour. The safety cognition system described in Figure 2 is insinuated as the mediated moderation factor between persona desire under specific external scenarios and the resulting motivation leading to a behavioural outcome. Furthermore, as workers gain more site experience and dexterity in perfecting their trade skills and routinely accomplish their work safely on a consistent level, safety awareness also increases at the same exponential knowledge of compliance. Therefore, it is more common to see workers being proactively and routinely safe by understanding how to conform to safety regulations. This is exhibited through increased avoidance of unsafe behaviours. Invariably, the antithesis is also actual. When workers behave unsafely, they are more likely to have sufficient safety awareness but exhibit low sensory understanding or anticipation of risks, hazards, and resulting harm or looming danger.

According to the Weber-Fechner Theory [73], human beings tend to become less sensitive to danger as their experience and skill grow, with less fear of danger. Almost befitting this theory is the expression that "familiarity breeds contempt" to warrant an effective response to compliance. There is virtually an infinite false sense of safety, qualified by unsafe behaviour. Expressing the same concern, Han et al. [37] compared their entry-level peers. They found that construction workers, in their middle careers, were more prone to underestimate the danger associated with site hazards. This conclusion is also prominent among workers who behave riskily but end up without encountering any negative consequences due to their behaviour. As for this group of workers, Kasperson et al. [74] have warned that the absence of negative experiences creates a false sense of safety. This predisposition to no harm leads to falsification of the actual benefits enshrined in full compliance, and conformance to safety standards has negative safety behaviour: workers become less sensitive to the potential risk-led dangers, are slow to be proactive, and become a danger to themselves and their fellow workers [74]. Workers' "fortunate" mindset would be strengthened under this scenario by relying on the superior supervision of foremen and sectional managers and the personal experience of co-workers. Holding the belief that accidents would not happen to themselves is what triggers or generates overconfidence and could deviate workers' safety perception and ability to improve their dexterities in their trade, and heighten the precipitation of perpetual acts of unsafe behaviours.

The factor of focusing on the end benefit (or benefit-driven) in addition to external pressure-induced desire is also a common trigger for unsafe behaviours. The explicit safety cognition (i.e., safety climate involving safe perception and safety awareness) plays a vital role as an intervening mediator to impact the behavioural decision. Under the proper mediation of safety cognition, workers could be equipped with sufficient safety awareness and sense of danger and hence not behaving unsafely. The occurrence of unsafe behaviour is not because of the internal personal desire but the failure of the mediated-moderation mechanism involving the safety cognition. Behaving unsafely but not causing accidents can strengthen and precipitate the "fortunate" behavioural syndrome mindset, thereby deteriorating the mediated moderation agent. Therefore, training workers with proper safety cognition to correct this bias of the "fortunate" attitude plays a key role.

5.2.3. The Dynamic Mechanism in the Formation of Behavioural Decision. It is workers themselves who decide their behaviours. In other words, they can self-direct their motivation and behaviours. Despite the sufficient safety knowledge, site experience, and level of safety awareness, as well as the sense of danger due to unsafe behaviours, the internal desire (e.g., gaining more income) and external inducer (e.g., tight project schedule) may affect the behavioural decision-making according to the analytic framework in Figure 2. This dynamic mechanism also means that which motivation dominates can keep changing. For example, workers may feel uncertain in weighing the benefits and risks. The mediated moderation from safety cognition aims to guide workers towards safety-dominating motivation. The Protection Motivation Theory (PMT) [75] indicates that human beings naturally tend to protect themselves from danger if they can correctly sense the danger. According to PMT [75], the key is to nurture the proper sense of danger for workers, besides the education on safety awareness.

On the other hand, the Risk Homeostasis Theory [76] proposes that human beings opt to take more risks if they have a strong sense of safety. Workers may behave at different risk levels depending on the external conditions [77]. It happens that workers work in a more risky way because they believe that the superior safety devices can protect them from injuries, hence underestimating the site risks due to their unsafe behaviours. Klen [78] reported that workers behaved more carelessly in a riskier manner when equipped with protective equipment. However, this is not to deny the importance of wearing safety equipment. Instead, it highlights that the malfunctioning safety cognition system as the mediated moderation mechanism should be corrected to prevent unsafe behaviours.

5.2.4. External Conditions That Affect Workers' Behavioural Decision. The adverse external conditions, such as high humidity and hot weather in summer construction and poor management commitment to safety, could exert a negative influence on workers' behaviours. This external influence cannot be ignored. The qualitative studies conducted in China's construction industry [10, 11] confirmed that workers are likely to be influenced by their peers' behaviours and the social values of their groups. If most other peers are working in an unsafe way, those minorities who behave in a standardized, safe manner may feel isolated and perhaps taken for granted. Safety management, therefore, plays a vital role in workers' behaviours. In some cases, workers quickly perform duties because they fear losing part of their income for failing to complete the job on time. Sometimes they must focus more on work efficiency to avoid being blamed by their managers.

Skinner's [79] theory indicates that timely and effective punishment for unsafe behaviour could prevent unsafe actions and motivations from reoccurring. However, insufficient safety monitoring and management system, which fails to handle safety violations timely and adequately, could motivate workers to behave unsafely and negatively affect their preestablished safety cognition system. A good safety management program is critical to forming a positive safety climate. The safety climate forms part of the safety cognition, which directly affects human behaviour [42]. A hostile site atmosphere (e.g., managers' emphasis on work efficiency and indifference to health and safety) could lead to the failure of the mediated moderation mechanism brought by the safety cognition system.

6. Conclusion

This study adopts a Grounded Theory approach to assist the investigation of the formation mechanism of construction workers' unsafe behaviour. Following site interviews with a total of 35 construction professionals, seven main categories were defined to describe workers' psychological needs or personal desires that led to unsafe behaviours. These seven categories, joint with the individual safety perception status, could lead to dangerous behaviours. The safety perception status measured by safety awareness and sense of danger could be incorporated into the explicit safety cognition. Individuals' psychological needs, activated by external scenarios and mediated by clear safety cognition, led to the behavioural outcome. The unsafe behaviour, according to the qualitative data obtained from this study, could be divided into proactive, passive, and reactive types, driven by different internal needs and external conditions on construction sites.

Following the data analysis adopting Grounded Theory, social psychology theories were applied in the context of construction safety behaviour. An analytic framework illustrating the formation of the behavioural decision was initiated by integrating the ideas of social cognitive psychology and safety cognition of construction workers. Social psychology highlighted the effects of two different factors (i.e., mediator and moderator) in affecting the behavioural outcome. The individual desire activated by an external scenario serves as one independent variable, which is one necessary but not sufficient condition for unsafe behaviours. The social psychology theories infer that construction workers' safety cognition system, consisting of implicit (e.g., safety knowledge and previous experience) and explicit (i.e., safety climate) cognitions, work as the mediated-moderation

mechanism affecting the behavioural outcome. This is a dynamic mechanism involving workers' safety awareness and sense of danger, which intervene in their individual desires activated by external scenarios workers.

By integrating the results from Grounded Theory and the analytic framework, a further diagram was developed to describe the formation process of construction workers' unsafe behaviours. This diagram was discussed in depth in terms of four main aspects, namely, the original desires causing unsafe behaviours, the effects of safety cognition in unsafe behaviours, the dynamic mechanism informing behavioural decisions, and external conditions that affect workers' behavioural decisions. By applying a variety of social psychology theories, the diagram provides practical suggestions to properly guide construction workers' behaviours, including (1) an effective safety management program to provide effective training addressing workers' personal needs instead of ignoring or denying these needs or desires; (2) establishing a positive safety climate to develop workers' safety perception with sufficient safety awareness and sense of danger; and (3) periodic safety orientation targeting individuals' safety cognition system, not only for new workers but also especially for experienced workers. More specifically, many construction workers might not have received a university-level education, and alternative training manners other than toolbox meetings could be adopted, e.g., virtual reality-based site tour and video plays of safety hazards/accidents. Other measures to increase the safety awareness and sense of danger could include but be not limited to a proper frequency of safety inspection of workers on-site and an established management scheme between incentive and punishment to regulate safety behaviours.

One limitation of this current study is that all interviews were conducted in China's most economically active region, where construction projects are mostly under tight schedules with productivity highly stressed. More future work could be done to evaluate these defined categories from Grounded Theory in different regions or countries. The developed analytic framework and diagram can also be further applied in other regions or countries' construction sites. More future work can also investigate the effects of safety incentives and punishment policies in safety cognition development.

Data Availability

Data generated or analyzed during the study are available from the corresponding author by request.

Conflicts of Interest

The authors confirm that there are no conflicts of interest involved in publishing this manuscript entitled "Grounded Theory and Social Psychology Approach to Investigating the Formation of Construction Workers' Unsafe Behaviour."

Acknowledgments

References

[1] R. Y. Sunindijo and P. X. W. Zou, "Political skill for developing construction safety climate," *Journal of Construction Engineering and Management*, vol. 138, no. 5, pp. 605–612, 2012.

[2] Y. Feng, E. A. L. Teo, F. Y. Y. Ling, and S. P. Low, "Exploring the interactive effects of safety investments, safety culture and project hazard on safety performance: an empirical analysis," *International Journal of Project Management*, vol. 32, no. 6, pp. 932–943, 2014.

[3] D. A. Hofmann, R. Jacobs, and F. Landy, "High reliability process industries: individual, micro, and macro organizational influences on safety performance," *Journal of Safety Research*, vol. 26, no. 3, pp. 131–149, 1995.

[4] F. W. Guldenmund, "The nature of safety culture: a review of theory and research," *Safety Science*, vol. 34, no. 1–3, pp. 215–257, 2000.

[5] Q. Chen and R. Jin, "Multilevel safety culture and climate survey for assessing new safety Program," *Journal of Construction Engineering and Management*, vol. 139, no. 7, pp. 805–817, 2013.

[6] X. Wu, Q. Liu, L. Zhang, M. J. Skibniewski, and Y. Wang, "Prospective safety performance evaluation on construction sites," *Accident Analysis & Prevention*, vol. 78, pp. 58–72, 2015.

[7] Q. Li, C. Ji, J. Yuan, and R. Han, "Developing dimensions and key indicators for the safety climate within China's construction teams: a questionnaire survey on construction sites in Nanjing," *Safety Science*, vol. 79, pp. 11–18, 2017.

[8] Evalued Toolkit, "Questionnaires," 2006, https://www.evalued.bcu.ac.uk/tutorial/4a.html.

[9] R. I. Lestari, B. H. W. Guo, and Y. M. Goh, "Causes, solutions, and adoption barriers of falls from roofs in the Singapore construction industry," *Journal of Construction Engineering and Management*, vol. 145, no. 5, Article ID 4019027, 2019.

[10] R. M. Choudhry and D. Fang, "Why operatives engage in unsafe work behavior: investigating factors on construction sites," *Safety Science*, vol. 46, no. 4, pp. 566–584, 2008.

[11] S. S. Man, A. H. S. Chan, and H. M. Wong, "Risk-taking behaviors of Hong Kong construction workers - a thematic study," *Safety Science*, vol. 98, pp. 25–36, 2017.

[12] M. Snyder and W. Ickes, "Personality and social behavior," in *Handbook of Social Psychology*, G. Lindzey and E. Aronson, Eds., pp. 883–948, Addison-Wesley, San Francisco, CA, USA, 1985.

[13] X. Li and H. Long, "A review of worker behavior-based safety research: current trends and future prospects," *IOP Conference Series: Earth and Environmental Science*, vol. 371, no. 3, Article ID 032047, 2019.

[14] G. Blomquist, "A utility maximization model of driver traffic safety behavior," *Accident Analysis & Prevention*, vol. 18, no. 5, pp. 371–375, 1986.

[15] T. D. Smith, K. Hughes, D. M. DeJoy, and M.-A. Dyal, "Assessment of relationships between work stress, work-family conflict, burnout and firefighter safety behavior outcomes," *Safety Science*, vol. 103, pp. 287–292, 2018.

[16] M. S. Sharifzadeh, G. Abdollahzadeh, C. A. Damalas, R. Rezaei, and M. Ahmadyousefi, "Determinants of pesticide

safety behavior among Iranian rice farmers," *The Science of the Total Environment*, vol. 651, pp. 2953–2960, 2019.

[17] H. W. Heinrich, *Industrial Accident Prevention: A Scientific Approach*, McGraw-Hill, New York, NY, USA, 1931.

[18] B. Sulzer-Azaroff, "The modification of occupational safety behavior," *Journal of Occupational Accidents*, vol. 9, no. 3, pp. 177–197, 1987.

[19] Y. M. Goh and M. J. Askar Ali, "A hybrid simulation approach for integrating safety behavior into construction planning: an earthmoving case study," *Accident Analysis & Prevention*, vol. 93, pp. 310–318, 2016.

[20] J. P. DePasquale and E. S. Geller, "Critical success factors for behavior-based safety," *Journal of Safety Research*, vol. 30, no. 4, pp. 237–249, 1999.

[21] H. Lingard and S. Rowlinson, "Behaviour-based safety management in Hong Kong's construction industry: the results of a field study," *Construction Management & Economics*, vol. 16, no. 4, pp. 481–488, 1998.

[22] H. Lingard and S. Rowlinson, "Behavior-based safety management in Hong Kong's construction industry," *Journal of Safety Research*, vol. 28, no. 4, pp. 243–256, 1997.

[23] D. J. Eckenfelder, "Behavior-based safety: a model poisoned by the past; based on obsolete thinking, behavior-based safety isolates safety instead of integrating it," *Risk and Insurance*, vol. 15, no. 12, p. 65, 2004.

[24] M. Lu, C. M. Cheung, H. Li, and S. C. Hsu, "Understanding the relationship between safety investment and safety performance of construction projects through agent-based modeling," *Accident Analysis & Prevention*, vol. 94, pp. 8–17, 2016.

[25] M. D. Cooper, "Behavior-based safety still a viable strategy," pp. 46–48, National Safety Council, Franklin, IN, 2003.

[26] R. M. Choudhry, "behavior-based safety on construction sites: a case study," *Accident Analysis & Prevention*, vol. 70, pp. 14–23, 2014.

[27] I. Hansez and N. Chmiel, "Safety behavior: job demands, job resources, and perceived management commitment to safety," *Journal of Occupational Health Psychology*, vol. 15, no. 3, pp. 267–278, 2010.

[28] B. H. W. Guo, T. W. Yiu, and V. A. González, "Identifying behaviour patterns of construction safety using system archetypes," *Accident Analysis & Prevention*, vol. 80, pp. 125–141, 2015.

[29] D. Zohar, "Safety climate in industrial organizations: theoretical and applied implications," *Journal of Applied Psychology*, vol. 65, no. 1, pp. 96–102, 1980.

[30] S. Cox and T. Cox, "The structure of employee attitudes to safety: a European example," *Work & Stress*, vol. 5, no. 2, pp. 93–106, 1991.

[31] A. Neal and M. A. Griffin, "A study of the lagged relationships among safety climate, safety motivation, safety behavior, and accidents at the individual and group levels," *Journal of Applied Psychology*, vol. 91, no. 4, pp. 946–953, 2006.

[32] S. Lyu, C. Hon, A. Chan, F. Wong, and A. Javed, "Relationships among safety climate, safety behavior, and safety outcomes for ethnic minority construction workers," *International Journal of Environmental Research and Public Health*, vol. 15, no. 3, p. 484, 2018.

[33] H. Lingard, T. Cooke, and N. Blismas, "Coworkers' response to occupational health and safety," *Engineering Construction and Architectural Management*, vol. 18, no. 2, pp. 159–175, 2011.

[34] M. T. Newaz, P. R. Davis, M. Jefferies, and M. Pillay, "Developing a safety climate factor model in construction

research and practice," *Engineering Construction and Architectural Management*, vol. 25, no. 6, pp. 738–757, 2018.

[35] G. Grote and C. Kunzler, "Diagnosis of safety culture in safety management audits," *Safety Science*, vol. 34, no. 1–3, pp. 131–150, 2000.

[36] J. L. Meliá, K. Mearns, S. A. Silva, M. L. Lima, and M. Luisa Lima, "Safety climate responses and the perceived risk of accidents in the construction industry," *Safety Science*, vol. 46, no. 6, pp. 949–958, 2008.

[37] Y. Han, Z. Feng, J. Zhang, R. Jin, and E. Aboagye-Nimo, "Employees' safety perceptions of site hazard and accident scenes," *Journal of Construction Engineering and Management*, vol. 145, no. 1, Article ID 04018117, 2019a.

[38] M. Duryan, H. Smyth, A. Roberts, S. Rowlinson, and F. Sherratt, "Knowledge transfer for occupational health and safety: cultivating health and safety learning culture in construction firms," *Accident Analysis & Prevention*, vol. 139, Article ID 105496, 2020.

[39] N. Marquardt, R. Gades, and S. Robelski, "Implicit social cognition and safety culture," *Human Factors and Ergonomics in Manufacturing & Service Industries*, vol. 22, no. 3, pp. 213–234, 2012.

[40] L. L. Jacoby and D. Witherspoon, "Remembering without awareness," *Canadian Journal of Psychology/Revue canadienne de psychologie*, vol. 36, no. 2, pp. 300–324, 1982.

[41] L. L. Jacoby, D. S. Lindsay, and J. P. Toth, "Unconscious influences revealed: attention, awareness, and control," *American Psychologist*, vol. 47, no. 6, pp. 802–809, 1992.

[42] P.-C. Liao, B. Liu, Y. Wang, X. Wang, and T. Ganbat, "Work paradigm as a moderator between cognitive factors and behaviors - a comparison of mechanical and rebar workers," *KSCE Journal of Civil Engineering*, vol. 21, no. 7, pp. 2514–2525, 2017.

[43] W. T. Chen, C. S. Lu, and Y. H. Huang, "Investigating the safety cognition of Taiwan's construction personnel," *Journal of Marine Science and Technology*, vol. 19, no. 4, pp. 398–408, 2011.

[44] E. Schein, *Organizational Culture and Leadership*, Jossey-Bass, Hoboken, NJ, USA, 2nd edition, 1992.

[45] J. Liu, "Study on the safety cognition deviation characteristics and formation mechanism of construction workers,"M.Sc. Thesis, pp. 12–16, Jiangsu University, Zhenjiang, Jiangsu, China, 2018.

[46] Y. Han, Z. Yin, J. Liu et al., "Initiating a safety cognition framework incorporating safety hazard perception," *Journal of Construction Engineering and Management*, vol. 145, no. 12, 2019b.

[47] W. C. Rowatt, L. M. Franklin, and M. Cotton, "Patterns and personality correlates of implicit and explicit attitudes toward Christians and Muslims," *Journal for the Scientific Study of Religion*, vol. 44, no. 1, pp. 29–43, 2005.

[48] J. Rowley, "Conducting research interviews," *Management Research Review*, vol. 35, no. 3/4, pp. 260–271, 2012.

[49] B. G. Glaser and A. L. Strauss, *The Discovery of Grounded Research: Strategies for Qualitative Research*, Aldine Transaction, New Brunswick (USA) and London (UK), 1967.

[50] T. R. Shalka, "Saplings in the hurricane: a grounded theory of college trauma and identity development," *The Review of Higher Education*, vol. 42, no. 2, pp. 739–764, 2019.

[51] Q. Cao, M. N. I. Sarker, and J. Sun, "Model of the influencing factors of the withdrawal from rural homesteads in China: application of grounded theory method," *Land Use Policy*, vol. 85, pp. 285–289, 2019.

[52] A. L. Non, G. León-Pérez, H. Glass, E. Kelly, and N. A. Garrison, "Stress across generations: a qualitative study of stress, coping, and caregiving among Mexican immigrant mothers," *Ethnicity and Health*, vol. 24, no. 4, pp. 378–394, 2019.

[53] A. Strauss and J. Corbin, *Basics of Qualitative Research Grounded Theory Procedures and Techniques*, Sage Publications, Thousand Oaks, CA, USA, 1990.

[54] A. Strauss and J. Corbin, *Basics of Qualitative Research Techniques and Procedures for Developing Grounded Theory*, Sage Publications, Thousand Oaks, CA, USA, 2nd edition, 1998.

[55] A. De Lucas Ancillo, M. T. Del Val Núñez, and S. G. Gavrila, "Workplace change within the COVID-19 context: a grounded theory approach," *Economic Research-Ekonomska Istraživanja*, vol. 34, no. 1, pp. 2297–2316, 2021.

[56] J. R. Cutcliffe, "Methodological issues in grounded theory," *Journal of Advanced Nursing*, vol. 31, no. 6, pp. 1476–1484, 2000.

[57] M. MacDonald, "Putting on and taking off the capulana: a grounded theory of how Mozambican women manage gender oppression," *Global Qualitative Nursing Research*, vol. 8, Article ID 23333936211051701, 2021.

[58] X. Li, J. Du, and H. Long, "Green development behavior and performance of industrial enterprises based on grounded theory study: evidence from China," *Sustainability*, vol. 11, no. 15, p. 4133, 2019.

[59] C. Dunne, "The place of the literature review in grounded theory research," *International Journal of Social Research Methodology*, vol. 14, no. 2, pp. 111–124, 2011.

[60] V. Timonen, G. Foley, and C. Conlon, "Challenges when using grounded theory: a pragmatic introduction to doing GT research," *International Journal of Qualitative Methods*, vol. 17, no. 1, 2018.

[61] iFLYTEK, "Education product," 2018, https://www.iflytek.com/en/about/down.html.

[62] L. A. Palinkas, S. M. Horwitz, C. A. Green, J. P. Wisdom, N. Duan, and K. Hoagwood, "Purposeful sampling for qualitative data collection and analysis in mixed method implementation research," *Administration and Policy in Mental Health and Mental Health Services Research*, vol. 42, no. 5, pp. 533–544, 2015.

[63] B. G. Glaser, *Doing Grounded Theory: Issues and discussion*, pp. 1–254, California Sociology Press, California, CA, USA, 1998.

[64] R. M. Baron and D. A. Kenny, "The moderator-mediator variable distinction in social psychological research: conceptual, strategic, and statistical considerations," *Journal of Personality and Social Psychology*, vol. 51, no. 6, pp. 1173–1182, 1986.

[65] M. F. Scheier, "Effects of public and private self-consciousness on the public expression of personal beliefs," *Journal of Personality and Social Psychology*, vol. 39, no. 3, pp. 514–521, 1980.

[66] M. Snyder, "The influence of individuals on situations: implications for understanding the links between personality and social behavior," *Journal of Personality*, vol. 51, no. 3, pp. 497–516, 1983.

[67] S. Korkmaz and D. J. Park, "Comparison of safety perception between foreign and local workers in the construction industry in Republic of Korea," *Safety and Health at Work*, vol. 9, no. 1, pp. 53–58, 2018.

[68] Q. Chen and R. Jin, "A comparison of subgroup construction workers' perceptions of a safety program," *Safety Science*, vol. 74, pp. 15–26, 2015.

[69] Q. Chen and R. Jin, "Safety4Site commitment to enhance jobsite safety management and performance," *Journal of Construction Engineering and Management*, vol. 138, no. 4, pp. 509–519, 2012.

[70] E. L. Deci and R. M. Ryan, *Intrinsic Motivation and Self-Determination in Human Behavior*, Plenum, New York, 1985.

[71] R. M. Ryan and E. L. Deci, "Intrinsic and extrinsic motivations: classic definitions and new directionsfinitions and new directions," *Contemporary Educational Psychology*, vol. 25, no. 1, pp. 54–67, 2000.

[72] S. Ove hansson, "Weighing risks and benefits," *Topoi*, vol. 23, no. 2, pp. 145–152, 2004.

[73] F. M. Urban, "The Weber-Fechner law and mental measurement," *Journal of Experimental Psychology*, vol. 16, no. 2, pp. 221–238, 1993.

[74] R. E. Kasperson, O. Renn, P. Slovic et al., "The social amplification of risk: a conceptual framework," *Risk Analysis*, vol. 8, no. 2, pp. 177–187, 1988.

[75] R. W. Rogers, "A protection motivation theory of fear appeals and attitude Change1," *Journal of Psychology*, vol. 91, no. 1, pp. 93–114, 1975.

[76] G. J. S. Wilde, "The theory of risk homeostasis: implications for safety and health," *Risk Analysis*, vol. 2, no. 4, pp. 209–225, 1982.

[77] G. J. S. Wilde, *Target Risk: Dealing with the Danger of Death, Disease and Damage in Everyday Decisions*, PDE Publications, Celbridge, Kildare, 1994.

[78] T. Klen, "Personal protectors and working behavior of loggers," *Safety Science*, vol. 25, no. 1–3, pp. 89–103, 1997.

[79] B. F. Skinner, *Beyond freedom and Dignity (No. 04; BF319. 5. O6, S5)*, Bantam Books, New York, NY, USA, 1972.

Research Article

Abnormal Target Detection Method in Hyperspectral Remote Sensing Image Based on Convolution Neural Network

Yun Liu [ID][1] **and Jia-Bao Liu** [ID][2]

[1]*School of Information Engineering, Chaohu University, Chaohu 238024, China*
[2]*School of Mathematics and Physics, Anhui Jianzhu University, Hefei 230601, China*

Correspondence should be addressed to Jia-Bao Liu; liujiabaoad@163.com

Abnormal target detection in hyperspectral remote sensing image is one of the hotspots in image research. The image noise generated in the detection process will lead to the decline of the quality of hyperspectral remote sensing image. In view of this, this paper proposes an abnormal target detection method of hyperspectral remote sensing image based on the convolution neural network. Firstly, the deep residual learning network model has been used to remove the noise in hyperspectral remote sensing image. Secondly, the spatial and spectral features of hyperspectral remote sensing images were used to optimize the clustering dictionary, and then the image segmentation containing target information is completed. Finally, the image was input into the deep convolution neural network with a dual classifier, and the network detects the abnormal target in the image. The test results of this algorithm show that the structural similarity of the denoised image is higher than 0.86, which shows that this method has good noise reduction performance, image details will not damage, segmentation effect is good, and it can obtain high-definition target image information and accurately detect abnormal targets in the image.

1. Introduction

Remote sensing images, also known as remote sensing images, include aerial photos and satellite photos. Therefore, the imaging methods of remote sensing images include aerial photography, scanning, or microwave radar scanning [1]. With the continuous development of remote sensing technology, the requirements for the imaging effect and quality of remote sensing images are gradually improved, from the basic monitoring application to the detection of abnormal targets through remote sensing images. Therefore, the resolution of remote sensing images needs to reach a certain standard. Based on this, hyperspectral is applied in the field of remote sensing and combined with remote sensing technology to obtain hyperspectral remote sensing images with better resolution [2]. Hyperspectral image refers to the resolution of $10-2\lambda$ for images of orders of magnitude, and spectral sensors are deployed on different space platforms to image the target area [3], which can obtain its

surface image and spectral image at the same time, to realize the combination of spectrum and remote sensing. The convolution neural network is a kind of network with the ability of convolution calculation and representation learning. It is widely used in image and object recognition, pose estimation, natural language processing, and so on. Moreover, the network has a good effect in processing the geometric, texture, and spatial distribution characteristics of remote sensing images and can identify the target objects in remote sensing images. In order to realize the detection of abnormal targets in hyperspectral remote sensing images [4], after relevant research in the literature [5] and [6], a correlation detection method based on spatial spectrum joint anomaly degree and spectral difference equalization interval screening is proposed. In the detection process, the above method has no segmentation effect and cannot accurately obtain the target area information. Therefore, there is a certain error in the detection result of the above method. Therefore, this paper proposes an abnormal target detection

method of hyperspectral remote sensing image based on the convolution neural network. Firstly, the high-frequency layer with noise information is studied in multiscale space by the residual network, and the residual remote sensing image is generated by residual mapping. Finally, the complete denoising result is obtained by jump connection. Then, the dictionary learning model is used to obtain the sparse representation of the brightness component and color image of the remote sensing image, reconstruct and compensate the missing high-frequency information in the remote sensing image, retain the high-resolution of the image, and retain the spectral information and spatial detail information in the remote sensing image. Finally, the convolution neural network is used to segment the hyperspectral remote sensing image after extracting the features and finally complete the image abnormal target detection.

2. Detection of Abnormal Targets in Hyperspectral Remote Sensing Images

2.1. Denoising of Hyperspectral Remote Sensing Image Based on Depth Residual Learning. In the process of imaging acquisition of hyperspectral, remote sensing images, under the influence of environment, equipment, and other factors, there will be noise in the acquired images, which will affect the detection results [7]. Therefore, in order to ensure the accuracy of abnormal target detection in hyperspectral remote sensing images, this paper uses depth residual learning to denoised the images.

Deep residual learning is a deep network model including residual module, which is composed of residual units. There is a mapping relationship between hyperspectral remote sensing images before and after noise reduction, which is nonlinear. The mapping relationship is realized by inputting the high-frequency band noise data in the image into the residual module technology. Multiple data nodes are connected by jumping, and each module can be effectively connected, so as to retain more edge information in the semantic feature difference information. The core of the network is the residual of the connection depth (shortcut connections), introducing branches to ensure smooth network data transmission and avoid under fitting caused by gradient disappearance and degradation.

2.1.1. Input Layer. The original hyperspectral remote sensing image $y\,(x)$ is used as the input of the model and input by the input layer.

2.1.2. Feature Extraction Layer. This layer completes the feature extraction of hyperspectral remote sensing image in the form of image block. In this process, the feature is extracted to ensure that the image features will not change after noise reduction. Map the image block originally located in the image space to the feature space, complete the learning of image features, and take the feature as a filter to participate in the convolution operation of the original hyperspectral remote sensing image. Its purpose is to obtain the activation value, which belongs to different positions and

features of the original image. In this layer, the activation function and convolution kernel are used to extract the eigenvalues of the image block, and the obtained neurons are transmitted to the residual module.

2.1.3. Residual Module. It mainly completes the residual learning between the input and output of the whole model. In order to ensure the integrity of image detail information in the learning process, this paper introduces local residual learning and recursive block and adjusts the residual module so that the input of identity branch and residual branch are in two states in the model and recursive block. The former is difference, and the latter is the same. In this way, the path between the input and output of recursive block is multi-path, which can effectively avoid the phenomenon of overfitting. To improve the learning performance of the model, formula (1) of the residual unit is as follows:

$$H^u = g\left(H^{u-1}\right) = \left(F_{H^{u-1}}, F_W\right) + H^0, \qquad (1)$$

where g represents the function, corresponding to the residual unit; F_W represents residual function; and both H^0 and H^u represent the output. The former corresponds to the first convolution layer, and the latter corresponds to the residual unit; $F_{H^{u-1}}$ is the input of the unit; u represents quantity, corresponding to residual unit. The original expectation mapping skips one or more layers of network structure and realizes identity mapping. With the increase of network depth, the weight of the convolution layer is constantly updated, and the weight value iterates in the direction of gradient descent.

2.1.4. Network Reconstruction Layer. After learning, the residual unit outputs the characteristic map of the image block and transmits it to this layer to form a hyperspectral mapping image, and its number is the same as the original image. After fusion processing through convolution calculation, a complete hyperspectral remote sensing image is formed. This layer can complete the prediction and removal of noise components in the image [8], so as to obtain the denoised hyperspectral remote sensing image. Then, the calculation formula is as follows:

$$X_x = x \times \left(H^u - s\right), \qquad (2)$$

where x represents the image after noise reduction; X_x represents the residual noise image after residual learning. The network learns the mapping from noise image to noise distribution. Using the characteristics of the neural network and global jump connection, x is subtracted to obtain a complete denoised image, and the multiplicative noise is removed indirectly by subtraction.

2.2. Feature Extraction of Hyperspectral Remote Sensing Image. In the abnormal target detection of hyperspectral remote sensing image, it is necessary to accurately extract the target information in the image. Therefore, this paper guarantees the definition of remote sensing image on the

basis of noise reduction and then carries out feature segmentation on x to remove the background in the image and retain the feature information. This paper uses the clustering dictionary learning method combined with the residual network model to complete the image pixel segmentation.

Determine the cluster center, use the dictionary representation, determine the category attribution, and complete the dictionary learning, which are completed according to the sparse representation and the elements in the cluster, respectively. In order to better characterize the image features [9], the dictionary atom is described based on the region image block. The dictionary is optimized by combining the two characteristics of wide band range and high-spectral resolution of hyperspectral remote sensing image, and the segmentation is completed by using the optimized DICTIONARY [10].

The purpose of clustering is to realize the division of clusters, which is completed according to the similarity of images, so that the elements with increased similarity are located in the same cluster, as shown in the following formula:

$$W_a = \min \sum_{i=1}^{K} R(x_i, v_i), \tag{3}$$

where K represents the number of clusters; x_i represents the i cluster, and v_i represents its cluster center; R represents the input hyperspectral remote sensing image, and $R(x_i, v_i)$ represents the distance, corresponding to the distance between x_i and v_i. The smaller the distance, the higher the degree of similarity between the two.

x_j is classified according to V_i. On this basis, a new clustering center is obtained, and the clustering is completed after complete convergence through cyclic iterative processing between them.

The center point is determined and represented by any pixel in x_j. In order to obtain the column vector set and contain n elements, the neighborhood image is processed by transformation, and the set is used as the input signal. The objective function of the method is shown in formula (1):

$$\min_{w_{ij}, D_j, C_j} J = \min_{w_{ij}, D_j, C_j} \sum_{j=1}^{k} \sum_{x_i \in C_j} (x_i - D_j w_{ij}), \tag{4}$$

where k represents the limit; J represents the sparse vector value; C_j represents the number of atoms; D_j stands for dictionary, corresponding to C_j; m_j represents the number of atoms, corresponding to D_j; w_{ij} represents sparse vector, corresponding to any signal x_i; T represents the limit, corresponding to sparsity; $R(D_j)$ represents the function, which is used to judge the consistency within D_j; δ means to set the fluctuation threshold. The smaller the value, the higher consistency of atoms in the dictionary.

After completing the construction of D_j, each w_{ij} has corresponding pixels in different clustering dictionaries. Therefore, the former can be determined according to the image signal corresponding to the latter. If you get $\|x_i - D_j w_{ij}\|$ with the smallest D_j, it indicates that the similarity

between D_j and x_i is high, you can classify the latter into the former.

During image segmentation [11], the neighborhood information of each pixel of hyperspectral remote sensing image is processed by transformation to form a one-dimensional vector x_i. In order to obtain the input signal set X, all signals are integrated to obtain x_i, which belongs to spectral remote sensing image. After the sparse representation of X is completed by sparse coding, X_i is segmented by clustering. In order to ensure the matching degree between the dictionary and the signal, the dictionary update needs to be completed, which is completed according to the signal in the cluster. After realizing the convergence of the energy function value J according to the cyclic interactive iteration, the clustering segmentation of hyperspectral remote sensing image is completed, and the segmented image $\tilde{X}$ containing target information is obtained.

2.3. Abnormal Target Detection Based on Deep Convolution Neural Network. After image clustering and segmentation, this paper uses the deep convolution neural network (DCNN) model to complete the final hyperspectral remote sensing image abnormal target detection. The model adopts dual classifier. The classifier is a machine learning method based on quadric surface and a general abnormal target linear classification method. Thus, the final abnormal target detection is completed, and the model structure is shown in Figure 1.

Take $\tilde{X}$ as the input of the model, and the convolution layer extracts the feature of $\tilde{X}$. Through convolution operation, the feature signal of the image can be enhanced, and the edge detection of the image can be sharpened and blurred [12]. The formula of convolution operation process is shown in

$$a_{j,l} = f \sum_{i \in M_j} \tilde{X} a_{j,l-1} * f \kappa_{i,j,l} f b_{j,l}, \tag{5}$$

where $a_{j,1}$ represents the activation value, corresponding to the output characteristic image j, and belongs to layer l; $k_{i,j,1}$ represents the kernel, which is used to connect two characteristic diagrams, which are located in layer l and layer $l-1$, respectively; $b_{j,1}$ represents the addition deviation, which corresponds to the output characteristic image j, and belongs to layer l; $f(\cdot)$ represents Relu function; M_j represents the characteristic diagram j and is linear.

The pooling layer can realize subsampling processing, which belongs to image features and needs to be based on the local correlation of the image, so that the valuable information in the image can be retained to the greatest extent [13]. The calculation formula of this layer is

$$a_{j,l} = f \beta_{j,l} \text{down}(a_{j,l-1}) \tilde{X} + f \alpha_{j,l} b_{j,l}, \tag{6}$$

where $\text{down}(\cdot)$ represents the function, corresponding to subsampling; $\beta_{j,1}$ and $\alpha_{j,1}$ represent multiplication bias, corresponding to the output characteristic image, and belong to the layer l.
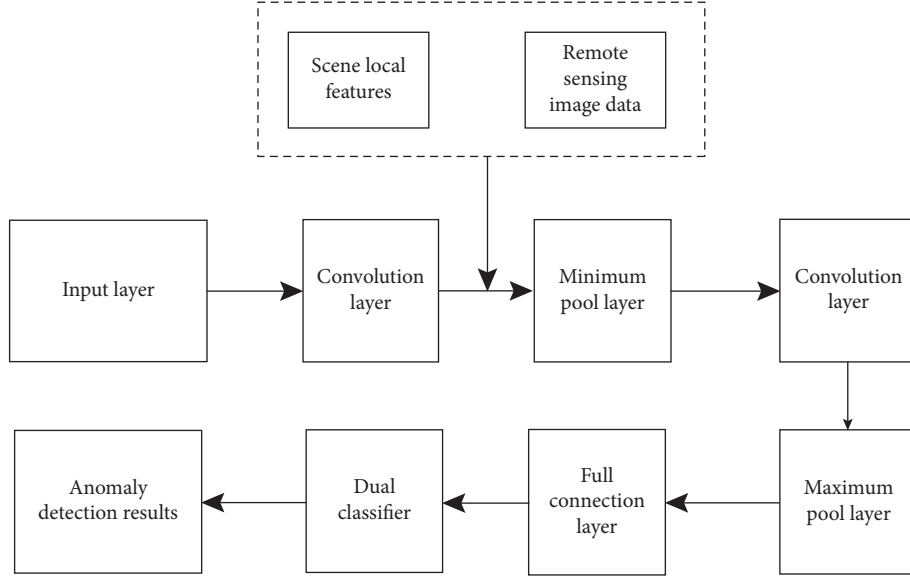
FIGURE 1: Abnormal target detection model based on DCNN hyperspectral remote sensing image.

When detecting abnormal targets in hyperspectral remote sensing images [14], there are obvious quantitative differences between classes. Therefore, in order to ensure the accuracy of detection results, weight is introduced to restrict each class of the image, larger weight is added to smaller classes, and smaller weight is added to larger classes; then, as shown in the following formula,

$$L(W, b) = \frac{1}{2}\left[\frac{\sum_{i=1}^{z}\mu_i\left\|y_j^{z_i} - \widehat{y}_j^{z_i}\right\|^2}{mn} + \lambda W^T W\right], \qquad (7)$$

where μ_i represents the weight, which is used for different types of constraints; L represents the deformation of norm; z_i represents the quantity, corresponding to the selected hyperspectral remote sensing image sample points; λ, m, and n are constants; W represents the weight matrix; $y_j^{z_i}$ and $\widehat{y}_j^{z_i}$ represent the feature value and feature approximation of the selected image, respectively.

The dual classifier in the model is a two-layer stack. The first layer is used as the training set of the second layer after completing the feature reconstruction of hyperspectral remote sensing image [15]. The dual classifier has the ability of spectral remote sensing image feature fusion, which can fuse the original features and extracted new features in the image, and process the fused features by means of standardization and normalization, to improve the detection accuracy of abnormal targets.

3. Experimental Analysis

In order to test the application performance and effect of this method on the abnormal target detection of hyperspectral remote sensing image, this method is used to detect the remote sensing image of land resource management in a province. The purpose of detection is to determine the abnormal illegal construction or illegal occupation of cultivated land based on hyperspectral remote sensing image
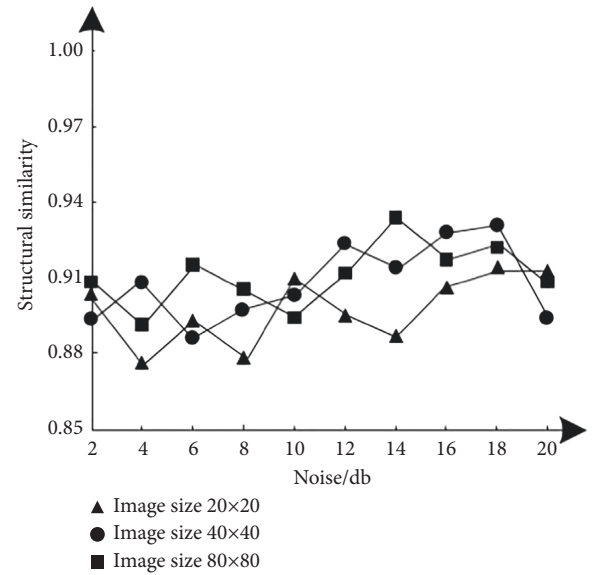
FIGURE 2: Test results of the structural similarity index.

and cooperate with relevant departments to complete land resource management. Hyperspectral remote sensing image detection is used to collect abnormal information. In the process of real-time abnormal target detection, line images need to be collected, so a 2-way blade server is used as the image server. Considering the running time, a disk array with a capacity of 8 t will be selected for the amount of data collected, so as to ensure the safety of abnormal target detection in hyperspectral remote sensing images.

3.1. Denoising Test. In order to test the drying performance of this method, structural similarity $S_{SSIM}(x, y)$, image information entropy H, and average correlation coefficient $\overline{C}$ are used as rating indicators, in which structural similarity
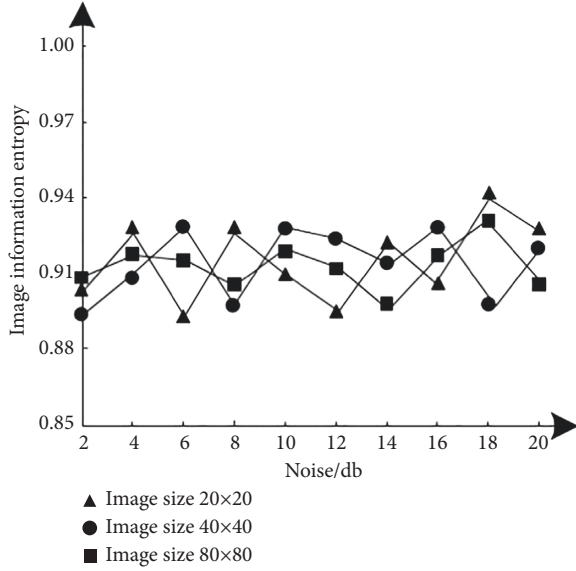
FIGURE 3: Test results of the image information entropy index.

FIGURE 4: Test results of the average correlation coefficient index.

refers to the measurement of macromolecular structural similarity; image information entropy refers to the average number of bits in the gray level set of hyperspectral remote sensing images; average correlation coefficient refers to the amount of linear correlation between abnormal target detection variables in hyperspectral remote sensing images, which usually represents an uncertain relationship. Test the results of three indexes after image denoising with different noise levels, as shown in Figures 2–4. The calculation formulas of the three indicators are as follows:

$$S_{\text{SSIM}}(x, y) = \frac{2\varepsilon_x \varepsilon_y}{(\varepsilon_x + \varepsilon_y)^2} \frac{2\sigma_{xy}}{(\sigma_x + \sigma_y)^2}, \tag{8}$$

$$H = -\sum_{i=0}^{1} p(i)^2 \ln, \tag{9}$$

$$\overline{\vartheta} = \frac{\sum_{i=1}^{m} \sum_{j=1}^{n} \vartheta_{od}(i, j)}{mn}, \tag{10}$$

where x and y represent two hyperspectral remote sensing images, and their mean values are represented by ε_x and ε_y, respectively. The covariance between them is σ_{xy}; $P(i)$ represents the probability density function, corresponding to the gray value i. $\vartheta(i, j)$ represents the correlation coefficient, which belongs to the spectral vector before and after noise reduction and corresponds to the pixel at (i, j) of the hyperspectral remote sensing image; m, n represent the number of rows and columns of hyperspectral data, respectively. The larger the value of the three index results, the better the noise reduction performance of this method, and the more the details and quality of the denoised image can be guaranteed. The expected standard is that the results of the three indexes are higher than 0.86.

According to the test results of Figures 2–4, under different image sizes, with the gradual increase of noise, the three indicators of this method show corresponding differential changes, but the change results meet the expected standard requirements, even if the image size is 80×80, when the noise is 20 dB, the results of the three indexes are 0.91, 0.90, and 0.88, respectively. Therefore, this method has good noise reduction performance.

In order to measure the noise reduction effect of this method, a remote sensing image of land resource management is randomly selected for noise reduction and the image results before and after noise reduction are obtained to judge the noise reduction effect of this method, as shown in Figure 5.

3.2. Image Classification and Evaluation.

In the experiment of remote sensing image classification, this paper uses 2DCNN, 3DCNN, and ResNet to compare and analyze the classical Indian pins set of remote sensing data, so as to further verify the training advantages of residual network. As shown in Table 1, the OA of remote sensing image classification completed by the reset model is as follows: the value is 0.966385; the value of AA is 0.967972; and the value of kappa is 0.960746.

Figure 6 shows the confusion matrix of the classification of Indian pins common data set. It is found that the position of each measured pixel shows better accuracy compared with the corresponding position of the actual image. Figure 7 shows the iterative values of loss, accuracy, val_loss, and val_loss, which further shows that this method has a good effect on the classification of multiband remote sensing images after noise removal.

According to the test results in Figures 5–7, it can be seen that there is noise influence in the image before noise reduction, and there is fuzziness in the image. After noise reduction, the clarity and brightness of the image are significantly improved. The results intuitively show that the noise reduction effect of this method is good, and the noise removal in the image can be completed on the premise of ensuring the quality of image details.
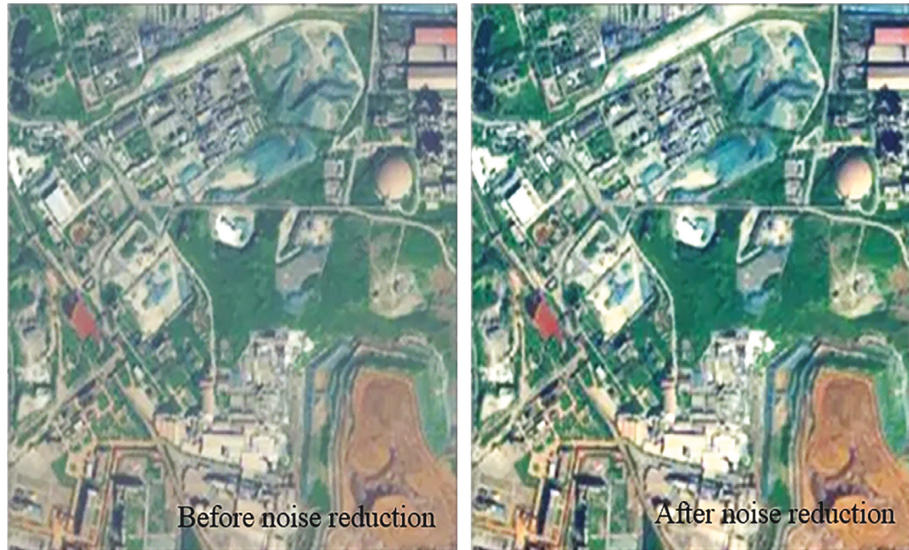
Figure 5: Test results of noise reduction effect.

Table 1: Comparison of classification accuracy of remote sensing images.

Network type classification criteria	OA	AA	Kappa
2DCNN	0.761929	0.767287	0.728459
3DCNN	0.949264	0.970596	0.940559
ResNet	0.966385	0.967972	0.960746
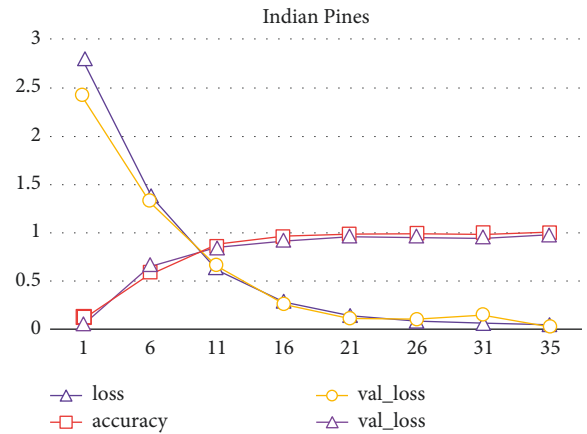
Figure 7: Precision contrast of the residual network.
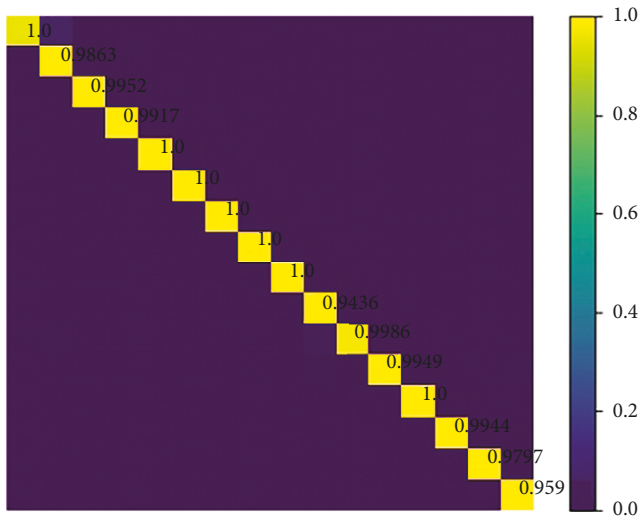
Figure 6: Confusion matrix of the residual network.

Figure 8: Test results of the gray mean index.

In order to test the image segmentation effect of the method in this paper, the gray mean and Jaccard similarity are used as evaluation indexes, and their calculation formulas (11)-(12) are as follows:
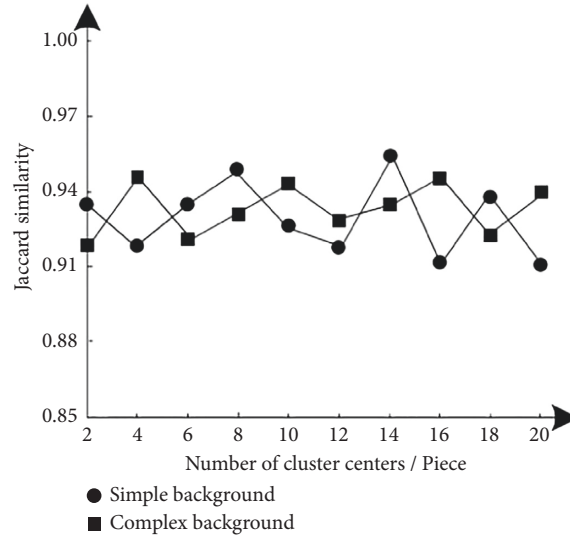
FIGURE 9: JAC similarity index test results.
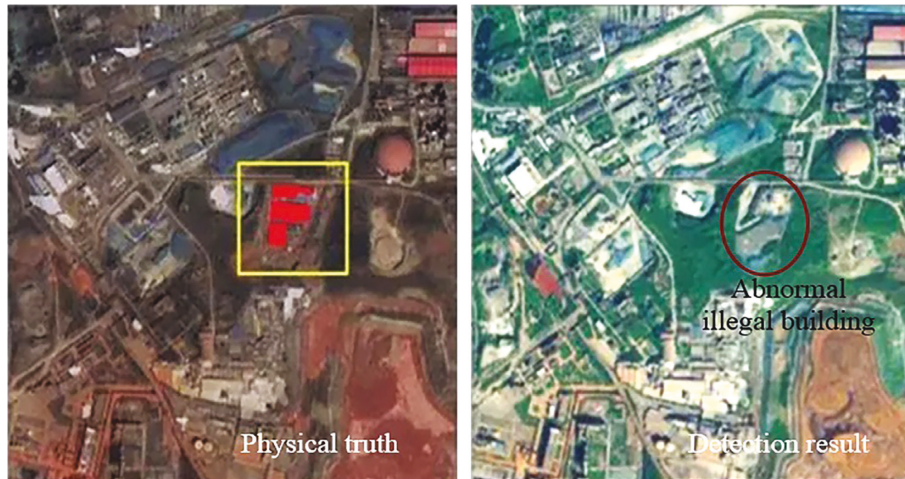
FIGURE 10: Abnormal target detection test results.

$$\mu = \frac{1}{mn} \sum_{i=1}^{m} \sum_{j=1}^{n} x_{ij}, \tag{11}$$

$$\text{JAC}(A, B) = \frac{|A \cap B|}{|A \cup B|}, \tag{12}$$

where x_{ij} represents the gray value of the image after noise reduction and corresponds to the pixel point at (i, j); A, B represent two different sets. The average gray level can reflect the gray level of the image, that is, the brightness of the image, and the expected standard is between 0.4 and 0.6. The closer the JAC similarity is to 1, the better the quality of the segmented image. The expected standard in this paper is more than 0.85.

The image segmentation results of the method in this paper are obtained according to formulas (9) and (10), as shown in Figures 8 and 9.

According to the test results of Figures 8 and 9, with the gradual increase of the number of segmentation of

hyperspectral remote sensing images, the results of gray mean fluctuate within the standard range. The results show that even if the number of segmentation is large, the basis can ensure the image quality. Therefore, it also indirectly shows that. The segmentation effect of this method is still good for images with complex background. In addition, with the gradual increase of clustering centers in the image, the results of JAC similarity fluctuate irregularly, but the variation range is about 0.9. Therefore, the image segmentation effect of this method is good and can obtain the target image information with high definition.

3.3. Target Monitoring Results. In order to test the abnormal target detection of hyperspectral remote sensing image in this method, this method is used to detect the abnormal target in the denoised image in Figure 5. There are abnormal illegal buildings in this image. The detection results of this method are obtained, as shown in Figure 10.

According to the test results in Figure 10, this method can complete the detection of abnormal targets in hyperspectral remote sensing images and obtain abnormal illegal buildings in the images. After confirmation, the detection results are consistent with the actual results. Therefore, this method has the effect of abnormal target detection in hyperspectral remote sensing images, and the detection results have good reliability.

4. Conclusion

Hyperspectral remote sensing images are used in more and more fields. It is an important detection method to complete abnormal target detection based on remote sensing images. In order to ensure the reliability of hyperspectral remote sensing image abnormal target detection, a hyperspectral remote sensing image abnormal target detection method based on the convolution neural network is proposed in this paper. The convolution neural network is used to classify the image to obtain the high-spectrum remote sensing image with target features, which is introduced into the convolution neural network with dual classifier to detect it. The results show that the abnormal target detection method of hyperspectral remote sensing image based on the convolution neural network has good noise reduction performance and can complete the noise processing in the image under the condition of ensuring the image quality and fine grain level. At the same time, it can also better complete the classification of target areas, and the display effect of various indicators is good. After segmentation, the quality of hyperspectral remote sensing image is intact, which plays an important role in accurately detecting abnormal targets in the image.

Data Availability

The datasets generated for this study are included within the article.

Conflicts of Interest

The authors declare that there are no conflicts of interest regarding the publication of this paper.

Acknowledgments

References

[1] Y. Miao, H. Zhao, and Y. Li, "Multi classification and recognition of hyper-spectral remote sensing features based on convolutional neural network," *Progress in Laser and Optoelectronics*, vol. 56, no. 2, pp. 191–198, 2019.

[2] J. Yang, J. Wu, and J. Zhi, "Research on aircraft target detection method in remote sensing image based on multi-scale circular frequency filtering and convolutional neural network," *Journal of Electronics and Information*, vol. 43, no. 05, pp. 1397–1404, 2021.

[3] Q. Yao, X. Hu, and L. Hong, "Research on remote sensing target detection based on multi-scale convolutional neural network," *Journal of Optics*, vol. 39, no. 11, pp. 346–353, 2019.

[4] H. Li, C. Li, and A. Anjubai, "Remote sensing image target detection based on improved convolution neural network with attention mechanism," *Chinese Journal of Image and Graphics*, vol. 24, no. 08, pp. 1400–1408, 2019.

[5] Y. Zhang, W. Hua, and F. Huang, "hyper-spectral anomaly target detection based on spatial spectrum joint anomaly degree," *Spectroscopy and Spectral Analysis*, vol. 40, no. 06, pp. 1902–1908, 2020.

[6] W. Wang, B. Zhao, and L. Tang, "hyper-spectral target detection based on spectral difference equalization interval screening," *Journal of Beijing University of technology*, vol. 39, no. 03, pp. 320–326, 2019.

[7] W. Jiang and L. Xiao, "Mei Shaohui Remote sensing image denoising algorithm based on convolutional neural network," *Microelectronics and Computer*, vol. 36, no. 08, pp. 59–62, 2019.

[8] J. Zheng, J. Huang, and M. Qin, "hyper-spectral image denoising based on nonlocal similarity and weighted truncated kernel norm," *Computer Science*, vol. 48, no. 09, pp. 160–167, 2021.

[9] Y. Liu and M. Xiao, "The door is facing the light hyper-spectral remote sensing image classification method based on multiple spatial information," *China Space Science and Technology*, vol. 39, no. 02, pp. 73–81, 2019.

[10] S. Li and Q. Wu, "Multi target detection and segmentation of remote sensing image based on improved mask r-cnn," *Computer Engineering and Application*, vol. 56, no. 14, pp. 183–190, 2020.

[11] J. Li, J. Cao, and B. Cheng, "Spectral clustering segmentation of high-resolution remote sensing images based on joint pixels and multi-scale objects," *Journal of Jilin University (Engineering Edition)*, vol. 49, no. 06, pp. 2098–2108, 2019.

[12] B. Cheng, "Zhao Chunhui Sparse RX hyper-spectral anomaly detection based on joint spatial preprocessing and bilateral filtering," *Journal of Harbin Engineering University*, vol. 40, no. 04, pp. 851–857, 2019.

[13] B. Sun, Z. Zhao, and B. Hu, "hyper-spectral anomaly detection based on 3D convolutional self codec and low rank representation," *Acta Photonica Sinica*, vol. 50, no. 04, pp. 262–274, 2021.

[14] D. Wang, W. Rao, and X. Sun, "hyper-spectral image anomaly detection combined with twin network and pixel pairing," *Chinese Journal of Image and Graphics*, vol. 26, no. 08, pp. 1860–1870, 2021.

[15] Z. Xu, "Zhang Ting Simulation of digital multimedia scene image accurate classification method," *Computer Simulation*, vol. 36, no. 07, pp. 385–388, 2019.

Research Article

Differentiation in Emotional Investments in Work Groups among Different Social Status of Construction Industry Practitioners: A Perspective from the Social Exchange Theory

Wenqing Zhang [iD] **and Dingzhou Fei** [iD]

Department of Psychology, Wuhan University, Wuhan, China

Correspondence should be addressed to Dingzhou Fei; feeding_psy@whu.edu.cn

The construction industry is characterized by a high level of mobility and a diverse range of practitioners from different social status, which can affect the industry's group management processes. The exploration of the mechanisms involved is an important task for theoretical research and a challenge for management practices. This study examines three relevant aspects of work-group behavior in the construction industry from a social exchange perspective: the individual's evaluation of the level of the emotional investment of members in the work team and their assessment of personal rewards and costs. The study of 71 construction industry workers through the development of a cost-benefit inventory questionnaire of individual-team exchange relationships revealed that their level of emotional investment in the work group can be predicted by assessing their awareness of personal rewards and costs. A further clustering algorithm revealed that an individual's social status had a significant impact on their level of affective investment, but there was no significant correlation between an individual's wage and their level of emotional investment in the work team. The findings deepen our understanding of group behaviors in the construction field by explaining the interactions between individuals and organizations in work groups while emphasizing the indispensable role of emotional factors in group development.

1. Introduction

1.1. The Current Situation of Construction Industry Workers.
After a long period of market system construction and effective regulation and rectification, the construction industry is steadily developing. At the same time, some social problems caused by the nature of the long project cycle, many projects, and complex environment have been exposed. Among them, the emotional problems of workers are coming to the fore more and more. Workers who are highly mobile due to site changes and need to move around all year round are usually far away from the city and their families and friends, and the resulting work-family conflicts can affect the social behavior of construction workers [1], and kinship plays an important role in the effectiveness of relational governance mechanisms in projects [2]. In addition, construction industry workers have a complex composition and diverse social backgrounds and are forced to accomplish

demanding and urgent tasks in an undesirable living environment and monotonous life. In such a work and life environment, it is imperative to pay attention to the emotional state of construction workers who are motivated by different social classes [3]. In addition, the current external competition of construction enterprises is becoming increasingly fierce, and in order to cope with the external pressure, enterprises need to give full play to their talents and mobilize the emotional engagement of their employees to cope with the market demands.

1.2. Social Exchange Theory. As one of the major theories of social interaction in the social sciences, theoretical and empirical applications involve extending the work of social exchange theory to the analysis of power and dependency, social networks, reciprocity, equity, social cohesion, and solidarity [4].

Airman and Taylor [5] studied relationship development from the perspective of social penetration, which led to the formulation of the well-known social exchange model of interpersonal interactions. Social penetration is viewed as a systematic process of self-revelation among individuals in interpersonal interactions in which people continually assess the quality of their interactions to determine whether they need to continue to invest. In contrast, the behaviors exhibited in social systems are the result of individual decision-making, where group members exchange various types of resources based on their assessment of and dependence on others. In previous research, the social exchange and exchange of information among construction industry practitioners can influence decisions on construction projects, which in turn affect work health and safety [6]. In addition, components of the emotional exchange model are often used to explain dynamic relationships such as emotional experience and expression [7]. It was also found that interpersonal relationships are continuously socially exchanged in a continuous developmental process and have a tendency to be increasingly rewarding.

1.3. Emotional Investment.
Emotional investment is a relational orientation in which individuals show loyalty and commitment to their work group and show mutual concern for their colleagues, and trusting interactions between participants help foster beneficial relational behaviors that in turn improve team performance [8]. It helps to improve team communication and thus effectively increases team effectiveness [9] As members' mutual interest increases, personal relationships accumulate and relationships with others become closer, and individuals make ongoing emotional investments in relationships [10], while each successful social exchange increases interdependence and commitment among work group members [11]. With increased interdependent communication, more and more team members have a higher level of emotional investment, which in turn leads to more effort for the team's goals and increases the satisfaction of other members. At the same time, the team environment evolves away from the previous mutual exchange of resources among group members to one in which the individual needs of members are met within the work group. Current research hot spots for emotional investment are applications to family groups of foster children [12, 13] and social media [14, 15], but we believe emotional investment can be applied to a broader range of domains.

1.4. Personal Rewards and Personal Costs.
Personal rewards refer to enjoyable or appreciated relational attributes that an individual receives in a relationship. Rewards are usually divided into six categories: money, status, love, information, things, and services. Each person defines rewards differently; what one person seeks may be worthless to another. Personal costs refer to the relationship attributes that individuals pay for in relationships that are annoying or disliked. For social exchange theory, successful resource exchange means that rewards can be maximized in exchange for the smallest possible personal cost. When this ideal social exchange is

achieved, group members increase their mutual contribution and commitment (e.g., [16]). Reciprocity signifies engagement and attachment among members, and the results of Xerri's [17] self-reported survey of 255 Australian engineering asset management employees indicated that the organizational support for members can positively predict employees' emotional attachment to the organization. Moreover, organizational support, emotional commitment to the organization, and employees' psychological well-being are mutually reinforcing, so individual rewards may be a more reliable predictor of reciprocity than costs. Therefore, we consider that personal rewards may be a better predictor of emotional investment than personal costs.

1.5. Adopting a Social Exchange Perspective to Analyze the Construction Industry.
To analyze in depth the attachment and especially the loyalty of construction workers to their groups, we applied social exchange theory to workers and managers in the construction industry, and to examine what characteristics this affective investment has due to the high mobility of the construction industry and how it relates to the social status of construction workers, an important aspect of construction project management theory has to be questioned. Our study is dedicated to find the correlation between social status and emotional investment in the context of a highly mobile profession like the construction industry. Behavior can be seen as the result of an individual's decision to make a trade-off between rewards and costs, a strategic framework for a game in which individuals or groups interact with society and the environment.

We emphasize the role of emotional investment in promoting work group survival and interdependence among team members, as quality relationships within the work group are the foundation for unlocking the individual potential for improved performance in the project environment [18]. In contrast, most studies on work groups emphasize group efficiency and output without examining the costs and rewards perceived by individual group members or the emotional investment members make in the group [19]. But an overemphasis on group output in the short term can have negative effects on group members' psychological well-being and performance and even on the long-term development of the group [20]. The reasons for this are as follows: first, if individuals feel a lot of pressure to perform in the short term and do not receive the emotional attention or personal rewards that are commensurate with the cost, group continuity is difficult to maintain and the long-term development of the group is not guaranteed [21], and group members may choose to leave, so long-term work group performance will be negatively affected. Second, if short-term team performance goals are overemphasized and members are required to sacrifice their personal interests to achieve them, members may reduce their efforts and knowledge contributions to the team [22], and in this case, although members do not terminate their ties to the group, their social interactions are reduced, individual emotional ties with other members are neglected, and the performance of the work group is similarly affected. Emotional support

such as motivation has been found to help with multiproject management in the industry, reduce burnout, and help retain project members [23].

As a human resource that needs to be developed in the current situation, the emotions of employees can have a significant impact on the dedication of corporate workers and the development and implementation of corporate systems [24]. In a study of the stress and burnout tendencies of members of different project groups, Pinto [25] found that project managers and construction workers had significantly higher levels of emotional exhaustion relative to other job types, so the construction industry should focus more on the social stratification of the practitioners in order to provide emotional de-escalation and management for groups vulnerable to psychological problems [3]. In view of the special characteristics of the work of employees in the construction industry, part of the employees are migrant worker groups with high job mobility and relatively high wage levels for some skilled workers with little room for promotion, and part of the employees are regular employee groups in construction enterprises with more stable jobs and relatively low wages, but with room for promotion within the enterprises. However, due to the inevitable existence of social prejudice, this paper classifies the group of migrant workers or contract workers as a group with relatively low social status and the group of regular employees within the enterprise as a group with relatively high social status. This paper examines team members' evaluations of personal costs and rewards and their own emotional investment in the work group and compares whether there are significant differences in the levels of emotional investment between the two groups and how their evaluations of personal costs and rewards affect their levels of emotional investment. In a social group, people with high social status usually interact emotionally with the group more than people with low status in the group.

In summary, this study focuses on the role of emotional investment generated by construction industry practitioners in the work group and its influencing factors. We consider the emphasis on affective investment and the focus on stratification of construction workers and the work environment as the main contributions of this study.

Based on the above statements, we build on the construction industry group and adopt a social exchange perspective to propose three hypotheses.

- (H1) People with high socioeconomic status have a higher level of emotional investment in the group
- (H2) High income does not affect the level of the emotional investment of individuals in the work group
- (H3) Personal rewards can be a better predictor of emotional investment than personal costs

2. Methods

The methods of this work consist of participants for surveys, questionnaires revised for Chinese contextures, and clustering analysis for defining the major factor affecting the emotional investments in the work groups.

Table 1: KMO and Bartlett test.

KMO measure of sampling adequacy		0.758
Bartlett's test of sphericity	Approx. chi-square	397.199
	df	36
	Sig.	0.000

Participants: due to the low participation of women in the architectural, engineering, and construction industry [26], a total of 71 (including 12 women) construction workers were selected to participate in this questionnaire for this study.

Objective of the surveys: to collect construction workers' level of emotional investment in work teams and team members' assessments of individual costs and personal rewards (including regular, contract, and migrant workers) by questionnaire survey method.

Study steps: this task focused on developing questionnaires and scales. The original scales and questionnaires were in English, and to translate all survey items from English to Chinese, we used the translation/back-translation procedure of Brislin [27] and then adapted them to the Chinese context. Finally, the adapted questionnaires and scales were tested for reliability and validity.

To test our proposed hypotheses, we conducted analyses at the individual level. We referred to Saavedra and Dyne [28] and selected three separate items from the cost-benefit inventory developed by [29, 30] based on social exchange in interpersonal relationships to assess individuals' perceptions of rewards and costs. Considering the purpose of this study is to examine the personal trait attributes and relational attributes of the different social status of practitioners within the construction industry, the items focus on the exchange of nonmaterial resources [28]. To measure affective investment, we used three items from Hackman's [21] assessment of members' perceptions of group well-being. A principal components analysis was conducted on nine items to ensure that the scale we used would achieve the predicted effect. The results indicated that the three factors, emotional investment, rewards, and costs, together accounted for 77% of the variance. Table 1 examines the suitability of the scales we used for principal components analysis, and Table 2 lists the individual items and the factor loadings for each item.

This study used the KMO (Kaiser–Meyer–Olkin) test to statistically compare the correlation coefficients between the variables, which yielded a KMO value of 0.758, which is greater than 0.7 (KMO takes values between 0 and 1, and the larger its value, the more suitable the original variables are for factor analysis). In addition, Bartlett's test $P < 0.05$, the above data indicate that it is appropriate to do factor analysis on the above items.

In addition, we conducted separate reliability analyses for the items measuring each factor in the scale, and Cronbach's α coefficients for each item measuring the three factors of emotional investment, personal cost, and personal reward were 0.857, 0.739, and 0.893, respectively, all greater than 0.7, meaning that the reliability of each item in the questionnaire was high.

TABLE 2: Factor analyses of self-report items.

Items	F1 personal rewards	F2 emotional investment	F3 personal costs
1. The members of my work team listen to me.	0.831	0.208	0.080
2. I feel needed by my work team.	0.863	0.376	0.068
3. I feel comfortable when I voice my work in work group.	0.835	0.348	079
4. Our team members have a strong sense of loyalty to the team.	0.235	0.925	0.010
5. Our work team members care about the collective and are committed to making it better.	0.370	0.888	0.021
6. I do not want to change the members of our work group.	0.442	0.597	0.128
7. Since I am friends with the members of my work team, I undertake a lot of extra responsibilities.	0.210	0.205	0.832
8. I often compromise my ideas by considering the preferences of other team members.	0.084	0.064	0.826
9. To integrate into the work group, I must sacrifice a great deal of personal independence.	0.223	0.043	0.765

3. Results

To test whether social status affects the level of individual affective investment, we conducted an independent sample t-test on the overall affective investment level between the regular and migrant worker groups, and the results are reported in Tables 3 and 4.

From the results of the independent sample t-test, it can be concluded that within the confidence interval of 99%, the level of emotional investment between regular and migrant worker groups is significantly different, and the level of the emotional investment of regular workers is significantly higher than the level of the emotional investment of migrant workers in work groups (The Emotional Investment Questionnaire items were selected on a seven-point scale, with a choice of 1 meaning strongly agree and a choice of 7 meaning strongly disagree). The formal worker group and the migrant worker group have different socioeconomic status, and it follows that socioeconomic status affects the emotional investment of individuals in the work group, and individuals with higher socioeconomic status have higher emotional investment in the work group; therefore, H1 is confirmed.

In order to describe the intergroup differences more intuitively in the overall level of emotional investment in different social status within the construction industry, we conducted a cluster analysis of the results of the emotional investment survey, the results of our survey on sentiment investment were analyzed in Origin using the K-mean algorithm for clustering. As a mainstream data analysis software, Origin has two main functions: data analysis and plotting. Origin's data analysis includes a variety of sophisticated mathematical analyses such as statistics, signal processing, image processing, peak analysis, and curve fitting. We use K-means, an unsupervised learning algorithm for solving clustering problems. The K-means method is a classical algorithm in clustering, one of the top ten classical algorithms for data mining; the algorithm receives the parameter k and then divides the n data objects entered in advance into k clusters, in order to satisfy that the objects in the clusters are more similar, while the objects in different clusters are less similar. The idea of the algorithm is to cluster

TABLE 3: Analysis of social status among construction workers.

	Overall emotional investment level			
	N	Mean	SD	Std. error mean
Regular worker	36	6.8333	3.48727	0.46601
Migrant worker	35	6.8857	3.28194	0.49477

the k points in the sample space, grouping the objects closest to them and updating each cluster centre one by one by iterative methods. The results are shown in Figure 1.

From the results of the cluster analysis, the distance of the vertical coordinate represents the difference in the level of emotional investment between the samples, and the horizontal coordinate represents the individuals; it can be seen that individuals belonging to the same social class are more aggregated and show more similarity in emotional investment, thus concluding that the social stratification in the construction field is obvious, and different groups based on different social classes differ in the characteristic of emotional investment level, while within the group, this characteristic is similar. The characteristics are similar within groups.

In addition, this study tested whether the level of personal income affects the emotional investment of individuals in the work group. The mean of the income levels of the 71 construction industry workers collected in this study was 1068.5 US$, so we used 1068.5 US$ as a cut-off for high- and low-income levels, with those below the mean income considered as a low-income group and those above the mean income considered as a high-income group, and conducted independent sample t-tests on the overall emotional investment levels of the two groups. The results are reported in Tables 5 and 6.

As can be seen in Table 6, the difference in the overall level of emotional investment between the high-income group and the low-income group is not significant at a confidence interval of 99%, indicating that there is no significant effect of high income on the level of the emotional investment of individuals; therefore, H2 is proved.

TABLE 4: Differentiation in the level of emotional investment across social classes is shown by t-test.

		t	df	Sig (2-tailed)	Mean difference	Std. error difference	99% confidence interval of the difference	
							Lower	Upper
Overall emotional investment level	Equal variances assumed	−5.76	69	0.000	−3.80049	0.66535	−5.5926	−2.0677
	Equal variances not assumed	−5.76	44	0.000	−3.80049	0.69693	−5.7071	−1.9532
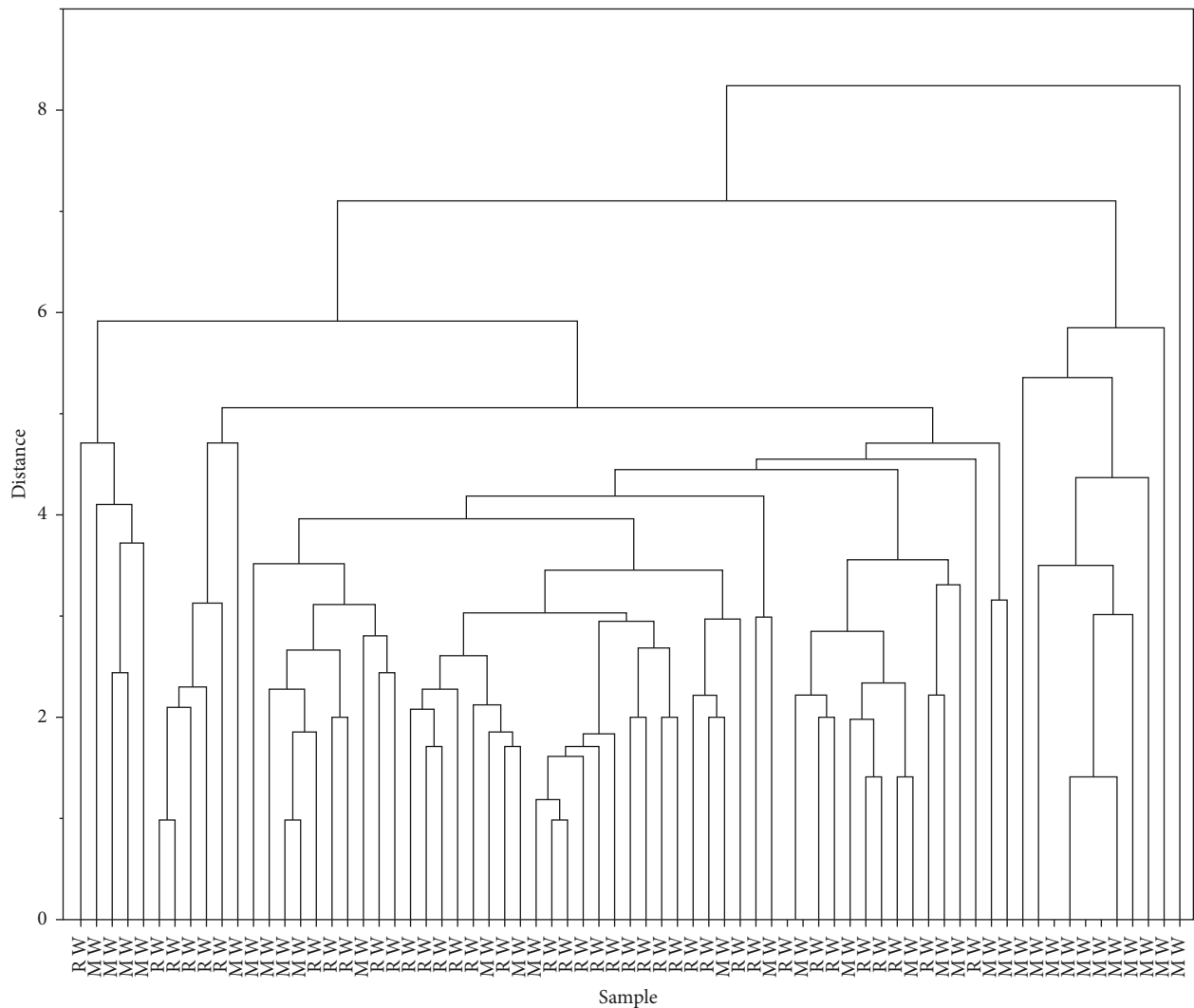
FIGURE 1: Intergroup differentiation in the level of emotional investment between regular workers and migrant workers through cluster analysis (RW = regular workers, MW = migrant workers).

We used hierarchical regression analysis to test H3, and the results are shown in Table 7. When both costs and rewards were regressed on affective investment, only rewards contributed unique and significant variance, indicating that individual rewards were the best predictor of affective investment among work groups in the construction industry; therefore, H3 is confirmed.

4. Discussion

Our goal is to illustrate the dynamics of relationships in the construction industry's work community on an emotional dimension, integrating concepts such as satisfaction, investment, and commitment. In the construction industry, construction workers are usually part of a work team, and

TABLE 5: Analysis of the income level of construction workers.

	Monthly income level	N	Overall emotional investment level		
			Mean	SD	Std. error mean
High-income group	≥1068.5 US	36	6.8333	3.48727	0.46601
Low-income group	<1068.5 US	35	6.8857	3.28194	0.49477

TABLE 6: The relationship between income level and emotional investment is illustrated by t-test.

		t-test for equality of means						
		t	df	Sig (2-tailed)	Mean difference	Std. error difference	99% confidence interval of the difference	
							Lower	Upper
Overall emotional investment level	Equal variances assumed	−0.7	69	0.98	−0.05238	0.80755	−2.1916	2.0868
	Equal variances not assumed	−0.7	69	0.948	−0.05238	0.80709	2.1903	−2.0856.

TABLE 7: Hierarchical regression analysis of emotional investment and personal costs and rewards.

Dv	IV	Adj. R^2	F	Beta for IV's
Emotional investment	Rewards	0.472	62.566	0.692
Emotional investment	Costs	−0.008	0.421	0.078
Emotional investment	Rewards Costs	0.464	30.883	0.690 0.022

poor work team relationships predict the work stress of construction workers, and their psychological perceptions greatly influence their behavioral and safety performance, and it is particularly important to study the impact of the work team on construction workers as key and indispensable contributors to each construction project [31]. Research sponsored by the American Society for Quality Control in conjunction with Fortune 500 companies shows that employees see teams as both a platform for personal development and a way to promote [32]. Studies have shown that construction workers with different levels of perception of group norms exhibit different personal safety behaviors at work. In addition, when construction workers were in different groups (e.g., work groups, projects), their perceptions of identity showed significant differences, thus introducing the idea that social identity with a group can moderate the effect of group norms on construction workers' personal safety behavior standards [33]. These findings also suggest new ideas for the management of the construction industry: improving the level of social identification and emotional investment of construction workers in their work group, which in turn improves communication in the team, and effective communication is an important factor in improving team effectiveness, thus enabling construction workers to have better emotional states while improving construction worker safety behaviors and increasing the efficiency of construction project completion.

Furthermore, most research on social exchange has focused on the cognitive aspects of relationships and has mostly examined binary exchanges between individuals, rarely addressing the affective aspects of social exchange. Therefore, this study examines the affective aspects of social exchange in structurally diverse pluralistic work groups within construction companies, extending the scope of the application of social exchange theory. However, excessive emotional attention may lead to a marked decrease in group members' openness to dissenting opinions [34]. By ignoring and excluding different insights and irreconcilable information, groups may make decisions that have serious adverse consequences. These problems are particularly evident in the construction industry, where the completion of projects in the construction industry relies on a variety of task environments such as raw materials, construction personnel, and market research in order to achieve them. Therefore, a balance between efficiency and emotion is needed to solve these problems.

The limitations of this paper are mainly reflected in the following aspects, which we will improve in our future research: firstly, due to the special nature of the sample of construction industry practitioners, the sample size we collected was not very large, but in future research, we will try our best to seek the cooperation of relevant construction companies in the hope that a larger sample size can be obtained. Also, during the data collection process, we discovered an interesting phenomenon: the vast majority of those working in the construction industry are men. This gap persists despite efforts to close the gender gap in the construction and engineering workforce and advocate for gender diversity over the past few decades [35, 36]. Outside of gender, age may have an impact on respondents' level of emotional investment [37], which needs to be refined in the future research. Perhaps in a more in-depth study in the future, we can make a more nuanced segmentation of construction industry practitioners to further explore the

social exchanges they engage within their work groups. Finally, this study did not include team performance in the overall structure, and in further research, we plan to explore the impact of emotional investment in work teams on team performance and create a more comprehensive research system considering that emotional investment may cause individuals to overestimate their actual abilities [38].

Data Availability

The [data type] data used to support the results of this study are available from the corresponding author upon request.

Conflicts of Interest

The authors declare that they have no conflicts of interest.

References

[1] Q. H. Xie, N. N. Xia, and G. Yang, "Do family affairs matter? Work-family conflict and safety behavior of construction workers," *Journal of Management in Engineering*, vol. 38, no. 1, Article ID 04021074, 2022.

[2] J. Xue, H. Yuan, and B. Shi, "Impact of contextual variables on effectiveness of partnership governance mechanisms in megaprojects: case of guanxi," *Journal of Management in Engineering*, vol. 33, no. 1, Article ID 04016034, 2017.

[3] G. Li, "An introduction to the emotional management of building construction enterprises," *Development*, no. 9, pp. 97-98, 2012.

[4] P. K. Jonason and J. P. Middleton, *The International Encyclopedia of the Social and Behavioral Sciences*, Elsevier, Amsterdam, Netherlands, 2015.

[5] I. Altman and D. A. Taylor, *Social Penetration: The Development of Interpersonal Relationships*, Holt Rinehart & Winston, New York, 1973.

[6] P. Pirzadeh and H. Lingard, "Understanding the dynamics of construction decision making and the impact on work health and safety," *Journal of Management in Engineering*, vol. 33, no. 5, p. 11, Article ID 05017003, 2017.

[7] J. L. Bevan, "Experiencing and communicating romantic jealousy: questioning the investment model," *Southern Communication Journal*, vol. 73, no. 1, pp. 42–67, 2008.

[8] X. Zheng, Y. J. Lu, and R. Chang, "Governing behavioral relationships in megaprojects: examining effect of three governance mechanisms under project uncertainties," *Journal of Management in Engineering*, vol. 35, no. 5, Article ID 04019016, 2019.

[9] K. G. Smith, K. A. Smith, J. D. Olian, H. P. Sims, D. P. O'Bannon, and J. A. Scully, "Top management team demography and process: The role of social integration and communication," *Administrative Science Quarterly*, vol. 39, pp. 412–438, 1994.

[10] W. W. Hartup and N. Stevens, "Friendships and adaptation in the life course," *Psychological Bulletin*, vol. 121, no. 3, pp. 355–370, 1997.

[11] I. Tallman, L. Gray, and R. L. Leik, "Decisions, dependency, and commitment: an exchange-based theory of group formation," in *Advances in Group Processes*, vol. 8, pp. 227–257, JAI Press, Greenwich, London, UK, 1991.

[12] N. Koren-Karie and R. Markman-Gefen, "Foster caregiver insightfulness and emotional investment in foster children," *Journal of Social Work*, vol. 16, no. 4, pp. 489–509, 2016.

[13] H. Jacobsen, H. Brabrand, S. Liland, T. Wentzel-Larsen, and V. Moe, "Foster Parents' Emotional Investment and Their Young foster Children's Socio-Emotional Functioning," *Children & Youth Services Review*, vol. 86, 2018.

[14] A. A. Alsunni and R. Latif, "Higher emotional investment in social media is related to anxiety and depression in university students," *Journal of Taibah University Medical Sciences*, vol. 16, no. 2, pp. 247–252, 2021.

[15] E. Lowe-Calverley, R. Grieve, and C. Padgett, "A risky investment? examining the outcomes of emotional investment in instagram," *Telematics and Informatics*, vol. 45, pp. 101299–101299.11, 2019.

[16] S. M. Drigotas and C. E. Rusbult, "Should I stay or should I go? A dependence model of breakups," *Journal of Personality and Social Psychology*, vol. 62, no. 1, pp. 62–87, 1992.

[17] M. J. Xerri, S. Nelson, and Y. Brunetto, "Importance of workplace relationships and attitudes toward organizational change in engineering asset-management organizations," *Journal of Management in Engineering*, vol. 31, no. 5, Article ID 04014074, 2015.

[18] M. M. Tuuli, S. Rowlinson, R. Fellows, and A. M. M. Liu, "Individual-level antecedents of psychological empowerment," *Journal of Management in Engineering*, vol. 31, no. 2, Article ID 04014036, 2015.

[19] L. Isaksson and T. Kiessling, "Corporate social responsibility (CSR) and engineering management: performance implications," *IEEE Transactions on Engineering Management*, vol. 7, pp. 1–11, 2021.

[20] J. E. McGrath, "Small group research, that once and future field: an interpretation of the past with an eye to the future," *Group Dynamics: Theory, Research, and Practice*, vol. 1, no. 1, pp. 7–27, 1997.

[21] I. R. Hackman, *A Set of Methods for Research on Work Teams (Tech. Rep. No. 1)*, Yale University, New Haven, CT, 1982.

[22] L. Argote and J. E. McGrath, "Group processes in organizations: continuity and change," in *International Review of Industrial and Organizational Psychology*, vol. 8, pp. 333–389, Wiley, New York, 1993.

[23] P. Patanakul, J. K. Pinto, and M. B. Pinto, "Motivation to perform in a multiple-project environment: the impact of autonomy, support, goal clarity, and opportunities for learning," *Journal of Engineering and Technology Management*, vol. 39, pp. 65–80, 2016.

[24] H. R. Wijaya and P. P. M. A. R. Heugens, "Give me a hallelujah! amen! institutional reproduction in the presence of moral perturbation and the dynamics of emotional investment," *Organization Studies*, vol. 39, no. 4, pp. 491–514, 2018.

[25] J. K. Pinto, P. Patanakul, and M. B. Pinto, "Project personnel, job demands, and workplace burnout: the differential effects of job title and project type," *IEEE Transactions on Engineering Management*, vol. 63, no. 1, pp. 91–100, 2016.

[26] V. Francis and E. Michielsens, "Exclusion and inclusion in the australian aec industry and its significance for women and their organizations," *Journal of Management in Engineering*, vol. 37, no. 5, Article ID 04021051, 2021.

[27] R. W. Brislin, "Handbook of cross-cultural psychology," in *Translation and Content Analysis of Oral and Written Material*, H. C. Triandis and J. W. Berry, Eds., vol. 2, pp. 349–444, Allyn & Bacon, Boston, 1980.

[28] R. Saavedra and L. Van Dyne, "Social exchange and emotional investment in work groups," *Motivation and Emotion*, vol. 23, no. 2, pp. 105–123, 1999.

[29] R. B. Hays, "The development and maintenance of friendship," *Journal of Social and Personal Relationships*, vol. 1, no. 1, pp. 75–98, 1984.

[30] R. B. Hays, "A longitudinal study of friendship development," *Journal of Personality and Social Psychology*, vol. 48, no. 4, pp. 909–924, 1985.

[31] M.-y. Leung, Y. S. Chan, and K. W. Yuen, "Impacts of stressors and stress on the injury incidents of construction workers in Hong Kong," *Journal of Construction Engineering and Management*, vol. 136, no. 10, pp. 1093–1103, 2010.

[32] M. D. Jones, *To succeed, work teams should benefit members and companies*, USA Today, 1996.

[33] B. Choi, S. Ahn, and S. Lee, "Construction workers' group norms and personal standards regarding safety behavior: social identity theory perspective," *Journal of Management in Engineering*, vol. 33, no. 4, Article ID 04017001, 2017.

[34] J. R. Hackman, "Group influences on individuals in organizations," in *Handbook of Industrial and Organizational Psychology*, M. D. Dunnette and L. M. Hough, Eds., pp. 199–267, Palo Alto, CA, USA: Consulting Psychologists Press, 2 edition, 1992.

[35] M. Baker, E. L. French, and M. Ali, "Insights into ineffectiveness of gender equality and diversity initiatives in project-based organizations," *Journal of Management in Engineering*, vol. 37, no. 3, Article ID 04021013, 2021.

[36] J. A. Maurer, D. Choi, and H. Hur, "Building a diverse engineering and construction industry: public and private sector retention of women in the civil engineering workforce," *Journal of Management in Engineering*, vol. 37, no. 4, Article ID 04021028, 2021.

[37] D. R. Johnson, M. E. Tynan, A. S. Cuthbert, and J. K. O'Quinn, "Metacognition in argument generation: the misperceived relationship between emotional investment and argument quality," *Cognition & Emotion*, vol. 32, no. 3, pp. 566–578, 2018.

[38] N. H. Zamzuri and Hamiza, "The role of emotional investment and social influence in predicting individual self-esteem for social media user among youth," *Advanced Science Letters*, vol. 23, no. 11, pp. 10542-10543, 2017.

Research Article

Correlation Study between Rural Human Settlement Health Factors: A Case Study of Xiangxi, China

Shuyuan Tong, Yafeng Zhu [ID], and Zhe Li [ID]

Department of Architecture, School of Architecture and Art, Central South University, Changsha 410075, China

Correspondence should be addressed to Zhe Li; lizhe88@csu.edu.cn

With the emergence of the Industry 4.0 era in China, more refined methods are being proposed for healthy living requirements for human settlements. Since the rural human settlements in China are relatively backward, this study aimed to investigate the influencing factors of human health. First, through field surveys and questionnaires conducted with villagers in Xiangxi's traditional villages in Hunan Province, we analyzed the factors affecting human health qualitatively and quantitatively using the SPSS software. We identified three main dimensions affecting human health in rural human settlements including human behavioral activities, physical environment, and natural environment. Then, we used correlation analysis and multiple linear regression analysis methods to analyze the correlation between environmental factors and human health. The results showed that human activities, building physical environment, and natural environment are significantly correlated with human health. Among them, human behavior has the strongest correlation with health. This research contributes to creating healthy human settlements and guiding the creation of a healthy environment in rural China.

1. Introduction

Under the backdrop of the Industry 4.0 paradigm, various industries around the world are gradually intelligent, integrated, and automated. Big data, interconnections, and artificial intelligence have been applied in the construction elements, which tend to develop in the directions of digitized, multifunctional, and health promotion [1–10]. Compared with traditional construction methods, Industry 4.0 has brought an innovation orientation and technological advancements to China's construction industry and improved the quality of human settlements, efficiency, and safety of construction processes [11–17]. With the increased emphasis on health performance in settlements, how to build a living environment that meets the needs of human health in the era of Industry 4.0 remained unclear, especially on environmental factors that affect health in different settings. Existing research on healthy architecture and living environments is valuable and involves multidimensional and multilevel fields, such as medicine, psychology, society, and planning [18–21].

In recent years, under the background of Industry 4.0, science and technology have developed rapidly in China. Research on the health of human settlements has been extensive, but most of it relates to urban settlements, while studies on the construction of traditional villages have been rare [22]. The production mode of construction industrialization has many advantages, including high production efficiency, good quality, low construction cost, saving resources, and protecting the environment. It can greatly improve the problems existing in rural housing, with the following positive effects:

① Improve the quality of housing construction

② Improve energy conservation and emission reduction

③ Improve the style of rural housing

④ Improve the construction speed

⑤ Improve the comfort of living environment

⑥ Reduce construction costs

⑦ Stimulate rural economic growth and resolve excess capacity [23, 24]

Therefore, the industrialized production of construction is the development trend of the construction mode of new rural construction in the future, and the state has issued a series of policies and measures to promote the industrialized construction and development of rural areas. To further promote the steady and healthy development of industrialization in rural areas, the healthy living environment in rural areas [23, 24]isfocused. Due to the acceleration of China's economic, social development, and process of urbanization, a large number of young laborers from rural areas have poured into cities, resulting in the widespread phenomenon of elderly people and children left behind in rural areas and even the emergence of "ghost villages." Numerous theoretical studies have shown that the living environment is directly related to the physical and mental health of the residents[25–27]. The rural environment in China is significantly different from the urban environment in terms of infrastructure, humanities and culture, and living conditions, thus resulting in significant differences in the physical and mental health levels of different groups of residents [28–30]. Generally, the village environment is rich in green resources and has good geography. In addition, the layout of the village and the housing structure follow the traditional idea of harmony between man and nature. These factors have a positive impact on human health. At the same time, bottlenecks in transportation, poor infrastructure construction, and physical environment need urgent improvements as such problems have a negative effect on people's physical and mental health. Therefore, to optimize rural human settlements and improve their physical and mental health, we aimed to conduct a correlation study on the influencing factors of health among rural humans.

2. Literature Review

Human health is a complex and comprehensive research topic involving multiple fields of study, such as medicine, sociology, and environmental science. Human settlement is a complex manifestation of many factors related to humanity, nature, and society. A healthy and comfortable human settlement can stabilize people's emotions and is conducive to physical and mental health; hence, building healthy human settlements is one of the trends of the construction industry under the background of Industry 4.0. In foreign countries, they have paid more attention to the construction of healthy human settlements earlier and have obtained substantial research results. Many international organizations, such as the World Health Organization, the European Environment Agency, and the United Nations Environment Program, have issued a series of guidelines and standards for healthy environments [31, 32]. In recent years, the WELL building standards released in the United States have established indicators for assessing the building environment across seven areas, namely air, water, nutrition, light, fitness, comfort, and mood. The associated research has presented various perspectives [33]. Previous research scholars have used different methodologies and techniques to systematically assess the health performance of living environments involving different spatial environments and

specific populations [34, 35]. In addition, previous mixed-methods studies have examined the interactions and feedback between multiple environmental physical factors and human health and propounded the possibilities and ways to achieve healthy living in an increasingly urbanized built environment [25, 36–44].

With the emphasis on healthy human settlements in China, deep and relevant research in multiple fields has been developed. Numerous scholars have analyzed in detail the health indicator systems of different urban environments, including transportation systems, infrastructure, air quality, sewage treatment, health care, social development, environmental management, and lifestyles. Many analysis methods have also been used to conduct relevant health assessments on environmental factors [45–52]. Most studies on healthy human settlements in China have focused on urban areas, whereas the rural environment in China has significant differences from urban areas in terms of spatial distribution, lifestyle, humanistic characteristics, infrastructure, and other environmental factors. Many studies have shown that various environmental factors with distinct rural characteristics influence people's lifestyles and behaviors at the social, humanistic, and material levels, which in turn have positive or negative effects on human physical and mental health [53–58]. Therefore, this work took Xiangxi's traditional villages in China as an example and conducted a correlation study on their human settlements related to human health.

3. Research Plan Design

3.1. Research Object. There are many traditional Chinese villages with obvious and different characteristics. With regard to the list of five batches of "Chinese traditional villages" published, the number of traditional villages distributed in Xiangxi has reached 172. At the same time, due to the special geographical and ecological environment and historical changes, Xiangxi still retains a relatively complete village form and humanistic tradition. Since ancient times, many ethnic groups, including Miao, Han, Tujia, Dong, and Yao, have been living in the area, with strong ethnic characteristics and living features. Therefore, we selected traditional villages with essentially complete settlement patterns as the main research focus. Our list comprised Lahao Village in the Duli Township of Fenghuang County, Laodong Village in the Machong Township, and Guantianshan Village (Figure 1). The long-term residents of the village were randomly selected as the study participants. Following uniform standards, we adopted methods such as the interview and participatory observation method to obtain information from the participants. Basic data were obtained by mapping and basic testing the human settlements of the villages.

3.2. Research Methods. To obtain the health indicators of the permanent residents in the Xiangxi rural environment, this study used the SF-36 scale to measure the eight dimensions of general health, physical function, physical role, somatic pain,

Figure 1: Area where the Xiangxi villages are located.

vitality, social function, emotional function, and mental health [59, 60]. The average of the total scores of the eight dimensions was used as the dependent variable y as an overall indicator for health evaluation. Second, according to the survey indicators of the human settlements, a questionnaire for the healthy villages' human settlements was constructed by reviewing the literature and consulting experts while considering the operability of data collection and the specificity of village lifestyles. When screening the evaluation indicators of the questionnaires, the first-level criteria layer was determined as the three dimensions of human behavior, natural environment, and physical environment by literature review. The secondary evaluation factors were 16 relevant environmental evaluation indicators based on existing studies, and after consulting with relevant scholars and experts by email in various fields such as architecture, planning and design, and landscape professionals, the evaluation feedback was filtered and modified based on expert feedback. After multiple additions and deletions of evaluation factors, a total of 18 factors were determined from three dimensions of human behavior, natural environment, and building physical environment. Related questions were set up around the 18 factors to form a structured questionnaire (Table 1). By designing a Likert scale, this study divided the evaluation factors of the environment into five evaluations based on the statements regarding the attitudes of approval or disapproval: very good, good, fair, poor, and very poor. We transformed the scale into a fixed-distance evaluation level of subjective evaluation [61, 62].

Correlation analysis was performed on the health self-assessment results and environmental influences. Subsequently, multiple linear regression analysis was used to establish regression equations to further explore the association between health and environment. All analyses were performed using SPSS.

3.3. Research and Analysis

3.3.1. Sample Characteristics. Of the 160 questionnaires distributed, 153 participants completed the assessment. The effective response rate was 95.6%. Among the 153 qualified

Table 1: Human settlement assessment factors of Xiangxi villages.

Dimension (A)	Evaluation factor (B)
Human behavior (A1)	B1 daily physical pattern and frequency B2 daily walking distance B3 frequency of communication with neighbors B4 daily hobbies and interests B5 daily cooking style B6 understanding of and access methods to health knowledge
Natural environment (A2)	B7 air quality of the natural environment B8 climate temperature and humidity comfort B9 daily noise pollution B10 waste disposal methods B11 medical level and care
Physical environment (A3)	B12 living house orientation B13 indoor temperature and humidity in summer and winter B14 construction methods and materials of the houses B15 indoor hygienic environment conditions B16 indoor ventilation and lighting conditions B17 indoor and outdoor vegetation and greenery B18 embodiment of regional culture decoration

participants, 73 (47.7%) were aged over 60 years and 83 (54.2%) were female (Table 2). In the SF-36 health assessment, 19 (12.4%) rated their overall health status as "excellent," 53 (34.6%) as "very good," 45 (29.4%) as "good," 35 (22.9%) as "fair," and 1 (0.7%) as "poor."

Xiangxi is in the northwestern part of Hunan Province, China, east of the Wuling Mountains areas of the Yungui Plateau. In total, 401 villages in Hunan Province are included in the fifth batch of the list of traditional villages in China, and Xiangxi accounts for 90 villages. Xiangxi is dotted with many Miao traditional villages of different forms and long histories. The climate in Xiangxi has four distinct seasons, with rainfall concentrated between April and June, accounting for 41–47% of the annual precipitation. Due to the complex terrain and the influence of airflow, the amount of solar radiation received varies, and the lighting and temperature of each region are different.

As an example, a typical local traditional residential building was mapped and tested for temperature, humidity, and light level. Using a French KIMO HD100S portable hygrometer thermometer with a temperature and humidity monitor, measurements were taken during the hours of 8 : 00–19 : 00 from January 15 to January 17 in a typical local winter season and from July 9 to 11 in a summer season, and the temperature and humidity of the measurement points (at 1.1 m from the ground) were recorded with an interval of 30 minutes. The measurement points were at five locations: outdoor courtyard, lobby, bedroom, kitchen, and fire pit, as shown in Figure 2 and Table 3. The results showed that the

TABLE 2: Summary of basic information of the questionnaire.

Statistical index		Frequency	Proportion (%)
Gender	Male	70	45.8
	Female	83	54.2
Age	≤18	8	5.2
	19–39	27	17.6
	40–59	45	29.4
	60–79	65	42.5
	≥80	8	5.2
Education level	Primary school and below	116	75.8
	Middle school	23	15.0
	High school/junior college	12	7.8
	College and above	2	1.3
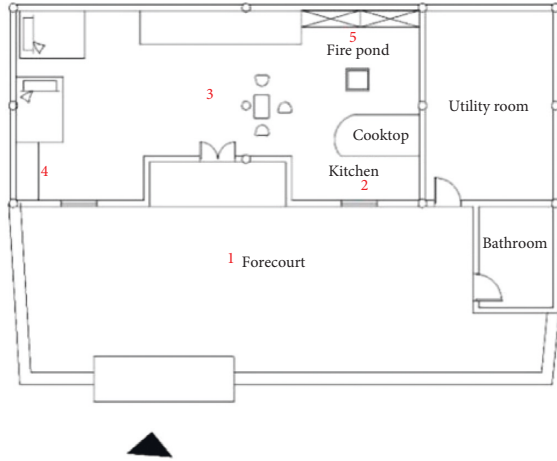
FIGURE 2: Temperature, humidity, and illuminance detection point of a typical traditional house.

TABLE 3: Temperature and humidity data of the measurement points in summer and winter.

Measurement point	Average summer temperature (°C)	Average summer humidity (%)
1	31.5	82.7
2	29.6	88.5
3	29.4	85.7
4	29.8	88.9
5	29.1	89.2
1	6.4	75.7
2	7.3	78.5
3	7.1	77.7
4	7.9	79.6
5	8.5	76.9

indoor and outdoor humidity was generally high, and the difference between the indoor and outdoor temperatures in summer and winter was within 3 °C due to the influence of the houses' construction materials and methods. The residential heating in winter mainly relied on firewood, which causes pollution.

TABLE 4: Illuminance data of the measurement points in summer and winter.

Measurement point	Summer illuminance (lux)	Winter illuminance (lux)
1	63701	3614
2	330	281
3	236	168
4	305	204
5	179	115
6	158	177

TABLE 5: Reliability test results.

Cronbach's coefficient	Number of terms
People 0.723	4
Building 0.972	10
Nature 0.849	4

To measure the indoor and outdoor illumination conditions, a Sigma AS82 handheld illuminance meter was used, and measurements were made at 12:00 noon on January 15 in winter and July 9 in summer. The weather we chose to measure was cloudy days without precipitation in winter and sunny days in summer, as shown in Table 4. Considering the different degrees of the influence of illumination on functional rooms, the measurement points included the outdoor courtyard, foyer, bedroom, kitchen, and fire pit. In addition to the five measurement points, the bathroom was also included as an illumination measurement point, as shown in Table 4. Due to the long scale of building depth and the limitation of building materials for the window and door openings, the indoor lighting was fair.

3.3.2. Reliability and Validity Test. This study used Cronbach's alpha coefficient to test the inherent reliability of the survey questionnaire. The range of Cronbach's alpha coefficient is between 0.00 and 1.00, with higher values indicating higher reliability and lower values indicating lower reliability. The survey results show that the overall Cronbach's alpha coefficient of the dimension of human behavior in the questionnaire was 0.723; the coefficient of the second dimension of the questionnaire of the physical environment of the building was 0.972; and the coefficient of the third dimension of the natural environment was 0.849, indicating that the questionnaire had good reliability and the measurement results were reliable (Table 5).

Validity tests were conducted using structural validity, and the KMO test and the Bartlett sphere test were used. When the KMO test coefficient is greater than 0.50 and the Bartlett sphere test, X2 has a P value less than 0.05, and the research questionnaire has structural validity. Validity tests were performed on the three dimensions, and the respective KMO test values were 0.702, 0.903, and 0.801, all of which were greater than 0.70. The corresponding P values were less than 0.05. The significant difference between the correlation coefficient and the unit matrix indicates that there is a

TABLE 6: Correlation analysis results.

		Gender	Age	Education level	People	Building	Nature	Y
Gender	Pearson's correlation	1	0.062	0.015	0.149	−0.054	−0.050	−0.012
	P (two-tailed)		0.448	0.859	0.067	0.508	0.542	0.882
	N	153	153	153	153	153	153	153
Age	Pearson's correlation	0.062	1	−0.355**	−0.140	−0.078	−0.235**	−0.495**
	P (two-tailed)	0.448		0.000	0.084	0.340	0.004	0.000
	N	153	153	153	153	153	153	153
Education level	Pearson's correlation	0.015	−0.355**	1	−0.009	−0.025	0.059	0.102
	P (two-tailed)	.859	0.000		0.913	0.758	0.470	0.211
	N	153	153	153	153	153	153	153
People	Pearson's correlation	0.149	−0.140	−0.009	1	−0.116	−0.012	0.520**
	P (two-tailed)	0.067	0.084	0.913		0.154	0.887	0.000
	N	153	153	153	153	153	153	153
Building	Pearson's correlation	−0.054	−0.078	−0.025	−0.116	1	−0.056	0.167*
	P (two-tailed)	0.508	0.340	−0.758	0.154		0.489	0.039
	N	153	153	153	153	153	153	153
Nature	Pearson's correlation	−0.050	−0.235**	0.059	−0.012	−0.056	1	0.211**
	P (two-tailed)	0.542	0.004	0.470	0.887	0.489		0.009
	N	153	153	153	153	153	153	153
Y	Pearson's correlation	−0.012	−0.495**	0.102	0.520**	0.167*	0.211**	1
	P (two-tailed)	0.882	0.000	0.211	0.000	0.039	0.009	
	N	153	153	153	153	153	153	153

**$P < 0.01$. *$P < 0.05$.

correlation among the survey data. Therefore, the questionnaire has structural validity.

3.3.3. Correlation Analysis.
Through the analysis of the questionnaire, the total score of the eight dimensions of the SF-36 health evaluation result was used as the dependent variable y, and the 18 environmental factor assignment calculations were divided into three dimensions using SPSS for correlation analysis. The Pearson correlation value is between [−1, +1]. A value greater than 0 means positive correlation, and a value less than 0 means negative correlation. The closer the absolute value is to 1, the stronger the correlation is. Since the data belonged to different populations, to decrease potential confounding of health status, gender, age, and education level were added to the correlation analysis as independent variables. In the correlation analysis results, the significance of the four variables of people, build, nature, and age is 0.000, 0.039, 0.009, and 0.000, all of which were less than 0.05 and statistically significant. Among population attributes, gender, education level, and health status had no significant correlation, while age and health status were significantly negatively correlated. In addition, the Pearson value corresponding to age is -0.495, indicating a negative correlation, and the older the age, the worse the health. In the three dimensions of people, build, and nature, the value of the Pearson correlation with y was 0.520, 0.167, and 0.211, all of which are positive numbers, suggesting that the variables of the three dimensions are positively correlated with the dependent variable y. Table 6 shows that human behavior has a stronger correlation with health status, whereas the correlation between the physical and natural environment of the building and health status is weak. Among these three dimensions, the factors that have the strongest correlation with health status are "daily physical activity level," "summer indoor temperature evaluation," and "housing orientation evaluation."

3.3.4. Regression Model Establishment.
The independent variables were quantitative and more than one in number in our research, so we choose the multiple linear regression analysis method to examine the relationship between the independent variables of the three dimensions and health status. The mathematical model of multiple linear regression is $E(y) = \beta_0 + \beta_1 x_1 + \beta_2 x_2 + \ldots + \beta_p$, where x_p explains the linear change in y caused by the change in variable x; $x_p (i = 1, \ldots, p)$ is the independent variable; p is the number of independent variables; β_0 is the constant term of the regression equation; and $\beta_p (i = 1, \ldots, p)$ is the regression coefficient.

The scores of gender, age, education level, mean values of the scores of human behavior, building physical environment, and natural environment were taken as the six independent variables, and regression analysis was performed with the dependent variable as health status. The results show that the D-W test value was 1.630 and its value tended to 2, indicating that there was no autocorrelation. That is, heteroscedasticity was considered not to exist (Table 7). R^2 was 0.508, which suggested that the independent variables of the three dimensions could jointly explain 50.8% of the dependent variable.

We performed the F test on the model, and the model's P value is less than 0.001, indicating that the model passed the F test, and the linear relationship was valid. At the same time, the statistical significance of the regression model also indicated that compared with the null model, the inclusion of independent variables helped to predict the dependent

TABLE 7: D-W test results.

Model	R	R^2	Adjusted R^2	Error in standard estimate	Durbin–Watson
1	0.713[a]	0.508	0.488	18.87590	1.630

a. Predictor variables: constant, nature, people, building, gender, age, and education level. b. Dependent variable: y.

TABLE 8: F test results.

Model		Sum of squares	Degree of freedom	Mean square	F	P
	Regression	53792.997	6	8965.500	25.163	0.000[b]
1	Residual	52019.735	146	356.300		
	Sum	105812.733	152			

(a) Dependent variables: y. (b) Predictor variables: constant, nature, people, building, gender, age, and education level.
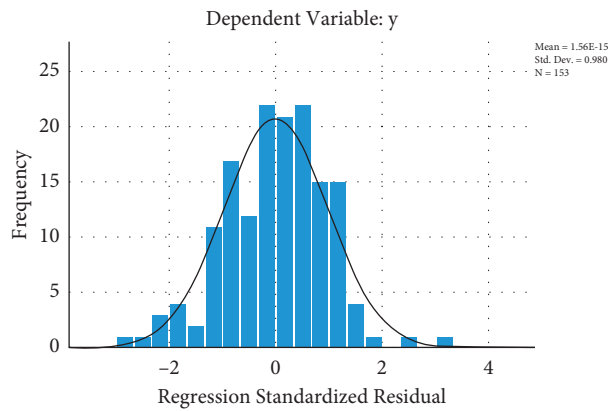
FIGURE 3: Histogram residual.
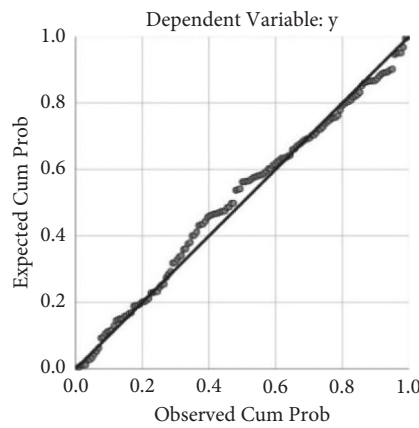
FIGURE 4: Normal P-P plot of regression standardized.

TABLE 9: Regression analysis results.

Model	Nonstandardized coefficient		Standardized coefficient	t	P
	B	Standard error	β		
Constant	122.422	12.203		10.032	.000
Gender	−2.320	3.115	0-.044	−0.745	.458
Age	−10.395	1.757	0-.387	−5.917	.000
Education level	−1.312	2.417	0-.034	−0.543	.588
People	12.095	1.464	0.496	8.259	.000
Building	4.259	1.266	0.199	3.363	.001
Nature	5.122	2.240	0.137	2.286	.024

Dependent variable: y.

variable, or that the model was better than the null model; that is, at least one of the six independent variables could affect the health status (Table 8).

Through the verification analysis, the results of the histogram showed that the curve was roughly normal distribution; the closer the distribution of each point in the normal P-P graph was to the diagonal line, the closer the data were to the normal distribution. Figures 3 and 4 depict that the residuals were approximately normally distributed, and the regression model was statistically significant.

In the regression, the dependent variable y was health status; the independent variables were gender, age, education level, people, building, and nature, which represented the four independent variables of age, human behavioral activities, building physical environment, and natural environment, respectively. The P value for each of these four independent variables was less than 0.05. The following equation was established:

$$\begin{aligned} Y = {} & 122.422 - \text{gender} * 2.230 - \text{age} * 10.395 \\ & - 1.312 * \text{education level} + \text{people} * 12.095 \qquad (1) \\ & + \text{building} * 4.259 + \text{nature} * 5.122. \end{aligned}$$

That is, for each additional person, y increased by 12.095 units; for each unit increase in building, y increased by 4.259 units; for each unit volume increase in nature, y increased by 5.122 units; and for every unit increase in age, y decreased by 10.395 units (Table 9).

4. Conclusions and Recommendations

With the acceleration of China's economic and social development and urbanization, the population structure of China is gradually changing into an aging population. In this study, 47.7% of the study participants were aged 60 years and above; most of the elderly were unaccompanied by children at home; and their physical functions have reduced over time. Some studies have shown that age is one of the main elements affecting health assessment, followed by gender, income, physical environment, health-related behaviors, and regional medical level. These are all factors relevant to health status [63–67].

The results of the univariate analysis in this study show that age was correlated with overall health negatively and significantly; that is, the higher the age, the lower the health self-assessment score. Income and education were not significantly correlated with health assessment results, and this result was related to the overall low income and low education level of the research subjects. At the same time, the results of this survey show that gender was not significantly correlated with health assessment results, because within the scope of the survey, gender differences are associated with cultural, social status, division of labor, living habits, etc., all of which can indirectly affect physical health [68, 69]. Among the eight dimensions of health assessment, older adults had lower mental health scores and generally were depressed and had negative emotional conditions due to lack of family companionship and recreational life. Some scholars have found that gender, age, ethnicity, hobbies, life satisfaction, and physical health were associated with mental health among the Xiangxi older adults [70–72].

Second, about 82.4% of the villagers among the research subjects needed to perform daily work activities and therefore maintained a certain amount of daily exercise. In the correlation analysis of this study, the factor "daily physical activity level" in the dimension of "human behavior" was significantly correlated with the health status. In the specific environment and cultural background of rural areas in China, work activity is an essential life support behavior, and this necessary lifestyle has a positive impact on the health of the research subjects. In the survey area, many medical records and surveys have shown that the lifestyle, medical condition, and labor intensity had a certain impact on human physical and mental health, and the health level of urban and rural residents is different [73–75].

The building physical environment has a direct impact on human perception, and the results of this study show that the "building physical environment" has a significant correlation with health status. We investigated the issues related to the setting of room temperature and humidity, kitchen drainage, and room spatial scale in the building physical environment. The strongest correlation with the dependent variable health status was the "summer indoor temperature evaluation." This is consistent with many existing research results such as indoor air pollution, heat, and humidity conditions affecting human health [76].

The natural environment is closely related to human health. In traditional Chinese culture, related theories emphasize the harmonious relationship between nature, architecture, and human beings. Our findings suggested that the natural environment and health status have a significant correlation, among which the univariate analysis showed that the "housing orientation evaluation" under the "natural environment" dimension had the strongest correlation [77–80].

Lastly, we proposed the following suggestions for healthy rural human settlements in Xiangxi. (1) Pay attention to the physical and mental health of the elderly living in the villages; increase the village infrastructure for adapting to the aged; improve the medical service system; enrich the recreational life of the middle-aged and elderly; and realize "healthy elderly care." At the same time, promote healthy lifestyles and popularize knowledge about healthy living for all. (2) Improve the living environment of villages and improve the comfort and convenience of the indoor environment of buildings. Modernize and renovate the pollution sources of the indoor environment and pay attention to the heat insulation performance of the houses. (3) Consider the orientation and the influence of light in the layout and site selection of the building. Draw lessons from the traditional village Taoist law of nature, the harmony between man and nature, and the movement according to time. Focus on the relationship between man and nature in urban architectural design to promote a positive impact on human health.

The questionnaire design in this study considered limited dimensions and factors. Considering the operability and practicality of the data, it mainly focused on architecture and environmental psychology, but many environmental impact factors were not included. Future studies should consider including more covariates.

Data Availability

The data used to support the findings of this study are included within the article.

Conflicts of Interest

The authors declare no conflicts of interest.

Authors' Contributions

S.T., Y.Z., and Z.L. conceptualized the study. S.T. and Y.Z. developed methodology, performed formal analysis, and wrote and prepared the original draft; S.T. and Z.L. reviewed and edited the manuscript. Y.Z. visualized the study; S.T. supervised the study and administered the project; and Z.L acquired funding. All authors have read and agreed to the published version of the manuscript.

Acknowledgments

References

[1] H. Lasi, P. Fettke, H.-G. Kemper, T. Feld, and M. Hoffmann, "Industry 4.0," *Business & Information Systems Engineering*, vol. 6, no. 4, pp. 239–242, 2014.

[2] D. Gorecky, M. Schmitt, M. Loskyll, and D. Zuhlke, "Human-machine-interaction in the industry 4.0 era," *Management Science*, vol. 23, no. 6, pp. 595–605, 2014.

[3] D. Kiel, J. M. Müller, C. Arnold, and K.-I. Voigt, "Sustainable industrial value creation: benefits and challenges of industry 4.0," *International Journal of Innovation Management*, vol. 21, no. 8, Article ID 1740015, 2017.

[4] M. Kozlovska, D. Klosova, and Z. Strukova, "Impact of industry 4.0 platform on the formation of construction 4.0 concept: a literature review," *Sustainability*, vol. 13, no. 5, p. 2683, 2021.

[5] N. Perrier, A. Bled, M. Bourgault et al., "Construction 4.0: a survey of research trends," *Journal of Information Technology in Construction*, vol. 25, pp. 416–437, 2020.

[6] G. D. Bona, V. Cesarotti, G. Arcese, and T. Gallo, "Implementation of Industry 4.0 technology: new opportunities and challenges for maintenance strategy," *Procedia Computer Science*, vol. 180, pp. 424–429, 2021.

[7] P. Dallasega, E. Rauch, and C. Linder, "Industry 4.0 as an enabler of proximity for construction supply chains: a systematic literature review," *Computers in Industry*, vol. 99, pp. 205–225, 2018.

[8] P. Murugaiyan and P. Ramasamy, "Analyzing interrelated enablers of industry 4.0 for implementation in present industrial scenario," *Management Research Review*, vol. 44, no. 9, pp. 1241–1262, 2021.

[9] A. Jimeno-Morenilla, P. Azariadis, R. Molina-Carmona, S. Kyratzi, and V. Moulianitis, "Technology enablers for the implementation of Industry 4.0 to traditional manufacturing sectors: a review," *Computers in Industry*, vol. 125, p. 103390, 2021.

[10] S. Qin and K. Cheng, "Special issue on future digital design and manufacturing: embracing industry 4.0 and beyond," *Chinese Journal of Mechanical Engineering*, vol. 29, no. 6, p. 1045, 2016.

[11] Z. You and L. Feng, "Integration of industry 4.0 related technologies in construction industry: a framework of cyber-physical system," *IEEE Access*, vol. 8, pp. 122908–122922, 2020.

[12] J. Li, H. Yang, and L. Zhao, "A research on development of construction industrialization based on BIM technology under the background of industry 4.0," *Matec Web of Conferences*, vol. 100, p. 2046, 2017.

[13] Z. Wang, T. Xu, and Q. Zhou, "Exploration on construction mode of training base under background of Industry 4.0," *Experimental Technology and Management*, 2015.

[14] L. Li, "China's manufacturing locus in 2025: with a comparison of "Made-in-China 2025" and "Industry 4.0"," *Technological Forecasting and Social Change*, vol. 135, pp. 66–74, 2018.

[15] S. Tian and Z. Pan, *Made in China 2025" und Industrie 4.0" – Gemeinsam in Bewegung*, Springer, Berlin Heidelberg, 2016.

[16] J. Wang, H. Wu, and Y. Chen, "Made in China 2025 and manufacturing strategy decisions with reverse QFD," *International Journal of Production Economics*, vol. 224, Article ID 107539, 2020.

[17] P. Zhang, H. Liu, L. I. Wenjing, and Z. H. O. Fanqin, "Industrial intelligent network: deepening and upgrading of industrial Internet," *Journal on Communications*, vol. 39, no. 12, p. 134, 2018.

[18] A. Zumelzu and M. G. Herrmann-Lunecke, "Mental well-being and the influence of place: conceptual approaches for the built environment for planning healthy and walkable cities," *Sustainability*, vol. 13, 2021.

[19] T. Yu, H. C. hen, Z. Li, Q. He, and B. Lin, "An efficient method of evaluating large scale urban residential skylight environment and an empirical study of Beijing main area," 建筑模拟(英文), vol. 14, no. 4, p. 13, 2021.

[20] C. Clavier, S. Gendron, L. Lamontagne, and L. Potvin, "Understanding similarities in the local implementation of a healthy environment programme: insights from policy studies," *Social Science & Medicine*, vol. 75, no. 1, pp. 171–178, 2012.

[21] C. Cheng-Chen, "[Incorporating smart technologies and resilience into healthy living environment designs]," . *Hu li za zhi The journal of nursing*, vol. 66, no. 3, pp. 23–28, 2019.

[22] Q. Wang, M. Chong, G. Li, and M. Liu, "Development concept,status and trend of healthy building in China," *Building Science*, vol. 9, pp. 12–17, 2018.

[23] S. Xiao, S. Y. Hao, and R. Xu, "A strategic analysis of developing prefabricated building in China's rural area," *Journal of Engineering Management*, 2018.

[24] Y. Zhang, Z. Chen, H. Sun, S. Zhang, K. Feng, and H. Liu, "Research on development countermeasures of prefabricated buildings in new rural construction -- A case study of longfeng village, hunan province," *E3S Web of Conferences*, vol. 136, p. 4056, 2019.

[25] A. Biswas, "A nexus between environmental literacy, environmental attitude and healthy living," *Environmental Science and Pollution Research*, vol. 27, no. 6, pp. 5922–5931, 2020.

[26] C. C. Bungău, I. F. Prada, M. Prada, and C. Bungău, "Design and operation of constructions: a healthy living environment-parametric studies and new solutions," *Sustainability*, vol. 11, no. 23, p. 6824, 2019.

[27] J. Morris, C. Deeming, P. Wilkinson, and A. D. Dangour, "Action towards healthy living--for all," *International Journal of Epidemiology*, vol. 39, no. 1, pp. 266–273, 2010.

[28] B. Guo, H. Cheng, and Y. Liu, "Study on influencing factors of health service utilization of rural elderly from the perspective of healthy aging," *Chinese Medical Ethics*, 2019.

[29] C. Peng and C. Zhang, "Rural residential environment quality and its influencing factors," *Journal of Macro-quality Research*, 2019.

[30] R. D. Groot, V. Katja, L. J. Schoonmade, W. L. de Kort, J. Brug, and J. Lakerveld, "Urban-rural differences in the association between blood lipids and characteristics of the built environment: a systematic review and meta-Analysis," *British Medical Journal Global Health*, vol. 4, no. 1, 2019.

[31] *Environmental Risk Assessment: Approaches, Experiences and Information sources[S]*, Europian Environment Agency, Copenhagen K Denmark, 2016.

[32] European Centre for Disease Prevention and Control, *Operational Guidance on Rapid Risk Assessment Methodology*, European Centre for Disease Prevention and Control, Solna Municipality, Sweden, 2011.

[33] *WELL Building Standard V1 with January 2017 Addenda*, IWBI, 2017.

[34] R. F. Zheng and J. H. Choi, "Analysis OF exploratory ON healthy building assessment abroad," *Architectural Technology*, 2019.

[35] A. Motaghifard, M. Omidvari, and A. Kaazemi, "Introducing a conceptual model for evaluating health safety environmental performance of residential buildings using the fuzzy decision-making approach," *Environmental Monitoring and Assessment*, vol. 192, no. 1, pp. 19.1–19.10, 2020.

[36] A. P. Hills, N. J. Farpour-Lambert, and N. M. Byrne, "Precision medicine and healthy living: the importance of the built environment," *Progress in Cardiovascular Diseases*, vol. 62, no. 1, pp. 34–38, 2019.

[37] C. Li, Q. Li, D. Tong et al., "Environmental impact and health risk assessment of volatile organic compound emissions during different seasons in Beijing," *Journal of Environmental Sciences*, vol. 93, pp. 1–12, 2019.

[38] W.-Ju Liao and Fu-C. Cheng, "Quality assessment of environmental hygiene and health of indoor bathroom design," *Architectural Journal, 2019(110_S:Special Issue on Innovative Low-Carbon and Green Buildings II)*, vol. 110, pp. 49–58, 2019.

[39] P. Carter, "Environmental health risk assessment for global climate change and atmospheric greenhouse gas pollution," *Climate Action*, pp. 413–423, 2020.

[40] K. C. O'Sullivan, "Health impacts of energy poverty and cold indoor temperature - ScienceDirect," *Encyclopedia of Environmental Health*, pp. 436–443, 2019.

[41] S. Basu and B. Banerjee, "Impact of environmental factors on mental health of children and adolescents: a systematic review," *Children and Youth Services Review*, vol. 119, Article ID 105515, 2020.

[42] M. Mannan, Y. W. Weldu, and S. G. Al-Ghamdi, "Health impact of energy use in buildings: radiation propagation assessment in indoor environment," *Energy Reports*, vol. 6, pp. 915–920, 2020.

[43] B. Zhang, R. Zeng, and X. Li, "Environmental and human health impact assessment of major interior wall decorative materials," *Frontiers of Engineering Management*, vol. 6, no. 3, pp. 406–415, 2019.

[44] J. Kallio, E. Vildjiounaite, J. Koivusaari et al., "Assessment of perceived indoor environmental quality, stress and productivity based on environmental sensor data and personality categorization," *Building and Environment*, vol. 175, p. 106787, 2020.

[45] J. T. Pang, Y. U. Qing-Long, and Y. H. Zou, "Analysis of status and strategies of healthy environment in shenzhen," *China Health Industry*, 2019.

[46] C. Mei, Q. Xin, and L. Zhang, "Public participation in environmental management in China: status quo and mode innovation," *Environmental Management*, vol. 55, no. 3, pp. 523–535, 2015.

[47] Y. Yi, Y. Liao, L. Zheng et al., "Health selectivity and rural-urban migration in China: a nationwide multiple cross-sectional study in 2012, 2014, 2016," *International Journal of Environmental Research and Public Health*, vol. 16, no. 9, 2019.

[48] S. Shao, H. Zhang, X. Chen et al., "Health education services utilization and its determinants among migrants: a cross-sectional study in urban-rural fringe areas of Beijing, China," *BMC Family Practice*, vol. 22, no. 1, pp. 1–19, 2020.

[49] X. He, G. Zhou, Y. Ma et al., "Winter vacation, indoor air pollution and respiratory health among rural college students: a case study in Gansu Province, China," *Building and Environment*, vol. 188, p. 107481, 2020.

[50] L. Lin and H. Jiang, "Healthy environment and healthy living in urban China: an emerging field in research (SPECIAL ISSUE: China's environmental challenges and sustainable development)," *The journal of contemporary China studies*, vol. 5, 2016.

[51] J. Shan and W. U. Zhanyun, "The healthy China initiative: reality, problems and remedies," *Chinese Journal of Urban and Environmental Studies (CJUES)*, vol. 6, 2018.

[52] W. Xueying and L. Wu, "PEST analysis of the comprehensive health industry industry in the context of healthy China," *Contemporary Social Sciences (English)*, 2018.

[53] T. Lu and T. Lu, "Health and rural-urban migration in rural China: a longitudinal analysis," in *Proceedings of the PPA 2018 Annual Meeting*, Denver, Colorado, April 2018.

[54] H. You, D. Zhou, S. Wu, X. Hu, and C. Bie, "Social deprivation and rural public health in China: exploring the relationship using spatial regression," *Social Indicators Research*, vol. 147, no. 3, pp. 843–864, 2020.

[55] Y. Li, B. Zeng, T. Wu, and H. Hao, "Effects of urban environmental policies on improving firm efficiency: evidence from Chinese new energy vehicle firms," *Journal of Cleaner Production*, vol. 215, pp. 600–610, 2019.

[56] X. J. Ding, L. I. Hong-Xing, and F. C. Fan, "Construction and evaluation indicator system of healthy village based on modified Delphi method and consensus meeting method," *Journal of Environment and Health*, 2019.

[57] L. M. Fang, L. U. Nan, and S. O. Insurance, "Can the middle-aged and the elderly achieve their health improvement from domestic energy consumption structure optimization in rural China," *China Population,Resources and Environment*, vol. 29, pp. 40–49, 2019.

[58] Li-na Deng, J.-heng Zhang, Ji-lin Wu et al., "Research on spatial and temporal distribution characteristics of traditional villages in Xiangxi prefecture and the influencing factors," *Hunan Agricultural Sciences*, vol. 8, pp. 108–113, 2020.

[59] J. E. Ware, C. D. Sherbourne, and C. D. Sherbourne, "The MOS 36-ltem short-form health survey (SF-36)," *Medical Care*, vol. 30, no. 6, pp. 473–483, 1992.

[60] J. R. F. Gladman, "Assessing health status with the SF-36," *Age and Ageing*, vol. 27, no. 1, p. 3, 1998.

[61] M. Á. Gil and G. González-Rodríguez, "Fuzzy vs. Likert scale in statistics," *Combining Experimentation and Theory*, pp. 407–420, 2012.

[62] A. Barua, "Methods for decision-making in survey questionnaires based on Likert scale," *Journal of Asian Scientific Research*, vol. 3, pp. 35–38, 2013.

[63] Q. Deng, Y. Yi, and K. Yu, "Influencing factors and countermeasures of the health of residents in the city clusters along the middle reaches of the yangtze river," *Healthcare*, vol. 8, no. 2, 2020.

[64] T. Shi and Y. Wang, "Heavy metals in indoor dust: spatial distribution, influencing factors, and potential health risks," *The Science of the Total Environment*, p. 755, 2020.

[65] L. M. Xu, L. F. Xie, X. Li, L. Wang, and Yu-meng Gao, "A meta-analysis of factors influencing health literacy among Chinese older adults," *Journal of Public Health*, no. 6, 2021.

[66] W. Pickett, N. King, C. Trask et al., "Factors related to self-perceived health in rural men and women," *Journal of Agromedicine*, vol. 20, no. 2, pp. 178–187, 2015.

[67] S. Miilunpalo, I. Vuori, P. Oja, M. Pasanen, and H. Urponen, "Self-rated health status as a health measure: the predictive value of self-reported health status on the use of physician services and on mortality in the working-age population," *Journal of Clinical Epidemiology*, vol. 50, no. 5, pp. 517–528, 1997.

[68] J. Xu, "Gender differences of the elderly health in China and its decomposition," *Journal of Northwest Normal University*, vol. 52, no. 01, pp. 139–144, 2015.

[69] D. Pan and X. Liu, "Effect of social participation on health with gender difference in rural China——econometric analysis based on propensity score matching model," *Journal of Agrotechnical Economics*, vol. 11, pp. 71–82, 2020.

[70] P. Sun, Y. Wang, J. Zhang, and C. Wang, "Support demand and its influencing factors among rural elderly people," *Nursing Journal of Chinese People's Liberation Army*, vol. 34, no. 03, pp. 13–17, 2017.

[71] W. Yao, S. Q. Yang, and W. H. Wang, "Relativity study on sleep disturbance and anxiety,depression for elderly People of Rural Areas in Hunan," *Journal of Hunan Normal University(Medical Sciences)*, 2016.

[72] Y. Bai, F. Bian, L. Zhang, and Y. Cao, "The impact of social support on the health of the rural elderly in China," *International Journal of Environmental Research and Public Health*, vol. 17, no. 6, p. 2004, 2020.

[73] Q. Yao, J. Hou, D. Zhu, K. Luo, Z. Chen, and Z. Lu, "Mental Health and social Security construction of the widowed elderly in western Hunan minority areas," *Chinese Journal of Gerontology*, vol. 38, no. 07, pp. 1759-1760, 2018.

[74] Z. H. Cao, X. U. Xiao-Sheng, and J. J. Ling, "Current status of health literacy and its influencing factors among 5,999 residents in some areas of hunan," *Practical Preventive Medicine*, 2011.

[75] Z. Song, "Research on the physical health status and influencing factors of the left-behind elderly in rural areas of western Hunan," *Sports World(Scholarly)*, vol. 8, p. 4, 2019.

[76] J. Shi and L. Tang, "Investigation and countermeasure research on health status of "empty nesters" in west Hunan," *Contemporary Sports Technology*, vol. 9, no. 10, pp. 200–202, 2019.

[77] Q. Zhong, "Analysis on the health risk factors of indoor living environment," *Value Engineering*, vol. 38, no. 27, pp. 195-196, 2019.

[78] Yu Chen, B. Chen, and C. Zeng, "SEM model of indoor environment associated health effects in residential buildings," *China Housing Facilities*, vol. 15, no. 5, pp. 88–91, 2016.

[79] J. Zhang and L. L. Pallasati, "Indoor air pollution and its health hazards in rural China," *Journal of Environment and Occupational Medicine*, vol. 24, no. 4, p. 5, 2007.

[80] X.-mei Wang, T. Huang, and Y.-hua Chen, "Environmental health hazard factors in rural areas of Hunan province in 2012-2014," *Journal of Environment and Health*, 2016.

Research Article

Research on Building Space Model Method Based on Big Data Map Visual Design

Qiang Xu[1] **and Long He** [2]

[1]*School of Architecture, Tianjin University, Tianjin 300072, China*
[2]*School of Architecture, Inner Mongolia University of Technology, Hohhot, Inner Mongolia 010050, China*

Correspondence should be addressed to Long He; hl20100000002@imut.edu.cn

In order to explore the architectural space model of design, a visualization method based on big data map is proposed. Referring to the tile pyramid model, a multidimensional aggregation pyramid model (MAP) is proposed, which extends the 2D spatial hierarchical aggregation of tile pyramid to the multidimensional of time/space/attribute and supports the multidimensional hierarchical aggregation of time, space, and attribute. Then, taking spark cluster as the parallel preprocessing tool and HBase distributed database as the persistent storage of map model data, an open-source distributed visualization framework (MAP-Vis) is realized. Then, the BIM model is reconstructed, and a component instance hierarchical splitting strategy based on IFC structure tree is proposed to separate the digital and analog of the original IFC file. The reconstructed IFC model file is transformed into glTF format file, and the dual relationship mapping of geometric space and semantic attributes is completed in the transformation process. Finally, the visibility detection algorithm of BS-AB scene components based on the hierarchical bounding volume (BVH) structure is proposed to eliminate the visibility of building components. The experimental results show that BIMviews is slow to load the IFC file of the experimental object and obtain the model data, with an average of about 40 s, and the Caton is obvious. However, it only takes about 7 s to load glTF file into big data map visualization design by Three.js. It is verified again that glTF format is more suitable for BIM model data than IFC format. The visualization design, display, and interaction based on big data map are based on glTF format. It proves the effectiveness of big data map visualization.

1. Introduction

With the maturity and diversification of data acquisition means such as personal intelligent devices, floating car GPS, Internet of things, and social media, the data sources are becoming richer and richer, and the amount of data collected is increasing explosively. These big data with huge volume, stream generation, numerous types, and value contain both space-time and high-dimensional characteristics [1]. Spatiotemporal features refer to data with spatial location and time tag or attribute fields that can reflect spatiotemporal location. High-dimensional feature refers to that the data contain other feature attributes except time and space, and the information law reflected by these attributes is often more valuable for research. Visualization is an important step and means of analyzing and mining spatiotemporal big data, which can directly reflect the patterns and

laws contained in the data. The building information model (BIM) provides advanced digital tools and information-sharing platform for the information management of the whole life cycle of construction projects. It solves the problems of information transmission fault and data-sharing difficulties faced by traditional facility engineering and has been widely used in architecture, engineering, construction, and facility management (AEC/FM) [2] (Figure 1). The greatest value of BIM lies in the efficient collaboration between multiple participants and multiple disciplines. With the continuous increase of building scale and the increasing complexity of building information data, its model visualization and massive data management become more and more difficult so that it cannot meet the current BIM localization application requirements of engineering construction information data management, sharing, and synchronization. Obviously, while meeting the
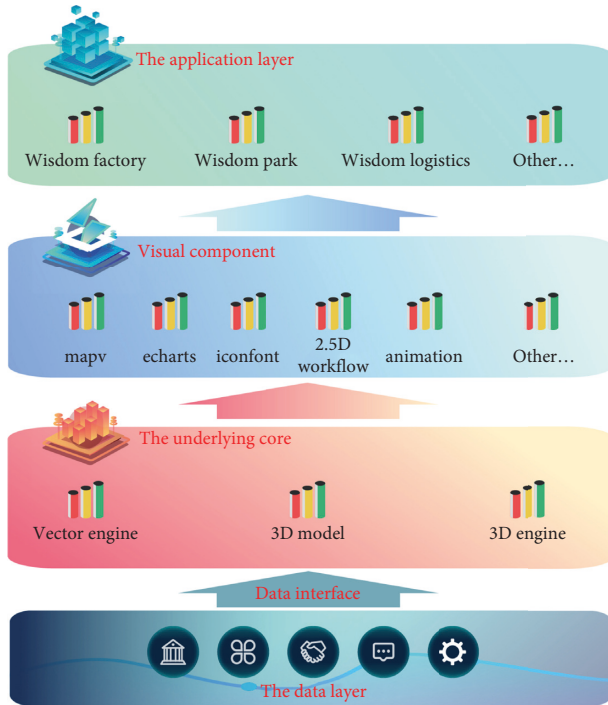
FIGURE 1: Big data map visual design.

needs of multiple users to access anytime and anywhere under different devices and different operating systems, it is particularly important to effectively ensure the integrity semantics of BIM model and data interoperability [3].

2. Literature Review

Zhu W. puts forward the general laws and characteristics of the thinking process of architectural creation and combined and summarized the visual expression and design tools [4]. Zhao L. divided the visual media of design into three aspects, drawing, solid model, and digital design, and analyzed how it affected the design information, so as to better complete and express the design [5]. MW Kowalczyk attempts to visualize the architectural design process from the perspective of computer programming [6]. Djari C. systematically summarized the development of relevant factors, information sources, design carriers, and expression tools of visualization technology and theory and discussed the specific application in different stages of the design process, to provide effective visual expression ways for designers in the process of architectural design [7]. Ladlf Su á rez proposed sequence snapshot and model in "time in GIS." The sequence snapshot model is the simplest spatiotemporal data model at present. It is widely used in various temporal GIS systems. This data model completely stores the state data at different times in the study area so that the objects that have not changed are repeatedly saved, resulting in data redundancy and reducing the use efficiency of the system [8]. Haiyan et al. proposed a ground state correction model on this basis, which only saves the initial state data and the change amount of the change part relative to the initial state in the study area, greatly reducing the data redundancy. However, these

models are only simple time simulation and do not really solve the problem of space-time combination [9]. Guan proposed a spatiotemporal composite model for the vector model, which divides space into a set of spatiotemporal composite units representing the same time process [10]. The spatiotemporal object model proposed by Zou Y. introduces the time dimension to make it orthogonal to the two-dimensional space and abstracts the real world into a discrete object set composed of spatiotemporal atoms. This kind of model mainly tends to the spatial change of geospatial entities with time, which is a simple simulation of the spatiotemporal change process of the research object [11]. Fu et al. proposed a three-domain model of space-time. They believed that simply introducing time as a new dimension into the space-time data model could not fully express and display the world, so they organized the space-time data from the perspectives of location, time, and object. With the emergence of object-oriented technology in computer, the real world is abstracted into a set composed of different types of objects (entities), and an object-oriented spatio-temporal data model is established. This model has great advantages in describing complex phenomena [12]. Mehta extended the spatiotemporal atomic structure by using Brisson lattice complex and proposed an object-oriented spatiotemporal data model based on lattice tuples [13].

Based on the current research, a method of map visualization based on big data is proposed. Referring to the tile pyramid model, a multidimensional aggregation pyramid model (map) is proposed, which extends the 2D spatial hierarchical aggregation of tile pyramid to the multidimensional of time/space/attribute and supports the multidimensional hierarchical aggregation of time, space, and attribute. Then, the BIM model is reconstructed, and a component instance hierarchical splitting strategy based on the IFC structure tree is proposed to separate the digital and analog of the original IFC file. The reconstructed IFC model file is transformed into glTF format file, and the dual relationship mapping of geometric space and semantic attributes is completed in the transformation process. Finally, the visibility detection algorithm of BS-AB scene components based on the hierarchical bounding volume (BVH) structure is proposed to eliminate the visibility of building components.

3. Visualization Design of Big Data Map

3.1. 2D Pyramid Model. In the geographic information system (GIS), the tile map pyramid model is often used for 2D map display. It is a multiresolution hierarchical model. From the bottom to the top, the resolution of pyramid is getting lower and lower. The pyramid contains multiple layers. Each layer is spliced by multiple square tiles, and each tile is composed of pixels (the default resolution is generally 256×256 pixels). In order to describe the construction process of the 2D pyramid model more accurately, the following concepts are defined in this study:

(1) Pixels: the pixel is the smallest data unit of the pyramid model; that is, a single pixel in the tile in the tile pyramid level is expressed as

$$\text{pixel} = \{l, x, y, p\}, \tag{1}$$

where l is the hierarchy of the pyramid, X and y are the spatial range contained in the pixel, and p represents the characteristic sampling values within the spatial range corresponding to the pixel, such as aggregate statistical values, such as mean and sum.

(2) Tiles: tiles in the tile pyramid model are a combination of pixels adjacent to space, and the default resolution is 256×256 pixels, which is expressed as

$$\text{tile} = \left\{l, X, Y, \overset{w \times w}{\underset{i=1}{\cup}} \text{pixel}\right\}, \tag{2}$$

where l is the hierarchy of the pyramid, X and y are the row and column numbers of the tiles, w is the resolution of the tiles, and the last union represents the set of pixels within the space of the tiles [14].

(3) Pyramid: pyramid is a spatial multiscale model composed of tiles at all levels and is expressed as

$$\text{pyramid} = \sum_{i=1}^{n} \sum_{j=1}^{M} \sum_{k=1}^{N} \text{tile}\left\{l_i, X_j, Y_k, \overset{w \times w}{\underset{i=1}{\cup}} \text{pixel}\right\}. \tag{3}$$

Based on the above concepts, the construction of the pyramid model also needs corresponding operations to jointly complete the hierarchical aggregation of spatial dimensions. The four basic operations defined are as follows:

(1) Extract operation: it is responsible for mapping each original record to the pixel unit. A pixel may correspond to one or more original records. The extract operation is

$$\text{Extract}\left(l_n, \{Lon, Lat\}, w\right) = \text{pixel}\{l_n, x, y, p\},$$

$$\begin{cases} x = \dfrac{Lon + 180}{360} \bullet 2^{l_n + r}, \\[2mm] y = \left(1 - \dfrac{(\tan(Lat \bullet \pi/180) + 1/\cos(Lat \bullet \pi/180))}{\pi}\right) \bullet 2^{l_n + r - 1}, \\[2mm] r = \log_2 w. \end{cases} \tag{4}$$

(2) Group operation: it is mainly to establish the corresponding mapping relationship between pixels and tiles, that is, to obtain the specific tiles to which the pixels should belong. The operation formula is

$$\text{Group}\left(\text{pixel}\{l_n, x, y, p\}\right) = \text{tile}\left\{l_n, X, Y, \overset{w \times w}{\underset{i=1}{\cup}} \text{pixel}\right\},$$

$$\begin{cases} X = \left(\dfrac{x}{w}\right), \\[2mm] Y = \left(\dfrac{y}{w}\right). \end{cases} \tag{5}$$

(3) Key value operation: the largest level of tiles and their aggregate data are obtained through group operation. The key can be the quadtree/space filling curve code of the tile, the value is the set of pixels of the tile, and its key value will be converted. The tiles will be stored in the form of key value pairs to establish the foundation for subsequent distributed storage.

(4) Aggregate operation: unlike the group operation, which combines pixels within a single tile, aggregate is the aggregation of tiles between levels. Extract, group, and key value operations obtain the tile set of the largest level of the pyramid. Next, they need to aggregate up level by level to get the tiles of each level and finally get the pyramid model. The aggregate operation formula is

$$\begin{aligned} Agg\Big(& \text{tile}\left\{l_n, X_{2i}, Y_{2i}, \overset{w \times w}{\underset{i=1}{\cup}} \right\}\text{pixel}\Big), \\ & \left(\text{tile}\left\{l_n, X_{2i}, Y_{2i+1}, \overset{w \times w}{\underset{i=1}{\cup}} \right\}\text{pixel}\right), \\ & \left(\text{tile}\left\{l_n, X_{2i+1}, Y_{2i}, \overset{w \times w}{\underset{i=1}{\cup}} \right\}\text{pixel}\right), \\ & \left(\text{tile}\left\{l_n, X_{2i+1}, Y_{2i+1}, \overset{w \times w}{\underset{i=1}{\cup}} \right\}\text{pixel}\right) = \left(\text{tile}\left\{l_{n-1}, X_i, Y_i, \overset{w \times w}{\underset{i=1}{\cup}} \right\}\text{pixel}\right). \end{aligned} \tag{6}$$

3.2. Multidimensional Aggregation Pyramid Model.

The multidimensional aggregation pyramid (map) model is a spatiotemporal multidimensional hierarchical aggregation model based on the traditional tile pyramid model. Among them, the temporal dimension and spatial dimension belong to positioning features. The whole composed of the two identifies a spatiotemporal unit and serves as the key of the spatiotemporal unit. The discrete attribute dimension aggregation tree is value, and the two correspond in the form of key value pair. In this way, while realizing spatiotemporal aggregation, attribute dimensions are also aggregated, and a multidimensional spatiotemporal aggregation pyramid model containing space, time, and attribute dimensions is obtained [15].

(1) Aggregation tree (faa_tree): attribute aggregation tree is a tree structure formed by aggregating each dimension unit of the attributes of spatiotemporal objects, which simplifies the actual storage space with the result of breadth first traversal. Obtain a fixed length 1-dimensional array that can be stored structurally, and the formula is

$$faa\_\text{tree} = \{a_{\text{all}}, a_1, a_2, \ldots, a_n\}, \tag{7}$$

where $a_{\text{all}}, a_1, a_2, \ldots, a_n$. The node array sequence is obtained by traversing the attribute aggregation tree according to the hierarchy. Compared with tree structure, the fixed length array structure provides great convenience for subsequent storage and processing.

(2) Spatiotemporal pixel (st pixel): different from the zero-dimensional characteristics of pixels in 2D map

tiles, spatiotemporal pixels are a one-dimensional structure, a container for attribute dimensional information, and the smallest data unit of the map model. Spatiotemporal pixels extend the connotation of the concept of tile pyramid pixels. In addition to the range of spatial coordinates, they also add time scale coordinates. The formula is

$$ST - \text{pixel} = \{l, x, y, t, faa\_\text{tree}\}, \tag{8}$$

where t represents the scale coordinates of the preset time granularity and tree is the attribute aggregation $faa\_$tree, which is the real source of visual content.

(3) St tile: the concept of spatiotemporal tile is like that of the 2D model, which is composed of spatiotemporal pixels. Spatiotemporal tiles contain spatiotemporal pixels. Spatiotemporal pixels mount the attribute dimension aggregation tree to form a spatiotemporal cube that can realize hierarchical aggregation. Spatiotemporal tile is the basic unit of map model display. It is a 5-tuple, defined as

$$ST - \text{tile} = \{L, X, Y, T, \text{Tile}\_faa\}, \tag{9}$$

where l is the level of pyramid, X and y are the row and column numbers of tiles, and T represents the scale coordinates with preset time granularity, and Tile _faa formula is

$$\text{Tile}\_faa = \{A_{\text{all}}, A_1, A_2, \ldots, A_n\}, \tag{10}$$

where $A_{\text{all}}, A_1, A_2, \ldots, A_n$ is the attribute aggregation tree at tile level obtained by accumulating the subscripts corresponding to the array sequence faa_tree of attribute aggregation trees of each pixel in the tile.

It can be seen from (10) that the defined space-time tile is no longer a two-dimensional plane in concept, so the basic operations in the two-dimensional need to be further expanded.

(1) Extract operation: in addition to extracting geographic location information, it is also necessary to extract time information and attribute dimensions, generate attribute aggregation tree, and list them in order. The operation is

$$\text{Extract}(l, Lon, Lat, w) = ST - \text{pixel}\{l, x, y, t, faa\_\text{tree}\}. \tag{11}$$

(2) Group operation: there are two steps. The first step is mainly to establish the corresponding mapping relationship between spatiotemporal pixels and spatiotemporal tiles, that is, to obtain the specific tiles to which the pixels should belong, so as to locate not only in space but also in time. The formula is

$$\text{Group}(ST - \text{pixel}\{l, x, y, t, faa\_\text{tree}\}) = ST - \text{tile}\left([l_n, X, Y, T, \text{Tile}\_faa]\right), \tag{12}$$

where t and T represent the time limit required for group operation. Therefore, the spatiotemporal unit to which each pixel belongs can be found through (12), and the spatiotemporal pixels can be mapped to specific spatiotemporal tiles.

The second step of group operation is to reduce all spatiotemporal pixels mapped to the same spatiotemporal tile and aggregate all pixels in the tile under the same time granularity and the same geographical range. At the same time, the aggregation tree tile of the spatiotemporal Tile_faa st tile is the accumulation of the corresponding positions of the 1-dimensional fixed length array faa_tree of all spatiotemporal pixels, and the formula is

$$ST - \text{Tile}\_faa = \sum_{i=1}^{N=n} ST - \text{pixel}.faa\_\text{tree}. \tag{13}$$

(3) Key value operation: split tile_. For each node in FAA, the node is jointly encoded with the quadtree and time t of the tile to generate the key. Then, take the pixel set corresponding to each node as a value to generate a key value pair. The true meaning of the key value operation is the statistical result of the event of an attribute node within the tile space within the time period T.

(4) Aggregate operation: it needs to be limited to the same time t, that is, aggregate the tiles after key valued and finally obtain the multidimensional pyramid model. The formula is

$$\begin{aligned}
&\text{Agg}\left(ST - \text{tile}\left(l_n, X_{2i}, Y_{2i}, T, \text{Tile}\_faa\right)\right), \\
&ST - \text{tile}\left(l_n, X_{2i}, Y_{2i+1}, T, \text{Tile}\_faa\right), \\
&ST - \text{tile}\left(l_n, X_{2i+1}, Y_{2i}, T, \text{Tile}\_faa\right), \\
&ST - \text{tile}\left(l_n, X_{2i+1}, Y_{2i+1}, T, \text{Tile}\_faa\right) = ST - \text{tile}\left(l_{n-1}, X_i, Y_i, T, \text{Tile}\_faa\right).
\end{aligned} \tag{14}$$

3.3. Scenario Management Strategy. In the actual rendering process, there are usually tens of thousands of building components in a rendered scene, and the network bandwidth, memory capacity, and rendering performance are often limited. If all components in the rendered scene are rendered indiscriminately, it will cause great performance sales to GPU and reduce the efficiency of graphics rendering. Therefore, it is very important to optimize the organization, management, and scheduling of rendering scenes. There are many solutions for the management and optimization of rendered scenes, such as visibility culling, region of interest setting, LOD index structure, and batch call rendering [16].

The view range of browser model data is composed of viewpoint position and view cone, which is usually only a part of the whole rendered scene. Therefore, the organization and management of rendering scene through visibility culling is a widely used scene management method. Visual cone culling, back face culling, and occlusion culling are three widely used visibility culling technologies. The technical comparison is shown in Figure 2.

The back culling is carried out in the rasterization stage. It improves the rendering performance by culling the pieces back to the viewpoint. It is a visibility culling algorithm supported by the native OpenGL. Occlusion elimination can eliminate invisible objects blocked by visible objects. Although it can reduce the performance overhead of rendering pipeline and GPU, it is implemented based on hardware and needs to collect the location information of occluded objects and occluded objects, which occupies CPU resources. Visual cone culling exists in many real-time renderings. It is used to cull polygons or objects outside the visual cone view and render only the geometric graphics within the visual cone view, to improve the efficiency of graphics rendering. Relatively speaking, the visual cone elimination algorithm is suitable for the organization and management of rendered scenes [17]. In this study, BSphere volume and AABB box collision detection algorithm are introduced to construct the visual cone elimination algorithm based on BVH.

3.4. Experimental Method and Process

3.4.1. Model transformation. The original IFC file usually contains geometric information (spatial position and spatial relationship, etc.) and nongeometric information (attribute type and material map, etc.), and in the process of model conversion, it will often cause the lack of architectural object semantic attribute information, resulting in the lack of model information integrity. Therefore, it is necessary to separate the BIM model from the digital model and store and load the geometric space information and semantic attribute information separately, to ensure the integrity and semantics of the BIM model. IFC organizes and manages the building and component information of the BIM model in the form of the tree structure. Each building component instance is a node on the IFC structure tree, and each node has spatial or attribute relationships such as inclusion and association with its parent node or through its parent node and other child nodes. For example, each IFC wall instance is included in the
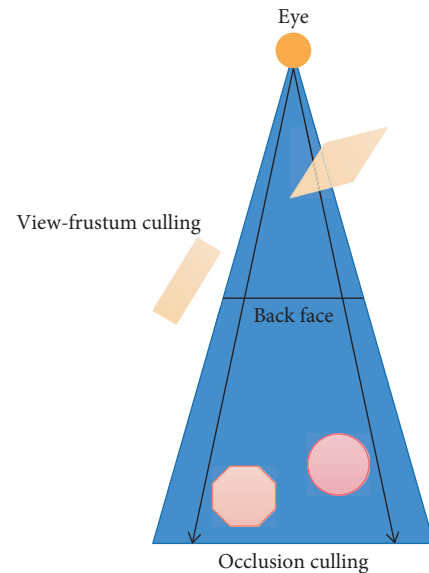
FIGURE 2: Comparison of common visibility culling techniques in rendering process.

IFC wall parent node as a child node, and similarly, the IFC wall parent node is included in the IFC building element as a child node, which is associated with the IFC door. By recursively accessing each node of the IFC structure tree and exporting the geometric attribute information of building component instances or other BIM scene information hierarchically, it can not only effectively manage IFC files and reduce IFC data redundancy but also lay a foundation for component batch rendering.

BIM server provides IFC file management, data analysis, formatted output, and other functions. This study will also traverse and retrieve the hierarchical relationship of the whole building model through the BIM server and split the building model into corresponding IFC model files and JSON text files through recursive access to the IFC structure tree. IFC model files store BIM spatial and geometric information, while JSON text files store BIM attribute and type information [18]. The digital analog separation process is shown in Figure 3.

In the past research studies, there are many solutions to convert IFC format files into GLTF format files. Select OBJ files as the intermediate format. First, call the IFC convert tool in the Ifc open shell library to convert IFC files into OBJ files and then convert OBJ into GLTF format files through the obj2gltf tool launched by AGI (analytical graphics, Inc.), so as to realize the overall conversion from IFC to glTF. By calling Revit API and inheriting IExternal Command and IExternal Application interfaces, this study constructs IFC glTF conversion framework based on c# language and realizes glTF model file output through Revit2gltf. The data conversion process is shown in Figure 4 [19].

Usually, in the process of BIM model transformation, it is necessary to complete the spatial relationship mapping from geometric information to WebGL. This is because the component position coordinate information in IFC file is defined by IfcLocalPlacement attribute, which usually
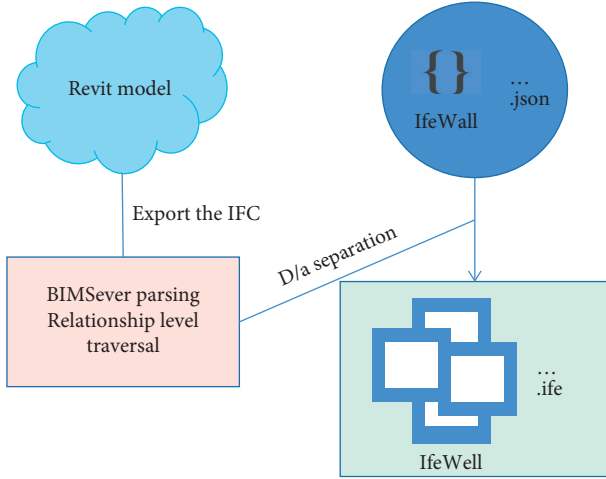
FIGURE 3: Digital analog separation process.

FIGURE 4: Data conversion process.

adopts the local coordinate system, while WebGL is the global coordinate system. Therefore, to establish the connection between IFC model components and WebGL camera, coordinate system space transformation must be carried out, mainly including model transformation and visual transformation. The coordinate transformation from the local coordinate system to the world coordinate system is the transformation of spatial geometry by translation, scaling and rotation alone or in combination [20]. Considering that the Cartesian coordinate system adopts the right-hand rule, take the z-axis as an example, as shown in Figure 5.

Usually, a point $V(x, y, z, 1)$ in space will pass through 4×4 matrix M transformation in (15) to get a new point $V'(x', y', z', 1)$:

$$\begin{bmatrix} a & b & c & d \\ e & f & g & h \\ i & j & k & l \\ m & n & o & p \end{bmatrix} \times \begin{bmatrix} x \\ y \\ z \\ 1 \end{bmatrix} = \begin{bmatrix} x' \\ y' \\ z' \\ 1 \end{bmatrix}. \tag{15}$$

If a vertex $V_{\text{Local}}(x, y, z, 1)$ in the local coordinate system translates the distance T_x, T_y, T_z on the x-axis, y-axis, and z-axis, respectively, to obtain $V_{\text{Global}}(x', y', z', 1) = V_{\text{Local}}(x + T_x, y + T_y, z + T_z, 1)$, and substituting it into (15), we can obtain the translation matrix, i.e.,

$$T = \begin{bmatrix} 1 & 0 & 0 & T_x \\ 0 & 1 & 0 & T_y \\ 0 & 0 & 1 & T_z \\ 0 & 0 & 0 & 1 \end{bmatrix}. \tag{16}$$

If the point is scaled with the origin as the base point and S_x, S_y, and S_z times are scaled in the x-axis, y-axis, and z-axis directions, respectively, the point $V_{\text{Global}}(x', y', z', 1) = V_{\text{Local}}(x + S_x, y + S_y, z + S_z, 1)$ will be obtained, which can be substituted into (15) to obtain the scaling matrix, i.e.,

FIGURE 5: Schematic diagram of translation, zoom, and rotation of spatial graphics.

$$S = \begin{bmatrix} S_x & 0 & 0 & 0 \\ 0 & S_y & 0 & 0 \\ 0 & 0 & S_z & 0 \\ 0 & 0 & 0 & 1 \end{bmatrix}. \tag{17}$$

If the figure rotates around the Z-axis, as shown in Figure 6, the Z value transformation can be ignored because the Z value remains unchanged. At this time, set R as the distance from the origin o to the point $V_{\text{Local}}(x, y, z)$. α is the angle the X-axis rotates to this point. According to the trigonometric function equation, the rotation matrix when the point $V_{\text{Local}}(x, y, z)$ rotates at angle β around the Z-axis can be obtained, i.e.,

$$R_z = \begin{bmatrix} \cos \beta_z & -\sin \beta_z & 0 & 0 \\ \sin \beta_z & \cos \beta_z & 0 & 0 \\ 0 & 0 & 1 & 0 \\ 0 & 0 & 0 & 1 \end{bmatrix}. \tag{18}$$

Similarly, the rotation matrix R_x when rotating angle B around the X-axis and the rotation matrix R_y when rotating angle ß around the Y-axis can be obtained.

To sum up, the geometric information of IFC model file can be transformed into the spatial coordinate system through (19) to complete the spatial relationship mapping from component geometric information to WebGL, that is,

$$V_{\text{Global}} = V_{\text{Local}} \times (T \times s \times r), \tag{19}$$

where $R = R_x R_y R_z$ is the rotation conversion matrix when the vertex rotates around the coordinate axis. After digital analog separation and data conversion, glTFmodel file and JSON semantic attribute file are introduced into the same scene object through the constructor "Loader" in Three.js to complete the loading of geometric model and semantic attribute information in WebGL [21].

3.4.2. Scene Management. Visual cone culling uses the spatial correlation in the rendered scene to judge whether the scene model is inside or intersecting with the visual cone. The viewing cone itself is usually composed of 6 cutting planes, and the right section of the cutting plane is shown in Figure 6. The opening angle is in the vertical direction of the apparent cone. Dn and Df are the distances from the viewpoint to the near clipping plane and the far clipping plane, respectively. Hn and Hf are the heights of the near clipping plane and the far clipping plane, respectively.

Suppose the aspect ratio of the camera is k and a vertex P (XO, Jo, Zo) is on the side of the right clipping plane. According to the geometric relationship, the distance between the vertex and the right clipping surface can be calculated through equation (6), to judge the spatial relationship between the vertex and the right clipping surface, i.e.,

$$d = \frac{|x_0 + k \tan \theta/2 z_0|}{\sqrt{1 + k^2 \tan^2 (\theta/2)}}. \tag{20}$$

If $d < 0$, the apex is outside the visual cone. If $d \geq 0$, the apex is inside the visual cone. This is because when the clipping space changes, the left- and right-hand coordinate system changes, and the normal vector of the clipping surface points to the viewing cone. According to the spatial relationship between all vertices of a component and the clipping surface, it can be determined whether the whole component and the viewing cone have an inclusion, intersection, or separation relationship, to determine whether to load and render the component.

(1) BVH-based visibility detection algorithm for BS-AB scene components: using the spatial data structure with hierarchical structure to organize the scene and build a bounding box approximate description component with
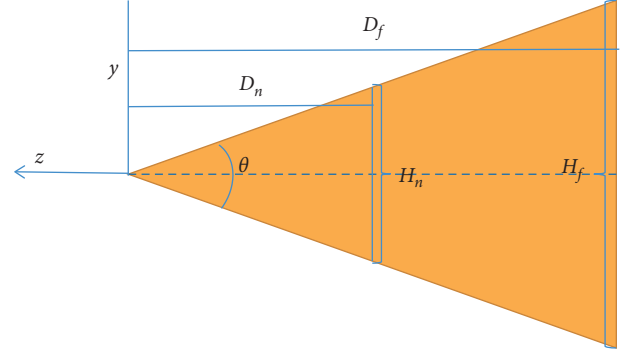
FIGURE 6: Section of the right cutting surface of the cone.

slightly large volume but relatively simple geometric features is a favorable way to solve the low efficiency of linear array traversal in complex scenes and the difficulty of visual cone intersection test of complex components. Hierarchical bounding volume (BVH) is a commonly used spatial data structure. It organizes and manages the objects in the scene in a hierarchical tree structure based on spatial information, including internal nodes and leaf nodes from the root node down.

Therefore, the BVH structure tree can be created according to the IFC component tree. Here, the cone scene is regarded as a root node, and each Ifc Building Element (such as IfcWall and IfcDoor) is placed in the internal node as a category; then, the family under each category is the leaf node. When there are still different components in the leaf node, continue to build the BVH tree according to the family and family type until the leaf node contains family instances. The purpose of adding enclosures in the scene is to filter the geometry outside the enclosure through accurate collision detection. Commonly used bounding bodies include BSphere body and AABB box. Bsphere volume algorithm is based on the sphere radius R and the distance d from the sphere center to the cutting surface of the viewing cone. If $d < r$, the sphere is separated from the visual cone without loading. If $|d| < r$, the sphere intersects with the visual cone for loading. If $d > r$, the sphere is loaded in the viewing cone, and its structure is shown in Figure 7. The AABB box algorithm is based on the distance between the vertex of the bounding box and the cutting surface of the viewing cone. Whether to load the bounding box is determined by judging whether the vertex of the bounding box is in the viewing cone or whether the connecting line between two points passes through the viewing cone. Its structure is shown in Figure 8.

When collision detection is performed between the visual cone and the hierarchical bounding body, BSphere predetection is performed first, and recursive access is performed to each node from the root node in turn. The separated internal nodes and leaf nodes are eliminated, and the leaf nodes contained in the internal nodes and the internal nodes intersecting with the visual cone are loaded. In addition, the leaf nodes that still intersect the visual cone in the internal nodes intersecting the visual cone are detected by AABB box, and the bounding boxes that are separated
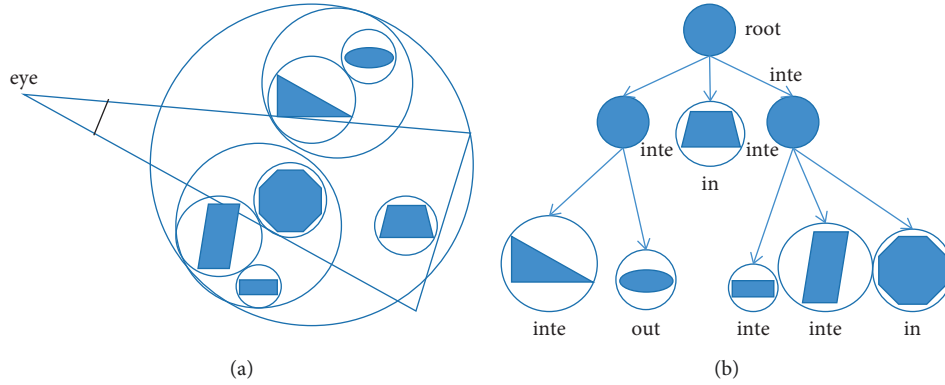
FIGURE 7: Schematic diagram of sphere hierarchical bounding box tree structure. (a) Surround scene components with spheres. (b) Hierarchy tree.

from the visual cone are eliminated. Based on ensuring the efficiency of visual cone elimination, this algorithm not only reduces the performance overhead of rendering pipeline but also improves the accuracy of visual component detection [22].

Sphere structure and intersection test are simple, but the tightness is too poor. Although AABB box supports dynamic update and detection is more accurate, the update efficiency is too low. Therefore, this study proposes to carry out sphere predetection on scene components, eliminate rough and loose components, and then further screen through AABB box detection to quickly achieve the optimal detection results.

4. Experiment and Result Analysis

In order to verify the effectiveness of model transformation strategy and scene management strategy, this study collects 10 experimental data of building scene composition from the open IFC model repository and BIM model databases for example verification. This example verifies that it is configured as Intel(R) Core (TM) i7-8700@3.20GHZ six core processor, 16 GB memory, NVIDIA GeForce GTX 1060 graphics card, and notebook computer with 64 bit Windows10 operating system is implemented based on Chrome browser and Three.js framework. The IFC version of all test data in the experiment is IFC2X3, as shown in Table 1.

4.1. Effectiveness Analysis of Model Transformation Strategy. In this study, glTF is proposed as the target format of model transformation to realize network loading. In this study, the model transformation experiment of IFC model file without semantic attribute is carried out. It can be seen from Figure 8 that, as the volume of model files increases, the volume of glTF increases slowly, while the growth of obj is larger and much larger than that of glTF files. This is because after digital to analog separation and format conversion of the original IFC file, only a small amount of information is stored in the glTF file, while most of the information is stored in the bin file.

It can be seen from Figure 9 that although the overall file size and conversion time of the converted model are
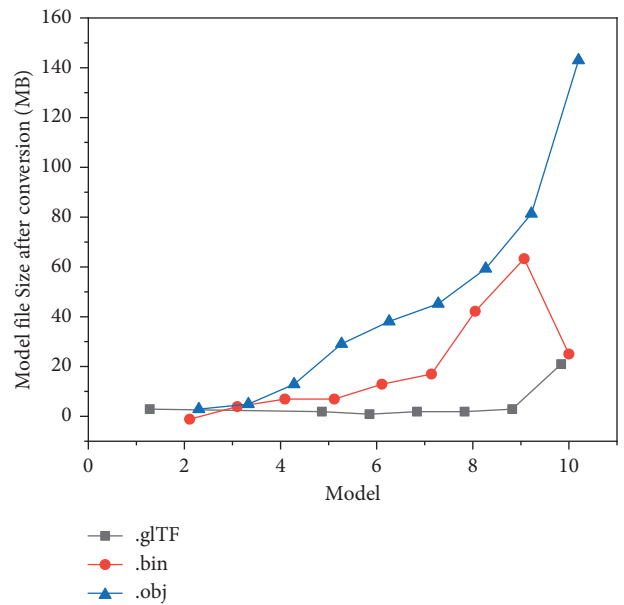
FIGURE 8: Size of the converted model file.

different due to different architectural scenes, the compression rate of gLTF format is more than 90%, which has obvious compression advantages compared with obj format. Therefore, taking gLTF as the target, the format of model conversion is effective to reduce the loading of 3D model data, and it will also be more conducive to the rapid loading of 3D model data on the web.

4.2. Effectiveness Analysis of Scenario Management Strategy. Aiming at the problem of low rendering frame rate caused by poor visibility detection effect of scene components, this study proposes to use BS-AB scene component visibility detection algorithm based on BVH to detect and eliminate the visibility of building components. In this study, Medel 10 is taken as the experimental object, and 10 cone scenes with the same angle and the same viewpoint but different distances between the viewpoint and the model are set, as shown in Figure 10. Then, in different cone scenes, the performance is compared with other rendering systems in

Table 1: Experimental test dataset.

Model ID	Model name	Size (MB)
1	231110AC11-institute-var-2	2.705
2	Autodesk_hospital_parking garage	6.110
3	20191126AZUMA9	10.001
4	Glodon building	27.315
5	HITOS_070308	61.127
6	PUIH-second phase	77.878
7	Humanized office building	90.514
8	Nihewan visitor center	116.766
9	TJ-taoy uanju-complex-architecture	171.011
10	Shr-office-building-structure	303.608

Figure 10: Model conversion results.

Figure 9: BIMServer FPS.

Figure 11: BS-AB FPS.

terms of FPS value and single rendering time, to verify whether this strategy is effective for scene visual component management.

In the experiment, the version of BIMviews that BIM-Server depends on is BIMServer1.5.88. Chrome web browser is a 64 bit version of 84.0.4147.89. During the experiment, start the FPS mater in the rendering listener of Chrome browser to monitor the rendering area of 3D scene. Use the stats.js library to monitor the rendering time of the scene area. In addition, BIMviews load IFC model files, and other methods load glTF files.

The experimental results are shown in Figures 9–14. It can be seen from Figures 11 and 12 that, as the distance between the viewpoint and the model decreases, the number of components in the visual cone decreases, and the overall FPS value is gradually increasing, but the increase of the other two methods is small and unstable. After Distance 5, the number of components in the visual cone is greatly reduced. The visual cone elimination effect of this method is obvious, and the rendering frame rate increases steadily. It can be seen from Figure 14 that, before Distance 5, there is little difference in the single rendering time of the two methods, but after Distance 5, the rendering time of the method used in this study decreases significantly. Through experimental comparison, the feasibility of the BS-AB scene

Figure 12: Three. js FPS.

Figure 13: Three.JS rendering time.
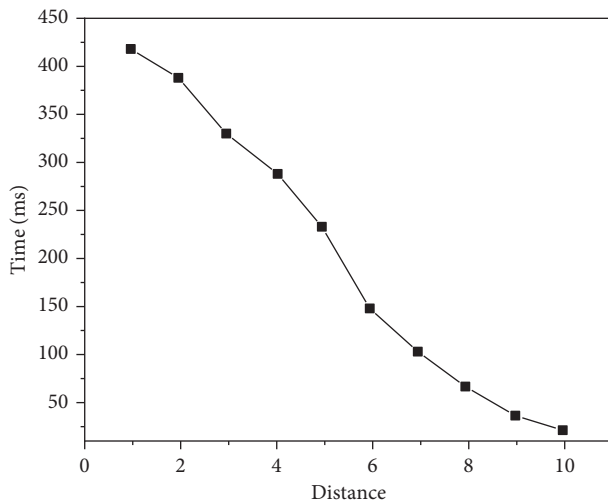
Figure 14: BS-AB rendering time.

component visibility detection algorithm and the effectiveness of the scene management strategy are verified, which can meet the smooth needs of BIM model data network visualization. In addition, during the experiment, it was found that BIMviews were slow to load the IFC file of the experimental object and obtain the model data, with an average of about 40 s, and the Caton was obvious. However, it only takes about 7 s to load the glTF file to the complete display of the big data map visualization design by using Three.js. It is verified again that the glTF format is more suitable for the display and interaction of BIM model data based on the big data map visualization design than the IFC format.

5. Conclusion

The visibility of scene components is eliminated by BS-AB scene component visibility detection algorithm based on BVH. The experimental results show that this method greatly reduces the amount of BIM model data, improves the

detection accuracy of visual components of the model, and has a good effect of web model loading and rendering. The visibility of components (e.g., building models) cannot be detected by different methods, but the visibility of components (e.g., building models) cannot be detected. The follow-up work will start with LOD and occlusion elimination algorithm to further optimize the performance overhead of rendering pipeline and GPU after rendering scene visual cone elimination.

Data Availability

The labeled dataset used to support the findings of this study are available from the corresponding author upon request.

Conflicts of Interest

The authors declare no conflicts of interest.

Acknowledgments

References

[1] Q. Zhou, "Research on architectural space design of coastal cities based on virtual reality technology," *Journal of Coastal Research*, vol. 115, no. sp1, 2020.

[2] W. Xiong, M. Tu, and X. Li, "Knowledge maps analysis of research on settlement landscape of qiang based on the citespace method," *IOP Conference Series: Earth and Environmental Science*, vol. 692, no. 4, Article ID 042078, 2021.

[3] Y. U. Fei and N. Norihito, "Research on the methodology of regional planning in the design of people's commune," *Journal of Architecture and Planning (Transactions of AIJ)*, vol. 84, no. 766, pp. 2669–2677, 2019.

[4] W. Zhu, Y. Hou, E. Wang, and Y. Wang, "Design of geographic information visualization system for marine tourism based on data mining," *Journal of Coastal Research*, vol. 103, 2020.

[5] L. Zhao and Z. Zhou, "Research on landscape information model construction based on visualization technology," *Journal of Physics: Conference Series*, vol. 1693, no. 1, Article ID 012126, 2020.

[6] M. W. Kowalczyk and A. Lewandowska, "Techniques of visual communiaction in architectural design," *Journal of Education, Culture and Society*, vol. 11, no. 2, pp. 376–383, 2020.

[7] C. Djari and A. Arrouf, "The impact of viewing images of precedents on the cognitive process of architectural idea generation," *Proceedings of the Design Society: International Conference on Engineering Design*, vol. 1, no. 1, pp. 209–218, 2019.

[8] L. Suárez, "Visualization of architectural experiences using heat maps," *The International Journal of Architectonic, Spatial, and Environmental Design*, vol. 13, no. 1, pp. 17–34, 2019.

[9] D. Haiyan, Z. Hong, H. Chunnan, and M. Bing, "Site planning and architectural conceptual design of a electronics factory based on the component method," *IOP Conference Series: Materials Science and Engineering*, vol. 1203, no. 2, Article ID 022096, 2021.

[10] X. Guan, C. Xie, and L. Han, "Map-vis: a distributed spatiotemporal big data visualization framework based on a multi-

dimensional aggregation pyramid model," *Applied Sciences*, vol. 10, no. 2, 2020.

[11] Y. Zou, Q. Zhan, and K. Xiang, "A comprehensive method for optimizing the design of a regular architectural space to improve building performance," *Energy Reports*, vol. 7, no. 211, pp. 981–996, 2021.

[12] Q. Fu, J. Lv, S. Tang, and Q. Xie, "Optimal design of virtual reality visualization interface based on kansei engineering image space research," *Symmetry*, vol. 12, no. 10, 2020.

[13] D. Mehta, "A review on challenges of daylight-based-classroom-studies and their methodology regarding architectural-design-process," *International Journal of Innovative Research in Science Engineering and Technology*, vol. 9, no. 10, Article ID 10112, 2020.

[14] S. Ceylan, "A case study on borders in retail spaces," *Archnet-IJAR: International Journal of Architectural Research*, vol. 14, no. 1, pp. 18–30, 2019.

[15] J. Sun and B. Z. Yuan, "Visualization analysis of research on rice with fertilizer from the 'agronomy' category based on citespace," *Current Science*, vol. 117, no. 9, 2019.

[16] X. Lu, Y. Wei, X. Hu, and J. Fang, "A research on the architectural design and its implementing of dong nationality in northern guangxi," *IOP Conference Series: Earth and Environmental Science*, vol. 525, no. 1, Article ID 012078, 2020.

[17] W. Wang and C. Lu, "Visualization analysis of big data research based on citespace," *Soft Computing*, vol. 24, no. 11, pp. 8173–8186, 2020.

[18] S. Yi and S. Gao, "Visualization analysis of online health care research based on citespace," *Open Journal of Social Sciences*, vol. 9, no. 7, pp. 311–325, 2021.

[19] T. Guo, "Research in the field of smart wearables from 2006 to 2019: a bibliometric analysis and visualization based on citespace," *Journal of Physics: Conference Series*, vol. 1790, no. 1, Article ID 012051, 2021.

[20] S. Basso, G. Botter, R. Merz, and A. Miniussi, "Phev! the physically-based extreme value distribution of river flows," *Environmental Research Letters*, vol. 16, no. 12, Article ID 124065, 2021.

[21] D. Liang, L. Yang, X. Cheng, and G. Song, "The visualization study on research progress of thermal comfort for indoor environment based on citespace," *IOP Conference Series: Earth and Environmental Science*, vol. 514, no. 3, Article ID 032033, 2020.

[22] S. Pushkarev, A. Plaksin, A. Sycheva, and P. Harlanova, "Geometric modeling of stress visualization tools based on the functional-voxel method," *Geometry & Graphics*, vol. 8, no. 3, pp. 36–43, 2020.

Research Article

Evaluation Index System of Economic and Social Development Pilot Area Based on Spatial Network Structure Analysis

Jing Tu (iD)

School of Economics, Xihua University, Chengdu 610039, China

Correspondence should be addressed to Jing Tu; 1220200008@mail.xhu.edu.cn

In order to improve the evaluation effect of the economic and social development pioneer area, this paper constructs the evaluation index system of the economic and social development pioneer area based on the spatial network structure analysis method and obtains an intelligent analysis system. Moreover, from the perspective of economic development information flow, this paper uses information flow direction analysis method and advantage flow analysis method to discuss the structural characteristics of urban economic development network in the economic belt, providing new methods and perspectives for the study of urban economic development flow. In addition, this paper attempts to propose a universal method for quantitative research on the "flow space" structure of urban economic development as the forward-looking content of urban economic development. According to the simulation test results, it can be seen that the evaluation index system of the economic and social development pilot area based on the analysis of the spatial network structure proposed in this paper has a good effect.

1. Introduction

The new development concept is an inseparable organic whole. In this organic whole, innovation is the internal driving force leading development and must be placed at the core of development, including innovation in theory, system, technology, culture, and other aspects. Coordination is the principal requirement of development, and the concept of coordinated development pays more attention to integrity, systematization, and balance and must correctly handle major relations in development and solve the problem of unbalanced and insufficient development [1]. At the same time, green is a necessary condition for development, and green development focuses on solving the problem of harmonious coexistence and coexistence between man and nature. While continuing and emphasizing adherence to the basic national policy of resource conservation and environmental protection, it is necessary to achieve synergy between economic and social development and ecological and environmental protection and create a good production and living environment for the people. Opening up is the environmental layout of development. To solve the problem

of developing internal and external linkages, a higher-level open economy must be developed to expand opening up and promote reform and development [2]. In addition, sharing is the fundamental purpose of development, focusing on solving social fairness and justice issues and continuously promoting the common prosperity of all people. The five development concepts are interconnected, and promote each other, constituting a brand-new concept and action guide to guide and lead today's development. Moreover, high-quality development under the guidance of new development concepts will surely become the normal state of development in the new era [3].

At present, the research on the airport economy at home and abroad is generally summarized from the aspects of case analysis and planning and construction, focusing on basic theoretical research such as basic concepts, characteristics, and development models at the macro level. However, there is a lack of specialized research on the airport economy industry from the perspective of regional economics, management, and industrial economics, as well as micro-subjects. It is necessary to select and plan the airport industry based on the development time sequence by using the

analytic hierarchy process in combination with the types of airport economic industries. At the same time, it is necessary to rationally plan and lay out the industrial space according to the industrial space structure layout of the airport area and combine the regional characteristics of the economic demonstration area so as to enrich the theoretical research system of the airport economy.

Based on the spatial network structure analysis method, this paper constructs the evaluation index system of the economic and social development pioneer area and obtains an intelligent analysis system, which provides a reference for the subsequent evaluation of the economic and social development pioneer area.

2. Related Work

The evaluation theory of economic and social development is a process of continuous evolution, and the evolution process is consistent with the development of the context and the theory of economic and social development. Through the study of relevant literature, it can be seen that the theory of economic and social development will affect the theory and connotation of measurement and evaluation. The changes of economic and social development theory with time and environment will inevitably lead to changes in the content of economic and social measurement and evaluation [4].

The social development concept of one-sided pursuit of economic growth has its profound and complicated historical reasons. The two world wars severely damaged the economy of the traditional capitalist powers. With the collapse of the world colonial system, the rise of independent democratic movements in the colonies directly shook the economic foundation of imperialism [5]. After the Second World War, the primary task of traditional capitalist powers was to restore and develop their own economies. Countries that have just gotten rid of the colonial system and become independent and countries that have just begun to industrialize have become developing countries. The primary task of developing countries is to develop their economies. In this way, the world is pursuing economic growth. Therefore, the development of this period mainly refers to the economic development. Due to special historical reasons, people at that time believed that the cause of social problems was the low economic aggregate, and rich material wealth could solve all social problems. Typical theories include Lewis's [6] dual structure theory, Rostow's economic development stage theory [7], Kuznets' statistical theory [8], and Chenery's econometric theory [9]. Under the guidance of this concept, the total economic volume has increased significantly, the progress of other aspects of society has been slow, or even counterproductive, and problems such as social unrest, political corruption, and unfair income distribution have emerged one after another. The concept of one-sided pursuit of economic growth began to be questioned.

Under the guidance of the one-sided pursuit of economic growth, other aspects of society have not achieved the expected progress, and people have begun to realize that simple economic growth cannot solve problems such as poverty, unemployment, and inequitable distribution [10]. The development theory has evolved from economics to a multidisciplinary comprehensive theory, which affirms the basic status of economic growth while taking into account other aspects of society. However, the focus of this period was mainly on social welfare, aiming to solve poverty, unemployment, and inequitable distribution. The focus is on raising the income of the poor, increasing the employment rate and improving the social security system [11]. Literature [12] believes that development should include economic, political, and cultural development and believes that as long as poverty, unemployment, and inequality are reduced, it belongs to development. Literature [13] proposed that development is a multidimensional process that includes the combination of the entire economy, society, culture, technology, ecology, and other elements and internal reorganization, including changes in economic aggregates, economic income growth, social systems, social structures, and even people's beliefs, habits, and other related content that cannot be regarded as a simple process.

In the process of industrialization, human beings have experienced an extensive economic development model. In this process, human beings exploit resources plunder, destroy the ecological environment, pursue short-term interests, and make economic development unsustainable [14]. Literature [15] believes that sustainable development mainly includes two cores, namely, the welfare problem in the economic growth period and the constraint problem of economic growth. The optimal growth path under different intergenerational goals and resource constraints is studied, and it is found that the optimal growth path is the path of sustainable development most of the time. Some scholars put forward another view. Literature [16] believes that the systematic interpretation of the connotation of "sustainable development" should be carried out from three aspects: economic sustainability, environmental sustainability, and social sustainability. With the deepening of research, the academic community has further enriched the theoretical framework of sustainable development and believes that the theoretical connotation of sustainable development includes five aspects: multidimensional development, common development, fair development, coordinated development, and efficient development. The indicator system of the United Nations Commission on Sustainable Development covers the four major systems of economy, society, environment, and system, including 142 indicators designed by driving force, state, and response model. The US Sustainable Development Indicator System consists of ten goals, including 54 indicators including health and the environment, equality, sustainable society, economic prosperity, public participation, protection of nature, and education. The UK sustainable development indicator system includes 21 aspects including economy, transportation, overseas trade, energy, land use, water resources, forests, atmosphere, waste, and radioactivity, with a total of 123 indicators [17].

3. Analysis Model of Spatial Network Structure

The city network mainly refers to the connection between cities. The relational data between cities is particularly critical to the study of urban networks, which can be roughly divided into attribute methods and relational methods. The data with realistic or abstract meanings that can reflect and carry various associations between cities, such as the flow of people, material exchange, and information exchange between cities, can be understood as relational data. The traditional urban network research is mostly carried out from the mode of urban hierarchy, scale, core-periphery, and so on. However, the urban network studied in this paper refers to the urban network in which the economic development information flow represents the abstract meaning perspective, and this paper reveals the connection between urban tourism through the abstract research perspective.

The central place refers to the place where goods and services can be provided to consumers in the surrounding area, such as a residential distribution point, a commercial center, or a city. Centrality is the degree to which a central place plays a central role relative to its surrounding areas, that is, its relative importance. Centrality can be expressed as follows [18]:

$$C = C_1 - C_2. \tag{1}$$

Among them, C_1 is the total amount of goods and services provided by the center, C_2 is the amount of goods and services provided by the center for itself, and C is the centrality, which refers to the amount of goods and services provided by the center to surrounding areas.

The central place theory is regarded as the basic theory of urban geography and regional economics research, as well as the foundational theory of urban system spatial structure research. The central place theory is a theory about the size of urban functions and the distribution of spatial structure in the region. It reveals the basic characteristics of the spatial structure of the central place system. In the tourism practice research, the urban tourism architecture mainly studies the system level division, the spatial layout in a certain area, and the connection between each other. The urban tourism grade is analyzed to provide support for the next regional tourism spatial structure.

The core idea of growth pole theory is that economic growth does not occur at the same speed in every location at the same time. Generally, the growth rate of a dominant economic sector or an innovative industry is the fastest, and these sectors and industries tend to gather in the best location. The location is usually a large- or medium-sized city within the region. Therefore, these large- and medium-sized cities gradually form regional growth poles and drive regional development through diffusion effects.

This theory provides a basis for the priority development of regional tourism. Due to the comprehensive characteristics of the tourism industry, the linkage effect of the tourism industry is extended to a larger area through the gathering and diffusion of regional tourism growth poles. In addition, regional tourism is not initially developed in a balanced way.

According to the development model of this theory, priority development areas can be used to drive tourism development in other regions so that it can play a role in the aggregation and diffusion of growth points and drive the economic growth of the entire regional tourism industry. The theory is mainly used in the two forms of the point axis structure and the network structure in the tourism space structure.

The point-axis theory is formed on the basis of the growth pole theory, which holds that the "point" is the node (city) at all levels, and the "axis" is the industrial belt formed by connecting the nodes at all levels in a certain direction. The point-axis structure is formed by a number of isolated nodes through the connection of the development axis and gradually develops to form a certain spatial network structure. Cities in a certain area are distributed hierarchically, so the development axis connecting each city is also hierarchical, and cities and axes with different levels have different attractiveness.

In the related research, the measurement methods used by most scholars to study the evolution law and trend of regional tourism development differences are basically based on the relevant methods of income distribution differences in economics. The specific measurement methods used in this paper are as follows:

(1) *Standard Deviation (VOC)*. It is the arithmetic square root of the ratio between the sum of squared deviations of the sample data and the total sample size. It reflects the absolute degree of dispersion between sample individuals and can be used to represent the absolute difference in economic scale between cities. The larger the value, the greater the absolute difference.

$$\text{VOC} = \sqrt{\frac{\sum_{i=1}^{n} (x_i - \overline{x})^2}{n}}. \tag{2}$$

(2) *Coefficient of Variation (CV)*. It is the quotient between the standard deviation and the mean. It can eliminate the interference of different sample averages on the degree of sample variation, reflect the relative dispersion of samples, and can be used to characterize the relative difference of tourism scale between cities. The smaller the value, the smaller the relative difference.

$$\text{CV} = \sqrt{\frac{\sum_{i=1}^{n} (x_i - \overline{x})^2 / n}{\overline{x}}}. \tag{3}$$

(3) *Gini Coefficient (G)*. It is combined with the coefficient of variation to determine the relative difference of urban tourism scale. The larger the value is, the larger the tourism scale gap between cities is.

$$G = 1 + \frac{1}{n} - \frac{1}{n^2 \overline{y}} (y_1 + 2y_2 + 3y_3 + \cdots + ny_n). \tag{4}$$

(4) *Growth Rate*. It can analyze the differences in the speed of regional tourism development, but the bases

of cities are different, and the same growth rate will lead to large differences in actual growth. In order to eliminate the above situation, this paper introduces the relative development rate (Nich) to measure the spatial difference of the relative development speed of urban tourism in the economic belt.

Nich is the relationship between the change of the economic development scale of each city in a certain period and the change of the average economic development scale of the whole region in the same period:

$$\text{Nich} = \frac{(Y_{2i} - Y_{1i})}{Y_1 - Y_2}. \tag{5}$$

In the formula, Y_{1i}, Y_{2i} is the economic development scale of city i at time 1 and 2, and Y_1, Y_2 is the average economic development scale of the region at time 1 and 2. Nich > 1 means that the growth rate of the economic development scale of city i is higher than the regional average level, $0 < \text{Nich} < 1$ means that the growth rate of the economic development scale of city i is lower than the regional average level, and Nich < 0 means that the economic development scale of city i has negative growth.

(5) *Herfindahl Coefficient (Hn)*. It is an index reflecting the scale and agglomeration degree of urban economic development. The larger the value, the higher the degree of concentration, and the more uneven the development.

$$H_n = \sum_{i=1}^{n} p_i^2. \tag{6}$$

(6) *First Degree (S)*. It is the quotient between the measures of the economic development scale of the first and second largest cities. It reflects the aggregation degree of urban economic development scale distribution. The larger the value, the more concentrated the distribution. When $S > 2$, the regional structure is considered unreasonable, and it is called the primacy distribution. When $S < 2$, the regional structure distribution is considered to be relatively reasonable.

$$S = \frac{P_1}{P_2}. \tag{7}$$

In formulae (1)–(6), X_i is the value of index i, $Y_1, Y_2, Y_3 \cdots Y_n$ is the index value from large to small, $\overline{X}$ and $\overline{Y}$ are the mean values of the indexes, and n is the total number of samples, P_i is the proportion of index i, and P_1, P_2 is the index value of the first and second largest cities.

3.1. Research Methods of Economic Development Scale Distribution. In order to better present the overall distribution of the economic development scale of cities in the economic belt. In this paper, the Rothko-type rank-scale distribution is used to measure the economic development scale distribution of cities in the economic belt. The formula is [19]

$$P = KR^{-q}. \tag{8}$$

Among them, P is the scale of urban economic development, R is the rank, K is the ideal scale of the first city, and q is the concentration index. According to the q-value, the scale distribution of urban economic development is divided into first type $(q \geq 1.2)$, concentrated type $(0.85 < q < 1.2)$, and balanced type $(q \leq 0.85)$.

In order to scientifically use the sample data for regression analysis, the natural logarithm of formula (7) is taken and sorted out:

$$\ln p = \ln k - q \ln R. \tag{9}$$

This paper uses the index of the total number of people received by the city's economic development to measure its functional scale and the index of the proportion of total economic development revenue to GDP to measure its functional status. Moreover, this paper uses Nelson's method to define the functional strength of each city. First, the sample mean $(\overline{X})$ of each city's functional indexes is calculated as the threshold for judging urban specialized departments; then, the sample standard deviation (σ) of each city's functional indexes is calculated, and then the coefficient (K_i) of each city's functional intensity is calculated.

$$\overline{X}_i = \frac{1}{n} \sum_{i=1}^{n} X_i,$$

$$\sigma_i = \sqrt{\frac{\sum_{i=1}^{n} (X_i - \overline{X})^2}{n}}, \tag{10}$$

$$K_i = \frac{X_i - \overline{X}}{\sigma}.$$

Each dimension is divided into 3 intervals according to the value of K_i. The specific description is as follows. In the dimension of functional scale, it is divided into small, medium, and large cities. In terms of functional status, cities are divided into low, medium, and high specialization cities.

The mean value of the total number of people received by the economic development of cities in the economic belt is expressed by $\overline{X}$, and the standard deviation is expressed by σ. After calculation, it is found that the original sample of functional scale is nonnormal. Therefore, this paper corrects it as follows:

$$T_i = \begin{cases} \text{small} - \text{scale } T_i \leq \overline{X}\tau, \\ \text{medium} - \text{sized } \overline{X}\tau < T_i < \overline{X}\tau + \sigma_i, \\ \text{large } T_i \geq \overline{X}\tau + \sigma_i, \end{cases}$$

$$S_i = \begin{cases} \text{Low specialization } S_i \leq \overline{X}_S, \\ \text{Specialization in secondary schools } \overline{X}_S < S_i \leq \overline{X}_S + \sigma_i, \\ \text{High specialization } S_i \geq \overline{X}_S + \sigma_i. \end{cases} \tag{11}$$

Among them, T_i is the functional scale of urban economic development, and S_i is the functional status of urban economic development.

The two dimensions are combined with each other to form 9 types of urban economic development functions (Figure 1).

With the rapid development of information technology, the popularization of the Internet and the economic development reservation system has largely changed the market conditions of the economic development industry. Moreover, the application of information technology in the economic development industry is becoming more and more extensive, and the influence of information flow on the economic development flow is gradually increasing. The guidance of economic development information flow to economic development flow is a process of information decision-making and implementation; in this process, "quasitourists" have been largely controlled by economic development information flow. On the one hand, the flow of economic development information enhances the flow of economic development, and on the other hand, the two can even replace each other in quantitative relationship. In the context of the rapid development of the Internet, the purchasing decisions and behaviors of economic developers are increasingly dependent on the Internet. Website information flow is the basic form and the only medium of Internet information transmission, and it plays a huge guiding role in the generation and change of people flow and is the most influential "flow" among many "flow" elements. Therefore, from the perspective of economic development information flow, this paper avoids the obstacles caused by the lack of statistics on domestic economic development flow data.

From the perspective of economic development information flow, this paper uses information flow direction analysis method and advantage flow analysis method to discuss the structural characteristics of urban economic development network in the economic belt, providing new methods and perspectives for the study of urban economic development flow. Moreover, this paper attempts to propose a universal method for quantitative research on the "flow space" structure of urban economic development as a forward-looking content of urban economic development so as to make up for the deficiencies of related research caused by the lack of information on the flow and flow of domestic actual economic development and to provide certain basic materials for later scholars to study the flow of economic development information. To a certain extent, it provides decision-making reference for economic development marketing, economic development e-commerce and economic development planning and provides a scientific basis for promoting the integrated construction and development of economic development.

This paper introduces C-value and D-value as two indicators to measure the status and level of each city in the urban economic development network. The formula is

$$C = \text{Ln} \frac{C_c}{C_s},$$

$$D = C_c - C_s. \tag{12}$$

Among them, C_c represents the amount of economic development information output by a city, and C_S
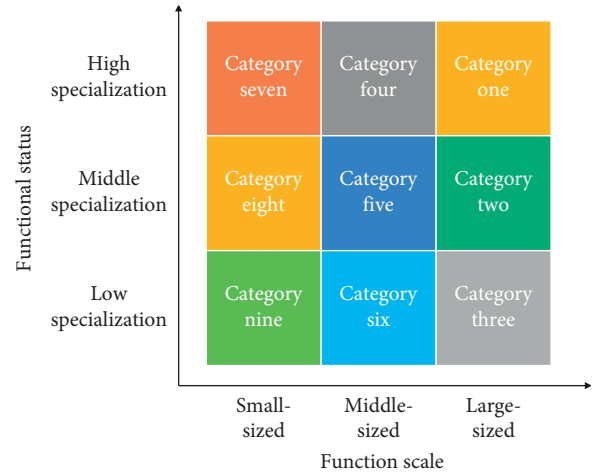
FIGURE 1: Types of urban economic development functions.

represents the amount of economic development information received by the city. If a city's economic development information output is greater than its information reception, that is, $D > 0$, the city is the control node (city) of the economic development information flow network. On the contrary, the city is considered as a subsidiary node (city).

In the process of data processing, it is found that, under normal circumstances, the amount of economic development information received by popular cities or cities with more developed economic development industries is often greater than the amount of economic development information output. The information flow of economic development from low to high is relatively large, while the amount of economic development information output from high to low is less. Therefore, C_c represents the amount of economic development information received by a city, and C_S represents the amount of economic development information output by the city.

The basic idea of the dominant flow analysis method is to judge the status of a city (A) in the urban system according to the maximum flow of economic development information of a city (A), the scale of urban economic development, and the flow between the city (A) and other cities. From this, the position of the city (A) in the network structure is obtained, and the position determines its influence in the spatial interaction. On this basis, Song Wei and other scholars divided cities into three types: dominant, subdominant, and subordinate cities. Based on the scale of urban economic development level obtained in the previous study, the level of the dominant stream is divided. The detailed contents are explained as follows. If the largest economic development information flow of city (A) is to city (B) with a smaller economic development scale, then city (A) is considered to be dominant. If city (B) has the largest economic development information flow to a city with a relatively large economic development scale, and at the same time there is one or more cities $(C_1, C_2 \cdots)$ whose economic development scale is smaller than the largest
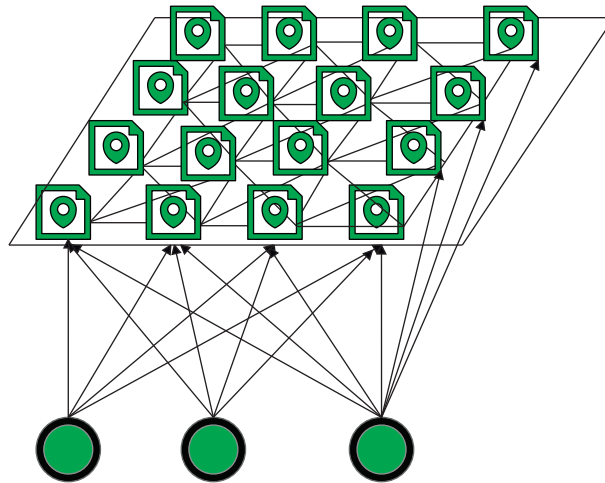
FIGURE 2: Kohonen network structure.
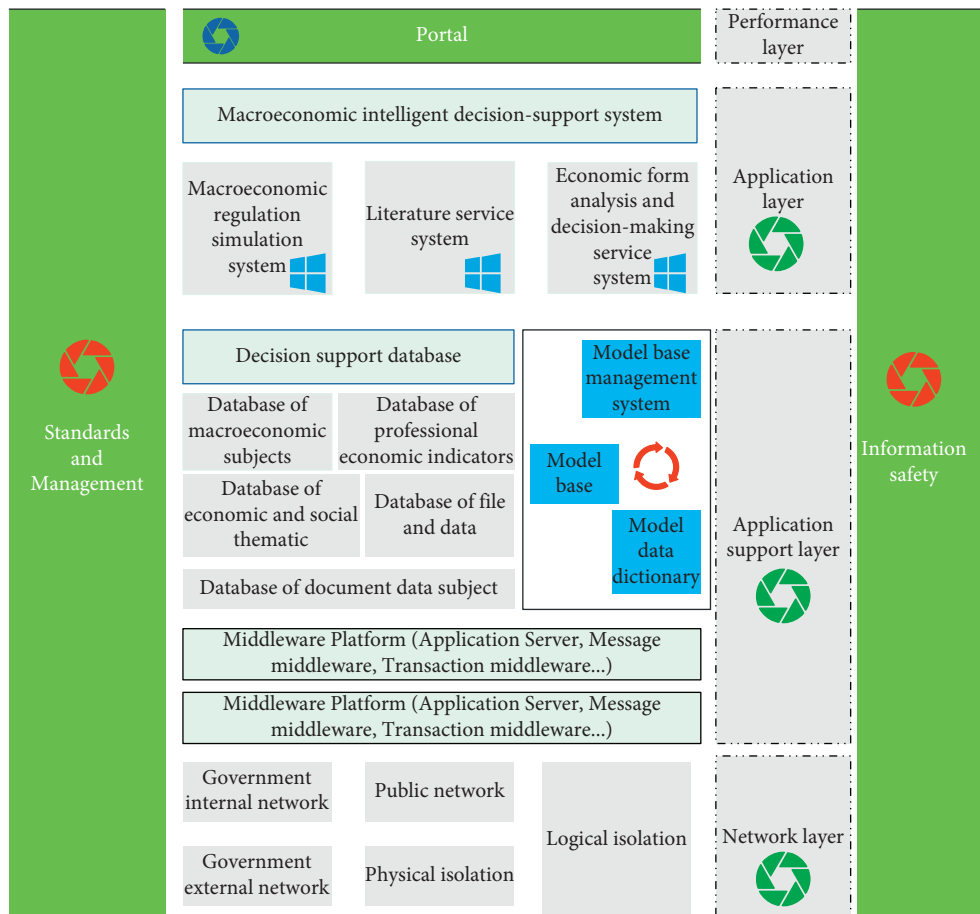
FIGURE 3: Overall architecture of the system.

economic development information flow to it (B), then city (B) is considered to have secondary dominance. If city (C) has the largest economic development information flow to the subdominant city (B), and there is no city (D) whose economic development scale is smaller than the largest economic development information flow to it (C), then it is determined that city (C) has a subordinate attribute.

4. Evaluation Index System of Economic and Social Development Pilot Area Based on Spatial Network Structure Analysis

The Kohonen network simulates the structure of neurons in the cerebral cortex as a two-dimensional spatial lattice. Functionally, through the interaction and competition
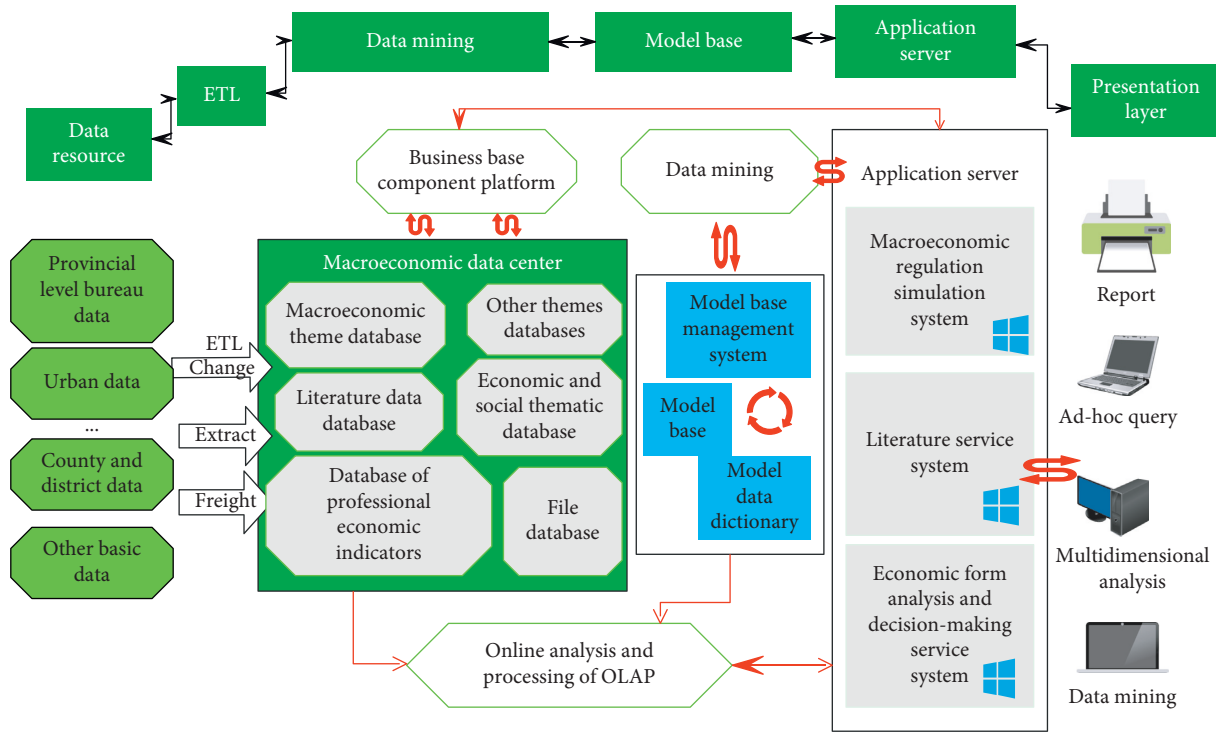
Figure 4: System flowchart.
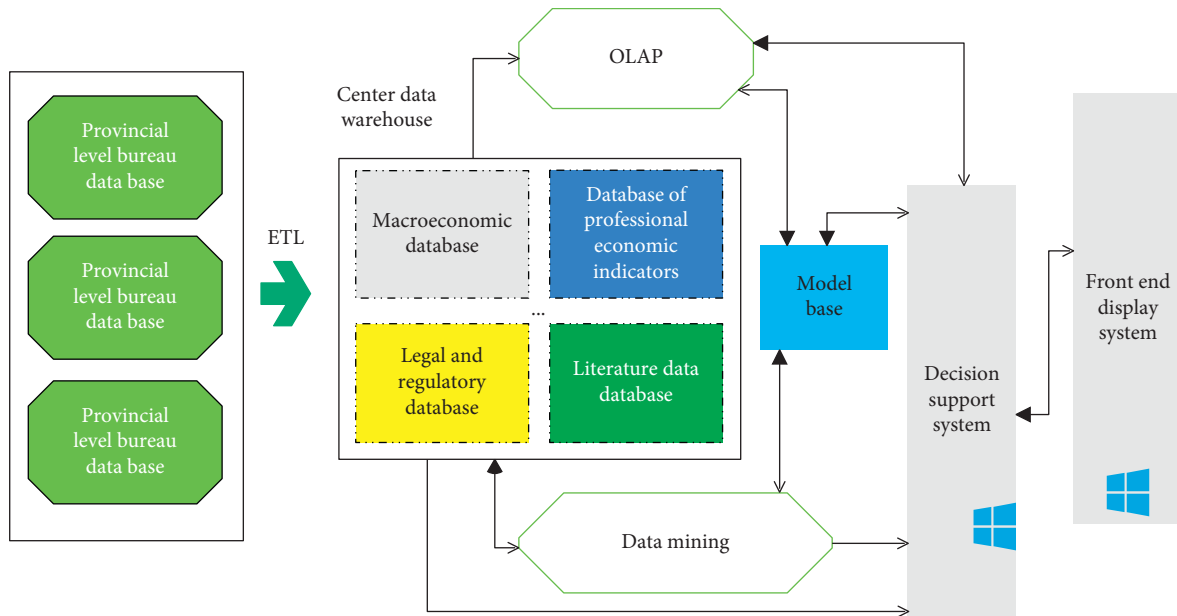
Figure 5: Schematic diagram of the decision support system based on data warehouse.

between neurons in the network, the clustering function and self-organization and self-learning functions of brain information processing are simulated. The Kohonen network structure is shown in Figure 2, which consists of an input layer and a competition layer.

This paper makes comprehensive use of multidisciplinary theories and technologies such as systems science, information science, dynamic econometrics, artificial intelligence, data warehouse, data mining, online analytical processing, and intelligent decision-making analysis tools and methods. Through the collection, storage, analysis, processing, and presentation of various data and related information, high-level information services and support are provided for leaders, and scientific and standardized decision-making is realized. The overall architecture of the system is shown in Figure 3.

The flowchart of the macroeconomic intelligent decision support system is shown in Figure 4.
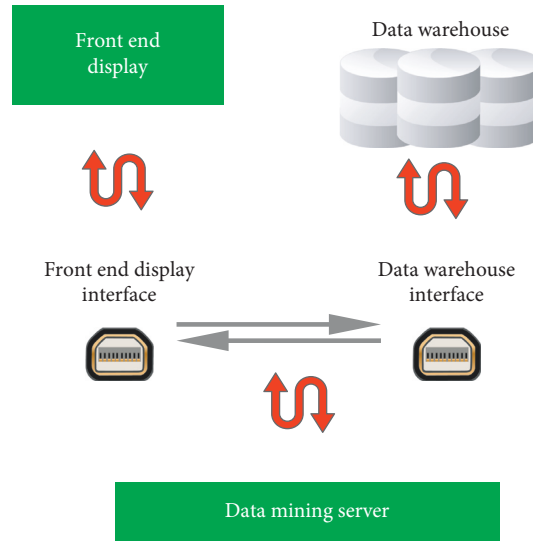
FIGURE 6: Interface design of data mining server.
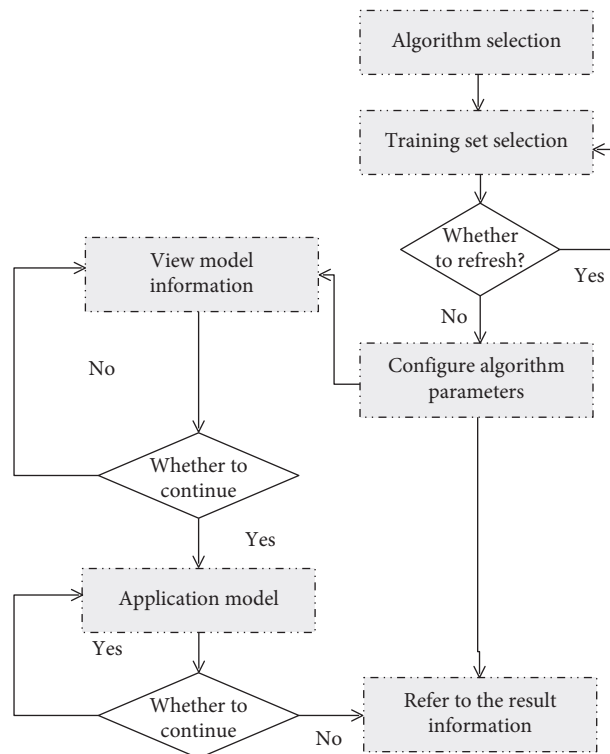
FIGURE 7: Overall activity diagram of data mining module.

The intelligent decision support system based on data warehouse takes data warehouse and model base (MB) as the main structure, supports online analytical processing, and applies data mining to knowledge discovery in the database, as shown in Figure 5:

The data mining server extracts data from the data warehouse and then sends the results to the front-end for display after mining and processing. The interface design of the data mining service is shown in Figure 6 below.

The mining steps of the data mining system are as follows: (1) The system selects an algorithm. (2) The system selects the training set and determines whether to refresh. If it needs to be refreshed, the system repeats step 2; otherwise, it goes to step 3. (3) The system configures the algorithm parameters. (4) The system checks the model information and chooses to continue to step 5; otherwise, it goes back to step 3. (5) The system uses the model to determine whether to refresh. If it needs to be refreshed, the system repeats step
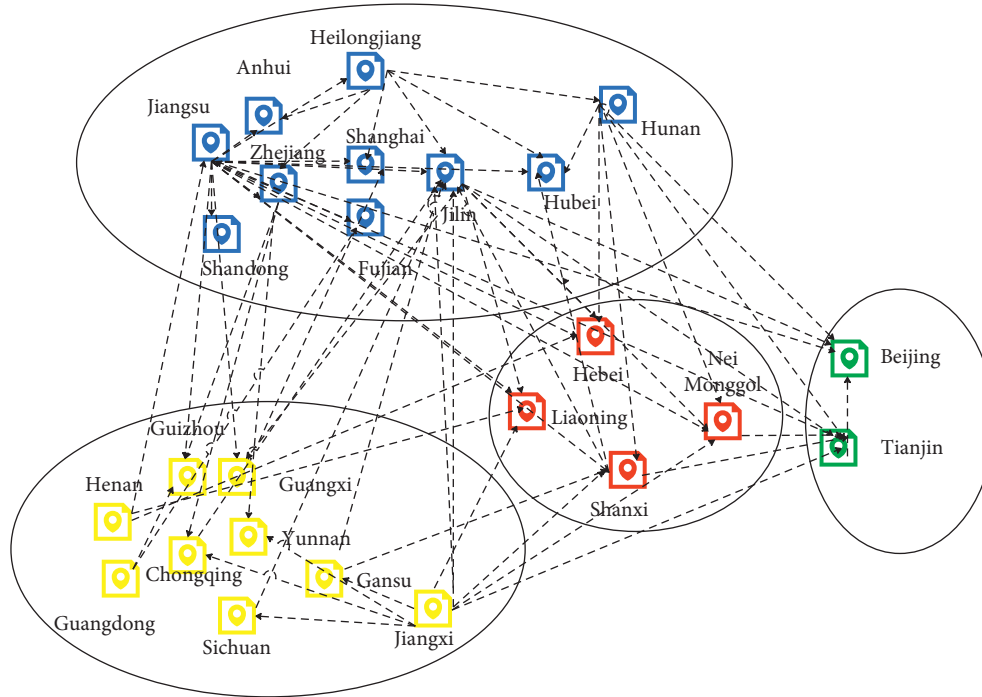
FIGURE 8: Analysis model of spatial network structure.

TABLE 1: Evaluation of the evaluation effect of the economic and social development pilot area.

Number	Evaluate the effect	Number	Evaluate the effect	Number	Evaluate the effect
1	85.04	20	80.86	39	71.63
2	81.19	21	87.61	40	75.90
3	86.35	22	79.78	41	73.16
4	80.73	23	71.85	42	78.66
5	71.80	24	75.74	43	81.58
6	71.07	25	84.73	44	74.08
7	76.79	26	86.22	45	73.76
8	79.12	27	77.03	46	72.41
9	76.22	28	72.53	47	74.15
10	76.56	29	71.51	48	87.06
11	85.82	30	76.00	49	80.16
12	72.76	31	78.15	50	71.73
13	86.10	32	77.13	51	86.23
14	78.13	33	81.22	52	74.45
15	82.19	34	79.27	53	71.64
16	83.32	35	82.48	54	87.36
17	84.48	36	74.20	55	75.99
18	84.74	37	78.38	56	77.32
19	84.83	38	75.16	57	84.74

5; otherwise, it goes to step 6. (6) The system checks the result information. The overall activity diagram of the data mining module is as shown in Figure 7.

Figure 8 shows the analysis model of the spatial network structure constructed in this paper.

This paper obtains a large amount of data from the network to verify the effect of the model in this paper and calculates the effect of the model constructed in this paper in the evaluation index analysis of the economic and social development pilot area and compares it through multiple sets of data. Moreover, this paper obtains the results shown in Table 1 and Figure 9.

From the above research, it can be seen that the evaluation index system of the economic and social development pilot area based on the analysis of the spatial network structure proposed in this paper has a good effect.
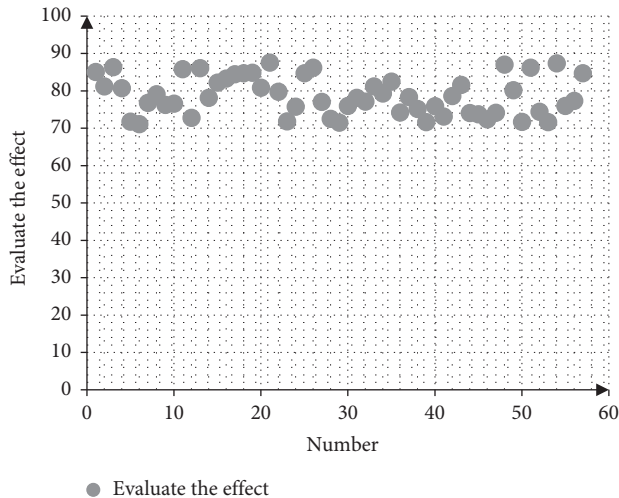
FIGURE 9: Statistical diagram of the evaluation of economic and social development pilot areas.

5. Conclusion

The construction and development process of the "two first districts" is the implementation of the five development concepts of innovation, coordination, greenness, openness, and sharing and is the development under the strategic guidance of the five development concepts. Therefore, the construction of the evaluation index system of the economic and social development pilot zone must be based on five development concepts. Moreover, it needs to take the five development concepts as the first-level indicators for evaluation and further select the second-level indicators and the third-level indicators according to their connotations and the actual construction. In addition, it provides a theoretical reference for the formation of the basic framework and the selection of specific indicators for the evaluation index system of the economic and social development pilot zone. At the same time, it can reveal the status quo, characteristics, and problems of economic and social development under the guidance of new development concepts and has certain practical value for guiding government departments to solve economic and social development problems according to the development requirements of new concepts. Based on the analysis method of spatial network structure, this paper constructs the evaluation index system of the economic and social development pilot area and obtains an intelligent analysis system. The simulation test study shows that the evaluation index system of the economic and social development pilot area based on the analysis of the spatial network structure proposed in this paper has a good effect.

Data Availability

The labeled dataset used to support the findings of this study are available from the corresponding author upon request.

Conflicts of Interest

The author declares that there are no conflicts of interest regarding the publication of this paper.

References

[1] S. Barde, "Back to the future: economic self-organisation and maximum entropy prediction," *Computational Economics*, vol. 45, no. 2, pp. 337–358, 2015.

[2] D. Bhattacharya, J. Mukhoti, and A. Konar, "Learning regularity in an economic time-series for structure prediction," *Applied Soft Computing*, vol. 76, no. 2, pp. 31–44, 2019.

[3] V. Daksiya, H. T. Su, Y. H. Chang, and E. Y. M Lo, "Incorporating socio-economic effects and uncertain rainfall in flood mitigation decision using MCDA," *Natural Hazards*, vol. 87, no. 1, pp. 515–531, 2017.

[4] A. Ferramosca, H. Alejandro, and D. Limon, "Offset-free multi-model economic model predictive control for changing economic criterion," *Journal of Process Control*, vol. 54, no. 3, pp. 1–13, 2017.

[5] A. Ferramosca, D. Limon, and E. F. Camacho, "Economic MPC for a changing economic criterion for linear systems," *IEEE Transactions on Automatic Control*, vol. 59, no. 10, pp. 2657–2667, 2014.

[6] Y. Geng, Z. Wei, H. Zhang, and M. Maimaituerxun, "Analysis and prediction of the coupling coordination relationship between tourism and air environment: yangtze river economic zone in China as example," *Discrete Dynamics in Nature and Society*, vol. 2020, no. 10, pp. 1–15, Article ID 1406978, 2020.

[7] N. Gordini, "A genetic algorithm approach for SMEs bankruptcy prediction: empirical evidence from Italy," *Expert Systems with Applications*, vol. 41, no. 14, pp. 6433–6445, 2014.

[8] F. Jahedpari, T. Rahwan, S. Hashemi et al., "Online prediction via continuous artificial prediction markets," *IEEE Intelligent Systems*, vol. 32, no. 1, pp. 61–68, 2017.

[9] P. Karanikić, I. Mladenović, S. Sokolov-Mladenović, and M. Alizamir, "Retraction Note: prediction of economic growth by extreme learning approach based on science and technology transfer," *Quality and Quantity*, vol. 53, no. 2, pp. 1095-1096, 2019.

[10] K. Ataka, "Prediction of election result and economic indicator," *Resuscitation*, vol. 96, no. 6, 84 pages, 2014.

[11] S. Lahmiri, "A variational mode decompoisition approach for analysis and forecasting of economic and financial time series," *Expert Systems with Applications*, vol. 55, no. 8, pp. 268–273, 2016.

[12] L. Liu, Q. Wang, J. Wang, and M Liu, "A rolling grey model optimized by particle swarm optimization in economic prediction," *Computational Intelligence*, vol. 32, no. 3, pp. 391–419, 2016.

[13] S. Nagy and J. Pipek, "An economic prediction of the finer resolution level wavelet coefficients in electronic structure calculations," *Phys.chem.chem.phys*, vol. 17, no. 47, pp. 31558–31565, 2015.

[14] J. Pipek and S. Nagy, "An economic prediction of refinement coefficients in wavelet-based adaptive methods for electron structure calculations," *Journal of Computational Chemistry*, vol. 34, no. 6, pp. 460–465, 2013.

[15] P. Rajsic, A. Weersink, and A. Navabi, "Economics of genomic selection: the role of prediction accuracy and relative genotyping costs," *Euphytica*, vol. 210, no. 2, pp. 1–18, 2016.

[16] C. Teljeur, M. Neill, L. Murphy et al., "Using prediction intervals from random-effects meta-analyses IN an economic model[j]," *International Journal of Technology Assessment in Health Care*, vol. 30, no. 1, pp. 44–49, 2014.

[17] H. L. Vu, K. T. W. Ng, and D. Bolingbroke, "Time-lagged effects of weekly climatic and socio-economic factors on ANN

municipal yard waste prediction models," *Waste Management*, vol. 84, no. 2, pp. 129–140, 2019.

[18] W. Yu and W. Huafeng, "Neural network model for energy low carbon economy and financial risk based on PSO intelligent algorithms," *Journal of Intelligent and Fuzzy Systems*, vol. 37, no. 5, pp. 6151–6163, 2019.

[19] L. Zhou, K. K. Lai, and J. Yen, "Bankruptcy prediction using SVM models with a new approach to combine features selection and parameter optimisation," *International Journal of Systems Science*, vol. 45, no. 3, pp. 241–253, 2014.

Research Article

Design and Implementation of Interactive Platform for Operation and Maintenance of Multimedia Information System Based on Artificial Intelligence and Big Data

Xin Yan [iD][1] **and Junhui Yan** [iD][2]

[1]*School of Management, Shanghai University, Baoshan, Shanghai 200444, China*
[2]*Maths & Information Technology School, Yuncheng University, Yuncheng, Shanxi 044000, China*

Correspondence should be addressed to Xin Yan; 201904217217@stu.zjsru.edu.cn

In order to cope with the challenges that operators face after the impact of diversified social channels in the field of interactive services, we actively build a new generation of intelligent interactive systems based on artificial intelligence technology, a semantic understanding, and intention recognition, covering rich media content, omnichannel coverage, high-frequency knowledge updates, consistent service response, high-quality, and low-cost intelligent interactive solutions is proposed. The solution provides overall business modeling for scenario design and a scenario-based knowledge expression system, with the function of fragmented knowledge processing. With complete text and voice information, combined with pictures, text, audio, video, and other multimedia, we intelligently interact with users, allowing users to obtain required information and solve problems in a pleasant and relaxing interaction. Therefore, the research and exploration of the intelligent interactive system architecture based on artificial intelligence is a useful practice and strong support for operators to redefine the connotation and elements of "smart service" in the process of building "smart operation." Through repeated tests, it can be seen that the language similarity has reached 0.75549, which is very close to 1.0000. It can be seen that the design of this platform has been successful.

1. Introduction

Since the 21st century, with the rapid development of computers and networks, artificial intelligence has become the most popular technology term today. The development of artificial intelligence affects the development of all walks of life. The development of robotics, autonomous driving technology, image recognition, and other technologies indicates that artificial intelligence is getting more and more attention from people, and its development has great potential. Big data plays a vital role in the development of artificial intelligence. Through the relationship between artificial intelligence and big data, starting from their development status, this article describes in detail the future development trend of artificial intelligence in the big data environment. The robot operating system ROS is easy to use

[1]. After determining the functional modules that the human-machine voice interaction system should have, we use the topics and services provided by ROS to realize the communication between related modules in the system and define the information format during communication. ROS originated from the cooperation between the STAIR project of the Stanford University Artificial Intelligence Laboratory in 2007 and the personal robot project of the robotics company Willow Garage. After 2008, Willow Garage promoted its development. ROS is an open-source meta-operating system suitable for robots. It provides the functions that the operating system should have, including hardware abstraction, low-level device control, realization of common functions, interprocess information transmission, and software package management. In addition, it also provides the tools and libraries needed to compile, write, and execute

programs across multiple computers [2]. ROS is similar to Player, YARP, Orocos, CARMEN, Orca, MOOS, and Microsoft Robotics Studio robot frameworks in some respects. The "blueprint" of the ROS runtime is a loosely coupled point-to-point process network based on the ROS communication infrastructure. ROS has several different communication methods, including a service mechanism based on synchronous remote procedure call protocol (Remote Procedure Call Protocol, RPC) communication, a topic mechanism based on asynchronous streaming media data, and a parameter server for data storage [3]. Figure 1 shows the flow chart of the intelligent interactive system management platform. Big data uses the increasingly mature cloud computing technology to obtain valuable information from the vast ocean of Internet information for information induction, retrieval, and integration, providing a software foundation for Internet information processing. Both require the participation of artificial intelligence, which is a commercial application after the order of the Internet information system. That is the real outlet for cloud computing and big data.

2. Literature Review

Tekerek A. and others said that the arrival of the era of intelligence and big data, and the social impact brought about by the industrial revolution in history, have inherent laws that are similar in appearance and similar in quality to the contradictions and mutual influences between productivity and production relations [4]. Ha T. and others stated that the era of intelligence and big data seems to have provided greater "convenience" for "distrust, disorder, and monopoly," and at the same time put forward higher requirements for "trust, order, and sharing [5]." Kyivska K. and others said that in the past 20 years, with the rapid development of artificial intelligence technology, especially the intelligence and big data information economy characterized by "Internet +," it has almost reshaped the production and operation models of enterprises and people's way of life has had a significant impact on the transformation of the paradigm of human "technology-economy-society" and the progress of social civilization [6]. Ongena et al. said that with the widespread application of computer technology, the continuous increase in data accumulation, and the continuous innovation and enhancement of algorithms and computing power, the current society has entered the era of intelligence [7]. Through research, Bhargava et al. have obtained the development of the "four major catalysts" of massively parallel computing, big data, deep learning algorithms, and smart chips, as well as the reduction of computing costs, which has enabled artificial intelligence technology to advance by leaps and bounds [8]. Fanea and others said that artificial intelligence has become the most exciting and most anticipated technology of this era, and it will become the focus of the development of the IT industry in the next 10 years and beyond [9]. Naghizade et al. found through investigations that the current operators are also facing the impact of the mobile Internet. Diversified service requirements, diversified service scenarios, and fragmented

social service models are all impacting the traditions of operators from all angles. *Service interaction mode* [10]. Zhang et al. said that the response speed and service satisfaction of interactive services force operators to innovate the service interaction model. The high-frequency requirements for service personnel knowledge update and training cost control have promoted the traditional interactive service model to the network. Development in the direction of automation, automation, and intelligence, through rich media and multichannels to achieve intelligent interaction with users, and effectively reducing service costs, improving service quality, and increasing user perception are the current urgent needs, which have been listed by operators as building the key issue of "smart operation" [11]. Elayyan and others said that with the development of artificial intelligence, the research of robots has also made great progress. Robots of various forms and functions have appeared one after another, and some robots have even entered people's homes and become members of the family [12]. Batarseh and others stated that the most important way for humans to interact with robots is through voice, which is more direct and convenient than other methods such as buttons, touch screens, and remote controls. Therefore, a human-machine with good performance is designed in the development of robots. The voice interaction system is very important. The intelligence of the robot must first be manifested in the smooth human-machine voice interaction function. The human-machine voice interaction system has become the most basic functional design requirement [13].

This paper combined with the requirements of information technology service-related standards and specifications, as well as the operation and maintenance project implementation experience and the key generic technology for information system operation and maintenance, provide system support for information system operation and maintenance specification, realize the information system operation and maintenance support system software industrialization and operational service interactive development pattern, drive the market demand of information system operational service, and promote the rapid formation and healthy development of operation and maintenance service industry chain.

3. Method

3.1. Use Bayesian Algorithm to Achieve Text Classification. Big data has now been summarized as having the characteristics of 4v: volume, velocity, variety, and value. The total data growth is shown in Figure 2.

Big data is a brand-new business model, life philosophy, and ideology developed on the basis of multiple data and cross-domain associations. This new approach to tools will have a huge disruptive impact on all aspects of our society. This is summarized on the basis of the characteristics of big data. With the continuous development of big data, when it reaches the advanced stage, it will generate new value and bring a qualitative leap to all aspects of society such as enterprises and schools [14]. There are many classic classification methods in machine learning, such as decision tree
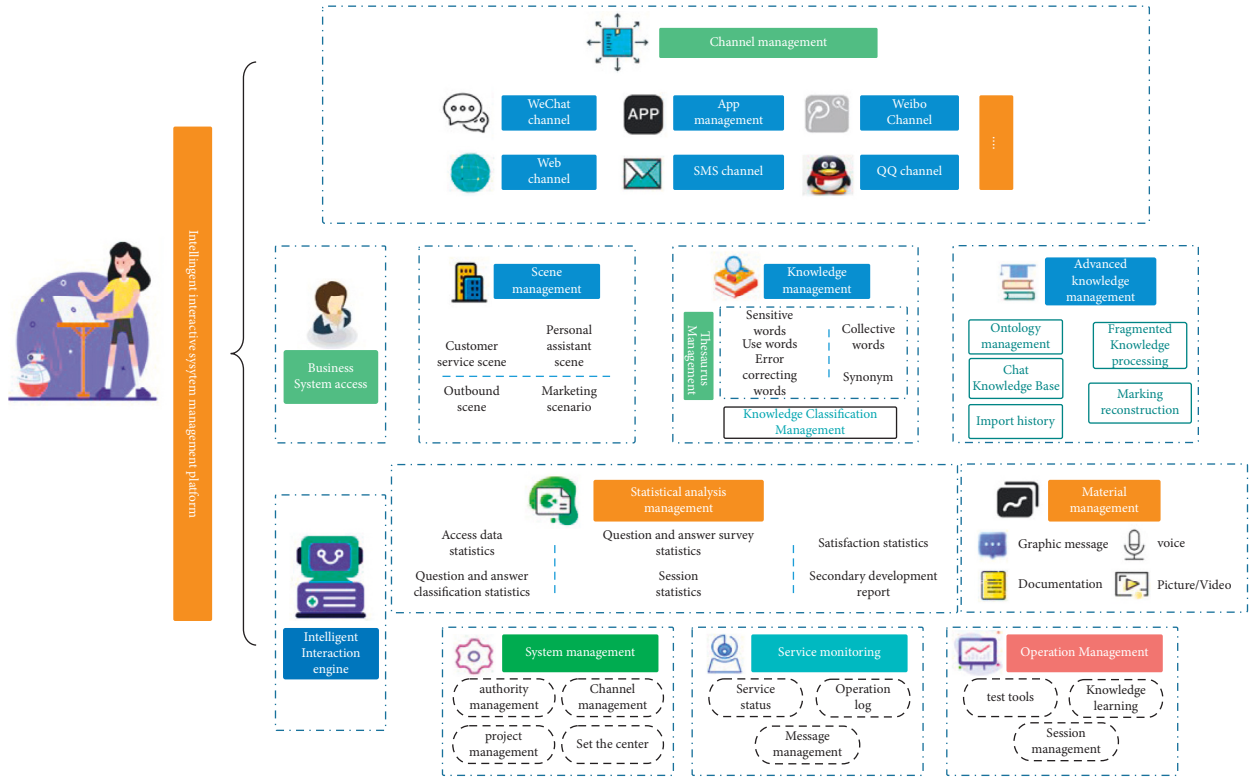
Figure 1: Flow chart of the intelligent interactive system management platform.

— The total amount of data grows
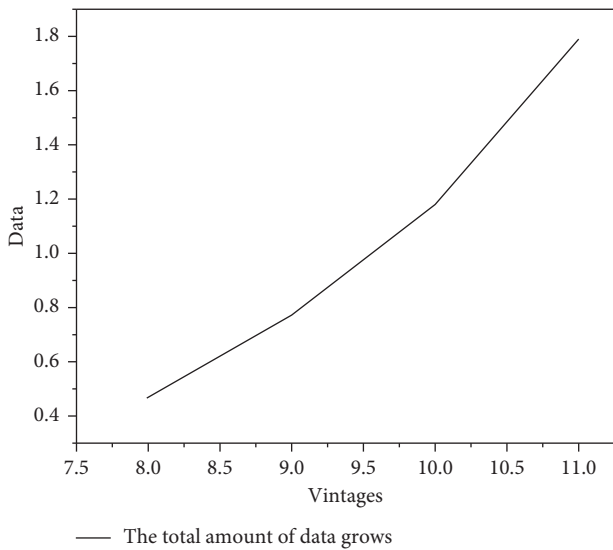
Figure 2: Growth graph of total data.

algorithms, support vector machines, Bayesian classification algorithms, artificial neural networks, and k-nearest neighbors. To process the text recognized by the speech recognition function, and to deal with the text classification problem, the naive Bayes classifier is one of the most effective algorithms. There are three reasons why Bayesian algorithm is often used to achieve text classification. First, the Bayesian algorithm is simple; second, it is easy to get the probability value required to train the Bayesian classifier based on the training text; third, naive Bayes classifier is comparable to other algorithms in most cases, and in some cases even better than other algorithms. The classification problem is the process of finding the best hypothesis from the hypothesis space given the training data. For sentence text Q, we can denote it as $\langle a_1, a_2, \ldots, a_n \rangle$ after word segmentation, where $a_i\,(1 \leq i \leq n)$ represents the word in sentence Q [15]. The classification of Q in this article is to divide it into a certain category of daily life frequently asked question and answer library, professional field frequently asked question and answer library, real-time question library, or control instruction library, that is, to deal with the following questions:

$$v_{\text{MAP}} = \arg\max_{v_j \in V} P(v_j | a_1, a_2, \ldots, a_n), \quad (1)$$

where v_{MAP} represents the maximum posterior value; V represents the category set of the library composed of the daily FAQ library, the professional field FAQ library, the real-time question library, and the control instruction library; and the v_j is the category that Q can be divided into [16]. Using Bayesian formula, formula (1) can be rewritten as

$$v_{\text{MAP}} = \arg\max_{v_j \in V} \frac{P(a_1, a_2, \ldots, a_n | v_j) P(v_j)}{P(a_1, a_2, \ldots, a_n)}$$

$$= \arg\max_{v_j \in V} P(a_1, a_2, \ldots, a_n | v_j) P(v_j), \quad (2)$$

where $P(v_j)$ represents the probability of each target value v_j and $P(a_1, a_2, \ldots, a_n | v_j)$ represents the probability of

5 under the condition of the target value v_j. We can get $P(v_j)$ by counting the number of frequently asked questions in daily life, frequently asked questions in professional fields, real-time question banks, or control instruction banks. But to get the value of $P(a_1, a_2, \ldots, a_n | v_j)$, a large training data set is required. In order to reduce the amount of calculation, it can be assumed that the words $a_i \, (1 \leq i \leq n)$ in the sentence are independent of each other, which reduces the problem to a naive Bayes classification problem. The corresponding formula (2) can be simplified as follows:

$$
\begin{aligned}
v_{NB} &= \arg\max_{v_j \in V} P(a_1, a_2, \ldots, a_n | v_j) P(v_j) \\
&= \arg\max_{v_j \in V} P(v_j) \prod_i P(a_i | v_j),
\end{aligned}
\tag{3}
$$

where v_{NB} represents the target value output by the naive Bayes classifier, $P(v_j)$ represents the probability of each target value v_j, and $P(a_i | v_j)$ represents the probability of word $a_i \, (1 \leq i \leq n)$ under the condition of the target value v_j. To use the naive Bayes classifier to deal with the sentence text classification problem, at this time, we only need to estimate $P(v_j)$ and $P(a_i | v_j)$ from the training data [17].

3.2. Human-Machine Voice Interaction System Based on ROS.
The execution process of the designed ROS-based human-machine voice interaction system is shown in Figure 3.

The main functions in the human-machine voice interaction process are described in detail below.

3.2.1. Voice Information Collection.
The voice information is collected through the external microphone of the robot, and the collected voice information is stored as an audio file. The quality of user voice information collected in a noisy environment will be disturbed by noise. In addition, it is impossible to know in advance when the user will speak to the robot, whether he is talking to the robot, and the duration of the speech. Therefore, the problems of noise interference, when to collect the user's voice information, and the collection time must be solved first [18]. These problems can be solved by voice activity detection (voice activity detection, VAD) technology. Voice endpoint detection technology is a basic link in speech recognition and speech processing, and it is also a popular field of speech recognition research. Its main purpose is to distinguish speech and nonspeech from the input speech. The main functions are automatic interruption, removal of silent components in the voice, obtaining effective voice in the input voice, and removing noise to enhance the voice. The open-source project pyVAD on GitHub is used to implement endpoint detection on the voice data read in real time.

3.2.2. Voice Recognition Node.
The voice recognition node is responsible for recognizing the collected voice information as text information. This article uses the REST API provided by Baidu voice to implement speech recognition. The speech recognition REST API provides developers with a universal HTTP interface that supports the POST method [19]. Based on this interface, developers can easily implement speech recognition functions. The API supports the recognition of the entire recording file; that is, the user needs to upload the entire voice, but the original voice file must conform to the specified format.

3.2.3. Speech Synthesis Node.
The speech synthesis node is responsible for synthesizing the requested information into audio. The speech synthesis is realized by using the REST API provided by Baidu voice. Speech synthesis REST API supports the synthesis of a paragraph of text, but the text must be encoded in UTF-8, and the text length must be less than 1024 bytes [20]. Currently, the interface supports both POST and GET methods.

3.2.4. Semantic Analysis Node.
The semantic analysis node has the function of understanding the request information received from the speech recognition node to determine what operation the robot should perform. The semantic analysis node must not only provide services to the speech recognition node but also must be able to request services provided by other nodes or publish information on specific topics [21].

3.2.5. Real-Time Information Acquisition Node.
Through real-time information acquisition nodes, real-time changing information content, such as time, date, weather, and news, can be obtained. Nodes that provide time and date information access services, and nodes that provide weather access services in major cities are now implemented [22].

3.2.6. Robot Control Function Node.
The robot control function nodes include nodes that control the robot to walk, avoid obstacles, and reach designated positions. These nodes need to be developed separately. On the PC side, the robot's walking function is tested and controlled by the turtlesim software package officially provided by ROS, and the function of playing music through voice control is also realized. On the built robot platform, the Python program that controls the movement of the motor is written through the GPIO port to realize the control of the robot [23].

4. Results and Analysis

Through analysis, the steps to classify sentence text Q are as follows:

Step 1. Collect and connect the question item in the FAQ database of daily life as a document and record it as category 1. Collect and connect the question item in the FAQ database of each professional field as a document and record it as category 2 (for convenience Explain that it is assumed that there is only one frequently asked question library in the professional field); the question item in the collection and connection real-time question library is a document, which is recorded as category 3; the question item in the collection
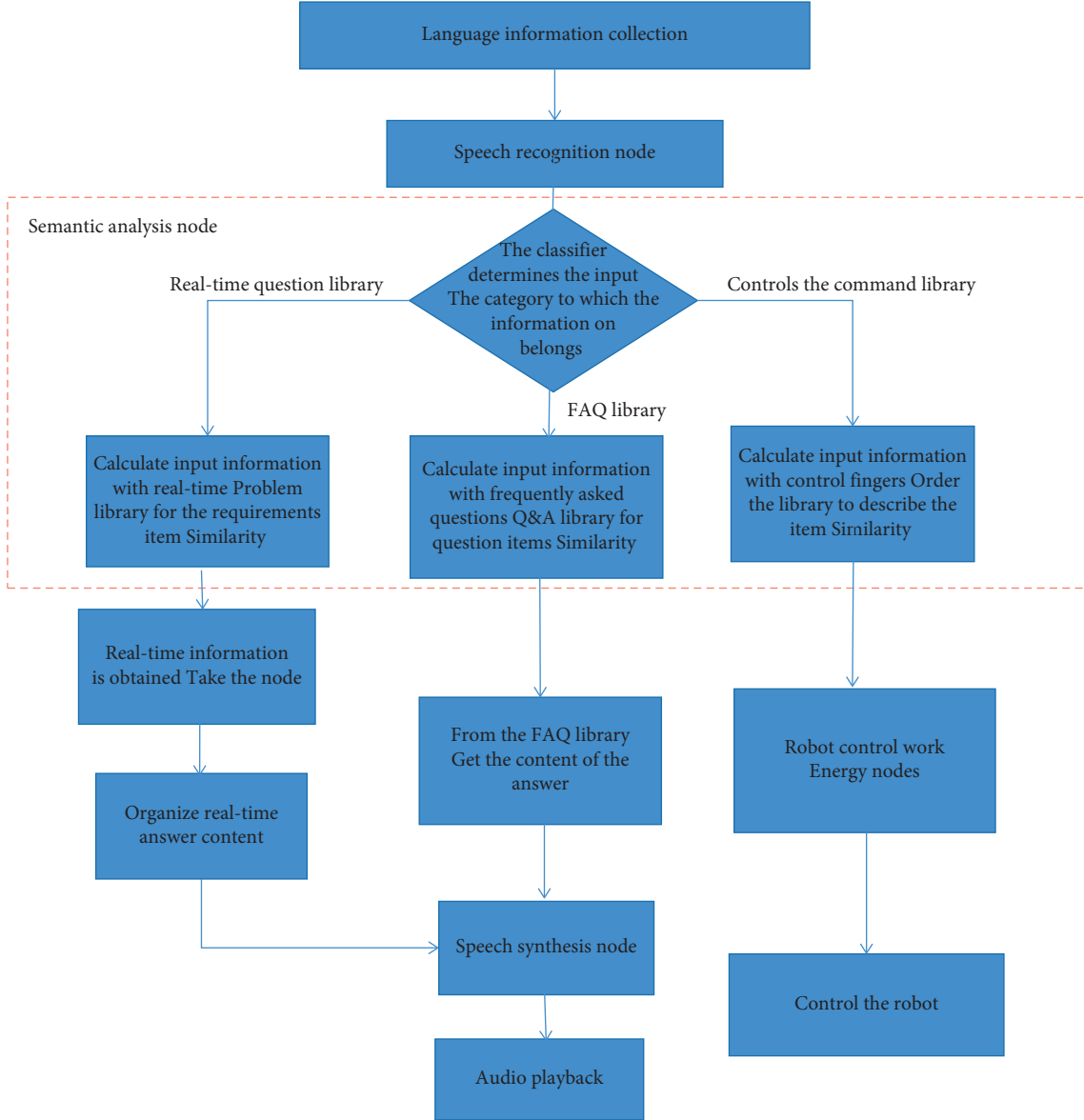
FIGURE 3: Human-machine voice interaction system execution process.

and connection control instruction library is a document, and is recorded as category 4 [24].

Step 2. Combine all categories of documents into a document, use Chinese word segmentation method to segment the Document, collect all the words in the Document, and form a collection Vocabulary. All categories form a set V, that is, $V = \{$category 1, category 2, category 3, category 4$\}$.

Step 3. For each target value v_j in V, calculate the probability term $P(v_j)$:

$$P(v_j) = \frac{|\text{docs}_j|}{|\text{Document}|}, \tag{4}$$

where docs_j is the subset of documents whose target value is in Document, $|\text{docs}_j|$ is the number of elements it

has, and $|\text{Document}|$ is the total number of category libraries that Document has [25].

Step 4. For each target value v_j in V, connect all members in docs_j to build a document Text_j, use Chinese word segmentation method to segment Text_j, and count the number n of different words in Text_j.

Step 5. For each word a_i in Vocabulary, calculate the probability term $P(a_i|v_j)$:

$$P(a_i|v_j) = \frac{n_k + 1}{n + |\text{Vocabulary}|}, \tag{5}$$

where n_k is the number of occurrences of word a_i in Text_j, and $|\text{Vocabulary}|$ is the total number of words that Vocabulary has [26].

Step 6. Use the Chinese word segmentation method to segment the sentence Q to get $\langle a_1, a_2, \ldots, a_n \rangle$, where a_i represents the word that appears at the i-th position in Q.

Step 7. Get the category v_{NB} to which Q belongs

$$v_{NB} = \arg\max_{v_j \in V} P(v_j) \prod_{i \in \text{positions}} P(a_i | v_j), \qquad (6)$$

where positions are the position where all words appear in Q. Any words that appear in Q but not in the documents in the training set will be simply ignored [7].

In order to verify the performance of the proposed ROS-based human-machine voice interaction system, experiments were carried out on the PC terminal and the robot platform built in the laboratory to test the human-machine voice question and answer function and the robot control function [27]. PC environment: Ubuntu 12.04, 32-bit operating system, the processor is Pentium(R) Dual-Core CPU E6500 @2.93 GHz 2. Install the robot operating system ROS on the Ubuntu system and choose Hydro as the ROS version. Sound collection device: USB microphone. Audio playback equipment: USB stereo. The robot platform is built on the HCR (Home Care Robot) omnidirectional wheel development platform. The central processor of the robot platform uses Raspberry Pi 2B, and the system installed on the Raspberry Pi is Raspbian wheezy. Install ROS on the Raspberry Pi, and the ROS version is Hydro. The GPIO port is used to control the rotation of the motor to make the robot walk. The motor drive module adopts SKU: DRI0018. Use a USB microphone to collect voice information and use a USB speaker to play audio.

As can be seen from Figure 4, after data smoothing, the obtained sample data are sorted from small to large. In order to ensure that all data are generated under nonabnormal conditions, the smallest and largest numbers need to be eliminated. The obtained data are as follows: [24, 34, 38, 39, 39, 39, 41, 41, 51, 53, 54, 56, 63, 63, 66, 67, 69, 73, 78, 79, 79, 79, 81, 87, 89, 91, 94 ,99, 102, 103]. Determine the range of 5 intervals, 103/5 = 21, namely, [0~21], [21~42], [42~63], [63~84], and [84~105]. Distribute the remaining 28 numbers after removing the abnormalities into these 5 intervals (interval minimum value ≤ N < interval maximum value). Interval 1 = []; Interval 2 = [34, 38, 39, 39, 39, 41, 41]; Interval 3 = [51, 53, 54, 56]; Interval 4 = [63, 63, 66, 67, 69, 73, 78, 79, 79, 79, 81]; interval 5 = [87, 89, 91, 94, 99, 102]. After interval allocation, it can be seen that the number of data in interval 4 is the largest. Therefore, the data in interval 4 and the upper and lower adjacent intervals 3 and 5 are taken. If there are no data in the upper and lower adjacent intervals, it is not necessary to take them. 21 data can be obtained [28].

The daily life frequently asked question and answer library established during the experiment contains 15 question and answer pairs, the library frequently asked question and answer library contains 50 question and answer pairs, the real-time question library contains 19 questions, and the control instruction library contains 30 instructions. The similarity value is a unitless real number in the interval of $[0, 1]$. The closer the value is to 1, the more similar the
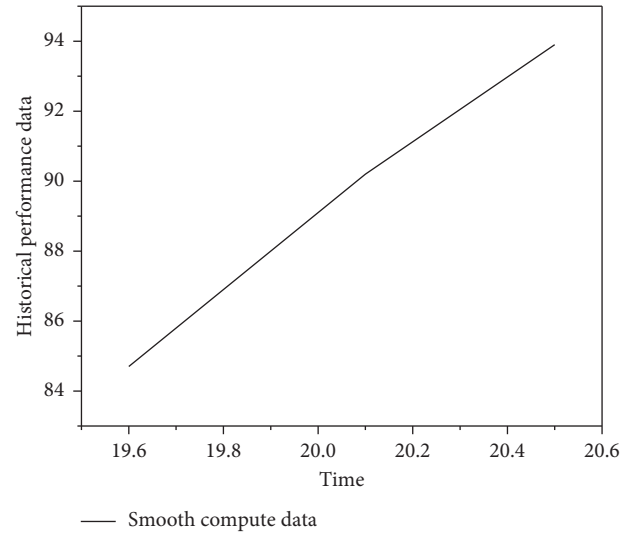
Figure 4: Data smoothing calculation data diagram.

meaning of the two sentences, and vice versa. Regarding the calculation of similarity, several existing basic methods are all based on vectors. In fact, it is to calculate the distance between two vectors. The closer the distance is, the greater the similarity. In the recommended scenario, in the two-dimensional matrix of user-item preferences, we can use a user's preference for all items as a vector to calculate the similarity between users, or use all users' preferences for an item as a vector A vector to calculate the similarity between items.

In order to test the performance of the similarity calculation method, three question items from the daily FAQ database were selected as "question sentences," and the similarity values between these three questions and each question item in the daily FAQ database were calculated. Table 1 lists the first three largest similarity values obtained in each calculation. The similarity value of each question in the table with itself is 1.00000.

Table 2 shows the similarity values between the three question sentences and the three question items in the library frequently asked questions and answers library.

Table 3 shows the similarity values between the question sentences expressing the same meaning and the question items in the library frequently asked questions. From the results in Table 3, it can be seen that for the same subject matter, if different questioning methods are used, it can also be well matched to the question item in the library. The adopted sentence similarity calculation method has strong adaptability to a variety of questioning methods.

Three question items are selected from the real-time question database as question sentences, and the similarity values between these three question sentences and each question item in the real-time question database are calculated, respectively. Table 4 lists the first three largest similarity values obtained in each calculation. The similarity value of each question in the table with itself is 1.00000.

The question "What's the time now?" is the same as the question item "What time is it now" and "Do you know what

Table 1: Examples of the calculation results of sentence similarity in the FAQ database of daily life.

Question	The question item in the frequently asked questions and answers library of daily life	Similarity value
What's your name?	What's your name?	1.00000
	What's your name?	0.74825
	Do you know what my name is?	0.68549
What do you do?	What do you do?	1.00000
	What can you do?	0.48597
	What's your name?	0.34859
Do you know me?	Do you know me?	1.00000
	Do you know what my name is?	0.75549
	Do you know who I am?	0.58165

Table 2: Example 1 of sentence similarity calculation results in the library frequently asked questions and answers database.

Question	The question item in the library frequently asked questions and answers library	Similarity value
What if the library does not have the books and periodicals I need?	What if the library does not have the books and periodicals I need?	1.00000
	Can I borrow books and periodicals in the reading room? How long can I borrow?	0.32812
	How to recommend a good book to the library for purchase?	0.16829
Do I need to submit a dissertation?	Do I need to submit a dissertation?	1.00000
	How to submit a paper dissertation?	0.58294
	How to check the electronic version of the dissertation review results?	0.35059
How to apply for one pass?	How to apply for one pass?	1.00000
	About the one pass card	0.45027
	The all-in-one card is reported to be lost or reissued	0.29153

Table 3: Example 2 of sentence similarity calculation results in the library frequently asked questions and answers database.

Question	The question item in the library frequently asked questions and answers library	Similarity value
What should I do if the library does not have the book I want to borrow?	What if the library does not have the books and periodicals I need?	0.63967
	My library personal information	0.54045
	Why cannot the book that has just been returned be lent out again by the person returning the book?	0.32829
What should I do if I do not find the book I need in the library?	What if the library does not have the books and periodicals I need?	0.72000
	My library personal information	0.51294
	How can I collect items lost in the library?	0.42059
What should I do if the journal I want to borrow is not in the library?	What if the library does not have the books and periodicals I need?	0.65000
	My library personal information	0.49027
	What is my library account password?	0.47153

Table 4: Examples of sentence similarity calculation results under the real-time question bank.

Question	The question item in the frequently asked questions and answers library of daily life	Similarity value
What time is it now?	What time is it now?	1.00000
	What time is it now?	0.88205
	Do you know what time it is now?	0.82591
Do you know what's the date today?	Do you know what's the date today?	1.00000
	What's the date today?	0.62517
	Tell me today's date?	0.28405
How's the weather today?	How is the weather today?	1.00000
	How is the weather tomorrow?	0.75755
	Tell me how is the weather today?	0.74058

time it is?" The question "Do you know today's date?" expresses the semantic content of "date query," and the question item "What is today's date?" The similarity value is 0.62517. The question item "Tell me today's date?" is the same as the semantic content of the question sentence, but the similarity value between the two is relatively small. It can also be seen from this that only relying on the Chinese knowledge dictionary and the number of identical words contained in the two sentences to measure the similarity between sentences cannot achieve very good performance, and the similarity calculation method can be further optimized.

5. Conclusion

From Table 1 above, it can be seen that the question "What is your name?" and the question item "What your name is it?" express the same semantic content, and the similarity value calculated by the experiment is 0.74825. And "Do you know what my name is?" is different from the semantic content of the question sentence, "Do you know what my name is?" is the user asking the robot his name, and "What is your name?" the user asking the name of the robot. Although the two sentences are intended to obtain names, the objects of the names to be obtained are different, so the calculated similarity value is relatively small. The question "What do you do?" and the question item "What can you do?" express the same semantic content, but the calculated similarity value is 0.48597, which shows that the sentence similarity calculation method adopted has room for improvement. The question "Do you know me?" and the question "Do you know what my name is?" are both the user asking the robot for his name. The calculated similarity value is 0.75549, which is very close to 1.00000.

The combination of interactive systems and artificial intelligence has greatly improved the accuracy and friendliness of interactive services. But at the same time, higher requirements are put forward for knowledge processing and learning, semantic intent recognition, interactive scenarios, and multiple channels. From the perspective of "achievable and deployable," the construction of an intelligent interactive system architecture based on artificial intelligence provides functional design and optimized solutions to current problems and challenges, so as to further make interactive services more intelligent and rich, humanized, and convenient. It lays the foundation for the subsequent formation of an intelligent interactive product system that can be promoted, replicated, and reduced in cost and increased efficiency. The experimental results show that the design achieves small positioning error; improves the system accuracy; greatly facilitates the installation, debugging, and maintenance of the positioning network; and reduces the labor cost of the network layout.

The implementation of the information operation and maintenance comprehensive supervision system has undergone a lot of preparations, but due to the large number and variety of information system equipment involved in the monitoring of the system, the realization of some functions in the implementation process is not satisfactory, and the system is still in application. There are areas that need further improvement, and its shortcomings are summarized as follows:

(1) The host, network, middleware, database, information security, and terminal equipment in the implementation of the information operation and maintenance comprehensive supervision system all involve alarm content. Due to the limited display interface, it cannot be displayed on the same interface. The real-time monitoring of information system monitoring personnel monitoring work increases the workload.

(2) Since there are many types of information system software and hardware that enterprises need to monitor, the display center needs to display network, application system, and performance data on multiple interfaces, which brings a lot to the daily monitoring work of operation and maintenance monitoring personnel of greater pressure.

Data Availability

The data used to support the findings of this study are available from the corresponding author upon request.

Conflicts of Interest

The authors declare no conflicts of interest.

References

[1] K. Chen, Y. Zu, and Y. Cui, "Design and implementation of bilingual digital reader based on artificial intelligence and big data technology," *Journal of Computational Methods in Science and Engineering*, vol. 20, no. 3, pp. 889–907, 2020.

[2] Y. Mori, S. E. Kudo, and K. Mori, "Implementation of artificial intelligence into colonoscopy: experience of research and development of computer-aided diagnostic system for endocytoscopy," *Nihon Shokakibyo Gakkai zasshi = The Japanese journal of gastro-enterology*, vol. 115, no. 12, pp. 1030–1036, 2018.

[3] H. Jing, H. Nikafshan Rad, M. Hasanipanah, D. Jahed Armaghani, and S. N. Qasem, "Design and implementation of a new tuned hybrid intelligent model to predict the uniaxial compressive strength of the rock using sfs-anfis," *Engineering with Computers*, vol. 37, no. 4, pp. 2717–2734, 2021.

[4] A. Tekerek and O. F. Bay, "Design and implementation of an artificial intelligence-based web application firewall model," *Neural Network World*, vol. 29, no. 4, pp. 189–206, 2019.

[5] T. Ha and H. Lee, "Implementation of application for smart healthcare exercise management based on artificial intelligence," *Journal of the Institute of Electronics and Information Engineers*, vol. 57, no. 6, pp. 44–51, 2020.

[6] K. Kyivska and S. Tsiutsiura, "Implementation of artificial intelligence in the construction industry and analysis of existing technologies," *Technology Audit and Production Reserves*, vol. 2, no. 58, pp. 12–15, 2021.

[7] Y. P. Ongena, M. Haan, D. Yakar, and T. C. Kwee, "Patients' views on the implementation of artificial intelligence in radiology: development and validation of a standardized

questionnaire," *European Radiology*, vol. 30, no. 2, pp. 1033–1040, 2020.

[8] A. Bhargava, M. Bester, and L. Bolton, "Employees' perceptions of the implementation of robotics, artificial intelligence, and automation (raia) on job satisfaction, job security, and employability," *Journal of Technology in Behavioral Science*, vol. 6, no. 1, pp. 106–113, 2020.

[9] L. Fanea, "Disease management strategy for direct and immediate implementation of artificial intelligence-based mri in radiology," *Journal of Biosciences and Medicines*, vol. 07, no. 09, pp. 38–50, 2019.

[10] S. Naghizade, S. Mohammadi, and H. Khoshsima, "Design and simulation of an all optical 8 to 3 binary encoder based on optimized photonic crystal or gates," *Journal of Optical Communications*, vol. 42, no. 1, pp. 31–41, 2021.

[11] W. Zhang, H. Ning, L. Liu, Q. Jin, and V. Piuri, "Guest editorial: special issue on hybrid human-artificial intelligence for social computing," *IEEE Transactions on Computational Social Systems*, vol. 8, no. 1, pp. 118–121, 2021.

[12] S. Elayyan, "The future of education according to the fourth industrial industrial revolution," *Journal of Educational Technology and Online Learning*, vol. 4, no. 1, pp. 24–30, 2021.

[13] F. A. Batarseh, L. Freeman, and C.-H. Huang, "A survey on artificial intelligence assurance," *Journal of Big Data*, vol. 8, no. 1, pp. 60–30, 2021.

[14] M. Lv, "Retracted article: agricultural climate change and multilingual GIS database translation system based on embedded database and artificial intelligence," *Arabian Journal of Geosciences*, vol. 14, no. 11, pp. 1048–1120, 2021.

[15] M. Maisonobe, "The Future of Urban Models in the Big Data and Ai Era: A Bibliometric Analysis (2000–2019)," *AI & SOCIETY*, vol. 37, no. 1, pp. 1–18, 2021.

[16] A. Bustamam, H. Hamzah, N. A. Husna et al., "Artificial intelligence paradigm for ligand-based virtual screening on the drug discovery of type 2 diabetes mellitus," *Journal of Big Data*, vol. 8, no. 1, pp. 74–21, 2021.

[17] S. Kar, A. K. Kar, and M. P. Gupta, "Industrial Internet of Things and Emerging Digital Technologies–Modeling Professionals' Learning Behavior," *IEEE Access*, vol. 99, p. 1, 2021.

[18] L. Fan and L. Zhang, "Multi-system fusion based on deep neural network and cloud edge computing and its application in intelligent manufacturing," *Neural Computing & Applications*, vol. 34, no. 5, pp. 3411–3420, 2021.

[19] S. K. Zhou, H. Greenspan, C. Davatzikos et al., "A review of deep learning in medical imaging: imaging traits, technology trends, case studies with progress highlights, and future promises," *Proceedings of the IEEE*, vol. 109, no. 5, pp. 820–838, 2021.

[20] X. Chai, J. Fu, J. Zhang, D. Han, and Z. Gan, "Exploiting preprocessing-permutation-diffusion strategy for secure image cipher based on 3D Latin cube and memristive hyperchaotic system," *Neural Computing & Applications*, vol. 33, no. 16, Article ID 10371, 2021.

[21] W. Yu, X. He, J. Pei et al., "Visually aware recommendation with aesthetic features," *The VLDB Journal*, vol. 30, no. 4, pp. 495–513, 2021.

[22] X. You, C. X. Wang, J. Huang et al., "Towards 6g wireless communication networks: vision, enabling technologies, and new paradigm shifts," *Science China Information Sciences*, vol. 64, no. 1, pp. 1–74, 2021.

[23] D. Messner, "Redefining and renewing humanism in the digital age [opinion]," *IEEE Technology and Society Magazine*, vol. 39, no. 2, pp. 35–40, 2020.

[24] S. Ranjbar, K. W. Singleton, P. R. Jackson et al., "A deep convolutional neural network for annotation of magnetic resonance imaging sequence type," *Journal of Digital Imaging*, vol. 33, no. 2, pp. 439–446, 2020.

[25] L. E. de Oliveira Aparecido, G. de Souza Rolim, J. R. da Silva Cabral De Moraes et al., "Machine learning algorithms for forecasting the incidence of coffea arabica pests and diseases," *International Journal of Biometeorology*, vol. 64, no. 4, pp. 671–688, 2020.

[26] A. White, "Ussocom 2019 programme updates an overview of ussocom's technology and materiel requirements for me next decade," *Military Technology*, vol. 43, no. 2, pp. 64–66, 2019.

[27] D. G. Lee, S. Oh, and H. I. Son, "Maintenance robot for 5-MW offshore wind turbines and its control," *IEEE*, vol. 21, no. 5, pp. 2272–2283, 2016.

[28] M. N. Habib, W. Jamal, U. Khalil, and Z. Khan, "Transforming universities in interactive digital platform: case of city university of science and information technology," *Education and Information Technologies*, vol. 26, no. 1, pp. 517–541, 2021.

Research Article

Influencing Factors of CO_2 Emissions in Chinese Power Industry: A Study from the Production and Consumption Perspectives

Qiang Liu [iD],[1] Chunmei Mao [iD],[2] and Fan Tian [iD][3]

[1]*School of Business, Hohai University, Nanjing 211100, China*
[2]*School of Public Administration, Hohai University, Nanjing 211100, China*
[3]*Lianyungang E-port Information Development Co., Ltd, Lianyungang 222042, China*

Correspondence should be addressed to Qiang Liu; 150208120020@hhu.edu.cn

China's huge regional differences are taken into consideration to study the influencing factors and their differences in CO_2 emissions of the power industry from different regions. This study aimed to improve the efficiency of CO_2 emission reduction policies. From the production and consumption perspectives, this study analyzes the influencing factors of CO_2 emissions and utilizes the Logarithmic Mean Divisia Index (LMDI) to decompose CO_2 emissions with consideration of the cross-regional power dispatching in the power industry. The results indicate that the trend of CO_2 emissions in the eastern, central, and western China seems similar during years 2005 to 2017 no matter from which perspective. From the production perspective, power consumption is the main factor in CO_2 emission increase and its affect extent may vary from different regions over a period of time. Energy efficiency inhibits CO_2 emission increase in all regions. The power structure and power distribution across regions affect CO_2 emissions significantly different in amount and direction from region to region. From the consumption perspective, economic activity plays a major role in CO_2 emission increase and plays a similar role in the trend of CO_2 emissions in three regions, but its affect extent on CO_2 emissions varies in different regions. Targeted policy recommendations are provided to reduce CO_2 emissions more effectively from China's power industry.

1. Introduction

Climate change caused by excessive carbon emissions is a serious threat to nature. China replaced the United States in 2006 to become the world's largest carbon emitter along with rapid economic development. After realizing the urgency of reducing CO_2 emissions, the Chinese government has decided to reduce carbon intensity by between 55% and 60% [1]. In addition, China committed to peak carbon emissions by 2030 at the Asia Pacific Economic Cooperation (APEC) in 2014 [2], but it is not easy for China to fulfill this commitment [3]. The power industry in China is high in energy consumption and emission, which accounts for 50% of coal consumption and 40% of CO_2 emissions in China [4]. Apparently, the power industry should therefore be the priority to reduce CO_2 emissions. However, China is with regional differences in natural resources, economy,

population, and technology. Taking this into account, we aimed to study the regional differences in CO_2 emissions in the Chinese power industry in order to improve the carbon emission efficiency.

It is noteworthy that more scholars began to pay attention to the influencing factors of regional differences in CO_2 emissions. Some scholars have analyzed carbon inequality between countries and explained the root reasons for global inequality during the sample period [5, 6]. Malla (2009) [7] discussed the factors influencing the evolution of carbon emissions from the power industry in several countries. Its results have shown that the influencing extent of factors on CO_2 emissions varied in different countries. Except for studies among countries, some research studies have examined differences among regions in emissions within a broad country such as China. Liu et al. [8] studied GHG emission characteristics, trends, and influencing

factors of four Chinese cities and concluded that emission reduction policies should vary in different cities. Chen et al. [9] studied regional differences in CO_2 emissions generated by coal consumption and explained that the root reason for emission differences is the disparity in economic growth. Moreover, some scholars have studied interregional differences in CO_2 emissions in the power industry. Wen and Yan [10] used a panel data model to study factors driving CO_2 emissions from the Chinese power industry from the regional and provincial perspectives. The results have shown that the impacts were different across regions. Zhou et al. [11] assessed the multiple factor impact of CO_2 emissions from power generation at the regional grid level from 2004 to 2010. The research found that the power grid in the northern China performed poorly. Yan et al. [12] further analyzed regional differences in power consumption and predicted CO_2 emissions for each region from 2013 to 2020 on the basis of Zhou et al.'s [11] paper.

Nevertheless, previous research studied the regional differences and driving factors of CO_2 emissions in the power industry only from a single perspective of production and did not consider the balance between producer responsibility and consumer responsibility in emissions, which to some extent weakens the emission reduction effect. Carbon leakage is likely to be caused when producer responsibility is employed to calculate CO2 emission of power industry which means CO2 emission from the power industry in each region is equal to direct CO2 emission from thermal power generation. This method ignores the phenomenon of carbon leakage in interprovincial power dispatching and characteristics of interregional power dispatching.

Scholars have studied regional carbon emissions from the consumption perspective due to power dispatching complexity. Wang et al. (2017) [13] extended the methods of Kang et al. (2012) [14] and Ji et al. (2016) [15] to propose a new estimation method, which is relatively accurate to measure CO_2 emissions of regional consumer. There is vast power dispatching around China with the power grid construction to solve the contradiction of power supply and demand. Some scholars have proved that CO_2 emissions are significantly different under different measurement perspectives. It is unilateral for either producers or consumers to undertake emission reduction obligations. The accounting scheme of carbon emission responsibility based on producers and consumers should be adopted to solve the imbalance of CO_2 emissions in the regional power industry [16].

The paper adopts the method of Wang et al. [13], Kang et al. [14], and Ji et al. [15] to calculate regional CO_2 from both production and consumer perspectives. The core idea of "carbon accounting" schemes is to consider the spatial transfer of emissions caused by power trading to fully reflect consumers' environmental responsibility. It is more conducive to reveal the real situation of carbon emission transfer among regions to study from both production and consumption perspectives and provide correct suggestions for carbon emission reduction. Therefore, this study employs Wang et al.'s [13] method to calculate regional CO_2 emissions from the production and consumption perspectives.

The commonly used approach in previous papers to study the impact of factors on carbon emissions from the energy industry is the LMDI due to its adaptability, availability, and easy interpretation of results (Ang 2004) [17]. The main driving factors at present affecting CO_2 emissions from the power industry are divided into economic and social factors (economic activities, population, etc.), structural factors (energy structure, industrial structure, etc.), and efficiency factors (energy efficiency, consumption efficiency, etc.) [4, 10, 18–20]. However, seldom scholars regard power dispatching as a factor affecting carbon emissions. With the power dispatching increase, it should be considered as an influencing factor of CO_2 emissions caused by power generation [20]. Even if some scholars have taken power dispatching as a driving factor in carbon emission, research was studied at the national level but without taking regional differences into account. We argue that there should be differences in the impact of power dispatching on carbon emissions in power import and export regions.

The current existing literature rarely considered power dispatching as a driving factor when studying regional differences in CO_2 emissions in the power industry. This usually leads to deviations in the accuracy of assessment results. On this basis, we first divide China into three regions based on different economic and geographic distributions and then calculate regional CO_2 emissions from the power industry from the production and consumption perspectives, respectively. Finally, we employ the LMDI method to determine the factors influencing the regional CO_2 emissions of China's power industry from two perspectives. Compared with existing research, we intend to contribute in two ways: (1) this study analyzes the variation trend of regional carbon emissions from both production and consumption perspectives under consideration of mass cross-regional power dispatching in China's power industry, which makes the analysis results more systematic and comprehensive. (2) Moreover, this study also divided CO_2 emission influencing factors from the power industry into production factor and consumption factor, which can determine influencing factors on CO_2 emissions from the regional power industry more accurately, and provided valuable suggestions for China to formulate more effective policies on carbon emission reduction.

The rest of the study is structured as follows. Section 2 introduces the main calculation method and data description. Section 3 presents the decomposition results and discussion. Section 4 summarizes the paper and provides policy recommendations.

2. Methods and Theory

2.1. Production Perspective

2.1.1. Estimate CO_2 Emissions from the Production Perspective. We apply the method provided by the Intergovernmental Panel on Climate Change (IPCC) to calculate CO_2 emissions from thermal power generation in one region from the production perspective without

considering power dispatching across regions. The CO_2 emission formula for the given region is as follows:

$$C^a = \sum_i C_i^a = \sum_i F_i \times K_i \times \varepsilon_i \times \gamma_i \times \frac{44}{12}, \quad (1)$$

where C^a is the CO_2 emission amount from burning of fossil fuels in one area. i is the fossil fuel type. F_i is the quantity of the ith fossil fuel in this area. K is the net heating value. ε_i is the oxidizer of carbon. γ_i is the carbon emission coefficient. 44/12 is the molecular weight ratio. We assume that the carbon emission coefficients of various fuels remain constant during the study period. Although the coefficients vary over time due to changes in fossil fuel grade, these changes are relatively small. Therefore, it can be ignored in the analysis of more important coefficients in CO_2 emissions [18].

2.1.2. Decomposition Method from the Production Perspective. Decomposition from the production perspective of CO_2 emission is expressed as follows:

$$C^a = \frac{C^a}{E} \frac{E}{Q_F} \cdot \frac{Q_F}{Q_P} \cdot \frac{Q_P}{Q_T} \cdot Q_T, \quad (2)$$

where E is the fossil fuel consumption for thermal power generation in the region. Q_F is the thermal power generation in the region. Q_P is the overall amount of power generated in the region (including thermal power and hydroelectric power). Q_T is the total power consumption in the region (including final consumption and transmission loss).

Equation (2) is equivalent as follows:

$$C^a = CC \cdot EE \cdot ES \cdot IO \cdot Q. \quad (3)$$

The function could be edited as follows according to the LMDI additive decomposition method:

$$\Delta C^a = C_{t_2}^a - C_{t_1}^a = \Delta C_{CC} + \Delta C_{EE} + \Delta C_{ES} + \Delta C_{IO} + \Delta C_Q. \quad (4)$$

According to the LMDI additive decomposition method, we decompose the overall change amount ($\triangle C$) of CO_2 emission from the power industry into five influencing factors based on the producer responsibility in the base year and target year. CC is the carbon emission coefficient. ΔC_{CC} is the impact of the fossil fuel structure change. EE is the energy efficiency of thermal power. ΔC_{EE} is the influence of the energy conversion efficiency change in thermal power. ES is the power structure. ΔC_{ES} is the change influence of power structure on CO_2 emission. IO is the power dispatching across regions. ΔC_{IO} is the impact of changes in power distribution across regions. Q is the power consumption. ΔC_Q is the impact of changes in power consumption on CO_2. t_2 and t_1 are base year and target year, respectively ($t_2 > t_1$).

We utilize the following formulas to calculate these driving factors:

$$\Delta C_{CC} = L\left(C_{t_2}^a - C_{t_1}^a\right) \cdot \ln\left(\frac{CC_{t_2}}{CC_{t_1}}\right), \quad (5)$$

$$\Delta C_{EE} = L\left(C_{t_2}^a - C_{t_1}^a\right) \cdot \ln\left(\frac{EE_{t_2}}{EE_{t_1}}\right), \quad (6)$$

$$\Delta C_{ES} = L\left(C_{t_2}^a - C_{t_1}^a\right) \cdot \ln\left(\frac{ES_{t_2}}{ES_{t_1}}\right), \quad (7)$$

$$\Delta C_{IO} = L\left(C_{t_2}^a - C_{t_1}^a\right) \cdot \ln\left(\frac{IO_{t_2}}{IO_{t_1}}\right), \quad (8)$$

$$\Delta C_Q = L\left(C_{t_2}^a - C_{t_1}^a\right) \cdot \ln\left(\frac{Q_{t_2}}{Q_{t_1}}\right). \quad (9)$$

L is the logarithmic mean value:

$$L(x, y) = \begin{cases} y - x/\ln y - \ln x, & x \neq y \\ x, & x = y \end{cases}.$$

2.2. Consumption Perspective

2.2.1. Decomposing CO_2 Emissions from Consumption Perspective. Local power consumption should be taken into account when calculating the overall CO_2 emissions in the region. CO_2 emissions from power utilization are estimated as follows:

$$C = C^a + C^b, \quad (10)$$

where C is the actual CO_2 emissions in the region based on consumer responsibility. C^b is the CO_2 emission allocation due to cross-regional power dispatching, which will be discussed in the next section. C^a is the CO_2 emissions from thermal power in the region. C^b is the CO_2 emission allocation in the region. We classify all provinces into two types according to Wang et al. (2017) [13].

$$\Delta = I - O, \quad (11)$$

where Δ is the net power consumption of one province. O is the output power from one province, while I is the input power from other provinces. $\Delta > 0$ means that the input power exceeds output power, and the province will be regarded as power import province. $\Delta < 0$ means that the output power exceeds input power, and then, the province will be regarded as power export province. We assume that each province gives priority to power production of its own.

2.2.2. Decomposing CO_2 Emissions in Power Export Provinces

$$C_m^b = \Delta \times \frac{Q_{F_m}}{Q_{P_m}} \times \frac{C_{F_m}}{Q_{F_m}}, \quad (12)$$

where C_m^b is the power export province. m is CO_2 emission dispatching. Q_{F_m} is the thermal power produced by province m. Q_{P_m} is the overall power produced by province m (including thermal power generation and hydroelectric power generation). Q_{F_m}/Q_{P_m} is the ratio of the thermal power

generation to total power generation in province m. C_{F_m} is the CO_2 emissions from thermal power generation in province m. C_{F_m}/Q_{F_m} is the emission factor of the thermal power generation.

2.2.3. Decomposing CO_2 Emissions in Power Import Provinces.

$$C_n^b = \Delta \times \frac{\sum_{m=1}^{m} |C_m^b|}{\sum_{m=1}^{m} Q_{F_m}} \times \frac{\sum_{m=1}^{m} Q_{F_m}}{\sum_{m=1}^{m} Q_{T_m}}, \tag{13}$$

where C_n^b is the dispatch of CO_2 emissions in the power import province.

$\sum_{m=1}^{m} |C_m^b| / \sum_{m=1}^{m} Q_{F_m}$ is the power emission factor of the total output thermal power generation, and Q_{F_m} is the thermal power generation distributed from province m.

$\sum_{m=1}^{m} Q_{F_m} / \sum_{m=1}^{m} Q_{T_m}$ is the ratio of dispatching amount on thermal power generation to total power dispatching. Q_{T_m} is the total export power of the power output province (including thermal power generation and hydroelectric power generation).

2.2.4. Decomposition Method from the Consumption Perspective.

According to Kaya (1989) [21] and considering the importance of industrial structure change, we decompose the exponent of CO_2 emissions from consumption perspective as follows:

$$C = \frac{C}{Q_T} \cdot \frac{Q_T}{GDP} \cdot \frac{GDP}{P} \cdot P. \tag{14}$$

Its abbreviation is as follows:

$$C = CI \cdot EI \cdot EA \cdot P. \tag{15}$$

GDP is the gross domestic product of the region. P is the resident population of the region. Similar to the above description, the annual rate of CO_2 increase can be decomposed into the following formula:

$$\Delta C = C_{t_2} - C_{t_1} = \Delta C_{CI} + \Delta C_{EI} + \Delta C_{EA} + \Delta C_P, \tag{16}$$

where CI is the carbon intensity of power consumption, reflecting the cleanliness of power consumption in the region. ΔC_{CI} is the influence of power consumption on carbon intensity changes. EI is the power intensity, which reflects the industrial structure. ΔC_{EI} is the impact of power intensity changes. EA is the economic activities. ΔC_{EA} is the impact of economic development and change. ΔC_P is the impact of population size fluctuations.

The right side of (15) can be computed as equations (5)–(9), which are not listed here due to limited space.

2.3. Data Description.

Considering the data accessibility and the impacts of COVID-19 pandemic on energy consumption in 2020, the Chinese power industry data from 2005 to 2019 were used in this study. We employ data on energy consumption caused by power generation in different provinces from the China Energy Statistical Yearbook (2005–2019).

Besides, population data and GDP data came from China Statistical Yearbook (2005–2019). Regional GDP from 2005 to 2019 was converted on the basis of the price level in 2005. The IPCC effective CO_2 emission factor and net calorific value of fuel were also considered. According to the geographical distribution and economic level, 30 provinces in China (Tibet, Taiwan, and Hong Kong were excluded) were divided into three parts. The detailed classification is listed in Table 1.

3. Results and Discussion

3.1. Outline of CO_2 Emissions from the Power Industry.

As shown in Figure 1, the CO_2 emissions in three regions from 2005 to 2017 mainly go through two phases, and their trends are also similar no matter from which perspective. The first phase is from years 2005 to 2011, and the CO_2 emissions in all regions increased significantly over time. The second phase is after 2011, and CO_2 emissions in each region are only slightly increased and even decreased in some years. The trend of CO_2 emissions in recent years proves that the Chinese green and low-carbon policies in the power industry have been effectively implemented. Although the overall trend of CO_2 emissions in three regions is almost the same, it is obvious that CO_2 emissions look higher from the consumption perspective than those from the production perspective in all tress regions.

The growth rate of CO_2 emissions in central China was lower than the other two regions from the production perspective. The CO_2 emissions in western China exceeded the central China from 2010 to 2011. This is mainly due to two main reasons: economic development is positively correlated with power consumption, so the developed eastern China requires a large amount of power to support its high economy. On the other hand, the economic development of western China is mainly extensive and it has carried on enterprise with high CO_2 emissions from other regions during industrial development and upgrading of China's industries.

The growth rate of CO_2 emissions in the eastern China was apparently the highest from consumption perspective. The current economic development needs power support, and the high economic aggregate in eastern China is precisely supported by large quantities of power consumption. This will become even more evident under the principle of "People who consume who take the responsibility." In general, the eastern China is with the highest carbon emissions from either production perspective or consumption perspective. Therefore, the eastern China should play a leading role in carbon reduction projects in the power industry. In addition, Figures 1(a) and 1(b) indicate that the regional amount and growth rate of CO_2 emissions are significantly different and the consumption side is higher than the production side in three regions from both perspectives.

Therefore, the analysis from two perspectives can provide a more systematic and comprehensive understanding of regional differences in CO_2 emissions in the power industry.

TABLE 1: Detailed classification of the Chinese regional divisions.

Regions	Provinces
East regions	Beijing, Tianjin, Hebei, Liaoning, Shanghai, Jiangsu, Zhejiang, Fujian, Shandong, Guangdong, Hainan
Central regions	Shanxi, Jilin, Heilongjiang, Anhui, Jiangxi, Henan, Hubei, Hunan
West regions	Chongqing, Sichuan, Guizhou, Yunnan, Shaanxi, Gansu, Ningxia, Qinghai, Xinjiang, Guangxi, Inner Mongolia
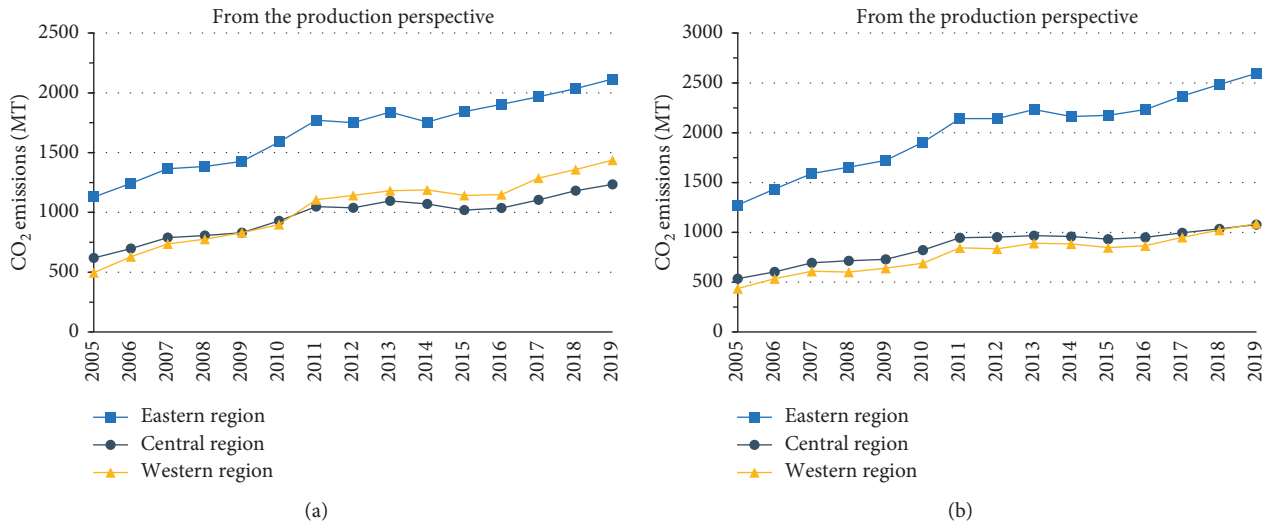
FIGURE 1: CO_2 emissions from the power industry in three regions from 2005 to 2017: (a) CO_2 emissions in three regions from the production perspective. (b) CO_2 emissions in three regions from the consumption perspective.

3.2. Results and Discussion from the Production Perspective. We discuss the impact of driving factors of three regions on CO_2 emissions from the Chinese power industry in this section. The power consumption is the most important factor for CO_2 generation in all regions, which is known from results (as shown in Figure 2 and Table 2). The energy efficiency is the major factor in restraining every region's CO_2 emissions even though the energy efficiency improvements in the west were not significant at the beginning of the study. The power generation structure and cross-regional power distribution have different effects on CO_2 emissions in terms of scale and direction in three regions. The carbon emission coefficient is not the main driving factor compared with other factors during the study period. We will discuss more details in the following parts.

3.2.1. Carbon Emission Coefficient and Energy Efficiency. Changes in carbon emission coefficient have a relatively low impact on CO_2 emissions compared with other factors in all regions. It reflects that the change in fossil fuel structure in the thermal power generation is small. The ratio of coal in total fossil fuel for the thermal power generation has always remained above 90% and has no signs of decline as shown in Table 3. Generally speaking, the fossil energy structure mainly depends on the overall regional resources. In China, the structure of fossil energy has been in a state of "more coal, less oil, and shortage of natural gas." The raw coal occupies 70% of energy consumption and will not change greatly in a short time [16]. The results show that the changes in fossil fuel structure affecting CO_2 emissions in the power

industry are weak. It also proves that there is still a long way to change the mix of fossil fuels in the thermal power generation in all regions.

The energy efficiency of thermal power generation is the main factor to restrain CO_2 emissions from the power industry in all regions. The CO_2 emission reductions in the eastern, central, and western China reached 43.25%, 39.86%, and 21.05%, respectively (Table 2). Although energy efficiency increased in all regions from 2005 to 2019, it had a smaller impact on CO_2 emission reduction in the western China than in the rest of the two regions. Additionally, we can see from Table 4 that the initial energy efficiency level is inconsistent in three regions during the study period and decreased from the east to the west. These phenomena are mainly caused by two reasons: (1) the economy of the central and western regions is relatively backward, which still keeps following the traditional extensive growth model. Both the central China and western China pay little attention to environmental protection; (2) it is also directly related to the resource they owned. For example, the environmental cost of hydro-rich provinces such as Sichuan and Yunnan is lower than the cost of coal-fired power. As a result, the production capacity of thermal power in these regions is not fully utilized and the energy efficiency of thermal power generation is low. Based on differences in energy efficiency in regions, the central China and western China have great potential to improve technologies of energy conversion.

3.2.2. Power Generation Structure and Cross-Regional Power Consumption. Hydropower is taken as the main comparison of power generation structure change. The power

(a)

(b)

(c)
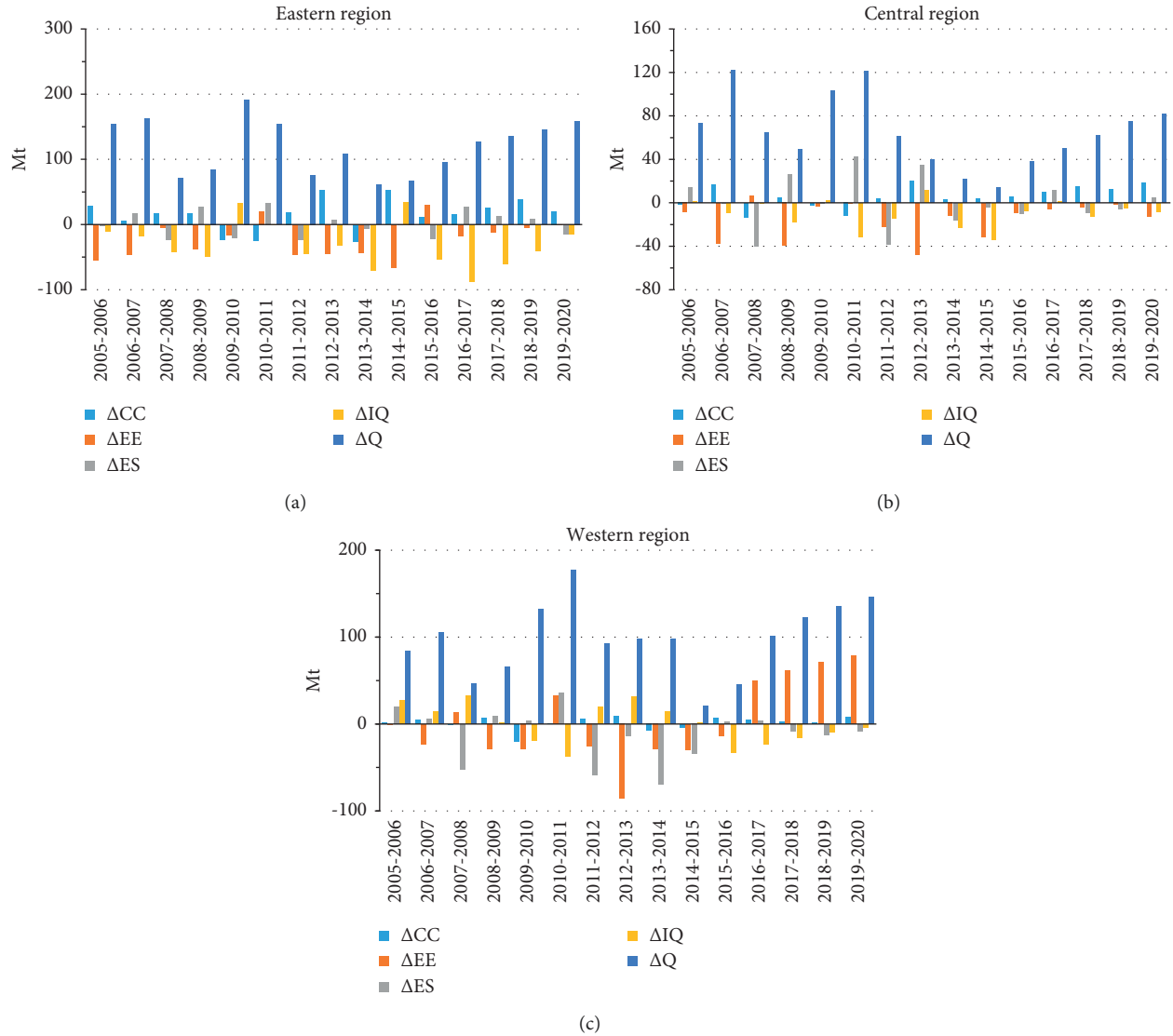
Figure 2: Contribution value of different factors on CO_2 emissions in three regions from the production perspective: (a) eastern China, (b) central China, and (c) western China.

Table 2: Changes in overall CO_2 emissions by different factors from the production perspective from 2005 to 2019 (unit: in metric tons).

Effect	Eastern China	Percent	Central China	Percent	Western China	Percent
$\triangle CC$ fuel structure	143.54	17.03%	29.52	6.02%	6.73	0.85%
$\triangle EE$ energy efficiency	−364.51	−43.25%	−195.32	−39.86%	−166.94	−21.05%
$\triangle ES$ electricity structure	26.04	3.09%	18.57	3.79%	−149.06	−18.79%
$\triangle IO$ interregional power dispatching	−320.89	−38.08%	−123.83	−25.27%	35.21	4.44%
$\triangle Q$ power consumption	1358.57	161.21%	761.03	155.32%	1067.27	134.55%

generation structure influences CO_2 emissions in three regions varied in scale and direction. The total CO_2 emission changes in the eastern, central, and western China are 3.09%, 3.79%, and -18.79%, respectively. As Figure 2 demonstrates, power generation structure changes slightly influence CO_2 emissions in eastern China, while greatly influencing fluctuations of CO_2 emissions in central China and greatly restraining CO_2 emissions in western China. These differences are mainly caused by uneven resource distributions in

regions. There is around 70% of hydroelectric power generated from western China from a national perspective. However, it is 40% of hydroelectric power generated from the west and less than 10% of hydroelectric power generated from the east from a regional perspective (Figure 3). Although the eastern China takes a low ratio in hydropower generation, it has little potential to increase this proportion (from technology perspective). The exploitable hydropower in the east coast of China only accounts for about 6% of the

TABLE 3: Ratio of raw coal in total fossil fuel consumption of the thermal power generation (unit: percentage).

Region	2005 (%)	2006 (%)	2007 (%)	2008 (%)	2009 (%)	2010 (%)	2011 (%)	2012 (%)	2013 (%)	2014 (%)	2015 (%)	2016 (%)	2017 (%)	2018 (%)	2019 (%)
Eastern region	93	94	94	94	94	95	95	94	95	94	94	93	94	94	93
Central region	97	96	96	95	95	92	93	94	93	94	93	92	93	92	92
Western region	97	98	98	97	97	97	95	95	95	95	95	93	94	94	93

TABLE 4: Energy efficiency of thermal power generation (unit: kJ/104 kW h).

Region	2005	2006	2007	2008	2009	2010	2011	2012	2013	2014	2015	2016	2017	2018	2019
Eastern region	10.22	9.75	9.42	9.38	9.14	9.03	9.14	8.9	8.68	8.47	8.17	8.3	8.07	8.21	8.17
Central region	11.6	11.45	10.89	10.98	10.46	10.42	10.42	10.19	9.75	9.64	9.35	9.27	9.33	9.31	9.58
Western region	12.12	12.11	11.7	11.91	11.49	11.11	11.47	11.21	10.42	10.16	9.91	9.79	10.2	9.83	10.06

(a)

(b)
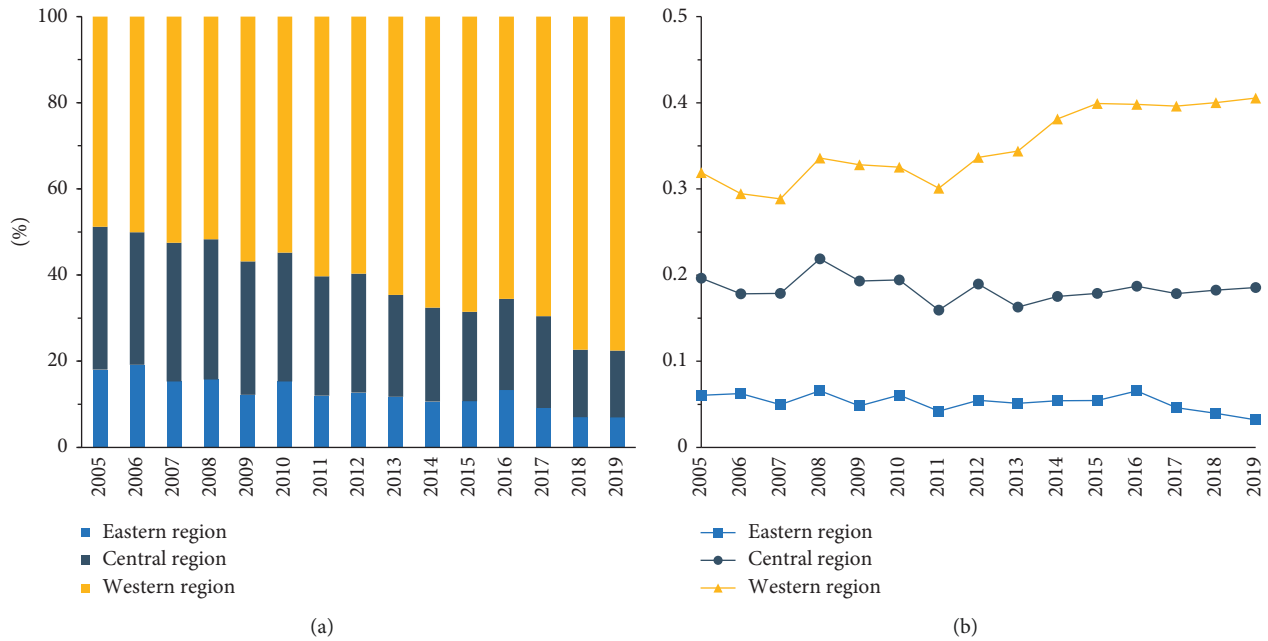
FIGURE 3: Hydropower generation ratio: (a) regional hydropower generation ratio in China and (b) hydropower generation ratio in overall power generation.

total power supply, while the exploitable power in the southwest, northwest, south, and central China accounts for 92%. Hence, by the end of March 2021, there is no room for hydropower exploitation on the east coast of China, compared with more than 50% exploitable space in the western China [22]. Therefore, China should focus on optimizing the energy structure of power generation in the central and western China, especially in the western China, which is rich in natural resources. Power generation structure improvement is an efficient measure to reduce emissions, which can not only ensure the power generation but also avoid environmental pollution.

The unbalanced distribution of regional natural resources is also one of the reasons affecting power dispatching. China has begun to implement power distribution measures since the 1990s to solve the mismatch problem of regional power supply and demand. Figure 2 illustrates that the impact on scale and direction of power distribution on CO_2 emissions is inconsistent among regions. The power dispatching increases CO_2 emission in eastern and central China while promoting the CO_2 emissions in western China.

Although power dispatching plays different roles in different regions, it is beneficial to restrain CO_2 emissions from the power industry. Thus, increased efforts will continue to make power dispatching. The suppression effect on CO_2 emission of power transfer in eastern China is mainly because power import can not only solve the problem of

insufficient power supply but also has a relatively low cost compared with power generation technology improvement. Therefore, the ratio of power imports is increasing year by year.

The effect of power dispatching on CO_2 emissions in western China is by promoting to suppress, and it is because the western China has already transferred natural resource advantage into economic advantage through power dispatching. With hydropower ratio growth, the western China benefits from providing clean energy to the east and reduces local environmental pollution as well [23, 24]. In addition, the import power of central China declines, indicating that power generation pressure in the central China has shifted in search of lower economic costs. China will continue to vigorously promote power dispatching to address the imbalance between supply and demand and reduce emissions by current policies. Thus, western China should accelerate the improvement of energy efficiency and power generation structure with increased power dispatching.

3.2.3. Power Consumption. Power consumption is the primary factor that increases CO_2 emissions of the power industry with an impact of 158.39%, 170.12%, and 147.91% on overall CO_2 emissions in eastern, central, and western China, respectively. According to Figure 2, the impact of power consumption on CO_2 emissions from the power industry is almost consistent with the economic cycle. Mi and Zhao (2012) [25] have verified the Granger causality between power consumption and economic development. They believe that economic development inevitably leads to power consumption, and power consumption will support economic development in turn. It is interesting to find out that although three regions are different in initial economic levels, the power consumption has almost the same tendency to affect CO_2 emissions from the power consumption. As a result, we could not simply assume that the CO_2 emission growth rate caused by power consumption is lower in central and western China because of the lower level of economic development.

Moreover, Figure 2 indicates that the enhancement effects of power consumption on CO_2 emissions in the power industry reduce in all regions since 2011, especially in the central China. Nevertheless, the power consumption restriction has its limitation in reducing CO_2 emissions due to tons of power required in regional development. High economic development and intensive population in eastern China lead to high power consumption demand. The acceleration of industrialization also required huge amounts of power in western China. Compared with western and eastern China, the central China is a transitional zone and its power consumption has a relatively lower impact on CO_2 emissions, but its power consumption, which remains stable, has no trend of decline.

3.3. Results and Discussion from Consumption Perspective. Economic activity is the main factor leading to CO_2 emission increase in three regions, and affecting trends in all regions seem similar, but CO_2 emissions in 2017 from economic activity in eastern China increased rapidly. Still, the carbon intensity and power intensity of power consumption are two key factors to restrain CO_2 emissions and these two factors influence CO_2 emissions, which vary from region to region. The population density has a relatively lower effect compared with other drivers.

3.3.1. Carbon Intensity of Power Consumption. The carbon intensity of power consumption is an intensity index to measure the cleanliness of regional power consumption from the consumption perspective. It plays a positive role in reducing CO_2 emissions, which accounts for -46.82%, -46.19%, and -61.83% of overall CO_2 emission changes in eastern, central, and western China, respectively, during the study period (Table 5). Contrary to the above energy efficiency factors, the carbon intensity of power consumption in western China is the lowest, indicating that power consumption in western China has the highest cleanliness (Table 6).

The western China has no responsibility to bear CO_2 emissions generated by power output, and its carbon intensity of power consumption can accurately measure the power consumption cleanliness. However, the power consumption cleanliness in western China decreased in 2017, which might be affected by extensive industry migration. Besides, the clean energy development in central and western China is also an important reason for the highest cleanliness of power consumption in the western China. As Figure 4 demonstrates, the carbon intensity of power consumption has a low impact on CO_2 emissions in three regions at the beginning of the study while increases significantly in the later stage, which is mainly attributed to the cleanliness improvement of power consumption due to the rapid growth of hydropower in the central and western China at the end of the study. The power consumption cleanliness improves greatly and plays a role in restraining CO_2 emissions in the eastern China due to the implementation of power transmission project. The carbon intensity of power consumption is an index influenced by multiple factors, including the cleanliness of region that only produced power and imported power. Everyone should work together to improve the power consumption cleanliness.

3.3.2. Power Intensity. Power intensity represents the dependence of GDP on power consumption. Its change reflects the influence of industry structure change. Although the power intensity promotes the CO_2 emissions in western China during the study period, it is the main factor in reducing CO_2 emissions in all regions. Compared with eastern and central China, the change in power intensity in western China has less impact on CO_2 emissions. This is mainly due to different industrialization levels in three regions. Table 7 demonstrates that there are significant differences in power intensity levels of three regions. The power intensity decreases progressively from east to west, which reflects the differences in the original industry structure among regions.

TABLE 5: Changes in CO_2 emission caused by drivers from the consumption perspective during 2005–2019 (unit: tons).

Effect	Eastern region	Percent	Central region	Percent	Western region	Percent
△CI	−512.7	−46.82%	−213.51	−46.19%	−314.76	−61.83%
△EI	−565.37	−51.63%	−325.69	−70.46%	−122.35	−24.03%
△EA	1943.71	177.50%	966.34	209.06%	908.42	178.44%
△P	229.42	20.95%	35.08	7.59%	37.78	7.42%

TABLE 6: Carbon intensity of power consumption (unit: $T/10^2$ kW h).

Region	2005	2006	2007	2008	2009	2010	2011	2012	2013	2014	2015	2016	2017	2018	2019
Eastern region	0.092	0.091	0.089	0.088	0.086	0.084	0.086	0.082	0.081	0.076	0.073	0.072	0.071	0.074	0.070
Central region	0.093	0.094	0.091	0.087	0.083	0.084	0.085	0.082	0.079	0.076	0.073	0.071	0.072	0.073	0.072
Western region	0.080	0.085	0.083	0.077	0.076	0.070	0.072	0.065	0.064	0.058	0.055	0.054	0.054	0.055	0.053

(a)

(b)

(c)
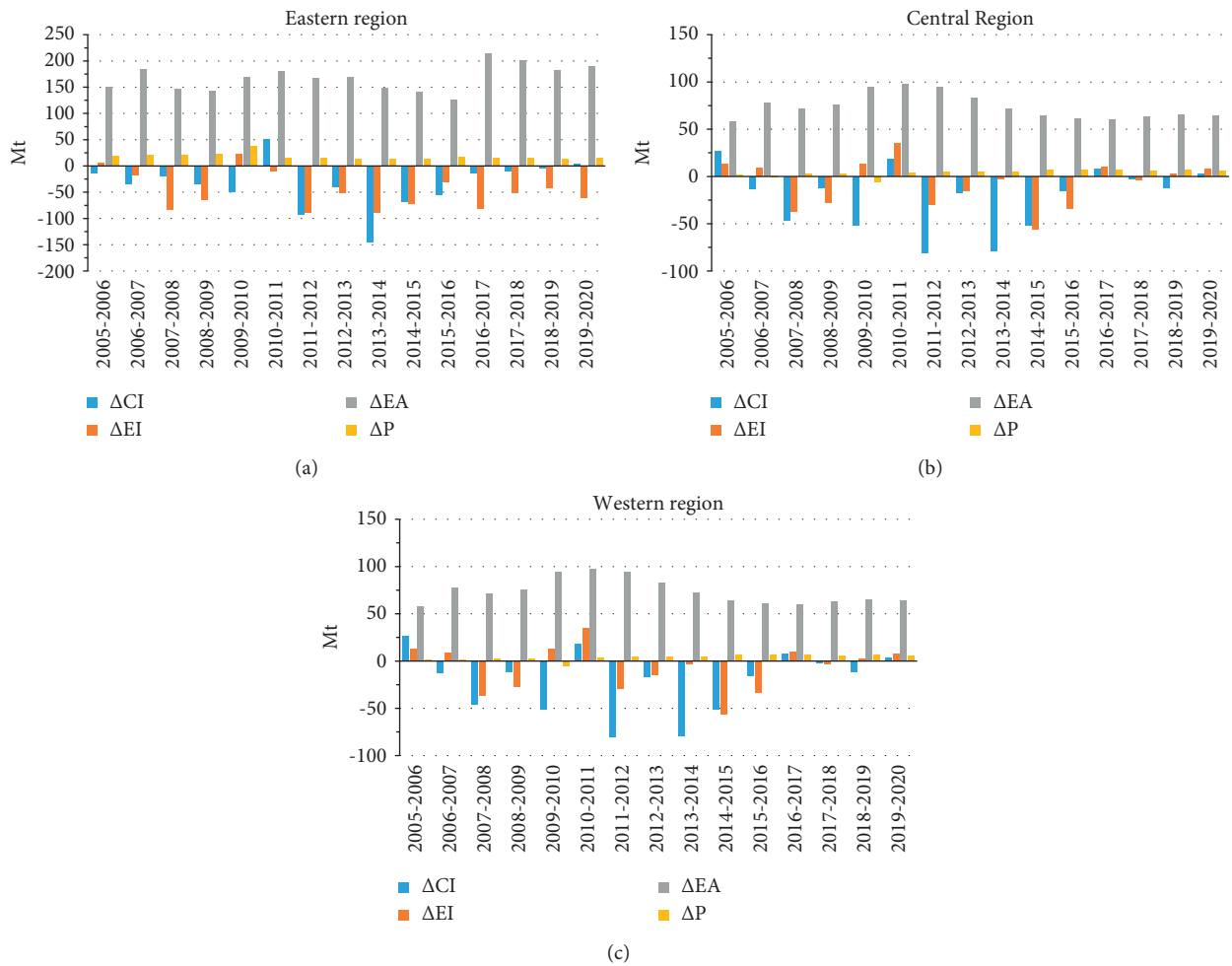
FIGURE 4: Contribution of different drives to CO_2 emissions in three regions from the consumption perspective: (a) eastern China, (b) central China, and (c) western China.

TABLE 7: Power intensity of the three regions (units: kW·h/yuan).

Region	2005	2006	2007	2008	2009	2010	2011	2012	2013	2014	2015	2016	2017	2018	2019
Eastern region	0.117	0.117	0.116	0.110	0.106	0.107	0.107	0.102	0.100	0.096	0.093	0.092	0.088	0.087	0.089
Central region	0.123	0.122	0.126	0.121	0.115	0.114	0.114	0.109	0.104	0.098	0.092	0.089	0.086	0.086	0.087
Western region	0.160	0.164	0.167	0.157	0.150	0.153	0.161	0.155	0.152	0.152	0.142	0.137	0.138	0.139	0.139

The greater the dependence of GDP on power consumption, the greater the ratio of secondary industry in the region.

After a series of national strategies issued, some high-consumption and high-polluting industries have been moved inland and the overall economic growth disparities among regions have been gradually reduced [26, 27]. The results indicate that the reduction in secondary power consumption in western China is not obvious, but the industry structure has gradually improved in the western China. Actually, the Chinese government acknowledges that the industry transfer can only eliminate regional economic differences, but not reduce total CO_2 emissions. Thus, the backward heavy industry technologies and industries in all regions should be eliminated to reduce total carbon emissions.

3.3.3. Economic Activity. The per capita GDP is a comprehensive indicator reflecting economic growth and quality of life. Figure 4 indicates that economic activity is the first driving factor for CO_2 emission increase from the power industry in all regions. The overall change in three regions increased by 177.50%, 209.06%, and 178.44%, respectively. This finding is in line with the results of Yang and Lin (2016) [4] and Zhang et al. (2013) [18]. The power generation, which is an essential element of productive activity, supports economic development. The economic development in turn gives rise to power demand and CO_2 emission increase. There are obvious economic level differences among regions in China since the reform and opening-up [28]. However, the influences of economic activity on driving CO_2 emissions in the three regions are in the same manner and fluctuate with the economic cycle. This is because economic activity (GDP/P) changes with the economy when the fluctuation of population scope in a region is very small. With the Chinese economy entering the new normal, the GDP growth has been transformed from rapid growth into medium-high-level growth since 2013. The economic activity makes a lower contribution to decreasing CO_2 emissions with the development of high-quality economy.

Scholars have proved that economic growth and environmental pollution have an inverted U-shaped relationship. There is still a long way for eastern China to reach the inflection point of inverted U shape of the most economically developed region in China. Thus, the economic activity will become the major driving factor in environmental pollution for a long time [29, 30], but economic activity can restrain CO_2 emissions from the power industry to some extent. For instance, officials in prosperous regions have a strong sense of environmental protection, while officials in impoverished regions are limited to economic development. Therefore, maintaining high-quality economic development is an effective way to slow down CO_2 emissions.

3.3.4. Population Size. The impact of population size on CO_2 emissions can be ignored compared with other influencing factors. The change in population size influences CO_2 emissions more obvious in eastern China compared with the rest of the two regions. The eastern China has a large population, which is mainly because of massive influx of people attracted by its blossom. Overall, population size has little effect in CO_2 emissions and it will not change much in the coming years [19].

4. Conclusions

This study aims to study regional differences in CO_2 emissions from China's power industry. Due to the universality of cross-regional power dispatching in the power industry, different regions have different CO_2 emission responsibility from the production and consumption perspectives. This study decomposes CO_2 emissions by LMDI and determines the factors affecting CO_2 emissions from both mentioned perspectives. Based on the decomposition results from 2005 to 2017, we observe significant differences in factors influencing CO_2 emissions from the power industry in scale and direction among regions. Therefore, measures to reduce CO_2 emissions from the power industry should vary from region to region.

This research has mainly discussed the impact of energy supply and demand distribution on carbon emissions from perspectives of energy supply and demand and power dispatching, and we aim to provide a reference for planning decision-makers and institution makers.

From the production perspective,

(1) Although power consumption has a decreased influence on CO_2 emissions in recent years, it remains the leading factor increasing CO_2 emissions in all regions. It is unrealistic in practice to control CO_2 emissions by restraining power consumption, especially in the eastern and western China. However, the Chinese government can enforce economic regulations to avoid excessive demand, which will contribute to reducing CO_2 emissions.

(2) Energy efficiency is the main factor restraining CO_2 emissions in all regions, but the initial levels of energy efficiency in different regions are significantly different. The central China and western China still have plenty of room to improve energy efficiency compared with the eastern China. Thus, the government should increase financial investment in energy efficiency in these two regions, such as continuing to restrict small-scale power generation enterprises and encouraging advanced energy conversion technologies.

(3) In addition, power structure and power distribution affect CO_2 emissions differently in scale and direction in three regions. Therefore, measures to reduce CO_2 emissions should vary from region to region. For example, the central and western China should take advantage of rich resources to optimize the power generation and thus reduce carbon emissions. Moreover, the eastern China should increase the dispatching of project to send power from the west to the east with the increase in hydroelectric power generation, so that the eastern China can fully benefit from hydropower of other regions.

From the consumption perspective,

(1) Economic activity is the major factor to increase CO_2 emissions in all regions, and its influences on increasing CO_2 emissions in all regions bear out the similar trend. As the economy grows, the local government should increase fiscal spending on environmental protection, especially in less developed areas where officials lack adequate awareness of environmental protection. In addition, China should always pay attention to the economic growth quality and accelerate the transformation of economic model from extensive to intensive.

(2) The power intensity should keep improving despite that the overall CO_2 emissions continue to rise. The carbon intensity of power consumption and power intensity are main restraining factors to CO_2 emissions in all regions, and their influences vary in different regions. It is wisdom for the Chinese government to implement industry transformation policies given that different regions are different in industrialization and economic development. The eastern China has transferred energy-intensive and heavily polluting industries to the central and western China as they have abundant natural resources and favorable markets, which can reduce the energy loss and cost during transportation.

However, the regions that industry moves into should reject the backward industries to avoid carbon leakage and achieve the overall goal of low CO_2 emissions. To sum up, reducing CO_2 emissions is not a simple unilateral action. The Chinese government should recognize regional differences and adopt targeted policies from the production and consumption perspectives to create a "low-carbon environment" for the power industry.

From the perspective of cross-region power dispatching policy:

(1) This study discussed the cross-region power allocation, which was viewed as an effective energy-carbon allocation measure. Currently, from the perspective of practice, the effectiveness of this allocation measure is mainly reflected in two aspects: (1) the cross-region power dispatching is in accord with the reality that the energy distribution does not match with the population and industry distribution in China. The energy supply in China is mostly located in the western region, while the major electricity demand from production and life is located in the coastal economic belt. Without long-distance power dispatching, most renewable energy could not be totally consumed by the local region. (2) In China, most of the renewable energy supply comes from underdeveloped regions, which have low payment capacity for energy consumption. The cross-region power dispatching could effectively improve the economy of renewable energy from the demand side, which would contribute to the carbon emission reduction process in China. This effectiveness could be viewed as the imbalance consideration of natural distribution on the supply and demand side in regional energy planning. Hence, cross-region power

dispatching is generally an irresistible choice, which is similar in developed regions such as Europe and the United States. In fact, although the new petrochemical power company in the western China would generate large carbon emissions, the cross-regional scheduling is beneficial due to the advanced energy efficiency and its contribution to the stability of the power system. This is also an episode in the process of technological change in the power industry.

4.1. Based on This, We Further Discuss Two Issues. When will this trans-regional power dispatching be ineffective? Apparently, it will result in an overall carbon emission increase to relocate power supply utilities from developed regions to underdeveloped regions simply because of carbon regulation. Moreover, the trans-regional power dispatching might result in comparative advantages of carbon permit only because of the difference in development among regions. To be specific, the carbon price is low in central and western regions thanks to abundant carbon sinks, while traditional power generation enterprises move westward because of the shortage of carbon permit. In this vein, trans-regional power dispatching should be assessed whether the increase in the economic development of western underdeveloped regions by this dispatching is worth the carbon emission generated by it. In the context of global carbon neutrality, this comparative advantage will disappear with the improvement of the balanced regional development and the diffusion of low-carbon technologies. As a result, the extent of trans-regional power dispatching will be suppressed.

Under what circumstances would this trans-regional power dispatching be more effective? In addition to the trans-regional power dispatching driven by high demand, the difference in the development intensity and potential of renewable energy among different regions are the natural driving factors for trans-regional power dispatching. From the perspective of supply side, preferential access, preferential dispatching, and preferential pricing of low-carbon power are the institutional motivation of trans-regional dispatching. From the demand side, the pricing system of integrated energy price, which includes carbon price, trading system of power system, and subsidy system of low-carbon electricity, will make it more feasible and efficient to promote trans-regional power dispatching of renewable energy power. Generally speaking, pricing market transactions and priorities of supply and demand can not only directly affect the supply and demand relationship of low-carbon power but also affect the possibility and utility of trans-regional power dispatching of low-carbon power.

Finally, we try to discuss the similarities and differences between China and Europe in power dispatching and relevant policies. Since the operation of ENTSO-E in 2009, the EU has established a unified power market in the form of an operator alliance, and the proportion of transnational exchange electricity is about 15%. In particular, typical countries include Denmark (dominated by thermal and wind power), Norway (dominated by hydropower), and Sweden (dominated by hydropower and nuclear power). Due to the differences in energy distribution and demand,

electricity exchange between countries is common. The unified grid connection and standard would be valuable for Europe, and a flexible electricity price system and even negative electricity price (encouraging users to use off-peak electricity) and accurate power accounting ability in Europe would be valuable for China. Besides, studies in Europe show that carbon tax, carbon price, and the improvement of cross-border transmission capacity could contribute to the production of low-carbon electricity [31, 32].

Data Availability

Conflicts of Interest

The authors declare that they have no known conflicts of interests or personal relationships that could have appeared to influence the work reported in this study.

Acknowledgments

References

[1] H. Wang, Y. Wang, H. Wang et al., "Mitigating greenhouse gas emissions from China's cities: case study of Suzhou," *Energy Policy*, vol. 68, pp. 482–489, 2014.

[2] S. Shao, J. Liu, Y. Geng, Z. Miao, and Y. Yang, "Uncovering driving factors of carbon emissions from China's mining sector," *Applied Energy*, vol. 166, pp. 220–238, 2016.

[3] Y. Zhao, H. Li, Z. Zhang, Y. Zhang, S. Wang, and Y. Liu, "Decomposition and scenario analysis of CO2 emissions in China's power industry: based on LMDI method," *Natural Hazards*, vol. 86, no. 2, pp. 645–668, 2017.

[4] L. Yang and B. Lin, "Carbon dioxide-emission in China′s power industry: evidence and policy implications," *Renewable and Sustainable Energy Reviews*, vol. 60, pp. 258–267, 2016.

[5] N. Cantore, "Distributional aspects of emissions in climate change integrated assessment models," *Energy Policy*, vol. 39, no. 5, pp. 2919–2924, 2011.

[6] C. Sauter, J.-M. Grether, and N. A. Mathys, "Geographical spread of global emissions: within-country inequalities are large and increasing," *Energy Policy*, vol. 89, pp. 138–149, 2016.

[7] S. Malla, "CO2 emissions from electricity generation in seven Asia-Pacific and North American countries: a decomposition analysis," *Energy Policy*, vol. 37, no. 1, pp. 1–9, 2009.

[8] Z. Liu, S. Liang, Y. Geng et al., "Features, trajectories and driving forces for energy-related GHG emissions from Chinese mega cites: the case of Beijing, Tianjin, Shanghai and Chongqing," *Energy*, vol. 37, no. 1, pp. 245–254, 2012.

[9] J. Chen, S. Cheng, M. Song, and J. Wang, "Interregional differences of coal carbon dioxide emissions in China," *Energy Policy*, vol. 96, pp. 1–13, 2016.

[10] L. Wen and F. Yan, "Regional differences and influencing factors in the CO2 emissions of China's power industry based on the panel data models considering power-consuming efficiency factor," *Environment, Development and Sustainability*, vol. 20, no. 5, pp. 1987–2007, 2018.

[11] G. Zhou, W. Chung, and Y. Zhang, "Carbon dioxide emissions and energy efficiency analysis of China's regional thermal electricity generation," *Journal of Cleaner Production*, vol. 83, pp. 173–184, 2014.

[12] Q. Yan, Q. Zhang, and X. Zou, "Decomposition analysis of carbon dioxide emissions in China's regional thermal electricity generation, 2000-2020," *Energy*, vol. 112, pp. 788–794, 2016.

[13] F. Wang, J. Shackman, and X. Liu, "Carbon emission flow in the power industry and provincial CO2 emissions: evidence from cross-provincial secondary energy trading in China," *Journal of Cleaner Production*, vol. 159, pp. 397–409, 2017.

[14] C. Kang, T. Zhou, Q. Chen, Q. Xu, Q. Xia, and Z. Ji, "Carbon emission flow in networks," *Scientific Reports*, vol. 2, no. 1, p. 479, 2012.

[15] L. Ji, S. Liang, S. Qu et al., "Greenhouse gas emission factors of purchased electricity from interconnected grids," *Applied Energy*, vol. 184, pp. 751–758, 2016.

[16] S.-C. Xu, Z.-X. He, and R.-Y. Long, "Factors that influence carbon emissions due to energy consumption in China: decomposition analysis using LMDI," *Applied Energy*, vol. 127, pp. 182–193, 2014.

[17] B. W. Ang, "Decomposition analysis for policymaking in energy," *Energy Policy*, vol. 32, no. 9, pp. 1131–1139, 2004.

[18] M. Zhang, X. Liu, W. Wang, and M. Zhou, "Decomposition analysis of CO2 emissions from electricity generation in China," *Energy Policy*, vol. 52, pp. 159–165, 2013.

[19] G. Chen, F. Hou, and K. Chang, "Regional decomposition analysis of electric carbon productivity from the perspective of production and consumption in China," *Environmental Science and Pollution Research*, vol. 25, pp. 1508–1518, 2017.

[20] J. Wang, S. He, Y. Qiu, N. Liu, Y. Li, and Z. Dong, "Investigating driving forces of aggregate carbon intensity of electricity generation in China," *Energy Policy*, vol. 113, pp. 249–257, 2018.

[21] Y. Kaya, *Impact of Carbon Dioxide Emission on GNP Growth: Interpretation of Proposed Scenarios*, Presentation to the energy and industry subgroup, response strategies working group of IPCC, Paris, France, 1989.

[22] J. P. Zhou, X. H. Du, and X. B. Zhou, "New situation and assignments of China′s hydropower development in the new phase," *Hydropower and Pumped Storage*, vol. 7, no. 4, pp. 1–6, 2021.

[23] L. Yang, "Study on environmental effects of emission reduction in west-to-East electricity transmission," *China Popul Environ*, vol. 20, pp. 36–41, 2010, (In Chinese).

[24] Y. Zeng, R. Zhang, and Z. N. Chen, "Electromagnetic lens-focusing antenna enabled massive MIMO," in *Proceedings of the 2013 IEEE/CIC International Conference on Communications in China (ICCC)*, pp. 454–459, Xi'an, China, August 2013.

[25] G. Mi and T. Zhao, "Research on the relationship among economic growth, electricity consumption and carbon emissions in China," *Sci Manag Res*, vol. 30, no. 1, pp. 89–91+116, 2012, (In Chinese).

[26] F. Song and X. Zheng, "What drives the change in China's energy intensity: combining decomposition analysis and econometric analysis at the provincial level," *Energy Policy*, vol. 51, pp. 445–453, 2012.

[27] J. Yin, M. Zheng, and X. Li, "Interregional transfer of polluting industries: a consumption responsibility perspective," *Journal of Cleaner Production*, vol. 112, pp. 4318–4328, 2016.

[28] K. W. Chan and M. Wang, "Remapping China's regional inequalities, 1990-2006: a new assessment of de facto and de jure population data," *Eurasian Geography and Economics*, vol. 49, no. 1, pp. 21–55, 2008.

[29] B. Lin and Z. J. Jiang, "Prediction of carbon dioxide environmental Kuznets curve and its influencing factors in China," *Management World*, vol. 4, no. 4, pp. 27–36, 2009, In Chinese.

[30] W. Zuo, "Test of carbon dioxide emission Kuznets curve (EKC) in China," *Stat Decis Mak*, vol. 11, pp. 22–24, 2014, In Chinese.

[31] C. B. Martínez-Anido, M. Vandenbergh, L. De Vries et al., "Medium-term demand for European cross-border electricity transmission capacity," *Energy Policy*, vol. 61, pp. 207–222, 2013.

[32] S. Mesfun, S. Leduc, P. Patrizio et al., "Spatio-temporal assessment of integrating intermittent electricity in the EU and Western Balkans power sector under ambitious CO2 emission policies," *Energy*, vol. 164, pp. 676–693, 2018.

Research Article

Analysis of Transient Response of ZPW-2000A Jointless Track Circuit Considering Frequency Variation

Bin Zhao ⬤, Guanghao Yu, Dong Wang, Lei Chen, and Jingning Ou

School of Automation & Electrical Engineering, Lanzhou Jiaotong University, Lanzhou 730070, China

Correspondence should be addressed to Bin Zhao; zhaobin@mail.lzjtu.cn

In order to accurately analyze the influence of electromagnetic transient signals on the jointless track circuit when the electromagnetic transient signal propagates in the rail, it is necessary to consider the frequency-variable load terminated in the ZPW-2000A jointless track circuit and the frequency-variable loss inside the rail. A method is proposed for calculating the transient response of transmission lines system with frequency-variable end load of jointless track circuit. Firstly, the transmission lines model of jointless track circuit is established, based on multiconductor transmission lines theory, the model equation is deduced and discretized by finite difference time domain (FDTD). The vector fitting method is used to express the admittance of the tuning region in the track circuit, and the rational approximation function of the tuning region is derived from the poles, residues, and constants. The voltage and current at nodes in the tuning region are calculated by piecewise linear recursive convolution algorithm. Combined with the discrete transmission line equation, the current and voltage expression of the transient electromagnetic signal at the receiving end of the track circuit in time domain is obtained. Compared with state variable method, the error is less than 6%, which verifies the correctness of the proposed method. Finally, this paper studies the influence laws of different factors on the overvoltage at the receiving end of jointless track circuit and the weak links of jointless track circuit under the influence of transient electromagnetic signal. It provides theoretical reference for fault research and anti-interference analysis of ZPW-2000A jointless track circuit.

1. Introduction

Jointless track circuit is the key equipment used to detect the occupancy of train section, the integrity of rail, and the transmission of running information in railway line, which is an important basic equipment to ensure the safe operation of high-speed railway [1]. With the increasing complexity of railway construction environment, the rail and signal transmission equipment laid outdoors are easily disturbed by strong electromagnetic signals. Electromagnetic interference signals use rail as transmission medium to produce conduction interference or radiation coupled interference on jointless track circuits [2]. The investigations show that lightning strikes can cause failures of trackside tuning matching units, signal transmission cables and lightning protection analog network disks, transmitters and receivers, etc. Jointless track circuit is easy to make wrong responses by

this disturbance, which will threaten the safety of train running. Therefore, it is important to analyze the interference of transient electromagnetic signal to track circuit.

The theory of multiconductor transmission lines is the theoretical basis of time-domain transient analysis of track circuits. Kunz and Luebbers [3] first solved the transmission lines equation by FDTD method, which provided a theoretical basis for time-domain solution of transmission lines. With the complex changes in transmission lines termination equipment, Wang et al. [4–6] respectively proposed a numerical algorithm based on Thevenin equivalent circuit method, state variable method, etc., to solve the terminal frequency-varying load and combined with the transmission line equation to solve the electromagnetic impulse response of the system. In the study of transient response of jointless track circuits. Mazloom et al. [7] proposed a method based on transmission line equation and ATP-EMTP simulation

model to analyze the voltage response of track circuit at the moment of train entering and clearing. Zhao et al. [8] obtained the general solution of current and voltage of rail line by Laplace transformation of the transmission line equation of track circuit, which simplified the calculation model and ignored the electrical insulation section; Yong-jian [9] used the state variable method to analyze the receiving end of the DC track circuit and solved equation of the track circuit by combining the transmission line equation, but it was difficult to write the state equation when the circuit structure was complex. Zhichao et al. [10] analyzed the overvoltage of each signal equipment during lightning strike catenary by establishing lightning strike simulation model of signal system.

ZPW-2000A jointless rack circuit includes parallel nonlinear equipment and rail with frequency variation characteristics. In order to accurately calculate the electromagnetic transient response of track circuit transmission line system, the influence of terminating frequency variation load and rail frequency variation loss must be considered. Firstly, according to the transmission characteristics of ZPW-2000A jointless track circuit, the transmission line model of track circuit is established. The model cannot be calculated directly due to the presence of parallel or terminated nonlinear lumped elements in the track circuit. Based on the multiconductor transmission lines theory, the model equation is solved by FDTD. The vector fitting method is a powerful tool for the modeling analysis of frequency-dependent systems, which is used to fit the admittance of the tuning region. The rational approximation function of the track circuit is derived from the poles, residues, and constants. The relationship between voltage and current at both ends of the admittance is derived by piecewise linear recursive convolution, which is submitted into the discrete equation of transmission lines. Finally, the time-domain expression of the current and voltage at the receiving end of the track circuit is obtained. Compared with the state variable method, the error is less than 6%, which verifies the correctness of the proposed method. This method is used to analyze the influence of lightning stroke distance, electromagnetic signal frequency, and track bed resistance on the overvoltage at the receiving end of track circuit; it provides a theoretical basis for the anti-interference analysis of track circuit.

2. Modeling of Transmission Line of Track Circuit with Frequency-Variable Load Terminated

The outdoor equipment of jointless track circuit is composed of steel rail, tuning unit (BA), air-core coil (SVA), signal cable, matching unit and compensation capacitor, etc. The tuning unit and the air-core coil part form an electrical insulation section to prevent cross-zone signal transmission from adjacent sections. The compensation capacitor is used to improve the transmission performance of the track circuit and increase the transmission distance of the track circuit

information. According to the transmission characteristics of track circuit, the rails are equivalent to uniform transmission lines [11]; it is characterized by two asymmetrical currents, one of which leaks into the ground, and the other flows from one rail to the other through ballast and sleepers. Taking a certain interval of track circuit as an example, the MTL equivalent model of jointless track circuit is established [12], as shown in Figure 1.

Here, r_1 and r_2 are the self-resistance of the rail; l_{11} and l_{22} are the self-inductance of the rail; l_{12} is the mutual inductance between rails; g_{11} and g_{22} are the leakage conductance between rails and Earth; g_{12} and g_{21} are the ballast resistance parameter of track characterized by conductance; c_{11} and c_{22} are the self-capacitance of the rail; c_{12} is the mutual capacity of the rails; and z_1 and z_2 represent the tuning region, respectively.

Transmission line losses are reflected in the conductor and the surrounding mediums; in general, these losses are frequency dependent, and the increase of frequency will lead to additional high-frequency losses. The most important is caused by the skin effect in the conductor and the polarization in the dielectric. Dielectric loss has little influence on transmission lines and can be ignored [12]. Therefore, the frequency domain expression of transmission line equation based on multiconductor transmission lines theory is

$$\frac{d\widehat{V}(z,w)}{dz} = \left[r(w) + jwl_i(w)\right]\widehat{I}(z,w) - jwl\widehat{I}(z,w)$$
$$= -\widehat{z}(w)\widehat{I}(z,w), \tag{1}$$

$$\frac{d\widehat{I}(z,w)}{dz} = -g(w)\widehat{V}(z,w) - jwc\widehat{V}(z,w)$$
$$= -\widehat{y}(w)\widehat{V}(z.w), \tag{2}$$

where impedance and admittance are, respectively, $\widehat{z}(w) = \widehat{z}_i(w) + jwl$, $\widehat{z}_i(w) = r(w) + jwl_i(w)$. $\widehat{y}(w) = g(w) + jwc$.

Converting the frequency domain equations of (1) and (2) is transformed by Laplace transform into the time domain given the convolution equation as

$$\frac{\partial \mathbf{V}(z,t)}{\partial z} = -z_i(t) * \mathbf{I}(z,t) - \mathbf{l}\frac{\partial \mathbf{I}(z,t)}{\partial t}, \tag{3}$$

$$\frac{\partial \mathbf{I}(z,t)}{\partial z} = -\mathbf{g}\mathbf{V}(z,t) - \mathbf{c}\frac{\partial \mathbf{V}(z,t)}{\partial t}. \tag{4}$$

In the case of high frequency, unit length resistance, internal inductance, and unit length conductance of conductor loss parameters are functions of frequency. The approximate formula $A + B\sqrt{s}$ for conductor losses is based on the transformation pair conversion; the inverse Laplace transform of the impedance in the conductor is

$$\widehat{z}_i(s) = A + B\sqrt{s} = A + B\frac{1}{\sqrt{s}}s \Leftrightarrow A + B\frac{1}{\sqrt{\pi}}\frac{1}{\sqrt{t}}\frac{\partial}{\partial t}, \tag{5}$$

where $A = r_{dc}$, $B = r_{dc}/\sqrt{\pi}\sqrt{f_0}$, r_{dc} is DC resistance.

The convolution of the calculation in (3) is expressed as

$$z_i(t) * I(z,t) = \int_0^t z_i(\tau)I(z,t-\tau)d\tau$$

$$= AI(z,t) + B\frac{1}{\sqrt{\pi}}\int_0^t \frac{1}{\sqrt{\tau}}\frac{\partial I(z,t-\tau)}{\partial(t-\tau)}d\tau. \tag{6}$$

The convolution term (6) is discrete with time step and divided by Δt segment. Discrete convolution is approximated in the following way:

$$\int_0^t \frac{1}{\sqrt{\tau}}F(t-\tau)d\tau \cong \int_0^{(n+1)\Delta t}\frac{1}{\sqrt{\tau}}F((n+1)\Delta t - \tau)d\tau$$

$$\cong \sum_{m=0}^n F^{n+1-m}\int_{m\Delta t}^{(m+1)\Delta t}\frac{1}{\sqrt{\tau}}d\tau \tag{7}$$

$$= \sqrt{\Delta t}\sum_{m=0}^n F^{n+1-m}Z_0(m),$$

where $F(t) = \partial I(z,t)/\partial t$, $Z_0(m) = \int_m^{m+1}1/\sqrt{\tau}\partial\tau$.

According to the FDTD algorithm, the position length of the transmission line is discretized by Δz, and the time length is discretized by Δt. The whole transmission lines are divided into NDZ segments, and the total solution times are divided into NDT segments. In order to ensure the stability of discrete calculation, the voltage of $NDZ + 1$ at discrete point $V_1, V_2, \ldots, V_Z, V_{NDZ+1}$ and the discrete point current $I_1, I_2, \ldots, I_{NDT}$ does interleaving calculation. Then, (3), (4), and (7) can be discretized as

$$\frac{\mathbf{V}_{k+1}^{n+1} - \mathbf{V}_k^{n+1}}{\Delta z} + \mathbf{l}\frac{\mathbf{I}_k^{n+3/2} + \mathbf{I}_k^{n+1/2}}{\Delta t} + A\frac{\mathbf{I}_k^{n+3/2} + \mathbf{I}_k^{n+1/2}}{2} +$$

$$\frac{\sqrt{\Delta t}}{\sqrt{\pi}}B\sum_{m=0}^n\left[\frac{\mathbf{I}_k^{n+3/2-m} + \mathbf{I}_k^{n+1/2-m}}{\Delta t}\right]Z_0(m) = 0, \tag{8}$$

$$\frac{\mathbf{I}_k^{n+1/2} - \mathbf{I}_{k-1}^{n+1/2}}{\Delta z} + \mathbf{g}\frac{\mathbf{V}_k^{n+1} + \mathbf{V}_k^n}{2} + \mathbf{c}\frac{\mathbf{V}_k^{n+1} - \mathbf{V}_k^n}{\Delta t} = 0.$$

The recursive relation of current at discrete points inside the transmission line is

$$\mathbf{I}_k^{n+3/2} = \mathbf{F}^{-1}\left(\mathbf{l}\frac{\Delta z}{\Delta t} - A\frac{\Delta z}{2} + B\frac{1}{\sqrt{\pi}}\frac{\Delta z}{\sqrt{\Delta t}}Z_0(0)\right)\mathbf{I}_k^{n+1/2}$$

$$- \mathbf{F}^{-1}B\frac{1}{\sqrt{\pi}}\frac{\Delta z}{\sqrt{\Delta t}}\sum_{m=1}^n\left[\mathbf{I}_k^{n+3/2-m} - \mathbf{I}_k^{n+1/2-m}\right],$$

$$Z_0(m) - \mathbf{F}^{-1}\left(\mathbf{V}_{k+1}^{n+1} - \mathbf{V}_k^{n+1}\right), \tag{9}$$

$$\mathbf{F} = \mathbf{l}\frac{\Delta z}{\Delta t} + A\frac{\Delta z}{2} + B\frac{1}{\sqrt{\pi}}\frac{\Delta z}{\sqrt{\Delta t}}Z_0(0).$$

3. Tuning Region Transient Modeling

In the ZPW-2000A jointless track circuit, the electrical insulation section realizes the electrical isolation of adjacent track and the stable output of local signal by forming series and parallel resonance for different carrier frequency signals. In the matching part, the rail impedance and cable impedance are matched to realize the output of high power signal to the rail [14]. The structure of electrical insulation section in jointless track circuit is shown in Figure 2.

Firstly, the transient model of tuning matching unit is established, and the drive point admittance of the tuning unit port is obtained by the short-circuit test method. The frequency domain admittance is fitted to a rational function expression by the vector matching method, as shown in (10). Secondly, the frequency domain rational function is transformed into time-domain expression by inverse Fourier transform. Finally, based on the piecewise linear recursive convolution method, the recursive iterative relation of admittance current is derived in (14). The admittance can be fitted to a rational function in the complex frequency domain by the vector matching method and the objective function $Y(s)$ expresses its s-domain admittance in pole and residue form [13]:

$$Y(s) = \sum_{i=1}^n \frac{a_i}{s - c_i} + sh + g = \sum_{i=1}^n Y_i(s) + Y_0(s), \tag{10}$$

where n is the order, i is an integer ($i = 1,2, \ldots, n$); a_i is the residue, and c_i is the pole, both are real numbers or conjugate complex number pairs, sh is the coefficient of the first term, and g is the constant term.

The fitting order of the poles in the tuning area is 12 to achieve appropriate fitting effect. The amplitude characteristic and phase angle characteristic function are fitted according to the pole and residue values. Compared with the admittance model of the tuning unit, the results are shown in Figures 3 and 4.

The results of admittance fitting of the tuning element are consistent with those of the exact value and meet the requirements of calculation. According to the admittance rational function, the current equation of the connection node is derived. The voltage current relationship of the tuning unit in time domain is expressed as $I_z(t) = Y(t) * V_z(t)$. Defining two parameter variables [5],

$$\chi_m = \int_{m\Delta t}^{(m+1)\Delta t} Y(\tau)d\tau,$$

$$\xi_m = \frac{1}{\Delta t}\int_{m\Delta t}^{(m+1)\Delta t} (\tau - m\Delta t)Y(\tau)d\tau. \tag{11}$$

Using piecewise recursive convolution integral, we know that if the two variables are satisfied,

$$\rho = \frac{\xi_m}{\xi_{m-1}} = \frac{\chi_m}{\chi_{m-1}}. \tag{12}$$

Then, the time-domain current I_z^n can be written in the recursive iterative form:

$$I_z^{n+1} = (\chi_0 - \xi_0)V_z^{n+1} + \xi_0 V_z^n + \rho I_z^n. \tag{13}$$

There are number of real numbers N_r and conjugate pairs N_g in the fitting residues of loads in residue regions and the poles, then the total current of the connected nodes is
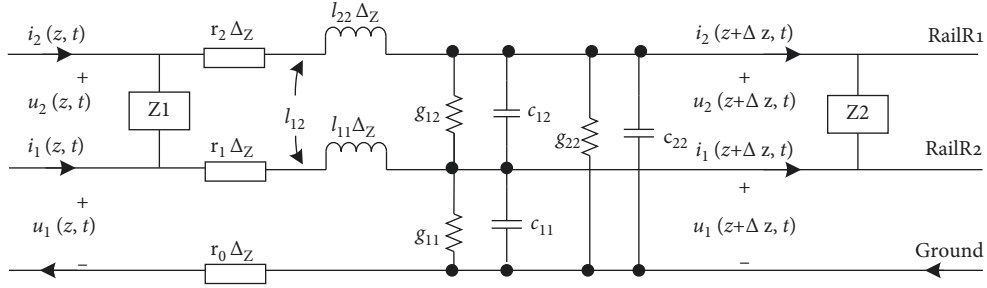
Figure 1: Equivalent circuit diagram of track circuit transmission line.
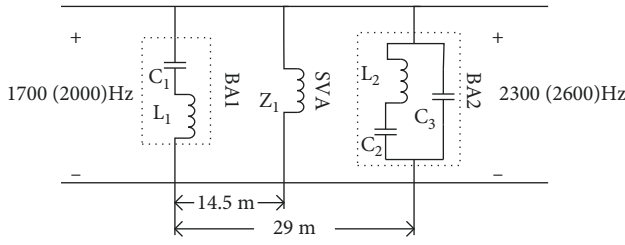
Figure 2: Structural schematic diagram of tuning unit.
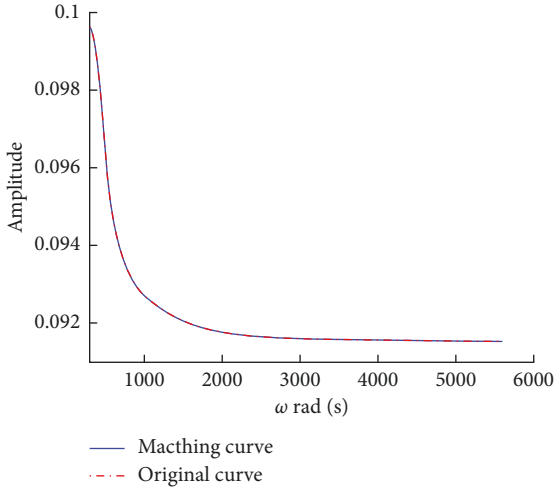
Figure 3: Vector fitting matches amplitude and model amplitude.

Figure 4: Vector fitting matches phase angle with model phase angle.

4. Transmission Line Voltage Equation of Track Circuit

When the transmission line load is pure resistance load, the current is $I_0 = (V_0 - V_1)/R$. The central difference method is used to discretize it.

$$\mathbf{I}_0^{n+1/2} = \frac{\left(\mathbf{V}_0^{n+1/2} - \mathbf{V}_1^{n+1/2}\right)}{R} = \frac{1}{2R}\left[\left(\mathbf{V}_0^{n+1} + \mathbf{V}_0^n\right) - \left(\mathbf{V}_1^{n+1} + \mathbf{V}_1^n\right)\right]. \tag{16}$$

According to the average value of power supply I_S current, (3) and (4) can be discretized:

$$\frac{1}{\Delta z/2}\left[\mathbf{I}_1^{n+1/2} - \frac{\mathbf{I}_0^{n+1} + \mathbf{I}_0^n}{2}\right] + \frac{1}{2}\mathbf{g}\left[\mathbf{V}_k^{n+1} + \mathbf{V}_k^n\right] + \frac{\mathbf{c}}{\Delta t}\left[\mathbf{V}_k^{n+1} - \mathbf{V}_k^n\right] = 0. \tag{17}$$

The initial voltage expression of the transmission line equation of the track circuit is

$$\mathbf{V}_1^{n+1} = \left(1 + \frac{\Delta z}{\Delta t}\mathbf{c}R_s + \frac{\Delta z}{2}\mathbf{g}R_s\right)^{-1}\left[\left(\frac{\Delta z}{\Delta t}\mathbf{Rc} - \frac{\Delta z}{2}R_s\mathbf{g} - 1\right)\mathbf{V}_1^n\right.$$
$$\left. - 2R_s\mathbf{I}_1^{n+1/2} + 2\mathbf{V}_0^{n+1/2}\right]. \tag{18}$$

$$I_z^{n+1/2} = PV_z^{n+1} + QV_z^n + I_t^{n+1}, \tag{14}$$

where $P = \chi_{0,t} - \xi_{0,t} + g/2 + h/\Delta t$, $Q = \chi_{0,t} + g/2 - h/\Delta t$;

$$\xi_{0,t} = \frac{1}{2}\sum_{i=1}^{Nr}\xi_{0,i} + \sum_{i=Nr+1}^{Nr+Ng}\mathrm{Re}\left(\xi_{0,i}\right)\chi_{0,t}$$

$$= \frac{1}{2}\sum_{i=1}^{Nr}\chi_{0,i} + \sum_{i=Nr+1}^{Nr+Ng}\mathrm{Re}\left(\chi_{0,i}\right), \tag{15}$$

$$I_t^n = \frac{1}{2}\sum_{i=1}^{N_r}\left(\rho_i + 1\right)I_{z,i}^n + \sum_{i=N_r+1}^{N_r+N_g}\mathrm{Re}\left[\left(\rho_i + 1\right)I_{z,i}^n\right].$$
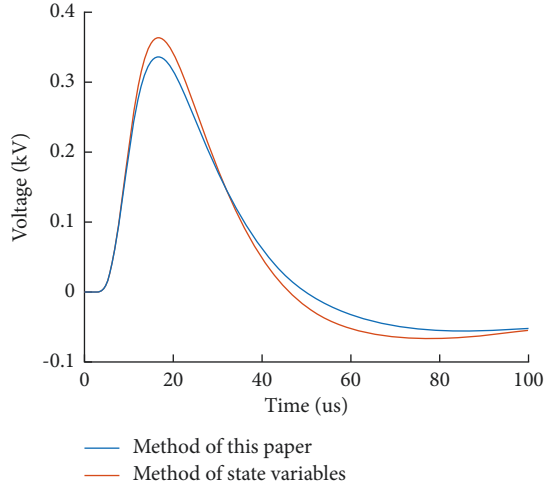
Figure 5: Comparison of calculation methods of overvoltage at receiving end of track circuit.

Figure 6: Error diagram of calculation results.

The internal point voltage iteration formula of the equation is

$$\mathbf{V}_k^{n+1} = \left(\frac{\Delta z}{\Delta t}\mathbf{c} + \frac{\Delta z}{2}\mathbf{g}\right)^{-1}\left[\left(\frac{\Delta z}{\Delta t}\mathbf{c} - \frac{\Delta z}{2}\mathbf{g}\right)\mathbf{V}_k^n - \left(\mathbf{I}_k^{n+1/2} - \mathbf{I}_{k-1}^{n+1/2}\right)\right]. \tag{19}$$

According to the average value of load current I_L at the load at the end of the transmission line, the transmission line equation can be discretized as follows:

$$\frac{1}{\Delta z/2}\left[\frac{\mathbf{I}_L^{n+1} + \mathbf{I}_L^n}{2} - \mathbf{I}_{\text{NDZ}}^{n+1/2}\right] + \frac{1}{2}\mathbf{g}\left[\mathbf{V}_{\text{NDZ}+1}^{n+1} + \mathbf{V}_{\text{NDZ}+1}^n\right]$$
$$+ \frac{\mathbf{c}}{\Delta t}\left[\mathbf{V}_{\text{NDZ}+1}^{n+1} - \mathbf{V}_{\text{NDZ}+1}^n\right] = 0. \tag{20}$$

When the nonlinear lumped element of a track circuit is terminated with a tuning unit as the terminal condition, the terminal condition gives the relation IL between voltage and current at the same time and position. According to (14), the current and voltage equation I_L at its endpoints is

$$\mathbf{I}_L^{n+1/2} = P\left(\mathbf{V}_{k+1}^{n+1} - \mathbf{V}_L^{n+1}\right) + Q\left(\mathbf{V}_{k+1}^n - \mathbf{V}_L^n\right) + \mathbf{I}_t^{n+1}. \tag{21}$$

The terminal voltage equation of the transmission line equation of the track circuit is

$$\mathbf{V}_{\text{NDZ}+1}^{n+1} = \left(P + \frac{\mathbf{c}\Delta z}{2\Delta t} + \frac{\mathbf{g}\Delta z}{4}\right)^{-1}\left[\left(\frac{\mathbf{c}\Delta z}{2\Delta t} - \frac{\mathbf{g}\Delta z}{4} - Q\right)\mathbf{V}_{\text{NDZ}+1}^n\right.$$
$$\left. + P\mathbf{V}_L^{n+1} + Q\mathbf{V}_L^n - \mathbf{I}_t^n + \mathbf{I}_{\text{NDZ}}^{n+1/2}\right]. \tag{22}$$

5. Method Validation

To verify the validity of the constructed track circuit model and the transient response formula, taking P60 rail carrier frequency signal 2300 Hz and 1.4 km track section as an example, the lightning wave adopted the double exponential lightning electromagnetic signal with wave head of $T_1 = 1.2\,\mu$s and wavelength of $T_2 = 50\,\mu$s, recorded as $1.2/50\,\mu$s standard lightning wave [15], and the amplitude was 30 kA for simulation. According to the transmission line model of track circuit, the overvoltage of track surface at the receiving end of track circuit is solved. The state variable method is used to compare the response results with the proposed method.

It can be seen from Figures 5 and 6 that the numerical algorithm for transient response of track circuit proposed in this paper is consistent with the calculation results of state variable method. The calculation error is less than 6%.

5.1. Impact Tolerance Level of Signal Equipment. When the electromagnetic field induced by lightning reaches a certain level, the signal equipment will work improperly or be damaged. The lightning tolerance level of signal equipment terminals is obtained through the destructive lightning shock tolerance experiment, which is the key factor to determine the lightning resistance of signal system equipment [10], as shown in Table 1.

6. Analysis of Influencing Factors

6.1. Influence of Lightning Transmission Distance on Rail Surface Voltage. When lightning strikes the rail, the change of track surface overvoltage with distance between the lightning point and the tuning area of the track circuit is shown in Figure 7.

It can be seen from Figure 7 that with the increase of the distance between the lightning point and the receiving end of the track circuit, the rail surface overvoltage decreases rapidly with the increase of the distance. Especially when the transmission distance is less than 700 m, the overvoltage generated by lightning will exceed the withstand voltage range of the tuning unit end, and there is a risk of breakdown of trackside electronic equipment.

6.2. Considering the Influence of Different Frequencies on Rail Surface Voltage. In ZPW-2000A jointless track circuit, the rail is used as the transmission channel of frequency shift

TABLE 1: Lightning resistance of signal system.

Device	Port	Shock withstands voltage/kV
Power box	Power terminal	$5 \sim 8$
Discrete component	(Resistance, capacitance) circuit	$3 \sim 5$
Tuning matching unit	Rail side to cable side	15
Signal cable	Core pair shielding layer	10
	Core pair	15
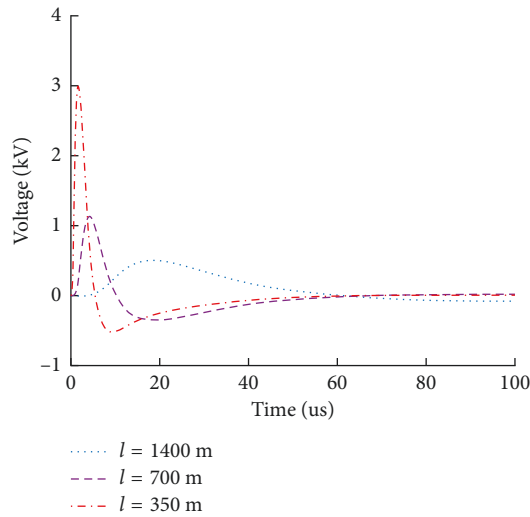
FIGURE 7: Influence of distance between lightning strike point and receiving end of track circuit on rail surface voltage.
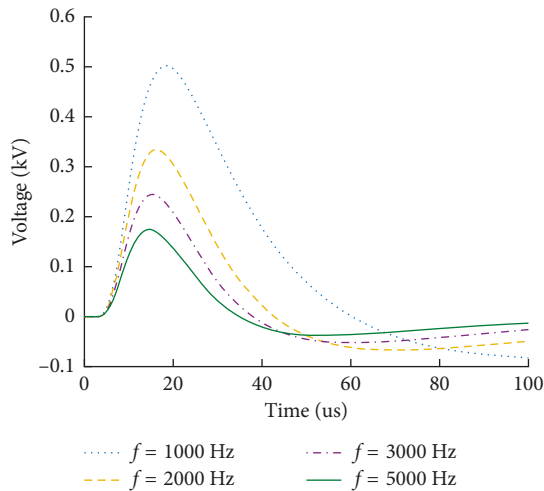
FIGURE 8: Rail surface voltage at receiving end of track circuit with different frequencies.

signal, and the rail parameters have the characteristics of frequency change. In the high-frequency electromagnetic environment, the load at the end of the transmission line usually shows the frequency change effect. In order to analyze the variation rules of signal overvoltage at the receiving end of track circuit when interference signals of different frequencies act on track circuit, the calculation results are shown in Figure 8.
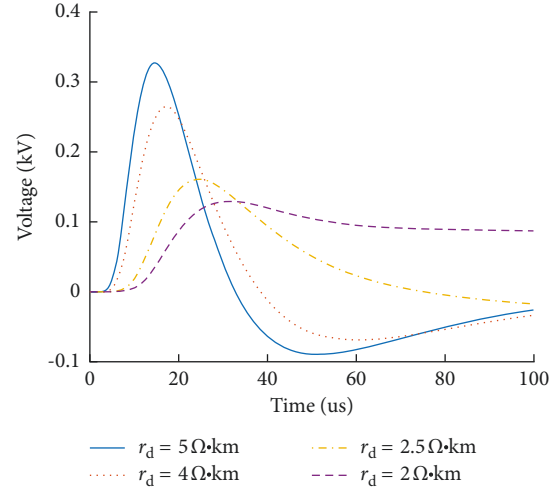
FIGURE 9: Influence of ballast resistance on rail surface overvoltage.

In Figure 8, the simulation results show that the frequency of electromagnetic interference signal has a great influence on the voltage amplitude at the receiving end of the rail surface. At the same time, the higher the frequency of the interference signal is, the smaller the amplitude of the rail surface voltage is at the receiving end. With the increase of signal frequency, the rail impedance increases, the loss of interference signal on the track circuit increases, and the rail voltage amplitude decreases at the receiving end. The internal frequency loss of the transmission line is very little affected by the change of frequency and can be ignored in the future research.

6.3. Influence of Track Bed Resistance on Rail Surface Voltage. The primary side parameters of the jointless track circuit will affect the transmission of interference signals on the rail. The P60 rail is selected, its impedance value is a certain value, while the resistance of the track bed will change with the difference of ambient temperature and humidity [16]. In order to study the influence rule of track bed resistance on rail surface voltage at the receiving end of track circuit, when the resistance value of track bed is $2\,\Omega\cdot$km, $2.5\,\Omega\cdot$km, $4\,\Omega\cdot$km, and $5\,\Omega\cdot$km, the influence rule of different track bed resistance on rail surface overvoltage is analyzed, as shown in Figure 9.

As shown in Figure 8, the greater the ballast resistance is, the greater the overvoltage is. Meanwhile, the faster the rate of rise and attenuation of overvoltage are. With the decrease of track ballast resistance, the amplitude of rail surface voltage decreases at the receiving end.

7. Conclusion

(1) The transient response model of track circuit is established. A numerical calculation method of transient electromagnetic response of track circuit transmission line system considering terminated frequency-varying load and frequency-varying loss is proposed, which is suitable for the analysis of transmission line model with terminated frequency-varying load. It provides theoretical reference for the transmission performance of jointless track circuits and the anti-interference design of track circuits.

(2) The frequency of electromagnetic interference signal has great influence on the amplitude of rail voltage at the receiving end. However, the frequency has little effect on internal loss of rail. The overvoltage and the time of signal attenuation to stability increase with increasing of the ballast resistance.

(3) According to withstand voltage level of the signal equipment, when the distance between the lightning strike point and the receiving end of the track circuit is small, there is a risk of insulation breakdown on the rail side of the tuning unit, so measures need to be taken to strengthen the protection of the signal equipment.

Data Availability

The data used to support the findings of this study are included within the article.

Conflicts of Interest

The authors declare that they have no conflicts of interest.

Acknowledgments

References

[1] H. Zhang, J. Zou, Z. Wang, J. Yang, and Z. Qiao, "Impedance decomposition method and its application in calculating the impedance of ballastless track," *Transactions of China Electrotechnical Society*, vol. 32, no. 12, pp. 164–170, 2017.

[2] N. Xiang, W. Chen, and C. Li, "Lightning transient model of isolation transformer for high-speed railway track circuit system," *High Voltage Engineering*, vol. 42, no. 05, pp. 1594–1599, 2016.

[3] K. S. Kunz and R. J. Luebbers, *The Finite Difference Time Domain Method for Electromagnetics*, CRC Press, New York, NY, USA, 1993.

[4] Z. Wang, G. Jin, Y. Zhang, S. Ning-xian, and M. Chen, "Transient analysis of ZPW-2000 track circuit based on FDTD interface method," *Journal of Southwest Jiaotong University*, vol. 54, no. 1, pp. 196–201+218, 2019.

[5] Z. Chen and C. Qing-xin, "Novel FDTD method for modeling arbitrary linear lumped networks," *Journal of XiDian University*, no. 2, pp. 262–266, 2008.

[6] C. Wang, R. Jia, Y. Zeng, and L. Wang, "A numerical algorithm for the transient response of a frequency-dependent transmission line system excited by EMP," *Journal of Beijing University of Posts and Telecommunications*, vol. 43, no. 2, pp. 52–58, 2020.

[7] Z. Mazloom, N. Theethayi, and R. Thottappillil, "Indirect lightning-induced voltages along a railway catenary-track multi-conductor transmission-line system with lumped components," *IEEE Transactions on Electromagnetic Compatibility*, vol. 54, no. 2, pp. 537–539, 2011.

[8] B. Zhao, Y. Zhang, and W. Lei, "Analysis on the time responses of track circuits," *Journal of the China Railway Society*, vol. 36, no. 9, pp. 68–72, 2014.

[9] Z. Yong-jian, *Some Theoretical Studies on Pantograph-Catenary Arc Electromagnetic Interference Propagation*, Zhejiang University, Hangzhou, China, 2013.

[10] Q. Zhi-chao, N. Xiang, Y. Jin, and L. Zhang, "Research of lightning transient model for high-speed railway signal system," *Journal of the China Railway Society*, vol. 4009, pp. 90–96, 2018.

[11] Z. Xu, *Study on at Network Model*, Southwest Jiaotong University, Chengdu, China, 2015.

[12] L. U. Xiao-qin and W. Xiao-ru, "State-space model of high-speed railway traction power-supply system," *Proceedings of the CSEE*, vol. 37, no. 3, pp. 857–869, 2017.

[13] B. Ngustavsen and A. Semlyen, "Rational approximation of frequency domain responses by vector fitting," *IEEE Transactions on Power Delivery*, vol. 14, no. 3, 1999.

[14] Z. Gao, S. Zhang, and L. Hao, "Modeling and analysis the effects of EMP on the balise system," *Computers, Materials & Continua*, vol. 58, no. 3, pp. 859–878, 2019.

[15] B. Zhao and Y. Zhang, "Transient analysis of track circuits based on FFT & Q-D algorithm," *Journal of the China Railway Society*, vol. 38, no. 3, pp. 78–83, 2016.

[16] Y. Zhang, W. Dong, B. Zhao, and Z. Jia, "Research on calculation of rail self-impedance of track circuit considering the influence of earth," *Journal of Railway Science and Engineering*, vol. 17, no. 11, pp. 2929–2937, 2020.

Research Article

Deep Neural Networks for Automatic Flower Species Localization and Recognition

Touqeer Abbas [ID],[1] **Abdul Razzaq** [ID],[1] **Muhammad Azam Zia,**[2] **Imran Mumtaz,**[2] **Muhammad Asim Saleem** [ID],[3] **Wasif Akbar,**[4] **Muhammad Ahmad Khan,**[2] **Gulzar Akhtar,**[5] **and Casper Shikali Shivachi** [ID][6]

[1]*Department of Computer Science, MNS University of Agriculture, Multan, Pakistan*
[2]*Department of Computer Science, University of Agriculture, Faisalabad, Pakistan*
[3]*School of Information and Software Engineering, University of Electronic Science and Technology of China, China*
[4]*Department of Computer Science, Numl, Multan, Pakistan*
[5]*Department of Horticulture, MNS University of Agriculture, Multan, Pakistan*
[6]*South Eastern Kenya University, Kitui, Kenya*

Correspondence should be addressed to Casper Shikali Shivachi; cshikali@seku.ac.ke

Deep neural networks are efficient methods of recognizing image patterns and have been largely implemented in computer vision applications. Object detection has many applications in computer vision, including face and vehicle detection, video surveillance, and plant leaf detection. An automatic flower identification system over categories is still challenging due to similarities among classes and intraclass variation, so the deep learning model requires more precisely labeled and high-quality data. In this proposed work, an optimized and generalized deep convolutional neural network using Faster-Recurrent Convolutional Neural Network (Faster-RCNN) and Single Short Detector (SSD) is used for detecting, localizing, and classifying flower objects. We prepared 2000 images for various pretrained models, including ResNet 50, ResNet 101, and Inception V2, as well as Mobile Net V2. In this study, 70% of the images were used for training, 25% for validation, and 5% for testing. The experiment demonstrates that the proposed Faster-RCNN model using the transfer learning approach gives an optimum mAP score of 83.3% with 300 and 91.3% with 100 proposals on ten flower classes. In addition, the proposed model could identify, locate, and classify flowers and provide essential details that include flower name, class classification, and multilabeling techniques.

1. Introduction

Flower identification is extremely important in agricultural production, forest management, and other allied sectors. Because of their enormous presence, complex structure, and unpredictable diversity of classes in nature, automated species identification was initially presented 17 years ago [1]. In recent years, the rapid development of technology, flower segmentation, and identification has been an interesting area of research in the image processing and computer vision community. Previous research mostly focused on flower recognition using a conventional detector and technique. Gaston and O'Neill [1] argued that advances in artificial intelligence and digital image processing might generate automated species identification a reality. The rapid development and growing prevalence of key information technologies, along with the widespread availability of compact devices such as digital cameras and smartphones, have resulted in a huge quantity of digital pictures that have been gathered in online databases. As a result, their vision is now almost tangible: mobile devices are utilized to photograph specimens in the field and then identify their species.

With the debut of smartphones and mobile applications, millions of plant pictures have been acquired [2]. Real-world social-based ecological surveillance [3], invasive exotic plant monitoring [4], environmental science popularization, and

other applications rely on mobile-based automated plant identification. Scholars and engineers are paying more attention to improving the effectiveness of mobile-based plant identification models [5]. On an extensive dataset, the researchers used a combination of characteristics to enhance flower classification efficiency. The local form/texture, the shape of the border, the overall geographical distribution of petals, and the color are all defined by distinct characteristics. A multiple support vector machine (SVM) classifier was utilized for classification. Fernando [6] developed an image classification-based approach for differentiating feature fusion, in which the color and shape characteristics are merged by the logistic regression strategy for flower picture classification. However, developing an automated flower category classification system remains a difficult challenge due to certain similarities within classes. The textural characteristics from the Gabor replies and the intensity co-occurrence matrix were utilized to automatically classify flowers using the K-nearest neighbor (KNN) classifier [7]. Color texture moments, gray-level co-occurrence matrix, and Gabor responses were used to classify flower pictures [8]. A classifier was built using a probabilistic neural network. The author [9] used a neural network for logistic regression on flower picture characteristics to solve the problem of flower classification. An aspect-based method for flower identification has been proposed in [10]. Visual characteristics were retrieved and generalized to fresh photographs of unidentified flowers to characterize flower pictures. A sparse representation classifier forecasted the characteristics of a particular flower picture. Several techniques depend on human participation [11]. Following years of research and development, smartphone applications like LeafSnap [12], Pl@ntNet [2], and Microsoft Garage's Flower Recognition app [13] are used to identify flowers rapidly.

The technique of flower identification is an essential component of conventional plant ecology research processes. In this research work, photos of various flowers using mobile devices or digital cameras subsequently have been acquired. The name and other information about the blooms from the horticultural expert of MNS-UAM were found uot. It would be really useful to accelerate this work and make it more accessible to nonexperts. Manual flower species identification may be difficult to scale to high-throughput needs even for specialists although it may be prohibitively time-consuming and erroneous for nonexperts. Furthermore, existing models only classify images, limiting the model's ability to recognize numerous flowers in a single image. In contrast, our proposed framework classifies with localization, allowing it to recognize countless flowers in a digital image by placing a boundary box around the identified flower with the label.

2. Proposed Methods

We used an eighth Generation Core i7 Quad-Core Processor with 8 GB RAM, 8 GB NVIDIA, and a 520 GB SSD hard drive for our research. This research is divided into four different sections. The first section discusses dataset collection. Image labeling is described in the second section. The third section contains the training of the model on different hyperparameters. The fourth and final section illustrates the model's testing and evaluation with varying inputs from different angles.

2.1. Implementation Detail. Some key hyperparameters are introduced to the proposed network, such as the anchor initialization, the maximum number of bounding boxes retained, and the learning rate decay. We initialize our anchors on each pixel of the feature map obtained from the base net. This equates to placing anchors every 16 pixels on each screen dimension. An initialized total of nine anchors will be created for each pixel of the feature map. Three different scales and three different height-width ratios are used to create the nine anchors in the image. 0.5, 1.0, and 2.0 are the scales we use. It has 0.5, 1.0, and 2.0 dimensions. We also need to use the target bounding boxes as labels to train our RPN. Anchors that overlap with the ground-truth box more than RPN POSITIVE OVERLAP = 0.60 are chosen as foreground labels. Anchors that overlap with any ground-truth box less than RPN NEGATIVE OVERLAP = 0.40 are chosen as negative or background labels. Table 1 shows the training hyperparameters for four nets we trained, inception V2, ResNet50, ResNet101, and MobileNet V2 SSD.

2.2. Image Acquisition. This research adopted specific techniques to collect datasets inspired by Michael Rzane and Zhenzhen Song's papers [1, 2]. An image-capturing scheme was developed to collect data on different classes of flowers. The dataset was collected by ourselves, and therefore no web scraping tool was used. A Canon EOS 2000D DSLR was employed to collect data and yield high-resolution images with 2976 × 1984 dimensions with a bit depth of 24. The ordinary lens of the Canon EOS 2000D DSLR with "IntelliAuto mode" was used to capture images. The color representation of each image is sRGB with 72dpi horizontal and vertical resolution. Out of 10 classes, seven classes were obtained from the university garden and 3 classes from the local park. The images were captured from different angles and lens focus (Zoom In, Out).

For an entirely distinct dataset, images of each class were taken at different periods (morning, afternoon, and evening) with different lighting conditions, direct sunlight, shadows, and flashlight in the evening. The images were saved in JPEG format. Each class comprises three images of the same flower from predefined perspectives (entire flower, frontal, and lateral view); (1) the whole flower: it is an image of the whole flower from its natural position on the plant; (2) although the side view of the flower in this group will be comparable to the entire flower image, this study primarily focused on the side view of the flower in this group; (3) flower top view: for this view, we used focus mode instead of "IntelliAuto mode" to focus on all the flower's leaves. Most of the images are of this type in the dataset.

The ten summer season classes are selected for the dataset category containing ten species of flowers as shown in Figure 1 such as Petunia, Dianthus, Jatropha, Periwinkle, Europhobia Milli Phlox, Ixora, Tacoma, Anthurium, Bounganwellia.

TABLE 1: Selected hyperparameters.

Net	Optimizer	Decay epoch	Total epoch	Bach size	GPU
Inception V2	Momentum	8	30k	4	2
ResNet50	SGD	8	50k	4	2
ResNet101	SGD	8	55k	4	2
MobileNet V2 SSD	Momentum	8	200k	4	2

FIGURE 1: Categories of flowers.

FIGURE 2: Dataset splitting ratio.

2.3. Data Labeling. In this study, 2000 pictures are captured. There are up to 15 target flowers objects in each picture, with a resolution of 2976×1984 pixels (ROI). To identify pictures with localization, we categorized the flower dataset with annotation comprising ten types of flowers, each with roughly 200 images. When we label the 2000 images, we get 3500 total objects. To acquire the ROI (Region of Interest), we used the GitHub application tools named tagging and marked the area to be selected and then identified photos one by one to offer information about the images. The data labeling is saved in an XML file once the image has been tagged. The XML file includes variables (w = width; h = height) that form a rectangle in the picture. Since these flowers are usually in the shape of a group, we labeled this composite flower a single flower head (i.e., Ixora). Each class's dataset is split into three folders at random: training, validation, and testing, as shown in Figure 2.

2.4. Data Augmentation. Data augmentation is a technique used to increase data size by adding slightly modified copies of existing data or creating new synthetic data from existing data. This technique is used to reduce overfitting when training machine learning models.

We have used adding noise, cropping, flipping, scaling, brightness, and rotation for data augmentation. In adding noise, we added some noise like a blur for viewing the data more accurately. In cropping, we select some parts, crop the image, and resize the original image size. While flipping, the images are flipped horizontally and vertically. While scaling, we scaled the images outward and inward; this way, an image can be more minor and more significant by its original size.

Brightness is a process in which we can change an image into brightness and darkness. This technique allows the model to view an image as brightness and lighter. In rotation, the idea is to rotate by a degree ranging from 0 to 360 degrees from its original position. Every rotated image will have a unique representation in the model. When we complete the data augmentation, we have 6540 whole ideas and obtain 10080 natural objects.

2.5. Construction of SSD MobileNetV2. The SSD (Single Shot MultiBox Detector) is a fast flower identification detection model based on a single deep neural network [14]. An SSD could simultaneously eradicate multiple target detection and forecast targeted segments and binding boxes.

The feedforward convolutional network is being used in the SSD model. Its backbone is VGG16, and it follows the primary network with six layers of different characteristics. The size of the inserted map is decreased layer by layer, employing six distinct feature layers to achieve a target of varied scales: low predictive levels and high predictive levels. To forecast the bounding box set of various sizes, the range of objects, and associated confidence, a substantial majority of multiple-choice selections are performed on distinct levels of information. To address the issue of excessive parameter size and training model efficiency, the convolution layer on the actual SSD is substituted by a mobile net splitting layer, which enhances the efficiency and performance of real-time flower recognition as shown in Figure 3.

Real-time object accessibility is also available in the app store, thanks to the MobileNetV2 developers. SSDLite, a hybrid of SSD Object Detector and MobileNetV2, was introduced. Remember how, in the CNN Model, we employed ssd_mobilenetv2 to identify a flower object in images? SSDLite is just the same way. The purpose of using an SSD is straightforward. Since the SSD lacks a whole network, conferences are substituted by a highly fragmented convolution. For MobileNetV2, the very first layer of SSDLite is attached to the extension of layer 15. The set of parameters required by the network to detect an item is substantially reduced when the usual combination is supplanted by intensely split convolution.

When we apply the construction of SSD MobileNetV2, first we apply Data Augmentation, which means the images will be trained in a different dimension; after that convolution filter will be used and the output image is obtained.
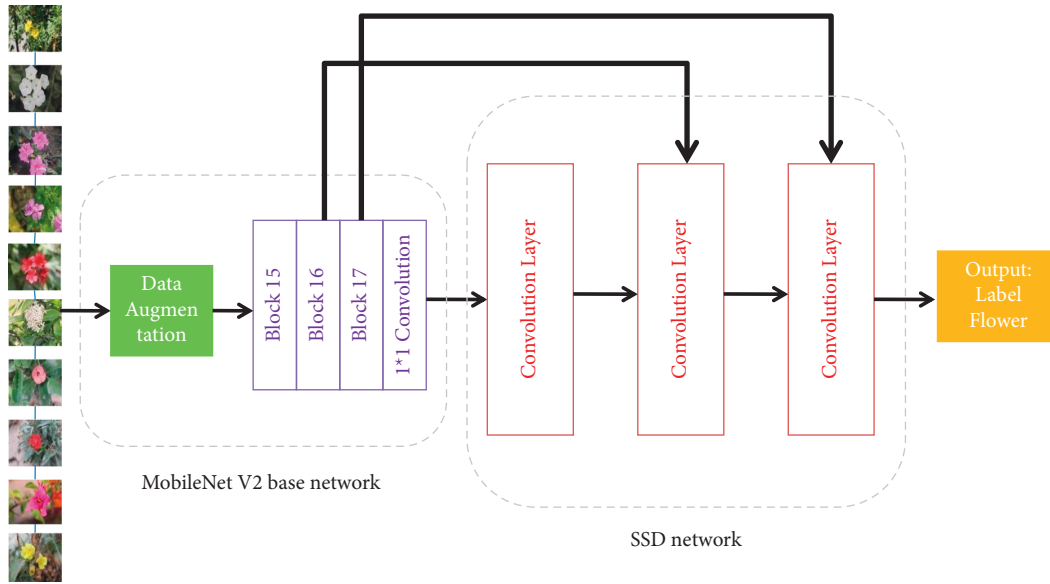
FIGURE 3: SSD mobile net V2 framework.

2.6. Construction of Faster R-CNN Inception V2. Faster region-based convolution neural network architecture is shown in Figure 4. This architecture was proposed by [15], and it uses Inception V2 for feature extraction, as explained in [16]. Each image was parted into subregions during the preprocessing of the model, as shown in Figure 4, "image division with overlay."

After that, inception V2 [15] generates the convolutional map feature that has been used in two stages Inception V2 [15] and Faster-RCNN [16]. In Regional Proposed Network (RPN), a convolutional network is used at the first stage that relays over the feature map, extracted by Inception V2, while anchors are placed on each point. Using two similar fully connected layers, the coordinates of the rectangular box around the flower and its probability of accuracy to matching class are determined. In the next step, the determined regions of the image are used to draw a feature map and classify each and every ROI (Region of Interest) with localization. After that, all extracted ROIs are passed through the pooling layer and fully connected layer to determine their probability of classification and localization [17]. These ROIs define the flower's location with a matching class in the output image, as shown in Figure 4.

At last, all output images are transposed and joined to show the original image as they are "divided with overlay" in Figure 1 and they came from training or testing datasets. The bounding boxes were refined and decreased in number by using the suppression algorithm [18]. All this was done by using Tensor Flow and anaconda prompt. Final selected hyperparameters for the next model Faster-RCNN are shown in Table 1 after refining. We give input image to the model Inception V2 applied on it, and feature extraction has been applied. RPN (Region Proposal Network) has been implemented using fully connected layers, activation

function, regression feature vector, and ROI pooling. After the proposed region is located in the image, it converts into a Box Classifier, in which two functions are performed: (1) Bounding Box Coordinates and (2) Object Probabilities. The output shows the classification of the input image with a boundary box around the flower.

The output shows the classification of an input image with a boundary box around the flower.

2.6.1. Inception V2. The Inception V2 package was created to decrease the intricacy of the convolution network in flower identification. This control system expands the convolution network rather than making it deeper. Functionalities in Inception V2 are classified into three modules: A, B, and C. It substituted a 3×3 convolution for the 5×5 convolution. This adheres to the idea that spatial aggregation may be performed over lower-dimensional embedding with little or no loss of representational capacity. Convolution performance was improved by using the 3×3 convolution. They discovered that dividing convolution filter size $n \times n$ into $1 \times n$ and $n \times 1$ convolutions made their technique 33% cheaper than a single 3×3 convolution. Additionally, the filter was enhanced to adhere to the concept that higher-dimensional depictions are simpler to process natively inside a network as shown in Figure 5.

2.6.2. ResNet 50. There are 48 Convolution layers in ResNet50 [19, 20], 1 MaxPool layer, and an Average Pool layer. The layers fitted a residual mapping and labeled it as $H(x)$, and the nonlinear layers fitted another mapping $F(x) = H(x) - x$, so the original mapping became $F(x) + x$. The total number of floating-point operations is $3.8 \times 10 * 9$.
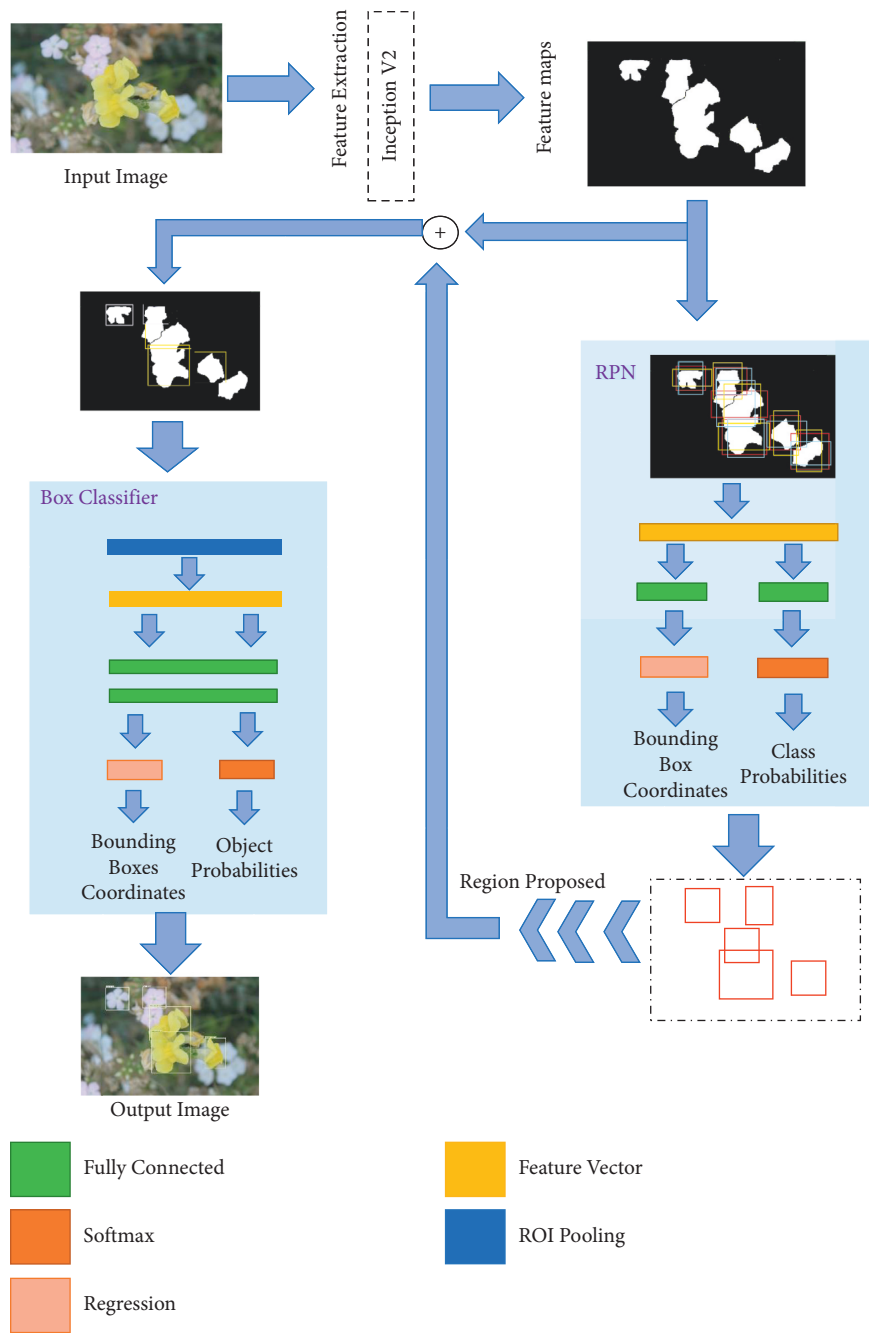
FIGURE 4: Faster R-CNN flower identification using Inception V2 architecture for feature extractor.

2.6.3. ResNet 101.

Residual connections can be divided into two categories:

(1) Identity shortcuts (x) may be directly used for inputs and outputs with the exact dimensions.

$$y = f(x, \{W_i\}) + X. \qquad (1)$$

Residual block function is with the same input and output dimensions as Equation (1).

(2) When the dimensions change, (A) identifiability mapping is still performed, with extra zero entries padded with the increased dimension. (B) Using a projection shortcut, the dimension can be matched (for example, by using $1 * 1$ Conv) using the following formula:

$$y = f(x, \{W_i\}) + W_s X. \qquad (2)$$
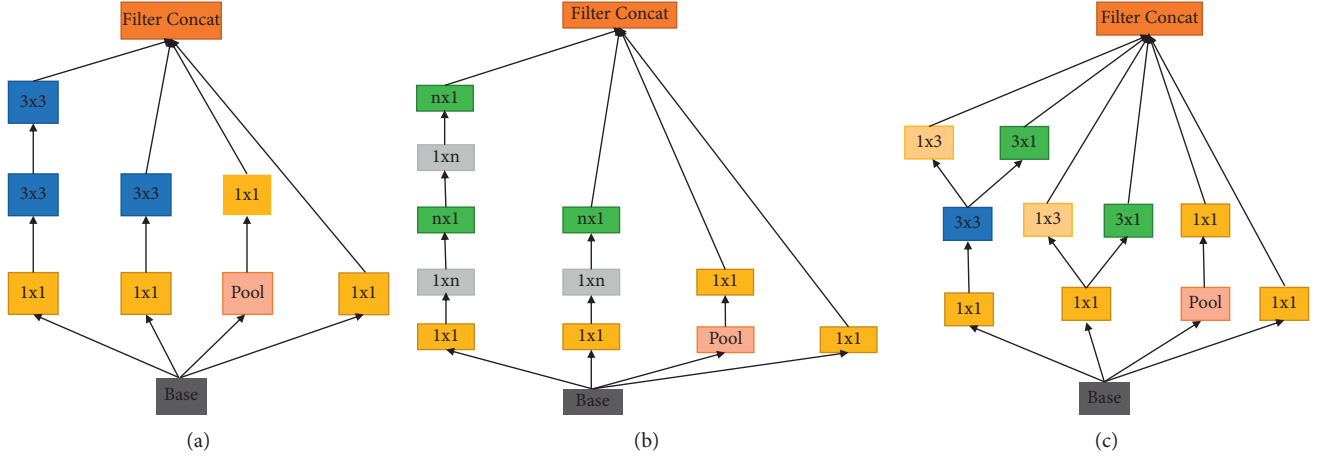
FIGURE 5: Inception V2 modules A, B, and C using 3×3 convolution.

Equation (2) deals with residual block function, which has different input and output dimensions.

3. Experiment Results and Performance Analysis

A series of comparisons of different object detection models have been conducted to evaluate the effectiveness of the proposed integrated approach. In this research, three object detection models are implemented. During the experiment, we have (1) trained the SSD and Faster-RCNN over ten flower clas images and analyzed its performance and (2) trained the object detection models using a transfer learning approach on different backbones that include Inception V2, ResNet 50, ResNet 101, and Mobile Net V2.

3.1. Quantitative Analysis of Flower Detection Performance. Furthermore, the performance of both approaches using qualitative and quantitative measurement methods has been compared. Several evaluation metrics were used to measure the effectiveness of flower detection for quantitative analysis, including the Mean Average Precision (mAP), Average Recall (AR), and average precision (AP). It is most commonly used to calculate the Precision and Recall of measurement systems based on the following equations:

$$Precision = \frac{TP}{TP + FP}, \tag{3}$$

$$Recall = \frac{TP}{TP + FN}, \tag{4}$$

$$F1 = \frac{2 * Precision * Recall}{Precision + Recall}. \tag{5}$$

TP stands for true positives, FP for false positives, and FN for false negatives. Further, the correctness of a positive is assessed through FPs and FNs evaluated by the intersection over union (IoU) overlap with the corresponding ground-truth bounding box [21]. It is calculated according to the following equation:

$$IoU = Area \frac{of \cap}{Area of \cup}. \tag{6}$$

Detected objects that were not matched to the ground-truth bounding box were considered false positives (FP). If the IoU (6) exceeded the threshold, it was considered a true positive (TP). Furthermore, a false negative (FN) is identified in the missed ground-truth bounding box. We have chosen 0.5 and 0.75 as the threshold values for this study. Detection performance has been determined by averaging the mean average precision (mAP) score and AP values from all classes [22]. As mAP increased, the overall performance of the flower dataset improved. Tables 2 and 3 show that these different object detection models have different detection performance results [20].

A summary of the Precision (given equation (3)) and Recall (given equation (4)) of different detection models is presented in Tables 1 and 2. With the different AP IoU (0.5: 0.95, 0.50, and 0.75) 0.81, 0.92, and 0.91, the proposed model Faster R CNN inception V2 with 100 proposals gives the best performances. Moreover, the values of different AR detections (1, 10, and 100) were 0.77, 0.91, and 0.89, respectively. We calculate $F1$-score using mean precision @0.5 IoU and recall @10 concerning 100 and 300 proposals, as shown in Table 4.

3.2. Qualitative Analysis for Different Flower Detection Experiment Results. The intersection qualitatively evaluates the correctness of a detected object over union (IoU) overlap with the corresponding ground-truth bounding box [14]. The ground-truth bounding boxes are those hand-labeled boxes from the training set indicating where the flowers are on the image. An example of the IoU overlap is seen in Figure 6, and this suggests that the prediction bounding box will be evaluated using IoU (i.e., prediction of object detection model).

Across all object detection models, the flower dataset has shown good performance. The red box indicates the ground-truth label, and the boxes of colored lines indicate prediction bounding boxes [23]. We compared the object detection model results to examine the effect of different pretrained CNN

TABLE 2: The performance of Average Precision (AP) for different object detection models.

Object detection model	Backbone pretrained model	AP, IoU					
		@ [IoU = 0.5 : 0.95]		@ [IoU = 0.5]		@ [IoU = 0.75]	
		@ 100 proposals	@ 300 proposals	@ 100 proposals	@ 300 proposals	@ 100 proposals	@ 300 proposals
Faster-RCNN	Inception V2	0.71	0.65	0.91	0.83	0.81	0.74
	ResNet 50	0.69	0.61	0.76	0.79	0.73	0.66
	ResNet 101	0.75	0.68	0.86	0.77	0.79	0.71
SSD	MobileNet V2	0.65		0.76		0.69	

TABLE 3: The performance of Average Recall (AR) for different object detection models.

Object detection model	Backbone pretrained model	AR, detections					
		@1		AR@10		AR@100	
		@ 100 proposals	@ 300 proposals	@ 100 proposals	@ 300 proposals	@ 100 proposals	@ 300 proposals
Faster-RCNN	Inception V2	0.81	0.77	0.83	0.79	0.84	0.80
	ResNet 50	0.8	0.71	0.81	0.76	0.84	0.78
	ResNet 101	0.72	0.58	0.74	0.59	0.76	0.61
SSD	MobileNet V2	0.65		0.66		0.67	

TABLE 4: The performance of F1-score for different object detection models.

Object detection model	Backbone pretrained model	F1-score	
		@ 100 proposals	@ 300 proposals
Faster-RCNN	Inception V2	0.87	0.81
	ResNet 50	0.78	0.77
	ResNet 101	0.79	0.66
SSD	MobileNet V2	0.71	

(a)

(b)

(c)

(d)
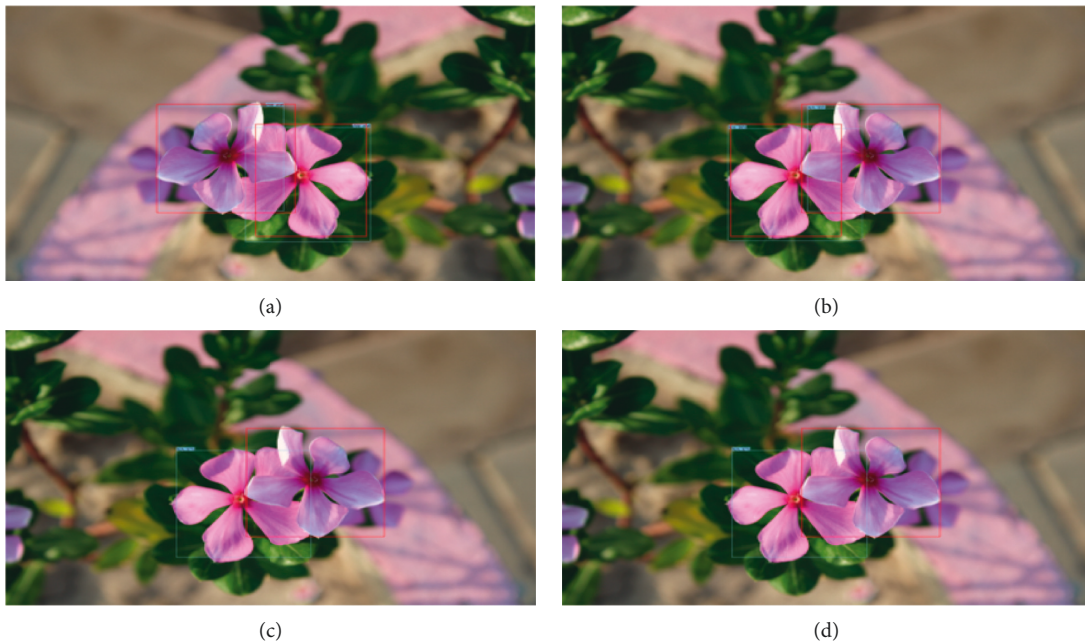
FIGURE 6: Performance of object detection models for Faster-RCNN using (a) Inception, (b) ResNet50, (c) ResNet101, and (d) SSD using MobileNet V2.
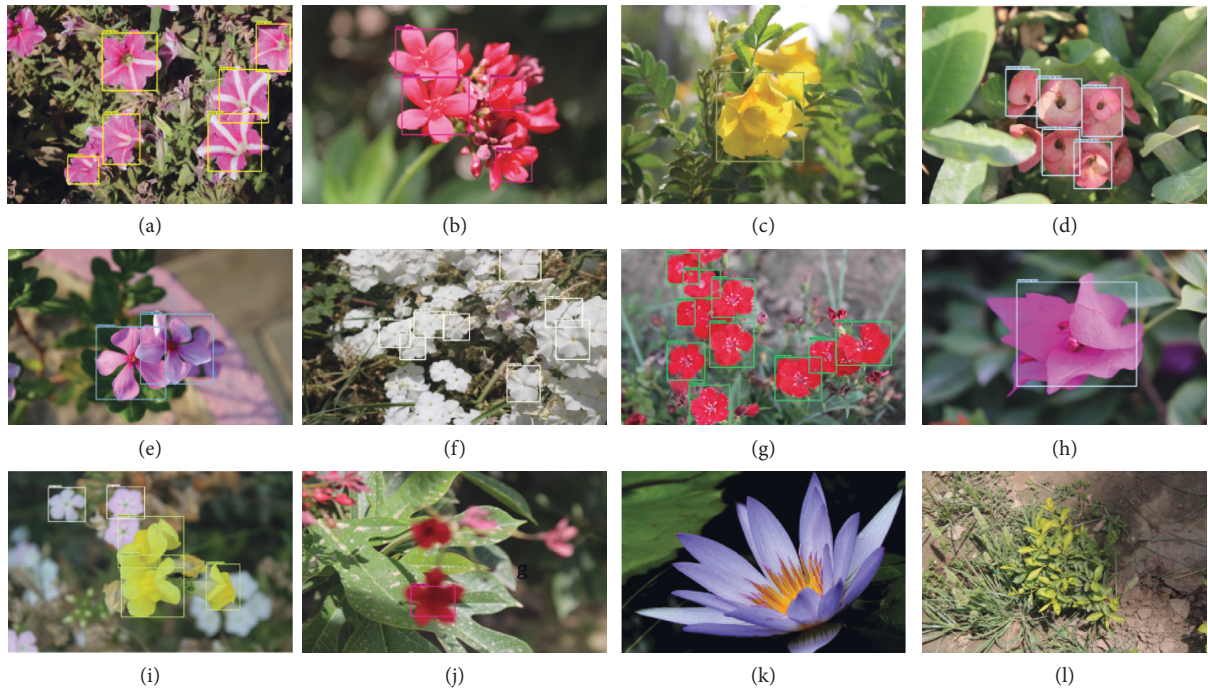
FIGURE 7: Output of testing images of different classes: (a) Petunia; (b) Jatropha; (c) Tacoma; (d) Europhobia milli; (e) Periwinkle; (f) Phlox; (g) Diahtus; (h) Bouganwelia; (i) Anthrium; (j) Jatropha; (k-l) Nulls.

architectures on flower detection performance [24]. Figure 6 shows some quantitative results for flower classes. Figure 7 shows the performance of Faster-RCNN. Figures 7(a) to 7(j) are part of the dataset, and Figures 7(k) and 7(l) are not part of the data used to determine the model generalization.

4. Conclusion

An efficient and generalized deep convolution neural network (DCNN)-based model for flower detection, localization, and classification has been proposed. The proposed model localization and recognition of flower species provide flower names, class classification, and multilabeling techniques. This study demonstrated that some classes are very similar in shape and color. In contrast, others can be distinguished better by their external shapes than their internal shapes and vice versa. Faster-RCNN and other object detection models have been evaluated using pretrained models of the COCO dataset. The proposed model provides an optimum mAP score of 83.3% with 300 and 91.3% with 100 proposals on the flower class dataset up to 100% accuracy confidence. However, it still has some limitations due to color similarity between the two classes of flowers, as shown in Figures 7(c) and 7(i). Furthermore, a multilabel classification model provides botanical information about a flower to help farmers, horticulture, and nonbotanists understand what type of flower it is. We should jointly train the models with visually similar classes as a future step.

Data Availability

The data used to support the findings of this study are available from the corresponding author upon request.

Conflicts of Interest

The authors declare that there are no conflicts of interest regarding the publication of this paper.

References

[1] K. J. Gaston and M. A. O'Neill, "Automated species identification: why not?" *Philosophical Transactions of the Royal Society of London - Series B: Biological Sciences*, vol. 359, no. 1444, pp. 655–667, 2004.

[2] A. Joly, H. Goëau, P. Bonnet et al., "Interactive plant identification based on social image data," *Ecological Informatics*, vol. 23, pp. 22–34, 2014.

[3] A. Joly, "LifeCLEF 2015: multimedia life species identification challenges," in *Proceedings of the International Conference of the Cross-jns of the Evaluation Forum*, 2016.

[4] H. Go¨eau, P. Bonnet, and A. Joly, "Plant identification in an open world (lifecycle 2016)," in *Proceedings of the CLEF: Conference and Labs of the Evaluation Forum*, pp. 428–339, Évora, Portugal, 2016.

[5] M.-E. Nilsback and A. Zisserman, "Automated flower classification over a large number of classes," in *Proceedings of the 2008 Sixth Indian Conference on Computer Vision, Graphics & Image Processing*, IEEE, Bhubaneswar, India, December, 2008.

[6] B. Fernando, "Discriminative feature fusion for image classification," in *Proceedings of the 2012 IEEE Conference on Computer Vision and Pattern Recognition*, IEEE, Providence, RI, USA, June, 2012.

[7] F. Mahmood, K. Abbas, A. Raza, M. A. Khan, and K. Pw, "Three-dimensional agricultural land modeling using unmanned aerial system (UAS)," *International Journal of Advanced Computer Science and Applications*, vol. 10, no. 1, pp. 443–449, 2019.

[8] E. Marchi, F. Vesperini, S. Squartini, and B. Schuller, "Deep recurrent neural network-based autoencoders for acoustic novelty detection," *Computational Intelligence and Neuroscience*, vol. 2017, Article ID 4694860, 14 pages, 2017.

[9] D. Guru, "Textural features in flower classification," vol. 54, no. 3-4, pp. 1030–1036, 2011.

[10] F. Siraj, M. A. Salahuddin, and S. A. M. Yusof, "Digital image classification for Malaysian blooming flowers," in *Proceedings of the 2010 Second International Conference on Computational Intelligence, Modelling and Simulation*, Bali, Indonesia, September, 2010.

[11] K. Cheng and X. Tan, "Sparse representations based attribute learning for flower classification," *Neurocomputing*, vol. 145, pp. 416–426, 2014.

[12] A. B. Mottos and R. S. Feris, "Fusing well-crafted feature descriptors for efficient fine-grained classification," *IEEE*, in *Proceedings of the 2014 IEEE International Conference on Image Processing (ICIP)*, Paris, France, October, 2014.

[13] N. Kumar, "Leafsnap: a computer vision system for automatic plant species identification," in *Proceedings of the European Conference on Computer Vision*, Springer, Berlin, Germany, 2012.

[14] M. He, "Research on face image digital processing and recognition based on data dimensionality reduction algorithm," *Computational Intelligence and Neuroscience*, vol. 2021, Article ID 3348225, 10 pages, 2021.

[15] D. Alamsyah and M. Fachrurrozi, "Faster R-CNN with inception V2 for fingertip detection in homogenous background image," *Journal of Physics Conference Series*, vol. 1196, 2017.

[16] S. Ren, K. He, R. Girshick, and J. Sun, "Faster R-CNN: towards real-time object detection with region proposal networks," *IEEE Transactions on Pattern Analysis and Machine Intelligence*, vol. 39, no. 6, pp. 1137–1149, 2017.

[17] Y. Ren, C. Zhu, and S. Xiao, "Object detection based on fast/faster RCNN employing fully convolutional architectures," *Mathematical Problems in Engineering*, vol. 2018, Article ID 3598316, 7 pages, 2018.

[18] A. Koirala, K. B. Walsh, Z. Wang, and C. McCarthy, "Deep learning - method overview and review of use for fruit detection and yield estimation," *Computers and Electronics in Agriculture*, vol. 162, pp. 219–234, 2019.

[19] N. Yu Peng Che, Y. Li, and G. Wang, "An Enhanced Region Proposal Network for object detection using deep learning method," *PLoS One*, vol. 13, 2018.

[20] K. He, X. Zhang, S. Ren, and J. Sun, "Deep residual learning for image recognition," 2015, https://arxiv.org/abs/1512.03385.

[21] A. Kamilaris and F. X. Prenafeta-Boldú, "Deep learning in agriculture: a survey," *Computers and Electronics in Agriculture*, vol. 147, pp. 70–90, 2018.

[22] K. Duan, B. Song, L. Xie, H. Qi, Q. Huang, and T. Qi, "CenterNet: keypoint triplets for object detection," 2019, https://arxiv.org/abs/1904.08189.

[23] T. Tazin, S. Sarker, P. Gupta et al., "A robust and novel approach for brain tumor classification using convolutional neural network," *Computational Intelligence and Neuroscience*, vol. 2021, Article ID 2392395, 11 pages, 2021.

[24] F. Mehmood, E. Chen, M. A. Akbar, and A. A. Alsanad, "Human action recognition of spatiotemporal parameters for skeleton sequences using MTLN feature learning framework," *Electronics*, vol. 10, no. 21, Article ID 2708, 2021.

Research Article

Collaborative Filtering Algorithm-Based Destination Recommendation and Marketing Model for Tourism Scenic Spots

Kejun Lin, Shixin Yang, and Sang-Gyun Na

College of Business Administration, Wonkwang University, 460 Iksandae-ro, Iksan, Jeonbuk, Republic of Korea

Correspondence should be addressed to Sang-Gyun Na; nsghy@wku.ac.kr

The information age of rapid development of tourism industry provides abundant travel information, but it also comes with the problem of information overload, which makes it difficult to meet the growing personalized needs of people. The traditional collaborative filtering recommendation algorithm (CFA) also suffers from the problem of data sparsity when the user population increases. Therefore, this study optimizes the CFA through the similarity factor and correlation factor and enhances the tourism sense of travel experience through the satisfaction balance strategy. The experimental results show that the improved CFA method has the highest average accuracy on the overall dataset and the best recommendation performance of the satisfaction balance strategy. Overall, the recommendation model in this study is useful for attraction selection of users and marketing optimization of travel companies.

1. Introduction

With the development of information technology and the Internet, network information is becoming an important source of information for the public to plan travel routes, and people are gradually entering the era of big data from the era of lack of information [1]. In the context of massive data, how to quickly find the information of the best value for users is of great significance, and various recommendation systems have emerged with the needs of users. The recommendation systems [2] involved in the existing literature mainly focus on a single user and have achieved good results in TV programs, music, movies, news, and so on. In the tourism industry, the recommendation system is still in the initial stage of development and needs to be continuously improved. Compared with recommendation systems such as movies and music, it is difficult to obtain the ratings of scenic spots in the tourism field, and the user's rating matrix is relatively sparse. In addition, the selection of travel routes usually needs to consider the preferences of multiple users, so a recommendation system that combines all users participating in travel is a research hotspot in the field of travel recommendation [3].

In the recommendation system based on collaborative filtering, the rating of a single user needs to be predicted first. However, when calculating the similarity between users or items, the traditional collaborative filtering algorithm does not consider the impact of the number of items jointly rated by users and the degree of correlation between ratings on the similarity. For example, two tourists with different interests may have fewer attractions at the same time. When the users have fewer common ratings, the traditional collaborative filtering algorithm cannot accurately measure the similarity of users [4]. Therefore, it is necessary to consider fusing the prediction results of a single user. Practice shows that the recommendation effect of mean value strategy and least pain strategy is better. The average strategy takes the user's average rating on the item as a comprehensive evaluation result, but does not consider the dissatisfaction of a few members. The least misery strategy selects the member's lowest rating on the item as the comprehensive evaluation result, which ignores the preference of the majority of members.

Recommendation system refers to defining a function F to calculate the probability that an item $i \in I$ (I am the set of all items) is recommended to a certain user $u \in U$ (U is the

set of all users) [5]. Recommendation algorithms find the most interesting items for users by calculating probabilities. Algorithms are the core of recommendation systems, and using efficient and accurate recommendation algorithms is the key to achieving good recommendation results. According to the different recommendation principles, it can be divided into popularity-based, social network-based, demographic-based, content-based, collaborative filtering-based, model-based, and hybrid recommendation algorithms. Recommendation based on popularity is to recommend hot content to users first, which can cover most of the content needs. Recommendations based on social networks include neighborhood-based social recommendation and graph-based social recommendation algorithms [6]. Demographic-based is to use the basic information of users, including age, gender, and place of residence, to calculate the degree of correlation between users and then make recommendations to users. The content-based recommendation algorithm recommends content like the items that they were interested in to users based on the attributes of the item itself [7]. The collaborative filtering algorithm proposed by Goldberg et al. is based on the assumption that if users X and Y rate t items similarly or have similar behaviors; then, users will rate or behave similarly to other items. It collects the user's past behavior to obtain the user's explicit or implicit information about the product, obtains the relevance of the product or user, and then recommends based on the relevance. Hybrid recommendation algorithms can combine the advantages of multiple algorithms to improve the performance of recommendation systems [8]. Hybrid recommendation algorithms include weighted type, switching type, intersection type, feature combination type, waterfall type, feature incremental type, and metalevel type [9]. According to the characteristics of travel recommendation and user needs, the recommendation algorithm based on collaborative filtering can better meet the recommendation requirements without causing excessive calculation. Nilashi et al. [10] used expectation maximization to construct a multicriteria collaborative filtering recommendation system for travel and tourism. Mehrbakhsh et al. [11] developed a collaborative filtering recommendation system based on ontology and dimensionality reduction techniques. Li et al. [12] proposed a combined recommendation algorithm based on improved similarity and forgetting curve.

In the process of travel recommendation, this study firstly improves the user-based and item-based collaborative filtering algorithms. The improved CFA combines the similarity factor and the correlation factor, which can better solve the problem of data sparsity in travel recommendation. Secondly, on the basis of average strategy and least misery strategy, a new user preference fusion strategy—satisfaction balance strategy—is defined. The strategy comprehensively considers the user's local satisfaction and overall satisfaction. Finally, through the experimental analysis based on the relevant tourism dataset of the city of Chongqing, it is verified that the improved method in this study can effectively improve the quality of tourism recommendation.

2. Recommendation Method

Collaborative filtering algorithm (CFA) is one of the most commonly used recommendation algorithms in the field of e-commerce recommendation, which does not require users to actively provide information about their personal needs, but obtains their potential preferences based on existing rating records. This study is based on the key techniques of recommendation for CFA applications, including fusion methods and fusion strategies. The fusion method is divided into model fusion and recommendation fusion. Model fusion generates recommendation combinations based on user preference models. Recommendation fusion, on the contrary, requires fusion based on prediction scores of each user after obtaining the prediction scores based on traditional algorithms and can also fuse the list of recommended items. The commonly used fusion strategies in recommendation key techniques include mean strategy, least pain strategy, and happiest strategy. Masthoff et al. [13] evaluated through a series of experiments that multiplication strategy, mean strategy, least pain strategy, and pain avoidance mean strategy are better. Zhang et al. [14] analyzed through literature studies and found that the most used strategies are mean strategy, pain mean value avoidance strategy, and minimum pain strategy, but the applicability of these strategies varies for clusters with different characteristics.

2.1. Recent Neighborhood Recommendations. CFA is often applied as a basic method in recommendation systems. The recommendation technique based on CFA includes four stages [15], such as similarity metrics, selecting neighbors, predicting ratings, and determining recommended items. Firstly, the similarity between every two users is calculated by the ratings of users in the rating matrix, then the ratings of current users for unknown items are predicted based on the K-nearest neighbor approach, and finally the recommendation list is generated by combining the preferences of all group members through a fusion strategy. The overall framework of the CFA-based recommendation technique is shown in Figure 1. Among them, CFA can be divided into user-based nearest neighbor recommendation and item-based nearest neighbor recommendation.

User-based nearest neighbor recommendation refers to the assumption that the current user will like the items liked by users with similar preferences. Currently, similarity calculation methods commonly used in practice include Cosine similarity and Pearson correlation coefficient. In this study, the main choice of similarity is defined as shown in the following equation:

$$c\text{sim}\,(p,q) = \frac{\sum_{i \in I_{pq}} R_{p,i} \cdot R_{q,i}}{\sqrt{\sum_{i \in I_p} R_{p,i}^2}\sqrt{\sum_{i \in I_q} R_{p,i}^2}}, \tag{1}$$

where $c\text{sim}\,(p,q)$ denotes the cosine similarity of users P and Q, $R_{p,i}$ and $R_{q,i}$ denote the ratings of user P and user Q for item i, respectively, I_p and I_q denote the set of items rated by user P and Q, and I_{pq} denotes the set of items jointly rated by user P and Q. By finding the set of users who have the
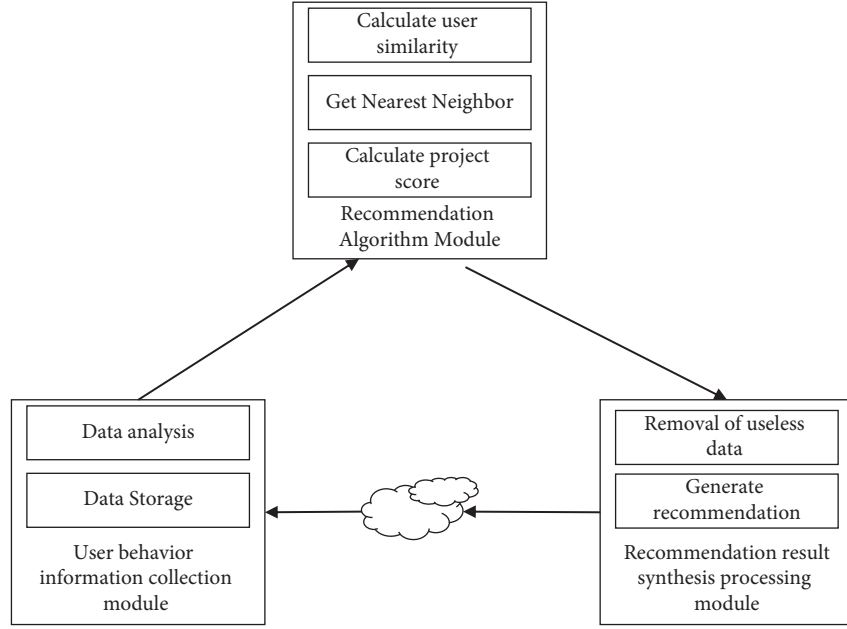
FIGURE 1: The framework of recommendation-based CFA.

similarity preferences to the current user P, as KQQ_a, then the predicted ratings of user P for item i are as in equation (2), where $\overline{R_p}$ and $\overline{R_q}$ denote the average ratings of user P and Q, respectively:

$$G_{p,i} = \overline{R_p} + \frac{\sum_{q \in KQQ_a} c\text{sim}(p,q) \times \left(R_{q,i} - \overline{R_q}\right)}{\sum_{q \in KQQ_a} \left|C_{\text{sim}(p,q)}\right|}. \tag{2}$$

The nearest collar recommendation based on the item uses the user's rating of the item to calculate the similarity, which is chosen in this study as shown in the following equation:

$$g\text{sim}(i,j) = \frac{\sum_{p \in R_{ij}} \left(R_{p,i} - \overline{R_i}\right)\left(R_{q,i} - \overline{R_j}\right)}{\sqrt{\sum_{p \in R_{ij}} \left(R_{p,i} - \overline{R_i}\right)^2} \sqrt{\sum_{p \in R_{ij}} \left(R_{p,j} - \overline{R_j}\right)^2}}, \tag{3}$$

where $g\text{sim}(i,j)$ denotes the Pearson similarity of item i and j, $\overline{R_i}$ and $\overline{R_j}$ denote the average scores of items i and j, and R_{ij} denotes the set of items that have scored both items i and j. By finding the set of items which have the similarity preferences to the current item i, as KQQ_i, then the predicted ratings of user Q for item i are as in the following equation:

$$G_{p,i} = \overline{R_i} + \frac{\sum_{j \in KQQ_i} g\text{sim}(i,j) \times \left(R_{a,j} - \overline{R_j}\right)}{\sum_{j \in KQQ_i} |g\text{sim}(i,j)|}. \tag{4}$$

2.2. Algorithm Improvement. Similarity is an important metric in CFA that determines how well a prediction is scored. In the travel field, the user's own combination of factors makes travel recommendations different from general e-commerce. For example, the frequency of users watching movies and online shopping in a year will be much greater than their frequency of travel. Therefore, the problem

of data sparsity is more prominent in travel recommendation. The traditional similarity calculation method can give good results when the rating data are abundant, but in travel recommendation, the traditional recommendation method may ignore the influence of the sparsity of user rating data on the similarity calculation result when calculating the similarity between users or items.

Chongqing is one of the most popular tourist cities in China. This study takes the scoring matrix of famous scenic spots in the city by different users as an example to discuss this issue.

From the data in Table 1, the number of attractions rated jointly by users A and B is more than that of users A and E. Therefore, the similarity of users A and B should be higher. However, the cosine similarity between users A and B is calculated to be 0.724 and the similarity between users A and E is 0.871. Therefore, traditional similarity calculation methods cannot correctly account for the correlation between user ratings. To solve this problem, this study uses the relationship between the number of common user ratings of attractions and the total number of user ratings of attractions to adjust the similarity between users, that is, the similarity influence factor s_i, and is defined as shown in the following equation:

$$s_i = 2\sqrt{\frac{I_{pq}}{I_p \cup I_q}} - 1, \tag{5}$$

where I_p is the set of attractions rated by user P and I_q is the set of attractions rated by user Q. The larger the number of attractions jointly rated by users P and Q in the total number of rated attractions is, the larger the corresponding similarity influence factor and the larger the value of similarity may be; conversely, the smaller the value of similarity may be.

TABLE 1: User rating matrix.

User	Hong Ya Dong	Dream Ordovician	Ciqikou ancient town	Wulong fairy mountain
A	5	3	3	1
B	3	3	0	4
C	4	5	4	0
D	3	5	0	2
E	5	0	4	0
F	5	3	0	0

User D and User F have a cosine similarity of 0.835, indicating that they have similar preferences, while their Pearson and modified cosine similarity calculations are negative, indicating that they have opposite preferences. Both calculations deviate from the actual situation. As the size of users and rating matrices increases, situations like this can also affect the accuracy of recommendation results. To solve such problems, this study uses the correlation of user ratings to adjust the similarity between users; the closer the common rating vectors of users are, the larger the value of similarity may be and vice versa, the smaller the value of similarity may be. The correlation factor s_i' is defined as the following equation:

$$s_i' = 1 - \sqrt{1 - \left[\frac{\sum 2R_{m,i}R_{n,i}}{\sum \left(R_{m,i}^2 + R_{n,i}^2\right)}\right]^2}. \tag{6}$$

The calculation of similarity is the most important step in collaborative filtering. The data sparsity problem faced by the travel domain makes it difficult for the original similarity methods to accurately measure the similarity among users. This is because in the case of sparse user rating data, traditional methods mainly consider the similarity between users' common ratings, but ignore the phenomenon that users are not necessarily similar on other items. Users' preferences can be considered similar only when they rate similarly on a relatively large number of items; moreover, traditional methods cannot accurately distinguish the similarity between some users with the same similarity but very different preferences.

The similarity influence factor s_i and correlation factor s_i' proposed in this study comprehensively consider the influence of common user rating items and rating correlation on the similarity measure, which can effectively alleviate the problem of inaccurate similarity calculation due to the data sparsity problem. Improved similarity $csim(p, q)_i = s_i[\theta \cdot csim(p, q) + (1 - \theta) \cdot s_i']$, and θ is a parameter of [0, 1]. Through substituting $csim(p, q)_i$ into equation (2), we can yield the user's predicted score for the scenic spot.

2.3. Modified Preference Fusion Strategy.
On the basis of individual users' prediction and scoring of items, the fusion strategy can fuse the user's preferences to obtain the overall evaluation value of each item and generate the final recommendation result according to the score. Since user preferences may vary, individual member preferences cannot represent overall preferences. How to obtain the common preferences of the overall users to alleviate the conflict is a problem that needs to be solved. Currently, the more commonly used preference fusion strategies include average strategy and least misery strategy. The average strategy selects the average of the user's rating on the item as the score of the item to be recommended. The calculation process is shown in the following equation:

$$R_{g,i} = \text{avg}\left(R_{a,i} : a \in g\right). \tag{7}$$

The least misery strategy refers to taking the minimum rating of the item among users as the score of the item to be recommended, as shown in the following equation:

$$R_{g,i} = \min\left(R_{a,i} : a \in g\right). \tag{8}$$

The average strategy only considers the average preference degree of users participating in the rating and may ignore the dissatisfaction degree of a few users. The least misery strategy is based on the minimum rating of the user to evaluate the project, which may be the feeling of the majority of households. To this end, this study considers the shortcomings of the above two strategies and defines a satisfaction balance strategy, which is used to balance the relationship between the user's local satisfaction and overall satisfaction. The definition is shown in the following equation:

$$B_{g,i} = \text{avg}\left(R_{a,i} : a \in g\right) + \frac{1}{S} \, avg\left(R_{a,i} : a \in g\right) * \min\left(R_{a,i} : a \in g\right), \tag{9}$$

where S denotes the number of users who evaluates the items. Based on the above strategies, we list four users and their evaluations of the five attractions, as shown in Table 2. The table shows the attractions scores under the average strategy, the least misery strategy, and the satisfaction balance strategy. According to the average strategy, S_2 and S_3 are equivalent for the surveyed users, but for S_1, the mean strategy does not consider the feelings of U_4. According to the least pain strategy, S_1 and S_2 are equivalent to the surveyed users. Compared with S_3, users are more interested in S_4. The least misery strategy only considers the minimum satisfaction of members but ignores them, the preference of most people. Obviously, the result calculated according to the satisfaction balance strategy can better reflect the user's overall interest in the scenic spots. According to the revised fusion strategy, the recommended list can be obtained as S_4, S_3, S_2, and S_1.

3. Experimental Design

3.1. Experimental Data.
There are no publicly available experimental datasets in the field of travel recommendation, and the data used in academic studies at home and abroad

Table 2: Different aggregation strategy examples.

Users	S_1	S_2	S_3	S_4
U_1	5	4	4	5
U_2	4	5	5	4
U_3	3	2	4	5
U_4	2	5	3	4
Average	3.5	4.00	4.00	4.50
Least misery	2.00	2.00	3.00	4.00
Satisfaction balance	5.25	6.00	6.00	6.75

Note: S_n denotes the different scenic spots; U_n denotes the different users.

are mainly from travel websites or questionnaires. There are two problems in the data obtained by means of questionnaires in terms of data volume and subjective bias. In this study, we have crawled 2874 travel notes related to "Chongqing" from https://Qunar.com and use 49,318 scores as the experimental dataset, with a score ranging from 1 to 5 points.

In order to reduce the error, this study preprocesses the acquired data, and users with duplicate records for the same user, attractions with unclear ratings, and users with less than 3 rating records are removed. The final number of valid users is 4072, the total number of ratings is 25894, and the sparsity level is 0.965.

3.2. Accuracy Evaluation. Mean absolute error (MAE) and root-mean-square error (RMSE) are the two most common metrics for continuous variables. MAE is a linear score that represents the mean of the absolute error between the predicted value and the observed value. RMSE represents the sample standard deviation of the difference between the predicted and observed values (called residuals) and is used to indicate the degree of dispersion of the sample. In this study, the accuracy of individual prediction results is tested using MAE and RMSE, as shown in the following equation:

$$\text{MAE}(X, R) = \frac{1}{m} \sum_{i=1}^{m} |R_i - y_i|; \text{RMSE}(X, R) = \sqrt{\frac{1}{m} \sum_{i=1}^{m} (R_i - y_i)^2},$$

(10)

where R and y denote the predicted and true user ratings of the items in the test set, respectively, and m is the number of ratings.

There are many evaluation metrics commonly used in recommendation systems. The main idea of Discounted Cumulative Gain (DCG) is that a user's favorite item being ranked in front of the recommendation list will increase the user experience to a greater extent than being ranked at the back, as defined in the following equation:

$$\text{DCG}(b, L) = \sum_{i=1}^{b} r_i + \sum_{i=b+1}^{L} \frac{r_i}{\log_b i},$$

(11)

where r_i indicates whether the product ranked i is preferred by the user, $r_i = 1$ indicates that the user likes the product, b is a free parameter, and L is the length of the recommendation list. Since DCGs are not directly comparable between

users, we normalize them by dividing the original DCG by the ideal DCG to obtain the normalized discounted cumulative gain (NDCG). NDCG is a number between 0 and 1. The larger the value of NDCG, the more accurate the ranking of the items in the recommendation list and the higher the accuracy of the recommendation.

4. Experimental Results and Analysis

We randomly select 70% of the rating records in the travel dataset as the training set and 30% as the test set and observe the performance of the recommendation algorithm when the number of neighbors K increases from 5 to 30 by 5 each time after several experiments, taking $\theta = 0$. From Figures 2 and 3, it can be obtained that, for the traditional user (uCFA)- and project (pCFA)-based methods, s_i and s_i' proposed in this study (uCFA-I; pCFA-I) are more effective in improving the CAF on MAE and RMSE. It shows that the improved method can provide better results in calculating the similarity between users or projects, which in turn improves the accuracy of prediction scores. The problem that traditional methods ignore the differences in users' interests for different attractions is reasonably solved.

Nowadays, people are more inclined to travel in groups, so it is important to fuse strategies for different users. Based on predictive scoring of users using a modified CFA, we compare the experimental results of the satisfaction balance strategy (SB) proposed in this study with the commonly used fusion strategies presented in Chapter 2.3 (AVE; LM) on a tour dataset. As can be seen from Figure 4, the NDCG values of the SB fusion strategy are the highest for different user sizes. AVE only considers the overall satisfaction of all members when recommending items to different users, but ignores the individuality of members' feelings; the LM strategy uses the opinions of a few members to decide the choice of the whole group, and the recommended items do not have a high probability of making the highest satisfaction of all members. And SB takes into account the relationship between overall and local user satisfaction, allowing the recommended projects to better reflect the preferences of the entire group.

Besides, regardless of the fusion strategy, the number of users at 4 makes NDCG take the highest peak. This also shows that, in the present social context, small groups of four are the most popular way to travel. On this basis, user satisfaction decreases as the number of people increases. This is also in line with the actual situation; as the more people there are, the greater the difference in interests is and the more difficult it is for the group to reach the peak of satisfaction with the same attraction.

Tourism market is very necessary for the development of cities. The model proposed in this study can help people to make decisions when traveling. Nowadays, there are various methods of travel recommendation, and only the method with outstanding accuracy and recommendation performance can stand out. In this study, we have proposed two improvement factors based on the common CFA, which can make the user get a better experience. Nowadays, travel companies should customize their marketing with full
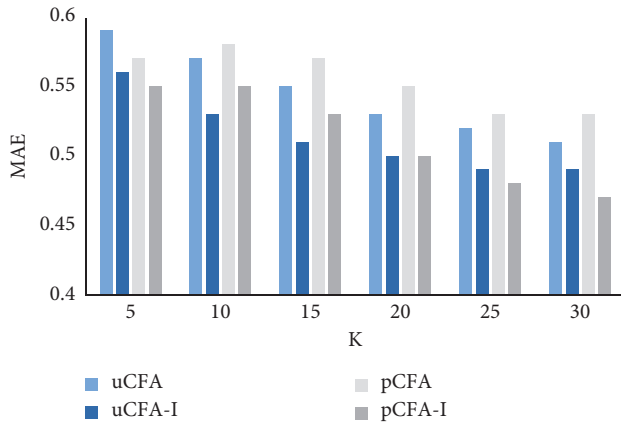
FIGURE 2: MAE comparison chart.
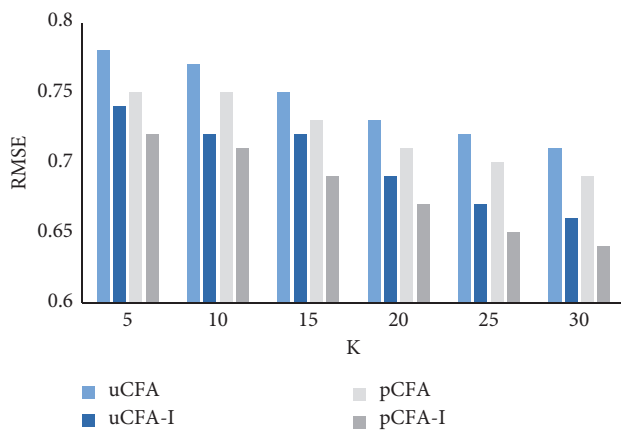
FIGURE 3: RMSE comparison chart.
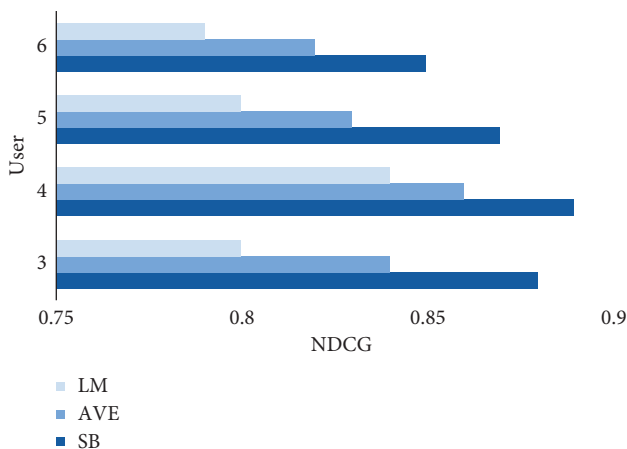
FIGURE 4: NDCG comparison chart.

consideration of user preferences, so the data source for this study's improved CFA method is web travel data that incorporate user interests. As society develops and incomes increase, marketing of tourism should adapt to the trend of increasing personalized demand by creating a user demand base. Also, tourism companies can use the method in this study to obtain the user satisfaction of different attractions

so that they can identify the attractions with more commercial value or business potential, improve their marketing and achieve greater economic benefits. For example, a group cruise or skiing program for four people can be developed at natural landscapes such as Fairy Mountain to make the tour small groups, reduce the probability of group members separating, and improve the overall satisfaction of the tour.

5. Conclusion

In response to the team-based nature of tourists, this study proposes a travel recommendation method that integrates users' personalized needs and maximizes team satisfaction based on the improved-CFA method. The method uses the massive rating information about tourist destinations on the web to build the basic framework of the travel recommendation method. The problem of sparsity of CFA data is solved by two factor corrections based on users and items. In the instance validation of https://Qunar.com, the improved CFA method in this study has significantly lower MAE and RMSE than the nonoptimized CFA method for different K. The satisfaction equalization strategy used in this study is also due to the conventional fusion strategy for different number of users. This shows the superiority of the method in this study and also greatly helps tourism companies to come up with better marketing strategies under complex market conditions. The recommendation algorithm in this study has room for improvement in accuracy, and future work will focus on the improvement of model accuracy and relevance of user preferences.

Data Availability

The labeled dataset used to support the findings of this study are available from the corresponding author upon request.

Conflicts of Interest

The authors declare no conflicts of interest.

Acknowledgments

References

[1] T. D. Pessemir, J. Dhondt, and L. Martems, "Hybrid group recommendations for a travel service," *Multimedia Tools and Applications*, vol. 76, no. 2, pp. 2787–2811, 2017.

[2] S. Dhelim, H. Ning, N. Aung, R. Huang, and J. Ma, "Personality-aware product recommendation system based on user interests mining and metapath discovery," *IEEE Transactions on Computational Social Systems*, vol. 8, no. 1, pp. 86–98, 2020.

[3] U. Kanimozhi, G. Sannasi, D. Manjula, and K. Arputharaj, "Retracted article: a user preference tree based personalized route recommendation system for constraint tourism and travel," *Soft Computing*, vol. 26, no. 3, p. 1499, 2022.

[4] Z. D. Zhao and M. S. Shang, "User-based Collaborative-Filtering Recommendation Algorithms on Hadoop," in

Proceeding of the 2010 Third International Conference on Knowledge Discovery and Data Mining, pp. 478–481, Phuket, Thailand, January 2010.

[5] H. Ko, S. Lee, Y. Park, and A. Choi, "A survey of recommendation systems: recommendation models, techniques, and application fields," *Electronics Times*, vol. 11, no. 1, 141 pages, 2022.

[6] A. Sajad, M. Majid, and A. Mohsen, "A social recommendation method based on an adaptive neighbor selection mechanism," *Information Processing & Management*, vol. 54, no. 4, pp. 707–725, 2018.

[7] C. Wang, A. Agrawal, X. Li et al., "Content-based top-N recommendations with perceived similarity," in *Proceesding of the 2017 IEEE International Conference on Systems, Man and Cybernetics*, pp. 1052–1057, Banff, AB, Canada, December2017.

[8] D. Nie, L. Hong, and T. Zhu, "Movie recommendation using unrated data," in *Proceeding of the 2013 12th International Conference on Machine Learning and Applications*, pp. 344–347, IEEE, Miami, FL, USA, December 2013.

[9] S. Zhao, M. Hu, Z. Cai, Z. Zhang, T. Zhou, and F. Liu, "Enhancing Chinese character representation with lattice-aligned attention," *IEEE Transactions on Neural Networks and Learning Systems*, pp. 1–10, 2021.

[10] M. Nilashi, O. B. Ibrahim, N. Ithnin, and N. H. Sarmin, "A multi-criteria collaborative filtering recommender system for the tourism domain using Expectation Maximization (EM) and PCA-ANFIS," *Electronic Commerce Research and Applications*, vol. 14, no. 6, pp. 542–562, 2015.

[11] N. Mehrbakhsh, I. Othman, and B. Karamollah, "A recommender system based on collaborative filtering using ontology and dimensionality reduction techniques," *Expert Systems with Applications*, vol. 92, pp. 507–520, 2018.

[12] T. Li, L. Jin, Z. Wu, and Y. Chen, "Combined recommendation algorithm based on improved similarity and forgetting curve," *Information*, vol. 10, no. 4, 130 pages, 2019.

[13] J. Masthoff, L. Rokach, and B. Shapira, "Group recommender systems: combining individual models," *Recommender Systems Handbook*, Springer, Boston, MA, USA, 2011.

[14] S. Zhao, M. Hu, Z. Cai, and F. Liu, "Dynamic modeling cross-modal interactions in two-phase prediction for entity-relation extraction," *IEEE Transactions on Neural Networks and Learning Systems*, pp. 1–10, 2021.

[15] J. Bobadilla, F. Ortega, A. Hernando, and A. Gutierrez, "Recommender systems survey," *Knowledge-Based Systems*, vol. 46, pp. 109–132, 2013.

Research Article

Research on Multicamera Photography Image Art in BERT Motion Based on Deep Learning Mode

Zhao Zhao,[1] **Mingyang Song,**[2] **and Hongyue Tang** [1]

[1]*School of Fine Arts, Hunan Normal University, Changsha 410006, China*
[2]*School of Physical Education, Hunan Normal University, Changsha 410006, China*

Correspondence should be addressed to Hongyue Tang; 202170173218@hunnu.edu.cn

In order to improve the artistic expression effect of photographic images, this article combines the deep learning model to conduct multicamera photographic image art research in BERT motion. Moreover, this article analyzes the external parameter errors caused in the calibration process and uses the checkerboard in the common field of view to calibrate the spatial coordinates of the corners of the board in multiple camera coordinate systems. In addition, this article aims to match the spatial coordinates of the corresponding points to each other and solve the rotation and translation matrix in the transformation process. Finally, this article uses the LM algorithm to optimize the calibration parameters of the camera and combines the deep learning algorithm to perform image processing. The experimental research results show that the research method of multicamera photography image art in BERT motion based on the deep learning mode proposed in this article can effectively improve the expression effect of image art.

1. Introduction

In people's daily life, as one of the main tools for image dissemination, photography has become ubiquitous to record and discover different visual possibilities. However, photography and photographic art are two completely different concepts, and photography is not related to all art. Photography is recognized as a relatively recent thing in the field of culture and art. In the 1970s, a large number of art festivals, periodicals, and galleries were launched in Western countries. Immediately afterwards, some colleges and universities set up professional photography colleges and photography departments. In addition, the research on the history of photography in the academic field is also deepening, a large number of photographic works have been included in the art collection, and more and more artists have begun to create photography. In short, the practice and dissemination of photography are no longer confined to a narrow field of practice but lead to the palace of art and culture. At the same time, people's concept of photography is constantly updated. When photography was invented, it was used only as a service tool. Today, however, it is increasingly being discussed and appreciated as the artwork itself. As a result, the public's attitude towards the practicality of photography has changed, attention has been drawn from the perceptual and rational nature of images, and the production, dissemination, and circulation of photography, as well as the form, value, and use of photography, have also changed accordingly.

Some people simply regard the art of photography as craftsmanship based on the principles of optics, chemistry, and mechanics with purity. To put it more frankly, they believe that photography is a kind of performance art of taking pictures, which leads them to ignore the lofty status of photography and its outstanding contribution to the development history of human society. In addition, the importance of photographic practice is generally ignored by some people, who only pay attention to theoretical knowledge and believe that it is enough to master the classic theories, such as visual aesthetics, cultural studies, and image expression in photographic art, and do not pay attention to photographic practice. These understandings of photography art are one-sided and not objective.

Photography art is a comprehensive artistic behavior. It is inclusive and has different connotations in different

situations. Sometimes it pays more attention to the connotation of the technical level, and sometimes it focuses more on the expression of culture and emotion. Today's photographic art is specifically a type of modern plastic art. A camera is a tool for photographic creation. Taking the photographer's creative concept as the basic starting point, they use the camera to take pictures of people or things in the real world and uses certain modern processing methods, perform artistic processing on the photographed things, and finally complete the creation of photographic works of art. Through the works showing the living conditions of human beings in the current society, at the same time, it can express the author's thoughts and feelings. Aesthetic features are more of an attribute, the presentation of their own aesthetic features. Photography, as one of many art categories, has aesthetic characteristics similar to other aesthetic activities, that is, the commonality of photography aesthetics and other aesthetic activities. In addition, photography art also has its own characteristics; it belongs to a branch of visual plastic art.

This article combines the deep learning model to study the multicamera photographic image art in BERT motion to improve the performance of photographic image art.

2. Related Work

From the perspective of the development process of image text description, it can be divided into three stages: template-based image text description method; retrieval-based image text description method; deep learning-based image text description method [1]. Before the deep learning method was proposed, most of the image description methods used template-based and retrieval-based methods. The template-based image text description method is mainly to annotate the image content, which is based on image annotation technology [2]. Template-based methods rely on visual perception of the relationship between image objects and components and describe images using representations of subject, predicate, environment, and preposition collocations [3]. Reference [4] used the method of image context subject, object, and their relationship to describe the image, used the neighbor similarity algorithm to calculate the matching degree between adjacent tuples, finally calculating the score, and the score is proportional to the matching degree. Reference [5] proposed a Conditional RaIldom Field (CRF) algorithm, the central idea of which is to generate text descriptions for predicted text labels according to template matching rules. Reference [6] improved the template in the image text description task and used the hidden Markov model to fill the template with sentences. Reference [7] applied syntactic analysis to the image text description task, used the VDR (Visual Dependency Representation) method to represent the object relationships contained in the graph with a dependency graph, and then represented the image as a VDR and then traversed the VDR, fully considering the VDR. Syntax tree relationships to fill in gaps in sentences. Template-based image text description methods may be grammatically correct in language descriptions, but the output descriptions are highly template-dependent, have

poor generalization performance, and generate text sentences that lack diversity. Due to the backwardness of this method, the image text description task is no longer used [8]. Searching for the relationship between matching text and images is the main purpose of the retrieval-based image description generation task. Retrieval-based image description also includes vision-based retrieval and multi-modal-based retrieval methods [9]. The retrieval method based on visual space is to obtain textual information from the features of similar parts in the image. The image retrieval dataset established by the literature [10], for each image, uses appropriate words to describe the image. Reference [11] proposed a large dataset, which includes attribute annotations of objects, which can be used to train attribute classifiers, predicted object attributes, and improved the quality of image text descriptions. The retrieval method based on multimodal space is to perform a multimodal representation of all images and text sentences in the training corpus. For the image to be tested, retrieval is performed in the multimodal space after the image and the text are jointly mapped. First, a set of similar images of the image to be tested is obtained, and the text description corresponding to the test image is obtained according to the text description of the similar image. In [12], the authors proposed to learn multimodal space representation, use kernel function calculation method to extract high-dimensional image features, in the multimodal space represented by image and text jointly, use a sorting algorithm according to the high-dimensional features of images, and find candidate text for the set of similar images of the target. Finally, the candidate text is screened according to a certain sorting algorithm, and the text description corresponding to the image is obtained. Reference [13] applied the neural network with stronger expressive ability in the field of image text description. It makes the image text description generated in the multimodal space more accurate and of higher quality. The retrieval-based method makes full use of the dataset, but the generated image text description largely depends on the dataset. When the gap between the target image and the training data set is large, the effect of the generated text description will be poor, and only the generated text description can be generated. Human-annotated sentences are already in the dataset. Retrieval-based image description methods have better expressiveness, mobility, and practicality. Although some excellent results have been obtained, the retrieval-based method still has dependencies. The production text description is highly dependent on the training corpus, and there are problems such as high complexity, which are seriously affected by human intervention, which makes the generated text description sentences simple and ineffective. With rich semantic information, researchers continue to explore new text description methods [14]. With the popularization of deep learning knowledge, researchers have proposed new methods based on deep learning methods. The advanced and commonly used method is the end-to-end model. On the one hand, deep convolutional neural networks can be used to create models for object features in images; on the other hand, recurrent neural networks can be used to create

language models for text [15]. Reference [16] proposed a deep semantic alignment model. The model echoes images and text descriptions by aligning them. In terms of images, a region-based convolutional neural network is used for pretraining, and the features of the images are mapped to the feature space of word vectors to match the two-part features. Descriptions are generated using recurrent convolutional networks in terms of language models. The NIC model based on the English dataset proposed in [17] uses the advanced Inception V3 network to extract image features and uses LSTM to generate descriptions in the language generation model stage. This method plays an important role in the image description task. Reference [18] proposed a hard attention mechanism and a soft attention mechanism, used the combination of the attention mechanism and the LSTM network to obtain the image information of each step, and improved the expressive ability of the image description.

3. Global Calibration Optimization of Multicamera System Based on Levenberg–Marquardt Algorithm

Camera calibration has two important functions. One is to construct the relationship between the image plane coordinates and the camera space coordinates, which is explained in detail in the principle of calibration and the principle of binocular stereo imaging. The other is to construct the rotation and translation relationship between the camera coordinate system and other camera coordinate systems.

As shown in Figure 1, there are two coordinate systems in space, (o-x-y-z) and (O-X-Y-Z), and o and O are the origins of the two coordinate systems, respectively. Moreover, there is a straight line between the two origins, and the same straight line forms different vectors at different coordinates. Among them, the o point and the O point are both (0, 0.0) in their respective coordinates, and the vector from the o point to the O point is (x_1, y_1, z_1). It can also be interpreted as the coordinate of the point O in the (o-x-y-z) coordinate system is (x_1, y_1, z_1).

In the same way, the vector from point O to point o is (x_2, y_2, z_2), which is interpreted as the coordinate of point o in the (O-X-Y-Z) coordinate system is (x2, y2, 2). Since the directions of each axis corresponding to the two coordinate systems are different, these two vectors are not two opposite vectors, but the length of the same straight line is unchanged. Therefore, the magnitudes of these two vectors are the same, as shown in the following formula:

$$x_1^2 + y_1^2 + z_1^2 = x_2^2 + y_2^2 + z_2^2. \tag{1}$$

A coordinate system with two origins that do not coincide cannot discuss rotation. Therefore, we first move the (o-x-y-z) coordinate system to the vector (x_1, y_1, z_1) until its origin coincides with the origin of the (O-X-Y-Z) coordinate system.

As shown in Figure 2, in order to make the two coordinate systems completely coincide, the o-x-y-z coordinates will be rotated around the origin, and the counterclockwise
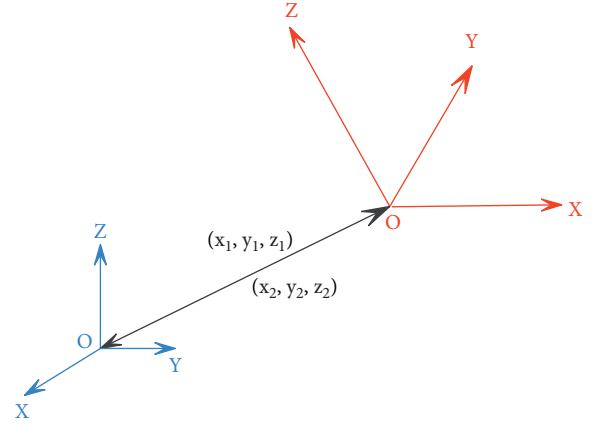
Figure 1: Coordinate system translation.
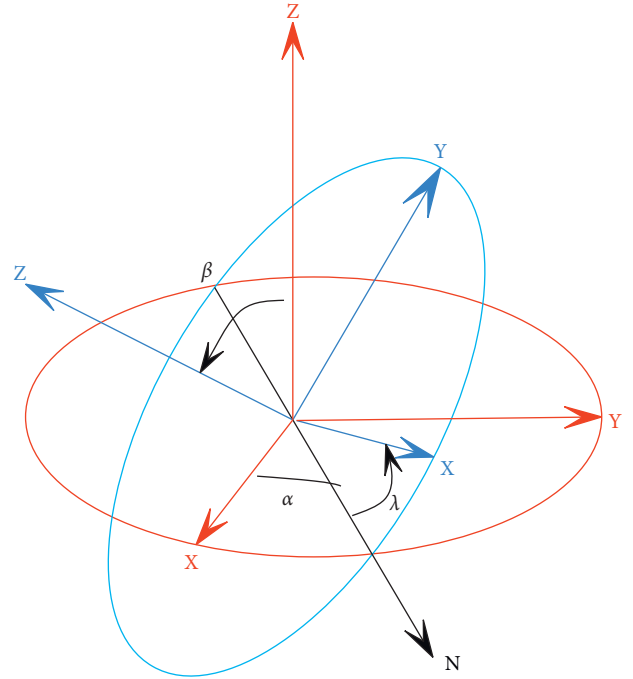
Figure 2: Coordinate system rotation.

direction is the direction of the rotation angle increment. The process is mainly divided into the following three steps.

The first step, which keeps the z-axis stationary, rotates the x-axis and the y-axis counterclockwise around the z-axis by an angle of a. At this time, x reaches the N-axis position, and a rotation variable $R_z(\alpha)$ is generated, and its matrix is shown in the following formula:

$$R_z(\alpha) = \begin{bmatrix} \cos \alpha & -\sin \alpha & 0 \\ \sin \alpha & \cos \alpha & 0 \\ 0 & 0 & 1 \end{bmatrix}. \tag{2}$$

In the second step, it keeps the x-axis stationary, which is the current N-axis, and the y-axis and the z-axis rotate counterclockwise around the x-axis by an angle of ß. The z-axis just coincides with the z-axis, and a rotation variable

$R_x(\alpha)$ is generated, whose matrix is shown in the following formula:

$$R_x(\alpha) = \begin{bmatrix} 1 & 0 & 0 \\ 0 & \cos \beta & -\sin \beta \\ 0 & \sin \beta & \cos \beta \end{bmatrix}. \tag{3}$$

The third step, which again keeps the z-axis stationary, rotates the x-axis and the y-axis counterclockwise around the z-axis by a y angle. At this time, the x-axis coincides with the X-axis, the y-axis coincides with the axis, and a rotation

variable $R_z(\gamma)$ is generated, whose matrix is shown in the following formula:

$$R_z(\gamma) = \begin{bmatrix} \cos \gamma & -\sin \gamma & 0 \\ \sin \gamma & \cos \gamma & 0 \\ 0 & 0 & 1 \end{bmatrix}. \tag{4}$$

The whole process consists of three independent rotations, generating a rotation matrix R, where R is the product of $R_z(\alpha)$, $R_x(\alpha)$, and $R_z(\gamma)$, and the calculation result is shown in the following formula:

$$R = \begin{bmatrix} \cos \alpha \cos \gamma - \cos \beta \sin \alpha \sin \gamma & -\cos \beta \cos \gamma \sin \alpha - \cos \alpha \sin \gamma & \sin \alpha \sin \beta \\ \cos \gamma \sin \alpha + \cos \alpha \cos \beta \sin \gamma & \cos \alpha \cos \beta \cos \gamma - \sin \alpha \sin \gamma & -\cos \alpha \sin \beta \\ \sin \beta \sin \gamma & \cos \gamma \sin \beta & \cos \beta \end{bmatrix}. \tag{5}$$

As shown in formula (6), the two vectors (x_1, y_1, z_1) and (x_2, y_2, z_2) in the above two camera coordinate systems can be converted to each other under the action of the rotation matrix R. It can be seen that the rotation-translation matrix is invertible, and the inverse matrix of the rotation matrix is its own transpose matrix, as shown in the following formula:

$$\begin{bmatrix} -x_2 \\ -y_2 \\ -z_2 \end{bmatrix} R = \begin{bmatrix} x_1 \\ y_1 \\ z_1 \end{bmatrix}, \tag{6}$$

$$R^{-1} = R^T. \tag{7}$$

When multiple cameras are calibrated, due to the accuracy of target positioning and the minimization of the global error of the pursuit, as shown in formula (8), there is a very small error in the external parameters, and the same point corresponds to different coordinates in the two camera coordinate systems. Among them, the coordinate of this point in a camera coordinate is (x_m, y_m, z_m). The other camera coordinate system is converted to this camera coordinate system through the rotation and translation matrix after calibration. The corresponding coordinate is (x_n, y_n, z_n). Because it is the same point in the real space, it should coincide in the unified coordinate system. If there is no coincidence, there must be an error in the rotation and translation matrix. Therefore, this error needs to be analyzed.

If the origin of the camera coordinate system coincides after the transformation, according to the coordinate transformation process, the relative position of the points in the same coordinate system does not change, then the distance between the two points and the origin should be equal. At this time, the point coordinate can be regarded as a vector; that is, the vector's modulus is equal, as shown in the following formula:

$$x_m^2 + y_m^2 + z_m^2 = x_n^2 + y_n^2 + z_n^2. \tag{8}$$

When the origins are coincident, there is no need to retranslate the camera coordinate system, and only the

parameters in the rotation matrix need to be calculated accurately. Finally, the translation vector is transformed once using (6) to reduce the error. Therefore, there is a very small angular rotation between the two coordinates, and the camera coordinate system that needs to be aligned is rotated by three angles in turn according to the rotation method shown in Figure 2.

We assume that the vectors (x_m, y_m, z_m) and (x_n, y_n, z_n) form a small angle θ. The relationship between the included angle θ and the two vectors is shown in the following formula:

$$\sin \frac{\theta}{2} = \frac{\sqrt{(x_m - x_n)^2 + (y_m - y_n)^2 + (z_m - z_n)^2}}{2\sqrt{x_m^2 + y_m^2 + z_m^2}}. \tag{9}$$

When the included angle θ is very small and approaches 0, the values of θ and $\sin \theta$ are equal, and its geometric meaning is the ratio of the distance between the two points to the vector modulus. Because the viewing angle of the camera is limited to a certain extent, in order to obtain a wider field of view, the camera will be arranged in a relatively far position, and the modulus of the camera coordinate vector will also increase accordingly. Moreover, the common field of view formed by binocular imaging is further compressed, and the measurement area will be divided into multiple segments, which will cause the measurement points in other camera coordinate systems to be converted into the global coordinate system and cause great errors. In order to avoid great errors, further optimization of the calibration external parameters must be carried out.

Another case is when the lengths of the two vectors (x_m, y_m, z_m) and (x_n, y_n, z_n) are not equal. Then, the relationship between the included angle θ and the two vectors is shown in the following formula:

$$\cos \theta = \frac{|x_m x_n + y_m y_n + z_m z_n|}{\sqrt{x_m^2 + y_m^2 + z_m^2} + \sqrt{x_n^2 + y_n^2 + z_n^2}}. \tag{10}$$

At this time, it is not only the rotation angle that causes the camera coordinate system error but also the translation

vector error. The allowable range of this error should consider the difference between the lengths of the two vectors and the distance between the two measurement points. In general, the optimization of the overall parameters of the camera during measurement will rarely cause a large change in the translation vector; that is, the distance between the origins of the two coordinate systems will not be very far. Therefore, the vector length difference will not exceed the measurement spread.

The conversion relationship between the two coordinate systems is calculated and obtained according to the geometric relationship between the coordinate systems of each camera in the process of constructing a large field of view in a multicamera system. Global calibration is to calibrate the overall measurement system to obtain the conversion relationship between all camera coordinate systems and reference coordinate systems. Taking a dual-camera station system composed of four cameras as an example, the multicamera global calibration process is described in detail with reference to Figure 3.

According to the definition of each coordinate system, it can be known that the transformation relationship between the camera coordinate systems of each camera in the entire measurement system is as follows:

The transformation of the A camera coordinate system and the B camera coordinate system of the measurement system 1 is as follows:

$$\begin{bmatrix} x_A \\ y_A \\ z_A \end{bmatrix} R_{BA} = \begin{bmatrix} x_B \\ y_B \\ z_B \end{bmatrix} + T_{BA}. \tag{11}$$

The conversion of the c camera coordinate system of the measurement system 2 to the D camera coordinate system is as follows:

$$\begin{bmatrix} x_C \\ y_C \\ z_C \end{bmatrix} R_{DC} = \begin{bmatrix} x_D \\ y_D \\ z_D \end{bmatrix} + T_{DC}. \tag{12}$$

In the above, R_{BA} and T_{BA}, R_{DC} and T_{DC} can be directly solved by the camera calibration principle. Among them, the R matrix and the T matrix can complete the inverse transformation of the two coordinate systems by formulas (6) and (7). In order to realize the coordinate conversion between the two measurement systems, the rotation matrix R_{CA} and translation vector T_{CA} of the A camera coordinate system and the C camera coordinate are directly solved by calibration. It can be solved indirectly by C camera calibration and B camera calibration rotation matrix R_{CB} and translation vector T_{CB}, or by constructing D camera and A camera calibration parameters rotation matrix R_{DA} and translation vector T_{DA}.

$$\begin{aligned} R_{CA} &= R_{BA} R_{CB}, \\ R_{CA} &= R_{DA} R_{CD}, \\ T_{CA} &= R_{DA} + T_{CD} + T_{DA}, \\ T_{CA} &= R_{BA} + T_{CB} + T_{BA}. \end{aligned} \tag{13}$$

The same target point exists in the common field of view, and the relationship between multiple target points $P_A(x_{Ai}, y_{Ai}, z_{Ai})$ in the A camera coordinate system and the corresponding target point $P_C(x_{Ci}, y_{Ci}, z_{Ci})$ in the C camera coordinate system is constructed, where $i = 1,2,3, \dots$. The parameters in the transformation matrix and transformation vector that satisfy multiple target points are solved.

$$\begin{bmatrix} x_{Ai} \\ y_{Ai} \\ z_{Ai} \end{bmatrix} = \begin{bmatrix} r_1 & r_2 & r_3 \\ r_4 & r_5 & r_6 \\ r_7 & r_8 & r_9 \end{bmatrix} \begin{bmatrix} x_{Ci} \\ y_{Ci} \\ z_{Ci} \end{bmatrix} + \begin{bmatrix} t_x \\ t_y \\ t_z \end{bmatrix}. \tag{14}$$

If it is assumed that there is a matrix A, then A^T represents the transposed matrix of A. Similarly, $\|A\|_2$ and $\|A\|_\infty$ represent the spectral norm and row sum norm of matrix A, respectively. The singular values of matrix A are to be solved, the largest of which is the spectral norm of the matrix A. The sum of the absolute values of the elements in each row of matrix A is calculated, the largest of which is the row sum norm of matrix A.

f is a functional relationship that maps the parameter vector $P \in R^m$ to the estimated measurement vector $\hat{x} = f(p), \hat{x} \in R^m$. An initial estimated parameter p and a measurement vector x are provided, and it is expected to find $p +$ the vector f that best satisfies the functional relationship, that is, minimize the squared distance $\varepsilon^T \varepsilon$, where $\varepsilon = x - \hat{x}$. The basis of the LM algorithm is to solve a linear approximation f in the neighborhood of δ_p. For a very small value of d, the Taylor series expansion approximation is as follows:

$$f(p + \delta_p) \approx f(p) + J\delta_p. \tag{15}$$

Among them, J is the Jacobian matrix $\partial f(p)/\partial p$. Like all nonlinear substitution methods, LM is iterative, starting from a chosen starting point p_0. This method generates a series of vectors $p_1, p_2, p_{3,\dots}$. These vectors converge to the local minima $p+$ with respect to the functional relation f. Therefore, at each step, it is necessary to find a suitable value δ_p to minimize the overall value $\|x - f(p + \delta_p)\| \approx \|x - f(p) - J\delta_p\| = \|\varepsilon - J\delta_p\|$, and finding δ_p is the solution to a linear least-squares problem. When the column space of $J\delta_p - \varepsilon$ and J is orthogonal, δ_p reaches the minimum value z and $f J^T(J\delta_p - \varepsilon) = 0$ can be obtained, and the resulting value 6 can be used as the solution of the normal equation.

$$J^T J \delta_p = J^T \varepsilon. \tag{16}$$

The $J^T J$ in the matrix on the left side of the equation is an approximation to the Hessian matrix, that is, to the second derivative matrix. The LM method actually solves for small changes in the equation, which can be called augmented regular equations.

$$N\delta_p = J^T \varepsilon. \tag{17}$$

Among them, the off-diagonal elements of N are the same as the corresponding elements in $J^T J$, and its diagonal elements are $N_{ii} = \mu + [J^T J]_{ii}$, where $\mu > 0$. The process of changing the diagonal elements of $J^T J$ is called damping,
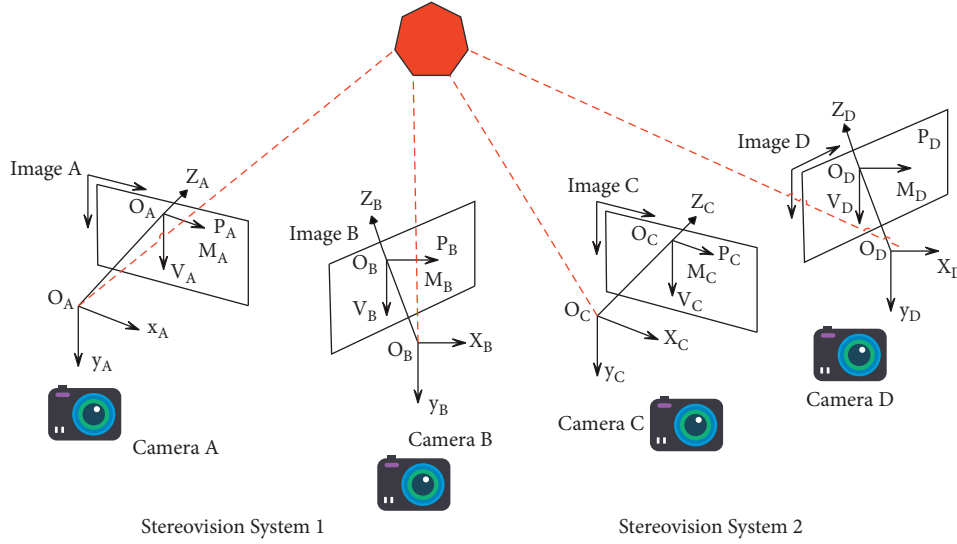
FIGURE 3: Schematic diagram of coordinate system transformation in a multicamera system.

and μ is the damping factor. In the iterative process, if a new parameter vector $p + \delta_p$ is obtained, which reduces the error ε, where δ_p can be calculated by the equation, the new parameter vector can be made closer to the optimal solution. Moreover, the iterative process is repeated with the aim of reducing the damping value.

If the new parameter vector $p + \delta_p$ is obtained and the error ε becomes larger or does not change, the damping value is increased, the augmented canonical equation is solved again, and the algorithm iterates until a value δ_p that reduces the error is found. In the equation, the solution is repeated for different damping factors μ until a parameter vector $p + \delta_p$ that is closer to the approximation is found. This update process corresponds to one iteration in the LM algorithm.

In the LM algorithm, the damping factor μ is adjusted during each iteration to ensure that the error can be reduced. If damping is set to a large value f, the matrix N in the equation used is almost on the diagonal and the LM update step value δ_p is close to the direction of the steepest descent. Also, the value of δ_p decreases in this case. Damping also handles the case of insufficient Jacobian elements, thus making $J^T J$ a singular matrix.

The LM algorithm terminates when at least one of the following conditions is met:

(1) The gradient size of $\varepsilon^T \varepsilon$ and $J\varepsilon$ on the right side of the equation will drop below a threshold.

(2) The relative change of the size of the step value δ_p falls below another threshold ε_2.

(3) The error $\varepsilon^T \varepsilon$ falls below another threshold ε_3.

(4) The maximum number of iterations k_{max} is completed.

$$ J^T \sum_x^{-1} J \delta_p = J^T \sum_x^{-1} \varepsilon. \tag{18} $$

If the covariance matrix Σ_x for the measurement vector x is available, $\sum_x^{-1}$ and the norm $\varepsilon^T \sum_x^{-1} \varepsilon$ can

be incorporated into the LM algorithm by minimizing squares instead of directly solving for $\varepsilon^T \varepsilon$. Therefore, a least-squares problem with minimum weights defined by weighted canonical equations is solved.

(4) Research on multicamera photography image art in BERT motion is based on the deep learning model

The image sentiment analysis model of sample selection and image content generation based on BERT features includes four parts: "image content generation," "text feature extraction," "sample selection based on BERT features," and "image sentiment analysis." The image is processed through deep learning, as shown in Figure 4.

The specific process of image content generation is shown in Figure 5.

Figure 6 shows the flowchart of the binocular stereo vision measurement procedure. The binocular cameras are synchronously triggered to capture a frame of pictures and then transfer them to the computer memory through the USB 3.0 interface. Then, it calls the image data to perform a series of tasks such as marker point detection and image point matching with the same name, then solves the pixel coordinates of the center of the marker point, and then performs 3D reconstruction to obtain the coordinates of the marker point in physical space and output the data.

According to the actual measurement needs, a CCD camera bracket and a fixed platform, lighting equipment, etc. are added to the system as auxiliary. The connection diagram of the main part of the system is shown in Figure 7.

The camera coordinate system and the imaging plane coordinate system are established. As shown in Figure 8, the world coordinate system in this section is selected on the target plane containing low-rank textures. For the convenience of description, the following two definitions are made first. When there is no rotation of the camera imaging plane coordinate system relative to the xw0wYw plane of the world coordinate system, the image captured at this time is called a
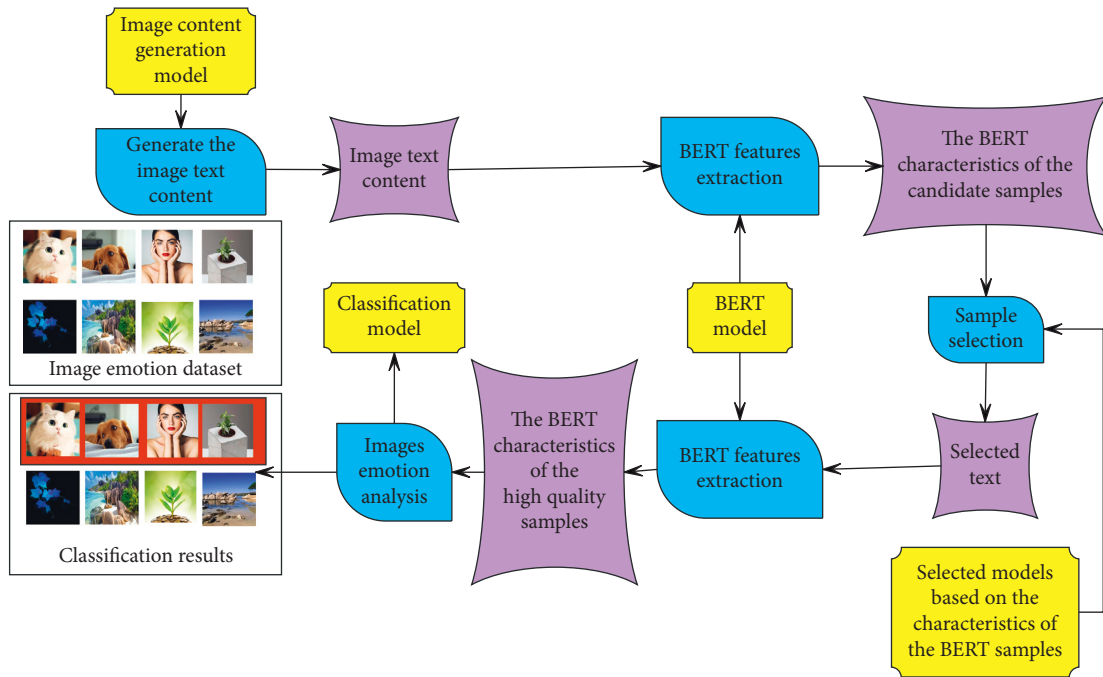
Figure 4: Image sentiment analysis process based on BERT feature sample selection and image content generation.
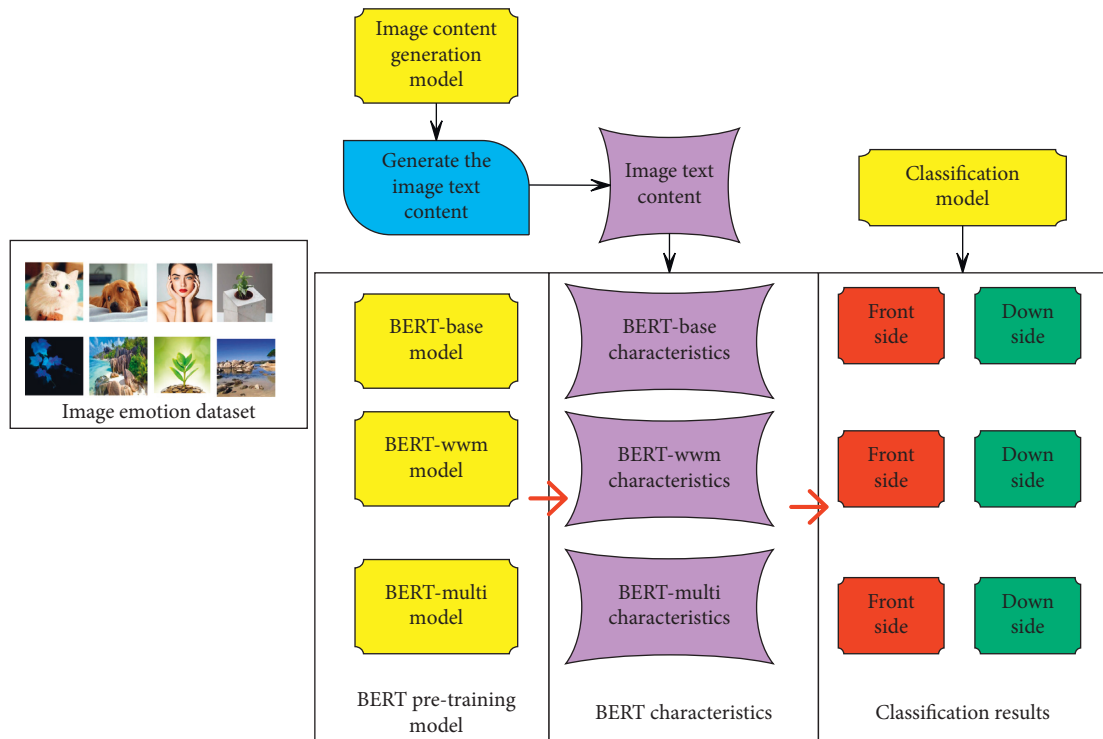
Figure 5: Flowchart of the use of the BERT model.
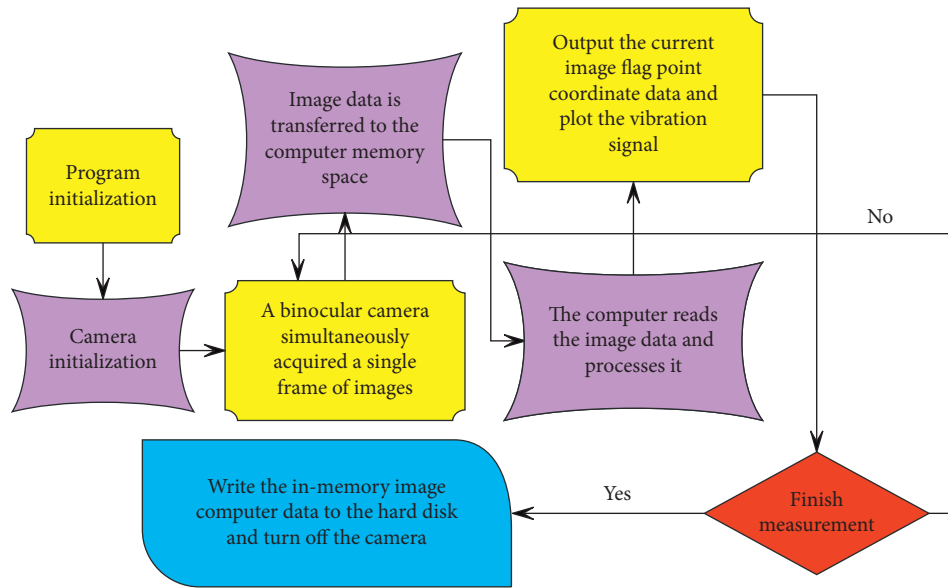
FIGURE 6: Program flowchart.
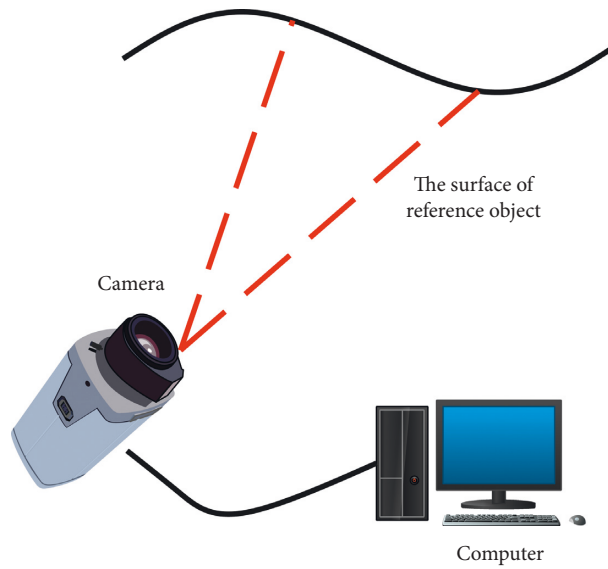
FIGURE 7: Schematic diagram of camera pose measurement system.
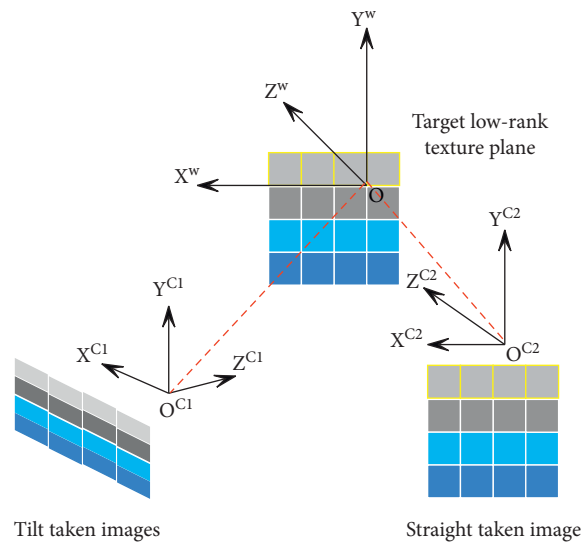
FIGURE 8: Front-facing images shot and oblique shot images.

TABLE 1: Expression effects of images obtained by multicamera photography.

Num	Image expression
1	88.18
2	88.99
3	89.51
4	92.73
5	93.77
6	93.81
7	90.25
8	93.21
9	95.29
10	94.59
11	89.42
12	90.74
13	94.84
14	91.28
15	93.75
16	89.30
17	90.44
18	90.00
19	88.68
20	95.94
21	93.01
22	95.17
23	95.38
24	89.76
25	92.51
26	94.99
27	94.53
28	90.61
29	95.25
30	91.77
31	90.05
32	89.88
33	90.56
34	89.46
35	89.66
36	90.74
37	91.43
38	92.86
39	95.43
40	89.85
41	94.19
42	95.16
43	94.74
44	88.54
45	91.94
46	95.36
47	88.43
48	93.64
49	95.12
50	89.44
51	95.78

TABLE 2: Artistic effects of images obtained by multicamera photography.

Num	Graphic arts
1	84.07
2	83.00
3	90.76
4	90.02
5	92.86
6	83.46
7	83.77
8	91.17
9	92.85
10	88.45
11	85.95
12	83.05
13	82.56
14	89.53
15	91.53
16	88.21
17	91.44
18	92.89
19	85.75
20	91.94
21	91.70
22	88.77
23	82.79
24	86.10
25	86.03
26	87.87
27	87.52
28	85.69
29	88.45
30	86.89
31	92.98
32	85.11
33	83.83
34	88.94
35	87.49
36	84.71
37	83.35
38	92.65
39	89.39
40	92.69
41	90.92
42	90.18
43	87.85
44	82.91
45	90.89
46	88.62
47	84.07
48	84.70
49	85.80
50	91.05
51	90.76

facing image. When the camera imaging plane coordinate system and XwDwYw, the plane has some unknown rotation and translation, the image captured at this time is called an oblique captured image. Obviously, compared with the original low-rank texture image, the front-facing image has no deformation, only scaling, and still retains the low-rank characteristic. When shooting at an angle, the image no longer retains low-rank properties due to projection distortion.

On the basis of the above research, the system model proposed in this article is verified, and the expression effect and image art of the multicamera image are evaluated, and the results shown in Tables 1 and 2 are obtained.

From the above research, it can be seen that the research method of multicamera photography image art in BERT motion based on the deep learning model proposed in this article can effectively improve the expression effect of image art.

4. Conclusion

Photography is a kind of visual art, but its expression must be carried out through forms, and different forms bring completely different visual experience. There are many forms of expression, and as one of the visual arts effects, ordering cannot be underestimated. "Ordering" as a guideline in graphic design can make the design more organized and normative. Similarly, for photography, "ordering" will make the photographic work have different formal meanings and show a strong sense of design order. There are many aspects to the formal expression of order in photography, such as symmetry and balance, repetition, and gradual change. These forms of order are often used in graphic art design, which can make the designed picture produce a visual experience of different orders. This article combines the deep learning model to conduct multicamera photographic image art research in BERT motion. The experimental research results show that the research method of multicamera photography image art in BERT motion based on the deep learning mode proposed in this article can effectively improve the expression effect of image art.

Data Availability

The labeled datasets used to support the findings of this study are available from the corresponding author upon request.

Conflicts of Interest

The authors declare no conflicts of interest.

References

[1] A. Martínez-González, M. Villamizar, O. Canévet, and J. M. Odobez, "Efficient convolutional neural networks for depth-based multi-person pose estimation," *IEEE Transactions on Circuits and Systems for Video Technology*, vol. 30, no. 11, pp. 4207–4221, 2019.

[2] M. Li, Z. Zhou, and X. Liu, "Multi-person pose estimation using bounding box constraint and LSTM," *IEEE Transactions on Multimedia*, vol. 21, no. 10, pp. 2653–2663, 2019.

[3] J. Xu, K. Tasaka, and M. Yamaguchi, "[Invited paper] fast and accurate whole-body pose estimation in the wild and its applications," *ITE Transactions on Media Technology and Applications*, vol. 9, no. 1, pp. 63–70, 2021.

[4] G. Szűcs and B. Tamás, "Body part extraction and pose estimation method in rowing videos," *Journal of Computing and Information Technology*, vol. 26, no. 1, pp. 29–43, 2018.

[5] R. Gu, G. Wang, Z. Jiang, and J. N. Hwang, "Multi-person hierarchical 3d pose estimation in natural videos," *IEEE Transactions on Circuits and Systems for Video Technology*, vol. 30, no. 11, pp. 4245–4257, 2019.

[6] M. Nasr, H. Ayman, N. Ebrahim, R. Osama, N. Mosaad, and A. Mounir, "Realtime multi-person 2D pose estimation," *International Journal of Advanced Networking and Applications*, vol. 11, no. 6, pp. 4501–4508, 2020.

[7] N. T. Thành and P. T. Công, "An evaluation of pose estimation in video of traditional martial arts presentation," *Journal of Research and Development on Information and Communication Technology*, vol. 2019, no. 2, pp. 114–126, 2019.

[8] I. Petrov, V. Shakhuro, and A. Konushin, "Deep probabilistic human pose estimation," *IET Computer Vision*, vol. 12, no. 5, pp. 578–585, 2018.

[9] G. Hua, L. Li, and S. Liu, "Multipath affinage stacked—hourglass networks for human pose estimation," *Frontiers of Computer Science*, vol. 14, no. 4, pp. 1–12, 2020.

[10] K. Aso, D. H. Hwang, and H. Koike, "Portable 3D human pose estimation for human-human interaction using a chest-mounted fisheye camera," in *Proceedings of the Augmented Humans Conference 2021*, pp. 116–120, Rovaniemi, Finland, February 2021.

[11] D. Mehta, S. Sridhar, O. Sotnychenko et al., "VNect," *ACM Transactions on Graphics*, vol. 36, no. 4, pp. 1–14, 2017.

[12] S. Liu, Y. Li, and G. Hua, "Human pose estimation in video via structured space learning and halfway temporal evaluation," *IEEE Transactions on Circuits and Systems for Video Technology*, vol. 29, no. 7, pp. 2029–2038, 2018.

[13] S. Ershadi-Nasab, E. Noury, S. Kasaei, and E. Sanaei, "Multiple human 3d pose estimation from multiview images," *Multimedia Tools and Applications*, vol. 77, no. 12, pp. 15573–15601, 2018.

[14] X. Nie, J. Feng, J. Xing, S. Xiao, and S. Yan, "Hierarchical contextual refinement networks for human pose estimation," *IEEE Transactions on Image Processing*, vol. 28, no. 2, pp. 924–936, 2018.

[15] Y. Nie, J. Lee, S. Yoon, and D. S. Park, "A multi-stage convolution machine with scaling and dilation for human pose estimation," *KSII Transactions on Internet and Information Systems (TIIS)*, vol. 13, no. 6, pp. 3182–3198, 2019.

[16] A. Zarkeshev and C. Csiszár, "Rescue method based on V2X communication and human pose estimation," *Periodica Polytechnica: Civil Engineering*, vol. 63, no. 4, pp. 1139–1146, 2019.

[17] W. McNally, A. Wong, and J. McPhee, "Action recognition using deep convolutional neural networks and compressed spatio-temporal pose encodings," *Journal of Computational Vision and Imaging Systems*, vol. 4, no. 1, p. 3, 2018.

[18] R. G. Díaz, F. Laamarti, and A. El Saddik, "DTCoach: your digital twin coach on the edge during COVID-19 and beyond," *IEEE Instrumentation and Measurement Magazine*, vol. 24, no. 6, pp. 22–28, 2021.

Hindawi

Research Article

An Improved Bearing Fault Diagnosis Model of Variational Mode Decomposition Based on Linked Extension Neural Network

Tichun Wang [ID] **and Jiayun Wang**

College of Mechanical and Electrical Engineering, Nanjing University of Aeronautics and Astronautics, Nanjing 210016, China

Correspondence should be addressed to Tichun Wang; wangtichun2010@nuaa.edu.cn

In bearing fault diagnosis, due to the insufficient obtained supervised data and the inevitable noise contained in the vibration signals, the problem of clustering bearing fault diagnosis with imbalanced data containing noise is caused. Thanks to the ability to quickly and fully learn boundary information in small samples, the extension neural network-type 2 algorithm (ENN-2) has the potential in imbalanced data clustering and has been gradually applied in fault diagnosis. Therefore, in order to improve the unstable clustering performance of ENN-2 caused by its heavy dependence on input order of samples, a novel algorithm called linked extension neural network (LENN) is developed by redesigning the correlation function and its iterative method, which greatly reduces the clustering iteration epochs of the algorithm. In addition, an evaluation index of clustering quality for this novel algorithm, extension density, is also proposed. After that, a bearing fault diagnosis model of variational mode decomposition (VMD) based denoising and LENN is proposed. Firstly, VMD is used to get intrinsic mode functions (IMFs), and the correlation coefficients of IMFs are calculated for signal denoising. Secondly, the features are extracted from denoised signals and selected by PCA algorithm, and the fault diagnosis is finally completed by LENN. Compared with ENN-2, K-means, FCM, and DBSCAN based models, the proposed model identifies the faults with different severities more accurately and achieves superior diagnostic ability on different imbalance degrees of datasets, which can further lay a foundation for clustering fault diagnosis based on vibration signals.

1. Introduction

Bearing is one of the most common connecting parts in rotating machinery, which is more likely to break down because of wear, fatigue, corrosion, or overload. Therefore, diagnosis timely and accurately of bearing conditions is of great significance to ensure the mechanical operation steady and reliable. Much study in recent years has focused on bearing fault diagnosis based on vibration signals, including signal acquisition and noise reduction, feature extraction and selection, and fault recognition. However, in industry, diagnostic data is often derived from monitoring signals, bringing great difficulties to record the machinery conditions by frequent downtime checking or manual labeling, which is time-consuming and laborious and resulting in insufficient labeled data for fault diagnosis [1]. Moreover, the number of obtained fault samples is always far less than that

of normal samples from monitoring signals, generating the diagnostic problem of imbalanced data.

Clustering analysis is especially suitable for fault recognition when there is no sufficient labeled data. Because of the nonlinear and unstable characteristics of bearing vibration signals, scholars preserve in their attempts to construct clustering diagnosis models with stronger identification ability. For example, after processing the data by ensemble empirical mode decomposition (EEMD) and linear discriminant analysis (LDA), Hou et al. [2] used Gath-Geva clustering algorithm (GG) to identify the faults of rolling bearing and got a satisfactory clustering result with better intraclass compactness. Chang et al.[3] achieved 96% accuracy of permanent magnet synchronous motors demagnetization fault diagnosis by auto-encoder and K-means algorithm. In addition, Li et al. [4] integrated K-means in the neural network architecture for unsupervised learning and

proposed a deep representation clustering-based diagnosis model to address the data sparsity issue in data-driven machinery fault diagnosis. Also, K-means was utilized together with K-nearest neighbor algorithm (KNN) to identify a transformer's fault category by cumulative votes [5]. On the other hand, for the algorithms which are unnecessary to set the number of fault categories before clustering, the study of Li et al. [6] describes a method to generate clustering template of rolling bearing so as to reduce the effect of noise on diagnostic accuracy using density-based spatial clustering of applications with noise (DBSCAN). This algorithm was also widely used in wind turbine condition monitoring [7] and diagnosis [8], photovoltaic power station fault detection [9], bolts with mission pins on transmission lines detection [10], and thermal runaway diagnosis of battery systems [11]. Moreover, Wei et al.[12] adopted affinity propagation clustering algorithm (AP) and a novel adaptive feature selection technique to identify different fault categories and severities of bearings successfully, and another bearing fault diagnosis model based on expectation maximization algorithm (EM) and wavelet packet was proposed by Zhang et al. [13] for coal cutter. Other clustering algorithms, including spectral clustering [14], fuzzy C-means (FCM) [15], clustering by fast search and find of density peaks algorithm (CFSFDP) [16], and extension neural network-type 2 (ENN-2) algorithm [17–19] were also applied to diagnosis. In conclusion, the clustering algorithms represented by K-means need to know the number of fault categories before clustering, which is contrary to the fact that clustering analysis does not require prior knowledge; however, the clustering algorithms represented by DBSCAN do not need to know the number of fault categories, but suffer a complex parameter adjustment process during training. Therefore, there remains a need for an efficient clustering method with less prior knowledge, simple parameter tuning process, and stable performance.

At the same time, considering the vibration signals used for fault diagnosis not only contain the running state signals of bearings but also contain a lot of aliasing signals with noises, signal denoising methods have generated considerable recent research interest. The commonly used denoising methods mainly include wavelet threshold denoising method, empirical mode decomposition (EMD), ensemble empirical mode decomposition (EEMD), and local mean decomposition (LMD). For example, Komaty et al. [20] introduced a signal-filtering method of EMD and a similarity measure. In their studies, white Gaussian and colored noises were almost removed from the signals by selecting the decomposed modes according to the similarity between the estimation of the probability density function (pdf) of the input signal and that of each mode, and combined EEMD with grey theory, Jia et al. [21] removed the noise of signals by evaluating noise levels of decomposed components of signals by grey relational analysis and selecting the noise-dominant components by grey model. Yang et al. [22] proposed an adaptive signal denoising method based on LMD. However, these decomposition methods have end-effect and modal aliasing phenomena and are more sensitive to sampling frequency, resulting in pretty large decomposition error. To overcome the defects above, Dragomiretskiy and Zosso [23] in 2014 have proposed variational mode decomposition (VMD), which is a new time-frequency analysis method with adaptive signal. Based on VMD, some research combined this method with other algorithms for signal denoising, such as singular value decomposition (SVD) [24], data-driven time-frequency analysis (DDTFA) [25], and wavelet threshold noise reduction [26], and there were also many studies that selected the decomposed modes in some evaluation methods and reconstructed the signal after VMD for noise reduction, such as kurtosis criterion [27], Bhattacharyya distance [28], and a novel parameter called signal clarity proposed by Li et al. [29]. In addition, Wang et al. [30] used VMD innovatively to eliminate outliers and noise points in features extracted from signals so as to achieve the purpose of signal-filtering and denoising.

However, few researchers have addressed the problem of bearing clustering fault diagnosis on imbalanced data with noise at the same time. Thus, in this paper, close attention is paid to develop an effective clustering algorithm on imbalanced data and construct a bearing fault diagnosis model dealing with the insufficient data contained noise. In our study, an improved clustering algorithm of ENN-2, called linked extension neural network (LENN), is proposed firstly, and based on this algorithm and VMD-based denoising method, a novel bearing fault diagnosis model is presented and applied to analyze the fault conditions and severities of bearings. To validate the effectiveness of the proposed algorithm and the model, three comparative experiments are designed and conducted on commonly used artificial clustering datasets and real bearing fault signals. The results manifest that the proposed model yields higher identification accuracy of minority fault clusters on imbalanced data with noise comparing with the models based on ENN-2, K-means, fuzzy C-means (FCM), and DBSCAN. Our study provides a promising method for machinery fault diagnosis based on insufficient labeled signals with imbalance, permitting an easier parameter adjustment process with less prior knowledge.

The rest of this paper starts with the novel LENN algorithm in Section 2. Section 3 provides a brief description of the proposed model, and the proposed algorithm and model are experimentally verified in Section 4. In Section 5, the concluding remarks are drawn.

2. Linked Extension Neural Network

Extension neural network-type 2 algorithm (ENN-2) is a new clustering algorithm based on extension theory [31]. With no need to set the number of clusters manually in advance, ENN-2 shows good clustering ability and fast convergence speed in simple construction. But in fact, the performance of ENN-2 relies heavily on the initial points and correct input order of the samples. To overcome these deficiencies, we develop a novel clustering algorithm called linked extension neural network (LENN).

2.1. Network Structure. Following the form of ENN-2, the structure of LENN contains only two layers, which is shown in Figure 1. The number of input layer nodes depends on the feature dimension of data, and the number of output layer
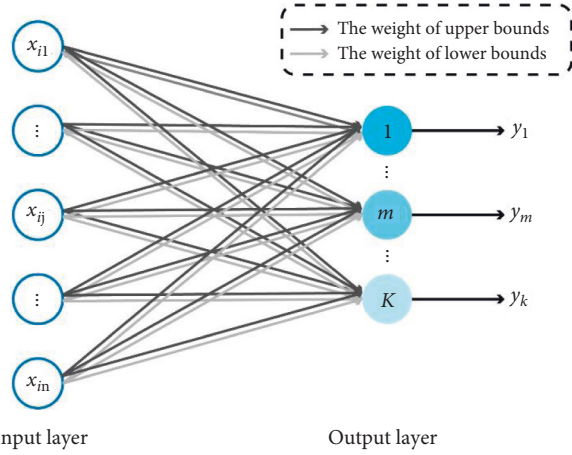
FIGURE 1: Structure of linked extension neural network (LENN).

FIGURE 2: Image of correlation function ED in ENN-2.

nodes is determined by the number of clusters. Between the two layers, the upper and lower bounds of the clusters connect the neurons as the connection weights, and output neurons are successively constructed in the process of iteration (represented by color shades in Figure 1), with only one node activated at a time to indicate the clustering result.

2.2. Improved Correlation Function

2.2.1. Correlation Function in ENN-2.
In ENN-2, the correlation function ED based on the extension distance is used to measure the distance between a sample and a target cluster. The extension distance in extension theory describes the distance between a point x and an interval $V = \langle a, b \rangle$ quantitatively, which is defined as

$$\rho(x, V) = \left| x - \frac{a+b}{2} \right| - \frac{a-b}{2}, \tag{1}$$

where a and b are the lower and the upper bounds of V, respectively.

Given the center of the kth cluster is $Z_k = [z_{k1}, z_{k2}, \cdots, z_{kn}]$, the boundary of the kth cluster can be represented by introducing a hyperparameter to measure the distance between the center and the ideal boundary as

$$\begin{aligned} W_k &= [\langle a_{k1}, b_{k1} \rangle, \langle a_{k2}, b_{k2} \rangle, \ldots, \langle a_{kn}, b_{kn} \rangle] \\ &= [\langle z_{k1} - \lambda, z_{k1} + \lambda \rangle, \langle z_{k2} - \lambda, z_{k2} + \lambda \rangle, \ldots, \langle z_{kn} - \lambda, z_{kn} + \lambda \rangle], \end{aligned} \tag{2}$$

Also, based on the definition of extension distance, the correlation function ED between a sample $X = [x_1, x_2, \cdots, x_n]$ and the boundary W_k of the kth cluster is defined as

$$ED_k = \sum_{j=1}^{n} \left[\frac{|x_{ij} - z_{kj}| - (b_{kj} - a_{kj})/2}{|b_{kj} - a_{kj}|/2} \right], \quad k = 1, 2, \ldots, K. \tag{3}$$

As shown in Figure 2, ED measures the extension relationship between a feature and its boundary. From

Figure 2, it can be seen that, for the jth dimension of the kth cluster, when $x_j \in \langle a_{kj}, b_{kj} \rangle$, $ED_{kj} \le 1$.

For a sample $X = [x_1, x_2, \cdots, x_n]$ with n-dimensional features, the sample X could be classified into the kth cluster if

$$ED_k \le n, \quad k = 1, 2, \ldots, K. \tag{4}$$

Thanks to this property of ED, the algorithm can estimate a sample belongs to which cluster and update the boundary and the center of the corresponding cluster to revise its information for iteration. Therefore, ENN-2 does not require the number of clusters K before learning and can obtain better clustering results by only adjusting the unique hyperparameter λ.

However, since the input order of samples determines the updating direction of clusters' boundaries and centers in the iteration process, ENN-2 is greatly affected by the initial point selection and the input order of samples and shows unstable clustering performances. Therefore, it is necessary to improve this algorithm.

2.2.2. Improved Correlation Function in LENN.
Different from ENN-2, each sample could be considered as a center during iteration in LENN. Take $X = [x_{11}, x_{12}, \cdots, x_{1n}]$ for example, its boundary W_{X1} can be represented as (4) with the hyperparameter λ:

$$\begin{aligned} W_{X_1} &= \left[\langle a_{x_11}, b_{x_11} \rangle, \langle a_{x_12}, b_{x_12} \rangle, \ldots, \langle a_{x_1n}, b_{x_1n} \rangle \right] \\ &= \left[\langle x_1 - \lambda, x_1 + \lambda \rangle, \langle x_2 - \lambda, x_2 + \lambda \rangle, \ldots, \langle x_n - \lambda, x_n + \lambda \rangle \right]. \end{aligned} \tag{5}$$

In order to measure the correlation distance between the sample $X = [x_{21}, x_{22}, \ldots, x_{2n}]$ and W_{X1}, the new correlation function is defined as

$$\begin{aligned} ED_{X_1, X_2} &= \sum_{j=1}^{n} \left[\frac{|x_{2j} - x_{1j}| - (b_{x_1j} - a_{x_1j})/2}{(b_{x_1j} - a_{x_1j})/2} + 1 \right] \\ &= \sum_{j=1}^{n} \left[\frac{\left| \|x_{2j} - x_{1j}\| \right|}{\lambda} \right]. \end{aligned} \tag{6}$$

The new correlation function is plotted in Figure 3. For the jth feature of the two samples, when $X_{2j} \in \langle a_{X_1j}, b_{X_1j} \rangle$, $ED_{X_1j, X_2j} \le 1$, and taking all features into account, the sample X_2 could be considered to belong to the same cluster as sample X_1 if
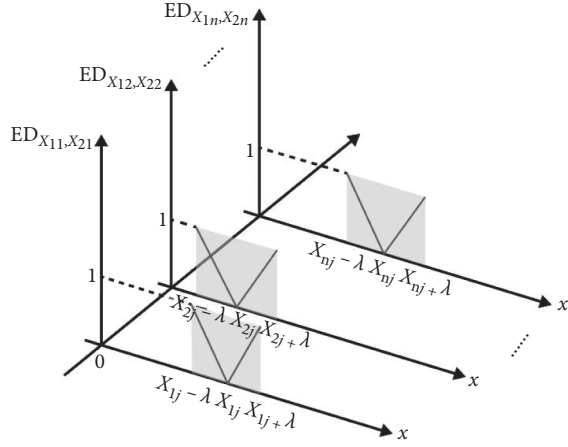
FIGURE 3: Image of new correlation function ED in LENN.

$$ED_{X_1, X_2} \leq n. \tag{7}$$

2.3. Learning Algorithm of LENN.

The learning process of LENN is an unsupervised learning. It takes a dataset $X = [x_1, x_2, \cdots, x_m]$ with samples as the input, and after calculating the correlation distances between samples level by level, the clustering results of the dataset are finally output in just one epoch. The specific learning steps are as follows:

(1) Set an optimal hyperparameter λ in $(0 \sqrt{\max(x_{ij})}]$.

(2) Input a sample $X_i = [x_{i1}, x_{i2}, \cdots, x_{im}]$ randomly and mark the cluster which belongs to as $k = 0$. Calculate the improved correlation function ED between X_i and all the other unmarked samples according to equation (5) and mark the samples which meet the requirements of $ED \leq n$ as $k = 0$. (3) For all the qualified samples in step (2), each sample is taken as the center to traverse, and EDs between this sample and all the remaining unmarked samples are calculated. Similarly, the samples that meet the condition of $ED \leq n$ are also marked as $k = 0$ until no qualified samples left. (4) A sample is randomly generated from the remaining unmarked samples for input to create a new cluster $k = k + 1$. Repeat steps (2) and (3).

(5) The learning process is finished until all samples are marked.

At the end of the iteration, if a cluster contains too few samples, it can be regarded as noise.

The iterative approaches of ENN-2 and LENN are both graphically presented in Figure 4. During the iteration, ENN-2 needs to update the central coordinates each time (represented by the orange dots), and the updating direction is significantly affected by the input order of the samples. Ideally, the input order of the samples should be sorted according to the distance between samples from small to large, which is pretty difficult to ensure for the unpretreated messy datasets. As can be seen from Figure 4(a) clearly, sample 6 is closer to the center

corresponding to sample 4 than sample 5. If sample 6 is input for calculation first according to (3), the result meets the requirement of (4), indicating sample 6 and samples 1~4 belong to the same cluster, and then the final clustering results of the whole dataset contain 2 clusters. But, if input sample 5 first for calculation, the result of (3) does not satisfy (4) because of the distant relationship of sample 5 and the current center, and then a new cluster is created for iteration, resulting in the final results of 3 clusters. However, in Figure 4(b) of LENN, one specific sample is regarded as the center each time, and all the qualified samples which satisfy (7) with the sample are found and marked in this iteration. Taking two-dimensional eigenspace as an example, the learning essence of LENN is to find the samples consecutively which fall in the square constructed by the initial center sample with 2λ as the side length. All the qualified samples are classified into the same cluster with their center. And then, the next iteration begins with a subsample of the cluster. Finally, all qualified samples of the same cluster are found by this iterative linkage method. Therefore, in Figure 5, samples 1, 4, 6, 5, and 10 are successively taken as the centers for iteration, and the final clustering result contains only 2 clusters with samples 1~9 belonging to the same cluster.

According to the learning process of the algorithm, LENN has the following remarkable advantages:

(1) Based on extension distance, LENN defines a new approach to categorization by distance calculation.

(2) There is no need to preset the number of clusters as in ENN-2; in addition, it is not necessary to initialize clustering center.

(3) The improved algorithm only needs one epoch to complete the clustering process and converges faster.

(4) LENN is not sensitive to the initial center and the input order of the samples and preserves more stable clustering ability than ENN-2.

Nevertheless, LENN is very sensitive to the hyperparameter λ, so it is necessary to select the optimal λ before learning.

2.4. Parameter Selection Method.

In LENN, the selection of the hyperparameter λ seriously affects the final number of clusters and the accuracy of clustering results. As shown in Figure 5, for a smaller λ (such as $\lambda = 7.2$ in Figure 5(a)), the constructed squares will be smaller with fewer qualified samples contained, resulting in more clusters in the end, and for a bigger λ (such as $\lambda = 8.7$ in Figure 5(b)), the constructed squares will be likewise bigger with more qualified samples contained, and fewer clusters are produced finally.

For clustering algorithms, silhouette coefficient is often used for evaluation with no real labels. However, this index is more suitable to analyze the clustering effectiveness of balanced data [32]. Considering this paper is primarily concerned with imbalanced data clustering problem, a novel evaluation index extension density EDe is developed to tune the hyperparameter λ based on extension distance, which is defined as
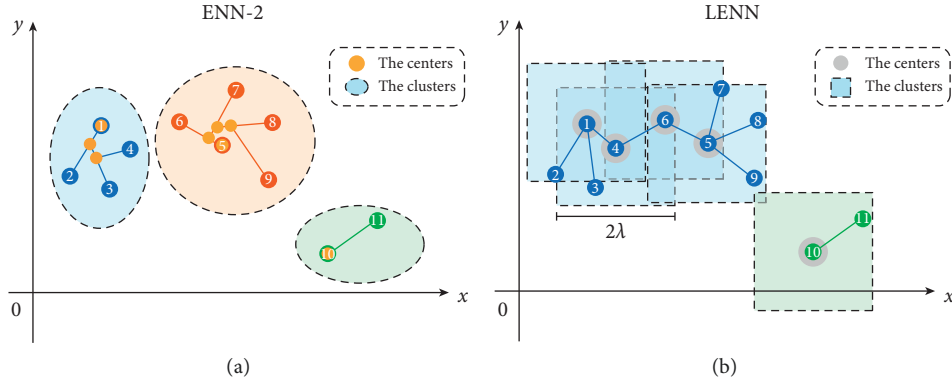
FIGURE 4: Iterative approaches: (a) ENN-2 and (b) LENN.
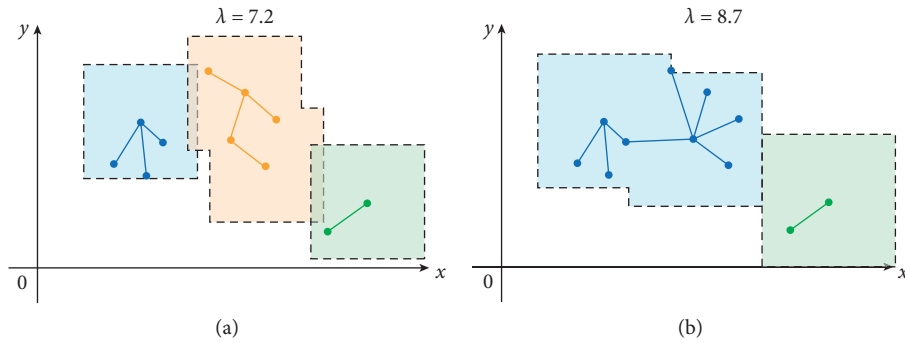
FIGURE 5: The influence of hyperparameter λ on LENN clustering process: (a) a smaller λ and (b) a bigger λ.

$$E\,De = \sum_{k=1}^{C} \frac{\sum_{x_i \in M_k, j=1}^{n} |x_{ij} - z_{kj}| - b_{kj} - a_{kj}/2}{m_k}, \qquad (8)$$

where m_k is the number of samples in the kth cluster, Z_{kj} is the center of the jth feature, and a_{kj} and b_{kj} represent the lower and upper bounds of the kth cluster respectively, a_{kj}, b_{kj} and can be computed by

$$a_{kj} = \min_{x_i \in M_k}(x_j),$$

$$b_{kj} = \min_{x_i \in M_k}(x_j), \qquad (9)$$

$$z_{kj} = \frac{b_{kj} - a_{kj}}{2}.$$

Typically, EDe declines with the increasing λ, and the optimal λ lies in the turning point of the curve.

3. Proposed Bearing Fault Diagnosis Model

3.1. Signal Denoising. Bearing vibration signals tend to present nonlinear and nonstationary characteristics with noise inevitably. Without signal denoising, the outliers in raw data will be transferred into the feature space through feature extraction and affecting the diagnostic results of the model. Compared with empirical mode decomposition (EMD) and ensemble empirical mode decomposition

(EEMD), variational mode decomposition (VMD) can effectively extract each frequency component of the signal and solve the problems of mode mixing and white noise. Therefore, VMD-based method is used for noise reduction in this paper.

3.1.1. The Principle of VMD. VMD is a variational problem solving process based on classical Wiener filter, Hilbert transform, and mixing, which can be written as the following constrained optimization form:

$$\min_{\{u_k\},\{\omega_k\}} \left\{ \sum_k \left\| \partial_t \left[\left(\delta(t) + \frac{j}{\pi t} \right) * u_k(t) \right] e^{-j\omega_k t} \right\|_2^2 \right\}$$

$$\text{s.t.} \sum_{k=1}^{K} u_k = f, \qquad (10)$$

where K is the number of modes to be decomposed, $\delta(t)$ represents Dirac function, *means the convolution operator, and $\{u_k\}$ and $\{\omega_k\}$ stand for the kth intrinsic mode function (IMF) and center frequency after decomposition.

The solution process of this problem is as follows:

(1) Transform the constrained variational problem to a nonconstrained variational problem by introducing the quadratic penalty factor α and Lagrange multiplier $\lambda(t)$:

$$L(\{u_k\},\{\omega_k\},\lambda) = \alpha \sum_k \left\| \partial_t \left[\left(\partial(t) + \frac{j}{\pi t} \right) * u_k(t) \right] \right\|_2^2 + \left\| f(t) - \sum_k u_k(t) \right\|_2^2 + \left\langle \lambda(t), f(t) - \sum_k u_k(t) \right\rangle. \tag{11}$$

(2) Solving the minimization problem of equation (12), alternating direction method of multipliers (ADMM) is adopted to seek the saddle point of the

augmented Lagrange expression by alternatively updating u_k^{n+1}, ω_k^{n+1}, and λ^{n+1}, and u_k^{n+1} can be obtained by

$$u_k^{n+1} = \underset{u_k \in X}{\arg\min} \left\{ \alpha \left\| \partial_t \left[\left(\delta(t) + \frac{j}{\pi t} \right) * u_k(t) \right] e^{-j\omega_k t} \right\|_2^2 + \left\| f(t) - \sum_i u_i(t) + \frac{\lambda(t)}{2} \right\|_2^2 \right\}, \tag{12}$$

where ω_k equals to ω_k^{n+1}, and $\sum_i u_i(t)$ equals to $\sum_{i\neq k} u_i(t)^{n+1}$.

Next, transform to frequency domain by Parseval/Plancherel Fourier isometric transform:

$$\hat{u}_k^{n+1} = \underset{\hat{u}_k, u_k \in X}{\arg\min} \left\{ \alpha \left\| j\omega \left[(1 + \operatorname{sgn}(\omega + \omega_k)) \hat{u}_k(\omega + \omega_k) \right] \right\|_2^2 + \left\| \hat{f}(\omega) - \sum_i \hat{u}_i(\omega) + \frac{\hat{\lambda}(\omega)}{2} \right\|_2^2 \right\}. \tag{13}$$

Replace ω in (13) with $\omega - \omega_k$ and then we can get

$$\hat{u}_k^{n+1} = \underset{\hat{u}_k, u_k \in X}{\arg\min} \left\{ \alpha \left\| j(\omega - \omega_k) \left[(1 + \operatorname{sgn}(\omega + \omega_k)) \hat{u}_k(\omega) \right] \right\|_2^2 + \left\| \hat{f}(\omega) - \sum_i \hat{u}_i(\omega) + \frac{\hat{\lambda}(\omega)}{2} \right\|_2^2 \right\}. \tag{14}$$

(14) is then converted to the form of nonnegative frequency interval integral:

$$\hat{u}_k^{n+1} = \arg\min \left\{ \int_0^\infty 4\alpha(\omega - \omega_k)^2 \left| \hat{u}_k(\omega) \right|^2 + 2 \left| \hat{f}(\omega) - \sum_i \hat{u}_i(\omega) + \frac{\hat{\lambda}(\omega)}{2} \right|^2 d\omega \right\}, \tag{15}$$

and set the first item in (15) to zero to obtain the quadratic optimization problem:

$$\hat{u}_k^{n+1}(\omega) = \frac{\hat{f}(\omega) - \sum_{i\neq k}\hat{u}_i(\omega) + \hat{\lambda}(\omega)/2}{1 + 2\alpha(\omega - \omega_k)^2}. \tag{16}$$

Similarly, the minimization problem of the center frequency can be obtained by converting the center frequency updating problem to frequency domain:

$$\omega_k^{n+1} = \frac{\int_0^\infty \omega \left| \hat{u}_k^{n+1}(\omega) \right|^2 d\omega}{\int_0^\infty \left| \hat{u}_k^{n+1}(\omega) \right|^2 d\omega}, \tag{17}$$

where $\hat{u}_k^{n+1}(\omega)$ is the Wiener filtering of $\hat{f}(\omega) - \sum_{i\neq k}\hat{u}_i(\omega)$, and ω_k^{n+1} represents the center of power spectrum.

Also, the learning process of VMD is as follows:

(1) Initialize $\left\{ \hat{u}_k^1 \right\}$, $\{\omega_k^1\}$, $\left\{ \hat{\lambda}^1 \right\}$ and n.

(2) Update u_k and $\overset{k}{\omega}$ according to equations (16) and (17).

(3) Update λ by

$$\hat{\lambda}^{n+1}(\omega) \leftarrow \hat{\lambda}^n(\omega) + \tau \left[\hat{f}(\omega) - \sum_k \hat{u}^{n+1}(\omega) \right]. \tag{18}$$

(4) For a given discriminant accuracy of $\varepsilon > 0$, if $\sum_k \|\hat{u}_k^{n+1}\| \sum_k \|\hat{u}_k^{n+1} - \hat{u}_k^n\|_2^2 / \|\hat{u}_k^n\|_2^2 < \varepsilon$, stop iteration, otherwise return to step (2).

3.1.2. VMD-Based Denoising Method. The VMD-based denoising method comprises two steps: (a) decompose the

vibration signal by VMD. (b) Calculate correlation coefficients of IMFs obtained by VMD for noise filtering and reconstruct the denoised signal. The parameters α, $\lambda(t)$, and K of VMD should be set before decomposition, which may affect the results noticeably.

Correlation coefficient is to describe the correlation degree between the original signal Y and its IMFs $X(i)$, which is defined as

$$\rho_i = \frac{COV(X(i), Y)}{\sqrt{D(X(i))}\sqrt{D(Y)}}. \tag{19}$$

The correlation coefficient also offers a means of measuring the degree of noise contained in IMFs. Thus, by selecting the sensitive IMFs according to (20) below [33], we are able to obtain the reconstructed denoised signal:

$$\mu_i = \frac{\max(\rho_i)}{10^* \max(\rho_i) - 3}, \tag{20}$$

where μ_i is the threshold of the ith IMF. Retain the IMFs of $\rho_i < \mu_i$ as sensitive IMFs for signal reconstruction, and remove the unqualified IMFs directly.

3.2. Feature Extraction and Selection

3.2.1. Bearing Fault Features. In feature extraction, to reflect the operation conditions of bearings accurately, objectively, and simply, statistical features are extracted from the denoised signals in this study, including 11 time domain statistical features $F_1 \sim F_{11}$ and 12 frequency domain statistical features $F_{12} \sim F_{23}$ shown in Table 1 [34]. For time domain statistical features extracted from raw signals, F_1 and $F_3 \sim F_5$ reflect the amplitude and energy of vibration in time domain; F_1 and $F_6 \sim F_{11}$ present the distribution of the signal in time series. For frequency domain statistical features extracted from FFT spectrums, F_{12} shows the vibration energy in frequency domain; $F_{13} \sim F_{15}$, F_{17}, and $F_{21} \sim F_{23}$ stand for the dispersion and concentration degree of the spectrum; F_{16} and $F_{18} \sim F_{20}$ represent the position variation of the main frequency band.

Here, $x(n)$ is a signal series in time domain, $n = 1, 2, \ldots, N$; N is the number of data points. $s(k)$ is a frequency spectrum of signal $x(n)$, $k = 1, 2, \ldots, K$, K is the number of spectrum lines, and f_k is the frequency value of the kth spectrum line.

3.2.2. Feature Selection Based on PCA. Although the multidomain features obtained above better describe the signals than using time domain or frequency domain features only, there may be feature redundancy, which will affect the diagnostic performance of the model. Considering the lack of labels of samples in clustering fault diagnosis, a commonly used unsupervised feature reduction algorithms principal component analysis (PCA) is adopted in the diagnosis model. The specific steps of PCA are as follows:

Let the multidomain characteristic matrix obtained above be $X_{n \times m} = [X_1, X_2, \cdots, X_m]$, where the number of

Table 1: Statistical features of time domain and frequency domain.

No.	Equation
Time domain features	
F_1	$\sum_1^N x(n)/N$
F_2	$\sqrt{\sum_1^N (x(n) - F_1)/N - 1}$
F_3	$(\sum_1^N \sqrt{|x(n)|}/N)^2$
F_4	$\sqrt{\sum_1^N (x(n))^2/N}$
F_5	$\max|x(n)|$
F_6	$\sum_1^N (x(n) - F_1)^3/(N-1)F_2^3$
F_7	$\sum_1^N (x(n) - F_1)^4/(N-1)F_2^4$
F_8	F_5/F_4
F_9	F_5/F_3
F_{10}	$F_4/1/N \sum_1^N |x(n)|$
F_{11}	$F_5/1/N \sum_1^N |x(n)|$
Frequency domain features	
F_{12}	$\sum_1^K s(k)/K$
F_{13}	$\sum_1^K (s(k) - F_{12})^2/K - 1$
F_{14}	$\sum_1^K (s(k) - F_{12})^4/KF_{13}^2$
F_{15}	$\sum_1^K (s(k) - F_{12})^3/K(\sqrt{F_{13}})^3$
F_{16}	$\sum_1^K f_k s(k)/\sum_1^K s(k)$
F_{17}	$\sqrt{\sum_1^K (f_k - F_{16})^2 s(k)/K}$
F_{18}	$\sqrt{\sum_1^K f_k^2 s(k)/\sum_1^K s(k)}$
F_{19}	$\sqrt{\sum_1^K f_k^4 s(k)/\sum_1^K f_k^2 s(k)}$
F_{20}	$\sum_1^K f_k^2 s(k)/\sqrt{\sum_1^K s(k)\sum_1^K f_k^4 s(k)}$
F_{21}	F_{17}/F_{16}
F_{22}	$\sum_1^K (f_k - F_{16})^3 s(k)/KF_{17}^3$
F_{23}	$\sum_1^K (f_k - F_{16})^4 s(k)/KF_{17}^4$

samples is m, and the dimension of features is n, then its covariance matrix C can be obtained by

$$C = \frac{1}{m}(X - \overline{X})(X - \overline{X})^T, \tag{21}$$

where $\overline{X}$ is a $n \times m$ matrix composed of row vectors of X, $\overline{X}_i = 1/m \sum_{j=1}^m x_{ij}, i = 1, 2, \cdots n$.

After that, the eigenvalues and the eigenvectors of the covariance matrix C are calculated by

$$|C - \lambda I_n| = 0, \tag{22}$$

where $\lambda_1, \lambda_2, \cdots, \lambda_n$ are the eigenvalues of C, and $P_1, P_2, \cdots, P_n$ are the corresponding eigenvectors of the eigenvalues.

Arrange the eigenvectors according to the magnitude of the corresponding eigenvalues, take the front k rows of eigenvectors to form the matrix P, and obtain the k-dimensional data Y by

$$Y = PX. \tag{23}$$

3.3. Bearing Fault Diagnosis Model of VMD-Based Denoising and LENN. Based on the above techniques, a bearing fault diagnosis model of VMD-based denoising and LENN is proposed in this paper, including three stages: (a) signal

denoising based on VMD and correlation coefficient calculation of IMFs; (b) feature extraction and selection by PCA; (c) clustering fault diagnosis on LENN. The specific diagnostic steps are as follows, which are shown in Figure 6.

(1) After signal acquisition, divide the raw signals into some segments of 2048 data points.

(2) For the sake of noise reduction, decompose each signal and calculate correlation coefficients and thresholds of IMFs according to equations (19)~(20). Reconstruct the signals by retaining the sensitive IMFs and removing the IMFs of $\rho_i \geq \mu_i$.

(3) Based on the denoised signals, 11 time domain statistical features are extracted from the signals and 12 frequency domain statistical features are extracted from their FFT spectrums according to Table 1.

(4) In order to avoid the influence of redundant features on the diagnosis results and improve the diagnostic speed of the model, PCA algorithm is used to obtain low-dimensional fault features for diagnosis.

(5) Finally, the proposed LENN algorithm will identify bearing fault conditions by clustering the obtained low-dimensional feature matrix into different clusters and achieve fault diagnosis.

4. Experimental Verification

4.1. Experiment of LENN Algorithm on Artificial Datasets. In order to verify the clustering effectiveness and stability of the proposed LENN algorithm on imbalanced data, LENN, ENN-2, and three commonly used clustering algorithms, namely, K-means, fuzzy C-means (FCM), and DBSCAN were experimented on three artificial datasets commonly used for clustering testing, which were Flame, Jain and Aggregation. These three datasets are all in two dimensions with different degrees of imbalance, which are summarized in Table 2. From Figure 7 of the real distributions of the datasets, it can be seen that Flame consists of a circle and a semiring, Jain contains two semirings, and Aggregation is composed of many rounded or crescent clusters with two clusters connected, which increase the difficulty of clustering.

Adopt Rand Index to evaluate the clustering results of the algorithms here, which is defined as

$$\mathrm{RI} = \frac{a+b}{a+b+h+g},\tag{24}$$

where a denotes the number of data pairs (x_i, x_j) whose clustering results and real labels are in the same category; b represents the number of data pairs (x_i, x_j) whose clustering results and real labels fall in the different categories; h denotes the number of data pairs (x_i, x_j) whose clustering results are of the same category while real labels are of different categories; and g represents the number of data pairs (x_i, x_j) whose clustering results turn to be of different categories while real labels turn to be of the same category.

In the experimental process of LENN, the optimal value range of λ was narrowed in each round of the experiment based on $(0, \sqrt{\max(x_{ij})}]$ to obtain the optimal λ, and the optimal λ

selection processes of LENN on three datasets are shown in Figure 8. As can be seen from the figure, RI reaches a peak at the inflection point of the EDe drop-down curve, and the corresponding value of λ is just the desired λ, and for ENN-2, the optimal λ was determined in the same way based on (0, 1]. The parameter K of K-means was set according to the real number of categories of each experimental dataset, and the parameter setting of FCM was the same as above. In the training process of DBSCAN, the optimal combination of the radius parameter ε and the field density threshold MinPts was searched for several times with the initial range of ε set as (0, 2] and the initial range of MinPts set as [2, 10]. In order to eliminate the influence of the sample input order on the experimental results, each experiment was conducted for ten times by disrupting the sample input order randomly to obtain RI score of the five algorithms, which are depicted in boxplots in Figure 9 and summarized in Table 3. Figure 10 presents the clustering performances of LENN graphically on three datasets.

In general, LENN achieved better performances in higher accuracy and stability on the three different datasets. Comparing Figure 9 and Table 3, it can be observed that, in terms of clustering accuracies, LENN and DBSCAN were not affected by the shape of data distribution, showing higher RI scores overall; while ENN-2, K-means, and FCM were highly affected by the shape of data distribution, all of them performed worse on semiorbicular clusters than rounded clusters, among which ENN-2 scored lowest on Flame and FCM scored lowest on Jain; in terms of clustering stability, which was visible in Figure 9, LENN showed extremely stable clustering performances on different input orders of samples, and there were small fluctuations in clustering stability of DBSCAN, K-means, and FCM, while ENN-2 showed the worst stability with the largest range of RI reaching 0.2436 on Flame. In particular, LENN scored highest on both Flame and Jain with nearly no impact of imbalanced data distribution on clustering, while scored slightly lower than that of DBSCAN on Aggregation. That was because, for Flame and Jain in Figure 10, all misclassified points of LENN, which were considered as noise, were individuals far away from their surrounding points; while for Aggregation, two clusters were closely connected distinctly by several data points, resulting in the algorithm which classified the two connected clusters as one cluster because of LENN's iterative distinguish mechanism; in spite of this, LENN could still fully identify the other minority clusters in Aggregation. As for ENN-2, only a small number of cases showed higher clustering accuracies on Aggregation, indicating that ENN-2 is better at processing rounded clusters, but still relies heavily on an appropriate sample input order. It could be concluded that the proposed LENN algorithm could deal with the clustering problem on imbalanced data in terms of higher accuracy and stability, addressing the limitations of dependency on input order of samples.

4.2. Bearing Fault Diagnosis Process of Proposed Model. The main purpose of this work was to establish an effective bearing fault diagnosis model on imbalance data with noise, so in this part, experiments were carried out based on
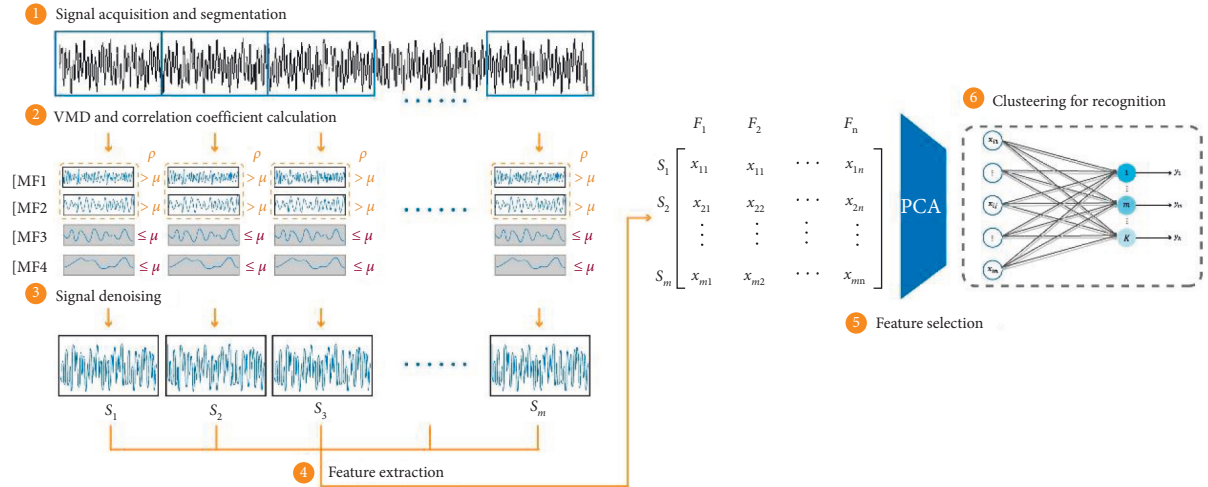
FIGURE 6: Flowchart of the proposed bearing fault diagnosis model.

TABLE 2: Description of the artificial datasets.

No.	Dataset	Degrees of imbalance	Feature dimensions	Number of categories	Number of samples
1	Flame	147 : 93	2	2	240
2	Jain	276 : 97	2	2	373
3	Aggregation	272 : 170 : 127 : 105 : 45 : 35 : 34	2	7	788
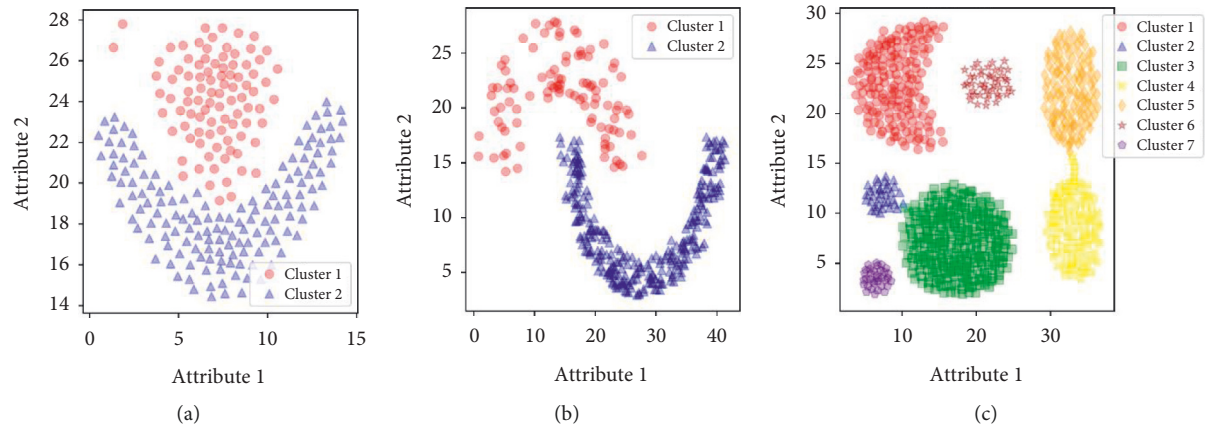
FIGURE 7: The real distributions of the datasets. (a) Flame. (b) Jain. (c) Aggregation.

bearing fault data from Case Western Reserve University [35, 36] to test the performance of the proposed VMD-based denoising and LENN model by comparing with the ENN-2-based model.

4.2.1. Experimental Data. The test rig for data acquisition is shown in Figure 11, which consists of a motor driving a shaft, a force meter, a torque transducer, and an electrical control device. In this part, we selected the data of a 6205-2RS deep-groove ball bearing from SKF Company, which were grouped into five categories, including normal, minor inner race fault (with the fault size of 0.1778 mm), serious inner race fault (with the fault size of 0.5334 mm), minor ball fault (with the fault size of 0.1778 mm), and serious ball fault (with the fault size of 0.5334 mm). After dividing the raw

signals into segments of 2048 data points, five datasets above comprised the whole data of this experiment with the imbalance degree of 2 : 1:1 : 1:1, which are listed in Table 4.

4.2.2. Signal Denoising and Feature Extraction and Selection. Firstly, VMD was carried out on the segmented fault samples. Here, set $\alpha = 2000$, $\lambda(t) = 1.5$, and the initial distribution of center frequency was uniform. Considering improper selection of the number of decomposition K will lead to excessive or insufficient decomposition, therefore, K was determined according to the change of the center frequency of each mode in this paper. Taking VMD results of minor inner race fault (MIF) for example, as shown in Table 5, there were similar center frequencies appearing when $K = 5$, which may be attributed to mode mixing and

(a)   (b)   (c)
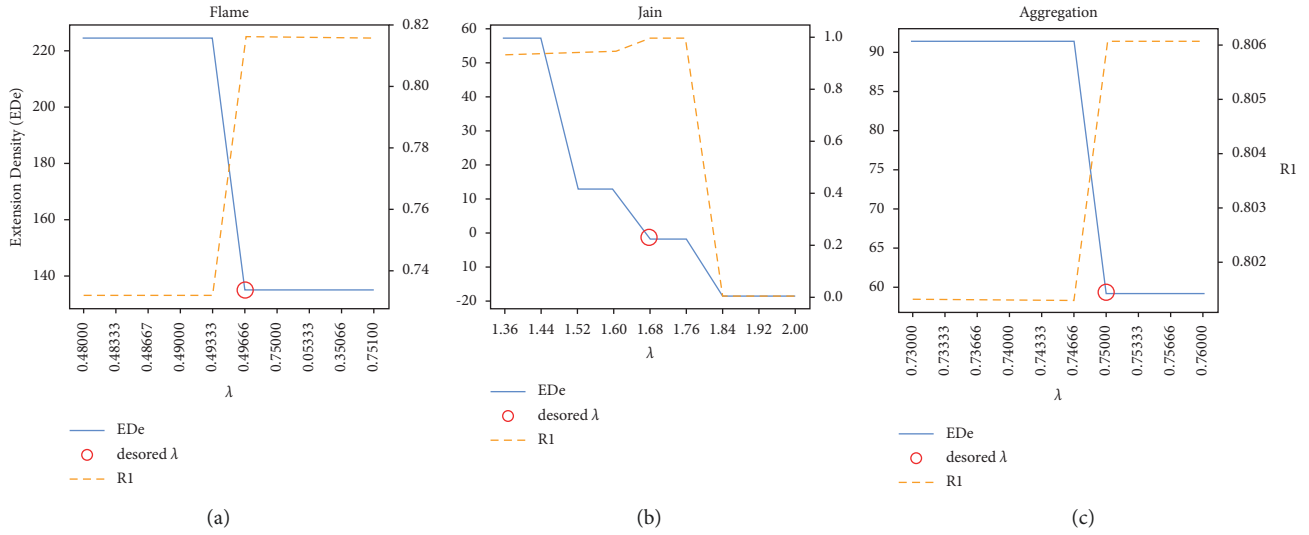
Figure 8: The optimal selection processes of LENN on three datasets. (a) Flame. (b) Jain. (c) Aggregation.

(a)   (b)   (c)
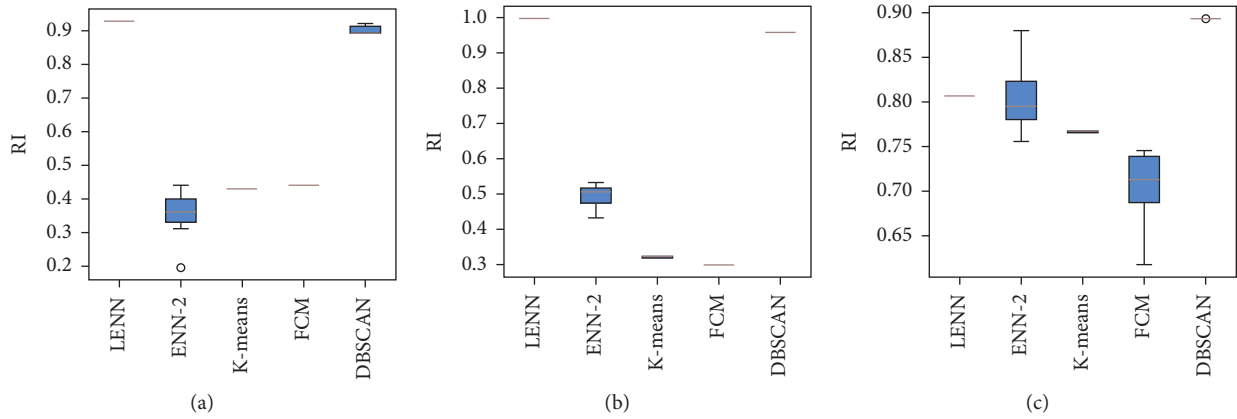
Figure 9: Boxplots of the results of five algorithms on three datasets. (a) Flame. (b) Jain. (c) Aggregation.

Table 3: RI scores of the five algorithms.

Algorithm	Target	Flame	Jain	Aggregation
LENN	Mean	0.9284	0.9971	0.8061
	Range	0	0	0
ENN-2	Mean	0.3547	0.4941	0.8033
	Range	0.2436	0.0998	0.1240
K-means	Mean	0.4311	0.3217	0.7663
	Range	0	0.0060	0.0024
FCM	Mean	0.4422	0.3004	0.7005
	Range	0	0	0.1276
DBSCAN	Mean	0.9028	0.9584	0.8934
	Range	0.0273	0	0.0003

excessive decomposition. Thus, K was set as four. Similarly, the number of decomposition K of other datasets was determined to be four, and the VMD results of a sample of five conditions are shown in Figure 12.

Then, the correlation coefficients and thresholds corresponding respectively to IMFs and the original signal were calculated according to equations (19)~(20). The obtained

results of all samples are graphically presented in Figure 13. Retain the corresponding IMFs whose correlation coefficient is above the red line and get the reconstructed signals.

Next, after signal denoising, extract the 23-dimensional features of each sample from both time and frequency domain according to Table 1, and PCA was used for feature selection and dimension reduction. By comparing the
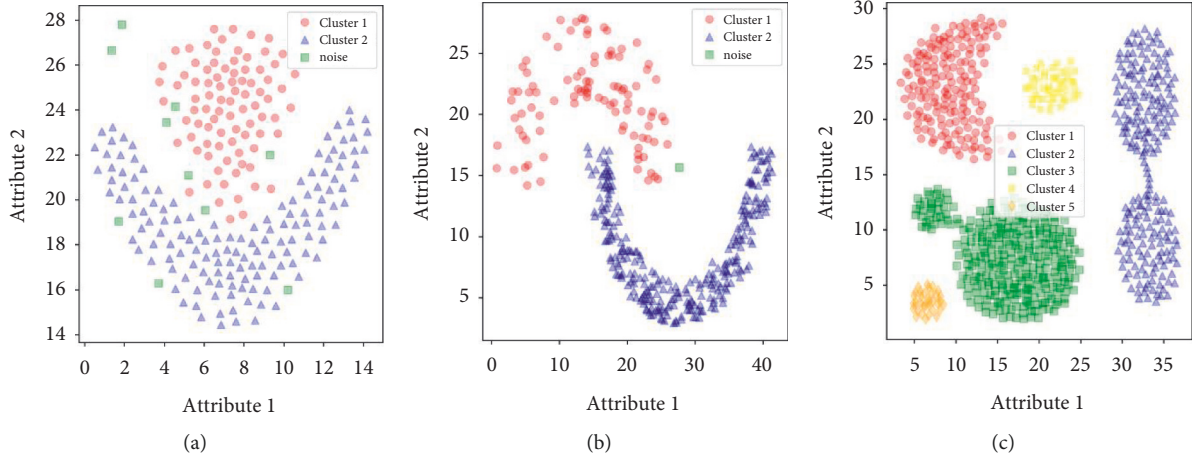
Figure 10: Clustering performances of LENN on three datasets. (a) Flame. (b) Jain. (c) Aggregation.
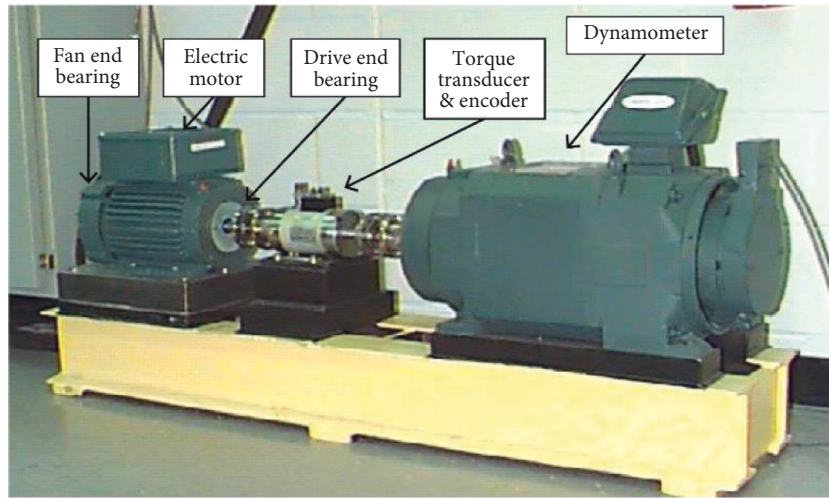
Figure 11: CWRU bearing test rig35.

Table 4: Description of bearing fault data.

Fault type	Motor speed (rpm)	Motor load (hp)	Sample frequency (kHz)	Fault size (mm)	Number of samples
Normal (N)	1797	0	12	-	119
Minor inner race fault (MIF)	1797	0	12	0.1778	59
Serious inner race fault (SIF)	1797	0	12	0.5334	59
Minor ball fault (MBF)	1797	0	12	0.1778	59
Serious ball fault (SBF)	1797	0	12	0.5334	59

dimensionality reduction results in two and three dimensions in Figure 14, it is visible that, in two dimensions, the cluster of normal is far away from others, while the other four clusters are pretty closer; moreover, the clusters of the same parts with different severities are very close to each other, with connected and overlapped points appearing in the clusters of minor and serious inner race fault, which is not conducive to fault diagnosis. In three dimensions, all the clusters could be well separated, and for the clusters of the same parts with different severities, there seem to be no overlaps among the clusters. Therefore, the feature matrix of three dimensions was selected and finally input into the proposed LENN and ENN-2 algorithms.

4.2.3. Fault Diagnosis Results and Analysis. At the end, the obtained matrix was input into LENN and ENN-2 using RI in (24) for comparison. Similarly, for the sake of eliminating the influence of sample input order on experimental results, each diagnosis experiment was conducted for 10 times by randomly shuffling the input order of samples. Two of the diagnosis results of ENN-2 and LENN-based models are depicted in Figure 15, with the detailed results summarized in Table 6.

It is particularly evident from the results that overall, there was a marked increase in the performance of LENN-based model than that of ENN-2-based model in terms of clustering accuracy and stability. As can be seen from Figure 15, both of

TABLE 5: Center frequencies corresponding to different values of K of minor inner race fault.

K	Center frequency (Hz)				
2	693	2776			
3	685	2740	3578		
4	615	1301	2745	3579	
5	615	1300	2729	3345	3616
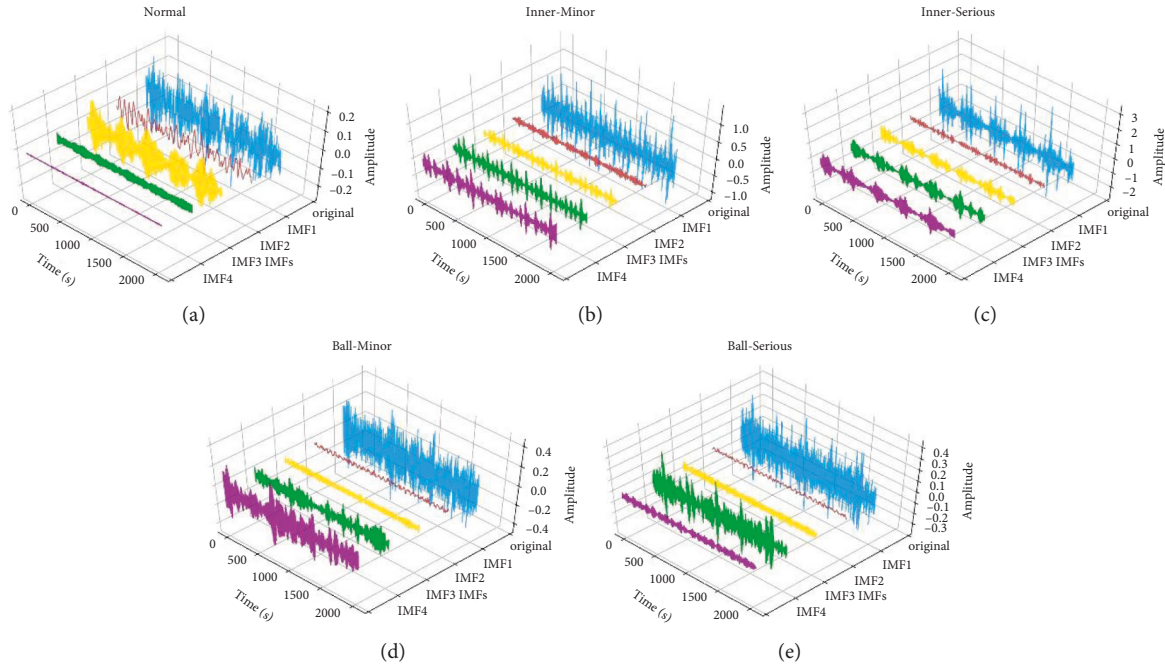
FIGURE 12: VMD results of a sample of five conditions: (a) normal, (b) minor inner race fault, (c) serious inner race fault, (d) minor ball fault, and (e) serious ball fault.
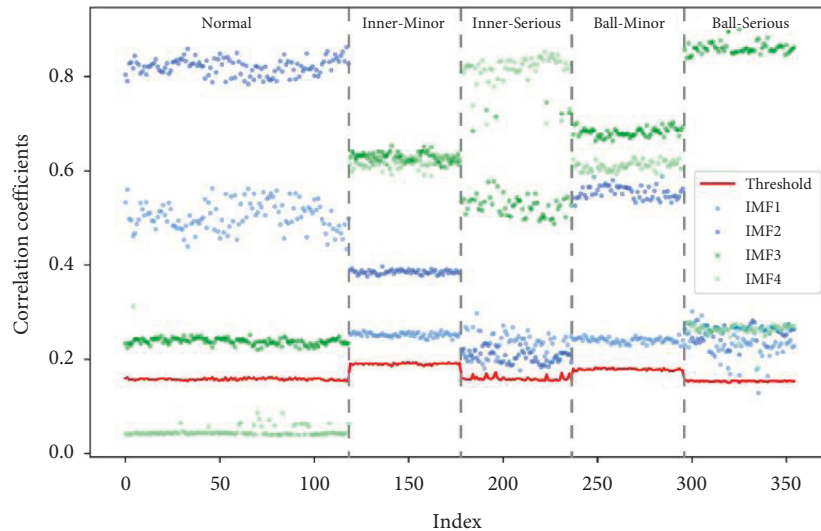
FIGURE 13: Results of correlation coefficient and threshold calculation.

the two models performed well on the data of MIF, SIF, MBF, and SBF because of the compact data distribution and good differentiation, with only three SIF points misclassified into MIF in ENN-2-based model. However, for the cluster in normal condition, its distribution was relatively loose, resulting

in ENN-2-based model which could not identify the whole cluster correctly and generated multiple clusters and noise points in the results, while LENN-based model only marked very few points at the edge of the cluster as noise which were far from their near points, and from Table 6, it can be observed that
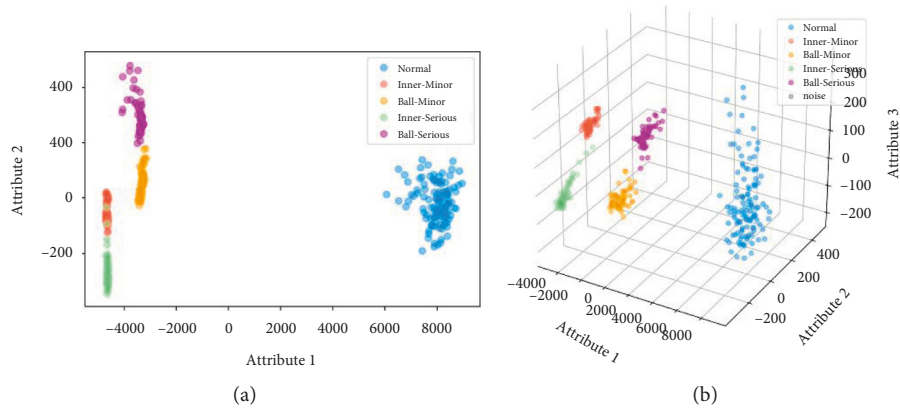
Figure 14: Dimensionality reduction results of bearing fault data: (a) in two dimensions and (b) in three dimensions.
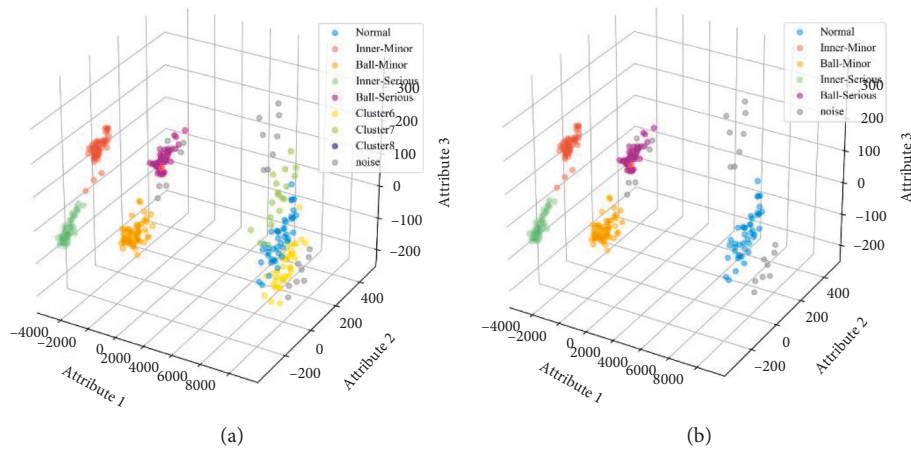
Figure 15: Diagnosis results of the models: (a) ENN-2-based model and (b) LENN-based model.

Table 6: Detailed results of ENN-2- and LENN-based models.

Model	Average epochs	Average score	Max score	Min score	Range
ENN-2	2	0.5835	0.6833	0.4520	0.2313
LENN	1	0.9754	0.9754	0.9754	0

ENN-2-based model needed an average iteration of two epochs to converge, while LENN-based model converged in only one epoch, and a significant improvement of RI score was obtained in LENN-based model (0.9754) than ENN-2-based model (0.5835). In addition, the clustering results of ENN-2-based model changed greatly with different sample input orders, while the performances of LENN-based model were very stable. All the results strongly confirm the proposed model preserves higher clustering accuracy and more stable performances.

4.3. Impact of Imbalance Degree of Datasets on Diagnostic Models. As outlined in the introduction, the problem of imbalanced data fault diagnosis in real industrial production increases the difficulty of clustering fault diagnosis. Thus, the impact of different imbalance degrees of datasets on diagnostic models was investigated experimentally. The bearing

fault data used in Section 4.2 was still adopted in this experiment, and based on the signal denoising and feature extraction and selection method proposed in this paper, four diagnostic models commonly used in clustering diagnosis were constructed and compared on datasets in different imbalance degrees selected randomly by certain proportions (shown in Table 7), which were models on LENN, K-means, FCM, and DBSCAN. The specific parameter settings of the models were in line with the settings in Section 4.1. To evaluate the performances and measure the ability of the models to deal with the clustering problem on imbalanced data, RI, macro-recall, and macro-F score were adopted in this experiment, and by conducting each experiment randomly for 10 times, we were able to get the average scores of each model.

Macro-recall measures the clustering performance of each class, especially the minority classes, which can be computed by

$$\text{macro} - R = \frac{1}{n} \sum_{i=1}^{n} \text{Recall} = \frac{1}{n} \sum_{i=1}^{n} \frac{\text{TP}_i}{\text{TP}_i + \text{FN}_i}, \quad (25)$$

where TP_i and FN_i represent the number of correctly and incorrectly predicted samples of the ith class, respectively.

Macro-F score is a comprehensive evaluation of the precision and recall of clustering results, which is defined as

TABLE 7: Imbalance degrees of experimental data.

No.	The number of samples in each condition (N : MIF : SIF : MBF : SBF)	Imbalance degree
Dataset 1	100 : 50 : 50 : 50 : 50	2 : 1 : 1 : 1 : 1
Dataset 2	100 : 30 : 30 : 30 : 30	3 : 1 : 1 : 1 : 1
Dataset 3	100 : 20 : 20 : 20 : 20	5 : 1 : 1 : 1 : 1
Dataset 4	100 : 10 : 10 : 10 : 10	10 : 1 : 1 : 1 : 1

TABLE 8: Average scores of models on datasets in different imbalance degrees.

No.	Target	LENN	K-means	FCM	DBSCAN
	RI	0.9485	0.5191	0.5301	0.8278
Dataset 1	Macro-R	0.9700	0.4960	0.4960	0.9140
	Macro-F1	0.9667	0.4933	0.4933	0.9333
	RI	0.9314	0.4806	0.4814	0.8113
Dataset 2	Macro-R	0.9510	0.4950	0.4950	0.8901
	Macro-F1	0.9487	0.4827	0.4827	0.9052
	RI	0.9250	0.4522	0.4376	0.6839
Dataset 3	Macro-R	0.9322	0.4950	0.4950	0.8130
	Macro-F1	0.9367	0.4827	0.4827	0.8486
	RI	0.8920	0.3822	0.2024	0.4329
Dataset 4	Macro-R	0.9100	0.4940	0.4860	0.7500
	Macro-F1	0.9357	0.4786	0.4500	0.8929

$$\text{macro} - F1 = \frac{\left(1 + \beta^2\right) \times \text{macro} - R \times \text{macro} - P}{\beta^2 \times (\text{macro} - R + \text{macro} - p)}, \quad (26)$$

where β denotes the relative importance of macro-R and macro-P, which is usually set as one, and macro-P can be obtained by

$$\text{macro} - P = \frac{1}{n} \sum_{i=1}^{n} \text{Precision} = \frac{1}{n} \sum_{i=1}^{n} \frac{\text{TP}_i}{\text{TP}_i + \text{FP}_i}, \quad (27)$$

where FP_i represents the number of samples which are misclassified into the ith class but do not belong to that class actually.

Table 8 collects the scores of the models on four datasets in different imbalance degrees. Two extreme cases with data imbalance degrees of $2 : 1 : 1 : 1 : 1$ and $10 : 1 : 1 : 1 : 1$ are taken to draw confusion matrices of the clustering results, which are shown in Figure 16.

It is apparent that, with the increase of data imbalance degrees, the clustering scores of all models showed a downward trend to varying imbalance degrees on the whole, among which LENN-based model performed noticeably best in all cases, while the configurations of K-means and FCM-based models were far from optimal. Comparing Table 8 and Figure 16, it can be observed that, the proposed model achieved considerably higher scores than other three models on all the datasets. Even on dataset 4 of the most extreme imbalance degree of $10 : 1 : 1 : 1 : 1$, LENN-based model also recognized four minority clusters precisely, with ten samples of minor inner race fault, nine samples of serious inner race fault, eight samples of minor

ball fault, and nine samples of serious ball fault identified correctly, DBSCAN-based model identified relatively few samples of these minor clusters; while K-means-based model regarded the samples of the same position but different severities as one cluster, failing to further subdivide the severities of samples, and FCM-based model directly identified all the four minority clusters as the same cluster, which scored lowest among the models. In addition, in the training process of LENN-based model on datasets with different imbalance degrees, the value of optimal λ grew gradually with the increase of data imbalance degree (shown in Figure 17). This was because, as the samples became more and more sparse, the distances between the samples increased, which required a larger λ to construct an extension correlation relationship between the samples, and this also indicated that the value of optimal λ was related to the final clustering results. In other words, the smaller of λ, the more precise the constructed extension relationship between samples would be, and the higher the accuracy of the proposed model could be obtained.

In conclusion, the imbalance degree of datasets increases the difficulty of fault diagnosis, especially for clustering algorithms relying on the selection of initial center points, and the appearances of minority clusters make it difficult for these algorithms to identify the fault categories correctly by distance calculation. At the same time, surprising outcomes of the experiments manifest that, by expressing the information of minority clusters more precisely through the constructed extension correlation function, the proposed LENN-based model shows good efficiency in identifying the minority clusters on imbalanced data.
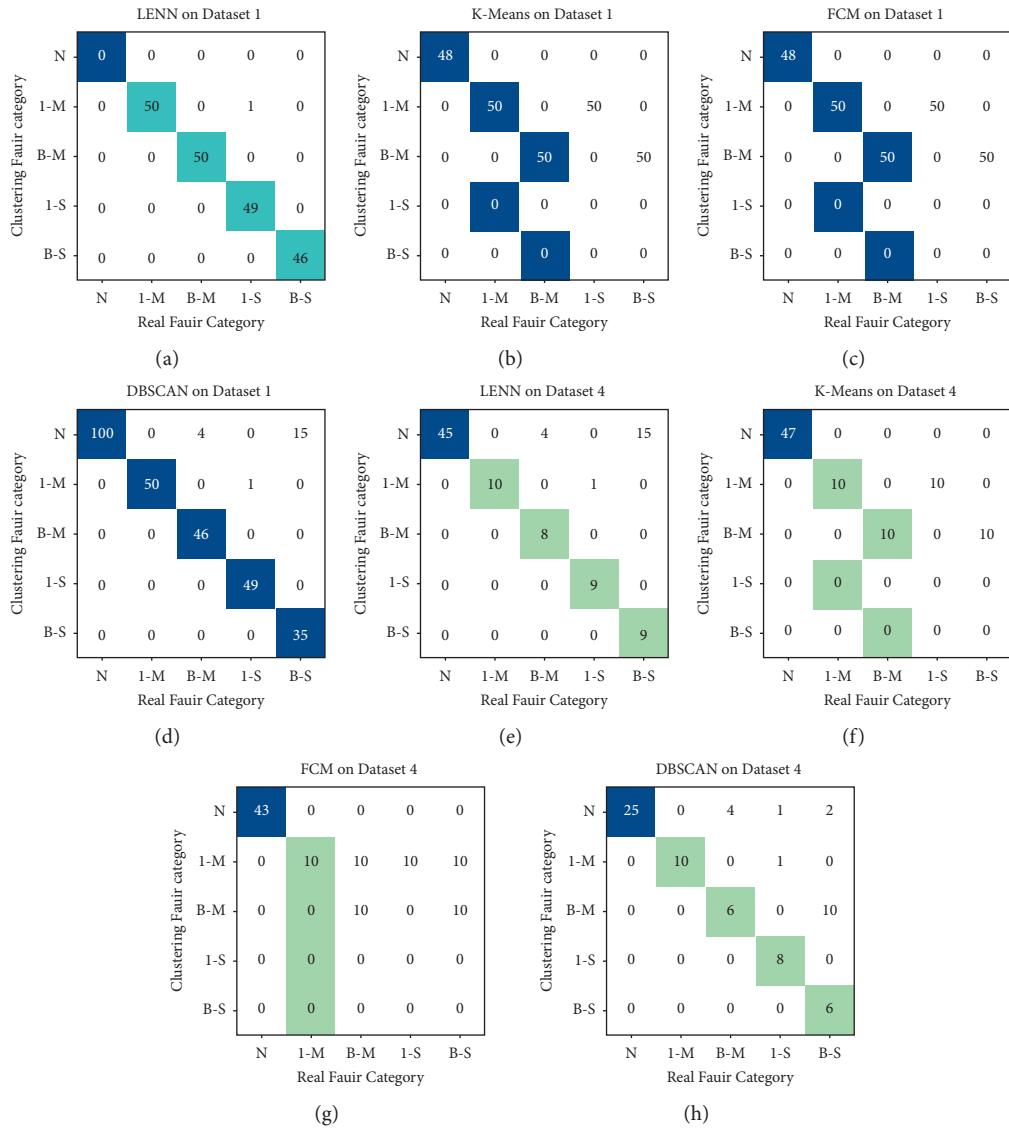
Figure 16: Confusion matrices of the results on two imbalance degrees of the datasets (2 : 1 : 1 : 1 : 1 and 10 : 1 : 1 : 1 : 1): (a) LENN on Dataset 1, (b) K-means on Dataset 1, (c) FCM on Dataset 1, (d) DBSCAN on Dataset 1, (e) LENN on Dataset 4, (f) K-means on Dataset 4, (g) FCM on Dataset 4, and (h) DBSCAN on Dataset 4.
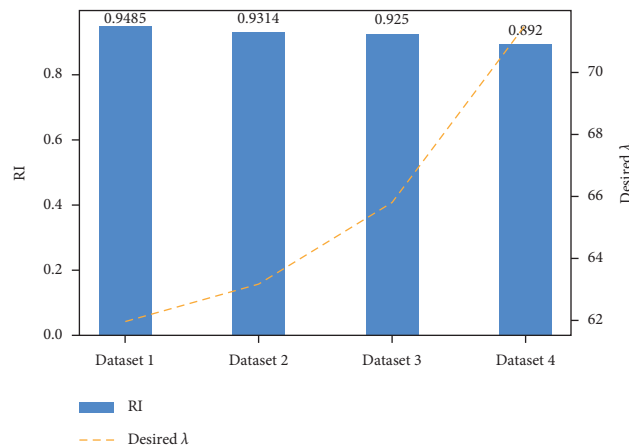
Figure 17: RI and optimal λ of LENN-based model on data with different imbalance degrees.

5. Conclusions

(1) A novel clustering algorithm called linked extension neural network (LENN) is developed based on extension neural network-type 2 (ENN-2), which is far less sensitive to initial point selection and sample input order by improved correlation function and new iterative method. Furthermore, to evaluate the clustering performance, extension density is proposed as an evaluation target for this algorithm.

(2) With the intention of improving the bearing fault diagnosis ability on imbalanced data with noise, a clustering fault diagnosis model of VMD-based denoising and LENN is constructed. The experimental results provide compelling evidence that the proposed model preserves powerful identification ability of minority fault clusters and achieves better diagnosis performance on imbalanced data with noise.

Data Availability

The labeled dataset used to support the findings of this study are available from the corresponding author upon request.

Conflicts of Interest

The authors declare no conflicts of interest.

Acknowledgments

References

[1] Y. Lei, B. Yang, Z. J. Du, and N. Lv, "Deep transfer diagnosis method for machinery in big data era," *Journal of Mechanical Engineering*, vol. 55, no. 7, pp. 1–8, 2019.

[2] J. B. Hou, Y. X. Wu, H. Gong, A. S. Ahmad, and L. Liu, "A novel intelligent method for bearing fault diagnosis based on EEMD permutation entropy and GG clustering," *Applied Sciences*, vol. 10, no. 1, 2020.

[3] L. K. Chang, S. H. Wang, and M. C. Tsai, "Demagnetization fault diagnosis of a PMSM using auto-encoder and K-means clustering," *Energies*, vol. 13, no. 17, pp. 1–12, 2020.

[4] X. Li, X. Li, and H. Ma, "Deep representation clustering-based fault diagnosis method with unsupervised data applied to rotating machinery," *Mechanical Systems and Signal Processing*, vol. 143, 2020.

[5] M. M. Islam, G. Lee, and S. N. Hettiwatte, "A nearest neighbour clustering approach for incipient fault diagnosis of power transformers," *Electrical Engineering*, vol. 99, no. 3, pp. 1–11, 2017.

[6] H. Li, W. Wang, P. Huang, and Q. Li, "Fault diagnosis of rolling bearing using symmetrized dot pattern and density-based clustering," *Measurement*, vol. 152, 2019.

[7] J. Y. Chen and Y. H. Chen, "Condition monitoring for wind turbines based on inner-DBSCAN and power curve pattern," *Electric Power Science and Engineering*, vol. 33, no. 8, pp. 27–34, 2017.

[8] F. F. Yin and Y. Gong, "DBSCAN and SVM for fault diagnosis of wind turbine based on SCADA data," *International Core Journal of Engineering*, vol. 6, no. 6, 2020.

[9] J. Ye, J. Zhu, Q. Lu, T. S. Li, S. Q. Chang, and Q. G. Wang, "A fault detection method of photovoltaic power station based on improved DBSCAN clustering algorithm," *Journal of Guangxi University(Natural Science Edition)*, vol. 44, no. 2, pp. 440–447, 2019.

[10] Z. B. Zhan, S. Zhang, W. Jiang, and P. Wu, "Detection method for bolts with mission pins on transmission lines based on DBSCAN-FPN," *Electric power*, vol. 54, no. 3, p. 10, 2021.

[11] D. Li, Z. Zhang, P. Liu, and Z. Wang, "DBSCAN-based thermal runaway diagnosis of battery systems for electric vehicles," *Energies*, vol. 12, no. 15, p. 2977, 2019.

[12] Z. Wei, Y. Wang, S. He, and J. Bao, "A novel intelligent method for bearing fault diagnosis based on affinity propagation clustering and adaptive feature selection," *Knowledge-Based Systems*, vol. 116, pp. 1–12, 2017.

[13] Z. G. Zhang, Q. Y. Chen, and J. Ma, "Fault diagnosis of shearer gear based on wavelet packet and EM clustering," *Coal Mine Machinery*, vol. 41, no. 9, pp. 183–186, 2020.

[14] N. Lu, G. T. Zhang, and F. X. Liu, "Vibrant fault diagnosis method for hydroelectric generating unit via ltsa and spectral clustering," *Engineering Journal of Wuhan University*, vol. 54, no. 296, pp. 1064–1069, 2021.

[15] M. Zhu, A. Q. Xu, R. F. Li, and J. L. Dai, "Diagnosis method for avionics based on membership and LMK-ELM," *Acta Aeronautica et Astronautica Sinica*, vol. 40, no. 12, pp. 202–214, 2019.

[16] Z. P. Gu, X. B. Liu, and Z. D. Han, "Aero engine fault diagnosis based on improved density peak clustering," *Computer Integrated Manufacturing Systems*, vol. 26, no. 5, pp. 1211–1217, 2020.

[17] H.-C. Chen, F.-C. Gu, and M.-H. Wang, "A novel extension neural network based partial discharge pattern recognition method for high-voltage power apparatus," *Expert Systems with Applications*, vol. 39, no. 3, pp. 3423–3431, 2012.

[18] T. Z. Wen, A. Q. Xu, and G. Cheng, "Multi-fault diagnosis method based on improved ENN2 clustering algorithm," *Control and Decision*, vol. 30, no. 6, pp. 1021–1026, 2015.

[19] M. H. Wang, M. L. Huang, and K. J. Liou, "Islanding detection method for grid connected photovoltaic systems," *IET Renewable Power Generation*, vol. 9, no. 6, pp. 700–709, 2015.

[20] A. Komaty, A. O. Boudraa, B. Augier, and D. Dare-Emivat, "EMD-based filtering using similarity measure between probability density functions of IMFs," *IEEE Transactions on Instrumentation and Measurement*, vol. 63, no. 1, pp. 27–34, 2013.

[21] Y. C. Jia, G. L. Li, X. Dong, and K. He, "A novel denoising method for vibration signal of hob spindle based on EEMD and grey theory," *Measurement*, vol. 169, 2021.

[22] M. Yang, S. H. Chen, H. Wu, and J. B. Yu, "An improved LMD-based denoising algorithm for fault diagnosis of rotating machinery," *Noise and Vibration Control*, vol. 35, no. 2, pp. 160–164, 2015.

[23] K. Dragomiretskiy and D. Zosso, "Variational mode decomposition," *IEEE Transactions on Signal Processing*, vol. 62, no. 3, pp. 531–544, 2014.

[24] X. Y. Luo, W. H. Lu, Y. P. You, and X. N. Hu, "A method for ball mill vibration signal random noise suppression based on VMD and SVD," *Noise and Vibration Control*, vol. 39, no. 6, pp. 169–175, 2019.

[25] F. Li, R. Li, L. Tian, L. Chen, and J. Liu, "Data-driven time-frequency analysis method based on variational mode

decomposition and its application to gear fault diagnosis in variable working conditions," *Mechanical Systems and Signal Processing*, vol. 116, pp. 462–479, 2019.

[26] Z. Guo, X. B. Li, T. Y. Yu, and X. Y. Fang, "Vibration signal denoising method of blast furnace opening machine based on improved VMD," *Machine Design and Research*, vol. 36, no. 5, pp. 174–179, 2020.

[27] Z. Q. Ma, X. Y. Liu, and J. J. Zhang, "Application of VMD-ICA combined method in fault diagnosis of rolling bearings," *Journal of Vibration and Shock*, vol. 36, no. 13, pp. 201–207, 2017.

[28] F. Xu, J. H. Chang, and B. G. Liu, "De-noising method research for lidar echo signal based on variational mode decomposition," *Laser & Infrared*, vol. 48, no. 11, pp. 1443–1448, 2018.

[29] J. Li, Y. Chen, and Z. H. Qian, "Research on VMD based adaptive denoising method applied to water supply pipeline leakage location," *Measurement*, vol. 151, 2020.

[30] Y. Wang, Z. Wei, and J. Yang, "Feature trend extraction and adaptive density peaks search for intelligent fault diagnosis of machines," *IEEE Transactions on Industrial Informatics*, vol. 15, no. 1, pp. 105–115, 2019.

[31] M.-H. Wang, "Extension neural network-type 2 and its applications," *IEEE Transactions on Neural Networks*, vol. 16, no. 6, pp. 1352–1361, 2005.

[32] L. J. Zhu, B. X. Ma, and X. Q. Zhao, "Clustering validity analysis based on silhouette coefficient," *Journal of Computer Applications*, vol. 30, no. 2, pp. 139–141, 2010.

[33] A. Ayenu-Prah and N. Attoh-Okine, "A criterion for selecting relevant intrinsic mode functions in Empirical Mode Decomposition," *Advances in Adaptive Data Analysis*, vol. 2, no. 1, pp. 1–24, 2010.

[34] Y. Lei, Z. He, Y. Zi, and Q. Hu, "Fault diagnosis of rotating machinery based on multiple ANFIS combination with GAs," *Mechanical Systems and Signal Processing*, vol. 21, no. 5, pp. 2280–2294, 2007.

[35] http://csegroups.case.edu/bearingdatacenter/pages/download-data-file.

[36] W. A. Smith and R. B. Randall, "Rolling element bearing diagnostics using the Case Western Reserve University data: a benchmark study," *Mechanical Systems and Signal Processing*, vol. 64-65, pp. 100–131, 2015.

Research Article

Comprehensive Evaluation on Teachers' Knowledge Sharing Behavior Based on the Improved TOPSIS Method

Xiaojuan Yu,[1] **Dianshun Hu** ,[1] **Na Li,**[1] **and Yan Xiao** [2,3]

[1]*School of Mathematics and Statistics, Central China Normal University, Wuhan 430079, China*
[2]*College of Mechanical Engineering, Chongqing University of Technology, Chongqing 400054, China*
[3]*School of Business, Macau University of Science and Technology, Macau 999078, China*

Correspondence should be addressed to Dianshun Hu; hdsh@ccnu.edu.cn and Yan Xiao; yxiao@cqut.edu.cn

Knowledge sharing among teachers is one of the important ways to improve their teaching and research ability. From the perspectives of teachers' knowledge sharing willingness, knowledge sharing ability, knowledge sharing environment, knowledge sharing technology support, knowledge sharing effect, and so forth, this paper constructs a teacher knowledge sharing behavior evaluation model, develops a knowledge sharing behavior evaluation index system, and proposes a comprehensive teacher's knowledge sharing behavior evaluation method based on the improved entropy-TOPSIS method. This is a comprehensive evaluation method combining subjective and objective weights, which avoids the subjectivity of traditional expert evaluation methods and other multilevel and multi-index weight determination methods and makes the evaluation results more objective, accurate, and more realistic. Finally, by taking the example of evaluating knowledge sharing behavior of teachers in a university of Chongqing, China, this paper verifies the feasibility and practicability of the proposed comprehensive teachers' knowledge sharing behavior evaluation system and method.

1. Introduction

With the advent of the knowledge economy era, knowledge resources and knowledge management ability have become an important source of core competitiveness of organizations and individuals [1, 2]. As practitioners in education, teachers are innovators and disseminators of professional knowledge, accumulating and creating knowledge in specific educational and teaching contexts through "cognition in action" and "reflection in action," which play important roles in the development of knowledge economy. With the continuous differentiation and depth of knowledge, teachers also need to constantly learn and supplement new knowledge to guarantee the competitiveness and value of their knowledge resources. Teachers' knowledge sharing not only helps to excavate and reveal teachers' individual knowledge and improve teachers' individual ability but also helps to realize the transformation of teachers' individual knowledge into group public knowledge and further enrich the practical knowledge base of the teacher community, thus providing important knowledge resources for the development of school organizations, which is of great significance to individual teachers, teacher groups, and school organizations [3, 4].

With the in-depth development of specialized subject, knowledge increasingly embodies the characteristics of complexity, intersection, and synthesis. Meanwhile, there are large knowledge gaps among teachers due to differences in educational background, knowledge stock, learning ability, thinking patterns, academic expertise, and personality traits [5]. Knowledge sharing among teachers is an important way to help teachers quickly understand, comprehend, and master knowledge, and, whether as individuals or as teacher community, its essence is the process of teachers transferring, communicating, and sharing knowledge [6]. However, compared with the attention paid to teachers' knowledge sharing, teachers' knowledge sharing behavior has encountered dilemmas such as absence, low

end, and ineffectiveness in real practice. Teachers are constrained by factors such as egoism and altruism, subjective sharing desire and objective conditions, self-worth of knowledge, and lack of resource facilitation, which hinder university teachers' willingness and action to share knowledge, thus leading to a lack of effective knowledge exchange and cooperation [7, 8]. Therefore, stimulating internal drive of teachers to participate in knowledge sharing and mobilizing their willingness to participate in knowledge sharing behavior can promote the effective realization of teachers' knowledge sharing, thus promoting their personal development and the improvement of school knowledge management capability. Among them, how to effectively and accurately evaluate teachers' knowledge sharing behavior is the key link to improve the level of knowledge sharing among teachers. While exploring various strategies to improve knowledge level of teachers, schools must first understand the development status of teachers' knowledge sharing behavior and take the current situation of teachers' knowledge sharing behavior as the focus of improving teachers' knowledge level, which requires clarifying the methods for monitoring and evaluating the behavior of teachers' knowledge sharing. Therefore, this paper focuses on the issue of evaluation of teachers' knowledge sharing behavior to clarify the current situation of teachers' professional knowledge, so as to improve the quality of teachers' development.

The results of literature retrieval show that although there are some achievements on knowledge sharing behavior evaluation, teachers' knowledge management performance evaluation, and teachers' knowledge sharing influencing factors, there are still few achievements of in-depth research on tacit knowledge sharing behavior evaluation of teachers. In addition, current research on teachers' knowledge sharing behavior is dominated by theoretical studies and less by quantitative empirical studies. Accordingly, based on the systematic study of the influencing factors and evaluation indicators of teachers' knowledge sharing behavior, this paper constructs an evaluation model of knowledge sharing behavior and implements empirical analysis using the entropy weight method and the TOPSIS method. This work is beneficial for managers to provide effective incentives and management measures for teachers' knowledge sharing behavior in the school, which can provide theoretical guidance for improving teachers' knowledge sharing ability.

The structure of this paper is organized as follows: Section 2 reviews the related works about evaluation of teachers' knowledge sharing behavior. Then, the indicator system of teachers' knowledge sharing behavior evaluation is developed in Section 3. In Section 4, the evaluation model of teachers' knowledge sharing behavior is proposed. Section 5 presents a real case to show the feasibility and effectiveness of the proposed evaluation method. Finally, Section 6 presents the conclusion and future work.

2. Literature Review

The issue of knowledge management in education has received increasing attention from the society and academia, and the researches related to teachers' knowledge sharing have become a research hotspot. In terms of knowledge sharing behavior and its influencing mechanisms, Cummings and Teng [9] argued through empirical studies that the degree to which knowledge can be expressed through words or graphics determines the difficulty and ease of knowledge sharing; that is, the easier it is to express, the more favorable it is to share. Hu and Liu [10] used the complete information game approach to find the subgame perfect Nash equilibrium solution for the game between each participant in the knowledge alliance. Tseng and Kuo [8] found that the knowledge sharing behavior of teacher groups in online communities was significantly influenced by social relationships and community affiliation management. Liu et al. [11] established a single-group and multigroup dynamic game model of knowledge sharing and analyzed the evolutionary stabilization strategy of this model. Caskova and Chudy [12] explored the effects of the school culture on teachers' career at the beginning of their teaching and pedagogical knowledge sharing. Wu et al. [13] established the sharing behavior model and shared utility function, based on which experimental simulations of the model were conducted to summarize and analyze the knowledge sharing and motivation rules of organizational individuals. Mollazehi and Karimi [14] identified and validated the factors affecting teacher's knowledge sharing through information and communication technology (ICT).

For the study on teachers' knowledge sharing behavior evaluation, Sun et al. [15] clarified the connotation and composition of tacit knowledge sharing ability of university teachers based on two levels of process and elements and thus constructed an index system for tacit knowledge sharing ability evaluation of university teachers. Zhang et al. [16] conducted a specific study on the knowledge sharing ability of teacher scientific research teams from a holistic network perspective, including network stickiness measurement, centrality measurement, core-edge measurement, cohesive subgroups, and structural hole measurement. McChesney and Aldridge [17] described the development and validation of a new instrument to assess teachers' perceptions of the impact of professional knowledge sharing. Zhao and Wang [18] constructed a tacit knowledge sharing model for university teachers based on their knowledge sharing intention, sharing ability, sharing atmosphere, and sharing effect and then used AHP method to measure and analyze the weights of the index system. Asghar and Naveed [19] evaluated the psychometric properties of the Knowledge Sharing Behavior Scale (KSBS) in an academic context, and the results indicated that KSBS is not a valid instrument for measuring knowledge sharing behavior within an academic environment. Li and Qin [20] provided a model framework for teachers to promote students' entrepreneurial motivation through knowledge sharing. Kularajasingam and Subramaniam [21] stated that university academics' knowledge sharing behavior and social intelligence are significant in improving their performance through their grasp of competencies, and they applied a mediation model among university teachers to investigate the impact of knowledge sharing behavior and social intelligence of university academics on their performance. Wang et al. [22]

examined factors explaining rural teachers' sharing behavior regarding digital educational resources, both within and outside school, as posited by combining motivation theory and the integrative model of behavior prediction.

The above research provides a very valuable reference for the evaluation of teachers' knowledge sharing behavior. However, due to the professional and tacit characteristics of teachers' knowledge, the evaluation of teachers' knowledge sharing behavior has multiobjective attribute, and it is usually difficult to balance between different goals; that is, it is difficult to have one evaluation scheme whose indicators are better than others [15]. Therefore, the evaluation of teachers' knowledge sharing ability needs a quantitative comprehensive evaluation method to improve the validity of the evaluation process and reduce subjectivity. Thus, this paper constructs an evaluation indicator system of teachers' knowledge sharing behavior and proposes a comprehensive evaluation method based on entropy weight method and TOPSIS method and then verifies the feasibility and effectiveness of this evaluation system and evaluation method through practical cases.

3. The Indicator System of Teachers' Knowledge Sharing Behavior Evaluation

The evaluation system of teachers' knowledge sharing efficiency is a complex evaluation system, and it is unrealistic to describe the essence and rule of the whole process of teachers' knowledge sharing to control it to reach the predetermined goals of individual teachers and school organizations, which requires the establishment of a massive index system [18]. One index can only reflect a certain attribute of the knowledge sharing behavior evaluation system. Therefore, a reasonable evaluation indicator system can only be formed by selecting the main indicators in a reasonable way to comprehensively evaluate the knowledge sharing behavior of teachers within a reasonable cost range.

Although the performance of knowledge sharing behavior is related to the contribution of individual teacher, knowledge sharing among individual teachers is more influenced by some difficult-to-quantify factors of interactions among members, and the results of knowledge sharing are not immediately apparent, showing a certain lag phenomenon [23, 24]. When evaluating knowledge sharing behavior, it is necessary to consider the impact of difficult-to-quantify interrelationships among teachers and their roles in the overall knowledge sharing process. Therefore, for teachers' knowledge sharing, outcome-based indicators can only reflect part of the final results of knowledge sharing behavior but less consider the process. In fact, the more important aspect of knowledge sharing behavior is the behavioral activities and the interactive coordination between individuals, which is extremely crucial. In addition, from the practice of teachers' knowledge sharing behavior, the cognitive gap between individual teachers and the knowledge sharing environment are objective factors that affect knowledge sharing behavior; thus the evaluation of teachers' knowledge sharing behavior should consider the above factors [25, 26].

Based on the above considerations, this paper comprehensively evaluates teachers' knowledge sharing behavior from five dimensions, namely, knowledge sharing willingness, knowledge sharing ability, knowledge sharing environment, knowledge sharing technology support, and knowledge sharing effect. The logical process of this index system is as follows: First, before the beginning of knowledge sharing, teachers' knowledge sharing willingness is the determining factor for their decision to implement knowledge sharing behavior. Second, in the process of knowledge sharing, teachers' individual knowledge sharing ability, external knowledge sharing environment, and knowledge sharing technology support are the key subjective and objective factors affecting knowledge sharing behavior. Third, all these subjective and objective factors are ultimately reflected in the effect of knowledge sharing behavior. When the knowledge sharing has produced certain effects, the knowledge sharing behavior of teachers can be reflected in its entirety. Further, through analyzing the characteristics and connotations of the five dimensions and following the principles of systemic, scientific, operability, and comparability of the evaluation indicator system, the evaluation indicator system of teachers' knowledge sharing behavior is constructed, as shown in Table 1.

4. Evaluation Model of Teachers' Knowledge Sharing Behavior

Teachers' knowledge sharing behavior is a complex systematic process, and the whole process involves various theories such as transaction cost theory, cognitive psychology, and organizational behavior [27]. Teachers' knowledge sharing behavior evaluation should realize the promoting function of the evaluation process and results on the knowledge exchange behavior among teachers and then improve teachers' individual knowledge ability and school knowledge management level through knowledge sharing behavior evaluation, which shows that teachers' knowledge sharing behavior evaluation is a multiobjective evaluation problem. Many multiobjective evaluation methods have been proposed [28, 29], and when teachers' knowledge sharing is used as the evaluation object, the evaluation conclusions obtained by various methods often differ largely since the rubric used is often subjective and ambiguous, which undoubtedly brings great difficulties to the evaluation of teachers' knowledge sharing behavior.

After the evaluation indicator system of teachers' knowledge sharing behavior is determined, its evaluation results mainly depend on two factors: one is the determination of evaluation index weights, and the other is the choice of comprehensive evaluation methods. Traditional knowledge sharing behavior evaluation methods often rely on the subjective judgments of organizers and experts to determine the weights of each index, and due to the great differences in professional personal experience and mastering information, which are subjective, the weight scores given by different individuals for the same evaluation index often differ greatly, resulting in great distortions of evaluation results and even wrong decisions [18]. Based on the

TABLE 1: The evaluation indicator system of teachers' knowledge sharing behavior.

Evaluation objects	Level 1 indicators	Level 2 indicators
Teachers' knowledge sharing behavior evaluation	Knowledge sharing willingness	Self-efficiency u11
		Interpersonal relationships u12
		Gaining respect u13
		Knowledge sharing recognition u14
		Position in the organization u15
	Knowledge sharing ability	Knowledge recognition ability u21
		Knowledge transfer ability u22
		Knowledge receiving ability u23
		Knowledge innovation ability u24
	Knowledge sharing environment	Knowledge exchange atmosphere u31
		Knowledge sharing incentive policy u32
		Knowledge sharing culture u33
		Trust among teachers u34
		Intellectual property policy u35
	Knowledge sharing technology support	Knowledge sharing platform u41
		Knowledge exchange medium u42
		Knowledge sharing map u43
		Knowledge base u44
	Knowledge sharing effect	Gaining valuable knowledge u51
		Knowledge sharing satisfaction u52
		Personal capability enhancement u53
		Colleague's approval u54
		Organizational performance improvement u55

above considerations, this paper combines the subjective judgment of experts with the objective situation of teachers' knowledge sharing behavior, determines the weights of the evaluation indexes of enterprise culture implementation by entropy weight method, and adjusts the subjective deviation of expert judgment by scientific weight coefficients and then adopts the improved ideal point (TOPSIS) as the comprehensive evaluation method to derive the final ideal evaluation results.

4.1. Entropy Weight Method and TOPSIS Method.

The concept of entropy originated from thermodynamics and was later introduced into information theory by Shannon. According to the definition and principle of entropy, the entropy value can be used as a measure of the amount of effective information provided by the system, representing the degree of disorder of the system. Entropy weight method is an evaluation method combining qualitative and quantitative analysis, which is an objective weighting method [30, 31]. The entropy weight method determines the indicator weights according to the amount of information conveyed to the decision-maker by each index. For an index, the entropy value can be used to judge the degree of dispersion of an index. If an index's information entropy value is smaller, the dispersion degree of the index is greater, and the influence of the index on the comprehensive evaluation is greater. If the values of an index are all equal, the index does not work in the comprehensive evaluation. For the evaluation problem, suppose that there are m evaluation objects and n evaluation indicators, and the initial evaluation matrix $R = (r_{ij})_{m \times n}$ is obtained, and r_{ij} denotes the value of the j evaluation indicator of the i

evaluation object; then the entropy value e_j of an indicator r_j is

$$e_j = -\frac{1}{\ln m} \sum_{i=1}^{m} \delta_{ij} \ln \delta_{ij}, \tag{1}$$

where $\delta_{ij} = r_{ij} / \sum_{i=1}^{m} r_{ij}$ and δ_{ij} denotes the proportion of the i participant to the indicator under the j indicator. According to the definition and principle of entropy weight method, when the entropy value of an index is larger, it means that the less effective information provided by the index, the smaller the role in the comprehensive evaluation, and its weight is smaller; conversely, the larger the entropy value, the more effective information provided by the index and the larger the role in the comprehensive evaluation, and its weight is larger [31]. Therefore, it is scientific and credible to use the entropy weight method to assign index weight during the analysis of multiple index evaluation problems.

TOPSIS method is a common method in system engineering, mainly for multiobjective evaluation and decision analysis of finite solutions, and it has many advantages, such as no requirement for sample content, no requirement for sample data distribution, simple calculation process, and intuitive and easy analysis of results, which makes TOPSIS method widely and effectively used in many fields, such as economy, management, and engineering technology. [28, 32, 33]. For the evaluation of teachers' knowledge sharing behavior, the TOPSIS method has no strict restrictions on data distribution and sample content indicators. It is suitable for small sample data and large-scale system data with multiple evaluation units and multiple indicators, which has the advantage of being real, intuitive, and reliable. The core idea and procedure of TOPSIS are as

follows: Firstly, the initial data is dimensionless processed to make the data objectively and truly reflect the gap between the evaluation objects; then, the positive and negative ideal values are determined according to the size of the standardized data of each index; next, the weighted Euclidean Distance between the evaluation objects and the positive and negative ideal values is calculated, from which the closeness of each evaluation object to the best state is derived; finally, the ranking of each evaluation object is measured. In this paper, when applying TOPSIS method for comprehensive evaluation, to address the problem of cumbersome calculation of Euclidean Distance from evaluation objects to the positive and negative ideal point, the decision matrix of TOPSIS method is normalized to simplify the calculation of the positive and negative ideal solution; meanwhile, the concept of relative closeness between the index value and ideal solution of each evaluation object is introduced, and each evaluation object is ranked according to the size of its relative closeness.

4.2. Comprehensive Evaluation Process of Entropy Weight-TOPSIS Method. The evaluation steps of the improved entropy weight-TOPSIS method are as follows:

For the evaluation problem with m teachers to be evaluated and n evaluation indicators, there is the initial data matrix $R = (r_{ij})_{m \times n}$.

(1) The normative matrix $Q = (q_{ij})_{m \times n}$ is obtained by dimensionless treatment of the R matrix; that is,

$$q_{ij} = \frac{r_{ij}}{\sqrt{\sum_{i=1}^{m} r_{ij}^2}}, \quad i = 1, 2, 3..., m, \ j = 1, 2, 3..., n. \quad (2)$$

(2) Calculate δ_{ij}, which is the weight of the j indicator of the i participant.

$$\delta_{ij} = \frac{q_{ij}}{\sum_{i=1}^{m} q_{ij}}. \quad (3)$$

(3) Calculate the entropy value e_j of the j indicator.

$$e_j = -\frac{1}{\ln m} \sum_{i=1}^{m} \delta_{ij} \ln \delta_{ij}, \quad (j = 1, 2, 3..., n), \quad (4)$$

where $0 \le e_j \le 1$.

(4) Calculate the difference coefficient e_j for the j indicator.

$$g_j = 1 - e_j. \quad (5)$$

For the j indicator, the larger the difference coefficient χ_j, the greater the role of the indicator in the program evaluation; conversely, the smaller χ_j is, the smaller the role of the indicator in the program evaluation is.

(5) Calculate the weight w_j of the j indicator.

$$w_j = \frac{g_j}{\sum_{j=1}^{n} g_j}. \quad (6)$$

(6) Construct the weighted data matrix $Z = (z_{ij})_{m \times n}$, where element z_{ij} is defined as follows:

$$z_{ij} = w_j q_{ij}. \quad (7)$$

(7) Determine the positive ideal value R^+ and the negative ideal value R^- of the index. The traditional TOPSIS method of the positive and negative ideals is more complex due to the values, which makes it difficult to calculate the Euclidean Distance of each evaluation scheme to the positive and negative ideals. For this reason, without affecting the evaluation problem to derive the final evaluation results, this paper makes improvements to the TOPSIS method to simplify the calculation. The value of q_{ij} in the normative matrix Q is taken as [0, 1]. Here we specify that the highest preferred target attribute value $q_{ij} = 1$ and the lowest preferred target attribute value $q_{ij} = 0$. Thus, it can be known that $z_j^* = w_j$ and $z_j^- = 0$; then the positive and negative ideal solutions are as follows:

$$\begin{aligned} Z^- &= \left(z_1^-, z_2^- ..., z_j^-\right) = (0, 0..., 0), \\ Z^* &= \left(z_1^*, z_2^* ..., z_j^*\right) = \left(w_1, w_2..., w_j\right). \end{aligned} \quad (8)$$

(8) Calculate the Euclidean Distance of each evaluation object to the positive and negative ideal points, and the distance formula uses Euclidean formula.

$$\begin{aligned} D_i^- &= \sqrt{\sum_{j=1}^{n} \left(z_{ij} - z_j^-\right)^2} = \sqrt{\sum_{j=1}^{n} w_{ij}^2 \left(q_{ij} - 0\right)^2}, \\ D_i^* &= \sqrt{\sum_{j=1}^{n} \left(z_{ij} - z_j^*\right)^2} = \sqrt{\sum_{j=1}^{n} w_{ij}^2 \left(q_{ij} - 1\right)^2}, \quad i = 1, 2, 3..., m, \ j = 1, 2, 3..., n. \end{aligned} \quad (9)$$

TABLE 2: Original data of expert panel scoring.

	u11	u12	u13	u14	u15	u21	u22	u23	u24	u31	u32	u33	u34	u35	u41	u42	u43	u44	u51	u52	u53	u54	u55
A	3	3	4	2	3	3	4	3	2	4	3	3	2	3	4	3	2	2	2	3	2	3	2
B	3	3	3	3	3	3	3	4	4	3	4	3	2	4	3	4	3	3	3	4	2	3	3
C	5	4	3	3	4	3	3	4	3	3	4	2	2	3	2	3	1	2	1	2	2	2	2
D	3	4	3	3	3	4	3	4	3	3	3	3	3	2	3	3	3	2	2	3	2	3	3

TABLE 3: The weight of the i participating teacher in the j indicator.

	u43	u44	u51	u52	u53	u54	u55	u43	u44	u51	u52		u53	u54	u55	u43	u44	u51	u52
A	0.214	0.214	0.307	0.181	0.231	0.231	0.307	0.202	0.168	0.307	......		0.250	0.249	0.250	0.273	0.249	0.231	0.200
B	0.214	0.214	0.231	0.273	0.231	0.231	0.231	0.266	0.334	0.231	......		0.375	0.334	0.250	0.273	0.334	0.231	0.300
C	0.358	0.286	0.231	0.273	0.307	0.231	0.231	0.266	0.249	0.231	......		0.125	0.168	0.250	0.181	0.168	0.231	0.200
D	0.214	0.286	0.231	0.273	0.231	0.307	0.231	0266	0.249	0.231	......		0.250	0.249	0.250	0.273	0.249	0.307	0.300

TABLE 4: Entropy values, variation coefficients, and weights of each evaluation index.

	u43	u44	u51	u52	u53	u54	u55	u43	u44	u51	u52		u53	u54	u55	u43	u44	u51	u52
Ej	0.979	0.992	0.994	0.99	0.994	0.995	0.98	0.994	0.992	0.99	......		0.953	0.98	1	0.99	0.98	0.994	0.985
Gj	0.021	0.008	0.006	0.01	0.006	0.005	0.02	0.006	0.008	0.01	......		0.047	0.02	0	0.01	0.02	0.006	0.015
Wj	0.057	0.022	0.016	0.027	0.016	0.014	0.055	0.016	0.022	0.027	......		0.128	0.055	0	0.027	0.055	0.016	0.041

(9) Calculate the relative closeness between the index value and the ideal solution of each evaluation object ψ_i.

$$\psi_i = \frac{D_i^{-}}{D_i^{*} + D_i^{-}}. \qquad (10)$$

(10) The schemes are ranked by the magnitude of relative closeness, and the greater the relative closeness ψ_i, the higher the level of knowledge sharing of the evaluated teachers; the greater ψ_i is, the lower the level of knowledge sharing of the evaluated teachers is.

5. Case Study

This paper selects a well-known university in Chongqing, China, as an example of teacher knowledge sharing evaluation work and illustrates the evaluation process of the teacher knowledge sharing evaluation model and method. This university is a multidisciplinary university with distinct engineering characteristics, and it focuses on cultivating application-oriented compound high-quality professionals with innovative spirit and practical ability. This university has more than 2300 teachers and staffs, and it strongly focuses on and supports knowledge sharing behaviors among teachers to improve individual teachers and the university's overall knowledge management. In the process of evaluating the knowledge sharing behavior of teachers in this university, the above evaluation system is used to comprehensively evaluate the knowledge sharing level of four teachers, A, B, C, and D, and then give the ranking of each teacher's knowledge sharing behavior.

In this paper, an expert panel is formed by several experts in higher education systems and knowledge management, and the expert panel scores each teacher individually according to the evaluation indicator system proposed in this paper. The range of scores is $1 - 5$, where higher scores indicate a higher level of knowledge sharing behavior of a teacher on an indicator. The final combined scores of the expert are obtained in Table 2.

(1) Since the scores in the expert rating scale are all dimensionless data, there is no need for dimensionless processing here.

(2) According to equation (3), the weight δ_{ij} of the i participating teacher in the j indicator is calculated to obtain Table 3.

(3) According to equations (4)–(6), the entropy value, variation coefficient, and weight of each evaluation index are obtained, and the results are shown in Table 4.

(4) As shown in Table 5, the weighted normalized data matrix is obtained from equation (7).

(5) As shown in Table 6, the relative closeness and its ranking table can be obtained from equations (8)–(10).

The ranking result of the relative closeness c_i shows that the four university teachers' knowledge sharing behavior level is B〉D〉A〉C in turn, which is consistent with the intuitive judgment of experts and school colleagues about the four teachers. Meanwhile, the results are consistent with those of the unsimplified traditional TOPSIS method, so the evaluation process of the improved TOPSIS method is more concise and efficient, and the evaluation results have higher credibility and practicality.

Table 5: Weighted normalized data matrix.

	u43	u44	u51	u52	u53	u54	u55	u43	u44	u51	u52	u53	u54	u55	u43	u44	u51	u52
A	0.172	0.065	0.065	0.055	0.049	0.0409	0.219	0.049	0.044	0.109	......	0.257	0.164	0	0.082	0.164	0.049	0.082
B	0.172	0.065	0.049	0.082	0.049	0.041	0.164	0.065	0.087	0.082	......	0.385	0.219	0	0.082	0.219	0.049	0.123
C	0.286	0.087	0.049	0.082	0.066	0.041	0.164	0.065	0.065	0.082	......	0.128	0.1099	0	0.055	0.109	0.049	0.082
D	0.172	0.087	0.049	0.082	0.049	0.055	0.164	0.065	0.065	0.082	......	0.257	0.164	0	0.082	0.164	0.065	0.123

Table 6: Relative closeness ψ_i and ranking results table.

Evaluation object	A	B	C	D
ψ_i	0.178566	0.323158	0.119644	0.213466
Ranking results	3	1	4	2

6. Conclusions

Knowledge sharing behavior evaluation can help schools and teachers to understand their knowledge sharing levels and thus provide decision-making input for better policy formulation, environment optimization, organization construction, and incentive behavior. Teachers' knowledge sharing behavior evaluation has become a hot focus of attention in education and academia at home and abroad, yet there is little research on the quantitative evaluation of teachers' knowledge sharing behavior. From a systematic perspective of combining process and result, this paper constructs an evaluation indicator system of teachers' knowledge sharing behavior containing five dimensions of knowledge sharing willingness, knowledge sharing ability, knowledge sharing environment, knowledge sharing technology support, and knowledge sharing effect, which is proved in practice to be able to evaluate teachers' knowledge sharing level scientifically, systematically, and comprehensively. The entropy weight method is used to revise experts' experience scoring results and determine the weights of knowledge sharing behavior evaluation index, which avoids the subjectivity of the traditional expert evaluation method and other multilevel and multi-index weight determination methods and makes the evaluation results more objective, accurate, and more in line with reality. Compared with the traditional TOPSIS method, the improved TOPSIS method has a more streamlined, efficient, and well-organized calculation process. In summary, the evaluation system and evaluation method of teachers' knowledge sharing behavior established in this paper are reasonable and practical, which can not only judge the comprehensive level of teachers' knowledge sharing ability but also analyze the strengths and weaknesses factors of each teacher's knowledge sharing, to provide a basis for decision-making to improve teachers' knowledge sharing level. Of course, the empirical research in this paper still has its limitations, such as insufficient sample sources and insufficient sample size. In the future work, the empirical analysis is needed to further verify the advantages of the evaluation model and method in this paper.

Data Availability

The data used to support the findings of this study are included within the article.

Conflicts of Interest

The authors declare that they have no conflicts of interest regarding the publication of this paper.

Acknowledgments

References

[1] Y. Sun, J. Liu, and Y. Ding, "Analysis of the relationship between open innovation, knowledge management capability and dual innovation," *Technology Analysis & Strategic Management*, vol. 32, no. 1, pp. 15–28, 2020.

[2] S. Jiafu, Y. Yu, and Y. Tao, "Measuring knowledge diffusion efficiency in R&D networks," *Knowledge Management Research and Practice*, vol. 16, no. 2, pp. 208–219, 2018.

[3] T. Kaya and B. Erkut, "The tacit knowledge capacity of lecturers: a cross-country comparison," *Electronic Journal of Knowledge Management*, vol. 16, no. 2, pp. 131–142, 2018.

[4] X. Gu and J. O'Connor, "Teaching 'tacit knowledge'in cultural and creative industries to international students," *Arts and Humanities in Higher Education*, vol. 18, no. 2, pp. 140–158, 2019.

[5] D. Yu and R. Zhou, "Tacit knowledge sharing modes of university teachers from the perspectives of psychological risk and value," *International Journal of Higher Education*, vol. 4, no. 2, pp. 214–224, 2015.

[6] N. Verloop, J. Van Driel, and P. Meijer, "Teacher knowledge and the knowledge base of teaching," *International Journal of Educational Research*, vol. 35, no. 5, pp. 441–461, 2001.

[7] K. Edge, "Rethinking knowledge management: strategies for enhancing district-level teacher and leader tacit knowledge sharing," *Leadership and Policy in Schools*, vol. 12, no. 3, pp. 227–255, 2013.

[8] F.-C. Tseng and F.-Y. Kuo, "A study of social participation and knowledge sharing in the teachers' online professional community of practice," *Computers & Education*, vol. 72, pp. 37–47, 2014.

[9] J. L. Cummings and B. S. Teng, "Transferring R&D knowledge: the key factors affecting knowledge transfer success," *Journal of Engineering and Technology Management*, vol. 20, no. 2, pp. 39–68, 2003.

[10] Y. Hu and X. Liu, "Game analysis of knowledge sharing in knowledge alliance," *Science & Technology Progress and Policy*, vol. 26, no. 7, pp. 143–145, 2009.

[11] C. Liu, W. Shan, and J. Yu, "Type and evolutionarygame model of knowledge sharing within organizations," *Science Research Management*, vol. 35, no. 2, pp. 145–153, 2014.

[12] K. Caskova and S. Chudy, "Influence of school culture on pedagogical knowledge sharing between an education student

and a training teacher," *SN Social Sciences*, vol. 1, no. 4, pp. 1–18, 2021.

[13] J. Z. Wu, S. Song, F. Zhi, and M. A. Guang, Games analysis and simulation in knowledge sharing based on knowledge contribution assessment and utility among organizational employees," *Journal of Industrial Engineering and Engineering Management*, no. 1, pp. 216–222, 2015.

[14] A. Mollazehi and F. Karimi, "Identification and validating factors affecting teachers' knowledge sharing through ICT," *Sciences and Techniques of Information Management*, vol. 4, no. 4, pp. 103–131, 2019.

[15] D. Sun, Y. Li, and D. Yu, "Ability evaluation model of university teachers' tacit knowledge sharing," *Information Science*, vol. 33, no. 4, pp. 46–52, 2015.

[16] W. Zhang, Q. Zhang, and W. Shan, "Research on measurement of knowledge sharing capabilities of university research team based on overall network perspective," *Science of Science and Management of S.& T.*vol. 33, no. 10, pp. 170–180, 2012.

[17] K. McChesney and J. M. Aldridge, "A review of practitioner-led evaluation of teacher professional development," *Professional Development in Education*, vol. 45, no. 2, pp. 307–324, 2019.

[18] L. Zhao and C. Wang, "A research on university teachers' tacit knowledge sharing model and evaluation index system," *China Educational Technology*, no. 10, pp. 100–105, 2014.

[19] A. Asghar and M. A. Naveed, "Psychometric Evaluation of Knowledge Sharing Behavior Scale in Academic Environment," *Library Philosophy and Practice*, pp. 1–15, 2021.

[20] J. Li and J. Qin, "Effect of teachers' knowledge sharing behavior on students' entrepreneurial motivation in social media environment," *International Journal of Emerging Technologies in Learning (iJET)*, vol. 17, no. 02, pp. 143–157, 2022.

[21] J. Kularajasingam, A. Subramaniam, D. K. Sarjit Singh, and M. Sambasivan, "The impact of knowledge sharing behaviour and social intelligence of university academics on their performance: the mediating role of competencies," *The Journal of Education for Business*, vol. 97, no. 1, pp. 54–61, 2022.

[22] J. Wang, D. E. H. Tigelaar, and W. Admiraal, "Rural teachers' sharing of digital educational resources: from motivation to behavior," *Computers & Education*, vol. 161, Article ID 104055, 2021.

[23] C. R. Trusson, N. F. Doherty, and D. Hislop, "Knowledge sharing using IT service management tools: conflicting discourses and incompatible practices," *Information Systems Journal*, vol. 24, no. 4, pp. 347–371, 2014.

[24] G. S. Erickson, H. Rothberg, and C. Carr, "Knowledge-sharing in value-chain networks: certifying collaborators for effective protection process," *Advances in Competitiveness Research*, vol. 11, no. 1, pp. 152–164, 2003.

[25] K. F. Hew and N. Hara, "Knowledge sharing in online environments: a qualitative case study," *Journal of the American Society for Information Science and Technology*, vol. 58, no. 14, pp. 2310–2324, 2007.

[26] S. E. Booth, "Cultivating knowledge sharing and trust in online communities for educators," *Journal of Educational Computing Research*, vol. 47, no. 1, pp. 1–31, 2012.

[27] Y. Charband and N. Jafari Navimipour, "Online knowledge sharing mechanisms: a systematic review of the state of the art literature and recommendations for future research," *Information Systems Frontiers*, vol. 18, no. 6, pp. 1131–1151, 2016.

[28] X. Zhang and J. Su, "A combined fuzzy DEMATEL and TOPSIS approach for estimating participants in knowledge-intensive crowdsourcing," *Computers & Industrial Engineering*, vol. 137, Article ID 106085, 2019.

[29] Y. Xiao, C. Li, L. Song, J. Yang, and J. Su, "A multidimensional information fusion-based matching decision method for manufacturing service resource," *IEEE Access*, vol. 9, Article ID 39839, 2021.

[30] Y. Zhu, D. Tian, and F. Yan, "Effectiveness of entropy weight method in decision-making," *Mathematical Problems in Engineering*, vol. 2020, Article ID 3564835, 5 pages, 2020.

[31] Y. He, H. Guo, M. Jin, and P. Ren, "A linguistic entropy weight method and its application in linguistic multi-attribute group decision making," *Nonlinear Dynamics*, vol. 84, no. 1, pp. 399–404, 2016.

[32] G. R. Jahanshahloo, F. H. Lotfi, and M. Izadikhah, "Extension of the TOPSIS method for decision-making problems with fuzzy data," *Applied Mathematics and Computation*, vol. 181, no. 2, pp. 1544–1551, 2006.

[33] X. Zhang and J. Su, "An integrated qfd and 2-tuple linguistic method for solution selection in crowdsourcing contests for innovative tasks," *Journal of Intelligent and Fuzzy Systems*, vol. 35, no. 1, pp. 1–14, 2018.

Review Article

A Comprehensive Review of Recent Deep Learning Techniques for Human Activity Recognition

Viet-Tuan Le ⓘ **, Kiet Tran-Trung** ⓘ **, and Vinh Truong Hoang** ⓘ

Ho Chi Minh City Open University, 35-37 Ho Hao Hon Street, Ward Co Giang, District 1, Ho Chi Minh City, Vietnam

Correspondence should be addressed to Vinh Truong Hoang; vinh.th@ou.edu.vn

Human action recognition is an important field in computer vision that has attracted remarkable attention from researchers. This survey aims to provide a comprehensive overview of recent human action recognition approaches based on deep learning using RGB video data. Our work divides recent deep learning-based methods into five different categories to provide a comprehensive overview for researchers who are interested in this field of computer vision. Moreover, a pure-transformer architecture (convolution-free) has outperformed its convolutional counterparts in many fields of computer vision recently. Our work also provides recent convolution-free-based methods which replaced convolution networks with the transformer networks that achieved state-of-the-art results on many human action recognition datasets. Firstly, we discuss proposed methods based on a 2D convolutional neural network. Then, methods based on a recurrent neural network which is used to capture motion information are discussed. 3D convolutional neural network-based methods are used in many recent approaches to capture both spatial and temporal information in videos. However, with long action videos, multistream approaches with different streams to encode different features are reviewed. We also compare the performance of recently proposed methods on four popular benchmark datasets. We review 26 benchmark datasets for human action recognition. Some potential research directions are discussed to conclude this survey.

1. Introduction

Human action recognition is one of the most crucial tasks in video understanding. This field has a wide range of applications, such as video retrieval, entertainment, human-computer interaction, behavior analysis, security, video surveillance, and home monitoring. In detail, we want to find handshake events in a movie or offside decisions in a football match and the results are returned automatically. The goal of human action recognition is to recognize automatically the nature of an action from unknown video sequences.

There are some challenges in human action recognition. The view invariance is one of the reasons that make human action recognition more complex. There are some simple datasets having a fixed viewpoint [1, 2] while most of the recent datasets have many viewpoints. In addition, each person has their size and shape as well as posture. They can

appear with various clothes and accessories. An action which is performed in an indoor environment with a uniform or static background is easy to recognize than an action that is recorded in a cluttered or dynamic background. In addition, lighting conditions or viewpoints contribute to increase or decrease of the accuracy of recognition. The next problem is intraclass and interclass variations. A human action recognition method must be able to generalize an action over variations within a class and distinguish between actions of different classes. For examples, people have different speeds when they run or walk. The occlusion problem is a hard issue in action recognition because some body parts of humans are disappeared temporarily. For example, some body parts cover other parts or a subject, or a person is hidden behind another person. Temporal variations are also an important challenge because actions are happening for a long time.

Deep learning methods have achieved state-of-the-art results on various problems of computer vision, especially

human action recognition. Convolutional neural networks (CNNs) [3] are the neural network that uses convolutional operator in their layers. Convolutional network is used for computing a grid of values such as images while recurrent neural networks (RNNs) [4] are a type of neural network for processing sequential data, such as text and video. In this survey, we focus on proposed methods for human action recognition using deep learning techniques.

1.1. Review of Related Survey Articles. Since human action recognition is an attractive problem, many surveys have been done over the last few years. The most popular survey of human action recognition is the work in [5]. Firstly, the authors discussed the local representation and global representation-based methods. Then, three types of action classification approaches were discussed, including direct classification, temporal state-space models, and action detection. However, this study have been conducted over ten years ago, and this survey reviewed methods using hand-crafted features.

Zhang et al. [6] provided an overview of human action recognition, interaction recognition, and human action detection methods. The whole part of the survey discussed human action feature representation methods. First, the authors discussed handcrafted action features for RGB, depth, and skeleton data. Then, they reviewed some deep learning-based methods. However, they focused on two-stream networks and long short-term memory methods.

A review of Singh and Vishwakarma [7] focused on human action datasets in the past two decades. They classified these datasets into two classes, namely RGB (Red-Green-Blue) and RGB-D (depth) datasets. They discussed 26 RGB and 22 RGB-D datasets. Two categories of existing methods (handcrafted and learned feature representations) were discussed; however, the main contribution of this work is dataset analysis.

RGB-D data plays a vital role in human action recognition because this data provide color, depth and skeleton data. The performance of human action recognition systems is improved significantly when they exploit depth and skeleton data. With a special focus on RGB-D data, Liu et al. [8] reviewed human action recognition and human interaction recognition based on hand-crafted features. Then, their survey discussed human activity recognition based on deep learning in the next part.

Zhu et al. [9] reviewed over 200 papers about human action recognition. Their survey focused on three different approaches for human action recognition. Firstly, two-stream networks were reviewed. The two-stream methods tried to exploit the temporal relationship between frames because motion information plays a vital role in human action recognition in video. The first stream encodes the spatial information and the second one encodes the optical flow. In this review, the authors focused on recurrent neural networks which were used as a part of a two-stream network while our work discusses RNNs-based methods for human action recognition. Next, 3D CNN-based methods were discussed. 3D CNNs exploit both spatial and temporal information by using a 3D tensor with two spatial and one temporal dimension. The two-stream networks require huge resources to compute, and the 3D CNNs are hard to train. Therefore, they reviewed efficient video modeling which try to reduce computational intensity.

Beddiar et al. [11] reported a survey which discussed human activity recognition approaches in the last ten years. The authors classified human activity recognition approaches into various categories. The first category is the feature extraction process. Both hand-crafted features and feature learning were discussed. Then, they discussed three stages of human activity recognition approaches, including detection, tracking, and recognition. Next, unimodel and multimodel approaches were surveyed. They classify human activity recognition methods into three classes of learning supervision, namely supervised, unsupervised, and semi-supervised methods. The review also provided different types of activities. However, the recent deep learning techniques for human activities recognition were not highlighted clearly.

In order to review many different challenges, Jegham et al. [10] reviewed methods which aimed to solve these challenges in human action recognition. Many challenges were discussed such as anthropometric variation, multiview variation, cluttered and dynamic background, interclass similarity, intraclass variability, low-quality videos, occlusion, illumination variation, shadow and scale variation, camera motion, and poor weather conditions. In the second part, the authors reviewed recent action classification methods and popular datasets. They focused on three types of methods, including template-based methods, generative model-based methods, and discriminative model-based methods.

A different survey [12] discussed human pose estimation and the role of it in human action recognition application. Firstly, the survey discussed various types of human pose estimation such as single person, multiperson, 3D human pose estimation, and human pose estimation in videos and depth images. In the remained part, they discussed human pose estimation for action recognition.

A review of single vision and multivision modalities was provided by Majumder and Kehtarnavaz [13]. In the single vision modality section, the authors discussed the approaches which used video data for action recognition. In the next section, the methods using RGB + Depth data were reviewed in multivision modality section. In each modality, both conventional and deep learning approaches were reviewed.

Table 1 provides a summary of recent related surveys. Moreover, some main contributions of this work are discussed.

1.2. Contributions of This Survey Article. Human action recognition has a wide range of applications; therefore, many approaches have been proposed using deep learning techniques. We aim to provide a comprehensive survey of recent deep learning techniques for human action recognition. In summary, our main contributions are listed here:

TABLE 1: Summary of the related survey articles.

Survey	Year	Handcrafted	2D CNN	RNN	3D single-stream	3D multistream	Convolution-free	Datasets	Contributions
					Scope				
[5]	2010	✓						✓	
[6]	2019	✓	✓	✓	✓	✓		✓	(i) We categorise five aspects of deep
[7]	2019							✓	learning methods for human action
[8]	2019	✓	✓	✓				✓	recognition
[9]	2020		✓	✓	✓	✓		✓	(ii) Convolution-free approaches are
[10]	2020							✓	first reviewed in our work
[11]	2020	✓						✓	(iii) A detailed review of popular
[12]	2021							✓	benchmark datasets for action
[13]	2021	✓	✓	✓				✓	recognition
Our	2021		✓	✓	✓	✓	✓	✓	

(i) We discuss the most recent deep learning techniques for human action recognition.

(ii) We provide the first review of convolution-free approaches in the human action recognition field.

(iii) We survey the most popular benchmark datasets for human action recognition

(iv) We provide a comprehensive analysis of proposed methods.

1.3. Roadmap of the Survey. As in Figure 1, the rest of the survey is organized as follows. In Section 2, we discuss the most recent deep learning techniques for anomaly detection. Then, we provide two accuracy comparisons of some popular datasets in Section 3. Section 4 reviews many popular benchmark datasets in the human action recognition field. Finally, we discuss some open research problems and give the conclusion of this survey.

2. Recent Deep Learning-Based Methods in Human Action Recognition

In this section, we review recent deep learning-based methods for human action recognition. With the development of large-scale datasets and deep learning, this leads a remarkable growth of models based on deep learning for human action recognition. There are four trends and a new trend has attracted some researchers recently. The first trend is 2D Networks which uses 2D convolutional neural networks in their models, such as TSM [14], TRN [15], and GSM [16]. The second trend is action recognition based on RNN, such as in [17–19]. The third trend is 3D Single Stream Network which uses 3D convolutional kernels in the networks, such as CSN [20] and TSN [21, 22]. The fourth trend is 3D Two-Stream Network which includes a spatial and a temporal stream to encode both structure and optical flow information, such as in [23–26]. Finally, convolution-free approaches based on attention mechanism are a new trend in human action recognition with efficient computation and performance, such as in [27–29] and TimeSformer [30].

2.1. Methods Based on 2D CNN. In this part, we will discuss the proposed methods that are based on 2D CNNs. One of the advantages of 2D CNNs is that the computation is cheap [14]. However, 2D CNNs often cannot exploit well the temporal information. Therefore, many approaches try to capture both spatial and temporal information [16, 31, 32]. Optical flow information plays a vital role in action recognition, but the computation cost is expensive. Therefore, in [33–35], the authors tried to compute optical flow with low cost and efficiency.

Two-stream networks are often trained individually with high computational cost. Jiang et al. [31] proposed an efficient method to exploit both spatiotemporal and motion features in a 2D framework, namely STM block. The STM block includes a channel-wise spatiotemporal module (CSTM) and a channel-wise motion module (CMN). The CSTM is used to extract spatiotemporal information. The input feature map $F \in \mathbb{R}^{N \times T \times C \times H \times W}$ is reshaped into $F^* \in \mathbb{R}^{NHW \times C \times T}$. Then, a channel-wise 1D convolution is applied on input feature maps. A 3D convolutional network can encode local spatial and temporal features. However, they cannot encode ordered temporal information of all clips. A channel-independent directional convolution (CIDC) [32] was introduced to solve this issue. Given input feature map with C channels, CIDC convolve each channel of input feature map with T' filter. The output feature map including spatial and temporal information is obtained by concatenating $C \times T'$ feature map. Another strategy in action recognition is frame selection. Gowda et al. [36] proposed a smart frame selection method that improved over many state-of-the-art models. The method includes two branches. The first computes a score δ_i for each frame, and the second computes a score γ_i of a pair of frames. Given n frames, top m frames are chosen using a final score which is multiplied both score δ_i and γ_i. Finally, a classifier is used for the final prediction. The authors used the Something-Something-V2 dataset [37] for ablation study. They also experienced on Kinetics [38], UCF101 [39], and HMDB51 [40].

According to the observation, movement variations at motion boundaries are very important in human action recognition. Zhang et al. proposed persistence of appearance

A Survey for Human Action Recognition
1. Introduction
  Review of related survey articles
  Contribution of this survey article
  Roadmap of the survey
2. Recent Deep Learning Based Methods in Human Action Recognition
  Methods Based on 2D CNN
  Methods Based on RNN
  Methods based on 3D Single-stream Network
  Methods based on 3D Multi-stream Network
  Convolution-free approaches
3. A Comparison of Methods
3. Benchmark Datasets
  Simple Datasets
  Clip-level Datasets
  Video-level Datasets
4. Open Research Problems
5. Conclusions

FIGURE 1: The structure of the survey.

(PA) [33] to obtain a map that encodes small motion variations at boundaries. The difference between the optical flow and PA is that PA captures the motion variation without encoding the direction of the movement. Given two frames, eight 7×7 convolutions are applied to obtain low-level feature maps F_1, F_2. The i-th PA component is computed as $PA_i(p, \Delta t) = F_i(p, t + \Delta t) - F_i(p, t)$, where F_i is the i-th feature map. All PA_i are aggregated to a channel PA. The PA maps the appearance to the dynamic motion because it maps from three-dimensional to two-dimensional tensor. To exploit motion information, Piergiovanni and Ryoo [34] proposed a convolutional layer to capture the flow of any channel for action recognition without computing optical flow. The proposed fully differentiable convolutional layer has learned parameters that enhance the performance of action recognition systems. Optical flow is an expensive method. Xu et al. [35] proposed a fast network to improve the extraction of optical flow. The optical flow is generated by MotionNet [41] which is an end-to-end trainable network. Moreover, OFF [42] is added to the network to get better optical flow features. The optical flow is computed directly from RGB frames without precalculation or storage. Therefore, both spatial and temporal information are learned by one network.

One of the most popular modules in human action recognition is temporal shift module (TSM) [14]. TSM has the complexity of a 2D CNN but obtains the performance of 3D CNN. In addition, this module can insert into a 2D CNN without extracomputation and parameters. Given a tensor with C channels and T frames. A part of the channels is shifted by -1, and another part is shifted by $+1$. The rest of the tensor is unshifted. The TSM can be inserted before convolutional layer or residual block, but the spatial features may be harmed because the information is lost. To deal with this problem, the TSM is inserted into a residual branch in a residual block. To exploit the temporal relations between frames in video, Zhou et al. [15] proposed a temporal relation network (TRN) which predict human-object interactions in the Something-Something dataset accurately. Their paper show that the TRN outperformed two-stream network as well as 3D convolution networks. The pairwise temporal relation is computed as $T_2(V) = h_\phi(\sum_{i<j} g_\theta(f_i, f_j))$, where $V = \{f_1, f_2, \ldots, f_n\}$ is the video with n frames. The functions h_ϕ and g_θ is used to fuse the frame features. Moreover, The function captured frames relations at different scale is described as $MT_N(V) = T_2(V) + T_3(V) + \cdots + T_N(V)$, where T_d is temporal relationship of d frames. A 2D convolution neural network (CNN) has smaller parameters and fast computation than a 3D CNN. However, a 2D CNN usually captures spatial information. Sudhakaran et al. proposed a gate shift module (GSM) [16] which is an 2D CNN to capture spatial and temporal features. The input is applied a spatial convolution. Then, a grouped spatial gating is computed. The 2D convolution ouput is split into group-gated features and residual. The gated features are group-shifted and fused with the residual. The spatial and temporal information is exploited by a learning spatial gating.

In a different approach to abovementioned methods, Zhang et al. [43] applied video super-resolution to human action recognition by introducing two video super-resolution (SR) modules, namely spatial-oriented SR (SoSR) and temporal-oriented SR (ToSR). The low-resolution input video is enhanced by two proposed modules. The input of the recognition network includes the output of the SoSR and the optical flow computed from the output of the ToSR module.

2.2. Methods Based on RNN.

CNNs are popular models for image representation. They are also used to learn action representation in videos [14–16]. However, they often work well with short videos [33, 34], since only spatial features are captured and motion information of action are not encoded. To encode longer motion in video, some approaches have used RNNs, and long-short term memory (LSTM), such as in [17–19]. RNN is widely used in sequence data like video, and text. LSTM is a special version of RNN with the capability of learning long-term information. In addition, LSTM is combined with an attention mechanism [44] or is used in a three-stream network [45, 46] for action recognition.

With video data, RNNs and LSTM requires high memory storage and computation cost. A compact LSTM model (TR-LSTM) [17] was proposed to solve this issue. The TR-LSTM use the tensor ring decomposition to reconstruct the input-to-hidden layer of the recurrent network. In the tensor ring decomposition, the first and last tensors are connected circularly and constructed in a ring-like structure. A densely-connected bi-directional LSTM (DB-LSTM) network [18] is used to represent the spatial and temporal information of human actions. The goal of DB-LSTM is to capture the spatial, short-term, and long-term patterns. The spatial and short-term patterns are extracted by a sample representation learner module, and the long-term patterns are exploited by a sampling stack. Another work, named correlational convolutional LSTM (C^2 LSTM) [19] aims to exploit both spatial and temporal information of human action video. The basic spatial features are extracted by two parallel convolutional networks, and then, these features are used as input for the C^2 LSTM module. The C^2 LSTM extracts the spatial and temporal information as well as the time relation by using cross-correlation inside the LSTM.

A three streams network was proposed by Liu et al. [45] for human action recognition. The network includes a spatial stream, a temporal stream, and a spatial-temporal saliency stream. These streams are used to extract appearance information of RGB frames, motion information of optical flow frames, and spatiotemporal foreground information of objects from spatiotemporal saliency maps. In addition, they proposed three attention-aware LSTMs to exploit the relationship between frames. Another three-stream network [46] processes different frame rates for human activity recognition. The first stream operates at a single frame rate and the second stream processes at low frame rates. Both streams are used to capture spatial features. The third stream processes at high frame rates to capture temporal features.

The output of the previous step is fed into two LSTM layers. This makes the proposed model deeper. Instead of using the LSTM layer, the authors use an attention mechanism to capture temporal information.

To extract the salient features of human action videos, Ge et al. [44] introduces an attention mechanism and convolutional LSTM. A convolutional network is used to extract features of the input video. Then, a combination of LSTM and a spatial transformer network extracts salient features. The final classification is obtained by a convolutional LSTM. The proposed combination can select salient localities effectively while getting higher accuracy than soft attention and using less calculation than hard attention.

2.3. Methods Based on 3D Single-Stream Network.

In this part, we will discuss 3D convolution-based models. These methods obtain good results since 3D CNN extracts spatial and temporal information from action video directly. Figure 2 is an example of single-stream network architecture. The input frames are fed into a 3D single-stream network to extract both spatial and temporal features.

Tran et al. [20] proposed a channel separated convolutional network (CSN) which employs 3D group convolution. The CSN is defined as 3D CNNs; however, only $1 \times 1 \times 1$ conventional convolutions or $k \times k \times k$ depthwise convolutions are used. In detail, the conventional convolutions are used for channel interaction and depthwise convolutions are used for local spatiotemporal interactions. In their work, a $3 \times 3 \times 3$ convolution from the bottleneck block by a pair of a $1 \times 1 \times 1$ convolution and a $3 \times 3 \times 3$ depthwise convolution to get a interaction-preserved channel-separated bottleneck block. Moreover, the $1 \times 1 \times 1$ convolution in the previous pair convolutions is removed to obtain interaction-reduced channel-separated bottleneck block. The authors also applied group convolution to ResNet blocks. Two $3 \times 3 \times 3$ convolutional layers of simple ResNet block are replaced by two $3 \times 3 \times 3$ grouped convolutions or a set of one $1 \times 1 \times 1$ convolution and two depthwise convolutions. 3D convolutional neural networks have high training complexity and huge memory cost. In order to resolve this problem, Zhou et al. [47] proposed a combination of 2D and 3D convolution, namely mixed convolutional tube (MiCT). The deep MiCT is an end-to-end network which receives RGB video sequences as inputs. The whole network includes four MiCTs and a global pooling in the last layer of the network. This pooling allows the network to accept any length videos as inputs. Each MiCT block receives an 3D signal. The input process by a 3D convolution to extract spatial-temporal feature maps. The extracted features are passed through a 2D convolution to compute the final feature maps. The MiCT-Net uses fewer 3D convolution, but it obtains deeper feature maps. Instead of combining 2D and 3D convolution, a new spatiotemporal architecture fused 2D and 3D architectures to improve spatiotemporal representation. Diba et al. proposed holistic appearance and temporal network (HATNet) [48] which exploits semantic information at different levels. HATNet uses 2D convolutional blocks to encode the appearance
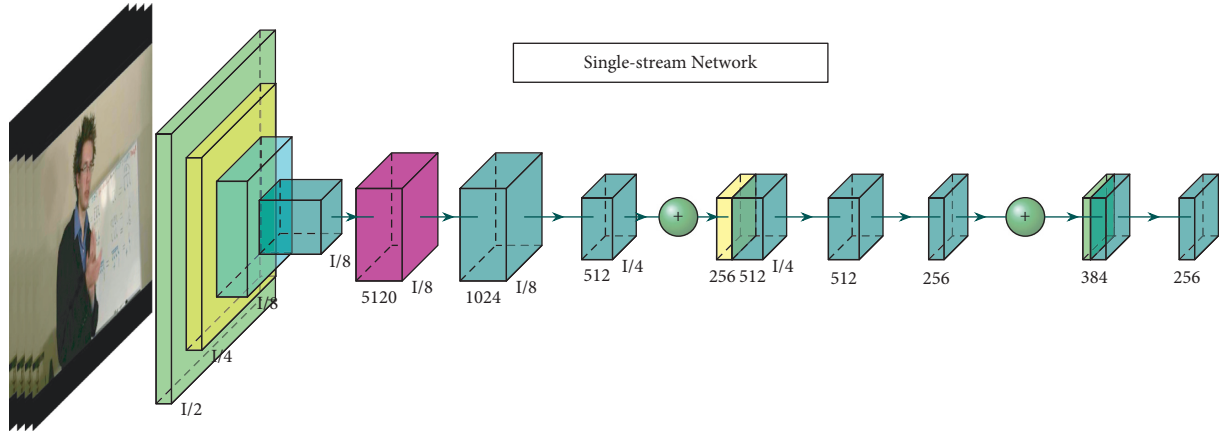
FIGURE 2: 3D single-stream network.

information of individual frames in a video clip. In addition, the 3D convolutions extract temporal information in a batch of frames. ResNet18 and ResNet50 was used in HATNet for 3D and 2D modules, respectively. The output feature maps of each 2D and 3D block are merged; then, a $1 \times 1 \times 1$ convolution is applied to reduce the channel of features. With prestraining on HVU dataset [48], the HATNet obtained 97.8% and 76.5% on UCF101 [39] and HMDB51 datasets [40], respectively.

The video usually has repeating information, and the temporal squeeze network [21] can map the movement information from a long video into a set of few frames. Given a video X with K frames, a frame-wize z is obtained by applying the squeeze operation. The output of squeeze operation is fed into a excitation operation. Global average pooling is used to implement the squeeze operation while the excitation operation is implement by two fully connected layers and two activation functions. The shorter sequence frames Y' is obtained by projecting the flattened vector of X onto the hyperplane $\mathbf{A}$, where $\mathbf{A}$ is computed from the output of the excitation operation. To reduce the computational cost of motion feature, a FASTER-GRU network [49] aggregates the temporal information. The FASTER framework uses an expensive model and a lightweight model to exploit the information of the action and scene, respectively. The FAST-GRU aims to learn the features from multiple models. This network maintains the resolution of feature maps to exploit more spatial-temporal information. A fully connected layer is replaced by a 3D $1 \times 1 \times 1$ convolution. The proposed method was evaluated on Kinetics [38], UCF101 [39], and HMDB51 datasets [40]. A combination of 3D convolution neural network and long-short term memory [50] is used to capture low-level spatial-temporal feature and high level temporal feature. The proposed network used Inception 3D CNN [38] to extract spatial features and low-level motion features from a sequence of frames. Then, the output of the I3D model is fed into a LSTM network to exploit high-level spatial features. Temporal information plays a vital role in human action recognition; however, this information still has challenging problems. A temporal difference network (TDN) [51] was

proposed to capture multiscale temporal information. In addition, TDN in an end-to-end model that captures both short-term and long-term motion information. Given T frames $I = [I_1, \ldots, I_T]$, a 2D CNN is used to extract features $F = [F_1, \ldots, F_T]$. A short-term and long-term TDM is applied to exploit short-term and long-term motion. To capture the short-term motion, a stacked RGB difference of frame I_i is downsampled using an average pooling, then extracted motion information with a 2D network. The feature is upsampled to match the size of RGB features. In the long-term TDM, the aligned temporal difference is computed, and then fed into a multiscale module to extract long-range motion information. Features are enhanced by a bidirectional cross-segment temporal difference. The TDN framework with ResNet backbone [52] was evaluated on Kinetics-400 [38] and Something-Something-V1-V2 [37]. Instead of computing the optical flow frame-by-frame, the proposed MotionSqueeze module [53] learned motion features by a light-weight learning technique. The module contains three parts, namely correlation computation, displacement estimation, and feature transformation. The correlation score is defined as $s(x, p, t) = F_x^{(t)} \cdot F_{x+p}^{(t+1)}$, where $F^{(t)}$ and $F^{(t+1)}$ are two input feature maps. Then, motion information is estimated in the displacement estimation module and a confidence map of correlation is obtained from the correlation. The concatenation of displacement map and the confidence map is used as the input of the feature transformation. The feature transformation converts the input into an effective motion feature. The MotionSqueeze module is inserted into ResNet and evaluated on Something-Something-V1, Something-Something-V2 [37], Kinetics [54], and HMDB51 datasets [40].

Kalfaoglu et al. [22] proposed a method which obtained highest accuracy on both HMDB51 [40] and UCF101 [39] datasets with 85.10% and 98.69%. The most important thing in this study is that the authors replace the conventional temporal global average pooling (TGAP) layer by the bidirectional encoder representations from transformers (BERT) layer. This replacement utilize the temporal information with BERT's attention mechanism. They declared that TGAP ignores the order of the temporal features, and

BERT can focus on the important temporal features. The proposed network removed temporal global average pooling at the end of the proposed 3D CNN architecture. A learned positional encoding was added to the extracted features to maintain the positional information. The two last parts of the architecture is multihead attention a classification. Then, they also proposed some features reduction blocks. Attention is a useful tool in many fields of computer vision. A novel W3 (what-where-when) video attention module [55] including a channel-temporal attention M^c and a spatio-temporal attention M^s was proposed for the action recognition problem. An average-pooling and a max-pooling are used to aggregate global spatial information. The output is fed into a shared MLP network to exploit the interchannel relationship. To model the temporal dynamics of objects, a channel temporal attention with two layers of 1D convolutions is computed. With spatiotemporal attention, an average-pooling and max-pooling are used as in channel-temporal attention to exploit spatial feature maps. The features are concatenated and fed into a 2D convolution to obtain frame-level spatial attention. To obtain the temporal attention, two 3D convolutional layers is applied with the frame spatial attention of previous step. The W3 attention module was integrated the ResNet50-based TSM [14].

The backbone CNN network plays a vital role in many recent action recognition systems. Martinez et al. [56] changes the last layers of the backbone network to improve the representation capacity. The important information is maintained in global feature branch. The global feature branch consists a global average pooling and a linear classifier. The average pooling aggregates the spatial and temporal information of the video. In the discriminative filter bank, the filters are includes 1×1 or $\times 1 \times 1 \times 1$ convolutions and global max pooling to compute the highest activation value. The third branch is local detail preserving feature branch. A bilinear upsampling operation are applied to double the resolution of the features. A skip connection is add from the features of stage 4. Two backbone networks (2D TSN [57] and inflated 3D [38]) were used to evaluate the proposed module with Something-Something-V1 [58] and Kinetics-400 [38]. The temporal modeling methods based on 3D CNN requires a large number of parameters and computations. Lee et al. [59] proposed VoV3D which is an 3D network with an effective temporal modeling module for temporal modeling. The module names temporal one-shot aggregation (T-OSA). The T-OSA use many 3D convolutions with different receptive fields. All the output features are concatenated and reduced dimension by a $1 \times 1 \times 1$ convolution. In addition, the authors proposed a depthwise spatial-temporal module which decomposes a 3D depthwise convolution into a spatial depthwise convolution and a temporal depthwise convolution for making a more light-weight and efficient network. Something-Something-V1, Something-Something-V2 [58], and Kinetics-400 [38] was used to evaluate.

Zhao and Snoek [60] proposed a single two-in-one stream network to reduce the complex computation of two stream network. The network processes both RGB and optical flow in a single stream. The most important contribution in this work is motion condition layer and motion modulation layer. The motion condition layer maps flow inputs to motion condition Ψ. Then, the motion condition Ψ is fed into the motion modulation to learn two affine transformation parameters (β, γ). These parameters are used to influence the appearance network as below formula $\mathcal{M}^2 (F^{rgb}) = \beta \odot F^{rgb} + \gamma$, where F^{rgb} is the RGB feature maps and $\odot$ is an element-wise multiplication operation. Instead of using deeply stacking convolution layers, Huang and Bors [61] proposed region-based nonlocal (RNL) to exploit long-range dependencies. The RNL operation is used to compute the relation between two positions based on their features and the neighboring features. The feature of each position is computed from all neighboring positions. The RNL operator is embed into a residual block as $z = yW_z + x$. In addition, the RNL block is combined with SE [62] block to exploit spatiotemporal attention and channel attention. Two backbone networks are used to implement the proposed RNL, including ResNet-50 [52] and temporal shift modules (TSM) [14]. The network was evaluated on Something-Something-V1 [37] and Kinetics-400 [38]. Furthermore, OmniSource [63] trains video recognition model using web data, such as images, short videos, and long videos. The methods train a 2D teacher network and a 3D teacher network to filter the the web data that have lo confidence scores. Hua et al. proposed a dilated silhouette convolutional network (SCN) [64] for human action recognition in video. The silhouette boundary curves of the moving subject are extracted, and then, the silhouette curves are stacked as a 3D curve volume. The curve volume is resampled to a 3D point cloud to represent the spatial and temporal information of actions.

2.4. Methods Based on 3D Multistream Network.
Multistream networks can exploit different types of features in human action recognition. Spatiotemporal and motion information are two important features of human action recognition. A two-branch network has two branches, including the RGB branch and flow branch. The RGB branch exploits the visual structure of scenes and objects, while the flow branch exploits the motion of objects. Many recent proposed methods use a 3D CNN to exploit spatiotemporal information and a flow stream to exploit motion information [24, 26, 38]. The two-stream network obtains state-of-the-art accuracy by using RGB and flow images as input. However, each stream is usually trained individually and the optical flow requires a heavy computation. Therefore, some approaches try to construct a two-stream network more efficiently [23, 65]. Figure 3 shows a two-stream network architecture that are used in many recent approaches.

To pay different types of attention, a two-stream attention [26] was proposed using the visual attention mechanism. The network contains two streams. The first stream is the temporal feature stream which inputs an optical flow image sequence. An LSTM and a temporal attention are used to aggregate the information of the optical flow image. The second stream is a spatial-temporal feature stream. This stream uses an LSTM architecture to encode the
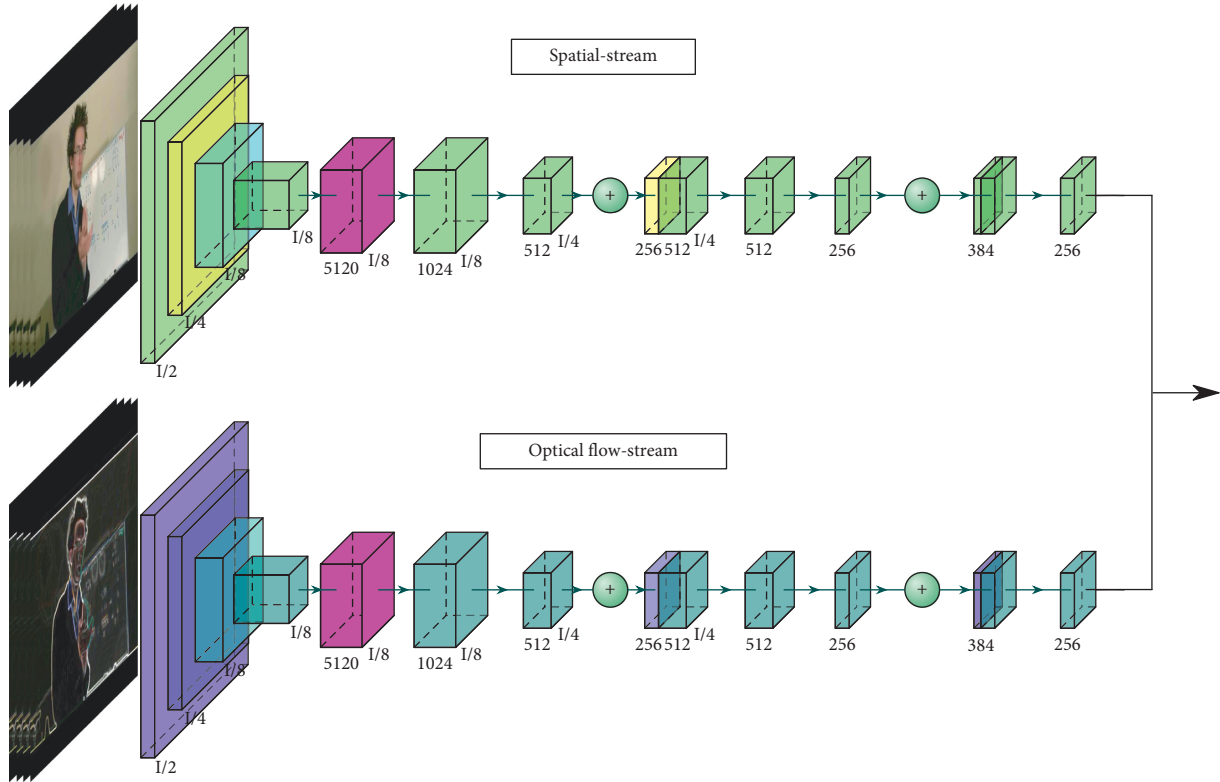
FIGURE 3: 3D two-stream network.

temporal relationship. The spatial features are extracted by some convolutions. Then, the spatial attention assigns an important location for the next step of feature generation and the temporal attention is used to focus the temporal frames. The method was evaluated on UCF11 [66], UCF Sports [67], and jHMDB [68]. An approach convert 2D classification networks into 3D ConvNets. The network is named as Two-Stream Inflated 3D ConvNets (I3D) [38]. They inflated all the filers and pooling kernels of the 2D architecture by enlarging a temporal dimension. To pretrain the 3D model on the ImageNet dataset, the authors converted an image into a video by copying it many times. The network has two streams. The first stream uses RGB inputs and the second one use flow inputs. The two networks are trained separately and the results are averaged. A two-pathway convolutional neural network [24] was proposed by Huang et al., namely Fine and Coarse. In the fine branch, motion information of raw input is extracted by a motion band-pass module. The extracted motion is fed into a backbone CNN [69] to learn the fine-grained motion features. On the other hand, the coarse branch is used to learn coarse-grained information. The raw frames are down-sampled and fed into a backbone CNN to exploit coarse-grained features. In order to merge the features from two branches, a lateral connection module was established. The proposed method was evaluated on Something-Something-V1 [37], Kinetics-400 [38], UCF101 [39], and HMDB51 dataset [40]. A combination of RGB, flow, pose, and pairwise stream [70] was proposed to improve the performance of the action recognition system. The network includes two branches. The first branch uses CD3 [71] and I3D [38] as backbone networks to extract spatial and temporal information. In the second branch, a pairwise stream learns the spatial relationship between the subject who perform the action and the surrounding objects. In addition, a pose stream inputs keypoint images. Keypoint images provide the connected key body parts of a person. The predicted results are obtained by using the late fusion method. The network was evaluated on UCF101 [39] and HMDB51 datasets [40].

Optical flow requires high computing. A proposed approach [23] mimics the motion stream using a standard 3D CNN. They introduced two learning strategies, namely Motion Emulating RGB Stream (MERS) and Motion-Augmented RGB Stream (MARS). In the first strategy, a flow network is trained to classify actions using optical flow clips. Then the MERS is trained to mimic the flow stream using only RGB frames. The last layer of MERS is trained by using the imitative flow features. In the second strategy, a flow stream (teacher) uses optical flow clips to train. Next, the teacher network is frozen its weight and MARS (student) is trained with RGB frames as input. Since only RGB frames are used as input in the testing phase, the network avoids the high computation of optical flow. The optical flow requires a high computation cost. Stroud et al. [65] introduced Distilled 3D Network (D3D) which obtained high performance without optical flow computation during inference. The D3D combines motion information in the temporal stream into the spatial stream. This leads the spatial to behave like the temporal stream. D3D trains two networks, including a teacher network and a student network. The teacher network

is a learned temporal stream of a two-stream network and the student network is a spatial stream. The knowledge of the teacher network is distilled into the student network during the training phase.

One of the problems of a two-stream network is to exploit the complementary information between two streams [25]. To solve this issue, Zhang et al. proposed a cross-stream network [25]. Two similar backbone networks are used to extract structure and motion features. Then, a cross-stream connection block is used to compute the correlation between the appearance and motion features. The classification scores are obtained by a classifier which inputs the extracted features of previous blocks. The cross-stream network is evaluated on UCF101 [39] and HMDB51 datasets [40] and Something-Something-V2 [58]. The most popular multimodality method fused its stream at the last stage of the model. A cross-modality [72] exchanges information between modalities in a more effective way. The proposed network has two branches. Instead of averaging the scores of the two branches, several cross modality attention (CMA) blocks are added after some stage of the network. The CMA matches a query of the first modality with key-value pairs of the second modality.

A very deep network [73] uses residual learning to encode spatial-temporal information human action recognition videos. The network, residual spatial-temporal attention network (R-STAN), includes two streams. Since the computation of optical flow has high cost, RGB Difference images are used to extract motion information. The RGB Difference images are computed by applying a element-wise subtraction operation between two frames. The network is constructed of many residual spatial-temporal attention blocks, including a residual block and a temporal and a spatial attention module. A feature map is processed as $M'(x) = M \odot A_T \odot A_S$, where M and M' are the input and output feature maps and A_T and A_S are the temporal and spatial attention, respectively. Two standard datasets (UCF101 [39] and HMDB51 [40]) was used to evaluate the proposed method. A proposed neural network [74] computed the local and global representations parallel. Therefore, the feature maps are processed in local path and global path. In the first path, the local features x_l are updated from x_{l-1} and global vector g_{l-1}. In the second one, the global vector is updated with local feature x_l. Next, they proposed a local and global combination classifier to make the final prediction by combining the local and global representations. Finally, they proposed two different local and global diffusion networks, namely LGD-2D and LGD-3D. The difference between the LGD-2D and LGD-3D is that the input of the first one is T noncontinuous frames while the input of the second is T consecutive frames. In addition, LGD-2D and LGD-3D use 2D convolution and 3D convolution, respectively. They evaluated on two datasets, namely Kinetics-400 [38] and Kinetics-600 [75]. They also experienced on two of the most popular video action recognition datasets UCF101 [39] and HMDB51 [40].

Instead of training different networks separately, Zhou et al. [76] constructed a probability space from which a spatial-temporal fusion strategy can be derived. The authors introduced spatial-temporal fusion strategies that obtained high performance on poplar datasets. To exploit the mutual correlations in the video, an attention mechanism [77] is used in the 3D convolutional network. The authors proposed a temporal and spatial attention submodule and then used these attentions to construct the temporal and spatial deformable 3D convolutional network. Both 3D convolutional networks can learn temporal and spatial information as well as static appearance. A proposed model [78] used pose information to predict actions. First, they used the PoseNet approach with ResNet backbone to obtain estimated pose keypoints for each human in a frame. The backbone network used is ResNet50 with a 3D version. They added a feature gating module and did not apply temporal downsampling in any layer of the backbone network to improve the performance. The authors tried to avoid training three models separately since the input included RGB, flow, and pose data. They proposed a multiteacher framework in which its input can be RGB, flow, or pose. They evaluated on three benchmark datasets, including Kinetics-600 [38], UCF101 [39], and HMDB51 [40],

2.5. Convolution-Free Approaches. The 2D network is very successful in capturing the spatial features. However, the motion information is still missed. 3D convolution network is used to encode spatial-temporal information in videos but it requires a high computation cost. Transformer was proposed for natural language processing and then adopted for computer vision. It does not require heavily stacked convolutions to encode information, such as in [27–30].

A convolution-free model [27] that requires a smaller number of frames for inference. The model is based on a self-attention mechanism for capturing both spatial and temporal information. The authors separate the spatial attention and the temporal attention to reduce the computation and exploit temporal information better. Each input frame ($H \times W$) of the network is split into nonoverlapping patches $N = HW/P^2$, where the size of each path is $P \times P$. Then, each patch representation is converted to query, key, and value vectors. To avoid expensive computation, spatial attention is applied between patches of the same image. The output representations of the spatial attention are applied to temporal attention. The proposed method was evaluated on Kinetics-400 [38]. They also reported the result on UCF101 [39].

To solve the heavy memory usage of the vanilla video transformer, a video transformer [28] was introduced to reduce the memory cost. The issue is solved by applying a spatial and temporal multihead separable-attention (MSA) sequentially $MSA(S) = MSA_s(MSA_t(S))$. Moreover, the authors solved the redundant information problem of the temporal dimension. Instead of using temporal average pooling or 1D convolutions with stride 2, they proposed a topK pooling which selects topK based highest standard deviation. They evaluated on 6 different datasets (Kinetics-400 [38], Kinetics-700 [79], Something-Something-V2 dataset [37], Charades [80], UCF101 [39], and HMDB51 [40]).

A convolution-free model is faster than 3D convolutional networks, namely, TimeSformer [30]. Each input

frame is split into N nonoverlapping patches same as in [27]. The spatiotemporal position of each patch is encoded by a learnable positional embedding $e_{(s)}^{pos} \in \mathbb{R}^D$. Each patch $X_{p,t}$ is mapped into an embedding vector $z_{(p,t)}^{(0)}$. The TimeSformer has L blocks and a set of query, key, and value vectors is computed from $\mathbf{z}_{(p,t)}^{(l-1)}$ for each block. In this study, the authors proposed a more efficient spatiotemporal attention. A temporal attention is applied, then, the output is fed into a spatial attention. The TimeSformer was evaluated on Kinetics-400 [38], Kinetics-600 [81], Something-Something-V2 datasets [37], and Diving48 [82].

Akbari et al. [29] introduced a convolution-free Transformer architecture, namely Video-Audio-Text Transformer (VATT). The input video clip is split into a sequence of $\lceil T/t \rceil \cdot \lceil H/t \rceil \cdot \lceil W/t \rceil$ patches. The position of each location (i, j, k) is encoded as $e_{i,j,k} = e_{\text{Temporal}_i} + e_{\text{Horizontal}_j} + V_{\text{ertical}_k}$, and Multi-Head-Attention applies the self attention on the input. Multilayer perceptron includes two dense linear projections with a GeLU activation. The common space projection contains a linear projection, and a two-layer projection with ReLU activation functions in between. The proposed method was evaluated on UCF101 [39], HMDB51 [40], Kinetics-400 [38], Kinetics-600 [75], and Moments in Time [83].

3. A Comparison of Methods

First, we compare recent methods on two benchmark datasets, including UCF101 [39] and HMDB51 [40]. These are the two most popular human action datasets that have been used to evaluate the performance of the proposed methods as shown in Table 2. We group the proposed methods by year. In 2019, the local and global diffusion network achieved the best result with 98.20% and 80.50% on UCF101 and HMDB51, respectively. Their network tried to learn local and global feature in parallel, and these features are diffused effectively. In 2020, Kalfaoglu et al. [22] obtained impressive results with 98.69% and 85.10% on UCF101 and HMDB51, respectively. The replacement of the conventional temporal global average pooling layer with the bidirectional encoder representations from the Transformers layer increase the performance of 3D convolutional neural networks. In 2021, a three-stream network obtained 99.00% on the UCF101 dataset. In this year, many approaches introduced a new model for human action recognition with a convolution-free architecture, such as VATT [29], VidTr [28], STAM [27], and TimeSformer [30].

Table 3 compares recent approaches on Something-Something-V1 and Something-Something-V2. TSM [84] is one of the most effective methods which obtains both high efficiency and high performance because it obtains the performance of a 3D network with the complexity of a 2D network. TSM uses a simple temporal shift module to exploit a temporal relationship with zero extra computation and zero extra parameters. It obtains 52.60% and 66.00% top-1 accuracy on Something-Something-V1 and Something-Something-V2, respectively. Another method TDN [51] obtained state of the art on the Something-Something-V1 and Something-Something-V2 with 56.80% and 68.20%.

TDN focus on capturing local and global motion for action recognition.

4. Benchmark Datasets

Benchmark datasets play a vital role in estimating the performance of proposed methods. The scope of the problem as well as a fairly comparison are provided by the dataset. For human action recognition, there is a wide range of benchmark datasets in common use. We briefly review the most well-known datasets and their information (size, average duration, action classes, and resolution) for human action recognition. These datasets are grouped into three categories such as simple, clip-level, and video-level. Table 4 provides a summary of these datasets.

4.1. Simple Datasets.
The two popular datasets which are most used with traditional methods are KTH [1] and Weizmann [2]. However, these datasets obtained absolute accuracy [102, 103] because the background is static and simple and one person performs an action in each video. Then, some more realistic datasets were proposed such as Hollywood [90] and Hollywood2 [91].

KTH [1] is a video dataset including 2391 videos. The dataset was performed by 25 different people in four different scenarios. The whole dataset (https://www.csc.kth.se/cvap/actions/) includes six human actions: walk, jog, run, box, hand-wave, and hand clap.

Weizmann [2] is a video dataset which was performed with nine people. Each participant performs 10 actions such as run, walk, jump, skip, jack, jump-forward, jump-in-place, side, wave-two-hand, and wave-one-hand. This dataset (http://www.wisdom.weizmann.ac.il/%20vision/SpaceTimeActions.html) includes 90 videos.

Hollywood [90] is a human action dataset taken from 32 movies. This dataset (https://www.di.ens.fr/%20laptev/download.html) has eight action classes with 233 training video samples and 211 testing video samples.

Hollywood2 [91] is a human action dataset with 3669 video clips. This dataset (https://www.di.ens.fr/%20laptev/actions/hollywood2/) includes 12 classes of actions and 10 classes of scenes with approximately 20.1 hours of video which is taken from 69 different movies.

4.2. Clip-Level Datasets.
The number of actions of previous datasets is small, and the actions are simple. Therefore, some datasets such as UCF101 [39], HMDB51 [40], and J-HMDB [68] were introduced to provide a higher variety of actions. However, the samples are short clips, and a single action is captured. Then, some large-scale datasets, such as Charades [80], Something-Something [37], Kinetics [54], Kinetics-600 [75], Kinetics-700 [79], Diving48 [82], Moments in time [83], HACS [93], HVU [48], and AViD [94], have been introduced. These datasets allow to train a deep convolutional neural network from scratch.

UCF101 [39] has 101 action classes and has split into five categories: human-object interaction, body-motion only, human-human Interaction, playing musical instruments,

Table 2: Accuracy of different methods on UCF101 and HMDB datasets.

Method	Year	Method	UCF101	HMDB
Carreira and Zisserman [38]	2017	Two-stream I3D	98.00	80.90
Zhou et al. [47]	2018	Mixed 3D CNNs, 2D CNNs	94.70	70.50
Zhang et al. [43]	2019	SoSR + ToSR (TSN [84], ResNet [52])	92.13	68.30
Ge et al. [44]	2019	Attention + ConvLSTM	92.39	66.37
Pan et al. [17]	2019	TR-LSTM (Inception-V3 [85])	93.80	63.80
Liu et al. [73]	2019	R-STAN(ResNet101 [52], temporal and spatial attention)	94.50	68.70
Wang et al. [50]	2019	I3D, LSTM	95.10	—
Lin et al. [14]	2019	TSM (TSN [84])	95.90	73.50
Jiang et al. [31]	2019	STM (CSTM, CMM, TSN [84], ResNet50 [52])	96.20	72.20
Chi et al. [72]	2019	CMA (attention)	96.50	—
Zhang et al. [25]	2019	CSN (TSN [84])	97.40	**81.90**
Hong et al. [70]	2019	I3D [38]/CD3 [71] (RGB, flow, pairwise and pose)	98.02	80.92
Crasto et al. [23]	2019	MARS + RGB + Flow	98.10	80.90
Qiu et al. [74]	2019	LGD-3D two-stream	**98.20**	80.50
Piergiovanni and Ryoo [34]	2019	Fully-differentiable convolutional layer	—	81.10
Kwon et al. [53]	2020	MSNet (ResNet50 [52])	—	77.40
Liu et al. [45]	2020	STS + attention LSTM	92.70	64.40
Majd and Safabakhsh [19]	2020	C^2LSTM	92.80	61.30
Huang and Bors [21]	2020	TSN (squeeze and excitation operation)	95.20	71.50
Li et al. [77]	2020	Attention (ResNeXt-101 [86])	95.90	72.20
Zhou et al. [76]	2020	Probability space	96.50	—
Zhu et al. [49]	2020	FAST-GRU	96.90	75.70
Diba et al. [48]	2020	HATNet (2D ResNet50, 3D ResNet18)	97.80	76.50
Zhang et al. [33]	2020	PANet (ResNet101 [52], TSM [14])	97.20	77.30
Duan et al. [63]	2020	2D network (ResNet50 [52]), 3D network (SlowOnly [87])	97.52	79.02
Stroud et al. [65]	2020	D3D (S3D-G [88])	97.60	80.50
Li et al. [32]	2020	CIDC (ResNet50 [52])	97.90	75.20
Li et al. [78]	2020	PoseNet, ResNet50 (3D), multiteacher network	98.20	82.00
Gowda et al. [36]	2020	MobileNet, MLP, LSTM	98.60	84.30
Kalfaoglu et al. [22]	2020	BERT, 3D convolution architecture	**98.69**	**85.10**
Akbari et al. [29]	2021	VATT	89.60	65.20
Xu et al. [35]	2021	MotionNet [41] + OFF [42]	91.50	67.90
Li et al. [28]	2021	VidTr (MSA, topK-based pooling)	96.70	74.40
Sharir et al. [27]	2021	STAM (spatial and temporal attention)	97.00	—
He et al. [18]	2021	DB-LSTM (ID3 [38])	97.30	81.20
Huang and Bors [24]	2021	FineCoarse (TSM R50 [69])	97.60	77.60
Hua et al. [64]	2021	SCN (Mask R-CNN [89])	98.30	**85.10**
Sheth [46]	2021	Three-stream network + LSTM/Attention	**99.00**	—

Bold represents the best performance.

Table 3: Accuracy of different methods on Something-Something-V1 and Something-Something-V2 datasets.

Method	Year	Method	Something-V1		Something-V2	
			Top-1	Top-5	Top-1	Top-5
Zhou et al. [15]	2018	TRN (2-stream TRN)	42.01	—	55.52	83.06
Jiang et al. [31]	2019	STM (CSTM, CMM, TSN [84], ResNet50 [52])	50.70	80.40	64.20	89.80
Lin et al. [14]	2019	TSM (TSN [84], ResNet50 [52])	52.60	81.90	66.00	90.50
Tran et al. [20]	2019	CSN (ResNet3D [52])	53.30	—	—	—
Martinez et al. [56]	2019	2D TSN [57], inflated 3D [38]	**53.40**	81.80	—	
Li et al. [32]	2020	CIDC (ResNet50 [52])	—	—	56.30	83.70
Zhou et al. [76]	2020	Probability space	—	—	62.90	88.00
Perez-Rua et al. [55]	2020	W3 (ResNet50-TSM [14])	52.60	81.30	66.50	90.40
Lee et al. [59]	2020	VOV3D-L (T-OSA)	54.70	82.00	67.40	90.50
Kwon et al. [53]	2020	MSNet (ResNet50 [52])	55.10	84.00	67.10	91.00
Sudhakaran et al. [16]	2020	GSM (InceptionV3 [85])	55.16	—	—	—
Zhang et al. [33]	2020	PANet (ResNet101 [52], TSM [14])	55.30	82.80	66.50	90.60
Wang et al. [51]	2020	TDN (short- and long-term TDM)	**56.80**	84.10	**68.20**	91.60
Huang and Bors [61]	2021	RNL (ResNet50 [52], TSM [14])	54.10	82.20	—	—
Huang and Bors [24]	2021	FineCoarse network (ResNet [52])	**57.00**	83.70	—	—

Bold represents the best performance.

TABLE 4: Some benchmark datasets for human action recognition.

	Dataset	Year	Samples	Mean length	Actions	Resolution
Simple	KTH [1]	2004	2391	4 sec	6	160 × 120
	Weizmann [2]	2005	90	Len	10	180 × 144
	Hollywood [90]	2008	430	Len	8	—
	Hollywood2 [91]	2009	3669	Len	12	—
Clip-level dataset	UCF101 [39]	2012	13,320	7.21 sec	101	320 × 240
	HMDB51 [40]	2013	6,766	—	51	—– × 240
	J-HMDB [68]	2013	31,838	1.4 sec	21	320 × 240
	MPII cooking [92]	2012	881,755	Len	65	1624 × 1224
	Charades [80]	2016	9,848	30 sec	157	671 × 857
	Something-Something-V1 [37]	2017	108,499	4.03 sec	174	—– × 100
	Something-Something-V2 [37]	2018	220,847	4.03 sec	174	—– × 240
	Kinetics-400 [38]	2017	306,245	10 sec	400	Variable resolution
	Kinetics-600 [75]	2018	495,547	10 sec	600	Variable resolution
	Kinetics-700 [79]	2019	650,317	10 sec	700	Variable resolution
	Diving48 [82]	2018	18,404	Len	48	—
	Moments in time [83]	2019	1,000,000	3 sec	339	340 × 256
	HACS [93]	2019	1.55M	2 sec	200	—
	HVU [48]	2020	572K	10 sec	739	—
	AViD [94]	2020	450K	3–15 sec	887	—
Video-level dataset	Sport1M [95]	2014	1,133,158	5 min 36 sec	487	—
	ActivityNet [96]	2015	28,108	(5–10) min	200	1280 × 720
	DALY [97]	2016	8133	3 min 45 sec	10	1290 × 790
	YouTube-8M [98]	2016	1.9B	226.6 sec	4,800	—
	EPIC-kitchens [99]	2018	11.5M	1.7 hrs	149	1920 × 1080
	AVA [100]	2018	392,426	15 min	60	451 × 808
	AVA-kinetics [101]	2020	624,430	—	60	—

and sports. It includes 13320 clips and 1600 minutes of video data. All videos (https://www.crcv.ucf.edu/data/UCF101.php) are downloaded from YouTube and have a fixed resolution of 320 × 240.

HMDB51 [40] has 51 action categories with 6,766 video clips (https://serre-lab.clps.brown.edu/resource/hmdb-a-large-human-motion-database/) which are extracted from different sources. There are five types of action, including general facial actions, facial actions with object manipulation, general body movements, body movements with object interaction, and body movements for human interaction. The height of all the frames is 240 pixels. To maintain the original aspect ratio of the video, the width was scaled accordingly to the height.

J-HMDB [68] is extracted from the HMD51 dataset [40]. Not only a dataset for human action recognition but also the J-HMDB is provided for pose estimation and human detection. The dataset (http://jhmdb.is.tue.mpg.de/) contains 21 classes with 31,838 annotated frames. Each action has 36–55 video clips, and each clip includes 15–40 frames.

MPII Cooking [92] is a dataset of cooking activities. The dataset (https://www.mpi-inf.mpg.de/departments/computer-vision-and-machine-learning/research/human-activity-recognition/mpii-cooking-2-dataset) contains 65 different cooking activities which are performed by 12 participants. In total, the dataset has 44 videos with 9 hours in length.

Charades [80] is a dataset of casual everyday activities of 267 people in their homes. The dataset has 9,848 videos with an average length of 30 seconds. It includes 157 action

classes and is split into 7,985 videos for training and 1,863 videos for testing (https://prior.allenai.org/projects/charades).

Something-Something [37] includes 108,499 videos (https://20bn.com/datasets/something-something/v1) in V1 and 220,847 videos (https://20bn.com/datasets/something-something) in V2. Both versions have 170 action classes. The duration of a video is from 2 to 6 seconds. The dataset is divided into three parts, including training, validation, and testing set.

Kinetics [54] (Kinetics-400 [38]) has 400 human action classes, and each class has at least 400 video clips. All clips were taken from YouTube. The actions in the dataset are the human-object interactions or human-human interactions. The dataset (https://deepmind.com/research/open-source/kinetics) has 306,245 videos and is split into three parts for training, validation, and testing.

Kinetics-600 [75] is a large-scale, high-quality dataset. The dataset (https://deepmind.com/research/open-source/kinetics) was taken from YouTube with 500K video clips. It has 600 human action classes with at least 600 video clips for each class. The length of each clip is about 10 seconds.

Diving48 [82] has 48 classes of 48 different diving actions. The dataset (http://www.svcl.ucsd.edu/projects/resound/dataset.html) has 18,404 video clips which contain 16,067 clips for training and 2,337 clips for testing. All clips were taken without background objects and the scenes contain a board, a pool, and a spectator in the background.

Kinetics-700 [79] is an extension of the human action dataset Kinetics-600 [75]. The extended dataset (https://deepmind.com/research/open-source/kinetics) has 700 classes and was taken from YouTube. Each class of dataset has at least 600 video clips which have a variable resolution as well as frame rate.

Moments in time [83] is a human-annotated dataset with 339 different classes. This is a large-scale dataset with one million videos, and each video corresponds with an event occurring in three seconds. The dataset (http://moments.csail.mit.edu/) is split into 802,264, 33,900 and 67,800 videos for training, validation, and testing, respectively.

HACS [93] is a large-scale dataset for human action recognition. It contains 1.5M clips which are sampled from 504K untrimmed videos. All clips (http://hacs.csail.mit.edu/) in this dataset have a two-second duration with 200 action categories.

HVU [48] is a multilabel and multitask video dataset which aims to describe the whole content of a video. The dataset includes approximately 572K videos with real-world scenarios. This dataset (https://holistic-video-understanding.github.io/) is split into 481K videos for training, 31K for validation, and 65M for testing.

AViD [94] is a video dataset for human action recognition. The main difference of this dataset is that it is collected from many different countries. This dataset (https://github.com/piergiaj/AViD) contains 410K training clips and 40K test clips. The duration of each clip is from 3 to 15 seconds.

4.3. Video-Level Datasets. With the development of deep models, some large-scale datasets were introduced such as Sport1M [95]. However, this dataset only focuses on Sports actions. Recently, other action datasets have been introduced with larger samples and temporal duration such as ActivityNet [96], AVA [100], AVA-Kinetics [101], DALY [97], EPIC-Kitchens [99], MPII Cooking [92], and YouTube-8M [98].

Sport1M [95] includes 1 million YouTube videos. The dataset (https://cs.stanford.edu/people/karpathy/deepvideo/) contains 487 classes of sports. There are 1000–3000 videos in each class.

ActivityNet [96] is a benchmark dataset for human activity understanding. The dataset (http://activity-net.org/index.html) contains human activities in their daily living. With 849 video hours, ActivityNet provides 200 activity classes. Each class has an average of 137 untrimmed videos. Most of the videos have a duration between 5 and 10 minutes and a half of the video has a resolution of 1280×720.

DALY [97] is a dataset for action localization in space and time. The dataset (http://thoth.inrialpes.fr/daly/) lasts about 31 hours of YouTube videos with 10 everyday human actions.

YouTube-8M [98] is a multilabel video classification dataset. The dataset (http://research.google.com/youtube8m/) includes 8,264,650 videos. With 500,000 hours of video, YouTube-8M contains over 1.9 billion video frames and 4,800 classes.

EPIC-Kitchens [99] was recorded by 32 participants in their kitchens. The participants comes from 10 different countries. The dataset (https://epic-kitchens.github.io/2020-55.html) has 55 hours of videos which include 11.5M frames. The videos have a resolution of 1920×1080; however, there are 1% of the dataset was recorded at 1280×720 and 0.5% at 1920×1440.

AVA [100] is a video dataset in which theactions are assigned in space and time. In addition, each person in the video is annotated with multiple labels. This dataset (https://research.google.com/ava/) contains 437 different videos of realistic scenes and action complexities. Each video is taken from the 15th to 30th minute time and has 900 frames. It is divided into 239 videos for training, 64 videos for validation, and 134 videos for testing, roughly a $55 : 15 : 30$ split.

AVA-Kinetics [101] is an extension of the AVA dataset [100] with new videos from the Kinetics-700 [79] annotated with the AVA action classes. The AVA-Kinetics (https://research.google.com/ava/) has 238,906 videos which is split into 142,475 videos for training, 32,529 videos for validation, and 64,902 videos for testing.

5. Open Research Problems

In the previous sections, we discuss the recent proposed methods and benchmark datasets for human action recognition with RGB data video. In this section, we will introduce some of the potential research problems in this field.

Data for human action recognition RGB videos are widely used in most methods for action recognition because these data are very popular and acquired with a low cost. However, other types of data provide more information for action recognition, such as skeleton, depth, infrared sequence, and point cloud. Skeleton data provide the trajectories of human body joints. Depth and point cloud data capture 3D structure and distance information. Infrared data provide data in a dark environment. Therefore, we cannot exploit color or texture in infrared data.

Pose estimation detects the location of human body joints in images. The skeleton data provide the body structure and pose of the object; therefore, we have more information for human action recognition. The skeleton data are obtained by using pose estimation on RGB videos or depth data.

Combination of different data types, such as RGB data with depth data or skeleton data with depth data, provides rich information for learning models. The RGB video data provide spatiotemporal features while depth data provide the 3D structure and depth information. We also combine different features of different models to get better performance.

6. Conclusions

In this survey, we provided a review of recent deep learning-based methods for human action recognition with RGB video data. We categorized recent approaches into five different groups, including 2D CNN-based methods, RNN-based methods, 3D single-stream network-based methods, 3D multistream network-based methods and convolution-free-based methods. More recently, a pure vision transformer with a convolution-free network has shown to be effective for human action recognition and various fields of computer vision. Therefore, we discussed recent transformer-based methods. We compared the accuracy of recent methods on four popular datasets, including UCF101, HDMB51, Something-Something-V1, and Something-Something-V2. We also discussed a wide range of benchmark datasets for human action recognition that are used in recently proposed methods. Lastly, we provide some potential research directions for human action recognition.

Data Availability

The datasets generated during and/or analysed during the current study are available from the corresponding author on reasonable request.

Conflicts of Interest

The authors declare that they have no conflicts of interest.

Acknowledgments

References

[1] C. Schuldt, I. Laptev, and B. Caputo, "Recognizing human actions: a local svm approach,"vol. 3, pp. 32–36, in *Proceedings of the 17th International Conference on Pattern Recognition, 2004. ICPR*, vol. 3, IEEE, Cambridge, UK, August 2004.

[2] M. Blank, L. Gorelick, E. Shechtman, M. Irani, and R. Basri, "Actions as space-time shapes,"vol. 1, pp. 1395–1402, in *Proceedings of the Tenth IEEE International Conference on Computer Vision (ICCV'05)*, vol. 1, IEEE, NW Washington, DC, USA, October 2005.

[3] Y. LeCun, P. Haffner, L. Bottou, and Y. Bengio, "Object recognition with gradient-based learning," in *Shape, Contour and Grouping in Computer Vision*, pp. 319–345, Springer, Heidelberg, Germany, 1999.

[4] D. E. Rumelhart, G. E. Hinton, and R. J. Williams, "Learning representations by back-propagation errors," *Nature*, vol. 323, no. 6088, pp. 533–536, 1986.

[5] R. Poppe, "A survey on vision-based human action recognition," *Image and Vision Computing*, vol. 28, no. 6, pp. 976–990, 2010.

[6] H.-B. Zhang, Y.-X. Zhang, B. Zhong et al., "A comprehensive survey of vision-based human action recognition methods," *Sensors*, vol. 19, no. 5, p. 1005, 2019.

[7] T. Singh and D. K. Vishwakarma, "Video benchmarks of human action datasets: a review," *Artificial Intelligence Review*, vol. 52, no. 2, pp. 1107–1154, 2019.

[8] B. Liu, H. Cai, Z. Ju, and H. Liu, "Rgb-d sensing based human action and interaction analysis: a survey," *Pattern Recognition*, vol. 94, pp. 1–12, 2019.

[9] Y. Zhu, X. Li, C. Liu et al., "A Comprehensive Study of Deep Video Action Recognition," 2020, https://arxiv.org/abs/2012.06567.

[10] I. Jegham, A. Ben Khalifa, I. Alouani, and M. A. Mahjoub, "Vision-based human action recognition: an overview and real world challenges," *Forensic Science International: Digital Investigation*, vol. 32, p. 200901, 2020.

[11] D. R. Beddiar, B. Nini, M. Sabokrou, and A. Hadid, "Vision-based human activity recognition: A Survey," *Multimedia Tools And Applications*, vol. 79, no. 41, pp. 30509–30555, 2020.

[12] L. Song, G. Yu, J. Yuan, and Z. Liu, "Human pose estimation and its application to action recognition: a survey," *Journal of Visual Communication and Image Representation*, vol. 76, p. 103055, 2021.

[13] S. Majumder and N. Kehtarnavaz, "A review of real-time human action recognition involving vision sensing," in *Real-Time Image Processing and Deep Learning*vol. 11736, , p. 117360A, International Society for Optics and Photonics, 2021.

[14] J. Lin, C. Gan, and S. Han, "Tsm: temporal shift module for efficient video understanding," in *Proceedings of the IEEE/CVF International Conference on Computer Vision*, pp. 7083–7093, Seoul, South Korea, April 2019.

[15] B. Zhou, A. Andonian, A. Oliva, and A. Torralba, "Temporal relational reasoning in videos," in *Proceedings of the European Conference on Computer Vision (ECCV)*, pp. 803–818, Munich, Germany, September 2018.

[16] S. Sudhakaran, S. Escalera, and O. Lanz, "Gate-shift networks for video action recognition," in *Proceedings of the IEEE/CVF Conference on Computer Vision and Pattern Recognition*, pp. 1102–1111, Seattle, WA, USA, June 2020.

[17] Y. Pan, J. Xu, M. Wang et al., "Compressing recurrent neural networks with tensor ring for action recognition," *Proceedings of the AAAI Conference on Artificial Intelligence*, vol. 33, pp. 4683–4690, 2019.

[18] J.-Y. He, X. Wu, Z.-Q. Cheng, Z. Yuan, and Y.-G. Jiang, "Db-lstm: Densely-connected bi-directional lstm for human action recognition," *Neurocomputing*, vol. 444, pp. 319–331, 2021.

[19] M. Majd and R. Safabakhsh, "Correlational convolutional lstm for human action recognition," *Neurocomputing*, vol. 396, pp. 224–229, 2020.

[20] D. Tran, H. Wang, L. Torresani, and M. Feiszli, "Video classification with channel-separated convolutional networks," in *Proceedings of the IEEE/CVF International Conference on Computer Vision*, pp. 5552–5561, Seoul, South Korea, October 2019.

[21] G. Huang and A. G. Bors, "Learning spatio-temporal representations with temporal squeeze pooling," in *Proceedings of the ICASSP 2020-2020 IEEE International Conference on*

Acoustics, Speech and Signal Processing (ICASSP), pp. 2103–2107, IEEE, Barcelona, Spain, May 2020.

[22] M. E. Kalfaoglu, S. Kalkan, and A. A. Alatan, "Late temporal modeling in 3d cnn architectures with bert for action recognition," in *Proceedings of the European Conference on Computer Vision*, pp. 731–747, Springer, Glasgow, Scotland, August 2020.

[23] N. Crasto, P. Weinzaepfel, K. Alahari, and C. Schmid, "Mars: motion-augmented rgb stream for action recognition," in *Proceedings of the IEEE/CVF Conference on Computer Vision and Pattern Recognition*, pp. 7882–7891, Long Beach, CA, USA, June 2019.

[24] G. Huang and A. G. Bors, "Video Classification with Finecoarse Networks," 2021, https://ui.adsabs.harvard.edu/abs/2021arXiv210315584H/abstract.

[25] J. Zhang, F. Shen, X. Xu, and H. T. Shen, "Cooperative Cross-Stream Network for Discriminative Action Representation," 2019, https://arxiv.org/abs/1908.10136.

[26] C. Dai, X. Liu, and J. Lai, "Human action recognition using two-stream attention based lstm networks," *Applied Soft Computing*, vol. 86, p. 105820, 2020.

[27] G. Sharir, A. Noy, and L. Zelnik-Manor, "An image is worth 16x16 words, what is a video worth?," 2021, https://arxiv.org/abs/2103.13915.

[28] X. Li, Y. Zhang, C. Liu et al., "Vidtr: Video Transformer without Convolutions," 2021, https://ui.adsabs.harvard.edu/abs/2021arXiv210411746Z/abstract.

[29] H. Akbari, L. Yuan, R. Qian et al., "Vatt: Transformers for Multimodal Self-Supervised Learning from Raw Video, Audio and Text," 2021, https://arxiv.org/abs/2104.11178.

[30] G. Bertasius, H. Wang, and L. Torresani, "Is space-time attention all you need for video understanding?," 2021, https://arxiv.org/abs/2102.05095.

[31] B. Jiang, M. Wang, W. Gan, W. Wu, and J. Yan, "Stm: spatiotemporal and motion encoding for action recognition," in *Proceedings of the IEEE/CVF International Conference on Computer Vision*, pp. 2000–2009, Seoul, South Korea, October 2019.

[32] X. Li, B. Shuai, and J. Tighe, "Directional temporal modeling for action recognition," in *Proceedings of the European Conference on Computer Vision*, pp. 275–291, Springer, Glasgow, Scotland, August 2020.

[33] C. Zhang, Y. Zou, G. Chen, and L. Gan, "Pan: Towards Fast Action Recognition via Learning Persistence of Appearance," 2020, https://arxiv.org/abs/2008.03462.

[34] A. Piergiovanni and M. S. Ryoo, "Representation flow for action recognition," in *Proceedings of the IEEE/CVF Conference on Computer Vision and Pattern Recognition*, pp. 9945–9953, Long Beach, CA, USA, June 2019.

[35] J. Xu, R. Song, H. Wei, J. Guo, Y. Zhou, and X. Huang, "A fast human action recognition network based on spatio-temporal features," *Neurocomputing*, vol. 441, pp. 350–358, 2021.

[36] S. N. Gowda, M. Rohrbach, and L. Sevilla-Lara, "Smart Frame Selection for Action Recognition," 2020, https://arxiv.org/abs/2012.10671.

[37] R. Goyal, S. Ebrahimi Kahou, V. Michalski et al., "The" something something" video database for learning and evaluating visual common sense," in *Proceedings of the IEEE International Conference on Computer Vision*, pp. 5842–5850, Venice, Italy, October 2017.

[38] J. Carreira and A. Zisserman, "Quo vadis, action recognition? a new model and the kinetics dataset," in *Proceedings of the IEEE Conference on Computer Vision and Pattern Recognition*, pp. 6299–6308, Honolulu, Hawaii, July 2017.

[39] K. Soomro, A. R. Zamir, and M. Shah, "Ucf101: A Dataset of 101 Human Actions Classes from Videos in the Wild," 2012, https://arxiv.org/abs/1212.0402.

[40] H. Kuehne, H. Jhuang, R. Stiefelhagen, and T. Serre, "Hmdb51: a large video database for human motion recognition," in *High Performance Computing in Science and Engineering*Springer, Heidelberg, Germany, 2013.

[41] P. Wu, S. Chen, and D. N. Metaxas, "Motionnet: joint perception and motion prediction for autonomous driving based on bird's eye view maps," in *Proceedings of the IEEE/CVF Conference on Computer Vision and Pattern Recognition*, pp. 11385–11395, Seattle, WA, USA, June 2020.

[42] S. Sun, Z. Kuang, L. Sheng, W. Ouyang, and W. Zhang, "Optical flow guided feature: a fast and robust motion representation for video action recognition," in *Proceedings of the IEEE Conference on Computer Vision and Pattern Recognition*, pp. 1390–1399, Salt Lake City, Utah, June 2018.

[43] H. Zhang, D. Liu, and Z. Xiong, "Two-stream action recognition-oriented video super-resolution," in *Proceedings of the IEEE/CVF International Conference on Computer Vision*, pp. 8799–8808, Seoul, South Korea, October 2019.

[44] H. Ge, Z. Yan, W. Yu, and L. Sun, "An attention mechanism based convolutional lstm network for video action recognition," *Multimedia Tools and Applications*, vol. 78, no. 14, pp. 20533–20556, 2019.

[45] Z. Liu, Z. Li, R. Wang, M. Zong, and W. Ji, "Spatiotemporal saliency-based multi-stream networks with attention-aware lstm for action recognition," *Neural Computing & Applications*, vol. 32, no. 18, pp. 14593–14602, 2020.

[46] I. Sheth, "Three-stream network for enriched action recognition," 2021, https://arxiv.org/abs/2104.13051.

[47] Y. Zhou, X. Sun, Z.-J. Zha, and W. Zeng, "Mict: Mixed 3d/2d convolutional tube for human action recognition," in *Proceedings of the IEEE Conference on Computer Vision and Pattern Recognition*, pp. 449–458, Salt Lake City, Utah, June 2018.

[48] A. Diba, M. Fayyaz, V. Sharma et al., "Large scale holistic video understanding," in *Proceedings of the European Conference on Computer Vision*, pp. 593–610, Springer, Glasgow, Scotland, August 2020.

[49] L. Zhu, D. Tran, L. Sevilla-Lara, Y. Yang, M. Feiszli, and H. Wang, "Faster recurrent networks for efficient video classification," *Proceedings of the AAAI Conference on Artificial Intelligence*, vol. 34, no. 07, pp. 13098–13105, 2020.

[50] X. Wang, Z. Miao, R. Zhang, and S. Hao, "I3d-lstm: a new model for human action recognition," *IOP Conference Series: Materials Science and Engineering*, IOP Publishing, vol. 569, no. 3, p. 032035, 2019.

[51] L. Wang, Z. Tong, B. Ji, and G. Wu, "Tdn: Temporal Difference Networks for Efficient Action Recognition," 2020, https://arxiv.org/abs/2012.10071.

[52] K. He, X. Zhang, S. Ren, and J. Sun, "Deep residual learning for image recognition," in *Proceedings of the IEEE Conference on Computer Vision and Pattern Recognition*, pp. 770–778, Las Vegas, NV, USA, June 2016.

[53] H. Kwon, M. Kim, S. Kwak, and M. Cho, "Motionsqueeze: neural motion feature learning for video understanding," in *Proceedings of the European Conference on Computer Vision*, pp. 345–362, Springer, Glasgow, Scotland, August 2020.

[54] W. Kay, J. Carreira, K. Simonyan et al., "The Kinetics Human Action Video Dataset," 2017, https://arxiv.org/abs/1705.06950.

[55] J.-M. Perez-Rua, B. Martinez, X. Zhu, A. Toisoul, V. Escorcia, and T. Xiang, "Knowing what, where and when to Look:

Efficient Video Action Modeling with Attention," 2020, https://arxiv.org/abs/2004.01278.

[56] B. Martinez, D. Modolo, Y. Xiong, and J. Tighe, "Action recognition with spatial-temporal discriminative filter banks," in *Proceedings of the IEEE/CVF International Conference on Computer Vision*, pp. 5482–5491, Seoul, South Korea, October 2019.

[57] L. Wang, Y. Xiong, Z. Wang et al., "Temporal Segment Networks for Action Recognition in Videos. Corr Abs/1705.02953 (2017)," 2017, https://arxiv.org/abs/1705.02953.

[58] F. Mahdisoltani, G. Berger, W. Gharbieh, D. Fleet, and R. Memisevic, "Fine-grained video classification and captioning," vol. 5, 2018, https://arxiv.org/pdf/1804.09235.pdf.

[59] Y. Lee, H.-I. Kim, K. Yun, and J. Moon, "Diverse Temporal Aggregation and Depthwise Spatiotemporal Factorization for Efficient Video Classification," 2020, https://arxiv.org/abs/2012.00317.

[60] J. Zhao and C. G. Snoek, "Dance with flow: two-in-one stream action detection," in *Proceedings of the IEEE/CVF Conference on Computer Vision and Pattern Recognition*, pp. 9935–9944, Long Beach, CA, USA, June 2019.

[61] G. Huang and A. G. Bors, "Region-based non-local operation for video classification," in *Proceedings of the 2020 25th International Conference on Pattern Recognition (ICPR)*, pp. 10010–10017, IEEE, Milan, Italy, January 2021.

[62] J. Hu, L. Shen, S. Albanie, G. Sun, and E. Wu, "Squeezeand-excitation Networks," 2017, https://arxiv.org/abs/1709.01507.

[63] H. Duan, Y. Zhao, Y. Xiong, W. Liu, and D. Lin, "Omni-sourced webly-supervised learning for video recognition," 2020, https://arxiv.org/abs/2003.13042.

[64] M. Hua, M. Gao, and Z. Zhong, "Scn: dilated silhouette convolutional network for video action recognition," *Computer Aided Geometric Design*, vol. 85, p. 101965, 2021.

[65] J. Stroud, D. Ross, C. Sun, J. Deng, and R. Sukthankar, "D3d: distilled 3d networks for video action recognition," in *Proceedings of the IEEE/CVF Winter Conference on Applications of Computer Vision*, pp. 625–634, Snowmass Village, CO, USA, March 2020.

[66] J. Liu, J. Luo, and M. Shah, "Recognizing realistic actions from videos "in the wild"" in *Proceedings of the 2009 IEEE Conference on Computer Vision and Pattern Recognition*, pp. 1996–2003, IEEE, Miami Beach, FL, USA, June2009.

[67] L. Shao, X. Zhen, D. Tao, and X. Li, "Spatio-temporal laplacian pyramid coding for action recognition," *IEEE Transactions on Cybernetics*, vol. 44, no. 6, pp. 817–827, 2013.

[68] H. Jhuang, J. Gall, S. Zuffi, C. Schmid, and M. J. Black, "Towards understanding action recognition," in *Proceedings of the IEEE International Conference on Computer Vision*, pp. 3192–3199, Sydney, NSW, December 2013.

[69] J. Lin, C. Gan, and S. Han, "Temporal shift module for efficient video understanding," in *Proceedings of the 2019 IEEE CVF International Conference on Computer Vision (ICCV)*, pp. 7082–7092, Seoul, Korea, November 2019.

[70] J. Hong, B. Cho, Y. Hong, and H. Byun, "Contextual action cues from camera sensor for multi-stream action recognition," *Sensors*, vol. 19, no. 6, p. 1382, 2019.

[71] D. Tran, L. Bourdev, R. Fergus, L. Torresani, and M. Paluri, "Learning spatiotemporal features with 3d convolutional networks," in *Proceedings of the IEEE International Conference on Computer Vision*, pp. 4489–4497, NW Washington, DC, December 2015.

[72] L. Chi, G. Tian, Y. Mu, and Q. Tian, "Two-stream video classification with cross-modality attention," in *Proceedings*

[73] Q. Liu, X. Che, and M. Bie, "R-stan: R-STAN: residual spatial-temporal attention network for action recognition," *IEEE Access*, vol. 7, pp. 82246–82255, 2019.

[74] Z. Qiu, T. Yao, C.-W. Ngo, X. Tian, and T. Mei, "Learning spatio-temporal representation with local and global diffusion," in *Proceedings of the IEEE/CVF Conference on Computer Vision and Pattern Recognition*, pp. 12056–12065, Long Beach, CA, USA, June 2019.

[75] B. Ghanem, J. C. Niebles, C. Snoek et al., "The Activitynet Large-Scale Activity Recognition challenge 2018 Summary," 2018, https://arxiv.org/abs/1808.03766.

[76] Y. Zhou, X. Sun, C. Luo, Z.-J. Zha, and W. Zeng, "Spatio-temporal fusion in 3d cnns: a probabilistic view," in *Proceedings of the IEEE/CVF Conference on Computer Vision and Pattern Recognition*, pp. 9829–9838, Seattle, WA, USA, June 2020.

[77] J. Li, X. Liu, M. Zhang, and D. Wang, "Spatio-temporal deformable 3d convnets with attention for action recognition," *Pattern Recognition*, vol. 98, p. 107037, 2020.

[78] Y. Li, Z. Lu, X. Xiong, and J. Huang, "Perf-net: Pose Empowered Rgb-Flow Net," 2020, https://arxiv.org/abs/2009.13087.

[79] J. Carreira, E. Noland, C. Hillier, and A. Zisserman, "A Short Note on the Kinetics-700 Human Action Dataset," 2019, https://arxiv.org/abs/1907.06987.

[80] G. A. Sigurdsson, G. Varol, X. Wang, A. Farhadi, I. Laptev, and A. Gupta, "Hollywood in homes: crowdsourcing data collection for activity understanding," in *Proceedings of the European Conference on Computer Vision*, pp. 510–526, Springer, Amsterdam, The Netherlands, October 2016.

[81] J. Carreira, E. Noland, A. Banki-Horvath, C. Hillier, and A. Zisserman, "A Short Note about Kinetics-600," 2018, https://arxiv.org/abs/1808.01340.

[82] Y. Li, Y. Li, and N. Vasconcelos, "Resound: towards action recognition without representation bias," in *Proceedings of the European Conference on Computer Vision (ECCV)*, pp. 513–528, Munich, Germany, September 2018.

[83] M. Monfort, A. Andonian, B. Zhou et al., "Moments in time dataset: one million videos for event understanding," *IEEE Transactions on Pattern Analysis and Machine Intelligence*, vol. 42, no. 2, pp. 502–508, 2019.

[84] L. Wang, Y. Xiong, Z. Wang et al., "Temporal segment networks: towards good practices for deep action recognition," in *Proceedings of the European Conference on Computer Vision*, pp. 20–36, Springer, Amsterdam, The Netherlands, October 2016.

[85] C. Szegedy, V. Vanhoucke, S. Ioffe, J. Shlens, and Z. Wojna, "Rethinking the inception architecture for computer vision," in *Proceedings of the IEEE Conference on Computer Vision and Pattern Recognition*, pp. 2818–2826, Las Vegas, NV, USA, June 2016.

[86] S. Xie, R. Girshick, P. Dollár, Z. Tu, and K. He, "Aggregated residual transformations for deep neural networks," in *Proceedings of the IEEE Conference on Computer Vision and Pattern Recognition*, pp. 1492–1500, Honolulu, Hawaii, July 2017.

[87] C. Feichtenhofer, H. Fan, J. Malik, and K. He, "Slowfast networks for video recognition," in *Proceedings of the IEEE/CVF International Conference on Computer Vision*, pp. 6202–6211, Seoul, South Korea, April 2019.

[88] S. Xie, C. Sun, J. Huang, Z. Tu, and K. Murphy, "Rethinking spatiotemporal feature learning: speed-accuracy trade-offs in

video classification," in *Proceedings of the European Conference on Computer Vision (ECCV)*, pp. 305–321, Munich, Germany, September 2018.

[89] K. He, G. Gkioxari, P. Dollár, and R. Girshick, "Mask r-cnn," in *Proceedings of the IEEE International Conference on Computer Vision*, pp. 2961–2969, Venice, Italy, October 2017.

[90] I. Laptev, M. Marszalek, C. Schmid, and B. Rozenfeld, "Learning realistic human actions from movies," in *Proceedings of the 2008 IEEE Conference on Computer Vision and Pattern Recognition*, pp. 1–8, IEEE, Anchorage, Alaska, USA, June 2008.

[91] M. Marszalek, I. Laptev, and C. Schmid, "Actions in context," in *Proceedings of the 2009 IEEE Conference on Computer Vision and Pattern Recognition*, pp. 2929–2936, IEEE, Miami Beach, FL, USA, June 2009.

[92] M. Rohrbach, S. Amin, M. Andriluka, and B. Schiele, "A database for fine grained activity detection of cooking activities," in *Proceedings of the 2012 IEEE Conference on Computer Vision and Pattern Recognition*, pp. 1194–1201, IEEE, Providence, Rhode Island, June 2012.

[93] H. Zhao, A. Torralba, L. Torresani, and Z. Yan, "Hacs: human action clips and segments dataset for recognition and temporal localization," in *Proceedings of the IEEE/CVF International Conference on Computer Vision*, pp. 8668–8678, Seoul, South Korea, April 2019.

[94] A. Piergiovanni and M. S. Ryoo, "Avid Dataset: Anonymized Videos from Diverse Countries," 2020, https://arxiv.org/abs/2007.05515.

[95] A. Karpathy, G. Toderici, S. Shetty, T. Leung, R. Sukthankar, and L. Fei-Fei, "Large-scale video classification with convolutional neural networks," in *Proceedings of the IEEE Conference on Computer Vision and Pattern Recognition*, pp. 1725–1732, Columbus, Ohio, June 2014.

[96] F. Caba Heilbron, V. Escorcia, B. Ghanem, and J. Carlos Niebles, "Activitynet: a large-scale video benchmark for human activity understanding," in *Proceedings of the Ieee Conference on Computer Vision and Pattern Recognition*, pp. 961–970, Boston, Massachusetts, June 2015.

[97] P. Weinzaepfel, X. Martin, and C. Schmid, "Human Action Localization with Sparse Spatial Supervision," 2016, https://arxiv.org/abs/1605.05197.

[98] S. Abu-El-Haija, N. Kothari, J. Lee et al., "Youtube-8m: A Large-Scale Video Classification Benchmark," 2016, https://arxiv.org/abs/1609.08675.

[99] D. Damen, H. Doughty, G. M. Farinella et al., "Scaling egocentric vision: the epic-kitchens dataset," in *Proceedings of the European Conference on Computer Vision (ECCV)*, pp. 720–736, Munich, Germany, September 2018.

[100] C. Gu, C. Sun, D. A. Ross et al., "Ava: a video dataset of spatio-temporally localized atomic visual actions," in *Proceedings of the IEEE Conference on Computer Vision and Pattern Recognition*, pp. 6047–6056, Salt Lake City, Utah, June 2018.

[101] A. Li, M. Thotakuri, D. A. Ross, J. Carreira, A. Vostrikov, and A. Zisserman, "The ava-kinetics Localized Human Actions Video Dataset," 2020, https://arxiv.org/abs/2005.00214.

[102] P. Natarajan and R. Nevatia, "Online, real-time tracking and recognition of human actions," in *Proceedings of the 2008 IEEE Workshop on Motion and Video Computing*, pp. 1–8, IEEE, NW Washington, DC, January 2008.

[103] D. Tran and A. Sorokin, "Human activity recognition with metric learning," *Lecture Notes in Computer Science*, Springer, in *Proceedings of the European Conference on Computer Vision*, pp. 548–561, October 2008.

Research Article

Emission Reduction Benefits and Economic Benefits of China's Pilot Policy on Carbon Emission Trading System

Zhijia Wang [ID],[1] **Lijuan Liang** [ID],[2] **Dong Cheng** [ID],[3] **Hujun Li** [ID],[4] and **Yongheng Zhang** [ID][2]

[1]*Research Center for Energy Economic, Henan Polytechnic University, Jiaozuo 454000, China*
[2]*School of Finance and Economics, Henan Polytechnic University, Jiaozuo 454000, China*
[3]*School of Business, Guilin Tourism University, Guilin 541006, China*
[4]*School of Civil Engineering, Henan Polytechnic University, Jiaozuo 454000, China*

Correspondence should be addressed to Dong Cheng; chengdong@gltu.edu.cn

As a market means to control nongreen behaviors of firms, the most expected incentive effect of the carbon emission trading system (CETS) is to achieve the dual economic and environmental effects. As a typical developing country, whether China's CETS has a positive incentive effect is significant to controlling greenhouse gas. Based on the quasinatural experiment of China's pilot policy on CETS in 2013, this study investigates its emission reduction and economic benefits using the difference-in-difference (DID) method. Then, the realization mechanism of CETS's incentive benefits is reversely studied with the idea that goals generate behavior. The results show that the following: (a) China's CETS has produced positive incentive effects of promoting both economic and emission reduction benefits. Furthermore, the results are still valid after using the instrumental variable to overcome the endogenous problem, placebo tests to eliminate sampling bias, and a series of robustness tests. (b) Further analysis shows that firms can choose to improve technology innovation and energy efficiency to get the positive incentive effects of CETS. (c) The incentive effects of CETS also have regional heterogeneity. The emission reduction and economic benefits are greater in provinces with deficient resource endowments and strict environmental law enforcement.

1. Introduction

Since the 21st century, climate warming has become a major obstacle to global sustainable development. Therefore, the United Nations proposed the carbon emission trading system (CETS) to regulate greenhouse gas emissions and alleviate the contradiction between ecological protection and economic development. According to "*Kyoto Protocol*," this market-oriented environmental regulation (ER) was first applied in developed countries. Since European Union (EU) launched the world's largest CETS in 2005, CETS has been widely recognized for its role in curbing greenhouse gas emissions and promoting economic development [1–3]. However, some scholars argued that CETS could fail to bring out its best incentive benefits due to the imperfect trading and management systems [4–6]. Therefore, current research still focuses on whether CETS can produce positive incentive

effects, especially how to produce and get the best incentive effects. Apart from developed countries, developing countries like China and India also need to reduce greenhouse gas emissions. After four decades of rapid economic growth, China became the world's second-largest economy in 2010. However, the rapid economic growth has also caused serious environmental problems. According to Carbon Brief, China emitted 10. 1 bn tons of CO_2 in 2018, the highest in the world, and 1.2 bn tons more than the sum of the US (5.4 bn tons) and the EU (3.5 bn tons). It can be seen that China plays a vital role in the world's economic and environmental problems. Studying the incentive benefits of China's CETS can provide substantial evidence for carbon reduction.

The research ideas of this article are as follows: Firstly, this study verifies whether China's CETS have positive incentive effects under the guidance of the new behavior theory. Secondly, the realization path is explored to obtain

positive incentive effects. Finally, the heterogeneity of incentive effects is analyzed to provide more accurate information for the effective implementation of CETS. The specific methods are as follows: Firstly, China's pilot policy on CETS in 2013 is used as a quasinatural experiment to analyze its emission reduction and economic benefits using the DID method. CO_2 emissions and total factor productivity (TFP) are used to represent the emission reduction benefits and economic benefits, respectively. Dynamic benefits analysis, instrumental variables, counterfactual test, placebo test, and other methods are used to test the robustness of the constructed econometric model. That is, to test whether the emission reduction benefits and economic benefits of the pilot policy on CETS are still significant after overcoming endogeneity, policy implementation time, and selection bias of pilot areas. Secondly, the mediation model is used to examine whether CETS's positive incentive effects can be achieved through technological innovation and energy efficiency. Finally, grouping regression is adopted to investigate CETS's incentive effects heterogeneity.

The marginal contributions of this study are as follows: (a) This study applies behavior theory to the research of ER. The role of China's market regulation is investigated from the perspective of the incentive effect. The realization path of incentive effect is discussed with the idea that goals generate behavior. This study provides a new vision for the formulation and implementation of ER. (b) This study includes emission reduction and economic benefits in a unified research framework. In the context of China, a more comprehensive evaluation of CETS's policy benefits is made. The ability of CETS to balance the environment and economy in developing regions is tested, which provides evidence for the decrease of greenhouse gas. (c) The empirical analysis based on the quasinatural experiment and DID avoid endogenous problems such as missing variables to a certain extent. However, it still could not eliminate the interference of regional characteristics that changed over time. Therefore, this paper further tests the robustness of the empirical results through instrumental variables, counterfactual test, and placebo test. It provides scientific evidence for studying emission reduction benefits and economic benefits of CETS.

The article is organized as follows. Section 2 presents the literature review. Section 3 analyzes the institutional background and theory. Section 4 discusses the results of the empirical research. Section 5 presents the results of the mechanism analysis. Section 6 presents highlights conclusions and the scope of future work.

2. Literature Review

2.1. Research on the Benefits of ER.
The relationship between ER and economics is controversial in academia. The neoclassical economic theory supports the view that ER internalizes pollution as cost and transfers resources from production to environmental protection [7, 8]. Therefore, the firms' production efficiency may regress in the short term [9]. However, economists represented by Porter raised objections. Porter and van der Linder [10] proposed the Porter hypothesis, which elaborates that strict and

appropriate ER can generate higher productivity through innovation. The hypothesis has been widely discussed. Lanoie et al. [11] and Peuckert [12] believed that the positive effects of ER through environmental technology could offset the short-term cost and ultimately benefit production efficiency. Testa et al. [13] found that more flexible ER significantly increased R&D investment and eventually improved firms' production efficiency. Using the steel industry data, Liu et al. [14] proved that economic incentives significantly boosted firms' profitability. Using panel data of 17 manufacturing industries, Rubashkina et al. [15] found that productivity increased only in industries under ER. With the increasing international status of China, scholars pay more attention to the environmental and economic benefits of ER in the context of China. Li et al. [16] found that the promotion effects of China's ER on production efficiency is only significant in the eastern provinces. Li and Chen [17] studied the promotion effects of China's air pollution prevention and control law on TFP by DID model. Wang and Liu [18] proved an inverted N relationship between China's ER and TFP.

2.2. Research on CETS.
Research on CETS focus on policy effects. They generally use developed countries as data sources. Scholars believed that CETS has positive policy effects. Anderson et al. [19] confirmed the emission reduction effects of EU's CETS in the manufacturing industry and firms participating in CETS are more likely to implement green technology innovation. However, some scholars believe that the policy effects of CETS are limited. Hoffmann [20] compared the emission reduction effects of the 2008 economic crisis and the CETS, and the results showed the former were far greater than the latter. Borghesi et al. [21] conducted an empirical study based on Italy's manufacturing industry and found that overly loose allocation of carbon quota limited the policy effects of the EU CETS. While China's CETS has a short running time, its emission reduction and economic benefits are unclear. Findings of the emission reduction benefits are inconsistent. Li and Zhang [22] proved that China's pilot policy on CETS significantly suppressed carbon emissions using industrial data. However, affected by the heterogeneity of objects, carbon quota, carbon price, and regional policies, the emission reduction benefits of CETS are not always significant [23, 24]. Findings of the economic benefits are also controversial. The empirical results from Liao et al. [25] suggested that the CETS generated green economic benefits by stimulating green innovation. Wang and Wang [26] found that China's CETS did not significantly affect the economic benefits measured by per capita GDP.

3. Institutional Background and Theoretical Analysis

3.1. Institutional Background.
CETS can be traced back to the "*Kyoto Protocol*" in December 1997. The protocol proposed a market-based approach to greenhouse gases, known as CETS. It also advocated that all signatories should reduce

emissions, but developed countries are greater than developing countries. Since then, developed countries, such as the UK, Germany, the EU, and Australia, have successively launched CETS, which means that CETS has changed from concept to practice. The EU CETS is the largest CETS in the world, who completed 80% of the global carbon trading volume. Furthermore, California and Tokyo have also established regional CETS. The existing CETS control local greenhouse gases and provide experience for the global CETS.

China needs to reduce emissions without harming the economy as a developing country. Therefore, the Chinese government has been committed to CETS in recent years. In October 2011, the Chinese government announced that CETS would pilot in seven regions, including Guangdong Province, Hubei Province, Beijing, Shanghai, Tianjin, Shenzhen, and Chongqing. From June 2013 to April 2014, the CETS was launched in seven pilot regions. Since then, the regional governments have continuously improved the supporting facilities of CETS, such as incentives and punishment system, cross-regional trading system, and offset system. At the same time, policies such as carbon mortgage, carbon finance, carbon funds, and carbon bonds have continuously strengthened the capital attributes of carbon emission rights. In December 2017, China began planning the national CETS. On July 16, 2021, the national CETS officially launched online trading. On the first day, the trading volume reached 4.1 million tons, with a turnover of 210.2 million yuan. So far, China's CETS has completed the spread from pilots to the entire nation. Although the national CETS only covers the power industry, it will radiate to electrolytic aluminum, cement, steel, petrochemical, chemical, papermaking, aviation, and other sectors in the future. At that time, the national CETS is expected to become the largest CETS in the world.

3.2. Theoretical Analysis. CETS is a market-based ER used to control nongreen behaviors of firms. New behaviorism theory holds that behavior depends not only on the perception of stimuli but also on behavior results. Similarly, whether firms can participate in CETS more actively depends on whether CETS has positive incentive effects. The Coase theorem emphasizes the property and market rules. The former makes public resources commodities, and the latter restrains participants' economic behavior [27]. CETS exerts incentive effects through the financial means of carbon emission trading. High-carbon firms can purchase carbon quotas to waive penalties for nonviolations. Low-carbon firms can sell carbon quotas to get additional economic benefits. In the end, a high level of emission reduction benefits can be achieved at a low economic cost. Moreover, Porter hypothesis argues that strict and flexible ER can promote economic growth while controlling pollution [10]. As an essential market-based regulatory tool, CETS uses market prices as a signal to enable firms to have higher flexibility [28]. Firms with more flexibility are more likely to increase productivity to alleviate and offset the additional costs of ER. Therefore, this article believes that CETS

ultimately produces positive incentive effects. That is, CETS has significant emission reduction benefits and economic benefits.

According to behaviorism theory, to achieve the dual effects of economy and emission reduction, the behavior adopted by firms must be conducive to both economy and environment, namely, green behaviors. This article analyzes the path of CETS to achieve positive incentive effects from two common green behaviors, as shown in Figure 1.

(1) CETS achieves economic and emission reduction benefits by promoting technological innovation. Because innovation has the characteristics of a long cycle, considerable investment, and high risk [29], whether a firm innovates depends on the external incentives it receives [21]. The analysis of CETS's policy benefits through technological innovation is as follows. (a) The surplus carbon quotas can be sold or used to offset the cost of violations. At this time, CETS provides firms with continuous and dynamic economic incentives. (b) CETS provides firms with market information about technological improvement, thereby reducing the uncertainty of technological innovation [30]. (c) CETS could increase firms' environmental and production costs as a legal pressure. As the pursuer of profit, firms' motivation to reduce cost by improving production technology will increase. Therefore, CETS can promote technological innovation and ultimately achieve economic and emission reduction benefits.

(2) CETS achieves emission reduction and economic benefits by improving energy efficiency. China's pilot policy on CETS adopts means of total control. First, the total quotas of national carbon emissions are determined, and then, certain carbon quotas are allocated to specific firms. If firms emit more than their quotas, they need to buy quotas from the carbon market or face default penalties. (a) Carbon emissions mainly come from the combustion of energy. The most direct means of emission reduction is to reduce energy consumption [31]. Nevertheless, this crude means greatly damage the economy [32]. Improving energy efficiency means using less energy with the same output, reducing carbon emissions without sacrificing the economy. (b) CETS make carbon quotas rare commodities. It makes capital flow to energy-saving industries, conducive to improving energy utilization efficiency [33]. Therefore, CETS is conducive to energy efficiency and ultimately to reduce CO_2 emissions and improve TFP.

4. Variables and Models

4.1. Variables

(1) CETS. China's pilot policy on CETS is an independent variable, represented by the dummy variable *TIME × TREAT. TIME* is a time dummy variable bounded by 2013 when the pilot policy started. The value is 0 from 2008 to 2012 and 1 from 2013 to 2017.
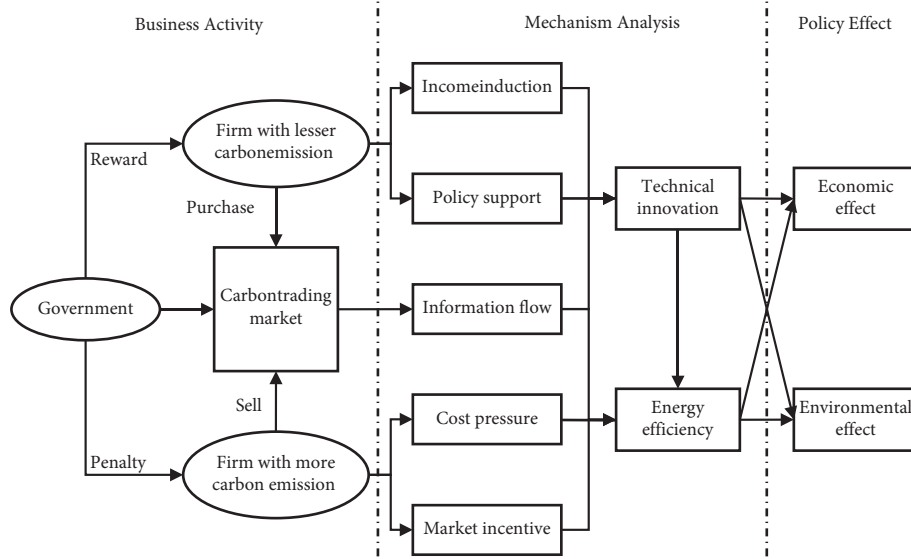
Figure 1: Theory frame.

Treat is a grouped dummy variable assigned to 1 if the province belongs to the pilot area and 0 otherwise. Among the seven pilot areas of CETS (Guangdong, Hubei, Beijing, Shanghai, Tianjin, Chongqing, and Shenzhen), Shenzhen is a city in Guangdong Province with a different administrative level from the other pilot areas, and its various data are a part of the Guangdong data. In addition, this article takes 30 provinces as samples for research. Therefore, the pilot areas mentioned in the subsequent study are Guangdong, Hubei, Beijing, Shanghai, Tianjin, and Chongqing.

(2) Emission reduction benefits. The emission reduction benefits measured by CO_2 emissions is a dependent variable, and the data come from the author's calculation. CO_2 mainly comes from the combustion of fossil energy. Therefore, the calculation of CO_2 emissions usually uses energy consumption data, as shown in formula (1). Carbon emission factor provided by IPCC (as shown in Table 1).

$$CO_2 = \sum_{j=1}^{7} E_j \times NCV_j \times CEF_j, \qquad (1)$$

where, CO_2 represents CO_2 emissions, and j represents seven kinds of energy: coal, coke, gasoline, kerosene, diesel, fuel oil, and natural gas. E is energy consumption, NCV represents net calorific value, CEF represents carbon emission factor.

(3) Economic benefits. Economic efficiency measured by TFP is another dependent variable. DEA-Malmquist calculates this index based on provincial data. (a) Capital input. "Permanent inventory" is used to estimate capital stock. Firstly, according to Zhang et al. [34], the total fixed capital formation is selected as the investment indicator for the current year. Then, the actual investment with

the constant price in 2000 is calculated through the investment product price index. Finally, the capital stock in 2008 is calculated according to Wang and Yan [35]. It can be referred to Wang et al. [36] to select the depreciation rate of each province. (b) Labor input. The number of employees is adopted as the labor input. (c) Energy input. Energy consumption is used to measure energy input. (d) Output. The real GDP with 2000 as the base period is selected as output.

(4) Control variables. Referring to Timothy et al. [2] and Akhmat et al. [31], the following variables are selected as control variables: the level of the service industry, optimization of industrial structure, level of foreign capital utilization, level of opening up, and level of education. The specific content is shown in Table 2.

4.2. Econometric Model. In order to test the emission reduction and economic effects of CETS, this paper constructs the DID model shown in formula (2).

$$Y_{it} = \alpha_0 + \alpha_1 \left(TIME_t \times TREAT_i \right) + \beta X + \gamma_t + \mu_i + \varepsilon_{it}, \qquad (2)$$

where, i is the province, and t is the year. Y represents dependent variables, i.e., CO_2 emissions and TFP. $TIME \times TREAT$ is the dummy variable representing China's pilot policy on CETS. The coefficient α_1 is the emission reduction and economic benefits of CETS concerned in this article. X is the vector of control variables. γ is the time fixed effects, which controls the common time factors of all samples, such as business cycle, monetary policy, macroeconomic shock, and fiscal policy. μ is the individual fixed effects that control the characteristics of each sample that do not change with time, such as geographical characteristics, climate, and resource endowment. ε is the random error term.

TABLE 1: Carbon emission factors of IPCC.

Energy types	Coal	Coke	Gasoline	Kerosene	Diesel	Fuel oil	Natural gas
NCV (kj/kg)	20908	28435	43070	43070	42652	43070	38931
CEF (kg/tj)	95333	107000	70000	71500	74100	77400	56100

TABLE 2: Variable design and description.

Variable types	Variable name	Code	Measure index
Independent variable	CETS	TIME × TREAT	China's pilot policy on CETS since 2013
Dependent variable	Emission reduction benefits	CO_2	CO_2 emissions
	Economic benefits	TFP	Total factor productivity
Control variable	Level of service industry	SI	Value-added service industry/GDP
	Optimization of industrial structure	OIS	Value-added tertiary industry/value-added secondary industry
	Level of foreign capital utilization	FDI	Actual utilization of FDI/GDP
	Level of opening up	OPEN	Total export/GDP
	Level of education	EDU	Total population of high school and above/total population at year end
Mediator variable	Technology innovation	TI	Turnover in the technology market
	Energy efficiency	EE	Total energy consumption/GDP

Note: the original data came from China Statistical Yearbook and China Environmental Statistical Yearbook. The data of TFP and EE were calculated by the authors.

5. Results and Discussions

5.1. Parallel Trend Analysis. The trends diagram of CO_2 emissions and TFP in pilot and nonpilot provinces are plotted in Figure 2. The emission reduction and economic benefits of pilot policy on CETS can be elementarily judged from the diagram. (a) CO_2 emissions in nonpilot provinces are higher than that in pilot provinces. In 2008–2012, CO_2 emissions in pilot and nonpilot areas showed an upward trend. After 2012, CO_2 emissions in nonpilot areas changed slightly but remained on the rise, while CO_2 emissions in pilot provinces showed a clear downward trend. (b) TFP in pilot provinces is higher than that in nonpilot areas. Before 2013, TPF in pilot and nonpilot provinces showed an upward trend. After 2013, the TFP growth of pilot provinces has increased, while nonpilot areas have shown a downward trend. Therefore, this article preliminarily speculated that compared with nonpilot areas, the decrease of CO_2 emissions, and the increase of TFP in pilot provinces might be caused by the pilot policy on CETS in 2013.

5.2. Results of Benchmark Regression. The results of CETS's emission reduction and economic benefits are shown in Table 3. The coefficients of CETS's emission reduction and economic benefits are −0.189 and 0.346, respectively, significant at 1%. After adding control variables, columns (3) and (4) are the results. The regression results change slightly, but the sign and significance remain the same, which shows that the regression results are stable. The above results indicate that China's pilot policy on CETS has produced significant emission reduction and economic benefits. This study refutes the view of foreign scholars such as Allen et al. [37] that all marketization mechanisms in China are invalid.

It is conducive to dispel the skepticism about China's marketization reform. As the central government's environmental and economic reform, CETS has political advantages in government guidance and market leadership. CETS provides an important direction for China to achieve green development through market-oriented means, under the dual pressure of environmental and economic.

5.3. Analysis of Dynamic Effects. The results of the benchmark regression only reflect the average emission reduction and average economic benefits of the pilot policy. In order to achieve the dynamic effects in CETS's emission reduction and economic benefits, a measurement model with reference to Jacobson et al. [38] is shown in formula (3), where φ represents a series of estimates for 2013–2017. $TIME_{2013}$ is assigned as 1 in 2013 and 0 in other years. Similarly, $TIME_{2014}$, $TIME_{2015}$, $TIME_{2016}$, and $TIME_{2017}$ take 1 in 2014, 2015, 2016, and 2017, respectively, and 0 in other years. Other variables are defined following formula (2).

$$Y_{it} = \varphi_0 + \sum_{t=2013}^{2017} \varphi_t \left(TIME_t \times TREAT_i \right) + \phi X + \gamma_t + \mu_i + \varepsilon_{it}. \tag{3}$$

Table 4 reports the results of dynamic analysis. It can be found that the absolute value and significance of $TIME \times TREAT$ gradually increase after the implementation of the pilot policy. It shows that the emission reduction and economic benefits of China's pilot policy on CETS increase with time. The possible reasons are as follows. CETS converts firms' emission reduction achievements into economic benefits through the carbon market. The longer the policy is
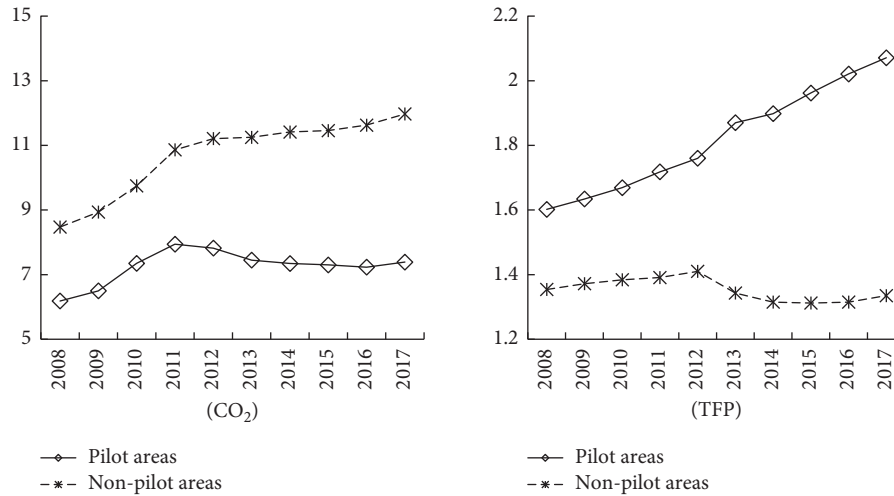
FIGURE 2: Means of CO_2 emissions and TFP in pilot and nonpilot areas.

TABLE 3: Results of benchmark regression.

VAR	(1) CO_2	(2) TFP	(3) CO_2	(4) TFP
TIME × TREAT	−0.189***	0.346***	−0.151***	0.213***
	(0.028)	(0.051)	(0.028)	(0.050)
OIS			−0.003***	0.003***
			(0.001)	(0.001)
SI			0.009***	−0.020***
			(0.004)	(0.006)
FDI			−0.045***	0.057**
			(0.015)	(0.026)
OPEN			−0.003**	−0.016***
			(0.002)	(0.003)
EDU			0.050***	−0.063***
			(0.013)	(0.023)
CONS	7.790***	2.164***	8.063***	2.945***
	(0.037)	(0.066)	(0.184)	(0.325)
PROV	YES	YES	YES	YES
YEAR	YES	YES	YES	YES
N	300	300	300	300
R^2	0.985	0.783	0.988	0.826

TABLE 4: Results of dynamic effects.

VAR	(1) CO_2	(2) TFP	(3) CO_2	(4) TFP
$TIME_{2013}$ × TREAT	−0.137***	0.233***	−0.104**	0.187**
	(0.049)	(0.088)	(0.045)	(0.081)
$TIME_{2014}$ × TREAT	−0.164***	0.289***	−0.141***	0.233***
	(0.049)	(0.088)	(0.045)	(0.081)
$TIME_{2015}$ × TREAT	−0.176***	0.356***	−0.130***	0.207**
	(0.049)	(0.088)	(0.047)	(0.083)
$TIME_{2016}$ × TREAT	−0.223***	0.412***	−0.192***	0.215**
	(0.049)	(0.088)	(0.048)	(0.085)
$TIME_{2017}$ × TREAT	−0.243***	0.441***	−0.214***	0.227***
	(0.049)	(0.088)	(0.048)	(0.086)
OIS			−0.003***	0.003***
			(0.001)	(0.001)
SI			0.008**	−0.020***
			(0.004)	(0.006)
FDI			−0.046***	0.057**
			(0.015)	(0.026)
OPEN			−0.004**	−0.015***
			(0.002)	(0.003)
EDU			0.050***	−0.064***
			(0.013)	(0.023)
CONS	7.790***	2.164***	8.110***	2.942***
	(0.037)	(0.066)	(0.186)	(0.331)
PROV	YES	YES	YES	YES
YEAR	YES	YES	YES	YES
N	300	300	300	300
R^2	0.986	0.787	0.988	0.826

implemented, the more complete the market construction will be, and the more emission reduction and economic benefits will be produced.

5.4. Results of Instrumental Variable.
DID can subtly overcome the endogeneity by comparing treat and control groups, but this requires that the pilot areas be chosen randomly. However, this is not the case. The pilot work is not easy because the pilot policy is of great significance, and there are specific requirements for carbon trading technology and supporting measures. It is not completely random when the government determines pilot areas. That is to say, the estimation results of the DID may be disturbed by potential factors. Therefore, drawing on Hering and Poncet [39], the instrumental variable is used to overcome the endogeneity as much as possible.

Instrumental variables need to be related to endogenous variables and not associated with the stochastic disturbance team. CETS aims to stabilize temperature by reducing carbon emissions. Temperature is affected by region and climate and is an exogenous factor. Therefore, referring to the practice of Hu and Ding [40], the annual average temperature is taken as an instrumental variable of the pilot policy on CETS. Temperature data comes from each province's statistical yearbook and China meteorological yearbook. The two-stage least square is used for regression.

After adding the instrumental variable, the results are shown in Table 5, where *IV* represents the instrumental variables. In the regression results of the first stage, the coefficient of $TIME \times IV$, the cross product of the instrumental variable and the time grouping variable, is significantly positive. It shows that the higher the temperature, the stricter the CETS is. The results of the weak instrumental variable show that the F value is 24.110, much higher than 10, rejecting the hypothesis of weak instrumental variables. In the regression results of the second stage, $TIME \times TREAT$, the pilot policy on CETS, still has significant inhibition effects on CO_2 emissions and significant promotion effects on TFP. The results indicate that the pilot policy on CETS still shows significant emission reduction and economic benefits after eliminating endogenous problems. That is, the results of the DID model are not caused by the bias in sample selection.

5.5. Results of Robustness Tests

(1) To replace the dependent variable, CO_2 emissions and TFP are replaced by pollutant emissions (*PE*) and GDP per capita (*PGDP*), respectively. Pollutant emissions are represented by the normalized indexes of total wastewater, exhaust gas, and general industrial solid waste production. Formula (2) is used for regression, and the results are shown in Table 6. The coefficient of pollutant emissions is still significantly negative, and the coefficient of economic benefit is still significantly positive. It suggests that the emission reduction and economic benefits of CETS do not depend on measures of dependent variables.

(2) To change the regression method, tobit method is adopted to conduct regression analysis on formula (2) again, and the results are shown in Table 7. The pilot policy on CETS has a significantly negative impact on CO_2 emissions and a significantly positive impact on TFP, consistent with the research results above. It shows that the regression method will not affect the estimation results. This result supports the robustness of the econometric model.

(3) Dynamic window test. The dynamic effects of CTES's emission reduction and economic benefits have been analyzed above. However, it only focused on changes after policy implementation and could not compare the differences before and after implementation. Therefore, dynamic window tests are carried out based on Shi and Li [41]. In addition to dynamically analyzing benefits gaps, this test can also test whether the DID model is affected by time horizons. Specifically, with 2013 as the time node of the policy introduction. One year, two years, three years, and four years are selected as the time window width to re-regress formula (2). The test results are shown in Table 8. The effects direction of CETS on CO_2 emissions and TFP does not change with the change of time window width. As the width of the time

window increases, the significance of the coefficients of emission reduction and economic benefits keeps improving. It is consistent with the results of dynamic effects analysis.

(4) Counterfactual test. The premise of DID is that the treatment and control groups are comparable. A year before the implementation of CTES is taken as the assumed impact point. If the assumed impact point coefficient is significant, there are significant differences between the experimental and control groups before implementing CETS. That is, the empirical model constructed in this article is not robust. On the contrary, if the coefficient is not significant, there is no significant difference between the experimental and control groups before implementing CETS. The difference between the two in the benchmark regression is caused by implementing CETS. The DID model constructed in this article is robust. In order to test this premise, referring to Hung et al. [42], the policy starting time of 2009, 2010, and 2011 is assumed as respectively, and formula (2) is used for regression. The results are shown in Table 9. The coefficient of $TIME \times TREAT$ is not significant when the start time is advanced to 2009, 2010, and 2011, respectively. It indicates that before the base year, the pilot policy of CETS cannot produce emission reduction and economic benefits. In other words, the actual policy year can indeed significantly reduce CO_2 emissions and improve TFP. Therefore, the previous conclusion has strong robustness.

(5) Placebo test. To further exclude the influence of unknown factors on the selection of pilot provinces and to ensure that the conclusions in this study are caused by the pilot policy on CETS, a placebo test is performed by randomly assigning pilot provinces [43]. In this article, 6 provinces are randomly selected as pilot areas of CETS from 30 provinces, and the other provinces are nonpilot areas. The placebo test should ensure that $TIME \times TREAT$, the independent variable, has no impact on CO_2 emissions and TFP. In other words, any significant findings will show that the results of this article are biased. 1000 random samples are taken using formula (2). The distribution of 1000 coefficients, and their *P* values are plotted in Figure 3. It can be seen that the distribution is mostly concentrated near the zero point, and the *P* value of most coefficients is bigger than 0.1. Therefore, the conclusions obtained in this article can pass the placebo test. The emission reduction and economic benefits of the pilot policy on CETS have no relationship with other unknown factors.

(6) To exclude the impact of other policies. In 2007, the Chinese government launched a pilot policy on emissions trading systems in 11 provinces, including Tianjin, Hebei, Shanxi, Inner Mongolia, Jiangsu, Zhejiang, Henan, Hubei, Hunan, Chongqing, and Shaanxi. Studies have shown that the policy also

TABLE 5: Results of the instrumental variable.

VAR	First stage		Second stage	
	(1) TIME × TREAT	(2) TIME × TREAT	(3) CO_2	(4) TFP
TIME × IV	0.028*** (0.006)	0.028*** (0.006)		
TIME × TREAT			−0.210** (0.089)	0.525*** (0.167)
OIS	0.005*** (0.001)	0.005*** (0.001)	−0.002*** (0.001)	0.002 (0.001)
SI	−0.014* (0.007)	−0.014* (0.007)	0.008** (0.004)	−0.015** (0.007)
FDI	−0.027 (0.032)	−0.027 (0.032)	−0.045*** (0.014)	0.054** (0.026)
OPEN	−0.010*** (0.003)	−0.010*** (0.003)	−0.004** (0.002)	−0.012*** (0.003)
EDU	−0.050* (0.028)	−0.050* (0.028)	0.046*** (0.014)	−0.039 (0.026)
CONS	0.002 (0.401)	0.002 (0.401)	8.088*** (0.174)	2.816*** (0.329)
PROV	YES	YES	YES	YES
YEAR	YES	YES	YES	YES
N	300	300	300	300
R^2	0.652	0.652	0.988	0.799

TABLE 6: Results of replacing dependent variables.

VAR	(1) PE	(2) PGDP	(3) PE	(4) PGDP
TIME × TREAT	−0.305*** (0.071)	1.027*** (0.134)	−0.178** (0.070)	0.754*** (0.122)
OIS			−0.006*** (0.002)	−0.003 (0.003)
SI			0.023** (0.009)	−0.034** (0.015)
FDI			−0.175*** (0.036)	0.053 (0.064)
OPEN			0.003 (0.004)	−0.064*** (0.007)
EDU			0.086*** (0.033)	−0.035 (0.057)
CONS	−1.236*** (0.093)	7.017*** (0.175)	−0.823* (0.461)	11.598*** (0.803)
PROV	YES	YES	YES	YES
YEAR	YES	YES	YES	YES
N	300	300	300	300
R^2	0.949	0.967	0.957	0.977

TABLE 7: Results of changing econometric model.

VAR	(1) CO_2	(2) TFP	(3) CO_2	(4) TFP
TIME × TREAT	−0.189*** (0.026)	0.346*** (0.047)	−0.151*** (0.026)	0.213*** (0.046)
OIS			−0.003*** (0.001)	0.003*** (0.001)
SI			0.009*** (0.003)	−0.020*** (0.006)
FDI			−0.045*** (0.013)	0.057** (0.024)
OPEN			−0.003** (0.001)	−0.016*** (0.003)
EDU			0.050*** (0.012)	−0.063*** (0.021)
CONS	7.790*** (0.034)	2.164*** (0.062)	8.063*** (0.169)	2.945*** (0.300)
PROV	YES	YES	YES	YES
YEAR	YES	YES	YES	YES
N	300	300	300	300

contributes to the reduction of pollutant emissions and the improvement of TFP. In order to identify the effects of CETS accurately, it is necessary to exclude the interference of similar policies. In addition, reward and punishment policies related to energy-saving technologies are also important factors affecting economic and environmental benefits. China's Ministry of Finance stated in document No.7 in 2016 that the central finance would continue to allocate funds to reward new energy technology-related issues from 2016 to 2020. Therefore, formula (2) is used for re-regression after removing policy cross-region and cross-time samples. The results in

Table 10 show that the coefficients of the two interaction terms are significant at the 1% level, and the influence direction of the CETS on these two dependent variables does not change. It indicates that the results are still robust after excluding the interference of other policies.

6. Further Analysis

6.1. Analysis of Mechanism. The above results show that China's pilot policy on CETS has positive incentive benefits. However, what behaviors should firms take under the stimulation of CETS to get positive incentive results? In

TABLE 8: Results of dynamic window tests.

VAR	One year		Two years		Three years		Four years	
	(1)	(2)	(3)	(4)	(5)	(6)	(7)	(8)
	CO_2	TFP	CO_2	TFP	CO_2	TFP	CO_2	TFP
TIME × TREAT	−0.087***	0.107**	−0.117***	0.153***	−0.137***	0.170***	−0.150***	0.198***
	(0.028)	(0.047)	(0.027)	(0.048)	(0.027)	(0.051)	(0.028)	(0.052)
OIS	−0.001	0.005	−0.000	0.003*	−0.002**	0.003**	−0.002***	0.002**
	(0.002)	(0.003)	(0.001)	(0.002)	(0.001)	(0.001)	(0.001)	(0.001)
SI	0.007	−0.033**	0.004	−0.031***	0.006	−0.025***	0.006	−0.017**
	(0.010)	(0.016)	(0.005)	(0.009)	(0.004)	(0.008)	(0.004)	(0.007)
FDI	−0.005	0.122**	−0.015	0.131***	−0.028*	0.069**	−0.040***	0.066**
	(0.033)	(0.055)	(0.027)	(0.049)	(0.017)	(0.031)	(0.015)	(0.027)
OPEN	−0.003	−0.012	−0.002	−0.012**	−0.002	−0.015***	−0.002	−0.017***
	(0.005)	(0.008)	(0.003)	(0.005)	(0.002)	(0.004)	(0.002)	(0.003)
EDU	0.031	0.006	0.033**	−0.020	0.037***	−0.045*	0.040***	−0.055**
	(0.020)	(0.033)	(0.016)	(0.028)	(0.013)	(0.024)	(0.014)	(0.025)
CONS	7.642***	3.138***	7.813***	3.494***	7.994***	3.281***	8.069***	2.875***
	(0.479)	(0.796)	(0.265)	(0.473)	(0.213)	(0.397)	(0.208)	(0.380)
PROV	YES	YES	YES	YES	YES	YES	YES	YES
YEAR	YES	YES	YES	YES	YES	YES	YES	YES
N	90	90	150	150	210	210	270	270
R^2	0.998	0.969	0.995	0.928	0.992	0.885	0.989	0.848

TABLE 9: Results of the counterfactual test.

VAR	2009		2010		2011	
	(1)	(2)	(3)	(4)	(5)	(6)
	CO_2	TFP	CO_2	TFP	CO_2	TFP
TIME × TREAT	−0.046	0.092	−0.029	0.094	−0.038	0.100
	(0.032)	(0.033)	(0.026)	(0.067)	(0.026)	(0.067)
OIS	−0.008***	0.005	−0.007***	0.000	−0.007***	−0.000
	(0.002)	(0.001)	(0.002)	(0.001)	(0.002)	(0.001)
SI	0.021***	0.009	0.020***	0.009*	0.020***	0.010*
	(0.006)	(0.005)	(0.006)	(0.005)	(0.006)	(0.005)
FDI	−0.076***	0.025*	−0.078***	0.026*	−0.078***	0.026*
	(0.024)	(0.014)	(0.024)	(0.014)	(0.024)	(0.014)
OPEN	−0.005**	0.004***	−0.005**	0.004***	−0.005**	0.004***
	(0.002)	(0.001)	(0.002)	(0.001)	(0.002)	(0.001)
EDU	0.038***	0.005	0.037***	0.005	0.033**	0.009
	(0.014)	(0.020)	(0.014)	(0.020)	(0.014)	(0.020)
CONS	8.966***	0.986***	8.924***	0.971***	8.892***	0.957***
	(0.276)	(0.134)	(0.277)	(0.129)	(0.278)	(0.128)
PROV	YES	YES	YES	YES	YES	YES
YEAR	YES	YES	YES	YES	YES	YES
N	150	150	150	150	150	150
R^2	0.995	0.940	0.995	0.943	0.995	0.943
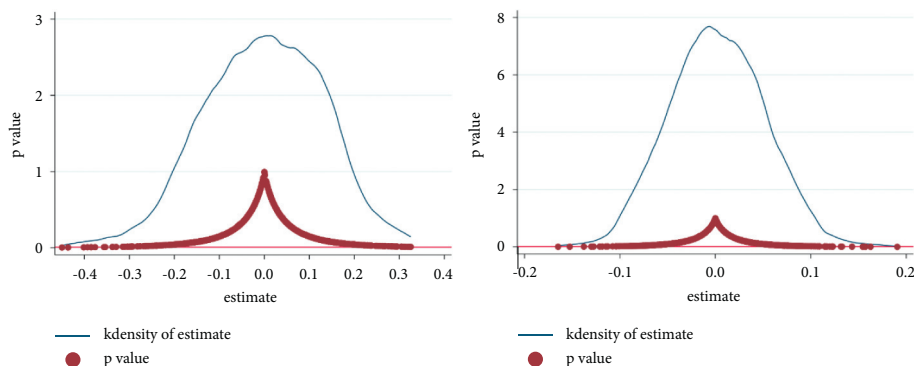
FIGURE 3: Results of placebo test.

TABLE 10: Results after excluding other policies.

VAR	(1) CO_2	(2) TFP	(3) CO_2	(4) TFP
TIME × TREAT	−0.196*** (0.040)	0.389*** (0.059)	−0.134*** (0.044)	0.187*** (0.064)
OIS			−0.003*** (0.001)	0.005*** (0.001)
SI			0.010** (0.005)	−0.031*** (0.007)
FDI			−0.068*** (0.020)	0.033 (0.030)
OPEN			−0.003 (0.002)	−0.013*** (0.003)
EDU			0.056*** (0.014)	−0.043** (0.020)
CONS	7.865*** (0.038)	2.031*** (0.056)	8.156*** (0.236)	2.971*** (0.346)
PROV	YES	YES	YES	YES
YEAR	YES	YES	YES	YES
N	216	216	216	216
R^2	0.989	0.828	0.991	0.860

order to verify the role of technological innovation and energy efficiency, the mediation model as shown in formulas (4) and (5) is constructed. The significance of the interaction terms' coefficient in formula (4) and the mediating variables' coefficient in formula (5) are the focus, where, *MEDIATOR* represents the mediating variable, namely, energy efficiency (*EE*) and technological innovation (*TI*). Other variables are defined as formula (2).

$$MEDIATOR_{it} = \theta_0 + \theta_1 \left(TIME_t \times TREAT_i\right) + \lambda X \\ + \gamma_t + \mu_i + \varepsilon_{it}, \quad (4)$$

$$Y_{it} = \delta_0 + \delta_1 \left(TIME_t \times TREAT_i\right) \\ + \delta_2 MEDIATOR_{it} + \eta X + \gamma_t + \mu_i + \varepsilon_{it}. \quad (5)$$

The three-step method is used to test whether the mediating effects are significant. Firstly, the impact of CETS on CO_2 emissions is significantly negative, and the impact on TFP is significantly positive (Table 3). Secondly, the effects of CETS on the mediating variable are tested. The results are significantly positive, as shown in columns (1) and (4) of Table 11. Finally, the effects of mediating variables on CO_2 emissions and TFP are tested, respectively. As shown in Table 11, technological innovation and energy efficiency have a significantly negative impact on CO_2 emissions and a significantly positive impact on TFP. Therefore, it can be concluded that CETS can stimulate firms to improve technological innovation and energy efficiency to obtain positive incentive effects.

6.2. Analysis of Heterogeneity

(1) Resource endowment. According to the resource curse hypothesis, regions with abundant resources have greater cost advantages. Therefore, they are not sensitive to the compliance cost pressure and the economic

incentives of CETS. Conversely, firms in poor resource endowment areas face higher illegal costs. They are more likely to gain additional economic benefits through carbon trading to cover environmental costs. A comprehensive index of the stock of 16 mineral resources, such as oil, natural gas, and coal, is used to measure the resource endowments of each province. The sample is divided according to the resource stock in 2012, one year before implementing the pilot policy on CETS. The provinces with resource stock higher than the average are defined as resource-rich provinces. The provinces with resource stock lower than or equal to the average are defined as resource-deficient provinces. In order to test the heterogeneity of the incentive effects of CETS under different resource endowments, formula (2) is used to regress the two samples separately. As shown in Table 12, CETS's emission reduction and economic benefits are greater in resource-deficient provinces than in resource-rich provinces. It suggests that the policy effects of CETS are also affected by the resource curse.

(2) Environmental law enforcement. The implementation of CETS needs a solid legal system, such as collecting carbon emission information and the punishment of noncompliance with trading rules. In order to protect local interests, some local officials allow polluters to discharge carbon emissions illegally, which leads to the failure of carbon emission trading. Tu and Chen [44] argued that strict environmental enforcement is necessary for China's market-oriented ER to achieve Porter's benefits. In theory, the greater the intensity of environmental law enforcement is, the higher the illegal cost is. There will be fewer violations, such as leakage and nonperformance. Also, firms are more likely to follow CETS. The sample was divided by the number of environmental administrative penalty cases in each

Table 11: Results of mechanism test.

	(1) TI	(2) CO_2	(3) TFP	(4) EE	(5) CO_2	(6) TFP
TIME × TREAT	4.018*** (0.528)	−0.090*** (0.030)	0.103* (0.053)	0.331*** (0.039)	−0.022* (0.027)	0.062* (0.048)
EE					−0.390*** (0.038)	0.704*** (0.066)
TI		−0.015*** (0.003)	0.027*** (0.006)			
OIS	0.095*** (0.011)	−0.001** (0.001)	0.000 (0.001)	0.002*** (0.001)	−0.002*** (0.001)	0.001 (0.001)
SI	−0.506*** (0.066)	0.002 (0.004)	−0.006 (0.007)	−0.031*** (0.005)	−0.003 (0.003)	0.002 (0.006)
FDI	0.538* (0.274)	−0.037*** (0.014)	0.042* (0.025)	0.090*** (0.020)	−0.010 (0.013)	−0.006 (0.022)
OPEN	−0.004 (0.029)	−0.003** (0.001)	−0.015*** (0.003)	−0.004* (0.002)	−0.005*** (0.001)	−0.013*** (0.002)
EDU	0.598** (0.246)	0.059*** (0.013)	−0.079*** (0.022)	−0.049*** (0.018)	0.031*** (0.011)	−0.029 (0.020)
CONS	25.549*** (3.461)	8.454*** (0.194)	2.248*** (0.343)	3.611*** (0.256)	9.472*** (0.206)	0.403 (0.361)
PROV	YES	YES	YES	YES	YES	YES
YEAR	YES	YES	YES	YES	YES	YES
N	300	300	300	300	300	300
R^2	0.912	0.989	0.840	0.964	0.991	0.879

Table 12: Results of heterogeneity in resource endowment.

VAR	Resource-deficient provinces		Resource-rich provinces	
	(1) CO_2	(2) TFP	(3) CO_2	(4) TFP
TIME × TREAT	−0.140*** (0.031)	0.271*** (0.064)	−0.195*** (0.063)	−0.078 (0.062)
OIS	−0.002*** (0.001)	0.002* (0.001)	−0.006** (0.003)	−0.006** (0.003)
SI	0.008* (0.004)	−0.027*** (0.009)	0.020* (0.012)	0.024** (0.011)
FDI	−0.052*** (0.018)	0.101*** (0.037)	−0.041 (0.025)	−0.021 (0.025)
OPEN	−0.002 (0.002)	−0.016*** (0.003)	−0.014*** (0.005)	0.006 (0.005)
EDU	0.007 (0.018)	−0.041 (0.037)	0.071*** (0.022)	−0.036* (0.021)
CONS	8.062*** (0.255)	3.556*** (0.520)	8.817*** (0.228)	1.135*** (0.222)
PROV	YES	YES	YES	YES
YEAR	YES	YES	YES	YES
N	180	180	120	120
R^2	0.992	0.841	0.975	0.773

Table 13: Results of heterogeneity in environmental enforcement.

VAR	Lax provinces		Strict provinces	
	(1) CO_2	(2) TFP	(3) CO_2	(4) TFP
TIME × TREAT	−0.026 (0.037)	0.037 (0.087)	−0.150*** (0.036)	0.127** (0.060)
OIS	−0.005*** (0.001)	0.008*** (0.001)	−0.000 (0.001)	−0.001 (0.002)
SI	0.038*** (0.006)	−0.083*** (0.014)	−0.001 (0.005)	0.003 (0.008)
FDI	0.043 (0.026)	−0.148** (0.062)	−0.047*** (0.016)	0.065** (0.027)
OPEN	−0.003 (0.002)	−0.021*** (0.005)	−0.003* (0.002)	−0.017*** (0.003)
EDU	0.001 (0.016)	0.035 (0.037)	0.068*** (0.017)	−0.136*** (0.028)
CONS	6.722*** (0.338)	6.100*** (0.797)	9.013*** (0.125)	1.627*** (0.209)
PROV	YES	YES	YES	YES
YEAR	YES	YES	YES	YES
N	220	220	80	80
R^2	0.995	0.913	0.985	0.786

province in 2012 (the year before the policy was implemented). Provinces with lower than the mean are defined as lax provinces, while those with higher or equal to the mean are defined as strict provinces. In order to test the heterogeneity of the incentive benefits of CETS under different environmental law enforcement, formula (2) is used to regress the two samples separately. The results in Table 13 show that the positive incentive effects of CETS are greater in provinces with strict environmental law enforcement. It indicates that the effective enforcement of China's CETS needs the support of local governments, especially environmental law enforcement departments.

7. Conclusion

Taking China's pilot policy on CETS in 2013 as a natural experiment, a DID model was constructed to control the potential endogenous problems. Under the guidance of

behavioral theory, a comprehensive study was conducted on the emission reduction benefits and economic benefits of China's CETS. The conclusions are as follows. (a) China's pilot CETS has produced significant emission reduction benefits and economic benefits. The results persisted after a series of robustness tests, including instrumental variable test, dynamic window test, counterfactual test, and placebo test of random sampling. (b) China's CETS can reduce CO_2 emissions and improve TFP through technological innovation and energy efficiency. (c) The results of heterogeneity analysis show that resource-deficient provinces and provinces with strict environmental law enforcement are more sensitive to CETS and have greater emission reduction and economic benefits.

Future research could focus on the following aspects. (a) Future research can investigate the impact of CETS on energy efficiency, industrial structure, and firm strategy to explore the firm's other responding behaviors to CETS. (b) Consumers are part of greenhouse gas emitters, and the following researchers can include them when formulating a more comprehensive carbon reduction policy system.

Data Availability

The data of this paper can be accessed by contacting the authors.

Conflicts of Interest

The authors declare that they have no conflicts of interest.

Acknowledgments

References

[1] N. O. Keohane, "Cap and trade, rehabilitated: using tradable permits to control U.S. greenhouse gases," *Review of Environmental Economics and Policy*, vol. 3, no. 1, pp. 42–62, 2009.

[2] L. Timothy, S. Misato, G. Michael, and C. Claudia, "The effects and side-effects of the EU emissions trading scheme," *Wiley Interdisciplinary Reviews: Climate Change*, vol. 5, no. 4, pp. 1–23, 2014.

[3] B. Cheng, H. Dai, P. Wang, D. Zhao, and T. Masui, "Impacts of carbon trading scheme on air pollutant emissions in Guangdong province of China," *Energy for Sustainable Development*, vol. 27, pp. 174–185, 2015.

[4] S. Fujimori, T. Masui, and Y. Matsuoka, "Gains from emission trading under multiple stabilization targets and technological constraints," *Energy Economics*, vol. 48, pp. 306–315, 2015.

[5] R. Calel and A. Dechezeprêtre, "Environmental policy and directed technological change: evidence from the European carbon market," *The Review of Economics and Statistics*, vol. 98, no. 1, pp. 551–574, 2012.

[6] G. Bel and S. Joseph, "Policy stringency under the European Union emission trading system and its impact on technological change in the energy sector," *Energy Policy*, vol. 117, pp. 434–444, 2018.

[7] W. B. Gray, "The cost of regulation: OSHA, EPA and the productivity slowdown," *The American Economic Review*, vol. 77, no. 5, pp. 998–1006, 1987.

[8] W. J. Baumol and W. E. Oates, *The Theory of Environmental Policy*, Cambridge University Press, Cambridge, 1988.

[9] D. W. Jorgenson and P. J. Wilcoxen, "Environmental regulation and U.S. Economic growth," *The RAND Journal of Economics*, vol. 21, no. 2, pp. 314–340, 1990.

[10] M. E. Porter and van der Linde, "Toward a new conception of the environment-competitiveness relationship," *The Journal of Economic Perspectives*, vol. 9, no. 1, pp. 97–118, 1995.

[11] P. Lanoie, M. Patry, and R. Lajeunesse, "Environmental regulation and productivity: testing the porter hypothesis," *Journal of Productivity Analysis*, vol. 30, no. 2, pp. 121–128, 2008.

[12] J. Peuckert, "What shapes the impact of environmental regulation on competitiveness? Evidence from executive opinion surveys," *Environmental Innovation and Societal Transitions*, vol. 10, pp. 77–94, 2014.

[13] F. Testa, F. Iraldo, and M. Frey, "The effect of environmental regulation on firms' competitive performance: the case of the building & construction sector in some EU regions," *Journal of Environmental Management*, vol. 92, no. 1, pp. 2136–2144, 2011.

[14] Z. Liu, X. Mao, J. Tu, and M. Jaccard, "A comparative assessment of economic-incentive and command-and-control instruments for air pollution and CO2 control in China's iron and steel sector," *Journal of Environmental Management*, vol. 144, no. 3, pp. 135–142, 2014.

[15] Y. Rubashkina, M. Galeotti, and E. Verdolini, "Environmental regulation and competitiveness: empirical evidence on the porter hypothesis from European manufacturing sectors," *Energy Policy*, vol. 83, no. 4, pp. 288–300, 2015.

[16] S. Li, X. Li, and X. Yang, "Environmental efficiency and environmental regulation in China based on the provincial data from 1986 to 2007," *Economic Research Journal*, vol. 36, no. 2, pp. 59–68, 2010.

[17] S. Li and G. Chen, "Environmental regulation and the growth of productivity in China: evidence from the revision of air pollution prevention and control law in 2000," *Economic Research Journal*, vol. 48, no. 1, pp. 17–31, 2013.

[18] J. W and B. Liu, "Environmental regulation and enterprises' TFP: an empirical analysis based on China's industrial enterprises data," *China Industrial Economics*, vol. 3, pp. 44–56, 2014.

[19] B. Anderson, T. C, and C. D. Maria, "Technological change and the EU ETS: the case of Ireland," *SSRN Electronic Journal*, vol. 216, no. 1, pp. 233–238, 2010.

[20] V. H. Hoffmann, "EU ETS and investment decisions:," *European Management Journal*, vol. 25, no. 6, pp. 464–474, 2007.

[21] S. Borghesi, G. Cainelli, and M. Mazzanti, "Linking emissions trading to environmental innovation: evidence from the Italian manufacturing industry," *Research Policy*, vol. 11, no. 4, pp. 669–683, 2015.

[22] G. Li and W. Zhang, "Research on industrial carbon emissions and emissions reduction mechanism in China's ETS," *China Population, Resources and Environment*, vol. 27, no. 10, pp. 141–148, 2017.

[23] W. Wang, P. Xie, C. Li, Z. Luo, and D. Zhao, "The key elements analysis from the mitigation effectiveness assessment of Chinese pilots carbon emission trading system," *China Population, Resources and Environment*, vol. 28, no. 4, pp. 26–34, 2018.

[24] L. Xue, X. Zhang, X. Hu, and H. Liu, "Spatial distribution of heterogeneous firms under the impact of carbon emissions trading market integration," *China Population, Resources and Environment*, vol. 28, no. 8, pp. 1–11, 2018.

[25] W. Liao, X. Dong, M. Weng, and X. Chen, "Economic effect of market-oriented environmental regulation: carbon emission trading, green innovation and green economic growth," *China Soft Science*, vol. 6, pp. 159–173, 2020.

[26] H. W and Z. Wang, "Research on the effects and influencing mechanism of carbon emission trading policy in Chinese pilot cities," *Urban Development Studies*, vol. 28, no. 06, pp. 133–140, 2021.

[27] J. H. Dales, *Pollution, Property & Prices: An Essay in Policy-Making and Economics*, University of Toronto Press, Toronto, 1968.

[28] S. Albrizio, T. Kozluk, and V. Zipperer, "Environmental policies and productivity growth: evidence across industries and firms," *Journal of Environmental Economics and Management*, vol. 81, no. 3, pp. 209–226, 2017.

[29] P. B and T. Hunter, "Strategic explanations for the early adoption of ISO 14001," *Journal of Business Ethics*, vol. 46, no. 3, pp. 289–299, 2003.

[30] L. H. Goulder and I. W. H. Parry, "Instrument choice in environmental policy," *Review of Environmental Economics and Policy*, vol. 2, no. 2, pp. 152–174, 2008.

[31] G. Akhmat, K. Zaman, T. Shukui, D. Irfan, and M. M. Khan, "Does energy consumption contribute to environmental pollutants? evidence from SAARC countries," *Environmental Science and Pollution Research*, vol. 21, no. 9, pp. 5940–5951, 2014.

[32] X. Zhang, L. Wu, R. Zhang et al., "Evaluating the relationships among economic growth, energy consumption, air emissions and air environmental protection investment in China," *Renewable and Sustainable Energy Reviews*, vol. 18, pp. 259–270, 2013.

[33] P. I. Hancevic, "Environmental regulation and productivity: the case of electricity generation under the CAAA-1990," *Energy Economics*, vol. 60, pp. 131–143, 2016.

[34] J. Zhang, G. Wu, and J. Zhang, "The estimation of China's provincial capital stock: 1952-2000," *Economic Research Journal*, vol. 10, pp. 35–44, 2004.

[35] B. W and P. Yan, "Technical efficiency, technical progress and East-Asian economic growth: empirical analysis based on APEC's view," *Economic Research Journal*, vol. 5, pp. 91–103, 2007.

[36] B. Wang, Y. Wu, and P. Yan, "Environmental efficiency and environmental total factor productivity growth in China's regional economies," *Economic Research Journal*, vol. 45, no. 5, pp. 95–109, 2010.

[37] F. Allen, J. Qian, and M. Qian, "Law, finance, and economic growth in China," *Journal of Financial Economics*, vol. 77, no. 1, pp. 57–116, 2005.

[38] L. S. Jacobson, R. J. Lalonde, and D. G. Sullivan, "Earnings losses of displaced workers," *The American Economic Review*, vol. 83, no. 4, pp. 685–709, 1993.

[39] L. Hering and S. Poncet, "Environmental policy and trade performance: evidence from China," *Journal of Environmental Economics and Management*, vol. 68, no. 4, pp. 296–318, 2014.

[40] Y. Hu and Y. Ding, "Can carbon emission permit trade mechanism bring both business benefits and green efficiency?" *China Population, Resources and Environment*, vol. 30, no. 3, pp. 56–64, 2020.

[41] S. D. and L. Li, "Emission trading system and energy use efficiency: measurements and empirical evidence for cities at above the prefecture level," *China Industrial Economics*, no. 9, pp. 5–23, 2020.

[42] M Hung, J. S, and Y. Wang, "The effect of mandatory CSR disclosure on information asymmetry: evidence from a quasi-natural experiment in China," *Social Science Electronic Publishing*, vol. 33, no. 5, pp. 1–17, 2013.

[43] X. Cai, Y. Lu, M. Wu, and L. Yu, "Does environmental regulation drive away inbound foreign direct investment? Evidence from a quasi-natural experiment in China," *Journal of Development Economics*, vol. 123, no. 1, pp. 73–85, 2016.

[44] Z. Tu and R. Chen, "Can emissions trading scheme achieve the porter effect in China?" *Economic Research Journal*, vol. 50, no. 7, pp. 160–173, 2015.

Research Article

Study on the Rural Revitalization and Urban-Rural Integration Efficiency in Anhui Province Based on Game Cross-Efficiency DEA Model

Shanhui Sun [ID],[1] Ni-Ni Zhang [ID],[2] and Jia-Bao Liu [ID][3]

[1]*College of Mathematics and Statistics, Suzhou University, Suzhou, Anhui 234000, China*
[2]*School of Management, Suzhou University, Suzhou, Anhui 234000, China*
[3]*School of Mathematics and Physics, Anhui Jianzhu University, Hefei 230601, China*

Correspondence should be addressed to Ni-Ni Zhang; ninizhang@ahszu.edu.cn

By taking the 16 cities in Anhui Province for evaluation, the main influencing factors and indicator system for integrated urban-rural development in the new era were explored, to build the BCC model, cross-efficiency model, and game cross-efficiency model of DEA. The above models were applied for empirical analysis and comparative study on the rural revitalization and urban-rural integration efficiency in Anhui Province, to summarize the conclusions efficiency and give suggestions based on the above calculations.

1. Introduction

City and countryside serve as two important constituents in social life, and the whole society's prosperity and development rest upon the sustainable development of these two parts. Rural revitalization and urban-rural integration supplement each other, so the study on their intrinsic logical relation shall be aimed at the complexity and dynamics of urban-rural regional system and exploring the construction plan, mode, and scientific method for eliminating urban-rural gap [1].

In September 2018, the issuance of the Plan for the Rural Revitalization Strategy (2018–2022) marked that rural revitalization stepped into the specific implementation stage and became the focus of attention of domestic scholars. Chinese government provides its scholars with the research direction of rural revitalization through land reform, socialism market system reform, and development of the beautiful village and modern agriculture [2]. Rural revitalization aims at establishing the system and mechanism for integrated urban-rural development and constructing the comprehensive development system for rural area, including the reformation, reconstruction, and innovation according to the requirements of thriving enterprises, pleasant living environment, convenance, civilized and effective governance, and prosperity.

Therefore, the urgent problem for rural revitalization is to objectively recognize the differences between urban living quality and rural living quality and identify the urban-rural integration degree, which is of important guiding significance to improving the living quality in urban and rural areas and promoting the formulation of the policies for integrated urban-rural development [3].

2. Current Situations of Domestic and Overseas Research

Along with the development of globalization and urbanization, different countries and regions are all faced with various problems and conflicts. Foreign countries mainly took the following policies for rural revitalization:

New Countryside Movement in South Korea, Comprehensive Village and Town Construction Demonstration Project in Japan, European Common Agricultural Policy (2014–2020), Japan's agricultural support policy and the study on rural economic development in Italy.

Rural-urban fringe zone refers to the transitional area combining the factors. As the border of urban expansion and the reserved land in rural area, rural-urban fringe zone has to solve the problem of urban-rural land use, which results in traffic jam, environmental pollution, and living quality degradation. Therefore, in order to effectively present the microdynamic development of the marginal area between city and countryside, it is necessary to guide the effective use of land. In Herberholz's opinion, urban-rural relationship is fundamental in the social development of human beings and also important to be solved in regional development [4]. Lysgard believes that theoretically, there are three main trends in the development of rural-urban relations: urban orientation, urban-rural interaction, and rural orientation [5]. Schmidt and Piloyan considered that the land element in the transitional area is one of the key points of the research by foreign scholars [6, 7]. Hachem successively proposed the concept of mixed community, which was strongly recommended and applied in the construction of modern integrated urban-rural development. It is used to promote the local economy by encouraging unity, supporting network, enhancing safety, and creating job opportunities [8].

The urban-rural dual structure gives priority to urban development, and labor force, resources, and capital are input for urban construction, resulting in a series of problems, such as village hollowing, environmental pollution, weakening of agriculture. Urban and rural areas are an interactive organism, and they are contradictory, coordinated, integrated, and equivalent, so rural revitalization is the only road for urban-rural integration.

Zheng et al. believe that pluralities of fields are covered for implementing rural revitalization strategy, including social governance, industrial development, and rural civilization, and all stakeholders shall develop top-level policy design for the rural revitalization strategy. We can really promote the integrated urban-rural development only by changing the development concept, allocating production factors efficiently, and optimizing the economic structure [9]. Li and Bo consider that it is necessary to put forward the overall plan for "development in five areas," seeking the inherent thought train for realizing the urban-rural integration [10]. Zhang and Zhao elaborate the basic frame of urban-rural integration from the consistency among objectives, essence, and space of rural revitalization strategy and integrated urban-rural development and put forth the result-based common development [11]. Li believes that the key to rural revitalization lies in urban-rural integration which is the objective law and also the effect form coping with risks and crises. Either-or thinking is not applicable to rural revitalization and urbanization; overall planning must be made for development in the process of promoting the rural revitalization strategy to realize integrated urban-rural development [12].

3. Research Methods, Data Source, and Index Construction

3.1. Research Methods. It analyzes the process and effect of rural revitalization and integrated urban-rural development by comprehensively applying the theory and method of system science and management. It analyzes indexes systemically with methods of statistics and operational research and builds scientific evaluation models and path selection models with data mining and mathematical modeling to provide a theoretical basis for path selection of rural revitalization and integrated urban-rural development.

3.2. Data Source and Index Construction. In this paper, the data are mainly from Anhui Statistical Yearbook, and the urban-rural integration is comprehensive and analyzed from the spatial arrangement, industry configuration, income gap, public service, and ecological environment. It makes crossover analysis on rural revitalization and urban-rural integration and finds their intersection combining with the statistical index of Anhui Statistical Yearbook. The analysis is detailed in the following Table 1.

In the table, $X1$ indicates the ratio between nonagricultural workers and agricultural workers, $X2$ refers to the ratio between nonagricultural production value and agricultural production value, $X3$ means the ratio of hospital bed, $X4$ refers to the ratio of the number of days with the air quality of and above Level II between urban and rural areas, $X5$ refers to the ratio of subsistence allowances amount per capita, $X6$ indicates the ratio of the number of students enrolled in middle schools, $X7$ means the green coverage ratio in built-up areas, $X8$ refers to the sewage treatment rate, and $X9$ refers to the ratio of disposable income. Moreover, $Y1$ is the variable and is expressed by the urbanization rate of residents [13].

4. Construction of Game Cross-Efficiency Model

First, it finds out the major influencing factors by factor analysis and carries out factor analysis for the original variables by data mining [14]. Second, it evaluates the efficiency by inputting three kinds of models of data envelopment analysis.

4.1. Principal Component Analysis. It means to classify variables based on the relevance of variables in systems and take the classified variables as the principal component to show the main system information with less principal component. n decision bodies and p evaluation indexes are provided, and the original data are

$$X = \begin{pmatrix} x_{11} & x_{12} & \dots & x_{1p} \\ x_{21} & x_{22} & \dots & x_{2p} \\ \dots & \dots & \dots & \dots \\ x_{n1} & x_{n2} & \dots & x_{np} \end{pmatrix}. \quad (1)$$

The correlation factor matrix is calculated as

TABLE 1: Index system of crossover analysis.

	Thriving business	Pleasant living environment	Rural civilization	Effective governance	Living in abundance
Spatial layout	X1	—	—	—	—
Industry configuration	X2	—	—	X3	—
Public service	X4	X5	X6	X7	—
Ecological environment	—	X7	—	X8	—
Income gap	—	—	—	—	X9

$$R = \begin{pmatrix} r_{11} & r_{12} & \cdots & r_{1p} \\ r_{21} & r_{22} & \cdots & r_{2p} \\ \cdots & \cdots & \cdots & \cdots \\ r_{n1} & r_{n2} & \cdots & r_{np} \end{pmatrix}, \tag{2}$$

where r_{ij} $(i, j = 1, 2, \ldots, p)$ is the correlation factor between the i th and the j th evaluation indexes.

$$r_{ij} = \frac{\sum_{k=1}^{n} (x_{ki} - \bar{x}_i)(x_{kj} - \bar{x}_j)}{\sqrt{\sum_{k=1}^{n} (x_{ki} - \bar{x}_i)^2 \sum_{k=1}^{n} (x_{kj} - \bar{x}_j)^2}}, \tag{3}$$

where

$$\bar{x}_i = \frac{1}{n} \sum_{k=1}^{n} x_{ki}, $$

$$\bar{x}_j = \frac{1}{n} \sum_{k=1}^{n} x_{kj}. \tag{4}$$

The eigenvalue and eigenvector of R are calculated. The equation $|\lambda I - R| = 0$ is solved to work out the eigenvalue λ_i, the eigenvalue λ_i in order of size $\lambda_1 \geq \lambda_2 \geq \ldots \geq \lambda_p \geq 0$ is arranged, the corresponding eigenvector $\vec{e}_i$ $(i = 1, 2, \ldots, p)$ is calculated; $\sum_{j=1}^{p} e_{ij}^2 = 1$, e_{ij} is the j th component of vector $\vec{e}_i$.

The contribution rate is

$$\frac{\lambda_i}{\sum_{k=1}^{p} \lambda_p} \ (i = 1, 2, \ldots, p). \tag{5}$$

The accumulative contribution rate is

$$\frac{\sum_{k=1}^{i} \lambda_k}{\sum_{k=1}^{p} \lambda_p} \ (i = 1, 2, \ldots, p). \tag{6}$$

Generally, the eigenvalue of the principal component with the accumulative contribution rate of 85%–95% is used; $\lambda_1, \lambda_2, \ldots, \lambda_m$ are, respectively, the 1st, 2nd, and $\ldots$, the $m(m \leq p)$th principal component.

The principal component load is calculated as follows:

$$l_{kij} = p(z_k, x_{ij}) = \sqrt{\lambda_i} e_{kij}, \tag{7}$$

where $k = 1, 2, \ldots, n$; $i, j = 1, 2, \ldots, p$.

Principle component is extracted, the load l_{kij}, $(k = 1, 2, \ldots, n; i, j = 1, 2, \ldots, p)$ of original variables x_{kj} $(k = 1, 2, \ldots, n; i, j = 1, 2, \ldots, p)$ on principle component z_k $(k = 1, 2, \ldots, n)$ is determined, and the representation of principle component of original data is

$$Z = \begin{pmatrix} z_{11} & z_{12} & \cdots & z_{1m} \\ r_{21} & r_{22} & \cdots & r_{2m} \\ \cdots & \cdots & \cdots & \cdots \\ x_{n1} & x_{n2} & \cdots & x_{nm} \end{pmatrix}, \tag{8}$$

where

$$z_{i1} = l_{1i_1} x_{i_1} + l_{1i_2} x_{i_2} + \ldots + l_{1i_p} x_{i_p}$$

$$z_{i2} = l_{2i_1} x_{i_1} + l_{2i_2} x_{i_2} + \ldots + l_{2i_p} x_{i_p}$$

$$\cdots \tag{9}$$

$$z_{im} = l_{mi_1} x_{i_1} + l_{mi_2} x_{i_2} + \ldots + l_{mi_p} x_{i_p}.$$

4.2. Envelopment Analysis Model. When the scale benefit is changeable, Banker, Charnes, and Cooper propose to evaluate the BCC model for decision-making unit U_0, and the oriented model is input in the type of

$$\min\left(\theta - \varepsilon\left(e^T s^- + e^T s^+\right)\right)$$

$$\text{s.t.} \sum_{i=1}^{n} (x_{ij} \lambda_i) + s^- = \theta x_{0j}, \quad j = 1, 2, \ldots, m,$$

$$\sum_{i=1}^{n} (y_{ir} \lambda_j) + s^+ = \theta y_{0r}, \quad r = 1, 2, \ldots, s, \tag{10}$$

$$\sum_{i=1}^{n} \lambda_i = 1,$$

$$\lambda_j \geq 0, s^+ \geq 0, s^- \geq 0.$$

x_{ij} and y_{ir} are the input and output factors, respectively, and θ is the effective value of U_0.

If $\theta = 1$, $s^+ = s^- = 1$, U_0 means DEA is effective; if $\theta = 1$, $s^+ \neq 1$ or $s^- \neq 1$, U_0 means weak DEA is effective; if $\theta < 1$, U_0 refers to non-DEA is effective.

4.3. Cross-Efficiency Evaluation. The linear programing (LP) type is as follows:

$$\max \sum_{r=1}^{s} u_r y_{rd} = \theta_d$$

$$\text{s.t.} \sum_{i=1}^{m} \omega_i x_{ij} - \sum_{r=1}^{s} u_r y_{rd} \geq 0, \quad j = 1, 2, \ldots, n,$$

$$\sum_{i=1}^{m} \omega_i x_{id} = 1. \tag{11}$$

$$\omega_i \geq 0, \quad i = 1, 2, \ldots, m,$$

$$u_r \geq 0, \quad r = 1, 2, \ldots, s,$$

We get a group of optimal weight value (multiplier) $\omega_{1\,d}^*, \ldots, \omega_{m\,d}^*, \mu_{1\,d}^*, \ldots, \mu_{s\,d}^*$ for each $DM\ U_d\,(d = 1, 2, \ldots, n)$ evaluation. The cross-efficiency of any $DM\ U_j\,(j = 1, 2, \ldots, n)$ can be expressed and calculated below with the weight chosen by DMU.

$$E_{dj} = \frac{\sum_{r=1}^{s} u_{rd}^* y_{rj}}{\sum_{i=1}^{m} \omega_{id}^* x_{ij}}, \quad d, j = 1, 2, \ldots, n. \tag{12}$$

As shown in Table 2, when we move along the line d in the cross-efficiency matrix E, each factor E_{dj} is the cross-efficiency of $DM\ U_d$ and $DM\ U_j$, and the main diagonal thereof is a special case for DMU self-evaluation [15].

Then, everyone averages the column of the cross-efficiency matrix in Table 1. The average value of all $E_{dj}\,(j = 1, 2, \ldots, n)$ for $DM\ U_j\,(j = 1, 2, \ldots, n)$, is $\overline{E_{dj}}$, namely, $\overline{E_{dj}} = 1/n(E_{1j} + E_{2j} + \ldots + E_{nj})$.

4.4. Game Cross-Efficiency.
During the calculation of game cross-efficiency, the efficiency of U_d is set as α_d; the optimal weight on the premise of ensuring no reduced α_d to maximize the self-efficiency [16] is obtained. The game cross-efficiency is

$$\alpha_{dj} = \frac{\sum_{r=1}^{s} u_{rjd} y_{rj}}{\sum_{i=1}^{m} v_{ijd} x_{ij}}. \quad d = 1, 2, \ldots, n \tag{13}$$

The corresponding model is

$$\max \sum_{r=1}^{s} u_{rjd} y_{rj},$$

$$\text{s.t.} \sum_{r=1}^{s} u_{rjd} y_{rj} - \sum_{i=1}^{m} v_{ijd} x_{ij} \leq 0,$$

$$\sum_{i=1}^{m} v_{ijd} x_{ij} = 1, \tag{14}$$

$$\alpha_d \sum_{i=1}^{m} \left(v_{ijd} x_{id} \right) - \sum_{r=1}^{s} \left(u_{rjd} y_{rd} \right) \leq 0,$$

$$u_{rjd}, v_{ijd} \geq 0.$$

5. Empirical Analysis on Game Cross-Efficiency

5.1. Principal Component Analysis (PCA) of Influencing Factors of Rural Revitalization and Urban-Rural Integration.

The influencing factors were analyzed with SPSS software. The results of the corresponding total variance explained are shown in Table 3.

The analysis results of the component scoring system matrix for the influencing factors are shown in the following Table 4.

Therefore, its corresponding regression equation is

$Z1 = 0.174 * X1 + 0.228 * X2 + 0.200 * X3 - 0.105 * X4 - 0.170 * X5 - 0.115 * X6 + 0.200 * X7 + 0.084 * X8 - 80.131 * X9$

$Z2 = -0.303 * X1 - 0.096 * X2 - 0.029 * X3 - 0.343 * X4 - 0.256 * X5 + 0.080 * X6 + 0.114 * X7 + 0.501 * X8 + 0.421 * X9$

$Z3 = 0.345 * X1 + 0.077 * X2 + 0.115 * X3 + 0.579 * X4 + 0.236 * X5 - 0.187 * X6 - 0.010 * X7 + 0.429 * X8 + 0.417 * X9.$

By the regression variance, we can calculate the results of three principal components of the influencing factors in 16 cities of Anhui Province. The specific condition is shown in Table 5.

5.2. Data Envelopment Model Analysis of Influencing Factors of Rural Revitalization and Urban-Rural Integration.
The MaxDEA software is used to calculate the above three efficiency values, and the calculation results are shown in Table 6.

By the above calculation results, we can derive a trend chart of efficiency indicators, as shown in Figure 1.

5.3. Result Analysis

5.3.1. Regional Development Is Unbalanced, and Echelon Distribution Is Significant.
From the efficiency results of 16 cities in Anhui Province, it can be seen that Hefei and Tongling belong to the first echelon; Ma'anshan, Huaibei, Huainan, and Wuhu belong to the second echelon; Bengbu, Xuancheng, Chuzhou, Chizhou, Anqing, and Huangshan belong to the third echelon; and Fuyang, Lu'an, Suzhou, and Bozhou belong to the fourth echelon.

5.3.2. The Results of BCC Efficiency and Cross-Efficiency Are Similar, but There Are Slight Differences.
From the comparison of the BCC efficiency and cross-efficiency results of 16 cities in Anhui Province, it can be seen that the ranking of efficiency values that are calculated by the two calculation methods has not almost changed. However, there are slight differences between the two groups of cities: Ma'anshan and Huaibei, and Anqing and Huangshan.

We can learn from the analysis that one of the main reasons for the above situation is that BCC efficiency and cross-efficiency are similar. The BCC efficiency in data envelopment analysis is mainly determined by the way that is most beneficial to the evaluated DMUs, while the cross-efficiency model evaluates all DMUs with each group of weights. In addition, the input and output indexes of Ma'anshan and Huaibei, Anqing and Huangshan are similar,

TABLE 2: General cross-efficiency matrix.

Evaluated units	1	2	3	. . .	n
1	E_{11}	E_{12}	E_{13}	. . .	E_{1n}
2	E_{21}	E_{22}	E_{23}	. . .	E_{2n}
3	E_{31}	E_{32}	E_{33}	. . .	E_{3n}
. . .	. . .	. . .	. . .	. . .	. . .
n	E_{n1}	E_{n2}	E_{n3}	. . .	E_{nm}
Average value	$\overline{E_1}$	$\overline{E_2}$	$\overline{E_3}$	. . .	$\overline{E_n}$

TABLE 3: Total variance explained of influencing factors of rural revitalization and urban-rural integration.

Component	Initial eigenvalue			Loading of quadratic sum extracted		
	Total	Variance	Accumulation	Total	Variance	Accumulation
1	4.175	46.386	46.386	4.175	46.386	46.386
2	1.365	15.164	61.550	1.365	15.164	61.550
3	1.084	12.047	73.597	1.084	12.047	73.597
4	0.876	9.730	83.327			
5	0.631	7.007	90.335			
6	0.406	4.515	94.850			
7	0.219	2.428	97.278			
8	0.202	2.247	99.524			
9	0.043	0.476	100.000			

TABLE 4: Component scoring system matrix for influencing factors.

	Component		
	1	2	3
$X1$ ratio of nonagricultural workers to agricultural workers	0.174	−0.303	0.345
$X2$ ratio of nonagricultural output value to agricultural output value	0.228	−0.096	0.077
$X3$ ratio of hospital bed in city and hospital bed in country (%)	0.200	−0.029	0.115
$X4$ air quality reaching or better than grade II (%)	−0.105	−0.343	0.579
$X5$ green coverage ratio of built-up area (%)	−0.170	−0.256	0.236
$X6$ ratio of urban subsistence allowance per capita and rural subsistence allowance per capita (%)	−0.115	0.080	−0.187
$X7$ ratio of urban middle school enrollment to rural middle school enrollment (%)	0.200	0.114	−0.010
$X8$ ratio of urban sewage treatment to rural sewage treatment (%)	0.084	0.501	0.429
$X9$ ratio of disposable income in rural towns	−0.131	0.421	0.417

TABLE 5: Calculation of the three principal components of influencing factors.

No.	City	Input variable			Output variable
		Principal component 1	Principal component 2	Principal component 3	
1	Hefei	2.92	35.55	102.66	76.33
2	Huaibei	15.00	24.41	107.22	65.88
3	Bozhou	27.96	26.91	113.56	42.22
4	Suzhou	25.73	22.45	112.68	43.96
5	Bengbu	23.10	16.24	124.91	58.58
6	Fuyang	22.88	26.29	107.68	44.62
7	Huainan	16.26	25.31	106.35	65.04
8	Chuzhou	16.38	21.00	117.36	54.54
9	Lu'an	25.64	15.55	125.85	47.09
10	Ma'anshan	6.64	30.74	106.02	69.12
11	Wuhu	8.24	32.36	113.30	66.41
12	Xuancheng	11.98	16.20	125.09	56.33
13	Tongling	5.91	2.06	101.12	57.16
14	Chizhou	15.69	18.58	125.60	54.92
15	Anqing	18.59	20.37	117.78	49.98
16	Huangshan	11.04	12.10	133.12	52.49

TABLE 6: Calculation and ranking of efficiency of rural revitalization and urban-rural integration.

No.	City	BCC model	Ranking	Cross-efficiency model	Ranking	Game cross-efficiency model	Ranking
1	Hefei	1.00	1	0.94	1	0.20	5
2	Tongling	1.00	1	0.96	2	0.49	1
3	Ma'anshan	0.91	3	0.83	3	0.20	5
4	Huaibei	0.91	3	0.81	4	0.21	4
5	Huainan	0.89	5	0.80	5	0.20	5
6	Wuhu	0.83	6	0.75	6	0.18	9
7	Bengbu	0.75	7	0.67	7	0.17	11
8	Xuancheng	0.72	8	0.65	8	0.23	3
9	Chuzhou	0.71	9	0.64	9	0.18	9
10	Chizhou	0.69	10	0.62	10	0.19	8
11	Anqing	0.65	11	0.58	11	0.16	12
12	Huangshan	0.65	11	0.59	12	0.25	2
13	Fuyang	0.60	13	0.54	13	0.12	14
14	Lu'an	0.60	13	0.54	13	0.13	13
15	Suzhou	0.59	15	0.52	15	0.12	14
16	Bozhou	0.54	16	0.48	16	0.11	16
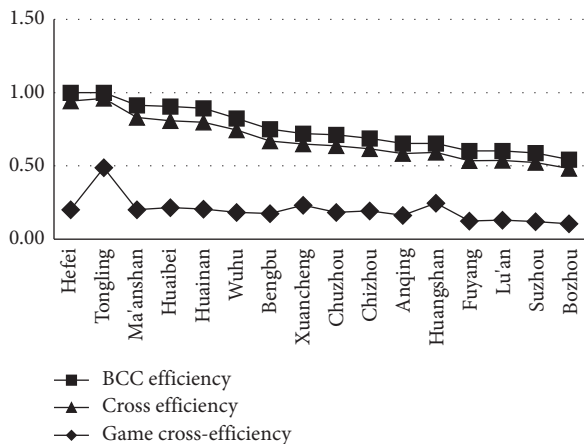
FIGURE 1: Trend chart of efficiency indicators.

so this is how the above analysis results are similar but slightly different.

5.3.3. Combined with the Analysis of Game Cross-Efficiency, the Differences among Cities in Anhui Province Are Obvious.

By combining with the analysis, it is found that the game cross-efficiency of Hefei, Xuancheng, and Huangshan fluctuates with BCC efficiency and cross-efficiency. From the comparison results of 16 cities in Anhui Province, it is found that the efficiency of urban-rural integration in Hefei in the first echelon declines significantly, while that in Huangshan and Xuancheng, the third echelon sees a rising trend, and especially, the rising extent of Huangshan is significant.

It is found from the above analysis that Hefei's attraction to the country is relatively insufficient. Tongling has done a good job in the urban-rural integration, because it is small, with little difference between city and country, and it has fewer difficulties than other cities [17]. Huangshan and Xuancheng have relatively strong competitiveness in potential and attractiveness in the future.

6. Conclusion and Suggestions

6.1. Strategic Direction of Building an Urban-Rural Integration System.

In order to implement the rural revitalization strategy, we should, by taking cities and countries as organic systems, build a coupling model and innovation system that integrates "human," "land" with "industry" in rural areas to promote gather of capital, talents, and other elements in rural areas, gradually break the urban-rural functional division pattern, and realize urban and rural areas support each other, integrate with each other and make progress simultaneously.

6.2. Overall Design of Urban and Rural Functional Planning.

A convenient and smooth transportation network system from the market to the field can be formed through the implementation of construction projects. The consolidation and upgrading project of urban and rural basic infrastructure can be implemented to improve and build an efficient network [18]. We should implement the overall design of functional planning, implement informatization construction projects, develop a safe and efficient information and communication network with reasonable urban and rural layout, balanced development and perfect functions, implement the digital rural strategy, and comprehensively promote the "Internet+."

6.3. Promote Cobuilding and Sharing of Urban and Rural Infrastructure.

The government should vigorously promote the network infrastructure construction that fits the demands of agriculture, rural areas, and farmers, adhere to overall planning, urban-rural integration, focus on weakness and break major problems, accelerate the upgrading of urban and rural infrastructure, and build a safe, efficient, and connective infrastructure network system [19]. According to local conditions, the government should implement a demonstration pilot project of integrated urban-rural development, promote upgrading and transformation of urban and rural infrastructure to realize joint construction and

sharing, and calmly realize the overall goal of building space that is suitable for both living and industry development and picturesque ecological scenery.

Data Availability

The data used to support the findings of this study are included within the article.

Conflicts of Interest

The authors declare there are no conflicts of interest regarding the publication of this paper.

Authors' Contributions

All authors contributed to this paper equally.

Acknowledgments

References

[1] Z. Zhang, *Research on the Development Path of Rural Vocational Education under the Strategy of Rural Vitalization" Nanjing*, Nanjing University of Posts and Telecommunications, Nanjing, China, 2020.

[2] Z. Tang, *Research on the Technology Development Problems and Solutions of Rural Revitalization Strategy in China"*, BOHAI University, Jinzhou, China, 2020.

[3] X. Wu, "Key points and risk prevention for the rural revitalization in the new era," *Journal of Guangdong Institute of Public Administration*, vol. 30, no. 6, pp. 92–98, 2018.

[4] C Herberholz and S Phuntsho, "Social capital, outpatient care utilization and choice between different levels of health facilities in rural and urban areas of Bhutan," *Social Science & Medicine*, vol. 211, no. 6, pp. 102–113, 2018.

[5] H. K. Lysgård, "The assemblage of culture-led policies in small towns and rural communities," *Geoforum*, vol. 101, no. 2, pp. 10–17, 2019.

[6] J. Schmidt and A. Hewitt, "Fuzzy land element classification from DTMs based on geometry and terrain position," *Geoderma*, vol. 121, no. 8, pp. 243–256, 2004.

[7] A. Piloyan and M. Konečný, "Semi-automated classification of landform elements in Armenia based on SRTM DEM using K-means unsupervised classification," *Quaestiones Geographicae*, vol. 36, no. 1, pp. 93–103, 2017.

[8] C. Hachem, "Design of A Base case mixed-use community and its energy performance," *Energy Procedia*, vol. 78, no. 11, pp. 663–668, 2015.

[9] R. Zheng, Z. Weng, and J. Huang, "Rural revitalization strategy: urban-rural integration, factors allocation and institutional arrangement - overview of the summit on "implementing rural revitalization strategy and deepening agricultural supply-side structural reform in the new era"," *Journal of Agro-Forestry Economics and Management*, vol. 17, no. 1, pp. 1–6, 2018.

[10] W.-H. Lin, W.-B. Wang, and L.-B. Ke, "On the problems and countermeasures of rural ecological culture construction from the perspective of the strategy of rural revitalization," *Proceedings of the 4th Annual International Conference on Management, Economics and Social Development (ICMESD 2018)*, vol. 120, no. 6, pp. 19–24, 2018.

[11] M. Zhang and M. Zhao, "Study on the framework and path for integrated urban-rural development from the perspective of rural revitalization strategy," *Journal of Northeast Agricultural University*, vol. 17, no. 5, pp. 1–7, 2019.

[12] D. Li, "Research on the path of promoting rural revitalization strategy in megacities from the perspective of integrated urban-rural development - guangdong as an example," *China Collective Economy*, vol. 21, no. 7, pp. 3-4, 2020.

[13] J.-B. Liu, J. Cao, A. Alofi, A. Al-Mazrooei, and A. Elaiw, "Applications of laplacian spectra for n-prism networks," *Neurocomputing*, vol. 198, pp. 69–73, 2016.

[14] C. Lai, J. Lv, and X. Li, "Port production efficiency research based on two-stage DEA game cross efficiency model," *Journal of Shanghai Maritime University*, vol. 39, no. 1, pp. 52–59, 2018.

[15] J.-B. Liu and X.-F. Pan, "Minimizing Kirchhoff index among graphs with a given vertex bipartiteness," *Applied Mathematics and Computation*, vol. 291, pp. 84–88, 2016.

[16] D. Zhang, "Analysis of the spatial spillover effect of new urbanization quality on agricultural economic growth - based on empirical data from 17 cities in shandong Province," *Journal of Shandong University*, vol. 4, no. 8, pp. 157–167, 2019.

[17] Q. Hongkai and Y. Lu, "Agricultural cultural heritage and rural revitalization: explanation and analysis based on the theory of new structural economics," *Journal of Nanjing Agricultural University*, vol. 21, no. 2, pp. 53–61, 2021.

[18] S. Sun and M. Zhou, "Analysis of farmers land transfer willingness and satisfaction based on SPSS analysis of computer software," *Cluster Computing*, vol. 22, no. 8, pp. 9123–9131, 2019.

[19] S. Shanhu, L. Hong, X. Liang, L. Zhuangzhuang, and Z. Bingqiu, "The model of the exploratory factor analysis about residents will of rural land transfer," *International Journal of Smart Home*, vol. 9, no. 8, pp. 63–72, 2021.

Research Article

Economic Analysis of Animal Husbandry Based on System Dynamics

Lei Wang [1,2] **and Hongwei Tan** [3]

[1]*Economics and Management School, Jilin Agricultural University, Changchun 130118, China*
[2]*Business School, Changchun Sci-Tech University, Changchun 130600, China*
[3]*Language and Culture School, Changchun Sci-Tech University, Changchun 130600, China*

Correspondence should be addressed to Lei Wang; wanglei@mails.jlau.edu.cn

In order to improve the effect of animal husbandry economic analysis, this article studies the animal husbandry economy based on system dynamics and studies how to define total factor productivity and its measurement method. Moreover, this article compares and analyzes the production function method, data envelopment analysis, and index method for measuring total factor productivity, selects decision-making units, and determines and processes input-output data. In addition, this article combines the system dynamics model to explore the causal relationship of the animal husbandry economy and builds an intelligent model to intelligently analyze the animal husbandry economy. Finally, this article analyzes the economy and performance of animal husbandry based on simulation experiments. The simulation test results show that the system dynamics model proposed in this article has a good performance in the economic analysis of animal husbandry.

1. Introduction

The living standards of residents are constantly improving, the consumption structure is constantly improving, and health awareness is also increasing. Therefore, people's demand for all kinds of healthy and nutritious animal products is growing rapidly, especially the demand for high-quality meat, eggs, and milk products. These shifts in food demand are also adding impetus to the development of animal husbandry. The national economy is a general term for various social production sectors and other labor sectors, including material production sectors such as industry and agriculture and nonmaterial production sectors such as transportation, finance, and commerce. These departments are both interrelated and independent, and together they form an organic whole of the national economy. However, the status of each sector in the national economy is not the same. Among them, agriculture, as the primary industry, plays a fundamental role in the national economy.

In human history, animal husbandry came into being before planting, and the emergence of nomadism separated animal husbandry from agriculture, realizing the first great division of labor in human history, which is a sign of the progress of human civilization. With the development of the times, animal husbandry is showing its important status and significance more and more. Planting and animal husbandry are two extremely important parts of agriculture, and they are interrelated and mutually reinforcing. On the one hand, planting provides essential fodder for the development of animal husbandry. Without the development of animal husbandry, planting is the basis for the development of animal husbandry; on the other hand, the development of animal husbandry provides the fertilizer, power, and funds needed for production, which in turn will promote the development of the planting industry. It can be seen that agriculture is the foundation of the national economy, embodied by both planting and animal husbandry. Both planting and animal husbandry are the basis for human survival and social development.

With the development of society and economy, the status of animal husbandry has become increasingly important, and

it is more closely related to the lives of the people. In the food consumption structure of many developed countries, animal products have become the theme of improving people's food structure and nutrition. The proportion of agricultural output value has exceeded that of the traditional planting industry, accounting for about 60%–80%. Driven by consumer demand, the labor force produced by the planting industry has begun to transfer to animal husbandry, which has promoted the industrialization and urbanization of rural areas. The development of animal husbandry has also greatly increased the demand for feed, changed the traditional planting structure, and transformed the traditional dual planting structure based on "grain-economic crops" into "grain-economic crops-feed crops" ternary planting structure has optimized the agricultural industry structure. It is undeniable that animal husbandry has many irreplaceable characteristics of other sectors, such as planting, and its correlation with other industries within agriculture is particularly high. Therefore, the development level of modern animal husbandry has become a measure of whether a country or a region's agricultural industry structure is reasonable. An important sign is the development of agricultural modernization that increasingly requires the support of strong animal husbandry.

This article studies the animal husbandry economy based on system dynamics and constructs an intelligent model to intelligently analyze the animal husbandry economy so as to improve the subsequent development effect of the animal husbandry economy.

2. Related Work

Literature [1] believed that due to the development of economic level and the continuous improvement of science and technology, the development of animal husbandry has been greatly impacted, and the traditional development mode of animal husbandry will face the elimination of the market. The application of science and technology to animal husbandry production can improve productivity and reduce costs, improve the ability of animal husbandry to respond to natural disasters or market changes, and promote the sustainable development of animal husbandry. Literature [2] pointed out that animal husbandry is a pillar industry of agriculture, which plays an important role in promoting the level of economic development and improving the comprehensive national strength. Developers should pay attention to the development of animal husbandry, which has an irreplaceable role in the development of the country. Therefore, the production and development of animal husbandry must be rationally arranged, and the construction of animal husbandry infrastructure must be strengthened. Attention must also be paid to fund support and policy guarantees. The sustainable development of animal husbandry is a challenge and an opportunity. Literature [3] found that poultry farms have been affected by the large-scale development of animal husbandry and suggested changing the development model of animal husbandry in order to realize the development of animal husbandry. The scale, standardization, and industrialization of the

development model need to meet the needs of the national residents for livestock products and to promote the development of agriculture and rural areas. Literature [4] pointed out that with the adjustment of the production structure of animal husbandry in the early days of the United Kingdom, the production of animal husbandry in the United Kingdom had undergone great changes and analyzed the importance of adjusting the production structure of animal husbandry. Literature [5] pointed out that the education level of the practitioners plays a very important role in the development of animal husbandry.

Literature [6] analyzed the output value and location quotient of modern grassland animal husbandry, studied the industrial advantages and scale, and proposed that the development of animal husbandry should follow the ecological priority, scientific ethics concept, modern pasture system, product differentiation design, synchronization, and the road to related industries. Literature [7] put forward suggestions for improving the development of animal husbandry by studying the coordination of grain production and animal husbandry development, aiming at different problems that arise, such as changing the development model, increasing grain output, and improving feed utilization. Reference [8] used the grey relational method to analyze the relevant data, and concluded that the factor with the highest correlation is the number of Internet users, and finally put forward countermeasures and suggestions to promote the development of animal husbandry. Literature [9] analyzed the output of animal husbandry, the output of animal products, and the number of slaughters and inventories, summarized the problems existing in the development of animal husbandry, and put forward development suggestions such as improving the efficiency of livestock and poultry breeding, improving the breeding system, and strengthening the control of livestock and poultry pollution. Literature [10], based on the analysis of animal husbandry market share, resource endowment coefficient, and product cost, summed up the road of combining agriculture and animal husbandry and industrial clusters, improving the competitiveness of animal husbandry, and promoting the development of animal husbandry. Reference [11] described the specific status of animal husbandry, analyzed the problems that restrict the development of animal husbandry, and put forward suggestions for sustainable development, including sustainable recycling mechanisms, the transformation of development models, and utilization of manure resources. For the development route, in [12], four suggestions for the sustainable development of the animal husbandry economy have been proposed, which are to increase the ideological emphasis on sustainable development of the ecological economy, improve the relevant policy support system for development, and expand the animal product market.

Reference [13] used the production layout index to illustrate the layout of the main production areas of raw milk and used empirical analysis to conclude that the factors affecting the layout change are resources, economy, non-agricultural employment, and the market. Reference [14] put forward suggestions for increasing or decreasing the

aquaculture scale in different regions. Reference [15] used the resource endowment index method and the comprehensive comparative advantage index method and used the principle of comparative advantage to research and analyze animal products. Literature [16] compiled and analyzed the relevant data on animal husbandry in the past 30 years, established the livestock and poultry breed structure index, and obtained the evolution process and characteristics of the breed structure index at different stages in the six major production areas of animal husbandry. The dominant varieties in the region are put forward, and countermeasures and suggestions for optimizing the production layout are put forward. Reference [17] used PIL to analyze the evolution process of changes in animal husbandry areas, combined with the principle of comparative advantage, and obtained the direction of layout changes and the advantageous breeding areas. Reference [18] used different indicators to calculate the industrial concentration based on the relevant production data of three years and finally identified the advantageous production areas.

3. Economic Calculation Model

DEA method is the most commonly used method in nonparametric frontier efficiency analysis. Farrell first proposed the DEA method, and then Charns further improved the CCR model. With the development of time, many scholars have improved the DEA method to make it more scientific and rational. Now, the DEA method has been relatively mature, and it has become a research method to study input-output efficiency with equal emphasis on traditional econometric methods.

The DEA method is used to scientifically evaluate the decision-making unit and measure the relative efficiency of the measurement unit according to the model. Decision-making unit (DMU) is a specific title; it can be the army, police station, prosecutor's office, or the same entity unit as a supermarket or coffee shop. Moreover, each decision-making unit has the same input and output indicators. DEA calculates input-output data to obtain quantitative indicators of decision-making units and comprehensive efficiency. According to this result, the decision-making units are sorted, the decision-making unit with the largest relative efficiency value is determined, and then the reasons and levels of the ineffectiveness of other decision-making units are analyzed. Finally, it provides suggestions for improvement and development direction of the decision-making unit system. The DEA method can also judge the scale return of each decision-making unit and put forward a scientific suggestion for a decision-making unit to adjust the industrial scale. Compared with other research methods, the DEA method has huge advantages in the research and analysis of multi-input-output systems, which are mainly manifested in the following:

(1) It is not necessary to determine the choice of the mathematical form of the production function before the research so as to avoid getting the wrong conclusion because of the wrong function selection;

(2) DEA research method does not have to collect price information of input products;

(3) In the study of complex systems, the DEA method does not need to sort out the relationship of each subsystem and also does not need to establish the comparability between the indicators;

(4) The DEA method does not need to determine the weight of the system and its input and output in advance, excludes the influence of subjective factors, and has the characteristics of simple and objective;

(5) DEA sorts out the data from an overall macro perspective to avoid the one-sidedness of the treatment of scattered indicators.

DEA has two models: the CCR model with constant returns to scale and the VRS model with variable returns to scale. CCR is used to calculate comprehensive technical efficiency (STE), including scale efficiency, and VRS is used to calculate technical efficiency (TE) without the effect of scale efficiency.

The CCR model assumes that there are N DMUn ($1 \leq n \leq N$), and each DMU has a kind of input and b kind of output, then the DMUn vector is expressed as follows:

$$X_j = \left(x_{1j}, x_{2j}, \ldots, x_{aj}\right)^T > 0, \quad j = 1, 2, \ldots, N,$$
$$Y_j = \left(y_{1j}, y_{2j}, \ldots, y_{bj}\right)^T > 0, \quad j = 1, 2, \ldots, N. \quad (1)$$

According to the above assumptions, the CCR model formula is as follows:

$$s.t. \begin{cases} \sum_{j=1}^{a} X_j \lambda_j \leq \theta x, \sum_{j=1}^{a} Y_j \lambda_j \leq Y_n, \lambda_j \geq 0, \quad j = 1, 2, \ldots, a. \quad (2) \end{cases}$$

In this system of equations, the economic meaning of DEA is that DMUn is valid for DEA if and only if $\theta = 1$ and all inequalities have equal signs. That is, in this system composed of N decision-making units, the output obtained by the current input level has reached the optimum. When $\theta = 1$ and the inequalities of formula (2) are all inequality signs, DMUn is weakly effective; that is, reducing the current input in this system can keep the output level unchanged or increase the output level under the current input level. When $\theta < 1$, DEA is invalid; that is, in this system composed of N decision-making units, the current output level can be maintained when the current input is reduced by θ times.

The CCR model calculates the overall efficiency under the premise that the scale benefit remains unchanged. This assumes that the decision-making unit can increase the output proportionally by increasing the input ratio. This situation is difficult to achieve in actual production, so scholars further study it. By adding a convexity assumption $\sum_n \lambda_j = 1$ to the CCR model, it becomes the aforementioned BBC model for calculating the removal of returns to scale, as shown in the following formula:

$$s.t. \left\{ \sum_{j=1}^{a} X_j \lambda_j \le \theta x_n, \sum_{j=1}^{a} Y_j \lambda_j \ge Y_n, \lambda_j \ge 0, \quad j = 1, 2, \ldots, a, \lambda_j \ge 0, \quad j = 1, 2, \ldots, a. \tag{3}\right.$$

By solving the BEC model, we can also obtain the technical efficiency θ of each decision-making unit. When $\theta = 1$, the decision-making unit technology is effective, and formula (3) is used to solve each decision-making unit, and the technical efficiency values of all DMUs are obtained.

Through the CCR and BCC models, we obtained the scale efficiency and technical efficiency of the object under investigation. Next, we will briefly introduce how to calculate pure technical efficiency (PTE). This calculation mainly uses the DEA model with crowded elements:

$$s.t. \left\{ \sum_{j=1}^{a} X_j \lambda_j \le \theta x_{j0}, \sum_{j=1}^{a} Y_j \lambda_j \ge \frac{1}{\theta} Y_{j0}, \sum_{j=1}^{a} \lambda_j = 1 \, (0 \le \theta \le 1). \tag{4}\right.$$

θ obtained in formula (4) is the pure technical efficiency we require. With regard to the introduction of the DEA model, we obtain the technical efficiency, pure technical efficiency, and scale efficiency of the decision-making unit. Lei Ming (1996) stated that management efficiency (ME) can be expressed by the following formula:

$$ME = PTE \cdot CE \cdot SE \cdot AE. \tag{5}$$

If TP is technological progress, then total factor productivity can be derived from the following formula :

$$\frac{\Delta TEP}{TFP} = \frac{\Delta TP}{TP} + \frac{\Delta ME}{ME}. \tag{6}$$

In traditional economics research, it is usually assumed that the cost is minimized to study the change of total input or that the profit is maximized to study the change of total output. Behind these assumptions, there is a perfectly competitive market, which is very demanding and difficult to achieve in empirical research. The emergence of the distance function perfectly solves the above problems. The distance function is a tool to study multiple input and output without making any assumptions about the production activities of the observer. How Farr et al. utilized the distance function will be described in detail below.

We assume that the vector X_j is the input vector of the DMU and Y_j is the output of the DMU. Because the minimum value of the distance function cannot be determined in the context of multiple outputs, the "inferior bound" is taken as the research object, and the distance function of the output angle is defined as $Do(X, Y) = \inf\{\theta: (X, Y|\theta) \in P(X)\}$. P(X) represents all feasible production combinations; that is, input X'' can

produce Y, and $\theta \in [0, 1]$ represents production efficiency. When $\theta = 1$, the resource allocation is reasonable, and when $\theta < 1$, it means that the research object is in a state of input redundancy. Under the premise of constant returns to scale, the distance function is single output (Figure 1(a)) or dual-output (Figure 1(b)), as shown in the figure below.

We assume that there is no efficiency loss in production, and the output point should be located at two points AC, but the actual situation may be located at two points BD. Under the premise of constant input, the object at BD two points can increase the output to AC two points; that is to say, from the perspective of output, the distance function represents the limit expansion of output to the production frontier.

The functions mentioned above do not take the time factor into account, so we consider the time factor as an independent variable. We assume that the input-output vectors in period t and period $t+1$ are (X_t, Y_t) and (X_{t+1}, Y_{t+1}), and the distance function diagram of single input and single output is shown in Figure 2. Then the Malmquist exponent with reference to time t is as follows:

$$M_t = \frac{D_t(X_{t+1}, Y_{t+1})}{D_t(X_t, Y_t)}$$
$$= \frac{l_{od}/l_{oe}}{l_{oa}/l_{ob}}. \tag{7}$$

The Manquist exponent expressed with reference to period $t+1$ is as follows:

$$M_{t+1} = \frac{D_{t+1}(X_{t+1}, Y_{t+1})}{D_{t+1}(X_t, Y_t)}$$
$$= \frac{l_{od}/l_{of}}{l_{oa}/l_{oc}}. \tag{8}$$

By borrowing Fisher's method of constructing the ideal index, we take the average of the above two formulas, and we get the Manquist productivity index as follows:

$$M_{t,t+1} = \left(\frac{D_t(X_{t+1}, Y_{t+1})}{D_t(X_t, Y_t)} \times \frac{D_{t+1}(X_{t+1}, Y_{t+1})}{D_{t+1}(X_{t+1}, Y_{t+1})} \right)^{1/2}. \tag{9}$$

By deforming formula (9), it can be seen that the total factor productivity change is composed of two parts, the technical efficiency change (EC) and the technical change (TC), that is, the following formula.

$$M_{t,t+1} = \underbrace{\left(\frac{D_t(X_{t+1}, Y_{t+1})}{D_t(X_t, Y_t)} \times \frac{D_{t+1}(X_{t+1}, Y_{t+1})}{D_{t+1}(X_{t+1}, Y_{t+1})} \right)^{1/2}}_{BC} \cdot \underbrace{\frac{D_{t+1}(X_{t+1}, Y_{t+1})}{D_t(X_t, Y_t)}}_{TC}. \tag{10}$$
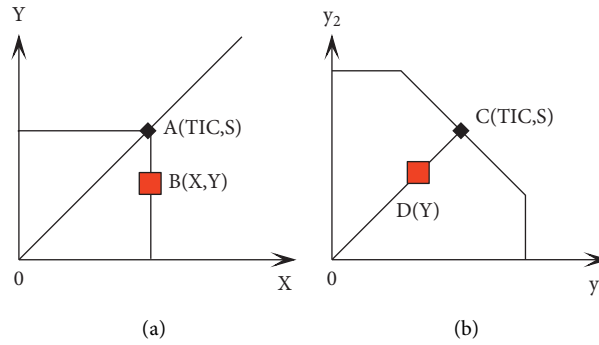
FIGURE 1: Distance function output. (a) Distance function for a single output. (b) Distance function for double output.
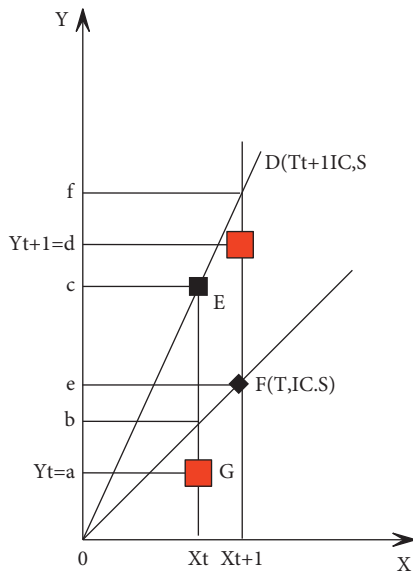
FIGURE 2: Manquist productivity index from an output perspective.

When $TC > 1$, it means technological progress; when $TC < 1$, it means technological regression; when $EC > 1$, it means that technical efficiency has improved, and when $EC < 1$, it means that technical efficiency has declined. The technical efficiency change is composed of pure technical efficiency change (PC) and scale efficiency change (SC); namely, $EC = PC \times SC$, so that $TFPch = TC \times PC \times Sc$ can be obtained.

4. Economic Analysis of Animal Husbandry Based on System Dynamics

System management is divided into classification management, membership management, and basic information management. Its main function is to set up the basic information, membership level, and different resource data categories of the entire platform in advance. At the same time, it has the functions of adding, modifying, and deleting, which is convenient for the future function expansion of the platform and the docking with other systems. Data management is mainly divided into animal husbandry economic statistical data management, scientific and technological achievements and literature resource management, and

member authority review management. The specific structure of the platform is shown in Figure 3.

The ecological economic system of animal husbandry cannot escape the influence of human beings. It is a complex system composed of customers, manufacturers, government, and other stakeholders, and it is reflected in the interrelationship of different subjects. In the era of a self-sufficient natural economy, the production mode of animal husbandry is mainly characterized by the natural regrowth of animals, and it drives the continuation and development of life according to the basic characteristics of the food chain and relies more on natural ecological laws for regulation. The conceptual structure of the animal husbandry ecological economic system is shown in Figure 4.

Residents' consumption behavior of livestock and poultry products constitutes the consumption subsystem of the animal husbandry ecological economic system, as shown in Figure 5(a). Residents' demand for livestock products depends on the population and per capita disposable income. The larger the population, the greater the demand for livestock products, and the higher the per capita disposable income, the higher the residents' demand for livestock products. When the supply is in short supply, the price of livestock products will rise, which will in turn affect residents' purchases of livestock products.

Under the current economic conditions, consumers cannot fully accept ecological livestock products but make a balanced choice between general livestock products and ecological livestock products. Therefore, in the consumption subsystem of the animal husbandry ecological economic development system, it includes both the consumption of general livestock products and the consumption of ecological livestock products (as shown in Figure 5(b)), and the two are substitute products for each other.

From an economic point of view (as shown in Figure 5(c)), residents' demand for animal husbandry products prompts animal husbandry enterprises to produce more animal husbandry products to meet the needs of customers. Animal husbandry enterprises can obtain more profits and require more raw materials for production, thus driving the development of raw material enterprises, thereby driving the development of the entire animal husbandry and other related industries, and promoting the GDP of the
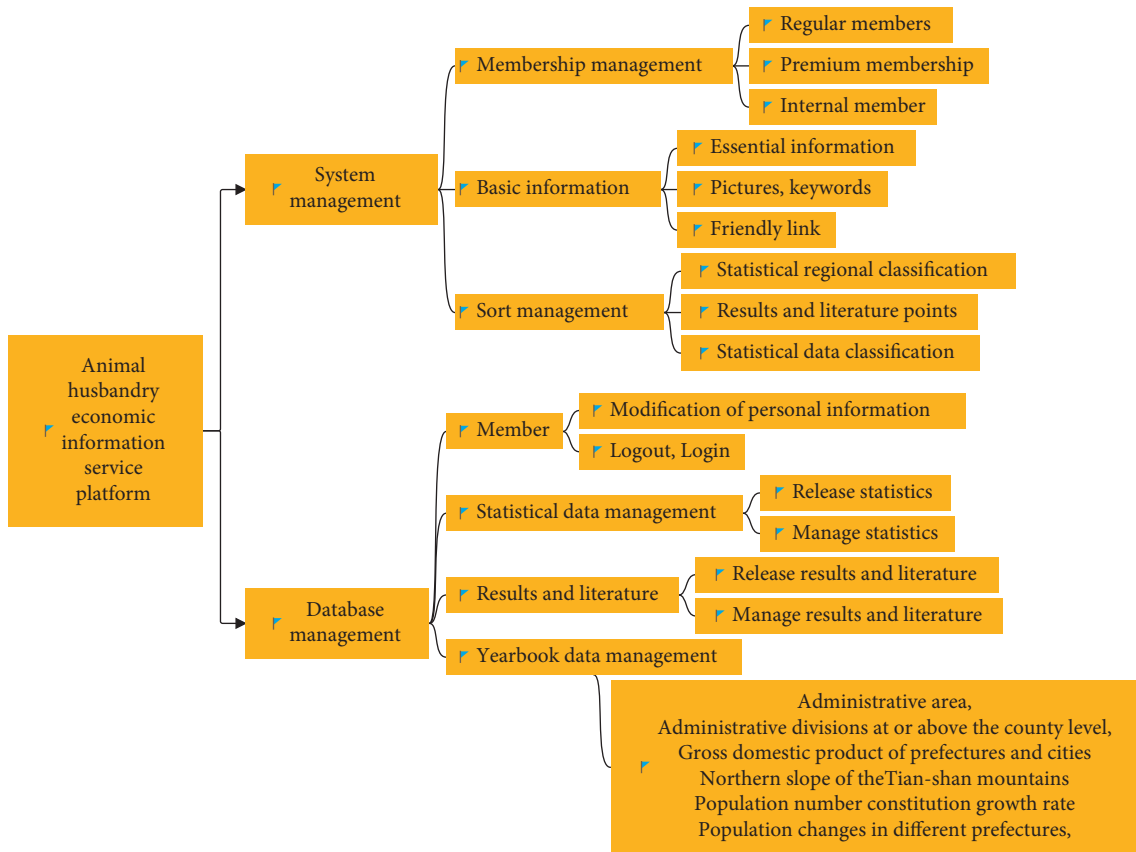
Figure 3: Platform structure diagram.
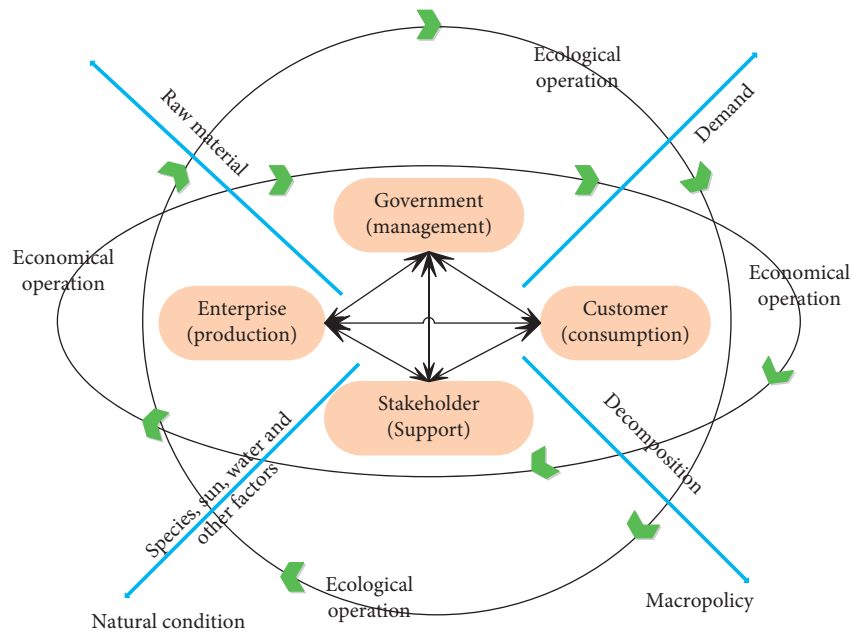
Figure 4: Conceptual structure diagram of animal husbandry ecological economic system.

entire country. At the same time, due to the increase in corporate assets, reinvestment is made to expand production.

With the development of the industry, the pressure from the natural environment continues to increase. The pressure from the natural environment is mainly manifested in the

(a)

(b)

(c)
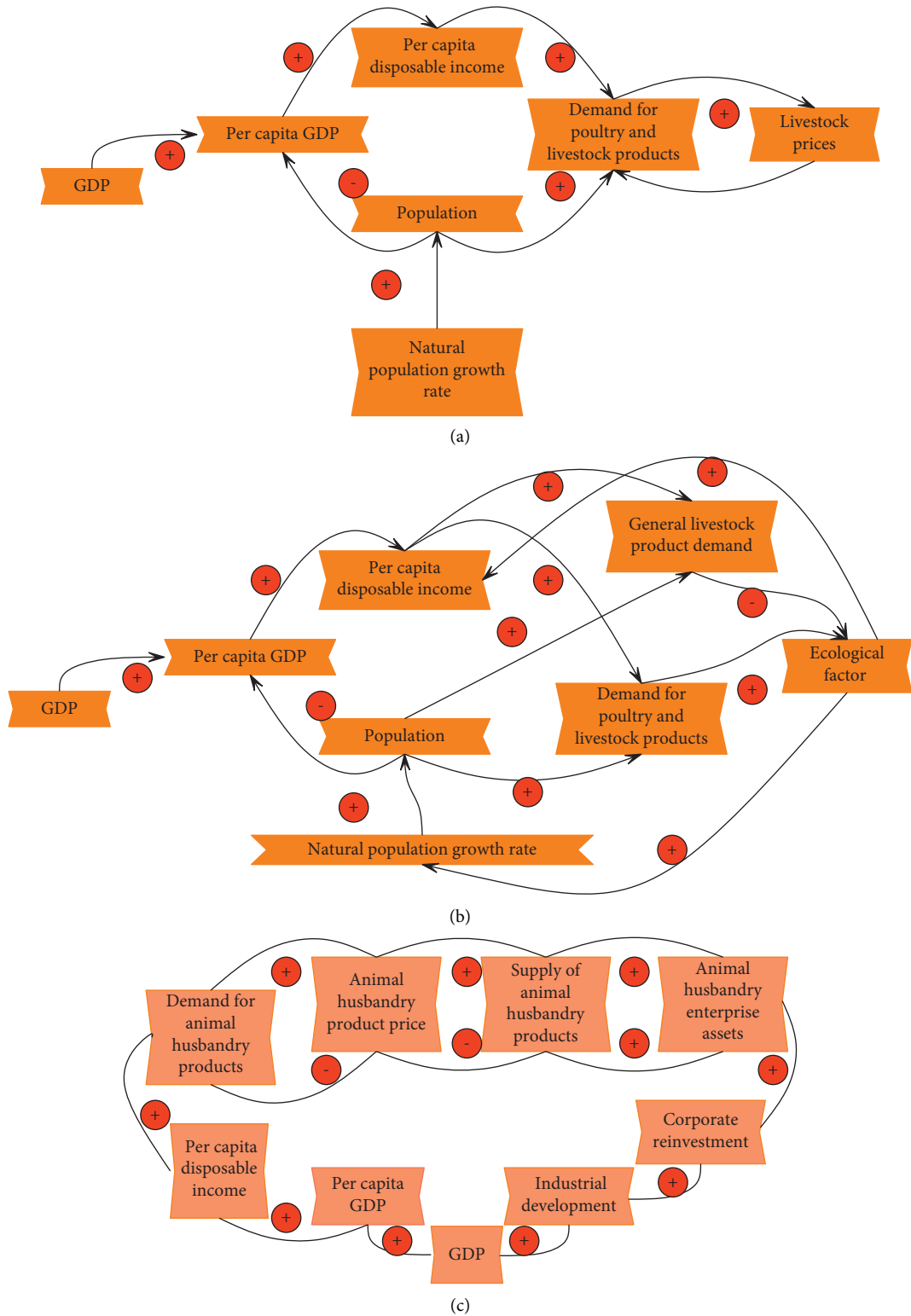
Figure 5: Continued.

(d)
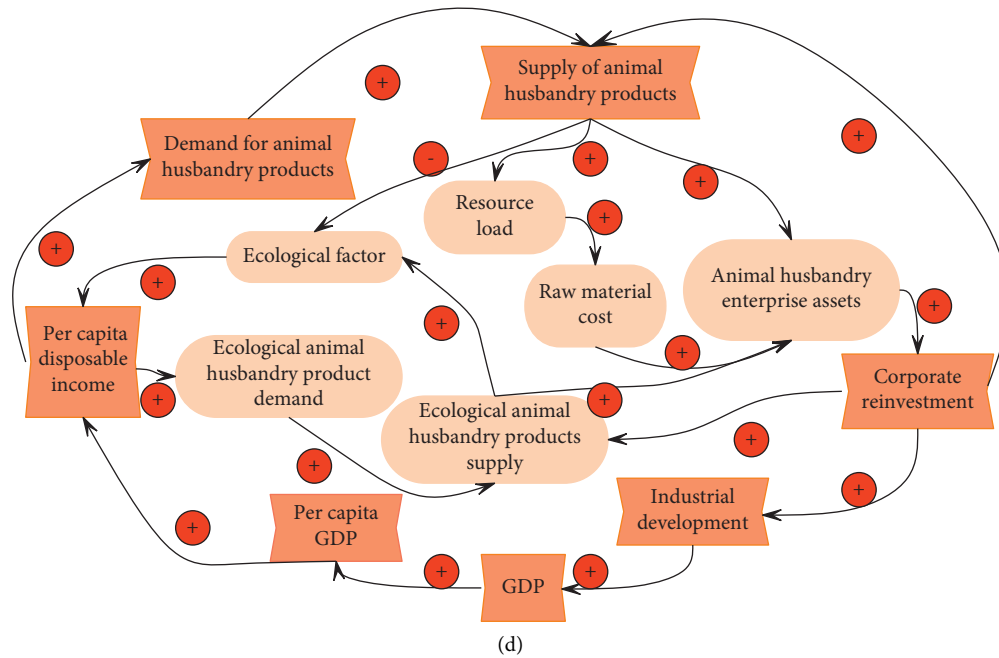
Figure 5: The causal relationship diagram of the animal husbandry economic system. (a) The causal relationship diagram of the demand subsystem from the economic point of view. (b) The causal relationship diagram of the ecological and economic demand subsystem of animal husbandry. (c) The causal relationship diagram of the production subsystem from the economic point of view. (d) The causal relationship diagram of the ecological and economic production subsystem of animal husbandry.

overuse and waste of raw materials and the pollution of the environment by excrement. In order to alleviate the pressure on the environment, it is necessary to invest more balancing funds, which causes the cost to rise, product prices to rise, and consequently the decline of the funds available for the industry to expand and reproduce, thus inhibiting the development of the industry (Figure 5(d)).

As shown in Figure 6(a), the ecological economic technology subsystem of animal husbandry is mainly reflected in three aspects of the consumption subsystem and economic subsystem of animal husbandry ecological economy. First, scientific and technological progress improves the spiritual and material life of human beings, and the increased disposable income of human beings can lead to more consumption of ecological animal husbandry products, which forms positive feedback. The second is the improvement of educational technology and the improvement of residents' educational level brought about by investment in science and technology. Humans realize the significance of ecological animal husbandry products for their own development, which can change consumption awareness and behavior, increase the consumption of ecological animal husbandry products, and form positive feedback. Third, the investment in science and technology has greatly improved the production technology of existing enterprises, improved the production efficiency of enterprises and the utilization rate of resources, and can produce ecological animal husbandry products at a lower cost, forming positive feedback. Conversely, if the technical orientation is wrong, it will exacerbate the negative feedback effect (as shown in Figure 6(b)). For example, the concentration of science and technology on the production and consumption of

nonecological products will inevitably increase the capital load and environmental degradation and make the system continue to deteriorate.

As shown in Figure 7(a), for nonecological economic behaviors, the government sets a higher threshold for customers and producers through economic penalties and direct supervision by regulatory authorities and turns to the production and consumption of ecological livestock products. For example, the government environmental monitoring department sets punitive consumption policies or thresholds according to environmental conditions, which increases the cost of general livestock products and reduces per capita disposable income.

Under the ecological economic behavior (as shown in Figure 7(b)), the government adopts more incentive policies to attract producers, consumers, and technology developers to switch from general animal husbandry products to ecological animal husbandry products, thereby promoting ecological animal husbandry products for nonprofit replacement of ecological livestock products and promoting a virtuous circle of positive feedback.

In order to further understand the operation law of the animal husbandry ecosystem, we combine nonecological economic products and ecological economic products together. Moreover, this article uses the proportion of ecological animal husbandry products in total animal husbandry products (the ratio of ecological animal husbandry products) to specifically express the choice of consumers, producers, and other subjects for ecological animal husbandry products and ecological behaviors. The SD causal relationship diagram of the whole animal husbandry ecological and economic development system is obtained as shown in Figure 8(a).

(a)

(b)
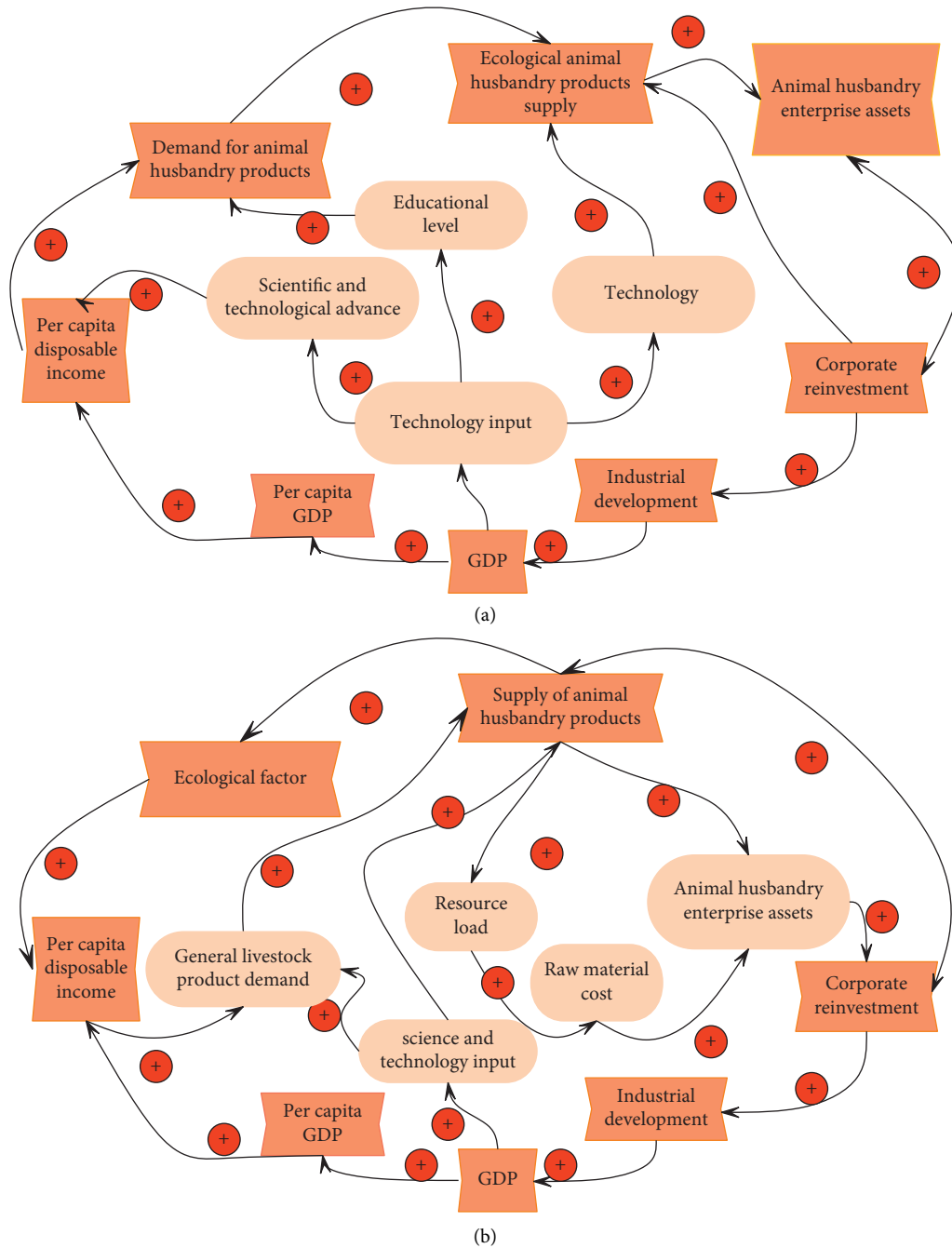
FIGURE 6: Causal diagram of technical subsystems. (a) The causal relationship diagram of the ecological economic technology subsystem of animal husbandry. (b) Negative feedback relationship diagram of technical subsystem.

Figure 8(b) shows the causal relationship diagram of the coordinated development of the ecological economic system of livestock and forestry. On the one hand, the development of animal husbandry requires forestry to provide more raw materials, so forestry enterprises increase the supply and can obtain more for their own expansion and reproduction. However, due to the constraints of the natural environment, the supply of forestry has a certain load limit, and if the load exceeds the load, it will have a negative impact on human beings and the environment. On the other hand, the development of forestry requires more organic fertilizers, which drives the development

of ecological animal husbandry enterprises, while investing in and expanding reproduction. Therefore, the development of forestry also drives the development of the ecological economy of animal husbandry.

Figure 8(c) shows the causal relationship diagram of the coordinated development of the ecological economic system of animal husbandry and crop farming. The relationship between the animal husbandry ecosystem and agriculture basically includes two aspects of coordinated development with forestry. However, unlike forestry, the products of planting not only meet the needs of ecological
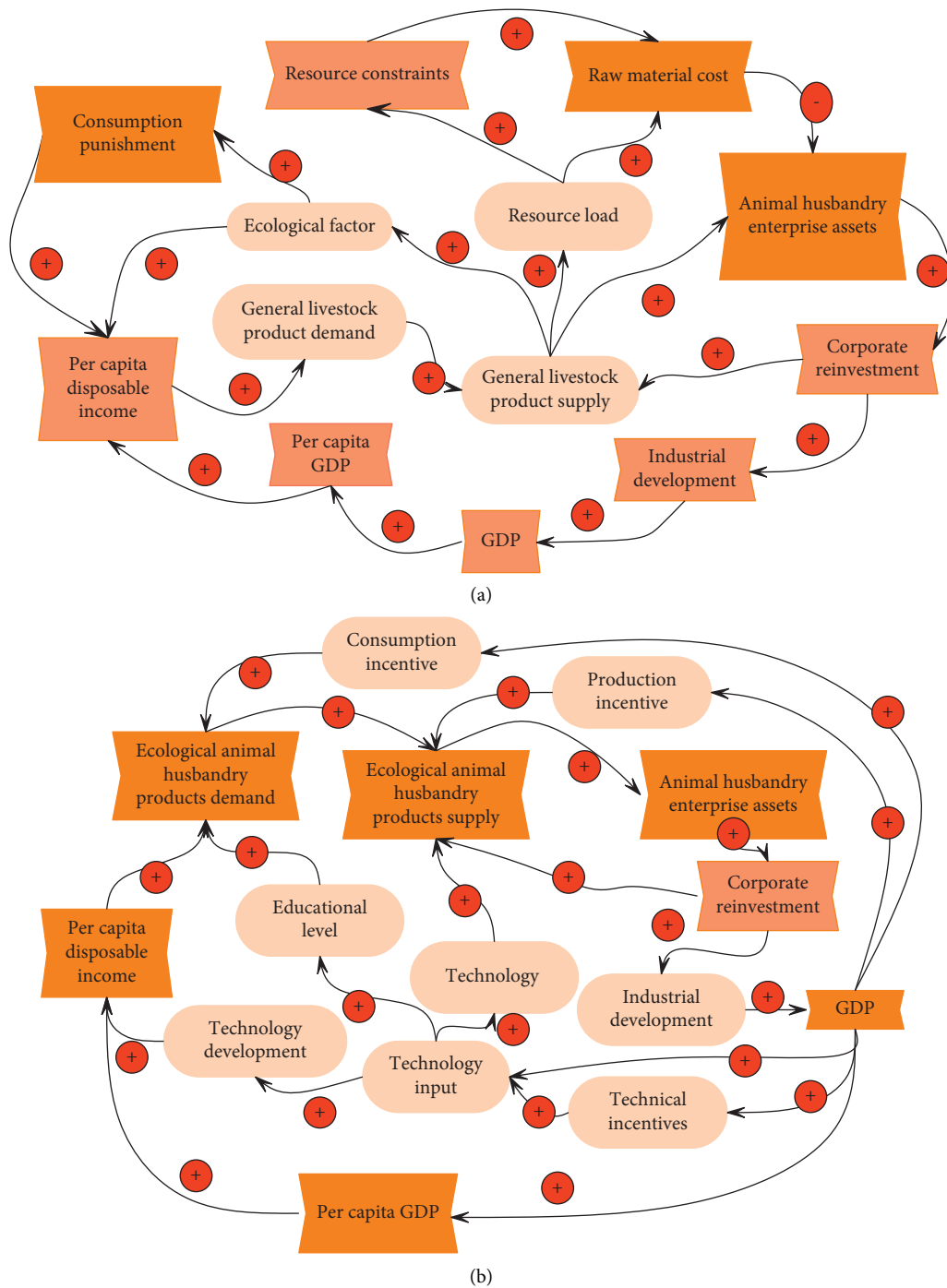
FIGURE 7: Relationship diagram of the management subsystem. (a) The causal relationship diagram of management subsystems under non-ecological economic behavior. (b) Relationship diagram of management subsystems under ecological economic behavior.

animal husbandry for raw materials but also meet the needs of people for food. Therefore, human needs aggravate the resource load of the planting industry, so that the ecological and economical operation of animal husbandry is more necessary to balance the needs of human and animal husbandry for the planting industry so as to alleviate and solve the resource load of the planting industry.

On the basis of the above research, the system dynamics model proposed in this article is simulated by the simulation software, and the analysis effect of the system dynamics model on the development of the animal husbandry economy is calculated. The effects in the ecological analysis of animal husbandry economy and the analysis of economic development effects are verified, and the results shown in Tables 1 and 2 are obtained.
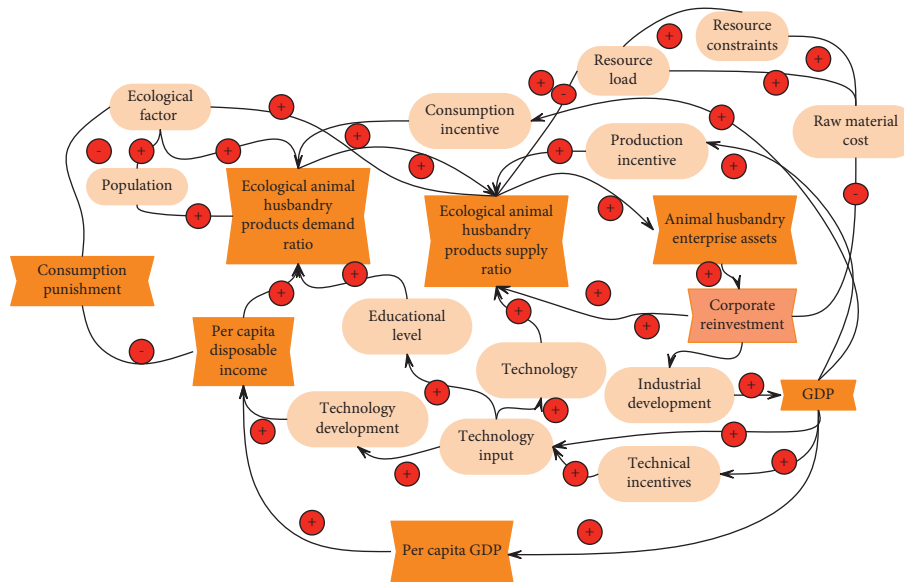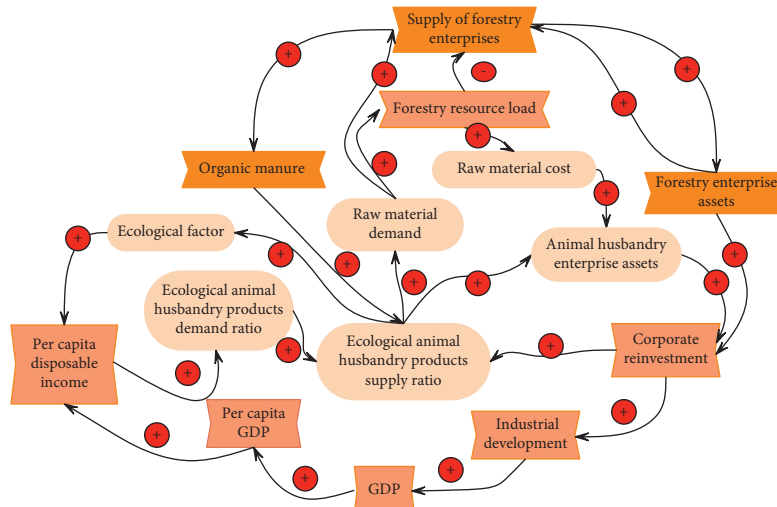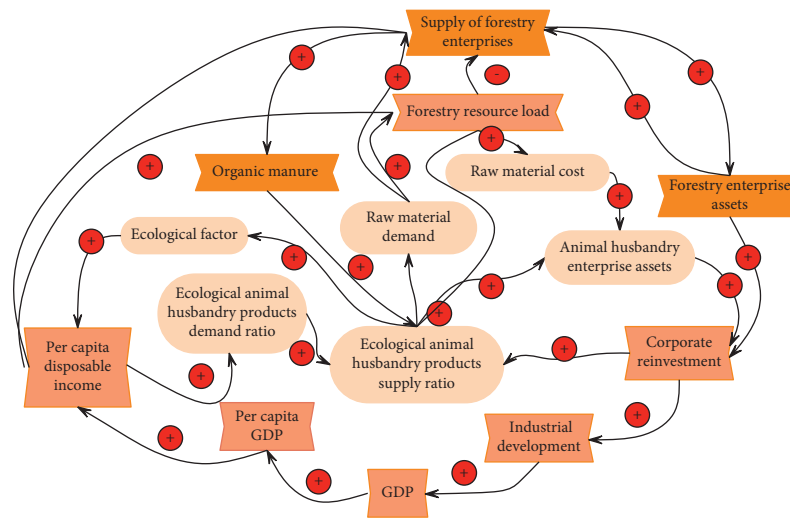
Figure 8: The relationship diagram between the coordinated economic development of animal husbandry. (a) The causal relationship diagram of the ecological and economic development system of animal husbandry. (b) The relationship diagram between the ecological economic development system of animal husbandry and the coordinated development of forestry. (c) The relationship diagram between the ecological and economic development system of animal husbandry and the coordinated development of planting.

TABLE 1: Evaluation of the effect of the system dynamics model in the economic and ecological analysis of animal husbandry.

Num	Ecological economic evaluation	Num	Ecological economic evaluation	Num	Ecological economic evaluation
1	81.51	23	84.57	45	89.92
2	88.18	24	81.88	46	80.16
3	87.69	25	86.58	47	81.01
4	79.07	26	83.75	48	81.21
5	91.45	27	86.56	49	80.95
6	85.30	28	83.66	50	83.49
7	79.55	29	88.37	51	91.37
8	90.74	30	87.66	52	90.22
9	86.98	31	88.34	53	83.76
10	86.44	32	81.35	54	86.13
11	90.42	33	82.38	55	82.03
12	88.07	34	83.03	56	91.79
13	79.89	35	89.97	57	83.04
14	82.71	36	80.46	58	81.62
15	80.73	37	91.15	59	79.22
16	85.29	38	81.65	60	82.57
17	89.71	39	91.59	61	91.07
18	85.28	40	89.22	62	87.26
19	84.68	41	81.25	63	80.71
20	83.35	42	82.16	64	79.54
21	83.67	43	84.09	65	89.17
22	89.09	44	82.62	66	86.21

TABLE 2: Evaluation of the effect of system dynamics model in the analysis of animal husbandry economic development.

Num	Economic development evaluation	Num	Economic development evaluation	Num	Economic development evaluation
1	76.95	23	87.23	45	78.95
2	79.59	24	88.89	46	84.70
3	83.53	25	76.70	47	80.84
4	74.96	26	75.61	48	84.62
5	75.21	27	81.21	49	76.94
6	79.91	28	80.08	50	85.93
7	87.83	29	88.23	51	77.91
8	83.53	30	79.68	52	75.02
9	78.10	31	84.34	53	84.48
10	86.27	32	82.07	54	82.79
11	85.28	33	87.96	55	79.88
12	76.13	34	80.86	56	87.02
13	80.30	35	87.14	57	88.51
14	88.45	36	81.38	58	81.47
15	74.82	37	77.26	59	88.62
16	83.34	38	81.58	60	81.51
17	83.22	39	86.58	61	87.24
18	74.85	40	76.20	62	75.06
19	75.23	41	83.29	63	82.17
20	83.85	42	79.43	64	74.73
21	76.51	43	78.32	65	79.22
22	80.37	44	85.29	66	85.52

It can be seen from the above research that the system dynamics model proposed in this article has a good performance in the economic analysis of animal husbandry and can provide a reference for the development of the animal husbandry economy.

5. Conclusion

There are many industries associated with animal husbandry, which influence each other to promote development, and animal husbandry integrates supply, production, and marketing. Among them, the planting industry is responsible for providing raw material feed, livestock and poultry use the feed for growth, and the produced manure is processed into organic fertilizer, which is recycled to the fields for use in the planting industry. The processing industry plays a key role in ensuring the quality of animal products and is an indispensable intermediate link in the output of animal husbandry. The logistics industry ensures the normal transportation and circulation of animal

products, and the service industry is indispensable in the process of animal product sales. This article studies the animal husbandry economy based on system dynamics and conducts an intelligent analysis of the animal husbandry economy by constructing an intelligent model. The simulation test study shows that the system dynamics model proposed in this article has a good performance in the economic analysis of animal husbandry and can provide a reference for the development of animal husbandry economy.

Data Availability

The labeled dataset used to support the findings of this study is available from the corresponding author upon request.

Conflicts of Interest

The authors declare no conflicts of interest.

Acknowledgments

References

[1] K. Ponnusamy and K. Pachaiyappan, "Strengthening extension research in animal husbandry: Review of issues and strategies," *Indian Journal of Animal Sciences*, vol. 88, no. 2, pp. 137–143, 2018.

[2] E. Guiry, B. M. Jones, S. DeFrance, J. E. Bruseth, J. Durst, and M. P. Richards, "Animal husbandry and colonial adaptive behavior: Isotopic insights from the La Belle shipwreck fauna," *Historical Archaeology*, vol. 52, no. 4, pp. 684–699, 2018.

[3] S. U. Minhaj, S. A. Khandi, R. A. Bafanda, B. Bhushan, F. Choudhary, and A. M. Khateeb, "Constraints perceived by dairy farmers in the adoption of improved animal husbandry practices in doda district," *International Journal of Livestock Research*, vol. 9, no. 2, pp. 319–326, 2019.

[4] J. R. Jones and J. A. Mulville, "Norse animal husbandry in liminal environments: Stable isotope evidence from the Scottish north Atlantic islands," *Environmental Archaeology*, vol. 23, no. 4, pp. 338–351, 2018.

[5] X. Hou and Y. Zhang, "Analysis on driving factors of improvement of quality and efficiency and transformation development of grasslands and animal husbandry industry," *Chinese Science Bulletin*, vol. 63, no. 17, pp. 1632–1641, 2018.

[6] A. Syakur, R. Azis, and Sukarsih, "Developing reading learning model to increase reading skill for animal husbandry students in higher education," *Britain International of Linguistics Arts and Education (BIoLAE) Journal*, vol. 2, no. 1, pp. 484–493, 2020.

[7] I. Grau-Sologestoa and U. Albarella, "The "long" sixteenth century: A key period of animal husbandry change in England," *Archaeological and Anthropological Sciences*, vol. 11, no. 6, pp. 2781–2803, 2019.

[8] R. Y. Banerjea, M. Badura, A. Brown et al., "Feeding the Crusades: Archaeobotany, animal husbandry and livestock alimentation on the Baltic Frontier," *Environmental Archaeology*, vol. 25, no. 2, pp. 135–150, 2020.

[9] I. Zhupley, T. Potenko, S. Gubarkov, N. Tretyak, and R. Grafov, "Structural shifts and reform of the agrarian sector of the Russian economy under the conditions of the import substitution policy," *Space and Culture, India*, vol. 6, no. 4, pp. 25–35, 2018.

[10] S. Ahmadi, "A study on effective factors on lack of tendency of agriculture graduate students college to employment and production in animal husbandry sector," *Agricultural Marketing and Commercialization Journal*, vol. 5, no. 1, pp. 90–99, 2021.

[11] L. C. G. Valentim, H. D. A. N. Lucena, I. B. C. Amaral, L. C. Couto, and A. B. Reis, "Short fiber fluff cellulose industry: Economic viability and energy potential," *Periódico Tchê Química*, vol. 16, no. 31, pp. 49–58, 2019.

[12] V. Patil, B. S. Reddy, S. S. Patil, and G. M. Hiremath, "Comparative economics of rural and periurban dairy farming in Kalaburagi district of Karnataka," *Journal of Applied and Natural Science*, vol. 11, no. 4, pp. 762–767, 2019.

[13] Y. Yang, L. Ren, G. Dong et al., "Economic change in the prehistoric hc), north-west China," *Archaeometry*, vol. 61, no. 4, pp. 957–976, 2019.

[14] A. Khaled, W. A. Moselhy, M. A. Ibrahim, A. R. Mahmoud, and R. R. A. El-Wahab, "Current trend on the economic and public health significance of sal-monellosis in Iraq," *Advances in Animal and Veterinary Sciences*, vol. 7, no. 6, pp. 492–497, 2019.

[15] S. N. Sirajuddin, I. Sudirman, L. D. Bahar, A. R. Al Tawaha, and A. R. Al Tawaha, "Social economic factors that affect cattle farmer's willingness to pay for artificial insemination programs," *Bulgarian Journal of Agricultural Science*, vol. 24, no. 4, pp. 574–580, 2018.

[16] A. A. M. Ibrahim and S. A. Elariane, "Feasibility tools for urban animal husbandry in cities: Case of greater Cairo," *Urban Research & Practice*, vol. 11, no. 2, pp. 111–138, 2018.

[17] W. M. Ramirez-Suarez, M. B. Hernandez-Chavez, A. A. Zurita-Rodriguez, and M. Navarro-Boulandier, "Performance of the edaphic macrofauna in animal husbandry systems, in a productive entity of the Yaguajay municipality, Cuba," *Pastos Y Forrajes*, vol. 41, no. 4, pp. 259–265, 2018.

[18] F. Tufaner and Y. Avsar, "Economic analysis of biogas production from small scale anaerobic digestion systems for cattle manure," *Environmental Research and Technology*, vol. 2, no. 1, pp. 6–12, 2019.

Research Article

Research on Brand Illustration Innovative Design Modeling Based on Industry 4.0

Yueyan Liu [iD] **and Zou Ping** [iD]

School of Academy of Arts, Qingdao Huanghai College, Qingdao, Shandong 266555, China

Correspondence should be addressed to Yueyan Liu; liuyy@qdhhc.edu.cn

With China's attention to the requirements of brand illustration innovative design, under the background of Industry 4.0, the advantages of applying 3D modeling method in the field of traditional illustration design are becoming more and more prominent. Based on this, this paper studies the modeling method of brand illustration innovative design based on Industry 4.0 and constructs a 3D analysis model of illustration design based on cattle cooperative hybrid algorithm. This paper innovates the innovative design method of brand illustration under the background of Industry 4.0 from the three aspects of illustration structure, illustration style, and illustration creation method, uses the cattle cooperative hybrid algorithm to quantify its innovation, and realizes the intelligent evaluation of its innovation and the quantitative representation of modeling method based on the illustration database. The experimental results show that the illustration innovative design analysis model based on cattle collaborative hybrid algorithm can effectively combine the industrial 4.0 background, realize the modeling innovation at the three-dimensional level, and significantly improve its innovative design efficiency and modeling success rate.

1. Introduction

Industry 4.0 is a division based on different stages of industrial development. According to the consensus, Industry 1.0 is the era of steam engine, Industry 2.0 is the era of electrification, Industry 3.0 is the era of information, and Industry 4.0 is the era of using information technology to promote industrial change, that is, the era of intelligence. In order to improve the core competitiveness of Germany's industrial revolution, the new concept of occupation machine appeared in Germany's Industrial Expo in 2013. In recent years, most illustration design masters have made many achievements in modeling the innovative design of brand illustration. Among them, the illustration design of traditional cultural style is the main, supplemented by the illustration design style of local and national characteristics [1]. Under the background of industry 4.0, new designers gradually began to combine illustration innovative design with industrial elements, such as illustration and advanced manufacturing technology, intelligent manufacturing

technology, robot technology, micro nano sensing technology, and other elements, so as to realize the innovative expression of their illustration [2]. On the other hand, with the emergence of a variety of modern 3D modeling methods, different types of brand illustration innovative design methods have gradually developed in a blowout way. The emergence of modern illustration design styles such as online illustration design scheme, multidimensional collaborative design, and two-dimensional and three-dimensional collaborative design provides a new direction for promoting "brand illustration innovative design" on a large scale [3]. Therefore, how to create more and better brand illustration works under the background of industry 4.0 has become an important feature of illustration design in China [4]. At present, although the existing illustration graphic design modeling method group provides a large number of reference design schemes, in terms of practical application, it is difficult to create more and more aesthetic illustration works in combination with the existing business characteristics of the actual brand company [5]. Under this

background, combined with the background of Industry 4.0, this paper proposes a modeling method of brand illustration innovative design based on cattle collaborative hybrid algorithm and studies the application of different types of 3D modeling and data analysis methods in the field of intelligent illustration 3D design.

This paper studies the modeling method of brand illustration innovative design based on Industry 4.0 and constructs an intelligent illustration design modeling strategy analysis model based on cattle cooperative hybrid algorithm. Compared with the traditional illustration design method with cultural elements as the main creative style, the innovation of this paper is to apply the cattle cooperative hybrid algorithm to the innovative design of brand illustration. On this basis, make full use of different types of 3D modeling data and collaborative multidimensional data analysis methods. Taking industry 4.0 as the background, combined with brand characteristics, realize the optimal and innovative design of illustrations, and use a variety of 3D modeling methods to represent different types of illustration works. Combined with the current illustration innovation analysis system, intelligent design and performance of different types of brand illustration works are carried out.

This paper studies the application of industrial 4.0 background in brand illustration innovation design modeling, which is mainly divided into four chapters. Chapter 1 briefly describes the background and necessity of this study. Chapter 2 discusses the brand illustration design method and existing research results on the application of cattle cooperative hybrid algorithm (domestic and foreign) analysis and summary. Chapter 3 constructs the analysis model of brand illustration innovative design based on cattle collaborative hybrid algorithm and uses the Laplace factor analysis method to create a 3D structure design method based on collaborative innovation and multidimensional analysis. Chapter 4 evaluates the optimization analysis model of brand illustration innovative design and the innovation of illustration constructed in this paper. Test the price index, analyze the test data, and draw a conclusion.

2. Related Work

At present, there are many problems in promoting the innovation of modeling methods in the field of intelligent illustration 3D design, especially in the brand elements of illustration design scheme, intelligent digital combination method, and collaborative design [6]. Chang and other scholars found that the current process of brand illustration design mainly takes the cultural value of the brand as the core and rarely reflects the industrial 4.0 background as the characteristic elements. Therefore, they proposed a free design method of illustration design based on the brand value communication method [7]. Hummel and other scholars proposed that attention should be paid to the development of three-dimensional illustration design methods. Through the use of 3D animation table technique based on modern style, it reflects the more affinity and appeal in the process of illustration design. By combining virtual and real works, it reflects the value circle

communication effect reflected by the brand through illustration [8]. According to the collaborative innovative design theory in illustration design, Qarariyah and other scholars put forward a new brand illustration innovative design system and intelligent integrated design scheme, analyzed the relationship between the traditional illustration design field and the integrated scheme of intelligent modern picture design, and realized its innovative and prominent design in the main features [9]. Aiming at the problem of slow modeling speed in illustration design, Ekman and Feng proposed an efficient illustration modeling method combined with intelligent collaborative hybrid algorithm based on illustration design theory. Through the analysis of illustration design effect, aesthetic requirements, and brand communication in different illustration design field schemes, multidimensional design is carried out according to its internal relevance. It realizes the efficient design of illustration at different levels [10]. Wang and other scholars put forward an illustration design module analysis method based on cloud comprehensive and unified distribution by analyzing the advertising illustration contents of multiple brands, combined with the actual illustration design methods, and aiming at the design commonalities of their internal correlation schemes. This method can effectively solve the low efficiency of illustration design, but it has limited-application scope and low data utilization [11]. Xu and other scholars combined with the illustration design culture and experience of local brands and used the deformed illustration design method to comprehensively analyze the traditional intelligent illustration design method. The results show that the illustration design field system has a good overall coordination effect and can be applied to different brand illustration designs and unconventional brand illustration innovative designs. It can effectively solve the problem of poor universality of illustration design methods [12]. Based on the traditional illustration design theory and illustration aesthetic structure design method, Li and other scholars proposed a panoramic brand illustration innovative design strategy. The results show that the strategy based on intelligent distribution of data flow can effectively reduce its comprehensive errors in the illustration design system and improve the overall illustration design effect. Later, it is optimized by combining Fourier function algorithm. The results show that the optimized method effectively reduces the differentiation problem in the process of illustration design [13]. In order to solve the problems of low efficiency of multi-illustration design cooperation and slow speed of multivariate analysis in the brand illustration innovation design system, Zhao and other scholars proposed an automatic design method of illustration design scheme based on genetic algorithm and particle swarm optimization algorithm. Experiments show that the automatic design method can effectively improve the innovative effect in the process of intelligent illustration design [14]. Aiming at the problem of low efficiency in traditional brand design methods, Deng and other scholars proposed a 3D modeling illustration design method combined with massive data information. This method can realize the innovative evaluation basis of brand illustration innovative design system

by simulating the three-dimensional structure diagram in illustration design, but it has the problem of low efficiency [15].

To sum up, it can be seen that the current research on brand illustration innovative design still focuses on the traditional illustration style design and the method based on low-dimensional data analysis strategy, mainly on the brand elements, intelligent digital combination method, and collaborative design of illustration design scheme, and rarely on the effective combination of intelligent algorithm and industrial 4.0 background [16–18]. On the other hand, in the modeling and optimization of illustration design style, most illustration design modeling and analysis models need to summarize the modeling data in different ranges first and then conduct unified analysis and processing, which leads to the overall illustration design efficiency becoming very low. And there is no research on optimization design and construction of relevant models for illustration design modeling [19–22]. Therefore, the research on the modeling method of brand illustration innovative design based on industry 4.0 has important practical significance.

3. Methodology

3.1. Application of Cattle Cooperative Hybrid Algorithm in Brand Illustration Innovative Design Analysis Model. In this study, in order to better quantify the data level of the intelligent illustration design process, a cattle cooperative hybrid algorithm based on color recognition strategy is adopted [23]. When studying the laws of different types of multidimensional information data, cattle collaborative mixing algorithm is a more commonly used one. Cattle collaborative mixing, also known as multilinear collaborative regression analysis, is a dynamic research model for comprehensive analysis based on the correlation between data and data, which is often used in big data analysis, cloud model verification, and so on [24]. In essence, collaborative hybrid algorithm belongs to two classification problems. Generally speaking, it is to carry out different degrees of classification process according to different types of problems, take the minimum error as the solution standard, and finally realize the optimal solution of the results [25]. Collaborative hybrid operation is also a basic method of self-learning and updating at the data level. In the process of data updating and analysis, through the accumulation of the characteristics of different types of data, it can realize the high relevance and coupling verification so as to solve the unknown complex multidimensional operation problem.

In this study, in order to build the brand illustration innovation design modeling and analysis model, the cattle cooperative hybrid algorithm is the core key point for the data information required for processing, and its corresponding data processing type is also obtained by multidimensional analysis and corresponding matrix operation. The data analysis and three-dimensional simulation operation process of its intelligent illustration innovative design is shown in Figure 1.

3.2. Establishment Process of Performance Analysis Model of Intelligent Illustration 3D Design Based on Cattle Cooperative Hybrid Algorithm. This intelligent illustration 3D design model based on cattle collaborative innovation algorithm combines the industrial 4.0 background and brand influence analysis mechanism to simplify the processing of complex data in intelligent illustration 3D information. Therefore, the intelligent 3D design performance analysis model needs to analyze many factors of illustration innovation so as to judge whether there are closely related factors in a variety of data. Therefore, this method can not only use the three-dimensional data required in the process of illustration design as the reference standard, but also use these comprehensive average indicators with closely related factors for data analysis or represent the modeling and analysis factors existing in intelligent illustration design through one of them. In addition, the information carried by these multidata (three-dimensional images) to be processed cannot be seriously distorted. The data analysis process of the intelligent three-dimensional description model of brand illustration is shown in Figure 2.

In the process of brand design of illustration, there is a data object to be processed (illustration innovative design modeling feature information). This process is called modeling the illustration model. In three-dimensional space, the position sequence expression in the illustration innovative design model is

$$
\begin{aligned}
Z_2 &= \frac{(z_2(1), z_2(2), \ldots, z_2(n))}{2n^2 + 3n - 1}, \\
Z_1 &= \frac{(z_1(1), z_1(2), \ldots, z_1(n))}{n^2 + n - 1}, \\
Y_2 &= \frac{(y_2(1), y_2(2), \ldots, y_2(n))}{2n^2 + 3n - 1}, \\
Y_1 &= \frac{(y_1(1), y_1(2), \ldots, y_1(n))}{n^2 + n - 1}, \\
X_2 &= \frac{(x_2(1), x_2(2), \ldots, x_2(n))}{2n^2 + 3n - 1}, \\
X_1 &= \frac{(x_1(1), x_1(2), \ldots, x_1(n))}{n^2 + n - 1}.
\end{aligned}
\tag{1}
$$

In the above formula, x, y, z refer to the three-dimensional coordinate information, X, Y, Z in the process of brand illustration innovative design refers to the design change position of brand illustration in the three-dimensional space, and n refers to the stacking product of feature points of different brand illustration innovative design. In this stage, in the processing of data groups with different dimensions, the simulation results of the three-dimensional space design change position with the cattle cooperative hybrid algorithm and the three-dimensional space change position without the cattle cooperative hybrid algorithm are shown in Figures 3 and 4, respectively.
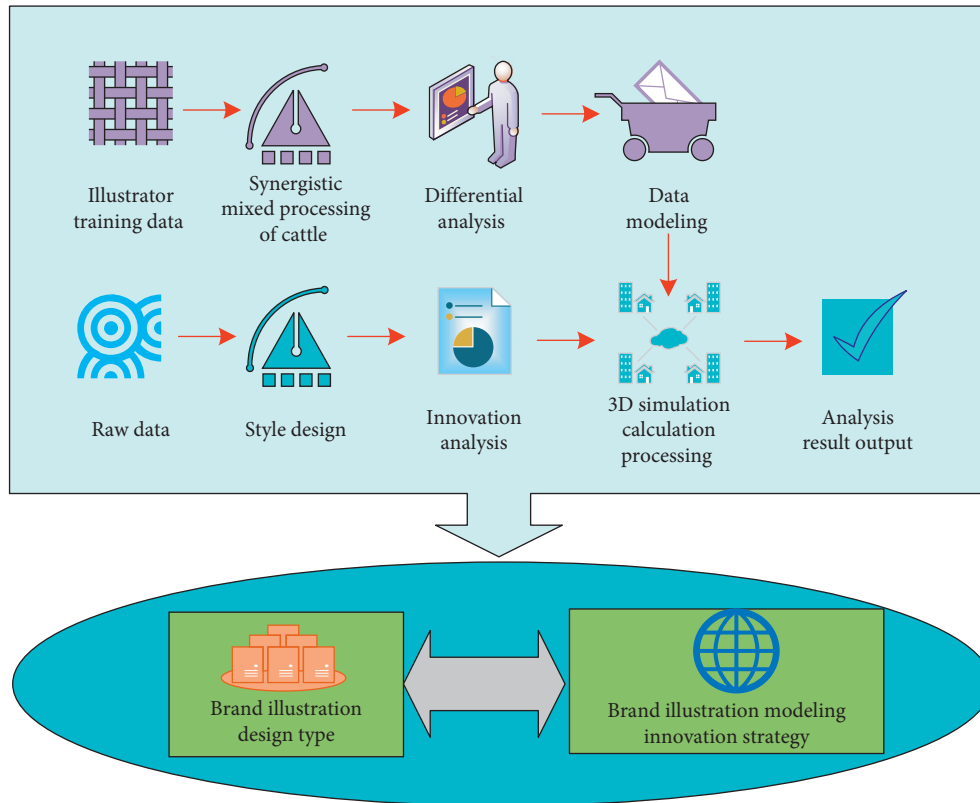
FIGURE 1: Data analysis and 3D simulation operation process of intelligent illustration creative design.
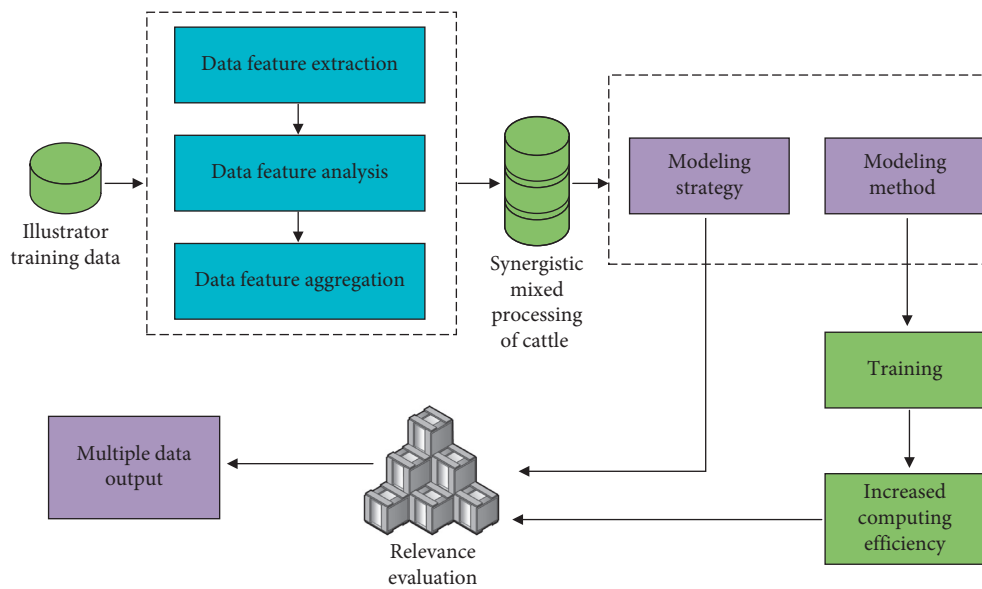
FIGURE 2: The data analysis process of the intelligent 3D description model of the brand illustration.

It can be seen from Figures 3 and 4 that under the cattle cooperative hybrid algorithm, with the increase of data operation speed, the difference between the data operation efficiency corresponding to the illustration design style and the internal correlation of the illustration three-dimensional spatial design position information is very obvious, because with the increase of the number of cattle cooperative operations, different types of illustration modeling impact graph indicators also show the same change law, which gradually decreases, and when the threshold is smaller, the impact
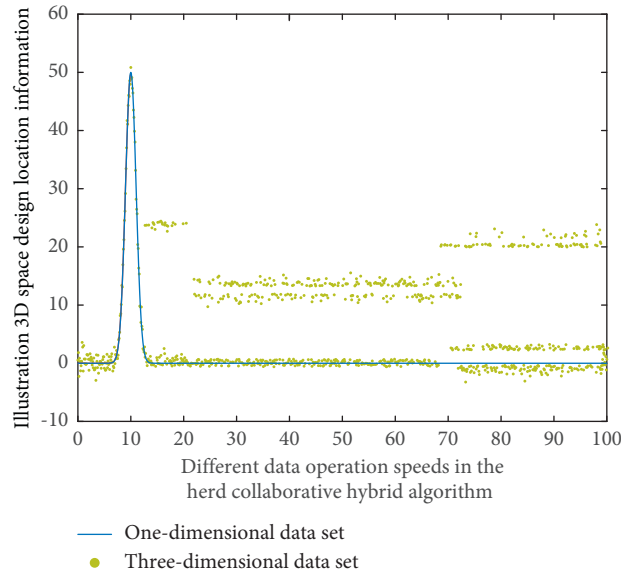
FIGURE 3: The spatial position change of the illustration design at different speeds without using the herd collaborative hybrid algorithm.
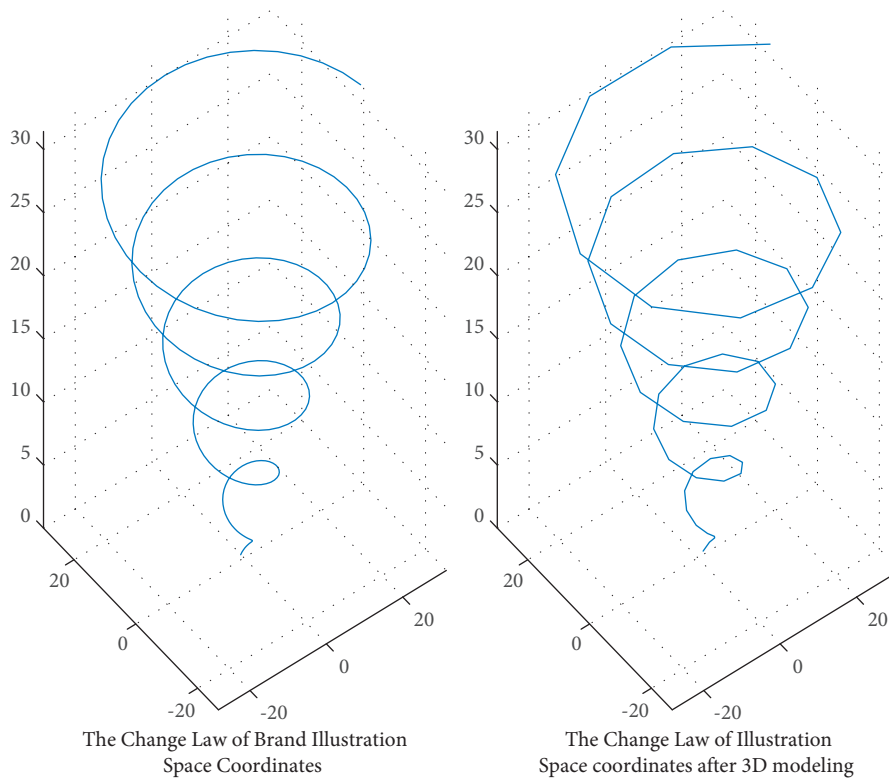
FIGURE 4: The spatial position change of the illustration design at different speeds using the herd collaborative hybrid algorithm.

indicator is smaller, because the smaller the threshold is, the weaker the impact degree is, and the better the corresponding stability is. Therefore, this means that the cattle collaborative hybrid method proposed in this study can effectively improve the modeling efficiency of illustration innovative design.

After combining the cattle cooperative mixed variable function $K(x, y, z)$ and the reinforcement machine learning mechanism rule function $L(x, y, z)$, the position expression of the corresponding illustration background 3D design modeling is

$$Z_2' = \frac{3n+5}{5n^2+7n-1} \frac{(z_2(1), z_2(2), \ldots, z_2(n))}{(n+1)^2 K(x,y,z) + (n+2)L(x,y,z)},$$

$$Z_1' = \frac{n+2}{n^2+n-1} \frac{(z_1(1), z_1(2), \ldots, z_1(n))}{n^2 K(x,y,z) + (n+1)L(x,y,z)},$$

$$Y_2' = \frac{3n+5}{3n^2+2n-1} \frac{(y_2(1), y_2(2), \ldots, y_2(n))}{K(x,y,z) + n^2 L(x,y,z)},$$

$$Y_1' = \frac{n+2}{n^2+n-1} \frac{(y_1(1), y_1(2), \ldots, y_1(n))}{K(x,y,z) + nL(x,y,z)},$$

$$X_2' = \frac{3n+5}{3n^2+2n-1} \frac{(x_2(1), x_2(2), \ldots, x_2(n))}{K(x,y,z) + 2L(x,y,z)},$$

$$X_1' = \frac{n+2}{n^2+n-1} \frac{(x_1(1), x_1(2), \ldots, x_1(n))}{K(x,y,z) + L(x,y,z)}.$$

$$(2)$$

The expressions of cattle cooperative mixed variable function $K(x,y,z)$ and reinforcement machine learning mechanism rule function $L(x,y,z)$ are, respectively,

$$L(x,y,z) = \frac{3x^4 - 3y^2 - 7z^3}{5x^2 + 7y^2 + 2z^3} \frac{zy^2 x^3 + xy^3 + x^{-1}y^{-1}z^3}{x^2 + y^2 + z^{-1}},$$

$$K(x,y,z) = \frac{x^4 - y^2 - z^3}{x^2 + y^2 + z^3} \frac{yx^2 + xy^2 + xyz^2}{x + y + z}.$$

$$(3)$$

X, Y, Z are the motion position function of brand illustration in three-dimensional space, n is the total number of feature points of different brand illustration innovative design schemes, and x, y, z are the spatial trajectory coordinate information of illustration three-dimensional design. When the set signal is different from the coordinate signal in the innovative design of illustration, combined with the analysis of signals by the function of reinforcement machine learning algorithm, the integral expression $Q(t)$ of the correlation comparison results between different types of data is as follows:

$$Q(t) = \frac{k_p \left[e(t) + 1/T_1 \int_0^t e(t)dt + T_D de(t)/dt \right]}{x^2 + y^2 + z^3},$$

$$(4)$$

where x, y, z are the three-dimensional coordinate information in the process of brand illustration innovative design, $e(t)$ represents the deviation, k_p represents the error increase of illustration three-dimensional design, and T represents the conventional modeling constant.

3.3. Application of Brand Illustration Innovation Analysis Model in Intelligent Illustration 3D Design.
Before completing the first draft of different types of brand illustration schemes, in the process of illustration design for different types of brands, after optimizing the innovative design methods of illustration, it is necessary to select different innovative countermeasures and methods of illustration design in combination with the characteristics of innovative design of brand illustration. In this process, by adopting the technical methods involved in different types of industrial 4.0 brands, taking the design brand illustration innovative design scheme and illustration design field as the core modeling goal, the process of the involved illustration design field will be comprehensively evaluated and analyzed to obtain the optimal illustration modeling design scheme. In this process, the internal relevance of different types of data will be analyzed through the 3D modeling method of the brand illustration innovation design system.

Secondly, the intelligent illustration 3D design method is to mine the collected illustration data types. For unknown cattle cooperative mixed data target (innovative design styles of different types of brand illustration), carry out fuzzy search and screening to realize data mining and feature analysis of the overall process of illustration design modeling, and transform the information of different types of intelligent illustration design schemes into data information that can be recognized by the system through a certain pattern. Data mining of different brands will produce different effects. The speed simulation results of the modeling method of innovative illustration design in the traditional illustration 3D design method and intelligent illustration 3D design method are shown in Figures 5 and 6, respectively.

Finally, after completing the above links, it is necessary to accumulate and stack the data generated by modeling under the cattle cooperative hybrid algorithm; that is, it is also necessary to estimate the error degree through the computer database information and the preset automatic innovative judgment program of illustration and then deeply mine and analyze some information in the field of illustration design so as to realize the secondary analysis and error analysis of the data after the initial linear analysis. The results of the illustration modeling simulation analysis method under different disturbing factors in this process are shown in Figure 7.

As can be seen from Figures 5–7, with the increase of illustration modeling and simulation times, its internal relevance is very obvious, especially in the aspects of modeling efficiency and illustration innovation. Moreover, under different thresholds, the change trends in modeling spatiotemporal differences are relatively similar, which are gradually increasing or decreasing, but the increase ranges are different, which shows that the cattle collaborative innovation method can well reduce the differences in illustration design methods. This is because the cattle cooperative hybrid algorithm has an inevitable correlation between data decision-making and state transition in illustration design, so its difference will be very small.

4. Result Analysis and Discussion

4.1. Experimental Results of Intelligent Illustration Modeling and Design Method Based on Cattle Collaborative Hybrid Innovation Model.
After constructing the performance analysis model of brand illustration innovative design, we need to evaluate its practical application effect in intelligent
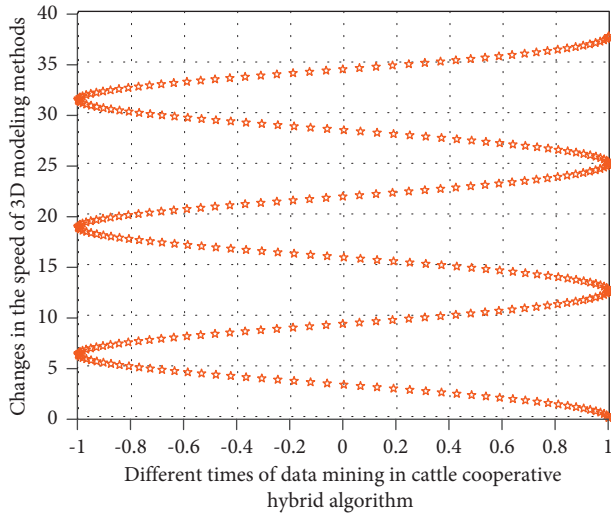
Figure 5: Simulation results of traditional illustration 3D design methods.
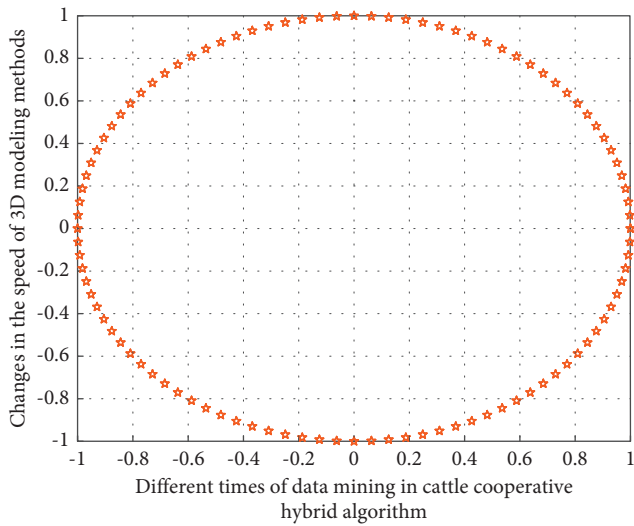
Figure 6: Simulation results of intelligent illustration 3D design method.

Figure 7: The results of illustration modeling simulation analysis under different disturbance factor values.
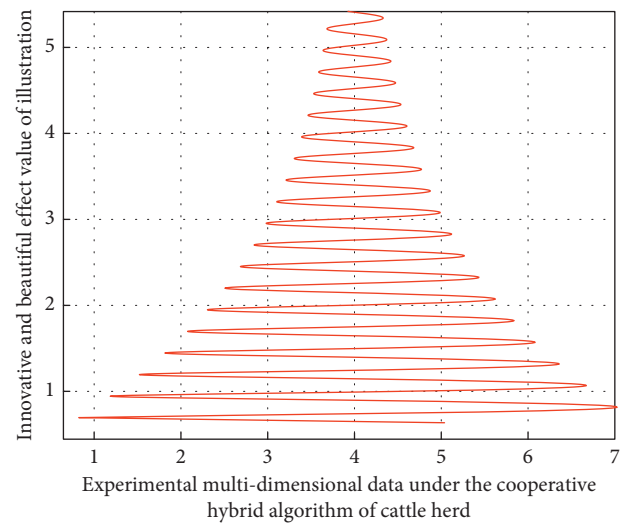
Figure 8: Preliminary analysis results of experiments under the cooperative hybrid algorithm of cattle herd.

illustration 3D design. When evaluating the data acquisition and analysis model of illustration innovative design based on Industry 4.0, it needs to be evaluated from many aspects. According to the needs of innovative illustration design of different brands, this study proposes several indicators to evaluate micro nano flexible sensors. This paper analyzes the application effect and quality of intelligent illustration in three-dimensional design in the process of illustration design. Therefore, it is necessary to analyze the data corresponding to multiple indicators of the three groups of experiments. The preliminary analysis results are shown in Figure 8, in which the horizontal axis is the number of multidimensional data. The vertical axis is the innovative and beautiful effect of illustration.

As can be seen from Figure 8, in the process of this experiment, in the verification process of intelligent illustration 3D modeling design experiment, in this study, the

above indicators can be properly classified, linear analysis and logistic regression through the observation results of known experimental object data. By deleting some unnecessary (i.e., less influential) impact indicators in the illustration design field. With the increase of the number of cycles of the conduction mechanism in the experiment, there are also great differences in the spatiotemporal delay accuracy of the illustration design structure under the corresponding collaborative innovation hybrid strategy, and the accuracy of the spatiotemporal difference of the experimental data of the three-dimensional financial structure will be higher. This is because the brand illustration innovation design analysis model of degree learning algorithm is optimized and classified according to the individual differences between different modeling 3D structures and technological innovation. Through the use of big data analysis and

intelligent fusion technology, the whole process monitoring of illustration innovation models of different brands in the illustration design process is realized, and the process is represented by data. Through the big data analysis system, the source data is transmitted to the system terminal, and then through the intelligent data depth mining technology and optimal analysis scheme based on cattle cooperative hybrid algorithm, a one-to-one analysis scheme is provided for the heterogeneity influence link of illustration innovative design modeling method. The above is the construction idea of brand illustration innovative design intelligent model.

4.2. Experimental Results and Analysis. Among the multiple data indicators used in this experiment to evaluate the three-dimensional design of intelligent illustration, some or several indicators do have correlation or mixed relationship. In order to analyze the experimental data more conveniently, the six comprehensive evaluation indexes involved in the experimental process and the correlation coefficient between the indexes are analyzed. Through the impact evaluation and application of the results of the experimental analysis of the known 9 different types of intelligent illustration design methods and the corresponding indicators in the illustration design, the performance optimization design and fiber flexibility effect of intelligent illustration modeling are realized. The corresponding image analysis is shown in Figure 9. The horizontal axis is the number of experiments and the vertical axis is the impact evaluation factor.

According to the result analysis in Figure 9, the correlation degree between the first index and the second index is 0.97; that is, the coupling relationship between the illustration design effect and the illustration style selected by the modeling method in the illustration design is very high because there is also a positive correlation between the design style and the 3D modeling method in the corresponding brand illustration innovation design system. There is also a positive correlation between design style and 3D modeling method. The relevant test results of six different types of evaluation indicators are passed in the corresponding brand illustration innovation design system. It can well reflect the effectiveness and timeliness of illustration design modeling and analysis model based on cattle cooperative hybrid algorithm. On the other hand, the experimental results show that the correlation degree between the second index and the third index is 0.96, which is very close to 0.9, which also shows that the aesthetics and symmetry in the field of illustration design are also very relevant, and its correlation value is more in line with the current practical experience, which also shows that there is a strong correlation between the two. It can be explained that the innovative modeling of illustration design and brand is also a strong correlation of positive synergy.

Therefore, the results of this study show that the intelligent illustration 3D design method based on big data analysis strategy and cattle collaborative hybrid algorithm can realize the efficient analysis of the internal information and external correlation degree between the data generated by different brands in the illustration design process. In
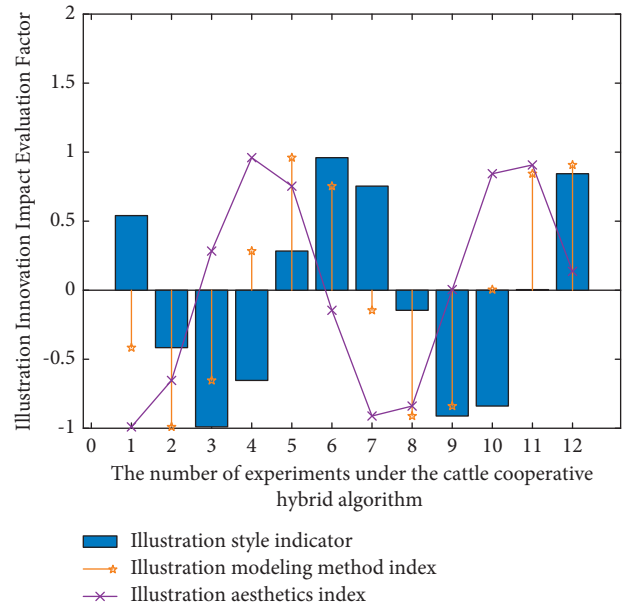
FIGURE 9: Analysis of experimental results under the synergistic hybrid algorithm of cattle.

addition, the relationship between brand illustration innovative design effect and external aesthetics can also be quantified and compared through the design modeling analysis model proposed in this study, and the degree of correlation is very small or even negligible, which is also in line with our life experience—under the background of Industry 4.0, the relationship between brand illustration design effect and external aesthetics is not large. This also shows the accuracy and objectivity of the results of this study in the application of brand illustration innovative design Industry 4.0 based on cattle collaborative innovation algorithm in innovative design.

5. Conclusion

In recent years, with the vigorous promotion of Industrial 4.0 technology, the application prospect of traditional illustration design in brand 3D modeling is becoming more and more obvious. Based on this, this paper studies the modeling method of brand illustration innovative design based on Industry 4.0 and constructs an intelligent illustration design and modeling strategy analysis model based on cattle cooperative hybrid algorithm. The collection of data and information in the process of brand illustration innovative design is realized from six aspects. The cattle cooperative hybrid algorithm is used to realize its data fusion. Combined with the quantitative evaluation method of multidimensional data, the illustration intelligent analysis model can comprehensively analyze and evaluate the data of different types of models. According to the relevant requirements in the field of illustration design and the general rules of modeling design method, the efficient modeling method in the process of brand illustration design is improved. Finally, relevant experiments are designed for verification. The experimental results show that the

intelligent illustration design modeling model based on cattle cooperative hybrid algorithm has the advantages of quantifiable evaluation and good stability. It can improve the efficiency of illustration three-dimensional design and strengthen the intelligence of brand illustration innovation design system. However, this study only analyzes the impact and relevance of modeling methods in intelligent illustration design and does not take other potential influencing factors in the implementation of intelligent illustration design methods into account. Therefore, the impact of other factors on the modeling effect of brand illustration innovative design needs to be further studied.

Data Availability

The data used to support the findings of this study are available from the corresponding author upon request.

Conflicts of Interest

The authors declare that they have no conflicts of interest regarding the publication of this paper.

References

[1] A. Nas, A. Eoh, and B. Aalka, "Ignoring competing events in the analysis of survival data may lead to biased results: a nonmathematical illustration of competing risk analysis," *Journal of Clinical Epidemiology*, vol. 122, pp. 42–48, 2020.

[2] A. Hartman, G. Antonini, J. Ekman, and M. D. Lauretis, "Bandlimited distortionless material design by an approximation of the heaviside condition," *IEEE Transactions on Electromagnetic Compatibility*, vol. 62, no. 2, pp. 1–10, 2019.

[3] A. Rru, B. Sfl, and C. Lt, "Variations in stepped-wedge cluster randomized trial design: insights from the patient-centered care transitions in heart failure trial," *American Heart Journal*, vol. 220, pp. 116–126, 2020.

[4] A. Qureshi and O. Hasan, "Formal probabilistic analysis of low latency approximate adders," *IEEE Transactions on Computer-Aided Design of Integrated Circuits and Systems*, vol. 38, no. 1, pp. 177–189, 2019.

[5] J. Karvanen, S. Tikka, and A. Hyttinen, "Do-search," *Epidemiology*, vol. 32, no. 1, pp. 111–119, 2021.

[6] M. Straka and M. Hricko, "Software System Design for Solution of Effective Material Layout for the Needs of Production and Logistics," *Wireless Networks*, vol. 28, pp. 1–10, 2020.

[7] C. Chang, Q. Lin, Z. Liao, J. Wang, and Y. Yang, "Globally optimal design of refinery hydrogen networks with pressure discretization," *Chemical Engineering Science*, vol. 247, no. 23, Article ID 117021, 2021.

[8] J. Hummel and W. Seim, "Displacement-based design approach to evaluate the behaviour factor for multi-storey CLT buildings," *Engineering Structures*, vol. 201, no. Dec.15, Article ID 109711.1, 2019.

[9] A. Qarariyah, T. Yang, and J. Deng, "Solving higher order PDEs with isogeometric analysis on implicit domains using weighted extended THB-splines," *Computer Aided Geometric Design*, vol. 71, no. MAY, pp. 202–219, 2019.

[10] J. Ekman and Y. Feng, "Effect of Sn addition on epitaxial GaAs nanowire grown at different temperatures in metal–organic chemical vapor deposition," *Crystal Growth & Design*, vol. 19, no. 9, pp. 5314–5319, 2019.

[11] Z. Wang, W. Jin, Y. Dong, and D. M. Frangopol, "Hierarchical life-cycle design of reinforced concrete structures incorporating durability, economic efficiency and green objectives," *Engineering Structures*, vol. 157, no. feb.15, pp. 119–131, 2018.

[12] L. B. Xu, X. S. Li, and Y. Guo, "Gauss-core extension dependent prediction algorithm for collaborative filtering recommendation," *Cluster Computing*, vol. 22, no. 4, 2019.

[13] Z. Li, H. Li, and Y. Feng, "Research on big data mining based on improved parallel collaborative filtering algorithm," *Cluster Computing*, vol. 22, no. 5, pp. 1–10, 2019.

[14] T. Zhao, J. Shi, D. Entekhabi et al., "Retrievals of soil moisture and vegetation optical depth using a multi-channel collaborative algorithm," *Remote Sensing of Environment*, vol. 257, no. 8, Article ID 112321, 2021.

[15] Z. Deng, T. Zhang, D. Liu, X. Jing, and Z. Li, "A high-precision collaborative control algorithm for multi-agent system based on enhanced depth image fusion positioning," *IEEE Access*, vol. 8, Article ID 34842, 2020.

[16] L. Meng, X. You, and S. Liu, "Multi-colony collaborative ant optimization algorithm based on cooperative game mechanism," *IEEE Access*, vol. 8, no. 99, p. 1, 2020.

[17] X. Han, Z. Wang, and H. J. Xu, "Time-Weighted collaborative filtering algorithm based on improved mini batch K-means clustering," *Materials, Computer Engineering and Education Technology*, vol. 105, pp. 309–317, 2021.

[18] J. Q. Ji and Y. Chung, "Collaborative filtering algorithm based on user–item attribute preference," *Journal of information and communication convergence engineering*, vol. 17, no. 2, pp. 135–141, 2019.

[19] J. Li, J. Ma, C. Li, Y. Wang, Z. Li, and J. Hong, "Multi-information collaborative cloud identification algorithm in Gaofen-5 Directional Polarimetric Camera imagery," *Journal of Quantitative Spectroscopy and Radiative Transfer*, vol. 261, no. L04701, Article ID 107439, 2020.

[20] Y. Wu, Y. Zhao, and S. Wei, "Collaborative filtering recommendation algorithm based on interval-valued fuzzy numbers," *Applied Intelligence*, vol. 50, no. 3, 2020.

[21] G. Zhang, H. F. Ng, W. Wen, and L. T. Hsu, "3D mapping database aided GNSS based collaborative positioning using factor graph optimization," *IEEE Transactions on Intelligent Transportation Systems*, vol. 22, no. 10, pp. 1–13, 2020.

[22] C. Yin, L. Shi, R. Sun, and J. Wang, "Improved collaborative filtering recommendation algorithm based on differential privacy protection," *The Journal of Supercomputing*, vol. 76, no. 7, 2020.

[23] X. Yu, F. Jiang, J. Du, and D. Gong, "A cross-domain collaborative filtering algorithm with expanding user and item features via the latent factor space of auxiliary domains," *Pattern Recognition*, vol. 94, pp. 96–109, 2019.

[24] T. Liang, Z. Jin, X. Qin, and K. Jing, "Supply chain scheduling in a collaborative manufacturing mode: model construction and algorithm design," *Annals of Operations Research*, vol. 275, no. 2, pp. 685–714, 2019.

[25] A. Laishram and V. Padmanabhan, "Discovery of user-item subgroups via genetic algorithm for effective prediction of ratings in collaborative filtering," *Applied Intelligence*, vol. 49, no. 11, pp. 3990–4006, 2019.

Research Article

Research on the Method of Acquiring Customer Individual Demand Based on the Quantitative Kano Model

Laihong Du [ID],[1,2] **Hua Chen** [ID],[1] **Yadong Fang** [ID],[1] **Xiaowei Liang** [ID],[1] **Yujie Zhang** [ID],[1] **Yidan Qiao** [ID],[1] **and Zhen Guo** [ID][1]

[1]*School of Mechanical and Electrical Engineer, Xi'an Technological University, Xi'an 710021, China*
[2]*School of Management, Xi'an University of Finance and Economics, Xi'an 710010, China*

Correspondence should be addressed to Laihong Du; dlh06@xaufe.edu.cn

In order to realize accurate marketing by analyzing customer individual demand, a new quantitative Kano model method is put forward, and it is helpful to provide customized products for heterogeneous customer classification groups. By improving the traditional Kano model, the customer satisfaction and the importance degree of products are defined, and the quantitative Kano demand model is established. Customers are classified as the price preference group, the brand preference group, and the service priority group, and decision-making of product attribute quality improvement for customer classification is realized. Lastly, electric vehicles (EVs) are selected as a study case, and their various demands for different classifications of customers are discussed by questionnaire survey and calculation of satisfaction and the importance degree. Furthermore, different customer group demands are classified as attractive demands, expected demands, nondifferential demands, or essential demands, and the important product attribute acquisition process for various customers is discussed to improve enterprise market competitiveness.

1. Introduction

With the continuous improvement of people's consumption levels and the diversification of product forms, more and more consumers no longer simply pay for the premium of the product brand but expect to achieve consumption upgrading on the basis of the price, which also brings huge opportunities and challenges for enterprises to design and customization of products and services. Many manufacturing enterprises have also been user-centered, driven by the demand side, and depicted the user portrait on the basis of big data mining and analysis, so as to realize personalized customized services to users. As early as 1998, Yeh and Pearlson proposed the concept of customer customization, providing the corresponding personalized design, production, and delivery of customer products or services according to their personalized needs [1, 2]. Foreign IKEA and BMW-Mini have launched user customization in product customization, while Amazon, Haier, and other websites have made personalized recommendations for use

[3]. Domestic red collar and WeiShang fully reflect the personalized personalization in the product application [4]. Enterprises can segment the market, regard the same type of users as a market segment, and provide them with the corresponding customized services to meet the personalized needs of users [5]. Personalized needs are to let products or services reflect their own unique needs and personality, not different needs from others. Therefore, while all users have common needs, the types of users can be distinguished through the personalized needs of users, and the products and services can be customized for different users' needs, which is of great significance to improving the competitiveness of enterprises in the same industry and the formation of precise marketing for customers.

At present, there is a certain vague uncertainty in the expression of user demand for products and services. How to maximize the personalized needs of users is the key to enterprise customization. There are two main ways to obtain information about users' needs: one is the data collection based on the Internet with the help of marketers. In [6], they

proposed a method of product personalized customization with a case-based reasoning theory to solve the problem of low matching between user requirements and product modules in the process of product personalized customization. A new method for KANO model classification was created in [7]. By collecting customer reviews and rating scores, the author builds a regression model between the score and the degree to which product attributes meet user needs according to their text expression. However, the cost of one-to-one communication with customers is high, and the expression of product demands in the process of independent selection is vague. Besides, the existing options and parameters are difficult to meet the needs of customers. In [8], they researched the user's personalized needs of smart health preserving pot based on the Kano model to guide the interaction design and make the interaction of smart health preserving pot more fit the user's real needs. In [9], they focused on investigating traditional garment enterprises' transformation from mass production to mass customization, and it probed deeply into the ways for the garment manufacturing industry to realize Internet-based mass customization and key problems to be solved. An approach of integration of the Kano model into QFD to examine customer satisfaction based on aesthetic sentiments was proposed in [10], and a sport utility vehicle has been selected for the study. The aesthetic attributes have been selected with the help of QFD and their importance and classification have been calculated using both the fuzzy Kano and the traditional Kano models. [11]aimed to examine consumer perspectives about service satisfaction in the domestic medical industry using Kano's two-dimensional model and employed the importance-satisfaction model to determine service items that need improvement. In [12], they estimated customer preference based on conjoint analysis and categorized service quality elements by the IPA-Kano model. A methodology that integrates the Kano model (KM), analytic hierarchy process (AHP), and quality function deployment (QFD) methods with intuitionistic fuzzy set (IFS) to solve decision-making problems in new product development and design was proposed in [13]. By the new method, the web crawler technology was first applied to e-commerce web sites to collect raw data, and the representative CRs were extracted through combining the LDA model with the Apriori algorithm. Second, the intuitionistic fuzzy Kano model (IFKM) is proposed to evaluate the adjustment coefficient of CRs and Kano categories via customer preference membership functions. In [14], they proposed the product feature KANO analysis method based on the emotional distribution of product features, and Kano analysis of product characteristics by using product review data can provide valuable reference information for companies to improve their products. Literature [15] classified the product functions mentioned in social media. In [16], they divided the design demands information of personal protective mask into several attributes initially and obtained the final Kano required attributes by the better-worse coefficient analysis method. In [17], they used the Kano model to identify and screen demand and built the quality demand hierarchy model of high-quality housing to calculate the importance

degree of each demand item. In the study [18], they defined the user requirements in the Kano model and classified user requirement hierarchies using the rough analysis hierarchy process method to calculate requirement weight. In [19], a hybrid Kano model with tools of SII and DDI was proposed.

Most of the existing customer demand determination methods are to calculate the importance degree of a customer's personalized demands and then determine the priority of the customer's demands, ignoring the existence of product satisfaction. Product satisfaction is an important and influencing factor of product upgrading, and it can realize product accuracy in marketing if the demands of customers are quantified with feedback on product importance and satisfaction. Therefore, this paper acquires the customer preferences for different types of demands by through a quantified Kano model classification according to the importance degree of customer demands. Furthermore, the satisfaction and importance evaluation of customer demands are combined to determine which types of demand items should be emphasized in the later update and upgrading of products so as to provide user groups with products that meet customer scenarios and actual demands in the future.

2. Related Work

The Kano model was formally proposed by Japanese scholar Yoshino. According to the subjective performance of the product and the customer subjective perception [11], the quality characteristics of the product were classified and screened. Among them, the customer's demand for products is divided into five categories, namely, necessity, expectation, charm, no difference, and reverse [20]. Must-be requirement refers to the basic requirements that the product should have. If the attribute is sufficient, the user will not be delighted, but if the point is absent, the user will be very dissatisfied. Attractive requirement, also known as excited demand, is a characteristic that can surprise or surprise customers. When it is sufficient, it can improve customer satisfaction to a large extent, but it will not cause dissatisfaction when it is insufficient. One-dimensional requirement is an essential factor for enterprises to evaluate competitiveness, which makes customers satisfied when the product has enough characteristics and causes dissatisfaction when it is not sufficient. Indifferent requirement, customers ignore factors, and whether it is satisfied does affect users' satisfaction with products. Reverse requirement, when product attributes are satisfied, customers are not satisfied, and when product attributes are not satisfied, customers are more satisfied. According to the objective performance of the product and customer satisfaction, the Kano model diagram is shown in Figure 1.

The Kano model requirement classification evaluation table designs the product attributes as positive and negative aspects and obtains the demand classification of product attributes by analyzing the Kano questionnaire filled by users. Among them, M represents the necessary demand, O represents the expected demand, A represents the charming demand, I represents the nondifference demand, R
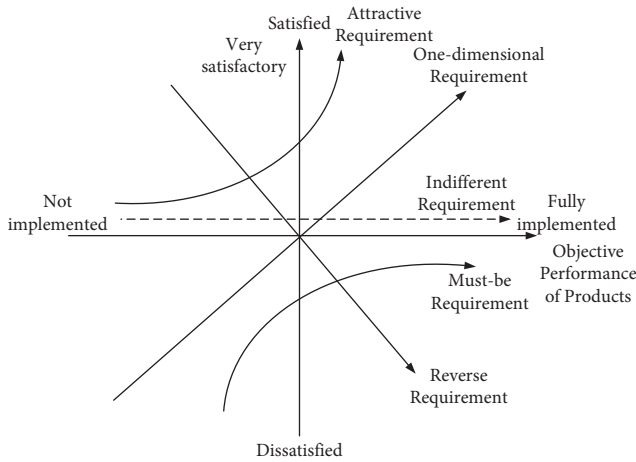
Figure 1: Kano model schematic.

Table 1: Kano model demand classification evaluation table.

Positive problem	Reverse problem				
	Like	Naturally	Never mind	Passable	Dislike
Like	Q	A	A	A	O
Naturally	R	I	I	I	M
Never mind	R	I	I	I	M
Passable	R	I	I	I	M
Dislike	R	R	R	R	Q

represents the reverse demand, and Q represents the problem demand (Table 1).

The traditional Kano model is essentially a qualitative analysis method, and its classification method is subjective. The preference of product characteristics is classified by the degree of selection of positive and negative problems in the Kano model demand classification evaluation table, which lacks quantitative standards. Therefore, it is of great significance to quantitatively improve the traditional Kano model and divide the user's demand preference after quantification, so as to realize the precise marketing of users.

3. Quantitative Kano Model Method

Different people have different demand expectations for the same product. The type of demand item can be determined according to the user's satisfaction degree and the importance degree of product services. Unlike the traditional Kano demand acquisition model, the quantitative Kano model will measure the user's expectation of the product through quantitative indicators, which can more objectively obtain the user's personalized demands.

The initial personalized hierarchical model is constructed. The quantitative Kano model is used to divide the initial demand according to the satisfaction index to determine the personalized demand category. Due to the heterogeneity of users, users are divided into different types. Users' evaluation of the importance of product services is added to improve the quality of personalized demands further and finally obtain the personalized priority demands of heterogeneous users. Getting personalized orders of heterogeneous users can be summarized in Figure 2.

The basic idea of quantifying users' satisfaction degrees and the importance degree of product service is as follows:

Step 1. Identify the initial personalized demand level.

The product specification is checked, and the relevant literature is read to understand the product characteristics that may be customized. At the same time, through face-to-face interviews with the sales staff, technicians, and customers, the requirements are obtained that the customer in the purchase process may mention the product. The original requirements are analyzed, deleted, and modified. The concept scope of the product is broad in the product instructions and interviews. The concept can be hierarchically sorted and summarized according to the affinity graph method, and Figure 3 of the initial personalized demand hierarchy model of the product is constructed ($PR = \{PR_1, PR_2, PR_i, ..., PR_n\}$, $PR_i = \{PR_{i1}, PR_{i2}, PR_{ik}, ..., PR_{is}\}$).

Step 2. Design of a quantitative Kano questionnaire.

Combined with Matzler's research, numerical indicators are set up in the user's product service satisfaction degree and importance degree. The user's demand options are quantified and counted when analyzing the questionnaire. At the same time, the quantitative Kano model is applied to different user groups, and the Kano demand types corresponding to different kinds of user groups are analyzed.

Because the positive answer is stronger than the negative answer, the index scale of satisfaction degree asymmetry can be set in the questionnaire to reduce the influence of negative evaluation and obtain the corresponding quantitative values for different personalized demands [12]. In addition, the importance degree of product services is divided into four degrees, the value is divided according to different levels, and the corresponding quantitative range is formulated. The Kano model requirements for classification evaluation table quantification criteria are shown in Tables 2 and 3.

Step 3. Calculation of customer satisfaction with product services.

Step 3.1. Assume variables.

According to the quantitative Kano model designed by the questionnaire data analysis,

Assume V represents a set of users, and v_j represents the jth user.

$$V = \{v_j | j = 1, 2, \ldots, n\}. \quad (1)$$

Assume F represents a collection with product service attributes, and f_i represents the ith product service attribute.

$$F = \{f_i | i = 1, 2, \ldots, m\}. \quad (2)$$

Assume that x_{ij} is the reverse product service satisfaction evaluation of jth users when the product service attribute f_i is not provided. y_{ij} is the positive product service satisfaction evaluation of user j when providing product service f_i. ω_{ij} is the importance evaluation of user j on product service
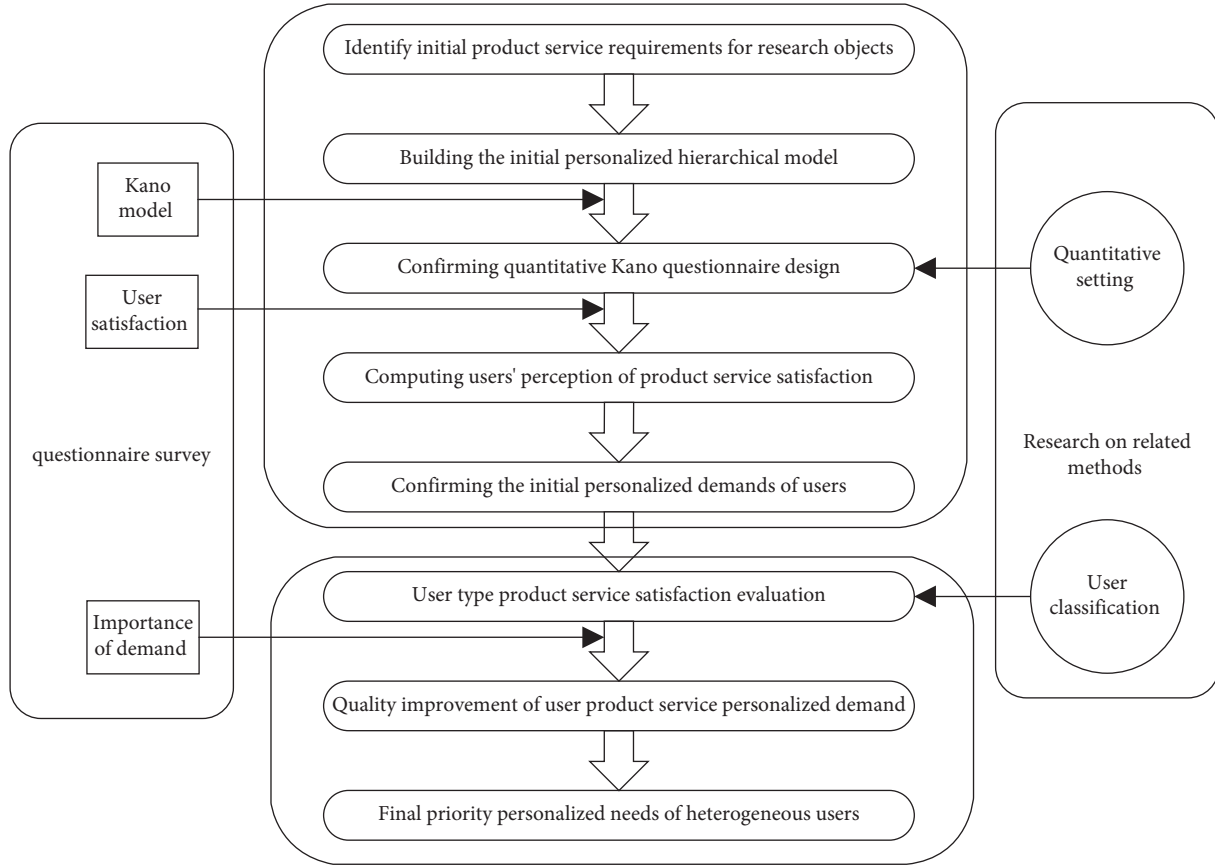
FIGURE 2: Process of obtaining personalized requirements for heterogeneous users.
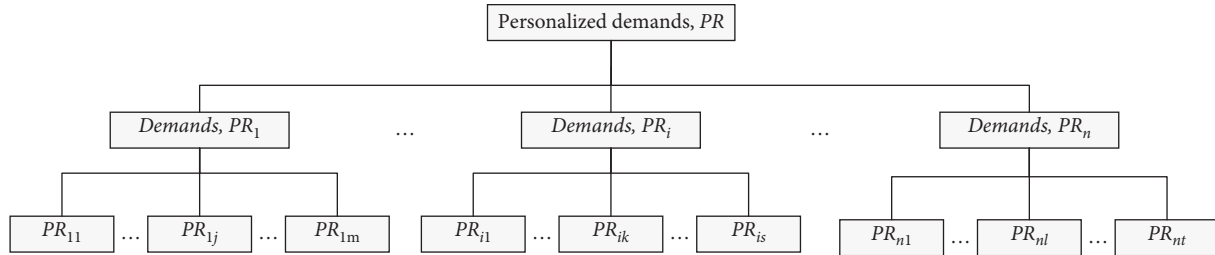
FIGURE 3: Initial hierarchy model of personalized requirements.

TABLE 2: Provision/nonprovision of satisfaction values for product and service attributes.

		Like	Naturally	Never mind	Passable	Dislike
Product attributes	Provides this attribute	1	0.5	0	−0.25	−0.5
	This attribute is not provided	−0.5	−0.25	0	0.5	1

TABLE 3: Importance degree of products and services.

Unimportant	Some important	Important	Very important
0–0.25	0.25–0.5	0.5–0.75	0.75–1

attribute f_i. For each user v_j, the evaluation of f_i can be expressed as follows:

$$e_{ij} = (x_{ij}, y_{ij}, \omega_{ij}). \qquad (3)$$

Step 3.2. Calculate the average value of users' positive and negative problems.

By designing a quantitative Kano questionnaire, the values of x_{ij}, y_{ij}, and ω_{ij} can be obtained by questionnaire analysis. $\overline{X}_i$ denotes the average level of user satisfaction with negative problems without providing f_i product service attributes; $\overline{Y}_{ij}$ represents the average level of user satisfaction with a forward problem when providing f_i product service attributes, which are as follows:

$$\overline{X}_i = \frac{1}{n} \sum_{j=1}^{n} \omega_{ij} x_{ij},$$

$$\overline{Y}_i = \frac{1}{m} \sum_{i=1}^{m} \omega_{ij} y_{ij}. \tag{4}$$

The value of $(\overline{X}_i, \overline{Y}_i)$ can be marked in the two-dimensional coordinate diagram. The abscissa is the user's dissatisfaction with the product service attribute f_i, and the ordinate indicates the satisfaction level. Most $(\overline{X}_i, \overline{Y}_i)$ values fall within the range of [0, 1] in the two-dimensional graph, and the negative value is reverse demand or problem demand, which is not included in the average value, as shown in Figure 4.

Step 3.3. Calculate the user product service importance degree and satisfaction degree index.

Product service attributes can be described as $f_i \sim \overrightarrow{r}_i = (r_i, a_i)$ in vector form, where r_i is the moment of vector $\overrightarrow{r}_i$, which represents the importance of the product service attribute f_i to the user and is the Kano importance degree index.

$$r_i = \left| \overrightarrow{r}_i \right| = \sqrt{\overline{x}_i^2 + \overline{y}_i^2}, \quad 0 \le r \le \sqrt{2}, \tag{5}$$

where a_i is the angle between the vector $\overrightarrow{r}_i$ and the horizontal coordinate axis, which determines the relative level of user satisfaction or dissatisfaction with the product service attributes and becomes the Kano satisfaction index.

$$\alpha_i = \text{arctg}\left(\frac{\overline{Y}i}{\overline{X}_i}\right), \quad 0 \le \alpha_i \le \frac{\pi}{2}. \tag{6}$$

Step 4. Decision on quality improvement of product service.

According to the quantitative Kano questionnaire, the user demands are divided into attractive demands, essential demands, expected demands, and nondifference demands, and the user groups filled in the questionnaire are classified. At the same time, the importance of product services filled out by users in the questionnaire is used to further improve the quality of personalized demand for product services. Taking Kano satisfaction degree and Kano importance degree as two dimensions, product service attributes are divided into four quadrants. As shown in Figure 5, $\overline{r}$ is the average value of product service attributes importance degree, and $\overline{\partial}$ is the average value of product service satisfaction degree.

According to the analysis of Figure 5, quadrant I can be summarized as an irrelevant region. The product service attributes of the region have little effect on customer satisfaction and importance degree. Enterprises do not need to spend too many resources to improve these attributes. Quadrant II is the oversatisfaction area. Customers have high satisfaction with the product service in the region, but the importance of this attribute is not high. Investment in the region's attributes can be moderated if companies demand to reduce costs. Quadrant III can be regarded as a performance
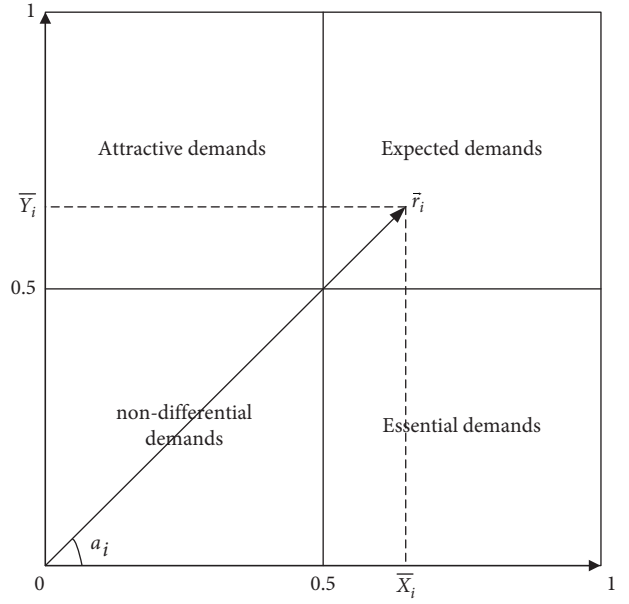
FIGURE 4: Quantitative standards for product and service requirements.
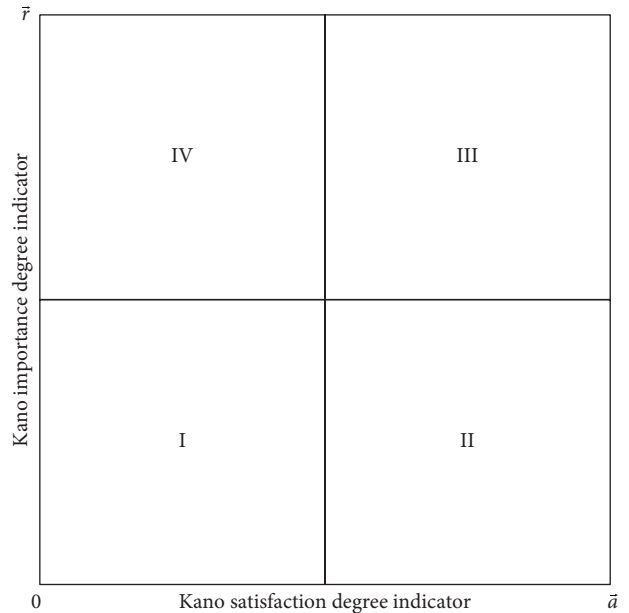
FIGURE 5: Decision on quality improvement of product service attributes.

improvement area, which has high satisfaction and an important degree of product and service attributes. Increasing investment in this regional details can improve customer satisfaction. Quadrant IV can be classified as a key promotion area, and it has a low satisfaction degree and a high importance degree. It shows that the product service attributes in the region play a significant role in user demands. If customer satisfaction with these attributes can be improved, the quality requirements of product services can be improved as a whole.

4. Case Study

Taking electric vehicles as an example, this paper establishes the initial demand item model of the electric vehicle, subdivides the customizable part of the electric vehicle, and determines the demand item problem of the quantitative Kano questionnaire. The personalized customization needs of different types of user groups for electric vehicles are obtained through a questionnaire. The quantitative Kano analysis method is used to quantify the satisfaction and importance of users to products and services. Then, the demand items are divided into corresponding types so that enterprises can carry out precision marketing for different demand types of heterogeneous users.

4.1. Construction of Initial Requirements Model for Electric Vehicle. The collected electric vehicle demand items are divided into four categories: internal appearance demand, software and hardware demand, functional demand, and service demand. Among them, the internal and external demand refers to the internal and external decoration, including the vehicle's external characteristics and internal design. The design of this part reflects the user's demand for the overall beauty and comfort of the vehicle. The software and hardware requirements involve the vehicle's software and hardware systems, which can ensure the safety of vehicle performance and the intellectualization of the system. Functional requirements include entertainment, transmission, and additional functions. These functions can satisfy users and meet users' expectations for the vehicle. The service demand can be used as the value-added service of the product. While providing users with product functions, the existence of these functions will make users more satisfied and enhance the value of the product. Therefore, the construction of the initial demand model of electric vehicles is shown in Figure 6.

4.2. Design of the Quantitative Kano Questionnaire. The questionnaire is designed based on the initial personalized demand hierarchy model of electric vehicles. The questionnaire is divided into two parts. The first part is to investigate the characteristics of customers and establish the relevant preferences of customers. The second part is designed in the form of selection (positive and negative problems) and filling (importance degree). The customers' EV demand items are shown in Table 4.

4.3. Analysis of Electric Vehicle Demand Items of Users. Combined with the Kano demand questionnaire of EV and Equations 1–4, the negative and positive satisfaction degree distribution is shown in Figure 7 and Figure 8. There are three customer groups and 25 demand items, and the satisfaction degrees of various preference customers and demand items are different. The results in Figures 7 and 8 demonstrate that the negative satisfaction degree of demand item f_{14} (wheel hub) is the highest, and the positive

satisfaction degree of demand item f_{11} (connection of vehicle networking data) is the highest.

In terms of the statistical results in the previous table, the satisfaction threshold is set to 0.5 for the product service attribute $x_i < 0.5$, $y_i < 0.5$ is divided into no difference. If $x_i \geq 0.5$, $y_i < 0.5$ is classified as an essential requirement. When $x_i \geq 0.5$, $y_i \geq 0.5$, it is considered an expected demand. Similarly, when $x_i \leq 0.5$, $y_i \geq 0.5$ can be divided into charismatic needs. Based on the abovementioned settings, by depicting the data in Figures 7 and 8, we can get the average satisfaction to scatter diagram of all users and different user groups on product service attributes. Different user groups are price advantage users, brand affects users, and service users before and after sales.

According to the scatter diagram in Figure 9, for the samples of all users, the size of trunk space, the setting of the speech recognition system, and the additional products of the vehicle are divided into charm requirements. The four attributes of battery life function, data connection of the Internet of vehicles, exclusive manual customer service, and remote charging are divided into expected requirements. Eight choices, including the choice of seat configuration, car suspension choice, and GPS positioning and navigation system, can be divided into necessary requirements. The other ten attributes, such as the customization of the vehicle color, the selection of sunroof type, and the type of key, can be classified as indifference requirements.

According to the heterogeneity characteristics of users, the perception of the same product service attributes is also different. Users can be subdivided into heterogeneous user groups. According to the description of the scatter diagram, the demand types of users can be classified and summarized according to different groups, and the following product service attributes (Table 5) of heterogeneous user groups about electric vehicles can be obtained.

It can be found from Table 5 that different user groups have heterogeneity on product and service attributes, and user stickiness and market influence can be enhanced by providing users with differentiated, personalized product and service attributes. For user groups that prefer price advantage, their user groups pay more attention to the cost performance of products and expect to use the least money to obtain higher quality products and services. They do not have too much expectation for products and services and can meet their basic needs. For the user groups that prefer brand effect, their users pay more attention to the product and service guarantees brought by the product brand and think that the greater the brand influence, the better the effectiveness of their products and services. Such subdivided users have higher standards for the attributes of products and services and expect the attributes of the products and services they use to pass the high-quality screening. This is consistent with the characteristics of the user preference brand effect. User groups who prefer sales services pay attention to the services provided in purchasing products and the sense of the experience of process services. The humanized services of user enterprises often move such users.
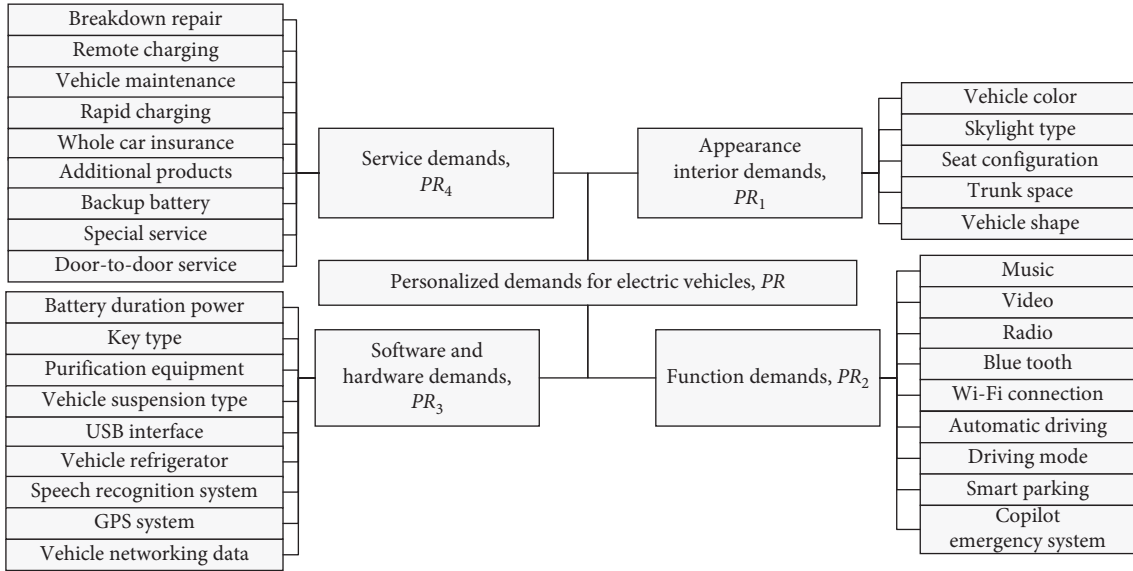
Figure 6: Construction of initial demand model of electric vehicle.

Table 4: Description of product/service attributes of electric vehicles.

Product/service attribute number	Product/service attribute number	Benefits for users
f_1	Custom vehicle colors	Personality and pleasure
f_2	The type of sunroof can be selected	Comfortable and safe
f_3	Selection of seat configuration	Comfortable and safe
f_4	Size adjustment of trunk space	Convenient and comfortable
f_5	Battery life function	Value-added and convenient
f_6	Type of key	Personality and convenience
f_7	Selection of onboard purification equipment	Safe and comfortable
f_8	Choice of automobile suspension	Personality and safety
f_9	Customization of entertainment functions	Personality and pleasure
f_{10}	The setting of the speech recognition system	Fast and convenient
f_{11}	Connection of vehicle networking data	Safe and fast
f_{12}	Selection of GPS positioning and navigation system	Personality and convenience
f_{13}	Vehicle additional products	Personality and value-added
f_{14}	Wheel hub	Personality and safety
f_{15}	Exclusive manual customer service	Added value and pleasure
f_{16}	Maintenance service	Fast and safe
f_{17}	Remote charging	Fast and value-added
f_{18}	Copilot emergency system	Safe and convenient
f_{19}	Intelligent parking	Fast and convenient
f_{20}	Automatic driving	Fast and convenient
f_{21}	Rear seat TV	Comfortable and pleasant
f_{22}	Hi-Fi equipment	Comfortable and pleasant
f_{23}	Lamp type	Personality and safety
f_{24}	Vehicle shape	Personality and value-added
f_{25}	Car refrigerator	Comfortable and pleasant

To sum up, users have heterogeneous characteristics for user groups with different purchase preferences. Considering the different needs of heterogeneous users, the classification of the same product and service attributes will also belong to different demand types. Enterprises can pay attention to the expected needs of heterogeneous user groups. Everyday needs are the key for enterprises to improve their competitiveness. Providing personalized, customized services for different users can effectively improve user satisfaction and stickiness to enterprise products and services.

4.4. User Demand Promotion Decision. According to the personalized needs of heterogeneous users, the quality of their product service attributes can be improved accordingly. The $|\overrightarrow{r}_i|$ and α_i values of all users and heterogeneous user groups are calculated. Electric vehicles product and service attributes are classified into four quadrants composed of demand, satisfaction, and importance. The distribution of various demands of overall customers is shown in Figure 10, and the quantitative Kano model decision matrix of customers who prefer price is illustrated in
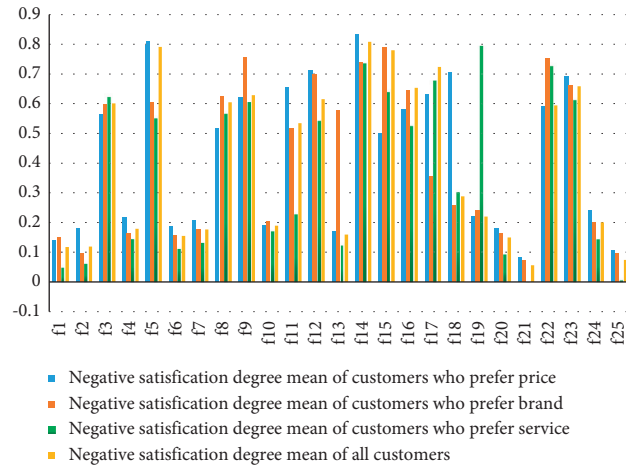
Figure 7: Negative satisfaction degree $\bar{x}_i$ statistical analysis of electric vehicle individual demand.
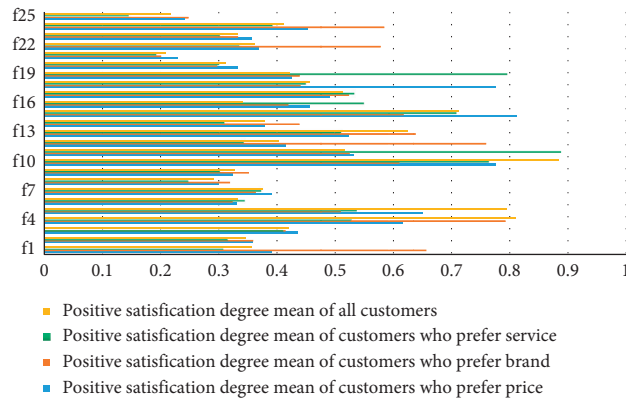
Figure 8: Positive satisfaction degree $\bar{y}_i$ statistical analysis of electric vehicle individual demand.
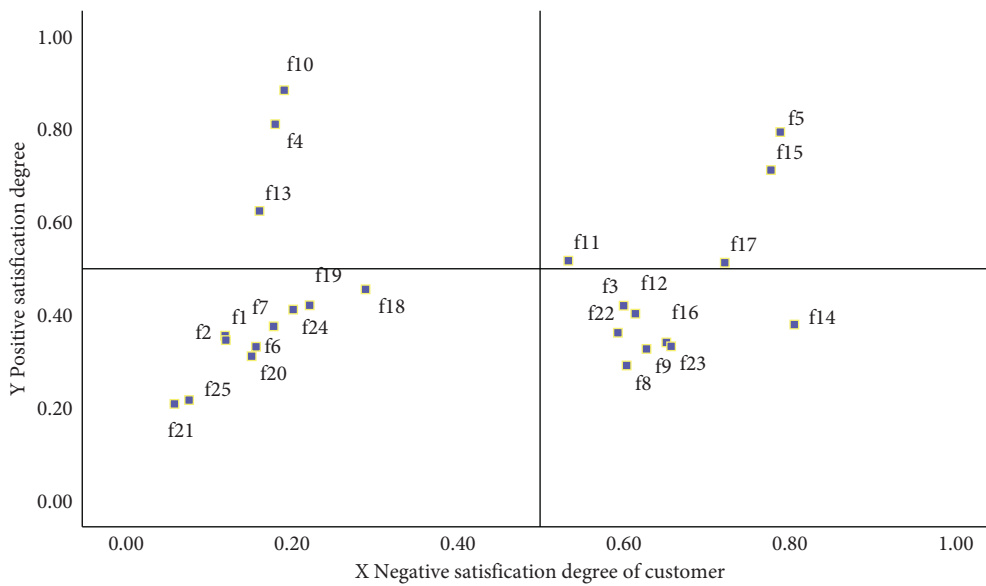
Figure 9: Scatter chart of mean satisfaction of overall customers with product attributes.

Table 5: Classification and summary of product/service requirements of heterogeneous users.

Product/service attributes	Users who prefer price advantage (73)	Users who prefer brand effect (66)	Users who prefer sales services (53)	All users (192)
f_1	I	A	I	I
f_2	I	I	I	I
f_3	M	M	M	M
f_4	A	A	A	A
f_5	O	O	O	O
f_6	I	I	I	I
f_7	I	I	I	I
f_8	M	M	M	M
f_9	M	M	M	M
f_{10}	A	A	A	A
f_{11}	O	O	A	O
f_{12}	M	O	M	M
f_{13}	A	O	A	A
f_{14}	M	M	M	M
f_{15}	O	O	O	O
f_{16}	M	M	O	M
f_{17}	O	A	O	O
f_{18}	I	I	I	I
f_{19}	I	I	O	I
f_{20}	I	I	I	I
f_{21}	I	I	R	I
f_{22}	M	O	M	M
f_{23}	M	M	M	M
f_{24}	I	A	I	I
f_{25}	I	I	I	I
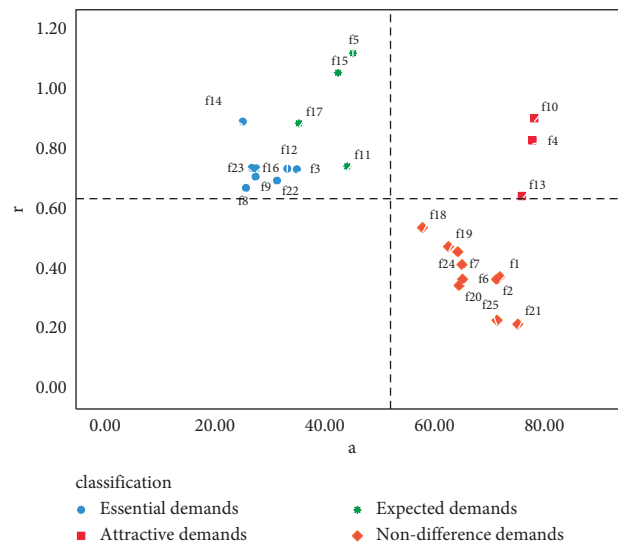
Figure 10: Quantitative Kano model decision matrix of overall customers.

Figures 11. Figure 12 describes the demand distribution of customers who prefer brand, and the quantitative Kano model decision matrix of customers who prefer service is shown in Figure 13.

According to the importance of demand attributes, the third quadrant and the fourth quadrant can be divided into performance improvement areas and critical improvement areas. The abovementioned figure shows that whether all users or different types of users, the demand attributes of the third and fourth quadrants are mostly necessary needs and expected needs. On the one hand, it expresses that good products can not only meet the most basic needs of users but also pay attention to the expected needs, that is, pay attention to the core competitiveness of enterprises, which is consistent with the classification of the quantitative Kano model mentioned above, which verifies the necessity of user demand classification. The product service attributes can be improved according to the quality decision matrix obtained
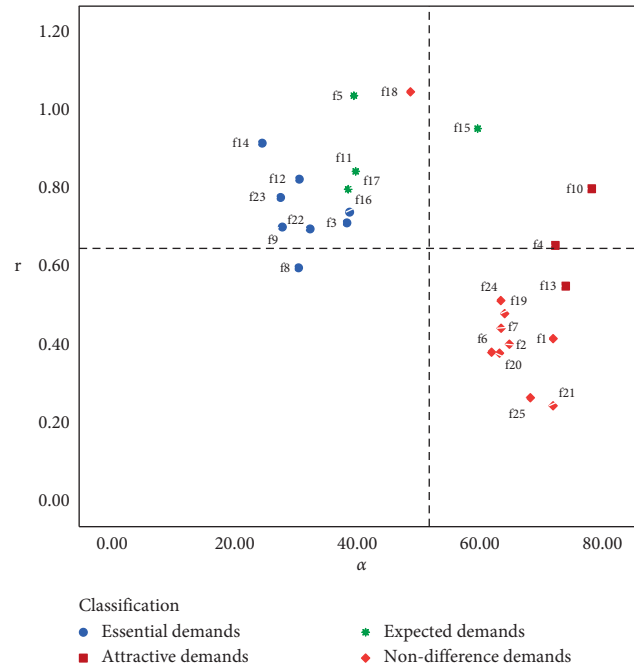
FIGURE 11: Quantitative Kano model decision matrix of customer who prefer price.
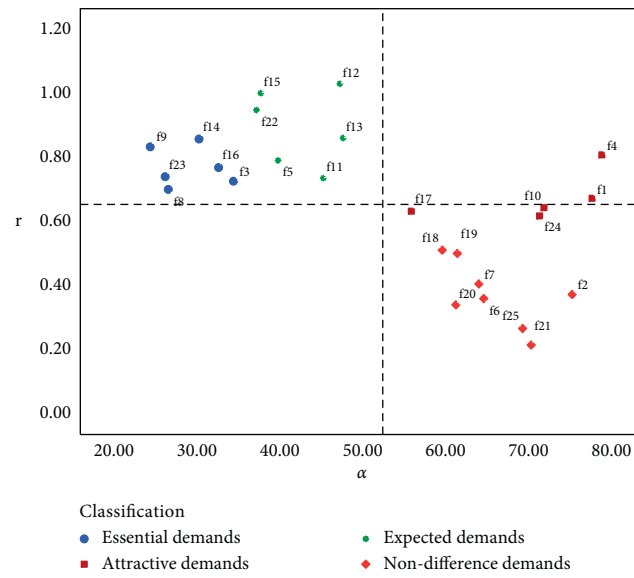
FIGURE 12: Quantitative Kano model decision matrix of customers who prefer brand.
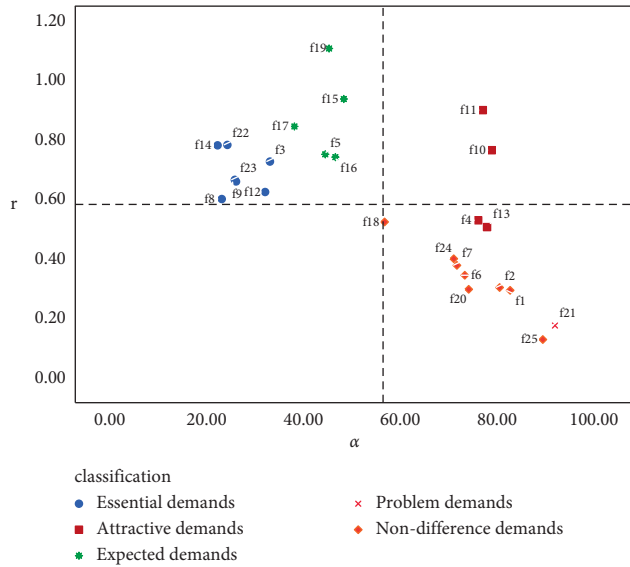
FIGURE 13: Quantitative Kano model decision matrix of customers who prefer service.

from the product service satisfaction and importance, and precise marketing can be carried out according to the user's pain points.

5. Conclusion

In the traditional Kano model, customer demand items are determined according to statistics of positive and negative problems that customers had with product attributes, and it ignores various customer demand classifications. Furthermore, the traditional Kano model leads to subjective demand classification results for its qualitative selection. Satisfaction and importance degree of customers are put forward to judge different demand preferences of different customers for the same product by the quantitative Kano model, and it is helpful to realize precise marketing of the product. The paper takes electric vehicles as an example. An initial demand model of product is first constructed, and then customer demand items are determined. It can get a quantitative perception evaluation of electric vehicle satisfaction and importance degree by the Kano demand questionnaire and Equations 1–5, and the result shows that it can improve demand matching quality. For heterogeneous customers, each product attribute may belong to various demand types. In the process of customer purchase, enterprises should focus on customer's expected demands and essential demands, which will change with different types of customers. The quality of those demands will affect the customer's purchase choice. At the same time, the research results can be applied to the process of customer demand type determination and demand quality decision-making in various industries, which is helpful to the enterprise demand management and upgrading for the corresponding customer. The focus of the further research in the paper is to transmit customer demands into EV product functions based on ontology technology.

Data Availability

The labeled dataset used to support the findings of this study are available from the corresponding author upon request.

Conflicts of Interest

The authors declare no conflicts of interest.

Acknowledgments

References

[1] R. Schuler, "A case study of the HR department at Swiss bank corporation," *Asia Pacific Journal of Human Resources*, vol. 26, no. 4, pp. 59–76, 2013.

[2] R. Tersing and M. Harvey, "Global customerization of markets has arrived," *European Management Journal*, vol. 16, no. 1, pp. 79–90, 1998.

[3] Y. Wang, H.-S. Ma, J.-H. Yang, and K.-S. Wang, "Industry 4.0: a way from mass customization to mass personalization production," *Advances in manufacturing*, vol. 5, no. 4, pp. 311–320, 2017.

[4] Y. Wu, Y. Sheng, and N. Chai, "Study on mass intelligent customization based on internet plus-case of Qingdao red-collar and Foshan weishang furniture," *China industrial economics*, vol. 1, no. 4, pp. 127–143, 2016.

[5] D. Zhong and Y. Huang, "Analysis of personalized needs for refrigerator based on Kano model," *Journal of hunan university of technology*, vol. 24, no. 2, pp. 48–53, 2019.

[6] W. Wang, J. Liu, and W. Pan, "Product personalized customization method based on case-based reasoning," *Packaging Engineering*, vol. 40, no. 20, pp. 187–194, 2019.

[7] A. P. Lu, Y. F. Sun, Z. Lei et al., "KKMA-A calculation method for Kano classification based on user reviews," *IOP Conference Series: Materials Science and Engineering*, vol. 1043, no. 2, pp. 1–9, 2021.

[8] M. Cao, K. Zhang, N. zhang, and Z. Hu, "Interaction design of smart health preserving pot based on individual demand," *Package Engineering*, vol. 38, no. 8, pp. 225–229, 2017.

[9] R. Guan, "Research on internet-based mass customization of traditional garment enterprises-a case study of Qingdao redcollar group," *Apparel Engineering*, vol. 1, no. 6, pp. 96–98, 2017.

[10] S. Avikal, R. Singh, and R. Rashmi, "QFD and fuzzy Kano model based approach for classification of aesthetic attributes of SUV car profile," *Journal of Intelligent Manufacturing*, vol. 31, no. 2, pp. 271–284, 2020.

[11] M.-C. Chen, C.-L. Hsu and L.-H. Lee, "Service quality and customer satisfaction in pharmaceutical logistics: an analysis based on Kano model and importance-satisfaction model," *International Journal of Environmental Research and Public Health*, vol. 16, no. 21, pp. 1–23, 2020.

[12] G. Huang and L. Shao, "Research on hotel service quality management based on online reviews and IPA-Kano model," *Shanghai management science*, vol. 43, no. 6, pp. 12–17, 2021.

[13] M. Li and J. Zhang, "Integrating Kano model, AHP, and QFD methods for new product development based on text mining, intuitionistic fuzzy sets, and customers satisfaction," *Mathematical Problems in Engineering*, vol. 2021, no. 5, pp. 1–17, 2021.

[14] B. Xu, J. Yu, S. He, P. Shi, and Y. Wu, "Research on Kano model analysis method based on product review data," *Productivity research*, vol. 1, no. 9, pp. 10–15, 2020.

[15] Y. Liu, C. Jiang, Y. Ding, Z. Wang, X. Lv, and J. Wang, "Identifying helpful quality-related reviews from social media based on attractive quality theory," *Total quality management & business excellence*, vol. 30, no. 15, pp. 1596–1615, 2019.

[16] Y. Qu, T. Zhang, Y. Wen, and X. Zhang, "Attribute research of personal protective mask designing demands based on Kano model," *Chinese Journal of Ergonomics*, vol. 26, no. 6, pp. 15–20, 2020.

[17] Z. Li and Q. Xiang, "Quality demand identification and importance degree analysis of high-quality housing based on Kano model," *Construction economy*, vol. 41, no. 8, pp. 110–115, 2020.

[18] Q. Yang, S. Li, W. Wang, J. Zhang, and R. Luo, "Product positioning design decision based on optimal Kano analysis," *Journal of Machine Design*, vol. 37, no. 6, pp. 129–133, 2020.

[19] G. Fan, T. An, and W. Li, "Service optimization approaches based on the improved Kano model," *Journal of Chongqing university of technology*, vol. 35, no. 5, pp. 233–237, 2020.

[20] J. Nassibeh and A. Shahin, "Product value analysis: a developed cost–benefit analysis ratio based on the Kano and PAF models," *TQM Journal*, vol. 33, no. 1, pp. 1163–181, 2021.

Research Article

Evolutionary Game and Simulation of Green Housing Market Subject Behavior in China

Yingmiao Qian,[1,2] **Mengyuan Yu** [iD],[1] **Tao Wang,**[3] **Ruijia Yuan** [iD],[1] **Zhenan Feng,**[4] **and Xing Zhao**[1]

[1]*School of Management Science and Engineering, Anhui University of Finance and Economics, Bengbu 233030, China*
[2]*School of Management, Hefei University of Technology, Hefei 230009, China*
[3]*School of Public Administration, Chongqing University, Chongqing 400030, China*
[4]*School of Built Environment, Massey University, Palmerston North 4442, New Zealand*

Correspondence should be addressed to Ruijia Yuan; ruijiayuan@outlook.com

In China, driven by the national "3060" double carbon targets (i.e., reaching peak carbon emissions by 2030 and carbon neutrality by 2060), green housing has become one of the major fields to reduce carbon emissions, facilitating the achievement of the double carbon targets. Promoting the growth of green housing is an important way for the real estate industry to achieve low-carbon transformation and improve the quality of housing. Meanwhile, the construction industry also can benefit from green housing to achieve its energy conservation and emission reduction targets. Therefore, it is critical to boost and maintain the sustainable growth of the green housing market in China. However, the literature has not focused attention on the market behavior of the green housing market in China. This study proposes a tripartite evolutionary game model to investigate the subject behavior of the green housing market in China. This model consists of three major subjects in a green housing market: developers, consumers, and governments. Based on this model, this study analyzes the stability of the strategy options for each stakeholder and identifies the stable conditions of strategy portfolios to reach the equilibrium points of the game system. The validity of the proposed tripartite evolutionary game model is tested through the simulation of the impacts from various factors on system evolution. According to the impacts of factors and the stable conditions of strategies, this paper puts forward relevant policy suggestions for the healthy and sustainable growth of China's green housing market.

1. Introduction

Natural resources are being consumed enormously as a result of human uncontrolled exploitation, the resulting series of environmental problems such as greenhouse effect and extreme climate disasters has become increasingly serious [1]. The construction industry is an important area of final energy consumption and carbon dioxide emissions. According to the report released by the United Nations Environment Programme (UNEP), the construction industry accounted for 36% of the global final energy consumption and 37% of the energy-related carbon dioxide emissions in 2020 [2]. Therefore, energy conservation and

emission reduction in the construction industry is crucial to curb global climate change and achieve carbon neutrality goals. The high consumption brought about by traditional buildings has a serious negative impact on the sustainable development of society. In order to reduce the environmental load and achieve the development strategy of buildings adapting to the ecological environment, the green building comes into being. Green buildings have the characteristics of energy conservation, environmental protection, and resource conservation, as well as high economic benefits [3–6], which have a broad market prospect in advocating sustainable development today. Green housing is an important branch of green building. It emphasizes the

harmonious coexistence of residential area and environment. Therefore, the impact on the natural environment is taken into account in all activities such as design, construction, and operation, and the negative impact is controlled to the minimum as far as possible [7]. It can be said that green housing is the key to promote the high-quality development of housing construction and promote the green and sustainable development of cities. However, in the context of the country's vigorous development of green buildings, the market development of green housing still faces many problems. First, the low level of technological innovation and high development cost fundamentally hinder the development process [8, 9]; Second, for consumers, they often do not understand the benefits and health value of green housing but are unwilling to buy it because of its incremental cost [10]. Moreover, for developers, the development of green housing faces the dilemma of mismatch between income and expenditure, which hinders the promotion of green housing to a large extent [11]. Therefore, although green housing has the advantages of environment, society, and economy, they will only be considered for the development and adoption of green housing if the interests of major market players are guaranteed.

At this time, using incentive as a driving tool can encourage the adoption of green building and green housing to a certain extent [12, 13]. In general, incentives can be divided into external incentives and internal incentives. External incentives mainly come from the forced promotion of the government, which requires beneficiaries to meet specific conditions or requirements before benefiting, while internal incentives refer to attracting beneficiaries to be incentivized out of volition due to the value of green buildings [14]. Despite their differences, the vast majority of scholars recognize the positive role of the two. Guo et al. [15] affirmed the importance of government incentives and pointed out that legislation is the most effective way to promote the development of green buildings in Hong Kong, while expedited permits and density bonus can encourage market players to adopt green environmental protection voluntarily. He and Chen [16] found that the government subsidy policy has a positive incentive effect for the development of green buildings. Simultaneously subsidizing both developers and consumers obtain the highest social welfare. Therefore, in order to improve the popularity of green buildings, incentives should be provided to both developers and consumers. Bond [17] argued that the government sees the benefits of sustainable construction more through social and environmental benefits, while the private sector is driven more by economic returns. Moreover, when some investors pay more and more attention to corporate social responsibility and social responsibility investment, they will be more willing to promote the construction of green buildings. Love et al. [18] confirmed the catalytic role of clients in driving the sustainability agenda through a specific green building case, where building performance can be significantly improved when the client have a sustained drive and commitment to innovation.

The abovementioned research supports the effectiveness of green building incentive, but mainly focuses on specific incentive measures and policies. In the green building market, the key stakeholders have complex relationships and different needs; it is thus necessary to study the behavior strategies among them. Meng et al. [19] studied the behavior evolution process of the two main stakeholders of green building (contractors and government departments) under different reward and punishment policy combinations, so as to provide useful suggestions for the government to formulate reasonable incentive policies. Cohen et al. [20] used the prisoner's dilemma model to point out that developers and consumers do not adopt green houses, which belong to a suboptimal equilibrium. The government should provide incentives to developers and consumers, so as to make the green housing market move toward the optimal balance. Feng et al. [21] found the interest equilibrium point among green building stakeholders (government, construction units and consumers) by building a game model, so as to provide reference for the development of green building led by the government. Chen [22] analyzed the economic benefits of green building by building a bilateral game model between green building developers, consumers, and the government. The research found that the incremental profit of developers is the primary factor affecting enterprise decision-making, followed by the government's incentive policy, and the final strategic choice will be stabilized to higher economic benefits. Most literature analyzed the behavior strategies and interest conflicts of various subjects in the green building market, where the game relationship between government and developers; government and consumers; developers and consumers; government, developers, and consumers are key topics [23–25].

Throughout the existing literature, it is either limited to a single perspective, such as the incremental costs or payoffs of a tripartite subject and the equilibrium points of interests of subjects in a market, which fails to comprehensively look into the evolutionary path of the subject behavior of a green housing market or it focuses on how to formulate incentive policies to promote the growth of a green housing market; however, the benefits brought by incentive policies and consequently, the impacts of these benefits on the decision-making of governments are overlooked. For instance, how will a government make decisions and other subjects behave if incentive policies fail to deliver more benefits? Meanwhile, some researchers have built relevant models to analyze the behavioral evolution of green housing market subjects, but there is still little theoretical understanding of these models. Furthermore, the dynamic simulation and validation of these models are lacking.

Therefore, in order to bridge this knowledge gap, this study proposes a tripartite evolutionary game model, which considers developers, consumers, and governments, to investigate the subject behavior of the green housing market in China. This study also simulates the evolutionary path of the green housing market to validate the proposed model. The paper consists of the following parts: Section 1 introduces the background and summarizes the relevant literature. Section 2 puts forward model assumption and establishes the game model. Section 3 analyzes the model formulation. Section 4 carries on the numerical simulation. Section 5 draws the conclusion and implication. This study will

provide some reference value to the healthy and sustainable development of the green housing market in China.

2. Model Assumption and Formulation

2.1. Model Assumption. It is well known that the development of green housing market involves multistage decision-making by multiple stakeholders, among which the developers[①], consumers[②], and government[③] are the core subjects. The evolutionary game with them has the following five assumptions.

Assumption 1. In view of the fact that green housing market subjects are not completely rational and accurate in the process of acquiring knowledge and information, all three subjects are participants of bounded rationality who constantly adjust their strategies in the process of interaction and stabilize to optimal strategies over a period of evolution.

Assumption 2. The developers' strategic space $\alpha = (\alpha_1, \alpha_2) = $ (developing green housing, developing ordinary housing); Developers have a probability of x to choose α_1 and a probability of $(1 - x)$ to choose α_2. The consumers' strategic space $\beta = (\beta_1, \beta_2) = $ (purchasing green housing, purchasing ordinary housing); Consumers have a probability of y to choose β_1 and a probability of $(1 - y)$ to choose β_2. The governments' strategic space $\gamma = (\gamma_1, \gamma_2) = $ (providing incentive policies, providing no incentive policies); Governments have a probability of z to select γ_1 and a probability of $1 - z$ to select γ_2. x, y and z all belong to [0, 1].

Assumption 3. A_P is the sales payoff of developers from ordinary housing, while C_P is the development cost of ordinary housing. Meanwhile, A_P is also the spending of consumers purchasing ordinary housing. In the case of green housing, the incremental sales payoff from green housing is A_Z, the incremental development cost on green housing is C_z, and the potential payoff brought by green housing for developers is A_Q. The potential payoff has several streams, including the increased brand value, social image, and reputation resulted from developing green housing, the preferential treatments of taxation and mortgage, and the savings of land use and building materials in the process of development. In addition, when governments provide subsidies as incentive polices, developers get a subsidy of θD_2 from developing green housing, where θ is the proportion of governments' subsidy D_2.

Assumption 4. The payoffs of consumers is S_P when they purchase ordinary housing, with a spending of A_P. When purchasing green housing, the incremental residential utility payoffs obtained by consumers is φS_{Z1}, which includes the financial benefits from the savings of energy and water in the use of green housing. The incremental perception gains obtained by consumers is ηS_{Z2}, which includes the satisfaction and comfort brought by green housing to consumers. The incremental spending paid by consumers on green housing is A_Z. In addition, when governments provide subsidies as incentive polices, consumers who purchase green housing get subsidies $(1 - \theta) D_2$, where θ is the proportion of governments' subsidy D_2 received by developers.

Assumption 5. Governments have two strategies: either providing incentive polices or not. In the case of providing incentive polices, a management cost D_1 will occur as governments have to spend on the propaganda for environmental protection and the regulation and monitoring on environment to facilitate the social promotion of green housing. Consequently, the utility of the use of D_1 is G_1. Meanwhile, the social and environmental benefits brought by green housing are G_2. When both developers and consumers choose green housing, the total amount of subsidies given by governments as incentive polices is D_2. When developers choose green housing and consumers purchase ordinary housing, governments bear social environmental risk costs, which are D_3.

2.2. Model Formulation. According to the previous literature [21–25], combining with the abovementioned relative assumption, the tripartite evolutionary game model of a green housing market has been constructed. Moreover, the logical relationship between each subject in the evolutionary game is shown in Figure 1. Whether or not government incentives, developers have two choices: to develop green housing or to develop ordinary housing; consumers similarly have two choices: to purchase green housing or to purchase ordinary housing, the strategies are marked with arrows. Meanwhile, the mixed strategy payoff matrix of developers, consumers, and governments is constructed with the assumptions stated in Section 2.1, as shown in Table 1.

3. Derivation and Analysis of the Model Formula

3.1. Replicator Dynamics Equations and Phase Diagrams of Each Game Subject's Decision-Making

3.1.1. Developers. The expected payoff E_{11} of developers developing green housing, E_{12} of developing ordinary housing, and the average expected payoff E_1 are given below:

$$\begin{cases} E_{11} = yz\left[(A_p + A_Z) - (C_P + C_Z) + \theta D_2 + A_Q\right] + y(1 - z)\left[(A_p + A_Z) - (C_P + C_Z) + A_Q\right] + (1 - y)z\left[-(C_P + C_Z) + \theta D_2 + A_Q\right] \\ \quad + (1 - y)(1 - z)\left[-(C_P + C_Z) + A_Q\right], \\ E_{12} = yz(-C_P) + y(1 - z)(-C_P) + (1 - y)z(A_P - C_P) + (1 - y)(1 - z)(A_P - C_P), \\ E_1 = xE_{11} + (1 - x)E_{12}, \end{cases} \quad (1)$$
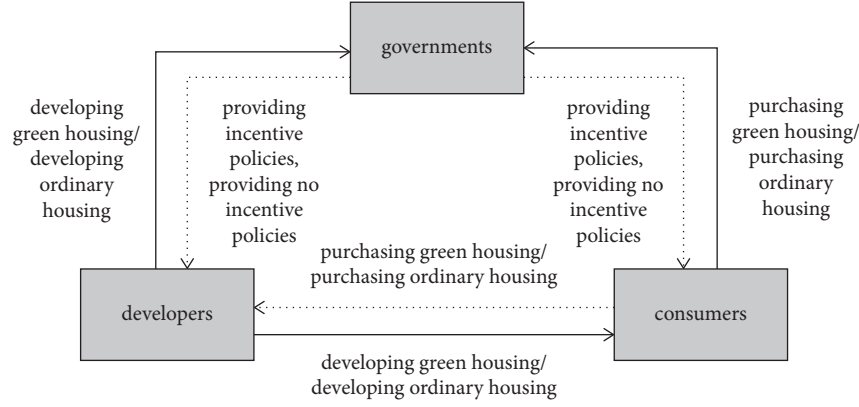
FIGURE 1: Logical relationship between each subject in the evolutionary game of a green housing market.

TABLE 1: Mixed strategy payoff matrix of developers, consumers, and governments.

The game party	Consumers[②]	Governments[③]	
		Providing incentive polices z	Providing no incentive polices$(1-z)$
Developers[①]			
Developing green housing x	Purchasing green housing y	①: $A_P + A_Z - (C_P + C_z) + \theta D_2 + A_Q$ ②: $S_P + \varphi S_{Z1} + \eta S_{Z2} - A_P - A_Z + (1-\theta)D_2$ ③: $G_1 + G_2 - D_1 - D_2$	①: $A_P + A_Z - (C_P + C_z) + A_Q$ ②: $S_P + \varphi S_{Z1} + \eta S_{Z2} - A_P - A_Z$ ③: G_2
	Purchasing ordinary housing $(1-y)$	①: $-(C_P + C_z) + \theta D_2 + A_Q$ ②: $S_P - A_P$ ③: $G_1 + G_2 - D_1 - \theta D_2 - D_3$	①: $-(C_P + C_z) + A_Q$ ②: $S_P - A_P$ ③: $G_2 - D_3$
Developing ordinary housing $(1-x)$	Purchasing green housing y	①: $-C_P$ ②: $S_P + \varphi S_{Z1} + \eta S_{Z2} - A_P - A_Z + (1-\theta)D_2$; ③: $G_1 - D_1 - (1-\theta)D_2$	①: $-C_P$ ②: $S_P + \varphi S_{Z1} + \eta S_{Z2} - A_P - A_Z$ ③: 0
	Purchasing ordinary housing $(1-y)$	①: $A_P - C_P$ ②: $S_P - A_P$ ③: $G_1 - D_1$	①: $A_P - C_P$ ②: $S_P - A_P$ ③: 0

The replicator dynamics equation of residential developers' decisions is as follows:

$$F(x) = \frac{d(x)}{dt} = x(E_{11} - E_1) = x(1-x)\left[y(2A_P + A_Z) + z\theta D_2 + A_Q - A_P - C_Z \right].$$ (2)

The first derivatives with respect to x and the set $G(y)$ are, respectively, as shown below:

$$\frac{d(F(x))}{dx} = (1-2x)\left[y(2A_P + A_Z) + z\theta D_2 + A_Q - A_P - C_Z \right],$$

$$G(y) = \left[y(2A_P + A_Z) + z\theta D_2 + A_Q - A_P - C_Z \right].$$ (3)

Based on the stability principle of differential equations, the probability of developers choosing developing green housing in a stable state must be satisfied by $F(x) = 0$, where $d(F(x))/dx < 0$. Because $\partial G(y)/\partial y > 0$, $G(y)$ is the increasing function of y. Therefore, when $y = [(A_P + C_Z) - A_Q - z\theta D_2]/(2A_P + A_Z) = y^*$, $G(y) = 0$; at this point, $d(F(x))/dx \equiv 0$, $F(x) \equiv 0$, which means that in a group of developers, any proportion of individuals

choosing developing green housing is a stable strategy. When $y < y^*$, $G(y) < 0$, $F'(x)|_{x=0} < 0$, $F'(x)|_{x=1} > 0$; at this point, $x = 0$ is the stable evolution point of developers, which means that when the proportion of consumers choosing purchasing green housing is less than $[(A_P + C_Z) - A_Q - z\theta D_2]/(2A_P + A_Z)$, developers will turn to ordinary housing. On the contrary, $x = 1$ is the stable evolution point of developers; in other words, developers will choose developing green housing. The decision-making

evolution phase diagrams of developers are shown in Figure 2.

3.1.2. Consumers. The expected payoff E_{21} of consumers for purchasing green housing, E_{22} for purchasing ordinary housing, and their average expected payoff E_2 are, respectively, as follows:

$$
\begin{cases}
E_{21} = xz\left[\left(S_p + \phi S_{Z1} + \eta S_{Z2}\right) - \left(A_P + A_Z\right) + (1-\theta)D_2\right] + x(1-z)\left[\left(S_p + \phi S_{Z1} + \eta S_{Z2}\right) - \left(A_P + A_Z\right)\right] \\
+ (1-x)z\left[\left(S_p + \phi S_{Z1} + \eta S_{Z2}\right) - \left(A_P + A_Z\right) + (1-\theta)D_2\right] + (1-x)(1-z)\left[\left(S_p + \phi S_{Z1} + \eta S_{Z2}\right) - \left(A_P + A_Z\right)\right], \\
E_{22} = xz\left(S_p - A_P\right) + x(1-z)\left(S_p - A_P\right) + (1-x)z\left(S_p - A_P\right) + (1-x)(1-z)\left(S_p - A_P\right), \\
E_2 = yE_{21} + (1-y)E_{22}.
\end{cases}
\tag{4}
$$

The replicator dynamics equation of consumers' decisions is as follows:

$$
F(y) = \frac{d(y)}{dt} = y(E_{21} - E_2) = y(1-y)\left[z(1-\theta)D_2 + \phi S_{Z1} + \eta S_{Z2} - A_Z\right].
\tag{5}
$$

The first derivatives with respect to y and the set $G(z)$ are, respectively, as follows:

$$
\frac{d(F(y))}{dy} = (1-2y)\left[z(1-\theta)D_2 + \phi S_{Z1} + \eta S_{Z2} - A_Z\right],
\tag{6}
$$

$$
G(z) = \left[z(1-\theta)D_2 + \phi S_{Z1} + \eta S_{Z2} - A_Z\right].
$$

Based on the stability principle of differential equations, the probability of consumers choosing purchasing green housing in a stable state must be satisfied by $F(y) = 0$, where $d(F(y))/dy < 0$. Because $\partial G(z)/\partial z > 0$, $G(z)$ is the increasing function of z. Therefore, when $z = (A_Z - \phi S_{Z1} - \eta S_{Z2})/(1-\theta)D_2 = z^*$, $G(y) = 0$; at this point, $d(F(y))/dy \equiv 0$, $F(y) \equiv 0$, which means that in a group of consumers, any proportion of individuals choosing purchasing green housing is a stable strategy. When $z < z^*$,

$G(z) < 0$, $F'(y)|_{x=0} < 0$, $F'(y)|_{x=1} > 0$; at this point, $y = 0$ is the stable evolution point of consumers, which means that when the probability of governments chooses providing incentive polices is less than $(A_Z - \phi S_{Z1} - \eta S_{Z2})/(1-\theta)D_2$, consumers will choose purchasing ordinary housing. On the contrary, $y = 1$ is the stable evolution point of consumers; in other words, consumers will choose purchasing green housing. The decision-making evolution phase diagrams of consumers are shown in Figure 3.

3.1.3. Governments. The expected payoff E_{31} of governments choosing incentive polices, E_{32} of governments choosing no incentive polices, and their average expected payoff E_3 are, respectively, as shown below:

$$
\begin{cases}
E_{31} = xy\left(G_1 + G_2 - D_1 - D_2\right) + x(1-y)\left(G_1 + G_2 - D_1 - \theta D_2 - D_3\right) \\
+ (1-x)y\left[G_1 - D_1 - (1-\theta)D_2\right] + (1-x)(1-y)\left(G_1 - D_1\right), \\
E_{32} = xyG_2 + x(1-y)\left(G_2 - D_3\right), \\
E_3 = zE_{31} + (1-z)E_{32}.
\end{cases}
\tag{7}
$$

The replicator dynamics equation of governments' decisions is as follows:
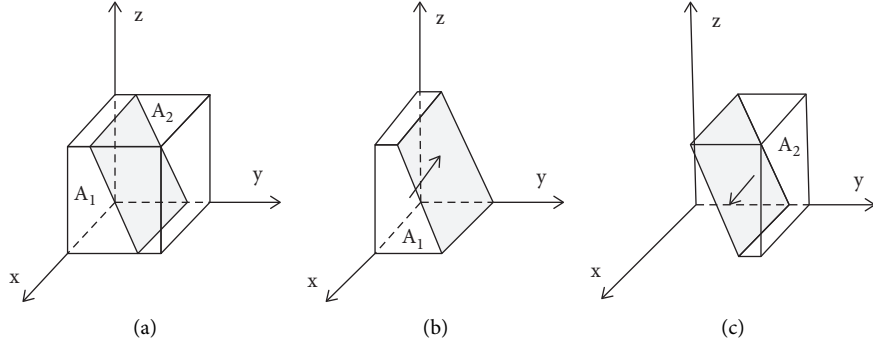
FIGURE 2: Evolution phase diagrams of developers' decisions in the case of develop green housing. (a) $y = y^*$, y is equal to the stable point. (b) $y < y^*$, y is less than the stable point. (c) $y > y^*$, y is greater than the stable point.
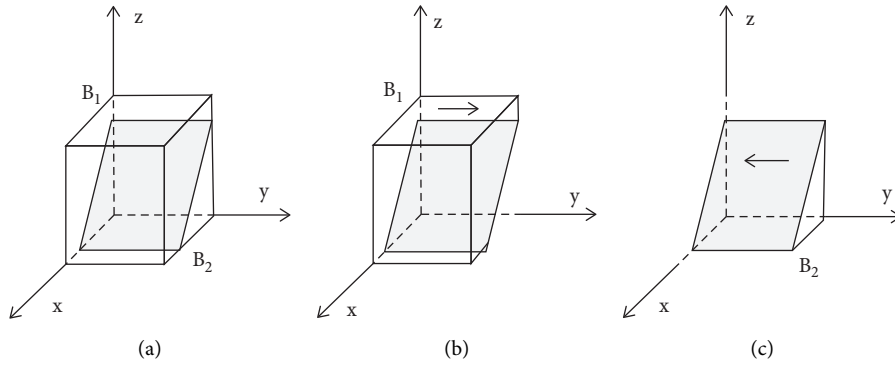
FIGURE 3: Evolution phase diagrams of consumers' decisions in the case of purchasing green housing. (a) $z = z^*$, z is equal to the stable point. (b) $z > z^*$, z is greater than the stable point. (c) $z < z^*$, z is less than the stable point.

$$F(z) = \frac{d(z)}{dt} = z(E_{31} - E_3) = z(1 - z)[G_1 - D_1 - x\theta D_2 - y(1 - \theta)D_2]. \tag{8}$$

The first derivatives with respect to z and the set $G(x)$ are, respectively, as shown below:

$$\frac{d(F(z))}{dz} = (1 - 2z)[G_1 - D_1 - x\theta D_2 - y(1 - \theta)D_2],$$

$$G(x) = [G_1 - D_1 - x\theta D_2 - y(1 - \theta)D_2]. \tag{9}$$

Based on the stability principle of differential equations, the probability of governments choosing incentive polices in a stable state must be satisfied by $F(z) = 0$, where $d(F(z))/dz < 0$. Because $\partial G(x)/\partial y < 0$, $G(x)$ is the decreasing function of x. Therefore, when $x = [G_1 - D_1 - y(1 - \theta)D_2]/\theta D_2 = x^*$, $G(x) = 0$; at this point, $d(F(z))/dz \equiv 0$, $F(z) \equiv 0$, which means that in governments, any proportion of individuals choosing incentive polices is a stable strategy. When $x < x^*$, $G(x) > 0$, $F'(z)|_{z=0} > 0$, $F'(z)|_{z=1} < 0$; at this point, $z = 1$ is the stable evolution point of governments, which means that when the proportion of developers choosing developing green housing is less than $[G_1 - D_1 - y(1 - \theta)D_2]/\theta D_2$, governments will provide incentive polices to encourage the development of green housing. On the contrary, $z = 0$ is the stable evolution point of governments; in other words,

governments will not choose incentive polices. The decision-making evolution phase diagram of governments is shown in Figure 4.

3.2. Stability Analysis of Each Game Subject's Decision-Making.
The simultaneous game of the replicator dynamics equations of three game subjects forms up a three-dimensional discrete dynamical system.

$$\begin{cases} F(x) = x(1 - x)[y(2A_P + A_Z) + z\theta D_2 + A_Q - A_P - C_Z] = 0, \\ F(y) = y(1 - y)[z(1 - \theta)D_2 + \phi S_{Z1} + \eta S_{Z2} - A_Z] = 0, \\ F(z) = z(1 - z)[G_1 - D_1 - x\theta_2^D - y(1 - \theta)D_2] = 0. \end{cases} \tag{10}$$

Thirteen strategic equilibrium points are obtained by solving the equilibrium points of the discrete dynamical system: $E_1[0, 0, 0]$, $E_2[0, 0, 1]$, $E_3[1, 0, 0]$, $E_4[0, 1, 0]$, $E_5[1, 1, 0]$, $E_6[0, 1, 1]$, $E_7[1, 0, 1]$, $E_8[1, 1, 1]$, $E_9[0, y_0, z_0]$, $E_{10}[1, y', z']$, $E_{11}[x_1, 0, z_1]$, $E_{12}[x_2, 1, z_2]$, and $E_{13}[x_3, y_1, z_3]$. Among them, E_1–E_8 are the pure strategic equilibrium points for the three subjects of a green housing market; E_9–E_{12} are the pure strategic equilibrium points for a single subject of a green housing market; and E_{13} is the mixed strategic equilibrium
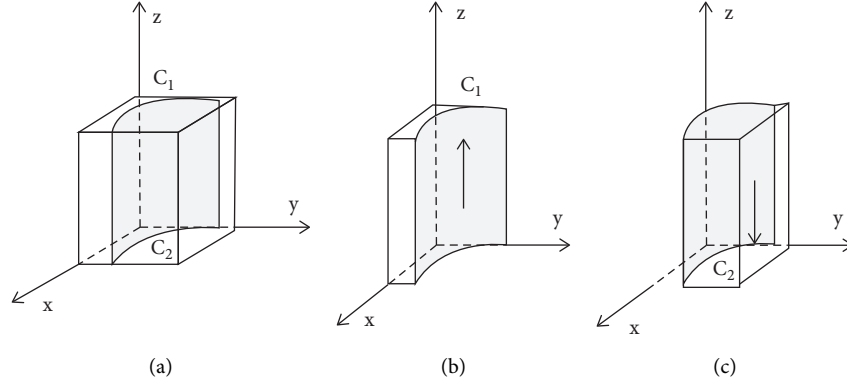
FIGURE 4: Evolution phase diagrams of governments in the case of choosing incentive polices. (a) $x = x^*$, x is equal to the stable point. (b) $x < x^*$, x is less than the stable point. (c) $x > x^*$, x is greater than the stable point.

point. Some scholars have pointed out that the stable solution of the replicator dynamics system in a multigroup evolutionary game is a strict Nash equilibrium solution. Therefore, except for the eight equilibrium points $(E_1–E_8)$, the remaining states are not asymptotically stable.

Based on the Lyapunov stability theory, the stability of a system at an equilibrium point is determined by the eigenvalues of a Jacobian matrix. When all the eigenvalues have negative real parts, an equilibrium point is asymptotically stable. When at least one of the eigenvalues has a positive real part, an equilibrium point is unstable. When all eigenvalues except those with zero real parts have negative real parts, an equilibrium point is in a critical state and the stability cannot be determined by the sign of an eigenvalue. Therefore, the Jacobian matrix of the discrete dynamical system can be obtained by integrating formula (10) as follows:

$$
J = \begin{vmatrix} \dfrac{\partial F(x)}{\partial(x)} & \dfrac{\partial F(x)}{\partial(y)} & \dfrac{\partial F(x)}{\partial(z)} \\[2mm] \dfrac{\partial F(y)}{\partial(x)} & \dfrac{\partial F(y)}{\partial(y)} & \dfrac{\partial F(y)}{\partial(z)} \\[2mm] \dfrac{\partial F(z)}{\partial(x)} & \dfrac{\partial F(z)}{\partial(y)} & \dfrac{\partial F(z)}{\partial(z)} \end{vmatrix} = \begin{vmatrix} J_{11} & x(1-x)(2A_P + A_Z) & x(1-x)\theta D_2 \\[2mm] 0 & J_{22} & y(1-y)(1-\theta)D_2 \\[2mm] z(z-1)\theta D_2 & z(z-1)(1-\theta)D_2 & J_{33} \end{vmatrix}, \tag{11}
$$

where

$$
J_{11} = (1-2x)\big[y(2A_P + A_Z) + z\theta D_2 + A_Q - A_P - C_Z\big],
$$
$$
J_{22} = (1-2y)\big[z(1-\theta)D_2 + \phi S_{Z1} + \eta S_{Z2} - A_Z\big],
$$
$$
J_{33} = (1-2z)\big[G_1 - D_1 - x\theta D_2 - y(1-\theta)D_2\big]. \tag{12}
$$

$E_1–E_8$ were substituted into the Jacobian matrix to obtain their eigenvalues and analyze the stability of equilibrium points. The detailed results are shown in Table 2.

Corollary 1. *When $A_Q - A_P - Cz < 0$ and $G_1 - d_1 < 0$, the replicator dynamical system has a unique stable equilibrium point $E_1[0, 0, 0]$.*

Proof. According to Chart 2, at this point, condition ① is met, $E_1[0, 0, 0]$ is the stable equilibrium point, and $C_Z + A_P - A_Q > 0$, $D_2 + D_1 - G_1 > 0$. Therefore, $E_3[1, 0, 0]$ and

$E_8[1, 1, 1]$ are also instable points. It is concluded that $E_1[0, 0, 0]$ is unique.

Corollary 1 shows that when the potential payoff of developers developing green housing is less than the sum of incremental payoffs and incremental costs, and the payoff of governments promoting green housing is less than the sum of incremental payoffs and incremental costs, both developers and governments will not choose developing and promoting green housing. Consequently, a green housing market will disappear. □

Corollary 2. *When $A_Q - A_P - C_Z > 0$ and $G_1 - D_1 - \theta D_2 < 0$, the replicator dynamical system has a unique stable equilibrium point $E_3[1, 0, 0]$. Corollary 2 can be proved following the same way to proof Corollary 1. Corollary 2 shows that when the potential payoff of developers developing green housing is greater than the sum of incremental payoffs and incremental costs, and the payoff of governments promoting green housing is less than the one without incentive policies,*

TABLE 2: Eigenvalues of the Jacobian matrix and local stability judgment of equilibrium point.

Equant equation	Eigenvalues of the Jacobian matrix $\lambda_1, \lambda_2, \lambda_3$	Real component symbol	Stability conclusion	Condition
$E_1[0, 0, 0]$	$A_Q - A_P - C_Z, \varphi S_{Z1} + \eta S_{Z2} - A_Z, G_1 - D_1$	$(\times, -, \times)$	Stable point	①
$E_2[0, 0, 1]$	$\theta D_2 + A_Q - A_P - C_Z, (1-\theta)D_2 + \varphi S_{Z1} + \eta S_{Z2} - A_Z, D_1 - G_1$	$(\times, +, \times)$	Instable point	—
$E_3[1, 0, 0]$	$C_Z + A_P - A_Q, \varphi S_{Z1} + \eta S_{Z2} - A_Z, G_1 - D_1 - \theta D_2$	$(\times, -, \times)$	Stable point	②
$E_4[0, 1, 0]$	$A_Q + A_P + A_Z - C_Z, A_Z - \varphi S_{Z1} - \eta S_{Z2}, G_1 - D_1 - (1-\theta)D_2$	$(+, +, -)$	Instable point	—
$E_5[1, 1, 0]$	$C_Z - A_P - A_Z - A_Q, A_Z - \varphi S_{Z1} - \eta S_{Z2}, G_1 - D_1 - D_2$	$(-, -, +)$	Instable point	—
$E_6[0, 1, 1]$	$\theta D_2 + A_Q + A_P + A_Z - C_Z, A_Z - \varphi S_{Z1} - \eta S_{Z2} - (1-\theta)D_2, (1-\theta)D_2 + D_1 - G_1$	$(+, -, -)$	Instable point	—
$E_7[1, 0, 1]$	$C_Z + A_P - \theta D_2 - A_Q, (1-\theta)D_1 + \varphi S_{Z1} + \eta S_{Z2} - A_Z, \theta D_2 + D_1 - G_1$	$(+, +, -)$	Instable point	—
$E_8[1, 1, 1]$	$C_Z - A_Z - A_P - \theta D_2 - A_Q, A_Z - \varphi S_{Z1} - \eta S_{Z2} - (1-\theta)D_2, D_2 + D_1 - G_1$	$(-, -, \times)$	Stable point	③

Note. x means the symbol is uncertain, ① $A_Q - A_P - C_Z < 0, G_1 - D_1 < 0$; ② $C_Z + A_P - A_Q < 0, G_1 - D_1 - \theta D_2 < 0$; ③ $D_2 + D_1 - G_1 < 0$.

developers will still be willing to develop green housing. The reason is that developers think highly of huge potential payoffs in the future. However, this strategy is only theoretically stable. When consumers choose purchasing ordinary housing, a green housing market does not grow.

Corollary 3. *When $D_2 + D_1 - G_1 < 0$, the replicator dynamical system has a unique stable equilibrium point $E_8[1, 1, 1]$.* Corollary 3 can be proved following the same way to prove Corollary 1. Corollary 3 shows that when the payoffs of incentive polices adopted by governments greater than their costs, developers will choose developing green housing, consumers will choose purchasing green housing, and governments will actively encourage them. The subjects of a green housing market jointly promote the sustainable and healthy growth of the market.

4. Numerical Simulation

In order to validate the stability of the evolution of green housing market subject behavior, the replicator dynamical system was assigned with numerical values for numerical simulation analysis. The determination method of numerical value is similar to the method of numerical selection in references [20–22], which is to obtain first-hand data by investigating consumers, developers, and leaders of government departments, and comparing the dimensions of the data to obtain the relative value [26]. Due to the limited length, this study selected numerical values, where $A_P = 50$, $A_Z = 40$, $\theta = 0.5$, $D_2 = 40$, $A_Q = 30$, $C_Z = 50$, $\varphi = 0.5$, $S_{Z1} = 30$, $\eta = 0.5$, $S_{Z2} = 30$, $G_1 = 160$, and $D_1 = 90$. The impacts of A_Z, A_Q, θ, η, and D_2 on the process and results of the system evolutionary game were analyzed when the conditions of $C_Z - A_Z - A_P - \theta D_2 - A_Q < 0$, $A_Z - \varphi S_{Z1} - \eta S_{Z2} - (1-\theta)D_2 < 0$, and $D_2 + D_1 - G_1 < 0$ were satisfied.

4.1. Impacts of Incremental and Potential Payoffs of Developers Choosing Developing Green Housing on the System Evolutionary Game. According to Figure 5, when a green housing market is approaching a state of stability, the incremental payoff of developing green housing for developers is
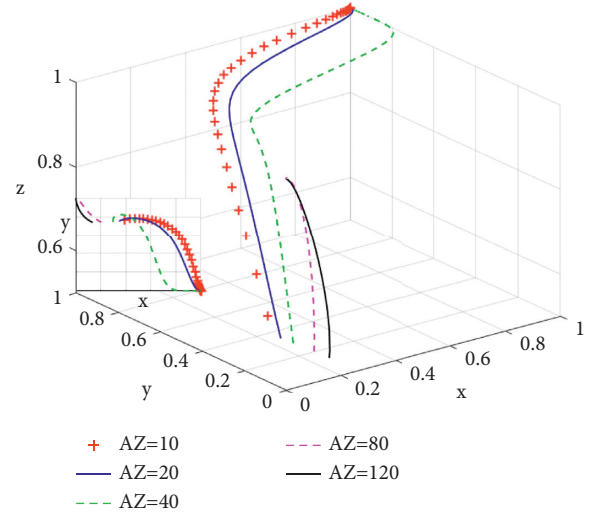
FIGURE 5: Influence of incremental income A_Z on the system evolutionary game.

increasing, and the evolutionary speed of green housing development is accelerating. With the increase of A_Z, the probability of developing green housing for developers is increasing. When A_Z reaches over 80, however, the system enters a state of instability. At this time, the increase of green housing incremental payoffs brings the increase of incremental costs for consumers purchasing green housing. When incremental costs reach a certain extent, consumers turn to ordinary housing, leading to a state of instability for a green housing market. This shows as a profitable enterprise, the developers excessively pass on the cost of green housing to consumers, thereby result in green housing market instability, which is in accord with Jiang and Payne [27].

As can be seen from Figure 6, when a green housing market is approaching a state of stability, the increase of potential income of green housing obtained by developers will accelerate the evolution speed of green housing development by developers. The application of green strategies such as the solar system and water saving technology can help contribute to building up developers' competitive advantages and bring a potential income for developers [28]. In
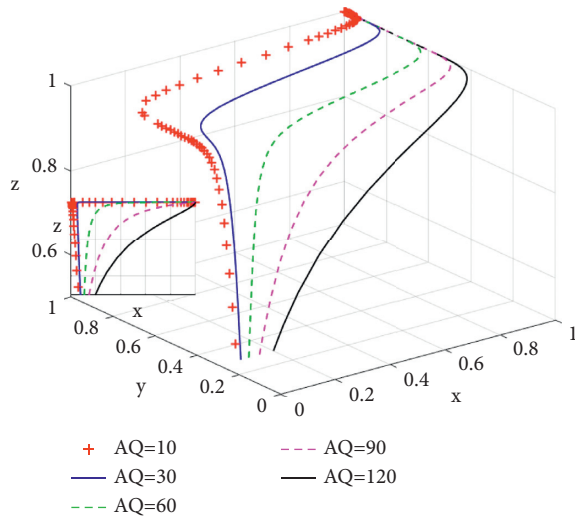
FIGURE 6: Influence of potential returns A_Q on the system evolutionary game.

FIGURE 7: Influence of incremental return coefficient $1 - \theta$ on the system evolutionary game.

other words, with the increase of A_Q, the probability of developing green housing for developers is increasing. In the case where governments provide incentive polices, the greater potential payoffs are the earlier a green housing market enters a stable state.

4.2. Impacts of Consumers' Green Housing Subsidies and Green Perception on the System Evolutionary Game.

According to Figure 7, when the total subsidy D_2 for green housing remains unchanged and $1 - \theta$ does not exceed 0.1 (i.e., the proportion of subsidies for consumers is low), the proportion of consumers choosing purchasing green housing drops from 0.3 to 0. However, when the proportion of subsidies $1 - \theta$ increases gradually, the proportion of consumers choosing purchasing green housing increases, and the evolutionary speed of consumers choosing green housing increases as well. He et al. [29] support the idea that the government encourages potential buyers of green houses to purchase through financial subsidies.

Green perception refers to consumers' satisfaction and comfort brought by green housing and essentially represents consumers' cognitive level of environmental protection, thereby determines the willingness to purchase, which is consistent with Guo et al. [30]. As shown in Figure 8, when green perception is low (i.e., η is less than 0.1), even if subsidies from governments for purchasing green housing are in place, the proportion of consumers choosing purchasing green housing drops from 0.3 to 0 at the beginning of system evolution. This means consumers only purchase ordinary housing. However, with the increase of green perception η, the proportion of consumers choosing purchasing green housing increases and the evolutionary speed of consumers choosing green housing increases as well.

4.3. Impacts of the Total Amount of Subsidies and Social Promotion for Green Housing on the System Evolutionary Game.

As shown in Figure 9, when the incremental payoff θ
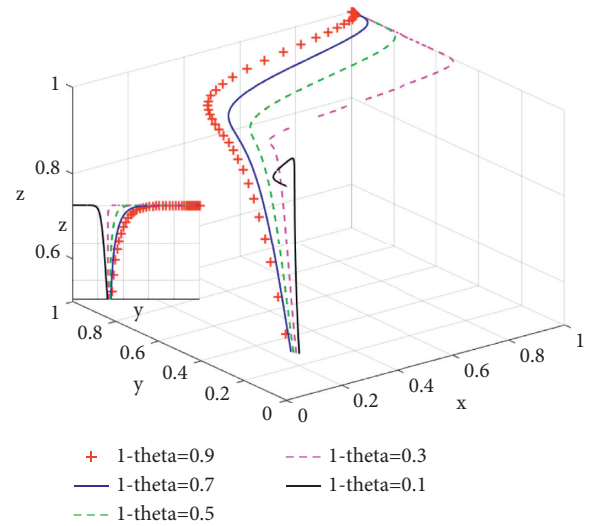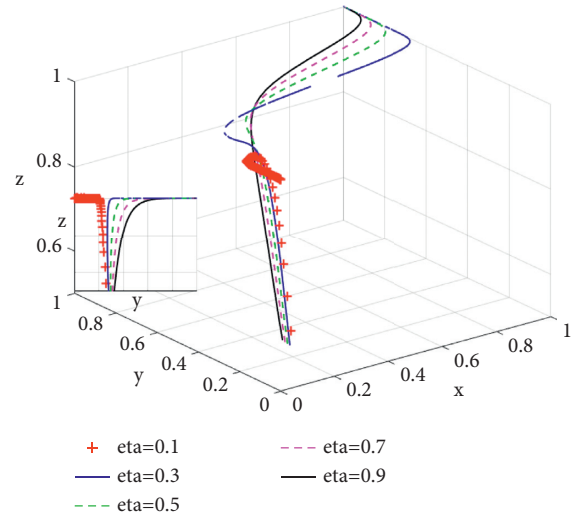
FIGURE 8: Influence of green perception coefficient η on the system evolution game.

is constant, the total amount of subsidies D_2 provided by governments as incentive polices has a significant impact on developers' decisions. When the total amount of subsidies D_2 is less than 10, the proportion of developers choosing developing green housing decreases from 0.3 to 0. When the total amount of subsidies D_2 is gradually increasing, the proportion of developers choosing developing green housing is gradually increasing from the initial value 0.3, and the evolutionary speed of developers choosing developing green housing is increasing as well, which is in line with the studies by He and Chen [16].

According to Figure 10, when governments use propaganda of environmental protection and deploy regulation and monitoring on environment, the social promotion effect of green housing is limited. In other words, when $G_1 = 100$, the proportion of developers choosing green housing gradually decreases from the initial value 0.3. When
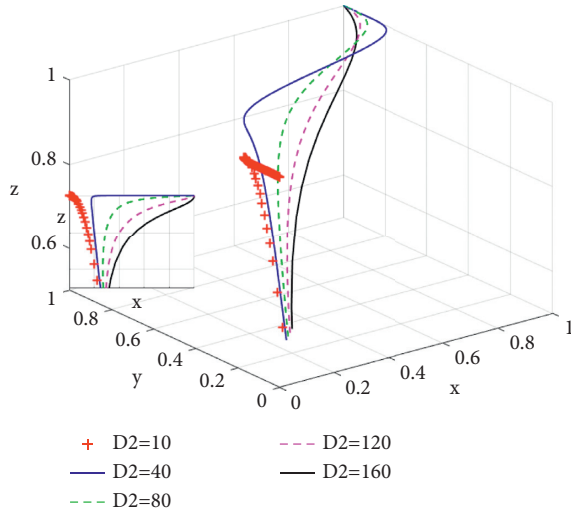
FIGURE 9: Influence of total green housing subsidy D_2 on the system evolution game.
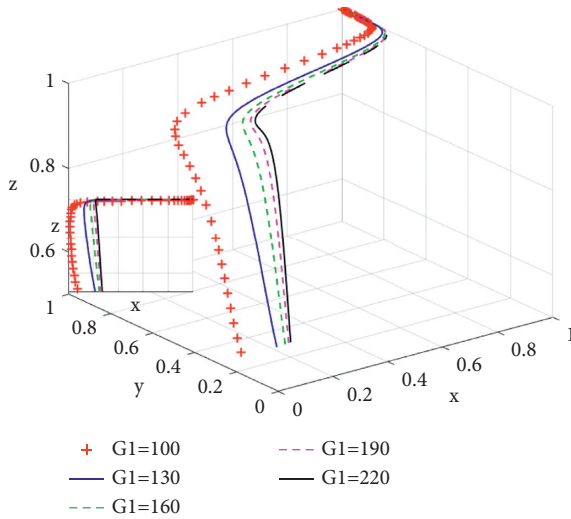
FIGURE 10: Influence of social promotion effect G_1 on the systematic evolutionary game.

intensive propaganda of environmental protection and strong environmental monitoring and regulation are in place, the social promotion of green housing becomes effective. With the increase of the proportion of government incentive policies, the proportion of developers choosing green housing increases and the evolutionary speed of the system increases.

5. Conclusion and Implications

The purpose of this research was to examine that how the behavioral decisions of developers, consumers, and governments among green housing market subjects affect the growth of green housing. First, this study builds a tripartite evolutionary game model to investigate a green housing

marketing, which includes developers, consumers, and governments. Second, this study obtains a three-dimensional discrete dynamic system and identifies the stable conditions of strategy portfolios to reach the equilibrium points of the game system based on the Lyapunov stability theory. Finally, this study assigns real-world values to the proposed tripartite evolutionary game model and conducts numerical simulation to test the influence and relationship of each factor on system evolution, validating the proposed model. Moreover, the results of this study reveal that developers should not blindly pursue the incremental payoffs brought by green housing; otherwise, consumers may turn to ordinary housing. Similarly, the potential earnings from green housing will make green housing more favorable to developers. Moreover, regarding consumers, the perception of green housing determines the demand intensity from consumers. Meanwhile, the more subsidies provided by governments, the more enthusiastic consumers will be in purchasing green housing. Furthermore, when governments do not provide or provide mild subsidies, both developers and consumers will embrace ordinary housing. In addition, governments can effectively increase the initiatives of developers and improve the awareness of consumers toward green housing through intensive propaganda of greenness and environmental protection and strong regulation of environment.

In addition, this study generates the following implications to the sustainable and healthy growth of green housing markets in China.

First, developers are the suppliers in a green housing market, who undertake the development task of green housing. In the process of green housing development, it is not feasible for developers to blindly pursue incremental payoffs brought by green housing. The increase of incremental payoffs for developers will result in the increase of incremental costs for consumers, where consumers may turn to ordinary housing as they cannot afford green housing. This is evident in our simulation when A_Z climbs over 80, the system of a green housing market enters a state of instability. Similarly, the increase of potential payoffs for developers will promote the development of green housing. There are various approaches to increase the potential payoffs for developers, such as taxation deductions and mortgage discounts. By applying these approaches, more developers will be encouraged to enter a green housing market.

Second, consumers are the demand side in a green housing market. Their perceptions toward green housing determines their demand intensity. Therefore, strengthening the publicity of green housing, improving consumers' understanding of green housing, and enhancing consumers' awareness of green housing are necessary measures to initiate the motivation of consumers to purchase green housing. At the same time, subsidies provided by governments to purchase green housing have a strong effect on the will of consumers to purchase green housing. This is demonstrated in our simulation where the increase of the subsidy $1 - \theta$ for consumers will lead to the increase of the

proportions of consumers who purchase green housing. Therefore, high subsidies can boost the demand side in a green housing market, facilitating the healthy and sustainable growth of green housing markets in China.

Lastly, governments are the facilitators and regulators in a green housing market. Governments formulate and implement relevant incentive polices to promote the growth of a green housing market. The incentives and subsidies provided by governments play a key role in cultivating and promoting a green housing market. If governments do not provide or provide little subsidies, both developers and consumers will turn to ordinary housing due to the large incremental costs of developing and purchasing green housing. Our simulation generates a similar result. When the total amount of the subsidy for green housing is less than ten units, developers will choose developing ordinary housing. In addition to subsidies, governments have other measures to stimulate the growth of a green housing market, such as intensive propaganda of environmental protection and strong regulations on built environment. By doing this, governments can boost the initiative of developers to develop green housing and the understanding of green housing for consumers. This is supported in our simulation where a higher effect of green housing promotion can result in a higher supply and demand of green housing. Therefore, intense incentives can accelerate the growth of green housing markets in China. While this study has two limitations such as considering merely the mainland Chinese greenhouse market, ignoring the difference of consumers' educational background and capital, which need to be further researched in the future.

Data Availability

The simulation part of this paper involves data, which are relative data and represent the degree of correlation. The data come from two parts: one is based on the research data of previous scholars and the other is obtained through interviews with relevant personnel of developers, consumers, and governments involved in the real estate market.

Conflicts of Interest

The authors declare that they have no conflicts of interest regarding the publication of this paper.

Acknowledgments

References

[1] Z. Wu, Q. He, Q. Chen, H. Xue, and S. Li, "A topical network based analysis and visualization of global research trends on green building from 1990 to 2020," *Journal of Cleaner Production*, vol. 320, 2021.

[2] United Nations Environment Programme, *Global Status Report for Buildings and Construction: Towards a Zero-Emission*, Efficient and Resilient Buildings and Construction Sector, Nairobi, 2021.

[3] B. Cheng, K. Lu, J. Li, H. Chen, X. Luo, and M. Shafique, "Comprehensive assessment of embodied environmental impacts of buildings using normalized environmental impact factors," *Journal of Cleaner Production*, vol. 334, 2022.

[4] L. N. Dwaikat and K. N. Ali, "The economic benefits of a green building - e," *Journal of Building Engineering*, vol. 18, pp. 448–453, 2018.

[5] L. Zhang, J. Wu, and H. Liu, "Turning green into gold: a review on the economics of green buildings," *Journal of Cleaner Production*, vol. 172, pp. 2234–2245, 2018.

[6] Z. Wu, M. Jiang, Y. Cai, H. Wang, and S. Li, "What hinders the development of green building? An investigation of China," *International Journal of Environmental Research and Public Health*, vol. 16, no. 17, 2019.

[7] N. Z. Abidin, N. Yusof, and H. Awang, "A foresight into green housing industry in Malaysia," *International Journal of Mechanical and Industrial Engineering*, vol. 6, no. 7, pp. 373–381, 2012.

[8] G. Seyfang, *Grassroots Innovations in Low-Carbon Housing*, pp. 1–29, University of East Anglia, Norwich, England, 2008.

[9] M. Sauer and K. Siddiqi, "Incentives for green residential construction," in *Proceedings of the 2009 Construction Research Congress*, pp. 578–586, Seattle, WA, USA, April 2009.

[10] M. H. Issa, J. H. Rankin, and A. J. Christian, "perception of research work investigating the cost premiums, long-term costs and health and productivity benefits of green buildings," *Building and Environment*, vol. 45, no. 7, pp. 1698–1711, 2010.

[11] Y. Deng and J. Wu, "Economic returns to residential green building investment: the developers' perspective," *Regional Science and Urban Economics*, vol. 47, pp. 35–44, 2014.

[12] E. Choi, "Green on buildings: the effects of municipal policy on green building designations in America's central cities," *Journal of Sustainable Real Estate*, vol. 2, no. 1, pp. 1–21, 2010.

[13] J. R. Dubose, S. J. Bosch, and A. R. Pearce, "Analysis of state-wide green building policies," *Journal of Green Building*, vol. 2, no. 2, pp. 161–177, 2007.

[14] O. A. Olubunmi, P. B. Xia, and M. Skitmore, "Green building incentives: a review," *Renewable and Sustainable Energy Reviews*, vol. 59, pp. 1611–1621, 2016.

[15] Z. Gou, S. S.-Y. Lau, and D. Prasad, "Market readiness and policy implications for green buildings: case study from Hong Kong," *Journal of Green Building*, vol. 8, no. 2, pp. 162–173, 2013.

[16] L. He and L. Chen, "The incentive effects of different government subsidy policies on green buildings," *Renewable and Sustainable Energy Reviews*, vol. 135, 2021.

[17] S. Bond, "Lessons from the leaders of green designed commercial buildings in Australia," *Pacific Rim Property Research Journal*, vol. 16, no. 3, pp. 314–338, 2010.

[18] P. E. D. Love, M. Niedzweicki, P. A. Bullen, and D. J. Edwards, "Achieving the green building council of Australia's world leadership rating in an office building in perth," *Journal of Construction Engineering and Management*, vol. 138, no. 5, pp. 652–660, 2012.

[19] Q. Meng, Y. Liu, Z. Li, and C. Wu, "Dynamic reward and penalty strategies of green building construction incentive: an evolutionary game theory-based analysis," *Environmental*

Science and Pollution Research, vol. 28, no. 33, pp. 44902–44915, 2021.

[20] C. Cohen, D. Pearlmutter, and M. Schwartz, "A game theory-based assessment of the implementation of green building in Israel," *Building and Environment*, vol. 125, no. 11, pp. 122–128, 2017.

[21] Q. Feng, H. Chen, X. Shi, and J. Wei, "Stakeholder games in the evolution and development of green buildings in China: government-led perspective," *Journal of Cleaner Production*, vol. 275, 2020.

[22] Z. Chen, "Economic benefit analysis of green building based on fuzzy logic and bilateral game model," *Journal of Intelligent and Fuzzy Systems*, vol. 37, no. 15, pp. 1–13, 2019.

[23] S. Yin, B. Li, and Z. Xing, "The governance mechanism of the building material industry (BMI) in transformation to green BMI: the perspective of green building," *The Science of the Total Environment*, vol. 677, pp. 19–33, 2019.

[24] X. Yang, J. Zhang, G. Q. Shen, and Y. Yan, "Incentives for green retrofits: an evolutionary game analysis on Public-Private-Partnership reconstruction of buildings," *Journal of Cleaner Production*, vol. 232, pp. 1076–1092, 2019.

[25] Q. Du, Y. Yan, Y. Huang, C. Hao, and J. Wu, "Evolutionary games of low-carbon behaviors of construction stakeholders under carbon taxes," *International Journal of Environmental Research and Public Health*, vol. 18, no. 2, 2021.

[26] Z. Wu, H. Li, Y. Feng, X. Luo, and Q. Chen, "Developing a green building evaluation standard for interior decoration: a case study of China," *Building and Environment*, vol. 152, pp. 50–58, 2019.

[27] H. Jiang and S. Payne, "Green housing transition in the Chinese housing market: a behavioural analysis of real estate enterprises," *Journal of Cleaner Production*, vol. 241, 2019.

[28] X. Zhang, L. Shen, and Y. Wu, "Green strategy for gaining competitive advantage in housing development: a China study," *Journal of Cleaner Production*, vol. 19, no. 2-3, pp. 157–167, 2011.

[29] C. He, S. Yu, Q. Han, and B. de Vries, "How to attract customers to buy green housing? Their heterogeneous willingness to pay for different attributes," *Journal of Cleaner Production*, vol. 230, pp. 709–719, 2019.

[30] X. Guo, Z. Fan, H. Zhu, X. Chen, M. Wang, and H. Fu, "Willingness to pay for healthy housing during the COVID-19 pandemic in China: evidence from eye tracking experiment," *Frontiers in Public Health*, vol. 10, 2022.

Research Article

Collaborative Supply Mechanism of Government-Subsidized Rental Housing from the Perspective of Tripartite Evolutionary Game in Metropolitan Cities of China

Xiaojun Liu ,[1] Jie Dong ,[1] Peng Cui ,[2] Mengmeng Wang ,[1,3] and Xiaotong Guo [1,3]

[1]School of Management, Xi'an University of Architecture and Technology, Xi'an 710055, China
[2]College of Civil Engineering, Nanjing Forestry University, Nanjing 210037, China
[3]Laboratory of Neuromanagement in Engineering, Xi'an University of Architecture and Technology, Xi'an 710055, China

Correspondence should be addressed to Xiaotong Guo; guoxiaotong@xauat.edu.cn

With the advancement of urbanisation, the inflow of population in China's large cities has been increasing and the demand for rental housing of "new citizens" with insufficient housing affordability has become increasingly strong. Therefore, the Chinese government proposes to provide government-subsidized rental housing (GSRH) different from public rental housing. At present, the supply mode of public rental housing in China is mainly government construction and operation, which has the problems of low supply efficiency and low service level. It is critical to explore an efficient supply model in the construction of the GSRH system. Therefore, this study, starting from the three supply subjects of government, market, and society, constructs an evolutionary game model and uses agent-based modelling simulation to explore how multisubjects achieve optimal collaboration in the supply process of GSRH. The results are as follows: First, the development of a collaborative supply system includes four stages: noncooperative behaviour, collaborative exploration, collaborative game, and three-subject collaborative supply. Second, the government is the core of realising multisubject coordination. Increasing government supervision will boost market participation, while increasing government subsidies can fully mobilise the enthusiasm of social subjects but cannot continuously improve the market's enthusiasm. Third, increasing the participation ratio of social subjects will help mobilise the enthusiasm of other subjects to participate, while the excessive participation ratio of market subjects may cause an imbalance in the collaborative supply system. This study provides theoretical support for the efficient supply of GSRH.

1. Introduction

China is currently experiencing the largest scale of urbanisation ever known in human history, with its ratio expected to reach 69 percent in 2030 [1]. The seventh census results show that the national floating population was 376 million in 2020, an increase of nearly 70 percent in 10 years [2]. The acceleration of China's urbanisation process has led to strong demand for housing rentals among "new citizens" in the net inflow of population of big cities such as Beijing and Shanghai. The concept of "new citizens" refers to the population that flows from other places and lives stably in cities, including groups of migrant workers, newly employed college students, and other groups. Owing to the lack of

housing affordability, the housing needs of this group are mainly concentrated in rental housing. However, for a long time, China's real estate market and housing security system have emphasised sales over rent, the housing rental market has not been fully developed, the structure of supply and demand is unbalanced, and the large-scale rental market has not been supported by special policies. Therefore, the new citizen group has become a "sandwich layer" group that neither is within the coverage of public rental housing (PRH) nor can afford commercial housing, bearing the housing pressure and crowding-out effect caused by high housing prices [3]; thus, it is a prominent problem that they cannot afford to buy a house or rent a good house at the present stage [4, 5]. To compensate for the obvious shortcomings of

the housing security system and break the housing dilemma of the new citizens, in July 2021, the General Office of the State Council issued the "Opinions on Accelerating the Development of Government-subsidized Rental Housing (GSRH)," which clearly proposed the concept of GSRH in the top-level design of the housing security system [6]. However, the current policy only proposes the basic concept of GSRH, and scholars and policymakers still need in-depth discussions on supply subjects and supply models.

GSRH is an institutional innovation to alleviate the housing difficulties of new citizens [7]. At present, China has established a housing security system with PRH, GSRH, and coownership housing as the main body. Among them, PRH has two standard lines of low income and housing difficulties and is mainly aimed at urban low-income families in difficulty. The supply mode of PRH is directly led by the government and built on the platform of state-owned enterprises, and the government undertakes the responsibility of the bottom guarantee. GSRH is mainly used to solve the housing difficulties of the new citizen group to make up for the institutional innovation of China's previous imperfect housing security system for the same group. In terms of supply mode, GSRH reconstructs a market-oriented and policy-supported security system and guides multisubject investment and multichannel financing of "small-sized, low-rent" rental housing. GSRH is an important measure with Chinese characteristics that promotes the steady development of the real estate market and stabilises the position of "housing not for speculation."

The single supply of the government subject has problems such as the obvious funding gap, the prominent contradiction between supply and demand, and weak construction enthusiasm caused by a one-sided view of political achievements. At present, the group of new citizens is large, and the shortage of rental housing is obvious. It is necessary for the housing security subject to change from government-based participation to the joint participation of the government, enterprises, and social forces to improve the efficiency and quality of supply. According to the policy background of GSRH, the supply subjects can be divided into government and nongovernmental institutions, in which the former refers to the public sector of local housing management institutions, while the latter are further divided into profit-oriented market subjects (including housing rental franchise enterprises, real estate development enterprises, and property service companies) and nonprofit social subjects (including large private enterprises, state-owned enterprises and institutions, industrial parks, research institutes, and rural collectives). The supply subject can be further abstracted as government, market, and society.

Therefore, this study focuses on how to cooperate with the government, market, and social subjects to participate in the rapid and effective supply of GSRH in large cities. Previous studies on PRH supply have mainly focused on four aspects as follows.

First, regarding the sustainability of PRH supply, [8] has enriched the knowledge of sustainable construction by proposing a building information modelling and life cycle assessment integration approach to comprehensively evaluate the life cycle-embodied environmental impacts of buildings at the design stage. Reference [2] constructs a sustainable development system of public housing project from the perspective of a complex eco-system, exploring the internal operation mechanism and the coupling mechanism among the ecological, economic, and social subsystems. Reference [9] assesses the financial viability of PRH projects in China from a private sector perspective. References [10, 11] propose the application of "green leasing" and "integrated design process" in low-cost housing. Reference [12] studies how to make affordable housing more sustainable from the perspective of stakeholders.

Regarding the relationship between central and local governments, some scholars have suggested that the central government delegates the responsibility of PRH supply to local governments, allowing these to obtain a set of administrative power in public engineering planning, maintenance, and commercial management [13]. Reference [14] believes that this decentralisation process shifts the burden of PRH supply from the state to local governments, with a view to creating new incentives at the microlevel to increase efficiency and productivity. Reference [15] studied the contradictions in China's PRH policy and found that the division of power, incentives, responsibilities, and income sources between the central and local governments runs counter to the national goal of affordable housing. Reference [16] researched campaign-style implementation and affordable housing provision in China, and the findings point to the defects of campaign-style implementation and China's need for more institutionalised mechanisms to implement policies prioritised by the national government.

With regard to local government supply problems, specific political and economic incentives for local governments played an important role in realising the scheme [17]. Many scholars have proposed that PRH brings negative effects such as a difficult integration into mainstream urban life, residential segregation, and job-housing balance [18, 19]. Reference [20] proposes that, driven by economic interests, local governments often construct high-capacity PRH communities in remote areas, thus potentially distorting the ambitious aims and principles of China's affordable housing scheme and negatively affecting the social interaction and life opportunities of the security objects. Reference [15] argues that, based on the interests of land, the spatial distribution of PRH development in China is biased towards the urban fringe to provide an institutional explanation. In view of China's intergovernmental relations, they believe that this discriminatory location approach is the result of urban government efforts to balance top-down political pressure and local fiscal interests.

Regarding changes in the supply mode of public housing, it is difficult for the government as a single subject to achieve the supply of PRH. Some scholars hold that the private sector has financial and professional advantages and can share risks with the public sector, reduce operating costs, introduce competition, increase options, and improve service quality [21, 22]. Using nongovernmental resources can create a more flexible structure to quickly adapt to rapidly changing environments [23]. Public-private partnerships (PPP) are

widely seen as a way to involve the private sector with rich capital and management experience in sharing the financial burden of governments and improving the efficiency and sustainability of the public housing supply [24, 25]. In Austria, the UK, and Italy, innovative mixed arrangements for the development, financing, and management of indemnificatory housing jointly developed by the state, the third sector, market, and community participants show that they can benefit from the participation of market participants and communities [26]. Around 2011, the central government launched an initiative to encourage local governments to cooperate with nongovernmental organisations in providing public housing [27]. Reference [28] evaluated the feasibility of PPP in social housing. Reference [23] studied the structure and mechanism of the role played by nongovernmental actors in public housing governance.

Previous research on PRH supply has mainly focused on its sustainability, clarifying the relationship between central and local governments in the supply process as well as the problems existing in the supply of local governments and exploring the feasibility of public-private cooperation. However, a research gap exists with regard to how a collaborative government, market, and society can supply PRH. In the complex, self-adaptive system of multisubject supply of GSRH, the plan chosen by any subject of the government, market, and society affects the interests of other subjects, and the relationship between different subjects may lead to different supply results. Behaviour is also influenced, to some extent, by the surrounding environment [29, 30]; therefore, it is not enough to only observe the participants in the research on the multisubject supply of GSRH and, more importantly, the research on the relationship between the participants and the interaction with the system environment [31].

The supply of GSRH by the government, market, and society is a science about collaboration. German scholar Haken proposed the synergy concept in system theory, which meant a subsystem's collaboration, cooperation, synchronous combined effect, and collective behaviour in the system, that the whole realised the effect via nonlinearity complex interaction among the subsystem which the individual cannot realise to produce the $1 + 1 > 2$ collaborative effect [32]. In the supply process, this synergy system is dynamic; that is, various factors influence each other through a relationship that is not only collaborative but also evolutionary [33]. Therefore, the supply of GSRH by government, market, and society is based on the coevolution theory. The coevolution theory follows the general analytical framework of Darwinism, which specifies the replicators and interactors in detail, and uses the "variation," "replication," and "selection" to describe the process of coevolution [34]. Evolutionary game theory (EGT) provides a useful method for Darwin's competition by defining a framework of competition, strategy, and analysis model [35].

EGT is based on the assumption of bounded rationality, taking the group as the research subjects, analysing its dynamic evolution process, and explaining why and how the group reaches the current evolutionary state [36, 37]. In the field of housing research, [38] built an evolutionary game model of the government and real estate operators in the housing rental market in the context of financial institutions and public participation in supervision and analysed the impact of different levels of supervision by financial institutions and the public on evolution. Reference [39] established an evolutionary game model between social forces and government to solve the problem of excessive participation of the former in housing rental projects leading to rising rents. Reference [40] constructed the interest game model between the central government and local governments in the process of developing rental housing, analysed the logic and dilemma of land reserve strategy and illegal land reserve problem, and determined the replication dynamic mechanism and evolutionary stability strategy of participants under various conditions. Therefore, this study explores the deep mechanism of supply system dynamic collaboration through a multisubject evolutionary game method based on coevolution theory.

In social systems, understanding a political or economic system requires more than an understanding of the individuals that comprise the system [41, 42]. It also requires understanding how the individuals interact with each other and how the results can be more than the sum of parts [43]. For this highly complex, nonlinear, and self-organising multiagent cooperative supply system based on an evolutionary game, agent-based modelling (ABM) can provide insights into dynamic interactions among real-world phenomena by capturing nonlinear interactions and feedback loops, thereby predicting outcomes that emerge out of complex dynamics in the real world [44–46]. ABM tools provide support for researchers and practitioners to study how the macrobehaviour of the system depends on the attributes, constraints, and rules at the microlevel and is increasingly recognised in ecology, economics, biology, sociology, social sciences, and many other STEM disciplines in simulating dynamic large-scale complicated systems and observing emergent behaviours [40, 47–49].

In summary, this study attempts to use EGT to explore the collaborative relationship of the three government-market-society subjects in the supply process, and it links the behaviour of agents with different information and decision rules with the macrobehaviour of the whole collaborative supply system with the help of the NetLogo multiagent simulation platform. Through large-scale policy experiments, it realises a bottom-up policy simulation of the game results and the collaborative supply mechanism of the three subjects; further, it explores the micromechanism of the evolution of the collaborative supply decision of GSRH under the condition of bounded rationality. The remainder of the paper is structured as follows. Section 2 analyses the evolutionary game model and ABM of GSRH. Section 3 establishes an asymmetric evolutionary game model of government, market, and society. Section 4 establishes an agent-based model based on the EGT model through the NetLogo simulation platform and conducts large-scale policy experiments to determine the evolution stage and collaborative supply mechanism of the three subjects. This study provides theoretical support for the formulation of a coordinated supply policy of GSRH in the pilot cities.

2. Materials and Methods

2.1. Evolutionary Game Theory. This study adopts a dynamic replication evolutionary game method to establish a three-group, two-strategy, asymmetric evolutionary game model to study the dynamic process of government-market-society in the collaborative supply of GSRH.

2.1.1. Game Agent Analysis. The supply subjects of GSRH can be abstracted into three categories: government, market, and society.

The government subject refers to the public sector of the local housing management institutions, including local government housing construction departments at all levels, housing security centres, and others. As quasipublic good, the supply of GSRH cannot and does not need to be fully borne by the government; however, as the executive department of state power, the government is fully responsible for guiding the supply of GSRH and has always been one of the main suppliers. Government participants rely on hierarchical guidance, mainly acting as nonprofit entities [23]. For the supply of GSRH, the state is at the top of the hierarchy, with the central government setting national supply policies and tasks and local governments acting as intermediaries responsible for establishing specific methods for local policy, project development and implementation, and negotiating with other actors to achieve housing construction and distribution [17, 50]. The authority and systematic organisation of government subjects can successfully promote the construction of GSRH, strengthen public services, ensure fair supply, and stabilise economic development. Moreover, the government subject is a key intermediary connecting other subjects [51].

The market subject refers to profit-making organisations that raise funds by themselves, including housing rental franchise enterprises, real estate development enterprises, property service companies, and others capable of directly or indirectly participating in the supply of GSRH. Market players use commercial principles to achieve efficiency, effectiveness, and innovation in providing public goods and social services [52]. The participation of market players reduces government costs and improves supply efficiency and supply effect. Moreover, it can avoid the psychological label effect of the centralised construction of GSRH on the security objects and achieve the goal of coordinating the layout of GSRH and ordinary commodity housing. The market subject is a key participant in effective supply; however, it is usually subject to the profit trend [19]. Compared with commercial projects, participation in GSRH projects has fewer returns and is not attractive to the market, and market subjects thus need certain incentives from the government. The incentive policies and measures are many, including reducing loan interest rates and providing tax relief and cheap or free land [2].

The social subject refers to nonprofit organisations that participate in supply on the principle of voluntary and mutual assistance. In China, these are large private enterprises, state-owned enterprises and institutions, industrial parks and rural collectives, and others. They build or reconstruct GSRH through self-construction, joint ventures, and shares or in other ways, using collectively operated construction land, idle land owned by enterprises and institutions, supporting land for industrial parks, and stock of idle houses. The social subject connects governments, collectives, and individuals and plays a complementary and balanced role in the multiagent collaborative supply system. Compared with government departments, social organisations are independent of the government system, which can get rid of the fixed pattern of the bureaucratic structure of government organisations and form their own unique diversity and flexibility, thus bringing low cost and high efficiency of supply. At the same time, it can effectively compensate for the lack of efficiency caused by the government's single supply or privatisation production mode. Compared with the private sector, the nonprofit goal of social organisations to participate in GSRH supply determines its more public welfare, the pursuit of high quality, and the efficiency of affordable rental housing supply.

2.1.2. Model Hypothesis. Many factors affect the collaborative supply of GSRH by the government, market, and society. This study draws upon several relevant studies and empirical research works. To simplify the problem, the model is constructed and analysed based on satisfying the following assumptions.

Assumption 1. The increased delegation of government tasks to other nongovernmental actors has made the GSRH provision a "governance" model [26]. Therefore, the government has two strategic choices in the process of GSRH supply; the strategy space is {intervention, no intervention} ({I, NI}), in which intervention is divided into subsidies and supervision. Subsidy refers to the use of land policy support, fiscal and taxation relief, financial support, and other policy means by the government subject, guiding the market and social subjects through new reconstruction, idle transformation, and other modes to participate in the supply of GSRH [52]. Supervision means that the government should supervise and correct the relevant behaviours of the market subject and social subject in the planning, construction, and operation of GSRH, establish and improve the housing rental management service platform, strengthen the supervision of the whole process of construction, rental, and operation management of GSRH, and enhance the supervision of engineering quality and safety, especially the problems of unqualified construction quality and indoor decoration health. Nonintervention refers to the free development of the supply system of GSRH without formulating or implementing any subsidy and supervision policies.

Assumption 2. If the government adopts the intervention strategy, the cost of policy subsidies is C_M for the market subject and C_S for social players. Compared with the market subject, social players are more willing to participate in supply because the provision of GSRH is conducive to attracting talents and improving productivity. In addition,

they generally maintain idle houses or land, and the construction costs are also small. Therefore, it is believed that $C_M > C_S$. The supervision cost generated in the process of government intervention is S_M as the market subject and S_S as the social subject. Considering that the supply object of the social subject is unit workers, the supply quality directly affects the unit's operation efficiency through residential satisfaction, the self-discipline level of high-quality supply is high, and the difficulty and cost of government regulation are low; thus, it is assumed that $S_M > S_S$.

Assumption 3. If the government takes a nonintervention strategy, local governments may obtain the leisure and governance resources, effective disposition, and so on, which bring extra gains to government subject as R_0. Economic growth used to be and still is the main criterion for the central government to assess the promotion of local officials [53]; in other words, local officials are more willing to allocate land resources to infrastructure and real estate construction projects that generate significant fiscal revenues to improve promotion opportunities [54]. To realise virtuous interactions between the central government and local governments in the field of housing construction and management, it is proposed that the central government should change the single evaluation system for local officials and establish a multiangle and comprehensive performance evaluation system for local officials [55]. This study abstracts the central government's overall control of the supply of GSRH such that when the government subjects choose the nonintervention strategy, they are punished by the higher authorities as P.

Assumption 4. According to the social contract theory, in addition to the need to fulfil the economic contract, the market and social subjects are obliged to fulfil the social contract. Their behaviour must conform to society's expectations; they must do their duty for social and economic improvement and adjust to the changes in social environment to respond to the stakeholders' interests [33]. Therefore, the strategic space of market and social subject is set as {participation, nonparticipation} ({P, NP}). For market subjects, participation refers to the development and operation of affordable rental housing projects, and the supply target refers to the whole society meeting the population's guarantee conditions. "Nonparticipation" refers to not participating in the GSRH supply and instead investing in the construction of commercial housing and other real estate development projects. For social subjects, participation refers to the use of their own land or idle houses to build or rebuild leased houses nearby, and the supply objects are generally employees and families of the unit. "Nonparticipation" refers to not participating in the supply of GSRH and using investment within social organisations.

Assumption 5. For market players, adopting a participation strategy allows obtaining government subsidy C_M and direct rental housing operating income such as rent; value-added service charges are set as R_{M0}, and indirect reputation gains such as corporate social responsibility are set as R_{M1}.

Investing in other projects, instead of participating in the supply of GSRH, yields R_{NM}. For the social subjects, the government subsidy C_S is obtained by taking the participation strategy. The GSRH supplied by the social subjects mainly uses the stock of land and housing to build in the industrial park and around the company to effectively solve the problem of job-housing balance, improve the enthusiasm of employees, generate a positive income R_{S0}, and bring a certain social reputation income R_{S1}. Social reputation is the higher satisfaction of staff and the social influence of suppliers brought by the physical supply of rental housing. Given the nonprofitability of the social subjects supplying GSRH, the operating income of rental housing is not considered here. Not participating in the supply of GSRH and instead using other investments within social organisations enable receiving R_{NS}, but for social subjects who do not participate, restraint measures shall be taken; that is, they need to pay a certain housing subsidy F to the unit's employees.

Assumption 6. GSRH belongs to the housing security system, which is essentially a certain degree of social welfare provided by the government. The main responsibility of it lies with the government, market, and social subjects through a collaborative supply. If market and social subjects participate in supply, government financial pressure is reduced, and the project's operation efficiency and quality, as well as are the government's reputation, are improved so that the contribution of the market subject participating in supply is GB_M and that of the social subject is GB_S.

Assumption 7. Game participants are bounded rational. Without considering other constraints, government, market, and society all have the bounded rationality characteristic; in other words, each subject cannot accurately calculate its own cost and the income, but it usually tries and imitates unceasingly over time and eventually tends to a stable strategy. Suppose that the proportion of the government choosing the intervention strategy is x, the proportion of the market choosing the participation strategy is y, and the proportion of society choosing the participation strategy is z ($0 \leq x$, y, $z \leq 1$). The specific dynamic game flow of collaborative supply among government, market, and society is shown in Figure 1.

It is worth noting that the impact of the policy environment is complex, and no unified housing policy is applicable to the housing market of each city [56]. The supply of GSRH implements the strategy of "one city, one policy." The key point of this strategy is to let the central government determine the basic principles and then allow local governments to determine the implementation details, which can make the real estate regulation of each city innovative and flexible and can, to a large extent, avoid the systemic risks arising from the unified regulation of the central government [55]. Therefore, this study does not make specific policy and institutional assumptions on the collaborative supply of government, market, and society, but it abstracts this supply as subsidies, benefits, and penalties to
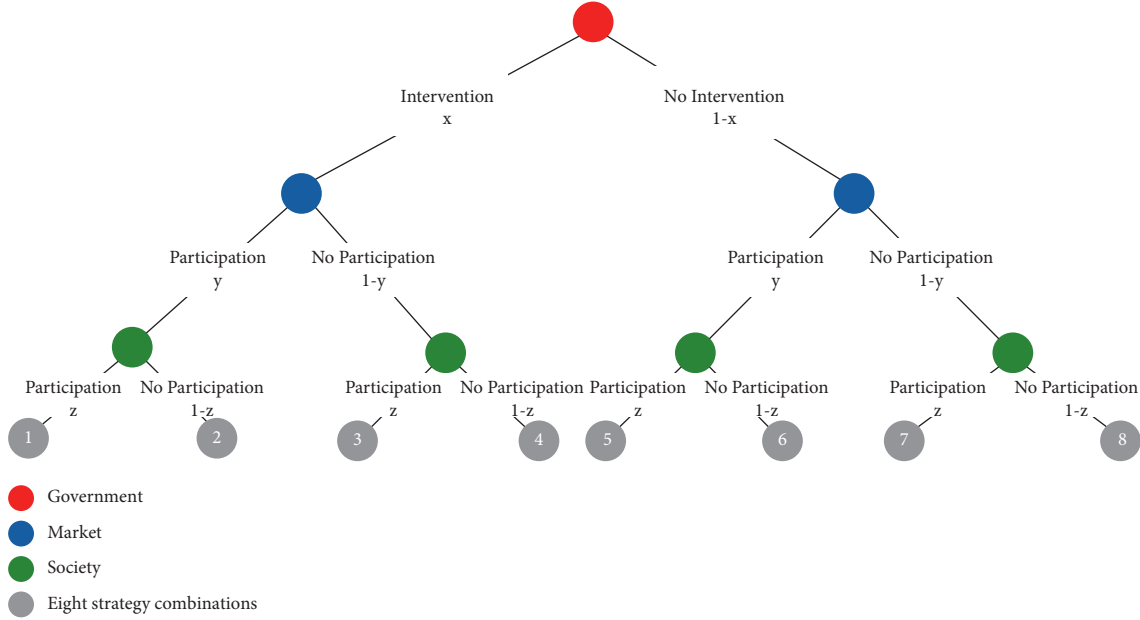
FIGURE 1: Dynamic flow of evolutional game among government, market, and social subject in GSRH supply.

discuss the synergy system. The summary and description of all model parameters are shown in Table 1.

2.1.3. Payoff Model.
In the course of the evolutionary game, according to individual bounded rationality and limited information principle and based on the above model assumptions, the payoff matrix of the government-market-society asymmetric cooperative game is shown in Table 2.

According to the benefits of the strategy combination in Table 2, the expected revenue of the intervention strategy $(G^{(1)})$, nonintervention strategy $(G^{(2)})$, and average benefits $(\overline{U_G})$ adopted by the government subject is, respectively,

$$
\begin{cases}
U_{G^{(1)}} = yz\left(GB_M + GB_S - C_M - S_M - C_S - S_S\right) + y(1-z)\left(GB_M - C_M - S_M\right) \\
\quad + (1-y)z\left(GB_S - C_S - S_S\right), \\
U_{G^{(2)}} = yz\left(GB_M + GB_S + R_0 - P\right) + y(1-z)\left(GB_M + R_0 - P\right) \\
\quad + (1-y)z\left(GB_S + R_0 - P\right) + (1-y)(1-z)\left(R_0 - P\right), \\
\overline{U_G} = xU_{G^{(1)}} + (1-x)U_{G^{(2)}}.
\end{cases}
\tag{1}
$$

The replication dynamics equation of the government subject is therefore

$$
\begin{aligned}
F_{(x)} = \frac{d_x}{d_t} &= x\left(U_{G^{(1)}} - \overline{U_G}\right) \\
&= x(1-x)\left[P - R_0 - y\left(C_M + S_M\right) - z\left(C_S + S_S\right)\right],
\end{aligned}
\tag{2}
$$

where $F(x)$ indicates the rate of change in government intervention strategies, $F(x) > 0$ means that the government tends to adopt an intervention strategy, and $F(x) < 0$ means that the government tends to adopt a nonintervention strategy.

Similarly, the expected revenue of the participation strategy $(M^{(1)})$, nonparticipation strategy $(M^{(v)})$, and average benefits $(\overline{U_M})$ adopted by the market subject is, respectively,

$$
\begin{cases}
U_{M^{(1)}} = xz\left(C_M + R_M\right) + x(1-z)\left(C_M + R_M\right) + (1-x)zR_M + (1-x)(1-z)R_M, \\
U_{M^{(2)}} = xzR_N + x(1-z)R_N + (1-x)zR_N + (1-x)(1-z)R_N, \\
\overline{U_M} = yU_{M^{(1)}} + (1-y)U_{M^{(2)}}.
\end{cases}
\tag{3}
$$

TABLE 1: Evolutionary game model parameters and variable descriptions.

Parameter	Description
GB_M	Benefits of market subject's participation in supply to government subject
GB_S	Benefits of social subject's participation in supply to government subject
C_M	The cost of policy subsidies for market subject by government intervention strategies
C_S	The cost of policy subsidies for social subject by government intervention strategies
S_M	Supervision cost of government intervention strategy for market subjects
S_S	Supervision cost of government intervention strategy for social subjects
R_{M0}	Direct operating income from market participation strategy
R_{M1}	Indirect reputation gains from market participation strategy
R_{NM}	Returns from market nonparticipation strategy to investment in other projects
R_{S0}	Positive benefits of social participation strategy
R_{S1}	Reputation gains of social participation strategy
R_{NS}	Benefits from social nonparticipation strategies to other projects in investment organisations
R_0	Government gains from the additional benefits of leisure and the efficient allocation of government resources when it takes nonintervention strategy
P	Governments that adopt nonintervention strategy will be punished by higher authorities
F	Housing subsidy paid by the society to employees of the unit without participation

TABLE 2: The payoff matrix of the evolutionary game among the government, market, and society.

Strategy combination	(Government, market, society)
(I, P, P)	$(GB_M + GB_S - C_M - S_M - C_S - S_S, C_M + R_{M0} + R_{M1}, C_S + R_{S0} + R_{S1})$
(I, P, NP)	$(GB_M - C_M - S_M, C_M + R_{M0} + R_{M1}, R_{NS} - F)$
(I, NP, P)	$(GB_S - C_S - S_S, R_{NM}, C_S + R_{S0} + R_{S1})$
(I, NP, NP)	$(0, R_{NM}, R_{NS} - F)$
(NI, P, P)	$(GB_M + GB_S + R_0 - P, R_{M0} + R_{M1}, R_{S0} + R_{S1})$
(NI, P, NP)	$(GB_M + R_0 - P, R_{M0} + R_{M1}, R_{NS} - F)$
(NI, NP, P)	$(GB_S + R_0 - P, R_{NM}, R_{S0} + R_{S1})$
(NI, NP, NP)	$(R_0 - P, R_{NM}, R_{NS} - F)$

The replication dynamics equation of the market subject is therefore

$$F_{(y)} = \frac{d_y}{d_t} = y\left(U_{M^{(1)}} - \overline{U_M}\right)$$

$$= y(1 - y)(xC_M + R_{M0} + R_{M1} - R_{NM}).$$

(4)

The replication dynamics equation of the social subject is therefore

$$F_{(z)} = \frac{d_z}{d_t} = z\left(U_{S^{(1)}} - \overline{U_S}\right)$$

$$= z(1 - z)(xC_S + R_{S0} + R_{S1} - R_{NS} + F).$$

(6)

Based on the nature of evolutionary stability strategy, the necessary condition for government subject to achieve evolutionary stability is $dF(x)/dx < 0$.

For the replication dynamic equation (2), when $z = (P - R_0 - y(C_M + S_M))/(C_S + S_S)$, x is a steady state.

The expected revenue of the participation strategy ($S^{(1)}$), nonparticipation strategy ($S^{(2)}$), and average benefits ($\overline{U_S}$) adopted by the social subject is, respectively,

$$\begin{cases} U_{S^{(1)}} = xy(C_S + R_S) + x(1 - y)(C_S + R_S) + (1 - x)yR_S + (1 - x)(1 - y)R_S, \\ U_{S^{(2)}} = R_{NS} - F, \\ \overline{U_S} = zU_{S^{(1)}} + (1 - z)U_{S^{(2)}}. \end{cases}$$

(5)

When $z < (P - R_0 - y(C_M + S_M))/(C_S + S_S)$, $x = 1$ is the evolutionarily stable strategy. When $z > (P - R_0 - y(C_M + S_M))/(C_S + S_S)$, $x = 0$ is the evolutionarily stable strategy. According to $z = (P - R_0 - y(C_M + S_M))/(C_S + S_S)$, a surface M can be drawn, as shown in Figure 2(a). The points on surface M are stable in the x-axis direction, the points above it evolve to $x = 1$, and the points below it evolve to $x = 0$. Similarly, for the point of market subject in surface V to stabilise in the y-axis direction, the point on the left side of surface V evolves towards $y = 0$, and the point on the right side of the surface tends to $y = 1$, as shown in Figure 2(b). For the stability of the social subject in the z-axis direction of
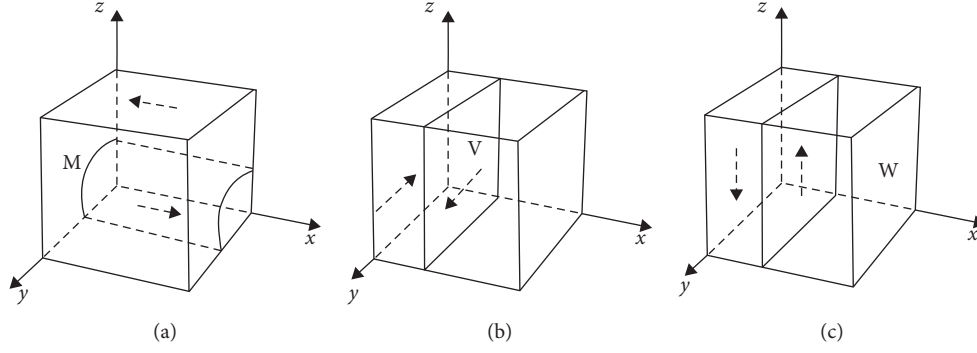
Figure 2: Replicated dynamic diagram of each subject. (a) Government. (b) Market. (c) Society.

the point in plane W, the point on the left side of plane W evolves to $z = 0$, and the point on the right side of it evolves to $z = 1$, as shown in Figure 2(c).

2.2. Agent-Based Modelling. Based on the above evolutionary game model and ABM simulation method, with a bottom-up, this part simulates the evolution process of multiagent supply of GSRH under the collaborative background from the perspective of microinteraction to macroemergence, and it attempts to reveal the micromechanism of collaborative supply of GSRH in the form of policy experiments in view of the advantages of the NetLogo 6.0.3 simulation platform, which can meet the simultaneous operation of multiple agents, set system variables, and parameters easily and quickly and provide a visual evolution interface. With the help of this platform, this study establishes the attributes of each subject, the number of agents in each subject, the selection mechanism of game objects, and the strategy update mechanism, and it compiles the government-market-society, three-agent game simulation programme. Through NetLogo, large-scale numerical experiments are conducted to show the dynamic game process of different subjects under different parameter conditions, verify the evolutionary game model of multiagent synergistic supply of GSRH, realise the simulation and effect evaluation

of relevant parameter and subject strategy selection changes, and provide verification for the effectiveness of policy recommendations.

2.2.1. Basic Variable Settings of the NetLogo Simulation Platform. This study constructs a three-group, asymmetric evolutionary game model composed of agents and game environment and generates a two-dimensional network space with periodic boundary. In a two-dimensional network space, the three-party game subjects are generated as government, market, and social subjects, respectively.

The parameter settings of each subject attribute are shown in Table 3.

The strategy of the government subject is $S_G(t) = \{0, 1\}$, where 0 means adopting a nonintervention strategy, and 1 means adopting an intervention strategy. The strategy of the market subject is $S_M(t) = \{0, 1\}$, where 0 means adopting a nonparticipation strategy, and 1 means adopting a participation strategy. The strategy of the social subject is $S_S(t) = \{0, 1\}$, where 0 means adopting a nonparticipation strategy, and 1 means adopting a participation strategy.

The expected return functions of the three subjects of government, market, and society to adopt their respective strategies are as follows:

$$\begin{cases} IR_G(t) = y_t(GB_M - C_M - S_M) + z_t(GB_S - C_S - S_S), \\ NIR_G(t) = y_t GB_M + z_t GB_S + R_0 - P, \\ PR_M(t) = x_t C_M + R_{M0} + R_{M1}, \\ NPR_M(t) = R_{NM}, \\ PR_S(t) = x_t C_S + R_{S0} + R_{S1}, \\ NPR_S(t) = R_{NS} - F. \end{cases} \tag{7}$$

2.2.2. Simulation Mechanism Design. Agent game and movement mechanism: agents can move randomly in the network space, assuming that the game range of each agent in the interaction process is in a neighbouring position. Initially, each agent selects the corresponding strategy with a random probability. In the simulation period t, according to

the agent's behaviour rules, the agent observes whether there are other agents around its eight neighbour positions. If there are no other agents, the agent moves to any neighbouring position randomly. If there are, it judges whether there are agents of other two types of subjects at the same time, and if this is the case, the game is randomly matched,

TABLE 3: Agent-based model parameters and variable descriptions.

Parameter	Description
$S_G(t)$	The strategic space of government subject
$S_M(t)$	The strategic space of market subject
$S_S(t)$	The strategic space of social subject
N_G	Number of government agents
N_M	Number of market agents
N_S	Number of social agents
$N_{S_G=1}t$	Number of government agents who choose intervention strategy in period t
$N_{S_M=1}t$	Number of market agents who choose participation strategy in period t
$N_{S_S=1}t$	Number of social agents who choose participation strategy in period t
$x(t)$	Probability of government intervention strategy at period t, $x(t) \in [0, 1]$
$y(t)$	Probability of market participation strategy at period t, $y(t) \in [0, 1]$
$z(t)$	Probability of social participation strategy at period t, $z(t) \in [0, 1]$
$FR_{G(i)}(t)$	The $Agent_i$ in the government subject benefits from the actual combination of strategies in the t-period game
$FR_{M(j)}(t)$	The $Agent_j$ in the market subject benefits from the actual combination of strategies in the t-period game
$FR_{S(k)}(t)$	The $Agent_k$ in the social subject benefits from the actual combination of strategies in the t-period game
$IR_G(t)$	Expected benefits of government intervention strategy
$NIR_G(t)$	Expected benefits of government nonintervention strategy
$PR_M(t)$	Expected benefits of market participation strategy
$NPR_M(t)$	Expected benefits of market nonparticipation strategy
$PR_S(t)$	Expected benefits of social participation strategy
$NPR_S(t)$	Expected benefits of social nonparticipation strategy

Note. The total number of agents in each agent remains unchanged.

and the strategy adopted at $t+1$ is determined by learning the algorithm according to the benefits of the game.

Strategy learning mechanisms: since the agent is and asymmetrical information, it is not strictly based on the principle of maximum utility to make decisions in the game. According to the view of biological evolution and replication dynamics, the subject with lower returns continues to learn, imitate, and compare different strategies, then chooses a strategy higher than the expected return of this strategy, always replaces the unsatisfied strategy with a satisfied one, and finally tends to a stable state [38, 57]. The agent takes the result of each game as the actual benefit of its strategic interaction and then compares it with the expected benefit of the two strategies at the same time to judge whether the strategy of the t-period is optimal and whether to update it.

For the government subject, when the strategy of individual i in $Agent_G$ at period t is $Str_{G(i)}(t) = 1$, if $NIR_{G(i)}(t) > IR_{G(i)}(t) > FR_{G(i)}(t)$ or $NIR_{G(i)}(t) > FR_{G(i)}(t) > IR_{G(i)}(t)$, then the strategy of $Agent_{G(i)}$ at period $t+1$ is $Str_{G(i)}(t+1) = 0$. When the strategy of individual i in $Agent_G$ at period t is $Str_{G(i)}(t) = 0$, if $IR_{G(i)}(t) > NIR_{G(i)}(t) > FR_{G(i)}(t)$ or $IR_{G(i)}(t) > FR_{G(i)}(t) > NIR_{G(i)}(t)$, then the strategy of $Agent_{G(i)}$ at period $t+1$ is $Str_{G(i)}(t+1) = 1$, the other cases keep the original strategy unchanged, and the formula is as follows:

$$Str_{G(i)}(t+1) = \begin{cases} 1 - Str_{G(i)}(t), & Str_{G(i)}(t) = 1 \text{ and} NIR_{G(i)}(v) > IR_{G(i)}(t) > FR_{G(i)}(t) \\ & \text{or} NIR_{G(i)}(t) > FR_{G(i)}(t) > IR_{G(i)}(t), \\ & Str_{G(i)}(t) = 0 \text{ and} IR_{G(i)}(t) > NIR_{G(i)}(t) > FR_{G(i)}(t) \\ & \text{or} IR_{G(i)}(t) > FR_{G(i)}(t) > NIR_{G(i)}(t), \\ Str_{G(i)}(t), & \text{other situation.} \end{cases} \tag{8}$$

Similarly, for the market subject, the strategy learning rules are as follows:

$$Str_{M(i)}(t+1) = \begin{cases} 1 - Str_{M(j)}(t), Str_{M(j)}(t) = 1 \text{ and} NPR_{M(j)}(t) > PR_{M(j)}(t) > FR_{M(j)}(t) \\ \text{or } NPR_{M(j)}(t) > FR_{M(j)}(t) > PR_{M(j)}(t), \\ Str_{M(j)}(t) = 0 \text{ and} PR_{M(j)}(t) > NPR_{M(j)}(t) > FR_{M(j)}(t) \\ \text{or } PR_{M(j)}(v) > FR_{M(j)}(t) > NPR_{M(j)}(t), \\ Str_{M(j)}(t), \text{othersituation.} \end{cases} \tag{9}$$

For the market, the strategy learning rules are as follows:

$$Str_{S(i)}(t+1) = \begin{cases} 1 - Str_{S(k)}(t), Str_{S(k)}(t) = 1 \text{ and} NPR_{S(k)}(v) > PR_{S(k)}(t) > FR_{S(k)}(t) \\ \text{or } NPR_{S(k)}(t) > FR_{S(k)}(v) > PR_{S(k)}(t), \\ Str_{S(k)}(t) = 0 \text{ and} PR_{S(k)}(t) > NPR_{S(k)}(t) > FR_{S(k)}(t) \\ \text{or } PR_{S(k)}(t) > FR_{S(k)}(t) > NPR_{S(k)}(t), \\ Str_{S(k)}(t), \text{othersituation.} \end{cases} \tag{10}$$

Evolutionary stable result output mechanism: the three types of agents go through a certain number of games in the simulation period (t) until the evolutionary equilibrium state of collaborative supply is finally reached. The output results of the final evolutionary stability of the government-market-society collaborative supply process are expressed as $x(t), y(t), z(t)$ through the estimation of different strategy proportions of each game party. Based on the complexity of the real world, the NetLogo simulation model established in this study introduces the consideration of uncertainty to deepen the simulation results of the three-subject evolutionary game.

Assuming that the simulation results based on NetLogo have ±10% error compared with the real world, the error terms of the government, market, and social agents are set as α, β, and γ, respectively, where $(\alpha, \beta, \gamma) \in (-0.1, 0.1)$ and $x(t), y(t), z(t)$ are calculated as follows:

$$\begin{cases} x(t) = \dfrac{N_{S_G=1}t}{N_G} \times (0.9 + \alpha), \\ \\ y(t) = \dfrac{N_{S_M=1}t}{N_M} \times (0.9 + \beta), \\ \\ z(t) = \dfrac{N_{S_S=1}t}{N_S} \times (0.9 + \gamma). \end{cases} \tag{11}$$

3. Results

3.1. The Equilibrium Analysis of the Model

3.1.1. Stability Analysis of the Evolutionary Game. By further solving the replicative dynamic equations composed of $dx/dt = dy/dt = dz/dt = 0$, 12 equilibrium points can be found in the cooperative game system of the government, market, and social subjects, which are $E_1 (0, 0, 0)$, $E_2(1, 0, 0)$, $E_3 (0, 1, 0)$, $E_4 (0, 0, 1)$, $E_5 (1, 1, 0)$, $E_6 (1, 0, 1)$, $E_7 (0, 1, 1)$, $E_8 (1, 1, 1)$, $E_9 ((F + R_{NS} - R_{S0} - R_{S1})/(C_S), 1, (C_M + P - R_0 - S_M)/(C_S + S_S))$, $E_{10} ((R_{M0} - R_{M1} + R_{NM})/(C_M), (P - R_0)/(C_M + S_M), 0)$, $E_{11} ((F + R_{NS} - R_{S0} - R_{S1})/(C_S), 0, (P - R_0)/(C_S + S_S))$, $E_{12} ((R_{M0} - R_{M1} + R_{NM})/(C_M), (C_S + P - R_0 - S_S)/(C_M + S_M), 1)$. According to the above assumptions, all initial points and evolution points must satisfy $0 \le x, y, z \le 1$ to have practical significance. The region surrounded by E_1-E_8 is the equilibrium solution of the evolutionary game. When condition $0 < (F + R_{NS} - R_{S0} - R_{S1})/(C_S) < 1$ is satisfied, it leads to $(F + R_{NS} - R_{S0} - R_{S1})/(C_S) > 1$, abandoning E_9 and E_{11}. When condition $P - R_0 < 0$ is satisfied, it leads to $(P - R_0)/(C_M + S_M) < 0$, abandoning E_{10}. When condition $C_M + S_M + C_S + S_S < P - R_0$ is satisfied, it leads to $(C_S + P - R_0 - S_S)/(C_M + S_M) > 1$, abandoning E_{12}. Therefore, the equilibrium point of the dynamic system is E_1-E_8, and these eight equilibrium points constitute the boundary of the evolutionary game domain. The stability of these equilibrium points in the evolutionary system can be

TABLE 4: Eigenvalues of Jacobi matrix corresponding to each equilibrium point.

Equilibrium point	Eigenvalue λ_1	Eigenvalue λ_2	Eigenvalue λ_3
$E_1(0, 0, 0)$	$P - R_0$	$R_{M0} + R_{M1} - R_{NM}$	$R_{S0} + R_{S1} - R_{NS} + F$
$E_2(1, 0, 0)$	$R_0 - P$	$C_M + R_{M0} + R_{M1} - R_{NM}$	$C_S + R_{S0} + R_{S1} - R_{NS} + F$
$E_3(0, 1, 0)$	$P - R_0 - C_M - S_M$	$-R_{M0} - R_{M1} + R_{NM}$	$R_{S0} + R_{S1} - R_{NS} + F$
$E_4(0, 0, 1)$	$P - R_0 - C_S - S_S$	$C_M + R_{M0} + R_{M1} - R_{NM}$	$-(R_{S0} + R_{S1} - R_{NS} + F)$
$E_5(1, 1, 0)$	$-(P - R_0 - C_M - S_M)$	$-(C_M + R_{M0} + R_{M1} - R_{NM})$	$C_S + R_{S0} + R_{S1} - R_{NS} + F$
$E_6(1, 0, 1)$	$-(P - R_0 - C_S - S_S)$	$C_M + R_{M0} + R_{M1} - R_{NM}$	$-(C_S + R_{S0} + R_{S1} - R_{NS} + F)$
$E_7(0, 1, 1)$	$P - R_0 - C_M - S_M - C_S - S_S$	$-(R_{M0} + R_{M1} - R_{NM})$	$-(R_{S0} + R_{S1} - R_{NS} + F)$
$E_8(1, 1, 1)$	$-(P - R_0 - C_M - S_M - C_S - S_S)$	$-(C_M + R_{M0} + R_{M1} - R_{NM})$	$-(C_S + R_{S0} + R_{S1} - R_{NS} + F)$

obtained by the local stability analysis of the Jacobian matrix [58].

$$
J = \begin{bmatrix}
\dfrac{dx/dt}{dx} & \dfrac{dx/dt}{dy} & \dfrac{dx/dt}{dz} \\[2mm]
\dfrac{dy/dt}{dx} & \dfrac{dy/dt}{dy} & \dfrac{dy/dt}{dz} \\[2mm]
\dfrac{dz/dt}{dx} & \dfrac{dz/dt}{dy} & \dfrac{dz/dt}{dz}
\end{bmatrix},
$$

$$
= \begin{bmatrix}
1 - 2x[P - R_0 - y(C_M + S_M) - z(C_S + S_S)] & -x(1-x)(C_M + S_M) & -x(1-x)(C_S + S_S) \\[2mm]
y(1-y)C_M & (1-2y)(xC_M + R_{M0} + R_{M1} - R_{NM}) & 0 \\[2mm]
z(1-z)C_S & 0 & (1-2z)(xC_S + R_{S0} + R_{S1} - R_{NS} + F)
\end{bmatrix}.
$$

(12)

The Jacobian matrix of the evolutionary game system is as follows:

Table 4 shows the eigenvalues of the Jacobi matrix corresponding to each equilibrium point.

3.1.2. Multiscenario Evolutionary Game Analysis. According to Lyapunov's stability theory, the asymptotic stability at the equilibrium point can be judged by the eigenvalues of the Jacobi matrix; that is, when all eigenvalues are negative, the equilibrium point is the stable point of the evolutionary game. It can be clearly judged from the eigenvalue results of the above equilibrium points that the stability of the synergic supply system of GSRH is affected by the value of the parameters; therefore, the evolutionary stable points of the system are discussed in eight cases as follows:

Scenario 1: $P - R_0 < 0$ and $-C_M < R_{M0} + R_{M1} - R_{NM} < 0$ or $R_{M0} + R_{M1} - R_{NM} < -C_M$ and $-C_S < R_{S0} + R_{S1} - R_{NS} + F < 0$ or $R_{S0} + R_{S1} - R_{NS} + F < -C_S$; that is, the additional benefit of the government subject in adopting a nonintervention strategy to transfer resources is greater than that of the higher-level punishment, and the benefit of the market and social subjects in adopting a participation strategy is less than that of the nonparticipation strategy regardless of whether there is an intervention subsidy of government

subjects. Therefore, the government tends to adopt a nonintervention strategy, and the market and social subjects adopt a nonparticipation strategy. The corresponding strategy stability point is $E_1(0, 0, 0)$. In this case, the three subjects cannot form a cooperative relationship.

Scenario 2: $P - R_0 < 0$ and $R_{M0} + R_{M1} - R_{NM} < -C_M$ and $R_{S0} + R_{S1} - R_{NS} + F > 0$; that is, the extra benefits of government subject transferring resources by adopting a nonintervention strategy are greater than the punishment of superior departments. When there is no government subsidy, the market subject's nonparticipation strategy benefits more than the participation strategy, while the social subject's participation in supply benefits more than nonparticipation. Therefore, the government tends to adopt the nonintervention strategy, the market adopts the nonparticipation strategy, and society adopts the participation strategy. The corresponding strategic stability point is $E_4(0, 0, 1)$.

Scenario 3: $P - R_0 < 0$ and $R_{M0} + R_{M1} - R_{NM} > 0$ and $-C_S < R_{S0} + R_{S1} - R_{NS} + F < 0$ or $R_{S0} + R_{S1} - R_{NS} + F < -C_S$; that is, the additional benefits of the transfer of resources by the government subject adopting the nonintervention strategy are

greater than the penalties of the higher authorities, and without government subsidies, the benefits of the market subject adopting the participation strategy are greater than those of the nonparticipation strategy, while the benefits of the social subject participating are less than those of the subject not participating. Therefore, the government tends to adopt the nonintervention strategy, the market adopts the participation strategy, society adopts the nonparticipation strategy, and the corresponding strategy stability point is $E_3 (0, 1, 0)$.

Scenario 4: $C_M + S_M < P - R_0 < C_M + S_M + C_S + S_S$ or $P - R_0 < 0$ and $R_{M0} + R_{M1} - R_{NM} > 0$ and $R_{S0} + R_{S1} - R_{NS} + F > 0$; that is, when the government subject chooses the nonintervention strategy, the punishment of the superior department is greater than the income, and the difference between punishment and income is greater than the cost paid by the intervention social subject and less than the cost paid by the intervention market and social subject. Alternatively, the benefits of nonintervention strategies adopted by government subjects are greater than the penalties imposed by higher authorities, and the benefits of participation in supply by market and social subjects are greater than those of nonparticipation in supply without government subsidies. Therefore, the government tends to adopt the nonintervention strategy, while market and social subjects adopt the participation strategy, and the corresponding strategy stability point is $E_7 (0, 1, 1)$.

Scenario 5: $C_M + S_M < P - R_0 < C_M + S_M + C_S + S_S$ or $C_M + S_M + C_S + S_S < P - R_0$ and $R_{M0} + R_{M1} - R_{NM} < -C_M$ and $R_{S0} + R_{S1} - R_{NS} + F < - C_S$; that is, under the condition of government subsidies, the benefit of market and social subject participating in the supply is less than that of not-participating subjects, and if the government subject adopts the nonintervention strategy, the punishment of the higher authorities is greater than the benefit of resource transfer and utilisation, and the difference between punishment and benefit is greater than the cost of government intervention in the market and social subjects. Therefore, the government subject adopts the intervention strategy, while market and social subjects adopt a nonparticipation strategy, and the corresponding strategic stability point is $E_2 (1, 0, 0)$.

Scenario 6: $C_M + S_M < P - R_0 < C_M + S_M + C_S + S_S$ or $C_M + S_M + C_S + S_S < P - R_0$ and $R_{M0} + R_{M1} - R_{NM} > 0$ or $-C_M < R_{M0} + R_{M1} - R_{NM} < 0$ and $R_{S0} + R_{S1} - R_{NS} + F < - C_S$; that is, the benefits of nonparticipation in supply are greater than participation, and the social subject tends to adopt a nonparticipation strategy. When the government subject adopts a nonintervention strategy, the loss is greater than the cost of intervening in the market subject. Alternatively, the government subject adopts an intervention strategy, and the benefit of a market subject participating in supply is greater than that of

nonparticipation. The government tends to adopt the intervention strategy, and the market tends to adopt the participation strategy. Thus, the corresponding policy stability point in this scenario is $E_5 (1, 1, 0)$.

Scenario 7: $C_M + S_M < P - R_0 < C_M + S_M + C_S + S_S$ or $C_M + S_M + C_S + S_S < P - R_0$ and $R_{M0} + R_{M1} - R_{NM} < -C_M$ and $R_{S0} + R_{S1} - R_{NS} + F > 0$ or $-C_S < R_{S0} + R_{S1} - R_{NS} + F < 0$; that is, the market subject tends to adopt a nonparticipation strategy when it benefits more from nonparticipation in supply than participation, when the loss of government subject without intervention is greater than the cost of interfering with the social subject and when the benefit of social subject participating in supply is greater than that of nonparticipation. When the benefit of social subject participating in supply is greater than that of nonparticipation under the intervention of the government subject, the government tends to adopt the intervention strategy, and society adopts the participation strategy. Thus, the corresponding policy stability point in this scenario is $E_6 (1, 0, 1)$.

Scenario 8: $C_M + S_M + C_S + S_S < P - R_0$ and $R_{M0} + R_{M1} - R_{NM} > 0$ or $-C_M < R_{M0} + R_{M1} - R_{NM} < 0$ and $R_{S0} + R_{S1} - R_{NS} + F > 0$ or $-C_S < R_{S0} + R_{S1} - R_{NS} + F < 0$; that is, when the loss of the government adopting a nonintervention strategy is greater than the cost of adopting an intervention strategy, the government subject must tend to adopt an intervention strategy. Under the intervention of the government subject, the benefit of the market and social subjects participating in supply is greater than that of not participating; thus, these subjects tend to adopt the participation strategy. Therefore, the corresponding strategy stability point in this scenario is $E_8 (1, 1, 1)$.

In conclusion, the collaborative supply of GSRH can be divided into five stages: noncooperative behaviour, invalid exploration stage, collaborative exploration, collaborative game, and three-subject collaborative supply. Among them, Scenario 1 corresponds to the stage of noncooperative behaviour, in which the central government has a low level of control over the supply of GSRH, and local governments are more inclined to transfer investment to other projects that can generate considerable fiscal revenue. In Scenarios 2–4, the central government's control is still insufficient, local governments still choose a nonintervention strategy, and the benefits of participation by the market or social subject are greater than nonparticipation. Based on the quasipublic goods properties of GSRH, the government subject is the core of the GSRH supply, and the market and social subject cannot actively participate in it without the government's guidance; therefore, Scenarios 2–4 represent an invalid exploration stage. As the central government further intensifies its control over the GSRH supply, the government subject begins to choose the intervention strategy; thus, the supply system enters the collaborative exploration stage, corresponding to Scenario 5. In the process of exploring the intervention strategy of the government subject,

intervention strategies are constantly adjusted to attract social or market subject to participate in supply, and the collaborative system enters the collaborative game stage, corresponding to Scenarios 6-7. In the collaborative game among government, market, and society, the three subjects constantly adjust their strategy choices and finally reach the collaborative supply stage of government intervention, market, and social participation, corresponding to Scenario 8. Given that GSRH is a kind of social welfare housing without government policy support and guidance, other subjects do not take the initiative to participate in the driving force. Therefore, the invalid exploration stage without the participation of the government subject is only a theoretical derivation result, which is not in line with the realistic logic of affordable rental housing supply and will not be discussed in subsequent research.

3.2. Simulation Analysis.

This section explores the characteristics of various mechanisms and a more effective mechanism configuration through scenario simulation [59]. Based on the aforementioned setting of government, market, and society, the number of government, market, and social subjects is approximated by county administrative area, real estate enterprises, state-owned enterprises, and institutions, respectively. According to the statistical yearbook, in 2019, there were 2,792 county-level administrative regions, 94,790 real estate enterprises (except state-owned and collective investment enterprises), and 20,486 state-owned enterprises and institutions (in all industries) [60]. It can be concluded that the proportion of government, market, and social agents can be roughly estimated as $1:34:7$. In this proportion, it is assumed that the initial state of the system is $\text{Agent}_G = 10$, $\text{Agent}_M = 340$, $\text{Agent}_S = 70$, and the initial strategy selection proportion of government, market, and social agents is 50%. On the NetLogo simulation platform, with a $t = 500$ simulation period and the probability of positive strategy selection of three game subjects as the main measurement standard, 50 policy simulation numerical experiments are conducted on the simulation parameters of each group. The following simulation results are obtained by analysing and visualising the experimental data.

3.2.1. Experiment 1: Simulation Results and Analysis of the Evolutionary Game of the Three Subjects of Government-Market-Society.

According to the above EGT derivation results, this section verifies the stability of the evolutionary equilibrium state of the GSRH collaborative supply system in each stage. The invalid exploration stage of EGT is only a theoretical derivation result that does not conform to the realistic logic of public housing supply in China. Therefore, this part only conducts a simulation analysis and discussion on the noncooperative behaviour stage, collaborative exploration stage, collaborative game stage, and collaborative supply stage. The parameter settings of each scenario are $P_S = (GB_M, GB_S, C_M, C_S, S_M, S_S, R_{M0}, R_{M1}, R_{NM}, R_{S0}, R_{S1}, R_{NS}, R_0, P, F)$, and the corresponding scenarios in each evolution stage are shown in Table 5.

When the government chooses the intervention strategy with a probability of 0.5 and the market and society choose the participation strategy with a probability of 0.5, the initial state of the evolutionary game system is (0.5, 0.5, 0.5). Throughout these four stages, in the stage of noncooperative behaviour, the punishment of the government subject for nonintervention by the higher authorities is less than the income, and the evolution result is that all the government agents tend to adopt the nonintervention strategy at a fast speed, and the final evolution is stable for the government subject to choose the intervention strategy with a probability of 0. With the decrease in the proportion of government agents taking intervention strategies, the probability of market and social agents taking that strategy tends to 0 at an approximate rate, as shown in Figure 3(a). When the central government pays more attention to the supply of GSRH and takes it as an important indicator for the performance evaluation or urban development of the government subject, the government subject tends to adopt the intervention strategy at a high rate, and the supply system of the city enters the stage of collaborative exploration. As the government subject has bounded rationality and obtains incomplete information in this phase, the enthusiasm of the market and social subjects to participate in the supply is not aroused; therefore, they will tend to adopt the nonparticipation strategy with a probability of 1 at a similar rate, as shown in Figure 3(b). Under the Further increase of subsidies and appropriate intervention by government subject on the market or society subject will attract the participation of the market or social subject and enter the cooperative game of the multisubject supply of GSRH, as shown in Figures 3(c) and 3(d)). In this stage, government agents need to adjust their strategy, actively intervene against nonparticipating agents, and conduct appropriate subsidies and supervision for active participation. In this process, each agent continues to learn and update its strategy; the intervention of the government subject successfully mobilises the enthusiasm of the market and social agents for participating, achieving the dynamic and stable state of the three-subject collaborative supply, as shown in Figure 3(e).

Note: in each evolution stage, the output results of the stability test of each equilibrium point are set as the average values of several parameters in the corresponding scenario.

3.2.2. Experiment 2: The Impact of Government Intervention on Supply Efficiency in the Collaborative Supply Phase.

In the collaborative supply stage of GSRH, different levels of government intervention may have different impacts on the efficiency of collaborative supply, in accordance with the hypothesis that the government's intervention strategy involves subsidies and supervision. To determine the impact of government intervention on supply efficiency, this section designs the following two sets of policy experiments.

The first experiment: for the supervision strategy, the government should increase or relax supervision to give full play to the market advantage to improve supply efficiency. Previous studies have asserted that strengthening

TABLE 5: Parameter values in corresponding scenarios at different evolution stages.

Stage	Scenario		GB_M	GB_S	C_M	C_S	S_M	S_S	R_{M0}	R_{M1}	R_{NM}	R_{S0}	R_{S1}	R_{NS}	R_0	P	F
1	1	1-1	5	5	2	1	2	1	3	2	6	2	1	5	5	4	1.5
		1-2	5	5	2	1	2	1	3	2	6	1	1	5	5	4	1
		1–3	5	5	1.5	1	1.5	1	3	1	6	2	1	5	5	4	1.5
		1-4	5	5	1.5	1	1.5	1	3	1	6	1	1	5	5	4	1
2	5	5-1	5	5	1.5	1	1.5	1	3	1	6	1	1	5	2	6	1
		5-2	5	5	1.5	1	1.5	1	3	1	6	1	1	5	1	7	1
3	6	6-1	5	5	1.5	1	1.5	1	3	2	4	1	1	5	2	6	1
		6-2	5	5	1.5	1	1.5	1	3	2	6	1	1	5	2	6	1
		6-3	5	5	1.5	1	1.5	1	3	2	4	1	1	5	1	7	1
		6-4	5	5	1.5	1	1.5	1	3	2	6	1	1	5	1	7	1
	7	7-1	5	5	1.5	1	1.5	1	3	1	6	2	2	5	2	6	2
		7-2	5	5	1.5	1	1.5	1	3	1	6	2	1	5	2	6	1.5
		7-3	5	5	1.5	1	1.5	1	3	1	6	2	2	5	1	7	2
		7-4	5	5	1.5	1	1.5	1	3	1	6	2	1	5	1	7	1.5
4	8	8-1	5	5	1.5	1	1.5	1	3	2	4	2	2	5	1	7	2
		8-2	5	5	1.5	1	1.5	1	3	2	4	2	1	5	1	7	1.5
		8-3	5	5	1.5	1	1.5	1	3	2	6	2	2	5	1	7	2
		8-4	5	5	1.5	1	1.5	1	3	2	6	2	1	5	1	7	1.5

government control can promote greater cooperation among various subjects in public housing supply [18], and the efficiency of public housing supply is a constraint of the government [17]; however, some scholars believe that it is necessary to provide the space for the market to play its advantage.

To clarify this problem, this part controls the subsidy strategy and conducts no supervision, low-supervision, and high-supervision as three groups of parameters, respectively, to conduct the policy experiment on the influence of supervision intensity on the supply system. With $t = 500$ as the cycle, 50 policy simulations are conducted. The parameter settings of the no supervision, low-supervision, and high-supervision strategies are $P_{S1-0} = (5, 5, 1.5, 1, 0, 0, 3, 2, 4, 2, 2, 5, 1, 9, 2)$, $P_{S1-1} = (5, 5, 1.5, 1, 1.5, 1, 3, 2, 4, 2, 2, 5, 1, 9, 2)$, and $P_{S1-2} = (5, 5, 1.5, 1, 3, 2, 3, 2, 4, 2, 2, 5, 1, 9, 2)$. Figure 4 shows the data analysis and visualisation of the output results of large-scale numerical experiments.

From the output results of the above large-scale policy simulation experiments, compared with the low-supervision strategy, when the government agents adopt the no supervision strategy, they do not have to pay the supervision cost, and the cost of participating in the supply is significantly reduced. Therefore, the proportion of government agents choosing the intervention strategy increases significantly during the simulation cycle. Compared with the low-supervision strategy, when the supervision is further increased, the proportion of government entities choosing intervention strategies decreases significantly as the intervention cost increases, and it is lower than the low-supervision strategy. In the early stage of three-subject collaborative supply ($T < 100$), no supervision, low-supervision, and high-supervision strategies have no significant effect on the strategy choice of market agents, and the market participation rate of the low-supervision strategy is higher relatively. With the development of the supply system ($100 < T < 400$), the participation rate of market agents choosing a high-supervision strategy is the highest, while the no supervision and low-supervision

strategies have no significant impact on the market participation rate. Conversely, as the collaborative supply system matures ($T > 400$), "high regulation" restrains the participation rate of market agents.

For the market agents, the simulation results show that, in the early stage of the GSRH collaborative supply, the government's adoption of the low-supervision strategy is relatively efficient and plays a market advantage while regulating the market. In the development stage of the collaborative supply, the government may choose the high-supervision strategy to strengthen its control over the market and promote greater cooperation between the government and market agents [17]. The simulation results also show a significant increase in market participation under the high-supervision strategy. In the mature stage of the collaborative system development, high-supervision restricts the market, while a low-supervision strategy is more efficient. For social agents, the influence of government supervision on their participation rate is not obvious, indicating that the choice of a government supervision strategy is not a key factor for social agents to participate in the supply of GSRH.

The second experiment: how much policy subsidy can realise the efficient synergy of GSRH supply by the government subject with the market and social subjects? To clarify this problem, three strategies of low subsidy, medium subsidy, and high subsidy are set up to conduct policy experiments on the effect of subsidy degree on the supply efficiency of affordable rental housing under the control of supervision. With $t = 500$ as the cycle, 50 policy simulations are conducted. The parameter settings of the "low, medium, and high" strategy are $P_{S2-0} = (5, 5, 1.5, 1, 1.5, 1, 3, 2, 4, 2, 2, 5, 1, 9, 2)$, $P_{S2-1} = (5, 5, 2, 1.5, 1.5, 1, 3, 2, 4, 2, 2, 5, 1, 9, 2)$, and $P_{S2-2} (5, 5, 3, 2, 1.5, 1, 3, 2, 4, 2, 2, 5, 1, 9), 2)$, respectively. Figure 5 shows the data analysis and visualisation of the output results of large-scale numerical experiments.

It can be seen from the output results of the large-scale policy simulation experiment that a medium-subsidy
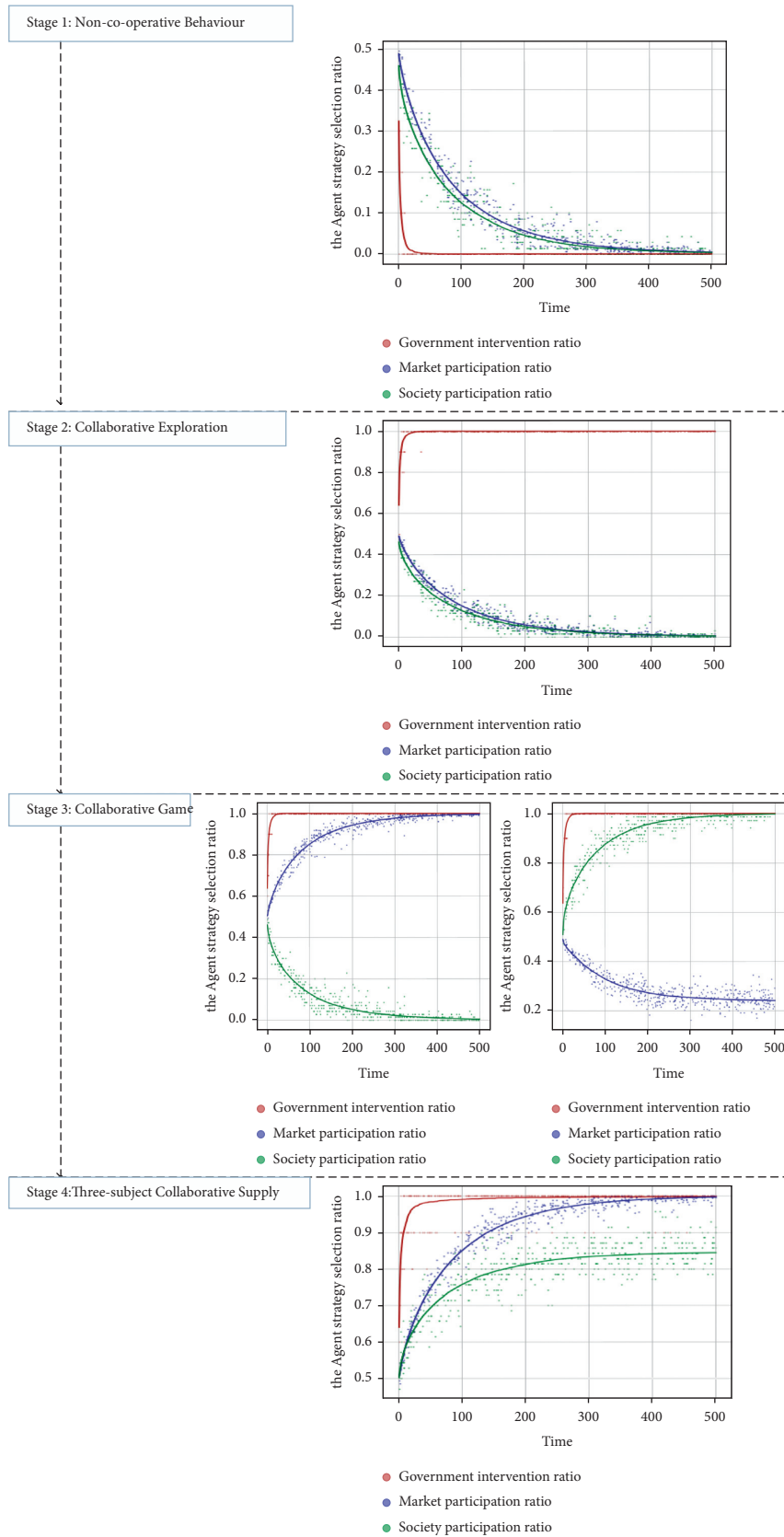
FIGURE 3: Four-stage simulation results of "government-market-society," three-subject collaborative supply. (a) Stability test of equilibrium point (0, 0, 0). (b) Stability test of equilibrium point (1, 0, 0). (c) Stability test of equilibrium point (1, 1, 0). (d) Stability test of equilibrium point (1, 0, 1). (e) Stability test of equilibrium point (1, 1, 1).
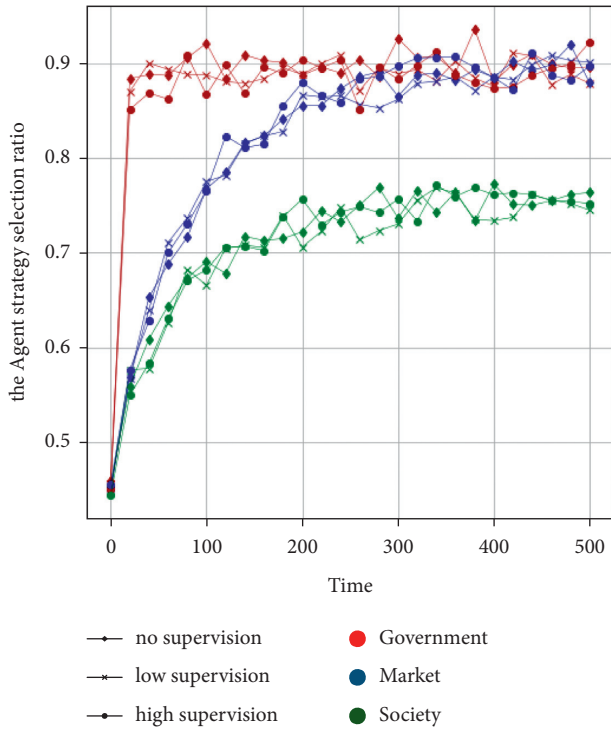
Figure 4: The influence of government supervision on the strategy selection of each agent.
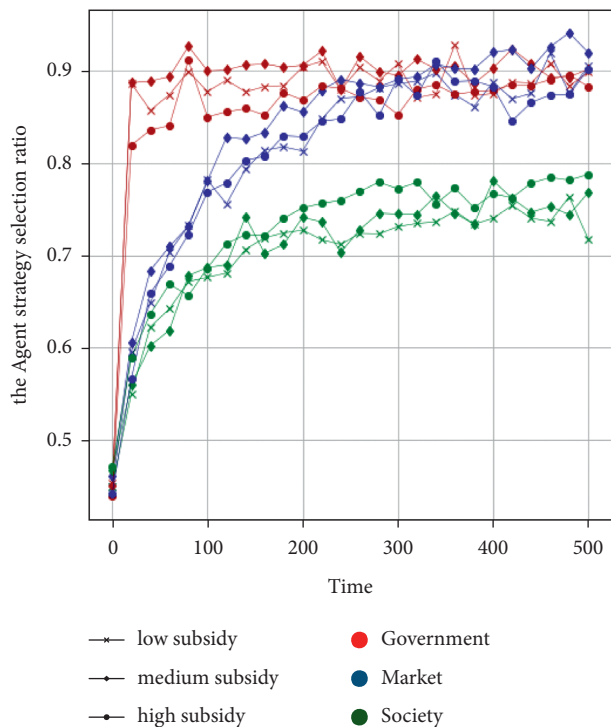
Figure 5: The influence of government subsidy on strategic selection of each agent.

strategy can mobilise the enthusiasm of various agents to participate compared with the low-subsidy strategy for government agents and the participation rate of government agents increases accordingly. While adopting the high-

subsidy strategy, the government's main body is involved in the supply of financial burden overweight, leading to a reduction in the participation rate of government agents. The medium-subsidy strategy has brought a greater guarantee to the income of the supply of affordable rental housing for market players compared with the low-subsidy strategy, and the market participation rate has significantly increased. The market participation rate is lower when the high-subsidy strategy, rather than the medium-subsidy strategy, is adopted, indicating that the government's blind increase of subsidies for the market subject cannot continuously stimulate the enthusiasm of market participation and that this increase should be reasonable. As the social subject participates in the nonprofit supply of GSRH, it is more motivated with a "high subsidy" than with a medium or low subsidy.

3.2.3. Experiment 3: Effects of Market and Social Participation on System Equilibrium. For different development stages of the collaborative GSRH supply system, the different initial strategy choices of the market and social agents may have different degrees of impact on the development of each stage of the collaborative supply system. To clarify this issue, this section designs the following two sets of experiments.

The first experiment: two groups of strategies of $y = 0.5$ and $y = 1$ are set to conduct the policy experiment on the influence of the initial proportion of market agents in the participation strategy on the GSRH supply efficiency. With $t = 500$ as the cycle, 50 policy simulations are conducted. Figure 6 shows the data analysis and visualisation of the output results of large-scale numerical experiments.

At every stage, when the probability of market participation is 1, compared with 0.5, the intervention rate of government agents is significantly reduced as the simulation results indicate that the participation rate of market agents increases in the collaborative supply stage (Stage 4). The participation rate of social agents is also greatly reduced at the same time, while there is no significant influence on the strategy choice of each subject in other stages, as shown in Figure 6(e). The simulation results show that the enthusiasm of market players is excessively aroused in the stage of collaborative supply, and the proportion of market agents occupy an excessively high proportion of the supply system, which leads to the relaxation of government intervention in supply and to social agents being squeezed out of the supply system by the market, resulting in the imbalance of the government-market-society collaborative supply system. The supply of GSRH is vulnerable to "market failure"; therefore, the government should take the initiative to regulate the participation ratio of market agents to avoid market-led supply imbalance in Stage 4.

The second experiment: two groups of strategies of $z = 0.5$ and $z = 1$ are set to conduct the policy experiment on the influence of the initial proportion of market agents in the participation strategy on the GSRH supply efficiency. With $t = 500$ as the cycle, 50 policy simulations are conducted. Figure 7 shows the data analysis and visualisation of the output results of large-scale numerical experiments.
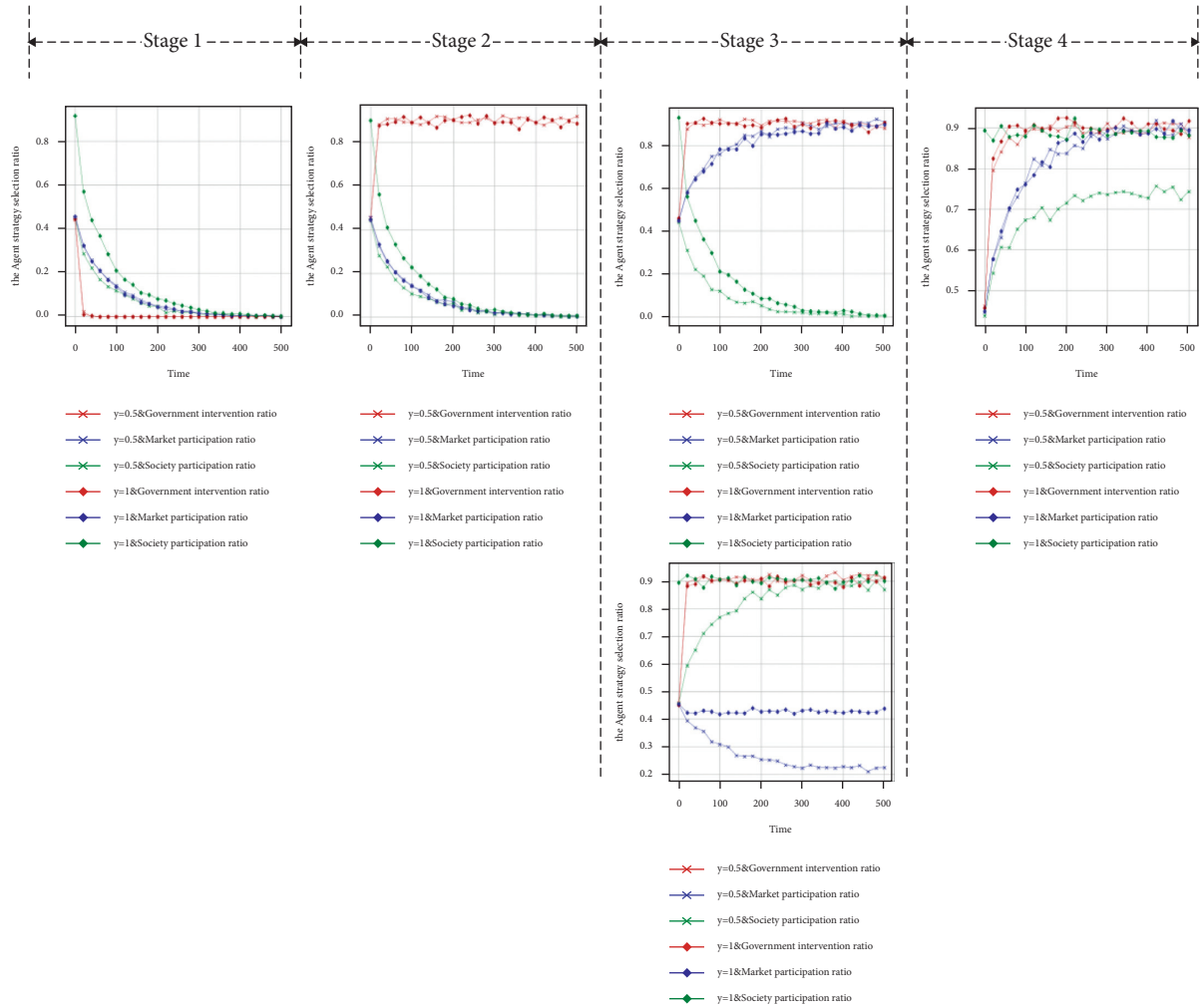
FIGURE 6: The influence of initial proportion of market agents' participation strategy on the supply system. (a) $y = 0.5$, $y = 1$, and stability test of equilibrium point $(0, 0, 0)$. (b) $y = 0.5$, $y = 1$, and stability test of equilibrium point $(1, 0, 0)$. (c) $y = 0.5$, $y = 1$, and stability test of equilibrium point $(1, 1, 0)$. (d) $y = 0.5$, $y = 1$, and stability test of equilibrium point $(1, 0, 1)$. (e) $y = 0.5$, $y = 1$, and stability test of equilibrium point $(1, 1, 1)$.

At every stage, the probability of social participation is 1, compared with 0.5 when the evolutionary stability strategy is $(1, 0, 1)$, namely, government intervention, market participation, and social participation, and the participation rate of market agents significantly improves with the increase of the participation rate of social agents in the collaborative game stage (Stage 3) from the simulation results, as shown in Figure 7(d). In the collaborative supply stage (Stage 4), as the participation rate of social agents increases, the market participation rate fluctuates, but the change is not significant, while the government intervention rate clearly increases, as shown in Figure 7(e). The impact on the strategy choice of each agent in other stages is not significant. The simulation results show that the increase of the proportion of social participation helps to mobilise the enthusiasm of market participants in the collaborative game stage and the government agents to intervene in the collaborative supply stage. Therefore, in the process of collaborative supply system development, mobilising the participation enthusiasm of social agents is conducive to the positive development of the collaborative supply system.

4. Discussion

On the basis of confirming previous studies, our results have obtained some new and more specific conclusions. First, the collaborative supply of GSRH can be divided into four stages: (i) noncooperative behaviour, (ii) collaborative exploration, (iii) collaborative game, and (iv) three-subject collaborative supply. Our division of the development stages of the multisubject collaborative supply system fills the gap of systematic research on the multisubject collaborative supply of public housing. The policy simulation of the four stages shows that the government is at the core of realising a multisubject collaborative supply, and the solution to housing affordability cannot rely solely on market forces. This result confirms the previous research conclusion on the important role of government subjects in the supply of affordable housing [26]. In the context of neoliberalism, Australia's study of the housing crises in Sydney and Melbourne also suggests that local governments must play a bigger role [61]. The policy's experimental findings further confirm the important role of specific political and economic
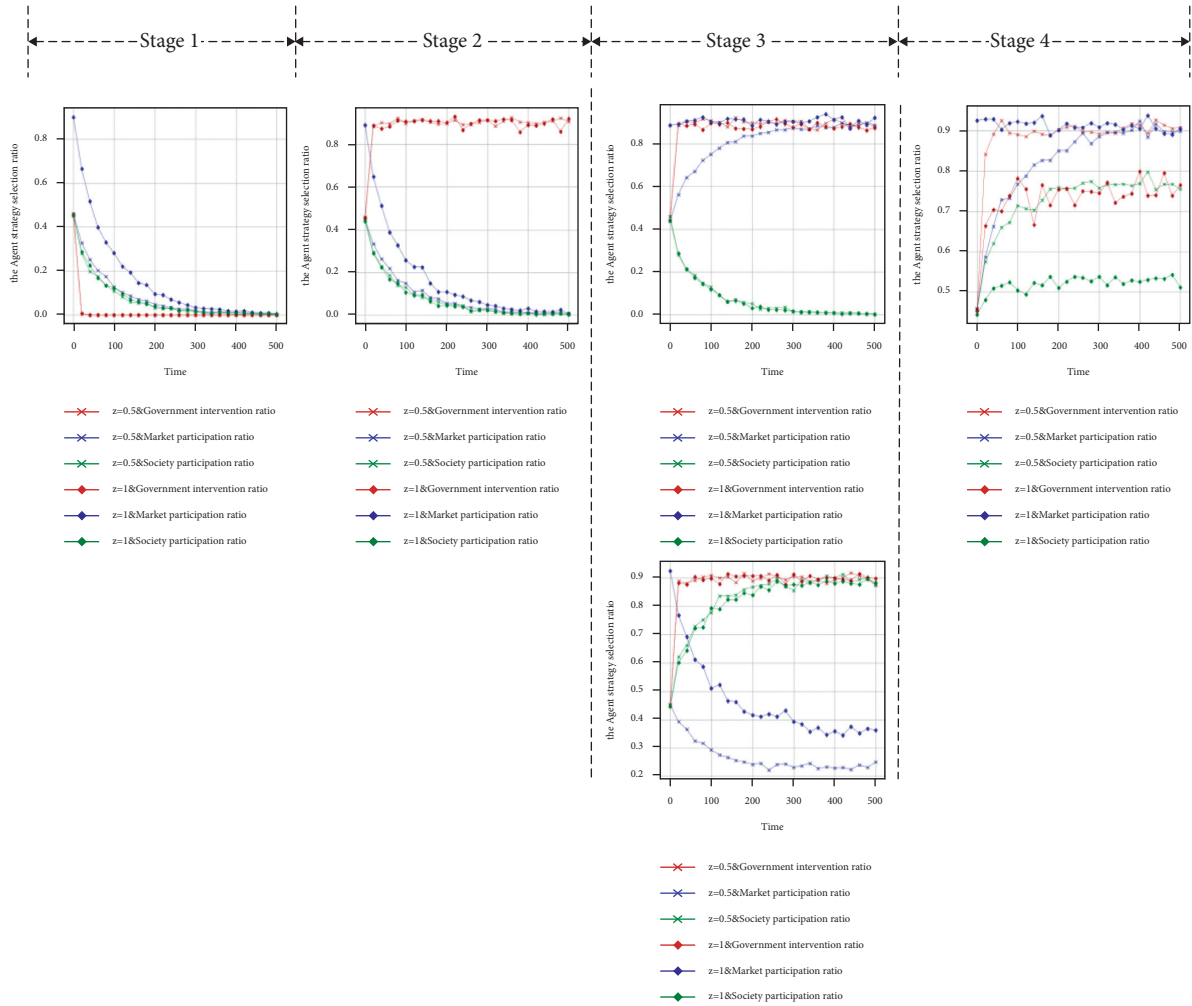
Figure 7: The influence of initial proportion of social agents' participation strategy on supply system. (a) $z = 0.5$, $z = 1$, and stability test of equilibrium point $(0, 0, 0)$. (b) $z = 0.5$, $z = 1$, and stability test of equilibrium point $(1, 0, 0)$. (c) $z = 0.5$, $z = 1$, and stability test of equilibrium point $(1, 1, 0)$. (d) $z = 0.5$, $z = 1$, and stability test of equilibrium point $(1, 0, 1)$. (e) $z = 0.5$, $z = 1$, and stability test of equilibrium point $(1, 1, 1)$.

incentives for local governments in achieving programmes [17]. The government should provide appropriate guidance for the market and social subjects, and it should be cautious in the intervention process. Improper intervention may create an uncontrollable and uncertain environment that affects market efficiency and fairness [62, 63]. And the government should determine the corresponding intervention measures according to the matching of supply and demand of GSRH in each city and the development stage of collaborative supply system so as to maximise the social benefits of these incentive mechanisms and ensure the financial feasibility of the market and social subjects [64].

Second, as the link for realising market and social synergy, how the government can efficiently realise the supply of GSRH is critical to the sustainable development of public housing at the stage of collaborative supply. The government's supervision and guidance strategy on the market and social subjects is equivalent to the "carrot" and "stick" initiative. A previous study discussed the feasibility of introducing housing affordability contributions and

incentives when developers entered the planning process and pointed out that optimum scenarios identified a balance of carrots and sticks [64]. Based on the previous related research, combined with the development stage of the collaborative GSRH supply system, this study determines the government's supervision and guidance of market and social subjects in different development stages of the supply system and obtains more detailed results. The incentive measures applicable to the supply of GSRH in all cities do not exist. Therefore, in the process of realising the multisubject collaborative supply of public housing, the development stage of the collaborative supply system should be determined according to the basic situation of the city, such as the specific population, economic situation, and policy background, combined with the exploration of the multisubject collaborative model of the city, such as public-private partnerships and inclusionary housing. And then, the specific supply policy applicable to the city should be determined according to the development stage of the collaborative supply system and the national support policy.

Finally, affordable housing is increasingly developed, financed, and managed by a mix of state, third sector, market, and community actors. Previous studies on public-private cooperation have focused more on the significance of cooperation among government and private and nonprofit organisations in increasing the supply of indemnificatory housing [26, 65], and private real estate developers have entered into partnerships with the Housing Authority to finance, design, build, and manage the new developments [66, 67]. Based on previous studies, through large-scale policy simulation experiments, this study draws microscopic and more instructive conclusions and discusses the positive and negative effects of different participation ratios of the market and social subjects in the multisubject, collaborative supply. For the different development stages of the collaborative GSRH supply system, the different initial strategy choices of the market and social agents have different degrees of influence on the development of each stage. In different stages, reasonable control of the proportion of the market and social subjects choosing participation strategies is conducive to the balance of the collaborative supply system and to avoid an imbalance caused by the insufficient or excessive participation enthusiasm of market and social subjects.

5. Conclusion

In large cities with a net population inflow, the supply of GSRH is an important measure to alleviate the staged housing difficulties of new citizens and young people, and it plays an important role in promoting new urbanisation and optimising the spatial allocation of human capital in China. The coordination degree of government, market, and society in the supply process directly affects the implementation of the urban GSRH supply plan. Based on the multisubject evolutionary game model, this study establishes an agent-based model with the help of the NetLogo simulation platform, conducts large-scale policy experiments to explore the development status of the collaborative supply system of GSRH and the influence of each agent's strategic choices on the balance of the supply system, and draws the following conclusions.

First, the collaborative supply of GSRH can be divided into four stages: (i) noncooperative behaviour, (ii) collaborative exploration, (iii) collaborative game, and (iv) three-subject collaborative supply. Second, this study determines the government's supervision and guidance of market and social subjects in different development stages of the supply system and obtains more detailed results. (a) Market agents are sensitive to the government's choice of supervision strategy. The government should adopt different levels of supervision strategies at different stages of the development of the collaborative supply system (Stages I–II: supervision; Stage III: increased supervision; Stage IV: supervision), but government supervision is not a key factor affecting the participation of social subjects in supply. Therefore, the government can appropriately increase the supervision of the market and relax the supervision of social subjects in the process of coordination. (b) For the choice of subsidy strategy, the reaction of market agents to the intensity of the government's subsidy strategy has certain limits, beyond which the increase of government subsidies cannot mobilise the market's enthusiasm, while increasing subsidies to social agents can fully mobilise their participation enthusiasm. Therefore, the government should appropriately increase subsidies to market subject and give full subsidies to social subject. Finally, the results of the policy simulation experiment indicate that increasing the participation ratio of social agents helps mobilise the enthusiasm of the government and of market agents to participate in Stage III. However, the excessive participation ratio of market agents leads to the imbalance of the collaborative supply system in Stage IV; thus, the government subject needs to limit the market participation ratio within a reasonable range.

This study has strong theoretical and practical implications for the establishment of collaborative supply system of various public housing. At the theoretical level, in view of the dilemma of the GSRH supply, this study attempts to explore the internal mechanism of the multisubject collaborative supply of GSRH based on the synergy theory and the methods of EGT and ABM. The study enriches the research achievements related to collaborative supply and provides a certain scientific basis for the pilot cities to formulate specific supply policies. In terms of practical implications, this study first clarifies the core status of government subject in the supply of GSRH and provides guidance for the intervention of government subject. Secondly, A "city-specific policies" approach must be followed to avoid distortion of policy results and improper allocation of government resources so as to achieve rapid and efficient GSRH supply [14]. Finally, this study is of great significance to protect the right of residence in human development opportunities.

This study suffers from some limitations that provide directions for future research. First, the supply of GSRH in each pilot city is currently in the planning stage; therefore, the simulation model in this study lacks testing of actual cases. Secondly, the policy simulation experiment lacks quantitative results, and there is no clear quantification of the degree of supervision and guidance strategies that government subjects should give to other supply subjects in different development stages of the collaborative supply system. Moreover, there is no clear quantification of the reasonable participation ratio of market and social subjects in each development stage of this system. Future research will focus on the pilot cities of GSRH, bringing the empirical analysis data into the policy simulation model, quantifying the model, and enriching the existing research conclusions. Further, it will make this research model a policy decision-making tool based on the background research on the pilot city's development, input the research results into the model, and then provide policy suggestions with direct guiding significance for the supply of GSRH in the city.

Data Availability

The data used to support the findings of this study are available from the corresponding author upon request.

Conflicts of Interest

The authors declare that there are no conflicts of interest regarding the publication of this paper.

Acknowledgments

References

[1] People, *China Steps up Development of Subsidized Rental Housing*, http://en.people.cn/n3/2021/1103/c90000-9914912.html, 2021.

[2] W. Shi, J. Chen, and H. Wang, "Affordable housing policy in China: new developments and new challenges," *Habitat International*, vol. 54, pp. 224–233, 2016.

[3] People, *China to Increase Gov't-Subsidized Housing in 2021-2025*, http://en.people.cn/n3/2021/0901/c90000-9890599.html, 2021.

[4] National Bureau of Statistic, http://www.stats.gov.cn/ztjc/zdtjgz/zgrkpc/dqcrkpc/ggl/202105/t20210519_1817698.html, 2021.

[5] X. Guo, X. Liu, S. Chen, L. Li, and H. Fu, "China's housing provision system: evolution, purchase -rental gap measurement and optimization strategy," *Journal of Urban Planning and Development*, vol. 147, no. 4, p. 04021054, 2021.

[6] X. Guo, L. Li, H. Xie, and W. Shi, "Improved multi-objective optimization model for policy design of rental housing market," *Sustainability*, vol. 12, no. 14, 2020.

[7] People, *Chinese Vice Premier Urges Development of Government-Subsidized Rental Housing*, http://en.people.cn/n3/2021/0723/c90000-9875896.html, 2021.

[8] B. Cheng, K. Lu, J. Li, H. Chen, X. Luo, and M. Shafique, "Comprehensive assessment of embodied environmental impacts of buildings using normalized environmental impact factors," *Journal of Cleaner Production*, vol. 334, 2022.

[9] D. Li, Y. Chen, H. Chen, E. Hui, and K. Guo, "Evaluation and Optimization of the Financial Sustainability of Public Rental Housing Projects: A Case Study in Nanjing, China," *Sustainability*, vol. 8330 pages, 2016.

[10] E. Yang, J. S. Guevara-Ramirez, and C. Bisson, "Finding evidence of green leasing in United States government-leased properties," *Journal of Green Building*, vol. 15, no. 1, pp. 55–72, 2020.

[11] M. Trebilcock-Kelly, G. Saelzer-Fica, and A. Bobadilla-Moreno, "An integrated design process of low-cost housing in Chile," *Journal of Green Building*, vol. 14, no. 3, pp. 81–93, 2019.

[12] X. Gun, J. Zuo, P. Wu, J. Wang, R. Chang, and T. Wen, "How affordable housing becomes more sustainable? A stakeholder study," *Journal of Science Cleaner Production*, vol. 162, pp. 427–437, 2017.

[13] G. C. George and A. Y. Zhang, "Emerging spaces of neoliberal urbanism in China: land commodification, municipal finance and local economic growth in prefecture-level cities," *Urban Studies*, vol. 52, no. 15, pp. 2774–2798, 2015.

[14] K. H. Mok and X. F. Wu, "Dual decentralization in China's transitional economy: welfare regionalism and policy implications for central-local relationship," *Policy and Society*, vol. 32, no. 1, pp. 61–75, 2013.

[15] Y. Zou, "Contradictions in China's affordable housing policy: goals vs. structure," *Habitat International*, vol. 41, pp. 8–16, 2014.

[16] X. Sun, "Campaign-style implementation and affordable housing provision in China," *The China Journal*, vol. 84, pp. 76–101, 2020.

[17] J. Zhou and R. Ronald, "The resurgence of public housing provision in China: the Chongqing programme," *Housing Studies*, vol. 32, no. 4, pp. 428–448, 2017.

[18] W. Sun, Y. Fu, and S. Zheng, "Local public service provision and spatial inequality in Chinese cities: the role of residential income sorting and land-use conditions," *Journal of Regional Science*, vol. 57, no. 4, pp. 547–567, 2017.

[19] J. Yu and Y. Liu, "Evaluation on residence satisfaction of affordable housing in Guangzhou in different periods—an empirical study on two typical cases (in Chinese)," *Journal of Guangzhou University*, vol. 17, no. 2, pp. 67–73, 2018.

[20] Z. Ma, C. Li, and J. Zhang, "Affordable housing brings about socio-spatial exclusion in Changchun, China: explanation in various economic motivations of local governments," *Habitat International*, vol. 76, pp. 40–47, 2018.

[21] P. Valkama, J. Kankaanpää, and AV. Anttiroiko, "Financial and structural impacts of quasi-marketization of the Helsinki Metropolitan Area's bus services," *Case Studies on Transport Policy*, vol. 6, no. 2, pp. 246–256, 2018.

[22] W. Xiong, X. Zhao, and H. Wang, "Information asymmetry in renegotiation of public–private partnership projects," *Journal of Computing in Civil Engineering*, vol. 32, no. 4, 2018.

[23] J. Yan, M. Haffner, and M. Elsinga, *Embracing Market and Civic Actor Participation in Public Rental Housing Governance: New Insights about Power Distribution*, Housing studies, United Kingdom, 2020.

[24] J. Song, Y. Li, Z. Feng, and H. Wang, "Cluster Analysis of the intellectual structure of PPP research," vol. 35, no. 1, 2019.

[25] H. C. Silvestre, R. C. Marques, and R. C. Gomes, "Joined-up Government of utilities: a meta-review on a public-public partnership and inter-municipal cooperation in the water and wastewater industries," *Public Management Review*, vol. 20, no. 4, pp. 607–631, 2018.

[26] G. Bortel and V. Gruis, "Innovative arrangements between public and private actors in affordable housing provision: examples from Austria, england and Italy," *Urban Science*, vol. 3, no. 52, 2019.

[27] M. L. R. MoF and MOHURD, *Notice of the Ministry of Finance, the Ministry of Land Resources, the Ministry of Housing and Urban-Rural Development and Other Departments on Adopting the PPP Mode to Promote the Investment*, Construction and Operation Management of Public Rental Housing, 2015, http://www.mohurd.gov.cn/wjfb/201506/t20150605_221098.html.

[28] M. R. Guarini and F. Battisti, "A model to assess the feasibility of public–private partnership for social housing," *Buildings*, vol. 7, no. 2, 2017.

[29] P. P. J. Driessen, C. Dieperink, F. Laerhoven, H. A. C. Runhaar, and W. J. V. Vermeulen, "Towards a conceptual framework for the study of shifts in modes of environmental governance - experiences from The Netherlands," *Environmental Policy and Governance*, vol. 22, no. 3, pp. 143–160, 2012.

[30] H. Liu, J. Li, H. Li, H. Li, P. Mao, and J. Yuan, "Risk perception and coping behavior of construction workers on occupational

health risks-A case study of nanjing, China," *International Journal of Environmental Research and Public Health*, vol. 18, no. 13, 2021.

[31] Q. Zhang, K. Jiang, M. Yan, and J. Ma, "A competitive multiattribute group decision-making approach for the game between manufacturers," *Computational Intelligence and Neuroscience*, vol. 2019, p. 8389035, 2019.

[32] Y. Gao, "On synergy of management innovation and technological innovation of enterprise, University and Research," *Applied Mechanics and Materials*, vol. 291-294, pp. 2968–2977, 2013.

[33] C. Li and S. Xu, *60 Theories Commonly Used in Management and Organization Research*, pp. 21–28, Peking University Press, Beijing, China, 2019.

[34] A. Y. Lewin and H. W. Volberda, "Prolegomena on coevolution: a framework for research on strategy and new organizational forms," *Organization Science*, vol. 10, no. 5, pp. 519–534, 1999.

[35] M. Smith and G. Price, "The logic of animal conflict," *Nature*, vol. 246, 1973.

[36] X. Zhang, H. Bao, and M. Skitmore, "The land hoarding and land inspector dilemma in China: an evolutionary game theoretic perspective," *Habitat International*, vol. 46, pp. 187–195, 2015.

[37] X. Jiang, Y. Ji, M. Du, and W. Deng, "A study of driver's route choice behavior based on evolutionary game theory," *Computational Intelligence and Neuroscience*, vol. 2014, 2014.

[38] L. Mu, X. Qin, Y. Li, and P. Liu, "Complex dynamic analysis for game model under different regulatory levels in China's housing rental market," *Complexity*, vol. 2020, 2020.

[39] J. Qiu, "The game of social forces participating in the evolution of the housing rental market and government regulation," *American Journal of Industrial and Business Management*, vol. 10, no. 1, pp. 99–109, 2020.

[40] J. Zhou, Y. Zhao, and F. Jv, "The static game and solution strategy in the development of housing rental market and its solution strategy," *See*, vol. 3, pp. 72–76, 2016.

[41] C. Hou, Y. Wen, Y. He et al., "Public stereotypes of recycled water end uses with different human contact: evidence from event-related potential (ERP)," *Resources, Conservation and Recycling*, vol. 168105464 pages, 2021.

[42] X. Liu, S. Chen, X. Guo, and H. Fu, "Can social norms promote recycled water use on campus? The evidence from event-related potentials," *Frontiers in Psychology*, vol. 13, p. 818292, 2022.

[43] S. Abar, G. K. Theodoropoulos, P. Lemarinier, and G. M. P. O'Hare, "Agent Based Modelling and Simulation tools: a review of the state-of-art software," *Computer Science Review*, vol. 24, pp. 13–33, 2017.

[44] M. W. Macy and R. Willer, "From factors to actors: computational sociology and agent-based modeling," *Annual Review of Sociology*, vol. 28, no. 1, pp. 143–166, 2002.

[45] J. Chhatwal and T. He, "Economic evaluations with agent-based modelling: an introduction," *PharmacoEconomics*, vol. 33, no. 5, pp. 423–433, 2015.

[46] F. Leon, "Stabilization methods for a multiagent system with complex behaviours," *Computational Intelligence and Neuroscience*, vol. 2015, 2015.

[47] N. Bahrami, A. Afshar, and M. Afshar, "An agent-based framework for simulating interactions between reservoir operators and farmers for reservoir management with dynamic demands," *Agricultural Water Management*, vol. 259, 2022.

[48] C. M. Macal, "Everything you need to know about agent-based modelling and simulation," *Journal of Simulation*, vol. 10, no. 2, pp. 144–156, 2016.

[49] A. Marvuglia, S. Rege, T. Navarrete Gutiérrez, L. Vanni, D. Stilmant, and E. Benetto, "A return on experience from the application of agent-based simulations coupled with life cycle assessment to model agricultural processes," *Journal of Cleaner Production*, vol. 142, pp. 1539–1551, 2017.

[50] J. Chen, L. Yao, and H. Wang, "Development of public housing in post-reform China," *China and World Economy*, vol. 25, no. 4, pp. 60–77, 2017.

[51] Q. Xing, "Governing housing in China: state, market and work units," *Journal of Housing and the Built Environment*, vol. 17, pp. 7–20, 2002.

[52] J. A. Kerlin, "A comparative analysis of the global emergence of social enterprise," *Voluntas: International Journal of Voluntary and Nonprofit Organizations*, vol. 21, no. 2, pp. 162–179, 2010.

[53] T. Liu, G. Cao, Y. Yan, and R. Y. Wang, "Urban land marketization in China: central policy, local initiative, and market mechanism," *Land Use Policy*, vol. 57, pp. 265–276, 2016.

[54] Y. Chen, D. Zhu, and L. Zhou, "A game theory analysis of promoting the spongy city construction at the building and community scale," *Habitat International*, vol. 86, pp. 91–100, 2019.

[55] L. Li, J. An, Y. Li, and X. Guo, "Multiattribute supply and demand matching decision model for online-listed rental housing: an empirical study based on shanghai," *Discrete Dynamics in Nature and Society*, vol. 2020, p. 4827503, 2020.

[56] C. Colleen and S. Zheng, "A burden or a tool? Rationalizing public housing provision in Chinese cities," *Housing Studies*, vol. 36, pp. 500–543, 2019.

[57] B. Xin and M. Sun, "A differential oligopoly game for optimal production planning and water savings," *European Journal of Operational Research*, vol. 269, no. 1, pp. 206–217, 2018.

[58] Y. Chen, S. Ding, H. Zheng, Y. Zhang, and S. Yang, "Exploring diffusion strategies for mHealth promotion using evolutionary game model," *Applied Mathematics and Computation*, vol. 336, pp. 148–161, 2018.

[59] M. Xing, F. Luo, and Y. Fang, "Research on the sustainability promotion mechanisms of industries in China's resource-based cities -- from an ecological perspective," *Journal of Cleaner Production*, vol. 315, 2021.

[60] National Bureau of Statistics of China, *China Statistical Yearbook*, http://www.stats.gov.cn/tjsj/ndsj/2019/indexeh.html, 2019.

[61] A. Morris, A. Beer, J. Martin et al., "Australian local governments and affordable housing: challenges and possibilities," *Economic and Labour Relations Review*, vol. 31, no. 1, pp. 14–33, 2020.

[62] X. Yu, Y. Tao, X. Tao, F. Xia, and Y. Li, "Managing uncertainty in emerging economies: the interaction effects between causation and effectuation on firm performance," *Technological Forecasting and Social Change*, vol. 135, pp. 121–131, 2018.

[63] X. Yu, T. Liu, L. He, and Y. Li, "Micro-foundations of Strategic Decision-Making in Family Business Organisations: A Cognitive Neuroscience Perspective," *Long Range Plan*, no. 102198, 2022.

[64] G. Warren-Myers, E. McRae, K. Raynor, and M. Palm, "Modelling the effects of affordable housing 'sticks' and 'carrots' for developer-delivered projects," *Pacific Rim Property Research Journal*, vol. 25, no. 3, pp. 195–215, 2019.

[65] P. Wakely, "Partnership: a strategic paradigm for the production & management of affordable housing & sustainable urban development," *International Journal of Urban Sustainable Development*, vol. 12, no. 1, pp. 119–125, 2020.

[66] X. Guo, Z. Fan, H. Zhu, X. Chen, M. Wang, and H. Fu, "Willingness to pay for healthy housing during the COVID-19 pandemic in China: evidence from eye tracking experiment," *Frontiers in Public Health*, vol. 10, p. 855671, 2022.

[67] M. L. Joseph, R. J. Chaskin, A. T. Khare, and J.-E. Kim, "The organizational challenges of mixed-income development: privatizing public housing through cross-sector collaboration," *Urban Research & Practical*, vol. 12, no. 1, pp. 61–83, 2019.

Research Article

New Quality Cost Framework (QCF) Based on the Hybrid Fuzzy MCDM Approach

Qiong Wu,[1,2,3] Jing Xuan [ID],[4] Fuli Zhou [ID],[5] Yuanfei Mei,[1] and Jiafu Su[6]

[1]*College of Management Science and Engineering, Chongqing Technology and Business University, Chongqing 400067, China*
[2]*Chongqing Research Center for Industrialization and Informatization Integration and*
 Logistics Information Technology Application, Chongqing, China
[3]*Postdoctoral Research station of Changzufeiyue (CZFY) Technology Development Co., Ltd, Chongqing 402360, China*
[4]*College of Language Intelligence, Sichuan International Studies University, Chongqing 400067, China*
[5]*College of Economics and Management, Zhengzhou University of Light Industry, Zhengzhou 450001, China*
[6]*International College, Krirk University, Bangkok 10220, Thailand*

Correspondence should be addressed to Jing Xuan; xuanjing8045@163.com and Fuli Zhou; deepbreath329@outlook.com

Quality cost framework (QCF), as a measurement tool and research method, has played a significant role on quality improvement procedure (QIP) and recognition on economics of quality. The four general QCFs are usually conceptually employed assist quality managers to measure the quality cost (QC/COQ) including PAF, intangible loss, process cost, and ABC framework. The question of how to select an appropriate quality cost framework for individual organization is of great significance for implementing quality improvement activities. Considering the *effectiveness* and *feasibility* of the alternative solution, a novel hybrid fuzzy MCDM approach integrating fuzzy DMEATEL, an antientropy weighting technique and FVIKOR method are employed to study the quality cost models and assist managers to select a best QCF for an auto factory. The combined weight from subjectivity and objectivity is embedded into fuzzy VIKOR procedure to obtain alternatives' ranking order. The case study in a Chinese automaker enterprise shows high robustness of the hybrid MCDM approach, and it assists quality mangers to perform quality cost practice. Different from the previous study, the preferred solution is the ABC quality cost framework when feasibility dimension dominates, while the intangible loss framework shows first priority when the organization focuses on effectiveness principle.

1. Introduction

With an increasing fierce marketing situation and multiple products in the auto industry, quality was treated as a crucial element and core competence for industrial organizations [1, 2]. Auto-makers began to focus on quality improvement programs and customer satisfactions' enhancement by quality tools such as total quality management (TQM), lean six sigma (LSS), 8D, and statistical process control (SPC) technique [3–8]. However, with continuous quality improvement practice (QIP), managers in self-brand auto firms show their interests on economics of quality improvement activities. Quality management (QM) practice, for instance,

supplier quality factor, processing technology, and procedure control have proven to be an effective method to promote quality performance [9]. As all industries exist, quality does not come for free as it bears extra inputs and investment. While there are few relative cost measurements during QM practice, especially for expenditures of the quality improvement program (QIP) in self-brand automotive firms. Besides, quality costing becomes an effective trigger and method to control quality improvement activities in the automobile industry [10].

The purpose of QIP is to improve the product performance with lower cost [11] to meet the requirement of customers, which stimulates the cost of quality model

development [12–14]. Freiesleben targeted profit maximization as the objective by taking quality investment, cost of poor quality and revenue effect of better quality into account instead of the cost minimization objective [15]. While the prerequisite work of all these quality innovations is the total quality related cost measurement, to collect quality costs an organization needs to adopt a framework to classify costs. Therefore, it is of great significance and urgency for managers to choose an appropriate quality cost framework (QCF) to recognize the economics of quality [11, 16].

Quality cost (QC) has proven to be an effective way for quality improvement and cost reduction. The concept of quality cost (QC), first proposed by Juran and Feigenbaum, has been studied and applied as an effective tool for cost reduction and quality improvement [11, 17]. Similar to the definition of lifecycle cost (LCC), the COQ focuses on the quality-related cost from product lifecycle perspective [18]. Cost of quality (COQ) represents the cost of not achieving good quality. Any expenditure due to substandard quality contributes to the cost of quality. The term is referred to as "quality related cost," "poor quality cost", or "cost of poor quality," all of which focus on the failure expenditure when the quality cannot meet the customer. Based on the definition of American Society for Quality Control (ASQC, 1971), cost of quality is a methodology that allows an organization to determine the extent to which its resources are used for activities that prevent poor quality that appraise the quality of the organization's products or services, and that result from internal and external failures [19–21].

Quality cost framework and accounting systems are part of every modern organization's quality improvement strategy, and help management plan for quality improvement by identifying opportunities for a greatest return on investment. While there is no general agreement on the definition of COQ, and the specific quality cost differs from author to author, as well as for different industry and organization. As quality scholars and experts advocate that quality cost framework should be tailor-made for particular industrial organization [16]. In order to identify the quality cost items, some organizations are trying to develop its quality cost system based on the quality cost framework (QCF) linking with its own financial accounting system. The cost items can be calculated based its specific activity and cost parameters. The quality cost program is a systematic task whose items need to be developed, modified, deleted, and adjusted according to quality improvement practice and the practical situation of the organization.

Because there are many conceptual quality cost frameworks can guide the organization to develop its COQ program, the appropriate QCF is the crucial step for its success. Moreover, it is important for different individual organizations to choose the most appropriate quality cost framework for better quality management practice. Because the quality cost framework selection is a complicated research problem subjecting to multiple criteria of the individual organization. The quality cost framework selection can be regarded as a multicriteria decision-making problem with respect to multiple conflicting criteria. The MCDM theoretical models have been regarded as truimple for

dealing with the comprehensive evaluation of industrial problems with multiple conflicting criteria [22]. Tsai initially explored a hybrid DEMTELA-ANP model to deal with this issue [16]. However, decision-making techniques are subjectivity-oriented, and it is difficult to collect the decision information with crisp value for the Chinese auto factories [23, 24]. Due to lack of researches in terms of quality innovation on QCF selection, this paper aims at assisting managers to evaluate and select the best quality cost framework to fill the gap by a hybrid fuzzy multi-criteria decision-making (MCDM) method considering the effectiveness and feasibility of alternative model. Meanwhile, the fuzzy-based method has been employed to deal with the uncertainty and vagueness of decision information which facilitates to the data collection for decision makers. This paper aims to enhance the capacity of auto factories to prioritize quality cost framework by a hybrid MCDM approach and address the quality cost innovation. The main contributions of this paper are as follows. First, the hybrid fuzzy multi-criteria decision-making approach integrating fuzzy DEMATEL, anti-entropy weighting technique and VIKOR method is employed for QCF selection, which facilitates data collection and easy implementation. Second, the seven criteria from effectiveness and feasibility of quality cost framework are addressed based on the barriers in COQ model, and the criteria relationship map (CRM) is illustrated in the two-dimension clusters. Third, the combined weighting technique from subjectivity and objectivity has been embedded into fuzzy VIKOR procedure, which makes the approach more flexible according to the decision makers' preference.

The rest of this paper is structured as follows. Section 2 provides the literature review on quality cost related topics. The hybrid MCDM approach integrating fuzzy DEMATEL, anti-entropy weighting technique, and fuzzy VIKOR method is employed to deal with the QCF selection in the next section. In Section 4, a case application is presented in a self-brand auto-factory and this paper is ended with conclusions in Section 5.

2. Literature Review

2.1. Development and Application of QCFs. The quality cost has experienced several decades by researchers and practitioner from all walks of life [21, 25–33], while the concept for different organization or industry has been argued by many researches, due to different considerations and specific procedures. The broad concept of "economics of quality" and "cost of quality" can be traced back to the early 1950s [33]. After the initial researches by Feigenbaum (1956), Juran (1951), and Crosby's (1979) etc., the basic philosophy of quality cost has been widely used and studied with high agreement and appreciation [34]. The prevailing four quality cost frameworks applied in the quality practice are prevention-appraisal-failure (PAF), the intangible loss framework, process cost framework and activity-based cost (ABC) [11, 16, 33, 34] are presented in Table 1.

The quality cost concept, first proposed in Juran's "quality control handbook" and in Feigenbaum's "total

TABLE 1: Four typical quality cost framework details.

	Prevailing QCF	Details and cost items	References
A1	PAF framework	Prevention + appraisal + failure cost	[35–40]
A2	Intangible loss framework	Prevention + appraisal + failure + hidden cost	[29, 41–45]
A3	Process framework	Conformance + non-conformance cost	[19, 28, 46]
A4	ABC framework	Value-added + non-value-added cost	[30, 37, 47]

quality control" [33]. The specific PAF framework is propounded and has been adopted by many researchers and practitioners. There are three categories in this cost framework including prevention cost, appraisal cost, and failure cost. Prevention cost consists of cost items are associated with activities launched to prevent poor quality in products or services. Appraisal costs are related to measurement, evaluation, or auditing products or service to guarantee conformance to quality specification and performance requirements. Failure cost includes cost items leading to products or services not conforming to customer needs from the defective's standpoint, and it can be divided into internal and external failure cost. The PAF cost framework, as a prevailing COQ model, has been applied into many industries for quality costing [31, 32, 48–50], and it is also employed to optimize the quality cost and obtain the optimal quality level [13, 40, 51–53].

With the concentration of customers' satisfaction, loyalty, and brand reputation, the intangible loss cost framework has been recently emphasized by extending the PAF model. Actually, in this group of models' intangible loss or opportunity loss cost is incorporated into a typical P-A-F model, which contained the revenue lost and profit not earned due to the customer complaints. Wang owed customer satisfaction and complaint after-sales to the intangible loss and the traditional COQ models has been illustrated [34]. Snieska et al. divided the hidden costs that are always neglected and usually hardly measured caused by failed quality, into three elements: customers' goodwill, brand value, and image of company [41]. As the quality cost measurement is a systematic work which need multi-department involvement, Yang redefined the "extra resultant cost" and "estimated hidden cost" on the basis of traditional PAF COQ model, which can be measured by quality cost account matrix and responsible weight of each department [45]. Liapis et al. studied intangible quality related cost in fuel supply chain including quality deficits, customer complaint, product mixtures, and negative impacts, etc. [46]. Palikhe studied the detailed quality cost construction considering opportunity cost in electric utility industry based on the PAF framework [54]. This group of models emphasizes the role of intangible cost within the overall quality cost scheme and focuses on the hidden loss, which helps quality managers to recognize the economics of quality and its products' performance better.

In view of a number of drawbacks of the PAF cost framework, the process cost framework developed by Crosby concentrated on the operation process rather than the products or services. The process cost framework has two segments that are cost of conformance (COC) and cost of un-conformance (CONC), and the quality term is treated as "conformance to customers' requirements." The conformance cost is the cost involved in making certain things are performed right at the first time, which is similar to actual prevention and appraisal costs, while the un-conformance cost is the expenditure wasted when the work fails to conform to customer requirements, calculated by recognizing the cost of reworking, correcting, scrapping activities, which is similar to failure cost. Daunorienė has studied the COQ model from the value added chain perspective, which provided an effective way to evaluate the quality cost of the value added chain's procedures [47]. Teli et al. has proven quality cost technique to be a significant tool to reduce total costs in the automobile industry without compromising quality, which presents a case study on failure cost analysis based on Crosby philosophy [50]. The cost items need to be measured based on specific processes and it is influenced by the conformance level. The application of process cost framework is suggested as a preferred method for quality costing under TQM environment due to its quick response on quality issues [34], and it helps quality mangers to identify the importance of process cost measurement and ownership with a more integrated framework [33, 55]. Understanding the related process sufficiently is the first step in quality costing program based on process cost framework; however, the complete concise activity analysis linked with specific process without duplication for an organization may be time-consuming compared with PAF framework.

Even though the above three quality cost frameworks provide management insight on quality costing based on the economics of quality; however, it still cannot provide appropriate methods to include overhead cost items. In other words, the three frameworks are effective enough to cover the cost items and reflect the quality actions in the continuous quality improvement procedure (CQIP), while all of them are category philosophy lacking of feasibility and specific calculation on overhead costs. In addition, due to the lack of quality related data and un-conformance of traditional accounting system, the three frameworks fail to measure the quality improvement benefits, as well as cost elements. Activity-based costing method, first developed by Cooper and Kaplan, filled this gap and was adopted to identify and assign every cost activity to products and services in an organization. It assigns more overhead expenditures into dire costs and is more compatible with cost measurement system. Jorgenson and Enkerlin [56] presented a quality cost program based on ABC framework to identify, quantify, and allocate cost by a manufacturing organization. The ABC method is an alternative way that can recognize the cost items, instead of a COQ model. Based on

the activity-oriented cost (ABC) framework, it is preferred for the auto factory to eliminate the nonvalue-added activities and invest much more effectively during its quality improvement procedure (QIP).

The abovementioned four quality cost frameworks have been widely used by experts and quality practitioners. In addition, some of the above cost frameworks have proven to be adopted by many standard organizations as presented in Table 2.

2.2. Criteria for QCF Selection.

Even though the quality cost framework provides an effective guidance on quality costing, there are many barriers for the quality cost practice due to the lack of quality related data and limited cost information, etc. It is a prevailing phenomenon that many departments usually ignore the importance of the quality cost reporting in Chinese auto factories. The quality manager always focuses quality improvement procedures and quality indexes such as failure frequency (R/1000). Customer complaints and things go wrong (TGW) indicator, ignoring economics of quality [20, 50]. Due to the difficulty on the benefit measurement and invisibility of the immediate improvement, financial manager does not show much interest on quality cost reporting. The less involvement and lack of management support or absence of management interests are the barriers in tracking such costs [20]. In addition, due to the lack of knowledge and cost un-conformance with traditional accounting system, the organization cannot perform quality costing program based on an appropriate quality cost framework (QCF). The well-organized data structure and multi-department involvement based on the appropriate quality cost framework can resolve the dilemma, which helps manager to identify the cost elements and data collection with higher efficiency. Therefore, an appropriate QCF is the crucial step for organizations. Based on previous studies [16, 38, 57, 58], seven criteria from two dimensions are categorized (illustrated in Table 3) to implement this research.

To recognize the most suitable quality cost framework for an organization, a hybrid fuzzy decision-making framework is employed to deal with this problem based on the established criteria hierarchy.

3. Fuzzy Hybrid MCDM Approach for QCF Selection

The purpose of this research is to select the most appropriate quality cost framework for an automotive organization with integrated fuzzy DEMATEL-AEW-FVIKOR approach. The quality cost framework selection is regarded as a *MCDM* problem subject to criteria set $C = \{C_1, C_2, \ldots, C_j, \ldots, C_n\}$, which includes decision makers $DM = \{DM_1, DM_2, \ldots, DM_k, \ldots, DM_K\}$ and alternative set $A = \{A_1, A_2, \ldots, A_i, \ldots, A_m\}$. Suppose $\tilde{x}_{kij}$ is the rating of i-th alternative with respect to j-th criterion provided by the k-th representative, which is represented by the triangular fuzzy number converted from linguistic terms. In addition, the criteria combined weight has been divided into

subjective and objective aspect. Let the relative subjective weight is presented as $\mathbf{w}^s = (w_1^s, w_2^s, \ldots, w_j^s, \ldots w_n^s)$, and the objective weight of criteria is $\mathbf{w}^o = (w_1^o, w_2^o, \ldots, w_j^o, \ldots, w_n^o)$. The φ index is the relative importance of subjective item, and the criteria combined weight is $\mathbf{w}^c = (w_1^c, w_2^c, w_3^c, \ldots, w_n^c)$ integrated with the subjectivity and objectivity. In order to figure out the cause and effect relationship among the criteria, every expert is asked to make a comparison with the direct effect of criterion C_i on criterion C_j with linguistic variables. There are five levels to express the influence degree (Table 4) and let $\tilde{p}_{kij}$ is the influence degree rating of criteria C_i on criteria C_j provided by the k-th expert [59].

3.1. Fuzzy-Based Techniques.

Linguistic variable has been utilized for the multicriteria decision-making problem for the uncertainty and vagueness of the decision information [62, 63]. It helps to collect decision information provided by investigated representatives and can transform the linguistic description into mathematical information. The fuzzy set, introduced by Zadeh in 1965, is an effective tool to deal with the uncertainty and ambiguity of human judgment and evaluation in decision-making science [60]. In practice, it is difficult to recognize the crisp numbered information of the investigated alternatives, which motivates the application of fuzzy-based techniques [64, 65]. It is much better to convert linguistic terms into qualitative fuzzy numbers [66, 67]. The triangular fuzzy number (TFN) has been adopted to quantify the corresponding linguistic term [68].

3.1.1. Triangular Fuzzy Number and Linguistic Variable

Definition 1 (Fuzzy set). Let X be the universe of discourse, and. the fuzzy set A can be regarded as order pairs, which are linked by a membership function that maps each element with the number. The function value is the membership degree for x. The fuzzy number is a particular case of a fuzzy set, which is used to represent the vague scale ratings of the objective.

Definition 2 According to the shape of membership function, the fuzzy numbers can be divided into several forms. Assume triangular fuzzy number $\tilde{A} = (a, b, c)$ and its membership function can be illustrated as Figure 1 shows.

$$\mu_{\tilde{A}}(x) = \begin{cases} \dfrac{(x-a)}{(b-a)}, & a \leq x \leq b, \\\\ \dfrac{(c-x)}{(c-b)}, & b \leq x \leq c. \\\\ 0, & \text{otherwise} \end{cases} \tag{1}$$

There are two kinds of linguistic terms that need to be defined for the measurement of criteria influence description (Table 4) and rating scales of four quality cost frameworks with respect to each criterion (Table 5). Linguistic variables and corresponding rating scales with TFNs are presented in the following two tables.

TABLE 2: General quality cost items by various nations.

Nations	QCF category	QCF items
ASQC (US)	A1-PAF	Prevention + appraisal + failure
BS6143 (UK)	A3-process cost	Conformance and non-conformance
ISO9004-1	A1-PAF	Prevention + appraisal + failure
GB/T13339 (CN)	A2-IL	Prevention + appraisal + internal/external failure

TABLE 3: Specific criteria for the requirement of a beneficial COQ framework.

Dimension	Criteria	Detail description
D1-effectiveness	C1	The selected alternative should support the continuous quality improvement procedures (CQIP)
	C2	The selected alternative should contain as many COQ items as possible
	C3	The selected alternative should be applicable to all the departments of the organizations
D2-feasibility	C4	The selected alternative should have an easy data collection and application
	C5	The selected alternative should have the clear form and type of data needed
	C6	The selected alternative should be based on the concept of production procedures
	C7	The cost item of selected alternative should be easily recognized, calculated and recorded by the organization

TABLE 4: Linguistic variables and corresponding TFNs for criteria influence degree.

Linguistic variables of influence description	Triangular fuzzy number (TFN)
No influence (NI)	(0, 0, 0.25)
Very low influence (VL)	(0, 0.25, 0.5)
Low influence (L)	(0.25, 0.5, 0.75)
High influence (HL)	(0.5, 0.75, 1)
Very high influence (VH)	(0.75, 1, 1)

Source: [59–61].
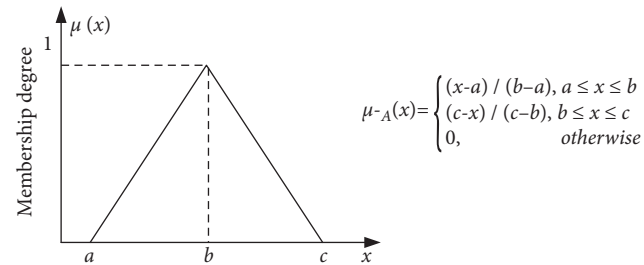
FIGURE 1: Membership function of triangular fuzzy number (TFN).

$$\mu_{\sim A}(x) = \begin{cases} (x-a)/(b-a), & a \le x \le b \\ (c-x)/(c-b), & b \le x \le c \\ 0, & otherwise \end{cases}$$

TABLE 5: Linguistic variables and corresponding TFNs for alternative evaluation.

Linguistic variables of influence description	Triangular fuzzy number (TFN)
Very low/poor (VL/VP)	(0, 0, 0.25)
Low/poor (L/P)	(0, 0.25, 0.5)
Medium (M)	(0.25, 0.5, 0.75)
High/good (H/G)	(0.5, 0.75, 1)
Very high/good (VH/VG)	(0.75, 1, 1)

Source: [69].

3.1.2. Fuzzy Operators and Defuzzification Method. Assume there are two triangular fuzzy numbers $A_1 = (a_1, b_1, c_1)$ and $A_2 = (a_2, b_2, c_2)$, the algebraic operations are implemented according to the fuzzy operators "⊖"

[70]. The common operations between these TFNs can be formulated as follows.

Addition operator: $A_1 \oplus A_2 = (a_1 + a_2, b_1 + b_2, c_1 + c_2)$
Subtraction operator: $A_1 \ominus A_2 = (a_1 - a_2, b_1 - b_2, c_1 - c_2)$
In addition,

$$\lambda A_1 = \begin{cases} (\lambda a_1, \lambda b_1, \lambda c_1), & \lambda \ge 0, \quad \lambda \in R \\ (\lambda c_1, \lambda b_1, \lambda a_1), & \lambda < 0, \quad \lambda \in R. \end{cases} \quad (2)$$

Through the abovementioned fuzzy operators, we can aggregate decision information provided by expert panels. The decision information aggregation can be formed based on the following equation:

$$\tilde{x}_{ij} = \frac{\left(\tilde{x}_{ij}^1 \oplus \tilde{x}_{ij}^2 \oplus \ldots \oplus \tilde{x}_{ij}^k \oplus \ldots \oplus \tilde{x}_{ij}^K \right)}{K}. \quad (3)$$

Fuzzy numbers usually require to be transferred into crisp value for ranking and prioritization purpose, whose process called defuzzification. The GMIR method was employed to transfer the TFNs into crisp values as equation (4) shows [71].

$$x_{ij} = \text{defuzzy}\left(\tilde{x}_{ij} \right) = \frac{x_{ij}^L + 4x_{ij}^M + x_{ij}^U}{6}. \quad (4)$$

3.2. Subjective Weight with the Fuzzy DEMATEL Method. The decision-making and trial evaluation laboratory (DEMATEL) method, first proposed in 1976, has been used to visualize the structure of complicated casual interactions. It helps decision makers to recognize and portray the causes and effects of the criteria with a diagraph map [59]. It has proven to be a big challenge for decision makers to provide crisp values of influence degree of the criteria. In that case, fuzzy logic has been embedded called fuzzy DEMATEL technique has been applied into the subjectivity weight study to address the uncertainty, vagueness, and information leaks. Implementation procedures of the fuzzy DEMATEL method are as follows [72]:

Step 1: Initial direct influence average fuzzy matrix $\tilde{P}$ construction

Based on the linguistic term and corresponding TFNs, the direct influence degree $\tilde{p}_{kij} = (p_{ijk}^L, p_{ijk}^M, p_{ijk}^U)$ can be converted that C_i on C_j by expert k. The diagonal element values of matrix P should be zero based on the definition of influence degree. After the fuzzy aggregation through fuzzy operators, the elements $\tilde{p}_{ij} = (p_{ij}^L, p_{ij}^M, p_{ij}^U)$ in the initial direct influence average fuzzy matrix $\tilde{P}$ can be generated as follows:

$$\tilde{p}_{ij}^L = \frac{1}{K} \sum_{k=1}^{K} p_{kij}^L,$$

$$\tilde{p}_{ij}^M = \frac{1}{K} \sum_{k=1}^{K} p_{kij}^M,$$

$$\tilde{p}_{ij}^U = \frac{1}{K} \sum_{k=1}^{K} p_{kij}^U,$$
$$\tag{5}$$

$$\tilde{P} = \left(\tilde{p}_{ij}\right)_{[n \times n]} = \begin{array}{c} \\ C_1 \\ C_2 \\ \\ \\ C_n \end{array} \begin{array}{c} C_1 \quad C_2 \quad \dots \quad C_n \\ \begin{bmatrix} 0 & \tilde{p}_{12} & \cdots & \tilde{p}_{1n} \\ \tilde{p}_{21} & 0 & \cdots & \tilde{p}_{2n} \\ \cdots & \cdots & \tilde{p}_{ij} & \cdots \\ \tilde{p}_{n1} & \tilde{p}_{n2} & \cdots & 0 \end{bmatrix} \end{array}.$$

Step 2: The normalized direct-influence fuzzy matrix $\tilde{M}$ construction.

The elements $\tilde{m}_{ij} = (m_{ij}^L, m_{ij}^M, m_{ij}^U)$ in the normalized direct-influence fuzzy matrix $\tilde{M}$ can be calculated through the following equation:

$$\tilde{m}_{ij} = \frac{\tilde{p}_{ij}}{s} = \left(\frac{p_{ij}^L}{s}, \frac{p_{ij}^M}{s}, \frac{p_{ij}^U}{s}\right) = \left(m_{ij}^L, m_{ij}^M, m_{ij}^U\right),$$
$$\tag{6}$$

$$s = \max_{1 \le i \le n} \left(\sum_{j=1}^{n} p_{ij}^U\right).$$

Step 3: The development of the total-influence fuzzy matrix $\tilde{T}$.

The total-influence fuzzy matrix $\tilde{T}$ can be obtained from the following equation:

$$\tilde{T} = \lim_{k \to \infty} \left(\tilde{M} \oplus \tilde{M}^2 \oplus \dots \oplus \tilde{M}^k\right) = \tilde{M}(I - \tilde{M})^{-1},$$
$$\tilde{T} = \left(\tilde{t}_{ij}\right)_{n \times n}, \tag{7}$$

where $\tilde{t}_{ij} = (t_{ij}^L, t_{ij}^M, t_{ij}^U)$ and

$$\begin{aligned}
\left[t_{ij}^L\right] &= M_L \times (1 - M_L)^{-1}, \\
\left[t_{ij}^M\right] &= M_M \times (1 - M_M)^{-1}, \\
\left[t_{ij}^U\right] &= M_U \times (1 - M_U)^{-1},
\end{aligned} \tag{8}$$

where I is the $n \times n$ square matrix with ones on its diagonal.

Step 4: Establishment of criteria influential relation map.

The sum of rows and columns are obtained from the total-influence matrix respectively expressed as $\tilde{D}_i$ and $\tilde{R}_i$ equation (9). The criteria in effect group and cause group can be calculated based on the ordered pairs of $(\tilde{D}_i + \tilde{R}_i, \tilde{D}_i - \tilde{R}_i)$.

$$\tilde{D} = (\tilde{D}_i)_{n \times 1} = \left[\sum_{j=1}^{n} \tilde{t}_{ij}\right]_{n \times 1}, \tilde{R} = (\tilde{R}_j)_{1 \times n} = \left[\sum_{i=1}^{n} \tilde{t}_{ij}\right]_{1 \times n}. \tag{9}$$

According to equation (3), the fuzzy ordered pairs $(\tilde{D}_i + \tilde{R}_i, \tilde{D}_i - \tilde{R}_i)$ are defuzzified to the crisp pairs $((\tilde{D}_i + \tilde{R}_i)^{\text{def}}, (\tilde{D}_i - \tilde{R}_i)^{\text{def}})$ through GMIR method, as well as the elements in total-influence fuzzy matrix where $(\tilde{D}_i + \tilde{R}_i)^{\text{def}}$ denotes the degree of the targeted attribute role that the factor plays in the network system and $(\tilde{D}_i - \tilde{R}_i)^{\text{def}}$ means the net effect that the element contributes to the network system. In order to obtain the criteria influential relation map, the threshold value p is established based on total-influence matrix T. Only those influential relationships whose value is greater than the established threshold value should be kept and chosen in the CRM [73]. In this paper, the arithmetic mean of all elements in matrix F is p value [16]. If $(\tilde{D}_i - \tilde{R}_i)^{\text{def}} > 0$, it means the criterion i has an effect on other criteria which will belong to the *cause group*, and if $(\tilde{D}_i - \tilde{R}_i)^{\text{def}} < 0$, the attribute i is being affected by others, which will belong to the *effect group*.

Step 5: Subjective weight calculation.

Based on the following equation (10), the subjective weight of criteria can be obtained through CRM as $\mathbf{w}^s = (w_1^s, w_2^s, \dots, w_j^s, \dots w_n^s)$.

$$w_{i0} = \left(\left[(\tilde{D}_i + \tilde{R}_i)^{\text{def}}\right]^2 + \left[(\tilde{D}_i - \tilde{R}_i)^{\text{def}}\right]^2\right)^{1/2};$$
$$w_i^s = \frac{w_{i0}}{\sum_{i=1}^{n} w_{i0}}. \tag{10}$$

3.3. Objective Weight by Antientropy Weight (AEW) Technique. Shannon Entropy is an effective method for uncertain information measurement formulated in terms of possibility theory. Liu has applied this technique into MCDM problem for the weights acquisition [74]. Objective weights based on entropy value can be realized through the following stages [75].

Step 1: Normalization of the decision-making matrix. The elements of the matrix can be calculated according to the following equation:

$$P_{ij} = \frac{x_{ij}}{\sum_{i=1}^{m} x_{ij}}. \tag{11}$$

Step 2: Calculation for the information entropy of each criterion based on the following equation:

$$e_j = -k \sum_{i=1}^{m} p_{ij} ln p_{ij} = -\frac{1}{lnm} \sum_{i=1}^{m} p_{ij} ln p_{ij}. \tag{12}$$

Step 3: The objective weight of each criterion can be obtained through the following equation:

$$w_j^o = \frac{1 - e_j}{\sum_{j=1}^{n}(1 - e_j)}. \tag{13}$$

3.4. Ranking Method Based on Fuzzy VIKOR Procedure. The VIKOR (VlseKriterijumska Optimizacija I Kompromisno Resenje) method has proven to be an effective method for multi-criteria prioritization problem [76–80]. The fuzzy VIKOR is the extension VIKOR method integrated with fuzzy-based techniques. The philosophy of VIKOR method is based on the particular measure of closeness to the ideal solution started with the following form of L_p-metric.

$$L_{p,i} = \left\{ \sum_{j=1}^{n} \left[\frac{w_i(f_j^* - f_{ij})}{f_j^* - f_j^-} \right]^p \right\}^{1/p}, \ 1 \le p \le +\infty, \tag{14}$$

$$i = 1, 2, \ldots, m.$$

It can be ranked by the index to choose the compromise solution. The implementation steps of FVIKOR method are as follows [75]:

Step 1: The normalized difference d_{ij} calculation.

The normalized difference d_{ij} is calculated based on the best value f_j^* and worst value f_j^- in following equation.

$$d_{ij} = \frac{f_j^* - x_{ij}}{f_j^* - f_j^-}, \tag{15}$$

where

$$f_j^* = \begin{cases} \max_i x_{ij}, \text{the more the better,} \\ \min_i x_{ij}, \text{the less the better,} \end{cases}$$
$$f_j^- = \begin{cases} \min_i x_{ij}, \text{the less the bad,} \\ \max_i x_{ij}, \text{the more the bad.} \end{cases} \tag{16}$$

Step 2: Compute S_i and R_i with criteria combined weight

The relative importance of subjective weight compared with objectivity is φ. According to equations (10) and (13), the combined weight of criteria $\mathbf{w}^c = (w_1^c, w_2^c, w_j^c, \ldots, w_n^c)$ can be calculated. Then the maximum group utility value S_i and minimum individual regret value R_i can be obtained in equation.

$$S_i = \sum_{j=1}^{n} (w_j^c d_{ij}),$$
$$R_i = \max_j (w_j^c d_{ij}), \tag{17}$$
$$w_j^c = \varphi w_j^s + (1 - \varphi) w_j^o.$$

Step 3: Calculation of the comprehensive utility value Q_i, $i = 1, 2, \ldots, m$.

$$Q_i = v \frac{S_i - S^*}{S^- - S^*} + (1 - v) \frac{R_i - R^*}{R^- - R^*}, \tag{18}$$

where
$S^- = \max_i S_i, S^* = \min_i S_i, R^- = \max_i R_i, R^* = \min_i R_i$. In order to reflect the attitude of decision makers, $v \epsilon (0, 1)$ represents the relative importance of maximum group utility, while the 1-v is the relative importance of individual regret.

Step 4: Alternatives ranking based on the three index value: S, R, and Q. The candidate $A^{(1)}$ will be regarded as the compromising solution, who has the minimum comprehensive group utility value Q, if the following two conditions (acceptance advantage and its stability) can be satisfied.

4. Case Study

4.1. Background and Data Collection. A real numerical case for the application of the hybrid MCDM approach integrating the fuzzy DEMATEL, anti-entropy method, and FVIKOR technique is presented in this section, and it has been applied into the quality cost framework selection of an automotive enterprise in China. The enterprise is a famous vehicle-assembly firm providing vehicle products such as cars, sport utility vehicles (SUVs), vans, and multipurpose vehicles (MPVs). With the implementation of quality improvement activities (8D and Six sigma), the quality index (PP100 and R/1000) is improved dramatically [67]. While, there is no appropriate quality cost framework helps managers to recognize the quality related cost and it is not enough to identify the COQ based on the financial report. In that case, it is of great urgency for CA Company to select the best quality cost framework to help its manager identify the COQ during the product whole lifecycle, especially for the continuous quality improvement procedure.

As the previous analyzed, there are four QCF alternatives in this study, which are evaluated from the two dimensions (effectiveness and feasibility). Expert panels include the quality manager, financial manager, and an expert on COQ. In order to obtain the required data, a questionnaire is prepared and distributed among the decision-making team, and each representative provide a judgment with linguistic variables for the direct influence of criteria (Table 6) and A1 alternative's performance subject to each criterion (Table 7), respectively.

In order to reflect the robustness of the proposed hybrid MCDM framework, the sensitivity analysis on the decision parameters φ and v are conducted in eleven experiment scenarios illustrated in Tables 8 and 9. In addition, in order to explore the best solution of the QCF under different consideration, the relative importance of the effectiveness (ρ) is defined with 11 experiment scenarios in Table 10.

4.2. Application of the Proposed Approach. The fuzzy DEMATEL method was used to recognize interdependence

TABLE 6: Initial direct influence degree of criteria given by representatives.

Effectiveness		C1	C2	C3	
C1	DM1	NI	VL	NI	
	DM2	NI	L	VL	
	DM3	NI	VL	VL	
C2	DM1	VH	NI	VH	
	DM2	HL	NI	VH	
	DM3	HL	NI	HL	
C3	DM1	VH	L	NI	
	DM2	L	VL	NI	
	DM3	VH	NI	NI	
Feasibility		C4	C5	C6	C7
C4	DM1	NI	VL	NI	L
	DM2	NI	L	VL	VL
	DM3	NI	L	VL	HL
C5	DM1	HL	NI	L	HL
	DM2	VH	NI	VL	VH
	DM3	VH	NI	NI	L
C6	DM1	HL	VL	NI	NI
	DM2	L	VL	NI	NI
	DM3	VH	NI	NI	VL
C7	DM1	HL	L	VL	NI
	DM2	VH	L	HL	NI
	DM3	VH	HL	L	NI

TABLE 7: Linguistic ratings of A1 QCF subject to criteria.

		C1	C2	C3	C4	C5	C6	C7
A1-PAF	DM1	G	M	VP	M	P	VP	P
	DM2	M	P	VP	P	M	G	M
	DM3	P	G	M	VP	P	P	VP

TABLE 8: Group utility weight setting (11 scenarios).

	SA1	SA2	SA3	SA4	SA5	SA6	SA7	SA8	SA9	SA10	SA11
v	0	0.1	0.2	0.3	0.4	0.5	0.6	0.7	0.8	0.9	1

TABLE 9: Relative importance of subjective weight (11 scenarios).

	SB1	SB2	SB3	SB4	SB5	SB6	SB7	SB8	SB9	SB10	SB11
φ	0	0.1	0.2	0.3	0.4	0.5	0.6	0.7	0.8	0.9	1

TABLE 10: Relative importance of "effectiveness" compared with feasibility principle (11 scenarios).

	SC1	SC2	SC3	SC4	SC5	SC6	SC7	SC8	SC9	SC10	SC11
ρ	0	0.1	0.2	0.3	0.4	0.5	0.6	0.7	0.8	0.9	1

and influence relationships among the criteria. The initial fuzzy direct influence matrix provided by the three representatives was collected by pairwise comparison in terms of influences (Table 5) and the fuzzy average direct influence matrix $\widetilde{P}$ was calculated based on equation (5). According to equations (6)–(9), the total-influence matrix $\widetilde{T}$ was derived and the threshold value p is established. The various indexes calculation results by FDEMATEL method are presented in Table 11 and criteria relationship map (CRM) was drawn based on the order pairs $(\widetilde{D}_i + \widetilde{R}_i)^{\mathrm{def}}$, $(\widetilde{D}_i - \widetilde{R}_i)^{\mathrm{def}}$, as shown

in Figure 2. In addition, the objective weight of criteria based on AEW method based on equations (12)–(14) is illustrated in Table 11. Let $\varphi = 0.5$, the combined weights can be calculated.

According to Table 11, the criteria weight can be obtained by fuzzy DEMATEL and antientropy method, which are embedded into fuzzy VIKOR procedures. The S, R and Q value and alternative ranking result can be obtained based on equations (15)–(18) as presented in Table 12.

As can be seen in the above table, the ranking order has the same sequence by S, R, and Q index. In addition, $Q(A^{(2)})-$

TABLE 11: Criteria weight item calculation result.

	$(\widetilde{D}_i + \widetilde{R}_i)$	$(\widetilde{D}_i - \widetilde{R}_i)$	Group	w_j^s	w_j^o	w_j^c
C1	(0.631, 1.267, 3.750)	(−1.371, −0.569, −0.514)	Effect	0.099	0.140	0.119
C2	(0.780, 1.861, 6.388)	(0.561, 0.772, 1.337)	Cause	0.148	0.161	0.153
C3	(0.665, 1.709, 6.027)	(−0.117, −0.051, 0.008)	Effect	0.129	0.109	0.119
C4	(1.010, 2.352, 9.064)	(−1.490, −0.780, −0.567)	Effect	0.193	0.117	0.155
C5	(0.680, 1.791, 7.913)	(0.121, 0.131, 0.169)	Cause	0.151	0.156	0.153
C6	(0.327, 1.170, 6.472)	(0.103, 0.140, 0.249)	Cause	0.110	0.159	0.134
C7	(0.830, 2.039, 8.548)	(0.294, 0.509, 1.120)	Cause	0.171	0.158	0.164
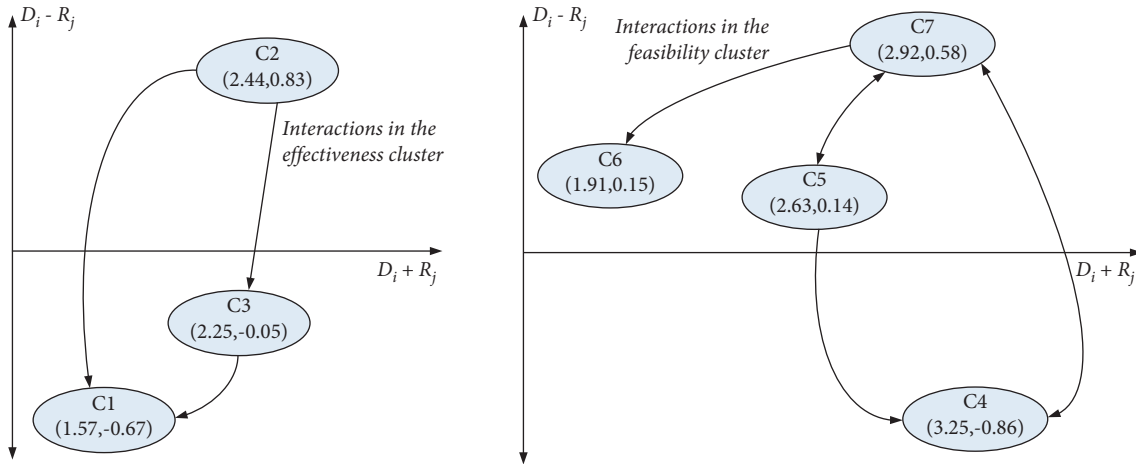
FIGURE 2: Criteria relationship map (CRM) in the two dimension clusters.

TABLE 12: Four QCF alternatives ranking result based on S, R and Q value.

Alternative	The proposed integrated framework				TOPSIS-based method	
	S value	R value	Q value	Ranking by $S/R/Q$	RC value by the TOPSIS steps	Ranking by RC
A1-PAFF	0.892	0.164	1	4	0.492	4
A2-ILF	0.513	0.155	0.563	3	0.523	3
A3-PF	0.370	0.153	0.420	2	0.758	2
A4-ABCF	0.319	0.119	0	1	0.952	1

$Q(A^{(1)}) = Q(A3) - Q(A4) = 0.42 \geq DQ = 0.33$. Therefore, the ABC quality cost framework (A4) is the best selection for its satisfaction on the two conditions. The research result shows high conformity with Tsai's study that the ABC model is the best choice for enterprise to recognize the economics of its quality improvement procedure [16]. Besides, the ranking lists show a high conformity with the TOPSIS-based method.

4.3. Sensitivity Analysis.
The abovementioned analysis shows the application of the proposed hybrid MCDM approach for the quality cost framework selection. In order to analyze the robustness of the proposed method, the sensitivity analysis is performed to understand effect on ranking result of the decision parameters. Established experimental scenarios are set in Tables 8–10.

4.3.1. Sensitivity Analysis on Relative Importance of Group Utility v.
The relative importance of group utility v reflects the optimistic attitude, and the Q value reflects the comprehensive group utility of compromising solution. The

calculated Q index values in different experimental scenarios (Table 8) are presented in the following Figure 3.

As Figure 3 shows, the best QCF selection is always the ABC model and the last one is PAF model (A1), even though there is a little fluctuation for the specific Q values of the middle two alternatives in different scenarios. The ranking order of the four quality cost framework alternatives keeps steady which means the group utility weight does not influence the decision result.

4.3.2. Sensitivity Analysis on Relative Importance of Subjectivity φ.
The defined decision parameter φ shows the relative importance of subjective weight, which reflects the weight of subjectivity in decision making. In this case, the sensitivity analysis on parameter φ (Table 9) is conducted to investigate the influence of subjectivity weight on the QCF alternative ranking results. The obtained Q values in established scenarios are illustrated in Figure 4.

The above figure shows high stability of the best solution (A4) when parameter φ varies. Similar to the sensitivity
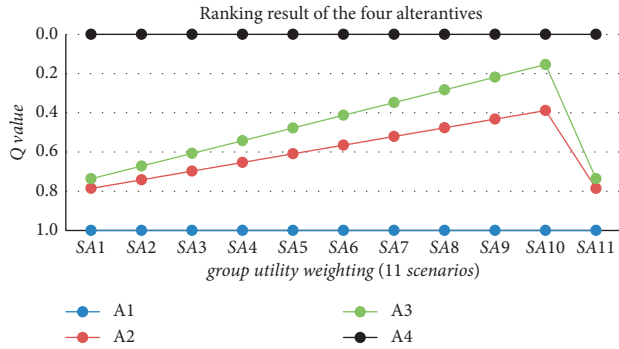
FIGURE 3: Sensitivity analysis on group utility weight v.
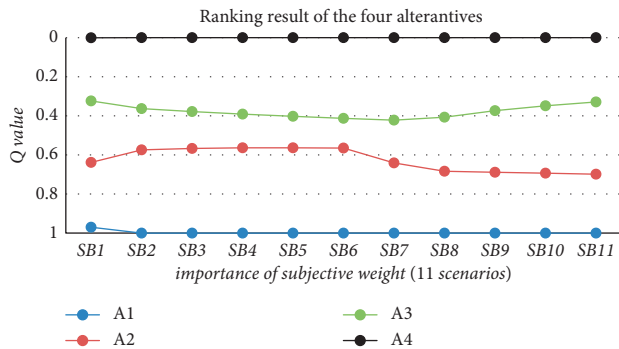
FIGURE 4: Sensitivity analysis on importance of subjective weight φ.

FIGURE 5: Sensitivity analysis on relative importance of two principles ρ.

analysis result of parameter v, the Q value of the middle two alternatives in established 11 scenarios keep a slight fluctuation which does not influence the ranking order.

4.3.3. Sensitivity Analysis on the Relative Importance of Effectiveness Dimension ρ. The decision parameter ρ reflects the attitude and validity of the representatives when the enterprise wants to select an appropriate quality cost framework. The conflict and paradox of the COQ model and traditional cost framework exist due to their unconformity. It is difficult for an organization to choose a best QCF with the two dimensions into consideration. In this part, the aim of sensitivity analysis is to explore the best solution variation when the firm focused on the different dimension.

As can be seen in the above Figure 5, the PAF quality cost framework is always the last alternative solution compared with other three ones. While the Q index values and ranking orders of other three alternatives fluctuate dramatically. When $\rho \leq 0.5$, the organization focuses on the feasibility of quality cost framework, and the best solution is ABC model catered to Tsai's research. However, when $\rho > 0.5$, the intangible loss quality cost framework shows its priority than other three alternatives due to the dominance of effectiveness dimension of QCF.

4.4. Discussion and Management Insight. The sensitivity analysis on the three decision parameters has been conducted to analyze the robustness of the proposed hybrid MCDM method. The analysis result shows that the best

solution keeps a stable priority in terms of parameter v or φ. However, best selection shifts from A4 to A2 with the increasing of parameter ρ. It is very interesting to find the different research conclusion compared with Tsai's research that the ABC model priors to other alternatives when the organization focuses on the feasibility of quality cost framework, while the intangible cost model shows its priority when it concentrates on effectiveness dimension. When the CA organization focus on the effectiveness dimension of quality cost framework, the intangible cost framework is more appropriate.

The best solution change means Chinese companies tend to focus on the importance of the hidden cost due to product unconformity, customer complaints and reputation loss, since they want to take these intangible cost items into consideration in its quality cost framework and costing report. However, it is really very difficult to quantify the cost item for either PAF model or intangible cost framework for manufacturing firms. Even some published papers have been studied on the quality cost calculation, the specific application was usually based on the organization's particular requirement. The QCF selection is a team task with all related departments involvement, and this paper presented a systematic procedure to establish an appropriate QCF integrating decision information from multigroups. The manager can select the appropriate quality cost framework based on the practical consideration of the organization. Actually, as Schiffauerova and Thomson studied [11], the quality cost framework alternative is only just a basic concept and the concrete costing systems or costing report still differ from company to company.

From the case application of the investigated organization in this paper, there occur two kinds of best solution, one is the ABC model and the other is the intangible loss framework. The intangible loss quality cost framework is the best choice when decision makers pay more attention on effectiveness principle and it can illustrate the quality related cost item from prevention, appraisal and failure term, as well as the hidden cost, which provides and extensive looking. While the best choice is the activity-oriented cost (ABC) measurement method when decision makers focus on feasibility dimension more, and it can help manager to investigate specific cost item. The new quality cost framework

from lifecycle and COQ dimension would be welcomed for both effectiveness and feasibility.

5. Conclusions

This paper employed a hybrid fuzzy multicriteria approach for quality cost framework selection from the typical four alternatives (PAF, intangible cost, process cost, and ABC), which helps the quality manager to develop quality cost practice based on appropriate QCF. The case study by the hybrid fuzzy MCDM approach integrating fuzzy DEMA-TEL, anti-entropy weighting technique, and fuzzy VIKOR method shows high robustness and flexibility on decision parameters. In addition, the fuzzy-based technique has been adopted to facilitate the decision makers to collect decision information. According to the model result, it caters to Tsai's study when the organization concentrates on feasibility principle, while the intangible loss cost framework shows the top priority when decision makers pay more attention to effectiveness for CA organization. This hybrid fuzzy MCDM approach shows its advantage on the flexibility of decision making and easy implementation due to the combined weighting technique and fuzzy method, and the auto-factory can perform quality costing practice based on this selection model. However, this study carries some limitations. First, the influential criteria can be extended based on different organizational industries by considering specific characteristics of individual requirements. Second, the decision-making information mainly comes from the judgements of experienced expert panels, and the big data driven techniques can be developed to make full use of operational information of objective firms. Finally, the AI-based decision-making framework could be explored to achieve smart determination and reduce the subjectivity.

Data Availability

The data used to support the findings of this study are included within the article.

Conflicts of Interest

The authors declare that there are no conflicts of interest regarding the publication of this paper.

Acknowledgments

References

[1] C. Madu, *Handbook of Total Quality Management*, Springer Science & Business Media, Berlin, Germany, 2012.

[2] C. H. Fine, "Quality improvement and learning in productive systems," *Management Science*, vol. 32, no. 10, pp. 1301–1315, 1986.

[3] S. A. Albliwi, J. Antony, and S. A. H. Lim, "A systematic review of Lean Six Sigma for the manufacturing industry," *Business Process Management Journal*, vol. 21, no. 3, pp. 665–691, 2015.

[4] Y. Xiao, C. Li, L. Song, J. Yang, and J. Su, "A multidimensional information fusion-based matching decision method for manufacturing service resource," *IEEE Access*, vol. 9, pp. 39839–39851, 2021.

[5] G. Büyüközkan and D. Öztürkcan, "An integrated analytic approach for Six Sigma project selection," *Expert Systems with Applications*, vol. 37, no. 8, pp. 5835–5847, 2010.

[6] F. Talib, Z. Rahman, and M. N. Qureshi, "Prioritising the practices of total quality management: an analytic hierarchy process analysis for the service industries," *Total Quality Management and Business Excellence*, vol. 22, no. 12, pp. 1331–1351, 2011.

[7] H. van de Water and J. de Vries, "Choosing a quality improvement project using the analytic hierarchy process," *International Journal of Quality & Reliability Management*, vol. 23, no. 4, pp. 409–425, 2006.

[8] F. Zhou, M. K. Lim, Y. He, and S. Pratap, "What attracts vehicle consumers' buying," *Industrial Management & Data Systems*, vol. 120, no. 1, pp. 57–78, 2019.

[9] S. Parvadavardini, N. Vivek, and S. R. Devadasan, "Impact of Quality Management Practices on Quality Performance and Financial Performance: Evidence from Indian Manufacturing Companies," *Total Quality Management & Business Excellence*, vol. 27, pp. 1–24, 2015.

[10] G. Giakatis and E. M. Rooney, "The use of quality costing to trigger process improvement in an automotive company," *Total Quality Management*, vol. 11, no. 2, pp. 155–170, 2000.

[11] A. Schiffauerova and V. Thomson, "A review of research on cost of quality models and best practices," *International Journal of Quality & Reliability Management*, vol. 23, no. 6, pp. 647–669, 2006.

[12] H. Zaklouta, *Cost of Quality Tradeoffs in Manufacturing Process and Inspection Strategy Selection*, Massachusetts Institute of Technology, Cambridge, MA, USA, 2011.

[13] C. Lim, H. D. Sherali, and T. S. Glickman, "Cost-of-Quality optimization via zero-one polynomial programming," *IIE Transactions*, vol. 47, no. 3, pp. 258–273, 2014.

[14] F. Zhou, X. Wang, M. Goh, L. Zhou, and Y. He, "Supplier portfolio of key outsourcing parts selection using a two-stage decision making framework for Chinese domestic auto-maker," *Computers & Industrial Engineering*, vol. 128, pp. 559–575, 2019.

[15] J. Freiesleben, "The economic effects of quality improvement," *Total Quality Management and Business Excellence*, vol. 16, no. 7, pp. 915–922, 2005.

[16] W.-H. Tsai and W. Hsu, "A novel hybrid model based on DEMATEL and ANP for selecting cost of quality model development," *Total Quality Management and Business Excellence*, vol. 21, no. 4, pp. 439–456, 2010.

[17] G. H. Hwang and E. M. Aspinwall, "Quality cost models and their application: a review," *Total Quality Management*, vol. 7, no. 3, pp. 267–282, 1996.

[18] F. Zhou, Y. He, P. Ma, M. K. Lim, and S. Pratap, "Capacitated disassembly scheduling with random demand and operation time," *Journal of the Operational Reserach Society*, 2021.

[19] S. Jiafu, Y. Yu, and Y. Tao, "Measuring knowledge diffusion efficiency in R&D networks," *Knowledge Management Research and Practice*, vol. 16, no. 2, pp. 208–219, 2018.

[20] V. E. Sower, R. Quarles, and E. Broussard, "Cost of quality usage and its relationship to quality system maturity," *International Journal of Quality & Reliability Management*, vol. 24, no. 2, pp. 121–140, 2007.

[21] P. D. Arenas, *Quality Costs Analysis in the Service Sector_ an Empirical Study of the Colombian Banking System*, CONCORDIA UNIVERSITY, Austin, Texas, 2014.

[22] S. Wan and Y. Zheng, "Supplier selection of foreign trade sourcing company using ANP-VIKOR method in hesitant fuzzy environment," *Industrial Engineering & Management*, vol. 4, no. 3, pp. 163–171, 2015.

[23] X. Huang, Y. Lin, F. Zhou, K. L. Ming, and S. Chen, "Agent-based modelling for market acceptance of electric vehicles: evidence from China," *Sustainable Production and Consumption*, vol. 28, 2021.

[24] F. Zhou, P. Ma, Y. He, S. Pratap, P. Yu, and B. Yang, "Lean production of ship-pipe parts based on lot-sizing optimization and PFB control strategy," *Kybernetes*, vol. 50, no. 5, pp. 1483–1505, 2021.

[25] J. M. Asher, "Cost of quality in service industries," *International Journal of Quality & Reliability Management*, vol. 5, no. 5, pp. 38–46, 1988.

[26] G.-H. Hwang and E. M. Aspinwall, "The development of a quality cost model in a telecommunications company," *Total Quality Management*, vol. 10, no. 7, pp. 949–965, 1999.

[27] M. A. Johnson, "The development of measures of the cost of quality for an engineering unit," *International Journal of Quality & Reliability Management*, vol. 12, no. 2, pp. 86–100, 1995.

[28] A. R. Pires, A. Cociorva, M. Saraiva, J. C. Novas, and Á. Rosa, "Management of quality-related costs. The case of Portuguese companies," *Total Quality Management and Business Excellence*, vol. 24, no. 7-8, pp. 782–796, 2013.

[29] M. E. Sellés, J. A. Rubio, and J. R. Mullor, "Development of a quantification proposal for hidden quality costs: applied to the construction sector," *Journal of Construction Engineering and Management*, vol. 134, no. 10, pp. 749–757, 2008.

[30] A. H. Khataie and A. A. Bulgak, "A cost of quality decision support model for lean manufacturing: activity-based costing application," *International Journal of Quality & Reliability Management*, vol. 30, no. 7, pp. 751–764, 2013.

[31] A. Zugarramurdi, M. A. Parin, L. Gadaleta, and H. M. Lupin, "A quality cost model for food processing plants," *Journal of Food Engineering*, vol. 83, no. 3, pp. 414–421, 2007.

[32] O. Akkoyun and H. Ankara, "Cost of quality management: an empirical study from Turkish marble industry," *Academic Journals. Scientific Research and Essay*, vol. 4, no. 11, pp. 1275–1285, 2009.

[33] N. Vaxevanidis and G. Petropoulos, "A literature survey of cost of quality models," *Journal of Engineering*, vol. 6, no. 3, pp. 274–283, 2008.

[34] M.-T. Wang, S. Wang, S. Wang, and A. Wang, "An introduction of COQ models and their applications," in *Proceedings of the 2010 International Conference on Engineering, Project, and Production Management*, 2010.

[35] P. Basak, "Analysis of economics of quality in manufacturing industries," *International Journal for Quality Research*, vol. 8, no. 1, pp. 121–138, 2014.

[36] K. K. Castillo-Villar, N. R. Smith, and J. L. Simonton, "A model for supply chain design considering the cost of quality," *Applied Mathematical Modelling*, vol. 36, no. 12, pp. 5920–5935, 2012.

[37] T. Arabian, S. M. Jourabchi, Z. Leman, and M. Ismail, "A research on the impact of cost of quality models and reporting system on managing cost of quality," *International Proceedings of Economics Development and Research*, vol. 59, no. 11, 2013.

[38] A. Šatanová, J. Závadský, M. Sedliačiková, M. Potkány, Z. Závadská, and M. Holíková, "How Slovak Small and Medium Manufacturing Enterprises Maintain Quality Costs: An Empirical Study and Proposal for a Suitable Model," *Total Quality Management & Business Excellence*, vol. 26, pp. 1–15, 2014.

[39] A. Chopra and D. Garg, "Behavior patterns of quality cost categories," *The TQM Journal*, vol. 23, no. 5, pp. 510–515, 2011.

[40] R. S. a. A. S. Arman Sadreddin, "Using System Dynamics Approach to Model Cost of Quality in the Procurement Process of the Construction Industry," *2014APCProceedings*, 2014.

[41] V. Snieska, A. Daunoriene, and A. Zekeviciene, "Hidden costs in the evaluation of quality failure costs," *Engineering Economics*, vol. 24, no. 3, 2013.

[42] G. Giakatis, T. Enkawa, and K. Washitani, "Hidden quality costs and the distinction between quality cost and quality loss," *Total Quality Management*, vol. 12, no. 2, pp. 179–190, 2001.

[43] M. Khaled Omar and S. Murgan, "An improved model for the cost of quality," *International Journal of Quality & Reliability Management*, vol. 31, no. 4, pp. 395–418, 2014.

[44] S. J. Cheah, A. Shah, M. Fauziah, Fauziah, and M. Taib, "Tracking hidden quality costs in a manufacturing company: an action research," *International Journal of Quality & Reliability Management*, vol. 28, no. 4, pp. 405–425, 2011.

[45] C.-C. Yang, "Improving the definition and quantification of quality costs," *Total Quality Management and Business Excellence*, vol. 19, no. 3, pp. 175–191, 2008.

[46] N. Liapis, D. Theodorou, and F. Zannikos, "Absence of TQM across the fuel supply chain: quality failure-associated costs," *Total Quality Management and Business Excellence*, vol. 24, no. 3-4, pp. 452–461, 2013.

[47] A. Daunorienė, "The quality costs assessment model in the aspect of value added chain," *Quality Innovation Prosperity*, vol. 20, no. 2, p. 119, 2014.

[48] A. Jafari and P. E. D. Love, "Quality costs in construction: case of qom monorail project in Iran," *Journal of Construction Engineering and Management*, vol. 139, no. 9, pp. 1244–1249, 2013.

[49] A. Jafari and S. Rodchua, "Survey research on quality costs and problems in the construction environment," *Total Quality Management and Business Excellence*, vol. 25, no. 3-4, pp. 222–234, 2013.

[50] S. N. Teli, V. S. Majali, U. M. Bhushi, L. M. Gaikwad, and V. G. Surange, "Cost of poor quality analysis for automobile industry: a case study," *Journal of the Institution of Engineers*, vol. 94, no. 4, pp. 373–384, 2013.

[51] N. V. R. Naidu, "Mathematical model for quality cost optimization," *Robotics and Computer-Integrated Manufacturing*, vol. 24, no. 6, pp. 811–815, 2008.

[52] B. Kiani, H. Shirouyehzad, F. Khoshsaligheh Bafti, and H. Fouladgar, "System dynamics approach to analysing the cost factors effects on cost of quality," *International Journal of Quality & Reliability Management*, vol. 26, no. 7, pp. 685–698, 2009.

[53] S. Shanshan, "Modeling and analysis of relationship between quailty cost and sales revenue using system dynamics," *Research Journal of Applied Sciences, Engineering and Technology*, vol. 7, no. 8, p. 6, 2014.

[54] H. Palikhe, *A Study of the Cost of Quality for Electric Utility Companies*, Texas Tech University, Lubbock, TX, USA, 2013.

[55] G. S. Weheba and A. K. Elshennawy, "A revised model for the cost of quality," *International Journal of Quality & Reliability Management*, vol. 21, no. 3, pp. 291–308, 2004.

[56] D. M. Jorgenson and E. M. Enkerlin, "Managing quality costs with the help of activity-based costing," *Journal of Electronics Manufacturing*, vol. 02, no. 04, pp. 153–160, 1992.

[57] X. Zhang and J. Su, "A combined fuzzy DEMATEL and TOPSIS approach for estimating participants in knowledge-intensive crowdsourcing," *Computers & Industrial Engineering*, vol. 137, Article ID 106085, 2019.

[58] X. Zhang and J. Su, "An integrated QFD and 2-tuple linguistic method for solution selection in crowdsourcing contests for innovative tasks," *Journal of Intelligent and Fuzzy Systems*, vol. 35, no. 6, pp. 6329–6342, 2018.

[59] J. Jassbi, F. Mohamadnejad, and H. Nasrollahzadeh, "A Fuzzy DEMATEL framework for modeling cause and effect relationships of strategy map," *Expert Systems with Applications*, vol. 38, no. 5, pp. 5967–5973, 2011.

[60] F. Zhou, X. Wang, and M. Goh, "Fuzzy extended VIKOR-based mobile robot selection model for hospital pharmacy," *International Journal of Advanced Robotic Systems*, vol. 15, no. 4, 2018.

[61] A. Jafarnejad Chaghooshi, A. Arab, and S. J. Hosseini Dehshiri, "A fuzzy hybrid approach for project manager selection," *Decision Science Letters*, vol. 5, no. 3, pp. 447–460, 2016.

[62] A. Awasthi and G. Kannan, "Green supplier development program selection using NGT and VIKOR under fuzzy environment," *Computers & Industrial Engineering*, vol. 91, pp. 100–108, 2016.

[63] F. Zhou, G. Wang, T. Chen, P. Ma, and S. Pratap, "Regional leading industry selection based on an extended fuzzy VIKOR approach," *International Journal of Decision Support System Technology*, vol. 14, no. 1, pp. 1–14, 2022.

[64] S. Vats, G. Vats, R. Vaish, and V. Kumar, "Selection of optimal electronic toll collection system for India: a subjective-fuzzy decision making approach," *Applied Soft Computing*, vol. 21, pp. 444–452, 2014.

[65] Y.-M. Wang, K.-S. Chin, G. K. K. Poon, and J.-B. Yang, "Risk evaluation in failure mode and effects analysis using fuzzy weighted geometric mean," *Expert Systems with Applications*, vol. 36, no. 2, pp. 1195–1207, 2009.

[66] E. Akyuz and E. Celik, "A fuzzy DEMATEL method to evaluate critical operational hazards during gas freeing process in crude oil tankers," *Journal of Loss Prevention in the Process Industries*, vol. 38, pp. 243–253, 2015.

[67] F. Zhou, X. Wang, Y. Lin, Y. He, and L. Zhou, "Strategic Part Prioritization for quality improvement practice using a hybrid MCDM framework: a case application in an auto factory," *Sustainability*, vol. 8, no. 6, p. 559, 2016.

[68] Y. Ju and A. Wang, "Extension of VIKOR method for multi-criteria group decision making problem with linguistic information," *Applied Mathematical Modelling*, vol. 37, no. 5, pp. 3112–3125, 2013.

[69] S. F. Alkhatib, R. Darlington, Z. Yang, and T. T. Nguyen, "A novel technique for evaluating and selecting logistics service providers based on the logistics resource view," *Expert Systems with Applications*, vol. 42, no. 20, pp. 6976–6989, 2015.

[70] H.-C. Liu, J. Wu, and P. Li, "Assessment of health-care waste disposal methods using a VIKOR-based fuzzy multi-criteria decision making method," *Waste Management*, vol. 33, no. 12, pp. 2744–2751, 2013.

[71] H. Zhao and S. Guo, "External benefit evaluation of renewable energy power in China for sustainability," *Sustainability*, vol. 7, no. 5, pp. 4783–4805, 2015.

[72] F. Zhou, X. Wang, M. K. Lim, Y. He, and L. Li, "Sustainable recycling partner selection using fuzzy DEMATEL-AEW-FVIKOR: a case study in small-and-medium enterprises (SMEs)," *Journal of Cleaner Production*, vol. 196, pp. 489–504, 2018.

[73] T. Kuo, C.-W. Hsu, and J.-Y. Li, "Developing a green supplier selection model by using the DANP with VIKOR," *Sustainability*, vol. 7, no. 2, pp. 1661–1689, 2015.

[74] H.-C. Liu, J.-X. You, X.-Y. You, and M.-M. Shan, "A novel approach for failure mode and effects analysis using combination weighting and fuzzy VIKOR method," *Applied Soft Computing*, vol. 28, pp. 579–588, 2015.

[75] F. Zhou, Y. Lin, X. Wang, L. Zhou, and Y. He, "ELV recycling service provider selection using the hybrid MCDM method: a case application in China," *Sustainability*, vol. 8, no. 5, p. 482, 2016.

[76] J. R. San Cristóbal, "Multi-criteria decision-making in the selection of a renewable energy project in Spain: the Vikor method," *Renewable Energy*, vol. 36, no. 2, pp. 498–502, 2011.

[77] G. Bakioglu and A. O. Atahan, "AHP integrated TOPSIS and VIKOR methods with Pythagorean fuzzy sets to prioritize risks in self-driving vehicles," *Applied Soft Computing*, vol. 99, Article ID 106948, 2021.

[78] N. G. Torlak, A. Demir, and T. Budur, "Using VIKOR with structural equation modeling for constructing benchmarks in the Internet industry," *Benchmarking: An International Journal*, vol. 28, 2021.

[79] E. Rafieyan, R. Khorsand, and M. Ramezanpour, "An adaptive scheduling approach based on integrated best-worst and VIKOR for cloud computing," *Computers & Industrial Engineering*, vol. 140, Article ID 106272, 2020.

[80] A. Kumar, A. A, and H. Gupta, "Evaluating green performance of the airports using hybrid BWM and VIKOR methodology," *Tourism Management*, vol. 76, Article ID 103941, 2020.

Retraction

Retracted: Sports Economic Operation Index Prediction Model Based on Deep Learning and Ensemble Learning

Computational Intelligence and Neuroscience

This article has been retracted by Hindawi following an investigation undertaken by the publisher [1]. This investigation has uncovered evidence of one or more of the following indicators of systematic manipulation of the publication process:

(1) Discrepancies in scope

(2) Discrepancies in the description of the research reported

(3) Discrepancies between the availability of data and the research described

(4) Inappropriate citations

(5) Incoherent, meaningless and/or irrelevant content included in the article

(6) Peer-review manipulation

The presence of these indicators undermines our confidence in the integrity of the article's content and we cannot, therefore, vouch for its reliability. Please note that this notice is intended solely to alert readers that the content of this article is unreliable. We have not investigated whether authors were aware of or involved in the systematic manipulation of the publication process.

Wiley and Hindawi regrets that the usual quality checks did not identify these issues before publication and have since put additional measures in place to safeguard research integrity.

We wish to credit our own Research Integrity and Research Publishing teams and anonymous and named external researchers and research integrity experts for contributing to this investigation.

The corresponding author, as the representative of all authors, has been given the opportunity to register their agreement or disagreement to this retraction. We have kept a record of any response received.

References

[1] C. Yang and J. Chen, "Sports Economic Operation Index Prediction Model Based on Deep Learning and Ensemble Learning," *Computational Intelligence and Neuroscience*, vol. 2022, Article ID 9085349, 12 pages, 2022.

Research Article

Sports Economic Operation Index Prediction Model Based on Deep Learning and Ensemble Learning

Chuangjian Yang [ID] [1] and Junmeng Chen [ID] [2]

[1]School of Physical Education and Health, East China Jiaotong University, Nanchang 330013, China
[2]Sangmyung University, Seoul 03016, Republic of Korea

Correspondence should be addressed to Junmeng Chen; chenjm11@st.btbu.edu.cn

In order to construct a prediction model of sports economic operation indicators, this paper combines deep learning and ensemble learning algorithms to integrate and improve the algorithms and analyzes the principles of the LightGBM ensemble learning model and the hyperparameters of the model. Moreover, this paper obtains appropriate intelligent algorithms according to the data analysis requirements of sports economic operation. The break-even analysis method of sports event operation is to find the critical point of the program's profit and loss by analyzing the relationship between the operating cost and profit of the sports event. In addition, this paper uses deep learning and ensemble learning to comprehensively evaluate sports events, constructs a summary evaluation structure of sports items, and evaluates the model in this paper combined with experimental research. The test results verify the reliability of the model in this paper.

1. Introduction

With the development of economy and the continuous growth of social material wealth, people began to pursue leisure consumption, and leisure consumption demand gave birth to the leisure industry. The leisure industry refers to the general term for the production of leisure goods and leisure service industries in the national economy triggered by leisure consumption demand [1]. It widely exists in the three major industries of the national economy, including the primary leisure industry, the secondary leisure industry, and the secondary leisure industry. The tertiary industry, of which the tertiary leisure industry is the main industry of the leisure industry, is mainly composed of tourism, culture, sports, and other leisure industries [2]. The transformation of the economic growth mode, especially the consumption-driven economic growth mode, has promoted the rapid development of the leisure industry. Leisure consumption has gradually become a new growth point for the national economy in many countries and regions, and some have even become the dominant region or country [3]. Leisure

industries, especially in some tourist cities, have become local pillar industries, and even the economic growth model has shifted from relying on a single leisure subindustry to relying on the overall development of the entire leisure industry. However, the development of China's leisure industry is relatively late, the development of subindustry is unbalanced, tourism and leisure are developing rapidly, out-of-the-box, and the economic effect of the industry is outstanding. The development of cultural leisure and sports leisure is obviously lagging, and the industrial effect is not obvious. This has caused the development of China's leisure industry. The overall level of development and competitiveness is not high; furthermore, tourism and leisure have experienced extensive development for two to three decades, and its development momentum and development space are obviously hindered, which further restricts the growth of China's leisure industry. It is particularly important to explore how to quickly and continuously promote the comprehensive and rapid development of China's leisure industry and make it a new pillar industry of the national economy.

The country's economy has taken off, and people's economic consumption levels have also taken a qualitative leap. More and more people have begun to put forward new requirements on their spiritual level, and they have begun to spend their leisure time by improving their aesthetics. Therefore, various top-notch domestic competitions have increasingly become a spiritual demand of people. In recent years, large-scale sports events have become more and more frequent on the world stage. However, the quality of my country's event services is uneven. As an important basis for running sports events, the organizers urgently need to make a big fuss about the quality of event services, because of the excellent service quality of large-scale sports events. Inferiority directly affects the quality and effect of the event. Good service quality will allow participants to continue to support the sport, and poor service quality will make participants feel disgusted and no longer support the sport.

Based on the previously mentioned analysis, this paper combines deep learning and ensemble learning to construct the sports economic operation index prediction model, evaluate the sports economic operation, and provide a reference for the subsequent development of the sports economy.

2. Related Work

Literature [4] believes that the distinguishing characteristics of large-scale festivals and ordinary events are as follows: first, this event must attract a large number of participants and viewers, forming a kind of global attention; second, large-scale festivals are also a kind of market strategy; for the tourism industry, especially, it can make organizers and regions receive extremely high attention in the international market; finally, large-scale festivals can create long-term heritage, which can still play a role after the event is over.

Literature [5] conducts a systematic literature review of the industry chain efficiency research from the five perspectives of industry chain competitiveness, efficiency (performance), ecological stability, sustainable development capability, and overall effect. Literature [6] adopts the concepts, methods, and means of performance evaluation to realize the process of performance evaluation of the government.

It has become a common phenomenon that sports events drive the development of the tourism industry. Literature [7] believes that hosting sports events can increase the visibility of a city, bring in a large number of visitors, and promote cultural exchanges between cities. Literature [8] explains the specific role of urban characteristics and how sports events shape the unique characteristics of the city and proposes to use the creation of sports events to shape urban characteristics and communicate the distinctive humanistic spirit through tourism. Sports events play an important role in shaping the image of the city and driving the development of the city. Literature [9] believes that the economic effects of sports events lead to the rapid development of urban economy and tourism. Literature [10] proposes that the shaping of sports landscape is also an important means of displaying the culture of the host city, and it has a positive

effect on the transmission of the city's image. Literature [11] mentioned the role of sports events in shaping and transmitting the image and brand of the city. Literature [12] proposes that sports events, as one of the most used cultural activities of the city, have a positive impact on the city's image and puts forward five strategies to convey and shape the image of the city.

Literature [13] takes urban sports as a research perspective and establishes a scientific evaluation system for the current situation of urban sports. Literature [14] established a sports rights evaluation system for college students. Literature [15] analyzes the job role and work process of referees and builds an evaluation index system for referee selection. Literature [16] studies sports tourism, gives an evaluation index system for sports tourism human resources, and develops a corresponding evaluation scale. Literature [17] has conducted research from the perspective of economic benefits. The indicators mainly include facility utilization rate, equipment integrity rate, venue revenue, venue self-sufficiency rate, and profit. Literature [18] assesses the economic benefits of stadiums and uses multifactor comprehensive analysis to construct a grading model of stadiums. The literature [19] mainly studies the two basic attributes of venues: "public welfare" and "business." Literature [20] constructs an evaluation index system for the normal operation of stadium operation and management after sports events are held.

3. Deep Learning and Ensemble Learning Prediction Algorithm

Ensemble learning is a machine learning technique commonly used in business and economic analysis. Machine learning algorithms usually cannot directly obtain models with better performance in all aspects, while ensemble learning can upgrade multiple weak individual learners with preferences to a strong learner to obtain higher accuracy. The essential idea is to first generate a set of learners, then use strategies to integrate them, and continuously optimize towards the objective function in the iterative process.

The GBDT algorithm consists of a gradient boosting algorithm (gradient boosting) and a decision tree algorithm (decision tree). It uses a decision tree as the base learner, uses the boosting algorithm to combine multiple weak learners into a strong learner through residual fitting, and uses the gradient information from the previous round to construct a decision tree in the iterative process.

3.1. Gradient Lifting Algorithm. The idea of the gradient boosting algorithm is an extension of the boosting method. In the iterative process, the loss function is optimized by adding submodels. If the loss function is extended to a differentiable function, and the boosting method and the gradient descent method are combined to obtain the gradient boosting method, the basic idea is as follows.

The formula of the compound model is shown in formula (1), where $f_i(X)$ is the submodel.

$$F_m(X) = \sum_{i=0}^{m} f_i(X). \tag{1}$$

We assume that the loss function is $L(Y, F_m(X))$, use a greedy way to ensure that the loss function is reduced every time a new submodel $f_m(X)$ is added, and use gradient descent to perform residual fitting.

$$F_m(X) = F_{m-1}(X) + f_m(X),$$
$$L(Y, F_m(X)) < L(Y, F_{m-1}(X)). \tag{2}$$

3.2. Decision Tree Algorithm. The decision tree algorithm uses a tree structure, the root node contains all the samples, the internal nodes represent the feature attribute test, and the leaf nodes are the results of the classification. The learning process of decision tree includes three steps: feature selection, decision tree generation, and pruning. The key point is the division of optimal attributes in the splitting process.

There are three criteria for feature selection: information gain, information gain ratio, and Gini coefficient. Among them, it is commonly used to perform top-down division according to the information gain criterion, and calculate the information gain of each feature during each division and select the maximum value.

The information Ent(D) is defined as formula (3), where P_k represents the proportion of the k-th sample in the sample set D.

$$\text{Ent}(D) = -\sum_{k=1}^{|y|} p_k \log_2 p_k. \tag{3}$$

In the information gain formula, D^v represents the value sample contained in the v-th attribute A in the V branch nodes, and the formula is as follows:

$$\text{Gain}(D, A) = \text{Ent}(D) - \sum_{v=1}^{V} \frac{|D_v|}{|D|} \text{Ent}(D^v). \tag{4}$$

The decision tree splitting method in the GBDT algorithm is divided into two, one is the method of leaf-wise growth according to the maximum profit, and the other is the method of direct level-wise growth.

According to the way of leaf growth, the required decision tree can be grown with a smaller computational cost. The advantage of this method is that it has high accuracy and can quickly and effectively complete the growth of the tree, but at the same time, it is easy to overfit and the growth process is sequential and cannot be directly accelerated in parallel. Figure 1 is the process of decision tree growth by leaves.

The way of layer growth means that each node of each layer must be split. Therefore, this method can directly perform parallel acceleration, but it will generate redundant split nodes, which requires a high computational cost. At the same time, each iteration needs to traverse the complete dataset, so higher running memory is required. Figure 2 is the growth process of a decision tree split by layer.

LightGBM is mainly based on the framework of decision tree algorithms such as GBDT to optimize the use of histogram algorithm, histogram difference optimization, tree growth based on restricted optimal leaf nodes, unilateral gradient sampling, and reordering of category feature histograms. Compared with other decision tree models, it has improved speed, memory consumption, and accuracy.

In order to reduce the computational cost and obtain better accuracy, the LightGBM model uses a tree growth method that splits according to the optimal leaf node. Algorithms can only be executed sequentially in principle, so three methods of feature parallelism, data parallelism, and voting parallelism are used, and parallel acceleration is performed from the three perspectives of feature, data, and communication.

3.2.1. Optimization of Histogram Algorithm. The basic idea is to divide continuous feature values into many #bins, use discrete values as indexes, and then search for the best split point on #bin, reducing the computational cost and storage cost. Moreover, the difference optimization of the histogram can be used to further speed up and get better performance. At the same time, due to the discrete nature, LightGBM can naturally handle category features.

The histogram algorithm only needs to store the discretized value #lbin, does not need the original feature value, and does not need to sort. The #bin value can use smaller data types to store training data, such as the uin8_t type, which can reduce memory consumption to 1/8 of the presorting algorithm. The memory optimization process is shown in Figure 3.

3.2.2. Gradient-Based Unilateral Sampling Algorithm (GOSS). The idea of GOSS algorithm was first applied to the AdaBoost model. The essential idea is to sort the gradients first, retain all instances with large gradients (errors) for sampling, and only randomly sample all instances with small gradients, so as to reduce the amount of information calculation for feature selection in the iterative process. At the same time, in order to reduce the accuracy of the loss, a certain weight value will be given to the small gradient of the sample.

O is the training data set on the fixed node of the decision tree, the instance is $\{x_1, x_2, ..., x_n\}$, and the gradient of the loss function is denoted as $\{g_1, g_2, ..., g_n\}$. Then, the traditional calculation of the variance gain of the split feature j of the node at d is defined as

$$V_{j|O}(d) = \frac{1}{n_O} \left[\frac{\left(\sum_{\{x_i \in O; x_{ij} \leq d\}} g_i\right)^2}{n_{l|O}^j(d)} + \frac{\left(\sum_{\{x_i \in O; x_{ij} > d\}} g_i\right)^2}{n_{r|O}^j(d)} \right]. \tag{5}$$
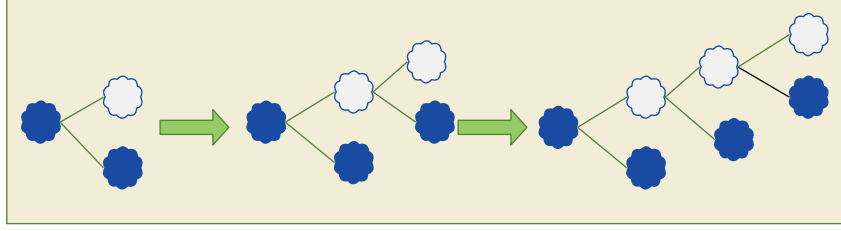
FIGURE 1: Decision tree divided by leaf growth.
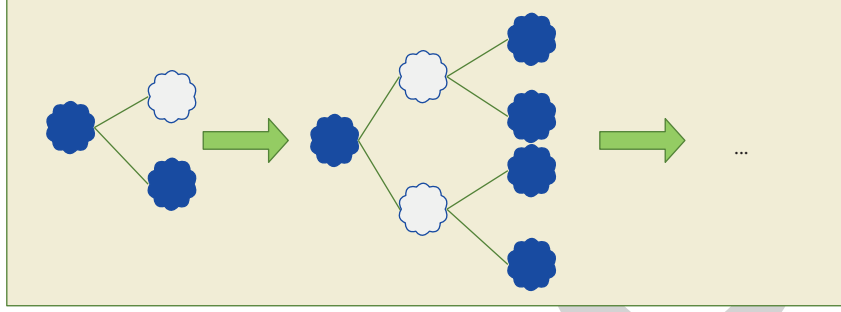
FIGURE 2: Decision tree split by layer.

On the left are int_32 store index and float_32 store values

The right is where uint8_8 stores the # bin value
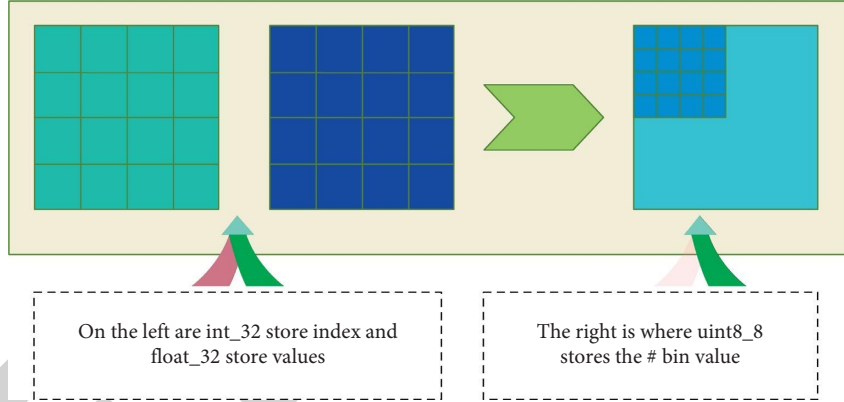
FIGURE 3: Schematic diagram of LightGBM histogram algorithm memory optimization.

Among them,

$$\begin{cases} n_O = \sum I[x_i \in O] \\ n_{l|O}^j(d) = \sum I[x_i \in O: x_{ij} \le d] \\ n_{r|O}^j(d) = \sum I[x_i \in O: x_{ij} > d] \end{cases}. \tag{6}$$

When using the idea of the GOSS algorithm, the algorithm first sorts the training examples in descending order

according to the absolute value of the gradient and composes the instance subset A by the larger gradient $\alpha \times 100\%$. After that, the algorithm samples the remaining set with a smaller gradient composed of $(1 - a) \times 100\%$ instances as a subset B of size $b \times |A^c|$. Finally, the gain $\tilde{V}_j(d)$ calculated according to the subset AUB is

$$\tilde{V}_j(d) = \frac{1}{n}\left[\frac{\left(\sum_{\{x_i \in A_r\}} g_i + 1 - a/b\sum_{\{x_i \in B_r\}} g_i\right)^2}{n_l^j(d)} + \frac{\left(\sum_{\{x_i \in A_r\}} g_i + 1 - a/b\sum_{\{x_i \in B_r\}} g_i\right)^2}{n_r^j(d)} \right]. \tag{7}$$

The definition of each subitem is as follows:

$$\begin{cases} A_l = \{x_i \in A: x_{ij} \le d\}, A_r = \{x_i \in A: x_{ij} > d\} \\ B_l = \{x_i \in B: x_{ij} \le d\}, B_r = \{x_i \in B: x_{ij} > d\} \end{cases}. \quad (8)$$

Using the estimated gain $\widetilde{V}_j(d)$ on a smaller subset of instances instead of the accurate gain $\widetilde{V}_j(d)$ on all instances to determine the split point can greatly reduce the computational cost. It is proved that GOSS will not lose much training accuracy, but the efficiency is better than random sampling.

3.2.3. Mutually Exclusive Sparse Feature Binding.
The optimal feature bundling problem can usually use a greedy algorithm to obtain an approximate solution to select the feature values that need to be combined. For the mutually exclusive feature merging process, since the histogram data is discrete, the original data can be distinguished by the offset to achieve the purpose of merging features.

3.2.4. Comparison of LightGBM and XGBoost Models.
Compared with another popular ensemble learning framework XGBoost model, the LightGBM model released later has made the following improvements, as shown in Table 1.

The most important parameter settings of the LightGBM model include the learning rate of the algorithm, the maximum depth limit of the decision tree, the number of leaves of a single decision tree, and the selection ratio of features in the iterative process.

The following are the main parameters for control and optimization of the LightGBM model.

(1) mum_leaves is the main parameter that controls the complexity of the tree model, representing the number of leaves per tree. Usually, it is considered that mum_leaves is less than 2mar_sdeph; otherwise, it is easy to cause overfitting problems. Among them, the corresponding relationship between the number of leaves of a full binary tree and the depth of the tree is

$$\text{num\_leaves} = 2^{\max\_depth}. \quad (9)$$

(2) learning_rate is the learning rate of the algorithm. If it is too small, the optimization efficiency of the model will be too low. If it is set too large, it may reduce the accuracy.

(3) max_depth refers to the maximum depth of the tree model, which can prevent overfitting when the data is small.

(4) max_bin is the maximum number of features stored in bin.

(5) min_data_in_leaf is the minimum amount of data that can be set on the leaf, and the small amount of data can also prevent overfitting.

(6) feature_fraction and bagging_fraction are the ratio of selected features to the total number of features and the ratio of selected data to the total data volume

respectively. The values of these two parameters are usually between 0 and 1, which can determine the speed of model training and can also deal with overfitting problems.

(7) mm_iterations represents the number of iterations of boosting.

It can be seen that some parameters overlap in improving the accuracy of the algorithm and dealing with the overfitting problem. Therefore, this paper selects the parameters that are relatively important to the model to optimize.

We configure parameters to obtain a better model from the balance of training speed, accuracy, and prevention of overfitting. The following are the hyperparameters that have a greater impact on model prediction:

(1) improving training speed: increasing learning_rate and decreasing max_bin

(2) improving accuracy: increasing max_bin, increasing mum_leaves, and decreasing learning_rate

(3) preventing overfitting: limiting the tree depth max_depth and reducing min_data_in_leaf and using smaller mum_leaves

Tuning machine learning model parameters through optimization algorithms is a common research content. After using the particle swarm algorithm to select the hyperparameters of the support vector machine, the optimized support vector machine is applied to the research of power load forecasting, and the optimization ability of the particle swarm algorithm is proved through experiments. However, the algorithm needs to adjust more parameters. Grid tuning is another common method of tuning machine learning model parameters. Through research, Cheng Chen et al. found that the method is relatively single and the parameter improvement range is limited, making it difficult to search for the best on a global scale. Therefore, a new quantum particle swarm algorithm is proposed to optimize the hyperparameters of the XGBoost model. In the research experiment of forecasting marketing data, compared with the XGBoost forecast based on the grid method tuning, the experiment proved that the new model has obtained higher forecast accuracy.

The Drosophila optimization algorithm is an excellent optimization algorithm suitable for machine learning tuning. Its advantages are simple implementation and fewer configuration parameters. The algorithm simulates the characteristics of the fruit fly colony capturing food in the air through smell and first collects various tastes in the air. The fruit flies in the colony obtain the place with the highest concentration of food taste according to their position information, and then, all the fruit flies fly to the smell point. After that, the algorithm also uses the olfactory characteristics of fruit flies to identify the location of the companions and iterates again, using the olfactory and visual characteristics of fruit flies, to gradually find the point with the largest odor concentration in the current area, and obtain the food location, that is, the global approximate optimal solution.

TABLE 1: Comparison of the details of the XGBoost and LightGBM models.

Model details	XGBoost	LightGBM
Tree growth pattern	Growth in layers	Growing by leaves restricted by depth
Split point search method	Feature presorting (default)	Histogram algorithm
Income calculation method during split	Data characteristics	Tbin container characteristics
Memory overhead	Big	Small
Categorical characteristics	One-hot encoding	Histogram data processing

Figure 4 is a schematic diagram of the optimization model of the standard fruit fly optimization algorithm.

The standard fruit fly algorithm is simple to implement, and its operation steps are as follows.

Step 1. The algorithm first initializes the fruit fly population, that is, initializing the population size Sizepop, setting the maximum number of iterations T, and randomly initializing (X_axis, Y_axis) as the initial position of the fruit fly population [21].

$$\begin{cases} X\_axis = random \times (top - bottom) + bottom \\ Y\_axis = randomx(top - bottom) + bottom \end{cases}. \quad (10)$$

Among them, random is a random number between [0, 1], and top and bottom are the upper and lower bounds of the search interval.

Step 2. The algorithm generates a random number within a certain range for each individual fruit fly and uses it as the direction and distance of the individual fruit fly in the random search process. The algorithm assigns values to the initialized fruit fly individuals to obtain the next position of the fruit fly. Among them, random value is the search distance.

$$\begin{cases} X_i = X\_axis + RandomValue \\ Y_i = Y\_axis + RandomxValue \end{cases}. \quad (11)$$

Step 3. The algorithm obtains the taste concentration determination value S_i by calculating the distance Dist between the current position of the fruit fly and the origin of the coordinate.

$$Dist_i = \sqrt{X_i^2 + Y_i^2},$$
$$S_i = \frac{1}{Dist_i}. \quad (12)$$

Step 4. The algorithm substitutes the obtained S_i into the taste concentration determination function, which is the corresponding fitness function, and calculates the taste concentration Smelli at the individual position of the fruit pupae.

$$Smell_i = Function(S_i). \quad (13)$$

Step 5. The algorithm finds the fruit flies with the best odor concentration (take the maximum value as an example) in the current fruit flies population and sets it as the best taste concentration point.

$$bestSmellIndex = SelectionMax(Smell_i). \quad (14)$$

Step 6. The algorithm judges whether the best taste concentration value is better than the previous best taste concentration. If it is better, the algorithm records the best taste concentration value and the position information bestSmellIndex and makes all fruit flies fly to this position.

$$\begin{cases} X\_axis = X(bestSmellIndex) \\ Y\_axis = Y(bestSmellIndex) \end{cases}. \quad (15)$$

Step 7. The algorithm starts iteratively to find the optimal solution. At the same time, it is judged whether the maximum number of iterations set by the algorithm is reached, and the conditions for satisfying other early termination algorithms are obtained. If the current best taste concentration obtained in the iterative process is better than the previous best taste concentration, Step 6 is executed; otherwise, Step 2 to Step 5 is repeatedly executed until the approximate optimal solution is obtained.

The execution flow of the FOA algorithm is shown in Figure 5.

It can be seen from the algorithm execution flowchart that the time required for each optimization of individual fruit flies in the FOA algorithm is T. At the same time, in the iterative process, each individual fruit fly needs to perform a search until the algorithm reaches the maximum number of iterations, so the time complexity of the standard fruit fly optimization algorithm is O(T' × Sizepop). Therefore, the key to the calculation cost of the control algorithm lies in the setting of the maximum number of iterations T and the size of the fruit fly population size.

Prediction evaluation refers to the evaluation of the accuracy of model prediction results or the measurement of prediction accuracy. In statistics, the magnitude of prediction error is commonly used to measure the quality of the prediction effect. Commonly used regression prediction evaluation methods include mean absolute error, mean square error, root mean square error, mean square log error, mean relative error, mean square log error, median absolute error, and coefficient of determination.

y_i is the actual value of a commodity price series, and $\widehat{y}_i$ is the predicted value.

(1) Mean Absolute Error (MAE). MAE is used to describe the difference between the predicted value and the true value. The smaller the value, the better. The average absolute error of *n* samples is as follows:
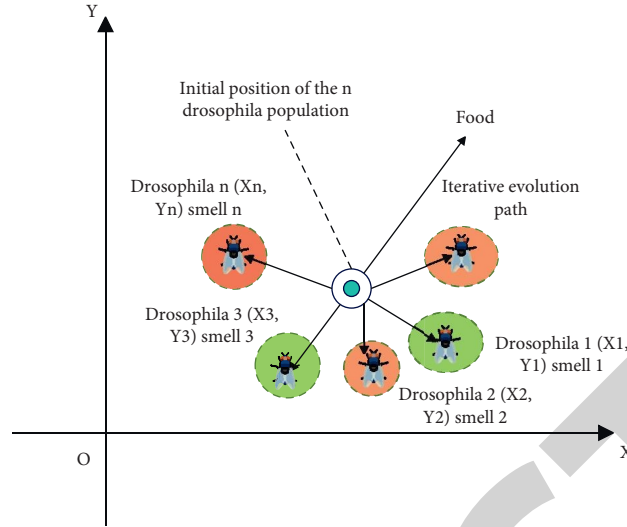
FIGURE 4: Schematic diagram of standard fruit fly optimization algorithm optimization.

$$MAE = \frac{1}{n} \sum_{i=1}^{n} |y_i - \widehat{y}_i|. \tag{16}$$

(2) Mean Square Error (MSE). The mean square error is calculated as the square error between the predicted value and the actual value. The MSE of *n* samples is calculated as follows:

$$MAE = \frac{1}{n} \sum_{i=1}^{n} |y_i - \widehat{y}_i|^2. \tag{17}$$

(3) Root Mean Square Error (RMSE). For the extremely large or extremely small error values in a set of prediction result data, using the root mean square error can well represent the deviation of the prediction result. The calculation is as follows:

$$RMSE = \sqrt{\frac{1}{n} \sum_{i=1}^{n} (f_i - y_i)^2}. \tag{18}$$

(4) Mean Square Logarithmic Error (MSLE).

$$MSLE = \frac{1}{n} \sum_{i=o}^{n-1} [\log_e (1 + y_i) - \log_e (1 + \widehat{y}_i)]^2. \tag{19}$$

When the target has the characteristics of exponential growth, this indicator is most suitable to use. MSLE is more sensitive to predictions below the true value.

(5) Median Absolute Error (MedianAE). The median absolute error uses the median of all absolute differences between the target and the forecast to calculate the loss, which can reduce the influence of outliers and is defined as

$$MedianAE = \text{median}(|y_1 - \widehat{y}_1|, ..., |y_n - \widehat{y}_n|). \tag{20}$$

(6) Coefficient of Determination (R^2 score). The best fit between the prediction model and the real data is judged to be 1, and it can be a negative value. The R^2 score of *n* samples is as follows:

$$R^2 = 1 - \frac{\sum_{i=1}^{n} (y_i - \widehat{y}_i)^2}{\sum_{i=1}^{n} (y_i - \overline{y}_i)^2}. \tag{21}$$

4. Sports Economic Operation Index Prediction Model Based on Deep Learning and Ensemble Learning

The break-even method is mainly to evaluate the uncertainty of the operating profit of sports events. The break-even analysis method of sports event operation is to find the critical point of the program's profit and loss by analyzing the relationship between the operating cost and profit of the sports event. The procedure for judging the impact of uncertain factors on the economic effects of the sports event operation plan is used to illustrate the degree of risk in the implementation of the sports event operation plan. This critical point is called the break-even point (BEP), as shown in Figure 6.

BEP is the break-even point of sports event operations, *s* is the income from sports event operations, and Q is the numerical value of sports event operation output. Ql is the numerical value of sports event operation output at the point of win-loss balance, *c* is the total cost of sports event operation, and Cr is the cost of sports event operation.

Based on the development standards of China's sports industry, this paper fully considers the general characteristics of the development of the sports industry to construct a first-level indicator system with the guidance of sports industry development theory. The specific content is shown in Figure 7.

This article uses deep learning and ensemble learning to comprehensively evaluate sports events. In the process of comprehensive evaluation, we often use a combination of
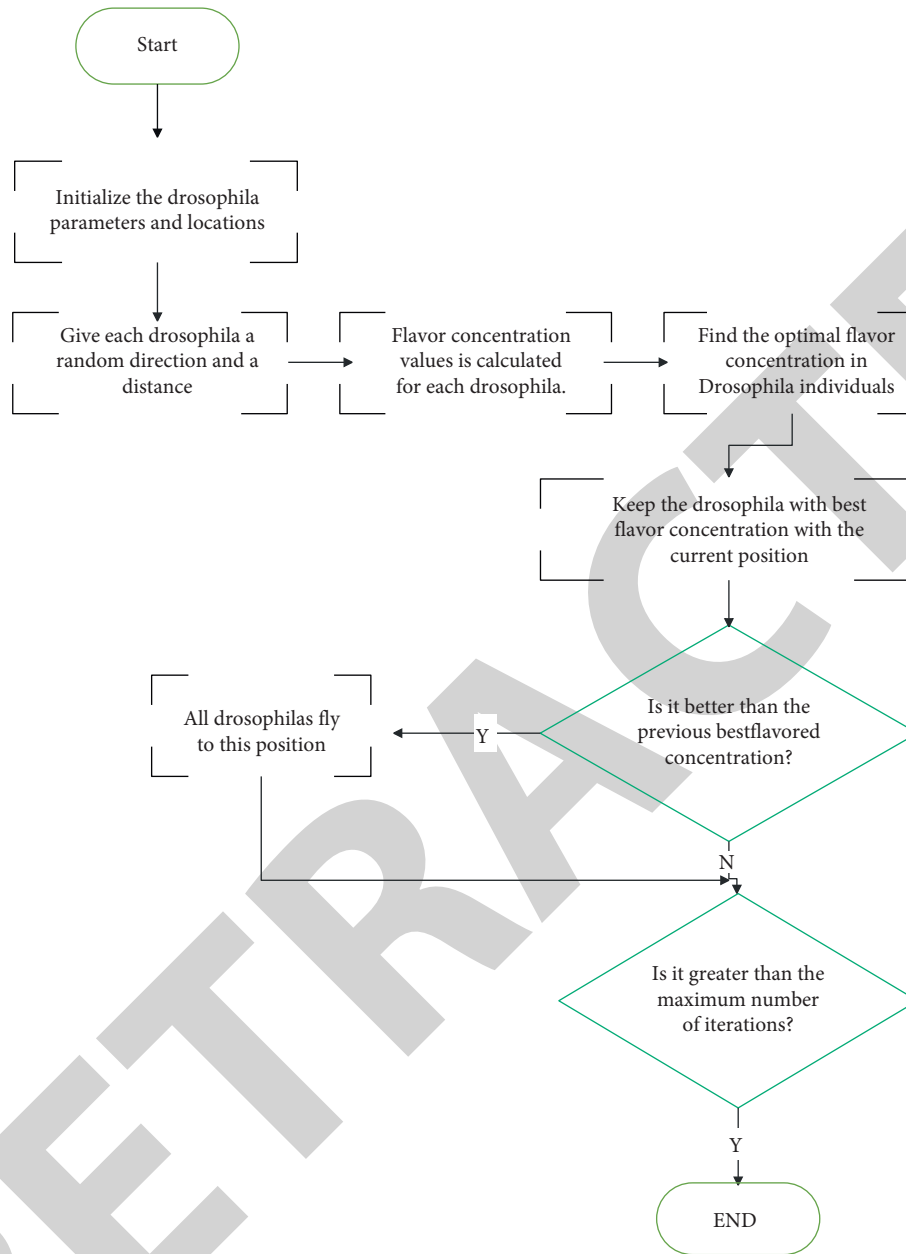
Figure 5: The execution flow chart of the standard fruit fly algorithm.
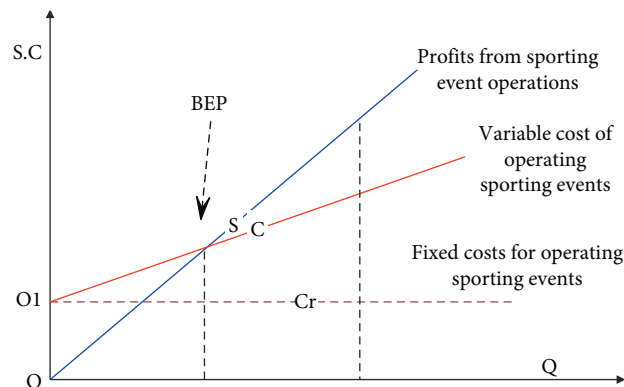
Figure 6: Break-even analysis.
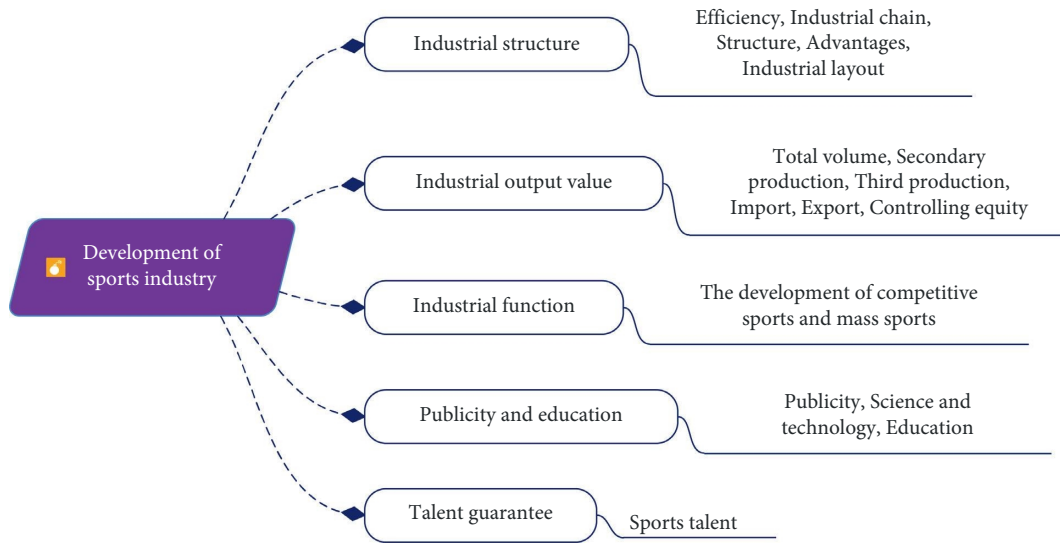
Figure 7: Schematic diagram of the development index of the sports industry.
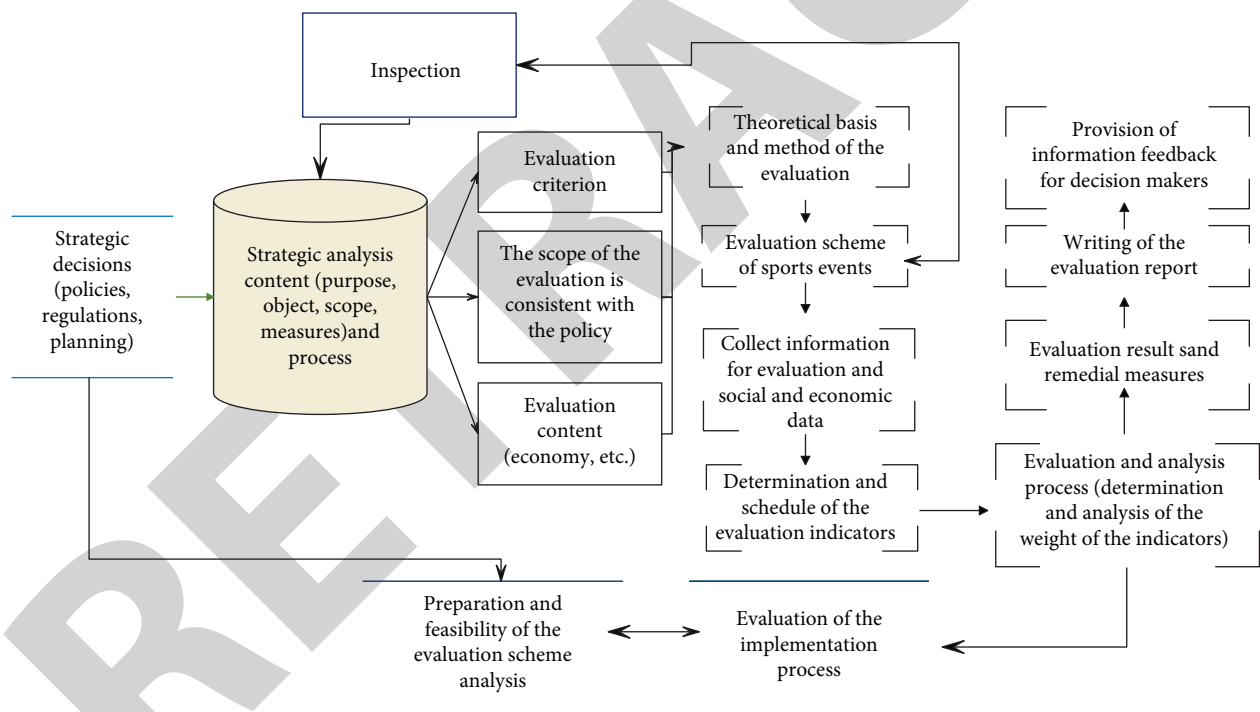
Figure 8: Evaluation program diagram of large-scale sports events.

qualitative and quantitative methods, or the analytic hierarchy process, for comprehensive evaluation. No matter which method or means is adopted, attention must be paid to the validity and reliability of the evaluation. The reason is that the purpose of comprehensive evaluation is ultimately to give an evaluation of whether the decision is feasible or not and the success or failure of sports events. From the previously mentioned main procedure, we can get the procedure of sports event evaluation as shown in Figure 8.

After constructing the above model, we evaluate the effect of the method in this paper. The data of the algorithm in this paper is processed through deep learning and ensemble learning. Therefore, first, the effect of the algorithm in this paper on the processing of sports economic operation indicators data is tested, and the results shown in Table 2 and Figure 9 are obtained.

From the previously mentioned analysis, it can be seen that the method proposed in this paper has a good effect in the data processing of sports economic operation indicators.

Table 2: The processing effect of sports economic operation index data.

Number	Data processing	Number	Data processing
1	96.00	17	92.20
2	92.13	18	96.89
3	91.03	19	91.52
4	91.07	20	93.76
5	88.08	21	88.99
6	89.12	22	96.99
7	95.35	23	96.75
8	89.62	24	96.38
9	95.48	25	92.51
10	92.43	26	92.83
11	88.61	27	89.14
12	95.13	28	90.05
13	90.73	29	90.26
14	90.02	30	93.22
15	94.67	31	96.98
16	96.30	32	95.71
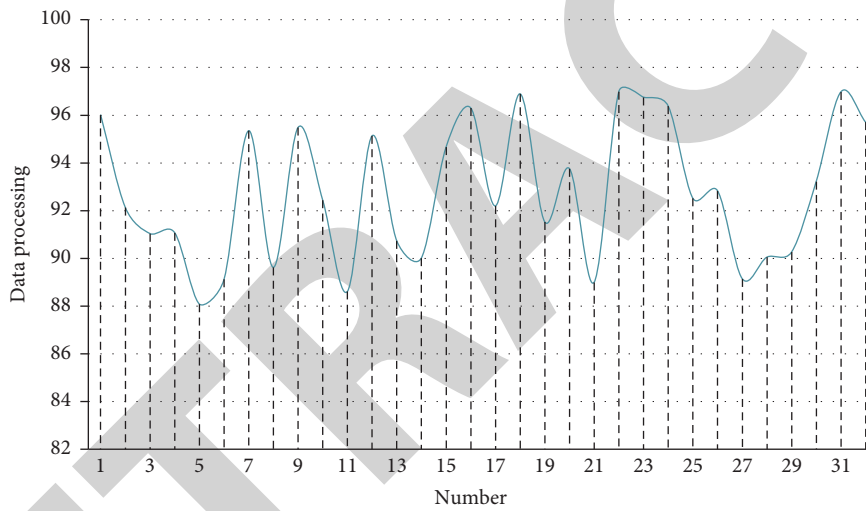
Figure 9: Statistical diagram of data processing effect.

Table 3: Predictive effects of sports economic operation index.

Number	Predictive evaluation	Number	Predictive evaluation
1	82.28	17	85.66
2	72.06	18	83.94
3	76.29	19	90.39
4	75.24	20	83.28
5	83.70	21	87.51
6	78.22	22	78.75
7	82.70	23	73.14
8	83.94	24	80.76
9	81.57	25	78.83
10	81.81	26	89.52
11	76.04	27	70.32
12	75.05	28	79.77
13	71.66	29	85.16
14	85.97	30	79.83
15	70.54	31	89.47
16	73.19	32	72.08
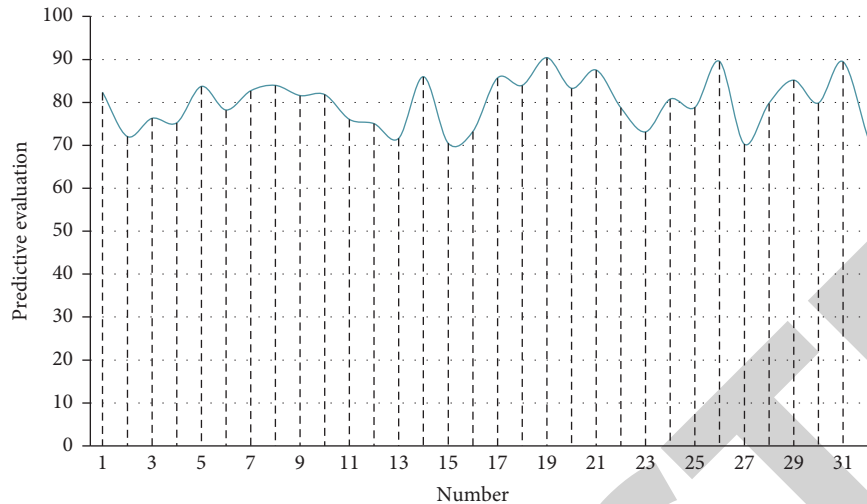
Figure 10: Statistical diagram of predictive evaluation of sports economic operation indicators.

After that, the prediction effect of the sports economic operation indicators of the model in this paper is evaluated, and the results shown in Table 3 and Figure 10 are obtained.

Through the previously mentioned research, we can see that the sports economic operation index prediction model based on deep learning and ensemble learning proposed in this paper has good results.

5. Conclusion

This article attempts to combine China's national conditions and the characteristics of large-scale sports events to construct an index system, which can diagnose and predict various service quality problems existing in the current events, and put forward constructive opinions. The improvement of the service quality of sports events can realize the faster and better development of the urban sports event industry, form a systematic and scientific sports event service quality evaluation system, and provide guidance for the holding of other large-scale sports series events. This article combines deep learning and ensemble learning to construct a sports economic operation index prediction model, evaluate the sports economic operation, and provide a reference for the subsequent development of the sports economy. Through experimental research, it can be known that the sports economic operation index prediction model based on deep learning and ensemble learning proposed in this paper has good results.

Data Availability

The labeled datasets used to support the findings of this study are available from the corresponding author upon request.

Conflicts of Interest

The authors declare no competing interests.

Acknowledgments

References

[1] J. Pipek and S. Nagy, "An economic prediction of refinement coefficients in wavelet-based adaptive methods for electron structure calculations," *Journal of Computational Chemistry*, vol. 34, no. 6, pp. 460–465, 2013.

[2] S. Nagy and J. Pipek, "An economic prediction of the finer resolution level wavelet coefficients in electronic structure calculations," *Physical Chemistry Chemical Physics*, vol. 17, no. 47, pp. 31558–31565, 2015.

[3] W. Yu and W. Huafeng, "Quantitative analysis of regional economic indicators prediction based on grey relevance degree and fuzzy mathematical model," *Journal of Intelligent and Fuzzy Systems*, vol. 37, no. 2, pp. 1–14, 2019.

[4] P. Karanikić, I. Mladenović, and S. Sokolov-Mladenović, "Retraction Note: prediction of economic growth by extreme learning approach based on science and technology transfer," *Quality and Quantity*, vol. 53, no. 2, pp. 1095–1096, 2019.

[5] K. Ataka, "Prediction of election result and economic indicator," *Resuscitation*, vol. 96, no. 6, p. 84, 2014.

[6] S. Barde, "Back to the future: economic self-organisation and maximum entropy prediction," *Computational Economics*, vol. 45, no. 2, pp. 337–358, 2015.

[7] A. Ferramosca, D. Limon, and E. F. Camacho, "Economic MPC for a changing economic criterion for linear systems," *IEEE Transactions on Automatic Control*, vol. 59, no. 10, pp. 2657–2667, 2014.

[8] L. Zhou, K. K. Lai, and J. Yen, "Bankruptcy prediction using SVM models with a new approach to combine features selection and parameter optimisation," *International Journal of Systems Science*, vol. 45, no. 1–3, pp. 241–253, 2014.

[9] D. Bhattacharya, J. Mukhoti, and A. Konar, "Learning regularity in an economic time-series for structure prediction," *Applied Soft Computing*, vol. 76, no. 2, pp. 31–44, 2019.

Research Article

Fault Diagnosis Method for Industrial Robots Based on DBN Joint Information Fusion Technology

Jian Jiao [ID] **and Xue-jiao Zheng**

Chongqing Water Resources and Electric Engineering College, Chongqing 402160, China

Correspondence should be addressed to Jian Jiao; jiaojian@st.btbu.edu.cn

Aiming at the problems of the traditional industrial robot fault diagnosis model, such as low accuracy, low efficiency, poor stability, and real-time performance in multi-fault state diagnosis, a fault diagnosis method based on DBN joint information fusion technology is proposed. By studying the information processing method and the deep learning theory, this paper takes the fault of the joint bearing of the industrial robot as the research object. It adopts the technique of combining the deep belief network (DBN) and wavelet energy entropy, and the fault diagnosis of industrial robot is studied. The wavelet transform is used to denoise, decompose, and reconstruct the vibration signal of the joint bearing of the industrial robot. The normalized eigenvector of the reconstructed energy entropy is established, and the normalized eigenvector is used as the input of the DBN. The improved D-S evidence theory is used to solve the problem of fusion of high conflict evidence to improve the fault model's recognition accuracy. Finally, the feasibility of the model is verified by collecting the fault sample data and creating the category sample label. The experiment shows that the fault diagnosis method designed can complete the fault diagnosis of industrial robot well, and the accuracy of the test set is 97.96%. Compared with the traditional fault diagnosis model, the method is improved obviously, and the stability of the model is good; the utility model has the advantages of short time and high diagnosis efficiency and is suitable for the diagnosis work under the condition of coexisting multiple faults. The reliability of this method in the fault diagnosis of the joint bearing of industrial robot is verified.

1. Introduction

Currently, automated production is developing rapidly in the direction of automation and intelligence. More and more companies use industrial robots to replace traditional manual operations, which significantly improves production efficiency while reducing labour costs [1, 2]. In automated production operations, the division of labour among the robots in each segment is relatively straightforward, and the synergistic relationship is close. When a robot malfunction occurs, it will inevitably lead to problems in the whole operation process, which has a significant impact on the progress and safety of the operation [3–5]. Therefore, it is necessary to judge the operation status of industrial robots in advance and deal with the initial failure in time to avoid various safety hazards caused by robot failure.

Based on this, some scholars used different methods to complete the fault diagnosis of industrial robots. Verma and Simmons [6] established a plan of robot fault diagnosis based on discrete-time observers by designing observers. The method achieves the fault diagnosis of robot joints through the co-operation of detection and diagnosis observers, which requires a large amount of joint sensor information. Jaber and Bicker [7] collected the vibration signal of the working state of the robot, used the methods of wavelet transformation time-frequency domain analysis to analyze the fault signal of the robot under various working conditions, and realized the fault diagnosis of the robot. Capisani et al. [8] established a fault diagnosis model for robots using a sliding observer and applied it to the fault diagnosis of Comau robots. This method can accurately diagnose a single fault, but it does not perform well in diagnosing robots with multiple responsibilities. Long et al. [9] used sparse

hybrid autoencoder (SAE) and support vector machine (SVM) to build a basic fault diagnosis model by learning fault information posture dataset, which can better complete the diagnosis of different faults of multi-joint industrial robots. However, it is difficult to implement large-scale sample training, and the accuracy of multi-fault classification is not high. Shan et al. [10] presented a fault diagnosis method for rolling bearings based on variable mode decomposition (VMD) and backpropagation (BP) neural networks. The energy of each component is obtained by decomposing the time-domain signal of bearing vibration into an intrinsic mode function, and the point is input as a feature into the training of the BP network. A diagnostic model for VMD-BP is established. The bearing fault type diagnosis can be completed well, but the accuracy of diagnosis is not ideal due to the boundary effect and the impact of sudden signals.

With the deepening of fault diagnosis research, the fault diagnosis method based on DBN has achieved good results in mechanical fault diagnosis such as bearing, gearbox, and motor [11–13]. Therefore, taking the joint bearing of industrial robot as the research object and the vibration signal as the starting point, this paper constructs the fault diagnosis method of industrial robot based on DBN. At the same time, considering that the accuracy of information fusion conclusion of traditional D-S theory is not ideal, the fusion problem of high conflict evidence is solved by improving D-S evidence theory. Taking the output layer of the model as fault evidence, the conflict between sample evidence is analyzed by using the improved D-S fusion rules and decision rules. Finally, a fault diagnosis model based on DBN joint improved D-S is established to improve the recognition accuracy of the fault model. It is of positive significance to further improve the service life and operation safety of industrial robots.

2. Related Knowledge

2.1. Information Fusion Technology. Information fusion technology is a multi-level and multi-faceted statistical process in its essence by detecting and combining the estimation of multiple sources of data to obtain information that information fusion can use [14]. Unlike simple signal processing techniques, multi-source information fusion techniques are suitable for handling multi-modal and conflicting forms of data and can achieve different levels and conditions of information fusion [15]. Thus, it performs well in improving the real time and reliability of mechanical systems, increasing the detectability of mechanical systems, and reducing the uncertainty of mechanical equipment.

According to the different levels of fusion processing, information fusion is mainly divided into three groups: data layer fusion, feature layer fusion, and decision layer fusion. Among them, the feature layer fusion technology extracts the corresponding features of the sensor data based on the type of the original signal, fuses the resulting feature information in the feature layer, and after normalization, forms a single feature vector to finally complete the classification of information and realize the identification of faults. The fusion process is shown in Figure 1.

2.2. Deep Belief Networks. Deep belief network (DBN) is a kind of neural network that can perform the tasks of feature recognition, data classification, and generation well. The scalability of the network is vital, so it is widely used in machine learning. DBN framework adopts the restricted Boltzmann vector machine (RBM) structure, and the model consists of visible, hidden, and output layers. In the DBN model, any two adjacent layers can be considered one RBM structure. The number of neurons in the visible layer is consistent with the dimension of the input data, which is mainly responsible for receiving the data from the bottom layer and outputting the computation results to the hidden layer. The BP artificial neural network (BPNN) in the top layer of the network classifies the features. It combines some of the labelling information to fine-tune the network parameters backwards to obtain the optimal network model [16, 17]. The DBN structure is shown in Figure 2.

The probabilistic generative model used in DBN differs from the discriminative model of traditional neural networks. DBN uses probability generation models to build the joint distribution of data and labels, train the hidden and visual layers of the network layer by layer, update and optimize the weights between layers and transfer parameters continuously so that the entire network model can generate training data with maximum probability, mine the correlation between higher-order data, and realize the extraction, classification, and identification of fault feature data [18]. The neurons in the same layer of the network are independent of each other and connected with the neurons in the adjacent layer, which makes the network have good conditional independence, which improves the parallel computing ability of the network and dramatically improves the training efficiency. Taking the DBN containing two RBMs as an example, the network training process is shown in Figure 3.

The training process of DBN consists of two main phases: unsupervised pretraining and supervised reverse fine-tuning.

(1) *Unsupervised Pretraining.* Multiple stacked restricted Boltzmann machines form a deep Boltzmann machine, and the output of the previous RBM is the input of the next RBM. Two steps carry out the training process of each RBM: forward computation and reverse reconstruction, and the optimal parameters of each RBM are finally obtained after multiple iterations in different batches.

(2) *Supervised Inverse Fine-Tuning.* After the pretraining, the RBM extracts the original data features, then classifies them using the top-level classifier, and finally fine-tunes all parameters top-down using the BP algorithm in combination with the label information to finally obtain the optimal model parameters.

3. Fault Diagnosis of Industrial Robot Based on DBN

3.1. Vibration Signal Preprocessing. The signal collected by the sensor contains the vibration of the joint itself and internal and external noise and non-smooth interference
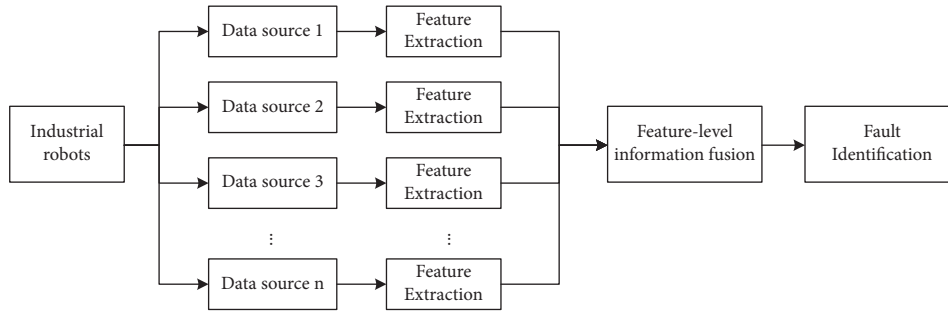
FIGURE 1: Feature layer fusion.
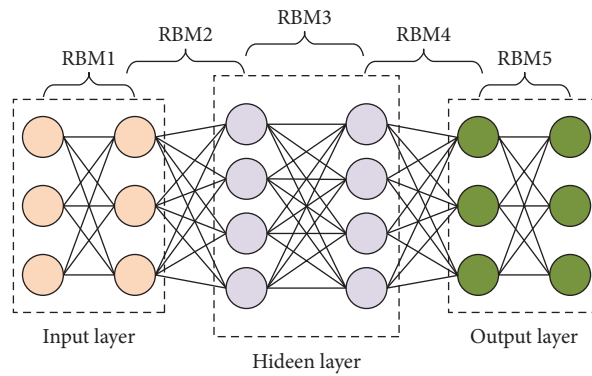
FIGURE 2: DBN structure.
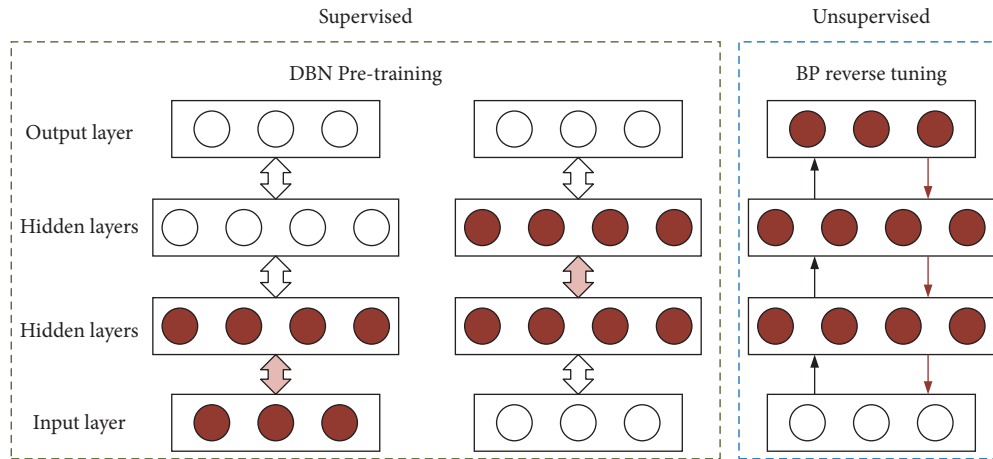
FIGURE 3: DBN training process.

signals such as resonance signals, so the vibration signal needs to be processed for noise reduction for the next operation. Wavelet packet transform (WPT) can divide the signal in a multi-level form and decompose the high-frequency part in depth, adaptively select the frequency band according to the characteristics of the analyzed signal, ensure the frequency band and the signal spectrum match each other, and thus improve the time-frequency resolution [19]. Therefore, in this paper, wavelet packets are used to complete the noise reduction of industrial robot vibration signals. The wavelet transform process and decomposition process are shown in Figure 4.

The steps of noise reduction based on wavelet packet transform signal are as follows.

Step 1. Select the wavelet basis according to the decomposition level of wavelets and decompose the signal.

Step 2. Determine the optimal wavelet packet basis and calculate the optimal tree after the entropy criterion.

Step 3. Select an appropriate threshold value for the high-frequency coefficients at different decomposition scales and perform threshold quantization. The wavelet coefficients larger than the threshold value are
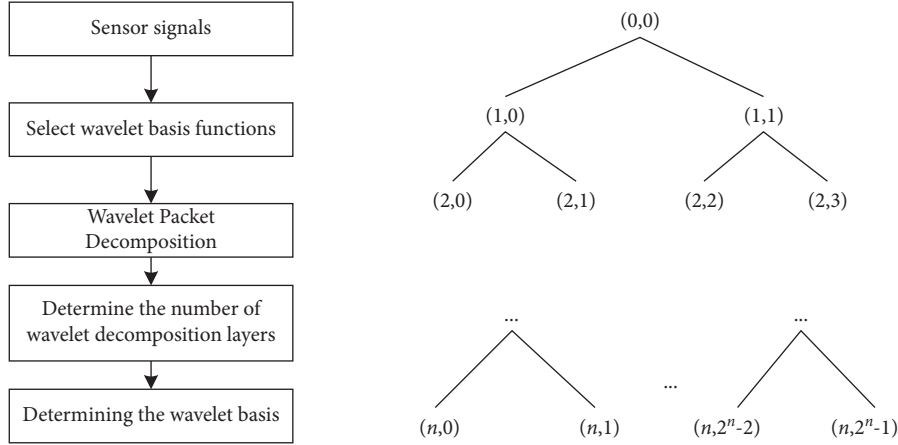
Figure 4: Wavelet transform flow and decomposition process.

considered to have signal generation and are retained; those smaller than the threshold value are deemed to be caused by noise and are set to zero, thus completing the purpose of noise reduction.

Step 4. Reconstruct the signal using the processed coefficients. The signal-to-noise ratio (SNR) and the root mean square error (RMSE) of the estimated signal and the original signal are often used to judge the merit of the denoising performance [20].

3.2. Energy Entropy Normalized Eigenvectors.

After the vibration signal is processed by wavelet transform, it is not suitable as the underlying input to the DBN due to the vast amount of information contained in the signal [21]. The signal's energy entropy normalized feature vector is further calculated, and the energy entropy normalized feature vector is used as the underlying input to the DBN model.

The energy entropy represents the measure of uncertainty [22]. It is defined as follows: if there is a system S containing multiple events $S = \{E_1, E_2, \ldots, E_n\}$ inside, each with a probability distribution $P = \{p_1, p_2, \ldots, p_n\}$, then the information of each event itself is

$$I_e = -\log_2 p_i. \tag{1}$$

The sum of the information entropy of all events in the whole system is the energy entropy, expressed as

$$E_s = \sum_{i=1} p_i I_e. \tag{2}$$

After the wavelet transform of the vibration signal, a total of 2^K nodes are reconstructed, and the energy entropy of each node is calculated to obtain a feature vector composed of 2^K elements. The energy entropy function is expressed as

$$E(u_K) = -\sum_J u_K \log(u_K). \tag{3}$$

The resulting energy entropy is normalized to [0, 1]. The energy entropy normalized eigenvector of the decomposed reconstructed signal is obtained as follows:

$$E(u_J) * = \frac{E(u_J) - E(u_J)_{\min}}{E(u_J)_{\max} - E(u_J)_{\min}}. \tag{4}$$

3.3. Improving Information Fusion with D-S Evidence Theory.

Dempster–Shafer (D-S) evidence theory is a kind of uncertainty inference, which effectively solves the influence of incomplete and uncertain information and other factors on the inference results by describing the uncertainty of the state of each part of the system from different perspectives and generalizing and estimating its probability. However, when the conflict between the evidence is severe, the traditional D-S theory information fusion accuracy is not satisfactory [23, 24]. To solve the fusion problem of high conflicting evidence, this paper uses the improved D-S evidence theory to complete the fusion of information to improve the identification accuracy of the fault model.

The inner vector product is added to the modification of the evidence combination rule. For any set of evidence, represented by a space vector, the average of each evidence vector is obtained by extending the evidence vector w to the n dimension as

$$\overline{w} = \frac{w_1 + w_2 + \cdots w_n}{n}. \tag{5}$$

The distance between each evidence vector and the average evidence vector is

$$DM = [c_1, c_2, \ldots c_n],$$
$$c_i = \frac{\sqrt{2}}{2} c(w_i, \overline{w}). \tag{6}$$

The similarity measure $Sw_i = 1 - c_i$ between two evidence vectors, i.e., the support of each evidence to evidence i, is calculated to represent the support of each evidence to evidence $Sup(w_i)$. Then, the weight $Crd(w_i)$ of evidence w_i is

$$\mathrm{Crd}(w_i) = \frac{\mathrm{Sup}(w_i)}{\sum_{i=1}^{n} \mathrm{Sup}(w_i)}. \tag{7}$$

By assigning a weighted average to the basic probabilities of each piece of evidence and then fusing the data, we can effectively solve the problem of conflicting evidence and further improve the accuracy of the fusion results.

4. Fault Diagnosis Model Based on DBN Joint Improved C-S Information Fusion

The DBN-based industrial robot fault diagnosis model is shown in Figure 5. The diagnosis model mainly contains the feature extraction part, DBN part, information fusion part, etc. Firstly, the vibration signal of the industrial robot joint is collected by the acceleration sensor. The wavelet packet transform is used to filter and reduce the signal's noise to avoid the deviation of the signal caused by the motion frequency and resonance frequency. The energy entropy normalized feature vector of the vibration signal is established using the information energy entropy theory. Secondly, the energy entropy normalized feature vector is divided into the training and test sets. The basic parameters of the DBN model are fine-tuned by unsupervised forward training and reverse supervised fine-tuning. The DBN model is constructed in this way. The output layer of the DBN model is used as the fault evidence for the evidence conflict factor analysis to check whether there is high conflict evidence, and the corresponding combination rules and decision rules are selected accordingly to realize the information fusion and complete the robot fault diagnosis.

5. Experimental Validation

5.1. Fault Dataset. The proposed method is used to construct a DBN classification model, and experiments are conducted to verify the effectiveness of the proposed method by acquiring vibration signals from the joint bearings of industrial robots. The experiments are shown on the Anaconda development platform running on the Windows 10 system as the base environment. The DBN deep learning model is built based on the Google deep learning framework TensorFlow.

Taking the FANUC Robot M-710C industrial robot as an example, set artificial fault on its joint bearing with $f = 12.5$ KHz frequency to collect collaborative vibration data. The data are divided according to the location and degree of the spot. Seven data types are obtained, including normal conditions and 350 sampled data points in each vibration cycle. Therefore, the original data of 7 categories are divided into 840 samples according to the window size, moving step of 1050 data points, and window moving step of 1050 data points to obtain the subseries sample space $R^{840 \times 1050}$, and each sample in the space is decomposed to calculate the time-frequency characteristics of each component to form a feature vector. According to the different fault categories corresponding to each feature vector, the category calibration is performed individually. The training and test sets are divided according to the ratio of 7 : 3. Table 1 shows the industrial robot joint bearings' fault data and category labels.

In the experiment, wavelet transform is used to reduce the noise of all data signals. Then, the energy entropy normalized feature vector and fusion features of the signals are calculated. The features' characteristics are analyzed, and finally, the different feature sets are input to the DBN-CS model for verification. Then, the fault diagnosis of industrial robot joint bearings is completed.

5.2. Experimental Results. Parameter setting of industrial robot fault diagnosis model is as follows: DBN network structure 128-100-36-7, network forward training is set to 100 times, and reverse optimization is set to 1000 times. The learning rate $\varepsilon = 0.05$, the momentum $m = 0.6$, the maximum number of iterations of the network is 50, and the training batch size is 100. Then, 180 rounds of training are carried out on the model using the training set, and the test set is used to verify the model's accuracy. The accuracy change curves of different sample sets are shown in Figure 6.

As shown in Figure 6, the accuracy rate increases with training rounds and stabilizes when the number of training rounds reaches 95. If we continue to train the data, it will not only not improve the accuracy significantly but also increase the computational time cost and even lead to the occurrence of overfitting. Therefore, the DBN model was tested after 95 rounds using the test set data, and the prediction results were compared with the actual category. Figure 7 shows the comparison between the predicted results and the actual categories.

In Figure 7, if the category labels obtained by the classification model overlap with the corresponding actual category labels, the classification result is correct; otherwise, it means that the classification fails. Of the 252 test samples, 5 were misclassified (points offset in Figure 7). Among them, one fault-free state was misclassified as outer ring light fault, two external ring light faults were misclassified as outer ring medium faults, one outer ring serious fault was misclassified as outer ring medium faults, and one inner ring medium fault was misclassified as internal ring light faults. To quantitatively analyze the accuracy of different fault classifications, the confusion matrix is used to represent the classification results of DBN on the test set, and the test statistics are shown in Table 2. The rows and columns in the table indicate the actual fault type and the diagnosed fault type, respectively.

To verify the stability and adaptability of the diagnostic model in the paper, the model is trained ten times with the same parameters, and the data are selected from the dataset without repetition as the training set and the test set in a random way to test the detection accuracy of the fault diagnosis model. The classification results are shown in Figure 8.

As can be seen from Figure 8, the diagnostic accuracy of the training set varies smoothly, with an average accuracy of 99.12%; the accuracy of the test set is lower than that of the training set, but the average accuracy still reaches 97.96%, which shows that the model designed in the paper has a high fault diagnosis rate and good stability. It is suitable for the diagnosis of joint bearings in multi-state coexistence.

5.3. Performance Comparison of Different Diagnostic Models. To make the industrial robot fault diagnosis models designed in this paper comparable, different fault
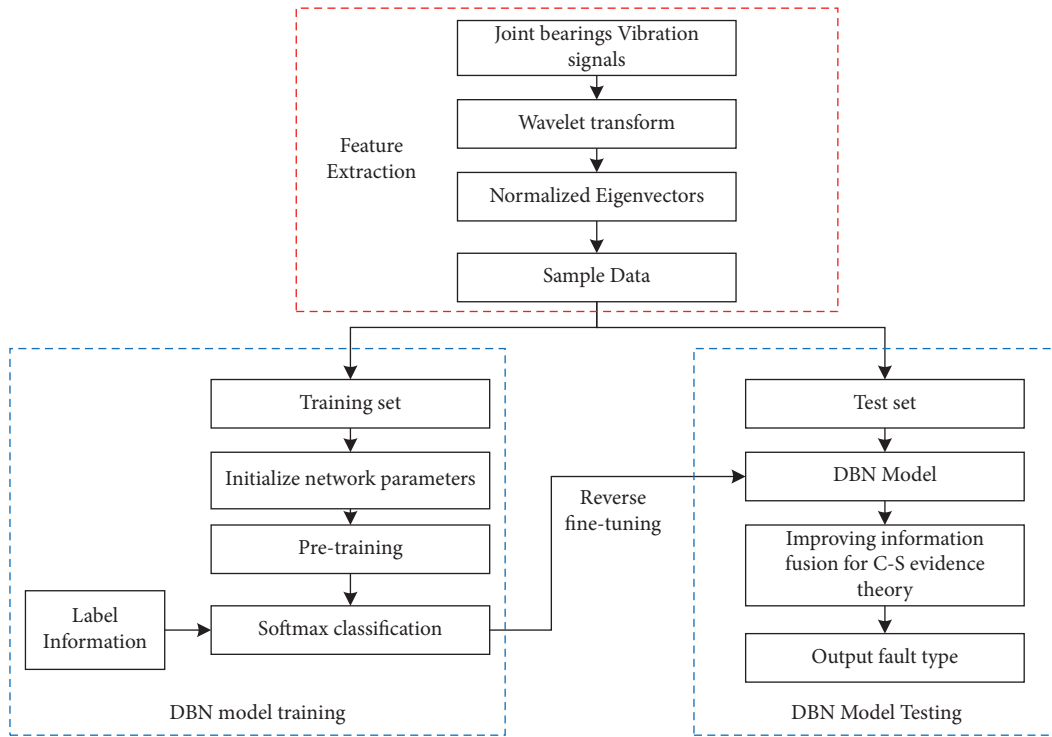
FIGURE 5: Industrial robot fault diagnosis model.

TABLE 1: Joint bearing data and category labels.

Fault location	Degree of failure	Depth of failure (inch)	Training set samples	Training set samples	Failure tags
Fault-free	No	0	84	36	0
Outer ring	Minor	0.004	84	36	1
	Moderate	0.008	84	36	2
	Severe	0.012	84	36	3
Inner ring	Minor	0.004	84	36	4
	Moderate	0.008	84	36	5
	Severe	0.012	84	36	6
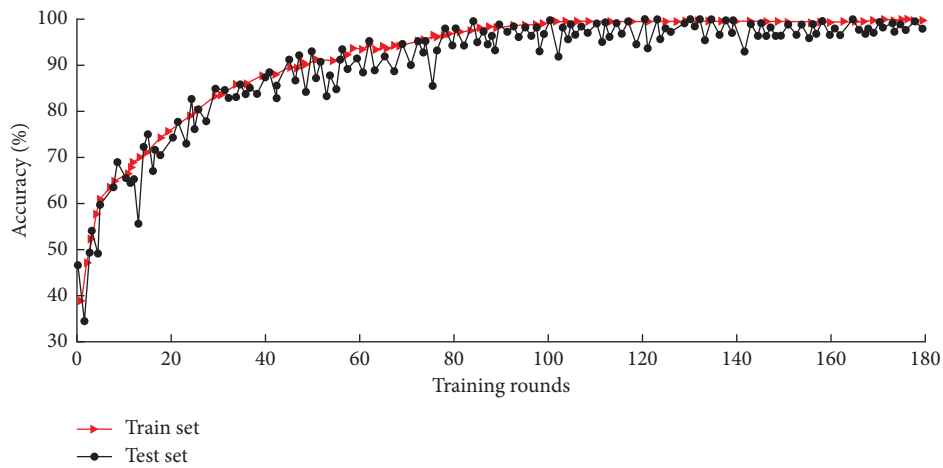
FIGURE 6: Accuracy variation curves of different sample sets.
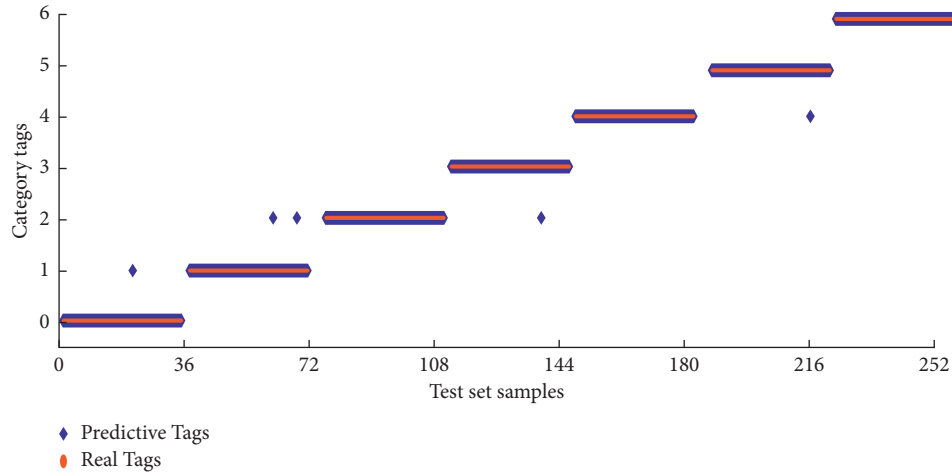
Figure 7: Comparison of predicted results and actual categories.

Table 2: Diagnostic accuracy of different faults.

Failure tags	0	1	2	3	4	5	6	Accuracy (%)	Average accuracy (%)
0	35	1	0	0	0	0	0	97.22	
1	0	34	2	0	0	0	0	94.44	
2	0	0	36	0	0	0	0	100	
3	0	0	1	35	0	0	0	97.22	98.01
4	0	0	0	0	36	0	0	100	
5	0	0	0	0	1	35	0	97.22	
6	0	0	0	0	0	0	36	100	
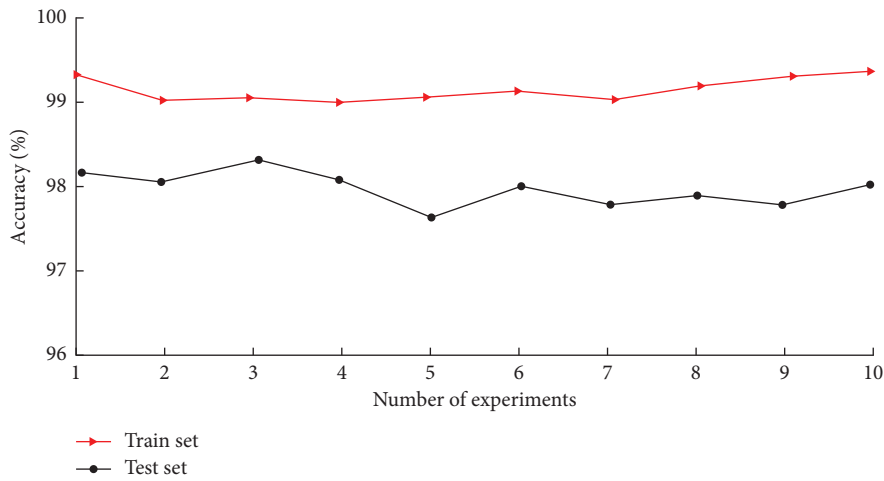
Figure 8: Accuracy of the experiment.

diagnosis models are constructed for testing with the same standard data, and the accuracy on the final test set is used as the evaluation criterion for model performance to verify the performance of the models in the paper. The fault diagnosis domain models involved are standard DBN, VMD + BPNN, VMD + SVM, EMD + DBN, and EMD + SVM models. The performance comparison results are shown in Table 3.

As can be seen from Table 3, compared with other algorithmic models, the diagnostic accuracy of the model designed in this paper is higher, and the standard deviation of the model is lower. Although the running time increases compared with VMD + SVM and EMD + SVM models, the increase is lower. It can better balance the relationship between diagnostic accuracy and real time to complete the fault diagnosis in complex fault states.

TABLE 3: Performance comparison of different fault diagnosis models.

Diagnostic models	Training set accuracy (%)	Test set accuracy (%)	Running time (s)	Standard deviation
DBN	87.34	81.66	61.63	0.0703
VMD + BP	92.72	86.58	39.17	0.0418
VMD + SVM	—	92.08	20.07	0.0658
EMD + DBN	90.21	86.17	48.55	0.0277
EMD + SVM	—	94.25	17.43	0.0491
The proposed method	99.12	97.96	23.46	0.0074

6. Conclusion

Taking industrial robot joint bearings as the research object, the problems of the current fault diagnosis methods are investigated by combining modern signal processing methods and deep learning theory. The accuracy rate is low when fault diagnosis is performed by the DBN alone, and it cannot meet real-time demand. Therefore, information fusion technology is combined to improve the performance of the fault diagnosis model to ensure the stability of the model and the accuracy of the diagnosis results. The experimental results show that the fault diagnosis accuracy of our method is higher than that of the traditional method and the average accuracy of the test set reaches 97.96%. The information fusion method with improved D-S evidence theory can effectively solve the evidence conflict problem and further improve the accuracy of the fusion results, suitable for handling the diagnosis of robot joint bearings under multiple fault states.

Data Availability

The labelled dataset used to support the findings of this study is available from the corresponding author upon request.

Conflicts of Interest

The authors declare that they have no conflicts of interest.

Acknowledgments

References

[1] V. Kuts, T. Otto, T. Tähemaa, K. Bukhari, and T. Pataraia, "Adaptive industrial robots using machine vision," in *ASME International Mechanical Engineering Congress and Exposition*vol. 52019, American Society of Mechanical Engineers (ASME), Article ID V002T02A093, 2018.

[2] P. Aivaliotis, S. Aivaliotis, C. Gkournelos, K. Kokkalis, G. Michalos, and S. Makris, "Power and force limiting on industrial robots for human-robot collaboration," *Robotics and Computer-Integrated Manufacturing*, vol. 59, pp. 346–360, 2019.

[3] S. Vallachira, M. Orkisz, M. Norrlöf, and S. Butail, "Data-driven gearbox failure detection in industrial robots," *IEEE Transactions on Industrial Informatics*, vol. 16, no. 1, pp. 193–201, 2019.

[4] E. Kulińska, M. Odlanicka-Poczobutt, and K. Kulińska, "Diagnosis of operational malfunctions and failures by the FMEA method in the industrial robots sector," *Research in Logistics & Production*, vol. 8, 2018.

[5] M. A. Costa, B. Wullt, M. Norrlöf, and S. Gunnarsson, "Failure detection in robotic arms using statistical modeling, machine learning and hybrid gradient boosting," *Measurement*, vol. 146, pp. 425–436, 2019.

[6] V. Verma and R. Simmons, "Scalable robot fault detection and identification," *Robotics and Autonomous Systems*, vol. 54, no. 2, pp. 184–191, 2006.

[7] A. A. Jaber and R. Bicker, "The optimum selection of wavelet transform parameters for the purpose of fault detection in an industrial robot," in *Proceedings of the 2014 IEEE International Conference on Control System, Computing and Engineering (ICCSCE 2014)*, pp. 304–309, IEEE, Penang, Malaysia, November 2014.

[8] L. M. Capisani, A. Ferrara, A. Ferreira de Loza, and L. M. Fridman, "Manipulator fault diagnosis via higher order sliding-mode observers," *IEEE Transactions on Industrial Electronics*, vol. 59, no. 10, pp. 3979–3986, 2012.

[9] J. Long, J. Mou, L. Zhang, S. Zhang, and C. Li, "Attitude data-based deep hybrid learning architecture for intelligent fault diagnosis of multi-joint industrial robots," *Journal of Manufacturing Systems*, vol. 61, pp. 736–745, 2021.

[10] M. Shan, W. Liu, and X. Wang, "A Novel Robot Joint Bearing Fault Diagnosis Method Based on VMD in BP Neural Network," in *Proceedings of the 2019 Sixteenth International Conference on Ubiquitous Robots (UR)*, June 2019.

[11] D. Han, X. Guo, and P. Shi, "An intelligent fault diagnosis method of variable condition gearbox based on improved DBN combined with WPEE and MPE," *IEEE Access*, vol. 8, Article ID 131299, 2020.

[12] J. Guo and P. Zheng, "A method of rolling bearing fault diagnose based on double sparse dictionary and deep belief network," *IEEE Access*, vol. 8, Article ID 116239, 2020.

[13] S. Shao, W. Sun, P. Wang, R. X. Gao, and R. Yan, "Learning features from vibration signals for induction motor fault diagnosis," in *Proceedings of the 2016 International Symposium on Flexible Automation (ISFA)*, pp. 71–76, IEEE, Cleveland, OH, USA, August 2016.

[14] H. Wang, X. Deng, W. Jiang, and J. Geng, "A new belief divergence measure for Dempster-Shafer theory based on belief and plausibility function and its application in multi-source data fusion," *Engineering Applications of Artificial Intelligence*, vol. 97, Article ID 104030, 2021.

[15] H. Habbouche, T. Benkedjouh, Y. Amirat, and M. Benbouzid, "Gearbox failure diagnosis using a multisensor data-fusion machine-learning-based approach," *Entropy*, vol. 23, no. 6, p. 697, 2021.

[16] G. Yuhai, L. Shuo, and H. Linfeng, "Research on failure prediction using dbn and lstm neural network," in *Proceedings of the 2018 57th Annual Conference of the Society of Instrument and Control Engineers of Japan (SICE)*, pp. 1705–1709, IEEE, Nara, Japan, September 2018.

[17] X. He and J. Ma, "Weak fault diagnosis of rolling bearing based on FRFT and DBN," *Systems Science & Control Engineering*, vol. 8, no. 1, pp. 57–66, 2020.

[18] P. B. Dash, B. Naik, J. Nayak, and S. Vimal, "Deep belief network-based probabilistic generative model for detection of robotic manipulator failure execution," *Soft Computing*, pp. 1–13, 2021.

[19] L. Wang, Z. Liu, H. Cao, and X. Zhang, "Subband averaging kurtogram with dual-tree complex wavelet packet transform for rotating machinery fault diagnosis," *Mechanical Systems and Signal Processing*, vol. 142, Article ID 106755, 2020.

[20] W. Yuan, "Study on noise elimination of mechanical vibration signal based on improved wavelet," in *Proceedings of the 2020 Twelveth International Conference on Measuring Technology and Mechatronics Automation (ICMTMA)*, pp. 141–143, IEEE, Phuket, Thailand, February 2020.

[21] H. Patel, A. Thakkar, M. Pandya, and K. Makwana, "Neural network with deep learning architectures," *Journal of Information and Optimization Sciences*, vol. 39, no. 1, pp. 31–38, 2018.

[22] S. Haidong, C. Junsheng, J. Hongkai, Y. Yu, and W. Zhantao, "Enhanced deep gated recurrent unit and complex wavelet packet energy moment entropy for early fault prognosis of bearing," *Knowledge-Based Systems*, vol. 188, 105022.

[23] J. Hu, T. Huang, J. Zhou, and J. Zeng, "Electronic systems diagnosis fault in gasoline engines based on multi-information fusion," *Sensors*, vol. 18, no. 9, p. 2917, 2018.

[24] E. Brumancia, S. Justin Samuel, L. M. Gladence, and K. Rathan, "Hybrid data fusion model for restricted information using Dempster-Shafer and adaptive neuro-fuzzy inference (DSANFI) system," *Soft Computing*, vol. 23, no. 8, pp. 2637–2644, 2019.

Research Article

Class-Incremental Learning on Video-Based Action Recognition by Distillation of Various Knowledge

Vali Ollah Maraghi and **Karim Faez**

Department of Electrical Engineering, Amirkabir University of Technology (Tehran Polytechnic), Tehran, Iran

Correspondence should be addressed to Karim Faez; kfaez@aut.ac.ir

Recognition of activities in the video is an important field in computer vision. Many successful works have been done on activity recognition and they achieved acceptable results in recent years. However, their training is completely static, meaning that all classes are taught to the system in one training step. The system is only able to recognize the equivalent classes. The main disadvantage of this type of training is that if new classes need to be taught to the system, the system must be retrained from scratch and all classes retaught to the system. This specification has many challenges, such as storing and retaining data and respending training costs. We propose an approach for training the action recognition system in video data which can teach new classes to the system without the need for previous data. We will provide an incremental learning algorithm for class recognition tasks in video data. Two different approaches are combined to prevent catastrophic forgetting in the proposed algorithm. In the proposed incremental learning algorithm, two approaches are introduced and used to maintain network information in combination. These two approaches are network sharing and network knowledge distillation. We introduce a neural network architecture for action recognition to understand and represent the video data. We propose the distillation of network knowledge at the classification and feature level, which can be divided into spatial and temporal parts at the feature level. We also suggest initializing new classifiers using previous classifiers. The proposed algorithm is evaluated on the USCF101, HMDB51, and Kinetics-400 datasets. We will consider various factors such as the amount of distillation knowledge, the number of new classes and the incremental learnings stages, and their impact on the final recognition system. Finally, we will show that the proposed algorithm can teach new classes to the recognition system without forgetting the previous classes and does not need the previous data or exemplar data.

1. Introduction

Recognition of human activity in the video has many applications, such as human interaction with computers, surveillance systems, and monitoring of human behavior in industrial environments. Approaches based on deep learning have reported excellent results in recognizing activity, especially human activity. But using these methods in real and dynamic environments such as urban space, wildlife, and industrial environments faces challenges. Because it is always possible to see new activities that the existing recognition system has not already seen, in this case, there is a need to update the system constantly.

Deep learning has significant achievements in terms of recognition and classification [1–3], but it also has some constraints. Training a model with a deep learning approach requires many annotated data and computational resources due to its increasing depth and complexity. Most successful methods restrict the batch setting: data are provided before training; hence, optimizing metaparameters and model selection is usually based on a complete dataset. Also, the training can rely on the assumption that the data and its underlying structure are static. But this is contrary to real-world scenarios. In the actual situation, training data is not available for all classes initially, and the number and nature of classes are not necessarily clear. A classification system in real environments should learn new classes incrementally when their training data becomes available and, of course, does not undermine the recognition of previous ones. But the main problem is that training a neural structure using

only new classes' data leads to forgetting previous classes, called catastrophic forgetting.

On the other hand, training a system from scratch to learn new classes faces challenges, including the high cost of training, storing previous class data for future training, and perhaps privacy restrictions for maintaining some data. So, as computer vision moves closer towards artificial intelligence, more flexible approaches are needed to handle the large-scale and dynamic situation more felt. The purpose of this work is to learn new categories to model without the need for previous data and without reducing the model's performance about previous classes, known as class-incremental learning in literature.

This paper provides a class-incremental learning method for recognizing human action in video data. The base model is an RNN-based deep neural structure, given the achievements of deep learning in classification, that should learn human action classes in video data. Class-incremental learning for RNN-based deep structures has rarely been done. The proposed method combines two common approaches in incremental learning (network sharing and network knowledge distillation). Using the proposed algorithm, we will show that new classes can be taught to a human action recognition system without data from previous classes. Of course, the system's overall performance will not be greatly impaired. We propose the distillation of network knowledge in two levels of classification and feature. The feature section can be decomposed into two sections of distillation of temporal and spatial features. We also proposed using Temporal Segment LSTM (TS-LSTM) for the temporal representation of the video instead of the usual use of LSTM. This technique helps to better temporally represent the video and improve the recognition system's performance. The proposed method will give comparable results to exemplar-based methods without the use of exemplar data. Meanwhile, in the Related Works section, we show that the class-incremental learning of action recognition in video is rarely done without the exemplars. We evaluate the proposed algorithm and compare it with other methods based on exemplar data, and we show that the proposed method has performed better. Under similar conditions, the recognition accuracy has improved by almost 8% and 6.5% compared to the existing methods on the UCF101 and HMDB51 datasets.

The innovation of this work is in three cases: first, network distillation at classification and feature levels, where distillation at the feature level is done separately for spatial and temporal features, second, providing class-incremental learning in video data without storing data or exemplars, and third, initializing new classifiers using previous classifiers to learn new classes faster and better. Also, our base model is an RNN-based structure, and other existing methods are not effective for these structures.

In the rest of the paper, we review some related works in Section 2. The proposed algorithm is presented in Section 3. We present the experimental results and evaluations in Section 4, discuss results in Section 5, and conclude the paper in Section 6.

2. Related Works

2.1. Incremental Learning on Video Data. Class-incremental learning means that a classifier architecture can accommodate new classes at any time during the training process without requiring access to all training data seen so far. The minor works in incremental learning in video data are almost related to domain-incremental learning [4]. Class-incremental learning to recognize human action in video data is suggested using a recursive-tree structure [5], which adds one class to the tree as each new class's data is added.

In deep learning, very little work has been done on class-incremental learning in video data, especially on action recognition in video. The adaptive RNN tree is proposed for large-scale action recognition, adapted to new classes by augmenting an existing model [5]. The ODN (Open Deep Network) [6] detects new categories by applying a multiclass triplet thresholding method and dynamically reconstructs the classification layer. It opens the deep network by continually adding predictors for new classes. The weights of the new classifiers are initialized from the average weights of the previous classifiers. The new model is fine-tuned using both new and old samples. The goal is to reduce the training energy from scratch and still require previous data. A temporally attentive knowledge distillation method is presented, which distills the network knowledge over the network and intermediate layers and uses it to prevent catastrophic forgetting [7]. Importance weights are estimated during training, and knowledge is distilled from these importance weights during incremental learning. This method also uses the storage of exemplar data for use in incremental learning. To improve the performance of incremental learning based on network distillation, the spatial-temporal feature decomposition into two parts, spatial and temporal features, is presented [8]. A dual granularity exemplar selection method is proposed to select exemplar data from previous classes for use in incremental learning [8].

As mentioned, little work has been done on incremental learning in video data. The exemplar data storage of previous classes is also usually used. On the other hand, the deep structures used for classification tasks in a single image are similar to video classification's deep systems. Therefore, catastrophic forgetting is a common phenomenon in the image and video domains. So, reviewing incremental learning in single images can give us a better insight into this issue.

2.2. Incremental Learning on Image Data. Mensink et al. [9] showed that the nearest class mean (NCM) classifier could do so. NCM represents each class by the average feature vector of all examples observed for the class so far. NCM has performed well for incremental learning and is more robust than other standard parametric classifiers [9–11]. The prototype-based classification idea of NCM was adapted for incremental classifier and representation learning (iCaRL) [12] where the average vector is computed only over a specifically chosen subset of all examples. The dilemma of

prototype-based methods deals with complex classification problems, where the number of classes increases and their nature becomes more complicated.

The recent success of deep neural networks can be mainly attributed to their suitable data representation [13–16]. The main problem in learning representation in the incremental learning mode is catastrophic forgetting, introduced by McCloskey and Cohen in 1989 [17]. Training a neural network with new data causes the previous data to be forgotten. Inspired by the idea of transfer learning [18], the previous model's knowledge can assist in learning new related classes. It has been shown that the features extracted in the lower layers of CNNs are general, which can be used in various domains, similar to Gabor filters and edge or corner detectors [19]. In contrast, the extracted features from the end layers are more abstract and specific for a class. This feature of CNNs is the basis of the transfer learning and partial sharing approach for incremental learning [20].

Much of what has been done recently for incremental learning in neural networks is based on the freeze/growth scenario [20–22]. Splitting the base network into various subnetworks and creating a tree structure are proposed to incrementally learn the new classes [23, 24]. An adaptive hierarchical network composed of DCNNs is proposed for incremental learning that grows and learns as new data becomes available [25]. In [26], the Bayesian transfer learning algorithm is proposed to avoid retraining the whole model from scratch. Selecting a portion of the initial exemplar data and storing it for training new classes are also provided to prevent catastrophic forgetfulness [12, 27, 28]. This scenario requires additional resources to store exemplar data. Using the generative adversarial networks (GANs) to create fake data is proposed [29, 30]. This approach eliminates the need for additional resources to store data but leads to additional training GANs. A method based on bias correction is proposed to solve the educational data unbalancing issue [31].

Network knowledge distillation has been used to reconstruct previous classes' features and train new classes to solve the catastrophic forgetting problem [32, 33]. In [32], the input is given to the previous model to extract the previous classes' information in the input image. The model responses to inputs are used as the ground truth for old classes during training the new classes to the system [14]. Castro et al. [34] proposed that, to train the new class, use network knowledge distillation to calculate the output of prior categories and generate a set of logits. These logits are then used to calculate the loss in training new classes to force the network to retain information from previous classes. An attentive feature distillation approach was proposed to distill necessary knowledge using both top-down and bottom-up attention for incremental learning object detection [35]. Incremental learning in the semantic segmentation of objects is also proposed with the same approach [36]. This approach is also used for incrementally object detection tasks [37] to train the class of new objects.

A review of related work suggests that if the main goal is to classify with one output class for each input, the appropriate approach is network sharing or storing and reproducing some of the data from previous classes [12, 20–24, 27–30]. For tasks with multiple outputs per input, such as multiple object detection, the use of network knowledge distillation may be a good approach, given the possibility of having information about multiple classes in a single input [35–37].

3. Proposed Approach

The purpose of this work is class-incremental learning for action recognition in video. A review of related work showed that the appropriate approach for class-incremental learning in single-output tasks is network sharing or storing and reproducing some of the data from previous classes [12, 20–24, 27–30]. The network distillation approach is more suitable for tasks where the input includes multiple classes, such as multiple object detection and multiclass segmentation. The new class data may consist of parts of some previous classes in these cases. So, the distillation network distills the information about those classes, which helps preserve previous network information in new training. However, these conclusions are for single-image data and may not be entirely valid for video data.

Our work is to recognize the action in the video, which is a single-class classification task. A specific action may consist of several subactions, some of which may be present in other activities. The way action recognition algorithms work in video is usually that first low- and high-level features are extracted from video frames (usually by a CNN). Recursive structures represent the temporal dependence of these features, and, finally, the classification is based on this representation. The extracted features in the first step are abstract visual features, and, due to a large number of frames in the inputs, the feature extraction module becomes general. In other words, the feature extraction module obtained from the training of the early classes also can extract the appropriate features from the data of the new classes. Therefore, the network sharing technique can be used for incremental learning in this work.

As mentioned, an action consists of its various components, including various subactions and abstract properties. The feature extraction module obtains abstract features in the first step. Subactions and their combinations are calculated to represent the action by recurrent structures in the second step. A new action may contain components that already exist in previous classes. Therefore, if a new action class data is applied to the model, the recurrent section may also represent different components of previous actions. In this case, the previous network information can be distilled using network distillation. Thus, although this is a one-class classification task, the network distillation approach can also be used for class-incremental learning.

3.1. Class-Incremental Learning. Our main goal in this work is to apply class-incremental learning to recognize the action in the video. Our proposed algorithm combines two approaches: network sharing and network distillation. After training the basic model with the data of some classes, it is

assumed that the feature extraction section (CNN) can extract appropriate properties of other classes. Therefore, the feature extraction module is fixed (frozen) for subsequent training efforts. This trick implements the concept of network sharing.

Distillation of network knowledge is the extraction of information learned from the network and applying this information to the network during incremental learning to prevent forgetfulness. In fact, the previously taught model as a teacher controls training the new model (student) not to forget the previous information. The teacher model is not updated during incremental learning. Distillation of network knowledge can be applied at the classification level (probabilities generated by the classification layer) or at the feature level (feature maps obtained in the middle layers). In a simple knowledge distillation algorithm, only the output of the classification layer is used to extract network knowledge and remind it in incremental training. In this case, the student network tries to preserve past information by reproducing the values generated by the teacher model. The last layer classifiers generate a probability for each class for each video input. Before new training, these probabilities are first calculated for the new class input, and, during the new classes training, the previous classifiers are forced to reproduce the previous probabilities. Therefore, when training the student model to train the new classifiers, the previous classifiers retain previous knowledge by being forced to reproduce their corresponding values in the teacher model. The task of preventing the forgetting of past knowledge in these circumstances is the sole responsibility of the classification layer.

But the information recorded in the network is available throughout the network. By extracting this information and reminding it to the network, it is possible to help preserve the network knowledge in new learning [7, 8]. In this situation, the teacher model controls the training of the student model throughout the model, not just in the classification portion. The feature maps obtained from the middle layers in 3D neural structures for video representation form a tensor with $T \times H \times W$ dimensions. This tensor contains spatiotemporal information obtained from video, including spatial information in dimensions H and W and temporal information in dimension T [8]. Separating spatial information and temporal information and distilling them has been shown to help improve incremental learning performance [8]. Pooling in temporal and spatial dimensions must be performed to decompose the tensor containing spatiotemporal information into spatial and temporal parts, respectively.

In our case, the model used to recognize action from the video is an RNN-based deep structure described in Section 3.2. In this type of structure, spatial features are first extracted at the frame level, and then temporal relations are represented by a recurrent part. Figure 1 shows this process. Therefore, spatial information is available separately from temporal information at the end of the first section (convolutional feature extraction module in Figure 1). Temporal representation is also available at the output of the recurrent part (LSTM module in Figure 1). Therefore, no process is required to parse spatial and temporal information.

According to the above, the network knowledge distillation technique is used to apply incremental learning by controlling the training of the student model by the teacher model. This control is applied at three levels: classification layer, spatial features, and temporal features. Figure 2 shows this control. Therefore, the knowledge of the network is distilled at three levels of classification, spatial characteristics, and temporal characteristics.

$$L_{cD} = \sum_{f=1}^{F} \left(-\frac{1}{N} \sum_{i=1}^{N} \sum_{j=1}^{C} \widehat{p}_{ij} \log \widehat{q}_{ij} \right), \tag{4}$$

The technique of distillation network knowledge and applying it during incremental learning is done by calculating the loss function and backpropagating it. The base network is trained using the common cross-entropy classification loss function (L_{cl}). The loss function in the incremental learning phase (L_{inc}) consists of two parts, one part related to classification and the second part associated with knowledge distillation. As for the base model training, the first part is a cross-entropy loss function (L_{cl}) and the second part is a distillation loss function (LD).

$$L_{inc} = L_{cl} + \gamma LD, \tag{1}$$

where γ is hyperparameter. The cross-entropy loss (L_{cl}) is as follows:

$$L_{cl} = -\frac{1}{Ns} \sum_{i=1}^{Ns} \sum_{j=1}^{C} p_{ij} \log q_{ij}, \tag{2}$$

where p_i is the grand truth for sample i and q_i is a softmax score of the logits of a classifier for sample i. Ns and C denote the numbers of samples and classes, respectively. The distillation loss function (LD) used to maintain previous classes consists of two parts, classification and feature:

$$LD = L_{cD} + \propto L_{fD}, \tag{3}$$

where L_{cD} and L_{fD} are the classification distillation loss and the feature distillation loss, respectively. The classification distillation loss is as follows:where $\widehat{p}_i$ and $\widehat{q}_i$ are the modified versions of p_i and q_i, which are obtained by raising p_i and q_i to the exponent $1/T$, as described in [38], where T is the distillation parameter. Distillation loss is calculated for all F previous classes. Choosing $T > 1$ forces the network to learn a more fine-grained separation between classes. This parameter is set to 2 for all experiments. Feature distillation loss can be calculated as fused spatiotemporal or separately in two parts: spatial and temporal. Due to the superiority of separate spatial and temporal distillation and separate access to these two features, we use separate distillation. So the feature distillation loss is formulated as follows:

$$L_{fD} = L_{tfD} + \beta L_{sfD}, \tag{5}$$

where L_{sfD} and L_{tfD} are the spatial and the temporal terms of the feature distillation loss. These losses are calculated as follows: the Euclidean distance between the features taken from the base model and the model under training.

FIGURE 1: Block diagram of the process in each processing stream. At first, the convolutional features of each frame are extracted. Then, the whole input video is represented by the LSTM block. Finally, the elements are aggregated.
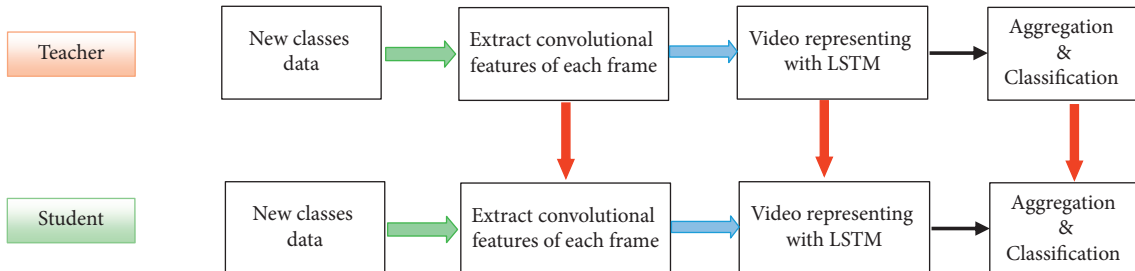
FIGURE 2: Control of student model training by teacher model at three levels of classification, temporal features, and spatial features. The teacher model is not updated during training the student model.

$$L_{fD} = \sum_{i=1}^{F} f_{ib} - f_{in}^{2}, \qquad (6)$$

where f_{ib} and f_{in} are the features obtained from the base model and new model, respectively.

So, the overall loss function formed as follows:

$$L_{inc} = L_{cl} + \gamma \left(L_{cD} + \propto \left(L_{tfD} + \beta L_{sfD} \right) \right). \qquad (7)$$

Therefore, the proposed class-incremental learning algorithm is as follows:

(i) A human activity recognition system is taught from scratch to recognize the initial classes. This trained model is used as the teacher model for the next training.

(ii) The new model (student model) is created by sharing the base model and adding classifiers for new classes.

(iii) The feature extraction module of the base model, except two last layers, freezes and is not updated during incremental learning. This work is derived from network sharing approaches.

(iv) The student model is taught using new class data under the supervisor of the teacher model. During this training, knowledge distillation is done by supervising the teacher model by calculating the loss function according to (7).

(v) The new taught model will be used as the teacher model for future training. In other words, the subsequent incremental learnings are done from step (ii) onwards.

We introduce an excellent neural structure for action recognition in video data in the following.

3.2. Action Recognition System.
An important feature of video data is temporal information in the video that can efficiently represent the video and identify the target class.

But what is the best way to exploit time information? Many previous methods, which follow a two-stream ConvNets [39], use optical flow images to take advantage of temporal information in one of the processing streams [40–44]. In these methods, visual appearance in spatial and temporal flows and their relationship are not considered, which is one of the essential components in activity recognition tasks. Therefore, they will not perform well for these tasks.

Therefore, we can consider a three-stream structure that the first and second streams process on RGB images, and the third stream includes the processing of optical flow images. This three-stream structure was previously introduced for action recognition in the video [45] and modified for verb recognition through zero-shot learning on human-object interaction (HOI) recognition [46]. We use this structure as a base model to investigate the proposed class-incremental learning algorithm. The operation of this structure and each of its three streams is described in full detail in [45]. We briefly introduce it below. Each stream has three main processing steps shown in Figure 1. The processing flows of the three streams are almost similar.

Patch-Based Representation. Activity-related areas are first estimated in each RGB frame in this processing path. These action patches are then used to extract the convolutional properties of each frame. The extracted feature map is given to the LSTM block to represent the temporal relationship. The resulting output vectors are aggregated to form the final representation vector for estimating the action class.

Focal Representation. In this path, the activity-related area is first estimated (like as first path), the other regions are blurred, and a new RGB image is obtained. The convolutional properties are extracted from each frame's resulting image, and the process's continuation is the same as the first stream.

Motion Representation. Short-term information in a video clip can be represented by optical flow. The RNN block can obtain long-term information. Therefore, the

third path can represent motion with optical flow. The convolution properties of each frame are extracted from the optical frame by a CNN network. The next steps are exactly like the other two streams.

The long short-term memory (LSTM) module is used as RNN to temporally represent the video. The LSTM module does the representation of the temporal relationship in the video. The extracted per frame CNN features are split into k-frame chunks in each input video and fed to the LSTM module. Each chunk fed to the LSTM module contains feature maps extracted from F/k consecutive frames of input video, where F is the total number of input frames and k is chunks number. Next, the LSTM outputs are fed into a densely connected feedforward neural network with a Softmax output layer, giving each chunk the probability of belonging to each C-action class. These probabilities are added for all chunks of each video to predict the class. The direct use of LSTM to consider temporal information is only similar to simple temporal pooling methods, such as mean or max pooling, due to the limited temporal dynamics of representing ConvNet-derived features [47]. It is shown that the features obtained from the frames of a video have similar representations [47]. Because a large portion of the video has the same feature representations over time, RNNs cannot learn the temporal information well. In the TS-LSTM method [47], the input sequence is divided into several temporal chunks, and their distinctive feature representations are learned. Each video is sampled into N frames and divided into M chunks. The features extracted from F input frames are split into F/k chunks. Temporary pooling is performed on each chunk, and then the pooled features of all chunks are fed to the LSTM module to represent the entire video. The output of this module will be used for recognition in the next dense layer. The TS-LSTM module learns the nonlinear feature combination and its segmental representation over time.

We substitute this TS-LSTM technique for the primary three-stream structure technique. The direct technique uses LSTM to represent each chunk typically, performs a recognition for each, and then sums the recognition results of all the fragments. The TS-LSTM technique, unlike the direct technique, uses all the video space for recognition, which will improve system performance. Due to the temporal pooling in each chunk, the total computations for recognizing a video are also reduced.

The results of the three introduced streams are merged to recognize the input video action class. The integration is as follows: A score is given to each class by a dense network in each stream. The total score of each class is calculated by summation of its scores in three streams. The class with the highest score is the recognized action class.

3.3. Initialization of new Classifiers.
Creating a new model (student model) for incremental learning is done by sharing the teacher model and adding new classifiers related to new classes. The initialization of the weights of these new classifiers is usually done randomly. Thus, in the created student model, the weights of the new classifiers are without any

initial training, while the previous classifiers are fully trained. To solve this imbalance, initializing the weights of the new classifiers with the previous weights can be helpful. The use of previous weighted averages to initialize new classifiers is proposed to reduce the learning time in the continuous training of categories for the open-set problems [6]. This work is not intended for class-incremental learning without the previous data and only makes learning the new model faster with more classes. Due to the nature of human action, which can consist of several subactions, using the information in the previous classifiers to initialize the new classifiers makes it easier to train and converge them.

We use this trick to initialize the weights of the new classifiers. Of course, we do not recommend the average of all the weights of the previous classifiers. It is best to use the average of the most similar classifiers for each new class. By feeding the data of each new class to the teacher model, the classifiers that produce the biggest probability for the input data are likely to be the most similar classifiers to the new class. Therefore, by estimating the most similar classifiers, the new classifier weights are initialized with the average of these weights as follows:

$$W_{N+1} = \frac{1}{M} \sum_{i=1}^{M} W_i, \tag{8}$$

where M denotes the M similar classifiers. The weights of the new classifier are denoted by W_{N+1} and W_i denotes the weights of previous classifiers (from the teacher model).

4. Results and Experiments

We present the results of our method in this section and compare them with those of some other class-incremental learning methods and the static training mode (training all classes to the model in one stage). Our proposed algorithm does not use exemplar data storage. At the time of doing this, there was no other similar method for comparison. Therefore the performance of the proposed method was compared with those of incremental learning methods based on exemplar data storage.

4.1. Datasets.
For human action understanding in videos, several appropriate datasets have been provided and published, such as UCF101 [48], HMDB51 [49], and Kinetics-400 [50]. We evaluated our method using the HMDB51, UCF101, and Kinetics-400 datasets.

HMDB51 includes 51 action classes with 6766 videos collected from various sources. There are three training/test splits, like the setting in [45], and, in each evaluation stage, the mean average accuracy is reported.

UCF101 consists of 101 action classes, 13k clips, and 27 hours of video data. This dataset contains the user's uploaded videos, including camera motion and cluttered background. The videos of each category are grouped into 25 different groups based on some characteristics such as environments and camera movement. The dataset is separated into three training/test splits; in each split, 18 groups are used for training and seven groups for testing.

The third dataset is Kinetics-400, a large-scale video classification dataset containing 400 human action categories. Kinetics-400 is a YouTube-type video dataset that provides 240k and 20k 10-second videos for training and validation, respectively.

4.2. Implementation Details. The recognizer system has three streams: two spatial streams and one temporal stream. The two spatial CNN streams use an AlexNet architecture pretrained on UCF sports. The first stream inputs are the estimated action patches, and the proposed focal representation is fed for the second stream. For the 3rd stream as motion representation, we used the CNN network like the network architecture used by Wu et al. [31]. This motion-CNN is pretrained on the optical flow images of UCF sports. There are many options for generating optical flow images. The two most common methods are Brox [51] and TV-L1 [52], in which TV-L1 performed slightly better based on the evaluation in [47]. So, TV-L1 is used as input for the temporal stream.

The FC7 layer of three CNNs extracts a 4096-dimensional feature vector for each input video frame. After obtaining feature vectors for all F frames of the input video in three CNNs, these feature vectors are used by the RNN module for temporal representation. For the RNN module, an LSTM block with 256 hidden units is used. Two FC layers, respectively, with the number of neurons equal to 256 and the number of action classes, are used as a classifier in each stream.

For training the base model with initial classes, the learning rates are initially set to 5×10^{-6} for two spatial streams and 5×10^{-3} for temporal stream. These learning rates are divided by 10 when the accuracy is saturated. The weight decay and momentum for all ConvNets are set to 1×10^{-4} and 0.9, respectively. The batch sizes for all ConvNets are 8. The LSTM module is trained with an Adam optimizer and learning rate of 5×10^{-5}.

The size of the input images is 224×224 for all streams. The number of sampled frames in each video is $N = 24$, and the number of temporal segments is selected as $M = 6$.

4.3. Experimental Results. In class-incremental learning scenario, To evaluate the proposed method, we follow the strategy used in [7]. First, the base model is trained with initial classes, and then the other classes are incrementally trained to model. For this purpose, all classes are sorted randomly, 50% classes (51 classes for UCF101 and 26 classes for HMDB51) are used to train the base model, and the remaining classes are used for incremental learning. The remaining 50 classes of the UCF dataset are taught to the model in 5 steps of 10 classes, ten steps of 5, and 25 steps of 2 in incremental learning. For the HMDB dataset, the remaining 25 classes are taught to the model in 5 stages of 5 classes and 25 stages of 1 class in incremental learning. Because the nature of the classes affects the result, these experiments are performed three times with randomly ordered classes. The model's classification accuracy is calculated on the seen classes in each step, and its average value is calculated.

The initialization of new classifiers is performed according to (8) with $M = 5$. First, the five most similar classifiers are calculated by calculating the teacher model's output on the new class's data for each new class. Their average weights are calculated and set as the initial values of the new classifier weights.

We test three scenarios for class-incremental learning based on using distillation knowledge and how much network sharing. These three scenarios are summarized in Table 1. The type of used distillation is depicted in the fourth column where cD represents distillation at the classification level and tfD and sfD represent distillation at the temporal and spatial features, respectively.

We train the model with the first available classes in experiments with the first scenario settings (3Stream-D). Then, the feature extraction module and the LSTM block are frozen, the classifiers corresponding to primary classes are discarded, classifiers for new classes are added, and the model is trained for new classes. During the training of new classes, only the new classifiers are taught. This experiment is just a network-sharing technique, and there is no distillation.

For the second scenario, as in the first scenario, the base model (teacher) is first trained for the primary classes. The student model is created by sharing the teacher model and adding the new classifiers. In this scenario, during incremental learning, the trained classifiers of the teacher model are not discarded. ConvNets is frozen in all streams. The distillation type is only a classification distillation. In other words, in (7), the alpha parameter is equal to 0.

The third scenario is similar to the second scenario and uses network knowledge distillation, except that, in this scenario, the distillation loss is calculated by classification and temporal features distillation. This increases the control of the teacher model on the student during incremental learning. In this case, spatial distillation is not used, and $\beta = 0 \propto$ in (7), while $\propto > 0$ is used.

Table 2 shows the class-incremental performance on UCF and HMDB datasets and compares the above scenarios with three other methods. The TCD [7] is proposed for video data, but UCIR [53] and PODNet are proposed for image datasets that are evaluated for video in [7]. All these three methods use exemplar data storage for incremental learning. The proposed algorithm does not use exemplar data. Still, for better comparison with the compared methods, the performance of the proposed method using exemplar data is also tested and is reported in Table 2.

The results of Table 2 show the efficiency of the proposed algorithm. The proposed algorithm has a much higher performance than other methods if it uses exemplar data. If exemplar data are not used, the proposed algorithm still performs better or is similar to the compared methods. Of course, part of this better performance is due to the structure used, which in static learning mode is more accurate than the compared methods. In other words, the accuracy of the used model before applying incremental learning is better than the compared models at the same time. However, Figure 3 shows that the rate of accuracy drop is acceptable by

TABLE 1: Three scenarios for class-incremental learning.

	Freeze ConvNets	Freeze LSTM	Distillation type	Update first classifiers
3Stream-D	Yes	Yes	—	No
3Stream + cD	Yes	No	cD	Yes
3Stream + cD + tfD	Yes	No	cD + tfD	Yes

TABLE 2: Class-incremental action recognition performance on UCF and HMDB datasets.

Methods	Exemplar	UCF101			HMDB51	
		10×5 stages	5×10 stages	2×25 stages	5×5 stages	1×25 stages
UCIR [53]	5	74.31	70.42	63.22	44.90	37.04
PODNet [54]	5	73.26	71.58	70.28	44.32	38.76
TCD [7]	5	74.89	73.43	72.19	45.34	**40.07**
3Stream + cD	5	80.65	78.33	76.84	52.35	45.63
3tream + cD + tfD	5	**83.24**	**81.24**	**79.2**	**54.28**	47.15
3Stream-D	0	69.34	64.32	59.86	45.23	—
3Stream + cD	0	74.23	69.51	67.12	48.2	—
3tream + cD + tfD	0	*77.05*	*74.12*	72.07	*50.75*	—
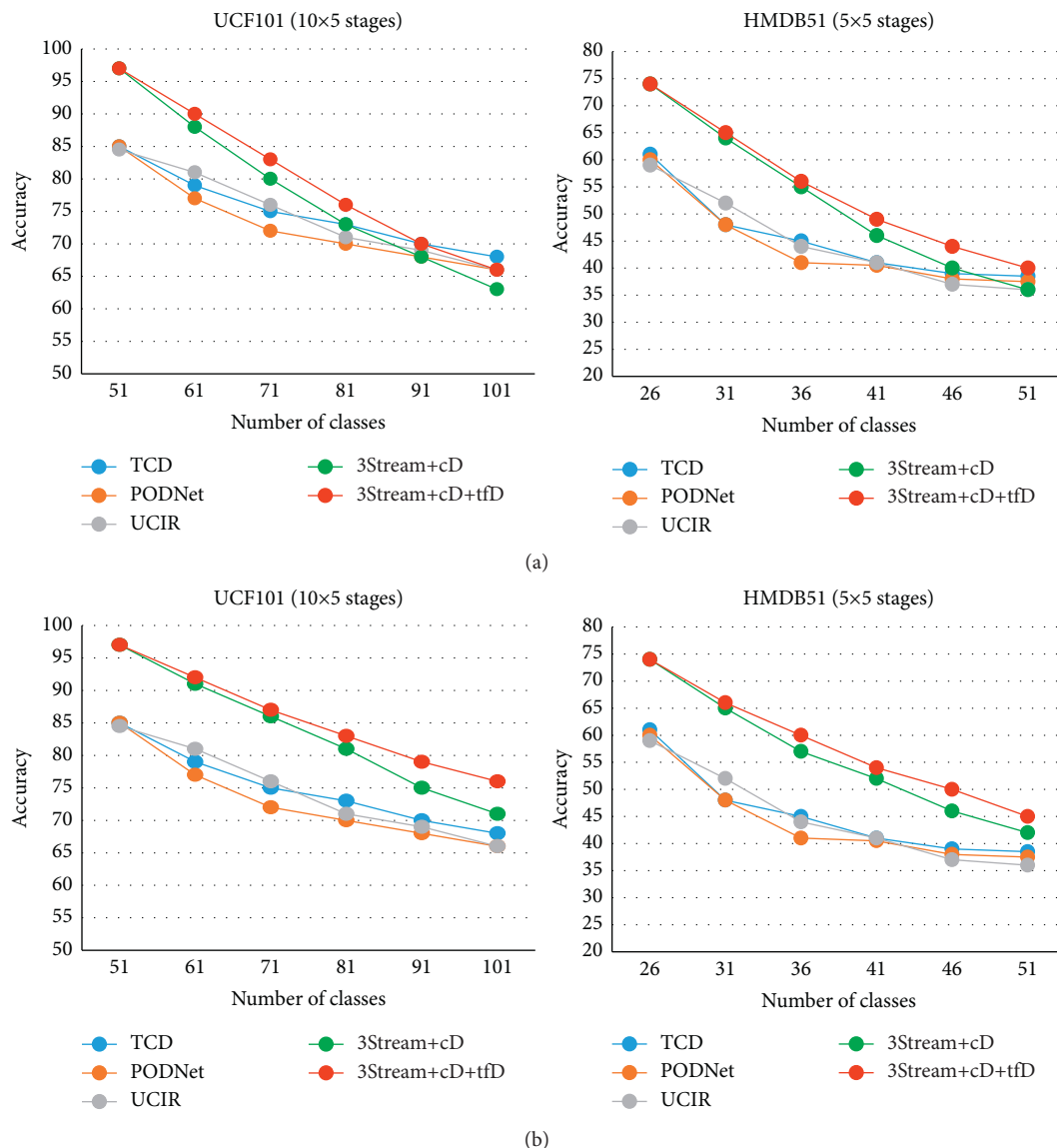
FIGURE 3: Accuracy chart in terms of incremental learning step. The top row does not use exemplar data for the proposed method, but, in the bottom row, the proposed method also uses exemplars. Compared methods use exemplar data in all cases. (a) 3Stream methods without using exemplars and (b) 3Stream methods use exemplars.

applying incremental learning despite not using the previous sample data. The curves in Figure 3 show that the final model obtained by the proposed algorithm performs better than other methods if the exemplar data are used. Also, if exemplar data are not used, the performance of the final model is acceptable compared to exemplar-based methods.

For the first scenario (3Stream-D), a large part of the network (ConvNets and LSTM) is frozen. Just the parameters of classifiers are updated, so the network learning capacity is reduced. Hence, the model's accuracy on the new classes is not very high. In the final model, the extractor modules and the primary classifiers have not changed during incremental learning, and the accuracy on the primary classes has been high. Still, in the final model, the classifiers related to the primary and secondary classes have not been trained relative to each other. If the model with all classifiers is considered, the error rate increases, and therefore the overall accuracy is not very high.

For the second scenario (3Stream + cD), the base model is precisely the same as the first one. The accuracy of the final model on all classes is increased. This improvement is because network knowledge distillation has been used, and primary classifiers have been updated against new classes. Updating the LSTM block probably reduces the model accuracy on the initial classes after incremental learning. Still, due to the distillation of network knowledge, this performance reduction is not expected to be very large. Of course, it should not be forgotten that this performance improvement is in exchange for a slight increase in training energy during incremental learning. However, the energy of the error backpropagation in the recursive structures is much less than that of the convolutional structures, and, due to the freezing of the convolutional parts, the training energy is much less than that of the static training. More control of the teacher model over the training of the student model in the third scenario (3Stream + cD + tfD) causes the previous information to be less affected by the new information, and the accuracy of the model decreases less.

4.3.1. Evaluation for Large Dataset.
The above tests and evaluations were performed on the common UCF101 and HMDB51 datasets. Still, these two datasets do not have a large number of classes, and a larger dataset is needed to conclude situations with a large number of classes. The Kinetics-400 dataset is a large dataset that contains 400 action classes. The evaluation of the presented algorithm on this dataset can be useful for examining conditions with a large number of classes. However, since other methods have not been evaluated on this dataset and their performance has not been reported, we evaluate the results only with the proposed method and the degree of the models' accuracy with incremental learning steps.

In this case, 300 classes have been randomly selected and used to train the base (teacher) model. The remaining 100 classes are taught in incremental learning in various steps to the model. The final models of incremental learning results are also compared with the results of static training in which all classes are taught in one step. The experiments were performed three times, and the average results were reported. Table 3 shows the evaluation results of the proposed method on this dataset.

The important columns in Table 3 are the results of the final models and their comparison with the base model and the static mode training. These results show that the use of knowledge distillation outperforms network sharing methods. Also, the knowledge distillation from different levels of the network reduces the attenuation of the model and increases the final accuracy. Reducing system performance is reasonable if the exemplar data are not used, but, given the knowledge distillation, the accuracy of the final model is not disappointing. Also, the results of Table 3 show that the number of incremental learning stages and the number of classes in each stage affect the performance of the final model. In general, the fewer incremental learning stages and the fewer new classes added to the model in fewer stages, the better the performance of the final model.

4.3.2. Effect of Initialization.
To initialize the new classifiers, we propose using the average weights of the most similar old classifiers. In this experiment, we evaluate the effect of this technique on system performance with equal epochs in training. We used the UCF101 dataset for this evaluation. Table 4 shows the recognition accuracy of the final model.

The results of Table 4 show that using the average weights of the most similar classifiers to initialize the new classifiers makes the final performance of the model better than the random initialization mode in equal training epochs.

4.3.3. Spatial Features Distillation.
In experiments performed so far, we have not used distillation of spatial features, and we have used distillation at the level of classification and distillation of temporal features. Here we also evaluate the impact of using spatial features on incremental learning. The exemplar data are not used in incremental learning. The results of recognition accuracy are reported in Table 5.

As expected, the results of Table 5 show the positive effect of spatial feature distillation on the system's final performance. Distillation of spatial features is applied only to the first part (CNNs), and its training is separate from the rest of the network. On the other hand, the spatial part of the system includes the convolution structure, which is costly to train. Therefore, it is not unjustifiable to put it aside by accepting the slight decline in final accuracy.

5. Discussion

This work's primary goal is to train new classes to a recognizing system, provided that the system's performance is not impaired for the previous classes. We tested three different scenarios and compared them with some other methods. Experiments and comparisons with other methods have shown that adding distillation of network knowledge at the feature level helps increase class-incremental learning accuracy. Distillation of knowledge at the feature level at both temporal and spatial feature levels increases

Table 3: Class-incremental action recognition performance on Kinetics-400 dataset. Mean-named columns show the average recognition accuracy (%) of all incremental learning steps. The other values report the recognition accuracy of one model.

Exemplar	Base model	20 × 5 stages		10 × 10 stages		5 × 20 stages		Static mode	Final
		Methods	Mean	Final	Mean	Final	Mean		
3Stream + cD	15	73.5	64.42	60.26	63.02	58.34	60.74	55.23	69.84
3Stream + cD + tfD	15	73.5	68.25	**65.78**	66.83	63.36	64.86	61.73	69.84
3Stream-D	0	73.5	55.3	46.32	52.26	43.54	48.73	39.6	69.84
3Stream + cD	0	73.5	60.4	56.86	58.7	54.21	55.38	51.63	69.84
3Stream + cD + tfD	0	73.5	63.9	**61.42**	62.43	60.12	60.9	58.35	69.84

Table 4: Effect of initialization on class-incremental action recognition accuracy on UCF101 dataset.

Exemplar	Methods	Random		Similar classifiers mean	
		10 × 5 stages	5 × 10 stages	10 × 5 stages	5 × 10 stages
3Stream + cD	5	70.14	67.23	71.32	68.86
3Stream + cD + tfD	5	75.31	72.7	76.47	73.76
3Stream-D	0	52.67	49.0	53.24	49.63
3Stream + cD	0	61.45	57.36	62.56	58.5
3Stream + cD + tfD	0	65.27	62.64	66.84	63.74

Table 5: Effect of spatial features distillation on class-incremental action recognition accuracy. Only the accuracy of the final model has been reported.

Methods	UCF101 10 × 5 stages	Kinetics-400 20 × 5 stages	HMDB51 5 × 5 stages
3Stream + cD	62.56	56.86	36.43
3Stream + cD + tfD	66.84	61.42	40.26
3Stream + cD + tfD + sfD	**68.17**	**62.97**	**41.14**

recognition accuracy (see Table 5). In the absence of exemplar data, our evaluations show that the proposed method can still have results comparable to exemplar-based methods (Tables 2–4).

We also investigated the effect of classifier initialization and showed that using the most similar classifiers is helpful for initialization (see Table 4).

Evaluation on large Kinetics-400 dataset showed that the fewer incremental learning stages and the fewer new classes added to the model in fewer stages, the better the performance of the final model. Although more classes in incremental learning lead to a greater decline in system accuracy, several incremental learning also increase system decline.

Experiments have shown that distillation from different model parts can help retain prior information during the training of new classes and reduce the model performance drop. Of course, this may increase the cost of training. Comparing the proposed method with other methods that use exemplar data, it has been observed that the proposed method has a similar or even better performance without using exemplar data.

6. Conclusion

In this research, we proposed an algorithm for class-incremental learning to an action recognition system based on deep learning that does not greatly impair the recognition accuracy of previous classes by training new classes to the system. The importance of this work is reflected in the reduction of system retraining energy for all classes and the lack of need to maintain data from previous classes for future training. In this research, a three-stream structure is used, swhere each stream includes the feature extraction section, a recurrent section, and classifiers. The main idea in this work is to maintain the network knowledge related to the previous classes and also to use this knowledge in training new classes, which helps the network not forget the previously learned information. Extracting network knowledge and reminding it to the model are done in different network parts and levels.

Our focus in this research is the distillation of network knowledge, during which the network knowledge is extracted using the training data of new classes. While learning new classes, this extracted knowledge is used to prevent the network from forgetting previous classes. Distillation of network knowledge is done at the level of classification and feature, which at the feature level can be decomposed into two parts, spatial and temporal. We also suggest that the average weights of the most similarly trained classifiers be used instead of random values to initialize new classifiers. We have shown that this low-cost work improves system performance.

Other basic structures that perform better for incremental learning for future work can be used. In this work, the classes added in the incremental learning phase are from the same dataset of classes used for initial training. Incrementally learning classes from one dataset to a system taught

with another dataset is a challenge that needs to be addressed. Also, we intend to integrate this work with our previous work in the field of zero-shot learning recognition of human-object interaction (HOI) recognition [46].

Data Availability

The datasets used to support the findings of this study are included in the article [48–50].

Conflicts of Interest

The authors declare that they have no conflicts of interest.

References

[1] S. Sadiq, M. Zmieva, M. L. Shyu, and S. C. Chen, "Reduced residual nets (red-nets): low powered adversarial outlier detectors," in *Proceedings of the 2018 IEEE International Conference on Information Reuse and Integration (IRI)*, July 2018.

[2] K. Kato, Y. Li, and A. Gupta, "Compositional learning for human object interaction," in *Proceedings of the European Conference on Computer Vision (ECCV)*, Munich, Germany, September 2018.

[3] Y. Qian, M. Bi, T. Tan, and K. Yu, "Very deep convolutional neural networks for noise robust speech recognition," *IEEE/ACM Transactions on Audio, Speech, and Language Processing*, vol. 24, no. 12, pp. 2263–2276, 2016.

[4] J. Cheng, H. Liu, F. Wang, H. Li, and C. Zhu, "Silhouette analysis for human action recognition based on supervised temporal t-SNE and incremental learning," *IEEE Transactions on Image Processing*, vol. 24, no. 10, pp. 3203–3217, 2015.

[5] W. Li, L. Wen, M. C. Chang, S. N. Lim, and S. Lyu, "Adaptive RNN tree for large-scale human action recognition," in *Proceedings of the IEEE International Conference on Computer Vision*, Venice, Italy, October 2017.

[6] Y. Shu, Y. Shi, Y. Wang, Y. Zou, Q. Yuan, and Y. Tian, "Odn: opening the deep network for open-set action recognition," in *Proceedings of the 2018 IEEE International Conference on Multimedia and Expo (ICME)*, July 2018.

[7] J. Park, M. Kang, and B. Han, "Class-incremental learning for action recognition in videos," in *Proceedings of the IEEE/CVF International Conference on Computer Vision*, Montreal, Canada, October 2021.

[8] H. Zhao, X. Qin, S. Su, Y. Fu, Z. Lin, and X. Li, "When video classification meets incremental classes," in *Proceedings of the 29th ACM International Conference on Multimedia*, Chengdu, China, October 2021.

[9] T. Mensink, J. Verbeek, F. Perronnin, and G. Csurka, "Metric learning for large scale image classification: generalizing to new classes at near-zero cost," in *Proceedings of the European Conference on Computer Vision*, October 2012.

[10] T. Mensink, J. Verbeek, F. Perronnin, and G. Csurka, "Distance-based image classification: generalizing to new classes at near-zero cost," *IEEE Transactions on Pattern Analysis and Machine Intelligence*, vol. 35, no. 11, pp. 2624–2637, 2013.

[11] M. Ristin, M. Guillaumin, J. Gall, and L. V. Gool, "Incremental learning of ncm forests for large-scale image classification," in *Proceedings of the IEEE Conference on Computer Vision and Pattern Recognition*, Columbus, OH, USA, June 2014.

[12] S.-A. Rebuffi, A. Kolesnikov, G. Sperl, and C. H. Lampert, "icarl: incremental classifier and representation learning," in *Proceedings of the IEEE Conference on Computer Vision and Pattern Recognition*, Honolulu, HI, USA, July 2017.

[13] Y. Bengio, A. Courville, and P. Vincent, "Representation learning: a review and new perspectives," *IEEE Transactions on Pattern Analysis and Machine Intelligence*, vol. 35, no. 8, pp. 1798–1828, 2013.

[14] Z. Li and D. Hoiem, "Learning without forgetting," *IEEE transactions on pattern analysis and machine intelligence*, vol. 40, no. 12, pp. 2935–2947, 2017.

[15] I. Misra, A. Shrivastava, A. Gupta, and M. Hebert, "Cross-stitch networks for multi-task learning," in *Proceedings of the IEEE Conference on Computer Vision and Pattern Recognition*, Las Vegas, NV, USA, June 2016.

[16] S. Saxena and J. Verbeek, "Convolutional neural fabrics," *Advances in Neural Information Processing Systems*, vol. 29, pp. 4053–4061, 2016.

[17] M. McCloskey and N. J. Cohen, "Catastrophic interference in connectionist networks: the sequential learning problem," *Psychology of Learning and Motivation*, Elsevier, vol. 24, pp. 109–165, 1989.

[18] S. J. Pan and Q. Yang, "A survey on transfer learning," *IEEE Transactions on Knowledge and Data Engineering*, vol. 22, no. 10, pp. 1345–1359, 2009.

[19] J. Yosinski, J. Clune, Y. Bengio, and H. Lipson, "How transferable are features in deep neural networks?," 2014, https://arxiv.org/abs/1411.1792.

[20] S. S. Sarwar, A. Ankit, and K. Roy, "Incremental learning in deep convolutional neural networks using partial network sharing," *IEEE Access*, vol. 8, pp. 4615–4628, 2019.

[21] T. Xiao, J. Zhang, K. Yang, Y. Peng, and Z. Zhang, "Error-driven incremental learning in deep convolutional neural network for large-scale image classification," in *Proceedings of the 22nd ACM International Conference on Multimedia*, Mountain View, CA, USA, June 2014.

[22] A. A. Rusu, N. C. Rabinowitz, G. Desjardins et al., "Progressive neural networks," 2016, https://arxiv.org/abs/1606.04671.

[23] D. Roy, P. Panda, and K. Roy, "Tree-cnn: A deep convolutional neural network for lifelong learning," vol. 3, 2018, https://arxiv.org/abs/1802.05800.

[24] R. Istrate, A. C. I. Malossi, C. Bekas, and D. Nikolopoulos, "Incremental Training of Deep Convolutional Neural Networks," 2018, https://arxiv.org/abs/1803.10232%20.

[25] D. Roy, P. Panda, and K. Roy, "Tree-CNN: a hierarchical deep convolutional neural network for incremental learning," *Neural Networks*, vol. 121, pp. 148–160, 2020.

[26] L. Li Fei-Fei, R. Fergus, and P. Perona, "One-shot learning of object categories," *IEEE Transactions on Pattern Analysis and Machine Intelligence*, vol. 28, no. 4, pp. 594–611, 2006.

[27] D. Lopez-Paz and M. A. Ranzato, "Gradient episodic memory for continual learning," *Advances in Neural Information Processing Systems*, vol. 30, pp. 6467–6476, 2017.

[28] S. Hou, X. Pan, C. C. Loy, Z. Wang, and D. Lin, "Lifelong learning via progressive distillation and retrospection," in *Proceedings of the European Conference on Computer Vision (ECCV)*, Munich, Germany, September 2018.

[29] Y. Wu, Y. Chen, L. Wang et al., "Incremental Classifier Learning with Generative Adversarial Networks," 2018, https://arxiv.org/abs/1802.00853.

[30] H. Shin, J. K. Lee, J. Kim, and J. Kim, "Continual Learning with Deep Generative Replay," 2017, https://arxiv.org/abs/1705.08690.

[31] Y. Wu, Y. Chen, L. Wang et al., "Large scale incremental learning," in *Proceedings of the IEEE/CVF Conference on*

Computer Vision and Pattern Recognition, Long Beach, CA, USA, June 2019.

[32] O. Tasar, Y. Tarabalka, and P. Alliez, "Incremental learning for semantic segmentation of large-scale remote sensing data," *Ieee Journal of Selected Topics in Applied Earth Observations and Remote Sensing*, vol. 12, no. 9, pp. 3524–3537, 2019.

[33] A. Rannen, R. Aljundi, M. B. Blaschko, and T. Tuytelaars, "Encoder based lifelong learning," in *Proceedings of the IEEE International Conference on Computer Vision*, Venice, Italy, October 2017.

[34] F. M. Castro and M. J. Marín-Jiménez, N. Guil, C. Schmid, and K. Alahari, End-to-end incremental learning," in *Proceedings of the European Conference on Computer Vision (ECCV)*, Munich, Germany, September 2018.

[35] X. Liu, H. Yang, A. Ravichandran, R. Bhotika, and S. Soatto, "Multi-task incremental learning for object detection," 2020, https://arxiv.org/abs/2002.05347.

[36] U. Michieli and P. Zanuttigh, "Incremental learning techniques for semantic segmentation," in *Proceedings of the IEEE/CVF International Conference on Computer Vision Workshops*, Seoul, Korea (South), Ocotober 2019.

[37] L. Guan, Y. Wu, J. Zhao, and C. Ye, "Learn to detect objects incrementally," in *Proceedings of the 2018 IEEE Intelligent Vehicles Symposium (IV)*, June 2018.

[38] G. Hinton, O. Vinyals, and J. Dean, "Distilling the Knowledge in a Neural Network," 2015, https://arxiv.org/abs/1503.02531.

[39] K. Simonyan and A. Zisserman, "Two-stream convolutional networks for action recognition in videos," 2014, https://arxiv.org/abs/1406.2199.

[40] J. Yue-Hei Ng, M. Hausknecht, S. Vijayanarasimhan, O. Vinyals, R. Monga, and G. Toderici, "Beyond short snippets: deep networks for video classification," in *Proceedings of the IEEE Conference on Computer Vision and Pattern Recognition*, Boston, MA, USA, June 2015.

[41] C. Feichtenhofer, A. Pinz, and A. Zisserman, "Convolutional two-stream network fusion for video action recognition," in *Proceedings of the IEEE Conference on Computer Vision and Pattern Recognition*, Las Vegas, NV, USA, June 2016.

[42] S. Zha, F. Luisier, W. Andrews, N. Srivastava, and R. Salakhutdinov, "Exploiting image-trained CNN architectures for unconstrained video classification," 2015, https://arxiv.org/abs/1503.04144.

[43] L. Sun, K. Jia, D. Y. Yeung, and B. E. Shi, "Human action recognition using factorized spatio-temporal convolutional networks," in *Proceedings of the IEEE International Conference on Computer Vision*, Santiago, Chile, December 2015.

[44] D. Tran, L. Bourdev, R. Fergus, L. Torresani, and M. Paluri, "Learning spatiotemporal features with 3d convolutional networks," in *Proceedings of the IEEE International Conference on Computer Vision*, Santiago, Chile., December 2015.

[45] V. Adeli, E. Fazl-Ersi, and A. Harati, "A component-based video content representation for action recognition," *Image and Vision Computing*, vol. 90, p. 103805, 2019.

[46] V. O. Maraghi and K. Faez, "Scaling human-object interaction recognition in the video through zero-shot learning," *Computational Intelligence and Neuroscience*, p. 2021, 2021.

[47] C.-Y. Ma, M.-H. Chen, Z. Kira, and G. AlRegib, "TS-LSTM and temporal-inception: exploiting spatiotemporal dynamics for activity recognition," *Signal Processing: Image Communication*, vol. 71, pp. 76–87, 2019.

[48] K. Soomro, A. R. Zamir, and M. Shah, "UCF101: a dataset of 101 human actions classes from videos in the wild," 2012, https://arxiv.org/abs/1212.0402.

[49] H. Kuehne, H. Jhuang, E. Garrote, T. Poggio, and T. Serre, "HMDB: a large video database for human motion recognition," in *Proceedings of the 2011 International Conference on Computer Vision*, November 2011.

[50] J. Carreira and A. Zisserman, "Quo vadis, action recognition? a new model and the kinetics dataset," in *Proceedings of the IEEE Conference on Computer Vision and Pattern Recognition*, Honolulu, HI, USA, July 2017.

[51] T. Brox, A. Bruhn, N. Papenberg, and J. Weickert, "High accuracy optical flow estimation based on a theory for warping," in *Proceedings of the European Conference on Computer Vision*, May 2004.

[52] C. Zach, T. Pock, and H. Bischof, "A duality based approach for realtime tv-l 1 optical flow," in *Proceedings of the Joint Pattern Recognition Symposium*, Springer, Heidelberg, Germany, September 2007.

[53] S. Hou, X. Pan, C. C. Loy, Z. Wang, and D. Lin, "Learning a unified classifier incrementally via rebalancing," in *Proceedings of the IEEE/CVF Conference on Computer Vision and Pattern Recognition*, Long Beach, CA, USA., June 2019.

[54] A. Douillard, M. Cord, C. Ollion, T. Robert, and E. Valle, "Podnet: pooled outputs distillation for small-tasks incremental learning," in *Proceedings of the Computer Vision-–ECCV 2020: 16th European Conference*, Springer, Glasgow, UK, August, 2020.

Research Article

Quantifying Carbon Emissions Generated by Monorail Transits: A Life Cycle Assessment Approach

Teng Li ⓘ **and Eryu Zhu** ⓘ

Department of Civil Engineering, Beijing Jiaotong University, No. 3 Shangyuancun, Beijing 100044, China

Correspondence should be addressed to Eryu Zhu; eyzhu@bjtu.edu.cn

The use of rail transits results in the generation of a large amount of carbon emissions. Throughout the life cycle of a rail transit system, huge amounts of carbon are emitted, which contributes to the threat posed by carbon emission on the city ecosystem. Despite the many methods previously proposed to quantify carbon emissions from rail transit systems, a method that can be applied to measure carbon emissions of monorail systems is yet to be developed. We have used the life cycle assessment (LCA) method to propose a method that can be used to quantify carbon emissions from monorail transits. The life cycle of a monorail transit system was divided into four stages (production, construction, use, and end-of-life). A monorail transit line segment in Chongqing, China, was selected for a case study. The results show that the "use" stage of the monorail transit line system significantly increases (93.2%) carbon emissions, while the "end-of-life" stage does not contribute significantly to the total carbon emitted. The processes of generation of steal, concrete, and cement are the three leading processes that contribute to the emission of carbon dioxide. The percentages of carbon emitted during these processes are 32%, 29.6%, and 13.3%, respectively. Prestressed concrete activity accounts for the largest proportion (91.1%) of the total carbon emissions. The results presented herein can potentially help in realizing sustainable development and developing green transportation.

1. Introduction

Global climate changes have aroused great concern worldwide as they have seriously affected social sustainability [1]. One important way to address the problem of climate change is to reduce carbon emissions [2]. The transportation sector facilitates human travel and helps in economic development. However, a large amount of energy is consumed during transportation, resulting in substantial carbon emissions. It has been reported that the transportation sector accounts for 14% of total carbon emissions worldwide [3]. Moreover, carbon emissions from the transportation sector have increased by 29% from 1990 to 2009 [4].

The monorail system uses a single rail instead of two rails as used in traditional rail systems during operation [5]. The monorail systems are low-noise systems that are safe to use. They are characterized by good climbing ability and small turning radii [6, 7]. At present, monorails are in operation in many countries worldwide, such as Japan, Germany, and the United States of America. Egypt, Thailand, Brazil, China, and a few other countries are actively building their monorail systems. This provides a glimpse into the great potential for further advances of monorail transits in the future. Huge quantities of raw materials (such as cement, concrete, and steel) are required for the efficient development of infrastructure required to build the monorail systems. The production of these raw materials is often accompanied by an enormous amount of carbon emissions. As large-scale construction of monorail systems will be realized in the near future, it is necessary to quantify carbon emissions to realize sustainable development.

Life cycle assessment (LCA) is a method of assessing the impacts exerted by products on the environment during their lifetime [8]. In general, process-based LCA consists of four steps: (1) goal and scope definition, (2) inventory

analysis, (3) environmental impact assessment, and (4) interpretation [8]. The LCA method has been widely used to evaluate the environmental performance of rail transits in recent years (Table 1).

Table 1 presents the data and research contexts of 25 selected works in which LCA was applied to research into transport systems. Among these 25 selected studies, 12 articles focused on HSR systems, 9 on metro or subways, and 6 on railways. Results obtained by studying light rail transits (LRTs) were reported in two papers. To the best of our knowledge, there are no reports on the carbon emissions from monorail transit systems. It has also been observed that the life cycle has been described and categorized differently by different research groups. Researchers chose the length of the life cycle based on the characteristics of the system. The results obtained in different cases were different. Researchers analyzed databases from their own country or nearby countries to match their local situation. For example, CLCD is generally used as the database for Chinese research. The object of research considered in this paper is a monorail transit in Chongqing, China. Hence, CLCD was selected as the database.

Table 1 demonstrates that LCA can provide a systematic framework to evaluate the life cycle environmental impacts of various rail transit systems. However, there are some research gaps:

(1) To date, researchers have widely focused on metro and HSR. To the best of our knowledge, carbon emission has not been quantified from the perspective of the whole life cycle for the case of monorail transit.

(2) Researchers have widely studied the four stages of rail transit systems (i.e., production, construction, use, and end-of-life), but a detailed study on the carbon emissions caused by materials production and construction works in the maintenance stage of the rail transit systems has not been conducted.

The aim of the present work is to quantify carbon emissions attributable to monorail transit systems using an LCA approach, with a monorail transit line in Chongqing, China, as a case study. The research work here is organized in four sections. Section 1 provides a brief introduction to the Chongqing monorail line 2 in China. Section 2 briefly introduces the methodologies of the LCA calculation. In Section 3, the case study for calculating the carbon emissions during the four stages of a monorail transit line in Chongqing is presented; the calculation results are interpreted; the observations are discussed; the uncertainty analysis and sensitivity analysis are conducted; recommendations are given. In section 4, the conclusions are derived and a summary of the key findings are presented. The results presented are expected to serve as a source of information and data that can be used to conduct LCAs in the future.

2. Materials and Methods

This study is based on a process-based LCA method. The different steps involved in the execution of the LCA method are defined in ISO 14040 [8]: goal and scope definition, life cycle inventory analysis, environment impact analysis, and interpretation. The results obtained following the LCA method reveal the potential environmental impacts of the monorail system (from cradle to grave). The methodology is shown in Figure 1.

2.1. Goal and Scope: Definition. The goal of this study is to assess the carbon emissions of a monorail transit line segment during the whole life cycle of its operation. The system boundary of the monorail transit was defined based on the guidelines presented in the EN 15978 standard [34]. Specifically, the process is divided into the production (associated with the extraction and upstream production, transport to a factory, and manufacturing processes), construction (associated with the processes of transportation to the working site and installation), use (associated with the use, maintenance, repair, and replacement of the system and the usage of operational energy), and end-of-life (associated with the processes of demolition, material transport, waste processing, and disposal) stages. The basic assumptions made have been presented:

(1) The life cycle length of the system is 50 years. The lifespan is the same as the lifespan assumed in previous works on a Chinese subway [22] and a light rail case [33].

(2) Vehicles were absent from the system, and this could be attributed to the lack of data. Studies have been previously conducted under similar situations, and the results have been reported [17, 19–22, 26–31].

(3) All the wastes are landfilled, and carbon emissions caused by waste transportation during the process of waste processing and waste disposal are primarily considered.

(4) Operational energy consumption remains the same every year (this assumption helps simplify the calculations).

(5) All the materials are locally available, and the transportation distance is 50 km.

The detailed system boundary is illustrated in Figure 2.

2.2. Inventory Analysis. The second step in LCA involves the process of inventory analysis. In this step, information on carbon emission factors associated with different materials and resource (material and energy) consumption at all stages is collected.

2.2.1. Carbon Emission Factors. We chose data presented in the Chinese Core Life Cycle Database (the most authoritative database for LCA in China) [35] to conduct our research to effectively reflect the Chinese conditions. The baseline emission factors of China's regional power grid (from 2011 to 2017) in Chongqing were obtained based on the data from the Ministry of Ecology and Environment of the People's Republic of China [36].

TABLE 1: LCA and its application in the field of transport.

Reference	Country, region	Type of rail	Lifespan (years)	Function unit	Data	Life cycle stages
[9]	USA	Railway, RTS, subway, and HSR	Varying	PMT and VMT	Sectors and literature	Vehicle (manufacture, operation, maintenance, insurance); infrastructure (construction, operation, maintenance); fuel consumption
[10]	USA	Railway, metro, CR, and LRT	—	PKT	Literature	Train manufacturing, train maintenance, station construction, track construction, station operation, station maintenance, electricity generation supply chains
[11]	USA, California	HSR	—	PKT	SimaPro	Vehicle, station, energy production
[12]	USA, California	HSR	20	PKT	Literature	Vehicle, infrastructure, energy production
[13]	Turkey	HSR and railway	40	PKM	SimaPro 7.3.3	Infrastructure (production of electrical energy, construction of lines, maintenance of lines, operation of lines, waste disposal); operation (production of electrical energy, production of train vehicles, maintenance of train vehicles, operation of train vehicles, waste disposal)
[14]	Italy, Rome	Metro	30	VKT	Operators and GaBi	Material acquisition, manufacturing, use, and end-of-life
[15]	China	HSR	20	SKM	Chinese Core Life Cycle Database (CLCD) and ecoinvent	Vehicle operation, vehicle manufacturing/maintenance/disposal, infrastructure construction
[16]	USA, New Jersey	Commuter	—	1 mile	Literature	Material manufacturing
[17]	Brazil, Rio de Janeiro	Metro	60		IPCC 2006	Infrastructure construction, train manufacture, maintenance, infrastructure operation, and train operation
[18]	Portugal	HSR	35	PKT	SimaPro and ecoinvent	Material, manufacturing, use, disposal
[19]	Austria, Vienna	Subway	100	PKT	Biding documents and GEMIS 4.5	Infrastructure construction, infrastructure operation
[20]	Spain, Bueno	HSR	60	PKM/year, TKM/year	Literature	Infrastructure construction, infrastructure maintenance, operation, 60 years
[21]	Canada, Toronto	Subway	8 (construction time)	Year	Literature, construction data	Infrastructure construction, operation
[22]	China, Shanghai	Metro	50	1 km	Observed data	Materials production, materials transportation, on-site construction, operation, and maintenance, 50 years, 1 km, PKT, VKT
[23]	India, Mumbai	Railway	25	PKT, VKT	Department data	Manufacturing, maintenance and operation, infrastructure construction, infrastructure maintenance
[24]	State of Qatar, Doha	Metro	—	1000 PKT	Company data and GaBi 6.0	Train operations, train stations operation
[25]	Turkey	Railway	—	TKM	SimaPro and ecoinvent	

TABLE 1: Continued.

Reference	Country, region	Type of rail	Lifespan (years)	Function unit	Data	Life cycle stages
[26]	China, Shanghai	HSR	100	-	Literature	Conception stage, construction stage, operation and maintenance stage, and disposal stage
[27]	China	HSR	100	T/km T/ vehicle	IO-LCA hybrid	Material production, construction
[28]	France	HSR	120	Travel of up to 17 metric tons per axle	Experts and ecoinvent 3.1	Production, maintenance, end-of-life
[29]	Belgium	Railway	6	TKM	Country-specific data and ecoinvent	Transport operation, rail equipment, and infrastructure
[30]	China, Fuzhou	Subway	Construction time	Km	In-service lines, regional database (IKE)	Infrastructure construction
[31]	Spain	HSR	100	Year	Google Earth	Construction, maintenance, one-year operation
[32]	USA, Houston	HSR	60	PKT VKT	Ecoinvent	Raw material extraction and processing, vehicle manufacturing, material distribution, construction, operation and maintenance, and end-of-life
[33]	Turkey, Kayseri	LRT	50	PKM	Company, SimaPro, and ecoinvent	Extraction and production of raw materials, transportation of the raw materials to construction sites, vehicle manufacture, transportation of vehicles, construction of infrastructure, operation, maintenance, and waste disposal
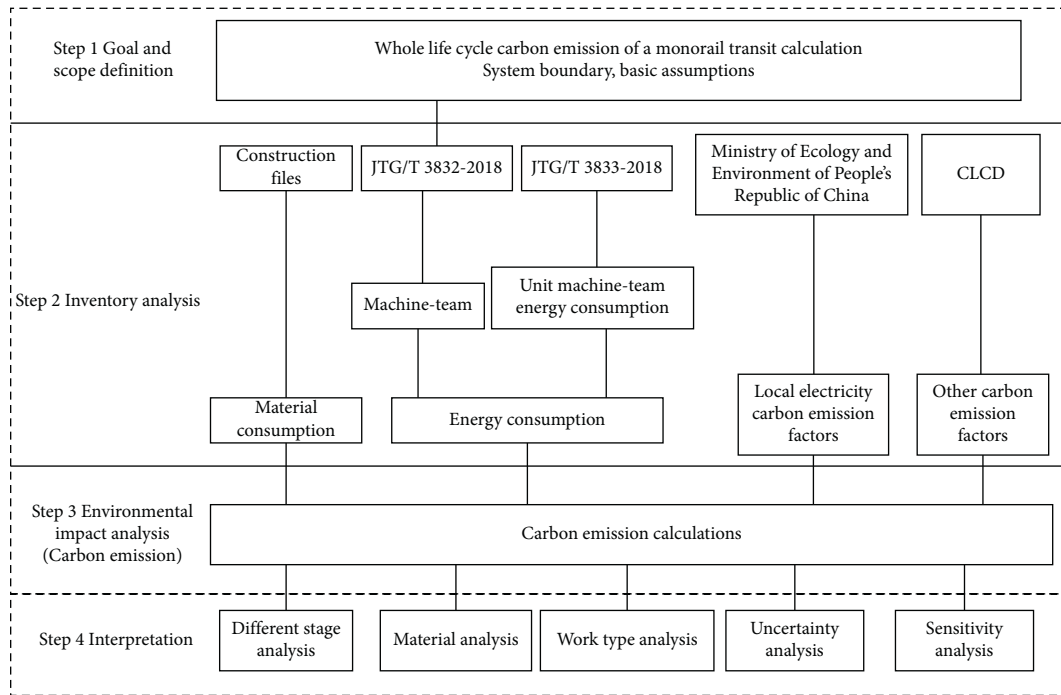
FIGURE 1: Methodology followed for carbon emission analysis.

2.2.2. Materials and Energy. Data on material consumption is obtained from construction files, which contain information on the types and quantities of materials used. The

Budgetary Norm of Highway Project (JTGT_3832-2018) [37] is studied to determine the machine-teams involved in the different working activities occurring in the construction
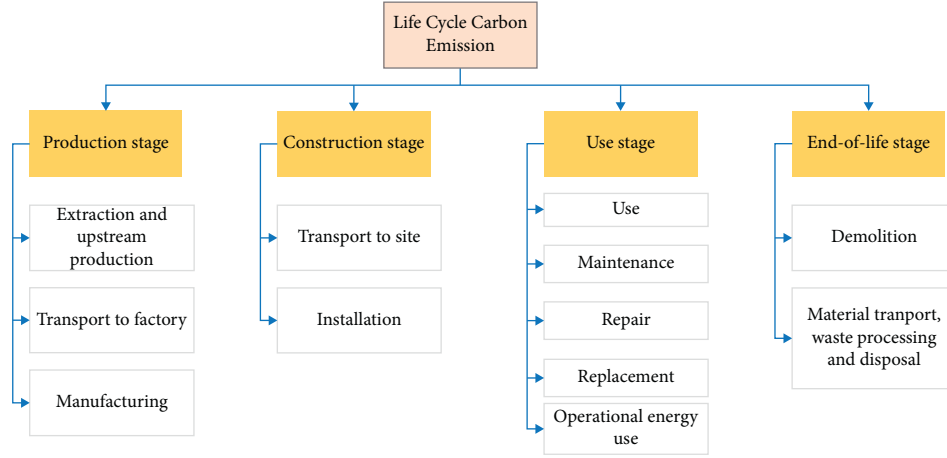
FIGURE 2: System boundary.

stage and during the process of demolition associated with the end-of-life stage. The Budget Norm of Maintenance and Strengthening of Highway Bridges (YNG/T B02-2011) [38] is considered to determine the machine-teams involved in the maintenance works associated with the use stage. The data presented in the Expense Standard of Machine-Team of Highway Project (JTGT_3833-2018) [39] are analyzed to obtain the unit energy consumption of different machine-teams. The China Urban Rail Transit Almanac 2019 [40] is referred to, to determine the amount of electricity consumed by the monorail transit lines and stations. The carbon emissions of the monorail transit line are obtained by multiplying the electricity carbon emission factors with the total quantity of electricity.

2.3. Environmental Impact Assessment.
The third step involves environmental impact assessment or life cycle impact assessment [41]. Results obtained using the various analytical methods reveal that carbon emission (for monorail transits) is realized in four stages. Total carbon emission is calculated using the following equation:

$$C_{tot} = C_{PD} + C_{CS} + C_{US} + C_{EL}, \quad (1)$$

where C_{tot}, C_{PD}, C_{CS}, C_{US}, and C_{EL} correspond to the amounts of carbon emitted during the life cycle, the production stage, the construction stage, the use stage, and the end-of-life stage, respectively.

The amount of carbon emissions produced in the production stage is equal to the carbon emission factors of various materials multiplied by the corresponding material quantities. This can be represented by the following equation:

$$C_{PD} = \sum_i CF_{MF,i} \times Q_{MF,i}, \quad (2)$$

where $CF_{MF,i}$ represents the carbon emission factors of the $i - th$ material and $Q_{MF,i}$ represents the consumed quantities of the $i - th$ material.

Carbon emissions produced during the construction stage are primarily generated during the transportation of the construction materials and consumption of energy (by different construction machines). The amount of carbon emissions generated in the construction stage can be represented by the following equation:

$$C_{MC} = \sum_i CF_{mt,i} \times Q_{mt,i} \times D_i + \sum_i CF_{cf,i} \times Q_{cf,i} + CF_e \times Q_{ce}, \quad (3)$$

where $CF_{mt,i}$ represents the carbon emission factor for the $i - th$ construction material transportation mode, $Q_{mt,i}$ represents the quantity of the $i - th$ transported construction materials, and D_i represents the distance between the production factory and the construction site. Here, it is assumed that road freight is the only transportation mode adopted. $CF_{cf,i}$ represents the carbon emission factor of the $i - th$ consumed fuel mode in the construction stage, $Q_{cf,i}$ represents the quantity of the $i - th$ fuel consumed in the construction stage, CF_e represents the regional carbon emission factor for electricity, and Q_{ce} represents the quantity of electricity utilized by the construction machines during the construction stage.

The carbon emissions during the use stage are primarily generated during maintenance works and the consumption of electricity by the vehicles and stations. The amounts of the carbon emissions produced during the use stage can be determined using the following equation:

$$C_{US} = C_{op} + C_{mt}, \quad (4)$$

where C_{US} represents the amount of carbon emissions generated from the monorail line in the use stage, C_{op} represents the carbon emissions produced during the operational phase, and C_{mtp} represents the carbon emissions produced during the maintenance phase.

$$C_{op} = C_{sy} \times Y, \quad (5)$$

$$C_{sy} = CF_e \times Q_{oe}. \quad (6)$$

In (5) and (6), C_{sy} represents the annual carbon emissions generated from the monorail line in the course of its operation, Y is the service life in the operational stage, and

Q_{oe} represents the amount of electricity consumed during the operational stage.

In the maintenance phase, the origin of carbon emissions can be attributed to the processes of material production and fuel consumption (consumed by construction machines). The amount of carbon emissions produced in the maintenance stage can be calculated using the following equation:

$$C_{mt} = \sum_i CF_{mt,i} \times Q_{mt,i} + \sum_i CF_{mfc,i} \times Q_{mfc,i} + CF_e \times Q_{me},$$

(7)

where $CF_{mt,i}$ represents the carbon emission factors of the $i-th$ material, $Q_{mt,i}$ represents the consumed quantities of the $i-th$ material, $CF_{mfc,i}$ represents the carbon emission factor for the $i-th$ consumed fuel (consumed by machines during the maintenance process), $Q_{mfc,i}$ indicates the quantity of the $i-th$ fuel consumed (realized during the maintenance process), and Q_{me} represents the quantity of electricity utilized by the construction machines during the maintenance process.

The carbon emissions generated during the end-of-life stage are produced during the consumption of energy by the construction machines during the processes of demolition and waste transportation. The amount of carbon emission produced during the end-of-life stage can be calculated using the following equation:

$$C_{EL} = \sum_i CF_{f\,d,i} \times Q_{f\,d,i} + CF_e \times Q_{de} + \sum_i CF_{dm\,t,i} \times Q_{dm\,t,i} \times D_i,$$

(8)

where $CF_{f\,d,i}$ represents the carbon emission factor corresponding to the consumed fuel mode (disposal process), $Q_{fc,i}$ represents the quantity of the $i-th$ fuel consumed during the disposal process, Q_{de} refers to the quantity of electricity utilized by the construction machines during the disposal process, $CF_{dm\,t,i}$ represents the carbon emission factor for the $i-th$ disposal transportation mode, $Q_{dm\,t,i}$ represents the quantity of the $i-th$ transported materials, and D_i indicates the distance between the construction site and the disposal area.

2.4. Interpretation.
In this step, the conclusions are arrived at based on the results obtained during inventory analysis and impact assessment. The key stages, working activities, and materials (used throughout the life cycle) that affect the extent of carbon emission produced during the functioning of a monorail transit were identified. The uncertainty analysis and sensitivity analysis methods were used, and the data were analyzed using Oracle Crystal Ball software to determine the possible range of life cycle carbon emissions of a monorail transit. The parameters that affect the results are also identified.

3. Results and Discussion

3.1. Monorail Transit Line: Background Information.
The monorail transit line 2 in Chongqing, China, is selected for a case study to demonstrate and validate the proposed LCA approach. It was inaugurated in December 2004 as the first straddle monorail line in China. It is one of the two straddle monorail lines that are currently in operation in China. Its operational mileage has reached 31.36 km. We have selected a section (from Niujiaotuo to Daping; length: 2409.09 m) of the entire route for our studies. We have quantified the carbon emissions produced in the selected section. The specific route under consideration is shown in Figure 3.

3.2. Calculating Carbon Emissions: Results

3.2.1. Carbon Emissions in the Production Stage.
According to equation (2), the carbon emissions produced during the production of the materials primarily used for production are shown in Table 2.

The total amount of carbon emissions produced during the production of main materials was 3,365.43 t.

3.2.2. Carbon Emissions Produced during the Construction Stage.
The carbon emissions produced during the construction stage are primarily generated during the processes of material transportation and construction. Equation (3) and the assumptions made were taken into consideration to calculate the amount of carbon emissions produced during the process of transportation of the materials (Table 3).

The total amount of carbon emissions produced during the transportation of materials was 113.49t. The amount of carbon emissions produced during the process of on-site construction was calculated (equation (3), Table 4). The carbon emission factors corresponding to electricity and diesel are 1.294 t CO_2/MWh and 3.664 kg/kg, respectively.

The amount of carbon emissions produced in the area of the chosen line segment was calculated to be 5,653.58 t. When the amount of carbon emissions produced during the transportation of the main material is taken into account, the total amount of carbon emissions generated during the construction stage is calculated to be 5,767.18 t.

3.2.3. Carbon Emissions Produced during the Maintenance Phase of the Use Stage.
The assumptions were taken into account, and the carbon emissions produced during the maintenance phase were calculated (equation (7), Table 5). The guidelines presented in the Budget Norm of Maintenance and Strengthening of Highway Bridges (YNG/T B02-2011) [38] were followed, and it was assumed that each time, one concrete treatment, 100 m-long expansion joint, 10 dm³-volume bearings, 1000 m-long cracked concrete, and 400 m³-area concrete beam section were maintained. According to the Budget Norm of Maintenance and Strengthening of Highway Bridges (YNG/T B02-2011) [38], the maintenance works are carried out once every ten years.

The total amount of carbon emissions produced during material, electricity, and fuel consumption during the construction of the machine was calculated to be 16.87 t/10 years. If the life cycle is considered to be 50 years long, the total carbon emission is calculated to be 60.51 t.

3.2.4. Amount of Carbon Emissions Produced during the Operation Phase of the Use Stage.
The data presented in the
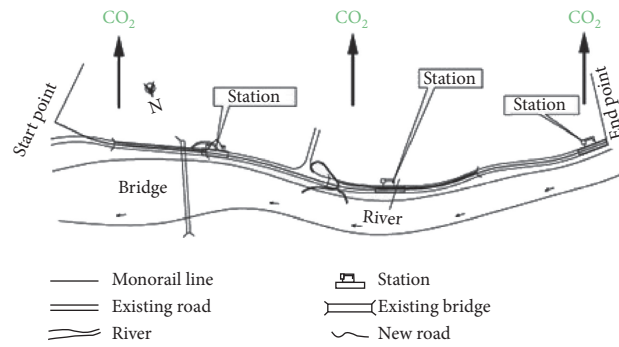
FIGURE 3: Case scenario.

TABLE 2: Carbon emissions generated during the production of materials primarily used for production.

Material	Unit	Quantity	Factor (kg/unit)	Carbon emissions (t)
Cement	t	622.30	719.62	447.82
C20 concrete	m^3	868.71	201.38	174.94
C25 concrete	m^3	105.07	250.54	26.32
C30 concrete	m^3	2,556.20	306.78	784.19
C40 concrete	m^3	6.04	391.03	2.36
C50 concrete	m^3	13.59	510.94	6.94
Sand	t	2,195.88	9.57	21.01
Gravel	t	1,728.33	12.69	21.93
Stone	m^3	35.94	6.05	0.22
Brick $200 \times 95 \times 53$	1000	474.83	504.00	239.31
Building blocks	m^3	789.65	146.00	115.29
Waterproofing	m^2	3,088.14	2.37	7.32
Coating	t	41.46	25.00	1.03
Steel Q235B	t	163.85	1,789.06	293.14
Other steel	t	29.97	1,789.06	53.61
Steel plate	t	0.29	1,789.06	0.52
Steel reinforcement	t	408.39	1,789.06	730.63
Wood	m^3	35.87	10.45	0.37
Aluminum	t	0.78	18.57	0.01
Mixed mortar (M5)	m^3	236.82	228.03	54.00
Mixed mortar (M2.5)	m^3	50.10	199.23	9.98
Cement mortar (1 : 1)	m^3	34.29	730.2	25.04
Cement mortar (1 : 2)	m^3	43.74	531.52	23.25
Cement mortar (1 : 2.5)	m^3	252.34	469.41	118.45
Cement mortar (1 : 3)	m^3	527.62	393.65	207.70
Total				3,365.43

TABLE 3: Carbon emissions produced during transportation of the materials during the construction stage.

Item	Means and energy	Distance (km)	Quantity	Carbon emissions (t)
Steel	Truck, diesel	50	1,376.36 t	4.88
Concrete	Mixer, diesel	50	3549.61 m^3	68.87
Aluminum	Truck, diesel	50	0.78 t	0.01
Sand and gravel	Truck, diesel	50	3,924.21 t	13.91
Stone	Truck, diesel	50	35.94 m^3	0.55
Brick	Truck, diesel	50	478.15 m^3	7.32
Building blocks	Truck, diesel	50	789.65 m^3	12.08
Wood	Truck, diesel	50	35.87 m^3	0.55
Coating	Truck, diesel	50	41.46 t	0.16
Cement	Truck, diesel	50	622.3 t	2.41
Mortar	Truck, diesel	50	1,144.91 m^3	2.75
Total				113.49

The total amount of carbon emissions produced during the transportation of materials was 113.49 t.

TABLE 4: Carbon emissions produced during on-site construction.

Working activities	Item	Construction machine	Energy	Energy consumption	Carbon emissions (t)
Foundation	Earth excavation	Crawler type mechanical single bucket excavator within 1.0 m³	Diesel	1,209.33 kg	4.44
	Stone excavation	Crawler type mechanical single bucket excavator within 1.0 m³	Diesel	766.86 kg	2.81
		Motorized air compressor within 9 m³/min	Electricity	1,433.42 kWh	1.66
	Impact drilling pile	Crawler type mechanical single bucket excavator within 1.0 m³	Diesel	114.23 kg	0.42
		Trucks within 10 t	Diesel	310.87 kg	1.14
		Truck crane within 16 t	Diesel	278.41 kg	1.02
		JK8 percussion drill	Electricity	10,157.69 kWh	13.10
		Mud separator	Electricity	74.55 kWh	0.10
		Mud mixer	Electricity	434.89 kWh	0.56
		Mud pump within Φ 100 mm	Electricity	1,275.30 kWh	1.65
		AC arc welder within 42 kV A	Electricity	331.52 kWh	0.43
	Manual digging pile	Single barrel slow winch within 50 kN	Electricity	15,087.19 kWh	19.46
Bridge substructure	Concrete	Concrete delivery pump within 60 m³/h	Electricity	18,372.52 kWh	23.70
		Truck crane within 25 t	Diesel	2,868.75 kg	10.53
	Steel	Truck crane within 25 t	Diesel	2,562.28 kg	9.40
		Automatic steel seam welder	Electricity	4,148.22 kWh	5.35
		AC arc welder within 32 kV A	Electricity	9,809.58 kWh	12.65
	Bearing	Truck crane within 20 t	Diesel	206.96 kg	0.21
		AC arc welder within 32 kV A	Electricity	178.36 kWh	0.23
Bridge superstructure	Concrete	Concrete delivery pump within 60 m³/h	Electricity	43,544.45 kWh	56.17
		Truck crane within 25 t	Diesel	40,285.13 kg	147.85
	Cast-in-place T-beam reinforcement	AC arc welder within 32 kV A	Electricity	44,693.70 kWh	57.66
		AC butt welder within 150 kV A	Electricity	20,485.11 kWh	26.43
	Centralized and standardized processing of rebar	CNC vertical rebar bending center	Electricity	711.17 kWh	0.92
		AC arc welder within 32 kV A	Electricity	44,693.70 kWh	57.66
		AC butt welder within 150 kV A	Electricity	20,485.11 kWh	26.43
	Prestressed concrete	Concrete delivery pump within 60 m³/h	Electricity	98,556.12 kWh	127.14
		Single-cylinder slow-motion winch within 30 kN	Electricity	2,681,021.27 kWh	3,458.52
		Single-cylinder slow-motion winch within 50 kN	Electricity	934,667.96 kWh	1,205.72
		Φ100 mm electric multistage water pump (≤120 m)	Electricity	204,479.87 kWh	263.78
	Steel strand	AC arc welder within 32 kV A	Electricity	51,668.13 kWh	66.65
		Prestressed steel tensile machine	Electricity	2,284.49 kWh	2.95
		Bellows rolling machine	Electricity	571.23 kWh	0.74
	Prestressed reinforcement	Prestressed stretching machine within 900 kN	Electricity	6980.95 kWh	9.01
		Bellows rolling machine	Electricity	621.10 kWh	0.80
		Single-cylinder slow-motion winch within 50 kN	Electricity	6,607.41 kWh	6.61
Other installation	Optical cable laying	Trucks within 10 t	Diesel	134.38 kg	0.49
		Engine-driven air compressor within 17 m³/min	Electricity	46.36 kWh	0.06
	Electric cable laying	Trucks within 10 t	Diesel	33.58 kg	0.12
		Truck crane within 5 t	Diesel	9.95 kg	0.04

Ministry of Ecology and Environment of the People's Republic of China [36] was analyzed to determine the baseline emission factors corresponding to the regional power grid in China. The data for different years were collected, and the carbon emission factors of different regions (time range: 2006–2017) were determined. Chongqing is situated in central China. The ARMA time series method was used to predict the electricity carbon emission factors of central

TABLE 5: Amount of carbon emissions produced during maintenance works.

Working activities	Items	Unit	Quantity	Carbon emission factors	Carbon emissions (t)
Concrete treatment	Polymer mortar	m^3	2.80	354.75 kg carbon emissions/m^3	0.99
	Concrete protective coating	kg	33.60	25 kg carbon emissions/t	0.00
	Electric concrete grinding machine within 3 kw	Machine-team	9	5 kWh/machine-team	0.06
	Handheld electric percussion drilling within 3 kw	Machine-team	18	98.28 kWh/machine-team	2.29
	Electric single-stage centrifugal clean water pump within 50 mm	Machine-team	56	23 kWh/machine-team	1.67
	Engine-driven air compressor within 0.3 m^3/min	Machine-team	15.20	16.1 kWh/machine-team	0.32
	Total carbon emissions	t	5.33		
Expansion joint repair and replacement (per 10 m)	Plain round bar	t	0.01	1789.06 kg/t	0.02
	Steel plate	t	0.05	1789.06 kg/t	0.09
	Petroleum asphalt	t	0.01	174.244 kg/t	0.00
	AC arc welder within 32 kV A	Machine-team	1.90	96.53 kWh/machine-team	0.24
	Total carbon emissions	t	0.35		
Bearing replacement (per 10 dm^3)	HRB400 steel rebar	t	0.10	1789.06 kg/t	0.18
	Steel plate	t	0.01	1789.06 kg/t	0.02
	AC arc welder within 32 kV A	Machine-team	0.02	96.53 kWh/machine-team	0.00
	Total carbon emissions	t	0.20		
Crack treatment (per 100 m)	Engine-driven air compressor within 0.3 m^3/min	Machine-team	3.6	16.1 kWh/machine-team	0.08
	Total carbon emissions	t	0.08		
Section enlargement (per 10 m^3)	C30 pump concrete	m^3	15	306.78 kg/m^3	4.60
	32.5 cement	t	7.65	719.62 kg/t	5.51
	Medium (coarse) sand	m^3	8.85	9.57 kg/m^3	0.08
	Gravel	m^3	8.40	12.69 kg/m^3	0.11
	Concrete mixer within 250 L	Machine-team	1.24	20.91 kWh/machine-team	0.03
	4–6 m^3/h concrete jet	Machine-team	3.17	15.4 kWh/machine-team	0.06
	Engine-driven air compressor within 9 m^3/min	Machine-team	2.78	51.50 kg diesel/machine-team	0.52
	Total carbon emissions	t	10.91		

China (for the years spanning 2002–2018) based on the existing data, as data for the years before 2006 and after 2017 were unattainable. The forecast results for 2002 and 2018 are 1.294 t CO$_2$/MWh and 0.5907 t CO$_2$/MWh, respectively.

The annual power consumption amounts and the annual passenger turnover were determined by analyzing the statistical data presented in the China Urban Rail Transit Yearbook 2019 [40]. The amount of carbon emission produced was calculated accordingly. The amount of carbon emissions produced by monorail line 2 (during its operation in 2018) was calculated to be 34,029.22 t. The total amount of carbon emissions produced during the 50-year-long life cycle was calculated to be 1,701,461 t. The amount of carbon emissions produced per unit length was 54255.77 t/km. The amount of carbon emissions produced by the chosen part of line 2 (length: 2.4 km) was 130,213.85 t. Equation (4) was used to calculate the total amount of carbon emissions generated during the whole use stage. The amount was calculated to be 130,274.36 t.

3.2.5. Carbon Emissions Produced during the End-of-Life Stage. Equation (8) was used, and the assumptions made were considered to calculate the amount of the carbon emissions produced during the process of structure demolition and waste disposal during the end-of-life stage. The engine-driven air compressor within 9 m^3/min was primarily used during the demolition process. The total amount of energy consumed during the demolition process was calculated to be 11,916.83 kWh. The total amount of carbon emissions generated during the demolition process was calculated to be 356.35 t. The total amount of carbon emissions generated during the process of waste transportation was calculated to be 113.49 t, and the total amount of carbon emissions produced during this stage was 469.84 t.

3.3. Amount of Carbon Emissions Produced during Different Stages. A comparison of the amounts of carbon emissions produced during different stages of the life cycle of the material is presented in Figure 4(a) and Figure 4(b). Analysis of the figures indicates that the maximum amount of the carbon emissions generated during the life cycle of the monorail transit is produced during the use stage (93.2%). The amount produced in this stage is significantly higher than the amount produced during the other stages. This can be primarily attributed to the fact that the amount of carbon emissions produced during the process of energy consumption during the entire 50-year-long operation period is considered during the study of the operational phase. A huge amount of carbon emissions is produced during this phase. Various maintenance works are carried out during the life cycle of the material. Each stage requires a certain amount of manpower and materials for completion. Different types of machinery are also required for the effective execution of the process. Maintenance work is carried out once every 10 years. Thus, a total of five maintenance cycles are carried out during the whole life cycle. This results in the generation of a large amount of carbon emissions in the use stage. A considerable amount of carbon emissions is also produced during the construction stage (4.1%). This can be attributed to the fact that a huge quantity of energy is consumed by different working machines during this process. The amount of carbon emissions generated during the production stage (2.4%) is slightly lower than the amount generated during the construction stage. It has also been observed that the amount of carbon emissions generated from the end-of-life stage is only 0.3% of the total amount generated, an insignificant amount as compared to emissions produced in other stages.

3.4. Carbon Emissions from Different Materials. Figures 5(a) and 5(b) provide a comparison of the amounts of carbon emissions produced during the use of different materials. As the figures show, there are significant differences in the amount of carbon emissions generated by different types of materials. The top 11 construction materials that contribute the most toward the production of carbon emissions are listed in Figure 5(a). The cumulative amount of the carbon emissions generated by these 11 materials is 3365.15 t, accounting for almost all of the total carbon emissions generated during the production stage. Specifically, the use of steel (32%), concrete (29.6%), cement (13.3%), and mortar (13%) results in the production of the maximum amount of carbon emissions during the production stage.

This can be attributed to the fact that a monorail line is a reinforced concrete structure that requires the use of a large amount of steel (1,376.36 t), concrete (3,549.61 m^3), cement (622.3 t), and mortar (1,144.91 m^3). The corresponding carbon emission factors are significantly high. The total amount of carbon emissions produced is large as the consumption and carbon emission factors of these materials are significantly high. Therefore, the key to improving the environmental performance of monorail transit lies in decreasing the amount of carbon emissions generated by these materials. It has been previously reported [42] that an efficient water reducing agent can be used to replace cement during the process of concrete production. This can help in reducing the amount of carbon emissions produced during the material production stage. The concrete strength can be improved simultaneously to reduce the amount of cement and concrete used. Furthermore, designers could consider using more amounts of renewable construction materials (such as renewable concrete) in the design stage [43]. Mortar, bricks, building blocks, gravel, sand, and other materials also contribute to the generation of carbon emissions in the production stage. The use of these materials results in the generation of insignificant amounts of carbon emissions.

3.5. Carbon Emissions: Analysis of Working Activities Occurring in the Construction Stage. A comparison of the amounts of carbon emissions generated at different stages of the construction stage is presented in Figure 6. Fifteen working activities are considered. The results reveal that prestressed concrete activity accounts for the largest proportion (91.1%) of the total carbon emissions produced in this stage. The amount of carbon emission produced during prestressed concrete activity is significantly higher than the amount produced during other construction activities. This can be primarily attributed to the fact that a huge quantity of electricity is consumed during the operation of machines single-cylinder slow-motion winch within 30 KN (2,681,021.27 kWh), single-cylinder slow-motion winch within 50 KN (934,667.96 kWh), Φ100 mm electric multi-stage water pump (≤120 m; 204,479.87 kWh), and concrete delivery pump (60 m^3/h; 98,556.12 kWh). In addition, a considerable amount of carbon emissions is generated during the construction of the beam concrete (3.6%). The amount of carbon emissions generated during the processes of beam reinforcement (1.5%) and rebar processing (1.5%) is slightly lower than the amount produced during the process of beam concrete construction. The amount of carbon emissions attributable to other construction activities accounts for less than 1% of the total carbon emissions originating from all construction activities. This indicates that these activities do not significantly affect the environment.

3.6. Uncertainty Analysis: Construction Stage and Production Stage. The uncertainty of carbon emissions corresponding to material and fuel consumption can be attributed to construction errors. Uncertainty analysis was conducted using the Oracle Crystal Ball (Figure 7) to evaluate the possible range of carbon emissions for a monorail segment during its life cycle. Standard normal distributions were assumed for the input parameters, and the number of testing times was set to 100,000. The probability distributions corresponding to the target variables were normal distributions. The variation range calculated for carbon emissions was 100,000–180,000 t.
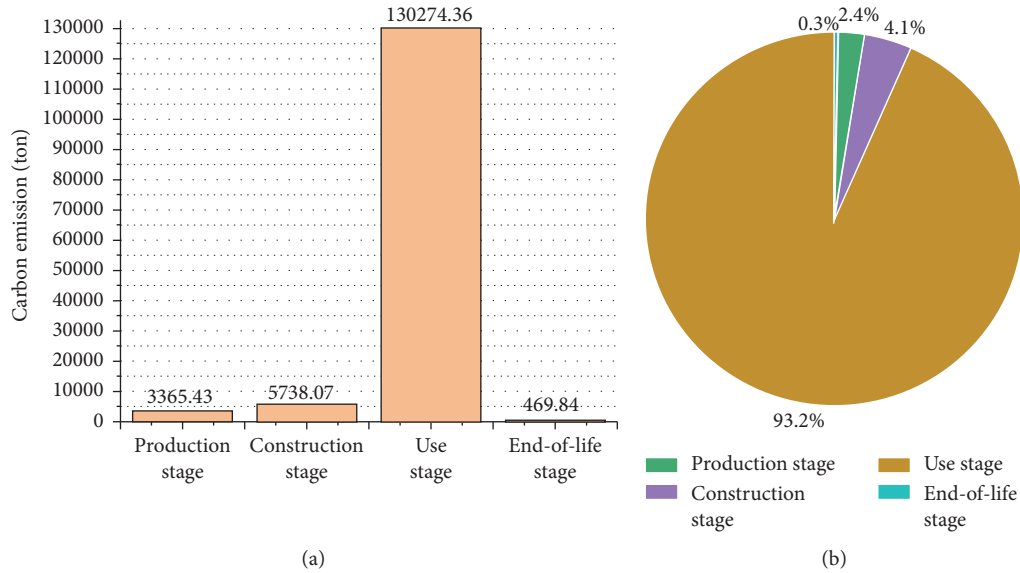
FIGURE 4: (a) Amounts of carbon emissions generated during different stages of operation throughout the life of the material. (b) Proportion of carbon emissions generated during different life cycle stages.
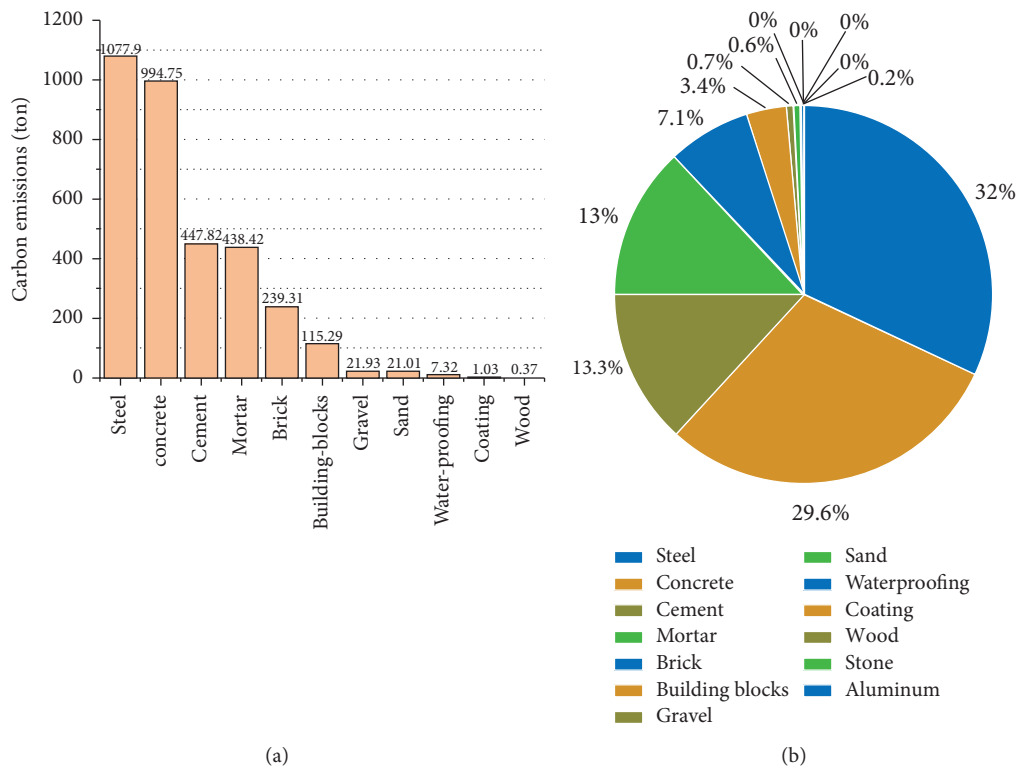
FIGURE 5: (a) Amounts of carbon emissions generated during the use of different materials. (b) Proportions of carbon emissions generated during the use of different materials.

3.7. Life Cycle: Sensitivity Analysis. The Oracle Crystal Ball was used to determine the sensitivity of carbon emissions during the life cycle of the monorail transit line. The results are shown in Table 6.

Analysis of the data presented in Table 6 reveals that the length of the life cycle, amount of electricity consumed annually, single-cylinder slow-motion winch within 30 KN quantity, single-cylinder slow-motion winch within 50 KN quantity, use of C40 concrete quantity, cement mortar (1 : 3) quantity, and brick 200 × 95 × 53 quantity are the sensitive factors that affect the final carbon emission results. The length of the life cycle and the amount of electricity
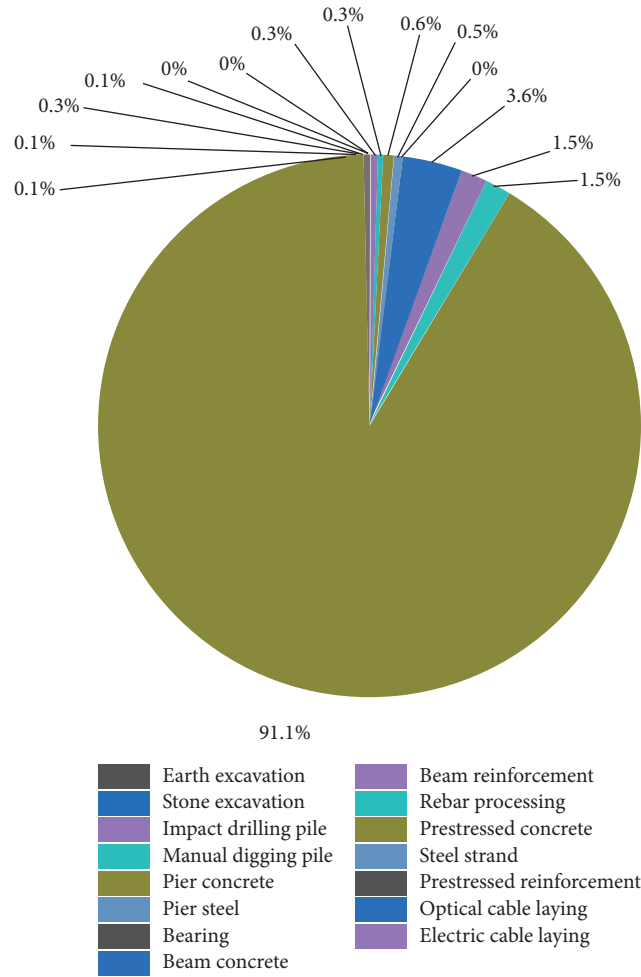
Figure 6: Proportions of carbon emissions generated during different construction activities.
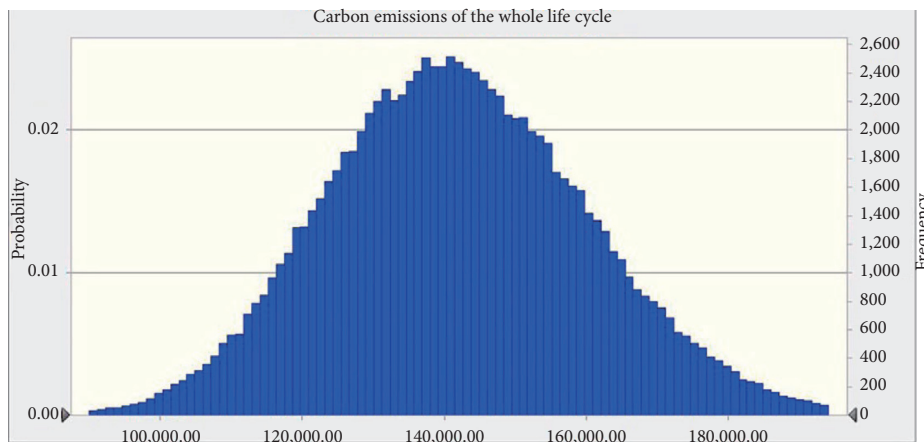
Figure 7: Uncertainty analysis conducted for carbon emissions produced during the life cycle of the material.

consumed annually during the operation of the system significantly influence the amount of carbon emission produced by the monorail system during its lifetime. In addition, the quantities of single-cylinder slow-motion winch within

30 KN, single-cylinder slow-motion winch within 50 KN, C40 concrete, cement mortar (1 : 3), and brick 200 × 95 × 53 also exert a certain influence on the results. It was observed that the degrees of influence were almost the same.

TABLE 6: Sensitivity analysis conducted for carbon emissions produced during the production stage.

Order	Parameters	Variance contribution (%)	Rank correlation
1	Life cycle length	47.0	0.69
2	Annual operation electricity consumption	46.9	0.68
2	Single-cylinder slow-motion winch within 30 KN	0.1	0.02
3	Single-cylinder slow-motion winch within 50 KN	0.1	0.01
4	C40 concrete quantity	0.1	0.01
5	Cement mortar (1 : 3) quantity	0.1	0.01
6	Brick 200 × 95 × 53 quantity	0.1	0.01
7	Others	0.1	-

3.8. Discussion of the Approach. This calculation framework can be used to calculate the amount of carbon emission produced by a monorail line during its lifetime, but it can also be used to calculate the amount of carbon emissions produced by ordinary railway, light rail, subway, and other rail transportation systems. The calculation results can help design the monorail transit system, and the results can help reduce the amount of carbon emission produced at the initial stages of the process.

As there are few monorail lines in operation in China, it is difficult to obtain field data. It is challenging to verify the universality of the results calculated from the only data available. More data can be obtained in the future as the construction of monorail traffic has been planned. Our model will be further optimized to make it universal.

3.9. Recommendations for Future Research. More attention should be paid to the following research directions:

(1) Verification and application of the approach used by us should be realized by analyzing fundamental data. Therefore, attention should be paid to obtaining more amounts of data to improve the developed approach.

(2) Some scenarios can be designed to simulate the carbon emission reduction effects based on the calculation results presented. This can potentially help in proposing helpful suggestions that can be exploited by designers and politicians for the sustainable development of the city.

4. Conclusions

We calculated the amount of carbon emissions produced during the operation of a monorail transit line (during its lifetime) using the LCA method. A segment of the Chongqing monorail line 2 was selected for the case study for validating the developed model. The following conclusions were drawn:

(1) The life cycle of the monorail transit line can be theoretically divided into four stages: the production, construction, use, and end-of-life stages. The use stage contributes >90% of the carbon emissions produced during the lifetime of the monorail transit line. A significant amount of carbon emissions is produced during the construction and production stages. The amount of emissions produced during the end-of-life stage is less than the amount produced in the other three stages.

(2) Steel, concrete, and cement are the most important sources of carbon emissions.

(3) Prestressed concrete activity accounts for the maximum proportion (91.1%) of the total carbon emissions. Significant amounts of carbon emissions are generated during the process of beam concrete construction (3.6%). The amounts of carbon emissions generated during the process of beam reinforcement (1.5%) and rebar processing (1.5%) are slightly lower than the amounts generated during the process of beam concrete construction.

In summary, the results presented herein can help gain a better understanding of the effects of the monorail transit industry on the ecosystem. The results can potentially help develop ideas that can be used by designers working in the rail transit industry to meet low carbon emission goals.

Abbreviations

ARMA: Autoregressive moving average
CE: Carbon emissions
CEF: Carbon emission factor
GHG: Greenhouse gas
HSR: High-speed rail
IO: Input-output
LCA: Life cycle assessment
LRT: Light rail transit
PKT: Passenger kilometer traveled
VKT: Vehicle kilometer traveled
PMT: Passenger mile traveled
RTS: Rapid transit system
SKM: Per seat per kilometer traveled
VMT: Vehicle mile traveled.

Data Availability

The data used to support the findings of this study are available from the corresponding authors upon request.

Conflicts of Interest

The authors declare no conflicts of interest.

Acknowledgments

References

[1] W. Cramer, J. Guiot, M. Fader et al., "Climate change and interconnected risks to sustainable development in the Mediterranean," *Nature Climate Change*, vol. 8, no. 11, pp. 972–980, 2018.

[2] Z. Mi, D. Guan, Z. Liu et al., "Cities: the core of climate change mitigation," *Journal of Cleaner Production*, vol. 207, pp. 582–589, 2019.

[3] IPCC, "Core writing team," in *Climate Change 2014: Synthesis Report. Contribution of Working Groups I, II and III to the Fifth Assessment Report of the Intergovernmental Panel on Climate Change*p. 151, IPCC, Geneva, Switzerland, 2014.

[4] G. Bueno, D. Hoyos, and I. Capellán-Pérez, "Evaluating the environmental performance of the high speed rail project in the Basque Country, Spain," *Research in Transportation Economics*, vol. 62, pp. 44–56, 2017.

[5] GB 50458-2008, *Code for Design of Straddle Monorail Transit*, China Building Industry Press, Beijing, China, 2008.

[6] K. Hwang, J.-D. Chung, K. Lee, J. Tak, and I.-S. Suh, "Feasibility analysis on ground-level stations and wireless power transfer technology applications for monorail system," *International Journal of Railway*, vol. 7, no. 3, pp. 71–79, 2014.

[7] X. He, "Application and prospect of straddle monorail transit system in China," *Urban Rail Transit*, vol. 1, no. 1, pp. 26–34, 2015.

[8] ISO 14040 International Standard, *Environmental Management - Life Cycle Assessment - Principles and Framework*, International Organization for Standardization, Geneva, Switzerland, 2006.

[9] M. V. Chester, *Life-Cycle Environmental Inventory of Passenger Transportation in the United States*, Ph.D. Dissertation, University of California Berkeley, Berkeley, CA, 2008.

[10] M. V. Chester and A. Horvath, "Environmental assessment of passenger transportation should include infrastructure and supply chains," *Environmental Research Letters*, vol. 4, pp. 237–266, 2009.

[11] M. V. Chester and A. Horvath, "Life-cycle assessment of high-speed rail: the case of California," *Environmental Research Letters*, vol. 136, pp. 123–129, 2010.

[12] M. Chester and A. Horvath, "High-speed rail with emerging automobiles and aircraft can reduce environmental impacts in California's future," *Environmental Research Letters*, vol. 7, no. 3, Article ID 034022, 2012.

[13] M. Banar and A. Özdemir, "An evaluation of railway passenger transport in Turkey using life cycle assessment and life cycle cost methods," *Transportation Research Part D: Transport and Environment*, vol. 41, pp. 88–105, 2015.

[14] F. Del Pero, M. Delogu, M. Pierini, and D. Bonaffini, "Life Cycle Assessment of a heavy metro train," *Journal of Cleaner Production*, vol. 87, pp. 787–799, 2015.

[15] Y. Yue, T. Wang, S. Liang et al., "Life cycle assessment of high speed rail in China," *Transportation Research Part D: Transport and Environment*, vol. 41, pp. 367–376, 2015.

[16] C. S. Hanson, R. B. Noland, and C. D. Porter, "Greenhouse gas emissions associated with materials used in commuter rail lines," *International Journal of Sustainable Transportation*, vol. 10, no. 5, pp. 475–484, 2015.

[17] C. E. S. d. Andrade and M. d. A. D'Agosto, "Energy use and carbon dioxide emissions assessment in the lifecycle of passenger rail systems: the case of the Rio de Janeiro Metro," *Journal of Cleaner Production*, vol. 126, pp. 526–536, 2016.

[18] H. Jones, F. Moura, and T. Domingos, "Life cycle assessment of high-speed rail: a case study in Portugal," *International Journal of Life Cycle Assessment*, vol. 22, no. 3, pp. 410–422, 2016.

[19] J. Lederer, C. Ott, P. H. Brunner, and M. Ossberger, "The life cycle energy demand and greenhouse gas emissions of high-capacity urban transport systems: a case study from Vienna's subway line U2," *International Journal of Sustainable Transportation*, vol. 10, no. 2, pp. 120–130, 2014.

[20] G. Bueno, D. Hoyos, and I. Capellán-Pérez, "Evaluating the environmental performance of the high speed rail project in the Basque Country, Spain," *Research in Transportation Economics*, vol. 62, pp. 44–56, 2017.

[21] S. Saxe, E. Miller, and P. Guthrie, "The net greenhouse gas impact of the Sheppard Subway Line," *Transportation Research Part D: Transport and Environment*, vol. 51, pp. 261–275, 2017.

[22] Y. Li, Q. He, X. Luo, Y. Zhang, and L. Dong, "Calculation of life-cycle greenhouse gas emissions of urban rail transit systems: a case study of Shanghai Metro," *Resources, Conservation and Recycling*, vol. 128, pp. 451–457, 2018.

[23] A. M. Shinde, A. K. Dikshit, R. K. Singh, and P. E. Campana, "Life cycle analysis based comprehensive environmental performance evaluation of Mumbai Suburban Railway, India," *Journal of Cleaner Production*, vol. 188, pp. 989–1003, 2018.

[24] F. E. Al-Thawadi and S. G. Al-Ghamdi, "Evaluation of sustainable urban mobility using comparative environmental life cycle assessment: a case study of Qatar," *Transportation Research Interdisciplinary Perspectives*, vol. 1, Article ID 100003, 2019.

[25] L. Bilgili, S. L. Kuzu, A. Y. Çetinkaya, and P. Kumar, "Evaluation of railway versus highway emissions using LCA approach between the two cities of Middle Anatolia," *Sustainable Cities and Society*, vol. 49, Article ID 101635, 2019.

[26] S. Kaewunruen, J. Sresakoolchai, and J. Peng, "Life cycle cost, energy and carbon assessments of beijing-shanghai high-speed railway," *Sustainability*, vol. 12, no. 1, p. 206, 2019.

[27] S. Cheng, J. Lin, J. Xu, D. Yang, J. Liu, and H. Li, "Carbon, water, land and material footprints of China's high-speed railway construction," *Transportation Research Part D: Transport and Environment*, vol. 82, Article ID 102314, 2020.

[28] A. de Bortoli, L. Bouhaya, and A. Feraille, "A life cycle model for high-speed rail infrastructure: environmental inventories and assessment of the Tours-Bordeaux railway in France," *International Journal of Life Cycle Assessment*, vol. 25, no. 4, pp. 814–830, 2020.

[29] A. L. Merchan, S. Belboom, and A. Léonard, "Life cycle assessment of rail freight transport in Belgium," *Clean Technologies and Environmental Policy*, vol. 22, no. 5, pp. 1109–1131, 2020.

[30] M. Liu, S. Jia, P. Li, X. Liu, and Y. Zhang, "Predicting GHG emissions from subway lines in the planning stage on a city level," *Journal of Cleaner Production*, vol. 259, Article ID 120823, 2020.

[31] A. Kortazar, G. Bueno, and D. Hoyos, "Environmental balance of the high speed rail network in Spain: a Life Cycle Assessment approach," *Research in Transportation Economics*, vol. 90, Article ID 101035, 2021.

[32] J. Chipindula, H. Du, V. S. V. Botlaguduru, D. Choe, and R. R. Kommalapati, *Life Cycle Environmental Impact of a*

High-Speed Rail System in the Houston-Dallas I-45 Corridor, Public Transport, Berlin, Germany, 2021.

[33] S. Gulcimen, E. K. Aydogan, and N. Uzal, "Life cycle sustainability assessment of a light rail transit system: integration of environmental, economic, and social impacts," *Integrated Environmental Assessment and Management*, vol. 17, no. 5, pp. 1070–1082, 2021.

[34] EN 15978:2011, *Sustainability of Construction Works Assessment of Environmental Performance of Buildings - Calculation Method*, European Committee for Standardization, Brussels, Belgium, 2011.

[35] Greenhouse Gas Protocol, "Chinese life cycle database (clcd)," 2012, http://www.ghgprotocol.org/Third-Party-Databases/CLCD.

[36] "Ministry of ecology and environment of the people's republic of china," 2018, http://www.mee.gov.cn/ywgz/ydqhbh/wsqtkz/201812/t20181220_685481.shtml.

[37] JTG/T 3832-2018, *Budgetary Norm of Highway Project*, Chinese standard, Beijing, China, 2018.

[38] YNG/T B02-2011, *Budget Norm of Maintenance and Strengthening of Highway Bridges*, Chinese standard, Yunnan, China, 2011.

[39] JTGT_3833-2018, *Expense Standard of Machine-Team of Highway Project*, Chinese standard, Beijing, China, 2018.

[40] Editorial Committee of the Yearbook of China Association of Metros, *2019 china urban rail transit almanac 2019*, Shanghai Bookstore Publishing House, Shanghai, China, 2019.

[41] M. Najjar, K. Figueiredo, M. Palumbo, and A. Haddad, "Integration of bim and lca: evaluating the environmental impacts of building materials at an early stage of designing a typical office building," *Journal of Building Engineering*, vol. 14, pp. 115–126, 2017.

[42] B. Cheng, J. Li, V. Tam, M. Yang, and D. Chen, "A bim-lca approach for estimating the greenhouse gas emissions of large-scale public buildings: a case study," *Sustainability*, vol. 12, no. 2, p. 685, 2020.

[43] B. Cheng, K. Lu, J. Li, H. Chen, X. Luo, and M. Shafique, "Comprehensive assessment of embodied environmental impacts of buildings using normalized environmental impact factors," *Journal of Cleaner Production*, vol. 334, Article ID 130083, 2022.

Research Article

Characterization of Group Behavior of Corruption in Construction Projects Based on Contagion Mechanism

Jingjing Li ⓘ**, Qiangqiang Shen** ⓘ**, and Wencan Gao** ⓘ

School of Traffic and Transportation Engineering, Changsha University of Science and Technology, Changsha 410114, China

Correspondence should be addressed to Qiangqiang Shen; 20101040131@stu.csust.edu.cn

With the rapid development of construction projects, more and more engineering corruption problems have emerged. Therefore, this paper proposes a SEIR (susceptible-exposed-infected-recovered) based corruption model to better understand the propagation process of corruption cases in construction projects. In this model, the data samples are collected from the 2018 Engineering Corruption Case Judgment Document, the propagation parameters are obtained through actual case analysis with the help of complex networks, the change process and key influencing factors of actual nodes in engineering corruption cases are simulated by Python. The study results indicate that the personnel conforms to the "4–9 transmission law," in which the early stage is a period of high incidence of corruption cases. The network of corruption cases is somewhat vulnerable, and its spread is about minus 8 times the change in crackdown rate and 10 times the change in infection rate. The variation range of the susceptible population S and the removed person R in the propagation simulation curve can predict the relationship between corruption infection rate and crackdown rate, which can provide theoretical guidance for preventing the occurrence of corruption.

1. Introduction

Corruption is extremely harmful to social stability, may hinder economic development, and affect the development of political parties [1, 2]. Corruption in construction projects has become a key factor affecting the construction market environment and the sustainable development of external construction [3]. How to effectively punish and prevent corruption in the construction projects has become a challenge all over the world [4], especially in developing countries such as China [5–12], Ghana [13–15], Turkey [16], Brazil [17], and Iran [18]. Moreover, the construction industry is one of the "disaster areas" prone to corruption, which has seriously restricted the economic development [10]. Corruption cases in the construction projects may cause greater losses and more serious social impacts than general corruption cases because of some of its characteristics, such as multiple and complex participants, clear division of labour, hidden exchange of interests, serious corruption, long incubation period and difficult to play a supervisory role in the power supervision mechanism [19].

The huge investment in infrastructure during China's rapid urbanization can also lead to corruption in the construction projects [7, 20, 21]. In order to prevent corruption in the construction projects, the government has continuously improved regulations and increased the intensity of filing and reviewing cases of violations of laws and disciplines. Advanced screening through the official website of China Judicial Documents revealed that the number of first instance judgments on corruption cases in the engineering industry dropped from 5062 in 2016 to 1718 in 2020. Although the number of related cases has been controlled to a certain extent, the related problems are still very serious [2]. In conclusion, it is imperative to explore the propagation mechanism of corruption in construction projects for better preventing corruption in the construction projects.

Previous studies have analysed the characteristics of corruption in construction projects from behavioral and sociological perspectives, mainly through the data collection methods such as interviews, case studies, and questionnaires. Yu [22] found that the corruption of Chinese construction industry by using association rules is age-related, with the

increase of corruption as managers approach retirement age. However, Zhang [23] pointed that the key factor affecting corruption in the real estate sector is not age growth, but abuse of power based on data from 135 cases. Emmanuel [19] summarized that the contract phase and the postcontract phase may be the main corruption prone stages of construction projects in many developing countries. It is notable that the professional backgrounds of corrupt elements are becoming more and more profound, the means of crime are diversifying, and the number of collective corruption is increasing [11, 23–26]. On the other hand, some scholars have analysed many cases to explore the criminal motives of corruption in the construction projects and the relationship of criminal personnel structure from the perspective of criminology. It is found that flawed legal systems, higher profits, and group complexity of construction projects are the key causes of corruption in construction projects [17]. Diviák [27] prompted that the criminal aggregation network of corruption presents a clear core-periphery structure in many cases, where all involved officials are located in the core of the network and have strong concealment in the corruption network. Wang [5] believed the corruption networks expand through brokerage activities in the form of spanning institutions and enlisting strategic resource holders. From the brief literature review, it can be found that many studies have explored the problem of corruption in construction projects from different perspectives, and illuminated the characteristics of corrupt behavior in construction projects such as complexity, dynamics, concealment, collective nature, and flexibility. It also verifies that individual characteristics have a strong correlation with the degree of corruption in both construction projects. However, these studies focused on the individual corruption characteristics from a behavioral or micro perspective, lacking group evolution context and macro insights. In addition, the research methods are still somewhat subjective such as questionnaires, expert interviews, literature reviews, which lack objectivity. Considering the dynamic nature of corruption behavior in construction projects, this study believes that it is also very important to explore the evolutionary relationship of corruption behavior propagation in construction projects from a macrogroup perspective.

To bridge the research gap, this study will explore the evolutionary process of the spread of corruption in construction projects by adopting the complex network theory and infectious disease SEIR model. This paper attempts to illuminate new ideas for preventing corruption in the construction industry from a macrogroup perspective. The parameters of the infectious disease model are obtained by actual corruption cases through the analysis of complex networks. The model can well describe the propagation mechanism of corruption behaviors in actual groups and is verified by actual corruption cases. The simulation results reveal the characteristics of corruption nesting in the engineering industry and the key factors of corruption governance, thus put forward governance recommendations for reference. Compared with the existing studies, the contributes of our research are highlighted as follows: (1) adopting a dynamic perspective to study the spread characteristics of corrupt behavior, (2) using a more objective

method to determine the model parameters by extracting the actual case data through network feature parameters, and (3) improving the infectious disease model to prevent the corrupt behavior of engineering construction.

2. Literature Review

2.1. Characteristics of Corruption in Construction Projects. Corruption in the construction sector has spread to other industries and almost all the construction phases [28], especially the land grant stage, the bidding stage, and the construction stage [23]. In addition, the corruption cases in construction projects may cause greater losses and more serious social impact than the general ones. Furthermore, it is found that the types of construction projects corruption are determined by the conditioning variables such as type of leadership, position level, region, and age [22, 23, 29]. Among which, the age of 46–50 and 55–60 are the high incidence of corruption cases [22, 23], and engineering corruption is more likely to breed in second-and third-tier cities than in first-tier cities [22, 23]. These characteristics of corruption in construction projects have become a common focus of attention and seriously affected the healthy development of the engineering industry.

In order to further study the characteristics of corruption and reveal the causes of construction corruption, many scholars often explored the influencing factors of corruption by using questionnaire surveys [6, 7], expert interviews [4, 30], literature reviews [4, 31], and multiple case studies [16, 28, 32]. The causes of construction corruption are mainly psychosocial specific reasons, organization-specific reasons [31], regulations specific reasons, and project-specific reasons [31]. Firstly, a flawed legal system may provide opportunities for corruption in the construction industry [7, 10, 11]. Secondly, higher profits may be the another reason for corruption in the construction industry [30]. Thirdly, the complexity of the construction industry, such as the long construction period of the project and the complexity of the participants, makes corruption prone to occur [24, 31]. Finally, government officials play multiple roles in public construction projects, such as decision-maker, approver, project fund owner, and arranger, is easy to intervene the implementation of normal construction projects such as bidding activities [15]. The factors influencing corruption in construction projects are complex and variable, which also reflects the value of exploring the dynamic evolutionary relationship of the analysis of the law of corrupt behavior in construction projects.

The people who are in the core network will also change over time due to the dynamics, complexity, and concealment of the corruption network of the construction project [29, 33, 34]. Similarly, some scholars found that the network structure adjusts with time in the evolution of drug crime networks, and roles have great flexibility and variability at different mission stages and at different times [34–36]. Nekovee [37] quantitatively analysed the infection of corruption within the organization from a dynamic perspective, and found the lower threshold of corruption infiltration in the organization with a flat structure compared with the higher

structured organization. Wang [5] found that the core of corrupt networks expanded by crossing institutions and securing strategic resource holders through brokering activities. Due to the versatility and flexibility of corrupt groups, corrupt groups spread through specific pathways within a certain spatial and temporal context [5], and such interactions against groups can be considered as the contagion of corrupt behavior [38]. Social contagion is similarly defined by scholars as "transmission among individuals in a group through interactions between individuals" [37, 38]. The current corruption phenomenon has shown a "fissile spread," which spreads from individuals to groups, and even to the whole organization according to management logic. Similarly, the research on corruption behavior in construction projects still focused on the static or micro perspectives such as individual behavioral characteristics, corruption behavior influencing factors, corruption governance measures, and corruption degree assessment. In fact, the corrupt behaviors among corrupt groups in construction projects are contagious, and the interactive, dynamic and complex nature of the spread of these behaviors need to be taken into account. It is also very important to explore the evolutionary relationship of corruption behavior propagation in construction projects from a macrogroup perspective.

2.2. Theory of Complex Networks and Infectious Disease Models. Complex network is a theoretical tool for evaluating the operating status of complex systems that has been widely applied to various fields of construction management industry [27]. Generally, the various elements and their relationships within a complex system are abstracted into a network structure diagram. The traditional construction method is to transform each entity of the complex system into a network node, and transform the connection of entities into the connection of nodes [5, 27]. Graph theory is a useful tool to further study the complex network structure such as complex system evolution mechanism, diffusion mechanism and governance strategy and other scientific problems that has emerged in recent years [39].

Complex network of epidemic spread model on has attracted great attention among researchers of physics, mathematics, and epidemiology due to its success in predicting and controlling epidemic spread in reality [40, 41]. Fundamentally, the traditional spread of public opinion, epidemics and violations are simulated by SIR and SEIR [42]. The outbreak of COVID-19 has initiated a large number of numerical studies by using epidemiology models [43–46]. The propagations of diseases, behaviors and information in real systems are rarely independent of each other, but they are coevolving with strong interactions [40]. Fan [47] proposed a contagion model as a simple and powerful mathematical approach for predicting the spatial-temporal evolution of the onset and recession of floodwaters in urban road networks. Nekovee [37] studied the contagiousness of corrupt behavior within the organization, and its transmission behavior is somewhat similar to rumours or infectious disease. It is feasible to use infectious disease models to study the evolutionary pattern of the spread of corrupt behavior.

A systematic review of the literature reveals that corruption in construction projects is a hot area of research for scholars nowadays. Due to the concealment, complexity and seriousness of corruption in construction projects, the management of corruption in construction projects is also the common goal of all countries nowadays. The dynamic nature of corruption networks is illustrated by the close division of labour and the mutual change of roles among the personnel of corrupt groups. At the same time, the infiltration of internal corrupt practices illustrates the contagious nature of corrupt practices. Intermediaries expanded the core of the corruption network, and transmitted the interactions between groups to jointly constitute the complex network of corrupt practices. In addition, infectious disease dynamics model with complex networks have proven to be a key approach for the study of behavioral transmission and have been widely used in various fields. The systematic discussion also provides a rich theoretical foundation and guiding direction for this study. However, the current research on behavioral communication mainly focused on the field of public opinion governance and infectious disease surveillance, and lacked the behavioral communication of corrupt groups in the construction projects field. Most scholars just concentrated on the individual characteristics and construction project corruption features from a behavioral perspective. Therefore, the spread characteristics analysis of construction corruption in this study is a new exploration of the regulation and governance of the construction management industry. Dynamic research on the changing characteristics of different periods is also the key point of this study. To address the research gap, this paper adopts the complex network theory and the SEIR model of infectious disease to study the propagation process pattern and governance measures of corruption cases in construction projects from a dynamic perspective.

3. Construction of an Infectious Disease Model for Corruption Nesting in Construction Projects

Infectious disease behavior on complex networks has been widely used by scholars in various fields. The method of infectious disease dynamics is a mathematical technique that has been developed into a rich interdisciplinary field. Scholars found that the transmission mechanism of infectious diseases is similar to information or human behavior [42]. Infectious disease models have been widely used in various fields such as the prediction and simulation of the new coronavirus [43, 48–50], the spread and intervention of unsafe behaviors of construction workers, flight operation risk spread analysis, panic spread research, the spatial spread and temporal evolution of the onset and recession of floodwaters in urban road networks [42, 47, 51, 52]. Besides, infectious disease models are used in the study of behavioral communication, which can reflect the propagation and evolution process of behavior at the microscopic level, and predict the trend of behavioral diffusion at the macroscopic level [53].

Corruption in construction projects has the characteristics of dynamic and contagious, and its evolutionary pattern can be analysed by infectious disease models. The emergence, replication, and spread of corruption in the engineering field are very similar to the transmission process of infectious diseases [42]. The spread of infectious diseases in the population requires the source of infection, latent persons, susceptible groups, and good conditions for transmission. Generally, the corruption nest of a construction project can be regarded as a transmission process from single individual corruption infection to group corruption infection. Considering that there are generally many people involved in the corruption case of a construction project, and the exchange of benefits is concealed, there may be an incubation period for individual corruption [19]. In addition, the corruption of construction projects has a certain latent nature because some corrupt groups or individuals would weigh the pros and cons before deciding to participate in corrupt practices. The traditional SIR model of infectious diseases does not consider the incubation period of corruption [54]. The spread study of corruption cases is based on the traditional SEIR model [55], which assumes that the overall propagation process of corruption nesters in construction projects conforms to a single process within a system from a state of vulnerability to corruption to participation in corruption and finally to being cracked down and caught. Therefore, this paper adopts an improved SEIR model and adds the incubation period parameter [47] to more reasonably explore the transmission mechanism of corruption behaviors in construction.

In formal rumor-spreading models, a closed population is subdivided into three groups; those who are ignorant of the rumor, those who have heard and actively spread it, and those who have heard but ceased to spread it [37, 42]. This paper designs a SEIR model for the propagation of corruption nests in construction projects with four populations, including susceptible population (S), exposed population (E), infectious population (I), and recovery population (R) [55]. The propagation state of the model is shown in Figure 1. Moreover, the evolutionary relationship of corruption transmission in this study is revealed by the SEIR model that integrated various external real factors to obtain the change rate of infectious diseases.

In this paper, it is assumed that the total number of nodes in the project corruption network is N and the number does not change throughout the propagation process, and the information propagation time is represented by t [50]. This study hypothesizes that corrupt behavior is generated through intergroup organizational interactions. The information propagation process in the SEIR model is described as follows.

(1) The susceptible population refers to the group who are prone to participate in the illegal and corrupt behavior of the construction projects.

(2) The latent population refers to the group who have been exposed to the corruption behaviors but have not yet decided to participate and has no transmission motivation.

(3) The people infected by corruption refers to the group who participate in the case of corruption or commit corruption and have the motivation to spread corruption.

(4) The dismissed people refer to the group that have been cracked down by external discipline inspection departments, courts, and other channels and are in a state of being dismissed.

(5) When $t = 0$, corruption of the initial project generated in the network. The susceptible nodes in the network first convert to exposed nodes with the probability of λ, and then the exposed nodes convert to the infected node with the Probability of u. Finally, the infected nodes can be converted into the Remove nodes with the probability of r[44].

(6) The overall process of spreading corruption in engineering projects can be expressed as follows: if the susceptible state individual m is considered to have corruption behavior with neighbouring corrupt individual j in the period $[t, t+1]$, then susceptible state individual m will be in latent state E by deciding whether to participate in corruption or not. When individual m in the latent state participates in corruption by choice, individual m will become a member of the corrupt group I in the construction projects. When individuals m in a corrupt state are under the supervision of external government departments and other relevant agencies, they are eventually arrested and become a removal group R [42]. In the whole process of corrupt spreading behavior in construction projects, each node may involve in corruption, which mainly depends on the comprehensive impacts of multiple factors.

(7) During the initial propagation of corruption in construction projects, it is assumed that the people in the group will be in one of the states where corrupt interactions occur with their neighbouring nodes during the beginning of corruption propagation.

The dynamic differential equation expression of the infectious disease model is shown in equation.

$$
\begin{cases}
\dfrac{\mathrm{d}S(t)}{\mathrm{d}t} = -\lambda * S(t) * I(t), \\[2ex]
\dfrac{\mathrm{d}E(t)}{\mathrm{d}t} = \lambda * S(t) * I(t) - \mu * E(t), \\[2ex]
\dfrac{\mathrm{d}I(t)}{\mathrm{d}t} = \mu * E(t) - \gamma * I(t), \\[2ex]
\dfrac{\mathrm{d}R(t)}{\mathrm{d}t} = \gamma * I(t), \\[2ex]
N = S + E + I + R.
\end{cases}
\tag{1}
$$

Among them, $S(t)$ represents the density of vulnerable nodes, $E(t)$ represents the density of latent nodes, $I(t)$
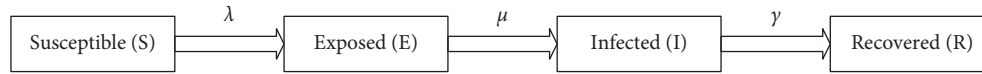
FIGURE 1: State transition diagram of the SEIR model.

represents the density of infected nodes, $R(t)$ represents the density of attack removal nodes, $S(t) + E(t) + I(t) + R(t) = 1$. λ, μ, γ represent the probability of conversion between personnel at each node, $0 \le \lambda$, μ, $\gamma \le 1$, λ is the corruption infection rate, μ is the potential decision rate, and γ is the crackdown rate.

The infection rate λ refers to the probability that an infectious disease will infect from a susceptible population to an individual in a complex network, mainly refers to the probability that a susceptible population becomes a potential individual node in the corrupt network. The incubation state refers to the incubation period of the infectious disease from the individual infection state to the outbreak stage of the group infection. In the corruption case network, the potential decision rate μ is used to express the probability that the potential individual corrupt personnel is willing to participate in the corruption case after the balance of income and expenditure analysis. The crackdown crate γ refers to the probability that the infected node is cured by some measures, which also means the probability that the official organization arrest the corrupt personnel.

4. Model Parameters

The parameter of the infectious disease model generally is a measurable indicator. Previous studies set the relevant parameters mainly through historical data, related literature, genetic algorithms and particle swarm optimization algorithms [42, 45, 46, 48, 56].

4.1. Data Collection. There are many news and network reports on corruption cases of construction projects, but there are two problems: description bias and selection bias [27]. Given the sensitiveness and implications of criminal proceedings, criminal intelligence and investigations strive for achieving the most accurate representation of each case [57]. China Judgments Online is an official platform sponsored by the Supreme Court [20], which provides numerous corruption cases including the construction projects. Moreover, the China Judgment Online records in detail the interaction of corrupt persons and other groups in the construction projects. In order to ensure the validity and authenticity, the data in this paper are derived from the legal judgment documents published in China Judgments Online.

This paper uses the advanced filtering function of the China Judicial Documents to obtain all the data. In the process of data screening, this study sets the case type, the trial procedure, court level, year, and document type as "criminal case," "criminal first instance," "all," "2018," and "judgment" respectively, and then conducts a full-text screening for "bribery," "acceptance of bribes," "construction projects" and "project corruption." After screening, analysing and sorting out specific content, a total of 2158

engineering corruption cases were found, involving people in 12 provinces and 1 municipality.

The cases of corruption in construction projects were filtered according to the following criteria: (1) The information of all judgment documents is complete, and the content of which is related to the field of construction projects. (2) All the judgment documents should be read in detail and adequately hand-screened to find interrelated cases. Based on the defined filtering rules. Then, a total of 109 cases with the most complex case relationship, large amount of corruption and long latency are selected for analysis. The cases selected in this paper are suspected of several charges, including bribery, acceptance of bribes, abuse of authority, collusion in bidding. All actors named in the selected adjudicative instruments as being involved in illegal activities are included in the detailed detail record. The earliest of the arrested core criminal officers began participating in corrupt activities in construction projects in November 2007 and were arrested and prosecuted in late 2017. Analysis of the data shows that nodes 2, 4, 5 and 34 are government department officials. The rest of the nodes are contractors except for the group of people associated with government officials. In addition, nodes 1, 2, 3, 4, and 5 are the key individuals who were eventually apprehended for participating in or committing corrupt acts on the construction projects. The selected cases involved 34 persons and institutions, more than 14 million single-person crime, and an incubation period of up to 10 years. The five adjudication documents of the selected cases are all first instance judgments of criminal cases, numbered (2018) Xiang 1224 No. 17, (2018) Xiang 1224 No. 64, (2018) Xiang 1224 No. 65, (2018) Xiang 1224 No. 196, (2018) Xiang 1281 No. 175 respectively.

In this paper, all names of personnel and company are replaced by numbers for conveniently analysing the relationship between corrupt personnel, then a $34 * 34$ one-dimensional adjacency matrix and a directed engineering corruption nest personnel relationship network are constructed to determine the parameters of the infectious disease model.

4.2. Partial Model Parameter Settings. This study determines the relevant parameters through the analysis of corruption cases in actual construction projects. Corruption contagion in actual construction projects can be initiated by several people or a small group; whereas the corruption spread of the construction projects involved in this case is initiated by one person and then gradually expands based on the detailed analysis of the five legal judgments involved in this study. Therefore, this paper selects one key person as the source group of corruption communication. The total number of people in the network is assumed to be $N = 34$ by analysing the actual case. S, E, I, and R represent the initial number of

personnel at each state node. Therefore, this study assumed the number of each group as $I = 1$, $E = 0$, $R = 0$, and $S = 33$ in the initial state, respectively. Due to the complexity, dynamics, concealment and sensitivity of corruption cases in construction projects, it is difficult to directly quantify the management measures such as supervision, close visits and talks in corruption cases in construction projects. For the setting of the crackdown rate of corruption in construction projects this study is replaced by the number of corrupt group members arrested and imprisoned. Considering that five people have been arrested in the organization's 34-person corruption network, the rate of attack is $r = 5/34 = 0.147$; The potential decision rate μ depends on the cost-benefit risk of corruption involved in the project, with a random possibility each time; The potential corruption decision rate u of corrupt personnel is taken as 0.5, in order to make this group of personnel have the same possibility each time. The analysis found that the incubation years of the five corruption offenders were 10 years, 9 years, 7 years, 5 years, and 4 years, respectively. The propagation time of 10 years in this study is the maximum incubation time for all groups of people and institutions involved in construction corruption projects. Therefore, this paper will use the incubation time as the parameter of the propagation time to describe the interaction of the group's corruption behaviors during the entire propagation period.

4.3. Corruption Infection Rate Parameter Setting.

This study attempts to determine the magnitude of personnel corruption contagion rate in the construction projects through complex network modelling. At the node level, degree centrality is used to represent the structural position of actors in a network [58]. The nodes with greater degree centrality in complex networks can be regarded as important conduction nodes [29, 58, 59]. In this study, the higher the degree of node centrality in the corruption network of the construction project, the more people have corrupt behavior. Therefore, this study reveals the number of corruption contagions in the corruption nesting network of construction projects according to the connection effect of several important nodes with greater centrality [29]. The corruption infection rate is defined as the average contact degree of the core personnel, as shown in equation.

$$\lambda = \frac{1}{n} \sum_{i=1}^{n} C_i. \tag{2}$$

Among them, λ is the corruption infection rate, C_i is the node ratio of the i-th core corrupt personnel to the corruption network, i is the i-th core corrupt personnel in the corruption network, and n represents the number of core personnel in the corrupt network.

4.3.1. Complex Network Model Construction.

Considering the complexity and interaction of corrupt behaviors among corrupt groups in construction projects, it is difficult to visualize the connections between nodes through textual narratives, and the use of complex networks can be a good

way to visualize the relationships among nodes. Based on the five selected adjudication documents, the relationship between groups of people is analysed in detail. If there is corruption between any two individuals in the corrupt group, a link is established. The corrupt personnel and the corruption relationship between personnel are abstracted as the network nodes, the edge of the network respectively, then the corruption relationship network is established [5, 60]. The corruption network can be represented by the adjacency matrix $An * n$, so that if there have been corrupt behaviors between personnel, then $a_{ij} = 1$, otherwise $a_{ij} = 0$. The adjacency matrix can reflect the relationship between groups in the complex network, as shown in Table 1. Ucinet software can build a corruption network for the corruption case group of construction projects based on the relationship of the adjacency matrix. A complex network of the personnel contact in the engineering corruption case is built by using Ucinet software, as shown in Figure 2. A detailed adjacency relationship matrix data is shown in the supplementary materials Annex 1.

4.3.2. Corruption Infection Rate in Complex Networks.

The nodes with larger out-degree and in-degree values can be considered as the important conduction nodes of the network in this study. In addition, it can be considered that the formation of corruption network is due to the corruption of a group or multiple individuals. Betweenness centrality is used to measure the transportation capacity of nodes in a complex network. The higher the betweenness centrality, the more influence the node has. It is believed that the nodes with high intermediary centrality in the corruption network of construction projects have strong corruption transmission capabilities. Closeness centrality is a characteristic value that reflects the distance between a node and the centre of the network [27, 29]. Thus, it is significant to calculate the degree centrality, betweenness centrality, closeness centrality, and core edge analysis of the corruption case network, so as to determine the key personnel in the corruption network [27, 39]. This study assumes that the corruption contagion rate of the corruption case is determined by the average degree centrality of the core personnel. The centrality indicators of each corrupt network node are shown in Table 2. Detailed data can be found in supplementary materials Annex 2.

Table 2 reveals that the top eight nodes with the highest total degree of centrality are: 5, 1, 3, 2, 22, 24, 4, and 11 respectively. The order of nodes with high betweenness centrality is 5, 2, 1, 22, 3, 4, 24, 8; The distribution of nodes with more tightness centrality is 2, 3, 1, 31, 5, 22, 4, 34. According to the degree of close connection between nodes in the complex network of the corruption case, the core and edge personnel in the corruption network are determined by using Ucinet software [35, 57, 59], as shown in Table 3.

According to the three-centrality analysis and core-edge structure of the corruption network personnel in Table 2 and Table 3, 7 people, namely Node 1, 2, 3, 4, 5, 22, and 24, are identified as the core personnel of the corruption network in this case. The corruption contagion rate of the project is $\lambda =$

TABLE 1: Corruption personnel node adjacency matrix (partly)).

	Node 1	Node 2	Node 3	. . .	Node 34
Node 1	0	1	0	. . .	0
Node 2	1	0	1	. . .	
Node 3	0	1	0	. . .	
. . .	. . .	. . .	. . .	. . .	
Node 34	0	0	0	. . .	
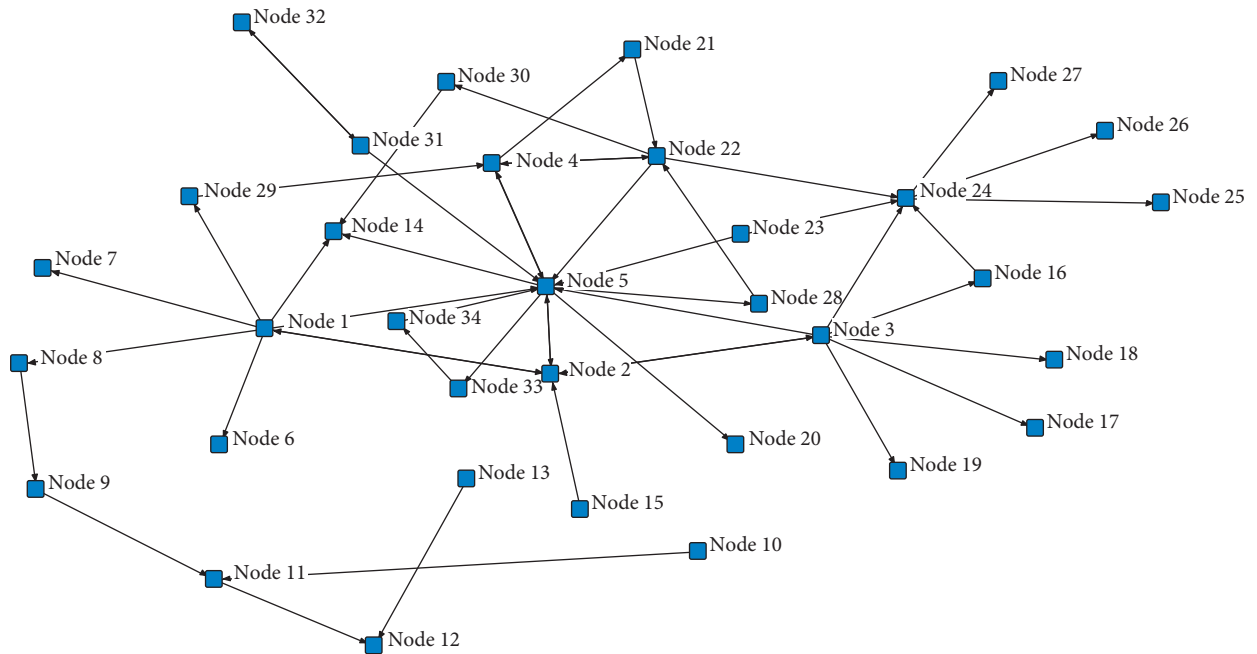
FIGURE 2: Personnel contacts of construction corruption case under complex network.

TABLE 2: Network centrality index of each corruption node.

Node	Degree centrality		Betweenness centrality	Closeness centrality	
	Out-degree	In-degree		Out-degree	In-degree
1	7	1	98	12.222	4.797
2	3	4	192.667	12.268	4.889
3	7	1	74.667	12.268	4.797
4	3	3	5	11.419	4.896
5	6	8	251.833	11.913	4.955
. . .	. . .	. . .	. . .	. . .	. . .
33	1	1	13	10.092	4.867
34	1	1	26	10.927	4.783

TABLE 3: Analysis results of core-edge structure.

Location	Core	Marginal
Personnel number	Node 1, 2, 3, 4, 5, 22, 24	Node 6, 7, 8, 9, 10, 11 et al.

0.239 according to the above assumption of equation (2). In summary, this paper uses the network characteristics of the case personnel to determine the improved SEIR model parameters, as shown in Table 4.

5. Simulation Verification and Analysis

5.1. Evolutionary Relationship of Corruption Contagion in Construction Projects under Actual Cases. This paper defines the total number of research groups as $N = S + E + I + R$. Where S, E, I and R represent the number of personnel at each status node in the process of corruption propagation. The corruption infection rate λ of initial corruption cases is 0.239. Potential decision rate μ, crackdown rate of the formal organization γ, and corruption propagation time t are 0.5, 0.147 and 10 years respectively. This paper use Python to simulate the infectious disease model in the state of corruption nest, then obtain the evolution results of people in each stage of the spread process of corruption nest, as shown in Figure 3.

Figure 3 shows that the number of corrupt personnel I node will first increase to a certain level and gradually decrease over time, then stabilize, and finally reach a peak in three years. The number of individuals at the latent node E is consistent with the changing trend of corrupt personnel as a whole, and the peak value is less than the number of corrupt personnel. It demonstrates that in a relatively closed network structure, the construction project-related personnel who would like to participate in corruption will eventually become a member of corruption to externally intervene in the construction project. The number of groups S in the perishable stage declines in a power law over time, indicating that the degree of corruption is relatively serious.

The number of R in an immune-strike state shows an increase in the power rate, which shows a good effect in combating corruption by the official organization. Throughout the propagation, the crackdown by official organizations and the spread of corruption coexisted, intersecting in about 4 years. Furthermore, the simulation curve of corruption propagation reveals that the effect of corruption cracking is significantly stronger than the level of corruption after 4 years, and the number of people in each state cluster is basically in a stable state after a latent period of about 9 years, which is consistent with corruption incubation period of around 10 years in the current construction project [23]. On the one hand, it illustrates the significant effect of the crackdown by official institutions in reducing corrupt practices during their dissemination online. On the other hand, it also shows that the complex and closed corruption network structure will eventually collapse by itself after a certain time of spreading due to the sparseness of the network and the multiple complexity of the personnel. This is also evidence of the vulnerability and poor flexibility of corruption case networks in long-term propagation.

The source data of five selected engineering corruption cases reflects that the time of 80% corruption criminal to form a group of corruption is less than 4 years. It also illustrates that the corruption criminal will quickly form a

TABLE 4: Probability of each parameter.

Parameters	λ	u	r	t
Range	0.239	0.5	0.147	10 years
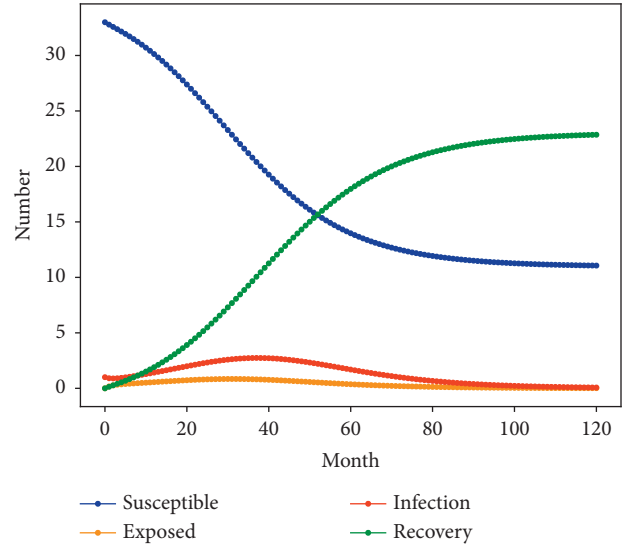
FIGURE 3: Variation in the nodes number of personnel during corruption with actual parameters.

network of corruption in various ways under the premise of satisfying the profit of all parties. In addition, it can also be found that the parameter settings are based on the actual construction project corruption cases in this study. The peak number of personnel for corruption propagation throughout the construction project is the same as the number of core personnel for corruption apprehension in the actual case. At the same time, by observing the evolution of the corruption propagation pattern, we can find that only five of the most central corrupt people in a corrupt network of 34 people were arrested, which is also consistent with our actual data of corruption cases in the magisterial documents. Other groups of people involved in corruption in construction projects may have been prevented from corruption by a variety of measures such as external supervision, confidential visits and interviews, combat and arrest only the most central key personnel, which is similar to the realistic measures to prevent corruption in construction projects.

The results show that the corruption and infectious disease model constructed in this paper is feasible and consistent with the actual situation. The "4–9 propagation law" of construction project corruption nest cases was discovered through actual case analysis.

5.2. The Impact of the Formal Organization's Crackdown Rate on the Spread of Corruption. This study sets the parameter of crackdown rate and others based on the specific construction projects corruption cases to investigate the effect of the crackdown rate on the contagion behavior in the construction project. Under the condition of constant corruption infection rate of 0.239 and other parameters, the crackdown rate γ of the formal organization is set to be [0, 1].

Variable parameters should be allowed to vary within a certain range to better reflect the real situations of corruption contagion behavior. However, when the parameters of corruption transmission behavior are freely changing, the simulation of corruption transmission behavior for construction projects does not truly reflect the correspondence under the changes of corresponding factors. More importantly, the factors under the infectious disease model are fixed parameter variation studies under transmission behavior analysis [42, 46, 48]. To overcome these shortcomings, this study uses sensitivity analysis to explore corruption contagion behavior under several relatively varying scenarios. Taking into account the actual crackdown rate of 0.147, the parameter values of the crackdown rate of the formal organization were set to 0.05, 0.1, 0.147, and 0.2, respectively, by sensitivity analysis of the crackdown rate [42, 61]. Based on the infectious disease model, Python is used to simulate the crackdown rate of personnel informal organizations. The change in the number of personnel at each node in the state of corruption is shown in Figure 4.

Figure 4 and Table 5 show that when the crackdown rate of formal organizations exceeds 0.2, corruption will hardly occur. With the increase of the crackdown rate, the peak value of corrupt personnel nodes I gradually decreases and the propagation time to reach the peak value gradually increases. When the corruption crackdown rate is increased from 0.05 to 0.1 by 5%, the degree of corruption is relatively reduced by 42.85%, and the peak propagation time of corruption is relatively increased by 8.57%. When the corruption crackdown rate increased by 9.7% from 0.05 to 0.147, the degree of corruption decreased by 78.57%, and the propagation time of corruption at its peak increased by 14.29%. It can be seen that the crackdown rate is negatively correlated with the degree of corruption in construction projects, and positively correlated with the peak propagation time of corruption. The corruption spread, the propagation time of corruption cases reaching the peak is about minus 8 times, 1.6 times of the crackdown rate respectively.

The number of perishable personnel S and the number of immune-strike personnel R also show power-law changes, and the magnitude of the change in the two curves reflects the relationship between corruption and crackdown in the corruption case. It can be seen from Figure 4 that when the crackdown rate is 0.05, 0.1, and 0.147, the susceptible S and the remover R intersect at 2.5 years, 3.2 years, and 4 years, respectively. The size of the intersection reflects the speed of the spread of personnel corruption in the corruption nest case. The whole corruption nest case network is in a stable state. When the crackdown rate increases by 5% and 9.7%, the increase of s of corrupt personnel in the project is 150% and 500%, respectively, which is 9.375% and 31.25% greater than the decrease of R of corrupt personnel in the project. With the increase of the crackdown rate, the increase of perishable personnel S in the construction project is greater than the decreased number of personnel removed from the immunization crackdown of the official organization of the construction project. It shows that the number of people involved in the spread of corruption is far smaller than the effect of the corruption crackdown, and the crackdown rate

of the corruption case of the project is also relatively high, which meets the crackdown requirements.

The analysis shows that the occurrence of corruption prevention cases can be reduced from the source through the dynamic monitoring of the project and strengthening the crackdown on the organization.

5.3. The Impact of the Infection Rate of Corrupt Personnel in the Engineering Corruption Case on the Spread of Corruption. Under the constant condition of crackdown rate (i.e., 0.147) and other parameters, the value of the corruption infection rate λ of the personnel in the engineering corruption network is [0, 1]. Considering the actual corruption transmission rate of 0.139, the values of corruption transmission rate parameters were set to be 0.139, 0.239, 0.339, and 0.439 by sensitivity analysis of the transmission rate [61]. Based on the infectious disease model, the extent of corruption nesting in construction projects under different corruption contagion rates is simulated by Python. The personnel change of each node in the state of corruption is shown in Figure 5.

According to the simulation results in Figure 5 and Table 6, it can be seen that corruption hardly occurs when the corruption infection rate of a construction project is less than the crackdown rate. When the corruption infection rate increases by 10% from 0.239 to 0.339, the transmission time of corruption nest cases reaching the peak decreases by about 25%, and the peak number of people involved in corruption increases by about 100%. When the corruption infection rate increases by 20% from 0.239 to 0.439, the propagation time of corruption cases reaching the peak is relatively reduced by about 50%, and the peak number of people involved in corruption is relatively increased by about 200%. The transmission scale and rate of corruption network increased with the increase of the change range of corruption infection rate. The infection rate is positively correlated (i.e., 0.1 times) with the corruption degree of the construction project, and negatively correlated (minus 0.4 times) with the time of the construction corruption reaching the peak of transmission. The infection rate of engineering project corruption has a great impact on the spread of corruption cases. The control of the infection rate of corruption must start from multiple aspects including real-time dynamic monitoring, reduce the spread of corruption, and ensure the normal implementation of the entire process of the project from the source.

In the whole process of corruption propagation, S curve and R curve show a power-law trend. Figure 5 shows that the simulation curves of the S curve and the R curve intersect at 4 years, 2.5 years, and 2 years, with intersection points of 6 people, 14 people, and 12 people respectively, as the infection rate increases. There will more perishable groups S and removed groups R over time. In a stable state of transmission, the relative reduction of personnel prone to corruption in the project is about 50% when the infection rate of corruption increases by 10%, which is greater than the increase of 27.27% by the formal organization of the project. The rate of decrease of perishable personnel in engineering projects is about 83.33% when the infection rate of

(a)

(b)

(c)

(d)
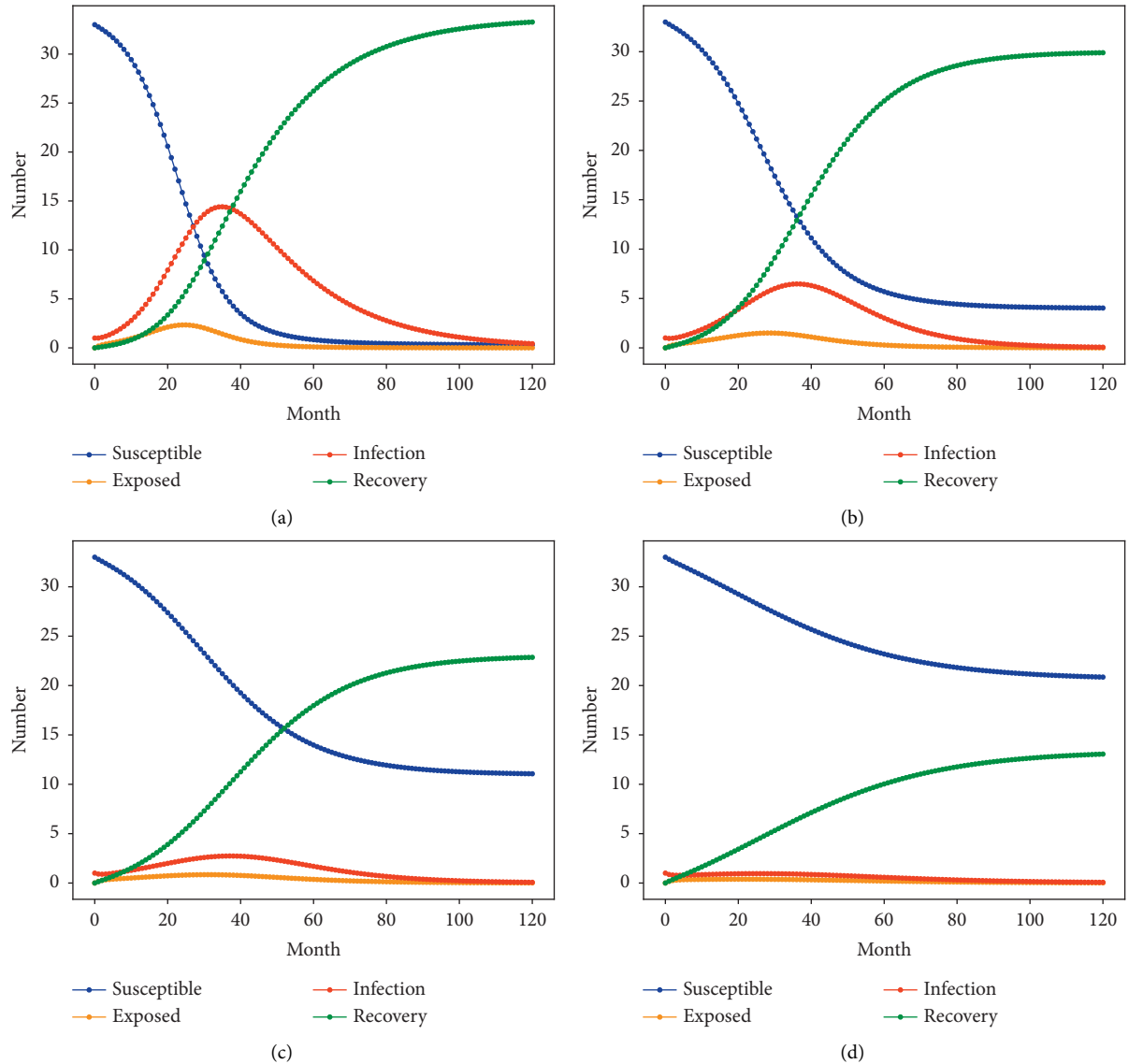
FIGURE 4: The relationship of changes under different crackdown rates. (a) $\gamma = 0.05$, (b) $\gamma = 0.1$, (c) $\gamma = 0.147$ (d)$\gamma = 0.2$.

TABLE 5: Parameter variation relationship of nodes at different crackdown rates.

γ	t	$S(t)$	t	$E(t)$	t	$I(t)$	t	$R(t)$
0.05	70	2	25	3	35	14	120	32
0.1	90	5	30	2	38	6	100	29
0.147	100	12	30	1	40	3	110	22
0.2	120	21	—	—	0	1	120	13

corruption increases by 20%, which is greater than the rate of 45.45% in the official organization of the project to crack down and remove the increased personnel. It can be seen that the spread of the number of people involved in corruption infection is far greater than the effect of corruption attacks with the increase in the infection rate. In addition, the impact of the intensity of corruption infection rate will be greater when the reduction of corruption prone personnel is greater than the increase personnel in the formal organization of the project.

5.4. The Impact of Changes in Latency Period on the Level of Corruption in Construction Projects. Parameters obtained from actual cases are taken as the corruption contagion rate and combating rate of construction projects. The influence of the evolutionary pattern of corruption nesting behaviors in construction projects under different incubation periods is studied separately. This paper selects the incubation period of 6 years, 8 years, 10 years and 12 years as the characteristic parameters to analyse the evolution relationship between the incubation period and the corruption degree of the project.

(a)

(b)

(c)

(d)
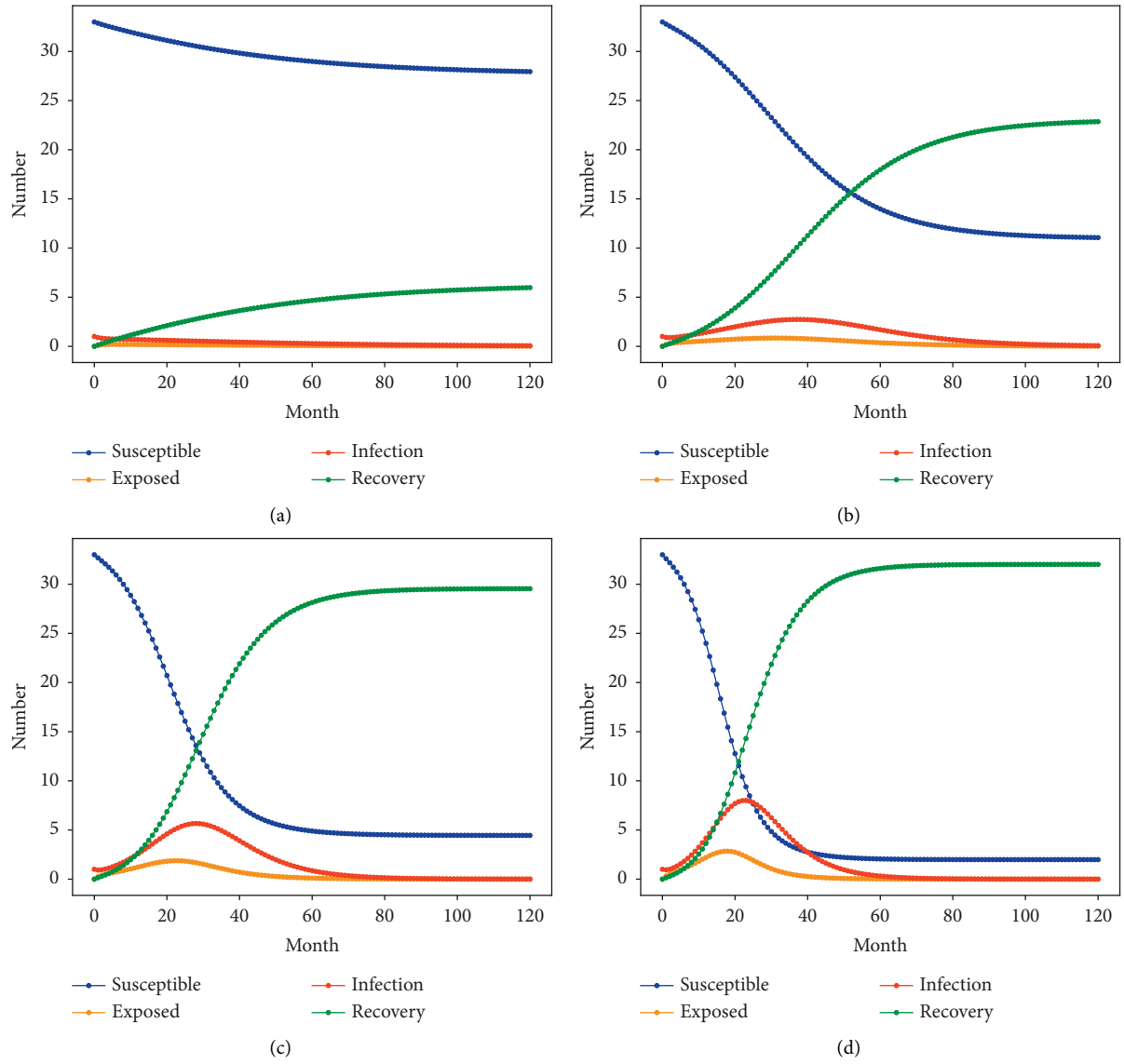
Figure 5: Relationship between changes under different infection rates. (a) $\lambda = 0.139$, (b) $\lambda = 0.239$, (c) $\lambda = 0.339$, and (d) $\lambda = 0.439$.

Table 6: Parameter variation relationship of nodes with different infection rates.

λ	t	$S(t)$	t	$E(t)$	t	$I(t)$	t	$R(t)$
0.139	100	28	—	—	—	—	110	6
0.239	90	12	30	1	40	3	110	22
0.339	60	6	22	3	30	6	80	28
0.439	50	2	18	4	20	9	60	32

Based on the infectious disease model, the extent of corruption nesting in construction projects under different corruption Latency Period are simulated by Python. The change of the personnel number at each node in the state of corruption is shown in Figure 6.

According to the simulation results in Figure 6 and Table 7, a very interesting phenomenon of corruption group evolution can be found when the rate of corruption contagion and the fight against corruption in construction projects are determined. The change of latency time has little effect on the peak value of group I in the construction projects corruption. When the incubation time is less than 10 years, the number of corruption-prone groups S and the number of removal-strike stage groups R are still in the process of propagation evolution. This also verifies the accuracy of the 10-year latency time for the five construction projects corruption adjudication documents selected in this study.

This is contrary to the traditional latency period of engineering projects and significant relationship between the degree of corruption. This is mainly because the number of corrupt groups in construction projects is relatively fixed
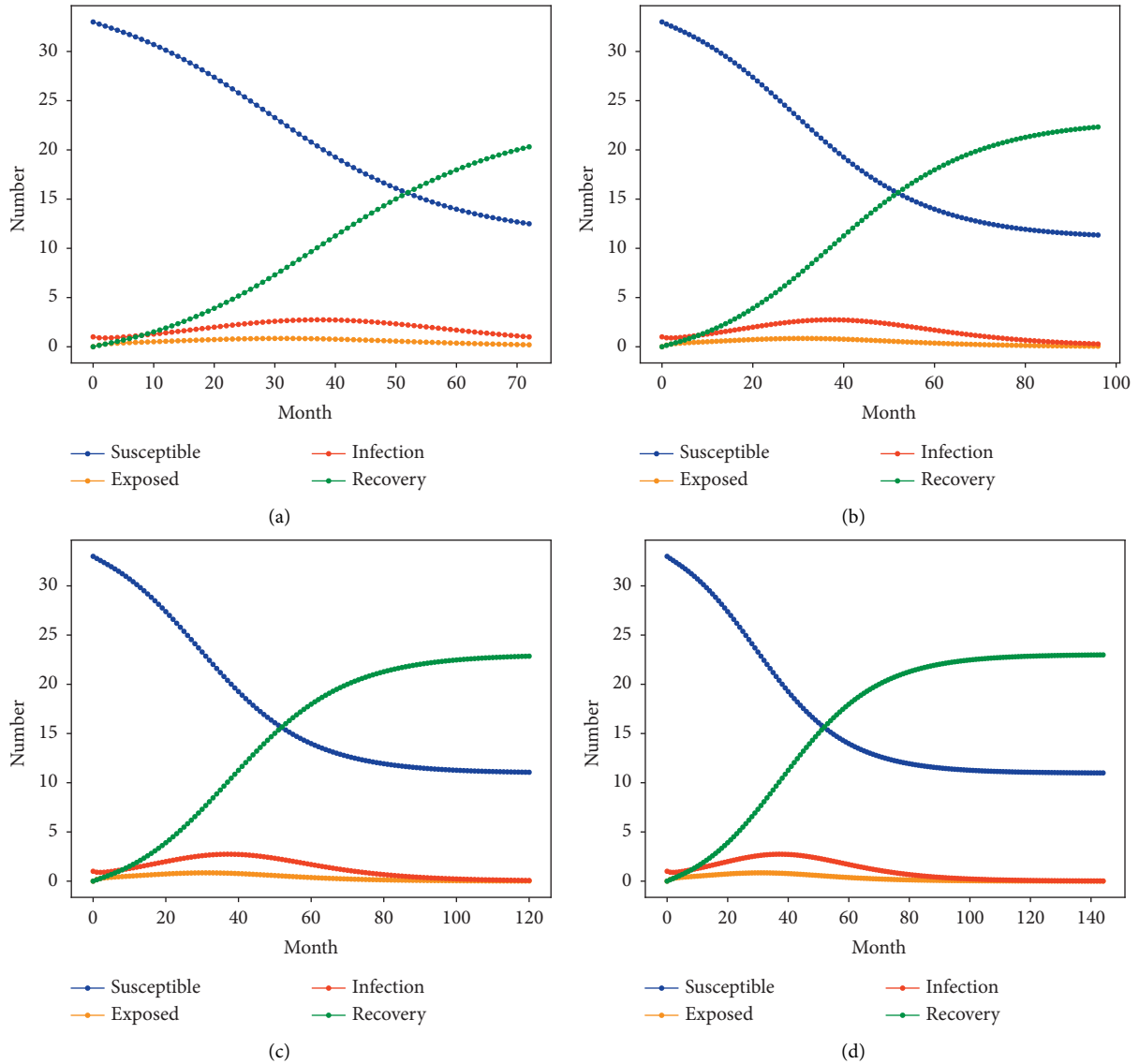
Figure 6: Relationship between changes under different latency periods. (a) $t = 6$ years, (b) $t = 8$ years, (c) $t = 10$ years, and (d) $t = 12$ years.

Table 7: Parameter variation relationship of nodes with different infection rates.

t	t	$S(t)$	t	$E(t)$	t	$I(t)$	t	$R(t)$
72	—	—	30	1	40	3	—	—
96	—	—	30	1	40	3	—	—
120	90	12	30	1	40	3	110	22
144	90	12	30	1	40	3	110	22

in this study, except the relatively fixed values of the contagion rate and strike rate parameters that affect the behavior of corruption transmission in construction projects. Similarly, this evolutionary relationship illustrates that the length of latency time cannot influence the peak state of corruption contagion behavior in construction projects when the propagation parameters are in a determined state, unless the latency time is short enough to influence the formation of corruption nesting networks in construction projects. This

also validates the infectious behavior of the corruption nest in construction projects will be rapidly infected to form a complex and hidden corruption network among the group in about 4 years.

This study demonstrates the behavior of corruption transmission in construction projects by changing the incubation time, and the simulation results also verify the rationality and scientific validity of the infectious disease model designed in this study.

6. Discussion

6.1. Findings. The construction and practical validation analysis of the construction projects corruption nesting SEIR model shows that the model constructed in this paper is scientific and reasonable in line with the actual situation. Due to the dynamics, complexity, and concealment of the corruption network of the construction projects, the people who are in the core network will also vary over time [27, 34, 36]. Zhang [42] proposed the MI-SEIR model considering the influence of media and interpersonal relationships on opinion dissemination based on the SEIR model. Nekovee [37] explored the mechanism of penetrating and spreading corrupt behavior within the organizations, and the behavioral interaction between corrupt group. The traditional spread of public opinion, epidemics and torts are generally based on models such as SIR and SEIR [42, 45]. The dynamic time dimension is used to study the propagation law of corruption in engineering projects according to the changing relationship of incubation time.

Because of the time lag between the occurrence of corruption and its apprehension, the length of the incubation period of corruption largely influences the extent of the spread of corruption in construction projects [19, 22, 23]. In the propagation model constructed in this paper, the relevant parameters are obtained from the actual case. The simulation results found that the level of corruption fight in a corruption network after a latency period of more than 4 years will be significantly stronger than the level of corruption propagation, and hardly exist after 9 years. Yu [22] found that the average latency period was significantly longer (i.e., 6.4 years) in construction-related corruption. There are 11 cases over 10 years, with the longest being 15 years. Zhang [23] also analysed the average corruption latency period of 8.02 years through actual data, which is also consistent with the nonexist corruption of about 9 years' latency time in this study. This shows that the corruption nest group in construction projects can quickly form a complex and flexible corruption network within the first 4 years. When the incubation period exceeds nine years, the corruption network of the construction project basically disintegrates and the core group in the corruption network will be hit.

The single factor analysis of corruption communication reveals that the corruption will hardly occur when the crackdown rate of formal organizations exceeds 0.2 or the rate of corruption infection is less than the crackdown rate, which shows that the corruption case network has certain fragility. There is a strong correlation between the crackdown rate, infection rate and the degree of corruption. Corrupt groups spread through specific pathways within a certain spatial and temporal context due to the versatility and flexibility, and such interactions against groups can be considered as the contagion of corrupt behavior [5, 38]. The increase of the crack-down inhibits the maximum scale and rate of corruption risks in the network, and the increase in the rate of infection determines the scale and rate of spread of the corruption case network. The spread scale of corruption cases, the propagation time reaching the peak is

about minus 8 times, 1.6 times of the crackdown rate respectively. The spread scale of corruption cases is about 10 times of the corruption rate, and the spreading time is about minus 2.5 times of the infection rate. The best way to reduce the incidence of corruption cases is to prevent corruption infection and strengthen the crackdown. The serious phenomenon of corruption spreads from individuals to groups and even to the whole organization, and from lower levels to higher levels according to management logic.

6.2. Theoretical Implications. On the one hand, we try to explain and discover the corrupt behavior of construction projects and its laws by using the contagion theory model. It enriches the theory and method of construction project corruption behavior research, while expanding the application scope of contagion model theory. This paper analyzes the evolution relationship of corrupt behavior in engineering projects, and focuses on the evolution law of corrupt behavior groups. This study broadens the research field of corruption behavior in construction projects, enriches the scope and conditions of application of the contagious disease model theory to the contagious behavior of corruption in construction projects, and applies the contagious disease SEIR model to the contagious behavior of corruption in construction projects. By analysing the evolutionary relationship of corruption contagion behavior in engineering projects, the paper focuses on the changing relationship of corruption contagion behavior under the influence of factors such as external corruption contagion behavior and crackdown under the change of latency time. The study breaks the traditional research for the degree of corruption in construction projects, the characteristics of corruption, corruption governance under a single perspective to consider the problem starting. The nature of corruption contagion behavior is analysed and sorted out, which helps to understand the inner evolution law of corruption contagion behavior in construction projects and expand the boundary area of corruption research in construction projects.

On the other hand, the complex network theory used in this paper combined with the contagion model theory explores the characteristics of the spread of corrupt behavior from a dynamic perspective. The method of determining model parameters through complex networks obtains more objective data than the questionnaires and expert interviews used in traditional studies. It also provides a theoretical reference for scholars to adopt new methods for data acquisition and consolidates the exploration of scientific governance in the field of corruption management of construction projects. At the same time, the evolutionary relationship of corruption contagion behavior in construction projects also breaks the tradition of analysing the relationship characteristics of corruption behavior mostly from a static perspective. It also reveals the changing characteristics of group behavior under the whole time of corruption transmission, and also provides a new theoretical exploration for the targeted fight against the occurrence of corruption.

6.3. Practical Implications. The study provides clearer target and compelling rationale for policy makers to select the right strategic tool in their fight. First of all, in view of the prevalence of such corruption in construction projects, the fight against corrupt groups should use a variety of means for full process control. Secondly, considering the simulation analysis of the actual case dissemination process in this study, the early stage is a high-frequency stage prone to corruption in construction projects. Therefore, the government supervision department should attach great importance to the control of small groups in violation of regulations in the early stage of the project such as the bidding process. Thirdly, the corruption hardly occurs when the strike rate of formal organizations exceeds 0.2 or the corruption infection rate is lower than the crackdown rate. Therefore, the government supervision department can choose appropriate crackdown and supervision strategies to improve the efficiency of project management according to the degree of corruption of local construction projects. Finally, government departments should pay more attention to the informal organization groups in the construction process of construction projects, and strengthen the control of the generation and dissemination of inter-group violations.

7. Conclusions and Future Study

7.1. Conclusions. This study proposes an improved SEIR model of corruption contagion behavior in construction projects based on the epidemic model considering the variation of latency time of group personnel. Five adjudication documents collected from the official website of Chinese adjudication documents were used to validate the propagation model test of corruption nesting cases in construction projects. This paper demonstrates that the model is consistent with the process of corruption propagation in construction projects, explores the evolutionary relationship of corruption propagation, and investigates the effects of changes in crackdown rate and contagion rate on the contagion time and the degree of corruption. Based on the simulation results, the following conclusions can be drawn.

(1) The improved SEIR model for infectious diseases proposed in this paper is scientifically and rationally compatible with the actual process. (2) A complex and hidden network of corruption in construction projects can be formed rapidly within four years or even less. When the latent period exceeds 9 years, the corruption network of construction projects will basically disintegrate and the core group in the corruption network will be crackdown. (3) If can target to Enhancement of the crackdown rate or even some regulatory measures by external regulatory agencies can effectively reduce the spread and proliferation of corruption behavior at the early stage of corruption contagion behavior in construction projects. Otherwise, if external regulators allow corruption to occur, corruption in construction projects will rapidly spread throughout the corrupt community. (4) There is a strong correlation between the crackdown rate, infection rate and the degree of corruption,

the increase of the crack-down inhibits the maximum scale and rate of corruption risks in the network, and the increase of the infection rate determines the scale and rate of spread of the corruption case network. The spread scale of corruption cases, the propagation time reaching the peak is about minus 8 times, 1.6 times of the crackdown rate respectively. The spread scale of corruption cases is about 10 times of the corruption rate, and the spreading time is about minus 2.5 times of the infection rate.

7.2. Limitation and Future Research Directions. Due to the limitation of the data source of corruption cases in construction projects, the dissemination process of corrupt behaviors in this study does not consider realistic issues from external factors such as investment in construction projects, local economic conditions, and government transparency. In addition, this study considers the parameter settings under real cases. However, the effect of free variation of factors in the interval is ignored because the parameters under the SEIR model of infectious diseases need to be fixed when analysing the effect of changing states of factors on the behavior of corruption transmission in construction projects.

The modelling analysis and feature disclosure in this article are based on a specific engineering corruption case; however, a complex network can be constructed with the help of big data techniques to determine the parameters of the infectious disease model.

In the context of Industry 4.0, the vigorous development of digital intelligence technology provides an efficient tool for the engineering management industry. In future research, the SEIR model of infectious diseases should be further improved when considering more influencing factors, such as the investment situation of construction projects, regional GDP, legal regulatory system, and local integrity index. The combination of digital intelligence technology and infectious disease models can dynamically predict the possibility of each behavior in real time. On the other hand, future research on corruption nests in engineering projects will consider multicase data to deeply analyse the evolutionary relationship of propagation behavioral.

Data Availability

The data used to support the findings of this study are available from the corresponding author upon request.

Conflicts of Interest

The authors declare that there are no conflicts of interest regarding the publication of this paper.

Acknowledgments

Supplementary Materials

The adjacency relationship matrix data used to construct the complex network of Figure 2 will be provided in supplementary materials Annex 1. The complete data of the three centralities used to analyse complex networks in Table 1 will be provided in supplementary materials Annex 2. The original judgment documents used by the literature research room will be provided in supplementary materials Annex 3. The supplementary material Annex 4 contains the source code of the manuscript. (*Supplementary Materials*)

References

[1] H. V. Ribeiro, L. G. A. Alves, A. F. Martins, E. K. Lenzi, and M. Perc, "The dynamical structure of political corruption networks," *Journal of Complex Networks*, vol. 6, no. 6, pp. 989–1003, 2018.

[2] Y. Zheng and X. Liao, "Corruption governance and its dynamic stability based on a three-party evolutionary game with the government, the public, and public officials," *Applied Economics*, vol. 51, no. 49, pp. 5411–5419, 2019.

[3] B. Cheng, K. Lu, J. Li, H. Chen, X. Luo, and M. Shafique, "Comprehensive assessment of embodied environmental impacts of buildings using normalized environmental impact factors," *Journal of Cleaner Production*, vol. 334, Article ID 130083, 2022.

[4] E. Kingsford Owusu and A. P. C. Chan, "Barriers affecting effective application of anticorruption measures in infrastructure projects: disparities between developed and developing countries," *Journal of Management in Engineering*, vol. 35, no. 1, Article ID 04018056, 2019.

[5] Y. Wang, "A network-exchange approach to corruption: brokers and institution spanning in A Chinese corruption network," *Deviant Behavior*, vol. 41, no. 12, pp. 1636–1649, 2019.

[6] X. Guo and W. Tu, "Corruption tolerance and its influencing factors-the case of China's civil servants," *Journal of Chinese Governance*, vol. 2, no. 3, pp. 307–328, 2017.

[7] Y. Le, M. Shan, A. P. C. Chan, and Y. Hu, "Investigating the causal relationships between causes of and vulnerabilities to corruption in the Chinese public construction sector," *Journal of Construction Engineering and Management*, vol. 140, no. 9, Article ID 05014007, 2014.

[8] E. K. Owusu, A. P. C. Chan, E. E. Ameyaw, and O.-K. Robert, "Evaluating the effectiveness of strategies for extirpating corrupt practices in infrastructure project procurement," *Journal of Infrastructure Systems*, vol. 26, no. 2, Article ID 04020004, 2020.

[9] E. K. Owusu, A. P. C. Chan, and A. Darko, "Evaluating the corruption susceptibility index of infrastructure procurement and management in the developed context: the case of Hong Kong," *Journal of Infrastructure Systems*, vol. 27, no. 2, Article ID 05021006, 2021.

[10] B. Zhang, Y. Le, B. Xia, and M. Skitmore, "Causes of business-to-government corruption in the tendering process in China," *Journal of Management in Engineering*, vol. 33, no. 2, Article ID 05016022, 2017.

[11] M. Shan, A. P. C. Chan, Y. Le, Y. Hu, and B. Xia, "Understanding collusive practices in Chinese construction projects," *Journal of Professional Issues in Engineering Education and Practice*, vol. 143, no. 3, Article ID 05016012, 2017.

[12] M. Shan, A. P. C. Chan, Y. Le, B. Xia, and Y. Hu, "Measuring corruption in public construction projects in China," *Journal of Professional Issues in Engineering Education and Practice*, vol. 141, no. 4, Article ID 05015001, 2015.

[13] E. E. Ameyaw, E. Parn, A. P. C. Chan, De-G. Owusu-Manu, D. J. Edwards, and A. Darko, "Corrupt practices in the construction industry: survey of Ghanaian experience," *Journal of Management in Engineering*, vol. 33, no. 6, Article ID 05017006, 2017.

[14] E. K. Owusu, A. P. C. Chan, and M. R. Hosseini, "Impacts of anti-corruption barriers on the efficacy of anti-corruption measures in infrastructure projects: implications for sustainable development," *Journal of Cleaner Production*, vol. 246, Article ID 119078, 2020.

[15] I. S. Damoah, C. A. Akwei, I. O. Amoako, and D. Botchie, "Corruption as a source of government project failure in developing countries," *Project Management Journal*, vol. 49, no. 3, pp. 17–33, 2018.

[16] T. Kaymak and E. Bektas, "Corruption in emerging markets: a multidimensional study," *Social Indicators Research*, vol. 124, no. 3, pp. 785–805, 2015.

[17] R. Signor, P. E. D. Love, A. T. N. Belarmino, and O. A. Olatunji, "Detection of collusive tenders in infrastructure projects: learning from operation car wash," *Journal of Construction Engineering and Management*, vol. 146, no. 1, Article ID 05019015, 2020.

[18] M. R. Hosseini, I. Martek, S. Banihashemi, A. P. C. Chan, A. Darko, and M. Tahmasebi, "Distinguishing characteristics of corruption risks in Iranian construction projects: a weighted correlation network analysis," *Science and Engineering Ethics*, vol. 26, no. 1, pp. 205–231, 2020.

[19] E. K. Owusu, A. P. C. Chan, and E. Ameyaw, "Toward a cleaner project procurement: evaluation of construction projects' vulnerability to corruption in developing countries," *Journal of Cleaner Production*, vol. 216, pp. 394–407, 2019.

[20] X. Wang, K. Ye, and D. Arditi, "Embodied cost of collusive bidding: evidence from China's construction industry," *Journal of Construction Engineering and Management*, vol. 147, no. 6, Article ID 04021037, 2021.

[21] Y. Le, M. Shan, A. P. C. Chan, and Y. Hu, "Overview of corruption research in construction," *Journal of Management in Engineering*, vol. 30, no. 4, Article ID 02514001, 2014.

[22] Y. Yu, I. Martek, M. R. Hosseini, and C. Chen, "Demographic variables of corruption in the Chinese construction industry: association rule analysis of conviction records," *Science and Engineering Ethics*, vol. 25, no. 4, pp. 1147–1165, 2019.

[23] H. X. Zhang, Y. Song, C. S. Li et al., "Exploring the impact of individual characteristics associated with government officials on the severity of real estate corruption," *Sustainability*, vol. 11, no. 12, Article ID 3351, 2019.

[24] E. K. Owusu, A. P. C. Chan, M. Shan, and E. Pärn, "An empirical study on construction process corruption susceptibility: a vignette of international expertise," *Science and Engineering Ethics*, vol. 26, no. 1, pp. 325–349, 2020.

[25] J. Lohne, N. E. Kjesbu, A. Engebo, B. Young, and O. Laedre, "Scoping literature review of crime in the AEC industry," *Journal of Construction Engineering and Management*, vol. 145, no. 6, Article ID 03119002, 2019.

[26] A. P. C. Chan and E. K. Owusu, "Corruption forms in the construction industry: literature review," *Journal of Construction Engineering and Management*, vol. 143, no. 8, Article ID 04017057,, 2017.

[27] T. Diviák, J. K. Dijkstra, and T. A. B. Snijders, "Structure, multiplexity, and centrality in a corruption network: the Czech Rath affair," *Trends in Organized Crime*, vol. 22, no. 3, pp. 274–297, 2018.

[28] B. van Schoor and C. Luetge, "Conditions of collective commitment in sector-specific coordinated governance initiatives," *Crime, Law and Social Change*, vol. 71, no. 2, pp. 129–150, 2017.

[29] Z. Chang, "Understanding the corruption networks revealed in the current Chinese anti-corruption campaign: a social network approach," *Journal of Contemporary China*, vol. 27, no. 113, pp. 735–747, 2018.

[30] J. Brown and M. Loosemore, "Behavioural factors influencing corrupt action in the Australian construction industry," *Engineering Construction and Architectural Management*, vol. 22, no. 4, pp. 372–389, 2015.

[31] E. K. Owusu, A. P. C. Chan, and M. Shan, "Causal factors of corruption in construction project management: an overview," *Science and Engineering Ethics*, vol. 25, no. 1, pp. 1–31, 2019.

[32] A. Jiménez, M. Russo, J. M. Kraak, and G. F. Jiang, "Corruption and private participation projects in central and eastern europe," *Management International Review*, vol. 57, no. 5, pp. 775–792, 2017.

[33] M. Reeves-Latour and C. Morselli, "Bid-rigging networks and state-corporate crime in the construction industry," *Social Networks*, vol. 51, pp. 158–170, 2017.

[34] D. Jancsics and I. Jávor, "Corrupt governmental networks," *International Public Management Journal*, vol. 15, no. 1, pp. 62–99, 2012.

[35] D. A. Bright, C. Greenhill, A. Ritter, and C. Morselli, "Networks within networks: using multiple link types to examine network structure and identify key actors in a drug trafficking operation," *Global Crime*, vol. 16, no. 3, pp. 219–237, 2015.

[36] D. A. Bright and J. J. Delaney, "Evolution of a drug trafficking network: mapping changes in network structure and function across time," *Global Crime*, vol. 14, no. 2-3, pp. 238–260, 2013.

[37] M. Nekovee and J. Pinto, "Modeling the impact of organization structure and whistle-blowers on intra-organizational corruption contagion," *Physica A: Statistical Mechanics and Its Applications*, vol. 522, pp. 339–349, 2019.

[38] S.-J. Kim and J. Lee, "A percolation-like process of within-organization collective corruption: a computational approach," *Business & Society*, vol. 60, no. 1, pp. 161–195, 2021.

[39] D. Bright, C. Whelan, and S. Harris-Hogan, "On the durability of terrorist networks: revealing the hidden connections between jihadist cells," *Studies in Conflict & Terrorism*, vol. 43, no. 7, pp. 638–656, 2018.

[40] W. Wang, Q.-H. Liu, J. Liang, Y. Hu, and T. Zhou, "Co-evolution spreading in complex networks," *Physics Reports*, vol. 820, pp. 1–51, 2019.

[41] W. Wang, M. Tang, H. Eugene Stanley, and L. A. Braunstein, "Unification of theoretical approaches for epidemic spreading on complex networks," *Reports on progress in physics. Physical Society*, vol. 80, no. 3, Article ID 036603, 2017.

[42] Y.-X. Zhang, Y.-X. Feng, and R.-Q. Yang, "Network public opinion propagation model based on the influence of media and interpersonal communication," *International Journal of Modern Physics B*, vol. 33, no. 32, Article ID 1950393, 2019.

[43] N. Piovella, "Analytical solution of SEIR model describing the free spread of the COVID-19 pandemic," *Chaos, Solitons & Fractals*, vol. 140, Article ID 110243, 2020.

[44] H. Alrabaiah, M. Arfan, K. Shah, I. Mahariq, and A. Ullah, "A comparative study of spreading of novel corona virus disease by ussing fractional order modified SEIR model," *Alexandria Engineering Journal*, vol. 60, no. 1, pp. 573–585, 2021.

[45] M. A. Acuna-Zegarra, M. Santana-Cibrian, and J. X. Velasco-Hernandez, "Modeling behavioral change and COVID-19 containment in Mexico: a trade-off between lockdown and compliance," *Mathematical Biosciences*, vol. 325, Article ID 108370, 2020.

[46] P. Yarsky, "Using a genetic algorithm to fit parameters of a COVID-19 SEIR model for US states," *Mathematics and Computers in Simulation*, vol. 185, pp. 687–695, 2021.

[47] C. Fan, X. Jiang, and A. Mostafavi, "A network percolation-based contagion model of flood propagation and recession in urban road networks," *Scientific Reports*, vol. 10, no. 1, Article ID 13481, 2020.

[48] S. He, Y. Peng, and K. Sun, "SEIR modeling of the COVID-19 and its dynamics," *Nonlinear Dynamics*, vol. 101, no. 3, pp. 1667–1680, 2020.

[49] C. Hou, J. Chen, Y. Zhou et al., "The effectiveness of quarantine of Wuhan city against the Corona Virus Disease 2019 (COVID-19): a well-mixed SEIR model analysis," *Journal of Medical Virology*, vol. 92, no. 7, pp. 841–848, 2020.

[50] X. Qian and S. V. Ukkusuri, "Connecting urban transportation systems with the spread of infectious diseases: a Trans-SEIR modeling approach," *Transportation Research Part B: Methodological*, vol. 145, pp. 185–211, 2021.

[51] Q. Liu, T. Li, and M. Sun, "The analysis of anSEIRrumor propagation model on heterogeneous network," *Physica A: Statistical Mechanics and its Applications*, vol. 469, pp. 372–380, 2017.

[52] L.-L. Xia, G.-P. Jiang, B. Song, and Y.-R. Song, "Rumor spreading model considering hesitating mechanism in complex social networks," *Physica A: Statistical Mechanics and its Applications*, vol. 437, pp. 295–303, 2015.

[53] M. Saberi, H. Hamedmoghadam, M. Ashfaq et al., "A simple contagion process describes spreading of traffic jams in urban networks," *Nature Communications*, vol. 11, no. 1, Article ID 1616, 2020.

[54] Y. Zhou, W. Zhang, and S. Yuan, "Survival and stationary distribution of a SIR epidemic model with stochastic perturbations," *Applied Mathematics and Computation*, vol. 244, pp. 118–131, 2014.

[55] I. A. Moneim, "An seir model with infectious latent and a periodic vaccination strategy," *Mathematical Modelling and Analysis*, vol. 26, no. 2, pp. 236–252, 2021.

[56] C. Zhao, M. Li, J. Wang, and S. Ma, "The mechanism of credit risk contagion among internet P2P lending platforms based on a SEIR model with time-lag," *Research in International Business and Finance*, vol. 57, Article ID 101407, 2021.

[57] G. Berlusconi, F. Calderoni, N. Parolini, M. Verani, and C. Piccardi, "Link prediction in criminal networks: a tool for criminal intelligence analysis," *PLoS One*, vol. 11, no. 4, Article ID e, 2016.

[58] C.-Y. Lee, H.-Y. Chong, P.-C. Liao, and X. Wang, "Critical review of social network analysis applications in complex project management," *Journal of Management in Engineering*, vol. 34, no. 2, Article ID 04017061, 2018.

[59] F. Troncoso and R. Weber, "Integrating relations and criminal background to identifying key individuals in crime networks," *Decision Support Systems*, vol. 139, Article ID 113405, 2020.

[60] L. A. Pal and J. Spence, "Event-focused network analysis: a case study of anti-corruption networks," *Policy and Society*, vol. 39, no. 1, pp. 91–112, 2020.

[61] G. Heravi and E. Eslamdoost, "Applying artificial neural networks for measuring and predicting construction-labor productivity," *Journal of Construction Engineering and Management*, vol. 141, no. 10, Article ID 04015032, 2015.

Research Article

A Gray Correlation Algorithm for Analysis of Influencing Factors of Film and Television Copyright Export

Bingchao Ren [1,2] **and Ting Jin** [3]

[1]*School of Intellectual Property, Nanjing University of Science & Technology, Nanjing 210094, China*
[2]*School of Literature, Journalism & Communication, Henan University of Economics and Law, Zhengzhou 450046, China*
[3]*School of Journalism and Communications, Henan University of Technology, Zhengzhou 450001, China*

Correspondence should be addressed to Bingchao Ren; renbingchao840205@163.com and Ting Jin; jinting840205@haut.edu.cn

In this paper, an intelligent model is constructed to facilitate real-time dynamic analysis of the factors affecting the export of film and television copyrights and to track the process of spatiotemporal context. The algorithm analyzes the factors affecting the export of film and television copyrights according to actual needs. Through the comparative analysis of experimental models, the influence and optimization of gamma correction and Laplace distribution weighting on spatial context information and confidence map update are verified. In addition, this paper uses the gray relational algorithm to construct an analysis system of factors affecting the export of film and television copyright. The research shows that the analysis model of the influencing factors of film and television copyright export based on the gray relational algorithm can play a very good role in the analysis of these factors.

1. Introduction

In the new normal economic environment, there is no doubt that China's export structure also needs supply-side reforms. In terms of film and television cultural works, our country has been in a state of deficit in international trade for a long time. With the development of economy, people began to pursue spiritual and cultural life after satisfying their material life. With the transformation of society and changes in consumption concepts and lifestyles, as well as the promotion of technological factors such as Internet technology and new media technology, film and television cultural works appear more and more frequently in people's lives, and people's expenditure on film and television cultural works is also increasing.

On the one hand, as a kind of copyright, film and television copyright has the characteristics of copyright, which can be summarized into three types: "exclusiveness," "territoriality," and "timeliness." "Exclusivity" means that copyright is as exclusive as ownership. Copyright is exclusively owned by the right holder, and this right of the right holder is strictly protected by law. Moreover, in addition to the exceptions provided by the law, the use of the work by others must obtain the permission of the right holder. "Territoriality" means that the effectiveness of copyright is restricted by space and only extends to the territory of the country, which is strictly territorial. Unless international conventions or bilateral treaties are signed between countries, intellectual property rights do not have extraterritorial effects, and anyone outside of the country can freely use the copyright. However, due to the accelerating process of today's world integration and the increasingly frequent exchanges between countries, transnational copyrights and transnational jurisdictions of copyrights and worldwide intellectual property protection organizations have emerged. Therefore, the characteristic of "territoriality" is gradually diminishing [1]. "Timeliness" means that the protection of copyright is limited by time. If the copyright exceeds the copyright protection period stipulated by law, it will no longer be protected. Generally speaking, the authorship right, the right to modify and, the right to protect the integrity of the work in the personal rights of copyright are not restricted by time and will not disappear due to the death of a person. The right of

publication in property rights and personal rights is restricted by the term of copyright protection [2]. On the other hand, film and television copyright also has its own characteristics. Film and television works are a collection of independent works such as music, songs, scripts, audio, and video. It is based on these independent works as a whole formed through the processing of modern technology and takes the whole as the object of copyright protection. At the same time, these independent works are separately protected by the law, and the protection of the copyright of these works does not prevent the film and television works as a whole from being protected by the law. Therefore, there is a unique problem of multiple copyrights in the protection of film and television copyrights [3].

In order to facilitate the analysis of the factors affecting the export of film and television copyrights, this paper constructs an intelligent model for real-time analysis of the factors affecting the export of film and television copyrights, which provides a theoretical reference for subsequent related research.

2. Related Work

In international trade, cultural trade is extremely special. It is based on cultural industries and involves trade in goods, trade in services, and intellectual property rights. The International Monetary Fund (IMF) describes international cultural trade as exchanges between countries and between residents and nonresidents, and personal, cultural, and entertainment service transactions are all within the category of cultural trade. It is subdivided into the following two categories: one is audiovisual and related services, and the other is other cultural and entertainment services [4].

The rise of cultural trade has attracted the attention and research of many economists, hoping to find a theoretical basis that can explain cultural trade [5]. Literature [6] believes that traditional trade theory can explain the rise of cultural trade. For example, the United Kingdom has a comparative advantage in Shakespeare's plays, and the United States has a comparative advantage in movies, so that the two countries can exchange works with each other. The United Kingdom concentrates on producing and exporting dramas and importing relatively disadvantaged movies, while the United States concentrates on producing and exporting movies and importing dramas. In this way, both countries can gain benefits in international trade. Literature [7] believes that traditional trade theories such as comparative advantage theory and factor endowment theory are more suitable for imitable cultural products. For example, the labor force in developing countries is relatively surplus and has a comparative advantage in the production of imitable cultural products, so that the export of labor-intensive cultural products can be profitable. However, traditional trade theories have no explanatory power for the trade of cultural products that cannot be imitated.

Literature [8] believes that there are external economies of scale in the cultural industry and the agglomeration of producers in the geographic location forms a large-scale operation. Several film and television companies in Hollywood, the United States, have concentrated on all the links of film production, showing a highly vertical integration

situation and forming an efficient external scale economy effect. This vertical integration can achieve large-scale operations; reduce unnecessary market circulation links, thereby reducing production costs; and help companies integrate their own advantages, realize resource sharing, and achieve good economic benefits. Literature [9] believes that there are also internal economies of scale in the cultural industry. Take the production of movies as an example. Copying ready-made templates can greatly reduce the production costs of movies. Large-scale film and television groups integrate small-scale scattered resources to reduce production costs in production, so as to obtain cost advantages in competition, thereby forcing small companies to withdraw from the market and gaining market share.

Literature [10] puts forward the so-called first actor advantage theory while considering the effect of economies of scale on international cultural trade. Literature [11] argues that the reason why the United States can occupy an absolute share of the global TV market and continuously export cultural products to the outside world is that it has economies of scale and first actor advantages. Large-scale production has given American TV production companies a stronger cost advantage, with the ability to share fixed costs; product upgrades; and relatively sufficient funds required for advertising, making it a greater advantage in the competition of similar cultural products. The first actor advantage considers certain technical conditions, and through actions such as first improving management, increasing labor productivity, improving marketing channels, and being familiar with the market conditions of the exporting country, American cultural production companies can obtain a "leading" advantage in the production of cultural products [12].

Literature [13] applies demand preference theory to cultural trade. Literature [14] believes that the consumption of cultural products can be understood as the satisfaction that people get from current consumption and the accumulation of future knowledge and experience. Therefore, the past consumption structure of cultural products largely determines the future consumption structure.

Literature [15] believes that the theory of comparative advantage can be used to analyze cultural trade. Literature [16] believes that factor endowments, production technology, production methods, and innovation capabilities can cultivate the comparative advantages of the cultural industry. With these comparative advantages, cultural trade can be carried out. Literature [17] used the theory of comparative advantage to explain cultural trade, specifically pointing out that the main advantages of cultural industry participating in international trade are the resource endowment on the supply side, the advantages of knowledge and technology, and the scale of demand.

Literature [18] agrees that the theory of economies of scale is applicable to cultural trade. Take American movies as an example; the formation of Hollywood has reduced the production and production costs of American movies to a large extent. This specialized assembly line and industrial chain have enabled American movies to dominate the world and win high profits. Literature [19] points out that cultural trade is intraindustry trade and uses demand preference

theory to analyze it. The vast majority of international trade in cultural products is carried out between a few countries and is highly concentrated in a few countries, which is a typical intraindustry trade. The theory of preference similarity can explain the phenomenon that the import and export of international cultural trade are highly concentrated between European and American countries with a common cultural background and between the United States and Canada in North America [20].

3. Factor Analysis Model Based on Gray Relational Algorithm

This paper mainly analyzes the influencing factors of film and television copyright export through gray relational algorithm and improves it based on the kernel K-means algorithm. By taking the nonlinear constraint of the kernel K-means algorithm as a penalty term, that is, taking the last term of the constraint in the formula as an independent penalty term, it is combined with the kernel K-means clustering algorithm. In order to extract more effective information in the process of clustering, orthogonality constraints and nonnegativity constraints are added to the proposed model at the same time, and the improved penalized K-means clustering model (PKKM) is obtained in this paper. The objective function is as follows:

$$\max_H Tr\left[H^T K H\right] - \alpha \left\|1_n^T - 1_n^T H H^T\right\|_F^2,$$
$$s.t.\, H \geq 0, H^T H = I. \tag{1}$$

Among them, K represents the kernel matrix, and α is a hyperparameter.

When H satisfies the orthogonality constraint, based on the properties of the Frobenius function and the trace function, the penalty term in (1) can be written as follows:

$$\left\|1_n^T - 1_n^T H H^T\right\|_F^2 = Tr\left[1_n 1_n^T\right] - Tr\left[H^T 1_n 1_n^T H\right]. \tag{2}$$

Therefore, (1) can be written in the following form:

$$Tr\left[H^T K H\right] - \alpha\left\|1_n^T - 1_n^T H H^T\right\|_F^2,$$
$$= Tr\left[H^T K H\right] + \alpha Tr\left\|H^T 1_n 1_n^T H\right\|_F^2 - \alpha Tr\left[1_n 1_n^T\right], \tag{3}$$
$$= Tr\left[H^T (K + \alpha E) H\right] - \alpha n.$$

Among them, $E = 1_n 1_n^T$ represents an $n \times n$ matrix, and all elements in the matrix are 1.

Because the proposed PKKM model has orthogonal and nonnegative constraints, in the process of optimizing the above objective function, the nonconvexity of the model itself makes the solution of the model an NP-hard problem. Therefore, this paper proposes a simple but robust numerical algorithm. The algorithm splits the original matrix variable into two variables through the splitting method and satisfies the orthogonality and nonnegativity constraints. The problem of solving the objective function is transformed into a problem of seeking extreme values of two variables. Furthermore, the algorithm uses an alternate iteration method to find solutions that meet

the constraints. The split model is a more relaxed model. The objective function of the model is as follows [21]:

$$\max_{x,H} Tr\left[H^T (K + \alpha E) H\right] - \frac{\mu}{2}\|H - X\|_F^2, \tag{4}$$
$$s.t.\, H \geq 0, H^T H = I.$$

Among them, the second term in formula (2) can be written as follows:

$$\frac{\mu}{2}\|H - X\|_F^2,$$
$$= \frac{\mu}{2}\left(\|X\|_F^2 - 2Tr\left[H^T X\right] + \|H\|_F^2\right), \tag{5}$$
$$= \frac{\mu}{2}\|X\|_F^2 - Tr\left[H^T (\mu I) X\right] + \frac{\mu k}{2}.$$

Therefore, the solution to the subproblem of H in the above problem can be described as follows:

$$\max_H\left[H^T (\mu I) X\right],$$
$$s.t.\, H^T H = I. \tag{6}$$

Among them, $K = K + \alpha E + \mu I$.

The above-mentioned problem is also called the orthogonal Plucker problem, which has a closed-form solution. Below, we solve it by alternating iterative method.

When the variable X is fixed, the original problem is transformed into the following: for any matrix $A \in R^{n \times k}$, the objective function of the related optimization problem for $H \in R^{n \times k}$ is as follows:

$$\max_H Tr\left[H^T A\right],$$
$$s.t.\, H^T H = I. \tag{7}$$

Formula (5) has a corresponding closed-form solution:

$$H^* = U(:, 1: k)V^T. \tag{8}$$

Among them, $A = U \sum V^T$ is the singular value decomposition of A.

The relevant proof is as follows:

First, $A = U \sum V^T$ is the singular value decomposition of A, and the solution of the H subproblem is as follows:

$$H^* = \arg\max_H Tr\left[H^T A\right]$$
$$= \arg\max_H Tr\left[U \sum V^T\right]$$
$$= \arg\max_H Tr\left[\left(U^T H V\right)^T \sum\right]$$
$$= U\left(\arg\max_H Tr\left[H^T \sum\right]\right)V^T \tag{9}$$
$$= U\begin{bmatrix} I_k \\ 0 \end{bmatrix}V^T.$$

The solution to the X subproblem is as follows: when the orthogonal matrix H cannot satisfy the nonnegativity constraint, the update rule for X is as follows:

$$X = \max(0, H). \tag{10}$$

Therefore, the entire process above is to update the variables between the Stiefel manifold and the nonnegative quadrant.

In this part, we will discuss the relationship between the proposed PKKM algorithm and some commonly used classic clustering algorithms, such as classic K-means algorithm, orthogonal nonnegative matrix factorization (ONMF) algorithm, spectral clustering, and projection nonnegative matrix factorization (PNMF) algorithm.

This relationship is shown in Figure 1. As can be seen from the figure, compared to the other three clustering algorithms, the model proposed in this paper is the closest relaxation model to the K-means model, and its scalability can be changed according to its model. The following part will discuss the relationship between PKKM model and K-means model, ONMF model, spectral clustering, and PNMF model.

When $\alpha = +\infty$, the PKKM algorithm is equivalent to the K-means clustering algorithm.

In the PKKM model, when the parameter $\alpha = +\infty$ of the penalty term in (1) is met, and the constraint condition $1_n^T - 1_n^T HH^T = 0$ is satisfied at the same time, (1) can be written in the following form:

$$\max_{H} Tr\left[H^T K H\right], \\ s.t. \, H \geq 0, H^T H = I_k, 1_n^T - 1_n^T HH^T = 0. \tag{11}$$

Formula (9) is equivalent to the objective function formula of the kernel K mean value.

When the parameter of the penalty term in (1) is $\alpha = 0$, the PKKM model can be written in the following form:

$$\max_{H} Tr\left[H^T K H\right], \\ s.t. \, H \geq 0, H^T H = I_k. \tag{12}$$

Equation (12) corresponds to the ONMF model.

Spectral clustering is the orthogonal relaxation of the proposed PKKM model. The objective function of the spectral clustering model is as follows:

$$\max_{X} Tr\left[X^T L X\right], \\ s.t. \, X^T X = I_k. \tag{13}$$

In formula (13) of the PKKM model, the kernel matrix $K + aE$ in the model is replaced by L, and then the non-negativity constraint in the model is removed. Then, the objective function of PKKM is equivalent to the model of spectral clustering.

The PNMF algorithm is a nonnegative relaxation of the proposed PKKM algorithm, and its objective function is as follows:
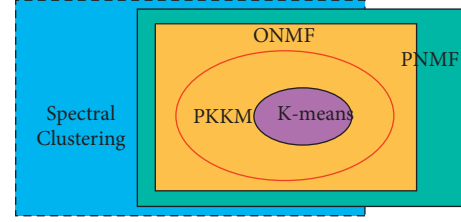
Figure 1: The relationship between PKKM algorithm and other clustering models.

$$\max_{x \geq 0} \left[M - MXX^T\right]_F^2. \tag{14}$$

In formula (1) of the PKKM model, $\alpha = 0$, and the orthogonality constraint is removed; then, the PKKM model and the PNMF model are equivalent.

4. Analysis of Influencing Factors of Film and Television Copyright Export Based on Gray Relational Algorithm

The export destinations of Chinese movies are mainly concentrated in two types of countries. One type is Southeast Asian and East Asian countries, which are close to our country's cultural distance and can have a better understanding of Chinese movies. Therefore, in the early stage of our country's film export, works were mainly exported to Southeast Asia, North Korea, and other countries. The other type is European and American countries, which have a developed domestic market and a wealth of domestic works, so there is not much demand for Chinese works. However, due to the relatively developed economies of European and American countries and the demand of local Chinese for domestic films, domestic films can also have some overseas income in Europe and the United States.

The film and television copyright management system creates an end-to-end streaming media content protection platform, while providing all the services needed from the content preparation stage to the delivery stage. The function flow chart of the film and television copyright management system is shown in Figure 2.

The film and television copyright management system uses the HLS protocol for video transmission. The HLS protocol is a streaming media transmission protocol based on HTTP, which can be used to realize video playback on terminal devices. It differs from the common RTP/RTCP and RTSP in that the client-side algorithm obtains complete media content. The content transmitted by HLS mainly includes M3U8 description files and continuous, equal-length TS format media files. Then, it uses the index file of M3U8 to play. The HLS work flow chart is shown in Figure 3.

The copyright tracking system of film and television works will extract and track the feature codes of the film and television works in the library to timely understand the relevant infringement status of the works on the Internet, provide a direction for combating copyright infringement of works, and provide technical support for the copyright protection of film and television works.
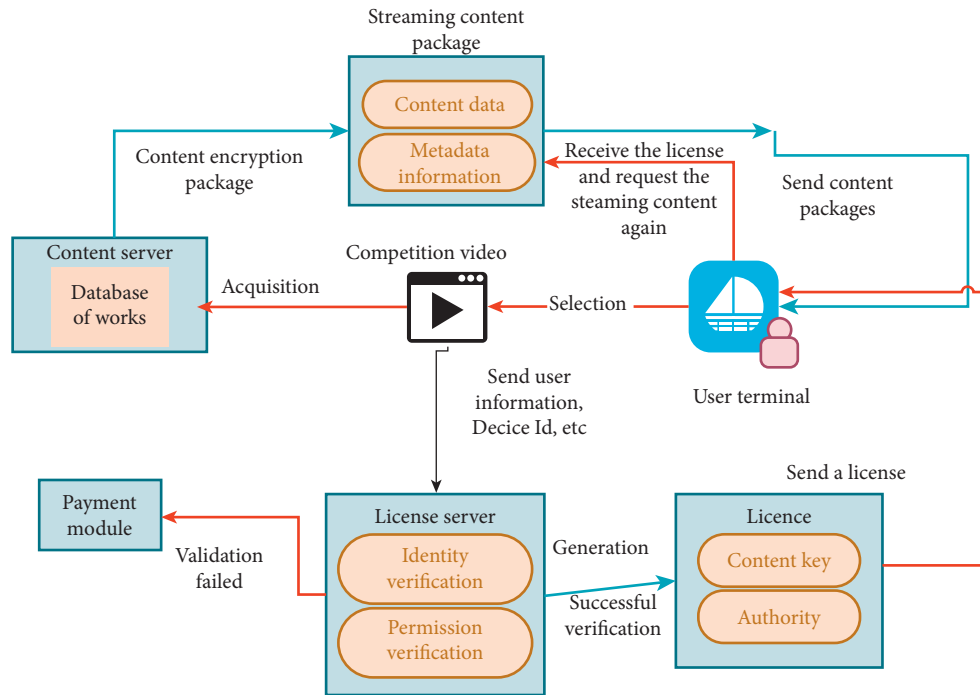
FIGURE 2: Function flow chart of film and television copyright management system.
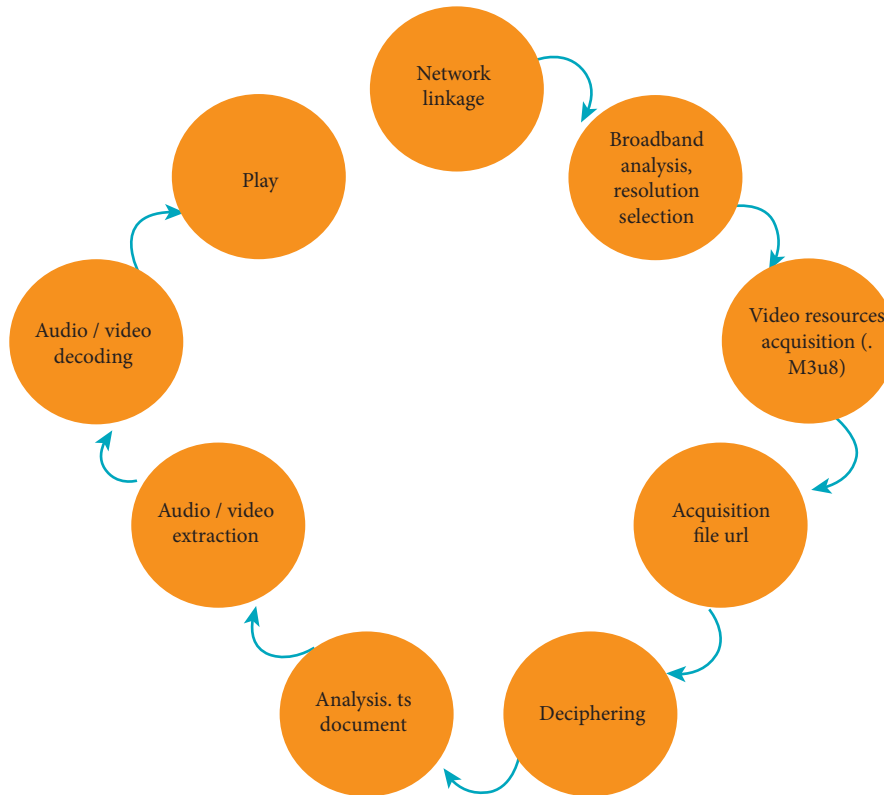
FIGURE 3: HLS flow chart.

After analyzing the needs of the copyright tracking system for text works, it is determined that the system is divided into the following three major modules: infringement information collection, statistical analysis, and auxiliary function modules. Among them, the collection of infringement information is a necessary function, which mainly includes the functions of system importing works, feature code extraction, web crawlers to collect infringement

information, and related process scheduling. The statistical analysis module mainly displays some analyzed data, mainly including functions such as hot infringement list, work infringement information query, and infringement information list. The auxiliary function module mainly configures some data of the system operation module, including authorized website management, key monitoring website management, parameter configuration, and domain name information management. The specific system function module structure diagram is shown in Figure 4.

Aiming at solving the problem of information asymmetry between the seller and the authorized party during the transaction of digital works, a trusted counting mechanism is proposed, as shown in Figure 5. Under this mechanism, trusted counters are introduced into the authorized party (authorization system), seller (sales system), and trusted third party (digital work transaction management platform system). Under the combined effect of the three counters, the supervision of digital works transactions is realized. After the sales system receives the order, it extracts the transaction information (including transaction time, seller ID, content provider ID, price, transaction quantity, and digital copyright identification) in the order and then calls the trusted counter of the sales-oriented system for processing. The sales system trusted counter first checks whether the format of the incoming data is legal and generates a transaction request number and a sales random number. Then, it assembles the data into sales permission request data according to the communication protocol in the counter and then signs the sales permission request data to form uploaded data. Finally, it puts the uploaded data into the data buffer pool, and finally the uploaded data is sent to the trusted counter for the management platform through the network. The authorization system obtains authorization-related information (including order information and authorization time) from the outside and calls a trusted counter for the authorization system to process the data. The trusted counter for the authorization system first checks whether the format of the incoming data is legal and generates an authorized random number. Then, the data is assembled into sales license data according to the communication protocol in the counter, and then the sales license data is signed to form upload data. Finally, the uploaded data is put into the data buffer pool and sent to the trusted counter for the management platform through the network. After the trusted counter in the trusted third party receives the uploaded data from the authorized end and the sales end, it first authenticates the data; the data that fails the authentication will be written into the log, and the data that is successfully authenticated will also be matched with the transaction data. Transaction data matching aims mainly to determine whether two uploaded data items belong to the same transaction. If the matching is successful, the uploaded data will be put into the matching database. If the matching fails, the uploaded data will be placed in the unmatched database. In addition, since there are locally generated random numbers in the two types of uploaded data, a certain degree of uniqueness of the data can be guaranteed, and the

data signature can ensure the nonrepudiation of the data. Therefore, the mechanism in Figure 5 is credible.

Figure 6 is a schematic diagram of the overall business architecture where the trusted counting system is located. The trusted counter for the sales system, the trusted counter for the authorization system, and the trusted counter for the platform constitute the trusted counting system. The trusted counter for the sales system is used by content sellers. The main function is to complete its own configuration, test the connectivity with the platform counter, complete the processing of transaction information, and upload it to the trusted counter for the platform. The trusted counter for the authorization system is used by integrators and content providers. In addition to completing its own configuration, connectivity testing, and uploading authorization data, it also supports querying the sales records of content sellers. The platform-oriented trusted counter is mainly responsible for the receipt, authentication, and final storage of the data uploaded by the sales and authorized ends (calling the relevant database interface). In addition, it is also responsible for managing the configuration information and usage status of the trusted counter for the sales system and the trusted counter for the authorization system and provides data for the sales record query of the authorized end (calling the relevant data query interface). The trusted transaction management platform conducts statistical supervision of transactions and provides external query services based on the data provided by the trusted counting system.

Figure 7 is a schematic diagram of the digital content publishing business process. First, the publishing unit processes the resources to be released and then releases it to the content provider. After the content provider obtains the resource, according to the nature of the resource and its own situation, it will carry out digital content services through direct sales or consignment by channel dealers. In the case of direct selling, the content provider acts as a content seller at the same time and directly deals with users. There is no issue of credible counting involved here. In the case of consignment sales by channel dealers, content providers have no control over content sellers. At this time, the role of a trusted counting mechanism is needed to help regulators supervise the transactions of data works through three types of counters: trusted counters for sales systems, trusted counters for authorization systems, and trusted counters for platforms. Users (including individual readers and institutions) obtain digital content through purchase and payment, and read or use it through a certain method (designated reading software). Throughout the transaction process, the supervisor monitors the information provided by the trusted counting system to ensure the fairness and credibility of the transaction.

On the basis of the above subsystems, this paper combines the gray correlation algorithm to analyze the factors affecting the export of film and television copyright and constructs the intelligent factor analysis model shown in Figure 8.

After constructing the above model, this paper evaluates the real-time monitoring effect of the film and television
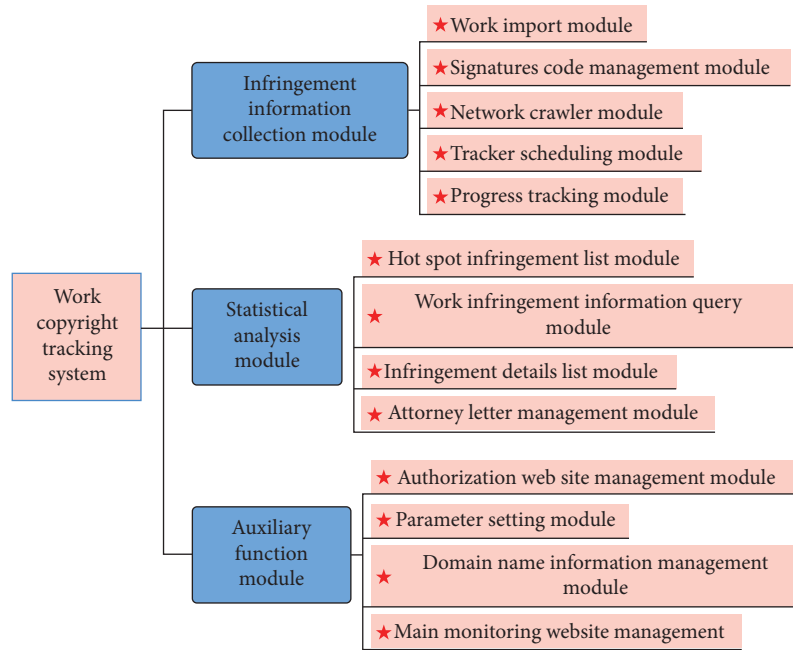
FIGURE 4: System function module structure diagram.
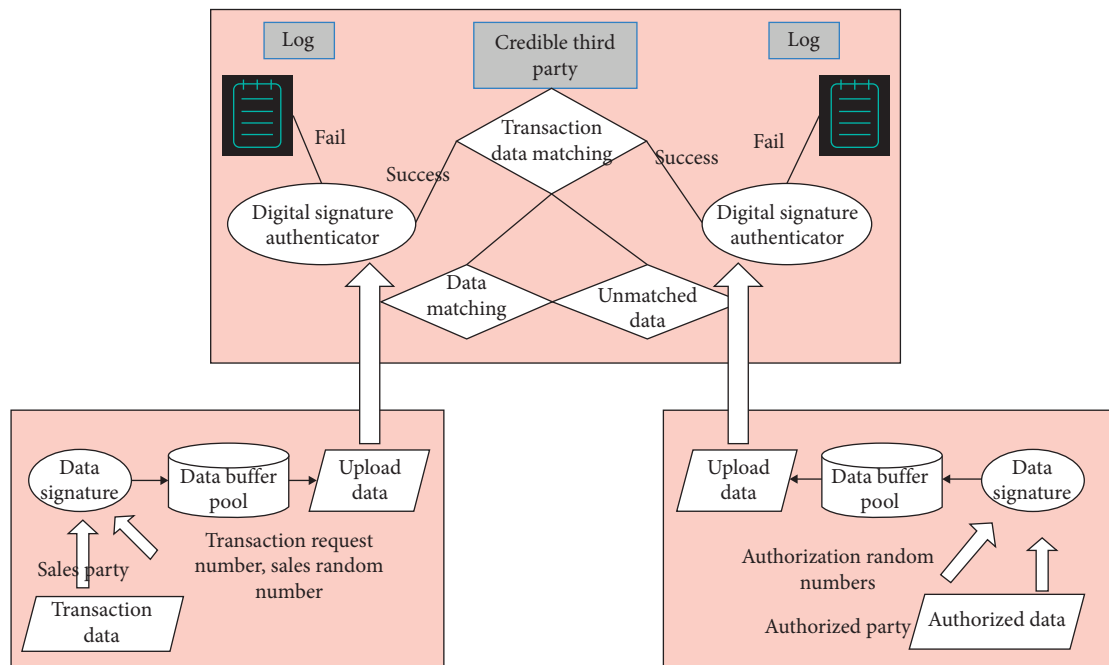
FIGURE 5: Trusted counting mechanism framework.

copyright export of this system and obtains the results shown in Table 1 and Figure 9.

On the basis of the above analysis, this article evaluates the measured effect of the analysis model of the influence factors of film and television copyright export based on the gray correlation algorithm, and the results are shown in Table 2 and Figure 10.

From the above research, it can be seen that the analysis model of influencing factors of film and television copyright

export based on gray correlation algorithm proposed in this paper can play a certain role in the analysis of these factors.

Through the analysis of the above model, we can see that different influencing factors have inconsistent degrees of influence on the import and export of our country's film and television cultural works. The increase in the number of movie screens represents the rapid development of our country's movie market in recent years, which means that the Chinese market's demand for film and television cultural
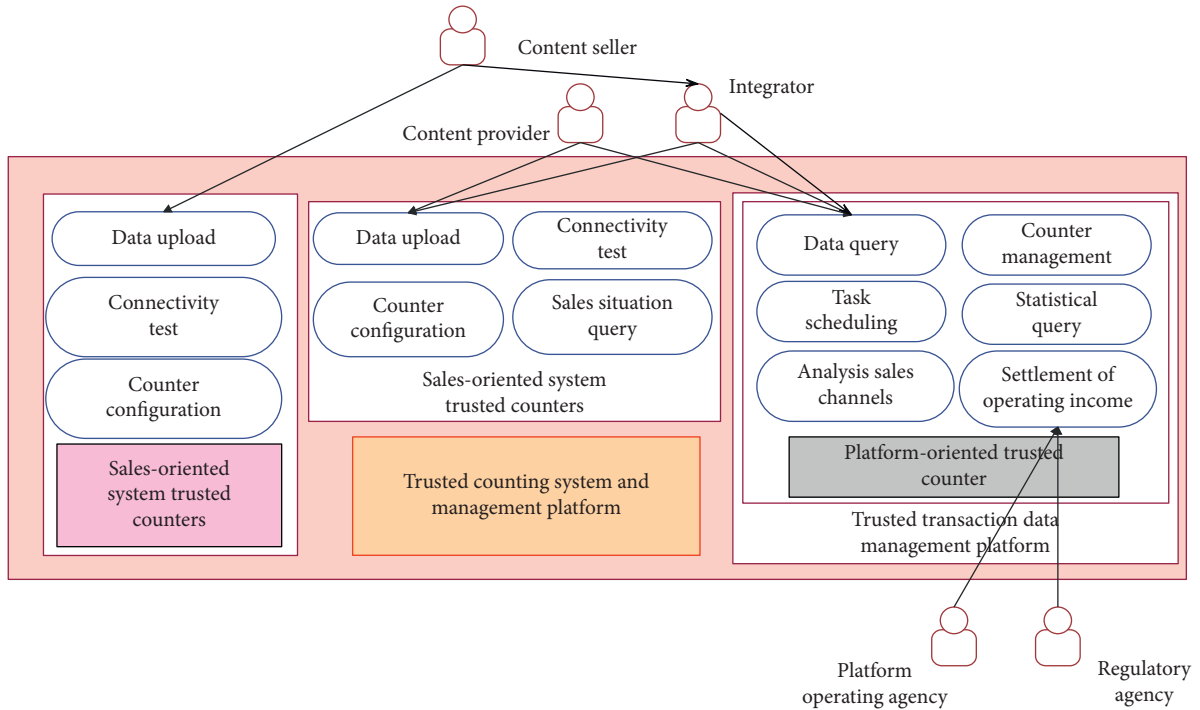
Figure 6: The overall business architecture where the trusted counting system is located.
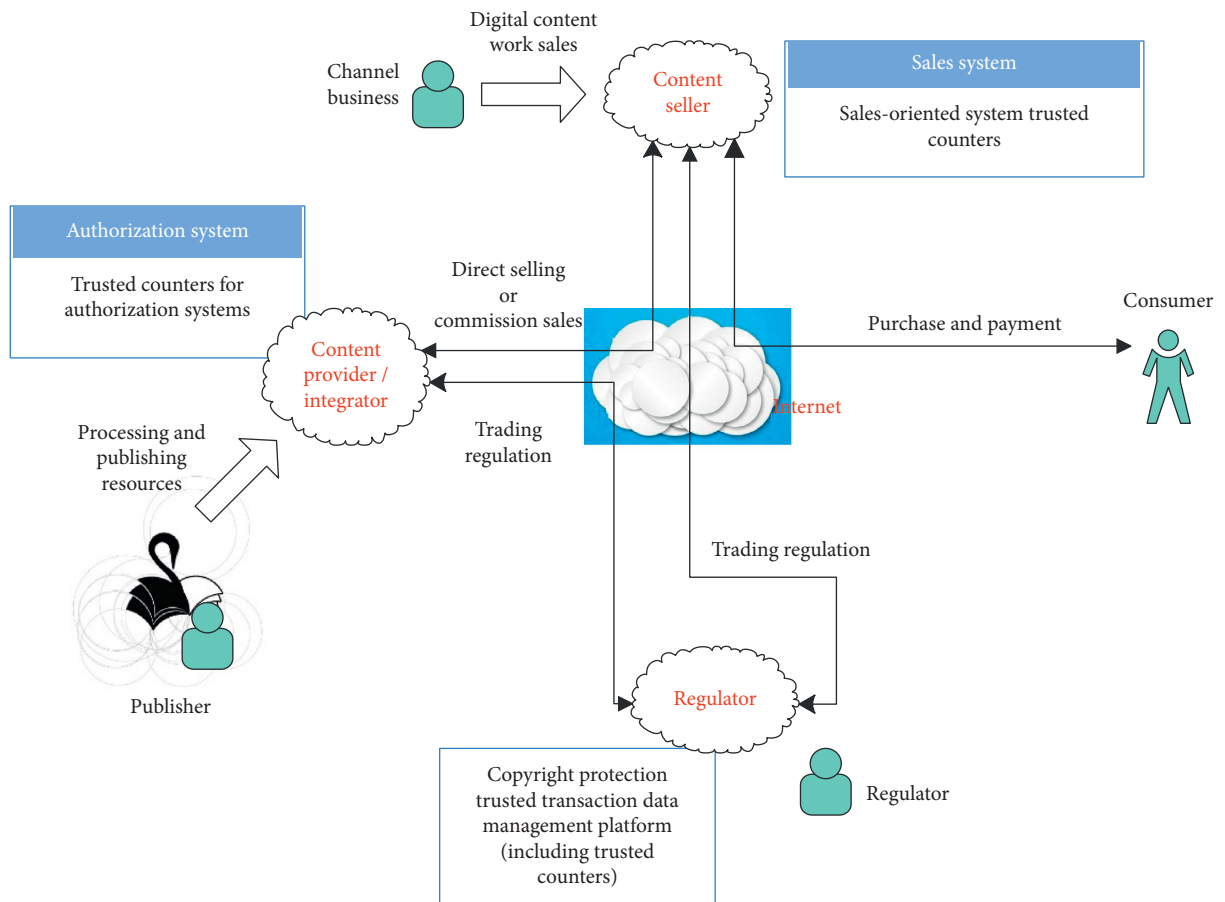
Figure 7: Digital content publishing business process.
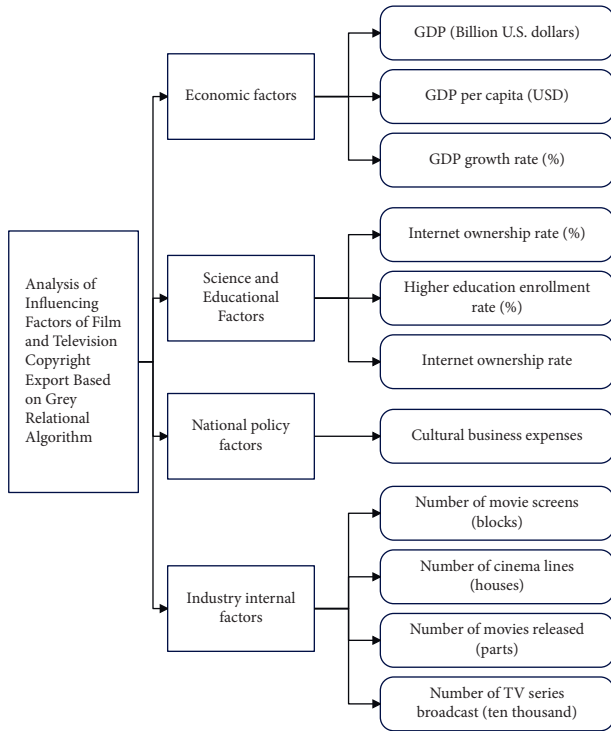
FIGURE 8: Analysis model of influencing factors of film and television copyright export based on gray relational algorithm.

TABLE 1: Real-time monitoring effect of film and television copyright export.

Number	Copyright monitoring
1	93.79
2	94.80
3	92.54
4	92.49
5	86.37
6	94.01
7	89.61
8	84.15
9	93.48
10	94.22
11	85.64
12	93.89
13	86.50
14	85.78
15	91.60
16	86.89
17	90.97
18	84.75
19	94.32
20	92.10
21	93.93
22	92.66
23	90.62
24	84.06
25	94.57
26	87.00
27	87.84

TABLE 1: Continued.

Number	Copyright monitoring
28	90.92
29	92.49
30	91.27
31	91.99
32	86.44
33	85.30
34	94.97
35	83.45
36	94.46
37	91.42
38	88.96
39	94.13
40	83.91
41	88.77
42	92.41
43	88.68
44	88.82
45	93.05
46	84.14
47	94.29
48	83.02
49	84.52
50	92.99
51	90.04
52	83.77
53	94.84
54	94.86
55	87.76
56	90.73
57	86.10
58	92.56
59	85.63
60	91.04
61	87.20
62	87.15
63	93.57
64	92.39
65	92.31
66	89.54
67	85.18
68	86.12
69	86.50
70	83.35
71	91.67
72	84.51
73	85.70
74	93.70
75	94.19
76	91.72
77	87.49
78	92.75
79	86.77
80	88.44
81	83.91

works has increased significantly. Moreover, domestic works can no longer meet the needs of the expanding market and consumers, so it is necessary to continuously import excellent works from abroad. The increase in the enrollment rate of higher education means that there are more people
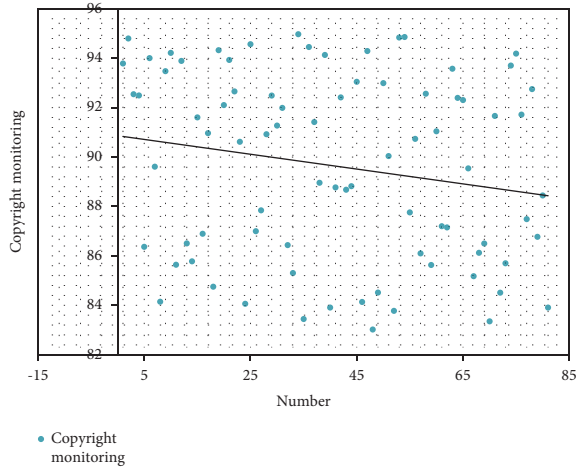
Figure 9: Statistical visual chart of the real-time monitoring effect of film and television copyright export.

Table 2: The actual measurement effect of the analysis model of factors affecting the export of film and television copyrights based on the gray correlation algorithm.

Number	Factor analysis
1	86.28
2	88.29
3	88.04
4	93.70
5	90.52
6	89.12
7	91.73
8	84.89
9	88.61
10	85.59
11	84.82
12	90.58
13	94.94
14	88.45
15	94.54
16	88.78
17	83.70
18	87.78
19	85.29
20	94.30
21	87.94
22	87.31
23	85.73
24	88.36
25	83.51
26	88.30
27	94.48
28	87.61
29	86.04
30	87.35
31	89.36
32	85.80
33	85.88
34	94.95
35	88.46
36	91.43

Table 2: Continued.

Number	Factor analysis
37	85.51
38	93.44
39	86.88
40	94.84
41	94.08
42	94.91
43	93.73
44	88.14
45	86.54
46	91.05
47	89.09
48	87.06
49	83.57
50	88.10
51	83.45
52	91.57
53	84.29
54	83.58
55	86.00
56	92.51
57	87.76
58	89.42
59	85.11
60	90.78
61	87.98
62	92.19
63	84.43
64	85.04
65	92.36
66	87.41
67	94.93
68	90.25
69	83.59
70	89.36
71	90.27
72	93.99
73	91.09
74	85.88
75	91.34
76	86.90
77	85.06
78	89.70
79	93.36
80	89.52
81	94.37

with higher education who have a stronger ability to consume spiritual and cultural products. Therefore, it will also increase the consumer group and consumption of film and television cultural works. In addition, other economic factors such as GDP, technological factors of Internet penetration rate, national policy factors of cultural undertakings, and growth of internal factors such as the number of movies and TV series will cause an increase in the import of film and television cultural works through their respective influence channels. Among the many influencing factors, the GDP growth rate has the strongest correlation with the export of film and television cultural works. The GDP growth rate reflects China's economic growth rate. Although it is a
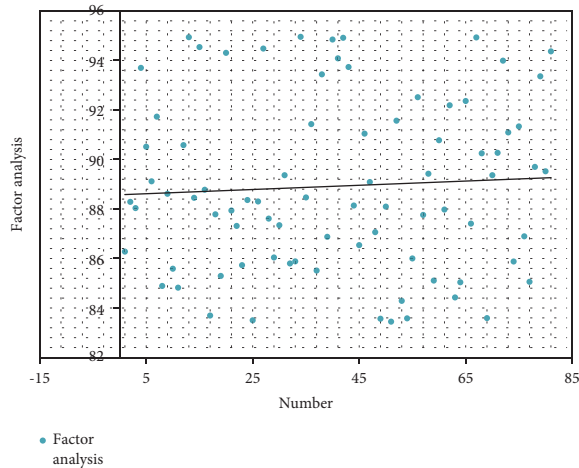
Figure 10: Visual diagram of the actual measurement effect of the analysis model of the factors affecting the export of film and television copyright based on the gray correlation algorithm.

macroeconomic indicator, the overall economic development is an economic environment for a small industry, which will also have a corresponding impact on its export volume.

5. Conclusion

Film and television copyright owners will be subject to certain restrictions in the process of exercising film and television copyrights. All countries in the world, including China with its copyright laws, have set certain restrictions on the exercise of copyright. It is mainly reflected in three legal systems: the fair use system, the statutory license system, and the compulsory license system. The fair use system is a basic system of copyright law. It refers to a system where the law allows others to freely use copyrighted works under certain conditions without having to obtain the copyright owner's consent or paying the copyright owner. The factors affecting the export of film and television copyright will continue to change with changes in the general environment, so they need to be studied in light of the actual situation. In order to facilitate the analysis of the export influencing factors of film and television copyright, this paper constructs an intelligent model for real-time analysis of these factors, which provides theoretical reference for subsequent related research. The research results show that the analysis model of film and television copyright export influencing factors proposed in this paper based on the gray correlation algorithm can play a certain role in the analysis of these factors.

Data Availability

The labeled dataset used to support the findings of this study is available from the corresponding author upon request.

Conflicts of Interest

The authors declare no conflicts of interest.

References

[1] C. S. Myers, "Plagiarism and copyright: b," *College & Undergraduate Libraries*, vol. 25, no. 1, pp. 91–99, 2018.

[2] J. H. Rooksby and C. S. Hayter, "Copyrights in higher education: motivating a research agenda," *The Journal of Technology Transfer*, vol. 44, no. 1, pp. 250–263, 2019.

[3] N. H. Sharfina, H. Paserangi, F. P. Rasyid, and M. I. N. Fuady, "Copyright issues on the prank video on the youtube," in *Proceedings of the International Conference on Environmental and Energy Policy (ICEEP 2021)*, pp. 90–97, Surakarta, Indonesia, January 2021, 2013.

[4] K. Nekit, H. Ulianova, and D. Kolodi, "Website as an object of legal protection by Ukrainian legislation," *Amazonia Investiga*, vol. 8, no. 21, pp. 222–230, 2019.

[5] V. Lunyachek and N. Ruban, "Managing intellectual property rights protection in the system of comprehensive seconday education," *Public Policy and Administration*, vol. 17, no. 1, pp. 114–125, 2018.

[6] S. Schroff, "An alternative universe? Authors as copyright owners- the case of the Japanese Manga Industry," *Creative Industries Journal*, vol. 12, no. 1, pp. 125–150, 2019.

[7] M. Finck and V. Moscon, "Copyright law on b: between new forms of rights administration and digital rights management 2.0," *IIC - International Review of Intellectual Property and Competition Law*, vol. 50, no. 1, pp. 77–108, 2019.

[8] N. K. S. Dharmawan, "Protecting traditional Balinese weaving trough copyright law: is it appropriate?" *Diponegoro Law Review*, vol. 2, no. 1, pp. 57–84, 2017.

[9] J. P. McSherry, "The labor of literature: democracy and literary culture in modern Chile by jane D griffin," *Journal of Global South Studies*, vol. 35, no. 2, pp. 448–450, 2018.

[10] G. Carugno, "How to protect traditional folk music? Some reflections upon traditional knowledge and copyright law," *International Journal for the Semiotics of Law - Revue internationale de Sémiotique juridique*, vol. 31, no. 2, pp. 261–274, 2018.

[11] R. Matulionyte, "Empowering authors via fairer copyright contract law," *Law Journal*, vol. 42, no. 2, pp. 681–718, 2019.

[12] E. Hudson, "The pastiche exception in copyright law: a case of mashed-up drafting?" *Intellectual Property Quarterly*, vol. 2017, no. 4, pp. 346–368, 2017.

[13] M. Sag, "The new legal landscape for text mining and machine learning," *Journal of the Copyright Society of the U.S.A*, vol. 66, no. 2, pp. 291–367, 2019.

[14] S. Geiregat, "Digital exhaustion of copyright after CJEU judgment in Ranks and Vasiļevičs," *Computer Law & Security Report*, vol. 33, no. 4, pp. 521–540, 2017.

[15] W. Slauter, "Introduction: copying and copyright, publishing practice and the law," *Victorian Periodicals Review*, vol. 51, no. 4, pp. 583–596, 2018.

[16] E. Rosati, "The Monkey Selfie case and the concept of authorship: an EU perspective," *Journal of Intellectual Property Law & Practice*, vol. 12, no. 12, pp. 973–977, 2017.

[17] I. Chatterjee, "Artificial intelligence and patentability: review and discussions," *International Journal of Modern Research*, vol. 1, no. 1, pp. 15–21, 2021.

[18] D. Jongsma, "Parody after d - a comparative overview of the approach to parody under copyright law in Belgium, France, Germany and The Netherlands," *IIC - International Review of Intellectual Property and Competition Law*, vol. 48, no. 6, pp. 652–682, 2017.

[19] I. G. Popescu, G. Sechel, and F. G. Leaşu, "Biomedical research ethics," *Romanian Journal of Morphology and Embryology*, vol. 59, no. 3, pp. 1001–1005, 2018.

[20] S. G. Rizzo, F. Bertini, and D. Montesi, "Fine-grain watermarking for intellectual property protection," *EURASIP Journal on Information Security*, vol. 2019, no. 1, pp. 1–20, Article ID 00942, 2019.

[21] Y. Vansover, "On the natural aspect of historical thinking in the classroom," *International Journal of Innovation, Creativity and Change*, vol. 4, no. 4, pp. 1–23, 2019.

Research Article

Study on Behavior and Bearing Capacity Computation Method of Shallow Rock-Socketed Short Piles Based on the Self-Balanced Loading Test

Junxiu Liu [1,2] **Xianfeng Shao** [3] **Xuhui Huang,** [2] **and Guangyong Cao** [1,2]

[1]*Anhui Province Key Laboratory of Building Structure and Underground Engineering, Anhui Jianzhu University, Hefei, Anhui 230601, China*
[2]*College of Civil Engineering, Anhui Jianzhu University, Hefei, Anhui 230601, China*
[3]*State Grid Anhui Electric Power Co., Ltd. Construction Company, Hefei, Anhui 230001, China*

Correspondence should be addressed to Junxiu Liu; tju_liu@hotmail.com

The self-balanced loading test is a state-of-art pile testing method, but its suitability to pile bearing capacity determination in transformer substation engineering in mountainous and hilly areas is not yet clear. In this study, a two-dimensional axisymmetric numerical model is established by the PLAXIS software to simulate the behavior and bearing mechanism of shallow rock-socketed short piles based on the self-balanced loading test. The model is first validated by simulating the field tests of two adjacent piles under self-balanced loading. Then the influence factors of the load-displacement curves of piles are analyzed. Thereafter, the mechanical mechanism of the self-balanced loading tests is simulated and compared with the conventional static loading tests. It is observed that the rock modulus, rock-socketed depth of piles, and burial depth of the Osterberg Cell affect the load-displacement significantly, but the cohesion of the rocks affects little. Moreover, compared with the conventional static loading tests, the shear stress of the pile-soil interface distributes less uniformly under self-balanced loading conditions. On this basis, a bearing capacity computation method of shallow rock-socketed short piles based on the self-balanced loading test is proposed.

1. Introduction

With the rapid and continuous urbanization, there are more and more transformer substation engineering, as important urban infrastructures, constructed in mountainous and hilly areas. Rock-socketed piles with small diameter (generally 600–800 mm), short length (generally 10–20 m), and shallow rock-socketed depth (generally 0.5–1.0 times the pile diameter) are usually adopted for transformer substations in these areas in China. The bearing capacity of these piles is usually obtained by the static loading test [1–8]. This method is to apply physical loads to the pile top at specific time intervals and monitor the displacement at the loading point until failure [9]. The static loading test is the most direct, reliable, and widely used testing method to obtain the bearing capacity of piles, but has some disadvantages such as

high cost, heavy workload, and long testing period in particular for high capacity piles [7–10]. For the mountainous and hilly areas with complex geological conditions, it is difficult to transport concrete blocks or sandbags needed for providing adequate reactive capacity for static loading tests. Besides, adverse environmental problems such as vegetation destruction, solid waste generation, energy consumption, and carbon emission may occur in the stacking loading process. Therefore, the application of the conventional static loading test in transformer substation engineering in mountainous and hilly areas is not cost-efficient and environmentally friendly. More economical and sustainable pile testing methods for transformer substation engineering in mountainous and hilly areas are needed.

The self-balanced loading test also referred to as the Osterberg Cell loading test, firstly introduced into

engineering practice by Osterberg in Northwestern University [11], is an advanced pile testing approach. When this method is used for pile testing, a particularly designed loading device called Osterberg Cell is placed at the specified position inside piles. The Osterberg Cell is a hydraulic jack-like device with displacement transducer wires extended to the ground surface. During the testing process, the Osterberg Cell is pressurized internally and expanded in a vertical direction [12–16]. Thus, an upward and a downward force inside the pile are generated, and the displacement of the two parts of the pile (above and below the Osterberg Cell) is measured. The actual applied load is in equilibrium with frictions between the upper segment of the pile and the soil, self-weight of the pile, frictions between the lower segment of the pile and the soil, and pile-end resistance. Therefore, dead weight or reaction frame is not required in the self-balanced loading test. The bearing capacity can be obtained from two load-displacement curves of the upper and the lower segment of the pile [17–31].

Compared with the conventional static loading test, the self-balanced method has many advantages. Firstly, because the multilevel Osterberg cell test is frequently employed and over one hydraulic jack can be installed on the same level, the capability of the self-balanced loading test can meet the requirements of almost all piles [22]. Secondly, for the piles with very high design loads, a conventional static loading test needs a very large weighted platform or very strong frame for reaction, which has been prohibitively costly and also difficult to arrange in the available time and space [13]. However, the self-balanced method is economic since a smaller testing area and less testing period and is particularly suitable for areas where a conventional static loading test is difficult to arrange in space. Thirdly, the self-balanced loading test has advantages even in the places where the conventional static loading test can be performed, such as less solid waste and other environmental impacts. Therefore, the self-balanced method is considered a more sustainable pile testing method [32].

Nowadays, the self-balanced loading test has been used for high-rise buildings, bridges, and offshore engineering projects [22–24]. However, there are still many problems not addressed. Firstly, when using the self-balanced loading test, the equilibrium point of the testing pile must be determined before Osterberg Cell placement. But engineering practice shows that it is difficult to estimate the equilibrium points accurately, which fails in the upper and lower segments of the piles to reach the ultimate bearing capacity simultaneously in the self-balanced loading test. Secondly, the loading point and loading mode of the self-balanced method is different from the actual stress condition, resulting in different frictional resistance distribution at the pile-soil interface [16, 17]. In addition, rock-socketed piles used in transformer substation engineering in mountainous and hilly areas usually have lower bearing capacity compared with other engineering projects because of smaller diameter, shorter length, and shallower rock-socketed depth. Therefore, the uplift bearing capacity of the pile will be obviously reduced if the Osterberg Cell is installed inside the pile body. In this study, a two-dimensional axisymmetric numerical model is established by the PLAXIS software to investigate the behavior and bearing mechanism of shallow rock-socketed short piles based on the self-balanced loading test. The model is first validated by simulating the field tests of two adjacent piles under self-balanced loading located in southern Anhui, China. Then the influence factors of the load-displacement curves of piles are analyzed. Thereafter, the mechanical mechanism of the self-balanced loading tests is simulated and compared with the conventional static loading tests. On this basis, a bearing capacity computation method of shallow rock-socketed short piles based on the self-balanced loading test is proposed. The simulation results and computation method should provide valuable information for managers to improve the efficiency of management of transformer substation engineering in mountainous and hilly areas.

2. Numerical Modeling

2.1. Description of the Field Test. The field tests were carried out to investigate the behavior of two adjacent cast-in-place concrete piles under self-balanced loading in a 500 kv transformer substation engineering located in southern Anhui, China. The length and diameter of the piles were 16.8 m and 0.6 m, respectively. The rock-socketed depth of the piles was 0.7 m.

The subsoil profile of the construction site consists of 4 soil layers. The 4 soil layers from top to bottom are as follows: compacted fill (10.8 m thick), clay (4.6 m thick), gravel (0.7 m thick), and limestone (3.6 m thick). There is no groundwater on the site. The material properties are illustrated in Table 1.

Figure 1 shows the details of the testing pile, ground condition, the Osterberg Cell, and the displacement monitoring system. The Osterberg Cell was located at the pile end and loaded through the loading system above ground. The displacement bars were connected to the upper or lower loading plates of the Osterberg Cell. Multi-stage loading was adopted for the pile testing. The first loading of the test was set to 260 kN, and the loading increment for each stage was set to 130 kN. During the test, each level of loading was maintained until the pile deformation was stable. For the Osterberg Cell selected for the field test, the maximum loading capacity was 2500 kN and the maximum loading stroke was 100 mm.

Figure 2 shows the measured upward displacement of pile bodies (UDPB) and downward displacement of pile ends (DDPE) of the two adjacent piles (A1 and A2) during the self-balanced loading test. It can be seen that their load-displacement curves were generally coincident, indicating that the self-balanced loading tests have good repeatability. During the field tests, when loaded to the 15th grade (2080 kN), the UDPB and DDPE of A1 were 4.10 mm and 77.06 mm; and the UDPB and DDPE of A2 were 4.81 mm and 71.88 mm. The total displacement nearly reached the maximum loading stroke of the Osterberg Cell and therefore the loading was stopped.

TABLE 1: Summary of the subsoil properties.

Material	Layer 1	Layer 2	Layer 3	Layer 4
γ (kN·m^{-3})	17.8	19.5	19.8	22.0
ω (%)	18.0	24.0	19.0	–
e_0	0.80	0.55	0.60	–
E_{50}^{ref} (MPa)	22.0	18.0	23.0	43.5
c (kPa)	16.0	20.0	25.0	23.0
φ (°)	30.0	27.0	30.0	42.0

Note: γ = unit weight; ω = water content; e_0 = initial void ratio; E_{50}^{ref} = secant modulus in standard drained triaxial testing; c = cohesion; φ = friction angle.

(a)

(b)
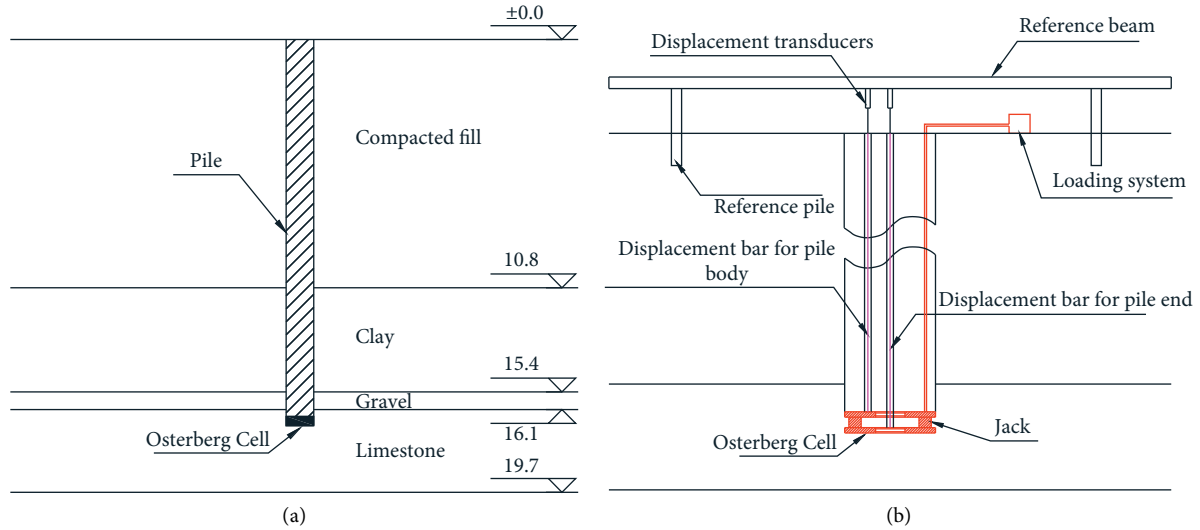
FIGURE 1: Details of the field test. (a) Pile and ground condition. (b) The Osterberg Cell and displacement monitoring.
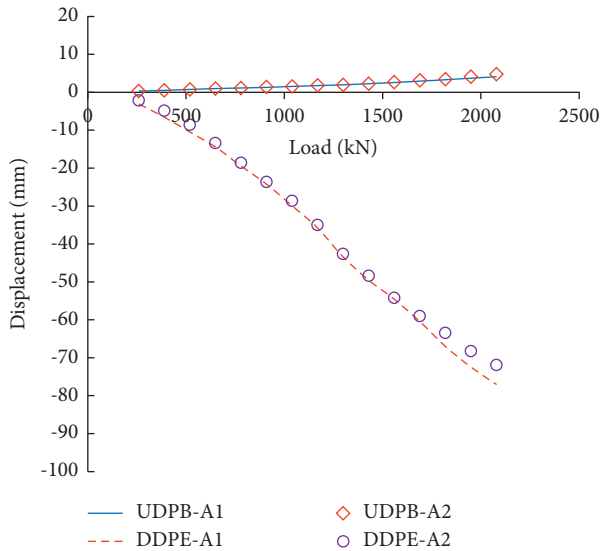
FIGURE 2: Measured load-displacement curves of the two adjacent piles.

FIGURE 3: Axisymmetric numerical model of the self-balanced loading test.

2.2. Finite Element Mesh and Boundary Conditions.

The finite element software PLAXIS is adopted in this study. PLAXIS is developed by the Delft University of Technology and could be used to simulate the nonlinear, time-dependent, and anisotropic behavior of soils and rocks [33]. Figure 3 shows the two-dimensional axisymmetric numerical model of the self-balanced loading test. The axis of symmetry is set at the axis of the pile. The boundary conditions are taken as rollers on the vertical boundary surfaces of the model and as fully fixed at the base of the model [34]. In the numerical model, the upper and lower loading plates of the Osterberg Cell are represented by two uniform distributed loads. In other words, the stress and displacement of the pile are simulated by applying upward and downward uniformly distributed loads to the upper and lower segments of the pile, respectively. The finite element mesh is set to be fine and automatically divided by the PLAXIS software. As

shown in Figure 3, the interface elements of PLAXIS are used to simulate the interaction between the pile body and soils.

2.3. Material Parameters.

The hardening-soil (HS) model is adopted for the soils and rock. The HS model is an advanced Duncan–Chang model. The yield surface of the HS model is not fixed but can expand with plastic straining, and the hardening modes consist of compression hardening and shear hardening [33, 35].

In the HS model, the confining stress dependent stiffness modulus E_{50}, which is corresponding to the 50% ultimate deviatoric stress, is used to account for the hyperbolic stress-strain relation in primary loading and is given by the equation:

$$E_{50} = E_{50}^{ref} \left(\frac{c \cos \varphi - \sigma_3' \sin \varphi}{c \cos \varphi + p^{ref} \sin \varphi} \right)^m, \qquad (1)$$

where p^{ref} is a reference pressure and the default setting of p^{ref} in PLAXIS is 100 kPa; E_{50}^{ref} is a reference stiffness modulus under the reference confining pressure of p^{ref}; σ_3' is the confining pressure in a triaxial test; m is the power for the stress-level dependency of stiffness.

The unloading/reloading stiffness (E_{ur}) can be expressed as

$$E_{ur} = E_{ur}^{ref} \left(\frac{c \cos \varphi - \sigma_3' \sin \varphi}{c \cos \varphi + p^{ref} \sin \varphi} \right)^m, \qquad (2)$$

where E_{ur}^{ref} is the reference unloading/reloading stiffness corresponding to the confining stress p^{ref}.

Table 2 summarizes the values of the constitutive parameters of the soils used in the numerical simulation. The constitutive parameters for the HS model are obtained by using the following empirical relationships: $E_{ur}^{ref} = 3E_{oed}^{ref} = 3E_{50}^{ref}$, in which E_{oed}^{ref} = tangent stiffness for primary oedometer loading [33]. For simplicity, m is assumed to be 0.5.

2.4. Modeling Procedure.

The modeling procedures were the same as the field tests: (1) Define the material properties of the numerical model; (2) Initiate the boundary and initial stress conditions, and the initial equilibrium state; (3) Activate the pile and the interface elements between the pile body and soils, and calculate to the equilibrium state; (4) Activate the upward and downward uniformly distributed loads to the upper and lower segments of the pile. The uniformly distributed load started at 260 kN and gradually increased to 2080 kN in 15 grades, that is, the corresponding stress on the loading surfaces increased from 920 kPa to 7360 kPa. Each grade of the loading was calculated until mechanical equilibrium and displacement stability.

2.5. Numerical Results

2.5.1. Deformation.

Figure 4 shows the computed displacement contour and deformed mesh of the numerical model under the self-balanced loading of 2080 kN, in which

TABLE 2: Model parameters of the subsoil.

Material	Layer 1	Layer 2	Layer 3	Layer 4
Material model	HS	HS	HS	HS
γ (kN·m^{-3})	17.8	19.5	19.8	22.0
E_{50}^{ref} (MPa)	22.0	18.0	23.0	43.5
E_{oed}^{ref} (MPa)	22.0	18.0	23.0	43.5
E_{ur}^{ref} (MPa)	66.0	54.0	69.0	130.5
m	0.5	0.5	0.5	0.5
ν_{ur}	0.2	0.2	0.2	0.2
c (kPa)	16.0	20.0	25.0	23.0
φ (°)	30.0	27.0	30.0	42.0

Note: E_{oed}^{ref} = tangent stiffness for primary oedometer loading; E_{ur}^{ref} = unloading/reloading stiffness; m = power for stress-level dependency of stiffness; ν_{ur} = Poisson's ratio for unloading-reloading.

the deformed mesh is magnified by 10 times. According to Figure 4(a), the largest displacement occurs at the pile end (over 100 mm) while the upward displacement of the pile body is very small (less than 10 mm). As shown in Figure 4(b), although there is relative sliding between the pile body and the surrounding soil along with the pile-soil interface, the sliding momentum is small. The rock at the pile end deforms greatly than the pile body, indicating that the end bearing resistance of the pile is more fully developed than the side friction resistance.

2.5.2. Load-Displacement Curves.

Figure 5 compares the displacement curves obtained from the field testing measurements and numerical simulations. It can be found that the DDPE (80 mm) is obviously larger than UDPB (10 mm) and the two groups of load-displacement curves are both approximately linear. The simulation results are in good agreement with the field testing measurements, indicating that the developed numerical model is reasonable and can be used to simulate the self-balanced loading test.

3. Sensitivity Analysis

The influences of different rock modulus, rock cohesion, rock-socketed depth of pile, and Osterberg Cell burial depth on the load-displacement curves of piles under self-balanced loading were analyzed. To simplify the analysis process, the foundation soil was assumed to contain two layers of soil: the upper layer was the 20 m thick soil and the lower layer was the 20 m thick rock. The length of the pile was 21 m, of which the rock-socketed depth was 1.0 m. The Osterberg Cell was located at the pile end initially. The parameters of the soil and rock are simplified and shown in Table 3.

3.1. Rock Modulus.

Figure 6 compares the load-displacement curves of the self-balanced loading test piles under different rock modulus. The representative modulus E is set to be 40, 80, 120, and 240 MPa, respectively. The secant and tangent stiffness (E_{50}^{ref} and E_{oed}^{ref}) of the HS model is assumed to be equal to the representative modulus E, and the unloading/reloading stiffness E_{ur}^{ref} is three times the representative modulus (i.e., 120, 240, 360, and 720 MPa). It can
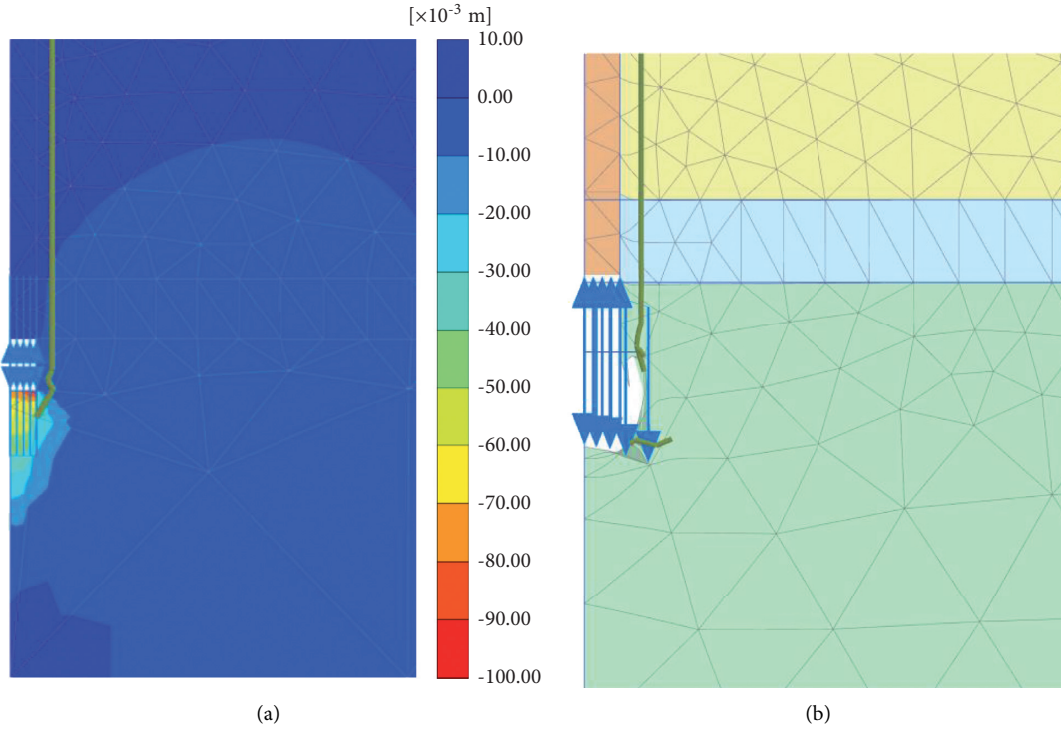
FIGURE 4: Simulated deformation of the testing pile and surrounding soils under self-balanced loading. (a) Displacement contour. (b) Deformed mesh.
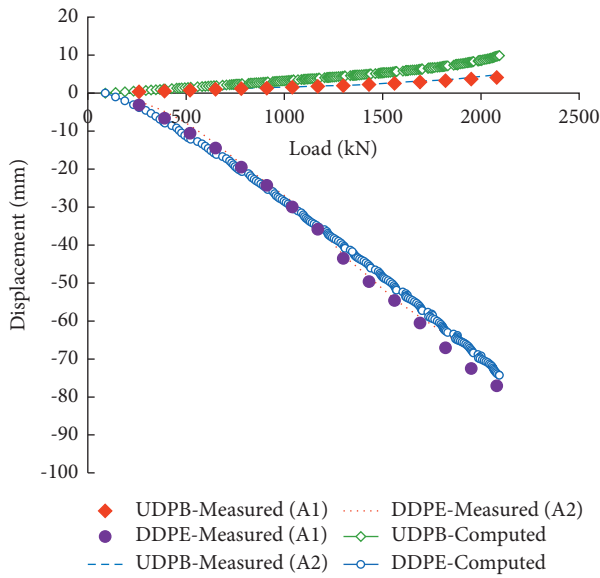
FIGURE 5: Load-displacement curves of the field testing measurements and numerical simulations.
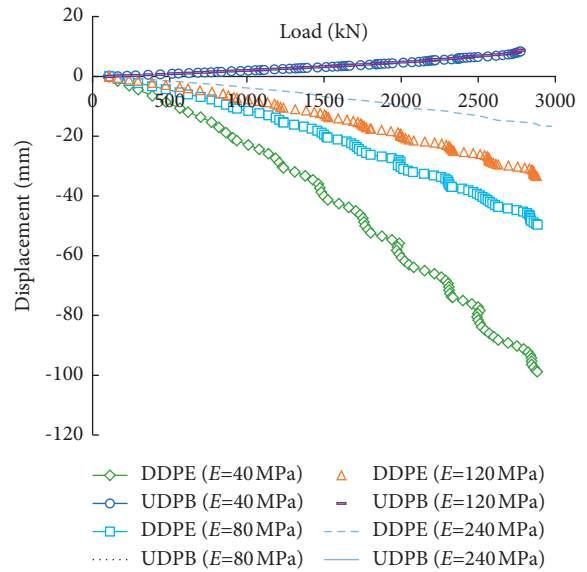
FIGURE 6: Load-displacement curves under different rock modulus.

TABLE 3: Simplified model parameters.

Material	γ (kN·m^{-3})	E_{50}^{ref} (MPa)	E_{oed}^{ref} (MPa)	E_{ur}^{ref} (MPa)	c (kPa)	φ (°)
Soil	17.8	22.0	22.0	66.0	16	30
Rock	22.0	40.0	40.0	120.0	23	42

be found that when the rock modulus increases from 40 MPa to 240 MPa, the DDPE decreases from 96 mm to 16 mm, while the curves of the UDPB approximately coincides. This means that the deformation modulus of rocks has significant impacts on the DDPE but little impact on the UDPB under the self-balanced loading.
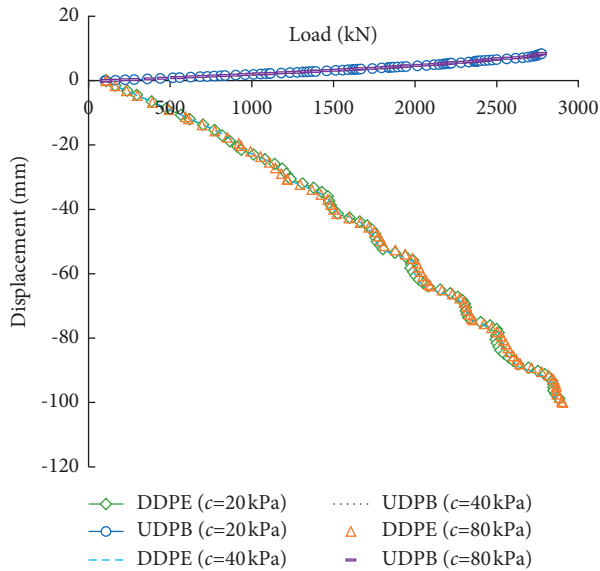
FIGURE 7: Load-displacement curves under different rock cohesion.

FIGURE 8: Load-displacement curves under different rock-socketed depths of the pile.

3.2. Rock Cohesion. Figure 7 compares the load-displacement curves of the self-balanced loading test piles under different rock cohesion. The value of the cohesion c is set to 20, 40, and 80 kPa, respectively. It can be seen that the load-displacement curves under different rock cohesion approximately coincide, indicating that only compression deformation is developed in the rocks but shear failure does not occur.

3.3. Rock-Socketed Depth of the Pile. Figure 8 compares the load-displacement curves of the self-balanced loading test piles under different rock-socketed depths. The rock-socketed depth is set to be 1.7D, 3.3D, 5.0D, and 6.7D (D is the diameter of the pile, and $D = 0.6$ m), respectively. It can be seen that the rock-socketed depth has a significant influence on the load-displacement curves of the self-balanced loading test piles. When the load is small, the load-displacement curves of different rock-socketed depths basically coincide. As the rock-socketed depth increases, the side resistance of the pile body and the end bearing capacity of the pile end increase correspondingly.

3.4. Osterberg Cell Burial Depth. Figure 9 compares the load-displacement curves of the self-balanced loading test piles under different burial depths of the Osterberg Cell. The burial depth of the Osterberg Cell (H) is set to be 20, 18, 16, and 14 m, respectively. It can be seen that the burial depth of the Osterberg Cell affects the load-displacement curves obviously. When the Osterberg Cell is located at the pile end, the UDPB is small and the downward displacement of the lower plate of the Osterberg Cell (DDLP) increases approximately linearly with the load. Both the side friction resistance of the upper segment of the pile and the end bearing resistance of the pile end have not reached the
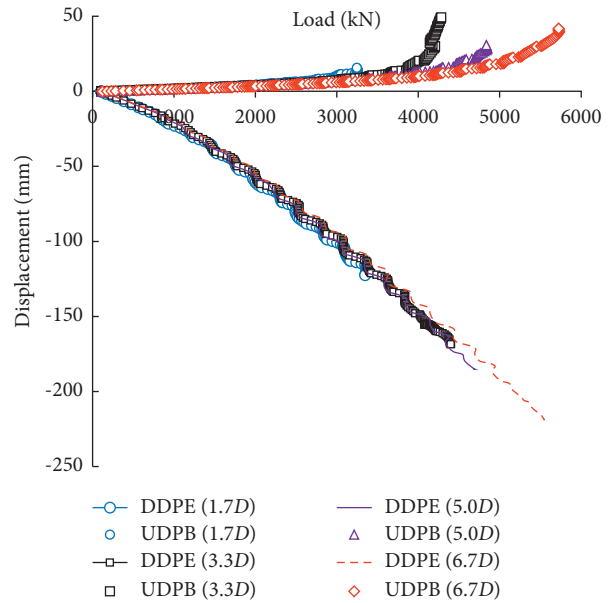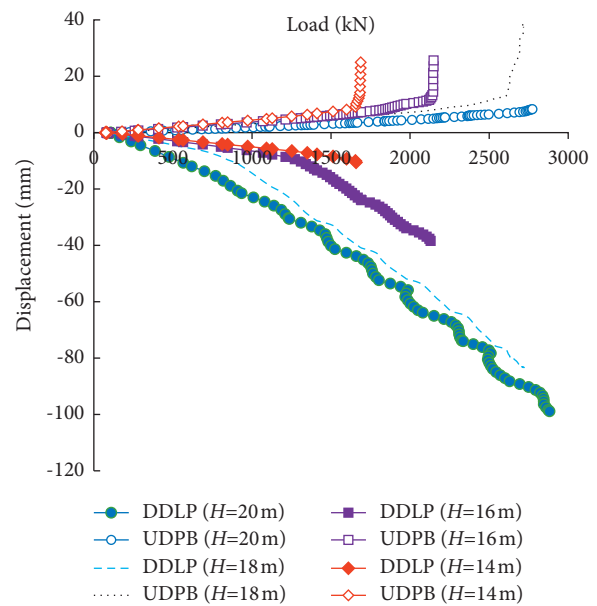
FIGURE 9: Load-displacement curves under different burial depths of the Osterberg Cell.

ultimate state. When the burial depth of the Osterberg Cell decreases, the DDLP is also decreased. The UDPB varies not obviously when the load is small with the burial depth of the Osterberg Cell decreasing. However, there exists a critical load. When exceeding the critical load, the upward displacement of the pile body increases significantly, indicating that the side friction resistance has reached the ultimate state. The shallower the Osterberg Cell set, the lower the critical load is.

4. Comparison with the Conventional Static Loading Test

The load-displacement curves and stress states of self-balanced loading test piles are different from the conventional static loading test piles. Comparative studies were carried out based on the validated numerical model to investigate the displacement and mechanical performance of the piles under self-balanced loading, static uplift loading, and static compressive loading. The geometric size of the numerical model was the same as those in Section 3, and the Osterberg Cell was located at the pile end. The static uplift loading and compressive loading were applied on the top of the pile. The constitutive parameters of the numerical model were shown in Table 3.

4.1. Self-Balanced Loading and Static Uplift Loading.
Figure 10 compares the upward displacement of piles under self-balanced loading and static uplift loading. It can be found that both curves are approximately linear when the load is not large. But when the load exceeds a critical value, the displacements of the piles suddenly increase. These critical loads, which are basically equal under the two loading conditions, can be regarded as the ultimate uplift bearing capacity of the piles. Therefore, the self-balanced loading test can precisely determine the uplift bearing capacity of shallow rock-socketed short piles.

In addition, the upward displacement of the pile under the self-balanced loading is slightly larger than that of the pile under the static uplift loading. Therefore, when the self-balanced loading tests are used to determine the displacement of piles under uplift loading, the results are biased towards safety.

Figure 11 compares the shear stress distribution of the pile-soil interface of the piles under the self-balanced loading and static uplift loading. The interface shear stresses under the two loading conditions are both downward. As shown in Figure 11, when the load is small, the distributions of the shear stress under the two loading conditions are basically coincident. Increasing the applied load will increase the interface shear stress. The minimum shear stress is located at the pile top and the maximum shear stress is at the pile end. This is because the shear stress of the pile-soil interface is related to the shear strength of the surrounding soil. The greater the depth, the greater the horizontal earth pressure, which increases the shear strength of the interface.

It can be also found that the shear stress of the pile-soil interface is distributed more uniformly under the static uplift loading when the load is less than 2080 kN. Specifically, the interface shear stress of the upper half part under the static uplift loading is larger than that under the self-balanced loading, and the lower half part is the opposite. This is because the shear stress of the pile-soil interface is also related to the relative displacement between the pile and soils. The static uplift loading is applied to the pile top, and the relative displacement between the pile and soils is the largest at the pile top and decreased with depth. However, the self-balanced loading is applied to the pile end and the relative displacement is also the largest at the pile end. Therefore, the interface shear stress of
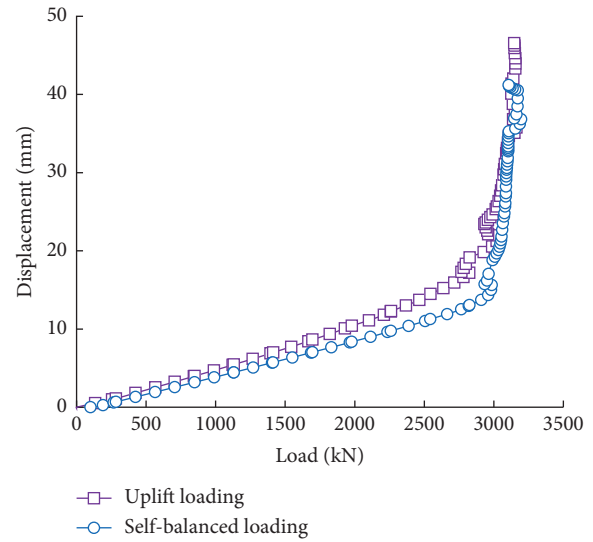
FIGURE 10: Load-displacement curves of piles under the self-balanced loading and uplift loading.
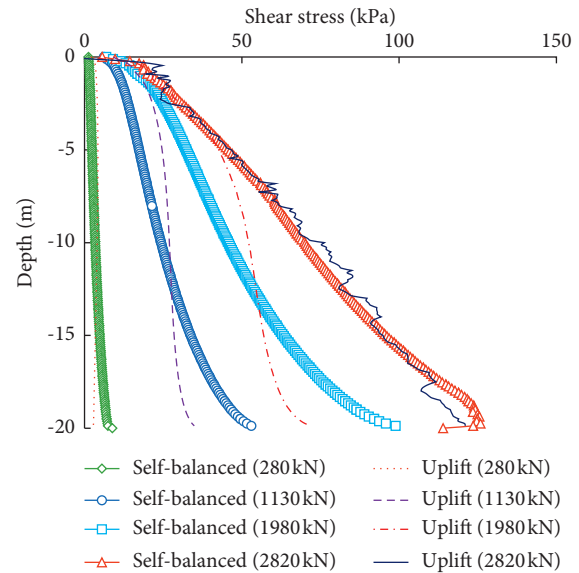
FIGURE 11: Shear stress distributions of the pile-soil interface under the self-balanced loading and uplift loading.

the lower half part under the self-balanced loading is larger than that under the static uplift loading.

When the load reaches 2080 kN, the interface shear stresses under the two loading conditions become a consistent distribution, indicating that the shear strength of the pile-soil interface is fully developed and the testing piles all reach the ultimate state. However, the curve of interface shear stress under static uplift loading is not smooth because a larger slip occurs between the pile and soil.

4.2. Self-Balanced Loading and Static Compressive Loading.
Figure 12 compares the load-displacement curves of the piles under the self-balanced loading and static compressive loading. It can be seen that the displacement
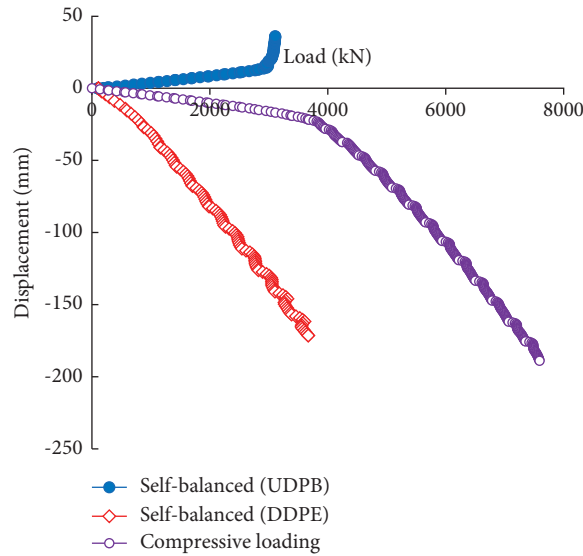
Figure 12: Load-displacement curves of piles under the self-balanced loading and compressive loading.
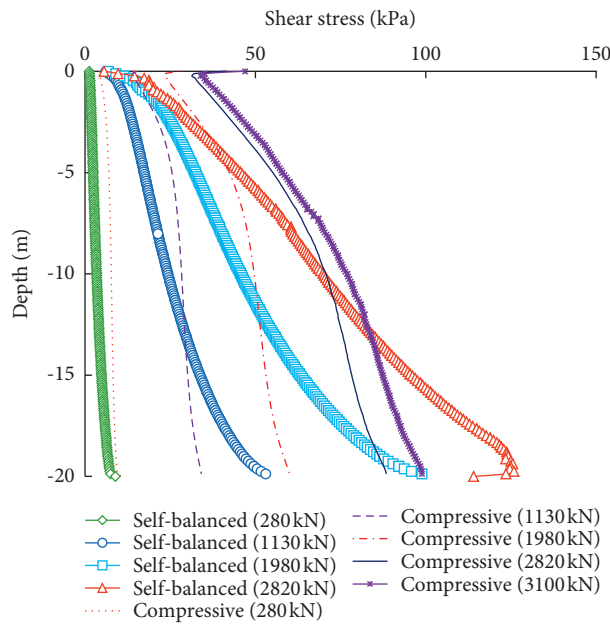
Figure 13: Shear stress distributions of the pile-soil interface under the self-balanced loading and compressive loading.

of the static compressive loading pile is significantly smaller than the DDPE of the self-balanced loading test pile. The UDPB of the self-balanced loading test pile keeps linear when the load is not large. But there exists an ultimate load, beyond which the displacement increases obviously.

Figure 13 compares the shear stress distribution of the pile-soil interface of the piles under the self-balanced loading and static compressive loading. The direction of the interface shear stress under the self-balanced loading is downward, while the direction of the interface shear stress under the compressive loading is upward.

As shown in Figure 13, when the load is small, the distributions of the interface shear stress under the self-

balanced loading and compressive loading are basically coincident. Increasing the applied loads will increase the interface shear stress. The minimum shear stress is located at the pile top and the maximum is located at the pile end. The shear stress of the pile-soil interface is distributed more uniformly under static compressive loading conditions. These are also because the shear stress distribution of the pile-soil interface is related to the shear strength of the surrounding soil and the relative displacement between the pile and soil.

However, when the load is increased from 2820 kN to 3100 kN, the interface shear stress of the piles under the compressive loading changes not significantly. This is due to the effect of the pile-end resistance.
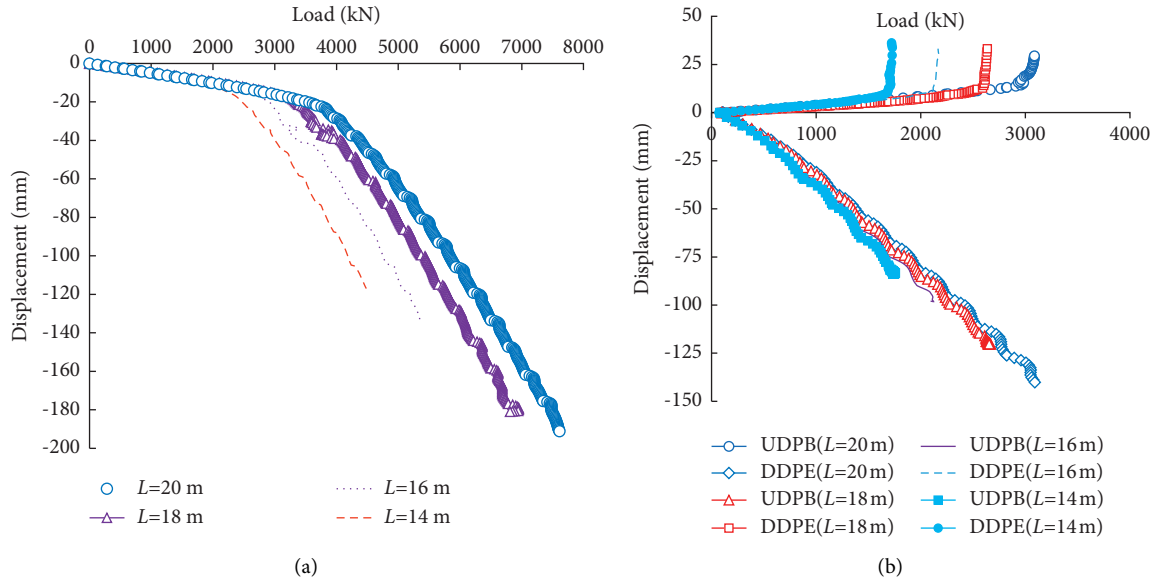
FIGURE 14: Load-displacement curves for different loading conditions. (a) Compressive loading. (b) Self-balanced loading.
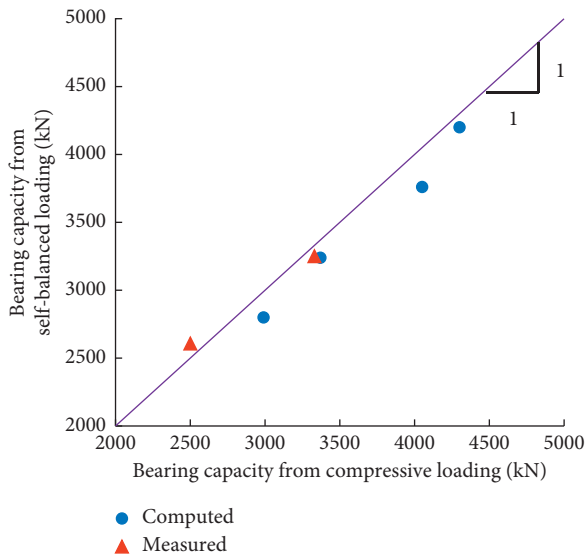
FIGURE 15: Comparison of the pile bearing capacity from the self-balanced and compressive loading tests.

5. A Bearing Capacity Computation Method of Piles

Based on the statistics of the numerical simulation results, a bearing capacity computation method of the shallow rock-socketed short piles under the self-balanced loading is established. In this method, the Osterberg Cell is set at the pile end and the ultimate compressive bearing capacity of the pile can be calculated by

$$Q_u = Q_{uu} + Q_{ud}, \tag{3}$$

where Q_u represents the compressive bearing capacity of the pile; Q_{uu} represents the ultimate side resistance of the pile

(the load corresponding to the inflection point of the load-displacement curve of UDPB); and Q_{ud} represents the pile end bearing capacity corresponding to the allowable settlement of 40 mm.

Figure 14 shows the load-displacement curves computed by the numerical modelings under the compressive and self-balanced loading conditions. The pile length varies from 14 m to 20 m. As shown in Figure 14(a), the static compressive test-based ultimate bearing capacities corresponding to the allowable settlement of 40 mm are 2990, 3370, 4050, and 4300 kN for the different pile lengths of 14, 16, 18, and 20 m. According to Figure 14(b), for different pile lengths of 14, 16, 18, and 20 m, the ultimate side resistances Q_{uu} are 1710, 2130, 2610, and 3000 kN, and the pile end bearing capacities Q_{ud} are 1090, 1110, 1150, and 1200 kN. The ultimate compressive bearing capacities of the piles determined by the proposed computation method are 2800, 3240, 3760, and 4200 kN.

Figure 15 shows the ultimate bearing capacity obtained from the numerical simulation results under the two loading conditions. The results based on the field test measurements are also shown in Figure 15. It can be seen that the ultimate bearing capacities of these two methods are approximately consistent. Therefore, the proposed bearing capacity computation method of the shallow rock-socketed short piles under the self-balanced loading is reliable.

6. Conclusions and Recommendations

In this study, a two-dimensional axisymmetric numerical model is established by the PLAXIS software to investigate the behavior and bearing mechanism of shallow rock-socketed short piles based on the self-balanced loading test. The model is first validated by simulating the field tests of two adjacent piles under self-balanced loading located in southern Anhui, China. Then the influence factors of the

load-displacement curves of piles are analyzed. Thereafter, the mechanical mechanism of the self-balanced loading tests is simulated and compared with the conventional static loading tests. On this basis, a bearing capacity computation method of shallow rock-socketed short piles based on the self-balanced loading test is proposed. The simulation results and computation method should provide valuable information for managers to improve the efficiency of management of transformer substation engineering in mountainous and hilly areas. The following conclusions can be drawn:

(1) The side resistance and end bearing of the pile increase with the rock-socketed depth. Downward displacement of pile end will decrease with the decrease of the burial depth of the Osterberg Cell. Increasing the rock modulus will also decrease the downward displacement of the pile end but has little impact on the upward displacement of the pile body. However, the rock cohesion has little effect on the load-displacement curve of the piles.

(2) Compared with self-balanced loading test piles, the shear stress of the pile-soil interface distributes more uniformly under static uplift or compressive loading conditions. The interface shear stress of the upper half part of the pile under the self-balanced loading test is larger than that under static uplift or compressive loading, and the lower half part is the opposite.

(3) For the self-balanced loading test of the shallow rock-socketed short piles, the Osterberg Cell is recommended to be set at the pile end. The ultimate uplift bearing capacity of the piles can be directly determined by the inflection point of the load-displacement curve of the pile body. The ultimate compressive bearing capacity of the piles is the sum of the ultimate side resistance and the end bearing capacity corresponding to the allowable settlement of 40 mm.

Data Availability

The data that support the findings of this study are available from the corresponding author upon reasonable request.

Conflicts of Interest

The authors declare that there are no conflicts of interest.

Acknowledgments

References

[1] P. Carrubba, "Skin friction on large-diameter piles socketed into rock," *Canadian Geotechnical Journal*, vol. 34, no. 2, pp. 230–240, 1997.

[2] S. Kim, S. Jeong, S. Cho, and I. Park, "Shear load transfer characteristics of drilled shafts in weathered rocks," *Journal of Geotechnical and Geoenvironmental Engineering*, vol. 125, no. 11, pp. 999–1010, 1999.

[3] C. W. W. Ng, T. L. Y. Yau, J. H. M. Li, and W. H. Tang, "New failure load criterion for large diameter bored piles in weathered geomaterials," *Journal of Geotechnical and Geoenvironmental Engineering*, vol. 127, no. 6, pp. 488–498, 2001.

[4] B. Livneh and M. H. El Naggar, "Axial testing and numerical modeling of square shaft helical piles under compressive and tensile loading," *Canadian Geotechnical Journal*, vol. 45, no. 8, pp. 1142–1155, 2008.

[5] M. Elkasabgy and M. H. El Naggar, "Axial compressive response of large-capacity helical and driven steel piles in cohesive soil," *Canadian Geotechnical Journal*, vol. 52, no. 2, pp. 224–243, 2015.

[6] K. Madhusudan Reddy and R. Ayothiraman, "Experimental studies on behavior of single pile under combined uplift and lateral loading," *Journal of Geotechnical and Geoenvironmental Engineering*, vol. 141, no. 7, Article ID 04015030, 2015.

[7] ASTM D1143-81, *Standard Test Method for Piles under Static Axial Compressive Load* Annual Book of ASTM Standards, West Conshohocken, PA, 1994.

[8] ASTM D1143-07, "Innovative load testing systems," *Research Rep. NCHRP 21-08, National Cooperative Highway Research Program*, Transportation Research Board of the National Academies, Washington, DC, USA, 2004.

[9] S. G. Paikowsky and T. A. Tolosko, *Extrapolation of Pile Capacity from Non-failed Load Test*, Federal Highway Administration (FHWA), Washington, D.C., 1999.

[10] S. G. Paikowsky, "Innovative load testing systems, National Cooperative Highway Research Program," Research Rep. NCHRP 21-08, Transportation Research Board of the National Academies, Washington, DC, 2004.

[11] J. Osterberg, "New device for load testing driven piles and drilled shafts separates friction and end-bearing," in *Proceedings of the international conference on piling and deep foundations*, pp. 421–427, london, May 1989.

[12] ASTM D8169-18, *Standard Test Methods for Deep Foundations under Bi-directional Static Axial Compressive Load* Annual Book of ASTM Standards, West Conshohocken, PA, 2018.

[13] B. H. Fellenius, A. Altaee, R. Kulesza, and J. Hayes, "O-cell testing and FE analysis of 28-m-deep barrette in Manila, Philippines," *Journal of Geotechnical and Geoenvironmental Engineering*, vol. 125, no. 7, pp. 566–575, 1999.

[14] M. W. O'Neill, D. A. Brown, F. C. Townsend, and N. Abar, "Innovative load testing of deep foundations," *Transportation Research Record*, vol. 1569, no. 1, pp. 17–25, 1997.

[15] J. O. Osterberg, "The Osterberg load test method for bored and driven piles-the first ten years," in *Proceedings of the 7th International Conference and Exhibition on Piling and Deep Foundations*, pp. 1–17, Deep Foundations Institute, Vienna, Austria, June 1998.

[16] J.-S. Lee and Y.-H. Park, "Equivalent pile load-head settlement curve using a bi-directional pile load test," *Computers and Geotechnics*, vol. 35, no. 2, pp. 124–133, 2008.

[17] H.-J. Kim and J. L. C. Mission, "Improved evaluation of equivalent top-down load-displacement curve from a bottom-up pile load test," *Journal of Geotechnical and Geo-environmental Engineering*, vol. 137, no. 6, pp. 568–578, 2011.

[18] J. L. C. Mission and H. J. Kim, "Design charts for elastic pile shortening in the equivalent top-down load-settlement curve from a bidirectional load test," *Computers and Geotechnics*, vol. 38, no. 2, pp. 167–177, 2011.

[19] M. England, "Bi-directional static load testing-state of the art," in *Proceedings of the 4th Geotechnical Seminar on Deep Foundations on Bored and Augered Piles*, pp. 309–313, Ghent, Belgium, June 2003.

[20] M. England, "Review of methods of analysis of test results from bi-directional static load tests," in *Proceedings of the 5th International Symposium on Deep Foundations on Bored and Auger Piles (BAP V)*, pp. 235–240, Ghent, Belgium, September 2008.

[21] M. G. England and P. F. Cheesman, "Optimum loading specifications for O-cell bi-directional static load testing," in *Proceedings of the 15th European Conference on Soil Mechanics and Geotechnical Engineering*, pp. 855–860, Delft, the Netherlands, January 2011.

[22] G. Dai and W. Gong, "Application of bi-directional static loading test to deep foundations," *Journal of rock mechanics and geotechnical engineering*, vol. 4, no. 3, pp. 269–275, 2012.

[23] W. Gong, G. Dai, Y. Jiang, and G. Xue, "Theory and practice of self-balanced loading test for pile bearing capacity," *Journal of Building Structures*, vol. 23, no. 1, pp. 82–88, 2002.

[24] G. L. Dai, W. M. Gong, Y. Cheng, and G. Y. Xue, "Application of self-balanced testing and post grouting to large diameter and super-long piles," *Chinese Journal of Geotechnical Engineering*, vol. 27, no. 6, pp. 690–694, 2005.

[25] Z. Muszyński, J. Rybak, and P. Kaczor, "Accuracy assessment of semi-automatic measuring techniques applied to displacement control in self-balanced pile capacity testing appliance," *Sensors*, vol. 18, no. 11, p. 4067, 2018.

[26] H. Xing, J. Wu, and Y. Luo, "Field tests of large-diameter rock-socketed bored piles based on the self-balanced method and their resulting load bearing characteristics," *European Journal of Environmental and Civil Engineering*, vol. 23, no. 12, pp. 1535–1549, 2019.

[27] C. He and C. Gong, "Comparison and analysis on self-balanced method and anchored pile method in Qingdao Gulf Bridge," in *Advanced Materials Research*, pp. 1024–1027, Trans Tech Publications, Switzerland, 2014.

[28] R. Afsharhasani, M. Karakouzian, and V. Farhangi, "Effect of competent caliche layers on measuring the capacity of axially loaded drilled shafts using the Osterberg test," *Applied Sciences*, vol. 10, no. 18, Article ID 6169, 2020.

[29] L. S. Cheng, T. B. Pin, C. M. Fai, H. Mohamad, A. K. An, and P. P. Rahardjo, "Application of distributed fibre optic sensor (DFOS) in bi-directional static pile load tests," *Geotechnical Engineering Journal of the SEAGC*, vol. 55, pp. 48–54, 2018.

[30] P. Asem and P. Gardoni, "A load-transfer function for the side resistance of drilled shafts in soft rock," *Soils and Foundations*, vol. 59, no. 5, pp. 1241–1259, 2019.

[31] P. Asem, "Base resistance of drilled shafts in soft rock using in situ load tests: A limit state approach," *Soils and Foundations*, vol. 59, no. 6, pp. 1639–1658, 2019.

[32] B. Cheng, K. Lu, J. Li, H. Chen, X. Luo, and M. Shafique, "Comprehensive assessment of embodied environmental impacts of buildings using normalized environmental impact factors," *Journal of Cleaner Production*, vol. 334, Article ID 130083, 2022.

[33] R. B. J. Brinkgreve, S. Kumarswamy, W. M. Swolfs, and F. Foria, *Material Model Manual*, Plaxis BV, Delft, Netherlands, 2018.

[34] J.-X. Liu, J. Yang, Y.-J. Liu, S. Zhu, and F. Laouafa, "Numerical investigation of tunnelling effects on existing piles in structured clay," *European Journal of Environmental and Civil Engineering*, vol. 2022, Article ID 2028192, 2022.

[35] J.-F. Chen, J.-X. Liu, J.-F. Xue, and Z.-M. Shi, "Stability analyses of a reinforced soil wall on soft soils using strength reduction method," *Engineering Geology*, vol. 177, pp. 83–92, 2014.

Research Article

Research on Human Behavior Modeling of Sports Culture Communication in Industrial 4.0 Intelligent Management

Zhihui Li (ID)

Department of Physical Education, Lvliang University, Lv Liang, Shanxi 033000, China

Correspondence should be addressed to Zhihui Li; lizhihuityx@llu.edu.cn

With the advent of the information age, Internet technology and computer technology are gradually applied in various fields. Human daily life is inseparable from the help of information technology. The progress and development of the times are also changing our industrial environment. The Internet of things, artificial intelligence, and digital production have been widely used in the industrial field. We need to integrate the new intelligent management concept in the industrial 4.0 era into the modern industrial system and media communication. In the communication of sports culture, how to integrate the intelligent technology under the background of industry 4.0 and realize the spatiotemporal modeling and analysis of human behavior and behavior characteristics is the main content of our research. Firstly, this study briefly analyzes the development and historical process of industry 4.0 era and explores the impact of Internet of things and information technology on sports culture communication. This study analyzes the development process of Chinese sports culture communication and probes into the influence and significance of sports culture communication on human behavior. Under the background of industrial 4.0 management, a model of human temporal and spatial behavior change in sports culture communication is established. Human behavior trajectory is analyzed by data mining, human behavior recognition algorithm, behavior quantitative analysis method, and behavior feature model. The results show that under the background of industry 4.0 management, human behavior modeling can clearly describe the basic characteristics and behavior state in the process of sports culture communication and can predict and analyze the human behavior performance of such social activities and phenomena. Through data mining, data preprocessing, and behavior quantitative analysis, human behavior trajectory is studied. It has a positive impact on the behavior trend in human daily life. The main factor affecting behavior change is whether to receive sports culture news.

1. Introduction

With the continuous renewal of the development of industrialization, we divide the different periods of the industrial age into grades [1]. At present, it is roughly in the "4.0" era. The development mode, scale, and speed of industry are different in different industrial environments [2]. From the 18th century, Jenny textile machine changed the production efficiency and provided effective help for the liberation of human hands. Until Watt improved the steam engine, every industrial revolution was to make human work easier and easier [3, 4]. Traditional manual labor has been gradually replaced, and mechanical development and mechanical production have gradually become the main pillars of the industrial era. In the industrial 1.0 era, mechanical equipment manufacturing has become the main content of production mode in the whole period [5]. This defect is that the equipment covers an excessive area, and the production space can ensure the production demand through the increase of the number of machinery. Until the 20th century, the development of electric power has brought new opportunities to the fields of communication and automobile [6]. Human civilization began to move towards the industrial 2.0 era. The emergence of wired, wireless communication, chemical knowledge, and fuel vehicles has led to a sharp increase in the number of human labor in the industrial field. In the production environment, the division of labor is gradually clear, and the scale is further expanding. The new industrial level and equipment can bring more profits to enterprises [7]. Assembly line production is the

main industrial process in this era. After World War II, the industrial 3.0 era began to enter people's lives. Machinery and equipment replace human labor and handicraft industry and become a substitute for assembly line enterprises [8]. The expansion of production scale no longer depends on the increase of the number of equipment but on the improvement of production methods and technical level. This era has further expanded the mode of mechanical equipment replacing human labor [9].

With the continuous development of human society and the progress of scientific and technological innovation and information technology, new opportunities have been brought to the industrial environment [10]. Scientific and technological innovation has led to great changes in human society. In order to accelerate the speed of scientific research achievements, many countries take the lead in setting up R&D centers such as scientific and technological manufacturing. Internet technology and information technology have also made great contributions to the advent of the industrial 4.0 era [11]. In project management, how to use big data technology to establish an intelligent management system is a key topic in each field. If managers cannot recognize the relationship between work needs and modern technology, they will not be able to adapt to the changes of the times. In the field of communication, the communication of sports culture in China has always been in a relatively weak link [12]. There is no deep-seated research on the impact of sports culture communication on human behavior.

This study is mainly divided into three structures: the first part briefly describes the development status of industry 4.0 model in various countries and analyzes the specific help provided by human behavior modeling research. The second part first explores the essence of sports culture communication in the industrial 4.0 environment and models the impact of sports culture communication on human behavior. Data mining and processing methods are used to analyze human behavior data, and modeling research is carried out from the spatial characteristics of human behavior. Finally, it analyzes the necessity of modeling human behavior characteristics in the communication of sports culture. The intelligent recommendation algorithm is used to actively realize the news prediction service of sports culture in the human behavior analysis model. The third part analyzes the research results of human behavior space modeling of sports culture communication under the environment of industry 4.0 and the research results of human behavior feature modeling.

2. Related Works

The core technology in the industrial 4.0 era is the field of Internet of things and information technology [13]. Communication technology and information development have played an important role in the industrial 4.0 era. Artificial intelligence can use electrified equipment and program calculation in Ronnie simulation to help analyze human behavior in the industry [14]. In the big data environment, processing huge information and complex data sets also

need to use big data for mining and processing. Big data technology can provide effective and accurate data for industrial 4.0 intelligent management, intelligent transportation, intelligent production, and other modes and help industrial development move forward steadily [15]. In Internet computing, cloud computing can provide information and software resources for management devices and analysis devices. When big data collects and analyzes information, heterogeneous distribution, measurement, and other functions can be realized by using cloud computing [16]. The above are the main technologies ahead of the industrial 4.0 era. They provide technical support for the progress of the industrial era. The analysis, detection, and modeling of human behavior are often complex, but the efficient management function can be realized by using various modern technologies in the industrial 4.0 environment. We analyze the development status of countries in the industrial 4.0 era as follows [17]:

With the implementation of the industrial 4.0 era, Germany has made new changes in talent training mode. The dual system can improve the selection of talent training objectives, structural system, and professional ability training [18]. It puts forward new challenges for the types of talent training. With the gradual reduction of the matching between postwork and actual ability, enterprises pay more and more attention to the ability level of recruiters. The optimization of talent training program in vocational education schools is also a major problem to be solved. Facing these challenges, German vocational schools put forward the dual system training management model. The industrial 4.0 environment complies with the development of the times, expands the direction of professional development, and transports professional talents for the country [19].

The development of information technology and modern industry in the United States is relatively advanced, and they have always been in a leading position in the process of industrial reform [20, 21]. With the continuous application of modern equipment, the manufacturing industry is also in urgent need of improving its own technology. Under the environment of industry 4.0, there is a higher demand for equipment manufacturing and equipment manufacturing industry. Intelligent reform has become the main direction of industrial 4.0 mode. The intelligent management of robot equipment in industrial operation has also become the main topic. They applied the sensor technology of Internet of things in the industrial 4.0 era to the transformation of industrial robots and realized the intelligent development to a certain extent [22].

The apprenticeship reform system in Italy has changed with the advent of the industrial 4.0 era [23, 24]. When the apprenticeship reform becomes the focus again in the world, Italy's national and regional management system puts forward new policies for the apprenticeship reform. In terms of system management, innovative measures have been taken in the application of industrial 4.0 intelligent management, curriculum development, and quality inspection. Under the industrial 4.0 environment, different types of apprenticeship systems can be positioned differently, realizing the effect of system optimization.

Taking Hong Kong and Macao as examples, China has transformed the manufacturing industry under the background of industry 4.0 to intelligent development [25]. Enterprises in the manufacturing industry are prone to many internal problems in the process of transformation. In this case, intelligent management in the era of industry 4.0 can help Hong Kong and Macao quickly change to the intelligent manufacturing industry. This study puts forward effective countermeasures and suggestions for its development path and solving problems. Based on industry 4.0 intelligent management environment, this study analyzes the human behavior modeling of sports culture communication.

3. Research on Human Spatiotemporal Behavior Modeling and Behavior Characteristics of Sports Culture Communication Based on Industrial 4.0 Intelligent Management

3.1. Intelligent Management of Sports Culture Based on Mobile Network. The main features of the industrial 4.0 era include interconnection. Connecting all things has always been the theme of the industrial 4.0 era. The universality of the connection scope can closely gather equipment, manufacturers, enterprises, communication institutions, users, and other objects together. In order to comply with the development trend of the Internet of things, the sensor equipment, intelligent management system, embedded equipment, mobile communication equipment, and intelligent communication equipment of the Internet of things constitute an intelligent network model. The production process of the factory can also be highly intelligent. Intelligent factories can be controlled by the Internet of things. That is, the production process is completely integrated by computer. The real-time production monitoring program knows what new materials and processes are needed to ensure the smooth progress of the production process. This is not a simple problem of production automation but the realization of intelligent control. If the system detects a sudden failure in the production process, the machine will automatically suspend operation and repair itself, rather than continue to operate and continuously produce defective products. Through information technology, the most effective utilization of energy can be ensured, which are the characteristics of intelligent chemical plants in the future.

It can integrate digital development with the physical world and connect with each other, so as to ensure that human society can live more conveniently. Every industrial revolution can help human progress. We analyze the process of industrial development in time and space, as shown in Figure 1.

As can be seen from Figure 1, industry 4.0 is a new era and its development time is expected to be long. With the advent of the new era, human behavior has gradually changed in diversity. We focus on sports culture communication.

Sports is a complex object in the development of social culture. It can combine the body and spirit as the basis of daily activities. With the continuous improvement of human growth and development, the mastery of sports and skills can ensure the healthy growth of physical quality. In order to achieve the all-round development of quality education, improve the physical quality of the whole people, and improve the way of life, we need to pay attention to the dissemination of sports culture. Although China's economic development is relatively rapid, it has not brought significant results to China's sports communication. We compare the gap between Chinese and foreign media in sports culture communication, as shown in Figure 2.

As can be seen from Figure 2, with the increase of years, China's attention to sports culture communication has gradually increased. But in 2010, it still cannot be compared with western countries. With the advent of the industrial 4.0 era, intelligent devices and the Internet have brought diversified development to human behavior. From the perspective of media communication mode, sports communication has an indispensable relationship with the development of Internet data. We make statistics on the data of Internet users and show the process of users obtaining sports and cultural news by means of mobile communication, wired Internet access, wireless Internet access, and virtual communication, as shown in Figure 3.

The continuous increase of survey behavior data is shown in Figure 3. From the beginning of mobile communication business, it has been transforming to wired Internet and wireless Internet. With the change of industry 4.0 era, virtual Internet also gradually exists in people's daily life. Therefore, the factors affecting human behavior by the dissemination of sports culture in the industrial 4.0 era are significant. We conduct modeling research on human behavior. Firstly, we analyze the range changes of individuals in time and space:

$$B := \{(s_i, t_i, c_i) | i = 0, 1, 2, \ldots\}. \tag{1}$$

In the formula, B represents the time-space behavior sequence, and (s_i, t_i, c_i) represents the element set. The range of each element in the collection is expressed as follows:

$$b = (s, t, c) \in B, \ s \in D^{|s|}. \tag{2}$$

We analyze that the spatial diffusion of human behavior change trajectory is decreasing. In the sample data, the data of users who are concerned about the dissemination of sports culture actively hiding information are analyzed. It can be found that the spatial change of human behavior is an exponential distribution. The mathematical formula can be expressed as follows:

$$p(\lambda) \sim (\lambda + \lambda_0)^{-b} \cdot e^{(\lambda/k)}. \tag{3}$$

The distribution of exponential function is between 0 and 2. Different cultural news takes different values. In the analysis of human spatiotemporal behavior, we need to
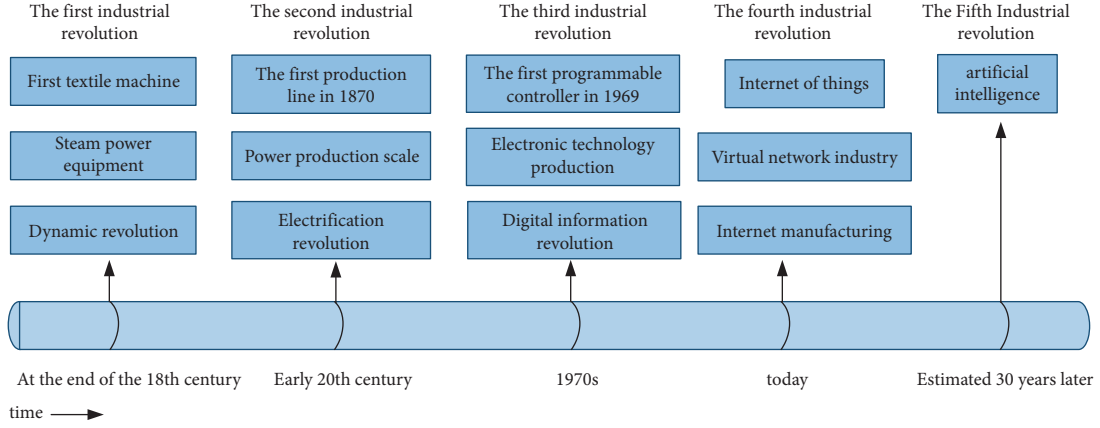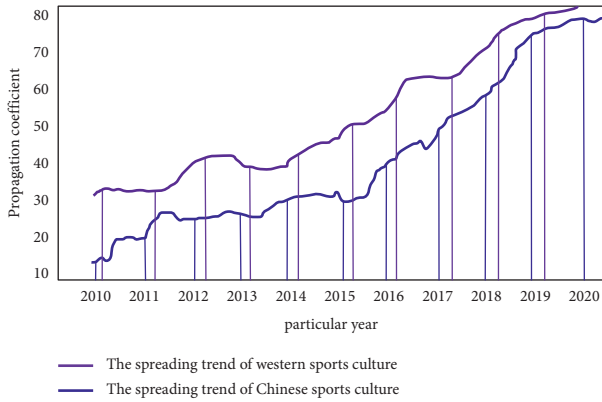
FIGURE 1: Industrial development process.

FIGURE 2: The gap between Chinese and foreign media in sports culture communication.

observe from multiple angles. The spatiotemporal movement variation of each individual can be defined as follows:

$$R_g^2 = \frac{1}{n} \sum_{k=1}^{n} (r_k - r)^2. \qquad (4)$$

In the formula, R_g^2 represents the characteristics of human behavior. We calculate the function law satisfied by the distribution of human behavior by using the transfer structure. The formula is as follows:

$$p(\lambda) = \int_0^\infty P(\lambda \mid R_g) P(R_g) dR_g. \qquad (5)$$

According to the above formula, the spatiotemporal pattern of human behavior can be determined. The law is calculated from the track data of the impact of sports culture communication on human behavior in the industrial 4.0 environment. Behavior pattern modeling can conform to the general process of human cognition. From the observed objects, it is found that many users have common characteristics. At present, more and more countries begin to pay attention to human behavior research. From the early stage of industry to 4.0, there are more and more technical means to study the human behavior model. We consulted relevant literature and analyzed the content release trend of human

behavior modeling research over the years, as shown in Figure 4.

It can be seen from Figure 4 that the development of the industrial age has a great impact on human behavior modeling. Since 2015, the number of human behavior modeling literature published in China has increased significantly. However, compared with the foreign release, it is still in a weak position. In order to further explore the impact of sports culture communication on human behavior, we also need to study from the analysis of behavior characteristics.

3.2. Research on Sports Culture Communication Based on Industry 4.0 Intelligent Management in Human Behavior Feature Modeling. In China's sports, table tennis and volleyball have always been the proud contents of the people. In the process of talking about sports news, the dissemination of cultural knowledge is realized. As China continues to win the Olympic Games, people all over the country begin to discuss sports news. People's attention to sports events is also the main manifestation of their attention to sports culture. Government communication and people's communication are the main channels. However, the way of sports culture communication should focus on itself. This communication effect is not only related to the development of national influence but also has an important impact on the performance of people's daily life and behavior.

Under the background of industry 4.0, the information communication model based on human behavior characteristics can more accurately describe the effect and process of sports communication. The main advantage is that it can choose the response after receiving information according to the set of human behaviors, including evaluation, forwarding, no response, and so on. Modeling human behavior can simulate the effect of data transfer in a variety of states. In sports culture communication, modeling based on human behavior characteristics can monitor the process of culture communication, which is a process from individual to collective modeling. It can take into account the personalized behavior judgment of users, so as to realize accurate information push and other functions. With the
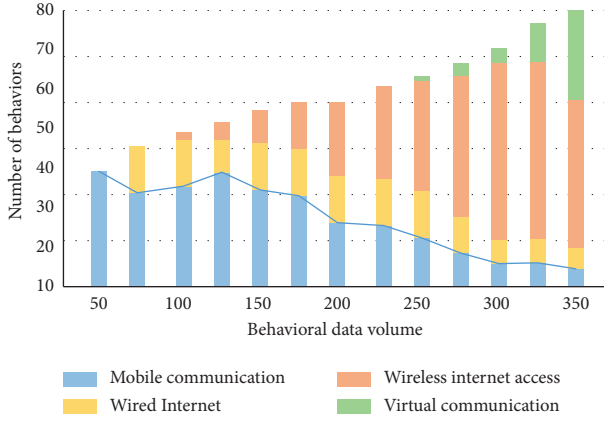
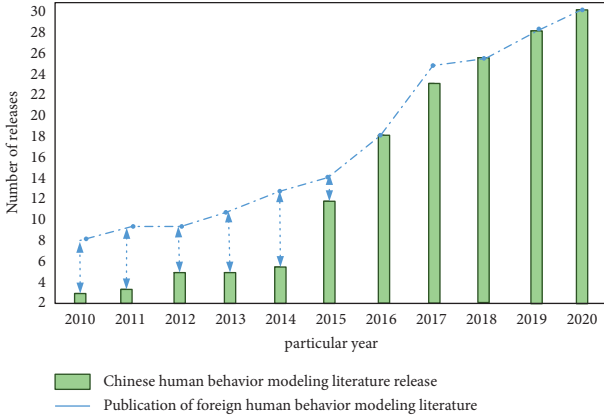FIGURE 3: The process of obtaining sports culture news in various ways.

FIGURE 4: The content release trend of human behavior modeling research over the years.

gradual application of industry 4.0 management in Internet information dissemination, network data and human behavior data indices increase. In order to facilitate accurate push of everyone's behavior data, we need to conduct personalized behavior feature modeling. Before behavior feature analysis and modeling, we compare the data acquisition speed of intelligent management system in industrial 4.0 environment with that of traditional data mining system, as shown in Figure 5.

As can be seen from Figure 5, with the increase of massive information in big data environment, the acquisition speed of traditional data mining system tends to decrease. The intelligent management data system in industrial 4.0 environment can effectively judge accurate data and useless data and realize the function of rapid acquisition. In the estimation of human behavior characteristics, we use mathematical formula as follows:

$$\text{Interest}(w) = f\big(\text{Interest}_{\text{Activit}}(w), \text{Interest}_{\text{Freq}}(w), \\ \cdot \text{Interest}_{\text{Time}}(w)\big). \tag{6}$$
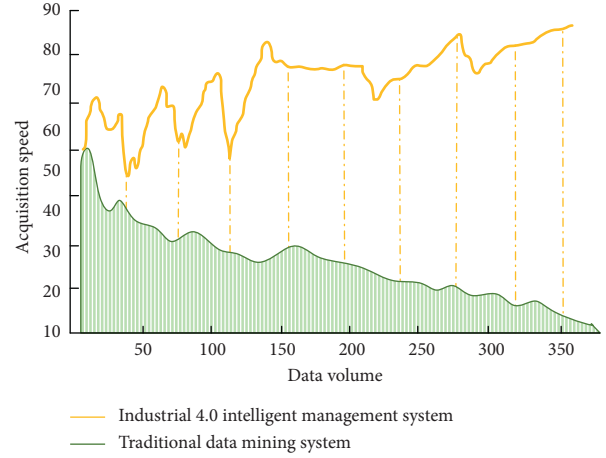
FIGURE 5: Comparison of data acquisition speed between the system and traditional data mining system.

$\text{Interest}_{\text{Activit}}$ is the actual action of human behavior, and $\text{Interest}_{\text{Freq}}(w)$ represents the number of information access. In order to study the number of human information browsing actions, we define the calculation function as follows:

$$\big(\text{Interest}_{\text{Activit}}(w) = f\,(\text{Sava}(w), \text{Keep}(w), \text{print}(w), \text{Copy}(w)\big). \tag{7}$$

Among them, they respectively represent the times of saving, collecting, and printing sports culture web pages and forwarding of information content. The browsing action can be represented by a binary function. The specific formula is as follows:

$$\text{Interest}_{\text{Activit}}(w) = \{0, \text{Sava}(w), \text{Keep}(w), \text{print}(w), \text{Copy}(w)\}, \tag{8}$$

$$\text{Interest}_{\text{Activit}}(w) = \{1, \text{Sava}(\varpi), \text{Keep}(\varpi), \text{print}(\varpi), \text{Copy}(\varpi)\}. \tag{9}$$

Investigation shows that most users rarely save and collect web pages when browsing sports culture news. Therefore, we cannot fully obtain the overall behavioral characteristics of human beings by using behavioral interest analysis. We need to calculate the number of visits and residence time respectively, so as to realize the feature modeling of human behavior. The number of behavior-based stops can be expressed by the following function:

$$\text{Stop}_{\text{Freq}(w)} = \frac{\text{Freq}(w)}{\max\limits_{E \in W}(\text{Freq}(w))}. \tag{10}$$

Among them, w represents the number of news visits by users in a certain period of time. With the increase of time, the number of behaviors is also accumulating. We update the number of visits in a cycle in the formula in proportion. In mathematical calculation, it can be calculated according to the following equation:

$$p = \frac{\left(\left|\mathrm{Freq}_{\mathrm{new}}\left(w\right) - \mathrm{Freq}_{\mathrm{old}}\left(w\right)\right|\right)}{\mathrm{Freq}_{\mathrm{old}}\left(w\right)}, \tag{11}$$

$$\mathrm{Freq}\left(w\right) = \left(\mathrm{Freq}_{\mathrm{new}}\left(w\right) + \mathrm{Freq}_{\mathrm{old}}\left(w\right)\right). \tag{12}$$

When the coefficient p less than 0, it represents human behavior, and the number of visits of users in the cycle does not change significantly. This study defines the browsing speed of each page of sports culture communication page as follows:

$$\mathrm{Speed}\left(w\right) = \frac{\mathrm{Size}\left(w\right)}{\mathrm{Time}\left(w\right)}, \tag{13}$$

where size (w) represents the storage size of the propagation interface and time (w) represents the time coefficient. Finally, the data delay in the management interface is calculated as follows:

$$\mathrm{Time}\left(w_i\right) = T\left(w_j\right) - T\left(w_i\right). \tag{14}$$

Next, the coefficient of influence on human behavior characteristics in the process of sports culture communication is calculated as follows:

$$R = \frac{\mathrm{Interet}_{(w)}}{\left(\mathrm{Speed}\left(w\right)/\max_{E \in W}\right)}. \tag{15}$$

According to the above formula, we can model the characteristics of human behavior and explore the impact of sports culture communication on human behavior under the management of industry 4.0. In the sports culture communication interface, we use the nonlinear normalization method to process the sample data. Compared with the traditional processing method, we compare the error coefficient, as shown in Figure 6.

As can be seen from Figure 6, the error coefficient of the traditional processing mode begins to increase with the increase of human behavior data. The data processed by nonlinear normalization can maintain basic accuracy.

4. Modeling of Human Spatiotemporal Behavior and Analysis of Behavior Characteristics Based on Sports Culture Communication in Industrial 4.0 Intelligent Management

4.1. Analysis of Research Results of Human Spatiotemporal Behavior Modeling of Sports Culture Communication Using Mobile Network in Industrial 4.0 Intelligent Management. In the industrial 4.0 environment, the intelligent management mode can liberate human labor and realize behavior interaction and industrial production on the basis of human wisdom. This model can optimize the traditional communication mechanism into intelligent communication mechanism in the field of communication and provides the core technology in human behavior analysis and modeling. Dealing with the invisible factors in the Internet era can change the performance and accuracy of human behavior model from uncontrollable to controllable under the
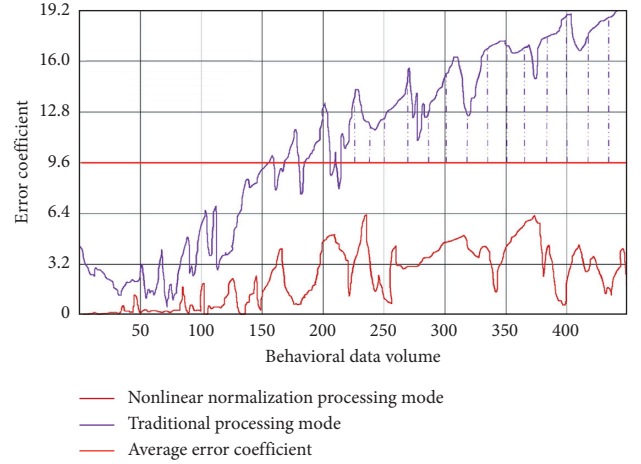
Figure 6: Comparison of error coefficient between traditional processing method and nonlinear normalization processing method.

premise of massive data. Firstly, we analyze the accuracy change of data in the process of human behavior modeling in the industrial 4.0 environment, as shown in Figure 7.

It can be seen from Figure 7 that the traditional human behavior model cannot guarantee the accuracy of data in the modeling process based on the massive data in the Internet age. The human behavior model in the industrial 4.0 environment can ensure the processing speed and control the accuracy above the standard range. In the mobile network environment, sports culture communication can be guaranteed. We build a human behavior model on mobile users. In the above calculation process, it is found that there are strong temporal and spatial characteristics and scene factors in the behavior participation characteristics of mobile networks. These scene factors are easily affected by many aspects. For example, the response of surrounding people to cultural news can indirectly affect individual behavior changes. We use objective quantitative method to map human behavior participation modeling. The response behavior influence coefficient of people in three states to sports cultural news is analyzed, as shown in Figure 8.

As can be seen from Figure 8, the influence coefficient of the crowd who obtains sports news is relatively stable, and the influence coefficient of the crowd who indirectly obtains news information is relatively severe. The influence coefficient of people who do not get sports news is low. The above trends of human behavior can well explain that the impact of sports culture communication on behavior characteristics is significant.

4.2. Analysis of Research Results of Sports Culture Communication of Industry 4.0 Intelligent Management in Human Behavior Feature Modeling. In an intelligent video surveillance system, the accuracy of background model has an important impact on the subsequent judgment of foreground detection, classification, tracking, and behavior understanding analysis. In other words, it largely determines the performance of the whole video surveillance system.
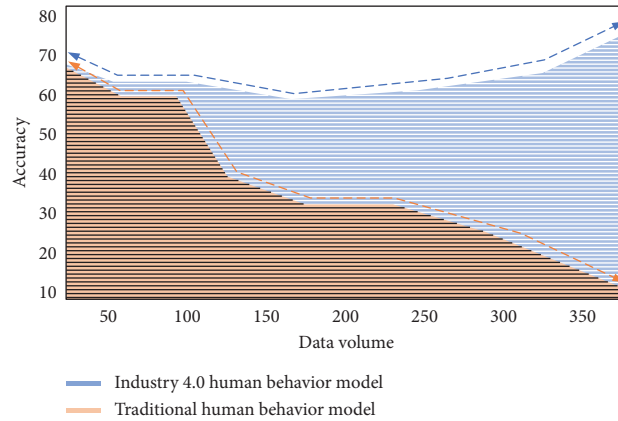
FIGURE 7: Accuracy changes of human behavior modeling data in industrial 4.0 environment and traditional models.
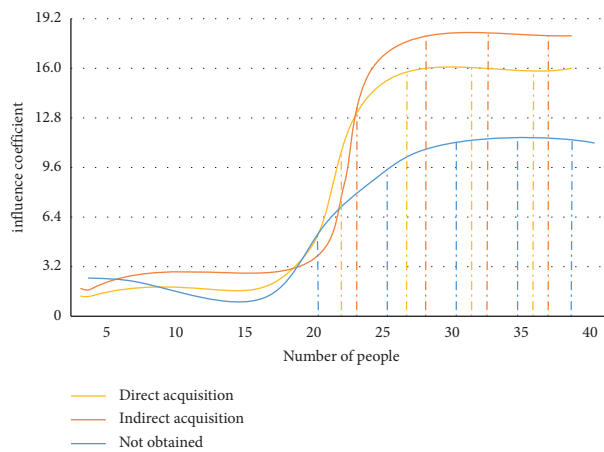
FIGURE 8: Influence coefficient of response behavior of people in three states to sports cultural news.

Complex scenes greatly increase the impact on the accuracy of model monitoring. The human behavior modeling process faces complex scenes in the industrial 4.0 environment, which will be affected and changed by many aspects of the outside world. Human beings may have a variety of behavior characteristics under the specified time and space sequence, or there may be no characteristic changes. Therefore, in the detection process, we need to locate and analyze from the initial cause to the behavior space. The calculation is based on the modeling of human behavior characteristics, including the judgment of the change of user interest. At different times, people staying in the same news can have different effects on the calculation results. With the increase of human behavior data, we need to study feedback efficiency in the model. The feedback speed of human behavior characteristic data before and after industrial 4.0 intelligent management is mainly compared, as shown in Figure 9.

As can be seen from Figure 9, the traditional management mode cannot meet the needs of efficient feedback in the dynamic change characteristics of data. The intelligent management mode in the industrial 4.0 environment can help the analysis model of human behavior characteristics to ensure the feedback efficiency. In the verification process of this study, the main flow of data feature processing is shown in Figure 10.
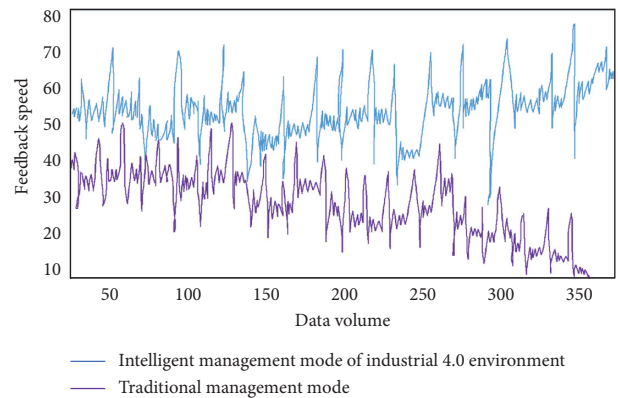
FIGURE 9: Feedback speed of human behavior characteristic data before and after industrial 4.0 intelligent management.

As can be seen from Figure 10, firstly, in data mining, we capture the main content of sports culture on an Internet platform. Secondly, the obtained data are preprocessed to facilitate the analysis of key features. The basic structure of the Internet is extracted, and the form of active behavior is taken as the general category of data statistics. Finally, the data distribution principle is used for visual analysis, and the
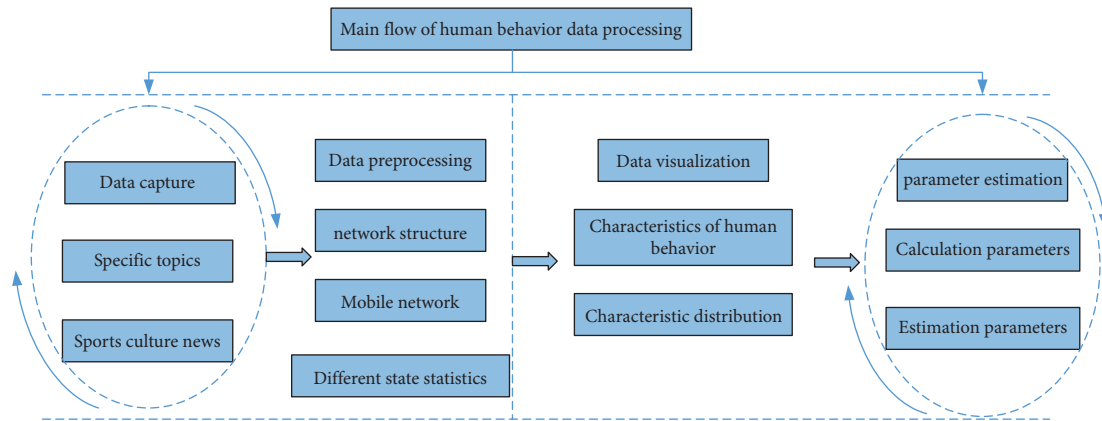
Figure 10: Main flow of data feature processing.

characteristic changes of human behavior are verified by hypothesis theory. In the final experimental results, we found that there are positive and negative trends in the impact of sports culture communication on human behavior under the industrial 4.0 Internet mode.

5. Conclusion

This study proposes to model the human behavior of sports culture communication in the industrial 4.0 intelligent management environment. Firstly, it analyzes the development process of industrial 4.0 environment and the current situation and difficulties of sports culture communication in China. Through data mining, data preprocessing, and behavior quantitative analysis, human behavior trajectory is studied. Under the condition of sports culture communication, the temporal and spatial changes of human behavior are modeled. The influencing factors of human behavior are divided into multiple models to calculate the data distribution of the temporal and spatial characteristics of individual behavior. Based on individual data set, it is transformed into the statistical analysis of group behavior. Finally, according to the track of human behavior and historical traces, the specific factors affecting behavior changes are analyzed. Search modeling is used to explore the characteristic changes of human behavior. The results show that in the industrial 4.0 environment, the communication mechanism and industrial process have changed by leaps and bounds. The results of this study have a positive impact on the behavior trend in human daily life. The main factor affecting behavior change is whether to receive sports culture news. It promotes the process of traditional culture communication and especially helps the communication of sports culture form a good cycle. In order to explore the process of the influence of sports culture news on human behavior. However, this study does not carry out simulation verification analysis on the model data, and further elaboration is needed in future research.

Data Availability

The data used to support the findings of this study are available from the corresponding author upon request.

Conflicts of Interest

The authors declare that they have no conflicts of interest.

## References

[1] C. Zhao, "Research on the construction of two-way practical teaching mode of Intelligent Manufacturing Specialty under the background of industry 4.0," *Light industry science and technology*, vol. 37, no. 11, pp. 112-113, 2021.

[2] L. F. B. Moraes, I. S. Rampasso, R. Anholon et al., "Assessing risk management in Brazilian social projects: a path towards sustainable development," *The International Journal of Sustainable Development and World Ecology*, vol. 28, no. 5, pp. 451–460, 2021.

[3] W. König, S. Löbbe, S. Büttner, and C. Schneider, "Establishing energy efficiency—drivers for energy efficiency in German manufacturing small-and medium-sized enterprises," *Energies*, vol. 13, no. 19, p. 5144, 2020.

[4] Li. Song and Li. Yang, "Governance innovation of occupational safety and health in China under the background of industry 4.0," *Industrial safety and environmental protection*, vol. 47, no. 09, pp. 79–82, 2021.

[5] X. Wang, "The impact of industry 4.0 on the development of traditional jade carving industry," *Light industry science and technology*, vol. 37, no. 9, pp. 96-97, 2021.

[6] S. Luo, "Exploration and practice of talent training mode of Intelligent Manufacturing Specialty in secondary vocational schools under the background of industry 4.0," *Journal of Yanbian Institute of education*, vol. 35, no. 04, pp. 48–51, 2021.

[7] L. Wang, Y. Liu, Q. Wang, J. Wang, and Z. Yang, "PLC course teaching method based on OBE teaching concept," *Advances in Educational Technology and Psychology*, vol. 4, no. 1, pp. 101–109, 2020.

[8] Y. Krykavskyy, O. Pokhylchenko, and N. Hayvanovych, "Supply chain development drivers in industry 4.0 in Ukrainian enterprises," *Oeconomia Copernicana*, vol. 10, no. 2, pp. 273–290, 2019.

[9] S. Gupta, S. Modgil, A. Gunasekaran, and S. Bag, "Dynamic capabilities and institutional theories for Industry 4.0 and digital supply chain," *Supply Chain Forum: International Journal*, vol. 21, no. 3, pp. 139–157, 2020.

[10] J. Holmström, M. Holweg, B. Lawson, F. K. Pil, and S. M. Wagner, "The digitalization of operations and supply

chain management: theoretical and methodological implications," *Journal of Operations Management*, vol. 65, no. 8, pp. 728–734, 2019.

[11] L. Sun, Y. Zhao, W. Sun, and Z. Liu, "Study on supply chain strategy based on cost income model and multi-access edge computing under the background of the Internet of Things," *Neural Computing & Applications*, vol. 32, no. 19, pp. 15357–15368, 2020.

[12] M. Westwood, "International faculty's perspectives on organizational culture and management: a three-step action plan," *United International Journal for Research & Technology*, vol. 3, no. 3, pp. 18–23, 2022.

[13] C. Bolling, S. D. Barboza, W. Van Mechelen, and H. R. Pasman, "Letting the cat out of the bag: athletes, coaches and physiotherapists share their perspectives on injury prevention in elite sports," *British Journal of Sports Medicine*, vol. 54, no. 14, pp. 871–877, 2020.

[14] C. Bolling, S. D. Barboza, W. Van Mechelen, and H. R. Pasman, "Letting the cat out of the bag: athletes, coaches and physiotherapists share their perspectives on injury prevention in elite sports," *British Journal of Sports Medicine*, vol. 54, no. 14, pp. 871–877, 2020.

[15] Y. Wang and X. Xu, "Exploration on the new business form and ethical dilemma of sports culture communication in 5g era," *Journal of Beijing University of physical education*, vol. 44, no. 07, pp. 132–142, 2021.

[16] L. R. Men and C. A. Yue, "Creating a positive emotional culture: effect of internal communication and impact on employee supportive behaviors," *Public Relations Review*, vol. 45, no. 3, p. 101764, 2019.

[17] Xi one. Cui, Y. Zhou, The one of the "one belt, one road" vision of sports culture transmission in China: based on Lasswell 5W communication mode," *Liaoning sports technology*, vol. 43, no. 4, pp. 16–19, 2021.

[18] X. Yang, Y. Yang, and N. Zhong, "Modeling and Simulation of human cognitive behavior under the influence of different emotions," *Computer Measurement and Control*, vol. 24, no. 12, pp. 188–190, 2016.

[19] P. Li, J. Shi, and X. Liu, "Competitive driving behavior modeling based on planned behavior theory," *Transportation system engineering and information*, vol. 16, no. 1, pp. 92–98, 2016.

[20] C. Zhou, Q. C. Zhao, and W. Lu, "Modeling of microblog user forwarding behavior based on interest change," *Journal of Tsinghua University*, vol. 55, no. 11, pp. 1163–1170, 2015.

[21] Fu. Ding, Li. Mingjiang, and Li. Lu, "Empirical research and modeling of human behavior dynamics based on value driven," *Journal of University of Electronic Science and technology*, vol. 44, no. 5, pp. 652–656, 2015.

[22] Du. Xiaoming, T. shuchao, Z. Xing, and Q. Huanren, "Human behavior modeling and research of ammunition support unit CGF (English)," *Journal of System Simulation*, vol. 26, no. 7, pp. 1440–1447, 2014.

[23] P. Wang, H. Peng, F. Xue, and Y. Xu, "Research and implementation of CGF human behavior model of self-propelled antiaircraft gun," *Modern electronic technology*, vol. 36, no. 2, pp. 100–102, 2013.

[24] D. Zhu and X. Zhao, "New characteristics of media communication and Digital Aesthetics of sports culture in 5g intelligent era," *Sports and science*, vol. 42, no. 1, pp. 61–66, 2021.

[25] T. Domínguez Vila, E. Alén González, and S. Darcy, "Accessible tourism online resources: a Northern European perspective," *Scandinavian Journal of Hospitality and Tourism*, vol. 19, no. 2, pp. 140–156, 2019.

Research Article

Exploring Technical Decision-Making Risks in Construction Megaprojects Using Grounded Theory and System Dynamics

Xiaoying Tang [iD],[1] **Mengjun Wang,**[1] **Qian Wang** [iD],[2] **Jingxiao Zhang,**[3] **Hujun Li,**[4] **and Juanjuan Tang**[1]

[1]*Department of Engineering Management, School of Civil Engineering, Central South University, Changsha 410075, China*
[2]*Department of the Built Environment, School of Design and Environment, National University of Singapore, Singapore 117566, Singapore*
[3]*School of Economics and Management, Chang'an University, Xi'an 710064, China*
[4]*Department of Engineering Management, School of Civil Engineering, Henan Polytechnic University, Jiaozuo 454003, China*

Correspondence should be addressed to Qian Wang; bdgwang@nus.edu.sg

Technical decision-makings (TDMs) are a vital part of the decision-makings in construction megaprojects, facing high risks brought by technical complexity, dynamic environment, and subject cognition. Identifying technical decision-making risks (TDMRs) and exploring their interactions are important in megaproject management. Due to the high complexity of TDMs in megaprojects, TDMRs are complex and diverse. However, there is a lack of research on exploring the systematic TDMRs in megaprojects. To address this gap in knowledge, this paper aims to better understand the dynamic complexity of TDMRs in megaprojects by identifying the risks and exploring their interactions from a dynamic and systematic perspective. Grounded theory (GT) and system dynamics (SD) were adopted for this research. First, the GT was used to identify TDMRs in megaprojects and create a conceptual model depicting the relationships among TDMRs. Then, an SD model characterizing the causal structure of the TDMRs system in megaprojects is developed in both qualitative and quantitative manners. The developed model involves interrelationships among environmental risks, decision-making process risks, and decision-making execution process risks. After the validation of the model, a model simulation is conducted to predict the dynamic evolution process of the TDMRs. As a result, a multilayer risk list consisting of 42 index layer risk indicators, 13 field layer risk indicators, and 3 standard layer risk indicators is identified. The SD modeling results show that these multilevel TDMRs interact dynamically and have intricate influences on the total risk level of TDMs in megaprojects. The results of this study could be useful for decision-makers to identify and mitigate TDMRs in megaprojects.

1. Introduction

Construction megaprojects are characterized by significant technical complexity that requires multitechnology integrations [1–3]. Hence, substantial technical decision-makings (TDMs) are required in megaprojects on almost all management hierarchies [4]. The TDMs refer to the process of identifying and analyzing key problems, as well as developing, selecting, and implementing technical schemes to resolve the problems. Hence, the TDMs include both long-term technology development strategies and short-term

technology selections [5, 6]. The outcome of a TDM process is a technical decision-making scheme, consisting of decision objectives, key variables, measures, and criteria [7]. The TDMs must be conducted properly to ensure the successful delivery of megaprojects [2, 7, 8].

Due to the high technical complexity of megaprojects, TDMs in megaprojects also have higher complexity. The complexity of TDMs comprises uncertainties and ambiguities (e.g., dynamic environment, ambiguities of decision-making goals, etc.), as well as the complex interrelationships among influencing factors in TDM issues (e.g., technical

complexity relating to the size and multitechnology integration of the project) [9–12]. Thus, TDMs are generally exposed to various risks. Technical decision-making risk (TDMR) is an extension of project risk and decision-making risk [13, 14]. TDMRs are potential hazards existing in the process and outcome of TDM, which negatively affect the TDM quality and project performance. These risks can cause project cost overruns, delays in delivery, and irreversible accidents [15–17]. For instance, in the Busan-Geoje Fixed Link Project, owing to the defective scheme for towing and mooring, the GINA gasket of standard tunnel element E16 was damaged during construction, resulting in a delay of three months and huge financial loss for repairing the GINA gasket [18]. Therefore, effective management of TDMRs in megaprojects plays an important role in successful decision-makings. Further, the TDM in megaprojects is an open environmental system involving multiple subsystems, which has dynamic and complicated relationships among the factors, rather than a series of normative and procedural activities [7, 19]. The dynamic complexity makes TDMRs in megaprojects highly interrelated, and the risks are transmitted between the internal and external environments of the system [20]. Many risk accidents in construction megaprojects occur due to the interactions of multiple risks rather than a single risk [13]. As such, it is imperative to examine the dynamic interactions among TDMRs.

Thus far, a few research efforts have been made to study decision-making risks of megaprojects using both quantitative and qualitative methods, such as optimism-based decision-making risk model for bridge projects [14], decision-making risk mitigation in megaprojects [21, 22], and identifying and assessing specific types of decision-making risks in megaprojects (i.e., design risks [23, 24], technology selection risks [25], social risks [26], and bidding risks [27, 28]). However, the first two kinds of studies were not focused on TDMR, and the last kind of studies was focused on only one specific risk belonging to TDMR (i.e., design risks and technology selection risks). Risks are interrelated and systematic through causal loops in megaprojects [28–30]. Negligence in considering such risk interrelations results in either underestimation or exaggeration of risk effects [12]. Thus, it is crucial to understand how risks are generated and how they transmit through their interactions. It is argued that research is still lacking to explore TDMRs from a systematic and dynamic perspective considering the whole process of decision-making-execution-feedback.

To address the aforementioned research gaps, this paper aims to identify the TDMRs in construction megaprojects and explore their interactions using the mixed method. The grounded theory (GT) is employed to identify all TDMRs in megaprojects, capturing the managers' perception of TDMRs in the practice of TDM in megaprojects. A conceptual framework depicting the relationships among these risks is provided. Then, a system dynamics (SD) model of TDMRs in megaprojects is constructed to explore the casual loops among TDMRs and simulate the interactions among these risks. The contributions of this study lie in two aspects. First, this study investigates TDMRs and their interactions systemically and dynamically for the first time to reveal the

dynamic nature of TDMRs, which deepens the understanding of TDM in construction megaprojects and enriches theories of construction decision-making and risk management. Second, the identified TDMRs and the simulation model proposed in this study could be adopted as a tool to evaluate and control TDMRs dynamically. The rest of this paper is structured as follows. Section 2 introduces the related work, followed by research methodology in Section 3. The results are presented in Section 4, and discussions and implications are illustrated in Section 5. Lastly, Section 6 summarizes and concludes this study.

2. Literature Review

2.1. Decision-Making Risks in Megaprojects. In recent years, many scholars have indicated the significance of identification and control of the complexity and risks of decision-makings in megaprojects [29, 30]. For example, Shi et al. [7] presented a comprehensive framework of decision-making complexity in megaprojects, which includes six dimensions which are technical, social, financial, legal, organizational, and time. Liu et al. [14] proposed an optimism-based decision-making risk model for bridge projects, where explicit benefits, implicit benefits, construction cost, and operation cost are considered. To mitigate decision-making risks in megaprojects, several researchers proposed risk mitigation strategies via degrading the uncertainty and complexity. Salet et al. [21] put forward three solutions to reduce the complexity and uncertainty of megaprojects to mitigate the decision-making risks, including changing organizational structure, enhancing organizational learning atmosphere, and controlling the number of alternative options for decision-makings.

Furthermore, efforts have been made to identify specific decision-making risks in projects, such as design risks [23, 24], technology selection risks [25, 31, 32], social risks [26], investment risks [33], and bidding risks [27, 28]. Although the aforementioned design risks and technology selection risks belong to TDMRs, each of these existing studies was focused on only one type of TDMRs. Some studies also attempted to assess decision-making risks. For instance, Kurhade and Wankhade [33] proposed a risk assessment framework for decision-making and identified four risk categories for infrastructure investment decision-making, covering political risk, economic risk, social/environmental/cultural risk, and technology risk.

Nevertheless, previous studies on decision-making risks are static without considering the dynamic nature of risks. Attention is lacking to systematically examine TDMRs in construction megaprojects considering the whole process of decision-making. This research gap is addressed in this paper by eliciting the perceptions of managers on what create and drive TDMRs and how they interact with each other by GT.

2.2. Risk Assessment Methods in Megaprojects. Risks can be interrelated, especially in megaproject [34]. Megaprojects are characterized by dynamic interactions of multiple

subsystems, extreme complexity, and technology challenges [35]. Such dynamic complexity makes the risks in megaproject a dynamic system, where the risks are highly interrelated [36]. To capture the dynamic nature of risks and their complex interactions in megaprojects, various risk analysis methods have been applied, such as interpretative structure models (ISM) [37], complex network (CN) [38, 39], social network analysis (SNA) [40], decision-making trial and evaluation laboratory (DEMATEL) [41], the analytic network process (ANP) [42], Bayesian network, and system dynamics (SD) [36, 43–45].

Among these methods, ISM is a qualitative method aiming to develop the hierarchy structure of the factors with direct and indirect correlation paths, and the developed model is influenced by the number of risk factors [37]. Different numbers of risk factors may result in different hierarchy structure of risk factors. Further, CN, SNA, and DEMATEL aim to analyze risk factors from the network perspective, whereas they failed to evaluate risk state in accordance with the interactions of factors. Meanwhile, ANP and Bayesian network (BBN) can be used to explore the interactions among risks and evaluate the risk state quantitatively, while they require large amounts of data. Wu et al. quantify the risk level of a subway station construction using fuzzy ANP via the synthesis of weight matrices, which requires much more computation for pairwise comparison between risk factors [46, 47]. BBN performs excellently to model complex relationships among risks on the bases of the conditional probabilities of the nodes [48]. However, it can only deal with discrete functions. In recent years, various artificial intelligence (AI) methods, such as machine learning and neural networks, have been utilized to identify, evaluate, and predict potential risks in constructions qualitatively and quantitatively [49]. For example, Yaseen et al. [50] developed an AI model integrating Random Forest classifier and Genetic Algorithm optimization to assess the risk of delay in construction, which indicated a robust and accuracy result for project delay risk prediction. Nevertheless, the above-mentioned risk assessment methods analyzed the relationships of risks based on the topology of the network rather than a dynamic and holistic description of the variations of risks. SD developed by Glaser and Strauss [51] is a modeling method dealing with complex causal relationships among components of the system [52]. The foundation of SD is the theory of system thinking, which holds on the view that everything is connected in a dynamic and complex system [53]. SD can not only study the dynamic relationships among risk factors but also simulate risk status during a time period [54]. Hence, SD has been widely used for megaproject risk assessment including modeling of the interrelationships and feedbacks of the risk system. For example, Boateng et al. [55] implemented SD to model the interactions among social, technical, economic, environmental, and political (STEEP) risks considering the complexity and dynamics of megaprojects. Xue et al. [36] proposed a risk coupling model based on SD for risk assessment of High-Speed Rail projects considering the interactions among risks. Wang et al. [56] developed an SD-based safety risk model that covered organizational processes and technical systems and demonstrated the model on an urban metro tunnel project. To identify and control the system risks of automatic metro, Zhao et al. [57] proposed an SD-based model embodying system risks and factors of organizational resource assignment, organizational experience, and avoidance of driver error to reveal the feedback mechanisms of automatic metro. In summary, SD can provide a powerful insight in understanding the complexity and dynamics of construction risk systems [54].

However, there have not been studies exploring the dynamic interactions among TDMRs in construction megaprojects. In this study, SD will be adopted to model the dynamics and interactions among TDMRs.

3. Methodology

A research framework based on a mixed method integrating GT, SD, and Shannon's entropy was proposed in this study to identify TDMRs and explore their dynamic interactions, as shown in Figure 1. Among the three methods, GT is widely used to identify risks from qualitative data [58], SD is an effective approach for modeling the dynamic relations among risks based on mathematical modeling techniques [59], and Shannon's entropy method is one of the various methods for objective weighting measures. GT, along with qualitative data collection techniques (e.g., case study, interviews, focus groups, etc.) and data analysis techniques (e.g., opening coding, axial coding, and selective coding), can be used to develop SD models based on qualitative data [60]. A mixed method is adopted to draw the advantages and minimize the disadvantages of both qualitative and quantitative methods [61–63]. Several studies have successfully implemented similar mixed methods with GT and SD [53, 64, 65]. For example, in [53], safety archetypes of construction workers were identified by GT and the behavior archetypes of safety involving construction workers were explored with SD.

Therefore, the mixed method was conducted in this study as follows. First, GT was employed to identify TDMRs in megaprojects and develop the conceptual model of these risks, as explained in Section Grounded theory. Then, an SD model of TDMRs in megaprojects was built, which involved qualitative modeling, quantitative modeling, model validation, and model simulation, as discussed in Section System dynamics. Further, the parameters involved in SD equations were determined based on the weights of risk indicators calculated by Shannon's entropy, as introduced in Section Shannon's entropy. Lastly, a simulation was conducted to understand the behavior of the system.

3.1. Grounded Theory.
This study uses GT to identify TDMRs and build the conceptual model. GT put forward by Forrester [52] as a qualitative research method linking concepts to generate meaningful theories [66], where concepts and their interdependencies are obtained from analyzing qualitative data (e.g., interview transcripts). GT could be applied by three approaches, namely, the Straussian
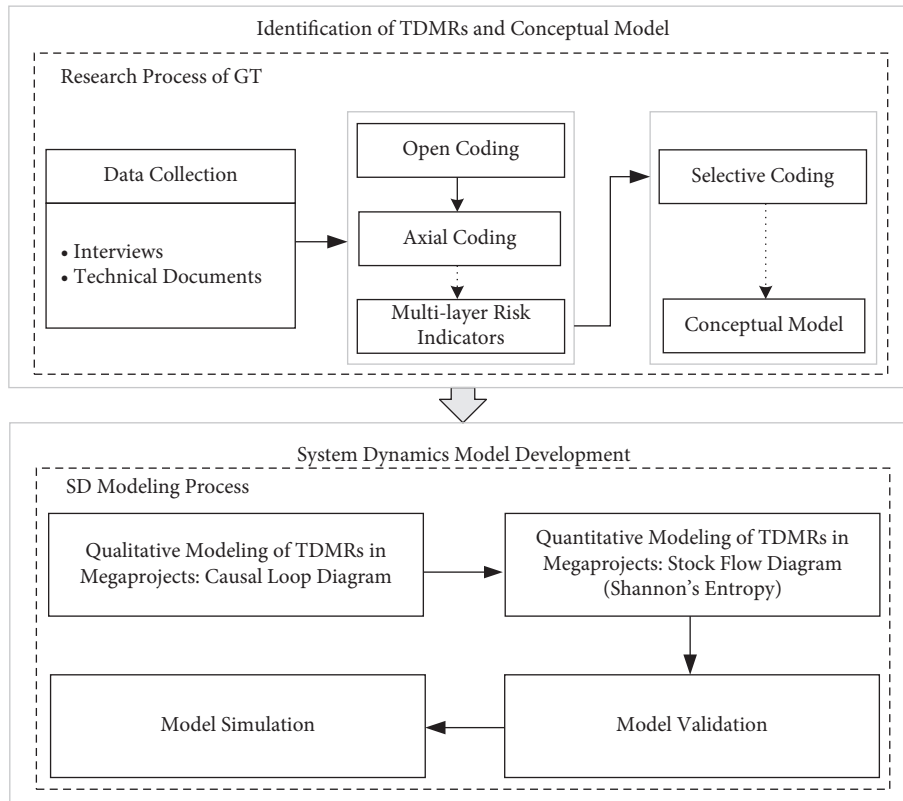
Figure 1: Research framework.

approach [67], the Glaswegian approach [68], and the Constructive approach [69].

Compared to other approaches, the Straussian approach is more prescriptive as it provides systematic procedure for data analysis including open coding, axial coding, and selective coding [70, 71]. On the other hand, the Glaswegian approach and the Constructive approach have no clear guidelines for data analysis. Therefore, the Straussian approach is adopted in this study to identify TDMRs from real megaprojects in a systematic way. Following the Straussian approach, the GT process of this study includes (1) data collection and (2) data analysis consisting of open coding, axial coding, and selective coding, as described in the following [67].

3.1.1. Data Collection. Qualitative data were collected based on a case study so that practical insights could be addressed to enable changes in practice to occur [72]. A case study can include either one single case or multiple cases, and there are different opinions on the required number of cases for understanding a phenomenon [72, 73]. The case study in this research was conducted on three megaprojects in China, namely, the Hong Kong-Zhuhai-Macao Bridge Island Tunnel Project (HZMBIT), the Foshan West Railway Station Comprehensive Transportation Hub Project (FWRSCTH), and the Kunming Comprehensive International Transportation Hub Project (KCITH), to enable generalizations on the TDMRs. These cases were selected because (1) the authors had access to the major stakeholders of these

projects, (2) these megaprojects were representative, characterized by multitechnology integrations and high technical complexity, and (3) these projects were under construction or completed less than three years during data collection. The selected cases covered different type of projects (tunnel, railway, and building), and they were all demonstration megaprojects jointly developed by national and local governments. All the cases had multitechnology decision-makings along project lifecycle, which made it possible to collect substantial qualitative data for TDMRs identification.

The case data were collected by semistructured interviews and review of technical documents. Semistructured interviews were conducted with experts from designers, contractors, consultants, and university partners of the three megaprojects. According to Bernard and Bernard [74] and Creswell and Poth [75], interviews with a sample size of 5 to 25 are appropriate for GT studies. In this study, 12 experts were selected for interviews, and the experts had 8 to 27 years of experiences in TDMR management in megaprojects, as shown in Table 1. The selected 12 experts provided meaningful insights that adequately represented the experiences of construction professionals on TDMR management. The interview questions were designed to collect relevant data about TDMRs in megaprojects. The interviewees were asked to elaborate their understandings on TDMRs, provide examples of TDMRs according to their working experience, describe the risk issues, and explain how they deal with risks in the TDM process. For example, the questions asked included (1) what factors drive TDMR events in megaprojects, and what factors contribute to a TDM failure? (2) Do

TABLE 1: The personal particulars of interviewees.

Job title	Working experience	Involved project
Project manager	17 years	KCITH
Project manager	17 years	KCITH
Project manager	25 years	HZMBIT
Project manager	22 years	FWRSCTH
Chief engineer	20 years	KCITH
Deputy chief engineer	22 years	HZMBIT
Designer	10 years	FWRSCTH
Designer	8 years	KCITH
Designer	18 years	HZMBIT
Consultant	15 years	HZMBIT
Consultant	13 years	KCITH
Professor	27 years	HZMBIT

TDMRs interact with each other and how? And (3) what happens if a TDMR event happens in megaprojects? Each of the 12 interviews lasted for 60 to 100 minutes.

In addition to interviews, technical documents of the three megaprojects were also collected to understand the TDMRs in these projects. Due to the large amount of TDMs, the three projects had a large number of technical documents including result-based documents (i.e., construction drawing, technical schemes, and contractual documents) and process-based documents (i.e., safety technical disclosure, environmental checklists and reports, records of technical scheme assessment meeting of the project). A total of 63 technical documents were selected as the raw data including 29 documents from HZMBIT project, 18 documents from FWRSCTH project, and 16 documents from KCITH project.

3.1.2. Three-Level Coding.
After data collection, all the collected data were analyzed based on three-level coding, namely, open coding, axial coding, and selective coding. Open coding is an analytic process that identifies the concepts and discovers their properties and dimensions through line-by-line analysis [67]. Hence, in the open coding step, the original data collected from interviews and technical documents were examined and coded to find major TDMRs in megaprojects (i.e., initial codes). Then, axial coding clusters the identified TDMRs into subcategories (i.e., focalized codes) and categories based on their properties and dimensions. Lastly, selective coding was to detect the relationships among different categories [67]. Selective coding is the last step of GT for theory refining and integrating. A conceptual model linking different categories to reveal their relationships was built during this step via reviewing the memos gathered during the analysis and interviews.

3.2. System Dynamics.
As presented in Section 2.2, SD is used in this study to model the interactions among TDMRs in megaprojects and to reveal how TDMRs interact dynamically and how these interactions contribute to the overall risk. The SD model is developed in the following four steps. In Step 1 (qualitative modeling), based on the identified TDMRs and the conceptual model, system analysis is conducted to draw the system boundary, and the logical structure of the system is defined with a causal loop diagram. Then, Step 2 (quantitative modeling) is performed to formulate the relationships among TDMRs with the stock-flow diagram. Next, Step 3 (model validation) is carried out through structure validation, behavioral validation, and sensitivity validation. Lastly, Step 4 (model simulation) simulates how the system reacts under diverse scenarios.

3.3. Shannon's Entropy.
Shannon's entropy is capable of measuring the uncertainty of a random process. It is widely used to calculate the weight of each risk indicator based on expert scores [76]. First, the expert scores are normalized using equations (1) and (2) for the-larger-the-better.

Criteria and the-smaller-the-better criteria are, respectively:

$$Y_{ij} = \frac{X_{ij} - \min(X_i)}{\max(X_i) - \min(X_i)}, \tag{1}$$

$$Y_{ij} = \frac{\max(X_i) - X_{ij}}{\max(X_i) - \min(X_i)}, \tag{2}$$

where X_{ij} is the score of the ith expert with regard to the jth risk indicator ($i = 1, 2, 3,\ldots,m; j = 1, 2, 3,\ldots,n$) and Y_{ij} is the normalization value of each risk indicator.

It is important to note in this paper that since the experts score based on the importance of each risk indicator, all scores of indicators are processed following the-larger-the-better criteria.

Subsequently, the entropy value E_j of each risk indicator is calculated as follows:

$$E_j = -\frac{1}{\ln m} \sum_{i=1}^{m} p_{ij} \ln p_{ij}, \tag{3}$$

where m is the number of experts; $p_{ij} = (Y_{ij}/\sum_{i=1}^{m} Y_{ij})$. If $p_{ij} = 0$, $\lim_{p_{ij} \to 0} p_{ij} \ln p_{ij} = 0$. Then, the weight W_j of each risk indicator can be calculated as

$$W_j = \frac{1 - E_j}{\sum_{j=1}^{n} (1 - E_j)}, \tag{4}$$

where E_j is the entropy value of each risk indicator, and n is the number of the indicators.

4. Results

4.1. Identification of TDMRs in Megaprojects.
According to the Project Management Institute (2008), a risk is "an uncertain event of condition that, if occurs, has a positive or negative effect on project's objectives." Following this definition, all the collected data were examined and TDMRs were identified through GT-based data analysis. In the open coding step, by identifying and describing overall constructs relevant to TDMRs based on the collected data, 97 key concepts were extracted through line-by-line and sentence-by-sentence analysis. Then, the 97 key concepts were summarized as 42 initial codes (A1-A42). Next, the axial

coding step identified connections between the initial codes and aggregated the initial codes into focalized codes and categories. As a result, the initial codes were grouped into 13 focalized codes (B1–B13) and further into three categories (BB1-BB3). Table 2 gives some examples of how the collected data were coded in open coding and axial coding.

Table 3 shows the coding results of TDMRs including 42 initial codes, 13 focalized codes, and 3 categories. Due to space limitation, the 97 key concepts are not shown in the table but can be obtained from the corresponding author upon request. According to the coding results, TDMRs in megaprojects are divided into three categories: decision-making process risk, decision-making execution process risk, and environmental risk.

Four layers of risk indicators (shown in Table 4) are established from the coding results including (1) target layer risk indicator (i.e., the total TDMR in a project), (2) standard layer risk indicators (i.e., corresponding to three categories), (3) field layer risk indicators (i.e., corresponding to 13 focalized codes), and (4) index layer risk indicators (i.e., corresponding to 42 initial codes). Risk indicators in each layer are determined by indicators in the lower layers. For example, B1 is determined by A1 to A5, and BB1 is determined by B1 to B5.

Decision-making process risk (BB1) represents risks within the process of identifying and analyzing problem and developing and choosing the technical solution. This process involves decision-makers, information, and procedure, and the outcome is a decision-making scheme. Five field layer risk indicators are related to BB1 including decision-making participants risk (B1), decision-making information risk (B2), procedure risk (B3), decision-making mechanism risk (B4), and decision-making scheme risk (B5).

Decision-making execution process risk (BB2) refers to risks associated with the execution process of the final technical decision-making scheme. Corresponding to the elements and characteristics of decision-making execution, executive, premanagement, in-process management, and technology management are key issues for successful execution of decision-making. Three field layer risk indicators are associated with BB2 including management risk (B6), executive risk (B7), and construction technical risk (B8).

Environmental risk (BB3) describes risks related to the external environment of TDM. The environment contains elements related to society, technology development, economy, and natural and political environment. Five field layer risk indicators are correlated to BB3 including technical environmental risk (B9), economic environmental risk (B10), natural environmental risk (B11), social risk (B12), and political environmental risk (B13).

In selective coding, three categories of risk indicators (BB1-BB3) were linked following a single storyline around which everything else was draped [77]. A conceptual model of their relationships was developed with grounded theory, as shown in Figure 2. The risk lies in the interaction between the subject and the environment [78]. The TDMR accidents in megaprojects occur under the joint influence of the environmental risks, the decision-making process risks, and the decision-making execution process risks. When environmental risks occur, there will be an increased tendency for the risk of the decision-making process and the risk of decision-making execution process. At the same time, the decision-making process risks may transmit to the decision-making execution process risks.

4.2. Dynamic Model of TDMRs in Megaprojects

4.2.1. Qualitative Modeling of TDMRs in Megaprojects. To qualitatively model TDMRs and understand the feedback loops among TDMRs, a causal loop diagram containing the three categories and 13 focalized codes of TDMRs is depicted, as shown in Figure 3. A causal loop diagram aids in visualizing how TDMRs and variables affect one another by arrows with positive or negative labels (Bala et al., 2017). The diagram is created based on the abovementioned coding results, especially the conceptual model of relationships among TDMRs in megaprojects, as well as the 12 interviews. Furthermore, a group interview was conducted with the abovementioned experts to validate the structure of the diagram. It is noted that the developed causal loop diagram aims to reveal the main causal loops among TDMR. Thus, the index layer risk indicators are not considered in the causal loop diagram since risk indicators in each layer are determined by indicators in the lower layers and the index layer risk indicators are the lowest layer. As presented in Figure 3, TDMRs interact with each other in 3 ways: (1) by the process of decision-making (i.e., the risks lie in decision-making process transmit to the decision-making execution), (2) by the life cycle of the project (i.e., the TDMRs lie in previous construction stage transmit to the next construction stage), and (3) from the external risk to the internal risk (i.e., environmental risks transmit to decision-making process and decision-making execution process). The decision-making process risks may transmit to the decision-making execution process risks. The diagram includes five balancing loops, which interact with each other.

Loop 1: Decision-making information risk--(+) Decision-making process risk--(+) Decision-making execution process risk--(-) Decision-making information risk. This is a balancing feedback loop meaning that the increase of decision information risk will stimulate the rise of decision-making process risk, with which decision execution process risk will grow, and then much attention will be paid to decreasing the risk of decision-making information risk. According to Pirzadeh and Lingard [79], technical decision-makings arise as the result of information exchanges between projects actors. Information is essential as an input of the decision-making process [23, 80].

Loop 2: Decision-making scheme risk--(+) Decision-making process risk--(+) Decision-making execution process risk--(-) Decision-making scheme risk. This is a balancing feedback loop indicating that the increase of decision-making scheme risk will result in a higher level of decision-making process risk, and then there will be a higher risk during the execution process of decision-making, which will attract more attention and the decision-making scheme will be checked and improved in turn. Decision-making

TABLE 2: Example of coding process in GT.

Collected data	Open coding		Axial coding	
	Key concepts	Initial codes	Focalized codes	Categories
Decision-maker lacks experience; the requirements of owner are beyond our ability; the chief decision-maker makes decisions based on their own knowledge, experience, and rationale, rather than information from other consulting subjects, which sometimes is impulsive, without enough information. Decision-maker cooperated with the consulting agency in the past; decision-maker usually prefers to choose the scheme he is familiar with rather than the more satisfying one; sometimes, it is hard to control the quality of scheme. Decision-making quality may deviate from the expectations; the consulting agency failed to provide proper advice. The lack of good communication and coordination ability among the decision-making participants leads to instability of the decision-making team. It is hard to coordinate the interests of all parties.	a01 decision-maker lacks ability and professional knowledge	A1 poor professional quality of decision-makers	B1 decision-making participants risk	BB1 decision-making process risk
	a02 the style of decision-maker is different a03 the psychological tendency of decision-makers matters a04 the value preference of decision-maker is different	A2 psychological tendency and value preference of decision-makers		
	a05 decision-making behavior changes	A3 risk of alienation of decision-makers' behavior		
	a06 the advice of experts is not adopted as expected a07 the consulting agency fails to support the decision-makers	A4 no prominent role of the decision support layer		
	a08 unreasonable sharing of risks among project participants in decision-making	A5 game risk of interest groups		

scheme is the outcome of a decision-making process, guiding the execution process [7]. Thus, the decision-making risk could transmit to decision-making execution process imperceptibly until the risk events happen. For example, in the HZMBIT project, the rib rubber mound was initially recommended as the structural design of the artificial island. However, it is found that the scheme may result in quality defects, delay, and pollution in execution process. Therefore, the initial design scheme was replaced by the large diameter deep inserted steel cylinder scheme, which sped up the schedule greatly [81].

Loop 3: Decision-making information risk--(+) Decision-making participants risk--(+) Decision-making process risk--(+) Decision-making execution process risk--(−) Decision-making information risk. This is a balancing feedback loop including a part of Loop 1. In addition to the information shown in Loop 1, Loop 3 also illustrates that the decision-making participants are more likely to make wrong decisions with incomplete and inaccurate information, which will result in a higher risk level of the decision-making execution process. Then it will provide feedback to improve the information quality. Research has shown that the knowledge to make a TDM resides in more than one decision-making participant [82]. TDM arises as the result of interactions and information exchanges among decision-making participants [79]. Hence, it is safe to claim that decision-making participants, such as project managers, play a pivotal role in successful TDM [83].

Loop 4: Decision-making information risk--(+) Decision-making scheme risk--(+) Decision-making process risk--(+) Decision-making execution process risk--(−) Decision-making information risk. **Loop 5:** Decision-making information risk--(+) Decision-making participants risk--

(+) Decision-making scheme risk--(+) Decision-making process risk--(+) Decision-making execution process risk--(−) Decision-making information risk. The balancing Loop 4 and Loop 5 include parts of Loop 1 to Loop 3. Loop 4 and Loop 5 further explain how risks transmit among decision-making information, decision-making scheme, and decision-making participants. The poor quality of decision-making information makes it more difficult for decision-making participants to make decision-making schemes [79]. The timely and effective exchange of information among participants is critical for the development of TDM schemes [84].

4.2.2. Quantitative Modeling of TDMRs in Megaprojects. To quantitatively model the interactions among TDMRs, it is essential to draw the system stock-flow diagram and build the dynamic equations. Based on the causal loop diagram of TDMRs in megaprojects as well as the characteristics of TDMRs in megaprojects, the system stock-flow diagram with four stock variables, four rate variables, 22 auxiliary variables, and 33 constant variables is built with three subsystems, namely, the decision-making process risk subsystem, environmental risk subsystem, and decision-making execution process risk subsystem. The meanings of SD variables in system stock-flow diagram are shown in Table 5. Arrows connect the four types of variables, indicating either substance or information flow between the two variables. As shown in Figure 4, a set of variables are involved in each subsystem. (1) Subsystem of decision-making process risk: decision-making process risk is quantified with the equations in Table 6. (2) Subsystem of decision-making execution process risk: decision-making execution process

TABLE 3: Coding results of TDMRs including 42 initial codes, 13 focalized codes, and three categories.

Core categories	Categories	Focalized codes	Initial codes
TDMR in construction megaprojects	BB1 decision-making process risk	B1 decision-making participants risk	A1 poor professional quality of decision-makers; A2 psychological tendency and value preference of decision-makers; A3 risk of alienation of decision-makers' behavior; A4 no prominent role of the decision support layer; A5 game risk of interest groups
		B2 decision-making information risk	A6 blocked access to information; A7 improper description of the decision problem; A8 insufficient precision and accuracy of basic data such as survey and design
		B3 procedure risk	A9 incompleteness of decision-making procedures; A10 compliance and legality of project approval procedures
		B4 decision-making mechanism risk	A11 unreasonable allocation of decision-making power; A12 unreasonable decision-making regulation and system
		B5 decision-making scheme risk	A13 decision-making method risk; A14 indicators risk for decision-making scheme comparison; A15 technology selection risk; A16 scheme design defects; A17 the legal risks of the scheme
	BB2 decision-making execution process risk	B6 management risk	A18 timing risk of plan execution; A19 insufficient member ability; A20 fuzzy organizational structure and allocation of rights, responsibilities, and benefits; A21 insufficient emergency response capability; A22 management system defects
		B7 executive risk	A23 insufficient professional ability of workers; A24 the executive's attitude risk
		B8 construction technical risk	A25 changes in geological and hydrological conditions at the construction site; A26 plan change risk; A27 construction and maintenance risks; A28 the risk of construction technology, mechanical equipment, and material
		B9 technical environmental risk	A29 different technical standard; A30 technology maturity risk; A31 technology policy risk
		B10 economic environmental risk	A32 financing difficulty; A33 unfavorable economic situation
	BB3 environmental risk	B11 natural environmental risk	A34 complex hydrological, geological, and meteorological conditions; A35 natural disasters; A36 regional ecosystem vulnerability
		B12 social risk	A37 public opinion risk; A38 social stability risk
		B13 political environmental risk	A39 government behavior; A40 legal risk; A41 government policy changes; A42 coup, war
Total	3	13	42

risk is a stock variable, which is influenced by the growth rate of decision-making execution with equations in Table 6. (3) Subsystem of environmental risk: environmental risk was determined by the growth rate of environmental risk with corresponding equations in Table 6. In terms of system of technical decision-making risk in megaprojects, technical decision-making risk is a stock variable and the growth rate of the technical decision-making risk in megaprojects as input of stock variable. Further, the growth rate of the technical decision-making risk in megaprojects was influenced by the decision-making process risk, decision-making execution process risk, and environmental risk. The relationships are depicted by equations in Table 6.

The mathematical equations of variables involved in each subsystem are established based on the stock-flow diagram. The coefficients of variables in each equation are established based on the weights of indicators. To determine the weights of indicators, questionnaires were distributed to seven experts engaged in megaproject management and risk management research at universities and practice fields. The experts included two professors engaged in megaproject risk management research at universities, two engineering managers engaged in whole process engineering consulting, two engineering managers from general construction contracting company, and one engineering manager from megaproject owner. They provide evaluations of the importance of each risk indicator in the index layer.

The experts were asked to score based on the controllability, possibility, and degree of loss of the risk. Responses are made based on a five-level Likert scale (1–5), where 1 represents lowest importance and 5 represents highest importance. In general, there are two categories of weighting methods, namely, subjective weighting methods and objective weighting methods [63]. Thereinto, subjective weighting approach is conducted on the basis of decision-maker's experiences and judgment, while the objective weights were calculated via mathematical computation [63]. According to Deng et al. [72], the method with objective weighting is more applicable when it is difficult to obtain the reliable subjective weights. In this paper, all the selected

TABLE 4: TDMRs in megaprojects.

| Target layer risk indicator	Standard layer risk indicators	Field layer risk indicators	Index layer risk indicators	Definitions
TDMR in construction megaprojects	BB1 decision-making process risk	B1 decision-making participants risk	A1, A2, A3, A4, A5	Inability of TDM participants to contribute to the decision-making activities and poor collaboration among them
		B2 decision-making information risk	A6, A7, A8	Inappropriate and inaccurate information, lack of documents
		B3 procedure risk	A9, A10	Incompleteness of procedure, lack of standardization, and process records
		B4 decision-making mechanism risk	A11, A12	Lack of rules and regulations
		B5 decision-making scheme risk	A13, A14, A15, A16, A17	Inadequate site investigation, mistakes in the TDM scheme, insufficient comparison, and selection of alternative scheme
	BB2 decision-making execution process risk	B6 management risk	A18, A19, A20, A21, A22	Poor management and supervision in implementation of TDM scheme. Inadequate coordination and collaboration on-site
		B7 executive risk	A23, A24	Inadequate experience and qualification of executive
		B8 construction technical risk	A25, A26, A27, A28	inferior quality and low safety level of the project, due to complex construction
		B9 technical environmental risk	A29, A30, A31	The uncertainty and immature of new technology. Industry technology is backward
		B10 economic environmental risk	A32, A33	Insufficient supply of capital and required resources and unfavorable macroeconomic situation
	BB3 environmental risk	B11 natural environmental risk	A34, A35, A36	Natural disasters, complex geographic and climatic conditions, and high environmental requirements for fragile ecological environment
		B12 social risk	A37, A38	The influence of bad public opinion and the instability of society caused by TDM scheme
		B13 political environmental risk	A39, A40, A41, A42	The uncertainty of the project construction caused by changes in the host country's domestic political situation, legal environment, and political relations with other countries
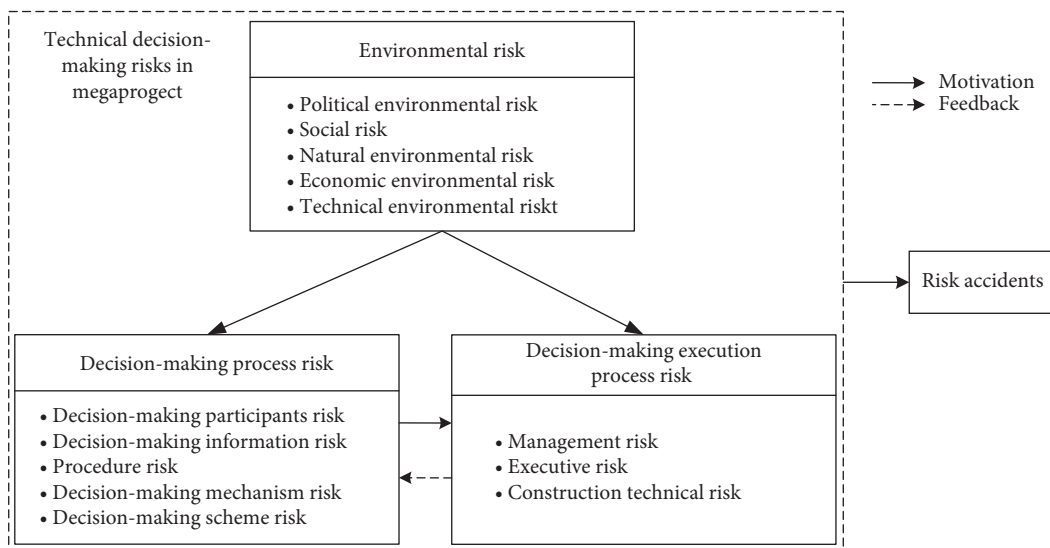
FIGURE 2: Conceptual model of the relationships among TDMRs in megaprojects.
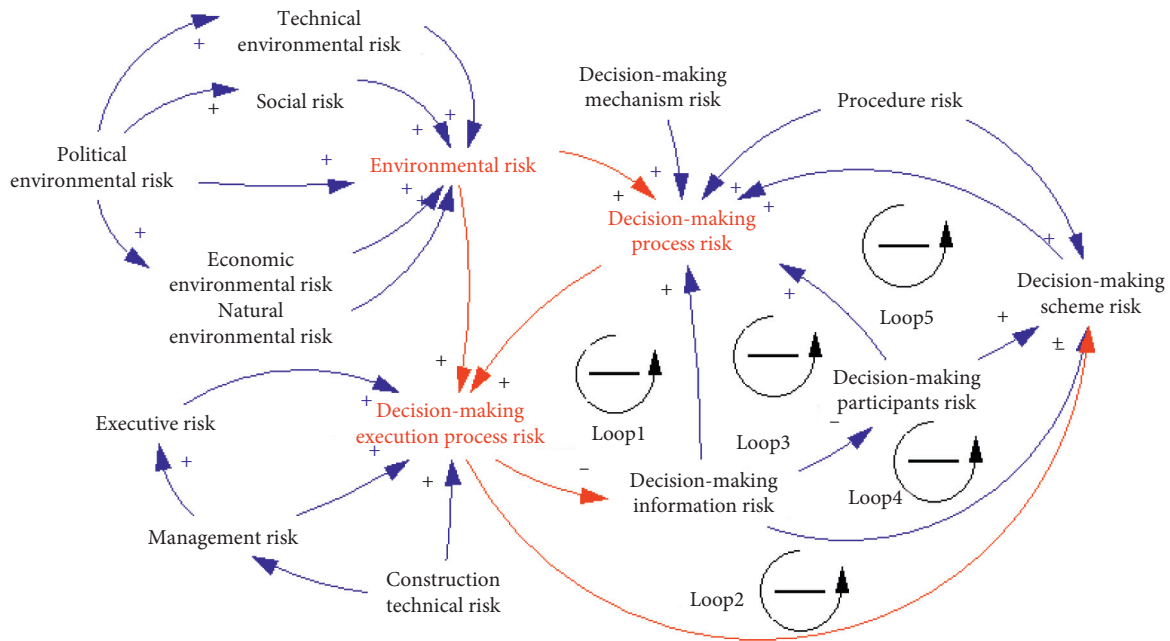
FIGURE 3: Causal loop diagram of TDMRs in megaprojects.

TABLE 5: Meanings of SD variables.

Variable	Variable type	Meaning
Technical decision-making risk in megaprojects L	Stock	State of technical decision-making risk in megaprojects
BB1 decision-making process risk LV1	Stock	State of decision-making process risk
RV1	Rate variable	The growth rate of the decision-making process risk
B1 decision-making participants risk	Auxiliary variable	
PPQDM	Constant	Poor professional quality of decision-makers
PTVPDM	Constant	Psychological tendency and value preference of decision-makers
RADMB	Auxiliary variable	Risk of alienation of decision-makers' behavior
NPRDSL	Auxiliary variable	No prominent role of the decision support layer
GRIG	Auxiliary variable	Game risk of interest groups
B2 decision-making information risk	Auxiliary variable	
BAI	Auxiliary variable	Blocked access to information
IDDP	Auxiliary variable	Improper description of the decision problem
IPABD	Constant	Insufficient precision and accuracy of basic data such as survey and design
B3 procedure risk	Auxiliary variable	
IDMP	Constant	The incompleteness of decision-making procedures
CLPAP	Constant	Compliance and legality of project approval procedures
B4 decision-making mechanism risk	Auxiliary variable	
UADMP	Constant	Unreasonable allocation of decision-making power
UDMRS	Constant	Unreasonable decision-making regulation and system
B5 decision-making scheme risk	Auxiliary variable	
DMMR	Constant	Decision-making method risk
IRDMSC	Constant	Indicators risk for decision-making scheme comparison
TSR	Constant	Technology selection risk

TABLE 5: Continued.

Variable	Variable type	Meaning
SDD	Constant	Scheme design defects
LRTS	Constant	The legal risks of the scheme
BB2 decision-making execution process risk LV2	Stock	State of decision-making execution process risk
RV2	Rate variable	The growth rate of decision-making execution process risk
B6 management risk	Auxiliary variable	
TRPE	Constant	Timing risk of plan execution
IMA	Auxiliary variable	Insufficient member ability
FOSBARRC	Constant	Fuzzy organizational structure and allocation of rights, responsibilities, and benefits
IERC	Constant	Insufficient emergency response capability
MSD	Constant	Management system defects
B7 executive risk	Auxiliary variable	
IPAW	Constant	Insufficient professional ability of workers
EAR	Constant	The executive's attitude risk
B8 construction technical risk	Auxiliary variable	
CGHCCS	Constant	Changes in geological and hydrological conditions at the construction site
PCR	Auxiliary variable	Plan change risk
CMR	Auxiliary variable	Construction and maintenance risks
RCTMEM	Auxiliary variable	The risk of construction technology, mechanical equipment, and material
BB3 environmental risk LV3	Stock	State of environmental risk
RV3	Rate variable	The growth rate of environmental risk
B9 technical environmental risk	Auxiliary variable	
DTS	Constant	Different technical standard
TMR	Constant	Technology maturity risk
TPR	Constant	Technology policy risk
B10 economic environmental risk	Auxiliary variable	
FD	Constant	Financing difficulty
UES	Constant	Unfavorable economic situation
B11 natural environmental risk	Auxiliary variable	
CHGMC	Constant	Complex hydrological, geological, and meteorological conditions
ND	Constant	Natural disasters
REV	Constant	Regional ecosystem vulnerability
B12 social risk	Auxiliary variable	
POR	Constant	Public opinion risk
SSR	Constant	Social stability risk
B13 political environmental risk	Auxiliary variable	
GB	Constant	Government behavior
LR	Constant	Legal risk
GPC	Constant	Government policy changes
CW	Constant	Coup, war

seven experts have much experience in TDMR management, and it is hard to quantify the subjective weights of experts. Therefore, the weights of indicators were obtained via objective weighting method, namely, Shannon's entropy, as illustrated in Section 3.3, ignoring the subjective weights of each expert. The obtained weights of risk indicators are shown in Table 7, and the mathematical equations of variables are presented in Table 6.

4.3. Model Validation. Structure validation, behavioral validation, and sensitivity validation are performed to test
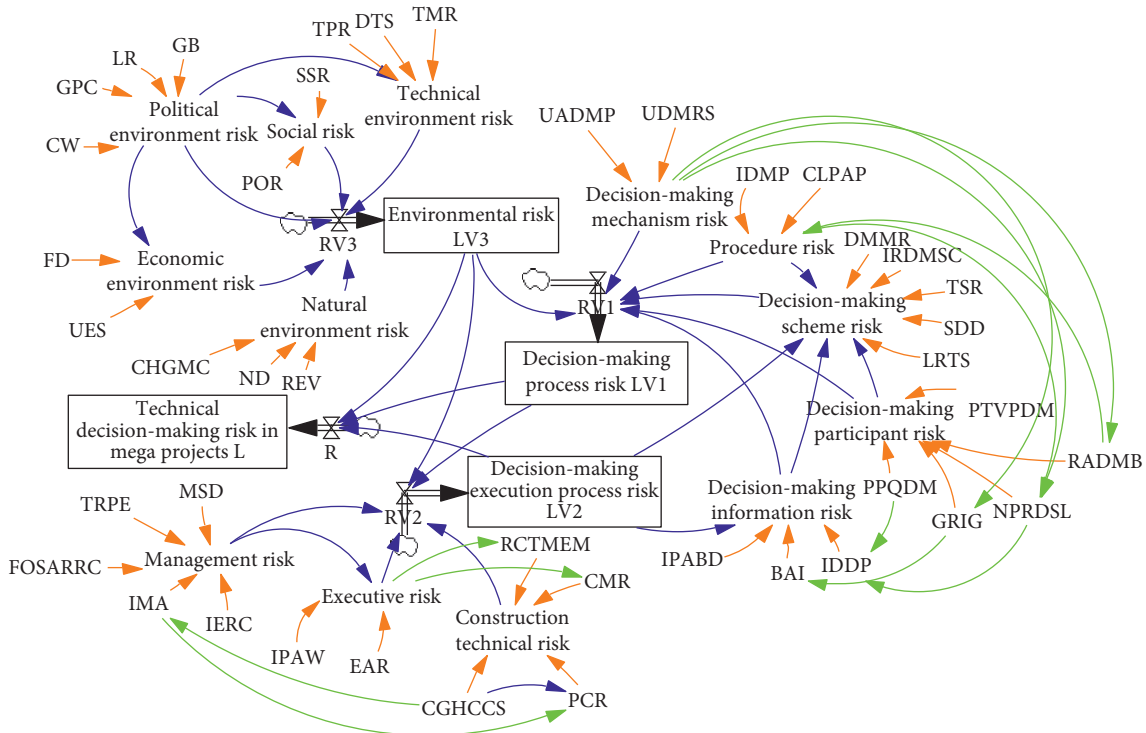
FIGURE 4: System stock-flow diagram of TDMRs in megaprojects.

the structure of the SD model and observe whether the model is consistent with the actual situation [85]. In this study, the structure validation aiming to assess the structural reliability of the model is conducted via structure verification test and dimension consistency test. The variables in the model are extracted from interviews and technical documents, and their relationships are confirmed with a structure verification through interviews with experts. Then, the behavioral validation test is conducted by running the simulation model for the period of one month and comparing the simulation results with the actual field data. The actual field data were collected from the KCITH project, and the comparison shows that the simulation model could produce similar results with the field data.

Furthermore, sensitivity validation is used to analyze the effects of the alteration of variables on model simulation results and identify critical TDMRs in megaprojects. Taking the decision-making process risk subsystem as an example, it is found that decision-making process risk is the most sensitive to psychological tendency and value preference of decision-makers (PTVPDM), unreasonable allocation of decision-making power (UADMP), and decision-making method risk (DMMR). The influence of PTVPDM on the decision-making process risk can be estimated by changing the initial values of PTVPDM. When the initial value of PTVPDM varies from 0.4 (run 1) to 4 (base run) and 40 (run 2), the decision-making process risk will increase significantly, as shown in Figure 5.

4.4. Model Simulation

4.4.1. Model Parameters. The model simulation of TDMRs was conducted based on case study of the KCITH project, which had an estimated investment of over 900 million USD. The project started in November 2017 and was expected to complete in February 2024. The KCITH project was selected since the TDMs of the project faced a variety of risks such as foundation pit collapse, impact of COVID-19, and policy change, due to the high standard of construction, dynamic external environment, and complex geology and climate conditions. Besides, the construction process involved many high-altitude operations and cross-disciplinary activities. At the time of data collection, the project was under construction and suffered time delays and other various risks in TDMs both internally and externally. Furthermore, the simulation results could help project manager to deal with the TDMRs.

According to the actual construction schedule of the project, the model simulation period was set to 73 months and the step length was one month. To determine the initial values of variables in the model, questionnaire surveys were conducted with seven experts participating in this project, including project managers, chief engineer, university experts, and managers of the project management firm. The questionnaire consisted of an introduction to the research aims and an introduction to the meanings of TDMRs and the scoring rules, which guided the experts to score the risk indicators according to the actual project situation and their experiences. Each risk indicator was scored based on a five-

TABLE 6: Equations of the variables in the system.

Variable	Equation
BAI	0.213 ∗ GRIG, initial value = 1
CMR	0.45 ∗ Executive, initial value = 3
Construction technical risk	0.1126 ∗ CGHCCS+0.2576 ∗ PCR+0.3722 ∗ CMR+0.2576 ∗ RCTMEM
LV2	INTEG (RV2, initial value), initial value = 0
Decision-making information risk	0.1564 ∗ Bai+0.3424 ∗ IDDP+0.2564 ∗ IPABD-0.2448 ∗ LV2
Decision-making mechanism risk	0.5372 ∗ UADMP+0.4628 ∗ UDMRS
Decision-making participants risk	0.0785 ∗ PPQDM+0.5196 ∗ PTVPDM+0.0836 ∗ RADMB+0.0825 ∗ NPRDSL+0.2358 ∗ GRIG
LV1	INTEG (RV1, initial value), initial value = 0
Decision-making scheme risk	0.0675 ∗ DMMR+0.0675 ∗ IRDMSC+0.1028 ∗ TSR+0.1319 ∗ SDD+0.1352 ∗ LRTS+0.113 ∗ Decision-making participants risk+0.2057 ∗ LV3+0.1146 ∗ Decision-making information risk+0.0662 ∗ Procedure risk
Economic environmental risk	0.3979 ∗ Political environmental risk+0.2198 ∗ FD+0.6021 ∗ UES
LV3	INTEG (RV3, initial value), initial value = 0
Executive risk	0.2637 ∗ IPAW+0.4548 ∗ EAR+0.4548 ∗ Management risk
GRIG	0.5431 ∗ Decision-making mechanism risk, initial = 4
IDDP	0.4876 ∗ PPQDM+0.5124 ∗ NPRDSL, initial value = 2
IMA	0.4213 ∗ CGHCCS, initial value = 3
Management risk	0.2367 ∗ FOSARRC+0.1427 ∗ MSD+0.3737 ∗ TRPE+0.1273 ∗ IMA+0.1196 ∗ IERC
Natural environmental risk	0.4853 ∗ CHGMC+0.1971 ∗ ND+0.3176 ∗ REV
NPRDSL	0.443 ∗ Decision-making mechanism risk+0.322 ∗ Procedure risk, initial value = 3
Political environmental risk	0.1416 ∗ GB+0.2687 ∗ LR+0.1912 ∗ GPC+0 ∗ CW
PCR	0.456 ∗ IMA+0.504 ∗ CGHCCS, initial value = 5
Procedure risk	0.2257 ∗ IDMP+0.5004 ∗ CLPAP+0.2738 ∗ RADMB, initial value = 3
R	0.3023 ∗ LV3+ 0.3319 ∗ LV1+0.3658 ∗ LV2
RADMB	0.5431 ∗ Decision-making mechanism risk, initial value = 2
RCTMEM	0.4332 ∗ Executive risk, initial value = 4
RV1	0.149 ∗ LV3+0.1928 ∗ Decision-making participants risk+0.1954 ∗ Decision-making information risk+0.1053 ∗ Procedure risk+0.117 ∗ Decision-making mechanism risk+0.2404 ∗ Decision-making scheme risk
RV2	0.2148 ∗ Management risk+0.1272 ∗ Executive risk+0.32 ∗ Construction technical risk+0.1611 ∗ Environmental risk LV3+0.1769 ∗ LV1
RV3	0.1825 ∗ Political environmental risk+0.2224 ∗ Natural environmental risk+ 0.1661 ∗ Economic environmental risk+0.2028 ∗ Social risk+ 0.2261 ∗ Technical environmental risk
Social risk	0.2454 ∗ POR+0.4538 ∗ SSR+0.3002 ∗ Political environmental risk
L	INTEG (R, initial value), initial value = 0
Technical environmental risk	0.1954 ∗ DTS+0.3159 ∗ TMR+0.2329 ∗ TPR+ 0.2557 ∗ Political environmental risk

level Likert scale (1–5), where 1 represented very low impact and 5 represented very high impact. Based on the responses, the initial value v_i of risk indicator i was calculated as the average score of all experts:

$$v_i = \frac{1}{k} \sum_{j=1}^{k} x_{ij}, \tag{5}$$

where x_{ij} was the score given by expert j for risk indicator i and k was the total number of the expert. The obtained initial values of all risk indicators required in the technical decision-making system are shown in Table 8.

4.4.2. Simulation Results. Model simulation was conducted to evaluate the evolution of the main stock variables (L, LV1,

LV2, and LV3) and rate variables (R, RV1, RV2, and RV3) in the TDMRs system, as shown in Figure 6. According to line 2 shown in Figure 6(a), the decision-making process risk LV1 increases faster at the beginning of the simulation period but then increases with a lower rate. The change of LV1 is consistent with the trend of RV1 (line 2 in Figure 6(b)), which increases at first and decreases after the 37th month. Typically, at the early stage of a megaproject, due to the complexity of the megaproject, decision-making participants lack sufficient cognition of the technical decision-making problem as well as the project information, which contributes to higher decision-making process risk. However, with the accumulation of decision-making execution process risk, some risk accidents may happen, which reveal the problems existing in the decision-making process, and measures (e.g., personnel adjustment and technical scheme

TABLE 7: Weights of risk indicators.

Target layer risk indicator	Standard layer risk indicators	Field layer risk indicators	Index layer risk indicators	Weight
Technical decision-making risk of megaproject	Decision-making process risk $W1 = 0.3319$	Decision-making participants risk $W11 = 0.2266$	Poor professional quality of decision-makers	0.0785
			Psychological tendency and value preference of decision-makers	0.5196
			Risk of alienation of decision-makers' behavior	0.0836
			No prominent role of the decision support layer	0.0825
		Decision-making information risk $W12 = 0.2297$	Game risk of interest groups	0.2358
			Blocked access to information	0.2071
			Improper description of the decision problem	0.5858
			Insufficient precision and accuracy of basic data such as survey and design	0.2071
		Procedure risk $W13 = 0.1238$	The incompleteness of decision-making procedures	0.3109
			Compliance and legality of project approval procedures	0.6891
		Decision-making mechanism risk $W14 = 0.1375$	Unreasonable allocation of decision-making power	0.5372
			Unreasonable decision-making regulation and system	0.4628
		Decision-making scheme risk $W15 = 0.2825$	Decision-making method risk	0.1116
			Indicators risk for decision-making scheme comparison	0.1116
			Technology selection risk	0.3353
			Scheme design defects	0.2180
			The legal risks of the scheme	0.2235
	Decision execution process risk $W2 = 0.3658$	Management risk $W21 = 0.3244$	Timing risk of plan execution	0.3737
			Insufficient member ability	0.1273
			Fuzzy organizational structure and allocation of rights, responsibilities, and benefits	0.2367
			Insufficient emergency response capability	0.1196
			Management system defects	0.1427
		Executive risk $W22 = 0.1921$	Insufficient professional ability of workers	0.4837
			The executive's attitude risk	0.5163
		Construction technical risk $W23 = 0.4833$	Changes in geological and hydrological conditions at the construction site	0.1126
			Plan change risk	0.2576
			Construction and maintenance risks	0.3722
			The risk of construction technology, mechanical equipment, and material	0.2576
	Environmental risk $W3 = 0.3023$	Technical environmental risk $W31 = 0.2284$	Different technical standard	0.2626
			Technology maturity risk	0.4245
			Technology policy risk	0.3129
		Economic environmental risk $W32 = 0.1579$	Financing difficulty	0.3188
			Unfavorable economic situation	0.6812
		Natural environmental risk $W33 = 0.2246$	Complex hydrological, geological, and meteorological conditions	0.4853
			Natural disasters	0.1971
			Regional ecosystem vulnerability	0.3176
		Social risk $W34 = 0.2048$	Public opinion risk	0.3507
			Social stability risk	0.6493
		Political environmental risk $W35 = 0.1843$	Government behavior	0.1416
			Legal risk	0.2687
			Government policy changes	0.1912
			Coup, war	0
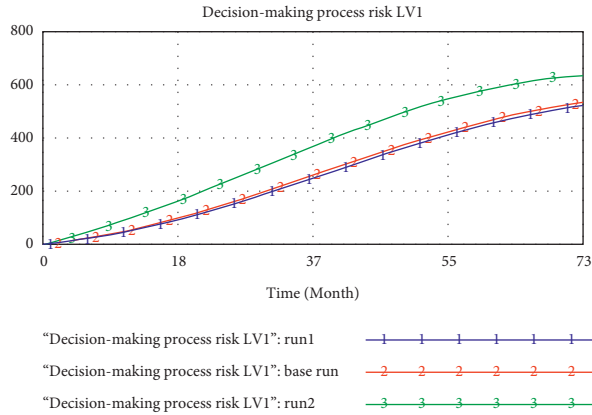
FIGURE 5: Sensitivity analysis of PTVPDM on the decision-making process risk.

TABLE 8: Initial risk values of the technical decision-making system.

Variable	Initial value	Variable	Initial value	Variable	Initial value
CGHCCS	2	IDMP	4	PTVPDM	3.13
CHGMC	2	IERC	3	REV	1
CLPAP	3	IPABD	2	SDD	2
CW	0	IPAW	3	SSR	3
DMMR	2	IRDMSC	2	TMR	2
DTS	2	LR	1	TPR	2
EAR	4.23	LRTS	4.3	TRPE	4
FD	1	MSD	2	TSR	3
FOSARRC	2	ND	4	UADMP	3
GB	2	POR	1	UDMRS	3
GPC	5	PPQDM	4.43	UES	4

(a)

(b)
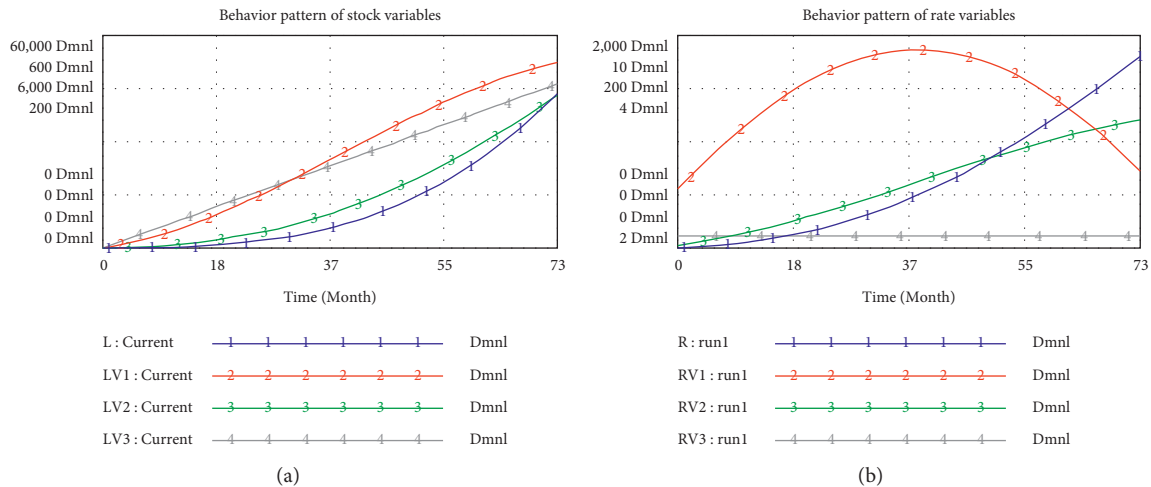
FIGURE 6: Simulation results of (a) stock variables and (b) rate variables.

adjustment) will be taken to lower the decision-making process risk.

As shown in line 3 in Figure 6(a), the decision-making execution process risk LV2 is very low in the initial several months and then increases with an increasing rate from the 9th month till the end. The corresponding rate variable (RV2) shows a constant increase throughout the period (line 3 in Figure 6(b)). Typically, at the early stage of a mega-project, many decision-making executions process risks are not obvious and the total effect of these risks on the project is

weak. Once the technical decision-making scheme is implemented, decision-making execution process risk will keep increasing and the increment rate LV2 also undergoes sustained growth unless the risks are controlled in time.

Furthermore, according to line 4 in Figures 6(a) and 6(b), the environmental risk LV3 keeps increasing at a fixed rate during the whole simulation period, which implies that the environmental risks are constant and not affected by other categories of risks.

Lastly, the L (technical decision-making risk in megaprojects) keeps increasing with an increasing rate, as shown in line 1 in Figures 6(a) and 6(b). The result indicates that the total risk will keep extending and lead to risk accidents unless risks are controlled in time. According to Figure 6(a), L remains very low before the 18th month and begins to increase faster afterwards, showing a similar trend with LV2. Hence, it can be inferred that LV2 is one of the most significant risk categories. There is also a strong two-way influence between LV1 and LV2. With the implementation of the decision-making scheme and the continuous effect of environmental risks, the decision-making execution process risks gradually accumulate and emerge, easily triggering risk accidents. Once the decision-making execution process is at a high-risk level, many measures will be taken to improve technical decision-making quality, such as to revise the decision-making scheme or to improve the quality of decision-making information.

4.4.3. Scenario Analysis. To provide policy implications for TDMR management in megaprojects, scenario analysis is conducted. For the purpose of clear illustration, only some major variables were selected to examine and describe their effects. First, two scenarios of PTVPDM and ND were selected as examples to conduct single variable analysis, detecting different effects of two variables on the overall TDMR in megaprojects. Second, a multivariate scenario analysis with three variables including PTVPDM, ND, and IPAW is carried out as an example to approximate to the real system.

For the single variable analysis of PTVPDM, three different values of PTVPDM are considered including 1 (run1), 4 (base run), and 7 (run2), respectively. As shown in Figures 7(a)–7(c), the increase of PTVPDM can increase the values of L, LV1, and LV2, which is in line with the study finding that risk derives from the interaction between people and the environment [86]. The personal characteristics of decision-makers can influence decision-making quality. If the decision-makers have a high tolerance of risk or have insufficient experience, the decision-making process and decision-making execution process may be subject to higher risks. Meanwhile, according to Figure 7(d), the environmental risk (LV3) does not change with different PTVPDM values, which is consistent with the characteristics of environmental risk. The environmental risk subsystem serves as the driver subsystem to the other two subsystems, and itself is hardly influenced by the other two subsystems. Hence, it is suggested that more attention should be paid to the behavioral risk of decision-makers.

For the single variable analysis of ND, three different values of ND, namely, 1 (run 1), 4 (base run), and 7 (run 2), were tested. As shown in Figures 8(a)–8(d), increase of ND will result in increases of all stock variables, which is in line with the influence path of the environment on decision-makings. The increase of ND, which belongs to the environmental risk subsystem, will certainly improve L and LV3, while LV3 will aggravate LV1 and LV2.

There are various complicated scenarios in the actual TDMRs system. It is the effect of risk interactions that inflates risk levels, which is the reason why this study explores the TDMRs in megaprojects systematically and dynamically. The multivariate analysis mainly observes the synthesis of PTVPDM, ND, and IPAW by setting the values of them as 1 (run 1), 4 (base run), and 7 (run 2). The results (Figure 9) show that the values of TDMRs are 42119.4 (run 1), 45348.1 (base run), and 48576.8 (run 2), respectively. Compared with the base run, the value of TDMRs decreases by 7.1% (run 1) and increases by 7.1% (run 2), respectively. However, under the scenario analysis of ND, the value of TDMRs decreases by 4.5% (run 1) and increases by 4.5% (run 2) compared with the base run, while under the scenario analysis of PTVPDM, the value of TDMRs decreases by 2.5% (run 1) and increases by 2.5% (run 2) compared with the base run. This implies that the increase of the TDMRs is not relying on the aggregate effects of individual parameters but the synthesis among them. Thus, it is suggested that decision-makers should fully consider how to mitigate the effect of environmental risks in TDM management of megaprojects. The results demonstrate the complex interactions among multilevel TDMRs. A combination of measures considering the comprehensive effects of risks would better control TDMRs in megaprojects.

5. Discussion and Implications

The main aim of this research is to identify TDMRs and examine their dynamic interactions. To attain the objective, a hybrid methodology consisting of GT and SD was implemented to explore TDMRs in megaprojects, which combines a qualitative content analysis approach and a quantitative simulation method. GT is used to elicit TDMRs in megaprojects from interviews and technical documents at first. Then an SD model of TDMRs is developed to describe how these TDMRs are interacting with each other, and the dynamic interactions among TDMRs are simulated with different scenarios.

As to the implications, this present research advances our understanding of TDMRs in megaprojects from a systematic and dynamic perspective and can serve as a decision-making management tool for the decision-makers in the following aspects. First, the identified list of TDMRs could be used to evaluate the overall risk level of TDM in megaprojects, which have both theoretical and practical contributions. Second, the SD model representing the interactions among multilevel risks of TDM shows that there are homogeneous and heterogeneous interactions within and among the environmental risk, decision-making process risk, and decision-making execution process risk
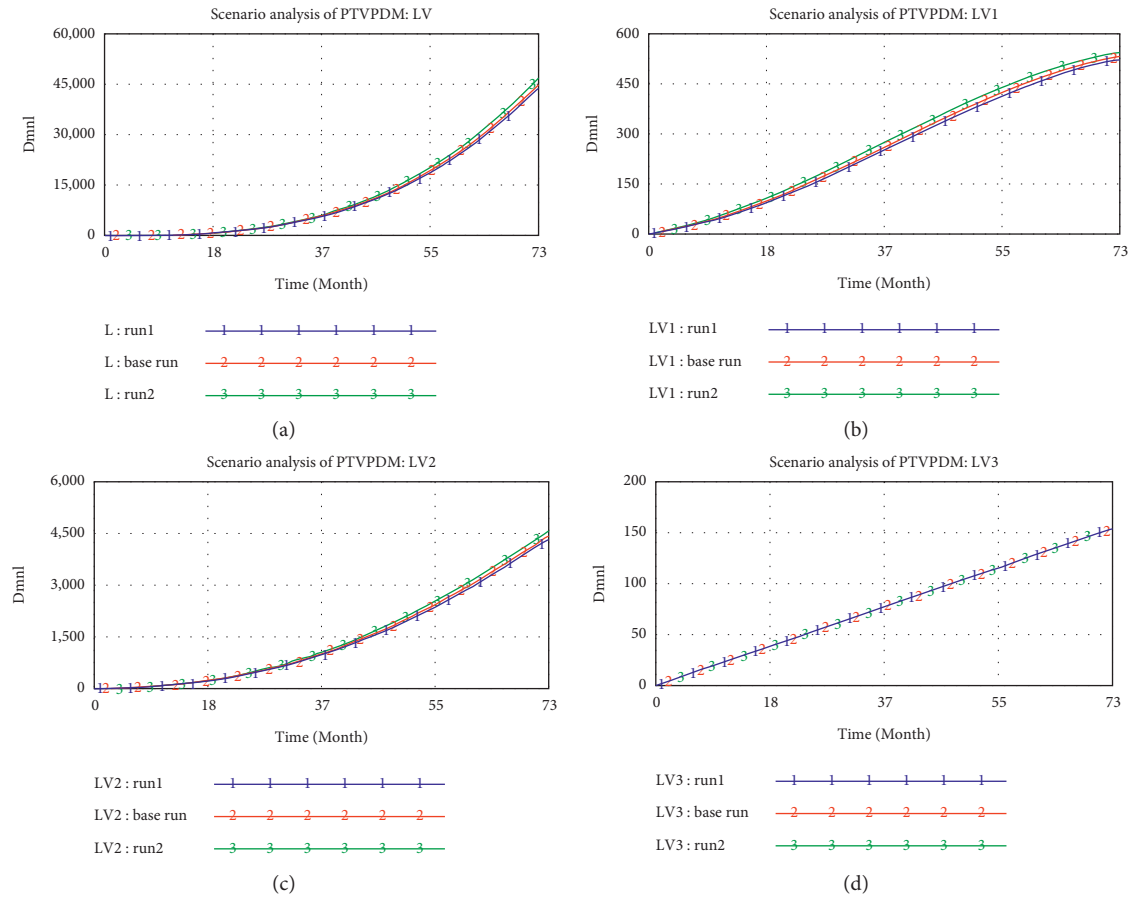
Figure 7: The results of scenario analysis of PTVPDM: (a) curves of L; (b) curves of LV1; (c) curves of LV2; and (d) curves of LV3.

Figure 8: Continued.

(c)
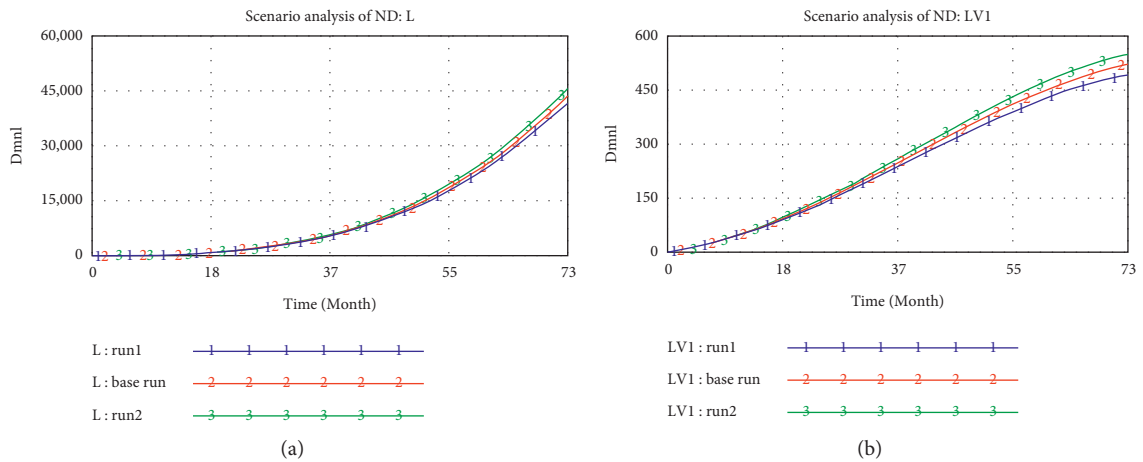
(d)
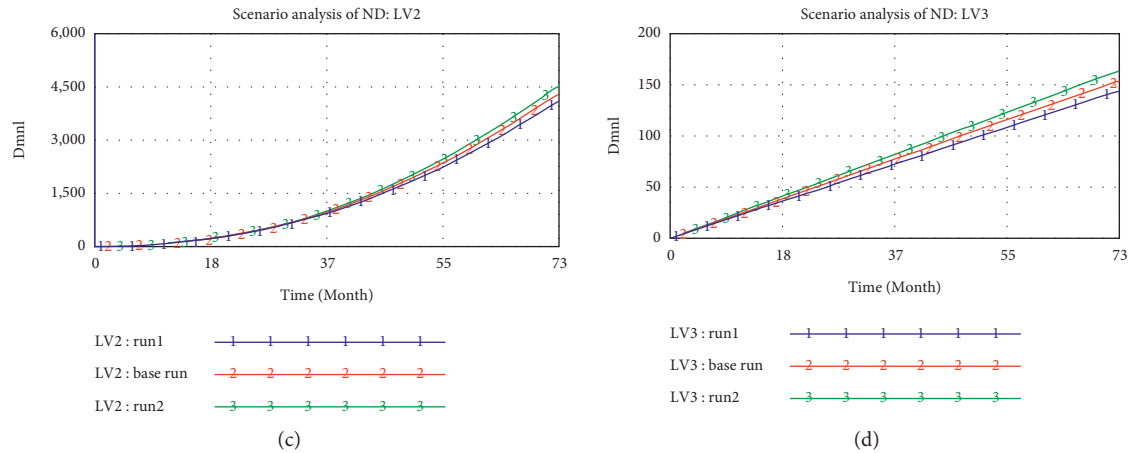
FIGURE 8: The results of scenario analysis of ND: (a) curves of L; (b) curves of LV1; (c) curves of LV2; and (d) curves of LV3.

(a)

(b)

(c)

(d)
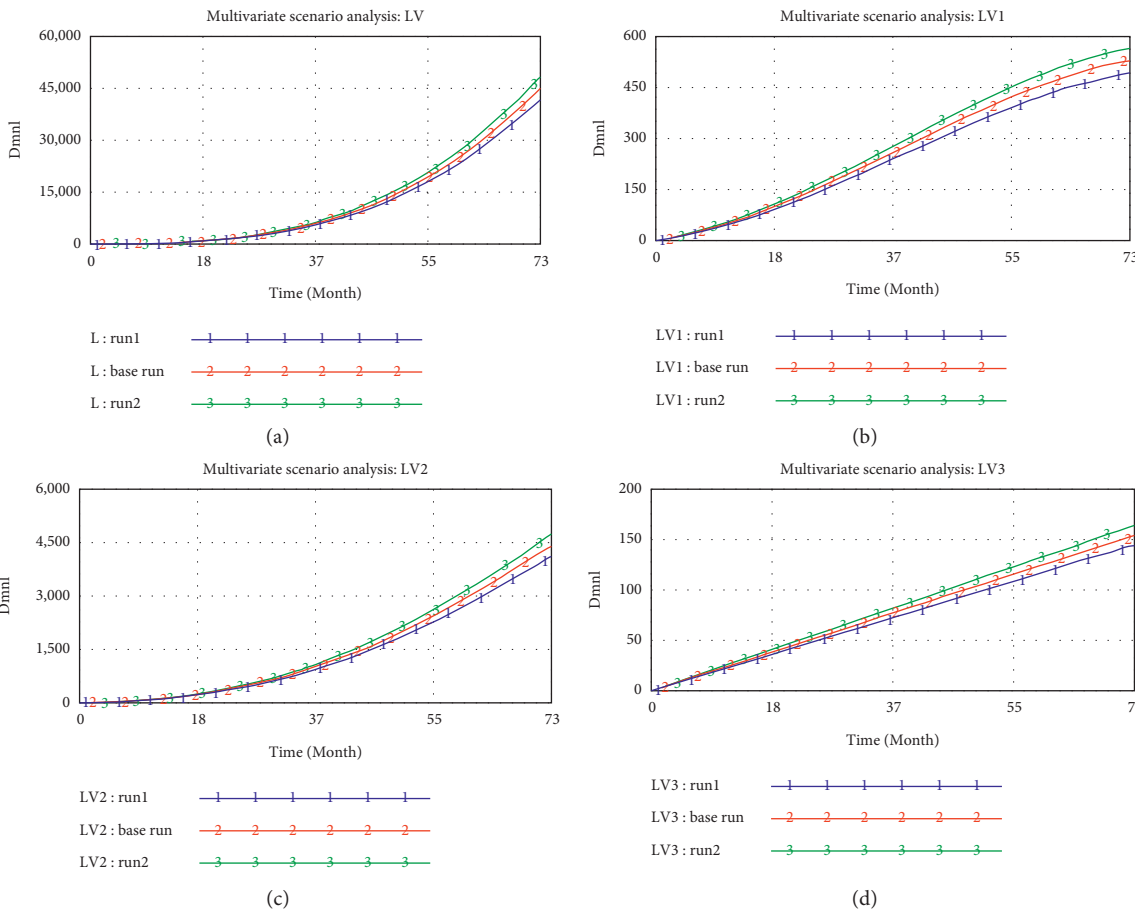
FIGURE 9: The results of the multivariate scenario analysis: (a) curves of L; (b) curves of LV1; (c) curves of LV2; and (d) curves of LV3.

subsystems. This means that these risk transmissions may aggravate the risk of certain subsystem. Specifically, the results of scenario analysis show that the overall risk level of TDM is inclined to be affected by the synthesis effects of risk interaction rather than the aggregate of individual risks. As such, multilevel measures considering the synthesis effects

are more effective to mitigate TDMRs in megaprojects. For example, it is recommended to establish a risk-management-based TDM process, integrating the iterative risk management and TDM process. For each TDM, firstly, identify the risk factors, then, make a decision-making scheme based on the risk status, and evaluate the risk level of the final

technical decision-making scheme and modify it dynamically until the risk level of the scheme is acceptable. Besides, a flatter organizational structure for decision-making and multiagent (i.e., the government, the owner, designer, contractor, scientific research institutes, the experts, and equipment suppliers) collaborative decision-making could speed up the information exchange efficiency and reduce risk. In addition, the decision-making information risk, decision-making scheme risk, and decision-making participants risk are three key variables indicated from the five casual loops, which is in line with studies of Sutrisna and Goulding [23] and Eweje et al. [80]. Thus, it is necessary to strictly control the quality of decision-making information and develop a reasonable comparison and selection process of alternative schemes. Finally, the simulation model presented in this paper can be adopted to (1) identify changes of TDMRs over time, (2) evaluate the effects of different risk factors on the total TDMR in megaprojects under different scenarios, and (3) take measures to respond to the project changes brought by TDMRs.

6. Conclusions and Limitations

The TDMRs in megaprojects and their interactions are complicated and dynamic, which makes them difficult to control. In the practice of TDMR management in megaprojects, project manager's perceptions of risks may be different from the identified risks in the literature. Therefore, exploring the dynamics of TDMRs fitting the practice of TDM in megaprojects is necessary for both scholars and project managers to gain a better understanding of the complexities of TDMRs in megaprojects. In this study, the TDMRs in megaprojects were identified and a multilayer risk list was determined based on GT. A total of 42 risk factors were identified and classified into 13 subcategories and 3 categories including decision-making process risk, decision-making execution process risk, and environmental risk. An SD model that depicted the dynamic interrelationships among multilevel risks of TDM in megaprojects was built. Rather than exploring single risk's effect, the developed SD model presented the risk-increasing synthesis effects of the interactions among risks.

The results show that the relationships among these TDMRs are complicated. The decision-making process risk and decision-making execution process risk are susceptible to environmental risk, whereas decision-making process risk will transfer to decision-making execution process and decision-making execution process risk may influence the decision-making process in turn. Besides, variables at different levels have varying effects on the total TDMR in megaprojects and the risk level of each subsystem. Among these effects, the synthesis effects of the interactions among risks have a great impact on TDMR in megaprojects. Therefore, it is suggested that a TDM mechanism driven by risk assessment should be established for megaprojects, where only when the risk is in control will the TDM process proceed. Specifically, decision-making execution process risk and decision-making process risk are the two most important risk categories, which need to be paid more attention to.

This study still has several limitations. Firstly, as GT is a qualitative method without quantification and there is a limited amount of original data, the identified TDMRs may be incomplete or inapplicable to other projects. Secondly, the mathematical equations and variable values used in the simulation model are established with from interview data, only considering the objective of each expert, which may not be applicable to other projects. Thirdly, the SD model presented in this paper only depicts the interactions among TDMRs in megaprojects without considering the risk mitigation strategies. Fourth, according to Box et al. [87], at least 50 observations are required to get a useful estimate of the correlation function, while the data used to simulate the model are obtained from the experts rather than practical observation data. Thus, more quantitative indicators and more objective methods (i.e., TOPSIS model for weighting the subjective weights and objective weights) determining the mathematical equations of variables are needed to assess TDMRs in megaprojects. Furthermore, the KCITH project is used for both data collection of GT and model simulation, which may limit the generalizability. Thus, more case studies are necessary to test the applicability and generalization of the presented simulation model [88].

Data Availability

The data used to support the findings of this study are available from the corresponding author upon request.

Conflicts of Interest

The authors declare that they have no conflicts of interest.

Acknowledgments

References

[1] R. J. Chapman, "A framework for examining the dimensions and characteristics of complexity inherent within rail megaprojects," *International Journal of Project Management*, vol. 34, no. 6, pp. 937–956, 2016.

[2] J. Lehtinen, A. Peltokorpi, and K. Artto, "Megaprojects as organizational platforms and technology platforms for value creation," *International Journal of Project Management*, vol. 37, no. 1, pp. 43–58, 2019.

[3] B. Cheng, K. Lu, J. Li, H. Chen, X. Luo, and M. Shafique, "Comprehensive assessment of embodied environmental impacts of buildings using normalized environmental impact factors," *Journal of Cleaner Production*, vol. 334, Article ID 130083, 2022.

[4] C. Beringer, D. Jonas, and A. Kock, "Behavior of internal stakeholders in project portfolio management and its impact on success," *International Journal of Project Management*, vol. 31, no. 6, pp. 830–846, 2013.

[5] X. Tang, M. Wang, Q. Wang, and N. Liao, "Research on mega infrastructure project technology decision-making mechanism with risk controllable," *Modernization of Management*, vol. 40, no. 4, pp. 70–73, 2020.

[6] W. K. M. Brauers, E. K. Zavadskas, F. Peldschus, and Z. Turskis, "Multi-objective decision-making for road design," *Transport*, vol. 23, no. 3, pp. 183–193, 2008.

[7] Q. Shi, M. Hertogh, M. Bosch-Rekveldt, J. Zhu, and Z. Sheng, "Exploring decision-making complexity in major infrastructure projects: a case study from China," *Project Management Journal*, vol. 51, no. 6, pp. 617–632, 2020.

[8] M. Bosch-Rekveldt, Y. Jongkind, H. Mooi, H. Bakker, and A. Verbraeck, "Grasping project complexity in large engineering projects: the TOE (Technical, Organizational and Environmental) framework," *International Journal of Project Management*, vol. 29, no. 6, pp. 728–739, 2011.

[9] D. Baccarini, "The concept of project complexity-a review," *International Journal of Project Management*, vol. 14, no. 4, pp. 201–204, 1996.

[10] A. Nieto-Morote and F. Ruz-Vila, "A fuzzy approach to construction project risk assessment," *International Journal of Project Management*, vol. 29, pp. 220–231, 2011.

[11] F. Guo, Y. Chang-Richards, S. Wilkinson, and T. C. Li, "Effects of project governance structures on the management of risks in major infrastructure projects: a comparative analysis," *International Journal of Project Management*, vol. 32, no. 5, pp. 815–826, 2014.

[12] W. G. Meyer, "The effect of optimism bias on the decision to terminate failing projects," *Project Management Journal*, vol. 45, no. 4, pp. 7–20, 2014.

[13] A. Mohammadi and M. Tavakolan, "Modeling the effects of production pressure on safety performance in construction projects using system dynamics," *Journal of Safety Research*, vol. 71, pp. 273–284, 2019.

[14] H. Liu, C. Jiang, Y. Liu, M. Hertogh, and X. Lyu, "Optimism bias evaluation and decision-making risk forecast on bridge project cost based on reference class forecasting: evidence from China," *Sustainability*, vol. 10, no. 11, p. 3981, 2018.

[15] J. Y. Wang and H. P. Yuan, "System dynamics approach for investigating the risk effects on schedule delay in infrastructure projects," *Journal of Management in Engineering*, vol. 33, 2017.

[16] B. Flyvbjerg, "Over Budget, over Time, over and over Again: Managing Major Projects," *The Oxford Handbook of Project Management*, Oxford, UK, 2011.

[17] B. N. Flyvbjerg and W. Rothengatter, *Megaprojects and Risk: An Anatomy of Ambition*, Cambridge University Press, Cambridge, UK, 2003.

[18] S. Jeong and J. Kim, "The immersed tunnel and bridges of busan- geoje fixed Link," *Structural Engineering International*, vol. 22, no. 1, pp. 20–25, 2012.

[19] T. Wang, S. Wang, L. Zhang, Z. Huang, and Y. Li, "A major infrastructure risk-assessment framework: application to a cross-sea route project in China," *International Journal of Project Management*, vol. 34, no. 7, pp. 1403–1415, 2016.

[20] C. Fang, F. Marle, E. Zio, and J.-C. Bocquet, "Network theory-based analysis of risk interactions in large engineering projects," *Reliability Engineering & System Safety*, vol. 106, pp. 1–10, 2012.

[21] W. Salet, L. Bertolini, and M. Giezen, "Complexity and uncertainty: problem or asset in decision making of mega infrastructure projects?" *International Journal of Urban and Regional Research*, vol. 37, no. 6, pp. 1984–2000, 2013.

[22] M. Giezen, W. Salet, and L. Bertolini, "Adding value to the decision-making process of mega projects: fostering strategic ambiguity, redundancy, and resilience," *Transport Policy*, vol. 44, pp. 169–178, 2015.

[23] M. Sutrisna and J. Goulding, "Managing information flow and design processes to reduce design risks in offsite construction projects," *Engineering Construction and Architectural Management*, vol. 26, no. 2, pp. 267–284, 2019.

[24] J.-G. Nibbelink, M. Sutrisna, and A. U. Zaman, "Unlocking the potential of early contractor involvement in reducing design risks in commercial building refurbishment projects - a Western Australian perspective," *Architectural Engineering and Design Management*, vol. 13, no. 6, pp. 439–456, 2017.

[25] C. DURáN, J. Sepulveda, and R. Carrasco, "Determination of technological risk influences in a port system using DEMATEL," *Decision Science Letters*, vol. 7, pp. 1–12, 2018.

[26] Z.-z. Liu, Z.-w. Zhu, H.-j. Wang, and J. Huang, "Handling social risks in government-driven mega project: an empirical case study from West China," *International Journal of Project Management*, vol. 34, no. 2, pp. 202–218, 2016.

[27] Y. Chao, "Projects Bidding Decision Risk Analysis Based on Multi-Factor Clustering Analysis," *Information Technology Journal*, vol. 12, pp. 6164–6168, 2013.

[28] P. W. Li, "Based on data analysis about risks of bidding decisions in engineering projects," in *Proceedings of the 2015 7th International Conference on Measuring Technology and Mechatronics Automation, ICMTMA 2015*, pp. 228–231, Nanchang, China, June 2015.

[29] M. N. Bakht and T. E. El-Diraby, "Synthesis of decision-making research in construction," *Journal of Construction Engineering and Management*, vol. 141, no. 9, Article ID 04015027, 2015.

[30] Z. Sheng, X. Xue, and S. An, "Constructing Theoretical System and Discourse System of Mega Infrastructure Construction Management with Chinese Characteristics," *Management World*, vol. 35, no. 4, pp. 2–16+51+195, 2019.

[31] J. E. Vinnem, "Evaluation of the Norwegian major hazard risk management approach for offshore installations in the concept selection phase," *ASCE-ASME J Risk and Uncert in Engrg Sys Part B Mech Engrg*, vol. 1, 2015.

[32] F. Zhao, Y. Xue, Y. Li, and H. Zhao, "A risk assessment system for hard rock TBM selection based on bayesian belief networks (BBN)," *Georisk: Assessment and Management of Risk for Engineered Systems and Geohazards*, pp. 454–467, Denver, CO, USA, 2017.

[33] M. Kurhade and R. Wankhade, "An overview on decision making under risk and uncertainty," *International Journal of Science and Research*, vol. 5, pp. 416–422, 2015.

[34] T. Williams, "The nature of risk in complex projects," *Project Management Journal*, vol. 48, no. 4, pp. 55–66, 2017.

[35] P. Boateng, *A Dynamic Systems Approach to Risk Assessment in Megaprojects*, Thesis for: PhDAdvisor, Citeseer, Princeton, NJ, USA., 2014.

[36] Y. Xue, P. Xiang, F. Jia, and Z. Liu, "Risk assessment of high-speed rail projects: a risk coupling model based on system dynamics," *International Journal of Environmental Research and Public Health*, vol. 17, 2020.

[37] X. Na, W. Jianping, L. Jie, and N. Guodong, "Analysis on relationships of safety risk factors in metro construction," *Journal of Engineering Science & Technology Review*, vol. 9, 2016.

[38] C. Zhou, L. Ding, M. J. Skibniewski, H. Luo, and S. Jiang, "Characterizing time series of near-miss accidents in metro

construction via complex network theory," *Safety Science*, vol. 98, pp. 145–158, 2017.

[39] D.-m. Zhang, F. Du, H. Huang, F. Zhang, B. M. Ayyub, and M. Beer, "Resiliency assessment of urban rail transit networks: shanghai metro as an example," *Safety Science*, vol. 106, pp. 230–243, 2018.

[40] Z. Zhou and J. Irizarry, "Integrated framework of modified accident energy release model and network theory to explore the full complexity of the Hangzhou subway construction collapse," *Journal of Management in Engineering*, vol. 32, no. 5, Article ID 05016013, 2016.

[41] S. Seker and E. Zavadskas, "Application of Fuzzy DEMATEL Method for Analyzing Occupational Risks on Construction Sites," *Sustainability*, vol. 9, no. 11, p. 2083, 2017.

[42] S. M. Hatefi and J. Tamošaitienė, "An integrated fuzzy dematel-fuzzy anp model for evaluating construction projects by considering interrelationships among risk factors," *Journal of Civil Engineering and Management*, vol. 25, no. 2, pp. 114–131, 2019.

[43] V. T. Luu, S.-Y. Kim, N. V. Tuan, and S. O. Ogunlana, "Quantifying schedule risk in construction projects using Bayesian belief networks," *International Journal of Project Management*, vol. 27, no. 1, pp. 39–50, 2009.

[44] Y. Li, B. Sankaranarayanan, D. Thresh Kumar, and A. Diabat, "Risks assessment in thermal power plants using ISM methodology," *Annals of Operations Research*, vol. 279, no. 1-2, pp. 89–113, 2019.

[45] J. Yuan, K. Chen, W. Li, C. Ji, Z. Wang, and M. J. Skibniewski, "Social network analysis for social risks of construction projects in high-density urban areas in China," *Journal of Cleaner Production*, vol. 198, pp. 940–961, 2018.

[46] L. Wu, H. Bai, C. Yuan, and C. Xu, "FANPCE technique for risk assessment on subway station construction," *Journal of Civil Engineering and Management*, vol. 25, no. 6, pp. 599–616, 2019.

[47] F. Afzal, S. Yunfei, M. Nazir, and S. M. Bhatti, "A review of artificial intelligence based risk assessment methods for capturing complexity-risk interdependencies: cost overrun in construction projects," *International Journal of Managing Projects in Business*, vol. 14, 2019.

[48] P. Vaz-Serra and P. Edwards, "Addressing the knowledge management "nightmare" for construction companies," *Construction Innovation*, vol. 21, no. 2, pp. 300–320, 2020.

[49] Y. Pan and L. M. Zhang, "Roles of artificial intelligence in construction engineering and management: a critical review and future trends," *Automation in Construction*, vol. 122, p. 21, 2021.

[50] Z. M. Yaseen, Z. H. Ali, S. Q. Salih, and N. Al-Ansari, "Prediction of risk delay in construction projects using a hybrid artificial intelligence model," *Sustainability*, vol. 12, no. 4, p. 1514, 2020.

[51] B. G. Glaser and A. L. Strauss, *The Discovery of Grounded Theory: Strategies for Qualitative Research*, Adline de Gruyter, Piscataway, NJ, USA, 1967.

[52] J. W. Forrester, "System dynamics, systems thinking, and soft OR," *System Dynamics Review*, vol. 10, no. 2-3, pp. 245–256, 1994.

[53] A. Mohammadi and M. Tavakolan, "Identifying Safety Archetypes of Construction Workers Using System Dynamics and Content Analysis," *Safety Science*, vol. 129, 2020.

[54] H. Bouloiz, E. Garbolino, M. Tkiouat, and F. Guarnieri, "A system dynamics model for behavioral analysis of safety conditions in a chemical storage unit," *Safety Science*, vol. 58, pp. 32–40, 2013.

[55] P. Boateng, Z. Chen, S. Ogunlana, and D. Ikediashi, "A system dynamics approach to risks description in megaprojects development," *Organization, technology & management in construction: An International Journal*, vol. 4, 2012.

[56] F. Wang, L. Ding, P. E. D. Love, and D. J. Edwards, "Modeling tunnel construction risk dynamics: addressing the production versus protection problem," *Safety Science*, vol. 87, pp. 101–115, 2016.

[57] B. Zhao, T. Tang, and B. Ning, "System dynamics approach for modelling the variation of organizational factors for risk control in automatic metro," *Safety Science*, vol. 94, pp. 128–142, 2017.

[58] P. Shojaei and S. A. S. Haeri, "Development of supply chain risk management approaches for construction projects: a grounded theory approach," *Computers & Industrial Engineering*, vol. 128, pp. 837–850, 2019.

[59] F. Nasirzadeh, A. Afshar, and M. Khanzadi, "System dynamics approach for construction risk analysis," *International Journal of Civil Engineering*, vol. 6, pp. 120–131, 2008.

[60] B. K. Akcam, S. Guney, and A. M. Cresswell, "Research design and major issues in developing dynamic theories by secondary analysis of qualitative data," *Systems*, vol. 7, no. 3, p. 40, 2019.

[61] R. B. Johnson and A. J. Onwuegbuzie, "Mixed methods research: a research paradigm whose time has come," *Educational Researcher*, vol. 33, no. 7, pp. 14–26, 2004.

[62] J. E. Symonds and S. Gorard, "Death of mixed methods? Or the rebirth of research as a craft," *Evaluation & Research in Education*, vol. 23, no. 2, pp. 121–136, 2010.

[63] J. W. Creswell and V. L. P. Clark, *Designing and Conducting Mixed Methods Research*, Sage publications, Thousand Oaks, CA, USA, 2017.

[64] J. W. Rudolph and N. P. Repenning, "Disaster dynamics: understanding the role of quantity in organizational collapse," *Administrative Science Quarterly*, vol. 47, no. 1, pp. 1–30, 2002.

[65] L. J. Black, P. R. Carlile, and N. P. Repenning, "A dynamic theory of expertise and occupational boundaries in new technology implementation: building on barley's study of CT scanning," *Administrative Science Quarterly*, vol. 49, no. 4, pp. 572–607, 2004.

[66] L. F. Luna-Reyes and D. L. Andersen, "Collecting and analyzing qualitative data for system dynamics: methods and models," *System Dynamics Review*, vol. 19, no. 4, pp. 271–296, 2003.

[67] A. Strauss and J. Corbin, *Basics of Qualitative Research*, Sage, Newbury Park, CA, USA, 1990.

[68] B. G. Glaser, *Emergence vs Forcing: Basics of Grounded Theory Analysis*, Sociology Press, Mill Valley,California,USA, 1992.

[69] K. Charmaz, "Constructivist and Objectivist Grounded Theory," *Handbook of Qualitative Research*, Thousand Oaks, CA, USA, 2000.

[70] H. Heath and S. Cowley, "Developing a grounded theory approach: a comparison of Glaser and Strauss," *International Journal of Nursing Studies*, vol. 41, no. 2, pp. 141–150, 2004.

[71] J. C. Van Niekerk and J. D. Roode, "Glaserian and Straussian Grounded Theory: Similar or Completely Different?" in *Proceedings of the 2009 Annual Research Conference of the South African Institute of Computer Scientists and Information Technologists*, pp. 96–103, ACM International Conference Proceeding Series, Times Square, NY, USA, October 2009.

[72] R. L. Baskerville, "Distinguishing action research from participative case studies," *Journal of Systems and Information Technology*, vol. 1, 1997.

[73] C. Hou, Y. Wen, Y. He et al., "Public stereotypes of recycled water end uses with different human contact: evidence from

event-related potential (ERP),” *Resources, Conservation and Recycling*, vol. 168, Article ID 105464, 2021.

[74] H. R. Bernard and H. R. Bernard, *Social Research Methods: Qualitative and Quantitative Approaches*, Sage, Thousand Oaks, CA, USA, 2013.

[75] J. W. Creswell and C. N. Poth, *Qualitative Inquiry and Research Design: Choosing Among Five Approaches*, Sage publications, Thousand Oaks, CA, USA, 2016.

[76] T.-C. Wang and H.-D. Lee, “Developing a fuzzy TOPSIS approach based on subjective weights and objective weights,” *Expert Systems with Applications*, vol. 36, no. 5, pp. 8980–8985, 2009.

[77] Z. Zhou, J. Irizarry, Q. Li, and W. Wu, “Using grounded theory methodology to explore the information of precursors based on subway construction incidents,” *Journal of Management in Engineering*, vol. 31, no. 2, Article ID 04014030, 2015.

[78] A. F. Farahani, K. Khalili-Damghani, H. Didehkhani, A. H. Sarfaraz, and M. Hajirezaie, “A framework for project risk assessment in dynamic networks: a case study of oil and gas megaproject construction,” *IEEE Access*, vol. 9, Article ID 88767, 2021.

[79] P. Pirzadeh and H. Lingard, “Understanding the dynamics of construction decision making and the impact on work health and safety,” *Journal of Management in Engineering*, vol. 33, no. 5, 2017.

[80] J. Eweje, R. Turner, and R. Müller, “Maximizing strategic value from megaprojects: the influence of information-feed on decision-making by the project manager,” *International Journal of Project Management*, vol. 30, no. 6, pp. 639–651, 2012.

[81] Y. Zhu, M. Lin, F. Meng, X. Liu, and W. Lin, “The Hong Kong-Zhuhai-Macao bridge,” *Engineering*, vol. 5, no. 1, pp. 10–14, 2018.

[82] J. B. Pocock, S. T. Kuennen, J. Gambatese, and J. Rauschkolb, “Constructability state of practice report,” *Journal of Construction Engineering and Management*, vol. 132, no. 4, pp. 373–383, 2006.

[83] R. A. Huff and V. R. Prybutok, “Information systems project management decision making: the influence of experience and risk propensity,” *Project Management Journal*, vol. 39, no. 2, pp. 34–47, 2008.

[84] A. N. Baldwin, S. A. Austin, T. M. Hassan, and A. Thorpe, “Modelling information flow during the conceptual and schematic stages of building design,” *Construction Management & Economics*, vol. 17, no. 2, pp. 155–167, 1999.

[85] J. Sterman, *Business Dynamics: Systems Thinking and Modeling for a Complex World*, McGraw-Hill, Manhattan, N, USA, 2000.

[86] G. Wu, H. Kai-Rong, and P. Bin, “The Evolution Mechanism and It’s Simulation Analysis of the Huge Transportation Infrastructure Projects Risk,” *Forecasting*, vol. 35, no. 3, pp. 69–74, 2016.

[87] G. E. P. Box, G. M. Jenkins, and G. C. Reinsel, *Time Series Analysis: Forecasting and Control*John Wiley & Sons, Hoboken, NJ, USA, 2008.

[88] B. Flyvbjerg, “What you should know about megaprojects and why: an overview,” *Project Management Journal*, vol. 45, no. 2, pp. 6–19, 2014.

Research Article

Construction of Relationship Model between College Students' Psychological Status and Epidemic Situation Based on BP Neural Network

Shuguang Yao (iD)

Anyang Normal University, Anyang 455000, China

Correspondence should be addressed to Shuguang Yao; hnysg@aynu.edu.cn

In view of the impact of COVID-19 on the mental health of college students, this paper proposes a study on the relationship between psychological status and epidemic situation of university students based on BP neural network, so as to provide theoretical basis for universities to take targeted mental health education. This paper investigates the effects of COVID-19 on the psychological emotions of college students. According to the behavior and psychological characteristics of college students, the relevant investigation results are obtained through event monitoring, early warning, and usual performance, and a relationship model between college students' psychological status and epidemic situation based on BP neural network is constructed. This paper studies several factors through the relationship model and uses the principal component analysis method to analyze the impact of various factors on college students' psychology. According to the model prediction and result analysis, it concluded that the influence of COVID-19 should focus on improving the professional quality, physical quality, humanistic quality, and moral quality of university students, so as to improve the stability of colleges and universities in the event of public health emergencies. The model constructed in this paper can provide reference for carrying out mental health education and formulating effective intervention programs.

1. Introduction

The COVID-19 epidemic is a global public health emergency, and some people will have a strong stress response and show obvious symptoms of anxiety and depression. Facing the COVID-19 epidemic, the group of college students will have a stress response, which will have a negative impact on their normal life and study, such as a decrease in outing activities, a decrease in communication, and a change in learning methods. Therefore, college students are prone to different levels of emotional problems, and the duration is longer.

In order to win the battle against the epidemic and respond to the call of the country, everyone has been quarantined at home. The development of the epidemic, the restriction of activities, and the changes in the original life state have made everyone anxious and fearful. For college

students who are unable to go to school normally, the continuous expansion of the epidemic has led to uncertain return to school time, home study has led to changes in learning styles, and the employment and graduation issues that graduating students worry about have increased the anxiety and depression of college students, which in turn affects their mental health. Therefore, various universities and the education department have issued guidance manuals on the mental health of college students during COVID-19 to carry out psychological crisis interventions in public health emergencies.

Some scholars have also conducted research on the psychological problems and protection of college students in major epidemics and published relevant results. The results are mainly concentrated in the following three aspects. The first is the investigation of the psychological status of college students under the background of the new crown epidemic

[1]. Many investigations and studies believe that the new crown epidemic has a significant impact on the psychology of college students, causing psychological problems such as panic, anxiety, anger, and stress among college students. Therefore, schools and society should strengthen the cultivation of college students' psychological quality in response to public health emergencies and improve their psychological endurance [2]. The second is the relationship between the awareness of the new crown epidemic and the physical and mental health of college students. The results of data analysis show that the cognitive level of COVID-19 is significantly related to the physical and mental health of college students. The education department should strengthen targeted publicity and education and strive to improve college students' cognitive level of the epidemic and enhance their physical and mental health [3].

Some scholars found in the investigation that the anxiety level of college students was higher than the norm during the epidemic prevention and control period. By summarizing the existing research results, it is found that its characteristics mainly have two scores [4]. One is that some of the results only focus on quantitative analysis of the psychological problems of college students under the background of major epidemics but lack qualitative research on the specific manifestations, characteristics, and effects of psychological problems. Second, some scholars only pay attention to presenting the psychological problems of college students in their research and make suggestions, but there are not many specific measures for the psychological protection of college students under the background of major epidemics.

The report of the 19th National Congress of the Communist Party of China clearly stated that a healthy China strategy should be implemented, and the policy of "prevention first, combined prevention and treatment" was advocated. The epidemic has caused people to experience anxiety, depression, and other emotions, and students' psychological and behavioral problems have also begun to become prominent. How to motivate college students to get rid of the trouble of bad emotions and integrate into college life as soon as possible, and to pose new challenges to college students' physical health education work, has also become an important topic for building a healthy Chinese background. First of all, doing a good job of mental health education for college students in the context of epidemic prevention and control is an important content and internal need for the development of the discipline of mental health education, and it is also an important work to effectively improve the overall level of psychological services. The second is the core task of ideological and political education in colleges and universities in response to the epidemic, which is of great significance to maintaining the stability of the campus and creating a civilized campus [5].

Contemporary college students are in a special period of physical, psychological development and maturity and are in a special stage of life development and have a special social environment and social norms. In this special group, there are many special stressors specifically for them. The stress of foreign college students mainly comes from study [6], social and emotional state or environment [7], personal aspects [8], including examination [9], competition, time, teachers, classroom environment [10], employment, parental relationships, close relationships, economic problems [11], interpersonal relationships, living conditions, appearance, etc. Domestically, it comes from learning troubles, personal worries, and negative life events [12], including study, employment, interpersonal relationships, life, romantic relationships [13], economy, society, family [14], examination, life, learning environment [15], future, ability, personal health [16], competition, etc. The pressure sources of college students at home and abroad are similar. The emergence of these problems has formed the unique characteristics of psychological activities of this group. The results of psychological surveys of college students show that many colleges are living with psychosomatic disorders, and stress is one of the important factors that affect their health [16]. Therefore, understanding the basic conditions and influencing factors of college students' behavior and psychological stress is the basis for further research on college students' behavior and mental health at present and in the future and is the key to formulating plans and implementation steps for college students' physical and mental development. Based on this far-reaching significance, it focuses on systematically elaborating the factors affecting college students' behavior and psychological stress [17].

College students are in an important stage of rapid physical and mental development and change, complex and changeable emotional response, self-consciousness from semi-independence to independence, and social role transition. They lack of understanding of public health emergencies, which is easy to affect their psychological state. It is known from the existing research that the research on the relationship between college students' psychological status and epidemic situation is not deep enough. Therefore, this paper proposes the construction of the relationship model between college students' psychological status and epidemic situation based on BP neural network.

2. BP Neural Network

Artificial neural networks (ANNs) are an algorithmic mathematical model that imitates the behavior characteristics of animal neural networks for distributed parallel information processing. At present, there are dozens of artificial neural network models with more applications, including BP neural network, Hopfield network, art network, and Kohonen network.

2.1. Neuron Model. BP neural network feeds back the error between the actual output value and the expected output value and then constantly trains and adjusts the model to reduce the error and make the prediction result of the model approach the actual situation. The basic component of BP neural network is neurons, which are connected with each other and transmit information through weighted connection channels. Neurons combine multiple received signals and then calculate the output results through the activation function, as shown in Figure 1.
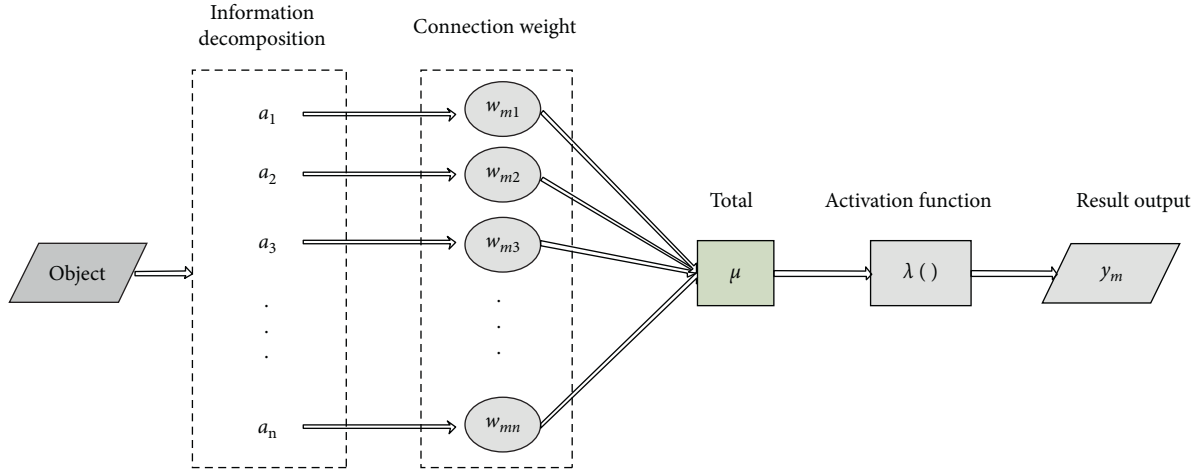
FIGURE 1: Structure diagram of neuron model.

The calculation formula of neuron output is as follows:

$$y_m = \lambda\left(\sum_{i=1}^{n} w_{mi}a_i - \mu\right), \tag{1}$$

where y_m shows the output value after processing, w_{mi} denotes the connection weight of each transmission signal, a_k represents the input signal of the upper layer, λ represents the activation function of neurons, and μ is the threshold of neurons.

2.2. Construction of Neural Network Model.

BP neural network is a three-layer structure (as shown in Figure 2), which is composed of input layer, output layer, and hidden layer. According to the different problems to be solved, the hidden layer of multilayered structure can be set, but the most classic is only one hidden layer, which makes it easy to understand the relationship between analog input and output. Each layer of BP neural network has multiple neurons, and their number is determined by a specific model, while the two neurons in the hierarchy are not interconnected. All neurons are connected with the nearby hierarchy through one-way connection, and the connected nodes interact through weight. When the signal enters the hidden layer through the input layer, the connection function will process the transmitted data, and then the hidden layer will transmit the processed data to the output layer of the neural network and finally get the output result.

2.3. Implementation Process of BP Neural Network.

The input layer described in this paper includes 3 nodes: basic information of students, epidemic information, and psychological information.

The output layer has only label degree; that is, the output layer is one node. The number of nodes in the hidden layer is l, which is obtained through the analysis of training experiments.

In order to eliminate the influence of different dimensions in the three evaluation indexes of student number,

epidemic severity, and psychological status, the data were standardized. The index variables are mapped to [0, 1] through normalization, and the formula is as follows:

$$q_i^k = \frac{Q_i^k - Q_{i\,\min}}{Q_{i\,\max} - Q_{i\,\min}}, \tag{2}$$

where q_i^k ($k = 300$) is the normalized data, $i = 1, 2, 3$, $k = 1, 2, \ldots, 300$, and $Q_{i\,\max}$ and $Q_{i\,\min}$ are the maximum and minimum values in the k-th original data. 80% of the data are randomly selected from the normalized data set as training data and the remaining 20% as test data.

Input the training data into the neural network, and the output value of the hidden layer can be obtained through equation (3), shown as follows:

$$h_m^k = \sum_{i=1}^{3} w_{im}^{(v)}Q_i^k + l_m^{(v)}, \tag{3}$$

where $m = 1, 2, \ldots, N$, N is the number of nodes in the hidden layer, $w_{im}^{(v)}$ is the connection weight between the input layer and the hidden layer, and $l_m^{(v)}$ is the threshold of the hidden layer.

In order to obtain better convergence effect and improve the accuracy of the model, Sigmoid function is introduced into the hidden layer, shown as follows:

$$p_m^k = \frac{1}{1 + e^{-\sum_{i=1}^{6} w_{im}^{(v)}Q_i^k + l_m^{(v)}}}, \tag{4}$$

where p_m^k is the output value of the hidden layer and k is 900. Take the output value of the hidden layer as the input data of the output layer, and calculate the output value of the output layer by using equation (5), shown as follows:

$$Z^k = \sum_{i=1}^{3} w_i p_i^k + l_i. \tag{5}$$

Among them, w_i is the connection weight, l is the output layer threshold, and Z^k is the output data of the output layer. In order to obtain better effect of the model, calculate the
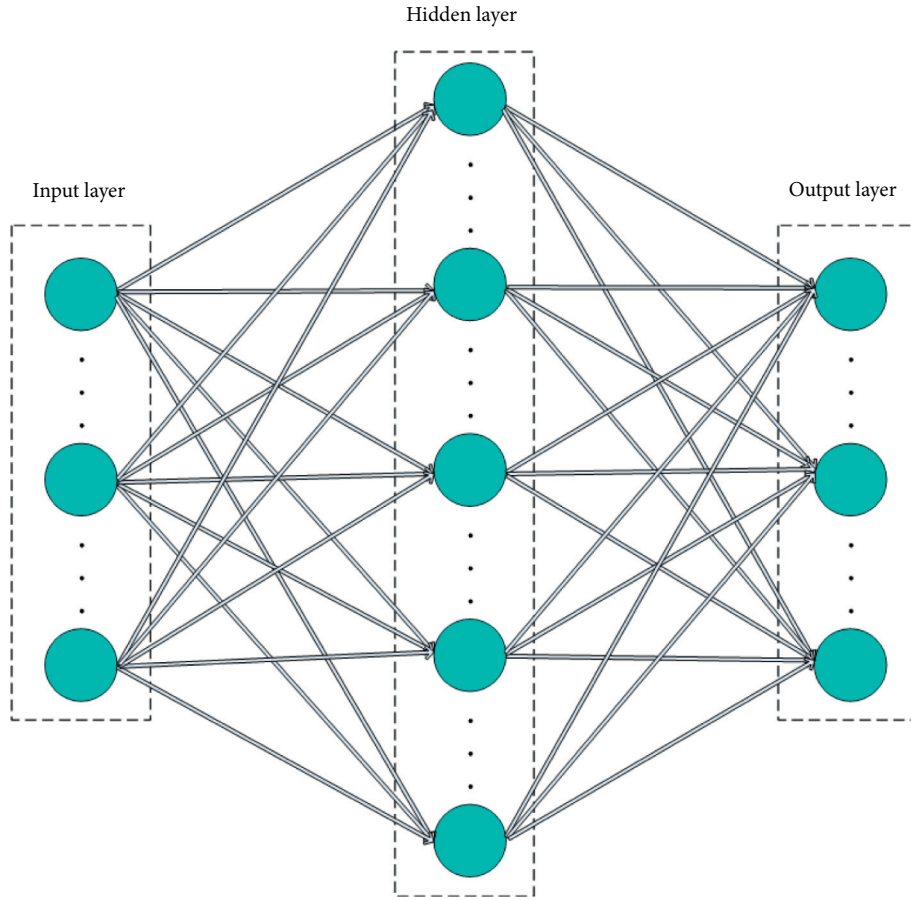
FIGURE 2: Structure diagram of neural network.

mean square error through equation (6), which is expressed as follows:

$$\text{Mean} = \frac{1}{900} \sum_{n=1}^{900} (Z^n - R^n). \qquad (6)$$

Among them, R^n is the actual value and Z^n is the predicted value. The gradient descent method is used to backpropagate the error, correct the connection weight and threshold of each layer, and stop training until the target accuracy or target training times are reached, which is shown as follows:

$$w_{N+1} = w_N - \theta \frac{\partial_{\text{Mean}}}{\partial_w},$$
$$S_{N+1} = S_N - \theta \frac{\partial_{\text{Mean}}}{\partial_S}, \qquad (7)$$

where S_N denotes the threshold of each layer, w_N represents the connection weight of each layer, S_{N+1} is the threshold correction value, w_{N+1} shows the correction value of connection weight, and θ is the learning rate.

3. Method and Modeling

3.1. Variables in Process. In order to discover and further explore the behavioral factors that affect college students

under public health emergencies, this paper proposes corresponding solutions and countermeasures and uses more precise statistical analysis methods to study them. Path analysis is used to study the ways in which earlier variables affect subsequent variables, reveal the hierarchical relationship between factors, and suggest the existence of causal or related relationships. This paper screens out various factors affecting the peak behavior of the new crown epidemic at the 0.05 level. On this basis, this paper establishes the restriction mode of path analysis and obtains the path analysis diagram of the restriction mode to show the hierarchical logical relationship that affects the peak behavior of the new crown epidemic, to provide a basis for improving the behavior of the peak of the COVID-19 epidemic. In path analysis, the path coefficient is a standardized partial regression coefficient, the sign reflects the direction of action, and the absolute value reflects the degree of direct influence between levels. Secondly, the degree of indirect influence can be reflected by the size of the product of the corresponding path coefficients. The standard coefficient of overall influence is the sum of the product of the standard partial regression coefficients of each channel in the path, that is, the sum of direct and indirect influences [18].

In the questionnaire design, this study adds some inverse questions and similar questions. The purpose is to facilitate the screening of invalid questionnaires to prevent misjudgment of the measurement results. A total of 878

complete questionnaires are collected in this survey, and these 878 questionnaires are screened one by one, and invalid questionnaires are eliminated. The principle of eliminating questionnaires are as follows: one is to eliminate questionnaires with inconsistent answers before and after similar questions; the other is to eliminate questionnaires with the same answer for all questions, including inverse questions. This questionnaire is set to submit permissions, so there will be no missing questionnaires.

Based on existing mental health, psychology should actively take the responsibility of maintaining social mental health in response to new problems and new trends in society. The scale was compiled by Derogates and has been modified many times during its use. There are 90 self-assessment items in the SCL-90 scale. The nine factors tested are somatization, obsessive-compulsive symptoms, interpersonal sensitivity, depression, anxiety, hostility, horror, paranoia, and psychosis. In addition, it also includes 1 other factor, which mainly reflects sleep and diet. In general research, it is classified as the tenth factor. At the same time, this paper also designs 13 questions including demographic characteristics. This questionnaire uses a five-level score of 1 (never), 2 (very light), 3 (medium), 4 (heavier), and 5 (very heavy). Moreover, it takes the score of one or more factors in the 10 factors of the SCL-90 scale ≥3 as the standard for testing positive symptoms of mental health. Cronbach's α coefficient of the SCL-90 scale in this study was 0.922 [19].

The contents of the self-made questionnaire are as follows:

(1) Basic information: school, grade, major, gender, age, ethnicity, whether it is an only child, physical condition, whether to serve as a student cadre, learning situation during school, relationship with classmates and teachers, hometown location, hometown new crown epidemic situation, etc.

(2) Coping style: In the standard scale-coping style questionnaire, according to the tendency of individual coping behavior types, it is divided into mature and immature types. The problems reflecting the six coping factors of "withdrawal," "fantasy," "self-blame," "seeking for help," "rationalization," and "solving problems" are selected separately: "Borrowing cigarettes or alcohol to dissipate sorrow"-"Retreat," "I hope that I have solved the problem facing"-"Fantasy," "Always blame oneself"-"self-blame," "Buried unpleasant things in one's heart"-"seeking for help," "calm down the troubles"-"rationalize," "try to see the good side of things"-"solve problems." Each has four options: "Never," "Occasionally," "Sometimes," and "Always." The corresponding scores are 1–4 scores, and the cumulative scores are 6–24 scores. The higher the score, the more mature the college students are in responding to public health emergencies.

(3) Behavioral and psychological investigations during the peak period of the COVID-19 epidemic: (1) Behavior survey: including personal hygiene habits:

hand washing conditions, according to frequency from low to high, it is recorded as 1–3 scores; spitting and throwing garbage anywhere, according to the frequency of occurrence from quotient to low, it is recorded as 1–4 scores; dining in small restaurants outside: according to the frequency of occurrence, it is recorded as 1–5 scores. Improve self-immunity: Whether to pay attention to the diet and nutrition, whether to work and rest on time, whether to exercise: According to the frequency of occurrence from low to high, they are all recorded as 1–5 scores. (2) Psychological investigation (focusing on the investigation of psychological stress): including the frequency of wearing masks, whether you have ever taken healthcare products, whether you have ever taken drugs to prevent the COVID-19 epidemic, whether you are worried about your family members being infected, and whether you feel suffocated in public, etc.

(4) Psychological investigation in the middle and late stages of the COVID-19 epidemic: (1) Anxiety state: In the standard scale—self-rating anxiety scale, we select six aspects of "anxiety," "unfortunate premonition," "fatigue," "can't sit still," and "sleep disorder," respectively. Each item has four options: "No or Rarely," "Sometimes," "Often," and "Always," which are recorded as 1, 2, 3, and 4 scores, and the total score is 5–20 scores. The higher the score, the higher the degree of depression. (2) Depressive state: In the standard scale—self-rated depression scale, three questions of "depressive mood," "irritability," and "emptiness" are selected, respectively. Each item has four options: "No or Rarely," "Sometimes," "Often," and "Always," which are recorded as 1, 2, 3, and 4 scores, and the total score is 5–20 scores. The higher the score, the higher the degree of depression.

(5) Behavioral and psychological investigations in the late stage of the COVID-19 epidemic: (1) Behavioral investigation: including the maintenance of personal hygiene habits: whether to spit and throw trash, whether to gather at a small restaurant, and how often to wash hands every day; improve self-immunity: whether you still pay attention to diet and nutrition, whether you still work on time, whether you still exercise, etc. (2) Psychological survey (focusing on the measurement of subjective feeling): After the COVID-19 epidemic is under control, whether students feel relaxed psychologically is divided into five levels: "not relaxed," "a little relaxed," "some relaxed," "relatively relaxed," and "completely relaxed."

(6) Survey of perceptions and knowledge during the occurrence and development of the new crown epidemic: it mainly involves (1) the communication between the school and the students: whether the students are satisfied with the various prevention and control measures taken by the school during the new

crown epidemic (hereinafter referred to as "Opinions to the School"). (2) Students' social support system: How to resolve the psychological tension caused by the COVID-19 epidemic (hereinafter referred to as the "resolving method"). (3) The impact of the COVID-19 epidemic on students' life and study.

3.2. Establishment of BP Neural Network Model. From the feasibility analysis, it is concluded that when BP neural network is applied to the research on the relationship between college students' psychological status and epidemic situation, it can effectively simplify the evaluation process and improve the evaluation efficiency and accuracy. In the process of creating the network model, it is necessary to maintain the good generalization ability of the model. In short, the network model must be able to widely adapt to different types of samples (i.e., different evaluation objects, indicators, etc.). Therefore, when constructing the BP neural network model, this paper will fully consider and reasonably set the key factors such as the structure, algorithm, number of neurons, and error accuracy of the network model (Figure 3).

In practical research, the number of neurons in the input layer depends on the number of variables contained in the problem. This study involves the evaluation index of the relationship between college students' psychological status and epidemic situation. According to the evaluation index system and the 10 secondary evaluation indexes involved in the questionnaire survey, this paper plans to record the number of neurons in the input layer as 10.

The output layer mainly depends on the actual needs of the studied object. The number of neurons in the output layer is selected after comprehensive analysis and judgment. In this study, the output content is the comprehensive evaluation result of the relationship between college students' psychological status and epidemic situation. Therefore, this paper sets the number of neurons in the output layer as 1.

The BP neural network with only one hidden layer is constructed this time. In order to ensure the effective training of the network model, the network structure needs to be simplified. Because the number of neurons in the hidden layer will directly affect the accuracy of network training, we need to be very careful when selecting the number of neurons. If the number of hidden layer neurons is too small, it will greatly reduce the fault tolerance of the network model and the accuracy of identifying samples. If the number of settings is too large, the network training time will be too long, and the fitting degree of the network model will be greatly increased, resulting in the problem of overfitting. We analyze or calculate the number of neurons contained in the input layer and output layer to determine how many neurons are needed in the hidden layer.

4. Experiment and Result

In this study, the convenience sampling method was used to investigate college students, and all respondents participated voluntarily. With the help of questionnaire star, the survey

list is included in the electronic questionnaire. The questionnaire uses unified guidelines to introduce the purpose and significance of the survey. After checking the collected data, input it into SPSS 20.0 software for data analysis and processing. The count data is expressed in cases and percentages. *T*-test, analysis of variance, correlation analysis, and multiple linear hierarchical regression analysis were used to explore the related factors and their interaction.

The basic status of the undergraduates participating in the survey is shown in Tables 1 and 2. From the questionnaire on the basic information of students and questionnaire on basic information of students affected by epidemic situation, the survey samples in this paper meet the needs of statistical surveys, which shows that the results of the experimental survey conducted in this paper are statistically significant.

Table 3 shows the survey statistics of students' personal behavior during the peak period of the COVID-19 epidemic. It can be seen from the table that, at the peak of the COVID-19 epidemic, although there are quite a few survey subjects who have never attracted attention in terms of hygiene habits and improving autoimmunity, the proportion is lower than that of students who sometimes, often, and always maintain good hygiene habits and pay attention to improving their own immunity.

Shown in Table 4 is the survey statistics of the personal behavior of students after the COVID-19 epidemic. In the later period of the COVID-19 epidemic, 7.21% of the survey respondents occasionally washed their hands, 64% of the survey respondents occasionally, sometimes, or often spit and throw garbage, and 2.35% of the survey respondents often or always dine in small restaurants outside. 8.25% of the survey respondents have never had the habit of regular work and rest. Less than half of the survey respondents sometimes, often, or always exercise their bodies, and 44.87% of the survey respondents never or only occasionally pay attention to the combination of diet and nutrition. Only 14.9% and 1.73% of the survey respondents always work and rest on time and exercise every day, respectively.

At the peak of the COVID-19 epidemic, among 780 students, 273 sometimes or often wear masks, accounting for 35.02%. 237 people have taken medicine to prevent the COVID-19 epidemic, accounting for 30.48%, and 160 people have taken healthcare products to increase their resistance, accounting for 20.50%. 66.75% of the survey respondents once felt suffocated in public, among which 220 people felt suffocated sometimes or often, as shown in Table 5.

The middle and late stages of the COVID-19 epidemic are between the peak of the COVID-19 epidemic and the latter part of the COVID-19 epidemic. As shown in Table 5, the psychological status during this period is measured using five anxiety and three depression items. 47.69%, 65.75%, 60.48%, 92.75%, and 80.76% of students have had obvious feelings of anxiety, premonitions of misfortune, fatigue, akathisia, and sleep disorders, respectively. 61.88%, 42.79%, and 82.48% of the survey respondents had significant depression, irritability, and feeling of emptiness, respectively, as shown in Table 6.
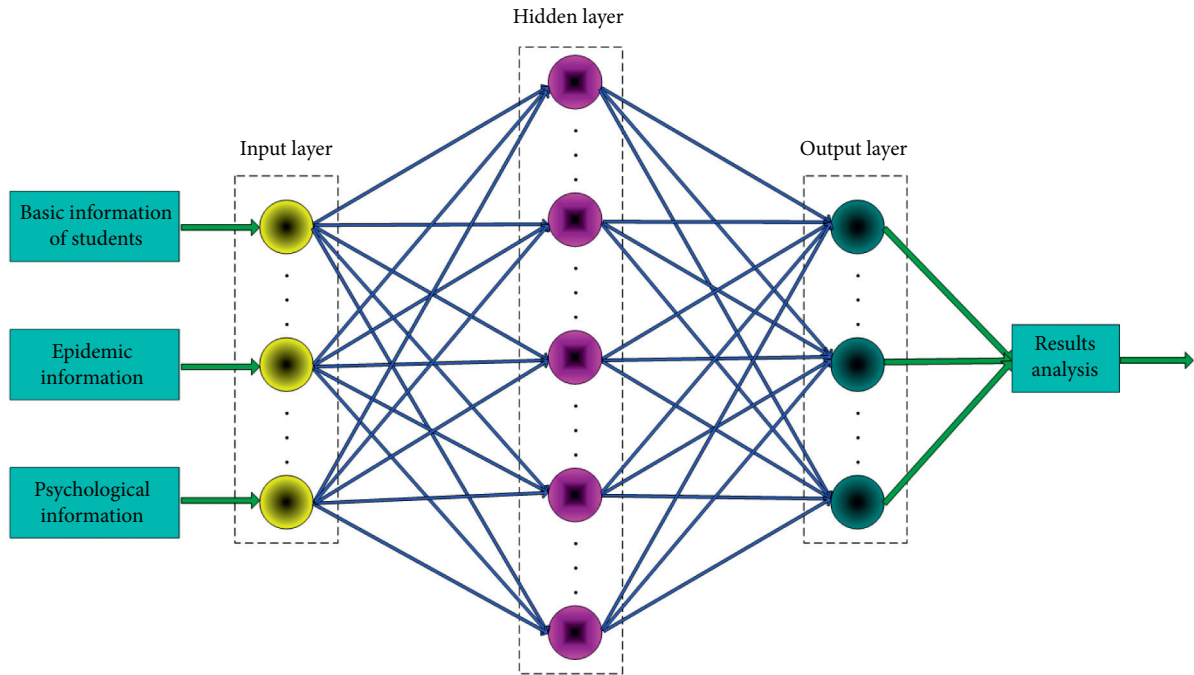
FIGURE 3: BP neural network model structure for analyzing the relationship between college students' psychological status and epidemic situation.

TABLE 1: Questionnaire on the basic information of students.

Project	Gender		Average age	Is it an only child		Physical conditions	
	Male	Female		Yes	No	Health	Unhealthy
Number of samples	482	298	20.52	502	278	758	22

TABLE 2: Questionnaire on basic information of students affected by epidemic situation.

Project	Whether to serve as a student leader		Epidemic situation in hometown		
	Yes	No	Serious	General	No
Number of samples	130	650	82	226	472

TABLE 3: Statistical table of the survey of the personal behavior of students during the peak period of the COVID-19 epidemic.

Item		Hygiene habits			Improve immunity		
		Hand washing frequency	Spitting/throwing garbage	Dining out	Reasonable diet	Standard schedule	Exercise
Never	Number of people	0	556	486	137	49	105
	Proportion (%)	0	71.25	62.35	17.56	6.32	13.52
Occasionally	Number of people	51	145	177	200	88	229
	Proportion (%)	6.52	18.6	22.65	25.61	11.26	29.31
Sometimes	Number of people	184	60	88	184	177	207
	Proportion (%)	23.54	7.65	11.26	23.58	22.69	26.54
Often	Number of people	510	10	15	177	301	192
	Proportion (%)	65.43	1.25	1.96	22.64	38.64	24.58
Always	Number of people	35	10	14	83	165	47
	Proportion (%)	4.51	1.25	1.78	10.61	21.09	6.05

TABLE 4: Statistical table of the survey of students' personal behaviors after the COVID-19 epidemic.

		Hygiene habits			Improve immunity		
Item		Hand washing frequency	Spitting/throwing garbage	Dining out	Reasonable diet	Standard schedule	Exercise
Never	Number of people	0	543	467	144	64	143
	Proportion (%)	0	69.58	59.84	18.52	8.25	18.35
Occasionally	Number of people	56	140	155	206	106	236
	Proportion (%)	7.21	18.01	19.85	26.35	13.65	30.21
Sometimes	Number of people	191	54	81	190	198	190
	Proportion (%)	24.53	6.98	10.35	24.35	25.35	24.35
Often	Number of people	518	10	18	164	295	198
	Proportion (%)	66.43	1.3	2.35	21.05	37.85	25.36
Always	Number of people	14	32	59	76	116	13
	Proportion (%)	1.83	4.13	7.61	9.73	14.9	1.73

TABLE 5: Statistical table of the survey of the psychological status of students in the early stage of the COVID-19 epidemic.

	Never		Occasionally		Sometimes		Often	
Item	Number of people	Proportion (%)	Number of people	Proportion (%)	Number of people	Proportion (%)	Number of people	Proportion (%)
Wear mask	120	15.35	197	25.31	190	24.32	273	35.02
Take medicine	542	69.52	168	21.54	41	5.32	28	3.62
Take supplements	620	79.52	119	15.23	16	2.1	25	3.15
Psychological depression in the crowd	259	33.25	300	38.51	174	22.35	46	5.89

TABLE 6: Psychological status of depression in the middle and late stages of the COVID-19 epidemic.

		No or rarely		Sometimes		Often		Always	
Item		Number of people	Proportion (%)	Number of people	Proportion (%)	Number of people	Proportion (%)	Number of people	Proportion (%)
Anxiety situation	Anxiety	408	52.31	285	36.52	62	7.98	25	3.19
	Unfortunate premonition	267	34.25	168	21.52	152	19.52	193	24.71
	Fatigue	308	39.52	336	43.12	103	13.25	32	4.11
	Can't sit still	57	7.25	212	27.12	337	43.25	175	22.38
Depression situation	Sleep disorder	150	19.24	242	31.02	244	31.24	144	18.5
	Depression	297	38.12	375	48.03	95	12.12	13	1.73
	Irritable	446	57.21	251	32.15	62	7.98	21	2.66
	Emptiness	137	17.52	297	38.14	242	31.02	104	13.32

The results of single-factor logistic regression analysis are shown in Table 7. Among them, the eight factors of gender, age, academic performance, peak behavior score, opinions on school measures to prevent the COVID-19 epidemic, resolving ways to confide in others, doing nothing, and coping style scores are significant.

This paper uses reliability to analyze the feasibility and effectiveness of the questionnaire. Reliability refers to the consistency and reliability of the results measured by the test or scale tool. In order to ensure the reliability of the questionnaire, this paper uses the Cronbach coefficient analysis method to analyze the internal consistency of the questionnaire data. For Cronbach coefficient the calculation formula is as follows:

$$\delta = \frac{M}{M-1}\left(1 - \frac{\sum f_i^2}{f^2}\right), \tag{8}$$

where M denotes the total number of items in the scale, f_i is the variance of score in question i, and f is the variance of the total score of all items. According to the formula and based on the data obtained from the questionnaire, the coefficient of this scale is 0.85, which proves that the questionnaire is stable and has high internal consistency and trust level.

TABLE 7: Results of single-factor logistic regression analysis of psychological conditions at the peak of the COVID-19 epidemic.

Influencing factors	Parameter value estimation	Standard error	χ^2	P	OR
Gender	0.20382	0.07828	6.85437	0.00929	1.23624
Age	−0.06555	0.02646	6.19342	0.01343	0.94637
Academic performance	0.08908	0.03868	5.35835	0.02151	1.10292
Peak behavior	0.06161	0.01172	27.98245	0.00002	1.07363
Opinions on the school	0.15736	0.04282	13.61965	0.00020	1.18069
Confide in others	0.21978	0.07777	8.07495	0.00475	1.25543
Doing nothing	−0.27937	0.14100	3.96880	0.04787	0.76558
Coping method	−0.10403	0.01667	39.21759	0.00004	0.91102

TABLE 8: Logistic multiple stepwise regression analysis results of psychological conditions at the peak of the COVID-19 epidemic.

Influencing factors	Parameter value estimation	Standard error	χ^2	P	OR
Intercept 1	−1.373196	0.653773	4.455918	0.036057	
Intercept 2	0.392284	0.650642	0.367135	0.552066	
Intercept 3	2.131201	0.652359	10.78074	0.001111	
Age	−0.071104	0.026664	7.182918	0.007777	0.94132
Opinions on the school	0.099384	0.044036	5.159282	0.024038	1.11403
Behavior at peak	0.086456	0.012524	48.512118	0.00020	1.09989
Confide in others	0.266539	0.079184	11.443603	0.000808	1.31502
Coping method	−0.1313	0.017271	58.107522	0.00004	0.88678

TABLE 9: Logistic multiple stepwise regression analysis results of psychological conditions in the late stage of the COVID-19 epidemic.

Influencing factors	Parameter value estimation	Standard error	χ^2	P	OR
Intercept 1	−1.29805	0.34017	14.70409	0.00010	
Intercept 2	−0.08797	0.33118	0.07121	0.79851	
Intercept 3	1.17433	0.33108	12.70964	0.00040	
Intercept 4	3.74811	0.33997	122.76671	0.00004	
Student leaders	−0.24684	0.08524	8.47723	0.00384	0.79083
The relationship between teachers	−0.15039	0.05232	8.37068	0.00414	0.86860
Anxiety	0.04020	0.01424	8.04233	0.00485	1.05141
Opinions on the school	−0.37905	0.04464	72.79363	0.00002	0.69387
Self-resolving	−0.29139	0.08141	13.00769	0.00030	0.75649

Fit the logistic avoidance model of multinomial ordinal classification to the factors in Table 7. Set the screening standard to 0.15 and reject to 0.05. The results are shown in Table 8. The younger you are, the more satisfied you are with the measures taken by the school, the higher your peak epidemic behavior score, the lower your choice of resolving ways to confide in others, and the lower your coping score, the more psychologically nervous you will be during the peak of the COVID-19 epidemic.

The regression results are shown in Table 9. Students who scored lower in anxiety in the middle and late stages of the COVID-19 epidemic were more satisfied with the measures taken by the school and chose self-resolving methods and felt more relaxed in the later stages of the COVID-19 epidemic.

According to the above experimental results, the following suggestions are put forward. First, multiple coordination is done to jointly protect students' mental health. COVID-19 epidemic should be published through key roles such as various media channels and counselors. On the one hand, it should reduce unnecessary fear and help students master the necessary preventive knowledge.

On the other hand, we can strengthen the health education of college students' lifestyle through a variety of information platforms to promote the generation and maintenance of their healthy behavior. Second, strengthen the construction of teachers and improve the combat effectiveness of epidemic prevention psychological work. In case of public health emergencies, students' cognition of epidemic situation knowledge is easy to deviate and students' psychological emotion is easy to fluctuate. Mental health education is facing new challenges. Therefore, it is essential to improve their psychological competence under the epidemic situation. Through online peer counselors' daily work discussion, supervisors are invited to conduct professional supervision and actively learn relevant knowledge of psychological maintenance under the epidemic, to lay a solid foundation for mental health work under the epidemic. In addition, popularize psychological epidemic prevention knowledge through mental health knowledge publicity, psychological network support, and psychological cloud classroom and improve students' psychological quality and open students' psychological self-help mode [20].

5. Discussion

As an important group in our country, the mental health of college students has always been a hot issue of social concern. The COVID-19 epidemic has affected the learning style, lifestyle, and communication styles of college students and also affected the mental health of college students to varying degrees. China's epidemic prevention and control is still in a tense stage of external defense import and internal defense rebound. The study life and interpersonal communication of college students will still be in a state of restraint and depression in the short term, and such long-term restraint and depression can easily lead to the transformation of some college students' mental health problems from nothing to existence, from small to large. Therefore, under the background of the COVID-19 epidemic, doing a good job in the mental health education of college students, preventing the occurrence of college students' psychological problems, and improving the level of college students' mental health are an urgent task for educators.

This paper combines the COVID-19 epidemic situation to investigate the current psychological emotions of college students through a questionnaire survey. Through investigation and analysis, it can be known that various behaviors of college students under public health emergencies are the result of a combination of multiple factors. This paper studies multiple factors in the research and combines factor analysis to finally get the influence of each factor on the psychology of college students.

6. Conclusion

In order to explore the impact of COVID-19 on college students' mental health, this paper proposes a BP neural network based model for the relationship between college students' psychological status and epidemic situation by evaluating the psychological status of college students and exploring the related factors. The relationship model constructed in this paper is used to analyze the psychological factors affecting college students, and the principal component analysis method is used to explore the factors affecting college students' psychology. From the model prediction and result analysis, it is known that the factors affecting college students' psychological status show multilevel and multifaceted characteristics. During the epidemic period, the psychological status of college students is not only related to demographic characteristics, but also affected by epidemic related factors. At the same time, their own behavior also has a more significant impact on their psychological status. On the premise of ensuring no infection, we should pay full attention to the intervention of college students' health behavior during the epidemic. In addition, the influence of COVID-19 on college students' psychology should focus on improving occupation quality, improving their physical quality, humanistic quality, and moral quality, and improving the stability of colleges and universities in public health emergencies. By evaluating the psychological status of college students and exploring the relevant influencing factors, this paper can provide reference for carrying out mental health education and formulating effective intervention programs.

Data Availability

The labeled datasets used to support the findings of this study are available from the corresponding author upon request.

Conflicts of Interest

The author declared that they have no conflicts of interest to this work. The authors declare that they do not have any commercial or associative interest that represents a conflict of interest in connection with the work submitted.

Acknowledgments

References

[1] L. L. Armstrong, S. Desson, E. JohnWatt, and E. Watt, "The DREAM program: developing resilience through emotions, attitudes, & meaning (gifted edition)–a second wave positive psychology approach," *Counselling Psychology Quarterly*, vol. 32, no. 3-4, pp. 307–332, 2019.

[2] F. Chakhssi, J. T. Kraiss, M. Sommers-Spijkerman, and E. T Bohlmeijer, "The effect of positive psychology interventions on well-being and distress in clinical samples with psychiatric or somatic disorders: a systematic review and meta-analysis," *BMC Psychiatry*, vol. 18, no. 1, pp. 211–217, 2018.

[3] X. Hu, J. Cheng, M. Zhou et al., "Emotion-aware cognitive system in multi-channel cognitive radio ad hoc networks," *IEEE Communications Magazine*, vol. 56, no. 4, pp. 180–187, 2018, Date of Publication:13 April 2018.

[4] F. Gander, R. T. Proyer, and W. Ruch, "A placebo-controlled online study on potential mediators of a pleasure-based positive psychology intervention: the role of emotional and cognitive components," *Journal of Happiness Studies*, vol. 19, no. 7, pp. 2035–2048, 2018.

[5] E. I. Gorlin, J. Lee, and M. W. Otto, "A topographical map approach to representing treatment efficacy: a focus on positive psychology interventions," *Cognitive Behaviour Therapy*, vol. 47, no. 1, pp. 34–42, 2018.

[6] J. He, Y. Zhao, H. Zhang, and Z. Lin, "Orthorexia nervosa is associated with positive body image and life satisfaction in Chinese elderly: evidence for a positive psychology perspective," *International Journal of Eating Disorders*, vol. 54, no. 2, pp. 212–221, 2021.

[7] S. Houge Mackenzie and E. Brymer, "Conceptualizing adventurous nature sport: a positive psychology perspective," *Annals of Leisure Research*, vol. 23, no. 1, pp. 79–91, 2020.

[8] P. Khanna and K. Singh, "Do All Positive Psychology Exercises Work for Everyone? Replication of Seligman et al.'," *Psychological Studies*, vol. 64, no. 1, pp. 1–10, 2019.

[9] I. Lopez-Gomez, C. Chaves, G. Hervas, and C. Vazquez, "Comparing the acceptability of a positive psychology intervention versus a cognitive behavioural therapy for clinical depression," *Clinical Psychology & Psychotherapy*, vol. 24, no. 5, pp. 1029–1039, 2017.

[10] J. Macfarlane, "Positive psychology: gratitude and its role within mental health nursing," *British Journal of Mental Health Nursing*, vol. 9, no. 1, pp. 19–30, 2020.

[11] P. D. MacIntyre, T. Gregersen, and S. Mercer, "Setting an agenda for positive psychology in SLA: theory, practice, and research," *The Modern Language Journal*, vol. 103, no. 1, pp. 262–274, 2019.

[12] C. Malboeuf-Hurtubise, G. Taylor, D. Lefrançois, I. Essopos, and E. Lacourse, "The impact of a mindfulness-based intervention on happiness: a reflection on the relevance of integrating a positive psychology framework within mindfulness research in youth," *International Journal of Applied Positive Psychology*, vol. 2, no. 1, pp. 23–37, 2018.

[13] S. C. Marques, J. L. Pais-Ribeiro, and S. J. Lopez, "The role of positive psychology constructs in predicting mental health and academic achievement in children and adolescents: a two-year longitudinal study," *Journal of Happiness Studies*, vol. 12, no. 6, pp. 1049–1062, 2011.

[14] D. P. Morton, "Combining lifestyle medicine and positive psychology to improve mental health and emotional well-being," *American Journal of Lifestyle Medicine*, vol. 12, no. 5, pp. 370–374, 2018.

[15] J. M. Nelson and B. D. Slife, "A new positive psychology: a critique of the movement based on early Christian thought," *The Journal of Positive Psychology*, vol. 12, no. 5, pp. 459–467, 2017.

[16] I. J. Raymond and C. M. Raymond, "Positive psychology perspectives on social values and their application to intentionally delivered sustainability interventions," *Sustainability Science*, vol. 14, no. 5, pp. 1381–1393, 2019.

[17] R. A. Roth, S. M. Suldo, and J. M. Ferron, "Improving middle school students' subjective well-being: efficacy of a multi-component positive psychology intervention targeting small groups of youth," *School Psychology Review*, vol. 46, no. 1, pp. 21–41, 2017.

[18] C. R. Stoner, M. Orrell, M. Long, E. Csipke, and A. Spector, "The development and preliminary psychometric properties of two positive psychology outcome measures for people with dementia: the PPOM and the EID-Q," *BMC Geriatrics*, vol. 17, no. 1, pp. 72–11, 2017.

[19] J. C. Vela, A. S. Lenz, G. S. Sparrow, and S. L. Gonzalez, "Using a positive psychology and family framework to understand Mexican American adolescents' college-going beliefs," *Hispanic Journal of Behavioral Sciences*, vol. 39, no. 1, pp. 66–81, 2017.

[20] G. Wang, Y. Zhang, J. Zhao, J. Zhang, and F. Jiang, "Mitigate the effects of home confinement on children during the COVID-19 outbreak," *The Lancet*, vol. 395, no. 10228, pp. 945–947, 2020.

Hindawi

Research Article

System Dynamics Analysis of Construction Safety Risk considering Existing Railway Lines

Xiaoye Zeng [iD],[1] **Naixin Huang,**[2] **Yang Han,**[1] **Yang Yin,**[1] **and Jianling Huang** [iD][1]

[1]*Department of Engineering Management, School of Civil Engineering, Central South University, Changsha 410083, Hunan, China*
[2]*College of Design, Construction and Planning, University of Florida, Gainesville, 32601, FL, USA*

Correspondence should be addressed to Jianling Huang; hjl1201@csu.edu.cn

Existing railway line (ERL) construction safety has received significant attention during the past decades due to the high accident rate and the difficulty of progress development under the limited synthesis construction time schedule (SCTS). However, the previous literature is dominated by the construction safety of new railway lines, while research on construction safety of ERLs is limited. This paper analyzed the interactions and causal relationships between construction safety risk (CSR) and multiple factors and classified feedback loops. Hence, a system dynamics model was developed, and a series of tests were conducted to simulate the evolution of CSR under different group environments. The results indicated that (1) the CSR considering ERLs is significantly relevant to the implementation degree of SCTS. For situations where there are more delays and more schedule pressure, construction safety accidents tend to have a higher level. (2) Work efficiency is negatively related to construction safety accidents probability. The increase of work intensity could reduce schedule pressure in the short term but could increase construction safety risk in a long time. Applying both appropriate work efficiency and work intensity may achieve an acceptable result. This paper adds to the knowledge of construction safety risk management in terms of implementation and offers lessons and references for future construction safety management considering ERLs.

1. Introduction

With the great improvement in train speed and operating conditions, some new railway projects will inevitably be built close to the existing railway lines (ERLs) [1]. Under the background of uninterrupted operation, to ensure the transportation of ERLs, the construction of new railway projects cannot be arranged randomly. It can only operate within a certain time called synthesis construction time schedule (SCTS) [2]. The SCTS is the time reserved in the train operation diagram, specifically used for the construction. No trains will be running during that time. The duration of SCTS should be more than 180 minutes when the construction is near a normal railway and 240 minutes at 0:00–6:00 when the construction is nearby a high-speed railway [3]. When the SCTS is long, the fluency of the transportation organization will be affected, thus affecting

the efficiency of the operation of ERLs. On the contrary, if the SCTS is too short, the normal construction schedule will be restricted, affecting the efficiency of construction operation and increasing the construction cost [4]. Due to the mutual interference between the construction of new railway projects and transportation of ERLs, the effective construction time and space are more and more limited, and the construction safety issues are more prominent [5]. Thus, it is challenging and demanding to ensure construction safety under the background that the transportation organization of ERLs affects the construction organization of the new railway projects.

Each country has different management modes for the construction and maintenance of ERLs. In Japan, for the traffic density of Shinkansen during the daytime, except for necessary patrol inspection, all construction and maintenance work will be arranged within the SCTS of 12:00~6:00 am, and

all trains in the SCTS will be suspended. 12:00~3:00 am is the time for construction or maintenance, and 3:00~6:00 am is the time of inspection and acceptance [6]. Construction and maintenance also adopt the 6 hours of SCTS in France, it is generally during 11:30 pm~5:30 am, and the actual operation time is controlled under 4 hours [7]. High-speed railways and general-speed railways are interlinked alternately into networks in Germany, and the railway lines are mixed passengers and freight trains. For the density and trains that run at night, the SCTS is arranged at 3:30~6:00 am. Only one line is blocked, and the other line is running normally. The express freight trains pass before the SCTS hours, during which only a small number of slow freight trains run. More construction and maintenance work will be carried out on weekends with no train traffic [8]. SCTS of construction and maintenance of ERLs in the above countries takes a long time, and there are no trains or only a few single lines of freight trains running during the SCTS. Transportation has a negligible impact on construction safety, and the construction safety of ERLs is not prominent as that of China. The setting of SCTS has constraints and impacts on the operation and the passing capacity of the railway. If the time of SCTS is too short, it cannot guarantee the completion of the construction task and will affect the quality and efficiency of the construction work, thus affecting the construction schedule.

Safety accidents during construction have been and continue to be a global problem [9], and they can cause casualties and huge economic losses [10]. Generally speaking, accidents are raised by many interacting systemic factors [11]. An accident or an unsafe event may be caused by some elusive causes [12, 13]. Since Heinrich realized that unsafe behavior was the dominant cause of safety accidents [14], there has been a growing amount of research concerning their contribution to accidents in recent years. Bird revised Heinrich's theory and proposed that the essential cause of accidents depends on management. Accidents were more likely to be caused by "unsafe acts of people" and "unsafe mechanical or physical conditions" [15, 16]. The "unsafe acts of people" and "unsafe physical or mechanical conditions" are collectively referred to as on-site errors. Management errors are the deep-seated reason that causes safety accidents [17]. Unsafe behavior can be defined as intentional or unintentional violations of safety compliance expectations [18]. An unsafe condition is when the physical layout, tools, equipment, and/or materials in a workplace or work location violate contemporary safety standards [19]. Avoiding unsafe behaviors and unsafe conditions can be effective in reducing the probability of safety accidents [20]. The majority of existing studies focus on the safety accidents in independent new rail projects [21, 22], and few studies consider CSR in the presence of ERLs. Furthermore, given the huge mediating effect of CSR considering ERLs, the mechanism of how CSR changes under the influence of multiple factors needs more attention. However, the evolution mechanisms of CSR considering ERLs are not yet clear, and it is necessary to be explored further. To fill the aforementioned research gap, this paper aims to investigate the laws and effects of influencing

factors in the safety management system considering ERLs, establishing a scientific causal model, and simulating the evolution of the system under different conditions to provide guidance for management decisions.

System dynamics is a system simulation method for analyzing production management and inventory management created by Jay Forrester and originally named Industrial Dynamics [23]. It has often been used for analyzing and understanding complex safety problems [24]. For example, researchers adopt SD to gain insight into the cause of major accidents [25–27]. SD was applied to gain insight into the complexity and coupling of project elements [28] and was shown as an efficient tool to simulate the dynamics of safety attitudes and behaviors [29] and to organizational learning [27, 30, 31]. As a systematic approach, SD emphasizes the feedback between variables in a system and understanding the behavior and dynamics of complex systems with time [32]. Therefore, it was used as a theory development tool [33]. SD emphasizes the holistic nature of systems and the nonlinear characteristics of complex systems and considers that the behavior patterns and characteristics of a system depend mainly on the internal dynamic structure and feedback mechanisms. The system develops and evolves according to certain laws under the action of internal and external dynamics and constraints. The approach of system dynamics to complex problems is a combination of qualitative and quantitative, and holistic and analytical thinking. It is a method of analysis, synthesis, and reasoning. This paper uses SD to investigate the complexity and coupling of project elements (e.g., construction schedule, safety cost, and safety) from a system thinking perspective considering ERLs.

The paper is organized as follows. Section 2 analyzes the relevant factors that influence the construction safety of new projects near ERLs and sets up the causal model. Section 3 sets up the SD model of construction safety considering ERLs, uses data collected from a construction site, and validates the model. In Section 4, tentative data are used to simulate the relationship between these variables and the occurrence of accidents. The results are analyzed and discussed to understand the dynamics of the management components. Finally, Section 5 provides concluding remarks.

2. Relevant Factors Influence on Construction Safety of ERLs

2.1. Identification of Feedback Loop for Construction Safety. This study is based on unsafe behaviors and unsafe conditions in those two perspectives and only considers the construction progress, cost, and safety factors. Other relevant factors were not considered. This study identifies and refines the factors affecting construction safety and analyzes the relationship between the various factors to establish a causal model. It can visually show the influence of each factor on construction safety and make the relationship among each factor clear. This paper made use of a large amount of literature involving railway construction safety in recent years to summarize while forming a preliminary

understanding of the identification of railway construction safety impact factors considering ERLs. Literature was based on Google Scholar, Elsevier, Web of Science, and Scopus, searched by entering keywords such as railway construction safety. Descriptions of construction safety influence factors considering ERLs in the literature were carefully extracted. According to the literature, the driving factors of construction safety can be categorized as follows:

(1) Construction schedule: if the schedule of the railway construction was out of control, economic and social losses would be inevitable [34]. It is important to note that excellent schedule management does not mean compressed schedules, which can lead to safety incidents [35, 36]. Management measures that are taken to expedite production put workers under pressure to increase productivity, which is negatively impacted[37]. When production pressure (e.g., excessive workload, required work pace, and time pressure) is perceived, workers perceive increased risks and barriers, leading them to be more likely to work with unsafe behaviors [38]. On the contrary, construction safety accidents are likely to cause project delays [39]. Therefore, previous studies have shown that schedule pressure is the critical link between scheduling and safety in construction.

(2) Cost: this paper does not consider the total production cost during the construction. It only analyzes the safety investment within the boundary range of the model. Safety investments generally refer to funds spent on workplace injury prevention measures or activities that aim to protect workers' health and physical integrity [40, 41]. In many previous studies, the components of safety investment have been discussed, such as safety training, safety supervision, and safety protection [42–44]. Since the vast majority of those engaged in the grassroots work of railway construction are migrant workers, they are poorly educated and lack safety awareness [45]. Safety training improves the safety awareness of workers to a certain extent. Safety supervision is a reflection of the management's attitude towards unsafe behaviors [46]. The more strict the supervision of safety managers at the construction worksite, the more the probability of discovering unsafe behaviors [47]. Severe punishment for unsafe behavior can also serve as an effective warning [48]. Not using personal protective is one of the leading phenomena of unsafe behaviors [49]. In view of the high incidence of falling accidents in railroad construction, safety measures can be effectively taken to reduce the rate and severity of accidents [50]. Providing safety protection is a crucial complement to other safety measures (e.g., safety training) and is considered a last resort for hazard control measures for workers [51].

(3) Safety subjects: the research on accident causation theory was pioneered by Heinrich [14], who analyzed 75,000 accident reports and developed a domino theory (model) of accident causation. The analysis led him to conclude that 88% of accidents are caused by unsafe behavior and 10% of accidents are caused by unsafe conditions. Unsafe behaviors and unsafe conditions can directly lead to the occurrence of accidents [52]. According to past statistics in China, more than 80% of accidents were caused by workers' unsafe behaviors [53]. Unsafe conditions on a construction site are events that are not related to people and are a natural part of the initial construction site conditions [19].

2.2. Causality Analysis of Construction Safety. In order to understand the causal relationships of construction safety considering ERLs, the causal loop diagram is proposed, as shown in Figure 1 (the polarities represent a positive or negative impact between variables). Due to the SCTS being fixed and limited, the construction must be executed strictly according to the plan. Owing to the complexity and uncertainty of the construction environment and conditions, schedule delays are inevitable [54–56]. The resulting schedule pressure (e.g., being pressed to work faster) leads to unsafe behaviors [57, 58]. Accidents caused by unsafe behaviors, in turn, lead to delays in production, thus creating production pressure [59]. With increased investment in safety comes increased safety training, supervision, and protection. Safety training and safety supervision are positively correlated with the improvement of safety consciousness and behaviors [60, 61]. Insufficient safety protection leads to the deterioration of cumulative unsafe conditions in the worksite and eventually to accident occurrences, which increases safety investment [62, 63]. In summary, the model reveals these feedback processes, and it is vital to consider schedule, safety cost, and safety on an operational level.

3. Modeling

System dynamics modeling is a typical simulation method, focusing on the interaction between factors of complex systems [64]. It predicts the changing trend of the system and summarizes the dynamic development law of the system by constructing a causal feedback loop to describe the dynamic adjustment process of construction safety considering ERLs, which is an ideal research method. System dynamics modeling requires three steps: determining the system boundaries, constructing the model structure, and quantifying the action paths. The analysis of feedback loops and simulation experiments are typical research methods.

3.1. System Boundary. The SCTS is the most important element in the construction of ERLs; the cost that construction enterprises pay special attention to is taken as the reference elements, while other elements such as quality and environment are not taken as the analysis object. According to the causal model of construction safety, safety accidents
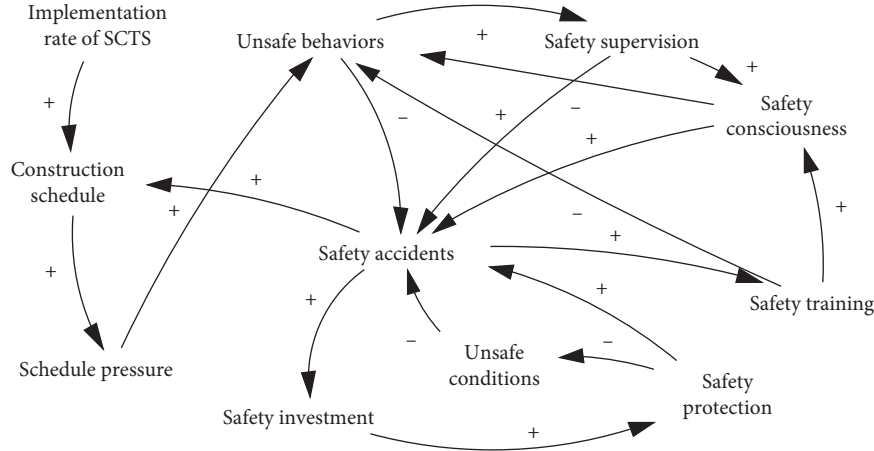
Figure 1: SD modeling for construction safety considering ERLs.

(SA), safety training (ST), safety investment (SI), safety supervision (SS), safety protection (SP), SCTS, schedule pressure, fatigue, unsafe conditions (UC), unsafe behaviors (UB), construction schedule (CS), and safety consciousness (SC) are defined as main systematic variables. This study focuses only on the relationships and interactions among the eleven variables.

3.2. Model Structure. Based on the causal model of construction safety under the context of ERLs, we further defined the stock, flow, and feedback loop in the dynamic system. A stock is the value or level of the core variables accumulated in a dynamic system that reflects the system's changing state. According to the dynamic regulation system of construction safety considering ERLs, the system stocks are the UB level of people and the UC level of physical or mechanical. A flow is an activity that changes the stock. In this study, the flows are the decrease and increase of UB of people as well as the decrease and increase of UC of physical or mechanical. According to the causal model, the reduction and improvement of UB are related to dynamic variables such as ST, SC, SS, fatigue, and schedule pressure. The improvement and reduction of UC are associated with dynamic variables such as SP, working platform restriction, and invasion barriers of equipment and materials. In addition, the auxiliary variables, such as working platform restriction and invasion barriers of equipment and materials which reflect the UC, are closely related to the dynamic regulation of SA and need to be defined separately. In conclusion, the structure of the dynamics model of construction safety considering ERLs is shown in Figure 2.

3.3. Model Hypothesis and Path Quantification. Construction safety considering ERLs may be interfered with by many factors. It is hard to enumerate and quantify all the interactions between variables. The rational assumptions of the system dynamics model allow itself to focus on the vital variables and their influence paths while ignoring the interference of other unimportant and small

probability events, thereby significantly reducing the complexity of the algorithm. In order to standardize the study, five hypotheses are proposed: (1) Only consider the relationship between unsafe behaviors, unsafe conditions, and safety accidents in the construction stage under the background of ERLs. (2) It does not consider the total production cost during the construction and only analyzes the safety investment. (3) The variables, such as total quantity, remaining quantities planned, daily actual quantities completed, daily planned quantities completed, actual quantities completed, planned quantities completed, and construction schedule, should be uniformly treated according to the progress unit. For example, the total quantity is 12,000 m, and the constructions schedule is 50 m/d. (4) Delay is set as a random function, and it is assumed that the delay occurs randomly. (5) Different lines have different actual situations. The values of relevant variables in this paper are derived from the production data of the case. The assigned values of correlation coefficients are the average values obtained after statistical analysis after collecting actual data.

Based on the above model assumptions, some mathematical functions are needed to describe the relationship between the key variables. Planned quantities completed (PQC) is the accumulation of daily planned quantities completed (DPQC); DPQC is related to planned quantities (PQ) and construction period (CP), which is an IF THEN ELSE function, and the specific description is shown in Table 1, so PQC is calculated as follows:

$$PQC = \sum_1^{CP} DPQC. \tag{1}$$

Similarly, the mathematical function of the calculation related to the actual quantities completed (AQC) can be obtained as formula (2), where daily actual quantities completed (DAQC) is related to the following three variables: WN stands for the number of workers per day, AHWW stands for the actual workload of workforce per hour, and WT stands for the work time per day, so the mathematical expression of DAQC is shown in formula (3).
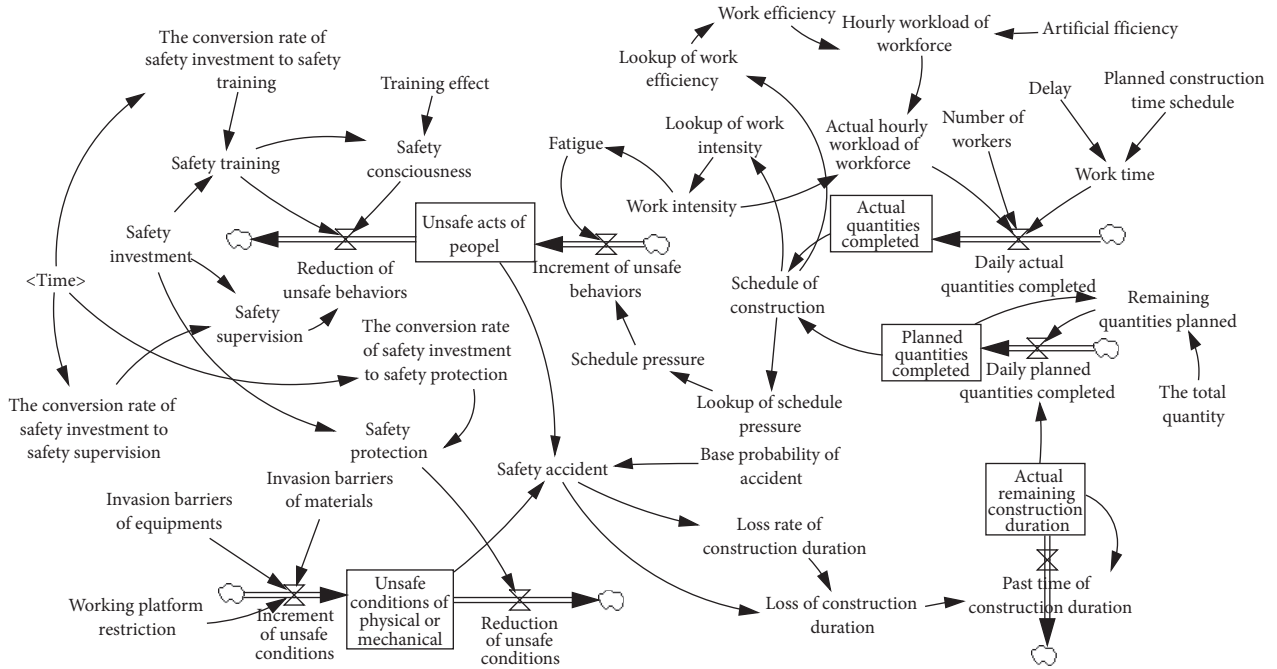
FIGURE 2: dynamics model of construction safety considering ERLs.

TABLE 1: Principal variables and constants description of the SD model.

Variables designation	Unit	Description
Schedule of construction	Dimensionless	IF THEN ELSE (actual quantities completed < planned quantities completed, (1− actual quantities completed)/ planned quantities completed, 0)
Schedule pressure	Dimensionless	1 * WITH LOOKUP (construction schedule ([(0, 0)-(1, 1)], (0, 0), (0.1, 0), (0.2, 0.1), (0.5, 0.7), (0.7, 1), (1, 1))
Work intensity	Dimensionless	1 * WITH LOOKUP (construction schedule ([(0, 0)-(1, 1)], (0, 0), (0.2, 0.3), (0.4, 0.5), (0.6, 0.7), (0.8, 0.9), (1, 1))
Fatigue	Dimensionless	WITH LOOKUP (work intensity ([(0, 0)-(1, 1)], (0, 0.045), (0.1, 0.21), (0.17, 0.3), (0.25, 0.37), (0.3, 0.4), (0.6, 0.4), (0.7, 0.45), (0.8, 0.58), (0.9, 0.76), (1, 1))
Reduction of unsafe behaviors	Dimensionless	0.33 * safety training + 0.33 * safety consciousness + 0.34 * safety supervision
Increment of unsafe behaviors	Dimensionless	0.35 * fatigue + 0.65 * schedule pressure
Increment of unsafe conditions	Dimensionless	0.38 * working platform restriction + 0.31 * invasion barriers of equipment + 0.31 * invasion barriers of material
Safety accidents	Dimensionless	Safety accidents probability (shown as Table 2), base probability of accidents * (unsafe behaviors + unsafe conditions)
Loss of construction period	d	Safety accident * loss rate of construction period
Daily actual quantities completed	m	Work time * actual hourly workload of workforce * number of workers
Daily planned quantities completed	m	IF THEN ELSE (actual remaining construction period ≤ 0, remaining quantities planned, remaining quantities planned/actual remaining construction period)
Hourly workload of workforce	m	Artificial efficiency × (1 + work efficiency)
Actual hourly workload of workforce	m	Hourly workload of workforce × (1 + labor intensity)
Work time	h	Planned construction time schedule−(delay/60)
Delay	min	RANDOM NORMAL (0, 20, 7, 15, 1)

$$AQC = \sum_{1}^{CP} DA\, QC. \tag{2}$$

$$DAQC = WN \times AHWW \times WT. \tag{3}$$

In the above formula, WT is actually determined by planned SCTS and delay per day. The detailed description is shown in Table 1, where the delay is a random function whose output is 0 or the actual delay time. Different delays are set to explore the influence of transportation organization of ERLs on construction safety in this study.

The increment of unsafe behaviors (UBI) is related to the following two variables: fatigue stands for the count of those unsafe behaviors caused by workers' fatigue, SP stands for the count of those unsafe behaviors caused by the schedule pressure of workers. Then, the decrement of unsafe behaviors (UBD) is related to ST, SC, and SS, which stand for the conversion of the safety investment to safety training, safety consciousness, and safety supervision, respectively. So the mathematical expression of the level of unsafe behaviors (UBL) is shown in formula (4), and the mathematical expression of the UBI and UBD is shown in formulas (5) and (6), where α_{1-5} is the influence weight of each variable.

$$UBL = UBI - UBD. \tag{4}$$

$$UBI = \alpha_1 F + \alpha_2 SP. \tag{5}$$

$$UBD = \alpha_3 ST + \alpha_4 SC + \alpha_5 SS. \tag{6}$$

Correspondingly, the increment of unsafe conditions (UCI) is related to the following three variables: MBI stands for the materials beyond the boundaries set for transportation safety, EBI stands for the equipment beyond the boundaries set for transportation safety, and WPR stands for the restrictions on work platforms set to ensure transportation safety. In this study, the decrement of unsafe conditions (UCD) is related to the SP, which refers to the conversion of the safety investment to safety protection. Therefore, the mathematical expression of the level of unsafe conditions (UCL) is shown in formula (7), and the mathematical expression of the UBI and UBD is shown in formulas (8) and (9), where β_{1-3} is the influence weight of each variable.

$$UCL = UCI - UC. \tag{7}$$

$$UCI = \beta_1 MBI + \beta_2 EBI + \beta_3 WPR. \tag{8}$$

$$UCD = SP. \tag{9}$$

The unsafe behaviors and unsafe conditions actually determine safety accidents (SA), but the former two are necessary not sufficient conditions for the latter. γ_s is set as a constant standing for the base probability of an accident. Therefore, SA is calculated as follows:

$$SA = \gamma_S (UCL + UBL). \tag{10}$$

All the previous formulas are the main mathematical functions in this study; more descriptions of variables and constants are shown in Table 1.

3.4. Model Validation. The validity tests of the model include mechanical error tests, dimensional consistency tests, and extreme condition tests. The model was built with Vensim in this study, which has passed the mechanical error tests, dimensional consistency tests, and extreme condition tests. The system model in this study included 35 variables and 10 constants. The main variables and function relationships in the model are described in Table 1.

Workers in the real world are faced with different situations every day and therefore make decisions accordingly. The conditions of the workplace vary day to day. As time goes on, the decision of workers and conditions of the workplace may be changed. To simulate this, the model sets some events (safety training, safety supervision, working platform restriction, etc.), which are triggered every day. According to the functions we set above, unsafe behaviors were performed, and unsafe conditions were accumulated. Consequently, the time step of the model was set to 200 days to ensure that a long enough observation time was available to show all possible trends. The initial value of safety accidents probability was set as 0. Vensim 8.2 was used to simulate the system dynamics in this study. And the input parameters of a railway cutting project close to the ERLs were designed. The main input parameters are shown in Table 3 and were determined by interviewing our industry workers involved in the data collection or based on available research literature and practical survey data. Relevant parameters were input into the model to conduct simulation analysis on the relationship between SCTS, construction schedule, UB, UC, and SA of the project. The simulation results are shown in Figure 3.

The construction risk degree and grade standards of existing lines were set by referring to "Technical Regulations for Risk Management of Railway Construction Engineering and Relevant Regulations," as shown in Table 2. The goal of the system safety management level was set as low risk.

Figure 3 shows that the safety accidents probability of the project reaches the maximum on the 31st day, which was a high-risk degree according to Table 2. It was reduced to medium risk on the 82nd day and low risk on the 187th day. Combined with the actual situation of the case project, it was found that the simulation result of the system dynamics was basically the same as the actual situation. That is, with the increase of construction schedule, unsafe behaviors and unsafe conditions rose to a high level at the end of the first month, which led to the rise of safety accidents. However, the safety investment came into play simultaneously. Various safety measures reduced the unsafe behaviors and unsafe conditions, which led to the reduction of safety accidents, so the safety risk was reduced to a low level on the 187th day. Figure 3 also indicates that the risk level would not decrease indefinitely with the increase of safety investment, which means there is no absolute zero safety risk.

TABLE 2: Degree and countermeasure for construction risk of existing railway lines.

Risk degree	Probability of casualty (0~1)	Countermeasure
Low	< 0.003	No measure
Medium	0.003~0.03	Strengthen daily management and increase investment in safety
High	0.03~0.3	Strengthen daily management and monitoring and increase investment in safety
Extreme high	> 0.3	Measures must be taken to reduce risks and increase investment in rectification

TABLE 3: Main parameters of the model.

| Parameter names	Parameter values	Parameter names	Parameter values
Total quantities	12,000 m	Planned construction time schedule	4 h
Number of works	100	Efficiency	0.075
Training effect	0.85	Safety investment	100 CNY/person·d
Working platform restriction	0.312	Invasion barriers of equipment	0.182
Invasion barriers of materials	0.236	Base probability of accident	0.03
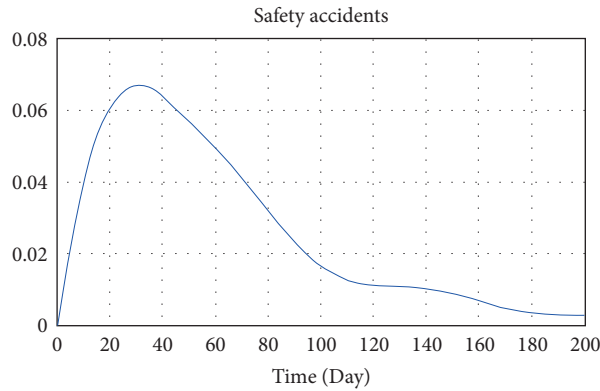
FIGURE 3: Simulation result of safety accidents probability of the case.

In general, it can be seen that the internal relationship among the parameters, the equations, and the parameters established in the system dynamics model established in this study are reasonable and can reflect the actual situation of engineering management.

4. Simulation and Discussion

4.1. Simulation Analysis in Different Delay. The influence of SCTS on safety accidents is essentially reflected in the work time. Although the time of SCTS is planned, which means the work time is fixed, delay on ERLs is inevitable, resulting in frequent changes of work time. To observe the correlation between SCTS and safety incidents, different assignments of delay are shown in Table 4. Different assignments of delay correspond to different implementation degrees of SCTS. The smaller the assignment, the higher the implementation degree. The simulation experiment results are shown in Figures 4–6.

From Figure 4, it can be observed that when the implementation degree of SCTS is high, the safety accidents probability of the project reaches the maximum on the 32nd day, and the valve is 0.066. It is reduced to medium risk on the 79th day and low risk on the 165th day. Eventually, the safety accidents probability is infinitely close to 0.

TABLE 4: Assignment of different implementation rates of synthesis construction time schedule.

Implementation degree of SCTS	Assignment of delay
High	RANDOM NORMAL (0, 20, 8, 15, 1)
Medium	RANDOM NORMAL (0, 30, 10, 8, 1)
Low	RANDOM NORMAL (0, 40, 17, 10, 1)

Correspondingly, when the implementation degrees of SCTS are medium and low, the safety accidents probability of the project reaches the maximum on the 32nd and 33rd days, and the valves are 0.0663 and 0.0772. It is reduced to medium risk on the 87th day and 108th day and kept at the medium risk level until the 200th day. From Figures 5 and 6, it can be seen that, with the increase of implementation degree, schedule pressure and loss of construction period are raised obviously. The reason behind this is that when the implementation degree of SCTS is low, the available working hours are limited. Due to the fact that the daily workload is planned, the schedule pressure increases rapidly. However, the workers will adjust the construction schedule according
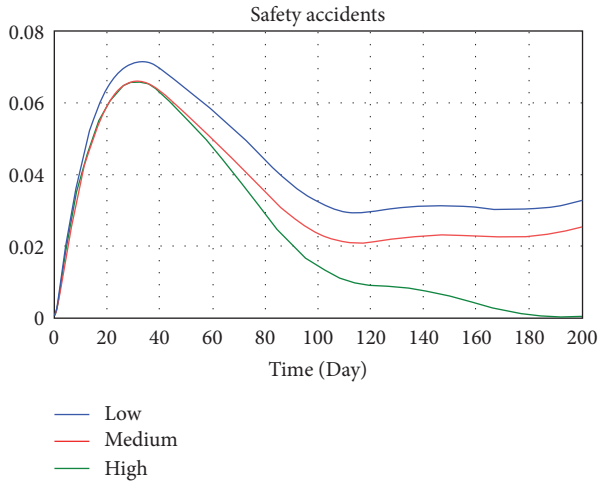
FIGURE 4: Comparison of safety accidents probability under different implementation degrees of SCTS.
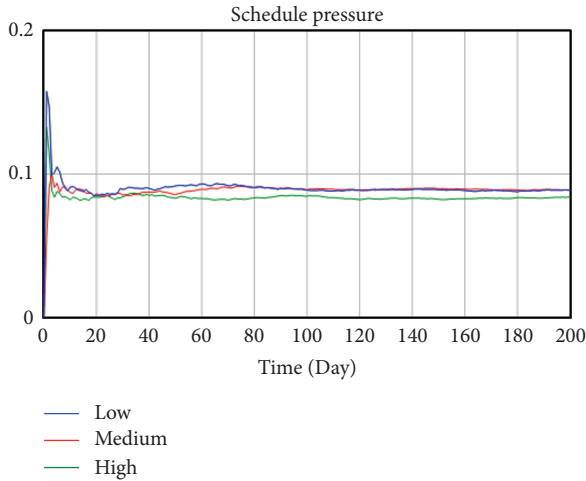

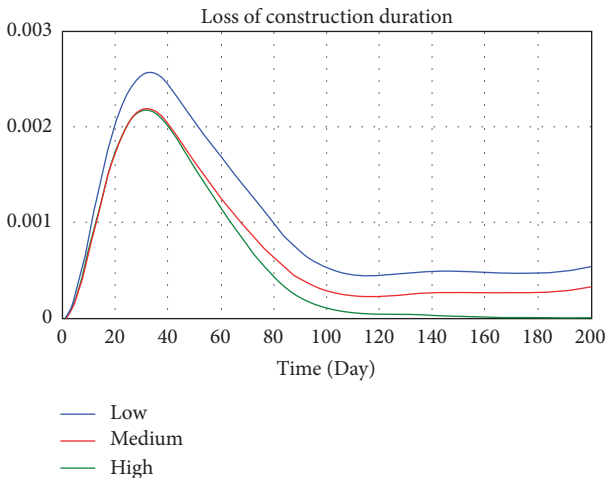FIGURE 5: Comparison of schedule pressure under different implementation degrees of SCTS.

FIGURE 6: Comparison of safety accidents probability under different implementation degrees of SCTS.

to the working hours and daily workload. As time goes on, the schedule pressure decreases and begins to level off. Loss of construction period is related to the safety accidents probability. A safety accident could lead to a construction shutdown and then result in loss of construction period.

4.2. Simulation Analysis in Different Safety Investment. Using the three major components categorized by existing researches [40, 65–67] as a point of departure, we chose to study three safety investments: (1) implementation of innovative technological tool proactive protection system, (2) employment of safety supervisor for conducting inspections, and (3) encouragement on being responsible for the safety of themselves and other coworkers with safety training. Three different safety investment assignments of 80, 100, and 120 (unit: CNY/person·d) were set to observe the relevance between safety investment and safety accidents. The simulation experiment result is shown in Figure 7.

The result from the simulation demonstrates the effectiveness of safety investment on construction safety risk. From Figure 7, it can be observed that when the safety investment is 120 CNY/person·d, the safety accidents probability of the project reaches the maximum on the 32nd day, and the valve is 0.0679. Correspondingly, when the implementation degree of SCTS is medium and low, the safety accidents probability of the project reaches the maximum on the 33rd and 35th day, and the valves are 0.0716 and 0.0756. In brief, higher safety investment may result in better safety performance.

4.3. Simulation Analysis of Construction Strategy. Improving work efficiency and increasing work intensity are common means to reduce schedule pressure. To observe the influence of those two factors on the whole model, 5 modes were set, respectively, as shown in Table 5. Different value assignments represented different strategies. Work efficiency and intensity in mode 1 were selected as 1.5 and 0, indicating that the construction was efficient and the work was easy. It would not cause physical and psychological discomfort to the workers. Mode 1 was the ideal mode. Similarly, mode 2 was the crushing mode, modes 3 and 4, respectively, represent some preference mode, and mode 5 was the equilibrium mode. That is, different modes represent different strategies. When other variables remain the same, the dynamics model simulates the evolution by changing the value assignments of the two variables mentioned above. According to the safety accidents probability, change of schedule pressure and loss of construction period after system runs to make rational decisions. The simulation results are shown in Figures 8–10.

According to the comparative analysis of Figures 8–10, mode 1 has the lowest safety accidents probability and loss of construction period but the highest schedule pressure. On the contrary, mode 2 has the most downward schedule pressure and the most increased safety accidents probability and loss of construction period. The result shows that it is unscientific to unilaterally improve work intensity to speed up the progress under the schedule pressure. This practice should be avoided in
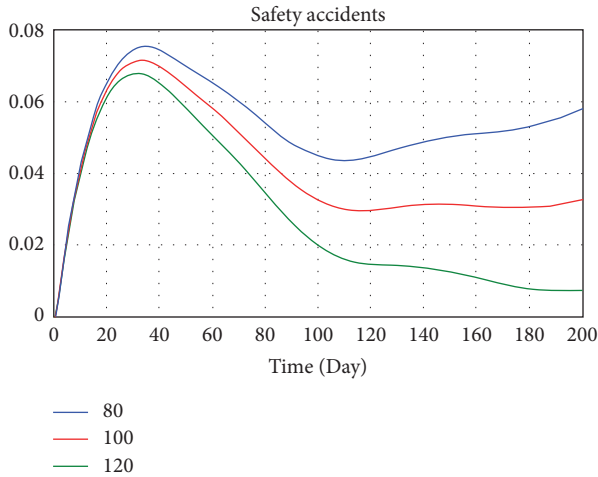
FIGURE 7: Comparison of safety accidents probability under different safety investments.

TABLE 5: Value assignments under different strategies.

	Work efficiency	Work intensity
Mode 1	1.5	0
Mode 2	0	1.5
Mode 3	1.5	0.5
Mode 4	0.5	1.5
Mode 5	1	1

the construction of ERLs. Advanced construction equipment and scientific construction methods should be actively promoted to improve construction efficiency. The construction of ERLs should be carried out in a planned and organized way. However, mode 1 can only be used as an ideal mode in management practice. Improving construction efficiency is limited under the current construction technology and method, and other satisfactory solutions can only be sought.

Compared with other modes, the safety accidents probability, schedule pressure, and loss of construction period of modes 3 and 5 all maintain low values, which can be a satisfactory solution. The safety accidents probability of mode 5 is relatively lower, and mode 3 performs better in terms of schedule pressure. However, the progress pressure of mode 4 in the first week is slightly lower than that of mode 3 and mode 5 and then increases significantly; the safety accidents probability and loss of construction period are also at a high level. It indicates that the strategy based on increasing work intensity can only accelerate the progress in the short term. When the fatigue degree of personnel reaches a certain value, the safety accidents probability will be increased, which will interfere with the progress and cause economic losses of accidents and rework.

5. Discussion

The results from the simulations demonstrate that the schedule pressure after stabilization and loss of construction period are proportional to the implementation degree of SCTS. With the decrease of implementation degree of SCTS, the schedule pressure, loss of construction period, and safety
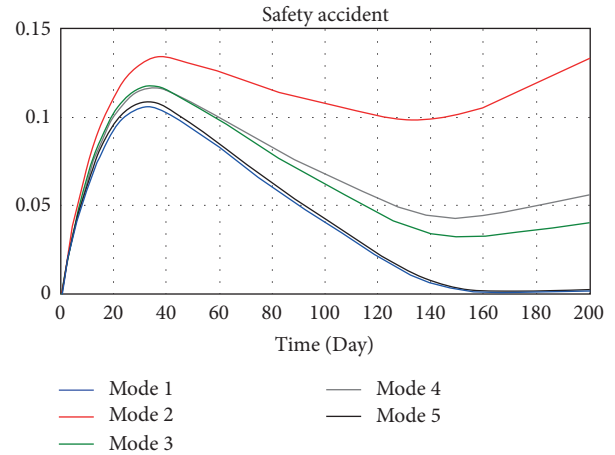

FIGURE 8: Comparison of safety accidents probability under different implementation degrees of SCTS.
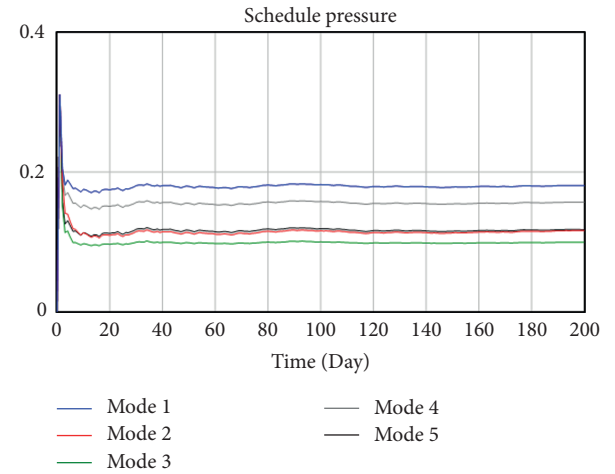

FIGURE 9: Comparison of safety accidents probability under different implementation degrees of SCTS.
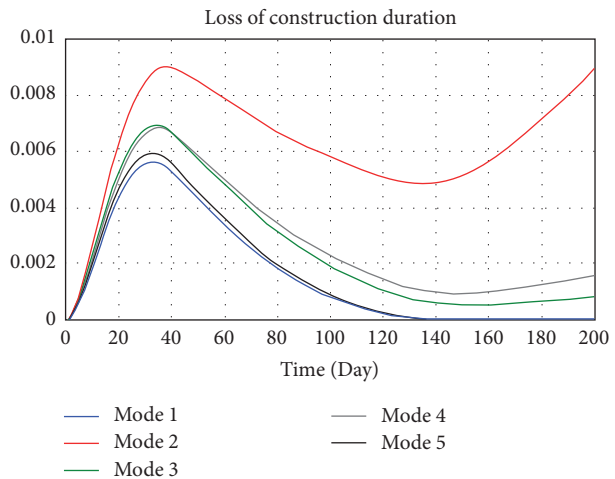

FIGURE 10: Comparison of safety accidents probability under different implementation degrees of SCTS.

accidents probability all increase to different degrees; especially, the safety accidents probability changes significantly. It can be seen that the evolution of the implementation degree of SCTS has a significant influence on the safety accident probability. To effectively enhance and improve the construction safety management of ERLs, the transportation organization should be optimized, and the implementation degree of SCTS should be improved.

Different safety investments have different effects on the safety accident probability, and safety investments have a positive effect on accident prevention. Good safety training not only raises the level of risk awareness but also persuades individuals to be less tolerant of risks. The findings of this study further showed that the interventions that combine good safety supervision with safety protection are more likely to reduce safety accident probability.

When the schedule pressure is low, it can be preferred to ensure safety. Increasing a certain amount of work efficiency can accelerate the schedule by reasonably arranging the working platform and optimizing equipment and processes. When the schedule pressure is high, increasing work intensity and work efficiency simultaneously is better. Under the condition of ensuring the low safety accidents probability, parallel construction can be organized as far as possible to expand the working platform. At the same time, construction organization and safety protection should be optimized to avoid interference between working platforms and construction procedures. When the construction period is nearing the end, appropriate consideration can be made to increase the work intensity, which can avoid the safety accidents and loss caused by fatigue accumulation in the later period and complete the planned project faster.

6. Conclusions

Based on the causal model of construction safety considering ERLs, a system dynamics model is proposed to simulate the construction safety evolution process, and a series of simulations are performed under different conditions. The results confirmed that the construction safety considering ERLs is significantly relevant to the implementation degree of SCTS. The incidence of construction safety incidents tends to be higher because the greater the possibility of construction delays, the greater the schedule pressure. However, even in each level of construction safety accidents probability, the evolution curve reached the maximum at about one month. As the countermeasure took effect, the evolution curve declined after reaching the maximum value and finally stabilized. Work efficiency has a negative impact on construction safety accidents probability. The increase of work intensity could reduce schedule pressure in the short term. Still, due to psychological and physiological factors, unsafe behaviors increased in a certain range. Interestingly, there is a marginal cost effect on the effect of work intensity on schedule pressure. The improvement in schedule pressure is not significant when work intensity increases to a certain level.

The main contribution of this study is that it is a major step forward in integrating system dynamics and safety in

the examination of construction safety management considering the ERLs. Theoretically, rather than studying construction safety considering ERLs in a static manner, this study examined the evolution as it unfolds over time. This study treats construction safety management considering the ERLs as a dynamic problem caused by "system structure" and a complex phenomenon. In this system, unsafety behaviors and unsafety conditions have significant impacts on construction safety risk considering ERLs. In contrast, almost all existing studies focus on construction safety risks relevant to new railway projects, with little research on construction safety management considering ERLs. Methodologically, a system dynamics approach can provide a rich dynamic perspective to visually explain the causes of construction safety risk changes. In general, this paper complements the body of construction safety management considering the ERLs in terms of theoretical foundations and implementation and offers references and lessons for the design and operation of construction safety management in the railway construction industry in the future.

The limitation of this study is the simplification of the interactions involved in construction safety. In fact, the mutual impacts are very complex, far more than those proposed in the hypothesis of this study. In fact, the vast majority of construction safety accidents are caused by people's unsafe behaviors. Furthermore, workers' hazard perception does play an essential role in the construction safety management considering ERLs. In the future, "how does the worker's hazard perception impact construction safety considering ERLs dynamically" should be studied further.

Data Availability

All datasets generated for this study have been included in the paper.

Conflicts of Interest

All authors declare no conflicts of interest.

Acknowledgments

References

[1] D. Yang and J. Huang, "Optimal allocation method of the railway skylight when adjacent to the existing line," *Journal of Railway Science and Engineering*, 2017.

[2] Z. Shen and L. Xu, "Dynamic analysis on influence of highspeed railway construction on existing adjacent railway lines and countermeasures," *Journal of the China Railway Society*, vol. 35, no. 6, pp. 82–90, 2013.

[3] J. Zhu and H. Yan, "Research on reasonable mode of skylight on wuhan-guangzhou passenger special line," *Journal of Northern Jiaotong University*, vol. 2, 2004.

[4] F. Wang, *Research On Construction Safety And Risk Management Of Bridges Over Existing Railway [Dissertation for the Doctoral Degree*, Central South University, Changsha, China, 2019.

[5] H. J. C. H. Tian Bi, "Multi-objective decision making in construction safety management of railway in service based on system dynamics," *Journal of Railway Science and Engineering*, vol. 16, no. 3, pp. 827–834, 2019.

[6] M. Taniguchi, *High Speed Rail in Japan: A Review and Evaluation of the Shinkansen Train*, https://escholarship.org/uc/item/5s48m11f, 1992.

[7] R. Vickerman, "High-speed rail in Europe: experience and issues for future development," *The Annals of Regional Science*, vol. 31, no. 1, pp. 21–38, 1997.

[8] E. Jänsch, "High-speed rail transport in Germany," *Railway Technical Review*, vol. 53, 1999.

[9] L. Ding, W. Fang, H. Luo, P. E. D. Love, B. Zhong, and X. Ouyang, "A deep hybrid learning model to detect unsafe behavior: integrating convolution neural networks and long short-term memory," *Automation in Construction*, vol. 86, pp. 118–124, 2018.

[10] S. Guo, B. Tang, K. Liang, X. Zhou, and J. Li, "Comparative analysis of the patterns of unsafe behaviors in accidents between building construction and urban railway construction," *Journal of Construction Engineering and Management*, vol. 147, no. 5, 2021.

[11] K. Li and S. Wang, "A network accident causation model for monitoring railway safety," *Safety Science*, vol. 109, pp. 398–402, 2018.

[12] H. Chen, H. Li, and Y. M. Goh, "A review of construction safety climate: definitions, factors, relationship with safety behavior and research agenda," *Safety Science*, vol. 142, Article ID 105391, 2021.

[13] E. Hollnagel, *Safety-I and Safety-II: The Past and Future of Safety Management*, CRC Press, 2018, https://www.google.com/search?rlz=1C1GCEB_enIN990IN990&q=Boca+Raton&stick=H4sIAAAAAAAAAOPgE-LUz9U3ME7LK09S4gAxk03LjLS0spOt9POL0hPzMqsSSzLz81A4VhmpiSmFpYlFJalFxYtYuZzykxMVghJL8vN2sDICAMcQcgZTAAAA&sa=X&ved=2ahUKEwj6-92hndX1AhVwxzgGHevCAU4QmxMoAXoECCgQAw.

[14] H. W. Heinrich, *Industrial Accident Prevention. A Scientific Approach*, 1941, https://www.ilo.org/global/topics/safety-and-health-at-work/normative-instruments/code-of-practice/WCMS_107829/lang--en/index.html, Second Edition.

[15] F. E. Bird, F. Cecchi, A. Tilche, and J. Mata-Alvarez, *Management Guide to Loss Control*, Institute Press, Vienna, Austria, 1974.

[16] F. E. Bird and R. G. Loftus, *Loss Control Management*, Institute Press, Vienna, Austria, 1976.

[17] E. E. Adams, "The quality revolution: a challenge to safety professionals," *Professional Safety*, vol. 36, no. 8, p. 22, 1991.

[18] J. L. Stratman and C. M. Youssef-Morgan, "Can positivity promote safety? Psychological capital development combats cynicism and unsafe behavior," *Safety Science*, vol. 116, pp. 13–25, 2019.

[19] T. S. Abdelhamid and J. G. Everett, "Identifying root causes of construction accidents," *Journal of Construction Engineering and Management*, vol. 126, no. 1, pp. 52–60, 2000.

[20] R. A. Haslam, S. A. Hide, A. G. F. Gibb et al., "Contributing factors in construction accidents," *Applied Ergonomics*, vol. 36, no. 4, pp. 401–415, 2005.

[21] C. Lu and C. Cai, "Challenges and countermeasures for construction safety during the Sichuan–Tibet railway project," *Engineering*, vol. 5, no. 5, 2019.

[22] W. Lin, L. Yaqi, and W. Enmao, "Research on risk management of railway engineering construction," *Systems Engineering Procedia*, vol. 1, pp. 174–180, 2011.

[23] J. W. Forrester, "Industrial dynamics," *Journal of the Operational Research Society*, vol. 48, no. 10, pp. 1037–1041, 1997.

[24] B. H. W. Guo, Y. M. Goh, and K. Le Xin Wong, "A system dynamics view of a behavior-based safety program in the construction industry," *Safety Science*, vol. 104, pp. 202–215, 2018.

[25] D. L. Cooke, "A system dynamics analysis of the Westray mine disaster," *System Dynamics Review*, vol. 19, no. 2, pp. 139–166, 2003.

[26] Y. M. Goh, H. Brown, and J. Spickett, "Applying systems thinking concepts in the analysis of major incidents and safety culture," *Safety Science*, vol. 48, no. 3, pp. 302–309, 2010.

[27] Y. M. Goh, P. E. D. Love, H. Brown, and J. Spickett, "Organizational accidents: a systemic model of production versus protection," *Journal of Management Studies*, vol. 49, no. 1, pp. 52–76, 2012.

[28] S. Han, F. Saba, S. Lee, Y. Mohamed, and F. Peña-Mora, "Toward an understanding of the impact of production pressure on safety performance in construction operations," *Accident Analysis & Prevention*, vol. 68, pp. 106–116, 2014.

[29] M. Shin, H.-S. Lee, M. Park, M. Moon, and S. Han, "A system dynamics approach for modeling construction workers' safety attitudes and behaviors," *Accident Analysis & Prevention*, vol. 68, pp. 95–105, 2014.

[30] D. L. Cooke and T. R. Rohleder, "Learning from incidents: from normal accidents to high reliability," *System Dynamics Review*, vol. 22, no. 3, pp. 213–239, 2006.

[31] Y. M. Goh, P. E. D. Love, G. Stagbouer, and C. Annesley, "Dynamics of safety performance and culture: a group model building approach," *Accident Analysis & Prevention*, vol. 48, pp. 118–125, 2012.

[32] Y. M. Goh and P. E. D. Love, "Methodological application of system dynamics for evaluating traffic safety policy," *Safety Science*, vol. 50, no. 7, pp. 1594–1605, 2012.

[33] E. D. Adamides, "System dynamics modelling in the development of management and organisational theory," in *Proceedings of the Paper presented at the International Conference of the System Dynamics Society*, The System Dynamics Society, Athens, Greece, July 2008.

[34] Q.H. Z. Qian, "The development of rail transit and the application of high and new technology," *Railway Construction Technology*, vol. 1, pp. 1–5, 2004.

[35] B. Cheng, K. Lu, J. Li, H. Chen, X. Luo, and M. Shafique, "Comprehensive assessment of embodied environmental impacts of buildings using normalized environmental impact factors," *Journal of Cleaner Production*, vol. 334, Article ID 130083, 2021.

[36] C. Webb, L. Gao, and L. Song, "Schedule compression impact on construction project safety," *Frontiers of Engineering Management*, vol. 2, no. 4, pp. 344–350, 2016.

[37] J. Hinze, *Construction Safety*, Prentice-Hall, 1997, https://www.google.com/search?rlz=1C1GCEB_enIN990IN990&q=Hoboken&stick=H4sIAAAAAAAAAOPgE-LUz9U3SMkxNi1U4gAxK_LMk7S0spOt9POL0hPzMqsSSzLz81A4VhmpiSmFpYlFJalFxYtY2T3yk_KzU_N2sDICAIsReflQAAAA&sa=X&sqi=2&ved=2ahUKEwigtOaTndX1AhXkzjgGHXqUDjsQmxMoAXoECBcQAw.

[38] D.-C. Seo, "An explicative model of unsafe work behavior," *Safety Science*, vol. 43, no. 3, pp. 187–211, 2005.

[39] D. N. C. Lai, M. Liu, and F. Y. Y. Ling, "A comparative study on adopting human resource practices for safety management on construction projects in the United States and Singapore," *International Journal of Project Management*, vol. 29, no. 8, pp. 1018–1032, 2011.

[40] S. L. Tang, H. K. Lee, and K. Wong, "Safety cost optimization of building projects in Hong Kong," *Construction Management & Economics*, vol. 15, no. 2, pp. 177–186, 1997.

[41] P. X. Zou, A. C. Sun, B. Long, and P. Marix-Evans, "Return on investment of safety risk management system in construction," Paper presented at the W099-Special Track 18th CIB World Building Congress, Salford United Kingdom, 2010.

[42] J. Hinze and J. Gambatese, "Factors that influence safety performance of specialty contractors," *Journal of Construction Engineering and Management*, vol. 129, no. 2, pp. 159–164, 2003.

[43] E. J. Jaselskis, S. D. Anderson, and J. S. Russell, "Strategies for achieving excellence in construction safety performance," *Journal of Construction Engineering and Management*, vol. 122, no. 1, pp. 61–70, 1996.

[44] T. M. Toole, "Construction site safety roles," *Journal of Construction Engineering and Management*, vol. 128, no. 3, pp. 203–210, 2002.

[45] R. M. Choudhry, "Behavior-based safety on construction sites: a case study," *Accident Analysis & Prevention*, vol. 70, pp. 14–23, 2014.

[46] D. Zohar and G. Luria, "A multilevel model of safety climate: cross-level relationships between organization and group-level climates," *Journal of Applied Psychology*, vol. 90, no. 4, pp. 616–628, 2005.

[47] S. Stiles, B. Ryan, and D. Golightly, "Evaluating attitudes to safety leadership within rail construction projects," *Safety Science*, vol. 110, pp. 134–144, 2018.

[48] D. Fang, Y. Chen, and L. Wong, "Safety climate in construction industry: a case study in Hong Kong," *Journal of Construction Engineering and Management*, vol. 132, no. 6, pp. 573–584, 2006.

[49] C.-F. Chi, T.-C. Chang, and H.-I. Ting, "Accident patterns and prevention measures for fatal occupational falls in the construction industry," *Applied Ergonomics*, vol. 36, no. 4, pp. 391–400, 2005.

[50] T. K. M. Wong, S. S. Man, and A. H. S. Chan, "Critical factors for the use or non-use of personal protective equipment amongst construction workers," *Safety Science*, vol. 126, Article ID 104663, 2020.

[51] J. Izudi, V. Ninsiima, and J. B. Alege, "Use of personal protective equipment among building construction workers in Kampala, Uganda," *Journal of environmental and public health*, vol. 2017, p. 7930589, 2017.

[52] D. P. Fang, F. Xie, X. Y. Huang, and H. Li, "Factor analysis-based studies on construction workplace safety management in China," *International Journal of Project Management*, vol. 22, no. 1, pp. 43–49, 2004.

[53] L. Ding and J. Xu, "A review of metro construction in China: organization, market, cost, safety and schedule," *Frontiers of Engineering Management*, vol. 4, no. 1, pp. 4–19, 2017.

[54] P. Mitropoulos, T. S. Abdelhamid, and G. A. Howell, "Systems model of construction accident causation," *Journal of Construction Engineering and Management*, vol. 131, no. 7, pp. 816–825, 2005.

[55] S. Mohamed, "Safety climate in construction site environments," *Journal of Construction Engineering and Management*, vol. 128, no. 5, pp. 375–384, 2002.

[56] A. Neal, M. A. Griffin, and P. M. Hart, "The impact of organizational climate on safety climate and individual behavior," *Safety Science*, vol. 34, no. 1-3, pp. 99–109, 2000.

[57] P. Mitropoulos and G. Cupido, "Safety as an emergent property: investigation into the work practices of high-reliability framing crews," *Journal of Construction Engineering and Management*, vol. 135, no. 5, pp. 407–415, 2009.

[58] L. Swanson and G. Swanson, "Modelling relationships between job stressors and injury and near-miss outcomes for construction labourers," *Work & Stress*, vol. 17, no. 3, pp. 218–240, 2003.

[59] M. Park and F. Peña-Mora, "Dynamic change management for construction: introducing the change cycle into model-based project management," *System Dynamics Review*, vol. 19, no. 3, pp. 213–242, 2003.

[60] H. Lingard, "The effect of first aid training on Australian construction workers' occupational health and safety motivation and risk control behavior," *Journal of Safety Research*, vol. 33, no. 2, pp. 209–230, 2002.

[61] A. Bena, P. Berchialla, M. E. Coffano, M. L. Debernardi, and L. G. Icardi, "Effectiveness of the training program for workers at construction sites of the high-speed railway line between Torino and Novara: impact on injury rates," *American Journal of Industrial Medicine*, vol. 52, no. 12, pp. 965–972, 2009.

[62] C. M. Tam, S. X. Zeng, and Z. M. Deng, "Identifying elements of poor construction safety management in China," *Safety Science*, vol. 42, no. 7, pp. 569–586, 2004.

[63] M. López-Alonso, M. P. Ibarrondo-Dávila, M. C. Rubio-Gámez, and T. G. Munoz, "The impact of health and safety investment on construction company costs," *Safety Science*, vol. 60, pp. 151–159, 2013.

[64] H. Ma, Z. Wu, and P. Chang, "Social impacts on hazard perception of construction workers: a system dynamics model analysis," *Safety Science*, vol. 138, Article ID 105240, 2021.

[65] C. Hou, Y. Wen, Y. He et al., "Public stereotypes of recycled water end uses with different human contact: evidence from event-related potential (ERP)," *Resources, Conservation and Recycling*, vol. 168, Article ID 105464, 2021.

[66] Y. Feng, "Effect of safety investments on safety performance of building projects," *Safety Science*, vol. 59, pp. 28–45, 2013.

[67] M. Lu, C. M. Cheung, H. Li, and S.-C. Hsu, "Understanding the relationship between safety investment and safety performance of construction projects through agent-based modeling," *Accident Analysis & Prevention*, vol. 94, pp. 8–17, 2016.

Hindawi

Research Article

A Novel Noncooperative Behavior Management Method for Multiattribute Large Group Decision-Making

Xiaoqin Dong,[1,2] Ying Yang,[1] Bo Shao ⓘ,[1] and Xianbin Sun[2]

[1]*College of Hydraulic & Environmental Engineering, China Three Gorges University, Yichang 443002, China*
[2]*School of Civil Architecture and Environment, Hubei University of Technology, Wuhan 430068, China*

Correspondence should be addressed to Bo Shao; shaobo910@whu.edu.cn

In multiattribute large-group decision-making (MALGDM), the ideal state indicates a high degree of consensus for decision-makers. However, it is difficult to reach a consensus because the conflict between various decision attributes and decision-makers increases. To deal with the problem, a novel consensus model was developed to manage the decision-making in large groups based on noncooperative behavior. The improved clustering method was used to take account of the similarities among different decision-makers, while similar decision-makers will be grouped into the same group. Moreover, the consensus threshold was determined from an objective and subjective aspect to judge whether the consensus reaching process continues. The noncooperative behavior and adjustment amount of decision-makers' opinions were investigated based on the proposed consensus model, and an emergency decision-making problem in flood disaster is applied to manifest the feasibility and distinctive features of the proposed method. The results show the proposed novel consensus model demonstrated strong applicability and reliability to the noncooperative subgroup problem and can be explored to manage multiattribute interactions in LGDM.

1. Introduction

Decision-making, which aims at identifying an ideal alternative based on the information described by decision-makers, is widely used in all aspects of modern life [1–3]. With the increase in the complexity of decision-making problems, many attributes relevant to decision-making problems have been explored [4]. Decision-makers need to consider all relevant aspects of the problem [5]. The decision-making behavior of decision-makers depends on many factors, including their personal and professional goals, interests, and the experience they pursue to develop themselves professionally [6]. Decision-makers need to know about Business, Management and Accounting, Engineering, Social Sciences, and Computer Science to inform the decision-making process [7]. Group decision-making (GDM) has attracted increasing attention due to its characteristic superiority of gathering knowledge of decision-makers from various fields [8–10]. Problems always involve many interconnected fields, and the decision-making results are related to the benefits of stakeholders. Thus, it becomes

uneasy for small-group decision-making to reach the demands of social development [11, 12]. As the number of people in the decision-making group increases, the problem of multiattribute large group decision-making appears [13].

Clustering processing, the essential part of large group decision-making, is a fundamental but indispensable process in multiattribute large-group decision-making (MALGDM) [14]. The clustering process in MALGDM can improve the efficiency of the decision process [15]. The C-means algorithm [16] and the k-means algorithm [17] are the most available clustering methods in applications. Xue used the Choquet integral (CI) operator to measure each attribute and then aggregated it [18]. Based on Shannon entropy, Li measured the uncertainty of discrete Z-numbers by a new technique [19]. The main features of these algorithms are the early decided clustering numbers and the effect of threshold selection on classification results. Having defined the shape similarity measure, Tapia-Rosero et al. developed a clustering method, in which similar-shaped membership functions are grouped by agglomerative hierarchical clustering technique [20]. However, this method did not

consider the similarity of decision-makers in the same cluster, and there exist errors for the shape similarity measure [21]. Besides, a clustering method based on vector space was proposed by Xu et al. This method considered the similarity of decision-makers' decisions [22, 23]. However, these methods classified the cluster by calculating the similarities between the decision-makers and the cluster. But those methods did not consider the similarities between two decision-makers in the same clusters. The similarities between decision-makers will decrease as the clustering processes develop.

The consensus level is selected to describe decision-makers' differences in opinion and preference. It can also measure the degree of agreement among different clusters in MALGDM [24]. There are many approaches to compute the consensus level [25–27]. In MALGDM, before making a group decision, a consensus reaching process is usually applied to reach the collective agreement [28, 29]. To reach a consensus, some decision-makers must modify their opinions in the dynamic and iterative group discussions [30]. For reaching a consensus process in MALGDM, many scholars do a lot of studies. Pérez et al. introduced a feedback mechanism and built a consensus model based on decision-makers' relevance or importance level [31]. For MALGDM problems, Xu et al. promoted the consensus reaching process in two stages. The novel method could appropriately adjust the preference of decision-makers and the weight of subgroups [32]. Jin et al. adopted a local adjustment strategy to retain preference evaluation of decision-makers as far as possible in group decision-making [33]. To reach consensus, Xu et al. proposed a dynamic consensus method based on an exit authorization mechanism. They thought the subgroup would be suggested to exit the decision-making process once the proximity index could not meet the requirement, and then the delegation mechanism is employed to reserve the cluster's influence by giving trust weights to other clusters [24]. Noncooperative behavior is common in the practical process of decision-making. However, these studies are lacking at considering the influence of noncooperative behavior. To reach a consensus, a suitable method should be adopted to manage the noncooperative behavior. Based on a self-management mechanism of noncooperative behaviors, Dong et al. introduced three kinds of noncooperative behaviors and developed a new consensus framework [34]. They also proposed a novel framework based on a self-management mechanism for noncooperative behaviors in large-scale consensus reaching processes [35]. Palomares provided a consensus model suitable to handle and detect the noncooperative behavior, and the consensus could be reached by decreasing the weight of noncooperative cluster [36]. Wu and Xu proposed a consensus model, in which the clusters can be changed. The clusters can modify if the individuals are able to change their preferences via the consensus reaching process [37]. Quesada et al. introduced a methodology to process noncooperative behaviors, in which a uniform-based weighting scheme was adopted to compute the weight of decision-makers in LGDM [38]. Nazari et al. used dynamic noncooperative games to model these conflicts when stakeholders appear noncooperative behavior

[39]. With the purpose of managing minority opinion and noncooperative behavior in MALGDM, Xu and put forward the concept of comprehensive adjustment coefficient and designed an improved consensus model [40].

To sum up, problems have evolved into many interrelated areas, and the decision-making of large groups needed to meet the requirements of social development. But regarding LGDM, it is not easy to reach the consensus level in decision processes. The goal of large group decision-making is to find a method that can reach consensus effectively in large groups, improve the consensus level in short time, and obtain the accurate decision-making result. In the previous literature, the subgroup obtained in these studies remains unchanged in the consensus reaching process. This is often untrue because decision-makers modify their available opinion. The subgroup opinion must be changed when decision-makers modify their opinion. This will lead to unacceptable results of large group decision making. Meanwhile, the decision-makers in the noncooperative subgroup who are willing to modify their decision opinion should not be penalized. Unlike previous literature, this paper protected individual decision opinion. And previous methods did not consider the similarity of decision-makers in the same cluster. This will reduce the consistency of the group. Mandal et al. acknowledged noncooperative behaviors and divided them with the experts' similar evaluations into a subgroup. But decision-makers were still unable to change subgroup [41]. Therefore, it is necessary to seek a large group decision-making method that can protect the opinions of decision-makers and improve the degree of consensus. The main contribution of the paper is a precise consensus reaching model that we proposed to manage noncooperative behaviors in MALGDM. And an improved clustering method is developed. This method considers the similarities among decision-makers.

The remaining part of the paper is structured as follows: firstly, decision-makers are clustered, and the group consensus level is obtained in Section 2. In Section 3, the noncooperative behavior is detected and managed. A typical example, applied to indicate the utility and applicability of this model, is shown in Section 4. Then, Section 5 discusses the advantages and innovations of the proposed methods in detail. Finally, conclusion and future researches are provided in Section 6.

2. Preliminaries

2.1. Problem Formulation.
MALGDM problems can be defined as a situation where a large number of decision-makers must make a high-quality decision result by choosing the n alternatives. The main parameters of MALGDM are as follows:

(1) A discrete finite set of alternatives $x = \{x_1, x_2, \cdots x_n\}$, where x_i represents alternative solution.

(2) A set of decision-makers can be denoted as $E = \{e_1, e_2 \ldots e_M\} (M \geq 2)$. The weight vector of decision-makers is $\omega = \{\omega_1, \omega_2, \cdots \omega_M\}$, where $\omega_j (j = 1, 2 \ldots M) \in (0, 1)$ and $\sum_{j=1}^{M} \omega_j = 1$. After collecting a

lot of previous literature, we can determine the range of the number of large groups of decision makers. Usually, when the number of experts in a group reaches 20, that is, $M \geq 20$, the group is considered as a large group. And the decision-making process in which they participate can be defined as large group decision-making [42, 43].

(3) A finite set of attributes $F = \{f_1, f_2 \ldots f_P\} (P \geq 2)$, the weight vector of attribute $\eta = \{\eta_1, \eta_2, \cdots \eta_P\}$, where $\eta_k \geq 0 \, (k = 1, 2, \ldots P)$, and $\sum_{k=1}^{P} \eta_k = 1$.

Each decision-maker will give a numerical decision matrix to express the opinion for the alternatives $A^j = (a_{ik}^j)_{n \times P}, j \in M$, where a_{ik}^j represents decision-maker e_j's preference of alternative x_i concerning attribute f_k. The premise of this paper is that there is disagreement among decision-makers in the group. So, it is not possible for all decision-makers to behave the same preference for x_i. This represents that $\max_i \{a_{ik}^j\} \neq \min_i \{a_{ik}^j\}$. Different attributes in MALGDM problems are often measured in different units, so the preference value should decision matrix $V^j = (v_{ik}^j)_{n \times P}$ as follows:

$$v_{ik}^j = \frac{a_{ik}^j - \min_i \{a_{ik}^j\}}{\max_i \{a_{ik}^j\} - \min_i \{a_{ik}^j\}}. \tag{1}$$

2.2. Clustering Method for Large-Group Members.
To simplify the decision-making processes, decision-makers are clustered by individual decision matrix A^j to transform into small-group decision making in LGDM. decision-makers are clustered into l clusters $(1 < Y < n)$ by the improved mean of preference clustering method, which is described in Algorithm 1.

2.3. Determination of Consensus Level.
Decision-makers' respective weights in the decision processes can be determined by the following definitions:

Definition 1. Experts in larger subgroups should be given larger weights based on the majority principle [37]. In line with the number and weight values of experts in the subgroup, the subgroup weight value can be defined as

$$\lambda_l = \frac{\left(\sum_{j=1}^{M} \omega_j \times \theta_{jl}\right)^2}{\sum_{l=1}^{Y} \left(\sum_{j=1}^{M} \omega_j \times \theta_{jl}\right)^2}, \tag{2}$$

where $\theta_{jl} = 1$ represents expert e_j belonging to the subgroup C^l; $\theta_{jl} = 0$ represents expert e_j not belonging to the subgroup C^l, where $l = 1, 2, \ldots, L$, and it is easy to know that $0 \leq \lambda_l \leq 1$ and $\sum_{l=1}^{Y} \lambda_l = 1$.

Definition 2. An individual decision matrix can be obtained by decision-makers' opinions, the subgroup decision matrix is computed by aggregating the individual matrices, considering the weights associated with each decision-maker, and the subgroup decision matrix can be calculated [44].

$$r_{ik}^l = \sum_{j=1}^{M} \omega_j \times v_{ik}^j \times \theta_{jl}. \tag{3}$$

By aggregating single subgroup decision matrixes, the normalized group decision matrix $R^c = (r_{ik}^c)_{n \times P}$ is obtained, where r_{ik}^c is represented as

$$r_{ik}^c = \sum_{l=1}^{Y} \lambda_l \times r_{ik}^l. \tag{4}$$

Definition 3. According to the gap subgroup decision matrix $R^l (l = 1, 2, \cdots, Y)$ and the group decision matrix R^c, the consensus level $CI(R^l)$ between the subgroups' decision matrices $R^l (l = 1, 2, \ldots, Y)$ and the group decision matrix R^c is defined as

$$CI(R^l) = 1 - d(R^l, R^c), \tag{5}$$

where $d(R^l, R^c)$ is the Manhattan distance between R^l and R^c; that is, $d(R^l, R^c)$ represents the similarity between subgroup C^l and C^C, which can be defined as

$$d(R^l, R^c) = \frac{1}{n} \times \sum_{i=1}^{n} \sum_{k=1}^{P} \eta_k \times \left| r_{ik}^l - r_{ik}^c \right|. \tag{6}$$

By calculating the average value of consensus level $CI(R^l)$, the group consensus level LGCI can be obtained:

$$\text{LGCI} = \lambda_l \times \sum_{l=1}^{Y} CI(R^l). \tag{7}$$

If $LGCI = 1$, it indicates that all decision-makers have reached consensus among the large groups. A $\overline{LGCI}$ indicates a higher level of consensus among all decision-makers. $\overline{LGCI}$, as the group consensus threshold, is set to determine whether the consensus reaching process should be carried out. If $LGCI \leq \overline{LGCI}$, the consensus process should be used to change decision-makers' opinions to reach a higher consensus level.

2.4. Determination of Consensus Threshold.
The consensus threshold $\overline{LGCI}$ should be determined to judge whether the consensus reaching process continues or not. The decision-making pressure of large groups often leads to the uncertainty and subjectivity of the opinion adjustment coefficient. In order to improve the accuracy of group decision making, both objective and subjective factors should be considered. And a coefficient should be set to adjust the subjective factors and objective factors.

2.4.1. Subjective Threshold.
For the particular problem, the decision-makers provide the consensus threshold $\overline{LGCI}$ according to the quality of the problem [45]. The consensus threshold $\overline{LGCI}$ reflects its attitude towards the group consensus level and opinion. If the consequence of the decision is important, the consensus threshold should be as high as possible. In this article, let the subjective consensus

---

Input: the individual matrix A^j and the threshold ζ, which is determined according to practical decision situation.

Output: the number of subgroup l and the subgroups $C_1, C_2, \ldots C_Y$.

Step 1. Construct the decision set U comprising all individual decision matrix, that is, $U = \{V^1, V^2, \ldots V^M\}$.

Step 2. Initialize $Y = 1$ as the number of subgroups, and select decision-maker e_1 as the member of this subgroup, this subgroup is defined as C^l, and S stands for a temporary set.

Step 3. Select decision-maker e_q sequentially from the set E and allocate them to the subgroup C^l. Then remove the decision matrix from the set U and let the number of members in subgroup C^l be z_l.

Step 4. Compute the gather degree between decision-maker e_q and each subgroup C^l, which can be denoted as :

$$\mu_{jl} = 1 - \max_{q=1}^{z_l} 1/n \sum_{i=1}^n \sum_{k=1}^P \eta_k \times |v_{ik}^j - r_{ik}^q| \, (j \neq q, e_q \in C^l, l \in Y)$$

where, z_l is the number of decision-maker in the subgroup C^l, μ_{jl} represents the gather degree of decision-makers e_j in the subgroup C^l, if the $\mu_{jl} \geq \zeta$, decision-maker e_j is allocated to the subgroup C^l, and remove it out from the set U, let $z_l = z_l + 1$. Otherwise, decision-maker e_j is allocated to the temporary set S.

Step 5. If S is not null, let $C^{L+1} = S$, $T = $ null and $Y = Y + 1$ respectively, and get back to Step 3; otherwise, go to Step 6.

Step 6. Record the results of clustering. The number of subgroups is recorded as Y, and the number of members is recorded as z_l in the subgroup C^l.

ALGORITHM 1:

---

threshold determined by the decision-makers' experience be $\overline{LGCI}_{sub}$. The subjective consensus threshold is the decision-maker's expected consensus level.

2.4.2. Objective Threshold. The objective consensus threshold $\overline{LGCI}_{ob}$ is determined to improve the feasibility of the consensus reaching process. The objective consensus threshold $\overline{LGCI}_{ob}$ represents that the large group can reach consensus level by the original decision matrices of decision-makers, which is defined as

$$\overline{LGCI}_{ob} = LGCI. \tag{8}$$

Definition 4. The consensus threshold should satisfy two conditions: one is that the consensus threshold meets the requirement of practical decision problem, which is described as subjective consensus threshold; the other is that the consensus threshold can be reached in the opinion adjustment scale, in which the decision-maker is willing to modify, which is defined as the objective consensus threshold. Thus, it is feasible to determine the consensus threshold by the objective consensus threshold and the subjective consensus threshold:

$$\overline{LGCI} = \alpha \overline{LGCI}_{ob} + (1-\alpha)\overline{LGCI}_{sub}, \tag{9}$$

where α is the consensus threshold adjustment coefficient and defined by the number and weight of decision-makers in the subgroup whose consensus level is less than the group consensus level calculated by the initial group decision matrix.

Definition 5. Let the subgroup set where consensus level is more than the group consensus level be G, which is described as

$$G = \{C^l \mid CI(R^l) > LGCI\}. \tag{10}$$

The adjustment coefficient α can be calculated as

$$\alpha = \frac{\sum_{\lambda=1}^Y \lambda_l \times \vartheta_{lg}}{\sum_{l=1}^Y \lambda_l}. \tag{11}$$

where ϑ_{lg} represents the subgroup l belonging to G.

3. Process of Noncooperative Behaviors

In this section, a consensus reaching model suitable for addressing noncooperative behavior in MAGDM problems is proposed. The innovative point of this model features in the abilities to detect and handle individual and subgroup noncooperative behaviors in the consensus reaching process, with the aim of improving the overall consensus reaching process performance.

3.1. Noncooperative Behavior Detection. In the consensus reaching model presented in this study, we define an approach to identify those noncooperative subgroups that exist as decision-makers who are reluctant to change their original preferences to reach a consensus, which is aiming at assisting the subsequent treatment of such decision-makers, so as to improve the performance of the consensus reaching process. The detection approach is first used in the second round of the consensus reaching process, because of its requirement of comparisons among subgroups obtained in the previous and current rounds of discussion. There exist three rules to detect the noncooperative subgroup according to the definition of noncooperative behavior. Let the noncooperative subgroup be C^{l*}. The detection method includes two steps:

Step 1. Determine the detection object

Before the noncooperative subgroup is detected, the detection object should be determined. The noncooperative subgroup includes two common characteristics according to the definition:

(i) The consensus level of the subgroup opinion is smallest, which can be denoted as

$$C^{l^*} = \min_{Y}^{l=1} \left\{ CI\left(R^{l(t-1)}\right) \mid l = 1, 2, \ldots, Y \right\}. \tag{12}$$

(ii) The number of decision-makers in these subgroups is small, in a general way, which is less than [M/n], described by the following formula:

$$\sum_{j=1}^{M} \theta_{jl^*}^{t-1} \leq \frac{M}{Y}. \tag{13}$$

For example, a large group consists of 15 decision makers, and there are three decision options. The number of people supported by the three decision schemes is 7, 5, and 3, respectively. Their CI value size relation is $CI_1 > CI_2 > CI_3$. According to characteristic (i), we can know that the third subgroup may be a noncooperative group. We can know that [M/n] is 5, the third group's number is 3, and 3 is smaller than 5. So, according to characteristic (ii), the third subgroup can be determined by the detection object.

Step 2. Detect the noncooperative subgroup

After the detection object is determined, the subgroup C^{l^*} will adjust their decision opinions by discussion in the $t-1$-th round, and the adjustment decision matrix of decision-maker $A^{j(t)}$ in the subgroup C^{l^*} is obtained, and the temporary subgroup decision matrices $R^{'l(t)}$, in which the form of subgroup is not changed, are calculated. For the noncooperative subgroup, there exists at least one decision-maker in the subgroup reluctant to adjust their own opinions, which is checked to determine whether decision-maker in the subgroup C^{l^*} is willing to adjust their opinions or not. To do this, the temporary subgroup consensus level $CI'\left(R^{l(t)}\right)$ and the temporary consensus level $LGCI'^{(t)}$ can be calculated by the temporary subgroup decision matrices $a^{'l(t)}$. Thus, there are three situations to define the noncooperative subgroup:

(i) Decision-makers in C^{l^*} are willing to adjust their opinions, but the decision opinion adjustment of decision-maker causes negative influence to the consensus level of C^{l^*}:

$$C^{l^*} = \left\{ C^l \mid CI'\left(R^{l(t)}\right) \right. \\ \left. < CI\left(R^{l(t-1)}\right); \ l = 1, 2, \ldots, Y \right\}. \tag{14}$$

(ii) Decision-makers in C^{l^*} do not change their opinions, that is, the consensus level of C^{l^*} in t-th round keeping correspondence with t-1-th round:

$$C^{l^*} = \left\{ C^l \mid CI'\left(R^{l(t)}\right) \right. \\ \left. = CI\left(R^{l(t-1)}\right); \ l = 1, 2, \ldots, Y \right\}. \tag{15}$$

(iii) The decision opinion adjustment of decision-maker causes positive influence to the consensus level of C^{l^*}, but there are only a small part of decision-

makers transforming their opinions, and there exist decision-makers who are not willing to modify their opinions. The noncooperative subgroup detection rule can be expressed as

$$C^{l^*} = \left\{ C^l \mid CI'\left(R^{l(t)}\right) > CI\left(R^{l(t-1)}\right); \sum_{j=1}^{n_l} \sigma_{jl} \neq z_{l,} l = 1, 2, \ldots, Y \right\}. \tag{16}$$

In the example in step (1), there are three decision-makers in the detection subgroup. If the subgroup has noncooperative behavior, then at least one person did not change his preference, or the decision opinion adjustment of decision-maker causes negative influence to the consensus level of C^{l^*}. If all decision-makers adjust their opinions, but $CI'\left(R^{l(t)}\right) < CI\left(R^{l(t-1)}\right)$, this is the first situation of noncooperative subgroup. If all decision-makers do not adjust their opinions, this is second situation. If at least one decision-maker did not adjust his opinion, despite the adjustments made by the rest of the decision-makers, and those adjustments have had a positive impact to the consensus level, subgroups are also considered as noncooperative subgroup. This is the third situation.

where σ_{jl} represents decision-maker e_j willing to change their opinions, and σ_{jl} is detected by change degree. The change degree is introduced to measure the decision-maker who modify his opinion [32]; it can be described as

$$\varphi_{jl}^t = \frac{1}{n} \sum_{i=1}^{n} \sum_{k=1}^{P} \eta_k \times \left| v_{ik}^{j(t)} - r_{ik}^{l(t-1)} \right| \times \theta_{jl}^t. \tag{17}$$

σ_{jl} can be computed by comparing the change degree between t-1-th round and t-th round, which is defined as

$$\sigma_{jl} = \begin{cases} 1, & \text{if } \varphi_{jl}^t - \varphi_{jl}^{t-1} \neq 0, \\ 0, & \text{if } \varphi_{jl}^t - \varphi_{jl}^{t-1} = 0. \end{cases} \tag{18}$$

3.2. Management Strategy of the Noncooperative Behavior. Through Step 3.1, we identified three different types of noncooperative behavior. But the core of this paper is to develop different strategies for different noncooperative behaviors. Thus, unlike the traditional adjustment method for noncooperative behaviors, a new strategy was devised in this study. The management strategy is determined by analyzing the noncooperative degree of noncooperative subgroup. And the noncooperative subgroup is allowed to change. The consensus level needs to be recalculated after the subgroup changed. The concrete process of management strategy is described as follows:

> Step 1: measure the noncooperative degree
>
> For the noncooperative subgroup, the degree of noncooperation is used to describe the decision-maker's willingness to change the decision to improve group consensus level. Thus, the degree of noncooperation is influenced by two factors: one is the number of decision-makers who have changed their views, and the other is whether the changed opinion can increase the level of consensus.

The number of policymakers who changed their minds first needs to be counted. In general, the LGCI can reflect whether the noncooperative subgroup modify their initial opinions or not, and the number of decision-makers who are willing to modify their opinions describe the adjustment degree of noncooperative subgroup, which is expressed as

$$\gamma_{l^*}^t = \sum_{j=1}^{M} \sigma_{jl^*} \times \theta_{jl^*}. \tag{19}$$

And then, Thus, the change of LGCI value can indicate whether a change in decision-makers' opinion has increased the level of group consensus. Thus, the noncooperative degree is measured by the value of *LGCI* and the number of decision-makers who are willing to modify their opinions, which is obtained as follows:

$$\phi_{l^*}^{(t)} = \frac{\left(\text{LGCI}^{'t} - \text{LGDI}^{t-1} \right) \gamma_{l^*}^t}{\left| \text{LGCI}^{'t} - \text{LGDI}^{t-1} \right| z_{l^*}}. \tag{20}$$

$\phi_{l^*}^{(t)}$ can represent the degree of noncooperation, and the number of experts in the MALGDM is odd, so $\phi_{l^*}^{(t)}$ is not equal to 0.5; there are three cases according to the calculation results.

(i) If $\phi_{l^*}^{(t)} \leq 0$, it means that the subgroup C^{l^*} manifests a very high degree of noncooperative behavior. A small number of decision-makers in noncooperative subgroup will change their opinions in the *t-1*-th round, and the changed result is negative for the consensus level.

(ii) If $0 < \phi_{l^*}^{(t)} < 0.5$, the subgroup C^{l^*} is considered as a partly noncooperative subgroup. A small part of the decision-maker in noncooperative subgroup modified their opinions in the *t-1*-th round, and the change result of subgroup is positive for consensus level.

(iii) If $0.5 < \phi_{l^*}^{(t)} \leq 1$, it indicates that the subgroup C^{l^*} is a cooperative subgroup, and more than half of decision-makers in the subgroup C^{l^*} change their opinions, and the change result of subgroup is positive for consensus level.

Step 2: process the noncooperative behavior

When the subgroup's noncooperative degree is got, the novel noncooperative behavior treatment method that considers the change of subgroup is developed. The following strategies are adopted for the three cases with different degrees of noncooperation.

(i) For the noncooperative subgroup, that is, $\phi_{l^*}^{(t)} \leq 0$, the decision-makers in subgroup C^{l^*} not only do not improve the group consensus, but also may cause the group consensus decrease. To speed up the decision-making processes and obtain proper results with a short period of time, the subgroup C^{l^*} will be suggested to withdraw from the decision process.

(ii) For the partly noncooperative subgroup, that is, $0 < \phi_{l^*}^{(t)} < 0.5$, a major part of decision-makers do not change their opinions in the subgroup C^{l^*}. It should be penalized by adjusting the weight of subgroup. But there are minor decision-makers willing to modify their decision opinion, and their opinions should be protected. Therefore, we need to determine whether the decision-maker who changes perspective belongs to the subgroup C^{l^*}. And then the form of subgroup C^{l^*} may be changed. Thus, the treatment method is determined by judging whether the decision-makers belong to the subgroup C^{l^*}.

Let the set of decision-makers who are unwilling to modify his opinion be $C^{'l^*}$ in the subgroup C^{l^*}, and the number is z_{l^*}', the set of decision-makers who are willing to modify his opinion is B^{l^*}. That is, $B^{l^*} = \left\{ e_{j^*} | e_{j^*} \in C^{l^*}, e_{j^*} \notin C^{'l^*} \right\}$. Based on the (17), we proposed a method to judge whether the decision-maker belongs to the subgroup C^{l^*}, which is denoted as

$$\varphi_{j^*l^*}^{'t} = \max_{\substack{q^*=1 \\ z_{l^*}'}} \frac{1}{n} \sum_{i=1}^{n} \sum_{k=1}^{P} \eta_k \times \sigma_{j^*l^*}^t \times \left| v_{ik}^{j^*t} - r_{ik}^{q^*t} \right| \tag{21}$$

$$\cdot \left(j^* \neq q^*, e_{q^*} \in C^{'l^*}, l^* \in Y \right).$$

where $\varphi_{j^*l^*}^{'t}$ represents the conflict degree between e_{j^*} and subgroup C^{l^*} in the *t*-th round.

If $\varphi_{j^*l^*}^{'t} \leq 1 - \varsigma$, it represents that the decision-maker e_{j^*} belongs to the subgroup C^{l^*} after his opinion is changed.

If $\varphi_{j^*l^*}^{'t} > 1 - \varsigma$, it represents that the decision-maker e_{j^*} does not belong to the subgroup C^{l^*} after his opinion is changed, and the decision-maker e_{j^*} can be clustered based on the procedure in Algorithm 1.

Although there are a little of decision-makers to modify their opinions in partly noncooperative subgroup, the subgroup C^{l^*} still expresses the lower cooperative level. Thus, in order to reduce its impact on the group consensus level, the weight of subgroup C^{l^*} also needs appropriate adjustment. The modified function is a decreasing function. To describe the interaction between the weight adjustment and the number of decision-makers, the weight adjustment function is developed based on the number of decision-makers who is willing to modify its own opinion, which is defined as

$$\lambda' l^*_{\ t} = \frac{z_{l^*}^t - z' l^*_{\ t}}{z' l^*_{\ t}} \lambda_{l^*}^t. \tag{22}$$

where $\lambda_{l^*}^{'t}$ is the weight of subgroup C^{l^*} after adjustment in the *t*-th round, and $\lambda_{l^*}^t$ is the weight of subgroup C^{l^*} in the *t*-th round. Generally speaking, subgroup weights reflect their contributions to the group consensus level. When the opinions of decision-makers in the subgroup C^{l^*} are modified, the subgroup' contributions are adjusted too. The greater the contribution of subgroup to consensus level, the more important it is. Individuals who have changed opinion

with negative effect to the group consensus level should reduce some weight [46]. Based on this rule, the contributions of the subgroup are introduced to measure the subgroup weight in the t-th round, which can be defined as

$$D_{l^*}^t = \text{LGCI}^t - \text{LGCI}_{\overline{l^*}}^t. \quad (23)$$

where $D_{l^*}^t$ represents the contributions of subgroup C^{l^*} for the group consensus level. $LGCI_{\overline{l^*}}^t$ denotes the group consensus level without the subgroup C^{l^*} in the t-th round, which is defined as

$$\text{LGCI}_{\overline{l^*}}^t = \sum_{l=1, l\neq l^*}^L \lambda_l^{t-1} \sum_{i=1}^n \frac{1}{n} \sum_{k=1}^P \eta_k \times \left| r_{ik}^{l(t)} - r_{ik}^{c(t)} \right|. \quad (24)$$

To protect the interest of decision-makers who are willing to modify its own opinion, we need to update the weights of the subgroup and recalculate the group-decision consensus level. The following equations show how to update the weights:

$$\lambda_{l^*}^t = \lambda_{l^*}^{t-1} \times \left(1 + D_{l^*}^t\right)^\xi. \quad (25)$$

ξ expresses the impact of the subgroups' contributions on their weights, which are usually given by the decision-makers in advance. If the decision problem is in urgency and has to be dealt with in time, it should be assigned less restrictive values. Otherwise, more restrictive values must be put into use.

(iii) For the cooperative subgroup, that is, $0.5 < \phi_{l^*}^{(t)} < 1$, more than half of decision-makers in this subgroup are willing to modify their initial opinions. This subgroup expresses a very high degree of cooperative behavior. Thus, the motivation mechanism should be adopted to protect the decision opinion of this subgroup. Similar to partly noncooperative subgroup, if the decision-maker e_{j^*} does not belong to the subgroup C^{l^*} after his opinion is changed, Algorithm 1 can be used to cluster the decision-maker e_{j^*} into a suitable subgroup. If the decision-maker e_{j^*} belongs to the subgroup C^{l^*} after his opinion is changed, the motivation mechanism is similar to the treatment process of partly noncooperative subgroup. When the number of decision-makers who modify their own opinions is more than the half of subgroup, the adjustment coefficient of the subgroup in equation (26) is not less than 1. Thus, the weight of subgroup will be enhanced.

3.3. Algorithm of Large Group Consensus.
Adopting consensus reaching model that the basic thought is to adjust decision information matrix, to enable the decision-makers to have a higher consensus level, the noncooperative subgroup is detected and addressed to obtain a higher consensus level. Algorithm 2 of the consensus reaching model is summarized as follows.

Let $t^* = t$. Output the final subgroups' decision matrices $R^{k(t^*)}(k = 1, 2, \ldots, n)$ and the final group decision matrix $R^{c(t^*)}$.

The process of consensus reaching model can be simply described in Figure 1.

4. Case Study

In this section, an example of emergency decision-making problem in flood disaster is applied to indicate the feasibility of the presented method.

4.1. Case Background.
There is a flood disaster hit Hu Nan Province, a south city in China, on July 3, 2018. After the flood disaster, the government carried out an emergency scheme based on instructions. As shown in Table 1, four preliminary plans were rapidly drawn up:

Twenty experts $E = (e_1, e_2, ..., e_{20})$ from different fields were asked to make decisions based on these four alternatives $X = (x_1, x_2, x_3, x_4)$. We consider three criteria for each alternative: (1) personnel security rate (f_1), the scale of evaluation value of personnel security rate is 0 to 1; (2) personnel injured rate (f_2), the scale of the evaluation value of the effectiveness of equipment is the same to personnel security rate; (3) the development of situation of flood disaster (f_3).

4.2. The Process of Group Decision-Making.
We set that the scale of evaluation value of development situation of flood disaster is 1 to 100. Each decision-maker opinion should be seriously taken into account. Suppose that there is no conflict of interest among the decision-makers. In order to obtain the best alternative(s), the following steps need to be performed.

Step 1. Cluster the initial normalized individual decision matrices.

To save space, the normalized individual decision matrices are omitted. Base on the clustering method, which is described in Algorithm 1, the clustering threshold is set as $\zeta = 0.8$, and the group can be divided into several smaller clusters. Table 2 shows the results, indicating that the original decision group can be divided into five clusters.
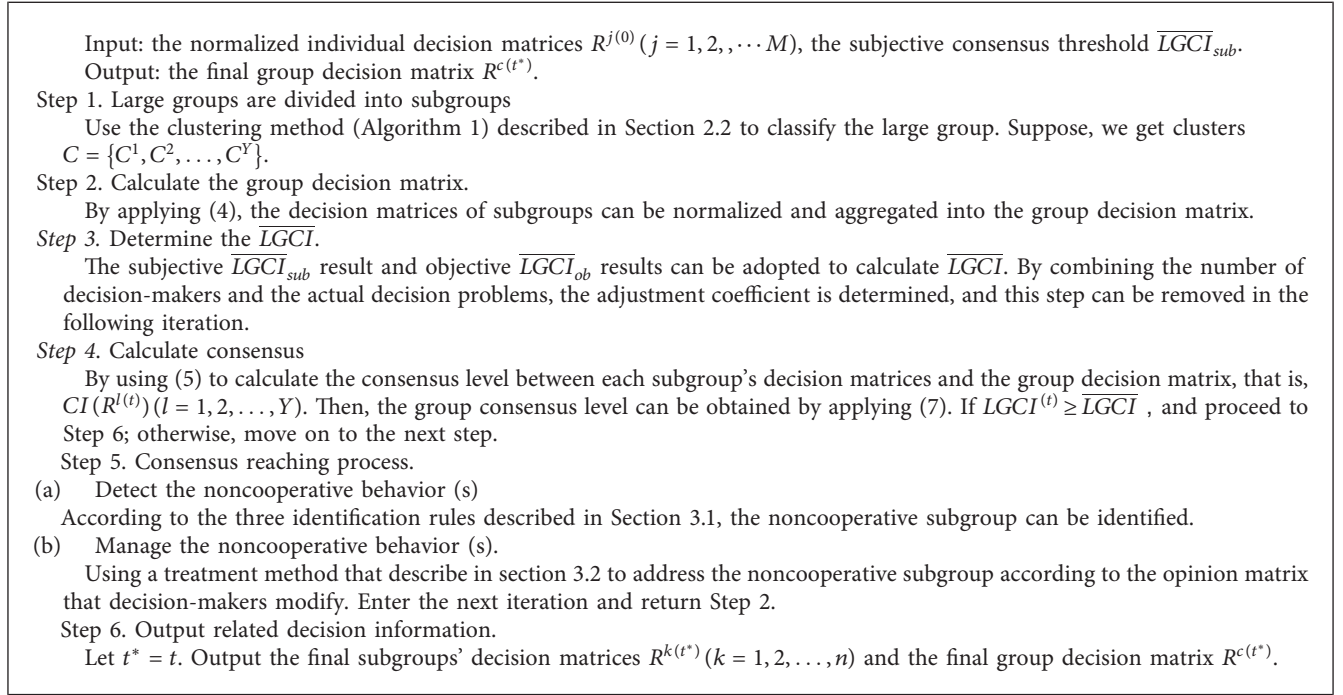
Step 2. Calculate the group decision matrix.

Aggregate the decision-makers' decision matrices into the subgroups' decision matrices by the (5). The weight of subgroup is calculated by the (2), and the group decision matrix is calculated by the individual decision matrices and the weight of cluster, which is adopted as

$$R^{c(0)} = \begin{bmatrix} 0.5099 & 0.8063 & 0.5721 \\ 0.6400 & 0.4345 & 0.3138 \\ 0.2837 & 0.7329 & 0.2879 \\ 0.4810 & 0.1408 & 0.7346 \end{bmatrix}. \quad (26)$$

Step 3. Consensus measure and calculate the consensus threshold.

Compute the subgroup consensus levels by the (5), that is, $CI(R^{1(0)}) = 0.7949$, $CI(R^{2(0)}) = 0.7388$, $CI(R^{3(0)}) = 0.6488$, $CI(R^{4(0)}) = 0.7263$ and $CI(R^{5(0)}) = 0.6141$. The initial group consensus level can be

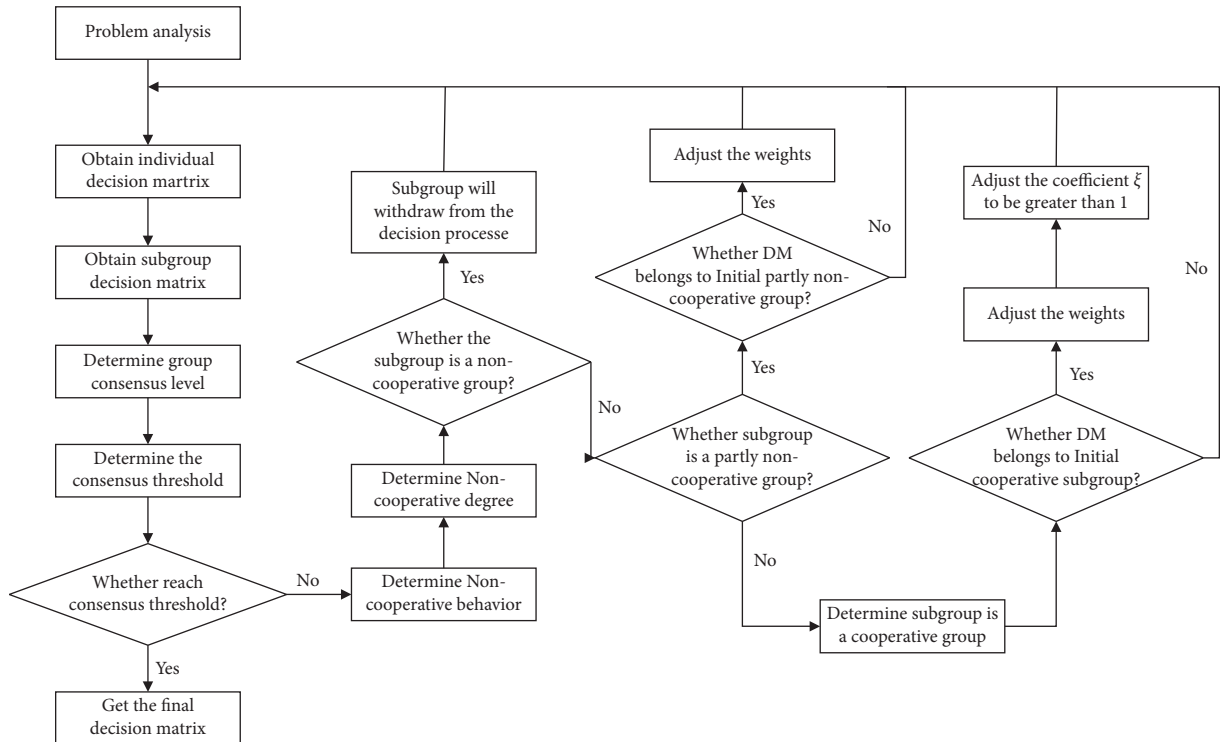Input: the normalized individual decision matrices $R^{j(0)}$ ($j = 1, 2, , \cdots M$), the subjective consensus threshold $\overline{LGCI}_{sub}$.

Output: the final group decision matrix $R^{c(t^*)}$.

Step 1. Large groups are divided into subgroups

Use the clustering method (Algorithm 1) described in Section 2.2 to classify the large group. Suppose, we get clusters $C = \{C^1, C^2, \ldots, C^Y\}$.

Step 2. Calculate the group decision matrix.

By applying (4), the decision matrices of subgroups can be normalized and aggregated into the group decision matrix.

Step 3. Determine the $\overline{LGCI}$.

The subjective $\overline{LGCI}_{sub}$ result and objective $\overline{LGCI}_{ob}$ results can be adopted to calculate $\overline{LGCI}$. By combining the number of decision-makers and the actual decision problems, the adjustment coefficient is determined, and this step can be removed in the following iteration.

Step 4. Calculate consensus

By using (5) to calculate the consensus level between each subgroup's decision matrices and the group decision matrix, that is, $CI(R^{l(t)})$ ($l = 1, 2, \ldots, Y$). Then, the group consensus level can be obtained by applying (7). If $LGCI^{(t)} \geq \overline{LGCI}$, and proceed to Step 6; otherwise, move on to the next step.

Step 5. Consensus reaching process.

(a)   Detect the noncooperative behavior (s)

According to the three identification rules described in Section 3.1, the noncooperative subgroup can be identified.

(b)   Manage the noncooperative behavior (s).

Using a treatment method that describe in section 3.2 to address the noncooperative subgroup according to the opinion matrix that decision-makers modify. Enter the next iteration and return Step 2.

Step 6. Output related decision information.

Let $t^* = t$. Output the final subgroups' decision matrices $R^{k(t^*)}$ ($k = 1, 2, \ldots, n$) and the final group decision matrix $R^{c(t^*)}$.

ALGORITHM 2:

FIGURE 1: The process of consensus reaching model.

TABLE 1: Different selection strategies.

x_i	Concrete measure
x_1	Find out trapped people and evacuate the seriously injured from the disaster areas to avoid further damage caused from flood disaster
x_2	Treat the injured and stop searching for trapped people until the rescue equipment arrived
x_3	Search for trapped people and treat the seriously injured in situ
x_4	Search for trapped people and cease treating the injured until the medical team arrived

TABLE 2: The information of subgroup.

C^k	n_k	e_i	$\lambda_k^{(0)}$
C^1	7	$e_1, e_6, e_7, e_{11}, e_{13}, e_{17}, e_{19}$	0.3500
C^2	5	$e_2, e_3, e_8, e_9, e_{18}$	0.2500
C^3	3	e_4, e_{10}, e_{20}	0.1500
C^4	4	$e_5, e_{12}, e_{15}, e_{16}$	0.2000
C^5	1	e_{14}	0.0500

calculated as $LGCI(R^{c(0)}) = 0.7416$. The consensus threshold can be calculated from the subjective and objective aspect, the subjective threshold is set as 0.8, and the objective threshold is 0.7416. The adjustment coefficient is obtained by the (11), which is expressed as 0.2234. Finally, the consensus threshold is computed as 0.7869. Because of $LGCI(R^{c(0)}) = 0.7416 < 0.7869$, the consensus process should be applied to change some opinions.

Step 4. Consensus reaching process.

(i) First consensus reaching iteration

The detection object of the noncooperative cluster is determined by (12) and (13), and the calculation result shows that the subgroup C^5 is the detection object. The decision-makers in the subgroup C^5 modify their initial decision opinions to reach the consensus, the decision-makers who needed to reconsider their preferences were determined, and the modification criterion of the decision-maker is the group decision matrix. The decision matrix of decision-maker $A^{j(1)}$ can be obtained after modification. The temporary subgroup decision matrix $R'^{5(1)}$ can be computed by the decision matrix of decision-maker $A^{j(1)}$. The consensus level of clusters is calculated by the temporary subgroup decision matrix $R'^{5(1)}$, which is expressed as $CI'(R^{5(1)})$. Comparing the temporary subgroup consensus level $CI'(R^{5(1)})$ with consensus level $CI(R^{5(0)})$, the result shows that the $CI'(R^{5(1)})$ is less than $CI(R^{5(0)})$, and the subgroup C^5 is noncooperative subgroup, which denotes that the subgroup C^5 expressed the high noncooperative behavior.

Based on the noncooperative management method, $\phi_{l^*}^{(t)} \leq 0$, the subgroup C^5 is suggested to quit the consensus process. Thus, the number of subgroups is null, and the decision matrix is 0, and there are four subgroups by clustering the decision-maker after management. Because of the change of subgroup number, the weight of cluster should be recalculated by (2), which is described as $\lambda^{(1)} = (0.350.3500, 0.2500, 0.2000, 0.2000, 0)$. Continuing consensus measure, the new cluster consensus levels are $CI(R^{1(1)}) = 0.7914$, $CI(R^{2(1)}) = 0.7425$, $CI(R^{3(1)}) = 0.7259$ and $CI(R^{4(1)}) = 0.7238$. The group consensus level is $LGCI(R^{c(1)}) = 0.7526 < 0.7869$. Thus, the consensus reaching process continues.

(ii) Second consensus reaching iteration

As $CI(R^{4(1)}) = \min\{CI(R^{i(1)}) | i = 1, 2, 3, 4\}$, the cluster C^4 can be regarded as detection object in the 2-th round iterations, and the decision-makers in the cluster C^4 are required to modify their own opinion. The decision-maker's decision opinion in the 2-th rounds can be obtained after discussion, which is described as $A^{j(2)}$, aggregating the individual decision matrices, obtaining the temporary group decision matrix. The temporary consensus level is determined by the temporary subgroup decision matrix $R'^{4(2)}$ and temporary group decision matrix. Comparing the temporary subgroup consensus level $CI'(R^{4(2)})$ with consensus level $CI(R^{4(1)})$, the result shows that the $CI'(R^{4(2)})$ is more than $CI(R^{4(1)})$, but only part of decision-makers in subgroup C^4 are willing to modify their opinions; thus, the subgroup C^4 is noncooperative subgroup.

The conflict degree of subgroup C^4 is calculated to denote the decision-makers who modify their decision opinion. Based on the result of the calculation, there are four decision-makers in the subgroup C^4 who are willing to modify their decision opinions. The noncooperative degree of subgroup is computed as $0.5 < \phi_{l^*}^{(t)} \leq 1$. According to (20), whether the decision-maker who modifies his opinion belongs to the initial subgroup can be judged. The result shows that the decision-maker e_5 does not belong to the subgroup C^4 after changing their initial decision opinion by the (21), and the decision-makers e_{15}, e_{16} belong to the initial subgroup C^4. The decision-maker e_5 is clustered by the Algorithm 1; the gathered degree between the decision-maker e_5 and the subgroup C^1 is $0.9135 > 0.8$; thus, the decision-maker e_5 belongs to the subgroup C^1. The weights of C^4 and C^1 are updated according to equation (2) and the number of decision-makers. The new subgroup weight can be denoted as $\lambda^{(2)} = (0.4517, 0.2438, 0.1976, 0.1069)$.

The new subgroup consensus levels are $CI(R^{1(2)}) = 0.8014$, $CI(R^{2(2)}) = 0.7956$, $CI(R^{1(2)}) = 0.7643$ and $CI(R^{1(2)}) = 0.7234$. The group consensus level is $LGCI(R^{c(2)}) = 0.7901 > 0.7869$. After two iterations, the decision-makers obtain consistency, and the final group consensus level meets the predefined requirement.

Due to the reaching of consensus threshold by group consensus level, the group decision matrix can be used to determine, which alternative is optimal, and the final calculation result of a group decision is expressed as

$$R^{c(2)} = \begin{bmatrix} 0.5119 & 0.8313 & 0.5596 \\ 0.6358 & 0.4491 & 0.2745 \\ 0.2753 & 0.6829 & 0.3379 \\ 0.4859 & 0.1408 & 0.7529 \end{bmatrix}. \quad (27)$$

According to the weight of the attribute, the decision vector is calculated as $(0.6343, 0.4531, 0.4321, 0.4599)$, and the value of alternative x_1 is 0.6343. Thus, the alternative x_1 is the most optimal.
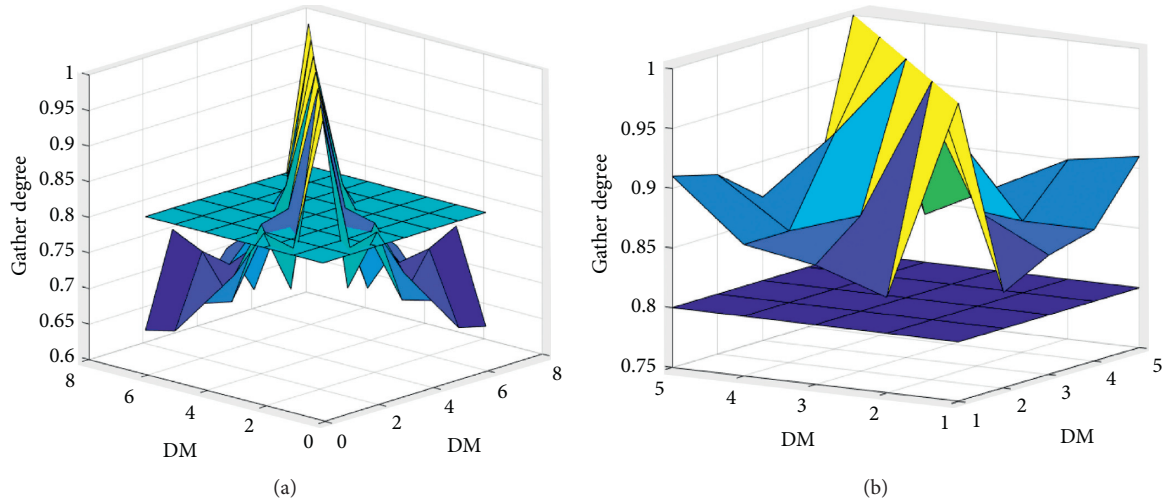
(a)

(b)

FIGURE 2: The effect of gather degree of decision-makers of different clustering methods. (a) The gather degree of traditional clustering method. (b) The gathered degree of improved clustering method.

5. Discussion

In this paper, we proposed a novel method to calculate the consensus threshold from the subjective and objective aspect. It is unlike the traditional determination method consensus threshold. Based on this consensus threshold and the traditional clustering method, the improved clustering method is developed. The improved method depends on the similarities between the decision-makers' decision opinions and subgroups' decision opinion. To better reflect the advantages of the clustering method, the case in Section 3 is adopted to compare the difference between the current clustering method and the traditional clustering method. We take the subgroup that includes the decision-maker e_1 as example, and the gathered degree of decision-makers for different clustering methods can be computed. And comparing the clustering thresholds, the effect of gather degree is shown in Figure 2.

From Figure 2, we can obtain that there are many decision-makers whose gathered degree is less than clustering threshold for the traditional clustering method (see Figure 2(a)); but it can be seen from Figure 2(b) that the gathered degree for any decision-makers is more than 0.8 after using the improved clustering method. The decision-makers using the improved method have higher gather degree than those using the traditional method. The result shows that the traditional clustering method considers the whole gather degree and omits the gather degree among decision-makers. Thus, the improved clustering method is more suitable to divide into the group.

Except for one group comparison, it can also compare the composition of different subgroups and the degree of subgroup clustering. The results of the comparison can be represented in Figure 3.

In Figure 3, groups are more concentrated. And compared to using traditional methods, each group has a higher degree of clustering after using the improved method in this article. The goal of MALGDM is to achieve a high degree of consistency. And the higher degree of clustering represents

that the large group has higher consensus level. Thus, the method used in this article is more effective than the traditional one in dealing with MALGDM problem.

Due to adherence to the principle that noncooperative behavior needs full consideration, the group consensus level increased from 0.7416 to 0.7901, which means that the management of the noncooperative behavior is helpful in reaching the consensus level. Generally, the noncooperative behavior can be addressed by two steps: the detection of the noncooperative behavior and the management of the noncooperative behavior. The current detection method uses the subjective adjustment result of subgroup to detect the noncooperative behavior. Unlike the current detection method, the practical adjustment result of subgroup is adopted to judge the noncooperative behaviors, that is, comparing the change degree of the subgroup decision matrix in the t-th rounds and $t-1$-th rounds.

For the management of the noncooperative behavior, the novel approach is explored to manage the noncooperative behavior. In general, the weight of the subgroup can be adjusted to manage the noncooperative behavior, and the decision matrix is transformed by the adjustment coefficient. In the practical decision problem, the adjustment opinion which the decision-maker is willing to accept should be respected. Thus, the noncooperative behavior is managed by adjusting the weight of subgroup, recalculating the subgroup decision matrix in this paper. In this study, the subgroups are allowed to modify. Generally, the number of subgroups is changed due to an enforced exit rule; nevertheless, the subgroups themselves remained the same. It is assumed that the decision makers can choose to modify their opinions under discussion, which makes it sensible that the subgroups they are classified into may also change. The example in Section 4 validated this point. Meanwhile, the weight of subgroup can be adjusted by the contribution of the cluster in the group consensus level and the number of the decision-makers who are willing to modify their initial opinion in the cluster.
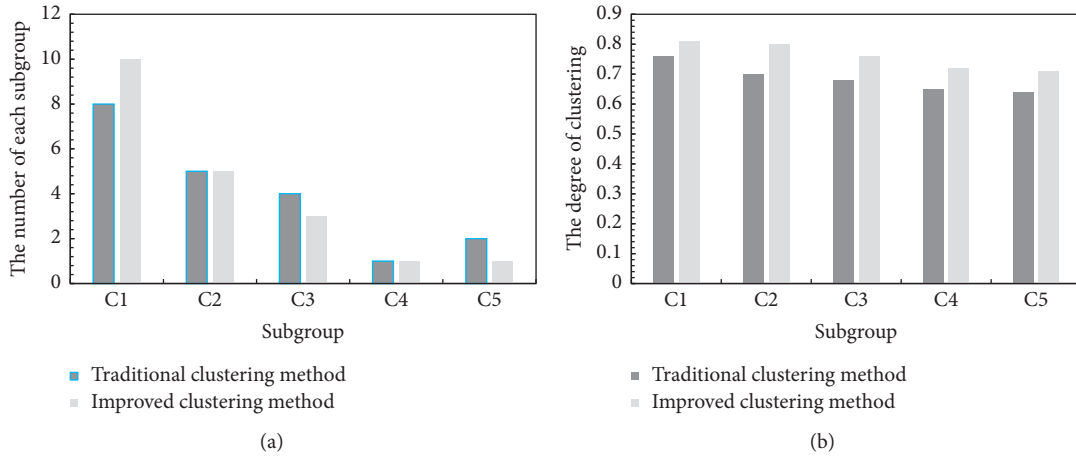
FIGURE 3: Comparisons between different groups under two different methods. (a) The number of each subgroup under two different methods. (b) The gathered degree of each subgroup under two different methods.

Different decision-making models have different emphasis. Therefore, there is no model that can be referred to as the best. Despite offered valuable methods to handle multiattribute large group decision-making problems, there are limitations in the proposed model: it is not easy to determine the subjective consensus threshold in this paper. Similar to other consensus models, the subjective consensus threshold needs to be decided by the moderator or group. Although empirical values for the consensus threshold can be given, the determination of the subjective consensus threshold depends on the actual problems and simulations. The subjective consensus threshold makes it free for the moderator and/or the group to grasp the decision processes.

6. Conclusion

The MALGDM problem becomes more and more significant for participants and stakeholders to make a consensus-based decision. The main contributions of the paper are as follows:

(1) A novel clustering method was adopted to divide the large group into several clusters. The similarity is calculated to express the gather degree of decision-makers, and the decision-maker can be classified by the gathered degree. The value of gathered degree decides the number of subgroups.

(2) A consensus framework for the consensus reaching process in a MALGDM is proposed. The consensus threshold is determined by the consensus level and subjective consensus threshold. Meanwhile, the noncooperative behavior of decision-makers is determined, and the subgroup that includes the decision-maker who expresses the noncooperative behavior is defined as the noncooperative subgroup.

(3) A novel consensus reaching process is designed to address the noncooperative subgroup. The noncooperative subgroup is detected by the number of decision-makers and the consensus level, and by determining three noncooperative behavior situations. The weight of the subgroup is adjusted to reach

the consensus level, and the subgroups in our proposed approach are allowed to change. Thus, there are three approaches to manage the noncooperative behavior: adjustment weight of subgroup, quitting the decision process, and changing the subgroups in each interactive round.

Further, some other clustering methods can be incorporated in the proposal to detect the influences of clustering on model convergence. For the classification of large groups, it may be a good alternative to adopt an automatic feedback strategy such as an optimization-based approach. However, some limitations exist in the research. Due to the difference of risk preference, decision-makers may make decisions that are difficult to coordinate, and this paper does not cover the psychological perception of decision makers, which may be an important research direction in LGDM problem in the future. Meanwhile, there are many factors that can influence the decision-making, and the interactions of factors may influence the results. Thus, the approach considering the interactions of factors will be used to explore multiattribute interactions of LGDM.

Data Availability

The data used to support the findings of this study are included within the article.

Conflicts of Interest

The authors declare that they have no conflicts of interest.

Acknowledgments

References

[1] Y. K. Hu, S. H. Yu, J. J. Chu et al., "A consensus-reaching approach to the evaluation of product design alternatives with multiple preference structures," *Computational Intelligence and Neuroscience*, vol. 2021, Article ID 6992648, 16 pages, 2021.

[2] P. Ren, Z. Xu, and H. Liao, "Intuitionistic multiplicative analytic hierarchy process in group decision making," *Computers & Industrial Engineering*, vol. 101, pp. 513–524, 2016.

[3] C. Hou, Y. Wen, Y. He et al., "Public stereotypes of recycled water end uses with different human contact: evidence from event-related potential (ERP)," *Resources, Conservation and Recycling*, vol. 168, Article ID 105464, 2021.

[4] B. Cheng, K. Lu, J. Li, H. Chen, X. Luo, and M. Shafique, "Comprehensive assessment of embodied environmental impacts of buildings using normalized environmental impact factors," *Journal of Cleaner Production*, vol. 334, Article ID 130083, 2022.

[5] H. Li, Y. Cao, L. Su, and Q. Xia, "An interval pythagorean fuzzy multi-criteria decision making method based on similarity measures and connection numbers," *Information*, vol. 10, no. 2, p. 80, 2019.

[6] F. Liu, J. W. Zhang, Q. Yu, Y. N. Peng, and W. Pedrycz, "On weak consistency of interval additive reciprocal matrices," *Fuzzy Optimization and Decision Making*, vol. 2020, no. 19, 175 pages, 2020.

[7] E. Abad-Segura, M.-D. González-Zamar, E. López-Meneses, and E. Vázquez-Cano, "Financial technology: review of trends, approaches and management," *Mathematics*, vol. 8, no. 6, 951 pages, 2020.

[8] N. M. Scala, J. Rajgopal, L. G. Vargas, and K. L. Needy, "Group decision making with dispersion in the analytic hierarchy process," *Group Decision and Negotiation*, vol. 25, no. 2, pp. 355–372, 2016.

[9] S. Cali and S. Y. Balaman, "A novel outranking based multi criteria group decision making methodology integrating ELECTRE and VIKOR under intuitionistic fuzzy environment," *Expert Systems with Applications*, vol. 119, pp. 36–50, 2019.

[10] J. Tang, F. Meng, F. J. Cabrerizo, and E. Herrera-Viedma, "A procedure for group decision making with interval-valued intuitionistic linguistic fuzzy preference relations," *Fuzzy Optimization and Decision Making*, vol. 18, no. 4, pp. 493–527, 2019.

[11] X.-B. Mao, M. Wu, J.-Y. Dong, S.-P. Wan, and Z. Jin, "A new method for probabilistic linguistic multi-attribute group decision making: application to the selection of financial technologies," *Applied Soft Computing*, vol. 77, pp. 155–175, 2019.

[12] J. Chu, X. Liu, Y. Wang, and K.-S. Chin, "A group decision making model considering both the additive consistency and group consensus of intuitionistic fuzzy preference relations," *Computers & Industrial Engineering*, vol. 101, pp. 227–242, 2016.

[13] A. Mahmoudi, S. Sadi-Nezhad, and A. Makui, "A hybrid fuzzy-intelligent system for group multi-attribute decision making," *International Journal of Fuzzy Systems*, vol. 18, no. 6, pp. 1117–1130, 2016.

[14] R. Krishankumar, K. S. Ravichandran, M. I. Ahmed, S. Kar, and X. D. Peng, "Interval-Valued probabilistic hesitant fuzzy set based muirhead mean for multi-attribute group decision-making," *Mathematics*, vol. 7, no. 4, p. 342, 2019.

[15] M. Przybyła-Kasperek and A. Wakulicz-Deja, "Global decision-making system with dynamically generated clusters," *Information Sciences*, vol. 270, pp. 172–191, 2014.

[16] A. Azadeh, M. Saberi, and M. Anvari, "An Integrated Artificial Neural Network Fuzzy C-Means-Normalization Algorithm for performance assessment of decision-making units: the cases of auto industry and power plant," *Computers & Industrial Engineering*, vol. 60, no. 2, pp. 328–340, 2011.

[17] L. Peide and L. Ying, "An improved failure mode and effect analysis method for multi-criteria group decision-making in green logistics risk assessment," *Reliability Engineering & System Safety*, vol. 215, Article ID 107826, 2021.

[18] Y. Xue, Y. Deng, and H. Garg, "Uncertain database retrieval with measure - based belief function attribute values under intuitionistic fuzzy set," *Information Sciences*, vol. 546, pp. 436–447, 2021.

[19] Y. Li, H. Garg, and Y. Deng, "A new uncertainty measure of discrete Z-numbers," *International Journal of Fuzzy Systems*, vol. 22, no. 3, pp. 760–776, 2020.

[20] A. Tapia-Rosero, A. Bronselaer, and G. De Tré, "A method based on shape-similarity for detecting similar opinions in group decision-making," *Information Sciences*, vol. 258, pp. 291–311, 2014.

[21] X. Xu, B. Wang, and Y. Zhou, "A method based on trust model for large group decision-making with incomplete preference information," *Journal of Intelligent and Fuzzy Systems*, vol. 30, no. 6, pp. 3551–3565, 2016.

[22] C.-g. Cai, X.-h. Xu, P. Wang, and X.-h. Chen, "A multi-stage conflict style large group emergency decision-making method," *Soft Computing*, vol. 21, no. 19, pp. 5765–5778, 2017.

[23] F. Meng, Q. An, and X. Chen, "A consistency and consensus-based method to group decision making with interval linguistic preference relations," *Journal of the Operational Research Society*, vol. 67, no. 11, pp. 1419–1437, 2016.

[24] X.-h. Xu, X.-y. Zhong, X.-h. Chen, and Y.-j. Zhou, "A dynamical consensus method based on exit-delegation mechanism for large group emergency decision making," *Knowledge-Based Systems*, vol. 86, pp. 237–249, 2015.

[25] M. Akram, A. Adeel, and J. C. R. Alcantud, "Multi-criteria group decision-making using an m-polar hesitant fuzzy TOPSIS approach," *Symmetry*, vol. 11, no. 6, p. 795, 2019.

[26] M. Zhao, X.-y. Ma, and D.-w. Wei, "A method considering and adjusting individual consistency and group consensus for group decision making with incomplete linguistic preference relations," *Applied Soft Computing*, vol. 54, pp. 322–346, 2017.

[27] H. Wang, Y. Ju, and P. Liu, "Multi-attribute group decision-making methods based on q-rung orthopair fuzzy linguistic sets," *International Journal of Intelligent Systems*, vol. 34, no. 6, pp. 1129–1157, 2019.

[28] M. Riaz and S. T. Tehrim, "Multi-attribute group decision making based on cubic bipolar fuzzy information using averaging aggregation operators," *Journal of Intelligent and Fuzzy Systems*, vol. 37, no. 2, pp. 2473–2494, 2019.

[29] F. Meng, S.-M. Chen, and J. Tang, "Group decision making based on acceptable multiplicative consistency of hesitant fuzzy preference relations," *Information Sciences*, vol. 524, no. 524, pp. 77–96, 2020.

[30] L. Martínez and J. Montero, "Challenges for improving consensus reaching process in collective decisions," *New Mathematics and Natural Computation*, vol. 2, no. 3, pp. 203–217, 2007.

[31] I. J. Perez, F. J. Cabrerizo, S. Alonso, and E. Herrera-Viedma, "A new consensus model for group decision making problems with non-homogeneous experts," *IEEE Transactions on*

Systems, Man, and Cybernetics: Systems, vol. 44, no. 4, pp. 494–498, 2014.

[32] Y. Xu, X. Wen, and W. Zhang, "A two-stage consensus method for large-scale multi-attribute group decision making with an application to earthquake shelter selection," *Computers & Industrial Engineering*, vol. 116, pp. 113–129, 2018.

[33] F. Jin, H. Garg, L. Pei, J. Liu, and H. Chen, "Multiplicative consistency adjustment model and data envelopment analysis-driven decision-making process with probabilistic hesitant fuzzy preference relations," *International Journal of Fuzzy Systems*, vol. 22, no. 7, pp. 2319–2332, 2020.

[34] Y. Dong, H. Zhang, and E. Herrera-Viedma, "Integrating experts' weights generated dynamically into the consensus reaching process and its applications in managing non-cooperative behaviors," *Decision Support Systems*, vol. 84, pp. 1–15, 2016.

[35] Y. Dong, S. Zhao, H. Zhang, F. Chiclana, and E. Herrera-Viedma, "A self-management mechanism for noncooperative behaviors in large-scale group consensus reaching processes," *IEEE Transactions on Fuzzy Systems*, vol. 26, no. 6, pp. 3276–3288, 2018.

[36] I. Palomares, L. Martinez, and F. Herrera, "A consensus model to detect and manage noncooperative behaviors in large-scale group decision making," *IEEE Transactions on Fuzzy Systems*, vol. 22, no. 3, pp. 516–530, 2014.

[37] Z. Wu and J. Xu, "A consensus model for large-scale group decision making with hesitant fuzzy information and changeable clusters," *Information Fusion*, vol. 41, pp. 217–231, 2018.

[38] F. J. Quesada, I. Palomares, and L. Martínez, "Managing experts behavior in large-scale consensus reaching processes with uninorm aggregation operators," *Applied Soft Computing*, vol. 35, pp. 873–887, 2015.

[39] S. Nazari, A. Ahmadi, S. Kamrani Rad, and B. Ebrahimi, "Application of non-cooperative dynamic game theory for groundwater conflict resolution," *Journal of Environmental Management*, vol. 270, Article ID 110889, 2020.

[40] X.-h. Xu, Z.-j. Du, and X.-h. Chen, "Consensus model for multi-criteria large-group emergency decision making considering non-cooperative behaviors and minority opinions," *Decision Support Systems*, vol. 79, pp. 150–160, 2015.

[41] P. Mandal, S. Samanta, and M. Pal, "Large-scale Group Decision-Making Based on Pythagorean Linguistic Preference Relations Using Experts Clustering and Consensus Measure with Non-cooperative Behavior Analysis of Clusters," *Complex & Intelligent Systems*, 2021.

[42] B. Liu, Y. Shen, X. Chen, Y. Chen, and X. Wang, "A partial binary tree DEA-DA cyclic classification model for decision makers in complex multi-attribute large-group interval-valued intuitionistic fuzzy decision-making problems," *Information Fusion*, vol. 18, pp. 119–130, 2014.

[43] Y. Liu, Z.-P. Fan, and Y. Zhang, "A method for stochastic multiple criteria decision making based on dominance degrees," *Information Sciences*, vol. 181, no. 19, pp. 4139–4153, 2011.

[44] Q. Dong and T. L. Saaty, "An analytic hierarchy process model of group consensus," *Journal of Systems Science and Systems Engineering*, vol. 23, no. 3, pp. 362–374, 2014.

[45] Y. Dong, Z.-P. Fan, and S. Yu, "Consensus building in a local context for the AHP-GDM with the individual numerical scale and prioritization method," *IEEE Transactions on Fuzzy Systems*, vol. 23, no. 2, pp. 354–368, 2015.

[46] D. Ben-Arieh and Z. F. Zhifeng Chen, "Linguistic-labels aggregation and consensus measure for autocratic decision making using group recommendations," *IEEE Transactions on Systems, Man, and Cybernetics-Part A: Systems and Humans*, vol. 36, no. 3, pp. 558–568, 2006.

Research Article

Intelligent Method for Real-Time Portable EEG Artifact Annotation in Semiconstrained Environment Based on Computer Vision

Xuesheng Qian [1,2] **Mianjie Wang,**[3] **Xinyue Wang,**[4] **Yihang Wang,**[5] **and Weihui Dai** [2]

[1]*Institute of Systems Engineering and Collaborative Laboratory for Intelligent Science and Systems,*
 Macau University of Science and Technology, Macao 999078, China
[2]*School of Management, Fudan University, Shanghai 200433, China*
[3]*Shanghai Ineutech Techonolgy Co., Ltd., Shanghai 200072, China*
[4]*College of Letters and Science, University of California, Berkeley, CA 94720, USA*
[5]*Steinhardt School of Culture, Education, and Human Development, New York University, New York, NY 10003, USA*

Correspondence should be addressed to Weihui Dai; whdai@fudan.edu.cn

As a convenient device for observing neural activity in the natural environment, portable EEG technology (PEEGT) has an extensive prospect in expanding neuroscience research into natural applications. However, unlike in the laboratory environment, PEEGT is usually applied in a semiconstrained environment, including management and engineering, generating much more artifacts caused by the subjects' activities. Due to the limitations of existing artifacts annotation, the problem limits PEEGT to take advantage of portability and low-test cost, which is a crucial obstacle for the potential application of PEEGT in the natural environment. This paper proposes an intelligent method to identify two leading antecedent causes of EEG artifacts, participant's blinks and head movements, and annotate the time segments of artifacts in real time based on computer vision (CV). Furthermore, it changes the original postprocessing mode based on artifact signal recognition to the preprocessing mode based on artifact behavior recognition by the CV method. Through a comparative experiment with three artifacts mark operators and the CV method, we verify the effectiveness of the method, which lays a foundation for accurate artifact removal in real time in the next step. It enlightens us on how to adopt computer technology to conduct large-scale neurotesting in a natural semiconstrained environment outside the laboratory without expensive laboratory equipment or high manual costs.

1. Introduction

Electroencephalography (EEG) has been proved to be a useful methodological tool for understanding brain activities, including the processes of perception, cognition, and decision, which are the basis of daily behaviors, business, and engineering activities.

With the great attention to human decision-making and the recognition of limitations of traditional psychological/ self-reported driven approaches [1–4], the neuromanagement on revealing the mechanism of human's behavior and decision-making based on brain imaging technology is promoted [5–7]. However, due to the high cost of purchasing and maintaining neurometric equipment and the complex operation and data analysis mode, brain technologies are limited to the laboratory environments and hindered from becoming widespread.

Neurophysiological measurements initially rely on high-cost equipment, complex systems, and many professional operations (e.g., measuring the size of the head, marking the position of electrodes on the scalp, placing electrodes on the scalp, and using conductive glue). Benefiting from the development of portable EEG technology (PEEGT), devices become cheaper and smaller, such as single-electrode

NeuroSky MindWave, four-electrode Muse, and fourteen-electrode Emotiv. What is more, with simple preparation, EEG data are collected through the wireless network. The PEEGT devices are suitable for nonclinical studies with better interactive experiences [8]. Nowadays, more and more research and commercial applications use PEEGT as a measurement tool. The utilization of PEEGT significantly expands the application of neurophysiological measurements and dramatically increases the practicability of neurometric equipment, such as in marketing [5], management [9], education [10], and engineering [11].

The PEEGT effectively reduces the threshold of the experimental environment in business and management situations. It is especially suitable for the volatile, uncertain, complex, and ambiguous (VUCA) environment. It makes large-scale and long-time neurophysiological measurements at the lowest cost possible. Moreover, subjects are allowed to have slight movements in position during a long-lasting experiment, for example, adjusting sitting or head posture like in a natural situation; we called this the semiconstrained environment. The semiconstrained environment is different from a constrained environment where subjects in the laboratory are under strict restrictions on autonomous activities. There is also a distinction between a semiconstrained and unconstrained environment where subjects have significant activity freedom. Nevertheless, fewer experimental restrictions in semiconstrained and unconstrained environments bring more artifacts by physical activities, which is difficult for artifacts operation.

Annotation of artifacts is a prerequisite for removing artifacts and EEG analysis. Existing methods of artifact annotation face the tradeoff between testing convenience and annotation accuracy, making it inapplicable in daily business scenarios where there are high requirements for both the convenience of collection and the accuracy of artifact annotation. The methods relying on additional reference signals or biological signal equipment are not applicable for the daily context that needs PEEGT. In contrast, methods relying on multiple algorithms have a long computing delay and are less accurate than methods with additional reference signals. Last but not least, most existing methods can only be used in postacquisition or offline settings, but real time is an essential demand of artifact annotation in business scenarios.

Considering existing methods, effectively annotating artifacts generated from physical activities usually requires manually annotating artifacts in postacquisition offline settings, which is extremely time-consuming and dependent on the data operator's expertise level. What is worse, to ensure the accuracy of the testing results and meet the requirements of business scenarios, tests with PEEGT usually need a larger sample size, a longer test time, and a more uncertain test environment. In a word, it is a great challenge to apply neuroscience in scenarios emphasizing "natural" due to the lack of adequate and suitable artifact processing technology. The artifact problem limits PEEGT to take advantage of portability and low test cost, which is a crucial obstacle for the potential application of PEEGT in the natural environment. It is worth noting that a challenge also exists in the laboratory EEG test, but the traditional experiment has more reference equipment assistance and more processing time. Therefore, in most laboratory cases, the limitation can be arranged by investing more resources.

Intelligent algorithms in computer vision (CV) bring new possibilities to solve the above difficulties. This article proposes one intelligent computing method on real-time portable EEG artifact annotations with computer vision, which changes the original artifact postprocessing mode based on signal recognition to the artifact preprocessing mode based on behavior recognition. It is especially suitable for artifact problems in semiconstrained environments involved in most real scenes in engineering and management. Besides, it provides the foundation for the subsequent artifact intelligent removal by the machine learning algorithm.

Our main contributions can be summarized as follows:

(1) We introduce a thought about changing the original signal recognition-based artifact postprocessing mode to the artifact preprocessing mode based on behavior recognition by the computer algorithm, making it possible to process artifacts in real time using only a camera instead of additional expensive neurological equipment and amounts of manual processing.

(2) We propose an intelligence method based on computer vision to automatically annotate the time segments and categories of artifacts caused by blinks and head movements in real time, which is of great importance for the large-scale application and real-time analysis of PEEGT and traditional EEG.

(3) We suggest a procedure about how to use large-scale neurological measurement in business and management scenarios with fewer restrictions on subjects' physical activities. The method ensures that the artifacts caused by the physical activities in blinks and head movements can be annotated in real time, which greatly expand neuroscience research into real applications environment including engineering and management.

2. Literature

2.1. EEG Artifacts. Electroencephalogram (EEG) is a standard method of measuring human brain activities that change over time in the form of electrograms. EEG data has shown great potential in research and commercial applications. It can be used as a diagnostic and monitoring tool for clinical applications, such as quantifying anesthesia levels before and during surgery [12], and film and advertising evaluation, such as film and television effect research [13]. However, there are many inherent challenges in EEG analysis, specifically the removal of various artifacts.

Generally, the artifacts of the EEG signal are mainly from the physiological activities of the participant and the additional noise artifacts introduced by the EEG acquisition instrument. The latter can be reduced or even eliminated by improving the operating performance of the EEG signal acquisition instrument. However, bioelectrical signals

generated by physiological activities are inevitably hidden in the EEG signals or even submerged in the EEG signals, which seriously affects the authenticity of the EEG signals and complicates the research work of feature extraction and EEG signal analysis. Blinks and head movements are two kinds of major signal artifacts. As a result, the research work of feature extraction and analysis of the EEG signals becomes complicated.

Figure 1 [14, 15] shows typical artifact waveforms with obvious and common interference to EEG signals. The blink artifact is generated by blinking eyes, while the head movement artifact is generated by head rotation or movements.

2.2. EEG Artifacts Annotation Methods.

EEG artifact annotation has always been a challenge in the EEG signals analysis process. Challenges come from the complexity of the method and the nonlinearity of the noise. For example, due to the "nonlinear" nature of the artifact, it is difficult to annotate the artifacts from the original EEG data without affecting the normal signal. In addition, some methods cannot be used for real-time applications. Until now, although researchers have been exploring lots of EEG artifact annotation methods, there is still no consensus on which algorithm is most suitable for a specific application.

In general, there are two categories of EEG artifact annotation methods: direct labeling of artifacts and indirect separation of artifacts [16].

2.2.1. Direct Labeling of Artifacts.

Direct labeling of artifacts refers to annotating artifact signals in real time when EEG signal is collected. However, it requires additional reference signals from reference electrodes channels or additional biological monitoring equipment. Li et al. [17] adopted additional channels of real EMG from neck and head muscles as input and realized the significant separation of EEG and EMG artifacts without losing the underlying EEG features. Mannan et al. [18] realized the simultaneous collection of EEG and EOG signals by adding the channels of EOG electrodes and combined independent component analysis (ICA), regression, and high-order statistics to identify and eliminate artifactual activities from EEG data. In terms of adding monitoring equipment, König et al. [19] used a laboratory-level eye tracker to annotate blink and eye movement artifacts in the constrained environment. Compared with the traditional manual artifact annotation, adding reference equipment has dramatically improved the accuracy and efficiency. Nevertheless, additional channels cause the additional possibility of artifacts. On the other hand, the additional expensive and complicated laboratory equipment will increase the burden of operators and participants and the terms of the test environment.

2.2.2. Indirect Labeling of Artifacts.

Indirect separation of artifacts refers to separating the mixed signals by multiple integrated algorithms without the reference electrodes or monitoring equipment. Jan et al. [20] improved the ICA method to better artifact removal. Chang et al. [21] used artifact subspace reconstruction (ASR) to preprocess EEG data and, combined with the ICA separation method, greatly improved the accuracy of artifact removal. Indirect separation of artifacts avoids extra electrodes, making it convenient in the test environment and reducing the extra noise. However, the method needs to integrate a variety of algorithms, increasing the algorithm's complexity and reducing the artifact annotation's real-time performance. Moreover, due to the lack of reference supervision of the artifact signals, the accuracy of the indirect artifact annotation is generally lower than those of the direct methods.

Although the two above-mentioned methods for artifact annotation have made explorations from different directions and achieved good results, they are based on sacrificing one aspect to improve the other, making it hard to apply in daily business scenarios. More specifically, the direct labeling of artifacts achieves better accuracy of artifact annotation with additional reference electrodes and laboratory equipment at the cost of the convenience in equipment operation and the comfort of participants. In contrast, the method of indirect separation of artifacts achieves more convenient signal acquisition with integrated algorithms at the cost of the accuracy of artifact annotation. Because the scenarios of daily business have high requirements for both the convenience in signal acquisition and the accuracy of artifact annotation, methods used in these scenarios should not only simplify the test environment and ease participant's test burden but also ensure the accuracy of artifact annotation and take the real-time requirements into account.

2.3. Semiconstrained Environment.

In neuroscience, research and experiments are conducted in two kinds of settings, laboratory settings and nonlaboratory settings. A laboratory test environment is carefully designed, in which researchers and participants need to follow strict restrictions and guidelines. Usually, other experimental settings outside laboratories are nonlaboratory settings. However, in most of the research articles, researchers either directly employ the term without further clarification [22] or use nonlaboratory settings to refer to a relatively broad idea [23]. For example, experiments conducted in the unattended home [24] and observational studies conducted in a community [25] are different in settings, but both are referred to as "nonlaboratory."

In the past literature, scientists did not specify how to set up neurological devices in conditions other than a laboratory. It is an unexpected gap in neural experiments. In many cases, it is unrealistic to keep participants motionless in a place with no distraction, especially in the natural environment using PEEGT. Therefore, to provide a more precise scope to clarify the application of our methods and algorithms, we define a term in our paper, a "semiconstrained environment," compared to a fully attended laboratory and an unattended natural setting. A semiconstrained environment describes an experimental setting where participants are required to wear a device; however, the research does not propose a highly restricted demand on participants
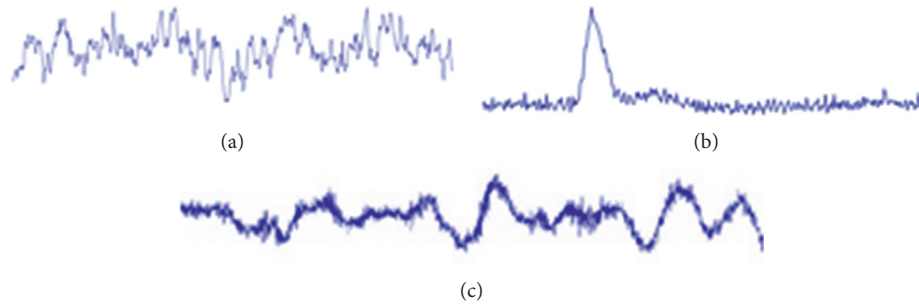
Figure 1: Typical artifact waveforms [14, 15]. (a) Clean EEG. (b) Blink artifact. (c) Head movement artifact.

(such as zero movements at all during measurement) since it is not always available to set up a lab-based environment.

3. Methodology

3.1. Method Proposed. In traditional EEG signal artifact processing without additional reference equipment, experienced signal processors must manually mark the abnormal signal period in the test signal after completing signal preprocessing, such as band-pass filtering. Usually, such an operation needs to be repeated 10–20 times for each subject, and more marks lead to a better operation effect. Then, the unique signal processing software will use algorithms such as ICA to automatically remove similar artifact signals according to the manually marked signal form. This method requires a long time and high personnel investment. In principle, such a manual postmarking and removal algorithm cannot ensure accuracy, and there is a certain degree of fuzzy space, even if it is existing in common practice.

In this paper, CV is introduced into neurological experiments. It can detect subjects' behaviors simultaneously during the experiment and mark the events that may produce artifacts from the source shown in Figure 2. Thus, it improves the real-time performance of artifact processing, avoids the later manual investment, and makes artifact marking no longer an ambiguous activity based on experience.

3.2. Process. The key to accurate artifact annotation in a semiconstrained environment is timely identifying the most common participants' physical activities that may cause artifacts, for example, blinks and head movements. In this paper, a method for annotating blink and head movement artifacts with computer vision in daily business scenarios is proposed, which meets requirements under this semiconstrained environment to a great extent. The method is shown in Figure 3. Firstly, it is necessary to collect the participants' initial state and calibrate the algorithm. Specifically, the subjects' eye-closing threshold is collected to measure blinking state during the test, and the subjects' initial sitting orientation is for the measurement of head movement state. Notably, the initialization of PEEGT equipment and standard commercial high-definition cameras, unlike the cumbersome operation of lab eye-

tracking equipment, performs the initial state check and calibration only to ensure the equipment availability and to collect the initial eye and head positions of the subjects.

Next, the PEEGT equipment and camera are used to synchronously collect participants' facial signals and EEG signals in real time. The blinks and head movements are detected with computer vision based on facial feature points. It is critical to note that the original EEG signals are downsampled in sync with the facial signal. Finally, the facial and the EEG signals in the same time series are analyzed and processed with the same analysis frequency. The EEG signals with blink and head movement artifacts are annotated.

The site-setting of the method is shown in Figure 4; the participant is wearing PEEGT devices and looking at the screen. In a semiconstrained environment, the participant can adjust his or her posture during the experiment. The camera ensures that head activity can be entirely recorded. Based on the computer algorithm with supervised real time and synchronization, the method can annotate the time segments of blinks and head movements that cause EEG artifacts.

3.3. Recognition Algorithm

3.3.1. Facial Feature Points Positioning. As mentioned above, the recognition algorithm first needs to collect the participant's facial signals and then monitor facial condition according to the specific facial features. The purpose of facial feature points positioning is to further define facial feature points (facial features and edge). The algorithms collect the baseline values of participants before the test, and the collected data and standards are unified. Therefore, the judgment threshold has corresponding calculations and standards for people of different face types.

The methods of facial feature point positioning can be categorized into the global method, the constrained local model (CLM) method, and the regression method, based on detecting face appearance and face shape information. The global method is to model the global face appearance and global face shape information explicitly [26]. The CLM explicitly models the local face appearance and the global face edge information [27]. The regression method uses global and local appearance information to implicitly embed global shape information for joint feature point detection
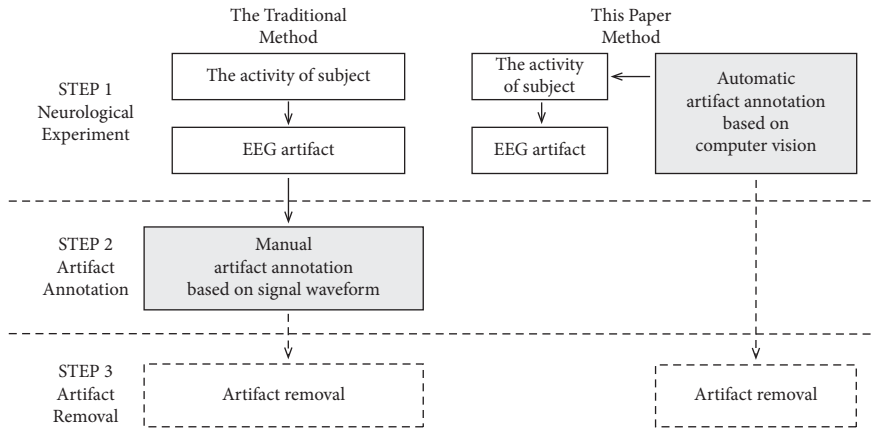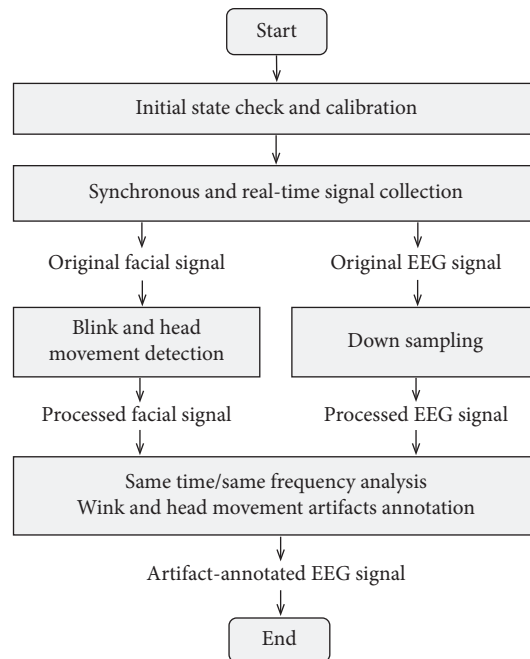
Figure 2: The proposed method.

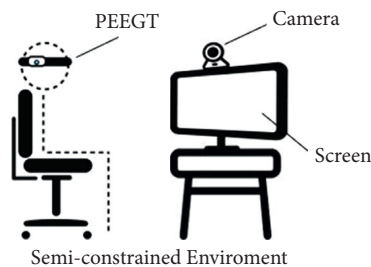Figure 3: Method of EEG artifact annotation with supervised computer vision.

Figure 4: The site-setting of blink and head movement artifacts annotation with supervised computer vision.

[28]. Generally, the regression method performs better because it contains more information compared to the other two. One representative algorithm of the regression method is Ensemble of Regression Trees (ERT) [29]. ERT is often used in facial feature point positioning because it is swift (it takes about 1 ms to detect each facial feature point) and can deal with the missing calibration of some key points in the training set.
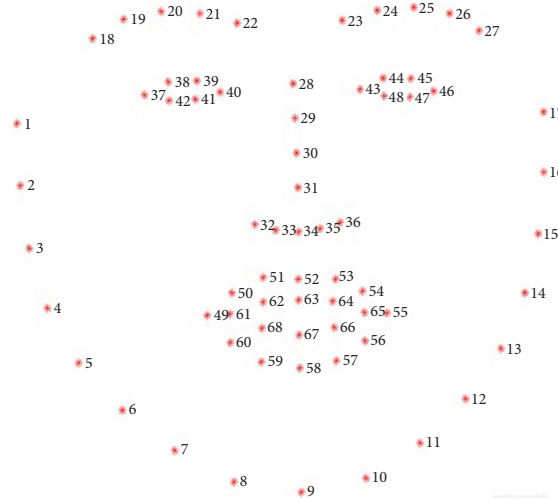
FIGURE 5: 68 key feature points of each face.

The method in this paper uses the ERT algorithm to position 68 key feature points (as shown in Figure 5) of each face within 1 ms through three steps: shape invariant split tests, choosing the node splits, and feature selection proposed by Kazemi and Sullivan [29], which can estimate the face's landmark positions directly from a sparse subset of pixel intensities, achieving super-real-time performance with high-quality predictions. The pseudocode for this program is as follows (Algorithm 1).

```
def face_landmarks ():
    predictor = dlib       initializes      shape_predictor
("shape_predictor_68_face_landmarks.dat")
    # cv2 is the OpenCv library
    cap = cv2 gets the first camera of the machine
    while (cap is opened):
        flag, im_rd = cap.read () builds 3D matrix
        img_gray = cv2.cvtColor                  (im_rd,
cv2.COLOR_RGB2GRAY)
        faces = detector (img_gray)
        for k, d in enumerate (faces):
            shape = predictor (im_rd, d)
    END face_landmarks
```

The implementation display of the recognition effect in the practical example of this method is shown in Figure 6.

3.3.2. Blink and Head Movement Detection

(1) Blink Detection. In Subsection 3.3.1, basic facial information and 68 key feature points of each face are positioned. In the method proposed, a participant's blink is detected by analyzing the closure degree of the eye region (six feature points forming a closed ellipse), as shown in Figure 7.

$$\mathrm{EAR}_L = \frac{\|p_{37} - p_{41}\| + \|p_{38} - p_{40}\|}{2\|p_{36} - p_{39}\|},$$

$$\mathrm{EAR}_R = \frac{\|p_{43} - p_{47}\| + \|p_{44} - p_{46}\|}{2\|p_{42} - p_{45}\|}. \tag{1}$$

Eye Aspect Ratio (EAR) is equal to the sum of the lengths of two vertical line segments divided by the double length of horizontal line segments. The EAR stands for the state of eyes' opening and closing, and p_i is one of the 68 feature points forming the eye region (as shown in formula (1)). Research shows that EAR can approach zero at the moment of closing eyes and return to the original value when opening eyes [30]. By monitoring whether the value of EAR fluctuates rapidly and approaches zero in real time, this method can identify whether the participant's eyes are closed. However, the threshold for blink detection is undefined in this method, introducing noises in the natural environment. Therefore, considering the sampling rate of CV, this paper monitors the blink state by setting the base value before measurement. That is, the data of eye-closed state for 1 minute before the test are collected, and the blink detection threshold $\mathrm{Blink_{threshold}}$ based on its average value is defined:

$$\mathrm{Blink_{threshold}} = \frac{1}{N} \sum_{i=1}^{N} B_i. \tag{2}$$

In the above equation, N represents the number of samples in 1 minute. Since the sampling rate of CV is 25, $N = 1500$. B_i is the data of eye-closed state collected at the ith time. After collecting and calculating the blink detection threshold $\mathrm{Blink_{threshold}}$, blinks are detected according to the value:

$$\mathrm{EAR_{per\_second}} = \min(\mathrm{EAR}_p),$$

$$\mathrm{Blink_{status}} = \begin{cases} 1, & \text{if} \quad \mathrm{EAR_{per\_second}} \leq \mathrm{Blink_{threshold}}, \\ 0, & \text{if} \quad \mathrm{EAR_{per\_second}} > \mathrm{Blink_{threshold}}, \end{cases} \tag{3}$$

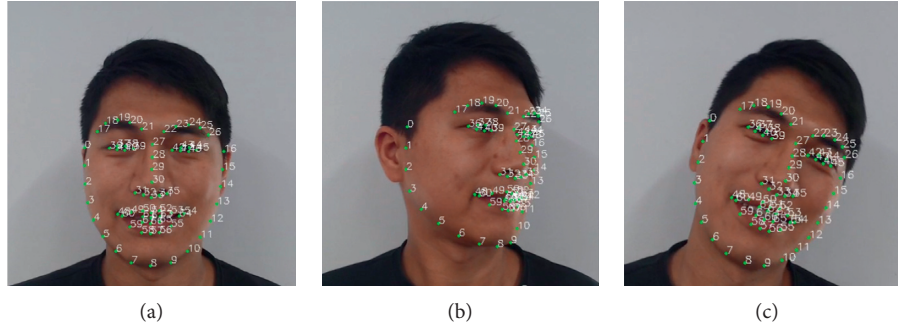(a)   (b)   (c)

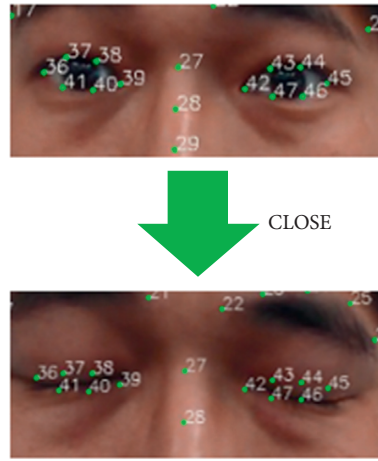FIGURE 6: The implementation display of recognition effect.

FIGURE 7: Method of blink detection.

where EAR_{per_second} is the minimum value of EAR in each cycle. If EAR_{per_second} is less than or equal to $Blink_{threshold}$, it is determined that there is blinking action within 1 second. If EAR_{per_second} is greater than $Blink_{threshold}$, it is determined that there is no blinking action within 1 second. The pseudocode for this program is as follows (Algorithm 2).

```
def face_ear ():
    if obtain 68 feature points of the face:
        ear_r_list.append (ear_r), ear_l_list.append
(ear_l)
        ear_r_status, ear_l_status = 0
        If N == 25:
            ear_r_persecond = min(ear_r_list),
ear_l_persecond = min(ear_l_list)
            ear_r_list.clear, ear_l_list.clear
            If                    ear_r_persecond ≤
blink_r_threshold:
                ear_r_status = 1
            else:
                ear_r_status = 0
            If        ear_l_        persecond ≤
blink_l_threshold:
                ear_l_status = 1
            else:
                ear_l_status = 0
        return ear_r_status, ear_l_status
    else return null
END face_ ear
```

(2) Head Movement Detection. Head movement (HM) detection is related to face orientation. In facial feature point positioning, 68 key feature points, including eyes and nose, are extracted from each facial image. In this paper, we refer to the center points of the eyes and nose to define the face orientation coordinates [31].

In (2), the eyes and nose have been correctly positioned. The three facial feature points determine an isosceles triangle by connecting lines between the three points. Considering the symmetry of the face, we can calculate the angle between the plane of the isosceles triangle and the image plane to determine the gaze direction. If one side of the triangle is located on the image plane, it is easy to calculate the angle of the gaze direction. The judgment of facial orientation is realized through the calculation of trigonometric function, as shown in Figure 8.

The triangle ABC is the projection of the isosceles triangle *ABE* on the image plane, which means that if the

(a)

(b)
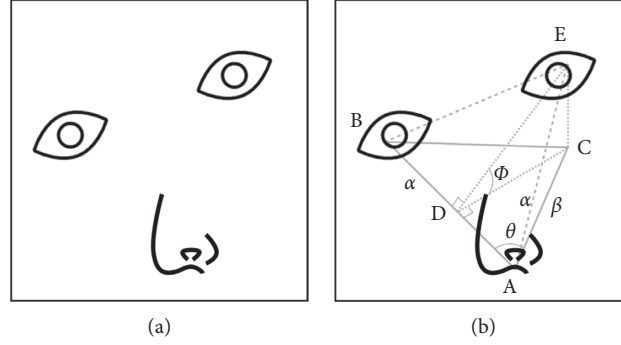
FIGURE 8: Facial image (a) and projection isosceles triangle model (b).

person in the picture looks straight ahead, the projection triangle will coincide with the isosceles triangle. The triangle CDE is located on the plane perpendicular to the image plane and isosceles triangle plane. If θ is the angle between line α and line β and ϕ is the angle between the image plane and the isosceles triangle plane, then

$$\cos \phi = \frac{|CD|}{|DE|},$$

$$|CD| = |AC|\sin \theta, |AD|$$

$$= |AC|\cos \theta, \tag{4}$$

$\cos \phi$ can be calculated by trigonometric function as follows:

$$\cos \phi = \frac{|AC|\sin \theta}{\sqrt{|AB|^2 - |AC|^2 \cos^2 \theta}}. \tag{5}$$

Therefore, determining the direction of the sight is to see how the isosceles triangle is projected on the image plane: the maximum distance from the eye to the mouth reveals the direction of the human gaze. After obtaining the participant's gaze direction, the attention direction is recorded, while the lateral (HM) of the participant is identified according to point A's coordinates.

Similarly, for head nodding, it is calculated as follows:

$$d = \|p_{27} - p_{30}\|. \tag{6}$$

d_i is obtained for each segment of detection. Thus,

$$D' = \text{Median}\{d_1, d_2, d_3, \ldots, d_N\}. \tag{7}$$

$N = 1500$ represents the number of samples in 1 minute. Then,

$$\phi' = \frac{\|D - D'\|}{D'} * 90. \tag{8}$$

In the above equation, ϕ' is the angle at which the subject's head is nodding, ranging from 0 to $90°$.

In addition, participants sit on the designated spot during the test in a semiconstrained environment and cannot move back and forth smoothly. Therefore, the above two detection conditions can meet the detection marks of

most HM artifacts, and the HM can be estimated by the angle difference between the two moments.

Instead of judging the absolute HM angle of the participant, the proposed method calculates the relative HM angle change in EEG artifact annotation.

Therefore, it is necessary to have

$$\psi = \frac{1}{N} \sum_{i=1}^{N} \varnothing_i,$$

$$\varnothing_{\text{relative}} = \psi_t - \psi_{t-1},$$

$$\text{Head}_{\text{status}} = \begin{cases} 0, \varnothing_{\text{relative}} \leq 10°, \\ 1, 10° < \varnothing_{\text{relative}} \leq 30°, \\ 2, \varnothing_{\text{relative}} > 30°, \end{cases} \tag{9}$$

where ψ is the real-time HM angle of the participant relative to the right ahead direction in a sampling period. $\varnothing_{\text{relative}}$ refers to the change of the HM angle of the participant in the current second relative to the previous second. If $\varnothing_{\text{relative}}$ is less than $10°$, it is judged to be relatively static and counted as 0. If $\varnothing_{\text{relative}}$ is greater than $10°$ and less than $30°$, it is judged as a micro-HM and counted as 1. If $\varnothing_{\text{relative}}$ is greater than $30°$, it is judged as a distinct HM and counted as 2. Head vertical and horizontal movements are calculated separately and $\text{Head}_{\text{status}}$ depends on the bigger one. Therefore, HM artifacts are detected and marked as different levels in the EEG artifact annotation.

The pseudocode for this program is as follows (Algorithm 3).

```
def face_angle ():
    if obtain 68 feature points of the face:
        head_angle_list.append (angle)
        current_angle = angle
        If N == 25:

head_change = current_angle–last_angle
        If head_change ≤ 10:
            head_status = 0
        else if 10 < head_change ≤ 30:
```
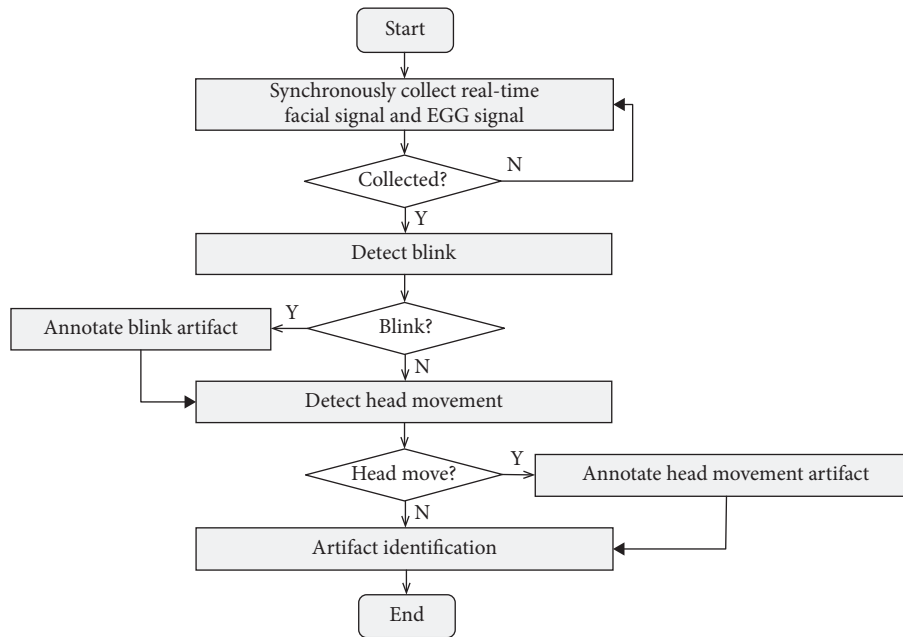
FIGURE 9: Process of EEG artifacts annotation with supervised computer vision.

```
                head_status = 1
        else:
                head_status = 2
        head_angle_list.clear
        return head_status
    else:
            last_angle = angle
    else:
        return null
END face_ angle
```

3.4. EEG Artifact Annotation with Supervised Computer Vision.
The process of blink and head movement artifacts annotation with supervised computer vision is shown in Figure 9. Firstly, the participant's facial and EEG signals are collected synchronously and in real time. Then, the blink detection algorithm is used to determine whether the blink action occurs. If there is a blink, the EEG signal in this state is annotated. Then the head movement algorithm, which determines whether a head movement occurs, is activated. If there is no head movement, the blink artifact is identified. If there is a head movement, the EEG signal in this state is annotated, and the head movement and blink artifacts are both identified.

It should be noted that the time window of the above process is 1 second. In a semiconstrained environment where tests generally take a long time, the 1-second time window can significantly reduce the time complexity and space complexity of data processing if enough EEG signals are retained and improve the efficiency of the whole test process. Real-time feedback also plays an important role in meeting the diverse business application needs.

3.5. Method Implementation.
Firstly, in algorithm implementation, we use Python 3.0 as the primary development language, and the development tool is PyCharm. The tool libraries used in the system development are Dlib, OpenCV, math, and NumPy. Specifically, Dlib is mainly used for face recognition and feature point labeling, OpenCV is mainly used for image processing and generation, math is used for mathematical algorithm calculation, and NumPy is used for feature point data processing.

Through the implementation, we verify the feasibility of the above method. In the example, we set the test environment and CV systems as in Figure 4 and performed the EEG acquisition for 24 seconds. In order to ensure the sensitive and accurate acquisition of EEG signals, we used the laboratory EEG equipment (ANT eego^{TM}mylab) instead of PEEGT to measure the example.

The model (by the author team) carried out four activities: blinking twice, towards two directions, and head movements twice, once slight and once severe. The implementation results indicated that all the activities were captured with the methods. All the artifacts were marked simultaneously by the 1-second time window, as demonstrated in Figure 10.

4. Experiment

4.1. Experiment Design and Participant.
We designed the experiment to verify whether the proposed intelligent computing method effectively recognizes and annotates the subject's activities in an authentic test environment.

The experiment recruited one participant that watched TV reality show programs for 15 minutes wearing PEEGT equipment and the test site-setting as in Figure 4. In the semiconstrained environment, the participant was not told
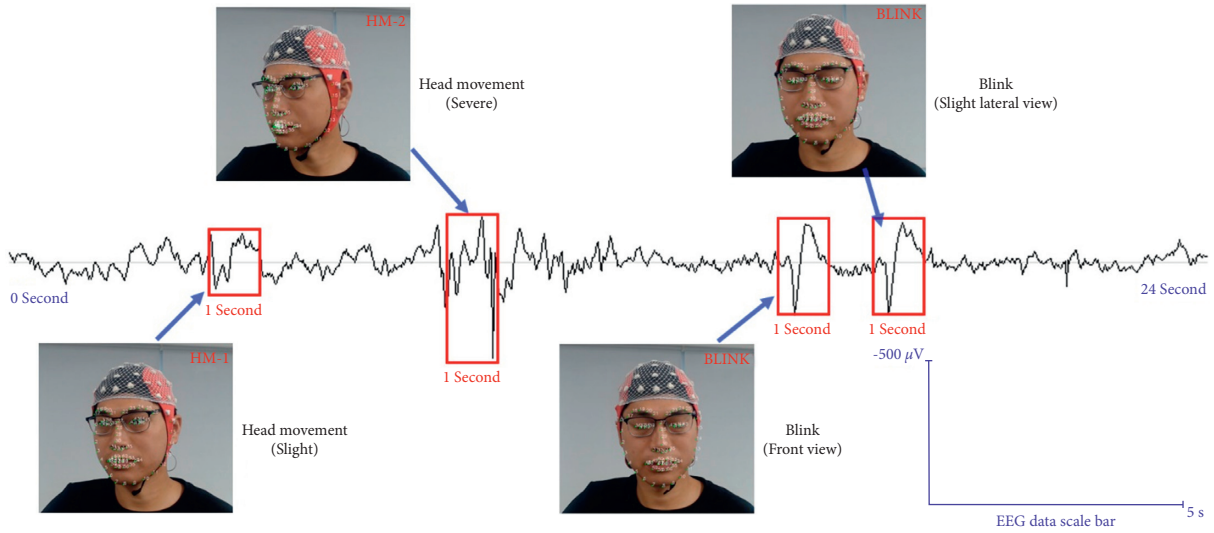
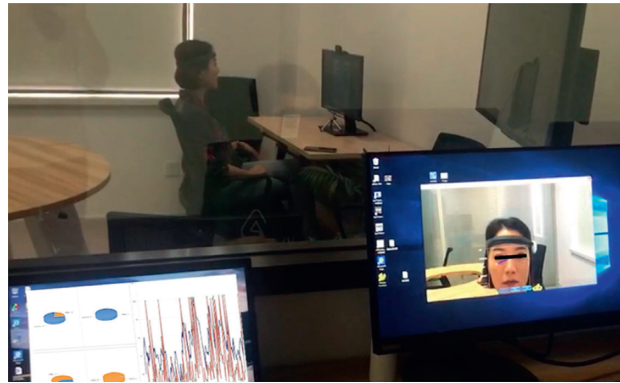FIGURE 10: The example of the method implementation.
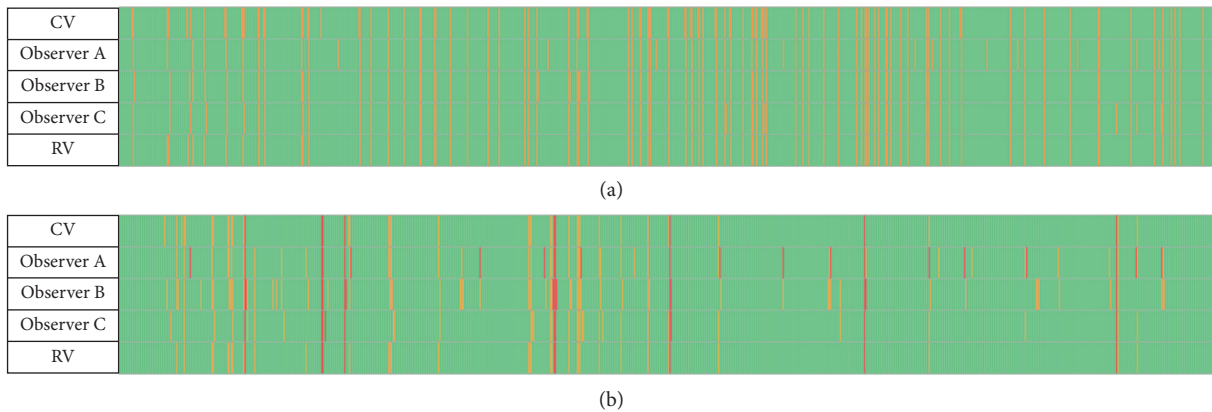

FIGURE 11: The experiment scene.

FIGURE 12: The original results of the experiment.

the requirement of body movement restriction, and no one else was present during the experiment. The camera above the screen recorded the participant's head movements and blinks. The experimenters were observed through one-way

glass and real-time system data. The scene picture is shown in Figure 11.

Three observers with EEG artifact processing experience watched the recorded video. They manually marked the

TABLE 1: Five groups of experimental result.

	Blink left					Blink right					Slight head movement					Severe head movement				
	Detection	Wrong	Miss	TPR (%)	SPC (%)	Detection	Wrong	Miss	TPR (%)	SPC (%)	Detection	Wrong	Miss	TPR (%)	SPC (%)	Detection	Wrong	Miss	TPR (%)	SPC (%)
CV	108	24	2	97.67	97.05	104	21	3	96.51	97.42	35	4	2	93.94	99.54	9	0	0	100.00	100.00
Observer A	91	11	6	93.02	98.65	91	11	6	93.02	98.65	40	15	8	75.76	98.27	22	13	0	100.00	98.54
Observer B	89	9	6	93.02	98.89	89	9	6	93.02	98.89	61	36	8	75.75	95.85	15	6	0	100.00	99.33
Observer C	88	10	8	90.70	98.77	88	10	8	90.70	98.77	32	4	15	84.85	99.53	11	2	0	100.00	99.86
Reference value	86	—	—	—	—	86	—	—	—	—	33	—	—	—	—	9	—	—	—	—

TPR represents the sensitivity of the data: the rate of real blinks or head movements. SPC represents the specificity of the data: the rate of real nonblinking or non-head-movements. TPR = (detection-wrong)/(detection-wrong + miss) × 100%. SPC = (total-detection-miss)/(total-detection-miss + wrong) × 100%.

participant's activity in the video, including blinks (left eye, right eye, and two eyes) and head movements (slight: rotation or tilt more than 10° and less than 30°; severe: rotation or tilt more than 30°). To simulate a large-scale artifact process task, the three observers perform a 30-minute irrelevant annotating task before the labeling task of this experiment. The participant's video is played at normal speed during the annotating process, and backward progress is not allowed.

The experimental team also manually marked the participant's movements as the reference value to ensure the accuracy of the marking. If necessary, the video can play slowly and repeatedly. For operability, the time granularity of all manual marking is 1 second.

4.2. Experiment Result. The activity markers of the participant were compared among the CV, three observers, and the reference value (RV, by experiment team). The original mark results are shown in Figure 12. The statistical result is shown in Table 1. The time granularity of all manual marking is 1 second, so the total represents 900 seconds, and each row has 900 horizontal grids in Figure 12. Note that the blinks here only refer to the ones detected by naked eyes.

5. Discussion

Overall, the experimental results show that the CV method in this paper got an ideal achievement, including sensitivity, specificity, and detection number. Moreover, the CV method has the advantages of real time and low cost.

For blink annotation, in general, the frequency of blinks correctly identified by the CV method is higher than that by the manual method, and the frequency of missed detections is lower under the close sensitivity and specificity. It is difficult for manual marking to maintain a high concentration and to notice the instant blink event for a long time, even with relevant data processing experience. In addition, the fuzziness of the human brain in judging events in unstructured data such as video will also lead to errors and omissions. The above reasons explain why the traditional artifacts processing cannot be applied to the business large-scale and long-time semiconstrained environment of PEEGT.

On the other hand, as for the CV method used in this experiment, the frequency of errors is slightly higher than that in the manual method in blink detection, which is due to categorizing the subject's eye-drooping activity as a blink event. From the perspective of bioelectrical signal interference, blinks and eye-drooping are the same. However, it is shown that even if the facial feature points can be captured all the time, the CV still has the possibility of recognizing some activity events incorrectly. Nevertheless, by optimizing the model, the false detection rate can be controlled, fully competent for the artifacts annotating long-time continuous EEG signal acquisition. In addition, there may be subtle differences between frequencies of two eyes' blinks in the CV method that independently detects binocular activity, which is distinguished from the

observer's overall observation style. Thus the difference may be more significant for participants with greater eye size differences. However, in large-scale and long-term tests, the influence of the above slight differences is almost negligible, especially in a semiconstrained test environment.

For head movements, the results are similar to the blinks. The CV recognition shows a significant advantage in efficiency, effectiveness, sensitivity, and specificity close to manual marking. Then it shows the great advantage of intelligent computing in a long-term mechanical task, and the method proposed in this paper is effective.

6. Conclusion and Future Work

The method proposed by this paper changed the original artifact postprocessing mode based on signal recognition to the artifact preprocessing mode based on behavior recognition by CV, which combined and optimized three efficient computer recognition algorithms. The paper also proved the method's effectiveness in the experiment. Through real-time monitoring of the participant's facial signals, the intelligent system can identify two main antecedent causes of the EEG artifacts, participant's blinks and head movements, and annotate the artifacts' time segments in real time. In a semiconstrained environment where PEEGT is generally used, the intelligent computing method makes PEEGT break through the current application bottleneck limited by artifacts, which meets the needs of processing large-scale test data with low cost and simple operation demands. The method introduces a new perspective to neurophysiological measurements. It utilizes the algorithm with a readily available commercial camera instead of expensive laboratory equipment or/and high manual costs. In addition, it enlightens us on conducting large-scale testing in a semiconstrained environment outside the laboratory.

The innovation of introducing the CV method into neurophysiological measurements is noteworthy:

(1) We proposed a new idea of detecting behavioral artifacts in EEG signals in real time. Therefore, the paper focuses on introducing the panorama of the method instead of the advantages of specific algorithms.

(2) Most of the machine learning algorithms in neuroscience and behavioral science run offline, but real-time detection is the innovation that the paper emphasized; and scenarios described in the paper are not the same as offline artifact mark recognition and thus are not comparable.

(3) We believe that interpretability is essential for a new method, and the algorithm black box is not conducive to trust and accept the innovation.

However, machine learning can effectively recognize blinking, head movement, and other behaviors in real time. Thus, in the specific recognition algorithms, we chose the method of logical judgment by feature points and achieved

ideal detection results. Nevertheless, with the acceptance of this method and continuous optimization of the algorithm, intelligent methods will be applied on a larger scale. The accuracy of the CV method will be promoted, which is the fundamental advantage of the algorithm compared with the manual annotation.

On the other hand, the efficient and accurate annotation of artifacts caused by the subject's activities is the critical precondition step for intelligent artifacts removal. The algorithm can accurately capture the individual physiological activity differences among participants in the same actions, such as blinks, thanks to the CV method. Thus, the supervised machine learning algorithm can be based on the individual differences for more accurate individual artifact removal and correcting, which will greatly improve the accuracy of EEG artifact signal processing. That is the goal of the next stage of this paper. In the future, it will be critical for PEEGT to start large-scale commercial applications in more complex experimental environments, such as the engineering management, the effects of film and television programs, advertising research, information flow research, aroma cognition test, and game interaction test.

Data Availability

Previously reported face feature selection data were used to support this study and are available at doi: 10.1109/CVPR.2014.241. These prior studies (and datasets) are cited at relevant places within the text as reference [29]. And the experiment data used to support the findings of this study are available from the corresponding author upon request.

Disclosure

The funders had no role in the study design, data collection, and analysis, decision to publish, or preparation of the manuscript.

Conflicts of Interest

The authors declare that the research was conducted in the absence of any commercial or financial relationships that could be construed as potential conflicts of interest.

Authors' Contributions

Xuesheng Qian and Weihui Dai conceived and designed this method and administered the project. Mianjie Wang completed the technology development. Xinyue Wang and Yihang Wang implemented the experiment and drafted the manuscript.

Acknowledgments

References

[1] D. Ariely and G. S. Berns, "Neuromarketing: the hope and hype of neuroimaging in business," *Nature Reviews Neuroscience*, vol. 11, no. 4, pp. 284–292, 2010.

[2] M. Hsu, "Neuromarketing: inside the mind of the consumer," *California Management Review*, vol. 59, no. 4, pp. 5–22, 2017.

[3] L. Hsu and Y. J. Chen, "Music and wine tasting: an experimental neuromarketing study," *British Food Journal*, vol. 122, no. 8, pp. 2725–2737, 2019.

[4] M. Piwowarski, U. Uma, and K. Nermend, "The cognitive neuroscience methods in the analysis of the impact of advertisements in shaping people's health habits," *European Research Studies Journal*, vol. 22, no. 4, pp. 457–471, 2019.

[5] C. Morin, "Neuromarketing: the new science of consumer behavior," *Society*, vol. 48, no. 2, pp. 131–135, 2011.

[6] M. Nilashi, S. Samad, N. Ahmadi et al., "Neuromarketing: a review of research and implications for marketing," *Journal of Soft Computing and Decision Support Systems*, vol. 7, no. 2, pp. 23–31, 2020.

[7] C. Yoon, A. H. Gutchess, F. Feinberg, and T. A. Polk, "A functional magnetic resonance imaging study of neural dissociations between brand and person judgments," *Journal of Consumer Research*, vol. 33, no. 1, pp. 31–40, 2006.

[8] P. Antonenko, F. Paas, R. Grabner, and T. Van Gog, "Using electroencephalography to measure cognitive load," *Educational Psychology Review*, vol. 22, no. 4, pp. 425–438, 2010.

[9] K. Yoshida, F. Hirai, and I. Miyaji, "Learning system using simple electroencephalograph feedback effect during memory work," *Procedia Computer Science*, vol. 35, pp. 1596–1604, 2014.

[10] J. Xu and B. Zhong, "Review on portable EEG technology in educational research," *Computers in Human Behavior*, vol. 81, no. 4, pp. 340–349, 2018.

[11] S. Anwer, H. Li, M. F. Antwi-Afari, W. Umer, and A. Y. Wong, "Evaluation of physiological metrics as a real-time measurement of physical fatigue in construction workers: state-of-the-art reviews," *Journal of Construction Engineering and Management*, vol. 147, no. 5, 2021.

[12] Y. Park, S.-H. Han, W. Byun, J.-H. Kim, H.-C. Lee, and S.-J. Kim, "A real-time depth of anesthesia monitoring system based on deep neural network with large EDO tolerant EEG analog front-end," *IEEE Transactions on Biomedical Circuits and Systems*, vol. 14, no. 4, pp. 825–837, 2020.

[13] U. Hasson, O. Landesman, B. Knappmeyer, I. Vallines, N. Rubin, and D. J. Heeger, "Neurocinematics: the neuroscience of film," *Projections*, vol. 2, no. 1, pp. 1–26, 2008.

[14] J. N. Knight, "Signal fraction analysis and artifact removal in EEG," Doctoral Dissertation, Colorado State University, Fort Collins, CO, USA, 2003.

[15] K. Onikura, Y. Katayama, and K. Iramina, "Evaluation of a method of removing head movement artifact from EEG by independent component analysis and filtering," *Advanced Biomedical Engineering*, vol. 4, pp. 67–72, 2015.

[16] R. J. Croft and R. J. Barry, "Removal of ocular artifact from the EEG: a review," *Neurophysiologie Clinique/Clinical Neurophysiology*, vol. 30, no. 1, pp. 5–19, 2000.

[17] Y. Li, P. T. Wang, M. P. Vaidya et al., "Electromyogram (EMG) removal by adding sources of EMG (ERASE)-A novel ICA-based algorithm for removing myoelectric artifacts from EEG," *Frontiers in Neuroscience*, vol. 14, Article ID 597941, 2021.

[18] M. M. N. Mannan, M. Y. Jeong, and M. A. Kamran, "Hybrid ICA-regression: automatic identification and removal of

ocular artifacts from electroencephalographic signals," *Frontiers in Human Neuroscience*, vol. 10, p. 193, 2016.

[19] P. König, M. Plöchl, and J. P. Ossandón, "Combining EEG and eye tracking: identification, characterization and correction of eye movement artifacts in electroencephalographic data," *Biomedical Engineering/Biomedizinische Technik*, vol. 57, no. SI-1, p. 392, 2012.

[20] S. Jan, R. Bortel, P. Sovka, and L. M. Ward, "Suppression of overlearning in independent component analysis used for removal of muscular artifacts from electroencephalographic records," *PLoS One*, vol. 13, no. 8, Article ID e0201900, 2018.

[21] C.-Y. Chang, S.-H. Hsu, L. Pion-Tonachini, and T.-P. Jung, "Evaluation of artifact subspace reconstruction for automatic artifact components removal in multi-channel EEG recordings," *IEEE Transactions on Biomedical Engineering*, vol. 67, no. 4, pp. 1114–1121, 2020.

[22] W. J. Sohn, R. Sipahi, T. D. Sanger, and D. Sternad, "Portable motion-analysis device for upper-limb research, assessment, and rehabilitation in non-laboratory settings," *IEEE Journal of Translational Engineering in Health and Medicine*, vol. 7, pp. 1–14, 2019.

[23] A. T. M. Van de water, A. Holmes, and D. A. Hurley, "Objective measurements of sleep for non-laboratory settings as alternatives to polysomnography-a systematic review," *Journal of Sleep Research*, vol. 20, no. 1, pp. 183–200, 2011.

[24] C. Iber, S. Redline, A. M. K. Gilpin et al., "Polysomnography performed in the unattended home versus the attended laboratory setting-sleep heart health study methodology," *Sleep*, vol. 27, no. 3, pp. 536–540, 2004.

[25] T. Blackwell, S. Ancoli-Israel, P. R. Gehrman, J. L. Schneider, K. L. Pedula, and K. L. Stone, "Actigraphy scoring reliability in the study of osteoporotic fractures," *Sleep*, vol. 28, no. 12, pp. 1599–1605, 2005.

[26] T. F. Cootes, G. J. Edwards, and C. J. Taylor, "Active appearance models," in *Proceedings of the European Conference on Computer Vision*, pp. 484–498, Freiburg, Germany, June 1998.

[27] J. M. Saragih, S. Lucey, and J. F. Cohn, "Deformable model fitting by regularized landmark mean-shift," *International Journal of Computer Vision*, vol. 91, no. 2, pp. 200–215, 2011.

[28] M. Dantone, J. Gall, G. Fanelli, and L. Van Gool, "Real-time facial feature detection using conditional regression forests," in *Proceedings of 2012 IEEE Conference on Computer Vision and Pattern Recognition*, pp. 2578–2585, Providence, RI, USA, June 2012.

[29] V. Kazemi and J. Sullivan, "One millisecond face alignment with an ensemble of regression trees," in *Proceedings of 2014 IEEE Conference on Computer Vision and Pattern Recognition*, pp. 1867–1874, Columbus, OH, USA, June 2014.

[30] J. Cech and T. Soukupova, "Real-time eye blink detection using facial landmarks," in *Proceedings of 21st Computer Vision Winter Workshop*, Rimske Toplice, Slovenia, February 2016.

[31] A. Nikolaidis and I. Pitas, "Facial feature extraction and pose determination," *Pattern Recognition*, vol. 33, no. 11, pp. 1783–1791, 2000.

Hindawi

Research Article

Myocardial Proteomics Based on Smart Fog Computing and Its Application in Sports

Fucai Zhang (ID) **and Yejin Wu** (ID)

School of Physical Education and Health, LinYi University, LinYi 276000, China

Correspondence should be addressed to Yejin Wu; wuyejin@lyu.edu.cn

How to strengthen physical fitness to improve the effect and efficiency of sports is an important research direction worthy of research. In response to these problems and limitations, Smart Fog Computing technology is introduced in this paper. Taking rats as the research object, the effective quantitative analysis and research of aerobic exercise on myocardial proteome are achieved through combining the business scope of myocardial proteomics, and connecting corresponding continuous aerobic exercises, verified by simulation analysis. The simulation research results show that the smart fog calculation is effective. For moderate-intensity aerobic exercise, the expression and intensity of the corresponding myocardial protein are changed significantly, and the corresponding heart becomes larger; meanwhile, moderate aerobic exercise can improve the metabolism and enhance digestive ability.

1. Introduction

With the continuous development of social economy, sports are increasingly valued and favored by people [1, 2]. However, because people have different physiques and cannot become sports athletes, for ordinary people, it can be achieved through corresponding food or nutritional supplements [3, 4]. It should be noted that some scholars have noticed the influence of related factors and then concentrated on the influence of myocardial mitochondrial protein [5, 6]. The emergence of aerobic exercise can gradually improve the related energy metabolism such as synthase in the corresponding myocardial protein tissue, further save the corresponding heart function, improve the corresponding pumping function, and accordingly meet the corresponding exercise needs. For different cells, the types of proteins are different under different pathological or physiological conditions [7, 8]. Therefore, the proteomics requires to be analyzed in terms of comprehensive and holistic analysis of dynamic changes in cells, so as to analyze protein composition, expression, modification, and other

states, further analyze the relationship between proteins, and reveal the laws of proteomics and cell activity [9, 10].

However, it should be noted that, with the increase of amount of exercise and practice, different exercise loads will be achieved, which will induce corresponding differences in the expression characteristics of the myocardial proteome, and thus discover different physiological and physical loads, which can achieve the differential expression of myocardial proteomics from the various factors such as load density and continuous training period [11, 12]. Therefore, it can be seen that exercise load may guide the recombination of myocardial proteomics to achieve the reshaping of the shape, state, and structure of the heart. In response to these needs and limitations, smart fog calculations is introduced in this paper, and the effective quantitative analysis and research of aerobic exercise on myocardial proteome are realized through combining the effects of aerobic exercise under a certain intensity on myocardial proteomics and taking rats as the research object, connecting corresponding continuous aerobic exercises in series, which is verified by simulation analysis, aiming to quantitatively analyze the influence law of myocardial proteomics.

2. Application Strategy of Motion Feedback System Based on Smart Fog Computing

The principle of network operation situation evaluation is to obtain the evaluation value of the current network operation situation through inference calculation based on the acquisition of operation data of various equipment and network operation and maintenance data, so as to reflect the overall operation of the network. From a mathematical point of view, the network operation situation evaluation is a mapping from the impact factor to the result value, and its mathematical model is

$$SA = f(x_1, x_2, \ldots, x_m). \tag{1}$$

In the formula, SA represents the network situation evaluation value, and the value is taken as $[0, 100]$; x_i is the influencing factor of network operation, that is, the evaluation index, where $i = 1, 2, \ldots, m$; f is the specific evaluation method, which is the realization of quantitative assessment of network operation situation proposed in this article based on the improved BP neural network model of entropy method and LM algorithm.

The entropy method and the Smart Fog Computing improved by the L-M algorithm are used in this paper to conduct the training process of situation assessment as shown in Figure 1.

The steps of determining the BP neural network structure, determining the index system, data preprocessing, and calculation of the index weight through entropy method as the model's initial parameters, BP neural network training model, and LM algorithm modification parameters are carried out successively. If the model error or the number of iterations meets the expected value, then the model training ends.

The square sum of the output resulting errors is taken as the objective function in the network model, and the parameter value is adjusted according to the gradient descent method to reduce the error. The model structure is shown in Figure 2.

Take the network situation assessment as an example.

$$y_j = f\left(\sum_{i=1}^{n} v_{ij} x_i - \theta_j\right). \tag{2}$$

In the formula, the function f is the selected activation function, which is usually expressed with the sigmoid function as

$$f(x) = \frac{1}{1 + e^{-x}}. \tag{3}$$

Similarly, for the kth neuron in the output layer, its output is

$$o_k = f\left(\sum_{j=1}^{m} w_{jk} y_j - r_k\right). \tag{4}$$

The error of the calculation result is expressed by the least square method:

$$E_k = \frac{1}{2} \sum_{k=1}^{l} (o_k - d_k)^2. \tag{5}$$

The above is the forward calculation process.

If the error does not meet the expected value, totaling $(N + L) \times M + M + L$ parameters. This process is a reverse calculation process.

In the reverse calculation process, the partial derivative of each parameter that needs to be adjusted is calculated, the parameter value is changed according to the gradient descent method, and the learning rate η is set to control the range of variation of parameter. w_{jk} is taken as an example, and the weight adjustment value is

$$\Delta w_{jk} = -\eta \frac{\partial E_k}{\partial w_{jk}}. \tag{6}$$

Realization of multiple iterations of forward and reverse directions is needed for Smart Fog Computing, and the number of iterations or allowable error range is set as the iteration termination condition to obtain the final model [13, 14].

The nonlinear mapping ability of Smart Fog Computing is extremely powerful, which can solve many practical application problems, and the network structure is flexible; but there are also some defects, such as slow learning speed, prone to fall into local optimal solutions, etc. These deficiencies may cause the lower accuracy and longer training time of situation assessment model based on the standard BP neural network. In response to these problems, an improved method based on Smart Fog Computing is proposed in this paper.

In the situation assessment method based on Smart Fog Computing, the final training effect of the BP neural network model is affected by the initial value of the model parameters. The index data of the network situation assessment is imported by the BP neural network model, so the index weights optimized by the entropy method are selected as the initialization parameters of the model.

To use the entropy method to calculate the index weight, the index system must first be determined.

For a total of n sample data and m indicators required for situation assessment, the j-th indicator value of the i-th data is denoted as x_{ij}. The normalized definition of data is shown in

$$x_{ij}' = \frac{x_{ij} - \min(x_j)}{\max(x_j) - \min(x_j)}. \tag{7}$$

For convenience, the data x_{ij}' after normalization is still recorded as x_{ij}.

Calculate the proportion of the i-th sample in the j-th index as

$$p_{ij} = \frac{x_{ij}}{\sum_{i=1}^{n} x_{ij}}. \tag{8}$$
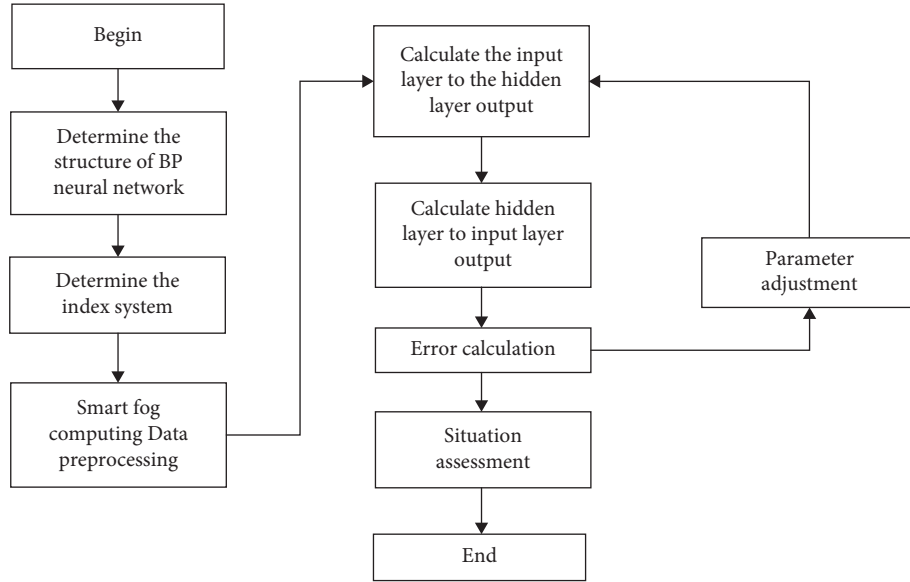
The calculation of entropy is

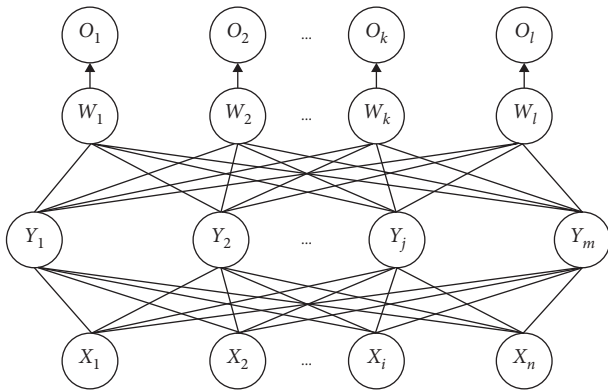FIGURE 1: Motion feedback evaluation process based on Smart Fog Computing.

FIGURE 2: Three-layer BP neural network model.

$$e_j = -k \sum_{i=1}^{n} p_{ij} \ln\left(p_{ij}\right). \tag{9}$$

In the formula, $k = 1/\ln n$ satisfies $e_j \geq 0$.

Calculate the information entropy redundancy of the j-th index as

$$d_j = 1 - e_j. \tag{10}$$

Calculate the weight of the j-th index as

$$w_j = \frac{d_j}{\sum_{j=1}^{m} d_j}. \tag{11}$$

Smart Fog Computing can deeply reflect the distinguishing ability of indicators, determine the weight of indicators, and have high credibility and accuracy. In the network situation assessment problem, the index weight calculated is used as the initial value of the parameters, which improves the credibility of the initial model and is conducive to the correct and rapid convergence [15].

Here, teachers can create a gamified teaching mode. Taking the 4×100 m relay run as an example, teachers can create different nodes on the sports field and place basketball, table tennis, badminton, boxing gloves, and other props at each node, separately before running. A separate instruction is issued for each club student. The instruction can include the name of a well-known athlete in a certain sport, sports rules, etc., so as to guide students to choose props based on the instruction and put them in the finish basket after finishing the run. The heartbeat, breathing rate, speed, and other data detected in the motion feedback system are scored as well as the correctness and wrong results of the instructions, which not only helps improve the fun of running training, but also realizes the training of students' basic sports knowledge and cultivates students' teamwork awareness and further improve students' enthusiasm for sports and enthusiasm for competition.

For sports, teachers are often accustomed to guiding traditional running and gymnastics to participate in collective exercise. However, due to the different physical fitness of students, the students are not often effectively supervised and guided by this model. Therefore, students' exercise is often conducted just in the classroom, but it cannot achieve the exertion of effect of sports. With the continuous development of technologies such as the Internet of Things, new technologies such as smart fog computing can fully cover and extend the corresponding smart watches and smart bracelets to achieve the full coverage and extension of the monitoring scope of sports. Meanwhile, big data analysis can be used to summarize the overall exercise behavior of students.

Big data intelligent analysis technology can generate instructive exercise information by processing the collected raw exercise data and provide an effective reference for the adjustment of the teacher's teaching plan and the setting of teaching priorities. Taking badminton training as an example, teachers can obtain information about different

students' movement postures, scores, hitting techniques, and sports area routes in the functional modules of the sports feedback system and use big data intelligent analysis technology to obtain the internal information between different indicators. Associate and then realize the quantification processing and calculation of sports information, presenting an intuitive evaluation of sports effects. Teachers need to use the exercise effect evaluation to judge the students' deficiencies in sports skills and technical programs and use this as a benchmark to adjust training content and methods, provide students with more professional and effective teaching guidance, and improve their sports skills and communicate effectively. At the same time, teachers can also use big data technology to comprehensively analyze the students' multiple training results and extract the progress curve around their original exercise level, which can be used as the benchmark for the evaluation of students' sports performance, so as to better improve the scientific nature of the evaluation of physical education and promote students' self-confidence in sports and the development of good exercise habits.

3. Application of Motion Feedback System in Middle School Physical Education Teaching

3.1. Promoting the Construction of Physical Education Informatization. For sports feedback, it is a kind of intelligent supervision that gathers big data analysis and intelligent IoT, which can effectively analyze sports behavior data and realize real-time or quasi-real-time analysis and monitoring of indicators, thus forming corresponding sports feedback forms, to realize dynamic analysis and evaluation during sports training, thereby reducing the cost of students' exercise analysis and promoting the in-depth application of smart fog computing.

3.2. Educational Requirements for Implementing Classified Guidance. The corresponding feedback system can be used to realize the collection, sorting, processing, analysis, and decision support of different individual motion modes, exercise speed, and other motion data, provide the corresponding teachers with personalized motion programs, and provide individual targeted guidance in different categories, thereby improving the overall effectiveness of physical education.

3.3. Promoting the Effective Improvement of Students' Physical Quality. The current sports feedback system is mainly embodied as wearable smart devices, including sports bracelets, smart wrist watch, and VR glasses, with functions such as exercise step counting, heart rate monitoring, and GPS positioning, to achieve effective capture of data on student movement trajectories, exercise time, etc. Physical education teachers can use their management authority to obtain the exercise data of different students, use big data intelligent analysis technology to collect the students' heart rate, speed, breathing frequency, and other parameters during exercise, and, at the same time, can judge whether the

student's exercise is in place and whether the trajectory is in place. Meet the requirements, in order to provide students with personalized guidance, with the help of the normative guidance of sports behavior, to better promote the effective improvement of students' physical fitness.

4. Simulation Experiment

4.1. Heart Weight Changes. In order to verify the effectiveness of smart fog computing, the corresponding fault diagnosis model is needed to be collected and constructed, and training can be conducted according to the corresponding data, and finally the online detection is realized in this paper. The specific fault diagnosis is shown in Figure 3:

Sports feedback is integrated; taking rats as an example, the results of their sports feedback are comprehensively compared, as shown in Figure 4. From the results, it can be seen that the heart weight and heart weight index of big data have corresponding changes, so you can see that, after a certain period of aerobic exercise, the rat's heart has undergone certain changes.

4.2. Mass Spectrum Identification Result. After a certain period of aerobic exercise, changes in the expression of myocardial protein in rats occur. Therefore, it is necessary to connect in series and use corresponding instruments for detection and identification to achieve quantitative analysis. As shown in Figure 5, it can be seen from the results that protein 7 is related to the metabolic energy of the myocardium.

4.3. Analysis of Changes in Heart Weight. Through corresponding experimental comparison, it can be seen that the rat's heart weight and heart weight index have increased. Therefore, the change of heart weight is used to analyze in this paper, and it can be obtained that, after a certain period of moderate aerobic exercise, the increase of myocardial physiology can be achieved, which results in a difference in the energy metabolism of some myocardial proteomics, which leads to an increase change in the level of myocardial metabolism, achieving myocardial contraction.

4.4. Analysis of Mass Spectrum Identification. In the process of heart remodeling during exercise, the pathway of cardiac energy metabolism has undergone corresponding changes. These proteins are mainly related to the tricarboxylic acid cycle and amino acid metabolism process in the aerobic oxidative metabolism of the myocardium.

The effect of moderate-intensity aerobic exercise on atrial myocardial tricarboxylic acid cycle: the expression of ACO2 may have expression difference of myocardium in different positions in different intensities, different continuous training periods, and different positions. The mechanism of its differential expression needs further experimental study. This experiment may increase the expression of
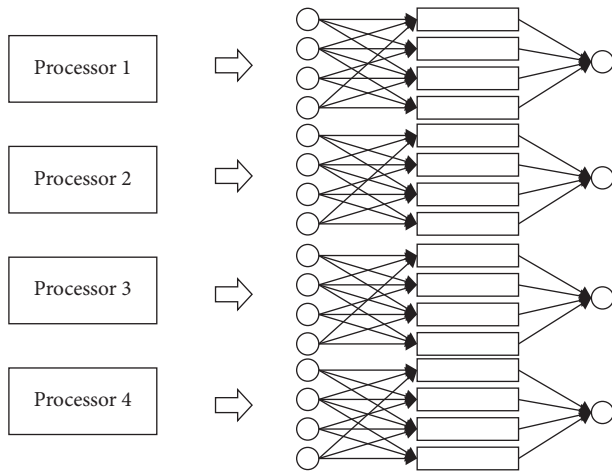
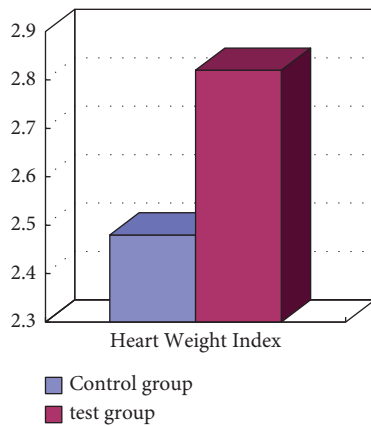FIGURE 3: Data parallelization process.

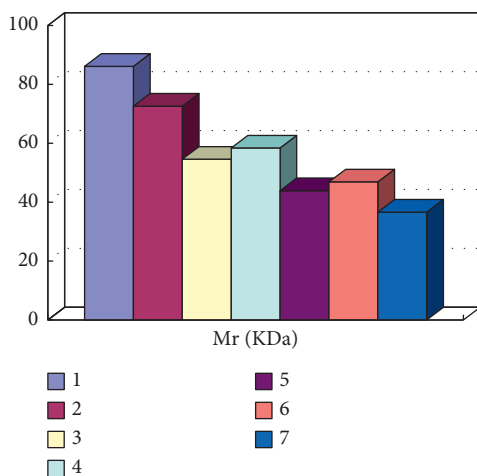FIGURE 4: Changes in heart weight index measurement.

FIGURE 5: Mass spectrometric identification of target protein spots related to myocardial energy metabolism.

aconitate hydratase through 4 weeks of moderate-intensity aerobic exercise, so as to improve the energy supply of the heart and enhance the contractility of atrial muscle.

First, collect the list of abnormal events in gateway measurement, and establish a database of abnormal events in metering equipment. Common abnormal events include electric energy meter error exceeding tolerance, PT secondary voltage drop exceeding tolerance, secondary circuit pressure loss, current loss, phase failure, and secondary load overrun, unbalanced current, overlimit demand, abnormal line loss, and unbalanced bus. Then, test typical measurement equipment, and verify the system's identification through the laboratory failure simulation platform to simulate various measurement abnormal events. According to the test results, the system's functions of distinguishing, recording, and alarming abnormal measurement events are verified, and meanwhile, the judgment rules and thresholds of abnormal measurement events are improved and standardized (Figure 6).

The mitochondrial succinate dehydrogenase coenzyme flavin subunit in atrial muscle declined by 7 times, and the expression of cytoplasmic malate dehydrogenase declined by 7.2 times after exercise. The difference in experimental results may be related to many factors. Therefore, a certain period of aerobic exercise can promote the increased expression of the myocardial protein of pyruvate dehydrogenase Elα1, realize the supply of heart energy, and enhance the contraction and pumping ability of the heart.

In this experiment, the mitochondrial succinate dehydrogenase coenzyme flavin subunit in atrial muscle was downregulated by 6.9 times, and the expression of cytoplasmic malate dehydrogenase was downregulated by 7.3 times after exercise. The difference in experimental results may be related to the intensity of exercise. The duration of exercise is related to the structure and function of myocardial tissue in different parts. The main function of the atrial muscle is not to contract and pump blood. Its ejection process is short, and the contraction work value is smaller than that of the ventricular muscle. In addition, there was a 4-week 60%–70% VO2max moderate-intensity aerobic exercise due to low exercise intensity and short exercise duration. It may be that the body is in the stage of exercise adaptation and may not produce strong oxidative stress on atrial muscle cells. Stimulate the expression of malate dehydrogenase and mitochondrial succinate dehydrogenase coenzyme flavin subunits of atrial muscle, but the reasons for the decrease in expression level need to be further explored and verified:

Point 265 is identified as pyruvate dehydrogenase Elα1, which belongs to the pyruvate dehydrogenase complex system. Pyruvate dehydrogenase complex (PDHc) is the key enzyme system that catalyzes the oxidation and decompression of ketone acid to form acetyl-CoA and plays an important role in the body's aerobic oxidation metabolism process.

The expression of pyruvate dehydrogenase Elα1 was "absent" in the right ventricular muscle of rats after 4 weeks of moderate-intensity aerobic exercise (70%–80% VO2max). There was no difference in its expression after 8 weeks of exercise, and its expression after 12 weeks of exercise. The expression level was upregulated by 33.3 times. The expression of this protein has a time effect. As the body slowly
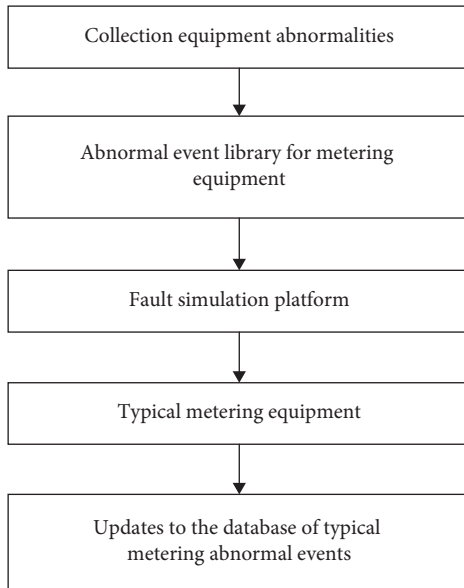
Figure 6: Establishment and verification of abnormal event database.

adapts to exercise intensity, it finally shows a high expression of adaptability to improve the myocardial oxidative metabolism capacity. Studies have found that the protein expression in right ventricular muscle is upregulated by 5.3 times after 8 weeks of exercise (60%–70% VO2max aerobic). In the results of this experiment, 4 weeks of moderate-intensity aerobic exercise induced an upregulation of the protein expression in atrial muscle and left ventricular muscle by 6.4 and 5.8 times, respectively. Based on the above research results, long-term moderate-intensity aerobic exercise can promote pyruvate dehydrogenase Elα1 increased expression in various parts of myocardial tissue and, as a result, accelerates the oxidative decompression of pyruvate in the body, provides sufficient acetyl-CoA for the myocardial triacyl acid cycle process, improves the energy supply of the heart, and enhances the contraction and pumping ability of the heart.

The effect of moderate-intensity aerobic exercise on the amino acid metabolism of atrial muscle: point 393 is identified as isovaleryl-CoA dehydrogenase. It is involved in the metabolic decomposition of leucine, an important catalytic enzyme for leucine metabolism. Point 236 is identified as mitochondrial dihydrolipoic acid dehydrogenase, which belongs to the multienzyme complex of glycine dehydrogenase and reductase and participates in the metabolism of glycine. In addition, it also works with pyruvate dehydrogenase and dihydrolipoic acid acetyltransferase. It constitutes the pyruvate dehydrogenase complex and belongs to the FAD-dependent enzyme.

After an acute exhaustive exercise intervention, isovaleryl-CoA dehydrogenase is "absent" expression in the atrial muscle, which may cause the accumulation of isovaleric acid, a metabolite of leucine, in the process of leucine degradation, and make the intracellular pH. When the value increases, the energy metabolism of myocardial cells is impaired, and the myocardial contractility decreases. This

experiment found that 4 weeks of moderate-intensity exercise reduced the expression of isovaleryl-CoA dehydrogenase in atrial muscle by 6.9 times, and the expression of mitochondrial dihydrolipoate dehydrogenase by 5.7 times. The oxygen demand is great, and the energy supply process of mature cardiomyocyte activity is mainly supplied by the aerobic oxidation of sugar, and the energy supply ratio of amino acid is very small. Hafstad's research shows that moderate-intensity treadmill exercise (65%–70% VO2max) improves the utilization of rat myocardial glucose and improves the aerobic capacity of the body. Therefore, the 4 weeks of moderate-intensity aerobic exercise in this study does not require a large amount of amino acid mobilization. It may be so in order to save the body's amino acids and protein. After exercise, the expression of the above two proteins in atrial muscle was inhibited. In this experiment, the downregulation of the expression of mitochondrial dihydrolipoate dehydrogenase may also be related to the upregulation of pyruvate deoxygenase Elα1. In order to optimize the energy supply structure, the upregulation of pyruvate deoxygenase Elα1 competitively inhibited dihydrolipoic acid dehydrogenation. For enzymes, the relationship between them in the metabolism of cardiomyocytes needs to be further explored.

The number point is identified as methylmalonate semialdehyde dehydrogenase [acyl], which plays a role in the metabolism of glycine and HI and belongs to the dehydrogenase family. There is no in-depth study of this protein in the field of sports medicine research: in this experiment, it was found that the expression level of this protein was upregulated by 6.3 times after 4 weeks of moderate-intensity aerobic exercise, which may bring new research content to the study of exercise to improve myocardial material and energy metabolism.

At present, with the continuous development of proteomics research technology, more and more researchers have applied proteomics and related technologies to the research of cardiovascular diseases and have made good progress, involving the expansion type proteomics research on cardiomyopathy, acute coronary syndrome, heart failure, hypertension, coronary heart disease, atrial fibrillation, myocardial infarction, vascular disease, and hyperlipidemia.

The research of sports heart proteomics is still in a preliminary stage of exploration. In recent years, the research on this topic is gradually increasing and deepening. The results of the study found that high-intensity exercise caused significant differences in the expression and quality of the proteome of rat myocardium. The effect of high-intensity exercise on the differential expression of the proteome of atrial and ventricular muscles in rats and exercise is studied. The duration of the load is related. With the extension of the duration of the exercise load, the rat's myocardial proteome changes adaptively, and the expression of more and more types and numbers of protein spots changes adaptively.

In this study, moderate-intensity aerobic exercise during a certain period of cycle does not require a large amount of amino acid to be mobilized for energy. After exercise, the expression of the above two proteins in atrial muscle
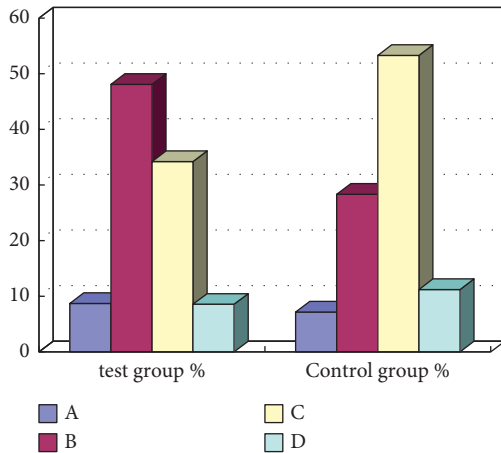
Figure 7: Comparison of physical fitness classification of middle school students after the intervention and during the backtest.

Figure 8: Comparison of changes in rats' physical exercise sensation after intervention and during backtesting.

probably was inhibited in order to save amino acids and protein in the body.

The research of sports heart proteomics is still in a preliminary stage of exploration. In recent years, the research on this topic is gradually increasing and deepening. Moder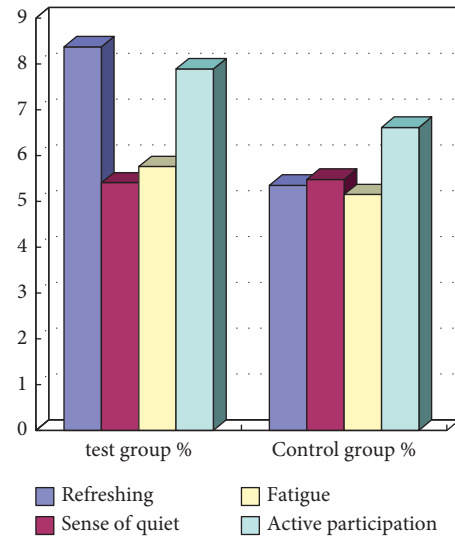ate-intensity aerobic exercise can make good adaptability changes in the heart. The study of the myocardium under this exercise intensity from the molecular level of protein can provide a theoretical basis for explaining the related mechanism as a whole. The changes in the myocardial proteome caused by long-term moderate-intensity exercise mainly occurred in the first 8 weeks, and different myocardial parts showed different differential expression characteristics.

Judging from the physical fitness classification of posttest and backtest, the physical fitness test results of the experimental group rats showed a phenomenon that the concentration of the rats in the test group rose from the "pass" level to the "good" level before the intervention, while, in the control group rats, all three physical fitness test results showed that they were gathered at the "pass" level (Figure 7). This also shows that intervention education has a good effect on improving the physical fitness of rats.

The exercise feeling test after the intervention showed (see Figure 8) that the comparison of the two dimensions of refreshment and active participation in the experimental group of rats was significantly higher than that of the control group ($P < 0.05$), and meanwhile, the quietness decreased, and fatigue sensation increased, but the difference between the groups was not significant (C0.05).

In this study, moderate-intensity aerobic exercise in a certain period of time does not require a large amount of amino acid mobilization for energy. It may be so in order to save amino acids and protein in the body; after exercise, the expression of the above two proteins in atrial muscle was inhibited.

The research of sports heart proteomics is still in a preliminary stage of exploration. In recent years, the research on this topic is gradually increasing and deepening. Moderate-intensity aerobic exercise can make good

adaptability changes in the heart. The study of the myocardium under this exercise intensity from the protein molecular level can provide a theoretical basis for explaining the related mechanism as a whole. The changes in the myocardial proteome caused by long-term moderate-intensity exercise mainly occurred in the first 8 weeks, and different myocardial parts showed different differential expression characteristics.

Long-term aerobic exercise can improve the heart and exercise capacity of the elderly to a certain extent, which in turn promotes the improvement of the cardiovascular skills of the elderly. From the perspective of proteomics, it can be seen that moderate aerobic exercise is beneficial to the heart and can provide a certain practical basis for cardiovascular rehabilitation and treatment of the elderly. Meanwhile, moderate-intensity and continuous practice can physiologically reshape the heart, guide the heart to transform to the direction of contraction and pumping function, and finally complete the continuous expression of differentiation.

5. Conclusions

The continuous development of social economy has promoted people's attention to the body more and more. How to effectively carry out physical exercise and enhance nutrition is extremely important. In response to these problems and limitations, aerobic exercise monitoring is performed for a certain period of time based on smart fog computing technology, through combining the business scope of myocardial proteomics, realizing the effective analysis of aerobic exercise on myocardial proteomics, and a certain verification is performed through simulation analysis. The experimental results show that the method is effective, can promote effective metabolism, and can achieve an effective improvement of digestive ability.

Data Availability

The labeled dataset used to support the findings of this study is available from the corresponding author upon request.

Conflicts of Interest

The authors declare no competing interests.

Acknowledgments

References

[1] N. Qvit, M.-H. Disatnik, E. Sho, and D. Mochly-Rosen, "Selective phosphorylation inhibitor of delta protein kinase C-pyruvate dehydrogenase kinase protein-protein interactions: application for myocardial injury in vivo," *Journal of the American Chemical Society*, vol. 138, no. 24, pp. 7626–7635, 2016.

[2] Y. Tsukamoto, "Takanari. Atrial fibrillation-mediated upregulation of miR-30d regulates myocardial electrical remodeling of the G-protein-gated K+ channel, I-K.ACh," *Circulation Journal*, vol. 4, no. 3, pp. 1–8, 2016.

[3] R. Zou, W. Shi, J. Tao et al., "SIRT5 and post-translational protein modifications: a potential therapeutic target for myocardial ischemia-reperfusion injury with regard to mitochondrial dynamics and oxidative metabolism," *European Journal of Pharmacology*, vol. 818, pp. 410–418, 2017.

[4] P. A. Fordjour, Y. Wang, Y. Shi et al., "Possible mechanisms of C-reactive protein mediated acute myocardial infarction," *European Journal of Pharmacology*, vol. 6, no. 5, pp. 101–108, 2015.

[5] M. Zhou, Y. Bao, H. Li et al., "Deficiency of adipocyte fatty-acid-binding protein alleviates myocardial ischaemia/reperfusion injury and diabetes-induced cardiac dysfunction," *Clinical Science*, vol. 129, no. 7, pp. 547–559, 2015.

[6] R. T. Gardner, L. Wang, B. T. Lang et al., "Targeting protein tyrosine phosphatase σ after myocardial infarction restores cardiac sympathetic innervation and prevents arrhythmias," *Nature Communications*, vol. 6, no. 4, pp. 6235–6245, 2015.

[7] M. Y. Heinke, C. H. Wheeler, J. X. Yan et al., "Changes in myocardial protein expression in pacing-induced canine heart failure," *Electrophoresis*, vol. 20, no. 10, pp. 2086–2093, 2015.

[8] R Garca, D Merino, J. M Gomez et al., "Extracellular heat shock protein 90 binding to TGF receptor I participates in TGF-mediated collagen production in myocardial fibroblasts," *Cellular Signalling*, vol. 28, no. 10, pp. 1563–1579, 2016.

[9] A. Sheriff, R. Schindler, B. Vogt et al., "Selective apheresis of C-reactive protein: a new therapeutic option in myocardial infarction?" *Journal of Clinical Apheresis*, vol. 30, no. 1, pp. 15–21, 2015.

[10] R. Sreedhar, S. Arumugam, R. A. Thandavarayan et al., "Depletion of cardiac 14-3-3η protein adversely influences pathologic cardiac remodeling during myocardial infarction after coronary artery ligation in mice," *International Journal of Cardiology*, vol. 54, no. 3, pp. 56–63, 2016.

[11] J. Winata, A. Supit, M. Rotty, K. K. Elka, H. A. Kuncoro, and R. A. Azis, "Comparing albuminuria and high sensitivity C-reactive protein as predictors of silent myocardial ischemia in hypertensive men without diabetes mellitus," *Journal of Hypertension*, vol. 33, no. 3, pp. 11–20, 2015.

[12] X. Wang, D. Liu, W. Chai, Y. Long, L. Su, and R. Yang, "The role of uncoupling protein 2 during myocardial dysfunction in a canine model of endotoxin shock," *Shock*, vol. 43, no. 3, pp. 292–297, 2015.

[13] K. C. Koskinas, S. Zaugg, K. Yamaji et al., "Changes of coronary plaque composition correlate with C-reactive protein levels in patients with ST-elevation myocardial infarction following high-intensity statin therapy," *Atherosclerosis*, vol. 247, no. 5, pp. 154–160, 2016.

[14] M. Morishima, E. Iwata, C. Nakada et al., "Atrial fibrillation-mediated upregulation of miR-30d regulates myocardial electrical remodeling of the G-protein-gated K+ channel, Ik.ACh," *Circulation Journal*, vol. 80, no. 6, pp. 1346–1355, 2016.

[15] R. Sreedhar, S. Arumugam, R. A. Thandavarayan et al., "Myocardial 14-3-3η protein protects against mitochondria mediated apoptosis," *Cellular Signalling*, vol. 27, no. 4, pp. 770–776, 2015.

Research Article

Research on Cold Chain Logistics Traceability System of Fresh Agricultural Products Based on Blockchain

Xinghua Zhang [iD],[1] Yongjie Sun,[2] and Yongxin Sun [iD][3]

[1]*Changchun Sci-Tech University, Changchun 130600, Jilin, China*
[2]*College of Life Science, Changchun Sci-Tech University, Changchun 130600, Jilin, China*
[3]*College of Physics and Electronic Information, Baicheng Normal University, Baicheng 13700, Jilin, China*

Correspondence should be addressed to Yongxin Sun; sunyongxin@bcnu.edu.cn

Xinghua Zhang and Yongjie Sun contributed equally to this work.

Traditional cold chain logistics has problems such as centralized data storage, low data reliability, easy data tampering, and difficulty in locating responsible persons, which leads to the inability to guarantee consumer rights. To solve these problems, a cold chain logistics traceability system is proposed for fresh agricultural products based on blockchain. Both alliance chain and private chain are used in the paper in order to ensure that the product traceability system not only has certain openness but also must contain enough privacy and security. Alliance chain is mainly used to query and share product traceability information. The private chain will be used to collect and store the product traceability information of each enterprise and then connected to the alliance chain via hash pointers. The proposed system is beneficial for reducing the burden of network transmission of alliance chain and improving the efficiency of consumer product data query. At the same time, the private chain ensures the security and privacy of enterprise product data, which not only has high data storage efficiency but also can meet the requirements of all participants for the traceability system. In the experimental part, the feasibility of this system is verified through simulation experiments, which provides a reference for the combination of blockchain technology and cold chain logistics traceability system.

1. Introduction

Agricultural products and cold chain logistics system from farmland to table involve production, processing, packaging, transportation, storage, sales, and other different links. Each link may have unsafe factors. In recent years, such incidents as "cadmium rice" [1], "aquatic crab," and "smuggled frozen meat" in Guangdong [2] and "malachite green" for bass [3] and "crayfish" in Nanjing have seriously damaged the interests of consumers [4]. At the same time, the production of fresh agricultural products and cold chain logistics enterprises also suffered a heavy blow. These events further triggered a crisis of trust between consumers and fresh agricultural products enterprises [5, 6]. Traceability system has become an effective means of supply chain quality management of fresh agricultural products by reducing

quality and safety risks, improving product recall efficiency, and ensuring public health [7, 8]. The research and establishment of cold chain logistics traceability system for fresh agricultural products, which can achieve effective supervision of the whole process from production to consumption, have become a hot issue of general concern.

The cold chain logistics traceability of fresh agricultural products involves agricultural supplies suppliers, farmers and other producers, processors, middlemen, and end consumers. Among them, middlemen further include logistics service providers, wholesalers, distributors, and retailers. Therefore, the cold chain logistics traceability system of fresh agricultural products is characterized by many points, long lines, wide areas, and intricate intersections [9, 10]. This makes food safety supervision and traceability particularly difficult in operation. The traditional traceability

system relies on the authority to manage the central database in practice, which has the problem of data centralization. Traceability data on each supply chain node is managed by the enterprise itself and is easy to be tampered with. At the same time, the reliability of information transmission among various roles in the supply chain remains to be solved.

Blockchain technology is characterized by tamability, distribution, decentralization, traceability, and high availability. Using these characteristics of blockchain, the combination of blockchain technology and cold chain logistics traceability of fresh agricultural products provides the possibility of solving the problems existing in the current traditional agricultural products traceability system. In recent years, domestic and foreign scholars [11–14] have carried out exploration and research in the field of agricultural product traceability. The existing methods are mostly based on the existing common blockchain systems such as Bitcoin, Ethereum, and Hyperledger Fabric system for application development. They have some bottleneck problems in data storage, such as low query efficiency, high data storage pressure, and poor data security. In practical applications, the following problems may occur when blockchain is used as a data management platform for traceability applications. As the quantity of nodes and data increases, the underlying storage system is frequently accessed by users. This puts forward high requirements on the function and performance of the data storage system.

Therefore, this paper proposed a cold chain logistics traceability system of fresh agricultural products based on blockchain, which is from the perspective of improving the efficient information storage and fast query efficiency of the cold chain logistics traceability system of fresh agricultural products. In order to ensure the high reliability of blockchain operation environment, the traceability system adopts the dual chain structure design of alliance chain and private chain. In the experiment, the feasibility of the system is verified by simulation experiment.

2. Related Work

2.1. Traceability to the Safety of Cold Chain Logistics.
Cold chain logistics generally refers to system engineering to ensure product quality and reduce product loss, keeping refrigerated and frozen products in a specified low temperature environment all the time. Production, storage, transportation, distribution, sales, and consumption before the purchase of each link are included among them. Studies have found that every $6°$ increase in temperature will double the growth rate of bacteria in food and shorten the shelf life by half [15]. When ambient temperatures rise at any point, bacteria multiply more quickly. This is the impact of temperature change on food safety that most people are not aware of.

The essence of traceability is to turn the physical circulation of industrial chain into information flow. The production and circulation information of products can be obtained according to the tracking and query of information flow [16]. Agricultural product safety traceability refers to

the ability to track the flow of products when there are safety problems in agricultural products, then recall the problematic food, cut off the source, and eliminate the harm. Therefore, each link needs to record the corresponding information from the production, circulation, and final consumption of agricultural products. For consumers, traceable agricultural products provide transparent product information. This enables consumers to fully enjoy the right to know when buying and to make the right purchase choice. It has always been regarded as the most complicated and difficult part of food traceability because of the wide circulation range, long chain, and many links of agricultural products.

The accurate and real-time whole process record provided by cold chain logistics provides conditions to trace agricultural product information accurately and effectively. The working principle of cold chain logistics relies on modern information technology with the help of advanced management methods and organization. Typically, a combination of RFID (Radio Frequency Identification), GPS (Global Positioning System), GIS (Geographic Information System), mobile communications, and temperature sensing technology is used [17]. Then, the record of temperature and humidity change is uploaded to the management platform for real-time management of product quality. This intelligent, information-based cold chain logistics process provides technical support for agricultural products traceability. However, in order to complete the traceability management of agricultural products, it is necessary to establish the necessary basic information base for its core information such as planting, storage, processing and distribution, sales, and consumer attention. Through the information management platform, the discovered problems can be queried, and the generated problems can be held accountable.

2.2. Basic Introduction to Blockchain

2.2.1. Blockchain.
Blockchain is a chain structure of blocks of data arranged in chronological order through cryptography algorithms. It can realize decentralized, tamper-proof, traceable, and multiparty jointly maintained distributed database [18]. Each party must agree to update the data according to the pre-agreed rules and implement information sharing and monitoring among the parties. Blockchain integrates P2P network, cryptography [19], smart contract [20], consensus mechanism [21], timestamp [22], blockchain structure, and other technologies. It can realize self-verification and management of data without relying on third parties.

2.2.2. Block Structure.
Blockchain is an ordered chain of data block structure with block as unit, and each block is composed of block head and block body [23]. As shown in Figure 1, each block header contains the hash value of the previous block header. The original block is connected to the current block and forms a chained data storage structure. The properties of the Merkle tree structure and the connection between timestamps and blocks are
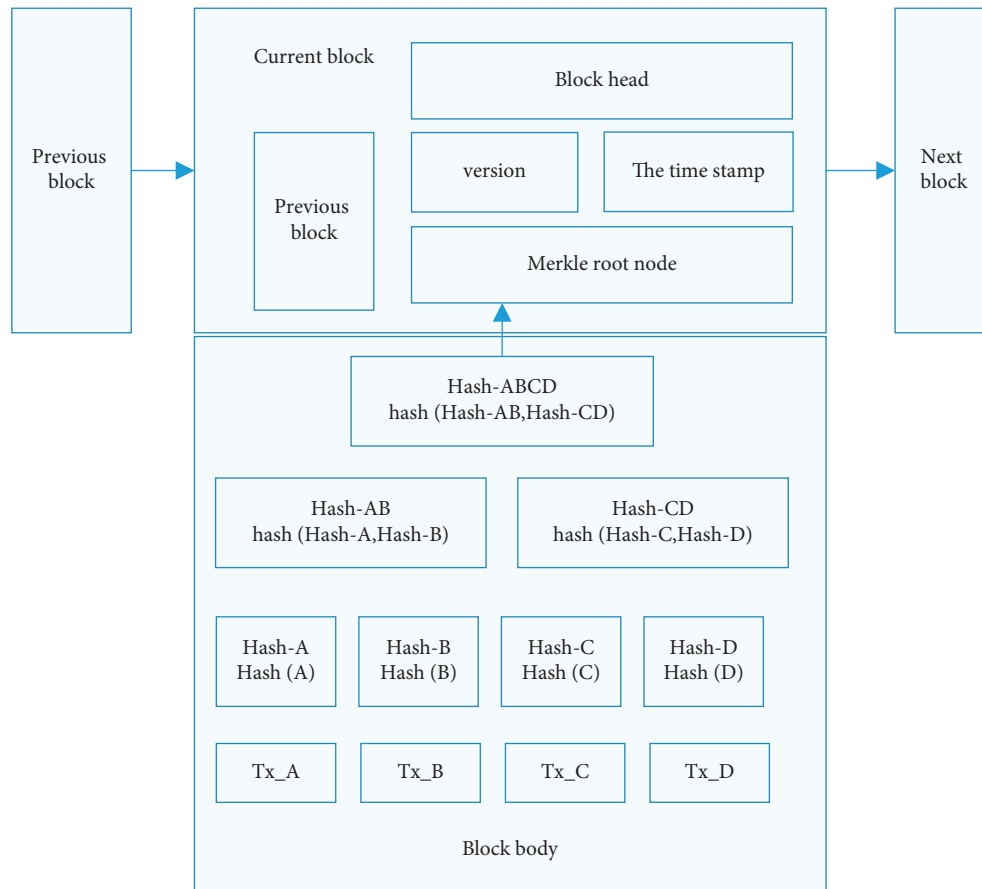
FIGURE 1: Structure diagram of block data.

utilized to ensure that each block is connected chronologically and the data is not susceptible to tampering [24]. Even if it is tampered with, it can be quickly located, which ensures the reliability and credibility of the traceability system data [25].

2.2.3. Hash Algorithm. The hash algorithm can map data of any length to a short-fixed length binary value through hash function [26, 27]. It is an irreversible mapping from plaintext to ciphertext; that is, the same input always yields the same output. Using the characteristics of hash function, it can not only verify whether trace data is tampered with, but also ensure the security of data. In practical applications, MD5 [28] algorithm is usually adopted, which generates a 32-bit hexadecimal sequence value for the input of arbitrary length string.

2.2.4. Blockchain Classification. According to the degree of regional decentralization, blockchain is mainly divided into public chain, alliance chain, and private chain [29]. In the traceability system, the responsible subjects of the agricultural supply chain belong to the cooperative relationship, but at the same time, they cannot be completely trusted. There is already association, horizontal interconnection and cooperation, or vertical transaction relationship. Therefore, alliance chain is usually used as

the technical framework for agricultural product traceability system research [30].

3. The Proposed Model in This Paper

3.1. Cold Chain Logistics Process Analysis of Fresh Agricultural Products. In order to design the traceability system of fresh agricultural products, the management mode of its generation to sales will be analyzed first, and then the traceability management method will be designed according to the characteristics of each link. The main body of "base-+ supermarket" agricultural cold chain logistics is clear, and the key points of traceability information flow are easy to define compared with other complex and diverse circulation forms of agricultural products. The specific process is as follows.

3.1.1. Planting and Harvesting. When agricultural products are still in the "field," their growth process will suffer from the soil pesticide residues, heavy metals, and other irreversible harm. Improper fertilization can also cause quality problems in agricultural products. Therefore, all production plots and greenhouses need to be numbered uniformly. The turnover box of picking agricultural products should also be managed by numbering, and strict and accurate records should be made. The harvest time of agricultural products is

short, and the process has little impact on the quality of agricultural products. In this stage, process records and quality testing reports are mainly carried out.

3.1.2. Storage and Processing. Harvested agricultural products that are not immediately listed need to be stored or circulated for processing. This link should strengthen production monitoring. The agricultural products cold storage requirements and the absolute safety of processing are ensured, depending on the temperature sensing technology. In this link, records of storage temperature, humidity, processing, and storage time should be made.

3.1.3. Transportation and Distribution. Transport vehicles for agricultural products shall comply with health requirements and be equipped with a continuous output of temperature records that cannot be artificially altered. The docking of agricultural product information should be carried out before transportation and distribution. In the process of distribution and transportation, GPS and GIS should be relied on to track and monitor the situation of agricultural products and refrigerated vehicles. This is to prevent damage to agricultural products caused by improper handling or microbial damage. In this link, records of transportation temperature, humidity, geographical location, and transportation time should be made. The logistics information recording process is shown in Figure 2.

3.1.4. Supermarket Sales. The sales of agricultural products still need refrigeration preservation technology to ensure the quality of agricultural products, which usually should be displayed and sold in accordance with the storage temperature and humidity of agricultural products. In this link, the refrigeration temperature, humidity, purchase and sale time, and other information should be well recorded.

The record of the above key points provides the prerequisite for the establishment of agricultural products traceability system. First, base operators generate retrospective two-dimensional code for the harvested agricultural products according to the production number and paste it on the packaging of agricultural products. The additional information is mainly the production experience of agricultural products, for example, the planting date; the fertilization date; the fertilization duration; and the use of pesticides, growth promoters, and other related auxiliary products. Record the names; sources; users; and pickers of pesticides, fertilizers, and regulators used. Upload production file information to the platform through information technology. In the subsequent cold chain logistics, the storage file, transportation file, and distribution file of each link should be recorded. Then, the cold chain logistics operator will upload them to the platform in real time. Finally, consumers who buy products at a supermarket scan a QR code on the package. Users can query the detailed information and quality test report of agricultural products from planting, production, transportation, storage, and sales through the platform. At the same time, the upstream subject can also track the information of agricultural products in each link of circulation through the platform. The traceability system of "base + supermarket" agricultural cold chain logistics integrates the records of planting, collection, and key points of cold chain logistics into the database information of the traceability system. Through the operation of the traceability service management platform, the main body of the agricultural supply chain can share information and achieve convenient and accurate traceability of agricultural products.

3.2. Data Structure of Private Chain and Alliance Chain

3.2.1. Participant Setting of the Anticounterfeiting Traceability System. The function and nature of product traceability determine that it has many participants, mainly including various manufacturers, relevant national departments, and consumers. Product traceability system must contain sufficient privacy and security while requiring certain openness. This paper proposes an anticounterfeiting traceability system using both alliance chain and private chain. The alliance chain is mainly used to query and share product traceability information. The private chain will be used to collect and store the product traceability information of each enterprise and then connected to the alliance chain through the hash pointer. This design method is beneficial for reducing the burden of network transmission of alliance chain and improving the efficiency of consumer product data query. The private chain ensures the security and privacy of enterprise product data. It not only has high data storage efficiency, but also can meet the requirements of all participants for the traceability system. The production department, transportation and storage department, sales department, information technology department, and national supervision department of each enterprise jointly maintain the private chain and add product traceability information and audit information of the supervision department to the private chain. Among them, the state supervision department, as the organizer of the private chain, will participate in the audit and authorization of enterprises. The information technology department is responsible for collecting information packaging blocks as the holder of billing rights for the private chain. Other departments in each enterprise and national law enforcement departments jointly maintain the alliance chain and provide external tracing information query function.

3.2.2. Product Traceability Information Structure. Blockchain does not prevent the initial data fraud; that is, it does not prevent companies from falsifying product raw materials, warehousing, and other information. Thus, companies will use IoT (Internet of Things) technology to monitor production, processing, and warehousing in real time and establish a set of intelligent production lines and storage lines to ensure the authenticity of the source data reliability.

As shown in Table 1, for a certain product, the production information P generated by the production department of the enterprise includes but is not limited to
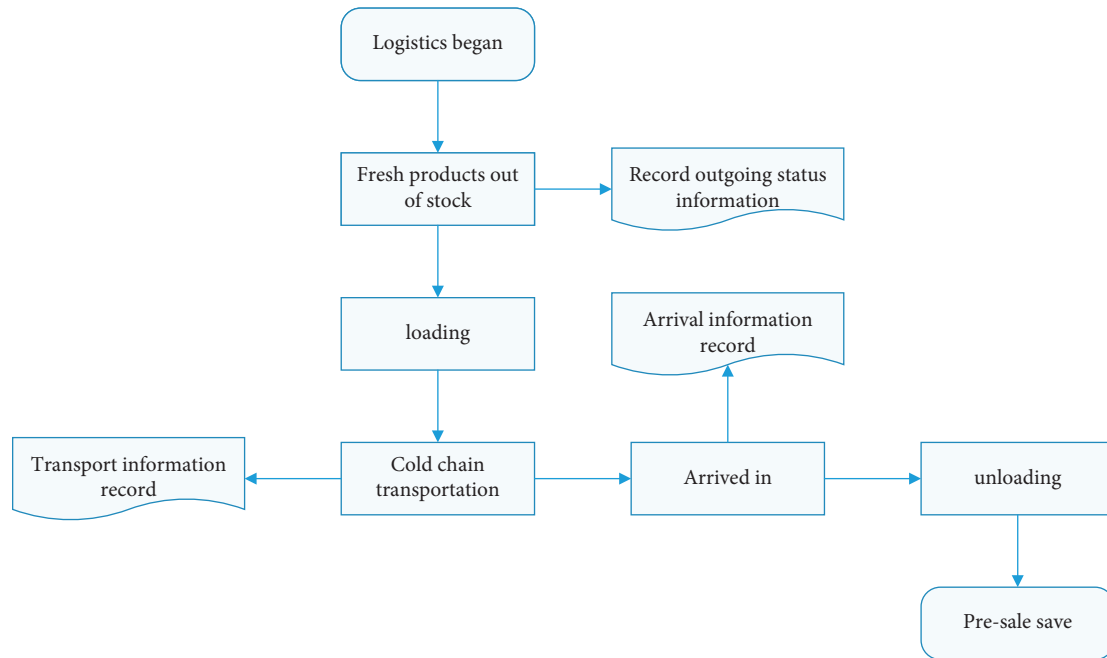
FIGURE 2: Logistics information recording process.

product ID, product name, raw material information (recorded by sensors and transmitted to the production department), signature S_x of the person in charge, and hash value $H(P)$ of the production information.

As shown in Table 2, for a certain product, the transportation and storage information T generated by the transportation and storage department of the enterprise includes but is not limited to transportation time, transportation mode, storage information (transmitted through temperature sensors, etc.), signature S_y of the person in charge, and hash value $H(T)$ of the transportation and storage information.

As shown in Table 3, for a certain product, sales information S generated by the sales department of the enterprise includes but is not limited to sales time, sales quantity, sales method, signature S_z of the person in charge, and hash value $H(S)$ of sales information S.

In order to prevent enterprises from tampering with their product traceability information, the above three types of traceability information should also be submitted to the national regulatory authorities for audit, and the audit information C can be obtained. Using the input sensitive property of hash function, check whether trace information is tampered with. In case of alteration, responsibility can be quickly confirmed according to the signature of the person in charge in each process to prevent the circulation of illegal products. If there is no alteration, it will be handled by the enterprise information technology department.

After the examination and verification by the national supervision department, the information technology department of the enterprise shall collect production information P, transportation and storage information T, sales information S, and audit information C, and then S_i is signed by the head of the information technology department. A transaction in a private chain block, the structure of which is shown in Table 4 is constituted.

After the above procedure is performed, a secure and reliable private chain of product traceability information will be generated. In order to prevent the leakage of enterprise privacy data, enterprises can only query the information of their own products on the private chain. Due to the large amount of data transmitted in the private chain, it is not suitable for transmission in the alliance chain that provides the query function. Therefore, it is not necessary to store complete product traceability information in the alliance chain block body, but to store the block header hash value of each block in the private chain. This can improve the efficiency of data transmission in the alliance chain. At the same time, according to the characteristics of Merkle tree and hash function, product traceability information items will correspond one by one, and there is no confusion of traceability information. The header of the block in the alliance chain consists of the current block hash, the hash of the previous block header, the timestamp, the Merkle root, and the associated responsible signature. The block body contains the hash value of each block header in the private chain. Figure 3 shows the data structure of the private and alliance chains.

3.3. The Proposed Cold Chain Logistics Traceability System

3.3.1. Storage Mechanism Design. There are many participating nodes in the blockchain-based agricultural supply chain, and the data collection volume of nodes in each link is large. If all the nodes are uploaded to the blockchain network at one time, in addition to the slow upload speed, the operation cost will be greatly increased, and the hardware requirements for nodes in each link will be high. Therefore,
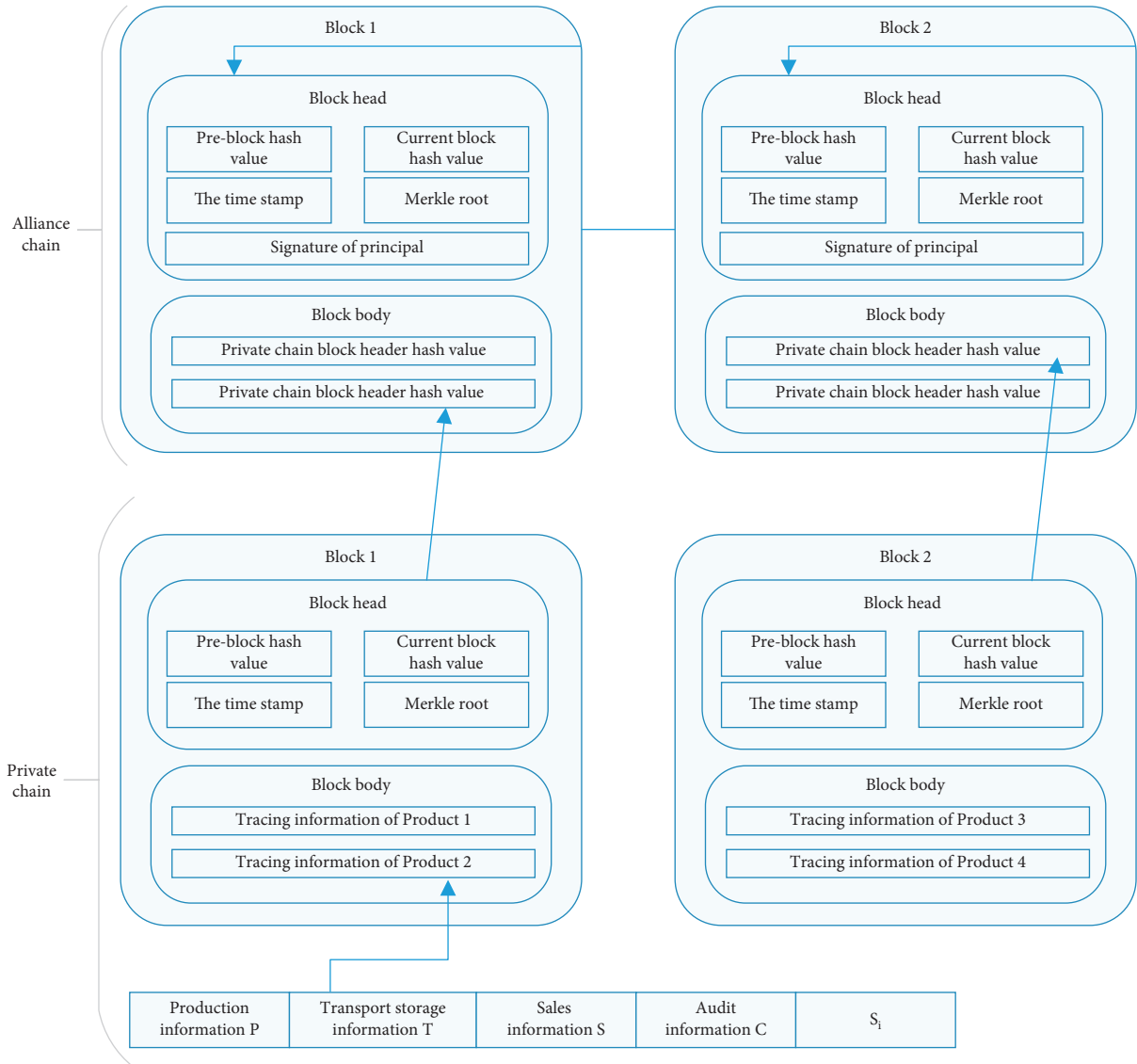
FIGURE 3: Data structure of private chain and alliance chain.

TABLE 1: Production information.

Product ID	Product name	Raw material information	S_x	$H(P)$

the dual-storage mechanism will be adopted in this paper; that is, the collected data information of nodes in each link will be stored together in the blockchain network and the relational database. However, the summary of information generated by SHA-3 (Secure Hash Algorithm 3) is stored in the blockchain network, while the complete information is stored in the database. This not only improves the operational efficiency of blockchain, but also solves the scalability problem faced by blockchain.

3.3.2. Design of the Traceability System of Fresh Agricultural Products. After the above process analysis and storage mechanism design of agricultural supply chain, the structure

diagram of agricultural product traceability scheme is designed, as shown in Figure 4.

The data stored in the traceability solution is stored by the blockchain system and the database. Introducing the relational database can solve the scalability problem of the blockchain system. Only a summary of the data is stored in a blockchain system, and the complete data is stored in a database. The database is maintained by the Administration for Industry and Commerce, while the blockchain system is jointly maintained by production enterprises, transportation enterprises, warehouse storage enterprises, sales enterprises, Food and Drug Administration, and Industry and Commerce Administration. The original intention of this system is to provide traceability inquiry services for consumers and provide more convenient and efficient supervision services for the regulatory authorities, so it also includes external users such as the regulatory authorities and consumers.

The information input process of the production enterprise, transportation enterprise, warehouse storage

TABLE 2: Transportation and storage information.

Transportation time	The mode of transportation	Storage information	S_y	$H(T)$

TABLE 3: Sales information.

Sales time	The sales amount	Sales way	S_z	$H(S)$

TABLE 4: Private chain transaction structure.

Production information P	Transport warehouse information T	Sales information S	Audit information C	S_i
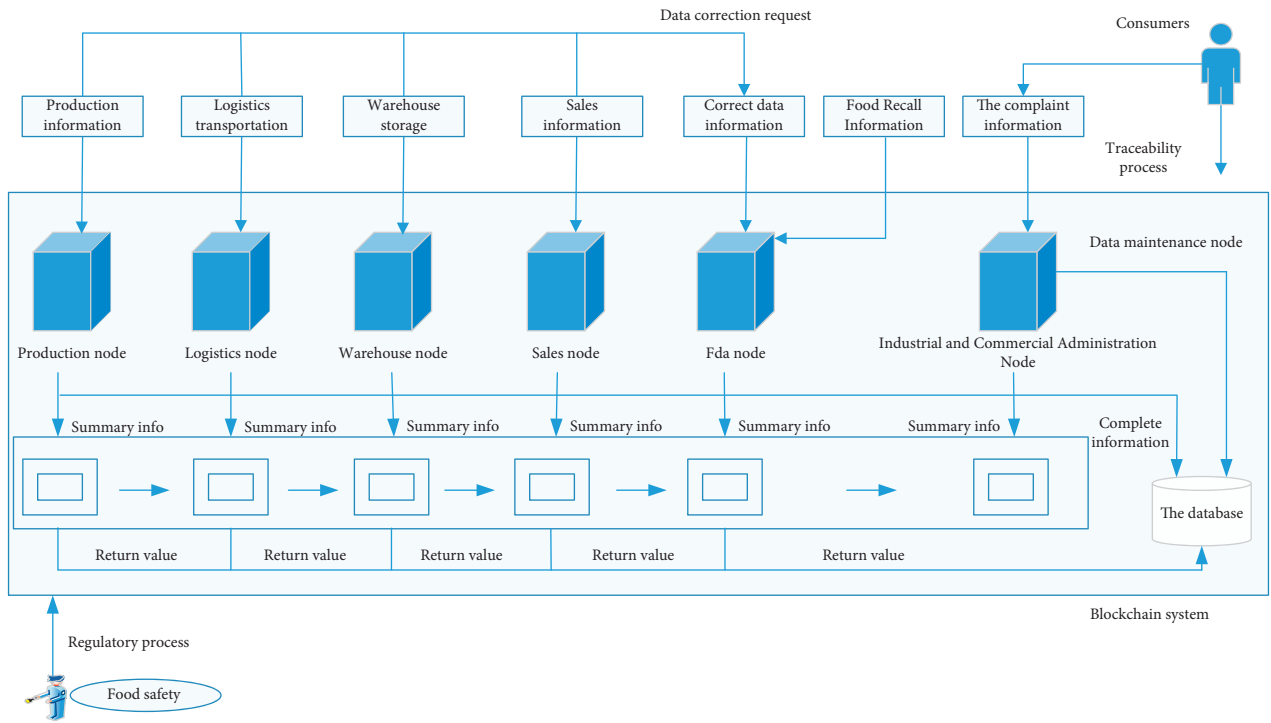
FIGURE 4: Structure of the proposed traceability system.

enterprise, and sales enterprise is the same. Taking the production enterprise as an example, the production enterprise packages the collected data and inputs it into the node and database at the same time. The production enterprise node generates a summary of the input data using SHA-3 and sends it to the blockchain. After reaching a consensus, the participating nodes write a summary of the information into the block. At this point, the block returns a hash value to be stored in the database, which can be used for data indexing. The Administration for Industry and Commerce and the Food and Drug Administration supervise the behavior of the above nodes.

Consumers purchasing food can use the code on the package in the database for traceability inquiry. If you have doubts about the queried information, you can query and compare the summary of the information in the blockchain to determine whether the data has been changed. If the information summaries are consistent, the data is true and unchanged. When it is found that the query data has been changed, consumers can complain to the Administration for Industry and Commerce. The complaint information will be

stored in the database and blockchain system in the same way as evidence.

Due to the large amount of data collected in each link of the agricultural supply chain, information may be omitted or incorrectly recorded due to manual error or other external interference during information input. In addition, once the information is entered into the blockchain system, the data cannot be changed, so the Food and Drug Administration is introduced into this scheme. If any node in the agricultural supply chain finds any error in the input information, it can send an information correction request to the Food and Drug Administration. After being verified by the Food and Drug Administration, the corrected information can be uploaded to the blockchain system by the FDA node. These methods can eliminate the huge loss of information input errors caused by human operation errors.

The design of agricultural product traceability scheme based on blockchain ensures that data cannot be tampered with and the centralized structure is removed. The traceability of information flow has realized the function of quick search and accurate positioning. According to the actual

needs of targeted introduction of Food and Drug Administration and Industry and Commerce Administration. The Food and Drug Administration can not only deal with information entry errors at all stages of the supply chain, but also provide data correction needs. It can also recall problematic food that may cause damage to human health. The Administration for Industry and Commerce is responsible for the timely acceptance of consumer complaints. Information about complaints that may damage consumers' health will be shared with the Food and Drug Administration in a timely manner, carrying out food recall work in a timely manner.

3.3.3. Traceability Architecture Based on Blockchain.

Figure 5 shows the traceability system hierarchy based on blockchain. The architecture is mainly divided into six layers from bottom to top, namely, operation layer, data acquisition layer, data layer, consensus and network layer, presentation layer, and user layer. The bottom layer is the operation layer, which refers to the production enterprises, transportation enterprises, warehouse storage enterprises, and sales enterprises that need to collect data. It is the source of the entire traceability data. Data acquisition layer refers to the use of radio frequency devices, information acquisition terminals, and application sensors to collect and transmit data at the operation layer and can improve the overall efficiency of agricultural supply chain. The data layer transfers data from the data acquisition layer to the data storage layer. It adopts the dual blockchain mechanism of alliance chain and private chain. Only a summary of the processed information is stored in a blockchain network, while the complete data and the hash values returned after the summarization are stored in a relational database. Consensus and network layer refers to key technologies of blockchain including P2P network, authentication mechanism, propagation mechanism, and PoW and PoS consensus mechanism. Presentation layer refers to the use of B/S architecture and JSP (Java Server Pages) technology to display data according to user needs. The top layer is the user layer, including production enterprises, transportation enterprises, warehouse storage enterprises, sales enterprises, regulatory departments, and consumers. Production enterprises, transportation enterprises, warehouse storage enterprises, and sales enterprises are responsible for information entry. Regulatory authorities and consumers can query product information in the system according to their needs.

4. Experiment

4.1. Experimental Environment.

In this simulation experiment, three PCs are mainly used to achieve traceability by building simulation private chain, alliance chain, and traceability platform. The experimental environment is shown in Table 5. The test is conducted in virtual machine simulation test, and its environment is based on CentOS 8.0. The operating memory is 8 GB, the hard disk is 500 GB, and the bandwidth is 200 Mb/s. The Fabric network contains four Peer nodes and one Orderer node. The default LevelDB database in the Fabric has a single query form. CouchDB meets real world needs and supports rich queries. Composite keys are modeled to support equivalent queries for multiple parameters. Therefore, this paper chooses CouchDB as the test database. Node SDK was used to develop test programs, and REST interface was used to call resources.

4.2. Analysis of Data Generation Efficiency.

In the experiment, a simple private chain system was built on PC1 to store detailed product traceability data, in which raw material information and storage information were roughly represented as product origin and raw material storage place. The traceability data of 20 kinds of products are simulated in the experiment, and the traceability function is realized by connecting them together according to previous_hash. At the same time, any modification of the data will destroy the chain structure and ensure that the data cannot be modified by changing.

Then, a simple alliance chain system is built on PC2 to store the hash value of the block header of the private chain.

Finally, a small product information traceability platform is built on PC3, and its data sources are from private chain and alliance chain. For the query of the traceability data of a product, the system will automatically take its hash value after the user enters the commodity name and then turn it over to the relevant block of the private chain for search after the processing of the alliance chain. The data will be returned to the platform matching request first and then to the user data. If the traceability information is not found, the user can submit feedback.

In terms of system performance, the running time of the anticounterfeiting traceability system proposed in this paper is mainly spent on the collection, transmission, and audit of traceability data. In the process of generating traceability data, the sensor can transmit accurate data in real time and consume less time. In addition, the information generated by each department depends mainly on network factors. As shown in Figure 6, under common network conditions, the system built in this paper was tested 20 times, in which the generation time of private chain transaction data ranged from 524 to 890 ms, with an average of 632 ms. The generation time of alliance chain transaction data ranged from 513 to 73 ms, with an average of 617 ms.

4.3. Query Efficiency Analysis.

Based on realizing the design of the above traceability system, it is necessary to show the information of the growth and circulation of agricultural products to consumers. Therefore, it is necessary to quickly trace the information of agricultural products batch. According to the different ways of storing blockchain traceability data, there are two commonly used query methods as follows:

(1) The first method is the key traversal query, namely, key method. Data information items about the growth, processing, logistics, and sales of agricultural products will be written into the blockchain one by
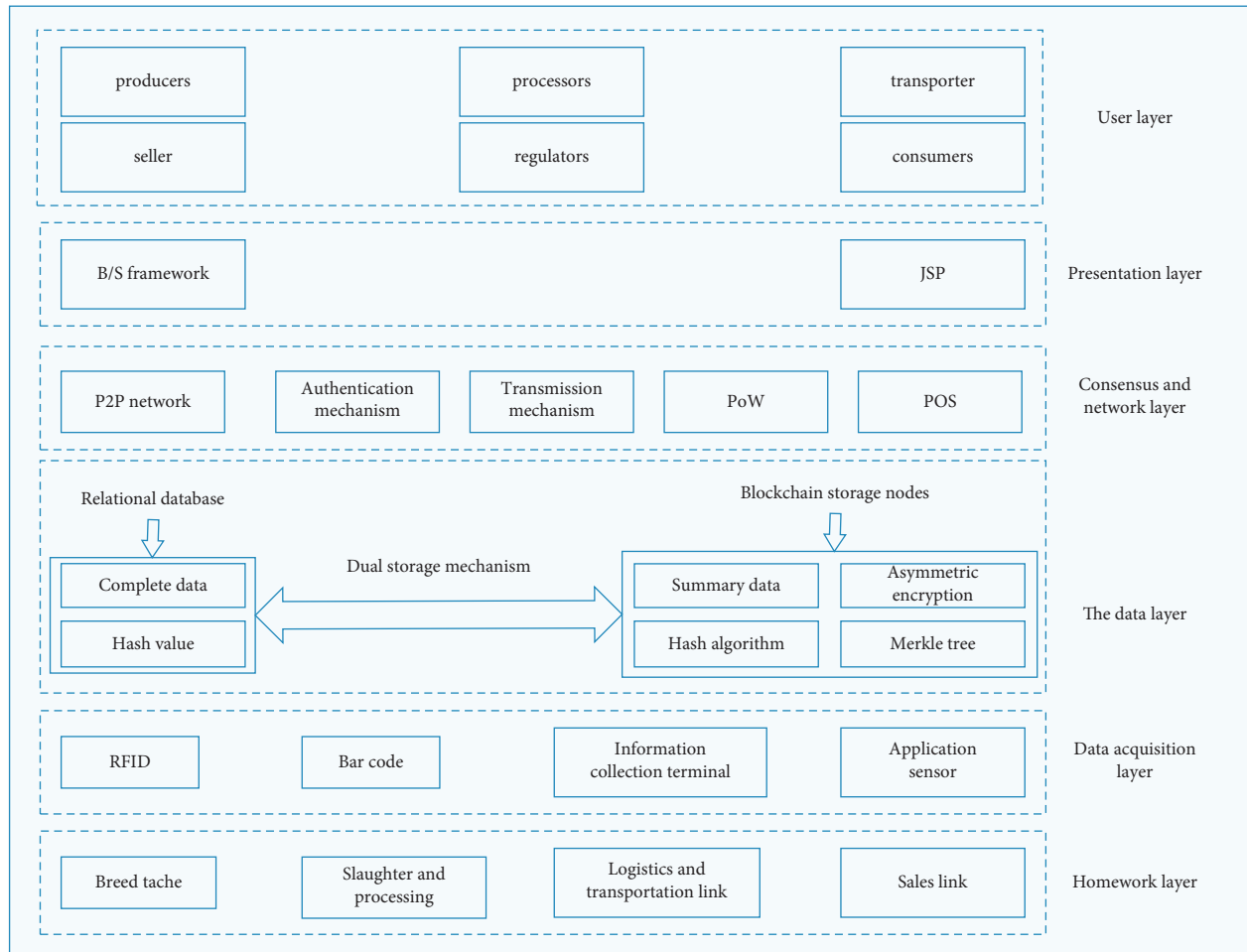
FIGURE 5: Hierarchy diagram of the proposed traceability system.

TABLE 5: Description of experimental environment.

Name	CPU/memory	Operating system	Main function
PC1	i7-9700/8 GB	CentOS 8.0	Deploying private chains
PC2	i7-9700/8 GB	CentOS 8.0	Deploying alliance chain
PC3	i7-9700/8 GB	CentOS 8.0	Building traceability platform

one. The ID of the traceability information is used as the key value, and the traceability information is stored in the blockchain as the value. The key is used as the index to traverse the previous block from the latest block to obtain the matching value during querying the traceability information. In addition to the fresh agricultural product traceability business, there are multiple traceability information uploading records of agricultural product batches. Batch information is usually obtained during query, requiring multiple traversals of the block by key. The number of iterations is related to the number of agricultural products batch traceability records.

(2) The second method is to query information by the field of batch number, namely, batch method. Specifically, the growth, processing, logistics, and sales of

agricultural products are written into the blockchain. The ID of the traceability information is used as the key value, and the traceability information is stored in the blockchain as the value. The query uses CouchDB's rich query to traverse from the latest block to the previous block by the batch number field in value. To obtain all the traceability information of a batch of agricultural products, you only need to traverse all blocks once to get all the traceability information of a batch of agricultural products.

This paper tests and compares the above two query methods. During the experiment, the same query operation is executed under the same circumstances, and the query time will fluctuate in a certain range. To ensure the objectivity of the data, each set of data is executed 10 times, and its average is calculated as the final value. The above methods were used to test the
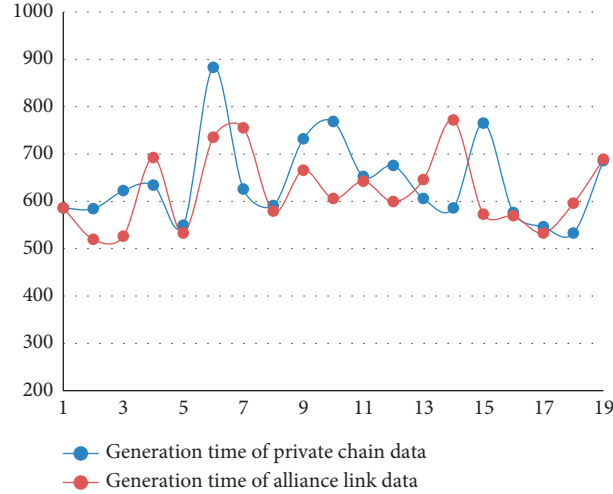
Figure 6: Time of data generation.

experiment, and the correlation analysis of the test results was carried out. The correlation coefficient can be calculated by

$$R_{(X,Y)} = \frac{\text{Cov}(X,Y)}{\sqrt{D(X)}\sqrt{D(Y)}}, \qquad (1)$$

where $\text{Cov}(X,Y)$ is the covariance of X and Y. $D(X)$ and $D(Y)$ are the variances of X and Y, respectively.

The comparison diagram of the relationship between the query time and the number of trace records under the specific total amount of trace records for these two query methods is shown in Figure 7. Figures 7(a)-7(c) show the comparison of query time in two different ways when the total number of retrospective records is 1×10^4, 5×10^4, and 9×10^4, respectively. The abscissa is the number of batch traceability records, which is 1, 200, 400, 600, 800, and 1000. The ordinate indicates the time it takes to query information. R represents correlation coefficient. Among them, the query time of key method is positively correlated with the number of batch traceability records. Correlation coefficients R were all >0.89. However, the correlation coefficients of time and trace records by batch method were all <0.5, showing a weak correlation.

Based on the above correlation analysis, the query efficiency improvement rate of the two methods is further analyzed, and its calculation equation is

$$n_{(A,B)} = \frac{t_B - t_A}{t_B} \times 100\%, \qquad (2)$$

where $n_{(A,B)}$ represents the efficiency improvement rate of A over B. t_B and t_A represent the time required by A and B, respectively.

As can be seen from Table 6, when querying a single traceability record, the query efficiency of batch query method fluctuates compared with that of key method. This is because the time required by a single query is small and the data fluctuation interval is large, resulting in a large difference in query time. When the number of batch traceability records is more than 200, the query efficiency of batch query method is basically stable at 60.77%–

72.42% compared with key method. In practice, agricultural product batches are recorded in the range of 200–400, while the total number of traceability records in the blockchain system increases with each node and time. When the number of batch traceability records is 200, and the total number of traceability records is 1×10^4, 3×10^4, 5×10^4, 7×10^4, 9×10^4, and 11×10^4, the query efficiency of batch method is improved by 70.77%, 71.43%, 69.53%, 69.58%, 69.2%, and 67.73%, respectively, compared with key method. When the number of batch traceability records is 400 and the total number of traceability records is 1×10^4, 3×10^4, 5×10^4, 7×10^4, 9×10^4, and 11×10^4, the query efficiency of batch method is improved by 70.35%, 73.33%, 70.91%, 69.82%, 69.16%, and 71.57%, respectively, compared with key method. From the perspective of the number of batch traceability records, the query efficiency of the content query method increases with the increase of the total number of traceability records.

4.4. System Security Analysis. The anticounterfeiting traceability system based on double blockchain and Internet of Things technology proposed in this paper has strong security, which is mainly reflected in the following aspects:

(1) Any modification of product traceability data will inevitably break the blockchain chain structure based on the security of blockchain itself, such as decentralization, immutability, and high fault tolerance. This increases the cost and difficulty of data modification and ensures the authenticity and reliability of traceability data. At the same time, it can also urge enterprises not to fabricate information in the process of product production to a certain extent.

(2) Use the Internet of Things technology to generate real and objective product data and transfer it to the product data of relevant departments to block the possibility of data source fraud. This measure improves the security and reliability of product traceability data.
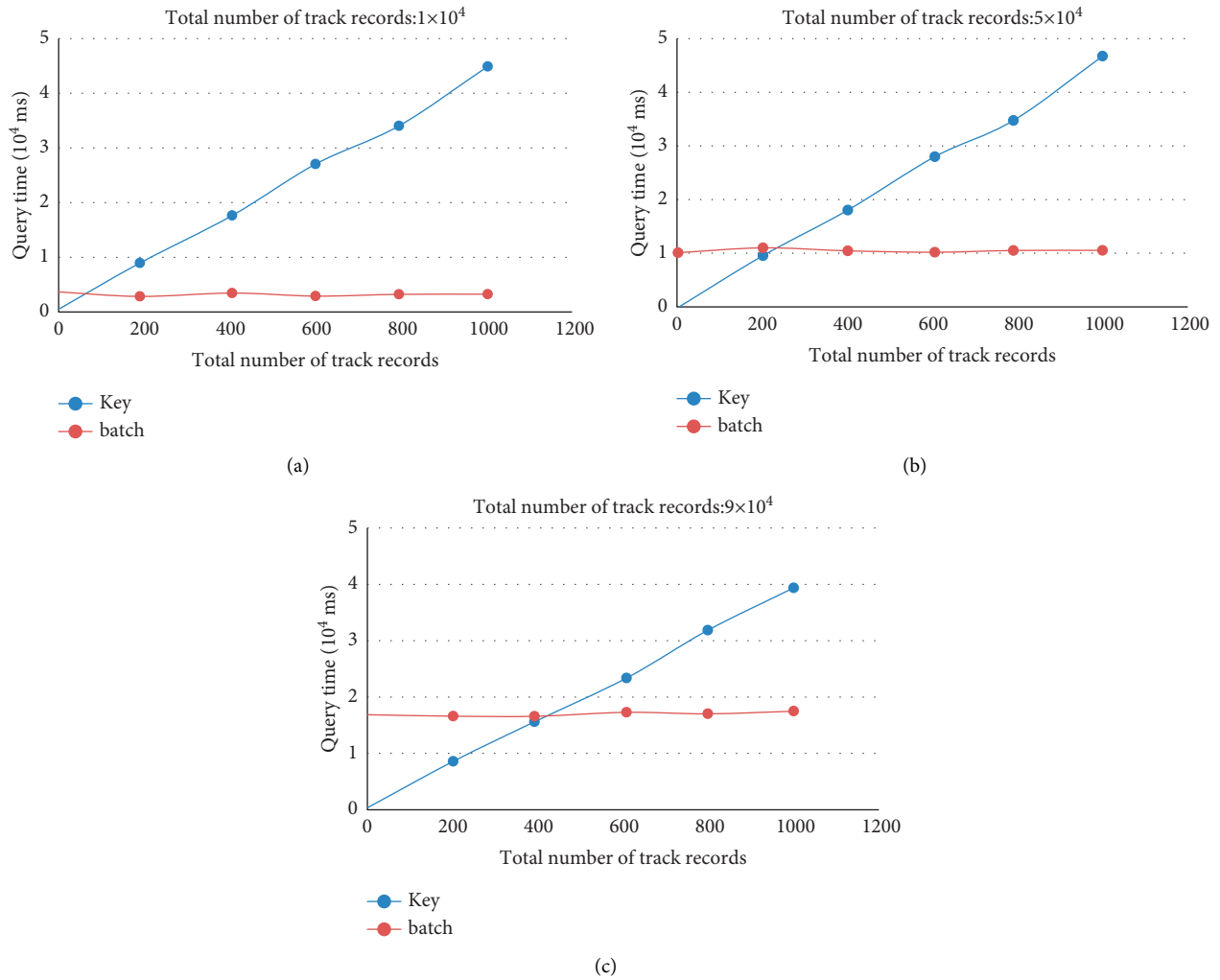
(a)

(b)

(c)

Figure 7: Time comparison between the two query methods.

Table 6: Percentage of efficiency improvement.

Total traceability record	Number of batch total traceability records (batch method is compared with key method)					
	1×10^4	3×10^4	5×10^4	7×10^4	9×10^4	11×10^4
1	34.07	7.1	11.96	8.86	21.78	-22.37
200	70.77	71.43	69.53	69.58	69.2	67.73
400	70.35	73.33	70.91	69.82	69.16	71.57
600	69.98	70.43	70.3	64.87	69.85	70.34
800	70.85	71.08	70.78	68.96	72.42	71.38
1000	60.77	68.74	64.21	61.92	60.23	65.85

(3) The double-chain structure of alliance chain and private chain can ensure the high reliability of blockchain operation environment. Alliance chains and private chains are built, deployed, and run based on a trusted partnership. All participants are vetted before joining the blockchain network, which greatly

reduces the possibility of malicious nodes in the system. This can also prevent internal attacks, further improving the security of the system.

5. Conclusion

On the premise that more and more people pay attention to product safety, many problems of traditional product traceability system, such as centralized storage, low reliability of data, easy data tampering, and difficulty in locating the responsible person, are analyzed in this paper. Besides, the related work of other scholars in the field of product traceability is sorted out, and the characteristics of information traceability and non-tampering of blockchain technology are expounded. In order to solve the security and privacy problems in the cold chain logistics traceability system of fresh agricultural products, a traceability system based on blockchain is proposed in the paper. Specific work includes the following: (1) The whole process of cold chain logistics of fresh agricultural products is systematically analyzed. (2) The data structure of private chain and alliance chain is analyzed. (3) Logistics traceability system based on private chain and alliance chain is designed. The alliance chain is mainly used to query and share product traceability information. The private chain will be used to collect and store the product traceability information of each enterprise and then connected to the federation chain via hash pointers. The feasibility of this system is verified by simulation experiments, which provides reference for the combination of blockchain technology and cold chain logistics traceability system. At present, the product anticounterfeiting traceability system using blockchain technology is still in the initial stage of exploration, and its applicable product types need further analysis. There are also some security issues with its integration with the Internet of Things. The next step will continue to refine the details of the combination of the two and improve the product traceability system.

Data Availability

The labeled dataset used to support the findings of this study is available from the corresponding author upon request.

Conflicts of Interest

The authors declare that they have no conflicts of interest.

Authors' Contributions

Xinghua Zhang and Yongjie Sun contributed equally to this work.

References

[1] Y. Wen, W. Li, Z. Yang, C. Guo, and J. Ji, "Evaluation of various approaches to predict cadmium bioavailability to rice grown in soils with high geochemical background in the karst region, Southwestern China[J]," *Environmental Pollution*, vol. 258, Article ID 113645, 2020.

[2] T. Vergne, C. Chen-Fu, and S. Li, "Pig empire under infectious threat: risk of African swine fever introduction into the People's Republic of China[J]," *The Veterinary Record*, vol. 181, no. 5, p. 117, 2017.

[3] L. Li, A. Peng, Z. Lin, H. P. Zhong, and X. M. Chen, "Biomimetic ELISA detection of malachite green based on molecularly imprinted polymer film[J]," *Food Chemistry*, vol. 229, pp. 403–408, 2017.

[4] B. Guo, G. Xie, X. Li et al., "Outbreak of Haff disease caused by consumption of crayfish (*Procambarus clarkii*) in Nanjing, China[J]," *Clinical Toxicology*, vol. 57, no. 5, pp. 331–337, 2019.

[5] S. Jin, Y. Zhang, and Y. Xu, "Amount of information and the willingness of consumers to pay for food traceability in China [J]," *Food Control*, vol. 77, pp. 163–170, 2017.

[6] J. Qian, L. Ruiz-Garcia, B. Fan et al., "Food traceability system from governmental, corporate, and consumer perspectives in the European Union and China: a comparative review[J]," *Trends in Food Science & Technology*, vol. 99, pp. 402–412, 2020.

[7] F. Tian, "A supply chain traceability system for food safety based on HACCP, blockchain & Internet of things," in *Proceedings of the 2017 International conference on service systems and service management*, pp. 1–6, IEEE, Dalian, July 2017.

[8] S. Cruz Introini, A. Boza, and M. D. M. Alemany Díaz, "Traceability in the food supply chain: review of the literature from a technological perspective[J]," *Dirección y Organización*, vol. 64, pp. 50–55, 2018.

[9] Y. Liao and K. Xu, "Traceability system of agricultural product based on block-chain and application in tea quality safety management[C]//Journal of Physics: conference Series," *IOP Publishing*, vol. 1288, no. 1, Article ID 012062, 2019.

[10] K. Wongpatikaseree, P. Kanka, and A. Ratikan, "Developing smart farm and traceability system for agricultural products using IoT technology," in *Proceedings of the 2018 IEEE/ACIS 17th International Conference on Computer and Information Science (ICIS)*, pp. 180–184, IEEE, Singapore, June 2018.

[11] J. Hua, X. Wang, M. Kang, H. Wang, and F. Y. Wang, "Blockchain based provenance for agricultural products: a distributed platform with duplicated and shared bookkeeping," in *Proceedings of the 2018 IEEE Intelligent Vehicles Symposium (IV)*, pp. 97–101, IEEE, Changshu, China, June 2018.

[12] K. Salah, N. Nizamuddin, R. Jayaraman, and M. Omar, "Blockchain-based soybean traceability in agricultural supply chain[J]," *IEEE Access*, vol. 7, pp. 73295–73305, 2019.

[13] D. Prashar, N. Jha, S. Jha, Y. Lee, and G. P. Joshi, "Blockchain-based traceability and visibility for agricultural products: a decentralized way of ensuring food safety in India[J]," *Sustainability*, vol. 12, no. 8, p. 3497, 2020.

[14] J. Li and X. Wang, "Research on the application of blockchain in the traceability system of agricultural products," in *Proceedings of the 2018 2nd IEEE advanced information management, communicates, electronic and automation control conference (IMCEC)*, pp. 2637–2640, IEEE, Xi'an, China, May 2018.

[15] F. Longo, L. Nicoletti, and A. Padovano, "Estimating the impact of blockchain adoption in the food processing industry and supply chain[J]," *International Journal of Food Engineering*, vol. 16, no. 5-6, 2020.

[16] T. K. Dasaklis, F. Casino, and C. Patsakis, "Defining granularity levels for supply chain traceability based on IoT and blockchain," in *Proceedings of the international conference on omni-layer intelligent systems*, pp. 184–190, COINS, Crete, Greece, May 2019.

[17] C. L. Chen, Z. Y. Lim, H. C. Liao, Y. Y. Deng, and P. Chen, "A traceable and verifiable tobacco products logistics system with GPS and RFID technologies[J]," *Applied Sciences*, vol. 11, no. 11, p. 4939, 2021.

[18] Q. F. Shao, C. Q. Jin, Z. Zhang, and W. N. Qian, "Blockchain, architecture and research progress[J]," *Chinese Journal of Computers*, vol. 41, no. 5, pp. 969–988, 2018.

[19] E. Fernando, D. Agustin, M. Irsan, D. F. Murad, H. Rohayani, and D. Sujana, "Performance comparison of symmetries encryption algorithm AES and DES with raspberry pi," in *Proceedings of the 2019 International Conference on Sustainable Information Engineering and Technology (SIET)*, pp. 353–357, IEEE, Lombok, Indonesia, September 2019.

[20] B. K. Mohanta, S. S. Panda, and D. Jena, "An overview of smart contract and use cases in blockchain technology," in *Proceedings of the 2018 9th International Conference on Computing, Communication and Networking Technologies (ICCCNT)*, pp. 1–4, IEEE, Bengaluru, India, July 2018.

[21] O. Alfandi, S. Otoum, and Y. Jararweh, "Blockchain solution for iot-based critical infrastructures: byzantine fault tolerance," in *Proceedings of the NOMS 2020-2020 IEEE/IFIP Network Operations and Management Symposium*, pp. 1–4, IEEE, Budapest, Hungary, April 2020.

[22] Y. Zhang, C. Xu, N. Cheng, H. Yang, and X. Shen, "Chronos+: an accurate blockchain-based time-stamping scheme for cloud storage[J]," *IEEE Transactions on Services Computing*, vol. 13, no. 2, pp. 216–229, 2019.

[23] Y. Lu, "The blockchain: state-of-the-art and research challenges[J]," *Journal of Industrial Information Integration*, vol. 15, pp. 80–90, 2019.

[24] H. Zhu, Y. Guo, and L. Zhang, "An improved convolution Merkle tree-based blockchain electronic medical record secure storage scheme[J]," *Journal of Information Security and Applications*, vol. 61, Article ID 102952, 2021.

[25] P. He, G. Yu, and Y. F. Zhang, "Survey on blockchain technology and its application prospects[J]," *Computer Science*, vol. 44, no. 4, pp. 1–7, 2017.

[26] L. A. Ajao, J. Agajo, E. A. Adedokun, and L. Karngong, "Crypto hash algorithm-based blockchain technology for managing decentralized ledger database in oil and gas industry," *D-J Series*, vol. 2, no. 3, pp. 300–325, 2019.

[27] B. Seok, J. Park, and J. H. Park, "A lightweight hash-based blockchain architecture for industrial IoT[J]," *Applied Sciences*, vol. 9, no. 18, p. 3740, 2019.

[28] S. Yaji, K. Bangera, and B. Neelima, "Privacy preserving in blockchain based on partial homomorphic encryption system for AI applications," in *Proceedings of the 2018 IEEE 25th International Conference on High Performance Computing Workshops (HiPCW)*, pp. 81–85, IEEE, Bengaluru, India, December 2018.

[29] X. Xia, X. Lin, W. Dong, and Z. He, "Design of traceability system for medical devices based on blockchain," *Journal of Physics: Conference Series*, IOP Publishing, vol. 1314, no. 1, , Article ID 012067, 2019.

[30] W. Xie, X. Zheng, X. Lu, X. Lin, and X. Fan, "Agricultural product traceability system based on blockchain technology," in *Proceedings of the 2019 IEEE Intl Conf on Parallel & Distributed Processing with Applications, Big Data & Cloud Computing, Sustainable Computing & Communications, Social Computing & Networking (ISPA/BDCloud/SocialCom/SustainCom)*, pp. 1266–1270, IEEE, Xiamen, China, December 2019.

Research Article

Research on Agricultural Product Traceability Technology (Economic Value) Based on Information Supervision and Cloud Computing

Rongkuan Wang [1] **and Xi Chen** [2]

[1]*School of Business Administration, Zhongnan University of Economics and Law, Wuhan, Hubei 430073, China*
[2]*Nanchang Business College of Jiangxi Agricultural University, Jiujiang, Jiangxi 332020, China*

Correspondence should be addressed to Rongkuan Wang; 202011080133@stu.zuel.edu.cn

Traditional agricultural product traceability system adopts centralized storage, and the traceability process is solidified, which results in the low reliability of traceability results and the poor flexibility of the system. Aiming to solve this problem, blockchain technology is applied to supply chain traceability, and a supply chain traceability system based on sidechain technology is proposed. Goods management, information sharing, and product traceability in supply chain are realized through Ethereum smart contract. The sidechain technology is adopted to expand Ethereum so that it can meet the needs of practical applications. The experiment results show that the proposed system has a transaction function and information sharing function. Compared with similar trading systems, the proposed system has more advantages in throughput and security.

1. Introduction

ptTraceability of agricultural products refers to the forward tracing and reverse tracing of all links of the industrial chain from production to circulation of agricultural products [1]. After years of development, the traceability system of agricultural products in China is becoming perfect. However, it still has some problems, such as low reliability of traceability results and poor system flexibility. From the very beginning, the agricultural product traceability system has attracted the attention of experts at home and abroad. As early as 2002, the US Congress passed the "Bioterrorism Act" to establish the traceability system of agricultural product quality and safety [2]. So far, the community has reached a consensus on the importance of traceability of agricultural product quality and safety. The construction of relevant systems and systems has also achieved initial results, but there are still many problems in practical work.

In the context of the rapid development of industry 4.0, many new technologies have been applied in the production,

management, and harvesting of agricultural products. The application of these technologies makes the production management of agricultural products more intelligent, efficient, and transparent. Among them, agricultural product traces technology also to ascend a new step. Literature [3] describes the possibility of realizing food quality testing during transportation from manufacturer to consumer. It uses a sensor remote monitoring system combined with the Internet of Things technology to propose a low-cost solution based on Internet of Things real-time food tracking and food transportation process monitoring. Although the Internet of Things technology is mature enough, the production and sales system of agricultural products involves many subjects, complicated uncertainties affecting the system, and large resource consumption for real-time monitoring with the help of sensors [4]. These will lead to difficult and inefficient management of quality and safety traceability system; especially, data storage security is still facing many challenges and problems.

In order to improve the reliability and flexibility of agricultural product traceability system, blockchain can

be used to replace the traditional centralized database. It ensures the safe storage of traceability data and non-repudiation of information source to achieve reliable traceability of agricultural products [5]. In addition, it can decouple the whole industrial chain into multiple independent links and combine them with independent channels in the super ledger into link modules. It can coordinate with the module allocation mechanism, dynamically adjust the traceability process according to the actual production, and finally realize the dynamic traceability of agricultural products. In literature [6], it is proposed to use blockchain distributed storage technology to solve the possibility of tampering or destroying data in the data storage stage by virtue of the irreversibility of blockchain.

Developed from the underlying technology of Bitcoin, blockchain is a distributed storage technology featuring decentralization, traceability, nontampering, openness and transparency, consensus mechanism, and transaction anonymity. However, compared with other industries, blockchain technology for agricultural product quality and safety traceability puts more pressure on the storage of IoT data. In order to achieve the consistency of distributed nodes, the block generation speed and transaction processing capability of blockchain are limited. Therefore, it is not possible to directly apply blockchain technology to process and store large amounts of sensor data. In order to solve the storage problem, cloud computing and cloud storage technologies are used in literature [7] to provide applications. As mentioned in literature [8], the traditional security problems still exist in cloud computing environment, and even traditional security mechanisms are no longer applicable to applications and data in cloud. In literature [9], the dual-chain structure of blockchain is proposed, which uses a chained data structure to store blockchain transaction hashes. It works with the blockchain to form double-chain storage that ensures that agricultural data cannot be tampered with or destroyed. As there are many standards involved in agricultural product traceability, effective policy control is needed for participating nodes. As the amount of data increases, the efficiency of blockchain transactions also increases. A complete public chain can no longer meet these variable needs. Compared with public chain, alliance chain has more advantages in high availability, high performance, programmability, and privacy protection. It is considered as the "partially decentralized" or "polycentric" blockchain. Alliance chain simplifies the number of nodes, which can make the system run more efficiently and cost less. It can confirm that the number of transactions per unit of time is much larger than the public chain, and it is easier to land in the agricultural product quality and safety traceability system.

There are two main problems in big data recording. The first is the issue of record speed caused by the blockchain consensus algorithm. While anyone is free to use Bitcoin's blockchain, only seven writes per second are the limit of its performance. The second is the boundary of the number of participating nodes. Even in participant-limited blockchains targeted at commercial use, the performance deteriorates

dramatically when the number of participating nodes exceeds a few dozen.

In view of the problems existing in the traditional agricultural supply chain system, such as difficulties in trust transmission, opaque transaction information, and difficult information sharing, this paper proposes an agricultural products traceability system of blockchain. In the agricultural product traceability system, the performance of the blockchain is affected as the agricultural product data increases. Sidechain technology can provide some functions such as smart contracts and privacy protection on top of the main chain. These features ensure that users can use them without affecting the performance of the main chain. Therefore, in order to improve the performance of the main chain, this paper uses sidechain technology to expand the capacity of Ethereum to meet the demand of supply chain traceability information on the chain. The innovations and contributions of this paper are listed as follows:

(1) Aiming to solve the problem that the traditional agricultural product traceability system has the low reliability of traceability results and poor flexibility, this paper proposes a supply chain traceability system based on sidechain technology.

(2) Goods management, information sharing, and product traceability in supply chain are realized through Ethereum smart contract. The sidechain technology is adopted to expand Ethereum so that it can meet the needs of practical applications.

The structure of this paper is as follows. The traditional agricultural products traceability system is described in the next section. The current state of blockchain traceability systems is described in Section 2. Section 4 focuses on the design of an agricultural product traceability system. Section 5 presents the experiment and analysis. Section 6 is the conclusion.

2. Traditional Agricultural Products Traceability System

2.1. Traditional Traceability Mode. In 2006, China proposed the establishment of agricultural product quality and safety traceability system [10], which has achieved fruitful results after years of development. Literature [11] proposed a technical system of agricultural product quality safety traceability system of "one core, two axes, and three chains" based on the characteristics of Internet of Things technology. Literature [12] proposed the traceability chain hierarchical model of the traceability system based on the food chain. Literature [13] designed a multilateral traceability system for agricultural product quality safety in view of the decentralized and noncentralized characteristics. Literature [14] constructed a design scheme of agricultural product quality traceability system based on Fabric blockchain implementation strategy. By analyzing the typical traceability system, the traceability model of traditional agricultural products is obtained, and its structure is shown in Figure 1.
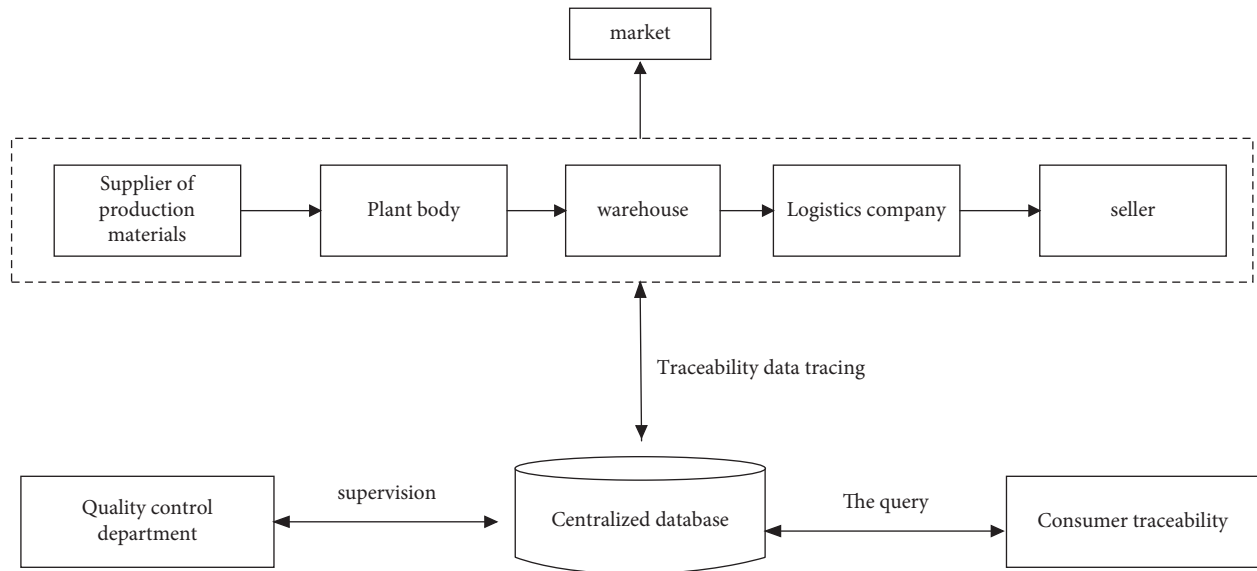
FIGURE 1: Structure of traceability model for traditional agricultural products.

Traditional agricultural product traceability system generally centers on a centralized database. In the actual production process, the supply, planting, storage, logistics, and sales of production materials in the industrial chain are arranged in sequence. Then, the traceability data is uploaded to the centralized database. The quality supervision department supervises the quality of agricultural products by collecting information from centralized databases. Consumers send a query request to the centralized database to obtain the traceability information of purchased agricultural products.

2.2. Existing Problems. In the early stage of agricultural product traceability research, researchers usually focus on the full collection of traceability data and complete coverage of the industrial chain. The research on data security storage and system dynamic traceability is relatively few, which leads to the lack of reliability and flexibility of traditional agricultural product traceability system. Some researchers apply blockchain technology to the traceability of agricultural products but seldom optimize the traceability process and system structure by combining the characteristics of both. While the traceability results obtained are reliable, there is still a lot of room for improvement in the flexibility of the system.

Traditional agricultural product traceability system stores data in a centralized database, which brings a series of data security problems. This reduces the credibility of the traceability system for agricultural products. Traditional traceability systems usually trace specific agricultural products in a narrow range. The limitation of traceability objects and production process leads to the solidified transaction processing process of the traceability system. It cannot dynamically adjust the sequence of production link combination according to the actual production scene, which is not conducive to system function expansion and

upgrade. These factors lead to poor flexibility of the traceability system.

3. The Current State of Blockchain Traceability Systems

3.1. Supply Chain Traceability System Based on Blockchain. At present, there are many researches and applications in academia and industry to realize supply chain traceability by using blockchain. Literature [15] applied blockchain to drug supply chain traceability system. It used affiliate link technology and quick response (QR) encrypted codes to establish full-chain traceability for drugs from manufacturer to seller. Literature [16] proposed a new two-step block-out method and designed a joint distributed ledger CoC (supply chain on blockchain) based on this method for supply chain management system. The experimental results show that the two-step block extraction method has good performance, which is faster, more efficient, and safer. Literature [17] used blockchain technology to enhance the elasticity of the supply chain and studied the basic framework of blockchain and its underlying technology. It analyzed the various risks facing the current supply chain and described the specific application scenarios of blockchain technology in the supply chain.

The above literature involves the research of supply chain traceability system but generally does not involve the underlying blockchain platform. In addition, it lacks running and testing on the blockchain. In industry, food industry giants are using blockchain technology to reform the food supply chain. Walmart, IBM, https://www.JD.com, and Tsinghua University set up a safe food blockchain traceability alliance. It uses blockchain technology to track the food supply chain and build safe tables. Among them, Hyperledger developed by IBM, as a kind of underlying blockchain technology, has been widely applied in various fields of supply chain by major companies. In China, Tmall

International products use ant blockchain independently developed by Alibaba for cross-border product traceability, which greatly increases the security of imported goods. The Institute of Intelligent Supply Chain Management of Tsinghua University cooperated with Yonghui Supermarket to use steel gash to trace the numbers of Xingcheng Turbot fish. It achieves one yard per fish to ensure food safety and has been promoted to more than 10 kinds of fresh products. Jingdong Y Business Department launched the Baas platform of "Zhizhen Chain" to realize the traceability of some commodities in Jingdong supermarket by using this platform.

At present, alliance chain technology is basically used in supply chain traceability projects. An affiliate chain is a blockchain network that allows only certain group members and limited third-party access. Because of the access mechanism, the small number of nodes, the use of a high-performance consensus algorithm, and other reasons, the alliance chain usually has higher transaction performance than the public chain. Moreover, the alliance chain can provide queries and other functions to the third party in the form of open API, which is more friendly to supervision. Therefore, it is called "Blockchain 3.0," which flaunts the future development direction of blockchain. The demand and background of the supply chain are consistent with the alliance chain: the members of the supply chain are limited and fixed. The up-chain of supply chain information requires faster transaction speed and lower transaction cost. Supply chain traceability needs the supervision of relevant departments. Therefore, alliance chain technology is suitable for supply chain traceability system. Currently, one of the more active and recognized open-source consortium projects is Hyperledger Fabric developed by IBM. Most blockchain platforms are improved and encapsulated based on Hyperledger.

However, relevant researches show that there are many difficulties in the realization of the alliance chain. Its main bottleneck lies in the weak financial strength of small and micro enterprises, that is, they are unable to maintain the servers required by the alliance chain. Consensus nodes are typically deployed in large enterprises and some third-party organizations. Small and microenterprises in the supply chain generally only have terminal or Internet of Things acquisition devices and do not configure a consensus server. This leads to the imbalance of consensus rights in the alliance chain and the failure of consensus strategies due to too few consensus nodes. In actual deployment, core enterprises gradually deploy consensus nodes in the same consensus domain. Docker container technology is used to generate four nodes on the same server for consensus, and other enterprises in the supply chain use clients to access the alliance chain. This operation saves costs and facilitates small applications and early commissioning. However, it violates the original intention and principle of the alliance chain and cannot play the role of the alliance chain. This system is developed based on Ethereum smart contract to realize supply chain traceability in a decentralized way to save costs for enterprises on the chain.

3.2. Sidechain Technology. To implement supply chain traceability on Ethereum, transaction costs must be considered. Suppliers, processors, and distributors shall chain raw material information, product processing information, and product sales information, respectively. This data can put a lot of pressure on the Ethereum main network and lead to high transaction fees, as well as high confirmation delays. In this paper, sidechain technology is used to expand Ethereum to meet the demand of supply chain traceability information.

The sidechain technology was first used in the expansion of Bitcoin. It is a protocol that allows Bitcoin to be safely transferred to other blockchains and safely returned to the main Bitcoin chain from other blockchains. The protocol moves some frequent, small transactions onto the sidechain. This not only improves the efficiency of Bitcoin's main network but also significantly reduces transaction fees. Therefore, the deployment of the corresponding sidechain technology on Ethereum can reduce the pressure on the main network of Ethereum and improve transaction efficiency. At present, common Ethereum sidechain protocols include Loom Plasma Chain and Snarky. The Loom PlasmaChain is a high-performance DPoS (delegated proof of stake) sidechain that implements the Plasma Cash framework model. It can gain security endorsement from Ethereum's underlying network, allowing users to enjoy the high-performance consensus of DPoS algorithms when using tokens supported by ERC 20 and ERC 721. Snark sidechain solution can expand Ethereum network transaction capacity up to 17000 TPS as a kind of down chain expansion. Snark allows users to transfer tokens and ETH outside Ethereum.

In the existing studies, the sidechain expansion schemes of Bitcoin and Ethereum only include token transfer. Token transactions are transferred to the sidechain for higher throughput and lower handling fees. This paper constructs a sidechain model of user data transfer to provide an expansion scheme for supply chain traceability information so that the supply chain traceability system based on Ethereum can be applied to the actual production.

4. The Design of Agricultural Product Traceability System

4.1. System Architecture. In this paper, aiming at the shortcomings of the existing agricultural supply chain traceability scheme, Ethereum and smart contract are used to design and implement a supply chain traceability system based on sidechain technology. Its architecture is shown in Figure 2. The smart contract module contains the business logic of the system. It deploys this module on the sidechain, which can greatly increase the efficiency of Ethereum usage, reduce transaction confirmation time, and reduce transaction costs. The data synchronization module is responsible for processing each batch of transaction data and using the Merkle tree algorithm to obtain the transaction hash value. It synchronizes the hash value to Ethereum for locking. When consumers and regulators query, the data synchronization
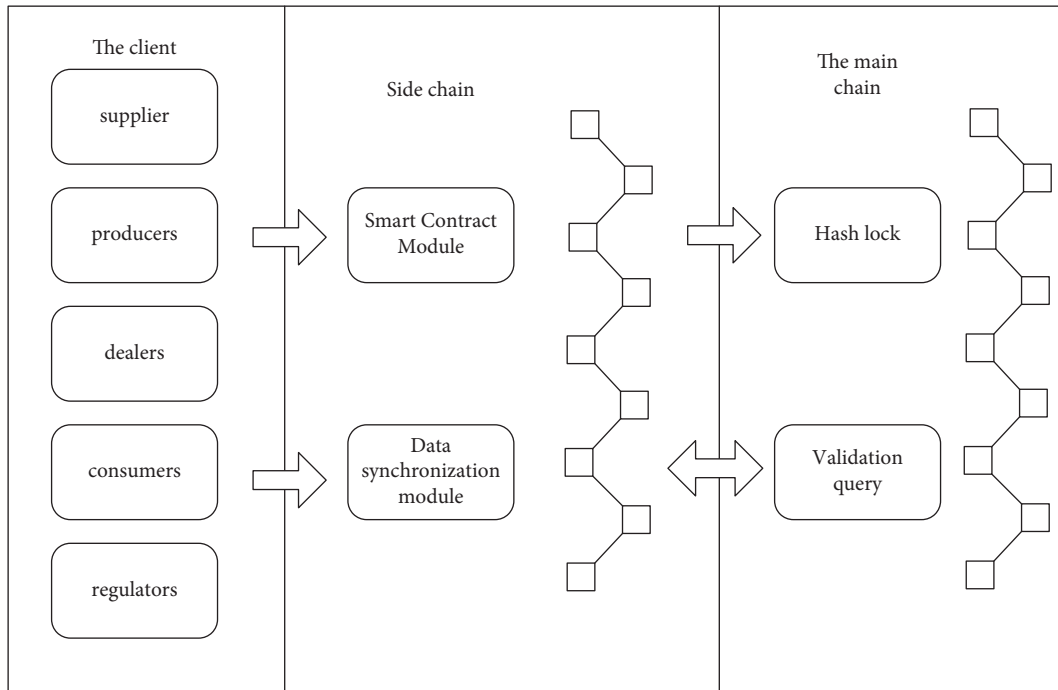
FIGURE 2: Supply chain traceability system architecture.

module can be used for calculation and verification to prevent data tampering.

In the blockchain supply chain traceability system network, enterprises such as suppliers, manufacturers, and distributors use the Internet of Things collection equipment to collect product information. It generates raw data, uses a terminal for data processing, and sends it to a sidechain server. The sidechain server is maintained by the core enterprise and runs the Ethereum sidechain process. It connects to the Ethereum public chain for data storage. The supervisor and the user use PC and mobile device, respectively, to access the sidechain server and verify the authenticity of the data on the Ethereum public chain.

4.2. Contract Design. There are five types of participants in the supply chain traceability system based on blockchain. As a raw material supplier, the supplier is the source of a batch of product information traceability. It requires the creation of an initial file and traceability number for the raw material. The manufacturer processes and distributes the raw materials and is the source of information for the smallest selling unit of the product. It needs to assign batch numbers and QR codes to traceability products, to achieve one code for one thing. Dealers buy from manufacturers and sell through different channels. It needs to provide information on warehousing, logistics, and so on. The supervisor supervises the production, circulation, and operation of commodities. Consumers can scan the QR code to view the traceability information of the whole life cycle of the product. The relevant operations and processes of participants on smart contracts are shown in Figure 3.

Smart contract includes the following five functions:

(1) User registration. Since the public chain itself has no identity authentication mechanism, it needs to realize user access through smart contract. Companies in the same supply chain need to agree on a number before entering information. The user is registered by executing the userRegister() function. This number groups these companies into a user group, and only the users in the group can add traceability information to the products on the chain. The pseudocode of the userRegister() function algorithm is shown in Algorithm 1.

(2) Input raw materials. As the information source of the supply chain, suppliers need to use the Internet of Things equipment to collect the data of the production environment, production cycle, and the person in charge of operation of raw materials. The rawRegister() function is then used to chain up the data, create an initial file for the raw material, and assign the raw material lot number. For example, a batch of raw material traceability file is modeled as <rawID, rawName, rawFac, produceTime, rawInfo>. The rawRegister() algorithm pseudocode is shown in Algorithm 2.

(3) Product production. The manufacturer processes the raw materials provided by the supplier to produce the minimum selling unit of the commodity. In this link, product files based on traceability source code are formally established and provided to consumers in the form of two-dimensional code for inquiry. The manufacturer needs to call the newProduct() function to integrate the raw material information. It can also write URLs to production environment,
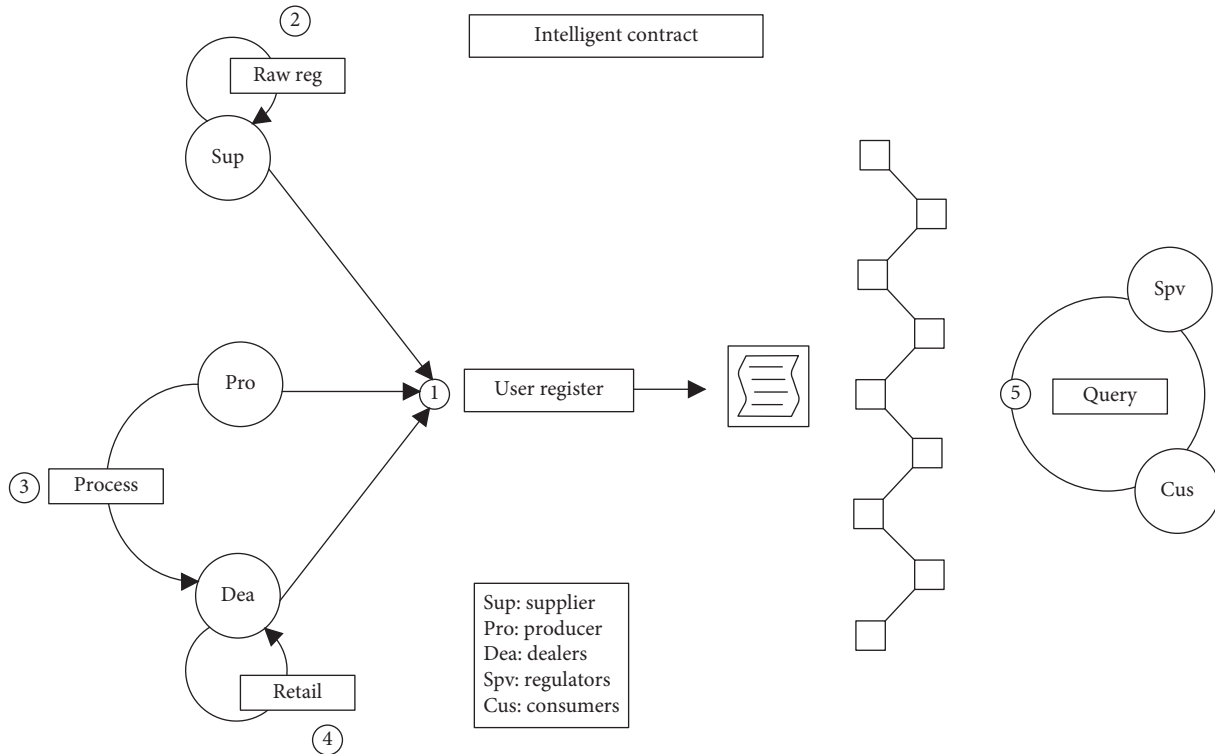
Figure 3: Operation flow of smart contract.

The input: Supply Chain Contract address base_addr, User group id user_group, user ID user_id, user role user_name, contract publisher owner
The output: The user registration is complete or failed
Require: the registered user_id is not in use
if msg.sender = = owner then
    The user group id is not occupied
    if user_group[msg.sender].occupied = = 0 then
        user_group[msg.sender].occupied = = 1
        Return Completes the user group registration
    end if
else
        The user group number is required to be registered
        user_group[user_group].add(user_id)
        user.id = user_id
        user.name = user_name
end if
final
return: The user registration is complete

Algorithm 1: userRegister() function.

production video, and other large files in the product_info field.

(4) Product distribution. This feature records the circulation of products, helps consumers to check the source of goods, and helps manufacturers to prevent the diversion of goods. After handling the goods, the distributor or logistics enterprise uses the product_deal() function to add the distribution information to the goods. Because one or more handling enterprises exist, product information is stored in the structure using the dynamic array Bytes32[] retailerNames. Since the code logic is like raw material entry, the pseudocode of the production and distribution functions will not be described here.

(5) Supervision and inquiry. Consumers can query the traceability information of the batches to which the goods belong, and supervisors have higher authority when querying the goods. In the query function, the

```
The input: supplyChain contract address base_addr, raw material name raw_name, raw material batch id raw_id, manufacturer
raw_factory, production information raw_info, timestamp
The output: raw material entry completed or failed
Require: the input raw_id is not occupied
Require: users are registered
if r.raw_id! = 0 ‖ supplierMap[msg.sender].id = = 0 then
    return FALSE;
end if
r.rawID = raw_id;
r.rawName = raw_name;
r.rawFac = raw_factory;
r.produceTime = timestamp;
r.rawInfo = raw_info; final return: true
```

ALGORITHM 2: rawRegister() function.

identity of the inquirer is first authenticated, and the batch file of the product is returned to the inquirer after passing.

4.3. Data Synchronization and Verification.

After the product traceability information is stored on the sidechain, the Merkle tree algorithm is used for hash locking, and the resulting Merkle Root is synchronized to the Ethereum main chain. Merkle Root changes when traceability information is tampered with.

After a round of trading, the information uploaded by suppliers, manufacturers, distributors, and other nodes in the sidechain is taken as the leaf nodes of the Merkle tree to calculate its hash value. If there are multiple suppliers or resellers, the information from the different nodes is processed as leaf nodes. After obtaining several hashes (H1, H2, ...), perform pairwise hash operation on (H1, H2, ...) to obtain the hash value. The pseudocode of the Merkle tree algorithm is shown in Algorithm 3.

Bind Merkle Root to the product batch number and synchronize it to the Ethereum main chain, which can be used as the traceability verification code of this batch of products. After the user queries the product traceability information, the same method is used to obtain Merkle Root. This can be compared to a reliable value on Ethereum to determine whether the traceability information for the product has been tampered with. Once the data is incorrect, regulators can use the Merkle tree algorithm to locate more quickly which branch the tampered data came from. Then, the accountability can be investigated in the corresponding supply chain links.

4.4. System Business Process.

The business process of supply chain traceability system designed in this paper is shown in Figure 4. Goods are traced back to their original raw materials. The process from rough machining by the supplier to finish machining by the manufacturer can be traced. The process from sales channels to consumers can also be traced back. All information can be tracked in an all-round, multiangle, and wide field. In this way, the origin and destination of products can be traced.

5. Experiment and Analysis

5.1. Fault Tolerance Test of Trading System.

The ability to operate stably when a system is attacked by a malicious node is called system fault tolerance. Therefore, the probability of a certain number of malicious nodes successfully destroying the normal operation of the system is taken as an index to evaluate the fault tolerance performance of the system. Considering the experimental effect and equipment performance, the number of nodes in the supply chain system was set to 50, and the number of malicious nodes gradually increased from 0 to 30. The successful rate of attack of malicious nodes in different states is obtained through several experiments under different number of malicious nodes.

In the supply chain system, the core enterprise will check the qualification of the enterprise applying to join the supply chain. Therefore, the probability that the number of malicious nodes exceeds 1/3 of the total number of nodes is low. At this time, according to Figure 5, the attack success rate is very low. The system has a high fault tolerance performance under the current conditions, but considering malicious attacks outside the system, the system fault tolerance performance needs to be further improved.

5.2. Throughput Analysis of Trading System.

Transaction Per Second (TPS) is used to evaluate system throughput. The transaction system undertakes the transaction function of the supply chain and has certain requirements on the real-time performance of the system. This paper analyzes the throughput of the supply chain transaction system through experiments, which provides a good foundation for system upgrade and deployment. The number of nodes of the trading system was taken as a variable in the experiment, and the number of nodes increased from 0 to 70. The experiment was repeated under different number of nodes. Finally, the TPS value of various nodes is used as the indicator of system throughput in various states.

```
The input: list info = [T1, T2, ..., t1, t2, ...]
The output: root hash merkle_root
Define hashed_info[] to hold the result of the hash operation
Define the array temp_info[] to hold the result of each layer of hash
for true do
    for index = 0; index < len(list_info); index+ = 2 do
        current = list_info[index];
        cur_right = list_info[index+1];
        cur_hash = sha256(current);
        cur_right_hash = sha256(cur_right);
        hashed_info[list_info[index]] = cur_hash;
        hashed_info[list_info[index + 1]] = cur_right_hash;
        Place (cur_hash + cur_right_hash) in temp_info[];
    end for
    if len(list_info) = = 1 then
        break;
    else
        list_info = temp_info;
    end if
end for
The last hash in the hashed_info array is merkle_root
return merkle_root
```

ALGORITHM 3: Merkle tree algorithm.
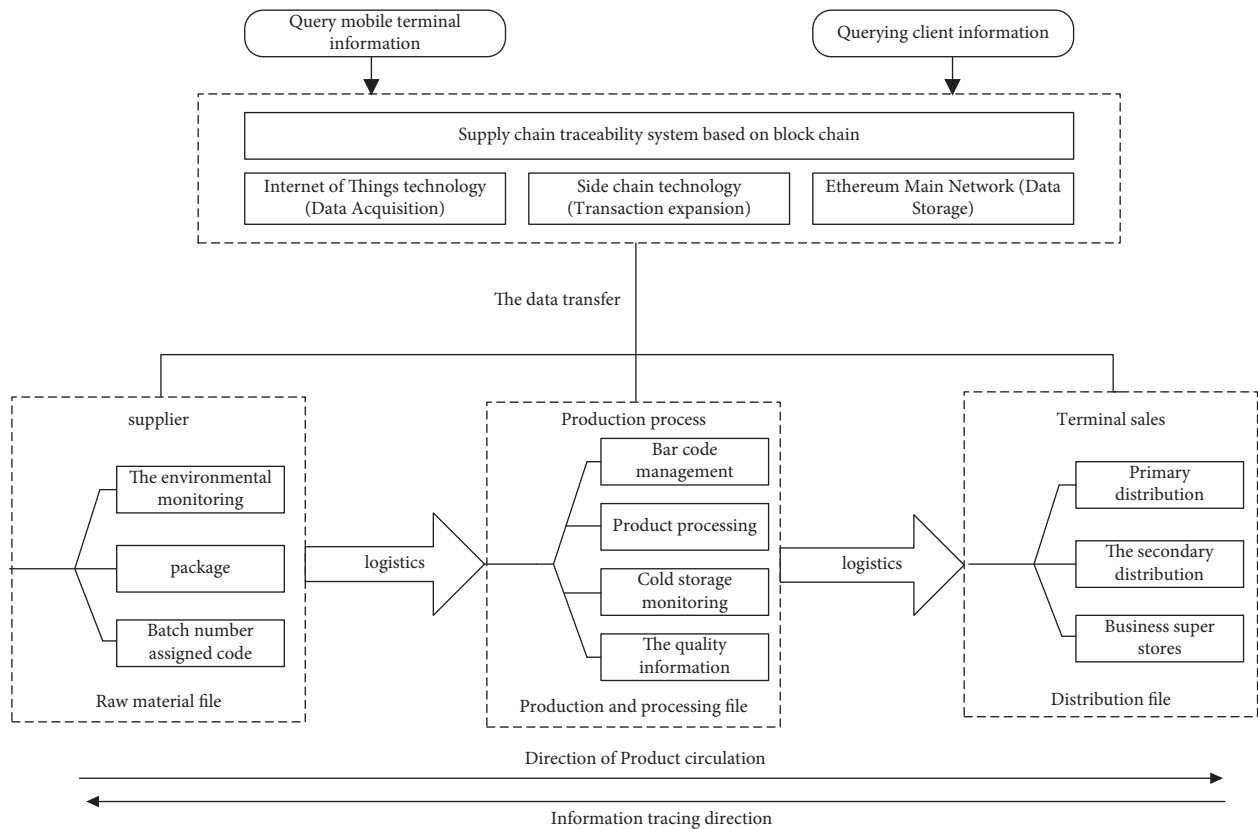
FIGURE 4: Business process of the traceability system.

It can be seen from Figure 6 that when the number of nodes is 5–45, the throughput of the transaction system rises with the increase of the number of nodes, and the upward trend remains basically unchanged. The throughput of the system in this paper is still small, even in the experimental environment where the operating environment is stable, and
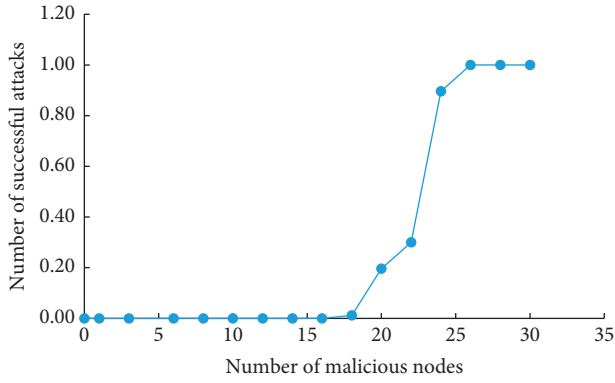
FIGURE 5: Success rate of trading system attack.
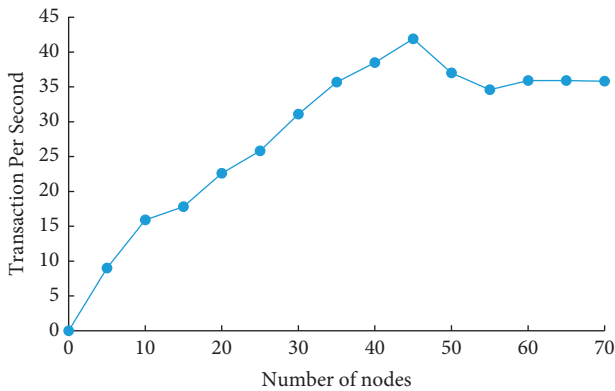
FIGURE 6: The throughput of the transaction system under different number of nodes.

the interaction content is simple. There is still a gap between this and the huge data transaction demand of the supply chain. Therefore, according to the actual demand of the supply chain, multichain and layered technologies will be combined to optimize the system architecture in the subsequent research. At the same time, the consensus algorithm is improved by using the advantages of the alliance chain and supply chain system to improve the consensus efficiency and increase the system throughput.

5.3. Comparison of Transaction Throughput. The throughput is an important indicator to evaluate the transaction system and blockchain system. Therefore, the throughput of the transaction system in this paper is compared with that of the transaction system in literature [18–20]. In the experiment, the number of nodes of the trading system was taken as a variable, and the number of nodes increased from 0 to 60. The experiment was repeated under different number of nodes, and the average value of TPS under different states was obtained as shown in Figure 7.

According to the experimental results, when the number of nodes is less than 40, the transaction system in this paper has certain advantages in throughput performance. However, the throughput of the transaction system in literature
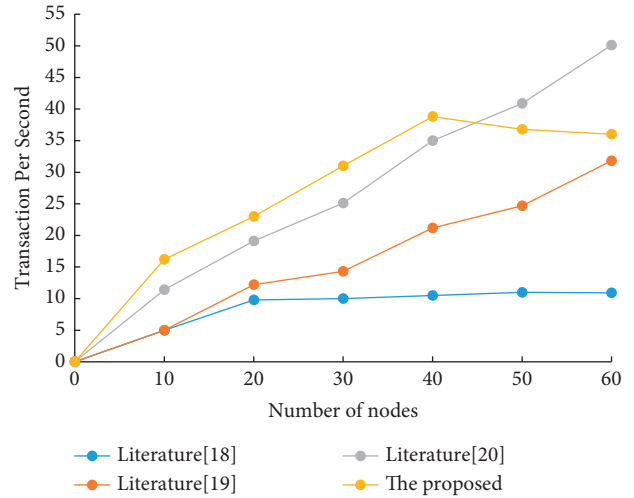
FIGURE 7: Throughput comparison of the trading system.

[18, 19] continues to rise and does not decline when the number of nodes reaches 60. Therefore, when the number of nodes in the transaction system is small, the transaction system in this paper has certain advantages in throughput performance. However, the system throughput peak value is small, which has a certain gap with the actual application demand of the supply chain system, and the system throughput performance has a large space to improve.

6. Conclusion

Traditional agricultural product traceability system is generally centered on a centralized database, which leads to the difficulty of traceability and inflexibility of the system. While blockchain technology is in the development stage, how to break through the technical bottleneck of blockchain and better apply it to the production of agricultural products has become the focus of the industry. In order to promote the cooperation between enterprises in the supply chain and improve the efficiency of supply chain cooperation, this paper designs a chain traceability system of agricultural products based on sidechain technology. It provides a trusted platform for data sharing, which is independent of third parties. The experimental results show that the system combines sidechain technology with supply chain traceability, and it provides an expansion scheme for nontransfer transactions. The future work is to compare and analyze different sidechain protocols and select the high-performance sidechain technology that is more suitable for supply chain traceability system to improve the transaction performance of the system.

Data Availability

The labeled dataset used to support the findings of this study is available from the corresponding author upon request.

Conflicts of Interest

The authors declare that they have no conflicts of interest.

References

[1] D. Prashar, N. Jha, S. Jha, Y. Lee, and G. P. Joshi, "Blockchain-based traceability and visibility for agricultural products: a decentralized way of ensuring food safety in India," *Sustainability*, vol. 12, no. 8, p. 3497, 2020.

[2] Z. Ning, X. Hu, Z. Chen et al., "A cooperative quality-aware service access system for social Internet of vehicles," *IEEE Internet of Things Journal*, vol. 5, no. 4, pp. 2506–2517, 2018.

[3] M. Maksimovic, V. Vujovic, and E. Omanovic-Miklicanin, "A Low-Cost Internet of Things Solution for Traceability and Monitoring Food Safety during Transportation," in *Proceedings of the HAICTA 2015, 7th International Conference on Information and Communication Technologies in Agriculture, Food and Environment*, pp. 583–593, Kavala, Greece, September 2015.

[4] R. Ostapenko, Y. Herasymenko, V. Nitsenko, S. Koliadenko, T. Balezentis, and D. Streimikiene, "Analysis of production and sales of organic products in Ukrainian agricultural enterprises," *Sustainability*, vol. 12, no. 8, p. 3416, 2020.

[5] J. F. Galvez, J. C. Mejuto, and J. Simal-Gandara, "Future challenges on the use of blockchain for food traceability analysis," *TRAC Trends in Analytical Chemistry*, vol. 107, pp. 222–232, 2018.

[6] S. Choi and J.-H. Lee, "Blockchain-based distributed firmware update architecture for IoT devices," *IEEE Access*, vol. 8, pp. 37518–37525, 2020.

[7] Z. Zhu, G. Qi, M. Zheng, J. Sun, and Y. Chai, "Blockchain based consensus checking in decentralized cloud storage," *Simulation Modelling Practice and Theory*, vol. 102, Article ID 101987, 2020.

[8] P. Sharma, R. Jindal, and M. D. Borah, "Blockchain technology for cloud storage: a systematic literature review," *ACM Computing Surveys*, vol. 53, no. 4, pp. 1–32, 2020.

[9] W. Liang, X. Lei, K.-C. Li, Y. Fan, and J. Cai, "A Dual-Chain Digital Copyright Registration and Transaction System Based on Blockchain technology," in *Proceedings of the International Conference on Blockchain and Trustworthy Systems*, pp. 702–714, Manhattan, NY, USA, December 2019.

[10] H. Peng, B. Hu, Q. Shi et al., "Removal of ocular artifacts in EEG-an improved approach combining DWT and ANC for portable Applications," *IEEE journal of biomedical and health informatics*, vol. 17, no. 3, pp. 600–607, 2013.

[11] X. Yang, J. Qian, C. Sun, and Z. Ji, "Key technologies for establishment agricultural products and food quality safety traceability systems," *Transactions of the Chinese Society for Agricultural Machinery*, vol. 45, no. 11, pp. 212–222, 2014.

[12] R. Shankar, R. Gupta, and D. K. Pathak, "Modeling critical success factors of traceability for food logistics system," *Transportation Research Part E: Logistics and Transportation Review*, vol. 119, pp. 205–222, 2018.

[13] C. Xie, H. Y. Guo, and D. F. He, "Research on the Construction of Traceability System for Ecommerce Agricultural Products Quality and Safety in China Based on blockchain," in *Proceedings of the 4th International Conference on Social Science and Contemporary Humanity Development (SSCHD 2018)*, Wuhan, Hubei, China, December 2018.

[14] K. Gao, Y. Liu, T. Han, and H. Xu, "Design and implementation of food supply chain traceability system based on Hyperledger Fabric," *International Journal of Computational Science and Engineering*, vol. 23, no. 2, pp. 185–193, 2020.

[15] Y. Dong, B. Ding, G. Zhang, G. Jin, and X. Zhao, "Quality and safety traceability system based on agricultural product supply chain," *Transactions of the Chinese Society of Agricultural Engineering*, vol. 32, no. 1, pp. 280–285, 2016.

[16] J. Sidhu, "Syscoin: A Peer-To-Peer Electronic Cash System with Blockchain-Based Services for e-business," in *Proceedings of the 2017 26th International Conference on Computer Communication and Networks (ICCCN)*, pp. 1–6, Vancouver, BC, Canada, July 2017.

[17] T.-M. Choi, X. Wen, X. Sun, and S.-H. Chung, "The mean-variance approach for global supply chain risk analysis with air logistics in the blockchain technology era," *Transportation Research Part E: Logistics and Transportation Review*, vol. 127, pp. 178–191, 2019.

[18] F. Jamil, L. Hang, K. Kim, and D. Kim, "A novel medical blockchain model for drug supply chain integrity management in a smart hospital," *Electronics*, vol. 8, no. 5, Article ID 505, 2019.

[19] I. Makhdoom, I. Zhou, M. Abolhasan, J. Lipman, and W. Ni, "PrivySharing: a blockchain-based framework for privacy-preserving and secure data sharing in smart cities," *Computers & Security*, vol. 88, Article ID 101653, 2020.

[20] C. Wang, S. Chen, Z. Feng, Y. Jiang, and X. Xue, "Blockchain-Based Data Audit and Access Control Mechanism in Service collaboration," in *Proceedings of the 2019 IEEE International Conference on Web Services (ICWS)*, pp. 214–218, Milan, Italy, July 2019.

Hindawi

Research Article

Selection and Exploration of Cultural and Creative Tourist Attractions Based on BP Network

Nian Xing (ID)

School of Journalism and Communication, Sichuan International Studies University, Chongqing 400031, China

Correspondence should be addressed to Nian Xing; 99002333@sisu.edu.cn

In order to improve the selection and exploration effect of cultural and creative tourist attractions, this paper applies BP network to the selection and search of cultural and creative tourist attractions. Moreover, this paper improves the algorithm to promote the interrelation of cultural and creative industries and tourism industries to promote each other to form a complex and changeable dynamic system and proposes a personalized recommendation model for tourist attractions based on domain adaptation. Domain adaptation can effectively reduce the distribution difference between different data. In addition, this paper combines experimental research to verify the system model of this paper. The research results show that the cultural and creative tourist attractions selection search system based on the BP network proposed in this paper has a good selection effect of tourist attractions and has an important role in promoting the development of cultural and creative tourism.

1. Introduction

At present, creative products based on regional culture are mostly concentrated in art exhibitions and high-end crafts, which make the audience group smaller. Tourism products on the traditional market have low cultural content and poor product quality, and a large part of the products are direct applications of pictures, so there is no innovation. Domestic and foreign scholars are doing more and more research studies on regional culture, but the design and application of regional cultural elements are in the initial stage. Therefore, it is necessary to start with cultural elements and develop and design tourism cultural and creative products based on regional culture as the research content. Moreover, it is necessary to analyze the cultural elements with the most regional characteristics through the study of regional culture, conduct research and analysis on them, and establish a material library of regional cultural elements, which is conducive to increasing the added value of products and is conducive to product serialization and branding.

At present, many tourism, cultural, and creative products centered on regional culture are seriously homogenized, and many products in scenic spots only replace the parts of the products that can be pasted, resulting in similar products with little difference. Most tourism products have no sense of design, messy types, and no special features. Except for the different pictures, the product modeling functions of the direct map products are almost the same. On the surface, it is because tourism products lack cultural connotation. At a deeper level, it is that the level of cultural excavation is not enough. New technologies and new media are used to rearrange and utilize the regional culture, build a regional cultural material library, and preserve the culture at the same time. More people know the regional culture. Second, the establishment of a regional cultural material library is conducive to the development of the cultural industry, thereby supporting the development and iteration of subsequent cultural creative products. Third, through the study of regional culture, establish a relevant cultural research system, explore relevant research methods and research models, and apply them to the design and research and development of cultural creative products to guide the development of cultural creative products, upgrades, and changes in the current market, so that the products are no longer low quality and low culture. Because of its particularity, regional culture also represents ancient Chinese

culture at a certain level. Using regional cultural elements to develop cultural and creative products will help promote the public to understand regional culture and history and understand Chinese culture. It can not only promote the development of local culture but also enhance tourists' awareness of local culture, thereby driving regional economic development. Development is more conducive to the establishment of national cultural self-confidence.

Regional culture refers to the cultural connotation with regional characteristics within a region containing material and spiritual characteristics, including the development form and social lifestyle of the place from time to time, as well as the unique cultural heritage and material heritage [1]. Natural resources and human resources are integrated into a cultural characteristic that can reflect national characteristics, thoughts, concepts, customs, beliefs, morals, ethics, and so on. Hundred schools of thought, piano, chess, calligraphy and painting, literature, drama, festivals, folk houses, architecture, characters, language, costumes, stories, characters, customs, dialects, singing and dancing, food, traditional Chinese medicine, religion, belief, philosophy, craftsmanship, martial arts, and other diverse regional cultures constitute the broad Chinese culture [2].

Packaging design research based on regional culture is to study the application of regional culture in packaging design. Taking Baminjin series packaging design examples as the starting point, it explores research approaches suitable for Baminjin packaging design, and through the inheritance and development of Bamin regional culture, it reflects the value of cultural innovation and wins a better investment market. It is necessary to apply regional culture in product packaging design and design according to consumers' cultural identity and emotional bonds of the brand, so as to enhance the cultural value of packaging design [3].

This paper applies the BP network to the selection of cultural and creative tourist attractions and builds an intelligent system based on the actual situation to promote the further development of cultural and creative tourism.

2. Related Work

For the study of cultural and creative industries, there have been relatively mature and systematic research results abroad. Literature [4] awakened the definition of the concept of creative industries based on the perspective of cultural economics. Literature [5] analyzed and compared the similarities and differences between the two terms "cultural entrepreneurship industry" and "creative industry" and pointed out that they have essentially the same characteristics. Literature [6] expanded the extension of the creative industry and collectively referred to the cultural industry and the art industry as the creative industry. Literature [7] analyzed the driving factors of innovation and pointed out that market demand plays a key role in guiding innovation, but it also restricts the development of innovation. Compared with technology, market demand has a greater driving role. Literature [8] put forward the "dual-factor theory" for the development of cultural and creative industries and believed that supply and demand are the two main driving

forces that promote the development of entrepreneurial industries. Literature [9] systematically proposed the theory of creative economics, which led to the vigorous development of theories of creative economics. Literature [10] studied the industrial characteristics of traditional handicrafts and pointed out that cultural creativity can give handicrafts more added value. Literature [11] combined creative industries with tourism and pointed out creative tourism, a new idea for the development of tourism. Literature [12] believed that under different economic environments, entrepreneurial industries should apply different development models and advocate different models. The former focuses on market orientation, while the latter believes that government leadership can better promote the development of creative industries. Literature [13] defined industrial agglomeration, took major cities in the world as the research object, and defined the new urban development model of "creative cities." Literature [14] compared several major cultural and creative industry development models. Literature [15] pointed out the evolution trend of Singapore's cultural and creative industries based on the perspective of potential mining. Literature [16] comparatively analyzed the creative industry, cultural industry, and cultural creative industry and sorted out the main similarities and differences of the three. Literature [17] analyzed the main influencing factors driving the development of cultural and creative industries based on the perspective of industrial competitiveness and further analyzed the value of cultural and creative industry chain research. Literature [18] studied the value chain creation mechanism of cultural and creative industries. Literature [19] pointed out that human resources, market demand, institutional environment, and basic environment are the key factors that promote the development of cultural and creative industries. On this basis, a framework of influencing factors of the cultural entrepreneurship industry is constructed. Literature [20] pointed out that the policy environment and cultural environment play a key role in the development of Beijing's cultural and creative industries.

3. Recommendation Algorithm Based on BP Neural Network Model

According to the above conclusions, it is known that the deep convolutional neural network cannot process data in non-Euclidean space and loses its effectiveness when encountering topological structure graph data. However, graph structures are common in real life, so more and more people are beginning to explore how to define convolution operations for graph data.

The main challenges of using convolutional neural networks for graph structures are as follows:

(1) The graph structure data do not satisfy the translation invariance; that is, the structure of each node is different, and the number of connected neighbor nodes is uncertain, so it is impossible to use a convolution kernel of the same size to perform convolution operations.

(2) The graph structure data have directionality. For example, users in social networks are connected.

The graph convolutional neural network for non-Euclidean spatial data is divided into two directions: spectral domain method and vertex domain method.

The vertex domain method of graph convolutional neural network has two ideas. One idea is to design convolution kernel and convolution operation based on graph structure data, and the other idea is to convert graph structure data into Euclidean space data structure.

Like the traditional convolutional neural network, the goal of the BP neural network model is to learn a function to extract features. Each neural network layer can be written as a nonlinear function:

$$H^{(l+1)} = f\left(H^l, A\right), H^{(0)} = X, H^{(L)} = Z. \tag{1}$$

Among them, L represents the number of layers, and $f(\cdot;)$ of each layer differs only in parameters, and Z represents the final output.

$$f\left(H^{(l)}, A\right) = \sigma\left(AH^{(l)}W^{(l)}\right). \tag{2}$$

The feature matrix, adjacency matrix, and weight matrix are subjected to matrix multiplication to reflect the physical meaning of convolution. Obviously the weight matrix is easy to understand. Multiplying the adjacency matrix and the feature matrix is to learn the traditional convolution operation. The traditional convolution operation is to sum the product of the convolution kernel and the corresponding element. The convolution operation of the graph structure also needs to meet the translation invariance; that is, the number of elements in the convolution kernel participating in the convolution operation must change according to the graph structure, and the translation invariance in the graph structure is reflected in the adjacency matrix. Graph structure data are as shown in Figure 1.

$$X = \begin{bmatrix} a_{11}, a_{12}, a_{13}, \ldots, a_{16} \\ a_{21}, a_{22}, a_{23}, \ldots, a_{26} \\ a_{31}, a_{32}, a_{33}, \ldots, a_{36} \\ a_{41}, a_{42}, a_{43}, \ldots, a_{46} \\ a_{51}, a_{52}, a_{53}, \ldots, a_{56} \\ a_{61}, a_{62}, a_{63}, \ldots, a_{66} \end{bmatrix},$$

$$A = \begin{bmatrix} 0, 1, 1, 0, 0, 0 \\ 1, 0, 1, 0, 0, 1 \\ 1, 1, 0, 1, 1, 0 \\ 0, 0, 1, 0, 1, 1 \\ 0, 0, 1, 1, 0, 0 \\ 0, 1, 0, 1, 0, 0 \end{bmatrix}. \tag{3}$$
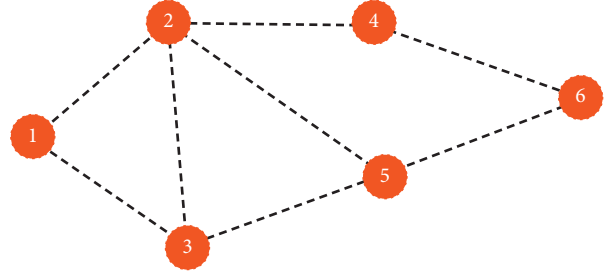
$Q = AX$, and we only list the first line of Q:

FIGURE 1: Graph structure data.

$$Q_{1\bullet} = \left[a_{21} + a_{31}, a_{22} + a_{32}, a_{23} + a_{33}, a_{24} + a_{34}, a_{25} + a_{35}\right]. \tag{4}$$

Q_1 can be expressed as the sum of the feature vectors of the two neighbor nodes of x_1. If the weight matrix is added, the meaning of weighted average can be expressed, which is the convolution operation in the traditional sense. However, there is one point that needs to be explained here. Since the convolution operation is a weighted average of the central node and the surrounding nodes, the above formula does not involve the central node, the adjacency matrix A is improved, and the original adjacency matrix A is added with its own node.

$$\widehat{A} = A + I. \tag{5}$$

$\widehat{A}$ is normalized to

$$\widehat{A} = \widehat{D}^{-1/2}\widehat{A}\widehat{D}^{-1/2},$$
$$f\left(H^{(l)}, A\right) = \sigma\left(\widehat{D}^{-1/2}\widehat{A}\widehat{D}^{-1/2}H^{(l)}W^{(l)}\right). \tag{6}$$

Although this model is very simple, the model effect is very powerful. Figure 2 shows the use of a simple GCN model on the famous Taekwondo club data set in this paper. After experimentation, it is found that only 3 levels are needed to classify club members. Moreover, the experimental result of using the identity matrix as the characteristic matrix when the characteristic matrix of the node is not known is also very impressive. For many graph networks, there may be no node characteristics, and graph convolutional neural networks can also be used at this time. The identity matrix I replaces the feature matrix X operation.

The second airspace method converts graph structure data into Euclidean space data. First, it selects a representative node sequence from the graph structure and second designs a neighborhood with a fixed convolution kernel size for each node. Then, it converts each graph structure data into Euclidean space data, which can be solved by using traditional convolution operations.

Each image can be regarded as a special graph, and each pixel in the image can be represented as a node. The convolution operation for each image is the weighted average of n central pixels and the surrounding pixels. Therefore, each
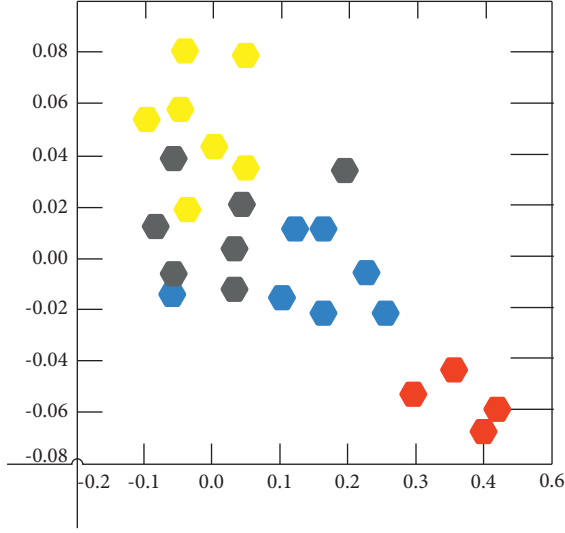
FIGURE 2: Diagram structure of Taekwondo club.

graph structure can also be regarded as a weighted average of n central vertices and corresponding neighborhoods, so that the graph structure can be converted into Euclidean space data. Traditional convolution operation is as shown in Figure 3, and graph structure transformation is as shown in Figure 4.

This paper selects n representative nodes, and the node selection is based on the Weisfeiler–Lehman algorithm. It can be understood as calculating the centrality of each node, sorting according to the size of the value, and then taking the first n representative nodes.

The neighborhood of the node is constructed by normalizing the neighborhood in the previous step. Normalization makes the nodes of the neighborhood graph have an order so that the unordered graph space is mapped to the vector space in a linear order. Moreover, this paper defines the optimal graph normalization problem and finds the optimal order by optimizing the function. The operation steps are shown in Figure 5.

$$\mathrm{argmin}_l \mathrm{E}_G \left[\left| d_A\left(A^l(G), A^l(G')\right) - d_G\left(G, G'\right) \right| \right]. \quad (7)$$

Each graph structure data can map the disordered neighborhood to the vector space through node selection and node neighborhood construction. Therefore, the method proposed in this paper is to build a bridge between graph structure data and convolutional neural network and solve the transformed Euclidean space data through traditional convolutional neural network.

In the traditional Fourier transform $\widehat{f}(\omega) = \int f(t)e^{-i\omega t}dt$, the integral operation here can be understood as a linear combination of $f(t)$ and basis function e^{-icx}. We only need to compare the basis function h used here to find the basis function on the graph.

The eigen decomposition of Laplacian matrix L is

$$L = U \begin{bmatrix} \lambda_1 & & \\ & \ddots & \\ & & \lambda_n \end{bmatrix} U^{-1}. \quad (8)$$

Because L is an orthogonal matrix,

$$L = U \begin{bmatrix} \lambda_1 & & \\ & \ddots & \\ & & \lambda_n \end{bmatrix} U^{\mathrm{T}}. \quad (9)$$

The characteristic matrix U of the Laplacian matrix L is the base matrix of the graph convolution, so the graph Fourier transform operation $\widehat{f}(\omega) = \sum_{i=1} f(i)u_l^*(i)$ is converted into a matrix form:

$$f^*g = \begin{bmatrix} u_1(1) & u_1(2) & \cdots & u_1(N) \\ u_2(1) & u_2(2) & \cdots & u_2(N) \\ \vdots & \vdots & \ddots & \vdots \\ u_N(1) & u_N(2) & \cdots & u_N(N) \end{bmatrix} \begin{bmatrix} f(1) \\ f(2) \\ \vdots \\ f(N) \end{bmatrix}. \quad (10)$$

Among them, f and g are the original signals, $F(f)$ is the Fourier transform of f, $\cdot$ represents the product, and * represents the convolution operation.

$$f^*h = F^{-1}\left(\widehat{f}(w)\widehat{h}(w)\right) = \frac{1}{2\pi} \int \widehat{f}(w)\widehat{h}(w)e^{iex}d\omega \, . \quad (11)$$

Analogy to $f^*h = U(\widehat{f}\widehat{h})$ in the graph, the Fourier transform $\widehat{h}(\lambda_l) = \sum_{i=1}^N h(i)u_l^*(i)$ of the convolution kernel h is written as a diagonal matrix as follows:

$$\widehat{h} = \begin{bmatrix} \widehat{h}(\lambda_1) & & \\ & \ddots & \\ & & \widehat{h}(\lambda_n) \end{bmatrix}. \quad (12)$$

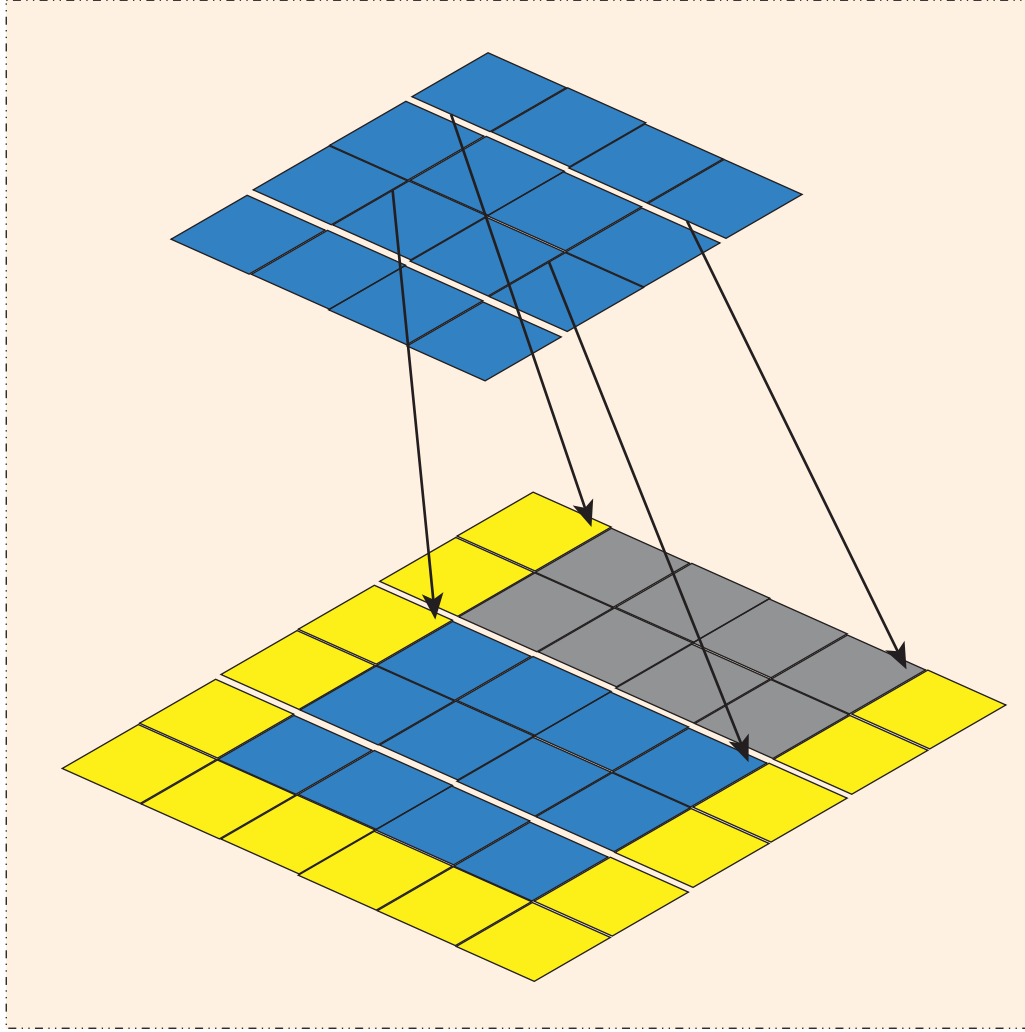Therefore, the generalized convolution on the graph is as follows:

FIGURE 3: Traditional convolution operation.

$$f^* g = U \begin{bmatrix} \widehat{h}(\lambda_1) & & \\ & \ddots & \\ & & \widehat{h}(\lambda_n) \end{bmatrix} U^T f, U = (\overrightarrow{u_1}, \overrightarrow{u_2}, \cdots, \overrightarrow{u_n}). \quad (13)$$

U is the unit eigenvector matrix of the Laplacian matrix. Later, in many spectral domain graph convolution papers, it is often represented by $(f^*h)_G = U((U^T h)\Theta U^T f))$, where Θ is the Hadamard product.

The setting of the first-generation convolution kernel directly selects the parameter diagonal matrix to represent.

$$g_\theta(\Lambda) = \begin{bmatrix} \theta_1 & & \\ & \ddots & \\ & & \theta_n \end{bmatrix}. \quad (14)$$

Among them, $\Theta(\theta_1, \theta_2 \cdots \theta_n)$ is n arbitrary parameters. It can be seen that the Laplacian matrix needs to be eigen-decomposed when seeking graph convolution.

Due to the large dimension of the Laplacian matrix of the graph data, calculating the eigenvalues will consume a lot of time. Moreover, because the first-generation convolution kernel does not have local features, many scholars have begun to modify the convolution kernel and proposed the second-generation convolution kernel.

$$g_\theta(\Lambda) = \begin{bmatrix} \sum_{j=0}^{K} \alpha_j \lambda_1^j & & \\ & \ddots & \\ & & \sum_{j=0}^{K} \alpha_j \lambda_n^j \end{bmatrix}. \quad (15)$$

The ingenious thing is

$$\Lambda^j = \begin{bmatrix} \lambda_1^j & & \\ & \ddots & \\ & & \lambda_n^j \end{bmatrix}. \quad (16)$$

When substituting it into the above formula, we can get

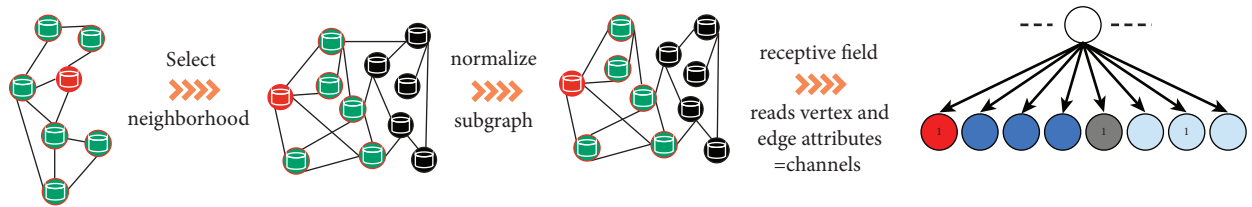(a)

(b)
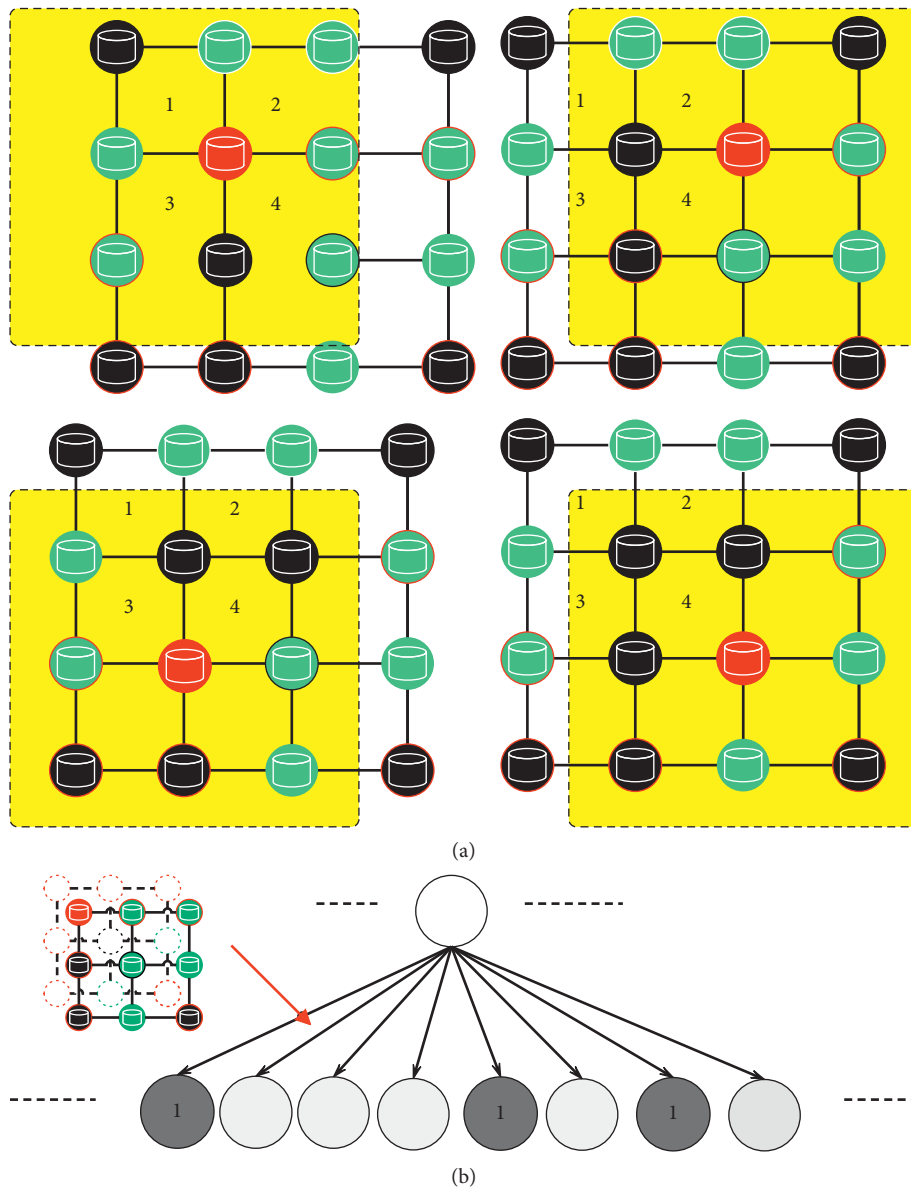
FIGURE 4: Graph structure transformation.

FIGURE 5: Operation steps.

$$g_\theta(\Lambda) = \begin{bmatrix} \sum_{j=0}^{K} \alpha_j \lambda_1^j & & \\ & \ddots & \\ & & \sum_{j=0}^{K} \alpha_j \lambda_n^j \end{bmatrix} = \sum_{j=0}^{K} \alpha_j \Lambda^j,$$

$$U \sum_{j=0}^{K} \alpha_j \Lambda^j U^T = \sum_{j=0}^{K} \alpha_j U \Lambda^j U^T = \sum_{j=0}^{K} \alpha_j L^j. \quad (17)$$

Therefore, the convolution operation is transformed into

$$y_{\text{output}} = \sigma\left(\sum_{j=0}^{K} \alpha_j L^j x\right). \quad (18)$$

Compared with the first-generation convolution kernel, the second-generation convolution kernel reduces the number of parameters, reduces the complexity of the parameters, and speeds up the calculation. The convolution operation avoids the eigen decomposition of the Laplacian matrix, and the convolution kernel adds the local features of each node.

In addition to cleverly designing the convolution kernel to avoid the eigendecomposition of the Laplacian matrix, Chebyshev polynomials can also be used to fit the convolution kernel, which is a widely used method in GCN papers. The third-generation graph convolutional network (GCN) is proposed.

The first-generation convolution kernel is

$$y_{\text{output}} = \sigma\left(U g_\theta(\Lambda) U^T x\right). \quad (19)$$

Among them, U is the matrix formed by the eigenvectors of the Laplacian matrix.

Using the Chebyshev polynomial instead of the original convolution kernel, we can get $g_\theta(\Lambda) = \sum_{k=0}^{K-1} \beta_k T_k(\widetilde{\Lambda})$, where $T_k(\cdot)$ is the k-order Chebyshev polynomial, β_k is the corresponding parameter, and Λ is the diagonal matrix of eigenvalues.

$$\widetilde{\Lambda} = \frac{2\Lambda}{\lambda_{\max}} - I. \quad (20)$$

It can be seen that the elements of the characteristic diagonal matrix are limited to [0, 1] at this time. The reason for this operation is that the Chebyshev polynomial has a domain of [−1, 1].

$$y_{\text{output}} = \sigma\left(U \sum_{k=0}^{K-1} \beta_k T_k(\widetilde{\Lambda}) U^T x\right),$$

$$y_{\text{owput}} = \sigma \sum_{k=0}^{K-1} \beta_k T_k\left(\widetilde{U\Lambda U^T})x\right), y_{\text{oupput}} = \sigma \sum_{k=0}^{K-1} \beta_k T_k(\widetilde{L})x\right). \quad (21)$$

Among them,

$$\widetilde{L} = \frac{2L}{\lambda_{\max}} - I, T_k(\widetilde{L}) = 2\widetilde{L}T_{K-1}(\widetilde{L}) - T_{k-2}(\widetilde{L}), T_0(\widetilde{L}) = I, T_1(\widetilde{L}) = \widetilde{L}, L = I - D^{-\frac{1}{2}} A D^{-\frac{1}{2}}. \quad (22)$$

We can see that

(1) Chebyshev polynomial as a convolution kernel avoids the eigen decomposition of the Laplacian matrix.

(2) By introducing the adjacency relationship of the graph, the convolution kernel has local features. Therefore, the graph convolution model based on the spectral domain method is a further promotion of the basis function of the Fourier transform and the convolution kernel of the convolution operation.

The data in the social recommendation system can be naturally expressed as a user-user social graph and a user-item graph, and the BP neural network can integrate the node information in the above two graph structures.

Therefore, BP neural network is widely used in product recommendation, movie recommendation, and other fields. User Modeling integrates the user information extracted from the user's social network (which can be understood as the characteristics of friends in the user's social relationship and reflects some of the characteristics of the user) with the user information extracted from the user-item graph structure (can be understood as the user's rating of the item and reflects the user's characteristics).

The Graphrec model includes User Modeling, Item Modeling, and Rating Prediction (Figure 6). Item Modeling integrates the characteristics of the item with the characteristics of the users participating in the evaluation of the item to reflect the characteristics of the item. Rating Prediction combines the user potential features extracted from
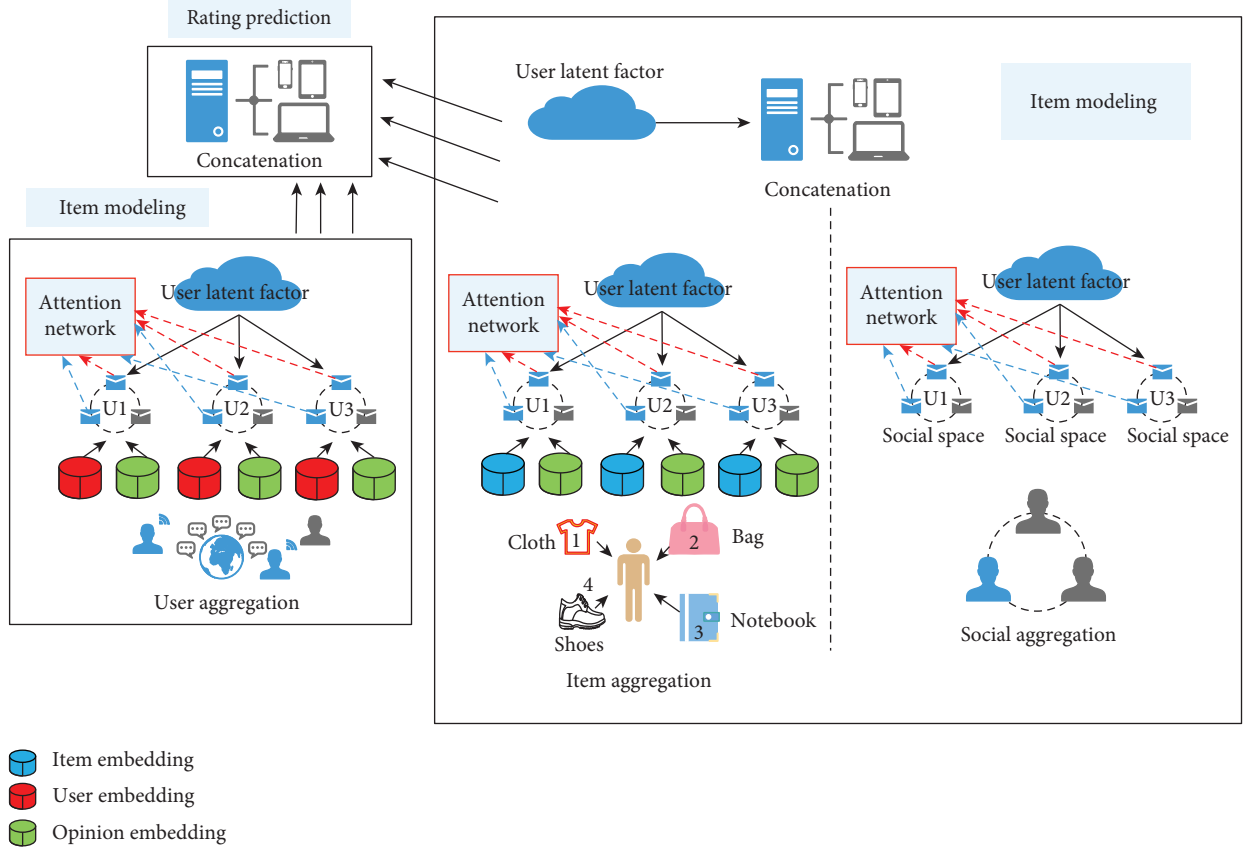
FIGURE 6: Graphrec model.

the User Modeling and Item Modeling described above with the potential features of the item to predict the rating of each item.

The following is a detailed introduction to the content of the paper.

3.1. User Modeling.
In order to understand the potential characteristics of users, the user model is divided into two parts, user-item graph and social network, and the two parts are described separately.

3.1.1. User-Item Graph Model

$$h_i^I = \sigma \left(W \cdot \text{aggre}_{\text{item}} \left(\{ x_{ia}, \forall a \in C(i) \} \right) + b \right). \tag{23}$$

Among them, $C(i)$ is the item evaluated by user $u(i)$, W, b is the weight and bias of the neural network, and σ is a nonlinear function.

Users will express their opinions when scoring items, so items and item scoring can help users model.

$$x_{ia} = g_v([q_a \oplus e_r]). \tag{24}$$

Among them, x_{ia} is the integration of users and items, x_{ia} is the interactive representation of each item and the score, q_a is the feature vector of the item, e_r is the feature of the five evaluation levels, and $\oplus$ is the connection of two vectors.

Generally, the abovementioned aggretions fusion function directly integrates multiple items evaluated by each user on an average basis, which as follows:

$$h_i^l = \sigma \left(W \cdot \left\{ \sum_{acc(t)} \alpha_i x_{ia} \right\} + b \right),$$

$$\alpha_i = \frac{1}{|C(i)|}. \tag{25}$$

Because the proportion of each item is different for users, it is not possible to directly calculate the average integration. In order to make up for the lack of average integration, the attention mechanism is introduced.

$$h_i^l = \sigma \left(W \cdot \left\{ \sum_{acC(i)} \alpha_{ia} x_{ia} \right\} + b \right), \tag{26}$$

where α_{ia} is the weight of the attention mechanism.

$$\alpha_{ia}^* = \left(w_2^T \cdot \sigma \left(W_1 \cdot [x_{ia} \oplus p_i] \right) + b_1 \right) + b_2,$$

$$\alpha_{ia} = \frac{\exp(\alpha_{ia}^*)}{\sum_{a \in C(i)} \exp(\alpha_{ia}^*)}. \tag{27}$$

Among them, p^i is the feature vector of user u_i, the interaction of items and ratings is connected with the feature
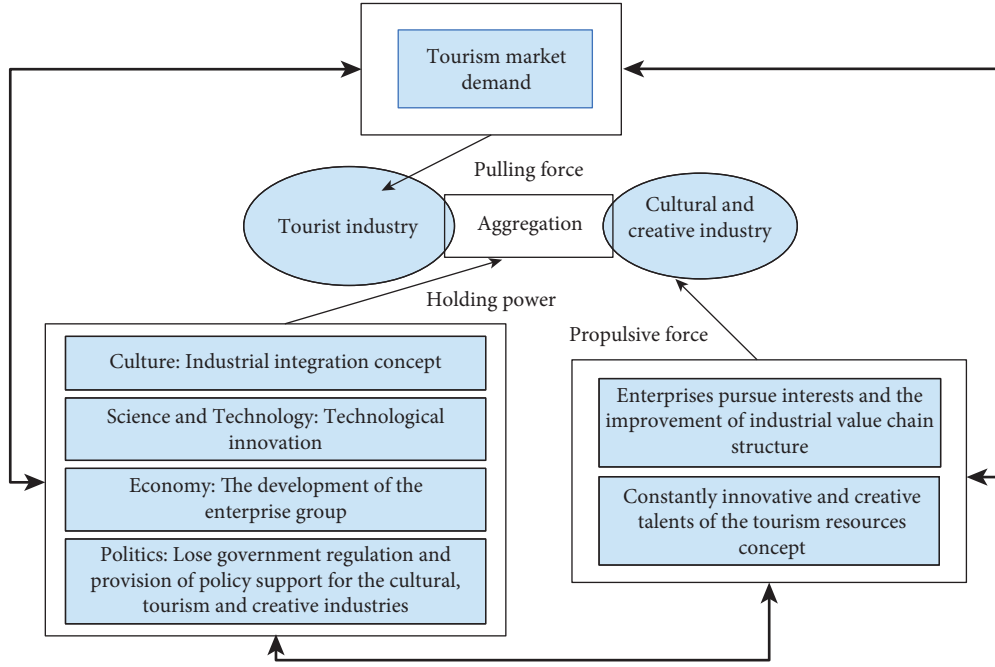
FIGURE 7: Integration mechanism of tourism industry and cultural creative industry.

vector of the user, and W_1 and w_2^T, b_1, and b_2 are weights and biases. The Softmax function is used to normalize the above attention weights to obtain the final attention weights, which can be understood as the contribution of the interaction to the user-item space user latent factor.

In the interaction between users and friends, it can be found that users' evaluations of products are similar to their own friends' evaluations. Therefore, this paper proposes to obtain the potential characteristics of the user by fusing the evaluation of the user's friends on the project and the characteristics of the project itself and design the following fusion function:

$$h_i^S = \sigma\left(W \cdot \text{Aggre}_{\text{neighhors}}\left(\left\{h_o^I, \forall o \in N(i)\right\}\right) + b\right),$$

$$h_i^S = \sigma\left(W \cdot \left\{\sum_{o \in N(i)} \beta_{io} h_o^I\right\} + b\right). \tag{28}$$

Since different friends have different influences on users, this paper introduces an attention mechanism to users' friends.

$$\beta_{io}^* = w_2^T \cdot \sigma\left(W_1 \cdot \left[h_o^I \oplus p_i\right] + b_1\right) + b_2,$$

$$\beta_{io} = \frac{\exp\left(\beta_{io}^*\right)}{\sum_{o \in N(i)} \exp\left(\beta_{io}^*\right)}. \tag{29}$$

The potential user characteristics obtained by the user-item graph model and the user potential characteristics obtained by the user social network model are merged, and the two parts of user characteristics are extracted through the full convolutional neural network to obtain the final user potential characteristics.

$$c_1 = \left[h_i^l \oplus h_i^s\right],$$

$$c_2 = \sigma\left(W_2 \cdot c_1 + b_2\right),$$

$$\cdots$$

$$h_i = \sigma\left(W_l \cdot c_{l-1} + b_l\right). \tag{30}$$

3.2. Item Modeling. The project model is to extract the potential features of the project and extract the potential features of the project by fusing the characteristics of the users participating in the project evaluation and the user's score.

$$f_{jt} = g_{ut}\left(\left[p_t \oplus e_r\right]\right). \tag{31}$$

Each user feature is fused, and the fusion function is designed as follows:

$$z_j = \sigma\left(W \cdot \text{Aggre}_{\text{users}}\left(\left\{f_{jt}, \forall t \in B(j)\right\} + b\right)\right),$$

$$z_j = \sigma\left(W \cdot \left\{\sum_{t \in B(j)} \mu_{jt} f_{jt}\right\} + b\right). \tag{32}$$

Since each user has a different proportion of item feature extraction, this paper adds an attention mechanism.

$$\mu_{jt}^* = w_2^T \cdot \sigma\left(W_1 \cdot \left[f_{jt} \oplus q_j\right] + b_1\right) + b_2,$$

$$\mu_{jt} = \frac{\exp\left(\mu_{jt}^*\right)}{\sum_{t \in B(j)} \exp\left(\beta_{jt}^*\right)}. \tag{33}$$
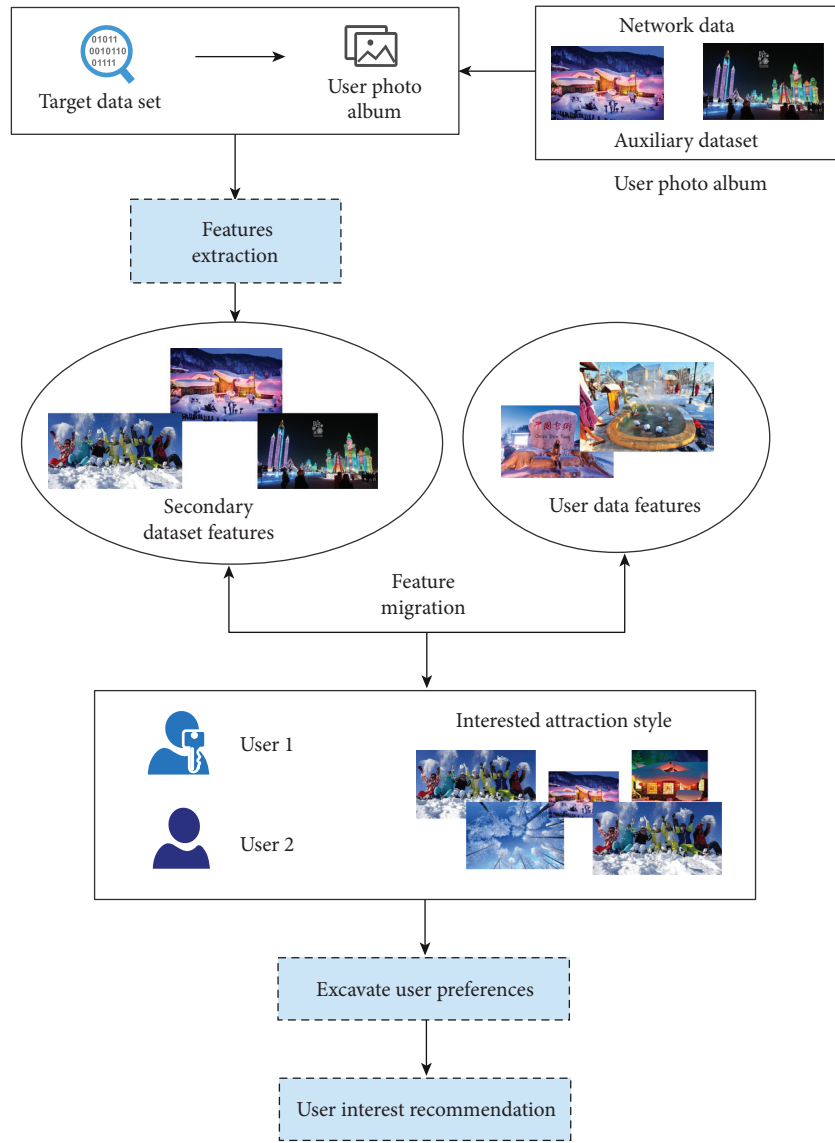
Figure 8: Block diagram of the personalized recommendation model for cultural and creative tourist attractions.
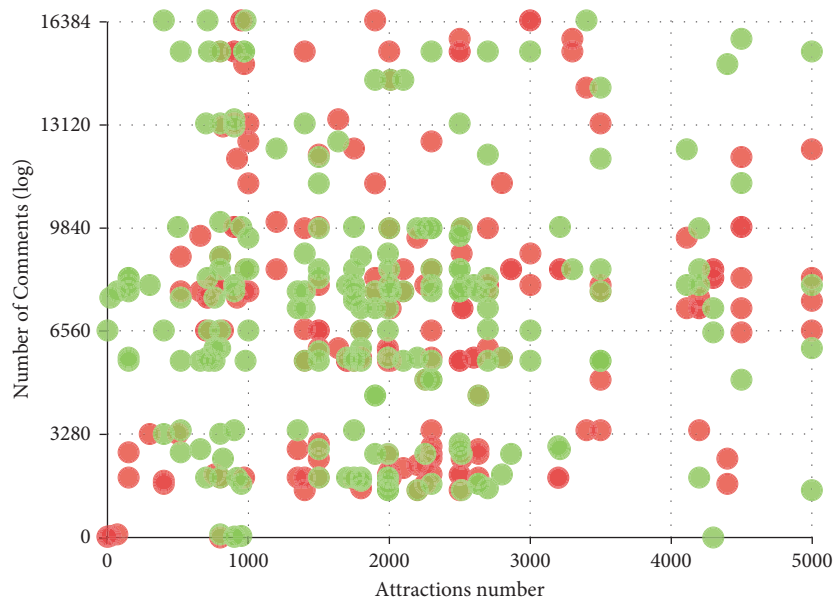

Figure 9: Reference diagram for setting the threshold of the dividing line of tourist attractions.

TABLE 1: Search results of the cultural and creative tourist attractions selection model based on BP network.

No.	Attractions search	No.	Attractions search
1	91.70	21	88.49
2	88.46	22	91.58
3	91.00	23	88.91
4	88.75	24	88.20
5	90.53	25	95.82
6	88.78	26	90.62
7	94.41	27	90.74
8	94.92	28	92.49
9	92.25	29	93.05
10	95.13	30	90.12
11	95.17	31	90.12
12	91.50	32	94.91
13	95.27	33	94.66
14	95.43	34	91.40
15	94.27	35	88.94
16	93.82	36	91.83
17	91.22	37	92.65
18	93.70	38	94.74
19	89.54	39	94.22
20	91.77	40	94.23

3.3. Rating Prediction.

Recommendation can be simplified as a matching problem between users and items, which matches suitable items for suitable users and derives users' predictions for items. Proved that the full convolutional layer (MLP) can approximate any measurable function with arbitrary accuracy, so similarity can also be learned using the full convolutional layer (MLP).

$$
\begin{aligned}
g_1 &= \left[h_i \oplus z_j \right], \\
g_2 &= \sigma \left(W_2 \cdot g_1 + b_2 \right), \\
&\cdots \\
g_{l-1} &= \sigma \left(W_l \cdot g_{l-1} + b_l \right), \\
r'_{ij} &= w^T \cdot g_{l-1}.
\end{aligned}
\tag{34}
$$

3.4. Loss Function

$$
L\text{oss} = \frac{1}{2|O|} \sum_{i,j \in O} \left(r'_{ij} - r_{ij} \right)^2.
\tag{35}
$$

Among them, O is the set of tuples (i, j), where the tuples represent the user u_i and the rated item v_j, so this loss function calculates the loss for all rated items and does not consider the loss for the unrated items.

4. Selection Model of Cultural and Creative Tourist Attractions Based on BP Network

From the above introduction to system theory, we can find that the essence of a system is a process. This process has always been in dynamic change and development, and the system structure is the manifestation of this dynamic change. Under the guidance of this theory, this paper combines the economic "supply-demand" structure theory to construct a dynamic process of the integration of cultural and creative

industries and tourism industries. Based on the perspective of system theory, the concept of industry is defined as a systematic combination of related elements such as technology, products, enterprises, markets, and systems. Different industrial factors interact with each other, continuously differentiate and restructure, and promote the development of the industrial system. It can be said that the integration mechanism of industries is the result of the evolution of different divisions of labor between industries or within industries. This evolution process is shown in Figure 7.

The interrelationship and mutual promotion of cultural and creative industries and tourism industries constitute a complex and changeable dynamic system. The main driving force of this dynamic system comes from the continuous expansion of the demand for tourism creativity and the continuous increase of the supply of tourism creativity products. This interactive dynamic system can better promote industrial integration with the support of regional cultural creativity and mature tourism market. The driving force generated by the interaction between the demand thrust and the supply pull and the interaction of various factors in the external market environment constitutes the main driving force for the industrial integration of the cultural and creative industries and the tourism industry.

The recommendation performance of the cultural and creative personalized tourist attraction recommendation system will be greatly reduced, and manual labeling of training data is time-consuming and laborious. Therefore, it is considered to introduce a labeled auxiliary data set related to the target data set to solve the problem of the lack of labeled data in the target data. However, there is a distribution difference between the auxiliary data set and the target data set, so the data distribution difference between the two must be eliminated before it can be used to train a personalized travel recommendation system. Therefore, a
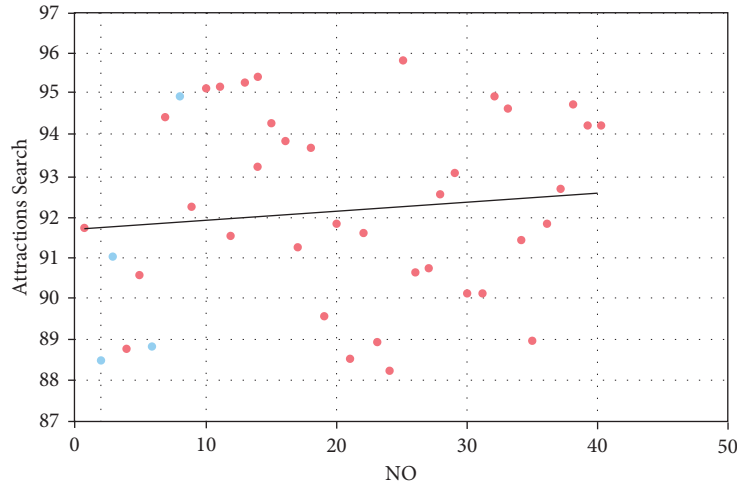
FIGURE 10: Statistics diagram of search results of the cultural and creative tourist attractions selection model based on BP network.

TABLE 2: User satisfaction of the model.

No.	Satisfaction	No.	Satisfaction
1	88.41	21	92.64
2	83.13	22	87.99
3	91.48	23	82.11
4	92.59	24	86.38
5	89.73	25	88.98
6	86.58	26	85.43
7	91.90	27	90.18
8	82.18	28	88.10
9	86.12	29	90.03
10	91.63	30	84.70
11	92.07	31	91.36
12	83.39	32	86.21
13	92.24	33	84.02
14	88.62	34	91.44
15	82.25	35	88.98
16	86.05	36	85.03
17	86.27	37	91.84
18	87.57	38	92.45
19	86.85	39	83.13
20	92.41	40	93.31

personalized recommendation model for tourist attractions based on domain adaptation is proposed. Domain adaptation can effectively reduce the distribution difference between different data. The block diagram of the personalized recommendation model for cultural and creative tourist attractions based on domain adaptation is shown in Figure 8.

Figure 9 is a schematic diagram of setting the time boundary threshold t and the popular/not popular boundary threshold b. It can be seen that the comment values of a large number of scenic spots are concentrated in the lower area of the figure. This distribution of the number of reviews is consistent with the "long-tail effect" in the distribution of scenic spots mentioned in Section 4 and is consistent with the setting of using the number of reviews to reflect the popularity of scenic spots. It is reasonable to set the b value in

the interval shown in the figure. In order to avoid the excessive subjective influence caused by the need to manually set the b value, this paper considers setting the experiment to select multiple thresholds b and analyzes the influence of the scenic spot popularity prediction under different b values.

Based on the above analysis, the effect of this model is verified. The system model in this paper is mainly applied to the selection and search of cultural and creative tourist attractions. Therefore, this paper conducts a simulation experiment on the search effect of the cultural and creative tourist attractions selection model based on the BP network and obtains the results shown in Table 1 and Figure 10.

The above research verifies the search effect of the cultural and creative tourist attractions selection system based on BP network. On this basis, a user satisfaction
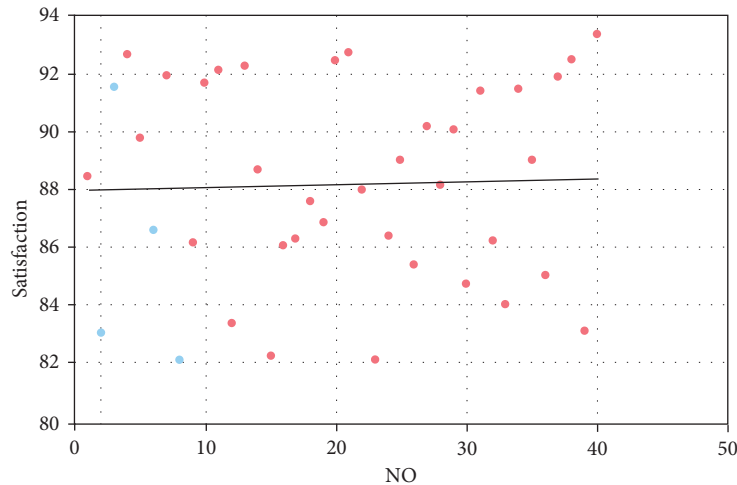
Figure 11: Statistical diagram of user satisfaction of the model.

survey is conducted on the model in this paper, and the results are shown in Table 2 and Figure 11.

From the above and the research results, we can see that the cultural and creative tourist attractions selection search system based on BP network has good user satisfaction. On the whole, the cultural and creative tourist attraction selection search system proposed in this paper based on the BP network has a good selection effect of tourist attractions and has an important role in promoting the development of cultural and creative tourism.

5. Conclusion

The development of China's cultural industry has entered a "new stage," and the innovative design of regional tourism cultural and creative products in the cultural industry has risen from corporate behavior to an important position in the national economy. For this reason, the focus of designers has shifted from traditional products to innovative products that highlight the five thousand years of Chinese culture and characteristic regional culture, which makes the cultural and creative industry hot. Chinese history and culture have a long history and a history of 5,000 years. The harmonious development of society and nature is based on the basic condition that the diversity of culture and nature is equally important. This paper applies the BP network to the selection and exploration of cultural and creative tourist attractions and builds an intelligent system based on the actual situation. Through experimental research, it can be seen that the cultural and creative tourist attraction selection search system proposed in this paper based on the BP network has a good selection effect of tourist attractions and has an important role in promoting the development of cultural and creative tourism.

Data Availability

The labeled dataset used to support the findings of this study is available from the corresponding author upon request.

Conflicts of Interest

The author declares that there are no conflicts of interest.

Acknowledgments

References

[1] Z. H. A. O. Juanjuan, X. U. Chengzhong, and M. E. N. G. Tianhui, "Big data-driven residents' travel mode choice: a research overview," *ZTE Communications*, vol. 17, no. 3, pp. 9–14, 2019.

[2] J. Bulchand-Gidumal, "big data and innovation in tourism, travel, and hospitality. Managerial approaches, techniques, and applications," in *Zeitschrift für Tourismuswissenschaft*, M. Sigala, R. Rahimi, and M. Thelwall, Eds., vol. 13, no. 2, pp. 309-310, 2021.

[3] I. Gallego and X. Font, "Changes in air passenger demand as a result of the COVID-19 crisis: using Big Data to inform tourism policy," *Journal of Sustainable Tourism*, vol. 29, no. 9, pp. 1470–1489, 2021.

[4] C. Anda, A. Erath, and P. J. Fourie, "Transport modelling in the age of big data," *International Journal on the Unity of the Sciences*, vol. 21, no. sup1, pp. 19–42, 2017.

[5] Y. Han, Y. Kim, and Y. Kim, "A study of measuring traffic congestion for urban network using average link travel time based on DTG big data," *The Journal of The Korea Institute of Intelligent Transport Systems*, vol. 16, no. 5, pp. 72–84, 2017.

[6] D. Fukuda, "Innovative travel survey methods and behavior modeling in the era of big data," *Asian Transport Studies*, vol. 5, no. 3, pp. 436–438, 2019.

[7] A. R. Alaei, S. Becken, and B. Stantic, "Sentiment analysis in tourism: capitalizing on big data," *Journal of Travel Research*, vol. 58, no. 2, pp. 175–191, 2019.

[8] T. Li, J. Wang, J. Huang, and X. Gao, "Exploring temporal heterogeneity in an intercity travel network: a comparative study between weekdays and holidays in China," *Journal of Geographical Sciences*, vol. 30, no. 12, pp. 1943–1962, 2020.

[9] M. Chen, J. Yang, L. Hu, M. S. Hossain, and G. Muhammad, "Urban healthcare big data system based on crowdsourced

and cloud-based air quality indicators," *IEEE Communications Magazine*, vol. 56, no. 11, pp. 14–20, 2018.

[10] P. D. Vecchio, G. Mele, V. Ndou, and G. Secundo, "Creating value from social big data: implications for smart tourism destinations," *Information Processing & Management*, vol. 54, no. 5, pp. 847–860, 2018.

[11] H. Wang, X. Tang, Y.-H. Kuo, D. Kifer, and Z. Li, "A simple baseline for travel time estimation using large-scale trip data," *ACM Transactions on Intelligent Systems and Technology*, vol. 10, no. 2, pp. 1–22, 2019.

[12] B. Li, M. C. Kisacikoglu, C. Liu, N. Singh, and M. Erol-Kantarci, "Big data analytics for electric vehicle integration in green smart cities," *IEEE Communications Magazine*, vol. 55, no. 11, pp. 19–25, 2017.

[13] H. Tian, M. Presa-Reyes, Y. Tao et al., "Data analytics for air travel data: a survey and new perspectives," *ACM Computing Surveys*, vol. 54, no. 8, pp. 1–35, 2021.

[14] C. M. Peak, A. Wesolowski, E. zu Erbach-Schoenberg et al., "Population mobility reductions associated with travel restrictions during the Ebola epidemic in Sierra Leone: use of mobile phone data," *International Journal of Epidemiology*, vol. 47, no. 5, pp. 1562–1570, 2018.

[15] A. I. Torre-Bastida, J. Del Ser, I. Laña, M. Ilardia, M. N. Bilbao, and S. Campos-Cordobés, "Big Data for transportation and mobility: recent advances, trends and challenges," *IET Intelligent Transport Systems*, vol. 12, no. 8, pp. 742–755, 2018.

[16] F. Chen, J. Zhang, Z. Wang, S. Shi, and H. Liu, "Passenger travel characteristics and bus operational states: a study based on IC card and GPS data in Yinchuan, China," *Transportation Planning and Technology*, vol. 42, no. 8, pp. 825–847, 2019.

[17] J. Ren, X. Luo, L. Dong et al., "Analysis on spatial-temporal features of taxis' emissions from big data informed travel patterns: a case of Shanghai, China," *Journal of Cleaner Production*, vol. 142, no. 2, pp. 926–935, 2017.

[18] P. Nitu, J. Coelho, and P. Madiraju, "Improvising personalized travel recommendation system with recency effects," *Big Data Mining and Analytics*, vol. 4, no. 3, pp. 139–154, 2021.

[19] P. Shi and Y. Long, "A research on complementary resources input decision of the travel agencies co-creating the O2O model," *Tourism Science*, vol. 31, no. 2, pp. 55–68, 2017.

[20] A. Kumari, S. Tanwar, S. Tyagi, and N. Kumar, "Verification and validation techniques for streaming big data analytics in internet of things environment," *IET Networks*, vol. 8, no. 3, pp. 155–163, 2019.

Research Article

Assessment on Changes of Ecosystem Carbon Storage in Reservoir Area due to Hydroproject

Shan Long [ID] [1] **and Shenbei Zhou** [ID] [2,3,4]

[1]*Management School, Hunan City University, Yiyang 413000, China*
[2]*Business School, Hohai University, Nanjing 211100, China*
[3]*Water Resources Economics Research Institute, Hohai University, Nanjing 211100, China*
[4]*Eastern Natural Resources, Environment and Sustainable Development Research Center, Nanjing 210098, China*

Correspondence should be addressed to Shenbei Zhou; shenbei@hhu.edu.cn

Hydropower offers significant value for global carbon peak and carbon neutrality. However, the construction of hydropower stations leads to significant changes in land use and cover structure in reservoir areas, which affect ecosystem services including carbon balance. Furthermore, the development and operation of hydropower project require vast investment. However, the reservoir ecosystem's carbon storage and carbon emission reduction caused by hydropower could offer economic benefits when the official carbon market trading in China was launched in 2021. Therefore, it is necessary to assess comprehensively the changes in carbon storage and its value to the ecosystem in reservoir areas. The evaluation is of great importance for carbon loss reduction, land management, and hydropower development. This study provides a comprehensive and effective framework for evaluating changes in carbon storage and has its value to the reservoir ecosystem. It combines land utilization classification data obtained from remote sensing image interpretation and the Integrated Valuation of Ecosystem Services and Tradeoffs (InVEST) carbon storage model. Based on the case study of the Xiluodu reservoir area, they were evaluated from two aspects: physical quantity and value quantity. The results show that the carbon storage in the Xiluodu reservoir area increased by 8,504.42 Mg from 2000 to 2018. The spatial distribution of the carbon storage shows a trend of high in the north and west, but low in the south and east. The construction of hydropower stations and the rise of reservoir water level covered a large amount of land, which led to the loss of carbon storage in reservoir areas. By implementing soil and water conservation and vegetation protection policies, parts of the cultivated land and grassland were converted into forestland, which was the main source for increasing the ecosystem's carbon storage. Moreover, carbon emission reduction was achieved by hydropower. In terms of the monetary value, the carbon storage value of the reservoir ecosystem increased to 19 million RMB during the construction period (2005–2015). The carbon storage value of the reservoir ecosystem increased to 611 million RMB during the operation period (2015–2018). The latter was greater than the maintenance cost of the hydropower station and exceeded the amortized cost of hydropower development, indicating the feasibility and economic benefits of hydropower development. These findings provide guidance for future hydropower development decisions in Jinsha River Basin and also others.

1. Introduction

Global warming is one of the biggest challenges to sustainable development of human society and natural ecosystem. It has gradually become a hot issue worldwide [1–3]. Previous studies show that carbon emissions caused by human activities are the main reason of climate change, mainly from burning of fossil fuels [2]. China is working on local and global environmental challenges [4]. These include a commitment to peak CO_2 emissions around 2030 according to the Paris Agreement signed in 2015 and a commitment to achieve carbon neutrality by 2060 at the 75th UN General Assembly in 2020 based on the Paris Agreement [5–7]. Considering the global carbon peak and carbon

neutrality deadlines, it is necessary to reduce dependence on fossil fuels, attach importance to clean energy development, and optimize energy structure.

As the largest share of clean energy (85%) and the most mature and sustainable power resource, hydropower continues to be the focus of future development [7, 8]. However, extensive hydropower development profoundly impacts the ecosystem, changing the local land use status, ecological diversity, and vegetation coverage [9, 10]. Previous studies showed that land use and cover change (LUCC) is the main cause of global carbon cycle imbalance and an important source of carbon emissions that ranks secondary after fossil fuels [11]. The impact of LUCC on the carbon cycle has become an important aspect of ecological benefit literature, mainly focusing on impacts of soil carbon storage and biomass carbon storage in specific ecosystems. However, the impact of LUCC on multiple carbon pools in composite ecosystems remains unclear [12].

Previous studies have confirmed the influence of hydropower station construction on changes of land use and cover type in the reservoir area. Zhang et al. found that the cultivated land, forestland, and grassland in the reservoir area kept decreasing, while the built-up area and the water area kept increasing during 1978–2005 due to the construction of the Three Gorges Dam and environmental protection policies after the completion of the dam [13]. Guan et al. believed that the construction of the Three Gorges Dam changed the land use structure. They used Logistic-CA-Markov and WLC-CA-Markov models to simulate Chongqing's future land use pattern in the Three Gorges Reservoir area. It was found that the grassland and cultivated land in the reservoir area would continue to decrease while the water area would remain stable, and the forestland and construction land would continue to increase [14]. Rufin et al. collected 178 cases of land use structure change caused by hydropower station construction and concluded that land cover change is mainly related to hydropower stations. Moreover, scholars have discussed the influence of hydropower station construction on soil carbon storage and forest carbon cycle in the reservoir area [15]. Kumar and Sharma and Pereira et al. studied the influence of water flooding of hydropower station on the soil carbon content in nearby forests [16, 17]. Dullah et al. discussed the influence of hydropower station construction on forest plant carbon. They believed that the carbon sequestration rate of the remaining forest in studied areas was still considerable, and the carbon sequestration potential was acceptable [18].

However, previous studies on influence of hydropower station construction on carbon storage were mainly concentrated on one or two carbon pools (plant carbon and soil carbon) of particular ecosystem. Therefore, it is necessary to comprehensively evaluate changes in various carbon pools in the reservoir area. Such an assessment is very important for carbon reduction, land management of future reservoir areas, and hydropower station management. The Integrated Valuation of Ecosystem Services and Tradeoffs (InVEST)

model can be linked to Geographic Information Systems (GIS) mapping to evaluate various service functions of ecosystem services [19–21]. The carbon storage and capture models in the InVEST model include four carbon pools: aboveground biomass, underground biomass, dead organic carbon, and soil carbon. They can accurately reflect changes in carbon storage caused by LUCC in terrestrial ecosystem.

The InVEST model has been widely used to evaluate and simulate carbon cycles of terrestrial ecosystems at different scales due to its visualization on evaluation results, data accessibility, and ease of operation [22–24]. However, previous studies with the InVEST model mainly focused on impacts of urban expansion, shelterbelt construction, and returning farmland to grassland on carbon storage. Few scholars used the InVEST model to study impacts of land use change caused by hydropower station construction on carbon storage in terrestrial ecosystems. Moreover, the development and operation of hydropower require vast investment. Taking the hydropower base in the Jinsha River Basin as an example, over 500 billion RMB has been invested in hydropower during past 20 years. With the official launch of carbon market trading in 2021, changes on carbon storage in the reservoir ecosystem and carbon emission reduction caused by hydropower during operation also have specific economic values. Therefore, this paper estimates the value of changes in ecosystems' carbon storage in the reservoir area from the perspective of carbon market value, considering carbon emission reduction caused by hydropower. Then, the value is compared with the hydropower investment and operating costs to evaluate the economic contribution to the reservoir area in different periods. The study provides guidance for decision-making of hydropower development and reservoir ecosystem management. Moreover, the study provides a comprehensive and effective framework for evaluating changes in carbon storage to reservoir ecosystems and their economic value which is based on integrating land use classification data obtained from remote sensing image interpretation and the InVEST carbon storage model.

The Jinsha River Basin has the largest hydropower resources in China. At present, three of the world's top ten hydropower stations are located here in terms of installed capacity and adequate resources for subsequent development. The Xiluodu hydropower station is the fourth largest station in the world and is located in the Jinsha River Basin. In the past 20 years, a large amount of land resources has been occupied by the construction, infrastructure, and immigrant resettlement along with the station development. The stored water has flooded the adjacent land causing the land use and cover of the reservoir area to change significantly. Functions of ecosystem service in the reservoir area have been affected, including carbon balance. Therefore, the Xiluodu reservoir area was selected for this study as a typical case. Particularly, four stages were selected: the period before hydropower station was built (2000); the beginning of construction (2005); the completion of construction (2015); the operation period (2018). Changes in carbon storage in the reservoir area from 2000 to 2018 were studied with an in-depth discussion on impacts of the station. Detailed topics show as follows:

(1) Distribution of land use and cover types in Xiluodu reservoir area in 2000, 2005, 2015, and 2018 due to hydropower station construction, combined with satellite data and environmental changes.

(2) Current changes of carbon storage in reservoir ecosystem and its main reasons, combined with land use, cover types, and carbon density data.

(3) Calculating economic value associated with carbon storage changes in the reservoir area with the market value method. The method accounts for carbon emission reduction caused by hydropower and compares the hydropower investment and operation costs to evaluate the economics of hydropower development.

2. Materials and Methods

2.1. Research Area. The reservoir area is located at $102°49'36''E$-$103°48'9''E$, $27°15'20''N$-$28°17'31''N$ (Figure 1). The reservoir area ($3,613,657\,hm^2$) is situated in a small watershed within the first ridgeline between the Baihetan hydropower station and the Xiluodu dam site. This location is within the first level watershed of Xiluodu hydropower station which is at the junction of Yunnan and Sichuan Province. There are nine counties (districts) in these two provinces. This area belongs to subtropical monsoon climate which is dry and hot. The annual precipitation ranges from 600 mm to 1100 mm. The annual average temperature varies from $10.1°C$ to $19.7°C$. The altitude ranges from 265 to 3,656 m (data source: Environmental Impact Assessment Report of Xiluodu Hydroproject, Edited by Chengdu Engineering Corporation Limited, April 2005). The reservoir is an ecologically sensitive area in China with steep slopes, high and middle gorge landforms.

The Xiluodu hydropower station is located in the Xiluodu Valley because of abundant water in this area which borders Yongshan County of Yunnan Province and Leibo County of Sichuan Province at the lower Jinsha River. The main program of the hydropower station was started in June 2004 and put into operation in October 2015. After Xiluodu hydropower station started operation, the water area in the reservoir area increased by approximately 10,000 hectares, and the cultivated land decreased by approximately 8,000 hectares.

2.2. Research Framework. The purpose of this study is to provide a framework for assessing impacts of hydropower programs on carbon storage of reservoir ecosystem and provide guidance for future hydropower construction and reservoir ecosystem management. Since the carbon trading market was officially launched in the Shanghai Environment and Energy Exchange (SEEE) in 2021, rights of carbon emission have been endowed with an economic value. Therefore, the evaluation of impacts of hydropower programs on carbon storage can be measured from two aspects: physical quantity and value quantity (Figure 2).

During the studied period from 2000 to 2018, the data obtained from remote sensing image interpretation were used to generate maps of the land use and cover type changes and the land use transfer matrix of the Xiluodu reservoir area from 2000 to 2018. Complementing in-situ monitoring of carbon storage changes, the InVEST model has advantages of data accessibility and visibility to results [25, 26]. It can simulate changes in the value of ecological services of various terrestrial, freshwater, and marine ecosystems. Therefore, the InVEST carbon storage model was used to evaluate physical changes in carbon storage in the reservoir ecosystem caused by hydropower programs.

A change in physical amount of carbon storage in the reservoir area reflects the situation of carbon sequestration and carbon emission. Therefore, a positive net change indicates that the ecosystem absorbs carbon from atmosphere, stores it in the ecosystem, and reduces the content of greenhouse gases in atmosphere. On the other hand, a negative net change indicates that the land use change leads to greenhouse gas emissions. Therefore, considering the carbon emission reduction caused by hydropower programs, the value of the reservoir ecosystem's carbon storage in this study refers to monetizing the carbon sequestration (or carbon emission) and emission reduction by hydropower in the reservoir area. The market value method has been widely used to measure the economic value of the forest carbon sink. Price per unit of the carbon sink is an important factor. This paper uses the market value method to calculate changes in the value of the reservoir ecosystem's carbon storage considering carbon emission trading price of the SEEE. In addition, the calculated value was compared with the carbon sink cost (hydropower investment and operation costs) to discuss the economics of hydropower development.

2.3. Calculation Method

2.3.1. Data Source and Processing. We employed the digital elevation model (resolution 30 m × 30 m) to process land use and cover data used obtained from the Data Center for Resources and Environmental Sciences, Chinese Academy of Sciences. The land use and cover data was sourced from Xiluodu reservoir area in 2000, 2005, and 2015, and data in 2018 were from the Landsat TM/ETM+/OLI satellite remote sensing images of the United States Geological Survey (USGS). The remote sensing images were preprocessed by radiometric correction, geometric correction, color enhancement, splicing, cutting, and then artificial visual interpretation. The accuracy of land use and the cover was greater than 85% which meets research requirements.

According to the classification standards issued by the Ministry of Natural Resources of China and the research needs of ecological environment of the Xiluodu reservoir area, the land use and cover types were divided into five types: (1) cultivated land (dry land, paddy land); (2) woodland (woodland, shrubbery, open woodland, and other woodland); (3) grassland (high coverage, medium coverage, and low coverage); (4) water area; and (5) construction land.

2.3.2. Carbon Storage Model: Application of the InVEST Model. In this paper, the carbon storage and capture model in the InVEST model (version 3.5.0) was used to estimate the
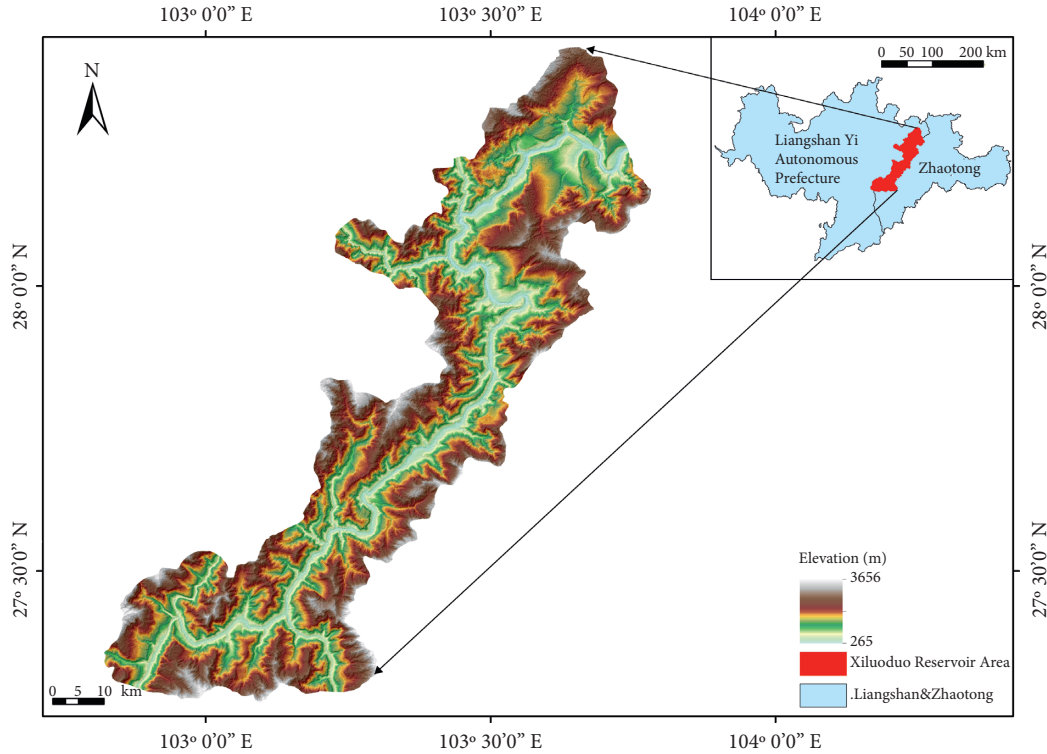
FIGURE 1: Geographic location of Xiluodu reservoir area.

carbon storage of the reservoir area over time, based on the spatial distribution map of land use at different times and carbon density of each land type. The InVEST model simulated the carbon storage of four carbon pools, including aboveground and underground biomass, dead organic carbon, and soil carbon. The top 20 cm layer of soil was studied in this paper. The calculation formula of carbon storage of reservoir ecosystem is as follows:

$$, , C_{total} = C_{above} + C_{under} + C_{dead} + C_{soil}. \tag{1}$$

2.3.3. Carbon Density. The carbon density data of the Xiluodu reservoir area mainly came from areas with a similar natural environment and same classification system as Xiluodu. Data about vegetation type, plant species composition, and vegetation coverage were collected by other scholars via field measurements in the reservoir and nearby areas. Previous studies showed that the conversion coefficient of the biomass to carbon of forest was 0.45–0.50, and that of grassland was 0.40–0.45. The carbon density of the underground root system was determined by ratios of the aboveground biomass to the underground biomass of different land types. The carbon density of the dead organic matter was determined by the ratio of aboveground dead matter to underground dead matter [27, 28]. The final organized data of carbon density of Xiluodu reservoir area are shown in Table 1.

2.3.4. Market Value. Carbon market trading was officially launched on SEEE on July 16, 2021. The closing price on that day was 51.23 CNY/Mg. The carbon in this paper refers to

elemental carbon, while the carbon trading in China uses CO_2eg per ton as trading object. According to the mass conversion coefficient of carbon per ton converted into CO_2eg, which is 3.67, the carbon trading price per ton in this study is converted to 188 CNY/Mg [40].

A previous study showed that the hydropower carbon footprint of the Xiluodu hydropower station is 7.6 gCO_2eg/(kW·h), while the coal-power carbon footprint is 822 gCO_2eg/(kW·h) [41]. The clean energy provided by hydropower station can effectively reduce carbon emissions. By the end of 2018, the cumulative power generation of the station exceeded 300 billion kW·h (date source: China's National Energy Administration, available online), with an emission reduction of 1856.83 million tons of CO_2eg, equivalent to 50.13 million tons of elemental carbon (C). Therefore, the value of carbon storage in the reservoir area can be calculated as follows:

$$V_c = (C_a + C_h) \cdot P_c. \tag{2}$$

V_c is value quantity, C_a is physical quantity change of carbon storage in the reservoir area, C_h is carbon emission reduction by hydropower, and P_c is carbon price (CNY/Mg).

3. Results and Analysis

3.1. LUCC of the Xiluodu Reservoir Area in 2000–2018

3.1.1. Spatiotemporal Pattern of LULC. The land use and land cover map (LULC) and area changes in the Xiluodu reservoir area from 2000 to 2018 are shown in Figure 3 and Table 2. Before the start of the construction in 2000, the
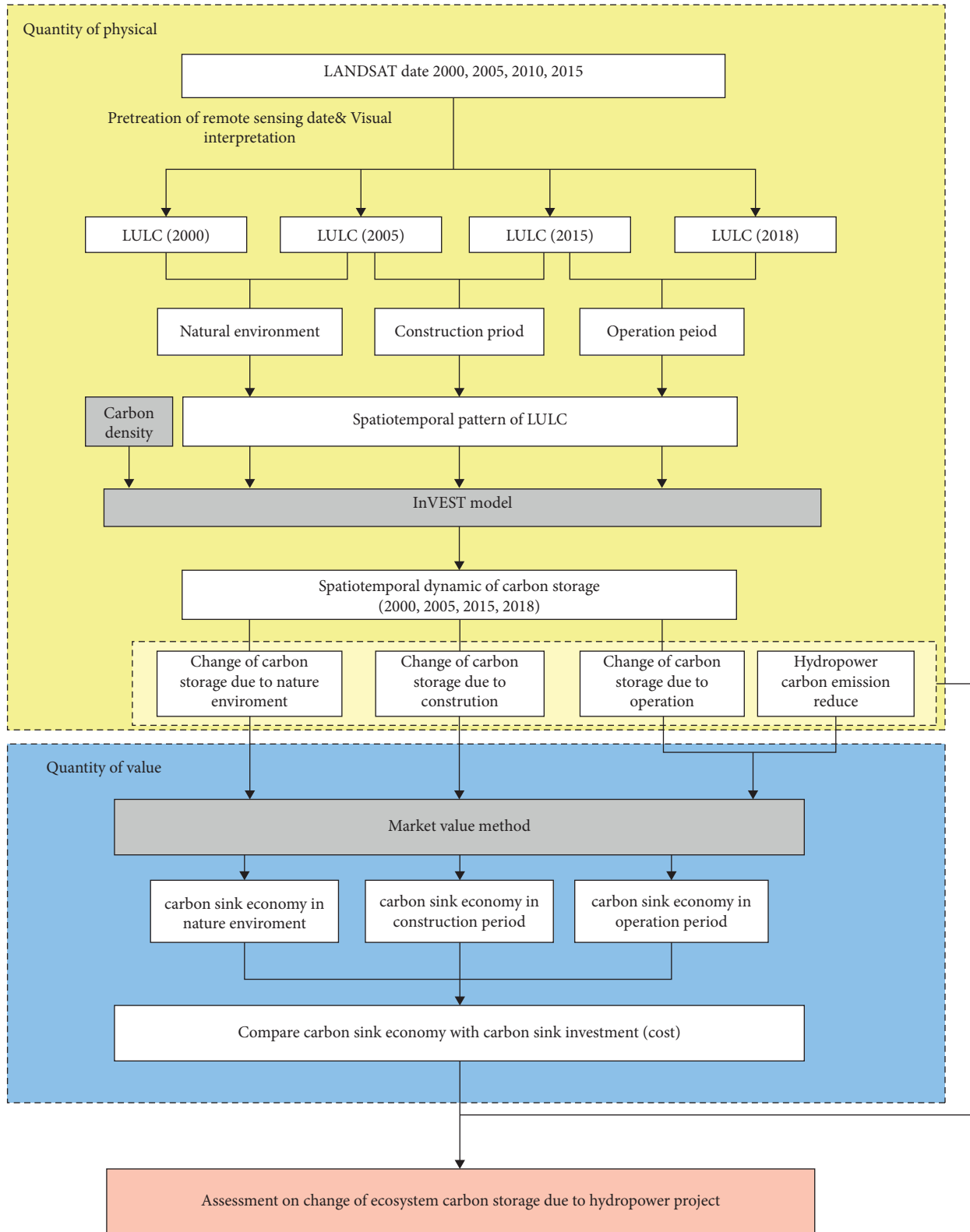
Figure 2: Methodological framework of the study.

forestland was the main land use and cover type, accounting for 38.91% of the total area of the reservoir area. It was mainly distributed in the mountainous area with a high elevation and a large slope. The grassland accounted for 32.75% of the total area and was distributed in the middle and low altitude areas along the lower Jinsha River. The water area and the construction land accounted for only 0.9% and 0.19% of the reservoir area, respectively. The water

TABLE 1: Carbon densities of different land use types in Xiluodu reservoir area.

Land use and cover types (Mg/hm^2)		$C_{i,\text{above}}$	$C_{i,\text{under}}$	$C_{i,\text{soil}}$	$C_{i,\text{dead}}$	Reference
Category	Type					
Woodland	Woodland	31.95	6.38	146.82	2.96	[29–31]
	Shrubwood	8.1	1.62	91.7	2.48	[31, 32]
	Open woodland	8.1	1.62	91.7	2.48	[29, 30, 33]
	Other woodland	35.03	7.01	142.58	3.75	[29, 30, 33]
Cultivated land	Paddy field	5.42	1.96	92.9	0	[34, 35]
	Dry land	3.64	0	33.46	13	[35, 36]
Grassland	High coverage	2.75	7.37	64.03	4.07	[37, 38]
	Medium coverage	2.205	5.365	48.41	3.035	[37, 38]
	Low coverage	1.66	3.36	25.79	2	[37, 38]
Water area	Water area	0.3	0	0	0	[39]
Construction land	Construction land	0	0	22.25	0	[39]

area was distributed in the river valley area with a low altitude level and a gentle slope, while the construction land was scattered in the upstream river.

During the initial stage of the station construction in 2005, no large-scale engineering construction was carried out since it is at the preparation stage of Xiluodu hydropower station. Therefore, the area was kept under the natural environment, and there were no significant changes in the various land use and cover types. After the station's construction in 2015, the area and distribution of the various land use and cover types changed significantly, with an area reduction of the cultivated land and the grassland. The cultivated land area decreased most, reaching 4732.92 hectares. The forestland area, water area, and the construction land area increased to 39.95%, 1.2%, and 0.2%, respectively. The forestland area increased most, reaching 3736.98 hectares. The increase of forestland was mainly on the west bank of Jinsha River in the hinterland, while the increase of construction land was mainly in the low altitude areas at the front and tail of the reservoir. The increase of the water area occurred mainly on both sides of the Jinsha River.

After the station was completed and put into operation in 2018, the cultivated land and grassland areas in the reservoir further decreased. The biggest reduction in the grassland area decreased to 30.77% and was mainly distributed in the middle and low altitude areas of the central region. The forestland and construction land areas decreased by 788.38 hectares and 293.85 hectares, respectively, compared to 2015, and the reduction was mainly distributed on both sides of the Jinsha River. Only the water area increased greatly, and its proportion increased to 3.7%, mainly distributed in the valley area with a low altitude and a gentle slope.

3.1.2. Land Use and Cover Type Change Directly Caused by Hydropower Station Construction. The land use and cover areas of the Xiluodu hydropower station during preparation (2000–2005), construction (2005–2015), and operation

(2015–2018) periods are shown in Figure 4. Due to construction, the cultivated land and grassland areas in the reservoir decreased considerably, while the water area increased the most, followed by the forestland and construction land area (Table 3). The following observations are noted:

(1) During the construction period, the woodland and construction land were mainly added to the reservoir area, while the cultivated land was mainly removed from the reservoir area. The increased area of both forestland and construction land came from cultivated land and grassland.

(2) Change in the construction land was the greatest, which was four times that in 2005. The increased area was mainly the engineering site of station at the head of reservoir and the immigrant resettlement area at the tail of reservoir.

(3) The forestland area increased by 3726.98 hm^2 downstream of the Jinsha River due to the vegetation restoration measures such as afforestation and natural forest closure during events such as "returning farmland to forest," engineering construction, and immigrant resettlement that began in 1998. Although some forestland was submerged due to water level rise during the station operation, the forestland area still increased compared to 2000. The construction of Xiluodu hydropower station did not cause severe damage to inland plants in the reservoir area.

(4) During the operation period, the water level was raised to inundate other lands in the reservoir area, resulting in a significant increase in water area. The cultivated land and grassland were main sources of the increased water area.

3.2. Carbon Storage in the Xiluodu Reservoir Area from 2000 to 2018

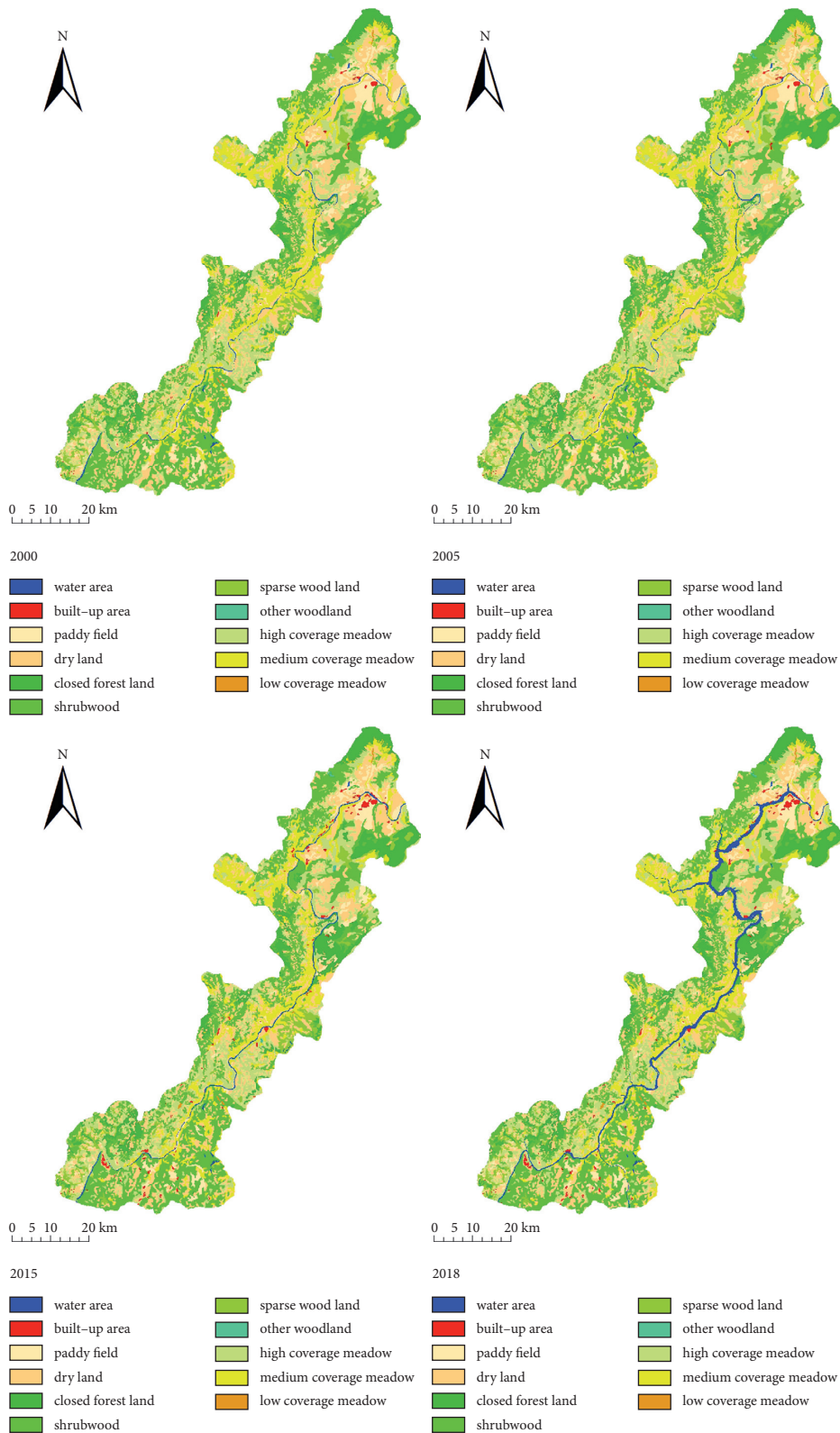*3.2.1. Spatial and Temporal Distributions of Carbon Storage.*

Figure 3: LULC of Xiluodu reservoir area for 2000, 2005, and 2015.

The total carbon storage of the Xiluodu reservoir area in 2000, 2005, 2015, and 2018 was 31,057,361 Mg, 31,955,862 Mg, 31,510,555 Mg, and 31,067,232 Mg, respectively (Figure 5). The corresponding average carbon densities were 85.94 Mg/hm^2, 85.93 Mg/hm^2, 87.19 Mg/hm^2, and 85.97 Mg/hm^2. SOC was the main carbon pool, followed by AGC, DOC, and BGC. The carbon storage of the reservoir ecosystem decreased by 1,499 Mg from 2000 to 2005. The

TABLE 2: Land use and cover change between 2000 and 2018.

Land use type	2000		2005		2015		2018	
	Area (hm^2)	Proportion (%)	Area (hm^2)	Proportion (%)	Area (hm^2)	Proportion (%)	Area (hm^2)	Proportion (%)
Woodland	140601.51	38.91	140651.28	38.92	144388.26	39.95	143599.88	39.73
Cultivated land	98495.55	27.26	98483.31	27.25	93750.39	25.94	90660.42	25.09
Grassland	118334.79	32.75	118250.82	32.72	116041.59	32.11	111189.33	30.77
Water area	3246.75	0.90	3287.25	0.91	4340.97	1.20	13364.82	3.70
Construction land	702.45	0.19	707.13	0.20	2859.93	0.79	2566.08	0.71
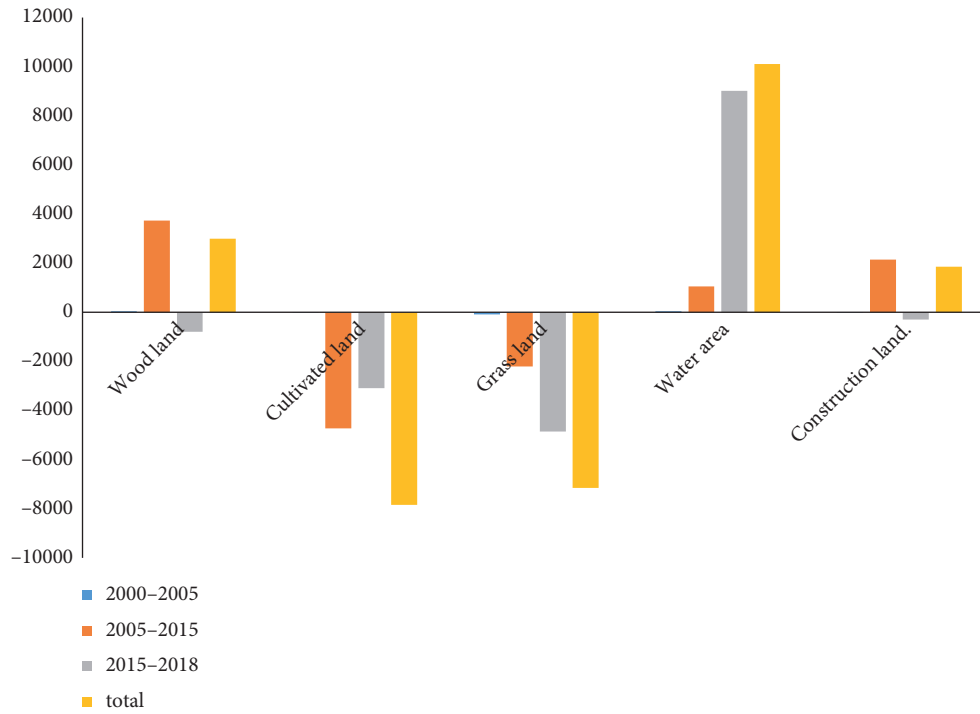
FIGURE 4: Change in each land use and cover type.

TABLE 3: The land use transfer matrix of the Xiluodu reservoir area from 2000 to 2018.

Time	Land use type	Woodland	Cultivated land	Grassland	Water area (hm^2)	Construction land
2000–2005	Woodland	139961.25	313.02	313.83	11.97	1.08
	Cultivated land	388.89	97684.92	389.34	23.13	9.09
	Grassland	292.59	472.77	117530.82	37.8	0.72
	Water area	7.2	8.37	16.02	3214.35	0.18
	Construction land	1.35	4.23	0.81	0	696.06
2005–2015	Woodland	137507	1101.69	1685	217.80	139.77
	Cultivated land	2513	91321.56	2606	467.73	1574.37
	Grassland	4265	1195.02	111614	661.05	516.15
	Water area	38	120.06	135	2993.58	0.81
	Construction land	65	11.88	1	0.36	628.83
2015–2018	Woodland	135881.64	3437.82	3821.22	1211.76	35.46
	Cultivated land	3532.86	82451.25	4587.84	2950.29	227.88
	Grassland	4086.55	4578.12	102558.87	4759.11	59.49
	Water area	66.16	40.5	50.76	4179.33	3.69
	Construction land	32.67	152.73	170.64	264.33	2239.56
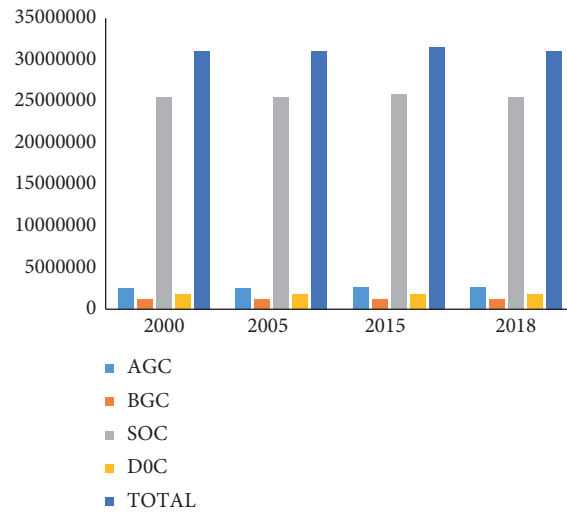
Figure 5: Carbon storage changes of different carbon pools.

carbon storage increased by 453,193 Mg during the construction period of 2000–2015. The carbon storage decreased by 443,322 Mg during the operation period of 2015–2018. The carbon storage increased by 8504.42 Mg in 2018 compared to 2000 when the hydropower station was not built.

From changes in proportions of land use carbon storage in the reservoir area (Table 4), the forestland was the largest carbon pool in Xiluodu reservoir area. The forestland had a high distribution density and high carbon density, accounting for 54.55%–57.2% of the total carbon storage of the reservoir area ecosystem, and its proportion continued to rise. The carbon storage of the grassland ranked next to the forestland. The grassland and the cultivated land accounted for 25.34%–26.66% and 17.15%–18.73% of the total carbon storage, respectively. The carbon storages of the grassland and the cultivated land continuously decreased each year. The carbon storage of the construction land and the water area ranked the lowest, which accounted for only 0.05%–0.22%. Although the water area increased significantly from 2000 to 2018, its carbon storage was still the lowest which is only 0.02% due to low carbon density.

In terms of spatial distributions, the carbon storage in the reservoir area was higher in the north and west, but lower in the south and east. The high carbon storage areas were mainly distributed in the high-altitude mountainous forest areas at the upstream and the western boundary of the reservoir. These areas had high vegetation coverage and good vegetation growth which is seldom affected by human activities. Therefore, their natural plants were well maintained. The second high carbon storage area was the grassland area in the south of the reservoir area. The water area was mainly distributed in the mainstream of the Jinsha River and its tributaries with the lowest carbon storage (Figure 6).

The carbon storage and spatial distribution did not change significantly from 2000 to 2005. However, with the construction of Xiluodu hydropower station, the carbon storage and spatial distribution changed significantly from 2005 to 2015 during the construction period. The carbon emission was mainly from the hydropower station construction area in the north and the immigrant resettlement area in the south. The carbon sequestration area was mainly the forestland on the western bank of Jinsha River in the middle of the reservoir area. As the station entered its operation period, the carbon storage along the mainstream and tributaries of Jinsha River decreased significantly from 2015 to 2018. Compared with the construction period in 2005–2015, the carbon emission area increased significantly, mainly due to the water level rise in the operation, which flooded vast grassland and cultivated land (Figure 7).

3.2.2. Carbon Storage Change Directly Caused by the Xiluodu Hydropower Station Construction. Due to the construction of Xiluodu hydropower station, the vegetation density, land use, and cover types in the reservoir area changed, which affect the carbon storage of ecosystem (Table 5). From 2000 to 2005, changes in vegetation densities of forestland, cultivated land, and grassland caused carbon densities to change from $120.499 \, \text{Mg/hm}^2$, $59.058 \, \text{Mg/hm}^2$, and $69.982 \, \text{Mg/hm}^2$ to $120.514 \, \text{Mg/hm}^2$, $59.070 \, \text{Mg/hm}^2$, and $70.123 \, \text{Mg/hm}^2$, respectively. The total carbon storage of the unchanged land use and cover types in the reservoir area increased by 5042.82 Mg. With the area conversion to different land use and cover types, the total increase of the carbon storage was 49,746.58 Mg, and the total decrease was 51,244.96 Mg, while the net decrease was 1,498.48 Mg. The annual carbon emissions of the ecosystem were 299.696 Mg/year.

During the construction period from 2005 to 2015, changes in the carbon densities of forestland, cultivated land, and grassland were $123.122 \, \text{Mg/hm}^2$, $58.913 \, \text{Mg/hm}^2$, and $70.123 \, \text{Mg/hm}^2$, respectively. The carbon storage of unchanged land use and cover types increased by 106,863.66 Mg. Due to the area conversion, the total increase of carbon storage was 827,971.28 Mg, and the total decrease was 373,278.88 Mg, while the net increase was

TABLE 4: Carbon storage of different land use and cover between 2000 and 2018.

Land use type	2000 Proportion (%)	2005 Proportion (%)	2015 Proportion (%)	2018 Proportion (%)
Woodland	54.55	54.56	56.42	57.20
Cultivated land	18.73	18.73	17.56	17.15
Grassland	26.66	25.65	25.83	25.34
Water area	0.00	0.00	0.00	0.02
Construction land	0.05	0.05	0.20	0.20
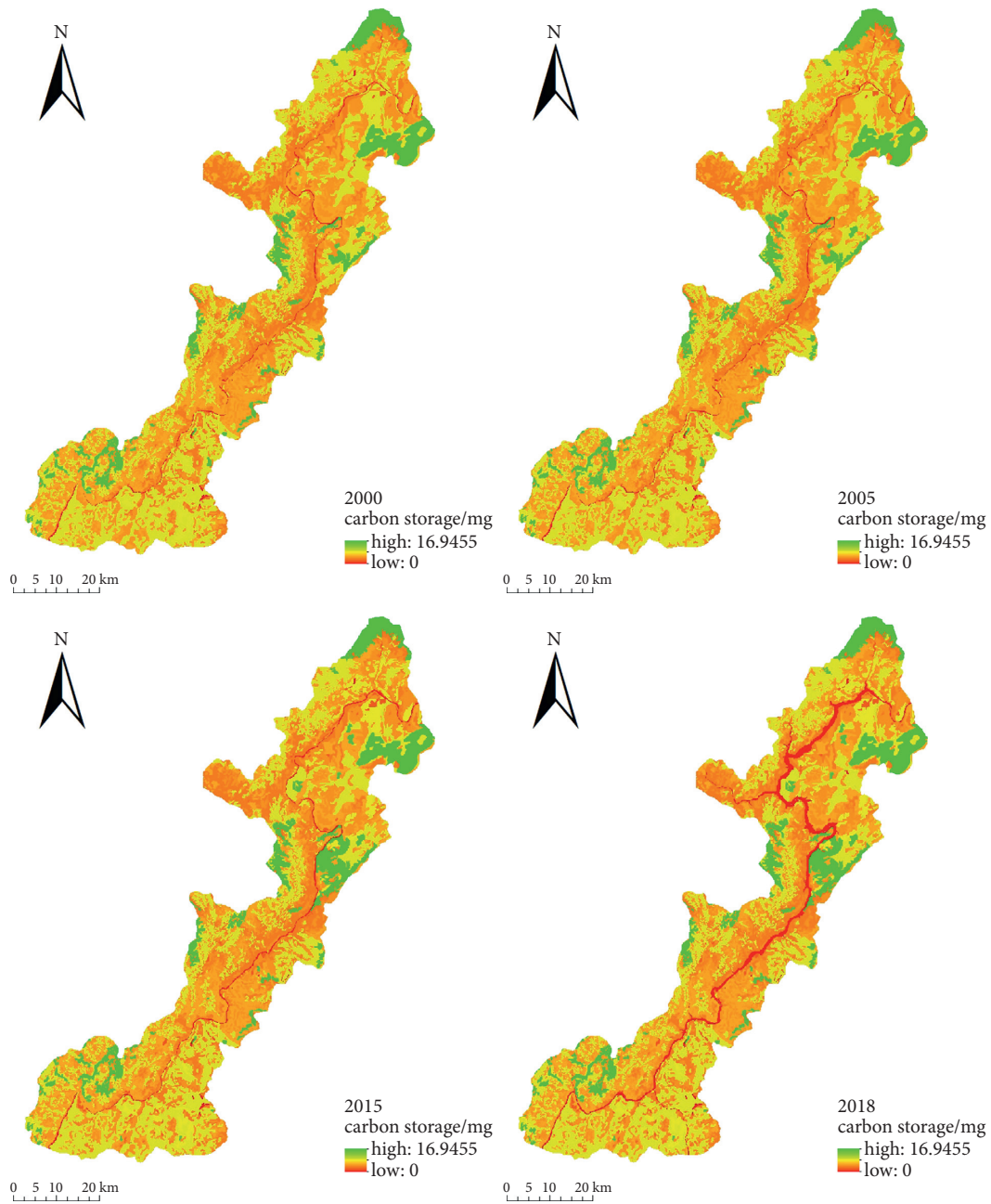
FIGURE 6: Spatiotemporal changes of carbon storage between 2000 and 2018 (Mg).

456,892.43 Mg. The annual carbon storage of ecosystem was 45,469.24 Mg/year.

During the operation period from 2015 to 2018, changes in carbon densities of forestland, cultivated land, and grassland were 123.722 Mg/hm^2, 58.911 Mg/hm^2, and 70.423 Mg/hm^2, respectively. The carbon storage of unchanged land use and cover types increased by 96,529.62 Mg. The total increase of the carbon storage caused by changes in
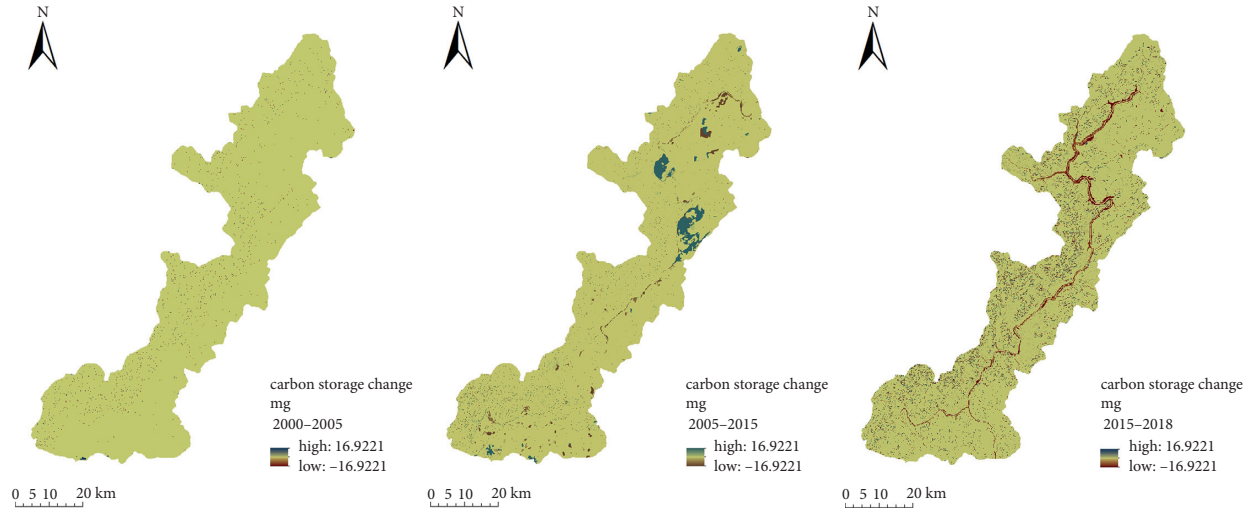
Figure 7: Carbon change between 2000 and 2018.

Table 5: Changes of carbon storage in the process of land use change from 2000 to 2018.

Time	Land use type	Woodland	Cultivated land	Grassland	Water area (Mg)	Construction land
	Woodland	2193.84	−19228.63	−18848.52	−1638.30	−104.67
	Cultivated land	22879.36	1134.07	4259.64	−1358.15	−322.54
2000–2005	Grassland	14769.21	−7078.17	1680.14	−2632.57	−33.41
	Water area	864.88	491.57	1115.94	0.00	4.18
	Construction land	130.86	150.35	37.64	0.00	34.80
	Woodland	160962.94	−14313.2	28801.23	−27469.83	−55890.3
	Cultivated land	366742.35	−67807.95	−84823.58	−26162.65	−13542.65
2005–2015	Grassland	227569.74	−13247.75	13708.67	−46048.19	−23964.42
	Water area	5665.72	7032.31	9420.57	0.00	18.81
	Construction land	7470.58	531.82	46.54	−8.36	0.00
	Woodland	228882.08	−113.63	55349.34	−172808.43	−8054.04
	Cultivated land	78510.50	−220115.17	−199255.54	−148782.57	−3530.12
2015–2018	Grassland	219199.17	−51320.75	87762.710	−331100.21	−2769.378
	Water area	8161.49	2372.16	3585.571	0.00	85.71
	Construction land	3271.24	5397.78	8089.65	−6140.38	0.00

land use and cover types was 700,667.40 Mg, and the total decrease was 1,143,990.22 Mg, while the net decrease was 443,322.82 Mg. The annual carbon emissions of ecosystem were 147,774.27 Mg/year.

During the entire study period from 2000 to 2018, the carbon storage of ecosystem caused by land use and cover type change was mainly due to the increase in forest area. The policies of "returning farmland to the forest" downstream of Jinsha River since 1998, the Changsha Shelterbelt Program, and the large-scale artificial planting and natural forest closure management since the hydropower program construction influenced the increase in forest areas. The forest areas converted from other types of land during period of 2000–2005, 2005–2015, and 2015–2018 were 38,644.31 Mg, 607,448.39 Mg, and 309,142.4 Mg, respectively, with ratios of 77.68%, 73.36%, and 44.12%. The carbon increase from 2000 to 2005 mainly came from converting cultivated land to forestland. The carbon increase from 2005 to 2015 mainly came from conversion of cultivated land and grasslands to forestland. The carbon increase from 2015 to

2018 mainly came from the conversion of grassland to forestland.

In these three periods, main sources of carbon loss were different. Before the construction (2000–2005), the carbon loss was mainly due to converting forestland and grassland to other land uses and cover types with a lower carbon density. During the construction (2005–2015) and operation (2015–2018) periods, the carbon losses were mainly due to the conversion of cultivated land and grassland to other land uses and cover types with a lower carbon density.

From 2000 to 2005, the main reason for carbon loss of reservoir ecosystem was the conversion of forestland to cultivated land and grassland. The carbon loss was 38,077.15 Mg, accounting for 74.30% of the carbon loss for that period. This was related to China's strict implementation of cultivated land protection policies, such as "Dynamic Balance of the Total Amount of Cultivated Land in the Region" and "Land Use Control," and some forestland has been reclaimed for cultivated land. Meanwhile, the regional ecological environment became fragile due to

TABLE 6: Carbon storage value and carbon sink cost evaluated at the 2000 price level.

Economic benefit and cost	2000–2005	2005–2015	2015–2018
Value (100 million RMB)	−0.001	0.19	19.87
Hydropower program cost (100 million RMB)	0	306.21	9.14
Amortized cost of hydropower program (100 million RMB)	0	0	18.28

cultivation of steep slopes and reclamation, and some forest vegetation was seriously destroyed and changed into grassland. The construction of Xiluodu hydropower station, immigrant resettlement, construction of supporting facilities, and water storage of the Xiluodu reservoir were important reasons for loss of cultivated land and grassland from 2005 to 2015.

During the construction period (2000–2015), the carbon losses caused by conversion of nonconstruction land and nonwater land into construction land and water area were 99,689.03 Mg and 93,397.37 Mg (corresponding to 26.70% and 25.02%), respectively. During the operation period (2015–2018), the carbon loss caused by conversion from nonwater area to water area was 652,691.21 Mg, accounting for 57.053% of the carbon loss in the same period. On the other hand, the carbon loss caused by conversion of nonconstruction to construction land accounted for 1.25%. It can be observed that, during the construction period, the carbon emission area of the reservoir was distributed in the converted area of nonconstruction to construction land and the submerged area with the rising water level. In contrast, during the operation period, the carbon emission area was only distributed in the submerged area with the rising water level.

3.3. Market Value. In order to make the carbon storage value in reservoir area comparable to the cost of the hydropower program from 2005 to 2018, CPI (consumer price index) was used to modify value and cost from 2000 to 2018. The monetary values in this study were prices in 2000. The discount rate of the capital market was assumed to be 8% [28, 42].

In this study, the economic value was evaluated based on the value of carbon storage of reservoir ecosystem during construction (2005–2015) and operation (2015–2018) periods of Xiluodu hydropower station by considering emission reduction. The carbon sink cost refers to the total investment of hydropower station in three periods. From 2005 to 2015, the total static investment of Xiluodu hydropower station was 44.993 billion Yuan in RMB evaluated at the price level of 2005. According to the estimated annual maintenance cost in the environmental assessment impact report of Xiluodu hydropower station, the annual maintenance cost was 1% of the total static investment, i.e., 449 million RMB (2005 price level) [41] (Table 6).

Before the station's construction (2000–2005), there were carbon emissions in the reservoir ecosystem under natural conditions, and the carbon storage value was −0.1 million Yuan in RMB. During the construction period (2005–2015), the carbon storage increased, and the value of carbon storage change was 19 million Yuan. During the

operation period (2015–2018), the carbon storage value increased significantly to 611 million Yuan considering the carbon emission reduction caused by hydropower. Moreover, during the construction period (2005–2015), the total investment of the station was 30.621 billion Yuan. We assumed the life of the station was 100 years [41], so the investment was evenly divided to 306 million Yuan per year from the first year of operation. During the operation period (2015–2018), the maintenance cost of the station was 914 million Yuan. With consideration of construction investment, the program cost was 1.828 billion Yuan.

It can be seen that the ecological protection measures during the construction period improved the carbon capture capacity and made a significant contribution to economy of the reservoir area. In addition, the rapid growth of carbon storage value of the reservoir ecosystem was mainly due to hydropower generation. From 2015 to 2018, the value brought by carbon storage was greater than cost on hydropower station's maintenance and slightly exceeded the amortized cost of the hydropower program. Even if the grid electricity price was not considered, the above analysis still demonstrates hydropower development's excellent feasibility and economic value. Furthermore, Xiluodu hydropower station has also played a substantial role in soil erosion prevention, flood control, sand control, and shipping transportation.

4. Discussion

Based on the InVEST model and the LULC data obtained from remote sensing images, this paper discusses in detail the physical and economic value changes of carbon storage in Xiluodu reservoir area from 2000 to 2018. The results show that the construction and operation of station generated significant changes in land use, cover types, and fluctuations in ecosystem carbon storage in the reservoir area. The hydropower program made positive contributions to economy of the reservoir area:

(1) The construction of hydropower station disturbed the reservoir ecosystem. However, after the construction completion, the ecological restoration measures brought the carbon storage level of the reservoir ecosystem higher than the preconstruction level even though a large amount of land was submerged in the water area. With the comparison of status of before and after station construction, it was found that the forestland, water area, and construction land in the reservoir area increased, while the areas of cultivated land and grassland decreased. The water area reached 10,118.07 hectares which increased most because of water storage in the

reservoir from 2015 to 2018. The water has inundated cultivated land and grassland along the Jinsha River and its tributaries. The cultivated land had the largest reduction in area, reaching 7,835.13 hectares, mainly due to water flooding, immigrant resettlement, land occupation for the station construction, and ecological conversion of farmland.

(2) In terms of physical quantity, the carbon storage in Xiluodu reservoir area increased by 8,504.42 Mg from 2000 to 2018. The spatial distribution of carbon storage exhibited a trend of higher in the north and west while lower in the south and west. During the construction period (2005–2015), the station occupied a large amount of nonconstruction land, and the water level rose to flood nonwater area resulting in the loss of carbon storage. Still, the forest area increased compared to 2005 due to implementation of water and soil conservation and vegetation restoration policies which increased the carbon storage of ecosystem. Considering all land use and cover area, the carbon storage of reservoir ecosystem increased during the construction period. During the operation period (2015–2018), the reservoir water level rose and flooded large cultivated land and grassland. This was the main reason for the loss of carbon storage of ecosystem. However, compared to 2000 when the construction was not started yet, the carbon storage in 2018 was more significant. The change of carbon storage mainly comes from the losses of carbon storage in the construction area in the north of the reservoir area, the resettlement area in the south, the main stream and tributaries of the lower Jinsha River, and the increase of carbon storage in the central and western bank of the Jinsha River. This change may be due to increased vegetation coverage, reduced soil erosion, and a stable terrestrial ecological environment after the construction of station.

(3) During the operation period (2015–2018), the value change of carbon storage of the reservoir ecosystem was greater than operation and maintenance cost on hydropower station and exceeded the station's amortized cost. Even if the income from grid electricity price was not taken into account, the analysis still showed that hydropower development is feasible and economical.

(4) Coal power (49.07%, from the year 2020 data) has been the largest energy source in China. It has become the main option of electrical power development due to low construction cost and fast production. However, the operation cost has increased and the profits have decreased with emergence of carbon emission. Although the initial investment cost of hydropower is higher and the construction period is longer, its sales income of carbon emission rights in the operation period is greater than the maintenance cost and even the investment cost. Therefore, the economic value of hydropower is significantly higher than that of coal power.

5. Conclusions

(1) This study proposes a framework for assessing impacts of hydropower programs on the reservoir ecosystem's carbon storage. It provides recommendations for future land management in the reservoir area and hydropower development management in Jinsha River Basin and other areas. The case study of Xiluodu reservoir area found that afforestation and forest restoration are main factors leading to the increase of carbon storage in reservoir area. Other effective measures to increase carbon storage of the reservoir system include a reasonable plan of the proportion of green and construction land in future land management; conversion from cultivated land to forest land; and increase of vegetation coverage and quality. Moreover, vegetation restoration measures such as natural forest closure management and afforestation in future hydropower development can effectively mitigate the disturbance to the reservoir ecosystem. The land use and cover type with a low carbon density should be selected as much as possible when determining the inundated area to reduce carbon loss caused by the rising water level in the reservoir. In addition, evaluating the carbon storage value of the reservoir ecosystem can help in decision-making of hydropower development.

(2) This paper has several limitations that are subject to future study. First, most carbon density data came from previous literature and were fixed values with which their time variations were disregarded. The constant assumption is different from real situation since the carbon densities are more complex in different land uses and cover types in different periods. Therefore, dynamic carbon densities need to be obtained in future through detailed field monitoring in the reservoir area to improve the accuracy of results. Secondly, the InVEST model can also be used to quantify the ecosystem services in the reservoir area in addition to carbon storage assessment, such as habitat quality and soil erosion. The impacts of hydropower programs on various ecological services in the reservoir area can be assessed in future studies.

Data Availability

The data used to support the findings of this study are included within the article. The original details of the data presented in this study are available on request from the corresponding author.

Consent

Not applicable.

Conflicts of Interest

Authors' Contributions

Acknowledgments

References

[1] J. Liu and X. Deng, "Impacts and mitigation of climate change on Chinese cities," *Current Opinion in Environmental Sustainability*, vol. 3, no. 3, pp. 188–192, 2011.

[2] C. Bamminger, C. Poll, and S. Marhan, "Offsetting global warming-induced elevated greenhouse gas emissions from an arable soil by biochar application," *Global Change Biology*, vol. 24, no. 1, pp. e318–e334, 2017.

[3] D. A. Ness and K. Xing, "Consumption-based and embodied carbon in the built environment: implications for apec's low-carbon model town project," *Journal of Green Building*, vol. 15, no. 3, pp. 67–82, 2020.

[4] Y. Mao, X. Gong, and Y. Ye, "Carbon emission-based measurement of floor area ratio bonus for residential green buildings in China," *Journal of green building*, vol. 13, no. 2, pp. 84–97, 2018.

[5] J. XI, "Statement at the general debate of the 75th session of the united nations general assembly[EB/OL]," 2020.

[6] S. Mallapaty, "How china could be carbon neutral by mid-century," *Nature*, vol. 586, no. 7830, pp. 482-483, 2020.

[7] Mitigation, Climate Change, "IPCC special report on renewable energy sources and climate change mitigation," *Renewable Energy*, vol. 20, p. 11, 2011.

[8] V. Chilkoti, T. Bolisetti, and R. Balachandar, "Climate change impact assessment on hydropower generation using multi-model climate ensemble," *Renewable Energy*, vol. 109, pp. 510–517, 2017.

[9] L. Huang, X. Li, H. Fang et al., "Balancing social, economic and ecological benefits of reservoir operation during the flood season: a case study of the Three Gorges Project, China," *Journal of Hydrology*, vol. 572, pp. 422–434, 2019.

[10] Y. Wu, L. Huang, C. Zhao, M. Chen, and W. Ouyang, "Integrating hydrological, landscape ecological, and economic assessment during hydropower exploitation in the upper yangtze river," *The Science of the Total Environment*, vol. 767, Article ID 145496, 2021.

[11] R. A. Houghton and A. A. Nassikas, "Global and regional fluxes of carbon from land use and land cover change 1850-2015," *Global Biogeochemical Cycles*, vol. 31, no. 3, pp. 456–472, 2017.

[12] J. Bae and Y. Ryu, "Land use and land cover changes explain spatial and temporal variations of the soil organic carbon stocks in a constructed urban park," *Landscape and Urban Planning*, vol. 136, pp. 57–67, 2015.

[13] J. Zhang, L. Zhengjun, and S. Xiaoxia, "Changing landscape in the Three Gorges Reservoir Area of Yangtze River from 1977 to 2005: land use/land cover, vegetation cover changes estimated using multi-source satellite data," *International Journal of Applied Earth Observation and Geoinformation*, vol. 11, no. 6, pp. 403–412, 2009.

[14] D. Guan, Z. Zhao, and J. Tan, "Dynamic simulation of land use change based on logistic-ca-markov and wlc-ca-markov models: a case study in three gorges reservoir area of chongqing, China," *Environmental Science and Pollution Research*, vol. 26, no. 20, pp. 20669–20688, 2019.

[15] P. Rufin, F. Gollnow, D. Müller, and P. Hostert, "Synthesizing dam-induced land system change," *Ambio*, vol. 48, pp. 1183–1194, 2019.

[16] G. H. A. Pereira, V. F. V. Silva, R. Camara, V. A. Fréo, and M. G. Pereira, "Artificial flooding changes soil chemistry and carbon dynamics in upland forests next to hydropower plant in Amazon basin," *Environment, Development and Sustainability*, vol. 23, no. 5, pp. 7537–7549, 2021.

[17] A. Kumar and M. P. Sharma, "Carbon stock estimation in the catchment of kotli bhel 1a hydroelectric reservoir, uttarakhand, India," *Ecotoxicology and Environmental Safety*, vol. 134, no. 2, pp. 365–369, 2016.

[18] H. Dullah, M. A. Malek, H. Omar, S. A. Mangi, and M. M. Hanafiah, "Assessing changes of carbon stock in dipterocarp forest due to hydro-electric dam construction in Malaysia," *Environmental Science and Pollution Research*, vol. 28, 2021.

[19] K. Pareta and U. Pareta, "Forest carbon management using satellite remote sensing techniques a case study of sagar district (m. p.)," *E-international Scientific Research Journal*, vol. III, 2011.

[20] M. Sahle, O. Saito, C. Fürst, and K. Yeshitela, "Quantifying and mapping of water-related ecosystem services for enhancing the security of the food-water-energy nexus in tropical data-sparse catchment," *The Science of the Total Environment*, vol. 646, no. 1-1660, pp. 573–586, 2019.

[21] E. Nelson, H. Sander, P. Hawthorne et al., "Projecting global land-use change and its effect on ecosystem service provision and biodiversity with simple models," *Plos One*, vol. 5, no. 12, p. e14327, Article ID e14327, 2010.

[22] X. Chu, J. Zhan, Z. Li, F. Zhang, and W. Qi, "Assessment on forest carbon sequestration in the three-north shelterbelt program region, China," *Journal of Cleaner Production*, vol. 215, no. APR.1, pp. 382–389, 2019.

[23] R. Lyu, L. Mi, J. Zhang, M. Xu, and J. Li, "Modeling the effects of urban expansion on regional carbon storage by coupling SLEUTH-3r model and InVEST model," *Ecological Research*, vol. 34, no. 3, pp. 380–393, 2019.

[24] S. Liu, W. Zhang, K. Wang, and S. Yirong, "Evaluation of carbon sequestration after conversion of cropland to forest and grassland projection in karst peak-cluster depression area of northwest Guangxi, China," *Acta Ecologica Sinica*, vol. 36, no. 17, pp. 5528–5536, 2016, http://en.cnki.com.cn/Article_en/CJFDTOTAL-STXB201617026.htm.

[25] F. Bottalico, L. Pesola, M. Vizzarri et al., "Modeling the influence of alternative forest management scenarios on wood production and carbon storage: a case study in the

Mediterranean region," *Environmental Research*, vol. 144, pp. 72–87, 2016.

[26] E. Zhu, J. Deng, M. Zhou et al., "Carbon emissions induced by land-use and land-cover change from 1970 to 2010 in zhejiang, China," *The Science of the Total Environment*, vol. 646, no. 1-1660, pp. 930–939, 2019.

[27] K. Mokany, R. J. Raison, and A. S. Prokushkin, "Critical analysis of root: shoot ratios in terrestrial biomes," *Global Change Biology*, vol. 12, no. 1, pp. 84–96, 2006.

[28] B. Manley and P. Maclaren, "Potential impact of carbon trading on forest management in New Zealand," *Forest Policy and Economics*, vol. 24, pp. 35–40, 2012.

[29] Z. Min and Z. Guangsheng, "Carbon storage of forest vegetation and its relationship with climatic factors," *Scientia Geographica Sinica*, vol. 24, no. 1, pp. 50–54, 2004, http://www.en.cnki.com.cn/Article_en/CJFDTOTAL-DLKX200401008.htm.

[30] Y. Yang, J. Xie, H. Sheng, G. Chen, X. Li, and Z. Yang, "The impact of land use/cover change on storage and quality of soil organic carbon in midsubtropical mountainous area of southern China," *Journal of Geographical Sciences*, vol. 19, no. 1, pp. 49–57, 2009.

[31] N. I. N. G. Chen, Y. A. N. Wende, and N. I. N. G. Xiaobo, "Biomass and carbon storage of shrub forests ecosystem in karst city," *Acta Ecologica Sinica*, vol. 35, no. 8, pp. 2555–2563, 2015, http://en.cnki.com.cn/Article_en/CJFDTotal-STXB201508017.htm.

[32] J. Cao, X. Zhang, R. Deo, Y. Gong, and Q. Feng, "Influence of stand type and stand age on soil carbon storage in China's arid and semi-arid regions," *Land Use Policy*, vol. 78, pp. 258–265, 2018.

[33] Z. Gong, Y. Tang, W. Xu, and Z. Mou, "Rapid sequestration of ecosystem carbon in 30-year reforestation with mixed species in dry Hot Valley of the Jinsha River," *International Journal of Environmental Research and Public Health*, vol. 16, no. 11, p. 1937, 2019.

[34] H. Luo, "Advances on carbon storage in crops of China," *Ecology and Environmental Sciences*, vol. 23, no. 4, pp. 692–697, 2014, http://en.cnki.com.cn/Article_en/CJFDTotal-TRYJ201404024.htm.

[35] S. Zhao, S. Liu, R. Yin et al., "Quantifying terrestrial ecosystem carbon dynamics in the Jinsha watershed, upper Yangtze, China from 1975 to 2000," *Environmental Management*, vol. 45, no. 3, pp. 466–475, 2010.

[36] W. She, Y. Wu, H. Huang et al., "Integrative analysis of carbon structure and carbon sink function for major crop production in China's typical agriculture regions," *Journal of Cleaner Production*, vol. 162, pp. 702–708, 2017.

[37] J. Ni, "Carbon storage in grasslands of China," *Journal of Arid Environments*, vol. 50, no. 2, pp. 205–218, 2002.

[38] K. Li, J. Cao, J. F. Adamowski et al., "Assessing the effects of ecological engineering on spatiotemporal dynamics of carbon storage from 2000 to 2016 in the Loess Plateau area using the InVEST model: a case study in Huining County, China," *Environmental Development*, vol. 39, Article ID 100641, 2021.

[39] X. Chuai, X. Huang, L. Lai, W. Wang, J. Peng, and R. Zhao, "Land use structure optimization based on carbon storage in several regional terrestrial ecosystems across China," *Environmental Science & Policy*, vol. 25, pp. 50–61, 2013.

[40] R. Sharp, R. Chaplin-Kramer, S. Wood, A. Guerry, and J. Douglass, "InVEST user's guide," 2018, https://invest-userguide.readthedocs.io/en/latest/index.html.

[41] Z. Li, H. Du, Y. Xiao, and J. Guo, "Carbon footprints of two large hydro-projects in China: life-cycle assessment according to iso/ts 14067," *Renewable Energy*, vol. 114, no. b, pp. 534–546, 2017.

[42] B. Cheng, K. Lu, J. Li, H. Chen, X. Luo, and M. Shafique, "Comprehensive assessment of embodied environmental impacts of buildings using normalized environmental impact factors," *Journal of Cleaner Production*, vol. 334, Article ID 130083, 2022.

Research Article

Research on Optimization Model of Multisource Traffic Information Collection Combination Based on Genetic Algorithm

Jianwei Guo and **Yongbo Lv**

School of Traffic and Transportation, Beijing Jiaotong University, Beijing 100044, China

Correspondence should be addressed to Jianwei Guo; 19114023@bjtu.edu.cn

In order to reduce the excessive use of multisource traffic information collection system, a multisource traffic information collection combination optimization mode is proposed based on genetic algorithm in this paper. This model is mainly used to analyze the traffic management data in the city. According to the collected data information, the characteristics of the traffic equipment can be effectively analyzed. Basing on the market demand and supply relationship, the multisource traffic information collection combination optimization model is used to complete the reorganization and optimization of the traffic information in this paper, to acquire the main convolution feature variables of the model. The data information combination processing is performed according to the acquired feature variables, and the genetic algorithm is used to adjust the multisource traffic information. During the process of information fusion data analysis, the multisource traffic information clustering and fuzzy constraint control can be performed effectively to realize the optimization of the team's traffic information collection combination. Finally, the simulation results show that the method proposed in this paper is more accurate in realizing the optimization process of multisource traffic information collection and combination and has a better degree of information fusion.

1. Introduction

At present, many large-scale cities in China have gradually increased their investment in urban transportation systems, especially in the collection of multisource traffic information [1, 2], wasting a lot of manpower and financial resources. as the foundation of urban traffic infrastructure, multisource traffic information can be used to effectively improve the During accuracy and efficiency of traffic information collection, laying the foundation for improving the urban intelligent traffic system [3, 4]. However, currently, due to the single structure of the existing acquisition system hardware in the use process, the collected data information is inaccurate, and the cost of investment is huge. The limitation of the single-structured traffic data acquisition equipment lies in the small acquisition range. Fixed information collection period and fixed types of acquired data information, resulting in large-scale investment and serious waste of resources. Meanwhile, all kinds of information collection equipment are damaged seriously leading to huge maintenance costs. The use of different types of information collection equipment will cause repeated collection of traffic information and increase the workload.

Based on genetic algorithm, a combined model of multisource traffic information collection is proposed in this paper. The model can be used to effectively analyze the results of the obtained multisource traffic information, genetic algorithms are combined to collect and combine the initial traffic information, complete the reconstruction of the multisource traffic information spatial structure, and obtain the convolutional characteristics of the traffic information. According to the characteristic variables, the fusion processing and combination of data information can be carried out. Complete distributed clustering of multisource information in the fusion space. Finally, the analysis of experimental simulation results shows that the method in this paper has superior performance and information collection ability in the process of extracting multisource traffic information collection combination.

2. Information Collection and Feature Preprocessing

2.1. Collection Combination Optimization System. The flow of mobile positioning and real-time monitoring system of road vehicle is shown in Figure 1, which mainly includes three parts: extraction and tracking of vehicle targets, road condition detection and real-time monitoring of traffic flow [5, 6]. The extraction and location of vehicle targets are mainly realized by the construction of the detection background to extract the characteristics of the moving vehicle, while monitoring the vehicle parameters in the implementation. The road background is based on for modeling the road condition monitoring, and the road surface can be divided by the acquired data information, and the vehicle detection area is extracted to obtain the conversion between the road plane coordinates and the left side of the multimedia spectrum plane. The data of the road and traffic flow obtained in previous times is integrated by the road traffic to complete the data analysis and statistics of the traffic flow on different lanes [7–11]. This system uses the traffic flow pictures collected by the cameras placed on the platform.

The main control software design is mainly composed of two main programs, which are the main control programs that can complete different business logics and the programs that can realize the user-side GUI process control. The main control program is mainly to receive external commands, and meanwhile send the obtained traffic flow information to the corresponding business module for processing, effectively realizing the business logic between systems.

The main process uses a message transfer mode including a communication module, a message transfer module, and a business module. The communication module mainly establishes a network link [12–14], and sends the received data information from the control information obtained to an arbitration level information commands are sent to the control center through the service interface. The control command center module executes in accordance with the message queue mechanism acquired by the GUI process system and the method of sending and receiving information between the corresponding processes. When the service module mainly processes specific services and all service modules are initialized, the service function module sends the command information that needs to be processed to the message control module. At the same time, when data information is received, the data control center will send the command information to the business module for sorting. The GUI process is developed based on the embedded graphics library mimugui, which is mainly a graphical user interface that realizes the needs of business logic. The GUI process communicates with the main process in the same way as the message queue [15].

The vehicle positioning detection module mainly communicates with the weight measurement platform and adopts the modbus protocol. This module is the master, and the vehicle volume measurement platform is mainly used as a slave device. The input of the vehicle positioning detection module is received using the RS485 interface, and the vehicle

volume detection module is used to extract vehicle volume-related data information, and at the same time, it is sent to the message arbitration module to obtain the quantity statistics operation command from the outside. The output of the detection module includes the transmission of the detection result data to the center via the network. The results of the quantity statistics are stored in the database. The detection of instructions are sent to the detection platform through the RS485 interface. the RS485 interface and the quantity statistics platform are used for the processing of the quantity statistics module to construct information and data associations. Meanwhile, the automatic fixed time is set at the RS485 interface to automatically and regularly read the vehicle information from the quantity statistics platform, and the analysis results are sent to the module for processing through data analysis. The interface to network is used by vehicle positioning detection module to send statistical results to the control center and stores them in the database. The processing steps of the detection module are shown in Figure 2.

The GPS module is used to obtain the geographic information parameters of the vehicle in this paper. When the vehicle image is acquired, and it is used in the system *l*, the processing of the above data can be displayed digitally, and the obtained results will be stored. The input GPS device of the GPS module is GPS information data sent via the network in this paper. The output of the GPS module's data information is encrypted and protected in the network center, and then the message arbitration module is used to store the vehicle-related data information in the GUI module. The warning information about GPS is stored in the database, and the data sent is mainly the warning information of GPS. The paper. GPS module is usually processed with a dedicated network to obtain the GPS device data information and use the GPS data analysis function module to realize the transmission of relevant information data and relevant alarm information by the network center GPS. As shown in Figure 3.

The data transmission task mainly includes the vehicle-mounted terminal transmitting data to the monitoring platform. In addition to the real-time data of the vehicle, it also includes sending the identification information and data mentioned in the link management task to the mainly includes branch of monitoring platform as supplement. The vehicle-mounted terminal can transmit information to multiple monitoring centers, so multiple data transmission tasks coexist. The data management is performed for coordinating multiple data transmission tasks to prevent conflicts and resource competition.

2.2. Collection of Multisource Traffic Information. In order to realize the optimal collection and fusion dispatching of traffic in a complex traffic network environment, first the design of a distributed data structure of multisource and multisource traffic information shall be carried out in the complex traffic network environment, and a multisource traffic information database structure is built in a complex
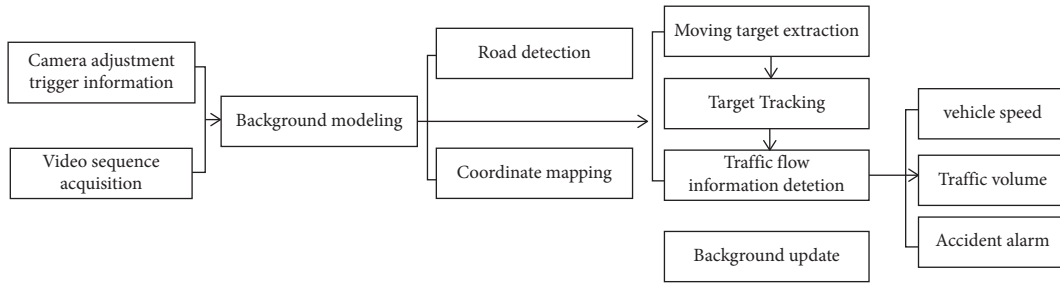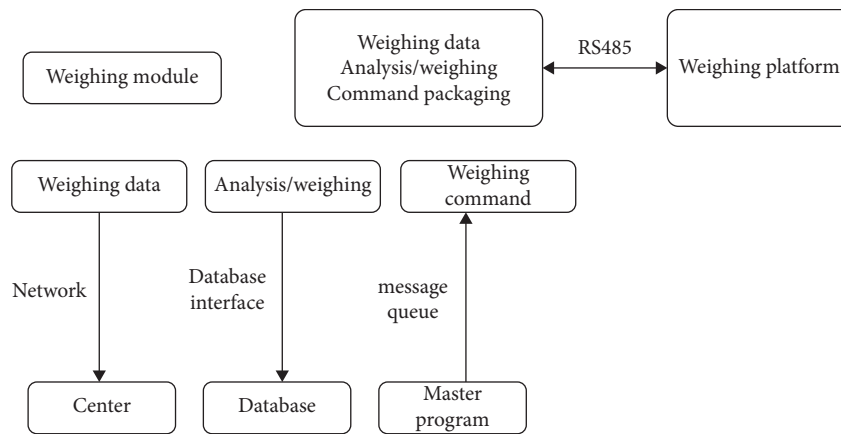
FIGURE 1: System flow chart.

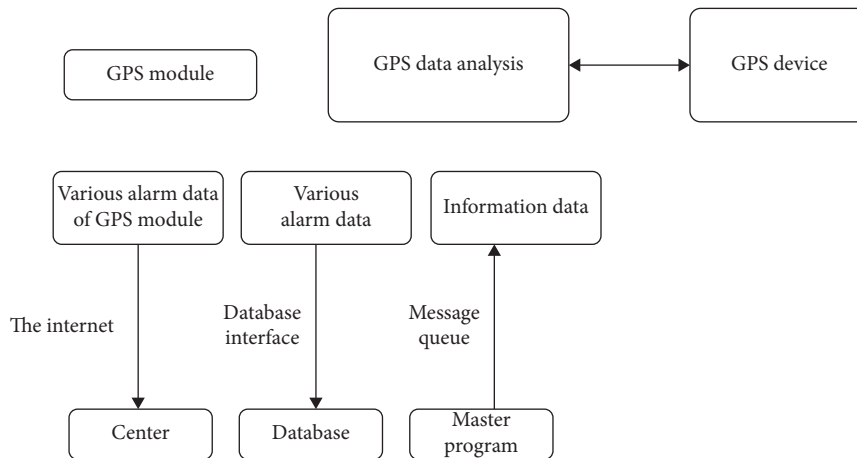FIGURE 2: Block diagram of quantity statistics module.

FIGURE 3: GPS module block diagram.

network environment,..0 + the fuzzy decentralized preservation center of multisource traffic information needs to be represented by 4 groups G. Suppose i is the feature space of the interaction of multiple sources of traffic information in a complex traffic network environment. The multisource traffic information is reconstructed in a high-dimensional feature space in a complex traffic network environment using the coupled statistical method of multiple non-linear components, combined with pattern recognition and adaptive clustering methods, to carry out the information fusion and feature extraction of source traffic information in multiple traffic network environments. Based on the above analysis, Figure 4 shows the overall structure model of building a combination of multisource traffic information collection and fusion collection in a complex traffic network environment.

According to Figure 4, the multisource traffic information collection process contains a large amount of
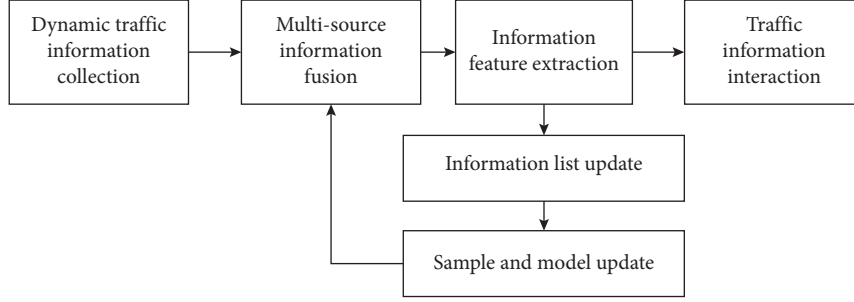
FIGURE 4: The overall structure model combined by multisource traffic information collection and fusion collection.

interference information and road condition information. This multisource traffic information indicates the data by spectral characteristics. The multisource and multisource traffic information contains n variables. $\{y_1, y_2, \ldots, y_n\}$ can be used to represent the variable threshold corresponding to a_j. The simplified mathematical model of multisource traffic information can be explained by the following formula.

$$
\begin{cases}
G_1 = b_{11}a_1 + b_{12}a_2 +, \ldots, b_{1n}a_n \\
G_2 = b_{21}a_1 + b_{22}a_2 +, \ldots, b_{2n}a_n \\
\ldots \\
G_n = b_{n1}a_1 + b_{n2}a_2 +, \ldots, +b_{nn}a_n
\end{cases}
\tag{1}
$$

Among them, a_j and G_k both have a strong correlation, which represents a distributed array of sensors that collect multisource traffic information in a complex traffic network environment, and use multisensor fusion recognition methods for effective information mining in multisource traffic in the Internet of Vehicles. The fuzzy adaptive clustering method is used to construct multisource in multi traffic information statistical feature quantity, combined with normalized feature extraction method, the multisource traffic information autoregressive analysis result is $u(x_j)\xi_j$, and the detection problem of multisource traffic information is transformed into a linear problem of measuring the dynamic distribution of multisources in a complex traffic network environment. According to the above design, the statistical result model of multisource traffic information is analyzed, and the statistical feature sampling method is used to carry out the acquisition of the information of the original multisource traffic [8].

2.3. Big Data Fusion of Traffic Information.
Based on the time-frequency coupling distribution of the multisource traffic bit sequence, the genetic algorithm method is used to remove the interference component and the feature set of the multisource traffic information [9] and realize the fuzzy clustering processing of the multisource traffic information of the automobile network: $k(x_i, x_j)$

$$
\left.
\begin{array}{l}
\min_{w,b,\xi} \dfrac{1}{2}\|w\|^2 + C \displaystyle\sum_{j=1}^{l} u(x_j)\xi_j \\[3mm]
\text{s.t. } y_j\big((w \cdot x_j) + b\big) + \xi_j \geq 1 \\[3mm]
\xi_j \geq 0, \; j = 1, 2, \ldots, l
\end{array}
\right\}.
\tag{2}
$$

Regarding the nonlinear collection and combination problem, based on the temporal variability and random change characteristics of traffic information, the fuzzy dynamic change kernel function $k(x_i, x_j)$ is introduced for dynamic feature separation. The following quadratic planning shows the information fusion of multisource and multisource traffic information problem.

$$
\left.
\begin{array}{l}
\min_{\alpha} \dfrac{1}{2} \displaystyle\sum_{i=1}^{l}\sum_{j=1}^{l} y_i y_j \alpha_i \alpha_j K(x_i, x_j) - \sum_{j=1}^{l} \alpha_j \\[4mm]
\text{s.t. } \displaystyle\sum_{j=1}^{l} y_j \alpha_j = 0 \\[4mm]
0 \leq \alpha_j \leq u(x_j)C, \; j = 1, 2, \ldots, l
\end{array}
\right\}.
\tag{3}
$$

Based on the results of feature extraction, statistical regression analysis is used to analyze the nonlinear structure group of multisource traffic information in a complex traffic network environment [10], and a linear coupling model is derived:

$$
x_k = \sum_{n=0}^{N/2-1} 2\left(a_n \cos \frac{2\pi kn}{N} - b_n \sin \frac{2\pi kn}{N}\right), \quad k = 0, 1, \ldots, N-1.
\tag{4}
$$

Among them, a_n represents the feature distribution of multisource traffic information linear programming in a complex transportation network environment. There are m multisource traffic information nodes $A_1, A_2, \ldots, A_m$ in a

complex transportation network environment to construct multisource traffic information fusion scheduling in a complex transportation network environment. Its mathematical expression is as follows:

$$\min(f) = \sum_{i=1}^{m} \sum_{j=1}^{n} C_{ij} X_{ij},$$

$$\text{s.t.} \begin{cases} \sum_{j=1}^{m} X_{ij} = a_i, \ i = 1, 2, \ldots, m \\ \sum_{i=1}^{m} X_{ij} = b_i, \ j = 1, 2, \ldots, n \\ X_{ij} \geq 0, \ i = 1, 2, \ldots, m; \ j = 1, 2, \ldots, n \end{cases} \quad (5)$$

Assuming that the number of multisource and multisource traffic information distribution nodes in the current complex traffic network environment is n, $N_1, \ldots, N_n$ the learning method of fuzzy convolutional neural network is adopted to realize the big data fusion of traffic information.

3. Collection Combination Configuration Model

When analyzing traffic conditions, a sufficient amount of multisource traffic information must be used as a database, but excessive traffic data will cause data duplication and redundancy [5]. Meanwhile, too many information collection devices have limited improvement in real-time monitoring of traffic conditions, which also causes a waste of social resources. Therefore, the basic idea of modeling in this paper is to comprehensively utilize the advantages of multiple multisource traffic information collection devices, make up for the shortcomings of different types of equipment, and form a multi-source traffic information collection system that constitutes an efficient and low-cost combination structure for correct collection and analysis of the data of the communication status.

A single multisource traffic information collection device is the basis of a composite configuration system. In order to make full use of the applicability of a single device, the principle of single configuration is first discussed.

3.1. Layout Based on a Single Multisource Traffic Information Collection Device.
General information collection devices are considered mainly in this article, which divides the types of devices into fixed and mobile types, and discusses their configuration methods.

3.1.1. Layout Method of Fixed Collection Equipment.
Set the road network as G (T, A), where T is the node in the road network and A is the road section in the road network. α_{ji} is defined as whether i multisource traffic information collection equipment is installed on the j section. If it is set, then $\alpha_{ji} = 1$, if not set, then $\alpha_{ji} = 0$. Based on the maximization of utility, the utility maximization model of collection equipment is established [6]:

$$\max U = \sum_{\alpha_i \in A} \alpha_{ji} f_i r_j,$$

$$\alpha_{ji} = 0 \text{ or } 1, \quad (6)$$

where U is the utility of the collection equipment; f_j is the traffic fluctuation coefficient of road section j; and r_j is the objectively important coefficient of road section j.

(1) Determination of Traffic Fluctuation Coefficient f_j. The traffic variation coefficients in different sections are different. The traffic variation coefficient is mainly affected by the traffic flow [7].

The traffic fluctuation coefficient is determined by the traffic volume. Take the observation sample h_k, $k = 1, 2, \ldots, l$, calculate the sample mean $\mu(h_k)$ variance $\mu(h_k)$, let

$$f_k = \frac{\delta(h_k)}{\mu(h_k)}. \quad (7)$$

The maximum is taken through computation, then

$$f_{\max} = \max(h_k), \ k = 1, 2, 3, \ldots, m,$$
$$f_{\min} = \min(h_k), \ k = 1, 2, 3, \ldots, m. \quad (8)$$

Based on equation (3) (9)

$$\sum_{k=1}^{l} \mu^2(h_k) = \sum_{k=1}^{l} \delta^2(h_k)/f_k^2. \quad (9)$$

Then,

$$\sum_{k=1}^{l} \delta^2(h_k)/f_{\min}^2 \geq \sum_{k=1}^{l} \mu^2(h_k) \geq \sum_{k=1}^{l} \delta^2(h_k)/f_{\max}^2. \quad (10)$$

Due to change in equal change, the following is obtained

$$f_{\max} \geq \left[\sum_{k=1}^{l} \delta^2(h_k)/ \sum_{k=1}^{l} \mu^2(h_k) \right]^{1/2} \geq f_{\min}. \quad (11)$$

Then the fluctuation coefficient of the road section is

$$f_j = \left[\sum_{k=1}^{l} \delta^2(h_k)/ \sum_{k=1}^{l} \mu^2(h_k) \right]^{1/2}. \quad (12)$$

(2) Determination of the Objective Importance r_j of Road Sections. The importance of different roads is almost inconsistent. The location of the bottleneck in the road network has a great impact on the road network. For example, sections with heavy traffic during peak hours and sections in busy streets are compared with the section with small traffic volume has relatively little impact on the road network. For example, unimportant sections near the suburbs.

The importance of the road network can be calculated according to the traffic volume [8]. The total traffic flow $Q = \sum_{j=1}^{r} q_j$ is defined, where r is the total number of intervals, q_j is the flow of interval j, $Q \leq L$ L is the network capacity, and Q is the historical data. Therefore, the objective importance T_j of segment j is

$$r_j = \frac{q_j}{Q}. \tag{13}$$

3.1.2. How to Determine the Sample Size of GPS Floating Car.
Different from fixed information collection equipment, mobile equipment mainly adjusts the input amount to ensure sufficient data collection [9]. This article chooses the floating lane network coverage. γ as an index to evaluate the adequacy of the input amount, there are

$$\gamma = \left(\frac{r}{R}\right) \times 100\%. \tag{14}$$

In the formula: r is the number of road sections that can be covered by the floating car and R is the total road section number in the road network.

The condition for judging whether a road is covered is that GPS floating car information can be obtained during the research cycle. With reference to previous research experience, there is the following relationship between the number of GPS floating vehicles in the road network and the capture rate.

$$\gamma = \exp\left\{-\left(a_0 + a_1 x_2 + a_2 x_2 + a_3 x_3 + a_4 x_4 + a_5 x_5 + a_6 x_6 + a_7 \ln(x_7)\right)^2\right\},$$

$$\begin{cases} \gamma \geq C_1 \\ x_7 \leq C_2 \\ \dfrac{d_r}{d_{x_7}} \geq C_3 \end{cases}, \tag{15}$$

where γ is the coverage of the road network; $x1$ is the area of road network, $100\,\text{km}^2$; $x2$ is the ratio of the expressway in the road network to the total road length; $x3$ is the ratio of the main arterial road to the total road length; $x4$ is the secondary arterial road to the total road length. $X5$ is the proportion of the length of secondary access road to the total road; $x6$ is the density of road network, km/km^2; $x7$ is the number of floating vehicles, (in hundreds); C1 is the minimum threshold of road network coverage, (in hundreds); C2 is maximum number threshold of GPS floating vehicles, (in hundreds); C3 is the minimum threshold of the marginal contribution of the number of floating cars to the coverage of the road network. In the model, a0, a1, a2, a3, a4, a5, a6, and a7 can be obtained by regression analysis.

3.2. Combination Configuration Principle for Multisource Traffic Information Collection.
The combination configuration of multisource traffic information collection shall satisfy the following principles:

(1) Ability to collect more effective multi-source traffic information;

(2) While minimizing the cost of the arrangement of the collection equipment, more effective multisource traffic information can be collected, and multi-function can be used to limit the overlap of data.

(3) The reduction of equipment input discussed in this paper is mainly based on the viewpoint of reducing the redundancy of data collection and subject to the optimization goals of other functions of the equipment.

3.3. Establishment of Model.
The set N is defined as the number of different types of multisource traffic information collection devices, and different collection devices can be put on the same road.

The defined variable a_{ji} indicates whether the ith multisource traffic information collection device is installed on the jth road. If is set, then $a_{ji} = 1$; if it is not set, then $a_{ji} = 0$, a_{ji} form matrix A.

3.3.1. Construction of Objective Function considering Economic Benefits.
Targeting at the lowest total configuration cost of collection equipment, with collecting the best multisource traffic information as the premise, there are various configuration methods for collection equipment. The cost of different equipment is different. In order to minimize the total cost of configuration, the most suitable layout plan can be obtained by optimizing the combination configuration.

In this article, we only considered general fixed and mobile collection equipment. In the construction of the function for the purpose of economic effect, the key variable of the device needs to be considered for the fixed information collection device, and only the number of equipment needs to be considered for the mobile type.

The definition φ_{ji} represents the factor variable of i kinds of multisource traffic information collection equipment on the j section, and the decisive factor is the characteristics of the collection equipment and the characteristics of the road section.

Assuming that there are r sections in the road network, the numbers of fixed and mobile equipment are l and e, respectively. In order to minimize the overall cost of the equipment, the objective function is

$$\min = \sum_{i=1}^{l}\sum_{j=1}^{r} a_{ji} \times \varphi_{ji} \times c_i + \sum_{i=1}^{e} n_i c_i. \tag{16}$$

In the formula: the value of a_{ji} is taken as 1; c_i is the cost of the ith type of equipment; and n_i is the number of the ith type of equipment.

3.3.2. Construction of Objective Function considering Comprehensive Benefits.
In order to meet the basic requirements for collecting data, a multifunctional comprehensive income function is also established to reduce the overall cost of the equipment.

The variables x_{ik} is defined as (x_{ik} 0–1 variables), x_{ik} indicating whether the kth data can be obtained by the ith multisource traffic information collection device, if it can be obtained, then $x_{ik} = 1\nabla(f, f')$, if it cannot be obtained, then $x_{ik} = 0$.

From the above analysis, the following matrix can be obtained:

$$P_{ijk} = [A] \begin{pmatrix} x_{11} & x_{12} & \cdots & x_{1g} \\ \vdots & \vdots & & \vdots \\ x_{(e+l)1} & x_{(e+l)2} & \cdots & x_{(e+l)g} \end{pmatrix} = \begin{pmatrix} b_{11} & b_{12} & \cdots & b_{1g} \\ \vdots & \vdots & & \vdots \\ b_{r1} & b_{r2} & \cdots & b_{rg} \end{pmatrix}, \tag{17}$$

where P_{ijk} is a collection of the kth multisource traffic information obtained by various collection devices on the j section; A is the matrix formed by a_{ji}; b_{jk} is the kth multisource traffic information obtained on the j section; g for multisource traffic information collection = the number of equipment categories, then

$$P_{ijk} = \begin{pmatrix} b'_{11} & b'_{12} & \cdots & b'_{1g} \\ \vdots & \vdots & & \vdots \\ b'_{r1} & b'_{r2} & \cdots & b'_{rg} \end{pmatrix}. \tag{18}$$

The effect maximization function of multisource traffic information collection equipment is

$$\max U = \sum_{j=1}^{r}\sum_{k=1}^{g} b'_{jk} f_j r_j, \tag{19}$$

where b'_{jk} is the k multisource traffic information jointly acquired by all collection equipment on the j section, when $b'_{jk} \geq 1$, $b'_{jk} = 1$, otherwise $b'_{jk} = 0$,. The coverage rate of mobile multisource traffic information collection equipment y is

$$\gamma_y = \frac{\sum_{j=1}^{r} a_{yj}}{r}, \tag{20}$$

where a_{yj} as the coverage rate of the Y multisource traffic information collection equipment in section j.

Finally, the sample supply of y is clarified. In addition, on the basis of benefit maximization and economic benefit optimization, the planning function of multiple objectives is

$$\begin{cases} \min Z = \sum_{i=1}^{l}\sum_{j=1}^{r} a_{ji} \times \varphi_{ji} \times c_i + \sum_{i=1}^{e} n_i c_i \\[2mm] \max U = \sum_{i=1}^{l}\sum_{j=1}^{r} b_{jk} f_j r_j \\[2mm] \text{s.t.} \begin{cases} a_{ji} \geq 0, \ a_{ji} = 0 \text{ or } 1 \\[2mm] b_{jk} = \sum_{i=1}^{l+e} a_{ji} \times x_{ik} \\[2mm] b'_{jk}, \text{ if } b_{jk} \geq 1, \ b'_{jk} = 1, \text{ otherwise, } b'_{jk} = 0 \\[2mm] n_y = \phi\left(\sum_{j=1}^{r} a_{yj}\right) \end{cases} \end{cases} \tag{21}$$

3.3.3. Solving Algorithm.
In order to solve the multiobjective planning function problem, the first step is to maximize the function

$$\begin{cases} \min Z = -\sum_{i=1}^{l}\sum_{j=1}^{r} a_{ji} \times \varphi_{ji} \times c_i - \sum_{i=1}^{e} n_i c_i \\[2mm] \max U = \sum_{i=1}^{l}\sum_{j=1}^{r} b'_{jk} f_j r_j \\[2mm] \text{s.t.} \begin{cases} a_{ji} \geq 0, \ a_{ji} = 0 \text{ or } 1 \\[2mm] b_{jk} = \sum_{i=1}^{l+e} a_{ji} \times x_{ij} \\[2mm] b'_{jk}, \text{ if } b_{jk} \geq 1, \ b'_{jk} = 1, \text{ otherwise, } b'_{jk} = 0 \\[2mm] n_y = \phi\left(\sum_{j=1}^{r} a_{yj}\right) \end{cases} \end{cases} \tag{22}$$

During the process of solving, due to existence of certain conflicts between multiple targets, it is difficult to obtain the ideal optimal solution, so intelligent algorithms can be used to obtain the optimal solution.

In this paper, we use a multisfunctional planning solution based on genetic algorithm to calculate [11]. First, the priority solution $f(x^*)$ is determined, and the solution is 337519; 39 can be found around the solution. (X^*) is the satisfaction solution of the model.

By checking the correlation between the two, two gray correlations can be expressed, that is, a single objective function converted into a solution

$$\begin{cases} \max \nabla(f, f') \\[2mm] \text{s.t.} \begin{cases} a_{ji} \geq 0, a_{ji} = 0 \text{ or } 1 \\[2mm] b_{jk} = \sum_{i=1}^{l+e} a_{ji} \times x_{ik} \\[2mm] b'_{jk}, \text{ if } b_{jk} \geq 1, \ b'_{jk} = 1, \text{ otherwise, } b'_{jk} = 0 \\[2mm] n_y = \phi\left(\sum_{j=1}^{r} a_{yj}\right) \end{cases} \end{cases}, \tag{23}$$

where the gray correlation $\nabla(f, f')$ is

$$\nabla(f, f') = \frac{\min|f'(x^*) - f(x^*)| + \xi \max|f'(x^*) - f(x^*)|}{|f'(x^*) - f(x^*)| + \xi \max|f'(x^*) - f(x^*)|}. \tag{24}$$

Assuming there are p objective functions in total, the solution model based on the gray relational degree algorithm is

$$\begin{cases} \max \sum_{p=1}^{k} \omega_p \dfrac{\min|f'(x^*) - f(x^*)| + \xi \max|f'(x^*) - f(x^*)|}{|f'(x^*) - f(x^*)| + \xi \max|f'(x^*) - f(x^*)|} \\ \\ \text{s.t.} \begin{cases} a_{ji} \geq 0, \ a_{ji} = 0 \text{ or } 1 \\ \\ n_y = \phi\left(\sum_{j=1}^{r} a_{yj} \right) \end{cases} \end{cases}. \tag{25}$$

The approximate optimal solution is obtained through genetic algorithm, and the final optimal solution is obtained through repetition.

3.4. Parking Lot Location Guidance Algorithm Based on Dijkstra Algorithm.

Generally speaking, Dijkstra's algorithm uses an adjacency matrix for storage. The adjacency matrix stores the relationship between each node. However, considering the actual situation of urban roads, although there are many nodes in the road graph, there are few directly connected points. Therefore, the actual road graph is a sparse graph, and the corresponding adjacency matrix is also a sparse matrix. Therefore, if the adjacency matrix is used to store the nodes, a lot of space will be wasted.

In this paper, the adjacency list is used to replace the adjacency matrix, which can reduce the space complexity of the algorithm. The comparison of the two storage methods is as follows:

If it is assumed that there are b nodes in the graph $G = (V, E)$, then its adjacency matrix A is a symmetric matrix.

If G is an unweighted graph, its adjacency matrix can be expressed as

$$A[i, j] = \begin{cases} 1, & (V_i, V_j) \in E(G), \\ 0, & (V_i, V_j) \notin E(G). \end{cases} \tag{26}$$

We believe that the actual city road map is an undirected weighted map. In the adjacency matrix of $G = (V, E)$, the elements are

$$A[i, j] = \begin{cases} \omega_{ij}, & (V_i, V_j) \in E(G), \\ 0, & (V_i, V_j) \notin E(G) \ \& \ i = j, \\ \infty, & (V_i, V_j) \notin E(G) \ \& \ i \neq j. \end{cases} \tag{27}$$

That is, the element on the symmetry line of the adjacency matrix is 0, where ω_{ij} is the weight between two points,
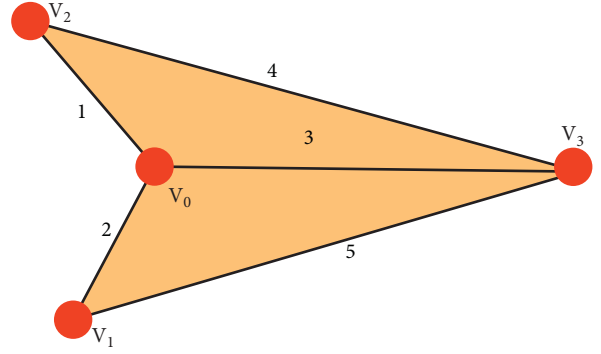
FIGURE 5: A typical undirected weighted graph.

and ∞ represents that i and j are not connected. A typical undirected weighted graph is shown in Figure 5:

The adjacency matrix is

$$A = \begin{bmatrix} 0 & 1 & 2 & 3 \\ 1 & 0 & \infty & 4 \\ 2 & \infty & 0 & 5 \\ 3 & 4 & 5 & 0 \end{bmatrix}. \tag{28}$$

On the one hand, the storage space of the adjacency matrix is only related to the number of nodes and contains n^2 elements in total. However, since the adjacency matrix is mostly a sparse graph, a lot of space is wasted. On the other hand, the time complexity of the Dijkstra algorithm using the adjacency matrix storage method is $O(n^2)$, and the time cost is too large.

The adjacency list is a very useful storage structure for sparse graphs. All the nodes in the graph are stored in a one-dimensional array, and then the edge with it as the end point is linked after each node to form a linked list. The linked list node is composed of three parts: the start point, the end point, and the weight of the edge. As shown in Figure 6, v_0 is a three-way intersection, and there are 3 sides with it as the endpoint. Then, we can build a singly linked list connecting these 3 edges and then connect it to v_0.

Figure 7 is stored as an adjacency list as follows:

The adjacency table storage requires only $n + m$ storage units, far less than n^2.

From the perspective of space complexity, the adjacency table only needs $n + 2m$ storage units, while the adjacency matrix requires n^2, and the storage efficiency advantage of the adjacency table is significant. In terms of time complexity, the complexity of the adjacency list $O(m + n)$ is also much lower than the complexity of the adjacency matrix $O(n^2)$.

In the research process, the graph is regarded as a plane graph, and the shortest path value from the temporarily marked node to the starting node and the Euclidean distance to the target node are added, and this value is regarded as the characteristic value of the marked node. In the selection process of permanent marked nodes, it is necessary to use this value as a theoretical basis to select among the set of temporary marked nodes, and permanent marked nodes can
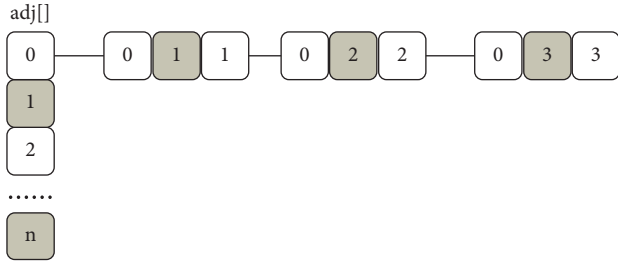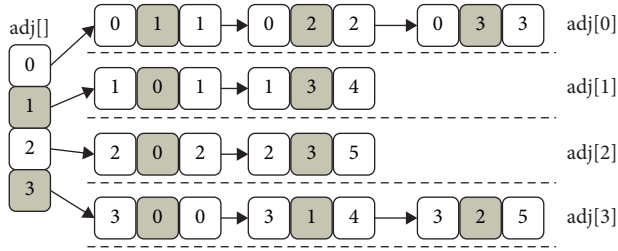
FIGURE 6: v_o example diagram.

FIGURE 7: Adjacency list of undirected weighted graph.

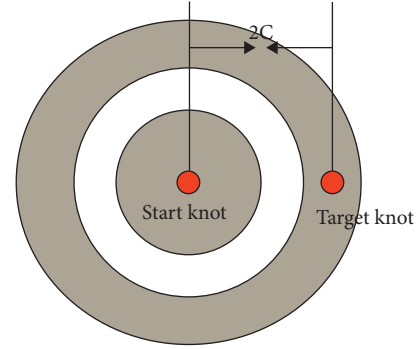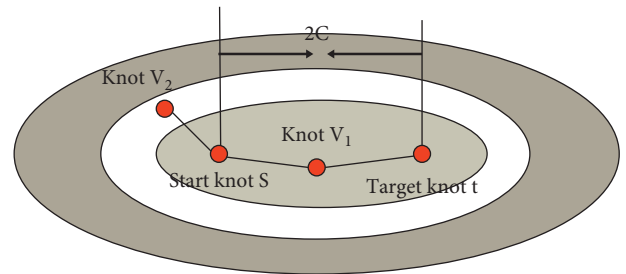

FIGURE 8: Classic Dijkstra algorithm.

FIGURE 9: The optimized Dijkstra algorithm.

FIGURE 10: Schematic diagram of optimized Dijkstra algorithm.

select the smallest temporary node of this value. This method can ensure that the target node can be found more accurately and quickly through the Dijkstra algorithm, and the search efficiency can be improved.

Through the above algorithm, the premise of determining the permanent mark point is that the above two values add to the minimum value. The concept of an ellipse here is a trajectory corresponding to a point in the surface where the distance between s and t is added to a constant $2c$. Among them, the point p is located on the trajectory, and the distances to the two points s and v are d_{sp} and d_{tp}, respectively, then $d_{sp} + d_{tp} = 2c$ can be obtained. Through this traversal method to find the shortest path method, the end point and the meta point can be regarded as two focal points, which can be regarded as a concentric ellipse. Before Dijkstra algorithm is optimized, the corresponding search process is shown in Figure 8:

After Dijkstra algorithm is optimized, the corresponding search process is shown in Figure 9:

If nodes v_1 and v_k are both temporarily marked nodes, s is the starting node, and t is the target node. It can be seen from Figure 10 that d_1 and d_k are the shortest path lengths between v_1 and v_k and s, respectively, and D_1 and D_k are the Euclidean distances between v_1 and v_k and t, respectively. The Euclidean distance between v_1 and v_k is C.

In the Dijkstra algorithm before optimization, in terms of selecting marked nodes, if $d_1 > d_k$, the marked node selects v_k, otherwise it is v_1. After the algorithm is optimized, if $d_1 + D_1 > d_k + D_k$, then mark the node selects v_k, otherwise it is v_1.

In summary, the search range of the latest algorithm is an ellipse. After optimization, the search efficiency is improved and the number of traversed nodes is reduced.

The ellipse limits the range of the search area, see Figure 11 for details. s is the starting node, v_1 is the boundary node, t is the target node, and $2a$ is the maximum limit distance. The Euclidean distance between s and v_1 is denoted by $|sv_1|$, and the Euclidean distance between v_1 and t is denoted by $|v_1t|$, and the specific search range is $|sv_1| + |v_1t| < 2a$. If $|sv_1| + |v_1t| > 2a$, then these nodes can be ignored in the algorithm. The reason is that the distance traveled by s from v_1 to t is greater than $2a$. In this way, an ellipse is formed, the ellipse is composed of all nodes that meet the condition of $|sv_1| + |v_1t| = 2a$, the focus is s and t, and the major axis is $2a$.
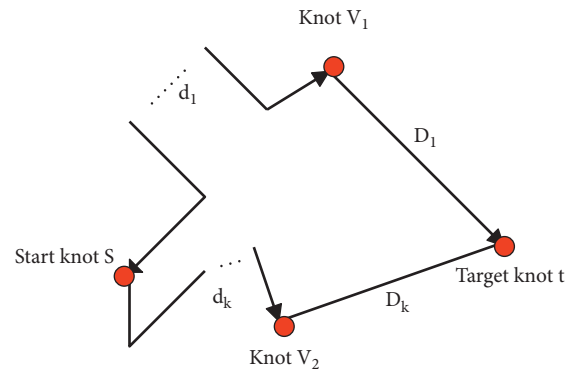
In summary, the parameters are set as follows: s and t are selected for the ellipse focus, and $\lambda|st|$ is selected for the length of the major axis. The Euclidean distance between s and t is represented by $|st|$, and the confidence coefficient is λ.
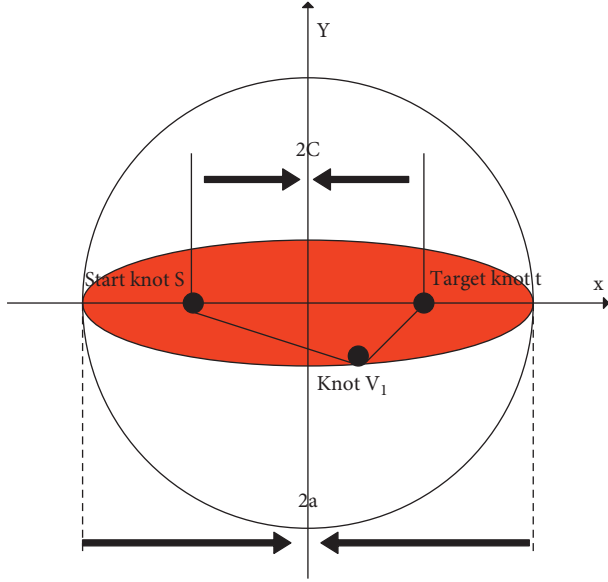
FIGURE 11: Search range restricted by ellipse.

In the process of setting parameters, the main purpose is to find a more reasonable long axis, that is, to calculate the most reasonable λ, and get the desired ellipse search interval.

The principle of finding λ: among the passing road network nodes, a group of nodes with strong representativeness is selected, and the starting node set and the target node are formed by multiplying A and B, which is the C composed of A and B of the required shortest path. C is also a set, that is,

$$C = A \times B$$
$$= \{(a,b) \mid aEA\alpha beB\}. \tag{29}$$

Among them, the starting node is represented by a_l, the target node is represented by b_l, the Euclidean distance between the two is represented by $E_{a_l b_l}$, and $P_{a_l b_l}$ is the specific value of the shortest path. Through $\lambda_i = P_{a_l b_l}/E_{a_l b_l}$, λ_i can be obtained. Regarding what kind of data is selected, the coefficient size of the specific ratio is obtained, and it is expressed in the form of a set, which is Γ. By studying the elements in it, λ_0 is obtained. Then, at $\lambda_i \le \lambda_0$, the confidence level is 95%. Then, λ_0 is the specific coefficient size, so the size of the major axis can be obtained: $2a = \lambda_0 |st|$.

It can be seen from Figure 12 that s belongs to any element in A, t belongs to any element in B, $\lambda = P_{st}/E_{st}$, and the shortest path between s and t is represented by P_{st}, which is $s \longrightarrow v_1 \longrightarrow v_2 \longrightarrow v_3 \longrightarrow \cdots \longrightarrow t$. The Euclidean distance between s and t is denoted by E_{st}. In the process of calculating λ, E_{st} is divided into segments, the number is n, and any segment is denoted as $E_{st1} = E_{st2} = \cdots = E_{st} = E_{stn} (i = 1, 2, 3, \ldots, n)$. According to the situation of segmentation, P_{st} is also segmented, the number is also n, and any segment is $P_{st1} = P_{st2} = \cdots = P_{sti} = P_{stn} (i = 1, 2, 3, \ldots, n)$, and there is $P_{sti} = E_{sti}/\cos \theta_i$.

The calculation process of λ is
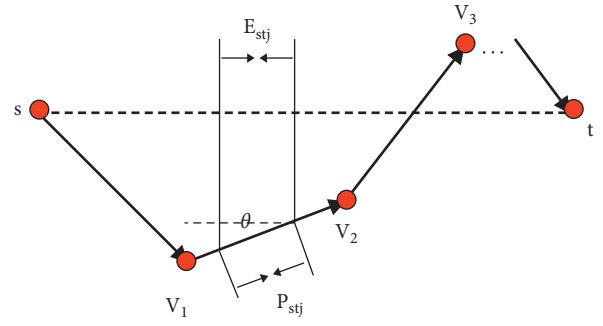
FIGURE 12: Schematic diagram of the research on the rule of λ value.

$$\begin{aligned}
\lambda &= \frac{P_{st}}{E_{st}} \\
&= \frac{P_{st1} + P_{st2} + \cdots + P_{sti} + \cdots + P_{stn}}{E_{st}} \\
&= \frac{1}{n}\left(\frac{1}{\cos \theta_1} + \frac{1}{\cos \theta_2} + \cdots + \frac{1}{\cos \theta_n}\right) \\
&= \frac{1}{n}\sum_{i=1}^{n}\frac{1}{\cos \theta_i}.
\end{aligned} \tag{30}$$

In urban roads, θ_i generally takes a value on $[0, \pi/4]$. The following three cases discuss the value of λ:

(1) If s and t have a relatively close distance, n has a smaller value. In order to prevent the shortest path from being found in the search range and to ensure that all valid nodes are included in the ellipse range, the maximum value of λ can be selected at this time.

$$\begin{aligned}
\lambda_{\max} &= \frac{1}{n}\sum_{i=1}^{n}\frac{1}{\cos \theta_i} \\
&= \frac{1}{n} \cdot n\sqrt{2} \\
&= \sqrt{2}.
\end{aligned} \tag{31}$$

(2) If s and t have a very long distance, n is infinite. On $[0, \pi/4]$, θ_i conforms to a uniform distribution, then λ is

$$\begin{aligned}
\lambda_{\infty} &= \int_0^{\frac{\pi}{4}} \frac{1}{\cos \theta}\frac{4}{\pi}d\theta \\
&= \frac{4}{\pi}\ln|\sec \theta + \tan \theta|\Big|_0^{\frac{\pi}{4}} \\
&= \frac{4}{\pi}\ln(\sqrt{2} + 1) \\
&\approx 1.122.
\end{aligned} \tag{32}$$

(3) If s and t have a longer distance, n has a larger value, and λ basically conforms to the normal distribution, then $N(\mu, \sigma^2/n)$, and the specific formula is

$$
\begin{aligned}
\mu &= E\left(\frac{1}{\cos \theta}\right) \\
&= \int_0^{\frac{\pi}{4}} \frac{1}{\cos \theta} \frac{4}{\pi} d\theta \\
&\approx 1.122,
\end{aligned}
$$

$$
\begin{aligned}
\sigma^2 &= D\left(\frac{1}{\cos \theta}\right) \\
&= E\left(\frac{1}{\cos^2 \theta}\right) - \left[E\left(\frac{1}{\cos \theta}\right)\right]^2 \\
&= \int_0^{\frac{\pi}{4}} \sec^2\theta \frac{4}{\pi} d\theta - \left[\int_0^{\frac{\pi}{4}} \frac{1}{\cos \theta} \frac{4}{\pi} d\theta\right]^2 \\
&= \frac{4}{\pi} - \left[\frac{4}{\pi}\ln(\sqrt{2}+1)\right]^2 \\
&\approx 0.01412.
\end{aligned}
\tag{33}
$$

It can be seen that the larger the value of n, the more normal distribution is obeyed. Therefore, in order to obtain more accurate data results, this paper chooses the ellipse with the largest area, then $\lambda = 1.414$. Moreover, when there is a long distance between s and t, when the study is conducted from the perspective of normal distribution, according to the confidence level query, the confidence level reaches 95%.

The performance analysis of the ellipse search algorithm is as follows:

(1) Algorithm validity analysis

In this regard: the main focus of attention is running time. The search range of the Dijkstra algorithm before optimization is

$$
\begin{aligned}
S_{\text{Diksrva}} &= \pi r^2 \\
&= \pi\left(\frac{\lambda+1}{2}|st|\right)^2.
\end{aligned}
\tag{34}
$$

The search range of the ellipse restricted area algorithm is

$$
\begin{aligned}
S_{\text{llipse}} &= \pi ab \\
&= \pi \frac{|st|}{2} \frac{\sqrt{(x^2-1)|st|}}{2}.
\end{aligned}
\tag{35}
$$

(2) Reliability analysis of the algorithm

The so-called reliability is to ensure that the path found belongs to the shortest path.

In a specific road network, nodes do not exist alone and have strong connectivity. There are basically paths connected between two points. If there is a small straight-line distance between the starting node and the target node, it will have a relatively small distance. The traversal range is small, and the path to China Unicom may not be found. In order to avoid this problem, in the research process of this paper, the eccentricity selected by the ellipse algorithm is the largest, that is, the ellipse area is the largest.

In summary, in the case of $\lambda = 1.414$, the confidence level is 95%, that is, only 5% may not be able to find the required shortest path.

(3) Algorithm applicability analysis

In the application process of the ellipse search algorithm, the search range is limited, the work efficiency is improved, and the traversal time is reduced. However, in order to make it clear that all newly appearing nodes are within this range through this method, it is necessary to perform many operations of product and square root extraction, so it takes a lot of time.

The algorithm flow is

The first step is to initialize the data. The algorithm clarifies s and t and calculates the straight-line distance $|st|$ between them based on their latitude and longitude calculations.

The second step is to define the ellipse area. The focus is s and t, $\lambda = 1.414$, from which the eccentricity can be known, and the elliptical area can be obtained.

The third step is to select the breadth-first search method to find the node and compare the value of the sum of the Euclidean distance between the node to b and t with the length of the long axis of the ellipse. If $|sv_1| + |v_1t| < 2a$, then this node is included in the area.

The fourth step is to find the shortest path st in the ellipse interval using Dijkstra's algorithm and then terminate the algorithm.

Through the understanding of the algorithm of the ellipse restricted search area, it is found that the calculation process has a slower speed, takes more time, and has lower work efficiency. Therefore, the algorithm is analyzed and researched. In the calculation process of the rectangular restricted search area algorithm, the required result can be obtained without a lot of calculation, and it has a good effect. The algorithm mainly calculates the circumscribed rectangle of the ellipse area and treats it as a restricted search area, so it achieves the effect of reducing the calculation amount of the algorithm.

The specific content is shown in Figure 13. s is the starting node, t is the target node, and the ellipse equation can be described by s, t, λ. In this process, in order to make the calculation easier, the center of the ellipse is assumed to be the origin of the coordinates, and the two focal points of
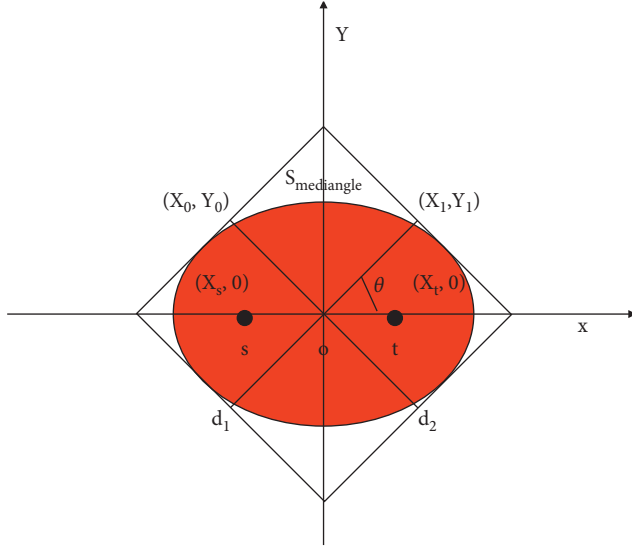
FIGURE 13: Schematic diagram of ellipse algorithm coordinates.

FIGURE 14: Comparison of ellipse and rectangular restricted areas.

the ellipse are above the g axis, then the coordinates $(-x_s, 0)$ of s and the coordinates $(x_t, 0)$ of m are obtained, and $x_e = x_t = c$.

The elliptic equation is

$$\frac{x^2}{a} + \frac{y^2}{b} = 1. \tag{36}$$

The parametric equation is

$$\begin{cases} x = a \cos \theta \\ y = b \sin \theta \end{cases} (\theta \in [0, 2\pi]) \tag{37}$$

In the above formula, $c^2 + b^2 = a^2, a = \lambda c$.
The elliptic equation is used to derive the derivative of x:

$$y' = -\frac{b^2}{a^2} \frac{x}{y}. \tag{38}$$

As shown in Figure 13, when a point (x_0, y_0) is taken, the tangent equation is

$$y = -\frac{b^2}{a^2} \frac{x}{y} (x - x_0) + y_0. \tag{39}$$

When $m = -b^2/a^2 x_0/y_0$, the tangent equation is

$$y = mx \pm \sqrt{a^2 m^2 + b^2}. \tag{40}$$

Then the distance between the two tangents is

$$d_1 = \frac{2\sqrt{a^2 m^2 + b^2}}{\sqrt{m^2 + 1}}. \tag{41}$$

As shown in Figure 14, we take a point (x_1, y_1) and its tangent is

$$y = -\frac{1}{m} x \pm \sqrt{\frac{a^2}{m^2} + b^2}. \tag{42}$$

Then the distance between the two tangents is

$$d_2 = \frac{2\sqrt{a^2 + b^2 m^2}}{\sqrt{m^2 + 1}}. \tag{43}$$

If the ellipse has a circumscribed rectangle with the smallest area, then the formulas (38) and (40) can be used to obtain $S_{rectangle}$:

$$S_{rectangle} = d_1 \cdot d_2 = \frac{4\sqrt{a^2 m^2 + b^2} \cdot \sqrt{a^2 + b^2 m^2}}{m^2 + 1}. \tag{44}$$

It can be seen from the above formula that if m^2 is equal to 0, that is, in the case of $m = 0$, the ellipse has a circumscribed rectangle with the smallest area. If the tangent line passes through (x_0, y_0), it is parallel to the axis, and if the tangent line passes through (x_1, y_1), it is parallel to the axis.

If $m = 0$, that is, in the case of $\theta = k\pi/2 \, (k = 0, 1, 2, 3, \ldots)$, the area of the rectangle is the minimum:

$$S_{rectargle} = 4ab = 4\lambda\sqrt{\lambda^2 - 1}|st|^2. \tag{45}$$

If $m = 1$, that is, in the case of $\theta = \pi + 2k\pi/2 \, (k = 0, 1, 2, 3, \ldots)$, the area of the rectangle is the maximum:

$$S_{rectargle} = 2(a^2 + b^2) = 2(2\lambda^2 - 1)|st|^2. \tag{46}$$

It can be seen from Figure 14 that the figure can be obtained as a standard ellipse rotation. The rotation angle is θ, and it translates x_c and y_c in the x and y directions, respectively. The elliptic equation can be obtained by the coordinate values of s and t:

$$\frac{[(x - x_c)\cos \theta + (y - y_c)\sin \theta]^2}{a^2}$$
$$+ \frac{[-(x - x_c)\sin \theta + (y - y_c)\cos \theta]^2}{b^2} = 1. \tag{47}$$

In the above formula, $c^2 + b^2 = a^2$, $x_c = x_s + x_t/2$, $y_c = y_s + y_t/2$, $\theta = \arctan y_t - y_s/x_t - x_s$. x and y:

$$x_m = x_c \pm \sqrt{a^2 \cos^2 \theta + b^2 \sin^2 \theta}, \qquad (48)$$
$$y_m = y_c \pm \sqrt{b^2 \cos^2 \theta + a^2 \sin^2 \theta}.$$

By reduction, the boundary of the rectangular area is obtained:

$$x_m = x_c \pm |st| \sqrt{\lambda^2 - \sin^2 \theta}, \qquad (49)$$
$$y_m = y_c \pm |st| \sqrt{\lambda^2 - \cos^2 \theta}.$$

Then, the area of the rectangular area is $S_{\text{rectargle}} \in [4ab, 2(a^2 + b^2)]$

Performance analysis of rectangle search algorithm:

3.4.1. Algorithm Validity Analysis. If the area of the rectangle is the smallest, the ratio of the search area of the rectangle and the ellipse is

$$\frac{S_{\text{rectargle}}}{S_{\text{ellipse}}} = \frac{4ab}{\pi ab} \approx 1.27. \qquad (50)$$

If the area of the rectangle is the largest, the ratio of the search area of the rectangle and the ellipse is

$$\frac{S_{\text{rectangle}}}{S_{\text{ellipse}}} = \frac{2(a^2 + b^2)}{\pi ab}$$
$$= \frac{4\lambda^2 - 2}{\pi \lambda \sqrt{\lambda^2 - 1}}. \qquad (51)$$

3.5. Parking Space Reservation Module. After the user finds the target parking lot, he may need to make a parking space reservation. Generally speaking, there are two ways to make a reservation: reserve a parking lot or reserve a parking space. The following is an analysis of possible reservation methods: (1) reserve a parking lot with precise reservation: if the reservation method provided to the parking lot of the parking lot means that it cannot fully guarantee that the user will leave a space for reserved vehicles after driving to the parking lot. Therefore, scientific traffic forecasting is required to ensure that a certain number of reserved vehicles arrive at the time of arrival. It can also guarantee a certain parking space. The calculation process of this method is too complicated, and for the peak parking period, the supply is often in short supply. Therefore, it is difficult to realize the reservation behavior of reserved parking. Fuzzy reservation: the parker makes a reservation for a fixed parking time. The parking lot guarantees that the parking space is free at the scheduled time and will not be illegally occupied. In order to ensure the above effects, it is necessary to ensure that there is a certain amount of vacant parking spaces that can be turned over. The berth cannot be used at the highest efficiency. (2) Precise reservation of the reserved parking space: the parking space and the start and end time are accurately reserved by the parker. The system needs to have parking space status detection equipment and parking space occupancy equipment. But for CBD commercial buildings, hospitals, and other areas, parking behavior is of high frequency and changeable. A parking person may delay parking and affect the next scheduled parking person to park the vehicle. Therefore, this kind of contradiction is difficult to solve, so stop. Accurate prediction of the position is not feasible. Fuzzy reservation + precise reservation: fuzzy means that you do not book an accurate parking start time, and precision means that the object of pleasure is the parking space. When a parker chooses a predetermined behavior, the general understanding is that the parker is worried that it is difficult to find a parking space within the arrival time or that the parking space best meets the user's expectations and wants to book in advance. Therefore, the system adopts this method. Specifically, the user has reserved a parking space in a parking lot, and since the reservation, the user's billing starts. In order to balance the user's affordability and the parking revenue, the reservation fee is set as 50% parking fee, the strategy can be optimized in the future, such as different charging standards in different time periods. In summary, only the fuzzy reservation + precise reservation mode for parking spaces is suitable for this system. Parkers can decide whether to reserve a parking space based on the predicted number of empty parking spaces mentioned in the previous chapter and their own needs. If there is a reservation in this mode, the reservation function can be designed with reference to the reservation business process, as shown in Figure 15:

When the user clicks on a parking lot in the reservation module, he enters the parking space reservation details page. The module has a parking space map of the parking lot, and the parking space map indicates the best parking space recommended by the system. The most important factor in the problem of the best parking space in the parking lot is the parking distance, which can be regarded as the shortest path problem (other factors have a weak influence and are not considered for the time being). That is to find the minimum value of stopping distance + driving distance away, so the shortest path algorithm is used to calculate the parking space and guidance path of the shortest path. This module can greatly improve the decision-making efficiency of parking seekers.

Suppose the entrance of the parking lot is E and the exit is S. If a certain free parking space is Pi ($i = 1, 2, \ldots, n$), the shortest path corresponding to the entrance process is $\text{path}(E, P)$, and the shortest path corresponding to the exit process is $\text{path}(p_i, s)$.

Then the entire shortest path length corresponding to the parking space is $d_{\text{path}}(E, p_i) + \text{path}(p_i, s)$

The shortest path length corresponding to the best parking space can be described as $\min\{d_{\text{path}}(E, p_1) + \text{path}(p_i, s), d_{\text{path}}(E, p_2) + \text{path}(p_2, s), \ldots, d_{\text{path}}(E, p_n) + \text{path}(p_n, s)\}$.

In other words, the core of this algorithm is to find the point and path of the minimum value of $d_{\text{path}}(E, p_i) + \text{path}(p_i, s)$.
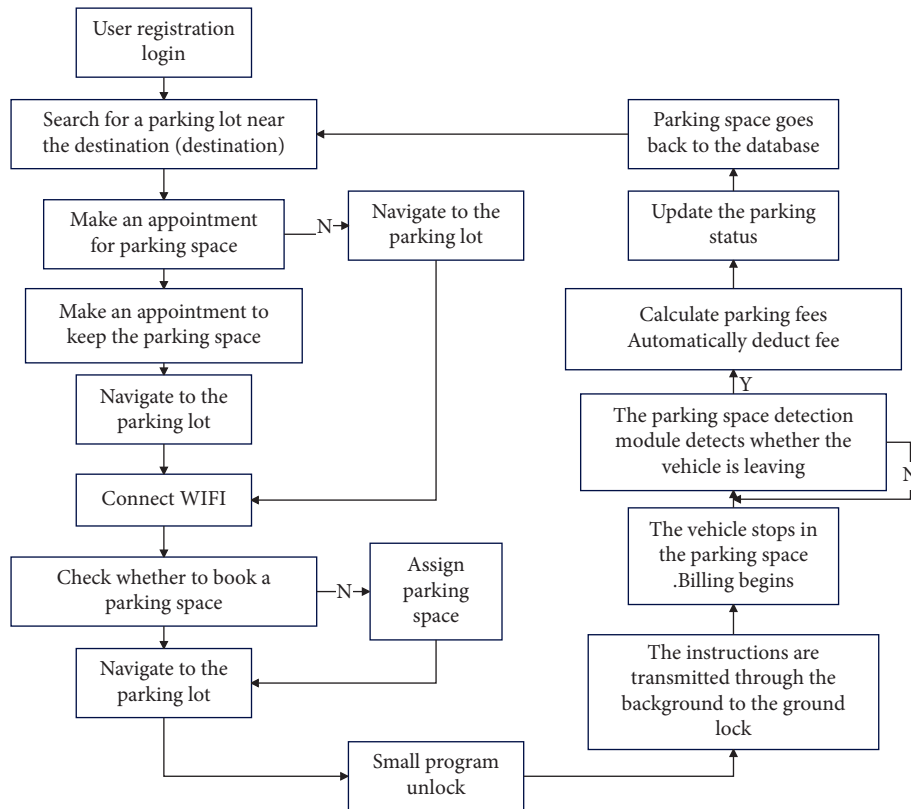
FIGURE 15: Business process of parking space reservation.

4. Development and Design of System Software

Based on the design of the above-mentioned multisource traffic information collection and combination algorithm, the intelligent multisource traffic information collection combination optimization model is designed for the network design and software design of the multisource traffic information collection combination optimization model, to carry out the network design of multisource traffic information collection combination optimization mode. ZigBee network technology is used to build a three-layer structure model of multisource traffic information collection and optimization model, and ITU-TH.323 and IETFSIP network signaling is used for multisource traffic information collection combination optimization model network control, to design human-computer interaction module, to realize multisource traffic information collection combination optimization mode human-computer interaction response design, an to build in a single network environment multisource traffic information fusion and information dispatch center (Figure 16).

In the MVB bus control protocol and embedded environment, the software development and design of the multisource traffic information collection combination optimization model is realized, and the ZigBee, GPRS, and other network technologies are used to carry out the network design of the multisource traffic information platform. Under the B/S structure system, the network design of the multisource traffic information collection combination optimization model is carried out, the process management and bus scheduling are carried out under the MVB bus control protocol, the Sip protocol stack is used to establish the session protocol of the multisource traffic information platform, and SIP is called. The call interface is used to create an INVITE message, and the data source is wrote to the multisource traffic information collection and combination optimization model DataSet. during Web programming, ADO. NET is used to query, update, and database management of the large-scale multisource traffic information collection and optimization model. Through the above analysis, the software development and design of the system can be realized.

The intelligent parking lot management system designed in this paper is mainly composed of parking lot server and mobile phone client. Communication methods include network communication based on TCP/IP protocol, Bluetooth communication, and Wi-Fi communication. The server uses a PC with Window 10 operating system as the socket communication and data storage device, responsible for socket communication with the mobile phone, and manages user information and parking lot information; adopts the ARM 6410-based development board as the core control of Bluetooth communication module, expand the Bluetooth module outwards, responsible for Bluetooth communication with mobile phones; use Wi-Fi routers to establish a local area network to simulate network communication between users and servers; and simulate the scene of opening the door when
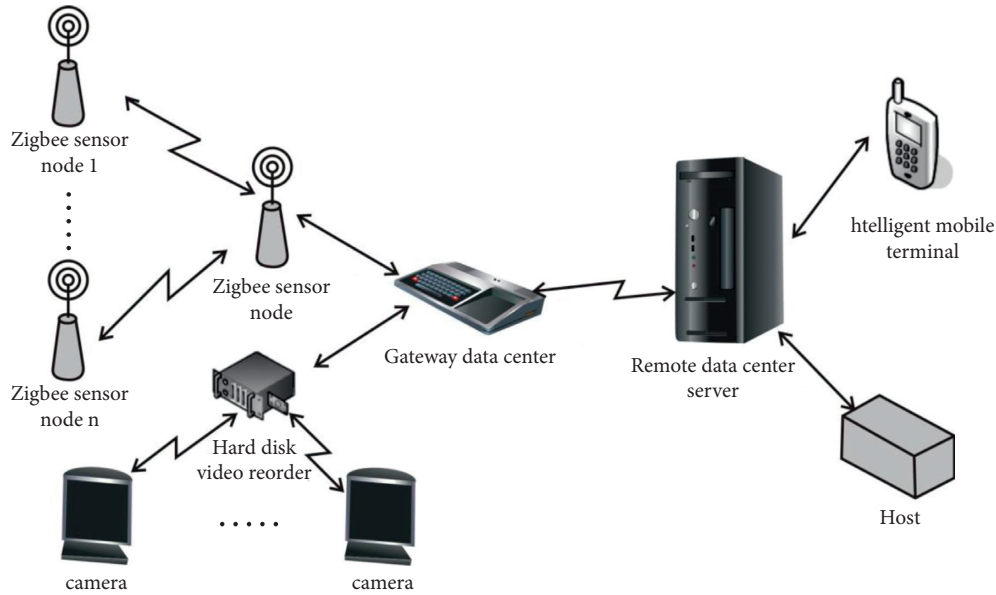
Figure 16: System network networking design.

users arrive at the entrance of the parking lot. The mobile client uses a smartphone with Android operating system, equipped with Wi-Fi function, Bluetooth function, and GPS positioning function, etc. The Wi-Fi function is used to detect Wi-Fi signals and communication within the local area network. The Bluetooth function is used to communicate with Bluetooth nodes in the parking space. GPS positioning is used to query the current position. The SDK provided by Baidu Maps gives the distance from the current position to the parking lot. The SDK provided by Baidu Maps gives the driving route from the current location to the entrance of the parking lot. The overall architecture of the intelligent parking lot guidance system designed in this paper is shown in Figure 17.

In order to prevent data loss during the communication process between the user and the server, this design adopts a connection-oriented and reliable TCP/IP protocol, and the communication process is implemented through the socket interface. The function of socket is mainly to provide an interface for data transmission between two different programs. Users only need to know the IP address and port of the server to establish a connection with the server and perform network communication. The workflow is shown in Figure 18.

In this design, the user's mobile phone first accesses the LAN Wi-Fi and automatically obtains an IP address. Establish a connection with the server through the server's IP address and port. The establishment of each connection requires the server to open a new socket thread to receive the registration, login, query, appointment, and other requests sent by the client to the server after the server receives the request, Through the operation of inserting and modifying the database, realize the functions of user registration and appointment; through the query operation to verify the correctness of the user information. The server returns the request result to the user through the user's IP address, as shown in Figure 19.

In this design, an independent Bluetooth node is installed in each parking space, and the Bluetooth node and the parking number are bound one-to-one and stored in the database. When the user receives the parking space address from the server, the Bluetooth on the mobile phone is automatically turned on and starts to detect the Bluetooth address on the parking space. Since the distance of Bluetooth communication is only within 10 m, when the user's car reaches the parking space, the pressure sensor detects the pressure signal. After turning on the Bluetooth module, the mobile phone Bluetooth can search for the address of the Bluetooth module, which can ensure that the user will park the car in the correct parking space and will not match the Bluetooth in other parking spaces. The Bluetooth matching process adopts an automatic matching method. Automatic matching requires program control on the mobile phone. This can reduce the user's operation on the mobile phone and improve the safety of the user's driving. The Bluetooth composition block diagram of this system is shown as in Figure 20.

Figure 21 is a schematic diagram of the entrance to the parking lot. According to the data, there is a negative correlation between Wi-Fi signal strength and distance. As shown in the figure, the distance between the user's mobile phone and Wi-Fi is equal to the distance between the cars plus the length of the car, and the distance between the first car and the second car from the Wi-Fi is one car length plus the distance between the cars. Generally, the length of a family car on the market is about 4 meters to 5.5 meters. The signal strength difference caused by this distance difference is huge. Therefore, it is not possible for two users to detect the same Wi-Fi signal strength.

The entire urban parking process can be represented as a circular ecosystem, as shown in Figure 22, which consists of three parts and two processes. Among them, the three parts are parking users, parking lots, and parking space recommendation systems. Contains the following entities,
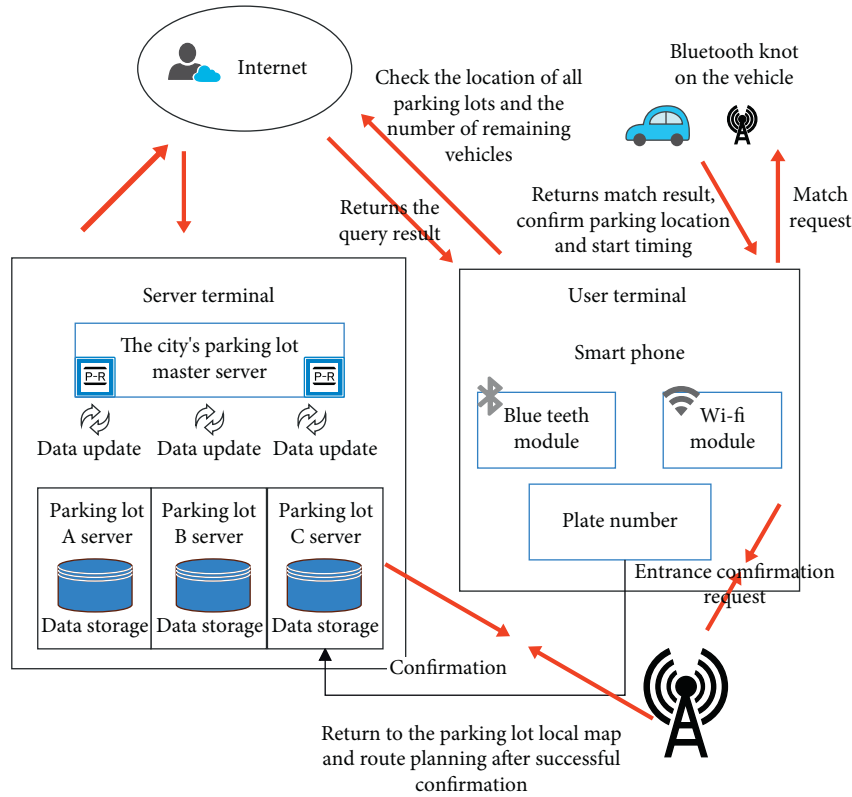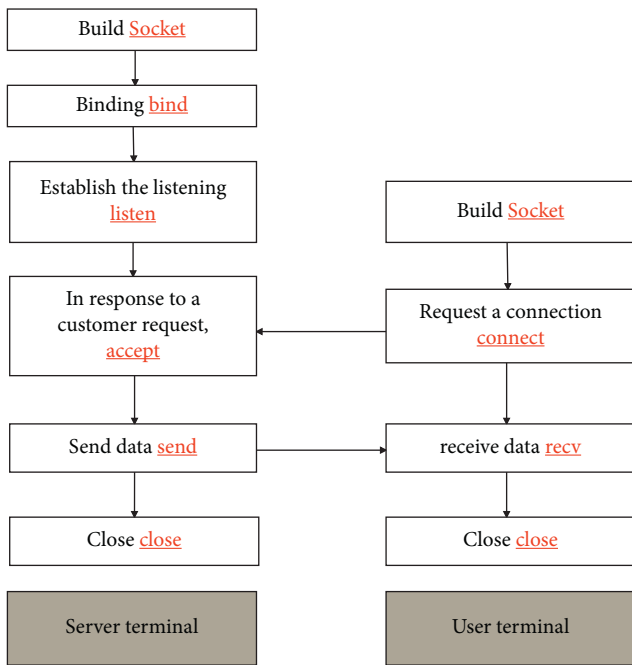
Figure 17: Overall system architecture.
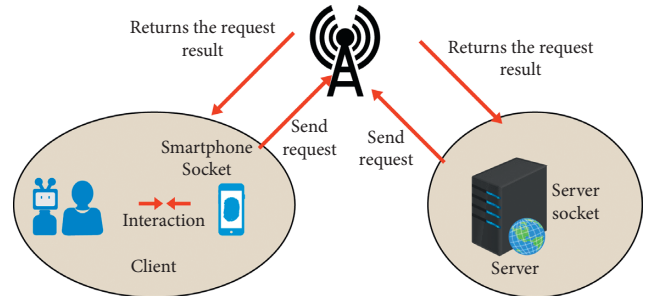

Figure 18: TCP/IP protocol workflow.

Figure 19: Schematic diagram of client accessing server.

parking drivers, vehicles, and various sensors on them, parking lot management systems and parking space detection equipment, and parking space recommendation

systems. The two processes are data flow and traffic flow. The traffic flow occurs on the road where the driver is looking for a parking space and when the vehicle arrives or leaves the parking lot, which is represented by the yellow double-headed arrow in Figure 22; the data flow occurs during parking. The process of interaction between the user and the parking lot and the parking space recommendation system is represented by a black arrow in Figure 22. The parking space sensor or parking lot management system installed on the roadside uploads the collected real-time parking space data to the parking space recommendation system. The driving vehicle uploads its real-time position, speed, and other status data, and the parking space recommendation system processes the data into effective information, release information on the availability of parking spaces in each parking lot, drivers can obtain the
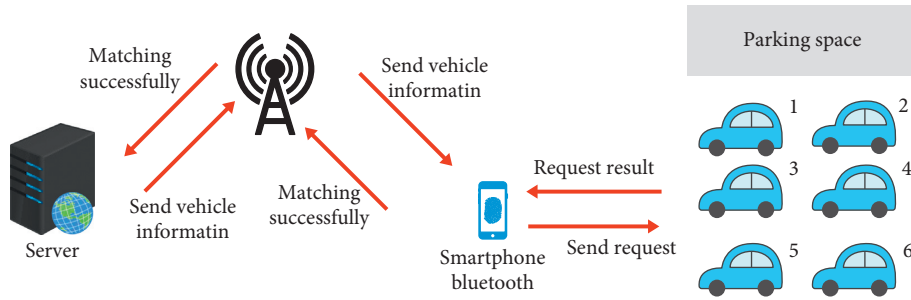
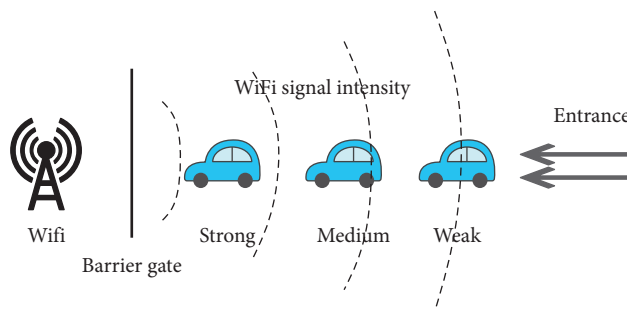FIGURE 20: System Bluetooth composition block diagram.

FIGURE 21: Wi-Fi signal diagram at the entrance of the parking lot.
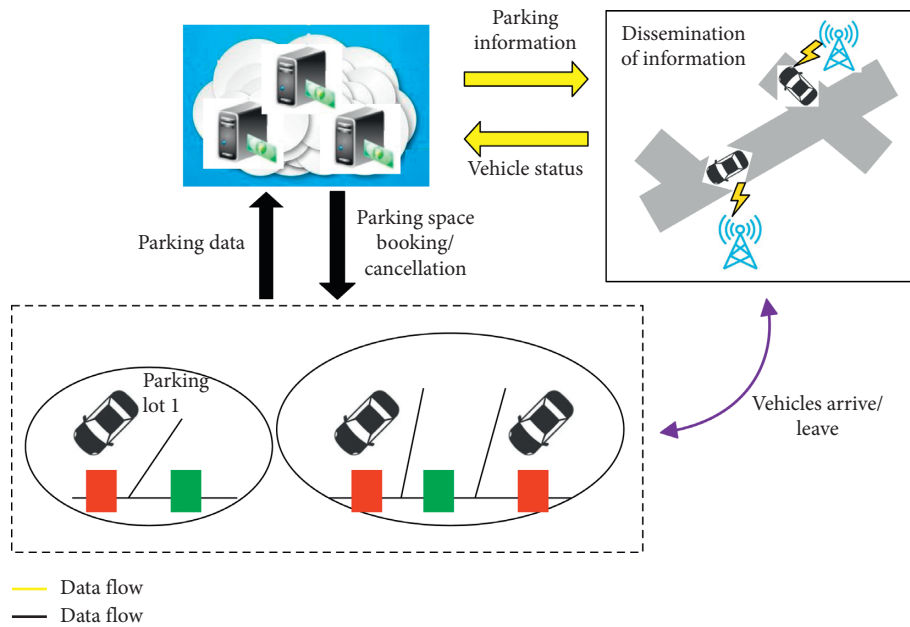

FIGURE 22: Urban parking process.

latest parking information from smart terminals that exchange information with base stations and other transceiver platforms, and turn to the parking area they want, and then park. When the vehicle arrives or leaves the parking space, the parking space sensor updates the parking space available information and uploads the information to the driver looking for the parking space through the intelligent terminal. Considering that when there are many drivers looking for parking spaces in a certain area, they can all receive parking space availability information. It is very likely that competition for a certain free parking space resource will result in parking conflicts. Therefore, the system should have a reservation mechanism. The reservation mechanism includes the reservation of free parking spaces, the cancellation or recycling of reservation orders, etc. The reservation operation causes data flow between the driver, the parking lot, and the parking space recommendation system.
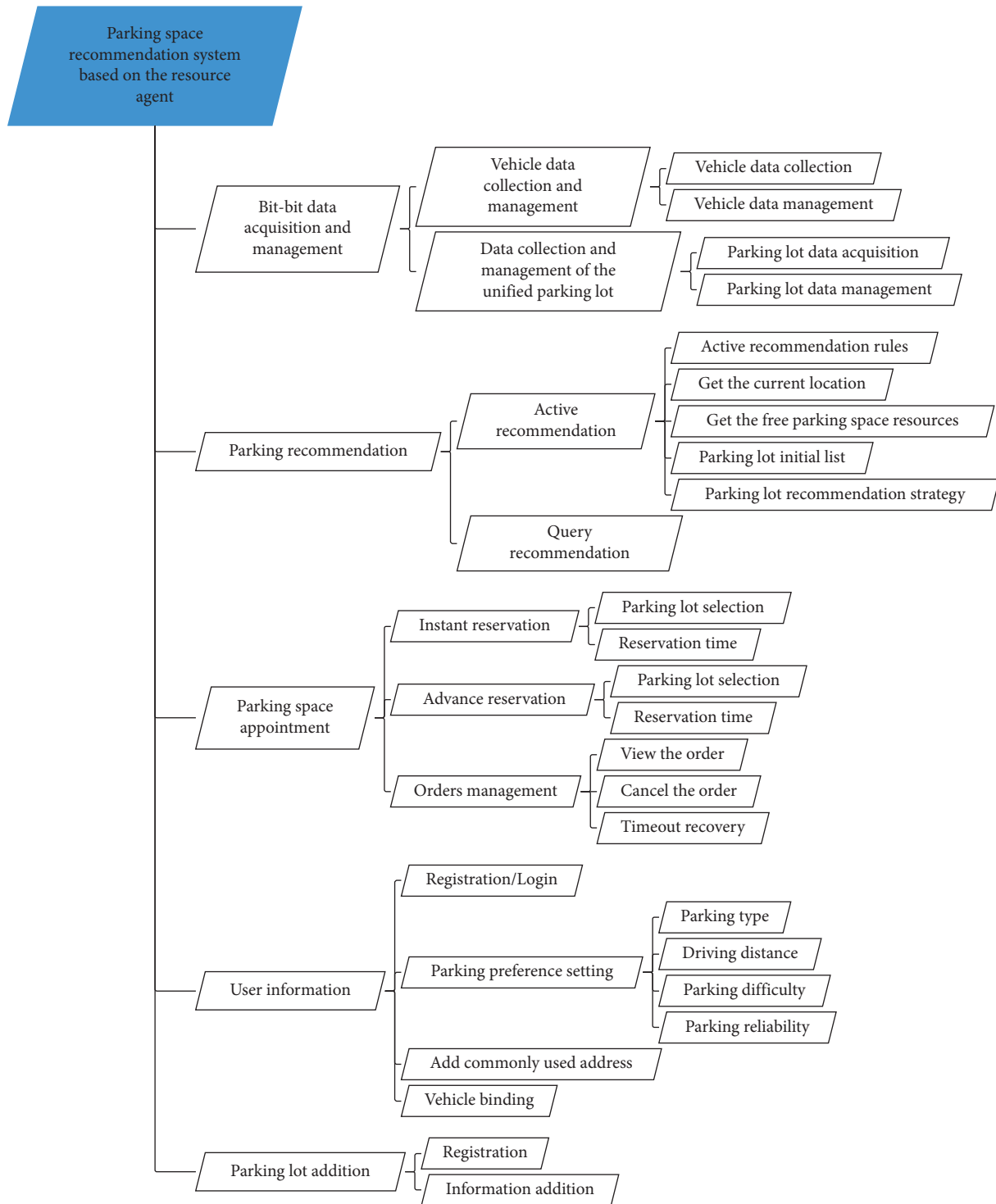
FIGURE 23: System data function structure.

TABLE 1: System parameter settings.

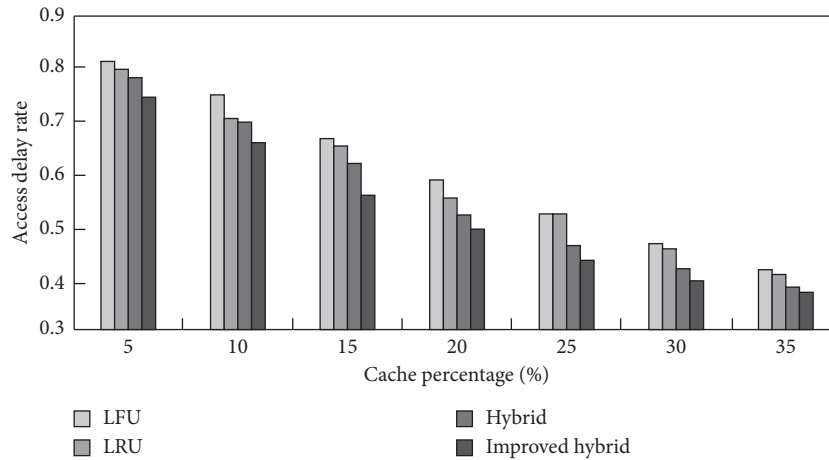| Dispatching data	Number of tasks	Percentage of dynamic traffic collection combination (%)
33	1–6	55
41	4–33	44
51	33–51	33
56	51–61	21

FIGURE 24: is the access delay rate of the traffic information collection combination in various cache percentages.
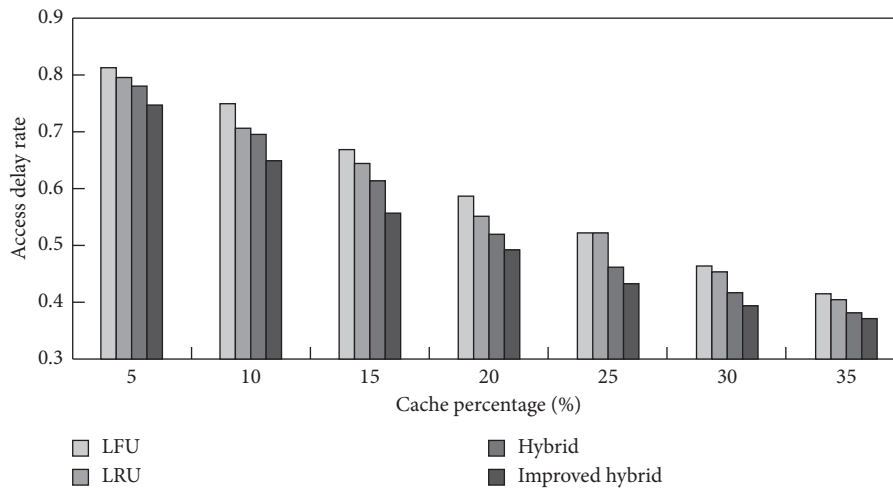

FIGURE 25: Access delay rate of traffic information collection combinations under various data sizes.

Recommending suitable parking lots and parking spaces for drivers with parking needs so that they can quickly find their own satisfactory parking spaces is the original intention of this research. From the above analysis and combined with the driver user use case diagram, it can be seen that the parking space recommendation system must have parking lot recommendation, parking space reservation, and order management after reservation. However, the realization of a parking application software for driver users requires some other functions, such as system login/registration, user information addition, etc. to be more complete. In addition, the analysis of the circular ecosystem formed by the above-mentioned urban parking process shows that the realization of the parking space recommendation system requires two key steps, namely, real-time data collection and management and parking-related services. Real-time data collection and management includes the collection and management of parking space data and vehicle data. Among them, data collection is the basis for the system to provide parking-related services. However, due to the different parking detection technologies used in the current parking lot, the parking lot application has not been unified. There is no unified standard for the data interface and exchange mechanism. The heterogeneity of parking space data makes the current parking application have a strong closedness, which has great limitations in data collection and use, and it is impossible to obtain more information. Comprehensive parking information provides users with good parking recommendations. At the same time, there are many types of user vehicles, and there are many types of sensors on them. Even sensors of the same type may have different data formats and transmission methods among vehicles, making it difficult to use vehicle data. The system needs to provide a processing method for raw data so that various heterogeneous data can be represented in the same way to support parking-related services. Therefore, the system should also have real-time data collection and management functions. In summary, the functions of the parking space recommendation system based on resource agents in this subject are proposed. The system function structure is shown in Figure 23.

5. Simulation Experiment and Result Analysis

In order to test the application performance of the combined optimization model for multisource traffic information collection designed in this paper, software debugging and simulation experiments are carried out. The multisource traffic information collection combination optimization model provides users with a simple and unified system call interface. The packet size is set to 24 kB/s, the weighting factor $w = 2.19$, the traffic information collection time is 1025, and the size of combined sequence training group is 2100 parameters.

According to the analysis results in Table 1, multisource traffic information collection is combined, as shown in Figure 24, to test the access delay rate of traffic information collection combinations in various cache percentages.

According to Figure 24, the access delay rate of the traffic information collection combination using this method is low. The delay rate of the traffic information collection combination of various data scales is tested, and the test results are obtained as shown in Figure 25.

After analyzing the above simulation results, it is found that using this method, the combined accuracy of multisource traffic information collection is high, the degree of information fusion is improved, and the delay is low.

6. Conclusions

In this paper, the combination ability of dynamic traffic information is improved. According to the improved information data, on the basis of collecting multisource traffic information, an information data processing system is developed combined with genetic algorithm. The multidimensional nonlinear joint statistical methods can be used to multiperform multidimensional feature space combination in the complex traffic network environment. In order to construct a multisource traffic information combination model, the genetic algorithm can be used to effectively collect the original traffic data information. According to the high-dimensional feature quantity, the obtained multisource traffic information is fused and combined to carry out the distributed clustering of traffic information and the effective control of fuzzy directivity constraints. Finally, the combined optimization model of traffic information collection has a high degree of intelligence, accurate information collection, and low delay in this paper.

Data Availability

The labeled data set used to support the findings of this study are available from the corresponding author upon request.

Conflicts of Interest

The authors declare no conflicts of interest.

Acknowledgments

References

[1] R. Zhang, P. Ge, X. Zhou, T. Jiang, and R. Wang, "An method for vehicle-flow detection and tracking in real-time based on Gaussian mixture distribution," *Advances in Mechanical Engineering*, vol. 5, no. 11, pp. 1–8, 2013.

[2] W. Shi and Y. Liu, "Real-time urban traffic monitoring with global positioning system-equipped vehicles," *IET Intelligent Transport Systems*, vol. 4, no. 2, pp. 113–120, 2010.

[3] F. Claude, Y. Wang, L. Leena, K. Elina, V. Jenni-Mari, and A. Petteri, "Empirical modeling of spatial 3d flow characteristics using a remote-controlled adcp system: monitoring a spring flood," *Water*, vol. 7, no. 12, pp. 217–247, 2015.

[4] W. Guan, X. Chen, M. Huang, Z. Liu, Y. Wu, and Y. Chen, "High-speed robust dynamic positioning and tracking method based on visual visible light communication using optical flow detection and bayesian forecast," *IEEE Photonics Journal*, vol. 10, no. 3, pp. 1–22, 2018.

[5] Y. Yin, H. Wang, Y. Gao, and X. Li, "Real-time monitoring and early warning of landslides at relocated wushan town, the three gorges reservoir, China," *Landslides*, vol. 7, no. 3, pp. 339–349, 2010.

[6] J. Y. Chen, C. W. Young, and C. Ay, "Design of a single-cell positioning controller using electroosmotic flow and image processing," *Sensors*, vol. 13, no. 5, pp. 6794–6811, 2013.

[7] M. Laumen, T. Kaufmann, D. Timms et al., "Flow analysis of ventricular assist device inflow and outflow cannula positioning using a naturally shaped ventricle and aortic branch," *Artificial Organs*, vol. 34, no. 10, pp. 798–806, 2010.

[8] M. Zhao and X. Li, "Deriving average delay of traffic flow around intersections from vehicle trajectory data," *Frontiers of Earth Science*, vol. 7, no. 1, pp. 28–33, 2013.

[9] R. Kanan, O. Elhassan, and R. Bensalem, "An iot-based autonomous system for workers' safety in construction sites with real-time alarming, monitoring, and positioning strategies," *Automation in Construction*, vol. 88, pp. 73–86, 2018.

[10] A. Curtis and R. Sarc, "Real-time monitoring of volume flow, mass flow and shredder power consumption in mixed solid waste processing," *Waste Management*, vol. 131, no. 2, pp. 41–49, 2021.

[11] A. Sharda, J. P. Fulton, T. P. McDonald, W. C. Zech, M. J. Darr, and C. J. Brodbeck, "Real-time pressure and flow dynamics due to boom section and individual nozzle control on agricultural sprayers," *Transactions of the ASABE*, vol. 53, no. 5, pp. 1363–1371, 2010.

[12] K. Terao, Y. Kitazawa, R. Yokokawa, A. Okonogi, and H. Kotera, "Open-access and multi-directional electroosmotic flow chip for positioning heterotypic cells," *Lab on a Chip*, vol. 11, no. 8, pp. 1507–1512, 2011.

[13] F. Sagala and R. T. Bambang, "Development of sea glider autonomous underwater vehicle platform for marine exploration and monitoring," *Indian Journal of Geo-Marine Sciences*, vol. 40, no. 2, pp. 287–295, 2011.

[14] S. Bekhor, T. Lotan, V. Gitelman, and S. Morik, "Free-flow travel speed analysis and monitoring at the national level using global positioning system measurements," *Journal of Transportation Engineering*, vol. 139, no. 12, pp. 1235–1243, 2013.

[15] P. P. Mathai, P. T. Carmichael, B. A. Shapiro, and J. A. Liddle, "Simultaneous positioning and orientation of single nano-wires using flow control," *RSC Advances*, vol. 3, no. 8, pp. 2677–2682, 2013.

Hindawi

Research Article

Research on Voice-Driven Facial Expression Film and Television Animation Based on Compromised Node Detection in Wireless Sensor Networks

Shi-Jiang Wen [1,2] **Hao Wu** [1,3] **and Jong-Hoon Yang**[1]

[1]*Department of Digital Image in Sangmyung University, Seoul 03015, Republic of Korea*
[2]*Department of Xinjiang Art and Sports, Ningbo Childhood Education College, Ningbo 315016, China*
[3]*School of Animation and Digital Arts, Communication University of Zhejiang, Hangzhou 310018, China*

Correspondence should be addressed to Hao Wu; 20030630@cuz.edu.cn

With the continuous development of social economy, film and television animation, as the spiritual needs of ordinary people, is more and more popular. Especially for the development of emerging technologies, the corresponding voice can be used to change AI expression. But at the same time, how to ensure the synchronization of language sound and facial expression is one of the difficulties in animation transformation. Relying on the compromised node detection of wireless sensor networks, this paper combs the synchronous traffic flow between the speech signals and facial expressions, finds the pattern distribution of facial motion based on unsupervised classification, realizes training and learning through neural networks, and realizes one-to-one mapping to facial expressions by using the rhyme distribution of speech features. It avoids the defect of robustness of speech recognition, improves the learning ability of speech recognition, and realizes the driving analysis of facial expression film and television animation. The simulation results show that the compromised node detection in wireless sensor networks is effective and can support the analysis and research of speech-driven facial expression film and television animation.

1. Introduction

With the continuous development of social economy, film and television animation is more and more sought after and favored by many people, especially rural people. It is not only the consumption of spiritual culture but also an embodiment of national culture [1, 2]. The development of artificial intelligence and other technologies has promoted the development of language pronunciation and facial expression, especially to meet different language pronunciation and interaction with different people; that is, language pronunciation is one person, and facial expression is another person [3, 4]. There is a close synchronous relationship between the two, but how to realize the seamless connection between the two and realize that language pronunciation directly drives facial expression is the research focus and difficulty of human-computer interaction under various

modes, and many industry experts have conducted corresponding research [5, 6]. Generally speaking, the driving of facial expression by speech can be mainly through speech pronunciation recognition and other types of recognition. For speech pronunciation recognition, the corresponding eigenvalues are mainly used for analysis, especially for the basic feature units of speech recognition based on factors and syllables. Mature empirical rules drive a whole set and use corresponding eigenvalues to compare corresponding lip shapes. This method is relatively simple and effective, but it is limited by rules. This rule requires manual definition by various experts and is limited to experts' experience and knowledge. Therefore, qualitative analysis is not accurate enough [7, 8]. At the same time, it is very difficult to realize accurate nonqualitative human speech recognition. This requires directly extracting the corresponding speech features and directly mapping them to the specific parameters

of the face. Therefore, this method can not only avoid the problems encountered in speech pronunciation to a certain extent but also effectively realize synchronization and realism [9, 10].

Some scholars proposed to use artificial intelligence and corresponding prediction to realize the training and learning from speech to facial expression and realize the tracking and relative position of facial expression by inputting relevant parameters [11, 12]. In addition, some scholars have proposed to use the relevant methods of neural networks to synthesize vision and speech, realize the recognition and analysis of speech and face motion parameters, and obtain a better feedback effect [13, 14]. Other scholars used the Markov chain for control analysis and introduced speech recognition for driving analysis of facial animation, that is, getting facial expression motion according to corresponding computer vision analysis technology and realizing learning and control facial expression model. This method can effectively solve visual synchronization on the one hand and human motion behavior on the other hand and realize the expression animation of face driven by voice pronunciation, but in the actual application process, there are still many limitations and specificities [15, 16].

In view of these limitations and requirements, this paper introduces wireless sensor network compromised node detection, combs the synchronous service analysis of voice pronunciation and facial expression, uses unsupervised classification technology to accurately analyze the corresponding facial expression, and realizes manual lip shape adjustment through voice level clustering analysis. At the same time, the video motion data can be used to train the voice to drive the face animation model, improve the authenticity and fidelity of the system, reduce the defects of artificial rules, and use the corresponding rhythm to directly add and map to the face pattern to realize the final driving analysis of face expression film and television animation.

2. Compromised Node Detection Method for Wireless Sensor Networks

By comparing the disadvantages and advantages of speech recognition and nonspeech recognition, this paper selects the latter so that neither the discreteness of speech samples nor the parameter mode of speech directly mapped to face motion needs to be considered [17, 18].

Detection using corresponding wireless sensor nodes can be mainly divided into the following steps:

(1) In the whole network, it is necessary to focus on deploying corresponding sensor nodes to ensure that sensor nodes have overlapping coverage. Therefore, it can be predicted that the occurrence or generation of an element may be detected by multiple nodes, and the node of one sensor can also detect multiple behaviors of other adjacent nodes [19, 20].

(2) For ordinary and distributed sensor nodes, they can only have limited ability and communication ability.

(3) For the transmission channel between the node and the base station, it is necessary to abide by the corresponding transmission routing protocol.

(4) For the base station, it is a computing device capable of representing location information.

(5) For the sensor node, it needs to have enough identifiers to represent it. In the whole deployed network, it needs to compromise according to the corresponding nodes.

(6) All messages are time stamped.

(7) The attacker needs to capture the physical address to obtain the corresponding site location and information.

For the base station site, if there are more resources, it is more secure and difficult to overcome. However, it should be noted that the network may transmit false data.

The whole system can be composed of two parts: one is a distributed network site system, and the other is a centralized system running in the so-called related base stations (Figure 1).

The so-called distributed component is relative to the deployment environment of the network. Each copy of its component runs on different network sensor nodes and is synchronized with the relevant transmission protocol and transmission app on the sensor. When each node detects the possible compromised behavior in adjacent nodes, it needs to report to the nearest base station for transmission in time. This detection method needs to rely on adjacent nodes for detection, and each node needs to detect and analyze adjacent nodes. However, due to the characteristics of wireless sensor networks, such deployment saves a certain cost.

For centralized components, they are higher-level computing devices, so it may be necessary to perform more complex behavior analysis to summarize whether there are corresponding compromised behaviors to the center and whether these compromised behaviors are legal. For the corresponding data collected by the whole network, these are collected and analyzed through their own network resources.

2.1. Distributed Component. Each sensor node has a distributed component running on it, which will record the data from adjacent nodes and establish a baseline based on these records. If a neighbor node continues to perform abnormal behavior, it will be identified as a compromised node and reported to the base station.

As shown in Figure 2, if the corresponding node A is attacked and considered by the attacker to imitate another node and if the neighbor node D does not detect A, then node A cannot directly imitate B or C. In this way, the node has enough neighbors to be solid with each other so that any attack and impersonation can be detected in time.

Considering instantaneous errors, such as collisions or other nonmalicious behaviors, ComDet has certain flexibility when determining a node as a compromised node and can tolerate certain abnormal behaviors. When judging whether a neighbor node behaves abnormally, there is no
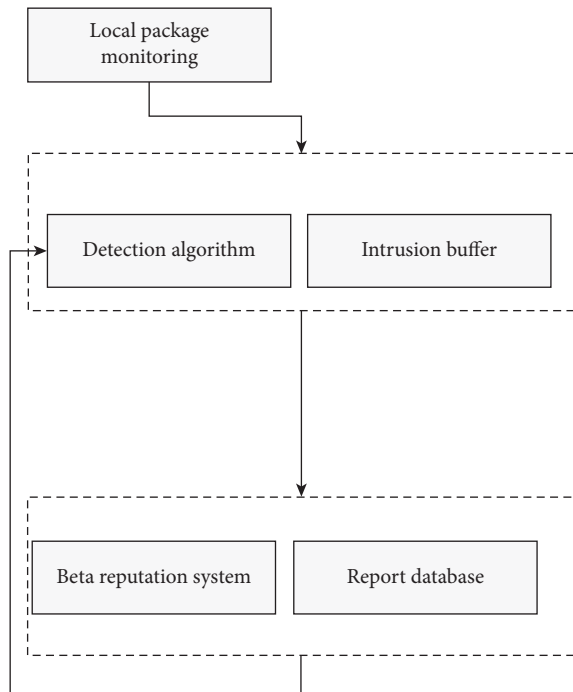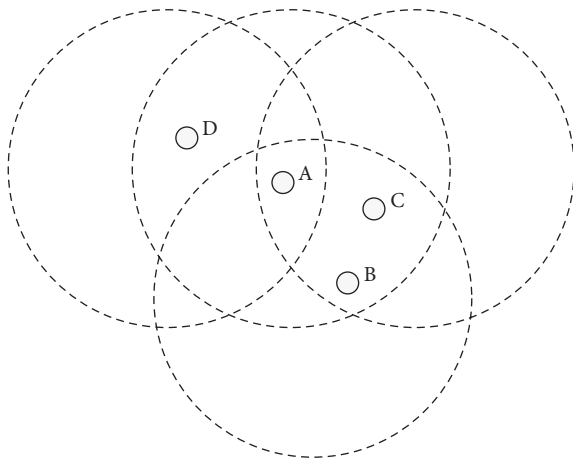
FIGURE 1: Frame structure.

FIGURE 2: If node *a* wants to impersonate any node, it must pass the detection of neighbor nodes.

cooperation between nodes. This independent decision-making process means that the compromised node cannot affect the perspective of the legitimate neighbor node.

2.1.1. Monitoring Indicators. The first step in designing any detection-based security system is to select the characteristics of the system that will be monitored. In order to support most wireless sensor networks, ComDet only monitors some common features of wireless sensor networks.

① Sensor readings: by monitoring sensor readings, attacks that attempt to distort the collected information can be detected.

② Received power: in a static network, the received power should remain unchanged. Fluctuations may be caused by changes in communication hardware or the location of corresponding nodes.

③ Sending rate: most applications read sensor readings and send them periodically. Any routing data packets will also be sent periodically. Therefore, the rate of data packets sent by a node should follow a consistent pattern. Most attacks, such as selective forwarding, Sybil attacks, and replay attacks, will cause measurement bias. In addition, the sudden idle period may be caused by the opponent's reprogramming of the node.

④ Receive rate: the ratio of incoming and outgoing data packets should be constant because the outgoing data packets can only be data packets routed by the node or generated by the node. A neighbor node that changes its receiving rate but does not change its sending rate may be a compromised node. It should be noted that regardless of whether the data is encrypted or not, the header of the data packet can usually be seen by all nodes.

Because most wireless sensor networks have these characteristics, ComDet has a wide range of applicability. However, these features may not be appropriate in two situations: (1) data packets can only be decrypted by the base station; (2) applications rarely exchange information with the base station.

When the confidentiality of information transmitted on the network is very important, the first scenario will appear. Since the compromised node cannot be detected and blocked immediately, some of the information sent may be eavesdropped on by the compromised node. Therefore, the data packet can be encrypted, and only the base station can decrypt it. Under such conditions, the defect of not being able to monitor sensor readings can be compensated by increasing the number of monitored neighbors so that ComDet can achieve corresponding performance by occupying more memory.

The second scenario is caused by the application of nonperiodic communication. For example, wireless sensor networks located in the quarantine zone only send information when an attack is detected, and they will not communicate in a secure environment. Because the monitored information is not sufficient, it is impossible to establish a baseline for most features. ComDet compensates by making the node send its unique identification code at a certain speed. In order to avoid prolonged silence and fail to discover that the node has been conquered by the attacker, a certain amount of communication overhead is necessary. This mode of behavior is only used when the application has very little communication volume.

2.1.2. Detection Algorithm. There are two types of algorithms for detecting abnormal behavior: anomaly detection and rule-based detection. They all use records of monitoring system characteristics. In anomaly detection algorithms, the existing records are first used to establish a baseline, and any

new records that deviate from the baseline to a certain extent are considered abnormal behaviors. On the contrary, rule-based detection requires the establishment of a specific standard. For example, if any two packets have the same header, it means that a replay attack has occurred. In the ComDet system, the main focus is on anomaly detection algorithms to meet ComDet's requirements for flexibility, rule-based algorithms target specific situations, and the rules they use must be updated continuously for each new situation.

ComDet's distributed components can be divided into five algorithms for attack detection: the first four are anomaly detection algorithms, which use network characteristics such as sensor readings, receiving power, sending rate, and receiving rate; the fifth is a rule-based detection algorithm.

For rule-based algorithms, if a node detects that a new neighbor meets the characteristics in the preset rule base based on the received message, it will consider the node to be a compromised node.

For anomaly detection, we need to identify the abnormal behavior. Based on the abnormal behavior of each node, we need to set different buffers, one is the buffer for normal packets, and the other is the buffer for abnormal behavior. When all detected abnormal phenomena are shared in the exception storage, the window is used for sliding analysis and compared with the corresponding limit. If it exceeds a certain security threshold, the data packet is considered abnormal. Abnormal behavior may have certain intrusion behavior, which will also cause the behavior report of the node.

The specific overview of the received power is shown in Figure 3, and the specific calculation equation is shown in the following formula:

$$\text{Power}_{\text{new}} - \text{power}_{\text{max}} > T, \text{if power}_{\text{max}} > \text{power}_{\text{max}},$$
$$\text{power}_{\text{min}} - \text{Power}_{\text{new}} > T, \text{if power}_{\text{new}} > \text{power}_{\text{min}}. \tag{1}$$

Compromised node detection in wireless sensor networks is used to analyze the maximum and minimum interval values of the received power of the packet buffer. When the received power of a new packet exceeds this interval, it is considered that the behavior is abnormal. Therefore, the abnormal data needs to be divided into abnormal packet buffer. After processing, the corresponding abnormal situation processing caused by environmental change is realized.

As shown in Figure 4, it is a conceptual diagram of using transmission power, which is mainly used to calculate the transmission rate of data packets and the transmission rate of data packets. When the ratio of the two rates exceeds the set threshold range, the adjacent neighbor nodes can be considered as compromised nodes.

The algorithm using the reception rate is different only in two aspects.

All the illegal behaviors of a node detected by the anomaly detection algorithm are stored in a shared illegal behavior buffer.

Once the abnormal behavior of a neighbor is detected, the weight of its abnormal behavior is calculated as shown in the following formula:
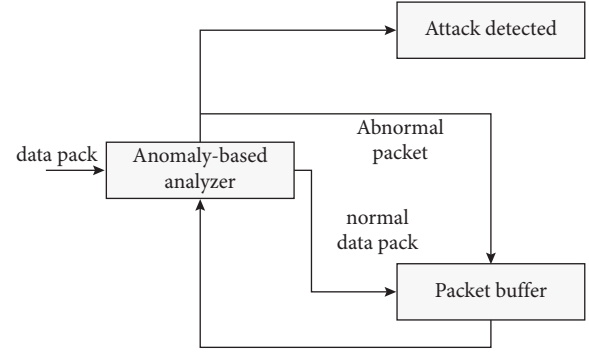

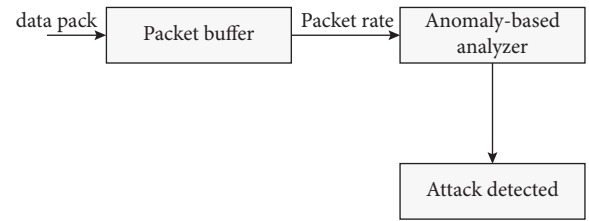Figure 3: Overview of detection algorithms using received power and sensor readings.

Figure 4: Overview of detection algorithm using transmission rate and reception rate.

$$\sum_M \left(t_{\text{current}} - t_{\text{stamp}} \right) + 0.3 \sum_m \left(t_{\text{current}} - t_{\text{stamp}} \right). \tag{2}$$

Once a node determines that a neighbor node a is compromised, it will send three reports about the compromised node to the base pair.

2.2. Centralized Component.
The centralized component runs on the base station and judges whether a reported node is really compromised based on the data from other nodes.

$f(\rho \mid \alpha, \beta)$ can be calculated with Γ function, and its calculation formula is shown in the following formula:

$$f(\rho \mid \alpha, \beta) = \frac{\Gamma(\alpha + \beta)}{\Gamma(\alpha) + \Gamma(\beta)} \rho^{\alpha-1} (1 - \rho)^{\beta-1}, \quad 0 \le \rho \le 1, \ \alpha > 0, \beta > 0. \tag{3}$$

The facial motion parameter FAP (facial animation parameter) defined by MPEG-4 is a set of parameters for realizing facial animation. FAP is based on the subtle movements of the face, and through detailed description and quantification of the actions of various parts of the face model, it can reproduce most natural facial expressions and lip movements. The MPEG-4 standard defines a total of 68 FAPs, including lip shape (viseme) FAP and expression (expression) FAP. For these two FAPs, some basic and different phantoms or expression data are stored in advance, and other phantoms or expressions can be formed by a linear combination of these basic phantoms or expressions. The function of lip shape and expression FAP is to accurately and conveniently express simple lip movements and expressions, but for complex and irregular lip movements and expressions, lip shape and expression FAP are difficult to describe

well. Therefore, in the MPEG-4 standard, in addition to lip shape and expression FAP, it is more convenient for users to describe. For subtle facial movements, general FAP definitions are also given. Generally, FAP is mainly used for movements in a specific area of the face, such as raising eyebrows and moving the upper lip up. The general FAP includes details of each part of the face motion description, which can generate more complete and complex animations than the 14 lip shapes and expression FAP defined by the standard. Therefore, the FAP mode in this paper is based on the general FAP. At the same time, it is different from the basic lip shapes and expressions defined by MPEG4. The FAP model described in this paper does not refer to hypothetical speech perception classification, such as cluster analysis of phonemes or words, but is directly obtained by cluster analysis from a large amount of real image data, so that the results obtained can be used more effectively. In face animation, we assume that all possible face poses belong to a certain state in a high-dimensional space plane, and complex face motion can be regarded as a transition between thousands of states.

Aiming at this diverse and complex face motion trajectory, our learning strategy is to use some FA patterns that can effectively characterize the face motion characteristics or represent a certain set of states to approximate this diversification in segments and then use linear interpolation to glue this segmentation to achieve high-fidelity facial animation. Of course, to achieve voice-driven facial animation, the acquisition of these FAP mode sequences must be obtained through a certain prediction method. At the same time, due to the complexity of face motion, only through the results learned from the large-scale audio and video library can we realize more natural face animation. Manual rules cannot meet the requirements. Because neural networks have better characteristics in processing input and output mapping relations and meet the characteristics of the human brain structure, we use neural networks to learn this mapping relationship.

2.3. System Framework. As shown in Figure 5, it is a specific step of synchronous processing of voice-driven facial animation. Using the corresponding technologies such as computer vision tracking, image processing, and wireless sensor network compromised node detection, the features of corresponding facial parameters and facial animation parameters are extracted from the video and calculated according to the corresponding eigenvalues, and the corresponding patterns are obtained by clustering method. By analyzing the learning context, the mapping relationship of learning is obtained, and the effective analysis and synchronization of speech and face animation are realized.

3. Data Preprocessing

3.1. Speech Signal Analysis. There are many kinds of speech signal processing. How to extract the feature elements in speech recognition is not completely effective for the prediction of facial expression, especially how to achieve synchronization, which is worth thinking and analyzing. Speech pronunciation and face behavior recognition may be related to speech and corresponding feature elements, which can ensure complexity and looseness. In the data preprocessing of this paper, different speech features are used for analysis and processing, and the association of prosody and facial expression in speech is used to obtain the pitch stream and ability analysis in speech segments, which are finally synthesized to form a unique feature vector.

3.2. Video Signal Analysis. In order to uniformly obtain the feature data of facial expression, this paper synchronously tracks many facial expression features, such as corners of the mouth, lips, and nose tip, but it is impossible to track the low texture area. Therefore, for a specific system, to effectively track the key low texture and obtain the coordinates of facial feature points and feature positions of each image, it is very important to form visual feature vectors.

4. Clustering and Learning

4.1. Clustering Algorithm. Different clustering results can be obtained by adjusting the clustering algorithm parameters, such as the desired number of clusters, maximum training times, minimum number of samples per class, separation parameter P, and merging parameter C. These specific parameter values can be changed and calculated by formula (4). The specific results are shown in Figure 6.

$$\text{Error Square}\,(X, Y) = \frac{\sqrt{(X - Y) * (X - Y)^T}}{\|X\|}, \tag{4}$$

where the real data matrix is represented by X, the matrix mapped from real data to category is represented by Y, and the matrix size is represented by $\|X\|$.

4.2. Artificial Neural Network. For artificial neural network, it is mainly learning-oriented input and output, which is used to reflect strong computational efficiency and corresponding robustness. The specific structure diagram is shown in Figure 7.

For each frame of speech, the 16-dimensional LPC and RASTA-PLP mixed vector and the 2-dimensional prosody parameters are calculated to form an 18-dimensional speech feature vector, and the front and back 8 frames are combined into an input vector. In this way, the input of each neural network is a vector.

5. Simulation Experiment

In order to cover the pronunciation of a single person as much as possible, this paper selects the sentence synchronous audio and video library in the Chinese speech synthesis library. By marking feature points, the motion data of lips, cheeks, and eyelids can be obtained. The camera converts the collected video into an image at 10 frames/S and uses the tracking program to process the image feature sequence.
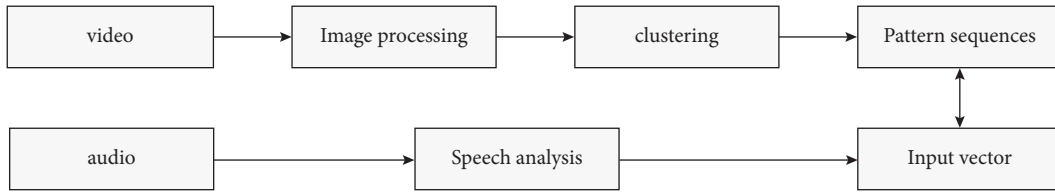
FIGURE 5: Speech-driven facial animation synchronization processing framework.
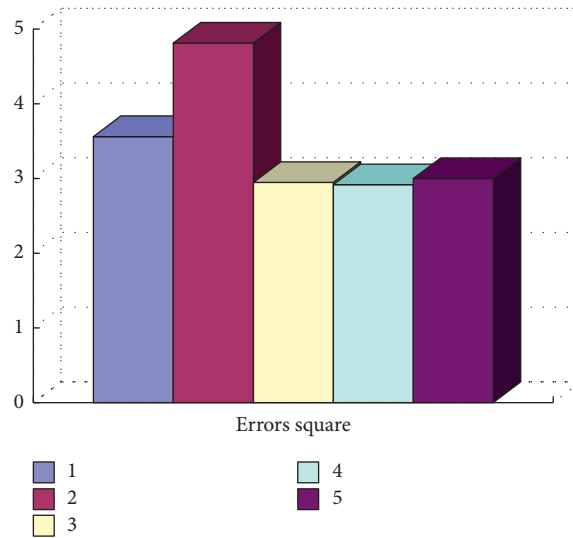

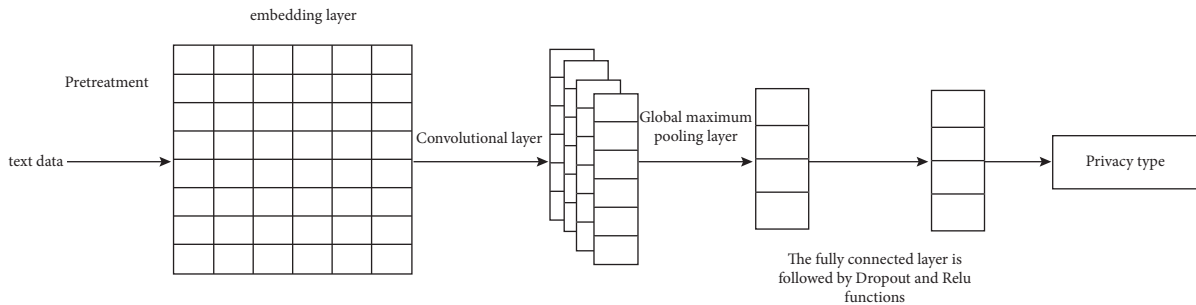
FIGURE 6: Comparison of clustering results.

FIGURE 7: Structure diagram of neural network.

Both qualitative and quantitative evaluation methods are used for the system. Quantitative testing is based on calculation to measure the error between predicted data and real data. Most machine learning systems should use quantitative methods. Qualitative testing is to judge whether the synthesized face motion is true through perception. For synthesis, qualitative testing is very important. In quantitative testing, the specific calculated variance is shown in Figure 8.

The simulation results show that the compromised node detection in wireless sensor networks can not only solve the dynamic change of the upper part of the face but also use the
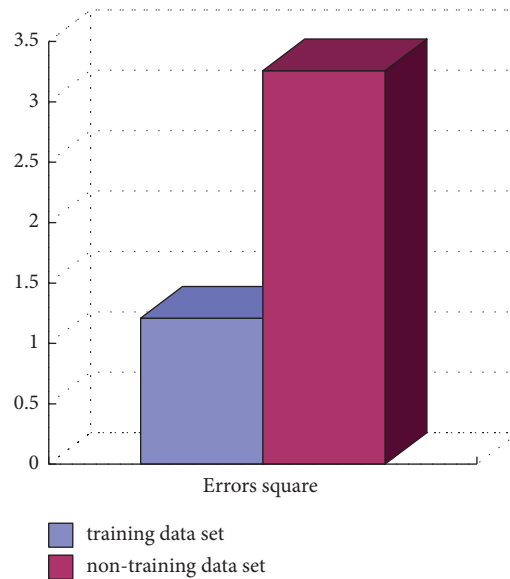
FIGURE 8: Variance comparison.

recorded original voice and can effectively solve the synchronization problem. Therefore, it has been highly evaluated and proved to be effective in practice.

6. Conclusions

The continuous development of artificial intelligence promotes the improvement and enrichment of film and television animation. People are increasingly pursuing the aesthetic and technical characteristics of film and television animation. Therefore, more technologies are introduced into the field of film and television animation. In view of these needs and limitations, based on the compromised node detection of wireless sensor networks, this paper combs the synchronous business relationship flow of voice signals and facial expressions, analyzes the process of voice processing signals, first detects abnormal behavior and voice using compromise, finds the basic pattern of facial expressions through cluster analysis, and seems to complete the one-to-one mapping from voice to facial expressions. At the same time, quantitative and qualitative evaluation methods are used for analysis and evaluation. The prosodic distribution of speech features is used to realize the one-to-one mapping to facial expression, which avoids the defect of the robustness of speech recognition, improves the learning ability of speech recognition, and realizes the driving analysis of human facial expression film and television animation. The simulation results show that the compromised node detection in wireless sensor networks is effective and can support the analysis and research of speech-driven facial expression film and television animation.

Data Availability

The labeled dataset used to support the findings of this study is available from the corresponding author upon request.

Conflicts of Interest

The authors declare that there are no conflicts of interest.

References

[1] E. Nakagami-Yamaguchi, K. Fujinaga, A. Batard et al., "The effect of an animation movie for inpatient fall prevention: a pilot study in an acute hospital," *Safety and Health*, vol. 2, no. 1, pp. 32–39, 2016.

[2] S. M. Wong, G. M. Ibrahim, A. Ochi et al., "MoviEEG: an animation toolbox for visualization of intracranial electroencephalography synchronization dynamics," *Clinical Neurophysiology*, vol. 6, no. 4, pp. 2370–2378, 2016.

[3] H. Critchley, E. Daly, M. Phillips et al., "Explicit and implicit neural mechanisms for processing of social information from facial expressions: a functional magnetic resonance imaging study," *Human Brain Mapping*, vol. 9, no. 2, pp. 93–105, 2015.

[4] M. L. Phillips, N. Medford, A. W. Young et al., "Time courses of left and right amygdalar responses to fearful facial expressions," *NeuroImage*, vol. 13, no. 6, p. 458, 2015.

[5] A.-R. Richoz, R. E. Jack, O. G. B. Garrod, P. G. Schyns, and R. Caldara, "Reconstructing dynamic mental models of facial expressions in prosopagnosia reveals distinct representations for identity and expression," *Cortex*, vol. 65, no. 5, pp. 50–64, 2015.

[6] H. Meng, N. Bianchi-Berthouze, Y. Deng, J. Cheng, and J. P. Cosmas, "Time-delay neural network for continuous emotional dimension prediction from facial expression sequences," *IEEE Transactions on Cybernetics*, vol. 46, no. 4, pp. 916–929, 2017.

[7] M. Wegrzyn, M. Riehle, K. Labudda et al., "Investigating the brain basis of facial expression perception using multi-voxel pattern analysis," *Cortex*, vol. 69, pp. 131–140, 2015.

[8] M. H. Siddiqi, R. Ali, A. M. Khan, Y.-T. Park, and S. Lee, "Human facial expression recognition using stepwise linear discriminant analysis and hidden conditional random fields," *IEEE Transactions on Image Processing*, vol. 24, no. 4, pp. 1386–1398, 2015.

[9] K. Strelnikov, J. Foxton, M. Marx, and P. Barone, "Brain prediction of auditory emphasis by facial expressions during audiovisual continuous speech," *Brain Topography*, vol. 28, no. 3, pp. 494–505, 2015.

[10] J. S. Dutt, D. S. Meena, and K. K. Sharma, "Facial expression recognition using the spectral graph wavelet," *IET Signal Processing*, vol. 13, no. 2, pp. 224–229, 2019.

[11] K. J. Jones, P. D. Storer, S. Drengler, and M. Oblinger, "Differential regulation of cytoskeletal gene expression in hamster facial motoneurons: effects of axotomy and testosterone treatment," *Journal of Neuroscience Research*, vol. 57, no. 6, pp. 817–823, 2015.

[12] K. Fisher, J. Towler, and M. Eimer, "Facial identity and facial expression are initially integrated at visual perceptual stages of face processing," *Neuropsychologia*, vol. 80, no. 5, pp. 115–125, 2016.

[13] K. Zhao, W.-S. Chu, F. De la Torre, J. F. Cohn, and H. Zhang, "Joint patch and multi-label learning for facial action unit and holistic expression recognition," *IEEE Transactions on Image Processing*, vol. 25, no. 8, pp. 3931–3946, 2016.

[14] F.-L. De Winter, Q. Zhu, J. Van den Stock et al., "Lateralization for dynamic facial expressions in human superior temporal sulcus," *NeuroImage*, vol. 106, no. 5, pp. 340–352, 2015.

[15] T. Diéguez-Risco, L. Aguado, J. Albert, and J. A. Hinojosa, Judging emotional congruency: explicit attention to situational context modulates processing of facial expressions of emotion," *Biological Psychology*, vol. 112, no. 4, pp. 27–38, 2015.

[16] N. Burra, C. Barras, S. Y. Coll, and D. Kerzel, "Electrophysiological evidence for attentional capture by irrelevant angry facial expressions," *Biological Psychology*, vol. 120, pp. 69–80, 2016.

[17] M. Schilder, J. Hooff, and C. J. Geer-Plesman, "A quantitative analysis of facial expression in the plains zebra," *Ethology*, vol. 66, no. 1, pp. 11–32, 2015.

[18] K. M. Mclennan, C. J. B. Rebelo, M. J. Corke, M. A. Holmes, M. C. Leach, and F. Constantino-Casas, "Development of a facial expression scale using footrot and mastitis as models of pain in sheep," *Applied Animal Behaviour Science*, vol. 176, no. 5, pp. 19–26, 2016.

[19] D. Milena, J. Corentin, and R. Bruno, "At a single glance: fast periodic visual stimulation uncovers the spatio-temporal dynamics of brief facial expression changes in the human brain," *Cerebral Cortex*, vol. 56, no. 8, pp. 8–14, 2016.

[20] M. Sormaz, A. W. Young, and T. J. Andrews, "Contributions of feature shapes and surface cues to the recognition of facial expressions," *Vision Research*, vol. 127, no. 4, pp. 1–10, 2016.

Research Article

Research on Management Efficiency and Dynamic Relationship in Intelligent Management of Tourism Engineering Based on Industry 4.0

Tianchen Hou [ID]

Physical Education College of Zhengzhou University, Zhengzhou 450044, Henan, China

Correspondence should be addressed to Tianchen Hou; houtianchen@peczzu.edu.cn

The digital age of artificial intelligence marks the rapid development of tourism engineering and the gradual improvement of intelligent management theory. This study aims to solve the problems of low efficiency of dynamic relationship analysis and low data utilization in traditional intelligent management methods of tourism engineering. This work studies the dynamic optimization model of tourism engineering management theory based on the artificial intelligence data analysis model and designs the dynamic analysis model of tourism engineering management data based on the convolution neural network. The model can collect dynamic data information of tourism management from many aspects and can also be used to study and analyze human behavior patterns based on the convolutional neural network algorithm. According to the human behavior data analysis model and convolution neural network algorithm, this study formulates the real-time management data scheme of tourism engineering and better extracts the characteristic information of the dynamic data of tourism engineering management. The results show that the topology optimization model of tourism intelligent management based on the convolutional neural network achieves high feasibility, high data accuracy, and high response speed. It can improve the collaborative coupling relationship between management efficiency and dynamic data in tourism engineering management based on big data analysis technology. It realizes the effective combination of tourism management, digital management, and artificial intelligence algorithm.

1. Introduction

At present, the traditional "many to many" cluster point information collection is the main data information of tourism project management in China [1]. Since the beginning of the 21st century, the rapid development of artificial intelligence technology in China has also led to the transformation of data analysis methods in tourism engineering management in China. The emergence of modern tourism engineering management analysis methods such as intelligent tourism management theory planning, efficient management data analysis, and coordinated utilization of software and hardware has contributed to the large-scale promotion of "intelligent management of industrial 4.0 tourism engineering" and provides opportunities [2]. Therefore, diversification and high efficiency have become important features of the intelligent degree of tourism

project management in China [3]. At present, although the existing intelligent management system of tourism engineering provides a large number of data information extraction schemes, it is difficult to select a targeted topological representation scheme according to its management dynamic theoretical system and the law of human behavior in the process of dynamic management, so as to achieve the optimal effect of topological analysis [4]. Based on this, this study proposes a theoretical topology analysis model of intelligent management of tourism engineering in the digital age based on big data and the convolutional neural network algorithm.

Aiming at the problems of low data analysis efficiency, low data storage efficiency, and low data classification efficiency existing in the current theoretical analysis model of intelligent management of tourism engineering, this work studies the data mining model scheme of discrete dynamic

analysis based on the convolution neural network algorithm and collaborative processing of big data in the cloud, which is mainly divided into four parts. Section 1 introduces the research background and the overall framework of this study. Section 2 introduces the research status of intelligent management theory and application methods of tourism engineering. Section 3 constructs the theoretical topology model of intelligent management of tourism engineering in the digital age based on big data and convolution neural network algorithm, adopts the multilayer convolution perception neural network factor method, and constructs the evaluation index system of tourism management data analysis and intelligent classification objectives of artificial intelligence analysis. In Section 4, the quantitative effect of data analysis of the industrial 4.0 tourism project intelligent management efficiency dynamic analysis model constructed in this study is experimentally analyzed and verified, and a conclusion is drawn in Section 5.

Compared with the data mining model established by the traditional intelligent management analysis model in tourism engineering, which takes the continuity of static management data as the main research object, the innovation of this study is that the discrete dynamic modeling technology and big data topology analysis strategy based on the convolution neural network algorithm are applied to the dynamic analysis model of industry 4.0 tourism engineering management. It can make full use of a large number of dynamic management data, extract appropriate management data feature information, realize the integrity approach at the simulation level, and quantitatively describe the quantitative representative eigenvalues, similarity of multidimensional management analysis modes, and expected evaluation indicators of different tourism projects in the process of employee management scheme allocation with multitransformed neural network factors. It can efficiently carry out customized analysis on the factors affecting management efficiency and accuracy.

2. Related Work

Although the domestic management theory analysis model has been developed for several years, there are still some deficiencies in the establishment, operation, and upgrading of the sports data mining model compared with some more developed countries [5]. Wei et al. optimized the data analysis process according to the management principle of three-dimensional space. His team proposed that attention should be paid to the development of the three-dimensional basic structure or dynamic theoretical decomposition method of tourism management based on Gaussian mixture [6]. Masterson et al. proved through experiments that the classified data analysis method can play a good role in differential learning, effectively improve the mining efficiency of big data, and use a number of indicators to evaluate the data analysis ability of the tourism management dynamic analysis model [7]. Greatbatch et al. have verified through repeated practice. The final results show that the establishment method based on human behavior discrete modeling technology can improve the data analysis efficiency of

the data mining model and the effectiveness of modifying data. It is suitable for the outside world to carry out continuous R&D planning for tourism engineering management data and find the optimal data structure scheme [8]. Mayro et al. put forward a new group tourism project management data model and database establishment method based on industry 4.0. The multidimensional spatial framework sequence is used to redistribute the data packets of each layer of the original management database, so as to realize the optimal determination of various mining methods in the process of management data capture [9]. According to the traditional establishment mode and practical experience of the data collection system in a general sense, Lang et al. found that the current data mining model has the problems of difficult dimension calculation and poor physical quantity in the process of managing tourism dynamic data analysis. Therefore, they developed a new intelligent data analysis technology based on deep learning [10]. Through logical analysis, adjustment, and summary of different data mining models, Egevad et al. finally established a new data mining system, which can realize delayed capture and real-time feedback of tourism engineering management data [11]. Scholars from Safarnejad L and other universities put forward a new data mining model establishment method based on the multirelationship recommendation algorithm according to the multifactor relationship theory in philology, analyzed the correlation of different modules in the traditional data mining model, and established a double factor analysis model [12]. Verganti et al. comprehensively evaluated the employee management data mining model of a tourism project from the aspects of the selection of the structure form of the tourism management storage database, the classification of the content, and the storage capacity of the database and realized the simulation of the working process of the model database by capturing different types of data [13]. The research results of Kai et al. show that the "data outside" interaction model based on discrete dynamic modeling technology is better than the traditional interaction model in terms of motion data information acquisition ability [14]. In order to improve the acquisition efficiency of tourism engineering management data and the maximum utilization of storage space, Liu et al. conducted various research studies and analyses on different tourism engineering management data and finally classified different data types into various types of data models to avoid storing duplicate data and increase the collection efficiency of tourism data [15]. Goodarzian et al. proved through experiments that the discrete data mining model established can realize the static segmentation of dynamic data and solve the problem that it is difficult to obtain dynamic data in management, but there is a problem of small application range [16].

To sum up, it can be seen that the current tourism engineering focuses on the data mining management analysis model with the continuity of static management data as the main research object in the establishment of the intelligent management analysis model, but there are some problems in this kind of model research, such as low intelligence and low data utilization [17–19]. On the other

hand, although China has done more theoretical analyses and research on the establishment method of the intelligent management and intelligent analysis system of tourism engineering, there is room for progress in the achievement transformation at the actual control level, and there is no establishment of the intelligent multimedia control system model [20, 21].

3. Methodology

The development of big data and artificial intelligence in the digital age has brought great opportunities for the digital development of intelligent management of tourism engineering [22]. The most typical algorithm in artificial intelligence technology based on big data idea is the convolution neural network algorithm [23]. The typical convolutional neural network structure is a feed forward network with three or more layers without feedback and no interconnection structure in the layer. The convolutional neural network is also a basic method for self-learning and updating at the data level. The first and last layers are called the input layer and output layer, respectively, and the middle layers are the hidden layer (also known as the middle layer) [24]. In the convolution neural network, the neurons in each layer are fully connected, and there is no connection between the neurons in each layer. The neural network algorithm used in the topological representation of management is an intelligent algorithm with "human biological characteristics" based on the overall structure of human neurons and the direct two-way regulation and automatic processing of neurons by the brain [25]. The data processing process of the convolution neural network algorithm is shown in Figure 1.

When the industrial 4.0 tourism engineering intelligent management data information is processed randomly, the mutual coupling analysis of two-way management information classification and the vector processing analysis of multiple coupling combinations are carried out through a single neuron structure with multiple neuron structure (synapse) characteristics, the management type with high modular demand is found from the total object to be processed, and the probability of being selected for secondary or multiple analysis is high. On the contrary, the probability of objects with low significance of management features being selected for secondary or multiple reusable framework processing is very low. The new generation of tourism project objectives has dynamic characteristics, which need to be compared and analyzed for many times to produce unified management. In this way, after several two-way information interaction cycles, mixed characteristic individuals conforming to the characteristics of artificial intelligence are finally generated, that is, modular unified processing for a certain type of tourism management data local optimization and feature extraction.

3.1. Establishment Process of the Multiple Grey Convolution Neural Network Model Based on Data Mining. By checking many factors of multimanagement data, we can judge whether there are closely related factors in various data of

intelligent management type of tourism engineering. Tourism information management is a process in which information personnel plan, organize, command, coordinate, and control the tourism information source utilizing information technology. From a microperspective, it includes the management of tourism information content. Macroscopically speaking, it includes the management of tourism information institutions and tourism information systems. In this way, we can not only use the comprehensive average index of these closely related factors or one of them to represent a variety of such factors. In addition, the information carried by these multidata to be processed cannot be seriously distorted. The data analysis process of the convolution neural network topology analysis model based on big data and artificial intelligence strategy is shown in Figure 2.

First, assume that there are n data objects to be processed (tourism engineering management information), which are called implementation objects, and each observation object has m characteristic data (management characteristic information); the sequence can be obtained as follows:

$$
\begin{aligned}
X_1 &= (x_1(1), x_1(2), \ldots, x_1(n)), \\
X_2 &= (x_2(1), x_2(2), \ldots, x_2(n)), \\
X_3 &= (x_3(1), x_3(2), \ldots, x_3(n)), \\
X_m &= (x_m(1), x_m(2), \ldots, x_m(n)).
\end{aligned}
\tag{1}
$$

Then, calculate the absolute correlation ε_{ij} between X_i and X_j for all $i \le j, i, j = 1, 2, \cdots, m$, and the calculation formula is

$$
\varepsilon = 1 - \sqrt{\frac{X_m + X_{m+1}}{X_m - X_{m-1}}}.
\tag{2}
$$

The corresponding coding function is obtained according to the correlation degree

$$
W(x) = \frac{7x^2 + x^4 + 1}{7x^2 + 8x^3 + 5x^4 + 2} \varepsilon_{ii},
\tag{3}
$$

where $\varepsilon_{ii} = 1; i = 1, 2, \cdots, m$ AA. In this process, the following results can be obtained from the simulation analysis of data types in different dimensions. The simulation results without big data coupling factors for different tourism projects are shown in Figure 3.

The simulation results of dynamic coupling quantity under level 1 big data coupling factor for intelligent management types of different tourism projects are shown in Figure 4.

The simulation results of the two-level big data coupling factor in dynamic characterization of intelligent management types of different tourism projects are shown in Figure 5.

For the intelligent management types of different industrial 4.0 tourism projects, the simulation results of three-level big data coupling factors in dynamic characterization are shown in Figure 5.

It can be seen from Figures 3–6 that the comprehensive utilization rate of the information of the corresponding
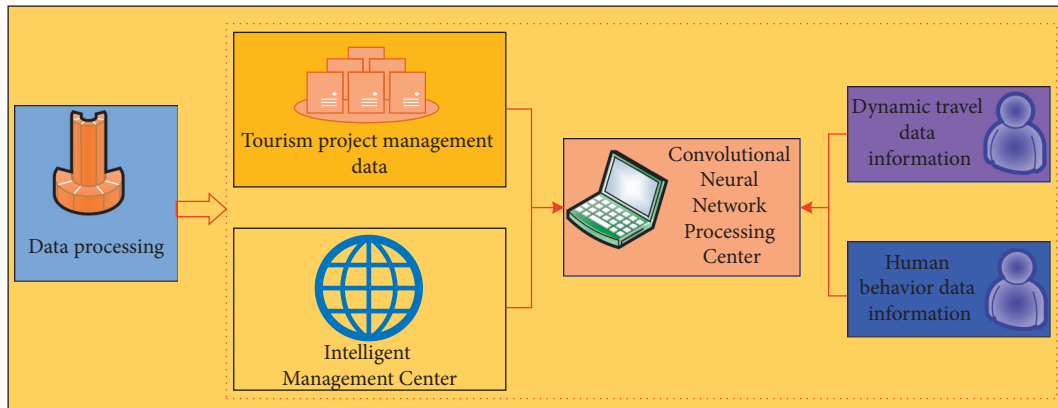
FIGURE 1: Data processing process of the convolutional neural network algorithm.
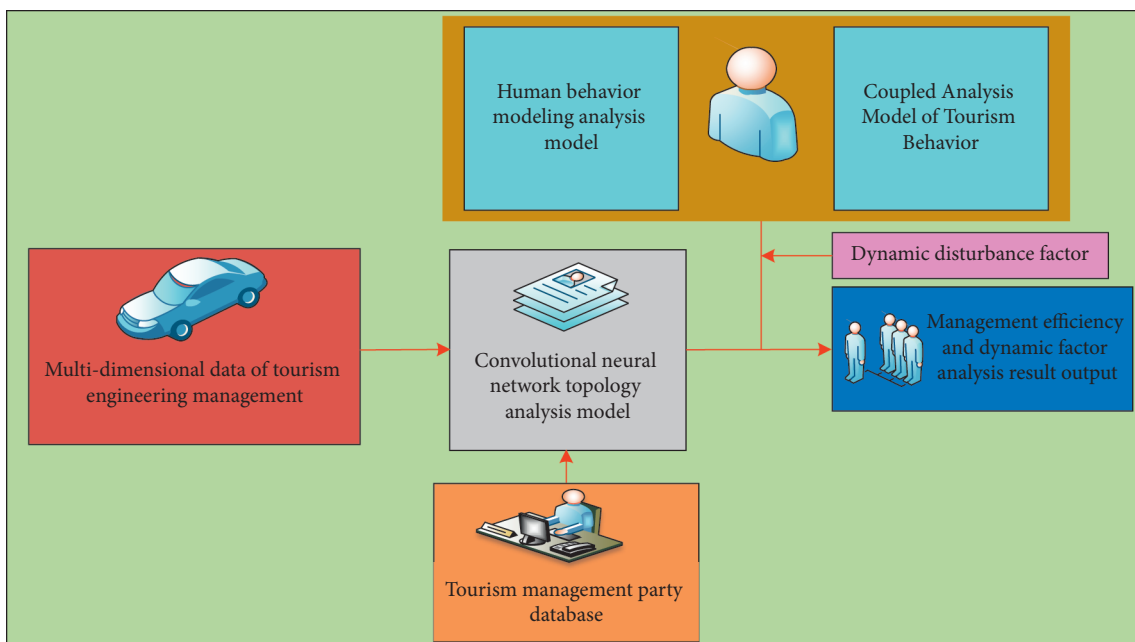

FIGURE 2: Data analysis process of the convolutional neural network topology analysis model based on big data and artificial intelligence strategies.
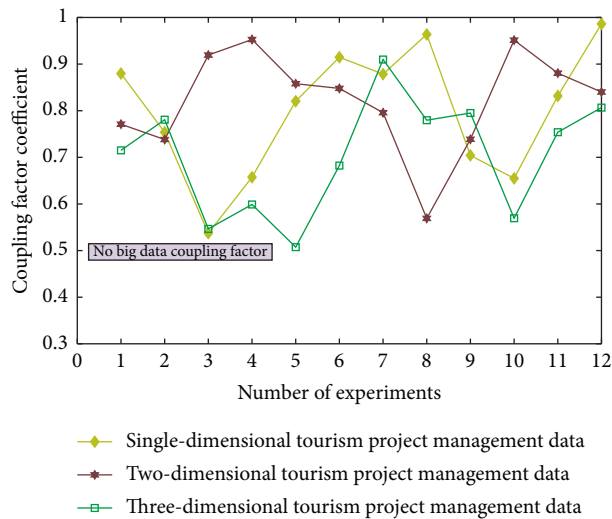

FIGURE 3: Simulation results of different tourism projects without big data coupling factors.
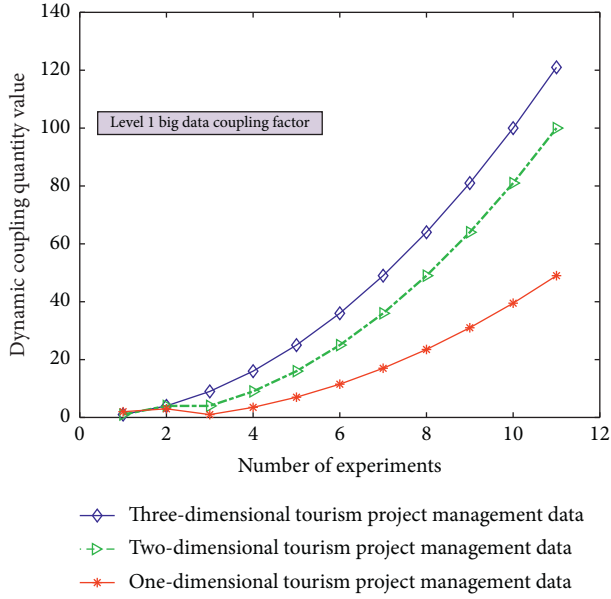
FIGURE 4: The simulation results of the dynamic coupling quantity value under the first-level big data coupling factor for the intelligent management types of different tourism projects.
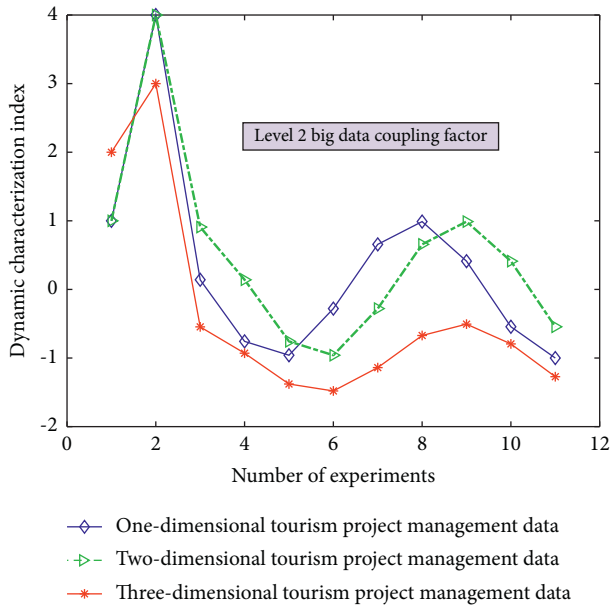

FIGURE 5: The simulation results of the dynamic characterization of the two-level big data coupling factor for the intelligent management types of different tourism projects.
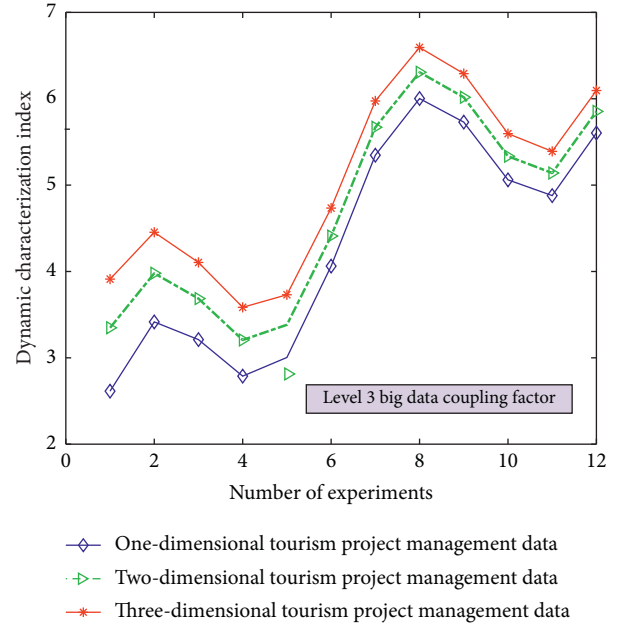

FIGURE 6: The simulation results of the dynamic characterization of the three-level big data coupling factor for the intelligent management types of different tourism projects.

management database changes with the change of the number of topology analyses when performing different degrees of association calculation and processing (level 0/1/2/3 big data coupling factor) for different data under the dynamic relationship topology model of the convolution neural network algorithm and when the level 3 big data coupling factor is added. There are more and more stable branches of its corresponding topological dynamic structure, and its stability utilization rate is also better and

better. This is because in the calculation process, through the computer database information and the preset linear judgment program, some data information can be deeply mined and analyzed, so as to realize the quadratic linear processing of the data after the initial linear analysis. After quadratic linear processing, its stability and data utilization are improved. In this study, the values of the analysis indexes of n data objects to be processed are divided into the class grey group, which is called j index subclass. The convolution network function of j index k subclass is recorded as $H_j^k(x)$.

$$H_j^k(x) = \frac{x + x_j^k(1)}{x_j^k(2) - x_j^k(1)}, \quad x \in \left[x_j^k(1), x_j^k(2)\right]. \quad (4)$$

Among them, $x_j^k(1)$ and $x_j^k(2)$ are the network nodes, and x is the data type.

If the function $H_j^k(x)$ does not have the first and second turning points $x_j^k(1)$ and $x_j^k(2)$, $H_j^k(x)$ is called the lower bound measure convolution network function, which is recorded as $H_j^k[-,-,x_j^k(3),x_j^k(4)]$. In this system, the corresponding lower bound measure function $f_j^k(x)$ is

$$f_j^k(x) = \frac{x_j^k(4) - x}{x_j^k(4) - x_j^k(3)}, \quad x \in \left[x_j^k(3), x_j^k(4)\right]. \quad (5)$$

The moderate measure function corresponding to this model is shown in formula (6), and the expression of the whitening weight function of the upper bound measure is formula (7).

$$Q_j^k(x) = f_j^k(x) = \frac{x_j^k(4) - x}{x_j^k(4) - x_j^k(2)}, \quad x \in \left[x_j^k(2), x_j^k(4)\right]. \quad (6)$$

$$W_j^k(x) = f_j^k(x) = \frac{x - x_j^k(1)}{x_j^k(2) - x_j^k(1)}, \quad x \in \left[x_j^k(1), x_j^k(2)\right]. \quad (7)$$

Among them, $x_j^k(1)$, $x_j^k(2)$, and $x_j^k(4)$ are the network nodes, and x is the data type.

3.2. Tourism Management Efficiency Based on the Convolutional Neural Network Gaussian Mixture Sparse Representation Data Processing Process of the Dynamic Optimization Model.

In this model, in order to better determine the specific significance of management data judgment index in the process of grey linear analysis, carry out factor analysis and provide basis for system decision-making. It is necessary to solve the problem of how to find correlation and measure from random time series. By determining the convolution variable weight linear coefficient, the accuracy of management data mining can be better improved. Therefore, the weighted linear coefficient σ_i^k can be expressed as

FIGURE 7: Stability changes of management efficiency under different topological structures.

$$\sigma_i^k = \sum_{j=1}^{m} f_j^k(x_{ij}) \cdot \eta_j^k,$$

$$\sigma_i = \left(\sigma_i^1, \sigma_i^2, \ldots, \sigma_i^s\right) = \left(\sum_{j=1}^{m} f_j^1(x_{ij}) \cdot \eta_j^1, \sum_{j=1}^{m} f_j^2(x_{ij}) \cdot \eta_j^2, \ldots, \sum_{j=1}^{m} f_j^s(x_{ij}) \cdot \eta_j^s\right). \quad (8)$$

The above formula is called the linear coefficient of the multilayer convolution neural network, and its corresponding linear coefficient matrix is

$$\Sigma = \left(\sigma_i^k\right) = \begin{bmatrix} \sigma_1^1 & \sigma_1^2 & \cdots & \sigma_1^s \\ \sigma_2^1 & \sigma_2^2 & \cdots & \sigma_2^s \\ \cdots & \cdots & \cdots & \cdots \\ \sigma_n^1 & \sigma_n^2 & \cdots & \sigma_n^s \end{bmatrix}. \quad (9)$$

In order to realize data mining of the convolutional neural network linear analysis process, the information of target data needs to be translated into language information that can be recognized by computer through a certain pattern. Therefore, after the feature sparse representation process of the Gaussian mixture industrial 4.0 tourism engineering intelligent management data of the management data, the simulation analysis results of the calculation efficiency of three different types of tourism engineering management data combined with human behavior are shown in Figure 7.

As shown in Figure 7, with the increase of the number of topologies, the stability and computational efficiency of the corresponding tourism engineering intelligent management database are also changing. Because some low-frequency or

meaningless management data information is intentionally deleted or deleted, the process is stored through a specific mode. To facilitate the data recovery required by posterror processing operations, form a special data information record and realize the conversion from data information to computer storage information, and its storage function can be expressed as $T(x)$.

$$T(x) = \frac{\sum_{j=1}^{m} f_j^1(x_j)}{\eta_j^1}. \quad (10)$$

Among them, η_j^1 is the storage coefficient, and its sparse representation can be expressed as $T'(x)$, which can be expressed as

$$T'(x) = \frac{\sum_{j=1}^{m} f_j^1(x_j)}{\eta_j^1 H(x)}. \quad (11)$$

where η_j^1 is the storage coefficient and $H(x)$ is the discriminant function.

Choosing different grey linear methods will make the data in the cluster have different correlation degrees. The topology analysis model based on the convolutional neural network is to fuzzy search and screen the unknown data targets (newly collected industry 4.0 tourism project

management information and known human behavior data) through data mining of multitarget data. The screening function is $P(x)$, and the expression is

$$P(x) = \frac{\sum_{j=1}^{m} (x_j - \overline{x})}{\eta_j^1 \overline{x}}, \tag{12}$$

where η_j^1 is the storage coefficient.

When it is necessary to classify different types of data indicators (such as relevant assessment data indicators of a tourism project), the evaluation model $Z(x)$ can be expressed as

$$Z(x) = \frac{1}{\eta_j^1 \sum_{j=1}^{m} (x_j - \overline{x})}, \tag{13}$$

where η_j^1 is the storage coefficient and $\overline{x}$ is the average number of management decomposition information.

$$Z(x) = \frac{1}{\eta_j^1 \sum_{j=1}^{m} (x_j - \overline{x})}. \tag{14}$$

In the optimal case, the convolution neural network analysis model can realize the recognition of multiple data under a certain similarity. However, there are still some problems in the data mining process and management dynamic algorithm. In order to improve the recognition degree of the association degree between management data information (feature information) and multiple data (management color channel and salient feature) by the multiple grey linear analysis model as much as possible, the expression of the association degree $R(x)$ is

$$R(x) = \frac{\eta_j^1}{\sum_{j=1}^{m} x_j - \overline{x}/x_{j+1} + \overline{x}}. \tag{15}$$

At present, the most commonly used method is to achieve accurate topological linear analysis through big data database statistics and data comparison between the same management types. The above dynamic flapping analysis method is also used to compare and determine the well-known feature recognition information and management sparse representation pattern information.

4. Result Analysis and Discussion

4.1. Experimental Design Process and Data Results. The input layer data used in this experiment are the known industry 4.0 tourism engineering management information data, the hidden layer is the artificial intelligence topology analysis strategy based on big data and the convolution neural network algorithm, the output layer is the dynamic optimal selection combination of tourism engineering management, and its convolution learning strategy is the tourism engineering intelligent management rules and regulations and employee level treatment. When evaluating the topological rate and change type of tourism engineering management data, it needs to be evaluated from many aspects. According to the needs of tourism engineering development, this study proposes 25 indicators to evaluate the quality of

management topology analysis. Through the observation results of 25 relevant data managing topological-mixed features, the above indicators are properly classified and sparse representation analysis, and the characterization standard is simplified by deleting some unnecessary (i.e., less influential) indicators, so as to realize the quantitative representation of the above data indicators, which is more convincing. During the experiment, the management data of three types (6 groups in total, 2 groups in each type) of different tourism projects are verified by topological analysis. The experimental results are shown in Figure 8.

4.2. Analysis of Experimental Results of Management Data Accuracy Based on the Convolutional Neural Network. The analysis results of data accuracy in the experimental results are shown in Figure 9.

From the experimental results shown in Figure 8 and the accuracy analysis results shown in Figure 9, it can be seen that after the analysis of three types of data (two groups each), the corresponding change of topology classification performance index is obvious. Among them, the topology performance of the third group of data is the highest, but the corresponding big data analysis data deviation is also the highest because with the increase of topology structure, the dimension of data analysis is also increasing, so its deviation will also change. On the other hand, among the above data indicators for evaluating the quality of topology analysis, some or several indicators do have correlation or mixed relationships.

In addition, it can be seen from the data shown in Figures 8 and 9 and the experiment that in the process of processing the experimental data, this study adopts an efficient and intelligent topological data analysis method. The model can realize the unified management of sparse representation demand data of different tourism management and different types of management representation method data. According to the local differences between data and the actual needs of sparse representation, the algorithm is used for intelligent optimization, analysis, and processing to realize the high-precision utilization and remote dynamic maintenance of data. Then, through the eigenvalues of the signals collected by the wireless nano data processing equipment and the structural characteristics of different management in the sparse representation process, according to the different eigenvalues such as vector difference and matrix difference, the intelligent optimization processing and deep information mining process based on the machine learning model and neural network algorithm are applied. Realize the classification level division of different management Gaussian mixture feature sparse representation methods in data analysis. Finally, through a series of data analysis processes represented by the neural network algorithm in the sparse representation of tourism management, classify according to the differences of information, realize the high classification of the similarity of different data, and realize the fitting analysis and simulation of approximate or the same data according to the different requirements for the sparse representation of different tourism
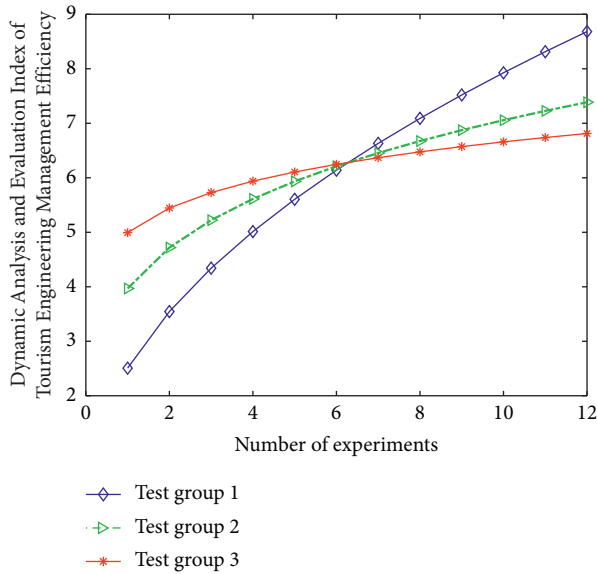
FIGURE 8: The results of topological analysis and verification on the management data of 3 types of different tourism projects.
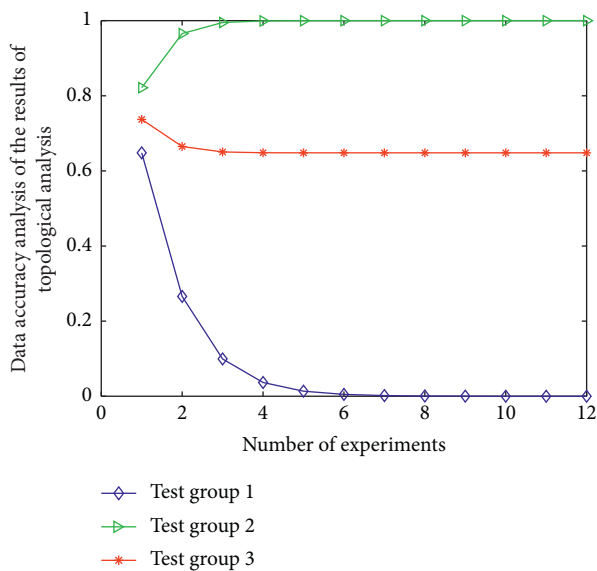

FIGURE 9: Analysis of the accuracy of the data in the experimental results.

management. Then, it completes the efficient and high-precision classification of the sparse representation optimization link of managing Gaussian mixture features.

5. Conclusion

This work studies the discrete dynamic analysis data mining model scheme based on the convolutional neural network algorithm and big data cloud collaborative processing. Compared with the traditional intelligent management analysis model of tourism engineering, which takes the continuity of static management data as the main research object, the innovation of this study is to apply discrete

dynamic modeling technology and big data topology analysis strategy based on the convolution neural network algorithm to the dynamic analysis model of industry 4.0 tourism engineering management. It can make full use of a large number of dynamic management data, extract appropriate management data feature information, realize the simulation level integrity method, quantitatively describe representative quantitative eigenvalues, the similarity of multidimensional management analysis modes and expected evaluation indicators of different tourism projects in the process of employee management scheme allocation, and adopt multiconversion neural network factors. It can efficiently customize and analyze the factors affecting management efficiency and accuracy. However, the algorithm only analyses the impact and correlation degree from the local analysis of management and does not consider other potential factors of sparse representation of management features. Therefore, the comprehensive analysis of the index evaluation system and the influence degree of other factors need to be further studied.

Data Availability

The data used to support the findings of this study are available from the corresponding author upon request.

Conflicts of Interest

The author declares that there are no conflicts of interest.

Acknowledgments

References

[1] S. Shen, M. Sotiriadis, and Y. Zhang, "The influence of smart technologies on customer journey in tourist attractions within the smart tourism management framework," *Sustainability*, vol. 12, 2020.

[2] P. G. Gonzáles-Mantilla and C. J. Leon, "Tourism management in south American geological areas: comparing two cases from Peru and Brazil," *Geoheritage*, vol. 12, no. 2, 2020.

[3] D. Cajiao, B. Albertos, P. Tejedo et al., "Assessing the conservation values and tourism threats in barrientos island, Antarctic peninsula," *Journal of Environmental Management*, vol. 266, Article ID 110593, 2020.

[4] R. Fang, J. Zhang, K. Xiong, K. S. Woo, and N. Zhang, "Influencing factors of residents' perception of responsibilities for heritage conservation in world heritage buffer zone: a case study of libo karst," *Sustainability*, vol. 13, 2021.

[5] L. B. Yan and M. Kasanin-Grubin, "Land degradation and management of red beds in China: two case studies," *Journal of Mountain Science*, vol. 16, no. 11, pp. 2591–2604, 2019.

[6] X. Wei, D. U. Junping, M. Liang, and Z. Xue, "Crowd density field estimation based on crowd dynamics theory and social force model," *Chinese Journal of Electronics*, vol. 28, no. 3, pp. 81–88, 2019.

[7] V. A. Masterson, J. P. Enqvist, R. C. Stedman, and M. Tengö, "Sense of place in social-ecological systems: from theory to empirics," *Sustainability science*, vol. 14, no. 3, pp. 555–564, 2019.

[8] O. Greatbatch, A. Garrett, and K. Snape, "The impact of artificial intelligence on the current and future practice of clinical cancer genomics," *Genetics Research*, vol. 101, p. e9, 2019.

[9] E. L. Mayro, M. Wang, T. Elze, and L. R. Pasquale, "The impact of artificial intelligence in the diagnosis and management of glaucoma," *Eye*, vol. 34, no. 5, pp. 1–11, 2020.

[10] Q. Lang, C. Zhong, Z. Liang et al., "Six application scenarios of artificial intelligence in the precise diagnosis and treatment of liver cancer," *Artificial Intelligence Review*, vol. 54, no. 7, pp. 5307–5346, 2021.

[11] L. Egevad, P. Ström, K. Kartasalo et al., "The utility of artificial intelligence in the assessment of prostate pathology," *Histopathology*, vol. 76, no. 6, pp. 790–792, 2020.

[12] B. Maille, M. Wilkin, M. Millon et al., "Smartwatch electrocardiogram and artificial intelligence for assessing cardiac-rhythm safety of drug therapy in the COVID-19 pandemic. The QT-logs study," *International Journal of Cardiology*, vol. 331, no. 2, 2021.

[13] R. Verganti, L. Vendraminelli, and M. Iansiti, "Innovation and design in the age of artificial intelligence," *Journal of Product Innovation Management*, vol. 37, no. 3, pp. 212–227, 2020.

[14] F. Kai, T. Nakamura, and K. Fukagata, "Convolutional neural network based hierarchical autoencoder for nonlinear mode decomposition of fluid field data," *Physics of Fluids*, vol. 32, no. 9, Article ID 095110, 2020.

[15] C. Liu, M. Pang, and R. Zhao, "Novel superpixel-based algorithm for segmenting lung images via convolutional neural network and random forest," *IET Image Processing*, vol. 14, no. 3, 2020.

[16] F. Goodarzian, V. Kumar, and A. Abraham, "Hybrid meta-heuristic algorithms for a supply chain network considering different carbon emission regulations using big data characteristics," *Soft Computing*, vol. 25, no. 11, pp. 7527–7557, 2021.

[17] Z. Liu, "Retracted article: mountain soil characteristics and agrotourism management optimization based on distributed collaboration," *Arabian Journal of Geosciences*, vol. 14, no. 15, p. 1447, 2021.

[18] A. D. Maio, A. Violi, F. Santoro, F. Santoro, and A. Violi, "Exploiting social data for tourism management: the SMARTCAL project," *Quality and Quantity*, no. 8–9, 2020.

[19] T. Zhang, Y. Yang, J. Wang et al., "Comparison between atlas and convolutional neural network based automatic segmentation of multiple organs at risk in non-small cell lung cancer," *Medicine*, vol. 99, no. 34, Article ID e21800, 2020.

[20] Y. Shi, Z. Liu, L. Chen, and W. Li, "Research on intelligent tourism management based on wireless network development," *Journal of Intelligent and Fuzzy Systems*, vol. 37, no. 7, pp. 1–8, 2019.

[21] S. Zhang, L. Zhong, H. Ju, and Y. Wang, "Land border tourism resources in China: spatial patterns and tourism management," *Sustainability*, vol. 11, no. 1, 2019.

[22] G. Lukoseviciute and T. Panagopoulos, "Management priorities from tourists' perspectives and beach quality assessment as tools to support sustainable coastal tourism," *Ocean & Coastal Management*, vol. 208, no. 7, Article ID 105646, 2021.

[23] P. Oleniewicz, S. Pytel, J. Markiewicz-Patkowska, A. R. Szromek, and S. Jandová, "A model of the sustainable management of the natural environment in national parks—a case study of national parks in Poland," *Sustainability*, vol. 12, 2020.

[24] C. Li, "Air pollution atmospheric environment detection and global tourism line planning management based on genetic algorithm," *Arabian Journal of Geosciences*, vol. 14, no. 17, 2021.

[25] F. Valls and J. Roca, "Visualizing digital traces for sustainable urban management: mapping tourism activity on the virtual public space," *Sustainability*, vol. 13, 2021.

Research Article

Industry 4.0 Engineering Product Life Cycle Management Based on Multigranularity Access Control Model

Longfei Yu [ID] and Shifan Zhu

College of Mechanical and Electrical Engineering, Harbin Engineering University, Harbin 150001, China

Correspondence should be addressed to Longfei Yu; yulongfei@hrbeu.edu.cn

In order to improve the management efficiency of the safety status of Industry 4.0 engineering products, the multigranularity access control model (MGACM) Industry 4.0 engineering product life cycle management (PLM) is adopted to optimize the safety management mode of Industry 4.0 engineering products in this paper. The multigranularity access control model is constructed in this paper, which has strong nonlinearity and better fault tolerance. In addition, the parameters of PLM are optimized through the multiparticle access control model, and PLM search is enabled. Taking into account the slow and easy convergence of the multigranular access control model, a niche technology with full life cycle heterogeneity and elimination mechanism is proposed to solve the premature convergence problem of the multigranular access control model. The final simulation results of this paper show that, compared with traditional algorithms, the proposed multigranularity access control model is more reliable and effective and has faster convergence speed and higher management efficiency.

1. Introduction

With the continuous advancement of society and unceasing enhancement of people's needs, data information has gradually become the basic technology for people's daily life, and the role of Industry 4.0 engineering product life cycle in people's lives has become more prominent. There are Industry 4.0 engineering products [1, 2], wireless communication Industry 4.0 engineering products, etc. Therefore, the Internet is usually used to transmit and receive data and information, and the quality of Industry 4.0 engineering products is more important. According to research at home and abroad, it is shown that the quality problems of industrial products are not simply solved by the use of preventive methods [3]. Under this circumstance, the security status perception of the integrated technology Industry 4.0 engineering products that need to obtain and process security information has attracted attention. However, Industry 4.0 engineering product safety situation management

is an emerging technology, and many research contents have not been resolved so far. In order to provide more effective and accurate management, an improved multigranularity access control model is introduced to optimize the life cycle management of Industry 4.0 engineering products in this paper. First of all, PLM with better nonlinear ability and approximation speed is adopted instead of BP or RBF neural Industry 4.0 engineering products for management. Secondly, the multigranularity access control model is used to optimize the parameters of the neural Industry 4.0 engineering product, which has strong global search capabilities.

By constructing a multigranularity access control model, the access host granularity and access level granularity are optimized and processed. Meanwhile, the life cycle granularity and authorization distribution control granularity of industrial products are used, to complete the optimization process of the model and complete the realization of multigranularity access control. Finally, the analysis of the experimental results shows that the constructed model can

effectively reduce the fault tolerance rate of the industrial product life cycle management system. Meanwhile, it can also strengthen the accuracy and completeness of model access control, which can better meet the special needs of PLM for access control.

2. Granularity Analysis of Access Control for Industry 4.0 Engineering Product Life Cycle Management

2.1. Granularity of Access Subject Composition. The subject that can be accessed by the multigranularity access control model only allows two dimensions: role and user. This article implements its subject by increasing the granularity diameter. Granular composition, as a collection of multiple users, can achieve the completion of its architecture through a combination of different forms. The full range of permissions for function groups and users is open. As the authorizer of the granularity of the access subject, ASD can assign its authority to the restricted relationship with the same structure. If a user is assigned to group A, then the role permissions of group B can be obtained. For example, technicians in the assembly process group can assign permissions to them in accordance with the engineering product management standards of Industry 4.0, and the same user can be assigned different users/assigned roles. Figure 1 shows the granularity of the access control subject and its relationship model.

The authorization of the access subject group can simplify the public permission distribution method for the unused functions in the same unit and can simplify the access control of the temporary project group. Because the user authorization can effectively improve the problems of personnel management, it is effective to reduce the confusion of the role. ASC and ASD are in a static relationship. At the same time, before assigning users to corresponding roles, their roles can be set according to the business rules of industrial products or possible problems can be solved in advance. ASC can make corrections when there is an error in the user's role assignment. The main function of ASD is to simplify the problem of repeated assignment of permissions for different roles. Therefore, the granularity of the access subject and its corresponding relationship can not only simplify its authorization procedure, but also avoid the probability of false authorization [4].

2.2. Access Object Level Granularity. The life cycle management analysis system uses the engineering product sequence information to analyze the life cycle management parameters of the camera based on a specific model. Most of the calculated amount of the engineering product stability algorithm is here, and the accuracy of life cycle management parameters affects the accuracy of the stable engineering product, so it is an important part of the engineering product stability system [5]. The multigranularity access control model MAC is shown in Figure 2 on the visitor layer. Operations (OpeRation, OPAR) can be used in different types of granularity groups. For any optimal granularity, the

achievable results can be used in special scenarios. During Industry 4.0 engineering product life cycle management process, due to the camera shaking during use, the engineering product sequence obtained by shooting will be jittered. The engineering product processing interference caused by this jitter will promote the engineering product life cycle management analysis technology emerging as the times require. Engineering product life cycle management analysis technology has been widely used in many fields of military and civilian use. From the perspective of military applications, large-scale guidance, fire control systems, and small self-seeking missile leading engineering products all involve engineering product life cycle management analysis technology. This technology can be used to improve the attack performance of weapon systems and for improvement of relevant indicators of other operations. In the photography of aviation field and terrain surveying and mapping instruments, in order to ensure that the corresponding measurement benchmarks for life cycle management analysis are obtained in the image plane of the instrument, the accuracy and processing speed of the measurement results are improved. As a new engineering product life cycle management analysis model that has gradually emerged in recent years, the multigranularity access control model can be used for the processing and analysis of Industry 4.0 engineering product life cycle management. The basic principle of this model is to use a different model for any Industry 4.0 engineering product data or perform multiple clustering operations on engineering products under different conditions and select the appropriate method for the calculation results obtained by the clustering operation, clustering and optimizing the data to obtain the best results.

2.3. License Allocation Control Granularity. As a bridge between the operation/object and the accessible subject, the license can realize comprehensive and neat distribution control. The particle progress control can ensure the consistency of the target to be visited. The distribution control particle size of the license can be distinguished according to the four aspects of the controllable control direction within the allowed range, the allowed access restriction, and the license priority. An Industry 4.0 engineering product life cycle management method is proposed. While transforming the two-dimensional engineering product life cycle management to one-dimensional engineering product data, it also evaluates and analyzes the deviation of the engineering product sequence in the life cycle management data, to eliminate the impact of engineering product quality due to lower sequence.

Allowable range, control direction, and access restrictions are static attributes, and allocation permissions need to be set (Table 1). Priority is a dynamic attribute, and the value before system execution is empty. If the system runs and loads all the permissions of the current user, the permissions are sorted according to the allowed source code and the priority of the above permissions. For example, the priority of direct permission from all users is 0, and the priority of permission from the user's group is 1.
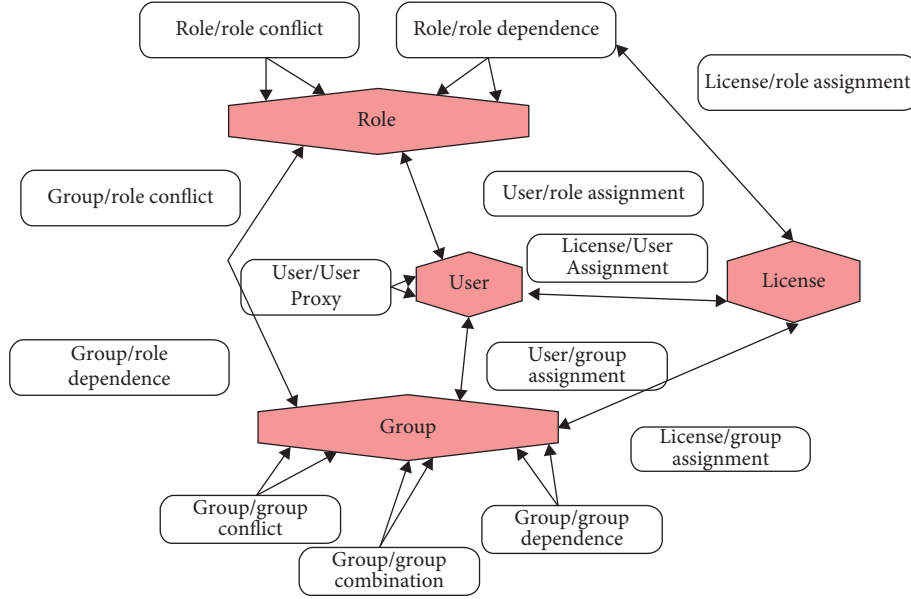
FIGURE 1: Access subject of multigranularity access control model MAC makes up the granular model.
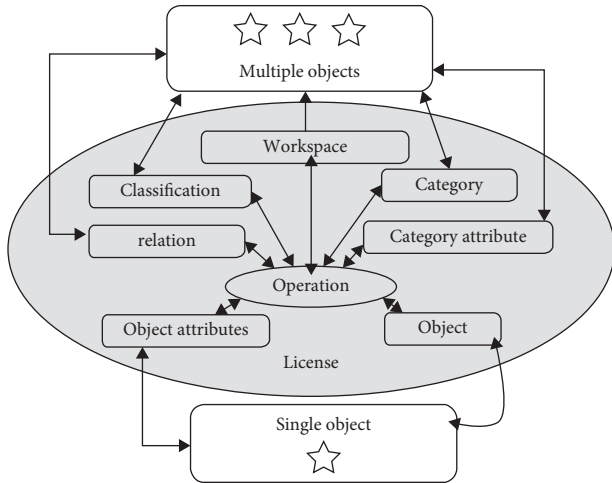
FIGURE 2: The process for multigranularity access control model MAC access to different object levels.

3. Multigranular Access Control Analysis

3.1. Control Subject and Object and Related Analysis.

TABLE 1: Access control direction combination relationship.

Control direction A	Control direction B	Combination result
Positive license	Negative license	Refusal
Positive license	Positive license	Allow
Positive license	Zero license	Allow
Negative license	Negative license	Refusal
Negative license	Zero license	Refusal
Zero license	Zero license	Refusal

First, the gradient descent training of error backpropagation is used to select and extract cluster members for the life cycle management of Industry 4.0 engineering products to provide an accurate data basis for subsequent cluster fusion. There is the actual sequence $\{x(t_0 + i\Delta t)\}$ of the information flow of the life cycle management Industry 4.0 engineering product data and $i = 0, 1, \ldots, N - 1$. After setting X and Y as the Industry 4.0 engineering product life cycle management attribute set, the cluster space state vector calculation formula of the Industry 4.0 engineering product life cycle management is

$$X = [x(t_0), x(t_0 + \Delta t), \ldots, x(t_0 + (K-1)\Delta t)] =$$

$$\begin{bmatrix} x(t_0) & x(t_0 + \Delta t) & \cdots & x(t_0 + (K-1)\Delta t) \\ x(t_0 + J\Delta t) & x(t_0 + (J+1)\Delta t) & \cdots & x(t_0 + (K-1)J\Delta t) \\ \vdots & \vdots & \vdots & \vdots \\ x(t_0 + (m-1)J\Delta t) & x(t_0 + (1 + (m-1)J\Delta t)) & \cdots & x(t_0 + (N-1)\Delta t) \end{bmatrix}. \quad (1)$$

In the formula, $x(t)$ represents the time series of the life cycle management information flow of Industry 4.0 engineering products. J represents the phase space time window function of the life cycle management reconstruction of the Industry 4.0 engineering product data and m represents the life cycle management cluster adjustment factor of the target engineering product data. Δt represents the sampling time interval of Industry 4.0 engineering product data.

Then the calculation expression of the discrete sample spectrum feature quantity for the life cycle management of Industry 4.0 engineering products is as follows:

$$X_p(u) = s_c(t)e^{j2\pi f_0 t} = \frac{1}{T}\text{rect}\left(\frac{t}{T}\right)^{j2\pi(f_0 t + Kt^2)/2}. \tag{2}$$

The formula $s_c(t)$ represents the characteristic scalar time series of the life cycle management of Industry 4.0 engineering products. $e^{j2\pi f_0 t}$ represents the discrete sample center of the Industry 4.0 engineering product life cycle management cluster.

$$u_{(i,d)}^{(k+1)} = \begin{cases} x_{(i,d)}^{(t+1)} & f_{\text{titness}}^t < f_{\text{fitness}}^*, \\ z_{(i,d)}^{(k+1)} & f_{\text{titness}}^t \geq f_{\text{fitness}}^*, \end{cases} \tag{3}$$

f_{fitness}^t is the expression representing the reliability coefficient of the life cycle management of Industry 4.0 engineering products. f_{fitness}^* represents the reliability interval coefficient for the life cycle management of Industry 4.0 engineering products.

According to the calculation of formulas (2) and (3), the best solution vector matrix formula for the life cycle management of Industry 4.0 engineering products centered on data clusters is

$$\Sigma_r = \text{diag}(\sigma_1, \sigma_2, \ldots, \sigma_r) \in R^{r \times r}. \tag{4}$$

The formula σ_r represents the position of Industry 4.0 engineering product life cycle management to $k+1$. $R^{r \times r}$ represents the actual matrix of Industry 4.0 engineering product life cycle management.

The diagonal vector indicator of the life cycle management of Industry 4.0 engineering products is close to the target solution, and the following conditions can be met:

$$\sigma_1 \geq \sigma_2 \geq \cdots \geq \sigma_r > 0. \tag{5}$$

According to the granularity fusion, the IEPLCM system can be divided into related extensions of the control main control, as shown in Figures 3 and 4.

3.2. Analysis of Relevant Elements of Multigranular Access Control.
Industry 4.0 engineering product life cycle management selection results, diversity and accuracy are used to define, comprehensive evaluate, and complete the selectivity of Industry 4.0 engineering product life cycle management. By searching the particle swarm in the Industry 4.0 engineering product life cycle management cluster to form the Industry 4.0 engineering product life cycle, the corresponding Industry 4.0 engineering product life cycle management data information feature vector χ_i is expressed as

$$l_\varepsilon(g) = (1 - \rho)l_\varepsilon(g-1) + \gamma f(\chi_i(g)). \tag{6}$$

In the above expression, f represents the corresponding adaptive function of the feature data feature vector χ_i of the life cycle management of Industry 4.0 engineering products. $\gamma \chi_i(g)$ represents the ε-th life cycle management corresponding media engineering product data optimization in the actual application process.

The expression of clustering π_p in Industry 4.0 engineering product life cycle management II is

$$\text{Acu}(\pi_p) = \text{NMI}(\pi_p, \pi^*). \tag{7}$$

In the formula, π_p and π_q represent the clustering integration of the life cycle management of Industry 4.0 engineering products. If there is less information shared with the Industry 4.0 engineering product life cycle management basic cluster, the accuracy of the basic cluster is low, and vice versa.

Based on the accuracy and diversity characteristics of the clusters based on the life cycle management of Industry 4.0 engineering products, the comprehensive evaluation criteria that define the clusters based on the life cycle management of Industry 4.0 engineering products include

$$\text{Eval}(\pi_p) = \lambda \text{Acu}(\pi_p) + (1 - \lambda)\text{Div}(\pi_p). \tag{8}$$

In the formula $\lambda \in [0, 1]$, the accuracy and diversity of the life cycle management of Industry 4.0 engineering products are an important degree in the comprehensive evaluation standard.

Based on the diversity $\text{Div}(\pi_p)$ of the basic clustering of Industry 4.0 engineering product life cycle management, formula (8) calculates the probability $\text{pro}(\pi_p)$ of selecting the basic clustering algorithm of each Industry 4.0 engineering product life cycle management as the optimized basic clustering. The calculation formula is as follows:

$$\text{pro}(\pi_p) = \frac{\text{Div}(\pi_p)}{\sum_{p=1}^{B} \text{Div}(\pi_p)}. \tag{9}$$

The $\text{pro}(\pi_p)$ calculation result of the benchmark formula (9) is used to use roulette to randomly select the cluster based on the life cycle management of the Industry 4.0 engineering product and obtain the integration cluster of the Industry 4.0 engineering product life cycle management.

If there are N data in the life cycle management of Industry 4.0 engineering products, the attribute dimension of the data can be represented by w, and the position and velocity matrix of Industry 4.0 engineering product data can be represented by N:

$$\delta_1^1 \delta_1^2 \cdots \delta_1^w \delta_1^1 \delta_1^2 \cdots \delta_2^w \cdots \delta_\tau^1 \delta_\tau^2 \cdots \delta_\tau^w \delta_1^1 \cdots \delta_1^w f. \tag{10}$$

Industry 4.0 engineering product life cycle management particle group overall fitness decentralized

$$\psi^2 = -\sum_{\eta=1}^{v} \left(\frac{f_i - f_{\text{avg}}}{f}\right). \tag{11}$$
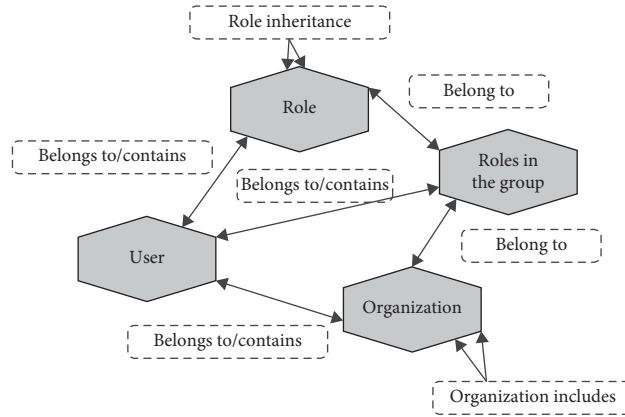
Figure 3: Correlative spread of common subjects.
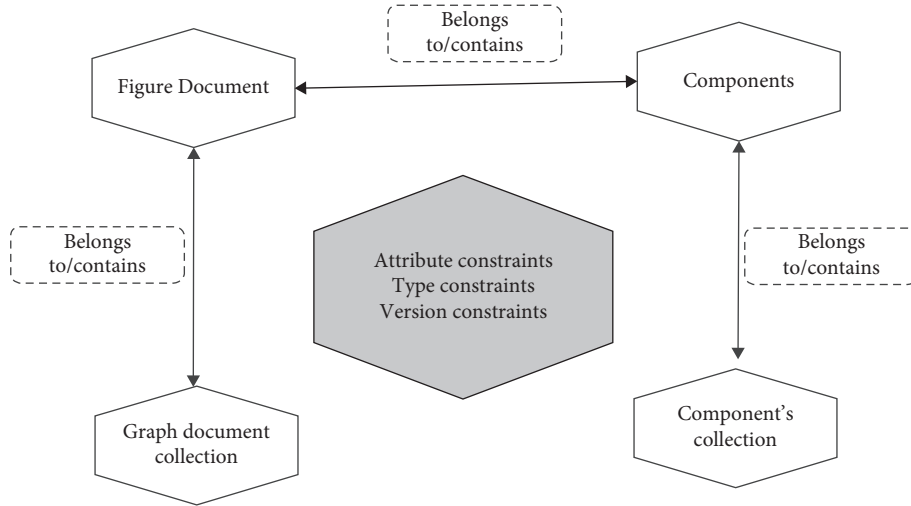
Figure 4: Correlative spread of common objects.

In the formula, v represents the number of particles of Industry 4.0 engineering product life cycle management. f_i represents the matching degree value of the ηth Industry 4.0 engineering product life cycle management particle. f_{avgA} represents the average fitness value of current particles in the life cycle management of Industry 4.0 engineering products.

$\psi^2 < \varphi$ represents the determination threshold of the Industry 4.0 engineering product life cycle management φ and can perform optimization of updating the position and velocity of Industry 4.0 engineering product data particles according to the following expressions:

$$v_t = \omega v_{t-1} + \kappa_1 \times \text{rand}_1 \left(\text{pbest} - x_{t-1}\right) + \kappa_2 \times \text{rand}_2 \left(\text{gbest} - x_{t-1}\right), \tag{12}$$

$$x_t = x_{t-1} + v_t. \tag{13}$$

3.3. Key Algorithms for Multigranular Access Control. As
mentioned above, to judge authority through access objects and related analysis, we must fully consider the spreading mechanism between access objects. This solves the set of equivalent access subjects associated with the detection target user and the set of equivalent control clients corresponding to the control target instance. It also provides a basis for authentication based on access control permissions.

Because the solver process that controls the set of equivalent access subjects and the set of objects is similar, the following only introduces the solver process of the set of equivalent access subjects. The pseudo-algorithm for solving the set of equivalent access subjects is described below.

The purpose of IEPLCM's multigranular access control is to temporarily allow or deny the request based on predefined permissions when a specific user requests access to

Input: user u and its context
Output: the equivalent access subject of user U $S_{eqv}(u)$
Begin
Initialize the equivalent access subject set;
Suppose the current detection visitor $s = u$;
According to the subject spread rule, obtain the subject spread set $P(s)$ of s;
Foreach ($p \in p(s)$)
Judge whether p is already in $S_{eqv}(u)$, if not, add p in it, and repeat the previous step with $s = p$;
After the recursive solution of the above process, the final complete result is obtained.
End

ALGORITHM 1: Equivalent access subject set solution.

specific product components or text data. When the access is determined to be a function, the entry parameter of the function is user u. In addition, the operation op performed by the requested access control client object functions as a function that returns b according to a predefined access rule. If the return value of the function is true, it can be executed [6, 7]. On the contrary, the access request is denied, and the corresponding access control is shown in Algorithm 2 based on the analysis of the abovementioned access control model components and masters, guests, and their related relationships pseudo-algorithm of the project process.

It can be seen from Algorithm 2 that the solver process for verifying access control authority is a process of multiple nested loops to ensure the efficiency of the algorithm. The number of permitted rule items sets common access control items for control guests (such as certain types of text, components) that have the meaning of data sets and sets special and individual access control items for specific control guests to achieve access control of data.

4. Product Life Cycle Management Process under the Multigranularity Access Control Model

4.1. Multigranularity Access Control Model.
It describes the composition granularity of the access subject, the level granularity of the access object, the granularity of the life cycle, and the license allocation control granularity from different aspects and levels to control the access to PLM. Based on the above analysis, as shown in Figure 5, a PLM access control model based on RBAC is constructed.

4.2. Formal Description of Multigranularity Access Control Model.
MGACM usually adopts a closed type with three layers of feedforward neural Industry 4.0 engineering products. In the model in this paper, it is assumed that the Industry 4.0 engineering product topology is shown in Figure 6, and there are m nodes in the input layer, h nodes in the hidden layer, and n nodes in the output layer. The input samples are represented by $X_1 \sim X_m$ and the output samples are represented by $Y_1 \sim Y_n$. The stretching and translation parameters are expressed by $a_1 \sim a_h$ $b_1 \sim b_h$, respectively. The link weights in Industry 4.0 engineering products between the input layer to the hidden layer and the hidden layer to the output layer are represented by $w_{11} \sim w_{mh}$ $w_{11}' \sim w_{hn}'$, respectively.

For the hidden layer, Morlet is selected as the main wavelet function and its equation is as follows:

$$\psi(x) = \cos(1.75x)\exp\left(-\frac{x^2}{2}\right). \tag{14}$$

The number h of hidden layer nodes is determined by the number m of input layer nodes. Calculation formula is

$$h = 2m + 1. \tag{15}$$

It follows that

$$g(x) = \frac{1}{[1 + \exp(-x)]}. \tag{16}$$

The x in (1) and (3) represents the data of the previous layer.

The output result of MGACM based on wavelet function is

$$Y_t = \sum_{s=1}^{h} w_{st}'\psi\left(\frac{\sum_{r=1}^{m} w_{rs} - b_s}{a_s}\right). \tag{17}$$

Generally, the gradient descent method is used to calculate the connection weight of Industry 4.0 engineering products, and the parameters in MGACM are more accurate than before. The extreme points of this method are only approximate values. Meanwhile, it is easily troubled by the problem of the best local Industry 4.0 engineering products. Therefore, this article intends to use an improved multigranularity access control model to optimize the parameters of local Industry 4.0 engineering products.

The increase of the fitness value determines the development direction of the multigranular access control model. The error E of MGACM is defined as an individual fitness function:

$$E = \frac{1}{2}\sum_{t=1}^{n}(Y_t - Y_t')^2, \tag{18}$$

$$f = \frac{1}{1 + E}, \tag{19}$$

Input: request user u, request access control object o and its current state os, request operation op
Output: the calculation result of F (u, op, o, os)
Begin
Solve the set of equivalent access F (subject set of u $S_{eqv}(u)$ and the set of equivalent access control object of o $O_{eqv}(o)$, refer to Algorithm 1 for the solution process;
foreach (o_i in $O_{eqv}(o)$))
{
Query the data access rule set R that satisfies the input condition constraints from the authorization rules associated with o_i
foreach (u_i in $S_{eqv}(u)$)
{
foreach (cs in R), where cs is the complex access subject corresponding to the access rule set
{
if ($u_i \in cs$)
{
return true
}
}
}
}
return false;
End

ALGORITHM 2: Access control authority verification solution.
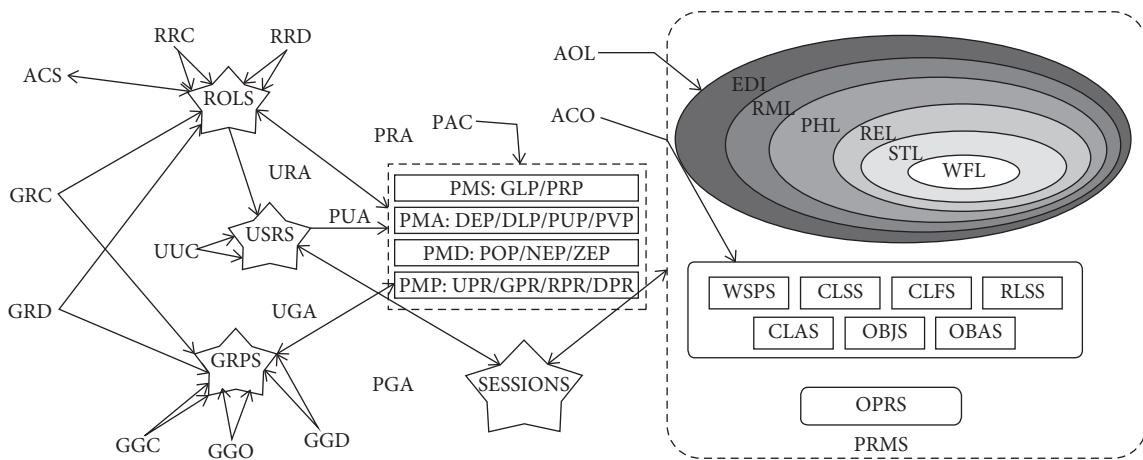

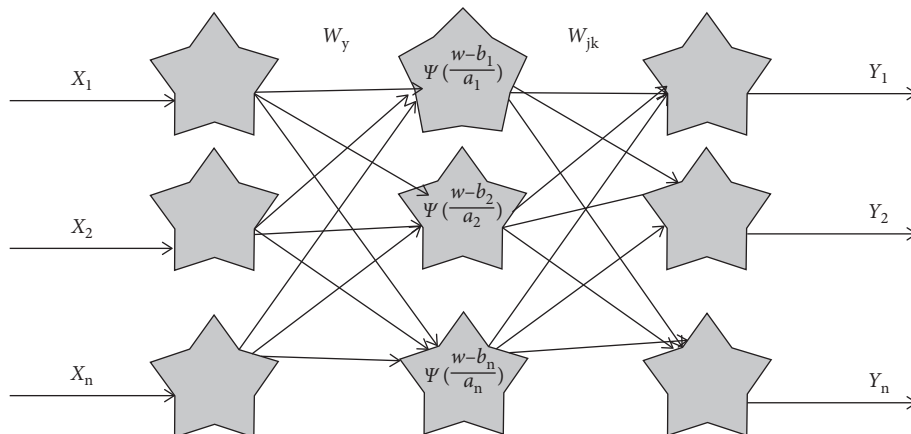FIGURE 5: Multigranularity access control model and its elements.

FIGURE 6: MGACM's Industry 4.0 engineering product topology.

where Y_t represents the real value of the t-th output node, and Y_t' represents the predicted output.

The most common selection operation is to choose roulette. However, the predictive model is selected with the expected value so as not to harm the best individual at the smaller number of samples [8, 9]. Expected value is calculated by (20). Therefore, the problem of probability is transformed into a problem of frequency. In the meantime, excellent personal retention institutions directly allow individuals to maintain the highest fitness value of the next generation of modern times.

$$q_i = \frac{f_i}{f_{\text{sum}}/N}, \quad i \leq N. \tag{20}$$

This represents the sum of the overall individual fitness values. f_{sum} represents the sum of all individual fitness values. f_i represents the ith personal health value. N represents the total number of people. In addition, rounding is required by q_i.

The choice of parameters is very important in the simulation process of the multigranularity access control model. For fixed values, the classic access control model always relies on crossover and mutation probabilities. However, it cannot dynamically adjust the probability of multigranularity in the evolution process, and the convergence speed is unstable. In addition, in order to deal with crossover operators and mutation operators, a multigranularity access control method is adopted in this paper. The multigranularity access control model probabilities p_c and p_m are defined in the following equations:

$$p_c = \begin{cases} \alpha_1 - \dfrac{(\alpha_1 - \alpha_2)(f_{\max} - f')}{f_{\max} - f_{\text{avg}}}, & f' \geq f_{\text{avg}}, \\[3mm] \alpha_2, & \text{else}, \end{cases} \tag{21}$$

$$p_m = \begin{cases} \beta_1 - \dfrac{(\beta_1 - \beta_2)(f_{\max} - f)}{f_{\max} - f_{\text{avg}}}, & f \geq f_{\text{avg}}, \\[3mm] \beta_2, & \text{else}. \end{cases} \tag{22}$$

Among them, α_1, α_2, β_1, β_2, respectively, represent random values between [0, 1]. In this paper, $\alpha_1 = 0.8$, $\alpha_2 = 0.5$, $\beta_1 = 0.05$, $\beta_2 = 0.001$ are assumed. $f_{\max}$ represents the largest individual fitness value in the population. The average personal fitness value is represented by f_{avg}. The parent fitness value before the crossover operation is expressed as f'. *f represents the fitness value suitable for the mutated individual.* Assuming that the initial multigranularity randomly generates $N \times m \times n$ data, the complexity of the algorithm is $O(m^2 \times n^2)$.

Suppose there are N individuals with multiple granular dimensions. Depending on the size of the genetic factor, problems sometimes arise in real numbers. Therefore, the real number multigranularity should be normalized by the following function:

$$\hat{x}_{pj} = \frac{(x_{pj} - x_{pj\min})}{x(x_{pj\max} - x_{pj\min})}, \tag{23}$$

where x_{pj} represents the multigranularity of the p-th individual at the j-th point in the genetic sequence.

After normalization by (23), the fuzzy similarity matrix R between individuals is created by

$$R_{pq} = \frac{\sum_{k=1}^{Chromlen} \min(\hat{x}_{pk}, \hat{x}_{qk})}{\sum_{k=1}^{Chromlen} \max(\hat{x}_{pk}, \hat{x}_{qk})} \tag{24}$$

The fuzzy similarity matrix satisfies reflexivity and symmetry. According to [10, 11], the ambiguous equivalent matrix solves the problem of ecology degree more effectively. Therefore, by searching the fuzzy minimum transmission limit of the similar matrix R, the corresponding ambiguity equivalent matrix T is obtained in this paper, and the matrix is clustered as a whole.

If the similarity coefficient λ is less than the coefficient T_{pq} of each pair of individuals, that is, $\lambda \leq T_{pq}$, the individuals x_p and x_q are divided into the same niche, until all individuals are divided into appropriate positions.

$$\text{Niche}(k) \Leftarrow \{x_p \cdots x_q\} (1 \leq k \leq \text{Chromlen}). \tag{25}$$

Based on the fuzzy equivalent matrix and the total number, the similarity coefficients λ are dynamically updated as follows:

$$\lambda_t = \frac{\sum_{j=1}^{N} T_{\max j}}{N}. \tag{26}$$

Among them, $T_{\max j}$ represents the equivalent coefficient between the individual with the maximum fitness value $x_{\max}$ and the individual x_j.

In order to use the improved multigranularity access control model to quantitatively analyze the diversity, equation (27) is defined to calculate the multigranularity diversity.

$$d_t = -\sum_{n=1}^{Q} p_n \log(p_n), \tag{27}$$

$$p_n = \frac{L_{mn}}{N}, \tag{28}$$

where Q represents the number of submultigranularities in the t-th generation, $T_{\max j}$ represents the number of n-th submultigranularities, and N represents the total number of individuals of the species. *The higher the d, the greater the diversity.*

If the fitness value for a certain ecological location is much smaller than other values

$$|f_i - f_{\max}| < f_{\text{default}}, \tag{29}$$

then

$$f_i = f_{niche}(i), \quad 1 \leq i \leq n, \tag{30}$$

$$f_{niche} = (f_1', f_2', f_3', \ldots, f_n'), \tag{31}$$

where f_{max} is the highest applicability value in the same generation. The default threshold of the adaptability value is $f_{default}$. $f_{niche}(i)$ represents the fitness of the i-th individual.

4.3. The Permission Consistency Control Operation of the Multigranularity Access Control Model. The session of the multigranularity access control model refers to the process in which a specific user registers and applies the permissions he owns. Through different login methods, the session includes the current user global authentication registration, proxy user global authentication registration, current user project registration, and proxy user project authorization registration. If the login user is set to u, then for any registration method, user u's permission distribution comes from the following 7 methods, allowing direct assignment to users.

$$PA_u(u) = u\_a\_ps(u). \tag{32}$$

The licenses owned by the user's group:

$$PA_{ug}(u) = \bigcup_{g \in u\_a\_gs(u)} g\_a\_ps(g). \tag{33}$$

The permissions owned by the user's role:

$$PA_{ur}(u) = \bigcup_{r \in u\_a\_rs(u)} r\_a\_ps(r),$$
$$PA_{gg}(u) = \bigcup_{g \in \left(\bigcup_{g_y \in u\_a\_gs(u)} g\_d\_gs(g_y) \right)} g\_a\_ps(g). \tag{34}$$

The permission of the user's group on which the user relies:

$$PA_{gr}(u) = \{(p, PAC)|PAC.PMA = DE \ P \lor PAC.PMA = PUP\},$$
$$PA_{rr}(u) \subseteq \bigcup_{r \in \left(\bigcup_{r_y \in u\_a\_r(u)} r\_d\_rs(r_y) \right)} r\_a\_ps(r). \tag{35}$$

The permission of the role that the user's group relies on, and

$$PA_{rr}(u) = \{(p, PAC)|PAC.PMA = DE \ P \lor PAC.PMA = PUP\},$$
$$PA_{rr}(u) \subseteq \bigcup_{r \in \left(\bigcup_{r_y \in u\_a\_r(u)} r\_d\_rs(r_y) \right)} r\_a\_ps(r). \tag{36}$$

The permission of the group on which the user's role depends:

$$PA_{rr}(u) = \{(p, PAC)|PAC.PMA = DE \ P \lor PAC.PMA = PUP\}. \tag{37}$$

Therefore, all the licenses of user u are allocated as

$$PA(u) = PA_u(u) \cup PA_{ug}(u) \cup PA_{ur}(u) \cup PA_{gg}(u) \cup PA_{gr}(u)$$
$$\cup PA_{rg}(u) \cup PA_{rr}(u). \tag{38}$$

License consistency control refers to the combined operation of all the licenses that have the same life cycle state, the same object, and the same operation, but the license distribution control combination operation of all permissions, to finally determine whether this operation is allowed to be executed [12, 13]. Let PA denote a single license distribution, and the license distributions in the four sessions are denoted as $PA_g(u)$, $PA_{dg}(u)$, $PA_p(u)$, and $PA_{dp}(u)$, respectively. The main flow of the permission consistency control algorithm is shown in Figure 7.

The main steps are described as follows:

(1) u log in and load all the license distribution $P(u)$ according to the seven aspects of license distribution. If the proxy is u', all the licenses loaded into u' are allocated to $P(u')$, and all the licenses that can be delegated to $P(u')$ need to be filtered out, that is, all the licenses owned by u as a proxy.

(2) According to whether it is a global authorization, filter with the condition pa.PAC.PMS = GLP to form the current user global permission $PA_g(u)$, current user project permission $PA_p(u)$, proxy user global permission $PA_{dg}(u)$, and proxy user project permission $PA_{dp}(u)$.

(3) If it is a global license, you only need to filter the license set according to the current ACO, AOL, and OPR and obtain all the license sets $P_{cur}(u)$ for the operation of the object in the current life state. If it is a project license, it must not only filter according to ACO, AOL, and OPR, but also filter according to pa.PAC.PMS = PRP, but if the obtained license set is null, the global license of the current object needs to be borrowed; that is, it will be filtered once based on ACO, AOL, and OPR filter again, to get $P_{cur}(u)$.

(4) In view of $P_{cur}(u)$, according to the priority of license allocation, select all the license allocations $P_{pri}(u)$ with the highest priority. Then let the positive license be 1, the negative license is −] (can be replaced by a larger negative number), the zero license is 0, and the pa.PAC.PMD is solved in the sum $P_{pri}(u)$. If the result is greater than zero, the execution is allowed; otherwise the execution is refused [14, 15].

5. Examples and Results Analysis

5.1. Data Preprocessing. In order to verify the validity of the predictive model, the real security provided by the laboratory Industry 4.0 engineering product life cycle management platform is adopted in this paper. The data, based on the evaluation of the safety status of Industry 4.0 engineering products, effectively realized the prediction of the value of the safety status of Industry 4.0 engineering products.

The 90-day continuous data is selected from the product lifecycle management platform for experiment. This data can
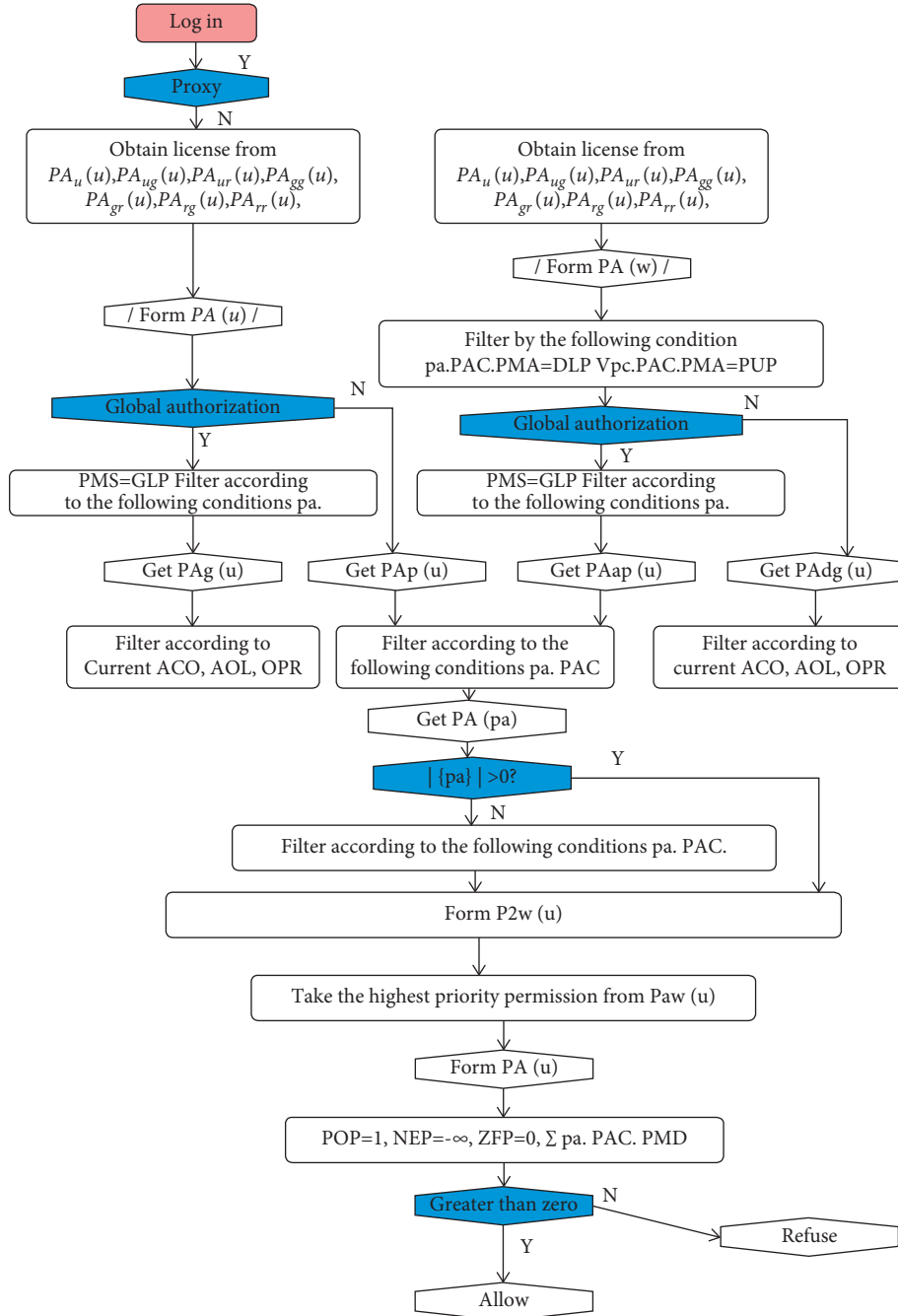
FIGURE 7: Multigranularity access control model MAC permission consistency control process.

be divided into two parts. As a training sample 76 days ago, the remaining 14 days were used as a test sample. According to the analysis of security data, deep attacks will be carried out regularly within 5 days. Therefore, this paper uses 5 days as the vector dimension input and 1 day as the vector dimension output. The selection of the dimension of the security situation is shown in Table 2. Confirm that the prediction model of MGACM Industry 4.0 engineering product structure is 5-11-1.

The magnitude difference in the value of the safety situation of Industry 4.0 engineering products will affect the education of Industry 4.0 engineering products. In order to

TABLE 2: Selection of security status dimensions.

Input sample	Output sample
X_1, X_2, X_3, X_4, X_5	X_6
X_2, X_3, X_4, X_5, X_6	X_7
...	...
$X_{71}, X_{72}, X_{73}, X_{74}, X_{75}$	X_{76}

avoid this phenomenon, the safety status values of Industry 4.0 engineering products within 90 days are standardized as follows:

$$\widehat{X} = \frac{(X - X_{\min})}{(X_{\max} - X_{\min})}. \tag{39}$$

This includes the minimum value of the sample and the maximum safety status value of the Industry 4.0 engineering product. X is the safety status value of the standardized Industry 4.0 engineering products successively.

Select the absolute error (AE), and define the mean relative error (MR) and mean square error (RMMSE) as the criterion for predicting accuracy.

$$AE = |Y_k - Y_k'|, \tag{40}$$

$$MRE = \frac{1}{N} \sum_{k=1}^{N} \left| \frac{Y_k - Y_k'}{Y_k} \right|, \tag{41}$$

$$RMSE = \sqrt{\frac{1}{N} \sum_{k=1}^{N} (Y_k - Y_k')^2}, \tag{42}$$

where N is the number of samples of the safety value of Industry 4.0 engineering products. It indicates the actual safety value of Industry 4.0 engineering products and displays the predicted value.

6. Results Analysis and Comparison

In order to prove the superiority of the proposed model, the MGACM, the performance of the multigranular access control model BP and that of the multigranular access control model MGACM are compared. Through the comprehensive training of these algorithms, we have selected convergence speed, diversity, and prediction accuracy to determine the advantages of these algorithms and verified the effectiveness of the proposed model.

In Figures 8 and 9, the horizontal axis represents the generation, and the vertical axis represents the squared error. It can be seen from this paper that different algorithms have different convergence speeds. The multigranularity access control model has the fastest convergence speed, converging to the 68th generation. The second high-speed algorithm is the multigranularity access control model PLM, which ended in the 118th generation. Multigranularity access control models BP and PLM stopped operating in the 139th and 359th generations, respectively, achieving convergence accuracy. Therefore, in this paper, we conclude that the combination of the modified small environment technology and the PLM model effectively reduces the convergence time and improves the prediction efficiency.

Therefore, this article attempts to increase product diversity to improve the premature problem of the multigranularity access control model. Equation (42) is the quantitative analysis of product diversity. It can be seen from Figure 9 that the diversity value of MGACM is stable in the early stage around 0.69. Comparing the classic and access control model, MGACM has great advantages in maintaining product diversity.
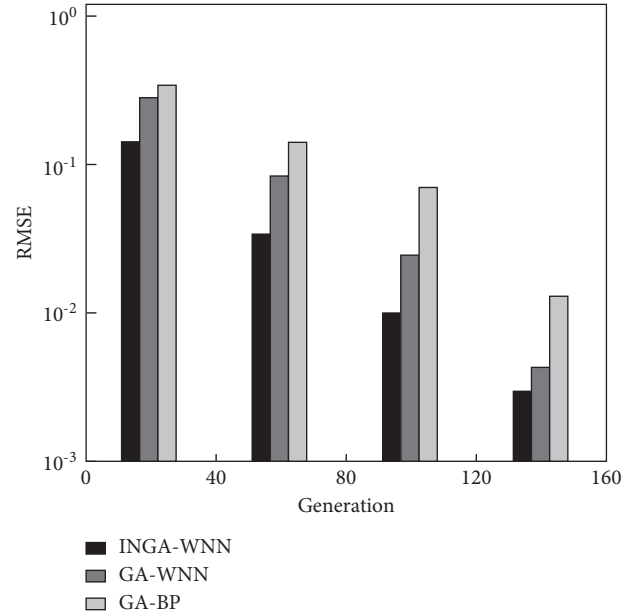
FIGURE 8: The convergence rate of the prediction model.
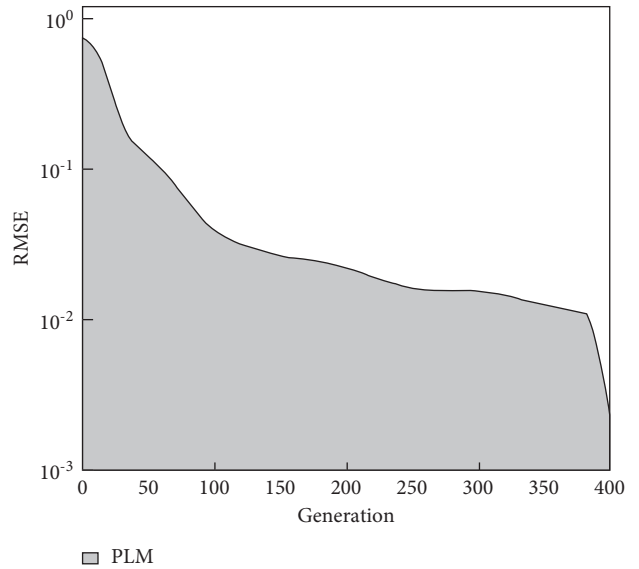
FIGURE 9: Convergence speed of PLM.

7. Conclusions

This paper proposes an MGACM security situation management model for Industry 4.0 engineering products, which uses an improved multigranularity access control model to optimize parameters. This management model combines an improved security situation analysis method with a multigranular access control model. Therefore, the new security situation analysis method has improved optimization capability and convergence speed of the multigranular access control model. In addition, the improvement of product diversity effectively solves the problems of premature and low convergence. The experiment proves the reliability and

validity of the multigranular access control model, which can also manage the security status of Industry 4.0 engineering products more accurately. Therefore, the multigranularity access control model MAC is suitable for large- and medium-sized enterprises, such as aviation and automobile enterprises, that have a wide variety of Industry 4.0 engineering products, complex structures, and strict access control.

Data Availability

The labeled dataset used to support the findings of this study is available from the corresponding author upon request.

Conflicts of Interest

The authors declare no conflicts of interest.

Acknowledgments

References

[1] F.-m. Zheng, L. Ma, N. Liu, and C. Jin-shan, "Assessment for distribution network planning schemes of urban electric power system," *Energy Procedia*, vol. 14, pp. 1067–1074, 2012.

[2] A. Anwar and A. N. Mahmood, "Anomaly detection in electric network database of smart grid: graph matching approach," *Electric Power Systems Research*, vol. 133, pp. 51–62, 2016.

[3] B. Tang, F. Li, Y. Yu, S. Feng, and Y. Wang, "Online static security analysis considering automatic device simulation for large power systems," *Dianli Xitong Zidonghua/Automation of Electric Power Systems*, vol. 35, no. 14, pp. 107–111, 2011.

[4] H.-G. Lee, J. Song, S.-S. Choi, and G.-H. Cho, "An advanced incident response methodology based on correlation analysis of polymorphic security events," *IEICE-Transactions on Communications*, vol. E96.B, no. 7, pp. 1803–1813, 2013.

[5] L. H. Liu, "Design and analysis of a power transmission network model of electric vehicle," *Key Engineering Materials*, vol. 693, pp. 45–52, 2016.

[6] V. Taratukhin and Y. Yadgarova, "Towards a socio-inspired multiagent approach for new generation of product life cycle management," *Procedia Computer Science*, vol. 12, no. 3, pp. 167–185, 2018.

[7] P. Hu and L. Wang, "Design of wireless local area network security program based on near field communication technology," *Lecture Notes in Electrical Engineering*, vol. 277, pp. 1109–1116, 2014.

[8] Z. H. Zhang, B. Y. Xu, Q. Chen, Y. Zhao, and C. Feng, "Optimal power flow control method of closed-loop distribution network with dual sources and fault seamless self-healing function," *Dianli Xitong Zidonghua/Automation of Electric Power Systems*, vol. 36, no. 12, pp. 101–106, 2012.

[9] H. Wang, G. Wang, J. Zhao, F. Wen, and J. Li, "Optimal planning for electric vehicle charging stations considering traffic network flows," *Dianli Xitong Zidonghua/automation of Electric Power Systems*, vol. 37, no. 13, pp. 63–69, 2013.

[10] W. R. Wessels and D. Sillivant, "Affordable reliability engineering: life-cycle cost analysis for sustainability & logistical support," *CRC Press*, vol. 38, no. 17, pp. 39–42, 2017.

[11] Z. Pan and Y. Zhang, "Index system and method for structure strength assessment of urban power network," *Zhongguo Dianji Gongcheng Xuebao/Proceedings of the Chinese Society of Electrical Engineering*, vol. 35, no. 16, pp. 3999–4005, 2015.

[12] Y. Guo, W. Wu, B. Zhang, and H. Sun, "Power system network parameter error identification by Lagrange multiplier based method," *Zhongguo Dianji Gongcheng Xuebao/Proceedings of the Chinese Society of Electrical Engineering*, vol. 33, no. 7, pp. 86–91, 2013.

[13] S. Song, X. Hu, J. Lu, and H. Li, "Power flow calculation of active distribution network based on fuzzy control theory," *Electrical Engineering*, vol. 14, no. 10, pp. 6–10, 2013.

[14] T. D. Hedberg, N. W. Hartman, P. Rosche, and K. Fischer, "Identified research directions for using manufacturing knowledge earlier in the product lifecycle," *International Journal of Production Research*, vol. 55, no. 4, pp. 819–827, 2017.

[15] N. Arena, P. Sinclair, J. Lee, and R. Clift, "Life cycle engineering of production, use and recovery of self-chilling beverage cans," *Journal of Cleaner Production*, vol. 142, no. 5, pp. 1562–1570, 2017.

Research Article

Four-Way Evolutionary Game Analysis of Government Project Bidding Collusion in a State of Limited Rationality Based on Prospect Theory

Chongsen Ma [ID], **Yun Chen** [ID], **and Sirui Nie** [ID]

College of Transportation Engineering, Changsha University of Science and Technology, Changsha, Hu Nan 410000, China

Correspondence should be addressed to Chongsen Ma; machongsen@stu.csust.edu.cn

Controlling collusion in government bidding is a prerequisite for ensuring social justice and the smooth operation of projects. Based on the prospect theory, this article establishes a four-party evolutionary game model for tenderers, enterprises with higher willingness to collude, enterprises with lower willingness to collude, and supervising enterprises. The study uses replication dynamics to analyze the stability of strategy selection after the evolutionary game. The results show that higher project base returns increase the probability of collusion, while lower market competition, higher risk aversion, and stronger collusive regulation all reduce the probability of collusion. When regulators adopt a strong regulatory strategy, the remaining project participants tend to choose a noncollusive strategy.

1. Introduction

Tendering is an effective way of acquiring and allocating resources developed over time in social and economic activities [1]. China's government investment projects primarily use bidding to determine the project builder. However, due to the asymmetry of information between the bidding parties, the trend of interests, and the imperfection of the restraint mechanism, the parties involved in the bidding process will produce collusion and other illegal and irregular behaviors to maximize their interests [2]. These behaviors will seriously affect the orderly development of China's construction market; therefore, it is of great theoretical and practical significance to control collusion in government investment projects' bidding processes.

The principal-agent theory and game theory are the main methods used by domestic scholars to analyze the engineering collusion phenomenon. Xie points out that although excessive competitive pressure in the construction market can induce collusion, its root cause is excessive returns and insufficient punishment [3]. According to Yu, information asymmetry caused by multiple entrustment relationships in

government-invested construction projects and the low cost of collusion are the main reasons for its emergence [4]. Cheng et al. argue that high profits in engineering projects' bidding processes are the leading cause of vertical collusion [5]. Miklos-Thal argues that collusion is possible without additional costs, but the presence of additional costs can facilitate its occurrence in cases of asymmetric collusion costs [6]. Through their investigation, Yun Chen et al. found that technical and environmental causes are more critical to creating vertical collusion [1].

Current research provides diverse solutions on control measures for collusion in bidding in government investment projects. For example, Wu et al. combined prospect theory and game theory to establish a collusion regulation deterrence model to regulate collusion in government investment projects [7]. Wang Xianjia et al. constructed a control model to prevent collusion between bidding agents and tenderers in the bidding process based on the "prisoner's dilemma" game [8]. Chen et al. used the cooperative game model to analyze the conditions of collusion and provide a reference for the policy formulation of collusion control [9]. Zhang and Wang constructed a two-sided game

model between owners and bid evaluation experts and established a control model to prevent collusion with bid evaluation experts [10].

The above literature review shows that although more scholars have researched vertical collusion in government investment project bidding, the research results have certain limitations due to the methods adopted, mainly focusing on game theory and principal-agent theory. The existing studies focus less on each participant's risk attitude and propensity on a behavioral decision. For simplification, the existing game models on the game behavior research process of vertical collusion process usually consider only two-party or three-party games, which cannot entirely reflect the actual situation [11–21]. In the bidding process of government investment projects, each participant shows different degrees of risk awareness and risk appetite due to different risk management behaviors in the face of complex and variable risk factors. The dynamic formation process of owners' and contractors' risk management behaviors can be seen as the process of both parties adjusting their strategies to form a final stable strategy through trial and error, summarization, and imitation. These methods are consistent with the characteristics of evolutionary games and can be analyzed by evolutionary game theory. This study helps each participant in the bidding process of government investment projects make reasonable risk management decisions by examining each participant's evolutionary behavior in the bidding process of government investment projects. The value function of prospect theory is introduced into the evolutionary game theory, based on the consideration of different collusion tendencies. The risk-benefit perception matrix is constructed to analyze the evolutionary process and inner law of the decision-making behaviors of bidding parties, subjects with high collusion tendencies, subjects with low collusion tendencies, and regulators. Based on MATLAB simulation, the influence of relevant factors on the evolutionary results is analyzed. Therefore, this article introduces prospect theory based on the original evolutionary game approach to analyze collusion in the bidding process. This article divides the bidders into high collusion willingness bidders and low collusion willingness bidders for analysis so that the model is more suitable to the actual situation.

The innovations of this paper are mainly in two ways:

(1) Most of the existing studies related to evolutionary games use two-party or three-party games, regardless of the topic and context of the paper's research. This study considers the game behaviour of four parties in the process of vertical collusive control of government investment project bidding. It has certain contribution in the model approach and broadens the existing research ideas and research perspectives.

(2) In the current research on vertical collusion in bidding for government investment projects in China, most of the parameters for the benefits and costs of each entity are set only considering the impact of penalties such as fines and penalties. Less consideration has been given to social recognition and the possible impact on future development

gains. The study introduces indicators such as the degree of market competition and loss of social recognition to provide an in-depth analysis of the benefits and costs of each subject. By diversifying the parameter model and introducing more detailed considerations, the results of the study are more relevant and reliable.

2. Simulation Model Construction

2.1. Simulation Analysis Model for the Evolution of Collusive Bidding Behavior. Vertical collusion is repeatedly prohibited in the bidding process of government investment projects. Existing studies usually view bidders as a whole, and they are considered to have a high degree of similarity in their behavior. However, in practice, different bid groups have different perceptions of factors such as potential benefits, penalties, and the probability of detection of vertical collusion, as well as large differences in the business philosophies of different companies. Even under the same external conditions, there are significant gaps in decision making between different bid groups. Therefore, this article divides bidders into two groups, high and low, according to their willingness to participate in collusion to improve the study's credibility. Bidders with high collusion willingness will actively seek collusion opportunities and promote collusive behavior. Firms with low collusion willingness are less likely to collude when faced with opportunities, and at the same time, may report collusive behavior.

In this study's evolutionary game-theoretical model, there are four game subjects: bidders, enterprises with a high willingness to collude, enterprises with a low willingness to collude, and regulators. The four parties influence each other in the bidding process. Some enterprises may choose to collude with the government to obtain a project, adopting forms such as bid-rigging and bid-rigging to obtain excessive profits; the regulator (including the regulator and the people) accepts the government's commission or spontaneously carries out supervision of the project. The government entrusts the regulators (including the regulator and the people), or they spontaneously supervise the project; the regulators' management also has a certain influence on the behavior of the government and enterprises. This article focuses on the vertical collusion in the bidding process of government investment projects. In government investment projects, the government side is the bidding side. In the bidding process, there is a bidding side to release the project; enterprises obtain the project by bidding. However, the bidding process involves inconsistency of different enterprises' business philosophies and decision-making tendencies. As such, enterprises with higher willingness to collude and those with lower willingness to collude will have a higher possibility of providing benefits to the bidders and seeking the opportunity to collude to obtain the project. Companies with a lower willingness to collude will not actively seek opportunities for collusion and will monitor and report any collusion found. Bidders, companies with a high willingness to collude, and companies with a low willingness to collude are all subject to the regulator's supervision. Due to the

incomplete symmetry of information and the imperfect rationality of the government and the parties involved in the game, all parties involved may act opportunistically in the project's construction process, making it impossible for all parties to obtain maximum utility. Figure 1 shows the relationship between the various interest subjects in the bidding process.

2.2. Model Assumptions

Assumption 1. The four main players in the game are the bidders, enterprises with higher willingness to collude, enterprises with lower willingness to collude, and the regulator. In the bidding process, the bidders prefer enterprises involved in collusion as the winning bidders. The colluding enterprises must pay a certain extra cost while fulfilling the contract conditions. The regulators monitor the enterprises involved in bidding to reduce corruption and collusion in the project. The enterprises not involved in collusion have a certain probability of reporting parties involved in collusion to ensure their rights and interests.

Assumption 2. In the project bidding process, all stakeholders are finite rational "economic agents," i.e., the parties involved in the project are not fully rational. In the game process, all four parties play a limited number of repeated games.

Assumption 3. Traditional evolutionary games are based on expected utility theory. They do not consider the influence of the various project participants in the decision-making process on the game's outcome due to psychological perception factors. This article addresses the problem by using the prospect theory proposed by Kahneman et al. to modify decision-makers' inconsistent risk preference behavior. The theory states that one cannot have an absolute perception of losses and gains but rather a relative value of perceived losses, expressed using $\Delta\omega 1$, the difference between the actual loss or gain $\omega 1$ and a reference point $\omega 0$. This reference point is subject to the influence of the decision-maker and is chosen differently across research areas. This paper chooses 0 as the reference point. In prospect theory, the expected total utility of a decision is measured using the value function $v(\Delta\omega 1)$ and the weighting function p. The prospect value is

$$V = \sum_{\iota} \pi(p\iota)v(\Delta\omega\iota). \tag{1}$$

Each participating subject makes a judgment on its next move based on its perceived value of the lost gain, and the value function is

$$V(\Delta\omega_i) = \begin{cases} (\Delta\omega_i)^\theta, & \Delta\omega_i \geq 0, \\ -\lambda(-\Delta\omega_i)^\theta & \Delta\omega_i < 0, \end{cases} \tag{2}$$

where θ is the risk attitude coefficient, indicating the game subject's marginal degree of diminishing perceived value of profit and loss. λ is the loss avoidance coefficient, indicating
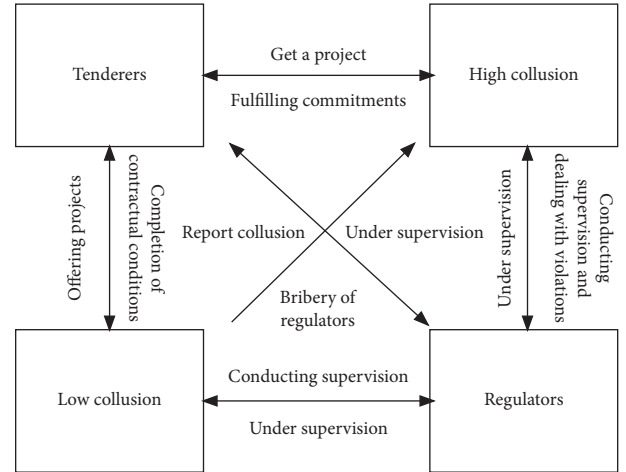

Figure 1: Four-way diagram of the game.

the game subject's sensitivity to loss; the larger the value, the greater the game subject's sensitivity to loss. At the same time, the game subject judges the weights according to the actual situation of the event, using the formula:

$$\pi(p_i) = \frac{p^\gamma}{(p^\gamma + (1-p)^\gamma)^{1/\gamma}}. \tag{3}$$

Except for minimal probability events, $\pi(p_i) < p_i$, $\pi(p_i) + \pi(1-p_i) \leq 1$ and $\pi(1) = 1$, $\pi(0) = 0$. In prospect theory, the probability of a low-probability event occurring is usually overestimated, and the probability of a high-probability event occurring is usually underestimated.

Assumption 4. The government has two strategies based on its interests and overall interests: participating in government-enterprise collusion or not participating in government-enterprise collusion. Similarly, enterprises with a high willingness to collude have two strategies: to participate in collusion actively or not actively participating in collusion. Enterprises with a low willingness to collude can either report collusion or not. Regulators also have two strategies: to strongly or weakly regulate collusion. A tenderer's probability of adopting a government-enterprise collusion strategy is x. The probability of a firm with a high collusion willingness implementing an active collusion strategy is y, the probability of a company with a low willingness to collude adopting a reporting collusion strategy is z, and the probability of a regulator adopting a strong regulatory model is m ($0 \leq x \leq 1$, $0 \leq y \leq 1$, $0 \leq z \leq 1$, $0 \leq m \leq 1$). Thus, the tenderer's probability of not participating in government-business collusion is $1 - x$. The probability of companies with high willingness to collude of not actively participating in collusion is $1 - y$, the probability of companies with low willingness to collude of not reporting collusion is $1 - z$, and the probability of regulators adopting the weak regulatory model is $1 - m$.

Assumption 5. The government's choice to engage in collusion means that, in the bidding process, it will give preference to a company willing to collude as the winning

bidder; if it chooses not to collude, the government will choose the best company as the winning bidder. Selecting a company with a high willingness to collude means that the company will actively seek collusion plans from the authorities, including bribes, etc., to obtain the project. Choosing not to participate in collusion actively means that, although the enterprise is willing to collude, it does not want to pay extra for collusion. Enterprises with a low willingness to collude that choose to report collusion indicate that this type of enterprise will inevitably report any discovered act for higher authorities to handle. The regulator's choice of a strong regulatory model for collusion can be costly, but collusion will be detected in all regulated projects. The choice of a weak regulatory model means that collusion in regulated projects will potentially go unnoticed.

2.3. Parameter Setting and Model Construction.

Suppose the government chooses to participate in the collusion with an enterprise. In that case, it will receive the social benefits of completing the project. However, it still has to bear the loss R_1 for the nonconformity of the capacity of the vertically colluding enterprise, with a probability of α. The probability of society discovering the collusion is β, and the loss of S_1 (including market distortion and the collusion will cause loss of trust, etc.). The government will receive the basic benefits of the completed project F regardless of whether it is involved in collusion. Still, because no corrupt practices occur during the project bidding process, the sociopolitical climate will increase along with people's trust in the government, with a gain of F_2.

The probability that a firm with a higher willingness to collude will choose to participate in the collusion strategy is β. The project's supply affects the probability that a firm with a higher willingness to collude will choose the collusion strategy. The degree of market competition affects SS, the more intense the competition, the higher the probability of choosing collusion and the higher SS. Suppose firms with a higher willingness to collude decide not to participate in collusion. In that case, the probability of their bid actively is reduced to R_3 while simultaneously reducing the possibility of firm expansion, bringing a loss of S_5.

A firm with a low willingness to collude chooses the strategy of reporting on collusion, in which case the gain is 0; there is a risk of resistance from the government and colluding firms, bringing a loss of S_6, but increased social recognition represented by F_4. The probability of the report being discovered by the government and colluding firms is D; choosing not to report on collusion yields an additional gain of F_5.

The supervising enterprise gains F_6 regardless of which model it chooses. Choosing to select a strong supervision model brings an increase in recognition, represented by F_7, but may be subject to hostility from the regulators involved in the collusion, bringing losses of S_6. Suppose the supervising enterprise does not collude with the enterprise and the bidder in the strong supervision model, choosing the weak supervision model gives a fixed gain of F_6, while there is a probability of G that the enterprise will choose to collude with the contractor. The firm has a G probability colluding with the offerer, which provides an additional F_7 gain (including the potential gain from more opportunities for cooperation between the offerer and the firm) and a D probability of being discovered, resulting in an S_7 loss.

The parameters and their explanations are shown in Table 1.

According to prospect theory, the decision-making group develops perceived utility when facing uncertain costs and benefits. This article assumes that the cost of expenditure and the legitimate monetized benefit obtained are deterministic. The remaining parameters are related to subjective perceptions, calculated using foreground values. Table 2 shows the payoff matrix of the bidding collusion evolution game.

2.4. Model Solution.

The steps for solving the model are shown in Figure 2.

According to Table 1, the prospective expectations and mean expectations for the bidders' sector to adopt the "engage in collusion" and "do not engage in collusion" strategies are

$$
\begin{aligned}
E_{11} = {} & y * z * m * \left(V(F) + \alpha * R_1 - \beta * V(S_1)\right) + (1 - y) * z * m * \left(V(F) + \alpha * R_1 - \beta * V(S_1)\right) + \\
& y * (1 - z) * m * \left(V(F) + \alpha * R_1 - \beta * V(S_1)\right) + y * z * (1 - m) * \left(V(F) + \alpha * R_1 - \beta * V(S_1)\right) + \\
& (1 - y) * (1 - z) * m * \left(V(F) + \alpha * R_1 - \beta * V(S_1)\right) + y * (1 - z) * (1 - m) * \left(V(F) + \alpha * R_1 - \beta * V(S_1)\right) \\
& + (1 - y) * (1 - z) * (1 - m) * \left(V(F) + \alpha * R_1 - \beta * V(S_1)\right), \\
E_{12} = {} & y * z * m * \left(V(F) + V(F_2)\right) + (1 - y) * z * m * \left(V(F) + V(F_2)\right) + \\
& y * (1 - z) * m * \left(V(F) + V(F_2)\right) + y * z * (1 - m) * \left(V(F) + V(F_2)\right) + (1 - y) * (1 - z) * m * \left(V(F) + V(F_2)\right) \\
& + y * (1 - z) * (1 - m) * \left(V(F) + V(F_2)\right), \\
\overline{E}_{13} = {} & x * E_{12} - (1 - x) * E_{12}.
\end{aligned}
\tag{4}
$$

TABLE 1: Parameters and explanation.

Parameter	Explanation
R_1	Risk of substandard capacity
F	Base earnings
F_3	Scale-up incentive
F_5	Nonreporting of collusive behavior gain
F_7	Regulator collusion gain
S_2	Winning bid gain
S_4	Collusion discovery loss
S_6	Losses from reported collusion being resisted
E	Probability of winning a bid by a firm with a high willingness to collude
D	Probability of detection of reported collusion
β	Probability of collusion being detected by the bidders
λ	Loss avoidance factor
R_3	Probability of winning a bid
F_2	Trust rising gain
F_4	Recognition gain
F_6	Regulatory gain
S_1	Tenderer collusion discovery loss
S_3	Collusion additional expense loss
S_5	Reduced expansion loss
S_7	Regulator collusion detected loss
SS	Degree of market competition
G	Probability of regulatory firms choosing to collude
α	Probability of colluding firms not meeting capacity standards
θ	Risk attitude coefficient

TABLE 2: Revenue matrix.

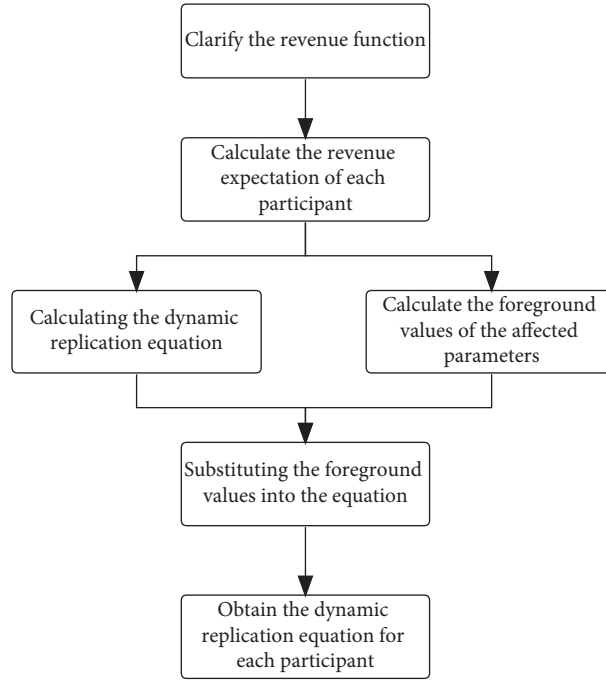| Strategy selection	Low collusion	Engage in collusion — Active collusion	Engage in collusion — Inactive collusion	Not engage in collusion — Active collusion	Not engage in collusion — Inactive collusion
Regulators — Strong regulatory model	Reporting collusion	$V(F)+\alpha*R_1-\beta*V(S_1)$ $E*SS*(V(F_3)-S_3-\beta*S_4+S_2)$ $V(F_4)-D*S_6$ $F_6+V(F_7)-V(S_6)$	$V(F)+\alpha*R_1-\beta*V(S_1)$ $R_3*S_2+S_5$ $V(F_4)-D*S_6$ $F_6+V(F_7)-V(S_6)$	$V(F)+F_2$ $E*SS*(V(F_3)-S_3-\beta*S_4)$ $V(F_4)-D*S_6$ $F_6+V(F_7)-V(S_6)$	$V(F)+V(F_2)$ $R_3*S_2+S_5$ $V(F_4)-D*S_6$ $F_6+V(F_7)-V(S_6)$
	Not reporting collusion	$V(F)+\alpha*R_1-\beta*V(S_1)$ $E*SS*(V(F_3)-S_3-\beta*S_4+S_2)$ F_5 $F_6+V(F_7)-V(S_6)$	$V(F)+\alpha*R_1-\beta*V(S_1)$ $R_3*S_2+S_5$ F_5 $F_6+V(F_7)-V(S_6)$	$V(F)+V(F_2)$ $E*SS*(V(F_3-S_3-\beta*S_4)$ F_5 $F_6+V(F_7)-V(S_6)$	$V(F)+V(F_2)$ $R_3*S_2+S_5$ F_5 $F_6+V(F_7)-V(S_6)$
Regulators — Weak regulatory model	Reporting collusion	$V(F)+\alpha*R_1-\beta*V(S_1)$ $E*SS*(V(F_3)-S_3-\beta*S_4+S_2)$ $V(F_4)-D*S_6$ $F_6+V(F_7)-V(S_6)+G*F_7-D*S_7$	$V(F)+\alpha*R_1-\beta*V(S_1)$ $R_3*S_2+S_5$ $V(F_4)-D*S_6$ $F_6+V(F_7)-V(S_6)+G*F_7-D*S_7$	$V(F)+V(F_2)$ $E*SS*(V(F_3)-S_3-\beta*S_4)$ $V(F_4)-D*S_6$ $F_6+V(F_7)-V(S_6)+G*F_7-D*S_7$	$V(F)+V(F_2)$ $R_3*S_2+S_5$ $V(F_4)-D*S_6$ $F_6+V(F_7)-V(S_6)+G*F_7-D*S_7$
	Not reporting collusion	$V(F)+\alpha*R_1-\beta*V(S_1)$ $E*SS*(V(F_3)-S_3-\beta*S_4+S_2)$ F_5 $F_6+V(F_7)-V(S_6)+G*V(F_7)-D*S_7$	$V(F)+\alpha*R_1-\beta*V(S_1)$ $R_3*S_2+S_5$ F_5 $F_6+V(F_7)-V(S_6)+G*F_7-D*S_7$	$V(F)+V(F_2)$ $E*SS*(V(F_3)-S_3-\beta*S_4)$ F_5 $F_6+V(F_7)-V(S_6)+G*V(F_7)-D*S_7$	$V(F)+V(F_2)$ $R_3*S_2+S_5$ F_5 $F_6+V(F_7)-V(S_6)+G*V(F_7)-D*S_7$

Figure 2: Calculation logic table.

The prospective expectations and mean expectations of firms with a high willingness to collude for "active collusion" and "inactive collusion" strategies are

$$
\begin{aligned}
E_{21} = {} & x * z * m * \left(E * \mathrm{SS} * V\left(F_3\right) - S_3 - \beta * S_4 + S_2\right) + (1 - x) * z * m * \left(E * \mathrm{SS} * \left(V\left(F_3\right) - S_3 - \beta * S_4\right) + \right. \\
& x * (1 - z) * m * \left(E * \mathrm{SS} * \left(V\left(F_3\right) - S_3 - \beta * S_4 + S_2\right) + x * z * (1 - m) * \left(E * \mathrm{SS} * V\left(F_3\right) - S_3 - \beta * S_4 + S_2\right) \right. \\
& + (1 - x) * (1 - z) * m * \left(E * \mathrm{SS} * V\left(F_3\right) - S_3 - \beta * S_4 + S_2\right) + \\
& (1 - x) * z * (1 - m) * \left(E * \mathrm{SS} * V\left(F_3\right) - S_3 - \beta * S_4 + S_2\right) + \\
& (1 - x) * (1 - z) * (1 - m) * \left(E * \mathrm{SS} * V\left(F_3\right) - S_3 - \beta * S_4 + S_2\right), \\
E_{22} = {} & x * z * m * \left(R_3 * S_2 + S_5\right) + (1 - x) * z * m * \left(R_3 * S_2 + S_5\right) + x * (1 - z) * m * \left(R_3 * S_2 + S_5\right) \\
& + x * z * (1 - m) * \left(R_3 * S_2 + S_5\right) + (1 - x) * (1 - z) * m * \left(R_3 * S_2 + S_5\right) \\
& + (1 - x) * z * (1 - m) * \left(R_3 * S_2 + S_5\right) + x * (1 - z) * (1 - m) * \left(R_3 * S_2 + S_5\right), \\
\overline{E}_{23} = {} & y * E_{21} - (1 - y) * E_{22}.
\end{aligned}
\tag{5}
$$

The prospective expectations and mean expectations of firms with low collusion intentions adopting the "report collusion" and "do not report collusion" strategies are

$$
\begin{aligned}
E_{31} = {} & x * y * m * \left(V\left(F_4\right) - D * S_6\right) + (1 - x) * y * m * \left(V\left(F_4\right) - D * S_6\right) + \\
& x * (1 - y) * m * \left(V\left(F_4\right) - D * S_6\right) + x * y * (1 - m) * \left(V\left(F_4\right) - D * S_6\right) + (1 - x) * (1 - y) * m * F_5 \\
& + (1 - x) * y * (1 - m) * \left(V\left(F_4\right) - D * S_6\right) + (1 - y) * (1 - m) * \left(V\left(F_4\right) - D * S_6\right)
\end{aligned}
$$

$$+ (1 - x) * (1 - y) * (1 - m) * (V(F_4) - D * S_6),$$

$$E_{32} = x * y * m * F_5 + (1 - x) * y * m * F_5 + x * (1 - y) * m * F_5 + x * z * (1 - m) * F_5$$
$$+ (1 - x) * (1 - y) * m * F_5 + x * (1 - y) * (1 - m) * F_5 + (1 - x) * (1 - y) * z * F_5 +$$
$$(1 - x) * (1 - y) * (1 - m) * F_5,$$

$$\overline{E}_{33} = z * E_{31} - (1 - z) * E_{32}.$$

(6)

The regulators' prospective expectations and mean expectations for a "strong regulatory model" and a "weak regulatory model" strategy are

$$E_{41} = x * y * z * (F_6 + V(F_7) - V(S_6)) + (1 - x) * y * z * (F6 + V(F_7) - V(S_6)) +$$
$$x * (1 - y) * z * (F_6 + V(F_7) - V(S_6)) + x * y * (1 - z) * (F_6 + V(F_7) - V(S_6))$$
$$+ (1 - x) * (1 - y) * z * (F_6 + V(F_7) - V(S_6)) +$$
$$(1 - x) * y * (1 - z) * (F_6 + V(F_7) - V(S_6))$$
$$+ x * (1 - y) * (1 - z) * (F_6 + V(F_7) - V(S_6)) +$$
$$(1 - x) * (1 - y) * (1 - z) * (F_6 + V(F_7) - V(S_6)),$$

$$E_{42} = x * y * z * (F_6 + V(F_7) - V(S_6) + G * V(F_7) - D * V(S_7) +$$
$$(1 - x) * y * z * (F_6 + V(F_7) - V(S_6) + G * V(F_7) - D * V(S_7)$$
$$+ x * (1 - y) * z * F_6 + x * y * (1 - z) * (F_6 + V(F_7) - V(S_6) + G * V(F_7) - D * V(S_7)$$
$$+ (1 - x) * (1 - y) * z * (F_6 + V(F_7) - V(S_6) + G * V(F_7) - D * V(S_7)$$
$$+ (1 - x) * y * (1 - z) * (F6 + V(F_7) - V(S_6) + G * V(F_7) - D * V(S_7) +$$
$$x * (1 - y) * (1 - z) * (F_6 + V(F_7) - V(S_6) + G * V(F_7) - D * V(S_7)$$
$$+ (1 - x) * (1 - y) * (1 - z) * (F_6 + V(F_7) - V(S_6) + G * V(F_7) - D * V(S_7),$$

$$\overline{E}_{43} = m * E_{41} - (1 - m) * E_{42}.$$

(7)

The replicated dynamic differential equation for the choice of an active strategy by bidders, high collusion willing firms, low collusion willing firms, and regulators can be expressed as

$$F(X) = \frac{dx}{dt} = x * (E_{11} - \overline{E}_{13}) = x * (1 - x) * (E_{11} + E_{12}) =$$

$$x * (1 - x) * (y * z * m (2V(F) + \alpha R_1 + V(F_2) - \beta V(S_1)) + (1 - z) * (2V(F) + \alpha R_1 + V(F_2) - \beta V(S_1))$$

$$+ z * m * (2V(F) + \alpha R_1 + V(F_2) - \beta V(S_1)) + y * z * (2V(F) + \alpha R_1 + V(F_2) - \beta V(S_1)),$$

$$F(Y) = \frac{dy}{dt} = y * (E_{21} - \overline{E}_{23}) = y * (1 - y) * (E_{21} + E_{22}) =$$

$$= y * (1 - y) * (z * x * m * (E * SS * V(F_3) - S_3 - \beta * S_4 + S_2 + R_3 * S_2 + S_5 - S_2)$$

$$+ (1 - z) * (E * SS * V(F_3) - S_3 - \beta * S_4 + S_2 + R_3 * S_2 + S_5 - S_2)$$

$$+ z * m * (SS * V(F_3) - S_3 - \beta * S_4 + S_2 + R_3 * S_2 + S_5)$$

$$+ x * z * (SS * V(F_3) - S_3 - \beta * S_4 + S_2 + R_3 * S_2 + S_5),$$

$$F(Z) = \frac{dz}{dt} = z * \left(E_{31} - \bar{E}_{33}\right) = z * (1 - z) * (E_{31} + E_{32}) =$$

$$= z * (1 - z) * (x * y * m * (V(F_4) - D * V(S_6) + F_5) + (1 - y) * (V(F_4) - D * V(S_6) + F_5)$$

$$+ (1 - y) * m * (V(F_4) - D * V(S_6) + F_5) + x * y * (V(F_4) - D * V(S_6) + F_5)),$$

$$F(M) = \frac{dm}{dt} = m * \left(E_{41} - \bar{E}_{43}\right) = m * (1 - m) * (E_{41} + E_{42}) = \tag{8}$$

$$= m * (1 - m) * (x * y * z * (2F_6 + 2V(F_7) - V(S_6) + G * V(F_7) - D * S_7)$$

$$+ (1 - y) * (2F_6 + 2V(F_7) - V(S_6) + G * V(F_7) - D * S_7)$$

$$+ y * z * (2F_6 + 2V(F_7) - V(S_6) + G * V(F_7) - D * S_7)$$

$$+ x * y * (2F_6 + 2V(F_7) - V(S_6) + G * V(F_7) - D * S_7)).$$

When the government party's probability of engaging in collusion is 1, the government party receives a base benefit of F. The prospective value of F is

$$V(F) = \pi(1) * V(F) = F^\theta. \tag{9}$$

When collusion is discovered, a loss of S_1 is obtained, and the prospective value of S_1 is

$$V(S_1) = \pi(1) * V(-S_1) = -\lambda S_1^\theta. \tag{10}$$

Similarly, the foreground values of F2, F3, F4, S6, and F7 can be obtained.

The positive strategy dynamic game equation of quadrilateral game can be obtained by substituting the prospect value:

$$F(X) = \frac{dx}{dt} = x * \left(E_{11} - \bar{E}_{13}\right) = x * (1 - x) * (E_{11} + E_{12})$$

$$= x * (1 - x) * \left(y * z * m\left(2F^\theta + \alpha R_1 + F_2^\theta + \lambda \beta S_1^\theta\right) + (1 - z) * \left(2F^\theta + \alpha R_1 + F_2^\theta + \lambda \beta S_1^\theta\right) +$$

$$z * m * \left(2F^\theta + \alpha R_1 + F_2^\theta + \lambda \beta S_1^\theta\right) + y * z * \left(2F^\theta + \alpha R_1 + F_2^\theta + \lambda \beta S_1^\theta\right)),$$

$$F(Y) = \frac{dy}{dt} = y * \left(E_{21} - \bar{E}_{23}\right) = y * (1 - y) * (E_{21} + E_{22}) =$$

$$= y * (1 - y) * \left(z * x * m * \left(E * SS * F_3^\theta - S_3 - \beta * S_4 + S_2 + R_3 * S_2 + S_5 - S_2\right) +$$

$$+ (1 - z) * \left(E * SS * F_3^\theta - S_3 - \beta * S_4 + S_2 + R_3 * S_2 + S_5 - S_2\right)$$

$$+ z * m * \left(SS * F_3^\theta - S_3 - \beta * S_4 + S_2 + R_3 * S_2 + S_5\right) + x * z * \left(SS * F_3^\theta - S_3 - \beta * S_4 + S_2 + R_3 * S_2 + S_5\right),$$

$$F(Z) = \frac{dz}{dt} = z * \left(E_{31} - \bar{E}_{33}\right) = z * (1 - z) * (E_{31} + E_{32}) = \tag{11}$$

$$= z * (1 - z) * \left(x * y * m * \left(F_4^\theta + \lambda\, D * S_6^\theta + F5\right) + (1 - y) * \left(F_4^\theta + \lambda\, D * S_6^\theta + F_5\right)$$

$$+ (1 - y) * m * \left(F_4^\theta + \lambda\, D * S_6^\theta + F_5\right) + x * y * \left(F_4^\theta + \lambda\, D * S_6^\theta + F_5\right),$$

$$F(M) = \frac{dm}{dt} = m * \left(E_{41} - \bar{E}^-_{43}\right) = m * (1 - m) * (E_{41} + E_{42}) =$$

$$= m * (1 - m) * \left(x * y * z * \left(2F_6 + 2F_7^\theta + \lambda S_6^\theta + G * F_7^\theta - D * S_7\right)\right.$$

$$+ (1 - y) * \left(2F_6 + 2F_7^\theta + \lambda S_6^\theta - D * S_7\right)$$

$$+ y * z * \left(2F_6 + 2F_7^\theta + \lambda S_6^\theta + G * F_7^\theta - D * S_7\right) + x * y * \left(2F_6 + 2F_7^\theta + \lambda S_6^\theta + G * F_7^\theta - D * S_7\right).$$

3. Equilibrium Analysis of the Four-Party Game in Transportation Infrastructure Project Operation

3.1. Game Player Unilateral Stability Strategy

3.1.1. Analysis of the Tenderer's Strategic Stability.
Let $F(X) = 0$ and solve for $x = 0$, $x = 1$, $y = (z - 1) - z * m/z * (m + 1) = Y^*$. It follows from the stability theorem for replicating dynamic differential equations that $F(y) = 0$, $\partial F(x)/\partial x < 0$, x is an evolutionary stabilization strategy. Since the range of values of z, m is [0, 1], in this article $Y* \leq 0$. Thus, there are only two cases, $y = Y*$ and $y > Y*$.

When $y = Y*$, $F(X) = 0$ is constantly established, and the stability point is $x = 0$, $x = 1$. Any value of x is a steady-state,

i.e., the strategy of the construction unit does not change over time.

When $y > Y*$, $F(X) = 0$ is constantly established, and $\begin{cases} \partial F(x)/\partial x > 0, x = 0 \\ \partial F(x)/\partial x < 0, x = 1 \end{cases}$ is established. The stability point is $y = 0$, and any value of x is steady-state, indicating that the perceived costs of the positive pole strategy outweigh the benefits for the bidders, who prefer to bear the penalty of uncertainty rather than investing more.

The bidders' replicated dynamic phase diagram is shown in Figure 3.

3.1.2. Analysis of the Progressive Stability of Firms with a High Willingness to Collude.
Let $F(Y) = 0$ and solve for $y = 0$, $y = 1$,

$$z = -\frac{E * SS * F_3^\theta - S_3 - \beta * S_4 + S_2 + R_3 * S_2 + S_5 - S_2}{x * m * \left(E * SS * F_3^\theta - S_3 - \beta * S_4 + S_2 + R_3 * S_2 + S_5 - S_2\right) - \left(E * SS * F_3^\theta - S_3 - \beta * S_4 + S_2 + R_3 * S_2 + S_5 - S_2\right) +} = Z^*. \tag{12}$$
$$m * \left(SS * V\left(F_3\right) - S_3 - \beta * S_4 + S_2 + R_3 * S_2 + S_5\right) + x * \left(SS * F_3^\theta - S_3 - \beta * S_4 + S_2 + R_3 * S_2 + S_5\right)$$

It follows from the stability theorem for replicating dynamic differential equations that $F(y) = 0$, $\partial F(y)/\partial y < 0$, x is an evolutionary stabilization strategy.

When $z = Z*$, $F(y) = 0$ is constantly established. The stability point is $y = 0$, $y = 1$, and any value of y is steady-state. The high collusion unit's strategy does not change over time.

When $z < Z*$, $F(y) = 0$ is constantly established, and $\begin{cases} \partial F(y)/\partial y > 0, y = 0 \\ \partial F(y)/\partial y < 0, y = 1 \end{cases}$ is established. The stability point is $y = 1$, and any value of x is steady-state. This suggests that parties with a high willingness to collude perceive the benefits of an aggressive strategy outweigh the costs. The benefits include a variety of gains. As shown by prospect theory, game subjects are usually reluctant to take losses when faced with gains, and parties with a high willingness to collude tend to adopt collusive strategies.

When $z > Z*$, $F(y) = 0$ is constantly established, and $\begin{cases} \partial F(y)/\partial y > 0, y = 0 \\ \partial F(y)/\partial y < 0, y = 1 \end{cases}$ is established. The stability point is $y = 0$, and any value of x is steady-state, indicating that the penalties and losses received by the building operator in providing low-quality services are less than the gains under this strategy. In this case, the building operator tends to choose a speculative strategy to obtain higher returns. The party willing to collude replicates the dynamic phase diagram, as shown in Figure 4.

3.1.3. Analysis of the Progressive Stability of Firms with a Low Willingness to Collude.
Let $F(Z) = 0$ and solve for $z = 0$, $z = 1$, $m = \lambda Y_1^\theta - \lambda Y_2^\theta + y/y - 1 = M^*$. It follows from the stability theorem for replicating dynamic differential equations that

$F(z) = 0$, $\partial F(z)/\partial z < 0$, z is an evolutionary stabilization strategy.

When $m = M*$, $F(Z) = 0$ is constantly established. The stability point is $z = 0$, $z = 1$, and any value of z is steady-state. The strategy of the low collusion unit does not change over time.

When $m < M*$, $F(Z) = 0$ is constantly established, and $\begin{cases} \partial F(z)/\partial z > 0, z = 0 \\ \partial F(z)/\partial z < 0, z = 1 \end{cases}$ is established. The stability point is $z = 1$, and any value of z is steady-state, suggesting that, for the low colluder, the perceived benefits of adopting an aggressive strategy outweigh the costs. In this case, the low colluding party tends to adopt a strategy of reporting the collusion.

When $z > Z*$, $F(Z) = 0$ is constantly established, and $\begin{cases} \partial F(z)/\partial z > 0, z = 0 \\ \partial F(z)/\partial z < 0, z = 1 \end{cases}$ is established. The stability point is $z = 0$, and any value of z is steady-state, suggesting that users have greater benefits from adopting nonreporting collusion. The low collusion willingness side tends to be associated with a nonreporting strategy. The low collusion willingness side replicates the dynamic phase diagram, as shown in Figure 5.

3.1.4. Progressive Stability Analysis of Regulators.
Let $F(M) = 0$ and solve for $m = 0$, $m = 1$, $x = (y - 1 + yz - ((1 - y)G * F_7^\theta)/(2F_6 + 2F_7 + \lambda S_6 + G * F_7 - D * S_7)/(yz + y)) = X^*$. It follows from the stability theorem for replicating dynamic differential equations that $F(m) = 0$, $\partial F(m)/\partial m < 0$, m is an evolutionary stabilization strategy.

When $x = X*$, $F(M) = 0$ is constantly established. The stability point is $m = 0$, $m = 1$, and any value of m is
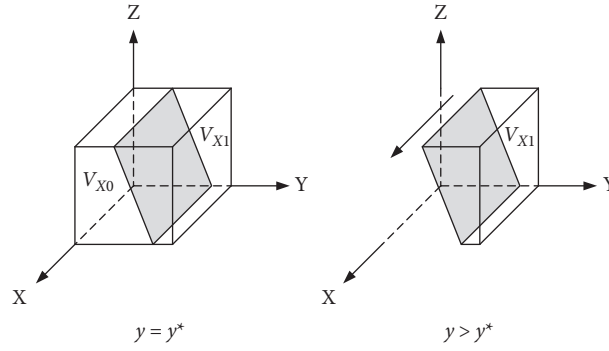
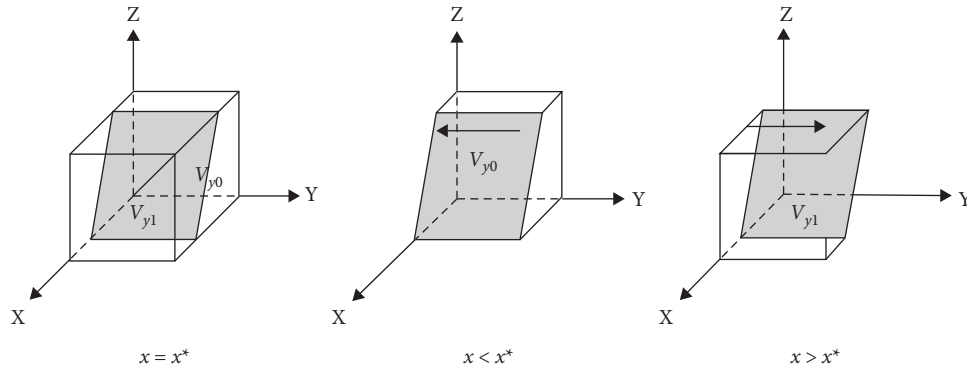Figure 3: Tenderer replicates dynamic phase diagram.

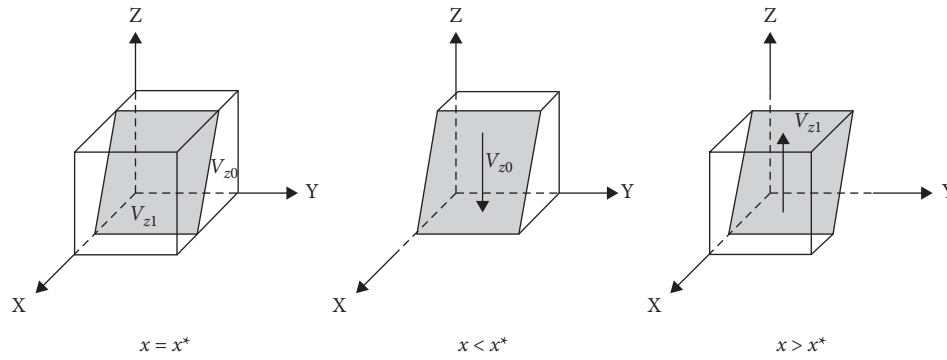Figure 4: High collusion replicates dynamic phase diagram.

Figure 5: Low collusion replicates dynamic phase diagram.

steady-state. The strategy of the low collusion unit does not change over time.

When $x < X*$, $F(M) = 0$ is constantly established, and $\begin{cases} \partial F(m)/\partial m > 0, m = 0 \\ \partial F(m)/\partial m < 0, m = 1 \end{cases}$ is established. The stability point is $m = 1$, and any value of m is steady-state, suggesting that the supervisory authority's perceived benefits outweigh the costs of an active strategy. In such cases, regulators tend to adopt strong regulatory measures against collusive behavior.

When $x > X*$, $F(M) = 0$ is constantly established, and $\begin{cases} \partial F(m)/\partial m > 0, m = 0 \\ \partial F(m)/\partial m < 0, m = 1 \end{cases}$ is established. The stability point is $m = 0$, and any value of m is a steady-state, suggesting a greater gain for the regulators in adopting a weak regulatory

strategy. In this case, there is a greater probability that the regulators will forgo regulation and choose not to regulate collusion. See Figure 6 for a phase diagram of regulator replication dynamics.

3.2. Strategy Portfolio Stability Analysis. Let $F(x) = F(y) = F(z) = F(m) = 0$. The equilibrium points can be obtained as follows: $E_1 (0, 0, 0, 0)$, $E_2 (1, 0, 0, 0)$, $E_3 (0, 1, 0, 0)$, $E_4 (0, 0, 1, 0)$, $E_5 (0, 0, 0, 1)$, $E_6 (1, 1, 0, 0)$, $E_7 (1, 0, 1, 0)$, $E_8 (1, 0, 0, 1)$, $E_9 (0, 1, 1, 0)$, $E_{10} (0, 1, 0, 1)$, $E_{11} (0, 0, 1, 1)$, $E_{12} (1, 1, 1, 0)$, $E_{13} (1, 1, 0, 1)$, $E_{14} (1, 0, 1, 1)$, $E_{15} (0, 1, 1, 1)$, $E_{16} (1, 1, 1, 1)$, $E_{17} (x^*, y^*, z^*, m^*)$; E_{17} is the mixed strategy equilibrium point. Suppose the equilibrium point in the three-way evolutionary game is ESS. In that case, it must be
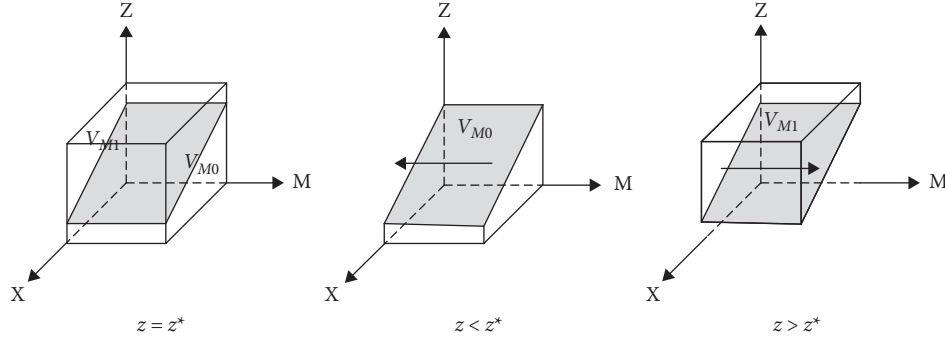
FIGURE 6: Regulators collusion replicates dynamic phase diagram.

satisfied that the equilibrium point is a pure strategy equilibrium, and therefore only the asymptotic stability of E_1 to E_{16} needs to be discussed. The asymptotic stability of the system can be obtained from the analysis of the Jacobian matrix, as proposed by Friedman:

$$ J = \begin{bmatrix} \dfrac{\partial F(x)}{\partial x} & \dfrac{\partial F(x)}{\partial y} & \dfrac{\partial F(x)}{\partial z} & \dfrac{\partial F(x)}{\partial m} \\[2ex] \dfrac{\partial F(y)}{\partial x} & \dfrac{\partial F(y)}{\partial y} & \dfrac{\partial F(y)}{\partial z} & \dfrac{\partial F(y)}{\partial m} \\[2ex] \dfrac{\partial F(z)}{\partial x} & \dfrac{\partial F(z)}{\partial y} & \dfrac{\partial F(z)}{\partial z} & \dfrac{\partial F(z)}{\partial m} \\[2ex] \dfrac{\partial F(m)}{\partial x} & \dfrac{\partial F(m)}{\partial y} & \dfrac{\partial F(m)}{\partial z} & \dfrac{\partial F(m)}{\partial m} \end{bmatrix}. \tag{13} $$

Each of the 16 equilibrium points is substituted into the Jacobian matrix. If the eigenvalues of the corresponding matrix are all negative, the equilibrium point is the system's ESS. The stability of each point is shown in Table 3.

The calculations reveal that this article should analyze the game's stabilization strategy in two scenarios.

Scenario 1: for all parties, the benefits of collusion are greater than the potential costs. In this case, M_2, M_3, $M_{5,}$ and M_6 are all greater than 0. In the game process, the benefits of the collusion process are greater than the costs incurred by the bidding parties, including direct costs, reputational losses, and potential expansion. In this case, the table shows that $E_{16}(1, 1, 1, 1)$ is the equilibrium point, and that the evolving equilibrium strategies are: engage in collusion, active participation in the collusion, report the collusion, weak regulatory model.

Scenario 2: the benefits of collusion are less than the potential costs for all parties. In this scenario, M_2, M_3, $M_{5,}$ and M_6 are all less than 0. In the game, the benefits of collusion to the bidding parties are greater than their costs, including direct costs, reputational damage, and potential expansion. Table 4 shows that there is no stable equilibrium in this case.

4. Analysis of Simulations

4.1. Initial Parameters Setting.
The model is assigned according to the real situation, and numerical simulation is carried out using Matlab 2020b. These choices intuitively demonstrate the influence of key factors on the evolutionary process and results of the multiparty game in the government project bidding process and verify the validity of the evolutionary stability analysis. The studied behavior is vertical collusion in the bidding process of government investment projects. As such, all parties are bound by relevant laws and regulations and hidden costs, and they tend to choose negative strategies at the beginning of the period. The probability of choosing positive strategies is less than 0.5. The probability of choosing the positive strategy is even lower due to the fear of loss and retaliation for reporting vertical collusion. According to the actual situation and this paper's assumptions, x, y, z, and m are set as 0.4, 0.3, 0.2, and 0.3, respectively, see Table 5.

4.2. Single-Factor Sensitivity Analysis

4.2.1. Impact of Changes in the Social Benefits of Project Completion Base.
When $F = \{12, 18, 24, 30\}$, the process and results of the evolution of the thematic strategy of the quadratic game are shown in Figure 7.

As seen in Figure 6, the increase in project completion benefits as the bidders collude impacts each of the four-party's evolutionary strategies. The more obvious change is for the bidders. With the increase of the social base gain, the probability of the bidders to adopt the collusion strategy shows an increase in the magnitude of the change, and the speed of evolution to a stable strategy becomes faster. However, the reduction of social base revenue can only reduce the occurrence of collusion in the short term and delay the evolution to a stable point. Still, it cannot control the occurrence of collusion.

4.2.2. Impact of Changes in Risk Attitude Factor.
When $\theta = \{0.8, 0.5, 0.3, 0.2\}$, the process and results of the evolution of the thematic strategy of the quadratic game are shown in Figure 8.

TABLE 3: Eigenvalues.

Equalization points	Eigenvalue λ_1	Eigenvalue λ_2	Eigenvalue λ_3	Eigenvalue λ_4
$E_1\,(0,0,0,0)$	M_1	M_2	M_4	M_6
$E_2\,(1,0,0,0)$	$-M_1$	M_2	M_4	M_6
$E_3\,(0,1,0,0)$	M_1	$-M_2$	0	0
$E_4\,(0,0,1,0)$	0	0	$-M_4$	M_6
$E_5\,(0,0,0,1)$	M_1	M_2	$2M_4$	$-\mathrm{M}_6$
$E_6\,(1,1,0,0)$	$-M_1$	$-M_2$	M_4	M_5
$E_7\,(1,0,1,0)$	0	M_3	$-M_4$	M_6
$E_8\,(1,0,0,1)$	$-M_1$	M_2	$2M_4$	$-\mathrm{M}_6$
$E_9\,(0,1,1,0)$	M_1	0	0	M_5
$E_{10}\,(0,1,0,1)$	M_1	$-M_2$	0	0
$E_{11}\,(0,0,1,1)$	M_1	M_3	$-2M_4$	$-M_6$
$E_{12}\,(1,1,1,0)$	$-M_1$	$-M_3$	$-M_4$	$3M_5$
$E_{13}\,(1,1,0,1)$	$-M_1$	$-M_2$	$2M_4$	$-M_5$
$E_{14}\,(1,0,1,1)$	$-M_1$	$M_2 + 2M_3$	$-2M_4$	$-M_6$
$E_{15}\,(0,1,1,1)$	$3M_1$	$-M_3$	0	$-M_5$
$E_{16}\,(1,1,1,1)$	$-3M_1$	$-M_2-2M_3$	$-2M_4$	$-3M_5$

$M_1 = 2F^\theta + \alpha R_1 + F_2^\theta + \lambda\beta S_1^\theta; M_2 = E * \mathrm{SS} * F_3^\theta - S_3 - \beta * S_4 + S_2 + R_3 * S_2 + S_5 - S_2; M_3 = \mathrm{SS} * F_3^\theta - S_3 - \beta * S_4 + S_2 + R_3 * S_2 + S_5; M_4 = F_4^\theta + \lambda\,D * S_6^\theta + F_5; M_5 = 2F_6 + 2F_7^\theta + \lambda S_6^\theta + G * F_7^\theta - D * S_7; M_6 = 2F_6 + 2F_7^\theta + \lambda S_6^\theta - D * S_7.$

TABLE 4: Stabilization table.

Equalization points	Scenario 1					Scenario 2				
	λ_1	λ_2	λ_3	λ_4	Stability	λ_1	λ_2	λ_3	λ_4	Stability
$E_1\,(0,0,0,0)$	+	+	+	+	−	+	−	+	−	−
$E_2\,(1,0,0,0)$	−	+	+	+	−	−	−	+	−	−
$E_3\,(0,1,0,0)$	+	−	0	0	−	+	+	0	0	−
$E_4\,(0,0,1,0)$	0	0	−	+	−	0	0	−	−	−
$E_5\,(0,0,0,1)$	+	+	+	−	−	+	−	+	+	−
$E_6\,(1,1,0,0)$	−	−	+	+	−	−	+	+	−	−
$E_7\,(1,0,1,0)$	0	+	−	+	−	0	−	−	−	−
$E_8\,(1,0,0,1)$	−	+	+	−	−	−	−	+	−	−
$E_9\,(0,1,1,0)$	+	0	0	+	−	+	0	0	−	−
$E_{10}\,(0,1,0,1)$	+	−	0	0	−	+	+	0	0	−
$E_{11}\,(0,0,1,1)$	+	+	−	−	−	+	−	−	+	−
$E_{12}\,(1,1,1,0)$	−	−	−	+	−	−	+	−	−	−
$E_{13}\,(1,1,0,1)$	−	−	+	−	−	−	+	+	+	−
$E_{14}\,(1,0,1,1)$	−	+	−	−	−	−	−	−	+	−
$E_{15}\,(0,1,1,1)$	+	−	0	−	−	+	+	0	+	−
$E_{16}\,(1,1,1,1)$	−	−	−	−	ESS	−	+	−	+	−

As shown in Figure 8, as the risk attitude increases, the probability of choosing collusion-related strategies decreases for each project participant. In the four-party game, with the change of risk attitude, the strategy change is more evident in the evolution trend of the bidding party and the party with high collusion willingness. As the risk attitude decreases, we find that the remaining conditions are unchanged. The initial degree of influence regarding the change in risk attitude on the parties' choice is greater than the social base gain. However, the change in risk attitude does not change each group's final choice. Only at the initial stage can the probability of collusive behavior be reduced between the bidding party and the party with high collusion willingness.

4.2.3. Impact of Changes in the Level of Competition in the Market. When $\mathrm{SS} = \{0.5, 0.75, 1, 1.25\}$, the process and results of the evolution of the thematic strategy of the quadratic game are shown in Figure 9.

As shown in Figure 9, the initial probability of bidders and parties with a high willingness to collude to choose collusion strategies also decreases as the degree of market competition continues to decline. However, the tenderers' willingness to collude decreases less in the initial period when the degree of market competition decreases. It decreases more sharply only after maintaining a smaller degree of market competition. However, a decrease in the degree of market competition does not affect each participant's final evolutionary outcome.

4.2.4. Impact of Changes in the Probability of Collusion Being Detected. When $\beta = D = \{0.8, 0.5, 0.3, 0.2\}$, the process and results of the evolution of the thematic strategy of the quadratic game are shown in Figure 10.

As shown in Figure 10, as the probability of detecting collusion rises, the probability that the high collusion willing
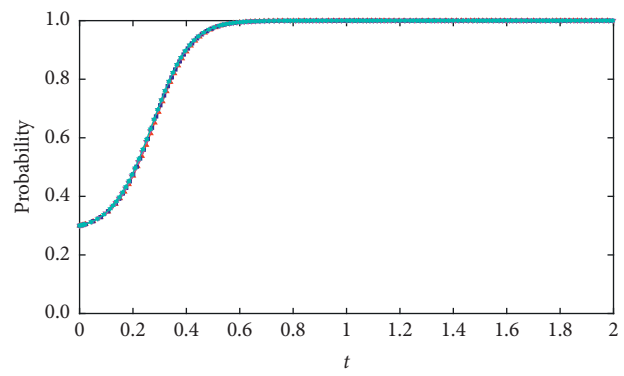
TABLE 5: Assignment table.

Parameters	Values
R_1	-2
F	12
F_3	2
F_5	3
F_7	1
S_2	8
S_4	2
S_6	4
E	0.5
D	0.5
β	0.5
λ	0.5
R_3	0.3
F_2	8
F_4	2
F_6	6
S_1	4
S_3	5
S_5	3
S_7	2
SS	0.5
G	0.5
α	0.7
θ	0.5

(a)
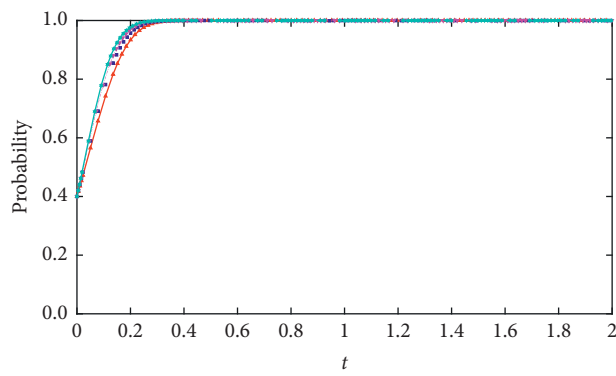
(b)

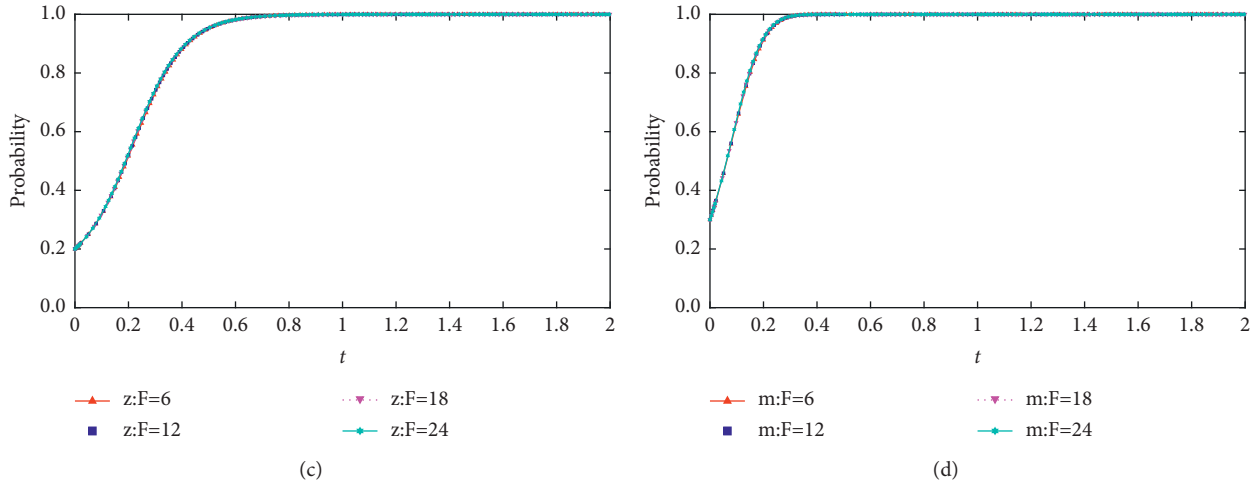FIGURE 7: Continued.

(c)

(d)

FIGURE 7: (a) Impact of changes in the social benefits of project completion base on the evolution of the high tenderers' strategy. (b) Impact of changes in the social benefits of project completion base on the evolution of the high collusion's strategy. (c) Impact of changes in the social benefits of project completion base on the evolution of the low collusion's strategy. (d) Impact of changes in the social benefits of project completion based on the evolution of the regulator's strategy.
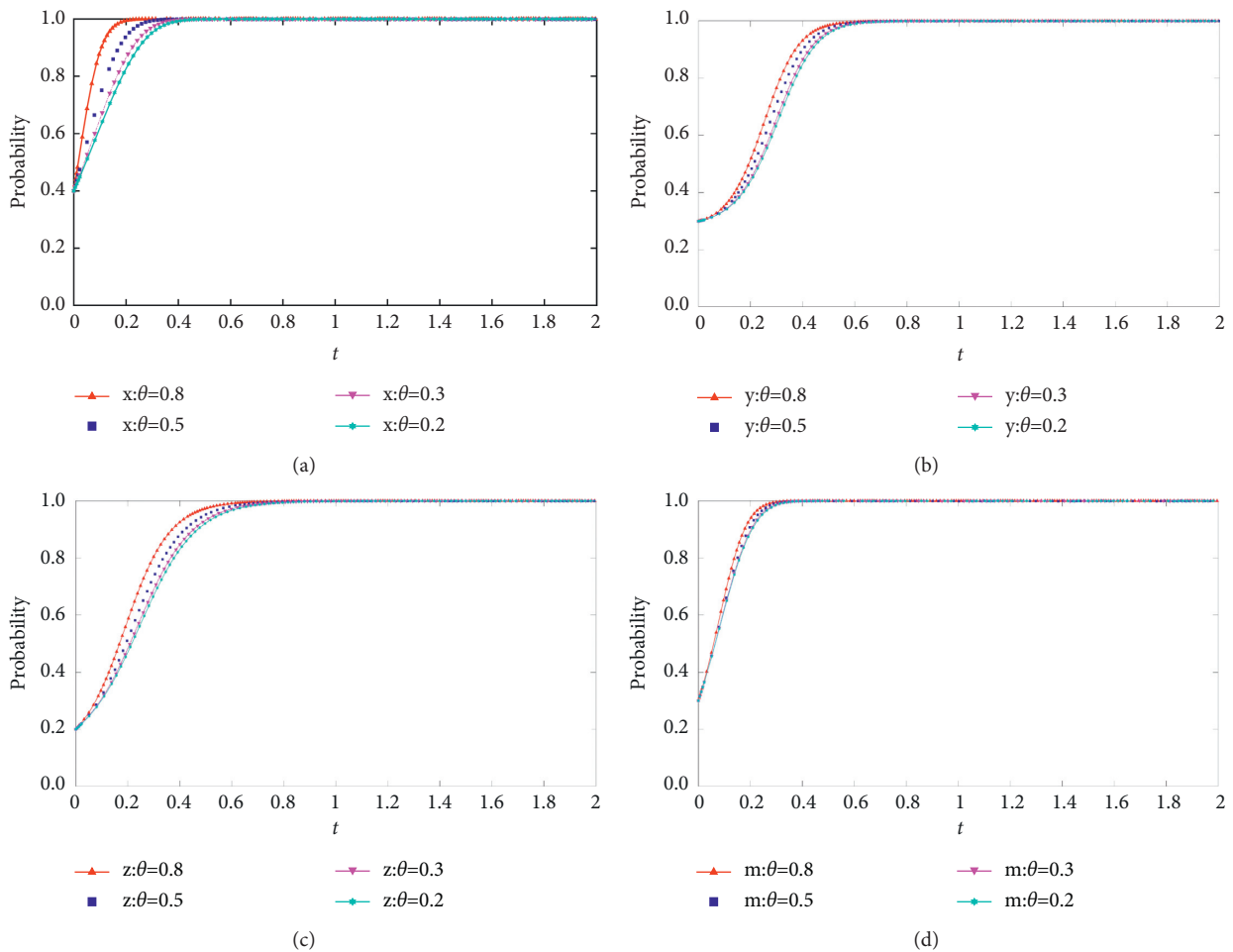

(a)

(b)

(c)

(d)

FIGURE 8: (a) Impact of changes in risk attitude coefficients on the evolution of the tenderers' strategies. (b) Impact of changes in risk attitude coefficients on the evolution of high collusion strategies. (c) Impact of changes in risk attitude coefficients on the evolution of low collusion strategies. (d) Impact of changes in risk attitude coefficients on the evolution of regulators' strategies.
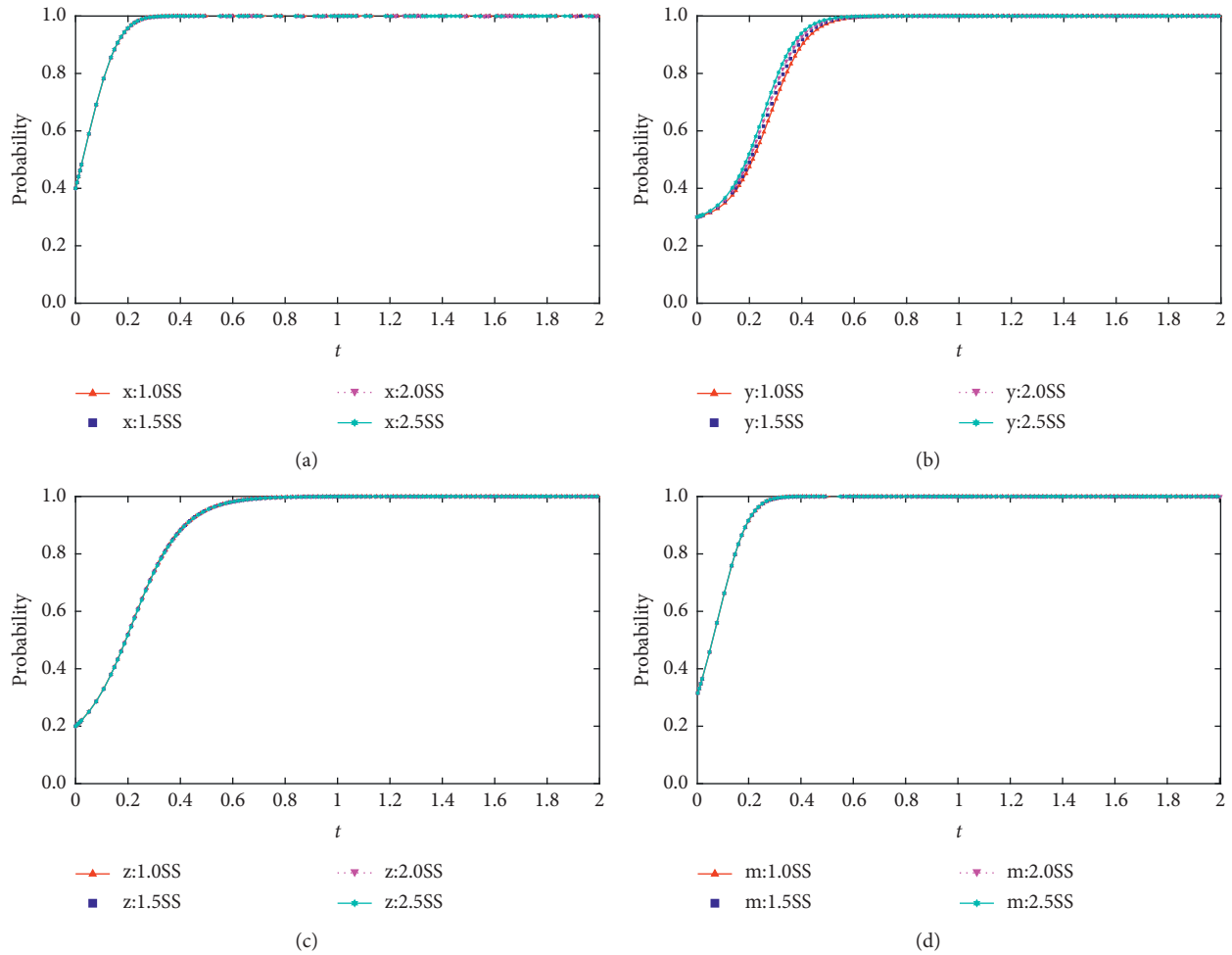
FIGURE 9: (a) The impact of changing levels of market competition on the evolution of tenderers' strategies. (b) The impact of changing levels of market competition on the evolution of high collusion strategies. (c) The impact of changing levels of market competition on the evolution of low collusion strategies. (d) The impact of changing levels of market competition on the evolution of regulators' strategies.

party and the tenderer will choose the collusion strategy decreases to some extent. Still, the high collusion willing party is more sensitive to the probability of collusion being detected. At the same time, as the probability of collusion detection being reported decreases, the probability of low collusion willing parties choosing to collude also decreases. Therefore, in controlling vertical collusion, it is essential to establish smooth reporting channels, protect the privacy of those who report violations, and avoid retaliation against whistleblowers. At the same time, it is important to increase supervision and establish a regular inspection and monitoring mechanism. The establishment of an effective monitoring system will improve the effectiveness of controls on collusion.

4.3. Impact of Internal Oversight Measures on Vertical Collusion.
To further investigate the influence of the internal supervision mechanism in government projects' bidding process, the simulation analysis was conducted by setting $z = 0$ and $z = 0.9$ to indicate the two states of the low collusion tendency group to report or not to report collusion. The

evolution process of different initial strategies was simulated for three parties, tenderers, high collusion willing parties, and supervisory agencies, and the results are shown in Figure 11.

From Figure 11, when $z = 0$, i.e., when low collusion-prone firms choose to engage in collusion without reporting, the stabilization strategy of the remaining participants in the bidding process is not unique due to the influence of many external factors. When $z = 0.9$, it has a unique stabilization evolution strategy (participation in collusion, active collusion, and strong regulatory model). Therefore, low collusion-prone firms are encouraged to report collusion; strengthening internal supervision has a better effect on the control of collusion.

4.4. The Impact of External Punishment Mechanisms.
The evolutionary strategy's impact was analyzed by setting the change in the punishment and supervision cost level when collusion was detected to investigate the effectiveness and feasibility of the external punishment mechanism in controlling collusion. Simulations were conducted to analyze the evolutionary process of different initial strategies of the
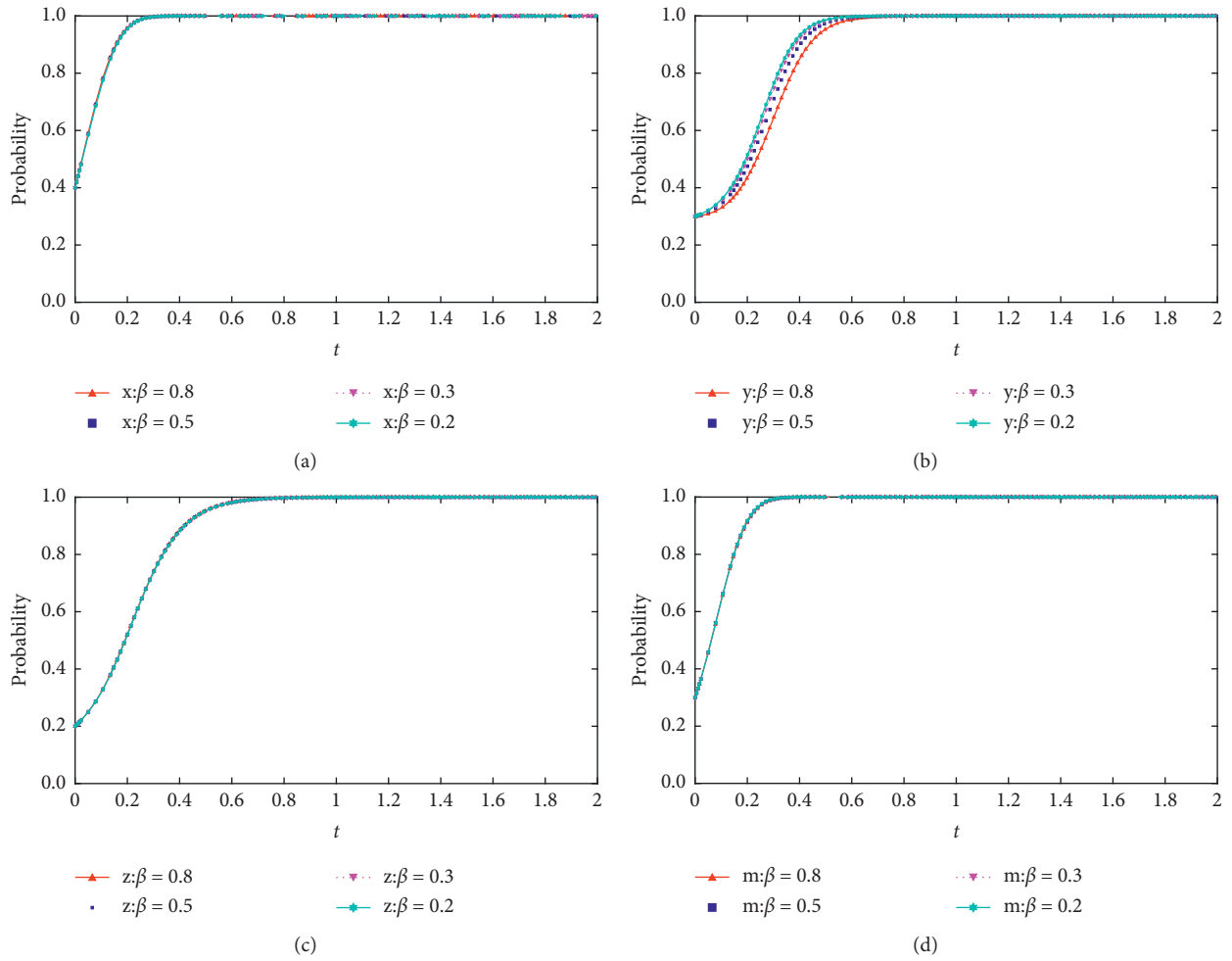
FIGURE 10: (a) The impact of changing levels of market competition on the evolution of tenderers' strategies. (b) The impact of changing levels of market competition on the evolution of high collusion strategies. (c) The impact of changing levels of market competition on the evolution of low collusion strategies. (d) The impact of changing levels of market competition on the evolution of regulators' strategies.
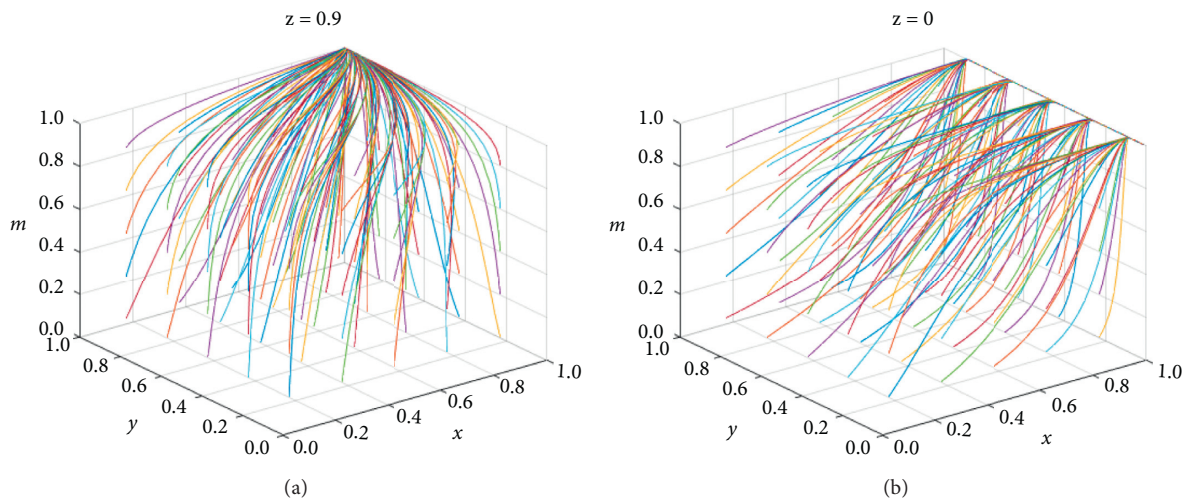

FIGURE 11: (a) The impact of strong supervision by internal oversight mechanisms on quadrilateral games. (b) Impact of nonoversight by internal oversight bodies on the quadrilateral game.
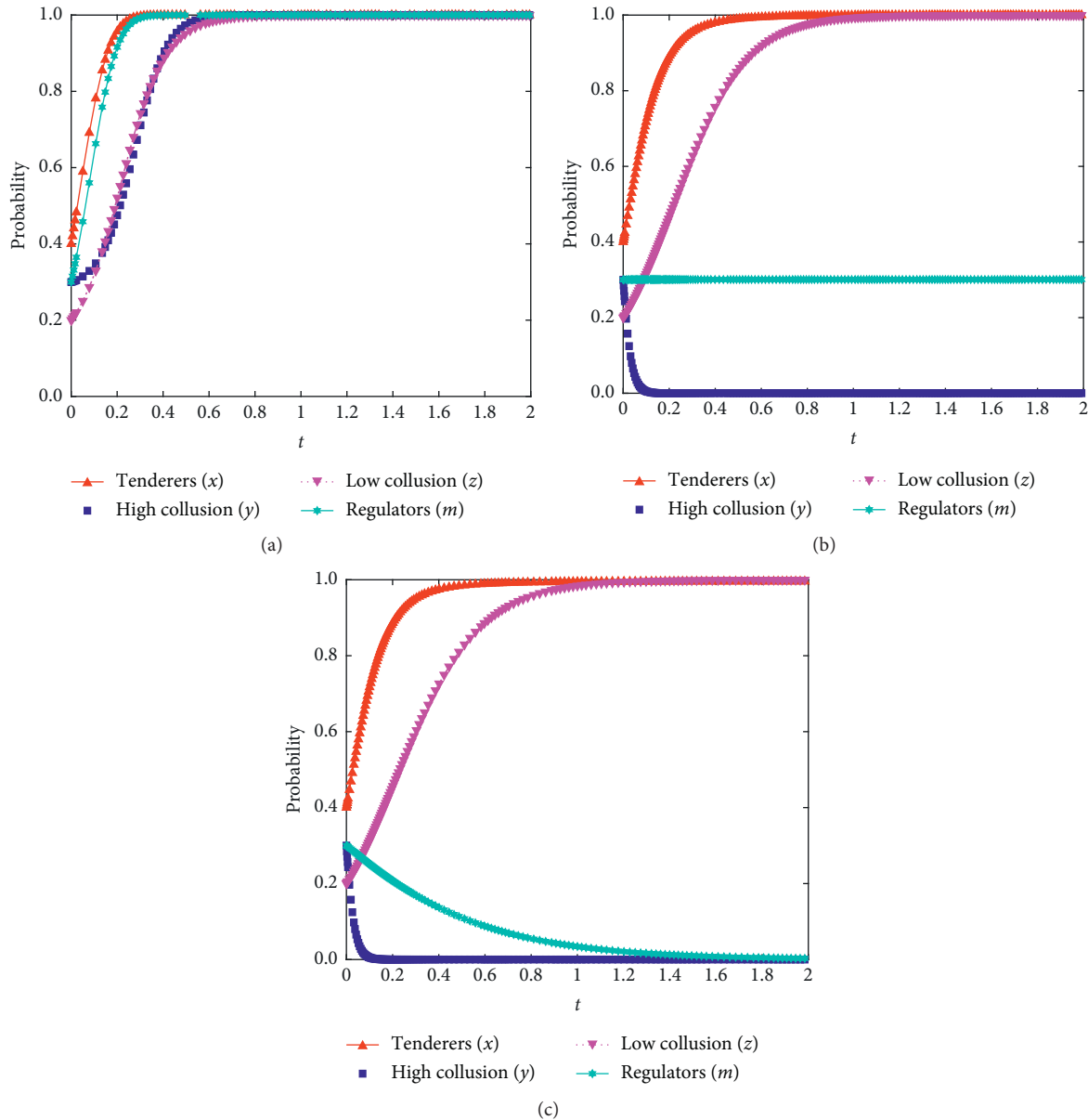
(a)

(b)

(c)

FIGURE 12: (a) Impact of changes in external penalty mechanisms (initial situation). (b) Impact of changes in external penalty mechanisms (medium penalty levels). (c) Impact of changes in external penalty mechanisms (high penalty levels).

three parties: the tenderer, the party with high willingness to collude, and the party with low willingness to collude. The results are shown in Figure 12.

As shown in Figure 12, as external penalties increase, the benefits gained by choosing to collude shift from higher than losses (low penalties) to medium penalties (the benefits of choosing to collude are equal to the losses when punished) and high penalties (the benefits of choosing to collude are lower than the losses when discovered). The probability of firms with higher willingness to collude engaging in collusion gradually decreases; however, as the cost of supervision increases, the probability of regulators adopting weak supervision also increases. Therefore, while increasing the intensity of control, attention should be paid to the equilibrium conditions. Such attention can avoid a decrease in

the supervisory body's willingness to supervise due to an excessive increase in external penalties.

5. Conclusions

This study focuses on the generation and control of collusion in the bidding process of government projects in China. It examines how to improve the quality of control of bidding collusion by considering different groups of enterprises and society's external supervision mechanism. The findings revealed the following.

(1) Establishing an effective external supervision mechanism and social supervision system can effectively reduce the probability of collusion among all

participants and achieve the quality of control over speculative behavior in the bidding process. The quality of the supervision system is closely related to the interests of the supervisory body, the benefits of reporting illegal behavior by social groups, and whether the report will bring retaliation from the tenderer and the colluding enterprises. In the control process, it is first necessary to reduce the cost of supervision and increase the incentives for supervisory bodies. Additionally, the application of deep learning, artificial intelligence, and other technologies should be vigorously promoted in the bidding process. Furthermore, a control mechanism should be established, combining artificial intelligence technology and manual auditing to reduce control costs.

(2) While establishing an effective regulatory mechanism, the reward and punishment mechanism should be improved to increase the punishment for law violations. Punishments can be imposed in the form of restrictions on bidding, social publicity, fines, and reduction of qualifications to increase the risk awareness of all participants in bidding and discourage those with a higher willingness to collude from participating in collusive behavior. At the same time, regular "look-back" inspections of phased government bidding projects should be carried out, with each region cross-checking the project's compliance to avoid concealment in the monitoring process.

(3) The bidding threshold and profitability of government bidding projects should be gradually raised under reasonable conditions. The level of competition in the market for government bidding projects should be reduced to control the willingness of project collusion participants. The simulation results show that the willingness of all parties to collude is low when the market is less competitive. Therefore, reasonably controlling the threshold and profitability of government projects can better control collusion. This will facilitate compliance and healthy operation of government bidding projects and the overall bidding market.

(4) Through research, we found that simply increasing the fines for illegal acts or improving the supervision cannot completely solve the vertical collusion in the bidding process of government investment projects. In the actual control process, we need to focus on the combination of internal supervision and external supervision system to enhance the law-abiding consciousness of each interest body, so as to realize that each interest body is unwilling to collude in thought and dare not collude in action, and to promote the effective operation of the bidding market of government investment projects.

The limitations of this study are the following two points.

(1) This study is based on the assumptions of non-fully rational economists and prospect theory. Still, in the government project bidding process, the decision of each game subject is influenced by random factors. Future research can examine the influence of random factors in the decision-making process and consider the influence of subjective emotions. Such an approach will make the results more in line with reality.

(2) This study examines vertical collusion in government investment projects, and the scope is not broad enough; widespread horizontal collusion is not considered. Future research may consider adding horizontal collusion to enhance the scalability of the research results.

Data Availability

The raw data supporting the conclusions of this article will be made available by the authors, without undue reservation.

Conflicts of Interest

The authors declare that they have no conflicts of interest regarding this work.

Acknowledgments

References

[1] Y. Chen and D. L. Cheng, "Analysis of the causes of vertical collusion in bidding for government investment engineering projects," *Journal of Changsha University of Technology (Natural Science Edition)*, vol. 15, no. 58, pp. 33–39, 2018.

[2] J. Wang and X. Qin, "Analysis of collusive motives of construction market actors under different regimes," *Construction Economics*, vol. S1, pp. 1–5, 2011.

[3] Y. Xie and W. J. Huang, "Incentives, supervision and collusion prevention of principal-agents in substitute establishments," *Mathematical Practice and Understanding*, vol. 01, pp. 42–47, 2008.

[4] X. Yu and H. Zhang, "Analysis of collusion game among owners, contractors and supervisors of government projects [J]," *Exploration on Economic Issues*, vol. 28, no. 11, pp. 86–92, 2008.

[5] S. Cheng, Q. Ge, Z. Sheng, and X. Liu, "Analysis of collusive game of large projects under tracking audit mode[J]," *Forecast*, vol. 31, no. 01, pp. 34–38, 2012.

[6] J. Miklós-Thal, "Optimal collusion under cost asymmetry," *Economic Theory*, vol. 46, no. 1, pp. 99–125, 2011.

[7] Y. Wu, Y. Peng, K. F. Chen, and Ru H. Xu, "A study of collusion regulation deterrence model for government investment proxy projects based on prospect theory," *Journal of Management in Engineering*, vol. 02, pp. 168–176, 2013.

[8] X. Wang and X. Lu, "Research on preventing collusion in engineering bidding based on the "prisoner's dilemma" game," *Technoeconomics*, vol. 32.007, pp. 65–68, 2013.

[9] J. Chen and H. Fu, "Research on collusive evolutionary game of multiple interest subjects in engineering project bidding," *Journal of Railway Science and Engineering*, vol. 16, no. 114, pp. 248–256, 2019.

[10] H. Zhang and H. Wang, "Game analysis of collusion phenomenon in the process of mutual evaluation of engineering bid evaluation experts," *Journal of Xi'an University of Technology*, vol. 3, pp. 232–236, 2014.

[11] Y. Chen and S. Deng, "Analysis of collusion conditions of construction project bidding based on cooperative game," *Journal of Railway Science and Engineering*, vol. 15, no. 95, pp. 275–280, 2018.

[12] Z. Yi, C. Xiang, L. Li, and H. Jiang, "Evolutionary game analysis and simulation with system dynamics for behavioral strategies of participants in crowd logistics," *Transportation Letters: The International Journal of Transportation Research*, vol. 5, pp. 1–15, 2020.

[13] J. I.-kun Kao and B.-ra Lee, "The Effect of Individual perceptions of social corruption levels and practices on corruption intentions: a Case study of Public Agency suppliers," *Korean Society and Administration Research*, vol. 23, no. 3, pp. 405–427, 2012.

[14] S. Brianzoni, R. Coppier, and E. Michetti, "Evolutionary effects of non-compliant behavior in public procurement," *Structural Change and Economic Dynamics*, vol. 51, 2019.

[15] Y. Fang, M. Perc, and H. Xu, "The Singaporean model in public goods dilemmas with benevolent leaders and bribery," *Journal of Theoretical Biology*, vol. 501, Article ID 110345, 2020.

[16] L. Liu, X. Chen, and A. Szolnoki, "Evolutionary dynamics of cooperation in a population with probabilistic corrupt enforcers and violators," *Mathematical Models and Methods in Applied Sciences*, vol. 29, 2019.

[17] J. He, Q. Yang, and Y. Gao, "Does multi-attribute bidding in public construction projects prevent corruption while tenderers' preferences are open? A study of China's practice," *Eurasia Journal of Mathematics, Science and Technology Education*, vol. 13, 2017.

[18] R. Clark, D. Coviello, J.-F.¿½ois Gauthier, and A. Shneyerov, "Corrigendum to: bid rigging and entry deterrence in public procurement: evidence from an investigation into collusion and corruption in quebec," *Journal of Law, Economics, and Organization*, vol. 35, no. 2, p. 454, 2019.

[19] P. Ballesteros-Pérez, M. Skitmore, E. Pellicer, and M. C. González-Cruz, "Scoring rules and abnormally low bids criteria in construction tenders: a taxonomic review," *Construction Management & Economics*, vol. 33, no. 4, 2015.

[20] H. Chunyan, *Research on Collusion and its Prevention in Engineering Project Bidding*, Henan University of Technology, MA thesis, 2020.

[21] R. Dou, *Research on the Problem of Bid-Rigging and Governance of Engineering Projects under the Background of Electronic Bidding*, Anhui University, MA thesis, 2020.

Hindawi

Research Article

Tourism Demand Forecast Based on Adaptive Neural Network Technology in Business Intelligence

Liangliang Wang (ID)

Xinyang Agriculture and Forestry University, Xinyang 464000, China

Correspondence should be addressed to Liangliang Wang; 2011300004@xyafu.edu.cn

In order to improve the effect of tourism demand forecast, the commercial development of the tourism industry, and the actual experience of users, this paper uses adaptive neural network technology to conduct tourism demand forecast analysis. Moreover, this paper improves the adaptive neural network algorithm so that it can handle multiple data for tourism demand forecast. After improving the algorithm, this paper employs the actual process of tourism demand forecast to construct a tourism demand forecast model based on adaptive neural network technology. After that, this paper combines travel time and space data analysis to determine the system's functional structure and network topology. Through experimental research, it can be seen that the tourism demand forecast model based on adaptive neural network technology proposed in this paper performs well in tourism demand forecast and meets the actual demand of modern tourism forecast.

1. Introduction

Since the beginning of the 21st century, the world's tourism industry has developed rapidly. Currently, many cities regard tourism as the pillar industry of their economic development, hoping to use the development of tourism to drive the development of the entire social economy. An obvious difference between tourism and industry, agriculture, and other production industries is the volatility of tourism, which is a huge challenge for enterprises and government planning departments in the tourism market. Therefore, in order to make a successful decision, we need to make an accurate forecast of the future demand of the tourism market. Modern tourism researchers have tried to use many mathematical methods and models to solve this problem. The main models commonly used at present are time series forecast models; regression models, including linear and nonlinear regression models; adaptive models; artificial neural networks; etc.

As a "green" driving force, tourism is not only related to the balance and coordination of resources and the environment, but also one of the important ways to achieve sustainable economic development [1]. Since the reform and

opening up, the development of China's tourism industry has experienced a historical leap from "shortage type" to "large country type." However, with the rapid growth of the tourism industry, the number of complaints about tourism experience is increasing, and the negative information exposed by the media and tourists through the Internet has a serious impact on the image of regional tourism [2]. In the Internet age, the dissemination of these negative information spans traditional geographic distance and time constraints [3] and has attracted more and more attention. Among them, the media and tourists' online attention to negative information such as travel complaints has become an important factor influencing tourists' decision-making and the development of regional tourism. At the same time, the massive amount of network information has made tourism routes more diverse, and the spatial associations between tourism demand-oriented regional tourism industries have become increasingly close and complex. Therefore, the spatial spillover effect of negative information network attention on regional tourism development cannot be ignored.

Some scholars divide the influencing factors into three types: thrust, pull, and resistance. Among them, push refers

to the factors that encourage people to travel, including population size, income trends, income distribution, and education level. Rally refers to the factors that attract people's subjective wishes to travel to a certain area, including climate, business, culture, marketing strategies, relatives, and friends. Resistance refers to the factors that hinder people from traveling to a certain area, including price, competitors, and supply capacity. When foreign countries use quantitative models to analyze influencing factors, they often take economic factors as the main research object. In the process of research, some scholars have discovered that the most critical factor affecting tourism demand and related decision-making is economy. Domestic scholars have also conducted research on the tourism demand of the source country of Hong Kong, showing that the tourism products, the economic level of the region, and the tourism costs are the most important factors. Special events include economic and noneconomic factors, such as social conflicts, sports events, and financial crises. In these three categories, it is generally believed that the influence of noneconomic factors is relatively small and that economic factors are more conducive to the establishment of tourism demand forecasting models; in-depth research was conducted on this basis. However, in terms of the actual situation in my country, my country's tourism demand is also greatly affected by family consumption habits, political and social factors, consumption concepts, and other factors. Therefore, the tourism demand forecasting method that only considers economic factors is not in line with my country's reality.

This paper uses adaptive neural network technology to carry out tourism demand forecast and analysis and build a business intelligence model to improve the forecast effect of subsequent tourism demand.

2. Related Work

Many scholars try to use different models to improve the accuracy and timeliness of demand forecasting, which can usually be divided into three categories: causality model, time series model, and artificial intelligence model. Literature [4] uses search keywords to establish a multiple linear regression function to predict the number of daily tourists and uses a single variable autoregressive moving average (ARMA) model to predict the tourism demand of 9 countries in the Asia-Pacific region. Sigalat Signes et al. [5] constructed a combined prediction model of autoregressive moving average model and BP neural network. Literature [6] applies support vector regression (SVR) model to tourism demand forecasting and combines it with autoregressive integrated moving average (ARIMA) model. Literature [7] uses an artificial neural network model to predict tourism demand in the Balearic Islands. Literature [8] uses a neural network-based fuzzy time series model as a prediction model to predict tourism demand during SARS. Literature [9] proposes a tourism flow forecasting SSVR-PSO (seasonal support vector regression particle swarm optimization) model that combines the seasonal support vector regression model and particle swarm optimization algorithm. Compared with the first two types of models, artificial intelligence

models show great advantages in terms of nonlinear fitting and adaptive learning, but traditional artificial neural networks have problems such as complex training process and long-time consumption. Therefore, finding efficient and accurate new neural network methods has become a hot research direction. Paper [9] proposed ESN (echo state network). Compared with traditional algorithms, the training process of echo state network is simple and efficient. It can approximate dynamic systems infinitely under general conditions and is widely used in various prediction problems. Literature [10] uses ESN to predict mobile communication traffic, and literature [11] uses it to deal with time series problems related to the prediction of certain eigenvalues of sunspots. However, ESN also has its own shortcomings and limitations. For example, ESN parameters and connection weights are randomly set, and only the output layer weights are adjusted during the training process, which is easy to fall into the local optimal solution. The common method currently used is to construct the ESN model when the network selects the optimal output multiple times, or select the parameters based on experience to construct the model. In this regard, many scholars have optimized the structure of the ESN. Literature [12] developed several new storage pool topologies for ESN and predicted the energy consumption of office buildings. Literature [13] proposed an echo state network prediction model with bifurcation structure to improve the prediction accuracy of ESN. Some scholars also use heuristic algorithms to optimize the parameters of ESN and obtain good experimental results. Literature [14] uses genetic algorithms to optimize the initial weights and thresholds of the forward feedback neural network, but there are relatively few studies of this kind at present. The fruit fly optimization algorithm (FOA) proposed by literature [15] has the advantages of low complexity, fast calculation speed, and strong solution ability. It has been applied in many combinatorial optimization and continuous optimization fields. Literature [16] uses FOA optimization for the structural parameters of the artificial neural network (ANN) model, and literature [14] uses FOA to optimize the penalty parameters and conversion coefficients of SVR and has achieved good experimental results. FOA itself has disadvantages such as low convergence accuracy and being easy to fall into local extreme values. Literature [17] proposed an adaptive mutation fruit fly optimization algorithm, according to the population fitness variance and the current optimal value; under the probability P, the mutation operator interferes with the replication to continue the optimization. Literature [18] increases the inertia to change the nonlinear decreasing characteristics and the relationship between individuals and groups, and an improved fruit fly optimization algorithm (IFOA) is constructed.

3. Tourism Demand Forecast Algorithm Based on Adaptive Neural Network

In order to achieve the control goal, the dynamic error system is defined as follows:

$$\tilde{x}_1 = x_1 - y\,d,$$

$$\tilde{x}_2 = \dot{\tilde{x}}_1,$$ (1)

$$\tilde{x}_3 = \dot{\tilde{x}}_2.$$

The design method of linear filter reduction is adopted, and filter variables are introduced to reduce the order of the system. The linear filter is defined as follows. The filter has the properties of exponential convergence, asymptotic convergence, and bounded transfer.

$$e1 = \tilde{x}_1,$$

$$e2 = \dot{e}_1 + 2e_1,$$ (2)

$$e3 = \dot{e}_2 + 2e_2.$$

We define $e = [e1^T, e2^T, e3^T]^T$, $\tilde{x} = [\tilde{x}1^T, \tilde{x}2^T, \tilde{x}3^T]^T$, and then there is the following relationship between e and $\tilde{x}$:

$$e = \left[\begin{pmatrix} I_2 & 0 & 0 \\ 2I_2 & I_2 & 0 \\ 4I_3 & I_3 & I_3 \end{pmatrix}\right] \tilde{x}.$$ (3)

In order to obtain the closed-loop dynamic equations of the three channels, the following equations are obtained by finding the first-order time derivative of $e3(t)$:

$$\dot{e}_3 = \frac{d}{dt}\left(\tilde{x}_3 + 4\tilde{x}_2 + 4\tilde{x}_1\right)$$

$$= \dot{\tilde{x}}3 + 4\dot{\tilde{x}}_2 + 4\dot{\tilde{x}}_1$$

$$= \overset{\text{\tiny t}}{\tilde{x}}1 - \overset{\text{\tiny t}}{\tilde{y}}\,d + 4\tilde{x}_3 + 4\tilde{x}_2$$ (4)

$$= F(x_1, x_2, x_3) + G(x_1, x_2)u - \overset{\text{\tiny t}}{\tilde{y}}d + 4\tilde{x}_3 + 4\tilde{x}_2.$$

By decomposing formula (4), $G(x_1, x_2)$, the following expression is obtained:

$$\dot{e}_3(t) = F(x_1, x_2, x_3) + S(x_1, x_2)DU(x_1, x_2)u - \overset{\text{\tiny t}}{\tilde{y}}d + 4\tilde{x}_3 + 4\tilde{x}_2.$$ (5)

By multiplying both sides of the above equation by $S^{-1}(x_1, x_2)$, we get

$$S^{-1}(x_1, x_2)\dot{e}_3(t) = S^{-1}(x_1, x_2)F(x_1, x_2, x_3)$$

$$+ DU(x_1, x_2)u + S^{-1}(x_1, x_2)\left(-\overset{\text{\tiny t}}{\tilde{y}}d + 4\tilde{x}_3 + 4\tilde{x}_2\right).$$ (6)

By adding and subtracting $(1/2)S^{-1}(x_1, x_2)e3$ at the same time in the right half of (6), we can get

$$S^{-1}(x_1, x_2)\dot{e}_3(t) = S^{-1}(x_1, x_2)F(x_1, x_2, x_3) + S^{-1}(x_1, x_2)\left(-\overset{\text{\tiny t}}{\tilde{y}}d + 4\tilde{x}_3 + 4\tilde{x}_2\right)$$

$$+ DU(x_1, x_2)u + \frac{1}{2}S^{-1}(x_1, x_2)e3 - \frac{1}{2}S^{-1}(x_1, x_2)e3.$$ (7)

Matrix D is a diagonal matrix, and the value of each item in the matrix is +1 or −1. The matrix form is

$$D = \begin{pmatrix} d_1 & 0 & 0 \\ 0 & d_2 & 0 \\ 0 & 0 & d_3 \end{pmatrix}.$$ (8)

The matrix U is an upper triangular matrix, in which each function above the main diagonal is an unknown function item. The matrix form is

$$U(x_1, x_2) = \begin{pmatrix} 1 & U_{12}(x_1, x_2) & U_{13}(x_1, x_2) \\ 0 & 1 & U_{23}(x_1, x_2) \\ 0 & 0 & 1 \end{pmatrix}.$$ (9)

In order to facilitate subsequent control design, a new auxiliary function variable is designed, and the auxiliary function is defined as

$$N\left(x_1, x_2, x_3, y\,d, \dot{y}d, \ddot{y}d, \overset{\text{\tiny t}}{y}d\right) = S^{-1}(x_1, x_2)F(x_1, x_2, x_3)$$

$$+ S^{-1}(x_1, x_2)\left(-\overset{\text{\tiny t}}{\tilde{y}}d + 4\tilde{x}_3 + 4\tilde{x}_2\right) + \frac{1}{2}S^{-1}(x_1, x_2)e3.$$ (10)

By substituting (10) into (7), the open-loop error dynamic system of $e3(t)$ is obtained as follows:

$$S^{-1}(x_1, x_2)\dot{e}_3(t) = N(\cdot) + DU(x_1, x_2)u - \frac{1}{2}S^{-1}(x_1, x_2)e3. \tag{11}$$

The hypersonic vehicle dynamics control signal is defined as $\Phi = u1, \delta e = u2, \delta c = u3$. According to the closed-loop dynamics equation in (10), in order to facilitate the subsequent stability analysis process, the control signal $u(t)$ is designed as follows:

$$u = [\Phi(t), \delta e(t), \delta c(t)]^T = [u1, u2, u3]^T. \tag{12}$$

Here, $u(t)$ is decomposed into

$$ui = uri + u\,di\,, i = 1, 2, 3. \tag{13}$$

uri is defined as follows:

$$uri = di(-ki)e3i. \tag{14}$$

By substituting matrix U, matrix D, and the resulting equation into (14), the closed-loop error dynamic equation is obtained:

$$S^{-1}(x_1, x_2)\dot{e}_3(t) = \begin{bmatrix} N1(\cdot) \\ N2(\cdot) \\ N3(\cdot) \end{bmatrix} - \frac{1}{2}\dot{S}^{-1}(x_1, x_2)e3$$

$$+ \begin{pmatrix} d_1 & 0 & 0 \\ 0 & d_2 & 0 \\ 0 & 0 & d_3 \end{pmatrix} \begin{pmatrix} 1 & U_{12} & U_{13} \\ 0 & 1 & U_{23} \\ 0 & 0 & 1 \end{pmatrix} \begin{bmatrix} ur_1 + ud_1 \\ ur_2 + ud_2 \\ ur_3 + ud_3 \end{bmatrix}. \tag{15}$$

By expanding (15), we can get

$$S^{-1}(x_1, x_2)\dot{e}_3(t) = \begin{pmatrix} N1(\cdot) + d1\left(u12\left(ur_2 + ud_2\right) + u13\left(ur_3 + ud_3\right)\right) \\ N2(\cdot) + d2\left[u23\left(ur_3 + ud_3\right)\right] \\ N3(\cdot) \end{pmatrix}$$

$$- \frac{1}{2}\dot{S}^{-1}(x_1, x_2)e3 + \begin{pmatrix} d1\left(ur_1 + ud_1\right) \\ d2\left(ur_2 + ud_2\right) \\ d3\left(ur_3 + ud_3\right) \end{pmatrix}. \tag{16}$$

The auxiliary function $M1, M2, M3$ is defined as the following form:

$$M1\left(x_1, x_2, x_3, y\,d, yd^{(1)}, yd^{(2)}, yd^{(3)}, ud_2, ud_3\right)$$

$$= N1(\cdot) + d1\left(u12\left(ur_2 + ud_2\right) + u13\left(ur_3 + ud_3\right)\right),$$

$$M2\left(x_1, x_2, x_3, y\,d, yd^{(1)}, yd^{(2)}, yd^{(3)}, ud_3\right)$$

$$= N2(\cdot) + d2\left[u23\left(ur_3 + ud_3\right)\right], \tag{17}$$

$$M3\left(x_1, x_2, x_3, y\,d, yd^{(1)}, yd^{(2)}, yd^{(3)}\right) = N3(\cdot).$$

By substituting (17) into (16), we can get

$$S^{-1}(x_1, x_2)\dot{e}_3(t) = \begin{pmatrix} M1 \\ M2 \\ M3 \end{pmatrix} - \frac{1}{2}\dot{S}^{-1}(x_1, x_2)e3 + \begin{pmatrix} d1(ur_1 + ud_1) \\ d2(ur_2 + ud_2) \\ d3(ur_3 + ud_3) \end{pmatrix}. \tag{18}$$

By using neural network approximation, $M1, M2, M3$ can be written as

$$M1 = \theta 1\phi 1^T(t) + \varepsilon 1,$$
$$M2 = \theta 2\phi 2^T(t) + \varepsilon 2, \tag{19}$$
$$M3 = \theta 3\phi 3^T(t) + \varepsilon 3.$$

Among them, $\theta 1^T\theta 1 \le \theta M$, $\theta 2^T\theta 2 \le \theta M$, $\theta 3^T\theta 3 \le \theta M$, $|\varepsilon 1| \le \varepsilon$, $|\varepsilon 2| \le \varepsilon$, $|\varepsilon 3| \le \varepsilon$, and θM is unknown constant.

ud_i is designed as follows:

$$ud_1 = -d1\hat{\theta}1\phi 1^T(t),$$
$$ud_2 = -d2\hat{\theta}2\phi 2^T(t), \tag{20}$$
$$ud_3 = -d3\hat{\theta}3\phi 3^T(t).$$

By substituting (14), (19), and (20) into (18), the closed-loop error dynamics equation can be obtained:

$$S^{-1}(x_1, x_2)\dot{e}_3(t)$$
$$= \begin{pmatrix} \theta 1\phi 1^T(t) + \varepsilon 1 \\ \theta 2\phi 2^T(t) + \varepsilon 2 \\ \theta 3\phi 3^T(t) + \varepsilon 3 \end{pmatrix} - \frac{1}{2}\dot{S}^{-1}(x_1, x_2)e3 - \begin{pmatrix} k_1 & 0 & 0 \\ 0 & k_2 & 0 \\ 0 & 0 & k_3 \end{pmatrix}e3 - \begin{pmatrix} \hat{\theta}1\phi 1^T(t) \\ \hat{\theta}2\phi 2^T(t) \\ \hat{\theta}3\phi 3^T(t) \end{pmatrix}$$
$$= \begin{pmatrix} \tilde{\theta}1\phi 1^T(t) \\ \tilde{\theta}2\phi 2^T(t) \\ \tilde{\theta}3\phi 3^T(t) \end{pmatrix} + \begin{pmatrix} \varepsilon 1 \\ \varepsilon 2 \\ \varepsilon 3 \end{pmatrix} - \frac{1}{2}\dot{S}^{-1}(x_1, x_2)e3 - \begin{pmatrix} k_1 & 0 & 0 \\ 0 & k_2 & 0 \\ 0 & 0 & k_3 \end{pmatrix}e3. \tag{21}$$

The proposed Lyapunov candidate function is defined as follows:

$$V = \frac{1}{2}e1^Te1 + \frac{1}{2}e2^Te2 + \frac{1}{2}e3^TS^{-1}(x_1, x_2)e3$$
$$+ \frac{1}{2}\tilde{\theta}1^T\Gamma 1^{-1}\tilde{\theta}1 + \frac{1}{2}\tilde{\theta}2^T\Gamma 2^{-1}\tilde{\theta}2 + \frac{1}{2}\tilde{\theta}3^T\Gamma 3^{-1}\tilde{\theta}3. \tag{22}$$

By deriving the Lyapunov function, the following equation can be obtained:

$$\dot{V} = -2e^2_{1,i} + e^T_{1,i}e_{2,i} - 2e^2_{2,i} + e^T_{2,i}e_{3,i} + e3S^{-1}(x_1, x_2)\dot{e}_3(t)$$
$$- \tilde{\theta}1^T\Gamma 1^{-1}\dot{\hat{\theta}}1 - \tilde{\theta}2^T\Gamma 2^{-1}\dot{\hat{\theta}}2 - \tilde{\theta}3^T\Gamma 3^{-1}\dot{\hat{\theta}}3 + \frac{1}{2}e3^T\dot{S}^{-1}(x_1, x_2)e3. \tag{23}$$

By substituting (21) into (23), according to the triangle inequality theorem, (23) can be transformed into the following form:

$$\dot{V} \le -2\|e1\|^2 - 2\|e2\|^2 + \frac{1}{2}\|e1\|^2 + \|e2\|^2 + 1/2\|e3\|^2$$
$$+ e3\left(\begin{pmatrix} \phi 1^T(t)\tilde{\theta}1 + \varepsilon 1 \\ \phi 2^T(t)\tilde{\theta}2 + \varepsilon 2 \\ \phi 3^T(t)\tilde{\theta}3 + \varepsilon 3 \end{pmatrix} - \frac{1}{2}\dot{S}^{-1}(x_1 x_2)e3 - \begin{pmatrix} k_1 & 0 & 0 \\ 0 & k_2 & 0 \\ 0 & 0 & k_3 \end{pmatrix}e3\right) \tag{24}$$
$$- \tilde{\theta}1^T\Gamma 1^{-1}\dot{\hat{\theta}}1 - \tilde{\theta}2^T\Gamma 2^{-1}\dot{\hat{\theta}}2 - \tilde{\theta}3^T\Gamma 3^{-1}\dot{\hat{\theta}}3 + \frac{1}{2}e3^T\dot{S}^{-1}(x_1, x_2)e3.$$

Next, the adaptive update rate $\dot{\hat{\theta}}1, \dot{\hat{\theta}}2, \dot{\hat{\theta}}3$ of neural network weights is designed as

$$
\dot{\hat{\theta}}1 = \Gamma 1 \phi 1\,(t)e3,1 - \Gamma 1\eta 1\hat{\theta}1,
$$

$$
\dot{\hat{\theta}}2 = \Gamma 2 \phi 3\,(t)e3,2 - \Gamma 2\eta 2\hat{\theta}2, \tag{25}
$$

$$
\dot{\hat{\theta}}3 = \Gamma 3 \phi 3\,(t)e3,3 - \Gamma 3\eta 3\hat{\theta}3.
$$

By substituting the adaptive update rate into the original inequality (25), after expansion, we can get

$$
\begin{aligned}
\dot{V} \le\ & -\frac{3}{2}\|e1\|^2 - \|e2\|^2 + \frac{1}{2}\|e3\|^2 \\
& + e3\left(\left(\begin{pmatrix} \phi 1^T(t)\tilde{\theta}1 + \varepsilon 1 \\ \phi 2^T(t)\tilde{\theta}2 + \varepsilon 2 \\ \phi 3^T(t)\tilde{\theta}3 + \varepsilon 3 \end{pmatrix} - \frac{1}{2}\dot{S}^{-1}(x_1,x_2)e3 - \begin{pmatrix} -(k1)e3,1 \\ -(k2)e3,2 \\ -(k3)e3,3 \end{pmatrix}\right)\right) \\
& - \tilde{\theta}1^T\Gamma 1^{-1}(\Gamma 1\phi 1(t)e3,1 - \Gamma 1\eta 1\hat{\theta}1) - \tilde{\theta}2^T\Gamma 2^{-1}(\Gamma 1\phi 1(t)e3,1 - \Gamma 1\eta 1\hat{\theta}1) \\
& - \tilde{\theta}3^T\Gamma 3^{-1}(\Gamma 1\phi 1(t)e3,1 - \Gamma 1\eta 1\hat{\theta}1) + \frac{1}{2}e3^T\dot{S}^{-1}(x_1,x_2)e3.
\end{aligned} \tag{26}
$$

After merging similar items, it is further transformed into the following form:

$$
\begin{aligned}
\dot{V} \le\ & -\frac{3}{2}\|e1\|^2 - \|e2\|^2 + \frac{1}{2}\|e3\|^2 + e3,1\phi 1^T(t)\tilde{\theta}1 + e3,2\phi 2^T(t)\tilde{\theta}2 \\
& + e3,3\phi 3^T(t)\tilde{\theta}3 + e3,1\varepsilon 1 + e3,2\varepsilon 2 + e3,3\varepsilon 3 - (k1)e3,1^2 \\
& - (k2)e3,2^2 - (k3)e3,3^2 - \tilde{\theta}1^T\phi 1(t)e3,1 + \tilde{\theta}1^T\eta 1\hat{\theta}1 \\
& - \tilde{\theta}2^T\phi 2(t)e3,2 + \tilde{\theta}2^T\eta 2\hat{\theta}2 - \tilde{\theta}3^T\phi 3(t)e3,3 + \tilde{\theta}3^T\eta 3\hat{\theta}3.
\end{aligned} \tag{27}
$$

Inequality (27) is reduced to the following form:

$$
\begin{aligned}
\dot{V} \le\ & -\frac{3}{2}\|e1\|^2 - \|e2\|^2 + \frac{1}{2}\|e3\|^2 + e3,1\varepsilon 1 + e3,2\varepsilon 2 + e3,3\varepsilon 3 - (k1)e3,1^2 \\
& - (k2)e3,2^2 - (k3)e3,3^2 + \tilde{\theta}1^T\eta 1\hat{\theta}1 + \tilde{\theta}2^T\eta 2\hat{\theta}2 + \tilde{\theta}3^T\eta 3\hat{\theta}3.
\end{aligned} \tag{28}
$$

At the same time, inequality scaling is performed on the residual term of the neural network approximation and the approximate value of the neural network weight, and the Lyapunov function inequality can be obtained as follows:

$$
\begin{aligned}
\dot{V} \le\ & -\frac{3}{2}\|e1\|^2 - \|e2\|^2 + \frac{1}{2}\|e3\|^2 + \frac{1}{2}\varepsilon_1^2 + \frac{1}{2}\varepsilon_2^2 + \frac{1}{2}\varepsilon_3^2 \\
& + \tilde{\theta}1^T\eta 1\hat{\theta}1 + \tilde{\theta}2^T\eta 2\hat{\theta}2 + \tilde{\theta}3^T\eta 3\hat{\theta}3.
\end{aligned} \tag{29}
$$

Considering $\|\theta i\| \le \theta M, \|\varepsilon i\| \le \varepsilon M, \|\tilde{\theta}i\| \le \tilde{\theta}M, i = 1,2,3,$, we set $ki - 1/2 > 1/2$, and it can be derived from the original inequality:

$$
\begin{aligned}
\dot{V} \le\ & -\frac{3}{2}\|e1\|^2 - \|e2\|^2 - \|e3\|^2 + \frac{1}{2}\varepsilon_1^2 + \frac{1}{2}\varepsilon_2^2 + \frac{1}{2}\varepsilon_3^2 + \frac{1}{2}\eta_1^2\theta_1^2 \\
& + \frac{1}{2}\eta_2^2\theta_2^2 + \frac{1}{2}\eta_3^2\theta_3^2 - \tilde{\theta}_1^T\eta 1\tilde{\theta}1 - \tilde{\theta}_2^T\eta 2\tilde{\theta}2 - \tilde{\theta}_3^T\eta 3\tilde{\theta}3.
\end{aligned} \tag{30}
$$

We assume that the maximum eigenvalue of $S^{-1}(x_1, x_2)$ is less than a constant λ, and the constant λ is greater than zero. The matrix $S(x_1, x_2)$ itself is a positive definite symmetric matrix with uniform positive definiteness. Therefore,

$$\dot{V} \le -\|e1\|^2 - \|e2\|^2 - \|e3\|^2 - \tilde{\theta}_1^T \eta 1 \tilde{\theta}1 - \tilde{\theta}_2^T \eta 2 \tilde{\theta}2 - \tilde{\theta}_3^T \eta 3 \tilde{\theta}3 + C. \tag{31}$$

Among them, $C = 1/2\varepsilon_1^2 + 1/2\varepsilon_2^2 + 1/2\varepsilon_3^2 + 1/2\eta_1^2\theta_1^2 + 1/2\eta_2^2\theta_2^2 + 1/2\eta_3^2\theta_3^2$.

$$V \le +\frac{1}{2}\left(\|e1\|^2 + \|e2\|^2 + \lambda\|e3\|^2 + \tilde{\theta}_1^T \Gamma 1^{-1}\tilde{\theta}1 + \tilde{\theta}_2^T \Gamma 2^{-1}\tilde{\theta}2 + \tilde{\theta}_3^T \Gamma 3^{-1}\tilde{\theta}3 \right). \tag{32}$$

According to the law of comparison, we have

$$\dot{V} \le \frac{-2\min(1, \eta 1, \eta 2, \eta 3),}{\max\left(1, \lambda, \Gamma 1^{-1}, \Gamma 2^{-1}, \Gamma 3^{-1}\right)}V + C. \tag{33}$$

By solving the differential inequality, we can get

$$V \le -\frac{c}{m} + \left(V(0) + \frac{c}{m}\right)e^{mt}. \tag{34}$$

Among them, $m = -2\min(1, \eta 1, \eta 2, \eta 3,)/\max(1, \lambda, \Gamma 1^{-1}, \Gamma 2^{-1}, \Gamma 3^{-1})$.

Therefore,

$$-\frac{c}{m}\|e\|^2 \le V \le -\frac{c}{m} + \left(V(0) + \frac{c}{m}\right)e^{mt}. \tag{35}$$

Thus, it is indicated that the tracking error $e1, e2, e3$ and the weight estimation error index $\tilde{\theta}1, \tilde{\theta}2, \tilde{\theta}3$ converge to zero.

4. Tourism Demand Forecast Based on Adaptive Neural Network Technology

In order to respond to the spatial increase of local tourism demand status, the short-sighted path dependence of the unidirectional flow view and the static destination market concept should be eliminated. Moreover, it is necessary to reconstruct a new tourist destination spatial system with both destination and tourist source functions from a more microscopic perspective (see Figure 1). The spatial reorganization of tourist destinations is explored under the continuous deepening of small- and medium-scale tourism spatial behavior. The system should be a specific organic whole composed of several interacting and interdependent tourism elements within a certain geographical space. It uses the existing borders of jurisdictions as the dividing lines between local and remote areas. This includes not only the part of the spatial system formed by the inflow of tourist from outside the region involved in the original space system into the tourist destination, but also the part of the regional tourism space system such as cities, towns, and rural areas. At the same time, it takes tourist destinations that have both the functions of tourist source and destination as the main body to form a space system with specific order and complementary internal and external space with factors such as regional tourism environment, tourism channels, tourism information, and tourism flow. It needs to be pointed out that the reconstruction of the new tourist destination space system is not a complete denial of the original tourist destination space system, but a supplement and improvement to its system.

When designing the system, the main direction is around the surrounding information of the scenic spot. For example, we need to add functions that allow users to search for, roam, navigate, collect, share, and pay for scenic spots to facilitate users to screen scenic spots and provide the readability of tourism quality and the convenience of transportation. In the process of searching and roaming at scenic spots, tourists can find relevant information such as the ticket limit of scenic spots, travel, and transportation costs. In addition, it should be noted that the platform must take into account both the emotional needs and consumer needs of users. On the one hand, after users have used the travel tools provided by the platform and browsed the target attractions, they will need to communicate with other people on the Internet. On the other hand, users also need to store and classify related information after using the platform. Therefore, we also need to provide a storage and classification function, so that users can save time when using the platform for the second time and quickly find the previously stored scenic spot information. The analysis of user needs is shown in Figure 2.

The analysis of platform function requirements is shown in Figure 3.

Before planning a trip, users need to search for resources effectively. It is necessary to classify the platform's attractions resources, and through the history function, users can easily call up the browsing history. Secondly, after the user has screened the destination, the user needs to understand the surroundings. At the same time, it is necessary to prompt peripheral information such as toilets, ATMs, and hotels during the virtual roaming process. When the platform constructs the framework, it needs to introduce data about city-related information. After the user has searched the surrounding information of the destination, the user needs to pay for the services that can be provided on the Internet. Therefore, the platform needs to add the function of Internet payment. After the travel experience, there must be follow-up emotional expressions, so the platform needs to have a comment function. The fishbone diagram of the platform function requirement analysis is shown in Figure 4.

The terminals involved in this paper include mobile devices and desktop devices. Mobile ports include tablet
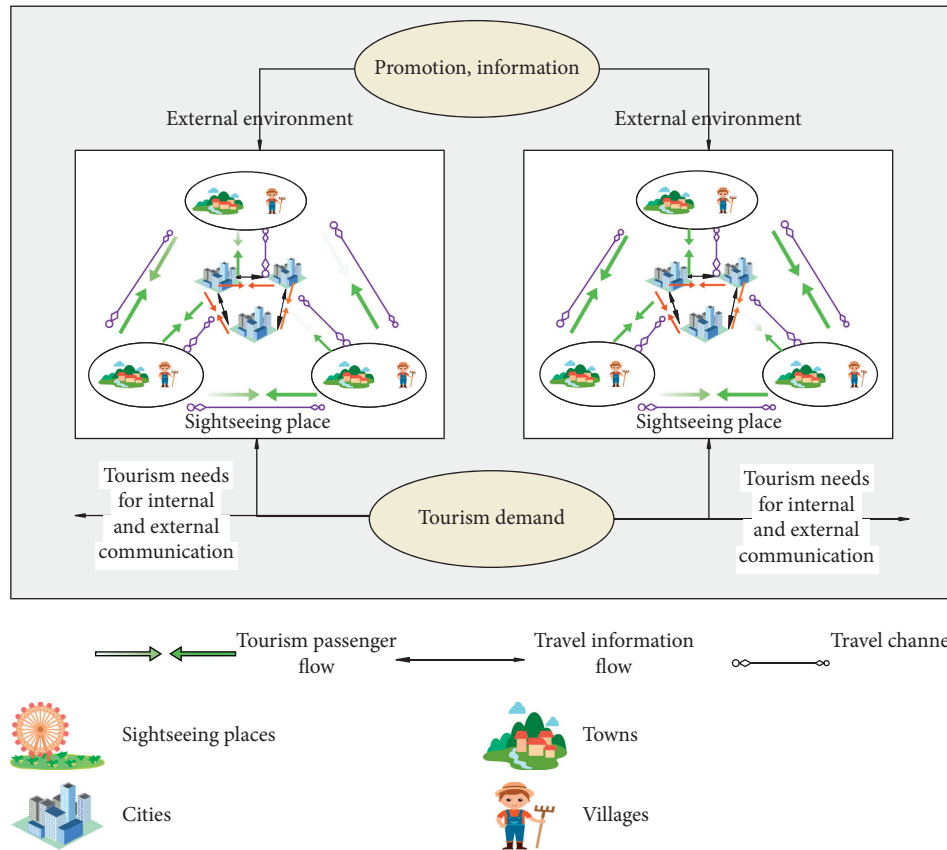
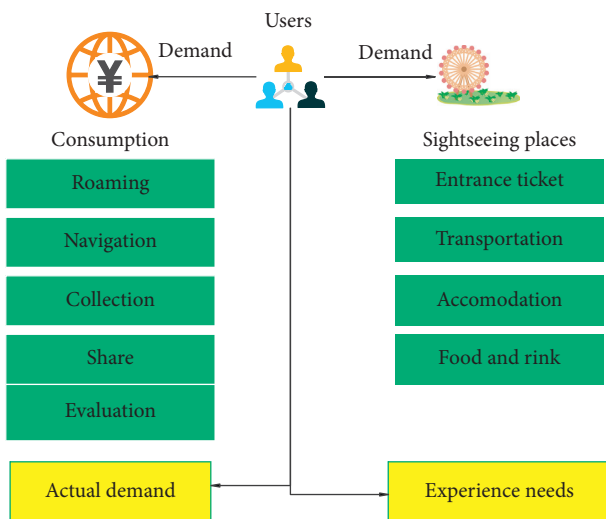FIGURE 1: Spatial system diagram of tourist destinations.

FIGURE 2: Analysis of user needs.

computers and mobile phones, and desktop devices are computer hosts. The network topology is shown in Figure 5.

Space, attribute, and time are the three basic characteristics of geographic phenomena and the three basic elements of geographic analysis. Time information is helpful to explore the movement laws of individual activities and predict future development trends. However, due to the lack of effective analysis methods for massive spatiotemporal data and other reasons, previous studies usually ignore time information. However, time geography introduces "time" and uses the concept of "time and space" to simultaneously analyze the three types of information of time, space, and attributes within the same framework, which bridges the traditional geography's neglect of time. It should be noted that time geography is not the geography of time, but a methodology for studying the relationship between the human behavior and the objective space-time environment. Temporal geography is the geography that studies the temporal and spatial characteristics of individual behavior under various constraints. It believes that the space-time range of individual activities is restricted by a variety of factors in itself and its surrounding environment, which can be summarized into three aspects: ability restriction, combination restriction, and authority restriction. At the same time, time geography borrows the concept of "space-time prism" to describe the space-time area in which individuals can carry out activities under various constraints. The space-time prism image represents the various possibilities of individual activities. The upper and lower vertices of the prism are determined by the time point, and the boundary of the prism is determined by the conditions of transportation.

With the quantitative development of time geography, probabilistic time geography began to appear and attracted attention. Although classical time geography borrows space-time prisms to express the uncertainty of individual movement in space-time regions, it assumes that individual objects are evenly distributed within the reach. However, according to the
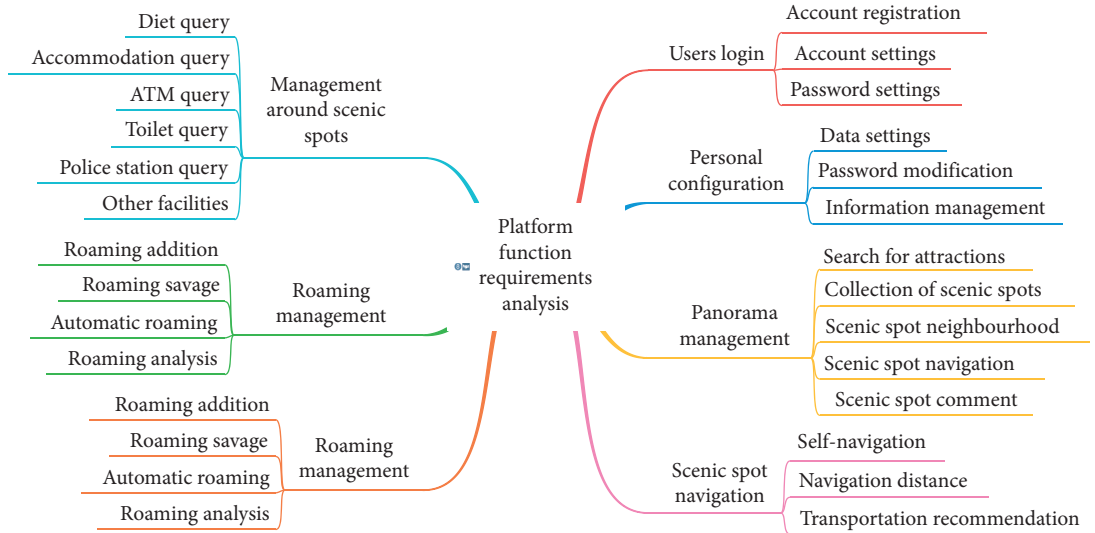
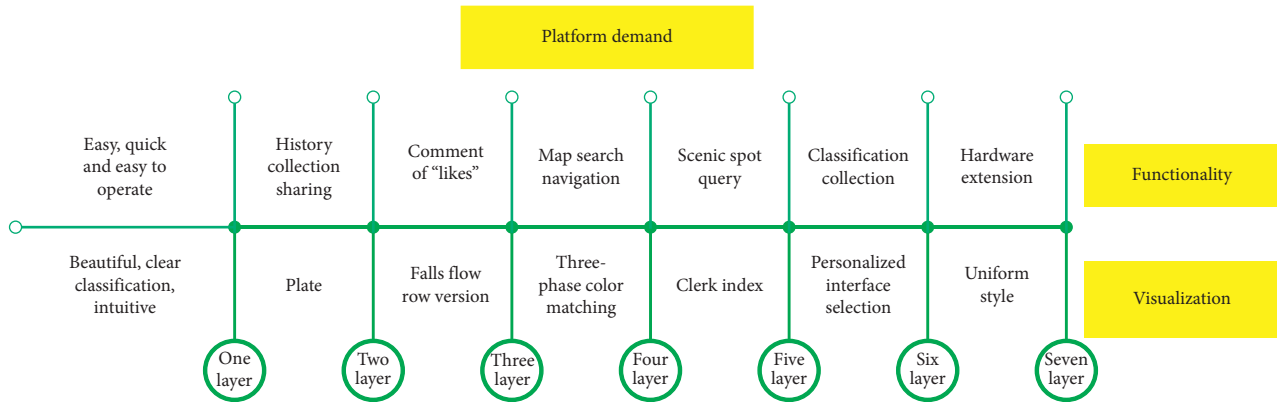FIGURE 3: Analysis of platform function requirements.

FIGURE 4: Fishbone diagram of the analysis of platform functional requirements.
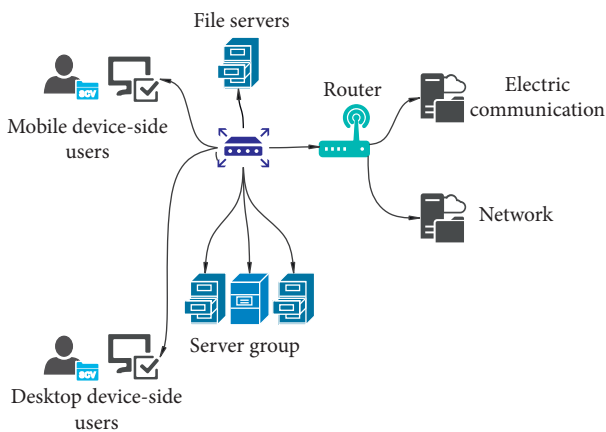

FIGURE 5: Network topology diagram.

first theorem of geography, it can be known that the possibility of individual moving objects in different reachable positions is not always uniform. Probabilistic time geography is based on this idea. It is believed that the possibility of moving objects distributed in each reachable position is not always equal, but is distributed within the reachable range with a certain probability value. Moreover, this probability value continues to change over time. Probabilistic time geography advocates the use of probabilistic methods to describe the nonequal possibilities of the reachable locations of mobile objects, which is an extension of classical time geography based on probability. Based on the probability characteristics of variance and other probabilities shown by time geography of different probability models, a time geography probability model of directional movement is constructed based on the Brown Bridge probability and the total probability formula, respectively. Probabilistic time geography is still immature and needs further improvement. However, the idea that the analysis of individual moving objects needs to consider the actual probability distribution provides a theoretical source for this paper to use the probability method to predict the temporal and spatial distribution of tourists in scenic spots. The schematic diagram of the space-time prism with the starting point and the end point in the same spatial position is shown in Figure 6, and the schematic diagram of the space-time prism with the starting point and the end point in different spatial positions is shown in Figure 7.
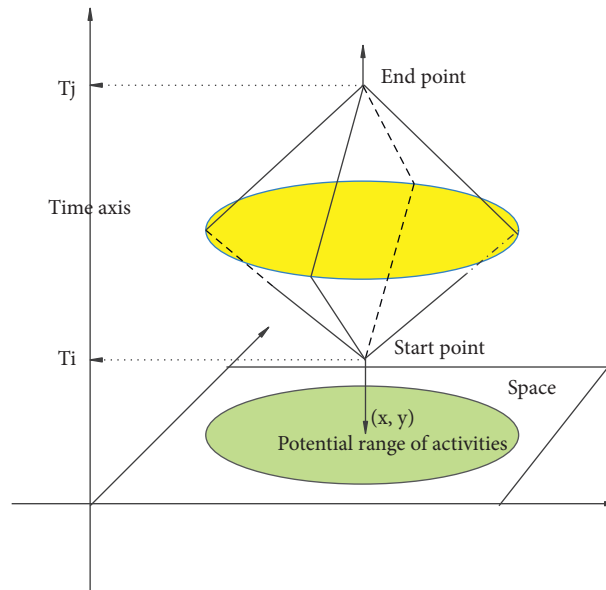
FIGURE 6: Schematic diagram of a space-time prism with the start and end points at the same spatial position (three-dimensional).
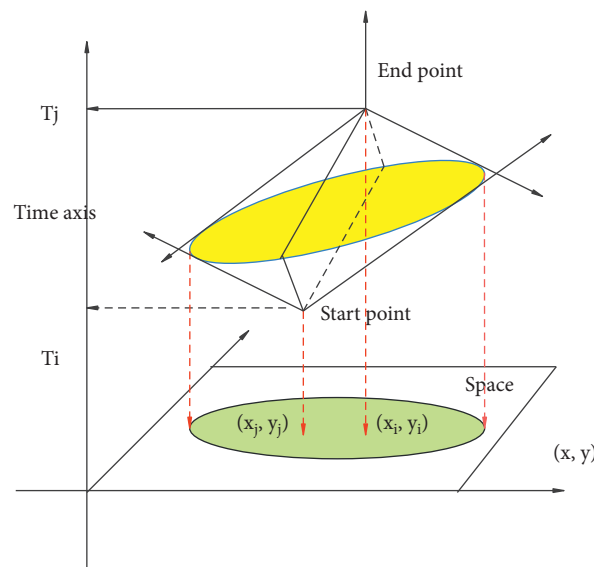

FIGURE 7: Schematic diagram of space-time prisms with start and end points at different spatial positions (three-dimensional).

This paper mainly studies tourism demand forecast based on adaptive neural network and realizes the heat forecast of tourist attractions by fusing the comfort index and specific adaptive neural network forecast algorithms. Moreover, this paper applies the research results to specific engineering practice and establishes a tourist attraction heat forecast system based on the comfort index. The establishment of the system can help tourists better understand the comfort and heat information of a scenic spot, help tourists choose scenic spots reasonably, and also benefit enterprises' decision-making on tourism projects, as well as their recommendation and management of tourists. The system should have three major functions: data collection, data calculation and analysis, and data management and display. The detailed functional modules are data collection

module, comfort index system module, tourism popularity forecast module, background management module, and result display module. The five major functional modules of the system are shown in Figure 8.

The data acquisition module mainly realizes data acquisition and data preprocessing. The data collection module performs related collection work according to different data requirements. After collection, the data is saved and backed up to the relevant server database, and a data interface is provided to enable other modules to use the travel data. The data collection module should be able to automatically obtain tourist data, weather data, environmental pollution data, road conditions around the scenic spot, etc. according to the configuration. The data acquisition module must have certain data preprocessing capabilities and realize data
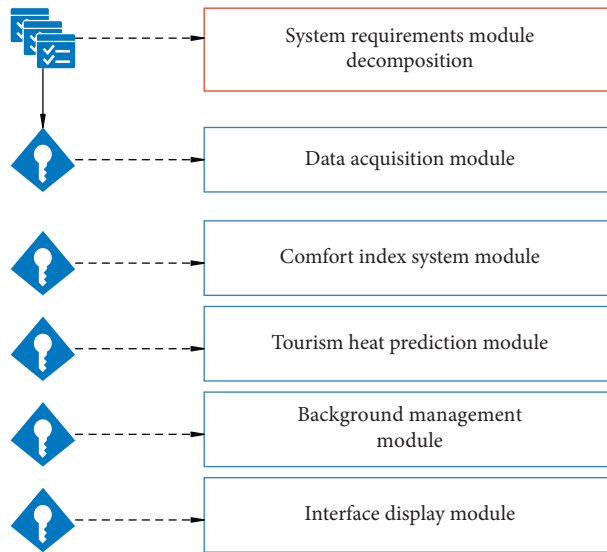
FIGURE 8: Functional decomposition of system requirements.
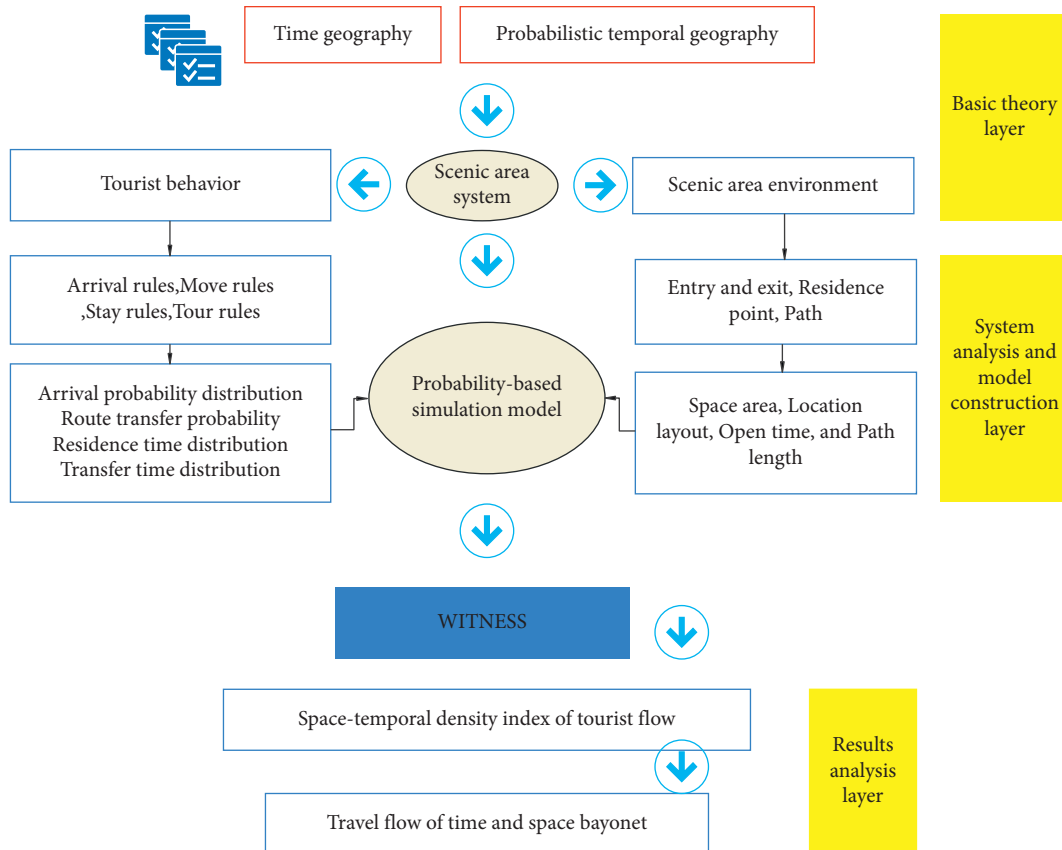
FIGURE 9: Forecast model of travel time and space bayonet.

cleaning and data integration work through programming. The data acquisition module must have a certain degree of anti-interference ability and response speed and provide multithreaded data acquisition and processing capabilities. The configuration administrator can view all the scenic spot information that the system can collect and the scenic spot information currently collecting data and can add and delete the scenic spots collected by the data collection module. When adding tourist attractions to the collection module, the configuration manager can set the time range and time interval for tourism data collection. When the configuration administrator deletes or adds tourist attractions to the data collection module, the delay will take effect until the next day. After adding the scenic spots where the data collection

TABLE 1: Processing effect of spatiotemporal tourism data.

Number	Data learning
1	92.51
2	91.70
3	90.67
4	93.20
5	92.19
6	92.67
7	88.08
8	91.39
9	88.70
10	89.38
11	88.31
12	89.65
13	92.42
14	92.79
15	88.56
16	88.56
17	89.05
18	93.77
19	93.95
20	92.71
21	93.49
22	91.95
23	90.20
24	91.49
25	91.58
26	90.63
27	91.36
28	90.01
29	90.27
30	90.53
31	91.16
32	92.01

TABLE 2: Results of tourism demand forecast.

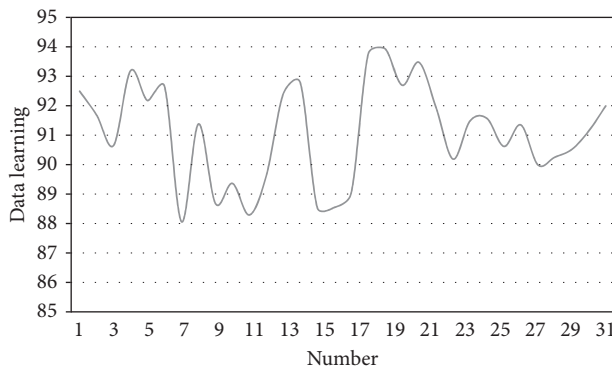| Number	Demand forecast
1	85.49
2	90.43
3	73.12
4	80.01
5	76.08
6	89.47
7	73.34
8	81.27
9	89.60
10	74.15
11	78.18
12	90.35
13	87.01
14	82.31
15	70.46
16	74.78
17	80.01
18	86.49
19	76.47
20	77.90
21	83.25
22	83.95
23	85.27
24	73.40
25	69.73
26	88.87
27	90.52
28	90.80
29	77.06
30	79.81
31	83.01
32	85.81

FIGURE 10: Statistical diagram of the processing effect of spatio-temporal tourism data.
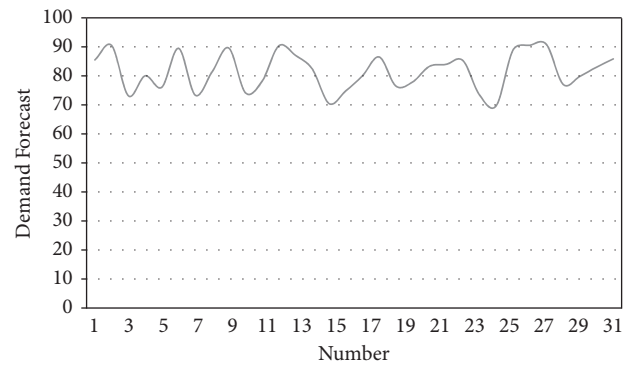
FIGURE 11: Statistical diagram of tourism demand forecast.

module works, the system will query all the URLs of the current scenic spots that collect data by default. The configuration administrator needs to confirm whether all the scenic spots URLs are valid. If they are invalid, they need to be added manually. At the same time, the data collection module requires a built-in web page analysis program. The previous analysis needs are only for China Weather Network, Green Breathing Network, Beijing Meteorological Bureau Network, Beijing Tourism Network, and Nanjing

Tourism Network. When confirming the URL of the scenic spot, we need to ensure that the system can parse the configured URL. At the same time, the configuration administrator needs to configure the collection of API interface information around the scenic spot to ensure accurate acquisition of the road situation around the scenic spot.

This paper integrates time geography and probability time geography theory, system analysis theory, and travel flow spatiotemporal bayonet theory and proposes a research framework based on WITNESS simulation system to predict

travel flow spatiotemporal bayonet. Among them, time geography and probabilistic time geography provide a theoretical basis for establishing a simulation model of a scenic spot system based on probability. According to the system analysis theory, the scenic spot system is analyzed from the two aspects of scenic spot environment and tourist behavior rules, and the scenic spot environment is abstracted and simplified into three categories: entrances and exits, paths, and stop points. The tourist behavior rules are divided into tourist arrival rules, mobile stay rules, and tour rules. According to the results of the system analysis, data on the area of the scenic area, location layout, path length, tourist arrival probability distribution, route transition probability, stay time probability distribution, and travel time of scenic spots are collected. These data provide initial parameters for the probability-based simulation system model, and the model is implemented on the WITNESS simulation software platform. Finally, according to the theory of travel flow time and space bayonet, it is proposed to use the time and space density index of tourism flow as an index to identify the time and space bayonet of tourism flow. The proposed research framework can provide reference and guidance for establishing the same simulation model for other types of scenic spots to predict the spatiotemporal bayonet of tourism flows, as shown in Figure 9.

After constructing a tourism demand forecast model based on adaptive neural network technology, the performance of this model is verified. Based on actual data, this paper uses the simulation platform proposed in this paper to process the time-space travel data, analyze the data processing effect, and obtain the results shown in Table 1 and Figure 10.

From the above analysis, it can be seen that the tourism demand forecast model based on adaptive neural network technology proposed in this paper has good spatiotemporal tourism data processing effects. After that, the tourism demand forecast model based on adaptive neural network technology is evaluated for the effect of tourism demand forecast, and the results shown in Table 2 and Figure 11 are obtained.

From the above research, it can be seen that the tourism demand forecast model based on adaptive neural network technology proposed in this paper performs well in tourism demand forecast and meets the actual demand of modern tourism forecast.

5. Conclusion

The study of factors affecting tourism demand is the key content of tourism demand forecasting. At present, domestic and foreign researches on this aspect have formed a more systematic theory. Quantitative analysis method is currently widely used in foreign countries to study the factors affecting tourism demand. Economic factors can be divided into income, price, leisure time, and marketing. Income includes the personal disposable income and the GDP of the source area; price includes the transportation expenses, the price of products and reading materials in tourist destinations, the price level of competing destinations, and the exchange rate.

Noneconomic factors include consumers' personal preferences, consumption habits, local political factors, travel restrictions, and other social and cultural factors. This article uses adaptive neural network technology to forecast and analyze tourism demand, build a business intelligence model, and improve the prediction effect of subsequent tourism demand. The experimental research results show that the tourism demand prediction model based on adaptive neural network technology proposed in this paper performs well in tourism demand prediction and meets the actual demand of modern tourism prediction.

Data Availability

The labeled datasets used to support the findings of this study are available from the corresponding author upon request.

Conflicts of Interest

The author declares no conflicts of interest.

Acknowledgments

References

[1] K. Nam, C. S. Dutt, P. Chathoth, and M. S. Khan, "Blockchain technology for smart city and smart tourism: latest trends and challenges," *Asia Pacific Journal of Tourism Research*, vol. 26, no. 4, pp. 454–468, 2021.

[2] C. D. Huang, J. Goo, K. Nam, and C. W. Yoo, "Smart tourism technologies in travel planning: the role of exploration and exploitation," *Information & Management*, vol. 54, no. 6, pp. 757–770, 2017.

[3] T. Brandt, J. Bendler, and D. Neumann, "Social media analytics and value creation in urban smart tourism ecosystems," *Information & Management*, vol. 54, no. 6, pp. 703–713, 2017.

[4] A. K. Tripathy, P. K. Tripathy, N. K. Ray, and S. P. Mohanty, "iTour: the future of smart tourism: an IoT framework for the independent mobility of tourists in smart cities," *IEEE consumer electronics magazine*, vol. 7, no. 3, pp. 32–37, 2018.

[5] E. Sigalat Signes, R. Calvo Palomares, B. Roig Merino, and I. García Adán, "Transition towards a tourist innovation model: the smart tourism destination," *Journal of Innovation & Knowledge*, vol. 5, no. 2, pp. 96–104, 2020.

[6] H. Lee, J. Lee, N. Chung, and C. Koo, "Tourists' happiness: are there smart tourism technology effects?" *Asia Pacific Journal of Tourism Research*, vol. 23, no. 5, pp. 486–501, 2018.

[7] C. Koo, L. Mendes Filho, and D. Buhalis, "Guest editorial," *Tourism Review*, vol. 74, no. 1, pp. 1–4, 2019.

[8] T. Zhang, C. Cheung, and R. Law, "Functionality evaluation for destination marketing websites in smart tourism cities," *Journal of China Tourism Research*, vol. 14, no. 3, pp. 263–278, 2018.

[9] M. A. C. Ruíz, S. T. Bohorquez, and J. I. R. Molano, "Colombian tourism: proposal app to foster smart tourism in the country," *Advanced Science Letters*, vol. 23, no. 11, pp. 10533–10537, 2017.

[10] W. Wang, N. Kumar, J. Chen et al., "Realizing the potential of the Internet of things for smart tourism with 5G and AI," *IEEE Network*, vol. 34, no. 6, pp. 295–301, 2020.

[11] I. Guerra, F. Borges, J. Padrão, J. Tavares, and M. H. Padrão, "Smart cities, smart tourism? The case of the city of porto," *Revista Galega de Economia*, vol. 26, no. 2, pp. 129–142, 2017.

[12] Y. Topsakal, M. Bahar, and N. Yüzbaşioğlu, "Review of smart tourism literature by bibliometric and visualization analysis," *Journal of Tourism Intelligence and Smartness*, vol. 3, no. 1, pp. 1–15, 2020.

[13] S. Joshi, "Social network analysis in smart tourism driven service distribution channels: evidence from tourism supply chain of Uttarakhand, India," *International Journal of Digital Culture and Electronic Tourism*, vol. 2, no. 4, pp. 255–272, 2018.

[14] F. Femenia-Serra, B. Neuhofer, and J. A. Ivars-Baidal, "Towards a conceptualisation of smart tourists and their role within the smart destination scenario," *Service Industries Journal*, vol. 39, no. 2, pp. 109–133, 2019.

[15] C. Koo, F. Ricci, C. Cobanoglu, and F. Okumus, "Special issue on smart, connected hospitality and tourism," *Information Systems Frontiers*, vol. 19, no. 4, pp. 699–703, 2017.

[16] H. Abdel Rady and A. Khalf, "Towards smart tourism destination: an empirical study on sharm el sheikh city, Egypt," *International Journal of Heritage, Tourism and Hospitality*, vol. 13, no. 1, pp. 78–95, 2019.

[17] T. Pencarelli, "The digital revolution in the travel and tourism industry," *Information Technology & Tourism*, vol. 22, no. 3, pp. 455–476, 2020.

[18] C. J. P. Abad and J. F. Álvarez, "Landscape as digital content and a smart tourism resource in the mining area of cartagena-La unión (Spain)," *Land*, vol. 9, no. 4, pp. 1–22, 2020.

Research Article

Coordinated Development of Population, Resources, Environment, Economy, and Society under Engineering Management Combined with Bilevel Optimization Model

Kai Chen and Yilin Chen [ID]

School of Economics and Trade, Northeastern University at Qinhuangdao, Qinhuangdao 066000, China

Correspondence should be addressed to Yilin Chen; 2110430@stu.neu.edu.cn

The in-depth analysis of the strategies for the coordinated and continuous development of population, resources, environment, economy, and society based on the engineering management model is highly important for the sustainable development of the regional economy and society. In this article, a population-economy-resources-environment bilevel optimization model is established based on the economic and social development in a provincial region. The method of bilevel optimization is adopted to introduce the specific bilevel optimization model. The concept and objectives of the bilevel optimization are explained, and its corresponding technical applications are described. In this article, the development in coordinated economic and social development of population, resources, and environment is analyzed and compared based on the bilevel optimization model. In particular, the evolution and changes before and after the implementation of engineering management are studied. Through the results, it can be observed that after the implementation of project management, the coefficient of industry location has presented a downward trend, and the coordinated development of population, resources, environment, economy, and society has become more coordinated.

1. Introduction

With the rapid economic development in recent years, the social resources acquired are getting greater and greater. As a result, it is impossible to sort out these resources based on the previous means and techniques [1]. In this context, the bilevel optimization model has become an important component in the coordinated economic and social development of population, resources, environment, with a low threshold and strong convergence characteristics possessing advantages [2, 3]. In the 21st century, people become more demanding for the relationships in the coordinated development of population, resources, environment, economy, and society. The previous simple economic growth can no longer meet their needs, and the coordinated development of population, resources, environment, economy, and society has slowly shifted from a single nature into an interactive

field [4, 5]. The coordinated development functions allow people to identify useful resources among massive resources. Hence, the combination of the coordinated development function and the coordinated economic and social development of population, resources, environment, and society are useful, and the combination of these two techniques can facilitate a better management of the coordinated economic and social development of population, resources, and environment.

The application of the bilevel optimization model can explain the previous concept of spatial location of production more effectively, while providing the corresponding way to new trade concepts and newly added concepts. After the analysis and evaluation of the basic concepts and techniques of the bilevel optimization model, a special study of the concept is conducted in this article on the situation of regional development in China. Through the study, it is

concluded that the bilevel optimization model has played a crucial role in promoting the coordinated development of population-resource-environment-economy-society regarding the differences in regional development. Finally, this article provides a theoretical basis for the future coordinated development degree of population-economy-resource-environment system in the province and puts forward a strategy to promote the coordinated development of socioeconomic and resource-environment scientifically and rationally, so as to provide a theoretical basis for the sustainable development of economy and environment in the province.

2. Bilevel Optimization Model

In this article, the bilevel optimization model is introduced, and it can be observed that the initialization of the bilevel optimization center can have a serious effect on the bilevel optimization model if the results are not reasonable. This effect requires massive computation time for engineering management under the population, resources, environment, economic, and social subjects intelligent search engine. At the same time, it will also greatly reduce the performance of bilevel optimization, which will eventually lead to inaccurate results obtained.

Based on the working principle of the bilevel optimization model cited in this paper, the method of small-sized samples and multiple sampling are dopated. Through the bilevel optimization model, the scientific and reasonable bilevel optimization center can be obtained so that the initialization stage of the bilevel optimization unreasonable phenomenon can be eliminated based on the big data bilevel optimization model to effectively improve the performance and accuracy of big data bilevel optimization model. The core idea of the model is based on small sample collection, followed by the bilevel optimization model analysis based on the Map-reduce model. The operational framework of the bilevel optimization model is shown in Figure 1.

In the next section, the optimization of the bilevel optimization model K-value is described in detail. The model consists of three main parts: separation model, subcenter elimination, and weight-K value optimization model.

It is assumed that that s stands for the number of samples, x stands for the coordinates, i stands for the ith sample, k stands for the number of clusters, and d stands for the data dimension, the result set of the ith sample cluster is represented in the following form:

$$\left(x^i_{11}, x^i_{12}, \ldots, x^i_{1\,d}\right)\left(x^i_{21}, x^i_{22}, \ldots, x^i_{2\,d}\right)\cdots\left(x^i_{k1}, x^i_{k2}, \ldots, x^i_{k\,d}\right). \quad (1)$$

The matrix form of the results obtained based on the bilevel optimization for all samples is shown as follows:

$$\begin{bmatrix} \left(x^1_{11}, x^1_{12}, \ldots, x^1_{1\,d}\right) & \left(x^1_{21}, x^1_{22}, \ldots, x^1_{2\,d}\right) & \cdots & \left(x^1_{k1}, x^1_{k2}, \ldots, x^1_{k\,d}\right) \\ \left(x^2_{11}, x^2_{12}, \ldots, x^2_{1\,d}\right) & \left(x^2_{21}, x^2_{22}, \ldots, x^2_{2\,d}\right) & \cdots & \left(x^2_{k1}, x^2_{k2}, \ldots, x^2_{k\,d}\right) \\ \vdots & \vdots & \cdots & \vdots \\ \left(x^s_{11}, x^s_{12}, \ldots, x^s_{1\,d}\right) & \left(x^s_{21}, x^s_{22}, \ldots, x^s_{2\,d}\right) & \cdots & \left(x^s_{k1}, x^s_{k2}, \ldots, x^s_{k\,d}\right) \end{bmatrix}. \quad (2)$$

In the above matrix, the arrangement of matrix elements corresponds one to the other based on the similarity of cluster centers. A column matrix corresponds to clusters, in which k clusters are shared. It is assumed that the kth cluster center of the first sample, the first cluster center of the second sample, and the second cluster center of the last sample are subcenters.

$$\begin{bmatrix} \left(x^1_{11}, x^1_{12}, \ldots, x^1_{1\,d}\right) & \left(x^1_{21}, x^1_{22}, \ldots, x^1_{2\,d}\right) & \cdots & \left(x^1_{k1}, x^1_{k2}, \ldots, x^1_{k\,d}\right) \\ \left(x^2_{11}, x^2_{12}, \ldots, x^2_{1\,d}\right) & \left(x^2_{21}, x^2_{22}, \ldots, x^2_{2\,d}\right) & \cdots & \left(x^2_{k1}, x^2_{k2}, \ldots, x^2_{k\,d}\right) \\ \vdots & \vdots & \cdots & \vdots \\ \left(x^s_{11}, x^s_{12}, \ldots, x^s_{1\,d}\right) & \left(x^s_{21}, x^s_{22}, \ldots, x^s_{2\,d}\right) & \cdots & \left(x^s_{k1}, x^s_{k2}, \ldots, x^s_{k\,d}\right) \end{bmatrix}$$
$$\Downarrow \quad (3)$$
$$\begin{bmatrix} \left(x^1_{11}, x^1_{12}, \ldots, x^1_{1\,d}\right) & \left(x^1_{21}, x^1_{22}, \ldots, x^1_{2\,d}\right) & \cdots & (0, 0, \ldots, 0) \\ (0, 0, \cdots, 0) & \left(x^2_{21}, x^2_{22}, \cdots, x^2_{2\,d}\right) & \cdots & \left(x^2_{k1}, x^2_{k2}, \ldots, x^2_{k\,d}\right) \\ \vdots & \vdots & \cdots & \vdots \\ \left(x^s_{11}, x^s_{12}, \ldots, x^s_{1\,d}\right) & (0, 0, \ldots, 0) & \cdots & \left(x^s_{k1}, x^s_{k2}, \ldots, x^s_{k\,d}\right) \end{bmatrix}.$$
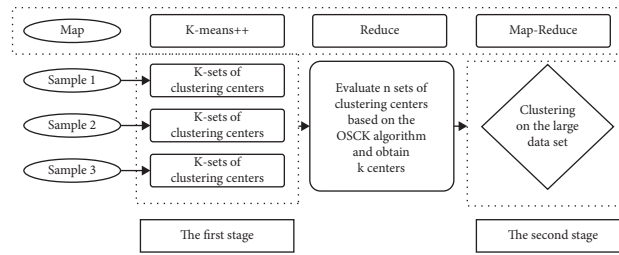
FIGURE 1: Framework of the method proposed in this paper at two stages.

In the above matrix (0, 0, ..., 0), which is the bilevel optimization center, is shown as a subcenter. In fact, it is still unknown what cluster centers are suboptimal. Hence, the next topic is to locate and remove the following suboptimal cluster centers.

3. Overview of the Study Area

The population of the province has shown an increasing trend since 1990, and the population growth rate has remained relatively stable, with a small downward trend during this period. The total production in the region of the province is characterized by obvious stage, presenting a gradual trend of growth in the fluctuating gross product of the province in the period from 1960 to 1980. In the period from 1981 to 2000, the gross production in the region showed a trend of annual growth, and in 1995, the gross production in the region exceeded 100 billion yuan with fluctuations. In the period from 2001 to 2014 with the implementation of the policy of revitalization of the old industrial bases in the region, the GDP showed significant growth characteristics until 2014 when the GDP reached RMB 1380.44 billion at the same time, the growth of the regional GDP was maintained at about 0.14%, and the regional economic growth gradually showed a growth trend (Figure 2).

The region is in a period of industrialization transformation and accelerating urbanization. The share of the three industrial structures in the region in 2014 was 11.1%, 52.7%, and 36.2%, respectively. Among them, the value of the primary industry in the regional industrial structure grew RMB 15.457 billion, corresponding to a growth rate of 4.7%. The growth value of the level 2 industry in the region is RMB 728.727 billion, with a corresponding growth rate of 6.7%, and the growth value of the tertiary industry in the region is RMB 499.198 billion, with a corresponding growth rate of 6.8%. The rapid development of industrialization and urbanization will lead to an increase in energy consumption in the city, from which it can be seen that in 2014 the energy consumption in the region was as high as 84.835 million tons, corresponding to a coal consumption rate of 72.5%, which is far above the national average. The majority of the end-use energy consumption is concentrated in the level 2 industry, mainly in coal consumption, while oil, electricity, and heat consumption are also relatively large.

4. Research Method and Data Sources

4.1. Regional Population-Economy-Resources-Environment Scheduling Forecast Model. The dynamics and complexity of the coordinated development of population, economy, and resources and environment in this region cannot be predicted based on a single conventional linear or nonlinear model of its future development trends. In this article, the parameters in the evaluation indexes are optimized by using a bilevel optimization model based on the scheduling and evaluation system of the population-economy-resource-environment association.

4.1.1. Establishment of the Index System and Determination of the Weights. In this article, the development evaluation index system of this region is mainly established with the goal of population-economy-resource-environment coordination, and the division of population development, economic development and resource-environment development is carried out based on bilevel optimization model. The corresponding indexes are combined by qualitative and quantitative methods, as shown in Table 1.

4.1.2. Coordination Degree Model. Coupling refers to the synergistic phenomenon due to the interaction and mutual influence between two or more systems and components, and the degree of bonding is a quantitative description of the degree of interaction and influence between systems and components. The synergistic forecast model for the population, economy, and resource environment established in this paper includes two parts: objective function and constraint conditions.

(1) Objective function: based on the concept of capacitive coupling in physics and the capacitive coupling coefficient model, the coordination degree model of population-economy-resource-environment (3-system) interaction is promoted.

$$D = (C \times T)^{1/2}. \tag{4}$$

In the above equation, D stands for the degree of coordinated development, which is [0, 1]. c stands for the degree of coupling, which reflects the level of synergy between the interactions of systems. T stands for the harmony index, which reflects the overall cooperative effect or

contribution of population, economy, and resource environment. C and T can be expressed as follows:

$$\begin{cases} C = \left\{ \dfrac{f(x) \cdot g(y) \cdot h(z)}{[f(x) + g(y)] \cdot [f(x) + h(z)] \cdot [g(y) + h(z)]} \right\}^{1/3}, \\[2em] T = \alpha \cdot f(x) + \beta \cdot g(y) + \gamma \cdot h(z). \end{cases} \tag{5}$$

In the above equation, the candidate quantities α, β, γ of the population-economic-resource-environment subsystem are finally set in this paper after the review of literature and the consultation of experts. $\alpha = 0.3$, $\beta = 0.2$, $\gamma = 0.5$; $f(x)$ is a function of population effect; $g(y)$ is a function of economic effect; and $h(z)$ is a function of resource-environment effect, which are shown in the following, respectively.

$$f(x) = \sum_{i=1}^{m} a_i x_i', \\ g(y) = \sum_{j=1}^{n} b_j y_j', \\ h(z) = \sum_{k=1}^{q} c_k z_k'. \tag{6}$$

In the above equation, x_i', y_j', and z_k' stand for positive numbers of specific indexes that represent the demographic-economic-resource-environmental characteristics, respectively. The weight of each index. The extreme value method is used for criterialization. The specific methods are described as follows:

$$x_i' = \begin{cases} \dfrac{x_i - \lambda_{\min}}{\lambda_{\max} - \lambda_{\min}}, & \lambda_{\min} \le x_i \le \lambda_{\max}, \quad x_i \text{ is a positive index } (i = 1, 2,), \\[2em] \dfrac{\lambda_{\max} - x_i}{\lambda_{\max} - \lambda_{\min}}, & \lambda_{\min} \le x_i \le \lambda_{\max}, \quad x_i \text{ is a positive index } (i = 1, 2,). \end{cases} \tag{7}$$

The original data processing method for y_j' based on the above method is $j = 1\ 2,3,4, k = 1,2,3,4,5,6$.

(2) Composition of constraint conditions: first, about the economic development constraints, the regional economic development status can be expressed as follows:

$$\text{GDP}_t = \text{GDP}_{t-1}(1 + k_{\text{GDP}}), \\ \text{GDP}_{rj_t} = \text{GDP}_{rj_{t-1}}\left(1 + k_{\text{GDP}_{rj}}\right), \quad \text{GDP}_{rj} \ge A_{\text{GDP}_{rj}}. \tag{8}$$

In the above equation, GDP_t stands for the regional GDP in year t, GDP_{t-1} stands for the regional GDP in year t-1, and k_{GDP} is the growth rate of regional GDP. With regard to GDP per capita in year t, $k_{\text{GDP}_{rj}}$ is the growth rate of GDP per capita, and $A_{\text{GDP}_{rj}}$ is the minimum GDP per capita required for the province.

Emission constraint of environmental pollutants: $W_t = W_{t-1}(1 + k_W), W_t \le W_{t-1}, W_t \le B_t$, in which W_t is the pollutant (SO_2/CO_2) emission in year t, W_{t-1} is the pollutant (SO_2/CO_2) emission in year t-1, k_W is the pollutant (SO_2/CO_2) emission growth rate, and B_t is the allowed pollutant emission in region in year t [4, 6].

Carbon emission intensity: $E_t = E_{t-1}(1 + k_E)$, $E_t \le E_{t-1}$, in which E_t is the carbon emission intensity in year t, E_{t-1} is the carbon emission intensity in year t-1, and k_E is the carbon emission intensity growth rate.

Forest coverage rate: $F_t = F_{t-1}(1 + k_F)$, $F_t \ge F_{t-1}$, in which F_t is the forest coverage in year t, F_{t-1} is the forest coverage in year t-1, k_F is the forest coverage growth rate, through ecological restoration and environmental protection and other measures, the regional forest cover in year $t \ge$ the regional forest coverage in year t-1.

(3) Division of the determination criteria for coordination degree: with regard to 3 major categories and 10 subcategories in the coordinated development of population, economy, and resources and environment association schedule, the transitional coordination, dysfunction and decline, each class based on the size of the population, economy, resources, and environment effect function is the population lag type, economic lag type, energy and environmental lag type, synchronous type four types (the details are shown in Table 2).

(4) Settings of the stages and index parameters: based on the current situation of the economy and society and the future development direction of resources and environment in the province, three stage schemes are established in this paper, that is, the standard stage, the stabilization stage, and the coordination stage, respectively.

(1) Baseline stage: rapid development of population and economy, with moderate improvement in the resources and environment

On the basis of the socioeconomic development in the 11th Five-Year Plan, the population regional production, rapid development of urbanization rate, industry and industry structure has a strong dependence on the level 2 industry coal, oil ratio also remains at a very high level. At this stage, the improvement in the energy efficiency has basically reflected the state of naturally oriented economic development and energy consumption, and it is relatively weak in the implementation of energy conservation and emission reduction measures. Environmental pollutants have yet to be controlled effectively.

- ⋆⋅⋅ population (in 10,000)
- —— Regional GDP (in 100 million yuan, based on the price in the current year)
- ⋅◆⋅ Growth rate of the population
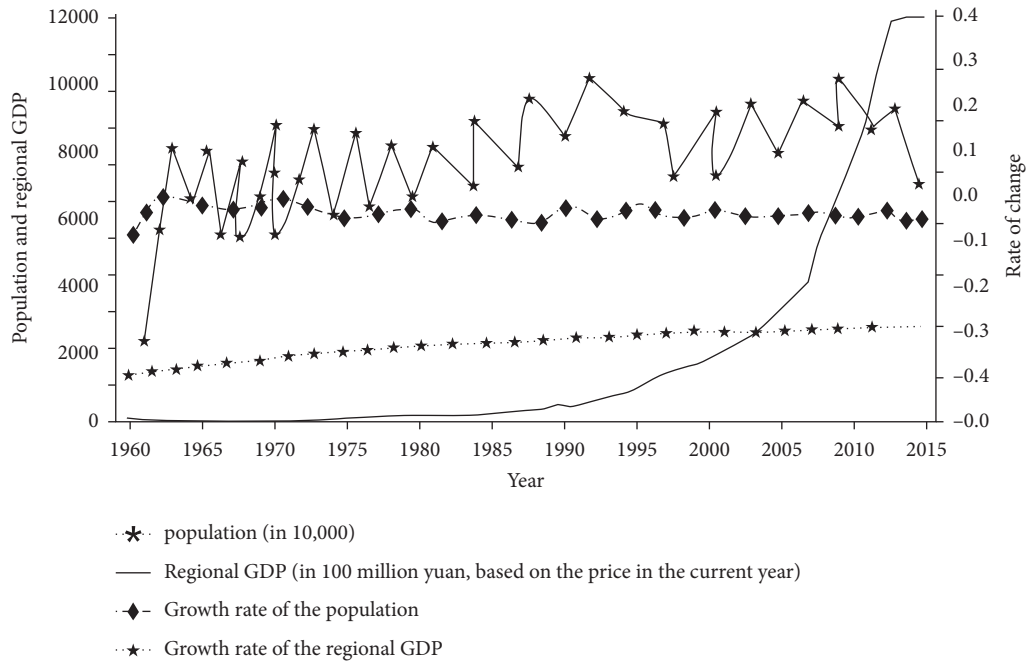- ⋅⋆⋅ Growth rate of the regional GDP

FIGURE 2: Diagram of demographic and economic development trends in the region.

TABLE 1: Scheduling evaluation index system and weights of the population-economy-resource-environment association in the province.

Target level	Criteria level	Index level	Nature of index	Weight
Comprehensive development level of population, economy, resources, and environment	Population development level	1. Population (million people)	−	0.8100
		2. Urbanization rate (%)	+	0.2100
	Economic development level 1. Gross regional product (in 100 million yuan)		+	0.2280
		2. GDP per capita (10,000 yuan/person)	+	0.1131
		3. Share of the secondary industry (%)	−	0.4710
		4. Share of the tertiary industry (%)	+	0.2280
	Resource and environment development level	1. Share of nonfossil energy (%)	+	0.1100
		2. Energy consumption intensity (t/10000)	−	0.2100
		3. Carbon emission intensity (in 10,000 yuan)	−	0.4100
		4. SO_2 emissions (million t)	−	0.1000
		5. CO_2 emissions (million t)	−	0.1000
		6. Forest coverage rate (%)	+	0.1100

(2) Robust development of population and economy, with a stable improvement of resources and environment: based on the standard stage, the growth rate of economy, population, and urbanization is slowed down, the reliance on industry and traditional primary energy is reduced, and energy-saving and low-carbon technologies are used to optimize the energy consumption structure and accomplish the goal of energy conservation and emission reduction. In this situation, the implementation of relevant energy conservation and emission reduction measures seeks to balance economic development and environmental improvement, which can basically reflect the state of economic development and resources and environment to be achieved by energy conservation.

(3) The coordination stage is highly similar to the stable development of population and economy, with the rapid improvement of resources and environment.

This stage is a comprehensive control stage, in which energy saving and emission reduction activities are carried out in the whole society, and the production and lifestyle of the population is comprehensively optimized. In addition, the economic development pattern and consumption pattern of the residents are improved. The energy structure and industrial structure are further optimized, and major breakthroughs are made in energy conservation and emission reduction measures and economic technologies on all fronts [7, 8]. This is basically an active effort to achieve the goal of economic development and the state of resources and environment.

Based on the above description, 12 index parameters such as population, urbanization rate, total regional production, GDP per capita, level 2 production ratio, tertiary production ratio, energy intensity, and nonfossil energy ratio are parameterized as stage elements (the details are shown in Table 3).

(1) Evaluation index system: based on the actual situation of the economic and environmental development and analytical modeling requirements of the county, the index decision follows the following principles: (1) Comparison of indexes is feasible; (2) identification of indexes is significant in the aspect of significance and differences; (3) indexes are highly independent of each other; and (4) the feasibility of index data collection. Based on the above principles, spatial variable analysis and correlation analysis were used to screen the indexes, as shown in the following equation:

$$C_{ij} = \frac{S_j}{X_j}, \quad (j = 1, 2, \ldots, 20). \quad (9)$$

In the above equation, C_{ij} stands for the coefficient of variation; S_j stands for the criteria deviation; and X_j stands for the mean value.

Based on equation (1) to determine the raw data belonging to the relevant indexes of each district and county, in addition to the indexes with large correlation coefficients, small spatial variation and identification of meaningful differences, the final 8 indexes that can reflect the economic environment and social interrelationship in the county. These are economic index system, environmental index system, and social development index system [9, 10]. The economic indexes include total industrial production ($X1$), gross domestic product per capita ($X2$), and GDP growth rate ($X3$). The environmental indexes include chemical oxygen demand emissions ($X4$), energy consumption per unit of GDP ($X5$), and pollutant emissions per unit of GDP ($X6$). The social development indexes include rural Engel coefficient ($X7$) and unemployment rate (%) ($X8$).

(2) Determination of the weighting of evaluation indexes: upon the determination of the weighting of

evaluation indexes, there will be increasing methods of subjective decision of weighting, such as the AHP method. The evaluation results are sometimes biased based on the subjective factors of human. Based on the information theory, the entropy value reflects the degree of disorder of information, the smaller its value, the smaller the disorder of the system, the greater the utility value of information; the larger that value is, the higher the disorder of the system and the smaller the utility value of the information.

For the initial matrix of n evaluation indexes for the m programs discussed in the above section, as the determination matrix is obviously an information carrier, the orderliness of the system information obtained through information entropy evaluation and its effects are used to determine the index weights eliminating the artificial interference of the weighting calculation if possible so that the evaluation results can be more practically consistent [11]. The calculation sequence is described as follows:

(1) The judgment matrix is established based on n evaluation indexes for m objects as follows:

$$R = (X_j)_{nm}, \quad (i = 1, 2, \ldots, n; j = 1, 2, \ldots, m). \quad (10)$$

(2) The decision matrix is normalized to obtain the normalized decision matrix as follows:

$$b_j = \frac{X_{ij} - X_{\min}}{X_{\max} - X_{\min}}. \quad (11)$$

In the above equation, each item is the most satisfied or the most dissatisfied under the same index (the smaller the better), that is, $X_{\max} X_{\min}$.

(3) Based on the definition of entropy, n evaluation index for m evaluation objects is the entropy of evaluation indexes as follows:

$$\mathrm{Hi} = \frac{1}{\ln m} \sum_{j=1}^{m} f_{ij} \ln f_{ij}. \quad (12)$$

In the above equation, $f_{ij} = b_{ij} / \sum_{j=1}^{m} b_{ij}$. When $f_j = 1$, $f_j \ln f_j$, different from the degree of disorder of information apparently reflected in the entropy, it is equal to 0 and does not match the actual situation. Hence, f_{ij} is further modified as follows

$$f_{ij} = \frac{1 + b_{ij}}{\sum_{j=1}^{m} 1 + b_{ij}}. \quad (13)$$

(4) The entropy weight of the evaluation index is calculated, which is in line with the actual situation.

(3) Establishment of the gray correlation model: for the convenience of analysis, the correlation model is established as follows:

TABLE 2: Determination criteria and classification system for the degree of coordinated development of regional population, economy, and resources and environment.

Classification	Degree of coordinated development	Level 1 criteria	Level 2 criteria
Interval of coordinated development	0.9~1	Superior coordination	
	0.80~0.89	Good coordination	
	0.70~0.79	Moderate coordination	
	0.60~0.69	Basically coordinated	
Interval of transitional reconciliation	0.50~0.59	Barely coordinated	
	0.40~0.49	On the verge of dysfunction and decline	① When $m = \min\{/(x), g(y), h(z)\}$, it is a lagged type, similar to $m = /(x)$, which is population lagged type.
	0.30~0.39	Mild dysfunction and decline	② When $/(x) = g(y) = h(z)$, it is a synchronous type for population, economy, and environment
Interval of dysfunction and decline	0.20~0.29	Moderate dysfunction and decline	
	0.10~0.19	Severe dysregulation and decline	
	0~0.09	Extremely severe dysfunction and decline	

(1) The optimal vector of the series is determined. As the original data are normalized and transformed into positive indexes, the optimal vector is obtained as follows:

$$G = (g_1, g_2, \ldots, g_n) = (f_{11} v f_{12} v \cdots v f_{1m}, f_{21} v f_{22} v \cdots v f_{2m}, \ldots, f_{n1} v f_{n2} v \cdots v f_{nm}). \tag{14}$$

In the above equation, v is the maximum operator.

(2) The gray correlation coefficient equation is used to calculate the correlation coefficient between the jth evaluation index and the optimal vector G, as shown in the following equation:

$$\xi_i(Y_i, G) = \frac{\min_i \min_j |f_{ij} - g_i| + \rho \max_i \max_j |f_{ij} - g_i|}{|f_{ij} - g_i| + \rho \max_i \max_j |f_{ij} - g_i|}. \tag{15}$$

In the above equation, the minimum difference between the two poles and the maximum difference between the two poles ρ-the decomposition coefficient is generally 0.5; that is, $\min_i \min_j |f_{ij} - g_i| \max_i \max_j |f_{ij} - g_i|$.

(3) The correlation R between the ith evaluation object b and the optimal vector G is calculated, as shown in the following:

$$R = \sum_{j=1}^{n} w_j \times \xi_i(Y_i, G). \tag{16}$$

(4) Output of the results: based on the economic environment data of the county in Shaanxi Province from 2000 to 2009, the original data of the indexes are processed dimensionless using official (2) and (3) to obtain the criteria data of the indexes. The entropy value assignment method is used to conduct calculation based on equations (12) and (13), in which

the weight of each index is shown as follows: $W_j = (0.114, 0.117, 0.123, 0.144, 0.128, 0.128, 0.140, 0.105)$.

Based on the normalized data, the series optimal vector $G = (1,1,1,1,1,1,1,1,1)$ tab is obtained. The above correlation coefficients are introduced into equation (16), and the correlation coefficient F is introduced into equation (15) to derive the status of the passing of the values of the coordination index of the economic, environmental, the social system subsystems, and the composite system from 2000 to 2009 (Figure 3).

5. Data Sources

The parameter values of evaluation indexes in this paper are set in accordance with the relevant literature such as the Statistical Yearbook of the Province, the economic and social development goals in the 12th Five-Year Plan, and the historical development experience of world economies.

5.1. Analysis of Results and Discussion. Based on the analysis of the overall development trend in this region, the growth trend in the standard stage and the stability stage from 2011 to 2030 presented a "U-shaped" trend. However, in the coordination stage, it mainly shows a development trend of increases year by year.

5.2. Analysis of Changes in the Time Series of the Coordinated Development Degree. With the gradual improvement of the economic level in the region, the level of science and

TABLE 3: Settings of the relevant parameters in the stage mode.

Classification	Degree of coordinated development	Level 1 criteria	Level 2 criteria
Interval of coordinated development	0.9~1	Superior coordination	
	0.80~0.89	Good coordination	
	0.70~0.79	Moderate coordination	
	0.60~0.69	Basically coordinated	
Interval of transitional reconciliation	0.50~0.59	Barely coordinated	
	0.40~0.49	On the verge of dysfunction and decline	① When $m = \min\{l(x), g(y), h(z)\}$, it is a lagged type, similar to $m = l(x)$, which is population lagged type.
	0.30~0.39	Mild dysfunction and decline	② When $l(x) = g(y) = h(z)$, it is a synchronous type for population, economy, and environment
Interval of dysfunction and decline	0.20~0.29	Moderate dysfunction and decline	
	0.10~0.19	Severe dysregulation and decline	
	0~0.09	Extremely severe dysfunction and decline	

Note: low, medium, and high stand for high growth rate, medium growth rate, and low growth rate, respectively. The parameters of the province are set based on the "12th Five-Year Plan"; the plan refers to the leapfrog plan of the key advantageous industries in the province, the establishment industry development plan of the province, the establishment industry development plan of the province in 2013, and the studies by scholars such as Lin Fude and Fu Jiafeng.

technology has also been developed in an unprecedented speed. In addition, the optimization of energy structure and energy utilization rate is also increasing year by year. In the situation of the coordinated development of the population-economy-resources-environment system, the growth of the regional economy in the standard stage and the stable stage has been improving from the historical low to zero in about 2030. Through comparison with the standard stage and the stable stage, the adjustment stage focuses more on energy saving and emission reduction activities in the whole society and proactively implements the rapid improvement of resources and environment through major breakthroughs in policy, economy, and technology in all aspects, and the degree of coordinated development has been maintaining an upward tendency [12, 13]. By 2030, the growth rate will be 0.64 (basically coordinated), which is 1.4 times that in 2010. The current stage represents the ideal model for the coordinated development of the regional population, economy, resources, and environment in this province (Figure 4).

5.2.1. Baseline Stage. The province is now in a period of steady urbanization. The population keep growing, with an average annual growth rate of about 0.2% and a declining population efficiency function (the details are shown in Figure 5). The economic development model at present is indispensable for the rapid development of industrialization. Under this background, the ratio of level 2 sector in the province is increasing with an average annual growth rate of about 0.6% industrial structure depends on level 2 sector. The economic efficiency is significantly lagging behind. Population and resource environment effects are not obvious. Until 2020, with the implementation of measures such as the improvement of energy use efficiency and nonfossil energy ratio, the emissions of SO_2 have been effectively suppressed with an annual average reduction of -1.14%. With this effect, the resource and environmental effect function increases slightly, reaching a peak in 2019.

However, with the economic and social development, CO_2 emissions increased significantly and offset the resource-environmental effect brought by the reduction of SO_2 emissions. Hence, the resource-environmental effect has been decreasing year by year subsequently.

Based on the analysis in the above sections, the economic development and energy consumption in the region are coordinated based on the baseline scenario development, which has ultimately kept the regional development in a low state, and the corresponding socioeconomic growth pattern is an extensive form. However, with the extension of time, the progress of resource and environment improvement lags far behind the economic and social growth rate, which makes the resource and environment growth efficiency unable to support, ultimately become a hindrance to the coordinated development of population-economy-resource and environment, and have a negative impact on the sustainable development of the whole society in the region.

5.2.2. Stability Stage. In the stability growth stage of the region, the population growth trend presents a U-shaped trend of gradual development, as shown in Figure 6. The urbanization rate can be effectively controlled to some extent, and the population growth function can achieve a level lower than the reference value to some extent. The industrial structure can be effectively adjusted. Based on the economic growth of GDP, GDP per capita and the proportion of tertiary industry show an increasing trend every year. The economic growth trend achieved the minimum level of 0.242% in 2020 and started to increase year by year in the later period [14, 15]. The utilization rate of nonfossil energy will be effectively improved, and the growth rate of pollutant emission will be suppressed. The annual average growth rate of SO_2 and CO_2 emission from 2010 to 2020 was reduced from −80% to 2.6%, which was a decrease of 20.5% and 37.2%, respectively, compared with the standard stage, with a more significant effect on resources and environment.
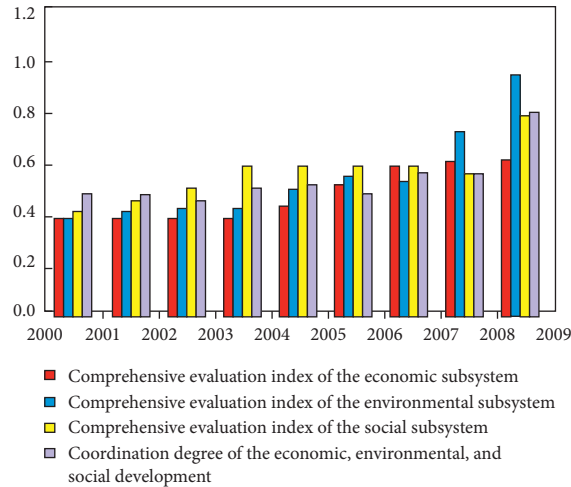
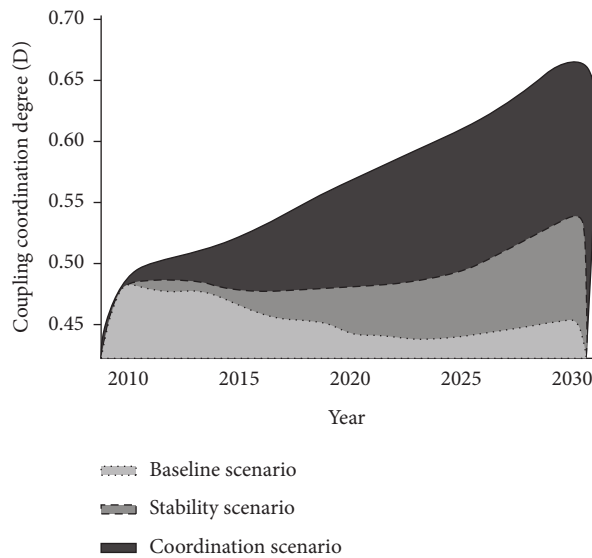FIGURE 3: Evolution of the economic-environmental-social system coordination index values in the county.

FIGURE 4: Changes in the time series of the coordination development degree at different stages: stages of population-economy-resources-environment scheduling and comparative analysis.

With the joint effect of population, economic, and resource-environmental effect functions, the stability stage of coordinated development degree has the same tendency of change as the baseline stage, with a U-shaped tendency of decreasing first and then increasing. Timing and size of its trough tips are significantly different from those in the baseline stage. Different from the criteria scenario, with the economic benefits of stable development, the value of the trough in 2020 was 0.478. However, by 2027, the value of development within the region will increase to 0.511, after which the development of the region will start to enter the stage of uncoordinated development, when the economic growth rate hits the lowest level among the three. This stage between 2010 and 2026 is on the verge of stagnation in the economic development.

5.2.3. Coordinated Development Stage. Through the overall optimization of production, change of lifestyle, and industrial structure in this region, the effective control of population growth in the region is carried out multiple times. In addition, under the premise of effective control while achieving the increase of urbanization level at the same time, the trend of population growth from 2010 to 2030 does not present a valley phenomenon. However, with the implementation of the resource and environmental improvement policies, the average annual growth rate of the emission of SO_2 and CO_2 is maintained at about -1.1%; and with the significant control of pollutant emissions, the energy efficiency function can always keep a significant growth trend, with the robust improvement in the annual growth. In 2027, the economic efficiency in this region is the lowest among
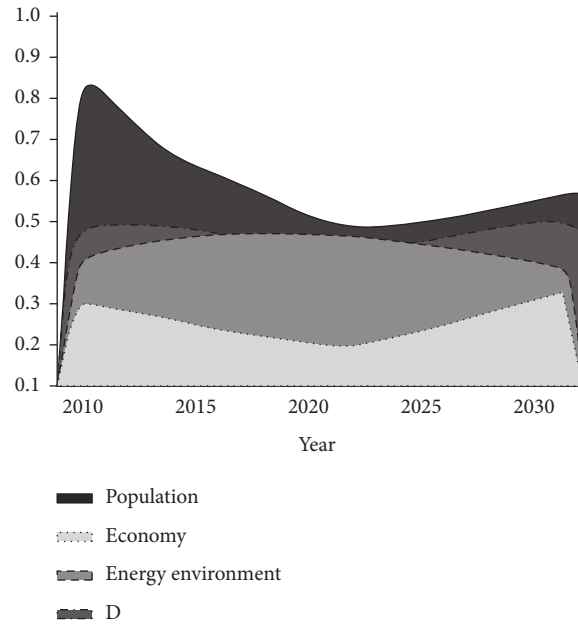
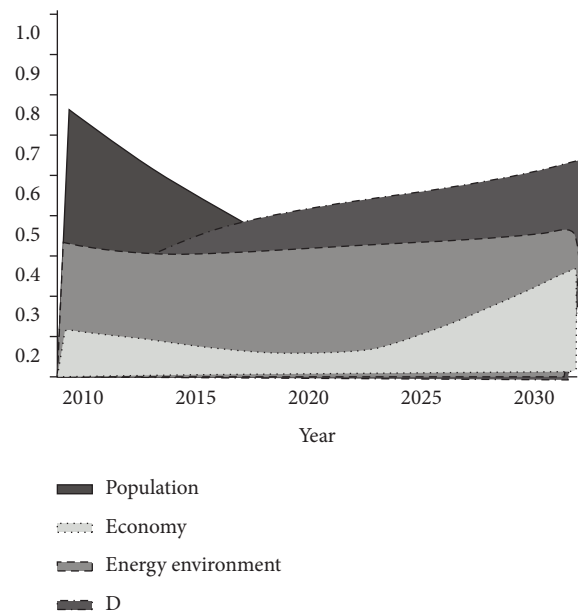Figure 5: Changes in the coordination degree at the baseline stage.

Figure 6: Changes in the coordination degree at the stability stage.

the three. However, in 2028 and 2030, the demographic effect and resource environment were eliminated. Hence, the development was the fastest among the three. From 2024 (0.0.6%) to 2026 (0.622%), it will be the period of relatively backward economic development; from 2027 to 2029, it will be the primary coordinated development with backward population, and 2030 will start to enter the primary coordinated development period with stagnant growth in the resources and environment (Figure 7).

Based on the trend diagram in Figure 7, the coordinated stage development phase occurs at different stages of production effects and profit lag can be obtained. However, as the development trend of population, economy, and resources and environment in the region gradually approaches 1, the evaluation indicates that the overall situation gradually moves towards coordinated development and eventually enters the model of coordinated development of population, economy, resources, and environment.
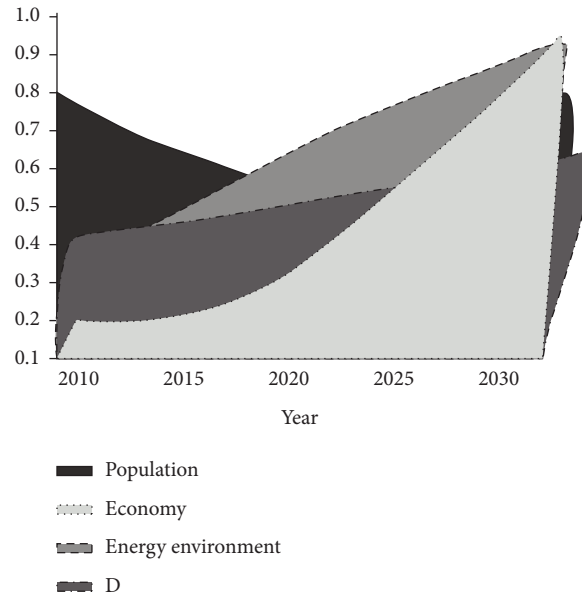
FIGURE 7: Changes in the coordination degree at the coordination stage.

6. Conclusions

In this article, a bilevel optimization model is used to establish an evaluation system for the coordinated development of population, economy, resources, and environment within the region, and the established evaluation index system is used to carry out accurate forecast for the economic development within this region. Through the experimental analysis, it can be known that for the purpose of achieving the coordinated development of population, economy, resources, and environment in this region, the effective regulation of urbanization development level should be carried out in the aspect of population growth. In the aspect of economic benefits, it is necessary to accelerate the speed of economic transformation in the region and optimize the industrial structure. In the aspect of resources and environment, it is necessary to develop and utilize nonfossil energy effectively and fully improve the utilization rate of resources and energy. In this way, the coordinated and rapid development among population, economy, resources, and environment in the region can be achieved gradually.

Data Availability

The labeled data set used to support the findings of this study is available from the corresponding author upon request.

Conflicts of Interest

The authors declare that there are no conflicts of interest.

Acknowledgments

References

[1] M. Biao, "Literature review on land carrying capacity of the coordinated development of population, resources, environment and economy," *AIP Conference Proceedings*, vol. 1890, no. 1, pp. 1–7, 2017.

[2] J. Zhu, "Population,resources,the environment and sustainable development," *Meteorological and Environmental Research*, vol. 10, no. 1, pp. 20–22, 2019.

[3] L. Binglin, J. Shengnan, X. Minghui, and X. Yun, "Coordinated development of population, economy and environment system and diagnosis of its obstacle factors in nanjing," *Meteorological and Environmental Research*, vol. 10, no. 5, pp. 42–46, 2019.

[4] L.-G. Zhang, L. Hui, C. Hua, and Z. Liu, "[Analysis on the coordinated development of ecology-economy-society in coal resource cities: a case study of huainan, China]," *Ying yong sheng tai xue bao = The journal of applied ecology*, vol. 30, no. 12, pp. 4313–4322, 2019.

[5] K. J. Gremillion, D. Shane miller, From Colonization to Domestication: Population, Environment, and the Origins of Agriculture in Eastern north america. salt lake city," *Antiquity*, vol. 93, no. 368, pp. 543-544, 2019.

[6] X. Cui, C. Fang, H. Liu, and X. Liu, "Assessing sustainability of urbanization by a coordinated development index for an urbanization-resources-environment complex system: a case study of jing-jin-ji region, China," *Ecological Indicators*, vol. 96, no. 9, pp. 383–391, 2019.

[7] C. Chen, Z. Ding, J. Kang, and L. I. Yanfei, "The coupling coordinated development of urbanization and resource-environment system in henan," *Journal of Henan University*, vol. 119, no. 6, p. 57, 2017.

[8] S. L. Zhu, H. Wang, W. T. Wang, X. Zhou, and Y. H. Liu, "Status of coordinated development between regional low-carbon economy and spatial land-use pattern in the 12~(th) five year plan," *China Population,Resources and Environment*, vol. 574, no. 7, pp. 914–923, 2017.

[9] X. Nie, T. Zhang, L. I. Zhu, and F. Feng, "Ecological civilization evaluation and coordinated development between

environment,economy and society in hubei," *Journal of Shanxi Normal University (Philosophy and Social Sciences edition)*, vol. 55, no. 12, pp. 24–30, 2018.

[10] Q. Sun, X. Zhang, H. Zhang, and H. Niu, "Coordinated development of a coupled social economy and resource environment system: a case study in henan province, China," *Environment, Development and Sustainability*, vol. 20, no. 1, pp. 1–20, 2018.

[11] H. E. Wei, "Relationship between economic development and environmental pollution in resource-based city——a case study of hengyang, hunan province," *Territory & Natural Resources Study*, vol. 24, no. 4, pp. 14–25, 2019.

[12] F. Wang and H. N. University, "Evaluation of coordinated development between water resources and ecological environment of wanjiang city belt," *Pearl River*, vol. 5, no. 5, pp. 3405–3407, 2017.

[13] H. Zhang, Z. Zhu, and Y. Fan, "The impact of environmental regulation on the coordinated development of environment and economy in China," *Natural Hazards*, vol. 8, no. 9, p. 1, 2018.

[14] X. J. Jiang, Q. S. Yang, Q. G. Geng, X. Y. Wang, and J. Liu, "Spatial-temporal differentiation and driving mechanism of coordinated development of ecological-economic-society systems in the yangtze river economic belt," *Resources and Environment in the Yangtze Basin*, vol. 27, no. 3, pp. 8–11, 2019.

[15] Y. U. Xiao-Yong, L. P. Zhang, X. C. Chen, K. Yang, and Y. Q. Huang, "Analysis of coupling and coordinated development between water resources and social economy in hubei province," *Resources and Environment in the Yangtze Basin*, vol. 27, no. 99, p. 1, 2018.

Hindawi

Research Article

Quality Evaluation Model for Smart City Social Sports Information Cloud Service

Lan Zhang [ID]

Department of Sports and Arts, Zhejiang Yuexiu University, Shaoxing 312000, China

Correspondence should be addressed to Lan Zhang; 19992009@zyufl.edu.cn

With the continuous development of social economy, social sport is more and more valued and favored by the people as a universal and nationwide sport, but it should be noted that social sport involves a wide range of aspects, but due to its particularity, it is also constrained by economic development. In view of these needs and limitations, three technical methods of entropy method, RSR (rank-sum ratio), and TOPSIS are introduced, to sort out the development of social sports, national physical development, social sports guidance, and the number of people to be measured in various places based on the relevant technologies of smart cities in this paper, realize the application analysis of social sports in the public service level. This paper aims to provide a scientific evaluation and evaluation method for social sports information cloud services. The results of simulation experiments show that the evaluation of social sports information cloud service quality based on smart cities is effective, and the comprehensive application of methods can be implemented perfectly, and the further promotion and popularization of social sports services can be realized.

1. Introduction

With the continuous development of social economy, physical exercise has become the main way of sports that people are more enthusiastic about, such as running, climbing, and cycling [1, 2]. On the one hand, sports can improve the physical fitness of everyone but also can ensure the popularization of sports methods. For social sports, it is a systematic project, covering a wide range; meanwhile, with the development of the economy, its connotation and corresponding content have changed, especially relative to the subjective judgment of the people [3, 4]. Therefore, how to effectively and objectively evaluate social sports is a problem to which industry scholars attach great importance [5, 6]. Many scholars have tried to conduct evaluation research of social sports from different perspectives, such as constructing a five-dimensional index system of government responsibility, investment, service benefits, social feedback, and value of social sports services. Through iterative calculation of methods, comprehensive evaluation is performed, such as constructing an index system covering

public participation satisfaction, public service input, efficiency, etc., using AHP method to evaluate social sports services, and providing corresponding decision support for government decision-making [1, 7]. In addition, some scholars conduct surveys, statistics, and analysis of different residents based on whether the audiences they serve are satisfied through questionnaires, visits, and consultations and other methods to reflect the popularity of social sports development from the perspective of the audience and whether there are many problems in the enjoyment of the audience, etc. [8, 9].

However, it is worth noting that, due to the restrictions and limitations of data sources, these studies are often conducted based on surveys, visits, questionnaires, etc. The audience's thinking time and response time are relatively concentrated or less, so the survey result may not completely represent their own true feelings [10, 11]. The development of cloud computing, Internet of Things, big data, and other technologies has promoted the continuous improvement of data collection, storage, analysis, mining, and other technologies. To a certain extent, it can solve the problem of

shortage of manpower, less data sharing, unbalanced equipment, and the limited right enjoyed by audience [12, 13]. Therefore, in view of these needs and limitations, the "Internet +" technology is introduced by trial in this paper, through the use of entropy method, rank-sum ratio method, TOPSIS, and other three technical methods, combining the status quo of social sports public services, in order to construct the corresponding social sports service evaluation index, to promote the transformation of social sports from traditional artificialization l to intellectualization, explore and solve the problems encountered by the people in social sports, and aim to improve the quality and effect of the public services of social sports for the people.

2. Research Objects and Methods

2.1. Research Object. The effectiveness of the method under the smart city technology can be verified through selecting certain 11 areas of the experimental area as the research object of the social sports public service level.

2.2. Research Method. By selecting the corresponding latest survey data, the development level of social sports, the number of people to be tested for national physique, the number of sports activities in the year, social sports groups, and other indicators are analyzed, compared, and calculated through selection and integration of corresponding current survey data, integration of Internet mobile phone signaling data, statistical yearbook data, and other data for summary, and the specific statistical results are shown in Figure 1.

For the analysis of social sports indicators, quantitative and qualitative analysis can be carried out in the following ways, including literature method, consultation and interview method, field investigation, and practical analysis method [12, 13]. Among them, the literature method is for summarizing, sorting, and analyzing, to provide a research basis and ideas for quantitative analysis of corresponding indicators by use of existing academic papers, public news reports, and other materials, while the interview method is to obtain the corresponding attitude and understanding of social sports services through the direct communication with audience or corresponding field experts about some questions [14, 15]. On-site inspections are to conduct on-site investigations of residents through visits and reading materials to obtain the most direct evaluation based on the distribution of equipment related to social sports [16, 17]. The logical approach is to conduct analysis and inverting according to the collected relevant data and finally get the corresponding index evaluation analysis.
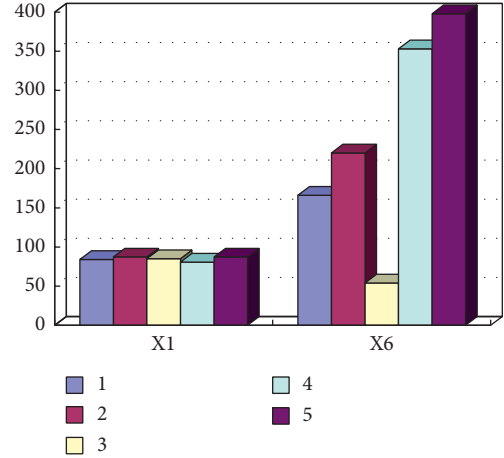

Figure 1: List of evaluation index values of social sports public service level in some regions.

Based on clarifying the relevant coverage of the index, the corresponding evaluation and analysis are carried out continuously.

2.2.1. Entropy Method. The entropy method is an objective and weight-based method, which is used to confirm and calculate the weight of the corresponding index. For diversified metrics, entropy is a specific method that can determine the weight. Because of these abovementioned characteristics, it can be used to clarify the weight determination of social sports and determine the weight evaluation value of social sports public services through the corresponding data sequence.

To conduct an effective social sports cloud service quality evaluation, the specific steps are mainly as follows:

(1) Orienting at the test area: a diversified evaluation index of social sports is constructed, and a matrix is used to make judgments, among which, $R = (X_{ij})_{nm}$, $(i = 1, 2, \ldots, n; j = 1, 2, \ldots, m)$.

(2) Normalize the judgment matrix R to obtain the normalized judgment matrix $R' = (Y_{ij})_{nm}$.

The larger the value of the evaluation index, the better in this research. Therefore, the calculation formula is shown as follows:

$$Y_{ij} = \frac{x_{ij} - x_{\min}}{x_{\max} - x_{\min}}. \tag{1}$$

According to formula (1), the normalized matrix is calculated as

$$Y_{ij} = \begin{bmatrix} 0.3011 & 0.5861 & 1.0000 & 0.0000 & 0.0203 & 0.3031 & 1.0000 & 1.0000 & 0.3832 \\ 0.5774 & 0.3483 & 0.2853 & 0.1792 & 0.1874 & 0.4492 & 0.0411 & 0.0432 & 0.5661 \\ 0.3962 & 1.0000 & 0.1982 & 0.0255 & 0.0911 & 0.0000 & 0.0072 & 0.0022 & 0.4152 \\ 0.000 & 0.3722 & 0.1113 & 0.7694 & 1.0000 & 0.8104 & 0.0593 & 0.1242 & 0.8862 \\ 0.5771 & 0.2412 & 0.0681 & 0.1532 & 0.0451 & 0.9321 & 0.1360 & 0.0483 & 1.0004 \\ 1.000 & 0.7011 & 0.8243 & 0.6151 & 0.0242 & 0.554 & 0.3392 & 0.3041 & 0.7865 \\ 0.9311 & 0.1511 & 0.0251 & 0.0253 & 0.0372 & 0.5882 & 0.0000 & 0.0000 & 0.4526 \\ 0.8445 & 0.1159 & 0.1586 & 1.0000 & 0.0000 & 0.3956 & 0.1053 & 0.0171 & 0.7422 \\ 0.3792 & 0.1443 & 0.1051 & 0.3331 & 0.0021 & 0.2875 & 0.0064 & 0.0021 & 0.4713 \\ 0.9911 & 0.3235 & 0.3972 & 0.9482 & 0.4011 & 1.0000 & 0.0172 & 0.0012 & 0.5413 \\ 0.3101 & 0.0000 & 0.0000 & 0.1021 & 0.0222 & 0.5314 & 0.0080 & 0.0063 & 0.0000 \end{bmatrix}. \tag{2}$$

(3) The calculation formula for calculating the entropy of the jth evaluation index is shown as follows:

$$H_j = \frac{1}{\ln n} \left(\sum_{i=1}^{n} f_{ij} \ln f_{ij} \right). \tag{3}$$

Among them, it can be calculated by

$$f_{ij} = \frac{1 + Y_{ij}}{\sum_{i=1}^{n} (1 + Y_{ij})}. \tag{4}$$

(4) Carry out the sparse calculation of entropy weight on the basis of formula (4). The specific calculation formula is shown as follows:

$$w_j = \frac{1 - H_j}{m - \sum_{j=1}^{m} H_j}, \tag{5}$$

($\sum_{j=1}^{m} w_j = 1$; $0 \le w_j \le 1$). The calculated entropy weight coefficient is the weight.

Based on the above calculation steps, the determined weights of the evaluation indicators are shown in Figure 2.

2.2.2. TOPSIS Method. The TOPSIS method is a diversified decision-making method, which uses the distance between the positive and negative TOPSIS and the object to be measured for quantitative evaluation and ranks them correspondingly in terms of superiority and inferiority, which is extremely effective in multiobjective decision-making [18, 19].

The TOPSIS method is a multiattribute decision-making method. Its basic idea is to sort the advantages and disadvantages by calculating the distance between the evaluation object and the TOPSIS (X^+) and negative TOPSIS (X^-). According to this method, only each utility function is required to have the monotone increasing (or descending) characteristics, which is a commonly used effective method in multiobjective decision analysis.

2.2.3. RSR Method. The rank-sum ratio method is to obtain a dimensionless statistic RSR through rank conversion in a matrix of N rows and M columns (M evaluation indicators) and rank the advantages and disadvantages of evaluation objects according to the RSR value.

First, a data analysis matrix for different evaluation indicators of social sports oriented at the experimental area is constructed. Because different evaluation indicators have different meanings and dimensions, the indicators are required to be normalized to achieve unified contrast and comparison. The specific normalization processing is shown in the following formula:

$$Z_{ij} = \frac{X_{ij}}{\sqrt{\sum_{i=1}^{16} (X_{ij})^2}}. \tag{6}$$

In the formula, the value range of i is [1, 11], and the value range of j is [1, 9]. According to the above formula and method, the matrix of the normalized evaluation index of social sports public service level is solved, and the specific expression is expressed by Z:
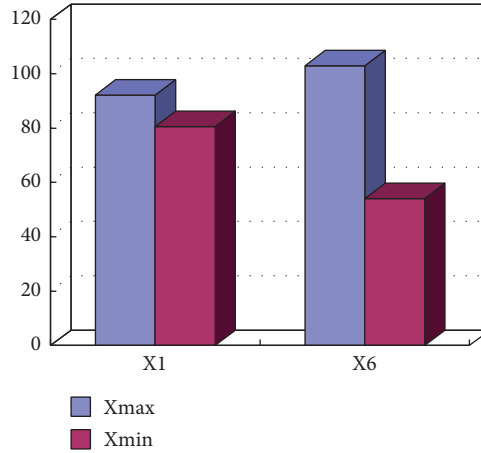
FIGURE 2: Entropy weight of evaluation index for sports public service level.

$$z = \begin{bmatrix} 0.2901 & 0.3844 & 0.7042 & 0.0253 & 0.0242 & 0.1842 & 0.9121 & 0.9453 & 0.1921 \\ 0.3012 & 0.2314 & 0.2013 & 0.1232 & 0.1752 & 0.2438 & 0.0622 & 0.0515 & 0.2752 \\ 0.2941 & 0.6504 & 0.1394 & 0.0413 & 0.0912 & 0.0611 & 0.0321 & 0.0132 & 0.2044 \\ 0.2782 & 0.2471 & 0.0795 & 0.4381 & 0.9023 & 0.3922 & 0.0853 & 0.1261 & 0.4221 \\ 0.3012 & 0.1624 & 0.0482 & 0.1092 & 0.0523 & 0.4424 & 0.1542 & 0.0513 & 0.4723 \\ 0.3181 & 0.4592 & 0.5815 & 0.3565 & 0.0321 & 0.2832 & 0.3352 & 0.2941 & 0.3714 \\ 0.3151 & 0.1062 & 0.0182 & 0.0412 & 0.0442 & 0.3013 & 0.0362 & 0.0141 & 0.2251 \\ 0.3124 & 0.0813 & 0.1121 & 0.5613 & 0.0111 & 0.2223 & 0.1231 & 0.0223 & 0.3523 \\ 0.2932 & 0.1032 & 0.0743 & 0.2054 & 0.0121 & 0.1761 & 0.0341 & 0.0123 & 0.2331 \\ 0.3181 & 0.2181 & 0.2806 & 0.5341 & 0.3632 & 0.4703 & 0.0452 & 0.0142 & 0.2642 \\ 0.2903 & 0.0072 & 0.0002 & 0.082 & 0.0312 & 0.2752 & 0.0362 & 0.0132 & 0.0242 \end{bmatrix}. \tag{7}$$

3. Simulation Experiment

It is not only a reform of business management, but also a reform and improvement of external services $z =$ to introduce cloud computing technology into the social sports management business. The improvement of these two aspects requires the transformation of traditional social sports and services from passive mode to active one. The corresponding social sports intelligent subject service system is designed in this paper, and the specific structure is shown in Figure 3.

According to the overall architecture shown in Figure 3, the social sports smart service system constructed in this article is mainly divided into three parts, which are distinguished as cloud providers, social sports management business personnel, and users according to different object-oriented aspects, respectively. When constructing a social sports smart public service system, full consideration should be given to the application requirements of users as the most basic and the largest number of users.

Based on the overall architecture, it is necessary to consider the hardware and software environment required for deployment. The infrastructure mainly includes hardware environments such as servers and storage, as well as operating network environments, disaster recovery backups, etc. These software and hardware environments need to be

fully utilized; construct the cloud service platform accordingly with this technology. The specific process diagram is shown in Figure 4.

As shown in Figure 5, the first is the cloud layer, which is the layer that relies on cloud infrastructure. It mainly provides storage, hardware, memory, and other environments. With these infrastructures, the integrity and security of the platform can be ensured. Transfer of service providers need to be carried out in the middle of the cloud for the social sports, to coordinate the management of users and service owners and provide external services on mobile terminals or PC terminals through the network environment.

The next is the library layer of the model. This part is to realize the relationship between social sports itself and users. The schematic diagram is shown in Figure 5. Through the analysis of user needs, it ensures that the service has comprehensively changed orientating at the actual social sports and user needs. For the services provided by social sports, users have highlighted individual needs, which requires cloud computing to give full play to its advantages and provide more demanding needs. In this context, based on cloud computing technology, the cloud platform of social sports can analyze user interests, adjust service goals of social sports, and optimize service methods and content based on habits and browsing history of users.
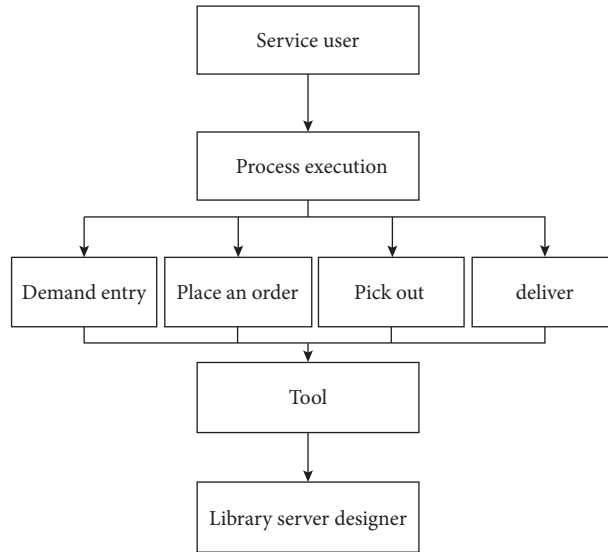
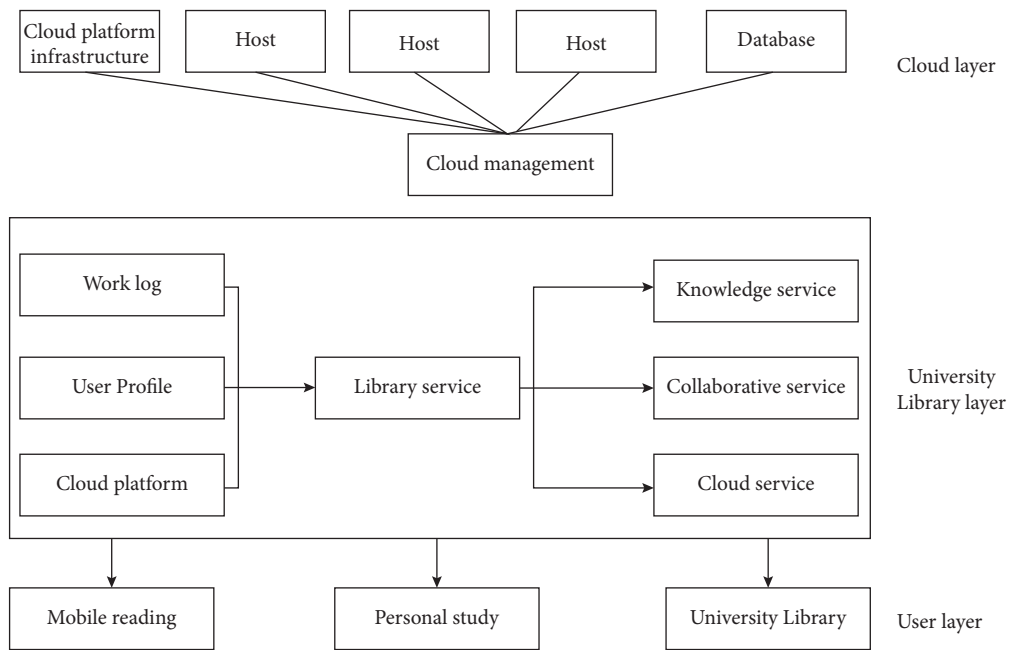Figure 3: The overall architecture of the cloud service platform.

Figure 4: Cloud service platform model.

The last is the user layer. For social sports, users are the foundation and core of the entire platform. According to users' information sharing and use, to achieve the purpose of learning and creation, their individual needs should be fully considered.

According to the data collected above, the ideal positive and negative solutions in the evaluation indicators of the social sports information cloud service quality of smart cities can be calculated.

3.1. The Low Actual Executive Force of Urban Community Sports Public Service Policies and Regulations. The public

service quality evaluation of social sports according to the corresponding community is shown in Figure 6.

From the results, it can be seen that the proportion of residents being very satisfied is less than 10%, the proportion of being relatively satisfied is about 30%, and the sum of general and dissatisfied residents has exceeded 50%. From the collected data, it can be seen that corresponding policies are not implemented for social sports, and there are some weaknesses in publicity and popularization. Therefore, the residents are not satisfied with the quality of public services of social sports.

It can be seen from Figure 7 that most of the funding sources of social sports are government investment and
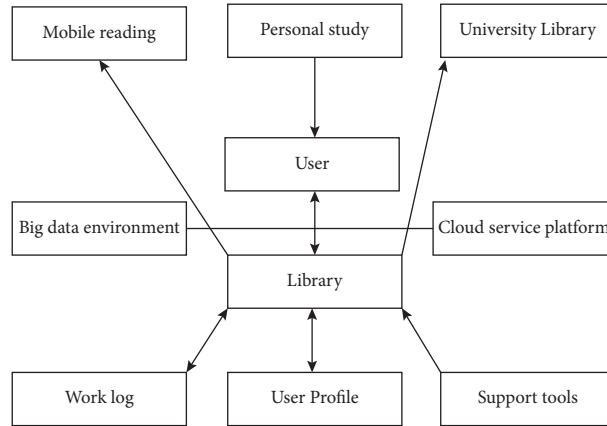
FIGURE 5: Schematic diagram of social sports interaction (taking borrowing sports books from library as an example).
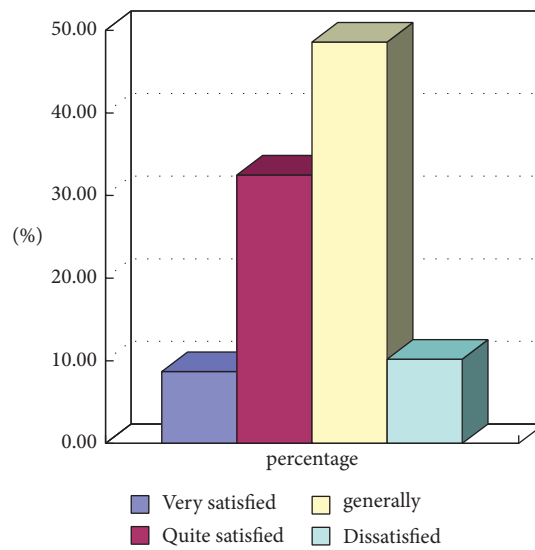

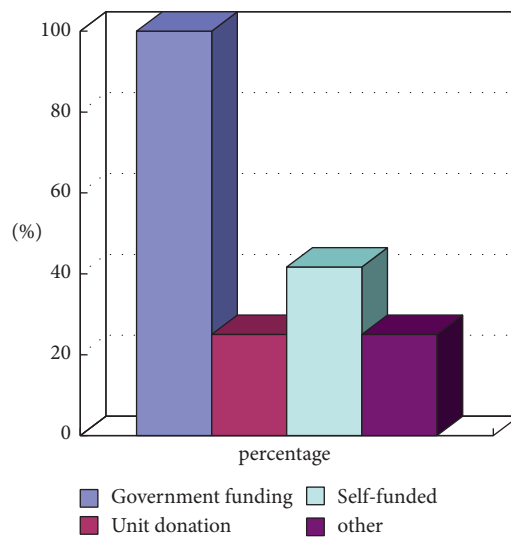FIGURE 6: Statistics of residents' satisfaction with the quality of public services of community sports ($N = 600$).

FIGURE 7: Main sources of service funding of community sports ($N = 12$).

support, and a small amount of funding comes from corporate donations. Therefore, most of the social sports venues still require a large amount of investment. It is precisely because of the insufficient funding that there are fewer public service facilities for social sports and the reduction of service experience.

3.2. The Low Implementation Speed and Efficiency of Urban Social Sports Public Services.

The so-called implementation efficiency of urban community sports public services refers to whether the principal part of urban community sports public services can efficiently satisfy the public's various sports needs in the process of providing various sports services to the public.

Through investigation and research, it is found that there are obvious regional differences in the quality of social sports public services in cities, which are restricted by local social development. For example, in areas with more developed economies, the efficiency and quality of public services for social sports are relatively satisfactory and can basically meet the needs of social sports of various audiences, but the relative execution efficiency in other areas is significantly lower.

In the construction of cloud service platform guarantee capacity, virtualization technology is the core technology for cloud resource management, scheduling, and transformation into platform guarantee capacity. In platform construction, virtualization technology should be used to realize on-demand allocation and unified scheduling of cloud resources, to strengthen the fine-grained division of infrastructure resources, cloud computing resources, cloud storage resources, cloud system platform resources, and cloud software resources, and to combine services. The characteristics of the object and service content, adopting different management standards, allocation strategies, packaging methods, and usage methods, really strengthen the management and control efficiency of virtual resources; secondly, the application security, reliability, and trustworthiness and reliability of the cloud service platform should be improved. Verification, under the premise of ensuring the cloud service provider has a high degree of credibility and security, realizes the dual identity authentication and security management of the cloud service provider and the platform user; third, the compatibility of the cloud service platform system and software should be strengthened. Availability, support of sports cloud services, availability of cloud applications and databases, cloud service migration capabilities, and capacity building ensure that traditional sports can efficiently, safely, orderly, and economically migrate to the cloud computing environment according to the athletes' cloud use needs. In the construction of the IaaS service platform, the user's ease of use and manageability of IaaS resources should be emphasized to ensure that users can obtain IaaS resources through Web application services. At the same time, administrators can use the IaaS platform monitoring and management system to quickly realize the creation, deployment, allocation, scheduling, management, and monitoring of IaaS resources

and ensure the load balance of the IaaS cloud service platform; secondly, the intelligence of the IaaS service platform resources should be strengthened. Dispatching and automated scheduling capabilities ensure that users can dynamically use resources in an efficient, flexible, scalable, and automatic way according to cloud application requirements and reduce usage costs by paying for usage; third, the IaaS service platform should have a larger system scale and application. Security, through the management and monitoring of resource pools, user resource allocation and scheduling, resource pool architecture optimization, and refined application operations of data transmission guarantee networks and the intensive management of IaaS cloud resources can be realized to ensure the security, efficiency, and efficiency of the IaaS platform, hostable and easy to expand. In the cloud computing environment, the data center has the characteristics of complex infrastructure structure, difficult management of cloud platforms and application systems, increased threats from the Internet, and cloud service platform resources shared by multiple users, and the cloud platform application service system is in a complex network environment middle. At the same time, cloud computing resources are logically divided and shared by multiple users in the distribution and use methods, leading to malicious users who may obtain control rights of the cloud system platform through illegal means and steal important data and user confidential information of the cloud system.

3.3. Failure to Give Full Play to the Role of Sports Clubs and Lack of Fitness Guidance.

With the development of social economy, social sports corporation plays an important role in the important process of sports popularization and sports reform.

As shown in Figure 8, social sports groups do not fully cover the audience. Many residents do not even know about such organizations, accounting for about 30%. A small number of people participate in social sports activities. From the results in Figure 8, it is found that the audience is not very enthusiastic about participating in the corresponding social organizations.

As the core of social sports, social sports instructors play an important guidance role in public services. From the summary results in Figure 9, it can be found that, in the actual guidance process, those exceeding 6 times account for about 15%, which shows the role of social sports instructors in the actual operation process is too weak, which restricts the audience's enthusiasm for participating in sports.

3.4. The Low Type, Frequency, and Participation of Urban Community Sports Public Service Activities.

The proportion in population of sports that young people like is relatively small. Due to the limitation of venues and equipment, the development of this type of sports is restricted. Community sports public service departments should consider increasing the construction of venues and equipment to increase the number of people participating in community sports, meet the needs of various groups of people, and
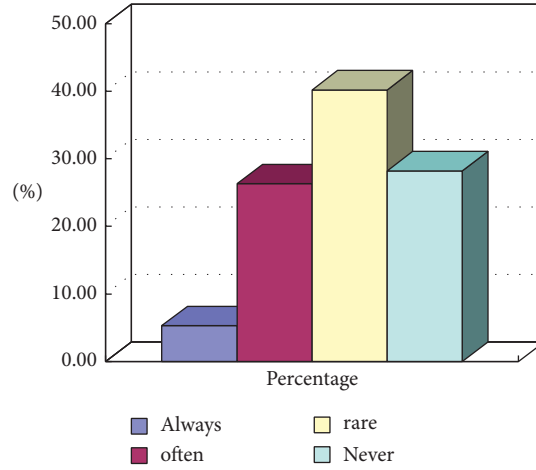
FIGURE 8: Statistics on the frequency of community residents participating in club activities.
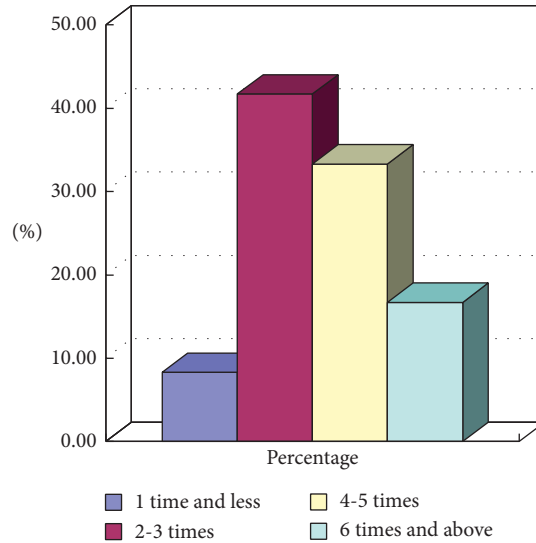
FIGURE 9: Statistics of the number of times that city community fitness instructors give community guidance.

continuously improve the quality of urban community sports services.

3.5. Calculate the Distance between Each Evaluation Index Data and X^+, X^-.
The calculation formula for the distance d_i^+, d_i^- between each evaluation index data and X^+, X^- is shown in the following formulae:

$$d_i^+ = \sqrt{\sum_{j=1}^{9} \left(Z_{ij}' - X_j^+ \right)^2}, \qquad (8)$$

$$d_i^- = \sqrt{\sum_{j=1}^{9} \left(Z_{ij}' - X_j^- \right)^2}, \qquad (9)$$

where $i = 1, 2, 3, \ldots, 16$ and $j = 1, 2, 3, \ldots, 8$.

Based on this, the public service level of sports is evaluated and ranked. The specific calculation is shown in formula (10), and some results are shown in Figure 10:

$$C_i = \frac{d_i^-}{d_i^+ + d_i^-}, \qquad (10)$$

where $i = 1, 2, 3, \ldots, 16$.

Through simulation experiments, the results show that the variance consistency between the classifications of each indicator is relatively good, and the differences between the files are statistically significant, and the evaluation of social information cloud service quality under the background of smart cities is effective.

(1) Build a national fitness social sports information service cloud platform that includes public and private clouds, and divide social sports cloud storage into corresponding public cloud storage and private cloud storage: public cloud is built on the Internet,

FIGURE 10: List of C_i values and rankings of sports public service levels in some regions.

and social sports management is built on a private cloud. In the government Intranet, all kinds of social sports management data are published on the Internet and Intranet through the form of services and can be integrate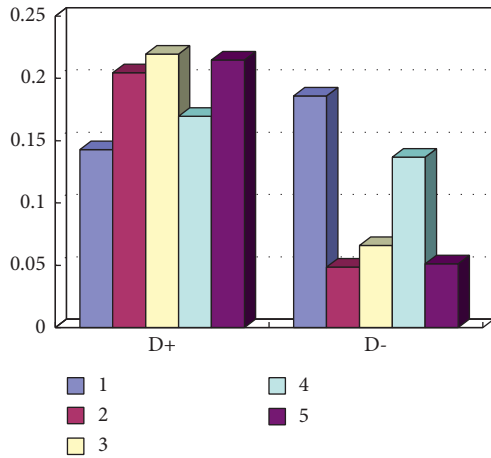d with various services such as government affairs and office running in the local area network and wide area network, so as to achieve the sharing of social sports management information and computing resources. The goal of the cloud platform can also provide a full range and multiangle for different users such as the State Sports General Administration, the Provincial Sports Bureau, the Municipal Sports Bureau, the Sports Guidance Center, the sports fitness site, the fitness team, the sports instructor, the seller, the sports venue, and the general public service.

(2) Build a national fitness social sports big data center, and store site information, social instructor information, training methods, training information, and other structured and unstructured information on a big data platform (HDFS, HBase, etc.) to form an authoritative large-scale database covering all aspects of national fitness and social sports to provide data sources for national fitness management, resource allocation, fitness guidance, and fitness evaluation. An authoritative large database covering all aspects of national fitness and social sports serves as a data source for national fitness management, resource allocation, fitness guidance, and fitness evaluation.

(3) Focus on the four core issues of fitness venues ("where to practice"), fitness people ("who will practice"), social instructors ("who to practice"), and fitness methods ("how to practice"), the design includes basic data management, information collection, data management, data query, data visualization, statistical analysis, data mining, decision support, and other major functions of the city's

national fitness social sports information service system.

(4) Use object-oriented programming language to develop the corresponding C/S mode background management system (C# language), B/S mode online service website (C# language), and mobile phone APP software (Java language), supporting two-dimensional code scanning is free to download and update automatically. Both the website and the mobile APP can quickly access various fitness project guidance materials ("how to practice"), and the management system is responsible for the maintenance and management of "where to practice," "with whom to practice," and "how to practice" related information. The actual application effect of the platform shows that the information platform has completed the foundation of 2,697 fitness sites and 21,295 social sports instructors at all levels in Dalian (84, 1731, 6,989, and 13,421 people at the national, first, second, and third levels). Information management greatly reduces the workload of managers and at the same time provides millions of intelligent information services for tens of thousands of fitness people. Users access the cloud platform through desktop systems, websites, and mobile apps (Android) and use cloud map services and cloud information services among them. In the subject of "who will practice," the public can use interactive applications such as online quick query to solve "where to practice" (find sites/venues), "with whom to practice" (recommend social instructors based on fitness programs), and "how to practice" (push learning materials according to fitness programs). Search for fitness sites, instructors, fitness paths, etc. based on location-based services through maps, and select the best fitness activities, fitness venues, and travel methods.

(5) The social sports service platform designed and constructed based on cloud computing, "Internet +," and other technologies is essentially a loosely coupled architecture, which can be flexibly connected with existing systems and new systems in the future and ultimately can achieve "data in the cloud." The new application service model of "sports by your side, applied in your hands" can satisfy the internal service model and external service model. "Unmanned guidance" issues practically introduce cloud computing, big data, Internet + and other thinking and technical methods into national fitness services, realize the transformation of national fitness services from artificial to intelligent, and effectively improve the public service quality of national fitness.

(6) Provide a reference for building an "Internet +" smart sports information service platform with authoritative data support and persistent services, and ultimately make it a part of smart sports and smart cities.

4. Conclusions

With the continuous development of social economy, people are paying more and more attention to sports. As a national sport, social sports public service industry is valued. Aiming at how to evaluate social sports public services, the relevant technologies of smart cities is introduced in this paper, based on TOPSIS, rank-sum ratio, entropy method, and other methods, social sports instructors, the number of people to be tested, and other analysis index systems are constructed by trial, and they are divided by classifying, to explore the public service level of social sports, aiming to explore the evaluation of cloud service quality of social sports information in the context of smart cities. The simulation results show that the relevant technologies of smart cities are effective, can support the quality evaluation of social sports information cloud service, and can promote the further popularization of social sports.

Data Availability

The labeled dataset used to support the findings of this study is available from the corresponding author upon request.

Conflicts of Interest

The authors declare that there are no conflicts of interest.

Acknowledgments

References

[1] X. Wang, B. Sheng, C. Zhang, Z. Xiao, H. Wang, and F. Zhao, "An effective application of 3D cloud printing service quality evaluation in BM-MOPSO," *Concurrency & Computation Practice & Experience*, vol. 30, no. 24, pp. 1–8, 2018.

[2] P. Manuel, "A trust model of cloud computing based on quality of service," *Annals of Operations Research*, vol. 233, no. 10, pp. 281–292, 2015.

[3] Y. Wang, J. Wen, X. Wang, and W. Zhou, "Cloud service evaluation model based on trust and privacy-aware," *Optik-International Journal for Light and Electron Optics*, vol. 134, no. 4, pp. 269–279, 2017.

[4] M. H. Yaghmaee, F. Banaee, and S. Seno, "Performance evaluation of CoAP proxy virtualization in cloud-assisted sensornetworks," *IET Wireless Sensor Systems*, vol. 10, no. 3, pp. 56–63, 2019.

[5] Q. Duan, "Cloud service performance evaluation: status, challenges, and opportunities-a survey from the system modeling perspective," *Digital Communications & Networks*, vol. 5, no. 6, pp. 101–111, 2016.

[6] Y. Xia, M. Zhou, X. Luo, Q. Zhu, J. Li, and Y. Huang, "Stochastic modeling and quality evaluation of infrastructure-as-a-service clouds," *IEEE Transactions on Automation Science & Engineering*, vol. 12, no. 1, pp. 162–170, 2014.

[7] H. Hao and J. Zhang, "The evaluation system for cloud service quality based on SERVQUAL," in *Proceedings of the 2012 International Conference on Information Technology and Software Engineering*, pp. 577–584, Beijing, China, December 2012.

[8] V. C. M. Leung, A. Shami, and L. Liao, "Distributed flowvisor: a distributed flowvisor platform for quality of service aware cloud network virtualisation," *Networks IET*, vol. 4, no. 5, pp. 270–277, 2015.

[9] T. Labidi, A. Mtibaa, and H. Brabra, "CSLAOnto: a comprehensive ontological SLA model in cloud computing," *Journal on Data Semantics*, vol. 5, no. 3, pp. 179–193, 2016.

[10] S. L. Greenspan, A. Singer, K. Vujevich et al., "Implementing a fracture liaison service open model of care utilizing a cloud-based tool," *Osteoporosis International*, vol. 5, no. 3, pp. 109–118, 2018.

[11] Y. Wang, Z. Xin, and D. Yang, "Evaluation methodology for fast switching cloud RAN systems," *IEEE Communications Letters*, vol. 4, no. 11, pp. 1–10, 2017.

[12] M. Anisetti, C. Ardagna, E. Damiani, and F. Gaudenzi, "A semi-automatic and trustworthy scheme for continuous cloud service certification," *IEEE Transactions on Services Computing*, vol. 13, no. 1, pp. 30–43, 2017.

[13] Y. Yang, B. Yang, S. Wang, W. Liu, and T. Jin, "An improved grey wolf optimizer algorithm for energy-aware service composition in cloud manufacturing," *International Journal of Advanced Manufacturing Technology*, vol. 105, no. 2, pp. 1–13, 2019.

[14] P. Cappanera, F. Paganelli, and F. Paradiso, "VNF placement for service chaining in a distributed cloud environment with multiple stakeholders," *Computer Communications*, vol. 133, no. 1, pp. 24–40, 2019.

[15] S.-E. Benbrahim, A. Quintero, and M. Bellaiche, "Live placement of interdependent virtual machines to optimize cloud service profits and penalties on SLAs," *IEEE Transactions on Cloud Computing*, vol. 7, no. 1, pp. 237–249, 2019.

[16] K. Mubarok, X. Xu, X. Ye, R. Y. Zhiong, and Y. Lu, "Manufacturing service reliability assessment in cloud manufacturing," *Procedia CIRP*, vol. 72, no. 4, pp. 940–946, 2018.

[17] R. Anitha and S. Mukherjee, ""MaaS": fast retrieval of data in cloud using metadata as a service," *Journal of Intelligent Manufacturing*, vol. 40, no. 6, pp. 1–21, 2015.

[18] S. Nastic, H. L. Truong, and S. Dustdar, "SDG-Pro: a programming framework for software-defined IoT cloud gateways," *Journal of Internet Services & Applications*, vol. 6, no. 1, pp. 1–17, 2015.

[19] A. K. Kar and A. Rakshit, "Flexible pricing models for cloud computing based on group decision making under consensus," *Global Journal of Flexible Systems Management*, vol. 16, no. 2, pp. 191–204, 2015.

Hindawi

Research Article

Video Content Analysis of Human Sports under Engineering Management Incorporating High-Level Semantic Recognition Models

Ruan Hui (iD)

Shanxi University, Shanxi, Taiyuan 030006, China

Correspondence should be addressed to Ruan Hui; rhui@sxu.edu.cn

In this paper, a high-level semantic recognition model is used to parse the video content of human sports under engineering management, and the stream shape of the previous layer is embedded in the convolutional operation of the next layer, so that each layer of the convolutional neural network can effectively maintain the stream structure of the previous layer, thus obtaining a video image feature representation that can reflect the image nearest neighbor relationship and association features. The method is applied to image classification, and the experimental results show that the method can extract image features more effectively, thus improving the accuracy of feature classification. Since fine-grained actions usually share a very high similarity in phenotypes and motion patterns, with only minor differences in local regions, inspired by the human visual system, this paper proposes integrating visual attention mechanisms into the fine-grained action feature extraction process to extract features for cues. Taking the problem as the guide, we formulate the athlete's tacit knowledge management strategy and select the distinctive freestyle aerial skills national team as the object of empirical analysis, compose a more scientific and organization-specific tacit knowledge management program, exert influence on the members in the implementation, and revise to form a tacit knowledge management implementation program with certain promotion value. Group behavior can be identified by analyzing the behavior of individuals and the interaction information between individuals. Individual interactions in a group can be represented by individual representations, and the relationship between individual behaviors can be analyzed by modeling the relationship between individual representations. The performance improvement of the method on mismatched datasets is comparable between the long-short time network based on temporal information and the language recognition method with high-level semantic embedding vectors, with the two methods improving about 12.6% and 23.0%, respectively, compared with the method using the original model and with the *i*-vector baseline system based on the support vector machine classification method with radial basis functions, with performance improvements about 10.10% and 10.88%, respectively.

1. Introduction

With the continuous development of information technology, the way people obtain and store massive video information keeps developing towards diversification, and video information gradually becomes the mainstream multimedia data carrier. In the context of huge video data resources, users face the challenge of how they can efficiently retrieve video resources according to their interests [1]. Therefore, it is necessary to classify and organize the massive video resources intelligently to facilitate users to retrieve according to their preferences. Video semantic analysis technology can annotate and classify important semantic information in videos, and users can retrieve it according to their preferred categories, which improves the efficiency of users' access to information. In addition, the host-based implementation of video semantic analysis technology can replace manual annotation work, reducing many human resources and improving information utilization. Video semantic concept analysis refers to the generalized description of video content after obtaining video sequences, and the content of events, scenes, objects, and so forth is the

multicategory semantic information contained in semantic concepts. A large amount of video data has large intraclass variations for the same action class, which may be caused by background clutter, viewpoint changes, and movement speed and style [2]. In particular, the feature information generated by the deep learning model is very large. Only when the attention mechanism is used in the huge feature space can the model extract more effective features and discard useless information. The high dimensionality and low resolution of the videos further increase the difficulty of designing efficient and robust recognition methods. Although traditional manual annotation methods can achieve the understanding and description of video semantic concepts to a certain extent, the time and labor cost of manual annotation are huge, subjective, and difficult to cross the semantic gap between the underlying features and the semantic understanding of video data, and its annotation speed cannot achieve efficient classification and organization of video data [3]. Therefore, in recent years, researchers have focused their research on how they can automatically access the semantic concepts of video data and annotate, classify, and organize rich video data. This research has significant academic and applied value and helps to improve video management techniques to make them more complete and more efficient.

Video semantic concept analysis is a key and difficult area in the field of machine learning and pattern recognition, where video data can be efficiently and intelligently retrieved and organized by recognizing and understanding the main events, scenes, and objects in the video. In recent years, with the rapid development of technology and the improvement of the computing power of hardware devices, the way of video acquisition has become faster [4, 5]. Video retrieval is the process of finding a match in the video database according to the user's textual description according to a specific algorithm and filtering all videos that match the user's needs according to some qualifying conditions. Group behavior recognition technology can derive labels for crowd scene images that can provide clues for retrieval of images and videos of group scenes. The advancement of group behavior recognition technology is a great boost to crowd scene classification, labeling, and retrieval. With the popularity of electronic devices, especially mobile electronic devices such as mobile phones, the change in people's lifestyles, and the need to record their productive lives, a large amount of image and video data has been generated. However, it is not a simple task to manage and utilize these huge amounts of images and data [6]. A good starting point can not only prevent the gradient descent algorithm from falling into the local extreme point which is difficult to jump out of but also reduce the time to find the global optimal solution, if the initialization point is close enough to the optimal solution. Current video retrieval technology relies heavily on users submitting and sharing videos along with video subject descriptions. This is difficult to achieve in real time, and it is difficult to get down to the specifics, as describing specific details is tedious and time-consuming, and only based on image and video analysis techniques can achieve real-time frame-by-frame analysis. Group behavior recognition techniques are of great interest for real-time frame-level video classification retrieval of crowd scenes.

Classification and detection of video-based actions is an important research topic in the field of computer vision, which has a very wide range of applications in intelligent human-computer interaction, video surveillance, telemedicine, and other fields. The difficulties of traditional action analysis tasks mainly come from several aspects: the differences arising from the same action performed by different people; the influence of environmental factors, such as occlusion, viewpoint changes, lighting differences, and dynamic background interference; and the ambiguity in defining the starting and ending points of the action. However, the existing recognition and detection performance still falls far short of the requirements for accuracy in practical applications. The reason for this is that, on the one hand, the number of action classes in the existing dataset is limited and cannot cover all actions in realistic scenes, and the definition of the classes is relatively coarse, so the models trained on the coarse-scale action classes are not able to analyze increasingly fine-grained action classes. Another important reason is that action classes in existing datasets are usually hand-selected and cropped, resulting in more significant episodic and motion differences between classes, while action boundaries in realistic scenes are usually fuzzy and uncertain, and similarities between actions are often large, often with only minor local differences in the actions. In such cases, more fine-grained action discrimination and detection are required. Therefore, we believe that fine-grained action analysis will facilitate further breakthroughs in the task of action classification and detection, thus promoting the advancement of abstract theoretical research to practical applications in realistic scenes.

2. Related Work

How to represent the behavior in the video is the core problem of behavior recognition research, which determines the recognition performance to a certain extent. There exist many feature representation methods, which can be divided into two categories according to the source of features: handcrafted features and features learned from samples [7]. Handcrafted features are features designed by research experts based on human visual principles. In contrast, features obtained from samples are learned without prior feature design, and suitable feature representations are found directly in training samples by various types of learning algorithms, among which deep learning methods have become the mainstream method for learning features due to their excellent performance [8]. It is pointed out that implicit knowledge is real in the practice of competitive sports, especially in the acquisition of motor skills where implicit cognition plays an important role, and a coping strategy is proposed on how implicit cognition and explicit cognition can be transformed into each other in motor skill learning. Large-scale image retrieval systems necessarily have high demands on the time overhead of retrieval [9]. The performance problem is a difficult problem that must be solved for retrieval on a collection of images of hundreds of millions of sizes [10]. The basis of image retrieval lies in the similarity

calculation between the query image and the database image in the feature space. Calculating the similarity between each vector following a linear traversal is very time-consuming [11].

How to ensure the efficiency of image retrieval systems has been a key research direction in the fields of information retrieval, machine learning, and computer vision [12]. Considering that the image features to be retrieved are not uniformly diffuse in the feature space but in some specific distribution pattern, it is sometimes not necessary to traverse the whole query space to query for the nearest neighbor feature vector. Based on this idea, many kinds of tree-based index structures were proposed to narrow the retrieval domain of the query vector by recursively partitioning the feature space. The vector quantization approach, on the other hand, lies in approximating the original features using quantization to certain representative elements [13]. Deep learning methods can learn multilayer feature hierarchies and automatically construct high-level representations of the original input. A large amount of data is used to drive network training and model optimization to extract more representative semantic features, thereby improving classification performance, making the limitations of traditional manually designed feature extraction methods largely avoided. Using quantization methods, the global features of an image are usually quantized to sparse storage, and the query features are associated with only a small number of relevant quantization points during the similarity calculation, which corresponds to a reduction in the dimensionality of the image features and therefore an increase in retrieval speed [14].

In terms of tacit knowledge measurement methods, most of the relevant results of hierarchical analysis and fuzzy integrated measurement methods are used for specific applications [15]. In recent years, many scholars have started to try to combine the relevant theories of discrete mathematics with multicriteria decision-making to characterize the weight information for multiple scenario comparisons and decision-making. The theory of partial order set, as an important element in discrete mathematical order theory, is a very attractive decision support tool, and the options can be compared and ranked by qualitative weight information. No systematic theoretical system has been developed. Many scholars have addressed the influence of nontechnical factors on athletes' performance from a psychological and philosophical perspective. There are more discussions about implicit learning in psychology, alienation, and sustainable development of competitive sports from a philosophical perspective. The literature applying knowledge management theory to the field of competitive sports practice is occasionally found to be more general. A systematic study of the basic theoretical issues of athletes' tacit knowledge will certainly make up for the lack of research in this field to a certain extent, thus promoting the enrichment and development of the theoretical system of athletes' tacit knowledge.

3. Video Content Analysis of High-Level Semantic Recognition Model Sports under Engineering Management

3.1. High-Level Semantic Recognition Model Design under Engineering Management. Interaction information is an important clue for the task of group behavior identification, and mining the interaction information between individuals is crucial for identifying individual behavior and group behavior. Group behavior can be identified by analyzing the behavior of individuals and the interaction information between individuals. Individual interactions in a cluster can be represented by individual representations, and analysis of the relationships between individual behaviors can be modeled by modeling the relationships between individual representations [16]. It is necessary to extract the appearance representation of individuals, to establish the relationship between individual interaction and individual representation, to analyze the behavior of individuals and to analyze the model of group behavior and individual interaction, and to obtain the group behavior by analyzing individual representation, individual behavior, and interaction between individuals. The attention mechanism is used in the individual fusion of interaction information. After completing the establishment of the index based on the random split rule, we input the automatically mined dance element into each random tree in turn and implement the top-down matching process to find its nearest neighbor in the feature space. By attention mechanism, we mean that the model devotes more attention to the important information and allocates more attention to it. The attention mechanism is essentially designed to pick out the most representative information and discard features with less information. In particular, the feature information generated by deep learning models is very large, and only by using the attention mechanism in large feature space can the model extract more effective features and discard useless information. Attention mechanisms can be used on different dimensions of features, spatial attention to determine which region in the image is more significant and should receive attention, temporal attention to determine which moment in the temporal sequence contains more information, and channel attention to highlight the important role of certain channels in the feature. Achieving attention can be done in both hard and soft ways; the hard attention approach is by completely retaining and completely discarding some information. The soft attention approach generates new states by calculating the weight of information in the new state. Through this form, it is possible to discover the cognitive differences between the two knowledge elements that directly affect the sports performance of the snow sports athletes to provide effective help for coaches to adopt targeted training methods and guidance strategies.

$$\max \phi(w) = \frac{1}{2}\left(w_1 \cdot w^2\right) \tag{1}$$

$$\text{subject to } y_i\left[(w \cdot x_i) - b\right] - 2 \geq 0, \quad i \in N,$$

where x_i and y_i^2 represent the i-vector of the i-th training language sample and the corresponding labels, respectively, and w and b are the parameters of the classification hyperplane to be trained. This is an optimization problem with constraints, and thus it can be optimized using the Lagrange multiplier method, so the following function is defined:

$$L(w, b, \alpha) = \frac{1}{2}\left(w \cdot w^2\right) - \sum_{i=1}^{n} \alpha_i \left\{y_i^2 [w \cdot x] - b\right\}. \tag{2}$$

Since the error back-propagation algorithm is, in fact, a search for states close to the extremum in a large numerical solution state space, a good starting point can both prevent the gradient descent algorithm from getting stuck in local extremes that are difficult to jump out of and reduce the time to find the global optimal solution, if the initialization point is close enough to the optimal solution. Moreover, the response threshold of the activation function is finite due to the nonlinear factor of the model [17]. A good initialization parameter can reasonably activate the activation function so that most parameters are involved in the training, allowing most neurons to participate in the expression without dying, as shown in Figure 1.

The data distribution of the dataset is often fixed and we cannot change the data distribution of the dataset, so the distribution of the parameters directly affects the output response of this network, and if the range of the region of the response is not in the expected interval, then the loss of the model is huge and hard to debug. The parameter-transformed output data should not appear in some uncommon zones, which will make it more difficult to fit the model and reduce its capacity.

$$\begin{cases} \max \|\alpha_i\|_1 & \text{s.t. } x_i = X\alpha_i^2, \\ I^T \alpha_i = 1. \end{cases} \tag{3}$$

The conceptual analysis of video semantics has been a more active research direction in recent years due to the potential applications of an effective understanding of human behavior in video and its interactions in the environment in a variety of domains. To accomplish this challenging task, several research areas have worked on modeling multiple aspects of video semantics (emotions, relational attitudes, behaviors, etc). The other subset contains all the remaining video clips as the natural dataset to be recommended.

In this context, understanding the underlying semantic concepts in videos becomes crucial in interpreting complex video events. In recent years, deep learning methods have played an important role and have been widely used in computer vision tasks such as image segmentation, detection, recognition, and retrieval. In the field of video semantic concept analysis, how to cross the "semantic gap" and establish a mapping relationship between underlying features

and high-level semantics to extract abstract features that are closer to the high-level semantics of video has become a core problem for researchers to solve. Deep learning methods can learn multiple layers of feature hierarchies and automatically construct high-level representations of the original input, using large amounts of data to drive the training of the network and optimization of the model to extract more representative semantic features, thus improving the classification performance, making the limitations of traditional manually designed feature extraction methods largely avoided. Since the feature construction process is fully automated, they are more general.

In our experiment, 10 video clips of each dance type are simulated to the video that the user has clicked on, and the final recommendation result is automatically obtained according to the degree of matching with the dance style excavated from the 10 input videos. Locality-sensitive discriminant analysis is a classical supervised dimensionality reduction algorithm that considers both the discriminant information in the data and the geometric structure of the data. By constructing intraclass and interclass graphs, the method can better characterize the original local features of the data manifold and preserve the original class labels of the data with good discriminability. The sparse constrained autoencoder enables the encoded learned feature representation to better obtain the sparse reconstruction relationship between data by introducing SPP-constructed graph constraints for the nonlinear autoencoder. This pretraining model not only effectively exploits the natural discriminative power of the sparse representation but also largely alleviates the difficulties in the selection of the nearest neighbor parameters.

$$J(f, g) = E(x, g(f(x))) - \frac{1}{2}\partial t \ r\left(H^T G_{\text{spp}} H^2\right). \tag{4}$$

In this framework, to exploit the structural information between images, we wish to obtain the flow information of the previous layer (which can be the input or pooling layer) by constructing locality and sparsity graphs and using the flow information to redesign the mapping relationships between adjacent layers. These graph construction methods make the learned features more stable and discriminative as the network depth deepens, further speeding up the convergence and improving the generalization of the model [18]. The objective function of the localization and sparsity-preserving embedding convolutional neural network of adjacent layers consists of two components: reconstruction error between feature graphs of adjacent layers and graph regularization. After completing the establishment of the random split rule-based index, we input the automatically mined dance elements into each random tree in turn and implement a top-down matching process to find their nearest neighbors in the feature space and recommend dances in the natural dataset based on the cumulative ranking of the matches of such features, as shown in Figure 2.

Then the impact of differences like this on the performance of the language recognition model is obvious.
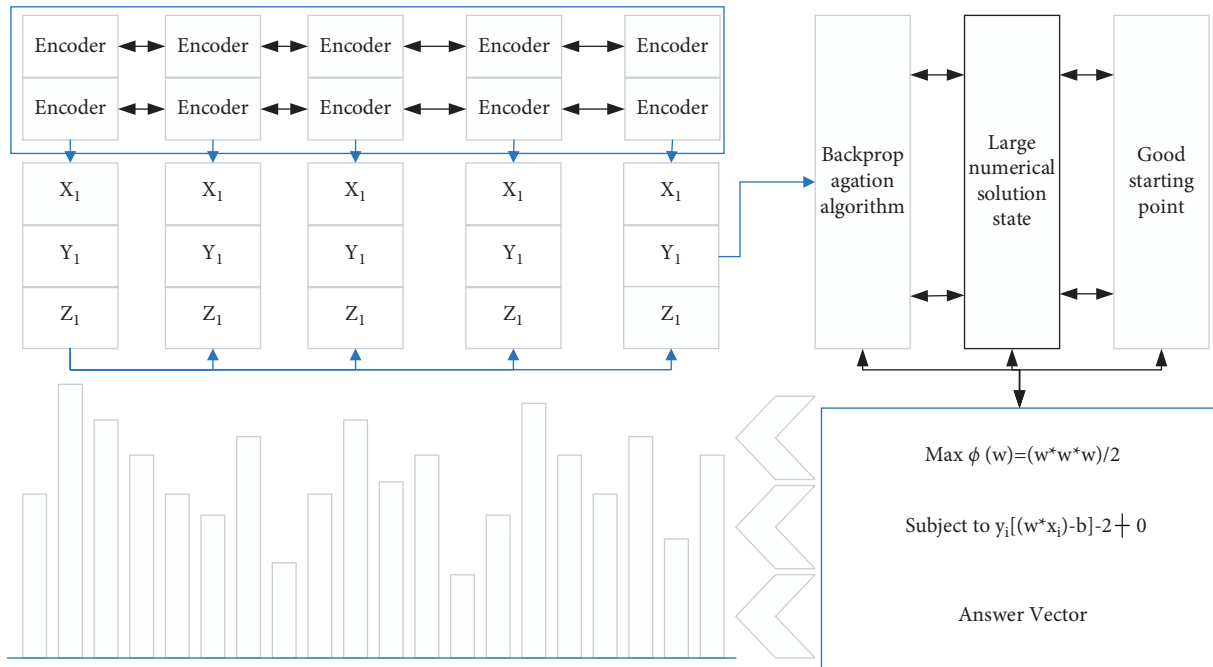
FIGURE 1: High-level semantic recognition model.
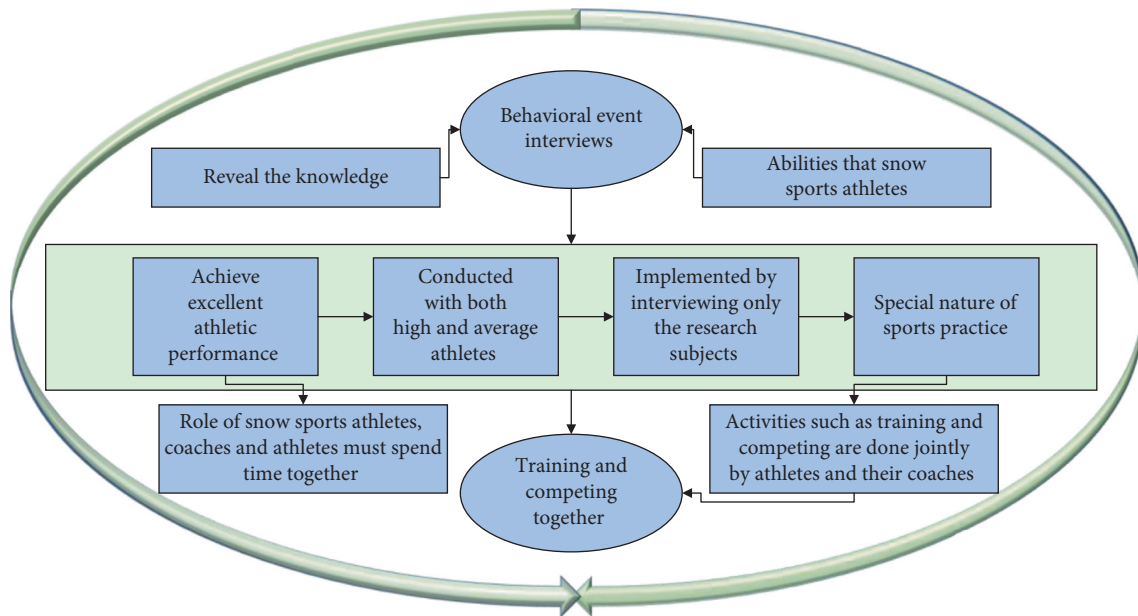
FIGURE 2: Campaign engineering management framework.

Depending on the method of selecting spatiotemporal interest points, the current mainstream methods can be divided into spatial-temporal interest point features and trajectory features. Feature detection of local spatial-temporal feature points usually selects spatial-temporal localization and scale by maximizing a specific saliency function, and different detectors usually differ significantly in the type and sparsity of the selected points. Feature descriptors capture shape and motion features in a neighborhood of the

selected point of interest using metrics such as spatial or spatial-temporal image gradients or optical flow.

$$R = \left(I^* g^* h_{gv}\right)^2 - \left(I^* g^* h_{o\ d}\right)^2. \tag{5}$$

Behavioral event interviews, conducted with both high and average athletes in snow sports, reveal the knowledge, qualities, and abilities that snow sports athletes must have to achieve excellent athletic performance, and this is often

implemented by interviewing only the research subjects themselves. However, due to the special nature of sports practice and the role of snow sports athletes, coaches and athletes must spend time together, not only training and competing together but also living together every day and "feeling and fighting" for a few years or more than ten years, and they are in contact with each other, and sports practice activities such as training and competing are done jointly by athletes and their coaches.

Considering the strong complementarity between spatial flow features and optical flow features, choosing a suitable fusion method can effectively improve the performance of video classification. This method first extracts video image frames to form image sequence and optical flow sequence. Therefore, coaches even know their strengths and weaknesses better than athletes. Based on the relevant knowledge information obtained by the snow sport athletes themselves, the behavioral event interviews with their coaches can not only provide a basis for the researcher to confirm the content elements of tacit knowledge but also find out the differences in the cognitive aspects of the knowledge elements that have a direct impact on the athletes' performance in snow sport, to provide effective help for the coaches to adopt targeted training methods and coaching strategies. This will help coaches to adopt targeted training methods and coaching strategies.

The processing of video presents more challenges compared to still images; for example, temporal sequencing is important for behavior recognition in video, but how to reflect temporal information in the representation of behavior still needs further research, as well as issues such as occlusion, background noise, and interclass differences, and further improvements in both hand-designed features and deep learning features, as well as how to fuse multiple features to improve recognition rates, require further research.

3.2. Experimental Design for Video Content Analysis of Sports.

The information in the two hidden layers can well contain the language-related identity information of the speech segment and reflect the nature of that speech segment; that is, it can be considered as the language-related identity information of that speech segment. This representation of speech segments is more exploitable than the LSTM network model. In fact, in the traditional language recognition approach, the i-vector itself is also a representation of the language vector after highly abstracting the high-level semantic information, which is very similar to the nature of the embedding vector. Moreover, the i-vector itself assumes that the sample distribution of language recognition conforms to a Gaussian distribution, whereas LSTM networks do not have such type of assumptions [19]. Therefore, if the i-vector, which reflects the nature of speech segments, can be replaced by the embedding vector and then the investor-based language recognition classification method can be used for classification and scoring, theoretically, it can achieve better results than the i-vector method.

The subset used for dance style mining consists of 10 video segments from each dance genre; another subset contains all remaining video segments as the natural dataset to be recommended. This unbalanced method of slicing the data exactly matches the reality. We know that a user browsing a video on a website selectively selects only a small number of videos to click through, while the amount of data to be recommended in the webspace is huge. A video recommender should then be able to efficiently select videos relevant to the video content that the user has clicked on for recommendation from a large amount of distracting data. In our experiments, 10 video clips of each dance genre are simulated as videos clicked by the user, and the final recommendation results are automatically obtained based on the match with the dance styles mined from the 10 input videos.

$$\text{MAP@}N = \frac{1}{N \sum_{i=1}^{n} (\theta(r_i)/i)} \left(\frac{1}{n} \sum_{i=1}^{n} \frac{\theta(r_i^2)}{i_1^2} \right). \qquad (6)$$

Its purpose is to guide the spatial stream to pay more attention to the foreground area of the human body and reduce the influence of background noise, to better obtain the changes and differences between temporal and spatial features, and to improve the rationality of the network to extract video features. In the AP17-OLR dataset description, the dataset provider also points out that there are some differences between the training data and the test data used for the experiments, and, in the cases of Japanese, Korean, and Russian, the dataset directly gives the sampling environments between the training and test sets, both in quiet conditions and in speech segments mixed with noise. Also, the provider of the dataset points out that the sampling environments of Kazakh, Tibetan, and Uyghur are completely different from the situations of all other languages, and there are some differences between the training and test sets. Whereas DNN-like networks (including LSTMs) are more sensitive to such issues, the impact of differences like these on the performance of language recognition models is obvious if there is no good method for channel compensation, or if existing channel compensation measures are not sufficient to solve the problem. In fact, in the models described in the previous sections of this paper, there is a significant degradation in the recognition accuracy of some of the languages; taking the LSTM-1-MFCC network as an example, the false rejection and false acceptance rates for each specific language in this network are shown in Table 1.

The video semantic concept analysis task is richer and more complex compared to recognition tasks such as image classification, and complex situations such as background dynamic information interference, angle transformation, and target blocking can occur in different scenes. Although convolutional neural networks have achieved great success in image classification and recognition tasks, how to model the spatial-temporal features of videos and obtain the spatial-temporal information contained in videos is still one of the main problems that need to be solved urgently for video semantic concept analysis using deep learning methods. Many works have designed various effective deep

TABLE 1: Network specific to each campaign.

Name	Ct-cn	Id-id	Kazak	Ko-kr	Tibet
Ct-cn	1233	11	0	23	0
Id-id	11	1234	11	0	0
Kazak	23	11	1234	11	23
Ko-kr	0	0	11	1234	11
Tibet	35	0	223	11	1234

convolutional neural networks for learning and extracting static frame appearance information and motion timing information of videos, such as adding a temporal dimension to the 2D convolutional kernel of convolutional neural networks and expanding it to the 3D convolutional kernel to extract both spatial and temporal dimensional features. Considering the strong complementarity between spatial flow features and optical flow features, choosing a suitable fusion method can effectively improve the video classification performance. As a result, a recognition rate of almost 100% is obtained. When the trajectory feature is used, the trajectory information of the limb movement is captured, which greatly enhances the expression of behavior. Especially when the MBH descriptor is used, the recognition rate of boxing and applause is increased by more than 20%. The method first extracts video image frames to form image sequences and optical flow sequences, then extracts spatial flow features and optical flow features by the convolutional neural network, and introduces optical flow attention layer from temporal flow network to spatial flow network by mining the nearest neighbor relationship and association information between features in the flow embedded spatial flow convolutional neural network to guide the spatial flow to pay more attention to the human foreground region and reduce the influence of background noise. Thus, the variations and differences between spatial-temporal features are better obtained, as shown in Figure 3.

The visual attention mechanism is a unique signal processing mechanism of the human brain; through the observation of the global sample to determine the focus area and area of interest, the key information closely associated with the target will be quickly accessed; attention mechanism frees people from the colorful and complicated information and improves the efficiency of information processing, and it is introduced into the field of computer vision to improve the computer to solve image, video, and other prediction and analysis tasks. Consider that optical flow can be used to direct human foreground attention when appropriate compensation is applied to the movement of the lens. We investigate the combination of spatial streaming embedding CNN and temporal streaming CNN to form a dual-stream convolutional neural network to learn video features [20]. The purpose of introducing an optical flow attention layer from the temporal network to the spatial network is to guide the spatial flow to pay more attention to the human foreground region and to reduce the effect of background noise. Thus, the variation and differences between spatial-temporal features are better obtained and the rationality of the network to extract video features is improved. Attention is a mechanism used to give more weight to a subset of elements,

and the optical flow attention map is directed to foreground regions and helps the spatial flow convolutional network to learn distributed feature representations around these regions to accomplish the label prediction task. In dual-stream convolutional networks, we propose an optical-stream attention layer to model the interaction of the two networks, which can be trained end-to-end using stochastic gradient descent and back-propagation algorithms.

Improve the efficiency of users to obtain information. In addition, the video semantic analysis technology based on the host computer can replace manual annotation work, reduce a lot of human resources, and improve the utilization rate of information. Considering the perceptual wildness of spatial information, the range of neighboring points can be expanded. When building a graph structure, the most extreme case, where the current node can be associated with all other nodes on the graph, can be achieved by the subsequent adoption of attention mechanisms or the amount of information passed. The inclusion of all nodes in the graph, as well as the interconnection of all nodes to each other, is a fully connected graph, constituting a complete graph that allows information about all locations to be perceived by each other. It allows each member to have a large enough perceptual field to recognize a larger range of spatial patterns.

4. Analysis of Results

4.1. Performance Results of High-Level Semantic Recognition Models under Engineering Management. By changing the length of the input sequence from 5 to 10 frames, the accuracy of the model was improved by 0.9%, but as we continued to increase the length of the input sequence to 15 and 20 frames, the accuracy of the model started to decrease. The reason for this phenomenon is that the size of the video dataset is relatively small and overfitting occurs when the input sequence is too long. Since each RGB image frame corresponds to 10 adjacent frames of the stacked optical flow image, the 10-frame input contains 100 consecutive frames of spatial-temporal information in the video clip, which is sufficient to represent the main semantic information of the video clip.

After the selection of the best input sequence is completed, the two-stream network stream embedding parameters and the confidence fusion parameters are set, and the experiments are firstly conducted to search the grid for the two parameters, and the best parameter for stream embedding is obtained as 0.2. After the stream embedding parameters are fixed, the experimental analysis of the effect of the confidence fusion parameter changes on the model
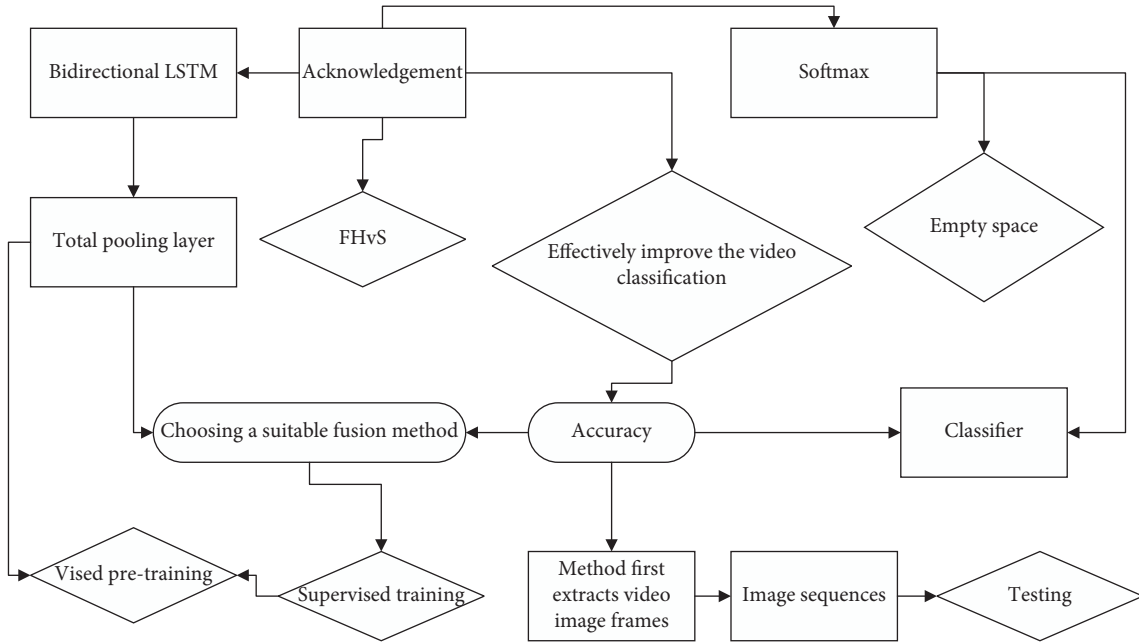
FIGURE 3: Network structure for compensating for mismatches between datasets.

performance is conducted, and the semantic concept detection accuracy based on different confidence fusion parameters is shown in Figure 4.

There is difficulty in designing an efficient and robust identification method. Although the traditional manual labeling method can realize the understanding and description of the video semantic concept to a certain extent, the time and labor cost of manual labeling is huge, and the subjectivity is strong. The vertical coordinate in the Cartesian coordinate system indicates the corresponding video semantic detection accuracy at different confidence parameters. The video semantic concept detection accuracy keeps improving when the values are taken in the interval [0.1, 0.7], which proves that the confidence of the classifier based on the probability error has an important contribution to the final category prediction. The model prediction performance is best when it is 0.7, so this chapter chooses to take a value of 0.7 as the confidence parameter of the dual-stream network classifier. The performance of feature engineering-based algorithms IDT remains competitive; in addition, many methods based on deep learning were combined with IDT to achieve better results, but several video semantic analysis methods with the best model performance are deep convolutional network-based algorithms, and CD methods do not have an advantage over traditional methods due to many model parameters and more difficult training. The basic dual-stream network model has achieved good results by emulating the human visual mechanism and has a better understanding of the spatial and temporal information of the video. The TSN method is built based on the dual-stream network model, which can learn video features efficiently by modeling long time scales and combining sparse sampling strategies and video supervision methods, and it has achieved good results. The proposed method in this paper has 0.4% higher accuracy than TSN.

This shows that the proposed method can better reflect the nearest neighbor relationship between samples and structural features, as well as the complementary relationship between images and optical flow, and the method of confidence fusion classification can effectively obtain video semantic concept features and improve the accuracy of video semantic concept detection, as shown in Figure 5.

The research has important academic significance and application value and helps to improve the level of video management technology, making it more complete and more efficient. In the process of optimal learning of video, features consider the nearest neighbor relationship between samples, association features, and so forth to construct stream shape constraint terms; optical flow attention mechanism was introduced to guide the spatial flow to pay more attention to the foreground region and reduce the influence of background noise, and, to better obtain the changes and differences between spatial-temporal features, in the acquisition of contextual information of video frame sequences, LSTM was introduced to construct stream shape embedding and optical flow attention based dual-stream CNN video semantic concept detection model. The proposed method can better reflect the nearest neighbor relationship and structural features between samples, as well as the complementary relationship between images and optical streams to obtain effective video semantic concept features, and the confidence fusion classification method for the category score results of the two-stream SoftMax layer can more effectively improve the accuracy of video semantic concept detection.

4.2. Experimental Results of Sports Video Content Analysis. As shown in Figure 6, the classification accuracies achieved by different coding and normalization methods are
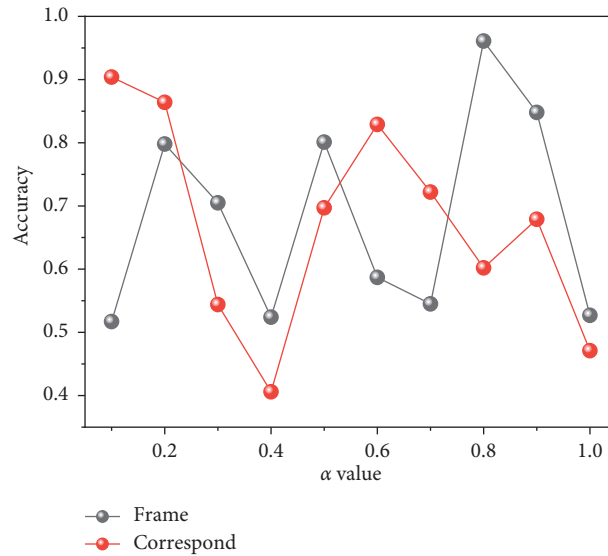
FIGURE 4: Effect of confidence parameters on model performance.

compared using spatial-temporal interest point features with the number of topics varying between 10 and 100. As the number of topics increases, all coding methods achieve significant performance gains, but after the number of topics is 60, the performance does not change much. The difference between the results obtained when using vector quantization and local soft assignment is small, and the different normalization methods make a limited contribution to the recognition rate, with exponential plus l normalization achieving the best classification accuracy for most of the number of topics. The performance mostly improved as the number of topics increased, and the best performance was obtained when the number of topics reached 80 and then decreased. For soft assignment coding, there was a more significant decrease in classification performance compared to the results for spatial-temporal interest points, and the performance fluctuated by a maximum of more than 15 percentage points using different normalization methods. For both classes of descriptors, soft assignment coding tended to achieve optimal performance in combination with l. Group behavior recognition technology can derive tags of crowd scene images and can provide clues for retrieval of pictures and videos of group scenes. The advancement of group behavior recognition technology has greatly promoted the classification, labeling, and retrieval of crowd scenes.

In Figure 7, the confusion matrix under different features is presented, and it is evident that walking and waving have the highest recognition rate among all cases, and, correspondingly, boxing and clapping have the lowest recognition rate. This is in line with the expectation that, in terms of form movements, boxing and clapping focused on upper limb movements and have a high degree of similarity, while walking and waving, which are more differentiated from the rest of the behaviors, obtain a recognition rate of nearly 100%. When trajectory features are used, the trajectory information of the limb movements is captured, which

substantially enhances the representation of the behaviors, especially when MBH descriptors are used, increasing the recognition rate of boxing and clapping by more than 20 percentage points at maximum.

We obtained a classification accuracy of 89.63% using spatial-temporal interest points, which results in a 6-percentage point improvement. It is reasonable to assume that similar behaviors have similar characteristics and thematic distributions. Describing behaviors with mixed topic probability distributions is superior to the approach of corresponding a topic to a class of behaviors. One advantage of the topic model is that topics can be considered as a mid-level semantic feature and then used to describe more complex behaviors. Inevitably, there are similar form movements in different behaviors; for example, boxing and clapping both have similar upper body movements. Thus, different behaviors share the same themes, and each behavior has its distribution of themes, which enhances the discriminative nature of the features.

Overall, principal component analysis preprocessing of raw features not only reduces the feature dimensionality, thus making it less demanding on computational resources, but also retains most of the discriminative primary information, while having a suppressive effect on noise caused by various reasons, and whitening was also performed in the experiments to reduce the correlation between features, further improving the robust performance of recognition. The difference in the performance of the same action by different people; the influence of environmental factors, such as occlusion, viewing angle changes, lighting differences, and dynamic background interference, etc; and the start and end points of the action are blurred. The use of principal component analysis to preprocess raw features has an important impact on improving the performance of recognition. The principal component analysis projects the original features onto the feature components, which objectively suppresses the
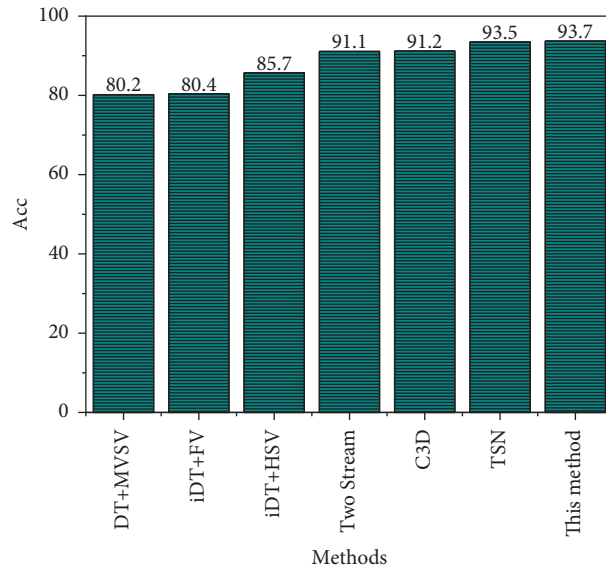
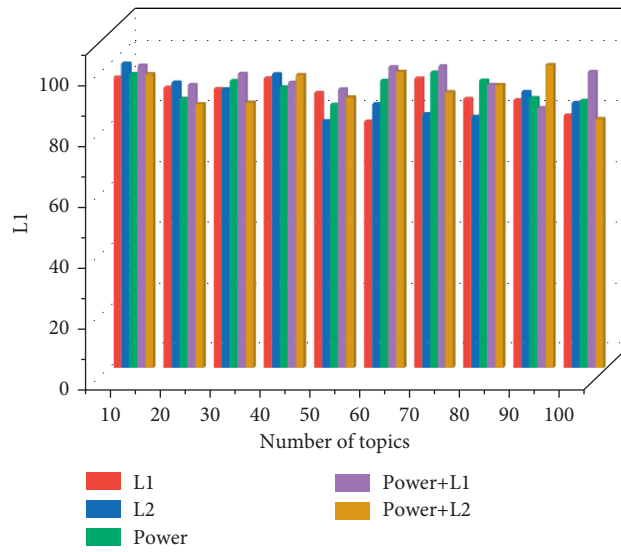FIGURE 5: Results of different methods on the UCF-101 dataset.

FIGURE 6: Performance comparison of different coding and normalization methods.
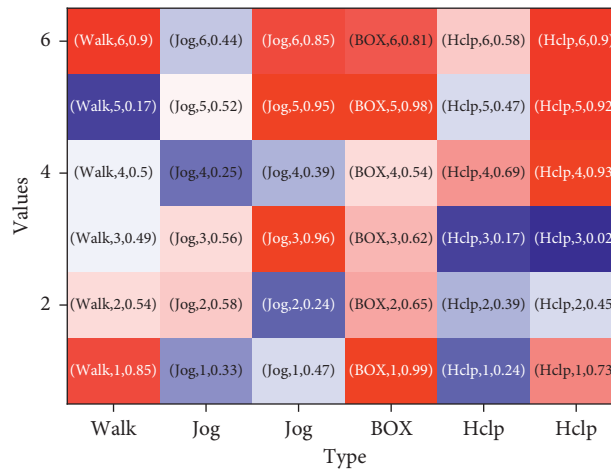

FIGURE 7: Content analysis results.

noise to a certain extent but, at the same time, inevitably brings about a loss of information. These two effects cancel each other out; if the noise component is large, the utility achieved by suppressing noise is large, which brings an increase in recognition rate, while the information loss effect is large and the corresponding performance is decreased. On the other hand, the performance of densely sampled features is superior, and the number of features to be processed is increasing, especially for video signals, which are particularly computationally intensive. If PCA is used to preprocess the original features, the number of feature dimensions is significantly reduced while retaining most of the information, resulting in little degradation in classification performance, which will greatly reduce the computational effort and improve the response speed, which is significant for applications that require real-time signal processing.

5. Conclusion

Better performance has been achieved after its introduction into the field of computer vision. In the word-packet framework, it has been shown that different feature encoding methods have an important impact on performance. Inspired by this, the impact of different coding methods combined with normalization methods on the classification performance of probabilistic implicit semantic analysis models is focused on, and it is found experimentally that local soft assignment coding combined with exponential normalization methods substantially improves the recognition performance; the impact of principal component analysis preprocessing raw features on performance is also examined, and when the features contain more noisy components, the computational effort is significantly reduced, while the classification recognition performance is even improved when the features contain more noisy components. However, the performance improvement of the fusion model for the language recognition model is limited. In addition, the idea of this paper is still stuck on the traditional pattern recognition task flow of the feature extraction-classification recognition model, and the two separated links may also affect the performance of the model to some extent. Therefore, a language recognition model based on an end-to-end approach is a very promising problem. Then the spatial flow features and optical flow features are extracted by the convolutional neural network, and the nearest neighbor relationship and association information between features are mined by stream shape embedded in spatial flow convolutional neural network, and the optical flow attention layer from the temporal flow network to spatial flow network is introduced to guide the spatial flow to pay more attention to the human foreground region and reduce the influence of background noise so that the variations and differences between spatial-temporal features can be better obtained. Then the features obtained from the two streams were input in temporal order to learn temporal features, and, finally, confidence fusion was performed on the classifier results of the two streams to detect the video semantic concept categories.

Data Availability

The data used to support the findings of this study are available upon request to the author.

Conflicts of Interest

The author declares that there are no known conflicts of financial interest or personal relationships that could have appeared to influence the work reported in this paper.

Acknowledgments

References

[1] Y. R. Pandeya and J. Lee, "Deep learning-based late fusion of multimodal information for emotion classification of music video," *Multimedia Tools and Applications*, vol. 80, no. 2, pp. 2887–2905, 2021.

[2] Y. Ou, Z. Chen, and F. Wu, "Multimodal local-global attention network for affective video content analysis," *IEEE Transactions on Circuits and Systems for Video Technology*, vol. 31, no. 5, pp. 1901–1914, 2020.

[3] A. Nadeem, A. Jalal, and K. Kim, "Automatic human posture estimation for sport activity recognition with robust body parts detection and entropy Markov model," *Multimedia Tools and Applications*, vol. 80, no. 14, pp. 21465–21498, 2021.

[4] L. Qin and L. Kang, "Application of video scene semantic recognition technology in smart video," *Tehnički Vjesnik*, vol. 25, no. 5, pp. 1429–1436, 2018.

[5] H. C. Shih, "A survey of content-aware video analysis for sports," *IEEE Transactions on Circuits and Systems for Video Technology*, vol. 28, no. 5, pp. 1212–1231, 2017.

[6] C. Liu, J. Hou, X. Wu, and Y. Jia, "A discriminative structural model for joint segmentation and recognition of human actions," *Multimedia Tools and Applications*, vol. 77, no. 24, pp. 31627–31645, 2018.

[7] T. Väisänen, V. Heikinheimo, T. Hiippala, and T. Toivonen, "Exploring human-nature interactions in national parks with social media photographs and computer vision," *Conservation Biology*, vol. 35, no. 2, pp. 424–436, 2021.

[8] P. Pareek and A. Thakkar, "A survey on video-based human action recognition: recent updates, datasets, challenges, and applications," *Artificial Intelligence Review*, vol. 54, no. 3, pp. 2259–2322, 2021.

[9] N. A. Rahmad, M. A. As'ari, N. F. Ghazali, N. Shahar, and N. A. J. Sufri, "A survey of video based action recognition in sports," *Indonesian Journal of Electrical Engineering and Computer Science*, vol. 11, no. 3, pp. 987–993, 2018.

[10] L. Greco, P. Ritrovato, and M. Vento, "On the use of semantic technologies for video analytics," *Journal of Ambient Intelligence and Humanized Computing*, vol. 12, no. 1, pp. 567–587, 2021.

[11] S. Hou, S. Zhou, W. Liu, and Y. Zheng, "Classifying advertising video by topicalizing high-level semantic concepts," *Multimedia Tools and Applications*, vol. 77, no. 19, pp. 25475–25511, 2018.

[12] M. Fourati, A. Jedidi, and F. Gargouri, "A survey on description and modeling of audiovisual documents," *Multimedia Tools and Applications*, vol. 79, no. 45, pp. 33519–33546, 2020.

[13] T. Singh and D. K. Vishwakarma, "Video benchmarks of human action datasets: a review," *Artificial Intelligence Review*, vol. 52, no. 2, pp. 1107–1154, 2019.

[14] N. A. Tu, T. Huynh-The, K. U. Khan, and Y.-K. Lee, "ML-HDP: a hierarchical bayesian nonparametric model for recognizing human actions in video," *IEEE Transactions on Circuits and Systems for Video Technology*, vol. 29, no. 3, pp. 800–814, 2018.

[15] H. Ji, D. Hooshyar, K. Kim, and H. Lim, "A semantic-based video scene segmentation using a deep neural network," *Journal of Information Science*, vol. 45, no. 6, pp. 833–844, 2019.

[16] V. Ellappan and R. Rajkumar, "Classification of cricket videos using finite state machines," *International Journal of Information Technology and Management*, vol. 20, no. 1-2, pp. 83–94, 2021.

[17] A. Prati, C. Shan, and K. I. K. Wang, "Sensors, vision and networks: from video surveillance to activity recognition and health monitoring," *Journal of Ambient Intelligence and Smart Environments*, vol. 11, no. 1, pp. 5–22, 2019.

[18] H. Liu, Q. Zheng, Z. Li, T. Qin, and L. Zhu, "An efficient multi-feature SVM solver for complex event detection," *Multimedia Tools and Applications*, vol. 77, no. 3, pp. 3509–3532, 2018.

[19] M. E. Abdulmunem and E. Hato, "Semantic based video retrieval system: survey," *Iraqi Journal of Science*, vol. 59, no. 2A, pp. 739–753, 2018.

[20] G. Bellitto, F. Proietto Salanitri, S. Palazzo, F. Rundo, D. Giordano, and C. Spampinato, "Hierarchical domain-adapted feature learning for video saliency prediction," *International Journal of Computer Vision*, vol. 129, no. 12, pp. 3216–3232, 2021.

Research Article

Cost Control of Mining Personnel Based on Wireless Communication Network from the Perspective of Operations Research

Hongyi Wang[1] **and Meichang Zhang** [2]

[1]*Management Science and Engineering, Liaoning Technical University, Fuxin 123000, China*
[2]*Mining Engineering, Liaoning Technical University, Fuxin 123000, China*

Correspondence should be addressed to Meichang Zhang; zhangmeichang@lntu.edu.cn

The sublevel caving method without sill pillar is used to improve the cost of mining. The analysis is performed according to unique geographical environment and the current mining technology of the mine. The wireless communication network is used to budget and control the work cost of mining. Simulation operation about unit explosive dosage, fan-shaped deep hole interval, hole bottom distance, and collapse step distance is performed. Experiments have shown that budget and control of the cost of mining workers with wireless communication technology can manage mining data and guide the design of mining data.

1. Introduction

The cost control by mining personnel is a relatively complex system. Due to the continuous changes in the production of mining factories, the cost control of mining personnel needs to consider the overall balance of different links, continuity, and uncertainty, in order to carry out effective identification and optimization, and control the cost of mining personnel of mine engineering. With the rapid development of science and technology, digitization and visualization technology have been widely used in various fields. As the main component of the mine, development plan for cost control of mining personnel is needed, digitizing and visualizing the mining activities, timely and accurately recording and expressing the engineering changes in the mine pit, and improving the mining level and work efficiency [1–3].

The construction of an integer model is used to optimize the location of fans in the network and the selection of structures in this paper. The cost of ventilation is normalized to minimize it. For the same problem, the nonlinear unmixed model covers special constraints and branch constraints, which are the basis for semiconstrained design, and optimizes the answer.

2. Establishment of Operational Research Model

The constrained flow network problem only includes the best deployment location of personnel and building selection to allocate personnel to all predetermined network branches [4–6]. The problem of nonholonomic constraints of the network will face a dual task. In addition to determining the best placement of personnel and the choice of structures, it is also necessary to control the people flowing into unclear branches.

2.1. Constrained Flow Network Problem. Because the distribution of personnel in the network is known, the constrained condition conditions do not need to be discussed, and then the objective function of this problem can be expressed by formula (3), and its constrained conditions are

$$\begin{cases} \sum_{j=1}^{b} \left(R_j |Q_j| Q_j + HR_j - HN_j - HF_j \right) = 0, \\ HR_j, HN_j \geq 0, \quad j = 1, \ldots, b. \end{cases} \tag{1}$$

Obviously, this is a nonlinear programming model, which is transformed into a linear programming model by introducing bivariate Y_j and the objective function is transformed by obtaining this value Y_j.

$$Y_j = \begin{cases} 1, & HF_j > 0, \\ 0, & \text{other}, \end{cases}, C_p Q_j = a_j,$$
$$\text{minimize } Z = \sum_{j \in L} a_j HF_j + \sum_{j \in L} C_j Y_j. \tag{2}$$

The constrained conditions are

$$\begin{cases} \sum_{j=1}^{b} b_{ij} \left(R_j |Q_j| Q_j + HR_j - HN_j - HF_j \right) = 0, \\ HR_j, HF_j \leq 0, \quad j = 1, \ldots, b, \\ HF_j \leq d_j Y_j, \quad j \in L, \\ Y_j = (0, 1). \end{cases} \tag{3}$$

In the formula, $d_j = \max HF_j$. When $HF_j \neq 0$, $Y_j = 1$; when $HF_j = 0$, $Y_j = 0$ 时. So when $Y_j = 1$, $Y_j = 0$, and a larger value may appear in Z.

2.2. Half Constrained Flow Network Problem.

Assume that the minimum value L_j and maximum values U_j of branchers, respectively, flow to ambiguous branchers and are represented by the objective function [7].

$$\text{Min} Z = \sum_{j=1}^{L} C_j Q_j HF_j + \sum_{j=1}^{L} C_j. \tag{4}$$

The constrained conditions are

$$\begin{cases} \sum_{j=1}^{b} a_{ij} Q_j = 0, \\ \sum_{j=1}^{b} b_{ij} \left(R_j |Q_j| Q_j + HR_j - HN_j - HF_j \right) = 0, \\ L_j \leq Q_j \leq U_j, \\ HR_j \geq 0, \\ X_j = (0, 1), \\ Q_j HF_j \geq P_j, X_j = 1, \\ Q_j HF_j = P_j, X_j = 0, \\ j = 1, \ldots, b, \end{cases} \tag{5}$$

where P_j is the minimum power allowed on branch j.

It can be seen from the previously mentioned objective function and constrained conditions that they are all nonlinear. So we need to transform it into a linear programming. During the transformation, the decompression is first

determined, and then, the solutions for each subset are established. All solutions need to form the elements that make up the aggregation L for X_j. Finally, this nonlinear programming is a linear programming, and then, the best solution is selected. The specific method is verified in the following example.

3. Specific Application of Operations Research

Figure 1 is a cost network diagram of a miner. It is composed of nine branches and six nodes, and each wind resistance is constant. According to the specific situation, the personnel can be configured for seven minutes when branching. On 8, the structures are at branches 3, 5, and 8.

The distribution of personnel on each branch is shown in Table 1.

3.1. Problem Solving for Constrained Flow Network.

We select the spanning tree {1, 2, 5, 6, 9}, and the matrix can be obtained b_{ij}

$$b_{ij} = \begin{bmatrix} 1 & 2 & 3 & 4 & 5 & 6 & 7 & 8 & 9 \\ -1 & 1 & 0 & 1 & 0 & -1 & 0 & 0 & 0 \\ 0 & 1 & 0 & 0 & 1 & 0 & 1 & 0 & 0 \\ 1 & 0 & 0 & 0 & 0 & 1 & 0 & 1 & 1 \end{bmatrix}. \tag{6}$$

Then, the objective function can be expressed as

$$\begin{aligned} \min Z = &\ C_p Q_5 HF_5 + C_p Q_7 HF_7 + C_p Q_8 HF_8 \\ &+ C_5 Y_5 + C_7 Y_7 + C_8 Y_8. \end{aligned} \tag{7}$$

The constrained conditions are

$$\begin{cases} -R_1 Q_1^2 + R_2 Q_2^2 + R_4 Q_4^2 - R_6 Q_6^2 = 0, \\ R_1 Q_1^2 - R_2 Q_2^2 + R_3 Q_3^2 + HR_3 - R_5 Q_5^2 - HR_5 + HF_5 = 0, \\ R_2 Q_2^2 + R_5 Q_5^2 + HR_5 - HF_5 + R_7 Q_7^2 - HF_7 = 0, \\ R_1 Q_2^2 + R_6 Q_6^2 + R_8 Q_8^2 - HF_8 = 0, \\ HF_5 \leq d_5 F_5, \\ HF_7 \leq d_5 F_7, \\ HF_8 \leq d_5 F_8, \\ Y_j = (1, 0), \quad j = 5, 7, 8, \\ HR_j \geq 0, \quad j = 3, 5, 8, \\ HR_j \geq 0, \quad j = 5, 7, 8. \end{cases} \tag{8}$$

After calculation, the best solution is to set up two personnel on branches 7 and 8, respectively, where the wind pressure on branch 7 is 11330.6 Pa, 840.8 Pa of which is shared by branch 8. The main auxiliary equipment is set on branch 3.

The best solutions are usually difficult to be found for the multifunctional optimization problems. Most of them adjust each target in a balanced manner and meet the requirements based on the problem to obtain the best balanced solution
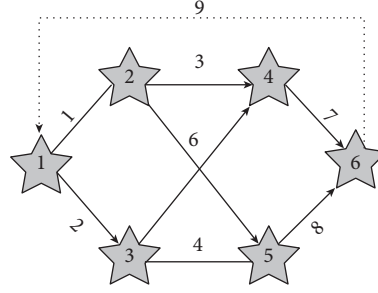
FIGURE 1: Cost network of mining personnel.

TABLE 1: Distribution of personnel in branches.

Branch	Wind resistance R_j	Personnel Q_j	Position of personnel	Structure placement
1	0.34	35.35		
2	0.41	37.02		
3	0.54	18.02		Allowable
4	0.91	20.02		
5	1.43	17.02	Allowable	Allowable
6	1.66	17.35		
7	0.22	35.02	Allowable	
8	0.17	37.35	Allowable	Allowable
9	0.01	72.25		

with certain accuracy and practical significance. Here, the decisive objective function and constraint conditions in the problem are shown. Fuzzy theory is combined with intelligent algorithms to solve chaotic optimization problems. The dark color of more than one thousand targets is most suitable for the best dextrin of the basic thousand single targets. In the fuzzy set of the optimal solution of each target, the solution of each target is satisfied as much as possible.

(1) The objective function of the formula MOP problem is complex and only provides a very large membership function. On the premise of satisfying the constraints as much as possible, the larger the objectives, the better, and there is an upper limit but no lower limit. The upper limit is the best value for each single goal optimization [8–10]. Therefore, the ray shape is selected as the correlation function for each target.

$$\mu(f_k(X)) = \begin{cases} 1, f_k(X) > c_{01}, \\ \dfrac{f_k(X) - c_{0k} + \delta_{0k}}{\delta_{0k}}, c_{0k} - \delta_{0k} < f_k(X) \leq x_{0k}, \\ 0, f_k(X) \leq c_{0k} - \delta_{0k}. \end{cases}$$

(9)

In the formula, $\mu(f_k(X))$ specifies the membership function $f_k(X)$ of the target. The target value $f_k(X)$ for the target optimization of the target monomer c_{0k}. This is the added value of target δ_{0k} accepted by policy makers, and it is determined by scaling to a certain extent on the basis of optimizing the target value into a single target (Figure 2).

The specific solution steps of the wireless communication network method are as follows:

Step 1. Use the following wireless communication network algorithm to find the optimal solution to the constraints of each single-objective function:

$$\begin{cases} \max f_i(X), i = 1, 2, \ldots, p, \\ g_i(X) \leq 0, i = 1, 2, \ldots, m, \\ h_j(X) = 0, j = 1, 2, \ldots, l. \end{cases}$$

(10)

Find the optimal solution of the constraint of the previously mentioned objective function.

Step 2. Stretch each single target value to a certain extent; that is, determine the added value

Step 3. The fuzzy of each objective function, that is, the function that determines the degree of membership of each objective function, is as follows:

$$\mu(f_k(X)), k = 1, 2, \ldots, p.$$

(11)

Define the satisfaction degree of all membership functions as

$$\lambda = \min\{\mu(f_i(X)), \mu(f_2(X)), \ldots, \mu(f_p(X))\}.$$

(12)

Step 4. Substitute c_{0k} δ_{0k} into (3) to obtain expression of p membership function.

Step 5. Based on the max-min law of the fuzzy set theory, the maximum satisfaction degree method is used to convert the multiobjective problem into a
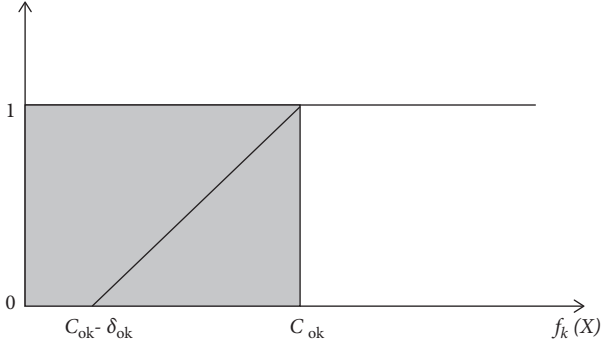
Figure 2: Membership function curve.

single-objective nonlinear problem. The mathematical model is as follows:

$$\begin{cases} \max \lambda, \\ f_1(X) - \delta_{01}\lambda \geq c_{01} - \delta_{01}, \\ \cdots \\ f_k(X) - \delta_{0k}\lambda \geq c_{0k} - \delta_{0k}, \\ \cdots \\ f_P(X) - \delta_{0P}\lambda \geq c_{0P} - \delta_{0P}, \\ 0 \leq \lambda \leq 1, \\ g_i(X) \leq 0, i = 1, 2, \ldots, m, \\ h_j(X) = 0, j = 1, 2, \ldots, l. \end{cases} \quad (13)$$

Step 6. The wireless communication network algorithm is applied to solve the previously mentioned single-objective fuzzy optimization model and find the optimal value of each objective function under a given satisfaction degree (90%).

3.2. Problem Solving for Half Constrained Flow Network. The personnel on branches 3, 4, and 7 are known to be $18.00 \, \text{m}^3/\text{s}$, $20.00 \, \text{m}^3/\text{s}$, and $35.00 \, \text{m}^3/\text{s}$, and a new matrix a_{ij} can be obtained.

$$a_{ij} = \begin{bmatrix} 1 & 2 & 3 & 4 & 5 & 6 & 6 & 8 & 9 \\ -1 & 1 & 0 & 1 & 0 & 1 & 0 & 0 & 0 \\ 1 & -1 & 1 & 0 & -1 & 0 & 0 & 0 & 0 \\ 0 & 1 & 0 & 0 & 0 & 0 & 1 & 0 & 0 \\ 1 & 0 & 0 & 0 & 0 & 1 & 0 & 1 & 0 \end{bmatrix}. \quad (14)$$

We define the personnel of branches 7 and 8 as surface personnel and branch 5 as a candidate for underground personnel. The objective function is

$$\min Z = Q_5 HF_5 + aHF_7 + Q_8 HF_8. \quad (15)$$

Suppose $Z_1 = (Q_i + HF_8)/2$, $Z_2 = (Q_8 - HF_8)/2$ and then introduce nonnegative special variables λ_k, u_k, and v_k, so that $\sum_k \lambda_k = 0$, $\sum_k u_k = 0$, $\sum_k v_k = 0$. Then, Z_1, Z_2, and Q_8 can be expressed as $Q_8 = \sum_K \lambda_k Q_{8k}$, $Z_1 = \sum_k u_k Z_{1k}$,

$Z_2 = \sum_k v_k Z_{2k}$. Then, the previously mentioned problem can be transformed into linear programming, and its objective function is

$$\min Z = Q_5 HF_5 + Q_7 HF_7 + \sum_k u_k Z_{1k}^2 - \sum_k v_k Z_{2k}^2. \quad (16)$$

After calculation, the wind pressure on branch 7 is 840.88 Pa, the wind pressure shared by branch 8 is 113.6 Pa, and the wind pressure on branch 5 is 374.35 Pa.

4. The Basic Function and Innovation of the Cost Control System for Mining Personnel

A simulation model of the mine's in-pit visual production system is built according to the actual situation of the specific mine at first, and simulation operation is performed after the model is verified and confirmed. The in-pit production process is observed dynamically in the mine. In addition, the operating status of each stage of the biological flow system of mine can be analyzed in real time. The development logic program of the dynamic optimization policy decision system for the three-dimensional dynamic visualization of underground mine engineering is as follows [11, 12].

(1) Information about mine production systems is collected for specific mines. It contains the parameters related to the tunnel formation system: the logistics process, production capacity, and technical parameters and capabilities of related equipment in the production system of coal mining, ventilation, transportation, drainage, and so on.

(2) Statistical analysis and integration is performed for the previously mentioned collected data related to the cost control system for underground mining personnel.

(3) Analyze the various influencing factors of mine production, define the boundaries of the mine logistics system, and divide the subsystems according to the functions of the logistics process of mine.

(4) On the basis of a large number of field investigations and statistical analysis, the statistical rules and parameters of each part of the mining system are determined.

(5) Through the mine layout system and production system of the built mine, the connection and conversion relationship between the various subsystems of the mine production is found out, the integration capability of the various equipment of the mine production system and the logistics system is established, and a fully visualized underground mine model of mining personnel cost control system is built.

(6) According to the simulation software of WITNESS, the cost control system model of the underground mining personnel of the mine is reasonably converted into a computer simulation model.

(7) The reliability simulation of the simulation model was verified, the interference of random factors was eliminated, the simulation results were statistically analyzed, and unreasonable factors in the system were found.

(8) The model is improved to make it more in line with the actual mine production system.

(9) According to the actual production of mine, the simulation operation of the mine logistics system is carried out. According to the simulation results, the mine logistics system is rationally optimized and integrated, to apply the improvement plan to the mine production practice and compare the improved demonstration operation result with the actual mine production practice effect for evaluation.

Among them, the key issues in the development of the mining personnel cost control system are as follows.

(1) Collect true information about mine production systems for specific mines: the parameters of the tunnel configuration system, coal mining, excavation, ventilation, transportation, drainage, and other logistics process, production capacity, and technical parameters and capabilities of related equipment

(2) Import mine development engineering drawings (Figure 3) into the WITNESS system. The imported engineering drawings will be imported to the prebuilt system modules based on the actual underground mining personnel cost control system process (Figure 4: the mine underground mining personnel cost control system process) to build a simulation model of the mine's in-pit visual production system.

(3) Perform the validity check of the simulation model of the in-pit visual production system in the mine. Transform the parameters of field survey and statistical analysis (including technical indicators such as underground logistics equipment capability, failure rate, repair rate, and other reliability indicators) into computer simulation models. Carry out simulation operation, analyze it combined with the actual logistics system operation, carry out validity check, and ensure the validity of the simulation system.

5. Realization of Cost Control of Mining Personnel

5.1. Projective Transformation. The functions of the wireless communication network-like calculation procedure library cannot directly generate arc surfaces. If the NURBS surface adopted cannot be correctly controlled, it cannot meet the need of explaining the lane. In addition, the complicated program leads to the low operation efficiency. In this study, an arched lane is made by adding a tangent plane. The arched lane is composed of two concentric cylinders with different radii and two concentric circular plates. Projective transformation is an important graphics conversion technique
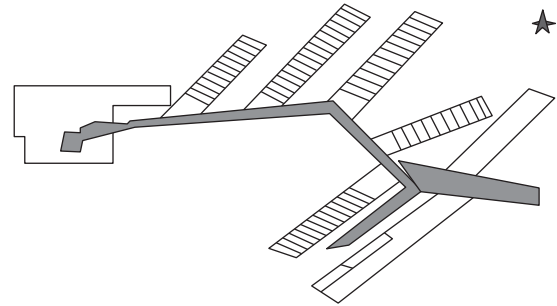

Figure 3: Mine development engineering drawing (partial).
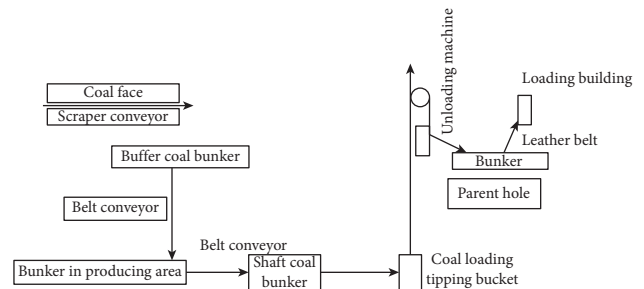
Figure 4: The process of the cost control system for underground mining personnel.

whose purpose is to define the view. The extra part outside the field of view is intercepted, and the final image is only the relevant part of the visual field.

In perspective projection, the projection close to the point is very large, the projection from the viewpoint is very small, and the projection that reaches the extreme point disappears and becomes the vanishing point. The projection is mainly used for meeting animation requests, visualization and other image display areas. In the mine mining intelligent analysis system, the proportional relationship between the alleys remains unchanged after the projection transformation for a more reasonable use of the relative spatial positions of different projects for the mining project layout of the mine.

5.2. Illumination Treatment. The illumination model of the algorithm is, for example, wireless communication network, radiation, ambient light, diffused light, specular light, and so on. The radiation is emitted directly from the object and is not affected by the light source. Ambient light is scattered multiple times from the light source through the environment, and light that cannot determine its direction is considered to come from all directions. The diffused light comes from a certain direction. It is brighter when it is perpendicular to the object than when it is tilted. After irradiating the object, it will be distributed evenly in all directions. Specular light comes from a specific direction and reflects in other directions.

The purpose of the illumination model is to make the generated graphic image be truly felt by performing complex calculations on normal, light sources, materials, and so on. The command to start the illumination model is glEnbale.

LIGHTING), gDiscable (GL_LIGHTING) turn off the current light.

5.3. Plane Normal Vector. The calculation vector strictly represents the direction between multiple countries. Open GL needs to use the normal vector to calculate the angle of light irradiating the object. In order to generate a three-dimensional image, the normal vector of the object must be defined. The wireless communication network algorithm uses two functions to define the normal vector. The first function means the three component values of the normal vector, respectively, given by the function. Second, define a pointer with three elements. The wireless communication network does not provide a function of the corona calculation method. Therefore, it is necessary to create a corresponding program for the developer. The normal vector algorithm designed in this research is verified by actual data and is accurate and effective.

5.4. Integrated Implementation. The characteristics of the following aspects are mainly reflected in the research and development process.

(1) In order to facilitate the development and use, this system adopts a modular design concept to construct a three-dimensional dynamic visualization system and related equipment modules for the engineering in the pit. Using this modular structure, different mines can be constructed: underground laborers and three-dimensional dynamic visualization simulation to determine the needs of the system.

(2) Regarding the logistics process and flow of the simulation system model, in the CAD engineering drawing of the actual mine production system, such as the introduction of mine development and mining plan, the structure configuration and construction of the simulation system can be fully adapted to the actual system (Table 2).

6. Examples and Results of the Analysis

Miner cost control is one of the important tasks of mining production. Through more accurate miner cost forecasting and control, parameters and mining parameters of the mine blocks are adjusted economically and reasonably, the personnel are arranged, and the personnel costs are reduced to improve results and benefits. The cost of mining personnel is closely related to the entire mining system and is affected by ventilation, drainage, transportation, and mining processes. The factors that affect the cost of mining personnel interact in a complex manner. Due to the complexity of the system, it is difficult to use traditional methods to build accurate and complete prediction and control models.

6.1. Mining Equipment. The equipment used in the mine development includes powdered ammonium nitrate explosive, light oil, detonating cords, explosive tubes, and detonators. The prices are shown in Table 3.

6.2. Mining Technology. When mining, the parameters of the mining process mainly include explosive unit consumption, row spacing, hole bottom distance, and collapse steps. Based on the theoretical and experimental research on the blastability evaluation of metal ore and the optimization of deep hole excavation parameters of the in-pit excavation sites, these parameters need to be considered in the optimal control model of production.

6.2.1. Preliminary Determination of Explosive Unit Consumption. All test blast holes are artificially filled. According to relevant data and experience, the unit consumption q value of the funnel test explosive is taken as $3.25 \, kg/m^3$ and detonated at the bottom of the hole with an explosive tube detonator. After the explosive is filled, it will be severely blocked by taphole clay. After the blast hole is mined, the falling part of the laccolith around the funnel mouth is subtracted to determine the boundary of the funnel mouth. Take the blast hole as the center, take the radii r of nine funnels in different directions directly at 45°, use the average value as the radius r of the collecting funnel, to measure the actual minimum resistance cord w, and calculate the mining action index n. The funnel test data based on test statistics and calculation benchmarks are shown in Table 4.

The average radius r of the mining funnel obtained from Table 4 is 0.88 m, the average minimum resistance cord is 0.65 m, and the actual mining action index $n = r/w = 1.38$. The explosive consumption q value in actual standard unit is in turn calculated as $1.68 \, kg/m^3$ according to the formula of Polis Aube.

The number of columns in each unit consumption value experiment is all 10 columns, and the number of tests is four times. The number of columns corresponding to each detonation is two columns, two columns, three columns, and three columns. The detonation is delayed in milliseconds between the columns, and the time interval should not be less than 50 ms. Table 5 shows the mining test results when different explosives are consumed separately.

Synthesizing the analysis and summary of the mining effect of multiple experiments, the reasonable unit consumption range of the mining area is 0.82–$0.88 \, km/m^3$, and the unit consumption value is set to $0.86 \, km/m^3$ in the mining design. The actual unit consumption is controlled within the range of 0.82–$088 \, kg/m^3$. The effect after mining is ideal, and the volume fraction is low (3%–25%). Afterwards, its impact on the construction is very small.

6.2.2. Selection of the Distance between the Row Spacing of Fan-Shaped Deep Hole and the Hole Bottom. In the collapse of mining place, the interval between the fan-shaped deep holes is the minimum resistance line, which is usually determined by the diameter of the hole, the characteristics of the ore, the power of the explosive, and the degree of rock fragmentation. The distance between the bottom of the hole is the vertical distance between relatively shallow hole bottom and the deep blast holes. The blast hole density factor is the ratio of the bottom hole distance to the minimum resistance line, that is,

TABLE 2: The modular structure of cost control for mining personnel.

Serial number	Module name	Module content	Module role
1	Mining equipment	Shearers, supports, roadheader, etc.	Used for selection and layout of equipment
2	Transportation equipment	Mine carts, belt conveyors, transfer conveyor, mine carts tippers, scraper conveyors, etc.	
3	Lifting equipment	Main and auxiliary shaft hoists, cages, small winches, etc.	
4	Ventilation equipment	Fans, dampers, air ducts, etc.	
5	Drainage equipment	Water pump, pipeline, drain, sump pit	
6	Underground personnel	Coal mining, tunneling, support personnel, maintenance personnel, management personnel, etc.	For personnel management
7	Laneway	Horizontal main alley, underground parking lot, transportation main alley, transportation dip entry, crossheading, etc.	Used for 3D dynamic visualization of underground engineering
8	Underground chamber	Coal bunker, gangue bunker, etc.	System layout
9	Main and auxiliary shaft	Main shaft, auxiliary shaft, air shaft	
10	Coal face	Comprehensive mining, general mining, etc.	Selection of coal mining method
11	Face of heading	Comprehensive mining, general mining, etc.	Selection of tunneling methods
12	Support module	Working face support module, laneway support module	Selection of support mode
13	Mine production cycle operation module	Cycle operations of coal mining, tunneling, auxiliary production, etc.	Selection of work organization form
14	Mine excavation plan	Layout drawing of underground mining, layout drawing of mining work surface, etc.	Base map of the simulation system layout
15	CAD module	CAD system, CAD library	Import and draw CAD drawings
16	JMP analysis module	System reliability analysis indicators, etc.	Analyze the reliability of the system
17	Auxiliary function	System maintenance and other module	Other auxiliary functions of the supplementary system

TABLE 3: Prices of mining equipment.

Composition	Price	Average price
Powdery ammonium nitrate explosive/(yuan/t)	4700~7000	5500
Diesel/(yuan/L)	709~760	728
Detonating cord/(yuan/m)	51~59	55
Nonel/(yuan/m)	10~16	126
Detonator/(yuan/send)	84~94	87

TABLE 4: Mining funnel test parameters.

Blast hole number	Explosion load (kg)	Loaded length (m)	Blockage length (m)	Funnel radius (m)	Design minimum resistance line (m)	Actual minimum resistance line	Mining effect evaluation	Data selection
1	087	04	05	084	065	066	Uniform lumpiness	Reserve
2	087	04	05	088	065	068	Uniform lumpiness	Reserve
3	087	04	05	—	065	—	Rushing stone	Reject
4	087	04	05	085	065	062	Uniform lumpiness	Reserve
5	087	04	05	074	065	073	Size of lump	Reject
6	087	04	05	118	065	055	Many chunk and fragment	Reject

$$m = \frac{a}{w}, \tag{17}$$

where m is the blast hole density coefficient; A is the bottom hole distance, m; w is the selection of the minimum resistance line.

The three parameters m, a, and w directly determine the hole density of the blast hole. The minimum resistance line reflects the density of the hole web between columns, and the bottom hole distance reflects the hole web density of the deep holes in the column, and the blast hole density coefficient reflects their mutual relationship. Whether the

TABLE 5: Mining test results of different explosive unit consumption.

Unit consumption/kg/ m3	Row spacing (m)	Hole bottom distance (m)	Mining effect	Open wiring condition	Top board situation	Two side-wall situation	Rear blast hole situation
091–095	16	20	Overgrind of ore	Damaged severely	Lots of falling lumps and pumice	More slanting side-wall	Serious blocking of holes and dislocation
086–091	16	20	Small lumpiness, partly fine ore	Small damage	More pumice	Less slanting side-wall	More plugged holes, less dislocation
082–086	16	20	Uniform lumpiness, less fine ore	Less damage	Partial pumice and falling lumps	Less slanting side-wall	Less plugged holes and dislocation
075–082	16	20	Uneven lumpiness, high lump rate	Less damage	Less pumice and falling lumps	Rarely slanting side-wall	Occasionally plugged or misplaced

selection of these three parameters is correct will directly affect the economic and technical indicators in the mining process.

Combining the experience of various metallurgical mines, the blast hole density coefficient can be $m = 1.0 \sim 2.0$. The relationship between the minimum resistance line w and the blast hole diameter d can be selected for reference from the actual data of the relevant mine. The value of the minimum resistance line used in mines is roughly as shown in Table 6 [13–15].

After the previously mentioned analysis, the design unit consumption is 0.85 kg/m^3, and the actual unit consumption is mining tests with different distances and intervals in the range of 082–087 kg/m^3. In the test, the hole bottom distances are divided into five groups, namely, 1.8 m, 2 m, 2.3 m, 2.4 m, and 2.5 m, respectively. Each group corresponds to seven kinds of intervals, 14 m, 15 m, 16 m, 18 m, 19 m, 20 m, and 21 m, respectively. The test site is located on the 2280 floor on the reexcavation channel of no. 23–25 detection line and the no. 19 detection line. Part of it is arranged on the return way of the no. 19 exploration line on the 2265 floor.

After mining, the mining effect records and analysis of seven different intervals are performed corresponding to five different hole bottom spacings. As the hole bottom distance and discharge interval increase, the impact of front row mining on the rear row of blast holes becomes more and more serious. The blast holes in the back row are blocked and misaligned more and more. The destruction of the eyebrow line gradually became apparent. The ceiling and the two groups will also be increased if they are missing. Obviously, the progress of the next mining project has slowed down. In the case of a certain hole bottom distance, as the cannon hole density coefficient increases, the volume rate after mining gradually decreases. If the big blast hole density coefficient increases to a certain range, a larger volume rate will be maintained. The relationship is shown in Figure 5.

Considering the comprehensive mining effect and project progress, the reasonable row spacing is 1.6–1.8 meters, and the reasonable hole bottom distance is 2–22 meters.

6.2.3. Determination of the Step Pitch of Ore Caving. According to the results of multiple mining tests and the determination of the loss of ore drawing poverty, if two roads are used for collapsed mines simultaneously, the step distance of collapsed mines should preferably be three rows in each direction; that is, the stepped distance of collapsed mines is about 53 m. When a one-way road falls into a mine, the collapsed mines steps are preferably four columns per road. In other words, the collapsed mine step is about 7 meters.

Through a large number of field mining tests, mining parameters can be selected from Table 7.

6.3. Design of Wireless Communication Network. Compare the ratio of the amount of ore mined at one time to the cost of material used for mining 1 m^3. The price performance ratio is considered as a measurement index, and cost performance is used as the output point of the model. In this way, the cost of equipment and personnel required for the volume of ore of the mining unit and the mining parameters are considered as the influencing factors of the system. This neural network model has nine input nodes. *Influence*. In other words, the model has nine input nodes. Due to the cost performance as the output of the model, the model has only one output node.

We collected a total of 20 learning samples, as shown in Table 8.

The first nine items in Table 6 are the input factors of the learning sample, and the last item is the output quantity. Use the samples in Table 8 to train the network. Before training, you should normalize the data not in [0, 1].

The model training, prediction, and appropriate program design calculations are carried out,. The model accuracy during training is 0.001, and the learning step is selected as 0.05. After 17 repetitions, the accuracy reached the requirement and the training was completed. Figure 6 shows the error variance curve during model training. At this point, the connection weight of each node of the model has been determined. The same type of samples can be predicted at any time.

According to the range of mining equipment and mining process parameters, each element of the model is valued

TABLE 6: Correspondence table of the relationship between the minimum resistance wire and the diameter of the blast hole.

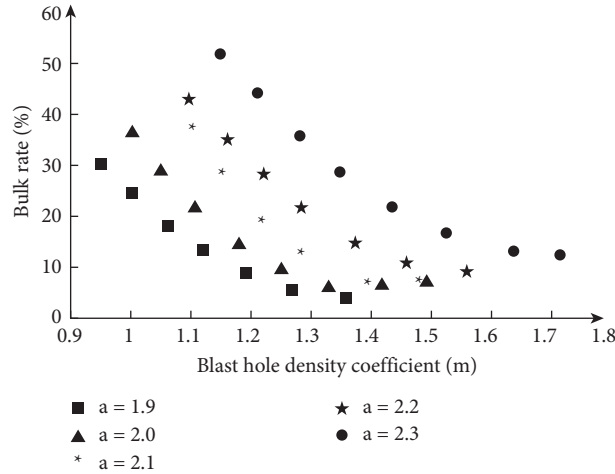| Blast hole diameter (mm)	Minimum resistance line (m)	Blast hole diameter (mm)	Minimum resistance line (m)
50–60	12–17	60–85	18–28
60–70	15–22	90–125	26–45

FIGURE 5: The relationship charts between the blast hole density coefficient and the yield rate of large lumps.

TABLE 7: Mining parameters.

Mining parameters	Explosive unit consumption/(kg/m^3)	Row spacing (m)	Hole bottom distance (m)	Ore drawing step pitch/row
Parameter value	0.83~0.873	5~1.9	1.8~24	2~5

TABLE 8: Learning sample.

Mining unit volume of ore mining equipment consumption					Operational parameter				
Powdery ammonia dynamite/ (yuan/m^3)	Diesel/ (yuan/ m^3)	Detonating cord/(yuan/ m^3)	Nonel/ (yuan/ m^3)	Detonator/ (kg/m^3)	Explosive unit consumption/ (kg/m^3)	Row spacing/ m	Hole bottom distance/ m	Ore drawing step pitch/ row	Performance price ratio/(m^3/ yuan)
457	50	235	39	53	85	170	20	4	2672
435	48	224	3	42	82	172	21	4	3128
459	49	228	32	45	85	172	20	2	2693
471	51	265	33	46	87	16	19	2	250
444	48	225	30	41	82	166	21	3	307
453	49	235	34	48	84	171	20	2	2579
464	50	230	33	46	86	171	22	4	2930
455	49	228	36	50	84	169	19	3	2155
449	48	217	34	47	83	178	22	2	2740
463	50	228	31	43	86	168	21	3	2832
451	47	223	30	42	83	176	20	2	2809
463	50	240	31	44	86	171	22	3	3224
464	50	226	38	44	86	177	21	3	3672
454	49	236	29	41	84	164	21	4	3079
460	46	215	32	42	85	176	21	3	3284
455	49	238	33	45	84	19	22	3	2915
461	50	246	31	43	85	178	22	3	3332
460	49	244	34	47	85	167	2	4	2816
447	48	237	29	41	83	166	21	4	3556
445	49	225	31	43	82	173	21	2	3166

FIGURE 6: Training error curve.

TABLE 9: Model prediction results.

Number	Mining unit volume of ore mining equipment consumption					Production process parameters				Performance price ratio	
	Powdery ammonium nitrate/ (yuan/m^3)	Diesel/ (yuan/ m^3)	Detonating cord/(yuan/ m^3)	Nonel/ (yuan/ m^3)	Detonator/ (kg/m^3)	Explosive unit consumption/ (kg/m^3)	Row spacing/ m	Hole bottom distance/ m	Ore drawing step pitch/ row	Predicted	Actual
1	459	51	241	40	53	86	161	21	5	2735	2690
2	459	48	223	31	41	85	170	21	3	3023	3071
3	459	48	228	33	45	86	176	22	4	3293	3374
4	459	49	230	35	43	85	165	21	3	3123	3141
5	471	49	238	34	46	88	176	22	4	3009	3034
6	464	51	264	33	45	86	18	22	4	3021	2993
7	470	48	224	30	40	87	155	22	4	336	3357

using interval intensive scanning technology in turn, which is used as the prediction sample of the model. Due to the large number of input factors and prediction samples, in order to ensure the comprehensiveness of the prediction samples, a computer is used to obtain values for the nine elements in sequence. Unsolicited data is automatically deleted. The selected prediction samples can be directly input into the model for prediction, and the performance-to-price ratio of all prediction samples can be obtained. Table 9 shows the results of the inverse normalization after the prediction of the seven groups of prediction samples of the model.

According to the prediction results in Table 9, the deviation between the prediction and the actual situation is relatively small, and the prediction and actual results of the third and seventh groups are relatively high. Multiple production practices and wireless communication networks are combined to predict and control the cost of miners. This lead mine uses the best mining parameter values of the collapse method without sill pillar division. The explosive unit consumption is 0.87 kg/m^3, the row spacing is 1.76 m, the hole bottom distance is 2.2 m, and the collapse step is 5.26 m. At this time, the actual price ratio of development reaches 33.78/yuan, which meets the production requirements.

7. Conclusions

In this paper, experiments on the budget and control of the cost of mining workers by wireless communication network technology have been carried out to prove that the characteristics of sandstone deposits are used to optimize the data, and the budget and control model of the cost of mining workers through wireless communication network technology are summarized. The method can accurately improve the mining work, guide the new direction of the mining design work, and provide favorable experience and data for mining similar mines.

Data Availability

The labeled datasets used to support the findings of this study are available from the corresponding author upon request.

Conflicts of Interest

Acknowledgments

References

[1] W. Yang, Z. Ai, X. Zhang, R. Gou, and X. Chang, "Nonlinear three-dimensional dynamics of a marine viscoelastic riser subjected to uniform flow," *Ocean Engineering*, vol. 149, no. 1, pp. 38–52, 2018.

[2] I. D. Moore and F. Guan, "Three-dimensional dynamic response of lined tunnels due to incident seismic waves," *Earthquake Engineering & Structural Dynamics*, vol. 25, no. 4, pp. 357–369, 2015.

[3] Y. Liu, Z. Wu, Q. Yang, and K. Leng, "Dynamic stability evaluation of underground tunnels based on deformation reinforcement theory," *Advances in Engineering Software*, vol. 124, pp. 97–108, 2018.

[4] D. Conroy and O. K. Matar, "Dynamics and stability of three-dimensional ferrofluid films in a magnetic field," *Journal of Engineering Mathematics*, vol. 107, no. 1, pp. 253–268, 2017.

[5] Y. Liang and Q. Liu, "Early warning and real-time control of construction safety risk of underground engineering based on building information modeling and internet of things," *Neural Computing and Applications*, pp. 1–10, 2021.

[6] S. A. Ghoreishi-Madiseh, A. P. Sasmito, F. P. Hassani, and L. Amiri, "Performance evaluation of large scale rock-pit seasonal thermal energy storage for application in underground mine ventilation," *Applied Energy*, vol. 185, no. 2, pp. 1940–1947, 2016.

[7] Z.-z. Liu, P. Cao, H. Lin, J.-J. Meng, and Y.-X. Wang, "Three-dimensional upper bound limit analysis of underground cavities using nonlinear baker failure criterion," *Transactions of Nonferrous Metals Society of China*, vol. 30, no. 7, pp. 1916–1927, 2020.

[8] P. Shan and W. Sun, "Analysis of thermal effect around an underground storage cavern with a combined three-dimensional indirect boundary element method," *Engineering Analysis with Boundary Elements*, vol. 95, no. OCT, pp. 255–265, 2018.

[9] D. S. S. Sandanayake, E. Topal, and M. W. Ali Asad, "A heuristic approach to optimal design of an underground mine stope layout," *Applied Soft Computing*, vol. 30, pp. 595–603, 2015.

[10] J. Menéndez, J. Loredo, M. Galdo, and J. M. Fernández-Oro, "Energy storage in underground coal mines in nw Spain: assessment of an underground lower water reservoir and preliminary energy balance," *Renewable Energy*, vol. 134, pp. 1381–1391, 2019.

[11] Y. A. Chirkunov and Y. L. Skolubovich, "Nonlinear three-dimensional diffusion models of porous medium in the presence of non-stationary source or absorption and some exact solutions," *International Journal of Non-linear Mechanics*, vol. 106, pp. 29–37, 2018.

[12] X.-D. Song, H.-Y. Wu, F. Liu et al., "Three-dimensional mapping of organic carbon using piecewise depth functions in the red soil critical zone observatory," *Soil Science Society of America Journal*, vol. 83, no. 3, pp. 687–696, 2019.

[13] A. Jahanbakhshzadeh, M. Aubertin, and L. Li, "Three-dimensional stress state in inclined backfilled stopes obtained from numerical simulations and new closed-form solution," *Canadian Geotechnical Journal*, 2018.

[14] A. Kapahi and H. S. Udaykumar, "Three-dimensional simulations of dynamics of void collapse in energetic materials," *Shock Waves*, vol. 25, no. 2, pp. 177–187, 2015.

[15] G. Prerna and S. David, "Three-dimensional multicomponent vesicles: dynamics & influence of material properties," *Soft Matter*, vol. 14, no. 1, pp. 1–7, 2018.

Retraction

Retracted: Value Proposition for Enabling Construction Project Innovation by Applying Building Information Modeling

Computational Intelligence and Neuroscience

This article has been retracted by Hindawi following an investigation undertaken by the publisher [1]. This investigation has uncovered evidence of one or more of the following indicators of systematic manipulation of the publication process:

(1) Discrepancies in scope

(2) Discrepancies in the description of the research reported

(3) Discrepancies between the availability of data and the research described

(4) Inappropriate citations

(5) Incoherent, meaningless and/or irrelevant content included in the article

(6) Peer-review manipulation

The presence of these indicators undermines our confidence in the integrity of the article's content and we cannot, therefore, vouch for its reliability. Please note that this notice is intended solely to alert readers that the content of this article is unreliable. We have not investigated whether authors were aware of or involved in the systematic manipulation of the publication process.

Wiley and Hindawi regrets that the usual quality checks did not identify these issues before publication and have since put additional measures in place to safeguard research integrity.

We wish to credit our own Research Integrity and Research Publishing teams and anonymous and named external researchers and research integrity experts for contributing to this investigation.

The corresponding author, as the representative of all authors, has been given the opportunity to register their agreement or disagreement to this retraction. We have kept a record of any response received.

References

[1] H. Liu, Q. Ju, N. Zhao, H. Li, and M. J. Skibniewski, "Value Proposition for Enabling Construction Project Innovation by Applying Building Information Modeling," *Computational Intelligence and Neuroscience*, vol. 2022, Article ID 2586307, 13 pages, 2022.

Research Article

Value Proposition for Enabling Construction Project Innovation by Applying Building Information Modeling

Hui Liu [ID],[1] Qianqian Ju [ID],[1] Na Zhao [ID],[2] Hujun Li [ID],[3] and Miroslaw J. Skibniewski [ID][4,5,6]

[1]*Department of Engineering Management, School of Management and Engineering, Zhengzhou University, Zhengzhou,*
 Henan 450001, China

[2]*Department of Engineering Management, School of Transportation, Changsha University of Science and Technology, Changsha,*
 Hunan 410114, China

[3]*Department of Engineering Management, School of Civil Engineering, Henan Polytechnic University, Jiaozuo,*
 Henan 454001, China

[4]*Center of Excellence in Project Management, Department of Civil and Environmental Engineering, University of Maryland,*
 College Park, MD, USA

[5]*Institute of Theoretical and Applied Informatics, Polish Academy of Sciences, Gliwice, Poland*

[6]*Chaoyang University of Technology, Taichung, Taiwan*

Correspondence should be addressed to Qianqian Ju; juqianqian800@126.com

Building information modeling (BIM) is evolving as a digital infrastructure model for innovation in the construction field. The innovation-enabling potential of BIM has been highly neglected in the literature. This study explores the innovative potential of BIM, specifically its value in enabling construction innovation (CI). Through reflective research and a literature review, the relationship between BIM and CI is redefined, BIM-CI's value spectrum and underlying mechanisms are mapped and their required resources and activities are illustrated. The results indicate that different BIM applications provide various proinnovation environments wherein CI may flourish. Extra attention should be paid to BIM-enabled systematic collaborative innovation and digital innovation ecosystems with BIM as the core infrastructure that integrates the physical space with cyberspace to accelerate radical innovation. This study extends BIM management research by considering digital innovation and providing a new perspective for CI management theory and practice. The results will provide academics with a solid point of departure for developing relevant research and serve as a reference for practitioners who intend to utilize BIM for efficient innovation in construction projects.

1. Introduction

Since it was first proposed in the 1970s, building information modeling (BIM) has become the newest trend in the construction field. An effort has been devoted to pursuing the potential of BIM. Some have focused on the functionality provided by BIM (e.g., clash detection and energy analysis), while others have emphasized productivity and efficiency achievements enabled by BIM, such as existing construction management tools being integrated with open BIM to extend their capabilities in construction ecosystems [1] as well as integrating and enabling BIM capabilities to improve

construction projects in combination with other innovations (e.g., new materials and new technologies such as three-dimensional (3D) printing, cloud computing, and robotics). These have led to advancements in the recognition and application of BIM.

However, regardless of the benefits related to productivity improvement in particular activities, the innovative capability of BIM has been highly neglected in the literature [2, 3]. Innovative capability involves the ability of BIM in enabling its user or organization/network to work differently (i.e., innovate) for improvement [2]. Evidently, construction innovation (CI) is pivotal to the ultimate success of

construction projects and is key to the sustainable development of the construction sector [4]. Although the construction industry is often perceived as conservative, its inertia characteristics (e.g., stakeholder complexity, fragmentation, low profit margins, and low productivity rates) render it "ripe for digitization" [5, 6]. It has been demonstrated that due to the characteristics of digital technologies (i.e., convergence and reprogrammability), tremendous benefits are expected from digital technologies for CI. There are very few researchers who have noticed this aspect of the potential of BIM, and most relevant research has used case studies to describe the process or the outcome of CI enabled by BIM through the application of specific functionality (e.g., 3D representation) during certain stages (e.g., the design phase) of construction projects [2, 6]. Systematic research on the innovative capabilities of BIM is extremely scarce.

The essential reason for this lack of academic research and untapped practical potential may be the absence of a holistic picture of the value of the innovative capability of BIM in construction projects. Thus, the purpose of this conceptual study is to map a value spectrum of the ability of BIM to enable innovation in construction projects. To achieve this goal, reflective research and a qualitative literature review were conducted to reidentify the relationship between BIM and CI. By coupling CI classifications and BIM application modes, a value spectrum depicting a holistic picture of the innovative capability of BIM is mapped and analyzed, and its underlying mechanisms and required resources and activities are also illustrated.

Innovation-related research in the BIM management field mostly considers BIM as an innovative application or technology and examines its adoption, application, and implementation based on innovation diffusion theory or the technology acceptance model [3, 7]. A BIM application is an evolving, dynamic, and complex sociotechnical process. Indeed, BIM is more like an innovation engine rather than simply a technological innovation in the construction field. By exploring the innovative value potential of BIM and analyzing the value spectrum of innovations that enable BIM in construction projects, this study contributes to the body of knowledge by extending the scope of BIM management research considering digital innovation management. Furthermore, this study provides a new perspective for CI management theory and practice. Reshaping the relationship between BIM and CI and creating a value spectrum of the innovative capability of BIM will serve as a solid departure point for developing relevant research and guiding practitioners in executing project management based on BIM to develop innovative solutions in order to address engineering problems, improve efficiency, and build better projects.

2. CI in the Digital Era

The construction industry is a diverse, project-based sector [8]. Architecture, engineering, and construction (AEC) projects are distributed (i.e., designed and constructed by multiple, autonomous actors), heterogeneous (i.e., comprising communities with distinct skills, expertise, and interests), and sociotechnical (i.e., requiring trust, values, and norms as well as information technology (IT) capabilities and complex fabrication processes) [6]. The construction industry has always been regarded as a conservative economic sector because it involves large volumes of repetitive work. However, the completion of iconic mega projects, such as the Burj Khalifa Tower in Dubai and the Hong Kong-Zhuhai-Macao Bridge, also underscores the immense innovative potential of this sector.

Currently, the digitization of the construction industry is overwhelming. The inertia characteristics of the construction industry (e.g., stakeholder complexity, fragmentation, low profit margins, and low productivity) render it "ripe for digitization" [5, 9]. In the new digital era, the construction industry is required to build better buildings and offer better service in a shorter time and with tighter budgets, which pose more challenges to CI and make the improvement of its efficiency imperative [3]. Under such circumstances, digital technologies claim to be a promising new path for improving CI efficiency. Today's construction technology landscape offers a wide variety of innovative digital solutions for optimizing project constraints in terms of scope, time, cost, quality, and resources [5]. Based on the findings reported by the World Economic Forum regarding the likely impact of new technologies and global drivers influencing the future of construction, digitization-enabled innovation—which includes a range of capabilities such as data creation, management, reality capture, analytics, and automation control and tracking—is one of two broad technical trends [10]. The other trend is innovation in building materials, which is not included in the scope of this study [11].

Digital innovation involves the use of digital technology during the innovation process. Nambisan et al. [12] conceptualized digital innovation as the creation of, and the consequent change in, market offerings, business processes, or models resulting from the use of digital technology. Boland and Lyytinen [6] indicated that the two fundamental properties of digital technology are their reprogrammability and data homogenization. Together, they provide an environment of openness and flexibility that is used to create convergent and generative innovations [6]. By overviewing the evolutionary process of CI, Skibniewski and Zavadskas [13] indicated that advanced information and communication technologies develop rigidly and rapidly to ensure the realization of innovative solutions for emergent, dynamic, and complex engineering problems. BIM appears to be at the center of most advancements in digital construction [11]. After the implementation of BIM, a series of innovations, whether incremental advancements toward design and construction management or more radical advancements toward robotics or direct digital construction, will emerge and thus improve management efficiency [11]. Up until this point, BIM has been a prospective solution for improving the efficiency of CI [5].

2.1. Innovative Capability of BIM in Construction Projects. In the digital economic era, BIM is considered the main paradigm of the construction industry's technological

transformation [14]. The BIM concept was originally proposed by Charles Eastman in the 1970s. Since then, issues related to BIM have attracted much attention. Research shows that innovation is one of the most popular topics in BIM management research [7].

Liu et al. [3] conducted a thorough bibliometric analysis of the BIM literature focused on innovation-related topics to investigate the latest status and trends. The results of the bibliometric analysis showed that the number of innovation-related articles in BIM research publications has increased over the past decade, while relevant research mostly depicted BIM as an innovative IT system and investigated its adoption, implementation, and performance based on innovation diffusion theory or the technology acceptance model from a technology-centered perspective. The characteristics of the ability of BIM to enable innovative action have generally been the focus of research. Innovative capability is the ability of technology to enable its users to pursue innovative activities [2]. Selçuk Çıdık et al. [2] highlighted that most relevant research still focused on what BIM technology can provide as a technological window of opportunity in construction projects. The topic of what and how people use BIM on a daily or routine operational basis to improve construction projects remains underresearched, which means that there is ambiguity regarding the innovative capability of BIM in construction projects. In other words, the ability of BIM to enable a construction project network to build or possess the ability to work differently (i.e., to innovate) in order to improve performance has been highly neglected. Thus, a clear illustration of the enabling capability of BIM for CI, that is, a clearly defined relationship between BIM and CI as well as a thorough analysis of the value level of the ability of BIM to enable CI, is highly necessary.

3. Methodology

Recently, there have been an increasing number of researchers claiming that divergent thinking and creative research methods are required for construction research [11]. In particular, conceptual advances are considered critical to the vitality of scientific research, which should be encouraged for prosperity [11, 15].

Research design and method selection are extremely effective and have the greatest potential for innovation when they match the nature of the research question [16]. In this study, the research question concerns the value spectrum of the ability of BIM in enabling CI. The purpose is to establish a conceptual or structural framework and detail, articulate, chart, describe, and depict the innovative capability of BIM. A conceptual study with a delineation goal can serve this research purpose [15].

Conceptual articles are devoted purely to thought-based conceptions and are devoid of data [15]. If inductive and deductive reasoning becomes difficult, and empirical data are either not available, are too costly for exploration, or are not particularly useful, then reflective research is a valid qualitative research method that is suitable for abductive topical reasoning and resolving this paper's research question [11]. Reflective research methodologies are frequently used in research groups; however, they are less often applied to academic research in the construction field. Nevertheless, Singh [11] claimed that this kind of exploratory research could benefit the research community by identifying outliers that are not limited by methodological rigor or statistical evidence [11]. In this research, the concept and characteristics of the innovative capability of BIM were perceived and constructed by thoroughly reviewing the relevant literature, including books, reports, and other sources. Given that CI enabled by BIM is a dynamically evolving, complex process, aside from literature reviews, authors have discussions with colleagues and attendees of international conferences to delineate the innovative value of BIM. Further, thought experiments have been utilized to map the value spectrum.

Actor network theory (ANT), path creation theory (PCT), trading zone theory (TZT), and digital innovation theory have been applied to assist the research process. Based on ANT, technology and other artifacts are regarded as actors shaping roles and relationships in networks [17]. Under this perspective, we can take BIM application in construction projects as a rearrangement of an innovation network. BIM, as the equivalent of other innovation actors, breaks the behavioral and interactional modes between innovation networks and provides a transparent and synchronizing information-sharing channel, thus cultivating propitious conditions for innovation to occur. Although the initial development of digital innovation theory in the context of an information system or the organizational science discipline is still in its infancy [12], the overwhelming development and application of pervasive digital technologies in various industries have challenged the underlying logic of traditional innovation theory. New logic for understanding the novel paradigm of innovation induced by pervasive digital technologies has been provided, for example, taking digital innovation management as a sporadic, parallel, and heterogeneous process of forking, merging, terminating, and refining problem-solution design pairs; shifts in participant cognition and sense-making in emerging distributed innovation as well as the importance of digital platforms with orchestration mechanisms [12, 18]. All the aforementioned examples provide a proper theoretical framework on which our reflective study may build. Regarding the driving mechanism under CI enabled by BIM, this study takes advantage of PCT and TZT to demonstrate how BIM stimulates innovation on the individual actor level and from the interaction perspective among multiple innovation network actors.

4. Redefining the Relationship between BIM and CI

Indeed, BIM is much more than a purely simple innovative technology; rather, it is an engine that promotes CI [19]. With the emergence of the digital economic era, BIM is considered the heart of smart/digital construction, and it will evolve as a digital infrastructure/platform for innovation in the construction field [9, 19]. Research has established BIM as a significant innovator [20]. The use of BIM can generate both technological and organizational innovation and

enable potentially radical innovation that could disrupt the entire industry [9].

The current innovative capability of BIM has attracted the attention of researchers. For instance, Selçuk Çıdık et al. [2] proposed a conceptual continuum by synergizing the polarized functionalist (i.e., technology-centered) and nonfunctionalist (i.e., human-centered) perspectives on BIM to analyze its innovative capability. Boland and Lyytinen [6] found that BIM implementation in Frank O. Gehry's projects instigated diverse innovations, each of which created a wake of innovation. They concluded that Gehry's adoption of 3D BIM as the representational tool disturbed the ecology of interactions and stimulated innovations in his project networks by providing path-creating innovation trajectories in separate communities of practice, creating trading zones in which communities could create knowledge about diverse innovations, and offering a means for intercalating innovations across heterogeneous communities [6].

The aforementioned research concerning the innovative capabilities of BIM primarily focuses on the scope of design practice. Increasingly, the enabling effect of BIM on CI has been expanded to the project life cycle or beyond. In a deductive case study, Holmström et al. [19] investigated how sociotechnical actions such as adoption, reuse, and recombination of designs and processes empower the users of BIM tools to not only achieve productivity improvement in particular activities but also build system capabilities that enable new ways of working. Recently, the incorporation of BIM within the life cycle project management system in the construction field has been highlighted [21, 22]. All of the evidence previously shown demonstrates that the collaborative application of BIM throughout the entire life cycle of a construction project will disrupt the CI ecosystem and provoke the emergence of new innovation patterns, the reduction of communication costs, and the creation of digital convergence that may lead to new interactions and relationships between innovators. New knowledge, skills, and innovative possibilities, accompanied by the associated cognitive and social translation, can occur through the penetration of boundaries [23]. Therefore, by considering the life cycle project management theory and aligning it with the analytical framework used by Boland and Lyytinen [6], this study redefines the relationship between BIM and CI (Figure 1).

CI represents the engineering of problem-oriented innovation activities on the construction project level, which are usually completed collaboratively. The path for CI can be illustrated as a dynamic problem-solution matching process from both an individual organizational perspective (i.e., path creation) and a cross-organizational perspective (i.e., collaborative innovation). During these processes, the embeddedness of BIM serves to activate an individual organization's subjective initiative and accelerates collaboration between organizations to support CI.

A CI network enabled by BIM can be considered a digital ecosystem, a concept that Sawhney et al. [24] defined as a complex intermeshing of an interdependent group of organizations, people, products, and things that work on a shared digital platform for a mutually beneficial purpose and value creation. In this digital ecosystem, BIM, as a shared digital platform or orchestrator, as claimed by Nambisan et al. [12], offers a convergent approach to make project data available for multiple construction technology use cases (e.g., design management, document management process simulation, and project scheduling), thus becoming a key driver of innovation, emergent ecosystem behavior, and value creation [24, 25].

As demonstrated in Figure 1, BIM provides a window of opportunity for people to work differently to improve (i.e., innovate) on an operational level in separate practice communities [26]; path creation enabled by BIM provides innovation trajectories for actors within their organizational boundaries. For example, triggered by the demands and opportunities of high-profile projects and the state of development within each firm, participants in innovation networks enabled by BIM could mindfully invent their own innovation trajectories at different paces. Moreover, some could be more collaborative in their project organization, whereas others could be more experimental with materials and work practices [6].

According to Galison [27], when community boundaries cross or overlap during a project, a trading zone emerges. Owing to certain occasions or specific project tasks, various innovations can be interplayed in trading zones supported by BIM at permeable boundaries (shown in Figure 1 as the circles of dotted lines). In these trading zones, owners, designers, and contractors take artifacts (e.g., the BIM model) authorized by BIM as boundary objects or a common language to constantly refine and mutually adjust their interrelationship, thereby establishing a new interdependent network system so they can work together to produce innovative solutions for various design, construction, and delivery tasks. For example, based on a BIM platform, a construction company can work with trade contractors and third-party software developers to develop a tool for the real-time monitoring of construction workers to track worker safety, productivity, and well-being [24]. Path creation and the interplay of various innovations in trading zones will together lead to the so-called "wakes of innovation" enabled by BIM among the construction project network [6]. During these processes, knowledge evolves, learning occurs, and new action patterns are constructed.

Although BIM is an overall approach, BIM application is a dynamically evolving elaboration, because there are various functional specifications that can be implemented at different phases of a project's life cycle that can bring distinctive benefits and costs [26]. In reality, the application of BIM shows various possibilities with different functions (i.e., what BIM can do)—depending on when, where, and how people use it—and the interactions among individuals during its implementation (i.e., what people can do with BIM) [2]. Therefore, different types of BIM implementation will provide various levels of enabling effects on CI. However, people realize that BIM application has innovative value for construction projects and its users; however, the problem lies in how much value it brings and, particularly, how and in which situation the application of BIM can contribute to improving innovation efficiency for actors and
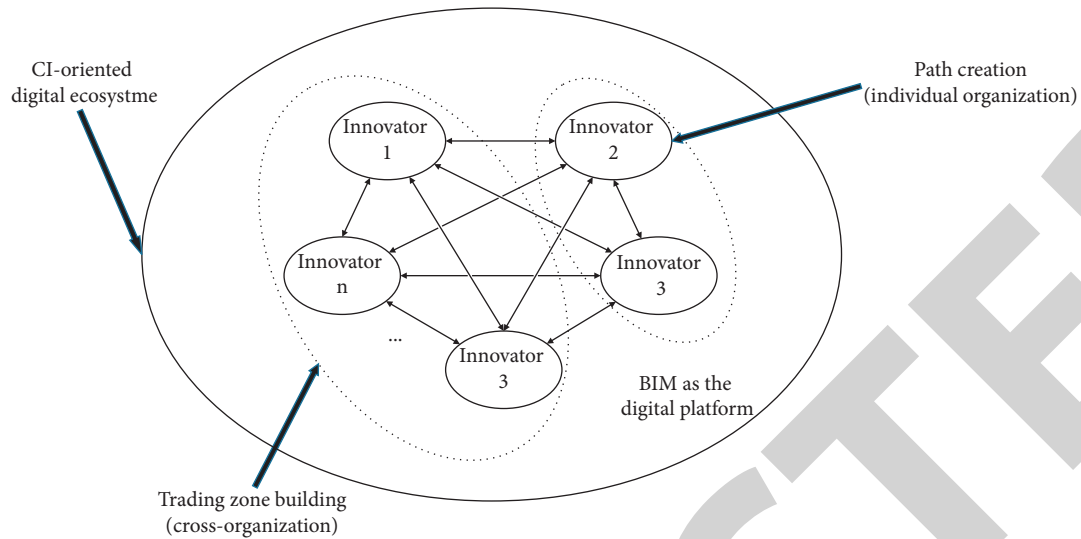
Figure 1: Relationship between BIM and CI.

networks of construction projects. This vagueness on the innovation value spectrum of BIM will consequently hinder construction projects in terms of taking full advantage of BIM to assist CI [26].

5. Value Spectrum of the Ability of BIM to Enable CI

5.1. Application Modes of BIM for Construction Projects. As previously mentioned, there are many possibilities of the application of BIM in construction projects, or various so-called "BIM application modes," which are highly dependent on the type of interactions and relationships between the participants and how BIM is used [28]. Based on a case study of 25 BIM projects, Taylor and Bernstein [29] identified 4 BIM application modes—the visualization, coordination, analysis, and supply chain integration modes—which are consequently incrementally involved in the BIM experience. From the interoperability perspective, Grilo and Jardin-Goncalves [28] acknowledged that various interaction styles between project network actors can lead to different kinds of BIM utility, namely, communication, coordination, cooperation, collaboration, and channels. To sum up, because of the heterogeneous and systematic characteristics of BIM, BIM allows various application statuses to coexist in the construction industry. In this study, grounded on the aforementioned literature coupled with validation from senior BIM experts, the BIM application modes finally include the visualization, coordination, analysis, collaboration, and infrastructure modes.

5.2. Classification of CI. The classification of CI made by Slaughter has been commonly acknowledged in this field [8, 20], which will be applied to be the framework measuring the innovation value level of BIM in this study. As per changes regarding the concept and its linkage to other components, Slaughter classified CI into five

clusters—incremental, modular, architectural, system, and radical—as shown in Figure 2.

According to Figure 2, incremental innovation is a small improvement to the standard practice based on existing experience and knowledge that influences the constraints of a specific element. Incremental innovation is usually more frequent in the construction industry than in other industries, such as the manufacturing industry. Actors from the entire value chain of a construction project can generate incremental innovation, for instance, by improving the products provided by a supplier or modifying the on-site construction process. Modular innovation is a relatively large change on the concept level within a component that has limited influence on the links to other elements or systems. The replacement of drawing with hands with computer-aided design (CAD) is a typical example of modular innovation, which only changes the way people design or draw in terms of the concept of design drawing; the changes to the relationships between design groups are very limited (i.e., they are still done using 2D paper drawings). Contrary to modular innovation, architectural innovation requires only trivial modification of concepts/elements but substantial revisions of the linkages with other elements/ systems, such as incorporating self-compacting concrete. There is no obvious change to the concrete technique itself; it is the fact that under gravity, the fluidity, density, and homogeneity of concrete can be achieved without additional vibrating process changes in the interaction and interconnection between the activities related to this work. To achieve new functions or levels of performance, system innovation involves the integrative innovation of multiple innovations that requires the effective rearrangement of the subsystems comprising the system and relative changes in corresponding elements/systems. One example is the application of ballastless tracks in railway construction. The realization of systematic innovation, such as a ballastless track, requires the integration and coordination of multiple independent innovations (e.g., new orbital technology, new
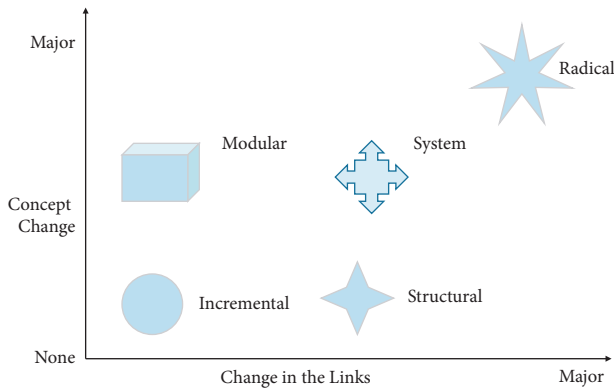
Figure 2: The classification of CI adapted from Slaughter [4].

roadbed construction technology, and new maintenance technology). Radical innovation is a rare and unpredictable breakthrough in science or technology that might lead to the essential reform of an entire industry. For instance, the realization of the so-called digital twins (DT) mode may overturn the overall working logic for the construction industry.

The five types of innovation presented through the model can be arranged as per the scale of required change from the current state-of-the-art practice as an incremental, modular, architectural, system, and radical [4] (see Table 1).

The innovation classification system proposed by Slaughter [4] is utilized as the innovation value metric for measuring the innovative capability of BIM. On the one hand, the enabling effect of the application modes of BIM on CI is highly dependent on the willingness of actors in distinct communities (innovation path creation for concept change) and the interaction mode and interrelationship between various project network communities (linkage changes based on trading zones). On the other hand, assuming that innovation provides improvement through change, an innovation classification model based on the degree of change is appropriate. As demonstrated in Table 1, it is easier to describe the specific resources and activities (e.g., the timing of commitment, degree of coordination within the project team, need for special resources, and type and level of active supervision) [4] required for the application of BIM to enable the relevant level of CI. The alignment of the application of BIM with the classification of CI in exploring the value of the innovative capability of BIM is demonstrated in Table 1.

5.3. Analyzing the Value Level of BIM in Enabling CI. Based on the combination of Slaughter's [4] CI classification system and the BIM application mode summarized in this study (as shown in Table 1), the value spectrum for the innovative capability of BIM will be analyzed as follows (Figure 3). In Figure 3, the x-axis represents the evolution of BIM application modes, while the value of the innovative capability of BIM is demonstrated on the y-axis. As the scope and maturity level of a BIM application evolves, BIM application modes become more innovation-friendly environments. In other words, in different application modes,

BIM provides different levels of innovation value. The wider the scope and the more mature the implementation of BIM, the higher the innovation value of its application in a construction project. Thus, the BIM application mode can be arranged according to the innovative value level of aspects such as visualization, coordination, analysis, collaboration, and infrastructure, as illustrated in Figure 3. This value proposition is not very solid and rigorous because incremental innovation to some actors may be considered modular or systematic innovation to other actors. Thus, the analysis and results herein are conducted on the construction project level and depart from the perspective of general project benefits.

5.3.1. Visualization. Since the 1990s, the visualization mode of BIM has been widely applied in the construction industry, mainly for marketing or aesthetic requirements. The application of BIM visualization demonstrates a great effect on the design and construction phase. First, 3D models of BIM designed on the basis of a 3D entity component provided by suppliers highly improve the designing efficiency. Second, the application of BIM makes communication between designers and owners regarding design intentions more convenient, thus enabling effective information to be correctly conveyed to the relevant team member. In a virtual environment based on BIM, many kinds of "what ifs" can be demonstrated and compared intuitively, which can accelerate the optimization of design solutions by smoothing the communication and cooperation targeting design objectives and solutions. On the construction stage, compared to two-dimensional (2D) painting, 3D models enable contractors to more easily and clearly understand the owner's actual design requirements and intentions, which consequently reduces changes and requests for information subsequently in the project's life cycle.

The BIM visualization mode is essentially the transformation from 2D to 3D presentation technology. Therefore, the visualization mode of BIM application accelerates incremental innovation in construction projects at any time during the project. Incremental innovation enabled by BIM based on the visualization mode only involves small improvements and most of time is constrained by the scope of a single organization with no special resources or coordination required. The related supervision of the individual task level focuses on improving the notification manner and the supervisory competencies of the specific improved product, process, or service.

5.3.2. Coordination. The coordination mode of BIM creates mutual benefits and avoids gaps and overlaps to connect various project activities and efficiently realize project objectives [28]. The coordination of the designing documents (e.g., structuring, plumbing, designing, and drawings) is an important example of this application mode. The coordination of complex systems is a common application in construction projects. The virtual 3D model is completed by various team members. No matter who the consultant is, a specialty manufacturer or a subcontractor, every team

Table 1: Alignment of innovative capabilities of BIM with innovation models for construction adapted from Slaughter [4] and Murphy [20].

| Type of CI	Definition	Scale of change	Example	Timing of commitment	Resource and activities required by BIM-enabled CI						BIM application mode
					Degree of coordination within the project team	Need for special resources	Supervision organizational level	Supervision type	Supervision competency	Enabling mechanisms	
Incremental	A small improvement to the standard practice based on existing experience and knowledge	Small	Modified construction process conducted on-site	At any time	None	None	At locus of improvement	Notification	Specific product or process		Visualization
Modular	A significant change in concept within a component but one that leaves the links to other components and systems unchanged		Computer-aided design (CAD)	At the design stage	None	For concept change	At design level	Notification, review	Technical competency	Path creation oriented	Coordination
Architectural	A small change within a component but a major change in the links to other components and systems		Self-compacting concrete	At the design-to-implementation stages	Among affected parties	For complementary changes	At the affected system level	Notification, agreement, review	System competency		Analysis
System	Multiple integrated innovations that complement each other to achieve new functions or levels of performance		Ballastless track	At the conceptual design stage	With all project team members	For integration of set of innovations	At top engineering management level	Project scope, agreement, review	Technical, system competency and organizational authority	Trading zone building oriented	Collaboration
Radical	A breakthrough in science or technology	Major	DT	At the technical feasibility stage	With top management from all involved organizations	For breakthrough	At top management level	Project objectives and scope	Specialized technical competency	Trading zone building + path creation oriented	Infrastructure
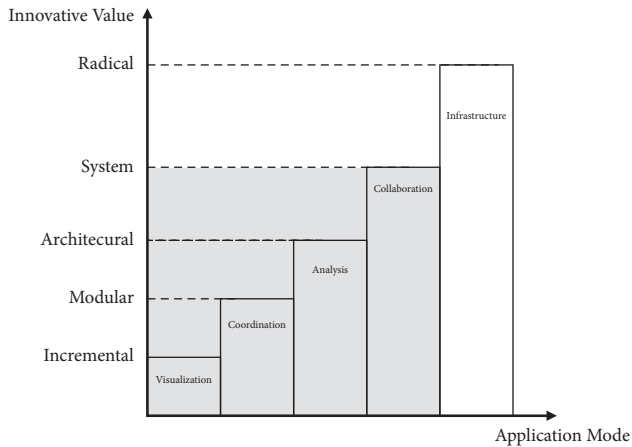
Figure 3: The value level of the innovative capability of BIM in construction projects.

member will create their own model for their work purpose in a project. The general contractor will integrate these independent models to form a more holistic composite model that represents the overall picture of the project. Based on the coordination of the constituent components of the composite model, possible conflicts can be identified and resolved before execution; thus, this mode is also known as the conflict detection mode.

The coordination mode of BIM application invokes conceptual change of coordination issues in construction projects (e.g., design checks and clash detection) while having little influence on other systems. In this mode, innovative solutions are likely to be created in order to realize conceptual goals. Thus, the value level is in modular innovation. Modular innovations enabled by BIM are usually created during the design and bid stages. Because changes to the links to other components or systems are rare, very little explicit or implicit coordination within the project team is required. The resources required for a conceptual change must be prepared to conduct modular innovation enabled by BIM, such as the training required to install and maintain a component embodying a modular innovation. Relative supervisory activities (i.e., notification and review and technical competency) are required on the design and bid levels to ensure modular innovations enabled by BIM meet project objectives.

5.3.3. Analysis. The analysis mode of BIM application realizes mutual benefits through sharing and cooperation. In the 3D virtual project environment based on BIM, the constructability and construction sequence can be clearly simulated. The entire arrangement of any specific task can be visualized in a 3D virtual environment based on BIM so that the schedule can be properly allocated. The BIM analysis mode provides the possibility to moderate and analyze construction costs and operations from the whole life cycle perspective. Moreover, BIM possesses many potential analytical capabilities for construction projects (e.g., energy consumption and lightning, wind flow patterns, and greenness). Theoretically, one central BIM model could be

formed with all of the information needed by all contractors and consultants—information that contractors previously had to create independently from an architect's 2D blueprints [6]. The application of the analytical functionality of BIM requires construction project stakeholders to correctly and timely renew the information in the BIM model and share relevant information, which overturns adversarial relationships between project team workers and persuades them to constantly optimize project solutions from a holistic perspective. Indeed, the BIM analytical mode has not changed the way relevant analysis is done; however, it changes the interactions and links between different analysis systems: the data used for analysis can be retrieved if team workers correctly and timely input and share the BIM model information rather than repeatedly manually measure and calculate them.

In this BIM application mode, there is more potential for architectural innovation to occur, which requires the support and encouragement of organizations at the system level with strong management and control capabilities. For major changes to system or component links, architectural innovation enabled by BIM may require a greater degree of supervision and coordination among the affected parties. To ensure high-level performance from the completed system, the supervisory activities required include notification, agreement, and constant review and revision. Coordination among project team members based on BIM includes both official contract changes (e.g., if architectural innovations based on BIM lead to new project deliverables) and unofficial coordination (e.g., commitment to cooperate). Small conceptual changes may lead to a wide scope of BIM-enabled architectural innovations, from design-to-implementation, with special resources associated with complementary changes.

5.3.4. Collaboration. The collaboration mode involves the full application of BIM in a construction project. Collaboration in a construction network based on BIM is a nonadversarial, team-based environment of mutual trust in which key participants are jointly involved in developing and augmenting the central BIM model throughout the life cycle of the project and where everyone understands and respects the input of others. The BIM model, as a central information resource, is a collaboration platform based on which the project's life-long activities are conducted (e.g., the owner develops an accurate understanding of the nature and needs of the project; the designer designs, develops, and analyzes the project; the contractor manages the construction of the project; the asset manager administers the operations of the project during the operation and decommissioning phase) [28, 30]. Through the collaborative application of BIM, the key participants jointly maximize the value of a construction project by mutually solving problems using proper contracts and fair risk/benefit sharing mechanisms. This application mode is pivotal to the formation and synergy of CI networks. The collaboration of a CI network based on BIM can bring about a synergistic effect that a single or a few functionalities or software programs

cannot establish. The integrative application of BIM over the whole life cycle of a construction project provides reliable information and a knowledge-sharing platform for decision-making. Based on this, joint goals, joint responsibilities, and mutual understanding and respect are easily formed; team workers can communicate fluently and work together for innovative solutions rather than simply for efficient and similar results as in traditional approaches, thus creating a context for system innovation [3, 28]. With the execution of the collaboration BIM application mode, systematic CI has rich grounds to flourish upon.

Commitment to systematic innovation enabled by BIM is usually made during the conceptual design phase because it often involves new functions or increased levels of performance of an entity or a facility as a whole [4]. During the conceptual design phase, the collaborative innovation network enabled by BIM was designed, which facilitates the integration of a set of innovations. Coordination among network actors is assigned through official contracts or unofficial negotiations to reach a common sensibility of the information sharing and resources related to each innovation and their integration. The integrated project delivery method, or the design assistant kind of contract, is used by all project team members. The risk associated with system innovation may require active supervision by top engineering managers who are concerned with incorporating it into the project scope, obtaining agreements, and constantly reviewing its implementation and performance. These supervisors require technical and system competencies to assess the complementary changes needed to effectively implement the system innovation combined with organizational authority in order to ensure collaboration and integration. Professionals not only need to possess knowledge related to the individual innovation and its integration but must also master relevant collaboration knowledge concerning system innovations enabled by BIM [30].

5.3.5. Infrastructure. With the coming digital economic era, the Internet 3.0 has enabled various possibilities for many different industries. In contrast to previous technological changes in the AEC industry, Morgan [9] claimed that the application of BIM has the potential to generate radical innovations that could disrupt the entire construction industry. The infrastructure application mode of BIM is more of a vision for the near future of the construction industry in the digitalized era wherein BIM is perceived as the most stable digital infrastructure [9, 19]. With BIM as the core digital infrastructure, the combination of divergent digital technologies (e.g., Internet of Things, 3D printing, and robotics) will thoroughly reform the productivity of the construction industry by welcoming the smart and digital construction era.

Radical innovation enabled by BIM entails not only financial and project risk but also the potential for technical failure, meaning that the commitment to this kind of innovation must be completed as early as possible, most often before the project is initiated (e.g., during the technical feasibility stage). Correspondingly, coordination of explicit and implicit cooperation and relative supervision requires the support of top management of all involved organizations. Consequently, the objective and scope of construction projects must be redefined, and the special resources required for radical innovation related to scientific or technological breakthroughs enabled by BIM might bring new challenges for top managers in terms of technical competencies in the specific scientific or technological area to monitor the implementation process and adjust the innovation activities accordingly [4].

6. Discussion and the Future BIM Agenda

Industry practitioners and academia mostly perceive BIM as a tool and an application and occasionally as a methodology. Consequently, research related to BIM mostly focuses on practice and application. BIM theory-building has been vastly limited [11]. Therefore, analogous to the development of management information systems as a discipline, Singh [11] claimed that there is a need to rethink the scope of BIM as a discipline emerging at the interface between construction, computer science, information management, and social science domains. The underpinning theoretical and conceptual questions regarding BIM have not been sufficiently investigated. Thus, our study joins this conversation by extending the BIM management research to the digital innovation management area by incorporating BIM into the domain of CI from a sociotechnical perspective [12]. In a CI network based on BIM, BIM may not only be an actor (i.e., a node) but also a relationship (i.e., a link) between elements or actors depending on the functionality used. This provides a new perspective for theory-building and practice of CI management. The underlying mechanisms for CI enabled by BIM will be analyzed based on path dependence theory and TZT in the following section. From the management information systems perspective, digital innovation and BIM-enabled digital innovation ecosystems will be utilized to describe the radical innovation value that BIM might be able to provide.

6.1. Mechanisms Underlying CI Enabled by BIM. As is depicted in Table 1, the enabling mechanism of incremental and modular innovation enabled by BIM based on the visualization and coordination modes is mainly path creation. The innovation trajectories of the involved actors are stimulated by the demands and opportunities of high-profile projects and the development status of each organization. Across the spectrum of engagement in path creation, actors may move at different temporal paces following their own logic and structure. The areas that incremental or modular innovation conduct are dependent on the professional identity and economic interests of the specific organization or community. Thus, they are sometimes more advanced in their use of technologies or are more experimental with their materials and work practices [6]. As the scope of change increases, the depth and width of the application of BIM in the analysis, collaboration, and platform modes rise. Aside from path creation, the innovating mechanism based on BIM focuses more on building trading zones. In these newly

created interactive trading zones, the innovative level is aligned with the intensity of the interactions enabled by BIM. The infrastructure mode of the application of BIM leads to brand new innovation paths and disturbs the existing construction industry ecosystem, bringing new interaction modes among construction project-level innovation networks. As the establishment of trading zones becomes the dominant innovating mechanism, innovators of the CI network enabled by BIM gradually tend to innovate based on a shared identity, common vocabularies, and mutual understanding. In this situation, the innovation trajectories of separate actors or communities cross with those of others. Such interplay of innovations not only invokes new knowledge and skills for system innovation but also provide occasions for further upgrading of their separate innovation paths. To achieve higher value levels from innovation activities enabled by BIM, their tempo, structure, and logic should be aligned with a coherent and synchronized plan [6].

6.2. Systematic Innovation Enabled by BIM Based on Collaboration.

The collaborative BIM application mode is the current goal of BIM implementation in a construction project. Collaborative BIM applications can reap value from incremental to system innovation, as shown in Figure 3. However, systematic innovation based on BIM through collaboration has not been thoroughly investigated in the literature [3].

BIM-CI is a dynamic problem-solution pairing process [12]. The implementation of BIM will change the interaction mode between the elements and actors involved and accelerate the formation and synergy between CI networks, thereby improving the innovative capabilities of BIM-CI networks [3]. BIM-CI networks are not designed but emerge from the interaction of individual social or technical elements or actors [31]. As an orchestrator, BIM plays the role of collaborative innovation platform, leading the innovation network to realize the synergistic effects of resource integration, effective communication, and common vision-building. The evolving and the emerging mechanism underlying this synergistic effect deserves further exploration.

Given the critical position of systematic innovation enabled by BIM in the value spectrum of the ability of BIM to enable innovation in construction projects, Liu et al. [3] proposed an inclusive systematic theoretical framework for collaborative CI enabled by BIM (also known as an "innovation pyramid"). This dynamic and evolving socio-technical system contains six interdependent subsystems—contexts, actors, artifacts, processes, structures, and innovative tasks—as illustrated in Figure 4. In this system, actors possessing varying attitudes, requirements, and abilities use a range of technologies and tools (classified as artifacts) and work within a context with structures and a regulatory framework to take advantage of all of the resources (processes) to achieve the assigned innovative tasks [3].

To reach the synergistic effect of a BIM-CI network, the subsystems must fulfill enormous emerging requirements
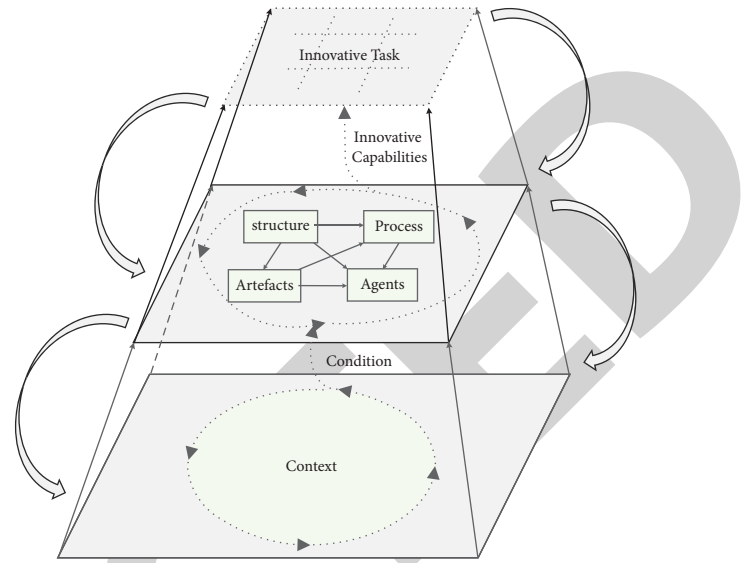

Figure 4: Collaborative innovation enabled by BIM in construction projects by Liu et al. [3].

and overcome many challenges [32]. For example, new professional roles and skills are needed; when innovative new tasks (e.g., some construction companies have started to sell "Building as a Service") for a new service emerge, the structure of the BIM-CI network (i.e., relationships and interrelationships, etc.) must be adjusted. Novel processes for the new form of business are required to implement workflow changes [33]. Further research should systematically examine the new problems faced by each subsystem. Additionally, the interactions, interrelations, and mutually adjusting effects of the subsystems on a macrolevel should also be investigated [3].

6.3. BIM as the Infrastructure for a Digital Innovation Ecosystem in Construction 4.0.

Through collaboration, CI enabled focuses on reaping the systematic innovation value of BIM within the confines of a construction project. The extensive digitization of the construction industry persuades us to consider the bigger picture on an interproject and an industrial level and beyond.

Industry 4.0 has introduced digital technologies, sensor systems, intelligent machines, and smart materials to the construction industry [1]. This transformation is known as "Construction 4.0" [34]. With the adoption of advanced technologies, the processes and outcomes of CI have been gradually digitalized, thereby upending existing theories on innovation management by calling fundamental assumptions into question, such as the following: Are innovation boundaries definitional? Can innovation actors be predefined? Can innovation processes and outcomes be separated? [12].

Under such circumstances, the CI enabled by digital technologies urgently requires specific attention. The concept of digital innovation proposed in the information systems management field can be applied here. As explained by Khin and Ho [35], digital innovation is the development

of new products, services, or solutions using digital technology (e.g., big data, Internet of Things, cloud computing, ontology, blockchain, data analytics, laser scanning, augmented and virtual reality, artificial intelligence, machine learning, and cyber-physical systems), in other words, in digital innovation, digital technologies and the associated digitizing processes form an inherent part of the new idea and its development, diffusion, or assimilation [12].

Digital innovation research brings digital technologies into the foreground of innovation management [31]. On the radical innovation value level, the DT mode is a revolutionary idea for realizing smart construction and Construction 4.0 [36, 37]. The key point for DT or Construction 4.0 is using BIM to connect virtual and actual building activities [35]. For the integration of this autonomous and synchronized cyber-physical system, BIM must collaborate with other cutting-edge Construction 4.0 technologies that embrace digital construction by transforming the construction industry into a dynamic environment [38].

To do so, a digital technologies ecosystem with BIM in the center as a common data infrastructure for enabling radical CI should be established. This "digital innovation ecosystem" refers to a dynamic, evolving network comprising heterogeneous elements [31]. The combined effects of several digital innovations in this ecosystem will bring about novel actors (and actor constellations), structures, practices, values, and beliefs that change, threaten, replace, or complement existing rules within organizations and fields [39]. How do we achieve an effective orchestration of these digital innovations? [12]. What is the structure of this complex, emerging, dynamic network? What are the emerging mechanisms underlying such digital innovation ecosystems? These are all equally significant issues that require examination. As digital technologies play an increasingly important role in construction and innovation activities, a challenging but fascinating set of security-related, ethical, legal, and regulatory issues also arise. How do we mitigate any potential negative influence while reaping the benefits of such digital technologies [40]? This is another research concern regarding digital innovation governance that should be investigated in future research.

7. Conclusions

This study explores a neglected area—the innovation-enabling potential of BIM in construction projects. Specifically, it analyzes and evaluates the value level of the ability of BIM to enable CI. The relationship between BIM and CI was redefined as shown in Figure 1. Besides the fact that BIM is often perceived as a typical construction innovation that offers efficiency and productivity improvements through its various functions or by extending BIM applications, BIM is instead an engine of CI. The main enabling mechanisms of BIM in terms of CI are path creation and trading zone building. Based on this fact, the value spectrum of the innovative capability of BIM was determined by coupling Slaughter's [4] CI classification system and BIM application modes in construction projects, as illustrated in Figure 3, with the resources and activities required to promote CI

enabled by BIM. Additionally, the underlying innovating mechanisms are described in detail in Table 1. Various BIM applications provide different proinnovation environments wherein various levels of innovation may occur and flourish. The results indicate that extra attention should be paid to systematic innovation enabled by BIM based on collaboration and digital innovation ecosystems with BIM as their core infrastructure that integrates cyberspace and physical space to accelerate radical innovation.

Theoretically, this research extends the scope of the BIM management research considering digital innovation management issues and provides a new perspective for CI theory-building and management practice. The relationship between BIM and CI and the mapping of the value spectrum of the innovative capability of BIM provides researchers in this field with a novel perspective on the innovative capabilities of BIM. Relevant research should take the relationship structure and value spectrum map as departing points to design and develop further research. For practitioners, the detailed resources and activities required and the enabling mechanisms for relative levels of BIM-enabled CI can serve as good reference points to guide and inspire BIM-based project management practitioners to develop innovative solutions, solve corresponding engineering problems, improve efficiency, and build better projects.

However, regardless of its contributions, this study also has some limitations. This conceptual study is an initial exploration of the value spectrum of the innovative capability of BIM. Because the goal of this study is to conceptually delineate the innovative capability of BIM, the main research methods applied in this study were the literature review, reflective thinking, and thought experiments, during which abductive and logical reasoning was required, and traditional qualitative research methods (e.g., ground theory) were not utilized, which may cause some concern regarding the validity of the results. Thus, future qualitative and quantitative exploration of the value spectrum map of the innovative capability of BIM is required. In other words, these also create future opportunities to research BIM-enabled CI or digital innovation in the construction field. For instance, further research can apply more quantitative or mixed-methods research to validate the corresponding relationships between BIM and CI and develop relevant research questions, such as the following: Is there a corresponding relationship between the BIM application mode and the level of CI? Do the strategy and resources for enabling relative BIM-enabled innovation illustrated in this study suffice? Is the match between BIM and CI influenced by the delivery mode or owner involvement? How can the innovative capability of BIM in construction projects be activated?

As overwhelming as the development of Industry 4.0 was, the new concept of Industry 5.0 has also been recently proposed [41]. Industry 5.0 highlights the importance of human-centricity, sustainability, and resilience in addition to digitalization itself. Accordingly, the new paradigm of Construction 5.0, the construction industry's version of Industry 5.0, should be put on the agenda. As BIM plays a core role in this transformation, BIM/digital innovation-

related research should pay extra attention to human-centered, environmentally friendly, and risk-related issues to promote the sustainable development of the construction industry.

Data Availability

No data were used to support this study.

Conflicts of Interest

The authors declare that there are no conflicts of interest regarding the publication of this paper.

Authors' Contributions

Conceptualization was done by Hui Liu and Qianqian Ju; methodology was provided by Hui Liu and Miroslaw J. Skibniewski; resources were provided by Na Zhao and Hujun Li; the original draft was prepared by Hui Liu; review and editing were done by all authors. The authors have read and agreed to the published version of the manuscript.

Acknowledgments

References

[1] R. Maskuriy, A. Selamat, K. N. Ali, P. Maresova, and O. Krejcar, "Industry 4.0 for the construction industry—how ready is the industry?" *Applied Sciences*, vol. 9, no. 14, p. 2819, 2019.

[2] M. Selçuk Çıdık, D. Boyd, and N. Thurairajah, "Innovative capability of building information modeling in construction design," *Journal of Construction Engineering and Management*, vol. 143, Article ID 04017047, 2017.

[3] H. Liu, M. J. Skibniewski, Q. Ju, J. Li, and H. Jiang, "BIM-enabled construction innovation through collaboration: a mixed-methods systematic review," *Engineering, Construction and Architectural Management*, vol. 28, no. 6, pp. 1541–1560, 2020.

[4] E. S. Slaughter, "Models of construction innovation," *Journal of Construction Engineering and Management*, vol. 124, pp. 226–231, 1998.

[5] O. Koseoglu, B. Keskin, and B. Ozorhon, "Challenges and enablers in BIM-enabled digital transformation in mega projects: the Istanbul new airport project case study," *Buildings*, vol. 9, no. 5, p. 115, 2019.

[6] R. J. Boland, K. Lyytinen, and Y. Yoo, "Wakes of innovation in project networks: the case of digital 3-D representations in architecture, engineering, and construction," *Organization Science*, vol. 18, no. 4, pp. 631–647, 2007.

[7] Q. He, G. Wang, L. Luo, Q. Shi, J. Xie, and X. Meng, "Mapping the managerial areas of building information modeling (BIM) using scientometric analysis," *International Journal of Project Management*, vol. 35, no. 4, pp. 670–685, 2017.

[8] B. Ozorhon, "Analysis of construction innovation process at project level," *Journal of Management in Engineering*, vol. 29, no. 4, pp. 455–463, 2013.

[9] B. Morgan, "Organizing for digitalization through mutual constitution: the case of a design firm," *Construction Management and Economics*, vol. 37, no. 7, pp. 400–417, 2019.

[10] P. R. de Almeida, M. Buhler, P. Gerbert, S. Castagnino, and C. Rothballer, *Shaping the Future of Construction: A Breakthrough in Mindset and Technology*, World Economic Forum (Together with the Boston Consulting Group), Cologny, Switzerland, 2016.

[11] V. Singh, "Digitalization, BIM ecosystem, and the future of built environment: how widely are we exploring the different possibilities?" *Engineering, Construction and Architectural Management*, 2019.

[12] S. Nambisan, K. Lyytinen, A. Majchrzak, and M. Song, "Digital innovation management: reinventing innovation management research in a digital world," *MIS Quarterly*, vol. 41, no. 1, pp. 223–238, 2017.

[13] M. J. Skibniewski and E. K. Zavadskas, "Technology development in construction: a continuum from distant past into the future," *Journal of Civil Engineering and Management*, vol. 19, no. 1, pp. 136–147, 2013.

[14] E. Papadonikolaki, "Loosely coupled systems of innovation: aligning BIM adoption with implementation in dutch construction," *Journal of Management in Engineering*, vol. 34, Article ID 05018009, 2018.

[15] D. J. MacInnis, "A framework for conceptual contributions in marketing," *Journal of Marketing*, vol. 75, no. 4, pp. 136–154, 2011.

[16] C. Janiszewski, A. A. Labroo, and D. D. Rucker, "A tutorial in consumer research: knowledge creation and knowledge appreciation in deductive-conceptual consumer research," *Journal of Consumer Research*, vol. 43, no. 2, pp. 200–209, 2016.

[17] H. C. J. Linderoth, "Understanding adoption and use of BIM as the creation of actor networks," *Automation in Construction*, vol. 19, no. 1, pp. 66–72, 2010.

[18] Y. Yoo, R. J. Boland, K. Lyytinen, and A. Majchrzak, "Organizing for innovation in the digitized world," *Organization Science*, vol. 23, no. 5, pp. 1398–1408, 2012.

[19] J. Holmström, V. Singh, and K. Främling, "BIM as infrastructure in a finnish HVAC actor network: enabling adoption, reuse, and recombination over a building life cycle and between projects," *Journal of Management in Engineering*, vol. 31, Article ID A4014006, 2015.

[20] M. E. Murphy, "Implementing innovation: a stakeholder competency-based approach for BIM," *Construction Innovation*, vol. 14, no. 4, pp. 433–452, 2014.

[21] T. O. Olawumi and D. W. M. Chan, "Building information modelling and project information management framework for construction projects," *Journal of Civil Engineering and Management*, vol. 25, no. 1, pp. 53–75, 2019.

[22] X. Ma, F. Xiong, T. O. Olawumi, N. Dong, and A. P. Chan, "Conceptual framework and roadmap approach for integrating BIM into lifecycle project management," *Journal of Management in Engineering*, vol. 34, Article ID 05018011, 2018.

[23] K. Lyytinen, Y. Yoo, and R. J. Boland, "Digital product innovation within four classes of innovation networks," *Information Systems Journal*, vol. 26, no. 1, pp. 47–75, 2016.

[24] A. Sawhney, M. Riley, and J. Irizarry, *Construction 4.0: An Innovation Platform for the Built Environment*, Routledge, London, UK, 2020.

[25] B. Keskin, B. Salman, and B. Ozorhon, "Airport project delivery within BIM-centric construction technology

Research Article

Smart Garden Planning and Design Based on the Agricultural Internet of Things

Yi Xun and Guangpei Ren (iD)

School of Art and Design, Guangdong University of Technology, Guangzhou, Guangdong 510060, China

Correspondence should be addressed to Guangpei Ren; ren20171220@gdut.edu.cn

To improve the effect of urban agricultural garden landscape planning and design, this paper combines the agricultural Internet of Things technology to construct a smart garden planning and design system. Moreover, this paper selects the LEACH protocol that can support monitoring for a long time according to actual application needs, introduces the latest swarm intelligence optimization algorithm, the gray wolf algorithm, to optimize some of the problems in the LEACH protocol, and conducts simulation experiments on the improved algorithm. The simulation experiment results show that the improved algorithm has obvious advantages in cluster head selection, data transmission within the cluster, and route maintenance. After constructing a smart garden planning system based on the agricultural Internet of Things, the effect of the agricultural Internet of Things data processing in this paper is evaluated. Finally, this paper constructs a garden simulation system and analyzes the performance of the system. The results verify that the agricultural Internet of Things has a good effect in the planning and design of smart gardens.

1. Introduction

Ecological culture is a new cultural outlook that represents new trends and trends in the world. It represents the awakening of human beings from the ignorant concept of ruling and conquering nature, seeking a way to respect and coexist in harmony with nature. It is the "ecological" and "natural" transformation of the central values of mankind [1].

Regarding the definition of the term landscape, many scholars have put forward different interpretations. In the field of landscape ecology, it studies the ecosystem of the entire natural world, and it focuses on the interaction between ecological subsystems such as climate, geology, soil, vegetation, hydrology, animal and human activities, and their impact on nature. In addition to studying the characteristics of the objective laws of the generation, development, and evolution of the landscape ecosystem itself, it also seeks measures and ways to rationally utilize, protect, and manage the landscape. The field of landscape geography focuses on the changes of natural landscape morphology,

emphasizes the natural characteristics of the landscape, and pays attention to the development and evolution of landscape morphology and landform. From the perspective of landscape architecture, it focuses on the relationship between humanity and nature from the relationship between human and landscape and social attributes. The connotation of the landscape shows obvious characteristics of dynamic changes with the influence of human activities and the change of regional form. From the perspective of the entire development history of human society, the landscape on the Earth is the result of human adaptation and transformation of the natural world [2]. From the definitions of the three major disciplines mentioned above, it can be summarized that landscape is the trace left on the land by human activities or the interaction between humans and nature. The landscape can be regarded as an organic collection composed of a series of symbolic landscape elements. The landscape elements are the unit elements that make up this large collection of landscapes. Therefore, landscape elements can be divided into two categories: natural landscape elements and artificial landscape elements. Natural landscape

elements include terrain, soil, vegetation, and Fengshui patterns, and artificial landscape elements include road paving, sketches, and buildings [3].

In recent years, rural revitalization has been a key work and policy measure in my country. Rural complexes are an important measure to realize rural revitalization. Since the concept of rural complexes was put forward, many cities and towns in my country have been put into practice. However, research on rural complexes and the development of on-site projects is not perfect, and the aspects involved are relatively limited, mainly including leisure and entertainment, physiotherapy, sightseeing agricultural picking, and specialty catering. There are relatively few research studies and analyses on building a smart pastoral complex from the perspective of global tourism combined with the Internet of Things. Global tourism is not the same as previous tourism, blindly pursuing the growth of tourist visits, but focusing more on the improvement of tourism quality. Above all, global tourism aims to build tourism into tourism that can improve people's quality of life and also pursue the value of tourism in people's new wealth revolution.

Taking the agricultural pastoral as the theme, this paper combines the agricultural Internet of Things technology to carry out smart garden planning and design, so as to promote the development of the industry and raise people's awareness of ecological protection and bring people a good pastoral scenery experience.

2. Related Work

With the continuous development of spatial geographic information acquisition technology and computer communication technology, the amount of geographic information data continues to expand, and the difficulty of information extraction and analysis continues to increase. Geographic information has gradually changed from a "digital city" to a "smart city" [4]. At present, various countries are developing smart city projects in line with their own national conditions, such as smart grids in the United States and smart communities in the European Union. With the gradual maturity of 3D geographic information technology, 3D geographic information data have finally entered a wide range of applications in recent years, new stage [5]. In terms of data acquisition methods, noncontact rapid batch acquisition of large-scale data has been achieved at home and abroad. Oblique photography technology, which uses multisensor or dynamic sensors to synchronously collect images from the air, can collect rich high-resolution texture data on the surface and side of buildings and is an upgrade to the traditional single-sensor acquisition method of aerial photography [6]. Literature [7] shows a 3D map made with oblique photography data. At present, the AOS system in the United States, the Penta-DigiCam system in Germany, the A3 system in Israel, and the RCD30 in Leica in Germany are widely used internationally [8].

With the popularization of drone technology, tilt photography technology has also shown explosive growth [9]. Now, in the smart city 3D modeling project, the oblique photography 3D modeling program has taken a place [10].

In addition, LiDAR technology, namely, laser scanning, has also emerged in many fields. It can quickly obtain high-precision point cloud data and is widely used in many fields such as surveying and mapping, architecture, deformation monitoring, mechanical engineering, archaeology, cultural relics protection, and autonomous driving [11]. At present, common international laser scanners include German ATOS 3D optical scanner, Swiss Leica 3D laser scanner, Austria RIEGL laser measurement system, and American Trimble 3D laser scanner [12].

In recent years, high-resolution satellite remote sensing technologies have also been continuously developed, such as QuickBird and WorldView in the United States. In my country, the Chinese "High Score Family" represented by Gaofen No. 2, No. 3, and No. 4 also provides reliable DOM (Digital Orthophoto) and DEM (Digital Elevation Model) for smart city 3D modeling projects data [13]. In the use of oblique photography data for 3D automatic modeling, there are foreign Smart3DCapture, Pixel Factory, PhotoMesh, PohtoScan, etc., which are all powerful tools suitable for the rapid production of smart city 3D models [14]. In the use of laser point cloud data for 3D automatic modeling, the current use of refined reverse engineering modeling software is mainly not suitable for the automatic production of large-area smart city 3D model data [15].

The massive data of smart cities need to be supported by software platforms with spatial management and analysis functions, such as SkylineGlobe, ArcGlobe, CityEngine, etc., which are all currently used smart city geographic information platforms [16].

Smart city 3D models have a wide range of data sources, different production methods, and data structures. Only when a unified standard specification is formulated, can the data interoperability be realized [17]. The Open Geospatial Consortium (OGC) has established the 13S standard as a new international three-dimensional standard, which is a standard specifically designed for three-dimensional spatial geographic information data [18].

3. Agricultural Wireless Sensor Network Model

In order to make the research on wireless sensor networks more targeted, the research content in this article is based on the following assumptions:

(i) The sink node is located in the monitoring area, and its energy is continuously supplied by an external power source. It has stronger computing and storage capabilities than ordinary nodes, can connect to the external network, send data to remote observers, and maintain communication with at least one node in the network.

(ii) The scale of the sensor network is designed to be 200 nodes, and they are randomly and evenly distributed in the monitored area. The nodes have limited energy and are supplied by their own batteries. They have certain computing and storage capabilities, and can sense their own remaining energy, and follow the network operation. As time progresses,

the energy consumption of each node is not the same, and the energy of the nodes will be inconsistent.

(iii) After the node is deployed, once the network is started, the position of the node will no longer change, and the node can know the distance between itself and other nodes through RSSI.

(iv) All nodes have similar communication capabilities and data processing capabilities, there is no super node, the channels between the nodes are symmetrical, the node's transmission power is limited, and it has a unique ID code.

(v) The communication success rate of all nodes conforms to formula (1). There is a communication path with a hop count of h in the network. If it is assumed that the communication distance of the i-th hop is d and the effective communication distance of the node is r, then the communication success rate obeys the following formula [19]:

$$P_{\text{suc}}(h) = \prod_{i=1}^{h} p(d_i) = \frac{(0.2)^h d^h, d^h, \ldots, d^h}{r^h} \leq 0.2^h. \quad (1)$$

It can be seen from formula (1) that the fewer the number of hops, the shorter the path and the higher the communication success rate [20].

The wireless sensor network communication channel is a random channel.

$$E_{\text{Tx}}(k\ d) = E_{\text{elec}}(k) + E_{mp}(k\ d) = \begin{cases} kE_{\text{elec}} + k\varepsilon d^2, & d \leq d_0, \\ kE_{\text{elec}} + k\varepsilon d^4, & d \geq d_0. \end{cases} \quad (2)$$

Here, E_{elec} is the receiving module to complete a complete transceiver, ε_{fs} and ε_{mp} depend on the parameters of the transmitting circuit and the receiving circuit, d is the distance between the transmitting node and the receiving node, and the calculation formula of d_0 is as follows:

$$d_0 = \sqrt{\frac{\varepsilon_{fs}}{\varepsilon_{mp}}}. \quad (3)$$

d_0 is the distance threshold. When d is less than d_0, the communication of the node obeys the free space model.

$$E_{rx}(k) = kE_{\text{elec}}. \quad (4)$$

The LEACH protocol is a WSN hierarchical routing protocol, which occupies a very important position in the research of WSN routing protocol. Figure 1 is a schematic diagram of LEACH protocol clustering. Clustering algorithms such as DCHS, TEEN, and APPTEEN, all borrow the idea of LEACH algorithm. The LEACH algorithm first puts forward the idea of "round." Each round is divided into two stages: cluster establishment and data transmission.

During the formation of the cluster, if the node randomly chooses a number between 0 and 1 and if the selected number is less than the threshold $T(n)$, it is selected as the cluster head. The calculation formula of $T(n)$ is as follows [21]:
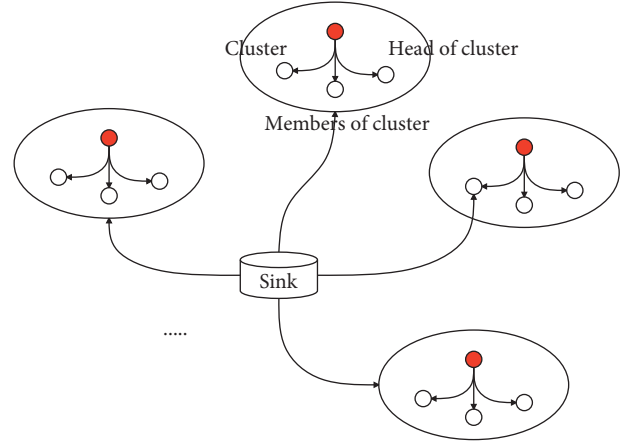

FIGURE 1: Schematic diagram of LEACH protocol clustering.

$$T(n) = \begin{cases} \dfrac{x}{1 - x(r \bmod (l/x))}, & \text{if } n \in S, \\ 0, & \text{otherwise.} \end{cases} \quad (5)$$

At this point, one cycle is over and preparations for the next cycle are started.

Figure 2 is the LEACH protocol flowchart. First, the algorithm selects the cluster head node. After this cluster head is determined, a broadcast message is sent to other nodes. The message includes the cluster head location, cluster head ID, and energy information. The noncluster head node selects the cluster head closest to its position to join according to the received message to form a cluster, and the cluster establishment phase is completed. The cluster head manages the nodes in the cluster, collects data collected by the members, and establishes a TDMA timing table for the member nodes. Then, send the timing table to the nodes in the cluster. All nodes send the collected data to the cluster head according to the time slot specified in the timetable. The cluster head performs simple preprocessing on the data in the cluster and then sends it to the upper node. At this point, one "round" is over and the next cycle begins.

Although the LEACH protocol has a very good performance in long-term monitoring, it also has some shortcomings, mainly including the following aspects:

(1) In each round of cluster establishment, all nodes must participate, and the amount of calculation is very large, which is a great waste of resources

(2) The selection of the cluster head is random

(3) All cluster capitals communicate directly with sink nodes and do not consider the resource loss caused by long-distance communication between cluster heads far away from sink nodes

This paper introduces a new meta-inspired optimization algorithm—gray wolf algorithm—to solve the above-mentioned problems of LEACH algorithm, so that it can better serve agricultural applications. Meta-heuristic algorithms are favored by researchers because of their simplicity and flexibility. The gray wolf (GWO) algorithm is currently the
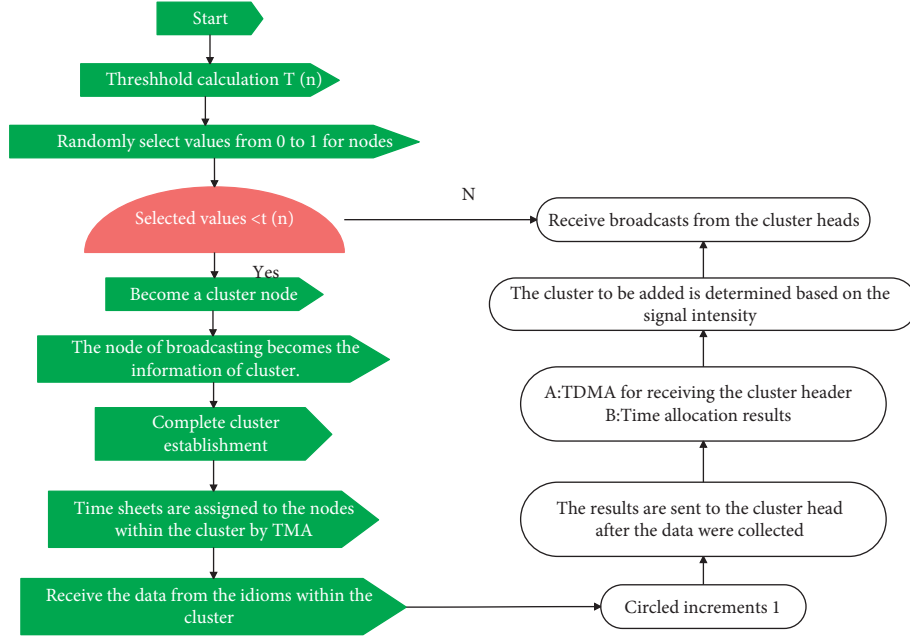
FIGURE 2: LEACH protocol flowchart.

most popular meta-heuristic algorithm in theoretical research. The main idea of the algorithm is to simulate the social hierarchy and group hunting behavior of the gray wolf family in nature. Gray wolves belong to the canine family and like to live in groups. On average, each group consists of 5–12 gray wolves and follows a strict hierarchy, as shown in Figure 3.

The social status of wolves in the gray wolf family can be divided into 4 levels from top to bottom, namely, α wolves, β wolves, δ wolves, and ω wolves. Alpha wolf is a wolf, mainly responsible for deciding the time and place of sleeping, hunting, and tactics. The second level of the gray wolf class is β wolves. β wolves are subordinate wolves, mainly responsible for assisting the wolves to manage the wolf pack. When the wolf pack lacks alpha wolves, beta wolves will replace alpha wolves. The delta wolf is on the third level. The delta wolf obeys the instructions of the alpha wolf and the beta wolf, but it can command the ω wolf at the bottom. The ω wolf is mainly responsible for balancing the relationships within the population.

The collective hunting of gray wolves is an important part of the social activities of gray wolves. Scholars such as Muro have introduced the hunting behavior of gray wolves in detail in the literature, as shown in Figure 4.

Mathematical model of gray wolf algorithm: (1) to establish a mathematical model of gray wolf's social hierarchy, we named the solution with the best fitness as α wolf. Therefore, the second and third best solutions are named β wolves as well as ω wolves, respectively.

3.1. Hunting Model.
In order to simulate the encircling behavior of gray wolves with a mathematical model, equations (6) and (7) are introduced.

$$\vec{D} = \left| \vec{C} \vec{X_P}(t) - \vec{X}(t) \right|, \tag{6}$$

$$\vec{X}(t + l) = \vec{X_p}(t) - \vec{A}\vec{D}. \tag{7}$$

The calculation formulas for vectors $\vec{A}$ and $\vec{C}$ are as follows [22]:

$$\begin{aligned} \vec{A} &= 2\vec{a}\vec{r_1} - \vec{a}, \\ \vec{C} &= 2\vec{r_2}. \end{aligned} \tag{8}$$

3.2. Attack Model.
GWO hunts are led by α, and β and δ occasionally participate. In order to mathematically simulate the hunting behavior of gray wolves, we assume that α (the best candidate solution) and β and δ have a more accurate understanding of the potential location of the prey. Therefore, the algorithm saves the first three optimal solutions obtained so far and forces other search agents (include o) to update their positions according to the position of the best search agent. And its update formula is as follows:

$$\vec{D_\alpha} = \left| \vec{C_1} \vec{X_\alpha} - \vec{X} \right|, \tag{9}$$

$$\vec{D_\beta} = \left| \vec{C_2} \vec{X_\beta} - \vec{X} \right|, \tag{10}$$

$$\vec{D_\delta} = \left| \vec{C_3} \vec{X_\delta} - \vec{X} \right|, \tag{11}$$

$$\vec{X_1} = \vec{X_\alpha} - \vec{A_1}\left(\vec{D_\alpha} \right), \tag{12}$$

$$\vec{X_2} = \vec{X_\beta} - \vec{A_2}\left(\vec{D_\beta} \right), \tag{13}$$
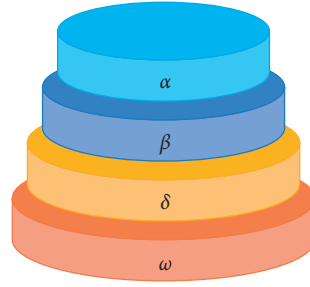
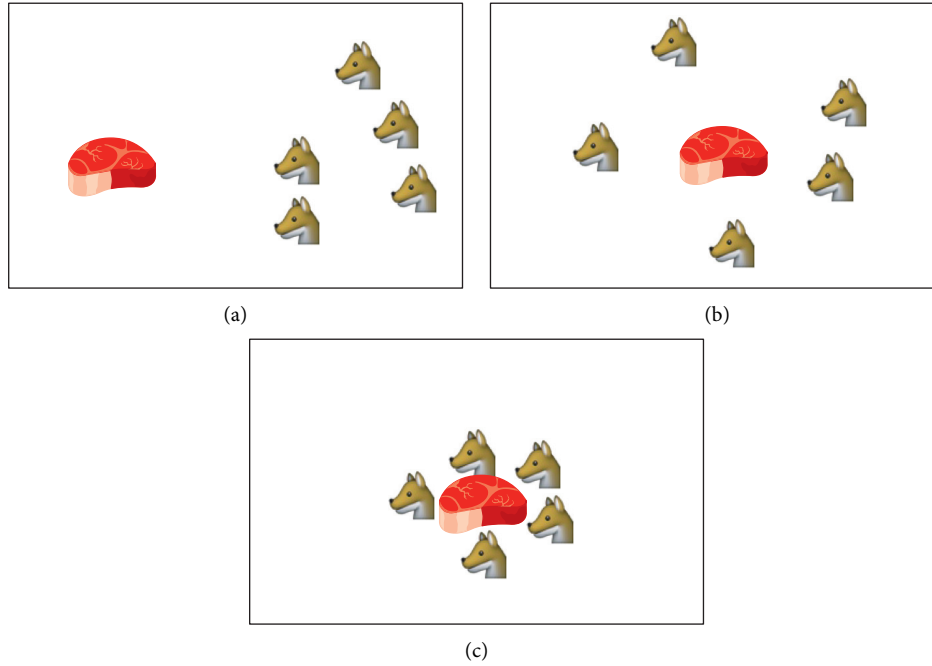FIGURE 3: Schematic diagram of the gray wolf population hierarchy.

FIGURE 4: Gray wolf hunting behavior. (a) Chasing, approaching, and tracking prey. (b) Pursuit, harassment, and encirclement. (c) Static state and attack.

$$\overrightarrow{X_3} = \overrightarrow{X_\delta} - \overrightarrow{A_3}\left(\overrightarrow{D_\delta}\right), \tag{14}$$

$$\overrightarrow{X}(t+l) = \frac{\overrightarrow{X_1} + \overrightarrow{X_2} + \overrightarrow{X_3}}{3}. \tag{15}$$

Equations (12) to (14) define the length and direction of the advancement of ω wolf toward α, β, and δ, respectively. Equation (15) represents the current α position. And the specific process is shown in Figure 5.

The general steps of the GWO algorithm are as follows:

Step 1: the algorithm initializes the wolf pack

Step 2: the algorithm calculates the fitness value of each wolf

Step 3: the algorithm selects the top three wolves with the best fitness as α, β, and 8

Step 4: the algorithm uses formulas (9) to (14) to update other wolves (ω)

Step 5: the algorithm updates parameters, a, A, and C

Step 6: if the end condition is not met, the algorithm goes to step 2

Step 7: the algorithm outputs the position of α

In this paper, sensor nodes represent individual wolves, and base station BS represents prey.

HCGW adopts a round-robin mechanism similar to LEACH, and each round performs the following steps: ①According to the relationship between signal reception and transmission and distance, the simulated gray wolf algorithm divides the network into multiple layers. Each node determines which layer it is in based on the distance between its position and the base station. ②The fitness function includes the remaining energy of the node. ③After the cluster head is determined, all member nodes choose the cluster head to form a cluster. ④ The GWO communication route is established between the cluster heads to avoid long-distance transmission. ⑤Establishes a new route for route maintenance.
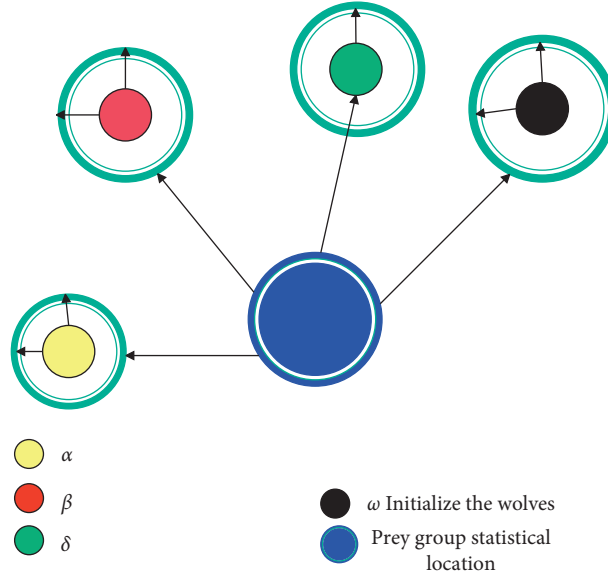
Figure 5: Schematic diagram of the gray wolf algorithm.

3.2.1. Network Layering. As shown in Figure 6, this paper assumes that the network can be divided into L layers. According to energy model formulas (2)–(4), nodes with a distance less than d_0 from the base station are classified as the first layer, and they are marked as layer α according to their priority. And the rest are β layer and 6 layer in order.

The node SN_i is in the lth layer:

$$l = \left[2 \times \frac{d_i}{d_0} \right]. \tag{16}$$

By layering the nodes, the communication distance between cluster heads is less than or equal to d_0 during data transmission, which can effectively avoid the energy loss caused by long-distance communication.

3.2.2. Cluster Head Selection Method Based on Fitness Principle. After the sensor nodes are layered, in each layer, the fitness function and fitness rules are used to calculate the fitness of the node, and one or several nodes with high fitness are selected as the cluster head of this layer.

(1) Node Remaining Energy. The node's remaining energy E_{RE} represents the maximum energy left by the node after a number of rounds in the network.

$$E_{RE} = E_{init} - E_r. \tag{17}$$

(2) Node Density. The greater the node density, the more neighbor nodes of the node, and the less energy it consumes when exchanging data with surrounding nodes. The node density is represented by P_{SN_i}, and its calculation company is as follows:

$$P_{SN_i} = \frac{N}{\pi \cdot d_0^2}. \tag{18}$$

Here, N is the number of nodes in the communication range of d_0.

(3) Node Centrality C. The centrality C represents the average distance between a certain node SN and its neighboring nodes. The smaller C is, the closer it is, the less energy is needed for communication, and vice versa.

$$C_i = \sqrt{\left(x_i - \frac{1}{n} \sum_{j}^{n} x_j \right)^2 + \left(y_i - \frac{1}{n} \sum_{j}^{n} y_j \right)^2}. \tag{19}$$

Here, x_i represents the abscissa of node SN_i, and y_i represents the ordinate of node SN_i.

(4) Fitness Function. The cluster head selection is determined by the fitness function. In the GWO algorithm, the fitness function plays a very important role in finding the prey mechanism. The input of this function is the characteristics of the node, including node residual energy (E_{RE}), node density, and node centrality. And, the output is the fitness value of whether the node can become the cluster head.

$$f(CH_i) = q_1 \left| \frac{P_{SN_i}}{C_i} \right| + q_2 \sum E_{RE}. \tag{20}$$

Here, q_1 and q_2 are random numbers in the range of [0, 1]. A certain threshold is set for the fitness, and the node with a fitness value greater than this threshold will be selected as the cluster head.

(5) Fitness Rules. The HCGW algorithm uses adaptive criteria for comprehensive evaluation. The nodes with more residual energy, higher node density, and higher centrality have very high priority. HCGW contains a total of 3 $3 * 3 * = 27$ fitness criteria, as shown in Table 1.
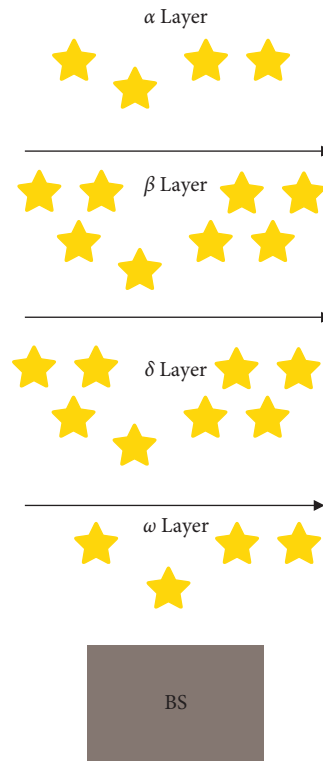
FIGURE 6: Schematic diagram of network layering.

3.2.3. Formation of the Family. After receiving the Invite.Msg message, the member node calculates the approximate distance d from itself to each CH and selects the cluster head with the smallest distance to join to form a cluster structure.

3.2.4. Route Establishment and Maintenance. The cluster head performs preprocessing steps such as compression and optimization of the data. Then, the algorithm sends the data head node of the upper layer with higher priority according to the priority order of the hierarchy and then transmits it in turn until the first layer. At this time, a multihop routing similar to the gray wolf hierarchy is established.

After a long enough time T, the routing of the entire network will be updated. Compared with the LEACH protocol's global mechanism, proposed by the HCGW algorithm, it can greatly save computational and broadcast costs and at the same time achieve local optimality.

4. Smart Garden Planning and Design Based on the Agricultural Internet of Things

The process for the smart garden information management platform to access and call basic geographic data is as follows: (1) The smart garden information management platform sends a graphical call request to the basic geographic information sharing service platform. (2) After receiving the graphic data query request, the basic geographic information sharing service platform will execute the relevant graphic data query process, package the query results (map images or JSON format attribute data), and return them to the smart garden information management platform. (3) After receiving the query result, the intelligent garden information management platform displays it in the map window of the platform. The thematic geographic data of landscaping is directly accessed and invoked on the platform and can be displayed superimposed with the basic geographic information sharing service. The schematic diagram of the business data interface model (process) of the smart garden information management platform is shown in Figure 7.

After constructing a smart garden planning system based on the agricultural Internet of Things, the effect of the data processing of the agricultural Internet of Things in this paper is evaluated, and a garden simulation system is constructed to analyze the performance of the system. The network nodes of the simulation system are shown in Figure 8.

Through the performance verification of the above model, the data processing effect of the agricultural smart garden is shown in Table 2 and Figure 9.

The above model verifies the data processing effect of the agricultural smart garden system.

On this basis, the planning and design effects of agricultural smart gardens are carried out, and the results shown in Table 3 and Figure 10 are obtained.

The above analysis verifies that the smart garden planning and design system has a good planning and design effect.

TABLE 1: Fitness rules.

| Fitness rules	Remaining energy	Node density	Centrality	Adaptability
1	Few	Secondary	Secondary	Very secondary
2	Few	Secondary	Commonly	Very secondary
3	Few	Secondary	High	Very secondary
4	Few	Commonly	Secondary	Very secondary
5	Few	Commonly	Commonly	Very secondary
6	Few	Commonly	High	Very secondary
7	Few	High	Secondary	Very secondary
8	Few	High	Commonly	Very secondary
9	Few	High	High	Very secondary
10	Commonly	Secondary	Secondary	Slightly secondaryer
11	Commonly	Secondary	Commonly	Slightly secondaryer
12	Commonly	Secondary	High	Commonly
13	Commonly	Commonly	Secondary	Slightly secondaryer
14	Commonly	Commonly	Commonly	Commonly
15	Commonly	Commonly	High	Slightly higher
16	Commonly	High	Secondary	Slightly secondaryer
17	Commonly	High	Commonly	Commonly
18	Commonly	High	High	Slightly higher
19	Many	Secondary	Secondary	Slightly secondaryer
20	Many	Secondary	Commonly	Commonly
21	Many	Secondary	High	Slightly higher
22	Many	Commonly	Secondary	Commonly
23	Many	Commonly	Commonly	Slightly higher
24	Many	Commonly	High	High
25	Many	High	Secondary	Commonly
26	Many	High	Commonly	High
27	Many	High	High	Very high
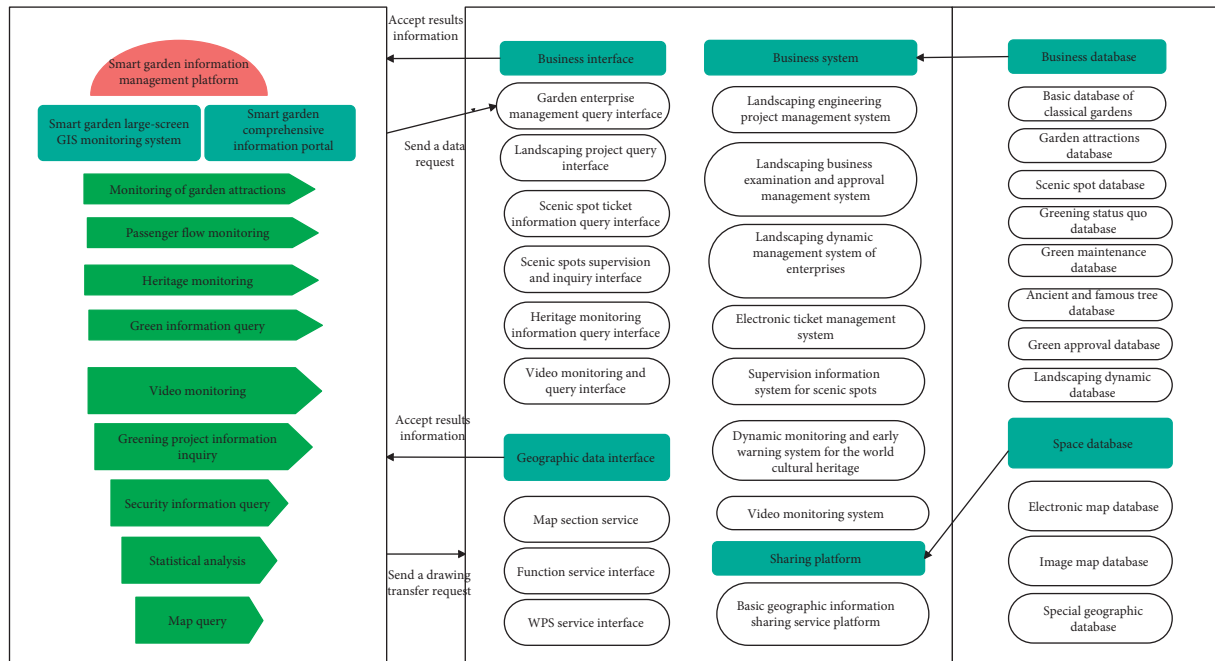
FIGURE 7: Schematic diagram of the data interface model of the smart garden business.
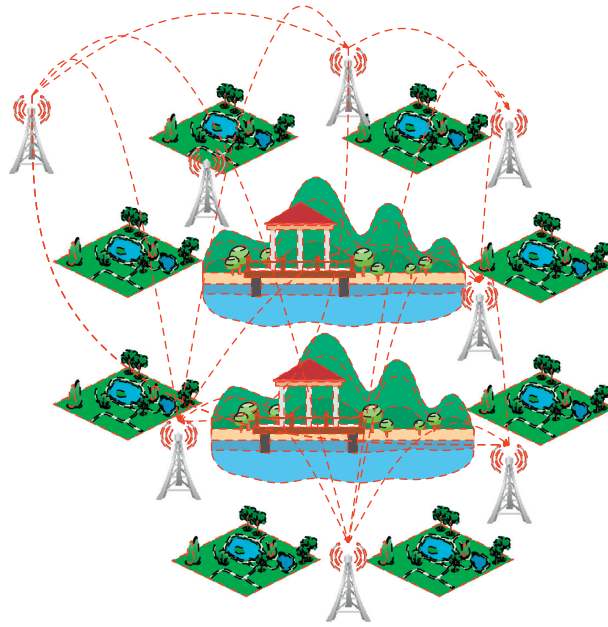
Figure 8: Model of the agricultural smart garden system.

Table 2: Data processing effect of agricultural IoT smart garden.

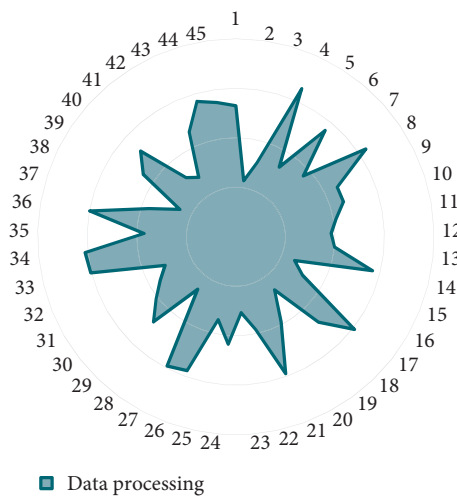| No.	Data processing	No.	Data processing	No.	Data processing
1	95.29	16	93.11	31	93.52
2	92.29	17	96.08	32	93.08
3	93.11	18	94.79	33	96.04
4	96.55	19	92.66	34	96.12
5	93.31	20	93.90	35	93.71
6	95.61	21	95.89	36	96.00
7	93.67	22	93.83	37	93.68
8	96.33	23	93.08	38	92.51
9	94.56	24	94.35	39	94.51
10	94.57	25	93.43	40	95.17
11	94.10	26	95.76	41	93.12
12	93.86	27	95.91	42	92.83
13	94.01	28	92.62	43	94.63
14	95.69	29	94.79	44	95.69
15	92.56	30	94.09	45	95.47

Data processing

Figure 9: Data processing statistics.

TABLE 3: Planning and design effects of agricultural smart gardens.

No.	Planning and design	No.	Planning and design	No.	Planning and design
1	86.45	16	82.77	31	81.62
2	74.26	17	80.81	32	89.68
3	80.49	18	88.72	33	77.24
4	89.06	19	86.27	34	88.22
5	82.10	20	80.38	35	83.12
6	84.06	21	86.88	36	74.41
7	85.45	22	74.03	37	80.85
8	89.51	23	82.76	38	91.39
9	74.47	24	74.25	39	78.90
10	86.67	25	80.52	40	79.56
11	83.42	26	80.94	41	74.14
12	78.27	27	82.41	42	90.94
13	73.73	28	85.22	43	87.79
14	88.74	29	84.31	44	81.33
15	77.87	30	82.94	45	88.75
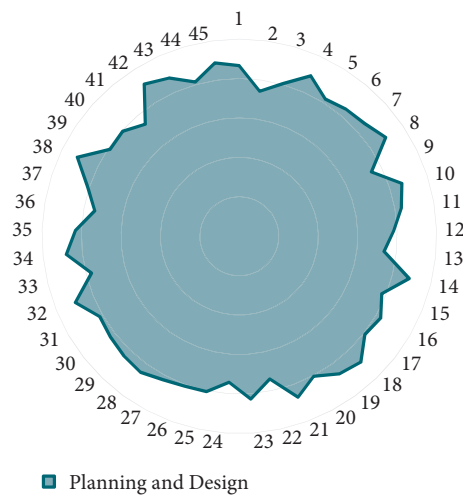
FIGURE 10: Statistical diagram of planning and design effects of smart gardens.

5. Conclusion

People can intuitively watch the objects in the real environment scene through the network platform and can select corresponding operations on the network client to perform corresponding operations on the real objects in the real environment. Virtual experience is dependent on computer and Internet of Things technology. Compared with real experience, virtual experience has some inherent characteristics, such as virtual experience, virtual experience with uncertainty, and virtual experience with globality. This paper combines the agricultural Internet of Things technology to carry out smart garden planning and design. With the theme of agricultural pastoral, it promotes industrial development and raises people's awareness of ecological and environmental protection and brings people a good pastoral scenery experience.

Data Availability

The data used to support the findings of this study are available from the corresponding author upon request.

Conflicts of Interest

The authors declare that there are no conflicts of interest.

Acknowledgments

References

[1] N. Suma, S. R. Samson, and S. Saranya, "IOT based smart agriculture monitoring system," *International Journal on Recent and Innovation Trends in Computing and Communication*, vol. 5, no. 2, pp. 177–181, 2017.

[2] P. P. Ray, "Internet of things for smart agriculture: technologies, practices and future direction," *Journal of Ambient Intelligence and Smart Environments*, vol. 9, no. 4, pp. 395–420, 2017.

[3] M. Roopaei, P. Rad, and K. K. R. Choo, "Cloud of things in smart agriculture: intelligent irrigation monitoring by thermal imaging," *IEEE Cloud Computing*, vol. 4, no. 1, pp. 10–15, 2017.

[4] K. L. Steenwerth, A. K. Hodson, A. J. Bloom et al., "Climate-smart agriculture global research agenda: scientific basis for action," *Agriculture & Food Security*, vol. 3, no. 1, pp. 1–39, 2014.

[5] G. N. Rameshaiah, J. Pallavi, and S. Shabnam, "Nano fertilizers and nano sensors–an attempt for developing smart agriculture," *International Journal of Engineering Research and General Science*, vol. 3, no. 1, pp. 314–320, 2015.

[6] P. Newell and O. Taylor, "Contested landscapes: the global political economy of climate-smart agriculture," *The Journal of Peasant Studies*, vol. 45, no. 1, pp. 108–129, 2018.

[7] H. Channe, S. Kothari, and D. Kadam, "Multidisciplinary model for smart agriculture using internet-of-things (IoT), sensors, cloud-computing, mobile-computing & big-data analysis," *International Journal of Computer Technology & Applications*, vol. 6, no. 3, pp. 374–382, 2015.

[8] L. Scherer and P. H. Verburg, "Mapping and linking supply-and demand-side measures in climate-smart agriculture. A review," *Agronomy for Sustainable Development*, vol. 37, no. 6, pp. 1–17, 2017.

[9] J. Liu, Y. Chai, Y. Xiang, X. Zhang, S. Gou, and Y. Liu, "Clean energy consumption of power systems towards smart agriculture: roadmap, bottlenecks and technologies," *CSEE Journal of Power and Energy Systems*, vol. 4, no. 3, pp. 273–282, 2018.

[10] R. B. Zougmoré, S. T. Partey, and M. Ouédraogo, "Facing climate variability in sub-saharan Africa: analysis of climate-smart agriculture opportunities to manage climate-related risks," *Cahiers Agricultures (TSI)*, vol. 27, no. 3, pp. 1–9, 2018.

[11] O. Elijah, T. A. Rahman, I. Orikumhi, C. Y. Leow, and M. H. D. N. Hindia, "An overview of internet of things (IoT) and data analytics in agriculture: benefits and challenges," *IEEE Internet of Things Journal*, vol. 5, no. 5, pp. 3758–3773, 2018.

[12] A. A. Kimaro, M. Mpanda, J. Rioux et al., "Is conservation agriculture "climate-smart" for maize farmers in the highlands of Tanzania?" *Nutrient Cycling in Agroecosystems*, vol. 105, no. 3, pp. 217–228, 2016.

[13] F. Terdoo and O. Adekola, "Assessing the role of climate-smart agriculture in combating climate change, desertification and improving rural livelihood in Northern Nigeria," *African Journal of Agricultural Research*, vol. 9, no. 15, pp. 1180–1191, 2014.

[14] A. K. Thakur and N. T. Uphoff, "How the system of rice intensification can contribute to climate-smart agriculture," *Agronomy Journal*, vol. 109, no. 4, pp. 1163–1182, 2017.

[15] C. J. Chae and H. J. Cho, "Smart fusion agriculture based on internet of thing," *Journal of the Korea Convergence Society*, vol. 7, no. 6, pp. 49–54, 2016.

[16] J. P. Aryal, T. B. Sapkota, D. B. Rahut, and M. L. Jat, "Agricultural sustainability under emerging climatic variability: the role of climate-smart agriculture and relevant policies in India," *International Journal of Innovation and Sustainable Development*, vol. 14, no. 2, pp. 219–245, 2020.

[17] K. Aliev, E. Pasero, and M. M. Jawaid, "Internet of plants application for smart agriculture," *International Journal of Advance Computer Science Application*, vol. 9, no. 4, pp. 421–429, 2018.

[18] A. Chandra, K. E. McNamara, and P. Dargusch, "Resolving the UNFCCC divide on climate-smart agriculture," *Carbon Management*, vol. 7, no. 5-6, pp. 295–299, 2016.

[19] M. Faling, R. Biesbroek, and S. Karlsson-Vinkhuyzen, "The strategizing of policy entrepreneurs towards the global alliance for climate-smart agriculture," *Global Policy*, vol. 9, no. 3, pp. 408–419, 2018.

[20] M. I. Alipio, A. E. M. Dela Cruz, J. D. A. Doria, and R. M. S. Fruto, "On the design of Nutrient film technique hydroponics farm for smart agriculture," *Engineering in Agriculture, Environment and Food*, vol. 12, no. 3, pp. 315–324, 2019.

[21] J. Verschuuren, "Towards an EU regulatory framework for climate-smart agriculture: the example of soil carbon sequestration," *Transnational Environmental Law*, vol. 7, no. 2, pp. 301–322, 2018.

[22] T. Hidayat, "Internet of things smart agriculture on zigbee: a systematic review," *Jurnal Telekomunikasi dan Komputer*, vol. 8, no. 1, pp. 75–86, 2017.

Research Article

Research on Artificial Intelligence Classification and Statistical Methods of Financial Data in Smart Cities

Xuezhong Fu [iD]

School of Economics, Hainan University, Haikou 570228, China

Correspondence should be addressed to Xuezhong Fu; xuezhongfu2572021@126.com

In order to improve the effect of financial data classification and extract effective information from financial data, this paper improves the data mining algorithm, uses linear combination of principal components to represent missing variables, and performs dimensionality reduction processing on multidimensional data. In order to achieve the standardization of sample data, this paper standardizes the data and combines statistical methods to build an intelligent financial data processing model. In addition, starting from the actual situation, this paper proposes the artificial intelligence classification and statistical methods of financial data in smart cities and designs data simulation experiments to conduct experimental analysis on the methods proposed in this paper. From the experimental results, the artificial intelligence classification and statistical method of financial data in smart cities proposed in this paper can play an important role in the statistical analysis of financial data.

1. Introduction

With the acceleration of economic globalization, financial information has become more transparent and authentic. In this context, accounting standards are converging faster and faster globally. According to incomplete statistics, there are nearly 120 countries and regions that have adopted the International Financial Reporting Standards (IFRS) in the global plan or have adopted the International Financial Reporting Standards (IFRS). The international financial crisis that broke out in 2008 made people realize that improving the transparency of accounting information and formulating a set of globally unified and high-quality accounting standards are vital to the stability and healthy development of the global financial system and capital markets. In this context, countries and regions have accelerated discussions and research on the international convergence of accounting standards [1].

Because keyword retrieval technology cannot meet the needs of some occasions, in recent years, some new researches have begun to focus on improving the efficiency and accuracy of information retrieval technology. Information extraction technology is one of the technologies for obtaining specific events or the relationship between events and events. It is a process of extracting structured and unambiguous information from unstructured free text or other information resources. Information extraction technology can not only filter out information that is not useful to users, but also generate specific information that users are interested in. Information extraction technology integrates artificial intelligence and natural language processing technology and plays an indispensable role in the field of information retrieval. To evaluate the market value of a company, such as the evaluation of intangible assets, all financial data of the company and the financial data of the industry are required, including the company's financial statements and notes to the statements, relevant industry financial news, and macro- and microeconomic data [2]. Most of these data are stored on the Internet in formats such as web pages (HTML) and PDF and are distributed on various websites that provide financial information. At present, people can only manually collect and sort relevant financial data from different data sources, carefully sort and analyze and filter out the data they want, but there is no place to directly get all the data they want. This takes a lot of manpower and time, and most of the work is repetitive work.

According to the preestablished evaluation model, the financial data evaluation results are obtained, which will greatly improve the efficiency of decision-making and provide support for financial-related decisions such as stock investment, mergers and acquisitions, and financial risk assessment [3].

This article combines big data technology to conduct financial data classification research and explores intelligent methods suitable for contemporary financial data classification.

2. Related Work

The literature [4] put forward some suggestions on the classification of financial assets. It includes two parts: one is the understanding of the different levels of financial transactions, and the other is how to deal with the various levels of relationships in the classification of financial instruments during the transaction process. The literature [5] conducted a comparative analysis on the four categories of financial assets and believed that financial assets should also be included in the foreclosed assets, and the financial assets in this part should be handled in accordance with the relevant regulations in the four categories. The literature [6] specifically analyzed and explained the revision of the classification of nonfinancial assets and financial assets in the national economic accounting system. The literature [7] studied the classification of financial instruments and the measurement model of financial instruments, explored the standard and root causes of the classification of financial instruments, and studied the future direction of the classification standard. According to the current classification standards of financial instruments, the literature [8] elaborated the classification standards of held-to-maturity investments in detail. The literature [9] believed that, under the current standards, the main reason for the strong subjectivity of the classification of financial assets lies in the intention of the management. Therefore, there may be errors in the classification of financial assets in actual work, and the relevant discrimination methods are given in the article.

With the changes in the economic environment, follow-up measurement issues and other related issues derived from the classification of financial assets have gradually emerged, and scholars have launched relevant discussions on these issues. Since the promulgation of the new accounting standards and the full implementation of the financial instrument standards, many scholars have begun to pay attention to whether the problem of financial asset classification will bring earnings management opportunities to enterprises. Therefore, most of the research and discussion on this issue have been concentrated in recent years. Literature [10] believes that the current research does not clearly define the criteria for the classification of financial assets, especially for transactional financial assets and available-for-sale financial assets, which only require classification according to the holding intention and ability of the enterprise. Therefore, companies can make full use of the subjectivity of financial asset classification to manipulate corporate profits. Literature [11] made a specific analysis on

the impact of the classification of equity financial assets on the basis of a full analysis of corporate equity financial assets. Literature [12] conducted an empirical study on the classification of listed companies' financial assets under the new standards. The research perspective is management, accounting policies, and earnings management. Studies have shown that when the initial classification of financial assets is performed, listed companies have obvious intentions to hold financial assets and can be clearly classified; however, during the holding period of financial assets, listed companies have more room for profit operation. The accounting treatment of available-for-sale financial assets can be managed according to the management's wishes. Literature [13] analyzed the classification standards of financial instruments of listed companies and concluded that because the classification of financial instruments is subjective and selective, holders will choose according to their own interests to maximize the reliability of financial information. Literature [14] investigated and studied the classification of financial instruments of listed companies and concluded that the classification of financial instruments of listed companies has a certain tendency according to the wishes of management. It can be found that many scholars have discovered in their research that the classification of financial assets will indeed bring opportunities for companies to manage earnings. The classification of financial assets is closely related to fair value measurement, and some scholars have discussed this. Literature [15] puts forward new insights in the classification, reclassification, and measurement of financial assets to prevent corporate management from adjusting corporate profits at will. Research in this area also exists in the field of practice. Literature [16], in studying the classification of financial instruments of securities companies and the fair value of financial instruments, concluded that the accounting information disclosure system of enterprises on financial instruments is still not perfect. Commercial banks hold the largest scale of financial assets, so some scholars have carried out research on the impact of financial asset classification on commercial banks' profits. Literature [17] analyzed the classification of financial instruments of commercial banks and concluded that the management of the enterprise has a risk appetite for the classification of financial instruments, and it replaces liquidity with robustness. Literature [18] uses the data of Liangmianzhen, Minmetals Development, and Qianjiang Biochemical Company as examples to discuss the earnings management of listed companies based on the perspective of financial asset classification and accounting confirmation differences. Literature [19] compares the differences between IFRS9 and the current accounting standards in the classification of financial assets and analyzes the differences between IAS39 and IFRS9 financial asset classification of 16 listed banks, showing the possible impact of commercial banks in the future. Financial asset standards are closely related to the financial environment. Literature [20] puts forward suggestions for strengthening supervision and protection. Literature [21] discusses the problems that financial asset reclassification may bring to corporate profits and losses, including the recognition of corporate profits and losses in

financial asset holdings, the impact of financial asset impairment on profits and losses, and the possible problems of financial asset reclassification.

3. Financial Data Intelligent Mining Classification Method

We assume that there are p indicators in the actual problem under discussion, and we regard these p indicators as p random variables, denoted as $X_1, X_2, \ldots, X_p$. Principal component analysis is to transform the problem of p indicators into a problem of discussing the linear combination of p indicators. These new indicators $F_1, F_2, \ldots, F_k (k \leq p)$ fully reflect the information of the original indicators in accordance with the principle of preserving the amount of main information and are independent of each other.

This process of reducing multiple indicators to a few comprehensive indicators is mathematically called dimensionality reduction. The usual method of principal component analysis is to seek the linear combination F_i of the original indicators.

$$
\begin{aligned}
F_1 &= \mu_{11}X_1 + \mu_{21}X_2 + \cdots \mu_{p1}X_p, \\
F_2 &= \mu_{12}X_1 + \mu_{22}X_2 + \cdots \mu_{p2}X_p, \\
&\cdots \\
F_p &= \mu_{1p}X_1 + \mu_{2p}X_2 + \cdots \mu_{pp}X_p.
\end{aligned}
\tag{1}
$$

It satisfies the following conditions:

(1) The sum of the squares of the coefficients of each principal component is 1, that is,

$$
\mu_{1i}^2 + \mu_{2i}^2 + \cdots \mu_{pi}^2 = 1.
\tag{2}
$$

(2) The principal components are independent of each other; that is, there is no overlapping information, that is,

$$
\mathrm{Cov}\left(F_i, F_j\right) = 0, \quad i \neq j, i, j = 1, 2, \ldots, p.
\tag{3}
$$

(3) The variance of the principal components decreases successively, and the importance decreases successively, namely,

$$
\mathrm{Var}\left(F_1\right) \geq \mathrm{Var}\left(F_2\right) \geq \cdots \geq \mathrm{Var}\left(F_p\right).
\tag{4}
$$

The conclusion of the two linear algebras is as follows:

(1) If A is a real symmetric matrix of order p, then an orthogonal matrix U must be found to make

$$
U^{-1}AU = \begin{bmatrix} \lambda_1 & 0 & \cdots & 0 \\ 0 & \lambda_2 & \cdots & 0 \\ \vdots & \vdots & \ddots & \vdots \\ 0 & 0 & \cdots & \lambda_p \end{bmatrix}_{p \times p}.
\tag{5}
$$

Among them, $\lambda_i (i = 1, 2, \ldots, p)$ is the characteristic root of A.

(2) If the unit eigenvector corresponding to the characteristic root of the above matrix is $\mu_1, \ldots, \mu_p$,

$$
U = \left(u_1, u_2, \ldots, u_p\right) = \begin{bmatrix} u_{11} & u_{12} & \cdots & u_{1p} \\ u_{21} & u_{22} & \cdots & u_{2p} \\ \vdots & \vdots & \ddots & \vdots \\ u_{p1} & u_{p2} & \cdots & u_{pp} \end{bmatrix}.
\tag{6}
$$

Then, the eigenvectors corresponding to different eigenvalues of the real symmetric matrix U are orthogonal, that is, $U'U = UU' = I$ [22].

Conclusion: $\sum x$ is the covariance matrix of the random vector $X = X_1 + X_2 + X_3 + \cdots + X_p$. It has eigenvalue $\lambda_1, \lambda_2, \ldots, \lambda_p$ and eigenvector $u_1, u_2, \ldots, u_p$, where $\lambda_1 \geq \lambda_2 \geq \cdots \geq \lambda_p$. Then, the principal components are

$$
\begin{aligned}
F_1 &= \mu_{11}X_1 + \mu_{21}X_2 + \cdots \mu_{p1}X_p, \\
F_2 &= \mu_{12}X_1 + \mu_{22}X_2 + \cdots \mu_{p2}X_p, \\
&\cdots \\
F_p &= \mu_{1p}X_1 + \mu_{2p}X_2 + \cdots \mu_{pp}X_p.
\end{aligned}
\tag{7}
$$

At this time, $\mathrm{Var}(F_i) = U' \sum xU = \lambda_i$, $i = 1, 2, \ldots, p$. $\mathrm{Cov}(F_i, F_j) = 0, i \neq j, i, j = 1, 2, \ldots, p$.

It is written in matrix form: $F = U'X$.

$$
U = \left(u_1, \ldots, u_p\right) = \begin{bmatrix} u_{11} & u_{12} & \cdots & u_{1p} \\ u_{21} & u_{22} & \cdots & u_{2p} \\ \vdots & \vdots & \ddots & \vdots \\ u_{p1} & u_{p2} & \cdots & u_{pp} \end{bmatrix},
\tag{8}
$$

$$
X = \left(X_1, X_2, \ldots, X_P\right).
$$

The two basic concepts are as follows:

(1) Contribution rate: the proportion of the variance of the i-th principal component in the total variance, $\lambda_i / \sum_{i=1}^{p} \lambda_i$, is called the contribution rate, which reflects how much information the original P indicators have and how comprehensive they are.

(2) Cumulative contribution rate: the comprehensive ability of the first k_i principal components is described by the variance of these k principal components and the proportion $\sum_{i=1}^{k} \lambda_i / \sum_{i=1}^{p} \lambda_i$ in the total variance, which is called the cumulative contribution rate.

One of the purposes of our principal component bond analysis is to replace the original p indicators with as few principal components $F_1, F_2, \ldots, F_k (k \leq p)$ as possible. In actual work, the number of principal components depends on the amount of information that can reflect the original variable, that is, the cumulative contribution rate.

Principal component analysis is a method that converts multiple indicators into a few indicators and can maintain the correlation of the largest original data. The more important variance contribution $\beta_i (i = 1, 2, \ldots, k)$ in principal component analysis represents the maximum value of the

variance contribution of the i-th common factor after eliminating the influence of $(i-1)$ common factors. It is mainly used to measure the importance of the i-th common factor. Therefore, the corresponding evaluation model can be established with β as the weight: $F = \beta_1 F_1 + \beta_2 F_2 + \cdots + \beta_k F_k$. Among them, $F_1, F_2, \ldots, F_k$ is the corresponding k common factors used to comprehensively describe the original indicators, and the comprehensive score is calculated and sorted.

In summary, the calculation process of finding the principal components has the following steps. We set n samples, where each sample has m data, denoted as

$$X = \begin{bmatrix} x_{11} & \cdots & x_{1m} \\ \vdots & \ddots & \vdots \\ x_{n1} & \cdots & x_{nm} \end{bmatrix}. \tag{9}$$

(1) Standardization of sample data: in order to achieve the standardization of sample data, the mean and variance of the sample data need to be required. The standardization of sample data is based on the mean and variance of the data. The essence of standardization is to transform the sample into standardized data with a mean value of 0 and a variance of 1. That is, the normalized transformation of the column is

$$x_{ij}^{\bullet} = \frac{\left(x_{ij} - \overline{x}_j \right)}{\delta_j}. \tag{10}$$

Among them,

$$i = 1, 2, \ldots, n,$$

$$j = 1, 2, \ldots, m,$$

$$\overline{x}_j = \frac{1}{n} \sum_{i=1}^{n} x_{ij}, \tag{11}$$

$$\delta_j^2 = \frac{1}{n} \sum_{i=1}^{n} \left(x_{ij} - \overline{x}_j \right)^2.$$

The resulting standardized matrix $X^{\bullet}$ is written as

$$X = \begin{bmatrix} x_{11} & \cdots & x_{1m} \\ \vdots & \ddots & \vdots \\ x_{n1} & \cdots & x_{nm} \end{bmatrix}. \tag{12}$$

(2) Calculation of the correlation matrix: for given n samples, we use a computer to calculate the correlation coefficient matrix of the indicator variables:

$$R = \begin{bmatrix} r_{11} & \cdots & r_{1m} \\ \vdots & \ddots & \vdots \\ r_{m1} & \cdots & r_{mm} \end{bmatrix} = \frac{1}{n} X' X. \tag{13}$$

Among them,

$$r_{ij} = \frac{1}{n} \sum_{i=1}^{n} X_{ij} X_{ik} = \frac{1}{n} x_j' x_k, \quad j, k = 1, 2, \ldots, m. \tag{14}$$

(3) Find eigenvalues and eigenvectors. The obtained correlation matrix is R to solve the characteristic equation:

$$|R - \lambda f| = 0. \tag{15}$$

By solving the characteristic equation, k eigenvalues $(i = 1 \sim m)$ and the eigenvector corresponding to each eigenvalue can be obtained:

$$Q_i = \left(a_{i1}, a_{i2}, \ldots, a_{ip} \right), \quad i = 1 \sim k. \tag{16}$$

And the eigenvectors corresponding to $\lambda_1 > \lambda_2 > \lambda_3 > \lambda_k > 0$ are orthogonal to each other.

By the above method, k $(k \leq p)$ principal components can be obtained. $\lambda_i / \sum_{i=1}^{k} \lambda_i$ is the contribution rate of the i-th principal component, denoted as β_i, which is

$$\beta_i = \frac{\lambda_i}{\sum_{i=1}^{k} \lambda_i}. \tag{17}$$

Among the k principal components, the sum of the contribution rates of the first q principal components is the cumulative contribution rate of the first q principal components, denoted as α:

$$\alpha = \frac{\sum_{i=1}^{q} \lambda_i}{\sum_{i=1}^{k} \lambda_i}. \tag{18}$$

The number of principal components can be determined by the cumulative contribution rate. Usually the cumulative contribution rate $\alpha \geq 0.85$ as the standard. For the selected q principal components, if the cumulative contribution rate reaches 85%, that is, $a \geq 0.85$, the principal components can be determined as q. It represents the selected q principal components and basically retains the information of the original p variables. When determining the number of principal components, the number of principal components should be minimized under the condition of the cumulative contribution rate constraint.

(4) Find the factor load α_i:

$$\alpha_i = \sqrt{\lambda_i} \alpha_i. \tag{19}$$

According to formula (19), we calculate the factor loading matrix and then calculate the score of each factor:

$$F_i = \alpha_i x, \quad i = 1, 2, \ldots, k. \tag{20}$$

(5) According to the numerator of the factor and the size of the contribution rate, we calculate the comprehensive score:

$$F = \beta_1 F_1 + \beta_2 F_2 + \cdots + \beta_k F_k. \tag{21}$$

Finally, it is sorted according to the comprehensive score. PCA analyzes the system with fewer q indicators instead of the original p indicators, which brings great convenience to the comprehensive evaluation of the system.

A large amount of original detection value data flow information is used to detect lag correlation using the BRAID method, and a series of time series with lag correlation can be found, and the lag time of each time series relative to the original reference series can be calculated.

We assume that there are n time series with a lagging correlation after the detection of the BRAID method. Each time series has a piece of data. Since the original detection data are data values obtained at equal intervals of time, a time variable t is introduced in the representation of the time series, and the data value corresponding to each time point is $x(t)$. Then the original multidimensional data flow is denoted as

$$X = (X_1(t), X_2(t), \ldots, X_n(t)), \quad t = 0, 1, \ldots, m - 1. \tag{22}$$

This can be written in matrix form, namely,

$$X = \begin{bmatrix} x_1(0) & x_1(1) & \cdots & x_1(m-1) \\ x_2(0) & x_2(1) & \cdots & x_2(m-1) \\ \vdots & \vdots & \ddots & \vdots \\ x_n(0) & x_n(1) & \cdots & x_n(m-1) \end{bmatrix}. \tag{23}$$

The lag time is recorded as $\Delta t_1, \Delta t_2, \ldots, \Delta t_n$.

Among them, $\Delta t_1 = 0$ (that is, x is the original reference sequence), and $\Delta t_2, \ldots, \Delta t_n$ is the lag time of the sequence $x_2, \ldots, x_n$ relative to the sequence x_1.

The first principal component analysis method is applied to "aligned" data streams; that is, the data is synchronized. This article discusses the lag-related multidimensional data flow. The data that needs principal component analysis is not synchronized, but has a certain lag time relative to the original time series. Therefore, it is necessary to perform principal component analysis on the detected multidimensional data stream with lagging correlation. The first task is to remove the lagging part of each time series, and "align" the data flow, that is, temporarily ignore the time parameters, and only keep the parts with similar changing trends in each time series, in order to achieve the purpose of multidimensional data flow synchronization. Figure 1 shows the unsynchronized time series, and Figure 2 shows the synchronized time series.

If the data corresponding to w time points in each data stream are obtained, the synchronized multidimensional data stream is recorded as

$$X = \begin{bmatrix} x_1(0) & x_1(1) & \cdots & x_1(w-1) \\ x_2(\Delta t_2) & x_2(\Delta t_2 + 1) & \cdots & x_2(\Delta t_2 + w - 1) \\ \vdots & \vdots & \ddots & \vdots \\ x_i(\Delta t_i) & x_i(\Delta t_i + i) & \cdots & x_i(\Delta t_i + w - 1) \\ \vdots & \vdots & \ddots & \vdots \\ x_n(t_n) & x_n(\Delta t_n + i) & \cdots & x_n(\Delta t_n + w - 1) \end{bmatrix}. \tag{24}$$

That is, $X = (X_i(\Delta t_i), X_i(\Delta t_i + 1), \ldots, X_i(\Delta t_i + w - 1))$, where $i = 1, 2, \ldots, n$.

For the above synchronized multidimensional data stream with delayed correlation, we apply the principal component analysis method to find the principal components. The steps of calculating the principal components include standardizing the sample data, calculating the correlation matrix, finding the eigenvalues and eigenvectors, and finding the principal components.

(1) Standardize multidimensional data streams. In order to achieve the standardization of multidimensional data streams, we should find the mean and variance of each data stream. The standardization of the data stream is based on the mean and variance of each data in the data stream. The essence of standardization is to transform the data stream into standardized data with a mean value of 0 and a variance of 1, which is to perform a standardized transformation on the column of X:

$$x_i^\bullet(j) = \frac{\left(x_i(j) - \overline{x(j)}\right)}{\delta_j}. \tag{25}$$

Among them,

$$i = 1, 2, \ldots, n,$$

$$j = 1, 2, \ldots, m,$$

$$\overline{x(j)} = \frac{1}{n} \sum_{i=1}^{n} x_i(j), \tag{26}$$

$$\delta_j^2 = \frac{1}{n} \sum_{i=1}^{n} \left(x_i(j) - \overline{x(j)}\right)^2.$$

Then we get the standardized matrix, denoted as

$$X = \begin{bmatrix} x_1(0) & x_1(1) & \cdots & x_1(w-1) \\ x_2(0) & x_2(1) & \cdots & x_2(w-1) \\ \vdots & \vdots & \ddots & \vdots \\ x_n(0) & x_n(1) & \cdots & x_n(w-1) \end{bmatrix}. \tag{27}$$

(2) Calculate the correlation matrix. For the w data streams with lagging correlations that have been detected, we use a computer to calculate the correlation coefficient matrix of the indicator variables:
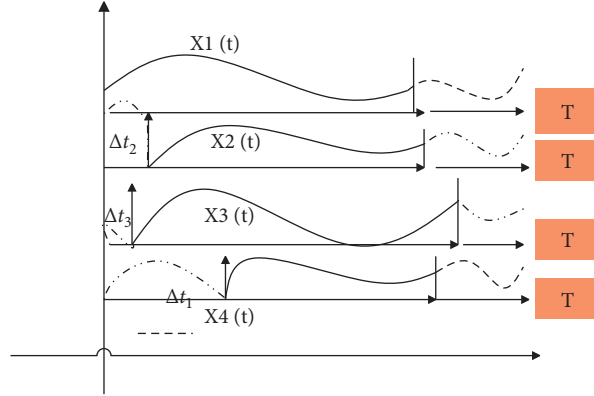
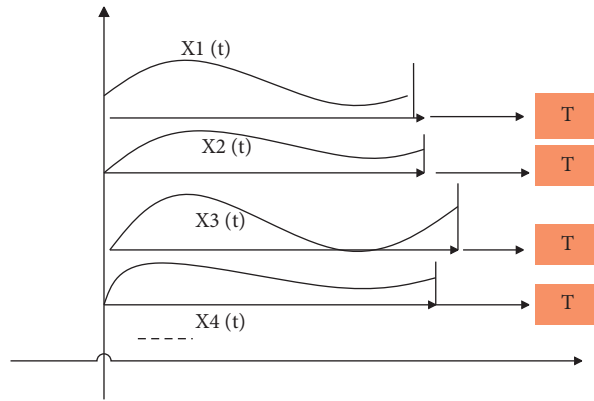FIGURE 1: Unsynchronized time series.

FIGURE 2: Synchronized time series.

$$R = \begin{bmatrix} r_{11} & \cdots & r_{1m} \\ \vdots & \ddots & \vdots \\ r_{m1} & \cdots & r_{mm} \end{bmatrix} = \frac{1}{n} X' X. \qquad (28)$$

Among them,

$$r_{ij} = \frac{1}{n} \sum_{i=1}^{n} X_{ij} X_{ik} = \frac{1}{n} x_j' x_k, \quad j, k = 1, 2, \dots, m. \qquad (29)$$

(3) Find eigenvalues and eigenvectors. The obtained correlation matrix is R to solve the characteristic equation: $|R - \lambda f| = 0$.

By solving the characteristic equation, w eigenvalues can be obtained, and the eigenvector corresponding to each eigenvalue: $U_i = (u_{i1}, u_{i2}, \dots, u_{iw})$, $i = 1 \sim w$, and $\lambda_1 > \lambda_2 > \cdots > \lambda_w > 0$, and its corresponding eigenvector are orthogonal to each other.

(4) Find the principal components. The algorithm can obtain w principal components by the above method. $\lambda_i / \sum_{i=1}^{w} \lambda_i$ is the contribution rate of the i-th principal component, denoted as β_i, namely,

$$\beta_i = \frac{\lambda_i}{\sum_{i=1}^{w} \lambda_i}. \qquad (30)$$

Among the w principal components, the sum of the contribution rates of the first k principal components is called the cumulative contribution rate of the first k principal components, denoted as α:

$$\alpha = \frac{\sum_{i=1}^{k} \lambda_i}{\sum_{i=1}^{w} \lambda_1}. \qquad (31)$$

The number of principal components can be determined by the cumulative contribution rate. This paper takes the cumulative contribution rate $\alpha \geq 0.85$ as the standard. For the selected k principal components, if the cumulative contribution rate reaches 85%, that is, $\alpha \geq 0.85$, then the principal components can be determined as k. It means that the selected k principal components basically retain the information of the original w variables. When determining the number of principal components, the number of principal components should be reduced as much as possible under the condition of $\alpha \geq 0.85$.

Using the obtained k principal components to linearly combine them can express the original multidimensional data flow of the lag correlation, namely,

$$
\begin{aligned}
F_1(t) &= u_{11}x_1(t) + u_{12}x_2(t + \Delta t_2) + \cdots + u_{1i}x_i(t + \Delta t_i) + \cdots + u_{1k}x_k(t + \Delta t_k), \\
F_2(t) &= u_{21}x_1(t - \Delta t_2) + u_{22}x_2(t) + \cdots + u_{2i}x_i(t + \Delta t_i - \Delta t_2) + \cdots + u_{2k}x_k(t + \Delta t_k - \Delta t_2), \\
&\cdots \\
F_i(t) &= u_{i1}x_1(t - \Delta t_i) + u_{i2}x_2(t - \Delta t_i + \Delta t_2) + \cdots + u_{ii}x_i(t) + \cdots + u_{ik}x_k(t - \Delta t_i - \Delta t_k), \\
&\cdots \\
F_n(t) &= u_{n1}x_1(t - \Delta t_n) + u_{n2}x_2(t - \Delta t_n + \Delta t_2) + \cdots + u_{ni}x_i(t - \Delta t_n + \Delta t_i) + \cdots + u_{nk}x_k(t + \Delta t_n - \Delta t_k).
\end{aligned}
\tag{32}
$$

Furthermore, the algorithm obtains a comprehensive evaluation function:

$$
F = \beta_1 F_1 + \beta_2 F_2 + \cdots + \beta_k F_k. \tag{33}
$$

It can be seen that, by performing principal component analysis (PCA) on the lag-related multidimensional data stream, the original multidimensional data stream represented by the data corresponding to the larger m time points can be converted into the smaller k principal components to represent the original multidimensional data stream, which brings great convenience to the storage and use of data stream and also provides help for the analysis and reconstruction of lag-related multidimensional data stream.

4. Classification and Statistics of Financial Data in Smart Cities Based on Artificial Intelligence

The overall framework of financial asset classification is shown in Figure 3.

There are three major factors in sequence analysis. (1) Sequence duration: it refers to the length of the analyzed sequence in the time dimension, such as the time period during which user behavior occurs. (2) Time folding window: it means that a series of actions occurring within a certain period of time will be regarded as occurring simultaneously. (3) Time interval: it refers to the time interval of the discovered time series model. An example of the data mining process is shown in Figure 4.

The fast hierarchical clustering algorithm based on root finding is based on the following assumption: a data set can be divided into several clusters, and there is a core point in each cluster, and this point can represent other points in the cluster. This core point is not necessarily the center of mass of the cluster; it exists in an area where the data is densely distributed. The area with dense data distribution here refers to the closest distance between the data points in this area relative to the surrounding neighborhood of this area. We call the core point of the cluster the root node, as shown in Figure 5.

The structure design of the financial data classification system is shown in Figure 6. The system obtains sample files from the sample database after data extraction and preprocesses the sample files into training samples and test samples. The training samples are used to train the classifier, and the test samples are used to evaluate the classification performance of the classifier, and the training process of the classifier is adjusted according to the evaluation results to obtain the final classifier.

The evaluation process of the classification effect is shown in Figure 7. The source of the test sample is the same as the training sample. It is taken from the sample database and preprocessed. The test sample also carries the actual category label.

The simple understanding of financial data classification task refers to the process of categorizing financial data of an unknown category based on its content when the classification system is known. Financial data classification is essentially a process of identifying the characteristics of financial data patterns. After the financial data is preprocessed and expressed as a feature vector, it is input into the classifier, and the model is trained. For the financial data to be classified, it is also expressed as a feature vector and then input into the classifier for classification. Figure 8 shows the principle of financial data classification. Financial data content processing will be introduced in detail later.

As shown in Figure 9, we have given a basic model framework based on rough set and KNN text classification. In this model framework, we can clearly see that this model is composed of three parts: rough set-related preprocessing module, KNN classification algorithm module, and quality evaluation module. First, in the text collection stage, the relevant web text data is obtained from the internet, and the relevant data is used as the training set and test set of the web text for subsequent operations, and then the next step is entered.

After constructing the above intelligent model, this paper conducts statistical analysis of the intelligent model and evaluates the effect of financial data mining and financial data classification, and the results are shown in Figure 10.

It can be seen from Figure 10 that the intelligent algorithm proposed in this paper can play a certain role in financial data processing. After evaluating the intelligent data decision in this paper, the results are shown in Figure 11.
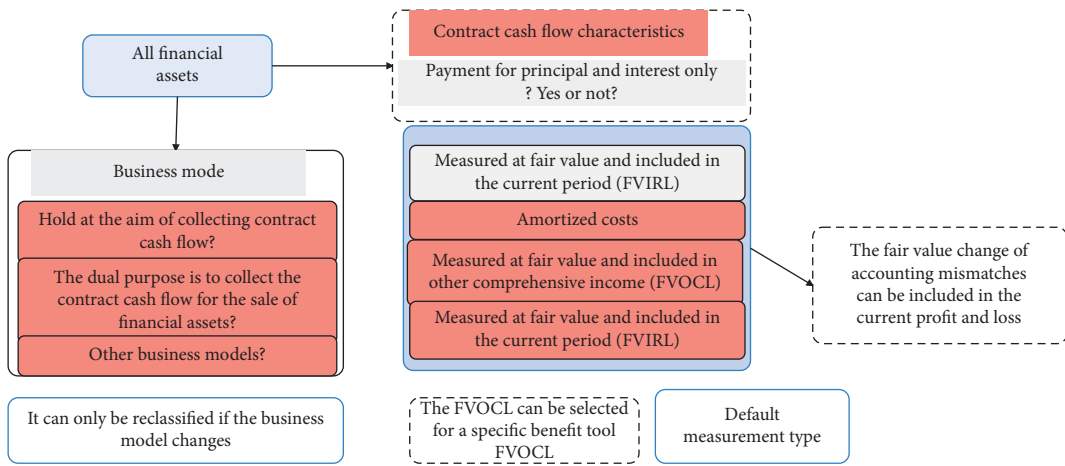
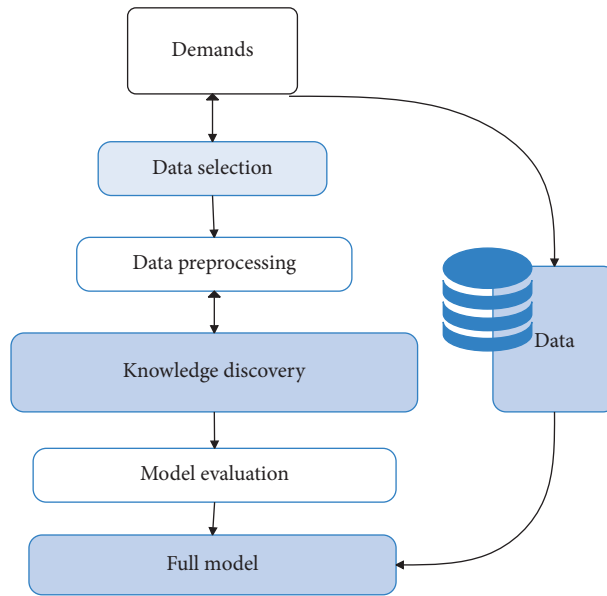FIGURE 3: The overall framework of financial asset classification.

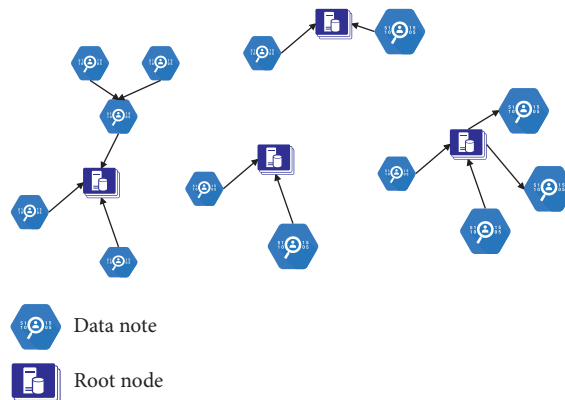FIGURE 4: The data mining process.

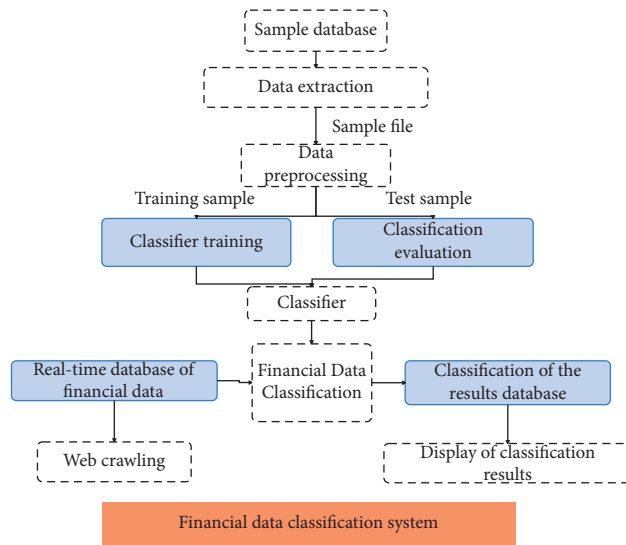FIGURE 5: A possible result of finding the root node on the sample data set.

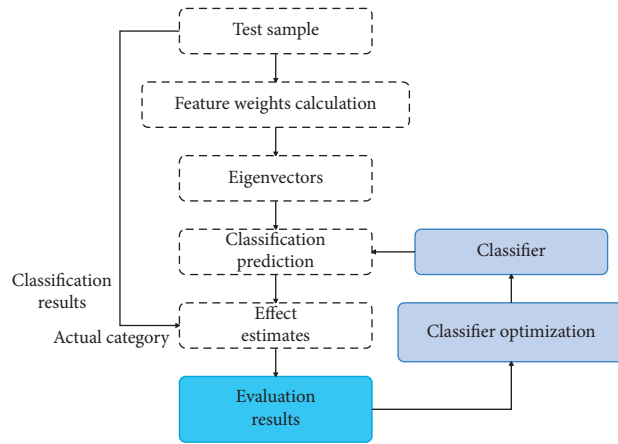Figure 6: Financial data classification system structure.

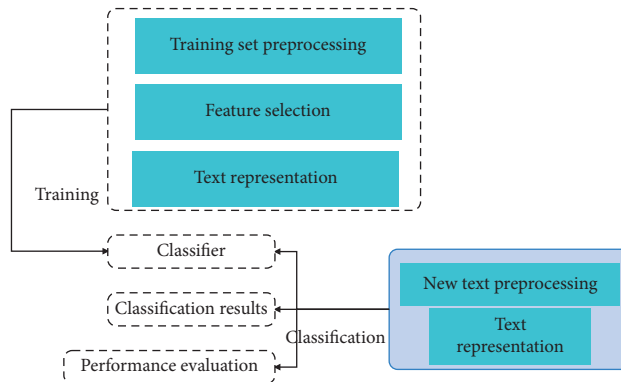Figure 7: Classification and evaluation process diagram.

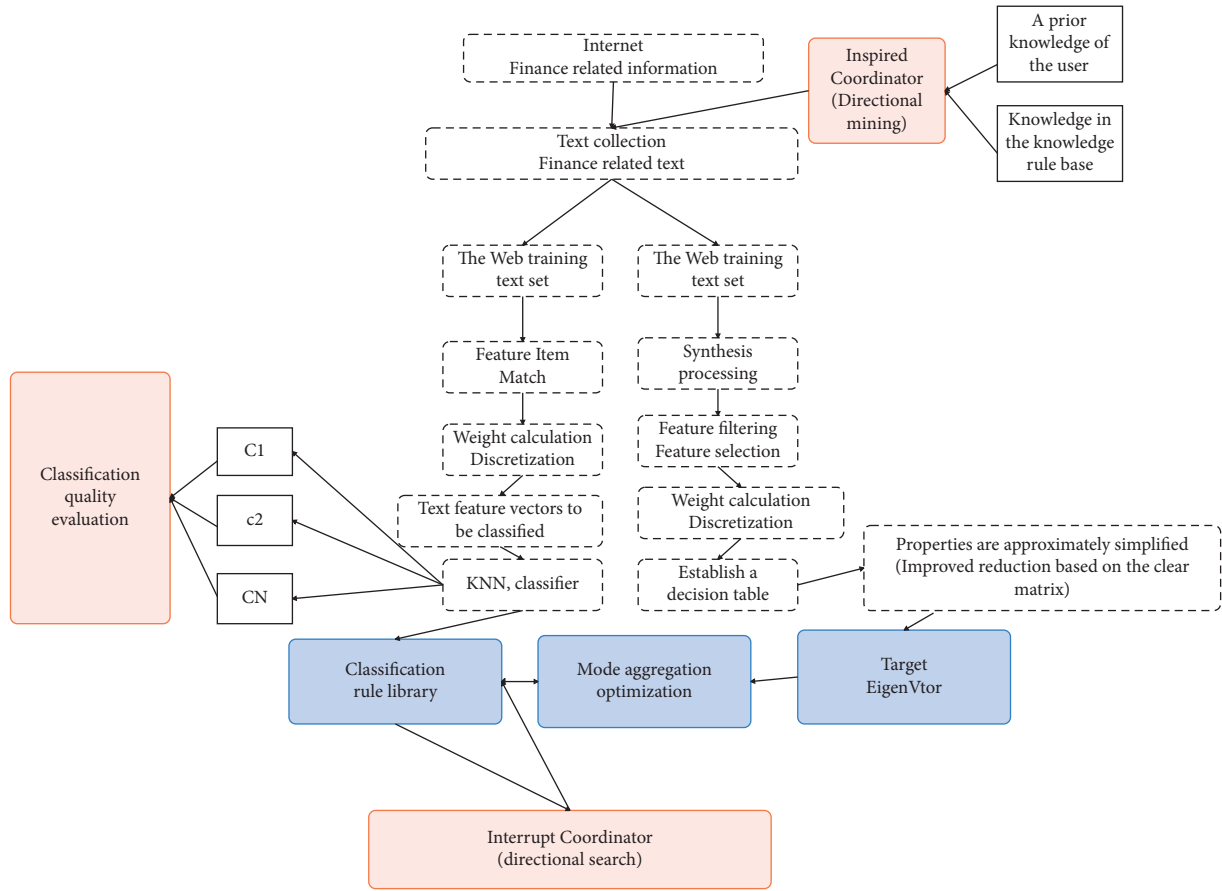Figure 8: Principles of financial data classification.

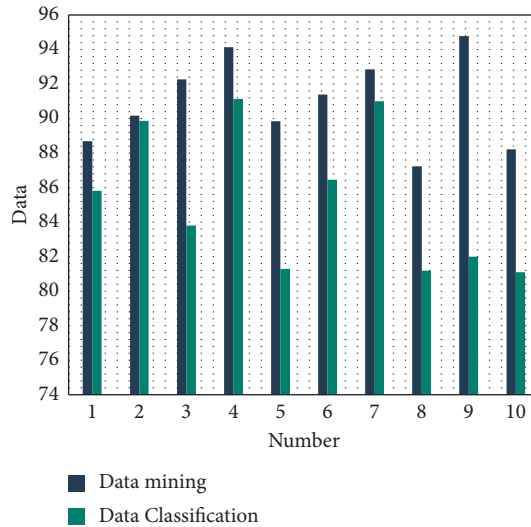FIGURE 9: Financial data subsystem model framework.

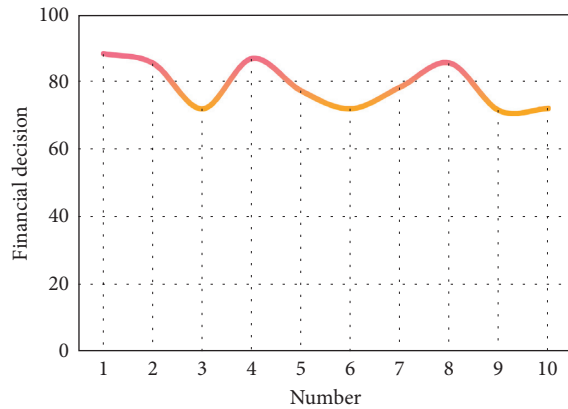FIGURE 10: Evaluation of financial data processing effect.

Figure 11: Intelligent data decision statistics.

From the above research, we can see that the artificial intelligence classification and statistical method of financial data in smart cities proposed in this paper can play a certain auxiliary role in financial decision-making.

5. Conclusion

The prediction problem of financial data processing is mainly the prediction of financial time series. Financial time series can be regarded as a special time series, which has the following three characteristics. (1) The generation process of financial time series is more complicated, and there are many influencing factors. (2) Most financial time series contain a large number of unpredictable influence factors. (3) The composition of the data in the financial time series is relatively complex and usually exhibits nonlinearity. Artificial intelligence information processing methods such as neural networks, chaos theory, and genetic algorithms can well adapt to these three characteristics, which have become advanced methods to solve financial data processing problems. This paper combines big data technology to carry out financial data classification research and extracts financial data from different data sources in an automatic and intelligent way. Users can not only get the data they want in the shortest time, but also improve the accuracy and effectiveness of the data. Through experimental research, we know that the artificial intelligence classification and statistical method of financial data in smart cities proposed in this paper can play a certain auxiliary role in financial decision-making.

Data Availability

The labeled dataset used to support the findings of this study is available from the corresponding author upon request.

Conflicts of Interest

The author declares no conflicts of interest.

Acknowledgments

References

[1] P. Rajsic, A. Weersink, A. Navabi, and K. Peter Pauls, "Economics of genomic selection: the role of prediction accuracy and relative genotyping costs," *Euphytica*, vol. 210, no. 2, pp. 1–18, 2016.

[2] F. Jahedpari, T. Rahwan, S. Hashemi et al., "Online prediction via continuous artificial prediction markets," *IEEE Intelligent Systems*, vol. 32, no. 1, pp. 61–68, 2017.

[3] V. Daksiya, H. T. Su, Y. H. Chang, and E. Y. M. Lo, "Incorporating socio-economic effects and uncertain rainfall in flood mitigation decision using MCDA," *Natural Hazards*, vol. 87, no. 1, pp. 515–531, 2017.

[4] S. Lahmiri, "A variational mode decompoisition approach for analysis and forecasting of economic and financial time series," *Expert Systems with Applications*, vol. 55, no. 8, pp. 268–273, 2016.

[5] N. Gordini, "A genetic algorithm approach for SMEs bankruptcy prediction: empirical evidence from Italy," *Expert Systems with Applications*, vol. 41, no. 14, pp. 6433–6445, 2014.

[6] A. Ferramosca, A. H. González, and D. Limon, "Offset-free multi-model economic model predictive control for changing economic criterion," *Journal of Process Control*, vol. 54, no. 3, pp. 1–13, 2017.

[7] C. J. Jane, "A hybrid model combined grey prediction and autoregressive integrated moving average model for talent prediction," *Journal of Grey System*, vol. 21, no. 2, pp. 91–102, 2018.

[8] A. Khadjeh Nassirtoussi, S. Aghabozorgi, T. Ying Wah, and D. C. L. Ngo, "Text mining for market prediction: a systematic review," *Expert Systems with Applications*, vol. 41, no. 16, pp. 7653–7670, 2014.

[9] M. Ellis and P. D. Christofides, "Integrating dynamic economic optimization and model predictive control for optimal operation of nonlinear process systems," *Control Engineering Practice*, vol. 22, no. 1, pp. 242–251, 2014.

[10] W. Schultz, W. R. Stauffer, and A. Lak, "The phasic dopamine signal maturing: from reward via behavioural activation to formal economic utility," *Current Opinion in Neurobiology*, vol. 43, no. 5, pp. 139–148, 2017.

[11] C. J. Lee and E. B. Andrade, "Fear, excitement, and financial risk-taking," *Cognition and Emotion*, vol. 29, no. 1, pp. 178–187, 2015.

[12] S. M. Bartram, G. W. Brown, and W. Waller, "How important is financial risk?" *Journal of Financial and Quantitative Analysis*, vol. 50, no. 4, pp. 801–824, 2015.

[13] W. W. Cooper, A. T. Kingyens, and J. C. Paradi, "Two-stage financial risk tolerance assessment using data envelopment analysis," *European Journal of Operational Research*, vol. 233, no. 1, pp. 273–280, 2014.

[14] W. Montford and R. E. Goldsmith, "How gender and financial self-efficacy influence investment risk taking," *International Journal of Consumer Studies*, vol. 40, no. 1, pp. 101–106, 2016.

[15] S. Muthii Wanjohi, J. G. Wanjohi, and J. M. Ndambiri, "The effect of financial risk management on the financial performance of commercial banks in Kenya," *International Journal of Finance and Banking Research*, vol. 3, no. 5, pp. 70–81, 2017.

[16] J. Magendans, J. M. Gutteling, and S. Zebel, "Psychological determinants of financial buffer saving: the influence of financial risk tolerance and regulatory focus," *Journal of Risk Research*, vol. 20, no. 8, pp. 1076–1093, 2017.

[17] E. S. Cole, D. Walker, A. Mora, and M. L. Diana, "Identifying hospitals that may be at most financial risk from medicaid

disproportionate-share hospital payment cuts," *Health Affairs*, vol. 33, no. 11, pp. 2025–2033, 2014.

[18] A. Zalik, "Resource sterilization: reserve replacement, financial risk, and environmental review in Canada's tar sands," *Environment and Planning A: Economy and Space*, vol. 47, no. 12, pp. 2446–2464, 2015.

[19] C. Lucarelli, P. Uberti, and G. Brighetti, "Misclassifications in financial risk tolerance," *Journal of Risk Research*, vol. 18, no. 4, pp. 467–482, 2015.

[20] E. Y. Chan, "Physically-attractive males increase men's financial risk-taking," *Evolution and Human Behavior*, vol. 36, no. 5, pp. 407–413, 2015.

[21] M. Banam and A. Mehrazeen, "The relationship of information asymmetry, institutional ownership and stock liquidity with income smoothing in tehran stock exchange," *Journal of Management and Accounting Studies*, vol. 4, no. 3, pp. 6–11, 2016.

[22] B. F. Jones, "The human capital stock: a generalized approach," *The American Economic Review*, vol. 104, no. 11, pp. 3752–3777, 2014.

Research Article

Association Mining of Near Misses in Hydropower Engineering Construction Based on Convolutional Neural Network Text Classification

Shu Chen,[1] Junbo Xi,[2] Yun Chen [iD],[1] and Jinfan Zhao[1]

[1]*Department of Engineering Management, College of Hydraulic and Environmental Engineering, China Three Gorges University, Yichang, Hubei 443002, China*
[2]*Department of Engineering Management, College of Economics and Management, China Three Gorges University, Yichang, Hubei 443002, China*

Correspondence should be addressed to Yun Chen; yunchen@ctgu.edu.cn

Accidents of various types in the construction of hydropower engineering projects occur frequently, which leads to significant numbers of casualties and economic losses. Identifying and eliminating near misses are a significant means of preventing accidents. Mining near-miss data can provide valuable information on how to mitigate and control hazards. However, most of the data generated in the construction of hydropower engineering projects are semi-structured text data without unified standard expression, so data association analysis is time-consuming and labor-intensive. Thus, an artificial intelligence (AI) automatic classification method based on a convolutional neural network (CNN) is adopted to obtain structured data on near-miss locations and near-miss types from safety records. The apriori algorithm is used to further mine the associations between "locations" and "types" by scanning structured data. The association results are visualized using a network diagram. A Sankey diagram is used to reveal the information flow of near-miss specific objects using the "location ⟶ type" strong association rule. The proposed method combines text classification, association rules, and the Sankey diagrams and provides a novel approach for mining semi-structured text. Moreover, the method is proven to be useful and efficient for exploring near-miss distribution laws in hydropower engineering construction to reduce the possibility of accidents and efficiently improve the safety level of hydropower engineering construction sites.

1. Introduction

Construction is a high-risk industry, and until recently, construction sites have continued to pose a serious threat to workers' lives and health [1]. In particular, hydropower engineering construction leads to various types of casualties due to the frequent cross-work of construction equipment, the dynamic construction work environment, and high-risk site operations [2]. For example, in March 2020 alone, there were two hydropower accidents in Sichuan Province: a scaffolding collapse and high falls caused by burnt-out safety belts led to 3 deaths and 4 injuries, according to China's National Energy Administration [3].

Near misses have been defined as a dangerous state in production that may lead to accidents, such as the unsafe behavior of people, an unsafe state of things, unsafe factors in the environment, and defects in management [4]. In particular, there is a wider variety of near misses in the construction of hydropower engineering, leading to a sharply increased probability of serious accidents. An accident is a fait accompli and cannot be undone. In contrast, near misses still have remedial leeway [5]. Therefore, to improve the safety situation, it is a key part of safety management to determine the potential laws of near misses and take safety measures to eliminate near misses in the construction of hydropower engineering projects.

With increasing attention to safety issues in the hydropower industry, the frequency of safety inspections has increased rapidly, and numerous near-miss text data have been accumulated. However, text data are both semistructured and unstructured; accordingly, traditional methods of mining text data are time-consuming and laborintensive. With the development of artificial intelligence (AI) technology, automatic mining and analysis of near misses will inevitably replace relying on manual work to structure text data and find near-miss laws [6]. Thus, it is of great significance to study the data mining of near-miss text data, especially the mining of near-miss distribution laws relying on AI technology.

In the field of construction, text mining application research mainly adopts text classification methods to classify housing construction accidents, subway construction near misses, and construction contract documents. Shallow machine-learning algorithms, such as the support vector machine (SVM), naive Bayes (NB), and K-nearest neighbor (KNN) algorithms, have been used to classify housing construction accidents [7] and construction contract documents [8]. Such algorithms require manually combining lexical, syntactic, and semantic features. These are limited by the domain knowledge of individuals, resulting in poor performance in feature representation.

In contrast, deep learning algorithms (e.g., convolutional neural networks (CNNs) [9], Bidirectional Encoder Representations from Transformers (BERT) for language understanding [10], and convolutional bidirectional long short-term memory (C-BiLSTM) [11]) can automatically identify features and use existing tagged data to train the classification model of house-building construction accidents and near-miss subway construction. The above research proves that deep learning has a better effect on the classification of construction of short texts than shallow machine learning.

Previous text information expression and big data mining technology have laid a very important foundation for intelligent analysis of text information. All kinds of text intelligent analysis technology have been widely used in housing construction, subways, and so on. However, there are few studies on the intelligent analysis of big data in the field of safety knowledge in hydropower engineering construction addressed in this study. Although the core algorithm of text big data analysis has not changed much, due to the unique characteristics of safety knowledge in hydropower engineering construction, the data analysis framework that focuses on hidden trouble needs to be reformulated. The main reason is that hydropower engineering construction involves a wide range of engineering types, and there are huge differences between different engineering types, leading to the necessity of reexploring the distribution of near misses in this kind of engineering. Moreover, these studies only classified the text without discussing how to further mine the more detailed construction knowledge contained in the classified text. Safety managers cannot intuitively and quickly acquire near-miss knowledge due to the poor visualization effect of near-miss distributions.

Against this contextual backdrop, we develop a near-miss classifier based on a CNN, associate the classified results, and visualize them with a network diagram [12] and a Sankey diagram so that safety managers can easily find the key points of massive near misses [13]. First, to structure text data, a CNN-based classifier that incorporates a deep learning method is developed to generate structured classification results of near-miss information within safety records. The classifier can capture semantic features in a near-miss text to automatically classify near-miss locations and the near-miss descriptions into predefined "location" and "type" categories, which can generate structured data for statistical analysis. An apriori algorithm is then used to quantify the frequency and trustworthiness of the association rule "location ⟶ type." The network diagram visualizes the quantification of the association rule "location ⟶ type." Finally, after integrating all texts corresponding to each category of strong association rules, the Chinese word segmentation is carried out on these texts. A Sankey diagram is drawn with word frequency as the size of the information flow.

A classifier based on deep learning and a CNN combined with the apriori algorithm and a Sankey diagram can automatically classify text and associate the "location" and "type" of the classification results. Consequently, safety management personnel can implement corresponding near-miss measures for specific near-miss locations, eliminate near misses in advance, and improve the safety level of hydropower project construction.

2. Related Work

2.1. Accident Prevention in Hydropower Engineering Construction. Hydropower engineering construction has the characteristics of a complex construction environment, including a wide range of cross-work and high labor intensity. Moreover, it has a low level of safety management and, more generally, a lack of safety supervision and personnel training [14]. Accidents occur frequently in hydropower project construction. There are many studies on accident prevention in hydropower engineering construction. Zheng et al. [15] applied the Human Factor Analysis and Classification System (HFACS) to study the evaluation of human factors in high-risk operations and finally obtained the evaluation value of faulty behavior risk (FBR) in hydropower engineering construction. Zhou et al. [2] integrated the methods of the decision-making trial and evaluation laboratory (DEMATEL) and the analytic network process (ANP), taking into account the interaction between factors and their self-feedback. The deduced causal diagrams provide suggestions for the safety management of high-risk working systems in several large hydropower projects. Zheng et al. [16] adopted the HFACS framework, collected 869 accident investigation reports, determined the first three accident types by frequency statistics, and determined the accident path by analyzing the correlation between different human factors. All the above studies focus on the prevention of accidents, but the study of near misses can advance the link of accident prevention and reduce the probability of accidents by eliminating near misses.

2.2. Text Classification and Machine Learning. Natural language processing (NLP) is a technology in which a computer is used to process and analyze human language, including text classification, information extraction, and information retrieval [17]. Text classification is a common task of NLP, which concerns training mathematical models to gain a certain generalization ability by inputting a group of texts with relevant classification labels so that the model can better predict the categories of other texts in the same field [18]. Text classification has been widely used in various fields as an efficient information processing technology [19].

Machine learning is a popular method to realize text classification [20]. For instance, Bertke et al. [21] identified the three "claim cause" categories of workers' medical compensation claims using the NB classifier. Ubeynarayana et al. (Ubeynarayana. and Miang., 2017) used a support vector machine (SVM) classifier to classify the Occupational Safety and Health Accident (OSHA) dataset. Similarly, Mahfouz [8] utilized an SVM to classify unstructured information in contract documents. Maia et al. [22] used the random forest (RF) method to classify complaint texts and achieved good results. All of the above studies used shallow machine learning, which can only obtain simple functions through a linear combination of feature parameters of training data. However, simple functions poorly classify the complex and changeable near-miss text of hydropower project construction.

Deep learning (DL) can learn complex functions and extract higher-dimensional features from input data. The DL method has been identified as an appropriate method to automatically extract features for text classification without manually creating features [23]. Compared to shallow machine learning, DL can effectively extract word order features and learn from the semantic information contained in text [24].

CNNs have been applied in NLP and have achieved good results in semantic processing [25], sentence modeling [26], and search query retrieval [27]. Researchers are increasingly interested in the application of CNNs in text classification. Arora et al. [28] proposed a text normalization algorithm based on deep convolutional character level embedding (the Conv-char-EMB neural network model) for sentiment analysis (SA) of unstructured data. He et al. [29] proved that CNN architecture with multiple pooling operations can extract the most significant features of a convolutional filter by convolution, activation, and pooling operations and effectively classify medical relations.

Do [30] proposed a CNN model that can use both a word vector adjusted for a specific task and a static pretrained word vector for the sentence-level text classification task. Yoon et al. [31] used a CNN to classify sentences preprocessed by word embeddings and suggested that only one layer of convolution can classify sentences effectively. The above studies have laid an important foundation for text big data mining, but the laws contained in text big data of near misses in hydropower project construction need to be further explored. Due to the large difference in the characteristics of various subprojects for hydropower projects, the types of near misses in different locations are also very different and present great trouble in the analysis of hidden danger data. The text intelligence analysis method commonly used in other projects has difficulty addressing this challenge.

2.3. Association Rules and Sankey Diagram. Association rules contain the rules of occurrence between things. It is imperative for people to understand detailed information about the research object. Agrawal [32] proposed an association rule algorithm for mining the potential association between transactions in a transaction database. The apriori algorithm is the most famous association rule algorithm. It can prune item set trees to prevent the exponential growth of candidate item sets, reduce the amount of data, and improve operation efficiency [33].

Association rule mining has been widely used in construction safety fields. Cheng et al. [34] used association rules in analyzing 1347 accidents to identify potential hazards in Taiwanese construction projects. Guo et al. [35] found the association rules of workers' unsafe behavior, worker type, and construction phase in the construction industry using the apriori algorithm. Qiu and Wang [36] proposed the "cause ⟶ emergency measure" association rule algorithm based on construction accident cases to find all possible accident cause chains. Mingyuan et al. [37] used the apriori algorithm to mine a dataset of near misses in construction and obtained the correlation between the hazard sources in the internal and external environments of a construction site.

Using the apriori algorithm for data mining, these researchers obtained valuable association rules that are difficult to find by subjective experience. The algorithm involves counting the number of terms. For unstructured text, items that have the same meaning but different expressions are considered different when they are counted. Therefore, items with the same meaning need to be classified into the corresponding preset categories to obtain structured text. Finally, the number of items in each category is counted as the operation data of the apriori algorithm. However, the association rule algorithm is only applicable to mining structured data, it is necessary to carry out structured data tasks to mine unstructured text, and text classification plays such a role. Since the near misses of hydropower projects are recorded artificially, they are random and nonstandard, and all belong to unstructured texts. To mine the association rules of near misses of unstructured texts, it is necessary to obtain structured texts that are easy to calculate by classifying near misses.

A Sankey diagram is a data flow diagram that shows the flow of information among multiple attributes [38]. The Sankey diagram is a fashionable tool in energy system analysis [39], and it can clearly show the energy flow process. There are also some applications of the Sankey diagram in civil engineering. For example, Abdelalim et al. [40] used a Sankey chart to carry out data visualization and analysis of energy flow at the multizone building scale. Goswein et al. [41] used a Sankey diagram to represent the relationship between building stock and its driving factors. Ioannidou

et al. [42] visualized the economic flow of construction projects through a Sankey diagram. These studies took advantage of the characteristic that the Sankey diagram can represent information flow. The distribution law of near misses also has the characteristics of information flow, so the Sankey diagram can be used to show the flow of specific near-miss objects between near-miss locations and near-miss types.

3. Data Preparation

The data preparation section is divided into 4 steps: (1) collecting near-miss data from the Crane Beach Hydropower Station projects and storing them in the database, (2) cleaning up noncompliance data and obtaining word segmentation, (3) labeling the training data, and (4) assigning the labeled dataset for training the model. This process is shown in Figure 1.

3.1. Source of Data.

The 32,370 safety records of the Crane Beach Hydropower Station from 2015 to 2020 were taken as the data source. The 24,325 collected semi-structured records were uploaded by the site construction operator through WeChat-based near-miss check software. The 8045 paper unstructured records were collected from the safety management personnel at the construction site and manually entered into the database. Some examples of raw data are shown in Table 1.

Each near-miss record includes its check date, near-miss description, and near-miss location. In the near-miss records, "description" and "location" belong to semi-structured data, which are characterized by lengthy sentences and inconsistent expressions. The fields of a semi-structured record are related to each other, but the data stored in the fields are unstructured text. The "description" contains the information of the type of near misses, and the "locations" contain the information of the near-miss places. However, the information is unstructured text and cannot be associated with the association rule algorithm. To automatically find the association rules between the near-miss type and the near-miss location, these two fields need to be transformed into structured text. The CNN DL algorithm is used to transform these two fields into structured data, which are 11 near-miss types and 35 near-miss locations.

3.2. Data Preprocessing.

The training effect of the model can be improved by preprocessing data to reduce data noise. The data preprocessing steps are as follows:

(i) Empty items, numbers, and punctuations such as "3#," "/," "," and "6–2" in a sentence are considered noise, and regular expressions (REs) are used in Python to remove the noise. In particular, "3#" describes the location information of hydropower projects in a more specific way. In different # hidden trouble locations, the impact

on hidden trouble types can be ignored, so 3# is not considered.

(ii) Jieba [45] (Chinese word segmentation software based on Python) is employed to carry out word segmentation to better express the features of Chinese sentences.

(iii) One-character words that are not rich in meaning are deleted.

3.3. Label Definition.

Since a supervised learning model is proposed, it is necessary to label the classified data accurately. According to 20 accident types that a near miss may cause [44] and combined with the description of the near misses in this study, the near misses are divided into 11 types for hydropower engineering construction. Due to the differences in construction organization plans in each near-miss location, we define a total of 30 near-miss location labels. The text datasets are manually tagged by experienced safety management personnel on-site and then reviewed by experts in the field of hydropower engineering construction to ensure the accuracy of the labels. Partial labels are listed in Table 2.

3.4. Dataset Division.

To obtain the classification model, the labeled datasets need to be divided into a training set, test set, and validation set. Among them, the training set optimizes the model, the validation set selects the parameters of the optimization model, and the test set evaluates the performance of the established model. The two datasets of "location" and "description" are arranged in proportion as follows: training set: test set: validation set = 10 : 1 : 1. The numbers of training sets, validation sets, and test sets for the "location" classifier are 14,995, 1515, and 1500, respectively. The numbers of training sets, verification sets, and test sets for the "type" classifier are 16,018, 1545, and 1580, respectively.

4. Near-Miss Text Mining Approach

The data mining model is divided into 3 parts: (1) CNN classification: the "type" classifier and "location" classifier are obtained by training the tag dataset. (2) Association analysis: the trained classifier classifies the "type" and "location" of new near misses to generate structured data of "type" and "location" for statistical analysis. An association rule network diagram is created to visualize the mining results. (3) Sankey diagram: the Sankey diagram adds detailed rules to the near-miss association rules. The specific steps are shown in Figure 2.

4.1. CNN-Based Classifier.

The CNN is a supervised learning method in DL. The weight sharing of a convolutional layer in a CNN can reduce the number of trainable parameters in the network and the complexity of the network model. A text classification method based on CNN can learn complex functions and related features from a given text without the need to select effective features through tedious manual text
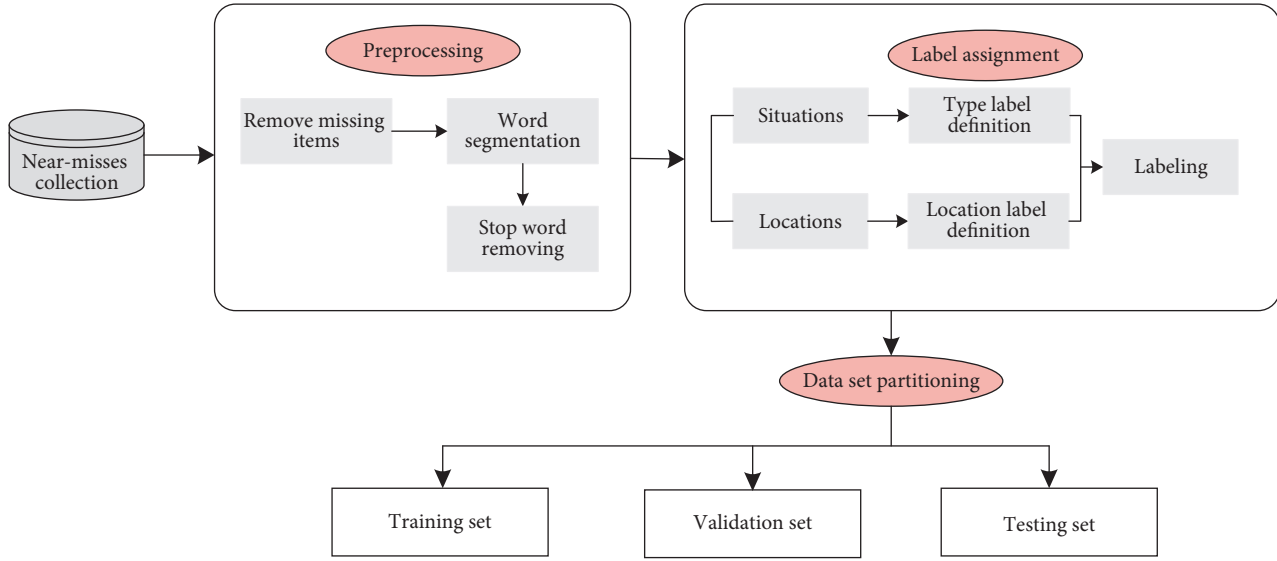
FIGURE 1: Data preparation process.

TABLE 1: Portion of safety records for hydropower engineering projects.

检查日期 (check date)	隐患描述 (near-miss description)	隐患部位 (near-miss location)
2016/08/27	顶拱挂网施工, 汽车吊吊装范围未警戒防护 (roof arch hanging net construction, car hoisting range without warning protection)	引水上平施工支洞(12#~13#之间)顶拱挂网施工, 汽车吊吊装范围未警戒防护 (construction of supporting tunnel (between #12 and #13) on the upper level of water diversion; construction of roof arch hanging net; no warning protection for the hoisting range of an automobile crane)
	......	
2017/05/09	洞内照明设施不满足现场施工要求 (the lighting facilities in the cave do not meet the requirements of site construction)	左岸泵房交通洞 (left bank pump room traffic hole)

TABLE 2: Examples of near-miss label.

NO.	Near-miss description	"Type" label	Near-miss location	"Location" label
1	基础分局锚索施工排架二端过道未贴反光条提示过住车辆。 (no reflective strip is attached to the second end corridor of the anchor cable construction rack in the basic subbureau.)	车辆伤害(vehicle injuries)	尾检北侧锚索施工排架 (construction of the anchor cable on the north side of the stern inspection)	排架 (bent)
2	现场电源线拆除后桩头裸漏 (after the removal of the power line on-site, the pile head is exposed to leakage.)	触电 (electric shock)	主变北侧交通洞洞口 (the main north side of the traffic hole)	洞口 (tunnel entrance)
3	一砂轮切割机无防护盖易造成操作人员伤害 (a grinding wheel cutting machine without a protective cover can easily cause injury to operators.)	机械伤害(mechanical injuries)	EL676马道 (EL676 berm)	马道 (berm)

analysis. This can greatly save on labor and time [9]. With the proposal of the word2vec method, word embedding training can be carried out on a large scale. This lays a foundation for CNN's extensive application in text classification [45].

The context information of each word in the near-miss text is crucial for the CNN model to capture the near-miss features. By introducing word2vec to the input layer, the near-miss text is transformed into a word embedded with a specific numeric expression containing the relationship between words in a near-miss text. This serves as the input layer of the CNN model. In the convolutional layer, the feature mapping of near-miss text is learned in parallel using different sizes of convolution kernels. A fixed-length near-miss feature mapping is acquired by performing the max pool operation at the pooling layer. The final near-miss
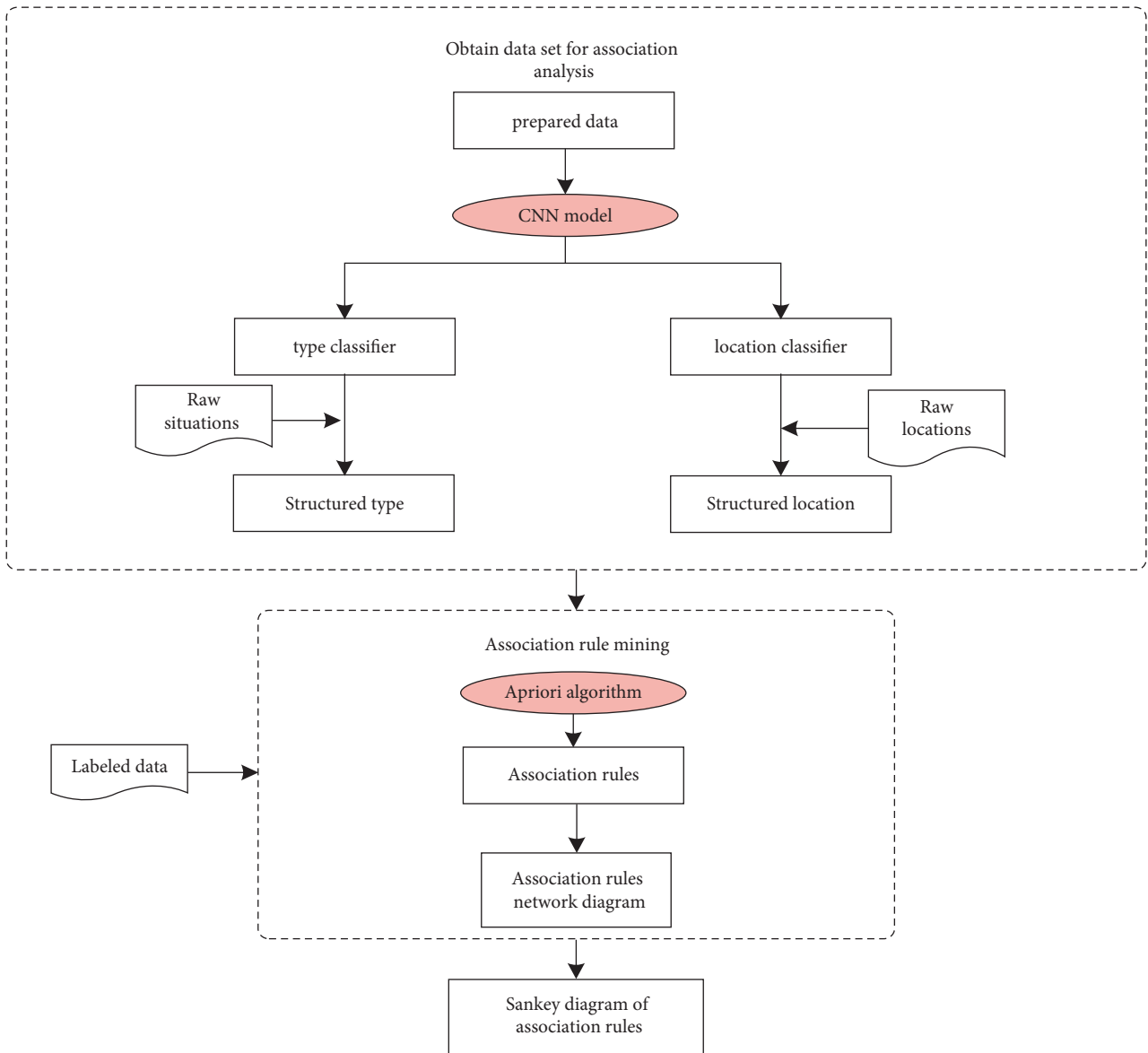
FIGURE 2: Text mining process of hydropower engineering construction near misses.

classification task is handled by the full connection layer. This is equivalent to classifying the features extracted by the convolution layer and pooling. The model structure is shown in Figure 3.

4.1.1. Word Representation. To make full use of the word characteristics, 19,143 "description" and 18,010 "location" instances in the dataset are divided into multiple words separated by line breaks with Jieba. Different words in the "description" and "location" datasets constitute the "description" word vector space and "location" word vector space, respectively. The numbers of words in the two word vector spaces are $V_{\text{description}} = 8001$ and $V_{\text{location}} = 1919$.

The text dataset of hydropower project construction near misses has the characteristics of a large word space, short sentences, and high frequency of professional vocabulary [46]. To better express the near-miss texts, we use word embedding to pretrain the near-miss words. In embedding spaces, different words that are semantically similar are likely to form semantic groups in which words with different properties are close together in distance. The continuous bag of words (CBOW) is a common model for word2vec [47]. The model is suitable for word embedding training in text datasets with fewer low-frequency words and more short sentences [48].

The main idea of the CBOW model is to use context words $\{x_1, x_2, ..., x_C\}$ to predict the central word W_i, where C is the window value (set to 5), W_i is the i word in word vector space, and $\{x_1, x_2, ..., x_C\}$ is the one-hot coding (the corresponding index position of the word is 1, and the others are 0). The model calculation is divided into two processes: forward propagation and back propagation.

(1) Forward propagation.

Figure 4 shows the calculation process of forward propagation, where "氧气(oxygen)/乙炔(acetylene)/瓶(bottle)/无 (no)/安全(safety)/距离(distance)" is taken as the
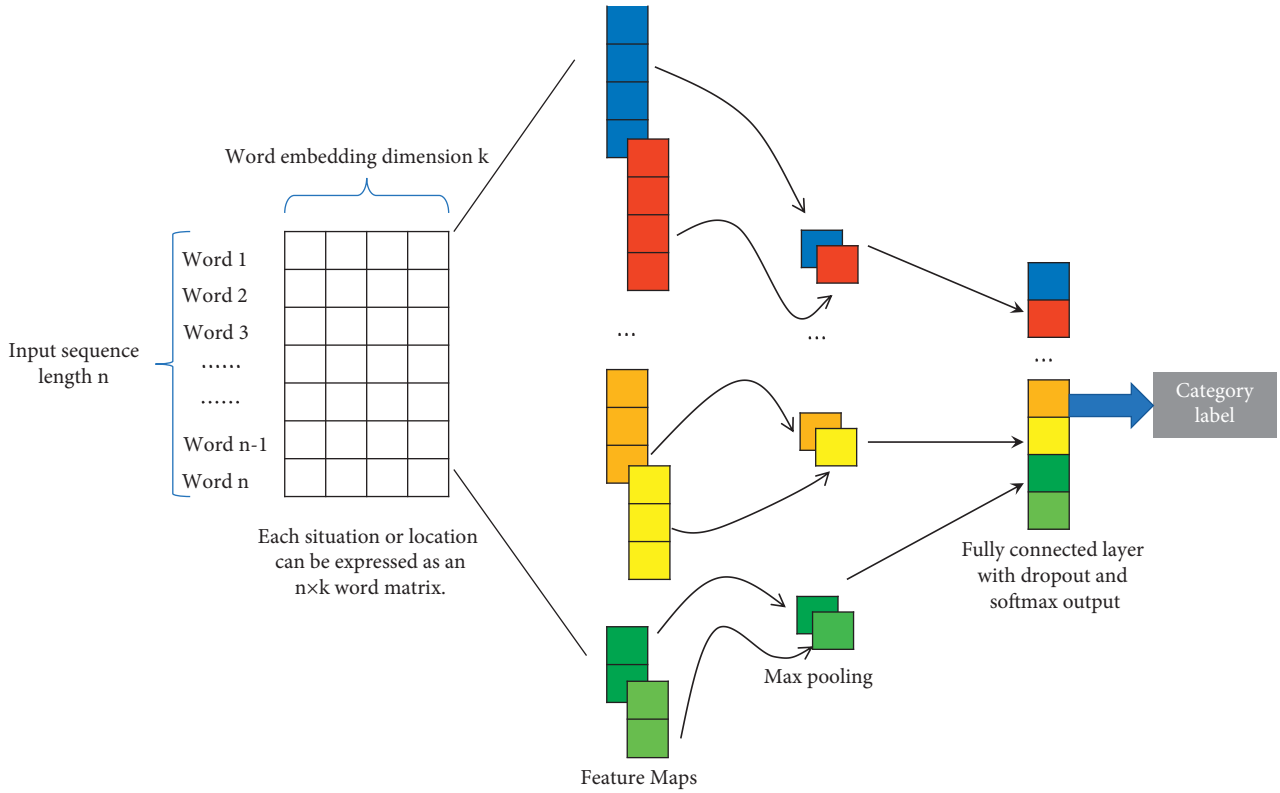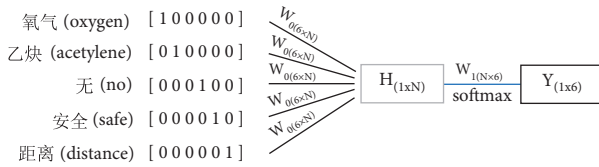
Figure 3: CNN classifier model framework.

Figure 4: CBOW forward propagation flowchart.

dataset for illustration, and "bottle" is the predicted central word. Forward propagation is divided into two steps.

Step 1: Calculate the hidden layer H, which is a $1 \times N$-dimensional vector. N is the dimension of each word vector. The value is set to 100. The calculation formula is described as follows:

$$H = \frac{1}{C} W_0 \cdot \left(\sum_{i-1}^{C} x_i \right), \tag{1}$$

where W_0 is a $V \times N$-dimensional matrix that connects the input vector and hidden layer, and V is the size of the word vector space. In the figure, the value is set to 6.

Step 2: Calculate the output vector Y of size $1 \times V$. Y (the word vector for "bottle" in this image) is a distributed representation of the predicted central word. To facilitate the calculation of errors during back propagation, the *softmax* function is used to normalize $H \times W_1$. The calculation formula is described as follows:

$$Y = \text{softmax}(H \cdot W_1), \tag{2}$$

where W_1 is the weight matrix with a size of $N \times V$ to connect the hidden layer and the output layer.

(2) Back Propagation. The back propagation error is calculated according to Y of the center word and the one-hot encoding vector of this word. The values of W_0 and W_1 are continuously adjusted using the gradient descent method. During the training, each word is used as a central word; that is, W_0 and W_1 are modified V times. After the training, the one-hot coding vector of each word is computed in steps 1 and 2 and united with the trained W_0 and W_1 to accomplish the word vector of all words in the entire dataset.

4.1.2. Convolution Layer. In the NLP domain, since the width of the convolution kernel is generally equal to the dimension k of the word embedding, the convolution kernel slides in only one dimension. We illustrate the process of convolution in Figure 4. In the example, the window value (the local word order length per convolution) h is set to 4. The process is divided into three steps. Step 1: the 4×4 matrix $X_{1:4}$ corresponding to "氧气(oxygen)"/"乙炔(acetylene)"/"瓶(bottle)"/"无(no)" and convolution kernel W are substituted into formula 1 to obtain the feature mapping C_1.

Step 2: due to the sliding step s = 1, the window slides down one slot. We perform the same calculation by replacing $X_{1:4}$ with $X_{2:5}$ corresponding to "乙

炔(acetylene)"/"瓶 (bottle)"/"无 (no)"/"安全 (safe)." Step 3: according to the first and second steps, an iterative operation is performed to obtain the feature mapping matrix C: 3×4. The calculation formula is described as follows:

$$c_i = f\left(w \cdot x_{i:\ i+h-1} + b\right), \tag{3}$$

where w is the convolution kernel matrix representing the shared weight, and $x_{i:\ i+h-1}$ is the connection matrix of the word embedding from the i word of a "description" or "location" to the $i + h - 1$ word. b is an offset term. f is a nonlinear function, and in this study, f is set to a rectified linear unit (ReLU). Figure 5 shows the convolution process.

4.1.3. Pooling Layer and Full Connection Layer. To represent richer features, the convolution kernel is set to different windows, and the same convolution kernel will run parallel operations [49]. Therefore, a sentence will generate feature vectors with different dimensions. The advantage of pooling is that it outputs a fixed-size matrix, reduces the dimensions of the output, and retains significant features with the maximum value $P_i (i = 1, 2, \ldots, m)$. P_i is the maximum value of the vector by the i convolution operation, and m is the number of convolution kernels.

Dropout technology is adopted in the fully connected layer to prevent hidden layer neurons from self-adapting and

to reduce overfitting [50]. The weight parameters of the fully connected layer are combined with $P = \{P_1, P_2, \ldots, P_m\}$ to calculate $Y = \{Y_1, \ldots, Y_t\}$. In this study, t is $t_{\text{description}}$ (the number of "descriptions" tags) and $t_{location}$ (the number of "locations" tags). After vector Y passes through the softmax layer, the probability distributions $L = \{L_1, L_2, \ldots, L_3\}$ of different labels are acquired by normalization calculations. Figure 6 shows the process of pooling to the fully connected layer.

4.1.4. Parameter Settings. According to the hyperparameter settings of CNN text classification in existing studies and through multiple comparison tests, the hyperparameters of this study are determined as shown in Table 3.

4.1.5. Evaluation Metric. In this study, accuracy, recall, precision, and F_1 score are used to evaluate the performance of the DL classification model. Formulas (4)–(7) define these metrics. Among them, recall can be understood as the ability to find crucial instances in the dataset, and precision represents the proportion of data points found by the model that is relevant to reality. The F_1 score is a comprehensive evaluation of the model combined with recall and precision [51].

$$\text{accuracy} = \frac{\text{the number of correctly classified categories}}{\text{the sum of classified data}} \times 100\%, \tag{4}$$

$$\text{precision} = \frac{TP}{TP + FP}, \tag{5}$$

$$\text{recall} = \frac{TP}{TP + FN}, \tag{6}$$

where TP is the number of positive samples predicted correctly, FP is the number of positive samples predicted incorrectly, and FN is the number of negative samples predicted incorrectly.

$$F_1\text{score} = \frac{2 \times precision \times \text{Recall}}{\text{precision} + \text{Recall}}. \tag{7}$$

4.2. Association Mining. This study utilizes the apriori association rule algorithm to analyze the associations between "type" and "location" classified by a CNN-based classifier. D is a set of all "types" and "locations." If there is an association rule "location1 $\longrightarrow$ type1" in which "location1" contains the "pipeline" item and "type1" contains the "electric shock" item, then there is a high probability of an electric shock accident occurring in the pipeline. "Location 1" and "type 1" (hereinafter abbreviated as P_1 and T_1) are both near-miss data item sets.

For association rule "$P_1 \longrightarrow T_1$," its support $\sup_{(P_1 \longrightarrow T_1)}$ is used to measure the frequency of

"$P_1 \longrightarrow T_1$," and the calculation formula is described as follows:

$$\sup_{(P_1 \longrightarrow T_1)} = \frac{\text{count}(P_1 \cap T_1)}{\text{count}(D)}, \tag{8}$$

where $\text{count}(P_1 \cap T_1)$ is the number of simultaneous transactions between P_1 and T_1, and $\text{count}(D)$ is the total number of transactions.

Confidence $\text{conf}_{(P_1 \longrightarrow T_1)}$ measures the degree of credibility of "$P_1 \longrightarrow T_1$":

$$\text{conf}_{(P_1 \longrightarrow T_1)} = \frac{\text{count}(P_1 \cap T_1)}{\text{count}(P_1)}, \tag{9}$$

where $\text{count}(P_1)$ is the number of transactions occurring in P_1.

Rules whose support and confidence are both greater than a given threshold are called strong association rules [52].

In this study, the front and back items of association rules are "locations" and "types," respectively, and each near-
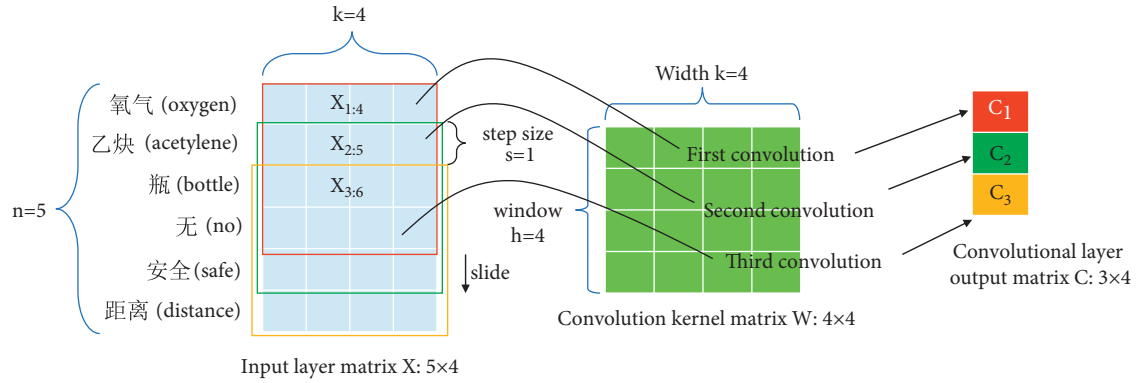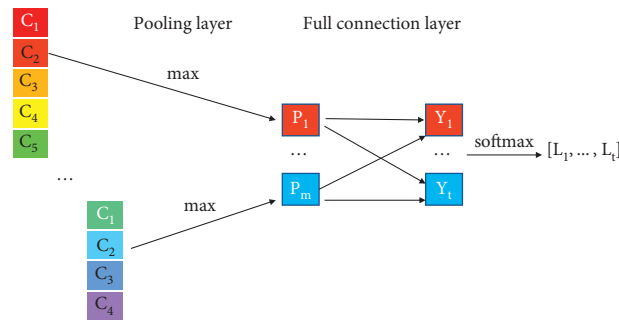
FIGURE 5: CNN convolution computation process.

FIGURE 6: Process of pooling to connection.

TABLE 3: Setting of CNN model hyperparameters.

Embedding dimension	Filter size	Number of filters	Dropout probability	Learning rate
100	5	128	0.5	0.8

miss record is a single safety check record. The front and back items of association rules are limited. That is, there is only one item. Therefore, the algorithm can be improved to reduce the time cost of scanning by lowering the number of scans.

This algorithm can be divided into two steps as follows:

(i) Step 1: When finding the frequent 1-item set (the number of items contained in the frequent item set is 1), different from the traditional apriori algorithm, only the "location" item set is scanned instead of the item sets of "type" and "location" at the same time, thus saving scanning time. The corresponding support degree of each item is calculated, and an item set below the support threshold value is cut off to obtain a frequent 1-item set. The frequent 1-item set is connected with the "type" item set to obtain the candidate frequent 2-item set, and the candidate frequent 2-item set below the support degree is screened out to obtain the frequent 2-item set and its item statistics.

(ii) Step 2: According to all frequent item sets mined in step 1, the confidence of each frequent item set is filtered whose value is greater than the small confidence; then, the frequent item set is a strong association rule.

This study explores what types of near misses may occur in a specific "location." To show the relationship between them more intuitively, a network diagram is used to visualize them, as shown in Figure 7. The thickness of the line in the network represents the degree of correlation, and the size of the circle indicates the frequency of occurrence. The thickness is determined by the weight calculated from the support and confidence of the association rule. The weight is calculated in two steps: (1) normalizing "support" and "confidence" and (2) calculating the sum of the normalized "support" and "confidence" and then normalizing the result of the sum. The normalization can be calculated by formula (10). This solves the problem of inaccurate evaluation caused by different orders of magnitude of evaluation indexes. The statistical quantity of near-miss locations and near-miss types in hydropower projects is evenly distributed. If the support degree and confidence degree are set higher, some rules with strong practical relevance will be lost. In addition, the data in this study are large, so more valuable association rules can be obtained by setting these two values to smaller values. We set the support degree and confidence degree to be lower at 0.001 and 0.01, respectively.
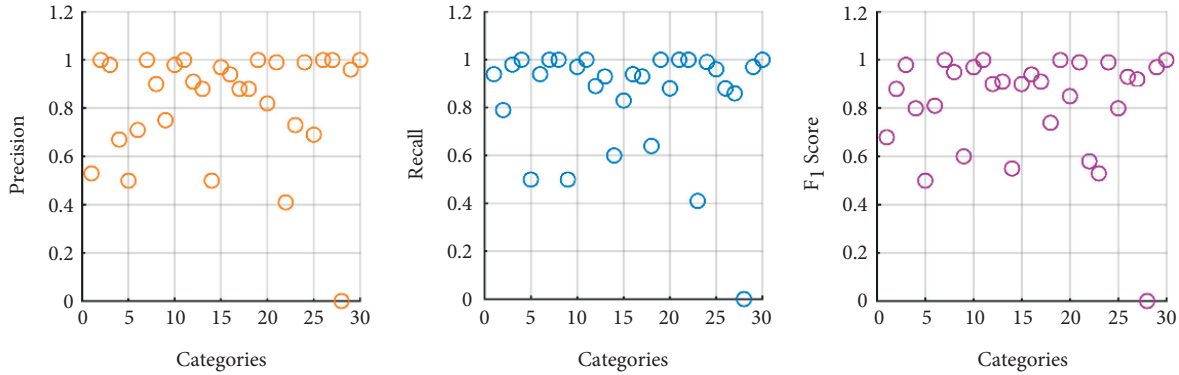
$$y = \frac{x - x_{\min}}{x_{\max} - x_{\min}}, \tag{10}$$

FIGURE 7: Precision, F_1 score, and recall of "location" classification results.

where x and y are the values before and after normalization, respectively, and x_{max} and x_{min} are the maximum and minimum values of the samples, respectively.

4.3. Sankey Diagram. The apriori algorithm can determine the strong association rule of "location $\longrightarrow$ type" but cannot determine the distribution law of specific near-miss objects. The text corresponding to categories in strong association rules is processed by the Chinese word segmentation to obtain a more detailed near-miss distribution. For example, for "dam shoulder slot $\longrightarrow$ fall from height," (1) all descriptions of this association rule are collected as shown in Table 4, (2) the Jieba word segmentation package is used to segment the description in Chinese, and (3) words with large word frequency and significance as specific near-miss objects are selected to connect "location" and "type." A Sankey diagram is drawn to describe the information flow of multiple strong association rules, in which the word frequency is used as the flow size.

5. Results and Discussion

5.1. CNN-Based Classification. To train the "location" and "type" classifiers with strong generalization ability, the dataset allocated according to section 3.4 is input into the constructed CNN DL text classification model. Furthermore, the model is evaluated by the accuracy, recall, precision, and F1 score.

The 8990 "description" data and the corresponding "location" data without labels generated in the Crane Beach Hydropower Station are taken to classify the "type" and "location," respectively, using the "type" classifier and the "location" classifier. The 8990 structured data are obtained for mining association rules "location $\longrightarrow$ type."

The average accuracy, average precision, average recall rate, and average F1 score rate of the "location" classifier were 90.19%, 81.90%, 84.43%, and 81.93%, respectively. The evaluation results of each category of the "location" classifier are shown in Figures 7 and8. The evaluation results of each category of the "type" classifier are shown in Table 5 and Figure 9.

In Figure 7, some categories are less effective, such as No. 28 "curtain" and No. 11 "drowning." The similarity of drowning words is high, and the sample size is extremely small, which leads to a higher precision but lower recall. The sample size of the "curtain" is very small, leading to all evaluation metrics being 0. No. 1, No. 4, and No. 6 have higher recall but lower precision. This is because the texts tagged in these categories are similar to the texts tagged in other categories, and more other tags are classified as these.

In Table 5, "mechanical damage," "collapse," and "drowning" have higher precision but lower recall. The reason is that these categories have strong text features; thus, the classification precision is better, but the small sample size leads to a low recall.

Although precision, recall, and F_1 scores indicate that the CNN performs better than other algorithms, they are unable to provide any information about how each category of "type" and "location" is misclassified. Thus, confusion matrices are introduced to focus on categories that are misclassified. In Figures 8 and 9, rectangles in the diagonal position represent the correct classification, while other rectangles represent the incorrect classification. Each row represents the actual category, and the column represents the predicted category.

As shown in Figure 8, since the descriptions of "No. 28" ("tunnel entrance") and "No. 13" ("inside tunnel") are extremely similar, it is easiest to misclassify them. The top misclassified "type" shown in Figure 9 is "drowning." The probability of "drowning" being misclassified as "civilized construction" (row 11, column 9) is 0.53. In the description of "civilized construction," there is a large amount of "surface ponding." Furthermore, the most striking feature that "drowning" describes is also "surface ponding," so CNN classifiers easily confuse "drowning" with "civilized construction." In addition, "collapse" has a 0.22 probability of being misclassified as "struck by objects" (row 8, column 10). After a collapse, there is a high probability of an object striking by accident. Therefore, the confusion between "collapse" and "struck by objects" can be explained by the symbiotic tendency. For a small number of categories that are easily confused, manual inspection is used for secondary classification to ensure classification accuracy.

5.2. Contrast Tests. Existing studies show that the short text classification effect of shallow machine learning is worse than that of DL [53]. Consequently, we do not consider shallow machine-learning algorithms and only compare

TABLE 4: Near-miss descriptions about "dam shoulder slot ⟶ fall from height."

| "Location"	Description	"Type"
Dam shoulder slot	坝肩槽EL635-EL625高程中间爬梯扶手焊点开裂2处, 存在安全隐患。(there are 2 cracked solder joints of the middle ladder handrail in the dam abutment grooves of EL635-EL625 that have safety risks.) 临边防护及警示缺失。(lack of border protection and warning.) … 坝肩槽EL74O通道端头未封闭开放, 存在坠落风险 (the end of the EL74°channel of the abutment groove is not closed and open, and there is a risk of falling.)	Fall from height
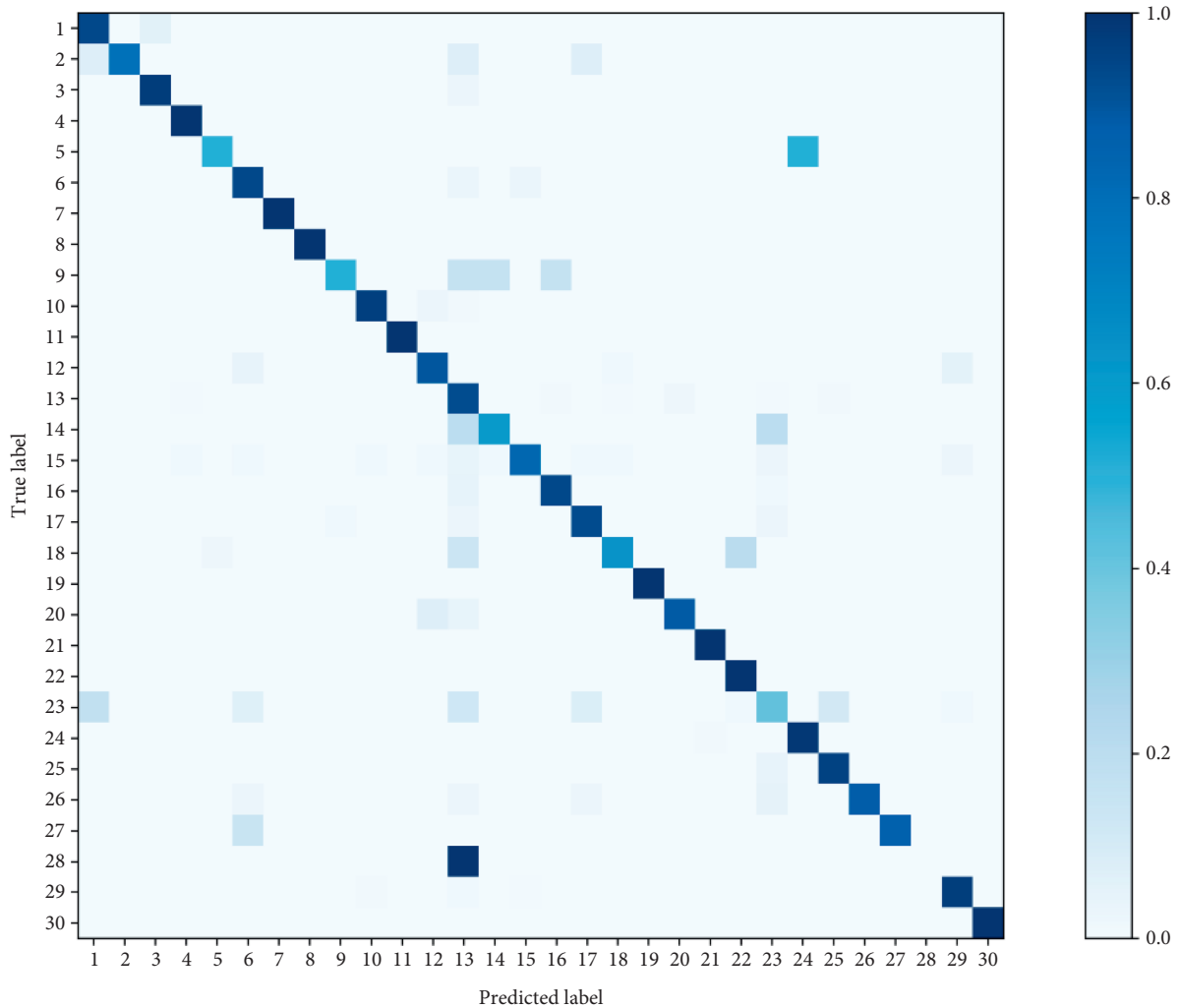
FIGURE 8: Confusion matrix of "location" classification results.

four typical DL classification algorithms: recurrent neural network (RNN) [54], BERT [10], fast text [55], and long short-term memory (LSTM) [56].

Near-miss short texts on hydropower engineering construction have the characteristics of limited sentence length, compact structure, and independent expression, which make it possible for CNNs to handle such tasks [57]. Five DL classification algorithms classify the same dataset in the comparison test, and the same trained word embedding layer is used as the input layer.

As the number of categories classified in this study is too high to fully display the evaluation metrics of each category, the average value of each evaluation metric of the classifier is

used for comparison with the CNN algorithm and other DL methods. As can be observed from Table 6, all metrics of the CNN algorithm are superior to those of other DL classification algorithms. Therefore, the CNN algorithm is adopted to classify the short text of near misses in hydropower engineering construction.

5.3. Association Rules. To acquire more objective association rules, labeled data are added to the association analysis dataset for more comprehensive data. Due to the large amount of data and the large number of label categories, the threshold of support and confidence were set at low levels of

TABLE 5: Precision, F1 score, and recall of "type" classification results.

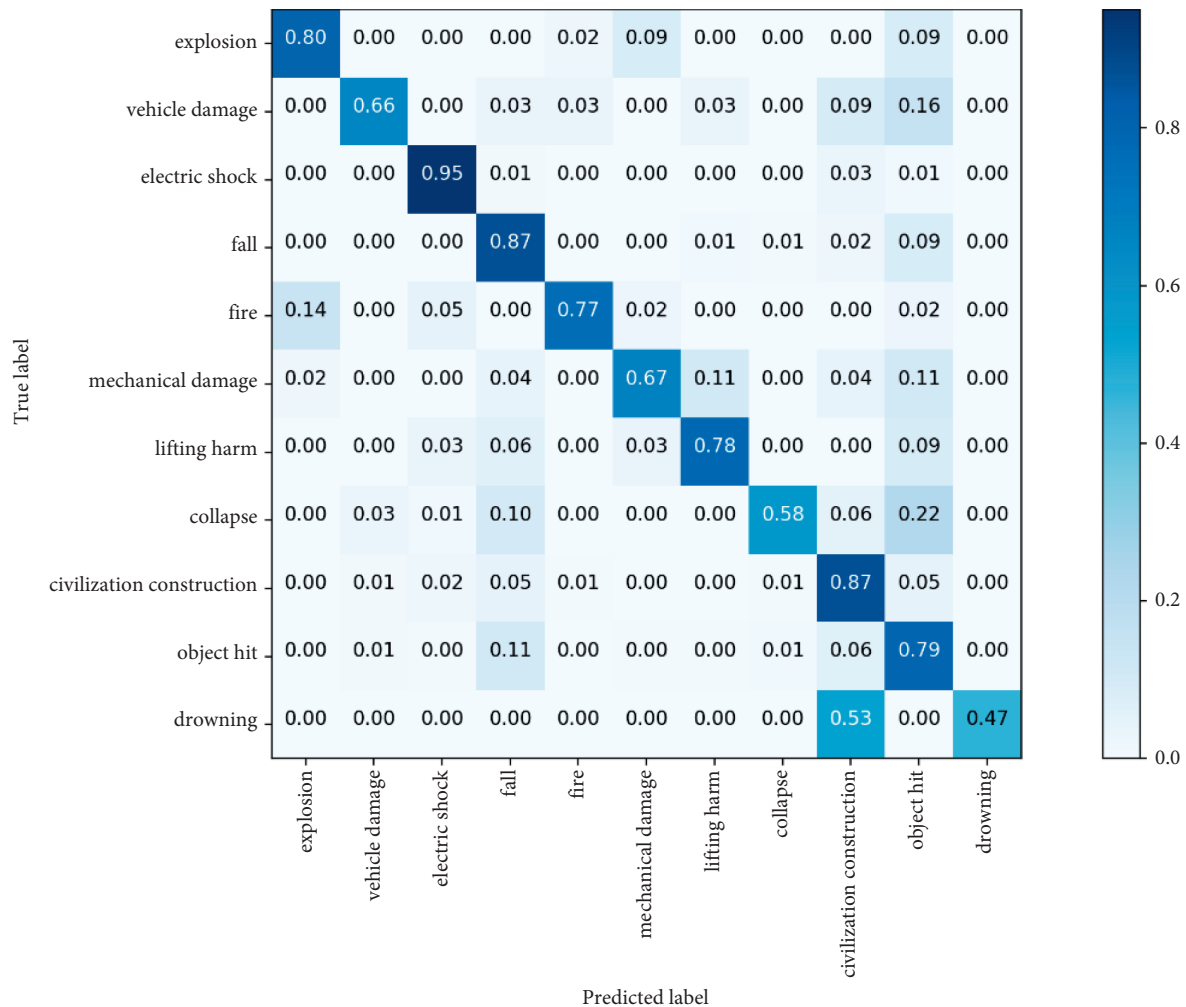| No.	Label	Precision	Recall	F1 Score
1	Explosion	0.82	0.80	0.81
2	Vehicle injuries	0.72	0.66	0.69
3	Electric shock	0.97	0.95	0.96
4	Fall from height	0.82	0.87	0.85
5	Fire	0.89	0.77	0.82
6	Mechanical injuries	0.82	0.67	0.74
7	Lifting injuries	0.69	0.78	0.74
8	Collapse	0.86	0.58	0.69
9	Civilization construction	0.86	0.87	0.86
10	Object hit	0.71	0.79	0.75
11	Drowning	0.88	0.47	0.61
	Average	0.82	0.75	0.77

FIGURE 9: Confusion matrix of "type" classification results.

0.02 and 0.20, respectively. A total of 31 strong association rules were mined. Some of the results are shown in Table 7.

To display more association information using a network diagram, we set the support degree and confidence degree lower at 0.001 and 0.01, respectively, and a total of 235 association rules are output. As shown in Figure 10, the larger circles of "civilized construction" and "struck by objects" indicate that these types of accidents are more likely to occur in the construction of hydropower engineering projects. According to the thickness of the line, "inside the tunnel" is prone to "collapse," "vehicle injury," "fire," and other accident types, while "underground chambers" are prone to "fall from height," "struck by objects," "fire," and other types of accidents.

Knowing which places are prone to accidents, safety managers can search for the corresponding original near-

TABLE 6: Comparison of CNN classification algorithm and other deep learning methods.

Dataset	Classifier algorithm	Metrics			
		Accuracy	Precision	Recall	F_1 score
	CNN	0.86	0.82	0.77	0.79
	RNN	0.85	0.79	0.74	0.76
Near-miss type	BERT	0.82	0.81	0.73	0.77
	Fast text	0.79	0.78	0.71	0.74
	LSTM	0.81	0.80	0.72	0.76
	CNN	0.90	0.82	0.84	0.83
	RNN	0.88	0.78	0.80	0.79
Near-miss location	BERT	0.85	0.75	0.78	0.76
	Fast text	0.81	0.73	0.75	0.74
	LSTM	0.86	0.77	0.78	0.77

TABLE 7: Results of association rule calculations.

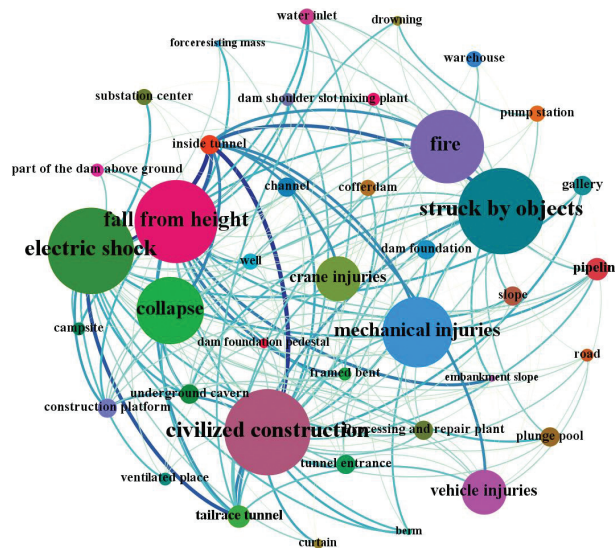| No.	Location	Type	Support	Confidence
1	Gallery	Electric shock	0.02	0.36
2	Tailrace tunnel	Electric shock	0.13	0.33
3	Dam shoulder slot	Fall from height	0.03	0.30
4	Tunnel entrance	Civilization construction	0.05	0.29
5	Water inlet	Fall from height	0.05	0.29
6	Pipeline	Electric shock	0.06	0.28
7	Embankment slope	Struck by objects	0.03	0.28

FIGURE 10: "Location ⟶ type" network graph.

miss description data and perform a more in-depth and detailed analysis based on the specific association rules. For example, a tunnel is prone to collapse due to arch cracking, no anchor, nonstandard support, and so on. More valuable near-miss prevention objects can be learned by combining raw near-miss data with an association rule network.

Compared with the network diagram, the Sankey diagram displays more detailed and specific content and visually presents the frequency distribution and information flow of the specific near-miss objects, near-miss locations, and near types. We exhibit one of the Sankey diagrams in Figure 11 using 6 pairs of strong association rules. Some

valuable hidden danger rules can be analyzed from the figure. For example, electric shock near misses are likely to appear in "dam shoulder slots" and "tailrace tunnels" due to the "inside of the distribution box." Referring to the original text related to "inside the distribution box," we can understand that "there is debris in the distribution box" is the cause of electric shock near misses, and it is more likely to appear in the "tailrace tunnel" and "dam shoulder slot."

In addition, the "traffic ladder" of the "dam shoulder slot" has great potential to cause near misses of "falling from height." Referring to the "traffic ladder" in the original text, we can find that the main reason for "fall from height" is that
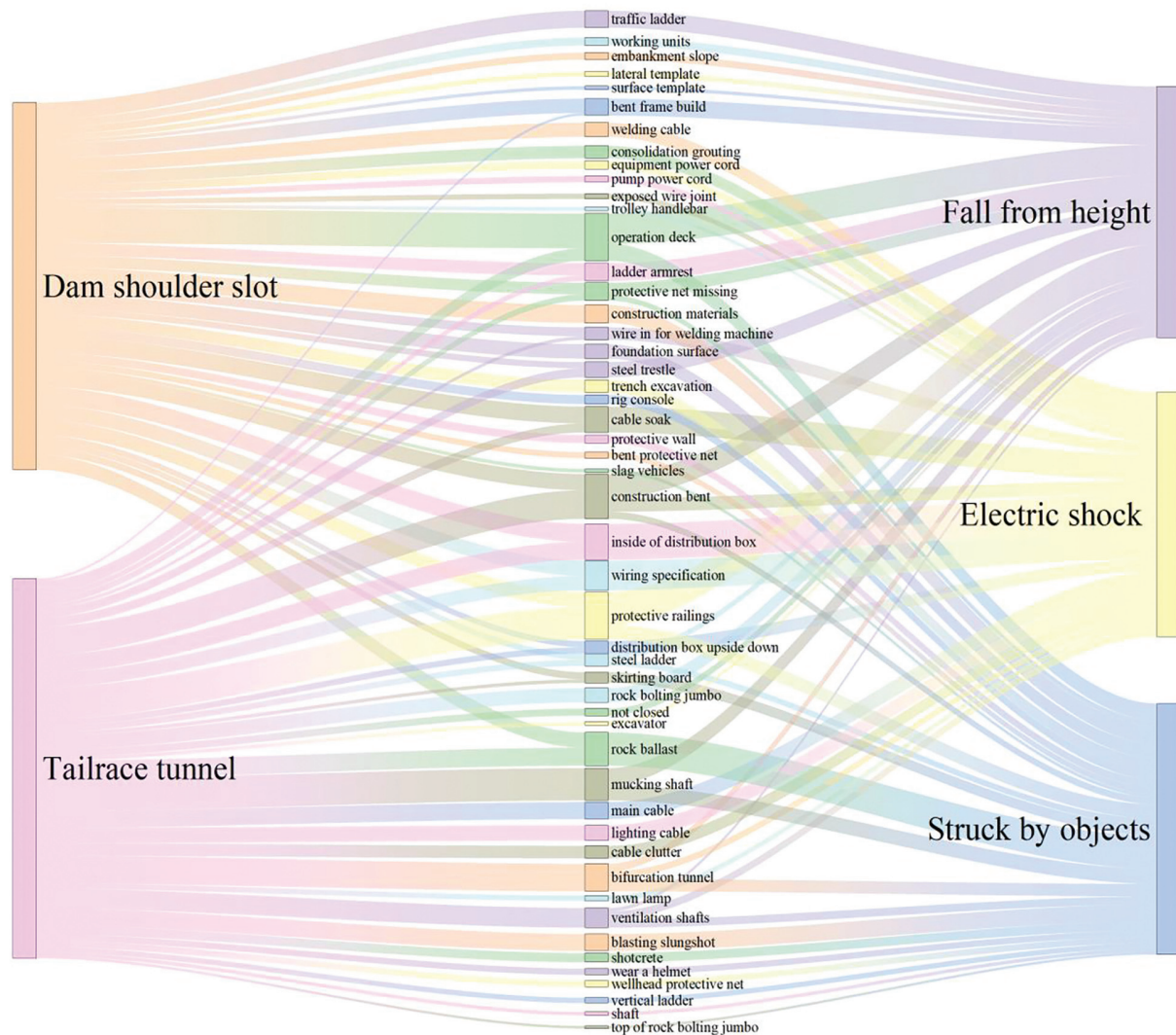
FIGURE 11: Sankey diagram of association rules.

"there is no traffic ladder," "the traffic ladder handrail is missing," and "the traffic ladder has no protective railing." Safety managers can quickly find the details of near misses and implement measures to prevent the emergence of these near misses through the Sankey diagrams combined with original text data.

6. Conclusion

The construction safety management of hydropower engineering is mainly based on the analysis of safety text data, but the recorded data are often inconsistent and messy data, so it is particularly difficult to directly obtain knowledge that can guide safety early warnings. In recent years, NLP technology combined with AI has provided the possibility for rapid and automatic analysis of text data in all walks of life.

To mine the valuable information hidden in the data of hydropower engineering construction near misses, this study developed a new model combining text classification

and association mining. The purpose of text classification is to aggregate near misses in the same category and lay the foundation for subsequent data statistics. The association algorithm can be used to calculate the results of structured classification and find the association rules with strong practical significance.

To overcome the shortcoming that the association algorithm cannot analyze the near-miss description field that contains the most near-miss information, the method of word segmentation combined with the Sankey diagram was used to add abundant near-miss information to the association rules. Intuitive near-miss distribution visualization helps safety managers quickly find the causes of near misses and take measures to control them to reduce the possibility of accidents and improve the safety level of hydropower engineering construction sites. The model can mine massive texts and obtain more detailed rules and is also applicable to other fields of text mining.

Our research can better examine near-miss associations, but there are still some limitations. First, the work of making

near-miss labels is completed by different people, which may lead to different classifications of the same near-miss types due to respective subjective opinions. Second, it is still necessary to manually check the near-miss classification results with poor performance in the classifier to ensure the accuracy of data involved in association rule mining. Third, the CNN-based model proposed was only used to evaluate the near-miss text dataset obtained from the Crane Beach Hydropower Station project. Future study is required to use unsupervised learning to improve the accuracy of near-miss data classification. In addition, the consistency of near-miss dataset classification models for different hydropower engineering projects can be further discussed.

Data Availability

The data generated and analyzed during this research are available from the corresponding author by request.

Conflicts of Interest

The authors declare that they have no conflicts of interest.

Acknowledgments

References

[1] H. Lingard, "Occupational health and safety in the construction industry," *Construction Management & Economics*, vol. 31, no. 6, pp. 505–514, 2013.

[2] J.-L. Zhou, Z.-H. Bai, and Z.-Y. Sun, "A hybrid approach for safety assessment in high-risk hydropower-construction-project work systems," *Safety Science*, vol. 64, pp. 163–172, 2014.

[3] National Energy Administration (China), http://www.nea.gov.cn/2020-2006/2010/c_139128997.htm, 2020.

[4] W. Wu, H. Yang, D. A. S. Chew, S.-H. Yang, A. G. F. Gibb, and Q. Li, "Towards an autonomous real-time tracking system of near-miss accidents on construction sites," *Automation in Construction*, vol. 19, no. 2, pp. 134–141, 2010.

[5] X. H. Wang, X. F. Huang, Y. Luo, J. J. Pei, and M. Xu, "Improving workplace hazard identification performance using data mining," *Journal of Construction Engineering and Management*, vol. 144, no. 8, p. 11, 2018.

[6] V. Maslej-Krešňáková, M. Sarnovský, P. Butka, and K. Machová, "Comparison of deep learning models and various text pre-processing techniques for the toxic comments classification," *Applied Sciences*, vol. 10, no. 23, p. 8631, 2020.

[7] C. U. Ubeynarayana and G. Y. Miang, "An ensemble approach for classification of accident narratives," in *Proceedings of the ASCE International Workshop on Computing in Civil Engineering*, Seattle, WA, USA, June 2017.

[8] T. Mahfouz, "Unstructured construction document classification model through support vector machine (SVM)," in *Proceedings of the International Workshop on Computing in Civil Engineering*, Miami, FA, USA, June 2011.

[9] B. Zhong, X. Xing, P. Love, X. Wang, and H. Luo, "Convolutional neural network: deep learning-based classification of building quality problems," *Advanced Engineering Informatics*, vol. 40, pp. 46–57, 2019.

[10] W. Fang, H. Luo, S. Xu, P. E. D. Love, Z. Lu, and C. Ye, "Automated text classification of near-misses from safety reports: an improved deep learning approach," *Advanced Engineering Informatics*, vol. 44, Article ID 101060, 2020.

[11] J. Zhang, L. Zi, Y. Hou, D. Deng, W. Jiang, and M. Wang, "A C-BiLSTM approach to classify construction accident reports," *Applied Sciences*, vol. 10, no. 17, p. 5754, 2020.

[12] F. Madani, T. Daim, and C. Weng, "Smart building technology network analysis: applying core-periphery structure analysis," *International Journal of Management Science and Engineering Management*, vol. 12, no. 1, pp. 1–11, 2017.

[13] B. Lehrman, "Visualizing water infrastructure with Sankey maps: a case study of mapping the Los Angeles Aqueduct, California," *Journal of Maps*, vol. 14, no. 1, pp. 52–64, 2018.

[14] P. Urgiles, M. A. Sebastian, and J. Claver, "Proposal and application of a methodology to improve the control and monitoring of complex hydroelectric power station construction projects," *Applied Sciences-Basel*, vol. 10, no. 21, 2020.

[15] X. Z. Zheng, F. Wang, and J. L. Zhou, "A hybrid approach for evaluating faulty behavior risk of high-risk operations using anp and evidence theory," *Mathematical Problems in Engineering*, vol. 2017, Article ID 7908737, 16 pages, 2017.

[16] X. Zheng, J. Zhou, F. Wang, and Y. Chen, "Routes to failure and prevention recommendations IN work systems OF hydropower construction," *Journal of Civil Engineering and Management*, vol. 24, no. 3, pp. 206–222, 2018.

[17] R. Collobert, J. Weston, L. Bottou, M. Karlen, K. Kavukcuoglu, and P. Kuksa, "Natural language processing (almost) from scratch," *Journal of Machine Learning Research*, vol. 12, pp. 2493–2537, 2011.

[18] B. Jang, M. Kim, G. Harerimana, S.-u. Kang, and J. W. Kim, "Bi-LSTM model to increase accuracy in text classification: combining Word2vec CNN and attention mechanism," *Applied Sciences*, vol. 10, no. 17, p. 5841, 2020.

[19] H. Wu, Y. Liu, and J. Wang, "Review of text classification methods on deep learning," *Computers, Materials & Continua*, vol. 63, no. 3, pp. 1309–1321, 2020.

[20] F. Sebastiani, "Machine learning in automated text categorization," *ACM Computing Surveys*, vol. 34, no. 1, pp. 1–47, 2002.

[21] S. J. Bertke, A. R. Meyers, S. J. Wurzelbacher, J. Bell, M. L. Lampl, and D. Robins, "Development and evaluation of a Nave Bayesian model for coding causation of workers' compensation claims," *Journal of Safety Research*, vol. 43, no. 5-6, pp. 327–332, 2012.

[22] P. Maia, R. Carvalho, M. Ladeira, H. Rocha, and G. Mendes, "Application of text mining techniques for classification of documents: a study of automation of complaints screening in a Brazilian federal agency," *Solid-State Electronics*, vol. 38, pp. 1461–1463, 2014.

[23] A. Hassan and A. Mahmood, "Convolutional recurrent deep learning model for sentence classification," *IEEE Access*, vol. 6, pp. 13949–13957, 2018.

[24] I. Banerjee, Y. Ling, M. C. Chen et al., "Comparative effectiveness of convolutional neural network (CNN) and recurrent neural network (RNN) architectures for radiology text report classification," *Artificial Intelligence in Medicine*, vol. 97, pp. 79–88, 2019.

[25] O. Sen and H. Y. Keles, "On the evaluation of CNN models in remote-sensing scene classification domain," *PFG-Journal of Photogrammetry, Remote Sensing and Geoinformation Science*, vol. 88, no. 6, pp. 477–492, 2020.

[26] H. X. Wen, X. H. Zhu, L. F. Zhang, and F. Li, "A gated piecewise CNN with entity-aware enhancement for distantly supervised relation extraction," *Information Processing & Management*, vol. 57, no. 6, p. 14, 2020.

[27] Z. Fu, F. Huang, X. Sun, A. V. Vasilakos, and C.-N. Yang, "Enabling semantic search based on conceptual graphs over encrypted outsourced data," *IEEE Transactions on Services Computing*, vol. 12, no. 5, pp. 813–823, 2019.

[28] M. Arora and V. Kansal, "Character level embedding with deep convolutional neural network for text normalization of unstructured data for Twitter sentiment analysis," *Social Network Analysis and Mining*, vol. 9, no. 1, p. 12, 2019.

[29] B. He, Y. Guan, and R. Dai, "Classifying medical relations in clinical text via convolutional neural networks," *Artificial Intelligence in Medicine*, vol. 93, pp. 43–49, 2019.

[30] H. H. Do, P. Prasad, A. Maag, and A. Alsadoon, "Deep learning for aspect-based sentiment analysis: a comparative review," *Expert Systems with Applications*, vol. 118, pp. 272–299, 2019.

[31] Y. Kim, "Convolutional neural networks for sentence classification," 2014, https://arxiv.org/abs/1408.5882.

[32] R. Agrawal, "Mining association rules between sets of items in large databases," in *Proceedings of the ACM SIGMOD Conference on Management of Data*, Washington, DC, USA, May 1993.

[33] A. Khalili and A. Sami, "SysDetect: a systematic approach to critical state determination for Industrial Intrusion Detection Systems using Apriori algorithm," *Journal of Process Control*, vol. 32, pp. 154–160, 2015.

[34] C.-W. Cheng, C.-C. Lin, and S.-S. Leu, "Use of association rules to explore cause-effect relationships in occupational accidents in the Taiwan construction industry," *Safety Science*, vol. 48, no. 4, pp. 436–444, 2010.

[35] S. Guo, P. Zhang, and L. Ding, "Time-statistical laws of workers' unsafe behavior in the construction industry: a case study," *Physica A: Statistical Mechanics and Its Applications*, vol. 515, pp. 419–429, 2019.

[36] G. Qiu and J. Wang, "Knowledge discovery of construction safety accidents based on concept lattice," *Journal of Safety and Environment*, vol. 19, no. 05, pp. 1625–1630, 2019.

[37] Z. Mingyuan, Z. Mi, and Z. Xuefeng, "Task-driven mining of association rules for hazard sources in construction sites," *Journal of Safety and Environment*, vol. 19, no. 01, pp. 14–20, 2019.

[38] C. Blume, S. Blume, S. Thiede, and C. Herrmann, "Data-Driven digital twins for technical building services operation in factories: a cooling tower case study," *Journal of Manufacturing and Materials Processing*, vol. 4, no. 4, 2020.

[39] K. Soundararajan, H. K. Ho, and B. Su, "Sankey diagram framework for energy and exergy flows," *Applied Energy*, vol. 136, pp. 1035–1042, 2014.

[40] A. Abdelalim, W. O'Brien, and Z. Shi, "Data visualization and analysis of energy flow on a multi-zone building scale," *Automation in Construction*, vol. 84, pp. 258–273, 2017.

[41] V. Göswein, J. Krones, G. Celentano, J. E. Fernández, and G. Habert, "Embodied GHGs in a fast growing city: looking at the evolution of a dwelling stock using structural element breakdown and policy scenarios," *Journal of Industrial Ecology*, vol. 22, no. 6, pp. 1339–1351, 2018.

[42] D. Ioannidou, S. Zerbi, B. García de Soto, and G. Habert, "Where does the money go? Economic flow analysis of construction projects," *Building Research & Information*, vol. 46, no. 4, pp. 348–366, 2018.

[43] M. Qiu, Y. R. Zhang, T. Q. Ma, Q. F. Wu, and F. Z. Jin, "Convolutional-neural-network-based multilabel text classification for automatic discrimination of legal documents," *Sensors and Materials*, vol. 32, no. 8, pp. 2659–2672, 2020.

[44] NBS (National Bureau of Standards), *Classification Standard for Casualty Accidents of Enterprise Workers*, NBS (National Bureau of Standards), Gaithersburg, MA, USA, 1986.

[45] T. Mikolov, K. Chen, G. Corrado, and J. Dean, "Efficient estimation of word representations in vector space," 2013, https://arxiv.org/abs/1301.3781.

[46] P. Wang, B. Xu, J. Xu, G. Tian, C.-L. Liu, and H. Hao, "Semantic expansion using word embedding clustering and convolutional neural network for improving short text classification," *Neurocomputing*, vol. 174, pp. 806–814, 2016.

[47] J. Li, J. Li, X. Fu, M. A. Masud, and J. Z. Huang, "Learning distributed word representation with multi-contextual mixed embedding," *Knowledge-Based Systems*, vol. 106, pp. 220–230, 2016.

[48] L. Shi, G. Cheng, S. R. Xie, and G. Xie, "A word embedding topic model for topic detection and summary in social networks," *Measurement + Control*, vol. 52, no. 9-10, pp. 1289–1298, 2019.

[49] J. Bruna and S. Mallat, "Invariant scattering convolution networks," *IEEE Transactions on Pattern Analysis and Machine Intelligence*, vol. 35, no. 8, pp. 1872–1886, 2013.

[50] D. Xu, Z. Tian, R. Lai, X. Kong, Z. Tan, and W. Shi, "Deep learning based emotion analysis of microblog texts," *Information Fusion*, vol. 64, pp. 1–11, 2020.

[51] M. Buckland and F. Gey, "The relationship between recall and precision," *Journal of the American Society for Information Science*, vol. 45, no. 1, pp. 12–19, 1994.

[52] B. Kavsek and N. Lavrac, "APRIORI-SD: adapting association rule learning to subgroup discovery," *Applied Artificial Intelligence*, vol. 20, no. 7, pp. 543–583, 2006.

[53] S. Li, J. Hu, Y. Cui, and J. Hu, "DeepPatent: patent classification with convolutional neural networks and word embedding," *Scientometrics*, vol. 117, no. 2, pp. 721–744, 2018.

[54] D. Q. Wei, B. Wang, G. Lin et al., "Research on unstructured text data mining and fault classification based on RNN-LSTM with malfunction inspection report," *Energies*, vol. 10, no. 3, p. 22, 2017.

[55] W. Zheng, H. Tang, and Y. Qian, "Collaborative work with linear classifier and extreme learning machine for fast text categorization," *World Wide Web*, vol. 18, no. 2, pp. 235–252, 2015.

[56] I. A. Kandhro, S. Z. Jumani, K. Kumar, A. Hafeez, and F. Ali, "Roman Urdu headline news text classification using RNN, LSTM and CNN," *ADSAA*, vol. 12, no. 2, p. 13, 2020.

[57] T. He, W. Huang, Y. Qiao, and J. Yao, "Text-attentional convolutional neural network for scene text detection," *IEEE Transactions on Image Processing*, vol. 25, no. 6, pp. 2529–2541, 2016.

Research Article

Research on Higher English Internationalization Education Model and Evaluation Index System Based on Multi-Source Information Fusion

Bei Yang,[1] **Huijun Tang,**[2] **and Lei Mou** [3]

[1]*School of Foreign Languages and Cultures, Chengdu University, Chengdu 610106, China*
[2]*School of Foreign Languages, China University of Geosciences, Wuhan 430074, China*
[3]*The Office of International Cooperation and Exchange, Chengdu University, Chengdu 610106, China*

Correspondence should be addressed to Lei Mou; mulei@cdu.edu.cn

With the continuous development of the global economy, the degree of internationalization and openness has gradually deepened. Higher English internationalization education also needs to keep pace with the times and keep pace with international development. At this time, it is necessary to build a multi-source information fusion algorithmic higher English international education model and evaluation index system to better adapt to the trend of higher English international education in the future. In the current higher English teaching process, it is necessary to change the traditional teaching concepts, change the previous teaching ideas, continuously expand the horizons, build an international and diversified English teaching training program, and actively absorb excellent education concepts from foreign excellent teaching models, which has better promoted the development of English teaching.

1. Introduction

English classroom education is mainly centered on the exchange activities between teachers and students. It is a system with significant social characteristics. The corresponding evaluation index system and teaching model together constitute the education level weighed by the higher English evaluation index [1–3], according to the principle of combining pre-teaching appointments and post-teaching satisfaction. At present, cloud computing, computer technology, big data analysis, and hypermedia technology are the basis for promoting the continuous development of modern information technology; it can provide English learners with virtualized teaching services and fast teaching services, which are generally interconnected, intelligent, and huge. Data-scale data information mining, image-friendly learning interface, and other data information technology services can not only effectively improve the environment of higher English teaching, but also change the previous views and

learning styles of English teaching. The relationship between teachers and students can apply higher English learning to the actual era of information development, and it has become the main factor that can realize the "structural reform" of higher English education. Education itself is to cultivate high-quality people, who are useful to society. Traditional education is centered on teachers. Teachers dominate and students passively participate. Students trained in this model rarely have innovative thinking. They are obedient and dependent. Learning is not so enthusiastic, and there is rarely a rich imagination, and scientific research and creation all need imagination as a support. Therefore, cultivating students' imagination and innovating their thinking ability is the motivation and purpose of our research. Through research, it is found that multimedia education is based on traditional education, which is obviously more advantageous and can stimulate students' enthusiasm. It is full of enthusiasm for learning and let students take the lead in learning. Therefore, multimedia support education is not

only a tool to assist education, but also a transformation of modern education for the improvement and reconstruction of learning methods, which is a leap in the quality of traditional education.

By constructing a higher English international education model and evaluation index system, this paper analyzes the key factors of the higher English international education system in the current information age in detail. It mainly initializes teaching information from the perspective of English teaching evaluation and analyzes the international English education in colleges and universities' level and quality.

2. Classroom Evaluation Health: A New Vision of "Effective Teaching" Evaluation Research

Learning is based on a certain English environment, with the help of others and multimedia, that is to say, the process of meaning construction achieved through cooperation activities between people. Therefore, in this mode, "condition, cooperation, dialogue, and meaning construction" are the four elements in the learning environment. The characteristics and functions of multimedia technology are conducive to fully embodying the four elements. In order to provide a supportive education model, it provides the necessary conditions for effective use in English classrooms. Based on the above viewpoints, the multimedia support English education model is the specific application of constructivist learning theory in multimedia English education. Multimedia support education is to teach knowledge before class in traditional classrooms, and the internalization of knowledge is to carry out work activities after the original class and then transfer to learning activities in the classroom. Combined with the concept of multimedia-supported education, a multimedia-supported education model with four stages of education preparation, memory, application analysis, and comprehensive evaluation of education was designed. Take university English as an example, try the composition, and establish higher vocational education. The college English multimedia-supported teaching model divides the college English multimedia-supported teaching into two stages: pre-education and classroom. Discussions on knowledge extraction, online learning, and classroom problem-solving are given in Figure 1. See the figure for the four links of evaluation and feedback.

The development of students is divided into two stages. The first stage is the individual differences of students. The results are different. The second stage of development is under the guidance of teachers, and students can dig out the potential level of development. Use this to verify. In the case of underachievers, some students have average grades at the beginning of their studies. As long as their teacher provides reasonable guidance, this student can make great progress. Therefore, the educational model has an important influence on the development of students. Therefore, teachers should formulate educational plans around students' learning conditions.

In the knowledge extraction link, the teacher selects the main points of knowledge according to the students' knowledge level, learning foundation, learning ability, and learning habits; determines the teaching goals, teaching difficulties, and learning tasks of each unit; and refines enlightening and guiding questions. The online learning link is under the guidance of the teacher's questions; students can watch teaching videos in groups or independently by themselves to learn the main language, sentence structure, cultural background, and text structure. At the same time, with the help of the group leader, they can understand the main knowledge points as much as possible and bring the unsolvable knowledge content to the classroom. In the classroom discussion problem link, students expand their self-learning language and culture knowledge in groups or individually and apply them to various activities and tasks of classroom teaching to promote the students to absorb, internalize, and apply the knowledge they have learned. In this link, students need to complete the exercises and exercises related to online learning tasks, as well as activities such as after-reading feelings, situational dialogues, role-playing, keynote speeches, and hot topic discussions. In addition, for common problems, teachers should organize students to collaboratively solve and summarize. For personality problems, teachers should inspire and guide students to solve them independently and give individual guidance; the evaluation feedback link is given after the completion of the first three links; then the teacher will conduct a summary evaluation of the strengths and weaknesses of the learning situation and performance and propose improvement measures and future directions for efforts. Through the implementation of this link, students can further consolidate and improve the knowledge they have learned and have a better understanding of the problem.

To accurately evaluate the internationalization of higher English education, we first need to build an evaluation model of English education model. Combining nonlinear information fusion methods and time series analysis methods, statistical analysis of the teaching ability of English international education is performed. Higher English internationalization education model and evaluation ability constraint index parameters are a set of nonlinear time series. Constructing a high-dimensional feature distribution space represents the distribution model of higher English analysis and evaluation parameters, and its main index parameters restrict the teaching ability of English international education, teachers' level, investment in educational facilities, and policy relevance. Construct differential equations and construct an information flow model that expresses the constraint parameters of English international education ranking ability [4–7].

$$x_n = x(t_0 + n\Delta t) = h[z(t_0 + n\Delta t)] + \omega_n. \tag{1}$$

In the formula, $h(\cdot)$ is the multiple value function of the analysis and evaluation of English international education. ω_n is an evaluation error measurement function. In the high-dimensional feature distribution space, the solution vector of
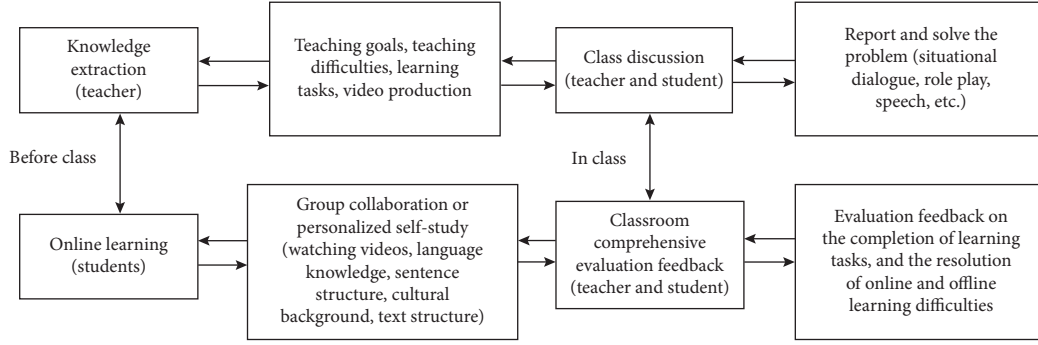
FIGURE 1: Multisource information fusion diagram of college English in higher vocational colleges.

the analysis and evaluation in the English international education teaching is calculated by the correlation fusion method, and the feature training subset $S_i (i = 1, 2, \ldots, L)$ of the education analysis and evaluation is obtained, and the following conditions are met:

(1) $\Sigma = \text{diag}(\delta_1, \delta_2, \ldots, \delta_r)$, $\delta_i = \sqrt{\lambda_i}, \forall i \neq j$

(2) $\cup_{i=1}^{L} S_i = V - v_s$

where $x_{n+1} = \mu x_n (1 - x_n)$ indicates that the evaluation index of higher English internationalization education adopts the conjugate solution of the statistical information model, which can reach the decomposition condition $U = \{u(t)|u(t) \in X, \|u\| \leq d, t \in I\}$ of the initial value, among which $(I_i)_{i \in N} = \{x_1, x_2, \ldots, x_m\}$. For multiple variable groups, the characteristic distribution sequence $x(n)$ corresponding to the evaluation statistics of higher English internationalization education can be used to construct a higher English internationalization education model based on the measured value of the previous teaching level.

$$c_{1x}(\tau) = E\{x(n)\} = 0,$$
$$c_{2x}(\tau) = E\{x(n)x(n+\tau)\} = r(\tau), \quad (2)$$
$$c_{kx}(\tau_1, \tau_2, \ldots, \tau_{k-1}) \equiv 0, \quad k \geq 3.$$

When $Q = 2$, the teacher's strength level and the distribution level of educational resources in the higher English classroom evaluation meet the $(2 + 1)$ dimensional continuous letter writing condition [8–10]. In other words, the courses of English internationalization education should be analyzed and evaluated.

$$\psi_x(\omega) = \ln \Phi_x(\omega) = -\frac{1}{2}\omega^2 \sigma^2. \quad (3)$$

The exclusive analysis and evaluation data information flow model of English international education it provides an accurate data input basis for the teaching analysis and evaluation of English international education and constructs a set of scalar sampling sequence components.

The multi-source information fusion algorithm is used to analyze the big data information model of the higher English international education model and the evaluation index system, and the control objective function for constructing the prediction and estimation of the ability of the higher English international education model is

$$\max_{x_{a,b,d,p}} \sum_{a \in A} \sum_{b \in B} \sum_{d \in D} \sum_{p \in P} x_{a,b,d,p} V_p, \quad (4)$$

$$\text{s.t.} \sum_{a \in A} \sum_{d \in D} \sum_{p \in P} x_{a,b,d,p} R_p^{bw} \leq K_b^{bw}(S), \quad b \in B. \quad (5)$$

Therefore, a specific analysis is made on the health evaluation index system of high school English teachers in the information learning environment.

3. The Health Evaluation Index and Measurement Analysis of College English Classroom Evaluation under the Information Environment

3.1. The Evaluation Index of College English Classroom Teaching System in the Information Learning Environment. According to the knowledge theory of health review, the motivation of the teaching system comes from the passage of English teachers and students in the system. The motivation of the English teaching and activity input system is mainly to promote the change of higher English international education mode, which needs to be measured indirectly through the obvious teaching mode of the outside world [11–13]. According to the analysis of the teaching process between the higher English teaching teachers and students, the types and characteristics of teaching activities are used to evaluate the health index system of higher English teachers. The higher English internationalization education model mainly prepares English teachers and English classroom education and provides special tutoring. The types of student education activities include students studying with teachers, and mutual help among students within teachers. The characteristics of higher English international teaching activities can use teacher enthusiasm and teaching. The time used by the process is measured. The characteristics of the student's learning model can be explained by the student's enthusiasm for learning and the amount of time spent on learning. The teaching enthusiasm of higher English teachers is used to evaluate the degree of effort of teachers in English teaching activities, and it is also an active psychological activity that appears in higher English teaching as a teaching model. Under the modern information, the motivation to input the evaluation system of higher teachers, in addition to the two

main teaching models of teachers and students, is the evaluation basis of the evaluation system under data informatization. In the past, higher English education needed a teaching model shared by teachers and students. As the teaching model of the education system, modern informatization mainly uses informationized teaching resources and higher English international teaching.

3.2. Organizational Structure Measurement Indicators for College English Classroom Teaching Evaluation in an Information Learning Environment. The higher English teaching evaluation index is used as a teaching model for English teachers and students individually, and the input energy from teaching is rationally allocated as an international teaching system. A certain teaching model can be constructed to ensure smooth energy flow and high efficiency. The teacher evaluation system can run the sequence in a healthy manner [14, 15]. In the modern information environment, the teacher evaluation system includes the interaction between the teachers, students, and teaching resources, and detailed teacher learning and classroom learning can explore the learning motivation of students and ensure that the input system energy meets the characteristics of all aspects in these mutual exchanges. The measurement is suitable for the organizational structure of higher English internationalization evaluation to construct teaching evaluation indicators. Teachers and students need to meet the needs of each other, and their mutual adaptability is very high. According to their own teaching activities to supervise each other's work, the way of energy transfer between each other has become more fluent, and the number of energy conversions has increased. On the whole, fitness satisfies the three aspects, namely, purpose fitness, content fitness, and method adaptation. Teaching attitude plays an important role in the evaluation system of higher English teachers. The purpose of different activities, teaching content, and learning attitudes are in line with the teaching levels of both parties.

3.3. Resilience Index of College English Classroom Teaching Evaluation in an Information Learning Environment. The resilience of the English curriculum evaluation system refers to the ability of the teaching evaluation system to be threatened by the outside world and to maintain the system's ability to create and function normally. In order to maintain the normal operation of teaching evaluation, the evaluation system can play an overall adjustment role and strengthen the protection elements to reduce the risk. This requires higher English teachers to have a sense of self-reflection in the teaching process and be able to consciously correct the existing risk factors in time. The main influencing factors in the evaluation system are the teaching fatigue of the English teachers in the teaching process, the lack of motivation of students, and the information incompatibility existing in the environment of globalization, and the teaching organization structure is threatened from the outside. This will be caused by teachers' fatigue, the interaction between student's learning and teacher's teaching activities, goals, teaching

content, teaching attitudes, and teaching methods that cannot meet their needs. It is not suitable to be applied to the modern information teaching environment. It needs to constantly overcome the existing problems. Teachers and students need to have the ability to reflect, detect the existing dangerous factors, and take corresponding measures to overcome the existing difficulties. This will enable teachers' and students' educational abilities to be effectively used, and the existing risk factors can be detected. The good state of learning motivation and organizational teaching structure is equivalent to the key protective factors in the English classroom evaluation system, in order to effectively promote English teachers, and the embodiment of the education level of the students ensures that the students have better learning ability.

4. Realization of Optimization of Higher English Internationalization Education Model and Evaluation System

Constructing a binding parameter index analysis system for higher English internationalization education model and evaluation analysis, using multisource information fusion for higher English internationalization education model and evaluation based on the analysis of big data information system, in order to improve the quantitative assessment ability of higher English classroom scheduling level, we propose a higher English classroom teaching analysis method based on a fuzzy greed algorithm and information fusion, analyze higher English classroom teaching, and transform the evaluation problem into a least-square estimation problem of the K-means cluster objective function. The least-squares problem is to find the consistent estimation value of the higher English internationalization education model and the evaluation resource constraint vector β so that $\|Y - X\beta\|$ can be minimized, where $\| \cdot \|$ is the F-norm in the European algebra norm, and obtains the constraint characteristics of the ability of advanced English classroom scheduling. The entropy feature extraction value of the information is

$$P_{\text{loss}} = 1 - \frac{1 - p_0}{\rho} = \frac{p_0 + \rho - 1}{\rho} = \sum_{n=1}^{N} p_{k,n}. \tag{6}$$

Given that d_i is the perturbation feature vector for teaching analysis and evaluation, the estimating formula of higher English classroom arranging ability is transformed into the least square solution

$$z(t) = x(t) + iy(t) = a(t)e^{i\theta(t)} + n(t), \tag{7}$$

where $x(t)$ is the real part of the time series for evaluating the distribution of big data, and $y(t)$ is the imaginary part of the higher English international education model and evaluation constraint index sequence.

Using surrogate data method to randomize the teaching ability of higher English classrooms can also disturb the empirical distribution data of the kth education analysis and evaluation of functional, and obtain the kth subgroup, which

represents the utilization rate of the resource distribution of higher English classrooms.

$$U_{\text{util}} = \gamma \overline{X}. \tag{8}$$

Constructing a hierarchical tree, using big data analysis methods, establishing the main component characteristics of the analysis and evaluation outside the teaching time of higher English classrooms, and using ambiguous close filling methods can solve the similarity of the distribution of educational resources.

$$\text{Sim}_1\left(d_i, d_{1j}\right) = \frac{\sum_{k=1}^{M} W_{ik} \times W_{1jk}}{\sqrt{\sum_{k=1}^{M} W_{ik}^2} \cdot \sqrt{\sum_{k=1}^{M} W_{1jk}^2}}, \tag{9}$$

where d_i is the prior distribution feature vector of higher English internationalization education model and evaluation and d_{1j} is the K-means clustering center vector of the first-level big data.

Combining the fusion method of linear correlation characteristics, the clustering, and integration of the index parameters of the higher English classroom teaching evaluation are realized, and the fusion formula of the output education resource information is as follows:

$$P(w|x) = \frac{P(x \mid w)}{P(x)}. \tag{10}$$

If the quantitative recursive feature $(N(i) \bmod L) < m$, the probability density feature $p(i) = \lfloor N(i)/L \rfloor$ of the distribution of teaching resources, the higher English internationalization education model, and the evaluation big data stream $X(i)$ are divided into $p(i)$ submatrices $N_{ij} \times m$ with the size of X_{ij}, and they are aggregated by index parameters, classes, and integration, and compile appropriate teaching evaluation contents, so as to realize the evaluation of international higher English education model.

5. Improvement Strategies for Higher English Internationalization Education under the Background of Multi-Source Information Fusion

5.1. Adjust Teaching Goals. If information processing methods and big data analysis methods are used to adjust teaching evaluation and resource utilization, the quantitative control of teaching progress will be improved and it will play an important role in the level of planning ability. Therefore, it aims at the background analysis of higher English teaching ability assessment. Because of the influence of many factors, the evaluation of higher English teaching ability first conducts experiments and researches on higher English teaching level, establishes a data system and resource analysis system for higher English teaching level, and uses information combination and clustering solutions to solve higher English. The evaluation of teaching ability and the establishment of the target and statistical system of English teaching ability evaluation can significantly improve the quantitative budget ability of higher English teaching ability evaluation. In the higher English international education model and evaluation index system, the effect of the international education model and evaluation index system is affected by the order of courses. It can be seen from the effect of the order of courses that the arrangement of higher English classrooms in a college is reasonable, and what is the effect of college education. The ranking of higher English classrooms represents the feasibility of the entire class schedule of this college.

5.2. Strengthen the Design of Higher English International Education Courses. For the traditional international education model and evaluation index system ability evaluation calculation, there is a situation of inaccurate classification. Based on this situation, research scholars have proposed an international education model and evaluation index system ability evaluation calculation method on the combination of fuzzy greedy calculation method and information. First, set up a research system for constrained parameter indicators, then use quantitative recursive methods to evaluate the ability of the data information system to achieve the ability to control the acquisition of characteristic resources, complete the classification and summary of the index parameters of the international education model and the ability of the evaluation index system, and edit the corresponding the teaching resource plan. Complete the evaluation of the ability of the evaluation index department. Using this calculation method to carry out the evaluation of the ability of the international education model and the evaluation index system, the information integration and analysis ability is high, the accuracy of the teaching ability evaluation is greatly improved, and the efficiency of the use of educational resources is improved.

5.3. Improve the Teaching Test and Evaluation System. For a long time, the evaluation of China's higher English internationalization education is based on final evaluation, with final exams and CET-4 and CET-6 as the main test methods, but students' evaluation of the English learning process is relatively neglected. Do not pay attention to the assessment and evaluation of students' learning methods, knowledge application ability training, and other key skills. CET-4, CET-6, CET-4, and CET-8 all emphasize achievement and pass rate. It has brought many negative effects to students' English learning. The question type of the college English test has a big flaw in its design. Not only is there a big deviation in the basic internationalization of college English education, but also the review of many contents cannot fully reflect the comprehensive language application ability of college students. In particular, the review of oral skills and translation skills has weakened. The phenomenon of dumb English with poor ears is still relatively serious. Therefore, it is necessary to reform the current higher English international education testing and evaluation system. On one hand, increase the proportion of formative evaluation and ask students to speak, read, write, and perform comprehensive test translation and other language skills to promote students' application skills of English knowledge. On the other hand, make corresponding changes in the form of

English examination questions and improve the effectiveness and accuracy of the review process. If objective problems can be reduced, questions such as conversational tests and subjective questions will be added, focusing on cultivating students' ability to use English language thinking skills and English knowledge to solve practical problems.

5.4. Pay Attention to the Construction of the Teaching Staff. In order to further accelerate the internationalization of higher English education and the process of internationalization of education, we must pay attention to the direct impact of the construction of the teaching staff. In the context of multisource information integration in higher education, the construction of the teaching team is ensured. The key to the smooth progress of the reform of higher English international education is to improve the professional quality of high school English teachers and to further improve the education level and quality of education. In order to better meet our country's actual needs for training international English talents. At present, college English teachers regularly participate in educational seminars, and training is the main way to build the teacher team. However, this is obviously insufficient for cultivating new international talents. On the basis of strengthening in-service teacher training, the university encourages students to participate in foreign language education seminars at home and abroad. If conditions permit, teachers can be given more opportunities for overseas exchanges and training. Expand the horizons of teachers' international education and form the ability of international thinking and practice in English education. In addition, on the basis of accumulating their own professional knowledge, college English teachers have been extensively involved in pedagogy, linguistics, psychology, sociology, anthropology, and other related subject knowledge, improving personal comprehensive quality and accelerating the accumulation and integration of and subject experience, so as to improve the quality of English international education.

6. Experimental Process and Results

This experiment will use this indicator system to analyze the results of the experiment. First, establish a hierarchy, based on the levels and elements of the learning ($a1$) part of the higher English international education model in Table 1; English learning input ($b1$) and English learning output ($b2$) are contained in it, and $c1$ is the visible learning level indicator. Adopt the sum of compulsory and elective hours, and the evaluation criteria are over 150A, 120–150B, 90–120C, 60–90D, E under 60, converted into a percentage system A 100 points, B 85 points, C 70 points, D 55 points, and E 40 points; $c2$, the invisible learning indicator calculates the level and number of students participating in competitions, participation in English-related lectures and activities, participation in international academic exchanges, and English-related practical activities, which are converted into a hundred-point

Table 1: *a-b* comparison judgment matrix.

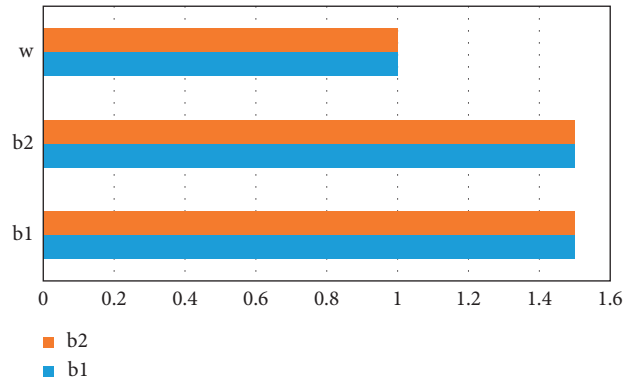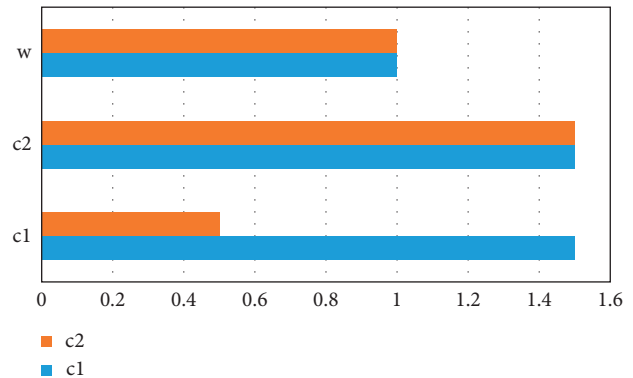| a_1	b_1	b_2	w
b_1	1.5	1.5	1
b_2	1.5	1.5	1

Figure 2: *a-b* matrix diagram.

Figure 3: b_1-*c* matrix diagram.

system; $c3$ indicators are degree courses and evaluation standards. It is a percentile system with a score of 7 : 3 on the roll and usual; $c4$ is the accumulation of other output such as awards in the National College English Contest and submission and publication of English papers (assigned according to ISTP, EI equal levels), etc. and is converted into a percentile system. Secondly, the corresponding questionnaire was compiled, and opinions were solicited from 20 teachers engaged in English teaching for non-English major graduate students to confirm the final judgment matrix and form the weight coefficient, as shown in Figures 2–4 and Tables 1–3.

When λmax = 1.5, when CI = 0 is satisfied, the obtained matrix has complete consistency (Figure 2).

When λ_{max} = 2.0, when CI = 0 is satisfied, the obtained matrix is completely consistent (Figure 3).

When λ_{max} = 2.5, when CI = 0 is satisfied, the obtained matrix has complete consistency (Figure 4).

The results of the 2019 higher English internationalization teaching courses are selected in order of 67–74 points, of which there are 50 students, 25 boys and 25 girls. The selected student targets have no significant difference
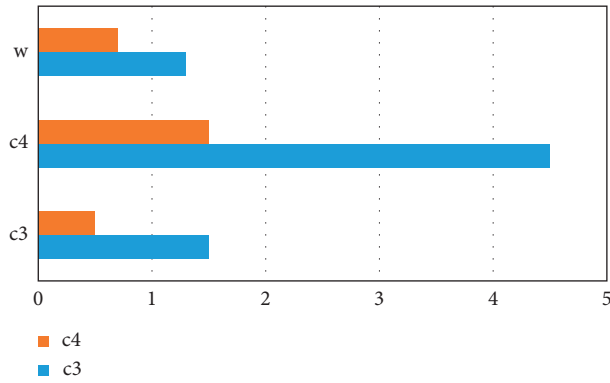
Figure 4: b_2-c matrix diagram.

Table 2: b_1-c comparison judgment matrix.

b_2	c_1	c_2	w
c_1	1.5	1.5	1
c_2	0.5	1.5	1

Table 3: b_2-c comparison judgment matrix.

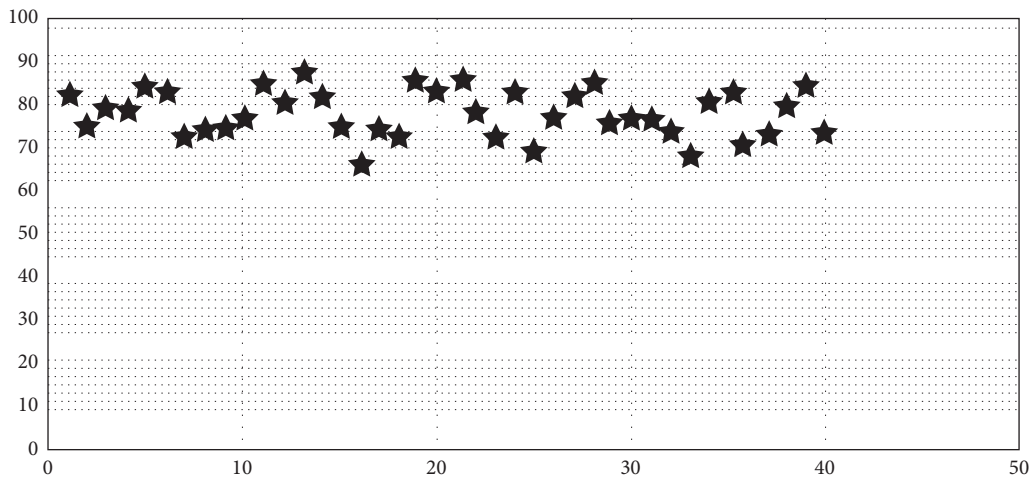| b_2	c_3	c_4	w
c_3	1.5	4.5	1.3
c_4	0.5	1.5	0.7

Figure 5: Distribution of English comprehensive ability assessment results.

in age. The detailed distribution is shown in Figure 5. As shown, in the evaluation of the quality of the teaching model, this single result obviously cannot be used to objectively evaluate the 50 students with insignificant differences in scores.

From the analysis of the experimental results, it can be seen that the higher English internationalization education index assessment constructed in this article has a good degree of discrimination, can more reasonably evaluate the higher English internationalization teaching ability, and can also make the evaluation process more objective and scientific. This provides a scientific basis for follow-up teaching quality evaluation.

7. Conclusions

According to the above analysis, it can be seen that there are many problems in the teaching process of higher English international education based on the multisource information fusion algorithm. The English teachers of colleges and universities need to reform according to the teaching level, mainly from the English teaching goals and English courses. Design standards, teaching content compilation, teaching quality evaluation, and English teacher team construction are analyzed from different perspectives to realize the adjustment and innovation of previous higher English nationalization teaching programs and effectively

enrich the role and functions of higher English international education. Improve the teaching level of English internationalization and better adapt to the development trend of the internationalization of higher education and economic globalization.

Data Availability

Data sharing does not apply to this article as no datasets were generated or analyzed during the current study.

Conflicts of Interest

The authors declare no conflicts of interest.

Acknowledgments

References

[1] X. Wu and S. Zhang, "Evaluation of computer assisted translation and its teaching application in English translation," *Kuram ve Uygulamada Egitim Bilimleri*, vol. 9, no. 4, pp. 157–178, 2018.

[2] T. Watanabe, "An evaluation of teaching English with an aet (team-teaching)," *Arele Annual Review of English Language Education in Japan*, vol. 1, pp. 125–134, 2017.

[3] R. Al-Mahrooqi and F. Al-Maamari, *English Education in Oman*, Springer, Berlin, Germany, Student evaluation of their english language teachers in omani basic education schools, 2018.

[4] T. C. Chen, "An overall evaluation of elementary English education in taiwan," *Journal of Asia Tefl*, vol. 66, no. 2, pp. 419–424, 2018.

[5] K. G. Krechetnikov and N. M. Pestereva, "A comparative analysis of the education systems in korea and Japan from the perspective of internationalization," *European Journal of Contemporary Education*, vol. 6, no. 1, pp. 77–88, 2017.

[6] T. Alsuliman, L. Alasadi, A. Mouki, and B. Alsaid, "Language of written medical educational materials for non-English speaking populations: an evaluation of a simplified bi-lingual approach," *BMC Medical Education*, vol. 98, no. 7, pp. 45–58, 2019.

[7] F. Altinay, G. Basari, M. Altinay, G. Dagli, and Z. Altinay, "An evaluation of strategies and policies in higher education management in internationalization process: new pedagogy," *Journal for Multidimensional Education*, vol. 37, no. 1, pp. 1–12, 2019.

[8] A. Usman, "An evaluation of middle basic education curriculum for English studies in Nigeria under the nine-year universal basic education curriculum," *Journal on English Language Teaching*, vol. 39, no. 6, pp. 1006–1011, 2017.

[9] T. Ohno, R. Kato, H. Itakura, H. Yanaguimoto, and N. Kurosawa, "A retrospective evaluation of the need for English education by hospital and community pharmacists," *Japanese Journal of Physical Education*, vol. 32, no. 4, pp. 376–384, 2019.

[10] L. Hongjing and L. Liwen, "A mixed methods evaluation of college English writing: a case study in China," *The Asia-Pacific Education Researcher*, vol. 26, no. 6, pp. 383–396, 2017.

[11] J. I. Liontas, T. I. Association, and M. Dellicarpini, "The tesol encyclopedia of English language teaching || terminology: assessment, evaluation," *The TESOL Encyclopedia of English Language Teaching*, vol. 23, no. 7, pp. 1–10, 2018.

[12] H. J. Kim and B. H. Kim, "Implementation of young children English education system by ar type based on p2p network service model," *Peer-to-Peer Networking and Applications*, vol. 23, no. 5, pp. 531–555, 2017.

[13] U. L. Igbokwe, E. N. Nwokenna, C. Eseadi, C. S. Ogbonna, and A. R. Ogbuagu, "Intervention for burnout among English education undergraduates: implications for curriculum innovation," *Medicine*, vol. 55, no. 11, pp. 548–554, 2019.

[14] X. Li, "Characteristics and rules of college English education based on cognitive process simulation," *Cognitive Systems Research*, vol. 57, no. 10, pp. 11–19, 2019.

[15] J. Han, "Empirical analysis of undergraduate students' learning satisfaction in college teaching evaluation: a case study of h university," *Boletin Tecnico/Technical Bulletin*, vol. 55, no. 8, pp. 592–599, 2017.

Research Article

Intelligent Building Construction Management Based on BIM Digital Twin

Yi Jiang (ORCID)

Henan Finance University, Zhengzhou 451464, China

Correspondence should be addressed to Yi Jiang; jiangyi@hafu.edu.cn

In order to improve the construction effect of intelligent buildings, this paper combines the BIM digital twin technology to construct the overall structure of the building construction operation and maintenance system driven by the BIM digital twin. Moreover, this paper conducts intelligent simulation of the construction process of the building and combines the construction process of the intelligent building to apply the BIM digital twin technology to the construction management of the intelligent building. In addition, this paper uses BIM to simulate the construction process. After the construction management plan is developed, BIM can be used to simulate the construction, find the problems in the construction, and formulate a reliable construction management plan in time. Through simulation experiment research, it can be known that the intelligent building construction management model based on BIM digital twin proposed in this paper can help the deployment of intelligent building construction process in many aspects and help improve the efficiency of building construction management.

1. Introduction

One of the largest network interconnection tools in the world is the Internet. The Internet uses some specific technical means and facilities connecting various types of related networks well and then connects these established connections to the Internet backbone network [1]. Generally speaking, the Internet technology we are talking about is the integration and synthesis of various technologies such as network, computer technology, multimedia technology, information data exchange, and communication technology, etc., to form a systematic information technology. Internet technology can be called a universal technology without exaggeration. It is a kind of integrated information technology. Moreover, it can perform a near-real simulation restoration of various activities, things, and situations in the real world, and it can also present various concepts of people on the computer in a virtual way [2].

The construction project management system is a newly built system. Therefore, the fourth-generation development environment construction system that can quickly generate prototypes is used in development, and it can be continuously improved and improved during operation, making it an ideal project management system [3].

BIM technology, simulation analysis technology, and monitoring technology have been widely used in the construction process of buildings [4]. BIM uses all the information of the engineering project as the database of the model, which can be used for visualization of the construction plan, construction simulation, and project management during the construction phase. Simulation analysis technology can simulate the mechanical performance and deformation state of the building structure at different times during the construction process. Large-scale finite element software is usually used to realize the simulation analysis of the structure, but the analysis of complex buildings requires secondary development. Moreover, through real-time construction monitoring of the construction process, especially the important parts and key procedures, it is possible to know the stress and operating status of the structure in time during the construction process. Whether the construction monitoring technology is advanced and reasonable, plays a vital role in construction control and is also an important part of the informationization of the construction process.

2. Related Work

Literature [5] defined BIM as integrating building component information into the building model by means of parametric modeling. At each node in the project life cycle, project participants can transmit and exchange project information through the model. BIM is used by all parties in the industry. With the continuous development of BIM standards, the continuous research of information exchange formats, and the continuous exploration of actual projects, BIM technology has been continuously improved [6]. For the intelligent management of construction sites, literature [7] is dedicated to the development of hybrid artificial intelligence tools, which have been successfully applied in many construction industries. In particular, in the field of construction management, CAPP software is used to determine important project success factors, and the developed Evolutionary Fuzzy Hybrid Neural Network (EFHNN) is used to evaluate project success. In terms of construction site informatization management, Japan has relatively standard regulations in the implementation of construction industry informatization, and Japan has fully implemented the full life cycle informatization of construction projects. On the basis of computer-aided design (CAD), a unified IT platform is provided for interaction, and electronic drawings and diagrams are used to illustrate the construction of the project, which proves that, in the case of three-dimensional electronic drawings, the realization of visualization is the most effective [8]. Literature [9] proposed a model for designing a visual management system. According to the degree of integration of the management process, the research proposed a set of guidelines for designing and implementing a visual management system and a virtual machine practice classification method.

Literature [10] proposed an Intelligent Scheduling System (ISS); project managers can use this system to find a near-optimal scheduling plan under project goals and project constraints. The ISS system integrates most important construction factors, including schedule, cost, space, manpower, equipment, and materials, etc. and uses simulation technology to allocate resources. The system assigns different levels of priority to different activities in each simulation cycle to find a near-optimal solution, so that the final progress is closer to the optimal. There are also various tools for the development of informatization in the construction industry in Germany. One of them is called the SWLMing project, which is called the energy-saving building information management semantic Web technology.

Using BIM, the construction process can be virtualized and visualized, and the construction progress, cost, resource allocation, etc. can be simulated, and the construction plan can be continuously improved, and the rationality of the construction can be improved [11]. Literature [12] proposed and verified the method of 4D model creation and the advantages of using 4D model; the use of 4D model in construction is conducive to project schedule and control. Finally, suggestions and precautions for using BIM in the process of 4D model creation are given. Literature [13] proposes a BIM-based automatic schedule plan generation method. Managers can use the schedule information model to compile a construction schedule. The two are linked for 4D simulation to increase the practicability of the schedule and reduce the number of managers and systems in subsequent construction. Literature [14] studied the BIM-based schedule planning model, which can automatically count the activity engineering quantity and calculate the duration and then schedule the schedule according to the duration. Based on the analysis of BIM-based schedule planning and BIM functions, a schedule planning method based on BIM to build an AEC + FM integrated framework is proposed.

Literature [15] deeply studied the benefits and value of applying BIM to prepare schedule and control the schedule and finally simulated the application of BIM technology to prepare schedule. Literature [16] conceived a BIM-based schedule management system framework. On the basis of this framework, a general and detailed secondary, weekly, and daily schedule plan was formulated. This action can realize the visualization of schedule management and the basis of information integration. Collaborative optimization to achieve multiple goals enriches schedule management theory, broadens schedule management practice ideas, and has guiding significance. Literature [17] uses BIM to study the automatic generation of schedule plans, with BIM technology as the main line and foundation, and on the basis of schedule planning process analysis, it integrates the establishment of expert knowledge and experience knowledge base in the field of construction and uses rules to conduct BIM-based automatic generation of schedule. BIM can be used as a database collection of component three-dimensional geometric information and other functional information. The advantage of RFID technology is that it can track and collect component progress status information, combine the advantages of the two to complement each other, and apply it to progress management, creatively solving the real-time progress. Tracking and progress monitoring are the core issues of construction progress management [18]. Literature [19] studied the application of the Internet of Things and BIM to the construction progress of the project, through radio frequency identification, global positioning, and remote understanding, command, and scheduling of construction.

3. Overall Structure of Building Construction Operation and Maintenance System Driven by BIM Digital Twin

Digital twin technology can be applied to a wide range of objects in the construction field, including buildings, work units, construction lines, workshops, etc. It should be noted that, in the digital twin general model architecture, when an object on the Y-axis (object level) is projected to the XOZ plane (system level-life cycle plane), it can be driven by the digital twin to realize the new idea of cyber-physical integration and intelligent operation of the object during its entire life cycle. Specifically, taking the building automation assembly construction line studied in this subject as an

example, when it is projected along the Y-axis XOZ plane in the three-dimensional digital twin architecture, the overall structure of the construction line operation and maintenance system driven by the digital twin can be obtained, as shown in Figure 1.

Among them, the building construction site as a physical entity layer is the basis for realizing virtual and real interaction. During the construction process, various sensors on the construction site transmit construction status information and equipment parameters to the virtual model layer through the digital tie layer. The virtual mirroring continuously updates the data and calls the geometry, physics, behavior, and rule models to simulate the status and performance of the construction line in real time and then feeds back the simulation analysis results to the physical layer and optimizes the control of the construction site through the controller. At the same time, the data link layer transmits the construction site conditions and simulation analysis results to the service application layer. On the one hand, the service application layer integrates modules such as building quality display, construction process monitoring, abnormal situation handling, construction progress feedback, equipment fault diagnosis, health status assessment, equipment life prediction, and maintenance plan generation. It displays the operation and maintenance status of the construction line on multiple platforms. On the other hand, enterprise management information systems such as ERP, MES, PDM, and PLM will also support various functional modules in the service application layer and provide them with construction-related information through data sharing. In addition, users can issue instructions through the service application layer to optimize the control of the building construction process, which also reflects from the side that the digital twin-driven construction line operation and maintenance system have good human-computer interaction performance.

In building construction activities, factors such as building structure, process flow, and technical indicators are closely related to construction efficiency and quality. Therefore, the focus of research and development of the building automation construction line is to reasonably carry out construction line layout, key mechanism structure design, and control system scheme design based on the analysis of construction elements and complete the automated construction of the building through the cooperation of reasonable and effective mechanical structure and stable and reliable control system. From the three aspects of construction element analysis, layout and structural design and hardware system design, the overall research and development idea of the design and development of the building automation construction line is shown in Figure 2.

The overall layout of the construction line is a prerequisite for development, so the overall layout of the construction line should be combined with the current situation and needs of the enterprise. As shown in Figure 3, the construction area is divided into areas such as storage of materials to be processed, storage of tooling and tools, and construction. Among them, the building construction area includes the main construction line and the automatic

feeding area, and the specific location of each station in the construction line can be determined according to the analysis of the process flow.

The virtual model of the traditional construction line mainly focuses on the visual expression, lacks the description of the characteristics, behavior, and rules of the construction line, cannot realize multidisciplinary, multiphysical, multiscale, and multiprobability simulation, and cannot meet the technical requirements of digital twins. Therefore, in the digital twin virtual model layer, researches are mainly conducted on the construction of geometric models, the standardized description of behavior models, and the evaluation of rule models.

As shown in Figure 4, in the construction of geometric models, the expression of key attributes such as physical entity size, shape, and assembly relationship is still the focus of research. Therefore, the node information will be planned based on the analysis of the structure and movement characteristics of the key elements of the physical construction line. And then use Open Inventor to build the geometric model of the object and express it visually. In terms of behavior model description, considering that the physical construction line is a construction system that integrates multidisciplinary and multidomain knowledge, there is currently no standardized description method for behavior models, and the modeling scope of AutomationML covers multidisciplinary data information, with descriptions. The ability of the behavior model and the construction line behavior model is related to the building, resources, and technology, so the standardized description of the behavior model will be studied based on AutomationML. Since the stability and reliability of the construction line's operating state are related to the key point information, the association rules of discrete data information will be mined, and the association rules will be quantified through the information entropy method, and the construction line health rule model will be established and collected through the construction site. The temperature data analyzes and evaluates the health of the construction line to verify the accuracy of the model.

At present, digital twin technology is still in its infancy, with few applications in services, and the advantages it brings are unclear. It can be seen that, through the development of the digital twin service application layer operation and maintenance system, it is very necessary to reflect the advantages of this technology in monitoring and evaluating the operation status of equipment in the construction field. The overall plan of the operation and maintenance system is shown in Figure 5. Based on the research of the physical entity layer and the virtual model layer, the key point data of the discrete construction line system is collected through the field bus to monitor the working conditions of the automated construction line at multiple construction sites. Establish a workshop Web network database server, integrate the physical entity layer construction database and the virtual model layer simulation database into the Web-core BS structure model, use the Web server to feed back the real-time construction situation and maintenance strategy of the construction site to the decision makers, and provide basic information query function. The construction information
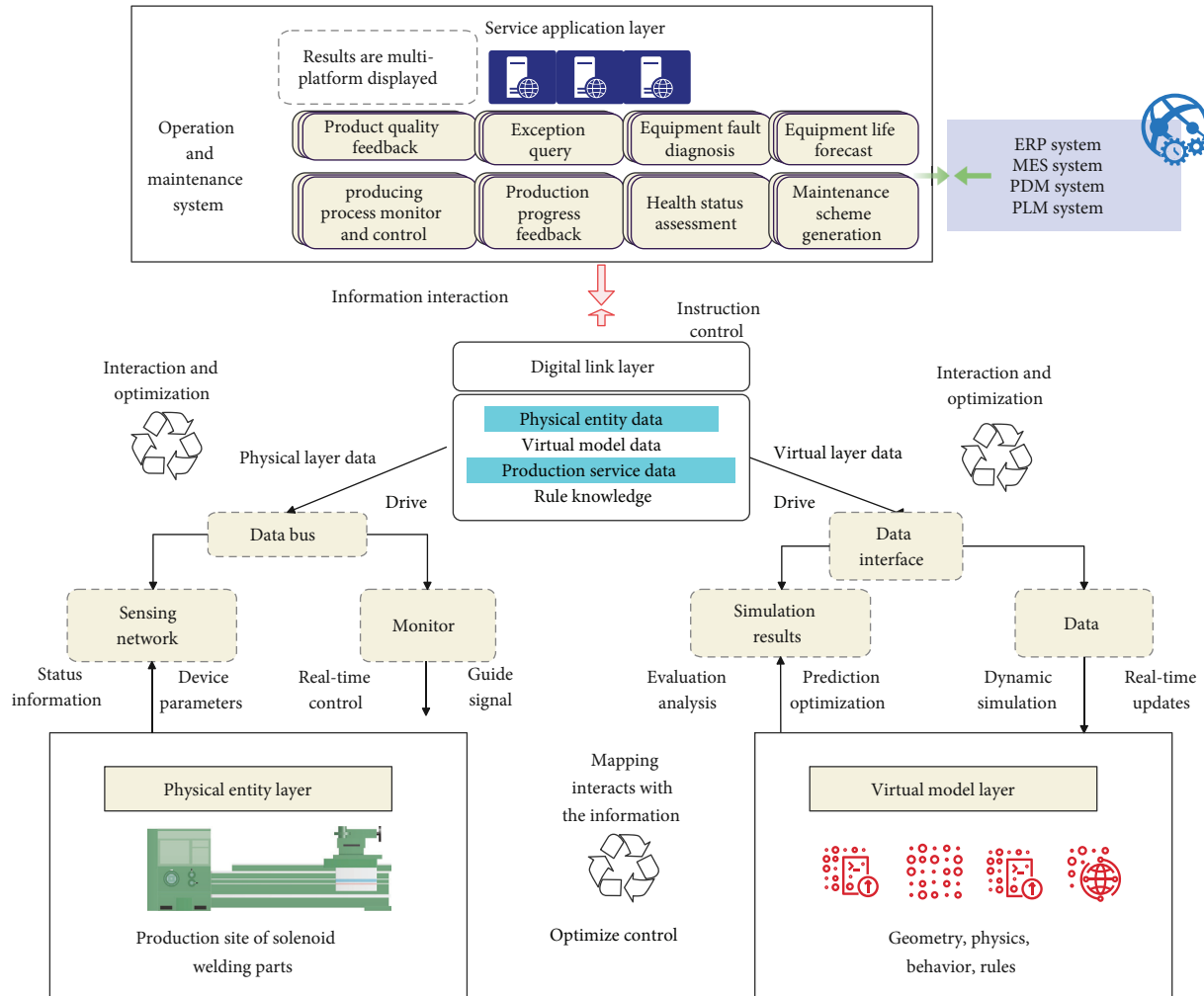
Figure 1: The overall structure of the construction line operation and maintenance system driven by digital twins.
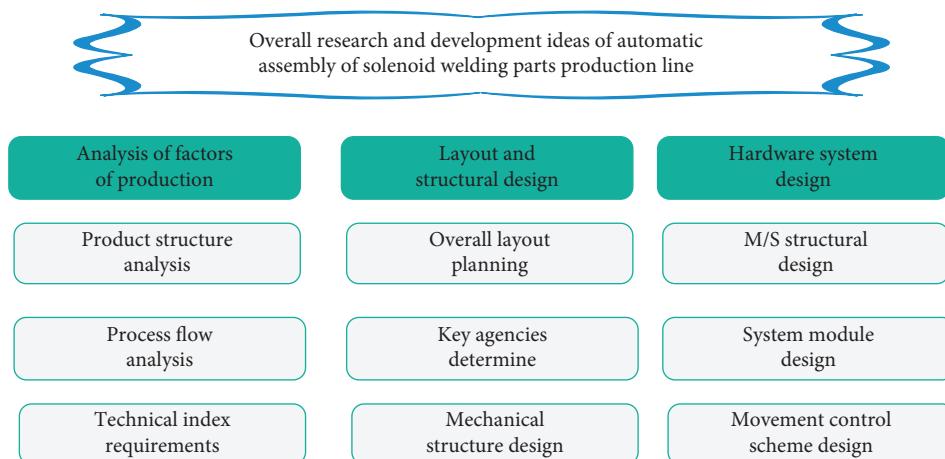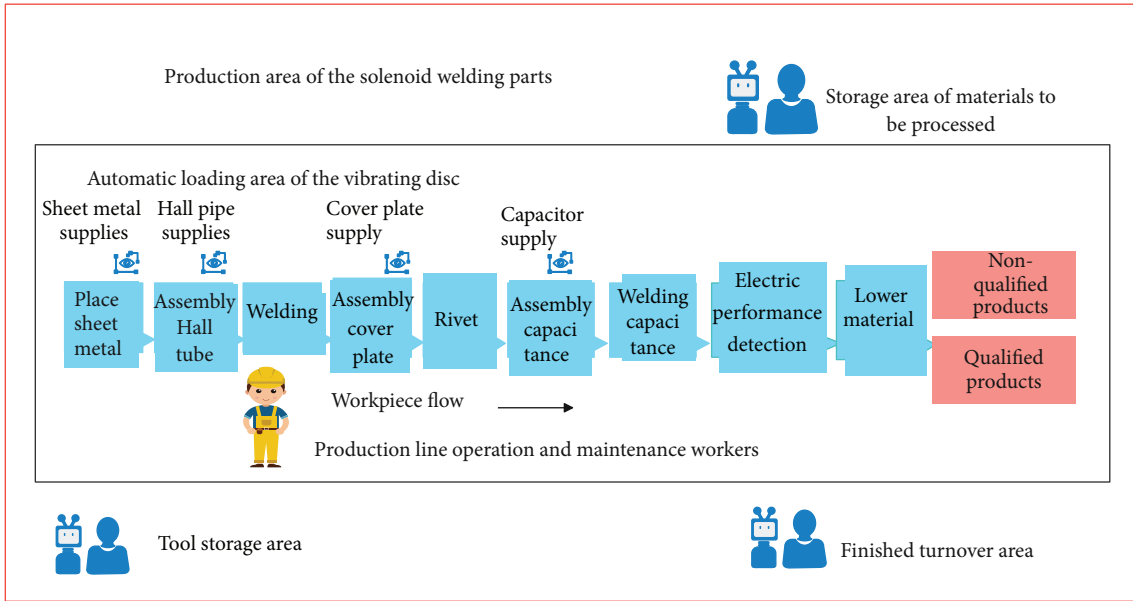

Figure 2: Overall research and development ideas of building automation construction line.

query and construction object information query functions build a unified and simple interaction method for the digital twin service application layer, physical entity layer, and virtual model layer that is independent of the user platform.

With the increase of construction line construction system equipment and the increase of uncertain factors in the construction environment, there will be complex coupling relationships within the system, which will seriously

FIGURE 3: Overall layout of building automation construction line.

$$MVE=\{Gy, By, Ry\}=\begin{Bmatrix} Bvl & Gvj & Rvj \\ Bva & Gvw & Rve \\ Bvt & Gwh & Rvo \\ .... & .... & .... \end{Bmatrix}$$

Construction of the production geometric model based on Open Inventor

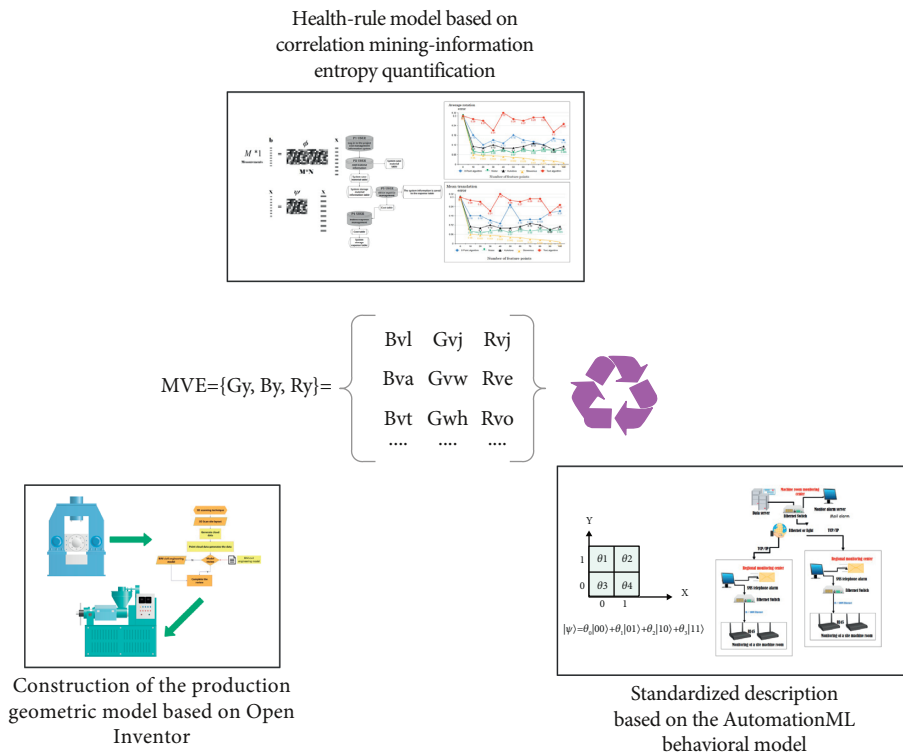Standardized description based on the AutomationML behavioral model

FIGURE 4: The main research content of the virtual model layer.

affect the reliability and stability of the construction system. Therefore, it is necessary to quantitatively evaluate the uncertain factors in the operation of the complex construction production line system. Taking into account that the digital twin rule model includes rules such as constraints, associations, and derivations, the mirroring of the virtual

space can be equipped with functions such as judgment, evaluation, prediction, and optimization. Therefore, this paper defines the digital twin rule model, combines it with the health assessment of the construction line system, and uses the real-time data collected by the physical entity layer sensor as the input of the rule model. Moreover, this paper
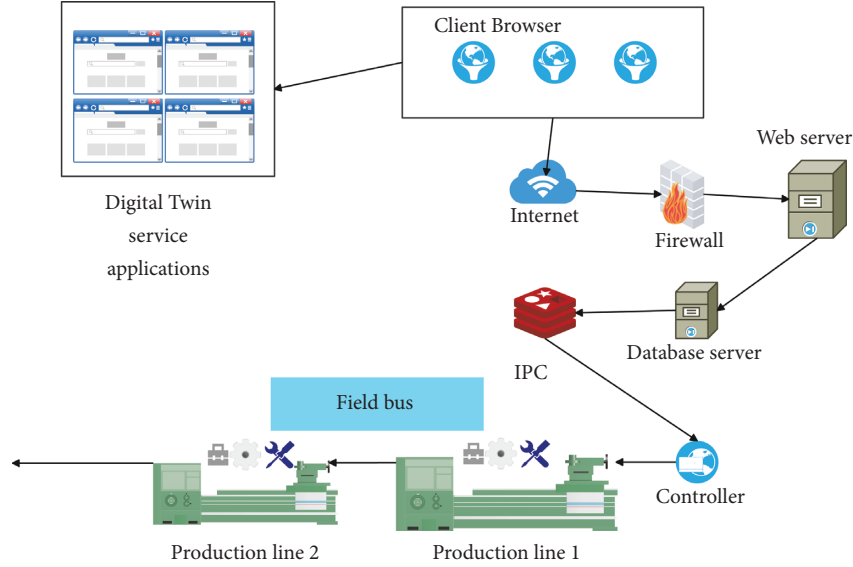
FIGURE 5: The overall scheme design of the service application layer operation and maintenance system.

uses quantitative association rules to output health and judge, evaluate, and optimize the working status of the construction line.

When any construction system works, there will be corresponding behavior patterns, and the collection of all behavior patterns represents the construction capability of the system. Although the behavior mode of the system is the result of the interaction of different attributes, the reliability of the system operation can be obtained by analyzing it, but the complex construction system often contains more attributes with coupling relationships, which increases the difficulty of identifying the internal behavior mode. It should be noted that the real-time data collected on the construction site can effectively reflect the construction status of the resource equipment. Therefore, it is the main research direction of the digital twin rule model to obtain the health of the construction system by analyzing the real-time data stored on the construction site and quantifying the relationship between different attributes.

Since the key point monitoring data of the construction line transmitted by the digital tie layer in real time is a data sequence $x_1, x_2, x_3, ..., x_n$ that arrives continuously at a fixed speed, the sliding window model can be used to evaluate the data, that is, to analyze the collected data updated over a period of time. The data to be processed in the digital tie layer can be expressed in the form of a matrix [20]:

$$D_{DT} = \begin{bmatrix} D_{DT\,1} & D_{DT\,2} & \cdots & D_{DT\,n} \end{bmatrix} = \begin{bmatrix} d_{11} & d_{12} & \cdots & d_{1n} \\ d_{21} & d_{22} & \cdots & d_{2n} \\ \vdots & \vdots & \vdots \\ d_{m1} & d_{m2} & \cdots & d_{mn} \end{bmatrix}.$$

(1)

.

In the formula, Dpr represents the digital tie layer data matrix, which is composed of n elements representing different attributes, which can describe the temperature, force, and other attributes of the key equipment of the construction line, and the value corresponding to the attribute is represented by d_{mn}. In the solenoid assembly line system, the digital tie layer data matrix mainly includes attributes such as welding temperature and hot riveting temperature.

Next, we use the digital tie layer data matrix to analyze the relationship between the data. Among the n attributes of the matrix ($n > 2$), two are selected arbitrarily as the X and Y axes to establish a two-dimensional scatter plot, and the extreme value in the data is used as the boundary of the two axes. At this time, a rectangular area containing all data points is obtained. According to the permutation and combination calculation formula, a data matrix with n attributes produces a total of $n(n-1)$ scatter plots. Since the data in the scatter chart represents the attributes of the object and its related operating modes, in this paper, the scatter chart is called the attribute pattern chart.

Because the continuous data stored in D_{DT} is not conducive to analysis and calculation, there is a problem of low calculation efficiency, which will affect the real-time simulation evaluation of the digital twin rule model, so these continuous attribute data need to be discretized.

This paper uses the equal interval method to discretize the data and divide the data area. First, this paper determines the number of intervals to be divided. The number of intervals usually takes a value of 5–9, which represents the health assessment accuracy (EA). To facilitate analysis, the coordinate axis of the data to be analyzed is divided into five intervals, which are represented by L1, L2, L3, L4, and L5, as shown in Figure 6(a). Next, this paper conducts correlation mining on variables to study the changing trend of the system state when a certain attribute is disturbed. The figure is divided into 25 cells, and the cells containing data may represent the next operating state of the system. Therefore, the cells can be selected in turn as the reference grid, and the
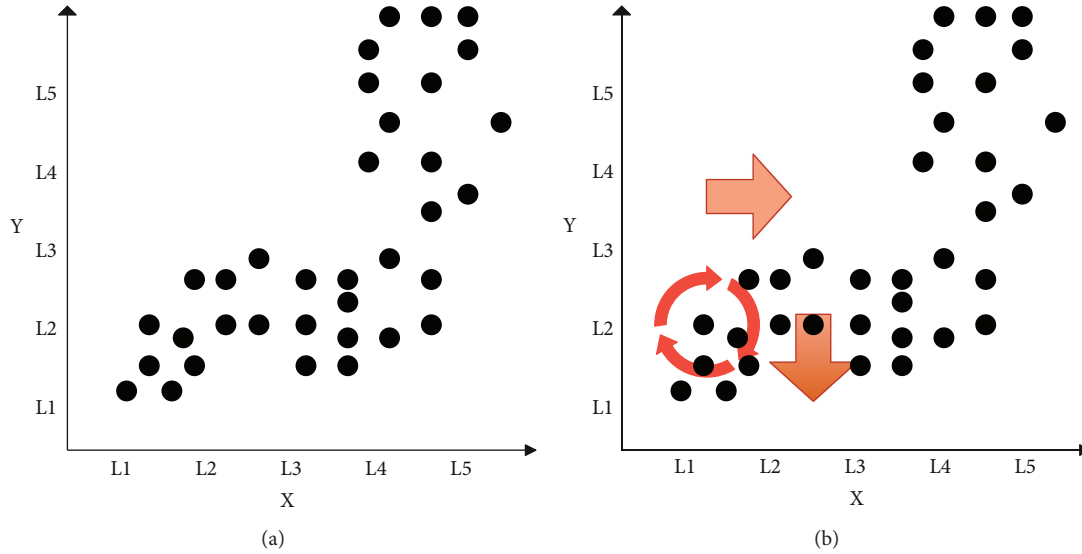
FIGURE 6: Attribute pattern diagram and association rule mining. (a) Attribute pattern diagram. (b) Association rule mining.

data can be disturbed, and the changes of other attributes can be analyzed. The mining of association rules can be expressed as [21].

$$X + \Delta X = \gg \Delta Y (\Delta X = \pm L). \tag{2}$$

This formula expresses applying a unit disturbance on the X-axis and observing the changes on the Y-axis. When mining association rules, relevant indicators need to be used to determine whether the rules are valid. Here, the two concepts of confidence coefficient (Con) and support coefficient (Sup) are introduced, which, respectively, represent the degree of reliability and the degree of support. Confidence coefficient and support coefficient can be expressed as the ratio of the number of data in the reference grid to the total number of data in the current data interval, and the ratio of the number of cell data after being disturbed to the total number of data intervals occupied. In the calculation process, the minimum values of the above two coefficients are both set to 2/EA, as shown in equations (3) and (4). Taking the above attribute pattern diagram as an example, since its evaluation accuracy is 5, the minimum confidence coefficient and support coefficient are set to 40%. If the minimum confidence coefficient is met, it means that the system has enough probability to fall into this state during operation. Satisfying the minimum support coefficient indicates that, after being disturbed, the system state has enough possibility to change to another operating state.

$$\min\_\mathrm{Con} = \frac{2}{\mathrm{EA}}, \tag{3}$$

$$\min\_\mathrm{Sup} = \frac{2}{\mathrm{EA}}. \tag{4}$$

Taking Figure 6(a) as an example, the selected cell (2, 3) is the reference grid, which contains 8 data points, and there are 16 data points in the X-axis L2 interval, so the confidence coefficient is 50%. It satisfies the minimum confidence

coefficient requirement; that is, during the operation, the state of the system may be the state pattern represented by the cell. When a positive disturbance is applied to the reference cell, the support coefficient of each cell on L3 is calculated, which is 6.25%, 62.5%, 31.25%, 0, 0, respectively. It can be seen that the cell (3, 2) meets the requirement of the minimum support coefficient. That is, when the system is in the state represented by cell (2, 3), if the attribute represented by the X-axis is disturbed in the positive direction, the system is likely to change to the state corresponding to cell (3, 2). By analogy, when negative interference is applied, the cells (1, 1) and (1, 2) meet the requirements of the support coefficient. The mining of the above association rules is shown in Figure 6(b).

After obtaining the association rules, in order to visually indicate the strength of the association rules, it needs to be quantified, and the health of the system can be obtained on this basis. Considering that entropy represents the degree of disorder of a data set and is directly related to the amount of information it contains, information entropy can be used to describe the strength of association rules. The information entropy of continuous variables can be expressed in the following form:

$$H(X) = -\int p(x)\log p(x)\mathrm{d}x. \tag{5}$$

However, to calculate the information entropy through this formula, the probability density function $p(x)$ needs to be obtained first, which is more difficult in some cases, so it needs to be discretized. The information entropy after discretization is

$$H(X) = -\sum_{i=1}^{n} p(x_i)\log_s p(x_i). \tag{6}$$

In the formula, $p(x_i)$ represents the probability when X takes the value xi, $i = 1, 2,...,n$.
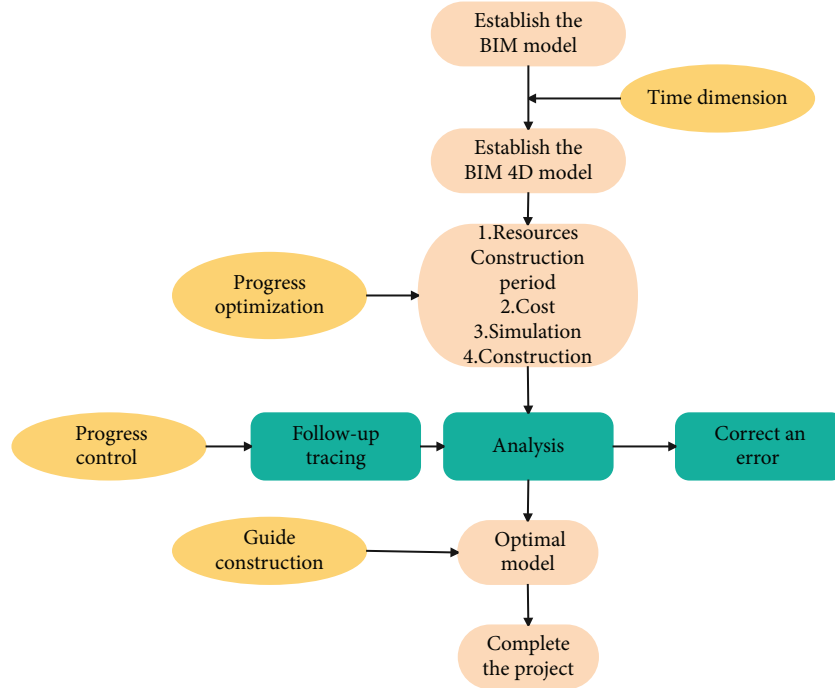
Figure 7: Flowchart of progress management based on BIM technology.

In addition, mutual information represented by entropy is a useful information measure in information theory, which can measure the degree of association between two variables, and its form is shown in formula (7). Among them, the mutual information of the two variables is equal to the sum of the respective entropy minus the joint entropy. Mutual information can describe not only linear correlations between variables but also nonlinear correlations, but its values are not normalized, so mutual information needs to be normalized. This article uses generalized correlation function to quantify the relationship, such as formula (8). Among them, the value of R_g is between 0 and 1. The closer R_g is to 1, the stronger the correlation between the two attributes.

$$I(X, Y) = H(X) + H(Y) - H(X, Y), \qquad (7)$$

$$R_g = \frac{I(X, Y)}{\sqrt{H(X)H(Y)}}. \qquad (8)$$

When different cells are used as the reference grid, the subpatterns mined may be the same effective area, so the confidence coefficient of each reference grid needs to be considered. For a certain mode, the health degree can be expressed by the sum of the product of each submode and the confidence coefficient:

$$U(D_x, D_y) = \sum_{i=1}^{EA} \sum_{j=1}^{EA} \text{con}(i, j) R_{i,j} | C_{D_x, D_y}. \qquad (9)$$

Among them, $R_{i,j}$ is the generalized correlation coefficient of the subpattern mined in the cell (i, j), and C_{D_x, D_y} indicates that the calculation comes from the coordinate system composed of the Dx and Dy attributes in the digital tie layer data matrix.

For any construction system, each variable will become a benchmark attribute for analyzing the possible association relationship with other variables, and at most $n\,(n-1)$ patterns can be obtained. The collection of the above modes can reflect the operating rules of the entire system. Therefore, the system health should be a collection of all modes

$$
\begin{aligned}
U &= \sum_{x=1}^{n} \sum_{y=1, y \neq x}^{n} U(D_x, D_y) \\
&= \sum_{x=1}^{n} \sum_{y=1, y \neq x}^{n} \left(\sum_{i=1}^{EA} \sum_{j=1}^{EA} \text{con}(i, j) R_{i,j} | C_{D_x, D_y} \right).
\end{aligned}
\qquad (10)
$$

4. Intelligent Building Construction Management Based on BIM Digital Twin

Compared with traditional schedule management, construction schedule management combined with BIM technology provides a communication platform that integrates multiparty information, including schedule, cost, and materials. When making schedules, it uses relevant software to simulate the project before construction to find and solve problems. During the implementation of the plan, it is possible to analyze and adjust the problems that occur efficiently and conveniently, so as to avoid missing the best time to solve the problems and affect the construction. The flowchart of the progress management based on BIM technology is shown in Figure 7.

The schedule preparation process is shown in Figure 8.

The schedule preparation and implementation procedure under BIM technology is shown in Figure 9 below. Under the BIM technology, through the early visual
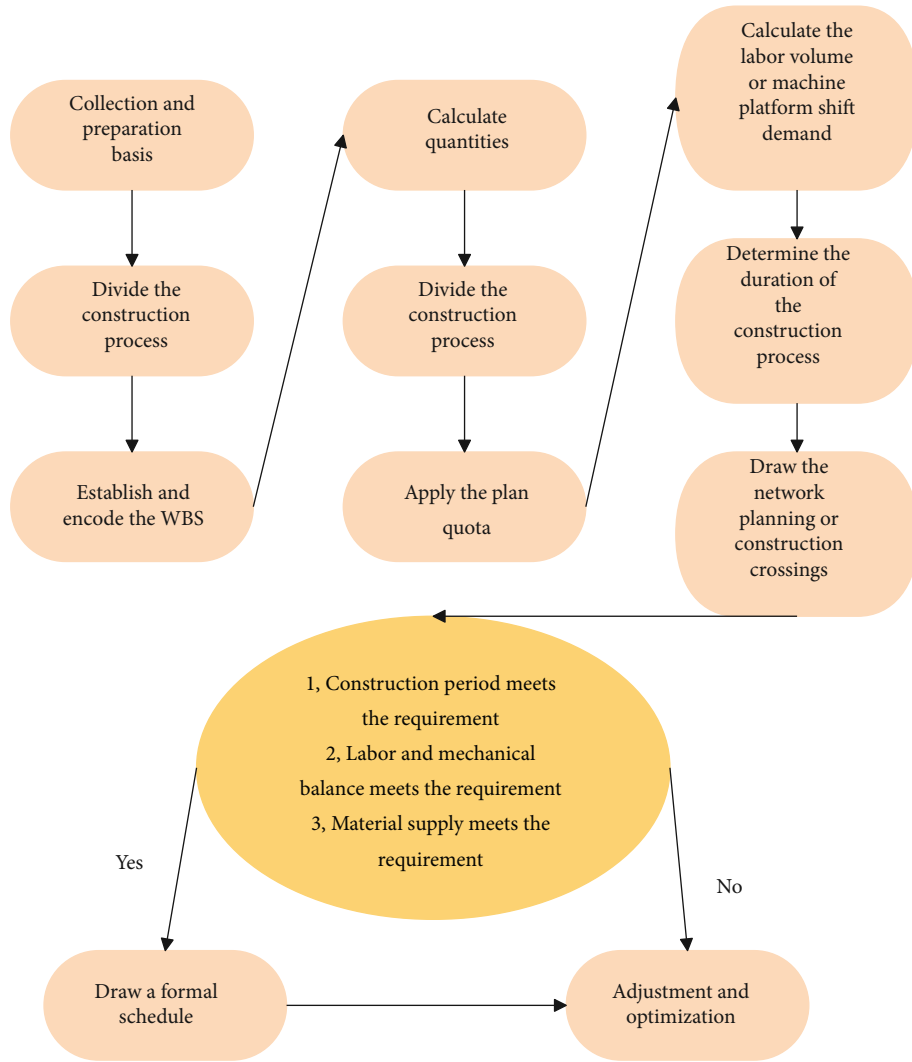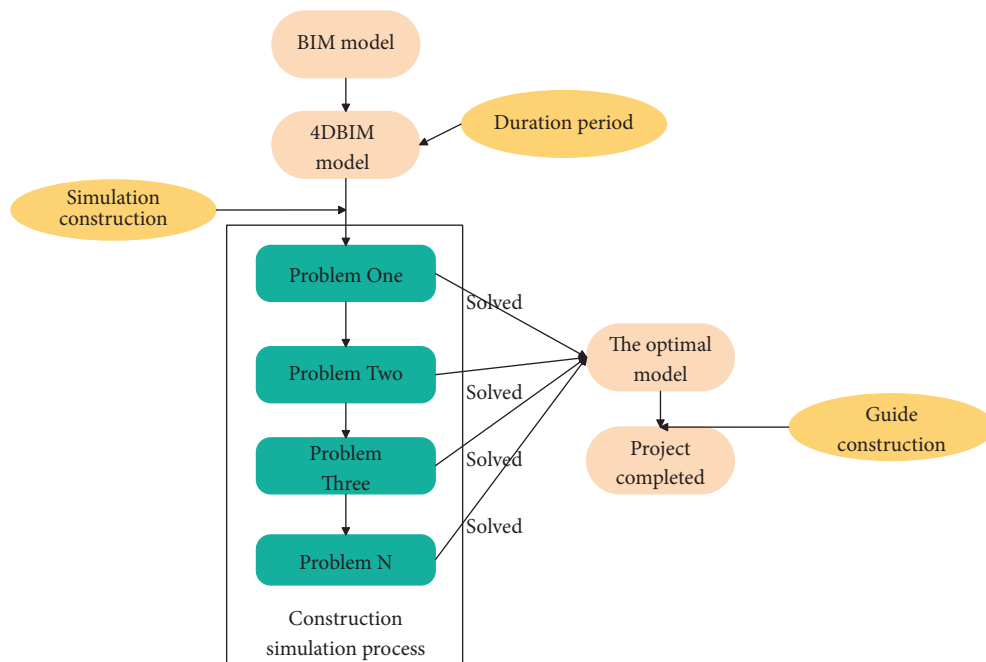
Figure 8: Schedule preparation process.

Figure 9: Schedule preparation and implementation procedures under BIM technology.

TABLE 1: Simulation test results.

| No	Construction safety	Equipment management	Material management	Site management	Job management	Quality control
1	93.11	90.29	76.68	82.68	92.72	87.65
2	93.65	89.66	90.82	81.02	93.64	91.72
3	93.96	82.48	82.34	92.21	93.46	90.64
4	93.45	86.70	76.97	86.53	90.92	95.75
5	93.42	84.18	90.42	87.51	91.37	86.61
6	92.90	84.16	79.76	92.49	92.44	91.91
7	93.07	84.67	88.04	97.46	91.03	90.06
8	92.34	86.46	76.92	94.99	94.17	95.62
9	92.38	82.89	77.35	86.68	93.83	95.38
10	93.49	82.23	92.06	92.41	91.08	89.00
11	93.66	82.58	90.31	90.85	93.63	95.72
12	93.00	89.50	84.30	93.66	92.86	94.63
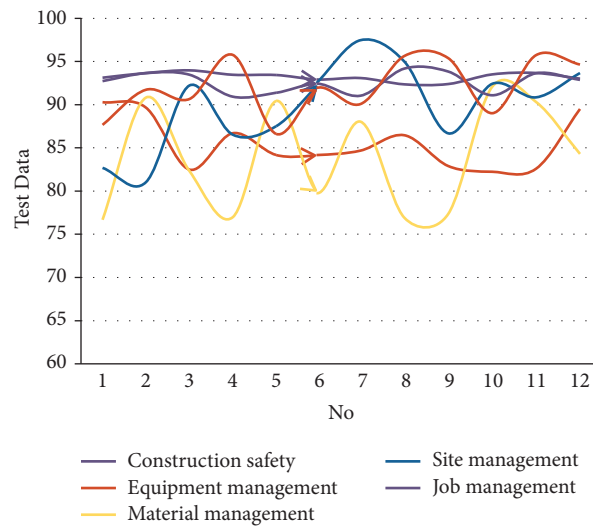
FIGURE 10: The effect of intelligent building construction management based on BIM and digital twins.

operation, the problem is first discovered, then rectified, and finally implemented.

After constructing the above model, the practical effect of the intelligent building construction management model based on the BIM digital twin is studied through experiments. This article explores the effectiveness of the intelligent building construction management model based on the BIM digital twin from the aspects of construction safety, equipment management, material management, site management, operation management, and quality management. The experimental results obtained through simulation research are shown in Table 1 and Figure 10.

It can be seen from the above research that the intelligent building construction management model based on BIM digital twin proposed in this paper can help the deployment of the intelligent building construction process in many aspects and help improve the efficiency of building construction management.

5. Conclusion

The calculation model, material properties, construction method, construction load, temperature change, etc. of the building structure from the start to the completion stage can affect the construction quality to varying degrees. This leads to a large deviation between the actual state of the structure and the ideal state, which requires strict control of the adverse effects during the construction process. For complex structures, the mechanical properties and safety control requirements during the whole construction process are no longer what the traditional construction control technology can meet. Then, how to consider the impact of unfavorable factors on the construction status during construction and carry out real-time identification and adjustment, how to reasonably and accurately simulate the time-varying process of the structural system in each stage of construction, how to arrange the construction and schedule reasonably, and how to control the stress and strain state of the structure during construction within the allowable range are the contents and technologies that are urgently needed in the current construction field. This paper applies BIM digital twin technology to intelligent building construction management and simulates the construction process through BIM. After the construction management plan is formulated, the construction simulation can be carried out through BIM, and the problems existing in the construction can be found, and a reliable construction management plan can be formulated in time.

Data Availability

Conflicts of Interest

Acknowledgments

References

[1] D. Chakraborty and H. Elzarka, "Advanced machine learning techniques for building performance simulation: a comparative analysis," *Journal of Building Performance Simulation*, vol. 12, no. 2, pp. 193–207, 2019.

[2] O. Guerra-Santin and S. Silvester, "Development of Dutch occupancy and heating profiles for building simulation," *Building Research & Information*, vol. 45, no. 4, pp. 396–413, 2017.

[3] T. Dodd, C. Yan, and I. Ivanov, "Simulation-based methods for model building and refinement in cryoelectron microscopy," *Journal of Chemical Information and Modeling*, vol. 60, no. 5, pp. 2470–2483, 2020.

[4] T. Abuimara, W. O'Brien, and B. Gunay, "Towards occupant-centric simulation-aided building design: a case study," *Building Research & Information*, vol. 47, no. 8, pp. 866–882, 2019.

[5] P. Remmen, M. Lauster, and M. Mans, "TEASER: an open tool for urban energy modelling of building stocks," *Journal of Building Performance Simulation*, vol. 11, no. 1, pp. 84–98, 2018.

[6] N. Endo, E. Shimoda, and K. Goshome, "Simulation of design and operation of hydrogen energy utilization system for a zero emission building," *International Journal of Hydrogen Energy*, vol. 44, no. 14, pp. 7118–7124, 2019.

[7] I. Beausoleil-Morrison, "Learning the fundamentals of building performance simulation through an experiential teaching approach," *Journal of Building Performance Simulation*, vol. 12, no. 3, pp. 308–325, 2019.

[8] C. Xiong, J. Huang, and X. Lu, "Framework for city-scale building seismic resilience simulation and repair scheduling with labor constraints driven by time–history analysis," *Computer-Aided Civil and Infrastructure Engineering*, vol. 35, no. 4, pp. 322–341, 2020.

[9] A. D. Black, "Wor (l) d-building: simulation and metaphor at the mars desert research station," *Journal of Linguistic Anthropology*, vol. 28, no. 2, pp. 137–155, 2018.

[10] K. Hanson, L. Hernandez, and J. A. Banaski, "Building simulation exercise capacity in Latin America to manage public health emergencies," *Health security*, vol. 16, 2018.

[11] E. K. Wati and N. Widiansyah, "Design of learning media: modeling & simulation of building thermal comfort optimization system in building physics course," *Jurnal Pendidikan IPA Indonesia*, vol. 9, no. 2, pp. 257–266, 2020.

[12] C. W. Lee and S. J. Cho, "The development of converting program from sealed geological model to Gmsh, COMSOL for building simulation grid," *Journal of the Korean Earth Science Society*, vol. 38, no. 1, pp. 80–90, 2017.

[13] C. Miller, D. Thomas, and J. Kämpf, "Urban and building multiscale co-simulation: case study implementations on two university campuses," *Journal of Building Performance Simulation*, vol. 11, no. 3, pp. 309–321, 2018.

[14] X. Xie and Z. Gou, "Building performance simulation as an early intervention or late verification in architectural design: same performance outcome but different design solutions," *Journal of Green Building*, vol. 12, no. 1, pp. 45–61, 2017.

[15] A. I. Adilkhodjayev, I. M. Mahamataliev, and S. S. Shaumarov, "Theoretical aspects of structural and simulation modeling of the macrostructure of composite building materials," *Journal of Tashkent Institute of Railway Engineers*, vol. 14, no. 2, pp. 3–14, 2019.

[16] S. Imam, D. A. Coley, and I. Walker, "The building performance gap: are modellers literate?" *Building Service Engineering Research and Technology*, vol. 38, no. 3, pp. 351–375, 2017.

[17] J. S. Pei, B. Carboni, and W. Lacarbonara, "Mem-models as building blocks for simulation and identification of hysteretic systems," *Nonlinear Dynamics*, vol. 100, no. 2, pp. 973–998, 2020.

[18] A. Brunelli, F. de Silva, and A. Piro, "Numerical simulation of the seismic response and soil–structure interaction for a monitored masonry school building damaged by the 2016 Central Italy earthquake," *Bulletin of Earthquake Engineering*, vol. 19, no. 2, pp. 1181–1211, 2021.

[19] P. Andrio, A. Hospital, and J. Conejero, "BioExcel Building Blocks, a software library for interoperable biomolecular simulation workflows," *Scientific data*, vol. 6, no. 1, pp. 1–8, 2019.

[20] G. Petrou, A. Mavrogianni, and P. Symonds, "Can the choice of building performance simulation tool significantly alter the level of predicted indoor overheating risk in London flats?" *Building Service Engineering Research and Technology*, vol. 40, no. 1, pp. 30–46, 2019.

[21] S. Gibeaux, C. Thomachot-Schneider, and S. Eyssautier-Chuine, "Simulation of acid weathering on natural and artificial building stones according to the current atmospheric SO_2/NO_x rate," *Environmental Earth Sciences*, vol. 77, no. 9, pp. 1–19, 2018.

Research Article

Construction of Smart City Street Landscape Big Data-Driven Intelligent System Based on Industry 4.0

Zhe Li [ID],[1] YuKun He,[2] XinYi Lu,[1] HengYi Zhao,[1] Zheng Zhou,[1] and YinYin Cao[1]

[1]*School of Architecture, Southeast University, Jiangsu 210096, China*
[2]*Graduate School of Engineering, Kyoto University, Kyoto 606-8501, Japan*

Correspondence should be addressed to Zhe Li; lizheseu@seu.edu.cn

With the application of engineering management in smart city construction under Industry 4.0, the intelligent design of urban street landscape has attracted extensive attention. Affected by the low intelligent level of traditional landscape design, the existing urban landscape composite system has difficulty in meeting the needs of smart city construction. Therefore, this paper proposes the construction of street landscape big data-driven intelligent decision support system based on Industry 4.0. Based on the complex network theory, this paper analyzes the structure, links, nodes, driving forces, and functional requirements of urban street landscape and then puts forward the construction content and implementation method of urban street landscape intelligent decision support system. The system consists of four aspects: intelligent infrastructure, service, protection and maintenance, and management and evaluation system. Its implementation not only reflects the cooperation and effective application of intelligent technology in each stage of street landscape construction, but also provides reference for the application of engineering management in other fields under Industry 4.0.

1. Introduction

Based on the connectivity provided by the Industrial Internet of Things (IIoT) and the use of a variety of digital technologies such as cloud computing, big data, and artificial intelligence, Industry 4.0 is proposed as a new stage of industrial maturity [1, 2]. These technologies have produced an industrial method of automation and interconnection involving objects, products, and people, thus achieving a higher level of industrial performance [3]. With the application of engineering management in smart city construction under Industry 4.0, the intelligent design of urban street landscape also rises and develops rapidly. Meanwhile, "intelligent" development has become the new trend in modern society due to the advancement of information technology represented by the Internet. The smart city emerges in this context, which can detect, analyze, and integrate the key information of urban core operating systems using information and communication technologies, thus making intelligent responses to various needs covering people's

livelihood, environmental protection, public security, urban services, and industrial and commercial activities [4]. The intelligent urban management and operation relying on advanced information technologies can effectively solve the complex urban problems and promote the harmonious and sustainable urban development [5].

As an important part of smart city construction, landscape architecture is also facing opportunities and challenges brought by the intelligent process. Smart gardens changing the construction, operation, and management modes of traditional gardens can effectively improve the efficiency in landscape garden industry, realizing the normalization, standardization, digitization, networking, and intelligence of garden construction [6]. The typical scenario of urban street landscape has significant effects on shaping the urban image. By selecting street landscape as the entry point of smart gardens, this paper aims to explore the needs of urban street landscape and discuss the intelligent system construction and implementation means, in order to provide reference for the construction of urban street intelligent systems [7, 8].

However, under Industry 4.0, in the process of intelligent city construction, how to effectively use new technologies such as big data and Internet of Things, as well as the interconnection between urban street landscapes after 5G network integration, has attracted people's attention to the security and anti-network attack stability of these systems.

2. Related Works

In the construction of urban street landscape intelligent system, "urban street" refers to the urban road equipped with sidewalks, municipal utilities, and various buildings on both sides in the overall length or most sections. As one of the subsystems under the future urban open complex giant system, the nature, function, form and structure of urban street are more complex than traditional urban road. Urban street serving as the most basic public urban space focuses on the citizens' life and humanized experience, which facilitates the interpersonal communication and interactions via emotional sustenance as well as playing an irreplaceable role in shaping the urban charms and vitalizing the economic development [9, 10].

Relying on the complex network theory and "Internet +" thinking, the smart landscape cooperates with new-generation information technologies such as Internet of Things, big data cloud computing, mobile Internet, remote sensing, and information intelligent terminal, obtains time-domain advantages, and responds quickly to social and natural activities carried in the landscape space. Integrating the spatial domain of modern ecological landscape into the large database achieves the intelligent connection between scattered social activities and needs of human beings, nature and landscape space for the interactive perception, and cognition and communication and improves the utilization and sharing rate of various scattered landscape resources, thus promoting the intelligent construction, service, and management of landscapes [11, 12].

The design of intelligent street landscape systems shall be based on the comprehensive consideration of user needs, greening landscapes, and basic street functions, through the Internet of Things, web services, and virtualization technology. The basic attributes, characteristic parameters, status, and other information of various street landscape elements are dynamically and intelligently sensed and accessed in real time, to build street space intensively. Through processing the information perceived by the landscape intelligent system, data collection, integration, analysis, processing, and feedback are realized under the mapping of landscape resources in urban streets. On the premise of ensuring the basic functions of the road, people's travel safety, life, and social security should be guaranteed, which provides conditions for the scientific, rapid, comprehensive, and visual development of urban street landscape design and management.

The construction of intelligent systems for urban street landscape based on complex network theory and the integration of smart landscape concept into the traditional urban street landscape indicate further improvement, which shall meet the requirements for intensive intelligent spaces, multiple interactive experience, and green ecology of energy conservation [13, 14].

3. Composition of Intelligent Systems for Urban Street Landscape

In order to cope with the multiple landscape needs under the complex system of urban streets, the intelligent street landscape system based on the complex network realizes the intelligent supply-demand matching of street landscape space services from the three levels of landscape facilities Internet of Things, service Internet, and user Internet.

The construction of street landscape intelligent system mainly involves four aspects: intelligent infrastructure, intelligent service, intelligent protection and maintenance, and intelligent management and evaluation.

3.1. Intelligent Infrastructure. Intelligent infrastructure is the physical layer and the foundation of street landscape intelligent systems. The infrastructure of street landscape intelligent systems shall proactively provide the information and services desired in addition to the basic functions and be available to correlate with other facilities and even users for the formation of a complete intelligent network featuring information interaction and function linkage, thus completing the virtualization and service-oriented information interaction and functional linkage of the intelligent information system.

3.1.1. Information Infrastructure. Information infrastructure is the basis of intelligent street landscape, covering the electric information screen shown in Figure 1, multimedia touch screen terminal shown in Figure 2, intelligent monitoring, intelligent broadcasting, help facilities, security facilities, and landscape performance facilities. The foundation of infrastructure construction lies in the sound network transmission and communication networks, and relevant facilities shall be arranged in the densely populated areas (e.g., road entrances, parking lots) to facilitate the service provision such as information inquiry and satisfy the important requirements of easy identification and convenient use. The service scope of facilities with special functions (e.g., help facilities and security facilities) shall cover the entire street area, as well as focusing on the locations along main/secondary trunk roads and various open spaces, activity sites, and surroundings of green landscapes [15].

3.1.2. Data Infrastructure. Data cognition is the core of intelligent street landscape development. The data infrastructure is used to collect and integrate street landscape data, achieving the intelligent street landscape construction by providing the users and managers with comprehensive and intuitive information based on the integration and analysis of multisource data (basic/business/service databases).

Figure 1: Electronic information screen.

Figure 2: Multimedia touch screen terminal.

Basic database clarifies the spatial location and surrounding environment of urban street landscape for the precise positioning of smart landscape. Business database has multiple subdatabases covering the special data, system planning and management, monitoring management, and industry management available for the precise and whole-process collection of street landscape data. Service database can provide the popular science knowledge about smart street landscape for the public and facilitate the review of various urban green spaces and scenic spots by potential travelers [16].

3.1.3. Observation Points of Street Green Space Ecosystem. Based on the ecological requirements of the street landscape intelligent system construction, ecological observation of the street is an effective measure to achieve this goal. Using RFID (radio frequency identification) technology, the real-time update of spatial ecological information of street landscape can be realized, and the location of vegetation, structures, and buildings can be monitored online. Special

sensors and wireless sensor networks for street landscape ecological observation can effectively realize real-time data acquisition and transmission. Real-time monitoring of the street green space ecosystem can help with maintenance and management of the green landscape. Furthermore, the obtained ecological econometric characteristic data can aid in the formation of quantitative analysis results of the street landscape space, resulting in better landscape and ecological effects from green space maintenance and management, Figure 3.

3.2. Intelligent Service. The service object of the intelligent street landscape systems is the streetscape users. The construction of intelligent service system is based on Internet functions, which can realize the dynamic matching of the user's needs. From the perspective of users, in the process of system construction, our goals and demand motivation can be evaluated, and the service content can be derived dynamically.

In terms of qualitative or quantitative data, managers could be provided with genuine feelings, opinions, and suggestions generated by the public in the service experience. With the help of dynamic characteristics analysis of smart infrastructure, a reliable method for demand forecast management is provided. Thus, public involvement can be achieved, and the quality of the service improves continuously [17].

3.2.1. Network Service Platforms. Network service platforms are the basis for intelligent service and the guarantee for intelligent linkage with other service facilities. The construction of portals serving the public shall cover various services such as bus routes, e-maps, traffic notices, travel tips, and road service calls. In addition, the construction of mobile-based network service platforms (e.g., mobile apps, WeChat public accounts) shall also be emphasized to ensure the real-time content update and provide mobile users with street information services based on the shared portal resources.

3.2.2. Basic Street Services. Basic street services are mainly the traffic, lighting, and other necessary basic services. For instance, the smart parking management system achieves the real-time monitoring of parking spaces and the intelligent guidance about available parking spaces based on the information inquiry of parking lots and spaces through various intelligent terminals such as smart phones. The construction of public transportation system shall ensure the timely release of bus information and certain functions (e.g., multimedia information release, passenger complaint) in combination with the special bus signal system for important bus corridors and the intelligent bus stations. The streets with heavy traffic flows shall be equipped with smart toilets, which are available for the information inquiry of location and real-time usage through various intelligent terminals (e.g., smart phones, multimedia touch screens). In addition, the intelligent lighting system subject to the independent

Figure 3: Ecosystem observation facility.

sensing, timing, voice control, or remote control of intelligent terminals shall also be arranged for the smart control of landscape lighting in different areas [18], Figure 4.

3.2.3. Road Navigation. The intelligent terminals (e.g., smart phones, multimedia touch screens) and multilanguage terminals for self-service navigation shall be arranged to facilitate the inquiry of street and surrounding-area e-maps and tour route planning as well as the scenic spot/plant introduction using QR code/RFID technologies [19].

3.2.4. Information Release. An interactive information system shall be established to provide life, service, business, and medical information for citizens, with various network service platforms serving as the channels for street information release, covering the street information, real-time road conditions, toilet usage, spare parking spaces, restaurant usage, and other basic information; climatic information (e.g., street temperature, humidity) and health information such as negative oxygen ion content in key areas Figures 5, flowering phase, and news and cultural event notices (e.g., lectures, exhibitions, festival activities, fitness events) at sites along the street; and information of emergency responses.

3.2.5. Personalized Services. Personalized services available at various network service platforms can meet the street use demands of different people [20], for instance, the online adoption of plants along the street, and regular pushing of plant growth status and daily conservation information; pushing of intelligent infrastructure, location awareness, environmental monitoring index analysis, online security, and health information via the Internet; and application of

intelligent technologies based on the users' different needs of travel and fitness.

3.2.6. Consulting/Complaint Services. Compared with the traditional consulting/complaint services, the services provided through the intelligent system are more convenient and efficient, and multiple channels (e.g., street intelligent terminals, consulting/complaint pages, mobile terminals) are available for the public. The intelligent system of linkage service can achieve the unified receipt and instant feedback/response to consultations and complaints from telephones and network terminals.

3.2.7. Virtual Experience. In order to improve the user experience, a multimedia experience center focusing on historical districts shall be constructed using multiple technologies (e.g., GIS, VR, and multimedia) for the display of historic landscapes, original natural features, and historical changes. The 3D panorama/reality enhancement display technology and 360°/720° real-life photos or videos can be utilized to create the virtual blocks for digital virtual tours that are available at portals and terminal devices (e.g., multimedia touch screens, smart phones) [16, 21].

3.3. Intelligent Protection and Maintenance. Intelligent protection and maintenance are the function expansion of the user Internet based on the Internet of Things of landscape facilities. Dynamically generate landscape maintenance needs based on smart infrastructure, and dynamically match landscape maintenance needs with landscape maintenance services through the Internet of Things technology. Realize the informatization and intelligence of the protection and maintenance process, provide visual guidance on daily maintenance process and key technology, and the responsible personnel and stages could be specified for the real-time recording of maintenance process and information [22].

3.3.1. Green Space Protection and Maintenance. Green space protection and maintenance are the key to intelligent protection and maintenance, covering the digital recording, monitoring, and control of boundaries and green resources including the main plants and facilities. The important spots and key facilities shall be equipped with 3D scenes for inspection and comparison via intelligent terminals, mainly involving the plant irrigation and fertilization, pest and disease and freezing damage management, and intelligent cultivation.

Environmental monitoring and intelligent irrigation system can provide effective services for intelligent plant irrigation and fertilization management. The digital data processing of soil nutrients can maximize the effects of water-saving and precise irrigation, scientific management, and low-carbon maintenance [23, 24]. The construction of soil monitoring subsystem is available for the real-time monitoring of ambient temperature and humidity, wind direction, rainfall, and illuminance in the
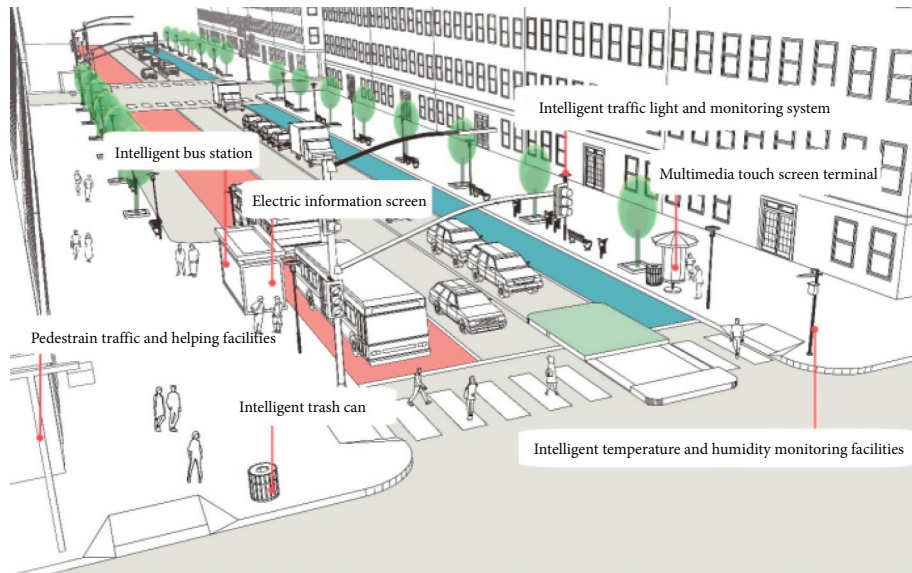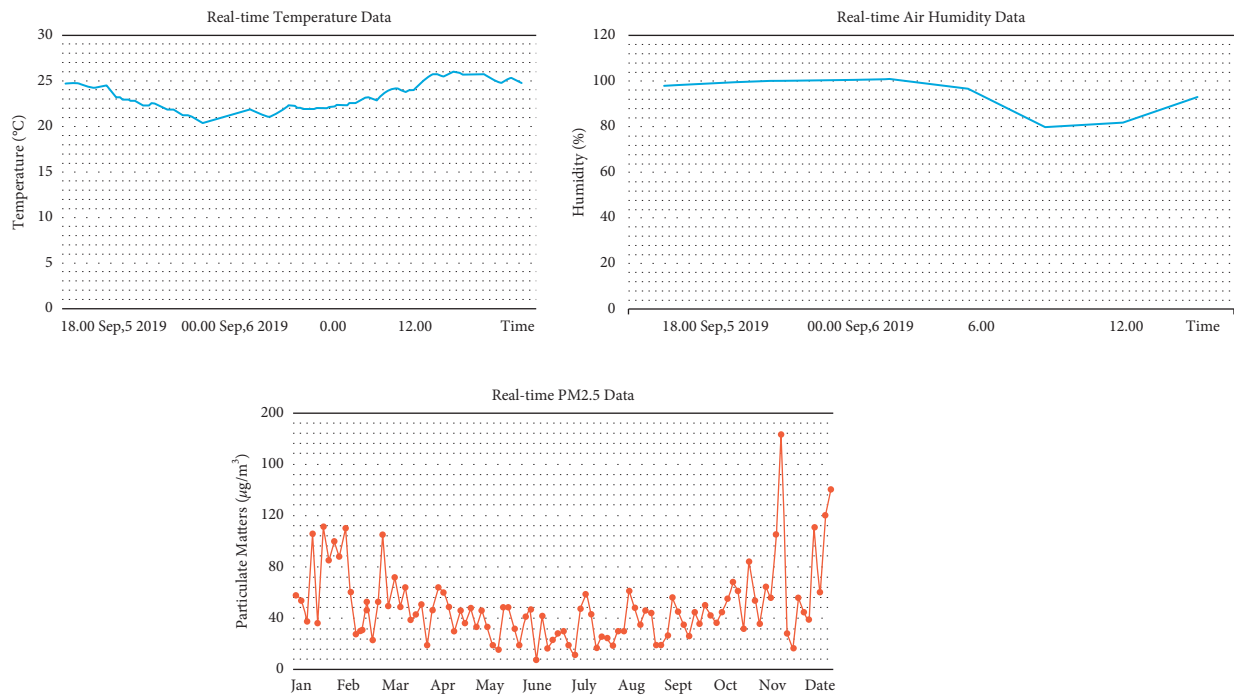
FIGURE 4: Basic street services.

FIGURE 5: Street climatic information and health information.

surrounding environment Figure 6, with the sensing facilities adopted for real-time detection of soil moisture, fertility, and other green space indexes. Maintenance decision-making depends on the IoT-based intelligent analysis and sorting of monitoring data received by servers [25]. In addition, the sprinkling and dropper systems are used for the automatic irrigation and fertilization and other intelligent applications, and the landscaping personnel can also search and receive monitoring data and warning information via computers and mobile phones Figure 7.

The GPS positioning and FRID technologies shall be adopted for the control of plant diseases and pests, with the dynamic tracking system established to ensure the dynamic protection and monitoring of green plants as well as help technicians locate the areas of pests and diseases at first time. The implementation of "prevention-first" principle by each institution responsible for plant management and protection targeting the necessary early warning of pests and diseases within all periods can greatly reduce the prevention costs and probability of large-scale pests and diseases [26]. Early warnings for the freezing damage management shall be
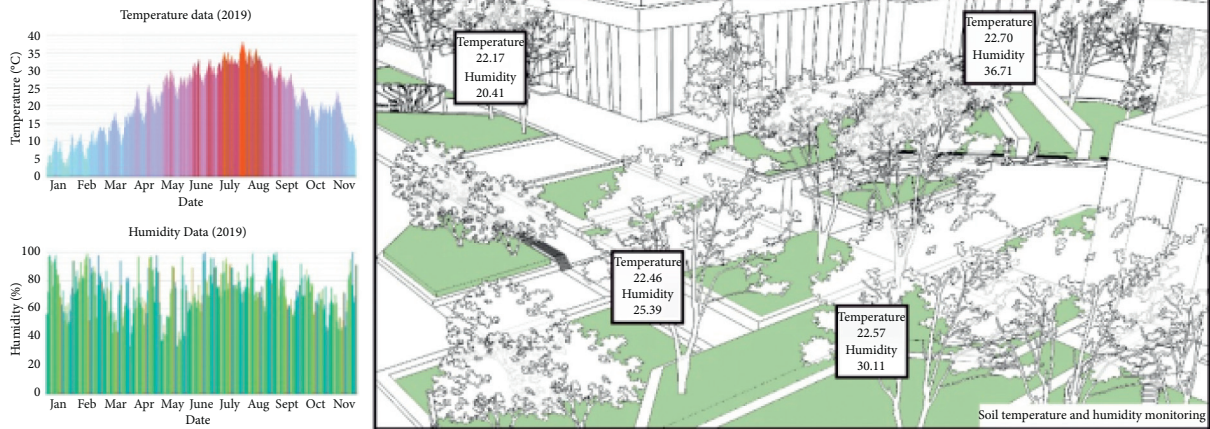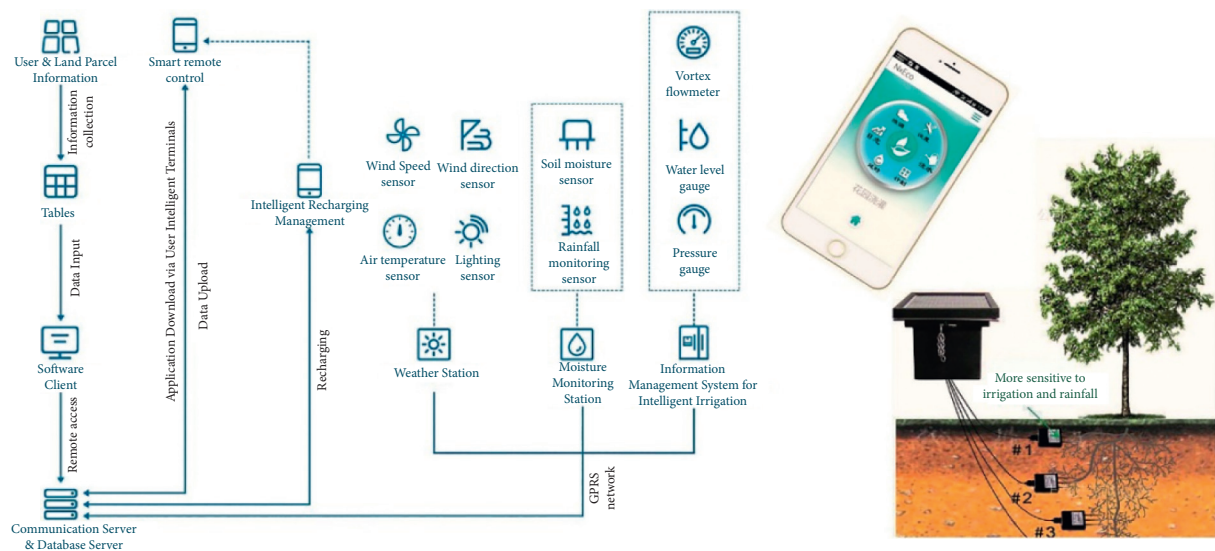
Figure 6: Soil monitoring subsystem.

Figure 7: Intelligent irrigation system.

issued in advance based on the weather conditions, providing the scientific basis and guidance for plant winter protection.

The intelligent technology-based seedling planting and cultivation shall make full use of the IoT and spatial information integration technologies. The partitional measuring of regional soil quality, hydrological conditions, and microclimate factors at the stage of planting planning provides the definite data basis for breeding and rapid formulation of cultivation schemes. At the same time, a tree full cycle database shall be established for plant tracking and data sorting in the whole process, as well as the records of seedling archives, tree transplantation, and maintenance information. Intelligent cultivation can effectively prevent the challenges faced by the traditional seedling cultivation (e.g., improper layout of trees, unsatisfactory production or waste of seedlings).

3.3.2. Heritage Protection and Maintenance.
Both natural heritage and cultural heritage involve heritage protection and maintenance, including ancient and famous trees and cultural relics. For the ancient and famous trees, the high-definition photos shall be obtained based on the precise coordinate positioning via monitoring and RFID technology in addition to the normal maintenance measures, and mastering relevant detailed information will facilitate the data calling, plant protection, document management, maintenance, and rejuvenation monitoring. Digital modeling based on the growth environment of ancient and famous trees also facilitates the accurate analysis of protection measures Figure 8. For the cultural relics and historical sites surrounding the street, the 3D data model shall be constructed to enhance the protection. The ancient buildings shall be equipped with stress-strain sensors for deformation monitoring and risk assessment [27].

3.4. Intelligent Management and Evaluation System.
Scientific and comprehensive management measures are an important prerequisite for realizing the sustainable development of streetscapes. Quantitative evaluation mechanism is an effective objective to judge the effectiveness of streetscapes.
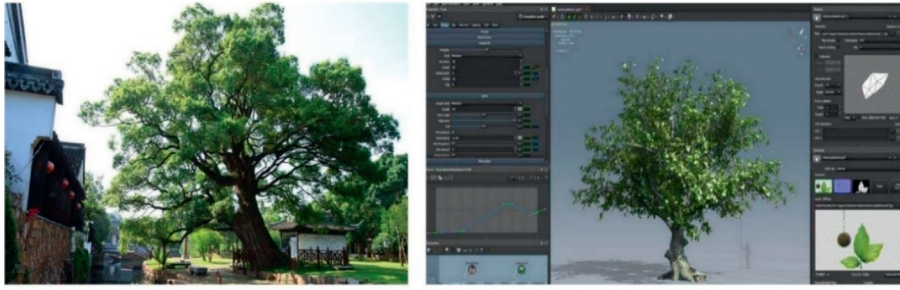
FIGURE 8: Digital monitoring of ancient and famous trees.

How to effectively integrate various scattered landscape management resources and coordinate various quantitative evaluation parameters to achieve the best match between street landscape management and demand is the key problem. Hence, quantitative data-driven evaluation and control system is ultimately conducive to the continuous optimization of landscape effects.

3.4.1. Intelligent Management. The comprehensive and scientific management shall take account of internal office work, gardening business, street security, and other related factors.

Office automation (OA) system can improve the overall efficiency of internal office work, covering process management, e-mail, document management, document circulation, approval management, working calendar, notice announcement, personal information maintenance, conference management, and attendance management.

In terms of the gardening business management, video monitoring, RFID, and infrared sensing technologies shall be adopted for the real-time perception of changes in street green resources, infrastructure, and traffic flows, as well as the automatic collection, adjustment, and update of street landscape data. The real-time monitoring of street landscape can achieve precise management and prevention against vandalism and damage caused by natural disasters.

Street security cannot be neglected considering the special traffic function of urban street with public spaces. The construction of integrated street control platform makes the daily operation monitoring and emergency command and dispatching possible, providing basic support for navigation and guidance based on the location services of GIS and satellite positioning systems [28]. Nowadays, the rapid development of information technology also facilitates the dynamic monitoring of public opinions released via key media, forums, blogs, and Weibo platform; extraction of relevant information; and timely warning/treatment of potential crisis events in accordance with predetermined strategies.

3.4.2. Intelligent Evaluation System. The evaluation of self-diagnosis by intelligent evaluation system aims to provide reference for further development. Moreover, reasonable performance evaluation can not only measure the achievements of street landscape construction and find out

the existing problems, but also provide important guidance for the continuous improvement of street landscape intelligent system.

Establishment of the complete, scientific, and effective evaluation system shall be based on the existing urban gardening standards, with the relevant street smart landscape indicators integrated into the system by means of spatial layers, forms/tables, document uploading, and image attachments for real-time computing and result judgment/analysis [29], Table 1.

4. Technical Means of Intelligent Systems for Urban Street Landscape

Intelligent technology refers to a specific technology or method used in the construction of an intelligent urban streetscape system. Internet of Things, spatial information integration, virtual reality and visualization technology, digital technology, etc. can solve the following problems in the construction of streetscape system under the condition of urban complex giant system:

(1) How to manage, digitize, and integrate information from scattered roads efficiently and precisely, in order to realize the effective distribution and dynamic overall grasp of the streetscape service capabilities.

(2) How to coordinate the relationship between the geographic space, data flow, time distribution, hardware network, and user needs of the streetscape intelligent system, in order to realize the spatial mapping between complex streetscape resources and intelligent system service capabilities [30].

Emergence of the most representative IoT technology in the intelligent process has led the transformation of information age into an intelligent era. The all-inclusive IoT technology involving radio frequency identification (RFID), infrared sensor, and sensor-laser scanner solves numerous urban problems via interconnection of things after the Internet-based information connection [31].

Spatial information reflects the spatial distribution characteristics of geographic entities, and the spatial information integration technology involving remote sensing (RS), geographic information system (GIS), and global positioning system (GPS) can reflect the topographical features of all sites more concretely and objectively at the

TABLE 1: Intelligent evaluation index.

Target layer	Control layer			
	Evaluation object	Weights	Indicator layer	Weights
Evaluation of intelligent urban street landscape (A)	Material element (B1)	0.38	Functional facilities (C1)	0.35
			Recreation facilities (C2)	0.3
			Plant landscape (C3)	0.15
			Paved landscape (C4)	0.2
	Open space (B2)	0.28	Spatial scale fitness (C5)	0.3
			Environment comfort (C6)	0.25
			Landscape interface suitability (C7)	0.23
			Activity type richness (C8)	0.12
			Activity time richness (C9)	0.1
	Environmental ecology (B3)	0.34	Landscape sensitivity (C10)	0.35
			Landscape suitability (C11)	0.33
			Landscape health (C12)	0.32

macro level and achieve precise quantification and data digitization for in-depth research and analysis [32].

VR technology integrates multiple techniques features in good experience of immersion, interaction, and conception, covering the real-time 3D computer graphics, 3D wide-angle (wide-field) display, tracking of the viewer's head/eyes/hands, tactile/force feedback, stereo effects, network transmission, and voice input/output [33].

The basic process of digitization involves the transformation of all complex and changeable information into measurable data, digital data modeling for binary code conversion, and input into the computer for unified processing [34]. At present, the digital technology is widely used in various industries, and the digitization serving as the predecessor of intelligent technologies shall be utilized continuously in the intelligent era.

5. Prospects of the Construction and Application of Intelligent Systems for Urban Street Landscape

To achieve the successful construction of street landscape intelligent systems, the mutual mapping of complex system and complex network of street landscape needs to be realized. Therefore, the above intelligent means must be implemented combined with the actual stages of street landscape construction in practice.

5.1. Planning and Design Stage. The early stage of planning and design provides direct guidance for the mid-term construction and post-management of landscape construction. The application of intelligent means such as the Internet of Things, virtual reality, and visualization technology at the planning and design stage can realize more scientific and rational street landscape design.

In terms of on-site investigation, the traditional investigation methods have large workload and large error, and most of them are completed on the basis of on-site inspection and surveying and mapping, combined with the existing data. In addition, the traditional street design focusing on-site plane lacks the 3D-space and humanized thinking in terms of vertical design, construction scale, and

detailed design. On the contrary, the intelligent landscape construction can realize the targeted integration of IoT and spatial information technologies into the site survey, with the precise positioning of street location and surrounding land uses utilizing the IoT sensing nodes [35]; moreover, the spatial information technology enables the designer to understand the connections between overall street appearance/style and urban image more comprehensively and accurately Figure 9.

5.2. Construction Stage. The construction quality directly affects the smooth implementation of the preliminary design and the cost of later maintenance and management. Due to the problems of inaccurate calculation of quantities, unconstrained construction, and limited professional quality of most construction personnel in traditional garden construction, there are often some deficiencies in construction quality compared with the expected effect.

The intelligent street landscape construction can ensure the rational resource allocation and construction efficiency through the in-depth survey of on-site environmental factors (e.g., soil quality, hydrological conditions, wind force, atmospheric pressure) using the sensing and RFID systems of IoT technology and the corresponding construction schemes and regulations. The application of spatial information integration technology and sensing system makes precise and rapid data positioning based on construction drawings possible at the stage of fixed point setting-out. The multispace model using VR technology enables the construction personnel to understand the design intention in an intuitive manner during construction, thus ensuring the realization of design effects. The application of IoT sensing system upon project acceptance for data measurement and quantitative analysis of engineering effects, combined with the direct data transmission to the auditor's mobile devices using mobile Internet technology, guarantee the strict project acceptance [36], Figure 10.

5.3. Green Plant Cultivation and Conservation Stage. Conservation management can maintain and guarantee the landscape effects after gardening construction. The
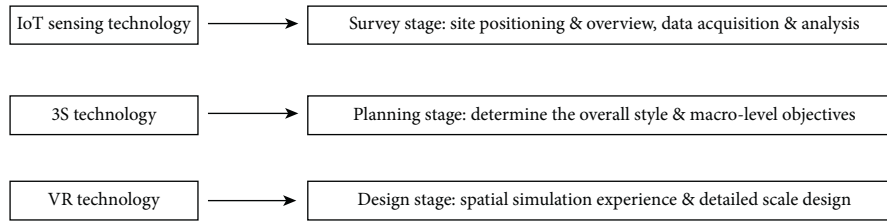
Figure 9: Application of intelligent technologies at the planning and design stage.
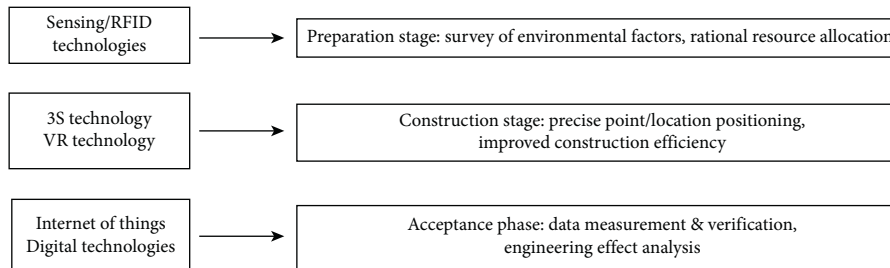

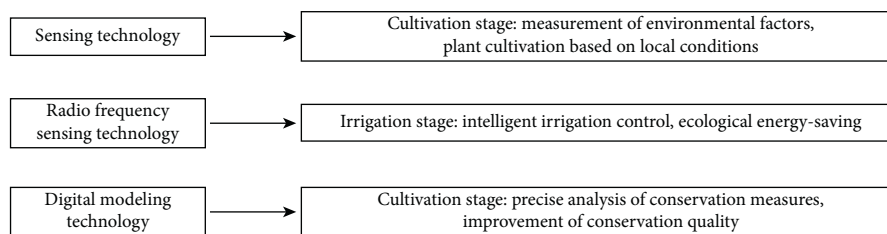Figure 10: Application of intelligent technologies at the construction stage.

Figure 11: Application of intelligent technologies at the green plant cultivation and conservation stage.

traditional plant cultivation and conservation have certain shortcomings, e.g., unsatisfactory professional quality of management personnel and conservation measures of low technical contents.

The intelligent plant cultivation and conservation integrating IoT technology ensure the effective improvement of conservation efficiency and effects with reduced cost. In order to make proper use of local conditions, the sensors shall be used to measure environmental factors (e.g., humidity and soil quality) at the cultivation stage, and the original manual sprinkling shall be replaced by the sprinkling/drip irrigation system with time-frequency sensors to detect the soil moisture and facilitate the intelligent control [37]. In terms of fertilization, winter protection, and wind protection, the digital model established based on the plant growth environment can realize the precise analysis of proper measures in different periods to ensure the normal plant growth and optimal effects Figure 11.

6. Conclusion

Applying intelligent means in urban street landscape design and integrating street landscape intelligent system into smart city construction can actively promote urban development. Procedures starting from scheme design and project construction to maintenance management,

technology introduction, and formulation of comprehensive and effective strategies are the key to the successful construction of street landscape intelligent system based on complex network. In addition, the construction of street landscape intelligent system also provides a platform for public participation and governance. The public can easily and quickly obtain information through such intelligent systems and use improved consultation/complaint services to give timely feedback to managers, which indicates that public participation has been significantly improved [7, 38, 39]. In short, the street landscape intelligent system based on complex network theory provides an advanced and sustainable construction mode for the future urban complex street system. In the context of Industry 4.0, with the rapid development of big data and the Internet of Things, more in-depth research in the future should aim to integrate the street landscape intelligent system into the construction of smart city and build a perfect street landscape intelligent system.

Data Availability

The labeled datasets used to support the findings of this study are available from the corresponding author upon request.

Conflicts of Interest

Acknowledgments

References

[1] L. S. Dalenogare, G. B. Benitez, N. F. Ayala, and A. G. Frank, "The expected contribution of industry 4.0 technologies for industrial performance," *International Journal of Production Economics*, vol. 204, pp. 383–394, 2018.

[2] A. G. Frank, L. S. Dalenogare, and N. F. Ayala, "Industry 4.0 technologies: implementation patterns in manufacturing companies," *International Journal of Production Economics*, vol. 210, pp. 15–26, 2019.

[3] J. M. Müller, D. Kiel, and K.-I. Voigt, "What drives the implementation of industry 4.0? The role of opportunities and challenges in the context of sustainability," *Sustainability*, vol. 10, no. 1, p. 247, 2018.

[4] A. Kamilaris, A. Pitsillides, F. X. Prenafeta-Bold, and M. I. Ali, "A Web of Things based eco-system for urban computing - towards smarter cities," in *Proceedings of the 24th International Conference on Telecommunications (ICT 2017)*, Limassol, Cyprus, May 2017.

[5] V. Albino, U. Berardi, and R. M. Dangelico, "Smart cities: definitions, dimensions, performance, and initiatives," *Journal of Urban Technology*, vol. 22, no. 1, pp. 3–21, 2015.

[6] G. De Francesco and R. Angelini, "Creative autotegulation: towards an interactive urban landscape," in *Proceedings of the 2014 International Conference on Intelligent Environments*, pp. 388–391, Shanghai, China, June 2014.

[7] X. Zhang, Z. Li, D. Li, and Y. He, "Marine environment distinctions and change law based on eCongnition remote sensing technology," *Journal of Coastal Research*, vol. 94, no. sp1, pp. 107–111, 2019a.

[8] F. Caprotti and R. Cowley, "Varieties of smart urbanism in the UK: discursive logics, the state and local urban context," *Transactions of the Institute of British Geographers*, vol. 44, no. 3, pp. 587–601, 2019.

[9] Z. Li, Y. N. Cheng, S. Song, and Y. K. He, "Research on the space cognitive model of new Chinese style landscape based on the operator optimization genetic algorithm," *Fresenius Environmental Bulletin*, vol. 28, no. 6, pp. 4483–4491, 2019.

[10] M. Carmona, "London's local high streets: the problems, potential and complexities of mixed street corridors," *Progress in Planning*, vol. 100, pp. 1–84, 2015.

[11] C. Perera, A. Zaslavsky, P. Christen, and D. Georgakopoulos, "Sensing as a service model for smart cities supported by Internet of Things," *Transactions on Emerging Telecommunications Technologies*, vol. 25, no. 1, pp. 81–93, 2014.

[12] O. A. Hosny, E. M. Dorra, K. A. Tarabieh et al., "Development of an automated optimizer for sustainable urban landscape design," *Automation in Construction*, vol. 94, pp. 93–103, 2018.

[13] Y. Bae and S. Lee, "A case study on the environmental color of urban regeneration in modern streets - focused on the color of historic and surrounding buildings on marunouchi street and Bashamichi street," *Journal of Korea Society of Color Studies*, vol. 33, no. 2, pp. 38–48, 2019.

[14] T. Alizadeh, "An investigation of IBM's Smarter Cites Challenge: what do participating cities want?" *Cities*, vol. 63, pp. 70–80, 2017.

[15] A. H. Sodhro, S. Pirbhulal, Z. Luo, and V. H. C. de Albuquerque, "Towards an optimal resource management for IoT based green and sustainable smart cities," *Journal of Cleaner Production*, vol. 220, pp. 1167–1179, 2019.

[16] Z. Li, Y. N. Cheng, and Y. Y. Yuan, "Research on the application of virtual reality technology in landscape design teaching," *Educational Sciences: Theory and Practice*, vol. 16, no. 5, pp. 1400–1410, 2018a.

[17] Y. Shen, "Create synergies and inspire collaborations around the development of intelligent infrastructure for human-centered communities," *Journal of the Association for Information Science and Technology*, vol. 70, no. 6, pp. 596–606, 2019.

[18] P. Mohandas, J. S. A. Dhanaraj, and X.-Z. Gao, "Artificial neural network based smart and energy efficient street lighting system: a case study for residential area in hosur," *Sustainable Cities and Society*, vol. 48, Article ID 101499, 2019.

[19] Z. Shen and M. Kawakami, "An online visualization tool for Internet-based local townscape design," *Computers, Environment and Urban Systems*, vol. 34, no. 2, pp. 104–116, 2010.

[20] S. Rinaldi, F. Bittenbinder, C. Liu, P. Bellagente, L. C. Tagliabue, and A. L. C. Ciribini, "Bi-directional interactions between users and cognitive buildings by means of smartphone app," in *Proceedings of the 2016 IEEE International Smart Cities Conference (ISC2)*, pp. 490–495, Trento, Italy, September 2016.

[21] L. Cheng, S. Chen, S. Chu et al., "LiDAR-based three-dimensional street landscape indices for urban habitability," *Earth Science India*, vol. 10, no. 4, pp. 457–470, 2017.

[22] S. Wolfert, L. Ge, C. Verdouw, and M.-J. Bogaardt, "Big data in smart farming—a review," *Agricultural Systems*, vol. 153, pp. 69–80, 2017.

[23] M. S. Munir, I. S. Bajwa, M. A. Naeem, and B. Ramzan, "Design and implementation of an IoT system for smart energy consumption and smart irrigation in tunnel farming," *Energies*, vol. 11, no. 12, p. 3427, 2018.

[24] F. Canales-Ide, S. Zubelzu, and L. Rodríguez-Sinobas, "Irrigation systems in smart cities coping with water scarcity: the case of Valdebebas, Madrid (Spain)," *Journal of Environmental Management*, vol. 247, pp. 187–195, 2019.

[25] J. M. Blonquist, S. B. Jones, and D. A. Robinson, "Precise irrigation scheduling for turfgrass using a subsurface electromagnetic soil moisture sensor," *Agricultural Water Management*, vol. 84, no. 1-2, pp. 153–165, 2006.

[26] L. Heeb, "Climate-smart pest management: building resilience of farms and landscapes to changing pest threats," *Journal of Pest Science*, vol. 92, no. 3, pp. 951–969, 2019.

[27] Z. Li, X. Han, X. Lin, and X. Lu, "Quantitative analysis of landscape efficacy based on structural equation modelling: empirical evidence from new Chinese style commercial streets," *Alexandria Engineering Journal*, vol. 60, no. 1, pp. 261–271, 2021.

[28] A. Costin and C. Eastman, "Need for interoperability to enable seamless information exchanges in smart and sustainable urban systems," *Journal of Computing in Civil Engineering*, vol. 33, no. 3, 2019.

[29] Z. Li, Y. Cheng, and R. Xiao, "Electroencephalogram experiment based analysis of aesthetic fatigue on Chinese traditional garden," *NeuroQuantology*, vol. 16, no. 5, pp. 356–362, 2018b.

[30] C. Balakrishna, "Enabling technologies for smart city services and applications," in *Proceedings of the 2012 Sixth International Conference on Next Generation Mobile Applications, Services and Technologies*, pp. 223–227, Paris, France, September 2012.

[31] K. Mandula, R. Parupalli, C. AS. Murty, E. Magesh, and R. Lunagariya, "Mobile based home automation using internet of things (IoT)," in *Proceedings of the 2015 International Conference on Control, Instrumentation, Communication and Computational Technologies (ICCICCT)*, pp. 340–343, Nagercoil, India, December 2015.

[32] F. Zhang, L. Wu, D. Zhu, and Y. Liu, "Social sensing from street-level imagery: a case study in learning spatio-temporal urban mobility patterns," *ISPRS Journal of Photogrammetry and Remote Sensing*, vol. 153, pp. 48–58, 2019b.

[33] L. Caneparo, "Shared virtual reality for design and management: the Porta Susa project," *Automation in Construction*, vol. 10, no. 2, pp. 217–228, 2001.

[34] J. Ching, D. Aliaga, G. Mills et al., "Pathway using WUDAPT's Digital Synthetic City tool towards generating urban canopy parameters for multi-scale urban atmospheric modeling," *Urban Climate*, vol. 28, 2019.

[35] C. R. Bruns and B. C. Chamberlain, "The influence of landmarks and urban form on cognitive maps using virtual reality," *Landscape and Urban Planning*, vol. 189, pp. 296–306, 2019.

[36] V. Gazis, M. Strohbach, N. Akiva, and M. Walther, "A unified view on data path aspects for sensing applications at a smart city scale," in *Proceedings of the 2013 IEEE 27th International Conference on Advanced Information Networking and Applications Workshops (WAINA)*, pp. 1283–1288, Barcelona, Spain, March 2013.

[37] H. Khachatryan, D. H. Suh, W. Xu, P. Useche, and M. D. Dukes, "Towards sustainable water management: preferences and willingness to pay for smart landscape irrigation technologies," *Land Use Policy*, vol. 85, pp. 33–41, 2019.

[38] N. Tcholtchev, P. Lammel, R. Scholz, Y. Rebahi, W. Konitzer, and I. Schieferdecker, "Enabling the structuring, enhancement and creation of urban ICT through the extension of a standardized smart city reference model," in *Proceedings of the 2018 IEEE/ACM International Conference on Utility and Cloud Computing Companion (UCC Companion)*, pp. 121–127, Zurich, Switzerland, December 2018.

[39] H. P. McKenna, "Innovating metrics for smarter, responsive cities," *Data*, vol. 4, no. 1, 2019.

Research Article

Urban Public Sports Information-Sharing Technology Based on Internet of Things

Youliang Li, Fenglei Li ⓘ, and Yujun Xiong

School of Physical Education, East China University of Technology, Nanchang 330013, China

Correspondence should be addressed to Fenglei Li; 201960251@ecut.edu.cn

With the continuous development of social economy, sports has become one of the important ways of physical exercise, and the demand for corresponding sports facilities is also increasing. The Internet of Things technology is introduced in this paper. Through combining the current status of urban public sports, an urban public sports sharing system is built by trial, to promote the sharing of urban public sports information through the continuous development of new technologies such as the Internet and improve the publicity and popularization of public sports information. Simulation experiments prove that the Internet of Things technology is effective and can effectively support the sharing of urban public sports information.

1. Introduction

With the continuous development of social economy, modern society has gradually transformed into a "data society," and all walks of life are subject to important influences and innovations related to informatization [1, 2]. The continuous progress of society has promoted the healthy development of human beings, but how to conduct sports or physical exercise is an issue that people are extremely concerned about, especially about the existence of surrounding stadiums and public welfare sports facilities, vacant venues for the badminton courts, etc. [3, 4].

From digital cities to smart cities, the construction of informatization has had a profound impact on various industries, and data have also grown in an explosive manner. However, disorderly and messy data often bring about important loads of hardware storage and network transmission and have become a burden on users [5, 6]. However, what needs to be valued is how to reasonably process, orderly process, and classify and extract these data, realize the reuse of data, tap its potential value, transmit potential information, realize the maximum sharing of data and information, and save the cost of data and information and various construction costs [7, 8]. The continuous construction and development of smart cities have gradually introduced a series of new technologies and methods such as the Internet of Things, the Internet, CloudNative, and Fog Computing, aiming to solve urban sickness such as urban congestion, environmental pollution, population agglomeration, and other cities in the process of urbanization [9, 10].

For sports, it is necessary to further consider its limitations and needs in the actual implementation process, how to select the location of sports facilities, how to release it to the public, when will the corresponding venue information be opened, how many visitors access the venues currently in real time, and so on [11, 12]. According to the different seasons, some information is extremely valued such as opening college swimming pools and badminton halls to the public, related matters, and public opening hours, to prevent the public from entering disorderly. In response to these needs and limitations, the new technologies such as the Internet of Things is introduced in this paper, and an urban public sports information-sharing architecture system is built by trial. Through the Internet and other technologies, information is continuously processed, extracted, and shared, and finally, information sharing is realized, aiming to improve the quality of public sports, realizing "one-time processing and analysis, and multiple times' sharing applications."

2. The Status Quo of the Co-Construction and Sharing of Sports Information Resources in China

The advent of the information age has given birth to the increase and enrichment of various information resources. As far as the sports industry is concerned, its information resources are an important branch of related information resources, which have the extensiveness and imbalance of traditional information resources. Similarly, sports resource information still contains a lot of content, but the quality is difficult to be guaranteed. Because sports has penetrated every walk of life, such as sports channels, sports pages of web news, sports sections in micromedia, sports bloggers, and various sports magazines, there are various carriers of sports information resources, even new media such as Douyin and Kuaishou, have a large amount of sports information resources. This aspect is due to the continuous development of information technology and the continuous enrichment of carriers. On the contrary, sports have become the focus of daily life and gradually attract more and more people's attention. How to provide important sports information to the public has become a problem and direction worthy of attention in the industry and academia [13, 14]. Therefore, it is necessary for all sports-related industries to work together to improve business capabilities and realize the sharing and co-construction of sports resources.

2.1. Outdated Concepts and Weak Consciousness. As a public welfare direction, usually sports does not receive too much guarantee in terms of policies, especially funding guarantees; it is difficult to be guaranteed completely. According to the research statistics of relevant experts, in the sports industry, construction of informatization for the related sports scientific research projects is hardly valued. On the one hand, the construction of sports facilities requires a high cost; on the other hand, it is difficult to keep up with management concepts and awareness. The relevant expert often meets with the trouble in calling for the strengthening of the co-construction and sharing of related information-based sports resources. On the one hand, information-based resources are less; even if they are shared, they cannot meet the requirements; on the other hand, institutions engaged in corresponding sports scientific research have few projects of related research and conducted few informatization research studies [15, 16]. In addition, managers in the actual sports industry still cannot have this kind of thinking or courage to realize the direct sharing of relevant information. On the one hand, the requirement and support from the relevant industry authorities are lacked. On the other hand, most industry managers believe that they have no obligation to provide information resources to other units. This has great limitations on information management and urban management, and it is not conducive to the sharing of sports resource information for urban residents.

2.2. Barriers Exists and Each Does Things in His Own Way. As far as the administrative authorities are concerned, the resource information is controlled by the corresponding competent authority; the physical education colleges for college students have relevant information resources, so the corresponding sports information center, scientific research institute, or university sports library are all carrying out their respective construction of informatization, in which there are not only technical gaps in the underlying system development but also differences in operating networks, all of which cause more trouble for information sharing to form an information barrier [17, 18].

2.3. Lack of Talents, Low Development, and Integration Capabilities. For a long time, because the construction and development of sports informatization have not been valued correspondingly, there are fewer composite talents with related sports knowledge in the field of sports informatization, including computer network technology, especially the high-quality sports services are less such as technical consultation sports characteristic databases and network academics [19, 20].

3. Conditions for Constructing a Platform for the Co-Construction and Sharing of Sports Information Resources in China

3.1. The Continuous Growth of Sports Digital Resources Provides a Resource Base. With the continuous development of the social economy, the sports information resource database has also been continuously enriched, which lays a solid foundation for the construction of a corresponding sports information resource-sharing platform. With the use of networked and electronic related technologies, the more demand emerges to use a unified portal for unrestricted access to corresponding information resources. Therefore, it is extremely important to establish corresponding sports shared information service platform. The continuous development of computer technology and network transmission technology can realize the integration of resources and one-stop fast service.

3.2. Coordination of Supply Entities. For most entities, the governance of collaborative information becomes possible because public sports services can involve multiple objects, such as the government, users, and markets, and require multiple parties to conduct collaborative management, which is mainly reflected in multiple aspects, such as under the background of informatization; multiple entities realize the supply and service of sports public services and realize the improvement of the overall quality of urban sports public services. Ensure that the form of government tends to be flat vertically; horizontally, we achieve coordination, unification, and cooperative management and governance between governments, focusing on solving the problem of fragmentation.

In addition, big data technology can ensure that online sports services are possible and clarify the further enhancement of the entity service. The traditional sports supply is managed by different administrative departments according to different responsibilities, giving full play to the

advantages of technology and knowledge, so that all aspects are all in the state of co-construction and sharing. However, what needs to be valued is that various factors such as the positions of various units, the cost of information sharing, and the different technical standards have caused various departments to form different service models. Therefore, the corresponding departments should be linked to realize the virtual cooperation in demand for sports public services, to ensure that the individual's management and service capabilities are improved, to achieve a more fragmented and detailed public sports services, to achieve the refinement of the tasks of the public service entity, to remove the traditional steps designated by the higher level, to optimize the organizational relationship, and to achieve flattening.

In the era of big data, there is a clear gap between the public and the actual supply of sports services. On the one hand, the public cannot accurately express the demand for sports facilities, and on the other hand, there is a structural dislocation in the demand for sports public services.

Before the era of big data, there is often a clear gap between people's expectations for public sports services and the supply of public sports services. The reasons are that the public's demand for public sports services is not fully and clearly expressed, the government's decision-making model is not sufficient, and there is a structural dislocation between the demand for sports public services and the supply. In the era of big data, public sports services are becoming more and more inventory oriented. The total public demand for sports and configuration needs of the people are clearly expressed, and they are realized through the intelligent perception of sports public service needs and service data decision-making.

First of all, the intelligent perception of sports public service needs. To fully and clearly express the people's sports service needs, the government can increase interaction with the society through open methods and can also use big data technology to intelligently acquire and perceive the people's public sports needs. The mainstream web3.0 technology of big data solves the inaccessibility of people's information technology and greatly reduces the cost of information and data transmission. The public can also use various terminals such as websites, Weibo, WeChat, and application software to express their needs for sports services; the government uses intelligent-sensing technology to gather these micro-data reflecting people's needs and aggregate them into the big data needed for statistics. Relying on big data analysis and mining technology, data are processed and people's specific needs are analyzed for sports public services. Second is data decision-making for the provision of sports public services. The total amount of services and the allocation of resources are the main content involved in the supply of sports public services; in the final analysis, it is a matter of decision-making. At present, the supply of sports public services is not balanced. The key factor is that the government's decision-making model is not perfect; the factor that the government's decision-making model is not perfect is that the decision-making body often makes decisions based on their own interests and preferences and does not fully consider the people's sports needs; with comparison of decision-

making methods, subjectively, it is difficult for the government to make scientific decisions in the absence of samples and data information. The use of big data largely solves the problems of data complexity, uneven levels, and in-depth data analysis. Data-driven decision-making has gradually become an important model for the precise supply of sports public services. Third, the supply of public sports services tends to be inventory based. The supply of sports public services covers the overlap between supply and demand. The supply is related to the financial situation of the local government, the level of social and economic development, and the realization of government functions. The cloud platform can be used to systematically integrate. The big data of the database are sorted out, and the supply of sports public services is accurately mined with the help of MapReduce technology. Demand refers to the type and quantity of people's needs for sports public services, which requires big data technology to collect social information more intelligently and comprehensively, such as through websites, Weibo, WeChat, and other terminals. With the help of big data technology and analysis technology, realize mining and evaluation.

With the help of big data resources and technology, we can effectively predict the total amount of sports public services and optimize their configuration to alleviate the problem of unbalanced supply on the demand side. At the same time, big data have also become an efficient and intelligent tool for the main body (government) on the supply side of sports public services, making the supply of sports public services more intelligent, precise, and simple, thereby realizing the government's modern governance goals.

First, the supply of sports public services is smarter. First of all, the auxiliary equipment for sports public services has realized intelligence. Big data promote APP-based terminal applications. By integrating government websites and government service AGM and other auxiliary equipment, the intelligent model can be used to reach all distances of sports public services. Secondly, the willingness to supply sports public services has become intelligent. Before the era of big data, government websites were mainly based on supply-oriented service models that only responded to requests. This model was relatively passive, and government supply usually did not match the people's sports needs. In the era of big data, the government can use online analysis tools such as Google Analytics, Urchin, and SiteCastalyst to collect and analyze data information such as the types and characteristics of search keywords and use Hadoop and other tools to analyze people's search behaviors, effectively based on people's points of interest. Push the corresponding sports service. Second, the supply of sports public services is more precise. Individual needs in the era of big data have become the focus of attention of enterprises, society, and government. Big data advocate the concepts of information openness, sharing, fairness, and information decision-making. Its mining analysis technology not only analyzes the sports public service database but also effectively analyzes the data of the Internet and mobile terminals and uses natural language decryption software to analyze unstructured data. The data can be used to identify the potential actions of users, so as to provide targeted sports services for them, and "let the data

speak" so that both the supplier and the demander can see the visualized results. Third, the supply of sports public services is more concise. Before the big data era, the supply of sports public services was based on the division of labor based on professionalism, and the operation process was constructed in the form of bureaucracy. In this way, a very complete sports public service chain was divided into countless broken links to make its service process more messy. The fragmented work process caused not only delays in service work but also an embarrassing situation in which operating costs exceeded benefits. Integrating resources is the important significance of the existence of big data, and the supply of sports public services under big data should also be transformed from the traditional multichannel model to a simplified model, integrating the application layer, data layer, and platform layer of different government functions in the background. In order to better provide resources and system support for the front end, we build an application system at the application layer to achieve connection and communication, establish a government department database at the data layer and open data information, establish a platform for government business support at the platform layer, and integrate sports at the front end. The public service client is integrated to provide a way of integration for the background. Unify the website port with the mobile port to provide simplified public sports services.

3.3. Principles of Sports Information Resource Sharing.
Assume that the subtask sample dataset of n platform data traffic shunt is

$$T(n) = \{t_1, t_2, \ldots, t_n\}. \tag{1}$$

Among them, $n \in N$ and t_i represents the ith shunt subtask $(i = 1, 2, \ldots, n)$ in the set. The corresponding attribute vector of the shunt task t_i is expressed by

$$t_i = \left(t_{id}^i, t_{mi}^i, t_{fee}^i, t_{deadline}^i, t_{memory}^i, t_{bw}^i, t_{submit}^i\right). \tag{2}$$

Among them, t_{id}^i represents the unique tag number of the task, t_{mi}^i represents the size of the platform data traffic task, which reflects the number of tens of millions of instructions (MI) of the task, t_{fee}^i represents the cost of the user's desired task, $t_{deadline}^i$ represents the deadline of the user's desired shunt task, t_{memory}^i represents the memory size requirement of the shunt task, t_{bw}^i represents the bandwidth requirement of the shunt task, and t_{submit}^i represents the time when the network user submits the shunt task.

Assume that the sample dataset of m virtual machine platform data traffic resources is

$$VM(m) = \{vm_1, vm_2, \ldots, vm_m\}(m \in N). \tag{3}$$

Among them, vm_j represents the jth virtual machine $(j = 1, 2, \ldots, m)$, to calculate the corresponding attribute vector of the virtual machine resource:

$$vm_j = \left(vm_{id}^j, vm_{capacity}^j, vm_{bw}^j, vm_{memory}^j\right), \tag{4}$$

where vm_{id}^j represents the unique tag number of the data traffic data center of the platform where the virtual machine is located, $vm_{capacity}^j$ represents the processing capacity of the virtual machine resources, vm_{bw}^j represents the bandwidth provided by the virtual machine, and vm_{memory}^j represents the memory size of the virtual machine, and ETC_{ij} is utilized to reflect the expected execution time of platform data traffic shunt subtasks t_i on virtual resources vm_i:

$$\text{ETC}_{ij} = \frac{t_{mi}^i}{vm_{capacity}^j}. \tag{5}$$

Let be_j represent the initial time for execution on different virtual machines and ETC_{ij} represent the expected completion time of the shunt task executed on the virtual machine vm_{ij}:

$$\text{ECT}_{ij} = be_j + \text{ETC}_{ij}. \tag{6}$$

The completion time of all platform data traffic shunt tasks is denoted as Makespan; then,

$$\text{Makespan} = \max\{\text{ECT}_{ij}\}. \tag{7}$$

Formula (8) is used to express the objective function and constraint conditions of the platform data traffic offload task:

$$\begin{cases} \min\{\text{Makespan}\}, \\ \begin{cases} t_{memory}^i \leq vm_{memory}^j, & i = 1, 2, \ldots, n, \\ t_{bw}^i \leq vm_{bw}^j, & j = 1, 2, \ldots, m. \end{cases} \end{cases} \tag{8}$$

In the form of linear programming, the objective function given by equation (8) is solved. Assuming that equation (8) is established, ω' is the optimal solution for the current platform data traffic shunt task, and equation (9) is used to establish a cloud platform data traffic management model:

$$\begin{cases} \omega' = \omega + \dfrac{(1-p)(1-\text{rand})}{e^y}, \\ 1/e^{\Delta y/(1+T_i)} > \text{rand}(), \end{cases} \tag{9}$$

where rand () is a random number in the interval $[0, 1]$, p is the mutation probability, and T_t represents the completion time of different subtasks in the objective function constraint condition determined by Makespan.

Assume that the set of platform data traffic shunt subtasks composed of sample data of k platform data traffic shunt subtasks is

$$c = [c(0), c(1), \ldots, c(e-1)]^k. \tag{10}$$

Among them, to satisfy the conditions of $a \sim g(c, s)$, $g(s|c)$ represents the distribution probability of subtasks in the shunt task, and we calculate the shunt task load of total platform data traffic:

$$\widehat{s} = \varepsilon \arg\min_{q \in \varepsilon} \sum_{s=1}^{+\infty} H(\widehat{s}, s) g(s|c), \tag{11}$$

where $H(\widehat{s}, s)$ represents the cost function in the shunt task and ε represents the set of all subtasks in the shunt task:

$$\varepsilon = \{\widehat{s}|c_1 + 2c_r \le \widehat{s} \le S\}, \tag{12}$$

where S represents the maximum value of the task in the process of shunting tasks, and the cost function is calculated using

$$H(\widehat{s}, s) = (\widehat{s}, s) = (\widehat{s} - s)^2, \tag{13}$$

where $\widehat{s}$ represents the mean value of the time required for the shunting process. Assuming that the diversion time meets the condition of $\sum_{s=1}^{s} \widehat{s}(s|c) = 1$, the estimated function can be obtained:

$$H(\widehat{s}, s) = |\widehat{s} - s|. \tag{14}$$

Substitute formula (13) into (11), the following results can be obtained:

$$\widehat{s} = \arg\min_{s} \widehat{s}\left(\sum_{s=1}^{s} s(s|s) - \sum_{s=s}^{s} s(s|c)\right). \tag{15}$$

Realize the calculation of the amount of subtasks in the process of platform data traffic shunting:

$$s = \arg\max_{s}(\overline{s}|c). \tag{16}$$

In summary, the amount of subtasks in the platform data traffic offloading task can be calculated, and the dynamic priority task of the platform data traffic shunt task can be obtained, which provides an accurate data foundation for the establishment of the data traffic optimization management model of the big data cloud platform.

To ensure that sports information play the role of co-construction and sharing, therefore, a co-construction and sharing platform is built by trial to realize the sharing of platform information in this paper.

According to the experience of various successful examples, the co-construction and sharing system platform is based on a library with rich digital resources and power (information centers) as the "leader" in a region (or industry), which leads everyone in the construction.

The first is to integrate existing digital resources, including local mirroring resources and remotely accessible resources, as shown in Figure 1, such as Chinese and foreign language collection catalogs, e-books, e-journals, and video materials.

The second is the division of labor and cooperation. The corresponding characteristic database is established based on different data. If the corresponding information resource database is constructed according to the sports items, the corresponding sports resource database will be formed, and continuous incremental updates will be carried out.

4. Simulation Experiment

4.1. Overall Objectives. Based on the development needs of the city, starting from the sharing of urban public sports information technology, technologies such as the Internet and the Internet of Things are introduced as an emphasis, to realize the relevant sharing of sports information by building a corresponding technical platform.

4.2. Overall Thinking. According to the urban public sports information sharing, the corresponding framework is realized, as shown in Figure 2.

In the higher vocational physical education class, the online and offline hybrid teaching mode is used, and the general process of using urban public sports information is carried out, as shown in Figure 2.

(1) The first stage: online learning before class.

According to the educational programs, the teacher before class organizes the learning materials online and uploads them to the learning and exchange group.

(2) The second stage: offline learning in class.

In the classroom, teachers can give targeted explanations based on students' preclass learning situation to improve classroom efficiency. Meanwhile, teachers should help the students carry out the explorative study, solve preclass questions, and consolidate knowledge and skills.

(3) The third stage: online consolidation after class.

After class, teachers continue to interact with students in the online learning platform to help students solve problems encountered in the learning process. Meanwhile, teachers improve and enrich learning materials and improve teaching methods based on students' feedback.

4.3. Establishment of Database. Using urban public sports information, the original data of 23,001 students from freshman to junior year are removed and cleaned and missing value data were purged, and data of 21,089 students were retained. A model of "the association between the physique test grade and each individual index" is established, as shown in Figure 3, to study the influence of each individual index of the physique test on the overall physical fitness assessment.

A large number of association rules are excavated, and the typical correlation rule is screened out, as shown in Figure 4, which will be beneficial to the decision support of this research goal.

41% of the senior girls are rated as with excellent physiques and with excellent speed and flexibility. Rule 2 shows that 48.5% of girls are rated as excellent with excellent speed and vital capacity and body mass index. Rule 3 shows that
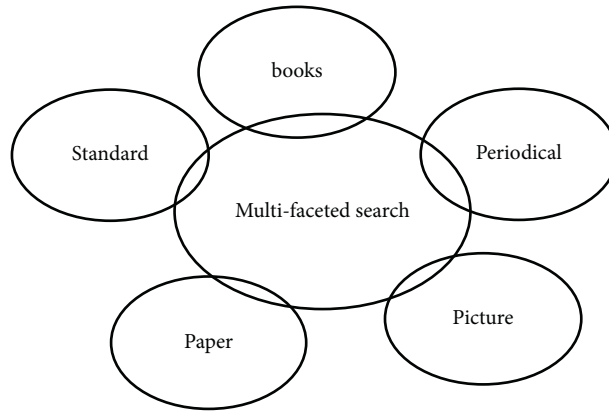
Figure 1: Searching and sorting out of existing digital resources.
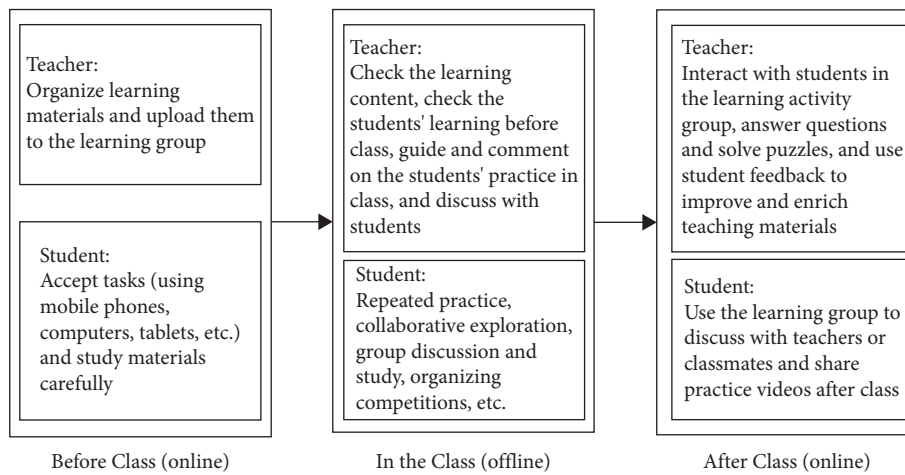

Figure 2: Procedure diagram of the online and offline mixed teaching mode of higher vocational physical education.
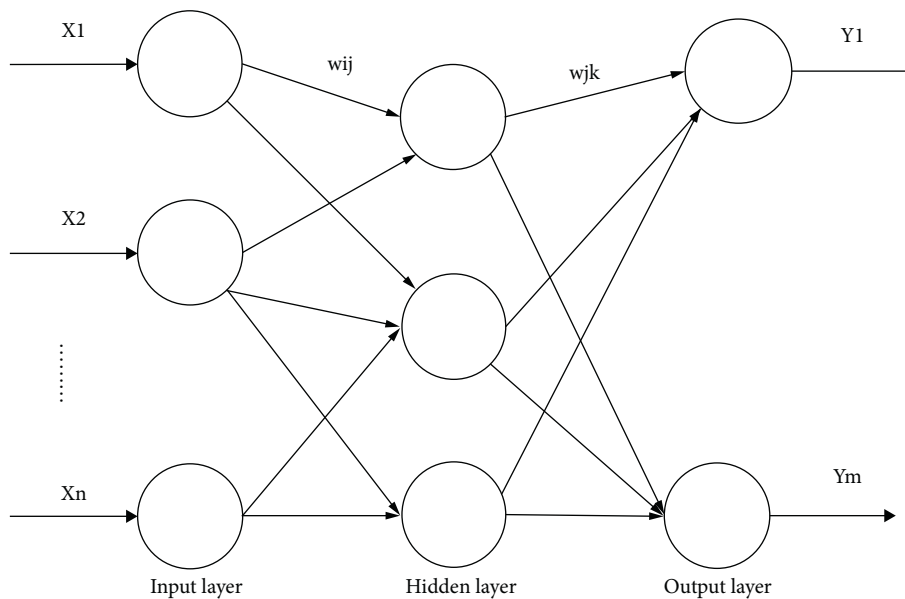

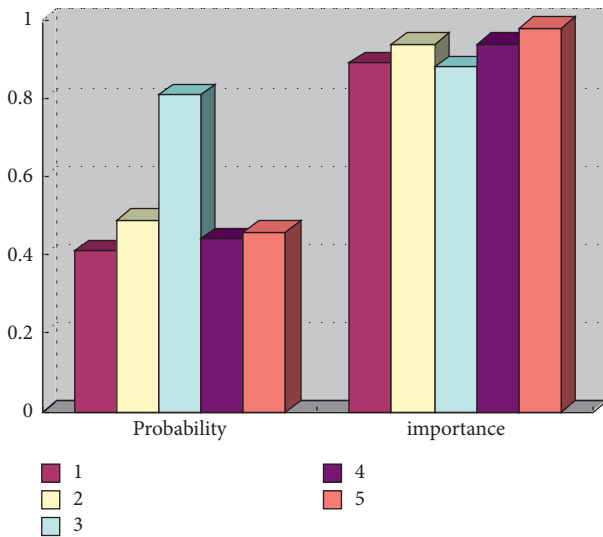Figure 3: Topological structure diagram.

Figure 4: Some part of the results of association rule mining.

82.4% of the senior girls who passed the overall evaluation score failed in speed, but had excellent flexibility, with an importance of 0.877025, indicating that even though the body has good flexibility, while the speed is poor, the overall evaluation results are only qualified. Rule 4 shows that the physical flexibility and BMI of the failed sophomore girls are both unqualified. The probability and importance are 0.44 and 0.94, respectively. It can be seen that the body shape and flexibility have a huge impact on the physical fitness test level. Rule 5 shows that even if the endurance score passes, the sophomore girl with poor vital capacity is unqualified and the probability and importance are 0.46 and 0.98, respectively. According to the comprehensive analysis of the results of urban public sports information sharing, girls with excellent physique evaluation have excellent speed, flexibility, and vital capacity. However, girls with poor physique evaluation are mainly caused by poor performance in speed, endurance, and vital capacity. Simulation experiments prove that technologies such as the Internet of Things and the Internet are effective and can support the sharing of urban public sports information.

5. Conclusions

With the advent of the era of big data, how to share urban public sports information has become an increasingly important issue. The status quo of the co-construction and sharing of sports information resources are sorted out by introducing related technologies such as the Internet of Things, the Internet, and artificial intelligence, and the needs and difficulties of co-construction and sharing of sports information resources are analyzed and constructed by trial in this paper. The aim is to promote the openness and popularization of public sports information by realizing the corresponding sharing scheme. Simulation experiments prove that the Internet of Things technology is effective and can effectively support the sharing of urban public sports information.

Data Availability

Data sharing is not applicable to this article as no datasets were generated or analyzed during the current study.

Conflicts of Interest

The authors declare no conflicts of interest.

Acknowledgments

References

[1] V. A. Korneeva, "The politicization of sports as a soft power public resource," *Indian Journal of Science and Technology*, vol. 9, no. 29, pp. 1–8, 2016.

[2] T. Zhang, H. Wen, and S. Hu, "The impact of using the visual multimedia presentation platform on the teaching effectiveness of public sports," *International Journal of Information Technology and Management*, vol. 13, no. 1, pp. 64–71, 2014.

[3] X. Zhang, "Construction of mass sports service information platform in Hebei based on media communication," *Revista de la Facultad de Ingenieria*, vol. 32, no. 9, pp. 617–623, 2017.

[4] C. Mou and Y. Cheng, "Research on information resource sharing and big data of sports industry in the background of OpenStack cloud platform," *Security and Communication Networks*, vol. 2021, no. 6, pp. 1–12, 2021.

[5] T. Jiang, "Urban public art and interaction design strategy based on digital technology," *Cluster Computing*, vol. 22, no. 4, pp. 1–8, 2019.

[6] S. Zhu, "Research on the sharing mode of sports information resources under big data environment," *Boletin Tecnico/Technical Bulletin*, vol. 55, no. 17, pp. 697–701, 2017.

[7] P. Ren, M. Nie, and H. Ming, "Optimization of sports good recycling management system based on Internet of Things," *Wireless Communications and Mobile Computing*, vol. 2021, no. 2, 11 pages, Article ID 6415136, 2021.

[8] D. Rockerbie and S. T. Easton, "Revenue sharing in professional sports leagues as a hedge for exchange rate risk," *International Journal of Sport Finance*, vol. 12, no. 4, pp. 342–358, 2017.

[9] Z. Huang, T. Mendis, and S. Xu, "Urban solar utilization potential mapping via deep learning technology: a case study of Wuhan, China," *Applied Energy*, vol. 250, PT.1, pp. 283–291, 2019.

[10] E. Nikitina, "Speech influence mechanisms and models in polycode and polymodal text (using the example of regional television sports coverage)," *Scientific Research and Development Modern Communication Studies*, vol. 5, no. 1, pp. 77–81, 2021.

[11] X. W. Xiong, "Study on the intelligent system of sports culture centers by combining machine learning with big data," *Personal and Ubiquitous Computing*, vol. 24, no. 15, pp. 1–7, 2019.

[12] J. Zhang and H. Cheng, "Evaluation of the government urban and rural information based on Choquet integral,"

International Journal of Computer Applications in Technology, vol. 20, no. 3, pp. 127–140, 2016.

[13] V. Mitrevski and A. Aceski, "Creation and transfer of knowledge management in sports institutions and organizations," *Indian Journal of Commerce and Management Studies*, vol. 6, no. 5, pp. 106–114, 2015.

[14] L. Kendall, B. Chaudhuri, and A. Bhalla, "Understanding technology as situated practice: everyday use of voice user interfaces among diverse groups of users in urban India," *Information Systems Frontiers*, vol. 22, no. 8, pp. 178–185, 2020.

[15] N. Erhardt and C. Martin-Rios, "Knowledge management systems in sports: the role of organisational structure, tacit and explicit knowledge," *Journal of Information and Knowledge Management*, vol. 15, no. 2, pp. 165–170, 2016.

[16] T. Peeters, "Profit-maximizing gate revenue sharing in sports leagues," *Economic Inquiry*, vol. 53, no. 2, pp. 1275–1291, 2015.

[17] S. Harvey, O. Atkinson, and B. P. Hyndman, "An investigation into sports coaches' Twitter use," *Journal of Teaching in Physical Education*, vol. 39, no. 4, pp. 1–10, 2020.

[18] K. Jin, "Operations management and reform combining with the principles of public service of the university sports venue," *International Journal of Technology, Management*, vol. 1, no. 99, pp. 1–10, 2015.

[19] C. Zhou, D. U. Zichun, and L. Gao, "Key technologies of a large-scale urban geological information management system based on a borwser/server structure," *IEEE Access*, vol. 2, no. 99, pp. 1–10, 2019.

[20] Y. I. Suh, T. Chung, and J. M. Kim, "The relationship between motivation of social viewing experiences, satisfaction, and loyalty in sports broadcasting," *International Journal of Computer Science in Sport*, vol. 18, no. 1, pp. 148–159, 2019.

Research Article

Research on Learning Evaluation of Online General Education Course Based on BP Neural Network

Zongbiao Zhang [iD]

Office of Academic Affairs, Zhejiang Shuren College, Hangzhou 310015, China

Correspondence should be addressed to Zongbiao Zhang; zzb33@zjsru.edu.cn

Network open curriculum provides a new solution for general education in local colleges and universities, which makes the network curriculum widely popularized and applied in colleges and universities. However, due to the lack of good curriculum learning evaluation, it is inconvenient for learners to choose. Therefore, this paper proposes to use the BP neural network model to evaluate the learning process of network general education course. Based on the course and user data provided by the existing platform, this paper constructs an online course learning evaluation model and studies the structure and effect relationship among learning experience, learning investment, and learning performance of ordinary online courses based on the preaging process product (3P) model and structural analysis method. Our research shows that curriculum quality is a key factor in analyzing and predicting learning results, which has a great impact on learning achievement. Learning experience is a direct factor affecting academic achievement. Learning experience, as an intermediary variable, indirectly affects e-learning performance. At the same time, it puts forward some suggestions to optimize the learning effect of ordinary online courses. On the one hand, the evaluation model provided in this paper can provide a reference for learners to select online courses; on the other hand, it can also be used as a supplement to the existing subjective evaluation model.

1. Introduction

General course aims in providing a broader and more comprehensive education for college students and enriches them with necessary knowledge and abilities for postgraduate practice. This concept originated from Europe, developed in the United States decades ago, especially after the Harvard committee established and published the "General Education in a Free Society" (the Harvard Redbook, 1945) [1, 2]. It caused an applauded response in the American higher education society and boomed around the world later. After the Chinese Economic Reform in 1978, the higher education in China started a progressive qualitative education reform and addressed the connection between vocational education and general education. Recently, colleges in China are exploring novelties and possibilities in general education theoretically and practically. Outstanding accomplishments were achieved, and some adapted general education models was established. These achievements have a significant impact in Chinese higher education [3].

Compared with first-class universities, regional colleges have some shared problems such as lacking faculty and staff, unbalanced course arrangement for different subjects, and setting up courses by number of students [4]. With the development of online open course, these problems are well relieved. Currently, there are more than 2000 universities, and more than 10 million students are using online learning platform in China. The online learning platform has become an important carrier for general education of regional college. However, challenges emerged with the succeeding of online teaching at the same time. For example, misunderstanding of course content during course selection, impure motivation in learning, imperfection of course assessment, assurance of course quality, marginalized course management, and plagiarisms. Based on a case study in our college, start from spring 2020, 400 modelized open general courses were offered for all students. Data for latest two years are given in Table 1. It is easy to find the "high selection rate-low complete rate-high excellent rate" pattern in Table 1. This led to questions on providing qualitative online general course.

TABLE 1: Operation data for online general course in Zhejiang Shuren College.

Semester	Course number	Course selection number	Pass rate (%)	Excellent rate (%)
Spring 2021	371	18836	88.67	71.46
Fall 2020	366	18745	89.86	71.38
Spring 2020	369	15184	86.29	68.96
Fall 2019	12	8278	92.81	71.92

How was the students' learning experience in the online general course? How to accurately control learning performance and its key factors? How to optimize the learning performance? Many scholars considered learning experience, learning engagement as the major factors for online learning [5, 6]. As a result, this study was theoretically based on the Dr. Bigg's "presage-process-product" model. We applied the structural equation modeling analysis method and discussed the structure and effect between learning experience, learning engagement, and learning performance for online general course. We were also aiming at optimizing the online learning performance, improving the general education quality, and providing future considerations on online general course in China.

2. Method and Modeling

Biggs pointed out that the early variables include student's personality and learning experience, and process variables include learning engagement and feeling to the course content in the learning process [7]. Based on the 3P theory, we provide an online general course learning relationship model (Figure 1). Taking the online learning experience as the main factor in the presage stage, taking the online learning engagement and course content quality as main factors in the process stage, and taking the online learning performance as the key factor in the product stage, the interaction between different factors forms a dynamic model.

2.1. Variables in Presage. Presage variables determine the attitude and method of the learner which further determines the learning product. As the direct participant and experiencer, students who attend the online course are affected by various factors such as the perception and experience for learning process and product.

Online learning experience positivity influences the online learning performance. Study shows strong correlation for the online learning experience and individual specialties of the students [8]. The individual specialties usually include willingness and motivation of learning, self-regulation ability, and information attainments [9, 10].

In this case, we propose that H1-H2, online learning experience has positive effect on online learning engagement and online learning performance.

2.2. Variables in Process. Process variables in online learning are mainly discussing whether the learning method could satisfy the learner's experience and whether the online learning performance could reach the preset goals. Course

content quality control is one of the key targets for the online learning management. Online learning engagement affects the learning quality greatly as well. Both of them affect the learning process significantly [11]. In this case, we investigated the online learning engagement and course quality as the major process variables.

Course content quality actively affects the online learning experience. Study shows the content and experience are in the relationship of demand and satisfaction [12]. Qualitative course content satisfies the learner with a higher learning experience, incites their mind and feeling, emotional, and positively gains them knowledge. Factors for online learning experience include online course anxiety, course content quality, perception of the usefulness of the course, flexibility of the course [13]. Course quality has positive impact on the online learning engagement. Study shows the interaction between learner and course content deeply reflects the degree of perception for learning engagement [14]. Modeling of online learning theory should focus on the positive learning experience and learning engagement concentration of the learner in an organic and unified information environment, paying attention to the thinking and interestingness of the content. Online course quality will have a positive impact on online learning performance. Research shows that appropriate course content is a key factor in the performance of teaching and online learning. Quality perception has a great impact on academic achievement. At the same time, the learning performance is directly affected by the perception of course value.

Online learning engagement has positive impact on online learning performance. Study shows increasing learner's learning engagement promote the learner's further in-depth processing, speculation, analysis reasoning, and argumentation of the learning content. It has significant impact on the learning performance as well [15–17]. Other classification research on the relationship between online learning engagement and performance in distance education shows positive relationship between online learning engagement and online learning performance in 60% of the learners [18].

Therefore, we assume (a) course content quality has positive effect on online learning experience, online learning engagement and online learning performance (H3-H5); (b) online learning engagement has positive effect on online learning performance (H6).

2.3. Variables in Product. Variables for learning product mainly include the performance and product of learner, they are directly affected by presage variables and process variables. Online learning performance, also called E-learning performance or digital learning performance, is both (a)
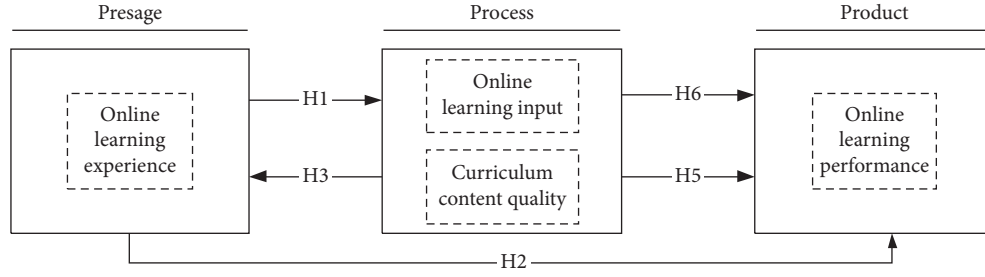
Figure 1: Online general course learning influential relationship model.

learning grade and performance achieved by the learner, and (b) information literacy consciousness, knowledge and skill improvement, learning experience satisfaction [19], etc. Currently, comprehensive, systematic, and in-depth studies on online learning performance have been carried out internationally. Overall, low online learning performance, low online course quality has significant long-term impact on college education. It is theoretically and practically important to figure out the factors for online learning performance [20]. This study uses online learning performance as the course product variable. We have added requirements for student abilities and emotions considering the online general courses are basic, accommodating, and profound. For instance, through the online general courses, students have formed general sense abilities, positive emotion, and attitude. This outcome aligns with our goal and highlights characteristics of general education.

The variable relationship among learners, learning process variables, and learning performance is shown in Figure 2.

2.4. Implementation Process of the BP Neural Network.
BP neural network, also known as back propagation neural network, its main working principle is to use machine learning to continuously iterate the training model, adjust the weight in the network structure, gradually optimize the model structure, make the error function decline along the negative gradient direction, and make the output value of the model constantly close to the expected value. The input layer described in this paper includes the following nodes: online learning experience, online learning engagement, course content quality, and online learning performance. The output layer has only label degree, that is, the output layer is one node. The number of nodes in the hidden layer is l, which is obtained through the analysis of training experiments.

In order to eliminate the influence of different dimensions among the four evaluation indicators: the number of course interaction, the number of course selection schools, the number of course selection and the number of viewers, the data are standardized. The index variables are mapped to [0,1] through normalization, and the formula is as follows:

$$p_i^m = \frac{P_i^m - P_{i\min}}{P_{i\max} - P_{i\min}}, \tag{1}$$

where $i = 1, 2, \ldots, 4$, $m = 1, 2, \ldots, 400$, $P_{i\max}$ and $P_{i\min}$ are the maximum and minimum values in the m-th original data, and p_i^m ($m = 400$) is the normalized data. 80% of the data are randomly selected from the normalized data set as training data and the remaining 20% as test data.

Input the training data into the neural network, and the output value of the hidden layer can be obtained through equation (2), shown as follows:

$$l_j^m = \sum_{i=1}^{4} w_{ij}^{(z)} P_i^m + h_j^{(z)}, \tag{2}$$

where $j = 1, 2, \ldots, n$, n is the number of nodes in the hidden layer, $w_{ij}^{(z)}$ is the connection weight between the input layer and the hidden layer, and $h_j^{(z)}$ is the threshold of the hidden layer.

2.5. Construction of the BP Neural Network Model.
In order to explore the internal relationship between different evaluation objects and indicators, the BP neural network model can be constructed based on the existing sample data. This paper will fully consider and reasonably determine the key factors such as the structure, algorithm, neuron number, and error accuracy of the network model and make the model have a certain generalization ability. The BP neural network model structure for analyzing the relationship among learners, learning process variables, and learning performance is shown in Figure 3.

Because the number of neurons in the input layer depends on the number of variables contained in the problem, this study involves learners, learning process variables, and learning performance. The output layer mainly depends on the research results. After comprehensive analysis and judgment, select the number of neurons in the output layer. The output of this study is the relationship among learning performance, learners and learning process variables. Therefore, this paper sets the number of neurons in the output layer to 1. From the above analysis, the BP neural network constructed in this paper contains only one hidden layer. Because the number of hidden layer neurons will directly affect the accuracy of network training, the number of neurons should be considered according to needs. If the number of hidden layer neurons is too small, it will greatly reduce the fault tolerance of the network model and the accuracy of sample recognition. If you set too many times, the network training time will be too long, and the fitting
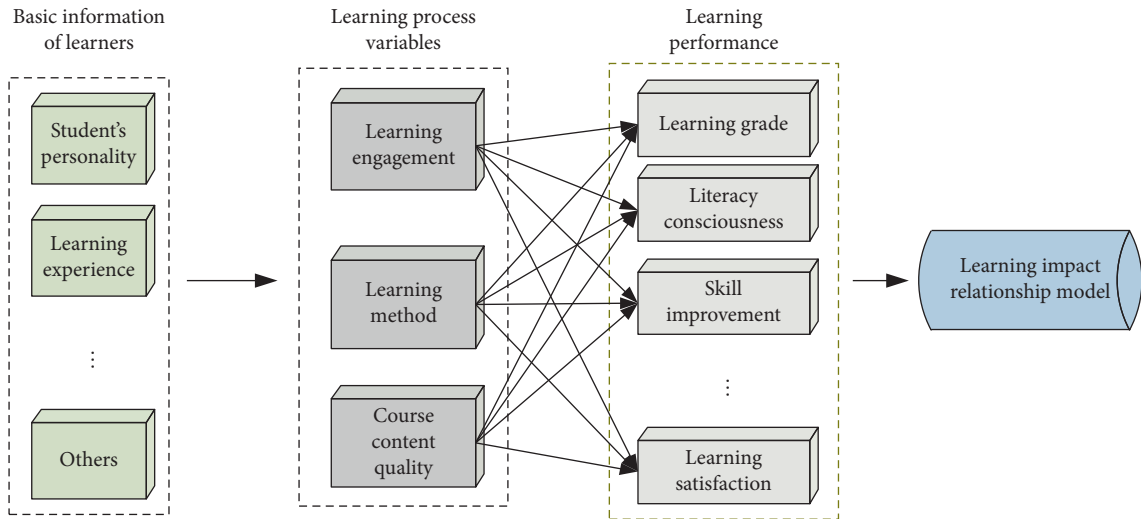
FIGURE 2: Schematic diagram of online learning impact relationship.
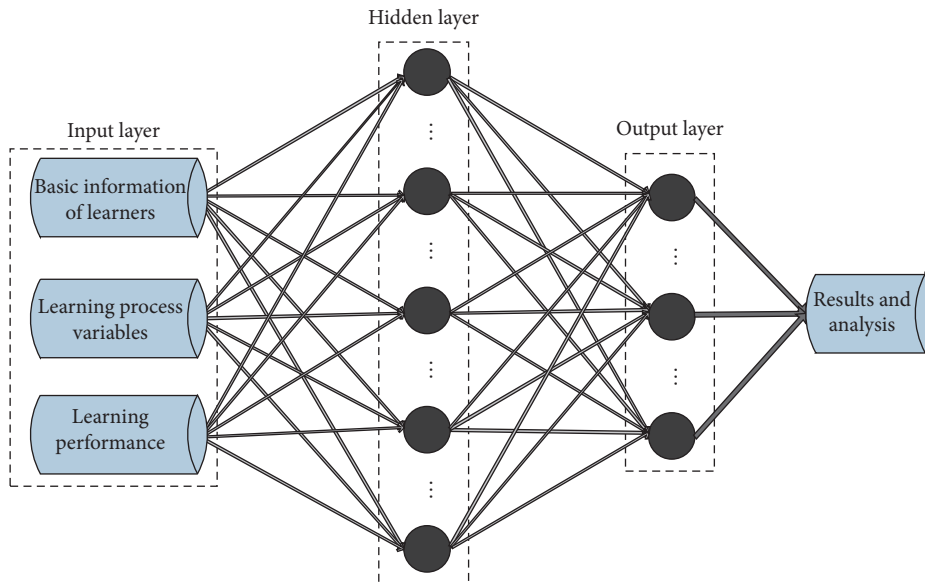
FIGURE 3: BP neural network model structure for analyzing the relationship between learners, learning process variables and learning performance.

degree of the network model will be greatly improved, resulting in overfitting problems.

3. Research Design

3.1. Research Content. Based on previous research results and 3P model, this study empirically explored the structural and effect relationship among online general learning experience, engagement, and performance in regional undergraduate schools from the perspective of general education, to explore ways and methods of which promoting teaching quality of online general course. This study focuses on the following issues: (a) validation of the theoretical model of online learning experience, online learning engagement, course content quality, and online learning performance; (b) if validated, the effects among each factor

in the model and the degree of effectiveness of the online general course.

3.2. Research Target. This study used convenience sampling on undergraduate students from five regional colleges in Zhejiang, China. We used the questionnaire survey method to collect relevant data and information. 685 questionnaires were successfully returned and analyzed. After screening by three standards: (1) no learning experience of online general course; (2) variable answers were all the same for variables; (3) answers for the variable items are missing, a total of 583 valid samples remained, with an effective rate of 85.11%.

Sample compositions are listed as follows:

Male: 257 (44.1%), female: 326 (55.9%)

Freshman: 162 (27.8%), Sophomore: 211 (36.2%)

Junior: 139 (23.8%), senior: 71 (12.2%)

Science and engineering: 189 (32.4%), literature/economics/financial/management: 154 (26.4%), agriculture and medicine: 78 (13.4%), art and edu: 92 (15.8%), law/history/philosophy: 70 (12%)

Course attended: 1 course: 75 (12.9%); 2-3 courses: 125 (21.4%); 4-5 courses: 245 (42%); more than 5: 138 (23.7%).

3.3. Research Method. SPSS 25.0 was used for data descriptive statistics and correlation analysis. AMOS 24.0 was used to establish the structural equation model. Maximum likelihood estimation method was used to evaluate the fitness of the model. Relative path analysis was combined to define the model.

3.4. Research Tool. In this study, a scale was developed to measure students learning status by literature reviews and student interviews. The scale includes two parts: learner's basic information (4 items) and survey on online general course (35 items). Each item in the second part was designed from the Likert's five-point scale (1 = strongly disagree, 5 = strongly agree). As shown in Table 2, the survey items are mostly referred to domestic influencing factor scales for various studies on general education.

To guarantee reliability and validity of the model, we used T-test for project analysis; we adopted internal consistency method for reliability evaluation; we used factor analysis method for construct validity test; we deleted one item from the learning engagement subscale, kept 34 items; and we deleted latent variables with a loading less than 0.5. Finally, dimensionality reduction was performed by calculating variables to determine 4 latent variables and 28 observed variables.

4. Results and Discussion

4.1. Measurement Model Testing. SPSS25.0 was used to perform reliability and validity test on the measurement model. In the model's reliability test, as shown in Table 3, from the view of average value, each latent variable is higher than the theoretical median (3 point). This indicates that learner's evaluation tends to be positive. Further improvement in online learning engagement is expected. From the view of standard deviation, the fluctuation of online learning engagement is high. Cronbach's α value is greater than 0.7, which implies data are reliable with high confidence. All average variance extracted (AVE) values are greater than 0.5, and all combination reliability (CR) is greater than 0.8, which indicate that the inherent quality of latent variables is good, and convergent validity is ideal. As a conclusion, the reliability of this measurement model is good.

In the model's validity test, as shown in Table 4, this model passed Bartlett's test. KMO >0.8, $P < 0.000$, and passed the significance test. This indicates the latent variables are suitable for factor analysis. The factor loadings of the observed variables are all greater than 0.7, eigenvalues are greater than 3, and cumulative variance explained rates are greater than 70%. As a conclusion, the overall validity of the measurement model is good.

4.2. Structural Model Testing. AMOS24.0 was used for confirmatory test on the structural model. The result shows the fitting index of the model is good. $X^2/df = 2.859$, RMSEA = 0.056, NFI = 0.868, RFI = 0.848, CFI = 0.903, IFI = 0.904, and TLI = 0.952. The discriminative validity test results for the structural model are shown in Table 5. The absolute values of the correlation coefficients of the observed variables are all less than 0.5 and are all less than the square root of the corresponding AVE. This indicates the model has an ideal discriminative validity.

4.3. Hypothesis Testing. This section uses hypothesis testing in the model to analyze the effect and relationship between course content quality, online learning experience, online learning engagement, and online learning performance. As shown in Table 6, course content quality has a significant positive impact on both online learning experience ($\beta = 0.724$, $P < 0.001$) and online learning performance ($\beta = 0.507$, $P < 0.001$), respectively, indicating that high-quality course content leads to high learning experience. This will not only help to improve the sense of achievement and satisfaction of learning but also improve general skills and better achieve knowledge, ability, and emotional goals. Course content quality has no significant effect on online learning engagement ($\beta = 0.124$, $P > 0.005$). Through communications and interviews with students, blind course section and the improper course selection phenomenon are existed. As a result, students have less course engagement or even drop the course in the midterm. These are the main reasons for the low completion rate of online general course. Online learning experience has a significant positive impact on both online learning engagement ($\beta = 0.493$, $P < 0.001$) and online learning performance ($\beta = 0.484$, $P < 0.001$). This indicates that good online learning experience can help students build a sense of self-worth, belonging, realize high-level cognitive activities, and improve learning performance. Online learning engagement has a significance positive effect on learning performance ($\beta = 0.671$, $P < 0.001$). This result indicates the positive attitude of learning engagement is an important cornerstone and guarantee for achieving excellent learning performance.

4.4. Effect Analysis. This section mainly analyzes the interaction mechanism between course content quality, online learning engagement, online learning experience, and online learning performance by total effect, direct effect, and indirect effect of the variables.

4.4.1. Overall Effect and Direct Effect Analysis. The total effect results between each variable in the modified structural model are shown in Table 7. Online learning engagement only has a direct effect on online learning

Table 2: Examples for survey item design and references.

1st dimension	2nd dimension
Online learning experience	Social interaction, support and service, evaluation method, input and output, teaching method [21]
Course content quality	Appropriateness, scientific, thinking, balance, fun, cutting-edge [12, 22]
Online learning engagement	Behavioral, cognitive, and emotional engagement, learning motivation [11]
Online learning performance	Self-efficacy, knowledge goals, ability goals, emotional goals, learning satisfaction [22]

Table 3: Measurement model's reliability test results.

Latent variable	Average	Standard deviation	Cronbach's α value	Average variance extracted (AVE)	Combination reliability (CR)
Course content quality	3.899	0.674	0.869	0.8419	0.8696
Online learning experience	3.819	0.751	0.913	0.7759	0.8453
Online learning engagement	3.618	0.802	0.840	0.7518	0.9135
Online learning performance	3.900	0.681	0.872	0.8665	0.8701

Table 4: Measurement model's validity test results.

Latent variable	Observed variable	Factor load	KMO	Approximate Chi-square and P	Eigenvalue	Cumulative variance explained rate (%)
Curriculum content quality	Appropriateness	0.874	0.892	874.048 ($P < 0.000$)	4.329	72.148
	Practicality	0.833				
	Cutting edge	0.840				
	Thinking	0.842				
	Systematicness	0.826				
	Fun	0.819				
Online learning experience	Social interaction	0.838	0.811	617.918 ($P < 0.000$)	3.321	71.424
	Input and output	0.784				
	Learning support and service	0.803				
	Evaluation methods	0.816				
	Teaching methods	0.811				
Online learning investment	Behavioral investment	0.846	0.844	595.826 ($P < 0.000$)	3.471	69.772
	Learning motivation	0.774				
	Cognitive investment	0.848				
	Emotional investment	0.893				
Online learning performance	Learning satisfaction	0.927	0.879	727.379 ($P < 0.000$)	3.707	74.136
	Self-efficacy	0.894				
	Knowledge goals	0.891				
	Ability goals	0.866				
	Emotional goals	0.917				

Table 5: Discriminative validity results.

	Course content quality	Online learning experience	Online learning engagement	Online learning performance
Course content quality	0.842			
Online learning experience	0.433	0.776		
Online learning engagement	0.394	0.383	0.752	
Online learning performance	0.429	0.413	0.433	0.867
Square root of AVE	0.918	0.881	0.867	0.931

performance ($\beta = 0.311$), indicating that the continuous and positive state displayed by students during learning is especially critical to achieve an excellent grade. The degree of total effect of online learning experience on each factor from high to low is online learning performance ($\beta = 0.637$) and online learning engagement ($\beta = 0.493$). And, it only has a direct effect on online learning engagement. This indicates that a successful online learning experience, such as learning

TABLE 6: Model parameter test values and research hypothesis testing results.

	S.E.	C.R.	P	Hypothesis testing
H1 Content quality ➔ learning experience	0.059	11.798	***	Yes
H2 Content quality ➔ learning engagement	0.123	0.203	0.839	No
H3 Content quality ➔ learning performance	0.111	4.267	***	Yes
H4 Learning experience ➔ learning engagement	0.142	3.634	***	Yes
H5 Learning experience ➔ learning performance	0.096	5.217	***	Yes
H6 Learning engagement ➔ learning performance	0.514	3.729	***	Yes

Note: $***P < 0.001$; $**P < 0.01$; and $*P < 0.05$.

TABLE 7: Total effect values between variables.

Dependent variable independent variable	Online learning experience	Online learning engagement	Online learning performance
Online learning engagement			0.311
Online learning experience		0.493	0.637
Course content quality	0.724	0.357	0.968

community, input and output, and learning support and service can help in reinforcing learning interest and motivation and getting a good grade by behavioral externalization. The degree of total effect of course content quality on each factor from high to low is online learning performance ($\beta = 0.968$), online learning experience ($\beta = 0.724$), and online learning engagement ($\beta = 0.357$). And, the total effect on online learning experience only has a direct effect, and the total effect on online learning engagement only has an indirect effect. This indicates that course content's appropriateness, practicality, cutting-edge, thinking, systematic, and fun are important to satisfy a good learning experience. Even if the result of course selection does not meet the expectation, it can also transform experience into self-driving force of learning, stimulate learning motivation, and improve learning achievement.

4.4.2. Medium Variables Effect Analysis. In the intervening effect variable analysis, the most used intervening effect value is the ratio of indirect effect by total effect. In this section, there are two intervening variables: online learning engagement and online learning experience (Table 8). In the intervening variable of online learning engagement, online learning performance changes by 0.637 standard deviations when online learning experience changes one standard deviation. Among these, online learning experience influences online learning performance through the intervening variable online learning engagement when effect value is 0.153. However, when effect value is 0.484, online learning experience has a direct effect on online learning performance. The intervening effect accounted for 24.02%, and this indicates the online learning engagement is a significant factor for the online learning performance. However, it is not the key role. In the intervening variable of online learning experience, online learning performance changes by 0.968 standard deviations when content quality changes

one standard deviation. Among them, 0.461 indicates the content quality influences online learning performance through the intervening variable online learning experience. However, the remaining 0.507 indicates the content quality has a direct impact on the online learning performance. The intervening effect accounted for 47.62%, which closes to the standard of important influential intervening variable, and this indicates the need to actively improve learning experience, motivate students to adopt in-depth learning ways, and improve learning performance in the online learning process.

4.4.3. Online Learning Performance Effect Analysis. As shown in Figure 4, from the perspective of total effect, the degree of effect of each factor on online learning performance from high to low is course content quality, online learning experience, and online learning engagement. From the perspective of direct effect, the degree of effect of each factor is consistent with total effect. From the indirect effect, the direct effect of curriculum content quality is higher than the intervention effect of e-learning experience. This result shows the key to the online learning performance of the online general course is course content quality and online learning experience. High-quality, satisfying, and demanding teaching content can enable learners to gain a high-level experience, spend more time and energy, and gain more.

5. Suggestions

5.1. Value the Effect of Course Content. Course content quality is the embodiment of course value. The result of this study revealed the course content quality plays a decisive role on the online learning performance of online general course. Additionally, the perceptual impact of content appropriateness is the most significant one. In another word, the course content should highly fit the learning goals.

TABLE 8: Intervening effect between online learning engagement and online learning experience.

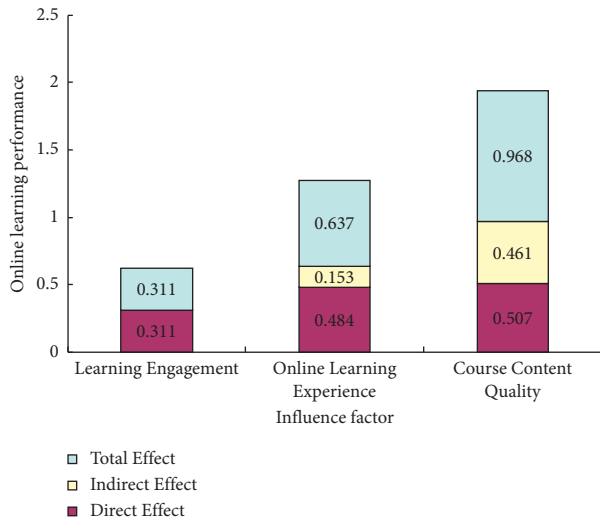| Intervening variable	Path	Effect value	Percentage (%)
Learning engagement	Learning experience ➡ learning performance	0.484	75.98
	Learning experience ➡ learning engagement ➡ learning performance	0.153	24.02
Learning experience	Content quality ➡ learning performance	0.507	52.38
	Content quality ➡ learning experience ➡ learning performance	0.461	47.62

FIGURE 4: Online learning performance factor's performance.

Therefore, firstly, set up "general education introduction course" for students to understand school's general education objectives, course system, courses selection strategy, and how to deal with general education, etc. Also, developing general literacy test and evaluation helps the students effectively understand their general literacy's advantage and disadvantage, gain personalized resource that can effectively remedy their shortcomings, and further guide course selection to fit their own learning goals. Secondly, value the thinking and cutting-edge facts in the course content when develops and introduces online general courses. Focusing on learning objectives, this paper discusses the evaluation value of learners' perspective in content perception. Moreover, design and research relevant quality analysis tools in order to improve the quality of curriculum content.

Carrying out a separate, specialized and normalized, precise online general course content quality evaluation comprehensively assesses the fitness and effectiveness of existing course and general literacy training in school. Sort by category on a basis of survival of the fittest, building "high-quality" general courses, establishing, and improving a general education course system that meets the quality requirements of the school's students. Practically improve teaching quality of general courses. For example, starting from the goal of talent training and actual school situation, Tianjin University explored a school-based course operation mode from various aspects such as course selection recommendation, process control, assessment setting, test paper customization, and teaching assistant. Lanzhou University used the general literacy assessment to grade the learning difficulties of the courses, let students "check their

seats," scientifically evaluated the implementation effect of general education and made timely adjustments. Sanjiang College took courses and activities as the starting point and constructed a "closed-cycle" application-oriented general education system in colleges and universities of "general course system + classic reading system + series of activities + cultural infiltration."

5.2. Focus on the Medium Effect of Online Learning Experience and Engagement. Results show that the online learning experience can not only directly affect online learning performance but also indirectly affect online learning performance through content quality as a key intervening variable. The most influencing factors on online learning experience are social interaction and evaluation methods. Therefore, firstly, the teachers should guide the students to participate in group discussion, learning, communication, sharing, strengthening their social connections, building a modular and diversified learning community for collaborative learning, and creating learning atmosphere of mutual assistance, mutual learning, and continuous interaction. The cultivation of a good learning community is of great significance to promote the general education, the students' overall training, and the teachers' growth. Secondly, according to course characteristic, clearly defining evaluation methods, designing a scientific course evaluation scale, adopting a multilevel and multitype dynamic assessment mode to evaluate students' comprehensive qualities comprehensively and objectively such as knowledge, abilities, and personal sentiments. Pay more attention to usual performance rather than test scores so that the students can truly enjoy general education.

The experimental results show that online learning investment not only directly affects online learning performance but also indirectly affects online learning performance through learning experience. The most influencing factors for online learning engagement are emotional engagement and cognitive engagement. Therefore, consideration of emotional elements is required while designing the course. Perform emotional design around sensory interaction, behavioral experience, and inner thinking to realize the intervention of learning, thereby promoting student's in-depth learning. In terms of cognitive engagement, using learning analysis technology to collect the feature vector of learner's personality cognition. Design different learning paths, recommending personalized resources and services. The cognition and attitude of learners towards general education are important factors affecting implementation and quality of general education. Good general education should be established on this foundation

and try its best to promote students' understanding and cognition towards general education; let them deeply understand the true value and significance of general education, to actively study and grow.

6. Conclusion

This paper takes online learning experience, online learning participation, course content quality, and online learning performance as the input layer of neural network and establishes the learning evaluation system of network general education course based on the BP neural network model. This study was based on the 3P model "Presage-Process-Product," a structural equation model was applied to analyze the structural and effect relationship among learning experience, learning engagement, and learning performance in the online general course. We found that the course content quality is the key factor on analyzing and predicting the early stage and product of learning, and it has the greatest impact on online learning performance. Appropriateness and thinking of content are the key factors affecting content quality. Online learning experience is the important factor which directly affects the online learning performance. It acts as a key intervening variable indirectly affects online learning performance through content quality. Social interaction and course evaluation methods are key factors which affect the online learning experience. Online learning engagement can have a direct and positive effect on the online learning performance. Emotional engagement and cognition engagement are key factors that affecting the online learning engagement. The above conclusions have a certain reference meaning for further optimization of learning effect of online general course. The experimental results show that the method proposed in this paper can effectively detect and evaluate the concentration of students in online course learning and analyze the relevant data. In future research, we will further enrich the variables of early stage and learning process from the aspects of general literacy, in-depth learning strategies, and knowledge acquisition, in order to make the learning impact relationship model of online general education curriculum more comprehensive [23]. In addition, we will combine simulation to prove the robustness of the method.

Data Availability

The data used to support the findings of this study are available upon request.

Conflicts of Interest

The author declares no conflicts of interest.

Acknowledgments

References

[1] Y.-y. Zhang, "The enlightenment of general education reform in harvard university on the construction of general education in Chinese universities," *Heilongjiang Researches on Higher Education*, vol. 2, pp. 59–63, 2021.

[2] X. Xie and S.-y. Wang, "General education curriculum in harvard university: the history, current situation and enlightenments," *Journal of Higher Education*, vol. 42, no. 3, pp. 100–109, 2021.

[3] F. Hui-min and X. Gan, "The situation and problems of general education in Chinese universities in the past 40 Years of reform and opening-up," *Theory and Practice of Education*, vol. 39, no. 9, pp. 3–5, 2019.

[4] M. A. Feng-qi, "Building "golden courses" is the key to improving the quality of general education," *Journal for Higher Education Management*, vol. 13, no. 4, pp. 57–63, 2019.

[5] M.-T. Wang and J. S. Eccles, "School context, achievement motivation, and academic engagement: a longitudinal study of school engagement using a multidimensional perspective," *Learning and Instruction*, vol. 28, pp. 12–23, 2013.

[6] K. Trigwell, P. Ashwin, and E. S. Millan, "Evoked prior learning experience and approach to learning as predictors of academic achievement," *British Journal of Educational Psychology*, vol. 83, no. 3, pp. 363–378, 2013.

[7] J. Biggs, D. Kember, and D. Y. P. Leung, "The revised two-factor study process questionnaire: R-SPQ-2F," *British Journal of Educational Psychology*, vol. 71, no. 1, pp. 133–149, 2001.

[8] W.-yuan Chen and W.-jun Jia, "Research on contributing factors of university students' online learning experience," *Journal of East China Normal University*, vol. 38, no. 7, pp. 42–53, 2020.

[9] B. J. Young, "Gender difference in student attitudes toward computers," *Journal of Research on Computing in Education*, vol. 33, no. 2, pp. 204–216, 2000.

[10] M. W. Cao, *Understanding Learners' Experience in MOOCs: A Review of Literature*, pp. 29–35, The University of Texas at Austin, Austin, Texas, 2014.

[11] R. Yin and H.-yun Xu, "Construction of online learning engagement structural model: an empirical study based on structural equation mode," *Open Education Research*, vol. 23, no. 4, pp. 101–111, 2017.

[12] L. Huang and X.-ning Pei, "A new study on the evaluation index system for content quality of online course: a perspective from learner experience and knowledge payment," *The Journal of Distance Education*, vol. 1, pp. 104–112, 2020.

[13] P.-C. Sun, R. J. Tsai, G. Finger, Y.-Y. Chen, and D. Yeh, "What drives a successful e-Learning? An empirical investigation of the critical factors influencing learner satisfaction," *Computers & Education*, vol. 50, no. 4, pp. 1183–1202, 2008.

[14] Z.-jun Wang and Li Chen, "Theory framework building of instructional interaction in connectivist learning context," *Open Education Research*, vol. 21, no. 5, pp. 25–34, 2015.

[15] T. Phan, S. G. McNeil, and B. R. Robin, "Students' patterns of engagement and course performance in a massive open online course," *Computers & Education*, vol. 95, pp. 36–44, 2016.

[16] M. Ronimus, J. Kujala, A. Tolvanen, and H. Lyytinen, "Children's engagement during digital game based learning of reading: the effects of time, rewards, and challenge," *Computers & Education*, vol. 71, pp. 237–246, 2014.

[17] E. T. Pascarella, T. A. Seifert, and C. Blaich, "How effective are the NSSE benchmarks in predicting important educational

outcomes," *Change: The Magazine of Higher Learning*, vol. 42, no. 1, pp. 16–22, 2010.

[18] Yi Gong and Bo Liu, "Empirical study of the relationship between online learning engagement and academic performance in distance educatio," *Adult Education*, vol. 38, no. 6, pp. 24–28, 2018.

[19] X.-yong Hu and H.-yun Xu, "The relationship between information literacy, online learning engagement and learning performance," *Distance Education and Online Learning*, vol. 3, pp. 77–83, 2020.

[20] C.-hui Duan and H. Jian-zhong, "The relationship between internet teacher-student interaction and online learning performance: the mediating effect of internet learning self-efficacy and internet learning motivation," *Psychological Development and Education*, vol. 35, no. 2, pp. 184–189, 2019.

[21] L.-jun Jiang and X.-mei Bai, "Research on the structural relationship of influencing factors of online learning experience," *Modern Distance Education*, vol. 1, pp. 27–36, 2019.

[22] F. Hui-min and H. Ming-dong, "University liberal educational teaching quality evaluation system and index design," *Educational Research*, vol. 11, pp. 61–67, 2012.

[23] W. Fuhl, N. Castner, and E. Kasneci, "Rule-based learning for eye movement type detection," in *Proceedings of the Workshop on Modeling Cognitive Processes from Multimodal Data*, pp. 1–6, Boulder Colorado, October 2018.

Research Article

A Product Styling Design Evaluation Method Based on Multilayer Perceptron Genetic Algorithm Neural Network Algorithm

Jie Wu [ID]

School of Anyang Institute of Technology, Anyang, Henan 45500, China

Correspondence should be addressed to Jie Wu; 20160735@ayit.edu.cn

Products no longer exist simply as carriers of useful functions, but more and more consumers are beginning to pay attention to the spiritual aspects of the feelings brought by products. This paper brings machine learning algorithms to the discipline of industrial design and proposes a method to evaluate the design of product shapes using a multilayer perceptron genetic algorithm neural network (GA-MLP-NN) algorithm, quantifying the product shape, using computer-aided design technology to achieve shape optimization, shape, and color scheme generation, and using interactive feedback with users to finally generate a product shape with market demand. In this paper, we use the combinatorial innovation method to arrange and combine the detail elements in the solution library to generate the modeling solution, combine the multilayer perceptron genetic algorithm neural network algorithm with product modeling, and establish the interactive genetic modeling system for the product, use this system to design the product modeling solution, and finally get the product modeling solution satisfied by the target users; using the multilayer perceptron genetic algorithm neural network method to evaluate the product modeling items. The mapping relationship model between morphological feature space and imagery cognitive space was constructed based on multiple linear regression equations, and the multiple regression model for each affective dimension was ideal. The results show that the model performance is reliable. The weights are calculated, and the appropriate people are selected to score and calculate the modeling scheme, and finally, the satisfactory product modeling scheme is obtained.

1. Introduction

Along with the progress of social history and the continuous improvement of human industrial civilization, people's living standards and consumption concepts have also undergone great changes. The esteem for material functions has gradually evolved into a strong pursuit of the field of spiritual consciousness. With the intersection and integration of various disciplines, many researchers have brought genetic ideas from biology to the discipline of industrial design; with the rapid development of computer and electronic information technology, the field of computer-aided industrial design has also gradually developed, and this design trend has led to more and more advanced algorithms to control the design process, resulting in many new design models [1]. These have brought a new idea in product design, i.e., how to assist in the design and optimization of product shape with the help of computers to produce products that are competitive in the market. Therefore, this thesis is based on a multilayer perceptron genetic algorithm neural network based on a computer-aided designer to design and optimize the product shape and find more possibilities and innovations to make the designed product more unique and selling point.

Neural networks are a research hotspot in the field of machine learning. Artificial neural networks have features such as massively parallel processing, distributed information storage, and good self-organization and self-learning ability. Artificial neural networks have been successfully applied to many fields such as signal processing, pattern recognition, and intelligent control [2]. At the same time, neural network learning also suffers from the disadvantages of easily falling into local minima, slow convergence of network learning, and complex network topology design,

which hinder its application. A multilayer perceptron neural network is a forward-structured artificial neural network also called a multilayer feedforward network, that maps a set of input variables to a set of output variables and gives a prediction of the outcome of the output variables as well as a prediction model based on the input variables. Structural characteristics of multilayer feedforward networks: (1) There is no connection between neurons in the same layer. (2) There is full connectivity between neurons in two adjacent layers. (3) There is directionality in information transfer. The feedforward computation is performed layer by layer from the input to the output. The idea of a genetic algorithm is derived from the biological evolutionary process in nature and is an optimization algorithm for solving complex problems. Intelligence and essential parallelism are the biggest differences between evolutionary computation and traditional optimization methods. Evolutionary computation does not require the objective function of the object to be continuous and differentiable, and these advantages it has made it more suitable for solving complex optimization problems, and it can also be used to avoid various defects of traditional neural networks themselves [3]. By combining the multilayer perceptron neural network algorithm with a genetic algorithm, different features are obtained by different feature extraction methods for the characteristics of product modeling design, and then the genetic optimization algorithm is used to optimize the selection of the extracted features, and the classifier is trained by MLP, and the results show that the combined model achieves the expected classification effect with a high accuracy rate. Nowadays, with the development of electronic information technology, the methods for signal processing are even more endless and become more and more efficient, and people will be more thorough in the study of feature signals to make new contributions to the future development of product modeling design [4].

2. Status of Research

There is a lack of information on the direction of machine learning algorithms combined with product form design. Many scholars and experts in the research of product morphology design theory and machine learning have made great contributions to these fields. Literature [5] first proposed a morphological analysis method, which encodes the main morphological elements and components of a product and forms different morphological products by arranging and combining them. This approach aims to generate new design solutions through "reconfiguration" and has since been widely used in product form design and related fields. Form quantization, proposed in [6], is characterized by the concept of averaging and complementing a set of similar product forms with low correlation, extracting representative forms, giving them different weights in the process, and then deriving new forms. In terms of morphological expansion, literature [7] considers the shape as a finite arrangement of lines and sets some conditions on the shape, such as position, size, and direction, through the concept of Euclidean transformation, to generate new shapes. The

imagery diagram method proposed by [8] suggested that the pictures and information can be studied by classifying them according to certain rules to establish the target scenario as a way to help the designer in designing. However, this method can only help designers to organize their thoughts to promote the association and is only an auxiliary technique before designing. Literature [9] proposes a product form design method based on the user's behavioral imagery capabilities, compared to traditional research methods that do not integrate user experience into product form design, through the study which found that the experience brought to the user by the product form has an impact on the consumer's purchase process and even plays a decisive role in the purchase decision. Literature [10] constructed a user semantic driven approach for product form prototyping and argued that semantics is the chain between people and things, and through the analysis of user semantics, it can improve user satisfaction with the product and promote the iteration of enterprise products. In addition, literature [11] proposed a theory of pan-community product form design approach based on shape literature and integrating anthropological and psychological theories. This theory first analyzes the product form elements and divides the homogeneous products and heterogeneous products and then deduces the shape grammar for both the homogeneous products and heterogeneous products and filters them to get a satisfactory solution. Literature [12] proposed a discrete neural network model with fully interconnected network topology and successfully solved the traveler problem using energy function. Literature [13] proposed a continuous neural network model, stating that neurons can be implemented with operational amplifiers and stating that the connections of all neurons can be simulated with electronic circuits, called continuous Hopfield networks. Literature [14] provides an exhaustive analysis of the error backpropagation algorithm for multilayer feedforward networks with nonlinear continuous transfer functions, which is known as the BP algorithm. Literature [15] simulates the consumer's imagery evaluation pattern for product color matching based on BP networks and generates offspring to optimize the color matching design by genetic algorithm to speed up the design process. Literature [16] incorporated genetic and biological coding methods into product color scheme design, proposed to form codes in terms of product formation, and created a PCIDBMT prototype system based on the above theory; based on interactive genetic algorithm, in [16] Yuan and Moayedi used techniques such as color merging and primary color extraction to establish an automatic mapping mechanism of color schemes from flat images to three-dimensional models of products; literature [17] introduced color matching case and grayscale correlation analysis into color matching design and used a scissor lift as an example to demonstrate that the described method can realize the conversion between case color matching and target color matching. Literature [18] proposes an orthogonal-interactive genetic algorithm, which reduces the genetic race space by orthogonal analysis to increase the convergence speed while reducing the psychological burden of fatigue to the user by reducing the number of user

interactions, producing a higher adaptation value that meets the needs of product styling design.

3. Product Styling Design Evaluation Method Based on Multilayer Perceptron Genetic Algorithm Neural Network Algorithm

3.1. Principle of Multilayer Perceptron Based Genetic Algorithm Neural Network Algorithm. A perceptron is a neural network with a single layer of computational units, which is a feedforward network with no connection between neurons within the same layer and no feedback between neurons between different layers, and the signal is transmitted from the lower-layer neurons to the upper-layer neurons. Its input and output are discrete values, and the neuron determines its output by a threshold function after the weighted summation of the inputs. The perceptron is a simple nonlinear neural network with a threshold function added to the linear neurons, also known as linear threshold elements. It can accept real type signals while outputting binary discrete quantities (0, 1). The main feature of the multilayer perceptron genetic algorithm neural network is to calculate the adaptation value based on the user's interaction evaluation rather than a function formula. Because of the combination of user evaluations as well as specific function formulas, it excels in problems where it is difficult to build adaptation functions, such as in the fields of product design, image retrieval, and design evaluation. The single-layer perceptron model has only two layers of neurons, the input and output layers, which are directly connected. It is designed as follows: first step: initialize the connection rights and thresholds; the initial values of both are generally set to smaller nonzero random numbers. Step 2: The input signals are fed into the network, the connection weights of all the input signals are weighted and processed, and the result of the calculation is used as the actual output of the network. Step 3: Adjust the weights. If the actual output of the network differs significantly from the desired output, the connection weights parameter is adjusted, and the adjustment process relies on the perceptron learning algorithm automatically [19]. Step 4: Perform step 3 repeatedly until the difference between the actual and desired outputs of the network meets the predesigned requirements.

In a neural network, perceptrons can be viewed as individual nodes in the neural network. The design idea of a parameter learning scheme for a multilayer perceptron network is that, in a multilayer perceptron network, the weights of all neurons except the last neuron are set in advance, and then the perceptron learning algorithm is used to learn the weights of the last neuron. Because the weights of the first layer neurons are set artificially, the degree of excellence of the first layer neuron design will directly affect the performance of the multilayer perceptron model. The design of the first layer neuron depends on the level of understanding of the problem faced and the data, which leads to the fact that there is no general approach to the design of parameters for the first layer neural network in solving a variety of different problems. As can be seen from Figure 1,

the structural characteristics of multilayer feedforward networks are (1) no connections between neurons in the same layer, (2) Full connectivity between neurons in two adjacent layers, and (3) there is directionality in information transfer. The forward calculation is done layer by layer from the input to the output [20].

The genetic algorithm improved multilayer perceptron neural network model is essentially the application of the genetic algorithm to extensively search the solution space of the target information, followed by locating the better multilayer perceptron neural network form searched by the genetic algorithm and then by training to obtain the optimal result of the prediction problem. Artificial neural networks are characterized by massively parallel processing, distributed information storage, and good self-organizing and self-learning capabilities. The process of genetic algorithm optimized multilayer perceptron neural network includes three parts: determining the multilayer perceptron neural network connection structure, determining the genetic algorithm optimized multilayer perceptron neural network weights and thresholds, and multilayer perceptron genetic algorithm neural network model prediction, the main steps are as follows (Figure 2): (1) determine the multilayer perceptron neural network structure based on the training sample data; (2) BP neural network hidden layers and layers are determined; (3) the length of the individual coding of the genetic algorithm is determined, and this value is determined by combining the number of parameters of the multilayer perceptron neural network; (4) the fitness value is optimized, and this value is optimized according to the error obtained from the training of the multilayer perceptron neural network; (5) the optimal solution is determined by the cyclic operation (4); (6) the optimal threshold weights are redetermined even more for the optimal solution; (7) the optimal weights and thresholds are assigned to the multilayer perceptron neural network model; (8) error calculation judgments on the new weights and thresholds are done to carry out multilayer perceptron neural network model training prediction; and (9) prediction result analysis is done, comparing the prediction results of multilayer perceptron neural network and genetic algorithm neural network.

Thresholds and weights of the multiperceptron neural network are cascaded according to a specific order, and the weights and thresholds of the multiperceptron neural network are cascaded according to the order; namely, N chromosomes are generated randomly; implicit and output layer thresholds; input and implicit layer thresholds; implicit and output layer weights; input and implicit layer weights; the fitness function selects the mean square error, and the fitness of the chromosomes is recalculated according to the mean square error function to judge whether the prediction results meet the target requirements and generate new individuals if they do not meet the requirements; the specific operation is to perform variation operation, crossover operation, and replication operation on the individuals that meet the requirements of the fitness value and judge whether the new individuals meet the requirements of the mean square error value function if they meet the requirements [21]. There are four mutation operations in the evolution of a multilayer perceptron genetic algorithm neural
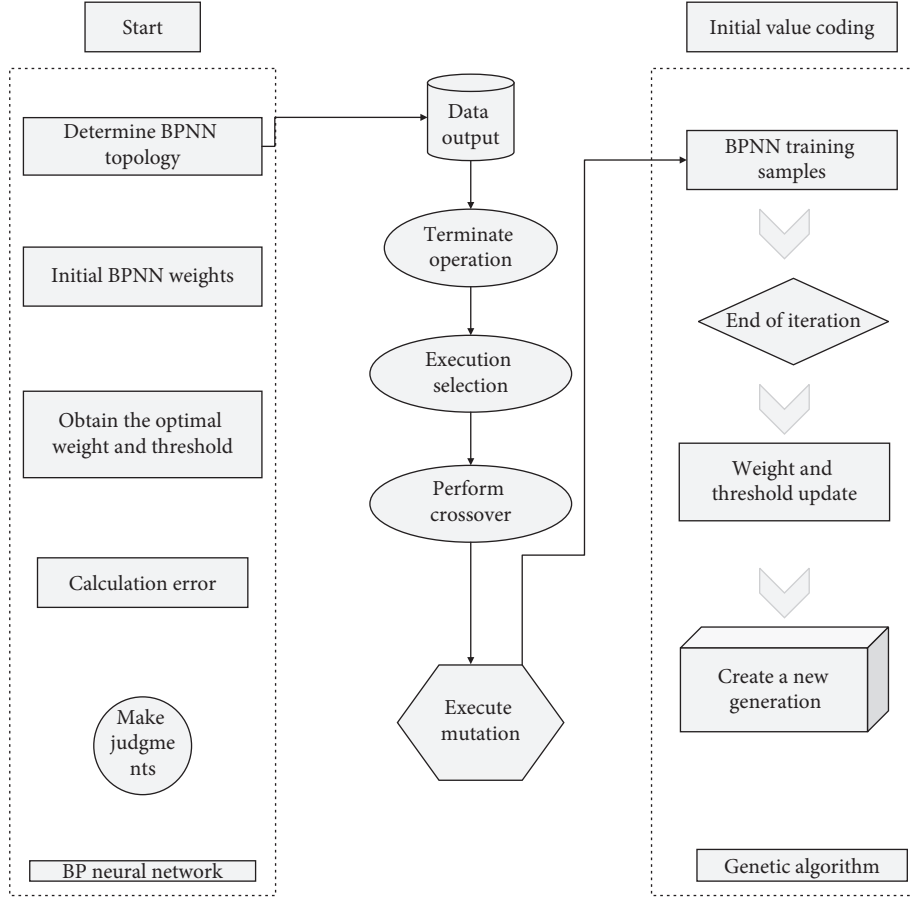
FIGURE 1: Topology of multilayer perceptron neural network.

network: adding connections, adding nodes, correcting connection weights, and changing the excitation function response. If the requirement is not met, the fitness of the chromosome is calculated again according to the mean square error function, and if the requirement is met, the optimal individuals are sequentially split and the threshold and weights applied to the multisensors neural network are updated; then the multisensors neural network is forward propagated, the global error is calculated, the weights and thresholds of the network parameters are adjusted and corrected, and the multisensors neural network learning training is cycled until the set learning times or accuracy requirements, the calculation is terminated, and the results are output.

Let the input layer of a multilayer perceptron genetic algorithm neural network have n one input neuron, the layer has m one output neuron, the hidden layer has q one hidden layer neuron, the connection weight between the hidden layer and the output layer is w_{ik} the v_{ik} connection weight between the input layer and the hidden layer is f_2, the transfer function of the hidden layer is f_1, and then the output of the hidden layer neuron is calculated as follows:

$$E(w_{ik}) = n \times f_1(q) \times f_2^m(v_{ik}) + C_v. \tag{1}$$

The output of the output layer neurons is calculated as follows:

$$\varphi_0 = F\left(f^P(i), f^Q(j+1)^2\right). \tag{2}$$

At this point, the multisensors genetic algorithm neural network completes the forward propagation process and establishes the mapping n from dimensional space vector to m dimensional space. For all the training samples in the BP neural network, the global error of the network is noted as G and is calculated as follows:

$$G = f^P(i) \oplus f^Q(j) = f(P_i) f^Q(j)^T. \tag{3}$$

The variation in the output layer weights of the multisensory layer genetic algorithm neural network is noted as L and is calculated as follows:

$$L = \sum_{(i,j,k)\in D} -\ln \sigma(z_{ij} - z_{ik}). \tag{4}$$

The formula for adjusting the weights of each neuron in the output layer is obtained as

$$R_{n+1} = R_n^2 - \sum P_{ij}. \tag{5}$$

Fixed topology evolution must be done artificially to design the topology of the neural network. In contrast, topological weight evolution methods can automatically evolve the correct network topology. In addition, there is no general set of laws that guarantee excellent performance of
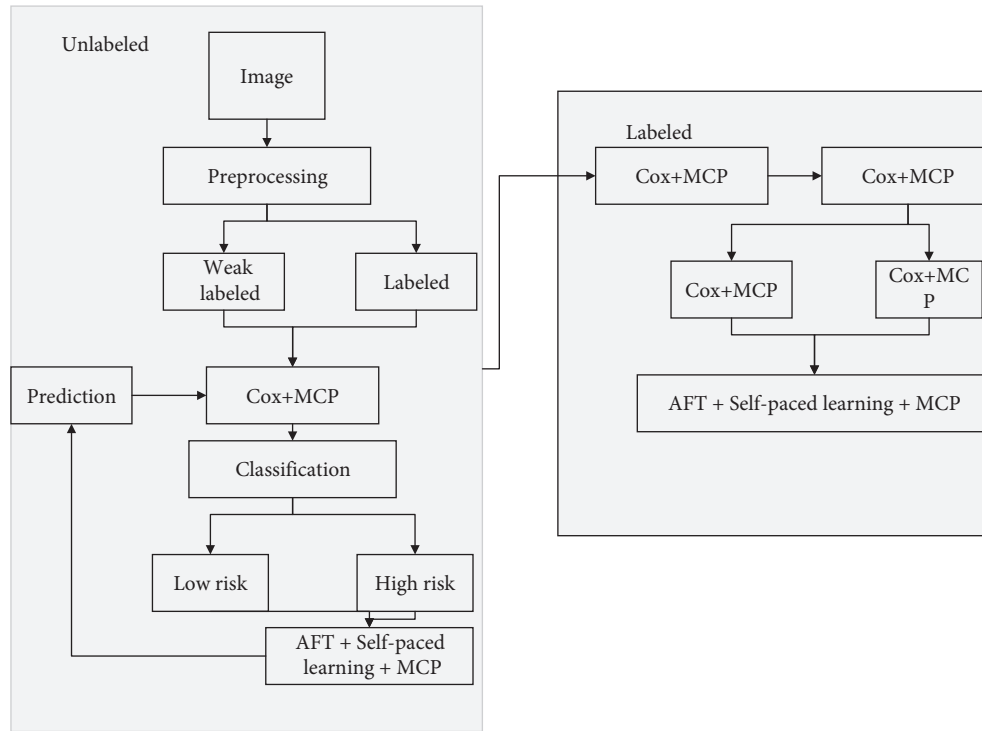
FIGURE 2: Computational flow of neural network of multilayer perceptron genetic algorithm.

artificially designed neural networks, so the topology of multisensory neural networks evolved based on genetic algorithms tends to outperform artificially designed solutions in terms of performance. This phenomenon is particularly evident in keeping network complexity to a minimum [22]. Although topology weight evolution methods perform better compared to fixed topology evolution methods, they also face many problems that do not exist in fixed topology evolution methods. There are four mutation operations in the evolution of a multilayer perceptron genetic algorithm neural network: adding connections, adding nodes, correcting connection weights, and changing the excitation function response. Before the mutation operation, we set a mutation probability, and the mutation of connection weights is done by correcting all connection weights according to the set mutation probability. In special cases, it is also possible to disregard the mutation probability and directly turn the original weight into a new weight. The mutation is used to change the weights and the network structure. Mutation of connection weights is done by adding a floating-point number (either positive or negative) to each weight with a fixed probability that matches a normal distribution. The network structure is mutated in two ways: mutation by adding nodes and mutation by adding a connection between two nodes.

3.2. Product Styling Design Evaluation Methods Based on Machine Learning Algorithms.
The so-called modeling is to point, line, surface as the basic elements, according to certain rules of mutual transformation, organic to produce new organic form. In the process of styling, the use of more

organic forms of free-form products can increase the uniqueness and innovation of products, of which, "selection" and "change," as two major modeling laws, are often applied. The so-called selection is to choose the basic type according to the use of function, maneuverability, and other conditions. There are two types of basic shapes, geometric and organic. Geometric forms are some common geometric shapes in mathematics, while organic forms are streamlined, bionic, or free-form. Transformation is the operation of dividing, cutting, accumulating, merging, stretching, extruding, bending, etc., in the form of the basic type. Splitting: It is in the form of "loss" or "separation." Usually, when cutting, it will be divided according to the golden ratio; for example, we commonly see the ratio of wheelbase to the total length of cars and the ratio of screen to the key distribution of flat panel products, etc., which are all golden ratios. Cutting: The basic type is partially cut to produce a face change in shape. The idea of the genetic algorithm comes from the biological evolution process in nature and is an optimization algorithm for solving complex problems. Intelligence and essential parallelism are the biggest differences between evolutionary computing and traditional optimization methods. The position, curvature, and depth of the cut all make the product produce different new shapes. Accumulation: The same or similar monoliths are stacked in size, position, number, and direction to produce a regular stack. The fruit plate, for example, is a shape produced by the accumulation of a basic type. (4) Merging: It is taking two separate individuals and creating a new shape by intersecting, cutting, or superimposing them. This type of shape can usually be seen in mechanical parts. (5) Stretching: As the name suggests, this is taking a base shape and dragging it

outward in a given direction to produce a new shape. This type of molding is seen everywhere in life; for example, refrigerator and cabinet air conditioner molding are applications of this method. (6) Extrusion: On the surface of a monolith, stretching in the direction of centripetal force is called extrusion.

With the vigorous development of computer technology, parametric and quantitative technology has become a hot spot for research in various academic fields and is also gradually applied to product form design. Most of the product form design is an improved design based on the original shape, and its parameters have a clear correspondence with the size of the design object. Therefore, the parametric design brings a more efficient design process to product design, which can use the previously accumulated and established models and modify them on this basis. The principle of parametric design is that the parameters of a line or a figure correspond to the control dimensions of the design object, and when different values of the parameter sequence are given, the design result changes, i.e., a new geometry is obtained under the drive of the parameters. At present, the application of parametric design in morphological design is more extensive, and its scope is gradually extended to the whole life cycle of the product, including two-dimensional organization, three-dimensional entities, accessories intermediate relations, product features expression, and other product-level designs.

Product styling is a process of multiple solution selection, and at the same time, styling is a field full of emotions. If traditional machine learning algorithms are involved in the design process, the nonoptimal individuals are completely discarded while the good individuals are retained. However, in the design domain, nonoptimal individuals can still have some influence and contribution to the final solution product even if they fail to satisfy some specific requirements. Therefore, this requires the introduction of multilayer perceptron neural networks to control the genetic algorithm. The main feature of the multilayer perceptron genetic algorithm neural network is to calculate the adaptation value based on the user's interaction evaluation rather than a function formula. Since users' visual cognition of products is mainly reflected in the form of perceptual information, designers should take the initiative to obtain information about users' perceptual preferences and understand how users decode their cognition of products and their perceptual preferences, to ensure success of design coding. Because of the combination of user evaluations as well as specific function formulas, it excels in problems where it is difficult to build adaptation functions, such as in the areas of product design, image retrieval, and design evaluation. For example, Figure 3 shows the flow chart of the product interactive styling design model.

In the conceptual stage of product design, the principle of combinatorial innovation is often used to generate new shapes. Combinatorial innovation, as it means, is the process of segmenting and analyzing a product based on a certain aspect, so that the modules can be combined to produce a new product shape, based on, but not limited to, function, shape, structure, man-machine, material, etc. The process of

design is always accompanied by many uncertainties, how to translate the subjective design activities into the digital language to analyze and quantify the emotions and demand preferences, need to analyze, process, and integrate all kinds of complex elements with the help of scientific and effective evaluation methods. Hierarchical analysis (AHP) is commonly used to measure the emotional factors of a product, simplifying complex decisions, or apply the principles of perceptual engineering theory to establish and determine the final evaluation index through semantic difference hierarchical evaluation. Product design evaluation is to use specific rules to evaluate the attribute values of each solution in a limited set of solutions and then use the specific rules to obtain a comprehensive evaluation value and finally rank all solutions based on the comprehensive evaluation value and obtain the optimal solution. It generally includes three steps: (1) normalize the evaluation matrix; (2) determine the weight size of each solution; (3) rank all alternatives. Commonly used design evaluation methods include the simple linear weighting method, efficacy coefficient method, hierarchical analysis method, approximate ideal solution ranking method, gray correlation analysis method, etc. The simple linear weighting method is a common multiobjective evaluation method; this method is based on the actual situation; first, determine the evaluation attribute weights, and then standardize the decision matrix, find out the average value of the linear weighting index of each option, and use it as the judgment basis of each feasible option ranking. The efficacy coefficient method converts the dissimilarity measures of each attribute into corresponding dimensionless efficacy coefficients and then performs a comprehensive evaluation. TOPSIS is a ranking method that approximates the ideal solution, which is characterized by full utilization of the original data, low error, and high reliability. The optimal solution is the one closest to the positive ideal solution and farthest from the negative ideal solution, to evaluate the optimal solution. The gray correlation method is a multifactor statistical analysis method, which is based on the sample data of each factor and analyzes the correlation size between each component factor and the whole and reflects the similarity of the solution to be evaluated and the optimal solution in terms of shape. Based on the multilayer perceptron genetic algorithm neural network, these evaluation indexes can be connected in series to evaluate the product shape design in a multifaceted way.

4. Experimental Verification and Conclusions

To verify the feasibility and effectiveness of the proposed method, a series of experiments are conducted to illustrate this paper. The main steps include the following: (1) constructing an evaluation system using perceptual engineering and hierarchical analysis; (2) using hierarchical analysis to obtain subjective weights; (3) using entropy weighting to obtain objective weights; (4) using game theory to obtain comprehensive weights; (5) using SD method to build a perceptual decision matrix; and (6) using KE-GRA-TOPSIS method to rank the alternative products.
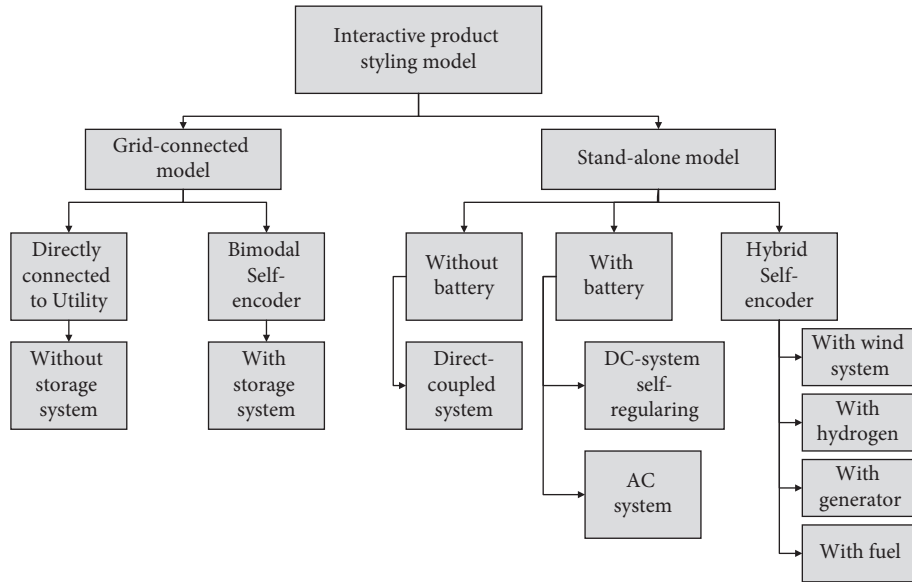
FIGURE 3: Flowchart of an interactive product styling model.

A comprehensive evaluation system for the product was developed using perceptual engineering and hierarchical analysis. The target level has only one element, i.e., the selection of the product solution. Six criteria and 12 indicators were identified based on the TF-EPA method. The product perceptiveness was evaluated in 6 dimensions: gender perspective, acceptance, structural characteristics, duration, weight characteristics, and technical characteristics, respectively. Two indicators were included under each criterion and the indicators consisted of a pair of perceptual words.

The relative closeness trends of the three methods MLP, GA, and GA-MLP-NN regarding the 14 alternatives were obtained based on the experiments, and the comparison graphs shown in Figure 4 were drawn. In the GA method, the relative closeness gap of the alternatives is larger because the GA method only considers the distance of the alternatives in space and magnifies the evaluation results; the gap of the alternatives in the MLP method is smaller because the method focuses on the association between indicators but ignores the distance of the evaluation alternatives in space. Introduce the preference information in the user's multidimensional perceptual preference space directly into the design conception. The information transfer and transformation efficiency in the process is improved. The GA-MLP-NN method is an integration of the GA method and MLP, which considers the relative closeness derived from this method is more realistic as it considers both the degree of association between evaluation options and the gaps between options.

The results of DM selection were also compared with those of the MLP method, GA method, GA-MLP-NN method, and TOPSIS method, and the comparison results are shown in Figure 5. The KE-GRA method was not included in this comparison test because its accuracy was too low. The GA-MLP-NN method had an accuracy of 78.6%, followed by the MLP method with 57.2%. Also, the accuracy
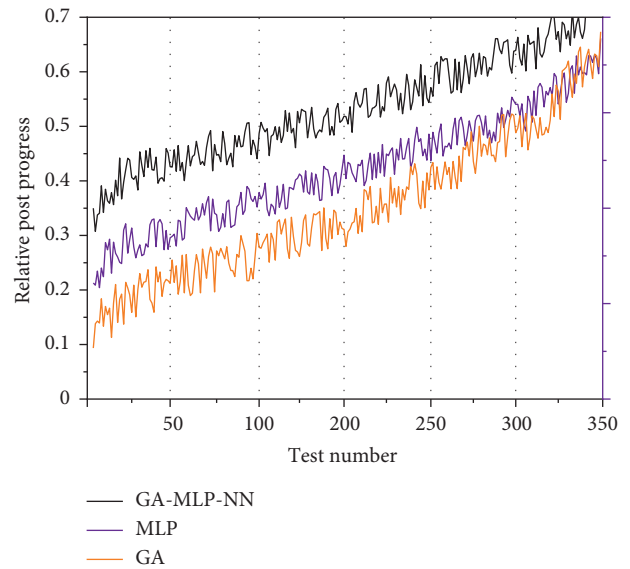

FIGURE 4: Comparison of relative posting progress trends.

of the GA method and TOPSIS method was 7.2% and 0. Observing Figure 5, it can be seen that the results of the GA-MLP-NN method and MLP method were similar, while the GA method and TOPSIS method were similar. In addition, the results of the GA-MLP-NN method and the MLP method are roughly consistent with the choice of DM. This experiment verifies that the TOPSIS method and its extensions cannot be directly used for the perceptual ranking of products.

To verify the validity of the proposed method, 10 additional participants were invited to repeat the experiment. Figure 6 shows the results of preferences and alternatives ranking given by the participants. It is worth noting that the subjective weights in the hierarchical analysis method are adjustable. The comparison results of the subjective choice
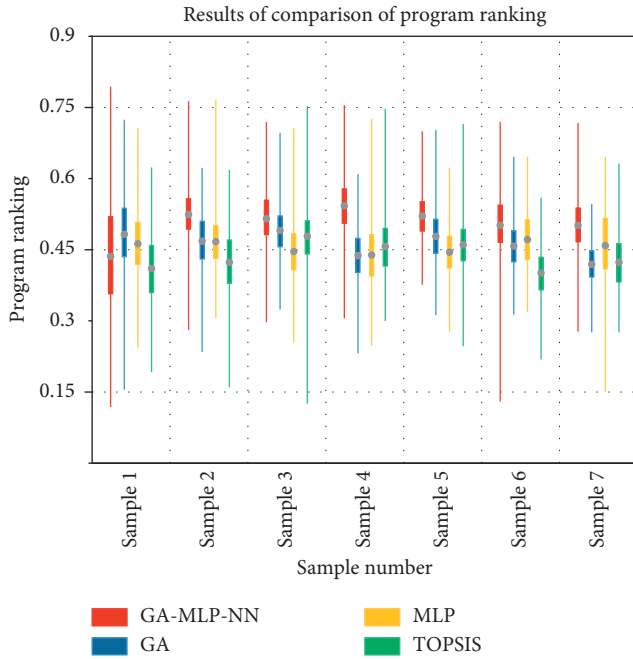
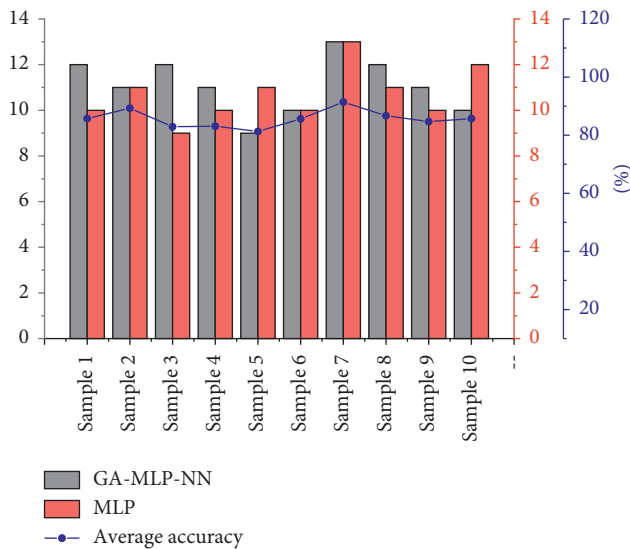FIGURE 5: Results of comparison of program ranking.

FIGURE 6: Results of participant preferences.

results of the 10 participants with the GA-MLP-NN method and the MLP method are shown in Figure 6, which contains the comparison of the number of correct rankings and the comparison of the accuracy rate. In this case, the bar graph represents the number of correct rankings and the line graph represents the accuracy rate. In the GA-MLP-NN method, the accuracy rates of U1 to U10 are 85.7%, 100%, 85.7%, 100%, 100%, 100%, 85.7%, 100%, 100%, and 100%, in that order. The average accuracy was calculated to be 95.7%. In the MLP method, the accuracy rates of U1 to U10 were 85.7%, 85.7%, 85.7%, 85.7%, 85.7%, 85.7%, 85.7%, 71.4%, 85.7%, 100%, and 85.7% in that order. The average accuracy rate was calculated to be 85.7%. In terms of accuracy, both

the GA-MLP-NN method and the MLP method performed well, and the GA-MLP-NN method was more accurate. The above results show the feasibility of the perceptual decision matrix and that the proposed GA-MLP-NN method can accurately rank products according to users' personalized preferences.

In Figure 7, True Positive (TP) indicates the number of positive samples classified as positive; True Negative (TN) indicates the number of negative samples classified as negative; False Positive (FP) indicates the number of negative samples classified as positive, and False Negative (FN) indicates the number of positive samples classified as negative. The commonly used evaluation metrics, including Accuracy, Precision, Recall, False Discovery Rate (FDR), and False Positive Rate (FPR), are listed in Figure 7. 30 product images are arbitrarily selected as a content map and 10 images as style map; 300 new product images were generated. After mixing 100 real images and 300 generated images, the 30 users in Section 3.4.2 were invited to distinguish the truth from the falsehood of 400 images. Since the product images generated by the GA-MLP-NN method are only used to inspire designers or users and are not final design renderings, to weaken the detailed features of the generated images, 30 users (with normal vision) observe the images at a distance of 1 m from the display (resolution of 2560×1440) with a maximum display size of about 8 cm on one side (width or height) of the images and each image. The dwell time does not exceed 2 s. The purpose of this experiment is to evaluate the user's ability to distinguish between real and generated images and to reflect the quality of the generated images. FDR is the proportion of actual negative samples among positive samples, and FPR is the proportion of actual negative samples among positive samples. FDR and FPR are positive indicators. The calculated FDR and FPR are 69% and 67%, respectively, indicating that the generated images are of good quality and can be used to display and inspire designers.

Due to the relationships of relevance, subordination, redundancy, and similarity between adjectives, two perceptual words with similar concepts and opposite meanings are more reflective of user psychology. Therefore, perceptual words are selected in this chapter to describe the user's psychological feelings. The importance of a word is proportional to the number of times it appears in a text, and if a word appears repeatedly in the text under study, it can be used to characterize the dominant tendency of the text. Considering the one-sidedness of the traditional method of selecting sentiment words by considering only word frequency or user preference in sentiment engineering, this chapter proposes a GA-MLP-NN-based method for selecting sentiment word pairs based on the characteristics of word frequency and EPA dimensions. Text sentiment analysis is the use of computer analysis of text with subjective feelings in user comments for polarity classification, which is usually classified as positive (positive), derogatory (negative), or neutral. Sentiment classification methods can be divided into two categories: machine learning-based methods and lexicon-based methods, the latter of which discriminate text sentiment by sentiment lexicons such as
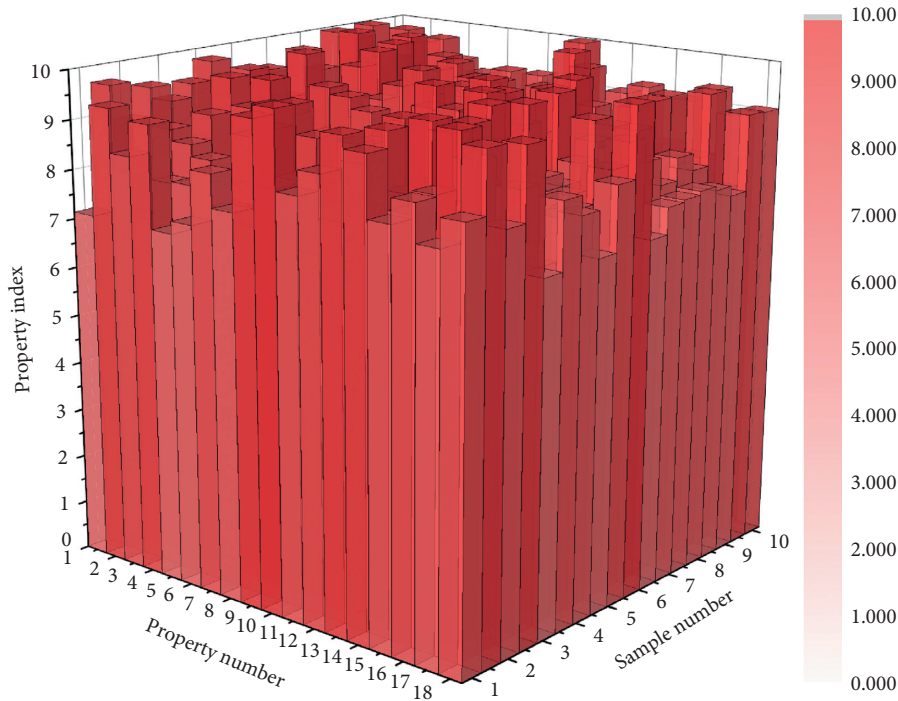
FIGURE 7: Partial sample attribute parameter rank distribution.

WordNet and HowNet, which rely on the quality and continuous improvement of sentiment lexicons. In this chapter, the sentiment dictionary-based approach is used to determine the sentiment tendency of sentiment words in online reviews. The HowNet dictionary and synonym word forests are searched to obtain the results of sentiment tendency judgment of sentiment words. The score of sentiment unit EO is the product of sentiment polarity EP and sentiment intensity EI, and the sentiment evaluation of the whole text is characterized by aggregating the sentiment units in the text. The sum of the sentiment tendency scores of independent positive and negative sentiment words in a sentiment pair is used as the evaluation value of a set of sentiment word pairs. Commonly used design evaluation methods include the simple linear weighting method, efficacy coefficient method, hierarchical analysis method, approximate ideal solution ranking method, gray correlation analysis method, etc. The perceptual evaluation values of the six sets of perceptual words are obtained by traversing the product reviews according to the perceptual evaluation value calculation process, where positive values indicate that the sample ratings are biased towards positive perceptual words, negative values indicate that the sample ratings are biased towards negative perceptual words, and the absolute values of the ratings indicate the degree of deviation. In the perceptual evaluation of the sample in Figure 8, the perceptual word "good-poor" is rated as 0.949, indicating the overall product evaluation preference; "beautiful-ugly" is rated as 2.133, indicating the product. The "smooth—sluggish" rating of −1.005 indicates that the system is sluggish to use. The perceptual rating for sample 2 was medium, with a "large-small" rating of 1.957, indicating a large product size. The perceptual rating for sample 3 was medium, with a "large-
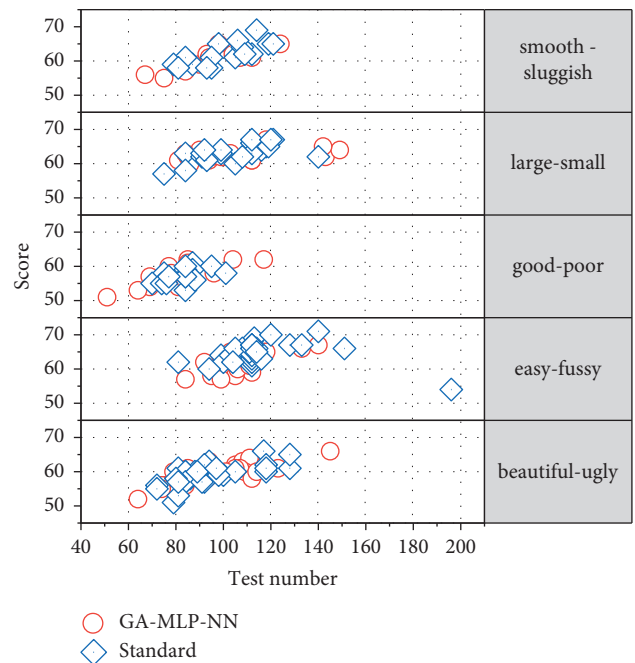
FIGURE 8: Partial sample perceptual evaluation.

small" rating of 2.127, indicating a large product size. Sample 4 had a medium perceptual rating of 4.0 on the "large-small" scale, indicating a large size, and a −1.121 on the "easy-fussy" scale, indicating that the product was fussy to use. The "Smooth-Sluggish" rating of 3.0 indicates that the system is smooth to use. The perceptual rating for sample 5 was medium, with a rating of 2.5 for "beautiful-ugly" indicating a beautiful product, and 2.589 for "large-small" indicating a

large product size. The "Flow-Sluggish" rating is 0.953, which indicates smooth system usage. The model predicted by GA-MLP-NN and the actual value model almost agree, indicating that the GA-MLP-NN model has high accuracy.

With the widespread application of the Internet of Things, Internet, and automation technologies, products are developing in the direction of intelligence and information technology, and the whole product life cycle process is becoming more and more open and transparent. The product life cycle is the whole process from product development to end-of-life, including product design, production and processing, transportation and supply, and sales and use. The data generated from the whole product lifecycle includes data in the database of enterprise information management system such as enterprise resource planning, CRM, manufacturing enterprise production process execution system, product data management, and supply chain management, as well as data generated by users in the Internet and e-commerce system such as browsing, clicking, purchasing, and reviewing, etc. These data have the typical characteristics of big data, i.e., many data types, large data volume, low-value density, and high commercial value. These data have the typical characteristics of big data, namely, many data types, large data volume, low-value density, and high commercial value. Among them, the data types include text data, image data, voice data, video data, and log data. These product-related data grow exponentially every day to form the product life cycle big data. The multilayer perceptual genetic algorithm neural network based on this paper can make full use of the characteristics of big data with low-value density and high commercial value to extract valuable information from large-scale data and the value of the most core part. The value of big data depends on the role that the data analysis results play in the application. The field of product design has received slightly less attention than other applications of big data, but there is no shortage of roles it can play. For example, by collecting product reviews in e-commerce systems, it is possible not only to detect changes in user needs but also to improve product defects based on user feedback, thereby increasing user satisfaction. Image big data can intuitively inspire designers and facilitate product styling.

5. Conclusion

This paper further develops an intelligent and systematic approach to product innovation design by exploring how to obtain information related to product design from the big data generated from the product life cycle and analyzing it in depth using techniques such as genetic algorithm neural network model based on multilayer perceptron, and the main research work is as follows. This paper analyzes the advantages and disadvantages of each multilayer perceptron neural network as well as genetic algorithm, and by combining genetic algorithm with multilayer perceptron neural network model, a set of multilayer perceptron genetic algorithm neural network models is formed, and product design domain knowledge is incorporated into it, and the method can automatically identify, extract, and reconstruct

the content and color features of images and migrate them to the product shape in the content map. Real-time generation of new product images is achieved. Among them, the training of the multilayer perceptron neural network migration model is an unsupervised training based on image data, and the trained model is used to automatically migrate the stylistic features of stylistic images; the genetic algorithm model is a supervised training, and the trained model is used to predict the product semantics in the content graph and guide the selection of the stylistic graph. The method alleviates the problems of poor image quality, uncontrollable content, and lack of theoretical guidance in the product design domain of the generated solution. The subjective imagery of users is ambiguous, and there is a "black box" problem between their subjective evaluation value and the elements of product form and shape. It is also not easy to improve the competitive advantage of the product. This paper also integrates product design domain knowledge into textual big data techniques to propose a data-driven perceptual engineering approach for online reviews. In terms of perceptual word collection, online reviews are used as a source of perceptual words; in terms of perceptual word acquisition, a GA-MLP-NN perceptual word extraction method combining three dimensions of word frequency and EPA is proposed; in terms of perceptual evaluation, a perceptual evaluation value calculation method combining degree adverbs with word clustering for online reviews is proposed, and the basic idea is to obtain users' emotional tendency towards the product by mining the emotional tendency of perceptual words. In terms of mapping model construction, a multilayer perceptron genetic algorithm neural network is used to construct a relationship model between users' difficult-to-quantify perceptual needs and product design elements, while the models constructed by multiple linear regression methods are compared to verify the effectiveness and feasibility of the proposed method.

Data Availability

The data used to support the findings of this study are available from the corresponding author upon request.

Conflicts of Interest

The authors declare that there are no conflicts of interest.

Acknowledgments

References

[1] M. Meenu Sreedharan, A. M. Khedr, and M. El Bannany, "A multi-layer perceptron approach to financial distress prediction with genetic algorithm," *Automatic Control and Computer Sciences*, vol. 54, no. 6, pp. 475–482, 2020.

[2] K. Bhattacharjee and M. Pant, "Hybrid particle swarm optimization-genetic algorithm trained multi-layer perceptron for classification of human glioma from molecular brain

neoplasia data," *Cognitive Systems Research*, vol. 58, pp. 173–194, 2019.

[3] J. A. Ramirez-Bautista, J. A. Huerta-Ruelas, L. T. Kóczy, M. F. Hatwágner, S. L. Chaparro-Cárdenas, and A. Hernández-Zavala, "Classification of plantar foot alterations by fuzzy cognitive maps against multi-layer perceptron neural network," *Biocybernetics and Biomedical Engineering*, vol. 40, no. 1, pp. 404–414, 2020.

[4] O. Osman, S. Sallem, L. Sommervogel, M. O. Carrion, P. Bonnet, and F. Paladian, "Distributed reflectometry for soft fault identification in wired networks using neural network and genetic algorithm," *IEEE Sensors Journal*, vol. 20, no. 9, pp. 4850–4858, 2020.

[5] A. C. Cinar, "Training feed-forward multi-layer perceptron artificial neural networks with a tree-seed algorithm," *Arabian Journal for Science and Engineering*, vol. 45, no. 12, pp. 10915–10938, 2020.

[6] M. Bahiraei, S. Nazari, H. Moayedi, and H. Safarzadeh, "Using neural network optimized by imperialist competition method and genetic algorithm to predict water productivity of a nanofluid-based solar still equipped with thermoelectric modules," *Powder Technology*, vol. 366, pp. 571–586, 2020.

[7] B. T. Pham, M. D. Nguyen, K.-T. T. Bui, I. Prakash, K. Chapi, and D. T. Bui, "A novel artificial intelligence approach based on multi-layer perceptron neural network and biogeography-based optimization for predicting coefficient of consolidation of soil," *Catena*, vol. 173, pp. 302–311, 2019.

[8] D. Akbari, "Improved neural network classification of hyperspectral imagery using weighted genetic algorithm and hierarchical segmentation," *IET Image Processing*, vol. 13, no. 12, pp. 2169–2175, 2019.

[9] A. Sharifi and K. Alizadeh, "A novel technique based on principal component analysis and multi-layer perceptron with genetic algorithm optimization for diagnosis of lung cancer," *Razi Journal of Medical Sciences*, vol. 26, no. 10, pp. 48–56, 2019.

[10] F. Golkhoo and O. Moselhi, "Optimized material management in construction using multi-layer perceptron," *Canadian Journal of Civil Engineering*, vol. 46, no. 10, pp. 909–923, 2019.

[11] M. Kaveh, M. Khishe, and M. R. Mosavi, "Design and implementation of a neighborhood search biogeography-based optimization trainer for classifying sonar dataset using multi-layer perceptron neural network," *Analog Integrated Circuits and Signal Processing*, vol. 100, no. 2, pp. 405–428, 2019.

[12] Y. Zhou, Y. Niu, Y. Niu, Q. Luo, and M. Jiang, "Teaching learning-based whale optimization algorithm for multi-layer perceptron neural network training," *Mathematical Biosciences and Engineering*, vol. 17, no. 5, pp. 5987–6025, 2020.

[13] L. Mallory and A. Sevkli, "Optimizing neural network architecture through a coarse genetic algorithm," *Journal of Computing Sciences in Colleges*, vol. 36, no. 4, pp. 71–82, 2020.

[14] R. Zhao, Y. Wang, P. Hu et al., "Selfish herds optimization algorithm with orthogonal design and information update for training multi-layer perceptron neural network," *Applied Intelligence*, vol. 49, no. 6, pp. 2339–2381, 2019.

[15] B. Turkoglu and E. Kaya, "Training multi-layer perceptron with artificial algae algorithm," *Engineering Science and Technology, An International Journal*, vol. 23, no. 6, pp. 1342–1350, 2020.

[16] C. Yuan and H. Moayedi, "The performance of six neural-evolutionary classification techniques combined with multi-layer perception in two-layered cohesive slope stability analysis and failure recognition," *Engineering with Computers*, vol. 36, no. 4, pp. 1705–1714, 2020.

[17] A. K. Dwivedi, "Radial basis function neural network with genetic algorithm for discrimination of recombination hotspots in saccharomyces cerevisiae," *International Journal of Medical Engineering and Informatics*, vol. 12, no. 2, pp. 108–118, 2020.

[18] M. Azhdari, A. Mahmoodzadeh, and M. Khishe, "Digital image watermarking using the combination of genetic algorithm and spread spectrum method in the field of discrete cosine transform," *Iranian Journal of Marine Science and Technology*, vol. 25, no. 1, pp. 14–33, 2021.

[19] J. Yang, V. V. Govindaraj, M. Yang, and S. H. Wang, "Hearing loss detection by discrete wavelet transform and multi-layer perceptron trained by nature-inspired algorithms," *Multimedia Tools and Applications*, vol. 79, no. 21, pp. 15717–15745, 2020.

[20] A. A. M. Lima, F. K. H. de Barros, V. H. Yoshizumi, D. H. Spatti, and M. E. Dajer, "Optimized artificial neural network for biosignals classification using genetic algorithm," *Journal of Control, Automation and Electrical Systems*, vol. 30, no. 3, pp. 371–379, 2019.

[21] Y. Yao, X. Yang, S. H. Lai, and R. J. Chin, "Predicting tsunami-like solitary wave run-up over fringing reefs using the multi-layer perceptron neural network," *Natural Hazards*, vol. 107, no. 1, pp. 601–616, 2021.

[22] S. J. Mousavirad, A. A. Bidgoli, H. E. Komleh, and G. Schaefer, "A memetic imperialist competitive algorithm with chaotic maps for multi-layer neural network training," *International Journal of Bio-Inspired Computation*, vol. 14, no. 4, pp. 227–236, 2019.

Research Article

Modeling Adoption Behavior of Prefabricated Building with Multiagent Interaction: System Dynamics Analysis Based on Data of Jiangsu Province

Zhen Li, Shaowen Zhang, and Qingfeng Meng (iD)

School of Management, Jiangsu University, Zhenjiang 212013, China

Correspondence should be addressed to Qingfeng Meng; mqf@ujs.edu.cn

In recent years, the development of prefabricated building (PB) mode in China has gradually attracted the attention of stakeholders. It is of great significance to explore the adoption behavior of PB mode by Chinese construction enterprises. Using the method of combining evolutionary game theory with system dynamics and considering the multiagent interaction of the government, construction enterprises, and consumers, as well as the influence of multiple factors, this paper constructs a model of construction enterprises' adoption behavior of PB mode. The purpose is to clarify the mechanism of Chinese construction enterprises' adoption behavior of PB mode and the evolution law of market share. The research results show the following. Firstly, government subsidy plays an important role in promoting the maturity of PB market, but it plays a relatively small role in the more mature and stable market. Secondly, the higher the initial acceptance probability of the construction enterprise, the greater the peak of the PB market share and the greater the volatility, but it has no differential impact on the balance of the PB market in the later stage. Thirdly, price factors and quality factors, respectively, have an important impact on the increase of the PB market share in the early and late stages of the formation of the PB market, but the delivery waiting time factor has no significant impact on the PB market share.

1. Introduction

The construction industry occupies a pivotal position in the national economy of all countries in the world, but it is also one of the industries with a high degree of energy intensiveness [1, 2]. It has always had problems such as high carbon emission and serious energy consumption. For example, the annual carbon dioxide generated by global construction accounts for more than 40% of the world's total carbon dioxide emission, and the annual energy consumed accounts for more than 30% of the world's total energy consumption [3–5].

The traditional construction mode has the problems of high pollution and high energy consumption during the construction period, which is not in line with the modern development concepts such as energy conservation and emission reduction and green and sustainable development [6]. In order to promote the green and sustainable development of the construction industry, the prefabricated building (PB) mode has been gradually introduced into China. PB mode not only has the advantages of improving production efficiency, reducing construction cost, and increasing construction safety but also has the functions of reducing carbon emission, reducing energy consumption, and reducing construction waste [7, 8]. Therefore, the Chinese government pays more and more attention to the transformation from traditional construction mode to PB mode and tries to promote the development of PB by means of encouraging technological innovation and policy incentives such as subsidies [5]. The Chinese government stipulates that by 2020, 15% of new buildings nationwide (according to the floor area) will be constructed using the PB mode each year, and this proportion will increase to 30% by 2025 [9]. However, the current application and promotion of the PB mode is not ideal.

In fact, the application and promotion of PB mode in China faces many obstacles. For example, in terms of the government, there is a lack of detailed government policy formulation and effective incentives [10]. In terms of the industry, there is a lack of specific construction specifications and construction standards for prefabricated buildings [11]. In terms of market demand, there are obstacles such as insufficient consumer awareness of PB and insufficient market demand [12, 13]. Therefore, considering the significance of promoting PB mode in China and many obstacles it faces in the development process, it is necessary to model and analyze the adoption behavior of the PB mode by construction enterprises in the context of multiagent interaction.

Modeling and analyzing the behavior of construction enterprises adopting PB mode and then understanding the mechanism of the adoption of PB mode play an inestimable role in the development of the whole industry. Some scholars have conducted relevant research on the factors affecting the adoption and promotion of the PB mode. For example, Li et al. [14] believe that the prefabricated component subsidies implemented by the government have a positive impact on the use of prefabricated components and the improvement of construction performance. Multiple policy measures are mutually complementary, and the combined effect of these policy measures is greater than the sum of the effects of individual policy measures. Wei et al. [15] believe that the promotion of government policies and the leadership of construction enterprises are the main driving factors to promote the development of PB. Research by Gan et al. [7] showed that strengthening policies and regulations has a strong stimulating effect on the promotion of PB and has a significant effect on solving organizational and environmental problems in the promotion process, but the effect on solving technical problems is not ideal. However, Xiahou et al. [16] found that in order to promote PB mode, China needs not only the promotion of the government and the pull of the market environment but also the self-driving of the PB industry. It is pointed out that the main way to promote the development of China's PB is to transform and upgrade the traditional construction industry and solve the development difficulties.

Some scholars believe that the government plays an important role in the process of whether the PB mode is adopted by the construction enterprise [5]. Government policy incentives have a positive effect on the promotion of PB mode, and reasonable policy incentives can help reduce opportunistic behavior [17, 18]. However, policy documents tend to favor the environment and supply and lack policy measures for other areas [7]. Currently, government subsidies are the main way to promote the development of PB mode, but in the long run, continuous government subsidies are not a long-term solution to maintain the steady development of the industry. At the same time, the government's publicity and guidance work is also gradually starting. For example, Xi'an, China, has begun to encourage consumers to purchase prefabricated commercial residential buildings and promote the development of prefabricated buildings from the consumer level.

Secondly, the construction enterprise is also one of the most influential stakeholders in the PB industry [19]. As the investor of a construction project, the construction enterprise's behavioral willingness and adoption behavior are highly correlated [20]. Therefore, whether the construction enterprise adopts the behavior and decision making of PB mode is very important for the development of the PB industry. The construction enterprise will make reasonable decisions on its own construction mode based on the economic benefits, environmental performance, maintenance cost, and other factors of the construction project [21, 22]. However, the high initial cost of adopting PB mode is one of the main factors that hinder the construction enterprise from adopting PB mode [7, 23]. The poor overall efficiency of PB industry also leads to the lack of motivation for some construction enterprises to adopt PB mode [13].

In addition, whether the PB mode is adopted is closely related to market demand [24]. The purchase motivation of consumers will have an important impact on the development of the PB market. Due to the lack of Chinese consumers' understanding of PB [12], Lee and Kim [25] believe that it is necessary to increase the correct publicity and guidance to change consumers' attitudes towards PB. Some scholars have studied consumers' attention to PB and the evolution trend of their attention content. For example, Wang et al. [26] pointed out that although consumers' attention to PB fluctuates greatly, it shows an overall upward trend, and the introduction of relevant government policies will significantly affect consumers' attention. Hu et al. [27] found that the content of PB that consumers are most concerned about mainly involves high-quality building performance.

In summary, the behavior and decision making of the construction enterprise adopting the PB mode are affected by multiple stakeholders. Existing research studies have identified the stakeholders who influence the adoption of the PB mode and analyzed the influencing factors and their effects. However, it rarely involves the influence of consumer group decision making on the adoption of the PB mode. In addition, less consideration is given to the complex interaction between a large number of factors and their nonlinear effects on the adoption behavior of PB mode.

In fact, first of all, consumers' cognition of PB and purchasing decisions are of great significance to the adoption of the PB mode. Consumers' purchase decision making is a more complex process, which considers many factors, such as price, quality, delivery waiting time, and so on. Previous studies generally regarded consumer demand as an exogenous variable to analyze its linear relationship with the adoption behavior of PB mode. This paper constructs a more realistic consumer decision-making model, which plays a vital role in revealing deeply the adoption behavior of PB and the evolution of market competition in the context of multiagent interaction. Secondly, the adoption behavior of PB mode by construction enterprises is also affected by many subjects and factors. They will comprehensively consider government policies, the status quo of the industry, market demand, and competitive pressure and adopt a suitable construction mode in the

pursuit of maximizing their own economic benefits. Therefore, there are relatively complex dynamic interactions between construction enterprises and between construction enterprises, government, and consumers. In the process of studying the adoption behavior and mechanism of PB mode, this dynamic and complex interaction and game relationship cannot be ignored [9].

To sum up, on the basis of considering more realistic consumer purchase decisions and more complex interaction among multiple subjects, this paper will focus on the analysis of the adoption behavior and mechanism of the construction enterprise to PB mode under the scenarios of government subsidies to the construction enterprise, government publicity and guidance to the market, PB products with different prices, qualities, and delivery waiting times, and different adoption intentions of the construction enterprise. This paper attempts to provide a theoretical basis for improving the market competitiveness of PB products and formulating reasonable policies and measures for the government. This is of great significance for the Chinese construction industry to achieve energy saving and emission reduction targets and to practice the concept of green and sustainable development.

This research considers the complex interactions among stakeholders (government, construction enterprises, and consumers) that influence the adoption of PB mode and the bounded rational behavior of decision-making. This research also considers many obstacles in the process of adopting PB mode, as well as the complex interaction and nonlinear feedback relationship between these factors. This research will use the method of system dynamics to model and analyze related problems. System dynamics are more suitable for analyzing complex systems. This method can be used to understand the behavior of the system over time and the relationship between the system structure and decision rules [28]. Also, in the process of Chinese construction enterprises adopting PB mode, the bounded rational game between them and industry competitors is continuous. Therefore, the behavior of both parties must be discussed from a dynamic perspective [9]. Evolutionary game theory has been widely used in the study of bounded rational behavior, such as the study of stakeholders in the construction industry [29]. Therefore, this paper will use the research method of combining evolutionary game and system dynamics to model and analyze the behavior and mechanism of PB mode adopted by construction enterprises in China. It hopes to provide a theoretical basis for the rapid and sustainable development of PB mode in China.

This paper attempts to solve the following three problems:

(1) What impact will government subsidies and government propaganda and guidance have on the adoption behavior of PB mode by construction enterprises?

(2) What impact will the initial willingness of Chinese construction enterprises to adopt PB mode have on the diffusion and evolution of the follow-up market of PB mode?

(3) What kind of evolutionary trend will the market proliferation of PB products under different prices, qualities, and delivery waiting times be?

2. Model

This paper combines evolutionary game theory with system dynamics to model and analyze the relationship and behavior of the three subjects involved in the adoption of PB mode: government, construction enterprises, and consumers.

2.1. Evolutionary Game Model. The construction enterprise will make decisions on the specific construction mode of the project. One is the adoption of traditional cast in situ buildings (TB) (hereinafter referred to as "D_N"). The second is the adoption of PB (hereinafter referred to as "D_Y"), including the selection of qualified and capable design institutions for modular design of drawings, the production of prefabricated components by prefabricated component manufacturers, and the assembly construction by construction organizations.

Whether the construction enterprise adopts PB mode will be mainly affected by government subsidies, competition from the same industry, consumer demand, and other factors. The interaction relationship and decision-making mechanism between agents are shown in Figure 1.

In order to clarify the competition mechanism among construction enterprises and then construct a system dynamics model with multiagent and multifactor comprehensive influence, this paper first uses the evolutionary game method to construct the behavior rules for construction enterprises to adopt PB mode. The construction enterprises are divided into two groups: initial adoption (Type Y construction enterprises) and initial nonadoption (Type N construction enterprises) of PB mode.

In the given situation, the two groups will take different strategies to play the game. This paper makes the following assumptions for model construction:

Hypothesis 1: assume that the overall number of construction enterprises remains unchanged. The construction enterprise will select a strategy that suits itself based on certain rules in each time unit.

Hypothesis 2: "D_Y" will increase the construction cost of the project. Use x_Y to represent the probability of the "D_Y" strategy and x_N to represent the probability of the "D_N" strategy, where $x_N = 1 - x_Y$, and x_Y and x_N are all functions of time t.

Hypothesis 3: the construction enterprise will choose its strategy according to its own profit level. The construction enterprise will compare its payoff with that of its competitors, so as to choose a strategy to make its expected payoff higher. Type Y construction enterprises and Type N construction enterprises will calculate their respective payoff differences. Taking Type Y construction enterprises as an example, if their payoff difference is greater than or equal to 0, Type Y
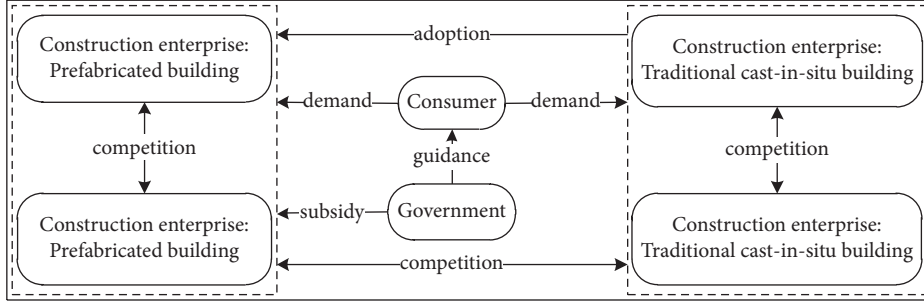
FIGURE 1: System analysis of construction mode selection of construction enterprise.

construction enterprises will maintain their existing strategy. When the payoff difference is less than 0, it will change its strategy with a certain probability [30]. The probability $\Phi(U_Y^D - U_N^D)$ of changing the strategy is shown in the following formula:

$$\Phi\left(U_Y^D - U_N^D\right) = \begin{cases} \dfrac{\left(U_Y^D - U_N^D\right)}{U_Y^D}, & U_Y^D < U_N^D, \\[3mm] 0, & U_Y^D \geq U_N^D. \end{cases} \tag{1}$$

Hypothesis 4: the expected average payoff of the construction enterprise that chooses the "D_Y" strategy is U_Y^{DA}, and the expected average payoff of the construction enterprise that chooses the "D_N" strategy is U_N^{DA}. Due to the different qualifications and capabilities of each construction enterprise, their real payoff will also be differentiated. Assume that the payoff of Type Y construction enterprise is $U_Y^D = \lambda_Y * U_Y^{DA}$, and the payoff of Type N construction enterprise is $U_N^D = \lambda_N * U_N^{DA}$. λ_Y, λ_N are the influence coefficients of expected average payoff.

Hypothesis 5: hypothesis p is the probability of the construction enterprise adopting PB mode. Using $\overline{x}$ to represent the derivative, the replication dynamic equation of the basic dynamic change rate at which the construction enterprise may choose to "D_Y" the strategy can be expressed as

$$\overline{x}_Y = x_Y * x_N \left[\Phi\left(U_Y^D - U_N^D\right) - \Phi\left(U_N^D - U_Y^D\right) \right] p. \tag{2}$$

2.2. System Dynamics Model Based on Evolutionary Game

2.2.1. Main Modules and Equations.
The system dynamics model based on evolutionary game is constructed by Vensim PLE. The model consists of three main modules: the construction enterprise decision-making module, the construction enterprise payoff module, and the consumer decision-making module. As shown in Figure 2, the construction enterprise decision-making module and the construction enterprise payoff module have an interactive relationship with each other, and the consumer decision-making module has an impact on the construction enterprise payoff module. Among them, the construction
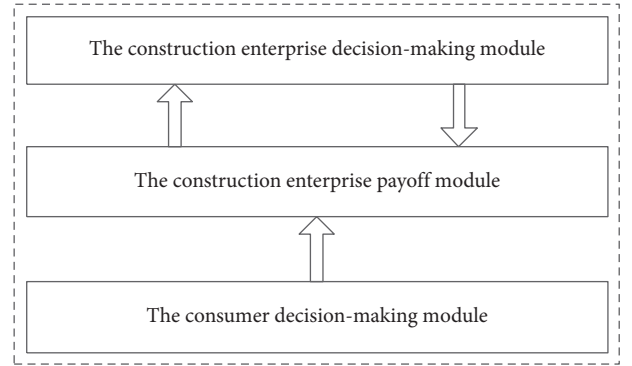

FIGURE 2: Interaction between modules.

enterprise decision-making module is constructed according to the assumption rules and logical relations of the evolutionary game part.

(1) The Construction Enterprise Decision-Making Module. In this module, each construction enterprise has different qualifications and abilities and will change its own decisions according to the development of the industry, so the time of their "D_Y" may be inconsistent. Each construction enterprise will go through a certain period of observation and then choose a strategy that suits itself. According to the plan of the Chinese government, the construction target of PB in the next stage is 2025. Therefore, the longest observation and consideration time of the construction enterprise is 5 years, and the average observation and consideration time is 1.5 years. Based on the above data, the dynamic change rate after D_Y (R_T) is set.

This model will use the relevant data of PB development planning in Jiangsu Province, China. According to statistics from the National Bureau of Statistics of China, the number of real estate construction enterprises in Jiangsu Province in 2018 was 6,723, of which 39 were state-owned real estate construction enterprises [31]. Since PB mode has been implemented in China for a short time, the priority to adopt PB mode is mainly state-owned real estate construction enterprises. Therefore, suppose that the number of construction enterprises that initially adopted PB mode is 39. This module includes two level variables, namely, the construction enterprise adopting PB mode (D_Y) and the construction enterprise not adopting PB mode (D_N). One

rate variable is the adoption rate of PB mode (D_R) obtained according to the replication dynamic equation R_B of evolutionary game. The model is shown in Figure 3, and the meaning of the symbols is shown in Table 1.

The main equations of this module are as follows:

$$D_R = D_T * R_T,$$
$$R_T = \text{Delay Fixed}\,(R_B, \text{Random Normal}\,(0, 5, 1.5, 0.1, 0), R_B),$$
$$R_B = \overline{x_Y}$$
$$D_Y = 0.039 + \int D_R,$$
$$D_N = 6.684 - \int D_R,$$
$$p = \text{Random Normal}\,(0, 1, 0.4, 0.3, 0).$$

$$(3)$$

(2) The Construction Enterprise Payoff Module. The construction enterprise payoff module mainly involves the payoff of the construction enterprise that selects the "D_Y" strategy (U_Y^D) and the "D_N" strategy (U_N^D). The payoff of the construction enterprise mainly includes construction payoff and government subsidies. Construction payoffs are realized through consumers' choice to purchase, and government subsidies are realized through government subsidies for construction projects that adopt PB mode. According to the current market conditions, government subsidies to construction enterprises are affected by factors such as subsidy factors, prefabrication ratio, and construction area of unit buildings. The model types of the payoff module of the construction enterprise that selects the "D_Y" strategy (U_Y^D) and the "D_N" strategy (U_N^D) are similar. Therefore, this module takes the module that the construction enterprise selects the "D_Y" strategy (U_Y^D) as an example. The model is shown in Figure 4, and the meaning of the symbols is shown in Table 1.

The main equations of this module are as follows:

$$U_Y^{DA} = \frac{\left[(P_1 - C_1) * A_R * C_1^C\right]}{D_Y} + S,$$

$$S = \begin{cases} A_C * s * f * 100, & Z \geq 0.5, \quad A_C * s * f * 100 \leq 1800, \\ 1800, & Z \geq 0.5, \quad A_C * s * f * 100 > 1800, \end{cases}$$

$$f = \begin{cases} (D_Y - \text{Delay1}\,(D_Y, \text{Time Step})), & (D_Y - \text{Delay1}\,(D_Y, \text{Time Step})) \geq 0, \\ 0, & (D_Y - \text{Delay1}\,(D_Y, \text{Time Step})) < 0. \end{cases}$$

$$U_Y^D = U_Y^{DA} * \lambda_Y,$$

$$\lambda_Y = \text{Random Normal}\,(0.9, 1.3, 1, 0.2, 0).$$

$$(4)$$

(3) The Consumer Decision-Making Module. The consumer decision-making module mainly characterizes the consumer's purchase decision for TB or PB, and its purchase decision mainly considers the price, construction quality, and delivery waiting time of construction products. Assuming that there are N types of developed construction products on the market, consumers will give priority to the construction products that can generate the greatest purchase motivation [32]. The consumer's purchase motivation function can be expressed by the following formula:

$$M_i = P_i * PS_i + Q_i * QS_i + W_i * WS_i + l_i. \quad (5)$$

The price sensitivity distribution model shows that the lower the price of a product is, the less price sensitivity the product produces, that is, the smaller the obstacle to consumers' purchasing motivation [33]. The consumer's price sensitivity is an exponential function of the difference between the actual product price P_i and the expected price P_e. Due to the different socioeconomic attributes k of different consumers, their expected price P_e is different. Therefore, the formula is as follows:

$$PS_i = -\alpha^{P_i - (P_e + k)},$$
$$k = \text{Random Uniform}\,(-0.2, 0.1, 0). \quad (6)$$

The quality sensitivity distribution model is used to measure the extent to which the quality of TB products and PB products affect consumers' motivation to purchase the products [34]. According to Taguchi quality theory and related research [35], consumers' perception of construction product quality mainly involves two aspects, including construction management level and information technology
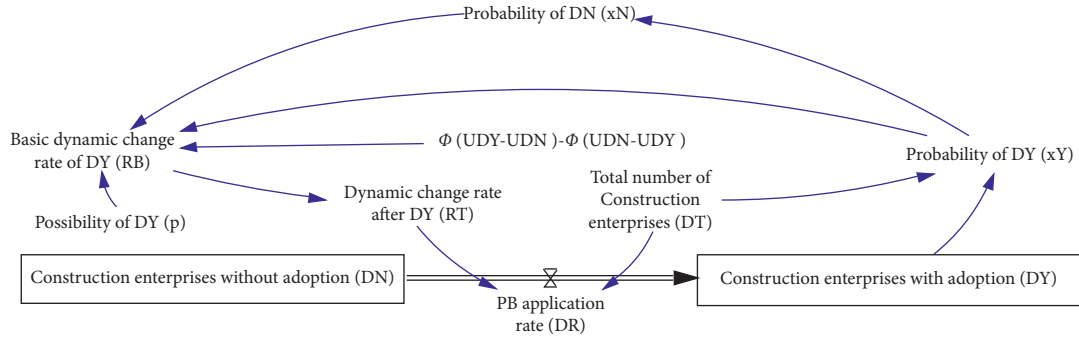
FIGURE 3: System diagram of the decision-making module of the construction enterprise.

TABLE 1: The symbolic meaning of the main equations.

Symbol	Implication
D_R	PB application rate
D_T	Total number of construction enterprises
R_T	Dynamic change rate after D_Y
R_B	Basic dynamic change rate of D_Y
p	Initial probability of D_Y
U_Y^{DA}	Average expected payoff of D_Y
C_i	Cost for per square meter of $i (i = 1$ is PB; $i = 2$ is TB)
P_i	Price for per square meter of i
S	Subsidies for D_Y
A_R	Average building area of per suite
A_C	Building area of unit building
C_i^C	Consumers of choosing i
Z	Prefabrication ratio
U_Y^D	Expected payoff of D_Y
s	Subsidy per square meter of D_Y
f	The amount of change of per unit time of D_Y
M_i	Consumers' motivation to purchase i
PS_i	Consumers' price sensitivity parameters for i
Q_i	Quality of i
QS_i	Consumers' quality sensitivity parameters for i
W_i	Delivery waiting time for i
WS_i	Consumers' delivery waiting time sensitivity parameters for i
l_i	The degree of external influence of consumers purchasing i
P_e	Consumer expected price for per square meter of building
k	Consumers' socio-economic attributes of price factors
μ_i	The quality to cost ratio of i
m_i	Management level in i construction
t_i	Information technology level in i construction
Q_e	Consumer expected quality for building
a, b, d	Constant
W_e	Expected delivery wait time for consumers
w	Consumers' socio-economic attributes of delivery waiting time factors
C_i^{CC}	Probability of consumers choosing i

level. Therefore, comprehensive consumers' perception of different quality factors will get consumers' overall quality evaluation of construction products. The overall quality evaluation formulas of different building modes are expressed as follows:

$$\mu_i = aQ_i^2 + bQ_i + d,$$
$$Q_i = m_i t_i, \qquad (7)$$
$$QS_i = \beta^{|Q_i - Q_e|}.$$

The delivery waiting time sensitivity distribution model is used to measure the extent to which the delivery time of different building modes affects consumers' motivation to purchase the product. WS_i is an exponential function of the difference between the actual delivery waiting time W_i and the expected delivery waiting time W_e of the building. Due to the different socioeconomic attributes w of different consumers, the expected delivery waiting time W_e is different. Therefore, the formula is as follows:
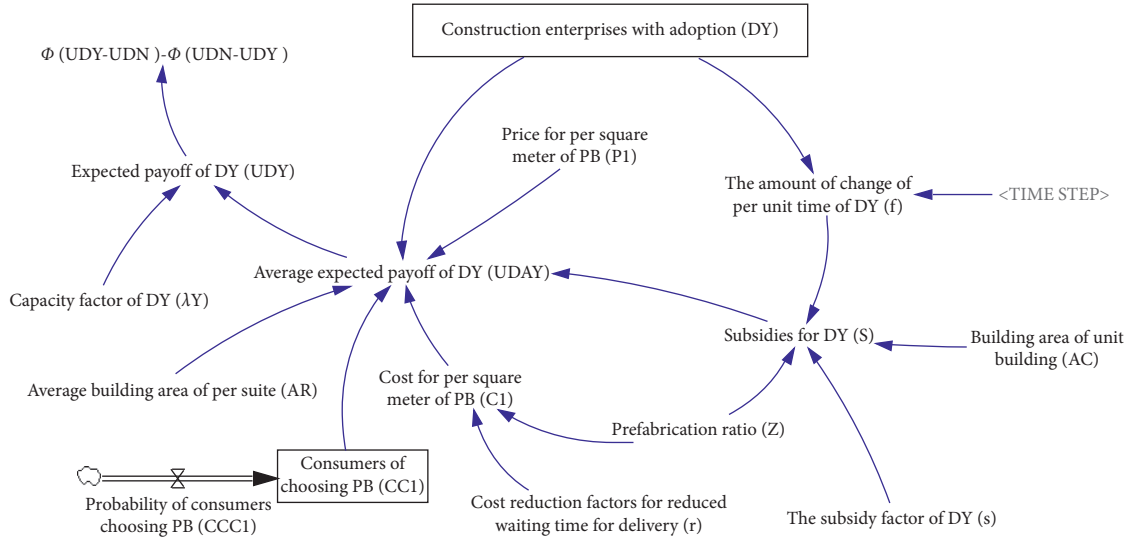
FIGURE 4: System diagram of the payoff module of the construction enterprise.

$$WS_i = \eta^{W_i - (W_e + w)}, \tag{8}$$
$$w = \text{Random Uniform}\,(-0.5, 0.5, 0).$$

The conditions for consumers to choose PB based on purchasing motivation are

$$C_1^{CC} = \begin{cases} 1, & M_1 \geq M_2, \\ 0, & M_1 < M_2. \end{cases} \tag{9}$$

Under this condition, the number of consumers purchasing PB is

$$C_1^C = 50 + \int C_1^{CC}. \tag{10}$$

The conditions for consumers to choose TB are

$$C_2^{CC} = \begin{cases} 1, & M_1 \geq M_2, \\ 0, & M_1 < M_2. \end{cases} \tag{11}$$

The number of consumers purchasing TB is

$$C_2^C = 100 + \int C_2^{CC}. \tag{12}$$

The model is shown in Figure 5, and the meaning of the symbols is shown in Table 1.

2.2.2. System Dynamics Model.
Based on the above three modules, the system dynamics model of PB mode adopted by Chinese construction enterprises is established. As shown in Figure 6, this model includes 4 level variables, 3 rate variables, 33 auxiliary variables, and 21 constants.

3. Model Simulation

3.1. Initial Value Setting and Simulation.
This paper sets the initial value based on the current data of PB in Jiangsu Province, China. According to the "Thirteenth Five-Year Development Plan for the Modernization of Construction Industry in Jiangsu Province," PB construction can apply for affordable housing projects, and for affordable housing projects built with PB, you can apply for a reward of no more than 300 yuan/m^2. When the prefabrication ratio of reinforced concrete structures is not less than 40%, the project will be subsidized, and the maximum subsidy for a single project will not exceed 18 million yuan per unit. Since China has determined that the minimum prefabrication ratio of PB is 50%, this paper sets the minimum prefabrication ratio as 50%. The prefabrication ratio set in the model has a linear relationship with the construction cost, in which the linear scale coefficient is 0.56 [36]. Based on the literature [37], when the prefabrication ratio of PB is greater than or equal to 50%, the cost of each additional 1% increase in the prefabrication ratio is about 29 yuan. This paper assumes that the construction area of the initial new construction project is 30000 m^2. According to the data query of China National Bureau of statistics in 2018, the average sales price of residential commercial housing is 10773.5 yuan/m^2. This paper uses Vensim PLE software to set TIME STEP to 0.0078125, and the initial value setting is shown in Table 2.

According to the setting of the initial value, the result of the adoption of PB mode in the construction enterprise is shown in Figure 7. The simulation results show that the adoption of PB mode by construction enterprises will reach a peak of 3.566 in the fourth year, that is, 3566 construction enterprises will adopt PB mode in engineering projects. However, after reaching the peak, the construction enterprises that adopted PB mode fluctuated in the form of shocks and eventually decreased gradually at a lower rate.

3.2. Analysis of Different Influencing Factors

3.2.1. Influencing Factors at the Government Level

(1) The Impact of Government Subsidies. In this experiment, we changed the value of the D_Y subsidy factor and set the
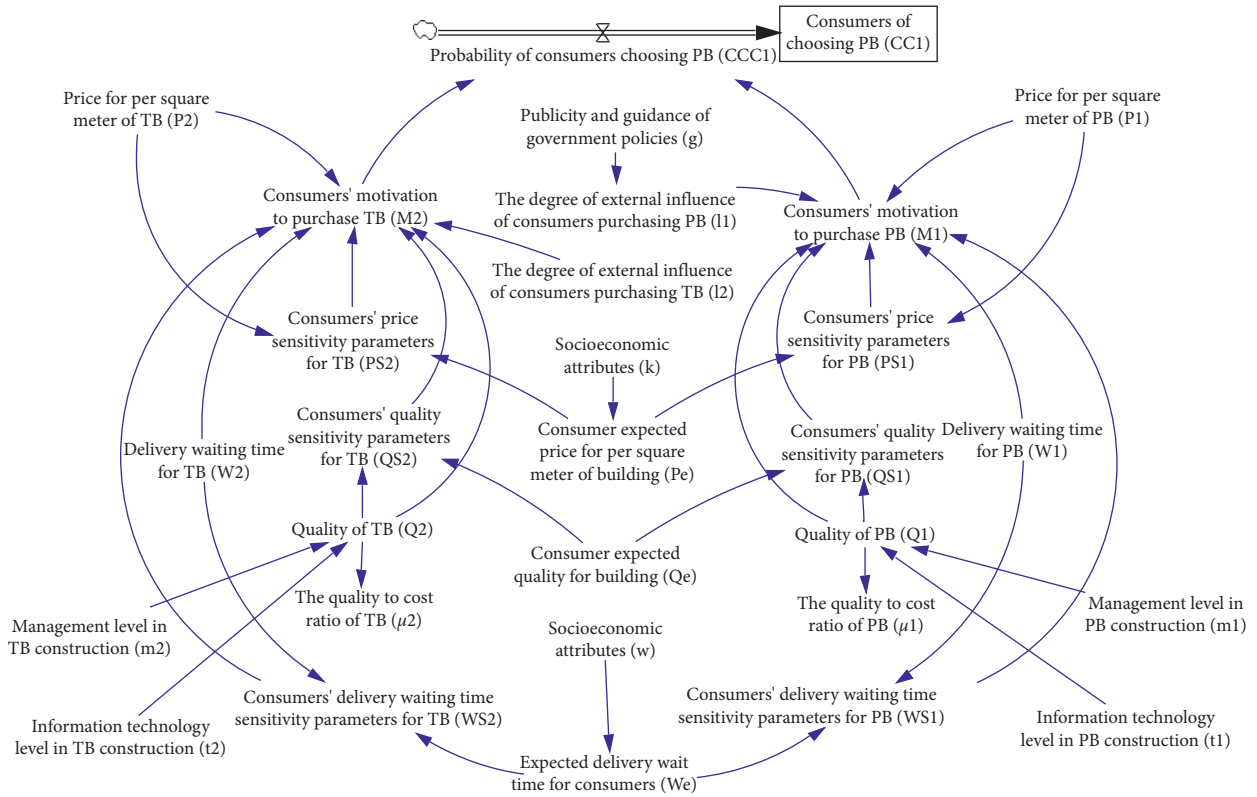
FIGURE 5: System diagram of consumer decision-making module.

value to 0, 0.01, and 0.02, respectively, that is, the subsidy of 0, 100, and 200 yuan per square meter for the PB project. The simulation results are shown in Figure 8. The higher the amount of subsidy, the higher the peak value of D_Y and the faster the growth rate.

The simulation results show that government subsidies play a relatively important role in promoting the maturity of PB market, but for an already mature stable market, the role of government subsidies is relatively small.

(2) The Impact of the Publicity and Guidance of Government Policies. In this experiment, we will analyze the impact of government policy propaganda and guidance on the adoption of PB mode by construction enterprises. We set the value of g to 0.1, 0.2, and 0.3, respectively, that is, the government has promoted consumers' favorability of PB mode by 10%, 20%, and 30% through publicity and guidance. The simulation results are shown in Figure 9. The government's publicity and guidance strength can play a positive role in promoting the results of the previous PB adoption, and the effects of different publicity and guidance strengths are not very different. However, in the later stages of the market, different publicity and guidance efforts will show differentiated promotion effects. The greater the strength is, the better the market will adopt PB.

Therefore, in the early stage of PB being introduced into the market, the government should adopt the way of subsidy to increase the market share of PB, while in the later stage of the market, the government should adopt the way of publicity and guidance to further promote the development of PB mode.

3.2.2. Influencing Factors at the Construction Enterprise Level

(1) The Impact of the Initial "D_Y" Probability of the Construction Enterprise. In this experiment, firstly, we set the probability of initial adoption of PB by the construction enterprise to 20%, 30%, 40%, and 50%, respectively. The simulation result is shown in Figure 10. At the initial stage of the formation of PB market, it is very important to improve the probability of the construction enterprise's initial adoption of PB mode to quickly improve the market share of PB, and the higher the initial adoption probability, the greater the peak value and fluctuation of the market share. However, the market share of PB will gradually reach a balanced and stable state. The probability that the construction enterprise initially adopts PB mode has no differential impact on the later market equilibrium. Therefore, the probability that the construction enterprise initially adopts PB mode does not have a first-mover advantage for the final market share of PB mode.

(2) The Impact of the Information Technology Level. In the scenario where m_1 in the quality factor is set to 1, we set the value of t_1 in the quality factor to 1, 1.5, and 2, respectively, which means that the information technology level in the PB product quality factor is increased by 0%, 50%, and 100%, respectively. The simulation result is shown in Figure 11.

The results show that in the early process of the adoption of PB mode, different information technology levels have little impact on the market share of PB. However, in the later stages of the market, different information technology levels
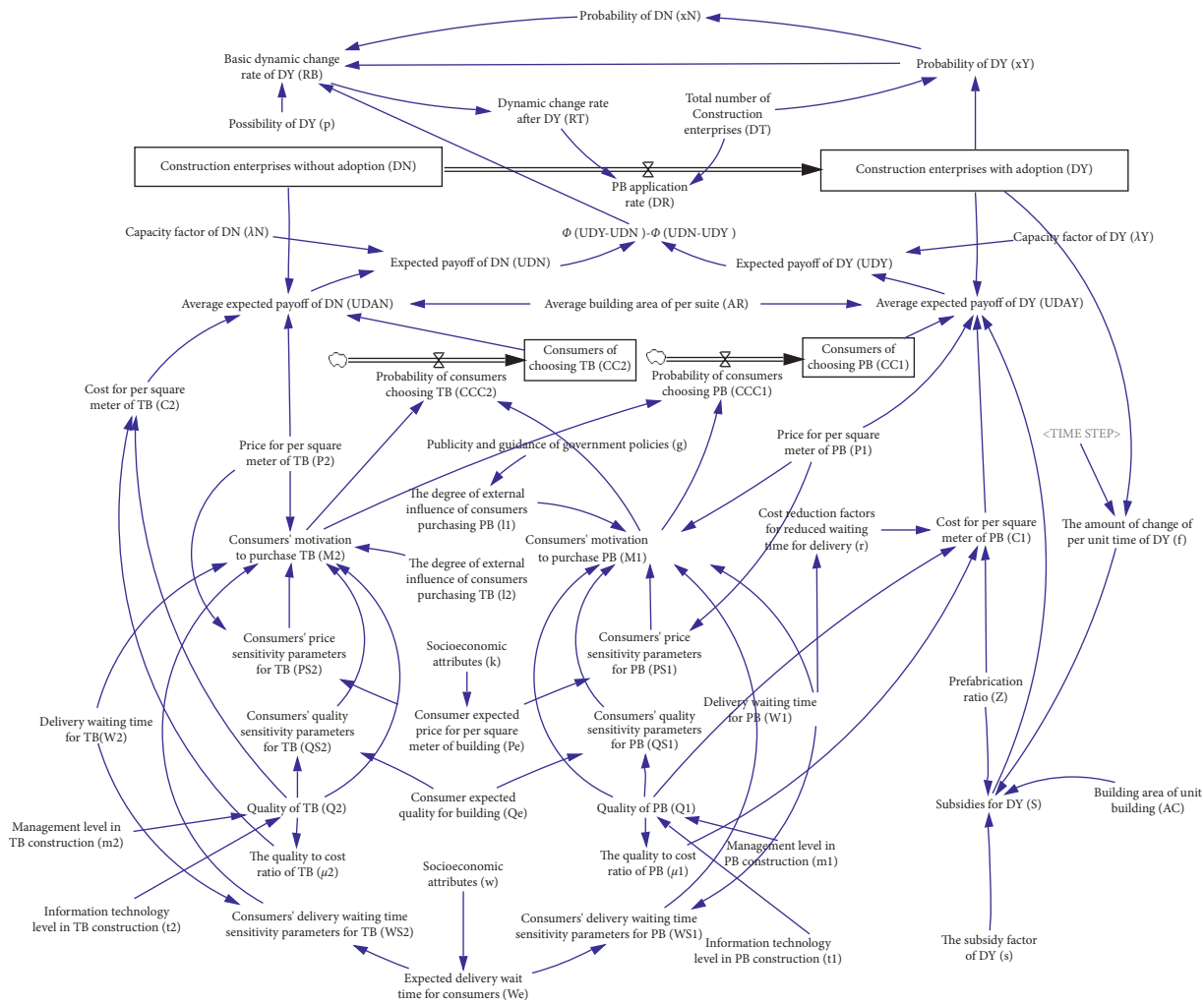
FIGURE 6: The system dynamics model of adoption behavior of PB mode by Chinese construction enterprises.

have had a different effect on the adoption of PB. When t_1 increases from 0% to 50%, the growth rate of PB market share is greater than that when t_1 increases from 50% to 100%. It can be seen that the construction enterprise should follow the principle of moderation when deciding on the information technology level, and that too high information technology level has a limited effect on advancing the PB market share.

(3) The Impact of Quality Factors. In this part, we will analyze the comprehensive influence of construction management level and information technology level on the adoption of PB mode. First, we set the value of m_1 to 1.5 (the initial value of m_1 is 1). On this basis, we set the value of t_1 to 1, 1.5, and 2, respectively. The simulation result is shown in Figure 12.

As can be seen from the figure, the market share of PB mode shows a rapid rise and then a decline and a slow rise. Compared with Figure 10, when the value of m_1 is set to 1.5, the overall D_Y number is further improved. In the scenario where the value of m_1 increases, a higher t_1 will bring a larger PB market share. When t_1 increases from 0% to 50%, the increase in PB market share is greater than the increase when

t_1 increases from 50% to 100%. It can be seen that increasing m_1 and t_1 will play a superimposed role in promoting the growth of PB market share.

(4) The Impact of Price Factors. In this experiment, we change the value of P_1 to $P_1 - 0.1$ and $P_1 + 0.1$, that is, the price of PB products per square meter is reduced by 1,000 yuan or increased by 1,000 yuan. The simulation results are shown in Figure 13, and the market share of PB mode shows an evolutionary trend of rapid rise and then slow decline.

Reducing the value of P_1 can quickly increase the market share of PB in a short period of time and enable it to reach a higher share. However, after reaching the peak, the market share of PB has shown a slow downward trend. It can be seen that adopting a low-price strategy will help PB mode to quickly penetrate the market, but for the later stage of the market, the ability of price to further enhance the market share of PB is limited.

(5) The Impact of Delivery Waiting Time Factors. We set the value of W_1 to 0.75, 1, and 1.25, respectively, that is, the delivery waiting time of PB is set to 0.75, 1, and 1.25 years.

TABLE 2: Setting of initial simulation value.

| Variable	Category	Initial value	Unit
Initial value of D_Y	Level	0.039	Thousand
Initial value of D_N	Level	6.684	Thousand
D_T	Constant	6.723	Thousand
λ_Y	Constant	1	1
λ_N	Constant	1	1
P_1	Constant	1.07735	Ten thousand yuan
P_2	Constant	1.07735	Ten thousand yuan
P_e	Constant	0.8	Ten thousand yuan
W_1	Constant	1.5	year
W_2	Constant	2	year
W_e	Constant	1	year
t_1	Constant	1	1
t_2	Constant	1	1
m_1	Constant	1	1
m_2	Constant	1	1
Q_e	Constant	3	1
A_C	Constant	30000	m^2
A_R	Constant	100	m^2
Z	Constant	0.5	1
s	Constant	0.03	Ten thousand yuan
g	Constant	0	1
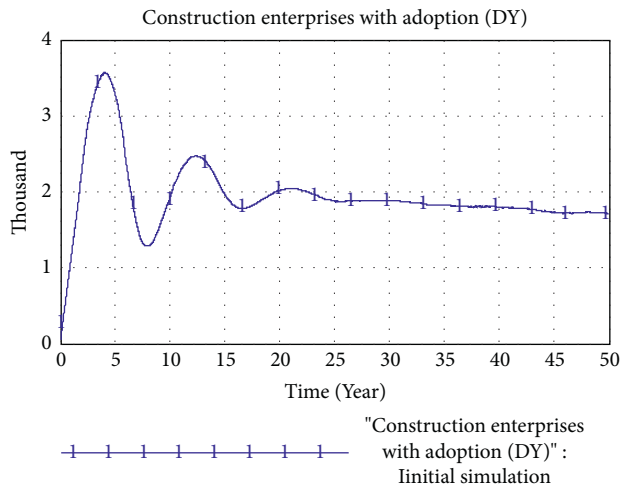
FIGURE 7: Initial simulation results.

The simulation result is shown in Figure 14. It can be seen from the figure that under the condition that consumers set in this paper have the same sensitivity to product price, quality, and delivery waiting time, different delivery waiting times have little difference on the market share of PB. However, in the early stage of the market, the delivery waiting time has a certain impact on the peak of the PB market share, but this differential impact is not very obvious.

4. Discussion

In the above simulation results and analysis, it can be found that the changes of different factors will have a different impact on the adoption strategy of the construction enterprise. It is necessary to analyze the most favorable aspects of different factors affecting the construction enterprise's adoption of PB mode from different angles. This paper will analyze the influencing factors from the following perspectives.

4.1. Influencing Factors at the Government Level. From the perspective of changing government subsidies, government subsidies play a positive role in promoting construction enterprises to adopt PB mode, especially in the initial stage of adopting PB mode by construction enterprises, which confirms Li et al.'s research results [14]. Also, the higher the government subsidy is, the higher the peak value of construction enterprises adopting PB mode is and the longer it will continue to grow. However, for the PB market that has gradually stabilized, government subsidies have no obvious promoting effect. Timely reduction or termination of government subsidies can effectively reduce fiscal expenditures and achieve good market effects.

From the perspective of improving the publicity and guidance of government policies, the government's positive guidance for PB mode has improved consumers' favorability of PB mode, which in turn promoted the long-term and steady development of the PB market, which is consistent with Wang et al.'s research results [26]. This effect is not obvious in the initial stage of the PB market but gradually widened the gap in the later stage. Positive publicity and guidance have a subtle effect on the development of the PB market, and the longer the time, the more obvious the effect.

In summary, in the early stage of PB mode entering the market, the government should use subsidies to increase the market share of PB. Although the publicity and guidance of government policies are more obvious in the later stage of the PB market, the government should still adopt positive publicity and guidance methods in the early stage of the PB market to further promote the development of PB mode.

4.2. Influencing Factors at the Construction Enterprise Level. From the perspective of changing the initial acceptance probability of the construction enterprise, higher initial acceptance probability of the construction enterprise is of great significance to the formation of the initial PB market, which is conducive to the rapid improvement of the maturity of the PB market. However, excessive pursuit of the probability of construction enterprises initially adopting PB mode is not conducive to the stable development of the PB market. In the long run, the adoption intention of the construction enterprise should follow a step-by-step process and maintain a relatively stable growth trend.

From the perspective of changing the level of information technology, the improvement of the level of PB construction information technology has significantly accelerated the rate at which construction enterprises adopt PB mode. However, the degree of improvement in the level of PB construction information technology is not linearly related to the rate at which construction enterprises adopt PB mode. When the PB construction information technology level is raised to a higher level, the impact of the increase in the PB construction information technology level on the increase in the rate of the construction enterprise
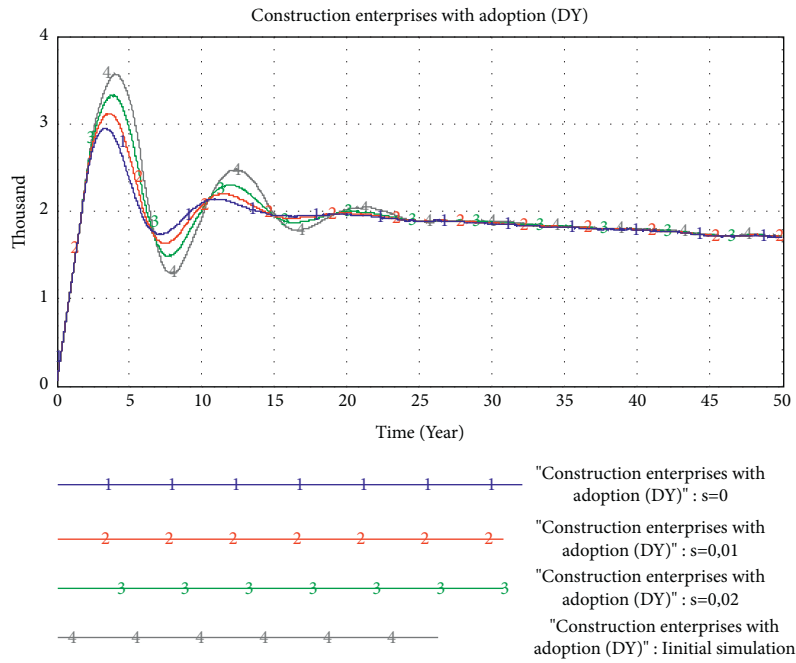
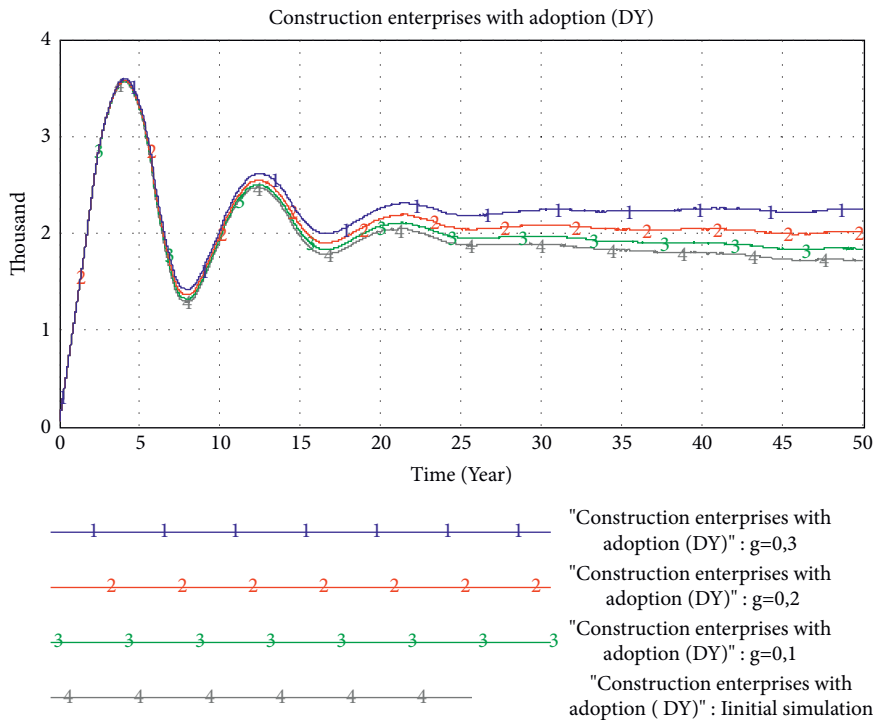Figure 8: Simulation results of changes in government subsidies.

Figure 9: Simulation results of changes in government policy publicity and guidance.

adopting PB mode will show a decreasing trend under the same proportion each time. Therefore, it is necessary to uphold the principle of moderation for the improvement of the information technology level, and blindly pursuing the unilateral improvement of the information technology level may not achieve the expected results.

From the perspective of changing quality factors, when the level of PB construction management improves, the corresponding improvement in the level of construction information technology will have a significant impact on accelerating the increase in the rate at which construction enterprises adopt PB mode. While maintaining the

FIGURE 10: The simulation result of the initial "D_Y" probability change.

FIGURE 11: Simulation results of changes in the information technology level.

improvement of the construction management level, the improvement of the same proportion of the information technology level will sharply reduce the increase in the rate of construction enterprises adopting PB mode. It can be seen that the improvement of the construction management level has a positive effect on the adoption of PB mode by the construction enterprise, and the improvement of the construction management level and the information technology

level at the same time will facilitate the rapid development of PB mode and maintain the PB market share for a long time.

From the perspective of changing price factors, compared with increasing the price of PB per square meter, the price reduction has shown an advantage in the early stage of the PB market. The price lower than the market price has been supported by more consumers, which has affected the construction enterprise's adoption of PB mode. Therefore,
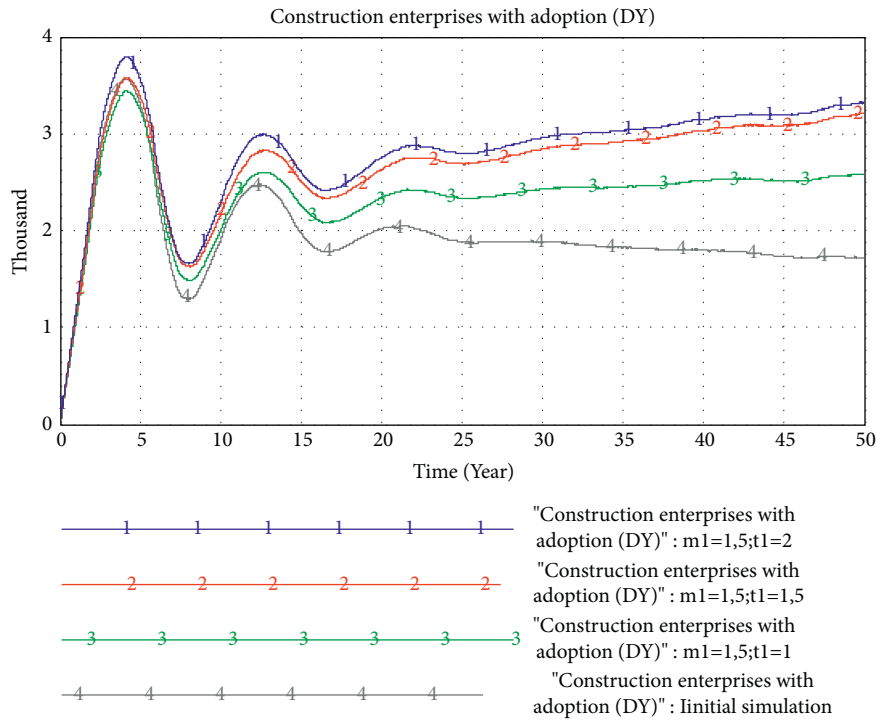
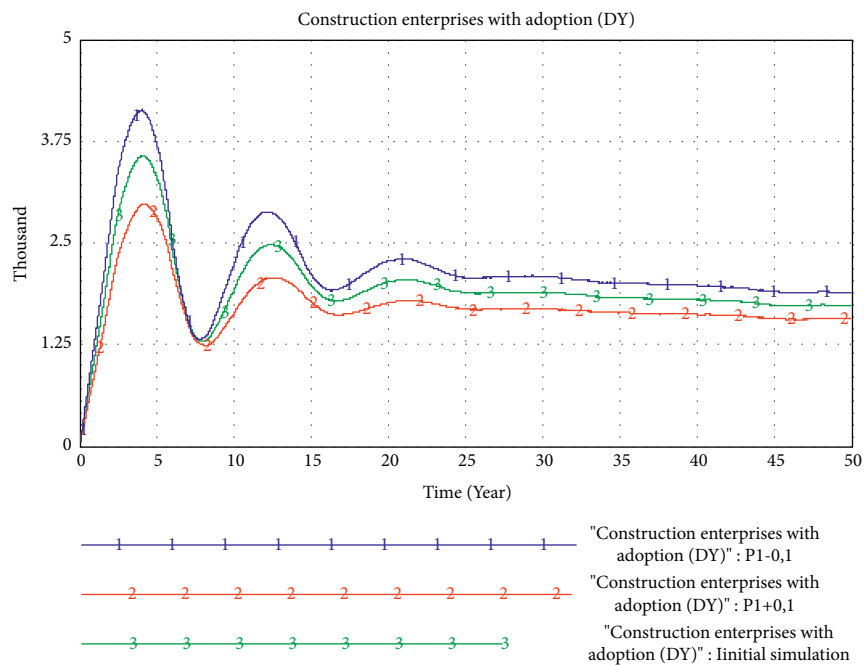Figure 12: Simulation results of quality factors.

Figure 13: Simulation results of changes in price factors.

the price factor has a more direct impact on the PB market, and the lower price indirectly stimulates the construction enterprises to improve the adoption of PB mode.

From the perspective of changing the delivery waiting time factor, the reduction in PB delivery waiting time does not significantly affect the rate at which construction enterprises adopt PB mode. This also shows to a certain extent

that when the delivery waiting time of the building is within the consumer's tolerance range, it will not cause strong rejection due to the long delivery waiting time. Therefore, the impact of the delivery waiting time factor on the construction enterprise's adoption of PB mode is not significant.

To sum up, we can draw the following conclusions. Firstly, the initial adoption intention of the construction
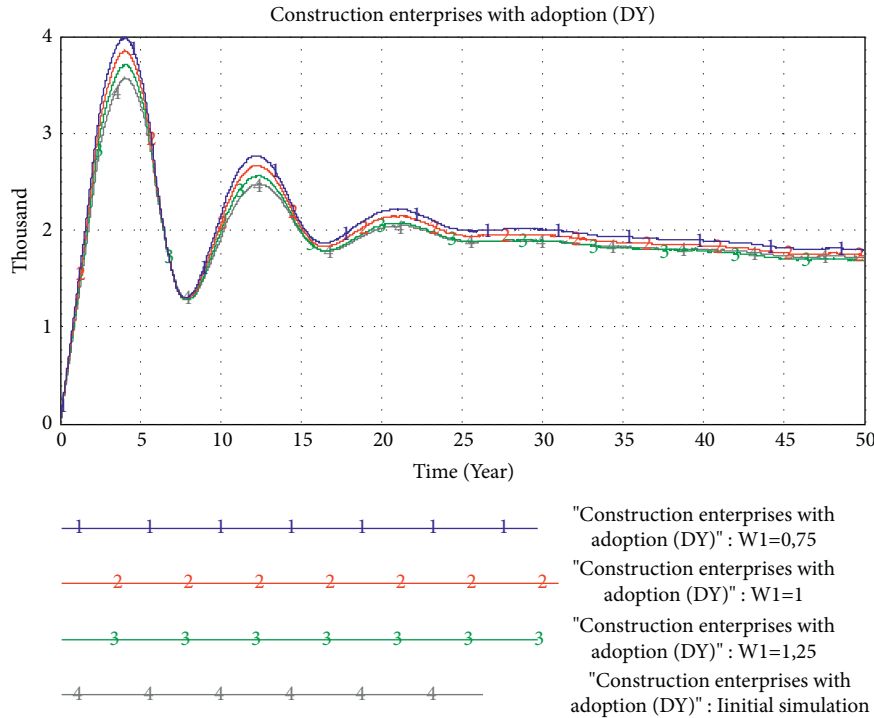
FIGURE 14: The simulation result of the change of the delivery waiting time factor.

enterprise should adopt the strategy of gradual improvement. Secondly, the construction management level and the information technology level in the quality factor of PB have complementary effects. At the same time, their improvement can not only quickly increase the PB market share but also maintain the stable and good development of the PB industry. Thirdly, the reduction of the price factor is conducive to the rapid increase of the PB market share in the short term. Fourthly, the delivery waiting time factor will not have a major impact on the construction enterprise's adoption of PB mode.

5. Conclusions and Recommendations

PB has developed earlier in some developed countries, such as the United Kingdom and the United States, and already has a certain market scale [38]. However, PB mode is still in the ascendant in China, but based on the needs of China's energy saving, emission reduction, and green development, PB mode has attracted the attention of many scholars in recent years.

Combined with evolutionary game theory, this study establishes a system dynamics model of Chinese construction enterprises' adoption behavior of PB mode under the scenario of multiagent interaction and uses the data of Jiangsu Province in China for simulation analysis. The purpose is to clarify the behavior mechanism of Chinese construction enterprises' adoption of PB mode and the evolution law of PB market share, so as to provide a certain theoretical basis for the vigorous development of PB mode in China. The corresponding conclusions and recommendations are as follows:

(1) Government subsidies play an important role in promoting the maturity of the PB market. Maintaining certain government subsidies can ensure a longer and more stable market share of PB mode. However, for the already more mature market, the role of government subsidies is relatively small. Therefore, government subsidies can be gradually reduced or cancelled after promoting the development of PB mode to achieve a good market effect. At the same time, the publicity and guidance of government policies have gradually produced the effect of promoting the market share of PB, which requires the accumulation of preliminary work. Therefore, in the early stage of the introduction of PB mode to the market, the government should simultaneously provide subsidies to construction enterprises and publicize and guide consumers to increase the market share of PB and further promote the development of PB mode.

(2) The initial acceptance probability of the construction enterprise should not be excessively pursued. The higher the initial probability of adoption, the greater the peak of the PB market share and the greater the volatility, which is not conducive to the stable development of the PB industry. Also, the probability that the construction enterprise initially adopts PB mode has no differential impact on the later market equilibrium state. Different initial acceptance probabilities of the construction enterprise will make the market share of PB reach a gradually balanced and stable state. Therefore, the probability that the construction enterprise initially adopts PB mode

does not have a first-mover advantage for the final market share of PB mode.

(3) The reduction of the price factor can quickly increase the market share of PB mode in a relatively short period of time. However, in the later stages of the market, lowering the price factor has limited ability to further increase PB's market share. The reduction of price factors cannot maintain the lasting and stable development of the PB market. The simultaneous improvement of the construction management level and the information technology level in the quality factors has an important impact on the market share of the later stage of PB mode and can maintain the steady growth of the PB market. Compared with price factors and quality factors, the delivery waiting time factor has no significant impact on the market share of PB mode. Therefore, the delivery waiting time factor does not need to be considered more by the construction enterprise in the decision to adopt PB mode. In summary, the PB industry still needs to promote the development of PB with the promotion of quality improvement as the main direction. Under the premise of small price fluctuations and stable quality improvement, the reduction in delivery waiting time should be gradually reduced, so that the PB industry can go more stable and go further.

This paper also has some limitations. For example, the model does not consider the specific components of construction cost, the relationship and behavior of other stakeholders, etc. In addition, this paper mainly studies the adoption behavior of PB mode by Chinese construction enterprises and comes to the conclusion that the universality and reference significance of management conclusions need to be strengthened. In the future, we can consider the relationships and behaviors between more stakeholders, add more abundant influencing factors, and promote the steady development of PB.

Data Availability

The data used to support the findings of this study are available from the corresponding author upon request.

Conflicts of Interest

The authors declare that they have no conflicts of interest.

Acknowledgments

References

[1] L. Jiang, Z. Li, L. Li, and Y. Gao, "Constraints on the promotion of prefabricated construction in China," *Sustainability*, vol. 10, no. 7, 2018.

[2] X. Lai, J. Liu, and G. Georgiev, "Low carbon technology integration innovation assessment index review based on rough set theory - an evidence from construction industry in China," *Journal of Cleaner Production*, vol. 126, pp. 88–96, 2016.

[3] Y. Dou, X. Xue, Z. Zhao, and Y. Jiang, "Measuring the factors that influence the diffusion of prefabricated construction technology innovation," *KSCE Journal of Civil Engineering*, vol. 23, no. 9, pp. 3737–3752, 2019.

[4] H. Zhou, Y. Lu, X. Liu, R. Chang, and B. Wang, "Harvesting wind energy in low-rise residential buildings: design and optimization of building forms," *Journal of Cleaner Production*, vol. 167, pp. 306–316, 2017.

[5] G. Wu, R. Yang, L. Li et al., "Factors influencing the application of prefabricated construction in China: from perspectives of technology promotion and cleaner production," *Journal of Cleaner Production*, vol. 219, pp. 753–762, 2019.

[6] M. K. Dixit, J. L. Fernández-Solís, S. Lavy, and C. H. Culp, "Identification of parameters for embodied energy measurement: a literature review," *Energy and Buildings*, vol. 42, no. 8, pp. 1238–1247, Aug 2010.

[7] X.-L. Gan, R.-D. Chang, C. Langston, and T. Wen, "Exploring the interactions among factors impeding the diffusion of prefabricated building technologies Fuzzy cognitive maps," *Engineering Construction and Architectural Management*, vol. 26, no. 3, pp. 535–553, 2019.

[8] Q. Du, Q. Y. Pang, T. N. Bao, X. Q. Guo, and Y. G. Deng, "Critical factors influencing carbon emissions of prefabricated building supply chains in China," *Journal of Cleaner Production*, vol. 280, Article ID 124398, 2021.

[9] X. J. Li, C. Wang, A. Alashwal, and S. Bora, "Game analysis on prefabricated building evolution based on dynamic revenue risks in China," *Journal of Cleaner Production*, vol. 267, Article ID 121730, 2020.

[10] C. Mao, Q. Shen, W. Pan, and K. Ye, "Major barriers to off-site construction: the developer's perspective in China," *Journal of Management in Engineering*, vol. 31, no. 3, Article ID 04014043, 2015.

[11] T. Tan, K. Chen, F. Xue, and W. Lu, "Barriers to Building Information Modeling (BIM) implementation in China's prefabricated construction: an interpretive structural modeling (ISM) approach," *Journal of Cleaner Production*, vol. 219, pp. 949–959, 2019.

[12] Y. Han and L. Wang, "Identifying barriers to OFF-site construction using grey dematel approach: case OF China," *Journal of Civil Engineering and Management*, vol. 24, no. 5, pp. 364–377, 2018 2018.

[13] Z. Rui and W. Yaowu, "Research on the constraints of the development of prefabricated building in dalian based on ISM (ICCREM 2019. Innovative construction project management and construction industrialization," in *Proceedings of the International Conference on Construction and Real Estate Management 2019*, pp. 461–474, Alberta, Canada, May 2019.

[14] Z. Li, G. Q. Shen, and M. Alshawi, "Measuring the impact of prefabrication on construction waste reduction: an empirical study in China," *Resources, Conservation and Recycling*, vol. 91, pp. 27–39, Sep 2014.

[15] P. Wei, Y. Yi, and Y. Lin, "High-rise modular building: tenyear journey and future development," in *Proceedings of the*

Construction Research Congress, pp. 523–532, Sustainable Design and Construction and Education, Lousiana, LO, USA, April 2018.

[16] X. Xiahou, J. Yuan, Y. Liu, Y. Tang, and Q. Li, "Exploring the driving factors of construction industrialization development in China," *International Journal of Environmental Research and Public Health*, vol. 15, no. 3, Article ID 442, 2018.

[17] X. Gan, R. Chang, and T. Wen, "Overcoming barriers to off-site construction through engaging stakeholders: a two-mode social network analysis," *Journal of Cleaner Production*, vol. 201, pp. 735–747, 2018.

[18] Y. Dou, X. Xue, Z. Zhao, and X. Luo, "Factors influence China's off-site construction technology innovation diffusion," *Sustainability*, vol. 11, no. 7, Article ID 1849, 2019.

[19] C. Mao, G. Liu, L. Shen, X. Wang, and J. Wang, "Structural equation modeling to analyze the critical driving factors and paths for off-site construction in China," *Ksce Journal of Civil Engineering*, vol. 22, no. 8, pp. 2678–2690, 2018.

[20] Y. Wang, F. Wang, P. Sang, and H. Song, "Analysing factors affecting developers' behaviour towards the adoption of prefabricated buildings in China," *Environment, Development and Sustainability*, vol. 23, no. 10, pp. 14245–14263, 2021.

[21] J. Wang and W. Pan, "Influencing parameters of the life cycle cost-energy relationship of buildings," *Journal of Green Building*, vol. 13, no. 4, pp. 103–121, 2018.

[22] D. A. Ness and K. Xing, "Consumption-based and embodied carbon in the built environment: implications for apec's low-carbon model town project," *Journal of Green Building*, vol. 15, no. 3, pp. 67–82, 2020.

[23] X. Zhang, M. Skitmore, and Y. Peng, "Exploring the challenges to industrialized residential building in China," *Habitat International*, vol. 41, pp. 176–184, 2014.

[24] Z. Xiaolin, R. Reed, and A. Mills, "Addressing sustainable challenges in China," *Smart and Sustainable Built Environment*, vol. 3, no. 3, pp. 261–274, 2014.

[25] J.-S. Lee and Y.-S. Kim, "Analysis of cost-increasing risk factors in modular construction in korea using FMEA," *Ksce Journal of Civil Engineering*, vol. 21, no. 6, pp. 1999–2010, 2017.

[26] Y. Wang, H. Li, and Z. Wu, "Attitude of the Chinese public toward off-site construction: a text mining study," *Journal of Cleaner Production*, vol. 238, Article ID 117926, 2019.

[27] X. Hu, H.-Y. Chong, and X. Wang, "Sustainability perceptions of off-site manufacturing stakeholders in Australia," *Journal of Cleaner Production*, vol. 227, pp. 346–354, 2019.

[28] J. Wang, Z. Li, and V. W. Y. Tam, "Identifying best design strategies for construction waste minimization," *Journal of Cleaner Production*, vol. 92, pp. 237–247, 2015.

[29] S. Guo, P. Zhang, and J. Yang, "System dynamics model based ON evolutionary game theory for quality supervision among construction stakeholders," *Journal of Civil Engineering and Management*, vol. 24, no. 4, pp. 318–330, 2018.

[30] Y. Tian, K. Govindan, and Q. Zhu, "A system dynamics model based on evolutionary game theory for green supply chain management diffusion among Chinese manufacturers," *Journal of Cleaner Production*, vol. 80, pp. 96–105, 2014.

[31] N. B. o. Statistics, http://www.stats.gov.cn/, 2018.

[32] T. Zhang and D. Zhang, "Agent-based simulation of consumer purchase decision-making and the decoy effect," *Journal of Business Research*, vol. 60, no. 8, pp. 912–922, 2007.

[33] B.-D. Kim, R. C. Blattberg, and P. E. Rossi, "Modeling the distribution OF price sensitivity and implications for optimal retail pricing," *Journal of Business & Economic Statistics*, vol. 13, no. 3, pp. 291–303, 1995.

[34] N. Zhang and X. Zheng, "Agent-based simulation of consumer purchase behaviour based on quality, price and promotion," *Enterprise Information Systems*, vol. 13, no. 10, pp. 1427–1441, 2019.

[35] J. M. Juran and F. M. Gryna, *Quality Planning and Analysis: From Product Development through Use*, McGraw-Hill, New York, NY, USA, 2001.

[36] N. Lou and J. J. Guo, "Study on Key cost drivers of prefabricated buildings based on system dynamics," *Advances in Civil Engineering*, vol. 2020, Article ID 8896435, 12 pages, 2020.

[37] C. Mao, F. Xie, L. Hou, P. Wu, J. Wang, and X. Wang, "Cost analysis for sustainable off-site construction based on a multiple-case study in China," *Habitat International*, vol. 57, pp. 215–222, 2016.

[38] I. Y. Wuni, G. Q. Shen, and R. Osei-Kyei, "Sustainability of off-site construction: a bibliometric review and visualized analysis of trending topics and themes," *Journal of Green Building*, vol. 15, no. 4, pp. 131–154, 2020.

Research Article

Application Analysis of Radial Basis Function Neural Network Algorithm of Genetic Algorithm for Environmental Restoration and Treatment Effect Evaluation of Decommissioned Uranium Tailings Ponds

Kun Wei [ID],[1,2] **Guokai Xiong** [ID],[1,3] **Zhenghua Xu** [ID],[2] **and Yong Liu** [ID][1,2]

[1]*School of Resource Environment and Safety Engineering, University of South China, Hengyang 421001, Hunan, China*
[2]*Decommissioning Engineering Technology Research Center of Hunan Province Uranium Tailings Reservoir,*
 University of South China, Hengyang 421001, Hunan, China
[3]*Hunan Provincial Key Laboratory of Emergency Safety Technology and Equipment for Nuclear Facilities, Hengyang 421001,*
 Hunan, China

Correspondence should be addressed to Yong Liu; 1992001751@usc.edu.cn

A new analysis method for the environmental stability of uranium tailing ponds is established in this paper, and the stability intervals and environmental stability rates of indicators are defined in precise mathematical language and analyzed with examples. The results show that the overall environmental stability of this uranium tailings pond is still in a poor state after the first phase of decommissioning treatment, and special decommissioning treatment should be carried out for factors such as pH and radionuclides Po and Pb. Using the powerful nonlinear mapping function of the artificial neural network, a radial basis function neural network algorithm was constructed to predict the environmental stability of the uranium tailing pond. It provides a new feasible method for the comprehensive evaluation technology of uranium tailings ponds. *Accuracy in DOA Estimation.* The research work in this paper mainly analyzed the environmental stabilization process and stability of decommissioned uranium tailings ponds, proposed a new concept of environmental stability with ecological and environmental protection concepts and gave it a new connotation, established an environmental stability evaluation index system for decommissioned uranium tailings ponds through index screening by using rough set theory, comprehensively considered the influence of environmental factors such as external wastewater and exhaust gas, and realized the multifactor. The system of evaluation indexes for the stability of decommissioned uranium tailings ponds was established by combining multiple factors, and the long-term monitoring and modeling of the environmental stabilization process of decommissioned uranium tailings ponds was carried out by using mathematical methods. The results show that the RBFNN-GA algorithm can reduce the training error of the random radial basis function neural network, improve the generalization ability of the network, and make it capable of handling large data sets.

1. Introduction

The goal for the governance and management of uranium metallurgical tailings is that the decommissioning environment must be restored to an acceptable level that allows for the protection of present and future personnel and the environment, with considerations for future generations that include potential radiation exposure, economic consequences, and requirements for monitoring and maintenance, and that do not place an undue burden on future generations. However, the current concept of stabilization of tailings ponds in China only considers their mechanical properties and uses only the mechanical stability of tailings dams as a criterion for judging the safety or otherwise of uranium tailings ponds, which obviously can no longer meet the needs of ecological and environmental

protection and sustainable development of uranium tailings pond decommissioning management [1]. From the perspective of protecting the ecological environment and safeguarding the safety of public life and property, it is of great significance to analyze and study the stabilization process and stable state of decommissioned uranium tailings ponds [2]. Therefore, it can better reflect the objective existence of ambiguity. For uranium tailings ponds, due to the complex environmental factors, how to define the stability of various environmental monitoring indicators and the overall stability of the environment is itself a difficult problem to determine. However, the current analysis and evaluation of the stability of uranium tailing ponds only consider the mechanical stability of tailings dams, and only the mechanical stability index of tailing pond dams as the evaluation index of the safety of decommissioned uranium tailing ponds obviously cannot meet the needs of ecological environmental protection and sustainable development of decommissioned uranium tailing ponds. In this paper, based on the systematic examination of the factors influencing the environmental stability of uranium tailings ponds, the analysis of the change pattern of environmental monitoring items of uranium tailings ponds over time, the analysis of the environmental stabilization process characterization of uranium tailings ponds, a new concept and connotation of the environmental stability of uranium tailings ponds in a comprehensive and systematic way, the establishment of the environmental stability evaluation index system of decommissioned uranium tailings ponds were proposed [3]. The analysis method of environmental stability of tailings was constructed, and the quantitative calculation of environmental stability rate was carried out, and the environmental stability grade of each month was divided, on this basis, the environmental stability of existing decommissioned uranium tailings ponds was evaluated and predicted, and a new method of environmental stability analysis and prediction of decommissioned uranium tailings ponds was systematically established, which further enriched and improved the comprehensive evaluation technology of decommissioned uranium tailings ponds, and has a positive impact. It has positive significance and impact on the decommissioning management and environmental protection of uranium tailings ponds [4].

It is generally believed that uranium mining and metallurgical tailings ponds do not cause great impact on the environment after decommissioning and treatment according to the design, but with the passage of time, influenced by external factors (including earthquakes, rainfall and human damage, etc.), the possibility and infiltration of radionuclides from uranium mine tailings ponds into the reservoir area and mine groundwater through the bottom and dam of the reservoir increases greatly with the growth of its age and the infiltration of radionuclides from the groundwater in the reservoir, causing pollution of the reservoir area and mine water environment, which then spreads to various organisms in the biosphere and causes serious ecological hazards, and this hazard has the characteristics of long-lasting, hidden, large degree of harm and difficult to repair; based on the above problems of

decommissioned uranium tailings ponds, the effect of treatment in the end needs to be scientifically assessed [5]. With time, some uranium metallurgical tailings ponds are inadequately monitored for safety and ineffective after decommissioning treatment. The leakage of toxic pollutants from uranium tailings dams in the nuclear industry can cause serious accidents, will have a significant impact on the natural environment, and negatively affect the safety of the living environment, and with the migration of radioactive elements, the impact will be further expanded and is difficult to recover. Therefore, strengthening the safety supervision of uranium tailings dams, the treatment of pollutants in uranium tailings dams, and the scientific assessment of the treatment effect are of great practical importance to help people understand the current situation of uranium tailings dams and the treatment effect and to inform people about the safety of nuclear production and social and environmental safety.

At present, there is no clear regulation and management for the effect of management of uranium mine tailings ponds after decommissioning in China, which leads to the lack of clarity of environmental protection departments at all levels on the issue of the effect of management of uranium mine tailings ponds after decommissioning, and the management of uranium mine tailings ponds after decommissioning is a comprehensive work, involving safety supervision, environmental protection, and many other departments. Only a scientific assessment of the effectiveness of the current situation of the tailing's ponds can improve their shortcomings and defects, improve the effectiveness of governance, and ensure the stability of the environmental impact of the uranium mine tailings ponds after decommissioning, which is of great significance to ensure the safety of people's lives and health. The environmental management of uranium tailings ponds is only based on whether the monitoring values of each item meet the standards; i.e., it is usually considered safe to be lower than the emission standards and unsafe to be higher than the emission standards; however, due to the special nature of uranium tailings ponds themselves, their surroundings are easily affected by various factors such as rainfall, earthquakes, dam structure, and human intervention, and the data obtained from monitoring at different moments often vary greatly. We perform 30 trials on each training set and test set and then take the median as the result to reduce the impact of random errors. The stabilization process of each environmental indicator needs to be considered comprehensively to make an objective and effective analysis and evaluation of the environmental stability state of uranium tailings ponds.

2. Status of Research

Uranium tailings ponds, as a major hazard source and a long-term potential source of huge radioactive pollution, are ranked 18th in the international ranking of disaster accidents, in which radionuclides, heavy metals, and other toxic and hazardous substances have caused serious pollution to the ecological environment around the tailings ponds through diffusion and migration, posing a serious threat to

the safety of downstream residents and facilities, and the quality of their environment is increasingly becoming a concern [6]. Because of the current research status of uranium tailings ponds and related problems of stability research, the author summarized the current research status of environmental stability analysis of uranium tailings ponds at home and abroad by reading a large amount of relevant literature on safety, environment, and stability of uranium tailings ponds at home and abroad [7]. It is important to focus on the three aspects of tailings dam seepage stability analysis, stability analysis of tailings dam deformation and mechanical characteristics, and comprehensive evaluation of uranium tailings pond environment [8]. The analysis methods for tailings dam stability mainly include numerical analysis method and limit equilibrium analysis method, the numerical analysis method is only applied to theoretical discussion and analysis, while the limit equilibrium method is more used in engineering practice; the comprehensive evaluation of the environment mainly applies fuzzy comprehensive evaluation, artificial neural network evaluation, and grey comprehensive evaluation methods [9]. Since radioactive waste is both radiation hazardous and chemically toxic, the treatment of uranium tailings should provide an acceptable level of environmental protection and must provide an acceptable level of human health protection, ensuring that it is within the limits set by the state and predicting that the impact of uranium mining and metallurgical facilities and radioactive waste treatment on the health of future generations is below the dose level of the relevant standards [10]. The residual uranium, needles, radium, etc. and decay substrates in uranium tailings have half-lives of several years, decades, centuries, or even tens of thousands of years and will have a long period of radioactive and chemical hazards to the surrounding atmosphere, water bodies, soil, vegetation, and other apparent environments, groundwater, and organisms, etc. Therefore, the decommissioning treatment of uranium tailings should adopt advanced technologies and methods, appropriate safety, and control measures as far as possible, to ensure that the treatment of uranium tailings the measures should be sufficiently stable and safe for a long period [11].

The environmental performance assessment method is now mainly applied to enterprise environmental performance, which mainly refers to the main achievements and effects achieved by enterprises in their business activities, due to environmental protection and management of environmental pollution; generally speaking, enterprise performance refers to the economic benefits of enterprises, comprehensive hierarchical analysis, and principal component analysis to build an index system to systematically assess the economic performance or environmental performance [12]. An assessment method in the systematic assessment and theoretical assessment results are more objective; the system construction is also more flexible; the disadvantage is that the implementation of a certain degree of difficulty requires a certain theoretical basis and scientific research capabilities to build the index system and determine the assessment scheme. In the stability study of tailings dam deformation and mechanical characteristics, the stability

analysis is mainly carried out using the limit equilibrium method [13]. Taking the tailings pond in Hunan Province as an example, the influence of tailings and its medium parameters on the stability and dynamic response of the tailings pond was analyzed by a combination of numerical simulation and model test, and the characteristics and laws of the seismic dynamic response of the tailings pond were summarized systematically by static analysis and dynamic calculation [14]. Baghaee et al. introduced the reliability theory into the stability of tailings dams based on the limit equilibrium theory and the traditional safety factor method. The feasibility and effectiveness of this method were verified [15]. The stability of tailings dams was analyzed based on the finite element method using ANSYS software, which verified the significant advantages of the numerical method in the stability calculation of tailings dams and effectively reflected the stability of tailings dam, providing a certain basis for the safety management of tailings ponds. The stability of the tailings pond accumulation dam was analyzed by using the circular arc bar division method, and the safety coefficient of the dam was calculated by the mechanical geometric model, which effectively reflects the current situation of the tailings dam stability. A three-dimensional numerical simulation study of the tailings dam was carried out using FLAC3D software, and the stress distribution laws of the tailings dam deformation were derived.

Based on the environmental monitoring data of uranium tailing ponds, the dynamic change pattern of environmental indicators over time was systematically analyzed, and the decommissioning management situation and stabilization trend of each environmental monitoring item were initially analyzed. The environmental stability evaluation index system of decommissioned uranium tailing ponds was constructed by considering three aspects, namely, external seepage water, atmospheric environment, and radioactive pollution, and the core index system of comprehensive environmental stability evaluation was finally determined by applying the method of rough set attribute simplification for index screening; the weights of each evaluation index were determined by using the GO method to construct a judgment matrix, and the stability grade of uranium tailing ponds was determined according to the weighted average principle. The environmental stability prediction model based on the BP neural network was established to predict the environmental stability rate and stability grade of a decommissioned uranium tailing pond by using its powerful nonlinear mapping function, and the prediction results were in good agreement with the actual situation.

3. Analysis of Radial Basis Function Neural Network Algorithm with Genetic Algorithm for Environmental Restoration and Treatment Effectiveness Evaluation of Decommissioned Uranium Tailings Ponds

3.1. Radial Basis Function Neural Network Algorithm Design for Genetic Algorithm. Most of the existing neural networks are improved in structural design and parameter

training; the more complex the structure, the more parameters are often required and the more demanding the correction algorithm. The radial basis (RBF) neural network has been chosen and widely used by most scholars because of its simple structure and its ability to approximate arbitrary nonlinear functions. RBF neural network is a novel and effective feedforward neural network with the best approximation and global optimum performance. RBF neural network is proposed based on the feature that neuronal cells in the human brain have a local response, which simulates the local tuning in the human brain. The generalization situation is also very good, and the generalization results are basically consistent with the test set data. It shows that the results of the random radial basis function neural network in the classification task are also satisfactory. The RBF neural network is a local approximation neural network structure with local tuning and mutual coverage of the receptive domain. The activation function is a radial basis function with multivariate interpolation, and the training method is fast and easy, without the problem of local optimality, which makes RBF neural networks have a wide range of applications in many fields, such as function approximation, classification, pattern recognition, regression problems, and prediction and signal processing. Structurally, RBF neural network has a simple topology and a simple and clear learning and training process [16]. It uses the radial basis function as the activation function, and the nodes in the hidden layer produce a larger output only when the input signal is near the center of the radial basis function. The RBF neural network consists of three layers: the input layer, the hidden layer, and the output layer. There is no weight connection between the input layer to the hidden layer, and the input vector is mapped directly to the hidden layer. The mapping from the input layer to the hidden layer is nonlinear; i.e., the transformation function of the hidden layer is nonlinear. There are connection weights between the implicit layer and the output layer, and the mapping from the implicit layer to the output layer is linear; i.e., the output of the entire network is a linear weighted sum of the outputs of the implicit layer. The topology diagram with structural RBF neural network is shown in Figure 1.

This layer is mainly to pass the input samples to the hidden layer. Before that, data normalization, such as normalization, needs to be done on the input samples so that the input values of each node are in the same order of magnitude to avoid the effect of magnitude. The second layer is the hidden layer, the number of neurons in the hidden layer J varies with the application to be solved, and the activation function of each hidden node uses a radial basis function. The radial basis function is a nonnegative nonlinear function that is symmetric about the centroid and decays radially, which has a local response function. The implicit layer performs a nonlinear transformation of the input vector to map the low-dimensional input vector into the high-dimensional space, where it solves problems that would otherwise be unsolvable in the low-dimensional space.

$$h_j(X) = \varphi\left(\frac{\|X - c_i\|}{\sigma_j}\right),$$

$$y_k = \sum_{j=1}^{J} w_{ik} h_j(X). \tag{1}$$

The main difference between RBF neural networks and other feedforward neural networks is the hidden layer. The "base" of the implicit layer space is a radial basis function so that once the center of the radial basis function of each implicit layer node is determined, the input vector can be mapped to the implicit layer space without the need to connect through weights. The diversity of neural networks is reflected not only in the network model determined by the number of nodes in the hidden layer but also in the radial basis functions selected. The radial basis function of the RBF network is nonlinear, and there are many parameters to be set in the process of building the RBF neural network model, including the center and width of the radial basis function and the connection weights of the connection layer. Moreover, solving the outer weight of the random radial basis function neural network by the least square method is a linear operation, and it is very fast in the calculation. Compared with solving the center and smoothing factor of the neural network through supervised learning, this method can effectively improve the learning efficiency of the network. The choice of the center and width of the radial basis function seriously affects the performance of the RBF neural network [17]. At the early stage of the development of RBF, many scholars have incorporated many optimization algorithms for the parameter optimization of RBF neural networks. It was found that once the center and width of RBF were determined, the RBF neural network became a linear system of equations about the connection weights from the input to the output, at which time the connection weights of the output layer could be obtained by solving with the least-squares method or by training with gradient algorithms such as the gradient descent method. How to select the center and what training weight method to use became the research direction of many scholars on RBF network learning.

$$p_K(f, f_{wn}) = \sqrt{\int_K [f(x) - f_{wn}(x)]^2 dx},$$

$$h_x(y, \theta) = g\{\theta \cdot [x + y] \cdot (x - y)\} \prod_{i=1}^{m} \sqrt{\theta_j}. \tag{2}$$

To explore the function approximation ability of the random radial basis function neural network, the thought method of convergence proof of random weighted feedforward neural network is applied to prove that the random radial basis function neural network can approximate any continuous function. The convergence error between the stochastic radial basis function neural network and the approximated function can be known from the analysis process. As the number of neuron nodes n increases, the convergence error gradually decreases tending to 0. It is easy to reach the error range that one can accept, so the neural
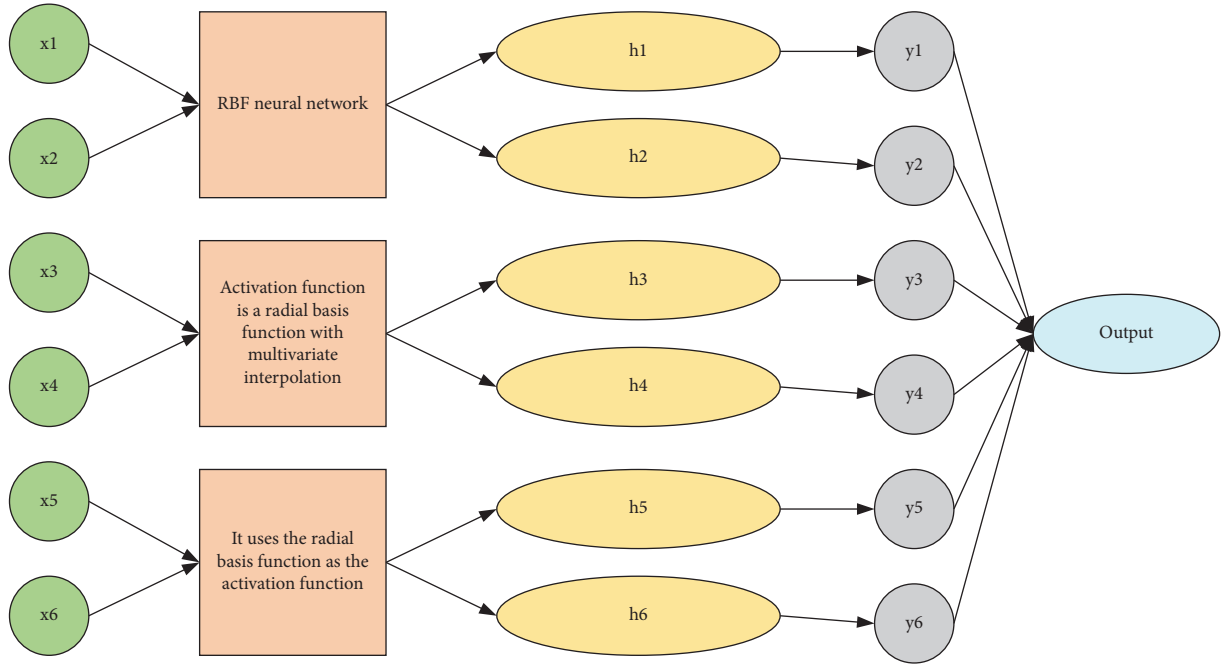
FIGURE 1: RBF neural network topology.

network is an efficient function approximator. The work has shown theoretically that the stochastic radial basis function neural network is capable of approximating arbitrary continuous functions and is also an efficient function approximator. To verify the above theoretical results, we give algorithms on how to solve for the weights of the output layer of the stochastic radial basis function neural network.

$$t_j = \sum_i^m \beta_i g\left(\frac{\|X_i + y_j\|}{\varsigma_i^2}\right),$$

$$H = \begin{bmatrix} g\left(\frac{\|X_i + y_j\|^1}{\varsigma_i^2}\right) & \cdots & g\left(\frac{\|X_i + y_j\|^3}{\varsigma_i^2}\right) \\ \cdots & \cdots & \cdots \\ g\left(\frac{\|X_i + y_j\|^2}{\varsigma_i^2}\right) & \cdots & g\left(\frac{\|X_i + y_j\|^5}{\varsigma_i^2}\right) \end{bmatrix}. \quad (3)$$

This idea has been used in several studies, such as the introduction of kernel methods for data classification in over-the-limit learning machines and stacked kernel networks (SKNs). However, a neural network model of the class of overdetermined learning machines, which essentially solves for a stochastic suboptimal solution of the network, is difficult to achieve the same results in large data. Stacked kernel networks, on the other hand, successfully apply kernel methods to classification tasks but also point out that the use of kernel methods can easily lead to overparameterization and overfit the network. Therefore, the introduction of kernel methods into deep learning models requires further exploration (Figure 2).

Therefore, instead of using these two ways of introducing kernel functions, this topic uses the ordinary radial base layer. Although this weakens the role of the kernel method, this cuts down the number of parameters in the model and makes it easier to avoid the problem of model overfitting due to overparameterization. In addition to the background related to the kernel method, the Gaussian function's properties are also of interest. In this way, the order of things based on the comparison feature is determined by the comparison result of a certain feature, and the order obtained from this comparison is used to judge the general situation of the membership function of these things for the specific feature, and then, the membership function is further constructed. To solve, the binary comparison ranking method is different according to the contrast measure. For example, the local approximation property, where the parameters associated with a local target space are only a small fraction of the total parameters, also fits some mechanisms of the organism. In terms of the mathematical nature of the function, the target of activation is not the data itself but the distance of the data from a particular central vector, and the fact that Gaussian functions have infinite order derivatives is also an advantage [18]. As a result, this topic proposes a radial basis self-encoder model, which consists of an input layer, a radial basis kernel function layer, and a self-coding layer, which is an improvement of the self-classical self-encoder model. Mathematically, in essence, the process of solving the model parameters is to solve the optimization problem shown in equation (4), which is often nonconvex, so it is important to choose a suitable solution. In this topic, we will combine the properties of Gaussian functions and use a gradient-based optimization algorithm for the parameter solution.
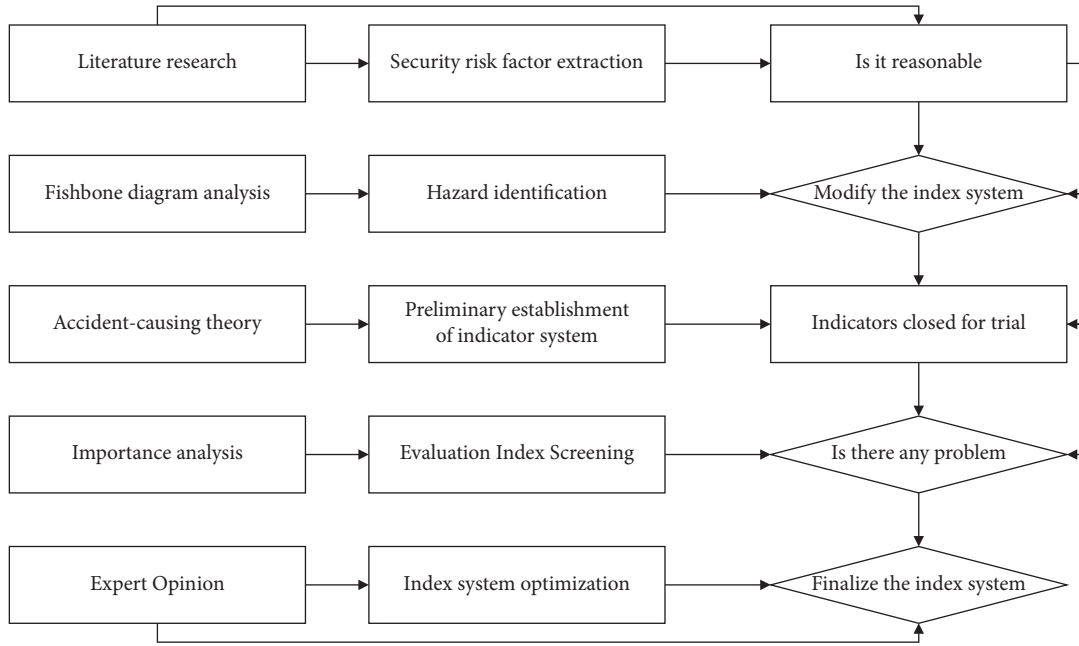
Figure 2: Flow of constructing safety risk assessment index system for tailing ponds.

$$\theta^* = \arg\max L\left(\theta^2, x_1, g^2\left(f\left(\phi\left(X\right)\right)\right)\right). \tag{4}$$

Like the classical self-encoder model, the training of the radial-based self-encoder model proposed in this paper also employs a back-propagation algorithm and uses a gradient-based training method. The data first go through a forward propagation process to get the output under the current model parameters, then, some loss function is used to measure the deviation of the current output from the true value, and then, the current model parameters are corrected and the next calculation is performed through a backward propagation process, and such an iterative process continues until a specific condition is satisfied and terminated. In this topic, the Gaussian function is chosen as the activation function for the radial basis function layer, and since the Gaussian function contains two hyperparameters center vector and variance, which can be selected in various ways, this section will discuss the methods for selecting these two hyperparameters as well as the overall network optimization methods (including loss function selection, activation function selection for the classical layer, and gradient-based methods for overall network parameter optimization).

3.2. Experimental Design for the Evaluation of Environmental Restoration and Treatment Effects of Decommissioned Uranium Tailings Ponds. ISO 14001 is the number of environmental management systems certified by the International Organization for Standardization. It is a standard developed in response to the global environmental damage and environmental pollution that is becoming more and more serious, global warming, destruction of the ozone layer, reduction of biodiversity, and other major ecological and environmental problems that threaten the future survival and sustainable development of mankind, to comply

with the development of international environmental protection, to take the road to sustainable development, and following the needs of international economic and trade development. ISO 14001 states that environmental performance is the measurable effectiveness of an organization's environmental management system based on environmental policies, objectives, and targets to control its environmental factors. The "organization" is the actor, which can be either a company or a government (department). The source of environmental performance varies from subject to subject [19]. Depending on the source of environmental performance, environmental performance is divided into organizational environmental performance and regional environmental performance.

Some scholars define environmental performance as an evaluation indicator of production efficiency that takes environmental issues into account and is used to analyze some of the problems of economic development in harmony with the environment, with its meaning being mainly the ratio of the economic value of products and services that meet human needs to the environmental load, i.e., the corresponding economic benefit per unit of environmental impact. The definition states that to improve environmental performance, people must take the initiative to control environmental pollution and protect the environment while carrying out development. Through the scientific and reasonable evaluation of the environmental efficiency of enterprises, individuals, or related organizations in the work of environmental management assessment, we can find out some necessary links between the situation of environmental protection and economic growth and some key problems of mutual constraints and influences between the two, to further provide new reference basis for managers or plan makers and then on a certain basis to revise. Obviously, it has been unable to meet the needs of ecological environment

protection and sustainable development for the decommissioning of uranium tailings ponds. Whether it is from the perspective of protecting the ecological environment or protecting the safety of public life and property, the analysis and research on the stabilization process and stability status of decommissioned uranium tailings ponds are of great research significance. Therefore, environmental performance assessment is a rather important way and assessment tool for individuals, enterprises, institutions, and projects, as shown in Figure 3.

As a systematic process for assessing and measuring environmental performance in all aspects of an organization's internal economy, environmental performance assessment provides a reliable and optimal guide for program design and implementation of economic investments, etc. within an organization. The process includes the selection of parameters, data collection and statistical analysis, information evaluation based on environmental performance guidelines, evaluation reports, and academic communication, and targeted periodic review and improvement of the evaluation process. As an internal implementation process and management tool, the purpose of environmental performance assessment is to provide managers with reliable and verifiable external environmental information of varying relevance to assess the gaps and shortcomings between an organization's environmental performance and the standards set by the organization's managers and to make further improvements and optimizations [20]. In the whole process of collecting and evaluating information, environmental performance assessment has a clear continuous (including past, present, and future) character compared to other methods. The purpose of environmental performance assessment is to provide a detailed description of the strengths and weaknesses of environmental conditions, to reveal the overall situation of environmental policies and environmental changes, to significantly improve the environmental awareness of all sectors of society, and to scientifically measure the level of management of organizations and their environmental managers. A sound environmental performance assessment is a prerequisite for the objective and effective management of organizations and projects.

The concept of stabilization of uranium tailings ponds only considers their mechanical properties, and only the mechanical stability index of tailings ponds as the evaluation index of the safety of decommissioned uranium tailings ponds can no longer meet the needs of ecological environmental protection and sustainable development of decommissioned uranium tailings ponds. The concept and connotation of environmental stabilization of decommissioned uranium tailings ponds proposed in this paper objectively reflect the necessity of evaluating the environmental stability of decommissioned uranium tailings ponds, which requires comprehensive consideration of environmental radiation, effluents, and other factors, to establish a reasonable evaluation index system, which is also the key to the evaluation of the stability of decommissioned uranium tailings ponds. The evaluation index system should be based on a system perspective, on the one hand, to grasp the key factors, and on the other hand to consider all other factors,
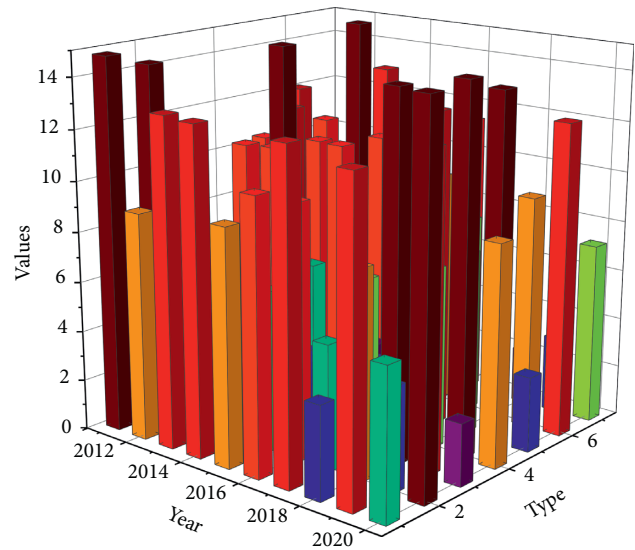

FIGURE 3: Statistics on environmental indicators.

so that the evaluation index system can reflect the actual situation of the evaluated object comprehensively and objectively. For the uranium tailings pond system, the index system should comprehensively include seepage water environmental indicators, atmospheric environmental indicators, and radiation environmental indicators (Figure 4).

The number of indicators in the indicator system should be reduced as much as possible, and the core impact indicators should be highlighted, so as not to make the evaluation indicator system too large and affect the accuracy of the evaluation results, and to avoid the interrelationship between indicators so that the selection of indicators is both adequate and necessary. For uranium tailing ponds, on the premise of including the main environmental monitoring indicators and the indicators with greater impact on the environment of uranium tailing ponds, irrelevant or harmless environmental indicators should be reduced as much as possible. The indicator system is used to describe social phenomena, and science is the premise and basis for the existence of the indicator system. Therefore, it is necessary to start from the actual situation, and the constructed indicator system should be able to objectively reflect the actual situation, while the indicators included should be in line with the scientific and theoretical basis. The uranium tailings pond is a complex system, and the indicator system should be able to analyze and compare with existing theories and methods, while the indicators with inclusive relationships should be deleted appropriately, and cross-over information should be avoided between each layer of indicators [21]. The process of constructing the indicator system is essentially the process of decomposing the top target layer by layer, so the evaluation indicator system is also a multilayer and multi-indicator system, analyzing the complex evaluation problems layer by layer, considering them comprehensively, grasping the key points, and considering both qualitative and quantitative indicators. Through the analysis of the change law of the environmental monitoring project of uranium tailings pond over time, the
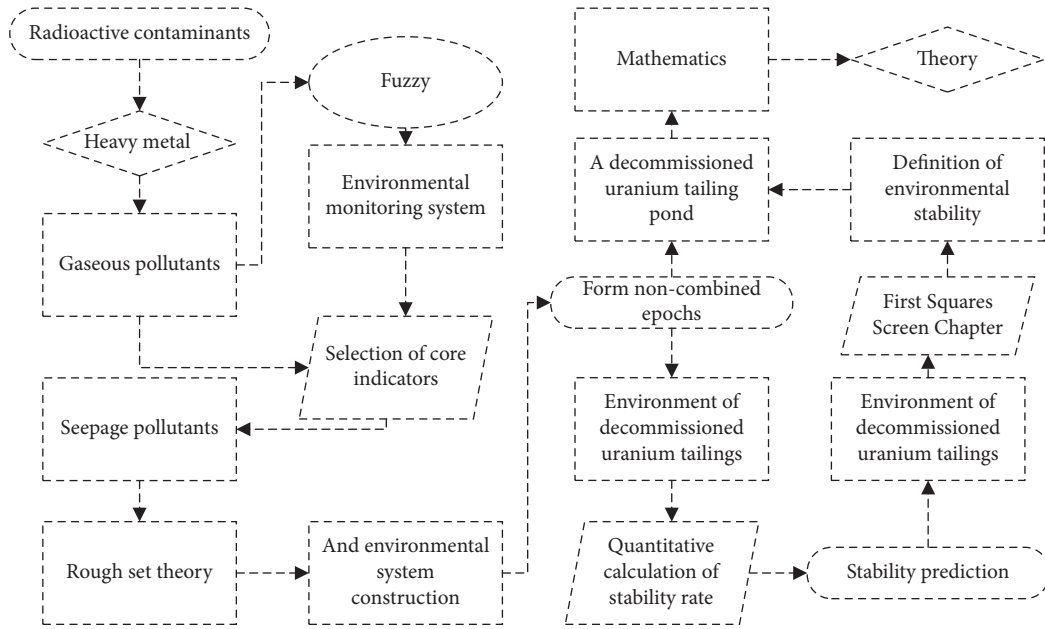
FIGURE 4: Technical roadmap for environmental stability analysis and prediction of decommissioned uranium tailings ponds.

characterization of the environmental stabilization process of the uranium tailing pond is analyzed, and the new concept and connotation of the environmental stability of the uranium tailing pond are comprehensively and systematically put forward. There is an environmental stability evaluation index system for decommissioned uranium tailings ponds. According to the actual situation of uranium tailings ponds, the environmental indicator system can usually be decomposed into three levels, and the decomposition process is from coarse to fine, from macro and micro, and from general to specific.

Fuzzy mathematics takes uncertainty as its research object; it uses precise mathematical language to describe fuzzy phenomena, so it can better reflect the objective fuzzy phenomena. For uranium tailings ponds, because of the complex environmental factors, how to define the stability of each environmental monitoring index and the comprehensive stability of the environment is itself a difficult problem to determine, and the use of fuzzy mathematical theory can make up for the shortcomings of exact mathematics and stochastic mathematics by making the fuzzy objects exact. In fuzzy mathematics, there are many branches such as fuzzy topology, fuzzy group theory, fuzzy graph theory, fuzzy probability theory, fuzzy linguistics, and fuzzy logic. After decades of development, they have been widely used in many neighborhoods. This thesis is theoretically feasible to use fuzzy mathematical theory to analyze the environmental stability of uranium tailing ponds.

4. Results and Analysis

4.1. Performance Results of Radial Basis Function Neural Network Algorithm with Genetic Algorithm. For these three datasets, we simplify the centroids of the hidden layer neurons in the random radial basis function neural network, and the smoothing factors uniformly distributed between

$[−1, 1]$ and $[0, 1]$, respectively. Thirty trials were conducted for each training and test set, and then, the median was taken as the result to reduce the effect due to random errors. The results of the performance test of the random radial basis function neural network are shown in Figure 5. During the task of fitting the cos (z) function of the random radial basis function neural network, the training error becomes smaller and smaller as the number of neuron nodes in the hidden layer gradually increases, and the fitting results become better and better. Observing Figure 5, it can be found that when the number of neuron nodes is small, the fit is inadequate, and as the number of neuron nodes increases, the fitting result of the random radial basis function neural network is gradually able to match the cos (a) function. It should be noted that the fitting results are not the same for each training here because of the random selection of some parameters in the network, and we have selected one of the cases for the graph.

To be able to better represent the performance of the stochastic radial basis function neural network, the Spectra dataset was selected to test its fit. Unlike the dataset with one-dimensional cos (z) functions for both input and output, the Spectra dataset has a higher dimensionality than the actual data. Figure 5 directly illustrates how the training error gradually decreases as the number of hidden layer neuron nodes increases during the fitting of the random radial basis function neural network to the Spectra training set.

The generalization of the random radial basis function neural network on this Spectra test set is also very good, and the generalization results can match the test set data. It illustrates the equally satisfactory results of the random radial basis function neural network in the classification task. In the classification dataset, the recognition rate in its training set can reach almost 100% with the increase of neuron nodes in the hidden layer of the network, and the highest
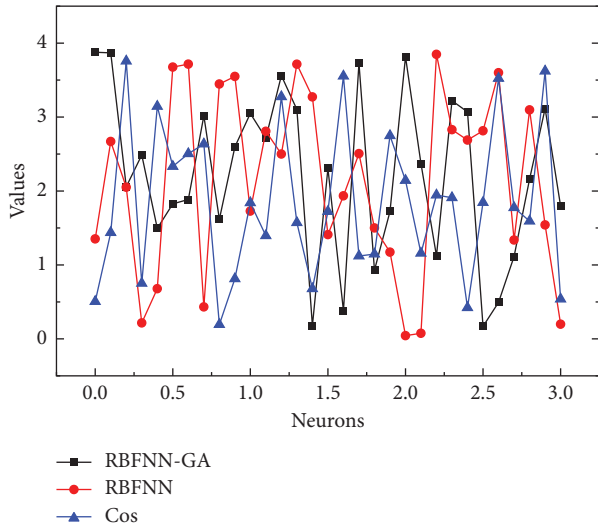
FIGURE 5: Results of the function training set fitting.

FIGURE 6: Training error and recognition rate of Spectra dataset under RBFNN algorithm.

recognition rate in the test set is close to 90%. Observation of the recognition rate in the test set reveals that the curve has a first increase and then decrease, which is because, with the increase of the number of hidden layer nodes, the weights of the output layer of the random radial basis function neural network derived by the simple RBFNN algorithm can easily lead to the overfitting phenomenon of the neural network. From Figure 6, the training time of the random radial basis function neural network is very short in the training tasks of both the Spectra dataset and Iris dataset, reflecting its fast-learning ability. According to the two curves toward the situation, the training time of the neural network increases gradually with the number of neuron nodes. The input dimension of Spectra is 401 dimensions and the output dimension of Iris is 4 dimensions. But the difference in training time between the two is only in the microsecond level, which is enough to show that the random radial basis function neural network has great potential to handle large data set tasks.

The random selection of some parameters in the radial basis function neural network is an important complement to the existing how to determine the radial basis function neural network center and smoothing factor. Improving its shortcomings and deficiencies, improving the governance effect, and ensuring the stability of the environmental impact after the decommissioning of the uranium mining and metallurgical tailings pond are of great significance to ensure the people's life, health, and safety. Unlike traditional BP neural networks, this random setting of radial basis function centers and smoothing factors makes it possible to calculate only one parameter, the output layer weight, in a radial basis function neural network with a three-layer network structure, which drastically reduces the number of parameters to be solved in the network. And solving the stochastic radial basis function neural network outer weights by least squares is a linear operation, which is very fast in computation. Compared to solving the center and smoothing factors of a neural network through supervised learning, taking this approach can effectively improve the learning efficiency of
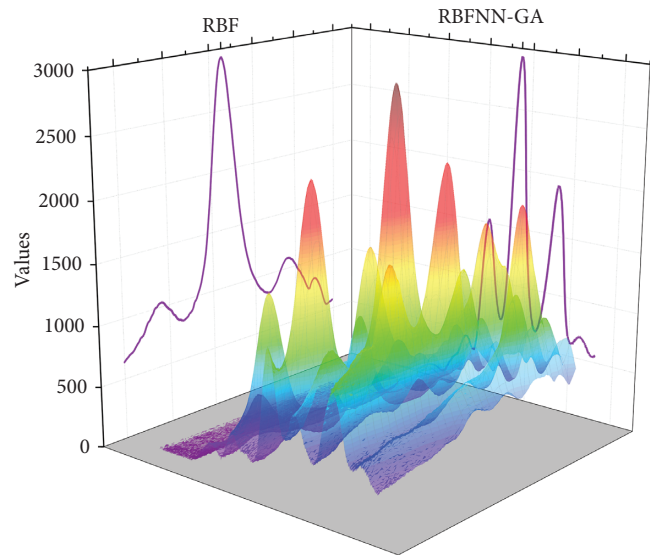
the network, making it a great potential for handling big data tasks. In this paper, we use the properties of generalized functions to construct a limit integral expression for the approximated function; secondly, we use Monte Carlo methods to compute the integrals in this expression and theoretically prove that this random radial basis functions neural network is not only capable of approximating arbitrary continuous functions but also an efficient function approximator. And the random radial basis function neural network is tested by fitting and classifying simulation by selecting different data sets. The results show that the stochastic radial basis function neural network does exhibit good performance.

4.2. Results of the Evaluation of the Environmental Rehabilitation and Treatment Effects of Decommissioned Uranium Tailings Ponds. Benchmarking, also known as benchmarking, is a method of environmental performance assessment in which an organization sets itself an example and a goal to strive for in its development process, with the basic idea of systematic optimization, continuous improvement, and continuous improvement. Benchmarking is unique in its assessment method, which is achieved through comparison. The first step in the benchmarking method is to identify a benchmark, usually a leading organization in the field, as a goal for the organization to strive for. At the end of each implementation phase, the results are compared with the identified benchmark, and a phase summary assessment is conducted to adjust the next phase of the approach until finally the benchmark level is reached and a higher benchmark is identified, as shown in Figure 7.

The binary comparison ordering method is more practical in the method of determining the affiliation function, which is implemented by making a reasonable two-by-two comparison of certain specific features between multiple things, to determine the order of things
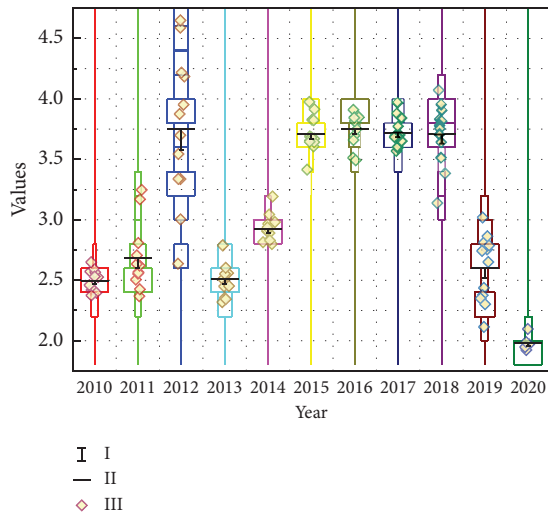
Figure 7: Classification of environmental performance benchmarking levels.

Figure 8: Changes in monitoring values.

based on this comparison feature with the comparison result of certain features, and the order obtained from this comparison is used to judge the approximate situation of these things for the affiliation function under this specific feature and further then construct the affiliation function for solving; the binary comparison ranking method can be divided into relative comparison method, comparison average method, priority relationship ordering method, and similar priority comparison method according to different comparison measures, as shown in Figure 8. The RBF neural network was proposed based on the characteristics of the human brain's neuronal cells that have a local response. It simulates the local approximation neural network structure of the human brain that is locally adjusted and covers the receptive domains.

As a result, a large amount of acidic wastewater is generated, which flows through a special pipeline to the wastewater treatment plant, where it is degraded and precipitated so that the heavy metals in it are precipitated and neutralized using lime, and then, the treated wastewater is discharged to the tailings pond. The wastewater migrates from the outfall to each section of the tailings reservoir, and the distance from each dam section to the outfall varies, resulting in different degrees of contamination. Dam B is located at the southwest end of the tailings dam, and due to the distance, the wastewater needs to flow for some time to reach this dam section, so the change in the pH of the water body is relatively flat, and because the wastewater contains more free state ammonia ions. The larger the concentration of ammonia ions, the more $H+$ produced by hydrolysis, and the more severe the acidification of the water body. The variation of pH values with time was plotted based on the monitored raw data. A new method for environmental stability analysis of uranium tailings ponds is proposed, and the stability intervals of indicators and environmental stability rates are defined in precise mathematical language, which is of positive significance for further
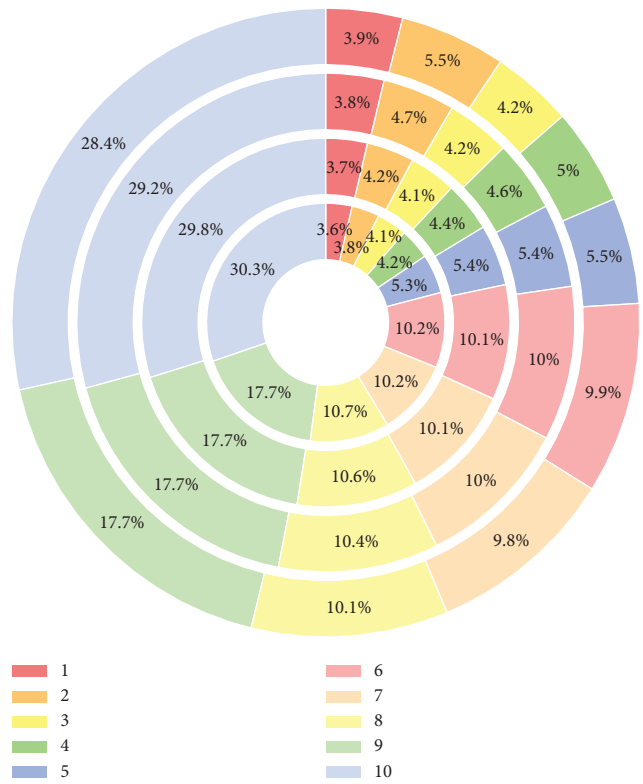
enriching and improving the comprehensive evaluation techniques of decommissioned uranium tailings ponds.

5. Conclusion

The research work in this paper mainly analyzes the environmental stabilization process and stability of decommissioned uranium tailing ponds, proposes a new concept of environmental stability with ecological and environmental protection concept and gives it a new connotation, establishes an evaluation index system of environmental stability of decommissioned uranium tailing ponds through index screening using rough set theory, integrates the influence of environmental factors such as external wastewater and exhaust gas, and realizes the multifactor. The system of evaluation indexes for the stability of decommissioned uranium tailing ponds was established by combining multiple factors; the long-term monitoring and model verification of the environmental stabilization process of decommissioned uranium tailing ponds were carried out by using mathematical methods, and the change law of the stability of environmental parameters over time was studied; the connotation of environmental stability was further deepened and supplemented; uncertainty theories such as statistical theory and fuzzy mathematics were applied to construct a comprehensive evaluation model for the stability of decommissioned uranium. There are an input layer, hidden layer, and output layer. There is no need for a weight connection between the input layer and the hidden layer, and the input vector is directly mapped to the hidden layer.

A comprehensive evaluation model of the stability of a decommissioned uranium tailings pond was constructed by applying statistical theory, fuzzy mathematics, and other uncertainty theories, and a prediction model of the environmental stability was established by using BP neural network. The average error rate of the predicted environmental stability rate was only 6.27%. Based on the principle of maximum affiliation, the predicted stability level was the same as the expected stability level of the sample, and the overall prediction results were consistent with the actual situation, which further verified the applicability and feasibility of the method. The degree of influence of environmental indicators on the environmental stability of uranium tailings ponds was also analyzed using the univariate method, which provides a new method and technique for the comprehensive evaluation and decommissioning management of uranium tailings ponds.

Data Availability

The data used to support the findings of this study are available from the corresponding author upon request.

Conflicts of Interest

The author declares that there are no conflicts of interest.

Acknowledgments

References

[1] E. S. Festin, M. Tigabu, M. N. Chileshe, S. Syampungani, and P. C. Odén, "Progresses in restoration of post-mining landscape in Africa," *Journal of Forestry Research*, vol. 30, no. 2, pp. 381–396, 2019.

[2] V.-B. Pentyala and S. Eapen, "High efficiency phytoextraction of uranium using Vetiveria zizanioides L. Nash," *International Journal of Phytoremediation*, vol. 22, no. 11, pp. 1137–1146, 2020.

[3] M. A. Trenfield, C. J. Pease, S. L. Walker et al., "Assessing the toxicity of mine-water mixtures and the effectiveness of water quality guideline values in protecting local aquatic species," *Environmental Toxicology & Chemistry*, vol. 40, no. 8, pp. 2334–2346, 2021.

[4] A. Sun and J.-F. Chang, "Application of radial basis function neural network to predict exchange rate with financial time series," *International Journal on Smart Sensing and Intelligent Systems*, vol. 10, no. 2, pp. 308–326, 2017.

[5] A. Hashemi Fath, F. Madanifar, and M. Abbasi, "Implementation of multilayer perceptron (MLP) and radial basis function (RBF) neural networks to predict solution gas-oil ratio of crude oil systems," *Petroleum*, vol. 6, no. 1, pp. 80–91, 2020.

[6] H. C. Huang and S. K. Lin, "A hybrid metaheuristic embedded system for intelligent vehicles using hypermutated firefly algorithm optimized radial basis function neural network," *IEEE Transactions on Industrial Informatics*, vol. 15, no. 2, pp. 1062–1069, 2018.

[7] M. Dua, R. Gupta, M. Khari, and R. G. Crespo, "Biometric iris recognition using radial basis function neural network," *Soft Computing*, vol. 23, no. 22, pp. 11801–11815, 2019.

[8] R. Sitharthan, T. Parthasarathy, S. Sheeba Rani, and K. Ramya, "An improved radial basis function neural network control strategy-based maximum power point tracking controller for wind power generation system," *Transactions of the Institute of Measurement and Control*, vol. 41, no. 11, pp. 3158–3170, 2019.

[9] L. N. Elisov, V. I. Gorbachenko, and M. V. Zhukov, "Learning radial basis function networks with the trust region method for boundary problems," *Automation and Remote Control*, vol. 79, no. 9, pp. 1621–1629, 2018.

[10] C. She, Z. Wang, F. Sun, P. Liu, and L. Zhang, "Battery aging assessment for real-world electric buses based on incremental capacity analysis and radial basis function neural network," *IEEE Transactions on Industrial Informatics*, vol. 16, no. 5, pp. 3345–3354, 2019.

[11] B. T. Pham, A. Shirzadi, D. Tien Bui, I. Prakash, and M. B. Dholakia, "A hybrid machine learning ensemble approach based on a radial basis function neural network and rotation forest for landslide susceptibility modeling: a case study in the Himalayan area, India," *International Journal of Sediment Research*, vol. 33, no. 2, pp. 157–170, 2018.

[12] M. Mohammadi, A. Krishna, S. Nalesh, and S. K. Nandy, "A hardware architecture for radial basis function neural network classifier," *IEEE Transactions on Parallel and Distributed Systems*, vol. 29, no. 3, pp. 481–495, 2017.

[13] B. H. Chen, S. C. Huang, C. Y. Li, and S. Y. Kuo, "Haze removal using radial basis function networks for visibility restoration applications," *IEEE transactions on neural networks and learning systems*, vol. 29, no. 8, pp. 3828–3838, 2017.

[14] A. Rubio-Solis, P. Melin, U. Martinez-Hernandez, and G. Panoutsos, "General type-2 radial basis function neural network: a data-driven fuzzy model," *IEEE Transactions on Fuzzy Systems*, vol. 27, no. 2, pp. 333–347, 2018.

[15] H. R. Baghaee, M. Mirsalim, G. B. Gharehpetian, and H. A. Talebi, "Unbalanced harmonic power sharing and voltage compensation of microgrids using radial basis function neural network-based harmonic power-flow calculations for distributed and decentralised control structures," *IET Generation, Transmission & Distribution*, vol. 12, no. 7, pp. 1518–1530, 2018.

[16] V. I. Gorbachenko and M. V. Zhukov, "Solving boundary value problems of mathematical physics using radial basis function networks," *Computational Mathematics and Mathematical Physics*, vol. 57, no. 1, pp. 145–155, 2017.

[17] W. Zhang and D. Wei, "Prediction for network traffic of radial basis function neural network model based on improved particle swarm optimization algorithm," *Neural Computing & Applications*, vol. 29, no. 4, pp. 1143–1152, 2018.

[18] L. Nie, J. Guan, C. Lu, H. Zheng, and Z. Yin, "Longitudinal speed control of autonomous vehicle based on a self-adaptive PID of radial basis function neural network," *IET Intelligent Transport Systems*, vol. 12, no. 6, pp. 485–494, 2018.

[19] L. Ortombina, F. Tinazzi, and M. Zigliotto, "Magnetic modeling of synchronous reluctance and internal permanent magnet motors using radial basis function networks," *IEEE Transactions on Industrial Electronics*, vol. 65, no. 2, pp. 1140–1148, 2017.

[20] Y. Chu, J. Fei, and S. Hou, "Dynamic global proportional integral derivative sliding mode control using radial basis function neural compensator for three-phase active power filter," *Transactions of the Institute of Measurement and Control*, vol. 40, no. 12, pp. 3549–3559, 2018.

[21] M. Smolik and V. Skala, "Large scattered data interpolation with radial basis functions and space subdivision," *Integrated Computer-Aided Engineering*, vol. 25, no. 1, pp. 49–62, 2018.

Research Article

Research on GDP Forecast Analysis Combining BP Neural Network and ARIMA Model

Shaobo Lu (ID)

Cardiff University Business School, Cardiff CF10 3AT, Wales, UK

Correspondence should be addressed to Shaobo Lu; lus14@cardiff.ac.uk

Based on the BP neural network and the ARIMA model, this paper predicts the nonlinear residual of GDP and adds the predicted values of the two models to obtain the final predicted value of the model. First, the focus is on the ARMA model in the univariate time series. However, in real life, forecasts are often affected by many factors, so the following introduces the ARIMAX model in the multivariate time series. In the prediction process, the network structure and various parameters of the neural network are not given in a systematic way, so the operation of the neural network is affected by many factors. Each forecasting method has its scope of application and also has its own weaknesses caused by the characteristics of its own model. Secondly, this paper proposes an effective combination method according to the GDP characteristics and builds an improved algorithm BP neural network price prediction model, the research on the combination of GDP prediction model is currently mostly focused on the weighted form, and this article proposes another combination, namely, error correction. According to the price characteristics, we determine the appropriate number of hidden layer nodes and build a BP neural network price prediction model based on the improved algorithm. Validation of examples shows that the error-corrected GDP forecast model is also better than the weighted GDP forecast model, which shows that error correction is also a better combination of forecasting methods. The forecast results of BP neural network have lower errors and monthly prices. The relative error of prediction is about 2.5%. Through comparison with the prediction results of the ARIMA model, in the daily price prediction, the relative error of the BP neural network prediction is 1.5%, which is lower than the relative error of the ARIMA model of 2%.

1. Introduction

GDP refers to the market value of all products and services produced by a country or region in a certain period of time using production factors. GDP not only is the accuracy of demand forecasting, but also provides a reference and basis for countries and regions in the deployment of strategic guidelines and the formulation of macroeconomic policies [1]. In addition, the statistics of GDP are more accurate and the calculation repeatability is small, so statistics are relatively easy [2]. GDP and economic growth rate, inflation rate, and unemployment rate are the main macroeconomic operation indicators that are closely related and are the most basic indicators [3]. In order to meet the requirements of social development and meet the needs of more accurate predictions, some prediction problems have introduced

computer technology, mathematical methods, and logical reasoning. The gradual development and maturity of these systems have led many countries in the world to establish various predictions. Research departments provide decision-making references for economic development, provide strength support for strategic research, and guide enterprises and the country's current and future social activities to maximize utility [4–6].

In GDP forecasting, a single model is used for forecasting. When generating forecast results, we often discard the forecast errors. We think that the useful information has been extracted. In fact, the error contains a small part of the information, and it is still desirable [7–9]. Therefore, some scholars integrate existing prediction methods and use the promotion and complementation of different information to improve the prediction accuracy of the model. Many

scholars have added error correction models when making GDP predictions [10]; the results show that the addition of the error correction model can significantly improve the accuracy of GDP prediction. Gao [11] et al. used a combination of ARIMA model and neural network in the forecast of tourism demand. Qin [12] et al. used SARIMABP to construct seasonal error correction time prediction model. In their article on carbon emissions prediction, they divided the data into linear and nonlinear parts, making full use of the good advantages of time series linear forecasting to make preliminary predictions, and then through the neural network implements error correction, the results show that the participation of the neural network is much better than the prediction effect of ARIMA alone. Yang [13] first used the adaptive filtering method to complete the preliminary prediction on the prediction data and then used Markov chain to correct the residuals generated after the preliminary prediction, and the result shows the feasibility of the method. Wang [14] further discussed the variable weight GDP forecast model and gave corresponding theoretical proofs and practical applications. Wang [15] proposed a generalized recursive reciprocal variance GDP prediction method on the basis of recursive equal weight GDP prediction and recursive reciprocal variance GDP prediction and deduced the iterative formula, starting from the GDP prediction accuracy. A combination model with the objective function as the predictive effectiveness index is established, and the optimal approximate solution of the weights is obtained. Some scholars comprehensively consider the mathematical expectation and standard deviation of GDP forecast accuracy, establish a multiobjective optimization GDP forecast model, derive its mathematical programming solution, and introduce entropy theory, and according to the degree of variation of the error sequence of the single forecast model, we obtain the weighting coefficient of each single model [16–19].

This paper studies and analyzes the artificial neural network model, especially the operating mechanism of BP neural network, compares its advantages with traditional forecasting methods, constructs a GDP forecast model, and discusses the setting rules of various parameters in the model. Experiments analyze the feasibility and superiority of artificial neural network in the field of GDP prediction and compare the prediction accuracy of BP neural network and traditional time series forecasting method. In the selection of prediction methods, the comparison is based on the superiority of the algorithm's BP neural network and the prediction accuracy of the BP neural network and the ARIMA prediction model. In order to reduce the prediction error and improve the accuracy of the model, this paper proposes a combination prediction model and a combination coefficient method to find a suitable model based on the information characteristics of the sequence value itself. From the final fitting results, it can be seen that the predicted value and the true value are very consistent; the true value falls within the 95% confidence interval, which fully shows that the model combination effect is good and the prediction accuracy is high. This empirical study shows that the ARIMA model and the ARIMAX model can be applied in actual work to make short-term macroforecasts.

2. Construction of the GDP Prediction Model Based on the BP Neural Network and ARIMA Model

2.1. BP Neural Network Spatial Sequence. The BP neural network is a computer-based processing system created by imitating the human brain. It is trained to understand the operating rules of the real system [20]. Figure 1 shows the spatial architecture of the BP neural network. Its outstanding ability is reflected in the prediction of nonlinear time series. It has strong predictive ability for exponentially increasing trend models, high accuracy, and strong fault tolerance, and fast information processing speed and can process quantitative and qualitative information at the same time, without the need to consider the system for problem of decoupling. The disadvantage is that the learning speed is very slow, the network training is very likely to fail, and it is more difficult to find the global minimum [21–24].

The establishment of the dynamic regression model is based on the assumption that there is a long-term equilibrium relationship between the response sequence and the independent variable sequence; that is to say, not all sequences can establish a dynamic regression model, only those sequences that have a long-term equilibrium relationship. It is suitable for establishing dynamic regression model [25, 26].

$$f(x \mid n) = \{x(1), x(2), \ldots, x(n) \mid n \in R\}, \tag{1}$$

$$Y(x) = \sum_{x=1, y=1}^{n} p(y \mid x) \times f(y \mid x). \tag{2}$$

According to the introduction of the one-time exponential smoothing model, it is suitable for stationary series without changing trend. In order to apply to the time series with obvious upward or downward trend, a double exponential smoothing model is proposed. The double exponential smoothing model uses the first exponential smoothing model to process the data after the first exponential smoothing model for the second time [27, 28].

$$|x(1) - f(x)| + |x(2) - f(x)| + \cdots + |x(n) \\ - f(x)| = n \times f(x), \tag{3}$$

$$\frac{g(x) - \sum_{i,j=1}^{n} [s(1, i) + s(2, i) + \cdots + s(j, i)]}{s(i, j)} = 0. \tag{4}$$

Since random fluctuations are not actually measurable, when we actually make a model, we usually set the value of the unobserved value to 0 and then perform the least squares. This estimation is called because of the addition of the preconditions. When we are building a model, it is impossible to try all models. The first thing we have to do is to determine the selected model form and then determine the order of the model. Generally for this step, we usually call it the model order. It can be determined based on the ACF diagram and the PACF diagram.
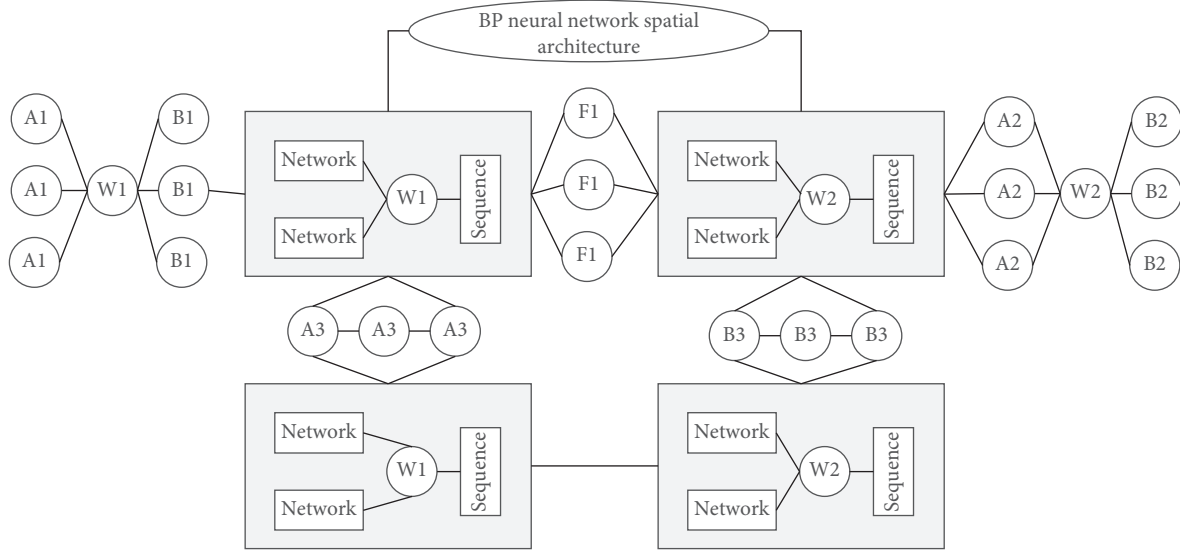
FIGURE 1: BP neural network spatial architecture.

$$\sigma(x, y) = \frac{1}{E} \times (\varepsilon(x, x) - t(\varepsilon(y, y))), \tag{5}$$

$$\{\sigma(x, x), \sigma(y, y), \sigma(z, z)\} \longrightarrow \{\varepsilon(x, y), \varepsilon(y, z), \varepsilon(z, x)\}. \tag{6}$$

With the observation sequence, we have to study the properties of these sequences, but the properties of random sequences cannot be obtained intuitively. In this way, we indirectly study the properties of his observation sequence and then infer randomness through the properties of the observations. When a group of data containing gray information is obtained, this group of data is usually irregular, but there is always some kind of generation to process the data to make it regular.

$$U = \frac{1}{2} \times \int_{\Omega} \sigma(z, x) \sigma(x, y) \sigma(y, z) d\Omega. \tag{7}$$

Based on this feature, we can process the data to build an equation generation model to achieve the fundamental mode of predicting the future. In general, the model constructed by the gray model is similar to a differential equation.

2.2. ARIMA Algorithm Structure Distribution. The Auto Regressive Integrated Moving Average model is abbreviated as the ARIMA (p, d, q) model, where p, d, and q represent the order of the autoregressive model, the order of the difference, and the order of the moving average model, respectively; ARIMA(p, d, q) model is essentially a combination of difference operation and autoregressive moving average. First, the sequence is subjected to d difference processing, transforms it into a stationary time series, determines the values of p and q according to the obtained stationary time series, and then uses the ARMA(p, q) model to predict and analyze the stationary time series. The aforementioned AR(p) model, MA(q) model, and ARMA(p, q) model are all stationary series. For nonstationary series, it is usually processed by difference processing several times first to convert them into stationary series. AR(p), MA(q), and ARMA(p, q) models are all established on the assumption that the time series are stationary. Table 1 shows the composition of the time series factors.

There are a large number of nonstationary series in practical problems, so it is necessary to use a time series model suitable for nonstationary series. That is, the nonstationary sequence becomes a stationary sequence after d-order difference processing; then it is called the d-order single integer sequence. If a sequence can be transformed into a stationary sequence after several difference operations, then the sequence is called a homogeneous nonstationary sequence, and the number of previous differencing operations is called the homogeneous order. In the actual economic situation, the time series we get are usually nonstationary. In real life, most time series are nonstationary, showing trend or periodic characteristics, such as economic development data, electricity consumption, and passenger travel volume. The characteristic of ARIMA is that when dealing with nonstationary time series, it is first differentiated into a stationary time series, and then AR, MA, and ARMA model theories are used for modeling and analysis. Figure 2 shows the structure topology of the ARIMA algorithm.

When predicting a stationary time series, the longer the prediction time is, the more the unknown information is represented. So a modified prediction is proposed; that is, as time develops, we can gradually get a real value, put this true value together with the previously known sequence value, refit the model, and then predict the value after again, and when the true value is obtained again, refit the model again, until the required predicted value until. If we use some methods to simplify the complex, convert the nonstationary

TABLE 1: Time series factor composition.

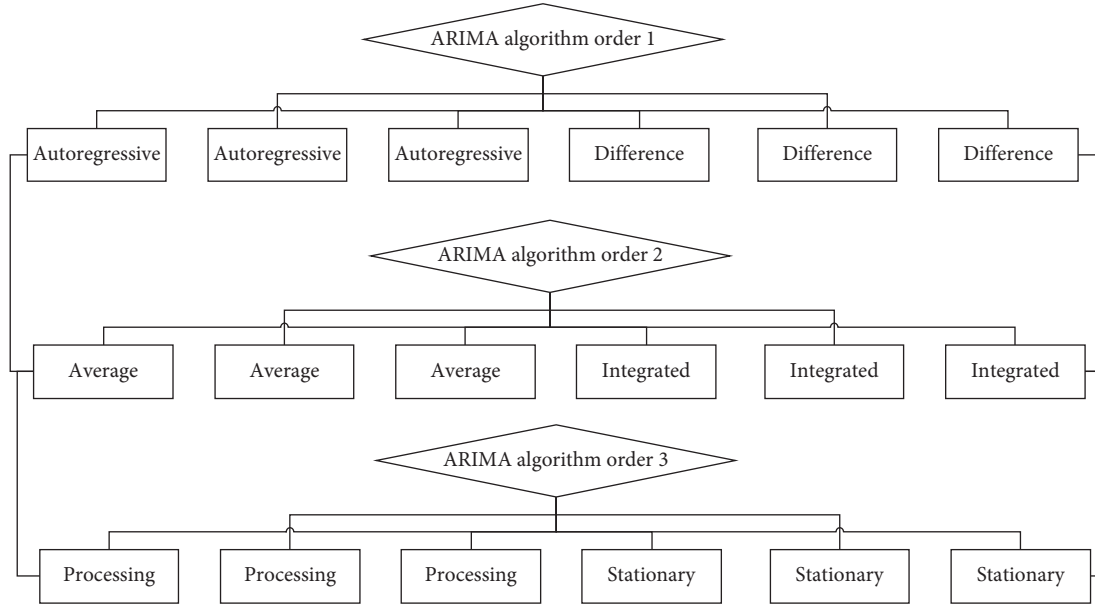| Factor index	Network sequence	Coefficient	Significance level
1	AR	1.71	0.58
2	MA	2.43	0.43
3	AR (D)	1.63	0.39
4	MA (Q)	1.56	0.54

FIGURE 2: ARIMA algorithm structure topology.

to the stationary, and then use the ARMA model for fitting, we can solve the above problems. In the exponential smoothing model, the parameter smoothing coefficient can not only reflect the speed of response to changes in the time series, but also affect the ability to correct random errors. The magnitude of a determines the degree of influence of the new and old data on the forecast results.

2.3. GDP Forecast and Evaluation Method. According to the differences in GDP forecast goals and characteristics, people divide GDP forecasts into qualitative forecasts and quantitative forecasts. Qualitative forecasting is a subjective forecasting method, which is mainly used in the absence of historical data. In the event of statistical data, it is suitable for short, medium, and long-term forecasting. Quantitative forecasting is mainly based on a large amount of data through a mathematical model to explore the law between the data. The fitting and prediction of the sequence are the ultimate goal of analyzing the time series. After the model has passed the significance test, the sequence can be fitted. Combining several methods with an appropriate weight, combining geometric empirical mode decomposition and support vector regression method, the prediction index has good fit and accuracy. If the fitting effect is good, the model can be predicted; that is, according to the experience summarized in the forecasting work, when the data series

shows a stable trend and no obvious fluctuations, it is more appropriate to choose between 0.1 and 0.3; when the data series shows a stable trend but there are obvious fluctuations, it should be between 0.3 and 0.5; when the data series has a clear trend and fluctuates, it is more reasonable to choose between 0.5 and 0.8. Figure 3 shows the prediction error ladder diagram of the BP neural network sequence.

Since the prediction method changes with time, place, and environment, the predicted value will be different with the change of the prediction method, and there will be unavoidable errors between the actual value and the predicted value, so it needs to be formulated. A certain standard evaluates the feasibility and rationality of the prediction method as a basis for measuring the pros and cons of the model. When the fitted model passes the above two significance tests, it can only show that the model is at this level of significance, but it cannot be said that this model is optimal. There are generally two criteria for model optimization, AIC criteria and SBC criteria. Using a certain prediction method to predict it, and the resulting sequence of prediction results, the prediction error can be expressed as T. If there is a correlation between the time series values, it should test whether there is a stationary correlation between the series. This test is called the stationarity test of the series. Commonly used testing techniques include time series graph testing, autocorrelation function graph testing, and unit root testing to plot the time series data in a rectangular coordinate
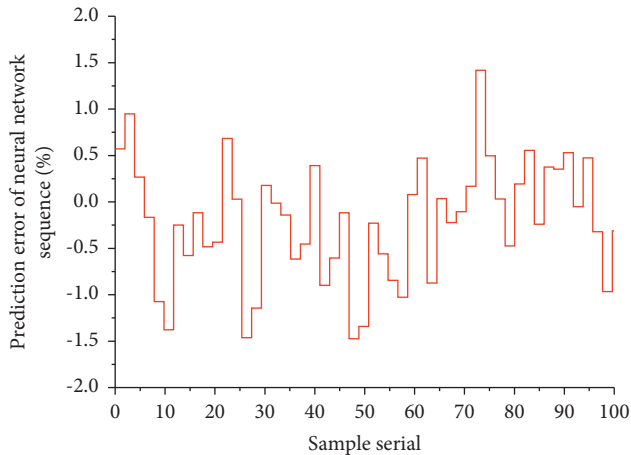
Figure 3: Prediction error ladder diagram of the BP neural network sequence.

system and observe whether the broken line has periodicity and trend. If it is a stable time series, then the graph should fluctuate randomly around a certain value with a small amplitude. By observing the autocorrelation function graph of the sequence, if the autocorrelation coefficient shows a rapid decay state as the order k increases, then it can be determined that the sequence is stationary; conversely, if the decay is very slow, then the sequence is nonstationary.

2.4. Model Weight Factor Analysis. The key to GDP forecasting is what criteria are used to obtain the weight coefficients, so that the GDP forecast has a higher forecast accuracy, but no matter how the guidelines are formulated, the measurement standards are considered from the perspective of error, and the forecast error is inversely proportional to the weight distribution. The weight coefficient is determined by the principle. The nonoptimal positive weight combination is to use the above theory to solve the weight coefficient with a simple principle. It is obviously inferior to the objective function of the optimal positive weight combination in terms of calculation difficulty, but some nonoptimal positive weights are currently better and the calculation is simple. Sort the variance sums of the prediction errors of each single model, and assign smaller weight coefficients to the single model corresponding to the error variance and too large or too small, and the single-term model in the middle is assigned a larger weight coefficient. Figure 4 shows the needle chart of the deviation of the individual weight coefficients of the BP neural network. The pros and cons of the prediction method can be reflected by the absolute value of the error. The maximum absolute value of the error is to be minimized based on the forecaster's needs, and the maximum absolute value of the GDP forecast error is minimized as much as possible, thereby improving the prediction accuracy.

For an observation time series, it is necessary to select the model that is most consistent with the actual development process from a variety of models, this is, the model identification process. That is to say, when predicting new

unknown values, this model is not used to predict forever, but after predicting the first new value, the first value that is the furthest in time in the sequence is removed, and then the predicted value is added to the sequence, a new model is reconstructed, and so on, so as to improve the whitening degree of the gray space. Based on the tailing and truncation of the calculated autocorrelation function and partial correlation function, combined with the identification rules of the model, we preliminarily determine the model type. In terms of time series, for annual data, we use a data for modeling, and b data mainly is to compare forecasts. In addition, c data is predicted. For quarterly data, because the data is relatively small, d data is used to fit the model, and e data is used to determine whether the model is good or bad. It can be summarized as follows: when the autocorrelation function is truncated at step q and the partial correlation function is tailing, then the MA(q) model should be selected; when the partial correlation function is truncated at step p, and the autocorrelation function is tailing, then the AR(p) model is selected; if both the autocorrelation function and the partial correlation function show tailing, then the ARMA model is selected. Therefore, the combination coefficient method combining the least square method and the MAE weight coefficient method is proposed in the selection method of the combination model weight, and the difference in nature between different combination methods is compared. The best criterion function method uses a criterion function, which can not only examine the degree of fit to the original sequence, but also consider the number of unknown parameters in the model. If the minimum value is obtained under the established criterion function, the order of the model can be determined.

3. Results and Analysis

3.1. Empirical Analysis of the BP Neural Network. This article has elaborated on the relevant theories of time series and now constructs the GDP time series forecast model, using EViews software to establish the ARIMA model and the exponential smoothing model, respectively. This paper uses the Box-Jenkings model identification method to conduct preliminary identification of the model. The main idea of this method is to visually judge the truncation and tailing of the sequence by observing the autocorrelation function graph and partial correlation function graph of the sample and screening series five suitable model types. Before applying the dynamic regression model, it is necessary to test the stationarity of each series to avoid the appearance of false regression. The stationarity of the sequence can be observed through the sequence diagram of the sequence, but it has a strong subjective impression. In order to improve the accuracy of the test, we usually perform a unit root test on the sequence, which is the most widely used statistical test method. First, the correlation analysis of the variables was carried out using the Pearson correlation coefficient. According to the results obtained, it was found that the selected variables all showed a high degree of positive correlation with GDP, and the variables also showed a strong correlation.
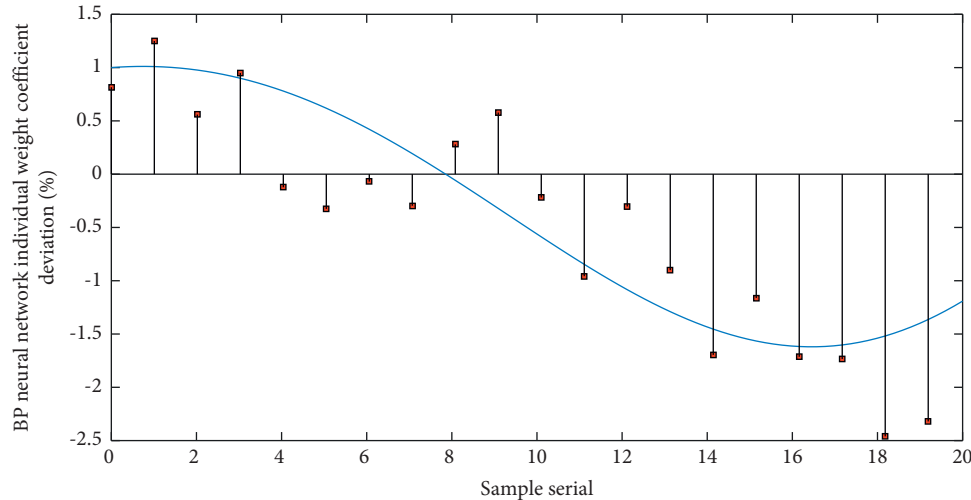
FIGURE 4: BP neural network individual weight coefficient deviation needle chart.

Figure 5 shows the distribution of each significance level curve of the BP neural network. From the figure, we can see that the GDP series has an obvious time trend, which is an exponential growth trend with time. It can be preliminarily judged that this is a nonstationary series. According to the ADF test, the test t statistic value is 1.493627, which is greater than the critical value at each significance level; that is, the null hypothesis cannot be rejected at the 1%, 5%, and 10% levels. Therefore, it can be judged that the original series is a nonstationary series. Since there are 6 independent variables in total, the input layer node is selected to be 6, the number of output layer nodes is 1, and the activation function is selected as a sigmoid type function. This is because it has good nonlinear mapping capabilities, and the hidden layer is selected as tan-sigmoid function; the output layer selects the linear purelin function. In order to eliminate the trend of the series and reduce the fluctuation of the series, we now take the logarithmic first difference of the original GDP series to get its series. According to the ADF test, the test t statistic value is -4.705133, which is less than the critical value under each significance level, that is, rejecting the null hypothesis, and it can be judged that the series is a stationary series at this time. Combining it can be seen that the sequence after the first difference of the logarithm of the original sequence is a stationary sequence, that is, $d = 1$. At this time, each parameter has a significant effect on the model, and the significance test of the parameter is passed. Then drawing the residual correlation diagram, it can be seen that there is no autocorrelation and heteroscedasticity in the residual, and it is normally distributed, and the model passes the test. Therefore, the established ARIMA(4, 1, 0) model meets the requirements.

3.2. Realization of GDP Prediction Model Simulation.

In this paper, statistical software SAS9.2 is used for ARIMA modeling of GDP total forecast; using the form of rolling window, the number of rolling windows is the number of forecast periods, and the data in the window is used to construct the ARIMA model. Sample 1 contains 18 windows
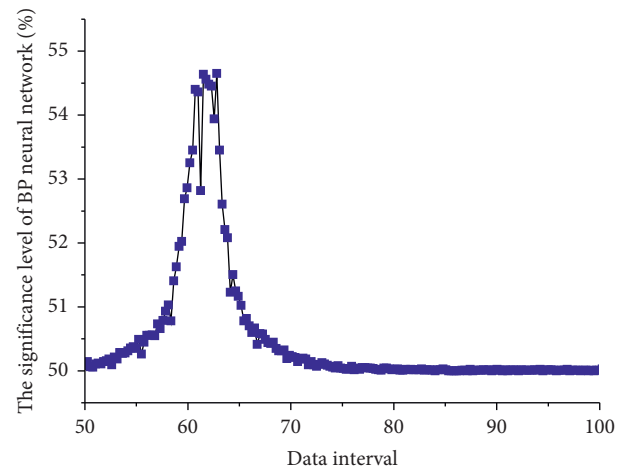
FIGURE 5: Distribution of saliency level curves of the BP neural network.

for building models, and sample 2 contains 20 windows for building models. Due to space limitations, sample 1 and sample 2 only describe the modeling process of the first window in detail. The error fluctuation range of ARIMA prediction alone is large, and the error of BP prediction alone is relatively small. However, the combined prediction error is the smallest, and the obtained prediction data is closest to the actual value. The ARIMA model has certain adaptability to nonstationary demand. Compared with the ARIMA model, the BP neural network based on genetic algorithm has a greater improvement in the prediction accuracy. This is mainly due to the fact that the generation of data is random and uncertain, and most of the data contains white noise. For stationary non-white noise sequences, the stationarity can be predicted. Stationary non-white noise sequence refers to the correlation between the sequences; that is, there are rules to follow in the sequence. The ARIMA model is a linear model, which has shortcomings and defects in the analysis and prediction of this nonlinear behavior of change. According to the results of the simulation analysis of

the calculation example, the combined model of the two methods can prove a great improvement compared with the single model. Figure 6 shows the histogram of the average absolute relative error of the GDP forecast model.

According to the GDP sequence diagram, it can be roughly judged that GDP is growing in a weak exponential form. If the double exponential smoothing method is used to predict GDP, then the original sequence can be processed by logarithm, and then the sequence can be fitted with double exponential smoothing. After the model is calculated, it is transformed into an exponential curve trend form, and the predicted value of the GDP series can be obtained. In general, low-order numbers are selected when building the model, so let $p = 1$ and $q = 1$. From a long-term perspective, the autocorrelation graph shows two 4th-order truncation, and the partial autocorrelation graph shows tailing. That is, $P = 1$, $Q = 1$ or 2, and because the first-order 4-step difference is started, $d = 1$, $D = 1$, and $S = 4$. Note that this article uses EViews software to build an exponential smoothing model. The initial smoothing value is the system default value. The Alpha and Beta values let EViews automatically choose to minimize the error.

Figure 7 shows the matchstick chart of the relative error of the ARIMA model fitting prediction. It can be seen from the autocorrelation graph of the quadratic difference sequence that the autocorrelation coefficients fall within 2 times the standard deviation after a delay of 3 orders, and the speed of attenuation to zero is faster, and after a delay of 9 orders, it fluctuates around the zero value. Based on the above two judgment methods, it can be considered that the sequence after the second-order difference is stationary. After the fitted model is determined, the model needs to be tested in two aspects, one is the adaptability test of the model, and the other is the significance test of the parameters. Each neuron on the hidden layer and the output layer corresponds to an activation function and threshold. The neurons on each layer are connected to the neurons on the adjacent layer through weights. For a nonstationary time series, the nonstationarity is usually eliminated by difference operation and relevant information is extracted. But you cannot blindly use the difference operation multiple times, because every time a difference operation is performed, the time series will lose part of the information. When multiple differences of the time series result in too much information loss, the estimated model parameters are unreliable, which will reduce the value of the model. This phenomenon is called overdifferential. In order to avoid excessive differences, when a low-order difference operation can be used to obtain a stationary sequence, there is no need to use high-order differences. It can be seen from the above results that if only one year's data is predicted, according to the time series method, the forecast error of quarterly data is smaller than that of annual data. Therefore, if the data is sufficient, if the ARIMA model is used to fit the forecast data, the number predicted by the quarterly data is better than the data predicted by the annual data, because the quarterly data is more seasonal than the annual data. The adaptability test of the model is mainly to determine whether the model is valid by checking whether the residual sequence is a white noise

sequence. The significance test of a parameter is to test whether the unknown parameter is significant to zero. If the independent variable corresponding to the parameter does not have a significant effect on the model, the variable should be considered to be eliminated.

3.3. Analysis of Experimental Results.

3.3. Analysis of Experimental Results. The nonlinear component of the total GDP sequence is added to construct an ARIMA-BP mixed model. The nonlinear component in the input layer is the residual of the ARIMA model's first-order delay. The ARIMA-BP hybrid model will simultaneously model the linear component and the nonlinear component in the GDP total sequence. The structure of the BP neural network in the sample 1 construction of the ARIMA-BP mixed model is $5 \times 6 \times 1$, and the structure in the sample 2 construction of the ARIMA-BP mixed model is $5 \times 11 \times 1$. The model is trained to predict the daily closing price of the total GDP. The actual values and predicted values of BP neural network and ARIMA-BP mixed model can be found in the article. First, the data input_train and data output_train are used as the data of the training learning sample, and the data input_test and data output_test are used as the input and output data of the test sample, respectively. According to the parameter-related setting theory and multiple tests of the model, the appropriate model is selected according to the prediction effect. The model parameters are set as follows: the normalization function of the data is mapminmax; the number of hidden layers is set to 8; the number of iterations is net.trainParam.epochs = 1000; learning rate net.trainParam.lr = 0.1; training target net.trainParam.goal = 0.00001; other parameters are the system default settings.

Figure 8 shows the BP neural network feasibility test deviation line chart. It is found from the result that when using all the data to test the feasibility of the model, the partial grade ratio does not fall within the tolerance interval, the data does not pass the feasibility test, and the gray model cannot be fitted. Cross-validation can evaluate the regression performance of LSSVM. It divides the data in the sample into multiple groups randomly. The training set trains LSSVM, and the validation set is used to test the prediction performance of LSSVM. After verification, a model that performs well in the sample can be used for out-of-sample predictions. RMSE measures the absolute error, and MAPE measures the relative error. RMSE and MAPE measure the accuracy of prediction from two different perspectives, and the two do not have similarities. For example, the RMSE index of the prediction effect of the A model is smaller than that of the B model, but the MAPE index of the prediction effect of the A model may be greater than that of the B model. Therefore, it is feasible to choose RMSE and MAPE to evaluate the predictive effects of different models in this paper. The smaller the two indicators, the closer the actual value to the predicted value, and the higher the prediction accuracy. When the level ratio test fails, one solution is to add a constant to the original sequence until the new sequence passes the level ratio test. The amount of change in the weight and threshold is equal to the amount of change in

FIGURE 6: Histogram of the average absolute relative error of the GDP forecast model.
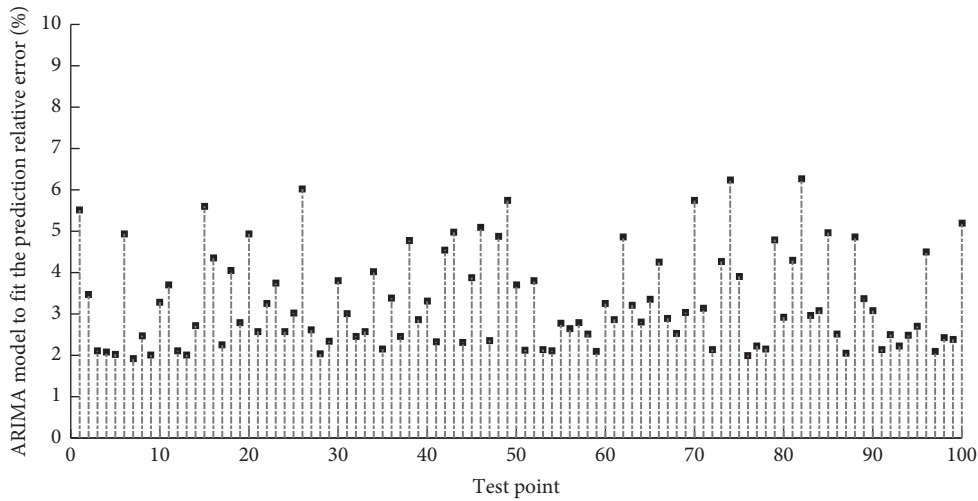
FIGURE 7: The matchstick chart of the relative error of the ARIMA model fitting prediction.

the previous moment. By increasing the momentum term, the network not only has a faster convergence speed, but also can effectively avoid the occurrence of local minimum problems in network training. Experiments show that if all the sequences are tested, only the constant is increased to 65000 or even more. The test can only be passed when it is large, and the predicted sequence, as shown in the text, can only roughly reflect a rising trend of GDP year by year, but the actual effect of predicting the future is very poor.

Table 2 shows the sequence-level comparison test of the neural network. It can be found that the process of ACF and

PACF attenuation to zero presents a tailing feature. The tailing order is the first order and the fourth order, which fits the ARMA(4, 1) model. Taking into account the process of first-order difference, the ARIMA(4, 1, 1) model was finally constructed on the basis of logarithms. The equation passed the significance test, but some coefficients failed the significance test. The reason is considered and compared, and the sparse coefficient model ARIMA((1, 3), 1, 1) is finally constructed, and the R language operation result is obtained. The prediction interval is trumpet-shaped, indicating that the prediction error is increasing with the growth of the

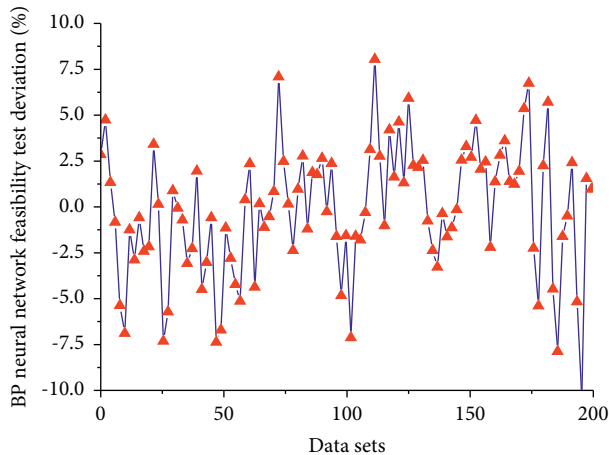FIGURE 8: BP neural network feasibility test deviation line chart.

TABLE 2: Sequence-level comparison test of the neural network.

Level number	Correlation coefficient	Weight	Error rate/%
1	0.97	0.32	9.17
2	0.86	0.34	5.43
3	0.88	0.21	6.77
4	0.91	0.13	3.54

prediction period. In addition to the significance test of the parameters, the adequacy of the model must also be verified; that is, the significance of the model is tested. If a model is significantly effective, it has extracted sufficient information from the time series, and the fitted residual series are no longer relevant. If the residual sequence is white noise, it indicates that the model is significantly effective; on the contrary, when the residual sequence is correlated, it indicates that the model does not sufficiently extract the correlation relationship in the time sequence. The logarithm operation was performed during the stationarity test of the original sequence at the beginning. Therefore, the predicted value obtained through the program on the basis of the logarithm needs to be exponentially operated to return to the actual required value. According to the formula for determining the weight of the correlation coefficient at the k time, the improved correlation coefficient matrix is obtained.

4. Conclusion

GDP forecast mainly includes two important aspects, one is the choice of a single model, and the other is the combination of models. In the choice of a one-way model, this article chooses the differential autoregressive moving average model (referred to as the ARIMA model), and BP neural network model and exponential curve model are studied. In terms of combination methods, this article combines weighted combination and error correction combination on the single model. After processing the sequence and identification, we use time series analysis theory 67ARIMA (p, d, q) model to predict GDP, and finally the graph is intuitively fitted well, and compared with the real

value of the GDP prediction result, the relative error is small, and the result is more reasonable. The predicted value of the time series is fitted to the GDP forecast, and the results are compared and analyzed with the ARMA model. First, an ARIMA model and an exponential curve regression model are established, and then MAPE and least squares are finally used to predict the GDP using a comprehensive weighted GDP prediction model based on MAPE and least squares. The simulation results show that the comprehensive weight is compared with a single weight. It is found that the forecasting effect of the combined model is better than that of a single model, and the combined weight coefficient method proposed in this paper is better than the combined model composed of other weight coefficient methods in the prediction error. In terms of the accuracy of GDP forecasting, the accuracy of GDP forecasting can be improved; in terms of error correction combination, this paper establishes gray adaptive filtering and ARIMA-BP according to the principle of complementary advantages and commonality of the model and establishes two error correction GDP forecasting models, which are verified by examples. The results show that the neural network has strong nonlinear mapping ability and good robustness, can identify and distinguish noisy samples, and is also a better GDP prediction model.

Data Availability

The data used to support the findings of this study are available from the corresponding author upon request.

Conflicts of Interest

The author declares that there are no conflicts of interest.

Acknowledgments

References

[1] Y. Du, "Application and analysis of forecasting stock price index based on combination of ARIMA model and bp neural network," in *Proceedings of the Control And Decision Conference*, pp. 2854–2857, Miami Beach, FL, USA, June 2018.

[2] F. Jiang, X. Yang, and S. Li, "Comparison of forecasting India's energy demand using an MGM, ARIMA model, MGM-ARIMA model, and BP neural network model," *Sustainability*, vol. 10, no. 7, p. 2225, 2018.

[3] X. Shi, "Tourism culture and demand forecasting based on BP neural network mining algorithms," *Personal and Ubiquitous Computing*, vol. 24, no. 2, pp. 299–308, 2020.

[4] Z. Yu, L. Qin, Y. Chen, and M. D. Parmar, "Stock price forecasting based on LLE-BP neural network model," *Physica A: Statistical Mechanics and Its Applications*, vol. 553, Article ID 124197, 2020.

[5] X. Zhao, M. Han, L. Ding, and A. C. Calin, "Forecasting carbon dioxide emissions based on a hybrid of mixed data sampling regression model and back propagation neural network in the USA," *Environmental Science and Pollution Research*, vol. 25, no. 3, pp. 2899–2910, 2018.

[6] Y. Weng, X. Wang, J. Hua, H. Wang, M. Kang, and F.-Y. Wang, "Forecasting horticultural products price using ARIMA model and neural network based on a large-scale data set collected by web crawler," *IEEE Transactions on Computational Social Systems*, vol. 6, no. 3, pp. 547–553, 2019.

[7] Z. Li and Y. Li, "A comparative study on the prediction of the BP artificial neural network model and the ARIMA model in the incidence of AIDS," *BMC Medical Informatics and Decision Making*, vol. 20, no. 1, pp. 143–213, 2020.

[8] D. Qi, "Study on the export of BP neural network model to China based on seasonal adjustment," *Advances in Intelligent Systems and Computing*, vol. 43, pp. 1672–1678, 2020.

[9] S. Ji, H. Yu, and Y. Guo, "Research on sales forecasting based on ARIMA and BP neural network combined model," *Intelligent Information Processing*, vol. 23, pp. 5-6, 2016.

[10] Y. Zhang, Y. Fu, and G. Li, "Research on container throughput forecast based on ARIMA-BP neural network," *Journal of Physics: Conference Series*, vol. 1634, no. 1, Article ID 012024, 2020.

[11] Y. Gao, C. Qu, and K. Zhang, "A hybrid method based on singular spectrum analysis, firefly algorithm, and BP neural network for short-term wind speed forecasting," *Energies*, vol. 9, no. 10, p. 757, 2016.

[12] J. Qin, Z. Tao, and S. Huang, "Stock price forecast based on ARIMA model and BP neural network model," *Big Data, Artificial Intelligence and Internet of Things Engineering*, vol. 36, pp. 426–430, 2021.

[13] H. Yang, X. Li, W. Qiang, Y. Zhao, W. Zhang, and C. Tang, "A network traffic forecasting method based on SA optimized ARIMA-BP neural network," *Computer Networks*, vol. 193, Article ID 108102, 2021.

[14] L. Wang, L. Zhan, and R. Li, "Prediction of the energy demand trend in middle africa-A comparison of MGM, MECM, ARIMA and BP models," *Sustainability*, vol. 11, no. 8, p. 2436, 2019.

[15] D. Wang, H. Luo, O. Grunder, Y. Lin, and H. Guo, "Multi-step ahead electricity price forecasting using a hybrid model based on two-layer decomposition technique and BP neural network optimized by firefly algorithm," *Applied Energy*, vol. 190, pp. 390–407, 2017.

[16] Y. Liu, Y. Tian, and M. Chen, "Research on the prediction of carbon emission based on the chaos theory and neural network," *International Journal Bioautomation*, vol. 21, no. 4, p. 339, 2017.

[17] L. Zhang, F. Wang, B. Xu, W. Chi, Q. Wang, and T. Sun, "Prediction of stock prices based on LM-BP neural network and the estimation of overfitting point by RDCI," *Neural Computing & Applications*, vol. 30, no. 5, pp. 1425–1444, 2018.

[18] Y. Yang, Y. Chen, Y. Wang, C. Li, and L. Li, "Modelling a combined method based on ANFIS and neural network improved by DE algorithm: a case study for short-term electricity demand forecasting," *Applied Soft Computing*, vol. 49, pp. 663–675, 2016.

[19] D. Wang, H. Luo, O. Grunder, and Y. Lin, "Multi-step ahead wind speed forecasting using an improved wavelet neural network combining variational mode decomposition and phase space reconstruction," *Renewable Energy*, vol. 113, pp. 1345–1358, 2017.

[20] W. Li and Y. Wang, "Dynamic evaluation of logistics enterprise competitiveness based on machine learning and improved neural network," *Journal of Ambient Intelligence and Humanized Computing*, vol. 42, pp. 12–15, 2021.

[21] L. Shao-Jiang, C. Jia-Ying, and L. Zhi-Xue, "A EMD-BP integrated model to forecast tourist number and applied to Jiuzhaigou," *Journal of Intelligent and Fuzzy Systems*, vol. 34, no. 2, pp. 1045–1052, 2018.

[22] J. Cao and J. Wang, "Exploration of stock index change prediction model based on the combination of principal component analysis and artificial neural network," *Soft Computing*, vol. 24, no. 11, pp. 7851–7860, 2020.

[23] D. Wang, Y. Liu, Z. Wu, H. Fu, Y. Shi, and H. Guo, "Scenario analysis of natural gas consumption in China based on wavelet neural network optimized by particle swarm optimization algorithm," *Energies*, vol. 11, no. 4, p. 825, 2018.

[24] Ö. Ö. Bozkurt, G. Biricik, and Z. C. Tayşi, "Artificial neural network and SARIMA based models for power load forecasting in Turkish electricity market," *PLoS one*, vol. 12, no. 4, Article ID e0175915, 2017.

[25] Y. Gao, Y. Cao, and Z. Jiang, "Investment forecast of power network infrastructure project based on BP neural network," *IOP Conference Series: Earth and Environmental Science*, vol. 332, no. 4, Article ID 042021, 2019.

[26] B. M. Al-Maqaleh, A. A. Al-Mansoub, A. A. Al-Mansoub, and F. N. Al-Badani, "Forecasting using artificial neural network and statistics models," *International Journal of Education and Management Engineering*, vol. 6, no. 3, pp. 20–32, 2016.

[27] P. Sutthichaimethee and H. A. Wahab, "A forecasting model in managing future scenarios to achieve the sustainable development goals of Thailand's environmental law: enriching the path analysis-varima-ovi model," *International Journal of Energy Economics and Policy*, vol. 11, no. 4, pp. 398–411, 2021.

[28] W. Sun and Y. Wang, "Short-term wind speed forecasting based on fast ensemble empirical mode decomposition, phase space reconstruction, sample entropy and improved back-propagation neural network," *Energy Conversion and Management*, vol. 157, pp. 11-12, 2018.

Research Article

Understanding the Impact of Transformational Leadership on Project Success: A Meta-Analysis Perspective

Na Zhao [1,2] **Dongjiao Fan,**[1] **and Yun Chen**[1]

[1]*School of Traffic and Transportation Engineering, Changsha University of Science and Technology, Changsha 410114, China*
[2]*Engineering Research Center of Catastrophic Prophylaxis and Treatment of Road and Traffic Safety of Ministry of Education, Changsha University of Science and Technology, Changsha 410114, China*

Correspondence should be addressed to Na Zhao; zhaona@csust.edu.cn

This paper aims to systematically analyze the reasons for the differences in the relationship between transformational leadership (TL) and project success and apply meta-analysis to summarize which dimensions of TL are the main driving forces for project success. Adopting the meta-analysis approach, we investigated 31 independent studies ($N = 6475$) and studied the theoretical moderators of this relationship from the perspectives of mediating variables, cultural background, and document type to test whether the moderating effects can explain the inconsistent research results. The results reveal that TL positively affects project success and leadership charm is the primary driver of TL. Also, the existence of a mediating mechanism has a more significant impact on the success of the leading project. Meanwhile, compared with project construction under the Western cultural background, countries with Eastern culture are more inclined to use a people-oriented philosophy for project management to promote project success. This research provides an empirical perspective to help project leaders select management talents, regulate leaders' words and deeds, and cultivate technical and soft leadership skills. Besides, this paper proposes a unique and nuanced view of the relationship between TL and project success, enhancing people's understanding of the TL's role in influencing project success.

1. Introduction

"Construction Industry 4.0," as a part of "Industry 4.0," is a specific application under the subdivision of the construction industry. It mainly contains two themes: "smart factory" and "smart production." With the emergence of the intelligent construction concept, a plenty of new-generation information technologies, such as 5G, construction robots, and BIM, have been applied in construction projects [1–3]. The integration of technologies has led to a gradual shift in project management from mechanization and digitalization to informatization and intelligence. However, many studies have shown that even with the increasing level of technology and management associated with project construction, the level of project success has not improved significantly due to the increasing complexity and uncertainty of the construction environment. For construction companies and project organizations,

changes in production models require far-reaching strategic decisions at all levels of the construction industry. Therefore, it is necessary to change the project organization to achieve a higher level of sustainable project success. It is well known that leaders play a dominant role in project organization reform, which is essential to increase organizational resilience and agility and develop high-reliability organizations [4]. Particularly in the last decade, an increasing number of project operations have developed under the project manager responsibility system. The project manager undertakes the leadership responsibility for the entire process of project implementation and overall management. This change will inevitably affect the leadership behavior of project managers and put forward higher requirements for their ability and comprehensive quality. Compared with other leadership styles, transformational leadership (TL) has advantages in enhancing project success. For example, it attaches great

importance to the leaders' standards of behavior and concerns for the needs of followers. Meanwhile, many reasons suggest that TL is indispensable in project organizational change [5–7]. Bass [8] argued that today's construction environment requires subordinates to perform beyond ordinary expectations, and TL can deliver. Therefore, both subordinates and superiors of the project believe that leaders with a transformational style are more productive and suitable for project managers [9].

In recent years, many scholars have conducted many empirical studies to explore the role of TL in project success [10, 11]. On the one hand, most researchers have shown that TL can promote project success. Zhang et al. [12] summarized the recent research results of some scholars and believed that TL plays a vital role in project success or failure. Appropriate TL is necessary for individuals or groups to carry out innovative behaviors [13]. Odusami et al. [14] conducted research to suggest a remarkable correlation between project managers' professional level, leadership style, team composition, and project success. Berssaneti et al. [15] pointed out that project success depends on many factors, including leadership ability, leadership style, and leadership skills of the project manager. However, on the other hand, some studies are reckoning that the project's successful realization will be hindered by TL [16–18]. Zhang [19] found an inhibitory relationship between the project manager's emotional intelligence and leadership style. Iqbal et al. [20] conducted surveys and interviews with engineering organizations in Malaysia. They believed that project leaders' high degree of psychological empowerment negatively impacted project performance due to their leadership style. Besides, Chen et al. [21] proposed an inverted U-shaped relationship between TL and project success, which suggests that it is most conducive to improving the project success rate when TL is at a medium level.

According to the discussion above, there are apparent conflicts in the strength, direction, and statistical significance of the relationship in most studies, which creates confusion in theory and practice. The scholars have not yet formed a consistent perspective on the relationship between TL and project success. Furthermore, the existing research lacks a more systematic and comprehensive integration of TL that contributes to project success, as well as fails to analyze and explain the differences in findings. Simultaneously, the impact of different dimensions of TL on the project's success has not yet been explored by scholars from the perspective of meta-analysis. Therefore, this paper intends to adopt a meta-analysis method through the comprehensive reanalysis of different individual research results to examine the overall effect of TL and other dimensions of TL on project success. Based on the literature collation results, this study explores mediating variables, cultural factors, and publication type factors as the moderating variables, focusing on identifying the reasons for the divergence between different research variables. The research conclusions are expected to comprehensively evaluate TL's theoretical and practical value in construction projects and inspire the sustainable development of project management practices in construction enterprises.

The remainder of the paper is structured as follows: Section 2 sums up the theoretical literature. Section 3 describes the methodology and the process of data collection. Section 4 analyses the results of the meta-analysis. A detailed discussion, implication, and limitation are provided in Section 5. Finally, Section 6 concludes this paper and points out the future research direction.

2. Literature Review and Hypotheses Development

2.1. Transformational Leadership. Burns proposed TL in 1978, and then Bass defined and quantified it in 1985 [8]. According to Bass, TL means that the leaders use words and actions to make subordinates realize the meaning and value of their work [22]. In this process, leaders also create a working atmosphere of trust and cooperation to inspire subordinates' enthusiasm for success and self-realization. In this way, the project manager can encourage them to surpass their interests for the organization's benefit to work more and improve their personal and organizational interests as well as the society's common well-being.

At present, most of the research on TL has been influenced by Bass. Although the multidimensionality of the transformational leader structure has been controversial [23, 24], with the gradual intensification of the discussion on TL, experts and scholars have extended the research from qualitative to quantitative and gradually presented different measurement dimensions of TL. Bass [22] initially proposed that the dimensions of TL have charm, intellectual stimulation, and individualized consideration. After that, Bommer [23] developed the integration, high-performance implementation, and personalized support. Also, Bass and Avolio [24] thought it includes charm, charisma, intellectual stimulation, and individualized consideration. Eventually, Li [25] proposed that TL can be divided into four dimensions: idealized influence, intellectual stimulation, leader charism, and individualized consideration, and they are widely accepted and used. Based on the discussion above, TL is embodied in four dimensions in this paper: (1) idealized influence, which draws a future blueprint for team members, and strengthens team beliefs; (2) intellectual stimulation, which clarifies team goals and encourages members to continue to cooperate in their work, practice, and innovation; (3) leadership charisma, which enhances the self-confidence, self-esteem, and autonomy of members; (4) individualized consideration, which can improve employee identification, loyalty, and enthusiasm.

2.2. Project Success. Nowadays, project management has become ubiquitous in the construction industry, capacity building, and social projects [26]. Project success was introduced in the research field of project management in the 1960s and was initially applied for project management performance. Many scholars have defined project success with deepening the research, but they have not yet come to a consistent conclusion. This article summarizes the opinions of essential project management scholars and practitioners

on the definition of project success based on the published literature (Table 1).

However, as project functions and the number of stakeholders has ascended, project success has a broader concept, which must be a multidimensional structure [34, 35]. Therefore, the Project Management Institute (PMI) defines project success to balance the competing demands for project quality, scope, time, and cost, as well as meet project stakeholders' changing concerns and expectations (PMI, 2008). Specifically, it includes the organization's benefits, user satisfaction, the benefits to project personnel, sustainability, and business success. Specific to the engineering project, the stakeholders have not formed a unified opinion on the project's success. The main reason is that many stakeholders involved in the project have inconsistent standards about project success and an extended project success evaluation period.

At the same time, scholars now no longer only focus on complex indicators such as quality, schedule, and cost for measuring project success but start to explore soft indicators, such as whether the partnership is enhanced, whether the company's capabilities have improved, and whether there is a willingness to cooperate next time, etc.

2.3. Transformational Leadership and Project Success.
Many scholars, such as Nam [36], Khawaja et al. [37], and Wang et al. [38], have supported leadership as a critical factor in promoting project success. Empirical evidence generally recognises the positive impact of TL on follower attitudes, effort, and performance. According to Bass and Avolio [39], TL motivates their subordinates to do things that not only exceed what they are simply asked to do, but also the effects often exceed their expectations. Simultaneously, in addition to directly affecting the performance of cross-level followers, TL can also indirectly affect project performance through direct subordinate leaders who contact cross-level followers [40]. Singh [41] postulated that the intellectual stimulation dimension of TL enhances exploratory thinking and communicates a clear vision of the project, motivating project members to generate new ideas.

Moreover, the leaders who demonstrate TL can gain their immediate followers [9] and are increasingly confident in trying new methods to complete projects with the support of their managers. Dulaimi [41] found that the leader's charisma and innovation support behavior are the main reasons for the investigated project's success in Singapore. Also, literature reviews show that project managers' individualized care and idealized influence play a vital role in achieving tremendous project success [42, 43]. Therefore, according to the findings above, this research proposes the following hypotheses:

H1: TL positively affects project success

H2a: leader charisma positively affects project success

H2b: idealized influence positively affects project success

H2c: intellectual stimulation positively affects project success

H2d: individualized care positively affects project success

2.4. Moderating Relationships.
Due to independent research's heterogeneity, certain potential control variables may affect the relationship between TL and project success. This paper summarizes the literature in this article and finds that the literature has differences in mediating variables, cultural background, and publication types.

2.4.1. The Existence of Mediating Variables.
Many studies have used mediating variables when discussing the relationship between TL and project success. Chou [44] used cognitive trust and collective effectiveness as intermediary variables to reveal the interrelationship between TL and team performance. Furthermore, García-Morales et al. [45] analyzed the impact of TL on organizational performance through organizational learning and innovation's dynamic capabilities. Aga and Vallejo [46] adopted a field survey with a sample of 200 development project managers in Ethiopian nongovernmental organization (NGO) departments. It adopted the structural equation model to find that team building plays a mediating role between TL and project success. Hassan et al. [47] saw that leaders apply their skills and abilities to contribute to the success of construction projects in Pakistan in project management. Thus, based on the existing literature, this study proposed the following hypothesis:

H3: the existence of mediating variables moderates the relationship between TL and project success

2.4.2. Document Type.
As the relationship between TL and project success varies across studies, the meta-analysis literature includes both published journal articles and unpublished papers. Therefore, the type of literature publication may be a source of variation. Furthermore, the earlier the published research, the more likely it will report significant training effects [48]. Meanwhile, the uncertainty and controversy gradually become clear through the indepth analysis. Compared to unpublished literature such as thesis, the journal papers are more inclined to describe significant results and distort the natural effect to avoid becoming drawer files [49]. Therefore, this paper proposes the following hypothesis:

H4: the document type moderates the relationship between TL and project success

2.4.3. Cultural Background.
Culture is a consciousness system gradually formed by human beings through coping with problems and adapting to the social development. It shapes not only humans' behavior but also influences humans' psychological needs. The leaders' attitudes, behaviors, and motivations towards their subordinates will vary depending on their culture [50].

These cultural differences will also impact the effectiveness of leadership behavior [51]. Western culture is mainly

TABLE 1: Definitions of project success.

Author	Definition
Edward [27]	Project success covers quality, time, cost.
Bryde and Robinson [28]	Project success includes pre-success, successful completion, and successful operation.
Kim and Reinschmidt [29]	The leading indicators of project success are customer satisfaction, quality, duration, cost, and other complex indicators.
Gabriella Cserháti [30]	There are five criteria for project success: efficiency, impact on a customer, impact on the team, business and immediate success, and preparation for the future.
Joslin and Müller [31]	Project success measurements include the iron triangle "time-cost-quality" and customer satisfaction.
Wang et al. [32]	Project success includes project efficiency, organizational benefits, project impact, stakeholder satisfaction, and future potential.
Luo et al. [33]	Project success includes time, cost, quality, health and safety, environmental performance, participants' satisfaction, user satisfaction, sustainability, and commercial value.

influenced by European and American cultures, which actively encourages people to express their visions and tendencies in organizations and promotes individualism. However, Eastern culture is more affected by Confucian patriarchal culture, and it advocates collectivism more than Western civilization, especially during the construction of large-scale projects [3]. The project teams can collaborate and cooperate based on task interdependence to promote the efficient integration of heterogeneous innovation resources. On the other hand, the samples used in different studies usually come from different countries. The differences in the countries' economic level and cultural environment where the models belong have a particular impact on the project's successful realization [52, 53]. Therefore, the following hypothesis is formulated:

> H5: cultural background moderates the relationship between TL and project success, and TL in developed countries has a more significant impact on project success

According to the above assumptions, this study proposed a theoretical research model, shown in Figure 1.

3. Method and Data

In recent years, meta-analysis has contributed prominently to the literature review as a new method of combining empirical research with research hypotheses. Specifically, meta-analysis can reanalyze multiple empirical research results with the same research purpose to obtain the fundamental relationship between variables. The advantage of meta-analysis is that it can systematically analyze many documents and evaluate the inconsistency of different research results [54]. This method can discover and explain the differences between various research results, systematically integrate the existing empirical research results, and further improve its reliability and validity. Therefore, this paper mainly uses Hunter and Schmidt's primary effect test as well as moderating effect test method. It adopts CMA 2.0 software to assist with the version bias heterogeneity test.

3.1. Literature Sources and Collection.
According to the following three steps, this research points to the literature collection to ensure the systematic literature collection.

Firstly, this study shows computerized keyword searches in the databases Web of Science, Google Scholar, Science Direct, Elsevier, and Springer before October 2020. The papers are searched by the following keywords: "transformational leadership," "project success," "project manager," and "Construction project success." Secondly, to avoid the omission of essential documents since some related studies on TL and project success are not included in the above databases, this research combines the collected records with the references of these documents, especially compared to the review literature one by one. Finally, the study manually searches the most essential and relevant journals, such as "*Journal of Cleaner Production*," "*The Leadership Quarterly*," and "*International Journal of Project Management*."

The process and results are shown in Figure 2.

3.2. Literature Inclusion Criteria.
The searched documents are filtered according to the following criteria: (1) It must be a survey or experimental empirical research, excluding pure theoretical and literature review articles. (2) It uses both the TL measurement scale and the project success measurement scale, and at least reports the correlation coefficient (r) between the dimension or total score of one scale and the dimension or total score of another scale. Or it can be converted into the F-value, t-value, or X^2 value of r. (3) The selected research is not only limited to journal papers, but also includes thesis, book chapters, etc. (4) If the data is published repeatedly, the published journal articles shall be taken. (5) Document effect value encodes an effect value based on each independent sample.

3.3. Document Coding Content and Results.
The subsamples included in the meta-analysis are also ordered as follows: firstly, the necessary information of the research (author name and publication time), sample size, and whether there are intermediate variables in the empirical research (divided into yes and no), the cultural background of the study (divided into Eastern culture, Western culture, and others) and the type of article (journal papers, thesis).

Secondly, the research should primarily discuss the total effect of TL on project success. This paper adopts the
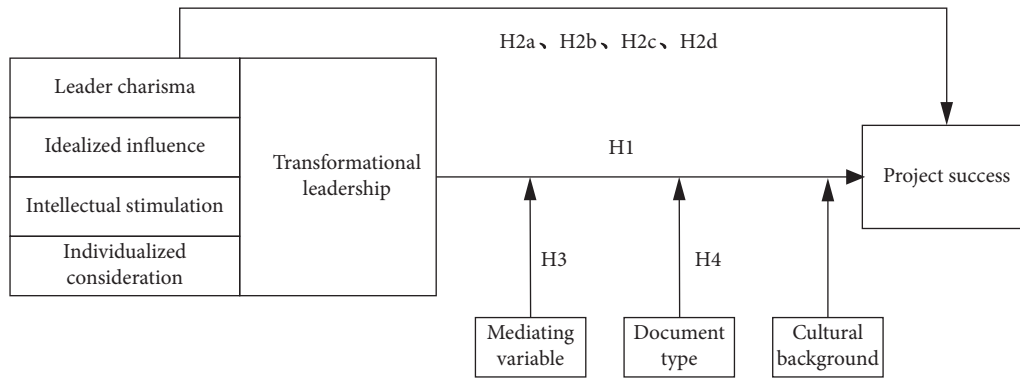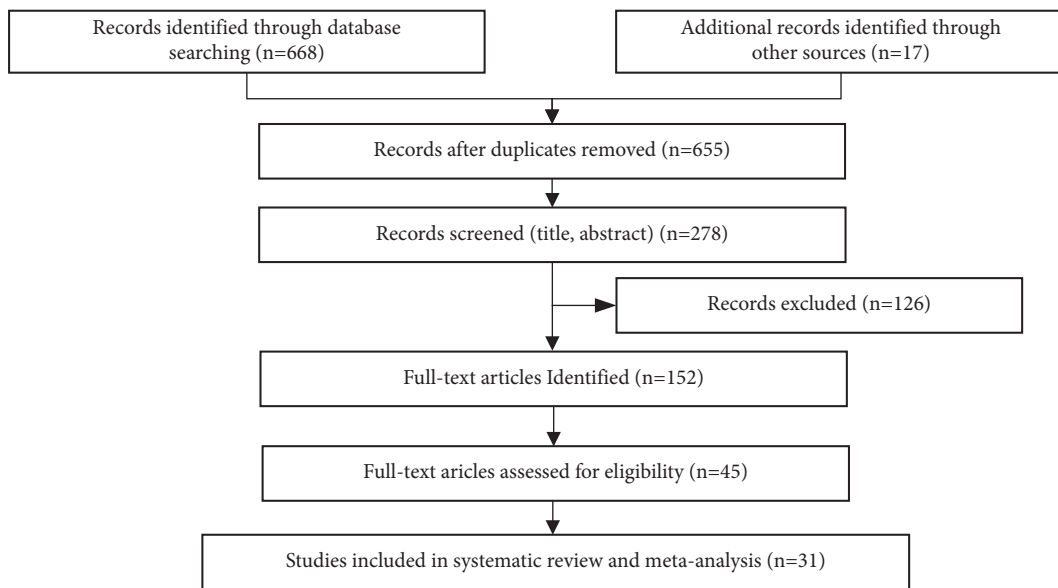
FIGURE 1: The theoretical research model.

FIGURE 2: The flowchart of study selection.

weighted average method for the influence coefficients of different dimensions of TL mentioned in the literature on project success. If they encounter the literature that discusses the disparate dimensions of TL on project success, the final effect value would be obtained by taking the average layer by layer. The necessary coding information of the main effects analysis is shown in Table 2.

4. Results

4.1. Test for Publication Bias. Funnel plots are the most commonly used approach to determine the presence of publication bias. Figure 3 shows the distribution of the effect value. It can be seen that most of the samples concentrate at the top of the funnel chart, and the scattered points distribute near the effect value [55]. Therefore, the possibility of publication bias in this study is relatively slight. Besides, this paper introduces a "file drawer" analysis according to Rosenthal [56] to estimate the severity of publication bias. The larger the coefficient, the greater the number of studies required to reverse this result, the more reliable the

conclusions of the meta-analysis, and the smaller the relative impact of bias. After calculation, when $P = 0.05$, Nfs = 10223, and $P = 0.01$, Nfs = 7945, the fail-safe coefficient of this study indicate that the conclusion is more reliable.

This paper adopts Fail-safe, Egger's test (regression intercept method), and rank correlation test for further testing to test the publication deviation more accurately. The results are shown in Table 3. The fail-safe factor is $N = 11495$, indicating that if people want to overturn the TL effect, 11,495 documents are needed to get the opposite result. Egger's test results show that the P value is 0.88, which is not significant, and there is no publication bias. The level correlation test results, Tau values being -0.09 ($P = 0.58$), suggest that there is no publication bias in the effect size.

4.2. Test of Heterogeneity. This study tests data for heterogeneity, which is a key step in synthesizing the global effect value from the practical value of a single study. The Q test results reflect the degree of heterogeneity of each

TABLE 2: Descriptive characteristics of the studies.

Author (time)	Category	Sample	Author (time)	Category	Sample
Odusami (2003)	(Y, J, W)	60	Xiang Ding (2017)	(Y, J, E)	162
Ralf Müller (2007)	(Y, J, W)	400	Yang Liu (2017)	(Y, T, E)	152
Arago'n-Correa (2007)	(Y, J, E)	408	Amin Akhavan (2017)	(N, J, W)	470
Anne Nederveen (2010)	(Y, J, E)	2	Yanchun Zhang (2018)	(Y, J, E)	251
Liu Xiaoyu (2011)	(N, J, E)	450	Jingting Shao (2018)	(Y, J, E)	79
Li-Ren Yang (2011)	(Y, J, E)	213	Lianying Zhang (2018)	(Y, J, E)	365
Kun-Shan Wu (2012)	(N, J, E)	106	Mustafa Raziq (2018)	(Y, J, W)	248
García-Morales (2012)	(Y, J, E)	168	Jae-Seung Hwang (2018)	(Y, J, E)	105
Susanne Braun (2012)	(Y, J, W)	360	Danting Li (2019)	(N, T, E)	201
Panagiotis Trivellas (2013)	(N, J, E)	97	Manandhar Sunitha (2019)	(N, J, E)	200
Huey-Wen Chou (2013)	(Y, J, W)	92	Floris (2019)	(Y, J, W)	37
John Kissi (2013)	(Y, J, E)	112	Li Danting (2019)	(N, T, E)	201
Muredeni Liphadzi (2015)	(N, J, E)	110	Doan (2020)	(N, T, W)	325
Assefa Aga (2016)	(Y, J, W)	224	Hassan Shah (2020)	(Y, T, E)	150
Zhang Lian-Ying (2016)	(N, J, E)	237	Jabran Khan (2020)	(N, J, W)	256
Aga (2016)	(Y, J, E)	200			

Note. Y: the existence of mediating variables; N: the absence of mediating variables; W: Western culture; W: Eastern culture; J: journal; T: thesis.
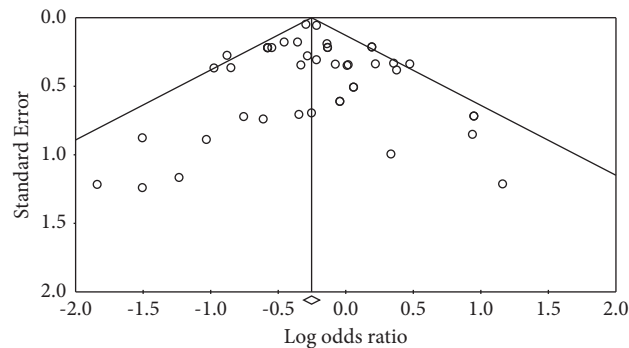

FIGURE 3: Funnel plot of standard error by Fisher's Z.

TABLE 3: Publication bias test.

| Leadership style | NFS | Egger's test | Tau | Trim and fill | | |
				Observations	Adjusted value	Change value
TL	11495	1.01 ($P = 0.88$)	0.09 ($P = 0.58$)	0.589	0.301	0.288

effect size. If each effect size is heterogeneous, it indicates that the true error causes the difference of each effect size in the meta-analysis. Since the combination of variables can lead to sampling errors, the random-effects model should be applied. The test results are shown in Table 4. It can be learnt that Q (19) = 1713.0, $P < 0.001$, and $I^2 = 98.89\%$, indicating that the effect size of each study is heterogeneous. Among them, I^2 greater than 75% means that the observed variation above 75% is caused by the true difference in effect size, reaching a high level of heterogeneity [56]. The values of Tau^2 are 0.317, which means that 31.7% of the inter-study variation can be used to calculate the weight.

The heterogeneity test results show that the correlation between TL and project success is heterogeneous in the selected studies. Therefore, the random effect model is used in this study since it is more accurate for meta-analysis.

4.3. Theoretical Model and Test of Direct Relations

4.3.1. Total Effect Size Test Result. According to the heterogeneity test results, the random-effects model was selected to test the main effects of the relationship between TL and project success (see Table 5). From the drawing, we can see that the overall test of the relationship between TL and project success, a total of 31 effect sizes ($N = 6475$), the overall correlation coefficient of TL and project success is 0.589 ($P < 0.001$), in 95% of the confidence interval is significant. When $|r| \leq 0.1$, it is low correlation, $0.1 < |r| < 0.4$ is medium correlation, and $|r| \geq 0.4$ is high correlation. Based on this judgment, TL is positively correlated with project success. Therefore, hypothesis 1 is supported.

4.3.2. Subdimension Effect Size Test Results. It can be seen from Table 6 that the Q test results of the heterogeneity of the relationship between each dimension of TL and project

TABLE 4: Results of the heterogeneity test.

| Leadership style | N | Heterogeneity test | | | | Tau² | | | |
		Q	Df (Q)	P	I²	Tau²	SE	Variance	Tau
Transformational leadership	31	1713	19	<0.001	98.891	0.317	0.132	<0.05	0.563

TABLE 5: Total effect size element analysis results as the test.

| Leadership style | Model | K | N | 95% CI | | | Z | P |
				Point estimate	Lower	Upper		
TL	Random	31	6475	0.589	0.398	0.732	5.187	<0.001

Note. K = number of studies; N = sample size; r = effect size; 95% CI = confidence interval around r.

TABLE 6: Dimensional meta-analysis results.

| H | Heterogeneity test | | | K | N | 95% CI | | | Two-tailed test | | NFS |
	Q	df	P			Point estimate	Lower	Upper	Z	P	
H2a	1589.59	10	<0.001	20	3243	0.731	0.612	0.817	8.366	<0.001	6376
H2b	824.79	10	<0.001	12	2948	0. 673	0.487	0.811	5.638	<0.001	5178
H2c	484.94	8	<0.001	8	2149	0.619	0.482	0.785	5.842	<0.001	3154
H2d	1093.4	9	<0.001	10	2543	0.721	0.576	0. 822	7.051	<0.001	6602

Note. K = number of studies; N = sample size; r = effect size; and 95% CI = confidence interval around r.

success are significant, indicating that each effect size is heterogeneous, and the random-effects model can be used. N's loss of safety factor is more powerful than 500, showing no publication bias in each dimension's effect value.

From the dimensional meta-analysis results, the four dimensions of TL have some differences in their effect size; in detail, leadership charm is the largest (0.731) while intellectual stimulation is the most minor (0.619). According to Cohen's scale for social science research, correlations with values close to 0.2, 0.5, and 0.8 correspond to weak, moderate, and decisive effect sizes. Thus, leadership charisma reasonably correlates with project success, while vision motivation has a fragile relationship. As a result, hypothesis 2a–d is accepted.

4.3.3. Moderation Analysis. As can be seen from the above, there is significant heterogeneity in the effect sizes for the meta-analysis in this paper. To further analyze the heterogeneity source, random-effects models are also adopted to test whether mediating variables, cultural background (Eastern culture, Western culture, and others), and literature publication types (journal papers, thesis).

The results in Table 7 show that whether to participate in the intermediary variables has a significant moderating effect on the relationship between TL and project success ($Q = 336.669$, $P < 0.001$). In the presence of intermediary variables, TL ($r = 0.649$, $P < 0.001$) and the correlation coefficients of project success were significantly higher than those of Western cultural background ($r = 0.452$, $P < 0.001$). Hence, hypothesis H3 is supported.

The cultural background also significantly moderates the relationship between TL and project success ($Q = 55.641$, $P < 0.001$). The empirical results indicate that TL in Eastern cultural backgrounds can play a more critical role in influencing project success. Thus, hypothesis H4 is supported.

Similarly, the literature publication has a significant moderating effect on the relationship between TL ($Q = 214.251$, $P < 0.001$) and project success. Under the dissertation type, the correlation coefficient between TL ($r = 0.765$, $P < 0.001$) and project success was significantly lower than that of the journal paper type ($r = 0.513$, $P < 0.001$). Therefore, it assumes that H5 is accepted.

5. Discussion and Implications

5.1. Discussion. This paper conducts an in-depth analysis of the empirical research on the relationship between TL and project success based on the meta-analysis method. It mainly focuses on the relationship between the various dimensions of TL and project success and the moderating role of the mediator variables, cultural background, and document type. Therefore, the following conclusions are drawn:

Firstly, the results suggest that TL can positively influence project success, in line with previous studies. The significant challenges of modern society and the increasingly different business environment require people to re-examine leadership research and change the traditional concepts and ways of thinking about leadership in the construction industry. A study by scholar Kissi [57] confirmed the necessity of project organizations to cultivate TL behavior to improve performance. By summarizing traditional team-building practices, Do [58] found that transformational leaders are more likely to enhance team members' understanding of project goals, roles, and responsibilities, interpersonal communication, and problem-solving skills, which will also help affect project success.

Secondly, this article's four dimensions of TL can improve project success in a cooperative-friendly way. To be

Table 7: Results of moderation analysis.

Moderating variable	Leadership style	Heterogeneity test			Sort	K	N	95% CI			Two-tailed test	
		Q	df	P				Point estimate	Lower	Upper	Z	P
Mediating variable	Transformational leadership	336.669	2	<0.001	Y	23	1254	0.573	0.622	0.817	8.546	<0.001
					N	8	1583	0.469	0.608	0.795	7.128	<0.001
Cultural background	Transformational leadership	55.641	2	<0.001	E	10	2319	0. 893	0.587	0.831	5.748	<0.001
					W	17	1826	0.759	0.452	0.776	5.682	<0.001
					O	4	1382	0.723	0.632	0.797	8.426	<0.001
Document type	Transformational leadership	214.251	2	<0.001	J	3	781	0. 611	0.467	0.834	5.678	<0.001
					T	28	2825	0.677	0.512	0.792	5.7843	<0.001

Note. Y: the existence of mediating variables; N: the absence of mediating variables; W: Western culture; E: Eastern culture; O: other; J: journal; T: thesis; K = number of studies; N = sample size; r = effect size; 95% CI = confidence interval around r.

specific, correlation strength is leadership charm, individualized consideration, idealized influence, and intellectual stimulation. Perhaps most empirical research on TL focuses on business operations, and the number of research samples in the construction context is relatively tiny. Stanislas [59] analyzed the indicators that affect sustainable construction and found that the personal charm of the project manager is one of the crucial indicators that can improve leadership effectiveness. Zia [60] reckoned that the emotional intelligence of project managers could improve partnerships and promote effective communication between project members. Maqbool [61] pointed out project managers with high emotional intelligence who bear the desired competencies and exhibit transformational leadership behavior are influential leaders and ensure higher success in projects than their counterparts. Also, Shafi [7] also indicated that idealized influence, intellectual stimulation, and inspirational motivation greatly influence organizational innovation. Many studies support this article's results [62, 63]. Therefore, the results of this article will help construction companies choose the right project manager for the project. At the same time, TL should pay attention to the rational use of the complementarity and dependence between various dimensions in the management process to promote project success.

Thirdly, mediating variables, cultural background, and document types are all sources of heterogeneity. Through a systematic review of meta-literature, this article finds one or more intermediary variables in most existing empirical models, such as knowledge learning, psychological capital, interorganizational relationships, and innovation atmosphere. Scholar Qaisar introduced psychological capital as an intermediary variable to construct a model and found that it negatively affected the relationship between the two. The existence of positive mediating variables will positively impact the relationship between project leadership style and performance, and vice versa. Under the East and the West's different cultural backgrounds, the influence of TL on project success is significantly different and regular. Under the environment of Eastern culture, the impact of TL on project success is higher than that of Western civilization. In particular, influenced by traditional Confucian culture [3, 64], high power distance, and collectivism, low-level project members in Chinese construction organizations are more likely to follow or accept organizational tasks assigned to leaders. However, the project members under a Western

cultural background are more inclined to individualism, reflecting their ability and value [65]. Therefore, the construction project members under different cultural backgrounds will have other internalized explanations when facing the same leadership style, resulting in differences. Under the experience of Eastern culture, TL has a more noticeable impact on project members than in Western countries, resulting in a higher project success rate. In journal papers, more studies have been found to study the relationship between the two, and a large number of research scholars tend to establish empirical models to explore the boundaries of the two through different variables, which is also the direction of future research.

5.2. Theoretical Implications. On the one hand, this research enriches and extends the development of TL and project success theory. Through a meta-analysis, the reasons for the inconsistent conclusions on the relationship between TL and project success in past studies have been identified, and a focused comparison of the impact of different dimensions of TL and project success is conducted. The research results show that TL has a positive and significant relationship with project success, which provides a new research perspective for improving project success. TL and its impact on the success of the project have been reviewed in previous studies, mainly from the perspective of the overall impact of TL on the success of the project; this is far from enough. Therefore, this article analyzes and explains the differences in previous research results as a whole and helps to clarify the indistinguishability of the project success relationship caused by the mixed use of TL concepts. It can provide more accurate estimates of TL performance in different dimensions and dig deeper. The essence of TL's influence on project success is analyzed, and the impact of TL's dimensions on project success is sorted.

On the other hand, this article enriches and refines the boundary conditions and scope of application that influence the success of the TL project. Based on the empirical data analysis of the former National People's Congress, by further refining the moderating effects of the existence of mediating variables, document type, and cultural background, on the relationship between the two, a detailed discussion of the mechanism of TL and project success can be realized. The research results reveal the precise path of transformational

leadership influencing project success, enriching and perfecting the existing project success model research. This article helps to understand TL-style project managers' internal laws of successful project operation and consolidates academic support for project management success in construction projects.

5.3. Practical Implications. This study provides several practical implications for construction companies and leaders. First of all, it helps construction companies preferentially select project managers. The results show that TL's leaders enhance team cohesion and mutual understanding, create a harmonious working atmosphere, promote the open exchange of ideas and analyses between project teams, and emphasize developing followers' self-management or self-leadership skills. In particular, selecting talents with strong leadership charm and abilities is more conducive to establishing a highly reliable organization for the project to cope with today's complex and changing international environment.

Then, the project managers should focus on their words and deeds on project members. Each project member can understand their mission and goal direction through vision incentives, translating into personal work goals. Inspiring leadership behavior through intelligence can create a challenging organizational atmosphere. This can make the project members more innovative and encourage them to express their ideas. The project manager actively cares about the organization's tasks and the needs of the project members, recognises the uniqueness and diversity of the beliefs and values of the project members, and provides corresponding support. Project managers should improve their own leadership charisma to enhance the self-confidence of members. At the same time, when making decisions, project leaders must have individualized considerations and seek more opinions from members to improve the identity and loyalty of project members. For example, in the Hong Kong-Zhuhai-Macao Bridge [66], well-trained professional subcontractors need better treatment, stable commitment, professional training, improved working conditions, genuine care, and on-site management for workers on-site. Therefore, it helps the Hong Kong-Zhuhai-Macao Bridge to achieve great success.

Finally, the construction project managers require to be trained in technical and soft leadership skills. The former ensures that project managers clearly understand and apply project management methods. The latter helps to adapt these methods to the specific social and cultural environment of the construction project. Thus, TL's leaders must make full use of the new generation of information technology, such as 5G, BIM, robots, etc. In the whole life cycle of project construction, they should lead the project members to achieve project success [67]. Also, they need to learn to use knowledge management and scenario deduction to make decisions, create a working environment that is most suitable for project members, and avoid limiting leaders' behaviors to a certain level. Meanwhile, as a survey concluded, different leadership styles are ideal for various projects [68].

So, it is necessary to adopt a diverse leadership style that adapts to the organizational environment to balance administrative tasks and meet the requirements of project members.

6. Limitation and Future Research Directions

There are several limitations that are worth mentioning. Firstly, the meta-analysis method only includes the analysis of the Pearson correlation coefficient when selecting samples, which will lead to the loss of some models. The removal of samples due to the inability to obtain effective effect sizes may affect the relationship in this article. Secondly, there is a limitation of potential moderating variable analysis. This study examines the potential moderating effects of situational features, design features, and measurement features, but different research samples will be affected by other factors. Future research can further explore other mediating factors, such as stakeholder relationships, psychological empowerment, individual values of project members, etc., to understand why certain construction activities can succeed while others fail.

7. Conclusions

There is a growing amount of research on the relationship between TL and project success, but the findings lack consensus. This meta-analysis provides more statistically valuable and accurate results for the general relationship between TL and project success by overcoming a single study's sampling error and sample size limitations. In addition, the moderating effects can be further tested to explore the influence of the existence of mediating variables, cultural background, and document types on the relationship of TL and project success and the inconsistent results of extant studies. In this way, a comprehensive theoretical framework is constructed for this study. The findings of this paper can provide better insights for choosing the right development strategy and improve leadership effectiveness to promote the project's sustainable development under the Industry 4. 0 era.

Data Availability

The data used to support the findings of this study are available from the corresponding author upon request.

Conflicts of Interest

The authors declare that there are no conflicts of interest regarding the publication of this paper.

Acknowledgments

References

[1] Z. Liu, Y. Lu, M. Shen, and L. C. Peh, "Transition from building information modeling (BIM) to integrated digital delivery (IDD) in sustainable building management: a knowledge discovery approach based review," *Journal of Cleaner Production*, vol. 291, pp. 1–23, 2021.

[2] M. Q. Huang, J. Ninić, and Q. B. Zhang, "BIM, machine learning and computer vision techniques in underground construction: current status and future perspectives," *Tunnelling and Underground Space Technology*, vol. 108, 2021.

[3] J. Dingle, "Cultural issues in the planning and development of major projects," *Risk Management*, vol. 9, 1991.

[4] G. Silvius and R. Schipper, "Exploring variety in factors that stimulate project managers to address sustainability issues," *International Journal of Project Management*, vol. 38, pp. 353–367, 2020.

[5] I. Ul Haq, A. T. Paracha, and W. Shakeel, "A multiple parallel mediation between transformational leadership and project-based performance—a process model," *International Journal of Financial Engineering*, vol. 7, 2020.

[6] A. Singh, "Implementation and evaluation of a transformational leadership education session for nurse leaders and nurse educators," *Journal of Doctoral Nursing Practice*, vol. 13, pp. 125–133, 2020.

[7] M. Shafi, Zoya, Z. Lei, X. Song, and M. N. I. Sarker, "The effects of transformational leadership on employee creativity: moderating role of intrinsic motivation," *Asia Pacific Management Review*, 2020.

[8] B. M. Bass, *Leadership and Performance beyond Expectations*, Free Press, New York, NY, USA, 1985.

[9] A. E. Keegan and D. N. Den Hartog, "Transformational leadership in a project-based environment: a comparative study of the leadership styles of project managers and line managers," *International Journal of Project Management*, vol. 22, pp. 609–617, 2004.

[10] J.-S. Hwang and J. Boo, "Impacts of PM's leadership type on project performance in PPP project," *Journal of Society of Korea Industrial and Systems Engineering*, vol. 41, pp. 41–49, 2018.

[11] J. W. Zheng, G. D. Wu, H. T. Xie, and H. Xu, "Ambidextrous leadership and sustainability-based project performance: the role of project culture," *Sustainability*, vol. 9, 2017.

[12] X. Zhang, Y. Zhang, Y. Sun, M. Lytras, P. Ordonez de Pablos, and W. He, "Exploring the effect of transformational leadership on individual creativity in e-learning: a perspective of social exchange theory," *Studies in Higher Education*, vol. 43, pp. 1964–1978, 2018.

[13] H. L. Chen and Y. L. Lin, "Goal orientations, leader-leader exchange, trust, and the outcomes of project performance," *International Journal of Project Management*, vol. 36, pp. 716–729, 2018.

[14] K. T. Odusami, R. R. O. Iyagba, and M. M. Omirin, "The relationship between project leadership, team composition and construction project performance in Nigeria," *International Journal of Project Management*, vol. 21, pp. 519–527, 2003.

[15] F. T. Berssaneti and M. M. Carvalho, "Identification of variables that impact project success in Brazilian companies," *International Journal of Project Management*, vol. 33, pp. 638–649, 2015.

[16] C. W. Langfred, "Too much of a good thing? negative effects of high trust and individual autonomy in self-managing teams," *Academy of Management Journal*, vol. 47, pp. 385–399, 2004.

[17] A. Tajasom, D. K. M. Hung, D. Nikbin, and S. S. Hyun, "The role of transformational leadership in innovation performance of Malaysian SMEs," *Asian Journal of Technology Innovation*, vol. 23, pp. 172–188, 2015.

[18] J. Zheng, G. Wu, and H. Xie, "Impacts of leadership on project-based organizational innovation performance: the mediator of knowledge sharing and moderator of social capital," *Sustainability*, vol. 9, 2017.

[19] L. Zhang, T. Cao, and Y. Wang, "The mediation role of leadership styles in integrated project collaboration: an emotional intelligence perspective," *International Journal of Project Management*, vol. 36, pp. 317–330, 2018.

[20] Q. Iqbal, N. H. Ahmad, A. Nasim, and S. A. R. Khan, "A moderated-mediation analysis of psychological empowerment: sustainable leadership and sustainable performance," *Journal of Cleaner Production*, vol. 262, 2020.

[21] J.-X. Chen, P. Sharma, W. Zhan, and L. Liu, "Demystifying the impact of CEO transformational leadership on firm performance: interactive roles of exploratory innovation and environmental uncertainty," *Journal of Business Research*, vol. 96, pp. 85–96, 2019.

[22] B. M. Bass, "Theory of transformation leadership redux," *The Leadership Quarterly*, vol. 6, pp. 463–478, 1995.

[23] P. M. Podsakoff, S. B. MacKenzie, and W. H. Bommer, "Transformational leader behaviors and substitutes for leadership as determinants of employee satisfaction, commitment, trust, and organizational citizenship behaviors," *Journal of Management*, vol. 2, pp. 259–298, 1996.

[24] B. J. Avolio and W. L. Gardner, "Authentic leadership development: getting to the root of positive forms of leadership," *The Leadership Quarterly*, vol. 16, pp. 315–338, 2005.

[25] S. Li Chaoping, "The structure and measurement of transformational leadership in China," *Acta Psychological Sinica*, vol. 37, pp. 803–811, 2005.

[26] S. Mišić and M. Radujković, "Critical drivers of megaprojects success and failure," *Procedia Engineering*, vol. 122, pp. 71–80, 2015.

[27] E. F. M. I. a. R. P. Leifer, "Effective control of new product projects: the interaction of organization culture and project leadership," *Journal of Product Innovation Management*, vol. 3, pp. 149–157, 1986.

[28] D. J. Bryde and L. Robinson, "Client versus contractor perspectives on project success criteria," *International Journal of Project Management*, vol. 23, pp. 622–629, 2005.

[29] B.-C. Kim and K. F. Reinschmidt, "Combination of project cost forecasts in earned value management," *Journal of Construction Engineering and Management*, vol. 137, pp. 958–966, 2011.

[30] G. Cserháti and L. Szabó, "The relationship between success criteria and success factors in organisational event projects," *International Journal of Project Management*, vol. 32, pp. 613–624, 2014.

[31] R. Joslin and R. Müller, "Relationships between a project management methodology and project success in different project governance contexts," *International Journal of Project Management*, vol. 33, pp. 1377–1392, 2015.

[32] Y. J. C. C. Chen, "Integrating knowledge activities for team innovation: effects of transformational leadership," *Journal of Management*, 2016.

[33] L. Luo, Q. He, J. Xie, D. Yang, and G. Wu, "Investigating the relationship between project complexity and success in complex construction projects," *Journal of Management in Engineering*, vol. 33, 2017.

[34] R. Ahmed and N. Azmi bin Mohamad, "Exploring the relationship between multi-dimensional top management support and project success: an international study," *Engineering Management Journal*, vol. 28, pp. 54–67, 2016.

[35] M. M. d. Carvalho, L. A. Patah, and D. de Souza Bido, "Project management and its effects on project success: cross-country and cross-industry comparisons," *International Journal of Project Management*, vol. 33, pp. 1509–1522, 2015.

[36] B. C. H. Nam, "Strategies for technology push: lessons from construction innovations," *Journal of Construction Engineering and Management*, vol. 118, pp. 507–524, 1992.

[37] A. N. Khawaja Fawad Latif, F. Shahzad, and M. Ullah, "Impact of entrepreneurial leadership on project success: mediating role of knowledge management processes," *Entrepreneurial leadership on project success*, vol. 41, pp. 237–256, 2020.

[38] D. Wang, H. Fu, and S. Fang, "The relationship between relational quality and megaproject success: the moderating role of incentives," *Engineering Management Journal*, vol. 25, pp. 1–13, 2019.

[39] J. Bruce and W. z. Avolid, "Transformational leadership and organizational commitment: mediating role of psychological empowerment and moderating role of structural distance," *Journal of Organizational Behavior*, vol. 25, pp. 951–968, 2004.

[40] K. M. R. Amin Akhavan Tabassi, A. H. Abu Bakar, and N. A. Yusof, "Linking team condition and team performance: a transformational leadership approach," *Project Management Journal*, vol. 48, pp. 22–38, 2017.

[41] M. F. Dulaimi, M. P. Nepal, and M. Park, "A hierarchical structural model of assessing innovation and project performance," *Construction Management & Economics*, vol. 23, pp. 565–577, 2005.

[42] C. M. Scott-Young, M. Georgy, and A. Grisinger, "Shared leadership in project teams: an integrative multi-level conceptual model and research agenda," *International Journal of Project Management*, vol. 37, pp. 565–581, 2019.

[43] A. u. Musawir, C. E. M. Serra, O. Zwikael, and I. Ali, "Project governance, benefit management, and project success: towards a framework for supporting organizational strategy implementation," *International Journal of Project Management*, vol. 35, pp. 1658–1672, 2017.

[44] H.-W. Chou, Y.-H. Lin, H.-H. Chang, and W.-W. Chuang, *Transformational Leadership and Team Performance*, SAGE Open, Newbury Park, CA, USA, 2013.

[45] V. J. García-Morales, M. M. Jiménez-Barrionuevo, and L. Gutiérrez-Gutiérrez, "Transformational leadership influence on organizational performance through organizational learning and innovation," *Journal of Business Research*, vol. 65, pp. 1040–1050, 2012.

[46] D. A. N. Aga and B. Vallejo, "Transformational leadership and project success: the mediating role of team-building," *International Journal of Project Management*, vol. 34, pp. 806–818, 2016.

[47] M. M. Hassan, S. Bashir, and S. M. Abbas, "The impact of project managers' personality on project success in NGOs: the mediating role of transformational leadership," *Project Management Journal*, vol. 48, pp. 74–87, 2017.

[48] R. Z. Z. C. B. C. Z. W. J. G. Z. Zhuohon, "Mechanisms of the acceptance and commitment therapy: a meta-analytic structural equation model," *Acta Psychologica Sinica*, vol. 51, 2019.

[49] M. Offord, R. Gill, and J. Kendal, "Leadership between decks A synthesis and development of engagement d resist ce theories of leadership based on evidence from practice in Royal Navy warships," *The Leadership and Organization Development Journal*, vol. 37, pp. 289–304, 2016.

[50] M. Mäkilouko, "Coping with multicultural projects: the leadership styles of Finnish project managers," *International Journal of Project Management*, vol. 22, pp. 387–396, 2004.

[51] R. M. Stock and G. Oezbek-Potthoff, "Implicit leadership in an intercultural context: theory extension and empirical investigation," *International Journal of Human Resource Management*, vol. 25, pp. 1651–1668, 2014.

[52] L. S. Henderson, R. W. Stackman, and R. Lindekilde, "Why cultural intelligence matters on global project teams," *International Journal of Project Management*, vol. 36, pp. 954–967, 2018.

[53] A. van Marrewijk and K. Smits, "Cultural practices of governance in the Panama canal expansion megaproject," *International Journal of Project Management*, vol. 34, pp. 533–544, 2016.

[54] F. Kong, C.-H. Tsai, F.-S. Tsai, W. Huang, and S. de la Cruz, "Psychological capital research: a meta-analysis and implications for management sustainability," *Sustainability*, vol. 10, pp. 1–9, 2018.

[55] C. S. Burke, K. C. Stagl, C. Klein, G. F. Goodwin, E. Salas, and S. M. Halpin, "What type of leadership behaviors are functional in teams? a meta-analysis," *The Leadership Quarterly*, vol. 17, pp. 288–307, 2006.

[56] S. G. T. Higgins, J. J. Deeks, and D. G. Altman, "Measuring inconsistency in meta-analyses," *BMJ*, vol. 327, pp. 557–560, 2003.

[57] J. Kissi, A. Dainty, and A. Liu, "Examining middle managers' influence on innovation in construction professional services firms," *Construction Innovation*, vol. 12, pp. 11–28, 2012.

[58] M. H. Do and A. Minbashian, "Higher-order personality factors and leadership outcomes: a meta-analysis," *Personality and Individual Differences*, vol. 163, 2020.

[59] M. Stanitsas, K. Kirytopoulos, and V. Leopoulos, "Integrating sustainability indicators into project management: the case of construction industry," *Journal of Cleaner Production*, vol. 279, 2021.

[60] N. U. Zia, "Knowledge-oriented leadership, knowledge management behaviour and innovation performance in project-based SMEs. The moderating role of goal orientations," *Journal of Knowledge Management*, vol. 24, pp. 1819–1839, 2020.

[61] Y. S. Rashid Maqbool, N. Manzoor, and Y. Rashid, "The Impact of emotional intelligence, project managers' competencies, and transformational leadership on project success: an empirical perspective," *Project Management Journal*, vol. 48, pp. 58–75, 2017.

[62] A. L. Allan Lee, D. Hughes, and A. W. Tian, "Alexander Newman & Caroline Knight. Leadership, creativity and innovation: a metaanalytic review," *European Journal of Work and Organizational Psychology*, 2019.

[63] J. Rowold, L. Borgmann, and M. Diebig, "A "Tower of Babel"?–interrelations and structure of leadership constructs," *The Leadership & Organization Development Journal*, vol. 36, pp. 137–160, 2015.

[64] W. W. Low, H. Abdul-Rahman, and N. Zakaria, "Organisational culture of Malaysian international construction organisations," *International Journal of Construction Management*, vol. 20, pp. 105–121, 2018.

[65] B. T. Atuahene and B. K. Baiden, "Organizational culture of Ghanaian construction firms," *International Journal of Construction Management*, vol. 18, pp. 177–188, 2017.

[66] Y. Hu, A. P. C. Chan, Y. Le, and R.-z. Jin, "From construction megaproject management to complex project management: bibliographic analysis," *Journal of Management in Engineering*, vol. 31, pp. 1–48, 2015.

[67] R. Borg, R. Dalli Gonzi, and S. Borg, "Building sustainably: a pilot study on the project manager's contribution in delivering sustainable construction projects—a Maltese and international perspective," *Sustainability*, vol. 12, 2020.

[68] R. Müller and R. Turner, "The Influence of project managers on project success criteria and project success by type of project," *European Management Journal*, vol. 25, pp. 298–309, 2007.